Cover Picture



Walter Schuh, Pierre Braunstein,* Marc Bénard, Marie-Madeleine Rohmer, and Richard Welter

What goes around comes around. The cover picture describes how a Pd center undergoes an oscillating motion along the Fe-Hg-Fe metal chain of a cluster that exhibits helically arranged diphenylphosphanylmethane ligands. The Pd^0 fragment was "captured" by a trimetallaphosphane that can easily adapt its conformation through rotation about a Hg–Fe bond. For more details of this unusual cluster, which exhibits an unprecedented Pd–Hg d^{10}–d^{10} interaction, see the Communication by P. Braunstein et al. on page 2161 ff.

Contents

Web Sites

http://www2.chemie.uni-erlangen.de/services ——— 2110 — Quantum Chemistry: A Playground with Hidden Treasures — *C. van Wüllen*

Books

Ionic Liquids in Synthesis ——— 2111 — Peter Wasserscheid, Tom Welton — *reviewed by M. Maase*

Encyclopedia of Catalysis ——— 2112 — Istvan T. Horvath — *reviewed by C. D. Frohning*

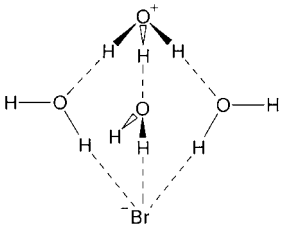
Highlights

Mechanisms of Acid Dissociation

A. F. Voegele, K. R. Liedl* — 2114 – 2116

Exploring HBr Ionization at the Molecular Level

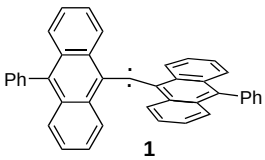
Cluster techniques and femtosecond spectroscopy has been used in a recent study to elucidate the mechanism of HBr dissolution and ionization. Complete dissolution is achieved by a cluster of five water molecules, while photoinduced electric excitation is necessary in clusters of four water molecules. The findings are in good agreement with ab initio results which propose that total dissolution can be achieved in clusters of four water molecules (see structure).



Stabilizing Carbenes

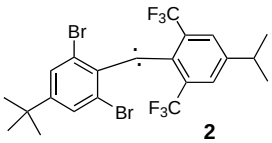
W. Kirmse* ——— 2117 – 2119

Persistent Triplet Carbenes



1

$t_{1/2}$ = 19 min at 20°C



2

$t_{1/2}$ = 9 min at 20°C

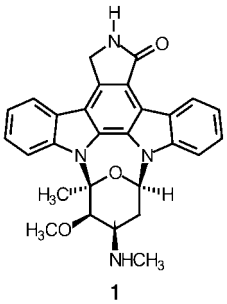
Unpairing carbenes with unpaired electrons: Triplet carbenes are prone to dimerization but can be stabilized kinetically. By means of steric shielding and electron delocalization, Tomioka and coworkers succeeded in preparing exceptionally long-lived triplet diarylcarbenes, such as **1** and the bromine- and trifluoromethyl **2**.

Reviews

Cyclin-Dependent Kinases

A. Huwe, R. Mazitschek, A. Giannis* ——— 2122 – 2138

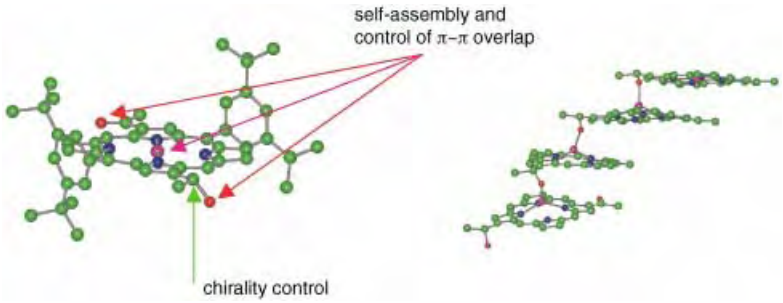
Small Molecules as Inhibitors of Cyclin-Dependent Kinases



1

A basic approach to cancer therapy: Cyclin-dependent kinases (CDKs) and their activating subunits, the cyclins, are the central pacemakers of the cell cycle. Virtually all malignant diseases are ascribed to a defect of these key players or their direct regulators. Therefore, great efforts have been made to synthesize compounds which modulate the activity of CDKs. This review provides an overview of the progress in the development of low-molecular-weight CDK inhibitors, such as the natural product stauosporin (**1**).

Communications

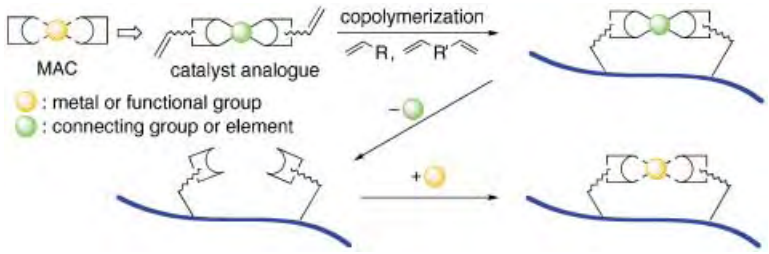


Artificial Light-Harvesting Antenna

T. S. Balaban,* A. D. Bhise, M. Fischer, M. Linke-Schaetzel, C. Roussel, N. Vanthuyne ——— **2140 – 2144**

Controlling Chirality and Optical Properties of Artificial Antenna Systems with Self-Assembling Porphyrins

In a biomimetic approach, the same groups that are responsible for the self-assembly of bacteriochlorophylls in the natural antenna systems of green photosynthetic bacteria, have been engineered onto desired positions of fully synthetic porphyrins. The architecture of the monomeric building block determines both the chirality and the optical properties of the supramolecular assembly, depicted right, as a tetramer. Neither the self-assembly, nor the chemisorption onto titania nanoparticles quenches the fluorescence of the aggregates, thus they may be of use in dye-photosensitized solar cells.



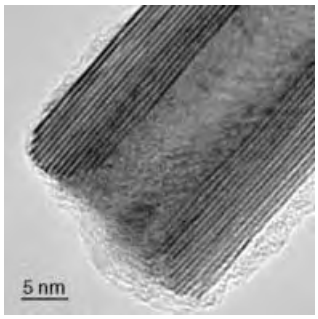
Multicomponent Asymmetric Catalysts

T. Arai, T. Sekiguti, K. Otsuki, S. Takizawa, H. Sasai* ——— **2144 – 2147**

"Catalyst Analogue": A Concept for Constructing Multicomponent Asymmetric Catalysts (MAC) by Using a Polymer Support

Big MAC news! A new concept for constructing multicomponent asymmetric catalysts (MACs) is proposed by use of a stable "catalyst analogue". After copolymerization of a catalyst analogue having olefinic moieties with a monomer (e.g., methyl methacrylate), the resulting polymer is used to prepare an active catalyst by exchanging the connecting group with a catalytically active metal (see scheme).

Filling the gaps: A low-temperature solution route was employed to successfully prepare multiwalled TiS_2 nanotubes with open-ended tips (see HRTEM image). The as-prepared nanotubes could be intercalated with lithium atoms by treating a solution of the TiS_2 nanotubes with *n*BuLi. The resulting homogeneous intercalated phase of $LiTiS_2$ exhibited a *c*-axis expansion of approximately 10.5% relative to the original TiS_2 material.



Li-Intercalated TiS_2 Nanotubes

J. Chen,* Z.-L. Tao, S.-L. Li ——— **2147 – 2151**

Lithium Intercalation in Open-Ended TiS_2 Nanotubes

For the USA and Canada:
ANGEWANDTE CHEMIE International Edition (ISSN 1433-7851) is published weekly by Wiley-VCH PO Box 191161, D 69451 Weinheim, Germany. Air freight and mailing in the USA by Publications Expediting Inc. 200 Meacham Ave., Elmont, NY 11003. Periodicals postage paid at Jamaica NY 11431. US POSTMASTER: send address changes to *Angewandte Chemie*, Wiley-VCH, 111 River Street, Hoboken, NJ 07030. Annual institutional subscription price for institutions: Europe € 2998.00/3148.00. Outside Europe US$ 3718.00/3904.00 (valid for print or electronic/print and electronic delivery); for individuals who are personal members of a national chemical society, or whose institution already subscribes, or who are retired or self-employed consultants, print only (including postage and handling charges): Europe € 248.00/Outside Europe US$ 348.00.

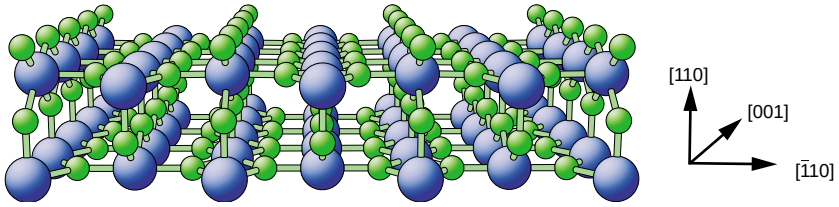
 © 2003 Wiley-VCH Verlag GmbH & Co. KGaA, Weinheim

Contents

Ruthenium Oxide Surface Chemistry

J. Wang, C. Y. Fan, Q. Sun, K. Reuter, K. Jacobi,* M. Scheffler, G. Ertl ——— **2151 – 2154**

Surface Coordination Chemistry: Dihydrogen versus Hydride Complexes on RuO_2(110)

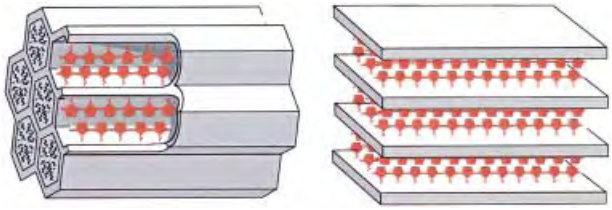


Both atomic and molecular hydrogen are found to chemisorb together at the rutile-structure RuO_2(110) single crystal surface (depicted) at 85 K. The combination of low-temperature ultrahigh vacuum vibrational spectroscopy in conjunction with DFT calculations provides detailed insight into the coordination chemistry of a solid oxide surface (O: green, Ru: violet).

Nanocomposite Films

M. Ikegame, K. Tajima, T. Aida* ——— **2154 – 2157**

Template Synthesis of Polypyrrole Nanofibers Insulated within One-Dimensional Silicate Channels: Hexagonal versus Lamellar for Recombination of Polarons into Bipolarons

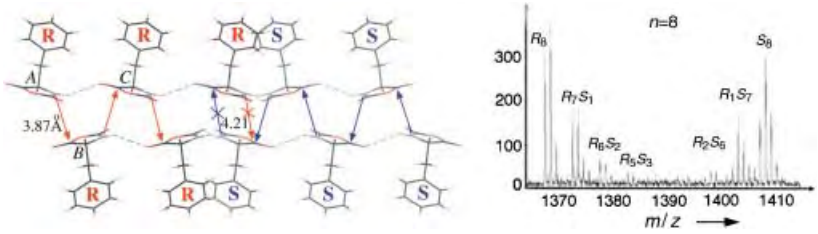


Very different electronic properties are found in the hexagonal and lamellar nanocomposite films (see schematic representations) prepared by dilution of a pyrrole-containing surfactant with non-polymerizable surfactants in a sol–gel-based template polymerization. The hexagonal composite film comprises a thin polypyrrole nanocable covered with an insulating silicate channel.

Oligopeptide Formation in Crystals

J. G. Nery, G. Bolbach, I. Weissbuch,* M. Lahav* ——— **2157 – 2161**

Generation of Oligopeptides with Homochiral Sequences by Topochemical Reactions within Racemic Crystals of Phenylalanine-*N*-carboxyanhydride



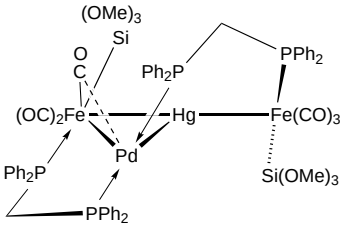
Reactions within crystals: Homochiral oligo(phenylalanine)s (see MALDI-TOF mass spectrum) were obtained from a racemic monomer by utilizing a "zipper-like" mechanism in the solid state (see packing diagram). By generating such species within crystalline architectures, the formation of oligopeptides of up to 17 units in length is plausible.

Dynamic Trimetallic Clusters

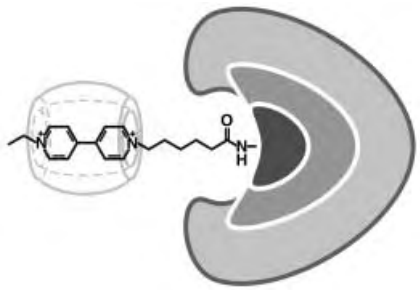
W. Schuh, P. Braunstein,* M. Bénard, M.-M. Rohmer, R. Welter ——— **2161 – 2164**

An Unusual Dynamic Fe-Hg-Pd Cluster with a Palladium(0) Fragment Stabilized by d^{10}–d^{10} Heterometallic Bonding

A heterometallic tetranuclear cluster resulting from an unprecedented metal–metal interaction is described in which a 14-electron PdL_2 fragment is bonded to a Fe-Hg-Fe chain through helically arranged diphenylphosphanylmethane ligands (see picture), along which it exhibits an oscillating motion. The cluster exhibits a close contact between the Pd^0 and Hg^{II} centers; the first such d^{10}–d^{10} interaction to have been observed.



 © 2003 Wiley-VCH Verlag GmbH & Co. KGaA, Weinheim

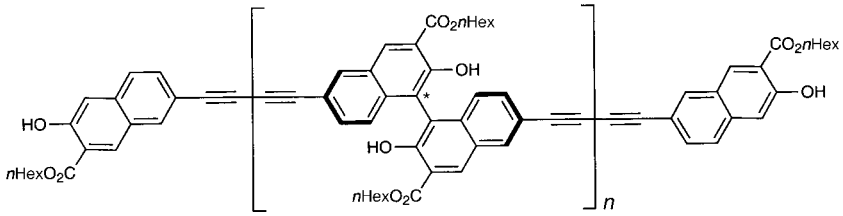


Dendrimers as guests: Dendrimers containing a single 4,4′-bipyridinium residue covalently attached to the focal points of carboxylate-terminated dendrons are strongly complexed by cucurbit[7]uril in aqueous solution (see schematic representation). The complexation has been monitored and quantified by NMR spectroscopic, UV/Vis spectroscopic, and mass spectometric techniques.

Host-Guest Binding Interactions

W. Ong, A. E. Kaifer* ——— **2164 – 2167**

Molecular Encapsulation by Cucurbit-[7]uril of the Apical 4,4′-Bipyridinium Residue in Newkome-Type Dendrimers

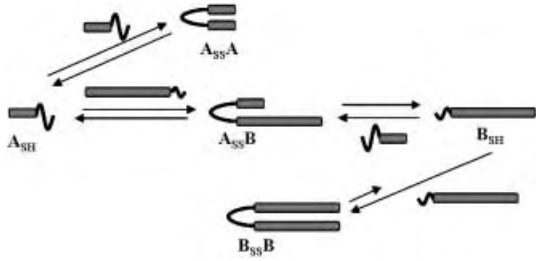


Unusually orderly! Alkynylnaphthols undergo two kinds of couplings stepwise, with high stereocontrol, and in one pot to give chiral binaphthyl polymers like that shown. Since the chemoselectivity of each coupling is remarkably high, this approach is useful for the organized assembly of multifunctional substrates in a single operation.

Cu-Catalyzed Couplings

X. Xie, P.-W. Phuan, M. C. Kozlowski* ——— **2168 – 2170**

Novel Pathways for the Formation of Chiral Binaphthyl Polymers: Oxidative Asymmetric Phenolic Coupling Alone and in Tandem with the Glaser–Hay Coupling



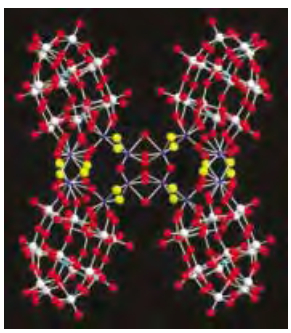
Driving peptides round the bend: Thiol-containing linear peptides ($\mathbf{A_{SH}}$ and $\mathbf{B_{SH}}$) are dimerized (see scheme) using dynamic covalent chemistry to preferentially form an energetically stabilized disulfide by a self-templating mechanism. NMR spectroscopy experiments on this disulfide show that the stabilization is a result of β-sheet formation with the disulfide bond acting as a turn scaffold yielding a peptide with a hairpin-type conformation.

Synthetic Peptides

Y. Krishnan-Ghosh, S. Balasubramanian* ——— **2171 – 2173**

Dynamic Covalent Chemistry on Self-Templating Peptides: Formation of a Disulfide-linked β-Hairpin Mimic

Fours for thought: The title compound was prepared by condensation of the preformed unit $\{Mo_2O_2S_2\}^{2+}$ as a linker on to the trivacant anion $[\alpha\text{-}P_2W_{15}O_5]^{12-}$. The self-assembled structure exhibits a modular arrangement (see structure). ^{31}P and ^{183}W NMR spectroscopy revealed that the structure of the supramolecular tetra-unit anion was maintained in solution.



A Polyoxothiometalate Tetramer

E. Cadot,* M.-A. Pilette, J. Marrot, F. Sécheresse ——— **2173 – 2176**

A Supramolecular Tetra-Dawson Polyoxothiometalate: $[(\alpha\text{-}H_2P_2W_{15}O_{56})_4\{Mo_2O_2S_2(H_2O)_2\}_4\{Mo_4S_4O_4(OH)_2(H_2O)\}_2]^{28-}$

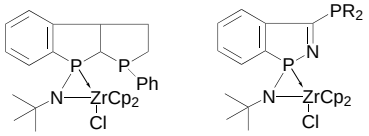
 © 2003 Wiley-VCH Verlag GmbH & Co. KGaA, Weinheim

Contents

Zirconium Spirophosphanes

K. Owsianik, M. Zablocka,* B. Donnadieu, J.-P. Majoral* ——— **2176 – 2179**

Metalla-Azaspirophosphanes: Synthesis, Structure, and Reactivity

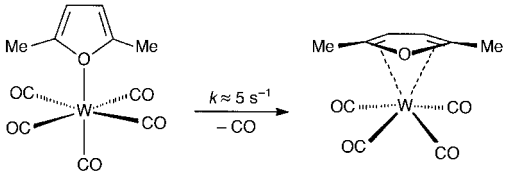


The reaction of a trichloro iminophosphorane ($Cl_3P{=}NtBu$) and either a zirconaindane phospholane or an azazirconaindane phosphane proceeds in an unexpected fashion, with the trapping of a transient chlorophosphaimine species ($Cl{-}P{=}NtBu$), and the formation of unique metalla-azaspirophosphanes (see picture).

Photolysis of Tungsten Complexes

R. Krishnan, H. E. Gottlieb, R. H. Schultz* ——— **2179 – 2181**

Furans Bound Face-On: Sequential Loss of CO in the Formation of $[W(CO)_4(\eta^4\text{-}2,5\text{-dimethylfuran})]$



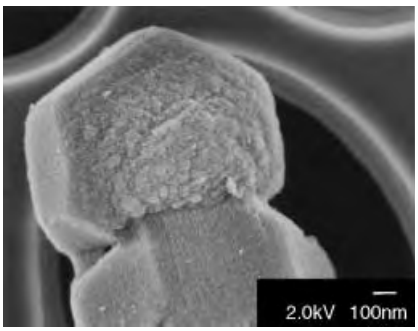
1 **2**

An unusual coordination mode is proposed for the furan ligand in the complex $[(CO)_4W(\eta^4\text{-}Me_2Fur)]$ (**2**; $Me_2Fur = 2,5$-dimethylfuran), which is produced by photolysis of a solution of $[W(CO)_6]$ in the presence of excess Me_2Fur. The kinetics and activation parameters of its formation from the unstable precursor $[(CO)_5W(\eta^1\text{-}Me_2Fur)]$ (**1**) are measured by using time-resolved infrared absorption spectroscopy.

Metal-Free Electron Microscopy

S. Che, K. Lund, T. Tatsumi, S. Iijima, S. H. Joo, R. Ryoo, O. Terasaki* ——— **2182 – 2185**

Direct Observation of 3D Mesoporous Structure by Scanning Electron Microscopy (SEM): SBA-15 Silica and CMK-5 Carbon

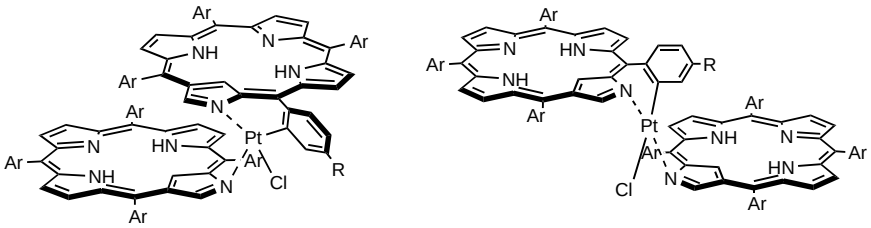


No metal jacket required: The surface structures of mesoporous materials were accurately determined by using electron-microscopy techniques—without the need for metal plating. The effectiveness of these techniques was demonstrated with SBA-15 mesoporous silica (see image) and its CMK-5 carbon replica, for which high-resolution images of the surfaces were obtained.

Pt Complexes of N-Confused Porphyrin

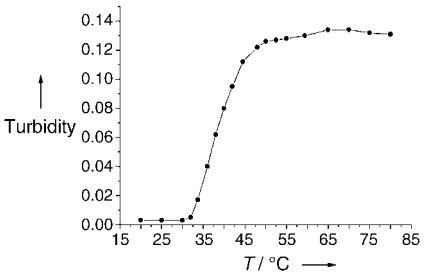
H. Furuta,* K. Youfu, H. Maeda, A. Osuka* ——— **2186 – 2188**

Facile Formation of *N*-Confused Porphyrin Dimers by Platinum(II) Coordination to the Outer-Nitrogen Atoms



Confusion but no doubt: Two types of Pt^{II} dimer complexes of *N*-confused porphyrin (depicted) were synthesized and the structures were unequivocally elucidated by X-ray crystal analyses. Both complexes contain a metallocycle that binds to a Pt center by an outer-nitrogen atom of the confused porphyrin, and by an *ortho*-carbon atom of a *meso*-aryl group.

 © 2003 Wiley-VCH Verlag GmbH & Co. KGaA, Weinheim

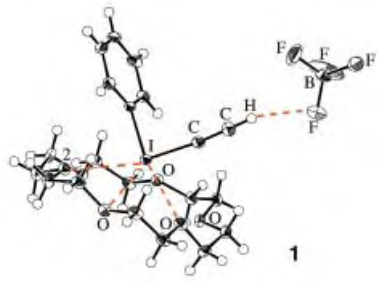


The gradual transition from cylindrical micelles to vesicles on increasing the temperature is demonstrated in the cationic–anionic surfactant system of sodium dodecylsulfate/dodecyltriethylammonium bromide. The transition has been studied by dynamic light scattering studies (see graph), a freeze-fracture technique with observation by electron microscopy, and rheology measurements.

Micelle to Vesicle Transition

H. Yin, Z. Zhou, J. Huang,* R. Zheng, Y. Zhang ——— **2188 – 2191**

Temperature-Induced Micelle to Vesicle Transition in the Sodium Dodecylsulfate/Dodecyltriethylammonium Bromide System



Iodine(III) crowned: Slow evaporation of solvents afforded the 1:1 complex **1** between $[H-C\equiv C-I-Ph]BF_4$ and [18]crown-6 (18C6). Both the solid-state and solution structures of **1** were determined. Reaction of **1** with methanol proceeds in a Michael-type fashion. The complexation with 18C6 increases the stability of labile λ^3-iodanes, such as **1**.

Methanol Additions and Iodanes

M. Ochiai,* K. Miyamoto, T. Suefuji, S. Sakamoto, K. Yamaguchi, M. Shiro ——— **2191 – 2194**

Synthesis, Characterization, and Reaction of Ethynyl(phenyl)-λ^3-Iodane Complex with [18]Crown-6



Amides of 2-iodoxybenzoic acid (IBX amides, **1**) are a new class of pentavalent iodine compounds with a pseudo-benziodoxole structure. These 2-iodoxybenzamides are useful reagents for the oxidation of alcohols, with a reactivity pattern similar to IBX ($R = CH(CH_3)CO_2CH_3$ or $CH(CH_2Ph)CO_2CH_3$ (in crystal structure shown)).

Oxidation of Alcohols

V. V. Zhdankin,* A. Y. Koposov, B. C. Netzel, N. V. Yashin, B. P. Rempel, M. J. Ferguson, R. R. Tykwinski* ——— **2194 – 2196**

IBX Amides: A New Family of Hypervalent Iodine Reagents

VIP Communications labeled with this symbol have been judged by two referees as being "very important papers".

The publication of Communications labeled with this symbol has been accelerated because of their topical or highly competitive nature.

Looking for outstanding employees?

Do you need another expert for your excellent team?
...Chemists, PhD Students, Managers, Professors, Sales Representatives...

Place an advert in the printed version and have it made available online for 1 month, free of charge!

Angewandte Chemie International Edition
Advertising Sales Department: Marion Schulz
Phone: 0 62 01 - 60 65 65
Fax: 0 62 01 - 60 65 50
E-Mail: MSchulz@wiley-vch.de

Service

Keywords ——— *2198*

Authors ——— *2199*

Vacancies ——— *2197*

Preview ——— *2201*

 © 2003 Wiley-VCH Verlag GmbH & Co. KGaA, Weinheim

Contents

Apology

In the Communication "Nanoporous Lanthanide–Copper(II) Coordination Polymers: Syntheses and Crystal Structures of $[\{M_2(Cu_3(iminodiacetate)_6)\}\cdot 8H_2O]_n$ (M = La, Nd, Eu)" by **Y.-P. Ren**, **L.-S. Long,** et al. (*Angew. Chem.* **2003**, *115*, 550; *Angew. Chem. Int. Ed.* **2003**, *42*, 532) the authors missed important references: "Synthesis, Crystal Structure and Magnetic Properties of a Series of Polymeric Lanthanoid–Copper Complexes $[Ln_2Cu_3\{O(CH_2CO_2)_2\}_6]\cdot nH_2O$ (Ln = La, Nd, $n = 9$; Ln = Er, $n = 6$)" (J. G. Mao, J. S. Huang, J. F. Ma, J. Z. Ni, *Trans. Met. Chem.* **1997**, *22*, 277–280), "Synthesis and Crystal Structure of a Novel Lanthanide–Copper Mixed Metal Complex: $Gd_2Cu_3\{O(CH_2COO)_2\}_6\cdot 9H_2O$" (J. G. Mao, L. Song, X. Y. Huang, J. S. Huang, *Polyhedron* **1997**, *16*, 963–966), "Synthesis and Structural Characterization of a Novel Polymeric Gadolinium(III)–Copper(II) Complex of Iminodiacetic Acid" (J. G. Mao, L. Song, J. S. Huang, *J. Chem. Crystallogr.* **1998**, *28*, 475–479), and "Synthesis and Crystal Structure of a New Praseodymiun(III)–Copper(II) Polymeric Complex: $[Pr_2(Cu_3(L^1)_6)_n]$ ($H_2L^1 = NH\{CH_2COOH\}_2$)" (J. G. Mao, L Song, J. S. Huang, *Chinese J. Struct. Chem.* **1999**, *18*, 4–8). The authors apologize for this oversight and thank Qinde Liu of Queen's University, Canada, and Prof. J. G. Mao, Fuzhou, China, for bringing it to their attention.

 © 2003 Wiley-VCH Verlag GmbH & Co. KGaA, Weinheim

Mechanisms of Acid Dissociation

Exploring HBr Ionization at the Molecular Level

*Andreas F. Voegele and Klaus R. Liedl**

Keywords:
ab initio calculations · femtochemistry · hydrogen bonds · hydrogen halides · proton transport

Many technical and methodological innovations in the last few years have resulted in a deeper understanding of mechanisms that occur in nature. For chemists it is essential to understand chemical processes at the atomic level. One of the fundamental theories in chemistry is the Brønsted concept, which describes the ionization of acid molecules in an aqueous environment. Even though much experimental and theoretical effort has been put into studying this phenomenon, there are still a few open questions concerning the mechanism. On a macroscopic scale, acid dissolution has been investigated in depth experimentally for many molecules, which is reflected in the wealth of tabulated thermodynamic data. However, on the molecular level, the basic steps of acid dissolution have for a long time only been accessible by computational methods.

In a recent study Castleman and coworkers[1] impressively demonstrated by using elaborate cluster techniques and femtosecond laser spectroscopy how acid ionization of HBr works at the molecular level. They concluded from their experiments that HBr is completely dissolved and ionized in water clusters consisting of five H_2O molecules and forms a supermolecule with a formal constitution of $H^+(H_2O)_5Br^-$. In smaller clusters with, for example, four water molecules, they found that in the ground state a large portion should exist as $HBr(H_2O)_4$ rather than as an ion pair. However, photoinduced electric excitation provides enough energy for the formation of the solvated ion pair $H^+(H_2O)_4Br^-$.

Castleman and co-workers also used ab initio calculations (Hartree–Fock and Møller–Plesset theory) to study the effect of H_2O complexation on the ionization potential (IP). Firstly, a $HBr{\cdot}H_2O$ hydrate has a slightly lower IP than pure HBr. Secondly, if the H_2O molecule is rearranged in the ionized $HBr{\cdot}H_2O^+$ complex to the proton-shifted $Br{\cdot}H_3O^+$ complex, the IP is once again lowered. These findings give rise to the conclusion that the two ions are separated by solvent within the complex. This complex can be formed by a water-mediated proton transfer, which was confirmed previously by theoretical studies.[2,3]

Conley and Tao studied HBr–water clusters by hybrid density functional theory (B3LYP with extended basis sets).[2] They found that in water clusters of constitution $HBr(H_2O)_3$ the non-ionic or molecular cluster is favored over the ion pair cluster by $-2.1\ kcal\,mol^{-1}$. However, the most stable form in clusters of constitution $HBr(H_2O)_4$ is the ion pair $H^+(H_2O)_4Br^-$, which is favored by $-5.3\ kcal\,mol^{-1}$ over the neutral form.[2] The two ions Br^- and H_3O^+ are separated by water molecules within the complex and form a diamond-like structure (Figure 1). This separation of the ions by water molecules is in agreement with the findings of Castleman and coworkers.[1] Such a complex can only be realized by a water-mediated proton-transfer mechanism, in which one of the H_2O molecules adjacent to HBr is used as a "proton wire" which accepts a proton from the HBr molecule and donates one of its own protons to the next water molecule, which then becomes a H_3O^+ ion.

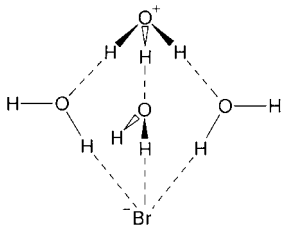


Figure 1. The most stable structure of the HBr–hydrate cluster with four water molecules. The molecule resembles a crownlike structure and the ions are separated by water molecules. Castleman and co-workers concluded from their experiments that a HBr–hydrate cluster forms by substitution of a water molecule according to the mechanism $(H_2O)_n + HBr \rightarrow (H_2O)_{n-1}{\cdot}HBr + H_2O$ followed by water-mediated proton transfer to form $H_3O^+(H_2O)_{n-2}{\cdot}Br^-$. (Adapted from Gertner et al.[3] and Conley and Tao.[2])

Even though the number of water molecules in the cluster determined by experiment ($n = 5$) and theory ($n = 4$) differs, these findings have to be considered as a good agreement because of the uncertainties in determining the temperature during the experiment[4] and as the theoretical results were determined at 0 K. While the computational findings of Conley and Tao[2] for the minimum structures have been confirmed by Gertner et al.,[3] the latter concluded that the cluster with $HBr(H_2O)_4$ is less stable at 180 K than the separated species HBr and $(H_2O)_4$. This result clearly reveals that temperature variations strongly influence the physicochemical properties of such clusters. All the theoretical studies indicate that small temperature variations have a huge influence on the occurrence of certain species of clusters as a consequence of the small energy differences between the single clusters.

[*] Prof. Dr. K. R. Liedl, Dr. A. F. Voegele
Institut für Allgemeine, Anorganische und Theoretische Chemie
Universität Innsbruck
Innrain 52a, 6020 Innsbruck (Austria)
Fax: (+43) 512-507-5144
E-mail: klaus.liedl@uibk.ac.at

 © 2003 Wiley-VCH Verlag GmbH & Co. KGaA, Weinheim DOI: 10.1002/anie.20021613

The study of the solvation and ionization processes of hydrogen halides is important for a number of reasons. First of all, they are readily soluble in water and at least HCl, HBr, and HI are strong acids that ionize easily. Secondly, as diatomic molecules they are the simplest models of a Brønsted acid. Thus, they are extremely well characterized, straightforward to handle, and spectroscopic data can also be interpreted almost unambiguously.

Of particular interest are the ionization processes of HBr and of HCl in the atmosphere, since both molecules are important reservoir species for halogens in the stratospheric. While gas-phase reactions of HCl and HBr play a minor role in stratospheric chemistry, heterogeneous reactions in polar stratospheric clouds (PSCs) convert these reservoir species into more reactive halogen compounds. PSCs form at cold temperatures below 200 K at an altitude of 12 to 25 km, which are conditions that are present in the stratosphere over the Antarctic. PSCs act catalytically by increasing the rates of transformation from inactive reservoirs into active species. The finally formed halogen atoms or halogen compound radicals are responsible for ozone destruction in the stratosphere.[5] Hence, detailed knowledge of the molecular processes occurring after adsorption of HX is of great importance for studying the heterogeneous reactions of PSCs.

To a first approximation, these PSCs can be classified into two major groups: type I and type II. Whereas PSCs of type I are of heterogeneous composition, PSCs of type II are considered to be solely composed of water ice.[6] Therefore, there is a large number of experimental[7–12] and theoretical[13–16] studies on the reaction and interaction of HCl and HBr with different ice samples that mimic PSCs of type II. Hudson et al.,[11] for example, studied the formation of H_2O/HBr hydrates in thin ice samples by FTIR and found hydrates with a formal stoichiometry of about 3.6:1. They thus proposed that the HBr hydrates formed in their samples were mainly a mixture of trihydrates and tetrahydrates. They were also able to confirm the formation of H_3O^+. Graham and Roberts[9] studied interactions between crystalline ice and HCl at a similar temperature but with slightly altered conditions and they reported the presence of several different states, including a hexahydrate ($HCl{\cdot}6H_2O$) at the surface and an ionized form in the bulk. Devlin et al.[12] studied the adsorption and solvation process of HCl on ice particles by means of FTIR, and used Monte Carlo simulations and ab initio calculations (Møller–Plesset) to analyze the different stages of HCl ionization (Figure 2). Possibly, in a first step the HCl molecule adsorbs almost perpendicularly at the ice surface with the hydrogen atom pointing towards an oxygen atom at the surface, thus forming one hydrogen bond. In the next step a free hydrogen atom at the ice surface binds the Cl entity of HCl to form a second hydrogen bond with the HCl molecule. The third step includes formation of a third hydrogen bond which induces spontaneous deprotonation of HCl. The proton is thus delocalized and diffuses into the ice. This proposal is in accordance with a theoretical study by Svanberg et al.,[17] who used a combined quantum mechanics and molecular mechanics method. They proposed that HCl ionization requires the formation of a total of three hydrogen bonds between ice and HCl, and the experimental findings of proton delocalization are again explained by a water-mediated proton-transfer mechanism.[17]

Studies such as those of Castleman and co-workers[1] and of Devlin et al.[12] reveal that chemical research has now reached a new level; experimentalists are no longer restricted to performing studies mainly on a macroscopic scale because of the limited resolution of their equipment at the molecular level. Modern cluster science and evolving techniques such as femtosecond spectroscopy nowadays allow the study of both molecular structure and orientation and even of transition states.[19–21] A few years ago these areas could only be accessed by computational methods, but now both experimentalists and theoreticians are able to access the molecular scale. The proper combination of both fields can now yield excellent and detailed microscopic pictures, as exemplified in several recent reports, which are more informative than those obtained soley from theory or experiment.[1,12,22]

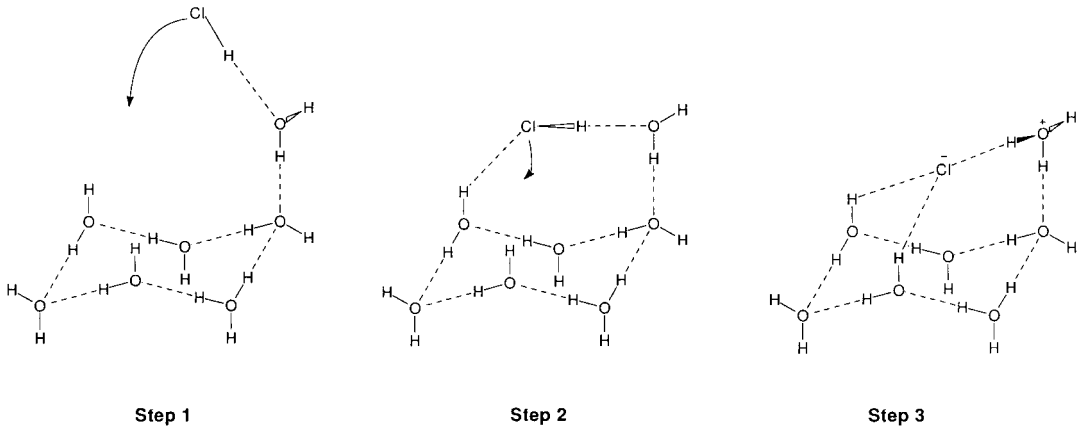


Figure 2. Single steps of HCl ionization on ice. In the first step a hydrogen bond is formed between HCl and a free oxygen atom at the surface. In the next step a second hydrogen bond is formed with a free hydrogen atom, and in the final step yet another hydrogen bond is formed which is accompanied by a proton-transfer step. The proton is considered to be delocalized, that is, it is transfered along the hydrogen bonds by a water-mediated proton transfer. (Adapted from Leutwyler[18] and Devlin et al.[12])

 © 2003 Wiley-VCH Verlag GmbH & Co. KGaA, Weinheim

Computational chemistry is evolving at an incredible pace in terms of both methodology and computation and is now entering the area of macroscopic chemistry. It is possible to study extended clusters at the border with the bulk phase by correlated ab initio methods.[23] Quantum-mechanical ab initio molecular-dynamic methods coupled with path integration have made it possible for theoreticians to study bulk-phase properties, such as proton transfer.[24–28] It is even possible to investigate macroscopic properties by computational methods as shown recently by Matsumoto et al.[29] In this study they described ice nucleation during the process of water freezing by a purely classical molecular dynamics simulation.

Even though it will still be a long time before it will be possible to investigate most of the chemical processes in detail both experimentally and theoretically, recent developments have made one thing clear: By careful and proper choice of methods it is not only possible to combine modern experimental with high-performance computational techniques to access the molecular level, but the combination of theory and experiment enables studies to be performed at the macroscopic level.

[1] S. M. Hurley, T. E. Dermota, D. P. Hydutsky, A. W. Castleman, Jr., *Science* **2002**, *298*, 202 – 204.

[2] C. Conley, F.-M. Tao, *Chem. Phys. Lett.* **1999**, *301*, 29 – 36.

[3] B. J. Gertner, G. H. Peslherbe, J. T. Hynes, *Isr. J. Chem.* **1999**, *39*, 273 – 281.

[4] S. M. Hurley, personal communication, **2003**; under the experimental conditions reported in Ref. [1], it is impossible to accurately determine the temperature range of the molecular beam, but an estimate of the temperature is possible. It is expected that the rotational temperature of the beam is a few Kelvin while the translational temperature should be near 0 K. An estimated vibrational temperature range is 100 – 200 K.

[5] M. J. Molina, T.-L. Tso, L. T. Molina, F. C.-Y. Wang, *Science* **1987**, *238*, 1253 – 1257.

[6] B. J. Finlayson-Pitts, J. N. Pitts Jr., *Chemistry of the Upper and Lower Atmosphere*, Academic Press, San Diego, **2000**.

[7] D. R. Hanson, A. R. Ravishankara, *J. Phys. Chem.* **1992**, *96*, 9441 – 9446.

[8] A. B. Horn, M. A. Chesters, M. R. S. McCoustra, J. R. Sodeau, *J. Chem. Soc. Faraday Trans.* **1992**, *88*, 1077 – 1078.

[9] J. D. Graham, J. T. Roberts, *J. Phys. Chem.* **1994**, *98*, 5974 – 5983.

[10] B. Fluckinger, L. Chaix, M. J. Rossi, *J. Phys. Chem. A* **2000**, *104*, 11739 – 11750.

[11] P. K. Hudson, K. L. Foster, M. A. Tolbert, S. M. George, S. R. Carlo, V. H. Grassian, *J. Phys. Chem. A* **2001**, *105*, 694 – 702.

[12] J. P. Devlin, N. Uras, J. Sadlej, V. Buch, *Nature* **2002**, *417*, 269 – 271.

[13] B. J. Gertner, J. T. Hynes, *Science* **1996**, *271*, 1563 – 1566.

[14] R. Bianco, B. J. Gertner, J. T. Hynes, *Ber. Bunsen-Ges.* **1998**, *102*, 518 – 526.

[15] B. J. Gertner, J. T. Hynes, *Faraday Discuss.* **1998**, *110*, 301 – 322.

[16] Y. A. Mantz, F. M. Geiger, L. T. Molina, M. J. Molina, B. L. Trout, *J. Phys. Chem. A* **2001**, *105*, 7037 – 7046.

[17] M. Svanberg, J. B. C. Petterson, K. Bolton, *J. Phys. Chem. A* **2000**, *104*, 5787 – 5798.

[18] S. Leutwyler, *Nature* **2002**, *417*, 230 – 231.

[19] K. Liu, J. D. Cruzan, R. J. Saykally, *Science* **1996**, *271*, 929 – 933.

[20] A. H. Zewail, *Angew. Chem.* **2000** *112*, 2688 – 2738; *Angew. Chem. Int. Ed.* **2000**, *39*, 2586 – 2631.

[21] J. S. Baskin, A. H. Zewail, *J. Phys. Chem. A* **2001**, *105*, 3680 – 3692.

[22] J. K. Gregory, D. C. Clary, K. Liu, M. G. Brown, R. J. Saykally, *Science* **1997**, *275*, 814 – 817.

[23] R. Ludwig, *Angew. Chem.* **2001**, *113*, 1856 – 1876; *Angew. Chem. Int. Ed.* **2001**, *40*, 1808 – 1827.

[24] M. E. Tuckerman, D. Marx, M. K. Klein, M. Parrinello, *J. Chem. Phys.* **1996**, *104*, 5579 – 5588.

[25] D. Marx, M. Parrinelle, *J. Chem. Phys.* **1996**, *104*, 4077 – 4082.

[26] D. Marx, M. E. Tuckerman, J. Hutter, M. Parrinello, *Nature* **1999**, *397*, 601 – 604.

[27] M. Benoit, D. Marx, M. Parrinello, *Nature* **1998**, *392*, 258 – 261.

[28] P. L. Geissler, C. Dellago, D. Chandler, J. Hutter, M. Parrinello, *Science* **2001**, *291*, 2121 – 2124.

[29] M. Matsumoto, S. Saito, I. Ohmine, *Nature* **2002**, *416*, 409 – 413.

 © 2003 Wiley-VCH Verlag GmbH & Co. KGaA, Weinheim

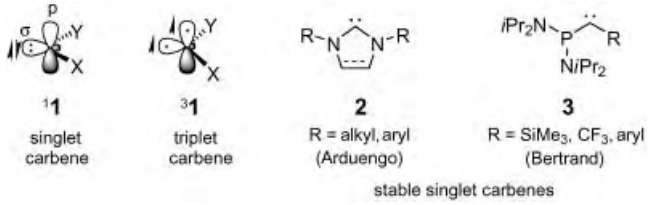
Stabilizing Carbenes

Persistent Triplet Carbenes

*Wolfgang Kirmse**

Keywords:
carbenes · dimerization · radicals · steric hindrance · substituent effects

Carbenes **1** are neutral, divalent derivatives of carbon.[1] The carbene carbon atom has two electrons not involved in bonding which can be spin-paired (singlet state) or unpaired (triplet state). As a rule, carbenes are highly reactive intermediates that can be isolated, at best, in solid matrices at very low temperatures.[2] However, with substituents, such as R_2N and R_2P, "bottleable" singlet carbenes have been prepared (for example, **2** and **3**, Scheme 1).[3] Some of these species are thermodynamically more stable than their alkene dimerization products.



Scheme 1. Electronic structure and stability of carbenes.

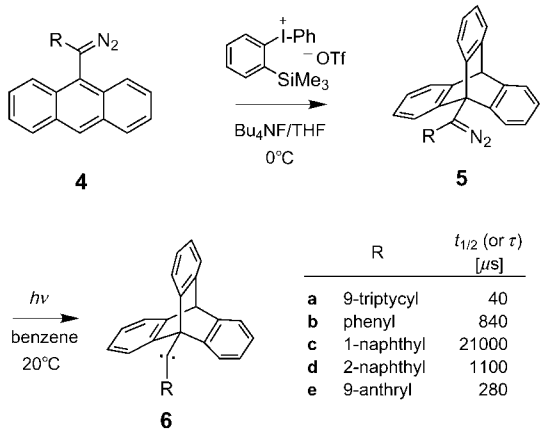
Long-lived triplet carbenes are more difficult to obtain. The dimerization reactions of triplet methylene, phenylcarbene, and vinylcarbene are exothermic by 728, 628, and 610 kJ mol^{-1}, respectively. These numbers indicate that conjugation with π systems will not lead to thermodynamically stable triplet carbenes. Steric congestion about the resulting double bond is also insufficient: the (hypothetical) dimerization of di(*tert*-butyl)carbene was computed to be exothermic by 308 kJ mol^{-1}.[4] Hence *kinetic stabilization* is the only promising approach to persistent triplet carbenes.

For more than a decade, Tomioka and his co-workers at Mie University, Japan, have explored the field of persistent triplet carbenes with remarkable success.[5] Some of the most fascinating results are summarized below.

The shielding of a divalent carbon atom is an ambitious task. Triplet carbenes readily abstract hydrogen from aliphatic C–H bonds. Although neighboring alkyl groups protect the carbene from external attack, intramolecular reaction pathways are opened that shorten its lifetime. Thus, triplet di(*tert*-butyl)carbene was detected by ESR spectroscopy at 20 K but decayed rapidly at temperatures above 70 K.[6] Moreover, steric hindrance will impede the synthesis of carbene precursors. Carbenes are usually generated from diazo compounds, which are obtained from ketones by way of hydrazones. With severe steric hindrance, these transformations proceed only sluggishly, if at all.

These problems were elegantly solved in Tomioka's recent work on triptycylcarbenes **6** (Scheme 2).[7] The desired carbene precursors **5** were made by adding benzyne to 9-anthryldiazoalkanes **4**, under neutral conditions at 0 °C. With two equivalents of benzyne, di(9-anthryl)diazomethane (**4e**) afforded di(triptycyl)diazomethane (**5a**).[7b] Triplet di(triptycyl)carbene (**6a**), generated by photolysis of **5a** and characterized by its ESR spectrum, was found to be the most persistent dialkylcarbene known. However, with a half-life of 40 μs at 20 °C, **6a** is still a rather elusive species.

The reactivity of the divalent carbon of a triplet carbene is also diminished by delocalization of the unpaired electrons. The longer lifetimes of aryl(triptycyl)carbenes **6b–6e**, relative to that of **6a**, attest to the efficiency of this approach.[7a] However, electron delocalization can create additional reactive sites which need protection. Di(9-anthryl)carbene (**7**; Scheme 3) provides a striking example of this effect: the half-life of **7** (0.5 μs at 20 °C) is shorter than that of diphenylcarbene. The unpaired electrons of **7** reside largely at the 10,10′-

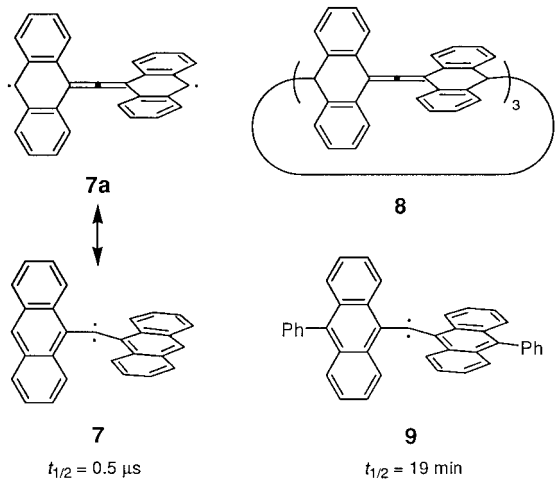


	R	$t_{1/2}$ (or τ) [μs]
a	9-triptycyl	40
b	phenyl	840
c	1-naphthyl	21000
d	2-naphthyl	1100
e	9-anthryl	280

Scheme 2. Generation and lifetimes of triplet 9-triptycylcarbenes (half-lives refer to degassed benzene at room temperature).

[*] Prof. Dr. W. Kirmse
Fakultät für Chemie
Ruhr-Universität Bochum
Universitätsstrasse 150, 44780 Bochum (Germany)
Fax: (+49) 234-321-4353
E-mail: kirmse@xenon.orch.ruhr-uni-bochum.de

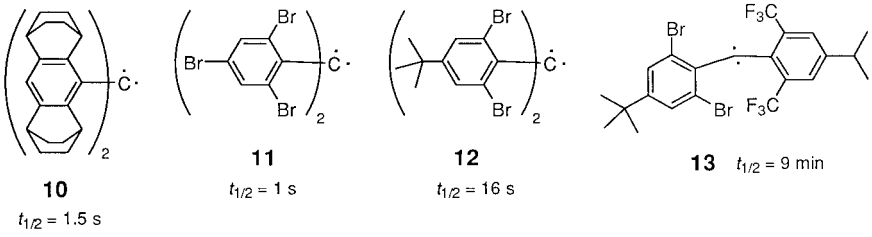
DOI: 10.1002/anie.200301638
© 2003 Wiley-VCH Verlag GmbH & Co. KGaA, Weinheim



Scheme 3. Triplet di(9-anthryl)carbene and its 10,10′-diphenyl derivative.

positions, as indicated by the resonance structure **7a**. In fact, the major product obtained from **7** is the trimer **8** arising by linking of the 10,10′-positions.[8] A dramatic change is brought about by phenyl substituents in these positions: carbene **9** has a half-life of 19 min at 20 °C and is the most persistent diarylcarbene known to date.[9]

The lifetimes of diphenylcarbene and di(1-napthylcarbene) are enhanced by factors of 10^4–10^5 if the *ortho* and *para* positions are substituted with methyl groups.[10] The half-lives of methyl-protected diarylcarbenes, which are in the ms regime, increase further, by factors of 3–10, upon replacement of *o*-CH_3 with *o*-CD_3. The isotope effect indicates that intramolecular hydrogen abstraction limits the lifetime of these triplet carbenes. The undesired formation of *o*-xylylenes is excluded by the bridged structure of **10** (Scheme 4). As



Scheme 4. Persistent derivatives of triplet diphenylcarbene.

to persistence, **10** ($t_{1/2}$ = 1.5 s) stands out among alkyl-protected diarylcarbenes.[11]

Bromine was found to be a good protecting group for the 2,6-positions of triplet diarylcarbenes while *tert*-butyl is preferable for the 4-position (compare **11** and **12**).[12] Trifluoromethyl is even better than bromine. Unfortunately, problems with the synthesis of carbene precursors have prevented the introduction of four *o*-CF_3 groups. So far, the best compromise is **13** the half-life ($t_{1/2}$ = 9 min) of which approaches that of **9**.[13] According to computations [B3LYP6-311G(d,p)], ^{3}**13** is destabilized by 26 kJ mol^{-1} relative to triplet diphenylcarbene.[14] The enormously enhanced lifetime of **13** (by a factor of approximately 10^8!) is entirely steric in origin. It should be emphasized that even the most persistent triplet carbenes react readily with oxygen. Careful exclusion of oxygen is mandatory to attain the half-lives given above.

Triplet carbenes are much more difficult to stabilize than radicals. Nevertheless, Tomioka has been able to prepare some fairly persistent species. The insights gained from his work should be extremely valuable for the construction high-spin polycarbenes and of molecular magnets.[15]

[1] Reviews: a) *Carbene Chemistry* (Ed.: G. Bertrand), Marcel Dekker, New York, **2002**; b) *Methoden Org. Chem. (Houben-Weyl) 4th ed. 1952–, Vol. E19b*, **1989**; c) C. Wentrup, *Reactive Molecules*, Wiley, New York, **1984**, chap. 4; d) R. A. Moss, M. Jones, Jr., *Carbenes (Vol. I)*, Wiley, New York, **1973**; R. A. Moss, M. Jones, Jr., *Carbenes (Vol. II)*, Wiley, New York, **1975**; e) W. Kirmse, *Carbene Chemistry, 2nd ed.*, Academic Press, New York, **1971**.

[2] Reviews: a) W. Sander in *Carbene Chemistry* (Ed.: G. Bertrand), Marcel Dekker, New York, **2002**, pp. 1–25; b) G. Maier in *Advances in Carbene Chemistry, Vol. 3* (Ed.: U. H. Brinker), Elsevier, Amsterdam, **2001**, pp. 115–157; c) H. Tomioka, *Bull. Chem. Soc. Jpn.* **1998**, *71*, 1501–1524; d) W. Sander, *Chem. Rev.* **1993**, *93*, 1583–1621.

[3] Reviews: a) R. W. Alder in *Carbene Chemistry* (Ed.: G. Bertrand), Marcel Dekker, New York, **2002**, pp. 153–176; b) G. Bertrand in *Carbene Chemistry* (Ed.: G. Bertrand), Marcel Dekker, New York, **2002**, pp. 177–203; c) D. Bourissou, O. Guerret, F. P. Gabbai, G. Bertrand, *Chem. Rev.* **2000**, *100*, 39–91; d) A. J. Arduengo, *Acc. Chem. Res.* **1999**, *32*, 913–921; e) W. A. Herrmann, C. Köcher, *Angew. Chem.* **1997**, *109*, 2256–2282; *Angew. Chem. Int. Ed. Engl.* **1997**, *36*, 2162–2187.

[4] H. M. Sulzbach, E. Bolton, D. Lenoir, P. von R. Schleyer, H. F. Schaefer III, *J. Am. Chem. Soc.* **1996**, *118*, 9908–9914.

[5] Reviews: a) H. Tomioka in *Carbene Chemistry* (Ed.: G. Bertrand), Marcel Dekker, New York, **2002**, pp. 103–152; b) H. Tomioka in *Advances in Carbene Chemistry, Vol. 2* (Ed.: U. H. Brinker), JAI Press, London, **1998**, pp. 175–214; c) H. Tomioka, *Acc. Chem. Res.* **1997**, *30*, 315–321.

[6] J. E. Gano, R. H. Wettach, M. S. Platz, V. P. Senthilnathan, *J. Am. Chem. Soc.* **1982**, *104*, 2326–2327.

[7] a) H. Tomioka, J, Nakajima, H. Mizuno, E. Iiba, K. Hirai, *Can. J. Chem.* **1999**, *77*, 1066–1076; b) E. Iiba, K. Hirai, H. Tomioka, Y. Yoshioka, *J. Am. Chem. Soc.* **2002**, *124*, 14308–14309.

[8] Y. Takahashi, M. Tomura, K. Yoshida, S. Murata, H. Tomioka, *Angew. Chem.* **2000**, *112*, 3620–3622; *Angew. Chem. Int. Ed.* **2000**, *39*, 3478–3480.

[9] H. Tomioka, E. Iwamoto, H. Itakura, K. Hirai, *Nature* **2001**, *412*, 626–628.

[10] a) H. Tomioka, H. Okada, T. Watanabe, K. Hirai, *Angew. Chem.* **1994**, *106*, 944–946; *Angew. Chem. Int. Ed. Engl.* **1994**, *33*, 873–875; b) H. Tomioka, H. Okada, T. Watanabe, K. Banno, K. Komatsu, K. Hirai, *J. Am. Chem. Soc.* **1997**, *119*, 1582–1593; c) Y.-M. Hu, K. Hirai, H.

 © 2003 Wiley-VCH Verlag GmbH & Co. KGaA, Weinheim

Tomioka, *J. Phys. Chem. A* **1999**, *103*, 9280 – 9284; d) K. Hirai, K. Yasuda, H. Tomioka, *Chem. Lett.* **2000**, 94 – 95; e) Y.-M. Hu, Y. Ishikawa, K. Hirai, H. Tomioka, *Bull. Chem. Soc. Jpn.* **2001**, *74*, 2207 – 2218; f) K. Hirai, T. Iikubo, H. Tomioka, *Chem. Lett.* **2002**, 1226 – 1227; g) T. Iikubo, K. Hirai, H. Tomioka, *Org. Lett.* **2002**, *4*, 2261 – 2264; h) T. Koshiyama, K. Hirai, H. Tomioka, *J. Phys. Chem. A* **2002**, *106*, 10261 – 10274.

[11] a) H. Tomioka, H. Mizuno, H. Itakura, K. Hirai, *Chem. Commun.* **1997**, 2261 – 2262; b) H. Itakura, H, Mizuno, K. Hirai, H. Tomioka, *J. Org. Chem.* **2000**, *65*, 8797 – 8806.

[12] a) H. Tomioka, T. Watanabe, K. Hirai, K. Furukawa, T. Takui, K. Itoh, *J. Am. Chem. Soc.* **1995**, *117*, 6376 – 6377; b) H. Tomioka, M. Hattori, K. Hirai, S. Murata, *J. Am. Chem. Soc.* **1996**, *118*, 8723 – 8724; c) H. Tomioka, T. Watanabe, M. Hattori, N. Nomura, K. Hirai, *J. Am. Chem. Soc.* **2002**, *124*, 474 – 482.

[13] K. Hirai, H. Tomioka, *J. Am. Chem. Soc.* **1999**, *121*, 10213 – 10214.

[14] H. L. Woodcock, D. Moran, P. von R. Schleyer, H. F. Schaefer III, *J. Am. Chem. Soc.* **2001**, *123*, 4331 – 4335.

[15] a) N. Koga, H. Iwamura in *Carbene Chemistry* (Ed.: G. Bertrand), Marcel Dekker, New York, **2002**, pp. 271 – 296, and references therein. See also: b) K. Tanaka, S. Nakazawa, K. Sato, D. Shiomi, T. Takui, Y. Nozaki, K. Hirai, H. Tomioka, *Mol. Cryst. Liq. Cryst.* **2002**, *376*, 489 – 494; c) K. Sato, D. Shiomi, T. Takui, M. Hattori, K. Hirai, H. Tomioka, *Mol. Cryst. Liq. Cryst.* **2002**, *376*, 549 – 554.



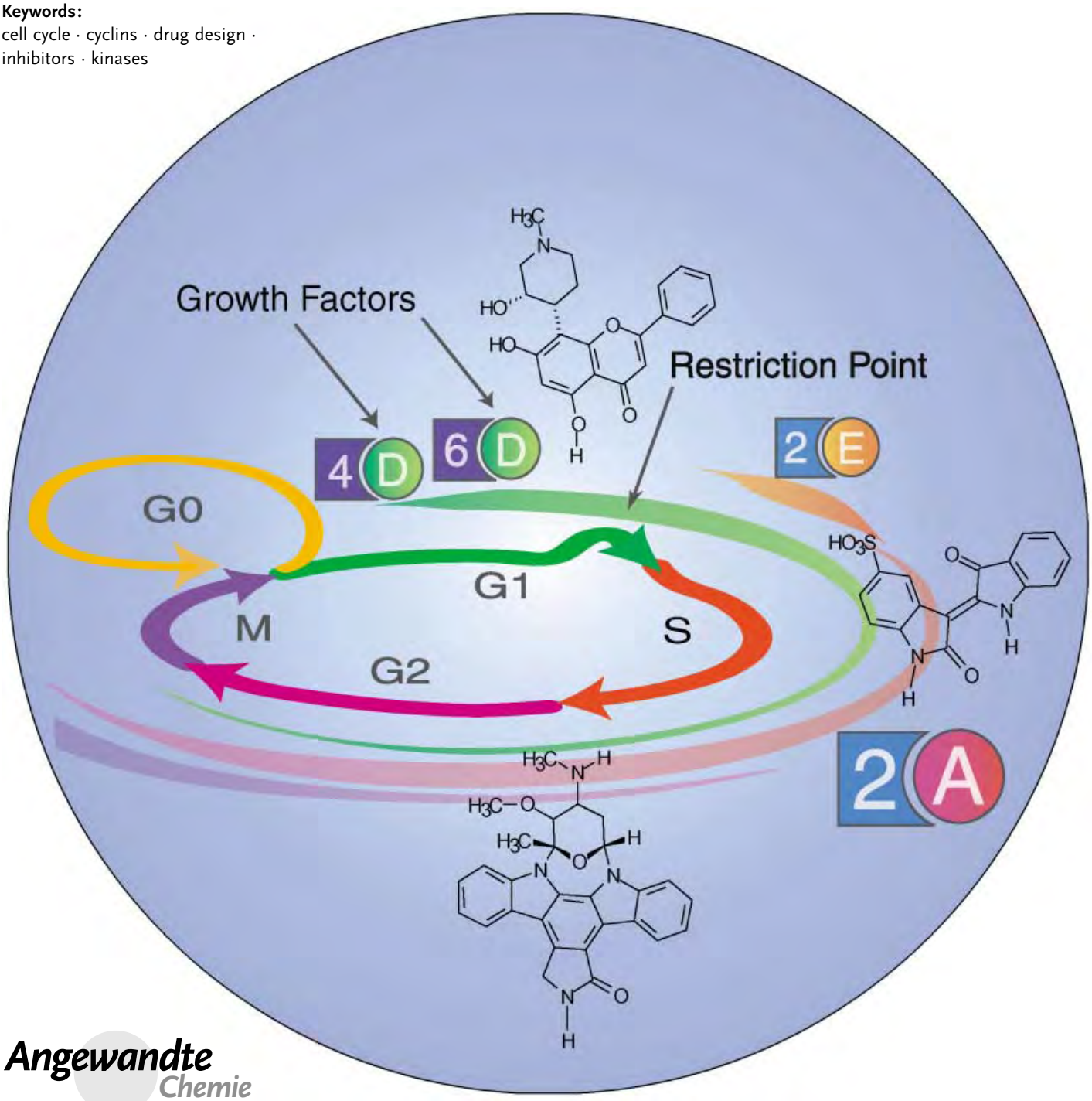
 © 2003 Wiley-VCH Verlag GmbH & Co. KGaA, Weinheim

Cyclin-Dependent Kinases

Small Molecules as Inhibitors of Cyclin-Dependent Kinases

*Axel Huwe, Ralph Mazitschek, and Athanassios Giannis**

Keywords:
cell cycle · cyclins · drug design · inhibitors · kinases



© 2003 Wiley-VCH Verlag GmbH & Co. KGaA, Weinheim
DOI: 10.1002/anie.200200540

Cell division (mitosis) is one of the basic requirements for multicellular oranisms. The capability of a cell to replicate enables a complex assembly to be created. Faulty regulation of the control mechanism in the cell cycle leads to an excessive cell proliferation and is the cause of cancer. The key position of the cyclin-dependent kinases (CDKs) and their direct partners, as well as the fact that the majority of malign illnesses show defects in at least one of these key players of the cell cycle, is of great interest for the development of low-molecular-weight CDK inhibitors. In this Review an overview of the different structural classes of ATP-competitive inhibitors of CDKs are given, whose devlopment was aimed at battling cancer. The Review shows how far the development of selective CDK inhibitors has progressed and to what extent the expectations for such drugs have so far been fulfilled.

From the Contents

1. Introduction 2123

2. Low-Molecular-Weight Inhibitors of Cycline-Dependent Kinases 2126

3. Conclusion 2134

1. Introduction

For the assembly and the survival of any multicellular organism, cell division (mitosis) is one of the basic requirements. It is only because cells are capable of replication that they can create a complex assembly and are able to replace apoptotic or necrotic cells. Since a creature is usually composed of billions of these tiniest components, a strict coordination and regulation of this process is necessary. The decision to proliferate is mostly the result of different mitogenic signals from surounding cells (tissue). Before the cell can reply to these requests and undergo replication, the cell mass must have reached a critical size. Furthermore, the DNA needs to be duplicated and the chromosomes must be seperated to ensure that both daughter cells receive a complete copy of genetic information. The whole process, starting from the response to extra cellular mitogenic signals and resulting in the generation of two daughter cells, is called the cell cycle.

The cell cycle can be devided into four distinct phases (Figure 1). At the onset of the first phase (G1 phase, G = gap), the progress of the cell cycle is dependent on stimulation by extra cellular growth factors, but the advancement can still be repressed by antiproliferative agents. The final decision is made late in the G1 phase by passing the so-called restriction point. Beyond this point the progression of the cell cycle is independent of external influence and the cell now makes elementary preparations, for example, enzymes and other proteins participating in DNA replication are synthesized. At the beginning of DNA synthesis the cell enters the S phase (synthesis) where the chromosomes are duplicated. After the S phase is completed the newly synthesized DNA is verified and eventually repaired during the G2 phase. Moreover, the cell is preparing for the transition to the M phase (mitose), in which the duplicated DNA is separated and the daughter cells are formed. After division, both cells can enter the G1 phase to traverse the cell cycle once more, or they can stay in a quiescent state named the G0 phase.

A succesfull division cycle implies there is a precise adherence of sequence and termination of each phase. This is guaranteed by control mechanisms that permit the transition to the next phase via distinct checkpoints only if certain critical events are fulfilled.[1,2] Cycline-dependent kinases (CDKs) are vitally important for the crossing of these checkpoints. The chronologic regulation of CDK activity is achieved by their association with cyclins and specific proteinogenic CDK inhibitors, their state of phosphorylation, and their ubiqutine-mediated degradation.[3–6] The key role of CDKs and their direct partners, as well as the fact that some of these central regulators of the cell cycle are defect in many maligne diseases, have raised great interest for the developement of CDK inhibitors.[7–9]

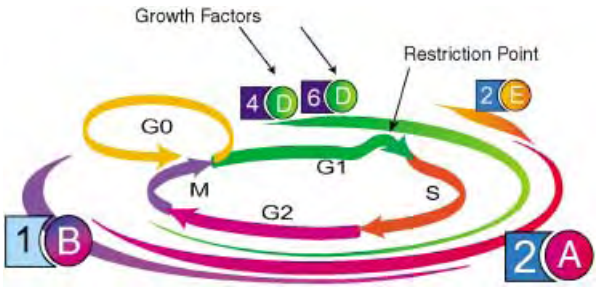


Figure 1. The four phases of the eukaryotic cell-division cycle comprises two phases G1 and G2, in which no morphologic changes are observed; the S phase, where the eukaryotypes are reduplicated; and the M phase in which formation of two daughter cells takes place. The M and S phases are separeted by the two G phases. An eukaryotic cell needs in general about 10–20 h for one division cycle. The quiescent state of the cell cycle is also called the G0 phase and some cells, depending on the cell type, can rest in this state for several years. The correct sequence of the respective phases are regulated by CDK1, 2, 3, 4, and 6. The prerequisite for enzymatic activity of the CDKs is the binding of specific regulatory subunits, the cyclins A, B, D, E. The concentration of the individual cyclins is symbolized by the thickness of the corresponding lines.

Ten cyclin-dependent kinases (CDK1–CDK10) are currently known, of which only CDKs1, 2, 3, 4, and 6 intervene

[*] Prof. Dr. A. Giannis, Dipl.-Chem. A. Huwe, Dr. R. Mazitschek
Institut für Organische Chemie
Universität Leipzig
Johannisallee 29, 04103 Leipzig (Germany)
Fax: (+49) 341-97-36-599
E-mail: giannis@chemie.uni-leipzig.de

 DOI: 10.1002/anie.200200540 © 2003 Wiley-VCH Verlag GmbH & Co. KGaA, Weinheim

directly in the cell cycle, while CDK7 plays only a indirect role as an activator of these CDKs.[6,10] Furthermore, like CDK8 and 9, CDK7 acts as a regulator of transcription.[11–16] CDK5 is important for neuronal developement and the function of gland cells and neurones.[17–19] Little is known about the function of the more recently identified CDK10. It interacts with transcription factor Ets2 and, like CDKs7, 8, and 9, it is involved in the further control of transcription.[20] CDKs obtain their basal enzymatic activity after binding to their corresponding cyclin, which functions as a positive regulatory subunit.[21] So far at least 15 cyclins have been identified.[22–24] Each phase of the cell cycle is characterized by the expression of distinct cyclins. The cyclins themselves underly a strict regulation by proteolytic degradation, whereas the CDKs are biosynthesized in constant concentrations and are comparably stable.[25–31]

As a result of mitogenic signals, the dormant cells react through the expression of cyclins D1, D2, and D3, which can then associate with the (cognate) CDK4 and 6 (Figure 2).[32–34] The expression pattern of the D-type cyclins vary from cell-type to cell-type. The existing complex of cyclin D and CDK4 or 6 is able to translocate into the cell nucleus, where it is phosphorylated by cyclin H/CDK7 (CAK, CDK activating kinase) at a specific threonine residue close to its ATP binding pocket and thereby achieves full enzymatic activity.[35–37] The main function of the active holoenzyme is the phosphorylation of the retinoblastoma proteins (pRb) during the G1 phase.[38] In its unphosphorylated state, pRb blocks the members of the E2F/DP transcription factor families by complexation. E2F/DP heterodimers can act as gene activators, but also as repressors.[39] The latter activity is derived through the binding of pRb and the recruitment of transcription repressors such as histone deacetylase (HDAC) at the promoters of certain genes.[40–43] In their uncomplexed form the E2F/DP proteins are responsible for the transcription of genes, the products of which are needed for G1/S transition and DNA synthesis.[4] The pRb phosphorylation by cyclin D/CDK4,6 leads to a separation of HDAC from the promotor and enables the transcription of cyclin E, which, subsequently, can activate CDK2. The hypophosphorylated pRb still complexes E2F, thus retaining the repression of the cyclin A promoter.[44] The catalytically active cyclin E/CDK2 complex is able to phosphorylate pRb at additional sites, which leads to total inactivation of pRb.[45,46] The hyperphosphorylated pRb is now no longer able to bind E2F/DP, which results in the further increase in the E2F concentration and the accumulation of cyclin E. In addition, E2F stimulates its own transcription.[4] Both results in a positive feedback and drives the cell cycle from the growth-factor-dependent state (cyclin D controlled) irreversibly to the growth-factor-independent state (cyclin E controlled).

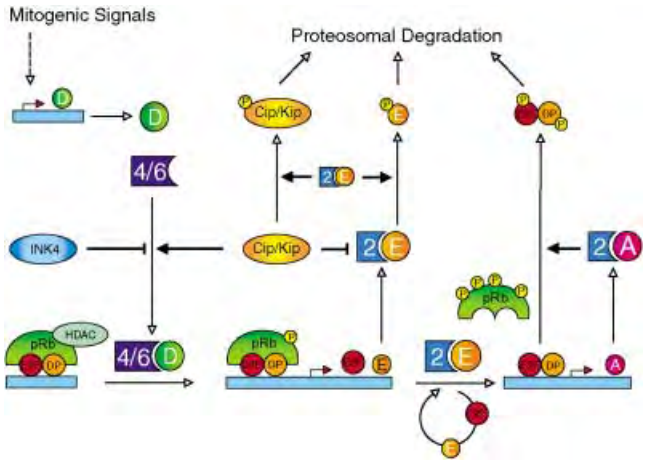


Figure 2. The translocation of the complexes of D-type cyclins and CDK4 and 6 into the nucleus is inhibited by INK4 and stimulated by Cip/Kip. See the text for further details.

The early S phase is not only characterized by the beginning of DNA synthesis, but also by the rapid ubiquitine-mediated degradation of cyclin E.[27,28] Cyclin E is



Athanassios Giannis was born in 1954 in Drama (Greece). From 1972–1980 he studied Chemistry and from 1979–1988 Medicine at the Universität Bonn. After his Diplomarbeit with Prof. M. T. Reetz he completed his PhD in 1986 with Prof. K. Sandhoff on the synthesis of C-glycosides. He completed his Habilitation in 1992 in Organic Chemistry and Biochemistry and moved to the Universität Karlsruhe. Since May 2002 he has been professor of Organic Chemistry and Natural Products at the Universität Leipzig. His interests concern the rational design and synthesis of bioactive natural products and their analogues as inhibitors of angiogenesis and as modulators of apoptosis and signal transduction.

Axel Huwe was born in 1972 in Landau/Pfalz. He studied Chemistry at the Universität Karlsruhe and completed his Diploma in May 1999. Since June 1999 he has been carrying out PhD studies in the research group of Prof. A. Giannis at the Institut für Organische Chemie der Universität Leipzig. His research concentrates on the synthesis of analogues of the natural products fumagillin and ovalicin as inhibitors of angiogenesis.

Ralph Mazitschek was born in 1971 in Karlsruhe. He studied Chemistry at the Universität Karlsruhe and completed his Diploma in 1999 and his PhD in 2002 with Prof. A. Giannis in Leipzig on the synthesis and biological evaluation of new anti-angiogenic drugs. Currently he works at the Institute for Chemistry and Cell Biology at Harvard Medical School where he is developing new methods for application in the area of Chemical Genetics.

 © 2003 Wiley-VCH Verlag GmbH & Co. KGaA, Weinheim

replaced by newly synthesized cyclin A. In contrast to the cyclin E containing analogue, the complex of cyclin A and CDK2 associates with the various E2Fs to phosphorylate their DP-1 subunits, which leads to the inhibition of DNA binding.[47–49] Additionally, cyclin A/CDK2 phosphorylates cdc6, an essential initiator of DNA replication, which induces its export out of the cell nucleus and thereby prevents the re-replication of DNA.[50] In addition to the above-mentioned regulators, other cyclin A/CDK2-specific substrates have been identified that participate in DNA replication.[51] Besides CDK2, cyclin A is also able to stimulate CDK1, but very little is known about the exact function of the cyclin A/CDK1 complex.[52,53] However, its importance for the progression of the cell cycle is commonly accepted.[54]

After the S phase is completed, the cyclin B/CDK1 complex, which is built during the G2 phase and the late S phase as a inactive dimer, is activated.[55–57] The inactivation is caused by phosphorylation of specific tyrosine/threonine residues (Tyr 15, Thr 14) by the bifunctional protein kinases Wee1 and Myt1, and prevents entry into mitosis before DNA synthesis has finished and possible replication errors have been repaired.[58–61] Activation is recovered by cleavage of these phosphate residues by members of the cdc25 phosphatases.[10,62] Structure proteins, which are necessary for the execution of mitosis, as well as regulatory proteins, which are required for the chronologic sequence and the control of the whole process, are both substrates of cyclin B/CDK1.[63] Furthermore cyclin B/CDK1 guarantees the global inhibition of protein biosynthesis, DNA replication, and DNA transcription.[64–67] In addition, cyclin B/CDK1 is involved in the stimulation of the proteolytic degradation mechanism, which allows the cell to eliminate M-phase proteins and to restore the initial status.[68,69] Apart from the regulation of kinase activity by varying the phosphorylation state of the CDKs and the sequential expression and degradation of cyclins, proteinogenous inhibitors (CKIs, CDK inhibitors) also participate in the regulation of CDK activity.[70] These inhibitors can be divided into two distinct families according to their specifity and sequence homology: the CIP/KIP and the INK4 families.[71,72]

The Cip/Kip family comprises $p21^{CIP1,WAF1}$, $p27^{KIP1}$, and $p57^{KIP2}$ and represents the first class of CDK inhibitors.[73–80] In contrast to p21 and p27, little is known about the exact biological function of p57. These proteins were originally thought to block all cyclin D, E, and A dependent kinases. However, recent results show that the simple picture of global inhibition of CDKs by members of the Cip/Kip protein family needs to be revised.[44,81–83] In fact, p21 and p27 inhibit CDK2 in the complex with cyclin E and cyclin A by trimerization, and an overexpression of the CIP/KIP inhibitors leads to an arrest of the cell cycle in the G1 phase.[84] Cyclin D dependent kinases are blocked by p21 and p27, albeit at much higher concentrations.[85] Surprisingly p21 and p27 also act as positive regulators for cyclin D dependent kinases. The CIP/KIP proteins are required for the binding of cyclin D and CDK4, the metabolic stability of the cyclin D/CDK4,6 complex, and for its translocation into the nucleus.[71,83] Accordingly, these CKIs should be considered as activators of CDK4 and 6 and inhibitors of CDK2.

The second class of CDK inhibitors is known as the INK4 family (inhibitors of CDK4) of CKIs, as a result of their specifity against CDK4 and 6. There are four structurally related members of this group: $p16^{INK4a}$, $p15^{INK4b}$, $p18^{INK4c}$, and $p19^{INK4d}$.[86–90] INK4 proteins can bind to CDK4 and 6 in place of cyclin D or can form a trimeric complex to block the enzymatic activity of the complex.[91,92] In the case of the binding of INK4 proteins to CDK4 and 6, they sequester potentially complexed CIP/KIP, which is responsible for the indirect inhibition of CDK2 by INK4. In this way these endogenous inhibitors ensure the stop of the cell cycle in the G1 phase. The property of INK4s to stop cells in this early phase of the cell cycle presupposes the presence of a functional pRb. Indeed over 60% of human tumors show defects in $p16^{INK4a}$ or pRb.[8,9]

Surprisingly, the INK4a gene locus encodes for a second potent tumor suppressor $p19^{ARF}$ by using an alternative reading frame (ARF). If mitogenic signals rise to a critical threshold, the expression of $p19^{ARF}$ is induced, which in turn stimulates arrest of the p53-mediated cell cycle.[93] The gene that encodes for the p53 protein is one of the most frequently mutated genes in tumors, thus stressing its importance in controlling the cell cycle.[94–97] In wild-type cells p53 is a protein with a very short half-life and it is only expressed tp a limited extent. However, when the DNA is damaged p53 is stabilized and accumulates in the cell.[98,99] p53 induces the expression of $p21^{CIP1,WAF1}$ and in this way causes arrest of the cell cycle, thus enabling the cell to repair the DNA damage. If the damage is irreparable, p53 will instead initiate the controlled cell death (apoptosis).[99,100]

The majority, if not all tumors show genetic defects in at least one of these key players of the cell cycle, which in a healthy organism guarantees the smooth process of cell division.[8,101] The most frequently observed mutations, besides the disfunction of p53, are the inactivation of endogenous inhibitors such as p16, the constitutive activation of CDK4, or the overexpression of its stimulating partner cyclin D1, and last but not least the loss of functional pRb.[8] These mutations render the cell independent of extracellular influences and signals (such as growth factors) and result ultimately in an uncontrolled cell proliferation.

This variety of reasons for unregulated cell proliferation means there are several posibilities to intervene in the cell cycle.[7] The different strategies target either directly the cyclin-dependent kinases or try to reduce CDK activity by indirect manipulation of regulating proteins. These indirect methods include, besides modulation of the phosphorylation state of CDKs, for example, by inhibition of activating enzymes (CAK, cdc25) or stimulation of inhibiting enzymes (Wee1, Myt1), activation of the proteolytic machinery and stimulation of CDK or cyclin degradation.

Direct inhibitors are preferably low-molecular-weight substances that block the enzymatic activity of CDKs. This review outlines the different structural classes of ATP-competitive inhibitors, which are synthesized for the purpose of intervening in malign diseases. It shows how far the developement has reached and to what extent the expectations of those compounds are justified.

 © 2003 Wiley-VCH Verlag GmbH & Co. KGaA, Weinheim

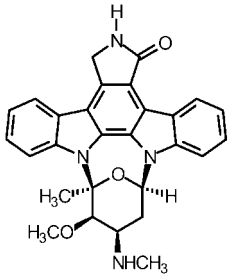
2. Low-Molecular-Weight Inhibitors of Cycline-Dependent Kinases

The ATP-competitive CDK inhibitors can be divided into two different classes according to their selectivity. The first class describes the unspecific kinase inhibitors, which can block CDKs and other unrelated serine/threonine and tyrosine kinases in similar concentrations. Among them one can find active compounds such as staurosporine (**1**) and its analogue UCN-01 (**2**). The second class is more complex in its structure. It covers selective CDK inhibitors which block all subgroups of this family in an equipotent manner (for example, flavopiridol (**4**)) and those that show a strong preference for one of these groups.

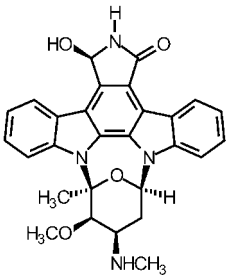
When considering and directly comparing IC_{50} values one always has to keep in mind that these agents act as ATP-competitive substances. These IC_{50} values directly depend on the ATP concentration, which can vary in different test systems, and generally are not comparable with each other. Furthermore the direct comparison with in vivo data is difficult, since the cellular ATP concentration lies in the millimolar range, whereas typical in vitro assays use concentrations between 2 and 40 μM. Nevertheless, the use of a low ATP concentration is sensible for the following two reasons. Firstly, even poorly soluble or less active compounds can be identified in the search for new lead structures, and secondly there are limitations that are well-founded in the nature of the assays. Since most assays commonly employ suitable antibodies to radioactively labeled ATP, radioactive contamination should be as low as possible.

2.1. Staurosporine

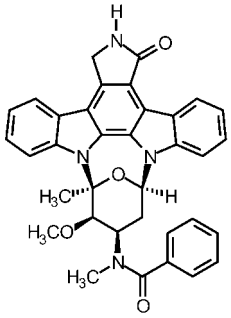
Staurosporine **1**, a metabolite from *Streptomyces* sp., is one of the few examples of an ATP-competitive natural product. The indolo[2,3-*a*]carbazole was originally identified as a highly potent compound ($IC_{50} = 1$ nM) in a screening study of inhibitors for proteinkinase C (PKC).[102] Further investigations demonstrate that staurosporine is an unspecific inhibitor that also blocks cyclin B/CDK1 with an IC_{50} value of 3.2 nM.[103] The poor selectivity of staurosporine can be explained from consideration of the crystal structures of staurosporine in different enzyme–inhibitor complexes.[104–106] The superimposition of ATP and staurosporine shows that the inhibitor is simply "too good" at imitating ATP. The heterocyclic ring system of staurosporine is almost congruent to the adenyl group of ATP, the lactam generates the same hydrogen bonds as the adenine residue to the enzyme, and the *N*-glycosyl-group is bound in the ribose pocket (Figure 3a and b). The structural analysis and the comparison with other derivates indicate the significance of hydrophobic interactions, which are responsible for the high affinity of the inhibitor **1** to the enzyme.



1



2



3

In spite of the low selectivity, staurosporine (**1**) has become "the" lead structure for the developement of novel PKC inhibitors, which should show a higher selectivity against PKC. Some of these derivates, such as UCN-01 (**2**, 7-hydroxystaurosporine; IC_{50}(PKC) = 6.9 nM) and CGP41251 (**3**, *N*-benzoxystaurosporine; IC_{50}(PKC) = 50 nM), show antitumor properties against different human cancer cell lines.[107–109] Further experiments have revealed, however, that PKC inhibition is not the only cause for antiproliferative efficiency. UCN-01 (**2**) at a concentration of 100 nM reduces the amount of phosphorylated pRb and blocks the G1/S transition in A549 lung adenocarcinoma cells. These results are consistent with the property of this compound to reduce the activity of CDK2, 4, and 6 to 50% at a concentration of 42, 32, and 58 nM, respectively.[107]

However, **2** not only has an inhibitory effect on the cell cycle. Orlandi and co-workers report that **2** can suspend a G2 arrest induced by DNA-damaging agents by activation of CDK1.[110] The stimulation can be attributed to the inhibition of the negative regulating kinase Wee1 and the simultaneous activation of phosphatase cdc25, and can be observed clearly below the IC_{50} values for the different CDKS.

The example of staurosporine (**1**) shows the difficulty in designing selective inhibitors of distinct kinases or kinase families, but also shows that complete selectivity is not a compelling criterion.

2.2. Flavones

Flavopiridol (**4**) and dechloroflavopiridol (**5**) are analogues of the naturally occuring alkaloid rohitukine (**6**).[111–113] Flavopiridol (**4**), as well as the stuctural related flavones genistein (**7**) and quercetin (**8**), shows inhibitory and cytotoxic properties against several tumor cell lines and is the first CDK inhibitor that entered clinical trials.[114]

Flavopiridol (**4**) was originally identified as a micromolar inhibitor for different proteinkinases, such as the receptor tyrosine kinases (RTKs; EGF receptor family $IC_{50} = 21$–25 μM),[115,116] receptor-associated kinases (src kinases 50 μM),[117] and cytosolic signal transduction kinases (protein

 © 2003 Wiley-VCH Verlag GmbH & Co. KGaA, Weinheim

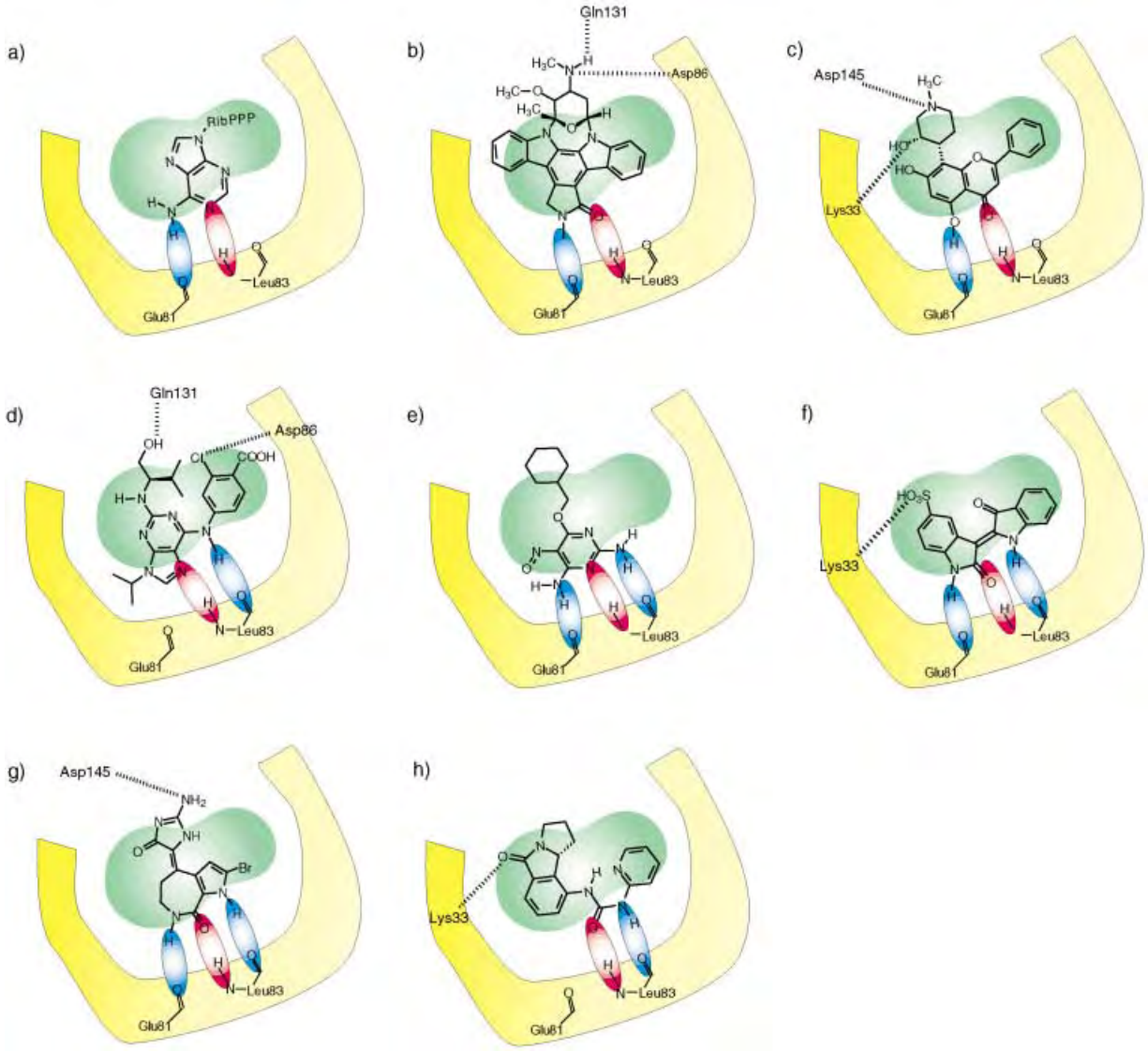
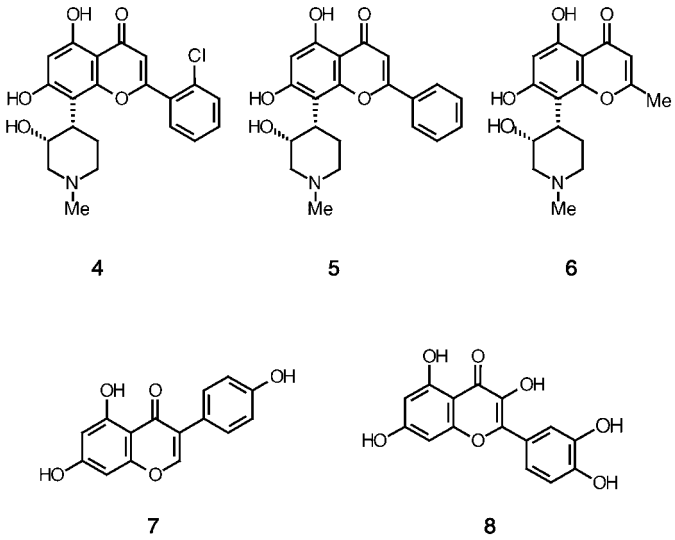


Figure 3. Schematic representation of the ATP binding pocket of CDK2 in the complex with different ligands. The hydrogen bonds to the peptide backbone are indicated in blue and red. The hydrophobic area of the binding region is depicted in green. The delimitation of the ATP binding pocket is shown in yellow. a) ATP, b) staurosporine (**1**), c) dechlorinated flavopiridol (**5**), d) purvalanol B (**21**), e) NU6027 (**22**), f) indirubin-5-sulfate (**32**), g) hymenialdisine (**49**), and h) diarylurea derivate **52**.



4 **5** **6**

7 **8**

kinase A 122–145 μM, PKC 6 μM, Erk-1 16 μM).[115,116,118] The highest activity of this compound is observed against the CDKs and the evolutionary related glycogen synthase 3β (GSK-3β, 450 nM).[119] Flavopiridol is moderately selective for cyclin D/CDK4 (20–40 nM), cyclin D/CDK6 (60 nM), and cyclin B/CDK1 (30–40 nM) in comparison to cyclin A/CDK2, cyclin E/CDK2 (100 nM), and cyclin H/CDK7 (100–300 nM).[115,117] The IC_{50} values that are detected against the isolated CDKs correlate with the results observed in cellular assays.[120] Further studies demonstrate that **4** induces an arrest of the cell cycle in the G1 or G2/M phase, which corresponds with its ability to block CDK1 and CDK2.[113]

Additional evidence of the potency of flavopiridol is shown in recent investigations which showed that it had an IC_{50} value of 6 nM against P-TEFb (positive transcription elongation factor b).[121] P-TEF-b, a complex consisting of

 © 2003 Wiley-VCH Verlag GmbH & Co. KGaA, Weinheim

CDK9 and cyclin T1, is a cellular cofactor for the HIV transactivator Tat. Interestingly, **4** blocks the activity of P-TEFb in a non-ATP-competitive manner, which is in contrast to other CDKs. Another effect of **4** is that it can suppress cyclin D1 transcription.[122] Thus, flavopiridol **4** is able to interfere in at least three ways in the cell cycle: by directly blocking the CDK activity, especially cyclin H/CDK7, which is necessary for the stimulation of other CDKs, and by suppression of the cyclin D1 expression.

A thorough insight into the selectivity of **4** for the distinct CDKs over other kinases is revealed by the crystal structure of CDK2 in complex with the unchlorinated analogue **5**.[123] Compound **5** essentially takes the same position as ATP (Figure 3a, c), with the flavonoid ring system and the adenine lying in identical planes, but twisted approximately 60° to each other. CDK2 binding is mainly achieved by hydrophobic interactions. Of special interest is the phenyl group of inhibitor **5**, since it points out of the ATP binding pocket of the enzymes and occupies an area that can not be utilized by ATP. This additional interaction seems to be responsible for the high affinity and selectivity of analogue **5** for CDK1 and CDK2 in comparison to other protein kinases, such as PKA. The chloro substituent (**4**→**5**) leads to a tenfold increase in activity. Its higher affinity is caused by an improved interaction with an isoleucine side chain.[124] Murthi et al. synthesized several flavopiridol derivatives to determine a structure–activity relationship. The results are summarized in Figure 4.[125]

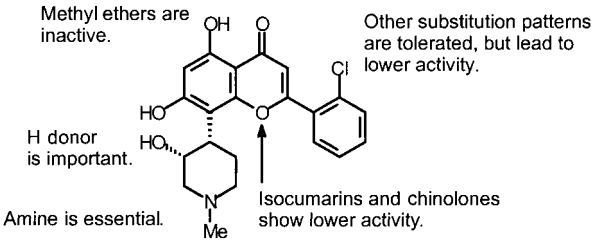
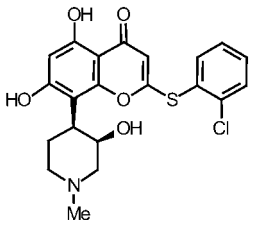


Figure 4. Structure–activity relationship of flavopiridol analogues.

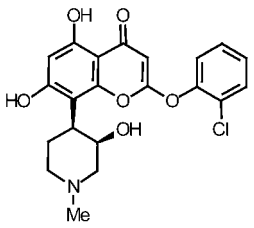
Smaller modifications of the phenyl residue are tolerated, but they do not result in improved activity. The hydroxy groups and the piperidine nitrogen atom are indispensable for the high affinity. Even substitution of the chromone structure by a isocumarin or chinol-4-one skeleton results in a reduction of activity. The introduction of a sulfur (**9**) or an oxygen linker (**10**) increases the selectivity towards CDK1/B over CDK2/E and CDK4/D1 (Table 1).[124] However, the enhanced selectivity is only a result of the reduced affinity.

The cytotoxic properties of flavopiridol (**4**) are not limited to proliferating cells, hence there are certainly additional mechanisms, besides the inhibition of CDKs, that contribute to its activity. Moreover, the flavone is able to enhance the impact of other chemotherapeutic drugs by sensibilization of tumor cells. This effect will be studied in clinical trials, in which **4** is tested in combination with different chemotherapeutics.[126]

Schoepfer et al. have recently shown that the 5-hydroxychromone skeleton of flavopiridol (**4**) can be replaced by a 4-hydroxybenzofuranone structure.[127] The authors designed



9

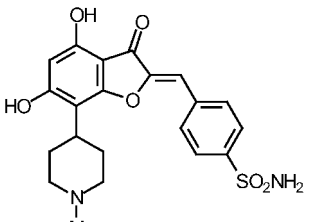


10

Table 1: Activity profile of flavopiridol (**4**) and its analogues **9** and **10** (IC_{50} values are in μM).

Inhibitor	CDK1/B	CDK2/E	CDK4/D1
9	0.11	2.10	16.2
10	0.13	2.11	6.15
4	0.03–0.04	0.1	0.02–0.04

corresponding mimetics of **4**, based on the crystal structure of CDK2 in the complex with **5**. The most potent compound was the sulfonamide **11**. The introduction of a chloro substituent in the *ortho* position of the phenyl ring does not result in an increased activity, as could be expected by comparison of the lead structures **4** and **5**. The members of this new class of CDK



11

inhibitors display a remarkable preference towards CDK1 and CDK2 versus CDK4 and GSK3 as shown by a simultaneous increased activity (Table 2). Unrelated receptor tyrosine kinases (RTKs) such as the vascular endothelium cell growth factor receptor 2 (VEGFR2) and the receptor for the epidermal growth factor (EGF) can also efficiently be blocked efficiently at higher concentrations. The inhibitors were tested in cellular proliferation assays against human colon carcinoma cells (HCT-116), however in this test system only slight activity could be detected.

Table 2: Activity profile of compound **11**.

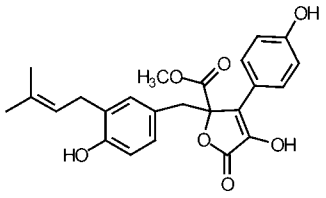
IC_{50} [μM]				% inhibition at 10 μM		
CDK1/B	CDK2/A	CDK4/D1	GSK3	PKCα	KDR	EGFR
0.009	0.03	1.87	3.7	42	25	36

2.3. Butyrolactone I

Kitagawa et al. have screened the culture media of several microorganisms for their capability to inhibit cyclin B/CDK1 (mouse cyclin B/cdc2) and discovered that the Aspagillus

 © 2003 Wiley-VCH Verlag GmbH & Co. KGaA, Weinheim

strain F-25799 expresses a substance with high inhibitory activity. The isolated active substance was identified as the metabolite butyrolactone I (**12**), which is able to block CDK1

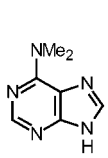


12

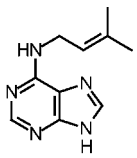
($IC_{50} = 0.68\ \mu M$) and CDK2 ($IC_{50} = 0.82\ \mu M$) in a submicromolar range.[128] The ATP-competitive metabolite inhibits CDK1 and 2, but does not interfere with other tested kinases, such as MAPK, PKC, casein kinase I and II, and EGFR. Compound **12** can also prevent the complete phosphorylation of pRb and histone H1. Cell-cycle arrest is observed during progression to the S phase and at the G1/M transition, which is consistent with its inhibitory effect on CDK1 and CDK2.[129] Higher concentrations of lactone **12** are clearly necessary to show its antiproliferative property ($IC_{50} =$ ca. 50 $\mu g\,mL^{-1}$) in cellular assays (lung tumor cells). This observation can be attributed to the low membrane permeability of the compound.[130]

2.4. Purines

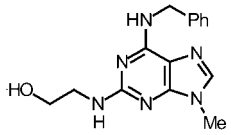
The first substance to be known as a CDK inhibitor was 6-dimethylaminopurine (**13**).[131] This compound was originally designed as a puromycine analogue—an inhibitor of protein biosynthesis—but it turned out that purine **13** inhibits the mitosis of sea urchin oocytes without blocking protein biosynthesis. Therefore, another mechanism had to exist and



13



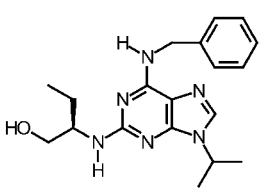
14



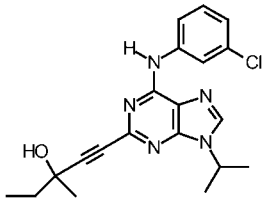
15

finally CDK1 ($IC_{50} = 120\ \mu M$) was identified as the actual target. Additional active purine derivates, including the more potent isopentenyladenine (**14**; $IC_{50} = 55\ \mu M$) and olomoucine (**15**), have been found using newly established in vitro kinase assays.[103,132] In particular, **15**—a moderate inhibitor of CDK1, 2 ($IC_{50} = 7\ \mu M$), and 5 ($IC_{50} = 3\ \mu M$)—showed a remarkable selectivity against other kinases (including CDK4, 6, and PKC) and served as a lead structure in the search for further 2,6,9-trisubstituted purines.

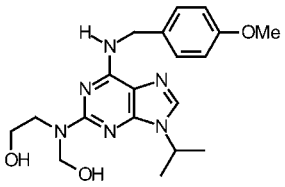
(*R*)-Roscovitine (**16**),[133,134] a slightly modified derivative of olomoucine (**15**), showed the same selectivity profile, but was approximately tenfold more active as the lead compound



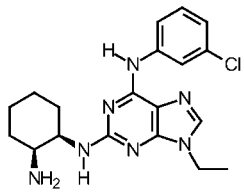
16



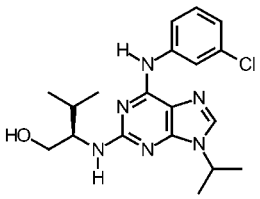
17



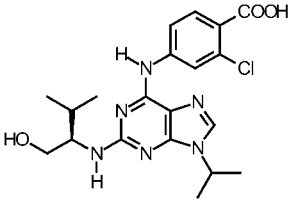
18



19



20



21

(Table 3). Crystal structures of **14**, **15**, and **16** in the complex with CDK2 reveal that the substances interact with the ATP binding side of the enzyme.[133,135] Interestingly, the orientation of the purine bicycle of the inhibitors do not correspond with the position of the adenine residues of ATP. Both heterocycles are coplanar, but are rotated almost 160° to one another. However, the interaction between the purine inhibitors and the peptide backbone is also based on a donor–acceptor motif, similar to ATP. In contrast to ATP, which interacts with Glu81 and Leu83 (Figure 3a), **16**

Table 3: Activity profiles of purin-based CDK inhibitors (IC_{50} values are given in μM).

Inhibitor	CDK1/B	CDK2/A	CDK2/E	CDK4/D	CDK5/p35
16	0.45	0.7	0.7	>100	0.16
17	0.06	–	–	–	–
18	4.2	0.5	0.5	215	–
19	0.025	–	–	–	–
20	0.004	0.07	0.035	0.850	0.075
21	0.006	0.006	0.009	>10	0.006

 © 2003 Wiley-VCH Verlag GmbH & Co. KGaA, Weinheim

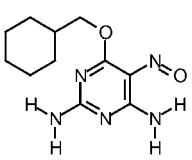
generates two hydrogen bonds to Leu 83. Unlike in the case of ATP, the H acceptor is not the pyrimidine nitrogen atom (N1), but the unsubstituted imidazole nitrogen atom (N7) of roscovitine, as shown in Figure 3d for purvalanol B (**21**).

The crystal-structure data have permitted a detailed characterization of the ligand–protein interaction and was a great advantage for the further planing of improved derivatives. By using combinatorial methods[136] and high-throughput screenings, additional purines were developed, among them 2-alkynylated derivatives such as **17**,[137,138] CVT 313 **18**,[139] diamine **19**,[140] purvalanol A (**20**), and purvalanol B (**21**, Table 3).[136]

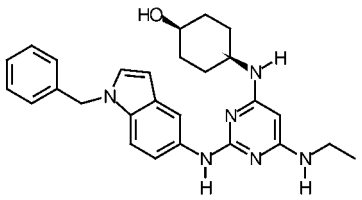
Purvalanol A causes an arrest of the cell cycle of human fibroblasts in the G1/S transition and during the G2/M phase, this is in line with the observed inhibition of CDK1 and CDK2. As investigations on the human cancer cell lines of the National Cancer Institute revealed, purvalanol A (with an average IC_{50} value of 2 μM) acts more like an antiproliferative agent than purvalanol B (**21**), probably because of its higher membrane permeability, although **21** is more active towards the isolated enzyme.

2.5. Pyrimidines

The pyrimidine NU 6027 (**22**) was designed as an analogue of the purine-based derivatives (see Section 2.4).[141] Compound **22** blocks, similar to olomoucine (**15**), CDK1 and CDK2 in an ATP-competitive way in the low micromolar range ($K_i = 2.5$ and 1.3 μM). The crystal structure reveals that the H-donor–acceptor–donor motif of **22** interacts with the



22



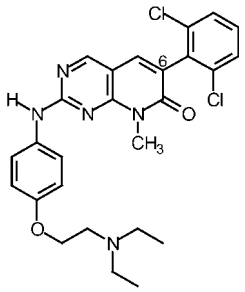
23

peptide backbone through three hydrogen bonds to CDK2 (Figure 3e). The 5-nitroso group is thereby essential for the conformational arrest of the pyrimidine, since it ensures the interaction of the 6-amino group with Glu 81. Compound **22** was even more active in cellular tests than the purine roscovitine (**16**) in cellular tests. This observation suggests there is a better bioavailability of the pyrimidine.

Soni et al. identified substance **23** (CINK4: chemical inhibitor of CDK4) in a high-throughput screening as an inhibitor of CDK4.[142] Besides CDK4 ($IC_{50} = 1.5$ μM) and CDK6 ($IC_{50} = 5.6$ μM), **23** also blocks CDK5 ($IC_{50} = 25$ μM) to a smaller extent. Other tested kinases (IGF-1R, insulin-R, v-abl, c-met) are affected at concentrations higher than 10 μM, while concentrations above 50 μM are necessary for the inhibition of CDK1 and CDK2. The pyrimidine derivative is able to inhibit pRb phosphorylation and causes an arrest in the cell cycle in pRb(+) cells during the G1 phase. Compound **23** decreased tumor growth similar to the endogenous inhibitor p16 in a mouse xenograft model and led to statistically significant smaller tumors.

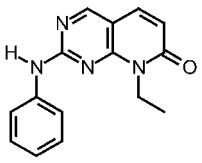
2.6. Pyrido[2,3-d]pyrimidinones

Pyrido[2,3-*d*]pyrimidinones were initially known as inhibitors of tyrosine kinases. In particular, the 6-aryl derivatives such as compound **24** showed a high affinity for several RTKs (EGFR, FGFR, PDGFR) and receptor-associated kinases (c-Src), but were inactive against CDKs.[143] Hollis Showalter and co-workers generated a binding model[144] to obtain insight into the molecular interactions between the inhibitors and the kinases. Their model ascribes the observed selectivity to the bulky 6-aryl substituent.

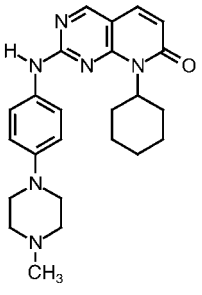


24

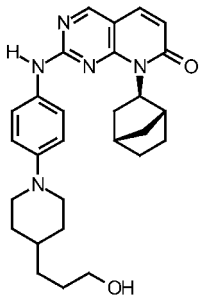
It was later shown that compounds missing the 6-aryl residue were also able to inhibit CDKs. Substance **25** blocked cyclin D/CDK4 in the submicromolar range ($IC_{50} = 0.62$ μM) and even showed a preference for CDKs over tyrosine kinases (cSrc and FGFR).[145] Encouraged by this result, Barvian et al. synthesized analogues of



25



26



27

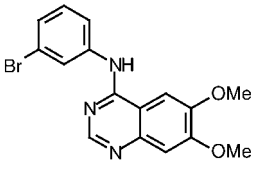
compound **25** and attained very potent and quite unselective kinase inhibitors, such as derivative **26**, as well as selective CDK4 inhibitors, such as compound **27** (Table 4).

The quinazolines, deaza analogues of the pyrido[2,3-*d*]pyrimidinones, were also originally reported to be inhibitors for RTKs.[146–149] The special role of these substances is mainly a result of their high activity with simultaneous selectivity.[150] The 3-(bromanilino)quinazoline **28**, a highly selective inhibitor for the EGF receptor, is one of the most potent kinase inhibitors, with an IC_{50} value of 29 pM (!).[149]

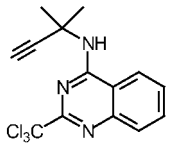
 © 2003 Wiley-VCH Verlag GmbH & Co. KGaA, Weinheim

Table 4: Activity profile of the pyrido[2,3-*d*]pyrimidinones **25**–**27** (IC_{50} values are given in μM).

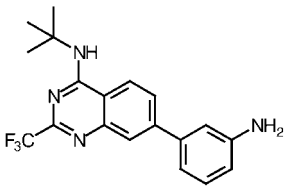
Inhibitor	CDK1/B	CDK2/A	CDK2/E	CDK4/D	FGFR
25	1.015	0.129	0.41	0.620	3.295
26	0.079	0.015	0.020	0.004	0.051
27	>40	0.209	0.165	0.008	8.62



28



29



30

However, CDK2 is only blocked ineffectively by this compound (IC_{50} = 250 μM).[150]

A detailed application of the quinazoline scaffold for developing CDK inhibitors is described by Sielecki et al.[151] Starting with compound **29**, which was identified in a screening study as being moderately potent towards CDK4/D1 (IC_{50} = 24 μM), CDK2/E (IC_{50} = 13,5 μM), and CDK1/B (IC_{50} = 15 μM), the authors generated a structure–activity relationship by systematic variations at positions 2, 4, and 6 (Figure 5).

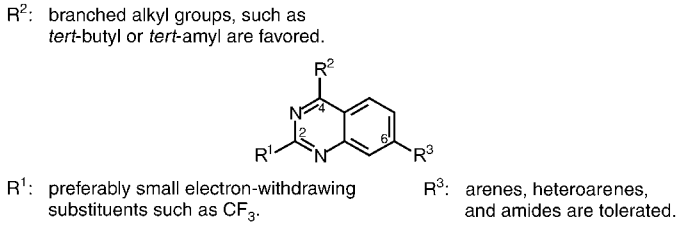
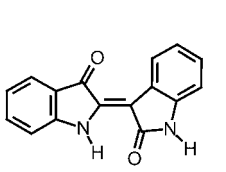


Figure 5. Structure–activity relationship of quinazoline-based CDK inhibitors.

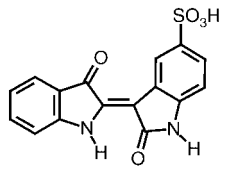
A small, electron-withdrawing substituent, such as trifluoromethyl or trichloromethyl, was found to be favored in position 2, whereas branched alkyl groups, such as *tert*-butyl or *tert*-amyl, are preferred in position 4. Position 6 tolerates several functional goups including arenes, heteroarenes, and amides. From these investigations compound **30** was identified as a potent inhibitor of cyclin E/CDK2. This substance shows, with an IC_{50} value of 0.6 μM, a slight selectivity towards CDK4 (IC_{50} = 2.1 μM). A comparison of the activity against different RTKs is not possible because of the absence of data. However, the notable preference of these compounds towards the EGF receptor and the general high affinity towards this RTK family makes this data of special interest.

2.7. Oxoindoles

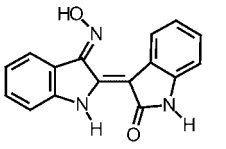
Traditional chinese medicine has been found to be a rich source for the identification of new biologically active substances. Indirubin (**31**, Table 5) is the active component



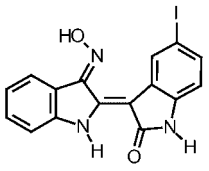
31



32



33



34

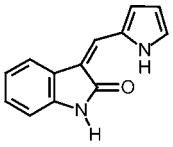
Table 5: Activity profiles of the indirubins **31**–**34** (IC_{50} values are given in μM).

Inhibitor	CDK1/B	CDK2/A	CDK2/E	CDK4/D IC_{50}	CDK5/p35	GSK-3β
31	10	2.2	7.5	12	5.5	0.6
32	0.055	0.035	0.15	0.3	0.065	0.28
33	0.18	0.44	0.25	3.33	0.1	0.022
34	0.025	–	–	–	0.02	0.009

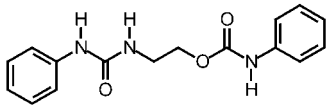
from Danggui Longhui Wan, a mixture of plants that was used for the treatment of chronic diseases, such as leukemia, four thousand years ago.[152] Indirubin (**31**) showed a high selectivity for CDKs compared to other protein kinases in different in vitro tests. Several derivatives with enhanced pharmacological properties were synthesized because of the poor water solubility and the low bioavailability of compound **31**. Analogues such as indirubin sulfate **32** and indirubin monoxime **33** were more active and showed a preference for CDK1, 2, and 5 versus CDK4. The crystal structure of compound **32** in the complex with CDK2 substantiate that the indirubins also act in a ATP-competitive way. The oxoindole **32** forms three hydrogen bonds to the peptide backbone (Glu 81 and Leu 83, Figure 3 f) and reaches deep into the ATP binding pocket.[153] The effect of the indirubins is clearly based on inhibition of CDKs, even though it is known to interact weakly with DNA.[154] Oxime **33** inhibits the proliferation of several cell lines in the late G1 and G2/M phases by blocking CDK1 and CDK2. Recent results reveal that indirubins are potent inhibitors of the related enzyme GSK-3β.[119] Of the most active indirubin derivatives some analogues, such as 5-iodoindirubin monoxime **34**, even showed a higher affinity towards GSK-3β.

Oxoindole **35** was identified, together with diarylketone **36** and the urea derivates **37** and **38** (Table 6), in a high-throughput screening as a moderate inhibitor of CDK4/D1.[155] In contrast to the more selective CDK4 inhibitors **36**,

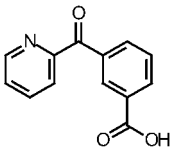
 © 2003 Wiley-VCH Verlag GmbH & Co. KGaA, Weinheim



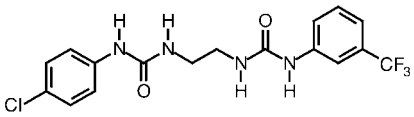
35



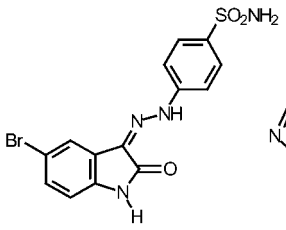
37



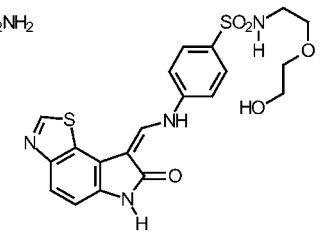
36



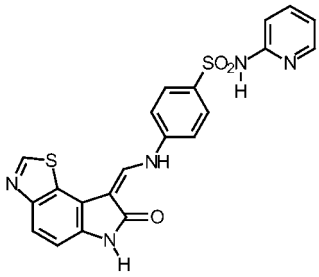
38



42



43

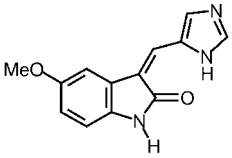


44

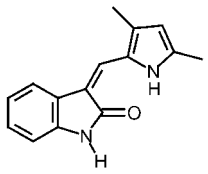
Table 6: Activity profiles of compounds **35**–**38** (IC_{50} values are given in μM).

Inhibitor	CDK1/B	CDK2/E	CDK4/D1
35	10.2	10.0	4.9
36	> 30	> 30	6.7
37	> 30	> 30	1.9
38	> 30	> 30	1.2

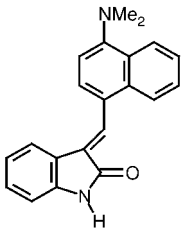
37, and **38**, compound **35** was able to inhibit the proliferation of human mammacarcinoma cells (MCF-7: $IC_{50} = 0.42$ μM and ZR-75-1: $IC_{50} = 0.1$ μM) in the submicromolar range and furthermore was less active against the pRb(−) cell line BT-549 ($IC_{50} = 13.9$ μM). This observation correlates with the postulated mechanism of action (inhibition of CDK1, 2, and 4). However, these data pose the question: Can a selective CDK4, 6 inhibitor itself block cell proliferation?



39



40



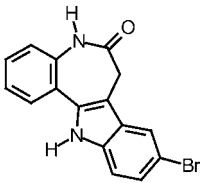
41

The 3,5-disubstituted oxoindole derivative SU9516 (**39**) shows a similar selectivity profile as **32** and blocks preferentially CDK2 ($IC_{50} = 0.022$ μM), CDK1 ($IC_{50} = 0.04$ μM), and CDK4 ($IC_{50} = 0.2$ μM).[156] Other protein kinases, such as PKC, p38, PDGFR, and EGFR, are affected by **39** at much higher concentration ($IC_{50} > 10$ μM). Unfortunately, the very interesting receptor tyrosine kinases, such as the VEGF receptors, were not considered, even though oxoindole compounds are known to be potent inhibitors of this receptor family. SU5416 (**40**) has already entered clinial trials as a selective inhibitor of VEGF-2.[157–159] MAZ51 (**41**), another oxoindole derivative, inhibits VEGFR-3 in the submicromolar range and was identified as the first low-molecular-weight inhibitor of lymph angiogenesis.[160]

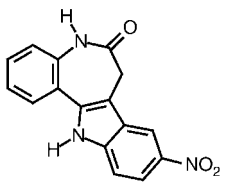
Further efforts have been made to develop new, selective protein kinase inhibitors on the basis of the oxoindole pharmacophore.[161] The hydrazone **42**, which was available in one step from commercial sources, inhibits CDK2 at a concentration of 60 nM ([ATP] = 1.4 μM) and was used as a lead compound to search for more potent analogues. The crystal structure of **42** in the complex with CDK2 provided detailed information about the inhibitor–enzyme interaction and was a prerequisite for developing a second generation of derivatives. The 4,5-annulated derivative **43** was one of the most potent compounds in the kinase assay (CDK2: $IC_{50} =$ 0.54 nM) and was about a factor of ten less active against CDK1 ($IC_{50} = 12$ nM). Selectivity against other kinases was demonstrated for compound **44**: in addition to CDK2 ($IC_{50} =$ 9.7 nM), **44** also showed a slight affinity for CDK1 ($IC_{50} =$ 100 nM), CDK4 ($IC_{50} = 130$ nM), GSK-3 ($IC_{50} = 56$ nM), and VEGFR-2 ($IC_{50} = 22$ nM).

2.8. Paullones

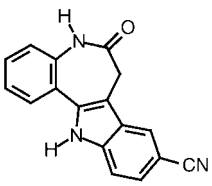
The benzazepine kenpaullone (**45**) was shown in a COMPARE search to have the same activity profile towards the 60 human cancer cell lines as the natural compound flavopiridole (**4**) and was identified in kinase assays as a selective inhibitor of CDK1, 2, and 5 (Table 7) .[162] However, **45** was far less active in the cellular assays than flavone. For further optimization and to gain structure–activity relation-



45



46



47

 © 2003 Wiley-VCH Verlag GmbH & Co. KGaA, Weinheim

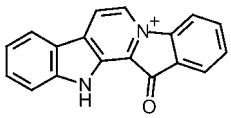
Table 7: Activity profiles of paullones **45**–**47** (IC_{50} values are given in μM).

Inhibitor	CDK1/B	CDK2/A	CDK2/E	CDK4/D	CDK5/p25	GSK-3
45	0.4	0.68	7.5	>100	0.85	0.023
46	0.035	0.015	0.2	>10	0.04	0.004
47	0.024	–	–	–	0.044	0.01

ship data analogues of the lead compound were synthesized and their inhibitory properties tested against cyclin B/CDK1 (starfish $p34^{cdc2}$/cyclin B^{cdc13}).[163] In fact, more potent substances, such as alsterpaullone (**46**) and the cyanide **47**, were found by variation of the bromo substituent. Introduction of additional substituents or the replacement of the lactam structure did not yield more active compounds, although substituents of the benzazepine scaffold especially at position 2 are tolerated.[164] Enzyme kinetic and molecular modeling studies revealed that paullones interact with the ATP binding pocket. Further targets of this substances were identified in subsequent studies and, besides the CDKs, GSK3α and β were inhibited in the nanomolar range.[165]

2.9. Fascaplysin

Yet another inhibitor with clear preference for CDK4 and 6 is the marine metabolite fascaplysin **48**. The red pigment fascaplysin was originally isolated from the sponge *Fascaplysinopsis* berquist and was identified as a antibiotic ingredient.[166] It was later shown that the diindole fascaplysine blocks CDK4/D1 and CDK6/D1 in the high nanomolar range.[167] Surprisingly, the inhibitory activity against the kinases was dependent on the bound cyclin partner (Table 8). Concentrations higher than 100 μM were necessary for 50% inhibition of CDK4/D2 and CDK4/D3, whereas non-cyclin-dependent kinases, such as v-abl, c-met, IGF-1R, and insulin-R, were not inhibited by concentrations lower than 10 μM.



48

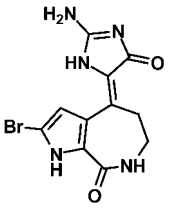
Table 8: Activity profile of fascaplysin (**48**; IC_{50} values are given in μM).

CDK–cyclin complex	IC_{50}	CDK–cyclin complex	IC_{50}
CDK1/B	>100	CDK4/D3	>100
CDK2/A	>50	CDK6/D1	3.4
CDK2/E	>50	CDK6/D2	>50
CDK4/D1	0.35	CDK5/p35	>20
CDK4/D2	>100		

Consistent with the inhibition of CDK4,6/D1 is the arrest of asynchronous growing MRC-5 and U2OS cells during the G1 phase by fascaplysine. Recently another mechanism of action of **48** was determined: the murine product intercalates in double-stranded DNA,[168] a property which diminishes its therapeutic use. Nevertheless, **48** is a valuable lead structure for the developement of new CDK4,6 inhibitors.

2.10. Hymenialdisine

A newly discovered inhibitor for CDKs is the pyrroloazepine alkaloid hymenialdisine (**49**).[169] This alkaloid was found as a component in several sponges and belongs to the class of aldisines. Meijer et al. recently demonstrated that hymenialdisine is a potent inhibitor of CDKs, for the closely related GSK-3β, as well as the caseine kinase 1 (CK1). Hymenialdisine is moderately selective towards cyclin B/CDK1, cyclin E/CDK2, CDK5/p25, GSK-3β, and CK1 (Table 9).



49

Table 9: Activity profile of hymenialdisine (**49**; IC_{50} values are given in μM).

CDK–cyclin complex	IC_{50}	CDK–cyclin complex	IC_{50}
CDK1/B	22	CDK5/p25	28
CDK2/A	70	CDK6/D2	700
CDK2/E	40	GSK-3β	10
CDK3/E	100	CK1	35
CDK4/D1	600		

Hymenialdisine blocks the investigated kinases in an ATP-competitive manner. Insight into the binding of the inhibitor at a molecular level results from the crystal structure of compound **49** in the complex with CDK2. As expected, hymenialdisine binds to the ATP pocket of the enzyme, where the pyrroloazepine replaces adenine. Interestingly, hymenialdisine is—just like indirubine (**31**)—able to built up three hydrogen bonds to the peptide backbone (Figure 3 g). Moreover, the guanidine group can form ionic interactions to the side chain of Asp 145, which enhances the affinity towards the enzyme. The van der Waals interactions between the inhibitor and the enzyme are essentially the same, and also observed with ATP, and are mainly based on the bicyclic system.

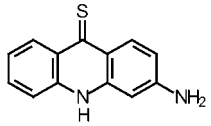
Recently (*E*)- and (*Z*)-hymenialdisine were identified as potent inhibitors of the Ras/Raf/MEK-1/MAPK signal transduction cascade.[170] Hymenialdisine blocks the phosphorylation of MAPK by MEK-1 in the low nanomolar range, which leads to inhibition of the signal transmission (IC_{50} = 3–9 nM). Since the oncogene form of Ras is associated with over 30% of all human cancers, hymenialdisine could accomplish a dual down-regulation of the cell cycle.

2.11. Acridones and Benzothiadiazines

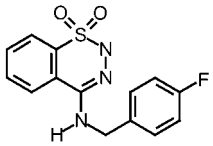
The loss of the function of $p16^{INK4}$, an endogenous inhibitor of cyclin D1/CDK4, is observed in a lot of tumors. Also, 47 out of the 60 cancer cell lines of the NIH panel showed changes in the acticity of $p16^{INK4}$. Kelley and coworkers assumed that it is most likely that selective inhibitors of CDK4 will be identified among those compounds that are capable of preferentially inhibiting the proliferation of these p16-deficient cell lines.[171] Two novel lead structures with the desired profile were discoverd by applying the COMPARE

 © 2003 Wiley-VCH Verlag GmbH & Co. KGaA, Weinheim

algorithm. In fact both compounds showed a clear selectivity for CDK4 over other CDKs. However, interactions with other kinases have not been investigated yet and other modes of action such as DNA intercalation are possible.[172] The two most potent compounds, NSC625987 (**50**) and NSC645787 (**51**), are suitable for further development (Table 10).



50



51

Table 10: Activity profile of **50** and **51** (IC_{50} values are given in μM).

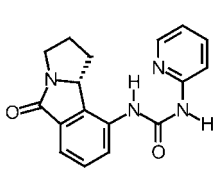
Inhibitor	CDK1/A	CDK2/A	CDK2/E	CDK4/D
50	88	>100	>100	3.1
51	>100	>100	>100	0.33

2.12. Diarylurea derivatives

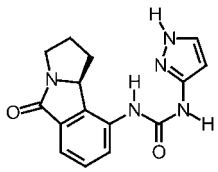
The initial design efforts for selective and potent inhibitors of CDK4 and 6 were hampered by the lack of suitable X-ray structures: The crystal structure of the complex of CDK6 and its endogenous inhibitor p16 is the only one described to date. Structural data of CDK4 and 6 with low-molecular-weight ATP analogues which enable a detailed description of the ATP binding site are still unavailable.

Honma et al. constructed a model for the CDK4 protein by taking advantage of the sequence homology of CDK4 and CDK2 (72% for the ATP binding pocket).[173,174] Based on the activated form of CDK2, this model was used for the conception of new lead structures. Four different scaffolds were identified by this approach and the authors chose diarylureas for further development, mainly because of the facile access to structurally diverse compound libraries and possibly as a result of the known preference of the aryl urea derivatives **37** and **38** (see Section 2.7). Finally, potent CDK inhibitors were yielded by varying both aryl substituents. CDK4 was inhibited by compound **52** at a concentration of 42 nM and displayed some selectivity towards non-CDKs, such as PKA, PKC, MEK1, Src, and EGFR. The pyrazolylurea derivative **53** was even slightly more active in an in vitro kinase assay (Table 11).

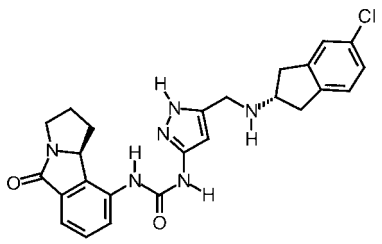
A CDK2 protein, in which the binding pocket was replaced by the one of CDK4, was expressed to validate the model of CDK4. Both, the "CDK4/CDK2" protein as well as the CDK2 wild-type protein could be successfully crystallized in a complex with the inhibitor **52** (Figure 3h).[175] The direct comparison of the crystal structures allowed the identification of CDK4-specific amino acid residues lining the ATP binding pocket and validated the homology model. This enabled the determination of structural characteristics, which faciliated further modifications of the lead structure of **52** with regard to increased selectivity for CDK4. Therefore, the existence of the selective inhibitor p16 was utilized: The pyridine ring of



52



53



54

Table 11: Activity profile of the urea derivatives **52**–**54** (IC_{50} values are given in μM).

Inhibitor	CDK1/B	CDK2/A	CDK4/D
52	0.120	0.078	0.042
53	–	–	0.029
54	1.8	0.44	0.002

compound **52** points towards the p16 binding site of the enzyme. Very potent and highly selective CDK4 inhibitors such as the pyrazolylurea **54** were obtained by introduction of additional substituents, which were capable of interacting with the p16 binding pocket (Gln98, Asp99, and Thr102).[174] Compound **54** arrested Molt-4, the pRB(+) cancer cell line, in the G1 phase at concentrations between 0.1 and 0.5 μM.

3. Conclusion

During recent years many novel and potent ATP-site directed inhibitors of CDKs been discovered and known inhibitors have been improved by using structure-based rational design. Thus, numerous structurally diverse compounds with remarkable activity and selectivity for individual CDK families are available today.

Unfortunately, in most cases only little or no attention was paid to the activity of these compounds against CDKs which are not directly involved in the control of the cell cycle. This includes in particular CDK5, which is involved in neuronal development and has been connected to Alzheimer diseases,[17–19,176] as well as CDK7, 8, and 9. In addition to an indirect participation in the regulation of the cell cycle, the latter are mainly involved in the transcriptional control of "housekeeping" functions. It is the high homology of the ATP binding domains found, for example, in CDK1, CDK2, and CDK9, which leads to the assumption that it will be difficult to evolve truly selective inhibitors for the cell-cycle machinery.[177] Additionally, many inhibitors, such as flavopiridol (**4**) or indirubin (**31**), show in vitro as well as in vivo effects which

 © 2003 Wiley-VCH Verlag GmbH & Co. KGaA, Weinheim

can not be exclusively explained by the inhibition of CDKs (see Section 2.2 and 2.7).

Furthermore, the question arises as to whether any of the known CDK inhibitors alone is suitable for use as a drug to reconstitute the cell-cycle machinery of degenerated cancer cells, or if these compounds can be employed in combination with conventional therapies. Here, CDK inhibitors could be used as a protective agent for healthy cells in the treatment of pRb-negative tumors. By blocking proliferating healthy cells in the G1 phase these cells could be rendered less sensitive towards chemotherapeutics while the tumor cells retain their susceptibility towards cyctotoxic agents which exert their activity during the S phase.[178] In this context, one application could result in the reduction of chemotherapy-induced alopecia (hair loss).[179] Moreover, the application of CDK inhibitors in other therapeutic areas are conceivable. Currently, such agents are under examination for the treatment of cardiovascular diseases, viral infections, and neuronal degeneration.[180,181] Undoubtedly, the known inhibitors are valuable tools for further investigation of the complex mechanisms of the cell cycle and for a more detailed analysis of the CDK-mediated transcriptional control.

Assuming that the problem of real selectivity can be solved, the question of the "most suited" CDK target remains unanswered. Although most mutations are found in CDK4, CDK6, or one of their regulators, research is currently mainly focused on the development of pan-CDK inhibitors or inhibitors of CDK2.[8] For two reasons this fact is not surprising: Firstly, compounds with apoptosis-inducing effects are of great interest from a pharmacological point of view and secondly only X-ray structures of CDK2 in complexes with small-molecule ligands have been solved to date, thus limiting structure-based design efforts mainly to this cyclin-dependent kinase.

However, recent results suggest that there is reasonable hope that chemists will succeed in the development of new compounds with suitable activity profiles, either by further improvement of known inhibitors or by the design of novel compounds based on structure–activity relationships. There will certainly be an increasing effort in the development of non-ATP-competitive inhibitors, since these molecules are promising an unrivaled increased selectivity for the individual kinases. In particular, the CDKs offer interesting starting points for the design of corresponding inhibitors as a result of their pleiotropic mechanisms of regulation.

Received: June 13, 2002 [A540]

[1] L. H. Hartwell, T. A. Weinert, *Science* **1989**, *246*, 629 – 634.
[2] A. G. Paulovich, D. P. Toczyski, L. H. Hartwell, *Cell* **1997**, *88*, 315 – 321.
[3] Y. Gu, J. Rosenblatt, D. O. Morgan, *EMBO J.* **1992**, *11*, 3995 – 4005.
[4] C. J. Sherr, *Science* **1996**, *274*, 1672 – 1677.
[5] M. Brandeis, T. Hunt, *EMBO J.* **1996**, *15*, 5280 – 5289.
[6] J. W. Harper, P. D. Adams, *Chem. Rev.* **2001**, *101*, 2511 – 2526.
[7] A. M. Senderowicz, E. A. Sausville, *J. Natl. Cancer Inst.* **2000**, *92*, 376 – 387.
[8] M. Malumbres, M. Barbacid, *Nat. Rev. Cancer* **2001**, *1*, 222 – 231.
[9] W. G. Kaelin, Jr., *J. Clin. Invest.* **1999**, *104*, 1503 – 1506.
[10] D. O. Morgan, *Annu. Rev. Cell Dev. Biol.* **1997**, *13*, 261 – 291.
[11] C. J. Hengartner, V. E. Myer, S. M. Liao, C. J. Wilson, S. S. Koh, R. A. Young, *Mol. Cell* **1998**, *2*, 43 – 53.
[12] H. Serizawa, T. P. Makela, J. W. Conaway, R. C. Conaway, R. A. Weinberg, R. A. Young, *Nature* **1995**, *374*, 280 – 282.
[13] J. Garriga, J. Peng, M. Parreno, D. H. Price, E. E. Henderson, X. Grana, *Oncogene* **1998**, *17*, 3093 – 3102.
[14] S. Akoulitchev, S. Chuikov, D. Reinberg, *Nature* **2000**, *407*, 102 – 106.
[15] P. Wei, M. E. Garber, S. M. Fang, W. H. Fischer, K. A. Jones, *Cell* **1998**, *92*, 451 – 462.
[16] J. P. Tassan, M. Jaquenoud, P. Leopold, S. J. Schultz, E. A. Nigg, *Proc. Natl. Acad. Sci. USA* **1995**, *92*, 8871 – 8875.
[17] G. Paglini, A. Caceres, *Eur. J. Biochem.* **2001**, *268*, 1528 – 1533.
[18] M. Nikolic, H. Dudek, Y. T. Kwon, Y. F. Ramos, L. H. Tsai, *Genes Dev.* **1996**, *10*, 816 – 825.
[19] J. Lew, R. J. Winkfein, H. K. Paudel, J. H. Wang, *J. Biol. Chem.* **1992**, *267*, 25 922 – 25 926.
[20] M. Kasten, A. Giordano, *Oncogene* **2001**, *20*, 1832 – 1838.
[21] M. J. Solomon, M. Glotzer, T. H. Lee, M. Philippe, M. W. Kirschner, *Cell* **1990**, *63*, 1013 – 1024.
[22] T. K. MacLachlan, N. Sang, A. Giordano, *Crit. Rev. Eukaryotic Gene Expression* **1995**, *5*, 127 – 156.
[23] J. Peng, Y. Zhu, J. T. Milton, D. H. Price, *Genes Dev.* **1998**, *12*, 755 – 762.
[24] M. C. Edwards, C. Wong, S. J. Elledge, *Mol. Cell. Biol.* **1998**, *18*, 4291 – 4300.
[25] A. Udvardy, *Eur. J. Biochem.* **1996**, *240*, 307 – 313.
[26] J. A. Diehl, F. Zindy, C. J. Sherr, *Genes Dev.* **1997**, *11*, 957 – 972.
[27] B. E. Clurman, R. J. Sheaff, K. Thress, M. Groudine, J. M. Roberts, *Genes Dev.* **1996**, *10*, 1979 – 1990.
[28] K. A. Won, S. I. Reed, *EMBO J.* **1996**, *15*, 4182 – 4193.
[29] V. Sudakin, D. Ganoth, A. Dahan, H. Heller, J. Hershko, F. C. Luca, J. V. Ruderman, A. Hershko, *Mol. Biol. Cell* **1995**, *6*, 185 – 197.
[30] A. Klotzbucher, E. Stewart, D. Harrison, T. Hunt, *EMBO J.* **1996**, *15*, 3053 – 3064.
[31] J. A. Diehl, M. Cheng, M. F. Roussel, C. J. Sherr, *Genes Dev.* **1998**, *12*, 3499 – 3511.
[32] H. Matsushime, M. F. Roussel, R. A. Ashmun, C. J. Sherr, *Cell* **1991**, *65*, 701 – 713.
[33] K. A. Won, Y. Xiong, D. Beach, M. Z. Gilman, *Proc. Natl. Acad. Sci. USA* **1992**, *89*, 9910 – 9914.
[34] C. J. Sherr, *Cell* **1994**, *79*, 551 – 555.
[35] J. Y. Kato, M. Matsuoka, D. K. Strom, C. J. Sherr, *Mol. Cell. Biol.* **1994**, *14*, 2713 – 2721.
[36] P. Kaldis, *Cell. Mol. Life Sci.* **1999**, *55*, 284 – 296.
[37] R. P. Fisher, D. O. Morgan, *Cell* **1994**, *78*, 713 – 724.
[38] J. Kato, H. Matsushime, S. W. Hiebert, M. E. Ewen, C. J. Sherr, *Genes Dev.* **1993**, *7*, 331 – 342.
[39] S. J. Weintraub, K. N. Chow, R. X. Luo, S. H. Zhang, S. He, D. C. Dean, *Nature* **1995**, *375*, 812 – 815.
[40] R. Ferreira, I. Naguibneva, M. Mathieu, S. Ait-Si-Ali, P. Robin, L. L. Pritchard, A. Harel-Bellan, *EMBO Rep.* **2001**, *2*, 794 – 799.
[41] A. Brehm, E. A. Miska, D. J. McCance, J. L. Reid, A. J. Bannister, T. Kouzarides, *Nature* **1998**, *391*, 597 – 601.
[42] Y. Takahashi, J. B. Rayman, B. D. Dynlacht, *Genes Dev.* **2000**, *14*, 804 – 816.
[43] H. S. Zhang, M. Gavin, A. Dahiya, A. A. Postigo, D. Ma, R. X. Luo, J. W. Harbour, D. C. Dean, *Cell* **2000**, *101*, 79 – 89.
[44] H. Zhang, G. J. Hannon, D. Beach, *Genes Dev.* **1994**, *8*, 1750 – 1758.

 © 2003 Wiley-VCH Verlag GmbH & Co. KGaA, Weinheim

[45] A. S. Lundberg, R. A. Weinberg, *Mol. Cell. Biol.* **1998**, *18*, 753 – 761.
[46] S. A. Ezhevsky, A. Ho, M. Becker-Hapak, P. K. Davis, S. F. Dowdy, *Mol. Cell. Biol.* **2001**, *21*, 4773 – 4784.
[47] M. Xu, K. A. Sheppard, C. Y. Peng, A. S. Yee, H. Piwnica-Worms, *Mol. Cell. Biol.* **1994**, *14*, 8420 – 8431.
[48] W. Krek, M. E. Ewen, S. Shirodkar, Z. Arany, W. G. Kaelin, Jr., D. M. Livingston, *Cell* **1994**, *78*, 161 – 172.
[49] B. D. Dynlacht, K. Moberg, J. A. Lees, E. Harlow, L. Zhu, *Mol. Cell. Biol.* **1997**, *17*, 3867 – 3875.
[50] B. O. Petersen, J. Lukas, C. S. Sorensen, J. Bartek, K. Helin, *EMBO J.* **1999**, *18*, 396 – 410.
[51] A. J. Obaya, J. M. Sedivy, *Cell. Mol. Life Sci.* **2002**, *59*, 126 – 142.
[52] M. Pagano, R. Pepperkok, F. Verde, W. Ansorge, G. Draetta, *EMBO J.* **1992**, *11*, 961 – 971.
[53] J. Pines, T. Hunter, *Nature* **1990**, *346*, 760 – 763.
[54] M. Santaguida, Q. Ding, G. Berube, M. Truscott, P. Whyte, A. Nepveu, *J. Biol. Chem.* **2001**, *276*, 45780 – 45790.
[55] P. Nurse, *Nature* **1990**, *344*, 503 – 508.
[56] G. Piaggio, A. Farina, D. Perrotti, I. Manni, P. Fuschi, A. Sacchi, C. Gaetano, *Exp. Cell Res.* **1995**, *216*, 396 – 402.
[57] T. Kishimoto, E. Okumura, *Prog. Cell Cycle Res.* **1997**, *3*, 241 – 249.
[58] C. H. McGowan, P. Russell, *EMBO J.* **1993**, *12*, 75 – 85.
[59] P. R. Mueller, T. R. Coleman, A. Kumagai, W. G. Dunphy, *Science* **1995**, *270*, 86 – 90.
[60] L. L. Parker, H. Piwnica-Worms, *Science* **1992**, *257*, 1955 – 1957.
[61] F. Liu, J. J. Stanton, Z. Wu, H. Piwnica-Worms, *Mol. Cell. Biol.* **1997**, *17*, 571 – 583.
[62] W. G. Dunphy, A. Kumagai, *Cell* **1991**, *67*, 189 – 196.
[63] V. A. Smits, R. H. Medema, *Biochim. Biophys. Acta* **2001**, *1519*, 1 – 12.
[64] P. J. Papst, H. Sugiyama, M. Nagasawa, J. J. Lucas, J. L. Maller, N. Terada, *J. Biol. Chem.* **1998**, *273*, 15077 – 15084.
[65] J. J. Long, A. Leresche, R. W. Kriwacki, J. M. Gottesfeld, *Mol. Cell. Biol.* **1998**, *18*, 1467 – 1476.
[66] M. Hendrickson, M. Madine, S. Dalton, J. Gautier, *Proc. Natl. Acad. Sci. USA* **1996**, *93*, 12223 – 12228.
[67] J. M. Gottesfeld, V. J. Wolf, T. Dang, D. J. Forbes, P. Hartl, *Science* **1994**, *263*, 81 – 84.
[68] L. Cerutti, V. Simanis, *Curr. Opin. Genet. Dev.* **2000**, *10*, 65 – 69.
[69] F. M. Townsley, J. V. Ruderman, *Trends Cell Biol.* **1998**, *8*, 238 – 244.
[70] N. P. Pavletich, *J. Mol. Biol.* **1999**, *287*, 821 – 828.
[71] C. J. Sherr, J. M. Roberts, *Genes Dev.* **1999**, *13*, 1501 – 1512.
[72] M. H. Lee, H. Y. Yang, *Cell. Mol. Life Sci.* **2001**, *58*, 1907 – 1922.
[73] K. Polyak, J. Y. Kato, M. J. Solomon, C. J. Sherr, J. Massague, J. M. Roberts, A. Koff, *Genes Dev.* **1994**, *8*, 9 – 22.
[74] K. Polyak, M. H. Lee, H. Erdjument-Bromage, A. Koff, J. M. Roberts, P. Tempst, J. Massague, *Cell* **1994**, *78*, 59 – 66.
[75] M. H. Lee, I. Reynisdottir, J. Massague, *Genes Dev.* **1995**, *9*, 639 – 649.
[76] S. Matsuoka, M. C. Edwards, C. Bai, S. Parker, P. Zhang, A. Baldini, J. W. Harper, S. J. Elledge, *Genes Dev.* **1995**, *9*, 650 – 662.
[77] H. Toyoshima, T. Hunter, *Cell* **1994**, *78*, 67 – 74.
[78] J. W. Harper, G. R. Adami, N. Wei, K. Keyomarsi, S. J. Elledge, *Cell* **1993**, *75*, 805 – 816.
[79] W. S. el-Deiry, T. Tokino, V. E. Velculescu, D. B. Levy, R. Parsons, J. M. Trent, D. Lin, W. E. Mercer, K. W. Kinzler, B. Vogelstein, *Cell* **1993**, *75*, 817 – 825.
[80] Y. Xiong, G. J. Hannon, H. Zhang, D. Casso, R. Kobayashi, D. Beach, *Nature* **1993**, *366*, 701 – 704.
[81] J. LaBaer, M. D. Garrett, L. F. Stevenson, J. M. Slingerland, C. Sandhu, H. S. Chou, A. Fattaey, E. Harlow, *Genes Dev.* **1997**, *11*, 847 – 862.
[82] J. W. Harper, S. J. Elledge, K. Keyomarsi, B. Dynlacht, L. H. Tsai, P. Zhang, S. Dobrowolski, C. Bai, L. Connell-Crowley, E. Swindell, *Mol. Biol. Cell* **1995**, *6*, 387 – 400.
[83] M. Cheng, P. Olivier, J. A. Diehl, M. Fero, M. F. Roussel, J. M. Roberts, C. J. Sherr, *EMBO J.* **1999**, *18*, 1571 – 1583.
[84] A. A. Russo, P. D. Jeffrey, A. K. Patten, J. Massague, N. P. Pavletich, *Nature* **1996**, *382*, 325 – 331.
[85] S. W. Blain, E. Montalvo, J. Massague, *J. Biol. Chem.* **1997**, *272*, 25863 – 25872.
[86] M. Serrano, G. J. Hannon, D. Beach, *Nature* **1993**, *366*, 704 – 707.
[87] G. J. Hannon, D. Beach, *Nature* **1994**, *371*, 257 – 261.
[88] K. L. Guan, C. W. Jenkins, Y. Li, M. A. Nichols, X. Wu, C. L. O'Keefe, A. G. Matera, Y. Xiong, *Genes Dev.* **1994**, *8*, 2939 – 2952.
[89] H. Hirai, M. F. Roussel, J. Y. Kato, R. A. Ashmun, C. J. Sherr, *Mol. Cell. Biol.* **1995**, *15*, 2672 – 2681.
[90] F. K. Chan, J. Zhang, L. Cheng, D. N. Shapiro, A. Winoto, *Mol. Cell. Biol.* **1995**, *15*, 2682 – 2688.
[91] M. Adachi, M. F. Roussel, K. Havenith, C. J. Sherr, *Blood* **1997**, *90*, 126 – 137.
[92] I. Reynisdottir, J. Massague, *Genes Dev.* **1997**, *11*, 492 – 503.
[93] C. J. Sherr, *Genes Dev.* **1998**, *12*, 2984 – 2991.
[94] J. M. Nigro, S. J. Baker, A. C. Preisinger, J. M. Jessup, R. Hostetter, K. Cleary, S. H. Bigner, N. Davidson, S. Baylin, P. Devilee, T. Glover, F. S. Collins, A. Weston, R. Modali, C. C. Harris, B. Vogelstein, *Nature* **1989**, *342*, 705 – 708.
[95] M. H. Hollstein, D. Sidransky, B. Vogelstein, C. C. Harris, *Science* **1991**, *253*, 49 – 53.
[96] S. P. Hussain, C. C. Harris, *Cancer Res.* **1998**, *58*, 4023 – 4037.
[97] S. P. Hussain, M. H. Hollstein, C. C. Harris, *Ann. N. Y. Acad. Sci.* **2000**, *919*, 79 – 85.
[98] M. B. Kastan, O. Onyekwere, D. Sidransky, B. Vogelstein, R. W. Craig, *Cancer Res.* **1991**, *51*, 6304 – 6311.
[99] X. Chen, L. J. Ko, L. Jayaraman, C. Prives, *Genes Dev.* **1996**, *10*, 2438 – 2451.
[100] T. M. Gottlieb, M. Oren, *Semin. Cancer Biol.* **1998**, *8*, 359 – 368.
[101] C. Sandhu, J. Slingerland, *Cancer Detect. Prev.* **2000**, *24*, 107 – 118.
[102] S. Omura, Y. Iwai, A. Hirano, A. Nakagawa, J. Awaya, H. Tsuchya, Y. Takahashi, R. Masuma, *J. Antibiot.* **1977**, *30*, 275 – 282.
[103] V. Rialet, L. Meijer, *Anticancer Res.* **1991**, *11*, 1581 – 1590.
[104] L. M. Toledo, N. B. Lydon, *Structure* **1997**, *5*, 1551 – 1556.
[105] A. M. Lawrie, M. E. Noble, P. Tunnah, N. R. Brown, L. N. Johnson, J. A. Endicott, *Nat. Struct. Biol.* **1997**, *4*, 796 – 801.
[106] L. Prade, R. A. Engh, A. Girod, V. Kinzel, R. Huber, D. Bossemeyer, *Structure* **1997**, *5*, 1627 – 1637.
[107] K. Kawakami, H. Futami, J. Takahara, K. Yamaguchi, *Biochem. Biophys. Res. Commun.* **1996**, *219*, 778 – 783.
[108] M. Begemann, S. A. Kashimawo, Y. A. Choi, S. Kim, K. M. Christiansen, G. Duigou, M. Mueller, I. Schieren, S. Ghosh, D. Fabbro, N. M. Lampen, D. F. Heitjan, P. B. Schiff, J. N. Bruce, I. B. Weinstein, *Clin. Cancer Res.* **1996**, *2*, 1017 – 1030.
[109] T. Meyer, U. Regenass, D. Fabbro, E. Alteri, J. Rosel, M. Muller, G. Caravatti, A. Matter, *Int. J. Cancer* **1989**, *43*, 851 – 856.
[110] L. Yu, L. Orlandi, P. Wang, M. S. Orr, A. M. Senderowicz, E. A. Sausville, R. Silvestrini, N. Watanabe, H. Piwnica-Worms, P. M. O'Connor, *J. Biol. Chem.* **1998**, *273*, 33455 – 33464.
[111] A. D. Harmon, U. Weiss, J. V. Silverton, *Tetrahedron Lett.* **1979**, 721 – 724.
[112] F. Arguello, M. Alexander, J. A. Sterry, G. Tudor, E. M. Smith, N. T. Kalavar, J. F. Greene, Jr., W. Koss, C. D. Morgan, S. F. Stinson, T. J. Siford, W. G. Alvord, R. L. Klabansky, E. A. Sausville, *Blood* **1998**, *91*, 2482 – 2490.

 © 2003 Wiley-VCH Verlag GmbH & Co. KGaA, Weinheim

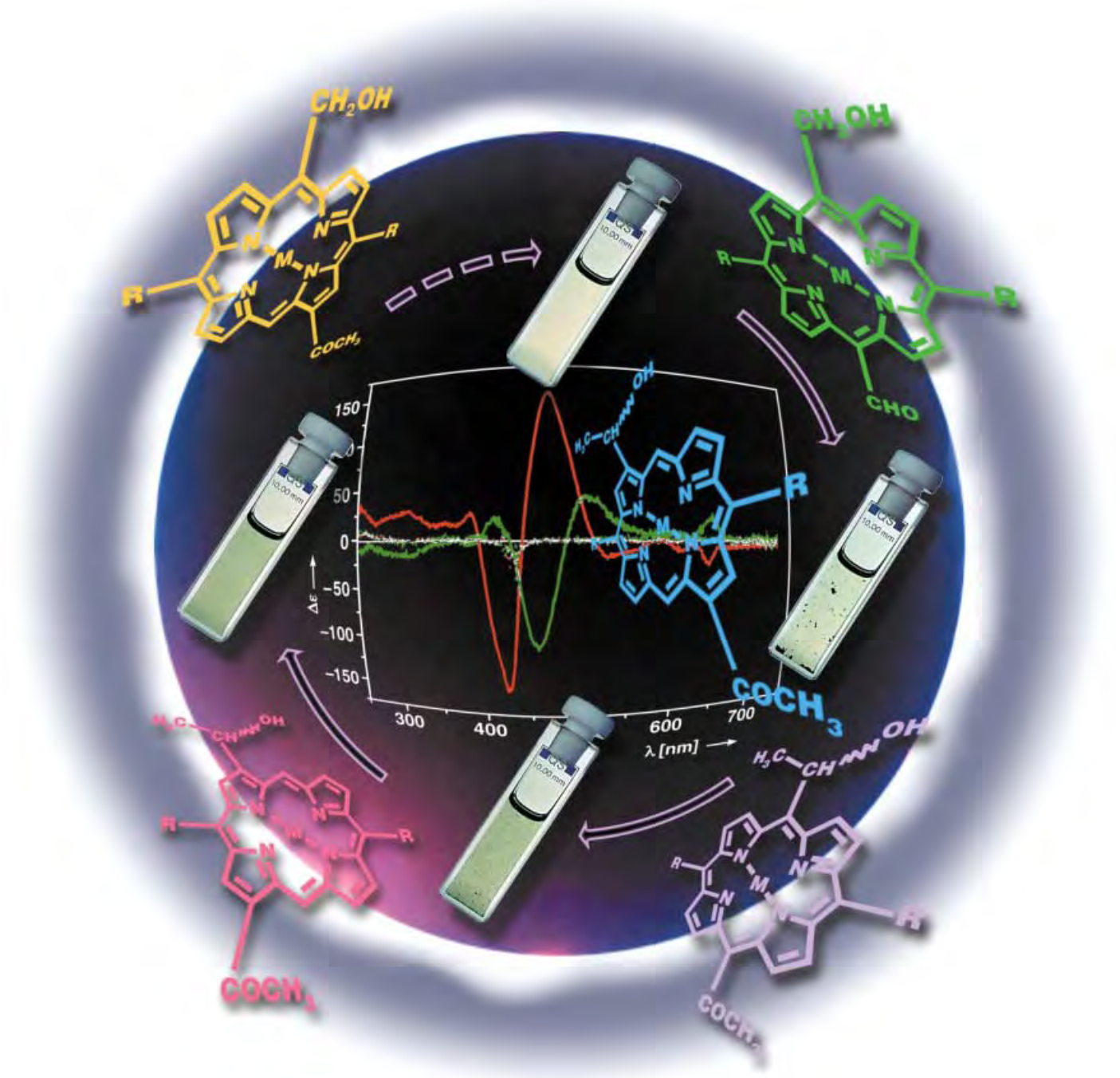
[113] G. Kaur, M. Stetler-Stevenson, S. Sebers, P. Worland, H. Sedlacek, C. Myers, J. Czech, R. Naik, E. Sausville, *J. Natl. Cancer Inst.* **1992**, *84*, 1736 – 1740.
[114] A. M. Senderowicz, *Invest. New Drugs* **1999**, *17*, 313 – 320.
[115] M. D. Losiewicz, B. A. Carlson, G. Kaur, E. A. Sausville, P. J. Worland, *Biochem. Biophys. Res. Commun.* **1994**, *201*, 589 – 595.
[116] H. H. Sedlacek, D. Hoffmann, J. Czech, C. Kolar, G. Seemann, D. Guessow, K. Bosslet, *Chimia* **1991**, *45*, 311 – 316.
[117] H. H. Sedlacek, *Crit. Rev. Oncol. Hematol.* **2001**, *38*, 139 – 170.
[118] J. Czech, D. Hoffmann, R. Naik, H.-H. Sedlacek, *Int. J. Oncol.* **1995**, *6*, 31 – 36.
[119] S. Leclerc, M. Garnier, R. Hoessel, D. Marko, J. A. Bibb, G. L. Snyder, P. Greengard, J. Biernat, Y. Z. Wu, E. M. Mandelkow, G. Eisenbrand, L. Meijer, *J. Biol. Chem.* **2001**, *276*, 251 – 260.
[120] H. H. Sedlacek, J. Czech, R. Naik, G. Kaur, P. Worland, M. Losiewicz, B. Parker, B. Carlson, A. Smith, *Int. J. Oncol.* **1996**, *9*, 1143 – 1168.
[121] S. H. Chao, K. Fujinaga, J. E. Marion, R. Taube, E. A. Sausville, A. M. Senderowicz, B. M. Peterlin, D. H. Price, *J. Biol. Chem.* **2000**, *275*, 28345 – 28348.
[122] B. Carlson, T. Lahusen, S. Singh, A. Loaiza-Perez, P. J. Worland, R. Pestell, C. Albanese, E. A. Sausville, A. M. Senderowicz, *Cancer Res.* **1999**, *59*, 4634 – 4641.
[123] W. F. De Azevedo, Jr., H. J. Mueller-Dieckmann, U. Schulze-Gahmen, P. J. Worland, E. Sausville, S. H. Kim, *Proc. Natl. Acad. Sci. USA* **1996**, *93*, 2735 – 2740.
[124] K. S. Kim, J. S. Sack, J. S. Tokarski, L. Qian, S. T. Chao, L. Leith, Y. F. Kelly, R. N. Misra, J. T. Hunt, S. D. Kimball, W. G. Humphreys, B. S. Wautlet, J. G. Mulheron, K. R. Webster, *J. Med. Chem.* **2000**, *43*, 4126 – 4134.
[125] K. K. Murthi, M. Dubay, C. McClure, L. Brizuela, M. D. Boisclair, P. J. Worland, M. M. Mansuri, K. Pal, *Bioorg. Med. Chem. Lett.* **2000**, *10*, 1037 – 1041.
[126] L. R. Kelland, *Expert Opin. Invest. Drugs* **2000**, *9*, 2903 – 2911.
[127] J. Schoepfer, H. Fretz, B. Chaudhuri, L. Muller, E. Seeber, L. Meijer, O. Lozach, E. Vangrevelinghe, P. Furet, *J. Med. Chem.* **2002**, *45*, 1741 – 1747.
[128] M. Kitagawa, T. Okabe, H. Ogino, H. Matsumoto, I. Suzuki-Takahashi, T. Kokubo, H. Higashi, S. Saitoh, Y. Taya, H. Yasuda, *Oncogene* **1993**, *8*, 2425 – 2432.
[129] M. Kitagawa, H. Higashi, I. S. Takahashi, T. Okabe, H. Ogino, Y. Taya, S. Hishimura, A. Okuyama, *Oncogene* **1994**, *9*, 2549 – 2557.
[130] K. Nishio, T. Ishida, H. Arioka, H. Kurokawa, K. Fukuoka, T. Nomoto, H. Fukumoto, H. Yokote, N. Saijo, *Anticancer Res.* **1996**, *16*, 3387 – 3395.
[131] I. Neant, P. Guerrier, *Exp. Cell Res.* **1988**, *176*, 68 – 79.
[132] J. Vesely, L. Havlicek, M. Strnad, J. J. Blow, A. Donella-Deana, L. Pinna, D. S. Letham, J. Kato, L. Detivaud, S. Leclerc, *Eur. J. Biochem.* **1994**, *224*, 771 – 786.
[133] W. F. De Azevedo, S. Leclerc, L. Meijer, L. Havlicek, M. Strnad, S. H. Kim, *Eur. J. Biochem.* **1997**, *243*, 518 – 526.
[134] L. Meijer, A. Borgne, O. Mulner, J. P. Chong, J. J. Blow, N. Inagaki, M. Inagaki, J. G. Delcros, J. P. Moulinoux, *Eur. J. Biochem.* **1997**, *243*, 527 – 536.
[135] U. Schulze-Gahmen, J. Brandsen, H. D. Jones, D. O. Morgan, L. Meijer, J. Vesely, S. H. Kim, *Proteins Struct. Funct. Genet.* **1995**, *22*, 378 – 391.
[136] N. S. Gray, L. Wodicka, A. M. Thunnissen, T. C. Norman, S. Kwon, F. H. Espinoza, D. O. Morgan, G. Barnes, S. LeClerc, L. Meijer, S. H. Kim, D. J. Lockhart, P. G. Schultz, *Science* **1998**, *281*, 533 – 538.
[137] M. Legraverend, O. Ludwig, E. Bisagni, S. Leclerc, L. Meijer, *Bioorg. Med. Chem. Lett.* **1998**, *8*, 793 – 798.
[138] M. Legraverend, P. Tunnah, M. Noble, P. Ducrot, O. Ludwig, D. S. Grierson, M. Leost, L. Meijer, J. Endicott, *J. Med. Chem.* **2000**, *43*, 1282 – 1292.
[139] E. E. Brooks, N. S. Gray, A. Joly, S. S. Kerwar, R. Lum, R. L. Mackman, T. C. Norman, J. Rosete, M. Rowe, S. R. Schow, P. G. Schultz, X. Wang, M. M. Wick, D. Shiffman, *J. Biol. Chem.* **1997**, *272*, 29207 – 29211.
[140] P. Imbach, H. G. Capraro, P. Furet, H. Mett, T. Meyer, J. Zimmermann, *Bioorg. Med. Chem. Lett.* **1999**, *9*, 91 – 96.
[141] C. E. Arris, F. T. Boyle, A. H. Calvert, N. J. Curtin, J. A. Endicott, E. F. Garman, A. E. Gibson, B. T. Golding, S. Grant, R. J. Griffin, P. Jewsbury, L. N. Johnson, A. M. Lawrie, D. R. Newell, M. E. Noble, E. A. Sausville, R. Schultz, W. Yu, *J. Med. Chem.* **2000**, *43*, 2797 – 2804.
[142] R. Soni, T. O'Reilly, P. Furet, L. Muller, C. Stephan, S. Zumstein-Mecker, H. Fretz, D. Fabbro, B. Chaudhuri, *J. Natl. Cancer Inst.* **2001**, *93*, 436 – 446.
[143] S. R. Klutchko, J. M. Hamby, D. H. Boschelli, Z. Wu, A. J. Kraker, A. M. Amar, B. G. Hartl, C. Shen, W. D. Klohs, R. W. Steinkampf, D. L. Driscoll, J. M. Nelson, W. L. Elliott, B. J. Roberts, C. L. Stoner, P. W. Vincent, D. J. Dykes, R. L. Panek, G. H. Lu, T. C. Major, T. K. Dahring, H. Hallak, L. A. Bradford, H. D. Hollis Showalter, A. M. Doherty, *J. Med. Chem.* **1998**, *41*, 3276 – 3292.
[144] S. Trumpp-Kallmeyer, J. R. Rubin, C. Humblet, J. M. Hamby, H. D. Hollis Showalter, *J. Med. Chem.* **1998**, *41*, 1752 – 1763.
[145] M. Barvian, D. H. Boschelli, J. Cossrow, E. Dobrusin, A. Fattaey, A. Fritsch, D. Fry, P. Harvey, P. Keller, M. Garrett, F. La, W. Leopold, D. McNamara, M. Quin, S. Trumpp-Kallmeyer, P. Toogood, Z. Wu, E. Zhang, *J. Med. Chem.* **2000**, *43*, 4606 – 4616.
[146] G. W. Rewcastle, W. A. Denny, A. J. Bridges, H. Zhou, D. R. Cody, A. McMichael, D. W. Fry, *J. Med. Chem.* **1995**, *38*, 3482 – 3487.
[147] A. J. Bridges, H. Zhou, D. R. Cody, G. W. Rewcastle, A. McMichael, H. D. Hollis Showalter, D. W. Fry, A. J. Kraker, W. A. Denny, *J. Med. Chem.* **1996**, *39*, 267 – 276.
[148] A. M. Thompson, D. K. Murray, W. L. Elliott, D. W. Fry, J. A. Nelson, H. D. Hollis Showalter, B. J. Roberts, P. W. Vincent, W. A. Denny, *J. Med. Chem.* **1997**, *40*, 3915 – 3925.
[149] D. W. Fry, A. J. Kraker, A. McMichael, L. A. Ambroso, J. M. Nelson, W. R. Leopold, R. W. Connors, A. J. Bridges, *Science* **1994**, *265*, 1093 – 1095.
[150] L. Shewchuk, A. Hassell, B. Wisely, W. Rocque, W. Holmes, J. Veal, L. F. Kuyper, *J. Med. Chem.* **2000**, *43*, 133 – 138.
[151] T. M. Sielecki, T. L. Johnson, J. Liu, J. K. Muckelbauer, R. H. Grafstrom, S. Cox, J. Boylan, C. R. Burton, H. Chen, A. Smallwood, C. H. Chang, M. Boisclair, P. A. Benfield, G. L. Trainor, S. P. Seitz, *Bioorg. Med. Chem. Lett.* **2001**, *11*, 1157 – 1160.
[152] R. Hoessel, S. Leclerc, J. A. Endicott, M. E. Nobel, A. Lawrie, P. Tunnah, M. Leost, E. Damiens, D. Marie, D. Marko, E. Niederberger, W. Tang, G. Eisenbrand, L. Meijer, *Nat. Cell Biol.* **1999**, *1*, 60 – 67.
[153] T. G. Davies, P. Tunnah, L. Meijer, D. Marko, G. Eisenbrand, J. A. Endicott, M. E. Noble, *Structure* **2001**, *9*, 389 – 397.
[154] G. Y. Wu, J. Z. Liu, F. D. Fang, J. Zuo, *Sci. Sin. Ser. B (Engl. Ed.)* **1982**, *25*, 1071 – 1079.
[155] L. L. Kent, N. E. Hull-Campbell, T. Lau, J. C. Wu, S. A. Thompson, M. Nori, *Biochem. Biophys. Res. Commun.* **1999**, *260*, 768 – 774.
[156] M. E. Lane, B. Yu, A. Rice, K. E. Lipson, C. Liang, L. Sun, C. Tang, G. McMahon, R. G. Pestell, S. Wadler, *Cancer Res.* **2001**, *61*, 6170 – 6177.
[157] L. Sun, N. Tran, F. Tang, H. App, P. Hirth, G. McMahon, C. Tang, *J. Med. Chem.* **1998**, *41*, 2588 – 2603.

 © 2003 Wiley-VCH Verlag GmbH & Co. KGaA, Weinheim

[158] L. Sun, N. Tran, C. Liang, S. Hubbard, F. Tang, K. Lipson, R. Schreck, Y. Zhou, G. McMahon, C. Tang, *J. Med. Chem.* **2000**, *43*, 2655 – 2663.
[159] T. A. Fong, L. K. Shawver, L. Sun, C. Tang, H. App, T. J. Powell, Y. H. Kim, R. Schreck, X. Wang, W. Risau, A. Ullrich, K. P. Hirth, G. McMahon, *Cancer Res.* **1999**, *59*, 99 – 106.
[160] V. Kirkin, R. Mazitschek, J. Krishnan, A. Steffen, J. Waltenberger, M. S. Pepper, A. Giannis, J. P. Sleeman, *Eur. J. Biochem.* **2001**, *268*, 5530 – 5540.
[161] H. N. Bramson, J. Corona, S. T. Davis, S. H. Dickerson, M. Edelstein, S. V. Frye, R. T. Gampe, Jr., P. A. Harris, A. Hassell, W. D. Holmes, R. N. Hunter, K. E. Lackey, B. Lovejoy, M. J. Luzzio, V. Montana, W. J. Rocque, D. Rusnak, L. Shewchuk, J. M. Veal, D. H. Walker, L. F. Kuyper, *J. Med. Chem.* **2001**, *44*, 4339 – 4358.
[162] D. W. Zaharevitz, R. Gussio, M. Leost, A. M. Senderowicz, T. Lahusen, C. Kunick, L. Meijer, E. A. Sausville, *Cancer Res.* **1999**, *59*, 2566 – 2569.
[163] C. Schultz, A. Link, M. Leost, D. W. Zaharevitz, R. Gussio, E. A. Sausville, L. Meijer, C. Kunick, *J. Med. Chem.* **1999**, *42*, 2909 – 2919.
[164] C. Kunick, C. Schultz, T. Lemcke, D. W. Zaharevitz, R. Gussio, R. K. Jalluri, E. A. Sausville, M. Leost, L. Meijer, *Bioorg. Med. Chem. Lett.* **2000**, *10*, 567 – 569.
[165] M. Leost, C. Schultz, A. Link, Y. Z. Wu, J. Biernat, E. M. Mandelkow, J. A. Bibb, G. L. Snyder, P. Greengard, D. W. Zaharevitz, R. Gussio, A. M. Senderowicz, E. A. Sausville, C. Kunick, L. Meijer, *Eur. J. Biochem.* **2000**, *267*, 5983 – 5994.
[166] D. M. Roll, C. M. Ireland, H. S. M. Lu, J. Clardy, *J. Org. Chem.* **1988**, *53*, 3276 – 3278.
[167] R. Soni, L. Muller, P. Furet, J. Schoepfer, C. Stephan, S. Zumstein-Mecker, H. Fretz, B. Chaudhuri, *Biochem. Biophys. Res. Commun.* **2000**, *275*, 877 – 884.
[168] A. Hormann, B. Chaudhuri, H. Fretz, *Bioorg. Med. Chem.* **2001**, *9*, 917 – 921.
[169] L. Meijer, A. M. Thunnissen, A. W. White, M. Garnier, M. Nikolic, L. H. Tsai, J. Walter, K. E. Cleverley, P. C. Salinas, Y. Z. Wu, J. Biernat, E. M. Mandelkow, S. H. Kim, G. R. Pettit, *Chem. Biol.* **2000**, *7*, 51 – 63.
[170] D. Tasdemir, R. Mallon, M. Greenstein, L. R. Feldberg, S. C. Kim, K. Collins, D. Wojciechowicz, G. C. Mangalindan, G. P. Concepcion, M. K. Harper, C. M. Ireland, *J. Med. Chem.* **2002**, *45*, 529 – 532.
[171] A. Kubo, K. Nakagawa, R. K. Varma, N. K. Conrad, J. Q. Cheng, W. C. Lee, J. R. Testa, B. E. Johnson, F. J. Kaye, M. J. Kelley, *Clin. Cancer Res.* **1999**, *5*, 4279 – 4286.
[172] I. Antonini, P. Polucci, T. C. Jenkins, L. R. Kelland, E. Menta, N. Pescalli, B. Stefanska, J. Mazerski, S. Martelli, *J. Med. Chem.* **1997**, *40*, 3749 – 3755.
[173] T. Honma, K. Hayashi, T. Aoyama, N. Hashimoto, T. Machida, K. Fukasawa, T. Iwama, C. Ikeura, M. Ikuta, I. Suzuki-Takahashi, Y. Iwasawa, T. Hayama, S. Nishimura, H. Morishima, *J. Med. Chem.* **2001**, *44*, 4615 – 4627.
[174] T. Honma, T. Yoshizumi, N. Hashimoto, K. Hayashi, N. Kawanishi, K. Fukasawa, T. Takaki, C. Ikeura, M. Ikuta, I. Suzuki-Takahashi, T. Hayama, S. Nishimura, H. Morishima, *J. Med. Chem.* **2001**, *44*, 4628 – 4640.
[175] M. Ikuta, K. Kamata, K. Fukasawa, T. Honma, T. Machida, H. Hirai, I. Suzuki-Takahashi, T. Hayama, S. Nishimura, *J. Biol. Chem.* **2001**, *276*, 27548 – 27554.
[176] L. Lilja, S. N. Yang, D. L. Webb, L. Juntti-Berggren, P. O. Berggren, C. Bark, *J. Biol. Chem.* **2001**, *276*, 34199 – 34205.
[177] E. A. Sausville, *Trends Mol. Med.* **2002**, *8*, S32 – S37.
[178] X. Chen, M. Lowe, T. Herliczek, M. J. Hall, C. Danes, D. A. Lawrence, K. Keyomarsi, *J. Natl. Cancer Inst.* **2000**, *92*, 1999 – 2008.
[179] S. T. Davis, B. G. Benson, H. N. Bramson, D. E. Chapman, S. H. Dickerson, K. M. Dold, D. J. Eberwein, M. Edelstein, S. V. Frye, R. T. Gampe, Jr, R. J. Griffin, P. A. Harris, A. M. Hassell, W. D. Holmes, R. N. Hunter, V. B. Knick, K. Lackey, B. Lovejoy, M. J. Luzzio, D. Murray, P. Parker, W. J. Rocque, L. Shewchuk, J. M. Veal, D. H. Walker, L. F. Kuyper, *Science* **2001**, *291*, 134 – 137.
[180] L. Meijer, S. Leclerc, M. Leost, *Pharmacol. Ther.* **1999**, *82*, 279 – 284.
[181] G. Brooks, N. B. La Thangue, *Drug Discovery Today* **1999**, *4*, 455 – 464.

 © 2003 Wiley-VCH Verlag GmbH & Co. KGaA, Weinheim

Communications



Several novel porphyrins mimicking the self-assembly ability of the natural bacteriochlorophylls *c*, *d*, and *e* have been synthesized in high yields. These artificial antenna systems should be able to harvest sunlight even under low-light illumination conditions, as implied by the eclipse of the sun shown in the background. For more information see the communication by T. S. Balaban et al. on the following pages.

DOI: 10.1002/anie.200250465
© 2003 Wiley-VCH Verlag GmbH & Co. KGaA, Weinheim

Artificial Light-Harvesting Antenna

Controlling Chirality and Optical Properties of Artificial Antenna Systems with Self-Assembling Porphyrins**

Teodor Silviu Balaban, Anil Dnyanoba Bhise, Matthias Fischer, Myriam Linke-Schaetzel, Christian Roussel, and Nicholas Vanthuyne*

Dedicated to Professors Klaus Hafner and Emanuel Vogel, magisters of chromophore chemistry, on the occasion of their 75th birthday

A fascinating example of self-assembly encountered in nature is provided by green photosynthetic bacteria. These bacteria developed early during evolution, under the pressure of synthetic and genetic economy, an organelle capable of capturing sunlight even at 10 m below the surface of water to trigger photosynthesis. In this organelle the so-called chlorosome, bacteriochlorophyll (BChl) molecules, self-organize without the use of proteinaceous scaffolding.[1,2] Later in evolution, purple bacteria and plants perfected their light-harvesting apparatus by assembling much more complicated (bacterio)chlorophyll-protein complexes.[3–6] These complexes are presently beyond the scope of synthetic chemistry. However, the earlier antennas, which are fully functional, can be mimicked with synthetic molecules by controlling their self-assembly in view of achieving artificial photosynthesis.

Essential for the self-assembly algorithm to be able to operate are 1) the ligation of the central magnesium atom by the 3^1-hydroxy group of another molecule; 2) cooperative hydrogen bonding of the same OH group to the 13^1-carbonyl group of a third BChl *c* molecule; and 3) π–π interactions between the chlorin macrocycles, which are organized into stacks. These supramolecular interactions are detailed in Figure 1.

The elucidation of the molecular mechanism, by which the self-assembly occurs has involved various spectroscopic techniques and studies on both natural chlorosomes and on isolated BChl *c*, which was induced to self-assemble. These studies included solid state NMR on ^{13}C-labelled samples,[2,7,8] FTIR,[9] circular dichroism (CD),[10] as well as visible absorption on semisynthetic mimics, in which the positions of the carbonyl and hydroxy groups have been reversed[11] and zinc is the central metal atom instead of magnesium.[12] However, the sole presence of these groups is not sufficient for engineering the self-assembly; a rather careful tailoring of the whole molecular architecture has to be assured, as shown in a previous study.[13] From single crystal X-ray crystallography one could conclude which interactions have to be favored and which interactions have to be inhibited or suppressed.[13] Remarkably, by sequencing the entire genome of *Chlorobium tepidum,* a photosynthetic green sulfur bacterium, genetic evidence was recently brought forth for the self-assembly process of BChls as a way of obtaining functional antenna systems.[14]

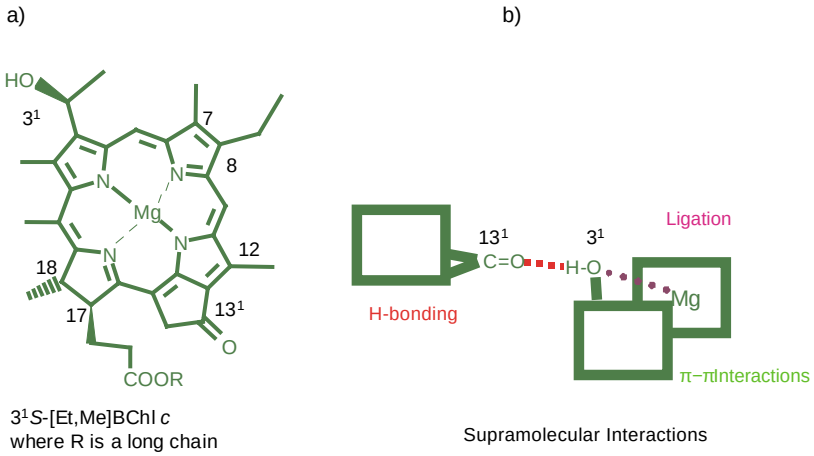


Figure 1. a) Molecular formula and atom numbering for a typical natural bacteriochlorophyll *c*—the 3^1-carbon atom may have either *R* or *S* configuration while the 17- and 18-carbon atoms are both *S*. Different substituents in the 8- and 12-positions (depicted are ethyl and methyl) as well as various long chain alcohols (such as farnesyl, stearyl, cetyl, oleyl, etc.) may esterify the 17-propionic acid side chain. b) The three important supramolecular interactions are presented schematically.

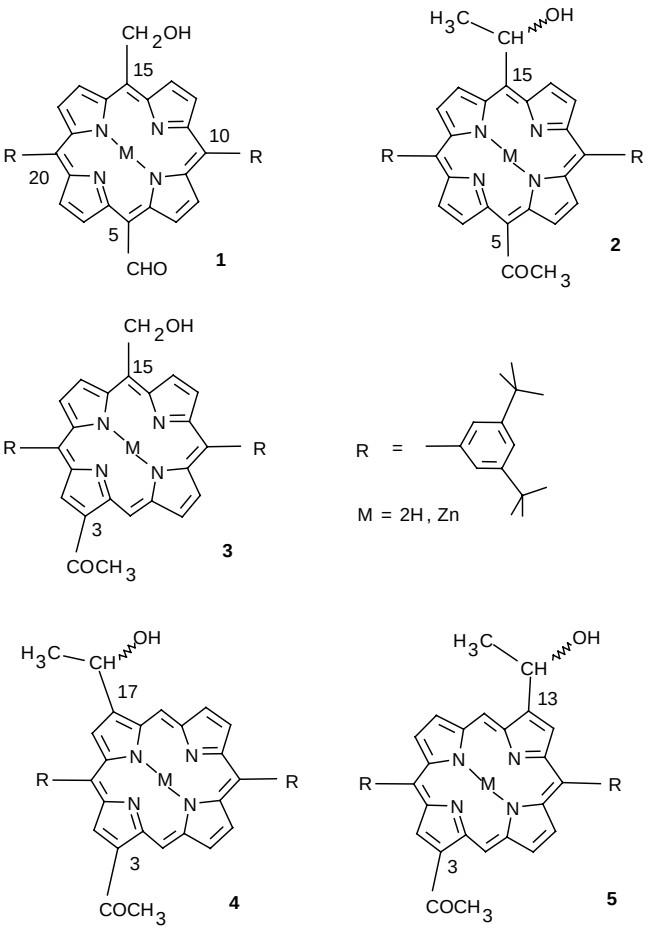
We have now developed very selective synthetic methods which have allowed us to synthesize the new porphyrinic systems **1**–**5** (Scheme 1), where R is a solubility-inducing group, namely the 3,5-di-*tert*-butylphenyl group. Both a hydroxy group, either as the achiral hydroxymethyl or as the chiral hydroxyethyl, and a carbonyl group, either as formyl or acetyl residues have been appended into desired positions onto the porphyrin periphery. In the self-assembled suprastructures, the interchromophoric interactions can now

[*] Priv. Doz. Dr. T. S. Balaban, A. D. Bhise, M. Fischer, Dr. M. Linke-Schaetzel
Institut für Nanotechnologie
Forschungszentrum Karlsruhe
Postfach 3640, 76021 Karlsruhe (Germany)
Fax: (+49) 724-782-6434
E-mail: silviu.balaban@int.fzk.de
Prof. Dr. C. Roussel, Dr. N. Vanthuyne
ENSSPICAM Université
Centre de Saint Jerome, 13397 Marseille CEDEX 20 (France)

[**] This work was partially supported by the Deutsche Forschungsgemeinschaft (DFG) through the joint project C3.2 of the Center for Functional Nanostructures involving FZK-INT and the University of Karlsruhe. We thank Prof. Horst Hahn and Dr. Branko Stahl for the preparation of nanocrystalline TiO_2, Dr. Hartmut Gliemann and Dr. Thomas Koch for fluorescence microscopic and AFM images, Prof. Volker Buß and Robert Knierim for CD measurements, Dr. Sergei Lebedkin for fluorescence spectra, Angelika Kernert and Ingrid Roßnagel for HR-FAB mass spectra.

Supporting information for this article is available on the WWW under http://www.angewandte.org or from the author.

 © 2003 Wiley-VCH Verlag GmbH & Co. KGaA, Weinheim DOI: 10.1002/anie.200250465



Scheme 1. The new porphyrins.

be fine tuned because of the slight but controlled variations in their geometry.

Different synthetic strategies were employed with full characterization of the intermediates (see Supporting Information). The structures of the new compounds were ascertained on the basis of their ^{1}H, ^{13}C NMR, FTIR and HRFAB mass spectra. NMR signals could be fully assigned on the basis of NOESY and COSY spectra.

The free bases **1**–**5** (M = 2H) could be metallated by using zinc acetate in a chloroform/methanol (4:1) mixture at room temperature with almost quantitative yields. Compounds **1**–**5** (M = Zn) are the first fully synthetic mimics of bacteriochlorophyll *c* that can self-assemble. The three structural elements responsible for the self-assembly, namely a hydroxy group, a central metal atom with affinity for a fifth ligand, and a carbonyl group are allowed to interact so that the algorithm leading to self-assembly is able to become operative. Previous attempts to program such self-assembly with porphyrins were not successful.[13] Semisynthetic products, which were derived from chlorophyll *a*, and which are also capable of self-assembly, were recently described.[15] If practical uses are envisaged, our synthetic strategies, which are high yielding and use cheap starting materials, are superior as the starting material, copper 10,20-bis-(3,5-di-*tert*-butylphenyl) porphyrin[16] is easily available in multigram quantities.

Compounds **1**–**5** self-assemble in nonpolar solvents such as *n*-heptane or *n*-hexane, just as the natural BChls *c*, *d* and *e* do. If the critically micellar concentration is surpassed, self-assembly leads to the separation of "fluffs" which are thermodynamically stable and usually settle at the bottom of the reaction vessel. These macroaggregates are visible to the eye, and upon gentle shaking are disrupted by shearing forces to nanoaggregates of about 100 nm, as indicated by dynamic light scattering and statistical analysis. This size shearing is illustrated in Figure 2 with self-assembled **1** (M = Zn) and is intriguingly similar both in general appearance and in the colors seen as the process that was reported for the natural BChl *c*.[17] After a few hours the macroaggregates reappear and this sequence may be repeated for several months because of their high stability in the absence of oxygen, even in the presence of light.

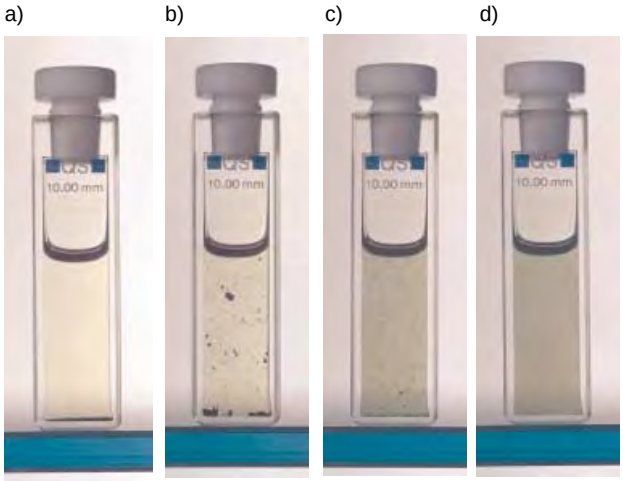


Figure 2. A quartz cuvette with self-assembled **1**. From left to right: a) the macroaggregates have settled to the bottom and the solution is only weakly colored. b) Gentle heating of the bottom of the cuvette leads to convection, the fluffs circulate slowly and are visible to the eye. c) The same cuvette after a longer period of convection. d) The same cuvette after shaking—a homogeneous, strongly colored solution is obtained, which arises from shearing forces.

The self-organization process is accompanied by drastic changes in the absorption spectra arising from electronic interactions between neighboring units within the supramolecular species. As only weak interactions are involved, the addition of small amounts of methanol, for example, leads to complete disassembly. This is illustrated in Figure 3 by means of UV/Vis absorption spectra. Very different behavior is encountered for each compound **1**–**5** because of the different positions at which the hydroxy and carbonyl groups are appended onto the porphyrin macrocycle. The supramolecular assemblies have different optical properties because of the fine tuning of the π–π overlap and the direction of the transition dipole moments.

Importantly, because of the self-assembly, the intense Soret band characteristic for porphyrins is "spread out" for **1**-**Zn**, **5**-**Zn**, and especially **2**-**Zn**; the much smaller Q bands are also affected. The absorption bands characteristic of the self-

 © 2003 Wiley-VCH Verlag GmbH & Co. KGaA, Weinheim

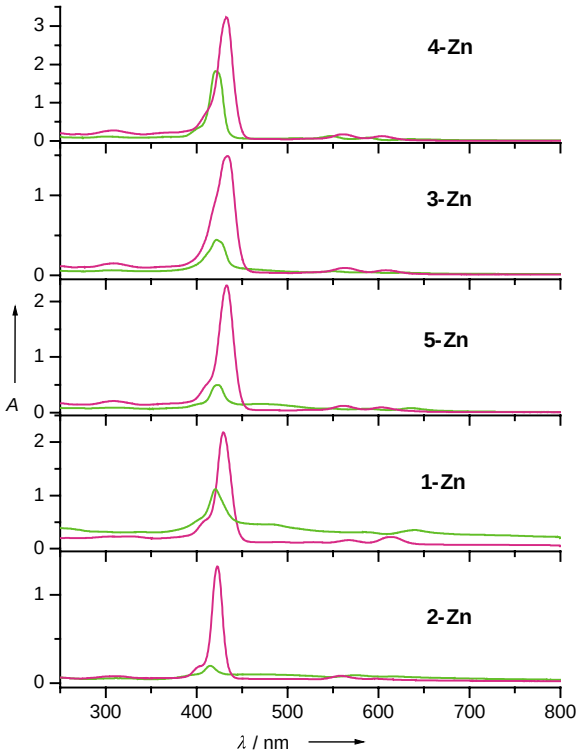


Figure 3. Visible absorption spectra of synthetic porphyrinic BChl *c* mimics. Green curves are samples after self-assembly in dry *n*-heptane (1.5 mL) obtained by dilution of a concentrated dry dichloromethane solution (30–100 μL). Magenta curves are measured in the same sample after the addition of methanol (50 μL) to the quartz cuvette with a path length of 0.5 cm and show complete disassembly of the aggregates to the monomeric zinc–methanol adducts. For the disassembly of **5-Zn**, which forms the most stable supramolecular structures, more methanol (100 μL) was needed. For **1-Zn** and **2-Zn** the solutions were strongly light-scattering. For **1-Zn** the magenta trace was recorded for the same solution as the green trace but with 1 mm path length. A similar experiment with a more concentrated solution of **2-Zn** and **5-Zn** are shown in the Supporting Information.

assembled species are red shifted in comparison to the monomers, as encountered in J aggregates,[18,19,20] or in the natural BChls *c*, *d* and *e*.[21] The Soret bands are shifted by about 50 nm, but because of the severe broadening they now overlap partially with the Q bands in the monomers. Thus these self-assembled species have a nonzero absorption coefficient between 400 and 700 nm, which is beneficial for light harvesting over a broad spectral range. In contrast to this behavior, in the self-assembled **4-Zn,** only a slight broadening and small red shift is encountered because of the limited π–π overlap, which perturbs only marginally the chromophores. In self-assembled **3-Zn** the situation is intermediate between **4-Zn** and the other cases. When methanol is added in very small amounts (but over the stoichiometric amount), the broad absorption bands completely disappear, and the Soret band drastically sharpens and red shifts by about 10 nm because of the formation of the monomeric Zn-methanol adducts. Methanol per se is not a better solvent, but competes for the zinc ligation and totally disrupts the hydrogen bonding network. This is clearly evident from FTIR spectra, in which the broad δ_{OH} vibrations between 3300 and 3200 cm^{-1} disappear upon methanol addition concomitantly with a shifting of the strong $\tilde{\nu}_{CO}$ arising from the acetyl group in compounds **2-Zn**–**5-Zn** from a very low frequency of 1639 cm^{-1} (in **5-Zn**), which we ascribe to a Zn–O–H···O=C< carbonyl group in conjugation with the porphyrin ring, to normal value of 1720 cm^{-1} (in **2-Zn**, where the acetyl group is forced out of the porphrin plane).[22] The self-assembly process is also responsible for the stacking of chromophores, as in J aggregates, which can be seen from the absorption spectra in dichloromethane at different concentrations (see Supporting Information). As the concentration decreases, the red-shifted aggregate peaks become less prominent and they are entirely absent in dilute solutions.

Racemates of **4-Zn** and **5-Zn** could be resolved satisfactorily on a chiral carbamate modified polysaccharide HPLC column (Chiralcel, OD-H), which provided fractions with enrichments varying between 78 and 95%. Compound **2-Zn** could not be separated into enantiomers under the same conditions. With both enantiomers of **5-Zn**, after the removal of any traces of 2-propanol and water (from the HPLC eluent), self-assembly was induced in *n*-heptane and the CD-spectra of both fractions were recorded at room temperature. Signals with intense ellipticity are encountered, which are mirror imaged in the two fractions (Figure 4). While a single Cotton effect is observed for the Q aggregate band at 635 nm, an excitonic couplet appears for the broadened Soret aggregate band. For the first fraction, which was more dilute and contained less self-assembled species, the couplet is not as symmetric as for the second fraction. In the latter case the longest wavelength Cotton effect of the couplet is positive, and has a maximum at 464 nm. The trough appears at 424 nm, thus indicating that indeed the rotary power stems

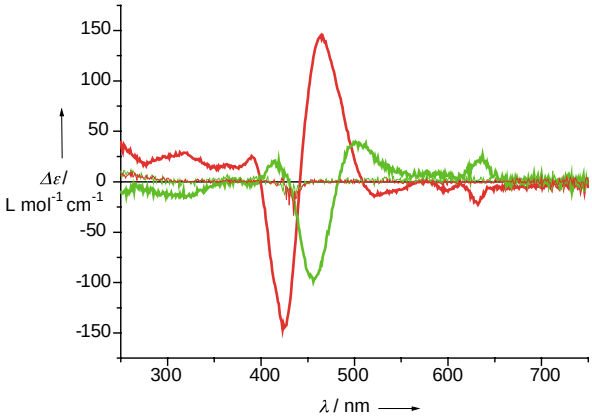


Figure 4. CD spectra of enantiomerically enriched **5-Zn** after self-assembly in *n*-heptane and after addition of methanol which disrupts the assemblies. The concentrations were 2.7 μmolar for the fraction of the firstly eluted enantiomer (green lines) and 4.7 μmolar for the fraction containing the secondly eluted enantiomer (red lines) which contained more self-assembled species as inferred from the absorption spectra. After addition of methanol the intense mirror imaged CD-signals disappear (thin red and green lines overlapping the 0 line). Pathlength was 1 cm and the averaging time was 2 s nm^{-1}. The spectra are corrected by subtracting the baseline which was measured in the same cuvette with *n*-heptane alone.

 © 2003 Wiley-VCH Verlag GmbH & Co. KGaA, Weinheim

from the red-shifted broad Soret band. The addition of methanol leads to complete disassembly, and the intense CD signals vanish, which indicates that the observed chirality is not because of the chirality of the monomeric porphyrins. However, the different configurations (*R* or *S*) of the hydroxethyl groups induce the different chirality in the self-assembled species. From the intense CD signals this chirality appears to be helical in origin, and opposite helicities (*M* or *P*) are generated from the two enantiomers. Giant CD, sometimes referred as Polymer and Salt Induced (PSI) CD may appear if the chiral objects (absorbing light at around 500 nm) are greater than 50 nm.[23,24] This also affects the overall shape of the CD curves, which can vary widely because of the different sizes of self-assembled species and the scattering contribution to the CD. However, the application of the exciton chirality method[25] leads the firstly eluted enantiomer to a self-assembled species in which the chirality of the transition dipole moments must be counterclockwise (defined as negative chirality). Whereas, the second eluted enantiomer leads to an aggregate with positive chirality (i.e. a clockwise arrangement of the transition dipole moments).

The very broad absorption of a film cast from self-assembling **5-Zn** is spectacular. If light harvesting is to be harnessed by artificial devices, a broad absorption with high extinction coefficients over the entire spectral range is beneficial. This is certainly the case with the aggregates of **5-Zn** and **2-Zn**. The fluorescence is not quenched and intense signals are observed as well in solution as from cast films (see Supporting Information), which is untypical for aggregated chromophores, and in our case arises from the well defined supramolecular architecture. This should allow photosensitization of a wide band semiconductor, such as nanocrystalline titania. Until now, photosensitization has been realized only with ruthenium polypyridine complexes in the most efficient artificial solar energy conversion devices, which were pioneered by Grätzel and coworkers[26,27] or very recently with phthalocyanine dyes.[28]

Confocal fluorescence microsocopy images of self-assembled **5-Zn** onto TiO_2 nanoparticles with average dimensions of 5 nm show bright spots proving that intense fluorescence is coming out from the porphyrin aggregates that have sizes of several hundred nm. This high fluorescence could be used in a solid device similar to the dry Grätzel solar cell[29] but with appreciably lower production costs and environmentally more friendly materials than the currently used ruthenium complexes. In a fully operational device in which a hole transporter is also present, part of this fluorescence should be quenched because of the competing electron injection into the conduction band of the TiO_2 semiconductor. Efforts employing our self-assembling porphyrins as photosensitizers in such photovoltaic devices are currently under way.

Received: November 4, 2002
Revised: February 12, 2003 [Z50465]

Keywords: chirality · light harvesting · photosynthesis · porphyrinoids · self-assembly

[1] R. E. Blankenship, J. M. Olson, M. Miller in *Anoxygenic Photosynthetic Bacteria* (Eds.: R. E. Blankenship, M. T. Madigan, C. E. Bauer), Kluwer Academic Publishers, The Netherlands, **1995**, pp. 399 – 435.
[2] T. S. Balaban, A. R. Holzwarth, K. Schaffner, G.-J. Boender, H. J. M. de Groot, *Biochemistry* **1995**, *34*, 15259 – 15266.
[3] G. McDermott, S. M. Price, A. A. Freer, A. M. Hawthornthwaite-Lawless, M. Z. Papiz, R. J. Cogdell, N. W. Isaacs, *Nature* **1995**, *374*, 517 – 521.
[4] W. Kühlbrandt, D. N. Wang, Y. Fujiyoshi, *Nature* **1994**, *367*, 614 – 621.
[5] A. Zouni, H.-T. Witt, J. Kern, P. Fromme, N. Krauss, W. Saenger, P. Orth, *Nature* **2001**, *409*, 739 – 743.
[6] P. Jordan, P. Fromme, H. T. Witt, O. Klukas, W. Saenger, N. Krauß, *Nature* **2001**, *411*, 909 – 917.
[7] B.-J. van Rossum, G.-J. Boender, F. M. Mulder, J. Raap, T. S. Balaban, A. R. Holzwarth, K. Schaffner, S. Prytulla, H. Oschkinat, H. J. M. de Groot, *Spectrochim. Acta Part A* **1998**, *54*, 1167 – 1176.
[8] B.-J. van Rossum, D. B. Steensgaard, F. M. Mulder, G.-J. Boender, A. R. Holzwarth, K. Schaffner, H. J. M. de Groot, *Biochemistry* **2001**, *40*, 1587 – 1595.
[9] J. Chiefari, K. Griebenow, F. Fages, N. Griebenow, T. S. Balaban, A. R. Holzwarth, K. Schaffner, *J. Phys. Chem.* **1995**, *99*, 1357.
[10] T. S. Balaban, A. R. Holzwarth, K. Schaffner, *J. Mol. Struct.* **1995**, *349*, 183 – 186.
[11] A. Jesorka, T. S. Balaban, A. R. Holzwarth, K. Schaffner, *Angew. Chem.* **1996**, *108*, 3019 – 3021; *Angew. Chem. Int. Ed. Engl.* **1996**, *35*, 2861 – 2863.
[12] T. S. Balaban, H. Tamiaki, A. R. Holzwarth, K. Schaffner, *J. Phys. Chem.* **1997**, *101*, 3424 – 3431.
[13] T. S. Balaban, A. Eichhöfer, J.-M. Lehn, *Eur. J. Org. Chem.* **2000**, 4047 – 4057.
[14] J. A. Eisen et al. , *Proc. Natl. Acad. Sci. USA* **2002**, *99*, 9509 – 9514.
[15] S. Yagai, T. Miyatake, H. Tamiaki, *J. Org. Chem.* **2002**, *67*, 49 – 58.
[16] a) A. A. Bhuiyan, J. Seth, N. Yoshida, A. Osuka, D. F. Bocian, *J. Phys. Chem. B* **2000**, *104*, 10757 – 10764; b) K. Susumu, T. Shimidzu, K. Tanaka, H. Segawa, *Tetrahedron Lett.* **1996**, *37*, 8399 – 8402; c) H. Tamiaki, Y. Nagata, S. Tsuduki, *Eur. J. Org. Chem.* **1999**, 2471 – 2473; d) A. Tsuda, A. Nakano, H. Furuta, H. Yamochi, A. Osuka, *Angew. Chem.* **2000**, *112,* 572 – 575; *Angew. Chem. Int. Ed.* **2000**, *39*, 558 – 561;e) N. Yoshida, N. Aratani, A. Osuka, *Chem. Commun.* **2000**, 197 – 198; f) T. E. O. Screen, I. M. Blake, L. H. Rees, W. Clegg, S. J. Borwich, H. L. Anderson, *J. Chem. Soc. Perkin Trans. 1* **2002**, 320 – 329.
[17] T. S. Balaban, J. Leitich, A. R. Holzwarth, K. Schaffner, *J. Phys. Chem.* **2000**, *104*, 1362 – 1372.
[18] L. Dähne, *J. Am. Chem. Soc.* **1995**, *117*, 12855 – 12860, and references therein.
[19] M. Wang, G. L. Silva, B. A. Armitage, *J. Am. Chem. Soc.* **2000**, *122*, 9977 – 9986.
[20] A kind referee indicated the similar behavior between cyanine dyes, which form J aggregates in water and are disassembled by methanol, and our porphyrin assemblies which, however, are formed only in nonpolar solvents. Furthermore, similar effects such as red-shifted and broadened absorption bands, as well as the precipitation of fluffs, which are disrupted upon shaking, were observed with a water insoluble porphyrin, which was slightly soluble in methanol. These latter aggregates could be seen with TEM and had dimensions between 50 and 110 nm. It appears that this same mesoscopic behavior can thus be engineered with different supramolecular interactions. In our case, because the same functional groups are present as those in the natural self-assembling BChls, we are surely mimicking these

 © 2003 Wiley-VCH Verlag GmbH & Co. KGaA, Weinheim

antenna systems only in the absence of solvents which can compete for hydrogen bonding or zinc ligation.

[21] a) M. I. Bystrova, I. N. Mal′gosheva, A. A. Krasnovskii, *Mol. Biol.* **1979**, *13*, 440 – 451; b) K. M. Smith, L. A. Kehres, J. Fajer, *J. Am. Chem. Soc.* **1983**, *105*, 1387 – 1389.

[22] a) Two factors are responsible for the shift to lower wavenumbers of the $\tilde{\nu}_{CO}$ frequency: 1) conjugation with the porphyrin macrocycle and 2) the presence of hydrogen bonding >C=O···H–O, which can occur either with or without simultaneous ligation of the central zinc atom. In the latter case a cooperative interaction occurs: because of zinc-atom coordination, the O–H bond becomes more polarized and is thus a better hydrogen bond donor. By comparison with the corresponding diacetyl compounds, either as free bases or as the Zn complexes, one can discern the individual contributions of factors 1) and 2). An acetyl group in a β-pyrrolic position, where it is coplanar with the porphyrin plane and thus strongly conjugated, has $\tilde{\nu}_{CO} \sim 1669\ cm^{-1}$ in **13** and $1666\ cm^{-1}$ in **14**, the diacetyl precursors of **4** and **5**, respectively (for their formulae see the Supporting Information). In the self-assembled species, obtained either in concentrated dry dichloromethane solutions or in *n*-heptane, this frequency is further shifted up to $1639\ cm^{-1}$ for **Zn-5**. This value corresponds well to that encountered in the epimers of the natural Mg complexed BChl *c* (1643 and $1653\ cm^{-1}$),[9] or even of the Zn complexed BChl *d* ($1651\ cm^{-1}$).[12] A different behavior is encountered for *meso*-acetyl groups, which are twisted out of the porphyrin plane as indicated also by their longest wavelength absorption. In the 5,15-diacetyl free base porphyrin (**12**), one band is encountered at $1697\ cm^{-1}$. In **12-Zn** two carbonyl bands appear at $1693\ cm^{-1}$ (with a shoulder). Also in self-assembled (*rac*)-**2-Zn** the carbonyl band is splitted (1696 and $1685\ cm^{-1}$). This latter case is indicative of diastereomeric assemblies, for example, a dimer, and may be present either as the *meso RS* dimer or as the enantiomorphic *RR* and *SS* dimers. In all cases the (Zn or H_2)-porphyrin breathing mode which appears between 1592 and $1605\ cm^{-1}$ serves as a marker band; b) T. S. Balaban, D. Moss, unpublished results.

[23] D. Keller, C. Bustamante, *J. Chem. Phys.* **1986**, *84*, 2972 – 2980.

[24] M.-H. Kim, L. Ulibarri, D. Keller, M. F. Maestre, C. Bustamante, *J. Chem. Phys.* **1986**, *84*, 2981 – 2989.

[25] N. Berova, K. Nakanishi in *Circular Dichroism. Principles and Applications 2nd ed.* (Eds.: N. Berova, K. Nakanishi, R. W. Woody), Wiley-VCH, New York, **2000**, pp. 337 – 382.

[26] B. O′Regan, M. Grätzel, *Nature* **1991**, *353*, 737 – 740.

[27] A. Hagfeldt, M. Grätzel, *Chem. Rev.* **1995**, *95*, 49 – 68.

[28] J. He, G. Benkö, F. Korodi, T. Polivka, R. Lomoth, B. Akermark, L. Sun, A. Hagfeldt, V. Sundström, *J. Am. Chem. Soc.* **2002**, *124*, 4922 – 4932.

[29] U. Bach, D. Lupo, P. Comte, J.-E. Moser, F. Weissörtel, J. Salbeck, H. Spreitzer, M. Grätzel, *Nature* **1998**, *395*, 583 – 585.

 © 2003 Wiley-VCH Verlag GmbH & Co. KGaA, Weinheim

Multicomponent Asymmetric Catalysts

"Catalyst Analogue": A Concept for Constructing Multicomponent Asymmetric Catalysts (MAC) by Using a Polymer Support**

*Takayoshi Arai, Tetuya Sekiguti, Kazuhiro Otsuki, Shinobu Takizawa, and Hiroaki Sasai**

Highly organized multicomponent asymmetric catalysts (MACs; Figure 1) have recently been developed as the result of work by numerous chemists.[1–3] In MAC catalyzed enantioselective reactions, synergistic cooperation between each component plays an important role in realizing highly stereoselective reactions.

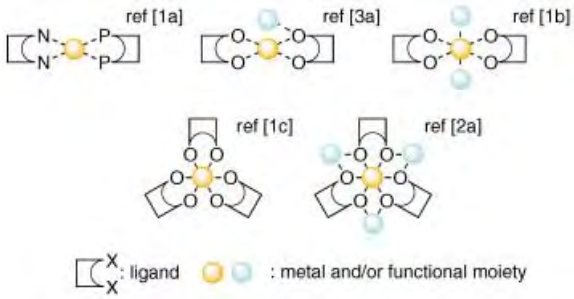


Figure 1. Schematic representation of typical multicomponent catalysts.

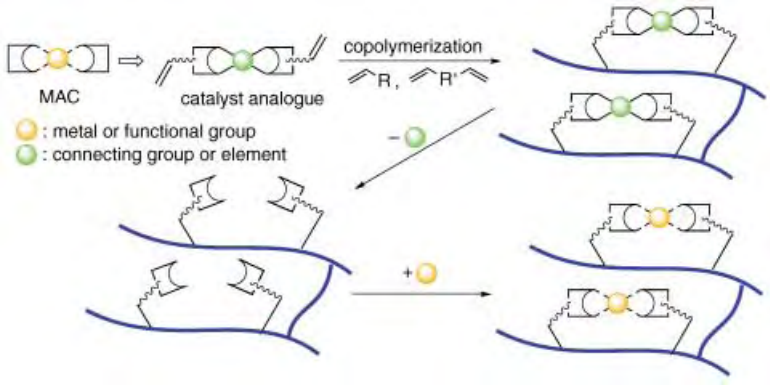
If ligands are attached to a polymer backbone and the position of each ligand in a catalyst is controlled appropriately to form a MAC, the polymer support would enhance MAC formation and stabilize the resulting catalyst. To that end a study of the polymer-supported catalysts would provide a general method for the construction of further useful MACs. However, conventional methods for the preparation of polymer-supported catalysts which rely on the random introduction of ligands into a sterically irregular solid polymer backbone (e.g., polystyrene resin) produce undesirable results for MACs because of the highly disordered orientation of the ligands along the polymer chain. To further the development of polymer-supported MACs, herin we report a new method for constructing polymer-supported MACs based on the use of a "catalyst analogue".

In the new procedure (Scheme 1), after the copolymerization of a catalyst analogue with a monomer in the presence

[*] Prof. Dr. H. Sasai, Dr. T. Arai, T. Sekiguti, K. Otsuki, Dr. S. Takizawa
The Institute of Scientific and Industrial Research (ISIR)
Osaka University
Mihogaoka, Ibaraki, Osaka 567–0047 (Japan)
Fax: (+81) 6-6879-8469
E-mail: sasai@sanken.osaka-u.ac.jp

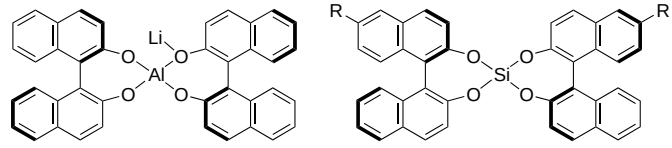
[**] This work was supported by a Grant-in-Aid for Scientific Research from the Ministry of Education, Culture, Sports, Science and Technology, Japan. We thank the technical staff in the Materials Analysis Center of ISIR, Osaka University.

 © 2003 Wiley-VCH Verlag GmbH & Co. KGaA, Weinheim DOI: 10.1002/anie.200250536



Scheme 1. Proposed construction of a MAC by using a polymer support.

of a crosslinker, the resulting polymer is used to prepare an active catalyst by exchanging the connecting group or element with the catalytically active metal atom or functional group. In this way, the position and orientation of each ligand in the resulting polymers can be controlled. The proposed method outlined in Scheme 1 was applied to AlLi-bis(binaphthoxide) complex (ALB), a MAC that we developed.[3] The connecting group in the catalyst analogue is expected to exchange readily with aluminum in the polymer matrix assuming that the analogue is stable under the required polymerization conditions. A Si-tethered binaphthol was employed as the catalyst analogue for this synthesis because of its structural similarity to ALB (Figure 2).



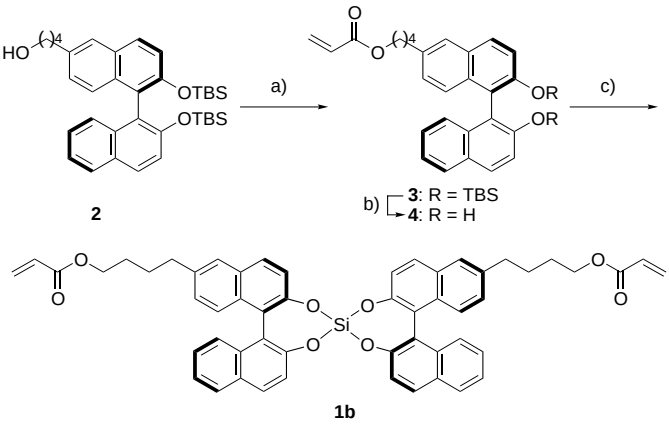
Al-Li-bis(binaphthoxide) complex (ALB)
original active catalyst

Si-tethered binaphthol (**1a**: R = H)
stable catalyst analogue

Figure 2. Target MAC and preferred catalyst analogue.

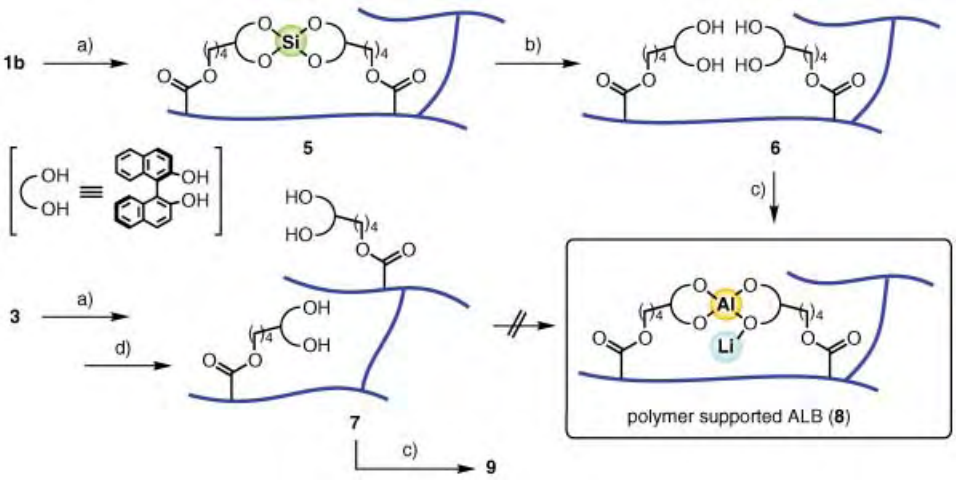
The Si-tethered binaphthol **1a** was found to be adequately stable under the conditions typical of radical polymerization (azobisisobutyronitrile (AIBN), 70 °C). A 6-substituted binaphthol derivative was used as the starting point for the synthesis of the soluble monomer **1b** (Scheme 2).

The binaphthol derivative **2**[4] was coupled with acryloyl chloride to give the ester **3**. After removal of the TBS group of **3**, the catalyst analogue **1b** was almost quantitatively prepared by the reaction of **4** with $SiCl_4$ in THF, and used directly in subsequent experiments.[5] The



Scheme 2. Synthesis of the catalyst analogue **1b** (TBS = *tert*-butyldimethylsilyl). a) Acryloyl chloride, Et_3N, THF, 0 °C; b) TBAF, RT, 30 min, obtained quantatively in two steps; c) $SiCl_4$, Et_3N, THF, 0 °C.

copolymerization of **1b** with methyl methacrylate (MMA) at a ratio of 1:20 was initiated by using 5 mol % of AIBN[6] with 1 mol % of ethylene glycol dimethacrylate (EGDMA) as a crosslinker. After completion of copolymerization, the Si–O bond in polymer **5** was cleaved by treatment with H_2O to give polymer-supported binaphthol **6A** (Scheme 3).

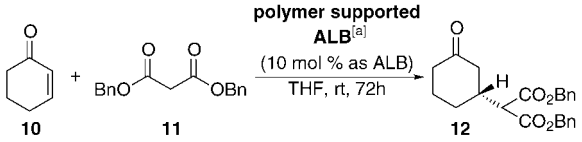


Scheme 3. Preparation of polymer-supported ALB. a) MMA, crosslinker, AIBN, THF, reflux; b) H_2O; c) $AlMe_3$, *t*BuLi, THF, −78 °C; d) TBAF, THF.

 © 2003 Wiley-VCH Verlag GmbH & Co. KGaA, Weinheim

The resulting polymer **6A** was characterized by gel-permiation chromotography (GPC; $M_w = 17\,800$, PDI = 2.03). The copolymerization of **3**, which has no Si tether, with MMA (**3**:MMA = 1:10) and EGDMA was also examined to afford **7A** as a reference. The polymer-supported AlLi-bis(binaphthoxide) catalyst (**8A**), generated by the treatment of a solution of **6A** in THF with $AlMe_3$ and *t*BuLi, promoted the Michael reaction of 2-cyclohexen-1-one (**10**) with dibenzyl malonate (**11**) to give the Michael adduct **12** in 73% yield with 91% *ee* (Table 1, entry 1).

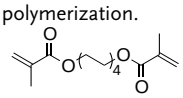
Table 1: Asymmetric Michael reaction catalyzed by polymer-supported ALB.



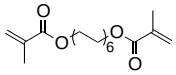
10 **11** **12**

Entry	Polymer-supported binaphthol[b]	Catalyst	Yield of **12** [%]	*ee* of **12** [%]
1	**6A** (**1b** + EGDMA)	**8A**	73	91
2	**7A** (**3** + EGDMA)	**9A**	77	21
3	**6B** (**1b** + **13**)	**8B**	84	80
4	**7B** (**3** + **13**)	**9B**	20	8
5	**6C** (**1b** + **14**)	**8C**	29	78
6	**7C** (**3** + **14**)	**9C**	42	34

[a] Polymers for entries 1, 3, and 5 were prepared in the ratio of **1b**:MMA = 1:20. Polymers for entries 2, 4, and 6 were prepared in the ratio of **3**:MMA = 1:10. [b] 1 mol% of crosslinkers was utilized in each polymerization.



C8DMA (**13**)



C12DMA (**14**)

As shown in entry 2 corresponding catalyst **9A**, which was constructed from polymer **7A**, gave **12** with only 21% *ee*, thus indicating that the use of a catalyst analogue is advantageous for constructing polymer-supported MACs.[7] The effect of the length of the crosslinker can also be seen in Table 1. The polymers **6B** and **6C** were also prepared by use of **13** and **14** as a crosslinker, respectively. The catalysts **8A, 8B**, and **8C**, prepared by using the catalyst analogue, exhibited better enantioselectivity for the formation of **12** than the corresponding catalysts **9A, 9B**, and **9C**.[8] In the case of the polymer-supported ALB experiments reported herein, an increase in the ratio of crosslinker in the polymer resulted in a reduction of the selectivity.[9] As an alternative approach towards the construction of polymer-supported MACs, the application of the method of molecular imprinting polymers (MIPs) might be fascinating.[10,11] In contrast to MIPs, our method using a "catalyst analogue" allowed chiral ligands to be arranged at suitable positions along the polymer chains even in the case of a flexible polymer.

In conclusion, a new and general approach for the efficient construction of polymer-supported MACs is proposed based on the use of a catalyst analogue. The polymer-supported MACs are readily obtained by a simple exchange of the connecting atoms in the polymer with catalytically active atoms.[12]

Experimental Section

3: NEt_3 (0.77 mL, 5.5 mmol) and acryloyl chloride (0.38 mL, 4.6 mmol) were added to a solution of (*R*)-4-[2,2′-bis(*tert*-butyldimethylsilyloxy)-1,1′-binaphth-6-yl]butan-1-ol (**2**) (2.5 g, 4.26 mmol) in THF (30 mL) at 0°C. The reaction mixture was stirred for 30 min, then quenched with H_2O (5 mL) at 0°C and the aqueous layer was extracted with AcOEt. The combined organic layer was washed with brine and dried over Na_2SO_4. After removal of the solvent under vacuum, the crude product was purified by flash column chromatography (SiO_2, AcOEt/hexane = 1:5) to give **3** (2.73 g, 4.26 mmol, quant.) as a pale-yellow oil. IR(neat): $\tilde{\nu}_{max} = 1070.4$, 1247.8, 1730.0 cm^{-1}; HR-MS (ESI) for $C_{39}H_{52}O_4Si_2Na^+$ $[M+Na]^+$: calcd: 663.3219, Found: 663.3236; ^1H NMR (270 MHz, $CDCl_3$): $\delta = 7.80$ (d, $J = 8.9$ Hz, 2H), 7.77 (d, $J = 8.9$ Hz, 1H), 7.72 (s, 1H), 7.14–7.58 (m, 6H), 7.05 (dd, $J = 1.6$, 8.6 Hz, 1H), 6.39 (dd, $J = 1.5$, 17 Hz, 1H), 6.11 (dd, $J = 10$, 17 Hz, 1H), 5.79 (dd, $J = 1.5$, 10 Hz, 1H), 4.18 (t, $J = 6.1$ Hz, 2H), 2.75 (d, $J = 6.8$ Hz, 2H), 1.72–1.77 (m, 4H), 0.47 (s, 18H), 0.01 (d, $J = 4.0$ Hz, 6H), −0.16 ppm (d, $J = 4.0$ Hz, 6H); ^{13}C NMR (67.7 MHz, $CDCl_3$): $\delta = 166.1$, 150.9, 150.4, 136.5, 134.4, 133.0, 130.3, 129.3, 129.1, 128.5, 128.0, 127.5, 127.1, 126.1, 125.9, 125.8, 125.7, 123.1, 122.1, 121.9, 120.4, 120.3, 64.5, 35.3, 28.2, 27.6, 25.1, 17.7, −4.2, −4.3, −4.4 ppm; $[\alpha]_D^{25} = +35.61$ ($c = 0.689$, $CHCl_3$).

4: TBAF in THF (1.0 M, 7.2 mL, 7.2 mmol) was added dropwise to a solution of **3** (1.9 g, 3.0 mmol) in THF (30 mL) at 0°C. The reaction mixture was stirred for 30 min, then quenched with H_2O (20 mL) at 0°C and the aqueous layer was extracted with AcOEt. The combined organic layer was washed with brine and dried over Na_2SO_4. After removal of the solvent under vacuum, crude product was purified by flash column chromatography (SiO_2, AcOEt/hexane = 1:3) to give **4** (1.23 g, 3.0 mmol, quant.) as a pale yellow oil. IR(neat) $\tilde{\nu}_{max} = 1714.6$, 3408.0 cm^{-1}; HRMS (ESI) for $C_{27}H_{24}O_4Na^+$ $[M+Na]^+$: calcd: 435.1572, Found: 435.1564; ^1H NMR (270 MHz, $CDCl_3$): $\delta = 7.88$–7.99 (m, 3H), 7.67 (s, 1H), 7.28–7.40 (m, 6H), 7.06–7.17 (m, 3H), 6.38 (dd, $J = 1.4$, 17 Hz, 1H), 6.10 (dd, $J = 10$, 17 Hz, 1H), 5.80 (dd, $J = 1.4$, 10 Hz, 1H), 4.18 (t, $J = 6.1$ Hz, 2H), 2.77 (d, $J = 6.8$ Hz, 2H), 1.73–1.76 ppm (m, 4H); ^{13}C NMR (67.7 MHz, $CDCl_3$): $\delta = 166.1$, 152.5, 152.1, 137.5, 133.3, 131.8, 131.1, 130.7, 130.5, 129.4, 129.3, 128.6, 128.3, 128.2, 127.3, 126.9, 124.2, 124.1, 123.8, 117.7, 117.6, 111.0, 110.8, 64.4, 35.3, 28.3, 27.6 ppm; $[\alpha]_D^{25} = -22.66$ ($c = 2.14$, $CHCl_3$).

1b: NEt_3 (0.11 mL, 0.8 mmol) and tetrachlorosilane in CH_2Cl_2 (1.0 M, 0.2 mL, 0.2 mmol) were added to a solution of **4** (165 mg, 0.4 mmol) in THF (2.0 mL) at 0°C. The reaction mixture was stirred for 30 min and used for the next polymerization. Selected physical properties of **1b**: ^1H NMR (270 MHz, $CDCl_3$): $\delta = 7.84$–8.01 (m, 2H), 7.57–7.69 (m, 4H), 7.49 (s, 2H), 7.26–7.40 (m, 2H), 6.82–7.18 (m, 12H), 6.19 (m, 2H), 5.97 (m, 2H), 5.65 (m, 2H), 4.04 (t, $J = 6$ Hz, 4H), 2.59–2.71 (m, 4H), 1.60–1.70 ppm (m, 8H); ^{13}C NMR (67.7 MHz, THF): $\delta = 165.8$, 149.0, 148.5, 139.5, 134.0, 132.5, 132.1, 131.8, 131.6, 131.2, 130.2, 129.4, 128.9, 128.8, 128.5, 128.4, 128.0, 127.6, 127.2, 127.1, 126.6, 125.4, 123.2, 121.7, 121.1, 120.8, 119.3, 64.6, 35.9, 29.2, 28.4 ppm.

Polymer **6A** from **1b**: EGDMA (8 μL, 0.044 mmol) and MMA (430 μL, 4 mmol) were added to a cooled solution (0°C) of **1b** (0.2 mmol) and AIBN (36 mg, 0.22 mmol) in THF (3.7 mL). The reaction mixture was heated at 70°C for 10 h under Ar, then H_2O was added to cleave the Si–O bonds. The aqueous layer was extracted with AcOEt and the combined organic layer was washed with brine and dried over Na_2SO_4. After removal of the solvent, the polymer was dissolved in about 2 mL THF, and this mixture was slowly added to stirring MeOH (30 mL). The precipitated polymer was collected by centrifugation at 3000 rpm for 10 min, and dried in vacuo to give light yellow polymer **6A**.

Typical procedure for the preparation of polymer supported ALB: Polymer **6A** (39.7 mg, 0.04 mmol as binol) was dried under

 © 2003 Wiley-VCH Verlag GmbH & Co. KGaA, Weinheim

reduced pressure at 45 °C for 2 h. A solution of $AlMe_3$ in hexane (0.98 M, 20.4 μL, 0.02 mmol) and *t*BuLi in pentane (1.48 M, 13.5 μL, 0.02 mmol) were added to a cooled (−78 °C) solution of **6A** in THF (0.4 mL). The reaction mixture was stirred at −78 °C for 10 min, then was warmed to room temperature. A clear gel was precipitated and used directly as a polymer-supported ALB **8A**.

Typical experimental procedure for polymer-supported ALB catalyzed asymmetric Michael reaction: 2-Cyclohexen-1-one (**10**; 25 μL, 0.22 mmol) and dibenzyl malonate (**11**; 50 μL, 0.2 mmol) were added to an insoluble polymer-supported ALB catalyst **8A** (10 mol %) in THF (0.5 M). The reaction mixture was stirred for 72 h, then quenched with HCl (1 N, 1 mL) at 0 °C and extracted with AcOEt. The combined organic extract was washed with saturated aqueous $NaHCO_3$ and brine, dried over Na_2SO_4, and concentrated in vacuo to give an oily residue. The mixture was dissolved in THF (≈ 1 mL) and this solution was slowly added to stirring MeOH (30 mL). The precipitated polymer was collected by centrifugation at 3000 rpm for 10 min, and the supernatant was evaporated to give a crude product. Purification by flash chromatography (SiO_2, acetone/hexane = 1:10) gave **12** in 73 % yield with 91 % *ee*. The enantiomeric excess of **12** was determined by chiral HPLC analysis (DAICEL CHIRALPAK AS, *i*PrOH/hexane = 1:4, 1.0 mL min^{-1}, 254 nm).

Received: November 13, 2002
Revised: February 14, 2003 [Z50536]

Keywords: · asymmetric catalysis · immobilization · polymerization · synthetic methods

[1] Representative examples of MACs: a) K. Mikami, T. Korenaga, M. Terada, T. Ohkuma, T. Pham, R. Noyori, *Angew. Chem.* **1999**, *111*, 517 – 519; *Angew. Chem. Int. Ed.* **1999**, *38*, 495 – 497; b) H. Ishitani, M. Ueno, S. Kobayashi, *J. Am. Chem. Soc.* **2000**, *122*, 8180 – 8186; c) H. Furuno, T. Hanamoto, Y. Sugimoto, J. Inanaga, *Org. Lett.* **2000**, *2*, 49 – 52; d) S. Kobayashi, H. Ishitani, *J. Am. Chem. Soc.* **1994**, *116*, 4083 – 4084. See also reference [2].

[2] For recent reviews, see: a) M. Shibasaki, H. Sasai, T. Arai, *Angew. Chem.* **1997**, *109*, 1290 – 1310; *Angew. Chem. Int. Ed. Engl.* **1997**, *36*, 1236 – 1256; b) G. J. Rowlands, *Tetrahedron* **2001**, *57*, 1865 – 1882; c) M. Shibasaki, N. Yoshikawa, *Chem. Rev.* **2002**, *102*, 2187 – 2209.

[3] a) T. Arai, H. Sasai, K. Aoe, K. Okamura, T. Date, M. Shibasaki, *Angew. Chem.* **1996**, *108*, 103 – 105; *Angew. Chem. Int. Ed. Engl.* **1996**, *35*, 104 – 106; b) T. Arai, Y. M. A. Yamada, N. Yamamoto, H. Sasai, M. Shibasaki, *Chem. Eur. J.* **1996**, *2*, 1368 – 1372; c) T. Arai, H. Sasai, K. Yamaguchi, M. Shibasaki, *J. Am. Chem. Soc.* **1998**, *120*, 441 – 442.

[4] D. J. Bayston, J. L. Fraser, M. R. Ashton, A. D. Baxter, M. E. C. Polywka, E. Moses, *J. Org. Chem.* **1998**, *63*, 3137 – 3140.

[5] The monomer **1b** was stable under neutral anhydrous conditions. The diasteroselectivity on **1b** was about 1:1.

[6] The amount of AIBN and the crosslinker is based on the total amount of **1b** and MMA.

[7] The polymer-supported ALB generated from the polymer prepared in the ratio of **1b**:MMA = 1:1 and **3**:MMA = 1:1 gave the Michael adduct **12** with 48 % *ee* and 2 % *ee*, respectively.

[8] The reusability of polymer **6A** was investigated by using another batch of polymer **6A** (M_w = 26000, PDI = 1.91). After the first and second run, **12** was obtained in 74 % yield with 89 % *ee*, and 76 % yield with 88 % *ee*, respectively. The polymer **6A** was recovered in 97 % after the second use (M_w = 24000, PDI = 1.81).

[9] The polymer-supported ALB prepared by use of 30 mol % and/or 90 mol % of crosslinker gave **12** in 32 % yield with 39 % *ee* and 32 % yield with 36 % *ee*, respectively.

[10] MIPs have been produced to order for the construction of chemo- and/or stereoselective receptors, sensors, columns, and/or artificial enzymes by using multisite recognition. In the application of MIPs to asymmetric metal catalysis, the molecular imprinting process is carried out using a chiral template of a transition state analogue, which is then removed for constructing a chiral cavity after the polymerization. Thus, the catalytic activities and selectivities are highly dependent on the efficiency of imprinting and the rigidity of the cavity. The requirement of a high loading of crosslinker for keeping the cavity rigid causes a serious decline in the activity of the catalyst.

[11] For recent reviews on MIP, see: a) *Molecularly Imprinted Polymers* (Ed.: B. Sellergren), Elsevier, Amsterdam, **2000**; b) K. Haupt, K. Mosbach, *Chem. Rev.* **2000**, *100*, 2495 – 2504; c) G. Wulff, *Chem. Rev.* **2002**, *102*, 1 – 27; Representative examples of MIPs of asymmetric metal catalysts: d) J. H. Koh, A. O. Larsen, P. S. White, M. R. Gagné, *Organometallics* **2002**, *21*, 7 – 9; e) K. Polborn, K. Severin, *Eur. J. Inorg. Chem.* **2000**, 1687 – 1692; f) M. R. Gagné, J. J. Becker, N. M. Brunkan, *Polym. Prepr. Am. Chem. Soc. Div. Polym. Chem.* **2000**, *41*, 404; g) F. Locatelli, P. Gamez, M. Lemaire, *J. Mol. Catal. A* **1998**, *135*, 89 – 98.

[12] Recent progress in reusable multicomponent asymmetric catalysts: a) T. Arai, Q.-S. Hu, X.-F. Zheng, L. Pu, H. Sasai, *Org. Lett.* **2000**, *2*, 4261 – 4263; b) Y. S. Kim, S. Matsunaga, J. Das, A. Sekine, T. Ohshima, M. Shibasaki, *J. Am. Chem. Soc.* **2000**, *122*, 6506 – 6507; c) S. Matsunaga, T. Ohshima, M. Shibasaki, *Tetrahedron Lett.* **2000**, *41*, 8473 – 8478; d) D. Jayaprakash, H. Sasai, *Tetrahedron: Asymmetry* **2001**, *12*, 2589 – 2595; e) T. Arai, T. Sekiguti, Y. Iizuka, S. Takizawa, S. Sakamoto, K. Yamaguchi, H. Sasai, *Tetrahedron: Asymmetry* **2002**, *13*, 2083 – 2087; f) T. Ohkuma, H. Takeno, Y. Honda, R. Noyori, *Adv. Synth. Catal.* **2001**, *343*, 369 – 375; g) H.-B. Yu, Q.-S. Hu, L. Pu, *J. Am. Chem. Soc.* **2000**, *122*, 6500 – 6501; h) G. Sundararajan, N. Prabagaran, *Org. Lett.* **2001**, *3*, 389 – 392; i) A. Fujii, M. Sodeoka, *Tetrahedron Lett.* **1999**, *40*, 8011 – 8014.

 © 2003 Wiley-VCH Verlag GmbH & Co. KGaA, Weinheim

Li-intercalated TiS_2 Nanotubes

Lithium Intercalation in Open-Ended TiS_2 Nanotubes**

Jun Chen, Zhan-Liang Tao, and Suo-Long Li*

There has been considerable recent interest in the synthesis and characterization of transition-metal disulfide nanotubes. The significant breakthrough in obtaining WS_2 and MoS_2

[*] Prof. Dr. J. Chen, Dr. Z.-L. Tao, Dr. S.-L. Li
Institute of New Energy Materials Chemistry
Nankai University, Tianjin 300071 (P.R.China)
Fax: (+86) 22-2350-9118
E-mail: chenabc@nankai.edu.cn

[**] The authors acknowledge support from the Trans-Century Distinguished Talent Project (Grant No. 200248) and the Scientific Research Foundation for the Returned Overseas Chinese Scholars (Grant No. 2002247; State Education Ministry). We are also thankful to Professors C. X. Cui and X. Q. Zhu, and Drs. Y. T. Shen and Q. Xu for their experimental assistance.

 DOI: 10.1002/anie.200250573 © 2003 Wiley-VCH Verlag GmbH & Co. KGaA, Weinheim

nanotubes by Tenne and co-workers[1,2] was accomplished through either the hydrosulfurization of a very thin film of tungsten or the gas–solid reaction between MO_3 (M = W, Mo) and H_2S in a reducing atmosphere at elevated temperatures (800–1000 °C). Methods, such as chemical transport,[3] solution routes,[4] in situ heating,[5] activation techniques,[6] and gas–solid reactions[7,8] can all be used to prepare MS_2 nanotubes. Recently, Remskar et al.[9] synthesized bundles of very long single-walled MoS_2 nanotubes (9.6 Å in diameter) using a C_{60}-catalyzed transport reaction. Furthermore, Nath and Rao[10,11] successfully prepared multiwalled transition-metal disulfide nanotubes of groups 4 and 5 through the thermal decomposition of metal trisulfides in a hydrogen atmosphere at 800–1000 °C. However, in comparison with their HfS_2 and ZrS_2 counterparts, TiS_2 nanotubes are more sensitive to electron beams,[11] and details of their characterization were not made available.

Layered transition-metal dichalcogenides MS_2 (such as TiS_2 and MoS_2) are of great interest as they act as host lattices by reacting with a variety of guest atoms or molecules to yield intercalation compounds, in which the guest is inserted between the host layers.[12] In layered MS_2 materials, atoms within a layer are bound by strong covalent forces, while the individual layers are held together by van der Waals (vdW) interactions. The weak interlayer vdW interactions allow foreign atoms or molecules to be introduced between the layers through intercalation.[13] Zak and co-workers[14] have accomplished the intercalation of alkali metals into fullerene-like MS_2 (M = W, Mo) nanoparticles, and have investigated the properties of these intercalation compounds. Their results show that the inert vdW surface of the closed nanoparticles presents a diffusion barrier for the intercalation process. Since the MS_2 nanotubes are formed through the folding of layered nanoparticles, it may be imagined that hollow multiwalled nanotubes with open-ended tips are suitable materials for atomic or molecular intercalation. Here, we report the low-temperature synthesis of open-ended TiS_2 nanotubes, and the subsequent intercalation of lithium into the nanotube by a solution-based chemical approach.

TiS_2 nanotubes were prepared by the following procedures: $Na_2S{\cdot}9H_2O$ (> 99 % purity, Aldrich) was dried under vacuum (~ 10^{-5} bar) at 200 °C for 24 h over P_2O_5 to remove the water of crystallization. THF was refluxed for 6 h in the presence of $LiAlH_4{\cdot}8$THF and subsequently distilled under argon. Only water-free Na_2S and THF were used in the subsequent reactions. A solution of $TiCl_4$ (3.8 g, 20 mmol, Aldrich) in THF (150 mL) was prepared in a glove box filled with pure argon (99.999 %) in the presence of an oxygen scavenger and a sodium drying agent. At 40 °C, crystalline Na_2S (3.1 g, 40 mmol) was added to the above solution while stirring. The mixture was then cooled after 30 min. The dark-brown solid was filtered, and washed with THF and methanol several times to remove NaCl formed during the reaction. The powder was then transferred into a teflon-lined stainless-steel tube, which was flushed with H_2 and maintained at 200 °C for 6 h to obtain pure TiS_2 nanotubes while removing the solvent. In a typical synthesis, about 2 g of the product was recovered. The process employed to obtain the TiS_2 nanotubes can be described thus:

$$TiCl_4 + 2\,Na_2S \xrightarrow{40\,^{\circ}C,\ THF} TiS_2 + 4\,NaCl \quad (1)$$

$$TiS_2\ (\text{nano/amorphous particles}) \xrightarrow[H_2]{200\,^{\circ}C} TiS_2\ (\text{nanotubes}) \quad (2)$$

The change in standard Gibbs free energy ($\Delta G°$) of reaction (1) is about $-431.5\ kJ\,mol^{-1}$, which implies that the reaction strongly favors the formation of TiS_2.

The as-prepared samples were characterized by scanning electron microscopy (SEM; JEOL JSM-5600 microscope), transmission electron microscopy (TEM; Philips Tacnai F20 microscope, 200 kV), energy-dispersive X-ray spectroscopy (EDXS), powder X-ray diffraction (XRD; Rigaku INT-2000 X-ray generator, $Cu_{K\alpha}$ radiation), X-ray photoelectron spectroscopy (XPS; Shimadzu Electron ESCA-3400 spectroscope, $Mg_{K\alpha}$ radiation), and Brunauer–Emmett–Teller (BET) nitrogen sorption (Shimadzu-Micromeritics ASAP 2010 Instrument).

Characterization of the as-prepared samples suggested that the low-temperature synthesis was successful in preparing open-ended nanotubes. Figure 1 shows a characteristic SEM image of the as-prepared products. It can be seen that a large number of nanotube filaments are distributed homogeneously over a wide area, and that they are a number of micrometers in length and several tens of nanometers in diameter. A significant proportion (> 95 %) of the sample exhibits a tubular structure.

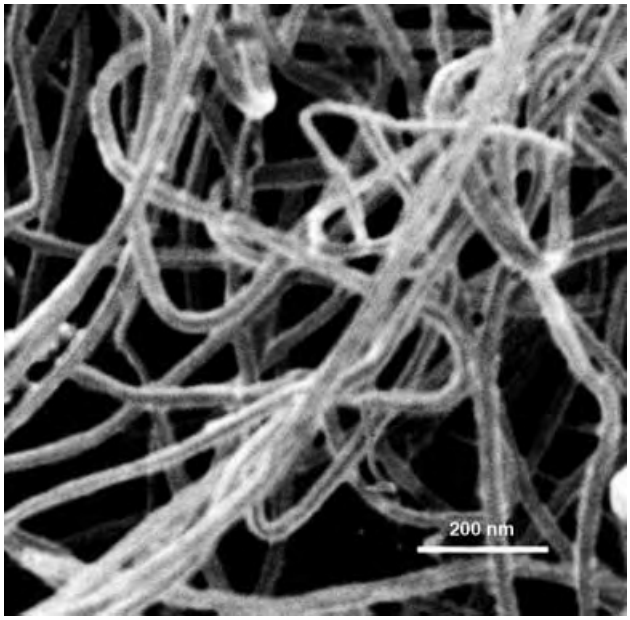


Figure 1. SEM image of the as-prepared TiS_2 nanotubes.

This low-temperature method also gave a satisfactory yield of multiwalled TiS_2 nanotubes with open-ended tips, as can be observed from TEM and high-resolution TEM (HRTEM) analyses (Figure 2). A low-magnification TEM image of a typical TiS_2 sample is shown in Figure 2a, from which it can be seen that the sample consists of single nanotubes and nanotube bundles. Both the single nanotubes and the nanotube bundles exhibit uniform tubular structures

 © 2003 Wiley-VCH Verlag GmbH & Co. KGaA, Weinheim

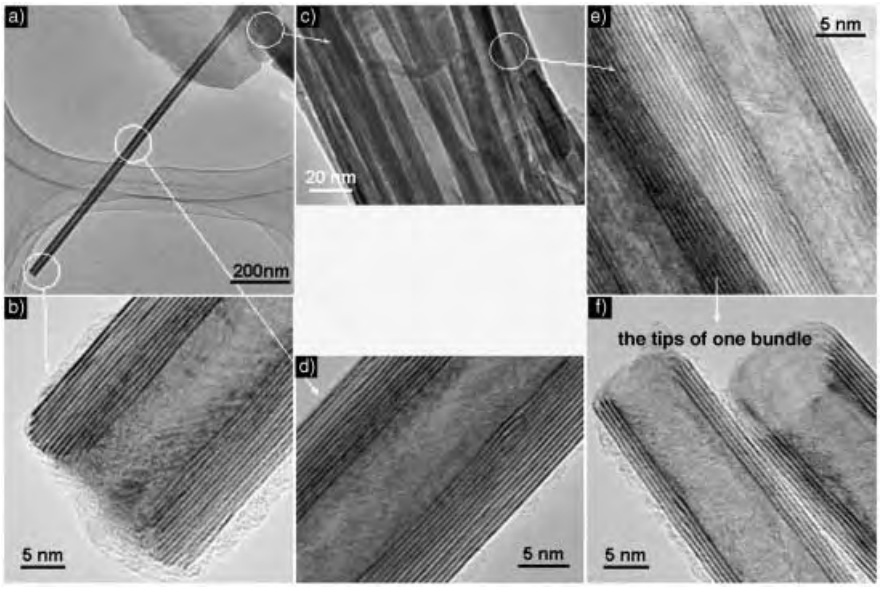


Figure 2. Representative low-magnification (a, c) and high-resolution (b, d, e, f) TEM images of multiwalled TiS_2 nanotubes.

with a length of approximately 2 μm, an outer diameter of approximately 30 nm, an inner diameter of approximately 10 nm, and an interlayer spacing of approximately 0.57 nm (Figure 2b, d, e, and f). Note that the nanotube tips are open and that there is little evidence for the coexistence of an amorphous phase at the tube tips (Figure 2b and f).

The chemical composition of both the individual nanotubes and the bundles was analyzed by EDXS, and both were shown to have a Ti/S atomic ratio of 1:2. XPS analysis demonstrates that the valence of the Ti centers within the nanotubes is +4, and the peak is assigned to Ti $2p_{3/2}$ orbital in TiS_2, which is characterized by a detected binding energy of 458 eV in a well-defined spin-coupled curve. Powder XRD analysis of the product confirmed that the sample was composed of the 1T-TiS_2 phase in high purity, with hexagonal lattice parameters ($a = b = 3.405$, $c = 5.697$ Å) that are in good agreement with those of polycrystalline TiS_2 ($a = b = 3.4049$, $c = 5.6912$ Å; ICDD–JCPDS card No. 15-0853). The c value from the XRD pattern is also consistent with the interlayer spacing observed from the HRTEM images shown in Figure 2. Thus, the EDXS, XPS, and XRD measurements have unambiguously demonstrated that the tubular structures in our sample are multiwalled TiS_2 nanotubes with open-ended tips.

Since multiwalled nanotubes with open-ended tips potentially have a lower diffusion barrier for the intercalation process than their closed counterparts, the introduction of lithium into the layers of the nanotubes was attempted by a solution-based approach. Lithium intercalation into TiS_2 nanotubes can be described thus:

$$TiS_2 + x\,Li^+ + x\,e^- \rightarrow Li_xTiS_2$$

Li_xTiS_2 samples ($x = 0.12$, 0.52, and 1.0) were prepared by the chemical intercalation of TiS_2 nanotubes using *n*BuLi (1.6 M, Aldrich) as the Li source.[15] The nanotubes were suspended in hexane, and *n*BuLi was added while stirring the reaction mixture. After 24 h of vigorous stirring, the samples were filtered, washed with THF, and dried in Ar at 40 °C for 5 h. The Li/Ti ratio was determined by chemical inductively coupled plasma (ICP) spectroscopy. The surface area of the $LiTiS_2$ and TiS_2 nanotubes was 32 and 25 $m^2 g^{-1}$, respectively, as determined by BET N_2 adsorption–desorption isotherms. All procedures for handling the materials (BET Bell tube, XRD and TEM specimen holders) were carried out in a glove box filled with pure Ar in order to prevent the reaction of Li with air. For XRD measurements, the Li_xTiS_2 nanotubes were coated with paraffin oil, smeared on a glass substrate, and then covered by an adhesive tape to prevent the sample from reacting with oxygen and/or moisture during the measuring process.[16] For TEM observations, the sample grid and specimen holder were prepared in the glove box and transferred to a glove bag (Cheltenham, Model X-27–27H). During the transfer of the specimen holder to the TEM chamber, special care was taken to minimize the exposure of the sample grid to the atmosphere.

XRD of the lithium-intercalated samples indicates that the nanotube structure of TiS_2 is maintained after intercalation. Figure 3a shows XRD patterns for the TiS_2 nanotubes before lithium intercalation, and for the resulting Li_xTiS_2 products. Upon intercalation, the (001) peak shifts to lower angles, which indicates an expansion of the interlayer spacing. Figure 3b shows the lattice parameters a and c obtained from the XRD for samples with different x values. It can be seen that only very slight differences were observed in the value of the lattice constant a, while the lattice spacing c is strongly correlated to the intercalated lithium quantity x. The largest interlayer spacing (6.3 Å) was observed when $x = 1$, which corresponds to an expansion in the c axis of approximately 10.5%. It has been previously reported that lithium intercalation in polycrystalline TiS_2 leads to a single homogeneous phase with a lattice expansion of approximately 10% for the entire intercalation range, up to $x = 1$ in Li_xTiS_2.[17] Therefore, lithium intercalation in the open-ended TiS_2 nanotubes was as effective as that of their polycrystalline counterparts.

The morphology of the lithium-intercalated TiS_2 nanotubes was further investigated by HRTEM. Figure 4 shows such images recorded for the $LiTiS_2$ sample. It was found that individual intercalated nanotubes were evenly aligned and distributed (Figure 4a). The observed interlayer spacing is about 6.3 Å, which is consistent with the XRD data shown in Figure 3. The lithium-intercalated TiS_2 nanotubes are somewhat sensitive to electron-beam irradiation during HRTEM investigations. This is believed to result from lithium being

 © 2003 Wiley-VCH Verlag GmbH & Co. KGaA, Weinheim

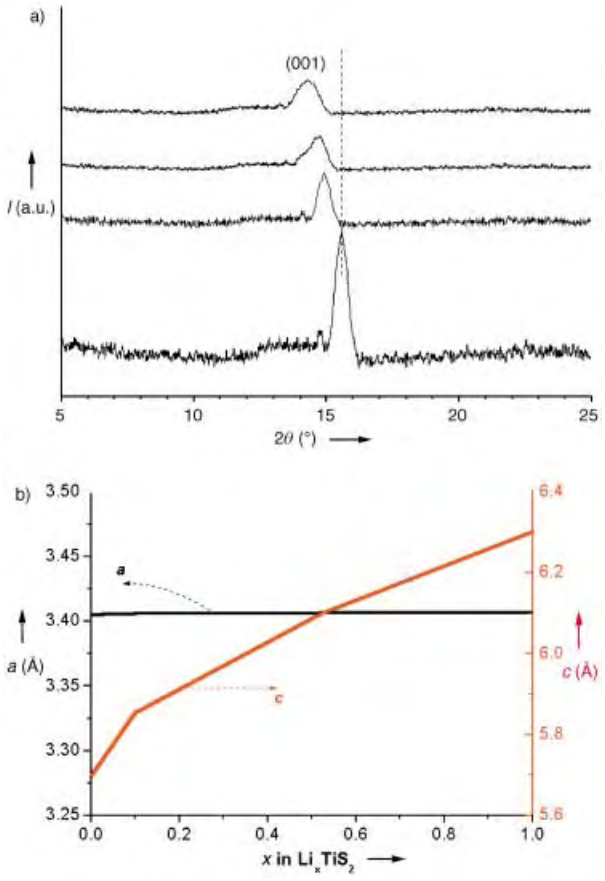


Figure 3. a) XRD patterns of lithium-intercalated Li_xTiS_2 nanotubes (bottom to top: $x = 0$, 0.12, 0.52, and 1.0, respectively); b) lattice parameters *a* and *c* of Li_xTiS_2 nanotubes.

"pumped out" from the nanotubes upon irradiation, which is consistent with qualitative analysis that shows a decrease in the interlayer spacing for the intercalated TiS_2 nanotubes after relatively long irradiation periods (Figure 4c and d). After irradiation for 5 s, the interlayer spacing of the nanotubes is about 6.3 Å (Figure 4b), while after 40 and 60 s of intensive electron-beam irradiation, the interlayer spacing of the nanotubes decreases to approximately 6.1 (Figure 4c) and 6.0 Å (Figure 4d), respectively.

It should be emphasized that some of the walls of the intercalated TiS_2 nanotubes were transformed to an amorphous phase and that more defects were observed after further subjection to intense beam irradiation (Figure 4e). The inset in Figure 4e shows the electron diffraction pattern, which exhibits a hexagonal arrangement of the remaining layers and indicates the axis of the tube is the perpendicular to the *c* axis. In addition, the halo pattern in the electron diffraction pattern reveals the strong incoherent scattering of the electron beam caused by the amorphous phase of TiS_2 around the tube walls. Since this beam sensitivity makes the electron-diffraction analysis difficult, further HRTEM and EDXS measurements were not carried out. Nonetheless, the present XRD and HRTEM observations confirm that the increase in basal spacing can be attributed to the intercalation of lithium. As is already known, the octahedral and tetrahedral interstitial sites in crystalline TiS_2 are available for the intercalation of lithium. In general, the octahedral sites are energetically more favored,[13,18] which leads to a possible maximum intercalation level of one lithium atom per formula unit. The intercalation of lithium within the vdW spacings results in the expansion of the host structure along the *c* axis.

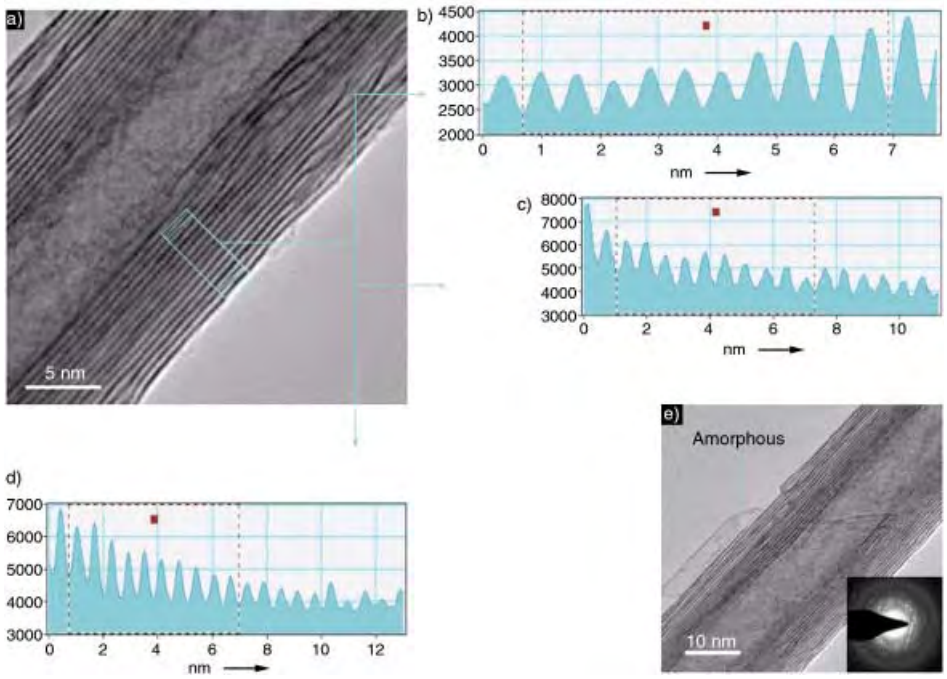


Figure 4. a) HRTEM image of an individual $LiTiS_2$ nanotube and charts of the interlayer spacing of the nanotubes after electron-beam irradiation of 5 (b), 40 (c), and 60 s (d) duration; e) HRTEM image of the $LiTiS_2$ nanotube shown in (a) after irradiation for 60 s (inset: the corresponding electron diffraction pattern).

 © 2003 Wiley-VCH Verlag GmbH & Co. KGaA, Weinheim

In conclusion, multiwalled TiS_2 nanotubes with open-ended tips have been successfully synthesized through a low-temperature solution route. It is believed that this rational route can be extended for the synthesis of other similar nanotubes, by starting from the layered structures in solution. Moreover, it can be shown that such TiS_2 nanotubes are very effective toward lithium intercalation while maintaining a homogeneous phase, despite their extreme sensitivity to electron-beam damage. Current work is directed towards further study of the intercalation–deintercalation of alkali metals, hydrogen, and organic molecules in TiS_2 nanotubes. In principle, such intercalated nanotubes should allow elucidation of the mechanism of superlattice formation, high-energy storage systems, and nanophase catalytic reactions.

Received: November 18, 2002 [Z50573]

Keywords: intercalations · lithium · nanotubes · sulfides · titanium

[1] a) R. Tenne, L. Margulis, M. Genut, G. Hodes, *Nature* **1992**, *360*, 444; b) L. Margulis, G. Salitra, R. Tenne, *Nature* **1993**, *365*, 113; c) M. Hershfinkel, L. A. Gheber, V. Volterra, J. L. Hutchison, L. Margulis, R. Tenne, *J. Am. Chem. Soc.* **1994**, *116*, 1914; d) Y. Feldman, E. Wasserman, D. J. Srolovitz, R. Tenne, *Science* **1995**, *267*, 222.

[2] a) R. Tenne, *Adv. Mater.* **1995**, *7*, 965; b) M. Homyonfer, B. Alperson, Y. Rosenberg, L. Sapir, S. R. Cohen, G. Hodes, R. Tenne, *J. Am. Chem. Soc.* **1997**, *119*, 2693; c) R. Tenne, M. Homyonfer, Y. Feldman, *Chem. Mater.* **1998**, *11*, 3225; d) A. Rothschild, R. Popovitz-Biro, O. Lourie, R. Tenne, *J. Phys. Chem. B* **2000**, *104*, 8976.

[3] a) M. Remskar, Z. Skraba, M. Regula, C. Ballif, R. Sanjines, F. Lévy, *Adv. Mater.* **1998**, *10*, 246; b) M. Remskar, Z. Skraba, R. Sanjinés, F. Lévy, *Appl. Phys. Lett.* **1999**, *74*, 3633.

[4] a) C. M. Zelenski, P. K. Dorhout, *J. Am. Chem. Soc.* **1998**, *120*, 734; b) H. W. Liao, Y. F. Wang, S. Y. Zhang, Y. T. Qian, *Chem. Mater.* **2001**, *13*, 6; c) Y. D. Li, X. L. Li, R. L. He, J. Zhu, Z. X. Deng, *J. Am. Chem. Soc.* **2002**, *124*, 1411.

[5] a) Y. Q. Zhu, W. K. Hsu, N. Grobert, B. H. Chang, M. Terrones, H. Terrones, H. W. Kroto, D. R. M. Walton, *Chem. Mater.* **2000**, *12*, 1190; b) W. K. Hsu, Y. Q. Zhu, C. B. Boothroyd, I. Kinloch, S. Trasobares, H. Terrones, N. Grobert, M. Terrones, R. Escudero, G. Z. Chen, C. Colliex, A. H. Windle, D. J. Fray, H. W. Kroto, D. R. M. Walton, *Chem. Mater.* **2000**, *12*, 3541.

[6] a) M. José-Yacamán, H. López, P. Santiago, D. H. Galván, I. L. Garzón, A. Reyes, *Appl. Phys. Lett.* **1996**, *69*, 1065; b) E. B. Mackie, D. H. Galván, E. Adem, S. Talapatra, G. L. Yang, A. D. Migone, *Adv. Mater.* **2000**, *12*, 495.

[7] M. Nath, A. Govindaraj, C. N. R. Rao, *Adv. Mater.* **2001**, *13*, 283.

[8] a) J. Chen, N. Kuriyama, H. T. Yuan, H. T. Takeshita, T. Sakai, *J. Am. Chem. Soc.* **2001**, *123*, 11813; b) J. Chen, S. L. Li, Q. Xu, K. Tanaka, *Chem. Commun.* **2002**, 1722.

[9] M. Remskar, A. Mrzel, Z. Skraba, A. Jesih, M. Ceh, J. Demsar, P. Stadelmann, F. Lévy, D. Mihailovic, *Science* **2001**, *292*, 479.

[10] M. Nath, C. N. R. Rao, *J. Am. Chem. Soc.* **2001**, *123*, 4841.

[11] M. Nath, C. N. R. Rao, *Angew. Chem.* **2002**, *114*, 3601; *Angew. Chem. Int. Ed.* **2002**, *41*, 3451.

[12] a) M. S. Whittingham, *Prog. Solid State Chem.* **1978**, *12*, 1; b) M. M. Thackeray, J. O. Thomas, M. S. Whittingham, *MRS Bull.* **2000**, *25(3)*, 39.

[13] M. Winter, J. O. Besenhard, M. E. Spahr, P. Novák, *Adv. Mater.* **1998**, *10*, 725.

[14] A. Zak, Y. Feldman, V. Lyakhovitskaya, G. Leitus, R. Popovitz-Biro, E. Wachtel, H. Cohen, S. Reich, R. Tenne, *J. Am. Chem. Soc.* **2002**, *124*, 4747.

[15] W. M. R. Divigalpitiya, R. F. Frindt, S. R. Morrison, *Science* **1989**, *246*, 369.

[16] a) W. Bronger, G. Auffermann, *Angew. Chem.* **1994**, *106*, 1144; *Angew. Chem. Int. Ed. Engl.* **1994**, *33*, 1112; b) M. Olofsson-Mårtensson, M. Kritikos, D. Noréus, *J. Am. Chem. Soc.* **1999**, *121*, 10908; c) J. Chen, N. Kuriyama, Q. Xu, H. T. Takeshita, T. Sakai, *J. Phys. Chem. B* **2002**, *105*, 11214.

[17] M. S. Whittingham, *Science* **1976**, *192*, 1126.

[18] B. van Laar, D. V. W. Ijdo, *Solid State Commun.* **1974**, *3*, 590.

 © 2003 Wiley-VCH Verlag GmbH & Co. KGaA, Weinheim

Ruthenium Oxide Surface Chemistry

Surface Coordination Chemistry: Dihydrogen versus Hydride Complexes on $RuO_2(110)$**

Jinhai Wang, Chao Yang Fan, Qiang Sun, Karsten Reuter, Karl Jacobi, Matthias Scheffler, and Gerhard Ertl*

Similarities between bond formation in transition metal complexes and chemisorption on solid surfaces form the basis of the relationship between homogeneous and heterogeneous catalysis. We find that hydrogen interacts in a complicated manner with the two sites that have an incomplete coordination environment—Ru^{cus} and O^{bridge}—on the $RuO_2(110)$ surface (Figure 1). Upon exposure at 85 K of the RuO_2 catalyst to hydrogen gas, a H_2 molecule, instead of dissociating at Ru^{cus}, weakly adsorbs as dihydrogen on top of the Ru^{cus} atom and interacts dissociatively with the O^{bridge} atom to form a metastable dihydride (waterlike) complex, which transforms into the stable monohydride when heated further. The combination of low-temperature ultrahigh vacuum experiments in conjunction with density-functional theory (DFT) calculations provides a detailed insight into the coordination chemistry of a solid surface, which exhibits a remarkable correlation with the chemistry of single-atom transition-metal complexes.

The binding of hydrogen, both with transition-metal complexes (i.e. hydride formation)[1] and with surfaces,[2] generally occurs concurrently with dissociation of the ligand. The discovery of η^2-H_2 (dihydrogen) complexes, in which the H–H bond remains intact, was surprising,[3] since

[*] Prof. Dr. K. Jacobi, Dr. J. Wang, Dr. C. Y. Fan, Dr. Q. Sun, Dr. K. Reuter, Prof. Dr. M. Scheffler, Prof. Dr. G. Ertl
Fritz-Haber-Institut der Max-Planck-Gesellschaft
Faradayweg 4–6, 14195 Berlin (Germany)
Fax: (+49) 30-8413-5106
E-mail: jacobi@fhi-berlin.mpg.de

[**] We gratefully acknowledge the help of A. Lafosse and Y. Wang in some experiments. Q.S. is thankful for an Alexander von Humboldt fellowship.

 DOI: 10.1002/anie.200250659 © 2003 Wiley-VCH Verlag GmbH & Co. KGaA, Weinheim

then the list of such compounds has been growing continuously.[4] Likewise the observation of nondissociative chemisorption of H_2 on transition-metal surfaces has so far been restricted to a few situations.[5,6] Herein we report that, remarkably, the particular atomic configuration of the $RuO_2(110)$ surface enables the coexistence of both nondissociated (dihydrogen) and dissociated (mono- and dihydride) species bound to different sites.

High-resolution electron energy-loss spectroscopy (HREELS)[7] with a resolution of 20 cm^{-1} was used to record vibrational spectra. The $RuO_2(110)$ surface was formed as a thin, stoichiometrically terminated epitaxial layer by exposing the Ru(0001) surface of a single crystal to O_2 (1×10^7 L; 1 L = 1.3×10^{-6} mbar s) at 700 K.[7,8] For DFT calculations the full-potential linear augmented plane wave scheme[9] was employed by using the following basis-set parameters: $R_{MT}^{Ru}=0.95$ Å, $R_{MT}^{O}=0.53$ Å, $R_{MT}^{H}=0.32$ Å, $E_{max}^{wavefunction}=27.54$ eV, $E_{max}^{potential}=5440$ eV, 18 **k**-points in the irreducible wedge of the (1×1) Brillouin-zone. The DFT calculations used the PBE[10] generalized gradient approximation for the exchange-correlation functional to solve the Kohn–Sham equations. The surface was modeled in a supercell geometry with three O–Ru–O trilayers where all atomic positions except those in the central Ru layer were fully relaxed.

The surface geometry of $RuO_2(110)$ (Figure 1) illustrates the two kinds of coordinatively unsaturated sites exhibited by the rutile(110) faces, (Ru^{cus} and O^{bridge}). The TD spectra of H_2

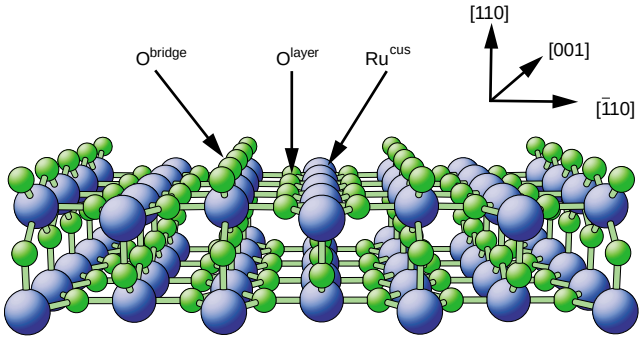


Figure 1. Ball-and-stick model of the bare stoichiometric $RuO_2(110)$ surface in perspective view (O: green, Ru: violet).

from the $RuO_2(110)$ surface exhibit two maxima centered at 95 K (α) and around 260 K (β) (Figure 2). The inset of Figure 2 shows the data for HD evolution after exposure of the $RuO_2(110)$ surface to D_2 (0.5 L) and then to H_2 (0.5 L); the intensity of the α peak is largely suppressed. This result indicates that there is almost no isotope exchange within the α state, which suggests that the peak originates from molecules that had not been dissociatively adsorbed. In contrast, the pronounced isotope scrambling of the β state is indicative of the recombination of chemisorbed atoms. In addition to H_2 molecules, above 400 K an appreciable quantity of H_2O molecules come off the surface, which indicates that apart from the recombinative desorption of H_2 in a different reaction, the whole surface entity H–O–H may be released.

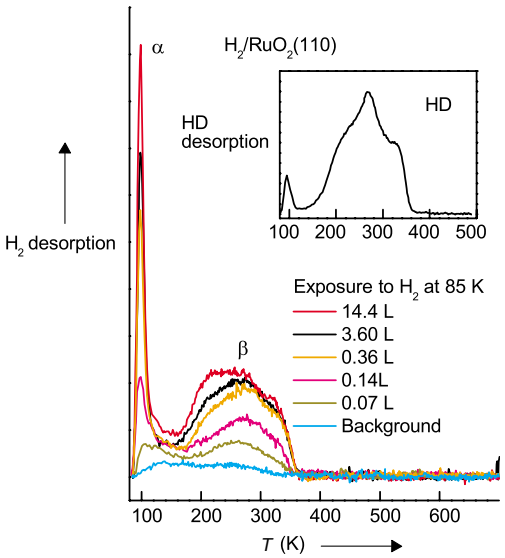


Figure 2. Thermal desorption (TD) spectra of H_2 (HD in the inset) after exposure to varying quantities of H_2 to the $RuO_2(110)$ surface at 85 K. The exposure is given in Langmuir units L (1 L = 1.3×10^{-6} mbar s).

A greater understanding of the nature of these surface hydrogen species is provided by the HREELS data (Figure 3). Spectrum A, obtained from the bare $RuO_2(110)$ surface, shows an intense fingerprint peak at $\tilde{\nu}=557$ cm^{-1} arising from the Ru–O stretch vibration of the O^{bridge} atoms.[11] After the $RuO_2(110)$ surface was saturated with hydrogen, the corresponding spectrum, B, reveals new intense peaks at $\tilde{\nu}=226$,

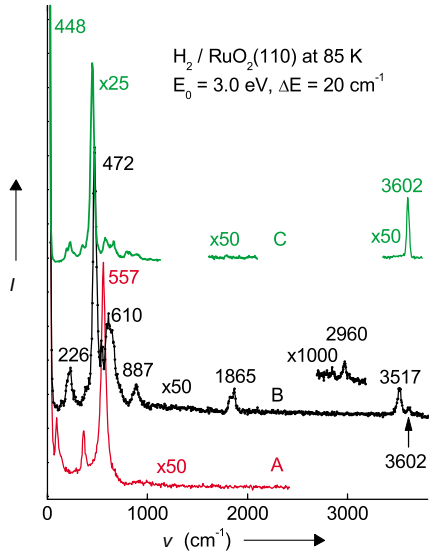


Figure 3. HREEL spectra for a primary electron energy E_0, at an energy resolution ΔE, in specular geometry at an angle of incidence of 60°. The factors ×50, etc. give the intensity enlargement with respect to the elastically scattered electrons (I = intensity, arbitary units). A) Bare stoichiometric $RuO_2(110)$ surface. b) After exposure of 1 L H_2 at 85 K. From the TD spectra it is concluded that about 75% of O^{bridge} sites are occupied by the dihydride complex and about 12% of Ru^{cus} by the dihydrogen species. C) After warming to 350 K complete transformation of the dihydride at O^{bridge} into monohydride occured.

 © 2003 Wiley-VCH Verlag GmbH & Co. KGaA, Weinheim

472, 610, 887, 1865, and 3517 cm^{-1}. These peaks remain in the spectrum after the sample has been heated to 150 K and hence have to be attributed to the β state, as at this moment the α state has been completely desorbed. The strong suppression of the Ru-O^{bridge} mode at $\tilde{\nu} = 557\ cm^{-1}$ suggests that in the β state hydrogen bonding takes place with the coordinatively unsaturated O^{bridge} atoms.

The data of spectrum B in Figure 3 strongly suggest an interpretation of this dissociative hydrogen channel in terms of the formation of a waterlike group at the surface, in which the measured frequencies would correspond to translational ($\tilde{\nu} = 226,\ 472\ cm^{-1}$), librational ($\tilde{\nu} = 610,\ 887\ cm^{-1}$), scissor ($\tilde{\nu} = 1865\ cm^{-1}$), and OH stretching ($\tilde{\nu} = 3517\ cm^{-1}$) modes. In our DFT calculations we tested several alternative configurations. Interestingly, the waterlike group is not symmetrical to the surface as H–O–H, because a scissor mode frequency above the gas phase value cannot be achieved for this configuration. It turned out that a more complex configuration is likely, where the H-O-H plane oriented towards the cus sites (compare Figure 4a and 4b). The OH bond lengths and bonding angle are indicated in Figure 4b. The calculated scissor frequency is $\tilde{\nu} = 1702\ cm^{-1}$, which is well above the gas phase value of $\tilde{\nu} = 1524\ cm^{-1}$.

This dihydride species formed from H_2 and an O^{bridge} surface atom exhibits some similarities with a water molecule: The back bonds of O^{bridge} are elongated from 1.91 to 2.27 Å with respect to the bare surface. Compared to a free water molecule some charge is transferred to the RuO_2 matrix, which makes the H-O-H angle larger and hypothetically reduces the scissor mode frequency. The latter effect is overcompensated by the hydrogen-bondlike interaction of one H atom with two O^{layer} and Ru^{cus}. This effect tilts the whole group so that one OH bond becomes nearly parallel (8°) to the surface (see Figure 4b), the OH bond length becomes further elongated, and the scissor mode increases even beyond the gas-phase value. The calculated adsorption energy of H_2 is 0.32 eV per H_2 molecule. Further details will be discussed elsewhere.

By warming the sample to 350 K, the dihydride complex is transformed into monohydride by releasing hydrogen, evidence for which is shown in the β peak of the TD spectra in Figure 2. All features arising from the dihydride species disappear (i.e. the peaks at $\tilde{\nu} = 887$ and 1865 (1815) cm^{-1}) or change slightly their frequency (472→448 cm^{-1} and 3517→3602 cm^{-1}) in full accordance with the formation of monohydride or hydroxyl groups with the O–H bond perpendicular to the surface (see Figure 4c). The DFT calculations show that under the experimental constraint of negligible O_2 partial pressure in the gas phase, this species indeed represent the thermodynamic ground state.

The only feature in the HREELS spectrum that disappears upon heating the corresponding sample to 150 K is a very weak peak at $\tilde{\nu} = 2960\ cm^{-1}$, which is hence attributed to the H–H stretch vibration of molecular hydrogen adsorbed on the α state. For D_2, the analogous peak is found at $\tilde{\nu} = 2073\ cm^{-1}$ and yields an isotope ratio of 1.42, which is in perfect agreement with the expectations for a (weakly held) molecular species. The value of the H–H frequency for adsorbed H_2 on the α state ($\tilde{\nu} = 2960\ cm^{-1}$) is considerably smaller than that for free H_2 ($\tilde{\nu} = 4407\ cm^{-1}$) or for physisorbed molecules (e.g. $\tilde{\nu} = 4121\ cm^{-1}$ for H_2/Ag(111)[12]), thus indicating that in the present case the rather strong binding to the surface appreciably weakens the H–H bond. The DFT calculations give an adsorption energy of 0.3 eV per H_2 molecule and show that such a molecular species can only be stabilized at the RuO_2(110) surface on top of the coordinatively unsaturated Ru^{cus} atoms in the side-on configuration (Figure 5), with a H–H stretch frequency of $\tilde{\nu} = 3331\ cm^{-1}$, which is in reasonable agreement with the experimental value. The H_2 molecule is separated by 1.8 Å from the Ru^{cus} atoms, while the H–H bond length is increased from 0.74 Å to 0.89 Å, again is very similar to results for η^2-H_2

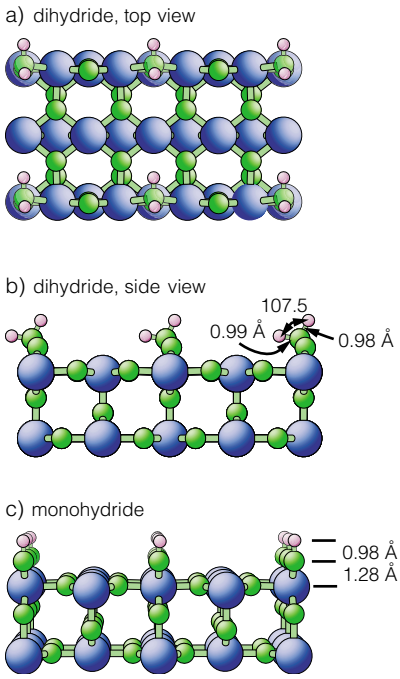


Figure 4. a) Top view and b) side view of the waterlike dihydride. c) Side view of the monohydride (O: green, Ru: violet, H: pink).

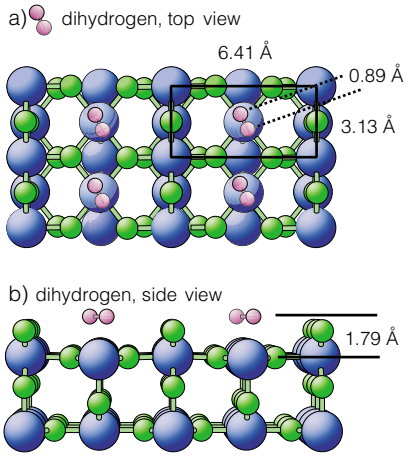


Figure 5. a) Top view and b) side view of dihydrogen bonded to Ru^{cus}. Note that the azimuthal orientation of dihydrogen is arbitrary as it is freely rotating. The (1×1) unit cell is indicated (O: green, Ru: violet, H: pink).

 © 2003 Wiley-VCH Verlag GmbH & Co. KGaA, Weinheim

complexes for which values in the range 0.8–0.9 Å have been reported.[13,14]

Analyzing the computed local density of states, we find the bonding is governed by the interaction between Ru-d_{z^2} and H_2-σ orbitals, as well as between Ru-d_{xz}/d_{yz} and H_2-σ* orbitals, respectively. As a consequence, the Ru-d_{z^2} hybridizes with the occupied H_2-σ leading to a small H→Ru charge transfer. On the other hand, there is some back-donation of electronic charge from the metal to the H_2-σ* orbital, whereby coupling to the surface is strengthened while the H–H bond is weakened and elongated. Correspondingly, the H–H stretch frequency gets significantly red-shifted, close to the values around $\tilde{\nu} = 2400$–$2800\ cm^{-1}$ known from dihydrogen complex chemistry.[15,16]

In summary, we have conclusively identified both dissociative hydride and non-dissociative dihydrogen species at the RuO_2(110) surface. Although we find strong similarities for both types of species with data from transition-metal complex chemistry, the major difference is that with the surface both atomic and molecular hydrogen types are related to different sites: the dissociated β state to O^{bridge} and the molecular α state to Ru^{cus} atoms.

Received: November 28, 2002 [Z50659]

Keywords: ab initio calculation · hydrogen · ruthenium oxide · surface chemistry · vibrational spectroscopy

[1] H. Brunner, *Applied homogeneous catalysis with organometallic compounds*, VCH, Weinheim, **1996**, p. 201.
[2] K. Christmann, *Surf. Sci. Rep.* **1988**, *9*, 1–163.
[3] G. J. Kubas, R. R. Ryan, B. I. Swanson, P. J. Vergamini, H. J. Wasserman, *J. Am. Chem. Soc.* **1984**, *106*, 451–452.
[4] G. J. Kubas, *Acc. Chem. Res.* **1988**, *21*, 120; R. H. Crabtree, *Angew. Chem.* **1993**, *105*, 828–845; *Angew. Chem. Int. Ed. Engl.* **1993**, *32*, 789–805.
[5] A. S. Mårtensson, C. Nyberg, S. Andersson, *Phys. Rev. Lett.* **1986**, *57*, 2045–2048.
[6] D. K. Schmidt, K. Christmann, G. Kresse, J. Hafner, M. Lischka, A. Groß, *Phys. Rev. Lett.* **2001**, *87*, 096103.
[7] J. Wang, C. Y. Fan, K. Jacobi, G. Ertl, *Surf. Sci.* **2000**, *481*, 113–118; C. Y. Fan, J. Wang, K. Jacobi, G. Ertl, *J. Chem. Phys.* **2001**, *114*, 10058–10062.
[8] H. Over, Y. D. Kim, A. P. Seitsonen, S. Wendt, E. Lundgren, M. Schmid, P. Varga, A. Morgante, G. Ertl, *Science* **2000**, *287*, 1474–1476.
[9] P. Blaha, K. Schwarz, J. Luitz, WIEN97, Technische Universität, Wien, Austria, **1999**, ISBN 3-9501031-0-4.
[10] J. P. Perdew, S. Burke, M. Ernzerhof, *Phys. Rev. Lett.* **1996**, *77*, 3865–3868.
[11] Y. D. Kim, A. P. Seitsonen, S. Wendt, J. Wang, C. Fan, K. Jacobi, H. Over, G. Ertl, *J. Phys. Chem. B* **2001**, *105*, 3752–3758.
[12] M. Gruyters, K. Jacobi, *Chem. Phys. Lett.* **1994**, *225*, 309–314.
[13] K. W. Zilm, R. A. Merrill, M. W. Kummer, G. J. Kubas, *J. Am. Chem. Soc.* **1986**, *108*, 7837–7839.
[14] L. S. Van der Sluys, J. Eckert, O. Eisenstein, J. H. Hall, J. C. Huffman, S. A. Jackson, T. F. Koetzle, G. J. Kubas, P. J. Vergamini, K. G. Caulon, *J. Am. Chem. Soc.* **1990**, *112*, 4831–4841.
[15] R. H. Crabtree, D. G. Hamilton, *J. Am. Chem. Soc.* **1986**, *108*, 3124–3125.
[16] G. J. Kubas, *J. Less-Common Met.* **1991**, *172*, 475–484.

 © 2003 Wiley-VCH Verlag GmbH & Co. KGaA, Weinheim

Nanocomposite Films

Template Synthesis of Polypyrrole Nanofibers Insulated within One-Dimensional Silicate Channels: Hexagonal versus Lamellar for Recombination of Polarons into Bipolarons**

*Midori Ikegame, Keisuke Tajima, and Takuzo Aida**

The nanoscale orientation of conjugated polymers is an interesting subject for the development of the next-generation optoelectronic materials. In this respect, an attractive approach is to utilize unidirectionally aligned nanoscopic channels or pores as templates for the synthesis of conjugated polymers.[1] Martin and co-workers have utilized porous membrane filters for the polymerization of pyrrole to give a polymer composite material with oriented, submicron-scale tubular-shaped polypyrrole domains, whose electronic conductivity is an order of magnitude higher than those of unprocessed bulk polymers.[2] However, the fabrication and properties of "insulated polypyrrole nanofibers" have not yet been explored.

We have exploited a novel approach toward macromolecular synthesis by using porous silica with ordered hexagonal arrays of uniformly sized nanoscopic channels.[3] Recently, we and other research groups succeeded in the fabrication of mesostructured silica consisting of conjugated polymers within aligned silicate nanochannels by using a sol–gel-based approach with diacetylenic surfactants as templates.[4] In contrast with post-loading approaches,[5] this new method guarantees a dense filling of the silicate channels with conjugated polymers. Herein we report the synthesis of a novel polypyrrole/silica nanocomposite material (**3a**), templated by a pyrrole-containing surfactant (**1a**), where polypyrrole domains are segregated and insulated by one-dimensional silicate nanochannels (Figure 1). In particular, we highlight a "nanoscopic confinement effect" of the hexagonal silicate channels on the recombination of polarons into bipolarons.

Surfactant monomers **1a** and **1b** were synthesized by an alkaline-mediated coupling reaction of 1,12-dibromododecane and 1,10-dibromodecane, respectively, with pyrrole, followed by subsequent transformation of the terminal hydroxy group into a quaternary ammonium ion. Pyrrole-containing mesostructured silica **2a** was successfully synthesized using **1a** according to a method reported by Ogawa for

[*] Prof. Dr. T. Aida, M. Ikegame, Dr. K. Tajima
Department of Chemistry and Biotechnology
School of Engineering, The University of Tokyo
7-3-1 Hongo, Bunkyo-ku, Tokyo 113-8656 (Japan)
Fax: (+81) 3-5841-7310
E-mail: aida@macro.t.u-tokyo.ac.jp

[**] We thank Dr. T. Fukushima and A. Kosaka for their active collaboration. We also acknowledge Prof. M. Ogawa for generous instruction on the preparation of mesoporous silica films.

Supporting information for this article is available on the WWW under http://www.angewandte.org or from the author.

 © 2003 Wiley-VCH Verlag GmbH & Co. KGaA, Weinheim DOI: 10.1002/anie.200250800

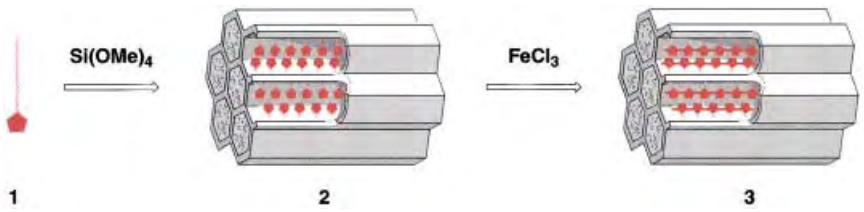
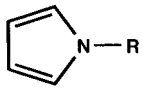


Figure 1. Schematic representation of the template synthesis of a polypyrrole/silica nanocomposite material (**3**) by oxidative polymerization of a pyrrole-containing surfactant (**1**) within a mesostructured silica (**2**).



R = $-(CH_2)_{12}-N^+Me_3\ Br^-$ **1a**

R = $-(CH_2)_{10}-N^+Me_3\ Br^-$ **1b**

the fabrication of mesoporous silica films.[6] Thus, tetramethyl orthosilicate (0.19 g) was added to 6 wt% of hydrochloric acid at 0°C with magnetic stirring to hydrolyze the Si–O bonds, followed by partial condensation of the resulting silanol functionalities. After 10 min, **1a** (0.1 g) was added to the above solution, and the mixture, after sonication for 1 min at 20°C, was spin-coated (3000 rpm) on a glass plate to afford a homogeneous, transparent film, which was then air-dried overnight at 25°C to promote the formation of the silica framework. The X-ray diffraction (XRD) pattern obtained for **2a** was characteristic of a hexagonal silicate structure, with (100) and (200) diffraction peaks and a *d* spacing of the former of 29.7 Å.[7] This value is close to a diameter expected for a single rod micelle of **1a**. When **2a** was calcined at 450°C for 8 h, the resulting material still showed a characteristic XRD pattern of the hexagonal structure, although the *d* spacing had decreased to 20.1 Å. Transmission electron microscopy studies on **2a** clearly showed regularly aligned hexagonal channels with a diameter of approximately 3 nm (Figure 2). The content of **1a** in the composite film was evaluated by thermogravimetric analysis (TGA) of **2a** to be

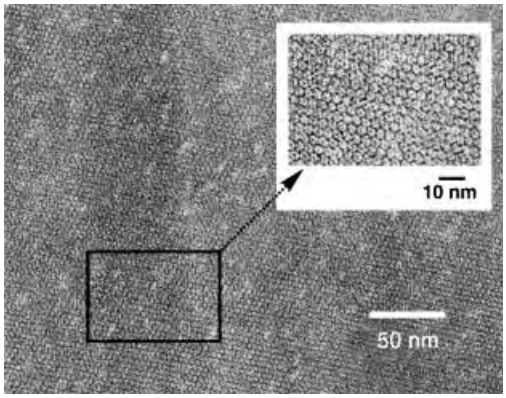


Figure 2. Transmission electron micrographs of pyrrole/silica nanocomposite film **2a**.

43 wt%,[7] which is as high as the values reported for ordinary mesoporous silica containing template surfactants. Therefore, the silicate channels of composite film **2a** are densely filled with **1a**. In contrast, when surfactant **1b**, which has a slightly shorter alkyl chain than **1a**, was used, the resulting composite film did not show any XRD diffractions.

When spin-coated film **2a**, after being air-dried overnight, was dipped for 1 min in a solution of anhydrous $FeCl_3$ (2 M) in diethyl ether at 20°C it immediately stained brown (Figure 3a), as a consequence of the oxidative polymerization of included **1a**.[8] The colored material **3a** thus obtained was found to retain essentially the same XRD profile[7] as that of **2a**. The absorption spectrum of **3a** showed a broad band centered at 1200 nm, which is characteristic of an electronic transition from a valence band of doped polypyrrole to a bipolaron (dication) band (Figure 4a). Etching the silica framework of **3a** with HF allowed isolation of the included polymer as a highly insoluble black precipitate, whose IR spectrum[7] over the range 900–1400 cm^{-1} was identical to that reported for a doped polypyrrole.[9] The complete polymerization of **1a** in composite film **2a** was confirmed by the absence of ^1H NMR signals arising from **1a** in the supernatant solution of the above extract.[7] All these observations demonstrate the formation of a nanocomposite material, in which each silicate channel contains a single, nanoscopic bundle of doped polypyrrole chains. Such a rapid, complete polymerization of **2a** is interesting, when the limited accessibility of included **1a** to the initiator ($FeCl_3$) is considered.

It is understood that oxidative polymerization of pyrrole derivatives is accompanied by the initial formation of polarons (radical cation species), which are then transformed into bipolarons (dicationic species) by recombination.[10] Each polypyrrole domain in composite material **3a** is nanoscopically segregated and insulated by the silicate channel, hence the transformation of polarons to bipolarons must occur within the individual silicate channels. We were motivated to explore the effects of this "nanoscopic segregation" on the recombination of polarons. Thus, **1a** was diluted with a nonpolymerizable surfactant (dodecyltrimethylammonium bromide, DTAB) at molar ratios of [**1a**]:[DTAB] = 1:3 and 1:6, and the mixtures were utilized for the sol–gel process. Consequently, transparent, thin films $\mathbf{2}_{\mathbf{1a}/DTAB}$ were obtained by spin coating which showed XRD patterns characteristic of hexagonal structures with *d* spacings of 32.3 and 32.6 Å.[7] These films, like **2a**, immediately stained brown when dipped in a solution of $FeCl_3$ (2 M) in diethyl ether for 1 min (Figure 3b,c). XRD analysis of these colored materials indicated the successful retention of their hexagonal silicate structures upon oxidative polymerization. Etching these nanocomposite silica films with HF allowed the isolation of insoluble black precipitates, whose IR spectra were characteristic of polypyrrole derivatives.[7] The polypyrrole-containing nanocomposite films ($\mathbf{3}_{\mathbf{1a}/DTAB}$) obtained at molar ratios [**1a**]:[DTAB] of 1:3 and 1:6 both exhibited two absorption

 © 2003 Wiley-VCH Verlag GmbH & Co. KGaA, Weinheim

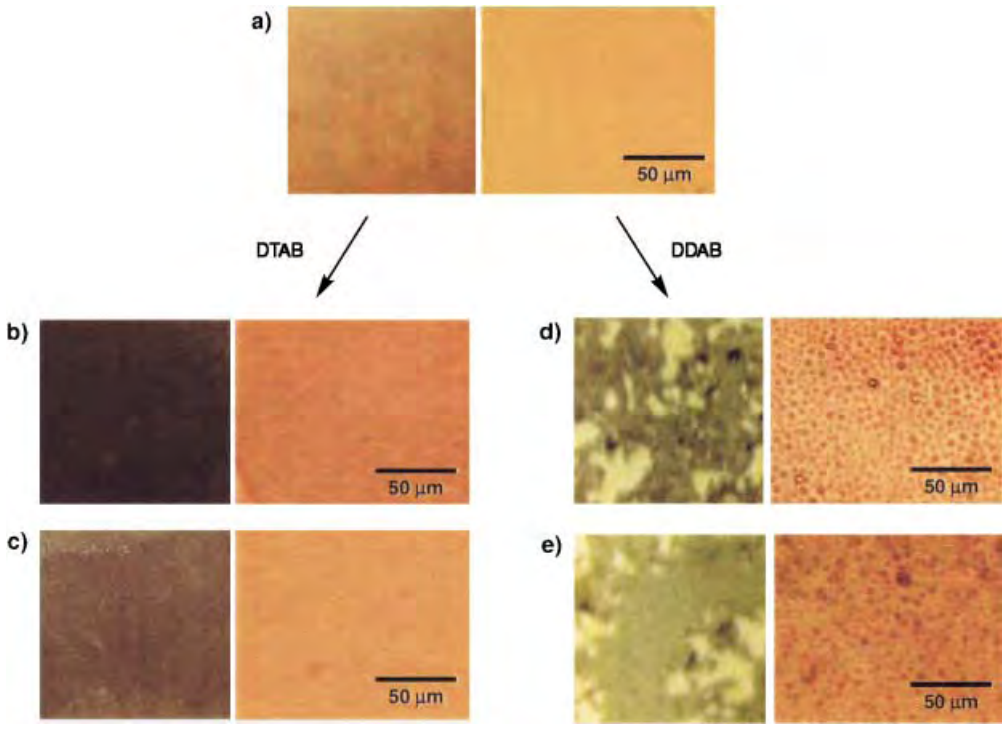


Figure 3. Pictures (left) and optical micrographs (right, ×400) of polypyrrole/silica nanocomposite films **3a**, $\mathbf{3}_{\mathbf{1a}/\mathrm{DTAB}}$, and $\mathbf{3}_{\mathbf{1a}/\mathrm{DDAB}}$. Compounds **3a** and $\mathbf{3}_{\mathbf{1a}/\mathrm{DTAB}}$ were prepared at [**1a**]:[DTAB] molar ratios of: a) 1:0, b) 1:3, and c) 1:6, while $\mathbf{3}_{\mathbf{1a}/\mathrm{DDAB}}$ were prepared at molar ratios [**1a**]:[DDAB] of: d) 1:3 and e) 1:6.

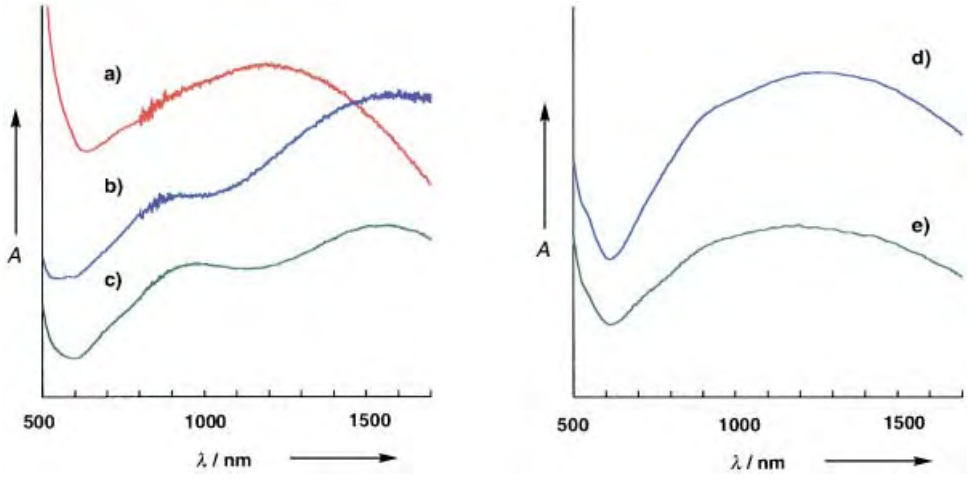


Figure 4. Electronic absorption spectra of polypyrrole/silica nanocomposite films **3a**, $\mathbf{3}_{\mathbf{1a}/\mathrm{DTAB}}$, and $\mathbf{3}_{\mathbf{1a}/\mathrm{DDAB}}$. Compounds **3a** and $\mathbf{3}_{\mathbf{1a}/\mathrm{DTAB}}$ were prepared at [**1a**]:[DTAB] molar ratios of: a) 1:0, b) 1:3, and c) 1:6, while $\mathbf{3}_{\mathbf{1a}/\mathrm{DDAB}}$ films were prepared at [**1a**]:[DDAB] molar ratios of: d) 1:3 and e) 1:6. All the spectra were taken 30 min after being dipped in a solution of $FeCl_3$ (2 M) in diethyl ether for 1 min at 20 °C. No spectral change occurred thereafter. The absorbance is given in arbitrary units.

bands centered at 900 and 1500 nm, with a small shoulder at 700 nm[11] (Figure 4b,c), which are typical of those reported for EPR-active polarons.[10] In sharp contrast, when the concentration of **1a** was higher (for example, [**1a**]:[DTAB] = 1:2), the resulting composite film $\mathbf{3}_{\mathbf{1a}/\mathrm{DTAB}}$, similar to **3a**, showed an absorption spectrum characteristic of bipolarons.[7]

We found that pyrrole-containing nanocomposite "lamellar" films $\mathbf{2}_{\mathbf{1a}/\mathrm{DDAB}}$ can be prepared by using didodecyldimethylammonium bromide (DDAB) as a co-template at [**1a**]:[DDAB] = 1:3 and 1:6. These composite films displayed characteristic XRD peaks with *d* spacings of 34.7 and 34.0 Å, respectively.[7] Similarly to hexagonal **2a** and $\mathbf{2}_{\mathbf{1a}/\mathrm{DTAB}}$, lamellar films $\mathbf{2}_{\mathbf{1a}/\mathrm{DDAB}}$ immediately stained black when dipped in a solution of $FeCl_3$ (2 M) in diethyl ether, thus indicating the successful polymerization of included **1a**. However, in sharp contrast to $\mathbf{2}_{\mathbf{1a}/\mathrm{DTAB}}$ ([**1a**]:[DTAB] = 1:3 and 1:6), the resulting polymeric composites ($\mathbf{3}_{\mathbf{1a}/\mathrm{DDAB}}$) both displayed only a broad

 © 2003 Wiley-VCH Verlag GmbH & Co. KGaA, Weinheim

absorption band centered at 1200 nm, which arises from bipolarons (Figure 4d,e). Analysis of these films by optical microscopy showed a macroscopic phase separation consisting of black-colored, doped polypyrrole domains dispersed in a continuous phase of nonpolymerizable DDAB (Figure 3d,e). These contrasting results clearly indicate that doped polypyrrole chains are highly constrained and insulated when incorporated within hexagonal nanoscopic channels and lose the possibility of the polarons (radical cations) recombining into bipolarons (dications), whereas those in two-dimensional lamellar interlayers possess a certain freedom for this electronic event.

In conclusion, we succeeded in the fabrication of a novel composite material (**3a**) consisting of "polypyrrole nanofibers" segregated and insulated by hexagonal silicate channels by using a sol–gel-based template polymerization of a pyrrole-containing surfactant monomer (**1a**). The dilution experiments with nonpolymerizable surfactants as co-templates with **1a** demonstrated an essential difference between one-dimensional and two-dimensional nanospaces for the electronic confinement of doped polypyrrole chains. The sol–gel-based synthetic approach reported herein in combination with lithographic technologies[12] would allow the nanoscopic patterning of aligned conductive cables with an insulating coat. Toward this end, studies on the electronic conductivity of the insulated polypyrrole nano domains would be one of the challenging subjects worthy of further investigation.

Received: December 19, 2002 [Z50800]

Keywords: materials science · polymerization · polypyrroles · silicates · sol–gel processes

[1] For a recent review, see K. Tajima, T. Aida, *Chem. Commun.* **2000**, 2399–2412.
[2] a) C. R. Martin, *Science* **1994**, *266*, 1961–1966; b) V. P. Menon, J. Lei, C. R. Martin, *Chem. Mater.* **1996**, *8*, 2382–2390; c) S. Demoustier-Champagne, P.-Y. Stavaux, *Chem. Mater.* **1999**, *11*, 829–834.
[3] a) K. Kageyama, T. Ogino, T. Aida, T. Tatsumi, *Macromolecules* **1998**, *31*, 4069–4073; b) K. Kageyama, J. Tamazawa, T. Aida, *Science* **1999**, *285*, 2113–2115; c) K. Tajima, G. Ogawa, T. Aida, *J. Polym. Sci. Part A* **2000**, *38S*, 4821–4825.
[4] a) T. Aida, K. Tajima, *Angew. Chem.* **2001**, *113*, 3919–3922; *Angew. Chem. Int. Ed.* **2001**, *40*, 3803–3806; b) Y. Lu, Y. Yang, A. Sellinger, M. Lu, J. Huang, H. Fan, R. Haddad, G. Lopez, A. R. Burns, D. Y. Sasaki, J. Shelnutt, C. J. Brinker, *Nature* **2001**, *410*, 913–917.
[5] For examples of porous inorganic/polypyrrole composite materials, see T. Bein, P. Enzel, *Angew. Chem.* **1989**, *101*, 1737–1738; *Angew. Chem. Int. Ed. Engl.* **1989**, *28*, 1692–1694.
[6] M. Ogawa, *Chem. Commun.* **1996**, 1149–1150.
[7] See the Supporting Information.
[8] J. A. Walker, L. F. Warren, E. F. Witucki, *J. Polym. Sci. Part A* **1988**, *26*, 1285–1294.
[9] a) S. Ghosh, G. A. Bowmaker, R. P. Cooney, J. M. Seakins, *Synth. Met.* **1998**, *95*, 63–67; b) R. G. Davidson, T. G. Turner, *Synth. Met.* **1995**, *72*, 121–128.
[10] a) J. L. Brédas, J. C. Scott, K. Yakushi, G. B. Street, *Phys. Rev. B* **1984**, *30*, 1023–1025; b) J. L. Brédas, G. B. Street, *Acc. Chem. Res.* **1985**, *18*, 309–315.
[11] The shoulder band at 700 nm was more apparent when $\mathbf{3}_{\mathbf{1a}/\mathrm{DTAB}}$ was prepared at a much lower concentration of **1a**, such as [**1a**]:[DTAB] = 1:9. See the Supporting Information.
[12] P. Yang, G. Wirnsberger, H. C. Huang, S. R. Cordero, M. D. McGehee, B. Scott, T. Deng, G. M. Whitesides, B. F. Chmelka, S. K. Buratto, G. D. Stucky, *Science* **2000**, *287*, 465–467.

 © 2003 Wiley-VCH Verlag GmbH & Co. KGaA, Weinheim

Oligopeptide Formation in Crystals

Generation of Oligopeptides with Homochiral Sequences by Topochemical Reactions within Racemic Crystals of Phenylalanine-*N*-carboxyanhydride**

José Geraldo Nery, Gérard Bolbach, Isabelle Weissbuch, and Meir Lahav**

Theories on the origin of life suggest that homochiral biopolymers were already being generated in prebiotic times from racemic mixtures of activated monomeric precursors;[1–3] various scenarios for their formation have been proposed.[4–7]

In our current program we promote a conceivable scheme for the formation of primitive homochiral polymers from mixtures of racemates or nonracemic mixtures of low enantiomeric imbalance, by their self-assembly within two-dimensional (2D) or 3D crystalline architectures of distinct packing motifs, followed by lattice-controlled polymerization reactions.[8–10] The overall process entails two different aspects: a) Generation of racemic mixtures of homochiral polymers from racemates, and b) only one of the two enantiomeric polymers are formed by spontaneous symmetry breaking or by asymmetric induction.

Polymerization reactions within rigid 3D crystals, initiated either thermally or by irradiation, are controlled by the crystal lattice, to the greatest extent, at the onset of the reaction, since the polymeric phase produced is generally much denser than the crystalline monomer reactant. Changes in density and heat release that occur at sites of chain propagation induce local disorder, which brings about the formation of nonstereospecific polymers. Consequently, after years of research, only a limited number of systems including dieth-

[*] Dr. I. Weissbuch, Prof. Dr. M. Lahav, Dr. J. G. Nery
Department of Materials and Interfaces
The Weizmann Institute of Science
76100-Rehovot (Israel)
Fax: (+972) 8-9344-138
E-mail: isabelle.weissbuch@weizmann.ac.il
meir.lahav@weizmann.ac.il

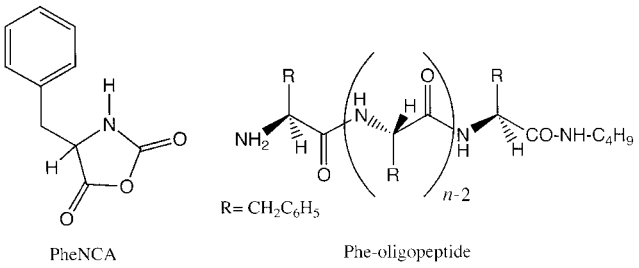
Dr. G. Bolbach
Laboratoire de Chimie Structurale Organique et Biologique
Université Pierre et Marie Curie
75252 Paris Cedex 05 (France)

[**] This work was supported by the Israel Science Foundation and The Petroleum Research Fund of the American Chemical Society.

 DOI: 10.1002/anie.200351114 © 2003 Wiley-VCH Verlag GmbH & Co. KGaA, Weinheim

ylenes, diacetylenes, and coordination complexes of nickel were reported that undergo lattice-controlled polymerization beyond dimers and trimers.[11–17] Heterogeneous solid–gas or solid–liquid reactions are even less stereospecific, since the reactant crystal is already damaged at the early stages of the chemical transformation.

Recently, we reported the synthesis of homochiral (isotactic) oligopetides by the polymerization of amphiphilic racemic amino acid derivatives within 2D monolayer crystallites at the air–water interface.[8–10] During these studies, we noticed that when *N*-carboxyanhydride (NCA) derivatives of α-amino acids, bearing long hydrocarbon chains, are arranged within 2D crystallites in a head-to-tail motif at the air–water interface, they undergo a most efficient "zipperlike" stereospecific polymerization reaction to yield syndiotactic (*S*/*R*) oligopeptides. Following these results, we supposed that this mechanism of polymerization should equally operate in the rigid 3D crystals of NCA–α-amino acids with related packing motifs, which would provide another plausible route for the generation of homochiral oligopeptides from racemates. We now report the formation of homochiral oligopeptides by a polymerization reaction in racemic crystals of phenylalanine-*N*-carboxyanhydride (PheNCA) initiated by *n*-butylamine.



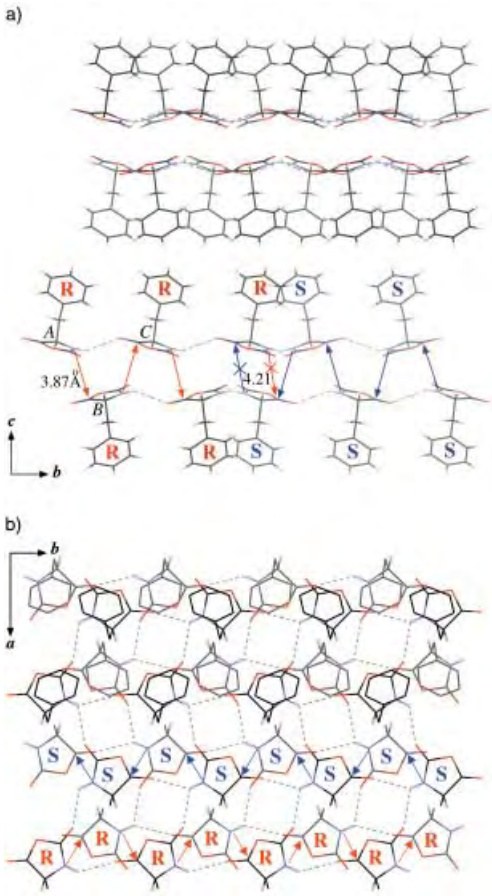


Figure 1. The packing arrangement of (*R*,*S*)-PheNCA crystals viewed along: a) the *a* axis, and b) the *c* axis. For clarity, some molecules in the lower parts of both images are not shown. The reaction pathway is indicated with red and blue arrows for the *R* and *S* molecules, respectively.

Kinetic and crystallographic studies by Kanazawa et al.[18–20] on the polymerization of several NCA monomers in the solid state have demonstrated that the rate of polymerization of these monomers is dependent on the packing arrangements of their crystals. However, since the diastereoisomeric composition of the oligopeptides was not available it was not possible to establish whether such crystals would be appropriate matrixes for the generation of oligopeptides with homochiral sequences. An inspection of the reported packing arrangement of racemic PheNCA[19] suggests that polymerization of this monomer via the zipperlike mechanism should furnish homochiral oligopeptides (Figure 1). The crystal contains two independent, almost identical, molecules per unit cell. The molecules form 2D hydrogen-bonded network layers arranged perpendicular to the *c* axis. For clarity we shall consider two rows of molecules, shown in the bottom bilayer in Figure 1a. Within each row the molecules are related by translation symmetry, and are arranged in a head-to-tail motif; the two rows are not symmetry related. The separation of the nitrogen atom of molecule A (*R* configuration) residing in one row and the carbonyl carbon atom adjacent to the chiral carbon of molecule B of the same handedness residing in the second row is short (3.87 Å), whereas the same nitrogen atom is separated further from the equivalent carbonyl carbon atom of a nearer *S*-configured molecule (4.21 Å). We anticipated that molecule A (first row) would interact with molecule B (second row), which would serve to bring the latter closer to molecule C, which has the same handedness and resides in the first row (Figure 1a). The propagation step will proceed preferentially by a zipperlike mechanism, where monomer units are added to the growing chains in an alternating sequential mode from monomers of the two rows. By virtue of symmetry, the enantiomeric monomers in the crystal should react to yield chains of the enantiomeric oligopeptides (Figure 1b).

To probe the veracity of this mechanism, it was essential to determine the composition of the oligopeptides formed in these crystals. We used racemic mixtures of monomers, in which the phenyl rings of the *S* enantiomer were deuterated.[7,8,21,22] The structure of this "quasi-racemic" crystal of PheNCA is identical to that of its unlabeled counterpart, and different from that of the pure enantiomorph, as determined by X-ray powder diffraction. The polymerization reaction was performed in crystals suspended in hexane and initiated with 0.5 mol% of *n*-butylamine, to yield a complex mixture of diastereoisomeric oligopeptides of various lengths, as determined by MALDI-TOF mass spectrometry. The distribution

 © 2003 Wiley-VCH Verlag GmbH & Co. KGaA, Weinheim

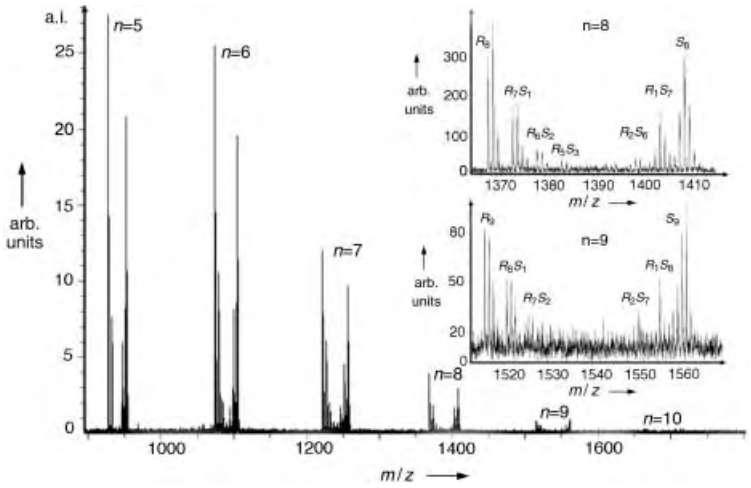


Figure 2. MALDI-TOF mass spectrum of the oligopeptides obtained in the polymerization of (*R*,*S*)-PheNCA at 22 °C showing the *m*/*z* range from penta- to decapeptides. The phenyl ring of the *S* enantiomer was pentadeuterated. The two insets show expanded spectra of the octamer and nonamer ranges. For analysis, samples were reacted with 2:1 (v/v) THF:trifluoroacetic anhydride; the *N*-trifluoroacetyl derivatives are soluble. Dithranol, mixed with NaI dissolved in THF, was used as the matrix.

of the products was analyzed directly after polymerization, or in the form of *N*-trifluoroacetyl derivatives. Figure 2 shows a MALDI-TOF mass spectrum of oligopeptides generated in crystals at 22 °C. Ion species deduced from mass/charge (*m*/*z*) ratios are *N*-trifluoroacetyl derivatives of the oligopeptides, which contain a single C_4H_9NH- group of the initiator, and are detected as Na ions. The intensity of the signals that correspond to different diastereoisomers of the same length are assumed to be proportional to their amount, as a result of identical ionization and detection efficiencies. The MALDI-TOF mass spectra provide a means of determining the relative abundance (r.a.) of the various diastereoisomers, defined as the ratio between the amount of a given diastereoisomer and the total amount of all the diastereoisomers of the same length. No measurable isotope effects were observed and the amount of oligopeptides decreased with an increase in length (Figure 2). The results were quite reproducible from sample to sample and very similar data were obtained using two different spectrometers. Usually, diastereoisomers as large as nonamers were detected but some samples showed also deca- and undecamers. Note that in the polymerization of unlabeled (*R*,*S*)-PheNCA samples, oligopeptides containing up to 17 repeat units were obtained.

Histograms describing the correlation between the r.a. and the composition of the oligopeptides of each length obtained from racemic PheNCA polymerized at 22 °C, 50 °C, and in the melt are shown in Figure 3a, b, and c, respectively. An oligopeptide of length *n*, where $n = h + d$ (*h* and *d* are the number of *R* and *S* repeat units, respectively) is labeled (*h*,*d*). Homochiral oligopeptides of each length *n* are represented at the wings, whereas the heterochiral species are represented in between them (Figure 3). Oligopeptides ($n = 4$–9), primarily exhibiting a homochiral sequence, were obtained in the racemic crystals of PheNCA at 22 °C (Figure 3a), as compared to a random polymerization obeying a binomial law (Figure 3e). Polymerization in the melt (Figure 3c) yielded shorter oligopeptides ($n = 7$), also with a primarily heterochiral sequence, and with an increase in length. Polymerization is still topochemically controlled at 50 °C (Figure 3b), although the degree of enantioselectivity is reduced. Further support for the topochemical nature of this solid-state reaction is gained from the observed different distribution of diastereoisomeric oligopeptides formed upon polymerization of racemic leucine-NCA[23] (Figure 3d), which crystallizes with a different structural motif.

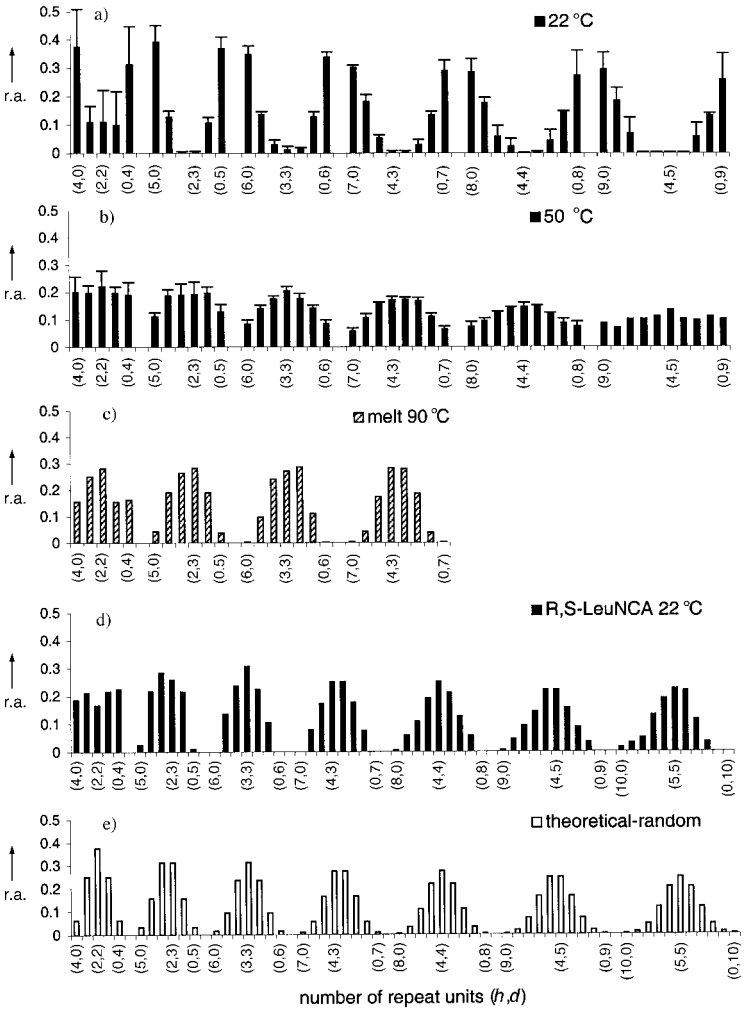


Figure 3. Histograms showing the experimental relative abundance of diastereoisomeric oligopeptides of various lengths obtained from the polymerization in: a,b,c) (*R*,*S*)-PheNCA crystals at 22 °C, 50 °C, and in the melt (90 °C in heptane); d) (*R*,*S*)-LeuNCA at 22 °C. e) The relative abundance calculated for a binomial distribution in a random process. Labels (*h*,*d*) represent the number of *R* and *S* repeat units of each oligopeptide. Histograms a) and b) show the average and standard deviation of three and four experiments, respectively. The nonamer in b) was obtained in one sample only.

 © 2003 Wiley-VCH Verlag GmbH & Co. KGaA, Weinheim

It is noteworthy that the r.a. of the homochiral fraction of the longer homochiral Phe-oligopeptides increases along with an increase of the chain length. Figure 4 shows the experimental r.a. (at 22 °C) of homochiral oligopeptides, normalized to that calculated in a theoretical random polymerization, for oligopeptides of various lengths. The results can be rationalized by supposing that a fraction of the short oligomers were formed at defect sites on the surface, which have not propagated towards the interior of the crystals.

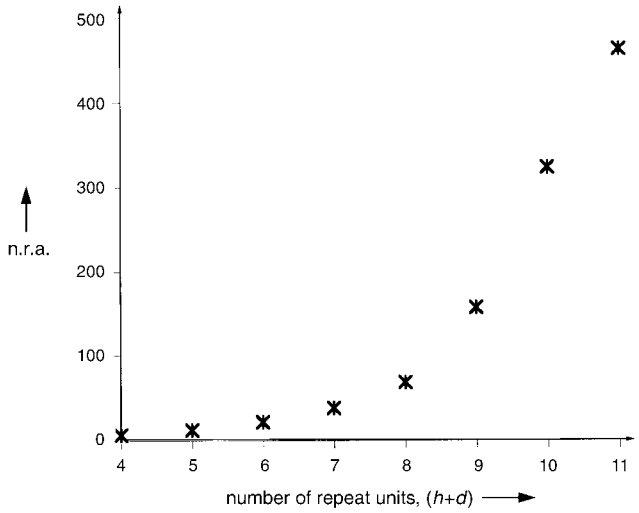


Figure 4. Enhancement of the experimental relative abundance of the homochiral [(*h*,0) + (0,*d*)] oligopeptides normalized to that calculated for a theoretical random process for molecules of any length $n = h + d$ (n.r.a. = normalized relative abundance). Note that deca- and undecapeptides were detected only in some of the polymerization experiments.

In conclusion, a process that comprises the self-assembly of activated α-amino acids into crystalline architectures, followed by lattice-controlled reactions, provides a plausible route for the formation of homochiral oligopeptides of 10–17 units in length. The generation of homochiral oligopeptides by this route is not confined for reactivity in 3D crystals, but should be also applicable within less organized architectures such as membrane bilayers and vesicles.

In the present study we have focused on the formation of racemic mixtures of homochiral oligopeptides. However, reactivity in crystals can be further exploited for the preparation of enantiopure oligopeptides, generated either by the polymerization of appropriate racemic monomers in the presence of small amounts of enantioselective initiators and inhibitors,[24] or by the amplification of chirality originating from nonracemic mixtures[8,25] of monomers of low enantiomeric imbalance that undergo phase separation.

Experimental Section

NCA monomers were prepared following a reported procedure.[26] *R*-Phe (1 mmol) and *S*-Phe (ring D5 98 % Cambridge Isotope Laboratories; 1 mmol) were suspended in dry THF and heated to 40 °C under argon. Solid bis(trichloromethyl) carbonate (3.5 mmol) was added gradually for about 1 h until a clear solution was obtained; the reaction then proceeded for additional 3 h. Hexane was then added and the NCA crystals were formed overnight at −5 °C. The thin platelike (*R*,*S*)-PheNCA crystals obtained after filtration were analyzed by IR spectroscopy and X-ray powder diffraction. (*R*,*S*)-LeuNCA was prepared in a similar way using deuterated (*S*)-[D_7]leucine.

Solid-state polymerization was performed (under argon atmosphere) in crystals suspended in hexane, using *n*-butylamine (0.5 mol %) as an initiator, for 12 and 72 h at 50 and 22 °C, respectively. The gel-like product was washed with dry THF and ethyl acetate until all the monomer was removed, as confirmed by infrared spectroscopy. The product in its final form was centrifuged and dried. Melt polymerization was performed in heptane, heated to 90 °C.

Samples for MALDI-TOF mass spectral analysis were prepared by either dissolving the dry material in a 2:1 (v/v) mixture of THF and trifluoroacetic anhydride (trifluroacetylation of the N-terminal of the oligopeptides) or THF:trifluoroacetic acid until a clear solution is obtained. 0.5 μL of this solution was deposited on to a matrix deposit (1:1 (v/v) mixture of dithranol solution in chloroform and a NaI saturated solution in THF) on the instrument holder. The MALDI-TOF positive-ion mass spectra were obtained in reflector mode from two different instruments at the Weizmann Institute (Bruker Biflex 3) and at the University of Paris VI (Perceptive Biosystems, Voyager Elite), both equipped with a N_2 laser.

Received: February 5, 2003 [Z51114]

Keywords: homochirality · oligo(phenylalanine) · solid-state polymerization · topochemistry

[1] P. Franck, W. A. Bonner, R. N. Zare in *Chemistry for the 21th Century* (Eds.: E. Keinan, I. Schechter), Wiley-VCH, Weinheim, **2000**, p. 175.
[2] F. F. Joyce, G. M. Visser, C. A. A. von Boeckel, J. H. von Boom, L. E. Orgel, J. von Westrenen, *Nature* **1984**, *310*, 602.
[3] A. Brack, G. Spach, *Origins Life* **1981**, *11*, 135.
[4] G. Wald, *Ann. N. Y. Acad. Sci.* **1957**, *69*, 352.
[5] E. R. Blout, P. Doty, J. T. Yang, *J. Am. Chem. Soc.* **1957**, *79*, 749.
[6] N. E. Blair, F. M. Dirbas, W. A. Bonner, *Tetrahedron* **1981**, *37*, 27.
[7] M. Blocher, T. Hitz, P. L. Luisi, *Helv. Chim. Acta* **2001**, *84*, 842.
[8] H. Zepik, E. Shavit, M. Tang, T. R. Jensen, K. Kjaer, G. Bolbach, L. Leiserowitz, I. Weissbuch, M. Lahav, *Science* **2002**, *295*, 1266.
[9] I. Weissbuch, G. Bolbach, H. Zepik, E. Shavit, M. Tang, J. Frey, T. R. Jensen, K. Kjaer, L. Leiserowitz, M. Lahav, *J. Am. Chem. Soc.* **2002**, *124*, 9093.
[10] I. Weissbuch, G. Bolbach, H. Zepik, E. Shavit, M. Tang, T. R. Jensen, K. Kjaer, L. Leiserowitz, M. Lahav, *Chem. Eur. J.* **2003**, in press.
[11] M. Hasegawa, *Chem. Rev.* **1983**, *83*, 507.
[12] L. Addadi, M. Lahav, *Pure Appl. Chem.* **1979**, *51*, 1269.
[13] G. Wegner, *Makromol. Chem.* **1971**, *145*, 85.
[14] K. Cheng, B. M. Foxman, *J. Am. Chem. Soc.* **1977**, *99*, 8102.
[15] M. J. Vela, V. Buchholz, V. Enkelmann, B. B. Snider, B. M. Foxman, *Chem. Commun.* **2000**, 2225.
[16] A. Matsumoto, T. Tanaka, T. Tsubouchi, K. Tashiro, S. Saragai, S. Nakamoto, *J. Am. Chem. Soc.* **2002**, *124*, 8891.
[17] T. Itoh, S. Nomura, T. Uno, M. Kubo, K. Sada, M. Miyata, *Angew. Chem.* **2002**, *114*, 4482; *Angew. Chem. Int. Ed.* **2002**, *41*, 4306.
[18] H. Kanazawa, Y. Ohashi, *Mol. Cryst. Liq. Cryst. Sci. Technol. Sect. A* **1996**, *277*, 45.
[19] H. Kanazawa, H. Uekusa, Y. Ohashi, *Acta Crystallogr. Sect. C* **1997**, *53*, 1154.

 © 2003 Wiley-VCH Verlag GmbH & Co. KGaA, Weinheim

[20] Y. Takenaka, Y. Ohashi, H. Kanazawa, *Acta Crystallogr. C* **1994**, *50*, 1950.
[21] L. Addadi, E. Gati, M. Lahav, L. Leiserowitz, *Isr. J. Chem.* **1977**, *15*, 116.
[22] M. Smrcina, S. Vyskocil, V. Hanus, M. Polasek, V. Langer, B. G. M. Chew, D. B. Zax, H. Verrier, K. Harper, T. A. Claxton, P. Kocovsky, *J. Am. Chem. Soc.* **1996**, *118*, 487.
[23] H. Kanazawa, T. Hayakawa, *Sci. Rep. Fukushima Univ.* **1999**, *63*, 27.
[24] M. Vaida, L. J. W. Shimon, Y. Weisinger-Lewin, F. Frolow, M. Lahav, L. Leiserowitz, R. McMullan, *Science* **1988**, *241*, 1475.
[25] M. Lahav, F. Laub, E. Gati, L. Leiserowitz, Z. Ludmer, *J. Am. Chem. Soc.* **1976**, *98*, 1620.
[26] W. H. Daly, D. Poché, *Tetrahedron Lett.* **1988**, *29*, 5859.

 © 2003 Wiley-VCH Verlag GmbH & Co. KGaA, Weinheim

Dynamic Trimetallic Clusters

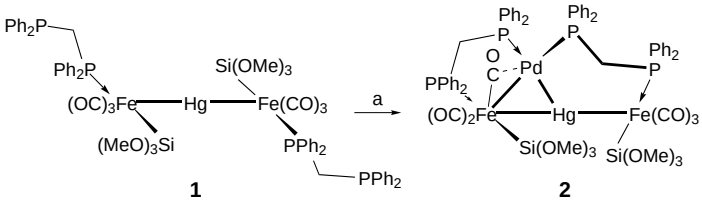
An Unusual Dynamic Fe-Hg-Pd Cluster with a Palladium(0) Fragment Stabilized by d^{10}–d^{10} Heterometallic Bonding**

Walter Schuh, Pierre Braunstein, Marc Bénard, Marie-Madeleine Rohmer, and Richard Welter*

Dedicated to Professor Achim Müller on the occasion of his 65th birthday

The nature of the bonding within metal clusters remains an area of continuing interest; electronic delocalization is often associated with the occurrence of isomeric metal cores and their possible interconversion.[1,2] There is a delicate energetic balance between metal–metal and metal–ligand interactions, and this is even more complex in heterometallic systems owing to the inherent diversity and polarity of the interactions. Unexpected features are therefore not uncommon, and we report here on a heterotetranuclear complex in which a coordinatively unsaturated 14-electron Pd^0 center is bonded to an Fe-Hg-Fe chain through helically arranged diphenylphosphanylmethane (dppm) ligands, along which it exhibits an oscillating motion. Extended Hückel calculations show that the two-electron three-centered Fe/Hg/Pd bonding, which involves interactions between the d^{10} centers Pd^0 and Hg^{II}, results partly from donation from the Fe–Hg σ bond to PdL_2, and mostly from back-bonding from the d^{10} Pd^0 center to the d^{10} Hg center and to a semibridging CO group.

The new compound $[Hg\{Fe[Si(OMe)_3](CO)_3(\mu\text{-dppm})\}_2Pd]$ (**2**) was obtained quantitatively (as calculated by ^{31}P NMR spectroscopy) by the reaction of the chain complex $[Hg\{Fe[Si(OMe)_3](CO)_3(dppm\text{-}P)\}_2]$ (**1**)[3] with a Pd^0 precursor (Scheme 1).[4]



Scheme 1. a) 1/2 $[Pd_2(dba)_3]\cdot CHCl_3$

A single-crystal structural determination[8] revealed that the tetranuclear $\{Fe_2HgPd\}$ core is nearly planar, with the Pd atom located at an asymmetric bridging position across one Hg–Fe bond and being much closer to the Hg center (269.15(8) pm) than to Fe1 (291.26(10) pm, Figure 1). The Pd–Hg bond length is shorter than in compounds with Pd–Hg d^8–d^{10} contacts (287.97(8)–309.8(1) pm).[10]

The P-Pd-P angle of 129.03(6)° and the Pd–P bond lengths of 232.2(2) and 233.2(2) pm are in the range found in trigonal-planar 16-valence-electron Pd^0 complexes.[11] Ignoring the Pd–Fe1 contact, the coordination geometry about each Fe atom may be described as distorted octahedral, with the

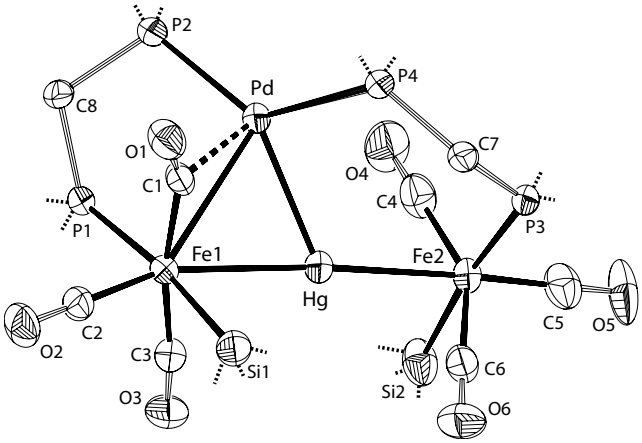


Figure 1. View of the molecular structure of **2**. Phenyl and MeO groups have been omitted for clarity. Ellipsoids enclose 50% of the electron density.

[*] Dr. P. Braunstein, Dr. W. Schuh
Laboratoire de Chimie de Coordination, UMR 7513 CNRS
Université Louis Pasteur
4, rue Blaise Pascal, 67070 Strasbourg Cédex (France)
Fax: (+33) 3-9024-1322
E-mail: braunst@chimie.u-strasbg.fr
Dr. M. Bénard, Dr. M.-M. Rohmer
Laboratoire de Chimie Quantique, UMR 7551 CNRS
Université Louis Pasteur
4, rue Blaise Pascal, 67070 Strasbourg Cédex (France)
Prof. R. Welter
Laboratoire DECMET, UMR 7513 CNRS
Université Louis Pasteur
4 rue Blaise Pascal, 67070 Strasbourg Cedex (France)

[**] This work was supported by the CNRS and the Ministère de la Recherche. We are grateful to the Fonds zur Förderung der wissenschaftlichen Forschung (FWF, Austria) for a postdoctoral grant to W.S. (Erwin-Schrödinger-Stipendium Proj. No. J2021) and to Prof. P. Peringer for access to WinDaisy facilities.

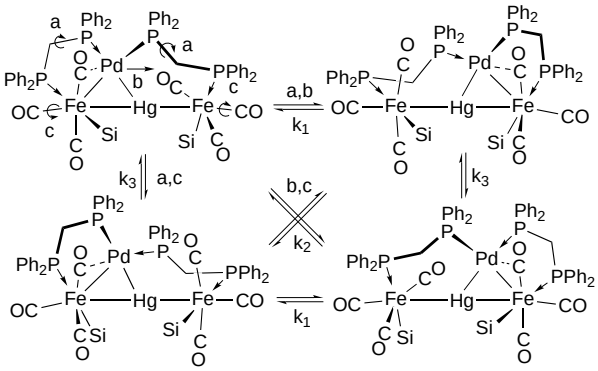
Supporting information for this article is available on the WWW under http://www.angewandte.org or from the author.

 DOI: 10.1002/anie.200250503 © 2003 Wiley-VCH Verlag GmbH & Co. KGaA, Weinheim

P and Si atoms *trans* to each other and the CO ligands in a *mer* arrangement. A semibridging carbonyl group, attached to Fe1 (Pd1–C11 213.8(6) pm) provides further stability, which was also established by theoretical calculations (see below) and accounts for a $\tilde{\nu}$(CO) vibration at 1821 cm^{-1} in the IR spectrum.[4] The dppm backbones and the Pd atom form a helical arrangement about the Fe-Hg-Fe axis (see Figure S-1 in the Supporting Information). As a result of the asymmetric position of the Pd center, the two dppm domains may be classified as heterotopic, in terms of helicate nomenclature.[12]

The Fe-Hg-Fe array is essentially linear (174.97(3)°) and the Hg–Fe1 bond, which is longer (266.80(9) pm) than the bond to Fe2 (262.12(9) pm), serves as a third "ligand" for the palladium center. The short separation between Pd and Hg suggests a bonding interaction between these two d^{10} metals, a feature related to the Cu^{I}–Hg^{II} interaction (268.9(2) pm) found in $[Hg\{Fe[Si(OMe)_3](CO)_3(\mu\text{-dppm})\}_2Cu]PF_6$ (**3**), which resulted in the 14-valence-electron Cu^{I} center possessing a Y-shaped coordination motif.[13] Here, in contrast, it is not a single atom (Hg) but a metal–metal single bond which allows the Pd^0 center to increase its formal 14-valence-electron count.

The bonding in complex **2** has been analyzed through extended Hückel calculations that were carried out on the model system $[Hg\{Fe[Si(OH)_3](CO)_3(PH_2CH_2PH_2)\}_2Pd]$ (**2′**), and its fragments $\{Pd(PH_3)_2\}$ (**5**) and $\{Hg[Fe\{Si(OH)_3\}(CO)_3(PH_3)]_2\}$ (**6**).[14,15] Palladium has a high-energy 5s/5p shell, whereas the 4d orbitals are fairly accessible at −12.0 eV. This means that Pd^0 will behave as a poor acceptor, especially when included in the PdL_2 fragment, but will tend to attach to the trimetallic complex through back-bonding. The donation interaction from the Fe1–Hg σ bond to PdL_2 does exist however, and can be evidenced from the population increase of the p_y orbital of Pd (from 0.05 to 0.14 e). The greater importance of the back-donation stems from the depopulation of the 4d shell of Pd, which is of the order of 0.48 e (Table S2 of the Supporting Information). Part of this population is transferred to Hg, whose p_y population increases from 0.06 to 0.18 e, and, to a lesser extent, to Fe1. However, the largest share of the density lost by the palladium center is donated to the π* orbital of the C1–O1 bond, which occupies a semibridging position between Pd and Fe1. Upon insertion of the Pd fragment, the C1–O1 bond becomes the most π-accepting carbonyl, with a net charge reversed from +0.09 to −0.11 e. The counterpart of this interaction gives rise to the LUMO+1 of complex **2′** (−9.0 eV) distributed over the π* orbital of C1–O1 (42%), Fe1 (10%), and Pd (23%). This is the only virtual MO with important weight on the d shell of palladium. The LUMO (−9.1 eV) is a combination of the iron π orbitals involved in back-donation towards the other carbonyl groups. The stabilization of complex **2** in the observed conformation should therefore be assigned to a multicentered anchoring of the PdL_2 fragment that involves donation interactions from the Fe1–Hg σ bond and back-donation to all atoms of fragment **6** that neighbor the Pd center, especially to the C1–O1 bond. This multicentric network of interactions is lost within the symmetric T-shaped structure, which is assumed to be an intermediate or a transition state in the dynamic exchange of **2** via pathway 1



Scheme 2. Dynamic exchange in **2** involving molecular motion via pathways 1–3: a) Flip of the dppm methylene groups; b) translational motion of Pd along the Fe-Hg-Fe axis; c) torsional motion about the Fe-Hg-Fe axis.

(Scheme 2). In this conformation, the electronic exchanges between the Pd fragment and the trimetallic moiety are only effective through the Hg atom, which becomes the only atom of **6** to remain in the vicinity of Pd. Both exchanges associated with donation to Pd and back-donation from Pd are strongly reduced in this conformation (0.03 e for donation to the sp shell of Pd, 0.23 e for back-donation from the d shell of Pd; Table S2), which explains that this structure does not correspond to an energy minimum, in contrast to the case of the copper compound **3**.

In solution, the kinetic lability of the bonding interactions between Pd and both the Fe–Hg bond and the semibridging carbonyl ligand in **2** is revealed by variable-temperature ^{1}H NMR spectroscopy (see Figure 2). In contrast to the low symmetry found in the crystal structure, there is only one resonance in the ^{1}H NMR spectrum (500 MHz, 310 K, CD_2Cl_2) for the $Si(OMe)_3$ and the dppm methylene protons, respectively. At 164 K however, four resonances for the CH_2 groups in dppm and two resonances for the methoxysilyl groups are observed, in accordance with the solid-state structure. In the temperature range 164–310 K, two distinct mutual exchange processes are observed, with activation

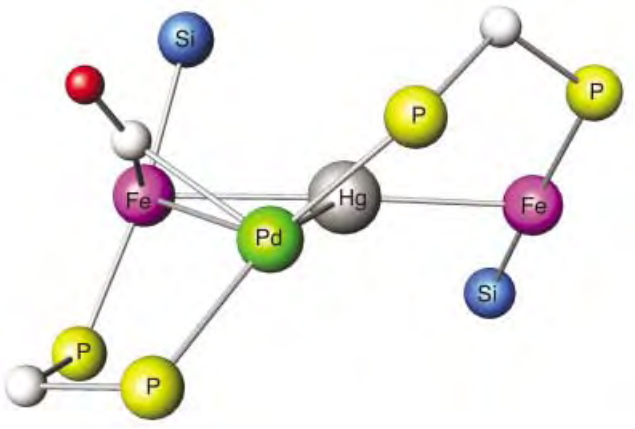


Figure 2. View of the core structure of **2** showing the helical arrangement of the diphosphane ligands.

 © 2003 Wiley-VCH Verlag GmbH & Co. KGaA, Weinheim

parameters $\Delta G^{\neq}_{182K} = 38 \pm 3\ kJ\,mol^{-1}$, $\Delta H^{\neq} = 43 \pm 2\ kJ\,mol^{-1}$ and $\Delta S^{\neq} = 27 \pm 9\ J\,K^{-1}\,mol^{-1}$, and $\Delta G^{\neq}_{270K} = 55 \pm 3\ kJ\,mol^{-1}$, $\Delta H^{\neq} = 45 \pm 2\ kJ\,mol^{-1}$ and $\Delta S^{\neq} = -37 \pm 6\ J\,K^{-1}\,mol^{-1}$, respectively, obtained by computational line-shape analysis of the spectra.[4,6,7] Since the exchange rates are retained when approximately 10% of **1** is added to a solution of **2**, the dynamic behavior may therefore be considered to proceed through an intramolecular mechanism.[16] The exchange pathways illustrated in Scheme 2 are discussed in the Supporting Information.

A comparison of the activation entropies reveals that the two dynamic processes must involve essentially different motions, since $\Delta S^{\neq}$ is clearly positive for exchange 1 and negative for exchange 2. The value of $\Delta H^{\neq}$ for exchange 1 is very similar to the activation enthalpy of the cyclohexane chair-conformation inversion, which also displays a positive $\Delta S^{\neq}$;[17] this strengthens the assignment of the low-energy dynamic process to pathway 1. Consequently, the torsional motion appears related to the negative activation entropy found for the high-energy dynamic process. This may be understood by considering that such a motion is a high-order concerted process. It may be hindered by increased random thermal motion or by molecular vibrations.

In conclusion, we have prepared an unprecedented heteropolymetallic complex by "capture" of a Pd^0 center by the trimetallodiphosphane **1**. Its metal–metal bonding has been analyzed in detail and shown to involve, for the first time to our knowledge, direct interactions between the d^{10} centers Pd^0 and Hg^{II}. The complex fluxional behavior of compound **2** has been shown to consist of an apparent "sliding" of the palladium along the trimetallic chain.[16] Further studies are in progress, and we can already indicate that Pt does not form a direct analogue of **2**, which emphasizes the delicate energetic balance that characterizes such complex molecules.

Received: November 7, 2002 [Z50503]

Keywords: cluster compounds · coordination modes · heterometallic complexes · metal–metal interactions · molecular dynamics

[1] a) "Reversible Skeletal Rearrangements in Transition Metal Clusters": P. J. Dyson in *Metal Clusters in Chemistry, Vol. 2* (Eds.: P. Braunstein, L. A. Oro, P. R. Raithby), Wiley-VCH, Weinheim, **1999**, p. 1028; b) "Skeletal Isomerism in Transition Metal Clusters": O. Rossell, M. Seco, G. Segalés in *Metal Clusters in Chemistry, Vol. 2* (Eds.: P. Braunstein, L. A. Oro, P. R. Raithby), Wiley-VCH, Weinheim, **1999**, p. 1053.

[2] a) R. Bender, P. Braunstein, A. Dedieu, P. D. Ellis, B. Huggins, P. Harvey, E. Sappa, A. Tiripicchio, *Inorg. Chem.* **1996**, *35*, 1223; b) P. Braunstein, C. de Méric de Bellefon, S.-E. Bouaoud, D. Grandjean, J.-F. Halet, J.-Y. Saillard, *J. Am. Chem. Soc.* **1991**, *113*, 5282.

[3] P. Braunstein, M. Knorr, A. Tiripicchio, M. Tiripicchio Camellini, *Inorg. Chem.* **1992**, *31*, 3685.

[4] Details for the synthesis are given in the Supporting Information. Selected spectroscopic data for **2**: IR (CH_2Cl_2): $\tilde{\nu} = 1994$ (s), 1978 (vs), 1930 (vs, br), 1821 cm^{-1} (m). $^1H\{^{31}P\}$ NMR (CD_2Cl_2, 164 K, 500 MHz, TMS): $\delta = 8.8$–6.5 (m, br, 40 H, Ph), 3.79 (br, 1 H, CH_2), 3.70 (s, 9 H, $(MeO)_3Si$), 3.61 (s, 9 H, $(MeO)_3Si$), 3.56 (br, 2 H, CH_2), 3.10 ppm (br, 1 H, CH_2). $^{31}P\{^1H\}$ NMR (CD_2Cl_2, 166 K, 202.5 MHz, 85% H_3PO_4): $\delta = 9.4$ ($^2J(P^2,P^4) = 80$ Hz, $^{2+4}J(P^3,P^4) = 55$ Hz, $^{3+4}J(P^1,P^4) = -18$ Hz, P^4), 9.6 ($^4J(P^2,P^3) = 11$ Hz, $^{2+3+4}J(P^1,P^2) = 197$ Hz, P^2), 45.9 ($^4J(P^1,P^3) = 0$ Hz, P^3), 59.3 ppm (P^1). For the numbering of the phosphorus atoms, see Figure 1. The assignment of the phosphorus resonances is based on the very large P–P coupling constant of 197 Hz between P^2 and P^3, which indicates a bonding interaction between the dppm-bridged metals Fe and Pd.[5] ^{199}Hg NMR (CD_2Cl_2, 298 K, 71.6 MHz, $HgMe_2$): $\delta = -134$ (s, br). Simulation of second-order spectra were performed with WinDaisy,[6] and computational line-shape analysis with SpinWorks.[7] More spectroscopic data, technical details, and Eyring plots are provided in the Supporting Information.

[5] a) P. Braunstein, C. de Méric de Bellefon, M. Ries, J. Fischer, *Organometallics* **1988**, *7*, 332; b) P. Braunstein, M. Knorr, A. Tiripicchio, M. Tiripicchio Camellini, *Angew. Chem.* **1989**, *101*, 1414; *Angew. Chem. Int. Ed. Engl.* **1989**, *28*, 1361.

[6] a) U. Weber, R. Spiske, H.-W. Höffken, G. Hägele, H. Thiele, Manual and Program system, Bruker Manual, **1993**; b) G. Hägele, P. Reinemer, M. Grzonka, Workshop Computer in der Chemie, Software-Entwicklung in der Chemie, Vol. 2, **1988**, p. 241.

[7] K. Marat, SpinWorks, University of Manitoba, **2002**.

[8] Crystal data for **2**·1/2 Et_2O·1/2 H_2O: Crystals suitable for X-ray diffraction were obtained upon slow evaporation of a solution of **2** in Et_2O that was in contact with air; monoclinic, space group *C2/c*, $a = 41.564(5)$, $b = 15.716(5)$, $c = 22.117(5)$ Å, $\beta = 95.715(5)°$, $V = 14375(6)$ Å^3, $Z = 8$, $T = 183(2)$ K, $Mo_{K\alpha}$ ($\lambda = 0.70930$ Å), 24981 data collected, 11149 data with $I > 2\sigma(I)$, θ min/max $= 0.998/32.032°$. The structure was solved by direct methods (SHELXS-97)[9a] and refined by full-matrix least-squares methods on F^2 (SHELXL-97).[9b] $R = 0.0583$, $wR2$(all data) $= 0.1446$, GOF $= 0.894$. CCDC-188689 contains the supplementary crystallographic data for this paper. These data can be obtained free of charge via www.ccdc.cam.ac.uk/conts/retrieving.html (or from the Cambridge Crystallographic Data Centre, 12, Union Road, Cambridge CB2 1EZ, UK; fax: (+44) 1223-336-033; or deposit@ccdc.cam.ac.uk).

[9] a) G. M. Sheldrick, SHELXS-97, Program for crystal structure solution, University of Göttingen, Göttingen (Germany), **1997**; b) G. M. Sheldrick, SHELXL-97, Program for refinement of crystal structures, University of Göttingen, Göttingen (Germany), **1997**.

[10] a) M. A. Bennett, M. Contel, D. C. R. Hockless, L. L. Welling, A. C. Willis, *Inorg. Chem.* **2002**, *41*, 844, and references therein; b) L. R. Falvello, J. Forniés, A. Martin, R. Navarro, V. Sicilia, P. Villarroya, *Inorg. Chem.* **1997**, *36*, 6166.

[11] R. U. Kirss, R. Eisenberg, *Inorg. Chem.* **1989**, *28*, 3372.

[12] C. Piguet, G. Bernardinelli, G. Hopfgartner, *Chem. Rev.* **1997**, *97*, 2005.

[13] M. Bénard, U. Bodensieck, P. Braunstein, M. Knorr, M. Strampfer, C. Strohmann, *Angew. Chem.* **1997**, *109*, 2890; *Angew. Chem. Int. Ed. Engl.* **1997**, *36*, 2758.

[14] a) R. Hoffmann, W. N. Lipscomb, *J. Chem. Phys.* **1962**, *36*, 2179; b) R. Hoffmann, W. N. Lipscomb, *J. Chem. Phys.* **1962**, *37*, 2872; c) R. Hoffmann, *J. Chem. Phys.* **1963**, *39*, 1397. The parameters used and the Mulliken orbital populations obtained for the metal atoms are available in the Supporting Information (Tables S1 and S2).

[15] The axis *x* is assumed to be collinear to Fe-Hg-Fe and *xy* is the average plane of the four metals. The chelating diphosphanes have been replaced by PH_3 in order to avoid unwanted interactions. In the trimetallic fragment **6**, neutral mercury (in the $d^{10}s^2$ configuration) acts as a donor by means of its deep 6s orbital (−13.7 eV) and as an acceptor through its 6p shell (−8.47 eV). The donation and the back-donation are operative

 © 2003 Wiley-VCH Verlag GmbH & Co. KGaA, Weinheim

respectively through the in-phase and the out-of-phase combinations of the Fe σ orbitals resulting from the approximate square-pyramidal conformation of the two {Fe[Si(OH)$_3$](CO)$_3$(PH$_3$)} moieties. The out-of-phase combination is stabilized and becomes the HOMO of fragment **6**, whereas the in-phase combination contributes to a low-energy MO with major weight on the mercury 6s orbital. The orbital populations of Hg in **6** are 1.29 e for 6s and 0.44 e, 0.06 e, and 0.07 e for the p_x, p_y, and p_z orbitals, respectively (Table S2 in the Supporting Information).

[16] We cannot state whether the intramolecular Pd motion corresponds to a contact sliding along the Fe-Hg-Fe chain or results from successive Pd detaching and reattaching to the Fe-Hg bond. At the moment, we have no way of separating the two enantiomers resulting from the presence of both *P* and *M* helical arrangements of the phosphanes.

[17] F. A. L. Anet, A. J. R. Bourn, *J. Am. Chem. Soc.* **1967**, *89*, 760.

 © 2003 Wiley-VCH Verlag GmbH & Co. KGaA, Weinheim

Host-Guest Binding Interactions

Molecular Encapsulation by Cucurbit[7]uril of the Apical 4,4′-Bipyridinium Residue in Newkome-Type Dendrimers**

*Winston Ong and Angel E. Kaifer**

Molecular recognition phenomena in biological systems often involve host or guest residues which are attached to the surface of organized assemblies (membranes) or incorporated into large macromolecular structures (proteins or nucleic acids). The high degree of structural complexity and molecular size that can be attained with dendritic structures can be utilized to model the complexity of biological systems. Therefore, the investigation of dendrimers as partners in host–guest binding interactions may have considerable biological relevance. Dendrimers have been used extensively as hosts, either by taking advantage of their inner cavities[1] or by designing and creating binding sites in their interior,[2] but their utilization as guests has been more limited.[3] We have previously reported the binding interactions of dendrimers containing organometallic guest units with cyclodextrin hosts,[4] as well as those of dendrimers containing a single dansyl residue with cyclodextrin and polyclonal anti-dansyl antibodies.[5] Here, we focus our attention on a new host–guest interaction recently reported both by Kim and coworkers[6] and our own research group,[7] which focuses on the strong complexation of 4,4′-bipyridinium (viologen) derivatives by cucurbit[7]uril[8] (**CB7**) in aqueous solution. The dendrimers selected as guests (**1-V^{2+}**, **2-V^{2+}**, and **3-V^{2+}**) contain a single viologen residue covalently attached to the focal points of carboxylate-terminated, Newkome-type dendrons (Scheme 1).

Dendrimers **1-V^{2+}**, **2-V^{2+}**, and **3-V^{2+}** were prepared by hydrolysis of their *tert*-butyl ester precursors with formic acid,[9] followed by ion exchange to their bromide salts. The resulting dendrimers were fully characterized by ^{1}H and ^{13}C, COSY, and HMQC NMR spectroscopies, FAB or MALDI-TOF mass spectrometry, UV/Vis spectroscopy, and electrochemical techniques. Host **CB7** was synthesized according to literature reports.[8] The water-soluble, viologen dendrimers **1-V^{2+}**, **2-V^{2+}**, and **3-V^{2+}** have 3, 9, and 27 surface carboxylic acid groups, respectively. As a consequence of their polyprotic acid character, the pH value of the solution is expected to influence the overall charge and the conformation of these dendrimers. Therefore, we decided to investigate their binding interactions with host **CB7** at two solution pH values, namely, pH 7 and 3, which were selected to bracket the average pK_a value of the carboxylic acid groups. Methylviologen (**MV^{2+}**) was used as a model compound to provide baseline values for the complexation of the viologen residues of **CB7** unhindered by dendritic components.

^{1}H NMR spectroscopic data readily confirm that the viologen dendrimers are complexed by **CB7**. For example, Figure 1 shows the spectra (in 0.1 M Na_2SO_4/D_2O) of **3-V^{2+}** in the absence and in the presence of one equivalent of **CB7**. Clearly, the host has a pronounced effect, primarily on the resonances of the bipyridinium protons. In fact, the bipyridinium β/β′ protons shift to higher fields and undergo considerable broadening, which is in agreement with the results that we had previously reported for the complexation of simple viologens by **CB7**.[7] Similar results were obtained with the other two viologen dendrimers, thus indicating that inclusion complexation of the viologen residue by the **CB7** host takes place regardless of the growth of the dendrimer (1st to 3rd generation).

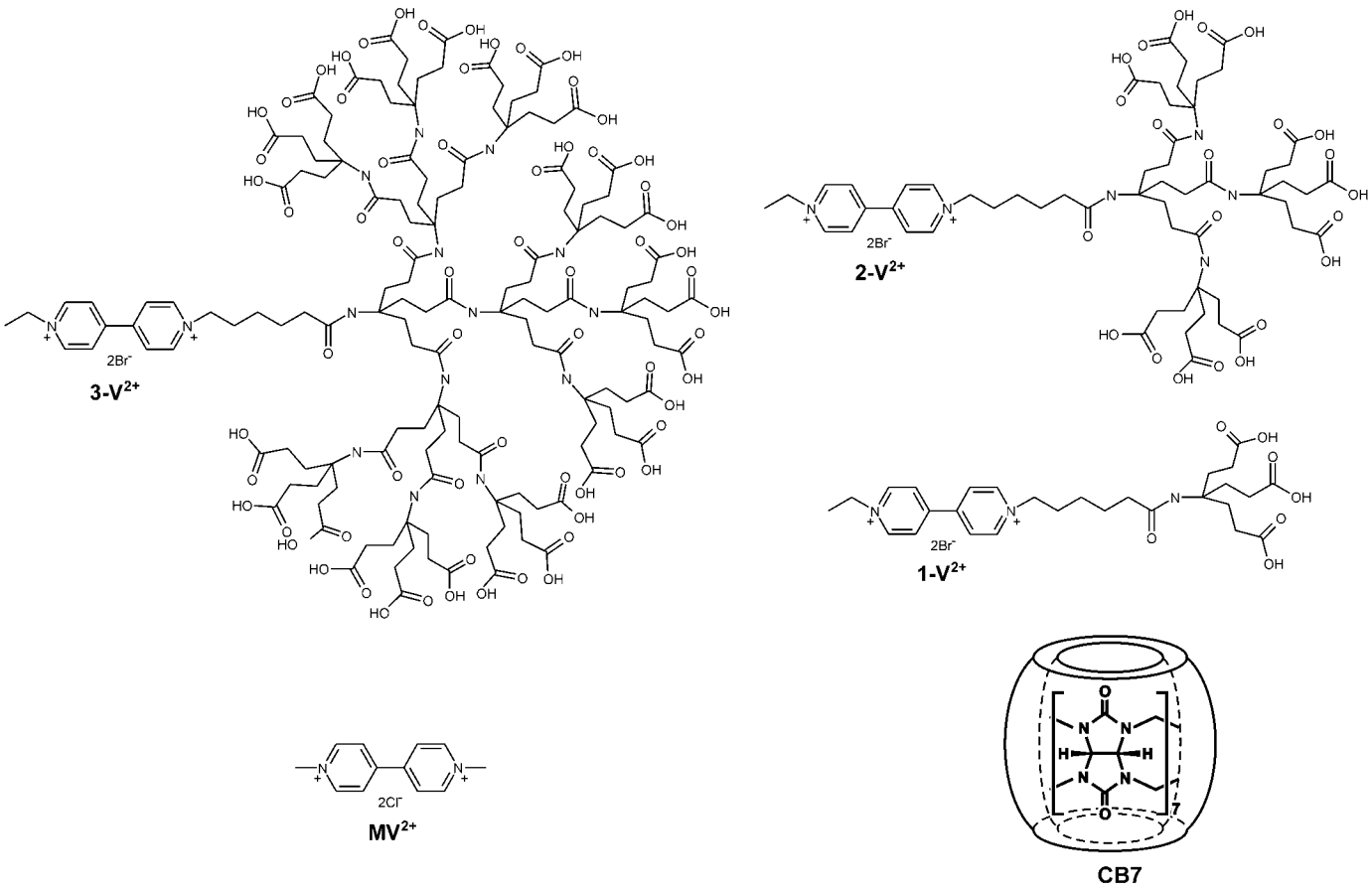
MALDI-TOF mass spectrometry also supplied strong evidence in support of complex formation between the viologen dendrimers and **CB7**. Figure 2 shows the spectra obtained from 1:1 mixtures of **CB7** and each of the viologen dendrimers using 2,5-dihydroxybenzoic acid matrices. In the case of the first generation dendrimer, the spectrum is dominated by a single signal at m/z 1691.3 (Figure 2A), which corresponds to the monocationic complex **CB7·1-V$^{+\cdot}$**. In the case of the second generation dendrimer, the spectrum contains two major signals (Figure 2B). The most intense peak again corresponds to the one-electron-reduced complex **CB7·2-V$^{+\cdot}$**, but the free dendrimer **2-V$^{+\cdot}$** is also clearly observed at m/z 1216.6. The spectrum for the third generation viologen dendrimer shows increased complexity, but all the major signals can be ascribed (Figure 2C). The most prominent signal observed still corresponds to the one-electron-reduced complex **CB7·3-V$^{+\cdot}$**. The clear spectroscopic detection of the radical cation complexes (**CB7·*n*-V$^{+\cdot}$**, $n = 1$, 2, and 3) reveals two things: 1) One-electron reduction of the viologen residues takes place under the mass spectrometric conditions, and 2) the resulting viologen cation radicals are

[*] Prof. A. E. Kaifer, W. Ong
Center for Supramolecular Science and Department of Chemistry
University of Miami, Coral Gables, FL 33124-0431 (USA)
Fax: (+1) 305-444-1777
E-mail: akaifer@miami.edu

[**] This work was supported by the NSF (to A.E.K.; CHE-9982014 and CHE-0240295).

Supporting information for this article is available on the WWW under http://www.angewandte.org or from the author.

 © 2003 Wiley-VCH Verlag GmbH & Co. KGaA, Weinheim DOI: 10.1002/anie.200250214



Scheme 1. Structures of the host and guest compounds.

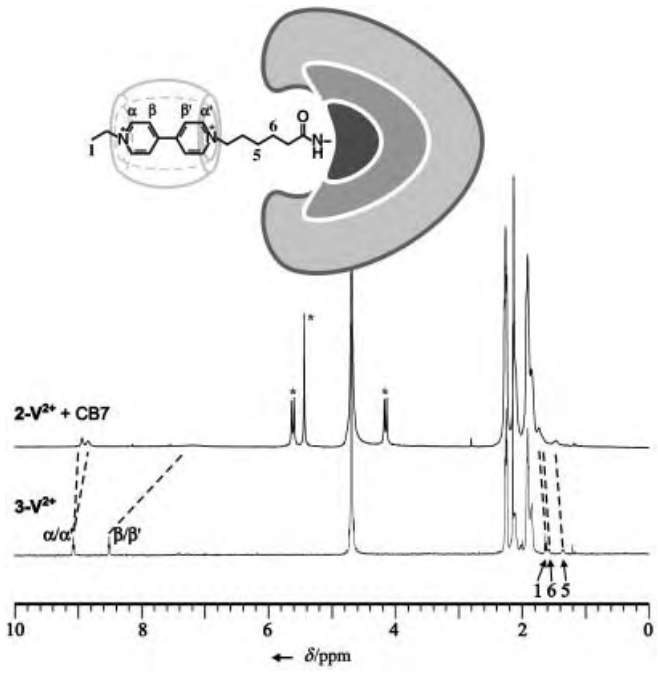


Figure 1. ^{1}H NMR spectra (500 MHz, 0.1 M Na_2SO_4/D_2O) of dendrimer **3-V^{2+}** in the absence (bottom) and in the presence (top) of one equivalemt of host **CB7**. Host resonances are labeled with an asterisk.

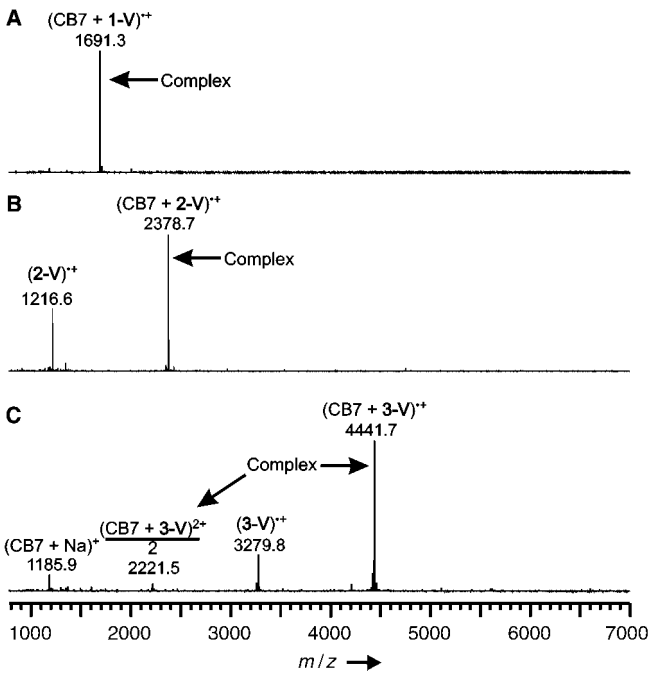


Figure 2. MALDI-TOF mass spectra obtained with 1:1 mixtures of each of the viologen dendrimers and host **CB7** in 2,5-dihydroxybenzoic acid matrices.

 © 2003 Wiley-VCH Verlag GmbH & Co. KGaA, Weinheim

also strongly bound by the **CB7** host. These findings have precedents in our previously reported data with simple viologen derivatives.[7]

The complexation equilibrium between any viologen derivative and the **CB7** host can be conveniently monitored by electronic absorption spectroscopy, since the molar absorptivity coefficient (ε) of the characteristic UV band of viologens (λ_{max} ca. 260 nm) is depressed upon formation of the **CB7** inclusion complex.[7] Figure 3 shows, for example, the

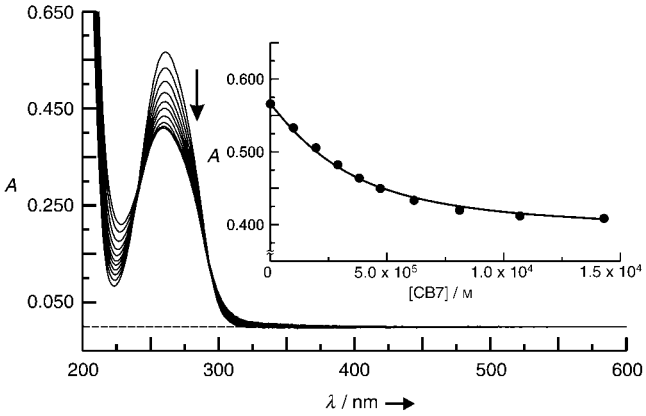


Figure 3. Electronic absorption spectra of aqueous solutions (0.03 M Tris buffer, pH 7.3) containing a fixed concentration (27 μM) of dendrimer **2-V^{2+}** and variable concentrations of **CB7**. The inset shows the experimental absorbances at 260 nm (filled circles) and the best fit line obtained with the parameters listed in Table 1.

UV spectra obtained with aqueous solutions (0.03 M tris(hydroxymethyl)aminomethane (Tris) buffer, pH 7.3) containing a fixed concentration of **2-V^{2+}** (27 μM) and variable concentrations of **CB7**. The absorption band of the viologen exhibits progressively lower absorbance as the concentration of host is increased. This observation reflects the increasing concentration of the **CB7·2-V^{2+}** complex and the decreasing concentration of free **2-V^{2+}** in the solution. The fitting of these data, using regression analysis, to a 1:1 binding isotherm model affords the corresponding binding constant (K) and the molar absorptivity coefficient of the complex (ε_c). The values obtained at the two surveyed solution pH values with methylviologen and the three viologen dendrimers are given in Table 1.

Table 1: Equilibrium association constants (K), free energies of complexation (ΔG^0), and molar absorptivity coefficients (ε_c) for the inclusion complexes formed between the viologen guests and host **CB7** in aqueous solutions at 25 °C.

	Medium					
	0.2 M formic acid buffer, pH 3.2			0.03 M Tris buffer, pH 7.3		
Guest	K [L mol^{-1}][a]	ΔG^0 [kcal mol^{-1}]	ε_c [M^{-1} cm^{-1}]	K [L mol^{-1}][a]	ΔG^0 [kcal mol^{-1}]	ε_c [M^{-1} cm^{-1}]
MV^{2+}	2.9×10^5	−7.45	11500	2.2×10^5	−7.28	11500
1-V^{2+}	5.9×10^5	−7.87	12900	5.5×10^4	−6.46	12900
2-V^{2+}	6.2×10^5	−7.90	14100	5.7×10^4	−6.49	14200
3-V^{2+}	3.4×10^5	−7.54	13600	1.3×10^4	−5.61	19200

[a] Estimated error margin: ±12%.

The first important fact that emerges from the data in Table 1 is that the binding affinity between the underivatized **MV^{2+}** guest and **CB7** depends on the composition of the medium. The 0.2 M formic acid buffer solution (pH 3.2) used in our experiments contains approximately 0.04 M Na^+ ions (introduced as NaOH in the preparation of the buffer). The binding constant measured in this medium ($K = 2.9\times10^5$ L mol^{-1}) is clearly larger than the value previously determined by us in unbuffered 0.2 M NaCl (1.0×10^5 L mol^{-1}).[7] Since neither the host or the guest are pH-sensitive and sodium ions are known to interact strongly with cucurbituril hosts,[10] we conclude that increasing concentrations of sodium ions depress the apparent K value for the binding of viologens by **CB7**. The binding constant measured in Tris buffer solution at pH 7.3 (2.2×10^5 L mol^{-1}) is very close to the value reported by Kim and co-workers in a similar medium (2.0×10^5 L mol^{-1} in 0.05 M Tris buffer, pH 7).[6] Since this medium does not contain any sodium ions, the measured K value indicates that protonated Tris also interacts with **CB7**.

The data in Table 1 reveal that dendrimer growth has a relatively small effect on the stability of the complexes formed between **CB7** and guests **1-V^{2+}, 2-V^{2+}**, and **3-V^{2+}**. In buffered formic acid solution, the K values are higher for the first and second generation dendrimers, while the binding constant for the third generation is closer to that measured with **MV^{2+}**. A reasonable explanation for these results takes two factors into account. First, one side of the viologen unit in the viologen dendrimers is connected to a large organic structure, which may partially hinder solvation by water molecules. This arrangement will enhance the ion–dipole interactions between the carbonyl portals of the host and the quaternary ammonium groups of the guest and will tend to increase the stability of the complex. Second, dendrimer growth may create some steric problems for the approach of the host to the viologen residue. This factor does not appear to be extremely important in these dendrimers, but it is probably responsible for the decrease in the K value from **2-V^{2+}** to **3-V^{2+}**. Finally, another trend clearly visible in Table 1 is that the binding constants between the viologen dendrimers and **CB7** are at least one order of magnitude lower in neutral solutions (pH 7.3) than in acidic solutions (pH 3.2). This pH effect is of a larger magnitude that can be attributed to medium effects, as evidenced by the much closer K values observed for the **CB7·MV^{2+}** complex. We rationalize the stronger pH effect detected with the **CB7·*n*-V^{2+}** ($n = 1$, 2, and 3) complexes as a result of the ionization of the peripheral carboxylic acid groups. The presence of the negatively charged carboxylates probably leads to some degree of intramolecular ion pairing with the positively charged viologen residue, which hinders the **CB7**–viologen interaction. This effect becomes stronger as the dendrimer generation (and the number of carboxylates) increases, which explains the lower K values observed and their relative variation from **1-V^{2+}** to **3-V^{2+}**.

We can define the thermodynamic free energy parameter $\Delta\Delta G^0$ as the difference

 © 2003 Wiley-VCH Verlag GmbH & Co. KGaA, Weinheim

$\Delta G^0_{3rd} - \Delta G^0_{st}$ to describe quantitatively the loss in complex stabilization from the first to the third generation of the dendrimer. From the values in Table 1, we obtain $\Delta\Delta G^0$ values of 0.33 and 0.85 kcal mol^{-1} at solution pH values of 3.2 and 7.3, respectively, for the host–guest system investigated in this work. These $\Delta\Delta G^0$ values are comparable to the value (0.61 kcal mol^{-1}) that can be obtained from our reported binding data on the host–guest system composed by dansyl-containing dendrimers and a polyclonal anti-dansyl antibody.[5] On the other hand, the values reported here are significantly smaller than the $\Delta\Delta G^0$ values calculated from our reported binding data on ferrocene-labeled dendrimers and β-cyclodextrin[4c] (1.74 kcal mol^{-1}), as well as from dansyl-labeled dendrimers and β-cyclodextrin[5] (2.91 kcal mol^{-1}). An important difference between the viologen dendrimer guests described in this work and the related ferrocenyl[4c] and dansyl[5] dendrimer guests reported before is the length of the tether connecting the guest residue to the Newkome-type dendron. While the ferrocenyl and dansyl residues were directly connected to the corresponding dendrons through a simple amide linker, the viologen residues in dendrimers **1-V^{2+}** to **3-V^{2+}** are separated by a 5-methylene chain from the amide group at the focal point of the dendrimer. However, in regard to the formation of inclusion complexes by guests at the focal point of Newkome-type dendrons, our $\Delta\Delta G^0$ data suggest that stable complexes ($K > 10^4$ L mol^{-1}) are less affected by dendrimer growth than weaker complexes ($K < 10^3$ L mol^{-1}). It is important to note that the literature contains reports on other dendrimer systems that exhibit different trends, such as large $\Delta\Delta G^0$ values for $K > 10^4$ L mol^{-1}[11] and small $\Delta\Delta G^0$ values for $K < 10^4$ L mol^{-1}.[12] Clearly, more thermodynamic binding parameters on host–guest systems involving dendrimers are necessary to fully rationalize the results presented here. Overall, this work underscores the complexity of host–guest binding interactions involving dendrimers and may suggest that the nature of the intermolecular forces between the host and the guest may be an important factor to determine the magnitude of dendrimer growth effects on the binding affinity.

Experimental Section

Dendrimers **1-V^{2+}, 2-V^{2+}**, and **3-V^{2+}** were prepared by hydrolysis of their *tert*-butyl ester precursors[9] (see Supporting Information for synthetic details and full spectroscopic characterization data). The host **CB7** was synthesized as reported by the research groups of Kim and Day.[8] ^{1}H NMR spectra were obtained on Bruker Avance 400 and 500 MHz NMR spectrometers. MALDI-TOF mass spectra were recorded in a Bruker Biflex IV system using either 2,5-dihydroxybenzoic acid or α-cyano-4-hydroxy

cinnamic acid as the matrix compounds. Electronic absorption spectra were recorded in a Shimadzu UV-2101PC spectrophotometer. The determination of the binding constants with the **CB7** host was done using the method previously reported for **MV^{2+}**.[7]

Received: September 23, 2002
Revised: November 19, 2002 [Z50214]

Keywords: cucurbituril · dendrimers · host–guest systems · self-assembly · thermodynamics

[1] a) A. Naylor, W. Goddard III, G. Kiefer, D. A. Tomalia, *J. Am. Chem. Soc.* **1989**, *111*, 2339 – 2441; b) J. F. G. A. Jansen, E. M. M. de Brabander-van den Berg, E. W. Meijer, *Science* **1994**, *266*, 1226 – 1229; c) M. Zhao, L. Sun, V. Chechik, L. Yeung, R. Crooks, *Acc. Chem. Res.* **2001**, *34*, 181 – 190.

[2] a) P. J. Dandliker, F. Diederich, M. Gross, C. B. Knobler, A. Loauti, E. M. Sanford, *Angew. Chem.* **1994**, *106*, 1821 – 1824; *Angew. Chem. Int. Ed. Engl.* **1994**, *33*, 1739 – 1742; b) S. Mattei, P. Seiler, F. Diederich, V. Gramlich, *Helv. Chim. Acta* **1995**, *78*, 1904 – 1912; c) G. R. Newkome, B. D. Woosley, E. He, C. N. Moorefield, R. Guther, G. R. Baker, G. H. Escamilla, J. Merrill, H. Luftmann, *Chem. Commun.* **1996**, 2737 – 2738; d) M. J. Hannon, P. C. Mayers, P. C. Taylor, *Angew. Chem.* **2001**, *113*, 1115 – 1118; *Angew Chem. Int. Ed.* **2001**, *40*, 1081 – 1084; e) S. Zimmerman, M. Wendland, N. Rakow, I. Zharov, K. Suslick, *Nature* **2002**, *418*, 399 – 403; f) G. M. Dykes, D. K. Smith, G. J. Seeley, *Angew. Chem.* **2002**, *114*, 3388 – 3391; *Angew. Chem. Int. Ed.* **2002**, *41*, 3254 – 3257.

[3] a) J. J. Michels, M. W. P. L. Baars, E. W. Meijer, J. Huskens, D. N. Reinhoudt, *J. Chem. Soc. Perkin Trans. 2* **2000**, 1914 – 1918; b) J. W. Lee, Y. H. Ko, S.-H. Park, K. Yamaguchi, K. Kim, *Angew. Chem.* **2001**, *113*, 768 – 771; *Angew. Chem. Int. Ed.* **2001**, *40*, 746 – 749; c) P. R. Ashton, V. Balzani, M. Clemente-León, B. Colonna, A. Credi, N. Jayaraman, F. M. Raymo, J. F. Stoddart, M. Venturi, *Chem. Eur. J.* **2002**, *8*, 673 – 684.

[4] a) R. Castro, I. Cuadrado, B. Alonso, C. M. Casado, M. Morán, A. E. Kaifer, *J. Am. Chem. Soc.* **1997**, *119*, 5750 – 5761; b) B. González, C. M. Casado, B. Alonso, I. Cuadrado, M. Morán, Y. Wang, A. E. Kaifer, *Chem. Commun.* **1998**, 2569 – 2570; c) C. M. Cardona, T. D. McCarley, A. E. Kaifer, *J. Org. Chem.* **2000**, *65*, 1857 – 1864.

[5] C. M. Cardona, J. Alvarez, A. E. Kaifer, T. D. McCarley, S. Pandey, G. A. Baker, N. J. Bonzagni, F. V. Bright, *J. Am. Chem. Soc.* **2000**, *122*, 6139 – 6144.

[6] H.-J. Kim, W. S. Jeon, Y. H. Ko, K. Kim, *Proc. Natl. Acad. Sci. USA* **2002**, *99*, 5007 – 5011.

[7] W. Ong, M. Gómez-Kaifer, A. E. Kaifer, *Org. Lett.* **2002**, *4*, 1791 – 1794.

[8] a) J. Kim, I.-S. Jung, S. Y. Kim, E. Lee, J. L. Kang, S. Sakamoto, K. Yamaguchi, K. Kim, *J. Am. Chem. Soc.* **2000**, *122*, 540 – 541; b) A. Day, A. P. Arnold, R. J. Blanch, B. Snushall, *J. Org. Chem.* **2001**, *66*, 8094 – 8100.

[9] W. Ong, A. E. Kaifer, *J. Am. Chem. Soc.* **2002**, *124*, 9358 – 9359.

[10] Y-M. Jeon, J. Kim, D. Whang, K. Kim, *J. Am. Chem. Soc.* **1996**, *118*, 9790 – 9791.

[11] Y. Tomoyose, D.-L. Jiang, R.-H. Jin, T. Aida, T. Yamashita, K. Horie, *Macromolecules* **1996**, *29*, 5236 – 5238.

[12] S. C. Zimmerman, Y. Wang, P. Bharathi, J. S. Moore, *J. Am. Chem. Soc.* **1998**, *120*, 2172 – 2173.

 © 2003 Wiley-VCH Verlag GmbH & Co. KGaA, Weinheim

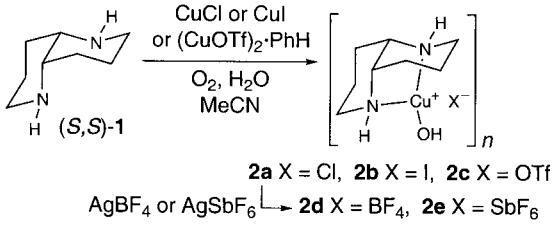
Cu-Catalyzed Couplings

Novel Pathways for the Formation of Chiral Binaphthyl Polymers: Oxidative Asymmetric Phenolic Coupling Alone and in Tandem with the Glaser–Hay Coupling**

*Xu Xie, Puay-Wah Phuan, and Marisa C. Kozlowski**

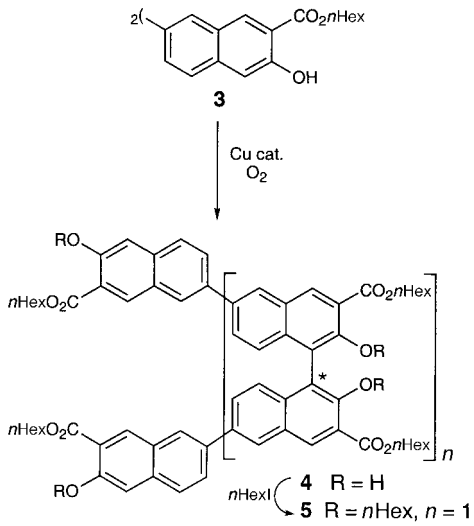
Conjugated polymers have exhibited a number of notable properties including high doped conductivity, electroluminescence, and optical nonlinearity.[1] Optically active versions are potentially important; however, few have been studied. Because of the important properties[2] that chiral polybinaphthyls[3] exhibit as well as their successful applications in asymmetric catalysis,[4] the synthesis of binaphthyl polymers with different functionality and the development of new methods for more efficient polymerization are important.

In this communication we describe the synthesis of new ester-functionalized chiral 1,1′-binaphthol polymers by oxidative coupling of achiral components with 1,5-diaza-*cis*-decalin catalysts **2** (Scheme 1).[5] Prior reports of the preparation of chiral binaphthyl polymers begin with chiral 1,1′-binaphthyl monomers. To our knowledge, the enantioselective synthesis of chiral polybinaphthyls has not been reported.[6]



Scheme 1. Preparation of chiral catalysts **2**. Tf = trifluoromethanesulfonyl.

Oxidative coupling of polymer precursor **3** with the achiral catalyst CuCl(OH)·TMEDA (**6**, TMEDA = tetramethylethylenediamine) yielded two fractions, **4a** and **4b**, with different molecular weight distributions (Scheme 2, Table 1, entry 1). The number-average molecular weights M_n from the integrations of the NMR signals for the internal and terminal units correlate with the data from gel-permeation chromatography (GPC).[7] When **3** was polymerized with the chiral CuI catalyst **2b** (Scheme 1) which we reported previously,[5] the reactivity was poor; a low molecular weight material **4c** (50–52% yield) was obtained which contained *ortho*-iodinated by-products.



Scheme 2. Polymerization of 6,6′-linked naphthalenes.

In a search for more reactive catalysts that would not cause substrate halogenation, we synthesized the new complexes **2c–e** (Scheme 1). It was necessary to effect halogen exchange to **2d,e** from the Cu^{II} complex **2a** as the metal complexes formed by in situ oxidation of the Cu^{I} diamine adducts with Ag^{I} salts were characterized by poor catalytic activity. Reactions with the resultant CuOTf and $CuSbF_6$ catalysts were relatively slow. However, the $CuBF_4$ catalyst was as selective as the CuI catalyst and substantially more reactive. With **3** (Table 1, entries 2 and 3), the yield and the degree of polymerization to give the new ester-functionalized polymers **4d** were substantially higher.

In undertaking these polymerizations, we were concerned whether the chiral biaryl from the first enantioselective coupling would influence the stereochemical outcome of the subsequent diastereoselective couplings. Work by Okamoto et al.[6] showed that such substrate diastereocontrol alters the stereochemical induction obtained with a chiral catalyst in related systems. To measure asymmetric induction in these polymerizations, **3** was treated with (*S,S*)-**2d** under milder conditions (3 h, 60 °C) to provide the dimer (*R*)-**4e** and trimer (*R,R*)-**4f**. CSP (chiral stationary phase) HPLC of the bisether **5** (Scheme 2) revealed that dimer **4e** formed with 85% *ee*. While HPLC resolution of the trimer was not possible, the ^{1}H NMR spectrum showed 70–75% *de*. Enantioselectivity of 85% *ee* in each biaryl coupling would lead to 72% *de* [85.5% (*R,R*)-**4f**, 14.0% (*S,R*)-**4f**, 0.5% (*S,S*)-**4f**], consistent with this NMR measurement. Thus, each biaryl coupling in the polymerization is independent, proceeding with 85% *ee*; stereocontrol from catalyst **2d** prevails over substrate diastereocontrol. The CD spectra[7] of the enantiomeric polymers **4d** show mirror Cotton effects, indicating that the enantiomeric catalysts indeed produce enantiomeric polymers. The spectra of the polymer are very similar to those of dimer **4e**

[*] Prof. M. C. Kozlowski, X. Xie, P.-W. Phuan
Roy and Diana Vagelos Laboratories
Department of Chemistry, University of Pennsylvania
231 South 34th Street, Philadelphia, PA 19104-6323 (USA)
Fax: (+1) 215-573-7165
E-mail: marisa@sas.upenn.edu

[**] Financial support was provided by the University of Pennsylvania Research Foundation and the National Science Foundation (CHE-0094187).

Supporting information for this article is available on the WWW under http://www.angewandte.org or from the author.

 © 2003 Wiley-VCH Verlag GmbH & Co. KGaA, Weinheim DOI: 10.1002/anie.200250325

Table 1: Treatment of **3** with selected Cu catalysts (Scheme 2).[a]

Entry	Cat.	Prod.	Yield [%]	M_w[b]	M_n[b]	PDI[b,c]	$[\alpha]_D^{RT}$	Int:term[b,d]
1	**6**	**4a**	37	4800	3100	1.56	–	4.7:1
		4b	25	8500	5800	1.48	–	9.6:1
2	(*R*,*R*)-**2d**	$(S)_n$-**4d**	74	10500	4900	2.14	+78	8.1:1
3	(*S*,*S*)-**2d**	$(R)_n$-**4d**	78	12300	5400	2.29	−89	8.9:1

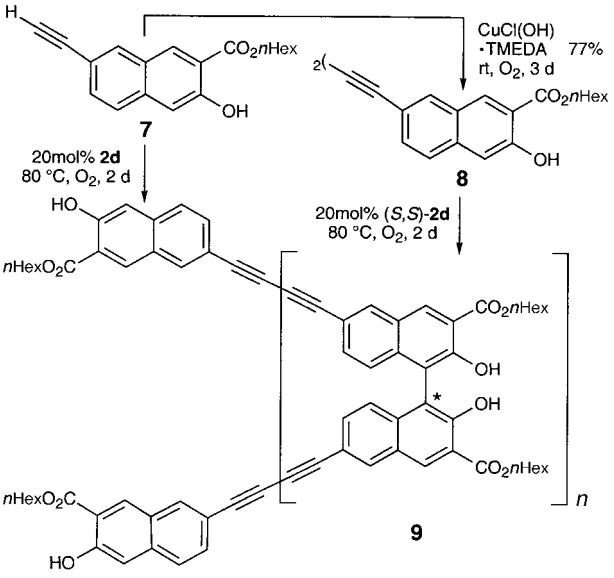
[a] Reactions were 2–5 d at 40–80 °C with 10–20 mol% catalyst. [b] Determined by GPC with a polystyrene standard. [c] PDI = M_w/M_n. [d] Ratio of internal to terminal units.

and trimer **4f** (same maxima and minima) except that the signals are more intense owing to the greater number of naphthalene units in the chain.[8]

Chiral polybinaphthyls typically contain naphthalene units that are linked by means of 1,1′-bonds and 2,2′-, 3,3′-, or 6,6′-connections. In prior reports and the work described above, polybinaphthyls are constructed from "monomers" in which one set of these linkages is already formed. A more efficient method for preparing such polymers would be to create both sets of linkages simultaneously. To test this proposal we prepared monomers **7** and **10**, which contain two sites that we hypothesized would react in the presence of **2d**—an alkyne terminus and a naphthol.

The Glaser–Hay coupling[9] of the terminal arylalkynes is very rapid and occurs prior to the phenolic coupling, as demonstrated by the formation of **8** (77% yield) upon treatment of **7** with CuCl(OH)·TMEDA (Scheme 3). Further polymerization by phenolic coupling was accomplished by subjecting diyne **8** to (*S*,*S*)-**2d** to provide **9** in 90% yield (Table 2). When monomer **7** was subjected to these same conditions, polymer **9** (73% *ee* for each biaryl coupling) was produced directly (Table 2). The UV and CD spectra[7] of polymer **9** generated from either **7** or **8** were identical, which indicates that catalyst **2d** can effect both the alkynyl and phenolic coupling cleanly (Figure 1). No cross-coupling and no interference by alkynylcopper intermediates on the stereochemical course of the biaryl coupling were observed. Finally, when a substituted 1,1′-binaphthol corresponding to the repeating unit of **9** (Scheme 3) was polymerized through alkyne–alkyne coupling, the structure of the resultant product was identical to that of polymer **9** from either **7** or **8** (Figure 1), even though the termini are alkynyl instead of naphthalenyl.

With alkyl alkynes we discovered that the Glaser–Hay coupling is slower than the phenolic coupling. For example, treatment of alkyl alkyne monomer **10** with 10 mol% CuCl(OH)·TMEDA at room temperature provided only the simple biaryl coupling product (±)-**11** (61% yield,



Scheme 3. Polymerization of arylalkynyl-2-naphthols.

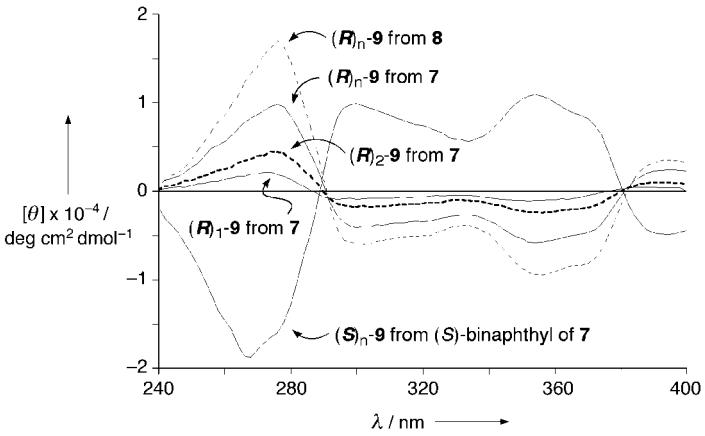


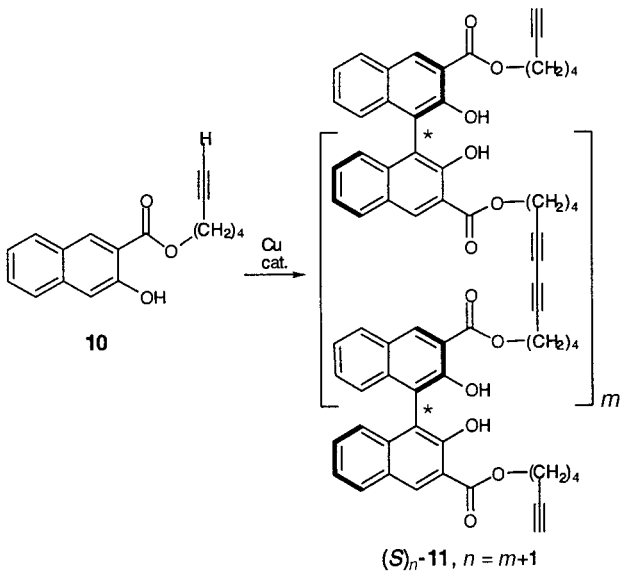
Figure 1. CD spectra of **9** (2×10^{-5} M in CH_2Cl_2).

Table 2: Treatment of **7**, **8**, and **10** with catalyst **2d** (Schemes 3 and 4).[a]

Monomer	**2d**	Product	Yield [%]	M_w[b]	M_n[b]	$[\alpha]_D^{RT}$
8	(*S*,*S*)	$(R)_n$-**9**	90	12900	4400	−248
7	(*S*,*S*)	$(R)_n$-**9**	80	9200	4900	−168
7	(*R*,*R*)	$(S)_n$-**9**	86	15100	6800	+174
10	(*R*,*R*)	$(S)_n$-**11**	60	10300	3900	−180

[a] Reactions were 2 d at 80 °C with 20 mol% catalyst. [b] Measured by GPC with a polystyrene standard.

 © 2003 Wiley-VCH Verlag GmbH & Co. KGaA, Weinheim



Scheme 4. Polymerization of alkylalkynyl-2-naphthols.

Scheme 4). The polymeric form incorporating both alkyl alkynyl and binaphthol coupling, $(S)_n$-**11**, could be generated directly from **10** by using 20 mol% (*R,R*)-**2d** (Scheme 4, Table 2, entry 4). Interestingly, the optical rotation of polymer $(S)_n$-**11** is negative while the optical rotation of the related polymer $(S)_n$-**9** (Scheme 3) is positive (Table 2, entry 3). Even though both compounds possess the same binaphthol configurations and a diyne unit, the optical absorption properties are substantially different due to the location of the linking units. This conclusion is supported by the CD spectra of these polymers; one negative absorption ($\lambda = 270$ nm) and two positive absorptions (302, 356 nm) are observed for $(S)_n$-**9**, while $(S)_n$-**11** is characterized by two strong negative absorptions (252, 262 nm) and one weaker positive absorption (308 nm).

The mirror Cotton effects from the CD spectra of polymers **9** (Figure 1) and **11** indicate that the enantiomeric catalysts indeed produce enantiomeric polymers. In addition, the CD spectra of **9** and **11** largely resemble those of their corresponding dimeric and trimeric forms, which indicates that the diyne-linked polymers described herein do not adopt a secondary helical conformation beyond the individual chiral binaphthyl units.

In conclusion, we report the first enantioselective synthesis of functionalized chiral polybinaphthyls from achiral starting materials. We use chiral copper catalysts to effect enantioselective oxidative biaryl coupling of 2-naphthols alone and in tandem with Glaser–Hay coupling. Since the functional group tolerance is high,[10] a large number of structures are accessible with this method. The CD and UV spectra (see Supporting Information) of the functionalized polybinaphthyls support the formation of chiral polybinaphthyls, with different linking units giving rise to different overall structures. The relative reaction rates of various substrates with the chiral catalysts follows the order: benzyl cyanides[11] $\gg$ aryl alkynes[9] > electron-rich 2-naphthols > electron-deficient 2-naphthols > alkyl alkynes.[9] Since the chemoselectivity of each coupling is remarkably high, substrates can be selected which assemble in a defined order under a single set of reaction conditions exposing selected terminal groups, allowing selective cross-linking, or generating more complex architectures.

Received: October 8, 2002 [Z50325]

Keywords: asymmetric catalysis · chirality · copper · coupling reactions · polymerization

[1] a) *Handbook of Conducting Polymers,Vol. 1–2* (Ed.: T. A. Skotheim), Marcel Dekker, New York, **1986**; b) J. L. Bredas, R. Silbey, *Conjugated Polymers: The Novel Science and Technology of Highly Conducting and Nonlinear Optically Active Materials*, Kluwer Academic, Boston, **1991**; c) *Conjugated Conducting Polymers* (Ed.: H. G. Kiess) Springer, New York, **1992**.
[2] Q. Hu, D. Vitharana, G. Liu, V. Jain, M. W. Wagaman, L. Zhang, T. R. Lee, L. Pu, *Macromolecules* **1996**, *29*, 1082–1084.
[3] For reviews see: a) L. Pu, *Chem. Rev.* **1998**, *98*, 2405–2494; b) L. Pu, *Tetrahedron: Asymmetry* **1998**, *9*, 1457–1477; c) L. Pu, *Chem. Eur. J.* **1999**, *5*, 2227–2232.
[4] a) Q. Hu, W. Huang, D. Vitharana, X. Zheng, L. Pu, *J. Am. Chem. Soc.* **1997**, *119*, 12454–12464; b) W. Huang, Q. Hu, X. Zheng, J. Anderson, L. Pu, *J. Am. Chem. Soc.* **1997**, *119*, 4313–4314; c) Q. Hu, X. Zheng, L. Pu, *J. Org. Chem.* **1996**, *61*, 5200–5201; d) T. Arai, Q. Hu, X. Zheng, L. Pu, H. Sasai, *Org. Lett.* **2000**, *2*, 4261–4263; e) H. Yu, Q. Hu, L. Pu, *J. Am. Chem. Soc.* **2000**, *122*, 6500–6501.
[5] For a report of the CuI catalysts see: X. Li, J. Yang, M. C. Kozlowski, *Org. Lett.* **2001**, *3*, 1137–1140.
[6] One example of a polymerization by diastereoselective oxidative biaryl coupling of chiral BINOL derivatives has been reported: S. Habaue, T. Seko, Y. Okamoto, *Macromolecules* **2002**, *35*, 2437–2439.
[7] We thank Andres Dulcey, Jonathon Ruddick, and Prof. Virgil Percec for assistance with the polymer characterization and Wai Leun Lau, Rachael S. Signarvic, and Prof. William DeGrado for assistance with the circular dichroism and UV measurements.
[8] For similar structural effects with related polybinaphthyls see: a) S. R. Wyatt, Q.-S. Hu, X.-L. Yan, W. D. Bare, L. Pu, *Macromolecules* **2001**, *34*, 7983–7988; b) L. Ma, P. S. White, W. Lin, *J. Org. Chem.* **2002**, *67*, 7577–7586.
[9] For a review see: P. Siemsen, R. C. Livingston, F. Diederich, *Angew. Chem.* **2000**, *112*, 2740–2767; *Angew. Chem. Int. Ed.* **2000**, *39*, 2632–2657.
[10] M. C. Kozlowski, X. Li, C. Mulrooney, J. B. Hewgley, J. Yang, *J. Org. Chem.*, in press.
[11] Our copper complex **2b** catalyzes the benyzl cyanide couplings described by de Jongh et al. in ~5 min at −78 °C: H. A. P. de Jongh, R. H. I. de Jongh, W. J. Mijs, *J. Org. Chem.* **1971**, *36*, 3160–3168.

 © 2003 Wiley-VCH Verlag GmbH & Co. KGaA, Weinheim

Synthetic Peptides

Dynamic Covalent Chemistry on Self-Templating Peptides: Formation of a Disulfide-linked β-Hairpin Mimic**

*Yamuna Krishnan-Ghosh and Shankar Balasubramanian**

The self-assembly of supramolecular structures is usually dependant on reversible noncovalent interactions.[1] Advantages of reversible self-assembly include mechanisms for error-correction through dynamic equilibration leading to the most stable structure and minimization of synthetic effort.[1b] However, thermodynamically stable assembled states often exhibit low kinetic stability. One approach to generate thermodynamic constructs that are kinetically stable is the concept of dynamic covalent chemistry where noncovalent interactions can be used to template covalent bond formation.[2] Dynamic covalent chemistry can generate an equilibrium mixture of interconverting molecules. The exchange mechanism may be stopped by changing the reaction conditions. The distribution of molecules shifts upon inclusion of a template to favor individual library members that bind to the template.[3] A specialized case of template-directed synthesis where the template is an integral part of the structure it helps to form has been termed "covalent capture".[4] Reversible covalent capture using dynamic chemistry to form stable peptide-based assemblies has been demonstrated for the oligomerization of helical peptide bundles.[5] Herein, we describe the first studies on the dimerization of β-sheet-forming peptides by covalent capture under both reversible and irreversible conditions.

The objective was to explore whether self-templating of β-sheet-forming peptides occurs during the process of dimer formation by dynamic covalent chemistry. We designed two peptides $\mathbf{A_{SH}}$ and $\mathbf{B_{SH}}$ of length 4 mer and 10 mer respectively (Figure 1) containing $(Leu–Lys)_n$ repeats[6] known to predispose the peptide to form β-sheets.[7] The cationic nature of the $(Leu–Lys)_n$ motif also disfavors aggregation.[8] As the length of the peptide would dictate the degree of noncovalent interactions[9] two different values of n were chosen; $n=1$ ($\mathbf{A_{SH}}$) and $n=4$ ($\mathbf{B_{SH}}$). Of the several possible covalent coupling motifs, we have chosen to exploit the coupling of the thiol–disulfide system since it is water compatible, relatively fast, and can be switched on or off by changing the pH value.[10] Thiols were incorporated into the peptides as N-terminal Cys residues with a Gly spacer to offer some conformational flexibility for disulfide bond formation.[5]

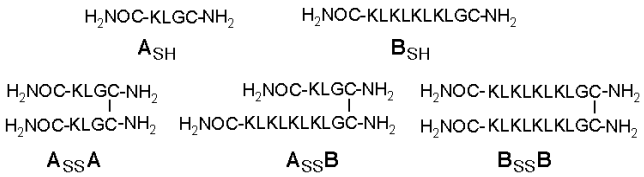


Figure 1. Sequences of peptides $\mathbf{A_{SH}}$ and $\mathbf{B_{SH}}$ and the various dimers potentially formed by covalent capture.

A mixture of $\mathbf{A_{SH}}$ and $\mathbf{B_{SH}}$ can dimerize to form two possible homodimers ($\mathbf{A_{SS}A}$ or $\mathbf{B_{SS}B}$) or a heterodimer ($\mathbf{A_{SS}B}$; Figure 2). We have investigated dimerization of equimolar solutions of $\mathbf{A_{SH}}$ and $\mathbf{B_{SH}}$ under irreversible and reversible conditions of covalent capture. Product distributions were analyzed from UV–HPLC traces of aliquots of the reaction mixtures (Figure 3) and quantified from a comparison of their areas under the traces with those of purified standards.[11] When a solution containing equimolar $\mathbf{A_{SH}}$ and $\mathbf{B_{SH}}$ in buffer

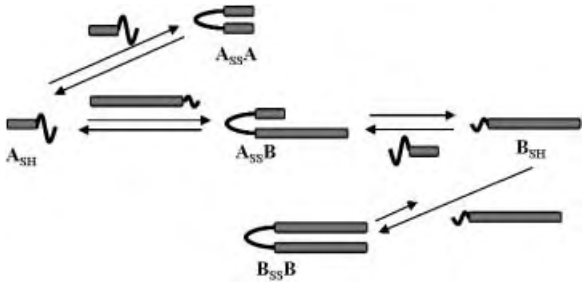


Figure 2. Schematic representation of reversible covalent capture in simple linear peptides leading to preferential formation of covalently linked peptide partners.

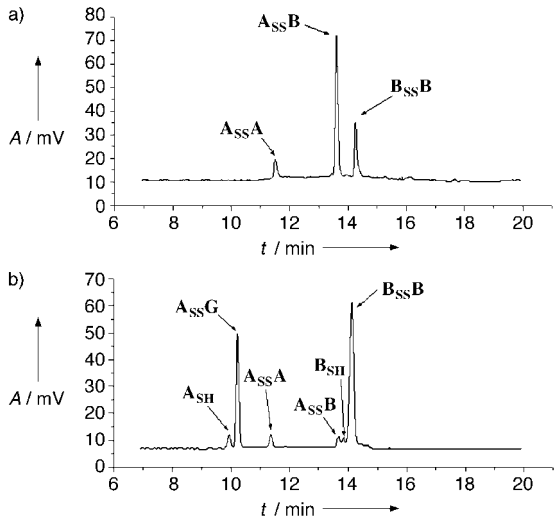


Figure 3. HPLC traces of aliquots of reaction mixtures where equimolar amounts of $\mathbf{A_{SH}}$ and $\mathbf{B_{SH}}$ were a) oxidized by air, b) equilibrated in buffer containing $\mathbf{G_{SH}}$ and $\mathbf{G_{SS}G}$ (where G = glutathione). Note that these raw data peaks have not been normalized for the difference in extinction coefficients at 220 nm for individual peptides.

[*] Dr. S. Balasubramanian, Y. Krishnan-Ghosh
University Chemical Laboratories
University of Cambridge
Lensfield Road, Cambridge CB2 1EW (UK)
Fax: (+44) 1223-336-913
E-mail: sb10031@cam.ac.uk

[**] YKG thanks the Royal Commission for the Exhibition of 1851 for a Research Fellowship. We thank Dr P. Grice for recording NMR spectra and Drs S. Otto and J. Christodoulou for helpful comments and suggestions.

Supporting information for this article is available on the WWW under http://www.angewandte.org or from the author.

 DOI: 10.1002/anie.200250551 © 2003 Wiley-VCH Verlag GmbH & Co. KGaA, Weinheim

was subjected to air oxidation[12] dimers $\mathbf{A_{SS}A}$:$\mathbf{A_{SS}B}$:$\mathbf{B_{SS}B}$ were obtained in a 1.0:2.4:1.1 molar ratio. This essentially statistical distribution reflects that dimer formation is not influenced by noncovalent interactions. Even when the completely oxidized reaction mixture was left stirring for 72 h, the change in product distribution was negligible. The same results were obtained when we oxidized the mixture of thiols using $K_3[Fe(CN)_6]$ in buffer.

To explore dimerization under reversible conditions we employed a redox buffer comprising oxidized ($\mathbf{G_{SS}G}$) and reduced ($\mathbf{G_{SH}}$) forms of glutathione.[5] As this peptide-based buffer was used in large excess over $\mathbf{A_{SH}}$ and $\mathbf{B_{SH}}$, it also serves as a competitor to reduce the effect of nonspecific interactions between other peptide components. Equimolar solutions of $\mathbf{A_{SH}}$ and $\mathbf{B_{SH}}$ were equilibrated in $\mathbf{G_{SH}}$/$\mathbf{G_{SS}G}$ redox buffer for 12 h. HPLC analysis of the products revealed only trace amounts of the statistically favored disulfide $\mathbf{A_{SS}B}$ and a dramatic increase in the quantity of $\mathbf{B_{SS}B}$ (Figure 3b).[13] A new peak corresponding to $\mathbf{A_{SS}G}$ where $\mathbf{A_{SS}G}$:$\mathbf{A_{SS}A}$ was 13:1 was also observed. This feature is attributable to a concentration effect (initial $[\mathbf{G_{SH}}]$:$[\mathbf{A_{SH}}] = 12.5:1$) because of the relatively low stabilization resulting from self-recognition of $\mathbf{A_{SH}}$. All the oxidized $\mathbf{B_{SH}}$ is present in the form of $\mathbf{B_{SS}B}$ with no $\mathbf{B_{SS}G}$ detected despite the 13-fold excess of $\mathbf{G_{SH}}$. This result is indicative of $\mathbf{B_{SS}B}$ being a particularly stabilized structure. The molar ratio of $\mathbf{A_{SS}B}$:$\mathbf{B_{SS}B}$ under reversible conditions was 1:86 which reflects a significant contribution of noncovalent stabilization energy resulting from self-recognition of $\mathbf{B_{SH}}$. The product distribution was unchanged when the reaction was left to equilibrate under argon for up to 2 weeks (data not shown), which suggests that this is a true thermodynamic distribution. To confirm that the system had indeed reached a thermodynamic equilibrium, a 1.0:2.4:1.1 mixture of $\mathbf{A_{SS}A}$:$\mathbf{A_{SS}B}$:$\mathbf{B_{SS}B}$ generated by air oxidation in buffer was re-equilibrated in the presence of $\mathbf{G_{SH}}$/$\mathbf{G_{SS}G}$ (500 μM/125 μM; Supporting Information). The product distribution was evaluated at various time intervals by HPLC. After equilibration for 36 h a product distribution identical to that shown in Figure 3b was obtained, which confirms our model. The same results were obtained when the equilibration was effected by a neutral redox reagent employing oxidized and reduced forms of β-mercaptoethanol (Supporting Information). Thus, for this system, the introduction of reversible conditions allows an error-correction step in the covalent capture of a peptide partner.

To determine the origin of stabilization in $\mathbf{B_{SS}B}$, the structure of $\mathbf{B_{SS}B}$ in water was studied using NMR spectroscopy. The influence of dimerization on structure was gauged by comparison with the monomer $\mathbf{B_{SH}}$, used as the reference compound. ^{1}H NMR spectra were recorded in 10% (v/v) D_2O and 90% (v/v) H_2O and assigned using a combination of TOCSY and NOESY 2D data sets (See Supporting Information for details of experiments and spectra). A comparison of the 1D spectra of dimer $\mathbf{B_{SS}B}$ (80 μM) and monomer $\mathbf{B_{SH}}$ (80 μM) revealed a high degree of similarity. Moreover, TOCSY on $\mathbf{B_{SS}B}$ clearly identified only eight Leu–Lys spin systems not 16 which indicates that the peptide backbones in $\mathbf{B_{SS}B}$ have C_2 symmetry (Supporting Information). Perturbations to the H_α and N–H chemical shifts are characteristic of secondary structure formation by peptides.[14,15] Substantial H_α upfield shifts ($\Delta\delta = 0.3$ ppm) were observed at C^{10} and C^{11} residues at the center of $\mathbf{B_{SS}B}$ which is indicative of a turn conformation at these residues. Keeping in mind the C_2 symmetry of $\mathbf{B_{SS}B}$, this suggests that the disulfide linkage is at the center of a turn with both the peptide backbones propagating in the same direction. The $^3J_{N\alpha}$ coupling constants of $\mathbf{B_{SS}B}$ and $\mathbf{B_{SH}}$ at 300 K are shown in Table 1 (see Figure 5 for numbering scheme). The $^3J_{N\alpha}$ coupling constants for $\mathbf{B_{SH}}$ are close to the ideal random coil value of 6.0 Hz. In contrast, for $\mathbf{B_{SS}B}$ the values for the $(Lys–Leu)_4$ residues are generally over 7.0 Hz some reaching even 9.0 Hz—characteristic of them being present in β-sheet conformation.[16] G^9 and G^{12} showed ΔJ values of −0.7 Hz indicating that they form part of the turn in $\mathbf{B_{SS}B}$. More evidence for folded structure is provided by the observation of long-range NOEs between residues in the two strands of $\mathbf{B_{SS}B}$. A number of cross-strand NH–NH interactions between hydrogen-bonded residues (L^2–K^{18}, K^{16}–L^6, L^6–K^{14}, K^{14}–L^8, L^8–G^{12}) were also observed.[17] (Figure 4). Furthermore, the temperature coefficients ($\Delta\delta/\Delta T$) of N–H protons on Lys residues at various points on the sheet decreased progressively from the N-terminus to the C-terminus (Supporting Information). Similar results were obtained for the corresponding Leu residues. This result demonstrates that N–H protons nearer the turn are more strongly hydrogen bonded than those near the C-

Table 1: Coupling constants ($^3J_{N\alpha}$) of various residues on $\mathbf{B_{SS}B}$ and the monomer $\mathbf{B_{SH}}$ at 300 K.

$\mathbf{B_{SH}}$ Residue	$^3J_{N\alpha}$ [Hz]	$\mathbf{B_{SS}B}$ Residue	$^3J_{N\alpha}$ [Hz]
K^1	6.83	K^1, K^{20}	7.80
L^2	6.60	L^2, L^{19}	7.26
K^3	6.43	K^3, K^{18}	7.65
L^4	6.54	L^4, L^{17}	6.95
K^5	6.34	K^5, K^{16}	9.14
L^6	6.10	L^6, L^{15}	6.97
K^7	6.62	K^7, K^{14}	7.39
L^8	6.54	L^8, L^{13}	9.68
G^9	5.81	G^9, G^{12}	5.11
C^{10}	–	C^{10}, C^{11}	–

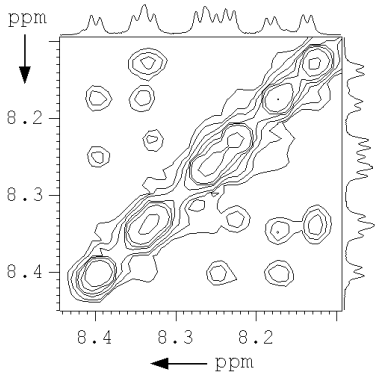


Figure 4. Portion of the NOESY spectrum of $\mathbf{B_{SS}B}$ at 300 K in 10% D_2O/90% H_2O illustrating cross-strand NH–NH NOEs that are consistent with the proposed folded structure.

 © 2003 Wiley-VCH Verlag GmbH & Co. KGaA, Weinheim

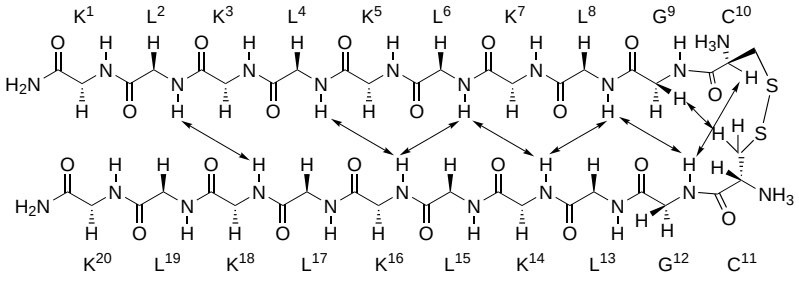


Figure 5. NOEs between non-adjacent residues observed in NOE NMR spectroscopy analysis of $\mathbf{B_{SS}B}$ at 300 K.

termini. This situation is completely consistent with $\mathbf{B_{SS}B}$ being present in a hairpin-type conformation as shown in Figure 5. Though disulfide linkages are known to stabilize β-hairpins[13] and have been proposed to act as turn scaffolds between helices,[18] this is the first example of a disulfide as a turn scaffold in a synthetic peptide yielding a β-hairpin-type conformation in water.

Biological systems frequently employ reversible covalent capture to stabilize inter- and intramolecular assemblies.[19] This is the first example of dynamic covalent chemistry applied to peptides to produce a thermodynamically stabilized β-sheet assembly.

Received: November 14, 2002
Revised: January 31, 2003 [Z50551]

Keywords: hydrogen bonding · peptides · self-assembly · template synthesis

[1] a) D. Philp, J. F. Stoddart, *Angew. Chem.* **1996**, *108*, 1242; *Angew. Chem. Int. Ed. Engl.* **1996**, *35*, 1154; b) J. S. Lindsey, *New J. Chem.* **1991**, *15*, 152.

[2] For selected reviews see: S. J. Rowan, S. J. Cantrill, G. R. L. Cousins, J. K. M. Sanders, J. F. Stoddart, *Angew. Chem.* **2002**, *114*, 938; *Angew. Chem. Int. Ed.* **2002**, *41*, 898; J.-M. Lehn, *Chem. Eur. J.* **1999**, *5*, 2455.

[3] I. Huc, J.-M. Lehn, *Proc. Natl. Acad. Sci. USA* **1997**, *94*, 2106; K. C. Nicolaou, R. Hughes, S. Y. Cho, N. Winssinger, H. Labischinski, R. Endermann, *Chem. Eur. J.* **2001**, *7*, 3824; V. Goral, M. I. Nelen, A. V. Eliseev, J.-M. Lehn, *Proc. Natl. Acad. Sci. USA* **2001**, *98*, 1347; C. Karan, B. L. Miller, *J. Am. Chem. Soc.* **2001**, *123*, 1074; R. L. E. Furlan, Y. F. Ng, S. Otto, J. K. M. Sanders, *J. Am. Chem. Soc.* **2001**, *123*, 8876.

[4] T. D. Clark, K. Kobayashi, M. R. Ghadiri, *Chem. Eur. J.* **1999**, *5*, 782; M. Royo, M. A. Contreras, E. Giralt, F. Albericio, M. Pons, *J. Am. Chem. Soc.* **1998**, *120*, 6639.

[5] A. Saghatelian, Y. Yokobayashi, K. Soltani, M. R. Ghadiri, *Nature* **2001**, *409*, 797; B. Bilgiçer, X. Xing, K. Kumar, *J. Am. Chem. Soc.* **2001**, *123*, 11815; M. A. Case, G. L. McLendon, *J. Am. Chem. Soc.* **2000**, *122*, 8089.

[6] W. F. DeGrado, J. D. Lear, *J. Am. Chem. Soc.* **1985**, *107*, 7684.

[7] H. Xiong, B. L. Buckwalter, H.-M. Shieh, M. H. Hecht, *Proc. Natl. Acad. Sci. USA* **1995**, *92*, 6349.

[8] P. I. Haris, C. H. Chapman, *Biopolymers* **1995**, *37*, 251–263; circular dichroism (CD) spectra of $\mathbf{B_{SH}}$ and $\mathbf{B_{SS}B}$ did not show evidence of extended β-sheet formation up to 300 μM, which indicates that there is no perturbation of the system by aggregation at the concentrations used for covalent capture experiments or NMR spectroscopy experiments.

[9] H. E. Stanger, F. A. Syud, J. F. Espinosa, I. Giriat, T. Muir, S. Gellman, *Proc. Natl. Acad. Sci. USA* **2001**, *98*, 12015.

[10] R. P. Szajewski, G. M. Whitesides, *J. Am. Chem. Soc.* **1980**, *102*, 2011.

[11] Concentrations of standards were determined by amino acid analysis. Errors in such estimation in our hands were within 3%.

[12] Air oxidation can yield thermodynamically stable products. See S. Otto, R. L. E. Furlan, J. K. M. Sanders, *J. Am. Chem. Soc.* **2000**, *122*, 12063.

[13] Peaks for $\mathbf{A_{SH}}$ and $\mathbf{B_{SH}}$ obtained in Figure 3b corresponded to the equilibrium concentrations of $\mathbf{A_{SH}}$ or $\mathbf{B_{SH}}$ alone when equilibrated in a redox buffer of $\mathbf{G_{SH}}/\mathbf{G_{SS}G}$. See A. G. Cochran, R. T. Tong, M. A. Starovasnik, E. J. Park, R. S. McDowell, J. E. Theaker, N. J. Skelton, *J. Am. Chem. Soc.* **2001**, *123*, 625.

[14] K. Wüthrich, *NMR of Proteins and Nucleic Acids*; Wiley, New York, **1986**.

[15] M. P. Williamson, T. Asakura, E. Nakamura, M. Demura, *J. Biomol. NMR* **1992**, *2*, 83; D. S. Wishart, B. D. Sykes, F. M. Richards, *J. Mol. Biol.* **1991**, *222*, 311.

[16] K. M. Fiebig, H. Schwalbe, M. Buck, L. J. Smith, C. M. Dobson, *J. Phys. Chem.* **1996**, *100*, 2661; A. J. Maynard, G. J. Sharman, M. S. Searle, *J. Am. Chem. Soc.* **1998**, *120*, 1996.

[17] The NOEs could arise between sequential residues. However, these NOEs were not observed in the case of $\mathbf{B_{SH}}$ suggesting that $\mathbf{B_{SS}B}$ is structured and the observed NOEs are a result of the presence of the second chain.

[18] I. Karle, D. Ranganathan, C. Lakshmi, *Biopolymers* **2001**, *59*, 301.

[19] T. Kogama, *Microbiol. Mol. Biol. Rev.* **1998**, *61*, 212; T. Kodadek, *Trends Biochem. Sci.* **1998**, *23*, 79; R. B. Freedman, *Curr. Opin. Struct. Biol.* **1995**, *5*, 85; T. Zhang, R. Alber, *Nat. Struct. Biol.* **1994**, *1*, 434.

 © 2003 Wiley-VCH Verlag GmbH & Co. KGaA, Weinheim

A Polyoxothiometalate Tetramer

A Supramolecular Tetra-Dawson Polyoxothiometalate: $[(\alpha\text{-}H_2P_2W_{15}O_{56})_4\{Mo_2O_2S_2(H_2O)_2\}_4\{Mo_4S_4O_4(OH)_2(H_2O)\}_2]^{28-}$

Emmanuel Cadot, Marie-Anne Pilette, Jérôme Marrot, and Francis Sécheresse*

The control of the aggregation processes in supramolecular inorganic chemistry is one of the keys for the targeted synthesis of mesoscopic materials with a high level of complexity. In this context, the self-assembly of modular inorganic systems into larger structures constitutes a rational

[*] Dr. E. Cadot, M.-A. Pilette, Dr. J. Marrot, Prof. F. Sécheresse
Institut Lavoisier, IREM, UMR 8637
Université de Versailles Saint Quentin
45 Avenue des Etats-Unis, 78035 Versailles (France)
Fax: (+33) 1-3925-4381
E-mail: cadot@chimie.uvsq.fr

 DOI: 10.1002/anie.200250663 © 2003 Wiley-VCH Verlag GmbH & Co. KGaA, Weinheim

approach to reach structures on the nanometer scale. Polyoxometalate (POM) chemistry has provided a huge diversity of compounds with a variety of exciting behaviors, such as catalytic, magnetic, and anti(retro)viral properties.[1] For several years, we have been exploring a fundamentally fruitful strategy, namely "the building-block strategy" which consists in the self-assembly of preformed building units.[2] Highly negatively charged polyvacant heteropolytungstates are strong nucleophilic groups which react quickly with the cationic oxothio fragment $[M_2O_2S_2]^{2+}$ (where M = metal center).[3] Several polyoxothioanions have been prepared by this way, the architecture of the resulting oxothio compounds is mainly governed by the stereochemistry of the parent lacunary polyanion.[4]

Herein, we report the structural and multinuclear NMR spectroscopic characterization (^{31}P and ^{183}W) of the first Dawson α-$[P_2W_{15}O_{56}]^{12-}$ thio derivative. The title compound **1** is a unique polyoxothiometalate-based macrocycle, about 30 Å in diameter, which results from direct connections between the complementary cationic fragment $[Mo_2O_2S_2]^{2+}$ and the basic trivacant α-$[P_2W_{15}O_{56}]^{12-}$ ion. In addition, the formation of Mo–OH–Mo bridges contributes to the build up of the tetrameric cluster, and shows that it is possible to generate elaborate architectures based on POM-incorporated cyclic oxothiomolybdates. The tetra-Dawson macrocycle **1** is the first multiunit POM compound to have pairs of hydroxy bridges that ensure the inter $\{Mo_2O_2S_2\}$-building-block connections.

Compound **1** was formed at pH 2 by the reaction of $[I_2Mo_{10}S_{10}O_{10}(OH)_{10}(H_2O)_5]^{2-}$ ions[5] with the trivacant Dawson anion α-$[P_2W_{15}O_{56}]^{12-}$ (30% yield). A recrystallization is necessary to obtain **1** as pure mixed sodium–potassium salt ($Na_{14}K_{14}$-**1**). The various attempts to prepare **1** by a one-pot procedure always produced a mixture of isomers, characterized by the presence of two multicomponent-sets of resonance signals in the ^{31}P NMR spectra. A recrystallization step is required for the preparation of the tetra-Dawson anion as single crystals of $Na_{14}K_{14}$-**1** suitable for X-ray crystallography.[6]

A crystallographically imposed inversion center is located in the center of the cluster. Nevertheless, the tetra-Dawson anion depicted in Figure 1, approaches the maximum possible C_{2h} idealized symmetry, the two α-$\{P_2W_{15}O_{56}\}$ moieties in the asymmetric unit are quasi-equivalent and present no local symmetry.

For clarity, the macrocycle will be described as the association of two formal dimers formed from two trivacant anions α-$[P_2W_{15}O_{56}]^{12-}$ connected to two $\{(H_2O)_2Mo_2O_2S_2\}^{2+}$ ions (hatched octahedra) as represented in Figure 2. One molybdenum atom of the $\{(H_2O)_2Mo_2O_2S_2\}^{2+}$ cation is singly bonded to a Dawson unit by a single Mo-μO-W bridge, while the second molybdenum atom is connected to the other Dawson unit by a double Mo-(μO-W)$_2$ bridge. A crystallographic C_2 axis passes through the center of the dimeric subunit while the two equivalent α-$[P_2W_{15}O_{56}]^{12-}$ moieties have no local symmetry.

The two pseudodimers are connected each others by two symmetric tetranuclear $\{Mo_4S_4O_4(OH)_4(H_2O)\}^{2+}$ moieties. This tetranuclear core can be viewed as a fragment of a cyclic molecular ring consisting of two $\{Mo_2O_2S_2\}$ fragment mutually linked by a double hydroxy bridge.[5] A water molecule completes the coordination sphere of each of the two central molybdenum atoms, ensuring a face-shared connection.

The P=O groups located near the vacancy of the α-$[P_2W_{15}O_{56}]^{12-}$ precursor (the O atoms of the P=O groups are noted *e* in Figure 2) are pointing towards the center of the six crown terminal oxygen. This orientation prevents the for-

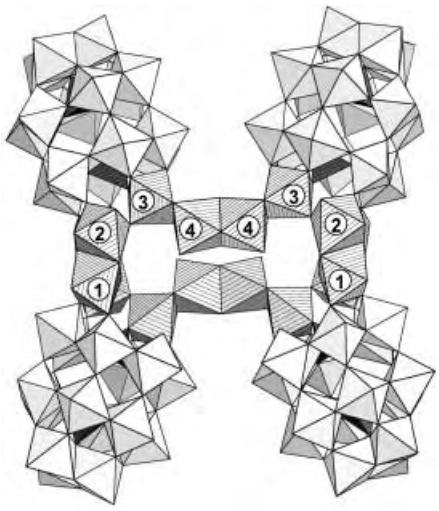


Figure 1. Polyhedral representation of **1**: the four α-$[P_2W_{15}O_{56}]^{12-}$ subunits (assemblies of nonhatched octahedra) are anchored to two $\{Mo_8S_8O_8(OH)_2(H_2O)_5\}^{6+}$ ribbons (hatched numbered octahedra) in which the $\{MoO_4S_2\}$ octahedra are connected through S-edge shared junctions (①–② and ③–④), by O-corner shared junctions (②–③), and by face-shared junctions (④–④). Gray WO_6 octahedra; dark gray PO_4 tetrahedra; hatched $\{MoO_4S_2\}$ octahedra.

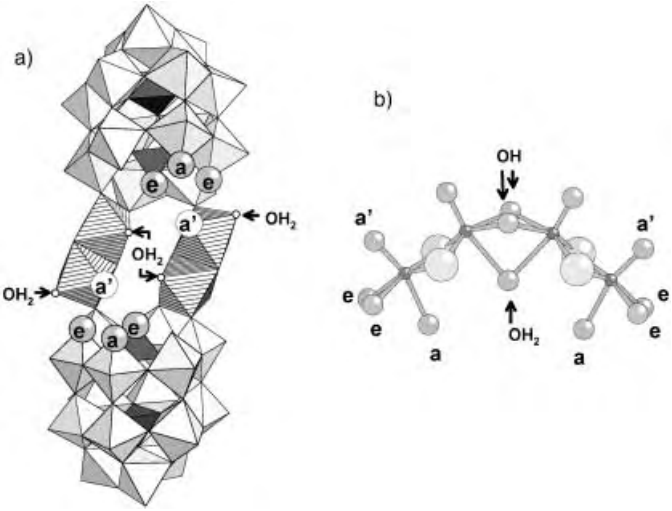


Figure 2. a) Pseudodimer in **1**: The two α-$[P_2W_{15}O_{56}]^{12-}$ subunits are directly connected by two $\{Mo_2O_2S_2(H_2O)_2\}^{2+}$ fragments (hatched octahedra). b) The $\{Mo_4S_4O_4(OH)_2(H_2O)\}^{2+}$ bridging core is linked to the two dimers by axial and equatorial junctions (labeled *a*, *a'*, and *e*). O Medium gray sphere; S big light-gray spheres; Mo little dark-gray sphere.

 © 2003 Wiley-VCH Verlag GmbH & Co. KGaA, Weinheim

mation of the typical sandwichlike structure previously reported for the Keggin α-$[(PW_9O_{34})_2\{Mo_2O_2S_2(H_2O)_2\}_3]^{12-}$ cluster. In the pseudodimer, each oxygen atom (noted *e* and *a* Figure 2) of the terminal P=O and W=O bonds of the trivacant Dawson anion is directly bonded to the corresponding equatorial (*e*) and axial (*a*) site of the $\{Mo_4S_4\}^{2+}$ fragment (Figure 2). In addition, the hatched $\{Mo_2O_2S_2(H_2O)_2\}^{2+}$ bridging fragment and the $\{Mo_4S_4O_4(OH)_2(H_2O)\}^{2+}$ central core are connected through a corner junction involving the molybdenum octahedra ② and ③ (Figure 1): the vacant axial site (ⓐ) in the $\{Mo_2O_2S_2(H_2O)_2\}^{2+}$ bridging groups (Figure 2a) is occupied by a terminal oxygen atom *a'* of the $\{Mo_4S_4O_4(OH)_2(H_2O)\}^{2+}$ linking group (Figure 2b) giving a long Mo···O separation (2.315(6)–2.301(8) Å). The two resulting symmetric cationic $\{Mo_8\}^{6+}$ octamers (formed by the eight numbered octahedra in Figure 1) resembles a ribbon decorated by four pendant Dawson units. This tetra-Dawson complex belongs to a series of planar compounds of high nuclearity exemplified by the macrocyclic cryptate $[As_4W_{40}O_{140}]^{28-}$.[7] Finally, the charge balance is ensured by eight protons which combine with oxygen units to form a coordinated H_2O molecule in each of the four α-$[P_2W_{15}O_{56}]^{12-}$ subunits. According to the valence-bond calculations, two protons are firmly trapped on the unshared oxygen atom of the six crown oxygen atoms surrounding the central P=O group (W–OH_2 separation of 2.146(7) and 2.180(6) Å). The other W–O bonds, involved in a W–O–Mo bridge are significantly shorter and are thus assumed to be unprotonated (1.764(6)–1.799(6) Å). The presence of the water ligand in the coordination sphere provokes the displacement of the W^{6+} ion concerned, away from the coordinated H_2O molecule, thus provoking the shortening of the *trans* W–O bond (1.789(6)–1.836(8) Å).

The solid-state structure of **1** (Figure 1) remains intact in aqueous solution. The ^{31}P NMR spectra of $Na_{14}K_{14}$-**1** in solution (Figure 3a) exhibit two sharp resonance signals of 1:1 relative integration at $\delta = -2.70$ and -13.05 ppm, as expected for four equivalent α-$[P_2W_{15}O_{56}]^{12-}$ subunits. Based on literature values, the $\delta = -2.70$ ppm signal is assigned to the $\{PO_4\}$ group near the vacancies while the $\delta = -13.05$ ppm resonance is attributed to the fully encapsulated phosphato group of the $\{PW_9\}$ Dawson anion.[8] The ^{183}W NMR spectrum consists of fifteen lines of equal integration (Figure 3b), which confirms the lack of symmetry of the four Dawson units. The ^{183}W chemical shift values of the fifteen lines are in the $\delta = -100$ to -300 ppm range, values usually observed for polyvacant or pseudovacant heteropolytungstates.[9]

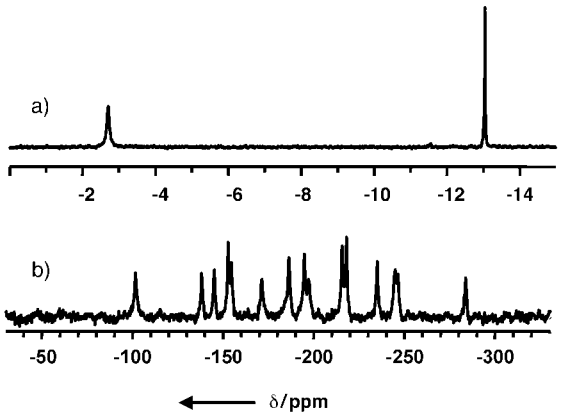


Figure 3. a) ^{31}P NMR spectrum of $Na_{14}K_{14}$-**1** (0.01 mol L^{-1} in D_2O) and b) ^{183}W NMR spectrum of **1** as the lithium salt (0.07 mol L^{-1} in D_2O).

Experimental Section

$K_{14}Na_{14}[(\alpha\text{-}H_2P_2W_{15}O_{56})_4\{Mo_2O_2S_2(H_2O)_2\}_4\{Mo_4S_4O_4(OH)_2(H_2O)\}_2]\cdot \approx 165\,H_2O$ ($K_{14}Na_{14}$-**1**$\cdot \approx 165\,H_2O$). Solid α-$[Na_{12}P_2W_{15}O_{56}]\cdot 23\,H_2O$ (10 g; 2.25 mmol) was added to a stirred solution of $K_2(N(CH_3)_4)_{0.75}I_{2.75}[Mo_{10}S_{10}O_{10}(OH)_{10}(H_2O)_5]\cdot 15\,H_2O$ (2.1 g; 0.9 mmol) dissolved in aqueous HCl (50 mL of 0.2 mol L^{-1}). The resulting red-brown solution was heated at 35 °C for 30 min and the pH value adjusted to 2.0 with about 3 mL of 2 mol L^{-1} aqueous HCl before addition of potassium chloride (7.5 g; 100 mmol. After 30 min at 25 °C, the brown precipitate was collected by filtration, washed with ethanol, and dried with diethyl ether, yield: 9.8 g of crude product. The solid was dissolved in aqueous 0.5 mol L^{-1} NaCl solution (65 mL). The resulting solution was allowed to stand for one week at 25 °C. About 3 g of well-formed red-brown crystals of $K_{14}Na_{14}$-**1**$\cdot \approx 165\,H_2O$ were collected (yield of crystals: about 30% based on α-$[Na_{12}P_2W_{15}O_{56}]\cdot 23\,H_2O$). FTIR (KBr pellet): $\tilde{\nu} = 1091$(m), 1048(w), 1031(w), 957(m), 923(m), 815(sh), 771(s), 705(sh), 596(vw), 557(vw), 519(w), 473(w), 427(vw), 365(sh), 322 cm^{-1}(m). ^{31}P NMR (121.496 MHz, 0.01 mol L^{-1} in D_2O; H_3PO_4): $\delta = -2.70$ (1P), -13.04 ppm (1P); elemental analysis (%) calcd for $Na_{14}K_{14}H_{32}P_8W_{60}Mo_{16}S_{16}O_{254}\cdot 165\,H_2O$: Na 1.54, K 2.61, P 1.18, W 52.7, Mo 7.34, S 2.45; found: Na 1.50, K 2.50, P 1.31, W 52.5, Mo 7.39, S 2.63. The water content was determined by thermogravimetric analysis.

Li_{28} salt for ^{183}W NMR spectroscopy: cationic exchange of $K_{14}Na_{14}$-**1** through a Dowex 50W-X2 resin (Li^+ saturated). ^{183}W NMR (12.5 MHz, 0.07 mol L^{-1} in D_2O; secondary standard: $H_4SiW_{12}O_{40}$ at $\delta = -103.8$ ppm): δ(1W) = -101.75, -138.12, -145.16, -152.76, -154.63, -171.44, -186.30, -194.86, -197.13, -215.70, -218.09, -235.04, -244.84, -246.38, -283.85 ppm.

Received: November 29, 2002 [Z50663]

Keywords: molybdenum · polyoxometalates · self-assembly · supramolecular chemistry · tungsten

[1] a) M. T. Pope, A. Müller, *Angew. Chem.* **1991**, *103*, 56; *Angew. Chem. Int. Ed. Engl.* **1991**, *30*, 34; b) M. T. Pope, A. Müller, *Polyoxometalates: From Platonic Solids to Anti-retroviral Activity*, Kluwer, Dordrecht **1994**; c) For an exhaustive rewiew: *Chem. Rev.* **1998**, *98*, 1–389 (Special Thematic Issue on Polyoxometalates, guest Ed. C. Hill).

[2] E. Cadot, F. Sécheresse, *Chem. Commun.* **2002**, 2189.

[3] E. Cadot, V. Béreau, S. Halut, F. Sécheresse, *Inorg. Chem.* **1996**, *35*, 551.

[4] E. Cadot, A. Dolbecq, B. Salignac, F. Sécheresse, *Polyoxometalates, From Topology to Industrial Applications* (Eds: A. Müller, M. T. Pope), Kluwer Academic, Dordrecht, **2001**.

[5] E. Cadot, B. Salignac, S. Halut, F. Sécheresse, *Angew. Chem.* **1998**, *110*, 631; *Angew. Chem. Int. Ed.* **1998**, *37*, 611.

[6] Crystal data for $Na_{14}K_{14}$-**1**$\cdot 165\,H_2O$: Siemens Smart CCD diffractometer, $Mo_{K\alpha}$ radiation ($\lambda = 0.71073$ Å. Red-brown paralepipedic crystal, dimensions $0.04 \times 0.02 \times 0.02$ mm^3, triclinic, space group $P\bar{1}$ (No. 2), $a = 14.4731(1)$, $b = 24.6433(1)$, $c = 29.5413(2)$ Å, $\alpha = 76.384(1)$, $\beta = 79.339(1)°$, $\gamma = 87.211(1)°$, $V = 10063.3(2)$ Å, $Z = 1$, $\rho_{calcd} = 3.351$ g cm^{-3}, $\mu(Mo_{K\alpha}) = 17.932$ mm^{-1}, $F(000) = 8964$, $T = 296(2)$ K. A total of 27541

 © 2003 Wiley-VCH Verlag GmbH & Co. KGaA, Weinheim

independent reflections, 20000 observed with $F_0 > 4\sigma(F_0)$, R(int) = 0.0644, $R_1 = 0.0579$, $wR_2 = 0.1181$, 1993 parameters. The structure was solved by direct methods, and refined by full-matrix-block least-squares procedure (SHELX-TL package); disorder in sodium–potassium cations and water molecules was found and partial occupancy factors were applied. Further details on the crystal structure investigations may be obtained from the Fachinformationszentrum Karlsruhe, 76344 Eggenstein-Leopoldshafen, Germany (fax: (+49) 7247-808-666; e-mail: crysdata@fiz-karlsruhe.de), on quoting the depository number CSD-412791.

[7] M. Leyrie, J. Martin-Frère, G. Hervé, *C. R. Seances Acad. Sci. Ser. C* **1974**, *279*, 895.

[8] S. P. Harmalker, M. A. Leparulo, M. T. Pope, *J. Am. Chem. Soc.* **1983**, *105*, 4286.

[9] R. Acerete, C. F. Hammer, L. C. Baker, *J. Am. Chem. Soc.* **1982**, *104*, 5384.

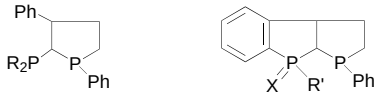
 © 2003 Wiley-VCH Verlag GmbH & Co. KGaA, Weinheim

Zirconium Spirophosphanes

Metalla-Azaspirophosphanes: Synthesis, Structure, and Reactivity**

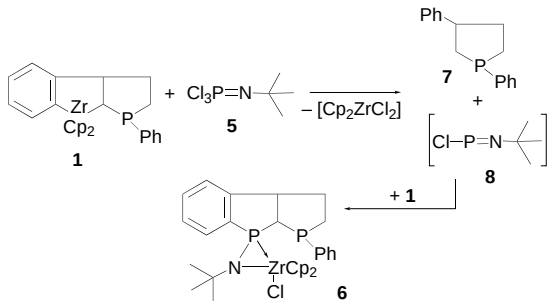
Krzysztof Owsianik, Maria Zablocka, Bruno Donnadieu, and Jean-Pierre Majoral**

Zirconium derivatives play central roles in a number of technologically important processes including, for example, the Ziegler–Natta-type polymerization of olefins.[1] The group IV metallocene derivatives have been the target of a range of studies directed either at the generation and trapping, or the isolation of a large number of significant species in organic and organometallic chemistry. A number of new methodologies in synthesis has been found that give easy access to useful starting materials, such as various heterocycles, chiral ligands, or more sophisticated molecules. Indeed the success of organozirconium reagents in organic, inorganic, and organometallic chemistry can be explained in terms of chemo-, regio-, diastereo-, and enantioselectivity. These reagents are generally able to discriminate between similar functionalities that differ only slightly in their steric and/or electronic environment.[2] However, studies of interactions between main-group elements and, more precisely, phosphorus derivatives and zirconium compounds have not been so frequently reported.[3,4] We recently reported the formation of mono- or tricyclic diphosphanes by exchange reactions between monochlorophosphanes or dichlorophosphanes and, for example, the zirconaindane phospholane (phospholanozirconaindane) **1** to obtain compounds **2** and **3** in good yields[5,6] and even in an enantiomerically pure form for one of these derivatives.[7] Functionalization of these ligands and their grafting on polymer supports or on dendrimers should open up interesting perspectives in catalysis. At first glance, an easy method of functionalization may involve the direct reaction of **1** with trichlorophosphane oxide or sulfide in order to synthesize monohalogenated tricyclic ligands such as **4**. However treatment of **1** with $(S)PCl_3$ or $(O)PCl_3$ gave numerous phosphorus species, as attested by the complexity of ^{31}P NMR spectra of the resulting mixtures. Unexpectedly, an unprecedented reaction was observed when **1** was treated with the trichloro iminophosphorane **5** leading to the first metallaspirophosphane **6**. We report here the full characterization of this unique compound including X-ray diffraction studies. The extension of this surprising reaction to the synthesis of another metalla-azaspirophosphane is described, as well as details concerning the mechanism of formation of these species and preliminary results concerning their reactivity.



2 **3** X = lone pair; R' = alkyl, NR_2, ...
4 X = O, S; R' = Cl

Treatment of the zirconaindane phospholane **1** (2 equiv) with $Cl_3P{=}N{-}t$Bu (**5**; 1 equiv) in toluene at room temperature resulted in the formation of two phosphorus species **6** and **7** and $[Cp_2ZrCl_2]$ (Scheme 1, $Cp = \eta^5\text{-}C_5H_5$). The $^{31}P\{^1H\}$ NMR spectrum of **6**, which was isolated in 52% yield, exhibits two doublets at $\delta = 3.7$ and 1.1 ppm ($^2J_{PP} = 22.4$ Hz), while a signal at $\delta = -10$ ppm is attributed to the phospholane **7**.[8] In addition to the signals from the carbon–phosphorus tricyclic



Scheme 1. Synthesis of the zircona–azaspirophosphane **6.** Solvent and conditions: toluene, 0°C, 30 min.

[*] Dr. J.-P. Majoral, B. Donnadieu
Laboratoire de Chimie de Coordination
CNRS
205 route de Narbonne, 31077 Toulouse cedex 4 (France)
Fax: (+33) 5-6155-3003
E-mail: majoral@lcc-toulouse.fr
Dr. M. Zablocka, K. Owsianik
Centre of Molecular and Macromolecular Studies
Polish Academy of Sciences
Sienkiewicza 112, 90-363 Lodz (Poland)

[**] This work was performed with the support of the Laboratoire Européen Associé (L.E.A) financed by C.N.R.S. (France), the Polish Committee for Scientific Research (KBN grant 3TO9A03619), and the European Community Marie Curie Fellowship (contract No. HPMT-CT-2001-00398).

Supporting information for this article is available on the WWW under http://www.angewandte.org or from the author.

 © 2003 Wiley-VCH Verlag GmbH & Co. KGaA, Weinheim DOI: 10.1002/anie.200250772

backbone and from the *tert*-butyl group linked to the nitrogen atom, two doublets are detected at $\delta = 6.05$ ($J_{HP} = 1.7$ Hz) and 6.09 ppm ($J_{HP} = 1.7$ Hz) in the ^{1}H NMR spectrum of **6**, which are characteristic of coupling of the cyclopentadienyl protons with a phosphorus atom when a direct phosphorus–zirconium bond is formed.[9,10] Other ^{1}H NMR data as well as ^{13}C NMR data are in agreement with the proposed structure for **6**, the first metalla-azaspirophosphane derivative reported to date. The solid-state structure of **6** has been corroborated by a single-crystal X-ray diffraction study.[11] An ORTEP diagram of **6** is shown in Figure 1 with selected bond lengths and angles.

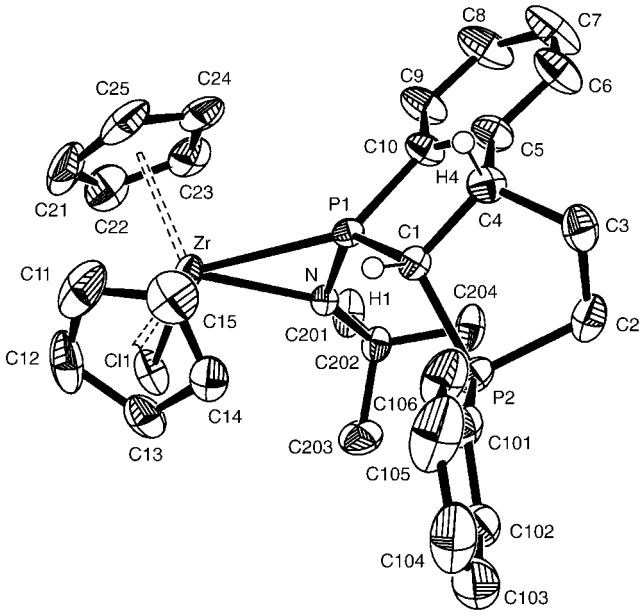
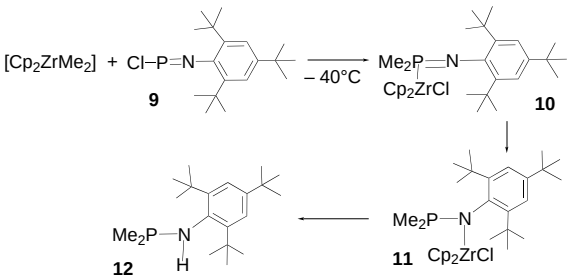


Figure 1. ORTEP drawing of complex **6**. Selected bond lengths [Å] and angles [°]: Zr-N 2.204(2), Zr-P(1) 2.5805(9), P1-N 1.615(2), P1-C1 1.865(2), P1-C10 1.807(3); N-Zr-P1 38.44(5), N-P1-Zr 58.05(7), P1-N-Zr 83.51(9), C10-P1-C1 92.9(12), N-P1-C1 123.54(11).

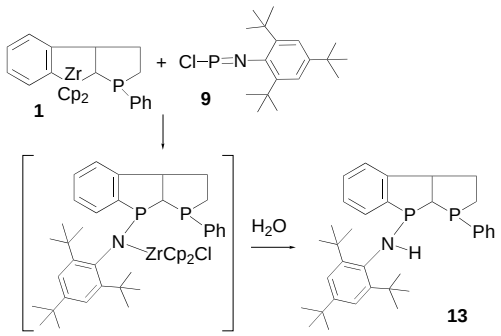
As a first approach, one can postulate that the trichloro iminophosphorane **5** reacts with the first equivalent of **1** (with removal of $[Cp_2ZrCl_2]$) to form the transient chlorophospha-imine Cl–P=N–*t*Bu (**8**), which reacts further with the second equivalent of **1** by insertion into an intracyclic Zr–C bond with concomitant migration of the chlorine atom from the phosphorus to the zirconium center. Rearrangement then leads to the stable 18 electron metalla-species **6**. Such an assumption is supported by previous work[10] in which the reaction of an analogous chlorophospha-imine **9** with $[Cp_2ZrMe_2]$ was reported. In this latter experiment the reaction proceeded by insertion of **9** into a Zr–Me bond followed by migration of the chlorine atom from the phosphorus to zirconium center and concomitant migration of the second methyl group in the opposite direction to give the kinetic product **10**, with the reaction observed only at −40 °C. Migration of a $\{Cp_2ZrCl\}$ fragment to nitrogen occurred, which led to the thermodynamic product **11** which is extremely water-sensitive and gave the final amino



Scheme 2. Addition of the chloro iminophosphane **9** to $[Cp_2ZrMe_2]$.

phosphane **12** through cleavage of the nitrogen–zirconium bond (Scheme 2).

In order to provide additional arguments in favor of the mechanism involving **1** and **5, 1** was reacted with the stable chlorophospha-imine **9** in a 1:1 ratio in toluene at 0 °C. Such a reaction allowed the isolation of the bisphosphane **13**, obtained as only one isomer, and arising from the insertion of **9** into a zirconium–carbon bond of **1** with release of a $\{Cp_2ZrCl\}$ fragment after mild hydrolysis of the nitrogen–zirconium bond (Scheme 3). Indeed, this experiment corroborates the proposed mechanism for the formation of **6** in which the trapping of an analogous chlorophospha-imine is postulated.



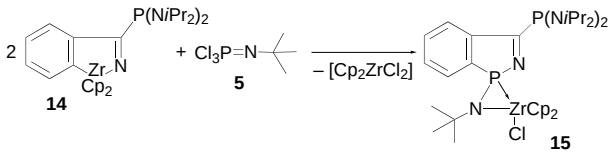
Scheme 3. Addition of the chloro iminophosphane **9** to the tricyclic system **1**.

As well as representing the preparation of an unique metalla-azaspirophosphane, these preliminary experiments show that in the presence of **1**, the trichloro iminophosphorane **5** can be regarded as a precursor of the unstable chlorophospha-imine **8**, a potentially useful new reagent in organophosphorus chemistry.

A question remains: Is it possible to generalize such a reaction? In other words, can other zircona complexes act in a similar fashion to **5**? To answer this question, the azazirconacyclopentene **14**[12] (2 equiv) was heated at 50 °C for 2 h in the presence of **5** (1 equiv); in these conditions the expected metalla-bisazaspirophosphane **15** was isolated in 49% yield (Scheme 4). Therefore, the presence of a N-Zr-C linkage in the starting reagent **14**, instead of the C-Zr-C unit in **1**, does not prevent the reaction from taking place.

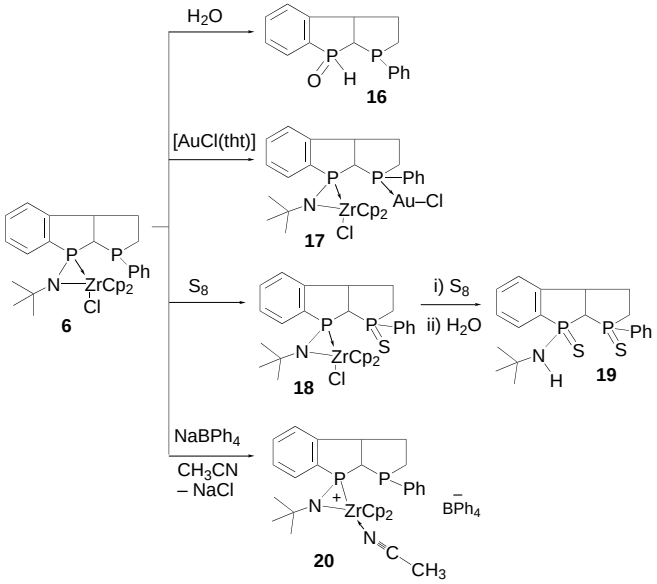
Such unusual complexes offer the opportunity to study their versatile behavior since several possible reactions can be

 © 2003 Wiley-VCH Verlag GmbH & Co. KGaA, Weinheim



Scheme 4. Synthesis of the zircona-bisazaspirophosphane **15**.

envisaged, including regiospecific reactions on one or both of the phosphorus atoms, selective cleavage of P–N or P–Zr bonds, and specific reactions at the zirconium center. Preliminary results obtained from experiments conducted with the metalla-azaspirophosphane **6** are shown in Scheme 5.



Scheme 5. Reactivity of the zircona-azaspirophosphane **6**.

Indeed, several observations can be made. Hydrolysis occurred, as expected, at the "central" phosphorus moiety with concomitant P–N and P–Zr bond cleavage that led to a new tricyclic ligand **16**, obtained as two isomers (*cis* and *trans* with respect to the position of the substituents on phosphorus atoms, that is, the proton and the phenyl group) in a 9:1 ratio and characterized by ^{31}P NMR (major product: $\delta = 3.4$ (br d, $^{2}J_{PP} = 143$ Hz, PPh) and 51.3 ppm (d of br d, $^{2}J_{PP} = 143$ Hz, $^{1}J_{PH} = 488$ Hz, PN); minor product: $\delta = -7.9$ (br d, $^{2}J_{PP} =$ 53 Hz, PPh) and 37.4 ppm (d of br d, $^{2}J_{PP} = 53$ Hz, $^{1}J_{PH} =$ 488 Hz, PN)), ^{1}H and ^{13}C NMR spectroscopy, as well as by mass spectrometry. Addition of [AuCl(tht)] (tht = tetrahydrothiophene) to **6** occurred at the phospholane ring, that is, on the external trivalent phosphorus atom, to form a unique bimetallic complex **17**. Treatment of **6** with two equivalents of sulfur initially afforded the derivative **18** resulting from sulfuration of the "external" phosphorus atom. The reaction can be monitored by ^{31}P NMR (doublets at $\delta = 60.3$ (P(S)Ph) and -0.5 ppm (PN) with $^{2}J_{PP} = 26$ Hz). Sulfuration of the central phosphorus moiety then occurred with cleavage of the dative P–Zr bond followed by mild hydrolysis of the N–Zr bond to form the disulfide adduct **19**, which was obtained as two isomers in a 9:1 ratio (major product: $\delta = 57.9$ (d, PPh) and 67.8 ppm (d, PN) with $^{2}J_{PP} = 7.8$ Hz; minor product: 57.5 (d, PPh) and 65.5 ppm (d, PN) with $^{2}J_{PP} = 4.4$ Hz). Dissociation of the strong zirconium–chlorine bond and retention of the ring system was observed when $NaBPh_4$ was added to a solution of **6** in acetonitrile. ^{31}P NMR spectra show the disappearance of the two doublets that arise from complex **6**, and two new doublets at $\delta = 4.4$ (PN) and 6.3 ppm (PPh) with $^{2}J_{PP} = 32$ Hz. Proof of ring retention is given by a small coupling constant ($J_{HP} = 1.5$ Hz) in the ^{1}H NMR spectrum that results from interactions between cyclopentadienyl protons and the phosphorus center. However, the resulting new cationic zirconium azaspirophosphane **20** is highly unstable and decomposes to several unidentified products. Indeed, the presence of P–Zr and N–Zr bonds does not significantly help in the stabilization of **20**. Nevertheless a specific reaction at the zirconium center can be emphasized at this stage.

In conclusion, the reaction of a trichloro iminophosphorane with two different zirconaindane complexes led to unique metallaspirophosphanes. The extension of such a methodology to other trichloro iminophosphoranes and to other zirconium complexes should provide a range of new metallaspirophosphanes; their versatile behavior would allow the preparation of useful reagents for organometallic chemistry and catalysis.

Received: December 16, 2002 [Z50772]

Keywords: bimetallic complexes · phosphanes · phosphorus · spiro compounds · zirconium

[1] See for example: a) "Metallocene and Single Site Olefin Catalysts": *J. Mol. Catal. A* **1998**, *128*, 1 (Ed.: R. F. Jordan); b) W. E. Piers, *Chem. Eur. J.* **1998**, *4*, 13, and references therein.

[2] See for example: a) "Recent Advances in the Chemistry of Zirconocene and Related Compounds:" *Tetrahedron* **1995**, *51, 15*, 4255 (Guest Ed.: E. I. Negishi); b) J. A. Labinger in *Comprehensive Organic Synthesis, Vol. 8* (Ed.: B. M. Trost, I. Fleming), Pergamon, Oxford, **1991**, p. 667; c) E. I. Neghishi in *Comprehensive Organic Synthesis, Vol. 5* (Ed.: B. M. Trost, L. A. Paquette), Pergamon, Oxford, **1991**, p. 1163; d) R. H. Grubbs, H. S. Pine in *Comprehensive Organic Synthesis, Vol. 5* (Ed.: B. M. Trost, L. A. Paquette), Pergamon, Oxford, **1991**, p. 1115; e) C. Ferreri, G Palumbo in *Comprehensive Organic Synthesis, Vol. 1* (Ed.: B. M. Trost, S. L. Schreiber), Pergamon, Oxford, **1991**, p. 139; f) A. D. Ryabov, *Chem. Rev.* **1990**, *90*, 403; g) J. E. McMurry, *Chem. Rev.* **1989**, *89*, 1513; G. Erker, M. Aulbach, M. Mena, R. Ptaff, F. Sosna, *Chem. Scr.* **1989**, *29*, 451; h) S. L. Buchwald, R. B. Nielsen, *Chem. Rev.* **1988**, *88*, 1047; i) E. I. Negishi, T. Takahashi, *Aldrichimica Acta* **1985**, *18*, 31.

[3] a) "New Aspects in Phosphorus Chemistry:" J. P. Majoral, A. Igau, V. Cadierno, M. Zablocka, *Top. Curr. Chem.* **2002**, *220*, 54; b) J. P. Majoral, P. Meunier, A. Igau, N. Pirio, M. Zablocka, A. Skowronska, S. Bredeau, *Coord. Chem. Rev.* **1998**, *178–180*, 145; c) J. P. Majoral, A. Igau, *Coord. Chem. Rev.* **1998**, *176*, 1.

[4] a) O. J. Scherer, M. Swarowsky, H. Swarowsky, G. Wolmershauser, *Angew. Chem.* **1988**, *100*, 738; *Angew. Chem. Int. Ed. Engl.* **1988**, *27*, 694; b) D. W. Stephan, *Angew. Chem.* **2000**, *112*, 322; *Angew. Chem. Int. Ed.* **2000**, *39*, 314; c) P. J. Chirik, J. A. Pool, E. Lobkovsky, *Angew. Chem.* **2002**, *114*, 3613; *Angew. Chem. Int. Ed.* **2002**, *41*, 3463.

 © 2003 Wiley-VCH Verlag GmbH & Co. KGaA, Weinheim

[5] M. Zablocka, A. Igau, B. Donnadieu, J. P. Majoral, A. Skowronska, P. Meunier, *Chem. Commun.* **1997**, 1239.
[6] M. Zablocka, N. Cenac, A. Igau, B. Donnadieu, J. P. Majoral, A. Skowronska, P. Meunier, *Organometallics* **1996**, *15*, 5436.
[7] M. Zablocka, B. Donnadieu, J. P. Majoral, M. Achard, G. Buono, *Tetrahedron Lett.*, in press.
[8] The phospholane **7** was isolated and characterized as its sulfide adduct. Main characteristic data: $^{31}P\{^1H\}$ NMR (C_6D_6, 162 MHz): $\delta = 55.1$ ppm. $^{13}C\{^1H\}$ NMR (C_6D_6, 100.6 MHz): $\delta =$ 29.8 (d, $^1J_{CP} = 66.8$ Hz; CH_2P), 32.7 (d, $^2J_{CP} = 3.7$ Hz; CH_2), 37.5 (d, $^1J_{CP} = 66.5$ Hz; CH_2P), 45.3 (d, $^2J_{CP} = 11.6$ Hz; CH), 126.7 (s), 127.0 (s), 128.8 (s), 128.9 (d, $J_{CP} = 11.1$ Hz; *o*-Ph or *m*-Ph), 129.9 (d, $J_{CP} = 9.8$ Hz; *m*-Ph or *o*-Ph), 131.9 ppm (s, *p*-Ph).
[9] a) M. Zablocka, F. Boutonnet, A. Igau, F. Dahan, J. P. Majoral, K. M. Pietrusiewicz, *Angew. Chem.* **1993**, *105*, 1846; *Angew. Chem. Int. Ed. Engl.* **1993**, *32*, 1735; b) V. Cadierno, M. Zablocka, B. Donnadieu, A. Igau, J. P. Majoral, A. Skowronska, *J. Am. Chem. Soc.* **1999**, *121*, 11086.
[10] A. Igau, N. Dufour, A. Mahieu, J. P. Majoral, *Angew. Chem.* **1993**, *105*, 76; *Angew. Chem. Int. Ed. Engl.* **1993**, *32*, 95.
[11] CCDC-199652 contains the supplementary crystallographic data for this paper. These data can be obtained free of charge via www.ccdc.cam.ac.uk/conts/retrieving.html (or from the Cambridge Crystallographic Data Centre, 12, Union Road, Cambridge CB21EZ, UK; fax: (+44) 1223-336-033; or deposit@ccdc.cam.ac.uk).
[12] V. Cadierno, B. Donnadieu, A. Igau, J. P. Majoral, *Eur. J. Inorg. Chem.* **2000**, 417.

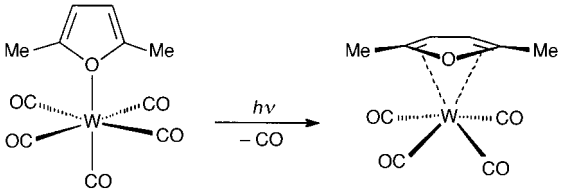
 © 2003 Wiley-VCH Verlag GmbH & Co. KGaA, Weinheim

Photolysis of Tungsten Complexes

Furans Bound Face-On: Sequential Loss of CO in the Formation of $[W(CO)_4(\eta^4\text{-}2,5\text{-dimethylfuran})]$**

*R. Krishnan, Hugo E. Gottlieb, and Richard H. Schultz**

While facially bound aromatic rings C_nH_n are ubiquitous in organometallic chemistry, complexes containing ligands of the type C_nH_nX (X = O or N) bound face-on are much less common. For example, although η^4-thiophene complexes are well-known,[1] and furan is known to bind in an η^4 fashion to surfaces,[2] as a ligand, furan normally prefers to bind in an η^2 fashion through one of its double bonds.[3] In fact, to our knowledge, only one complex containing an η^4-furan ligand has been reported, $[Cp^*Ru(\eta^4\text{-}C_4H_4O)]^+$.[4] We report here the observation of a carbonyl-containing η^4-furan complex, $[W(CO)_4(\eta^4\text{-}Me_2Fur)]$ **2** (Me_2Fur = 2,5-dimethylfuran), and the results of a kinetic study of its formation from $[W(CO)_5(\eta^1\text{-}Me_2Fur)]$ **1** [Eq. (1)].



1 **2** (1)

It has long been known that photolysis of $[M(CO)_6]$ (M = Cr, Mo, W) in the presence of a bischelating ligand (L_2) produces $[M(CO)_4(L_2)]$.[5] Technological advances made over the past two decades have made it possible to investigate the details of the reaction by means of the techniques of "fast kinetics." Such studies have shown that the reaction proceeds in several steps: first, the pentacarbonyl complex formed by the initial photolysis reacts within tens of picoseconds to form a solvated intermediate $[M(CO)_5(solv)]$ (solv = a molecule of solvent).[6] This solvated intermediate reacts with a molecule of L_2 to produce a monodentate complex $[M(CO)_5(L\text{-}L)]$, which then undergoes a thermally activated intramolecular ligand exchange, on a much slower timescale, to form the bidentate complex $[M(CO)_4(L_2)]$.[7–9]

The majority of the research in which the sequential chelation steps have been observed directly by fast kinetics techniques has concentrated on formation of $[M(CO)_4(\eta^1,\eta^1\text{-}L_2)]$ complexes, where L_2 is a bischelating phosphane or bipyridyl ligand. To our knowledge, the only report in the literature concerning the kinetics of the formation of an $[M(CO)_4(\eta^2,\eta^2\text{-}L_2)]$ complex from $[M(CO)_5(\eta^2\text{-}L\text{-}L)]$, where the ligand is a bischelating diene, is a study of the formation of $[Mo(CO)_4(\eta^2,\eta^2\text{-NBD})]$ (NBD = norbornadiene) following photolysis of $[Mo(CO)_6]$ solutions containing excess NBD.[10]

We have previously reported[11c] that in the presence of excess Me_2Fur, $[W(CO)_5(CyH)]$ (CyH = cyclohexane) reacts rapidly (second-order rate constant of 2.46×10^6 L mol^{-1} s^{-1} at 20 °C) to form $[W(CO)_5(Me_2Fur)]$. Based on the similarity of the C–O stretching region of its IR spectrum (two strong stretches at 1927 and 1941 cm^{-1} and a weak one at 2075 cm^{-1}) to those of other $[W(CO)_5L]$ complexes (L = cyclic ether),[11c] we assigned to it the η^1 structure **1**, that is, the ligand is bound to the metal through the lone pair of the O atom. We also determined the activation parameters for the reaction to be $\Delta H^{\neq} = 26.4 \pm 1.7$ kJ mol^{-1} and $\Delta S^{\neq} = -41.0 \pm 4.2$ J mol^{-1} K^{-1}. $[W(CO)_5(Me_2Fur)]$ is unstable in CyH solution, however. Over the course of a few seconds, its IR absorbtions begin to decay, while simultaneously, new peaks appear in the C–O stretching region of the IR spectrum at 1957, 1991, 2030, and 2097 cm^{-1}. This behavior contrasts with that of the analogous complexes with furan or 2-methylfuran, which are stable for several minutes in a room-temperature CyH solution con-

[*] Dr. R. H. Schultz, Dr. R. Krishnan, Dr. H. E. Gottlieb
Department of Chemistry, Bar-Ilan University
Ramat-Gan (Israel)
Fax: (+972) 3-535-1250
E-mail: schultr@mail.biu.ac.il

[**] This work was supported in part by the Israel Science Foundation, founded by the Israel Academy of Arts and Sciences. We would like to thank Dr. Vered Marks for assistance with collection of the NMR spectra. R.K. would like to acknowledge Bar-Ilan University for financial support.

Supporting information for this article is available on the WWW under http://www.angewandte.org or from the author.

 DOI: 10.1002/anie.200250804 © 2003 Wiley-VCH Verlag GmbH & Co. KGaA, Weinheim

taining a moderate excess of free ligand, but then decompose to unidentified products.

The only other $[W(CO)_5(\eta^1\text{-L})]$ (L = cyclic ether) complexes that we had previously observed to be unstable on a time scale of seconds are those in which the ligand also contains a double bond.[12] Following their initial formation from $[W(CO)_5(CyH)]$, these complexes undergo an intramolecular linkage isomerization to yield $[W(CO)_5(\eta^2\text{-L})]$, in which the ligand is bound to the metal by means of its double bond. Although η^2 binding is normally seen in furan complexes,[3] this kind of linkage isomerization cannot account for the behavior of $[W(CO)_5(Me_2Fur)]$, since the observed IR spectrum, which contains four C–O stretches, is inconsistent with a $[W(CO)_5L]$ structure. Rather, the IR spectrum is typical of that of a *cis*-$[M(CO)_4L_2]$ complex.[10,13] We assign this new complex the structure $[W(CO)_4(\eta^4\text{-}Me_2Fur)]$ **2**, produced by an intramolecular replacement of a second CO ligand and rearrangement of the Me_2Fur ligand from O-bound to π-bound at the ring face [Eq. (1)].

This structural assignment is supported by ^{1}H NMR spectroscopy. When a CyH solution containing 2×10^{-3} mol L^{-1} $[W(CO)_6]$ and 0.15 mol L^{-1} Me_2Fur is placed in a quartz NMR tube and exposed to the output of a XeCl excimer laser (308 nm), two new peaks appear in the ^{1}H NMR spectrum. The intensities of these peaks grow with additional photolysis, and the relative integrations are consistent with those of Me_2Fur, indicating that they arise from a photolysis product that contains Me_2Fur. In this product, the peak corresponding to that of the ring protons has shifted upfield relative to free Me_2Fur, from $\delta = 5.68$ to $\delta = 4.49$, while that corresponding to the methyl protons has shifted downfield, from $\delta = 2.15$ to $\delta = 2.36$. Upfield shifts in ring proton resonances but downfield shifts in methyl proton resonances upon complexation are typical for a facially bound methyl-substituted aromatic ligand, e.g., η^6-mesitylene.[14] Although the NMR data indicate that approximately 20% conversion of $[W(CO)_6]$ to this product had taken place, and the complex is stable for hours in CyH solution, we have not yet succeeded in isolating it. $[Cp^*Ru(\eta^4\text{-}C_4H_4O)]^+$ has also been reported to be stable only in solution.[4]

In order better to understand what is occurring in our system, we performed a kinetic study in which we used time-resolved IR absorption spectroscopy to monitor the conversion of $[W(CO)_5(\eta^1\text{-}Me_2Fur)]$ **1** to the final product. We observed that under the conditions of our experiment, the conversion occurs with clean first-order kinetics, and the rate of the decay of the intensities of the peaks corresponding to $[W(CO)_5(\eta^1\text{-}Me_2Fur)]$ **1** is equal, to within experimental error, to that of the growth of the product.[15] Furthermore, to within experimental error, the observed first-order rate constant is independent of $[Me_2Fur]$ and of $[W(CO)_6]$ in the initial solution. The independence of the rate on the reactant concentrations is clear evidence of an intramolecular process, consistent with our assigment of the structure $[W(CO)_4(\eta^4\text{-}Me_2Fur)]$ **2** to the product of the reaction. It also precludes the two other structures for the complex that might explain the spectral data: *cis*-$[W(CO)_4(Me_2Fur)_2]$, which would also have four IR-active CO stretches, or a dimeric complex in which a molecule of Me_2Fur bridges two $W(CO)_x$ fragments, which is consistent with the ^{1}H NMR spectrum. Since those two species would necessarily be formed in bimolecular reactions, the reaction rate constant for their formation would depend on the concentrations of the reactants. We also note that, to within experimental error, the reaction rate constant for formation of $[W(CO)_4(\eta^4\text{-}Me_2Fur)]$ **2** is the same whether the reaction takes place under Ar or in a CO-saturated solution under 1 atm of CO, implying that the reaction is irreversible under our experimental conditions.

Figure 1 shows an Eyring analysis of the temperature dependence of the rate constants that yields activation parameters of $\Delta H^{\ddagger} = 61.9 \pm 1.3$ kJ mol^{-1} and $\Delta S^{\ddagger} = -33.5 \pm 4.6$ J mol^{-1} K^{-1}. These activation parameters are similar to

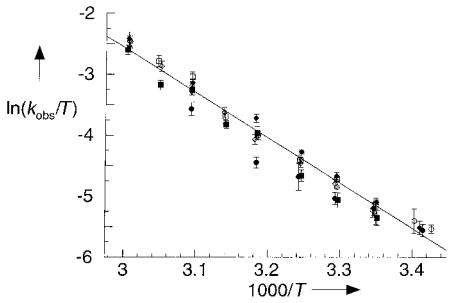


Figure 1. Eyring plot for the conversion of $[W(CO)_5(\eta^1\text{-}Me_2Fur)]$ **1** to $[W(CO)_4(\eta^4\text{-}Me_2Fur)]$ **2**. Shown are experimentally measured first-order rate constants with 1 σ uncertainties. Different symbols represent measurements made at different concentrations of Me_2Fur and $[W(CO)_6]$. The solid line is a weighted least-squares linear fit to the data corresponding to $\Delta H^{\ddagger} = 61.9$ kJ mol^{-1}, $\Delta S^{\ddagger} = -33.5$ J mol^{-1} K^{-1}.

those of chelate ring closure in $[W(CO)_5(L\text{-}L)]$, where L_2 is a bischelating N donor such as a bipyridyl, phenanthroline, or diazabutane ligand.[9] The low value of $\Delta H^{\ddagger}$ relative to the [W]–CO bond dissociation energy[16] and the negative $\Delta S^{\ddagger}$ indicate that the second CO replacement, like the first, is associative,[11] in which the Me_2Fur rearrangement and CO loss are concerted. Once again, this behavior is typical of intramolecular chelate ring closure.

As mentioned above, neither furan nor 2-methylfuran produces $[W(CO)_4(\eta^4\text{-L})]$ under the experimental conditions that yield $[W(CO)_4(Me_2Fur)]$ **2** within several seconds of the initial photolysis. We have previously noted that more strongly electron-donating ligands tend to react more rapidly with $[W(CO)_5(CyH)]$ because they can more readily stabilize the transition state for the ligand exchange.[11b,c] Presumably, similar considerations are at work in the present case. Me_2Fur, being more electron rich than furan or MeFur, can better stabilize a complex with electron-withdrawing ligands. Thus, the $[W(CO)_5(\eta^1\text{-}Me_2Fur)]$ complex **1** will be the most thermodynamically stable of the three, making competition from dissociation less significant than in the other two cases. Not only that, but for the same reason, formation of $[W(CO)_4(\eta^4\text{-L})]$ from $[W(CO)_5(\eta^1\text{-L})]$ should have the lowest activation barrier for $L = Me_2Fur$, which can best stabilize a transition state in which a bond is being broken. Hence, it is not surprising that $[W(CO)_4(Me_2Fur)]$ is much

 © 2003 Wiley-VCH Verlag GmbH & Co. KGaA, Weinheim

more readily formed and observed than the analogous furan and MeFur complexes.

Further studies are underway to isolate [$W(CO)_4(\eta^4$-$Me_2Fur)$] **2**, to elucidate the kinetics of the analogous furan and MeFur systems, and to produce and identify [$M(CO)_4$-(η^4-L)] complexes with these ligands as well.

Experimental Section

The spectrometer with which the kinetic experiments were performed has been described in detail previously.[11a] An Ar-degassed CyH solution containing $0.5–1 \times 10^{-3}$ mol L^{-1} [$W(CO)_6$] and a large excess of Me_2Fur was prepared. The solution flowed through a temperature-controlled (± 0.8 °C) CaF_2 IR cell (pathlength 0.5 mm), where it was exposed to a pulse (~20 ns, typically 60–80 mJ/pulse) of 308-nm light emanating from a XeCl excimer laser. The flow was maintained to ensure that each laser pulse irradiates fresh solution. The reaction kinetics were determined from the time dependence of the change of the absorption of the output of a Pb-salt diode laser. For these experiments, the laser was tuned to 1957 cm^{-1}, corresponding to a C–O stretch of the product complex **2**. Measurements were also made of the decay of the C–O stretch of [$W(CO)_5(\eta^1$-$Me_2Fur)$] **1** at $\lambda =$ 1942 cm^{-1}, and were consistent with those obtained from the growth of the product. Because the output of our laser is not as strong at $\lambda = 1942$ cm^{-1}, these transients were of lower quality and were not used for the kinetic analysis. The raw transients were converted to ΔA ($A =$ absorbance). First-order rate constants were obtained by fitting the time dependence of ΔA to a single exponential and by linear fits to $\ln|\Delta A_t - \Delta A_\infty|$. The reported rate constants (see Supporting Information) are the averages of several independent fits to the data, and are given with 1 σ uncertainties to the fits.

Static IR spectra of reaction products were obtained by photolyzing a [$W(CO)_6$]/Me_2Fur solution with 1–100 laser shots, taking an aliquot of the solution, and measuring its IR spectrum in a Bruker Equinox 55 FTIR spectrometer. NMR spectra were obtained on a Bruker DPX-300 instrument with presaturation of the resonance of the C_6H_{12} solvent protons. The chemical shift of the protons in neat CyH was measured in a separate experiment and found to be $\delta =$ 1.443 relative to the TMS internal standard.

CyH was obtained in spectrophotometric- or HPLC-grade purity and distilled from Na/benzophenone to remove remaining H_2O. [$W(CO)_6$] was obtained in 98% purity from Strem Chemicals and used without further purification. Me_2Fur was obtained from Aldrich in >99% purity (confirmed by NMR), distilled from a drying agent, and stored over KOH.

Received: December 20, 2002 [Z50804]

Keywords: IR spectroscopy · kinetics · photolysis · tungsten

[1] a) R. J. Angelici, *Acc. Chem. Res.* **1988**, *21*, 387; b) B. Chaudret, F. Jalón, F. M. Pérez-Manrique, F. Lahoz, F. J. Plou, R. Sánchez-Delgado, *New J. Chem.* **1990**, *14*, 331; c) K. E. Janak, J. M. Tanski, D. G. Churchill, G. R. Parkin, *J. Am. Chem. Soc.* **2002**, *124*, 4182.

[2] a) A. B. Sexton, *Surf. Sci.* **1985**, *163*, 99; b) R. M. Ormerod, C. J. Baddeley, C. Hardacre, R. M. Lambert, *Surf. Sci.* **1996**, *360*, 1; c) F. Q. Yan, M. H. Qiao, X. M. Wei, Q. P. Liu, J. F. Deng, G. Q. Xu, *J. Chem. Phys.* **1999**, *111*, 8068.

[3] a) R. Cordone, W. D. Harman, H. Taube, *J. Am. Chem. Soc.* **1989**, *111*, 5969; b) H. Chen, L. M. Hodges, R. Liu, W. C. Stevens, Jr., M. Sabat, W. D. Harman, *J. Am. Chem. Soc.* **1994**, *116*, 5499; d) L. A. Friedman, M. Sabat, W. D. Harman, *J. Am. Chem. Soc.* **2002**, *124*, 7395.

[4] B. Chaudret, F. A. Jalon, *J. Chem. Soc. Chem. Commun.* **1988**, 711.

[5] S. S. Sandhu, A. K. Mehta, *J. Organomet. Chem.* **1974**, *77*, 45.

[6] a) J. A. Welch, K. S. Peters, V. Vaida, *J. Phys. Chem.* **1982**, *86*, 1941; b) J. Simon, K. S. Peters, *Chem. Phys. Lett.* **1983**, *98*, 53; c) L. Wang, X. Zhu, K. G. Spears, *J. Am. Chem. Soc.* **1988**, *110*, 8695; d) M. Lee, C. B. Harris, *J. Am. Chem. Soc.* **1989**, *111*, 8963; e) X. Xie, J. D. Simon, *J. Phys. Chem.* **1989**, *93*, 4401; f) A. G. Joly, K. A. Nelson, *Chem. Phys.* **1991**, *152*, 69; g) T. Lian, S. E. Bromberg, M. C. Asplund, H. Yang, C. B. Harris, *J. Phys. Chem.* **1996**, *100*, 11994.

[7] a) J. A. Connor, G. A. Hudson, *J. Organomet. Chem.* **1974**, *73*, 351; b) J. A. Connor, P. I. Riley, *J. Organomet. Chem.* **1975**, *94*, 55; c) J. A. Connor, G. A. Hudson, *J. Chem. Soc. Dalton Trans.* **1975**, 1025.

[8] a) S. Oichi, *Organometallics* **1988**, *7*, 1237; b) K. Bal Reddy, R. Hoffman, G. Konya, R. van Eldik, E. M. Eyring, *Organometallics* **1992**, *11*, 2319; c) Q. Ji, C. R. Lloyd, E. M. Eyring, R. van Eldik, *J. Phys. Chem. A* **1997**, *101*, 243.

[9] a) M. J. Schadt, A. J. Lees, *Inorg. Chem.* **1986**, *25*, 672; b) D. E. Marx, A. J. Lees, *Inorg. Chem.* **1987**, *26*, 620; c) K. Bal Reddy, R. van Eldik, *Inorg. Chim. Acta* **1990**, *169*, 13; d) S. Zhang, V. Zang, G. R. Dobson, R. van Eldik, *Inorg. Chem.* **1991**, *30*, 355.

[10] S. Zhang, G. R. Dobson, *Inorg. Chem.* **1990**, *29*, 598.

[11] a) R. Paur-Afshari, J. Lin, R. H. Schultz, *Organometallics* **2000**, *19*, 1682; b) A. Lugovskoy, R. Paur-Afshari, R. H. Schultz, *J. Phys. Chem. A* **2000**, *104*, 10587; c) R. Krishnan, R. H. Schultz, *Organometallics* **2001**, *20*, 3314.

[12] a) R. Elgamiel, I. Huppert, E. Lancry, Y. Yerucham, R. H. Schultz, *Organometallics* **2000**, *19*, 2237; b) A. Shagal, R. H. Schultz, *Organometallics* **2002**, *21*, 5657.

[13] a) M. H. B. Stiddard, *J. Chem. Soc. Dalton Trans.* **1962**, 4712; b) J. H. Darensbourg, H. H. Nelson III, M. A. Murphy, *J. Am. Chem. Soc.* **1977**, *99*, 896.

[14] a) E. L. Muetterties, J. R. Bleeke, A. C. Sievert, *J. Organomet. Chem.* **1979**, *178*, 197; b) T. Szymańska-Buzar, K. Kern, *J. Organomet. Chem.* **2001**, *622*, 74.

[15] A table of first-order rate constants for the reaction is given in the Supporting Information.

[16] K. E. Lewis, D. M. Golden, G. P. Smith, *J. Am. Chem. Soc.* **1984**, *106*, 3905.

 © 2003 Wiley-VCH Verlag GmbH & Co. KGaA, Weinheim

Metal-Free Electron Microscopy

Direct Observation of 3D Mesoporous Structure by Scanning Electron Microscopy (SEM): SBA-15 Silica and CMK-5 Carbon**

*Shunai Che, Kristina Lund, Takashi Tatsumi, Sumio Iijima, Sang Hoon Joo, Ryong Ryoo, and Osamu Terasaki**

Mesoporous silica has attracted much attention in recent years, because of its potential for advanced applications in catalysis, separation technologies, electronic engineering, and manufacturing of optical devices.[1,2] The highly nanoporous structures with good thermochemical stability are suitable for the synthesis of new materials such as nanoparticles, wires and networks of platinum and carbon within the pore system.[3,4] In the case of the carbon synthesis, the fabrication technique has been fully developed so that ordered mesoporous carbons exhibiting Bragg X-ray diffraction (XRD) lines similar to those of the MCM-41-type mesoporous silica can be obtained after the complete removal of the silica template.

Recently, an electron crystallographic analysis method based on transmission electron microscopy (TEM) has been developed to solve 3D structures of mesoporous silica crystals.[5] The structural solution provided direct information on detailed structures inside the mesoporous crystals such as pore diameter, shape and connectivity. But, the detailed structures at the crystal surfaces, such as the manner of channel openings at external surface and the accessibility to internal pores, were not clarified. Scanning electron microscopy (SEM) has advantages over TEM for the determination of the surface structures. SEM is a relatively simple experiment and requires minimum sample preparation, and solid information on surface structures can be obtained from "nonprojected" images in three dimensions because of the long focal depth of the objective lens.[6] However, because of "charging problems" common for insulators and low resolution, ordinary SEM has been unsuitable for accurate determination of the detailed surface structures of the mesoporous materials.

Herein, we report that we can visualize directly the detailed surface structures of the SBA-15 mesoporous silica and its CMK-5 carbon replica, by using high resolution SEM and scanning transition electron microscopy (STEM) without metal coating. The high-resolution 3D SEM images clearly show the presence of interconnections between the hexagonally packed mesoporous channels, as suggested in previous works based on TEM imaging of the Pt replica.[4,7] Interestingly, the images show that the surfaces perpendicular to the direction of the channels (*c* direction) are intricately composed of tubes with closed ends, open ends, and channels that are curled back to the inside of the particles. Furthermore, we can distinguish two types of pores in the CMK-5 carbon, that is, the tubelike pores formed by carbon tubes and pores formed by removal of the silica wall.

The SBA-15 silica and CMK-5 carbon samples observed in the SEM investigation were obtained by following procedures described elsewhere.[3a] Typical synthesis conditions and properties obtained from N_2 adsorption–desorption measurement are given in Table 1.

Figure 1 shows SEM images and STEM image of the calcined SBA-15 silica sample. The silica particles in the SEM image exhibit hexagonal cylinderlike morphologies with curvatures along the *c* direction, which is consistent with the 2D hexagonal mesostructures. The high-resolution SEM images reveal that the external surfaces parallel to the *c* direction are composed of a uniform array of bisectional parts of channels. The channel walls exhibit "wiggling" along the *c* direction to form random interconnections between adjacent channels. However, compared to the surfaces parallel to the *c* direction, the external surfaces perpendicular to the *c* direction is composed of intricately curved channels. Many of the channels are curled to join back with others at the surfaces.

The STEM analysis was performed with microtomed cross sections of the particles. The STEM image confirms that the channels are hexagonally arranged within the hexagonal cylinder, and that the channels at surfaces along the *c* direction have a concaved open cross-sectional shape (Figure 1e). The image analysis gave the SBA-15 pore diameters in the range of 7.5 ± 0.3 nm and the thickness of the pore wall to be 2.5 ± 0.3 nm. A schematic model of the structure is given in Figure 2, the interconnections of channels are not shown for simplicity. It can be considered that the surface of the

[*] Dr. O. Terasaki
Department of Physics
Graduate School of Science
Tohoku University
Sendai, 980-8578 (Japan)
Fax: (+81) 22-217-6475
E-mail: terasaki@struc.su.se
E-mail: terasaki@msp.phys.tohoku.ac.jp

S. Che, S. Iijima
ICORP-JST
c/o NEC
34 Miyukigaoka, Tsukuba, Ibaraki, 305-8501 (Japan)

Dr. O. Terasaki, K. Lund
Arrhenius Laboratory
Stockholm University
10691 Stockholm (Sweden)

S. Che, T. Tatsumi
Division of Materials Science & Chemical Engineering
Faculty of Engineering
Yokohama National University
79-5 Tokiwadai, Yokohama 240–8501 (Japan)

S. H. Joo, R. Ryoo
National Creative Research Initiative Center for Functional Nanomaterials and
Department of Chemistry (School of Molecular Science-BK21)
Korea Advanced Institute of Science and Technology
Daejeon, 305-701 (Korea)

[**] The authors are grateful to Messrs Makoto Watanabe (Hitachi Science System) and Yasushi Nakaizumi (Hitachi High-Technologies Corporation) for taking scanning electron micrographs. S.C. thanks Dr. M. Yudasaka (ICORP-JST) for giving advise and comments.

 © 2003 Wiley-VCH Verlag GmbH & Co. KGaA, Weinheim DOI: 10.1002/anie.200250726

Table 1: Properties of tubelike mesoporous carbon materials with different tube diameters.

Sample	Synthesis conditions		Unit cell *a* [nm]	Surface area S_{BET} [$m^2 g^{-1}$][a]	Tube diameter d_{BJH} [nm][b]
	FA/SiO_2	Polymerization time			
SBA-15	–	–	9.8	597	8.2[c]
a	1.5	2 h	9.4	1750	5.0
b	1.5	3 h	9.8	1640	4.6
c	2.0	4 h	9.4	1578	4.2
d	2.5	6 h	9.6	1368	3.6
e	2.75	–[e]	9.4	1354	3.6
f[d]	3.25	–[e]	9.4	1118	3.0

[a] Calculated by the BET method. [b] Calculated from the adsorption branch of the N_2 isotherm of the CMK-5 without removing silica wall by using the BJH method. [c] Mesopore diameter of SBA-15. [d] Synthesized with two-step FA polymerization. [e] Synthesized without evacuation.

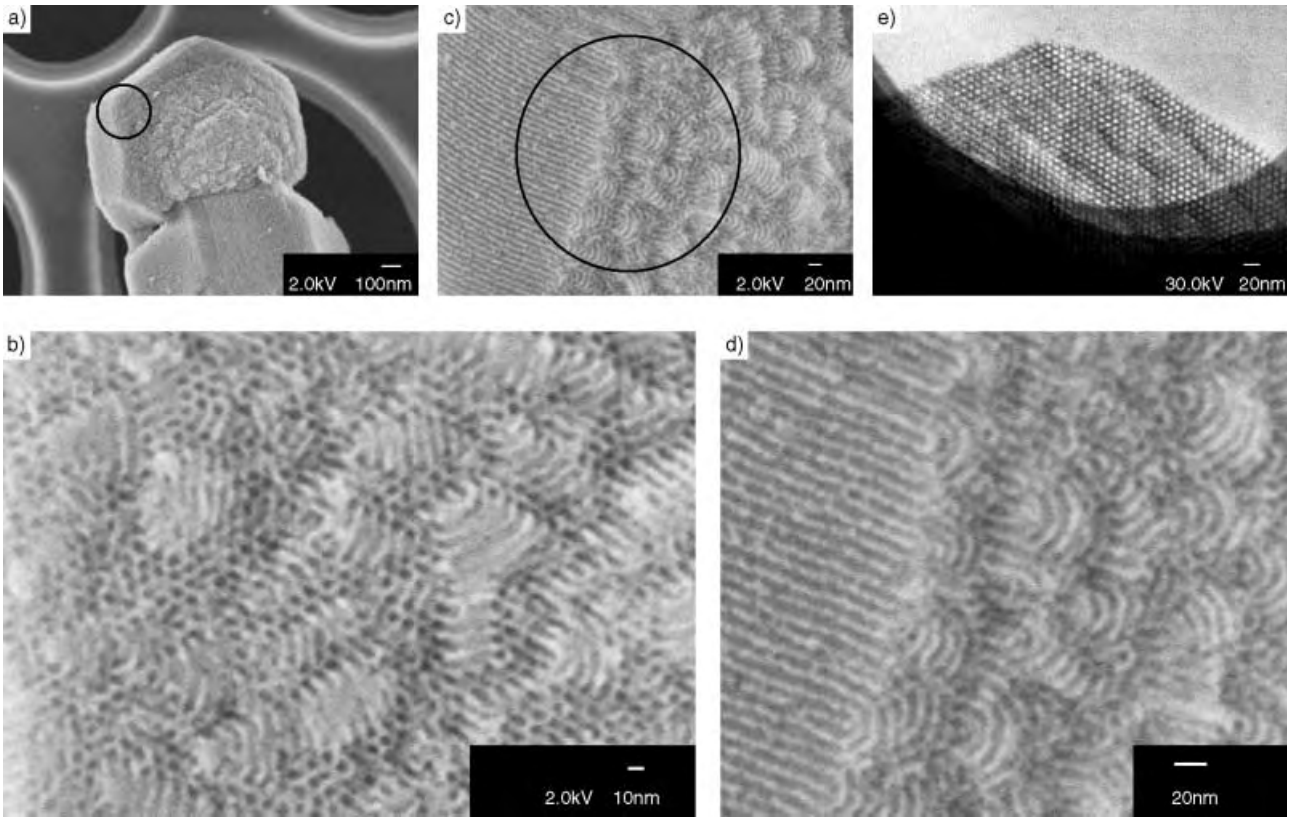


Figure 1. SEM (a, b, c and d) and STEM (e) images of SBA-15 mesoporous silica. Circled areas in a) and c) are enlarged in b) and d) respectively.

hexagonal cylinders along the *c* direction is always formed by the cut along the center of the pores. If the surfaces were formed by cuts along the pore walls (dotted line in Figure 2), we would not be able to observe the open concave channels. Initially, SBA-15 was considered to be an extra-large pore MCM-41 analogue with 2D hexagonal *p6mm* structure. Later, the replication studies using platinum and carbon have revealed that the main channels of SBA-15 can be interconnected into the form of a 3D porous network,[3,4,7] particularly when the synthesis mixture is heated after the mesophase formation.[8]

Figure 3A and 3B show the XRD patterns of SBA-15 silica and CMK-5 carbons, which were synthesized with various ratios of furfuryl alcohol (FA)/silica and different times for FA polymerization. We found out that the tube inner diameter of the carbon product depended not only on the FA/silica ratio but also on the polymerization time before evacuation. At present, by using SBA-15 with pore diameter of 8.2 nm we were able to control the inner diameters of the CMK-5 carbon in the range of 3.0–5.0 nm (see Table 1). This result indicates that the thinnest possible tubes were 1.6 nm in wall thickness. Interestingly, it was difficult to prepare carbon

 © 2003 Wiley-VCH Verlag GmbH & Co. KGaA, Weinheim

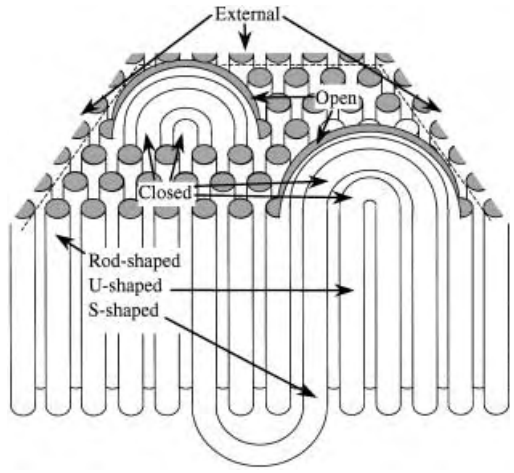


Figure 2. Schematic representation of the mesostructure of the SBA-15. Interconnections between adjacent channels are omitted for clarity.

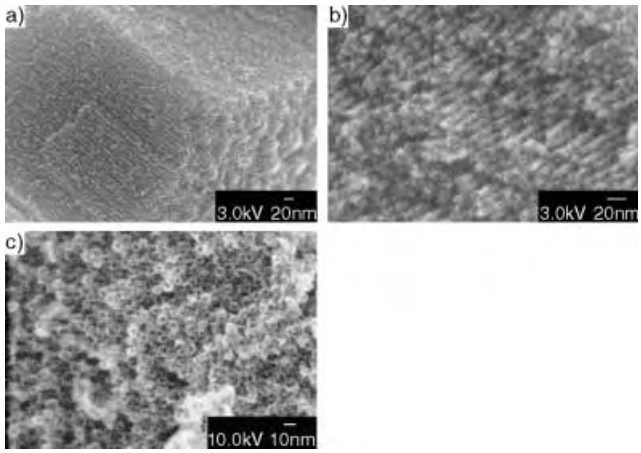


Figure 4. SEM images taken along different directions, at different magnifications and accelerating voltages from CMK-5 with tube inner diameter of 4.2 nm.

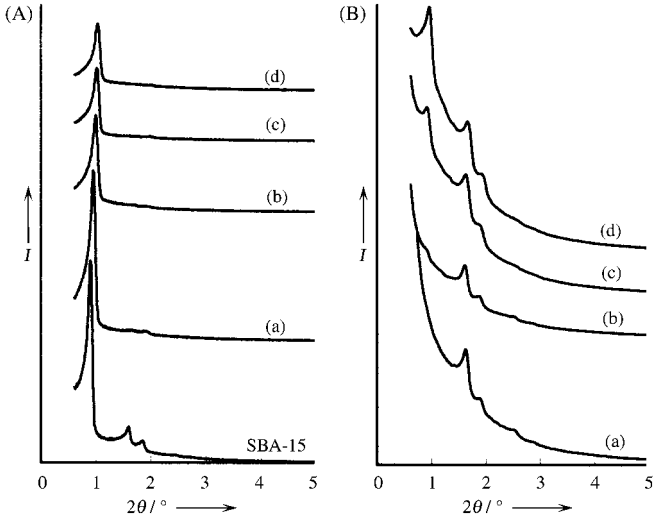


Figure 3. XRD patterns of SBA-15 and CMK-5 carbons obtained before (A) and after (B) removing silica wall. The FA/SiO_2 ratio and other synthesis conditions are a) 1.25:1, without evacuation; b) 1.5:1, with 3 h polymerization; c) 2.5:1, with 6 h polymerization; d) 3.25:1, with two steps FA polymerization; I = relative intensity.

tubes less than 3.6 nm in diameter by a single-step FA polymerization even by using a large amount of FA and without evacuation. When FA polymerization was performed in two steps, the tube diameter of the resultant CMK-5 was decreased to 3.0 nm. Oxalic acid was used as an acid catalyst for FA polymerization in the second step. We clearly observed that powder XRD intensity of the silica/carbon composite (i.e., samples just before removal of the silica framework) varied significantly depending on the thickness of the carbon tubes formed within the silica channels. More systematic studies on this point are continuing and the results will be reported separately.

Figure 4 shows the high-resolution SEM images of the CMK-5 sample with the inner diameter of 4.2 nm. The SEM images of the carbon exhibit very similar morphologies to those for the SBA-15 silica template. Interestingly, most of the carbon nanotubes are open at the surfaces of the porous crystals. This SEM investigation confirms that the carbon replication with FA can be perfectly achieved throughout the entire volume of the silica particle.

In conclusion, we have demonstrated for the first time that the resolution of the present SEM (taken directly from silica without gold plating) and STEM is sufficiently high for accurate determination of the surface structures of the mesostructured SBA-15 silica and CMK-5 carbon materials. We believe that these EM techniques can also be used for other mesoporous materials. The accurate information thus obtained will be highly useful for gaining new insights into the molecular factors governing the formation and growth of the inorganic–organic mesophases, and also for the development of various applications.

Experimental Section

SBA-15: SBA-15 mesoporous silica was synthesized by using the triblock copolymer Pluronic P123 ($EO_{20}PO_{70}EO_{20}$, $M_{av} = 5800$, BASF) as a surfactant and tetraethoxylsilicon (TEOS) as a silica source. In a typical synthesis experiment, TEOS (20.8 g) was added to a mixture of P123 (10 g), TMB (0–20 g), HCl (62.57 g, 35 wt %), and deionized water (319 g)under static condition at 35 °C. After the mixture was stirred for 24 h, the mesostructured product thus formed was cured at 100 °C for an additional 24 h. The products were filtered, dried without washing, and calcined at 823 K.

CMK-5: CMK-5 was synthesized by using SBA-15 as the template and furfuryl alcohol (FA, $C_5H_6O_2$) as the carbon precursor. The SBA-15 silica was converted to an aluminosilicate form with a Si/Al ratio of 20:1, following the postsynthesis incorporative procedure. The pore volume of SBA-15 was filled with different amount of FA by the incipient-wetness technique. The aluminosilicate SBA-15 containing the FA was heated for different polymerization times (see Table 1) at 80 °C and then at 150 °C for 8 h, which resulted in the aluminosilicate acid-catalyzed polymerization of the FA in the form

 © 2003 Wiley-VCH Verlag GmbH & Co. KGaA, Weinheim

of a layer coated on the pore walls. The remaining FA in the core of the template pores was removed by heating the sample at 80 °C with evacuation (Table 1 samples a, b, c, d) or without evacuation (Table 1 samples e, f). To obtain the smaller tube diameter, a two-step method was employed for the filling of FA. Oxalic acid was used as an acid catalyst in the second step, because the aluminosilicate wall was covered with FA polymer in the first step and therefore could not catalyze the polymerization further. The polymerized FA was converted to carbon inside the SBA-15 template by pyrolysis at 900 °C for 6 h under an Ar flow. The porous carbon was obtained after subsequent dissolution of the silica framework in 5 % HF acid at room temperature.

XRD measurement: XRD patterns were recorded by using an MX Labo powder diffractometer equipped with $Cu_{K\alpha}$ radiation (40 kV, 20 mA) at the rate of 1.0° min^{-1} over the range of 1.5–10.0° (2θ). The samples were prepared as thin layers on glass slides.

SEM and STEM measurement: The microscopic features of all samples (Aluminated SBA-15, CMK-5 with different tube diameter) were observed with SEM (Hitachi, S-5200). To observe genuine pore structures on the external surface, the samples were observed without any metal coating for SEM. By using a low accelerating voltage, we can obtain selective information from the surface region. In addition, the "charging problems common for insulators" are not serious. The resolution is limited by an effective electron probe size on the specimen, and is determined from spreads owing to a) diffraction of an aperture (Airy pattern), b) spherical aberration, and c) chromatic aberration in addition to electron source size, therefore to obtain high-resolution images at low accelerating voltage an electron source with high brightness and coherence, and small spherical and chromatic aberrations of the objective lens are important.[6] An accelerating voltage, 2 kV (resolution: ca. 1.2 nm) was chosen for SBA-15, because this was the highest possible without charging problem, and 10 kV (resolution: ca. 0.6 nm) for CMK-5 to optimize a relation between surface information and image resolution. To observe internal structures of the samples, STEM images were taken from thinly sectioned samples, mesoporous silica or carbon particles, obtained with an ultramicrotome.

N_2 adsorption-desorption measurement: The surface area and the pore size were measured at −196 °C on a Belsorp 28SA sorptionmeter. Samples were pretreated for 2 h at 200 °C and 1.33×10^{-4} Pa. The BET specific surface area, S_{BET}, was calculated by using adsorption branches in the relative pressure range from 0.04 to 0.1. The primary mesopore volume V_p was obtained by using the high-resolution t-plot method. The pore size distribution was calculated from adsorption branches of isotherms using the BJH method.

Received: December 9, 2002 [Z50726]

Keywords: carbon nanotubes · electron microscopy · mesoporous materials · self-assembly · zeolite analogues

[1] a) T. Yanagisawa, T. Shimizu, K. Kuroda, D. Kato, *Bull. Chem. Soc. Jpn.* **1990**, *63*, 988; b) C. T. Kresge, M. E. Leonowicz, W. J. Roth, J. C. Vartuli, J. S. Beck, *Nature* **1992**, *359*, 710; c) J. S. Beck, J. C. Vartuli, W. J. Roth, M. E. Leonowicz, C. T. Kresge, K. D. Schmitt, C. T.-W. Chu, D. H. Olson, E. W. Sheppard, S. B. McCullen, J. B. Higgins, J. L. Schlenker, *J. Am. Chem. Soc.* **1992**, *114*, 10834.

[2] A. Monnier, F. Schüth, Q. Huo, D. Kumar, D. I. Margolese, R. S. Maxwell, G. D. Stucky, M. Krishnamurty, P. Petroff, A. Firouzi, M. Janicke, B. F. Chmelka, *Science* **1993**, *261*, 1299.

[3] a) S. H. Joo, S. J. Choi, I. Oh, J. Kwak, Z. Liu, O. Terasaki, R. Ryoo, *Nature* **2001**, *412*, 169; b) R. Ryoo, S. H. Joo, S. Jun, *J. Phys. Chem. B* **1999**, *103*, 7743; c) S. Jun, S. H. Joo, R. Ryoo. , M. Kruk, M. Jaroniec, Z. Liu, T. Ohsuna, O. Terasaki, *J. Am. Chem. Soc.* **2000**, *122*, 10712.

[4] a) Z. Liu, O. Terasaki, T. Ohsuna, K. Hiraga, H. J. Shin, R. Ryoo, *ChemPhysChem* **2001**, *2*, 229; b) O. Terasaki, Z. Liu, T. Ohsuna, H. J. Shin, R. Ryoo, *Microsc. Microanal.* **2002**, *8*, 35; c) H. J. Shin, C. H. Ko, R. Ryoo, *J. Mater. Chem.* **2001**, *11*, 260.

[5] a) A. Carlsson, M. Kaneda, Y. Sakamoto, O. Terasaki, R. Ryoo, S. H. Joo, *J. Electron Microsc.* **1999**, *48*, 795; b) Y. Sakamoto, M. Kaneda, O. Terasaki, D. Y. Zhao, J. M. Kim, G. Stucky, H. J. Shin, R. Ryoo, *Nature* **2000**, *408*, 449; c) M. Kaneda, T. Tsubakiyama, A. Carlsson, Y. Sakamoto, T. Ohsuna, O. Terasaki, S. H. Joo, R. Ryoo, *J. Phys. Chem. B* **2002**, *106*, 1256.

[6] "Structure and Structure Determination": O. Terasaki in *Electron Microscopy Studies in Molecular Sieve Science in Molecular Sieves-Science and Technology, Vol. 2* (Eds.: H. G. Karge, J. Weitkamp), Springer, Heidelberg, **1999**, p. 71 – 112.

[7] R. Ryoo, C. H. Ko, M. Kruk, V. Antochshuk, M. Jaroniec, *J. Phys. Chem. B* **2000**, *104*, 11465.

[8] A. Galarneau, H. Cambon, F. Di. Renzo, R. Ryoo, M. Choi, F. Fajula, *New J. Chem.* **2003**, *27*, 73.

 © 2003 Wiley-VCH Verlag GmbH & Co. KGaA, Weinheim

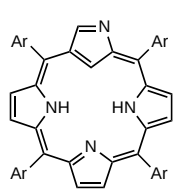
Pt Complexes of N-Confused Porphyrin

Facile Formation of *N*-Confused Porphyrin Dimers by Platinum(II) Coordination to the Outer-Nitrogen Atoms

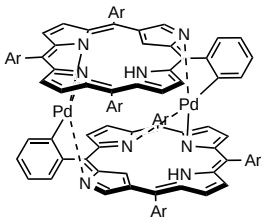
Hiroyuki Furuta, Katsuyuki Youfu, Hiromitsu Maeda, and Atsuhiro Osuka**

Recently, metal assisted porphyrin assembly has attracted much interest as one of the useful strategies employed to create polyporphyrin architectures in supramolecular chemistry.[1] For such studies, a combination of Pd^{II} or Pt^{II} ions, and amines such as pyridine, which can form stable tetracoordinated square-planar complexes, are frequently used as external bridging metal ions and ligands, respectively.[2] The edge-to-edge distances between two adjacent porphyrin rings in these systems depend on the size of the linker, thus, one way of generating the shortest connection might be to form a bond between the bridging metal atom and the porphyrin framework in which the coordinating atom is embedded.

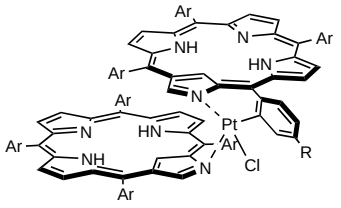
In the course of studying *N*-confused porphyrin (NCP, **1**),[3,4] we discovered the formation of a doubly linked Pd^{II}–NCP-dimer complex, or "double decker" (**2**), in which two Pd centers were directly bonded to an outwardly pointing nitrogen atom of the confused pyrrole ring, an *ortho*-carbon atom of *meso*-aryl group, and two inner core nitrogens of the countered porphyrin.[5] The unique structure of **2** was derived as the result of the distortion from planarity of both the porphyrin ring and the coordinated Pd^{II} center. In this regard, we have been interested in Pt^{II}-ion complexation because rigid square-planar Pt^{II} complexes are known.[6] This attribute might force the porphyrin ring to be distorted significantly if the NCP formed a similar type of dimer to that of complex **2** with Pt^{II} ions. Interestingly, the Pt dimer complexes (**3, 4**) were singly linked dimers with the ratio of Pt to NCP being 1:2. Herein, we report the syntheses and structural characterization of novel Pt^{II}–NCP dimer complexes and an inner coordinated monomer complex (**5**). To the best of our knowledge, the complexes **3** and **4** are the first NCP dimers linked by a metal at the peripheral core nitrogens.



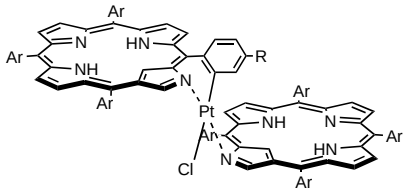
1



2



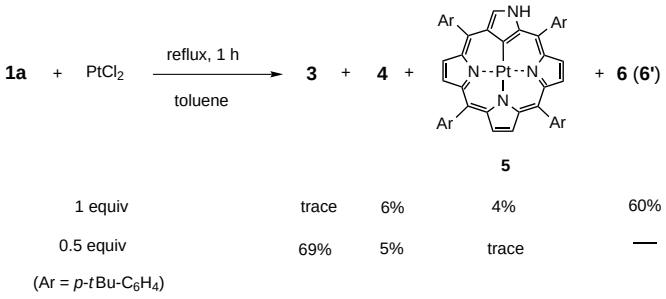
3



4

When *N*-confused 5,10,15,20-tetrakis(4′-*tert*-butylphenyl)-porphyrin (**1a**)[7] was treated with one equivalent of $PtCl_2$ in refluxing toluene for 1 h, green dimer complexes **3** and **4** were isolated in trace and 6% yield, respectively. Apart from these, inner coordinated monomer complex **5** and an isomeric mixture of reddish dimer complexes **6** and **6′** (see below) were produced in 4 and 60% yields, respectively. On the other hand, when 0.5 equivalents of $PtCl_2$ was subjected to the reaction, the dimers **3** and **4** were isolated in 69 and 5% yields, respectively, but the monomer **5** was obtained only in trace amounts and the formation of neither **6** nor **6′** were observed (Scheme 1).

The structures of dimer complexes **3** and **4** were established by single crystal X-ray analyses (Figure 1).[8] Both complexes consist of one Pt atom, two NCP units, and one chloride atom. The Pt center was connected with two outer-nitrogen atoms of NCP molecules, an *ortho*-carbon atom of a



Scheme 1. Reactions of NCP **1a** with $Pt^{II}Cl_2$.

[*] Prof. Dr. H. Furuta[+]
Department of Chemistry and Biochemistry
Graduate School of Engineering
Kyushu University
Fukuoka 812-8581 (Japan)
Fax: (+81) 92-651-5606
E-mail: hfuruta@cstf.kyushu-u.ac.jp
Prof. Dr. A. Osuka, K. Youfu, H. Maeda
Department of Chemistry
Graduate School of Science
Kyoto University
Kyoto 606-8502 (Japan)
Fax: (+81) 75-753-3970
E-mail: osuka@kuchem.kyoto-u.ac.jp
[+] PRESTO
Japan Science and Technology Corporation (JST) (Japan)

Supporting information for this article is available on the WWW under http://www.angewandte.org or from the author.

 © 2003 Wiley-VCH Verlag GmbH & Co. KGaA, Weinheim DOI: 10.1002/anie.200350995

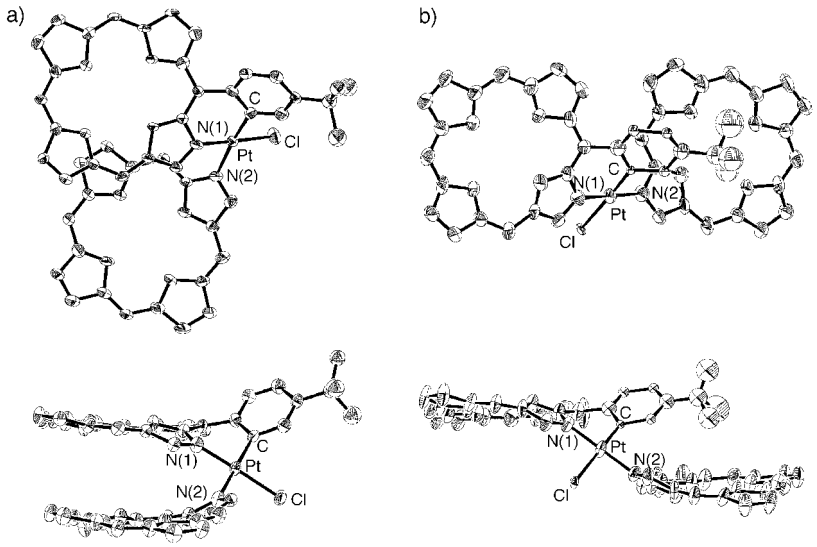


Figure 1. Molecular structure and coordination geometries of a) **3** and b) **4**; top view (top) and side view (bottom; ORTEP drawing, ellipsoids set at the 50% probability level). Uncoordinated *meso*-aryl groups were omitted for clarity. Selective bond lengths [Å] and angles [°]: a) Pt-N(1) 1.97(1), Pt-N(2) 2.12, Pt-C 1.98(1), Pt-Cl 2.313(4), N(1)-Pt-N(2) 91.8(5), N(1)-Pt-C 87.8(5), N(2)-Pt-Cl 88.3(3), C-Pt-Cl 92.4(4); b) Pt-N(1) (=Pt-N(2)) 2.007(9), Pt-C 1.892(8), Pt-Cl 2.512(5), N(1)-Pt-C 85.6(5), N(2)-Pt-Cl 86.9(1).

meso-aryl group, and a chloride atom in a square-planar fashion. The two confused pyrrole rings in **3** and **4** were located around the Pt center in a *cis* and *trans* configuration, respectively. The confused pyrrole rings, which were serving as metallocyclic ligands, were tilted 20.94° for **3** and 28.72° for **4** to the mean planes consisting a core of 24 atoms. In both the complexes, the two core planes were nearly parallel with dihedral angles of 7.71 and 7.42°, respectively, and in the case of **3**, these planes were partially overlapped. Noteworthy, the binding mode of the second NCP molecule to a Pt center is a simple outer-N coordination, in just the same fashion as nucleobase adducts to cisplatin.[9] In fact, this NCP ligand was quantitatively replaced with triphenylphosphane in toluene at room temperature.[10] The structure of **5** was also established from the X-ray analysis of the corresponding NCP derivative,[11] which showed Pt^{II} ion in the center of the NCP core with a carbon–metal atom bond similar to that of Pd^{II} monomer complex (see Supporting Information).

The ^{1}H NMR spectrum of *cis* **3** showed the two inner-CH signals at $\delta = -5.08$ and -4.76 ppm in $CDCl_3$ at room temperature. At -40 °C, the two pairs of inner N-bonded H atoms were observed unequivocally at $\delta = -3.25$, -2.05 ppm, and $\delta = -1.09$, -0.68 ppm, respectively. The folded arrangement of the two porphyrin rings in **3** was reflected in the outer-CH signals of confused pyrrole rings at $\delta = 4.26$ and 9.60 ppm, in which the diamagnetic shielding effect of the former proton was manifested because it partially overlaps the countered porphyrin. The ^{1}H NMR spectrum of *trans* complex **4** showed the two inner-CH signals at $\delta = -4.38$ and -4.32 ppm, but the outer-CH signals were observed in the normal aromatic region at $\delta = 8.84$ and 9.44 ppm, which is also consistent with the extended arrangement of the two porphyrin rings shown by the molecular structure of **4**. In both the complexes, the ^{1}H signals of *meso*-aryl groups above the NCP planes were observed in the range from $\delta = 3$ to 4.5 ppm at -40 °C owing to the ring-current shielding effect. These data suggest that the structures of the dimers **3** and **4** in the $CDCl_3$ solution are rigid and similar to those observed in the solid states.

The absorption spectra of **3** and **4**, recorded in $CHCl_3$, were similar and displayed the Soret band at $\delta = 447$ and 458 nm, and Q bands in the region of 563–820 and 580–820 nm, respectively (Figure 2). In comparison with the free base **1a**, the Soret band and the Q band at the longest wavelength transition of **3** were 4 and 84 nm red-shifted probably because of the interaction between the two NCP rings and the distortion of the NCP planes.

With regards to the structures of unseparated **6** and **6′**, we believe the complexes are an isomeric pair of bisplatinum complexes as depicted in Scheme 2. Quantitative transformation of the mixture to triphenylphosphane complex **7** and **7′** (Scheme 2, path A), the similar absorption spectrum to that of **7** (**7′**), the inner CH signals at $\delta = -4.27$ and -4.07 ppm in the same

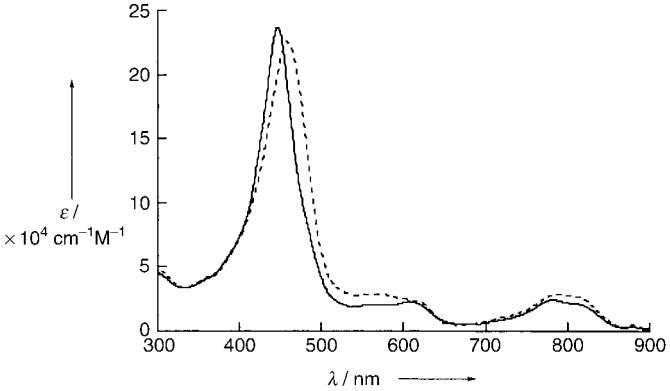
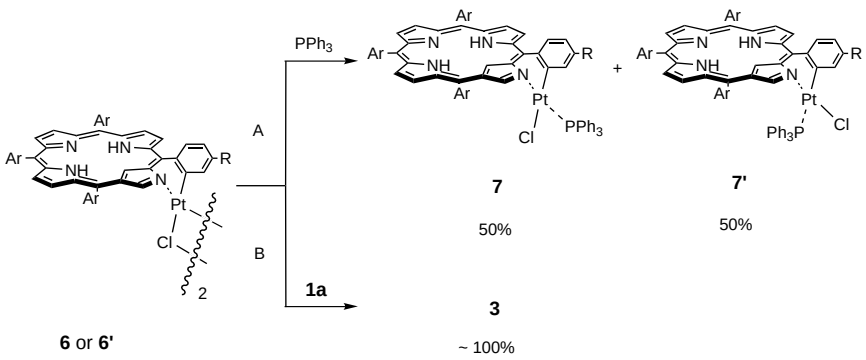


Figure 2. Absorption spectra of **3** (——) and **4** (-----) recorded in $CHCl_3$.



Scheme 2. Reactions of **6** (**6′**) with triphenylphosphane (path A) and **1a** (path B).

 © 2003 Wiley-VCH Verlag GmbH & Co. KGaA, Weinheim

region to that of **7** (**7′**) at $\delta = -4.07$ (-4.11) ppm, and the FABMS peak at m/z 2137.7, all these data support the structures suggested for **6** (**6′**). The lower yield of **3** in the reaction with one equivalent of $PtCl_2$ arises from the formation of intermediates **6** (**6′**) because these intermediates are transformed into **3** quantitatively by the reaction with free base **1a** (Scheme 2, path B).[12] From a mechanistic point of view, outer-N coordination and succeeding *ortho* platination seem to be faster than the inner coordination as judged by the lower yield of **5**, especially in the reaction with 0.5 equivalents $PtCl_2$.

In summary, we have synthesized the NCP dimer complexes with Pt^{II} ions and shown that the outer nitrogen of the confused pyrrole in NCP can serve as a good coordinating ligand and that the formation of a metallocycle using an *ortho*-carbon atom of the *meso*-aryl group is not only restricted to Pd^{II} metal. By introducing a second confusion in the NCP ring,[13] the NCP oligomers with Pt^{II} connectors may be accessible. Such a strategy would be useful to build porphyrin arrays for the study of molecular wires, which are of current interest.[14]

Received: January 22, 2003 [Z50995]

Keywords: macrocycles · macrocyclic ligands · N ligands · platinum · porphyrinoids

[1] a) T. Imamura, K. Fukushima, *Coord. Chem. Rev.* **2000**, *198*, 133–156; b) J. Wojaczynski, L. Latos-Grażyński, *Coord. Chem. Rev.* **2000**, *204*, 113–171.

[2] a) C. M. Drain, J.-M. Lehn, *J. Chem. Soc. Chem. Commun.* **1994**, 2313–2315; b) A. P. H. J. Schenning, F. B. G. Bennerker, H. P. M. Geurts, X. Y. Liu, R. J. M. Nolte, *J. Am. Chem. Soc.* **1996**, *118*, 8549–8552; c) H. Yuan, L. Thomas, L. K. Woo, *Inorg. Chem.* **1996**, *35*, 2808–2817; c) P. J. Stang, J. Fun, B. Olenyuk, *Chem. Commun.* **1997**, 1453–1454; d) C. M. Drain, F. Nifiatis, A. Vasenko, J. D. Batteas, *Angew. Chem.* **1998**, *110,* 2478–2481; *Angew. Chem. Int. Ed.* **1998**, *37*, 2344–2347; e) J. Fan, J. A. Whiteford, B. Olenyuk, M. D. Levin, P. J. Stang, E. B. Fleischer, *J. Am. Chem. Soc.* **1999**, *121*, 2741–2752; f) A. Ikeda, M. Ayabe, S. Shinkai, S. Sakamoto, K. Yamaguchi, *Org. Lett.* **2000**, *2*, 3707–3710; g) N. Fujita, K. Biradha, M. Fujita, S. Sakamoto, K. Yamaguchi, *Angew. Chem.* **2001**, *113,* 1768–1771; *Angew. Chem. Int. Ed.* **2001**, *40*, 1718–1721.

[3] a) H. Furuta, T. Ogawa, T. Asano, *J. Am. Chem. Soc.* **1994**, *116*, 767–768; b) P. J. Chmielewski, L. Latos-Grażyński, K. Rachlewicz, T. Głowiak, *Angew. Chem.* **1994**, *106,* 805–807; *Angew. Chem. Int. Ed. Engl.* **1994**, *33,* 779–781.

[4] a) L. Latos-Grażyński, *The Porphyrin Handbook, Vol. 2* (Eds: K. M. Kadish, K. M. Smith, R. Guilard), Academic Press, San Diego, **2000**, chap. 14; b) H. Furuta, H. Maeda, A. Osuka, *Chem. Commun.* **2002**, 1795–1804.

[5] H. Furuta, N. Kubo, H. Maeda, T. Ishizuka, A. Osuka, H. Nanami, T. Ogawa, *Inorg. Chem.* **2000**, *39*, 5424–5425.

[6] *Advanced Inorganic Chemistry*, 6th ed. (Eds.: F. A. Cotton, G. Wilkinson, C. A. Murillo, M. Bochmann), Wiley, New York, **1999**, chap. 18.

[7] 4-*tert*-Butylphenyl-substituted NCP (**1a**) was used to increase the solubility of the Pt^{II} complexes.

[8] Crystal data for **3**: $C_{120}H_{123}N_8PtCl{\cdot}3\,CH_2Cl_2$, $M_W = 2162.69$, triclinic $P\bar{1}$ (No. 2), $a = 10.5849(5)$, $b = 18.0888(9)$, $c = 30.344(2)$ Å, $\alpha = 80.344(2)$, $\beta = 90.992(2)$, $\gamma = 79.960(1)°$, $V = 5633.4(5)$ Å^3, $T = 123$ K, $\rho_{calcd} = 1.275$ g cm^{-3}, $Z = 2$. For 18054 reflections measured; $R = 0.090$, $wR = 0.112$ for 12171 reflections with $[I > 3\sigma(I)]$, $GOF = 0.131$. Crystal data for **4**: $C_{120}H_{123}N_8PtCl{\cdot}3\,C_6H_{14}{\cdot}CH_2Cl_2$, $M_W = 2253.37$, monoclinic $C2/c$ (No. 15), $a = 15.739(1)$, $b = 23.184(2)$, $c = 34.791(2)$ Å, $\beta = 91.927(3)°$, $V = 12687.4(1)$ Å^3, $T = 123$ K, $\rho_{calcd} = 1.180$ g cm^{-3}, $Z = 4$. For 19858 reflections measured; $R = 0.099$, $wR = 0.120$ for 8349 reflections with $[I > 3\sigma(I)]$, $GOF = 1.652$. CCDC-200335 (**3**) and 200334 (**4**) contain the supplementary crystallographic data for this paper. These data can be obtained free of charge via www.ccdc.cam.ac.uk/conts/retrieving.html (or from the Cambridge Crystallographic Data Centre, 12 Union Road, Cambridge CB2 1EZ, UK; fax: (+44) 1223-336-033; or deposit@ccdc.cam.ac.uk).

[9] E. R. Jamieson, S. J. Lippard, *Chem. Rev.* **1999**, *99*, 2467–2498.

[10] When **3** was stirred with triphenylphosphane for 1 h at room temperature, the dimer complex was completely converted to the monomer to afford free base **1a** and the triphenylphosphane-coordinated monomer complex **7**, quantitatively. See Supporting Information.

[11] A single crystal with good quality for X-ray analysis was obtained from 3,5-di-*tert*-butylphenyl substituted NCP complex. K. Ariga, T. Kunitake, H. Furuta, *J. Chem. Soc. Perkin Trans. 2*, **1996**, 667–672.

[12] The porphyrin ring interaction might be active in the selective formation of the *cis* dimer.

[13] H. Furuta, H. Maeda, A. Osuka, *J. Am. Chem. Soc.* **2000**, *122*, 803–807.

[14] a) S. Richeter, C. Jeandon, R. Ruppert, H. J. Callot, *Chem. Commun.* **2002**, 266–267; b) K. Ogawa, T. Zhang, K. Yoshihara, Y. Kobuke, *J. Am. Chem. Soc.* **2002**, *124*, 22–23.

 © 2003 Wiley-VCH Verlag GmbH & Co. KGaA, Weinheim

Micelle to Vesicle Transition

Temperature-Induced Micelle to Vesicle Transition in the Sodium Dodecylsulfate/Dodecyltriethylammonium Bromide System**

Haiqing Yin, Zukang Zhou, Jianbin Huang, Rong Zheng, and Yongyi Zhang*

Amphiphilic molecules have the ability to form organized assemblies such as micelles, vesicles, and lamellar structures in solution. Different kinds of assemblies can be transformed by the change of various environmental factors.[1] Temperature often plays an important role in such transitions.[2] The

[*] Prof. Dr. J. Huang, H. Yin, Z. Zhou, R. Zheng, Y. Zhang
State Key Laboratory for Structural Chemistry
of Unstable and Stable Species
College of Chemistry and Molecular Engineering
Peking University, Beijing 100871 (P. R. China)
Fax: (+86) 10-6275-1708
E-mail: jbhuang@chem.pku.edu.cn

[**] This work was supported by the National Natural Science Foundation of China.

Supporting information for this article is available on the WWW under http://www.angewandte.org or from the author.

 © 2003 Wiley-VCH Verlag GmbH & Co. KGaA, Weinheim DOI: 10.1002/anie.200350913

transition from an ordered state to a disordered one[3] or from a higher ordered state to a lower ordered one (such as the transition from a vesicle to a micelle[4]) on increasing the temperature usually occurs among organized assemblies. However, studies of the reverse temperature-induced transitions, such as micelle to vesicle transition (MVT), are so far rare. Herein, we report for the first time a temperature-induced MVT in a cationic–anionic surfactant system.

The sodium dodecylsulfate (SDS)/dodecyltriethylammonium bromide (DEAB) system was prepared in a molar ratio of 2:1 and a total concentration (C_{total}) of 10 mM. The results of the turbidity measurements are shown in Figure 1a. A clear increase in turbidity was observed as the temperature increased from 30 to 50 °C, which suggests the growth of aggregates in the system. No phase separation or precipitate was observed during the transition, which is different from the "cloud point" phenomena seen in some ionic surfactant systems.[5]

Dynamic light scattering (DLS) studies, a freeze fracture technique with observation by electron microscopy (FF-EM), and rheology measurements were used to investigate the temperature-induced transition in the system. The aggregate has an average hydrodynamic radius ($\langle R_h \rangle$) of 25 nm at 20 °C (Figure 2a). A steady flow curve (Figure 3) revealed the non-Newtonian nature of the system and thus indicated the existence of asymmetric aggregates. A remarkable shear-thickening feature was also evident in the flow curve. It has been well documented[6] that the growth or flow alignment of cylindrical micelles was responsible for the shear-thickening behavior in dilute surfactant solutions. However, a few small spherical vesicles were also observed by FF-EM (Figure 4a). Thus, we can conclude that cylindrical micelles are the major aggregates which coexist with a few small spherical vesicles in the system. Similar results were obtained at 25 °C from DLS (Figure 2b) and rheology curves, which indicate there was no apparent change between 20 and 25 °C.

However, the situation became different as the temperature increased to 30 °C. A DLS plot (Figure 2c) showed that the peak corresponding to the small aggregates ($R_h \sim 25$ nm) shrank relative to that at 25 °C, while another peak appeared ($R_h \sim 100$ nm). The polydispersity index (PI, calculated by the Cumulant method) grew from 0.282 (25 °C) to 0.339 (30 °C), which was indicative of the increase in the vesicle/micelle ratio in the system.[7] Vesicles with a diameter of 150–200 nm were observed by FF-TEM (Figure 4b), which coincides with the newly appeared peak in the DLS plot. Moreover, there

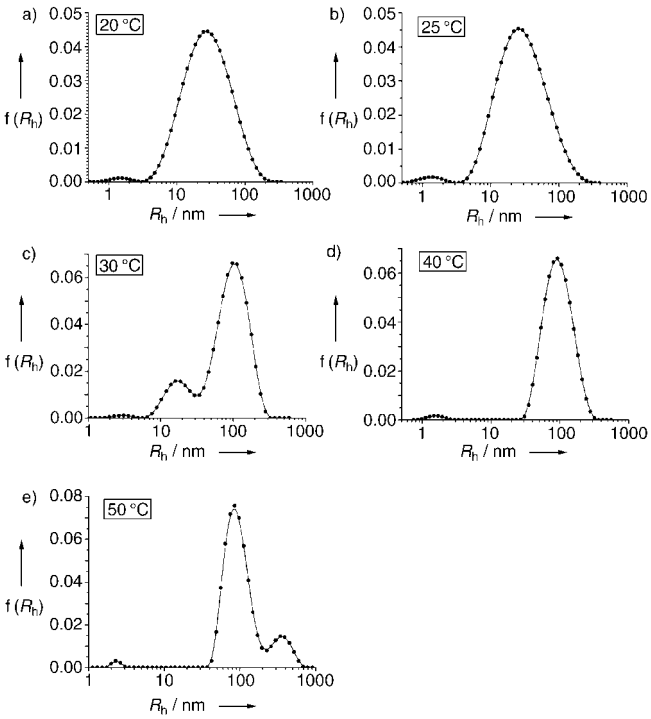


Figure 2. Hydrodynamic radius (R_h) distributions of SDS/DEAB (2:1, $C_{total} = 10$ mM) at 20 °C (a), 25 °C (b), 30 °C (c), 40 °C (d), and 50 °C (e) calculated by the Contin method.

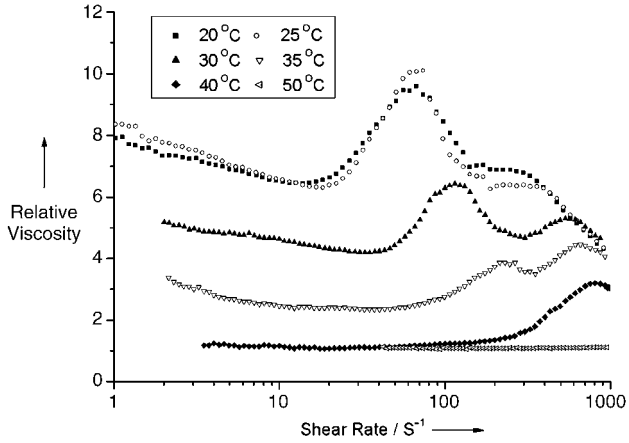


Figure 3. Steady flow curves as a function of temperature in SDS/DEAB (2:1, $C_{total} = 10$ mM).

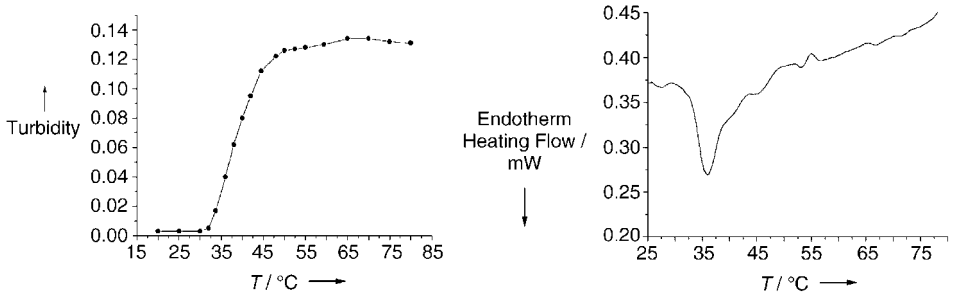


Figure 1. Turbidity curve (a) and DSC heating curve (b) of the SDS/DEAB (2:1, $C_{total} = 10$ mM) system as a function of temperature.

 © 2003 Wiley-VCH Verlag GmbH & Co. KGaA, Weinheim

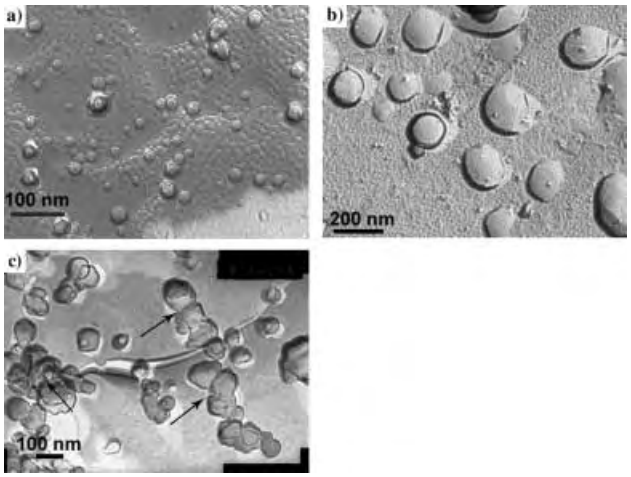


Figure 4. Vesicles of the system SDS/DEAB (2:1, $C_{total} = 10$ mM) observed by FF-EM at 20 °C (a), 30 °C (b), and 50 °C (c). Solid arrows show the aggregation of vesicles.

was a dramatic decrease in the relative viscosity at low shear rate. All these results confirm that the increase in turbidity with increasing temperature is actually caused by the transition from cylindrical micelles to vesicles in the system.

The MVT process continued as the temperature was further increased. At 40 °C, the system showed approximate Newtonian characteristics under low shear rate despite shear-thickening behavior still being present at a high shear rate. This result suggests that the aggregates in solution become more symmetrical. In the DLS plot, the R_h peak at approximately 25 nm assigned to cylindrical micelles almost disappeared, to leave the R_h peak of about 100 nm assigned to vesicles (Figure 2d). The low PI value (0.195) also indicates that vesicles are the dominating aggregates in the system. Further heating to 50 °C resulted in the system becoming a completely Newtonian fluid (Figure 3) and its relative viscosity was approximately unity ($\eta_r = 1.08$). Large vesicles still existed in the system (Figure 4c). Thus, it can be concluded that the cylindrical micelles were almost completely transformed into vesicles at this temperature. Consequently, the turbidity remained nearly constant upon further heating. However, another peak emerged with an R_h value of 200–300 nm in the DLS plot (Figure 2e), and the PI value correspondingly increased to 0.21. The formation of these larger aggregates may be attributed to the aggregation of the vesicles (Figure 4c).

The transition between the micelle and the vesicle is often accompanied by a heat effect.[8,9] Therefore, DSC measurements were employed to monitor the temperature-dependent transition. An endothermic peak can clearly be observed in the heating curve (Figure 1b). Compared with the turbidity curve, this peak appeared during the interval of transition (from ca. 30 °C to ca. 50 °C). It is possibly a result of the positive transfer enthalpy of micelle to vesicle transition, which was elucidated to extensively in another study.[9] The result of the DSC studies also provides strong support for our conclusion.

Several heating–cooling cycles were performed on the same sample and the results obtained were reproducible, which indicates the reversibility of the transition. Such a transition was also remarkably influenced by the molar ratio of the anionic/cationic surfactants and the total surfactant concentration.

In summary, cylindrical micelle to vesicle transition upon an increase in the temperature was demonstrated in the system of SDS/DEAB (2:1, $C_{total} = 10$ mM). A clear transition occurred between 30 and 50 °C. Although temperature-induced MVT was previously reported in some lipid/surfactant,[9] non-ionic surfactant,[10] and ionic surfactant/cosurfactant[11] systems, the transition in our case can not be explained simply with the interpretations for the above systems, and seems to come from a more complex origin. However, the temperature-dependent interaction of the oppositely charged surfactant molecules should play a key role in this case.

Experimental Section

Materials: SDS was bought from ACROS ORGANICS Co. (99% purity). DEAB was synthesized from dodecyl bromide and triethylamine. The purity of all the surfactants was examined and no surface tension minimum was found in the surface tension curve.

Turbidity measurements were carried out using a Shimadzu UV-250 spectrophotometer at 514.5 nm.

DLS measurements were performed with a spectrometer (ALV-5000/E/WIN Multiple Tau Digital Correlator) and a Spectra-Physics 2017 200 mW Ar laser (514.5 nm wavelength). The scattering angle was 90°, and the intensity autocorrelation functions were analyzed by using the methods of Contin and Cumulant.

Samples for electron microscopy were prepared by freeze-fracture replication according to standard techniques with a high vacuum freeze-etching system (FED.B-JEE-4X). Replicas were observed with a JEM-100CX electron microscope.

The rheological properties of the samples were measured with a ThermoHaake RS300 rheometer. A double gap cylinder sensor system was used with an outside gap of 0.30 mm and an inside gap of 0.25 mm.

DSC measurements were carried out 1 °C min^{-1} using Micro DCS III (Setaram-France) instrument.

Received: January 9, 2003 [Z50913]

Keywords: micelles · self-assembly · surfactants · temperature effects · vesicles

[1] a) J. C. Hao, H. Hoffmann, K. Horbaschek, *J. Phys. Chem. B* **2000**, *104*, 10144–10153; b) P. A. Hassan, S. R. Raghavan, E. W. Kaler, *Langmuir* **2002**, *18*, 2543–2548; c) M. Mao, J. B. Huang, B. Y. Zhu, J. P. Ye, *J. Phys. Chem. B* **2002**, *106*, 219–225; d) C. Z. Wang, J. B. Huang, S. H. Tang, B. Y. Zhu, *Langmuir* **2001**, *17*, 6389–6392.

[2] a) R. Bott, T. Wolff, K. Zierold, *Lanmguir* **2002**, *18*, 2004–2012; b) N. Gorski, J. Kalus, *Langmuir* **2001**, *17*, 4211–4215; c) S. Kumar, D. Sharma, Z. A. Khan, K. U. Din, *Langmuir* **2001**, *17*, 5813–5816; d) H. Q. Yin, M. Mao, J. B. Huang, H. L. Fu, *Langmuir* **2002**, *18*, 9198–9203.

[3] S. Förster, T. Plantenberg, *Angew. Chem.* **2002**, *41*, 712–739; *Angew. Chem. Int. Ed.* **2002**, *41*, 688–714.

[4] a) E. Mendes, R. Oda, C. Manohar, J. Narayanan, *J. Phys. Chem. B* **1998**, *102*, 338–343; b) R. T. Buwalda, M. C. A. Stuart, J. B. F. N. Engberts, *Langmuir* **2000**, *16*, 6780–6786; c) P. A. Hassan, B. S. Valaulikar, C. Manohar, F. Kern, L. Bourdieu, S. J.

 © 2003 Wiley-VCH Verlag GmbH & Co. KGaA, Weinheim

Candau, *Langmuir* **1996**, *12*, 4350 – 4357; d) J. Narayanan, E. Mendes, C. Manohar, *Int. J. Mod. Phys. B* **2002**, *16*, 375 – 382.
[5] a) S. R. Raghavan, H. Edlund, E. W. Kaler, *Langmuir* **2002**, *18*, 1056 – 1064; b) Z. J. Yu, G. Z. Xu, *J. Phys. Chem.* **1989**, *93*, 7441 – 7445; c) G. G. Warr, T. N. Zemb, M. Drifford, *J. Phys. Chem.* **1990**, *94*, 3086 – 3092.
[6] a) R. Bruinsma, W. Gelbart, A. B. Shaul, *J. Chem. Phys.* **1992**, *96*, 7710 – 7727; b) S. Q. Wang, *J. Phys. Chem.* **1990**, *94*, 8381 – 8384; c) S. Hofmann, H. Hoffmann, *J. Phys. Chem. B* **1998**, *102*, 5614 – 5624; d) Cl. Oelschlaeger, G. Waton, S. J. Candau, M. E. Cates, *Langmuir* **2002**, *18*, 7265 – 7271.
[7] S. U. Egelhaaf, P. Schurtenberger, *J. Phys. Chem.* **1994**, *98*, 8560 – 8573.
[8] a) M. R. Wenk, J. Seelig, *J. Phys. Chem. B* **1997**, *101*, 5224 – 5231; b) M. Bergsma, M. L. Fielden, J. B. F. N. Engberts, *J. Colloid Interface Sci.* **2001**, *243*, 491 – 495; c) H. Heerklotz, G. Lantzsch, H. Binder, G. Klose, A. Blume, *Chem. Phys. Lett.* **1995**, *235*, 517 – 520; d) A. Hildebrand, P. Garidel, R. Nerbert, A. Blume, *Langmuir* **2002**, *18*, 2836 – 2847.
[9] P. R. Majhi, A. Blume, *J. Phys. Chem. B* **2002**, *106*, 10753 – 10763.
[10] G. Wanka, H. Hoffmann, W. Ulbricht, *Colloid Polym. Sci.* **1990**, *268*, 101 – 117.
[11] H. Hoffmann, K, Horbaschek, F. Witte, *J. Colloid Interface Sci.* **2001**, *235*, 33 – 45.

 © 2003 Wiley-VCH Verlag GmbH & Co. KGaA, Weinheim

Michael Additions and Iodanes

Synthesis, Characterization, and Reaction of Ethynyl(phenyl)-λ³-Iodane Complex with [18]Crown-6

Masahito Ochiai, Kazunori Miyamoto, Takashi Suefuji, Shigeru Sakamoto, Kentaro Yamaguchi, and Motoo Shiro*

Because of the powerful electron-withdrawing nature of the phenyl-λ³-iodanyl group,[1] ethynyl(phenyl)-λ³-iodane (**1**) [HCCI(Ph)X] (where X = heteroatom ligand) the parent member of the family of alkynyl(aryl)-λ³-iodanes,[2] is highly electron deficient and hence serves as a good Michael acceptor towards a variety of nucleophiles. Commercially available ethynyl(phenyl)(tetrafluoroborato)-λ³-iodane (**1a**: X = BF_4)[3] induces direct ethynylation of alkali-metal enolates derived from 1,3-dicarbonyl compounds and nitroalkanes under mild conditions.[4] Analogous ethynyl-λ³-iodane **1b** (X = OTf; CF_3SO_3)[5] also affords ethynylation products by the reaction with sodium *p*-toluenesulfinate, sodium diethyl phosphate, and sulfonylamides.[6] These direct ethynylations of nucleophiles with λ³-iodanes **1** probably involve tandem Michael addition/alkylidene–carbene rearrangement pathway.[2]

Synthetic use of ethynyl-λ³-iodanes **1** with these prominent reactivity, however, is limited because of their relatively low thermal stability: for instance, the iodane **1a** gradually decomposes when left to stand at room temperature. The heteroatom ligand BF_4 is weakly nucleophilic and, therefore, its coordination (through a fluorine atom) to the iodine(III) center by hypervalent bonding is relatively loose,[7] which in turn increases the positive charge on the iodine atom of **1a**. These features tend to enhance the reactivity of **1a** toward nucleophiles as well as to decrease its stability. Introduction of more nucleophilic ligands, such as halogens, instead of BF_4 is expected to decrease the susceptibility of **1a** to decomposition, because of the decreased positive charge on the iodine(III) center; however, the attempted ligand exchange of ethynyl-λ³-iodane **1a** with halide ions results in the Michael addition to the β carbon atom, instead of the formation of ethynyl(phenyl)(halo)-λ³-iodanes.[8] To increase the stability of **1a,** development of a new type of heteroatom ligand that efficiently coordinates to the iodine(III) but not undergoes Michael additions is highly desirable.

Recently, we found that [18]crown-6 (18C6) forms a discrete complex with diphenyl(tetrafluoroborato)-λ³-iodane, in which the iodine(III) center forms contacts with the three adjacent oxygen atoms of 18C6 through two hypervalent secondary bonding and a weak interaction.[9] Herein, we report synthesis and characterization of supramolecular complex **2** formed between ethynyl(phenyl)-λ³-iodane **1a** and 18C6. The complexation with 18C6 not only stabilizes **1a** but also maintains its high reactivity toward nucleophiles. We also found that the presence of the ligand 18C6 in **2** makes it possible to synthesize the highly labile (*Z*)-(β-alkoxyvinyl)-phenyl-λ³-iodanes as stable complexes with 18C6.

Slow evaporation of a dichloromethane/diethyl ether solution of a 1:1 mixture of **1a** and 18C6 at −20 °C afforded an 89% yield of single crystals of a 1:1 complex **2**. The complexation with 18C6 dramatically changed the solubility of **1a** in organic solvents: thus, **1a** is sparingly soluble in dichloromethane and chloroform, while the complex **2** is highly soluble in these solvents. More importantly, the stability of **1a** was much improved by the complexation and almost no decomposition of **2** was observed when it was left standing under ambient conditions over one month.

The X-ray crystal structure (Figure 1)[10] illustrates that, in the 1:1 complex **2**, the ethynyl(phenyl)-λ³-iodanyl group protrudes above one face of 18C6. The iodine(III) center has contacts with three adjacent oxygen atoms (O2, O3, and O4) of 18C6 and the complex **2** adopts a distorted pentagonal-planar geometry about the iodine, with root-mean-square deviation of 0.355(9) Å for I1, C2, C3, O2, O3, and O4 from their least-squares plane and the sum of the iodine-centered bond angles $\Sigma°I = 363.0(4)°$.

[*] Prof. M. Ochiai, K. Miyamoto, T. Suefuji
Faculty of Pharmaceutical Sciences
University of Tokushima
1–78 Shomachi, Tokushima 770-8505 (Japan)
Fax: (+81) 88-633-9504
E-mail: mochiai@ph2.tokushima-u.ac.jp
S. Sakamoto, Prof. K. Yamaguchi
Chemical Analysis Center, Chiba University
Yayoi-cho, Inage-ku, Chiba 263–8522 (Japan)
M. Shiro
Rigaku Corporation, 3-9-12 Matsubara
Akishima, Tokyo 196–8666 (Japan)

 DOI: 10.1002/anie.200250866 © 2003 Wiley-VCH Verlag GmbH & Co. KGaA, Weinheim

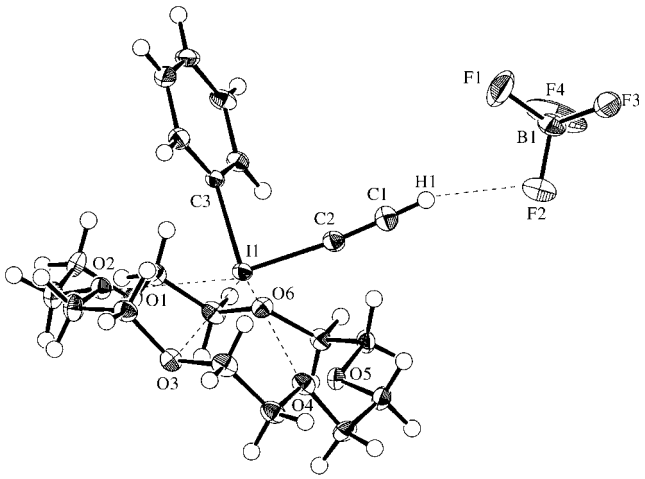


Figure 1. ORTEP drawing of **2**. Selected interatomic distances [Å] and angles [°]:I1-C2 2.009(4), I1-C3 2.116(4), I1···O2 2.918(3), I1···O3 3.120(3), I1···O4 2.923(3), H1···F2 2.34(5), C2-I1-C3 91.0(2), C2-I1···O2 164.0(5), C3-I1···O4 167.8(2), C1-H1···F2 160(5).

The I1···O2 and I1···O4 separations (2.918(3) and 2.923(3) Å) are considerably longer than the average covalent bond length (2.14 Å)[11] but shorter than the van der Waals distance (3.50 Å).[12] Both C2-I1···O2 and C3-I1···O4 are near-linear and therefore these close contacts are indicative of hypervalent secondary interactions, in which each oxygen atom donates an electron pair into an I–C σ* orbital. The other I1···O3 contact is weak and considerably deviates from the linearity of three-center, four-electron (3c–4e) σ bonding.[13] The symmetry of the crown ether approximates to D_{3d}, the most frequently observed conformation in supramolecular complexes of 18C6.[14]

The heteroatom ligand BF_4 shows a close contact with the acetylenic hydrogen atom. The H1···F2 distance 2.34(5) Å is shorter than their combined contact radii (2.67 Å)[12] and the C1-H1···F2 bond shows a nearly linear conformation with an angle of 160(5)°. Hydrogen bonding reduces the thermal vibrations of the engaged residues. The ratio of isotropic displacement parameters (U(C1)/U(C2) = 1.23) is close to 1, which probably reflects H1···F2 hydrogen bonding.[15] Small isotropic displacement parameter of F2 (U = 0.0377(8)) compared to those of the other fluorine atoms (U(F1), 0.068(1); U(F3), 0.047(1); U(F4), 0.084(1)) also indicates reduction of the acceptor vibration through the hydrogen bonding.[16]

In general, C_{sp}–H groups act as good donors in hydrogen bonding, a directional interaction with a preference for linear geometry.[17] The highly acidic nature of H1 in **2** is responsible for the C–H···F hydrogen bonding.[18] The C_{sp}–H stretching frequency of **2** provides spectroscopic evidence for this interaction: it appears as a single sharp band at $\tilde{\nu}$ = 3208 cm^{-1} (Nujol), whereas that of **1a** appears at higher frequency of $\tilde{\nu}$ = 3242 cm^{-1}.

In solution, ethynyl-λ³-iodane **1a** forms 1:1 complex with 18C6. ^{1}H NMR spectroscopic analyses showed that a solution of 18C6 in $CDCl_3$ (0.01 M) dissolve 0.9 equivalents of solid λ³-iodane **1a** at 23 °C, and the methylene singlet is shifted upfield by 0.06 ppm on complexation with **1a**, as observed in the Ph_2IBF_4·18C6 complex.[9] Irradiation of the methylene protons of 18C6 gives rise to nuclear Overhauser effects (NOEs) for the *ortho* protons of **1a,** but not for the *meta* and *para* protons. The cold-spray ionization (CSI) MS spectrum for the complex **2** in dichloromethane showed the most prominent ion peak of 1:1 complex [**2**–BF_4]$^+$ at m/z 493 (Figure 2).[19] The binding constant was measured by ^{1}H NMR spectroscopic titrations of $CDCl_3$ solutions of 18C6 with **1a** at 23 °C. The resulting binding curve gave an excellent fit with a 1:1 binding model and was analyzed by nonlinear least-squares method to give a binding constant (K_a) value of 1.92×10^3 M^{-1} (correlation coefficient 0.99).

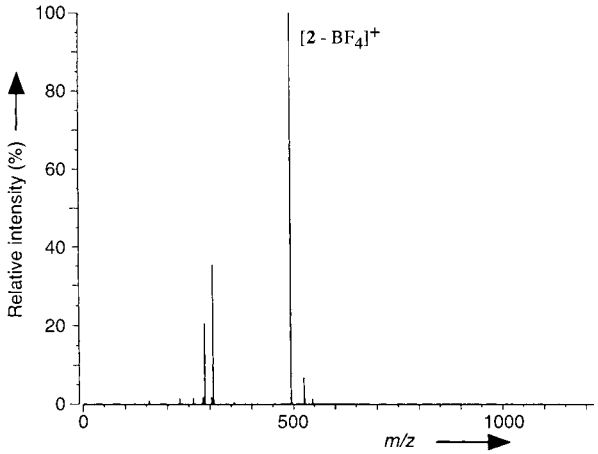
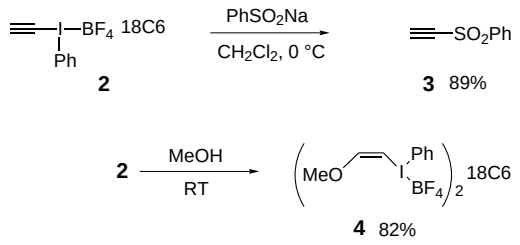


Figure 2. CSI-MS spectrum of **2** in CH_2Cl_2.

The 1:1 complex **2** has the desired high reactivity towards attack of nucleophiles and serves as a good Michael acceptor. Thus, on exposure to sodium benzenesulfinate in dichloromethane, **2** undergoes tandem Michael addition/alkylidene–carbene rearrangement to give the ethynyl sulfone **3** in a high yield under mild conditions (Scheme 1).[6a,20] Very interestingly, it is possible to synthesize the highly labile (*Z*)-(β-methoxyvinyl)-λ³-iodane as a crown-ether complex **4**, directly from the complex **2** (Scheme 1):[21] thus, reaction of **2** with methanol at room temperature results in *anti* Michael addition yielding the 2:1 complex **4**, with a small vicinal coupling constant 3.7 Hz between vinylic protons, stereoselectively in 82% yield. Ethanol and *tert*-butanol similarly undergo the Michael addition to give the analogous 2:1 complexes. In these reactions, 18C6 functions as a stabilizing ligand not only for the reactant ethynyl-λ³-iodane **1a** but also



Scheme 1. Reaction of the 1:1 complex **2** with nucleophiles.

 © 2003 Wiley-VCH Verlag GmbH & Co. KGaA, Weinheim

for the products (*Z*)-(β-alkoxyvinyl)-λ³-iodanes, which have not been synthesized before. Without use of 18C6, the isolation and the purification of (*Z*)-(β-alkoxyvinyl)-λ³-iodanes are very difficult, probably because of the facile *anti*-β-elimination[22] of the phenyl-λ³-iodanyl group with remarkable nucleofugality.[23]

In conclusion, 18C6 was shown to be an excellent polydentate ligand of ethynyl- and (*Z*)-(β-alkoxyvinyl)-λ³-iodanes. The X-ray crystal structure of the ethynyl(phenyl)-λ³-iodane 18C6 complex **2** shows that the iodine(III) interacts with three adjacent oxygen atoms of 18C6 with a distorted pentagonal-planar geometry. Most importantly, the complexation with 18C6 increases the stability of these labile λ³-iodanes.

Experimental Section

2: **1a** (103 mg, 0.33 mmol) and 18C6 (86 mg, 0.33 mmol) were dissolved in dichloromethane (1 mL) and the solution was stirred for 30 min at room temperature. After addition of diethyl ether (0.75 mL), a slow evaporation at −20 °C of the solvent by exposure to the atmosphere yielded **2** (169 mg, 0.29 mmol, 89 %) as colorless plates: m.p. 133–134 °C; ^{1}H NMR (300 MHz, CD_2Cl_2, 0.01 M, 24 °C, TMS): $\delta = 3.48$ (s, 1 H; CCH), 3.63 (s, 24 H; 18C6), 7.59 (dd, $^3J(H,H) = 8.2$, 7.4 Hz, 2 H; *m*-H), 7.71 (t, $^3J(H,H) = 7.4$ Hz, 1 H; *p*-H), 8.20 ppm (d, $^3J(H,H) = 8.2$ Hz, 2 H; *o*-H); ^{13}C NMR (75 MHz, [D$_6$]acetone, 0.09 M, 24 °C, TMS): $\delta = 30.4$ (*C*CH), 70.7 (18C6), 98.1 (C*C*H), 116.6 (*ipso*-C), 133.2 (*m*-C), 134.1 (*p*-C), 137.0 ppm (*o*-C); IR (Nujol): $\tilde{\nu} = 746$ s, 835 s, 957 s, 1053 vs, 1108 vs, 2042 w, 3208 s cm^{-1}; CSI-MS (CH_2Cl_2): *m*/*z* 493 [(*M*−BF_4)$^+$]; elemental analysis calcd (%) for $C_{20}H_{30}BF_4IO_6$ (580.16): C 41.41, H 5.21; found: C 41.25, H 5.03.

4: **2** (25 mg, 0.042 mmol) was dissolved in methanol (1.2 mL) under argon and the solution was stirred for 18 h at room temperature. Evaporation of the solvent under reduced pressure, followed by repeated decantation at 0 °C with *n*-hexane and then with diethyl ether, gave **4** (16.7 mg, 0.017 mmol, 82 %) as colorless prisms after recrystallization from dichloromethane/*n*-hexane: m.p. 92–93 °C; ^{1}H NMR (400 MHz, $CDCl_3$, 24 °C, TMS): $\delta = 3.68$ (s, 24 H; 18C6), 4.02 (s, 6 H; MeO), 6.02 (d, $^3J(H,H) = 3.7$ Hz, 2 H; CHI), 6.96 (d, $^3J(H,H) = 3.7$ Hz, 2 H; CHOMe), 7.49 (dd, $^3J(H,H) = 7.7$, 8.4 Hz, 4 H; *m*-H), 7.65 (t, $^3J(H,H) = 7.7$ Hz, 2 H; *p*-H), 7.94 ppm (d, $^3J(H,H) = 8.4$ Hz, 4 H; *o*-H); IR (Nujol): $\tilde{\nu} = 742$ w, 1054 vs, 1104 s, 1257 w, 1614 s, 3110 w cm^{-1}; elemental analysis calcd (%) for $C_{30}H_{44}B_2F_8I_2O_8$ (960.08): C 37.53, H 4.62; found: C 37.41, H 4.50.

Received: December 30, 2002 [Z50866]

Keywords: crown compounds · hydrogen bonds · iodine · Michael addition · supramolecular chemistry

[1] For Hammett substituent constant ($\sigma_p = 1.37$) of Ph(BF$_4$)I—see: A. A. Mironova, I. I. Maletina, S. V. Iksanova, V. V. Orda, L. M. Yagupolskii, *Zh. Org. Khim.* **1989**, *25*, 306.

[2] For reviews of alkynyl(aryl)-λ³-iodanes see: a) M. Ochiai in *Chemistry of Hypervalent Compounds* (Ed.: K. Akiba), Wiley-VCH, New York, **1999**, p. 359; b) G. F. Koser in *The Chemistry of Halides, Pseudo-halides and Azides, Supplement D2* (Eds.: S. Patai, Z. Rappoport), Wiley, New York, **1995**, p. 1173; c) P. J. Stang, *Angew. Chem.* **1992**, *104*, 281; *Angew. Chem. Int. Ed. Engl.* **1992**, *31*, 274; d) A. Varvoglis, *The Organic Chemistry of Polycoordinated Iodine*, VCH, New York, **1992**.

[3] a) M. Ochiai, T. Ito, Y. Takaoka, Y. Masaki, M. Kunishima, S. Tani, Y. Nagao, *J. Chem. Soc. Chem. Commun.* **1990**, 118; b) M. Ochiai, Y. Masaki, Y. Nagao, *J. Synth. Org. Chem. Jpn.* **1990**, *48*, 970; c) T. Suzuki, Y. Uozumi, M. Shibasaki, *J. Chem. Soc. Chem. Commun.* **1991**, 1593.

[4] For direct ethynylation of silyl enol ethers see: M. Arisawa, R. Amemiya, M. Yamaguchi, *Org. Lett.* **2002**, *4*, 2209.

[5] P. J. Stang, A. M. Arif, C. M. Crittell, *Angew. Chem.* **1990**, *102*, 307; *Angew. Chem. Int. Ed. Engl.* **1990**, *29*, 287.

[6] a) R. R. Tykwinski, B. L. Williamson, D. R. Fischer, P. J. Stang, A. M. Arif, *J. Org. Chem.* **1993**, *58*, 5235; b) B. Witulski, M. Gosmann, *Chem. Commun.* **1999**, 1879; c) B. Witulski, T. Stengel, *Angew. Chem.* **1999**, *111*, 2521; *Angew. Chem. Int. Ed.* **1999**, *38*, 2426; d) J. A. Nanzon, J. M. Kuo, B. W. Miles, D. R. Fischer, P. J. Stang, F. M. Raushel, *Biochemistry* **1995**, *34*, 743.

[7] For solid-state structures of tetrafluoroborato-λ³-iodanes see: a) M. Ochiai, Y. Kitagawa, N. Takayama, Y. Takaoka, M. Shiro, *J. Am. Chem. Soc.* **1999**, *121*, 9233; b) M. Ochiai, K. Sumi, Y. Takaoka, M. Kunishima, Y. Nagao, M. Shiro, E. Fujita, *Tetrahedron* **1988**, *44*, 4095.

[8] M. Ochiai, K. Uemura, Y. Masaki, *J. Am. Chem. Soc.* **1993**, *115*, 2528.

[9] M. Ochiai, T. Suefuji, K. Miyamoto, N. Tada, S. Goto, M. Shiro, S. Sakamoto, K. Yamaguchi, *J. Am. Chem. Soc.* **2003**, *125*, 769.

[10] Crystal data for **2**: $C_{20}H_{30}BF_4IO_6$, colorless block of dimensions of $0.40 \times 0.20 \times 0.10$ mm^3, monoclinic, $P2_1$ (No. 14), $a = 8.0240(5)$, $b = 10.9067(7)$, $c = 13.980(1)$ Å, $\beta = 96.569(3)°$, $V = 1215.4(1)$ Å^3, $Z = 2$, $\rho_{calcd} = 1.585$ g cm^{-3}. Data collected on a Rigaku RAXIS-RAPID Imaging Plate diffractometer with $Mo_{K\alpha}$ radiation ($\lambda = 0.71069$ Å) at $T = 93$ K, $2\theta_{max} = 59.9°$, 13627 reflections measured, of which 3683 unique ($R_{int} = 0.034$), $\mu = 13.80$ cm^{-1}. Structure was solved by heavy-atom Patterson methods[24a] and expanded using Fourier techniques,[24b] $R = 0.044$, $R_w = 0.077$. Hydrogen atoms were included but not refined. CCDC-199570 (**2**) contains the supplementary crystallographic data for this paper. These data can be obtained free of charge via www.ccdc.cam.ac.uk/conts/retrieving.html (or from the Cambridge Crystallographic Data Centre, 12 Union Road, Cambridge CB2 1EZ, UK; fax: (+44) 1223-336-033; or deposit@ccdc.cam.ac.uk).

[11] F. H. Allen, O. Kennard, D. G. Watson, L. Brammer, A. G. Orpen, R. Taylor, *J. Chem. Soc. Perkin Trans. 2* **1987**, S1.

[12] a) A. Bondi, *J. Phys. Chem.* **1964**, *68*, 441; b) R. S. Rowland, R. Taylor, *J. Phys. Chem.* **1996**, *100*, 7384.

[13] a) N. W. Alcock, *Adv. Inorg. Chem. Radiochem.* **1972**, *15*, 1; b) N. W. Alcock, *Bonding and Structure*, Ellis Horwood, Chichester, **1990**; c) J. Starbuck, N. C. Norman, A. G. Orpen, *New J. Chem.* **1999**, *23*, 969; d) G. A. Landrum, R. Hoffmann, *Angew. Chem.* **1998**, *110*, 1989; *Angew. Chem. Int. Ed.* **1998**, *37*, 1887.

[14] Crown ether IR frequencies ($\tilde{\nu} = 957$ cm^{-1} for CH_2 rock and $\tilde{\nu} = 835$ cm^{-1} for C–C stretch) in **2** are consistent with approximate D_{3d} symmetry. See: A. Elbasyouny, H. J. Brugge, K. von Deuten, M. Dickel, A. Knochel, K. U. Koch, J. Kopf, D. Melzer, G. Rudolph, *J. Am. Chem. Soc.* **1983**, *105*, 6568.

[15] T. Steiner, *J. Chem. Soc. Chem. Commun.* **1994**, 101.

[16] D. Braga, F. Grepioni, K. Biradha, V. R. Pedireddi, G. R. Desiraju, *J. Am. Chem. Soc.* **1995**, *117*, 3156.

[17] For C-H···F hydrogen bonding see: a) J. Parsch, J. W. Engels, *J. Am. Chem. Soc.* **2002**, *124*, 5664; b) L. Shimoni, H. L. Carrell, J. P. Glusker, M. M. Coombs, *J. Am. Chem. Soc.* **1994**, *116*, 8162; c) T. Steiner, *Chem. Commun.* **1997**, 727.

[18] The pK_a value for **1b** was estimated to be in the range of 2–5.[5]

[19] S. Sakamoto, M. Fujita, K. Kim, K. Yamaguchi, *Tetrahedron* **2000**, *56*, 955.

[20] M. Ochiai, M. Kunishima, S. Tani, Y. Nagao, *J. Am. Chem. Soc.* **1991**, *113*, 3135.

[21] For the synthesis of (*E*)-(β-ethoxyvinyl)-λ³-iodane see: M. Ochiai, M. Kunishima, K. Fuji, M. Shiro, Y. Nagao, *J. Chem. Soc. Chem. Commun.* **1988**, 1076.

 © 2003 Wiley-VCH Verlag GmbH & Co. KGaA, Weinheim

[22] For facile *anti*-β-elimination of (*Z*)-(β-alkylvinyl)-λ^3-iodanes see: M. Ochiai, K. Oshima, Y. Masaki, *J. Chem. Soc. Chem. Commun.* **1991**, 869.
[23] T. Okuyama, T. Takino, T. Sueda, M. Ochiai, *J. Am. Chem. Soc.* **1995**, *117*, 3360.
[24] a) PATTY: P. T. Beurskens, G. Admiraal, G. Beurskens, W. P. Bosman, R. de Gelder, R. Israel, J. M. M. Smits, *The DIRDIF-94 program system,* Technical Report of the Crystallography Laboratory, University of Nijmegen, The Netherlands, **1994**; b) DIRDIF94: P. T. Beurskens, G. Admiraal, G. Beurskens, W. P. Bosman, R. de Gelder, R. Israel, J. M. M. Smits, *The DIRDIF-94 program system,* Technical Report of the Crystallography Laboratory, University of Nijmegen, The Netherlands, **1994**.

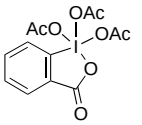
 © 2003 Wiley-VCH Verlag GmbH & Co. KGaA, Weinheim

Oxidation of Alcohols

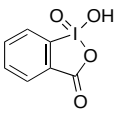
IBX Amides: A New Family of Hypervalent Iodine Reagents**

Viktor V. Zhdankin, Alexey Y. Koposov, Brian C. Netzel, Nikolai V. Yashin, Brian P. Rempel, Michael J. Ferguson, and Rik R. Tykwinski**

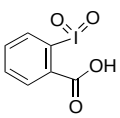
Organic derivatives of pentavalent iodine have found wide application as oxidizing reagents in the synthesis of biologically important complex organic molecules.[1] The most important representatives of this class of compounds, Dess–Martin periodinane (DMP, **1**) and its precursor 1-hydroxy-1,2-benziodoxol-3-(1*H*)-one-1-oxide (**2a**), have emerged as the reagents of choice for the oxidation of alcohols to carbonyl compounds and for other synthetically useful oxidative transformations.[1,2] Reagent **2a** is commonly referred to as 2-iodoxybenzoic acid (IBX, **2b**), although the tautomeric form **2a** is the best representation of the actual structure of this compound. This has been confirmed by X-ray crystallographic analysis, which also indicated that IBX has a polymeric structure formed through an extended linkage of intermolecular secondary I···O bonding interactions.[3] The polymeric structure of IBX renders it essentially insoluble in all nonreactive media. Its low solubility and potentially explosive nature restrict the practical application of this reagent. Herein we report the preparation and structure of novel derivatives of 2-iodoxybenzoic acid, namely 2-iodoxybenzamides **4**, which are stable, soluble reagents with oxidizing properties similar to IBX and DMP. These synthetically valuable characteristics of compounds **4** are best explained by their pseudocyclic structure in which intramolecular secondary I···O bonds partially replace the intermolecular I···O secondary bonds that give rise to the polymeric structures of other reported iodylarenes.



1

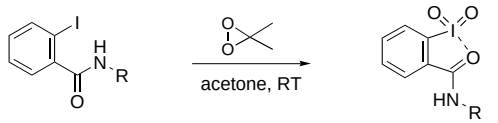


2a



2b

The new 2-iodoxybenzamides **4a–g** were prepared by dioxirane oxidation of the readily available 2-iodobenzamides **3** (Scheme 1) and isolated in the form of stable, white, microcrystalline solids. This procedure allows the preparation of compounds **4** derived from numerous types of amino compounds, such as esters of natural α-amino acids (**4a, 4c**, and **4d**) and non-natural amino acids (**4b**), β-amino acids (**4e** and **4f**), and (*R*)-1-phenylethylamine (**4g**). Optical rotation measurements showed substantially greater $[\alpha]_D$ values for the chiral products **4** relative to the respective amino acids, and, as expected, the values for oxidants **4a** and **4b**, derived from L- and D-alanine, respectively, were opposite in sign and nearly equal in magnitude.[4] It is interesting to note that the dioxirane oxidation of ester derivatives **3a–d** does not result in the formation of cyclic benziodazoles, as has been observed in the oxidation of 2-iodobenzamides derived from α-amino acids[5a] and some other precursors.[5b–d]



3a-g → **4a-g** (45-73%)

a: R = (*S*)-CH(CH$_3$)CO$_2$CH$_3$
b: R = (*R*)-CH(CH$_3$)CO$_2$CH$_3$
c: R = (*S*)-CH(CH$_2$Ph)CO$_2$CH$_3$
d: R = (*S*)-CH(*i*-Bu)CO$_2$CH$_3$
e: R = CH$_2$CH$_2$CO$_2$H
f: R = CH(CH$_3$)CH$_2$CO$_2$H
g: R = (*R*)-CH(Ph)CH$_3$

Scheme 1. Preparation of 2-iodoxybenzamides **4a–g**.

Products **4** were characterized by elemental and spectroscopic analysis, as well as single-crystal X-ray analysis in the case of **4c**.[6,7] IR spectra of all compounds showed an N-H absorption at about $\tilde{\nu} = 3300\ cm^{-1}$, a carbonyl stretch at $\tilde{\nu} =$

[*] Prof. Dr. V. V. Zhdankin, A. Y. Koposov, B. C. Netzel, N. V. Yashin
Department of Chemistry, University of Minnesota Duluth
Duluth, Minnesota 55812 (USA)
Fax: (+1) 218-726-7394
E-mail: vzhdanki@d.umn.edu
Prof. Dr. R. R. Tykwinski, B. P. Rempel
Department of Chemistry, University of Alberta
Edmonton, Alberta, T6G 2G2 (Canada)
Fax: (+1) 780-492-8231
E-mail: rik.tykwinski@ualberta.ca
Dr. M. J. Ferguson
X-Ray Crystallography Laboratory
Department of Chemistry, University of Alberta
Edmonton, Alberta, T6G 2G2 (Canada)

[**] This work was supported by a research grant from the National Institutes of Health (R15 GM065148-01), the National Science and Engineering Research Council of Canada, and the University of Alberta.

Supporting information for this article is available on the WWW under http://www.angewandte.org or from the author.

 © 2003 Wiley-VCH Verlag GmbH & Co. KGaA, Weinheim DOI: 10.1002/anie.200351018

1610–1620 cm^{-1}, and an I=O absorption at $\tilde{\nu} = 780–740\ cm^{-1}$. The signals of the N-H protons in the ^1H NMR spectra of compounds **4** were observed as a characteristic doublet (broad singlet for **4e**) centered at about $\delta = 9.6$ ppm. The most characteristic signals in the ^{13}C NMR spectra of compounds **4** were those of the carbon atom of the amide carbonyl group at $\delta = 165–166$ ppm and C-IO_2 at $\delta =$ ca. 149 ppm. All products **4** have moderate solubility in common organic solvents, such as chloroform, dichloromethane, and acetonitrile.

A single crystal of **4c** suitable for X-ray crystallographic analysis was obtained through the slow evaporation of an acetonitrile solution and was analyzed as the respective solvate. The unit cell consists of four crystallographically independent molecules that are pseudocentrosymmetrically arranged in a tetrameric structure (Figure 1). Strong secondary I···O bonding interactions between neighboring molecules of this tetramer (e.g., I1–O42 2.690(5) Å, I1–O32(5) 2.594 Å, shown as dashed lines) enforce this arrangement. Hydrogen bonding (shown as dotted lines) between the amide proton of molecules 1 and 3 and an oxygen atom of molecules 2 and 4 link adjacent tetramers together. An additional intramolecular close contact of the hypervalent iodine center with the oxygen atom of the amide group (e.g., I1–O13 2.571(6) Å) within each molecule enforces a planar geometry on the resulting five-membered ring, a geometry that is analogous to that observed for IBX and other benziodoxoles.[3,8]

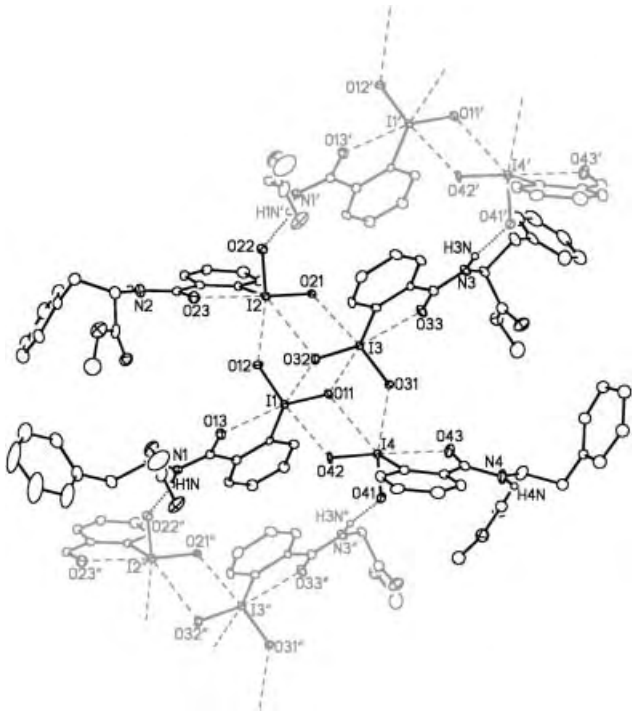
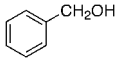


Figure 1. Perspective view of the four crystallographically independent molecules of **4c**·CH_3CN (shown in black, CH_3CN removed for clarity) and extended lattice (shown in gray). Selected distances [Å] and angles [°]: I1–O11 1.823(5), I1–O12 1.807(5), I1–O13 2.571(6), I1–O32 2.594(5), I1–O42 2.690(5), I1–C1 2.114(8); O11–I1–C1 92.4(3), O12–I1–C1 98.4(3), O13–I1–C1 71.0(3).

The solid-state structure suggests that the partial replacement of intermolecular I···O bonds with intramolecular I···O bonds through the introduction of an *ortho* substituent is crucial for stabilization and improved solubility.[9,10] Furthermore, intermolecular I···O interactions in other iodyl benzene derivatives afford structures best described as polymeric, which accounts for their more limited solubility in comparison to **4c**, with its discrete tetrameric structure. The significance of secondary I···O bonding interactions in previously reported iodylbenzene derivatives,[9] including a 2-sulfonyl-substituted iodylbenzene, has recently been discussed by Protasiewicz and co-workers.[10a]

Preliminary experiments demonstrate that 2-iodoxybenzamides show aspects of reactivity similar to both IBX and DMP, but consistent with neither. As outlined in Table 1, a range of alcohols were oxidized to the respective carbonyl compounds under mild conditions. For example, the reaction of benzyl alcohol with **4c** gave benzaldehyde cleanly, as the only product detected by ^1H NMR spectroscopy (Table 1, entry 1). A variety of secondary alcohols were converted into the corresponding ketones in good yields with **4a–c** (Table 1, entries 2, 3, and 5), although reaction times varied as a function of the reagent used. The oxidative kinetic resolution of racemic *sec*-phenethyl alcohol was also investigated with reagents **4a–c**. The reaction mixture containing 0.5 equivalents of the respective oxidant was analyzed by gas chromatography (GC) on a chiral stationary phase. Whereas analysis of the reactions with **4a** and **4b** indicated no enantiomeric enrichment of the alcohol remaining in the product mixture (Table 1, entries 5 and 6), in the reaction with **4c** the alcohol starting material was enriched to a very modest 9% *ee* (Table 1, entry 7). Reagent **4b**, in contrast with DMP, effected

Table 1: Reaction of IBX amides **4a–c** with alcohols.[a]

Entry	Alcohol	Reagent (equiv)	*t* [h]	Yield [%]
1		**4c** (1.02)	2	100
2		**4c** (1.04)	18	98
3		**4c** (1.03)	18	89
4		**4b** (0.50)	24	26[b,c]
5		**4b** (0.50)	72	94[b,c]
6		**4a** (0.51)	72	100[b,c]
7		**4c** (0.46)	18	96[b,d]
8		**4c** (1.00)	48	309[e]

[a] Reactions were carried out in $CDCl_3$ at room temperature. [b] Yield of ketone based on oxidant. [c] Remaining alcohol is racemic, as determined by GC. [d] Remaining alcohol shows 9% *ee*, as determined by GC. [e] Yield of 1,6-hexanedial.

 © 2003 Wiley-VCH Verlag GmbH & Co. KGaA, Weinheim

oxidative cleavage of *cis*-1,2-cyclohexanediol to give hexanedial in 30% yield (Table 1, entry 8). It should be emphasized that, according to literature data,[1] iodylbenzene ($PhIO_2$) and other noncyclic iodylarenes do not react with alcohols in the absence of acid catalysis. In agreement with their structural features, the oxidizing reactivity of 2-iodoxybenzamides **4** is closer to that of the benziodoxole-based pentavalent iodine reagents.

In conclusion, we have reported the preparation and structure of novel 2-iodoxybenzamides **4**, which are stable and soluble compounds with unique and synthetically valuable oxidizing properties. X-Ray data on **4c** reveals a pseudobenziodoxole structure in which intramolecular I···O secondary bonds partially replace the intermolecular I···O secondary bonds, thus disrupting the polymeric structure characteristic of $PhIO_2$ and other previously reported iodylarenes. This structural characteristic substantially increases the solubility and stability of these reagents relative to other I^V reagents.

Received: January 24, 2003 [Z51018]

Keywords: alcohols · hypervalent compounds · iodine · oxidation · synthetic methods

[1] a) A. Varvoglis, *Hypervalent Iodine in Organic Synthesis*, Academic Press, London, **1997**; b) V. V. Zhdankin, P. J. Stang, *Chem. Rev.* **2002**, *102*, 2523; c) T. Wirth, *Angew. Chem.* **2001**, *113*, 2889; *Angew. Chem. Int. Ed.* **2001**, *40*, 2812; d) H. Tohma, Y. Kita, *Top. Curr. Chem.* **2003**, *224*, 209.

[2] a) R. Mazitschek, M. Mulbaier, A. Giannis, *Angew. Chem.* **2002**, *114*, 4216; *Angew. Chem. Int. Ed.* **2002**, *41*, 4059; b) K. C. Nicolaou, T. Montagnon, P. S. Baran, *Angew. Chem.* **2002**, *114*, 1035; *Angew. Chem. Int. Ed.* **2002**, *41*, 993; K. C. Nicolaou, D. L. F. Gray, T. Montagnon, S. T. Harrison, *Angew. Chem.* **2002**, *114*, 1038; *Angew. Chem. Int. Ed.* **2002**, *41*, 996; K. C. Nicolaou, T. Montagnon, P. S. Baran, Y.-L. Zhong, *J. Am. Chem. Soc.* **2002**, *124*, 2245; K. C. Nicolaou, P. S. Baran, Y.-L. Zhong, S. Barluenga, K. W. Hunt, R. Kranich, J. A. Vega, *J. Am. Chem. Soc.* **2002**, *124*, 2233; e) K. C. Nicolaou, K. Sugita, P. S. Baran, Y.-L. Zhong, *J. Am. Chem. Soc.* **2002**, *124*, 2221; K. C. Nicolaou, P. S. Baran, Y.-L. Zhong, K. Sugita, *J. Am. Chem. Soc.* **2002**, *124*, 2212.

[3] P. J. Stevenson, A. B. Treacy, M. Nieuwenhuyzen, *J. Chem. Soc. Perkin Trans. 2* **1997**, 589.

[4] In addition to the chirality of the amino acid derived moiety, the iodine is also a potential stereogenic center, as is seen in the solid state. As the preferred conformation/configuration about the iodonium center in solution is not known, the enantiomeric/diastereomeric relationship between **4a** and **4b** can not be established.

[5] a) V. V. Zhdankin, A. E. Koposov, J. T. Smart, R. R. Tykwinski, R. McDonald, A. Morales-Izquierdo, *J. Am. Chem. Soc.* **2001**, *123*, 4095; b) V. V. Zhdankin, R. M. Arbit, B. J. Lynch, P. Kiprof, V. G. Young, *J. Org. Chem.* **1998**, *63*, 6590; c) H. J. Barber, M. A. Henderson, *J. Chem. Soc. C* **1970**, 862; d) T. M. Balthazar, D. E. Godaz, B. R. Stults, *J. Org. Chem.* **1979**, *44*, 1447.

[6] Representative procedure: A freshly prepared solution of dimethyldioxirane in acetone (0.1M, 90 mL, 9 mmol) was added to a stirred mixture of **3c** (1.23 g, 3.0 mmol) in dry dichloromethane (15 mL) at 0°C, upon which the solution immediately turned light yellow. The reaction mixture was stirred at room temperature for an additional 8 h, then filtered, and the precipitate collected was washed with diethyl ether and dichloromethane, and dried under vacuum to afford **4c** (0.86 g, 65%) as a white microcrystalline solid. M.p. 156°C (decomp); $[\alpha]_D^{RT} = -34$ ($c = 0.0023$, CH_3CN); ^{1}H NMR (300 MHz, [D$_6$]DMSO, 25°C): $\delta = 9.66$ (d, ^3J(H,H) = 7.8 Hz, 1H; NH), 8.27 (m, 2H; Ar), 7.95 (t, ^3J(H,H) = 7.6 Hz, 1H; Ar), 7.76 (t, ^3J(H,H) = 7.6 Hz, 1H; Ar), 7.27 (m, 5H; Ph), 4.74 (m, 1H; CH), 3.67 (s, 3H; OCH_3), 3.21 ppm (m, 2H; CH_2); ^{13}C NMR (75.5 MHz, [D$_6$]DMSO, 25°C): $\delta = 171.2$, 166.1, 149.1, 137.1, 133.1, 131.3, 128.9, 128.3, 127.9, 127.2, 126.6, 123.1, 54.7, 52.1, 35.8 ppm; IR (KBr): $\tilde{\nu} = 3220$ (NH), 1744 (C=O), 1620 (C=O), 760 cm^{-1} (I=O); elemental analysis: calcd for $C_{17}H_{16}INO_5$: C 46.28, H 3.66, N 3.17, I 28.76; found: C 46.07, H 3.69, N 3.17, I 28.47; MS(CI): m/z (%): 410.0 $[M-MeOH+H]^+$ (78). See Supporting Information for additional synthetic and characterization details.

[7] X-ray diffraction data were collected on a Bruker PLATFORM/SMART 1000 CCD diffractometer with graphite monochromated $Mo_{K\alpha}$ radiation (0.71073 Å). Crystal data for **4c** $C_{68}H_{64}I_4N_4O_{20}\cdot C_7H_{10.50}N_{3.50}$: $M_r = 1908.52$, colorless, $0.46 \times 0.22 \times 0.07$ mm^3, monoclinic, $P2_1$ (No. 4), $a = 11.1810(8)$, $b = 30.221(2)$, $c = 12.0210(9)$ Å, $\beta = 100.468(2)°$, $V = 3994.2(5)$ Å^3, $Z = 2$, $\rho_{calcd} = 1.587$ g cm^{-3}, $\mu = 1.634$ mm^{-1}. Data collection and refinement: ω scans (0.2°; 20 s exposures), $T = -80$°C, 2θ max = 52.80°, total data collected = 25445, independent reflections = 15852 ($R_{int} = 0.0366$). The data were corrected for absorption with a multiscan model by using *SADABS* (transmission factors: 0.8942–0.5203). The structure was solved by direct methods (*SHELXS-86*) and full-matrix least-squares refinement on F^2 of 904 variables (*SHELXL-93*) converged to $R_1 = 0.0451$ (for 13250 observed data with $F_o^2 \geq 2\sigma(F_o^2)$), $wR_2 = 0.1093$, and $S = 1.036$ (all data, $F_o^2 \geq -3\sigma(F_o^2)$); Flack parameter = 0.01(2). Non-hydrogen atoms were refined anisotropically; hydrogen atoms were included in calculated positions using a riding model. Residual electron density = 1.413 and −0.696 e Å^{-3}. CCDC-200547 (**4c**) contains the supplementary crystallographic data for this paper. These data can be obtained free of charge via www.ccdc.cam.ac.uk/conts/retrieving.html (or from the Cambridge Crystallographic Data Centre, 12, Union Road, Cambridge CB21EZ, UK; fax: (+44) 1223-336-033; or deposit@ccdc.cam.ac.uk).

[8] V. V. Zhdankin, *Rev. Heteroat. Chem.* **1997**, *17*, 133.

[9] a) N. W. Alcock, J. F. Sawyer, *J. Chem. Soc. Dalton Trans.* **1980**, 115; b) A. R. Katritzky, G. P. Savage, G. J. Palenik, K. Qian, Z. Zhang, H. D. Durst, *J. Chem. Soc. Perkin Trans. 2* **1990**, 1657; c) D. G. Naae, J. Z. Gougoutas, *J. Org. Chem.* **1975**, *40*, 2129.

[10] a) D. Macikenas, E. Skrzypczak-Jankun, J. D. Protasiewicz, *Angew. Chem.* **2000**, *112*, 2063; *Angew. Chem. Int. Ed.* **2000**, *39*, 2007; b) D. Macikenas, E. Skrzypczak-Jankun, J. D. Protasiewicz, *J. Am. Chem. Soc.* **1999**, *121*, 7164; c) U. H. Hirt, M. F. H. Schuster, A. N. French, O. G. Wiest, T. Wirth, *Eur. J. Org. Chem.* **2001**, 1569; d) U. H. Hirt, B. Spingler, T. Wirth, *J. Org. Chem.* **1998**, *63*, 7674.

 © 2003 Wiley-VCH Verlag GmbH & Co. KGaA, Weinheim

Cover Picture



Daniel Krüger, Roger Rousseau, Harald Fuchs, and Dominik Marx*

"Mechanochemistry" is the use of mechanical forces to induce and control molecular reactions. This link between chemistry and nanophysics is illustrated by D. Marx et al. on page 2251 ff. in a theoretical study: thiolate molecule is employed to stretch a gold cluster into a nanowire. The cover picture follows clockwise the isomerization steps that occur under the application of an external pulling force, such as that exerted by an atomic force microscope.

Contents

News

Main Group Chemistry: F. Mathey Moves to USA ____ 2214

Organic Chemistry: S. Danishefsky Recognized ____ 2214

Books

Combinatorial Library ____ 2215 — Lisa Bellavance English — *reviewed by K. Knepper, S. Bräse*

Dendrimers and Other Dendritic Polymers ____ 2215 — Jean M. J. Fréchet, Donald A. Tomalia — *reviewed by H. Frey*

Dendrimers and Dendrons ____ 2216 — George R. Newkome, Charles N. Moorefield, Fritz Vögtle — *reviewed by B. Meijer*

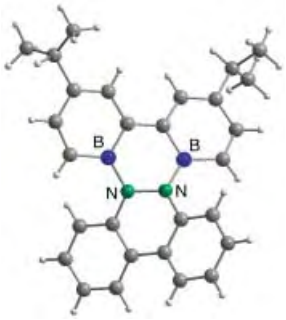
Highlights

Polydentate Lewis Acids

F. P. Gabbaï* ____ 2218 – 2221

The Charge-Reverse Analogy as an Inspiration for the Preparation of Polydentate Lewis Acidic Boranes

Reversing the charge: The recent preparation of a masked version of a 2,2′-diborabiphenyl (the radical anion of its adduct with benzo[*c*]cinnoline is shown) constitutes a noticeable achievement on the way to bidentate Lewis acidic boranes with optimized properties as ligands and opens up the chemistry of this unique class of bidentate Lewis acids.

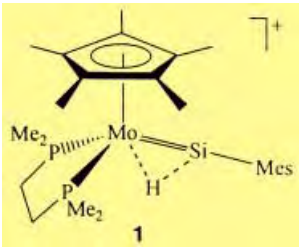


Multiple Bonds with Si/Ge/Sn/Pb

M. Weidenbruch* ____ 2222 – 2224

Triple Bonds of the Heavy Main-Group Elements: Acetylene and Alkylidyne Analogues of Group 14

Carbon copies? Compounds containing homo- and heteronuclear multiple bonds involving the heavier Group 14 elements have become available in the past few years. The most recent example is the cationic complex **1** (Mes = mesityl = 2,4,6-trimethylphenyl), for which the structural analysis and DFT calculations indicate a pronounced silylidene character and a nonclassical H···Si interaction.



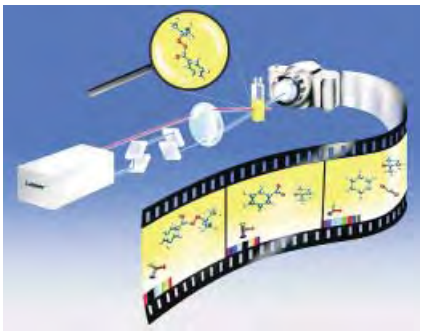
Reviews

Femtosecond Spectroscopy

J. Aßmann, M. Kling, B. Abel* ____ 2226 – 2246

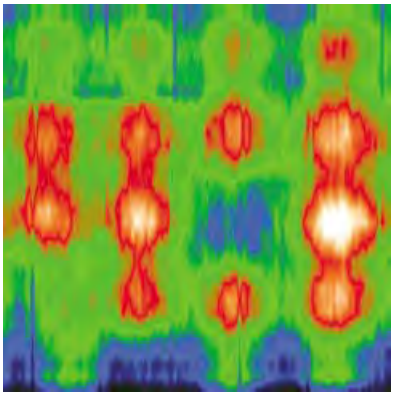
Watching Photoinduced Chemistry and Molecular Energy Flow in Solution in Real Time

Intramolecular vibrational energy redistribution and intermolecular vibrational energy transfer govern the rates, pathways, and yields of chemical transformations in solution. Powerful experimental approaches of femtosecond spectroscopy allow the direct observation of photoinduced chemistry on an ultrafast timescale and of molecular energy flow in solution.



© 2003 Wiley-VCH Verlag GmbH & Co. KGaA, Weinheim

Communications



Surface cartography: The combination of microcontact printing and local electrochemical surface modification enables a new approach for the creation of complex functional thin films containing several interacting biomolecules within defined regions. Scanning electrochemical microscopy could indicate the local conversion rates for any position within the pattern formed by horseradish peroxidase and glucose oxidase layers (see picture).

Complex Functional Thin Films

T. Wilhelm, G. Wittstock* — **2248 – 2250**

Analysis of Interaction in Patterned Multienzyme Layers by Using Scanning Electrochemical Microscopy

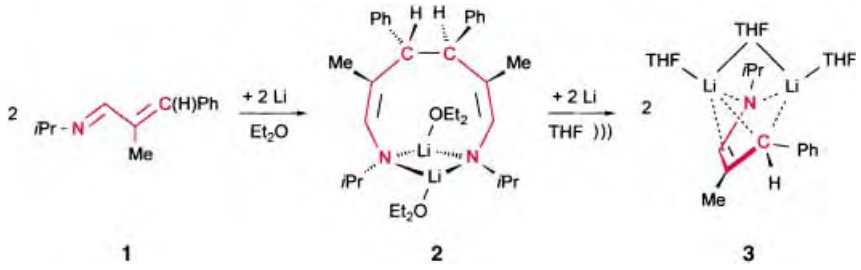


Stretching the imagination: Based on simulations it is proposed that atom-manipulation techniques, such as atomic force microscopy (AFM), could be used to draw and manipulate monoatomic nanowires using thiolates anchored to gold clusters on surfaces (see picture, gold Au, yellow S). At the same time, the force-versus-extension curve is diagnostic for the isomerizations of the underlying covalently bound species.

Gold Nanowires

D. Krüger, R. Rousseau, H. Fuchs, D. Marx* — **2251 – 2253**

Towards "Mechanochemistry": Mechanically Induced Isomerizations of Thiolate–Gold Clusters



A suprising intermediate during the reduction of the 1-aza-1,3-diene **1** with lithium is the dilithium hexa-1,5-dien-1,6-diamide **2**, which probably forms by dimerization of the initially generated radical anion of **1**. However, the new C–C bond of **2** is not very resistant to the alkali metal and is reductively cleaved, which leads to the formation of the dark red (1-azabut-2-en-1,4-diyl)dilithium compound **3**.

Monoazadiene Complexes

V. Lorenz, H. Görls, J. Scholz* — **2253 – 2257**

Reduction of a 1-Aza-1,3-diene to a 1-Azabut-2-ene-1,4-diyl Dianion: An Unusual Reaction Course

For the USA and Canada:
ANGEWANDTE CHEMIE International Edition (ISSN 1433-7851) is published weekly by Wiley-VCH PO Box 191161, D 69451 Weinheim, Germany. Air freight and mailing in the USA by Publications Expediting Inc. 200 Meacham Ave., Elmont, NY 11003. Periodicals postage paid at Jamaica NY 11431. US POSTMASTER: send address changes to *Angewandte Chemie*, Wiley-VCH, 111 River Street, Hoboken, NJ 07030. Annual institutional subscription price for institutions: Europe € 2998.00/3148.00. Outside Europe US$ 3718.00/3904.00 (valid for print or electronic/print and electronic delivery); for individuals who are personal members of a national chemical society, or whose institution already subscribes, or who are retired or self-employed consultants, print only (including postage and handling charges): Europe € 248.00/Outside Europe US$ 348.00.

 © 2003 Wiley-VCH Verlag GmbH & Co. KGaA, Weinheim

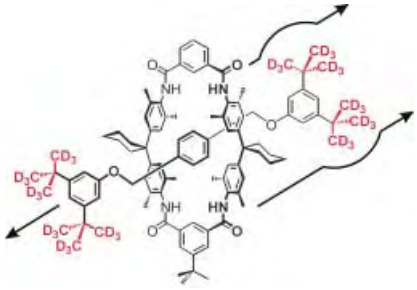
Contents

Kinetics of Rotaxane Deslippage

T. Felder, C. A. Schalley* ____ **2258 – 2260**

Secondary Isotope Effects on the Deslipping Reaction of Rotaxanes: High-Precision Measurement of Steric Size

A supramolecular measuring instrument for determining steric size: The deslipping reaction of the rotaxane shown with deuterated stopper groups senses the smaller steric size of the deuterium atom and proceeds with a 10% higher reaction rate than the reaction of the unlabeled rotaxane. This result sheds new light from a supramolecular point of view on the classical problem of determining steric demand.

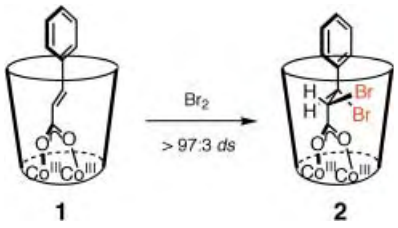


cis-Bromination of Alkenes

G. Steinfeld, V. Lozan, B. Kersting* ____ **2261 – 2263**

cis-Bromination of Encapsulated Alkenes

Inside changes! In striking contrast to the *trans*-bromination of the free acid, bromination of the bridging cinnamato ligand in **1** proceeds highly diastereoselectively to give the *syn*-brominated complex **2**. A possible explanation for this is that the bromination of **1** proceeds within a confined environment. Since the brominated products can be liberated from the binding pocket of the dinuclear complexes, the metal complexes can be used as reagents

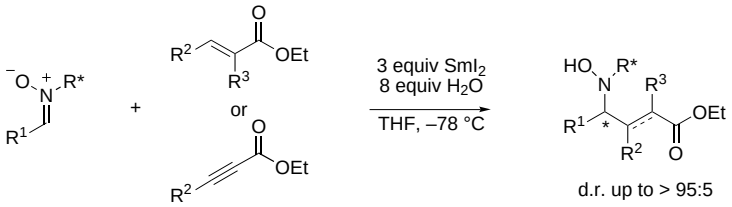


for the *cis*-bromination of olefins with anchoring RCO_2^- functions.

Umpolung of C-N Bonds

G. Masson, P. Cividino, S. Py,* Y. Vallée* ____ **2265 – 2268**

SmI_2-Induced Umpolung of the C=N Bond: First Reductive Conjugate Addition of Nitrones to α,β-Unsaturated Esters

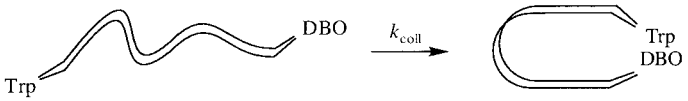


Enantioselective approach to γ-amino acid derivatives: Umpolung of the C=N bond of nitrones by reduction with SmI_2, generates a species that adds smoothly to α,β-unsaturated esters. The corresponding γ-*N*-hydroxyamino esters are obtained with excellent stereoselection (see scheme).

Amino Acid Flexibility

F. Huang, W. M. Nau* ____ **2269 – 2272**

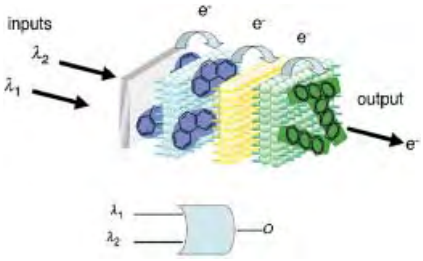
A Conformational Flexibility Scale for Amino Acids in Peptides



The end-to-end collision frequency of short polypeptides labeled with a fluorescent probe (DBO) at one end and an efficient contact quencher (Trp) at the other end (see scheme) provides an absolute measure of the time scale of conformational changes in short structureless peptides as a function of the amino acid type. A general correlation with secondary structure propensity applies, with the most flexible amino acids being most abundant in β turns and the most rigid ones in β sheets.

 © 2003 Wiley-VCH Verlag GmbH & Co. KGaA, Weinheim

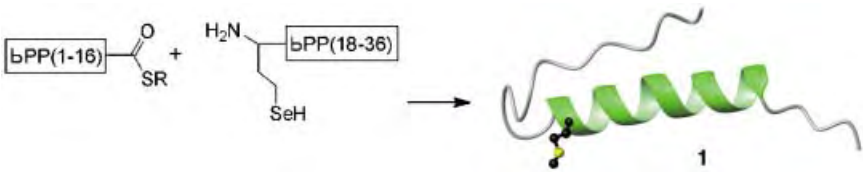
Many ANDs make light work: A novel optical AND logic gate based on an assembly of polymer Langmuir–Blodgett (LB) films is proposed. The device is composed of four polymer LB layers, which contain phenanthrene, anthracene, electron-donor, and electron-acceptor polymers (see scheme). In this optical logic device, the input signals are photoirradiation with the wavelengths for excitation of phenanthrene ($\lambda_1 = 300$ nm) and anthracene ($\lambda_2 = 380$ nm), and the output is the photocurrent.



Molecular Electronics

J. Matsui, M. Mitsuishi, A. Aoki, T. Miyashita* ——— 2272 – 2275

Optical Logic Operation Based on Polymer Langmuir–Blodgett-Film Assembly



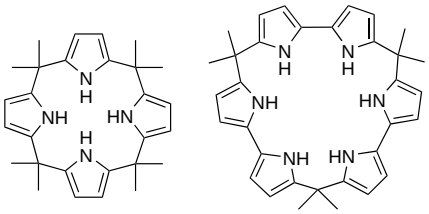
Site-selective incorporation of selenomethionine into proteins in place of methionine provides a unique spectroscopic probe of local protein structure and dynamics. This was demonstrated with seleno-bPP **1**, a synthetic variant of a peptide hormone prepared by ligation of a C-terminal peptide thioester with a peptide fragment containing an N-terminal selenohomocysteine, followed by methylation of the resulting selenol (see scheme; bPP = bovine pancreatic peptide).

Probing Protein Folding

G. Roelfes, D. Hilvert* ——— 2275 – 2277

Incorporation of Selenomethionine into Proteins through Selenohomocysteine-Mediated Ligation

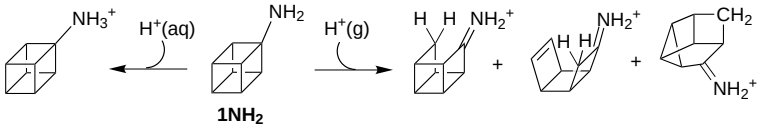
Bigger is better: Preliminary anion-binding studies reveal that bipyrrole-containing macrocycle calix[3]bipyrrole **2** binds large halide anions (for example, Br^-) with affinities that are substantially enhanced relative to those of the smaller pyrrole-containing calix[4]pyrrole **1**. The complexation has been studied by ^1H NMR spectroscopy, isothermal titration calorimetry, and X-ray crystallography. In addition, the synthesis of the even larger calix[4]bipyrrole was achieved.



Anion Binding by Calix[n]bipyrroles

J. L. Sessler,* D. An, W.-S. Cho, V. Lynch ——— 2278 – 2281

Calix[*n*]bipyrroles: Synthesis, Characterization, and Anion-Binding Studies



The cubic structure of cubylamine ($\mathbf{1}NH_2$) is maintained on protonation in aqueous solution, but in the gas phase $\mathbf{1}NH_2$ is irreversibly protonated on the carbon framework, leading to the formation of iminium ions through ring opening (see scheme).

Protonation of Cubylamine

J.-L. M. Abboud,* I. A. Koppel,* I. Alkorta, E. W. Della, P. Müller, J. Z. Dávalos, P. Burk,* I. Koppel, V. Pihl, E. Quintanilla ——— 2281 – 2285

Stereoelectronic, Strain, and Medium Effects on the Protonation of Cubylamine, a Janus-like Base

 © 2003 Wiley-VCH Verlag GmbH & Co. KGaA, Weinheim

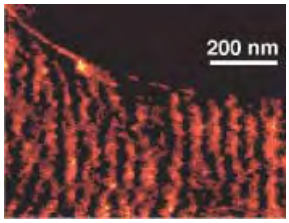
Contents

Multiple-Scale Self-Organization

T. Hayakawa,* S. Horiuchi — **2285 – 2289**

From Angstroms to Micrometers: Self-Organized Hierarchical Structure within a Polymer Film

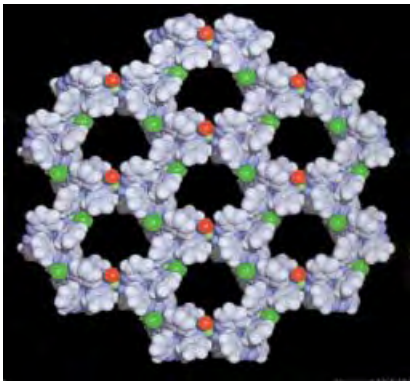
Self-organization on three length scales is exhibited by a block copolymer of styrene and an oligothiophene-bearing isoprene in cast films. For example, a phase-separated nanostructure consisting of π-conjugated oligothiophene molecules is self-aligned perpendicular to the substrate, as revealed in a TEM image of a section through the film (see picture).



A 2D Molecule-Based Magnet

J. R. Galán-Mascarós, K. R. Dunbar* — **2289 – 2293**

A Self-Assembled 2D Molecule-Based Magnet: The Honeycomb Layered Material $\{Co_3Cl_4(H_2O)_2[Co(Hbbiz)_3]_2\}$

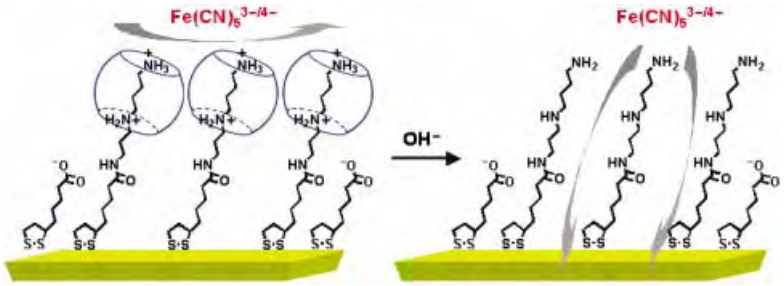


A novel 2D coordination compound, $\{[Co_3Cl_4(H_2O)_2[Co(Hbbiz)_3]_2 \cdot 3\,C_7H_8 \cdot 9\text{-}CH_3OH\}_\infty$ has been prepared and characterized. The compound (see picture) consists of a honeycomb structural motif of twelve-membered rings composed of alternating octahedral and tetrahedral Co^{II} ions and the bridging ligand 2,2′-bibenzimidazole (Hbbiz). Magnetic ordering is observed below $T_c = 9$ K (T_c = Curie temperature).

Pseudorotaxanes on Gold

K. Kim, W. S. Jeon, J.-K. Kang, J. W. Lee, S. Y. Jon, T. Kim, K. Kim* — **2293 – 2296**

A Pseudorotaxane on Gold: Formation of Self-Assembled Monolayers, Reversible Dethreading and Rethreading of the Ring, and Ion-Gating Behavior



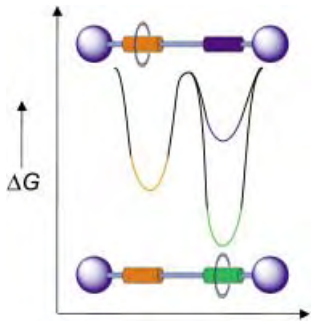
Machinelike behavior—reversible dethreading and rethreading of a molecular bead—is demonstrated in a self-assembled monolayer (SAM) of a pseudorotaxane on gold. Furthermore, unprecedented ion-gating behavior associated with threading and dethreading is observed; the SAM blocks or allows the access of electroactive species to the electrode surface depending on the presence or absence of the threaded molecular bead (see picture).

Bistable Molecular Shuttles

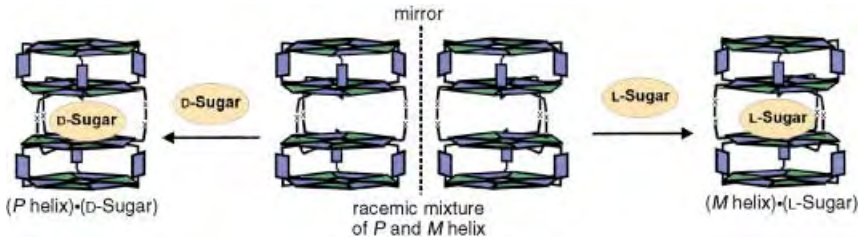
A. Altieri, G. Bottari, F. Dehez, D. A. Leigh,* J. K. Y. Wong, F. Zerbetto* — **2296 – 2300**

Remarkable Positional Discrimination in Bistable Light- and Heat-Switchable Hydrogen-Bonded Molecular Shuttles

A tale of two stations: Molecular shuttles, in which a macrocyclic unit can move between two stations over a relatively large distance (1.5 nm), exhibit bistability that can be induced using either light or heat as stimuli, and exhibit large required variations in ΔG between the two stations (see diagram). This is achieved with remarkable positional integrity, which originates from the self-binding of non-fumaramide stations.



 © 2003 Wiley-VCH Verlag GmbH & Co. KGaA, Weinheim

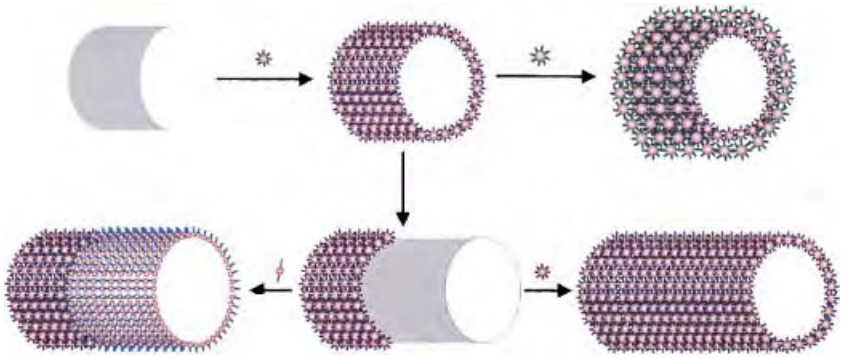


Sweet selection: Stereoselective recognition of carbohydrates has now been achieved by a receptor self-assembled through hydrogen bonds. The receptor, which is present as a racemic mixture of the *P* and *M* helices, is amplified in the mixture by the addition of a chiral guest (see schematic representation).

Saccharide Recognition

T. Ishi-i, M. A. Mateos-Timoneda, P. Timmerman, M. Crego-Calama,* D. N. Reinhoudt,* S. Shinkai ____ **2300 – 2305**

Self-Assembled Receptors that Stereoselectively Recognize a Saccharide

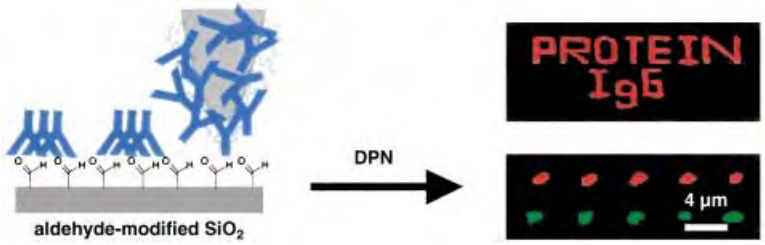


Dynamic control over the nano-, micro, and macroscopic architectures of materials can be achieved by using living fungi templates for the assembly of DNA-functionalized Au nanoparticles into ordered structures (see scheme). After assembly of one type of particle, a second type of particle can be assembled along the growing direction of the hyphae templates simply by changing the culture solution.

DNA-Functionalized Au Nanoparticles

Z. Li, S.-W. Chung, J.-M. Nam, D. S. Ginger, C. A. Mirkin* _ **2306 – 2309**

Living Templates for the Hierarchical Assembly of Gold Nanoparticles



Pen a nanoletter: Direct-write dip-pen nanolithography (DPN) has been used to generate protein nanostructures on modified silicon oxide surfaces. This technique offers control over feature size at the 50–550 nm scale. The bioactivity of the proteins remains intact and has been studied by fluorescence microscopy (see picture).

Protein Nanostructures

J.-H. Lim, D. S. Ginger, K.-B. Lee, J. Heo, J.-M. Nam, C. A. Mirkin* ___ **2309 – 2312**

Direct-Write Dip-Pen Nanolithography of Proteins on Modified Silicon Oxide Surfaces

VIP Communications labeled with this symbol have been judged by two referees as being "very important papers".

The publication of Communications labeled with this symbol has been accelerated because of their topical or highly competitive nature.

 © 2003 Wiley-VCH Verlag GmbH & Co. KGaA, Weinheim

Looking for outstanding employees?

Do you need another expert for your excellent team?
... Chemists, PhD Students, Managers, Professors, Sales Representatives...

Place an advert in the printed version and have it made available online for 1 month, free of charge!

Angewandte Chemie International Edition
Advertising Sales Department: Marion Schulz
Phone: 0 62 01 - 60 65 65
Fax: 0 62 01 - 60 65 50
E-Mail: MSchulz@wiley-vch.de

Service

Keywords ____ *2314*

Authors ____ *2315*

Vacancies ____ *2213*

Preview ____ *2317*



➤ journals ➤ books ➤ reference work
➤ databases ➤ management resources

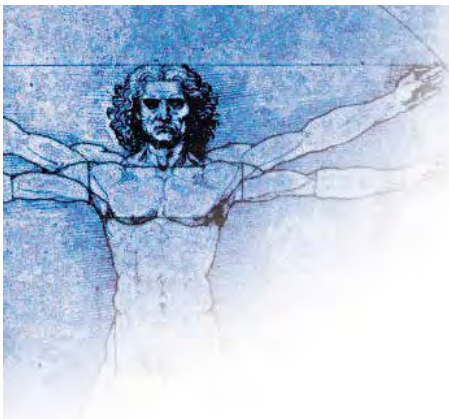
Wiley Interscience is designed
to be an integral part
of your discovery process.
Whether you are conducting original
research across multiple disciplines,
looking for practical solutions, or seeking
professional growth,
Wiley InterScience helps you...

www.interscience.wiley.com

WILEY InterScience®
www.interscience.wiley.com
Discover something great

discover
something
GREAT.

 © 2003 Wiley-VCH Verlag GmbH & Co. KGaA, Weinheim



F. Mathey: A Parisian in America

Later this year, François Mathey (Ecole Polytechnique, Palaiseau, France), will move to the University of California at Riverside (UCR) to take over a position as Distinguished Professor in the Department of Chemistry. He was born in Paris (France) in 1941, and studied chemistry at Paris VI University (today Université Pierre et Marie Curie). He received his doctorate from this university in 1971 and worked in industry until 1988. Then, he was appointed Professor at the Ecole Polytechnique in Palaiseau near Paris (founded in 1794) and Research Director at the CNRS.



F. Mathey

The research of his group is focused on phosphorus and transition-metal chemistry as well as homogeneous catalysis. Mathey is especially interested in the analogy between the chemistry of low-coordinate carbon and phosphorus species. He is a co-author of a book on this subject and his overview of achievements in phosphaorganic chemistry was recently published as a Review in *Angewandte Chemie*.[1] Therein, he reports on the synthesis, reactivity, and coordination modes of the most fundamental low-coordinate units, the phosphorus analogues of alkenes, alkynes, and carbenes. "This analogy is deep, specific, and fertile," he writes. Together with his new colleagues Guy Bertrand (joint UCR–CNRS laboratory) and Chris Reed, Mathey will make Riverside one of the preeminent places for research on main-group chemistry in the world.

Mathey has been a full member of the chemistry department of the French Academy of Sciences since 1998. Having been in office since 2000, he will continue to serve as a President of the French Chemical Society (Société Française de Chimie, SFC) until the end of the year. He is also a member of the Editorial Board of *Chemistry—A European Journal*.

S. Danishefsky: An American in Darmstadt

The Emanuel Merck Lectureship, awarded by Merck KGaA, Darmstadt, Germany (Pharmaceuticals and Chemicals), is given to Prof. Samuel J. Danishefsky from New York. It is worth 10000 €.

Danishefsky obtained his Ph.D. in 1962 at Harvard University under the direction of Peter Yates. From 1961 to 1963, he was a Postdoctoral Fellow at Columbia University (New York) under the mentorship of Gilbert Stork. He then joined the faculty at the University of Pittsburgh, PA, before moving to Yale in 1980. In 1993, he returned to New York as a Professor of Chemistry at Columbia University and is currently Head of Bioorganic Chemistry at the Memorial Sloan–Kettering Cancer Center in Manhattan. The roots of this institution go back as far as 1884, and the basic-research arm was founded in 1948. It is the world's oldest and largest private institution devoted to patient care, education, and research into cancer.



S. J. Danishefsky

Danishefsky's research interests are centered around the strategy and methodology of organic synthesis and its application to problems of biological importance—challenging and thought-provoking organic chemistry at the interface of plausible biological and medical applications. In particular, his group works on the syntheses of antitumor and anti-infective natural products, analogues thereof, and syntheses of fully synthetic carbohydrate epitope vaccines whose goal is suppression of tumor recurrence. Furthermore, oligosaccharides are investigated as potential analogues of cancer cell surfaces. Clinical tests have yielded promising results with patients. Fittingly, the title of the prize lecture is "On the Power of Organic Synthesis". It will provide an insight into the potential of modern medicinal chemistry and drug design and will be delivered at Darmstadt University of Technology on May 26, 2003. In addition to this lecture, Danishefsky will give two seminars for students at Darmstadt University of Technology.

In 2002, the Danishefsky group published no less than five Communications in *Angewandte Chemie*, three of which were recognized as being either Very Important or Hot Papers by the referees or editors, respectively. His Review on the total synthesis of gelsemine was featured on the cover of Issue 1/2003.[2] Gelsemine was picked as a target for its interesting structure, rather than biological activity. "It is in the solution of such problems that much new chemistry is often learnt," Danishefsky points out.

[1] a) K. B. Dillon, F. Mathey, J. F. Nixon, *Phosphorus: The Carbon Copy*, John Wiley and Sons, Chichester, **1997**; b) F. Mathey, *Angew. Chem.* **2003**, *115*, 1616; *Angew. Chem. Int. Ed.* **2003**, *42*, 1578.

[2] H. Lin, S. J. Danishefsky, *Angew. Chem.* **2003**, *115*, 38; *Angew. Chem. Int. Ed.* **2003**, *42*, 36.

 © 2003 Wiley-VCH Verlag GmbH & Co. KGaA, Weinheim

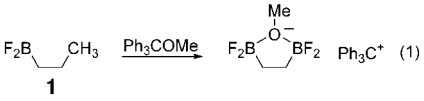
Polydentate Lewis Acids

The Charge-Reverse Analogy as an Inspiration for the Preparation of Polydentate Lewis Acidic Boranes

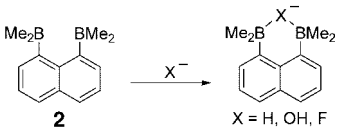
*François P. Gabbaï**

Keywords:
adduct formation · anions · boraarenes · Lewis acids · organoboron chemistry

Polyfunctional Lewis acids contain several Lewis acidic sites that can readily accept electron pairs from incoming basic substrates.[1] Thus, their chemical nature is the reverse of polyfunctional Lewis bases, which incorporate in their molecular skeleton a given number of Lewis basic sites available for coordination of electrophilic substrates (Scheme 1). This analogy was recognized almost four decades ago by Shriver and Biallas, who showed that methoxide anions are effectively chelated by 1,2-bis(difluoroboryl)ethane (**1**), a charge-reverse analogue of ethylenediamine [Eq. (1)].[2] While a global and long standing research effort engraved polydentate Lewis bases on the tables of our chemical tradition, the chemistry of polydentate Lewis acids remains in its infancy. The slow emergence of these polydentate Lewis acids results, at least in part, from the difficulties associated with their syntheses. With promising applications in the fields of molecular recognition, material synthesis, and catalysis, this class of compounds is generating an increased interest. By aiming at a greater control of their properties as ligands, much effort has been placed on the architectural design of these compounds, along with a fine-tuning of the electronic and steric environments of the Lewis acidic centers. In this regard, the recent preparation of 2,2′-diborabiphenyl[3] as an analogue of 2,2′-bipyridine constitutes a noticeable achievement, which will be presented in this highlight.

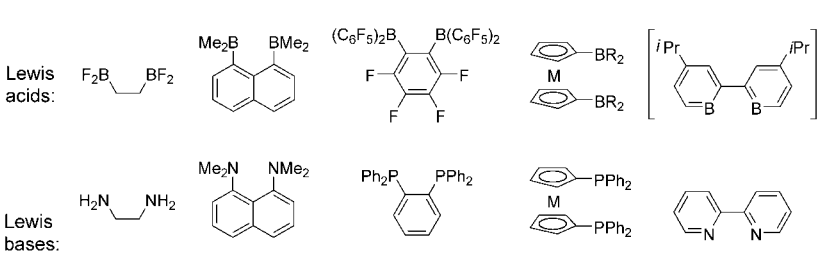


Whereas several tin[4] and mercury[1a,b,5] analogues of crown ethers exist, most of the boron systems investigated to date feature open-framework structures. Their design is inspired from bidentate Lewis bases that incorporate rigid aromatic backbones. 1,8-Diborylnaphthalenes are prototypical examples of such polyfunctional Lewis acids.[1e] Their synthesis usually involves the metathesis reaction of 1,8-dilithionaphthalene with the appropriate boryl halide or alkoxide reagents. Of this category, 1,8-bis(dimethylboryl)naphthalene (**2**) is one of the most studied examples.[6,7] In the presence of potassium hydride in THF, **2** forms a kinetically and thermodynamically stable 1:1 hydride complex that fails to reduce benzaldehyde [Eq. (2)]. The formation



of a B-H-B three-centered two-electron bond in this hydride complex is responsible for the unusual acidity of **2**. As a result, this molecule is commonly referred to as the "hydride sponge", which indicates its charge-reverse relationship to the well known 1,8-diaminonaphthalene proton sponges.

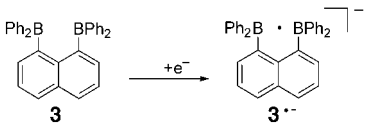
The chemistry of **2** has been further explored in the context of anion complexation. In addition to abstracting hydrides from a variety of substrates, which include superhydride ($LiBHEt_3$) or zirconocene chloride hydride, **2** forms bridged adducts with fluoride and hydroxide ions [Eq. (2)]. The reduction chemistry of these diboranes has also been studied. The reaction of 1,8-bis(diphenylboryl)naphthalene (**3**) with K/[18]crown-6 leads to the formation of a radical species that features a transannular boron–boron one-electron σ bond [Eq. (3)].[8] An interesting parallel exists between $\mathbf{3}^{\bullet-}$ and the radical cation obtained by oxidation of biden-



Scheme 1. Bidentate boranes[2,3,6,12,15,16] and some of their arbitrarily chosen Lewis basic analogues.

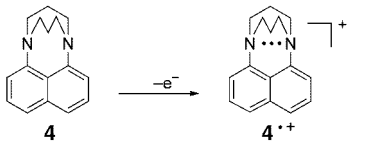
[*] Prof. Dr. F. P. Gabbaï
Department of Chemistry
Texas A&M University
P.O.Box 30012
College Station, TX 77842-3012 (USA)
Fax: (+1) 979-845-4719
E-mail: gabbai@mail.chem.tamu.edu

 © 2003 Wiley-VCH Verlag GmbH & Co. KGaA, Weinheim DOI: 10.1002/anie.200301630



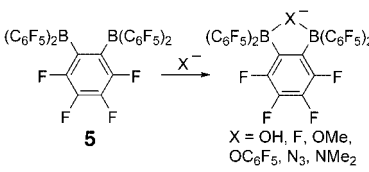
(3)

tate Lewis bases such as the naphtha[3.3.3]diamine (**4**) [Eq. (4)].[9] In the latter case, the heteroatoms are involved in a three-electron σ interaction, which also formally results in a bond order of 0.5.



(4)

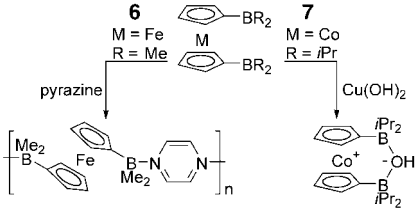
Ortho-phenylene diboranes constitute another important class of polydentate Lewis acids. With structures that parallel that of *ortho*-phenylene diamines or diphosphanes, these derivatives have been considered for the complexation of both neutral[10] and anionic[1d,11–13] electron-rich substrates. In the context of anion complexation, most efforts have centered on the synthesis of strongly electrophilic boranes and their behavior as ligands. Among several compounds,[11] 1,2-bis(bis(pentafluorophenyl)boryl)tetrafluorobenzene (**5**) constitutes a notable example,[12] the synthesis of which involves the use of trimeric perfluoro-*ortho*-phenylene mercury as a starting material. This organomercury reagent can be converted into the target molecule by successive treatment with boron tribromide and bis(pentafluoro)phenylzinc. Like **2**, compound **5** chelates small anions very efficiently [Eq. (5)]. Reported examples



(5)

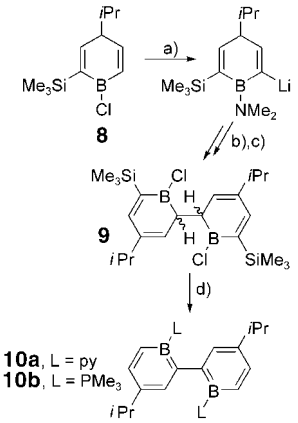
include fluoride,[12] hydroxide,[12] methoxide,[13] pentafluorophenyl oxide,[13] dimethylamide,[1d] and azide[1d] complexes in which the negative charge is shared by two borate centers. The pentafluorophenyl oxide-bridged complex is a weakly coordinating anion, whose robustness makes it ideally suited for the generation of metallocenium olefin polymerization catalysts.[13] By contrast to the aforementioned anionic complexes of **5**, which all feature a bridged structure, methide complexation triggers a ligand redistribution reaction and subsequent formation of a nonbridged borate anion.[14]

In addition to bidentate boranes that feature purely organic backbones, derivatives in which the boryl moieties are linked by metallocene units have also been studied (Scheme 2) and can be regarded as analogues of 1,1′-bis(diphenylphosphanyl)ferrocene. As imposed by the sandwich structure, the boryl moieties of these derivatives feature a relatively large separation. 1,1′-Diborylferrocenes are remarkable building blocks that have been incorporated in various supramolecules.[15] For example, 1,1′-bis(dimethylboryl)ferrocene (**6**) reacts with pyrazine to afford a coordination polymer that displays an intense metal-to-ligand charge-transfer absorption (Scheme 2).[15c] 1,1′-Diborylcobaltocenium complexes have also received attention and have been used as anion chelators.[16] Treatment of 1,1′-bis(diisopropylboryl)cobaltocene (**7**) with $Cu(OH)_2$ results in oxidation of the cobalt center and formation of a hydroxide chelate complex (Scheme 2).[16a] While a methoxide chelate complex has also been detected, the larger and softer chloride anion undergoes simple monotopic complexation at one of the boron centers.



Scheme 2. Boryl-substituted metallocenes as bidentate Lewis acids.

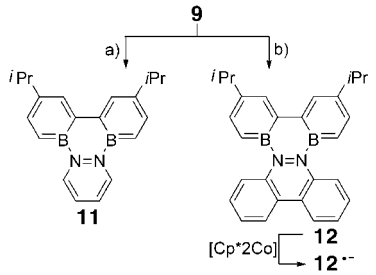
As illustrated above, the study of polydentate boranes has been limited to the case of bidentate derivatives which are analogues of diamines or diphosphanes. The recent report of a 2,2′-diborabiphenyl by Piers and co-workers[3] obliges us to review this situation, now that a charge-reverse analogue of 2,2′-bipyridine has been isolated. Combining the methodologies developed for the synthesis of 1-chloro-2-trimethylsilyl-1-bora-2,5-cyclohexadiene[17] and 4-substituted 1-chloro-1-bora-2,5-cyclohexadiene,[18] compound **8** was first prepared (Scheme 3). In one pot, this compound was converted into an aminoborane derivative and lithiated. The resulting anion undergoes an oxidative coupling reaction in the presence of a Cu^I species to afford a diamino diborane derivative, as was previously observed for the case of a pinene-fused boratabenzene.[19] Subsequent treatment with BCl_3 yields the dichloro derivative **9**, a masked version of a 2,2′-diborabiphenyl.



Scheme 3. a) Lithium dimethylamide, 2 equiv; b) CuCl, 2.1 equiv; c) BCl_3, 2 equiv; d) L.

In the presence of pyridine or trimethylphosphane, elimination of trimethylsilylchloride occurs (Scheme 3). This reaction is accompanied by a 1,3-shift of the 1 and 1′ hydrogen atoms, which finally affords Lewis adducts of the 2,2′-diborabiphenyl (**10a**,**b**). The crystal structure of the trimethylphosphane adduct **10b** shows that the connectivity of the two boraphenyl rings places the boron centers in the 2 and 2′ positions. Reactions of **9** with 1,2-diazines proceed in an analogous fashion and afford, in the case of pyridazine, a diazadibora analogue of triphenylene (**11**, Scheme 4). Unlike triphenylene, this compound features intense absorptions at $\lambda_{max}(CH_2Cl_2) = 509$ and 545 nm. These absorption bands presumably re-

 © 2003 Wiley-VCH Verlag GmbH & Co. KGaA, Weinheim



Scheme 4. a) pyridazine; b) benzo[*c*]cinnoline.

sult from charge transfer between the pyridazine nucleus and the 2,2′-diborabiphenyl moiety. This proposal is reinforced by theoretical calculations, which suggest a strong localization of the HOMO and LUMO on the pyridazine and the 2,2′-diborabiphenyl moiety, respectively. An analogous observation is made with the adduct formed between the 2,2′-diborabiphenyl and benzo[*c*]-cinnoline (**12**; Scheme 4).

Interestingly, both adducts display two reversible one-electron reduction events. Adduct **12**, which is more easily reduced than **11**, reacts with $[Cp^*_2Co]$ to afford the radical anion **12**$^{\bullet-}$. This radical anion displays a featureless EPR signal at $g = 2.003$ and has been prepared as crystals of its decamethylcobaltocenium salt. Its crystal structure reveals the existence of a strongly twisted backbone, which results from intramolecular steric interactions of the face-to-face aromatic protons (Figure 1). The relatively short B–N bonds (1.466(4) and 1.482(4) Å) indicate that the $C_2B_2N_2$ heterocycle retains some degree of aromaticity. However, the N–N distance (1.430(4) Å) is much longer than in benzo[*c*]cinnoline (1.292(3) Å), which, as indicated by the authors, is likely to result from the N–N antibonding character of the singly occupied molecular orbital (SOMO).

The synthesis of a masked 2,2′-diborabiphenyl demonstrates that the charge-reverse analogy continues to serve as an inspiration for the preparation of polydentate Lewis acidic boranes. By their incorporation in a borabenzene ring, the boron centers of 2,2′-diborabiphenyl are forced in a geometry that directs their accepting orbitals outward. This situation also leads to an increase in the s character of these orbitals. As a result, the boron centers experience a dramatically enhanced Lewis acidity that impedes isolation of the base-free bidentate Lewis acid. By isolating a masked, yet reactive, version of this derivative, Piers and co-workers have been able to circumvent this problem. Their strategy provides a realistic and convenient precursor to a 2,2′-diborabiphenyl, which will open up the chemistry of this unprecedented bidentate Lewis acid.

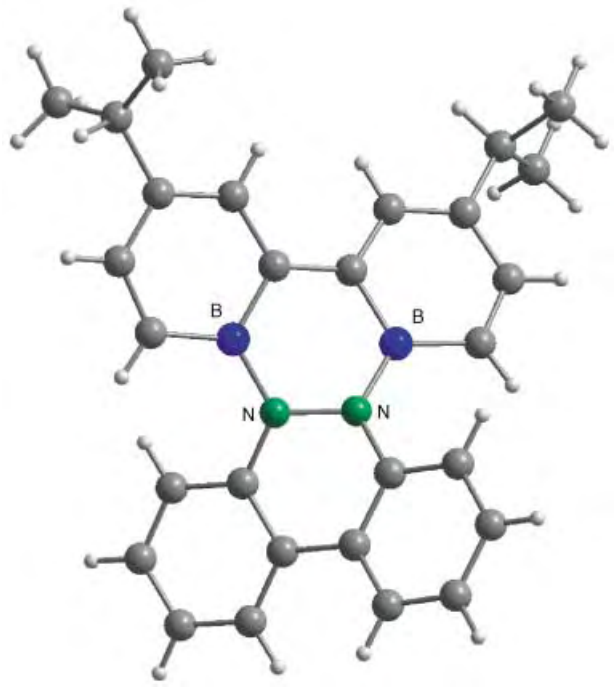


Figure 1. Molecular structure of **12**$^{\bullet-}$ in the crystal of the $[Cp^*_2Co]^+$ salt.

[1] a) F. P. Schmidtchen, M. Berger, *Chem. Rev.* **1997**, *97*, 1609–1646; b) M. F. Hawthorne, Z. Zheng, *Acc. Chem. Res.* **1997**, *30*, 267–276; c) J. D. Wuest, *Acc. Chem. Res.* **1999**, *32*, 81–89; d) W. E. Piers, G. J. Irvine, V. C. Williams, *Eur. J. Inorg. Chem.* **2000**, 2131–2142; e) J. D. Hoefelmeyer, M. Schulte, M. Tschinkl, F. P. Gabbaï, *Coord. Chem. Rev.* **2002**, *235*, 93–103.

[2] D. F. Schriver, M. J. Biallas, *J. Am. Chem. Soc.* **1967**, *89*, 1078–1081.

[3] D. J. H. Emslie, W. E. Piers, M. Parvez, *Angew. Chem.* **2003**, *115*, 1289–1293; *Angew. Chem. Int. Ed.* **2003**, *42*, 1251–1255.

[4] M. Schulte, G. Gabriele, M. Schürmann, K. Jurkschat, A. Duthie, D. Dakternieks, *Organometallics* **2003**, 22, 328–336, and references therein.

[5] a) E. S. Shubina, I. A. Tikhonova, E. V. Bakhmutova, F. M. Dolgushin, M. Y. Antipin, V. I. Bakhmutov, I. B. Sivaev, L. N. Teplitskaya, I. T. Chizhevsky, I. V. Pisareva, V. I. Bregadze, L. M. Epstein, V. B. Shur, *Chem. Eur. J.* **2001**, *7*, 3783–3790; b) J. B. King, M. R. Haneline, M. Tsunoda, F. P. Gabbaï, *J. Am. Chem. Soc.* **2002**, *124*, 9350–9351.

[6] H. E. Katz, *J. Org. Chem.* **1985**, *50*, 5027–5032; H. E. Katz, *J. Am. Chem. Soc.* **1985**, *107*, 1420–1421.

[7] For a study concerning 1,8-bis(dichlorboryl)naphthalene, see: H. E. Katz, *Organometallics* **1987**, *6*, 1134–1136.

[8] J. D. Hoefelmeyer, F. P. Gabbaï, *J. Am. Chem. Soc.* **2000**, *122*, 9054–9055.

[9] R. W. Alder, *Tetrahedron* **1990**, *46*, 683–713.

[10] a) K. Nozaki, M. Yoshida, H. Takaya, *Bull. Chem. Soc. Jpn.* **1996**, *69*, 2043–2052; b) K. Nozaki, M. Yoshida, H. Takaya, *Angew. Chem.* **1994**, *106*, 2574–2576; *Angew. Chem. Int. Ed. Engl.* **1994**, *33*, 2452–2454.

[11] a) M. V. Metz, D. J. Schwartz, C. L. Stern, P. N. Nickias, T. J. Marks, *Angew. Chem.* **2000**, *112*, 1368–1372; *Angew. Chem. Int. Ed.* **2000**, *39*, 1312–1316; b) E. Y.-X. Chen, T. J. Marks, *Chem. Rev.* **2000**, *100*, 1391–1434.

[12] V. C. Williams, W. E. Piers, W. Clegg, M. R. J. Elsegood, S. Collins, T. B. Marder, *J. Am. Chem. Soc.* **1999**, *121*, 3244–3245.

 © 2003 Wiley-VCH Verlag GmbH & Co. KGaA, Weinheim

[13] a) V. C. Williams, G. J. Irvine, W. E. Piers, Z. Li, S. Collins, W. Clegg, M. R. J. Elsegood, T. B. Marder, *Organometallics* **2000**, *19*, 1619 – 1621; b) L. D. Henderson, W. E. Piers, G. J. Irvine, R. McDonald, *Organometallics* **2002**, *21*, 340 – 345.

[14] V. C. Williams, C. Dai, Z. Li, S. Collins, W. E. Piers, W. Clegg, M. R. J. Elsegood, T. B. Marder, *Angew. Chem.* **1999**, *111*, 3922 – 3926; *Angew. Chem. Int. Ed.* **1999**, *38*, 3695 – 3698.

[15] a) L. Ding, K. Ma, G. Duerner, M. Bolte, F. Fabrizi de Biani, P. Zanello, M. Wagner, *J. Chem. Soc. Dalton Trans.* **2002**, 1566 – 1573; b) R. E. Dinnebier, M. Wagner, F. Peters, K. Shankland, W. I. F. David, *Z. Anorg. Allg. Chem.* **2000**, *626*, 1400 – 1405; c) M. Grosche, E. Herdtweck, F. Peters, M. Wagner, *Organometallics* **1999**, *18*, 4669 – 4672.

[16] a) G. E. Herberich, A. Fischer, D. Wielbelhaus, *Organometallics* **1996**, *15*, 3106 – 3108; b) G. E. Herberich, U. Englert, A. Fischer, D. Wielbelhaus, *Organometallics* **1998**, *17*, 4769 – 4775.

[17] D. A. Hoic, J. Robbins-Wolf, W. M. Davis, G. C. Fu, *Organometallics* **1996**, *15*, 1315 – 1318.

[18] A. J. Ashe III, S. Al-Ahmad, X. Fang, J. W. Kampf, *Organometallics* **1998**, *17*, 3883 – 3888.

[19] G. E. Herberich, U. Englert, B. Ganter, M. Pons, R. Wang, *Organometallics* **1999**, *18*, 3406 – 3413.

 © 2003 Wiley-VCH Verlag GmbH & Co. KGaA, Weinheim

Multiple Bonds with Si/Ge/Sn/Pb

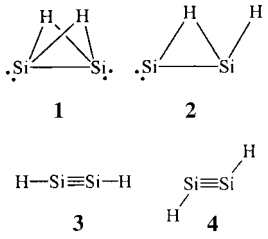
Triple Bonds of the Heavy Main-Group Elements: Acetylene and Alkylidyne Analogues of Group 14

*Manfred Weidenbruch**

Keywords:
alkyne analogues · germanium · multiple bonds · silicon · tin

The unique position of carbon in chemistry is in part a result of its ability to form homo- and heteronuclear multiple bonds. In contrast, silicon and its heavier congeners exhibit a much less pronounced tendency to form multiple bonds. This aspect has been the subject of intensive research in the past decades that has resulted in, not only the formation of compounds with homonuclear double bonds between all elements of Group 14,[1] but also, in the meantime, the first molecules with heteronuclear double bonds between these elements have also been isolated.[2] The existence of homo- and heteronuclear triple bonds remains a challenge although remarkable progress has been made in the past few years.

The main difficulty in the construction of these triple-bond systems is illustrated by the acetylene homologue disilyne, Si_2H_2. By means of submillimeter spectroscopy of a silane plasma cooled to −196°C, Bogey et al. found, in excellent agreement with theoretical calculations,[3] the doubly hydrogen-bonded molecule **1** as a global minimum with an Si–Si bond length of 220.79 pm and, as a local minimum, the singly bridged compound **2** with a very short Si–Si separation of 211.3 pm.[4] On the other hand, the acetylene analogue molecule **3** with $D_{\infty h}$ symmetry is not a minimum on the potential hypersurface[5] and distorts to the C_{2h}-symmetrical *trans*-bent form **4**. Although this bending is accompanied by a loss of π-bond strength and a lowering of the bond order,[6] these effects are more than compensated by a marked increase in the σ-bond strength.[7]

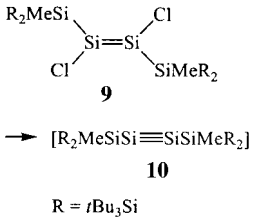


1 **2**

3 **4**

According to DFT calculations the presence of bulkily substituted silyl groups R_3Si[8] or voluminous aryl groups[9] should be highly suited to stabilize the Si≡Si triple bonds in compounds of the type **3** or **4** and so render them synthetically accessible. The dehalogenation of the molecules **5** and **7** investigated in this context presumably proceeded via the respective disilynes that proved, however, to be unstable and underwent dimerization to **6**[10] or isomerization to **8**.[11]

The steric shielding in the proposed disilyne is apparently not sufficient to stabilize the species from subsequent reactions. A much more promising candidate for the realization of the first Si≡Si bond could be the disilene **9** containing two extremely bulky $(tBu_3Si)_2MeSi$ groups. Dehalogenation of **9** with naphthalene/lithium furnished a chlorine-free product for which the ^{29}Si NMR spectroscopy chemical shift of $\delta =$

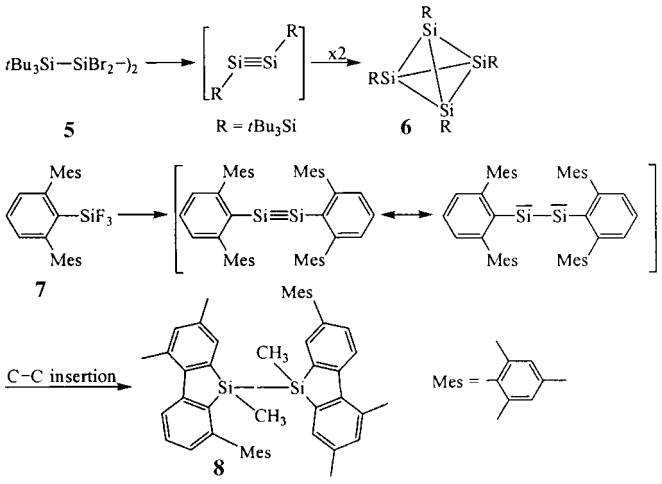


9

→ $[R_2MeSiSi{\equiv}SiSiMeR_2]$

10

$R = tBu_3Si$



5 $R = tBu_3Si$ **6**

7

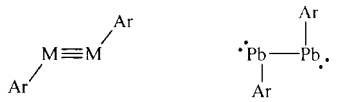
8

[*] Prof. Dr. M. Weidenbruch
Fachbereich Chemie der
Universität Oldenburg
Carl-von-Ossietzky-Strasse 9–11, 26111
Oldenburg (Germany)
Fax: (+49) 441-798-3352
E-mail:
manfred.weidenbruch@uni-oldenburg.de

 © 2003 Wiley-VCH Verlag GmbH & Co. KGaA, Weinheim DOI: 10.1002/anie.200301635

91.5 ppm is suggestive of the existence of the disilene **10**.[12] Although the final structural elucidation of **10** has not yet been achieved, DFT calculations support the existence of this molecule for which an Si–Si bond length of 207.2 pm and an R–Si–Si angle of 148° have been determined. In addition, these calculations revealed that **10** should be very stable not only to isomerization but also to dimerization.[13]

The situation with germanium and tin is less ambiguous since Power et al. have prepared and structurally characterized both the digermyne **11**[14] and the



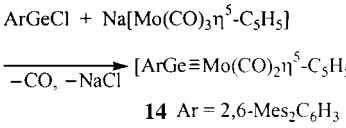
11 M = Ge; **12** M = Sn **13**

Ar = 2,6-(2,6-*i*Pr$_2$C$_6$H$_3$)$_2$C$_6$H$_3$

distannyne **12**.[15] In **11** the Ge–Ge bond length is 228.50 pm and the *trans*-bent angle C–Ge–Ge is 128.7°. This bond length is significantly shorter than a Ge–Ge single bond (244 pm) and lies in the region typical for digermenes.[1] DFT calculations for a slightly different digermyne containing additional isopropyl groups in the *para*-positions of the terphenyl substituents are indicative of a similar structure (Ge–Ge = 227.7 pm, C–Ge–Ge = 131.2°) to that determined experimentally for **11**.[16] As a consequence of its short Sn–Sn bond length of 266.75 pm and *trans*-bent angle of 125.24°, the ditin compound **12** should have a similar multiple-bond system to that of **11**. However, in contrast to **11**, the results of DFT calculations do not agree with the observed parameters.[16]

While the molecules **11** and **12** contain homonuclear multiple bonds with a bond order of about 2.5,[17] the corresponding lead compound **13** should rather be considered as a diplumbylene with a Pb–Pb single bond and a free electron pair on each of the lead atoms. This situation is indicated by the Pb–Pb bond length which, at 318.81 pm, is markedly longer than the Pb–Pb single bond length of 284.4 pm in hexaphenyldiplumbane[18] and by the *trans*-bent angle of 94.26° for the C–Pb–Pb fragment.[19] These experimental observations are supported by quantum-chemical calculations that unequivocally show the diplumbylene form **13** to be an energy minimum.[20] The results available to date demonstrate that germanium and probably also silicon prefer the structure type **11** whereas for lead the diplumbylene form is more favorable. The situation for tin is more interesting since calculations indicate that a ditin compound of the type **13** should be possible[16,17] as well as the observed structural type **12**. Experimental conformation for the former isomer has not yet been obtained.

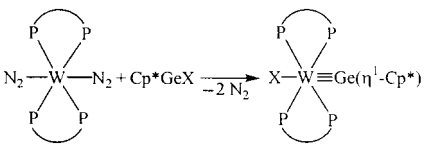
Just like the formal, homonuclear triple bonds between elements of Group 14, triple bonds between these atoms and transition-metal atoms were unknown until recently. Although transition-metal–carbyne or -alkylidyne complexes have been known since the work of Fischer and co-workers in 1973,[21] it was not until 1996 that Power et al. achieved the synthesis, by the surprisingly simple route of salt elimination, and characterization of the germylyne–molybdenum complex **14**.[22] In the mean time the corresponding complexes of all the elements of Group 6



14 Ar = 2,6-Mes$_2$C$_6$H$_3$

have been prepared.[23] The formulation of a Ge≡M bond (M = Cr, Mo, W) is justified since the three frontier orbitals of the 15-electron fragment M(CO)$_2$(η^5-C$_5$H$_5$) and the three valence electrons of the RGe unit can combine to form a stable 18-electron complex.

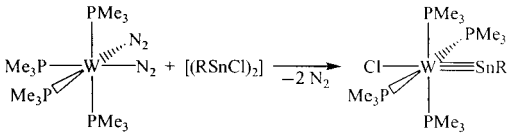
A route to the germylyne–transition-metal complexes **16** involving the reaction of the bis(dinitrogen)tungsten complex **15** with the pentamethylcyclopentadienylgermanium halide [Cp*GeX] (X = Cl, Br, I; Cp* = C$_5$Me$_5$)[24] was developed by Filippou



15 **16**

et al. In all cases, the pronounced shortening of the Ge≡M bond lengths and the almost planar arrangement of the R-Ge≡M units support the existence of genuine triple bonds.[22–24] This situation is corroborated by DFT calculations for the model compounds [Cp(CO)$_2$M≡GeMe] for which, in excellent agreement with the experimental values, a bond order of three is predicted.[25]

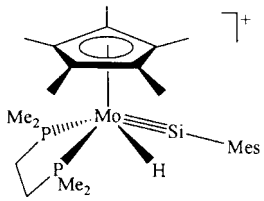
Although, triple bonds between the heavier atoms of Group 14 and transition-metal fragments were previously restricted to germanium, recent reports have shown that other elements of this group are also able to form such bonds. Using a route similar to that employed successfully to prepare compounds **16**, Filippou et al. realized the synthesis of the first stannylyne complex **17** (Mes = mesityl = 2,4,6-trimethylphenyl) which,



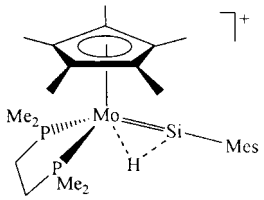
R = 2,6-Mes$_2$C$_6$H$_3$ **17**

in agreement with the germylyne complexes, is characterized by a short W≡Sn bond and an almost linear coordination of the tin atom.[26]

The cationic complex **18** in which the silicon atom exhibits appreciable silylyne character represents the provisional terminus in the field of multiple bonds of these types. Of the proposals for the bonding situation, both X-ray crystal-structure analysis and the preliminary



18a



18b

 © 2003 Wiley-VCH Verlag GmbH & Co. KGaA, Weinheim

DFT calculations indicate that the form **18b**, in which the hydridic Mo–H hydrogen atom participates in a nonclassical interaction with the electrophilic silicon atom, is more probable than the form **18a**.[27]

Thus, in the series of Group 14 analogues of alkylidyne–transition-metal complexes only the corresponding lead compound and a silicon compound in which the silylyne character is more pronounced than that of compound **18** are still lacking.

[1] Recent reviews: a) P. P. Power, *Chem. Rev.* **1999**, *99*, 3463; b) M. Weidenbruch, *J. Organomet. Chem.* **2002**, *646*, 39.

[2] $R_2Si{=}GeR'_2$: a) V. Y. Lee, M. Ichinohe, A. Sekiguchi, N. Tagaki, S. Nagase, *J. Am. Chem. Soc.* **2000**, *122*, 9034; b) V. Y. Lee, A. Sekiguchi, *J. Am. Chem. Soc.* **2000**, *122*, 12604; c) M. Ichinohe, Y. Arai, A. Sekiguchi, N. Tagaki, S. Nagase, *Organometallics* **2001**, *20*, 4141; b) $R_2Ge{=}SnR_2$: A. Schäfer, W. Saak, M. Weidenbruch, *Organometallics* **2003**, *22*, 215.

[3] a) H. Lischka, H. Köhler, *J. Am. Chem. Soc.* **1983**, *105*, 6646; b) B. T. Colegrove, H. F. Schaefer, *J. Phys. Chem.* **1990**, *94*, 5593; c) R. S. Grev, H. F. Schaefer, *J. Chem. Phys.* **1992**, *97*, 7990.

[4] a) M. Bogey, H. Bolvin, C. Demuynck, J. L. Destombes, *Phys. Rev. Lett.* **1991**, *66*, 413; b) M. Cordonnier, M. Bogey, C. Demuynck, J. L. Destombes, *J. Chem. Phys.* **1992**, *97*, 7984; c) Review: M. Karni, Y. Apeloig, J. Kapp, P. von R. Schleyer in *The Chemistry of Organic Silicon Compounds, Vol. 3* (Eds.: Z. Rappoport, Y. Apeloig), Wiley, Chichester, **2001**, p. 1.

[5] Review: R. S. Grev, *Adv. Organomet. Chem.* **1991**, *33*, 161.

[6] a) A. J. Bridgeman, L. R. Ireland, *Polyhedron* **2001**, *20*, 2841; b) J. Grunenberg, *Angew. Chem.* **2001**, *113*, 4150; *Angew. Chem. Int. Ed.* **2001**, *40*, 4027.

[7] D. Danovich, F. Ogliaro, M. Karni, Y. Apeloig, D. L. Cooper, S. Shaik, *Angew. Chem.* **2001**, *113*, 4146; *Angew. Chem. Int. Ed.* **2001**, *40*, 4023.

[8] a) K. Kobayashi, S. Nagase, *Organometallics* **1997**, *16*, 2489; b) S. Nagase, K. Kobayashi, N. Tagaki, *J. Organomet. Chem.* **2000**, *611* 264.

[9] a) K. Kobayashi, N. Tagaki, S. Nagase, *Chem. Lett.* **2001**, 966; b) K. Kobayashi, N. Takagi, S. Nagase, *Organometallics* **2001**, *20*, 234.

[10] N. Wiberg, C. M. M. Finger, K. Polborn, *Angew. Chem.* **1993**, *105*, 1140; *Angew. Chem. Int. Ed. Engl.* **1993**, *32*, 923.

[11] R. Pietschnig, R. West, D. R. Powell, *Organometallics* **2000**, *19*, 2724.

[12] N. Wiberg, W. Niedermayer, G. Fischer, H. Nöth, M. Suter, *Eur. J. Inorg. Chem.* **2002**, 1066.

[13] N. Takagi, S. Nagase, *Eur. J. Inorg. Chem.* **2002**, 2775.

[14] M. Stender, A. D. Phillips, R. J. Wright, P. P. Power, *Angew. Chem.* **2002**, *114*, 1863; *Angew. Chem. Int. Ed.* **2002**, *41*, 1785.

[15] A. D. Phillips, R. J. Wright, M. M. Olmstead, P. P. Power, *J. Am. Chem. Soc.* **2002**, *124*, 5930.

[16] N. Takagi, S. Nagase, *Organometallics* **2001**, *20*, 5498.

[17] G. Frenking, M. Lein, P. Spuhler, M. Holthausen, L. W. Han, unpublished results. I thank Prof. Frenking, Marburg, for this advance information.

[18] H. Preut, F. Huber, *Z. Anorg. Allg. Chem.* **1974**, *419*, 92.

[19] L. Pu, B. Twamley, P. P. Power, *J. Am. Chem. Soc.* **2000**, *122*, 3524.

[20] Y. Chen, M. Hartmann, M. Diedenhofen, G. Frenking, *Angew. Chem.* **2001**, *113*, 2108; *Angew. Chem. Int. Ed.* **2001**, *40*, 2052.

[21] E. O. Fischer, G. Kreis, C. G. Kreiter, J. Müller, G. Huttner, H. Lorenz, *Angew. Chem.* **1973**, *85*, 618; *Angew. Chem. Int. Ed. Engl.* **1973**, *12*, 564.

[22] R. S. Simons, P. P. Power, *J. Am. Chem. Soc.* **1996**, *118*, 11966.

[23] L. Pu, B. Twamley, S. T. Haubrich, M. M. Olmstead, B. V. Mork, R. S. Simons, P. P. Power, *J. Am. Chem. Soc.* **2000**, *122*, 650.

[24] a) A. C. Filippou, A. I. Philippopoulos, P. Portius, D. U. Neumann, *Angew. Chem.* **2000**, *112*, 2881; *Angew. Chem. Int. Ed.* **2000**, *39*, 2778; b) Highlight: P. Jutzi, *Angew. Chem.* **2000**, *112*, 3953; *Angew. Chem. Int. Ed.* **2000**, *39*, 3797.

[25] K. K. Pandey, M. Lein, G. Frenking, *J. Am. Chem. Soc.* **2003**, *125*, 1660.

[26] A. C. Filippou, P. Portius, A. I. Philippopoulos, H. Rohde, *Angew. Chem.* **2003**, *115*, 461; *Angew. Chem. Int. Ed.* **2003**, *42*, 445.

[27] B. V. Mork, T. D. Tilley, *Angew. Chem.* **2003**, *115*, 371; *Angew. Chem. Int. Ed.* **2003**, *42*, 357.

 © 2003 Wiley-VCH Verlag GmbH & Co. KGaA, Weinheim

Femtosecond Spectroscopy

Watching Photoinduced Chemistry and Molecular Energy Flow in Solution in Real Time

*Jens Aßmann, Matthias Kling, and Bernd Abel**

Keywords:
density functional calculations · femtochemistry · intermediates · molecular dynamics · transition states



© 2003 Wiley-VCH Verlag GmbH & Co. KGaA, Weinheim
DOI: 10.1002/anie.200200541

Energized molecules are the essential actors in chemical transformations in solution. As the rearrangement of bonds requires a movement of nuclei, vibrational energy is often the driving force for a reaction. Vibrational energy can be redistributed within the "hot" molecule, or relaxation can occur when molecules interact. Both processes govern the rates, pathways, and quantum yields of chemical transformations in solution. Unfortunately, energy transfer and the breaking, formation, and rearrangement of bonds take place on ultrafast timescales. This Review highlights experimental approaches for the direct, ultrafast measurement of photoinduced femtochemistry and energy flow in solution. In the first part of this Review, we summarize recent experiments on intra- and intermolecular energy transfer. The second part discusses photoinduced decomposition of large organic peroxides, which are used as initiators in free radical polymerization. The mechanisms and timescales of their decarboxylation determine the initial steps of polymerization and the microstructure of the polymer product.

From the Contents

1. Introduction 2227

2. Probing Intramolecular and Intermolecular Energy Flow of Molecules in Solution 2228

3. Ultrafast Dissociation in Solution: Photoinduced Decarboxylation of Organic Peroxides 2237

4. Summary and Outlook 2243

1. Introduction

Since the invention of flash photolysis 50 years ago,[1] chemical reactions have been studied with continuously improving time resolution. Norrish, Porter, and Eigen were among the first to resolve elementary reaction steps and rates of simple "immeasurably fast" chemical reactions.[1–3] It was soon realized, however, that the most relevant timescales of chemical reactions often lie in the range between the duration of molecular vibrations and motions (i.e., between ten femtoseconds and several tens of picoseconds), and those were by far not accessible at that time. What may be straightforward for isolated molecules[4,5] is more difficult in solution owing to complex interactions with the molecular environment and broad spectra often preventing unambiguous assignments.[6] Nevertheless, bond fission,[7–13] structural isomerization,[14,15] intramolecular rearrangements,[16,17] solvation,[18,19] inter- and intramolecular energy transfer,[20–38] internal conversion,[19,39] as well as electron[39–41] and proton transfer[42–44] are only few of the numerous elementary processes in the condensed phase that have been studied recently by time-resolved femtosecond (fs) spectroscopy. Good overviews that highlight important work and pioneering experiments are given in references [5,6,45,46]. The systems under investigation so far range from simple model systems to relatively complicated large molecules.[5,6]

In contrast to the situation in the gas phase, a quantitative understanding of chemical reactions and competing processes in the condensed phase is still missing.[45] The main reason for this is that competing energy-transfer processes in solution, which have a strong influence on the outcome of a chemical transformation, are not quantitatively understood. *Intra*molecular vibrational energy redistribution (IVR) is often simply assumed to be a sufficiently fast and statistical process that is over well before the reaction. This may or may not be true for the actual system under investigation. As we will demonstrate in the first part of this Review, such long-standing conjectures can be tested with modern laser-based time-resolved spectroscopic techniques. Moreover, even the coupling of an initially excited nonstationary state to other modes of the molecule and the role of the solvent can be directly investigated. Unfortunately, the mechanisms of *inter*molecular vibrational energy transfer (VET) have also remained largely unclear in the past. Chemists regard this process to be necessary for the thermal activation of the molecule, but finer details of its role in the outcome of a chemical reaction are often ignored because of the lack of more specific information. When physical chemists are asked about mechanisms, the common statement is that low-frequency modes of the molecule dominate timescales and mechanisms of VET. With state-of-the-art femtosecond spectroscopy it is now possible to shed more light on this issue and to test convenient but unjustified assumptions in separate experiments in which VET is decoupled from reactive processes. Finally, a further obstacle is that even when competing processes (IVR, VET, solvation, etc.) are known, spectral overlap as a result of broad absorptions and the presence of many species at the same time often prevents the unambiguous identification of reaction intermediates and products, even for very simple reactions in solution.

In the second part of this Review, we show how this problem may be overcome by using femtosecond spectroscopy. The broad spectral tunability enables the systematic search for unperturbed spectral windows and the investigation of competing processes separately. Our strategy is based on the investigation of reactions, competing processes, and their solvent dependence for a large set of structurally different molecules in combination with high-level quantum theory and modeling. This puts us in a position to shed some light on the mechanisms of the processes so that we can

[*] Prof. Dr. B. Abel, Dr. J. Aßmann, Dr. M. Kling
Institut für Physikalische Chemie, Universität Göttingen
Tammannstrasse 6, 37077 Göttingen (Germany)
Fax: (+49) 551-393-150
E-mail: babel@gwdg.de

 DOI: 10.1002/anie.200200541 © 2003 Wiley-VCH Verlag GmbH & Co. KGaA, Weinheim

critically test assumptions and concepts in the field. Based on these results, we can then suggest models that not only reproduce data for a large family of molecules but also have some predictive power. This is the ultimate goal and the link between the investigations highlighted in this Review, which focuses on recent results mainly from our group in two fields: condensed-phase femtochemistry and intramolecular and intermolecular vibrational energy flow in solution.

2. Probing Intramolecular and Intermolecular Energy Flow of Molecules in Solution

Most experiments in the past on intermolecular VET in solution have focused on large organic molecules, which undergo an internal conversion after electronic excitation.[37,47–60] Mechanisms of IVR in competition with intermolecular relaxation can best be investigated in (vibrationally) state-specific experiments. Of particular importance are experiments in which the vibrational energy is initially deposited with some degrees of freedom in the molecule, and is then dissipated into lower-energy vibrations and into the solvent.[20–23,25,26,28–36,61–70] Several time-resolved techniques such as IR absorption spectroscopy,[20,24,62,71–73] anti-Stokes Raman spectroscopy,[28–30,35,65,74–77] and UV absorption spectroscopy[25–27,56,61] have been successfully applied to measure rates of IVR and VET of organic molecules. IVR and VET in halogenated hydrocarbons,[20,21,24,27,34,62,63,78] benzene,[65] nitromethane,[30] acetonitrile,[28] alcohols,[35,36,66,67] and water[78,79] have been studied in considerable detail in the time domain employing different techniques of (state-selective) pump-and-probe spectroscopy. Each of these techniques opens a different window on the vibrational population distribution of an ensemble of relaxing molecules. Nevertheless, since almost all the above experiments studied the relaxation of the fundamental vibrations, not much is known about IVR and VET at higher internal energies or about the influence of structure, mode, and solvent on the relaxation dynamics.[23,25,26,61] Moreover, in spite of the importance of IVR and VET for chemistry in solution a quantitative understanding of their most elementary features and mechanisms is still missing.

Recently, we measured intra- and intermolecular relaxation in solution for several molecules of different size and structure and with different functional groups.[25,26,61,80] One of the major motivations for our studies was to understand the relationship between the chemical structure of the molecules and their relaxation dynamics, in particular the rates of IVR. Progress in an understanding of these trends may help to design molecules in which IVR rates in solution can be controlled by (temporary) chemical modification.

2.1. Time-Resolved Near-IR Overtone Pump and UV Probe Spectroscopy: Concept and Experimental Approach

The experimental setup, ideas, and concepts of our experiments have been described in detail elsewhere.[25,26,61] Briefly, the technique was introduced recently by Crim and co-workers to measure the relaxation of CH_2I_2 in organic solvents.[23] In the meantime, it has been further developed to measure IVR and VET in fundamentals, in overtones, and in combination bands of several alkyl iodides.[23,25–27,61,80] We recently extended these studies to aromatic molecules and showed that the experimental approach is very general and not limited to molecules containing C–I bonds.[81]

For the selective excitation and probing of molecules in solution in our experiments we employed femtosecond (fs) IR-pump and UV-probe transient absorption spectroscopy. The probe laser is tuned to the red wing of the electronic absorption of the molecule in the near-UV spectral range. This method measures changes in the electronic absorption spectrum after selective overtone excitation as relaxation populates Franck–Condon (FC)-active vibrational modes in the ground state. This aspect of IR/UV transient absorption spectroscopy makes the technique complementary to infrared absorption and anti-Stokes Raman spectroscopy. In comparison to the techniques mentioned earlier, transient electronic absorption spectroscopy can be regarded to be selective because it is only sensitive to the FC-active modes of the molecule, however, it is also nonspecific to some extent because it cannot distinguish among these modes. A significant advantage over other techniques is its overall sensitivity, which permits studies of dilute solutions and solutions in supercritical CO_2.[82]

Because the initially excited "state" is a nonstationary state of the molecular Hamiltonian it evolves in time, and vibrational energy flows from the C–H bond to other degrees



Bernd Abel was born in 1960 in Delmenhorst (Germany). He studied chemistry at the University of Göttingen. After his PhD in Physical Chemistry in 1990, he spent two years at the MIT (Cambridge MA, USA). Since 1994 he has been at the Institute of Physical Chemistry of the University of Göttingen, where he was appointed Associated professor in 2002. He is also a group leader at the Max-Planck-Institute of Biophysical Chemistry in Göttingen. In 1999 he received the Sir Harold Thompson Memorial Award (Elsevier Science), and in 2001 the Nernst-Haber-Bodenstein Prize (Deutschen Bunsengesellschaft for Physical Chemistry)



Jens Aßmann was born in 1973 in Rehren (Germany). He studied chemistry at the University of Göttingen. In 1998 he spent a research semester at the University Joseph-Fourier in Grenoble. In 1999 he received the Gustav-Tammann Prize (Chemistry Faculty, University of Göttingen) for his diploma thesis on "Experimental Investigation and Wavepacket Calculations of the Dissociation Dynamics of HgI_2". He was fellow of the Studienstiftung des deutschen Volkes and the Fonds der chemischen Industrie. His PhD (2002) work was in the field of femtosecond spectroscopy of organic molecules in solution.

 © 2003 Wiley-VCH Verlag GmbH & Co. KGaA, Weinheim

of freedom, including the FC-active modes (for the electronic transition) that were not excited initially. The successive population of these FC modes causes an increasing absorption of the UV probe pulse. Resonance Raman and dispersed fluorescence experiments help to identify such modes. For molecules with a C–I bond, experiments (in the gas and liquid phase) show that the dominant mode in the Raman spectra is the C–I stretch.[54,83–87] For molecules with an aromatic chromophore, only a limited number of low-frequency ring-deformation modes are FC-active.[88–91] The pump and probe schemes for C–I-containing molecules and aromatic molecules are depicted schematically in Figures 1 a and b, respectively. Finally, during and after IVR, vibrational energy transfer to the solvent takes place and in turn decreases the absorption. The characteristic rapid increase followed by a distinctly slower decrease in UV absorption on a significantly longer timescale is interpreted as IVR and VET as a result of intermolecular interactions with the solvent. Another special feature of the experiment is that energy–time profiles can be calculated from transient absorption traces by using high-temperature absorption spectra measured in shock waves.[26] In this Review we will call this procedure "energy calibration". After a careful optimization of λ_{probe} only one probe wavelength and calibration is sufficient to probe the internal energy of the molecules in this experiment. We would like to emphasize at this point that the technique is sensitive to (and measures) the rate-determining step in an extended relaxation cascade, that is, relaxation in the cases discussed here is very likely not a single-step process. This implies that other timescales (e.g. an ultrafast timescale much below 1 ps for the relaxation of the C–H stretch) may be hidden.

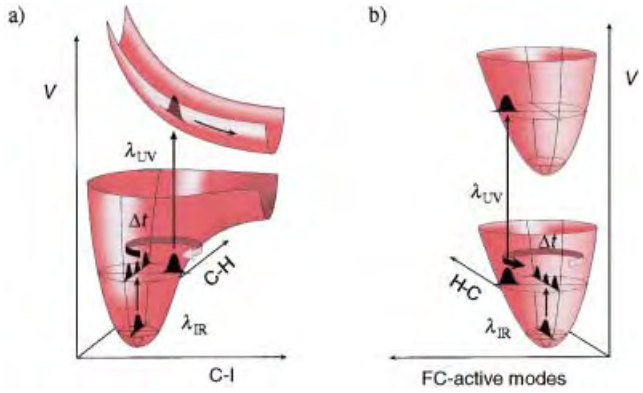


Figure 1. Schematic representation of the pump and probe process: a) alkyl iodides with dissociative electronic excitation and b) aromatic molecules in which the final state is bound. Only two degrees of freedom of the molecules are considered.



Matthias F. Kling was born in 1972 in Hannover (Germany). He studied physics at the University of Göttingen and laser physics at the University of Jena. He received his diploma in 1998 for studies in the field of ps IR spectroscopy. As a graduate student at Göttingen and at the Lawrence Berkeley National Laboratory in Berkeley (USA), he investigated the fs dynamics of the decomposition of organic peroxides. He received the Otto-Wallach Prize in 2001 (Chemistry Faculty, University of Göttingen) for these studies. He completed his PhD in 2002 and is currently a postdoctoral researcher in the group of Prof. M. Buback.

In the experiments we used fs laser pulses from a home-built regeneratively amplified titanium–sapphire laser system pumping two optical parametric amplifiers (TOPAS from Light Conversion and a home-built noncollinear optical parametric amplifier, NOPA) with a pulse width of ~50 fs and a bandwidth $\tilde{\nu}$ of ~300 cm^{-1}.[25,26,61] The relatively weak transient difference absorptions with signal amplitudes in the range 50–1000 μOD (OD: optical density) were measured at 1 kHz with a noise level of about 5–10 μOD.

2.2. Variation of the Structure and Functional Groups of Aliphatic Molecules: Effect of Chemical Substitution

The molecules investigated with the present technique are shown in Figure 2 a–l. Initial studies were focused on the model systems diiodomethane (CH_2I_2) and allyl iodide (C_3H_5I).[25,26] We employed near-IR fs laser pulses tuned to the relevant spectral absorption features (see Figure 3 a for the case of CH_2I_2) and selectively excited both molecules in the first C–H-overtone region (2 quanta of C–H stretch) and in combination vibrations of the C–H stretch vibration in solution. The probe laser was tuned to the long wavelength range of the electronic absorption of both molecules at 400 nm (see Figure 3 b for CH_2I_2). For the energy calibration we used high-temperature absorption spectra measured in our laboratory.[91] The time-delayed rise and subsequent decay of the transient absorption in the UV spectral range at 400 nm induced by the IR-pump (1700 nm) for CH_2I_2 is shown in Figure 4. To extract overall rate constants for IVR and VET from the data, we adopted the simple model introduced in references [25,26]. Since the rise and the decay of the signal was interpreted to be associated with IVR and VET, we assumed a first-order energy-decay process of an energy E_{loc} (i.e., a coherent superposition of states that resembles the zeroth-order bright state), which is "localized" in the initial excitation, to the background states of CH_2I_2. The sum of the energies of the background states was termed "redistributed" energy E_{red}. This energy could be measured directly, as our calibration procedure enabled us to use the FC-active modes of the molecule and their time-dependent population as intramolecular probes. For the VET process we also assume a simple first-order decay. The time dependence of E_{red} is then given by Equation (1) (τ_{IVR} and τ_{VET} are global IVR and VET relaxation coefficients, $E_0 = h\nu_{IR}$ is the initial excess excitation energy of the solute molecules).

$$E_{red}(t) = E_0\left[\frac{1/\tau_{IVR}}{1/\tau_{IVR}-1/\tau_{VET}}\right](\exp(-t/\tau_{VET})-\exp(-t/\tau_{IVR})) \qquad (1)$$

 © 2003 Wiley-VCH Verlag GmbH & Co. KGaA, Weinheim

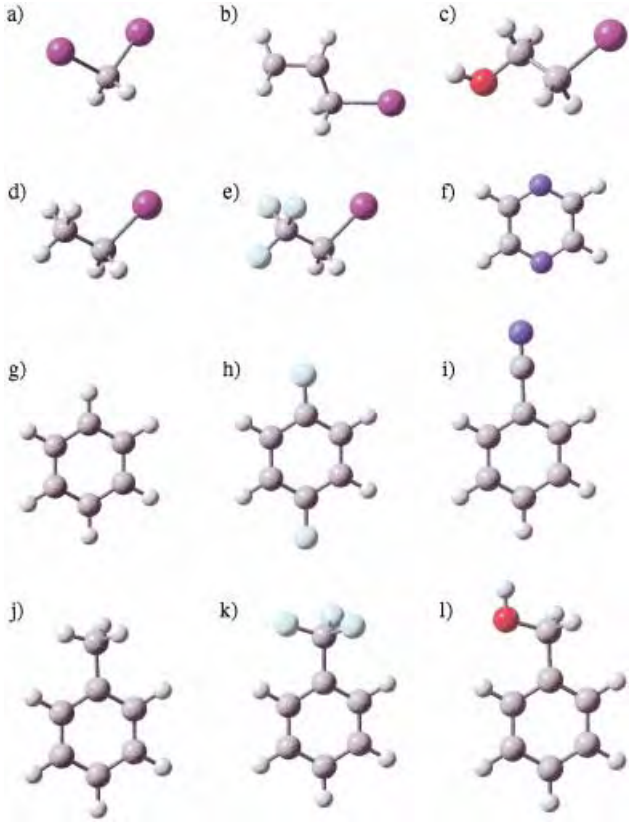


Figure 2. Aliphatic and aromatic molecules investigated with selective near-IR/UV fs absorption spectroscopy. a) diiodomethane, b) allyl iodide, c) 2-iodoethanol, d) iodoethane, e) 1,1,1-trifluoro-2-iodoethane, f) pyrazine, g) benzene, h) *para*-difluorobenzene, i) benzonitrile, j) toluene, k) α,α,α-trifluorotoluene, l) benzyl alcohol.

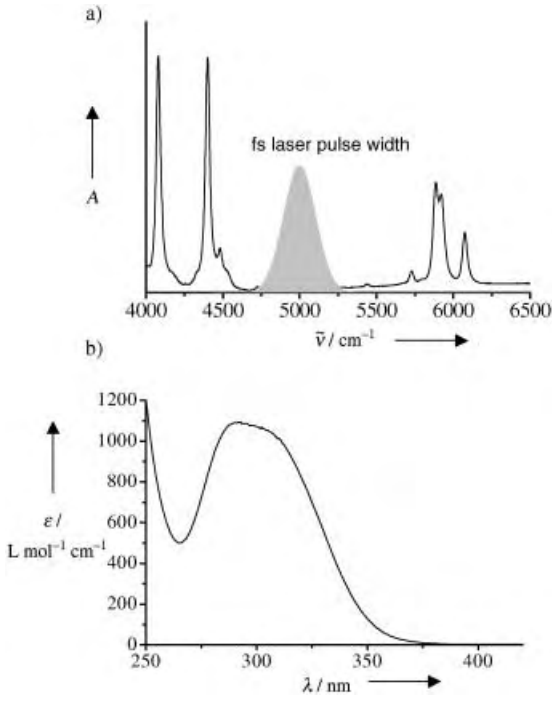


Figure 3. a) Near-IR spectrum of CH_2I_2 in CCl_4. The bandwidth of the IR excitation pulse is indicated (A = absorbance); b) absorption spectrum of CH_2I_2 in CCl_4 in the range 250–400 nm.

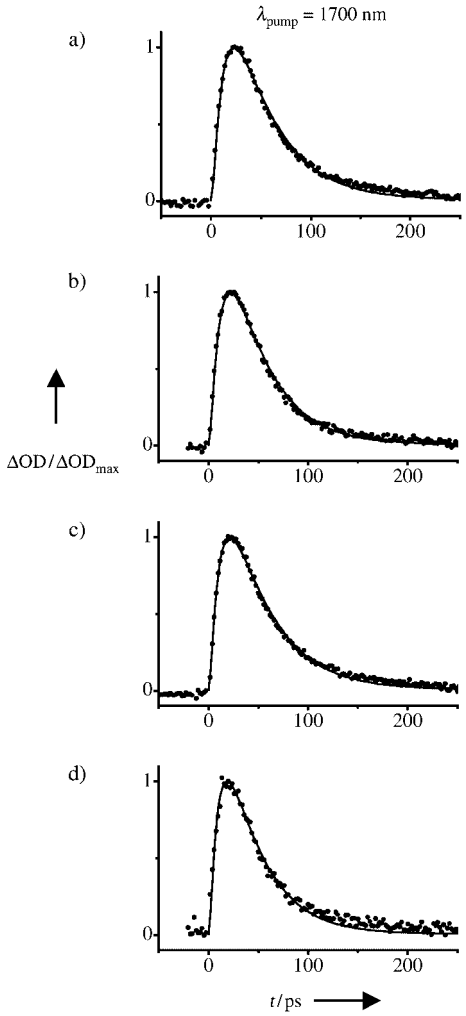


Figure 4. Experimental results (●) for the excitation of CH_2I_2 at 1700 nm in various solvents (a) CCl_4, b) $CDCl_3$, c) C_2Cl_4, d) C_3Cl_6), and results from a simulation (——) using the simple model described in the text. For details, see reference [25].

The signal is then readily calculated from Equation (2) (ε_λ = absorption coefficient at the corresponding probe wavelength).

$$\Delta\mathrm{OD}(t) \propto \varepsilon_\lambda(E_{\mathrm{red}}(t)) - \varepsilon_\lambda(E_{298\mathrm{K}}) \qquad (2)$$

Such a model with τ_{IVR} and τ_{VET} as adjustable parameters has been found to describe the rise and the decay of the transients well. Together with the measured $\varepsilon(E)$ it was used to fit the experimental traces (see Figure 4 for the case of CH_2I_2) and to determine overall time constants for the IVR and VET processes (Table 1).

In a further study we extended the group of model systems to include CF_3CH_2I and CH_3CH_2I[61] to determine the effect of chemical substitution on IVR and VET in solution. Near-IR fs laser pulses (1.7 μm wavelength) were used to excite the molecules in the C–H overtone region. For energy calibration, again high-temperature absorption spectra were used. Figures 5a and b show the "absorption coefficient" ε of both molecules at $\lambda_{\mathrm{probe}} = 335$ nm and $\lambda_{\mathrm{probe}} = 340$ nm, respectively,

 © 2003 Wiley-VCH Verlag GmbH & Co. KGaA, Weinheim

Table 1: Relaxation coefficients τ_{IVR} and τ_{VET} for different molecules after excitation of the first overtone of the C–H stretching mode ($v_{CH}=2$).

Molecule	τ_{IVR} [ps]	τ_{VET} [ps]
CH_2I_2	10 ± 1	63 ± 8
C_3H_5I	2 ± 1	17 ± 2
CH_3CH_2I	1.5 ± 1	20 ± 2
CF_3CH_2I	3.5 ± 1	50 ± 10
$HOCH_2CH_2I$	1.2 ± 0.5	17 ± 3

as a function of internal energy E. The time-delayed rise and subsequent decay of the transient absorption of both molecules in the UV spectral range at 335 nm and 340 nm induced by the IR pump is displayed in Figure 6. The model described above was again used to determine overall rate constants for IVR and VET (see Table 1). Interestingly, τ_{IVR} and τ_{VET} are both larger for the fluorinated species. As the excitation energy and the solvent is the same for both molecules, the differences on the timescales are directly related to the chemical substitution. Additional studies have shown that the timescales do not change significantly in other weakly interacting solvents. As the normal modes frequencies of both molecules were not available in the literature, we calculated these for isolated molecules with density functional theory (DFT) at the B3LYP6–311G level.[92] These frequencies were used to calculate densities of states for both molecules by using a standard harmonic counting routine (Figure 7).

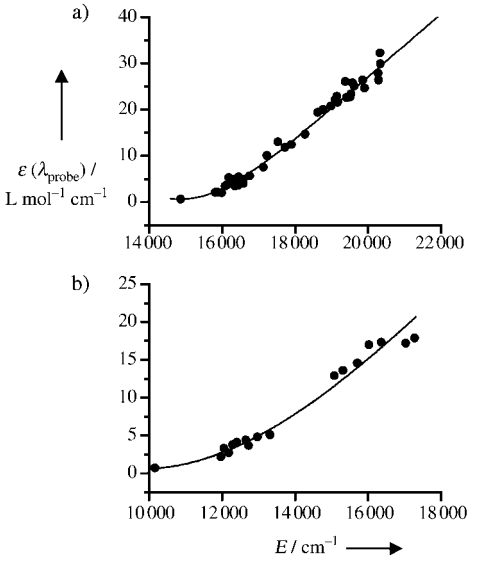


Figure 5. a) Molar absorption coefficient ε of CH_3CH_2I (gas phase) as a function of internal energy E (E includes a zero-point energy of 14557 cm^{-1}) for $\lambda_{probe}=335$ nm measured in a shock tube experiment; b) ε of CF_3CH_2I as a function of E for $\lambda_{probe}=340$ nm (E includes a zero-point energy of 9448 cm^{-1}). The solid line is a polynomial fit of the data.[61]

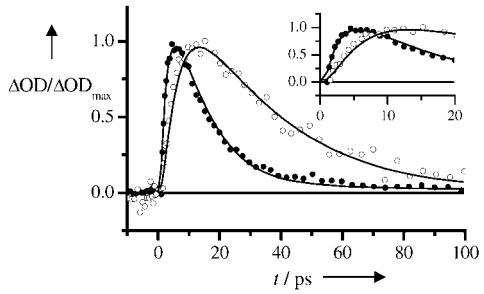


Figure 6. Normalized transient absorbance–time profiles ($\Delta OD/\Delta OD_{max}$ as a function of delay time) for CH_3CH_2I (●) and CF_3CH_2I (○) in CCl_4 with excitation at 1715 nm (●) and 1695 nm (○). Also shown is a fit using the model described in the text (——). The inset shows the same traces on a shorter timescale.

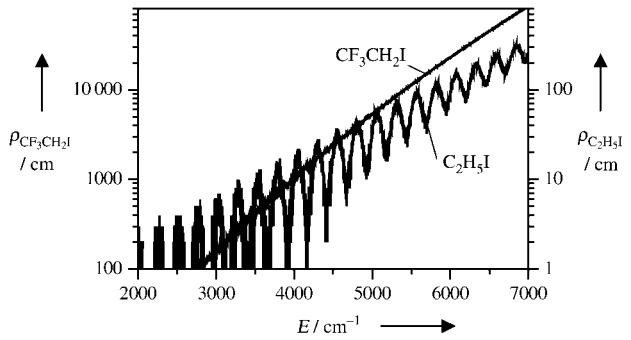


Figure 7. Density of states $\rho(E)$ for CH_3CH_2I and CF_3CH_2I. The right axis corresponds to $\rho(CH_3CH_2I)$, whereas the left axis corresponds to $\rho(CF_3CH_2I)$.

Our experimental findings that IVR is significantly faster for the molecule with the considerably lower overall density of states (Figure 6 and 7) may at first be surprising. This observation is a strong indication for hierarchical IVR[93] (Figure 8) in these molecules in solution, which is governed by specific low-order intramolecular interactions and which can be rationalized with a simple low-order coupling model. It is based on a tier model, which is well-known for isolated molecules. A characteristic feature is that energy decays into the quasi-continuum of molecular states through a chain of low-order couplings.[94,95] Only those resonances that couple a few quanta into other modes from the initially excited C–H stretch are of primary importance, implying an early bottleneck for this process. The number of possible low-order

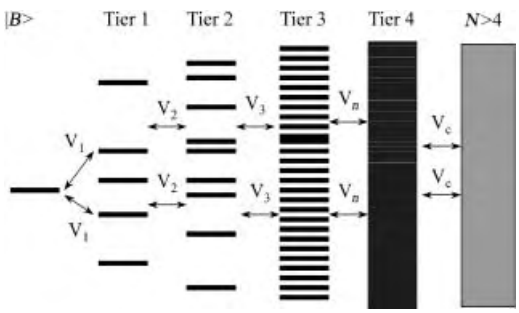


Figure 8. Schematic representation of the zeroth-order quantum states ordered in tiers that couple to a zeroth-order bright state through low-order coupling terms in the molecular Hamiltonian.

© 2003 Wiley-VCH Verlag GmbH & Co. KGaA, Weinheim

Table 2: τ_{IVR} for different molecules in CCl_4 upon excitation of the first overtone ($\upsilon_{CH}=2$) and number of low-order interactions of the C–H stretch ($\upsilon_{CH}=2$, $\pm 100\ cm^{-1}$) to states in the first tiers.

Molecule	τ_{IVR} [ps]	Number of low-order resonances 3rd order	4th order	5th order
CH_2I_2	10	1	4	19
C_3H_5I	2	5	87	258
CH_3CH_2I	1.5	7	45	100
CF_3CH_2I	3.5	1	50	298
$CH_2(OH)CH_2I$	1.2	5	73	263

resonances for CH_3CH_2I and CF_3CH_2I, in comparison with those for CH_2I_2 and C_3H_5I is given in Table 2. If we assume that the rate of IVR from the initially excited zeroth-order bright state to the (final) bath of states with energy E_{red} is larger for the molecule with the larger number of lowest-order interactions,[95] the qualitative trends for both molecules and the difference to diiodomethane and allyl iodide can be explained. Support for this picture comes from a closer inspection of the density of states plot in Figure 7. As opposed to the state density $\rho(E)$ of CF_3CH_2I, that of CH_3CH_2I shows a characteristic clustering, indicating polyads of similar well-coupled zeroth-order states. It is interesting to note that also the trends observed for the excitation of different combination vibrations in CH_2I_2 are predicted surprisingly well by the simple model.

While the relaxation constants and timescales of VET for both molecules are in the range observed for other alkyl iodides, the effect of chemical substitution on the rates of VET is rather surprising. Since it is a common belief that the intermolecular vibrational energy transfer is dominated by the low- (or even the lowest-) frequency normal mode(s) in a molecule, we expected that the introduction of a significant number of modes with much lower frequencies (by fluorination of the methyl group of CH_3CH_2I) would enhance the rate of VET. Instead, our present finding is that the VET in CF_3CH_2I is slower than in CH_3CH_2I. The results may be rationalized if we consider incomplete IVR in these molecules with the consequence that the lowest-frequency modes are not populated significantly on the timescale of relaxation. Molecular-dynamics simulations showed that in such a case the modes cannot contribute significantly to the overall VET.[96] Another explanation invokes the different intermolecular pair potentials for hydrogen and fluorine and the corresponding different spectral densities at the corresponding (changed) oscillator frequencies.[61]

To increase the intermolecular interaction and to study the impact of the presence of OH groups on the vibrational relaxation in solution we also investigated 2-iodoethanol (ICH_2CH_3OH).[80]

2.3. Aromatic Model Systems: Impact of a Methyl "Rotor" and Chemical Substitution

The influence of a (hindered) methyl rotor on the rates of IVR for isolated molecules has attracted much experimental and theoretical attention.[97–101] Most of the experimental results, especially the work of Stone and Parmenter[97] and Lehmann et al.,[103] suggest that the methyl group can enhance the IVR of isolated molecules. Since almost all investigations in this direction are experiments in the gas phase, it is not clear what should be expected in solution. Although interesting, the impact of chemical substitution at a side chain as opposed to substitution directly at the aromatic ring is not known. To investigate this effect systematically, we measured IVR and VET for several aromatic molecules depicted in Figures 2 f–l. In our first studies we focused on toluene and α,α,α-trifluorotoluene.[81] With properly tuned near-IR fs laser pulses, we excited the molecules in the C–H overtone region and in combination vibrations of the C–H stretch. In the case of toluene, the C–H stretches of the ring are excited preferentially over those of the methyl group as a result of significantly larger IR-absorption cross sections. The probe laser was again tuned to the long-wavelength range of the electronic absorption of both molecules, that is, 280 nm. The experimental results for toluene and α,α,α-trifluorotoluene together with a fit for the determination of the relaxation constants τ_{IVR} and τ_{VET} are shown in Figures 9 and 10. The corresponding relaxation constants are given in Table 3. For all aromatic molecules, high-temperature spectra were measured for the energy calibration of the measured traces. These aromatic systems constitute a group of molecules with systematic chemical substitutions at the aromatic ring and at the side chain, which allowed us to study the impact of chemical substitution on the IVR of aromatic molecules in solution. The investigation of benzyl alcohol enabled us to

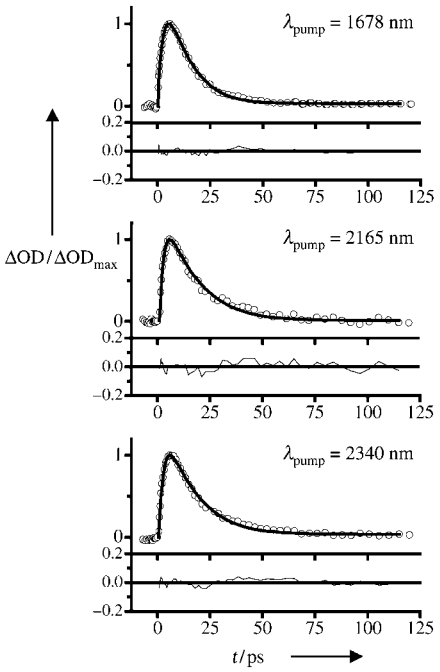


Figure 9. Experimental traces for toluene with excitation in $\upsilon_{CH}=2$ (C–H overtone at 1678 nm) and in two combination vibrations with one quantum of C–H stretch and *n* quanta of a lower-frequency vibration (excitation at 2165 nm and 2340 nm, respectively). Also displayed is a fit using the simple model described in the text.

 © 2003 Wiley-VCH Verlag GmbH & Co. KGaA, Weinheim

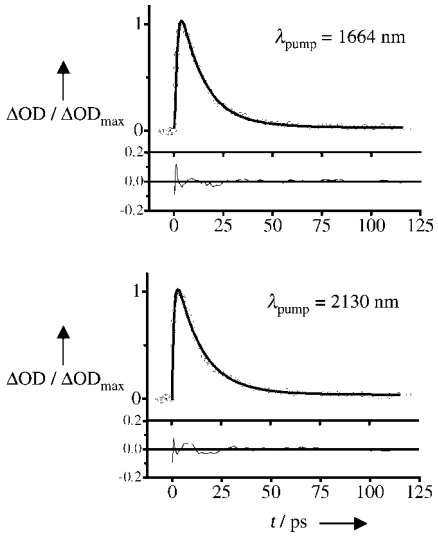


Figure 10. Experimental traces for α,α,α-trifluorotoluene with excitation in $v_{CH}=2$ (C–H overtone at 1664 nm) and in a combination vibration of one quantum of C–H stretch and *n* quanta of lower-frequency vibration (excitation at 2130 nm). Also shown is a fit using the simple model described in the text.

Table 3: τ_{IVR} and τ_{VET} for different aromatic molecules in $CF_2ClCFCl_2$.

Molecule	λ_{pump} [nm]	τ_{IVR} [ps]	τ_{VET} [ps]
benzonitrile	1661	1.7±0.5	19±4
	2140	1.9±0.5	19±3
p-difluorobenzene	1655	1.7±0.5	24±5
	2130	0.8±0.2	30±3
	2330	0.6±0.2	30±3
pyrazine	1684	0.2[a]/5.2±0.5	26±3
	2210	0.2[a]/5.1±0.5	28±3
benzene	1664	2.2±0.5	70±5
	2139	1.8±0.5	69±5
toluene	1668	2.9±0.5	13±2
	2165	2.0±0.5	18±2
	2340	2.3±0.5	17±2
α,α,α,-trifluorotoluene	1664	1.2±0.3	20±3
	2130	1.1±0.3	21±3
benzyl alcohol	1670	0.4±0.3	9±2
	2140	0.4±0.3	9±2

[a] Instantaneous and slower component of the signal, as described in reference [81].

study the impact of hydrogen bonding on IVR and VET, a topic that is beyond the scope of the present article.[91]

At first glance the variations of IVR rates upon chemical modification (see Table 3) of the aromatic ring or the side chain are difficult to judge and appear to be erratic. The wavelength and/or mode dependence is rather small in general, except for *p*-difluorobenzene. The observed trends do not correlate with the total density of states of the molecules or with the number of lowest-order interactions of the zeroth-order bright state. However, the results from our previous study could indicate that in aromatic molecules also the large number of higher-order (as opposed to the small number of strong lowest-order) anharmonic resonances may play a prominent role.[81] The (small) enhancement of the overall relaxation rate for the excitation of several combination bands of the aromatic molecules as opposed to the dynamics for pure overtone excitation may be attributed to the delocalization of the initial pump energy and to an enhanced number of (low-order) coupling possibilities of combination modes. Remarkably, the opposite trend was found for CH_2I_2.[25]

All molecules from Table 3 (except benzyl alcohol) can be divided into two groups: one with substitution at the side chain (benzonitrile, toluene, trifluorotoluene) and the other with substitution at the aromatic ring (benzene, *p*-difluorobenzene, pyrazine). The time dependence of the traces for excitation in the pure C–H overtone region is displayed in Figure 11. The trend for the fluorination of a methyl group in comparison with benzene has already been discussed.[81] Upon comparing benzonitrile with toluene and trifluorotoluene, it is clear that the methyl group does not play a significant role for IVR in solution. When the IVR rates of benzene are compared with those of *p*-difluorobenzene it is evident that fluorine substitution directly at the aromatic ring may also accelerate IVR, as does fluorination of the methyl group in toluene. Pyrazine appears to have a unique role. We showed recently[81] that the increase in absorption, which we attributed to IVR, could only be fitted with a two-exponential function that correlated with an instantaneous rise and a slower increase in absorption. The simplest explanation for this observation is a direct population (excitation) of FC-active modes in pyrazine by the near-IR excitation laser.

Despite the observed changes in the IVR rates upon systematic chemical substitution, the overall variations for all aromatic systems investigated are only moderate. In fact, the variations of the IVR timescales are all within a factor of five

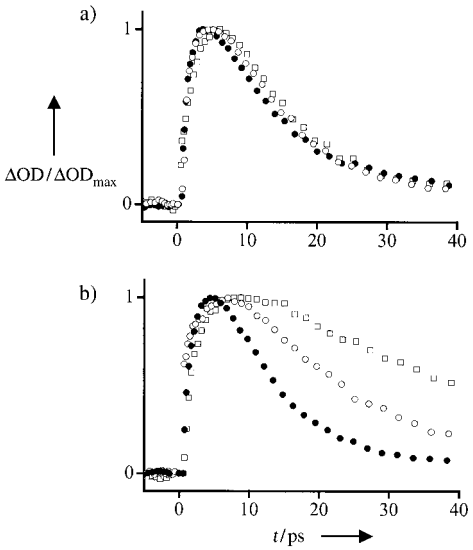


Figure 11. Normalized absorbance–time profiles of different aromatic model systems (separated into groups) after excitation of the C–H stretch overtones ($\lambda_{pump}\approx1660$ nm). a) □ toluene, ○ benzonitrile, ● α,α,α-trifluorotoluene; b) □ benzene, ○ pyrazene, ● *p*-difluorobenzene.

 © 2003 Wiley-VCH Verlag GmbH & Co. KGaA, Weinheim

(Table 3). In general, the IVR timescales are shorter for aromatic than for aliphatic systems. Why do the observed relaxation rates not vary dramatically? From high-resolution spectroscopic studies of substituted "acetylenes" in the gas phase by Nesbitt and Field as well as Lehmann and co-workers, it is known that in the gas phase, IVR lifetimes of C–H chromophores are surprisingly insensitive to the nature of the substituent. The huge reservoir of state density provided by the larger substituents has essentially little or no coupling with the zeroth-order bright C–H stretch state.[104,105]

For the present case of substituted aromatic molecules, the zeroth-order C–H stretch modes of the aromatic ring were excited preferentially, and the characteristic FC-active modes of the aromatic ring were also probed. Therefore, we may consider the aromatic ring as the pumped and probed "chromophore", which is chemically modified. Evidently, the rates of IVR of zeroth-order C–H stretches of the aromatic ring are relatively insensitive to chemical substitution at the aromatic ring or at a side chain (methyl group).

This result is perhaps not surprising: In all the molecules, similar FC-active states were observed, which are all probably at a similar "distance" from the zeroth-order bright state in "state space". This insensitivity can probably be found for a series of systems in which substitutions do not perturb the energy-level structure of the aromatic ring too much and therefore do not significantly change the pattern of low-order resonances and thus overall relaxation pathways.

Unfortunately, most of the available studies on VET in solution mentioned earlier cannot be compared with the present results because very different molecules with significantly higher internal energies were investigated. As previously reported[81] only the VET time constants for benzene can be directly compared with those from a recent IR–Raman experiment of Dlott and co-workers in which C–H fundamentals are pumped and IVR as well as VET processes could be monitored in real time.[65] In their experiments, the VET rate coefficient was determined to be close to 80 ps, which is in good agreement with our results if we assume a small or negligible energy dependence of the VET. As can be seen in Table 3, benzene transfers energy to the solvent much less efficiently than do the other aromatic molecules, presumably as a result of the smaller number of low-frequency modes in benzene. This result is easily explained by classical Landau–Teller and energy gap type arguments.[25,46,106,107] Since the rate of intermolecular energy transfer is expected to depend significantly on the number of low-frequency modes in the molecule, we expected that the chemical substitutions would introduce significantly different numbers of low-frequency modes such that the VET should be sufficiently different for the systems under investigation. Instead, the chemical substitution $X = CN \rightarrow CF_3 \rightarrow CH_3$ in our model systems C_6H_5X had no pronounced effect on the energy transfer by the molecule to the surrounding liquid. A comparison of the relaxation of C–H stretch overtones in *p*-difluorobenzene and benzene reveals the effect of chemical substitution at the aromatic ring on the VET. In this case, fluorination significantly promotes the VET, whilst the IVR is much less affected. This effect can readily be attributed to the additional low-frequency modes that are introduced upon fluorination. However, a similar simple correlation can not be found for the other molecules in Table 3.

Although the trends of the VET rates of different aromatic molecules on chemical substitution are difficult to rationalize in general, an interesting correlation is clear (Figure 11). If we consider the two groups of molecules (benzene, pyrazine, *p*-difluorobenzene and benzonitrile, toluene, trifluorotoluene), it is striking that VET appears to be affected only if the substitution is directly at the aromatic ring. The side chain seems to be a mere spectator in the VET of the molecule, which appears to be dominated by the low-frequency ring modes. It appears that only chemical substitution directly at the ring changes these modes and in turn accelerates VET of the molecule. This observation may be important for an understanding of dynamic aspects and efficiencies of single collisions in solution.

2.4. Theoretical Approaches to IVR and VET in Solution

As outlined in the introduction, a straightforward approach for the theoretical treatment of IVR in solution does not exist, although the importance of the processes has stimulated theoretical work.[96,102,106–112] Recent developments have allowed molecular-dynamics (MD) simulations of polyatomic systems to play a role in the understanding of experimental data.[96] Although advances in computer power have made direct non-equilibrium MD simulations feasible, the calculations are still expensive and by no means standard. Furthermore, the inter- and intramolecular potentials are simply not known well enough and introduce significant uncertainty and ambiguity. These limitations and the present experimental results, which suggest that mechanisms of IVR in isolated molecules[113] may to some extent survive in solution, encouraged us to propose a model, originally developed for the gas phase. This model can be used to explain and partly predict IVR in weakly interacting solvents. In Section 2.2 we introduced a simple low-order coupling model to rationalize the trends in the measured IVR constants. Recently, we developed a more sophisticated theoretical model for IVR in weakly interacting solvents in which IVR is described as a quantum energy flow (diffusion) in quantum number space (QNS) with a straightforward scaling of relevant low-order interactions. The basis of this model is the work of Wolynes and co-workers[114–116] and Gruebele and co-workers,[117–120] who proposed a similar approach for IVR in the gas phase. The QNS for a triatomic molecule is depicted schematically in Figure 12. For convenience we use a normal mode basis for the quantum number space.[117] For a basis with N degrees of freedom, each state of the molecule can be represented on a Cartesian lattice of the QNS as a point, and the vibrational ground state is located at the origin. Pure overtone states can be regarded as edge states, and these states are less well connected to other states because they have fewer coupling opportunities than the larger number of interior states (combination states).[117] Isoenergetic states lie close to a given energy shell (corresponding to the triangle in Figure 12). States that have wavefunctions with similar nodal structures have small values

 © 2003 Wiley-VCH Verlag GmbH & Co. KGaA, Weinheim

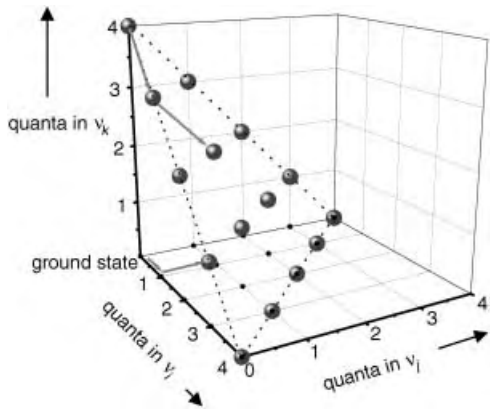


Figure 12. Schematic illustration of the quantum number space (QNS) for a triatomic molecule. Shown is the first step in the relaxation of an overtone "state" in an isoenergetic shell. The ground state is at the origin. For more details see the text.

of Δn, the difference in quantum numbers of the two states being considered [Eq. (3)].

$$\Delta n = \sum_i \Delta v_i \tag{3}$$

It is therefore immediately apparent which states are most strongly coupled: those whose connecting vector is short and has its largest components along QNS axes corresponding to small vibrational frequencies (see Figure 12). It is also clear that the structure of the QNS influences the IVR. At $t = 0$ we may start with a pure state or a superposition of states in the QNS. The evolution of the "wavepacket"(a coherent superposition of states) in the time domain is reflected in the time dependent coefficients c_i of each state in QNS. The state-to-state population-transfer coefficients are expressed in Equation (4) (ΔE_{ij} = energy gap between states i and j, γ and λ = scaling factors, V_0 = constant characteristic matrix element (not known a priori), which is scaled by the exponential factors of the equation).[114]

$$k_{ij} = \frac{2\pi}{\hbar}\frac{\lambda}{4}|V_0|^2\, e^{-\gamma|\Delta n_{ij}|}\, e^{-\lambda|\Delta E_{ij}|} \tag{4}$$

The sum of k_{ij} over the energy range $\Delta E = E \pm \delta$ with $\delta = 2/\lambda$ provides an expression that resembles Fermi's golden rule [Eq. (5)].

$$k = \frac{2\pi}{\hbar}|V_0|^2 \rho_{loc} \tag{5}$$

It implies a local density of states, ρ_{loc}, which is significantly smaller than the total density of states ρ and limits the molecular energy flow, as was already discussed by Wolynes and Schofield.[114] A propagation of the population distribution in the QNS is provided by the solution of Equation (6) (K is the rate coefficient matrix that connects all relevant energy levels).

$$\dot{N} = K N \tag{6}$$

Taken into account are all states within an energy interval $\Delta\varepsilon$ that is chosen to be large enough for the problem and small enough for the corresponding matrices to be manipulated with the available computer power. The time-dependent populations in the QNS can be projected back onto the normal mode basis to be compared with mode-selective experimental data. Other approaches for IVR in isolated molecules employ shifted update rotation (SUR) propagators.[118] The fundamental idea of this approach is that the impact of the weakly interacting solvent is reflected in the matrix element $|V_0|^2$. For a family of weakly interacting solvents, we have found only small differences in the IVR timescales such that, in the absence of more detailed information, we assume $|V_0|^2$ to be of the same order of magnitude for different molecules in similar solvents. In principle, $|V_0|^2$, λ, and γ are adjustable parameters, but they appear to be of similar magnitude for different molecules. Figure 13 displays our simulations for different excitations of

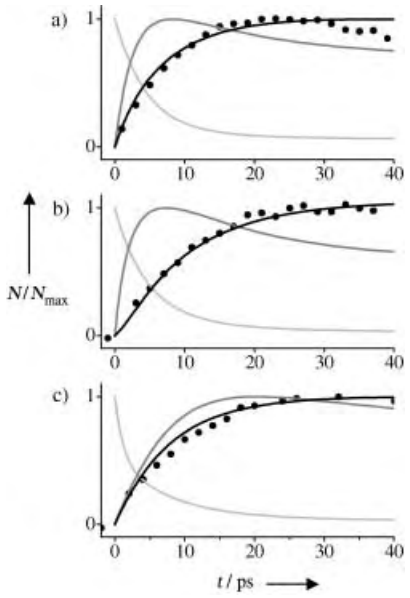


Figure 13. Simulations of experimental traces (●) for CH_2I_2 with the simple IVR model described in the text for different excitation wavelengths. a) $\lambda_{pump} = 1700$ nm, b) $\lambda_{pump} = 2275$ nm, c) $\lambda_{pump} = 2450$ nm. Color code: a) light grey: CH_2 s-stretch, dark grey: CH_2 wag, black: CI_2 a-stretch; b) light grey: CH_2 s-stretch, dark grey: CH_2 wag, black: CI_2 a-stretch; c) light grey: CH_2 s-stretch, dark grey: CH_2 scissor, black: CI_2 a-stretch. The dynamics of the FC-active CI_2 antisymmetric stretch (CI_2 a-stretch) should be compared with the absorbance—time profiles.

CH_2I_2. We found it remarkable that with a parameter set that is close to that for CH_2I_2 (given in Table 4) we were able to *quantitatively* model the whole relaxation cascade of CH_3NO_2 in $CHCl_3$, that is, all mode- and time-resolved populations recently found in an experiment by Dlott and co-workers,[30] without further assumptions.

Our current investigations into other molecules and solvents suggest that the partially statistical and partially molecular detail-based model we propose here actually appears to be able to explain semiquantitatively, but at least

 © 2003 Wiley-VCH Verlag GmbH & Co. KGaA, Weinheim

Table 4: Parameters of the simple IVR model describing IVR as an energy-diffusion process in QNS.

	V_0 [cm^{-1}]	γ	λ [cm]
CH_2I_2			
$2\nu_1 1\nu_2$ ($\lambda_p = 1700$ nm)	12	2	0.16
$1\nu_1 1\nu_3$ ($\lambda_p = 2275$ nm)	10	2	0.16
$1\nu_2 1\nu_4$ ($\lambda_p = 2450$ nm)	10	2	0.16
CH_3NO_2[30]			
$1\nu_3$	6	2	0.3

qualitatively, most of the available data from this type of experiment as well as from other experiments.[30]

While the development of models and the application of theory for IVR in solution is still in its infancy, the situation is somewhat different for intermolecular VET. In the Landau–Teller approach, the VET rate of a molecule in solution is directly related to the frequency-dependent friction $\xi(\omega)$ at the oscillator frequency ω, which is calculated from the time-correlation function of the solvent forces acting on the vibrational coordinate of the solute.[46,106,107,111,112,121] In general, $\xi(\omega)$ has a maximum at very low frequencies and decays exponentially with increasing ω, such that VET is dominated by the lowest-frequency modes of the solute.[111,122] However, it is also well-known that collisions that are characterized by a low order are favored, that is, only states of the molecule that differ by a small number of quanta and that excite the least number of quanta in the solvent are accessible. It is thus the trade off between a low-order process and a small energy gap that is important for effective VET. As a result of this balance, VET is mostly determined by $\xi(\omega)$ at frequencies $\omega > \sim 100$ cm^{-1}, that is, the range beyond the lowest-frequency modes describing complex collective motions of the liquid.[69,123,124] $\xi(\omega)$ is defined in Equation (7) ($C(t)$ is proportional to the force autocorrelation function).

$$\xi(\omega) = \mathrm{Re} \int_0^\infty \mathrm{d}t\, \mathrm{e}^{-i\omega t}\, C(t) \tag{7}$$

A classical MD simulation based on a model potential function can be used to determine the forces exerted by the solvent on the solute vibrational coordinate. As shown by Hochstrasser and co-workers,[46] the rate constant for the VET (for a diatomic molecule with one oscillator) is then given by Equation (8) ($\beta = 1/k_B T$; μ = reduced mass).

$$k_{\mathrm{VET}} = \frac{2\tanh(\beta\hbar\omega/2)}{\mu\beta\hbar\omega}\,\xi(\omega) \tag{8}$$

This quantity can, in principle, also be calculated for polyatomic systems by MD calculations, and thus VET rates could be estimated in solution. However, to date this approach has only been feasible for very simple systems such as diatomic molecules or breathing-sphere model systems.[46,112] Beyond such an approach, flexible MD calculations should be able to treat IVR and VET in solution, even for polyatomic systems. Recently, VET of azulene in solution and supercritical fluids[122–124] and VET as well as IVR of diiodomethane in solution was investigated in full MD simulations.[96] The latter study has accompanied our recent experimental investigations of the intra- and intermolecular vibrational energy flow of CH_2I_2 in solution. The theoretical background of classical MD calculations is provided elsewhere.[96,123,124] Direct non-equilibrium MD simulations have been found to reproduce important features of the energy gain and loss of FC-active CI_2 stretch modes observed in the experiments. A key finding of the studies of Kaeb et al. is that most of the excess energy deposited by the IR pump is dissipated into the solvent through the lowest-frequency C–H mode (CH_2 rocking vibration), while the lowest-frequency mode (CI_2 bending) is merely a spectator in the overall process of energy redistribution and relaxation and is not significantly populated at all on the timescale of the relaxation. Figure 14 shows the time-dependent kinetic-

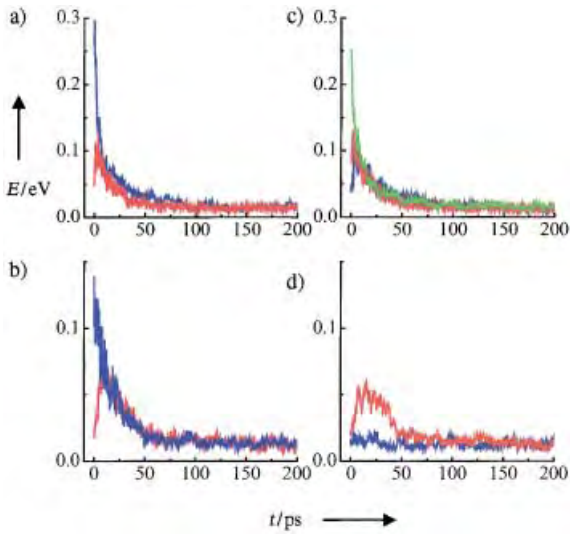


Figure 14. Time-dependent vibrational kinetic energy of different normal modes of CH_2I_2 in chloroform calculated in classical MD simulations.[96] a) blue: ν_6 (CH_2 a-stretch), red: ν_7 (CH_2 rock); b) red: ν_3 (CI_2 s-stretch), blue: ν_8 (CH_2 wag); c) green: ν_1 (CH_2 s-stretch), red: ν_2 (CH_2 bend), blue: ν_5 (CH_2 twist); d) blue: ν_4 (CI_2 bend), red: ν_9 (CI_2 a-stretch).

energy content of the degrees of freedom of diiodomethane.[96] Notably, mainly the asymmetric CI_2 stretch is probed in the experiment such that the energy profile of ν_9 (red) (Figure 14d) should be compared with the experimental traces in Figure 4. The advantage of such studies is that they can provide insight into the mechanisms of IVR and VET beyond experimental observables. However, it should be noted that the absolute timescales for IVR and VET still differ from the experiment a factor of 2–3. This could, in principle, be corrected by the modification of the inter- and intramolecular potentials. This points to an inherent problem of such studies: the choice of the intramolecular and intermolecular potential function is by no means trivial or unambiguous in these simulations.

 © 2003 Wiley-VCH Verlag GmbH & Co. KGaA, Weinheim

3. Ultrafast Dissociation in Solution: Photoinduced Decarboxylation of Organic Peroxides

Large organic peroxide molecules are of fundamental as well as of practical importance because they are used as initiators for free radical polymerizations.[125–127] From this point of view it appears important to investigate the mechanism of initiator dissociation, which releases CO_2 either in a prompt or delayed manner, and can thus be correlated with different time-dependent concentrations of carbon- or oxygen-centered free radicals.[11,128] A large body of literature is focused on the thermal decomposition of peroxides.[11,126,128] Until recently, the photochemical decomposition of peroxides has been investigated almost exclusively in the nano- and microsecond time domain by flash photolysis and visible absorption or EPR spectroscopy.[129–131] These studies revealed the principal reaction channels and some structural aspects of the peroxide decomposition, however the mechanistic details of the photodissociation were not understood very well.[131,132] Whereas in early ps studies short-lived species could be detected,[133,134] the formation of CO_2 and its vibrational cooling in solution has been monitored recently on a ps timescale with transient IR spectroscopy.[9–11] These studies revealed that an improvement of the time resolution is still necessary, because many of the peroxides decompose on an even shorter timescale. Just recently, a study on decarboxylation of carbonyloxyl radicals, intermediates in the decomposition of organic peroxides, was published with fs-time resolution.[135] Unfortunately, the wealth of experimental data about the thermal and photochemical decomposition of peroxides did not lead to a model that is able to explain the dependence of the dissociation dynamics on the molecular structure, internal energy, and molecular environment.[11,128]

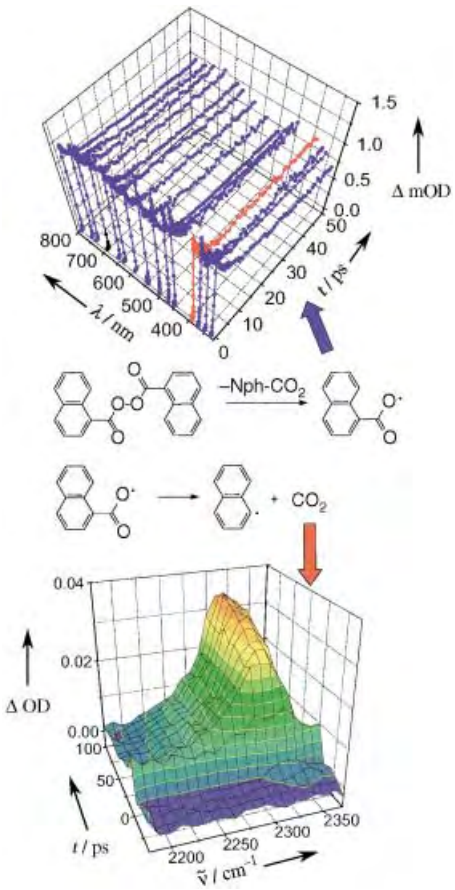


Figure 15. Schematic representation of the decarboxylation of di(1-naphthoyl)peroxide at 266 nm. Top: time-resolved traces (difference in optical density) of the 1-naphthoyloxyl radical at 300–800 nm. Bottom: transient spectra of "hot" CO_2 at 2340 cm^{-1} as a function of time.[10] Time-dependent concentrations are obtained by integrating over the entire ν_3 band of CO_2.

3.1. Direct Observation of Primary and Secondary Bond Dissociation, Transient Intermediates, and Products: Experimental Approach

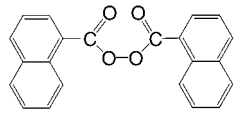
As schematically shown in Figure 15 for the decomposition of di(1-naphthoyl) peroxide (DNPO), the lifetimes of transient intermediates such as the naphthoyloxy radicals and the formation of products can be probed with transient fs absorption spectroscopy. In this particular case, the intermediate aroyloxy radicals absorb strongly in the visible spectral range and can be monitored by fs visible absorption spectroscopy (see Figure 15, upper trace). Likewise the formation of the CO_2 product as well as its vibrational cooling, which manifests itself in a narrowing and shifting of the transient IR spectra of the ν_3 mode, can be monitored by transient IR spectroscopy at 4.3 μm (Figure 15, lower trace).[10] In this particular case, the absorption of the second fragment (naphthyl) was covered by the absorption of the parent molecules and was thus not detectable. For other peroxides (see example below) the product can be detected because the absorption of the product radical undergoes a strong red shift. Unfortunately, the "simple" decarboxylation of peroxides in solution can be accompanied by several competing processes, for example, intermolecular VET or solvation. Moreover, absorptions of parent molecules, intermediates, and products often overlap and spectral congestion in general can be challenging. Therefore it is important to identify spectral windows free of other unwanted absorptions by scanning the probe wavelength over a broad spectral range.

The experimental setup for the time-resolved study of peroxide decomposition is detailed in the literature.[136,137] Briefly, in the present experiments the pump wavelength was tuned between 250 and 300 nm to a broad electronic absorption of the $S_1 \leftarrow S_0$ transition of the peroxides and the probe wavelength was varied between 290 and 1000 nm. Both laser pulses were weakly focussed ($f = 200$ mm) and overlapped temporally and spatially in nearly collinear pump/probe geometry (5°) in a fast-flow cell (0.1–0.2 mm thickness). Relative polarization at magic angle was chosen for the pulses. Transient difference absorption at 1 kHz repetition rate was recorded. The experimental setup for the transient IR absorption spectroscopy with ps time resolution was described recently.[11,138].

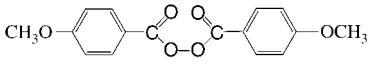
 © 2003 Wiley-VCH Verlag GmbH & Co. KGaA, Weinheim

3.2. Time-Resolved Decarboxylation of Organic Peroxides in Solution

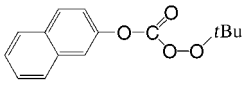
Over the past two years we have investigated a significant number of peroxides with different structures. In this Review we are only able to highlight a limited number of molecules (Figure 16), which serve as illustrative examples that show the general trends and features observed. The first two systems are diaroyl peroxides (DNPO and DMBP), a group of peroxides that has been extensively studied but is not necessarily well-understood.[11] This group of molecules has not yet been investigated by fs spectroscopy. The third system in Figure 16 is a *tert*-butyl aryl peroxy carbonate with general structure R^1-X-C(O)-O-O-R^2 (X = O, R^1 = aromatic ring, R^2 = *tert*-butyl).[11] All molecules considered here were excited between 250 and 300 nm ($S_1 \leftarrow S_0$ transition) and probed in the wavelength range between 290 nm and 1000 nm.



di(1-naphthoyl) peroxide (DNPO)



di(4-methoxybenzoyl) peroxide (DMBP)



tert-butyl-2-naphthylperoxycarbonate (TBNC)

Figure 16. Selected peroxides.

An overview of the transient spectra recorded after the photolysis of di(1-naphthoyl) peroxide (DNPO) in propylene carbonate is given in Figure 15. In the 3D plot (upper graph) we show the time-resolved traces (optical density versus time) for the intermediate 1-naphthoyloxy radical at various probe wavelengths. A characteristic feature of all traces is the instantaneous rise and the subsequent slower decay of absorption, which we attribute to the fast formation of "hot" naphthoyloxy radicals (in the photolysis of the parent peroxides) and their reaction (dissociation) on a ps timescale in competition with vibrational cooling. This decay correlates nicely with the time scale of CO_2 formation.[136] The "offset" of the traces reflects the much slower thermal reaction on a longer timescale. For longer delay times two broad absorption bands can be identified, which can be assigned to the absorption spectrum of the intermediate 1-naphthoyloxy radicals published by Tateno and co-workers.[139] From a detailed analysis of the traces, we found two nearly ideal wavelength ranges at around 390 nm and 620 nm for the sensitive and unperturbed observation of intermediates.[136] Transient spectra between 290 and 1000 nm, which mapped out dominant spectral changes caused by solvation and VET, helped us to identify these spectral windows.[137]

Transient absorption traces after the decomposition of di(4-methoxybenzoyl)peroxide (DMBP) in the wavelengths region 290–1000 nm after excitation at 266 nm in propylene carbonate are shown in Figure 17. In contrast to the case with DNPO, we found large variations in the kinetic traces, and evidently the wavelength dependence of the transients is more complicated. However, also in this case a fast rise and a slower decay in the traces can mostly be attributed to the fast formation and subsequent decay of a methoxybenzoyloxyl radical. A slow increase of absorption similar to the decay of the methoxybenzoyloxyl radical must be assigned to the formation of product, that is, the methoxyphenyl radical. The absorptions at longer time delays again correspond to the measured spectra of Misawa et al. after flash photolysis of DMBP at 308 nm.[140] It is clear that the time-resolved traces at many wavelengths are likely a superposition of several transient spectra of different species. In this particular case the observation window that allows us to monitor the sequential dissociation reaction is quite small and located approximately between 450 nm and 550 nm. Likewise, the product formation can be best observed at 320 nm and 830 nm. Its formation rate at these wavelengths is equal to the

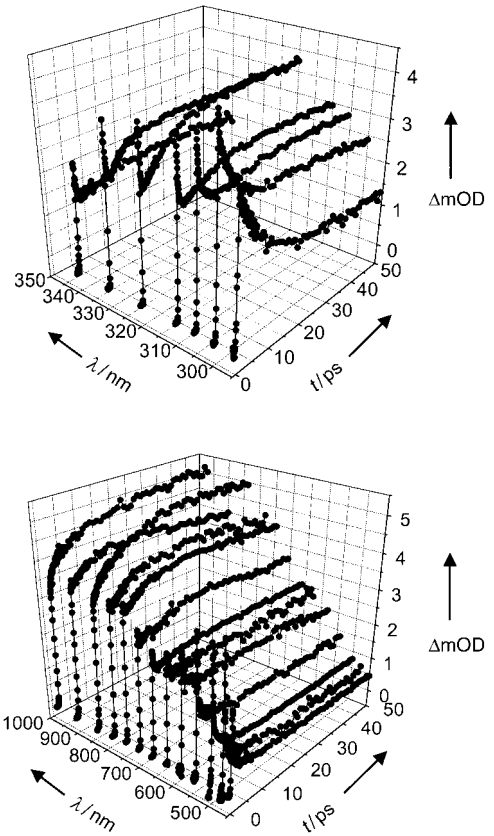


Figure 17. Photolysis of DMBP at 266 nm in propylene carbonate. Time-resolved traces (difference in optical density) in the wavelength range between 300 and 1000 nm. The different features of the traces at different probe wavelengths are evident.

 © 2003 Wiley-VCH Verlag GmbH & Co. KGaA, Weinheim

decay of the signal at 450 nm or 500 nm, the preferred observation window for the intermediate. The relatively weak absorption in the 500-nm range can therefore be attributed solely to the methoxybenzoyloxyl radical, which is in good agreement with its measured spectrum and absorption coefficient measured by Oishi et al.[141]

The third molecule we want to highlight is *tert*-butylperoxy-2-naphthylcarbonate (TBNC). In the wavelength range above 400 nm an immediate increase in less than a picosecond and a decay on a ps timescale can be observed, which we attribute to the absorption of the intermediate 2-naphthyloxycarbonyloxyl radical.[129] Characteristic experimental traces for 594 nm and 766 nm are shown in Figure 18. In addition, a trace at 297 nm shows the absorption of the 2-naphthyloxyl product radical[142] on a similar timescale to that of the decay of the intermediate. It is interesting to see and very convincing that all the experimental traces at different wavelengths above 400 nm show exactly the same kinetic behavior (decay), except amplitude modulations. To make this point clearer, we superimposed all normalized traces. We found that in the wavelength region 400–830 nm, the decays of the intermediate 2-naphthyloxycarbonyloxyl radical (see Figure 19) are the same, as one would expect for the (kinetically) unperturbed observation of the intermediate radical. In Figure 20 we superimposed the decay of different experiments for slightly different excitation wavelengths and a number of different solvents. Remarkably, they are all very similar, which implies that the excitation wavelength and solvent dependence is small. Finally, in Figure 21 a we show the two experimental traces at 297 nm (open circles) and 766 nm (filled circles). In the latter, product absorption was subtracted. Both are complementary and show intermediate decay and product formation on the same timescale. As can be seen in the inset of Figure 21 a, about half the product is already formed in much less than 1 ps, whereas the other half is formed on a ps timescale. We will discuss the origin of this "prompt" and "delayed" CO_2 formation in Section 3.3.

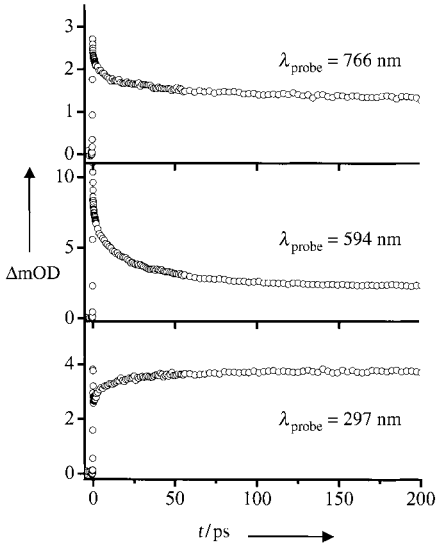


Figure 18. Photolysis of TBNC at 266 nm in propylene carbonate. Transient absorbance as a function of time at different probe wavelengths.

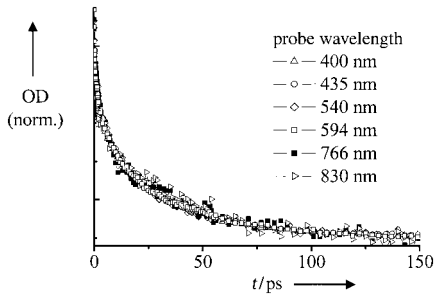


Figure 19. Photolysis of TBNC at 266 nm in propylene carbonate. Transient difference absorption (normalized, see text) of the 2-naphthyloxycarbonyloxyl radical as a function of time at different probe wavelengths.

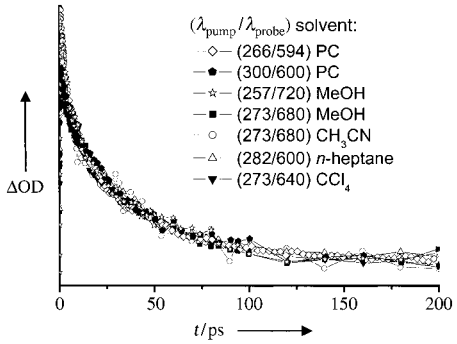


Figure 20. Photolysis of TBNC at 250–300 nm. Transient difference absorbance traces (normalized, see text) of the naphthyloxycarbonyloxyl radical as a function of time at different probe wavelengths and in various solvents (PC = propylene carbonate). Pump and probe wavelength are indicated in the figure legend.

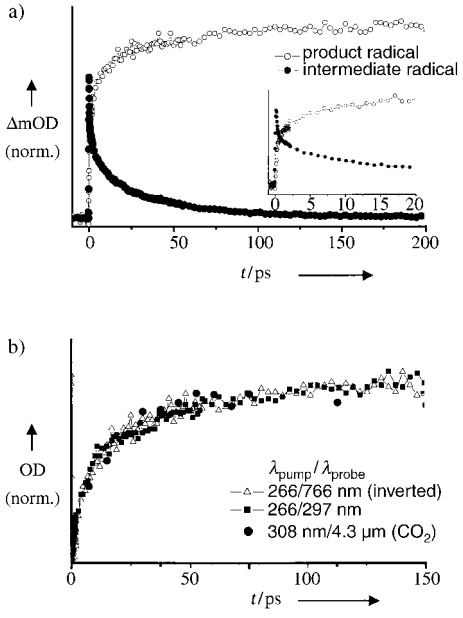


Figure 21. a) Photolyis of TBNC at 266 nm in propylene carbonate. Transient absorbance of the 2-naphthyloxycarbonyloxyl radical at 766 nm (●), and of the naphthyloxyl radical (○) at 297 nm. b) Superimposed decay of the intermediate (inverted), product formation, and CO_2 formation from different experiments. △: 2-naphthyloxycarbonyloxyl (inverted); ■: 2-naphthyloxyl radical (product); ●: integrated absorbance at 4.3 μm monitoring nascent CO_2 (product).

 © 2003 Wiley-VCH Verlag GmbH & Co. KGaA, Weinheim

To show that the time constants for the decay of the intermediate and the formation of the product (■) in Figure 21a are the same, within experimental error, we superimposed the traces in Figure 21b (subtraction of the offset and scaling of the amplitude). In this case, the trace of the intermediate decay was inverted (▲). Also included is a trace from an experiment in which the nascent CO_2 product after excitation of TBNC at 308 nm was probed as a function of time delay (●) from the time-resolved integrated absorption of the ν_3 band of CO_2 at 4.3 μm (see Figure 15).[9] This is a nice demonstration that the different spectroscopic techniques provide complementary information.

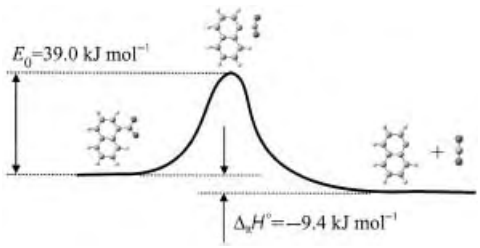


Figure 22. DFT calculations of the energy profiles (barrier E_0 and reaction enthalpy $\Delta_R H^0$(298 K)) for the decomposition of naphthoyloxyl radicals (from the photolysis of DNPO).

3.3. Quantitative Model for the Sequential Decomposition of Peroxides Based on Quantum Chemistry and Statistical Unimolecular Rate Theory

A rigorous theoretical treatment of chemical transformations in solution is still a significant challenge.[45,46] For the development of any model one has to make certain assumptions and approximations about the processes under consideration. The main ideas of the present approach can be summarized as follows: First, we assume that absorption at 266 nm excites the parent peroxide in the repulsive S_1 state.[143] We further assume that the concerted elimination of CO_2 (that is, the simultaneous dissociation of different bonds) is rather unlikely, and that a fast sequential dissociation is the rule rather than the exception for the decomposition of organic peroxides.[144] Within a vibrational period, the peroxide molecules decompose and may form vibrationally excited intermediates in the $\tilde{X}$ ground state and in the second electronically excited $\tilde{B}$ state (as well as another hot fragment). For convenience we use the trivial assignment $\tilde{X}$, $\tilde{A}$, and $\tilde{B}$ for labeling the ground , first excited, and second excited state of the molecules of different symmetry groups (e.g. the correct symmetry label of the $\tilde{B}$ state is $^2A'$ for C_s symmetry and ^2A for C_1 symmetry). Since the $\tilde{B}$ state of the intermediate radicals in most cases correlates with the ground state of the final radical product,[145] radicals in this excited state can react in a fast barrier-free "downhill reaction" to the vibrationally excited products. On the contrary, the (very) low-lying first excited $\tilde{A}$ state usually does not correlate with the reaction products in their ground state and is therefore not considered. The energy of the excited $\tilde{B}$ state of the intermediate radical can be probed through the optical transition in the near IR spectral range. In the present case it is in fact the upper state in our probe transition.[145] Coupling of the states in this energy region is assumed to be strong. However, if the excess energy suffices for the excited state reaction channel it will become the preferred one. This process releases "hot" CO_2, which has been experimentally observed.[9–11]

For many of the diaroyl peroxides the excited $\tilde{B}$ state in the primary fragment radicals has been found to be too high in energy to be populated in the dissociation at 266 nm. Thus, vibrationally excited intermediate radicals are formed in the electronic ground state. These have a longer lifetime and equilibrate and dissociate in a statistical unimolecular barrier reaction to the products. The situation for DNPO and the intermediate 1-naphthoyloxyl radicals in their ground state potential energy surface (PES) is depicted schematically in Figure 22. This dissociation can be treated rigorously by statistical unimolecular rate theory,[146] if the barrier height and the frequencies of the parent molecule as well as the transition state are obtained from high-level quantum chemical calculations. The simplest assumption about the energy distribution of the radicals is that the excess energy is redistributed statistically among the fragments and that a temperature can be assigned to the products and intermediates. Finally, we assume that the (weakly interacting) solvents used in the present studies have only a minor influence on the dynamics of the peroxide decomposition, such that we only need to consider the energy profile of the isolated molecule. However, this is a bold assumption in the absence of proof. Therefore, we investigated the solvent and viscosity dependence of the kinetics of several peroxides in various solvents. We have found no significant influence of the solvent on the dissociation dynamics of this type of molecule, except for a variation in the intermolecular energy transfer efficiency. Evidently, the CO_2 fragment is too small to show appreciable viscosity dependence in the dissociation reaction as opposed to other systems.[8] We also find no indication for a significant contribution of geminal recombination to the observed signal.

The resolvable time-dependent signals can be calculated and compared with the experimental values. Our approach is actually a forward modeling of experimental traces. The crucial input data for this approach are the barrier height and the frequencies of the parent intermediate radicals and transition states (for the isolated system). Density functional theory (DFT) has been used to calculate energies and structures of the parent molecules, intermediates, products, transition states, as well as their frequencies. Kieninger et al. recently calculated the energy profiles of HCOO and CH_3COO radicals with DFT (B3LYP and B3PW91) and higher level techniques (CASPT2/ANO and MP2) and found that DFT calculations give good results, even in comparison with higher-level techniques for the systems under investigation.[147] This was also proved in our own calculations for the significantly larger benzoyloxyl radical, which is formed in the decay of dibenzoyl peroxide, Ph-C(O)O-O(O)C-Ph.[137] We therefore assume that DFT calculations also give results with reasonable accuracy for the decomposition reactions of peroxides highlighted in this article.

 © 2003 Wiley-VCH Verlag GmbH & Co. KGaA, Weinheim

The microcanonical (statistical) specific rate constant for a molecule reacting over a distinct barrier to the products is defined in Equation (9)[146] ($W^{\#}(E-E_0)$ = number of energetically accessible transition state energy levels, $\rho(E)$ = density of states at energy E).

$$k(E) = \frac{W^{\#}(E-E_0)}{h\rho(E)} \tag{9}$$

We used the calculated barrier heights $E_0 = 39.0\ \mathrm{kJ\,mol^{-1}}$ and $46.9\ \mathrm{kJ\,mol^{-1}}$, the ground- as well as the transition-state frequencies of the 1-naphthoyloxyl radical ($1NphCO_2$ from DNPO dissociation) and the 4-methoxybenzoyloxyl radical ($4MeOPhCO_2$ from DMBP dissociation), respectively (Tables 5 and 6), to calculate the specific rate constants

Table 5: Calculated barriers E_0 and reaction enthalpies $\Delta_R H^0$ (298 K) for the decomposition of intermediate radicals.

	$\Delta_R H^0$ [kJ mol^{-1}]	E_0 [kJ mol^{-1}]
$1NphCO_2$	−9.4[a]	39.0[b]
$4MeOPhCO_2$	12.0[c]	46.9[d]
$2NphOCO_2$	−131.7[c]	12 ± 2[e]

[a] B3LYP6-311+G(2d,p)//6-31+G(d,p). [b] B3LYP6-311+G(2d,p)//6-31G(d). [c] B3LYP6-311+G(2d,p). [d] B3LYP6-311+G(2d,p)//6-311+G(d,p). [e] Determined experimentally (see text).

$k(E)$ as a function of internal energy E for both cases without any fitting parameters. From the excess energy $E_{h\nu}-E_0$ and statistical thermodynamics,[146] the initial internal energy $\langle E\rangle_{\mathrm{ini}}$ was estimated under the assumption that the excess energy is distributed statistically among the fragments. We determined that $\langle E\rangle_{\mathrm{ini}} = 172\ \mathrm{kJ\,mol^{-1}}$ and $167\ \mathrm{kJ\,mol^{-1}}$ and $T_{\mathrm{ini}} = 910$ K and 950 K, for the vibrationally excited 1-naphthoyloxyl and 4-methoxybenzoyloxyl radicals, respectively. The time-dependent "decay" of the energy distribution (with $n(i,t)$ as the level populations, see Equation (10) can be modeled within a relatively simple stepladder model, assuming microscopic state i to state j energy-transfer rates, $k(j,i)$, of standard exponential form for activating and deactivating "collisions" in solution.[146,148]

$$\frac{\mathrm{d}n(i,t)}{\mathrm{d}t} = \sum_j k(i,j)n(j,t) - \sum_j k(j,i)n(i,t) - k_i(E)n(i,t) \tag{10}$$

The time constants $k(j,i)$ were fit to reproduce a phenomenological (global) relaxation constant, $\tau_{VET} = 7.5 \pm 1.5$ ps, of the energy distribution $P(E)$ of the hot intermediates. It was found to be in agreement with experimental results for molecules of similar complexity and degrees of freedom,[37] and was kept constant for all molecules in the simulations in a particular solvent (e.g., propylene carbonate; for less efficient solvents such as CCl_4 τ_{VET} was close to 10 ps). The initial intermediate radical energy distribution was assumed to be thermal. Finally, theoretical concentration versus time profiles, $S(t)_{\mathrm{norm}}$, were obtained by using Equation (11), with subsequent convolution with the cross-correlation function of the system.

Table 6: Calculated frequencies of the normal modes (in cm^{-1}), intermediate radicals, and their transition states.[a]

	Ground state	Transition state[b]
$1NphCO_2$	29, 90, 180, 180, 217, 337, 368, 400, 469, 479, 510, 537, 578, 617, 641, 714, 730, 757, 789, 807, 825, 870, 882, 949, 962, 991, 1000, 1032, 1060, 1108, 1179, 1181, 1197, 1199,1246, 1256, 1299, 1395, 1407, 1435, 1490, 1507, 1564, 1575, 1628, 1650, 1680, 3184, 3188, 3196, 3204, 3210, 3218, 3222[c]	313i, 45, 74, 155, 173, 192, 222, 377, 409, 425, 466, 520, 521, 537, 594, 645, 656, 739, 772, 780, 793, 802, 875, 907, 921, 960, 972, 998, 1053,1073, 1140, 1182, 1191, 1212, 1248, 1260, 1288, 1376, 1398, 1406, 1470, 1499, 1539, 1599, 1654, 1674, 2056, 3183, 3189, 3198, 3207, 3212, 3239, 3251[c]
$4MeOPhCO_2$	69, 100, 136, 169, 212, 265, 293, 327, 427, 481, 506, 516, 606, 639, 641, 718, 780, 818, 822, 873, 985, 994, 1002, 1029, 1041, 1136, 1167, 1168, 1203, 1210, 1288, 1326, 1351, 1459, 1473, 1484, 1495, 1501, 1532, 1572, 1632, 3024, 3090, 3148, 3190, 3203, 3206, 3218[d]	274i, 36, 64, 107, 142, 216, 246, 273, 291, 401, 424, 453, 505, 601, 618, 621, 686, 783, 784, 829, 937, 970, 976, 1042, 1053, 1116, 1168, 1179, 1200, 1249, 1273, 1304, 1337, 1410, 1471, 1494, 1494, 1503, 1599, 1616, 1998, 3009, 3070, 3140, 3190, 3203, 3221, 3222[d]
$2NphOCO_2$	57, 61, 82, 156, 179, 286, 330, 352, 402, 434, 446, 482, 523, 534, 583, 635, 646, 729, 764, 765, 778, 782, 789, 836, 883, 903, 933, 969, 983, 985, 998, 1048, 1121, 1154, 1166, 1183, 1224, 1259, 1286, 1302, 1372, 1379, 1412, 1475, 1485, 1533, 1553, 1593, 1612, 1633, 3167, 3172, 3174, 3183, 3194, 3203, 3223[e]	257i, 58, 70, 104, 159, 198, 285, 341, 364, 407, 449, 483, 518, 535, 557, 616, 643, 708, 758, 764, 770, 777, 785, 835, 880, 900, 935, 970, 980, 987, 999, 1050, 1120, 1153, 1169, 1185, 1225, 1262, 1294, 1324, 1367, 1372, 1418, 1474, 1496, 1539, 1586, 1599, 1610, 1628, 3168, 3172, 3175, 3184, 3195, 3203, 3232[e]

[a] Frequencies for $1NphCO_2$ from reference [136] (Supporting Information). Frenquencies for $2NphOCO_2$ from reference [158]. [b] The normal mode with the imaginary frequency corresponds to the reaction coordinate. [c] B3LYP6-31G(d). [d] B3LYP6-311+G(2d,p). [e] B3LYP6-311+G(d,p).

$$S(t)_{\mathrm{norm}} = \frac{\sum_i n(i,t)}{\sum_i n(i,t=0)} \tag{11}$$

Experimental traces and simulations for 1-naphthoyloxyl and 4-methoxybenzoyloxyl radicals at probe wavelengths of 390 nm and 532 nm, respectively, are given in Figures 23 and 24. The solid line is the simulation of the traces with the parameters given in Tables 5 and 6. In both cases, the agreement between experiment and theory is very satisfying. Notably, a significant "spike" of the signal at $t = 0$ ps is mainly a coherence artifact rather than a real signal and need not be considered in the fit. The cross-correlation in Figures 23 and 24 is a measure of the effective time resolution in the experiment. We emphasize that the "offset" in the signals reflects the slower thermal decomposition on the ns timescale, which must also be simulated correctly.

 © 2003 Wiley-VCH Verlag GmbH & Co. KGaA, Weinheim

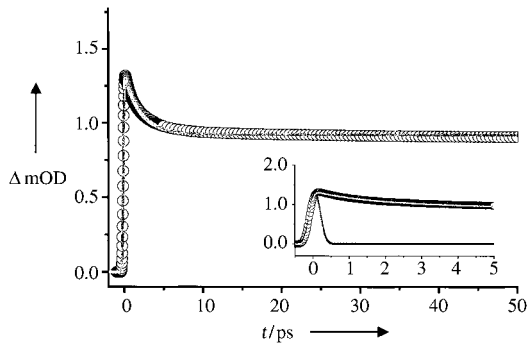


Figure 23. Comparison of the experimental trace (probe: 390 nm) for the decomposition of 1-naphthoyloxyl radicals from the photodissociation of DNPO at 266 nm in propylene carbonate (○) and model calculations (——) using the simple model described in the text. The inset shows the signal up to 5 ps and the cross-correlation of the experiment. Parameters of the model: $\langle E\rangle_{int} = 172\ kJ\,mol^{-1}$ (initial intermediate radical energy), $E_0 = 39\ kJ\,mol^{-1}$, $\tau_{VET} = 7.5$ ps.

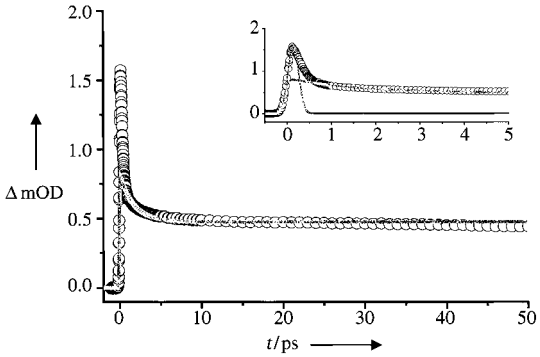


Figure 24. Comparison of the experimental trace (probe: 532 nm) for the decomposition of methoxybenzoyloxyl radicals from the photodissociation of DMBP at 266 nm in propylene carbonate (○) and model calculations (——) using the simple model described in the text. The inset shows the signal up to 5 ps and the cross-correlation of the experiment. Parameters of the model: $\langle E\rangle_{int} = 167\ kJ\,mol^{-1}$ (initial intermediate radical energy), $E_0 = 46.9\ kJ\,mol^{-1}$, $\tau_{VET} = 7.5$ ps.

The two systems above are members of a family of molecules in which excited states are not significantly involved in the dissociation process of the intermediate radicals. However, as already mentioned, the electronically excited states of the intermediate radicals in some systems are low enough in energy and thus are accessible in the photodissociation of the parent peroxides. A typical member of this family is the 2-naphthyloxycarbonyloxyl radical from the photodissociation of the *tert*-butyl-2-naphthylperoxycarbonate (TBNC). As is illustrated in Figure 25 the overall intermediate radical dissociation after the ultrafast primary peroxide bond dissociation in this case can be characterized by two contributions: The fast, direct excited-state dissociation and the slower reaction of the 2-naphthyloxycarbonyloxyl radical via the ground state over a small barrier. The branching ratio depends on the energy of the excited state of the intermediate radical (ΔE) relative to the center of gravity and width of the initial energy distribution of the intermediate

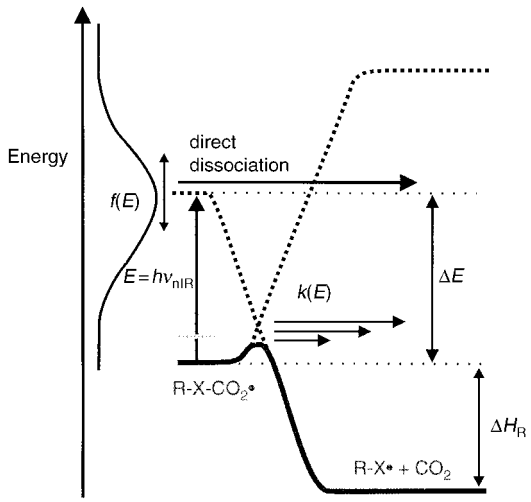


Figure 25. Generalized energy level and correlation scheme of the energy profile in the decomposition of nascent radical intermediates from the photodissociation of R-X-CO_2-OR-type peroxides. The grey solid barrier potential was used for the calculations of specific rate constants $k(E)$ (statistical unimolecular rate channel). $f(E)$ is the vibrational energy distribution of the intermediates, resulting from the photodissociation of the parent peroxides. The second electronically excited state is the upper state in the probe transition.

radical. We assume here that mixing of the ground and electronically excited state is strong in the high-energy region and that whenever the energy of the radicals is above that of the excited state, the molecules react through the excited state in a direct, barrier-free reaction. For a detailed discussion of the labelling and features of the ground and excited states of this type of radicals, see reference [145]. This fast direct decarboxylation reaction depletes the population in the high-energy part of the energy distribution, and the solvent is not able to repopulate this part significantly during reaction. After the fast reaction of the high-energy intermediate radicals, the remaining radicals (now with a significantly lower average energy E) reacts on the ground state PES statistically over the barrier to the products. As can be seen in Figure 21, the yield for the latter reaction in this particular case is about 50%.

A simulation of the dissociation dynamics of the 2-naphthyloxycarbonyloxyl radical in propylene carbonate and *n*-heptane is represented in Figure 26 (the absorbance of the naphthyloxyl product radical has been subtracted. The parameters of the simulation are given in Table 5 and 6. In contrast to the calculation of the geometries and frequencies, the calculation of the rather small barrier for the 2-naphthyloxycarbonyloxyl radical was very difficult for several reasons. One reason lay in the flatness of the PES close to the saddle point. Because the reliability of our most costly calculations (B3LYP6-311 + G(2d,p)) was not sufficient for a precise determination of the barrier height in this case, we used the calculated value as a starting point and adjusted it within the uncertainties of the calculations to reproduce our experimental data. Finally, a barrier height of $E_0 = 12 \pm 2\ kJ\,mol^{-1}$ (Table 5) is consistent with the calculations[158] and our experimental data. The internal energy of the

 © 2003 Wiley-VCH Verlag GmbH & Co. KGaA, Weinheim

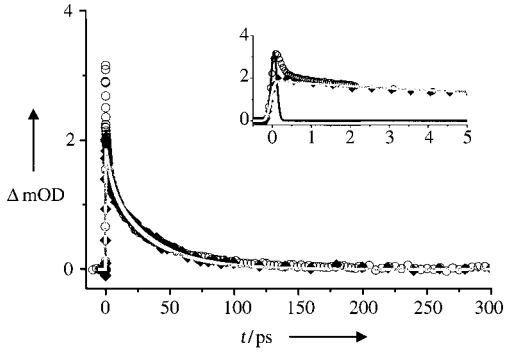


Figure 26. Comparison of experimental traces for the decomposition of naphthyloxycarbonyloxyl radicals (after subtraction of residual absorption from naphthyloxyl radicals) from the photodissociation of TBNC in propylene carbonate (○, 266 nm pump/594 nm probe) and *n*-heptane (◆, 282 nm pump/600 nm probe) and model calculations (——). The inset shows the signal and the cross-correlation of the experiment. Parameters of the model: $\langle E\rangle_{int} = 32\ kJ\,mol^{-1}$ (initial intermediate radical energy), $E_0 = 12\ kJ\,mol^{-1}$, $\tau_{VET} = 7.5$ ps.

reacting intermediate radicals is relatively low in this case (32 kJ mol^{-1}, which corresponds to a temperature of 370 K). This observation is a direct consequence of the low energy of the (second) electronically excited state of the carbonyloxyl radical. We emphasize that the simulation fits the results for *n*-heptane and propylencarbonate very well (neglecting contributions from the coherence artifact at $t = 0$ ps), although the viscosity for the two solvents differs by a factor of 7. This simulation was also carried out with an overall energy transfer time constant τ_{VET} of about 7.5 ps.

4. Summary and Outlook

In this Review we have highlighted experiments for the direct measurement of IVR in simple and more complex organic molecules in solution. A key feature is that IVR following selective overtone excitation is not statistical. Instead, specific couplings tend to survive in weakly interacting solvents, which can be rationalized within a generalized tier model. It should be pointed out again that the reported experiments are sensitive to the rate-determining step in a relaxation cascade. This implies that other timescales may be hidden, for example, the ultrafast timescale ($t < 1$ ps) in which the C–H stretches are known to couple to in-plane modes of the aromatic ring. To provide a balanced description of IVR, we also emphasize that IVR in general depends strongly on the particular excitation of the molecule. The situation encountered in Sections 2.2 and 2.3 is a special case in which local, well-isolated modes of a molecule are excited at relatively low energies. The picture we obtained appears to be characteristic for overtone excitation experiments. We expect the situation to be very different from intramolecular relaxation of large molecules (e.g., azulene) after electronic excitation and internal conversion.[19,37] In the case of internal conversion, states in strongly coupled tiers of the molecule are most likely to be excited, a situation that should be accompanied by much faster IVR than that observed for overtone or fundamental excitation. Although, the timescales may be very different in such a case, the underlying mechanisms for IVR should be the same as outlined in Section 2.2. From the data in Section 2.2 and 2.3, one may be tempted to speculate about a change and control of IVR and in turn of reactivity by (temporal) structural modification. A minimum requirement for laser-directed chemistry is, however, that the nonstatistical nature of the excitation should live long enough for the desired reaction to occur. In the case of bimolecular chemistry (in solution), this requires that the energy must be localized at least for the duration of the mean collision time (transport phenomena not considered). One possibility is to use structural modifications or substitutions to modify (slow down) the IVR rate. This pragmatic approach to laser chemistry seeks to use the well-developed methods of synthetic chemistry to engineer molecules with long-lived, bond-localized excitations.[149,150] In this manner, IVR-blocking groups or heavy atoms[151] may be suitable modifications to direct a reaction at a specific site.

What is the impact of our findings on the concept of molecular VET in solution? It has been known for some time that VET depends to some extent on the low-frequency modes of the molecules. We have found that this is not necessarily true if IVR competes with VET, which means that low-frequency modes may not be populated sufficiently on the timescale of the relaxation process. Nevertheless, in other excitation schemes such as optical excitation followed by internal conversion, the situation is likely to be quite different. In this case the low-frequency modes are expected to be populated on the timescale of relaxation. In this case, structural changes will enhance VET only if additional low-frequency modes ("gateway modes") are induced, no matter what the size, structure, and internal energy of the molecule is. This is the reason why VET rate constants can be quite similar for molecules of very different structure and excitation energies. The ultrafast IVR and our understanding of VET in organic molecules is the reason why statistical approaches and VET models are so successful in the case of the theoretical modeling of the photodissociation of peroxides in the second part of this review.

Based on chemical intuition and experience, polymer chemists have known for some time that the mechanism for the decomposition of peroxides may be determined by the structure of the parent peroxide compounds and the stability of the radical intermediates or products.[131] However, to date, the structure dependence has not been identified sufficiently well and no quantitative or even predictive model has been suggested. The systematic investigation of a large family of molecules and the strategy outline above enabled us for the first time to develop a relatively simple model that not only explains existing data, but is actually able to predict the decarboxylation of organic peroxides in a semiquantitative manner, based on thermodynamic data and quantum chemistry. It also helps to find criteria to group them into families and to predict kinetics on much longer timescales. Finally, it may be useful for chemists who want to control the initial steps of a light-induced polymerization, that is, the initiator efficiency and the transfer activity of primary initiator-

 © 2003 Wiley-VCH Verlag GmbH & Co. KGaA, Weinheim

derived free radicals, as well as the microstructure of the corresponding final polymer.

In this Review we have shown that an understanding of ultrafast chemistry depends on the knowledge of fast competing processes, and that both can be studied through the use of powerful femtosecond absorption spectroscopy. Nevertheless, the two areas of research covered in this review, namely femtochemistry and fast competing processes in solution, are still in an early stage of understanding, as opposed to similar processes in the gas phase. For a better understanding of chemistry in solution at the molecular level, further intensive research is necessary. Both fields will certainly benefit from new powerful developments in time-resolved spectroscopy such as ultrafast electron[152,153] and X-ray diffraction,[154] multidimensional IR spectroscopy,[155] photon echo spectroscopy,[156] and X-ray spectroscopy,[157] as well as advances in theory and computer power in the near future.

We thank the Deutsche Forschungsgemeinschaft for financial support within the SFB357 ("Molekulare Mechanismen Unimolekularer Prozesse"), as well as Prof. M. Buback, Prof. P. Botschwina, Dr. A. Charvat, Priv.-Doz. Dr. S. Schmatz, Prof. J. Schroeder, Prof. D. Schwarzer, and Prof. J. Troe for stimulating discussions on various aspects of this work. Many results highlighted in this Review were obtained in collaborations with our colleagues Prof. D. Schwarzer, Prof. M. Buback, and Prof. J. Schroeder, as well as Prof. P. Botschwina and Priv.-Doz. Dr. S. Schmatz within the SFB357 in Göttingen (Projects A4, A13, B3, and B7). B.A. and J.A. thank the Fonds der Chemischen Industrie for financial support and a graduate student fellowship. We thank Dr. K. Henning, R. Bürsing, and Dr. C. Kappel for measurements of high-temperature spectra. Finally, we thank Akzo Nobel for kindly providing the peroxide samples and for financial support.

Received: June 13, 2002 [A541]

[1] R. G. W. Norrish, G. Porter, *Nature* **1949**, *164*, 658.
[2] M. Eigen, *Angew. Chem.* **1963**, *75*, 489; *Angew. Chem. Int. Ed. Engl.* **1964**, *3*, 1.
[3] M. Eigen, *Nobel Lectures (Chemistry)*, Elsevier, Amsterdam, **1972**, p. 170.
[4] A. H. Zewail, *Angew. Chem.* **2000**, *112*, 2688; *Angew. Chem. Int. Ed.* **2000**, *39*, 2586.
[5] J. Manz, L. E. Wöste, *Femtosecond Chemistry 1 + 2*, VCH, New York, **1995**.
[6] F. C. De Schrywer, S. De Feyter, G. Schweitzer, *Femtochemistry*, Wiley-VCH, Weinheim, **2001**.
[7] J. C. King, J. Z. Zhang, B. J. Schwarz, C. B. Harris, *J. Chem. Phys.* **1993**, *99*, 7595.
[8] J. Schroeder, J. Troe, *Annu. Rev. Phys. Chem.* **1986**, *38*, 163.
[9] J. Aschenbrücker, M. Buback, N. P. Ernsting, J. Schroeder, U. Steegmüller, *Ber. Bunsen-Ges.* **1998**, *102*, 965.
[10] J. Aschenbrücker, M. Buback, N. P. Ernsting, J. Schroeder, U. Steegmüller, *J. Phys. Chem. B* **1998**, *102*, 5552.
[11] M. Buback, M. Kling, M. T. Seidel, F.-D. Schott, J. Schroeder, U. Steegmüller, *Z. Phys. Chem.* **2001**, *215*, 717.
[12] S. Hess, H. Hippler, T. Kühne, P. Vöhringer, *J. Phys. Chem. A* **1999**, *103*, 5623.
[13] T. Lian, S. E. Bromberg, M. Asplund, H. Yang, C. B. Harris, *J. Phys. Chem.* **1996**, *100*, 11994.
[14] J. Schroeder, D. Schwarzer, J. Troe, F. Voß, *J. Chem. Phys.* **1990**, *93*, 2393.
[15] J. Schroeder, J. Troe, P. Vöhringer, *Z. Phys. Chem.* **1995**, *188*, 287.
[16] C. K. Payne, P. T. Snee, H. Yang, K. T. Kotz, L. Schafer, T. D. Tilley, C. B. Harris, *J. Am. Chem. Soc.* **2001**, *123*, 7425.
[17] K. T. Kotz, H. Yang, P. T. Snee, C. K. Payne, C. B. Harris, *J. Organomet. Chem.* **2000**, *596*, 16303.
[18] S. A. Kovalenko, N. Eilers-König, T. A. Senyushkina, N. P. Ernsting, *J. Phys. Chem. A* **2001**, *105*, 4834.
[19] S. A. Kovalenko, R. Schanz, V. M. Rarztdinov, H. Henning, N. P. Ernsting, *Chem. Phys. Lett.* **2000**, *323*, 312.
[20] H. J. Bakker, P. C. M. Planken, A. Langendijk, *Nature* **1990**, *347*, 745.
[21] H. J. Bakker, P. C. M. Planken, A. Langendijk, *J. Chem. Phys.* **1991**, *94*, 6007.
[22] H. J. Bakker, *J. Chem. Phys.* **1993**, *98*, 8496.
[23] D. Bingemann, A. King, F. F. Crim, *J. Chem. Phys.* **2000**, *113*, 5018.
[24] M. Bonn, M. J. P. Brugmans, H. J. Bakker, *Chem. Phys. Lett.* **1996**, *249*, 81.
[25] A. Charvat, J. Aßmann, B. Abel, D. Schwarzer, *J. Phys. Chem. A* **2001**, *105*, 5071.
[26] A. Charvat, J. Aßmann, B. Abel, D. Schwarzer, K. Henning, K. Luther, J. Troe, *Phys. Chem. Chem. Phys.* **2001**, *3*, 2230.
[27] C. M. Cheatum, M. M. Heckscher, D. Bingemann, F. F. Crim, *J. Chem. Phys.* **2001**, *115*, 7086.
[28] J. C. Deàk, L. K. Iwaki, D. D. Dlott, *J. Phys. Chem. A* **1998**, *102*, 8193.
[29] J. C. Deàk, L. K. Iwaki, D. D. Dlott, *Chem. Phys. Lett.* **1998**, *293*, 405.
[30] J. C. Deàk, L. K. Iwaki, D. D. Dlott, *J. Phys. Chem. A* **1999**, *103*, 971.
[31] H. Graener, A. Lauberau, *Appl. Phys. B* **1982**, *29*, 213.
[32] H. Graener, *Chem. Phys. Lett.* **1990**, *165*, 110.
[33] H. Graener, R. Zürl, Hofmann, *J. Phys. Chem. B* **1997**, *101*, 1745.
[34] I. Hartl, W. Zinth, *J. Phys. Chem. A* **2000**, *104*, 4218.
[35] A. Lauberau, W. Kaiser, *Rev. Mod. Phys.* **1978**, *50*, 607.
[36] A. Lauberau, G. Kehl, W. Kaiser, *Opt. Commun.* **1974**, *11*, 74.
[37] D. Schwarzer, J. Troe, M. Zerezke, *J. Chem. Phys.* **1997**, *107*, 8380.
[38] S. A. Kovalenko, R. Schanz, H. Henning, N. P. Ernsting, *J. Chem. Phys.* **2001**, *115*, 3256.
[39] A. Hertwig, H. Hippler, H. Schmid, A.-N. Unterreiner, *Phys. Chem. Chem. Phys.* **1999**, *1*, 5129.
[40] D. A. V. Kliner, J. C. Alfano, P. F. Barbara, *J. Chem. Phys.* **1993**, *98*, 5375.
[41] K. Wynne, C. Galli, R. M. Hochstrasser, *J. Chem. Phys.* **1994**, *100*, 4797.
[42] B. J. Schwarz, L. A. Peteanu, C. B. Harris, *J. Phys. Chem.* **1992**, *96*, 3591.
[43] T. Elsässer in *Femtochemistry* (Eds.: J. Manz, L. Wöste), VCH, New York, **1995**, p. 563.
[44] J. Weiß, V. May, N. P. Ernsting, V. Farztdinov, A. Mühlpfordt, *Chem. Phys. Lett.* **2001**, *346*, 503.
[45] R. M. Stratt, M. Maroncelli, *J. Phys. Chem.* **1996**, *100*, 12981.
[46] J. C. Owrutsky, D. Raftery, R. M. Hochstrasser, *Annu. Rev. Phys. Chem.* **1994**, *45*, 519.
[47] U. Sukowski, A. Seilmeier, T. Elsässer, S. F. Fischer, *J. Chem. Phys.* **1990**, *93*, 4094.
[48] S. L. Shultz, J. Quian, J. M. Jean, *J. Phys. Chem. A* **1997**, *101*, 1000.
[49] N. H. Gottfried, A. Seilmeier, W. Kaiser, *Chem. Phys. Lett.* **1984**, *111*, 326.

 © 2003 Wiley-VCH Verlag GmbH & Co. KGaA, Weinheim

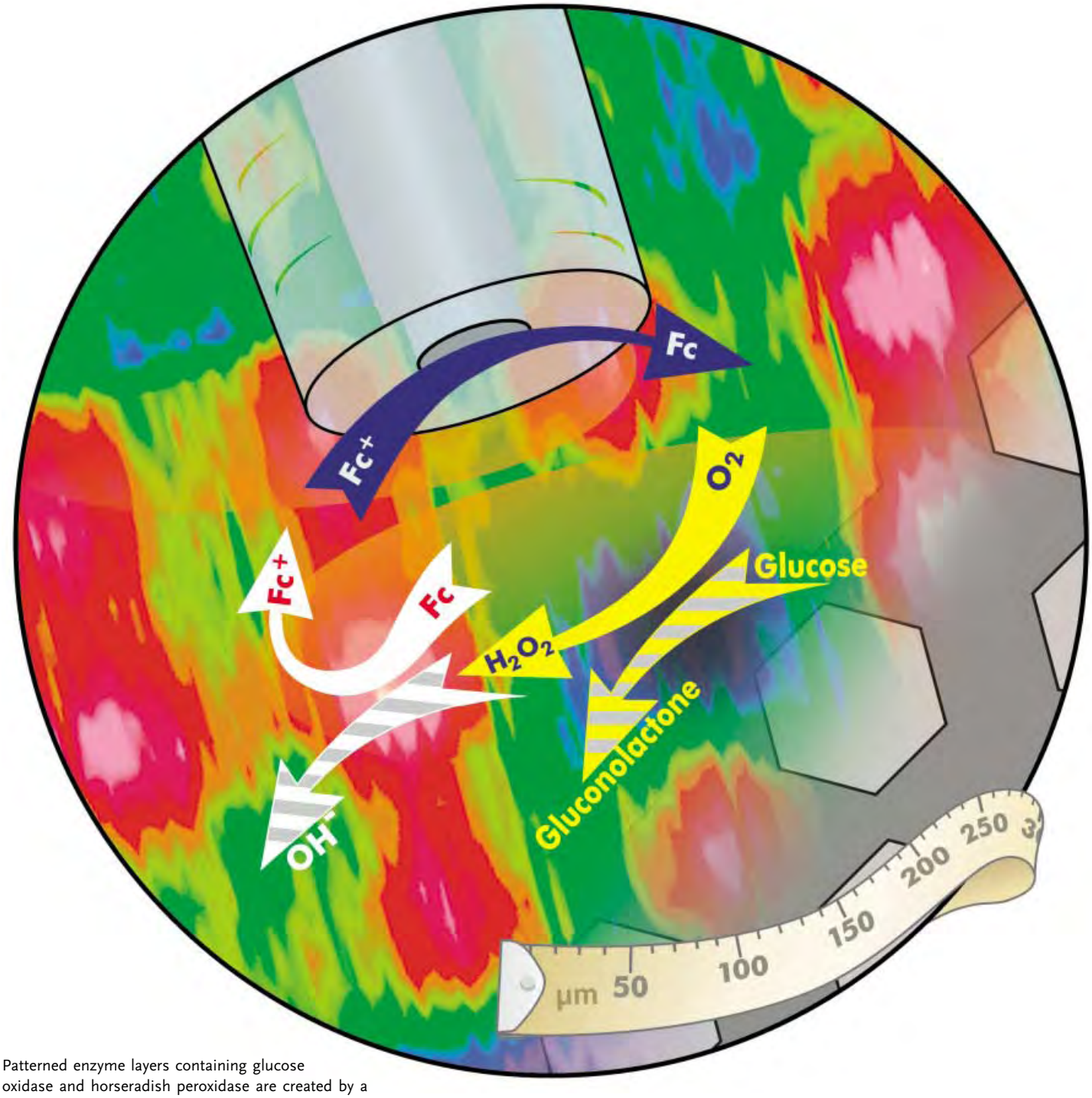
[50] J. Benzler, S. Linkerdoerfer, K. Luther, *J. Chem. Phys.* **1997**, *106*, 4992.
[51] R. J. Sension, S. T. Repinec, A. Z. Szarka, R. M. Hochstrasser, *J. Chem. Phys.* **1993**, *98*, 6291.
[52] T. Nakabayashi, H. Okamoto, M. Tasumi, *J. Phys. Chem. A* **1998**, *102*, 9686.
[53] L. Nikova, D. Schwarzer, J. Troe, *Chem. Phys. Lett.* **1995**, *233*, 303.
[54] D. L. Phillips, J. M. Rodier, A. B. Myers, *Chem. Phys.* **1993**, *175*, 1.
[55] K. E. Schultz, D. J. Russell, C. B. Harris, *J. Chem. Phys.* **1992**, *97*, 5431.
[56] F. Emmerling, M. Lettenberg, A. Lauberau, *J. Phys. Chem.* **1996**, *100*, 19251.
[57] A. Seilmeier, P. O. J. Scherer, W. Kaiser, *Chem. Phys. Lett.* **1984**, *105*, 140.
[58] F. Laerner, T. Elsässer, W. Kaiser, *Chem. Phys. Lett.* **1989**, *156*, 381.
[59] G. Angel, R. Gagel, A. Lauberau, *Chem. Phys. Lett.* **1989**, *156*, 169.
[60] H. J. Hubner, M. Worner, W. Kaiser, A. Seilmeier, *Chem. Phys. Lett.* **1991**, *182*, 315.
[61] J. Assmann, A. Charvat, C. Kappel, D. Schwarzer, K. Luther, B. Abel, *J. Phys. Chem. A* **2002**, *106*, 5197.
[62] H. J. Bakker, P. C. M. Planken, L. Kuipers, A. Langendijk, *J. Chem. Phys.* **1991**, *94*, 1730.
[63] H. J. Bakker, *J. Chem. Phys.* **1993**, *98*, 8496.
[64] H. Graener, G. Seifert, *J. Chem. Phys.* **1993**, *98*, 36.
[65] L. K. Iwaki, J. C. Deak, S. T. Rhea, D. D. Dlott, *Chem. Phys. Lett.* **1999**, *303*, 176.
[66] R. Laenen, K. Simeonidis, *Chem. Phys. Lett.* **1999**, *299*, 589.
[67] R. Laenen, C. Rauscher, *Chem. Phys. Lett.* **1997**, *274*, 63.
[68] G. Seifert, R. Zürl, H. Graener, *J. Phys. Chem. A* **1999**, *103*, 10749.
[69] A. Tokmakoff, M. D. Fayer, *J. Chem. Phys.* **1995**, *103*, 2810.
[70] P. Hamm, M. Lim, R. M. Hochstrasser, *J. Chem. Phys.* **1997**, *107*, 10523.
[71] G. Seifert, T. Patzlaff, H. Graener, *J. Chin. Chem. Soc.* **2000**, 667.
[72] G. Seifert, R. Zurl, T. Patzlaff, H. Graener, *J. Chem. Phys.* **2000**, *112*, 6349.
[73] M. A. F. H. van den Broek, H. J. Bakker, *Chem. Phys.* **2000**, *253*, 157.
[74] L. K. Iwaki, D. D. Dlott, *Chem. Phys. Lett.* **2000**, *321*, 419.
[75] L. K. Iwaki, D. D. Dlott, *J. Phys. Chem. A* **2000**, *104*, 9101.
[76] X. Y. Hong, S. Chen, D. D. Dlott, *J. Phys. Chem.* **1995**, *99*, 9102.
[77] S. Chen, X. Y. Hong, J. R. Hill, D. D. Dlott, *J. Phys. Chem.* **1995**, *99*, 4525.
[78] S. Woutersen, U. Emmerichs, H. J. Bakker, *Science* **1997**, *278*, 658.
[79] H.-K. Nienhuis, S. Woutersen, R. A. Santen, H. J. Bakker, *J. Chem. Phys.* **1999**, *111*, 1494.
[80] J. Assmann, A. Charvat, R. von Benten, B. Abel, in *Ultrafast Phenomena XIII, Proceedings of the 13th International Conference* (Eds.: R. D. Miller, M. M. Murnane, N. F. Scherer, A. M. Weiner), Springer, Heidelberg, **2003**, p. 490.
[81] J. Assmann, R. v. Benten, A. Charvat, B. Abel, *J. Phys. Chem. A* **2003**, *107*, 1904.
[82] K. Sekiguchi, A. Shimojima, O. Kajimoto, *Chem. Phys. Lett.* **2002**, *356*, 84.
[83] W. M. Kwok, D. L. Phillips, *J. Chem. Phys.* **1996**, *104*, 2529.
[84] W. M. Kwok, D. L. Phillips, *Chem. Phys. Lett.* **1995**, *235*, 260.
[85] F. Markel, A. B. Myers, *Chem. Phys. Lett.* **1990**, *167*, 175.
[86] D. L. Phillips, B. A. Lawrence, J. J. Valentini, *J. Phys. Chem.* **1991**, *95*, 7570.
[87] D. L. Phillips, A. B. Myers, *J. Chem. Phys.* **1991**, *95*, 226.
[88] M. L. N. Sastri, H. Sponer, *J. Chem. Phys.* **1952**, *20*, 1428.
[89] W. T. Cave, H. W. Thompson, *Discuss. Faraday Soc.* **1950**, *9*, 35.
[90] A. M. Bass, *J. Chem. Phys.* **1950**, *18*, 1403.
[91] J. Aßmann, PhD Thesis, Universität Göttingen, **2002**.
[92] Gaussian 98 (Revision A.7), M. J. Frisch, G. W. Trucks, H. B. Schlegel, G. E. Scuseria, M. A. Robb, J. R. Cheeseman, V. G. Zakrzewski, J. A. Montgomery, R. E. Stratmann, J. C. Burant, S. Dapprich, J. M. Millam, A. D. Daniels, K. N. Kudin, M. C. Strain, O. Farkas, J. Tomasi, V. Barone, M. Cossi, R. Cammi, B. Mennucci, C. Pomelli, C. Adamo, S. Clifford, J. Ochterski, G. A. Petersson, P. Y. Ayala, Q. Cui, K. Morokuma, D. K. Malick, A. D. Rabuck, K. Raghavachari, J. B. Foresman, J. Cioslowski, J. V. Ortiz, B. B. Stefanov, G. Liu, A. Liashenko, P. Piskorz, I. Komaromi, R. Gomperts, R. L. Martin, D. J. Fox, T. Keith, M. A. Al-Laham, C. Y. Peng, A. Nanayakkara, C. Gonzalez, M. Challacombe, P. M. W. Gill, B. G. Johnson, W. Chen, M. W. Wong, J. L. Andres, M. Head-Gordon, E. S. Replogle, J. A. Pople, Gaussian, Inc., Pittsburgh, PA, **1998**.
[93] P. R. Stannard, W. M. Gelbart, *J. Phys. Chem.* **1981**, *85*, 3592.
[94] E. L. Sibert III, W. P. Reinhardt, J. T. Hynes, *J. Chem. Phys.* **1984**, *81*, 1115.
[95] J. E. Gambogi, K. K. Lehmann, B. H. Pate, G. Scoles, X. Yang, *J. Chem. Phys.* **1992**, *97*, 1748.
[96] G. Kaeb, C. Schroeder, D. Schwarzer, *Phys. Chem. Chem. Phys.* **2002**, *4*, 271.
[97] C. S. Parmenter, B. M. Stone, *J. Chem. Phys.* **1986**, *84*, 4710.
[98] V. A. Walters, S. D. Colson, D. L. Snavely, K. B. Wiberg, B. M. Janison, *J. Phys. Chem.* **1985**, *89*, 3857.
[99] J. M. Jasinski, *Chem. Phys. Lett.* **1984**, *109*, 462.
[100] D. B. Moss, C. S. Parmenter, G. E. Ewing, *J. Chem. Phys.* **1987**, *86*, 51.
[101] C. C. Martens, W. P. Reinhardt, *J. Chem. Phys.* **1990**, *93*, 5621.
[102] R. E. Larsen, R. M. Stratt, *J. Chem. Phys.* **1999**, *110*, 1036.
[103] J. E. Gambogi, R. P. L'Esperance, K. K. Lehmann, B. H. Pate, G. Scoles, *J. Chem. Phys.* **1993**, *98*, 1116.
[104] K. K. Lehmann, G. Scoles, B. H. Pate, *Annu. Rev. Phys. Chem.* **1994**, *45*, 241.
[105] D. J. Nesbitt, R. F. Field, *J. Phys. Chem.* **1996**, *100*, 12735.
[106] D. W. Oxtoby, *Adv. Chem. Phys.* **1981**, *47*, 487.
[107] D. W. Oxtoby, *Annu. Rev. Phys. Chem.* **1981**, *32*, 77.
[108] S. Velsko, D. W. Oxtoby, *J. Chem. Phys.* **1980**, *72*, 2260.
[109] A. Nitzan, J. Jortner, *Mol. Phys.* **1973**, 713.
[110] B. M. Ladanyi, R. M. Stratt, *J. Phys. Chem. A* **1998**, *102*, 1068.
[111] S. A. Egorov, J. L. Skinner, *J. Chem. Phys.* **1996**, *105*, 7047.
[112] S. A. Egorov, J. L. Skinner, *J. Chem. Phys.* **2000**, *112*, 275.
[113] B. Abel, A. Charvat, S. F. Deppe, H. H. Hamann, *Ber. Bunsen-Ges.* **1997**, *101*, 329.
[114] S. A. Schofield, P. G. Wolynes, *J. Chem. Phys.* **1992**, *97*, 1123.
[115] D. M. Leitner, P. G. Wolynes, *J. Chem. Phys.* **1996**, *105*, 11226.
[116] D. E. Logan, P. G. Wolynes, *J. Chem. Phys.* **1990**, *93*, 4994.
[117] M. Gruebele, R. Bigwood, *Int. Rev. Phys. Chem.* **1998**, *17*, 91.
[118] R. Bigwood, M. Gruebele, *Chem. Phys. Lett.* **1995**, *233*, 383.
[119] R. Bigwood, M. Gruebele, *Chem. Phys. Lett.* **1995**, *235*, 604.
[120] V. Wong, M. Gruebele, *J. Phys. Chem. A* **1999**, *103*, 10083.
[121] D. Rostkier-Edelstein, P. Grad, A. Nitzan, *J. Chem. Phys.* **1997**, *107*, 10470.
[122] V. S. Vikhrenko, C. Heidelbach, D. Schwarzer, V. B. Nemtsov, J. Schroeder, *J. Chem. Phys.* **1999**, *110*, 5273.
[123] C. Heidelbach, I. I. Fedchenia, D. Schwarzer, J. Schroeder, *J. Chem. Phys.* **1998**, *108*, 10152.
[124] C. Heidelbach, V. S. Vikhrenko, D. Schwarzer, I. I. Fedchenia, J. Schroeder, *J. Chem. Phys.* **1999**, *111*, 8022.
[125] K. Fujimori, *Organic Peroxides* (Ed.: W. Ando), Wiley, New York, **1992**, p. 319.
[126] Y. Sawaki in *Organic Peroxides* (Ed.: W. Ando), Wiley, New York, **1992**, p. 425.
[127] C. A. Barson, J. C. Bevington, *J. Polym. Sci. A* **1997**, *35*, 2955.
[128] M. Buback, J. Sandmann, *Z. Phys. Chem.* **2000**, *214*, 583.

 © 2003 Wiley-VCH Verlag GmbH & Co. KGaA, Weinheim

[129] J. Chateauneuf, J. Lusztyk, K. U. Ingold, *J. Am. Chem. Soc.* **1988**, *110*, 2877.
[130] J. Hashimoto, K. Segawa, H. Sakuragi, *Chem. Phys. Lett.* **1999**, *314*, 261.
[131] J. Wang, T. Tateno, H. Sakuragi, K. Tokumaru, *J. Photochem. Photobiol. A* **1995**, *92*, 53.
[132] A. Kitamaru, H. Sakuragi, M. Yoshida, K. Tokumaru, *Bull. Chem. Soc. Jpn.* **1980**, *53*, 1393.
[133] D. E. Falvey, G. B. Schuster, *J. Am. Chem. Soc.* **1986**, *108*, 7419.
[134] E. A. Morlino, M. D. Bohorquez, D. C. Neckers, A. A. J. Rodgers, *J. Am. Chem. Soc.* **1991**, *113*, 3599.
[135] T. M. Bockman, S. M. Hubig, J. K. Kochi, *J. Org. Chem.* **1997**, *62*, 2210.
[136] B. Abel, J. Aßmann, M. Buback, M. Kling, S. Schmatz, J. Schroeder, *Angew. Chem.* **2003**, *115*, 312; *Angew. Chem. Int. Ed.* **2003**, *42*, 300.
[137] B. Abel, J. Assmann, P. Botschwina, M. Buback, M. F. Kling, R. Oswald, S. Schmatz, J. Schroeder, T. Witte, unpublished results.
[138] J. Aschenbrücker, M. Buback, N. P. Ernsting, J. Jasny, J. Schroeder, U. Steegmüller, *Appl. Phys. B* **1997**, *65*, 441.
[139] T. Tateno, H. Sakuragi, K. Tokumaru, *Chem. Lett.* **1992**, *20*, 1883.
[140] H. Misawa, K. Sawabe, S. Takahara, H. Sakuragi, K. Tokumaru, *Chem. Lett.* **1988**, *23*, 357.
[141] S. Oishi, H. Tsubaki, H. Matsuzawa, *Chem. Lett.* **1999**, *365*, 805.
[142] J. G. Radziszewski, M. Gil, A. Gorski, J. Spanget-Larsen, J. Waluk, J. Mroz, *J. Chem. Phys.* **2001**, *115*, 9733; J. G. Radziszewski, M. Gil, A. Gorski, J. Spanget-Larsen, J. Waluk, J. Mroz, *J. Chem. Phys.* **2002**, *116*, 5912.
[143] J. C. Scaiano, G. G. Wubbels, *J. Am. Chem. Soc.* **1981**, *103*, 640.
[144] C. Maul, K.-H. Gericke, *Int. Rev. Phys. Chem.* **1997**, *16*, 1.
[145] J. Pacansky, D. W. Brown, *J. Phys. Chem.* **1983**, *87*, 1553.
[146] T. Baer, W. L. Hase, *Unimolecular Reaction Dynamics: Theory and Experiments*, Oxford University Press, New York, **1996**.
[147] M. Kieninger, O. N. Ventura, S. Suhai, *Int. J. Quantum Chem.* **1998**, *70*, 253.
[148] R. G. Gilbert, S. C. Smith, *Theory of Unimolecular and Recombination Reactions*, Blackwell, Oxford, **1990**.
[149] S. P. Wrigley, B. S. Rabinovitch, *Chem. Phys. Lett.* **1983**, *82*, 386.
[150] P. Rogers, D. C. Montague, J. P. Frank, S. C. Tyler, F. S. Rowland, *Chem. Phys. Lett.* **1982**, *89*, 9.
[151] E. R. T. Kerstel, K. K. Lehmann, T. F. Mentel, B. H. Pate, G. Scoles, *J. Phys. Chem.* **1991**, *95*, 8282.
[152] J. C. Williamson, J. Che, H. Ihee, H. Frey, A. H. Zewail, *Nature* **1997**, *386*, 159.
[153] V. A. Lobastov, R. Srinivasan, B. M. Goodson, C.-Y. Ruan, J. S. Feenstra, A. H. Zewail, *J. Phys. Chem. A* **2001**, *105*, 11159.
[154] C. Rischel, A. Rousse, I. Uschmann, P.-A. Alboury, J.-P. Geindre, P. Audebert, J.-C. Gauthier, E. Förster, J.-L. Martin, A. Antonetti, *Nature* **1997**, *390*, 490.
[155] P. Hamm, M. Lim, R. M. Hochstrasser, *J. Phys. Chem. B* **1998**, *102*, 6123.
[156] D. Zimdars, A. Tokmakov, S. Chen, S. R. Greenfield, M. D. Fayer, T. L. Smith, H. A. Schwettman, *Phys. Rev. Lett.* **1993**, *70*, 2718.
[157] F. Raksi, K. R. Wilson, Z. Jiang, A. Ikhlef, C. Y. Cote, J.-C. Kieffer, *J. Chem. Phys.* **1996**, *104*, 6066.
[158] M. Kling, S. Schmatz, unpublished results.

 © 2003 Wiley-VCH Verlag GmbH & Co. KGaA, Weinheim

Communications



Patterned enzyme layers containing glucose oxidase and horseradish peroxidase are created by a combination of microcontact printing and local electrochemical modification. The conversion at such structures depends on the position within the pattern and can be measured by scanning electrochemical microscopy. For more information see the following communication by T. Wilhelm and G. Wittstock.

DOI: 10.1002/anie.200250578
© 2003 Wiley-VCH Verlag GmbH & Co. KGaA, Weinheim

Complex Functional Thin Films

Analysis of Interaction in Patterned Multienzyme Layers by Using Scanning Electrochemical Microscopy**

*Thomas Wilhelm and Gunther Wittstock**

Microstructured biochemically active layers constitute a key component in a number of new and prospective applications. These include biochemical sensors, sensor arrays, and chip-based testing systems. While such systems are already commercially marketed in case of DNA chips, realization of similar highly integrated systems based on proteins is more difficult because proteins tend to be less stable and can denature upon contact with solid surfaces (in particular with metals). However, because of the large variety of protein functions, a broader range of applications is expected than with DNA chips. When immobilizing enzymes into microstructures, such as in arrays of enzyme sensors or enzyme labels in affinity sensors, new problems are encountered. The continuous conversion of a substance is maintained by the catalytic activity of the enzyme and gives rise to diffusion layers of enzyme substrates and products in the adjacent liquid phase. Overlapping diffusion layers may result if the distances between microstructures are short. For possible applications this situation may lead to undesired cross-talk in arrays of enzyme microsensors if different sensors rely on the detection of the same product (e.g. H_2O_2 for different oxidases).[1] While such effects are of central importance for microstructured transducer arrays, some effects may be advantageous and can be exploited for macroscopic sensors or reactive interfaces. Macroscopic, yet microcompartmentalized interfaces may contain regions optimized to support enzymes and other, uncovered regions, for fast electron transfer. This arrangement could be used to optimize a sensor's response time.[2] Also conceivable are functionalized regions for the attachment of different enzymes, which require different local environments, but that interact with each other by cofactor recycling or through catalytic amplification cycles[3] involving the products of an enzymatic reaction, to give a signal enhancement.

To date such effects could be discussed only as concepts because experimental realization was limited to a few examples. The characterization of these effects was mainly based on integral measurements, that is, signals from a macroscopic interface having a microstructured pattern. The development of scanning electrochemical microscopy (SECM) has established a method that enables the mapping of reactivities at solid–liquid interfaces.[4] In addition to imaging electrochemical reactivities, it is particularly suited for the local investigation of activities of immobilized enzymes.[5] Herein the application of the technique for the investigation of *different* enzymes within a *complex* pattern and their interactions is demonstrated.

Extended enzymes layers with defined geometries and periodicities in the micrometer range are accessible by a variety of methods.[6] The immobilization of different proteins in microscopic arrangements is challenging because several modification steps need to be performed without compromising the activity of the proteins. For this purpose a large variety of sequential procedures have been proposed, some of which make use of scanning probe techniques.[7]

In this study, because of their high reproducibility, lithographic strategies were used for the rapid generation of periodic microstructures. This technique was combined with the flexibility of a sequential procedure to fabricate variable prototypes. Our model systems were generated by a combination of microcontact printing (MCP) and local electrochemical desorption followed by chemisorption of functionalized thiols or disulfides. The enzymes horseradish peroxidase (HRP) and glucose oxidase (GOx) were selected because their reactions can be coupled to each other by common products and substrates, and the reactions of each individual enzyme can be easily imaged by SECM. First a polycrystalline gold surface was modified by MCP with ω-mercapto hexadecanoic acid[8] to yield periodic arrangements of hexagonal regions of a self-assembled monolayer (SAM) (Figure 1a). Following the chemisorption of cystaminium dihyrochloride at the regions not modified by MCP, HRP was bound to the aminofunctionalized surface.[9] Afterwards the ultramicroelectrode (UME) of the SEC microscope was positioned relative to the pattern by horizontal line scans in the SECM feedback mode (Figure 1b). The monolayers from ω-mercapto hexadecanoic acid are so densely packed that the redox mediator hydroxymethyl ferrocene (Fc) or its oxidized form (Fc^+) cannot undergo an electron transfer with the gold surface. Therefore, the diffusion of Fc towards the UME is hindered and the diffusion-controlled currents decreased compared to that in the bulk phase of the solution (Figure 1c). In contrast the HRP layers are permeable to low-molecular-weight compounds and Fc^+ can reach the gold surface. Recycling of the mediator at the gold surface causes an enhanced current at the UME (Figure 1c, $y = 65$, 215, 365 μm).

After positioning the UME above the center of a HRP-modified region, a defined small region of the gold surface was regenerated by local electrochemical desorption of the HRP.[7b] The sample was then wetted with a solution containing GOx into which terminal thiol groups had been introduced.[8] The pattern resulting after binding of the modified enzyme is shown in Figure 2a. In a solution containing dissolved O_2, glucose, and Fc the reactions at the patterned multienzyme layer were studied in the generation-collection (GC) mode. Under consumption of glucose and O_2 the GOx

[*] Prof. Dr. G. Wittstock, Dr. T. Wilhelm
Fachbereich Chemie und
Institut für Chemie und Biologie des Meeres
Carl von Ossietzky Universität Oldenburg
26111 Oldenburg (Germany)
Fax: (+49) 441-798-3486
E-mail: gunther.wittstock@uni-oldenburg.de

[**] This work was supported by the Deutsche Forschungsgemeinschaft (DFG) under grant Wi1617/1-3. T.W. was a scholar and associated fellow of the DFG graduate course 152 "Physical Chemistry of Surfaces and Interfaces" at the University of Leipzig. The frontispiece on the preceding page was designed by Oleg Sklyar.

 © 2003 Wiley-VCH Verlag GmbH & Co. KGaA, Weinheim DOI: 10.1002/anie.200250578

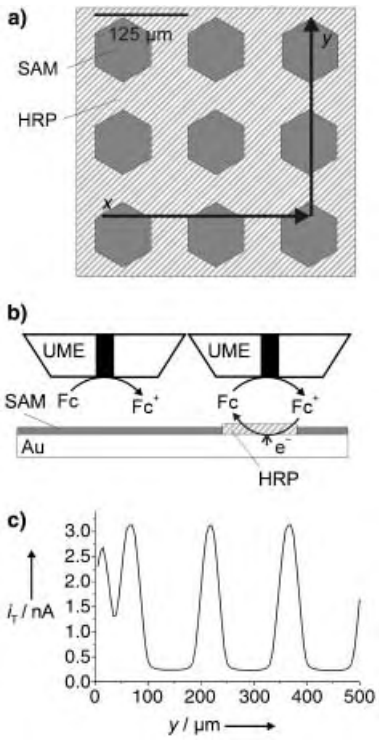


Figure 1. a) Schematic representation of the stamped surface, b) schematic representation of the SECM feedback experiment for lateral positioning of the UME prior to the local electrochemical desorption, c) SECM line scan along the line indicated in Figure 1 a.

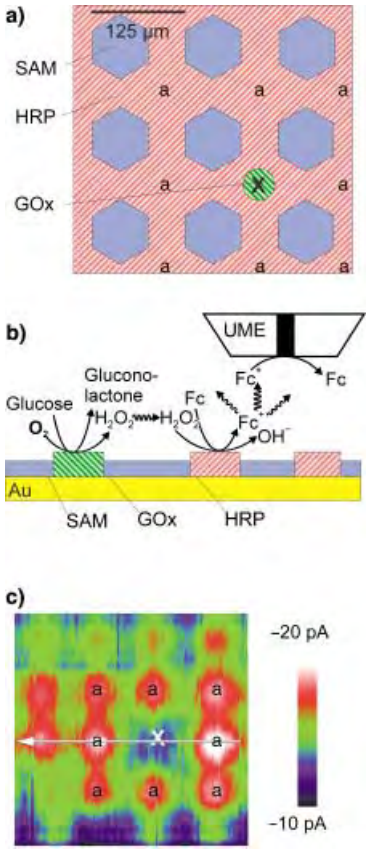


Figure 2. a) Scheme of the patterned surface after electrochemical desorption and attachment of GOx, b) schematic representation of the SECM GC experiment, c) experimental results in the presence of O_2, glucose, and Fc; image frame $500 \times 500\ \mu m^2$.

forms gluconolactone and H_2O_2. H_2O_2 is a substrate for HRP, and is reduced to water with Fc acting as the electron donor. The corresponding ferrocinium derivative Fc^+ is formed from Fc. Fc^+ can be reduced at the UME at a potential $E_T = 0$ mV (Figure 2 b). At this potential no other solution constituent is converted. High currents for Fc^+ reduction therefore correlate to high local reaction rates at the HRP. The two-dimensional SECM GC measurement shows the dependence of the conversion at the HRP layer on the distance from the region with immobilized GOx, the center of which is at the position marked by "x" in Figure 2 c. The eight HRP regions in the immediate vicinity ("a") are distinguished by high currents (therefore, high rates). No significant reaction at the HRP was detected perpendicular to the scan direction of the UME (arrow in Figure 2 c). The HRP-modified layers effectively suppress the diffusive transport of H_2O_2. Parallel to the line shown, a reaction outside regions labeled with "a" was observed, probably because the scanning UME carries H_2O_2-containing solution in this direction.

Even more detailed information about the interface is accessible using the GC mode of the SECM. After exchanging the solution, the activities of the two immobilized enzymes can be mapped independently. The local formation of H_2O_2 can be detected at the UME by oxidation at $E_T = 750$ mV in a solution containing glucose and O_2, but no Fc (Figure 3 a). A scan along the line in Figure 2 c shows the formation of H_2O_2 at $x = 220$ μm and hence the location of the immobilized GOx (Figure 3 b). If, on the other hand, H_2O_2 and Fc, but no glucose, is present in solution, a reaction occurs at the HRP-

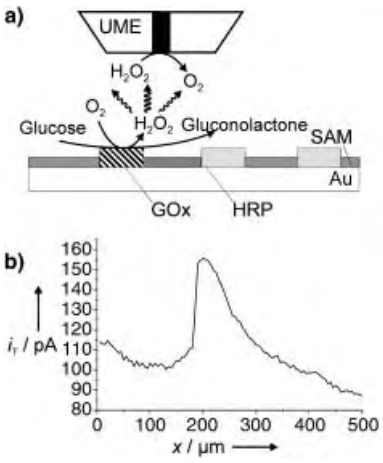


Figure 3. a) Schematic representation of the SECM GC experiment for recording the GOx activity, b) SECM line scan along the line indicated in Figure 2 c while detecting the formation of H_2O_2 in a solution initially containing glucose and O_2.

modified regions independent of this regions position relative to the GOx region. The conversion was monitored by reduction of the formed Fc^+ at $E_T = 0$ mV (Figure 4 a). A corresponding scan along the line in Figure 2 c displays the periodic sequence of the HRP-modified regions by corre-

 © 2003 Wiley-VCH Verlag GmbH & Co. KGaA, Weinheim

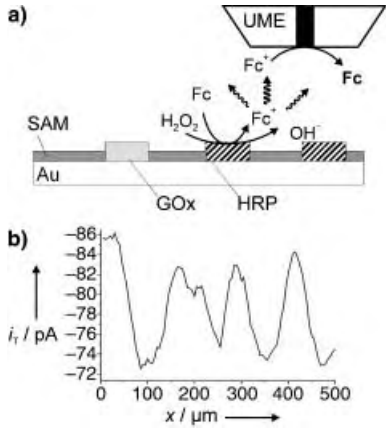


Figure 4. a) Schematic representation of the SECM GC experiment for recording the HRP activity, b) SECM line scan along the y line indicated in Figure 2c while detecting the formation of Fc^+ in a solution initially containing H_2O_2 and Fc.

sponding maxima of the reduction currents at $x = 20$ µm, 170 µm, 300 µm, and 420 µm. The magnitude of the signal was comparable between regions, which shows that the HRP was catalytically active on the entire surface. The confinement of the reactions in Figure 2c to regions in the vicinity of the GOx-modified region is, therefore, because of the suppression of the diffusion of H_2O_2.

The approach described for structuring surface layers can be applied to other systems as well and, in connection with SECM, introduces a new experimental method for the investigation of interactions within enzymatically active microstructures. Different reactivities can be mapped individually or as a combined effect.

Experimental Section

The SECM used has been described elsewhere and was applied in the three-electrode setup.[8] All potentials are referred to the saturated calomel electrode (SCE). The Pt UME had a diameter of 25 µm. The PDMS stamp printed hexagons with an edge length of 43 µm and a periodicity of 125 µm in the *x* direction and 150 µm in the *y* direction. HS-$C_{15}H_{30}$COOH from a 1 mM solution was printed using this stamp, as described elsewhere.[8] After several rinsing steps cystaminium dihydrochloride was chemisorbed and HRP was bound to the aminated surface regions.

The UME of the SECM was positioned 10 µm above the sample using O_2 reduction and calculated current–distance curves[10] for hindered diffusion. A 2 mM solution of Fc in 0.1M KCl and 0.1M phosphate buffer (PB; pH 7), and a potential $E_T = 400$ mV was applied for lateral positioning of the UME above individual elements of the stamped pattern. a square-wave voltage (2 V peak-to-peak, 5 kHz, 38 s) was directly applied between the UME and the macroscopic gold support for electrochemical desorption.[7b] For attachment of GOx, the electrolyte solution was exchanged for 30 min against a solution of SATA-GOx-conjugate (1.5 mg mL^{-1}; SATA = *S*-acetylthioglycolic acid *N*-hydroxy succinimidyl ester) in 0.1M PB. After rinsing with 0.2% polyoxyethylene sorbitan monolaureate (Tween 20) in PB and rinsing five times with PB the cell was filled with a solution of 2 mM Fc, 50 mM Glucose, and 0.1M KCl in PB. The UME was brought to 40 µm above the sample and an image at $E_T = 0$ mV (reduction of Fc^+) in the GC mode was recorded. Afterwards the cell content was exchanged five times by emptying and refilling. The localized formation of H_2O_2 by GOx was mapped in the GC mode at $E_T = 750$ mV (oxidation of H_2O_2) in 50 mM glucose, and 0.1M KCl in PB, while the local reduction of H_2O_2 by HRP was recorded in the GC mode at $E_T = 0$ mV (reduction of Fc^+) in 2 mM Fc, 0.5 mM H_2O_2, and 0.1M KCl in PB.

Received: November 19, 2002 [Z50578]

Keywords: enzymes · pattern formation · scanning electrochemical microscopy · self-assembly · thin films

[1] G. A. Urban, G. Jobst in *Frontiers in Biosensorics, Vol. II* (Eds.: F. W. Scheller, F. Schubert, J. Fedrowitz), Birkhäuser, Basel, **1997**, pp. 161 – 171.
[2] W. B. Nowall, N. Dontha, W. Kuhr, *Biosens. Bioelectron.* **1998**, *13*, 1237 – 1244.
[3] C. G. Bauer, A. V. Eremenko, E. Ehrentreich-Förster, F. F. Bier, A. Markower, H. B. Halsall, W. R. Heineman, F. W. Scheller, *Anal. Chem.* **1996**, *68*, 2453 – 2458.
[4] *Scanning Electrochemical Microscopy* (Eds.: A. J. Bard, M. V. Mirkin), Marcel Dekker, New York, **2001**.
[5] a) G. Wittstock, *Fresenius J. Anal. Chem.* **2001**, 370, 303 – 315; b) H. Shiku, T. Matsue in *Sensor Updates, Vol. 6* (Eds.: H. Baltes, W. Göpel, J. Hesse, M. Esashi, H. Fujita, N. Miura, T. Moriizumi), Wiley-VCH, Weinheim, **2000**, pp. 231 – 240.
[6] a) S. Sukeerthi, A. Q. Contractor, *Anal. Chem.* **1999**, *71*, 2231 – 2236; b) C. Kurzawa, A. Hengstenberg, W. Schuhmann, *Anal. Chem.* **2002**, *74*, 355 – 361; c) D. J. Pritchard, H. Morgan, J. M. Cooper, *Angew. Chem.* **1995**, *107*, 84 – 86; *Angew. Chem. Int. Ed. Engl.* **1995**, *34*, 91 – 93; d) N. Dontha, W. B. Nowall, W. Kuhr, *Anal. Chem.* **1997**, *69*, 2619 – 2625; e) D. T. Chiu, N. L. Jeon, S. Huang, R. S. Kane, C. J. Wargo, I. S. Choi, D. E. Ingber, G. M. Whitesides, *Proc. Natl. Acad. Sci. USA* **2000**, *97*, 2408 – 2413; f) M. N. Yousaf, B. T. Houseman, M. Mrksich, *Proc. Natl. Acad. Sci. USA* **2001**, *98*, 5992 – 5996; g) R. D. Egeland, F. Marken, E. M. Southern, *Anal. Chem.* **2002**, *74*, 1590 – 1596; h) E. Delamarche, A. Bernard, H. Schmid, A. Bitsch, B. Michel, H. Biebuyck, *J. Am. Chem. Soc.* **1998**, *120*, 500 – 508.
[7] a) G. Wittstock, W. Schuhmann, *Anal. Chem.* **1997**, *69*, 5059 – 5066; b) T. Wilhelm, G. Wittstock, *Electrochim. Acta* **2001**, *47*, 275 – 281; c) I. Turyan, T. Matsue, D. Mandler, *Anal. Chem.* **2000**, *72*, 3431 – 3435; d) S. Xu, G.-Y. Liu, *Langmuir* **1997**, *13*, 127 – 129; e) J. K. Schroer, R. M. Crooks, *Langmuir* **1997**, *13*, 2323 – 2332; f) J. R. Kenseth, J. A. Harnisch, V. W. Jones, M. D. Porter, *Langmuir* **2001**, *17*, 4105 – 4112; g) R. D. Piner, J. Zhu, F. Xu, S. Hong, C. A. Mirkin, *Science* **1999**, *283*, 661 – 663; h) S. Gaspar, M. Mosbach, L. Wallmann, T. Laurell, E. Csoeregi, W. Schuhmann, *Anal. Chem.* **2001**, *73*, 4254 – 4261; i) C. A. Wijayawardhana, G. Wittstock, H. B. Halsall, W. R. Heineman, *Anal. Chem.* **2000**, *72*, 333 – 338.
[8] T. Wilhelm, G. Wittstock, *Langmuir* **2002**, *18*, 9485 – 9493.
[9] A surface-grafted and cross-linked gel is formed with an thickness of 60 nm.[8]
[10] J. L. Amphlett, G. Denuault, *J. Phys. Chem. B* **1998**, *102*, 9946 – 9951.

 © 2003 Wiley-VCH Verlag GmbH & Co. KGaA, Weinheim

Gold Nanowires

Towards "Mechanochemistry": Mechanically Induced Isomerizations of Thiolate–Gold Clusters**

*Daniel Krüger, Roger Rousseau, Harald Fuchs, and Dominik Marx**

The investigation of the electrical, mechanical, and chemical properties of atomic gold wires and the nanopoint contacts connecting two metallic surfaces with a view to developing molecular electronic devices based on nanoscale metallic wires is an increasingly popular field of research.[1–6] An intriguing possibility is to use mechanical energy as a tool to construct such nanoscale architectures. For example, suspended monoatomic gold nanowires[7–9] have been detected by using mechanically controllable break junctions or atomic force microscopy. Recent theoretical work has focused on the modulation of mechanical and electrical conduction properties of such nanowires bridging two gold surfaces by the inclusion of defects, such as sulfur atoms and thiolate molecules.[10,11] However, the role of these defects in the formation and growth, as well as their implications for the isomerization chemistry, of these wires remains an open issue. We recently reported ab initio molecular-dynamics simulations that, surprisingly, also lead to such a nanowire.[12] In this simulation a single chemisorbed thiolate molecule was pulled from a gold surface, a situation akin to corresponding experiments.[13] Thus, these simulations suggest that a single thiolate molecule may be used as a moleculer "hook" which allows the controllable extraction of monoatomic gold nanowires from bulk metallic surfaces. However, for this effect to be of practical importance it must be transferable to other nanoscale materials, such as gold nanoparticles deposited or grown on semiconducting substrates.[2,14] Relevant to this discussion is the observation[12] that the pulling process resulted first in the temporary formation of a "localized gold cluster" which was initially pulled from the surface along with the thiolate. This situation suggests that the underlying mechanism for drawing monoatomic gold wires may be the reorganization of the metal–metal bonds within the gold-cluster "intermediates" and would suggest that the process is transferable to interfaces other then those involving flat surfaces. In principle, this could open up possibilities for "mechanochemical wiring" of hybrid molecular–metallic nanostructures at will.

Is it easy to estimate if the above-mentioned processes might be possible on small clusters instead of surfaces? The bonding of thiolates to gold clusters offers a wide variety of structures including some in which there are fewer, but stronger, Au–S bonds than found with bulk surfaces.[15,16] In addition to the coordination-number issue there are also energetic considerations which are more difficult to judge. Typical thiolate–gold-cluster binding energies (from gradient corrected density functional calculations) are in the range 2.5–3 eV,[15] which is between the Au–Au bond energy in Au_2 (about 2.3 eV) and the cohesive energy of the face-centered-cubic (f.c.c.) solid (approximately 3.8 eV). Furthermore, the chemisorption energy on bulk terminated surfaces is of the order of 1.5–1.8 eV[16] depending on the method used and the binding site. Still, it is possible to draw nanowires from surfaces because the decrease in coordination number occurs in conjunction with dynamic restructuring.[12] Thus, simple estimates do not lead to a faithful assessment, so we performed electronic-structure calculations based upon Kohn–Sham density functional theory.[17]

To mimic a typical mechanical pulling experiment involving a molecule attached to a supported cluster we have used Au_3–SCH_3 and Au_5–SCH_3. Such small species represent limiting cases of molecular bonding in which the few Au–S and Au–Au bonds present are strong. Thus, these low-coordination cases are very different from the situation encountered at extended surfaces. The following constrained geometry relaxation model was applied (Figure 1, see refs. [18,19] for related approaches): one gold atom was constrained to move in a plane P1 whereas the methyl carbon

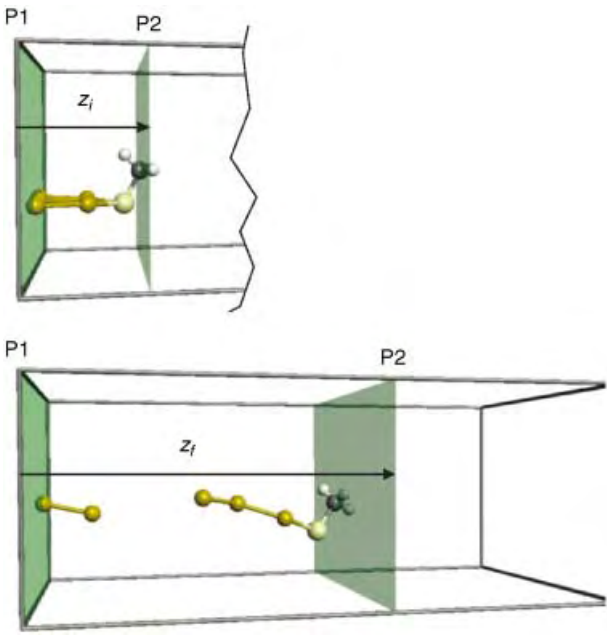


Figure 1. Initial (top) and final (bottom) configurations of the rupture calculations of Au_5–SCH_3. The planes P2 and P1 constrain the carbon atom and the most distant gold atom, respectively, and z_i is the initial and z_f the final distance between these planes.

[*] Prof. Dr. D. Marx, Dr. R. Rousseau
Lehrstuhl für Theoretische Chemie
Ruhr Universität Bochum
44780 Bochum (Germany)
Fax: (+49) 234-321-4045
E-mail: office@theochem.ruhr-uni-bochum.de
Dr. D. Krüger, Prof. Dr. H. Fuchs
Physikalisches Institut
Westfälische Wilhelms-Universität Münster
Wilhelm-Klemm-Strasse 10, 48149 Münster (Germany)

[**] We gratefully acknowledge computer time provided by SSC Karlsruhe, Bayer AG, and RUB, as well as partial financial support by FCI.

 DOI: 10.1002/anie.200351000 © 2003 Wiley-VCH Verlag GmbH & Co. KGaA, Weinheim

atom was confined to another parallel plane P2. Starting from the fully optimized structure of the cluster–thiolate adduct, $z_i = 0$ Å, the distance between the planes z was increased stepwise in increments of $\Delta z = 0.05$ Å. At each step z_n the entire system was reoptimized ensuring that the two atoms were confined to their respective planes. The extension force, which would correspond to the experimentally measured pulling force, is obtained from the slope of the total energy versus the extension (z_n): $F = -dE/dz \approx -\Delta E_n/\Delta z_n$. Finally, the calculation for the smaller adduct was checked using both spin-polarized and unpolarized calculations, which gave identical results.

Both cluster sizes yielded qualitatively similar findings: transformation of the compact gold cluster to an open monoatomic wire followed by rupture of a gold–gold bond within the wire. Hence, we can focus our discussion on the larger, and more complex, Au_5–SCH_3 system (Figure 2). The

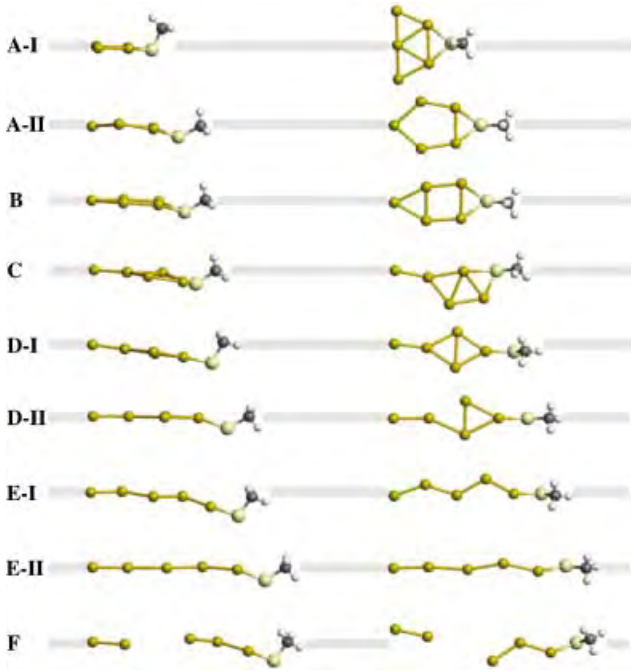


Figure 2. Side view (left) and top view (right) of the configuration of the Au_5–SCH_3 system at the elongations as marked in Figure 3. The bold gray lines are parallel to the constraint force.

calculation is initiated with the lowest-energy isomer,[15] in which the Au atoms assume a planar closest packing structure (**A-I**) and the thiolate is bound symmetrically to two gold atoms. Upon pulling, this twofold coordination of the sulfur atom remains intact initially, whereas the five gold atoms of the cluster itself gradually adopt a circular structure (**A-II**). As shown by a clear change in the slope of $F(z)$ at $z \approx 1.1$ Å (Figure 3), there is a smooth transformation from a closest-packed triangular structure to the open Au_5 ring, **A-II**. This family of structures **A** is stable upon elongation of up to about 3.8 Å where there is a discontinuous rearrangement with the five-membered ring collapsing into a four-membered ring with a capping atom, (structure **B**), which induces a jump in

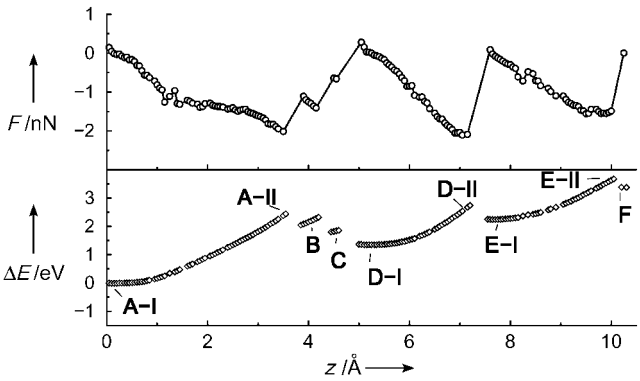


Figure 3. Evolution of the total energy (bottom) of Au_5–SCH_3 relative to the fully relaxed initial configuration **A-I** and the corresponding extension force F (top) as a function of z. Views of the labeled structures are displayed in Figure 2. Estimated computational errors in F are of the order of 0.1 nN; note that the sign convention of the force is different from the one used in ref. [12].

the force-versus-extension curve. Thus, both these gradual and sudden changes in the structure of the cluster can be discerned by distinct features in the force profile (Figure 3). After another isomerization of the cluster at $z \approx 4.3$ Å leads to structure **C**, the coordination number of the sulfur atom reduces from two to one at $z \approx 4.8$ Å (structure **D-I**). The transformation from **D-I** to **D-II** can also be detected in the $F(z)$ profile. Most importantly, the next transition is to a wirelike structure **E**, which is similar to the species reported in our surface simulations.[12] Finally, wire rupture occurs leaving two fragments, a gold dimer (Au_2) and a bent Au_3 molecule which is anchored to the thiolate (Au_3–SCH_3; structure **F**). Importantly, this entire sequence of "isomerizations" can be readily detected in the force profile.

Overall, the force curve of this transformation process (Figure 3) is qualitatively and even quantitatively similar to those that are typically observed in rupture experiments using pure gold–gold nanojunctions.[9] Specifically, our cluster calculations reproduce the general saw-tooth behavior, the vanishing force $F \approx 0$ nN when wire formation begins, a maximum force of around 2 nN before breaking, and a smaller rupture force of about 1.5 nN. Our calculations also underscore an important observation: it is possible to employ external mechanical forces to create high-energy chemical species, as demonstrated by the formation of stable configurations (such as, **D-I** and **E-I**, which are 1.36 eV and 2.25 eV above the ground state **A-I**, respectively) where the total force is zero.

In addition, the energetics and corresponding structures generated in the rupture process give some unique insights into the complex chemistry occurring during the drawing. The rich isomerization chemistry of gold clusters[15] allows the system to adopt substantially different configurations during the elongation process as a result of rearrangements in the chemical bonding pattern. More precisely, the rupture of the smaller adduct, Au_3–SCH_3, results in the final fragments, Au_2 and Au–SCH_3, in their ground state with $\Delta E_{rupture}(Au_3\text{–}SCH_3) \approx E_{min}(Au_2) + E_{min}(Au\text{–}SCH_3) - E_{min}(Au_3\text{–}SCH_3) = 1.67$ eV. Similarly, for Au_5–SCH_3, $\Delta E_{rupture}(Au_5\text{–}SCH_3) =$

 © 2003 Wiley-VCH Verlag GmbH & Co. KGaA, Weinheim

3.38 eV is in excellent agreement with the value of $E_{min}(Au_2) + E_{min}(Au_3{-}SCH_3) + \Delta E^* - E_{min}(Au_5{-}SCH_3) = 3.41$ eV, where, $\Delta E^* = 0.48$ eV is the energy difference between $Au_3{-}SCH_3$ with a bent Au_3 unit and the lower-energy triangular Au_3 isomer.[15] Thus, the overall picture that emerges is that the mechanical pulling force literally induces a series of isomerization reactions to stable intermediates which ultimately lead to energetically favorable fragmentation of the cluster itself.

In conclusion, by examining small thiolate–gold cluster adducts we have demonstrated that under an applied pulling force the cluster unfolds from a compact form to an extended wirelike configuration. Supplemented by earlier findings of an analogous nanowire formation from bulk metal surfaces, this result implies that monoatomic wires may be drawn from a wide variety of gold-based nanoscale architectures including molecular and nanoscale clusters as well as macroscopic leads. Taken together, this opens up possibilities to use gold clusters, firmly attached to an insulating or semiconducting support, to construct nano-electronic assemblies by atom-manipulation techniques. Most interestingly, wire formation in the sense of a sequence of chemical transformations is found to proceed along a well-defined reaction coordinate, which is externally imposed by the applied force. Along this preselected path a series of mechanically induced isomerization reactions occurs, which can be monitored by the behavior of the force–elongation curve. These observations could serve as a general method for future investigations where mechanical rather than thermal, light, or electrical energy is used to induce controlled chemical reactions involving covalent bonds.

Received: January 22, 2003 [Z51000]

Keywords: chemisorption · cluster compounds · gold · molecular electronics · nanostructures

[1] N. I. Kovtyukhova, T. E. Mallouk, *Chem. Eur. J.* **2002**, *8*, 4355.
[2] F. Patolsky, Y. Weizmann, O. Lioubashevski, I. Willner, *Angew. Chem.* **2002**, *114*, 2429; *Angew. Chem. Int. Ed.* **2002**, *41*, 2323.
[3] V. Paraschiv, S. Zapotoczny, M. R. de Jong, G. J. Vancso, J. Huskens, D. N. Reinhoudt, *Adv. Mater.* **2002**, *14*, 722.
[4] T. O. Hutchinson, Y.-P. Liu, C. Kiely, C. J. Kiely, M. Brust, *Adv. Mater.* **2001**, *13*, 1800.
[5] T. Hassenkam, K. Nørgaard, L. Iversen, C. J. Kiely, M. Brust, T. Bjørnholm, *Adv. Mater.* **2002**, *14*, 1126.
[6] S. Hoeppener, R. Maoz, S. R. Cohen, L. F. Chi, H. Fuchs, J. Sagiv, *Adv. Mater.* **2002**, *14*, 1036.
[7] H. Ohnishi, Y. Kondo, K. Takayanagi, *Nature* **1998**, *395*, 780.
[8] A. I. Yanson, G. Rubio-Bollinger, H. E. van den Brom, N. Agraït, J. M. van Ruitenbeek, *Nature* **1998**, *395*, 783.
[9] G. Rubio-Bollinger, S. R. Bahn, N. Agraït, K. W. Jacobsen, S. Vieira, *Phys. Rev. Lett.* **2001**, *87*, 026101.
[10] H. Häkkinen, R. N. Barnett, U. Landman, *J. Phys. Chem. B* **1999**, *103*, 8814.
[11] F. D. Novaes, A. J. R. da Silva, E. Z. da Silva, A. Fazzio, *Phys. Rev. Lett.* **2003**, *90*, 036101.
[12] D. Krüger, H. Fuchs, R. Rousseau, D. Marx, M. Parrinello, *Phys. Rev. Lett.* **2002**, *89*, 186402; for an animation see www.theochem.ruhr-uni-bochum.de/go/afm.html.
[13] M. Grandbois, M. Beyer, M. Rief, H. Clausen-Schaumann, H. E. Gaub, *Science* **1999**, *283*, 1727.
[14] *Metal Clusters at Surfaces* (Ed.: K.-H. Meiwes-Broer), Springer, Berlin, **2000**.
[15] D. Krüger, H. Fuchs, R. Rousseau, D. Marx, M. Parrinello, *J. Chem. Phys.* **2001**, *115*, 4776.
[16] Y. Yourdshahyan, A. M. Rappe, *J. Chem. Phys.* **2002**, *117*, 825.
[17] D. Marx, J. Hutter in *Modern Methods and Algorithms of Quantum Chemistry*, (Ed.: J. Grotendorst), NIC, FZ Jülich, **2000**, pp. 301–449; for downloads see www.theochem.ruhr-uni-bochum.de/go/cprev.html. These plane-wave pseudopotential calculations were carried out using CPMD and the BP86 density functional (using Troullier-Martins pseudopotentials for C and S, an 11-electron scalar-relativistic dual space pseudopotential for Au, and a 40-Rydberg plane-wave energy cutoff). The performance of this particular approach was scrutinized in a preliminary study[15] where computational details can also be found.
[18] A. M. Saitta, P. D. Soper, E. Wasserman, M. L. Klein, *Nature* **1999**, *399*, 46.
[19] D. Aktah, I. Frank, *J. Am. Chem. Soc.* **2002**, *124*, 3402; U. F. Röhrig, I. Frank, *J. Chem. Phys.* **2001**, *115*, 8670.

 © 2003 Wiley-VCH Verlag GmbH & Co. KGaA, Weinheim

Monoazadiene Complexes

Reduction of a 1-Aza-1,3-diene to a 1-Azabut-2-ene-1,4-diyl Dianion: An Unusual Reaction Course**

*Volker Lorenz, Helmar Görls, and Joachim Scholz**

We have been searching for a rather simple method for the synthesis of 1-aza-1,3-diene complexes of early transition metals for quite some time. This search is motivated by some remarkable applications of these compounds: For example, (1-aza-1,3-diene)zirconocene complexes react diastereoselectively with carbonyl compounds to form seven-membered zirconacycles,[1a] from which highly substituted five-membered oxygen heterocycles, which are applied in the synthesis of natural products and active agents, can be separated.[1b] Titanium 1-aza-1,3-diene complexes in turn offer a simple approach to novel metallacyclic alkylidene complexes. For example, in attempts to methylate (1-aza-1,3-diene)titanium complexes even under mild conditions, an α-agostic Ti←H–C interaction on the terminal methine group of the 1-aza-1,3-diene ligand triggers an α-methane elimination that results in

[*] Prof. Dr. J. Scholz, Dr. V. Lorenz
Institut für Chemie der Universität Koblenz-Landau
Universitätsstrasse 1, 56070 Koblenz (Germany)
Fax: (+49) 261-287-2251
E-mail: scholz@uni-koblenz.de
Dr. H. Görls
Institut für Anorganische und Analytische Chemie
der Friedrich-Schiller-Universität Jena (Germany)

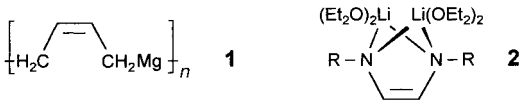
[**] Monoazadiene Complexes of Early Transition Metals: Part 4. This work was supported by the Deutsche Forschungsgemeinschaft. We are grateful to Prof. D. Steinborn, Universität Halle-Wittenberg, for providing laboratory facilities. Part 3: Ref. [2].

 DOI: 10.1002/anie.200250116 © 2003 Wiley-VCH Verlag GmbH & Co. KGaA, Weinheim

the formation of the Ti=C double bond.[2] Furthermore, we found that different (1-aza-1,3-diene)titanium and -zirconium complexes catalyze the polymerization of olefins with high activity.[3]

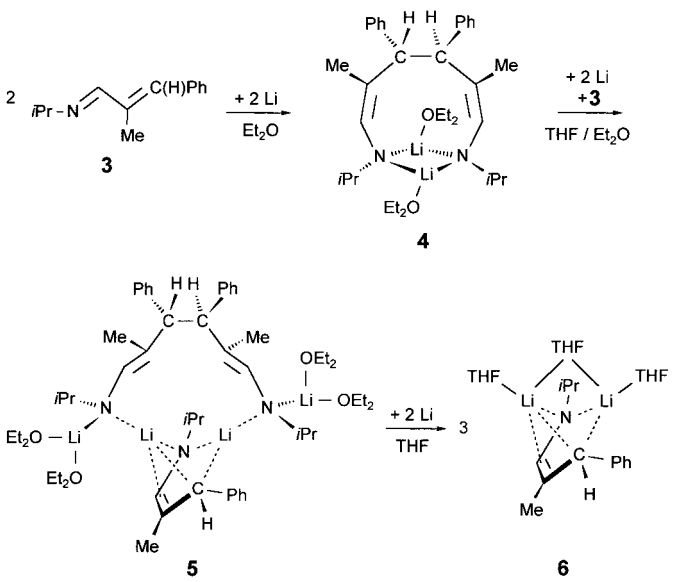
Despite these interesting applications 1-aza-1,3-diene complexes of the early-transition metals, in contrast to the "related" buta-1,3-diene or 1,4-diaza-1,3-diene complexes, are still rare, and corresponding complexes of lanthanides have not yet been described at all.[4]

The reason for this is quite clear: While with the (but-2-ene-1,4-diyl)magnesium complex ("magnesium butadiene") **1**[5] and the (1,4-diazabut-2-ene-1,4-diyl)dilithium complexes **2**[6] (Scheme 1) there are readily available dianion equivalents



Scheme 1. Readily available dianion equivalents **1** and (1,4-diazabut-2-ene-1,4-diyl)dilithium compounds **2** for the synthesis of the buta-1,3-diene and 1,4-diaza-1,3-diene complexes.

for the synthesis of buta-1,3-diene and 1,4-diaza-1,3-diene complexes, corresponding (1-azabut-2-ene-1,4-diyl)magnesium or -dilithium complexes are still unknown. To fill the gap we studied the behavior of 1-aza-1,3-dienes towards alkali metals. Herein we report on the reduction of a 1-aza-1,3-diene with lithium, which initially takes an unexpected reaction course but finally leads to the desired (1-azabut-2-ene-1,4-diyl)dilithium compound (Scheme 2).



Scheme 2. Reaction of the 1-aza-1,3-diene **3** with lithium. Treatment with ultrasound is necessary for the formation of **5**.

For our investigations we chose the 1-aza-1,3-diene **3**, which was synthesized by a condensation reaction of α-methyl cinnamaldehyde with 2-propylamine.[7] Compound **3** is a yellowish oil that congeals at 5 °C. Its solid-state structure shows the typical configuration of the planar N=C–C=C framework (N-C1-C2-C3 175.6(1)°) that was found in other 1-aza-1,3-dienes as well (Figure 1).[8,9]

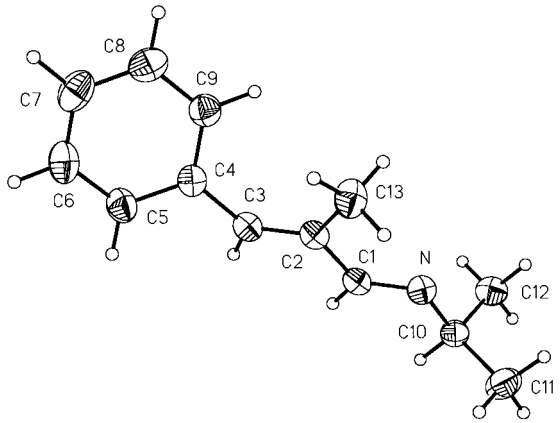


Figure 1. Molecular structure of **3**. Selected bond lengths [Å] and angles [°]: N-C1 1.269(2), N-C10 1.466(2), C1-C2 1.470(2), C2-C3 1.341(2), C3-C4 1.475(2); N-C1-C2 122.5(1), C1-C2-C3 117.6(1), C2-C3-C4 128.0(1); N-C1-C2-C3 175.6(1).

If a solution of **3** in diethyl ether is mixed with an excess of lithium then immediately an exothermic reaction is initiated. After the reaction has subsided and subsequent separation of unreacted lithium, pale yellow crystals precipitate out of the orange solution. Surprisingly, the crystal structure analysis reveals the precipitate to be the *N*,*N*′-dilithium-hexa-1,5-diene-1,6-diamide **4** (Figure 2).[8] Hence, we conclude that under the influence of lithium in the first step of the reaction the 1-aza-1,3-diene **3** is reduced to a radical anion, which stabilizes by dimerization. The formation of the C–C bond occurs between the terminal carbon atoms (C3–C4 1.532(4) Å). As both isolated C=C double bonds of the new hexa-1,5-diene structure C1=C2 (1.357(4) Å) and C5=C6 (1.367(4) Å) are *cis*-configured, the terminal amide groups approach close enough to be bridged by the two lithium atoms. Overall, the result is the boat-shaped ring structure of **4**.[10]

The formation of C–C bonds as a result of an electron transfer step are not unusual and belong to the standard repertoire of organic synthetic chemistry. Thus, there are numerous examples for the reductive coupling of imines, and some are of preparative use for the synthesis of vicinal diamines.[11] Nevertheless, the formation of **4** is unprecedented, because the reductive C–C coupling of the 1-aza-1,3-dienes **3** does not occur as expected via the imine but instead via the terminal β-carbon atoms. Evidently, in agreement with the principle of vinylogy,[12] during the reduction of **3** on the phenyl-substituted terminal carbon atom C3 a sufficiently stable benzyl radical is formed, whose longevity allows a recombination to **4**.

If **3** is reduced with lithium in THF and if additionally the reaction mixture is treated with ultrasound for a few hours, its color changes to dark red and the extremely air- and moisture-sensitive lithium compound **5** is formed. Evidently, the extent of the reduction of **3** strongly depends on the

 © 2003 Wiley-VCH Verlag GmbH & Co. KGaA, Weinheim

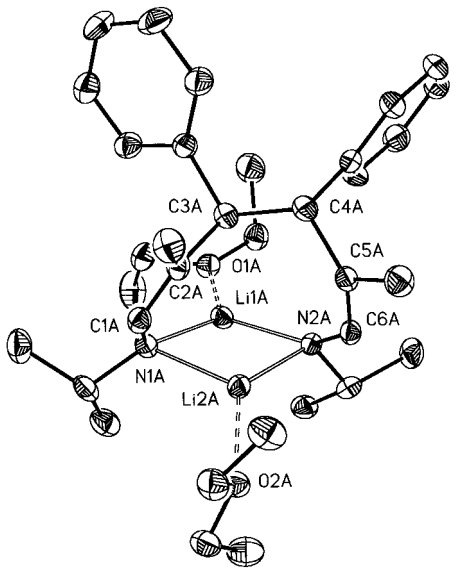


Figure 2. Molecular structure of one of the two crystallographically independent molecules of **4** (molecule A). Hydrogen atoms are omitted for clarity. Selected bond lengths [Å] and angles [°]: Li1A-N1A 1.989(5), Li1A-N2A 1.982(5), Li2A-N1A 2.101(5), Li2A-N2A 2.058(5), Li2A-C1A 2.260(5), Li2A-C6A 2.320(5), Li1A-O1A 1.967(5), Li2A-O2A 2.024(5), N1A-C1A 1.378(4), N2A-C6A 1.376(3), C1A-C2A 1.357(4), C2A-C3A 1.536(4), C3A-C4A 1.532(4), C4A-C5A 1.517(4), C5A-C6A 1.367(4); N1A-C1A-C2A 128.4(2), C1A-C2A-C3A 122.9(2), N2A-C6A-C5A 130.9(2), C4A-C5A-C6A 127.9(2); C2A-C3A-C4A-C5A 53.8(2), N1A-C1A-C2A-C3A 12.8(2), N2A-C6A-C5A-C4A −14.2(2), Li1A-N1A-Li2A-N2A 5.2(2).

reaction conditions. Many NMR signals of **5** are largely consistent with those of the coupling product **4** (Table 1). However, several new signals indicate that there is another 1-aza-1,3-diene unit in this compound, but there is no strong hint upon its structure. A marked high-field shift of the significantly broadened phenyl proton signals ($\delta = 6.45$, 5.28, and 5.08 ppm) indicates that the phenyl substituent of this 1-aza-1,3-diene unit is also involved in the coupling process.

These findings are also confirmed by the results of the X-ray structure analysis of **5** (Figure 3).[8] Suitable single crystals of **5** were obtained by recrystallization from a solution in diethyl ether. The molecular structure of **5** is exceptionally complex and can be described as an aggregate of **4** and a novel (1-azabut-2-ene-1,4-diyl)dilithium compound. Thus, did we really succeed in reducing the 1-aza-1,3-diene **3** into the dianion? The answer lies in the major structure parameters of the (1-azabut-2-ene-1,4-diyl)dilithium unit. The N–C=C–C backbone is *cis*-configured and planar (N3-C27-C28-C29 −9.7(2)°). The comparison of the sequence of N–C and C–C bond lengths ("long–short–long") in the 1-azabut-2-ene-1,4-diyl units with that of **3** ("short–long–short") leaves no doubt that a two-electron reduction has occurred. The two lithium atoms Li3 and Li4 bridge the terminal atoms N3 and C29 of the 1-azabut-2-ene-1,4-diyl unit (Li3–C29 2.574(5), Li3–N3 1.962(5), Li4–C29 2.419(5), Li4–N3 2.057(5) Å). The distance between the lithium atom Li4 and the two inner carbon atoms C27 and C28 is even shorter (Li4–C27 2.213(5), Li4–C28 2.318(5) Å). According to the structure principles of organometallic compounds of alkali metals,[13] the lithium atom Li4 is placed directly above the point of highest charge density of the 1-azabut-2-ene-1,4-diyl dianion. In contrast, the lithium atom Li3 lies in the plane of the 1-azabut-2-ene-1,4-diyl backbone and thus compensates its charge deficit by an additional interaction with the π-electron system of the phenyl group (Li3–C34 2.406(5), Li3–C35 2.478(5) Å). In spite of this special bonding situation of Li3 the structure of the (1-azabut-2-ene-1,4-diyl)dilithium unit is very reminiscent of the molecular structures of related compounds (see reference [14] and **2**, Scheme 1).[6]

Indeed, the route by which the (1-azabut-2-ene-1,4-diyl)dilithium unit in **5** is formed still requires clarification.

Table 1: NMR spectroscopic data of **3**–**6**.[a]

3: ^{1}H NMR ($CDCl_3$): $\delta = 7.99$ (s, 1H; CH=N), 7.42–7.32 (m, 4H; *o*/*m*-Ph), 7.29–7.22 (m, 1H; *p*-Ph), 6.75 (s, 1H; C*H*=CMe), 3.47 (sept, $^3J(H,H) = 6.3$ Hz, 1H; NC*H*Me$_2$), 2.17 (s, 3H, CH=C*Me*), 1.24 ppm (d, $^3J(H,H) = 6.3$ Hz, 6H; NCH*Me*$_2$); ^{13}C NMR ($CDCl_3$): $\delta = 162.97$ (CH=N), 138.20 (*C*H=CMe), 136.99 (*i*-Ph), 136.62 (CH=*C*Me), 129.16 (*o*/*m*-Ph), 128.13 (*o*/*m*-Ph), 127.37 (*p*-Ph), 61.14 (*N*CHMe$_2$), 24.12 (NCH*Me*$_2$), 13.30 ppm (CH=C*Me*).

4: ^{1}H NMR ([D$_8$]THF): $\delta = 7.49$ (br d, 4H; *o*-Ph), 6.92 (br t, 4H; *m*-Ph), 6.79 (br t, 2H; *p*-Ph), 6.10 (s, 2H; C*H*=CMe), 4.07 (br s, 2H; C*H*Ph), 3.35 (q, $^3J(H,H) = 7.0$ Hz, 8H; OC*H*$_2$CH$_3$), 2.99 (sept, $^3J(H,H) = 6.3$ Hz, 2H; NC*H*Me$_2$), 1.54 (s, 6H; CH=C*Me*), 1.12 (d, $^3J(H,H) = 6.3$ Hz, 6H; NCH*Me*$_2$), 1.09 (t, $^3J(H,H) = 7.0$ Hz, 12H; OCH$_2$C*H*$_3$), 1.05 ppm (d, $^3J(H,H) = 6.3$ Hz, 6H; NCH*Me*$_2$); ^{13}C NMR ([D$_8$]THF): $\delta = 148.26$ (*i*-Ph), 147.62 (CH=*C*Me), 128.59 (*o*,*m*-Ph), 127.06 (*o*,*m*-Ph), 124.79 (*p*-Ph), 97.01 (*C*H=CMe), 66.07 (OCH$_2$CH$_2$), 57.71 (NCHMe$_2$), 52.50 (*C*HPh), 27.90 (CH=C*Me*), 27.32 (br, NCH*Me*$_2$), 21.80 (br, NCH*Me*$_2$), 15.54 ppm (OCH$_2$*C*H$_3$).

5: ^{1}H NMR ([D$_8$]THF): $\delta = 7.50$ (br d, 4H; *o*-Ph), 6.93 (br t, 4H; *m*-Ph), 6.80 (br t, 2H; *p*-Ph), 6.45 (br m, 3H; *o*,*m*-Ph), 6.10 (s, 2H; C*H*=CMe), 6.04 (s, 1H; C*H*=CMe), 5.28 (br t, 2H; *p*-Ph), 5.08 (br m, 1H; *o*,*m*-Ph), 3.38 (q, $^3J(H,H) = 7.0$ Hz, 16H; OC*H*$_2$CH$_3$), 3.06 (sept, $^3J(H,H) = 6.3$ Hz, 1H; NC*H*Me$_2$), 3.00 (sept, $^3J(H,H) = 6.3$ Hz, 2H; NC*H*Me$_2$), 2.93 (br s, 1H; C*H*Ph), 1.63 (s, 3H; CH=C*Me*), 1.54 (s, 6H; CH=C*Me*), 1.12 (q, $^3J(H,H) = 7.0$ Hz, 16H; OCH$_2$C*H*$_3$), 1.15 (d, $^3J(H,H) = 6.3$ Hz, 6H; NCH*Me*$_2$), 1.05 (d, $^3J(H,H) = 6.3$ Hz, 6H; NCH*Me*$_2$), 0.99 ppm (d, $^3J(H,H) = 6.3$ Hz, 6H; NCH*Me*$_2$); ^{13}C NMR ([D$_8$]THF): $\delta = 148.39$ (*i*-Ph), 147.84 (*i*-Ph), 141.18 (*C*H=CMe), 130.4 (br, *o*,*m*-Ph), 128.72 (*o*,*m*-Ph), 128.5 (br, *o*,*m*-Ph), 127.13 (*o*,*m*-Ph), 124.84 (*p*-Ph), 118.7 (br, *o*,*m*-Ph), 106.1 (br, *o*,*m*-Ph), 103.32 (*p*-Ph), 97.04 (*C*H=CMe), 60.88 (*N*CHMe$_2$), 57.82 (*N*CHMe$_2$), 55.06 (*C*HPh), 52.62 (*C*HPh), 28.30 (NCH*Me*$_2$), 27.92 (CH=C*Me*), 27.4 (br, NCH*Me*$_2$), 22.85 (CH=C*Me*), 21.8 ppm (br, NCH*Me*$_2$).

6: ^{1}H NMR ([D$_8$]THF): $\delta = 6.60$–5.90 (br m, 3H; *m*,*o*-Ph), 6.06 (s, 1H; C*H*=CMe), 5.29 (br t, 1H; *p*-Ph), 5.05 (br m, 1H, *o*-Ph), 3.62 (m, 12H; THF), 3.05 (sept, $^3J(H,H) = 6.3$ Hz, 1H; NC*H*Me$_2$), 2.95 (s, 1H; C*H*Ph), 1.77 (m, 12H; THF), 1.61 (s, 3H; CH=C*Me*), 1.03 ppm (d, $^3J(H,H) = 6.3$ Hz, 6H; NCH*Me*$_2$); ^{13}C NMR ([D$_8$]THF): $\delta = 147.01$ (s; *i*-Ph), 140.78 (d, $^1J(C,H) = 146.0$ Hz; *C*H=CMe), 131.6 (br d; *o*,*m*-Ph), 128.3 (br d; *o*,*m*-Ph), 118.4 (br d; *o*,*m*-Ph) 105.9 (br d; *o*,*m*-Ph) 102.66 (d, $^1J(C,H) = 157.2$ Hz; *p*-Ph), 97.01 (s; CH=*C*Me), 68.42 (t, $^1J(C,H) = 144.6$ Hz; OCH$_2$CH$_2$, THF), 62.66 (d, $^1J(C,H) = 141.5$ Hz; *N*CHMe$_2$), 55.08 (d, $^1J(C,H) = 127.1$ Hz; *C*HPh), 28.36 (q, $^1J(C,H) = 125.3$ Hz; NCH*Me*$_2$), 26.26 (t, $^1J(C,H) = 131.7$ Hz; OCH$_2$CH$_2$, THF), 23.27 ppm (q, $^1J(C,H) = 124.3$ Hz; CH=C*Me*).

[a] The NMR spectra were recorded at 25 °C in [D$_8$]THF at 300.075 (^{1}H) and 75.462 MHz (^{13}C) with a Varian Gemini 300 BB. Correct elemental analysis was obtained for all compounds.

 © 2003 Wiley-VCH Verlag GmbH & Co. KGaA, Weinheim

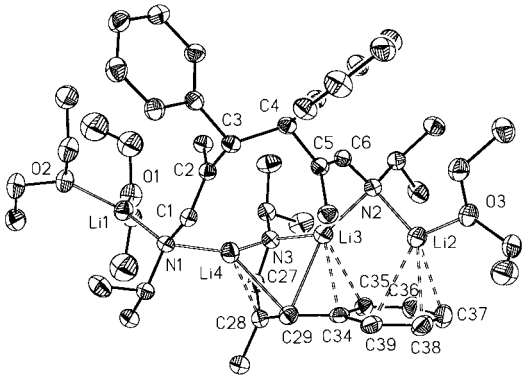


Figure 3. Molecular structure of **5**. Hydrogen atoms are omitted for clarity. Selected bond lengths [Å] and angles [°]: Li1-N1 1.987(4), Li4-N1 2.027(5), Li2-N2 1.983(5), Li3-N2 2.012(5), Li3-N3 1.962(5), Li4-N3 2.057(5), Li1-O1 1.932(5), Li1-O2 1.927(5), Li2-O3 1.957(5), Li2-C37 2.555(6), Li2-C38 2.428(5), Li2-C39 2.711(5), Li3-C29 2.574(5), Li3-C34 2.406(5), Li3-C35 2.478(5), Li4-C27 2.213(5), Li4-C28 2.318(5), Li4-C29 2.419(5), N1-C1 1.382(3), N2-C6 1.379(3), C1-C2 1.347(3), C2-C3 1.521(3), C3-C4 1.553(3),C4-C5 1.519(3), C5-C6 1.352(3), N3-C27 1.381(3),C27-C28 1.363(3), C28-C29 1.481(3), C29-C34 1.405(3); N3-Li3-C29 79.1(2), N3-Li4-C29 81.3(2), N3-C27-C28 124.6(2), C27-C28-C29 121.3(2); N1-C1-C2-C3 176.8(2), C2-C3-C4-C5 −49.1(2), N2-C6-C5-C4 177.5(2), N3-C27-C28-C29 −9.7(2).

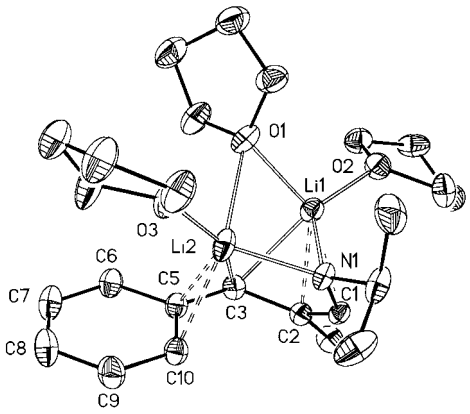


Figure 4. Molecular structure of **6**. Hydrogen atoms are omitted for clarity. Selected bond lengths [Å] and angles [°]: Li1-N1 2.027(4), Li2-N1 1.963(4), Li1-O1 2.009(4), Li1-O2 1.904(4), Li2-O1 2.424(6), Li2-O3 1.945(4), Li1-C1 2.183(4), Li1-C2 2.273(5), Li1-C3 2.386(5), Li2-C3 2.722(5), Li2-C5 2.395(5), Li2-C10 2.363(6), N1-C1 1.375(3), C1-C2 1.355(3), C2-C3 1.470(3), C3-C5 1.408(3); N1-C1-C2 125.0(2), C1-C2-C3 123.2(2), N1-Li1-C3 83.8(2), N1-Li2-C3 76.4(1); N1-C1-C2-C3 −10.4(2).

We assume that **4** reacts further with the excessive lithium, which results in the reductive cleavage of its C3–C4 bond. Initially, the lithium atoms of the new (1-azabut-2-ene-1,4-diyl)dilithium units are coordinated by the amide groups of the remaining **4** because their donor strength certainly exceeds that of the solvent THF. Furthermore, the two C=C double bonds of the hexa-1,5-diene-1,6-diamide unit of **5** are now, in contrast to those of the coupling product **4**, *trans*-configured. Hence, the two amide groups reach a sufficient distance to enable them to function as "molecular brackets" and thereby stabilize the lithium atoms Li3 and Li4 and thus the central dilithium 1-azabut-2-ene-1,4-diyl unit.

Longer reaction times in THF and a large excess of lithium are sufficient to completely convert the intermediate **5** into the (1-azabut-2-ene-1,4-diyl)dilithium compound **6** by reductive cleavage of the C–C bond of the hexa-1,5-diene-1,6-diamide unit. After several hours red cubic crystals of **6** precipitate directly from the reaction mixture.

The result of the crystal structure analysis[8] (Figure 4) shows that the geometry of **6** is nearly unchanged compared with that of the 1-azabut-2-ene-1,4-diyl unit of the intermediate **5**. In place of the amide groups of the hexa-1,5-diene-1,6-diamide brackets of **5** two THF molecules are coordinated to the lithium atoms with a third molecule of THF additionally bridging the two alkali metals.[6,15] Notably, the characteristic interaction between the lithium atom Li2 and the π-electron system of the phenyl group remains the same as in **5** (Li2–C5 2.395(5), Li2–C10 2.363(6) Å). Considering the line-broadening and the striking high-field shift of the ^{1}H and ^{13}C NMR signals of the phenyl group in the NMR spectra of **6** (Table 1) it becomes evident that this contact is not broken even by the donor solvent THF.

The presented findings on the reaction of the 1-aza-1,3-diene **3** with lithium are of interest for two reasons: On the one hand the isolated intermediate products allow an insight into important fundamental steps of this unexpected reaction course and hence contribute to the general understanding of the redox reaction of alkali metals with unsaturated hydrocarbons. On the other hand the successful synthesis of the (1-azabut-2-ene-1,4-diyl)dilithium compound **6** now provides an opportunity to demonstrate the much wider synthetic potential of the 1-aza-1,3-diene complexes and to include even the lanthanides. This is all the more valid as recently we even found that **3** can be converted quickly and directly into the dianion equivalent **6** if lithium powder is used for the reduction reaction.

Experimental Section

All work was carried out under argon and in carefully dried and degassed solvents.

3: According to reference [7] 2-propylamine (40.0 g, 676.7 mmol) were added to a solution of α-methyl cinnamaldehyde (50.0 g, 342.0 mmol) in diethyl ether (100 mL) at room temperature. During the reaction molecular sieves (ca. 40 g with color indicator) were added in portions to adsorb the resulting water. After 12 h the reaction was complete and the solvent and the excess 2-propylamine were evaporated in vacuo. Compound **3** is a pale yellow oil that crystallized at +5 °C and was kept under argon. Yield: 60.0 g (94 %).

4: Small pieces of lithium (1.0 g, 142.8 mmol) was added at room temperature to a solution of **3** (20.0 g, 106.8 mmol) in diethyl ether (100 mL). The reaction mixture was stirred for 24 h. Afterwards, the excess lithium was filtered off and the filtrate was reduced to one-half of its volume. At a temperature of −5 °C, pale yellow crystals of **4** precipitate (23.0 g, 42.7 mmol; 80 %).

5: Application of ultrasound for 3 h to the reaction of **3** (20.0 g, 106.8 mmol) with lithium (2.0 g, 285.6 mmol) in THF (100 mL) at room temperature led to a color change to red. After a reaction time of 48 h the excess lithium was filtered off, the solvent THF was removed under vacuum, and the residue was taken up in diethyl ether. Red crystals of compound **5** (21.0 g, 77 %) separated when the solution was left to stand at −5 °C.

 © 2003 Wiley-VCH Verlag GmbH & Co. KGaA, Weinheim

6: When the reaction mixture was kept in the ultrasound bath for three more hours its color deepened to dark red. After the reaction was complete, the unreacted lithium was filtered off, and the dark red THF solution was cooled down to −20 °C. After a longer period of time red cubic crystals of **6** (30.3 g, 68 %) precipitated. If highly active lithium powder (Firma UD-FC/MO, Merseburg) was used instead of the compact lithium pieces for the reduction of **3**, then within five hours the dark red compound **6** was formed.

Received: September 6, 2002 [Z50116]
Publication delayed at authors's request

Keywords: amides · heterodienes · lithium · reduction

[1] a) J. Scholz, M. Nolte, C. Krüger, *Chem. Ber.* **1993**, *126*, 803 – 809; b) D. Enders, M. Kroll, G. Raabe, J. Runsink, *Angew. Chem.* **1998**, *110*, 1770 – 1773; *Angew. Chem. Int. Ed.* **1998**, *37*, 1673 – 1675.

[2] St. Kahlert, H. Görls, J. Scholz, *Angew. Chem.* **1998**, *110*, 1958 – 1962; *Angew. Chem. Int. Ed.* **1998**, *37*, 1857 – 1861.

[3] S. Becke, H. Windisch, J. Scholz, St. Kahlert (Bayer AG), US Pat. 5 965 678, **1999** [*Chem. Abstr.* **1999**, *130*, P125529p].

[4] a) J. M. Davis, R. J. Whitby, A. Jaxa-Chamiec, *J. Chem. Soc. Chem. Commun.* **1991**, 1743 – 1745; b) J. Scholz, St. Kahlert, H. Görls, *Organometallics* **1998**, *17*, 2876 – 2884; c) K. Mashima, Y. Matsuo, S. Nakahara, K. Tani, *J. Organomet. Chem.* **2000**, *593–594*, 69 – 76; d) Y. Matsuo, K. Mashima, K. Tani, *Organometallics* **2002**, *21*, 138 – 143.

[5] a) K. Fujita, Y. Ohnuma, H. Yasuda, H. Tani, *J. Organomet. Chem.* **1976**, *113*, 201 – 213; b) S. S. Wreford, J. F. Whitney, *Inorg. Chem.* **1981**, *20*, 3918 – 3924; c) Y. Kai, N. Kanehisa, K. Miki, N. Kasai, K. Mashima, H. Yasuda, A. Nakamura, *Chem. Lett.* **1982**, 1277 – 1280.

[6] a) J. Scholz, B. Richter, R. Goddard, C. Krüger, *Chem. Ber.* **1993**, *126*, 57 – 61; b) M. Haaf, A. Schmiedl, T. A. Schmedake, D. R. Powell, A. J. Millevolte, M. Denk, R. West, *J. Am. Chem. Soc.* **1998**, *120*, 12714 – 12719.

[7] O. Doebner, W. Miller, *Ber. Dtsch. Chem. Ges.* **1883**, *16*, 1664 – 1668. See also Experimental Section.

[8] Crystal structure analyses: **3**: $C_{13}H_{17}N$, $M_r = 187.28\ g\,mol^{-1}$, colorless cubes, crystal size $0.10 \times 0.09 \times 0.08\ mm^3$, orthorhombic, space group *Pbca*, $a = 9.4632(3)$, $b = 11.2806(3)$, $c = 21.7174(7)$ Å, $V = 2318.3(1)$ Å^3, $T = -90$ °C, $Z = 8$, $\rho_{calcd} = 1.073\ g\,cm^{-3}$, $\mu(Mo_{K\alpha}) = 0.62\ cm^{-1}$, $F(000) = 816$, 4678 reflections collected, $h(-12/12)$, $k(-14/14)$, $l(-28/28)$, range $2.86° \le \Theta \le 27.49°$, $\Theta_{max} = 99\,\%$, 2641 symmetry-independent reflections, $R_{int} = 0.033$, 1812 observed reflections with $F_o > 4\sigma(F_o)$, 195 refined parameters, 0 restraints, $R1_{obs} = 0.047$, $wR^2_{obs} = 0.101$, $R1_{all} = 0.082$, $wR^2_{all} = 0.117$, GOOF = 1.007, max. residual electron density: 0.133/−0.184 e Å^{-3}. **4**: $C_{34}H_{54}Li_2N_2O_2$, $M_r = 536.68\ g\,mol^{-1}$, colorless cubes, crystal size $0.12 \times 0.12 \times 0.10\ mm^3$, orthorhombic, space group $Pca2_1$, $a = 21.1701(4)$, $b = 9.7292(2)$, $c = 32.8356(7)$ Å, $V = 6763.1(2)$ Å^3, $T = -90$ °C, $Z = 8$, $\rho_{calcd} = 1.054\ g\,cm^{-3}$, $\mu(Mo_{K\alpha}) = 0.63\ cm^{-1}$, $F(000) = 2352$, 13208 reflections collected, $h(-27/27)$, $k(-12/12)$, $l(-42/42)$, range $1.92° \le \Theta \le 27.48°$, $\Theta_{max} = 96.9\,\%$, 13208 symmetry-independent reflections, 8820 observed reflections with $F_o > 4\sigma(F_o)$, 765 refined parameters, 1 restraint, $R1_{obs} = 0.064$, $wR^2_{obs} = 0.168$, $R1_{all} = 0.093$, $wR^2_{all} = 0.1828$, GOOF = 0.974, Flack parameter 0.4(10) (merohedral twin), max. residual electron density: 0.420/−0.247 e Å^{-3}. **5**: $C_{51}H_{81}Li_4N_3O_3 \cdot 0.5\,C_4H_{10}O$, $M_r = 843.97\ g\,mol^{-1}$, red cubes, crystal size $0.12 \times 0.12 \times 0.10\ mm^3$, monoclinic, space group $P2_1/n$, $a = 15.423(3)$, $b = 20.970(4)$, $c = 16.826(3)$ Å, $\beta = 100.15(3)°$, $V = 5356.8(19)$ Å^3, $T = -90$ °C, $Z = 4$, $\rho_{calcd} = 1.046\ g\,cm^{-3}$, $\mu(Mo_{K\alpha}) = 0.63\ cm^{-1}$, $F(000) = 1840$, 17050 reflections collected, $h(-18/18)$, $k(-25/23)$, $l(-20/20)$, range $1.94° \le \Theta \le 25.32°$, $\Theta_{max} = 99.6\,\%$, 9760 symmetry-independent reflections, $R_{int} = 0.041$, 5154 observed reflections with $F_o > 4\sigma(F_o)$, 562 refined parameters, 0 restraints, $R1_{obs} = 0.058$, $wR^2_{obs} = 0.156$, $R1_{all} = 0.116$, $wR^2_{all} = 0.181$, GOOF = 0.963, max. residual electron density: 0.388/−0.288 e Å^{-3}. **6**: $C_{25}H_{41}Li_2NO_3$, $M_r = 417.47\ g\,mol^{-1}$, orange cubes, crystal size $0.10 \times 0.08 \times 0.06\ mm^3$, monoclinic, space group $P2_1/c$, $a = 18.2920(4)$, $b = 9.4405(2)$, $c = 15.2487(3)$ Å, $\beta = 103.976(1)°$, $V = 2555.28(9)$ Å^3, $T = -90$ °C, $Z = 4$, $\rho_{calcd.} = 1.085\ g\,cm^{-3}$, $\mu(Mo_{K\alpha}) = 0.68\ cm^{-1}$, $F(000) = 912$, 15928 reflections collected, $h(-23/23)$, $k(-10/12)$, $l(-9/19)$, range $2.67° \le \Theta \le 27.45°$, $\Theta_{max} = 98.9\,\%$, 5777 symmetry-independent reflections, $R_{int} = 0.027$, 4193 observed reflections with $F_o > 4\sigma(F_o)$, 280 refined parameters, 0 restraints, $R1_{obs} = 0.067$, $wR^2_{obs} = 0.189$, $R1_{all} = 0.092$, $wR^2_{all} = 0.215$, GOOF = 1.001, max. residual electron density: 0.516/−0.286 e Å^{-3}. CCDC-191595 (**3**), CCDC-191596 (**4**), CCDC-191597 (**5**) and CCDC-191598 (**6**) contain the supplementary crystallographic data for this paper. These data can be obtained free of charge via www.ccdc.can.ac.uk/conts/retrieving.html (or from the Cambridge Crystallographic Centre, 12 Union Road, Cambridge CB2 1EZ, UK; Fax: (+44) 1223-336033; or deposit@ccdc.cam.ac.uk).

[9] a) R. F. Childs, G. S. Shaw, C. J. L. Lock, *J. Am. Chem. Soc.* **1989**, *111*, 5424 – 5429; b) J. Wunderle, J. Scholz, E. Hovestreydt, *Z. Kristallogr.* **1993**, *208*, 274 – 276; c) W. Imhof, A. Göbel, D. Braga, P. DeLeonardis, E. Tedesco, *Organometallics* **1999**, *18*, 736 – 747.

[10] Running the reductive C–C coupling of 1-aza-1,3-dienes with sterically demanding N-substituents (i.e. 2,6-(iPr)$_2$C$_6$H$_3$) leads to the formation of two diastereomeric *N,N′*-dilithium-hexa-1,5-diene-1,6-diamides (according to NMR spectroscopy). In contrast to **4** their molecular structures have a linear hexa-1,5-diene skeletal structure. J. Scholz, V. Lorenz, H. Görls, unpublished results.

[11] D. Lucet, T. Le Gall, C. Mioskowski, *Angew. Chem.* **1998**, *110*, 2725 – 2772; *Angew. Chem. Int. Ed.* **1998**, *37*, 2580 – 2627.

[12] K. Schwetlik, *Organikum*, 21st ed., Wiley-VCH, Weinheim, **2001**, p. 592.

[13] W. N. Setzer, P. von Ragué Schleyer, *Adv. Organomet. Chem.* **1985**, *24*, 353 – 451.

[14] a) D. Wilhelm, T. Clark, P. von Ragué Schleyer, H. Dietrich, W. Mahdi, *J. Organomet. Chem.* **1985**, *280*, C6-C10; b) L. D. Field, M. G. Gardiner, B. A. Messerle, C. L. Raston, *Organometallics* **1992**, *11*, 3566 – 3570; c) M. G. Gardiner, C. L. Raston, F. G. N. Cloke, P. B. Hitchcock, *Organometallics* **1995**, *14*, 1339 – 1353.

[15] Important structure principles of **6** are comparable to those of the *N,N′*-dilithium-but-2-ene-1,4-diamide [(4-CH$_3$C$_6$H$_4$)-LiNC(Ph)=C(Ph)NLi(4-CH$_3$C$_6$H$_4$)]·3THF[6a] or those of the *N,N′*-dilithium ethylenediamide [PhLiNCH$_2$CH$_2$N-LiPh]·3HMPA (HMPA = hexamethylphosphoramide), in which three HMPA ligands provide coordinative saturation of the lithium atoms. D. R. Armstrong, D. Barr, A. T. Brooker, W. Clegg, K. Gregory, S. M. Hodgson, R. Snaith, D. S. Wright, *Angew. Chem.* **1990**, *102*, 443 – 445; *Angew. Chem. Int. Ed. Engl.* **1990**, *29*, 410 – 411.

 © 2003 Wiley-VCH Verlag GmbH & Co. KGaA, Weinheim

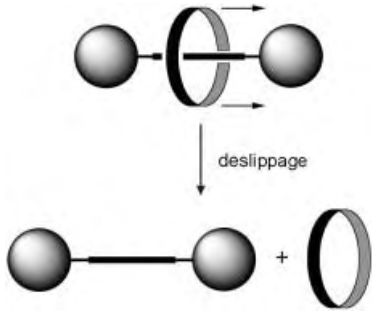
Kinetics of Rotaxane Deslippage

Secondary Isotope Effects on the Deslipping Reaction of Rotaxanes: High-Precision Measurement of Steric Size**

*Thorsten Felder and Christoph A. Schalley**

Small structural changes can cause unexpectedly large effects on the deslipping reaction[1] of rotaxanes[2] (Scheme 1). A particularly striking example[3] is the replacement of the isophthalaldehyde unit in **6a** (Scheme 2) by a 2,6-pyridinedicarboxamide, that is, the simple exchange of a CH group by an isoelectronic N atom to yield **6b**. Without any other changes in the rotaxane structure, the barrier for the passage of the wheel over one of the stopper groups increases from approximately 80 to 135 kJ mol^{-1} as a result of the formation of intramolecular hydrogen bonds. This increase is reflected in a more than 10^4-fold increase in the half-life.

Probably one of the smallest steric changes which can be made in a molecule is the replacement of hydrogen atoms by deuterium atoms.[4] According to electron-diffraction studies and calculations, the time-averaged length of the C–D bond is approximately 0.005 Å shorter than that of the C–H bond.[5] In addition, the C–D bond has a lower vibrational frequency and vibrational amplitude than the C–H bond.[6] This difference is reflected in a smaller van der Waals radius. Further experimental evidence comes from the isomerization reactions of suitably substituted biaryls[7] and [2.2]metacyclophanes,[8] as well as from the reactions of 2,6-dimethylated pyridines with Lewis acids and electrophiles.[9] The smaller steric size of the C–D bond is reflected in a tighter crystal packing of deuterated molecules[10] and in the ^{13}C NMR chemical shifts of groups located in the proximity of deuterated substituents.[11] Herein, we describe the results of deslipping experiments performed with unlabeled rotaxanes **9a** and **10a** and their isotopologues **9b** and **10b** that have deuterated stopper groups (Scheme 2).



Scheme 1. The deslipping reaction of rotaxanes: the mechanical bond is broken and the free components liberated without cleavage of a covalent bond.

The deuterated di-[D_9]*tert*-butylphenol stopper **5b** was synthesized according to established literature procedures[12] as depicted in Scheme 2. Threefold Friedel–Crafts alkylation of benzene **1** is followed by replacement of one of the *tert*-butyl groups in **2b** by an acetyl substituent in a Friedel–Crafts acylation which deactivates the aromatic system and prevents it from further reaction. A Baeyer–Villiger oxidation of intermediate **3b** with *m*-chloroperbenzoic acid (MCPBA) followed by hydrolysis of ester **4b** yields stopper **5b**. The rotaxanes **9a**,**b** and **10a**,**b** can be prepared from the corresponding stoppers **5a**,**b**, one of the axle center pieces **7** or **8**, and wheel **6** by an anion template effect in a yield of 25–30 %.[13] The degree of isotopic labeling could be determined to be greater than 95 % from the ^{1}H NMR spectra as well as from the isotope patterns of the MALDI mass spectra (see Supporting Information).

The deslipping reaction is unimolecular and follows a first-order rate law. It is easily monitored by ^{1}H NMR spectroscopy because of the sizeable chemical shift differences ($\Delta\delta$) between the rotaxane signals and those of the free axle (Figure 1). The largest values for $\Delta\delta$ are found for the

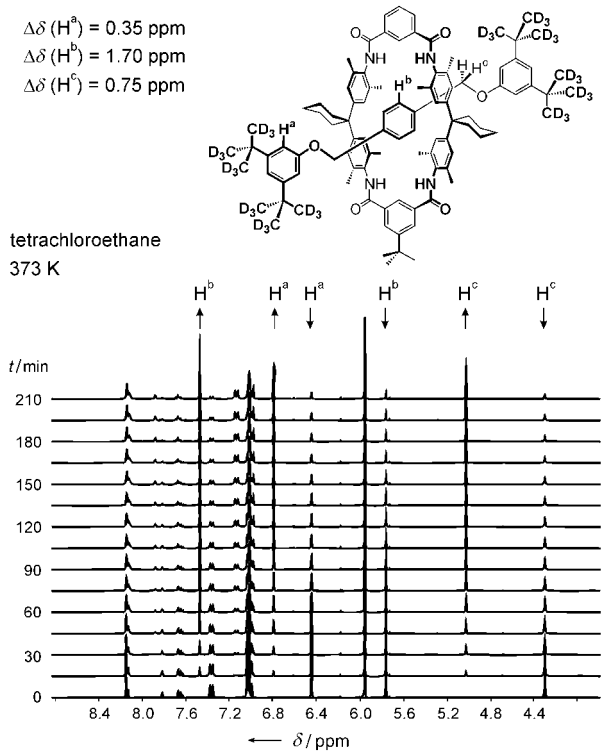


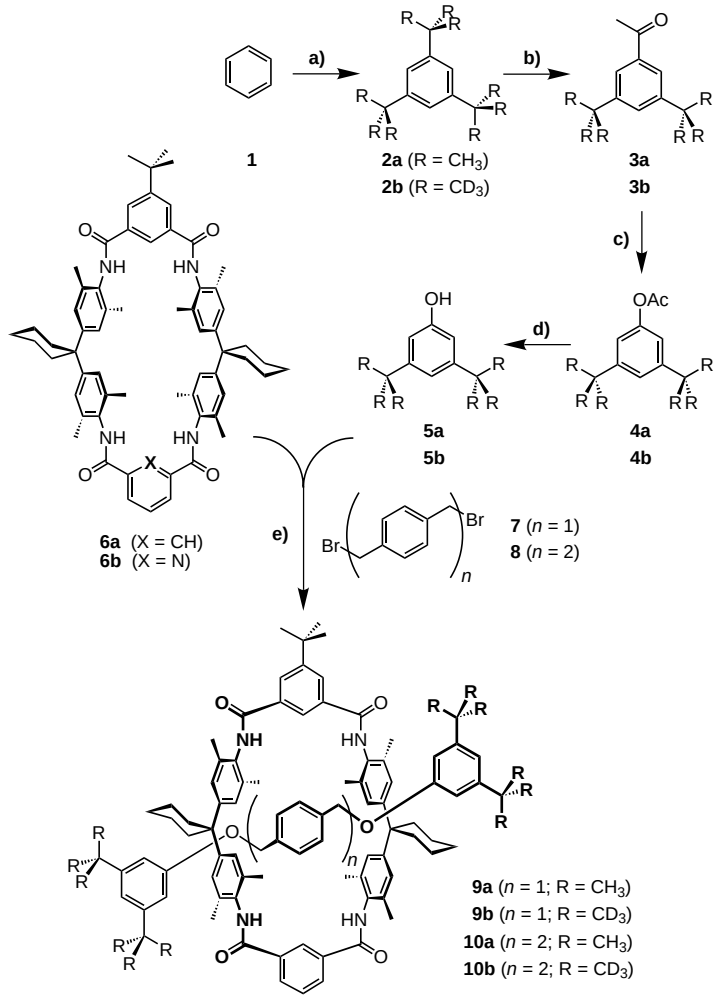
Figure 1. ^{1}H NMR spectra of a 4 mM solution of **9b** in [D_2]tetrachloroethane recorded every 15 min after heating the sample to 373 K. Three different proton signals have been assigned to the rotaxane (decreasing signal intensity; down arrows) and the free axle (increasing signal intensity; up arrows).

[*] Dr. C. A. Schalley, Dipl.-Chem. T. Felder
Kekulé-Institut für Organische Chemie und Biochemie
Universität Bonn
Gerhard-Domagk-Strasse 1, 53121 Bonn (Germany)
Fax: (+49)-228-735-662
E-mail: c.schalley@uni-bonn.de

[**] We thank Prof. Fritz Vögtle and Dipl.-Chem. Sonja Müller for continuous support and inspiring discussions, and Claus Schmidt and Hannelore Spitz for their help with recording a large number of ^{1}H NMR experiments. The Fonds der Chemischen Industrie and the Deutsche Forschungsgemeinschaft are gratefully acknowledged for financial support.

Supporting information for this article is available on the WWW under http://www.angewandte.org or from the author.

 © 2003 Wiley-VCH Verlag GmbH & Co. KGaA, Weinheim DOI: 10.1002/anie.200350903



Scheme 2. Synthesis of deuterated rotaxanes and their unlabeled analogues: a) *t*BuCl or [D_9]*t*BuCl, $AlCl_3$, −40 °C → −10 °C, 3 h, 90%; b) CH_3COCl, $AlCl_3$, 15%; c) MCPBA, 2 h, 85%; d) KOH, H_2O/EtOH (2:1), reflux, 4 h, 67%; e) K_2CO_3, dibenzo[18]crown-6, CH_2Cl_2, 25–30%.

protons of the axle center piece (H^b: $\Delta\delta = 1.7$ ppm), which is most affected by the anisotropy of the aromatic rings incorporated in the wheel. Smaller shifts are observed for protons more remote from the center (H^c: $\Delta\delta = 0.75$ ppm, H^a: $\Delta\delta = 0.35$ ppm). This behavior is typical for rotaxanes of this type.[3] All the rotaxanes were simultaneously subjected to the same conditions so that a direct comparison was possible and systematic errors were reduced to a minimum. Figure 2 shows the results of the deslipping reactions of **9a**,**b** and **10a**,**b** at 373 K in the form of a plot of $\ln(c/c_0)$ versus reaction time *t*. The rotaxanes **10a**,**b** with the longer axles deslip more quickly relative to their shorter counterparts **9a**,**b**—a finding which has been analyzed in detail before.[3] Of particular interest in the present study is the fact that the deuterated rotaxanes **9b** and **10b** liberate the free components at a rate about 10% higher than the nonlabeled analogues **9a** and **10a**. The rate constants and isotope effects obtained from deslipping experiments at different temperatures are summarized in Table 1. Average inverse, secondary kinetic isotope effects (KIE) of 0.91 for **9a**/**9b** and **10a**/**10b** are obtained. These results can be attributed to the smaller steric demand of the deuterated stoppers.

A study of the temperature dependence of the isotope effects should enable the separate enthalpic and entropic contributions to be determined.[14] Equation (1) expresses the KIE in terms of the differences in free-activation enthalpies ($\Delta\Delta G^{\neq}$), activation enthalpies ($\Delta\Delta H^{\neq}$), and activation entropies ($\Delta\Delta S^{\neq}$; see Supporting Information).

$$\ln \mathrm{KIE} = \ln \frac{k_H}{k_D} = -\frac{\Delta\Delta G^{\neq}}{RT} = -\frac{\Delta\Delta H^{\neq}}{RT} + \frac{\Delta\Delta S^{\neq}}{R} \qquad (1)$$

The results in Table 1 suggest that the isotope effects observed for the deslipping reaction do not

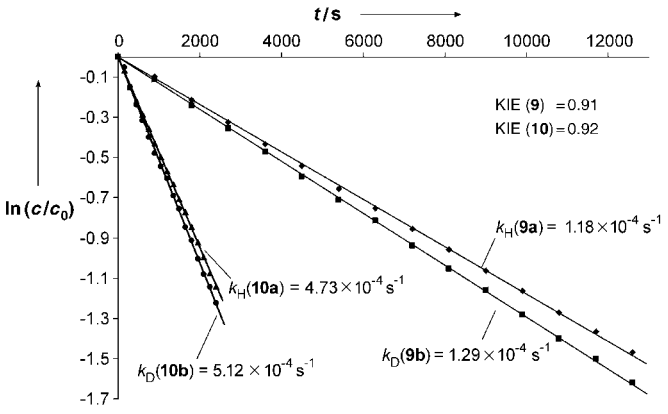


Figure 2. Plot of $\ln(c/c_0)$ versus reaction time *t* for the evaluation of the reaction rate constants *k* (in s^{-1}) of rotaxanes **9a**,**b** and **10a**,**b** at 373 K in [D_2]tetrachloroethane. The rate constants and the kinetic isotope effects are shown ($\mathrm{KIE} = k_H/k_D$). Excellent correlation coefficients were obtained for all linear regressions ($R^2 > 0.997$).

Table 1: Rate constants *k*, kinetic isotope effects KIE, and free activation enthalpies $\Delta G^{\neq}$ for rotaxanes **9a**,**b** and **10a**,**b**.[a]

T [K]	Rotaxane	*k* [s^{-1}]	KIE	$\Delta\Delta G^{\neq}$ [J mol^{-1}]
333	**9a**	$(2.09 \pm 0.03) \times 10^{-6}$	0.92	221
	9b	$(2.26 \pm 0.02) \times 10^{-6}$		
353	**9a**	$(2.06 \pm 0.03) \times 10^{-5}$	0.91	277
	9b	$(2.26 \pm 0.03) \times 10^{-5}$		
373	**9a**	$(1.18 \pm 0.02) \times 10^{-4}$	0.91	292
	9b	$(1.29 \pm 0.02) \times 10^{-4}$		
383	**9a**	$(6.74 \pm 0.06) \times 10^{-4}$	0.91	300
	9b	$(7.44 \pm 0.06) \times 10^{-4}$		
313	**10a**	$(2.44 \pm 0.02) \times 10^{-6}$	0.89	303
	10b	$(2.73 \pm 0.04) \times 10^{-6}$		
333	**10a**	$(1.95 \pm 0.02) \times 10^{-5}$	0.90	292
	10b	$(2.17 \pm 0.02) \times 10^{-5}$		
353	**10a**	$(1.27 \pm 0.03) \times 10^{-4}$	0.93	213
	10b	$(1.36 \pm 0.03) \times 10^{-4}$		
373	**10a**	$(4.73 \pm 0.04) \times 10^{-4}$	0.92	259
	10b	$(5.12 \pm 0.04) \times 10^{-4}$		

[a] See also the Supporting Information.

 © 2003 Wiley-VCH Verlag GmbH & Co. KGaA, Weinheim

change with temperature, within experimental error (although there seems to be a very minor trend to higher KIE values at higher temperatures for rotaxanes **10a**,**b**). Thus, $\Delta\Delta H^{\neq}$ must be close to zero. A more precise evaluation of the $\Delta\Delta H^{\neq}$ and $\Delta\Delta S^{\neq}$ values would require a larger temperature range, which is not possible for technical reasons. Consequently, we refrain from such a deconvolution of our data and for the time being restrict ourselves to the following semiquantitative discussion: If $\Delta\Delta H^{\neq}$ is approximately 0 J mol^{-1}, the isotope effects are mostly entropic in nature with $\Delta\Delta S^{\neq}$ values of about -0.8 J K^{-1} mol^{-1} for **9a**,**b** and about -0.6 J K^{-1} mol^{-1} for **10a**,**b**. These results can be understood in terms of the vibrational freedom in the transition structures of the deslipping reactions. The larger vibrational amplitude of the C–H bonds means that the vibrations of the nonlabeled stoppers suffer from tighter restrictions upon passage through the wheel than those of the deuterated stopper which benefits here from the lower vibrational amplitude of the C–D bonds. Larger vibrational freedom is expressed in a slightly higher and, thus more beneficial, activation entropy for the deslipping reaction of the deuterated rotaxane. This effect is much less pronounced in the local minima of the rotaxanes on the potential energy surface, since the stoppers are located remote from the wheel.

In conclusion, the deslipping reaction of a rotaxane is very sensitive, even to extremely small changes in the molecular architecture and the steric demand of its components—despite their large size, their complex molecular structure, and the high flexibility of the mechanical bond. The present work provides a novel supramolecular and highly precise approach to the classical problem of determining and comparing steric demand. The fact that the two "reaction partners", that is, the axle and the wheel, are already independent molecules and only mechanically interlocked before the reaction excludes all isotope effects arising from hyperconjugative or inductive effects which have been intensely discussed in earlier work[15] and were not always easy to distinguish from steric isotope effects.

Received: January 7, 2003 [Z50903]

Keywords: isotope effects · kinetics · reaction mechanisms · rotaxanes · supramolecular chemistry

[1] a) P. R. Ashton, I. Baxter, M. C. T. Fyfe, F. M. Raymo, N. Spencer, J. F. Stoddart, A. J. P. White, D. J. Williams, *J. Am. Chem. Soc.* **1998**, *120*, 2297–2307; b) F. M. Raymo, K. N. Houk, J. F. Stoddart, *J. Am. Chem. Soc.* **1998**, *120*, 9318–9322; c) for a review, see "Slippage and Constrictive Binding": M. C. T. Fyfe, F. M. Raymo, J. F. Stoddart in *Stimulating Concepts in Chemistry* (Eds.: F. Vögtle, J. F. Stoddart, M. Shibasaki), Wiley-VCH, Weinheim, **2000**.

[2] a) G. Schill, *Catenanes, Rotaxanes and Knots*, Academic Press, New York, **1971**; b) *Molecular Catenanes, Rotaxanes, and Knots* (Eds.: J.-P. Sauvage, C. Dietrich-Buchecker), Wiley-VCH, Weinheim, **1999**.

[3] a) A. Affeld, G. M. Hübner, C. Seel, C. A. Schalley, *Eur. J. Org. Chem.* **2001**, 2877; see also: b) G. Hübner, G. Nachtsheim, Q.-Y. Li, C. Seel, F. Vögtle, *Angew. Chem.* **2000**, *112*, 1315–1318; *Angew. Chem. Int. Ed.* **2000**, *39*, 1269–1272; c) H. W. Gibson, S. Liu, P. Lecavalier, C. Wu, Y. X. Shen, *J. Am. Chem. Soc.* **1995**, *117*, 852–874; d) C. Heim, A. Affeld, M. Nieger, F. Vögtle, *Helv. Chim. Acta* **1999**, *82*, 746–759.

[4] For a review on isotope effects on noncovalent interactions, see D. Wade, *Chem.-Biol. Interact.* **1999**, *117*, 191–217.

[5] a) K. Kuchitsu, L. S. Bartell, *J. Chem. Phys.* **1962**, *36*, 2470–2481; b) P. Pulay, W. Meyer, J. E. Boggs, *J. Chem. Phys.* **1978**, *68*, 5077–5085.

[6] D. J. Lacks, *J. Chem. Phys.* **1995**, *103*, 5085–5090.

[7] a) L. Melander, R. E. Carter, *J. Am. Chem. Soc.* **1964**, *86*, 295–296; b) K. Mislow, R. Graewe, A. J. Gordon, G. H. Wahl, Jr., *J. Am. Chem. Soc.* **1964**, *86*, 1733–1741; c) C. Heitner, K. T. Leffek, *Can. J. Chem.* **1966**, *44*, 2567–2570; d) R. E. Carter, L. Melander, *Adv. Phys. Org. Chem.* **1973**, *10*, 1–27.

[8] S. A. Sherrod, R. L. da Costa, R. A. Barnes, V. Boekelheide, *J. Am. Chem. Soc.* **1974**, *96*, 1565–1577.

[9] a) H. C. Brown, G. J. McDonald, *J. Am. Chem. Soc.* **1966**, *88*, 2514–2519; b) H. C. Brown, M. E. Azzaro, J. G. Koelling, G. J. McDonald, *J. Am. Chem. Soc.* **1966**, *88*, 2520–2525; see also: c) W. Gałęzowski, I. Grześkowiak, A. Jarczewski, *J. Chem. Soc. Perkin Trans. 2* **1998**, 1607–1611.

[10] N. E. Heimer, D. L. Mattern, *J. Am. Chem. Soc.* **1993**, *115*, 2217–2220.

[11] a) F. A. L. Anet, A. H. Dekmezian, *J. Am. Chem. Soc.* **1979**, *101*, 5449–5451; b) J. Abildgaard, S. Bolvig, P. E. Hansen, *J. Am. Chem. Soc.* **1998**, *120*, 9063–9069; b) K. Ibrom, G. Kohn (né Wentzel), K.-U. Boeckmann, R. Kraft, P. Holba-Schultz, L. Ernst, *Org. Lett.* **2000**, *2*, 4111–4113.

[12] A. W. Burgstahler, P.-L. Chien, M. O. Abdel-Rahman, *J. Am. Chem. Soc.* **1964**, *86*, 5281–5290.

[13] a) G. M. Hübner, J. Gläser, C. Seel, F. Vögtle, *Angew. Chem.* **1999**, *111*, 395–398; *Angew. Chem. Int. Ed.* **1999**, *38*, 383–386; b) C. A. Schalley, G. Silva, C. F. Nising, P. Linnartz, *Helv. Chim. Acta* **2002**, *85*, 1578–1596; c) P. Ghosh, O. Mermagen, C. A. Schalley, *Chem. Commun.* **2002**, 2628–2629.

[14] a) L. Melander, R. E. Carter, *Acta Chem. Scand.* **1964**, *18*, 1138–1149; b) R. E. Carter, L. Dahlgren, *Acta Chem. Scand.* **1969**, *23*, 504–514; c) R. E. Carter, L. Dahlgren, *Acta Chem. Scand.* **1970**, *24*, 633–643.

[15] a) V. J. Shiner, Jr., *J. Am. Chem. Soc.* **1956**, *78*, 2653–2654; b) V. J. Shiner, Jr., *J. Am. Chem. Soc.* **1960**, *82*, 2655–2656; c) K. Mislow, R. E. O'Brien, H. Schaefer, *J. Am. Chem. Soc.* **1960**, *82*, 5512–5513; d) G. J. Karabatsos, G. C. Sonnichsen, C. G. Papaioannou, S. E. Scheppele, R. L. Shone, *J. Am. Chem. Soc.* **1967**, *89*, 463–465; e) A. J. Kresge, R. J. Preto, *J. Am. Chem. Soc.* **1967**, *89*, 5510–5511.

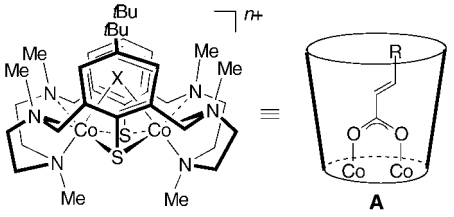
 © 2003 Wiley-VCH Verlag GmbH & Co. KGaA, Weinheim

cis-bromination of alkenes

cis-Bromination of Encapsulated Alkenes**

*Gunther Steinfeld, Vasile Lozan, and Berthold Kersting**

Metalated container molecules are currently attracting much interest, since their properties are often different from those of their constituent components.[1–3] Several groups have already reported that such assemblies show a higher chemical reactivity than their unmodified analogues,[4–6] but so far it is unclear, whether they are also applicable in stereoselective transformations.[7,8] This led us to study the bromination of encapsulated alkene ligands in complexes of the type **A** (Scheme 1); we hoped that the binding pocket would exert an



X = Cl⁻, RCO_2^-, n = 1–3

Scheme 1. Structures of dicobalt complexes $[(L^{Me})Co_2(\mu\text{-}X)]^{n+}$ (X = binding site). The cavity representation of the ligand $(L^{Me})^{2-}$ in **A** should not be confused with the one used for the calixarenes.

effect on the stereochemical course of the reaction. We report here the synthesis and structures of a series of dicobalt complexes of the type $[(L^{Me})Co_2(\mu\text{-}O_2CR)]^{n+}$ bearing α,β-unsaturated carboxylate ligands (Table 1) and demonstrate the remarkable *cis*-bromination of the encapsulated substrates.

The acrylato-bridged dicobalt(III) complex **3** was selected in orienting experiments (Scheme 2). Complex **3** can be readily prepared in high yields by the reaction of the μ-Cl species **1** with sodium acrylate in methanol, followed by a two-electron oxidation of the intermediate $Co^{II}Co^{II}$ species **2**. The kinetically inert complex **3** was subsequently found to undergo the bromination reaction without interference by side reactions. Thus, reaction of **3** with a tenfold excess of Br_2 proceeded smoothly and produced complex **4**, which was identified by IR and NMR spectroscopy, as the sole product.[9]

[*] Priv.-Doz. Dr. B. Kersting, Dipl.-Chem. G. Steinfeld, Dr. V. Lozan
Institut für Anorganische und Analytische Chemie
Universität Freiburg
Albertstrasse 21, 79104 Freiburg (Germany)
Fax: (+49) 761-203-5987
E-mail: berthold.kersting@ac.uni-freiburg.de

[**] This work was supported by the Deutsche Forschungsgemeinschaft (Project No. KE 585/3-1). B. K. thanks Prof. Dr. H. Vahrenkamp for his support of this work.

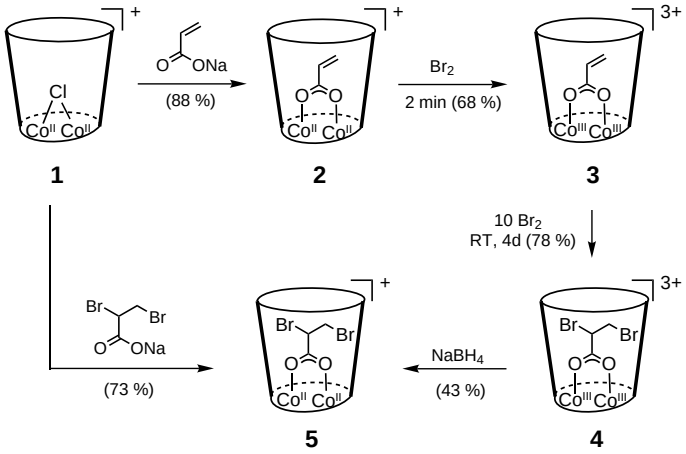
Supporting information for this article is available on the WWW under http://www.angewandte.org or from the author.

Table 1: Synthesized complexes and selected analytical data.[a]

Complex	$\tilde{\nu}(RCO_2^-)$ [cm^{-1}][b]	E^1, E^2 [V][c]
$[(L^{Me})Co_2^{II}(\mu\text{-}Cl)]^+$ **1**		
$[(L^{Me})Co_2^{II}(\mu\text{-}O_2CCH{=}CH_2)]^+$ **2**	1578, 1430 (1639)	0.22, 0.59
$[(L^{Me})Co_2^{III}(\mu\text{-}O_2CCH{=}CH_2)]^{3+}$ **3**	1519, 1428 (1635)	0.22, 0.60
$[(L^{Me})Co_2^{III}(\mu\text{-}O_2CCHBrCH_2Br)]^{3+}$ **4**	1559, 1386	0.31, 0.70
$[(L^{Me})Co_2^{II}(\mu\text{-}O_2CCHBrCH_2Br)]^+$ **5**	1627, 1394	0.30, 0.69
$[(L^{Me})Co_2^{III}(\mu\text{-}O_2CCH{=}CHPh)]^{3+}$ **6**	1505, 1388 (1631)	0.20, 0.60
$[(L^{Me})Co_2^{III}(\mu\text{-}threo\text{-}O_2CCHBrCHBrPh)]^{3+}$ **7**	1560, 1384	0.32, 0.69
$[(L^{Me})Co_2^{II}(\mu\text{-}threo\text{-}O_2CCHBrCHBrPh)]^+$ **8**	1627, 1390	0.32, 0.70
PhCHBr–CHBr–CO_2H (*threo-dl* pair) **9**		
PhCHBr–CHBr–CO_2H (*erythro-dl* pair) **10**		
$[(L^{Me})Co_2^{II}(\mu\text{-}erythro\text{-}O_2CCHBrCHBrPh)]^+$ **11**	1623, 1393	0.30, 0.68
$[(L^{Me})Co_2^{III}(\mu\text{-}erythro\text{-}O_2CCHBrCHBrPh)]^{3+}$ **12**	1550, 1390	0.30, 0.68

[a] The complexes were isolated as ClO_4^- or BPh_4^- salts. [b] The values in parentheses refer to the IR band poisitions of the C=C stretches. [c] The redox potentials [$E^1(Co^{III,II}/Co^{II,II})$, $E^2(Co^{III,III}/Co^{III,II})$] were determined for the perchlorate salts in CH_3CN and are referenced to the saturated calomel electrode (SCE).

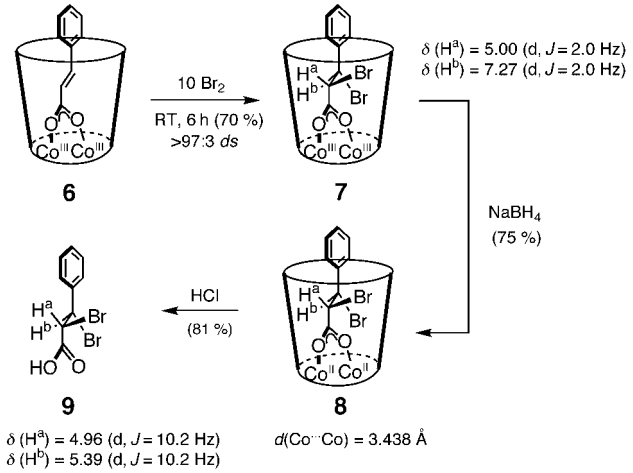
The fact that the reduction of **4** with $NaBH_4$ and the reaction of **1** with sodium 2,3-dibromopropionate yield the same complex **5** (Scheme 2) is also in accord with the formulation of **4**.



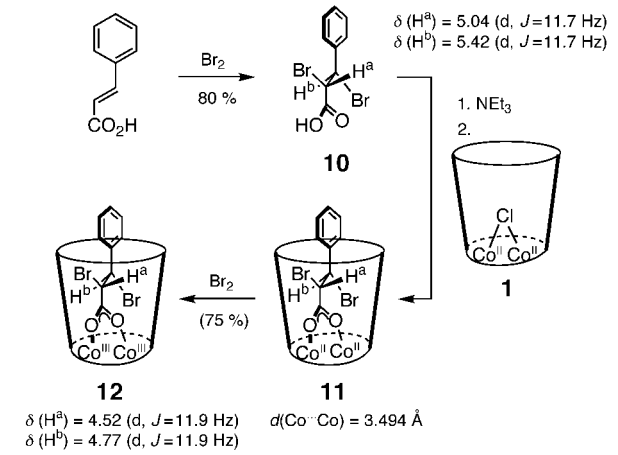
Scheme 2. Preparation of dicobalt complexes **2**–**5**. Numbers in parentheses refer to yields of isolated products.

The cinnamato-bridged dicobalt(III) complex **6**, whose synthesis and structure were reported earlier,[10] was examined next. In this case the bromination reaction was complete after 6 h at ambient temperature and yielded a single addition product **7** in nearly quantitative yield (Scheme 3). NMR-spectroscopic studies of **7** and a single-crystal X-ray structure determination of the reduced $Co^{II}Co^{II}$ complex **8** revealed the presence of a bridging 2,3-dibromo-3-phenylpropionato ligand (threo *dl* pair).[9] The expected complex **12** of the *erythro* form of 2,3-dibromo-3-phenylpropionate, which was prepared for comparative purposes according to the route depicted in Scheme 4, is only produced in low yields (< 3 %). Therefore, the bromination of the alkene encapsulated in **6** is a highly diastereoselective *syn* addition.

 DOI: 10.1002/anie.200351131 © 2003 Wiley-VCH Verlag GmbH & Co. KGaA, Weinheim



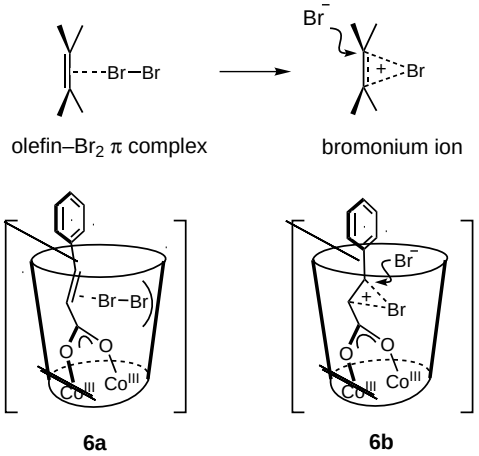
Scheme 3. Preparation of compounds **7**–**9** with details of key NMR data.



Scheme 4. Preparation of compounds **10**–**12** with details of key NMR data.

This is rather unusual and is in striking contrast to the bromination of the free acid, which is an *anti* addition.[9] Also the bromination of the encapsulated alkene is 2–3 orders of magnitude slower. The decrease in the rate can be ascribed to steric effects. This is true in particular, when one recalls that the bromination of free alkenes begins with the formation of olefin–Br_2 π complexes with T-shaped structures.[11] In our case, such a π complex (**6a**) can not form due to steric interactions with the ligand matrix.

To get some preliminary insights into the reaction mechanism, we have carried out the bromination of **6** at four different temperatures.[9] This gave a set of rate constants from which the entropy of activation could be determined. The calculated $\Delta S^{\neq}$ value of $-220\,J\,mol^{-1}\,K^{-1}$ is much more negative than in the case of the free alkenes ($\Delta S^{\neq} \lesssim -80\,J\,mol^{-1}\,K^{-1}$), [12] which indicates a well-ordered transition state. This result nicely corroborates with the observed *syn* addition. The bromination of **6** presumably involves a tight bromonium ion/Br^- contact-ion pair **6b**, in which one face of the olefin is sterically shielded by the aryl ring of the ligand $(L^{Me})^{2-}$. However, a mechanism involving a π complex between the bromonium ion and the arene, in which the soft bromonium ion interacts with a phenyl ring of the spectator ligand, cannot be ruled out at the moment.[13] It should be remembered that Ag^+ or Cs^+ ions can form coordinative bonds with the π electrons of calixarenes.[14]



The electrophilic bromination of olefins almost invariably yields *trans*-1,2-dibromides, and there are currently no reagents available that readily *cis*-brominate olefins.[15] It is therefore worth mentioning that the brominated products can be liberated from the binding pocket of the dicobalt(II) complexes. For example, complex **8** decomposes under acidic conditions to give the hydrochloride salt of the ligand ($H_2L^{Me}\cdot 6\,HCl$), a water-soluble cobalt(II) complex, and the acid **9**, which can be separated from the reaction mixture in analytically pure form by extraction into an organic solvent (Scheme 3). The new method is currently only applicable to olefins with anchoring groups (RCO_2^-), but expansion of the container approach to a general concept for the *cis*-bromination of olefins appears to be in reach.

We have described the stereochemical course of the bromination of α,β-unsaturated carboxylate ligands. The reaction is dictated by the size and form of the binding cavity of the complexes and this results in a highly diastereoselective *syn* addition of the Br_2 molecule to the carbon–carbon double bond. We are currently probing the possibility whether this and related transformations can be made enantioselective.

Received: February 7, 2003 [Z51131]

Keywords: alkenes · bromination · container molecules · diastereoselectivity · reaction mechanisms

[1] S. Hecht, J. M. J. Fréchet, *Angew. Chem.* **2001**, *113*, 76–94; *Angew. Chem. Int. Ed.* **2001**, *40*, 74–91.
[2] Y. Rondelez, G. Bertho, O. Reinaud, *Angew. Chem.* **2002**, *114*, 1086–1088; *Angew. Chem. Int. Ed.* **2002**, *41*, 1044–1046.
[3] E. Engeldinger, D. Armspach, D. Matt, P. G. Jones, E. Welter, *Angew. Chem.* **2002**, *114*, 2705–2708; *Angew. Chem. Int. Ed.* **2002**, *41*, 2593–2596.

 © 2003 Wiley-VCH Verlag GmbH & Co. KGaA, Weinheim

[4] M. T. Reetz, S. R. Waldvogel, *Angew. Chem.* **1997**, *109*, 870 – 873; *Angew. Chem. Int. Ed. Engl.* **1997**, *36*, 865 – 867.
[5] V. F. Slagt, J. N. H. Reek, P. C. J. Kramer, P. W. N. M. van Leeuwen, *Angew. Chem.* **2001**, *113*, 4401 – 4404; *Angew. Chem. Int. Ed.* **2001**, *40*, 4271 – 4274.
[6] B. Kersting, *Angew. Chem.* **2001**, *113*, 4109 – 4112; *Angew. Chem. Int. Ed.* **2001**, *40*, 3987 – 3990.
[7] M. Yoshizawa, Y. Takeyama, T. Kusukawa, M. Fujita, *Angew. Chem.* **2002**, *114*, 1403 – 1405; *Angew. Chem. Int. Ed.* **2002**, *41*, 1403 – 1405.
[8] T. Ooi, Y. Kondo, K. Maruoka, *Angew. Chem.* **1998**, *110*, 3213 – 3215; *Angew. Chem. Int. Ed.* **1998**, *37*, 3039 – 3041.
[9] For details of the experimental procedures, characterization data, results of kinetic measurements, control experiments and crystal structure determinations (CCDC-202751 (**8**), CCDC-202752 (**11**) contain the supplementary crystallographic data for this paper. These data can be obtained free of charge via www.ccdc.cam.ac.uk/conts/retrieving.html (or from the Cambridge Crystallographic Data Centre, 12, Union Road, Cambridge CB21EZ, UK; fax: (+44)1223-336-033; or deposit@ccdc.cam.ac.uk).) see Supporting Information.
[10] B. Kersting, G. Steinfeld, *Inorg. Chem.* **2002**, *41*, 1140 – 1150.
[11] a) R. Herges, *Angew. Chem.* **1995**, *107*, 57 – 59; *Angew. Chem. Int. Ed. Engl.* **1995**, *34*, 51 – 53; b) R. Bianchini, C. Chiappe, D. Lenoir, P. Lemmen, R. Herges, J. Grunenberg, *Angew. Chem.* **1997**, *109*, 1340 – 1343; *Angew. Chem. Int. Ed. Engl.* **1997**, *36*, 1284 – 1287.
[12] G. Bellucci, C. Chiappe, G. L. Moro, *J. Org. Chem.* **1997**, *62*, 3176 – 3182.
[13] Prof. G. Erker (University of Münster), private communication.
[14] J. W. Steed, J. L. Atwood, *Supramolecular Chemistry*, Wiley, Chichester, **2000**, p. 169.
[15] R. M. Carman, R. P. C. Derbyshire, K. A Hansford, R. Kadirvelraj, W. T. Robinson, *Aust. J. Chem.* **2001**, *54*, 117 – 126.

 © 2003 Wiley-VCH Verlag GmbH & Co. KGaA, Weinheim

Umpolung of C-N Bonds

SmI_2-Induced Umpolung of the C=N Bond: First Reductive Conjugate Addition of Nitrones to α,β-Unsaturated Esters**

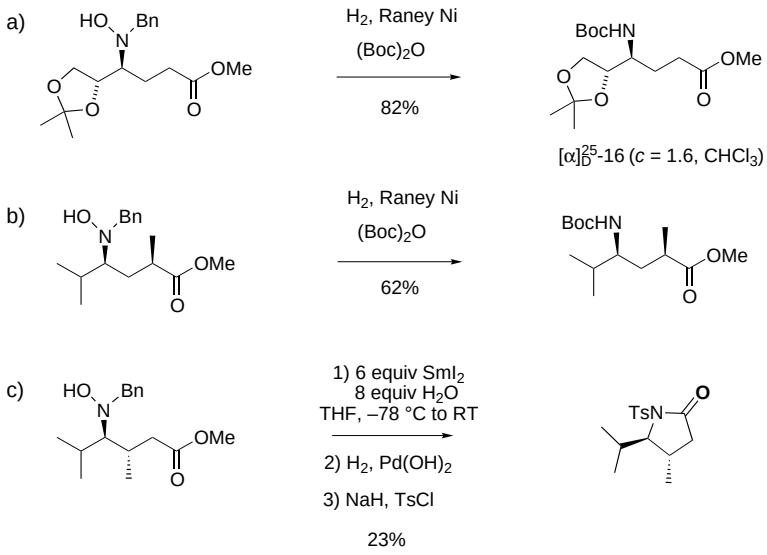
Géraldine Masson, Pascale Cividino, Sandrine Py, and Yannick Vallée**

Polarity inversion of organic functional groups is of great interest because it allows added flexibility in the design of complex synthetic schemes. While the umpolung of carbonyl groups is well documented,[1] a similar inversion of the C=N bond has been demonstrated in significantly fewer examples.[2,3] We have recently reported a general and high-yielding pinacol-type heterocoupling of nitrones with aldehydes and ketones in presence of SmI_2 that produces the corresponding β-*N*-hydroxyamino alcohols.[4] In that work, nitrones proved to be far superior to imines,[5] oximes,[6] and hydrazones[7] for the *intermolecular* cross-coupling reaction with carbonyl partners. Concerning the mechanism of this coupling, evidence was found that SmI_2 first reduces the nitrone, as opposed to the carbonyl component, to generate an α-aza-nucleophilic species (radical or anion), which then adds to the C=O bond of the aldehyde or ketone. Herein we demonstrate that *nitrone umpolung* chemistry can be extended to other electrophiles, namely α,β-unsaturated esters, to generate important γ-amino ester derivatives.

Owing to its finely tunable reactivity, samarium(II) diiodide has found wide application in organic synthesis[8] since the seminal work by Kagan and co-workers in the early 1980s.[9] In particular, this mild reducing agent has become a popular reagent for the reductive addition of carbonyl compounds to a variety of electrophilic species, as exemplified by the conjugate addition to α,β-unsaturated acid derivatives.[10] Owing to the apparent persistency of the nitrone-derived species generated upon treatment with SmI_2, it appeared that they might undergo addition to electron-deficient alkenes and alkynes.

Indeed, when a solution of an aliphatic nitrone and ethyl acrylate in THF at −78 °C was treated with two equivalents of SmI_2, the γ-*N*-hydroxyamino ester resulting from conjugate addition was isolated in about 75% yield (Table 1, entries 1, 2, and 4). An attempt to accelerate the addition by running the reaction at higher temperature led to the corresponding oxazinanone as the main product (Table 1, entry 3). However, the desired products were obtained with dramatically increased reaction rates by addition of a proton source such as water (Table 1, entries 5, 6, 8, and 9). The effect of water[9,11] was particularly significant in the reductive additions of a hydroxy-containing nitrone (Table 1, entry 5) and a ketonitrone (Table 1, entry 6) to ethyl acrylate. In both examples, reaction times were shorter (7-fold and 12-fold, respectively) and yields were much better in the presence of this safe and convenient additive.

The possibility of 1,2-diastereomeric induction was next addressed by using carbohydrate-derived nitrones as substrates. A recently described D-mannose-derived (*E*)-aldonitrone[12] reacted with ethyl acrylate (Table 1, entry 7) to afford a 75:25 mixture of diastereomers, thus offering a new, reasonably stereoselective route to diversely substituted sugar mimics (azasugars).[13] Similarly, the (*R*)-2,3-*O*-isopropylidene-D-glyceraldehyde-derived nitrone[14] added to ethyl acrylate with good diastereoselectivity (Table 1, entry 8) and yielded an important intermediate[15,16] for the synthesis of Vigabatrin,[17] a potent and selective GABA-transaminase inhibitor used for treatment and prevention of epilepsy. The relative stereochemistry displayed in the product in entry 8 of



Scheme 1. Determination of the stereochemistry of the products in entries 8 (a), 9 (b), and 11 (c) of Table 1. See text for details. Boc = *tert*-butyloxycarbonyl.

Table 1 was determined by reduction of the hydroxylamine and carbamoylation to give a known[15a] Boc-protected γ-amino ester (Scheme 1a).

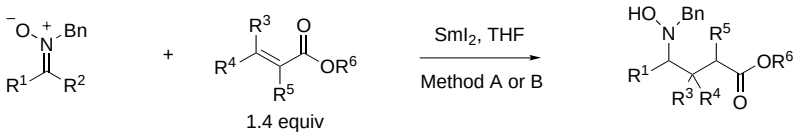
Following these encouraging results, the addition of nitrones to substituted acrylates was studied. Both methyl methacrylate (Table 1, entries 9, 10), and (*E*)-methyl crotonate (entry 11) proved to be good acceptors. Furthermore, their reactions displayed excellent diastereoselectivities, and afforded the 2- and 3-substituted-γ-*N*-hydroxyamino acid derivatives respectively, in > 95% purity. The relative stereochemistry (Table 1, entry 9) was assigned by hydrogenation/

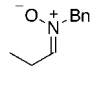
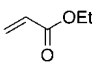
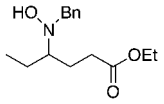
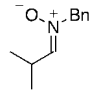
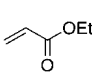
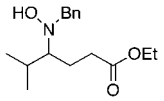
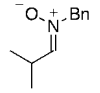
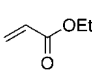
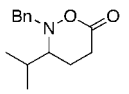
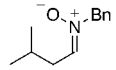
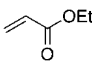
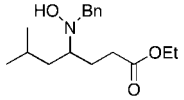
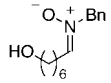
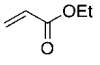
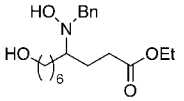
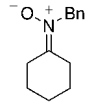
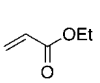
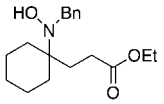
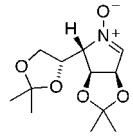
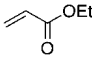
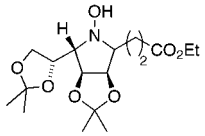
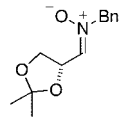
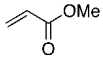
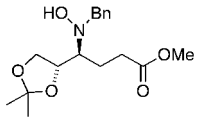
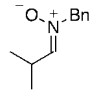
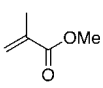
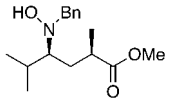
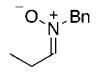
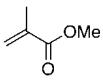
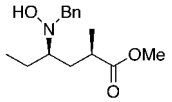
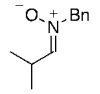
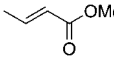
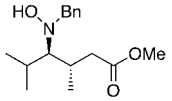
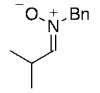
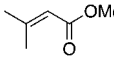
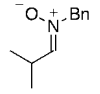
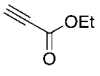
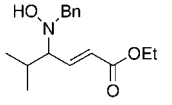
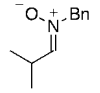
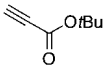
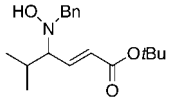
[*] Dr. S. Py, Prof. Y. Vallée, G. Masson, P. Cividino
LEDSS, UMR 5616
Université Joseph Fourier-CNRS; BP53
38041 Grenoble Cedex 9 (France)
Fax: (+33) 04-7663-5983
E-mail: sandrine.py@ujf-grenoble.fr
syrca.ledss@ujf-grenoble.fr

[**] We thank Drs. Andrew E. Greene and C. Morin for helpful discussions and encouragement, and Dr. M. Christian Philouze for the X-ray structure analysis. This work was supported by the Centre National de la Recherche Scientifique (CNRS) and the Université Joseph Fourier. G.M. thanks the French Ministry of Education, Research, and Technology (MENRT) for a doctoral fellowship.

 DOI: 10.1002/anie.200250480 © 2003 Wiley-VCH Verlag GmbH & Co. KGaA, Weinheim

Table 1: Preparation of γ-*N*-hydroxyamino esters by reductive conjugate addition of nitrones to α,β-unsaturated esters.



Entry	Nitrone	Electrophile	Product	Method[a]	*t* [h]	Yield [%][b] (d.r.)[c]
1				A	10	76
2				A	10	75
3				A[d]	7	58
4				A	9	74
5				A B	7 1	60 73
6				A B	96 8	45 55
7				B	5	63 (75:25)
8				A B	7 1	72 (90:10) 81 (85:15)
9				A B	7 2	29 (>95:5) 74 (>95:5)
10				B	3	76 (>95:5)
11				B	2.5	66 (>95:5)
12				B	3	54
13				A B	8 0.5	<10 71
14				B	7	58

carbonylation reactions of the product (Scheme 1b) and comparison to a known carbamate.[18] In the case of the product in entry 10 (Table 1), although the proposed assignment should be considered tentative, it is most likely as depicted by analogy with that in entry 9 (Table 1). To determine the stereochemistry of the product in entry 11, the product was cyclized into a pyrrolidinone (Scheme 1c) in which the observed coupling constant ($J_{4,5} = 7.7$ Hz) is indicative[19] of a *trans* relationship. The method, however, seems to reach a limit with β,β-disubstituted esters, as no addition product was detected with 3,3-dimethyl acrylate (Table 1, entry 12); the starting nitrone merely undergoes reduction. The outcome of this reaction strongly suggests a mechanism for these additions that involves initial reduction of the nitrone followed by conjugate addition, rather than initial reduction of the α,β-unsaturated ester and addition of the resulting radical anion to the nitrone.

While intramolecular SmI_2-induced conjugate additions to α,β-acetylenic esters have been reported to be sluggish[20] and have allowed only the elaboration of five-membered rings,[21] no examples of the intermolecular version of these additions have been disclosed. It is noteworthy that the conjugate addition of nitrone-derived α-azanucleophilic species to propiolates in presence of water proceeded smoothly (Table 1, entries 13, 14)

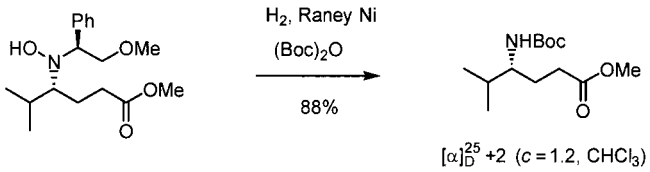
[a] Method A: A solution of the nitrone and α,β-unsaturated ester in THF at −78 °C was treated with two equivalents of SmI_2, and the reaction mixture was then kept at −78 °C for the indicated reaction time. Method B: A solution of the nitrone, α,β-unsaturated ester and degassed water (8 equiv) in THF at −78 °C was treated with three equivalents of SmI_2, and the reaction mixture was then kept at −78 °C for the indicated reaction time. [b] Yields of isolated product after column chromatography. [c] According to ^{1}H NMR analysis of the crude products. [d] The reaction mixture was allowed to reach −50 °C over 7 h.

 © 2003 Wiley-VCH Verlag GmbH & Co. KGaA, Weinheim

to produce the corresponding γ-*N*-hydroxyamino-α,β-ethylenic esters as single isomers (100% *E*). The effect of water in these additions was even more dramatic than in those above: the presence of eight equivalents of water resulted in both a remarkable acceleration of the reaction and an improvement of the yield (<10% to 71%). The products represent versatile intermediates for the synthesis of a variety of naturally occurring γ-amino-α,β-ethylenic and γ-amino-α,β-dihydroxy acid derivatives.[22]

To achieve enantioselectivity in the synthesis of γ-amino acid derivatives, nitrones bearing a chiral auxiliary at the nitrogen center were prepared and treated with ethyl acrylate (Table 2).[23] These additions proceeded in good yield[24] to afford diastereomeric γ-*N*-hydroxyamino esters, which could be separated by column chromatography (Table 2, entries 1–4). In the case of entry 4 (and by analogy entry 5), the major diastereomer was assigned the depicted stereochemistry from its conversion to a known derivative (Scheme 2).[25]

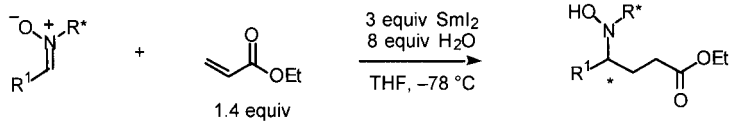
When the 1-(triisopropylphenyl)ethyl auxiliary[26] was used, an excellent diastereoselectivity (>95:5) was observed (Table 2, entry 6); a single-crystal X-ray crystallographic analysis of the major diastereomer provided its relative configuration.[27]

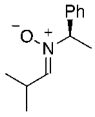
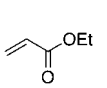
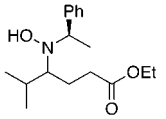
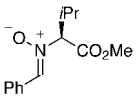
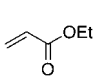
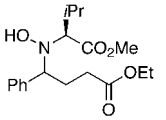
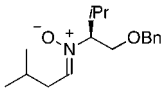
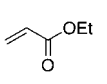
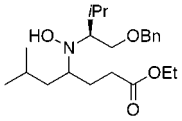
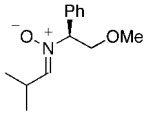
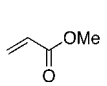
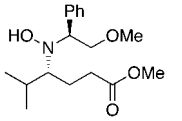
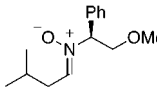
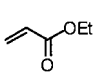
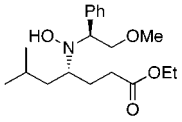
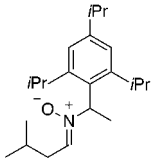
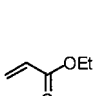
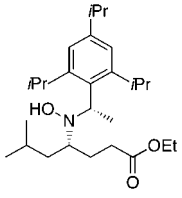


Scheme 2. Determination of the stereochemistry of the product in entry 4 of Table 2.

In conclusion, reduction of nitrones by SmI_2 yields α-azacarbon nucleophiles that undergo efficient and highly selective intermolecular conjugate addition to acrylic and propiolic esters. Outstanding diastereoselectivities are observed and the use of chiral auxiliaries at the nitrogen center provides an expedient, enantioselective approach to γ-amino acid derivatives. The 4-substituted, 2,4-disubstituted, and 3,4-disubstituted γ-*N*-hydroxyamino and γ-amino acid derivatives[16] produced by this novel, direct method should find considerable application, both as synthetic intermediates and as precursors of conformationally defined, protease-resistant γ-peptides.[28] Current work is aimed at extending this method to other unsaturated systems.

Table 2: Reductive conjugate addition of chiral nitrones to ethyl acrylate.



Entry	Nitrone	Electrophile	Product	*t* [h]	Yield [%]	d.r.[a]
1				2	78	75:25[b]
2				0.5	36	70:30
3				4.5	56	60:40
4				3	96	85:15
5				3.25	84	85:15
6[c]				11.5	73	>95:5

[a] According to ^{1}H NMR analysis of the crude product. [b] In this case the diastereomeric ratio (d.r.) could not be determined from ^{1}H NMR analysis of the crude material because of signal overlap and was therefore based on the yields of the isolated diastereomers. [c] In this case the chiral nitrone was used as a racemic mixture.

Experimental Section

Preparation of 0.1M SmI_2 in THF:[29] A suspension of samarium powder (4 g, 26.6 mmol) and I_2 (5 g, 19.7 mmol) in dry THF (200 mL) was vigorously stirred at room temperature for at least 2 h, during which time the color changed from yellow-brown to green and finally to blue. Titration of this SmI_2 solution was performed with a 0.1M solution of I_2 in THF (the end point is reached when the solution turns yellow and SmI_3 precipitates).

General procedure for intermolecular conjugate addition of nitrones to acrylic and propiolic esters: A stirred and carefully deoxygenated solution of the nitrone (*N*-alkylidenebenzylamine-*N*-oxide) (0.5 mmol) in dry THF (10 mL) was cooled to −78°C under argon. The unsaturated ester (0.7 mmol), water (4 mmol, degassed by boiling under a stream of argon for 30 min) when method B was employed, and a solution of SmI_2 (ca. 0.1M, 10 mL, 1 mmol) in THF were then added. The temperature was kept at −78°C until the reaction was judged to be complete by TLC, whereupon a saturated aque-

 © 2003 Wiley-VCH Verlag GmbH & Co. KGaA, Weinheim

ous solution of $Na_2S_2O_3$ (30 mL) was added. The yellow mixture was extracted with AcOEt (3 × 50 mL) and the combined organic layers were washed with a saturated aqueous solution of NaCl, dried over $MgSO_4$, filtered, and concentrated in vacuo. Purification of the resulting residue by chromatography on silica gel afforded the expected γ-*N*-hydroxyamino ester as a single product (or a mixture of diastereomers). All new compounds gave spectroscopic and analytical data in agreement with the assigned structures.

Received: November 5, 2002
Revised: January 1, 2003 [Z50480]

Keywords: amino acids · chiral auxiliaries · nitrones · samarium · umpolung

[1] a) D. Seebach, *Angew. Chem.* **1979**, *91*, 259; *Angew. Chem. Int. Ed. Engl.*. **1979**, *18*, 239; b) D. J. Ager in *Umpoled Synthons: A Survey of Sources and Uses in Synthesis* (Ed.: T. A. Hase), Wiley, New York, **1987**.

[2] For examples of α-amino anion equivalents from sterically hindered hydrazones, see: a) R. M. Adlington, J. E. Baldwin, J. C. Bottaro, M. W. D. Perry, *J. Chem. Soc. Chem. Commun.* **1983**, 1040; b) R. Fernandez, J. M. Lassaletta, *Synlett* **2000**, 1228, and references therein.

[3] For generation of α-amino radicals from other C=N bonds, see: a) S. F. Martin, C. P. Yang, W. L. Laswell, H. Rueeger, *Tetrahedron Lett.* **1988**, *29*, 6685; b) P. Renaud, L. Giraud, *Synthesis* **1996**, 913, and references therein; c) J. M. Aurrecoechea, A. Fermandez, J. M. Gorgojo, C. Saornil, *Tetrahedron* **1999**, *55*, 7345; d) C. E. McDonald, A. M. Galka, A. I. Green, J. M. Keane, J. E. Kowalchick, C. M. Micklitsch, D. D. Wisnoski, *Tetrahedron Lett.* **2001**, *42*, 163.

[4] G. Masson, S. Py, Y. Vallée, *Angew. Chem.* **2002**, *114*, 1850; *Angew. Chem. Int. Ed.* **2002**, *41*, 1772.

[5] a) E. J. Roskamp, S. F. Pedersen, *J. Am. Chem. Soc.* **1987**, *109*, 6551; b) T. Imamoto, S. Nishimura, *Chem. Lett.* **1990**, 1141; c) T. Shono, N. Kise, N. Kunimi, R. Nomura, *Chem. Lett.* **1991**, 2191; d) D. Guijarro, M. Yus, *Tetrahedron* **1993**, *49*, 7761; e) A. Clerici, L. Clerici, O. Porta, *Tetrahedron Lett.* **1995**, *36*, 5955; f) J.-N. Denis, A. Fkyerat, Y. Gimbert, C. Coutterez, P. Mantellier, S. Jost, A. E. Greene, *J. Chem. Soc. Perkin Trans. 1* **1995**, 1811; g) F. Machrouhi, J.-L. Namy, *Tetrahedron Lett.* **1999**, *40*, 1315; h) N. Taniguchi, M. Uemura, *J. Am. Chem. Soc.* **2000**, *122*, 8301.

[6] a) T. Shono, N. Kise, T. Fujimoto, *Tetrahedron Lett.* **1991**, *32*, 525; b) T. Hanamoto, J. Inanaga, *Tetrahedron Lett.* **1991**, *32*, 3555.

[7] T. Shono, N. Kise, T. Fujimoto, A. Yamanami, R. Nomura, *J. Org. Chem.* **1994**, *59*, 1730.

[8] a) G. A. Molander, C. R. Harris, *Chem. Rev.* **1996**, *96*, 307; b) T. Skrydstrup, *Angew. Chem.* **1997**, *109*, 355; *Angew. Chem. Int. Ed. Engl.* **1997**, *36*, 345; c) G. A. Molander, C. R. Harris, *Tetrahedron* **1998**, *54*, 3321; d) A. Krief, A.-M. Laval, *Chem. Rev.* **1999**, *99*, 745.

[9] a) P. Girard, J. L. Namy, H. B. Kagan, *J. Am. Chem. Soc.* **1980**, *102*, 2693; b) H. B. Kagan, J. L. Namy, P. Girard, *Tetrahedron Suppl.* **1981**, *37*, 175.

[10] a) A. Gansauer, H. Bluhm, *Chem. Rev.* **2000**, *100*, 2771; b) P. G. Steel, *J. Chem. Soc. Perkin Trans. 1* **2001**, 2727, and references therein.

[11] E. Hasegawa, D. P. Curran, *J. Org. Chem.* **1993**, *58*, 5008.

[12] O. Tamura, A. Toyao, H. Ishibashi, *Synlett* **2002**, 1344.

[13] For a review on natural occurrence, biological activity, and prospects for therapeutic applications of sugar-mimic glycosidase inhibitors, see: N. Asano, R. J. Nash, R. J. Molyneux, G. W. J. Fleet, *Tetrahedron: Asymmetry* **2000**, *11*, 1645.

[14] P. DeShong, C. M. Dicken, J. M. Leginus, R. R. Whittle, *J. Am. Chem. Soc.* **1984**, *106*, 5598.

[15] a) M. Alcon, M. Poch, A. Moyano, M. A. Pericàs, A. Riera, *Tetrahedron: Asymmetry* **1997**, *8*, 2967; b) C. Dagoneau, A. Tomassini, J.-N. Denis, Y. Vallée, *Synthesis* **2001**, 150.

[16] *N*-hydroxylamines can be easily reduced to amines by using excess SmI_2 in the presence of a proton source: A. S. Kende, J. S. Mendoza, *Tetrahedron Lett.* **1991**, *32*, 1699; see also ref. [4].

[17] S. M. Nanavati, R. B. Silverman, *J. Am. Chem. Soc.* **1991**, *113*, 9341.

[18] M. Brenner, D. Seebach, *Helv. Chim. Acta* **2001**, *84*, 2155.

[19] H. Nagashima, H. Wakamatsu, N. Ozaki, T. Ishii, M. Watanabe, T. Tajima, K. Itoh, *J. Org. Chem.* **1992**, *57*, 1682.

[20] Z. Zhou, D. Larouche, S. M. Bennett, *Tetrahedron* **1995**, *51*, 11623.

[21] G. A. Molander, C. R. Harris, *J. Org. Chem.* **1997**, *62*, 7418.

[22] For examples of biologically active natural products see: a) A. B. Smith III, G. K. Friestad, J. Barbosa, E. Bertounesque, J. J. W. Duan, K. G. Hull, M. Iwashima, Y. Qiu, P. G. Spoors, B. A. Salvatore, *J. Am. Chem. Soc.* **1999**, *121*, 10478; b) A. K. Ghosh, A. Bischoff, J. Cappiello, *Org. Lett.* **2001**, *3*, 2677; c) A. Zampella, M. V. D'Auria, L. G. Paloma, A. Casapullo, L. Minale, C. Debitus, Y. Henin, *J. Am. Chem. Soc.* **1996**, *118*, 6202.

[23] Following the submission of this manuscript, a paper appeared describing chiral ester induced diastereoselection, D. Riber, T. Skydstrup, *Org. Lett.* **2003**, *5*, 229.

[24] When nitrones with *C*-aryl substituents were used as substrates, products resulting from reductive dimerization of the nitrone were also isolated.

[25] U. Schmidt, B. Rield, G. Haas, H. Griesser, A. Vetter, S. Weinbrenner, *Synthesis* **1993**, 216.

[26] P. Delair, A. M. Kanazawa, M. B. M. de Azevedo, A. E. Greene, *Tetrahedron: Asymmetry* **1996**, *7*, 2707.

[27] CCDC-201303 contains the supplementary crystallographic data for this paper. These data can be obtained free of charge via www.ccdc.can.ac.uk/conts/retrieving.html (or from the Cambridge Crystallographic Center, 12 Union Road, Cambridge CB21EZ, UK; Fax: (+44) 1223-336033; or deposit@ccdc.cam.ac.uk).

[28] a) J. Frackenpohl, P. I. Arvidsson, J. V. Schreiber, D. Seebach, *ChemBioChem* **2001**, *2*, 445; b) D. Seebach, M. Brenner, M. Rueping, B. Jaun, *Chem. Eur. J.* **2002**, *8*, 573, and references therein.

[29] a) T. O. M. Imamoto, *Chem. Lett.* **1987**, 501; b) D. P. Curran, W. Zhang, P. Dowd, *Tetrahedron* **1997**, *53*, 9023.

 © 2003 Wiley-VCH Verlag GmbH & Co. KGaA, Weinheim

Amino Acid Flexibility

A Conformational Flexibility Scale for Amino Acids in Peptides**

*Fang Huang and Werner M. Nau**

The molecular flexibility of proteins is a crucial factor in determining their biological activity,[1] including binding affinity,[2] antigenicity,[3] and enzymatic activity.[4] The identification of regions in proteins with the highest conformational flexibility and rigidity is essential for predicting the mechanism of protein folding,[5,6] for understanding domain motions in proteins,[1,7,8] and for predicting the rate of nonlocal interactions as well as intramolecular reactions, including electron and proton transfer[9] and cyclizations.[10] Consequently, there is considerable interest in predicting the flexibility or, conversely, the rigidity of peptides from their amino acid sequence.[11–13] The prediction of peptide flexibility has additional implications for the de novo design of peptides[14] and for the theoretical understanding of peptide dynamics.[15]

We now report a novel scale for the flexibility of amino acids, which provides an absolute measure for the time scale of conformational changes in short structureless peptides as a function of the amino acid type. This experimental scale is derived from kinetic measurements of the collision frequency between the two ends of short random-coil polypeptides.

The present experiments provide the first application of our recently introduced fluorazophore method for measuring the kinetics of end-to-end collision in polypeptides.[16,17] In essence, 2,3-diazabicyclo[2.2.2]oct-2-ene (DBO) is attached as a fluorescent probe at one end of the peptide and tryptophan is placed at the other end as an efficient quencher (Figure 1). The unique features of this probe/quencher pair are the exceedingly long fluorescence lifetime of the probe (several hundred nanoseconds) and the contact quenching mechanism, which differentiates it from conventional fluorescence resonance energy transfer (FRET) donor/acceptor pairs. The fluorescence lifetimes of DBO/Trp peptides provide the quenching rate constants (k_q), which measure the end-to-end collision frequency (k_{coll} in Figure 1).[17] Such collisions occur on the ns–μs time scale according to recent studies.[17–20]

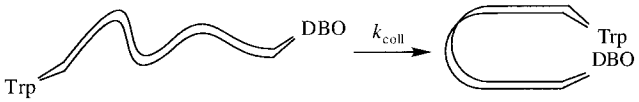
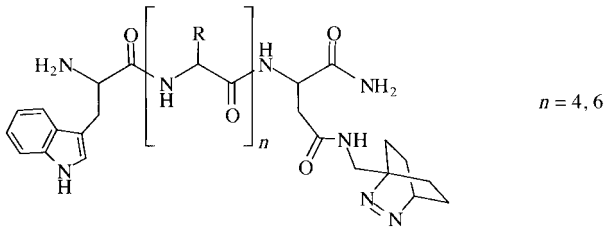


Figure 1. End-to-end collision in peptides labeled with DBO as a fluorescent probe at the *C* terminus and Trp as a fluorescence quencher at the N terminus.

We reasoned that the collision frequency of peptides, in which Trp and DBO are separated by a sequence of identical amino acids (Scheme 1), should be an excellent measure of the conformational flexibility of the backbone.[21] These peptides adopt random-coil conformations according to CD measurements.[22] Since the conformational changes required for end-to-end contact derive from fast rotations about the N–C^{α} and C^{α}–C bonds,[23] and since different α substituents are expected to hinder these bond rotations to a different degree, we expected different collision frequencies when the probe and the quencher are separated by different amino acids. This arrangement should allow us to correlate the collision frequency with the type of amino acid and thereby build up a flexibility scale (Table 1). It should be stated that this scale reflects the global or conformational flexibility of the amino acids in peptides. This scale is unrelated to previously introduced local or positional flexibility scales[24] obtained from X-ray diffraction crystallographic data.[11–13] The latter scales provide measures of the average displacements of atoms in amino acid residues from their equilibrium geometry, which are derived from vibrations on the femtosecond time scale and reflect the shallowness of the potential centered around an energy minimum.



Scheme 1. General structure of the peptides.

The quenching rate constants in Table 1, which were obtained from the fluorescence decays (Figure 2), show variations of 1–2 orders of magnitude for the various amino acids. Lower quenching rate constants correspond to lower end-to-end collision frequencies and indicate a lower flexibility (or higher rigidity). The following order of flexibility applies:

Gly > Ser > Asp, Asn, Ala > Thr, Leu > Phe, Glu, Gln > His, Arg > Lys > Val > Ile > Pro

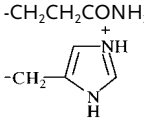
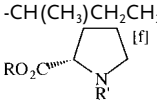
The above order was also preserved in the presence of 6 M guanidinium chloride, except that Leu appeared to give rise to a somewhat less flexible peptide. Guanidinium chloride is an efficient denaturant, which should destroy any remaining secondary structure as well as aggregation between hydro-

[*] Prof. Dr. W. M. Nau
School of Engineering and Science
International University Bremen
Campus Ring 1, 28759 Bremen (Germany)
Fax: (+49) 421-200-3229
E-mail: w.nau@iu-bremen.de
Prof. Dr. W. M. Nau, Dipl.-Chem. F. Huang
Departement Chemie
Universität Basel
Klingelbergstrasse 80, 4056 Basel (Switzerland)

[**] This work was supported by the Swiss National Science Foundation within the NFP 47 "Supramolecular Functional Materials".

 DOI: 10.1002/anie.200250684 © 2003 Wiley-VCH Verlag GmbH & Co. KGaA, Weinheim

Table 1: Fluorescence quenching rate constants in Trp-X_6-DBO-NH_2 peptides.

X	Residue (R)	k_q [10^6 s^{-1}] without additive[a]	with denaturant[b]
Gly	-H	39	23
Ser	$-CH_2OH$	25	19
Asp[c]	$-CH_2CO_2H$	21	
	$-CH_2CO_2^-$	19	12
Asn	$-CH_2CONH_2$	20	14
Ala	$-CH_3$	ca. 18[d]	ca. 14[d]
Thr	$-CH(OH)CH_3$	11	9.3
Leu	$-CH_2CH(CH_3)_2$	ca. 10[d]	ca. 5.1[d]
Phe	$-CH_2Ph$	ca. 7.6[d,e]	ca. 7.5[d]
Glu[c]	$-CH_2CH_2CO_2H$	8.8	
	$-CH_2CH_2CO_2^-$	7.4	5.4
Gln	$-CH_2CH_2CONH_2$	7.2	4.8
His[c]		4.8	4.0
Arg	$-(CH_2)_3NHCNH_2NH_2^+$	4.6	2.6
Lys[c]	$-(CH_2)_4-NH_2$	4.0	
	$-(CH_2)_4-NH_3^+$	2.8	1.9
Val	$-CH(CH_3)_2$	ca. 3.0[d,e]	ca. 2.6[d]
Ile	$-CH(CH_3)CH_2CH_3$	ca. 2.3[d,e]	ca. 1.6[d]
Pro		< 0.1	< 0.1

[a] Measured in D_2O. [b] Measured in H_2O with 6 M guanidinium chloride. [c] The unprotonated forms were studied at pD 12, the protonated ones at pD 2. [d] Extrapolated from the kinetics of the shorter peptide ($n = 4$), see Experimental Section. [e] Measured with 30% acetonitrile. [f] Entire amino acid.

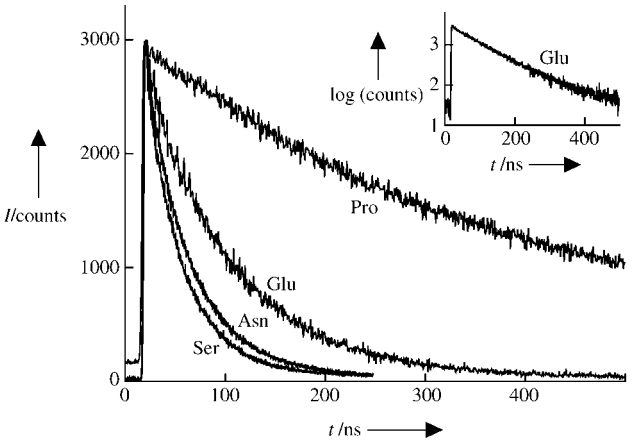


Figure 2. Fluorescence decays for selected Trp-X_6-DBO-NH_2 peptides in aerated D_2O measured by single photon counting. The inset shows a representative decay on a semi-logarithmic scale.

phobic peptides.[25] The consistency of the results in the absence and presence of this denaturant provides strong evidence that the property which is being reflected by the kinetic measurements is indeed conformational flexibility. Note also that the rate of end-to-end collision in the presence of the salt is reduced throughout the entire series of peptides; this reflects the increased viscosity of the solution which limits the mutual diffusion of the chain ends.

According to the conformational flexibility scale, the introduction of Gly into the peptide increases the conformational flexibility, while Pro makes it more rigid. This is in line with expectations from conformational space,[26] with Gly being the amino acid with the least limited rotational freedom and Pro being the one with a frozen N–C^α bond. The sequence found for the other amino acids cannot be predicted in a straightforward manner. There is a general trend between the residue size and the kinetics: larger residues lead to lower collision frequencies, which indicates a lower flexibility; for example, Gln < Asn; Thr < Ser; Phe, Leu < Ala < Gly; Ile < Val. This result is presumably related to the larger rotational barriers imposed by the larger residues and the decrease in the diffusion coefficient of the peptide chain with increasing residue size. The effect of residue charges was also examined; there appears to be a tendency for the neutral residues to allow a slightly greater flexibility, namely, unprotonated Lys > protonated Lys, protonated Glu > unprotonated Glu, and protonated Asp ≧ unprotonated Asp. The observed charge effect is not very large, but is in line with the intuitive expectation that Coulombic repulsions reduce the overall flexibility by limiting the conformational freedom.

β Branching is well known to increase the activation barriers for bond rotations of an amino acid and therefore decreases the accessible conformational space in a peptide significantly.[27] Indeed, the peptides with β-substituted amino acids (Val and Ile) are amongst the least flexible ones on our scale. Particularly instructive is the comparison of the two constitutional isomers Leu and Ile, where the latter one imposes a higher rigidity. The β-branched Thr gives rise to more flexible peptides than Val and Ile. Nevertheless, the flexibility of the Thr peptides is slightly decreased compared to those composed of β-unsubstituted amino acids with even larger residues, for example, Thr < Asn, Asp. Evidently, the β-hydroxy group somewhat limits the flexibility, but much less severely than the β-methyl group in Val and Ile. The special effect of hydroxy substitution is also evident with Ser, which gives rise to a more flexible peptide than Ala, although it is larger as a result of the additional hydroxy group.

We did not observe a clear-cut relationship between the flexibility and the hydrophobicity of the residue. Val and Ile are very hydrophobic amino acids, but the high rigidity of the related peptides appears to be mainly a consequence of the β-substitution pattern, since there is a large differentiation from Leu, which is similarly hydrophobic. On the other hand, His and Arg are quite hydrophilic, but their peptides are less flexible than that based on the hydrophobic Phe. The hydrophobicity of the residues, therefore, does not emerge as a common denominator of peptide flexibility.

A long-standing question in peptide chemistry is which properties of an amino acid are decisive for the protein secondary structure. Statistical,[28–30] theoretical,[31] and experimental[32,33] analyses have revealed relative abundances of particular amino acids in secondary protein structures such as α helices, β strands, and β turns. According to the statistical results,[28] Met, Glu, Leu, Ala, Gln, Lys, His, and Cys are α-helix-forming amino acids, Val, Ile, Phe, Tyr, Thr, and Trp tend to form β-sheet structures, and Pro, Gly, Asp, Ser, and Asn favor β turns. A correlation between conformational

 © 2003 Wiley-VCH Verlag GmbH & Co. KGaA, Weinheim

flexibility and the propensity of an amino acid to occur in a secondary structure emerges if one disregards the α-helix-forming amino acids and Pro (see below). Accordingly, the most flexible amino acids, including Gly, Ser, Asn, and Asp, are β-turn-forming amino acids, while the most rigid amino acids, namely Val and Ile, are β-sheet-forming amino acids. In addition, when comparing the β-branched amino acids, Thr is not only the most flexible one on our scale, but it also has a much higher tendency than Val and Ile to occur in β turns.[28]

We consider that this agreement between the flexibility and the β-turn and β-sheet propensity is significant and suggest that both properties are the result of the same underlying reason: namely, the (energetically unfavorable) angular arrangements which are required in β turns may be the same as those which need to be reached for collision-induced quenching (Figure 1). In other words, the conformations required for quenching are turnlike. Large α substituents and in particular β branching do not favor β turns because of steric interactions,[27] and this avoidance also manifests itself in the kinetic measurements where a similar conformation is required for quenching. It appears that flexible amino acids, in particular Gly and Ser, promote stable β turns, although one must keep in mind that the abundance of an amino acid also depends strongly on the specific position within a β turn.[34] Rigid amino acids have a higher tendency to occur in β-sheet structures than in β turns, but they may also favor the formation of α helices. α-Helix formation is dominated by additional interactions between non-adjacent amino acids,[35] which are unlikely to be related to chain flexibility. In fact, a relationship between α-helix propensity and flexibility cannot be recognized, although it is evident that the α-helix-forming amino acids adopt an intermediate position on the proposed flexibility scale.

A clear exception is Pro,[22] which gives rise to the most rigid peptide, but which is also favored in β turns. The high rigidity is imposed by its cyclic structure, which prevents rotations about the N–C^{α} bond. The high β-turn propensity, on the other hand, is related to the restricted $-60°$ ϕ angle, which presents an ideal arrangement in the $i+1$ position of β turns.[36]

In summary, the following trends emerge for the conformational flexibility of amino acids in peptides as assessed by our method: 1) Large residues reduce the flexibility; 2) β-alkyl branching greatly reduces flexibility, while β-hydroxy substitution retains a high flexibility; 3) charge repulsions between residues decrease the flexibility slightly; 4) the conformationally frozen amino acid Pro is the least flexible while the simplest amino acid Gly is the most flexible; 5) a correlation with β-turn propensity applies, with the most flexible amino acids also being those with high β-turn propensity; 6) rigid amino acids appear to be favored in β sheets; and 7) there is no clear-cut relationship between flexibility and hydrophobicity or the α-helix propensity of amino acids. Finally, one must note that the present flexibility scale is based on a set of synthetic peptides with a backbone composed of identical amino acids. Whether the flexibility of native random-coil peptide sequences can be predicted from this scale in an incremental fashion or depends strongly on the specific sequence, will be the subject of future studies applying the same methodology.

Experimental Section

The peptides were commercially synthesized in >95% purity (Affina, Berlin). Details on the synthesis of the probe and its suitability in solid-phase peptide synthesis have been reported.[17] The choice of the peptide length (number of amino acids as spacers of the probe and the quencher) is essential since the peptide should not be too long to enable measurement of significant quenching and to maintain water solubility, and neither should it be too short to maintain sufficiently long lifetimes for accurate measurement and to ensure that the measured rates reflect an intrinsic property of the backbone, namely, the amino acid. Six amino acids ($n=6$) provided a good balance between these factors, but peptides of this chain length with the most hydrophobic amino acids (Ala, Leu, Phe, Val, and Ile) were poorly soluble in pure water, thus causing complications in both peptide synthesis as well as fluorescence measurement. For these cases, a shorter sequence of four amino acids ($n=4$) was chosen, and the known length dependence of the kinetics of end-to-end collision[17] allowed extrapolation of the rates to the value for $n=6$.

Fluorescence decays were measured by single photon counting (FLS900, Edinburgh Instruments) under air, either in D_2O or in H_2O containing 6 M guanidinium chloride. All peptides were sufficiently soluble in the presence of guanidinium chloride, but peptides based on the hydrophobic amino acids Phe, Val, and Ile were not sufficiently soluble without this denaturant. In these three cases, 30% acetonitrile was added to D_2O to achieve the same working concentration (10 μM) as for the other peptides and these solutions were deaerated. The co-solvent did not have a major effect on the measured rates, which could be demonstrated through control experiments in neat D_2O at lower peptide concentration (ca. 1 μM).

The decay kinetics were monoexponential in all cases (Figure 2), such that it was possible to assign a characteristic fluorescence lifetime (τ) to each peptide and amino acid backbone.[21] The quenching rate constants k_q were obtained from the experimental fluorescence lifetimes as $k_q = 1/\tau - 1/\tau_0$, where τ_0 corresponds to the intrinsic fluorescence lifetime of the probe in the absence of quenchers, for example, as measured for the free parent fluorophore as well as for peptides lacking a quencher. This value amounts to 500 ns in aerated D_2O and to 360 ns in H_2O containing 6 M guanidinium chloride. Subject to the assumption of a random coil conformation[22] and subject to the assumption of diffusion-controlled intramolecular quenching,[17,20] the quenching rate constant (k_q) can be directly interpreted as end-to-end collision frequency (k_{coll} in Figure 1).

Received: December 3, 2002 [Z50684]

Keywords: amino acids · fluorescence · peptides · protein folding · secondary structure

[1] R. Huber, *Biochem. Soc. Trans.* **1987**, *15*, 1009–1020.
[2] D. T. Braddock, J. M. Louis, J. L. Baber, D. Levens, G. M. Clore, *Nature* **2002**, *415*, 1051–1056.
[3] N. Taschner, S. A. Müller, V. R. Alumella, K. N. Goldie, A. F. Drake, U. Aebi, T. Arvinte, *J. Mol. Biol.* **2001**, *310*, 169–179.
[4] P. Závodszky, J. Kardos, A. Svingor, G. A. Petsko, *Proc. Natl. Acad. Sci. USA* **1998**, *95*, 7406–7411.
[5] P. Hammarström, U. Carlsson, *Biochem. Biophys. Res. Commun.* **2000**, *276*, 393–398.
[6] A. R. Fersht, *Curr. Opin. Struct. Biol.* **1997**, *7*, 3–9.
[7] Y. Q. Qian, G. Otting, K. Furukubo-Tokunaga, M. Affolter, W. J. Gehring, K. Wüthrich, *Proc. Natl. Acad. Sci. USA* **1992**, *89*, 10738–10742.
[8] S. Hayward, *Proteins* **1999**, *36*, 425–435.
[9] D. Pogocki, E. Ghezzo-Schöneich, C. Schöneich, *J. Phys. Chem. B* **2001**, *105*, 1250–1259.

 © 2003 Wiley-VCH Verlag GmbH & Co. KGaA, Weinheim

[10] M. Mutter, *J. Am. Chem. Soc.* **1977**, *99*, 8307 – 8314.
[11] P. A. Karplus, G. E. Schulz, *Naturwissenschaften* **1985**, *72*, 212 – 213.
[12] R. Bhaskaran, P. K. Ponnuswamy, *Int. J. Pept. Protein Res.* **1988**, *32*, 241 – 255.
[13] M. Vihinen, E. Torkkila, P. Riikonen, *Proteins* **1994**, *19*, 141 – 149.
[14] S. H. Gellman, *Acc. Chem. Res.* **1998**, *31*, 173 – 180.
[15] W. F. van Gunsteren, R. Bürgi, C. Peter, X. Daura, *Angew. Chem.* **2001**, *113*, 363 – 367; *Angew. Chem. Int. Ed.* **2001**, *40*, 351 – 355.
[16] W. M. Nau, X. Wang, *ChemPhysChem* **2002**, *3*, 393 – 398.
[17] R. R. Hudgins, F. Huang, G. Gramlich, W. M. Nau, *J. Am. Chem. Soc.* **2002**, *124*, 556 – 564.
[18] O. Bieri, J. Wirz, B. Hellrung, M. Schutkowski, M. Drewello, T. Kiefhaber, *Proc. Natl. Acad. Sci. USA* **1999**, *96*, 9597 – 9601.
[19] L. J. Lapidus, P. J. Steinbach, W. A. Eaton, A. Szabo, J. Hofrichter, *J. Phys. Chem. B* **2002**, *106*, 11 628 – 11 640.
[20] I.-C. Yeh, G. Hummer, *J. Am. Chem. Soc.* **2002**, *124*, 6563 – 6568.
[21] Most amino acids have been shown not to act as quenchers. Only Trp, Tyr, Cys, and Met are themselves quenchers (ref. [17]) and these four amino acids could consequently not be included in the present study; the fluorescence lifetimes of peptides containing these amino acids in their backbone would be too short. Also His becomes a fairly strong quencher in its unprotonated form (above pH 6, ref. [17]), such that His could only be studied at low pH values in its protonated form.
[22] CD measurements were performed for all peptides (including measurements at different pH values, for example, for protonated and unprotonated Lys and Glu). The CD patterns are characteristic of random-coil conformations, which excludes the occurrence of sizable amounts of secondary structures in any of the investigated short peptides, including the peptides composed of amino acids with known α-helix propensity. The only exception was the Pro-derived peptide since, according to the CD spectrum, it adopts its characteristic PPII helix.
[23] D. V. Mikhailov, L. Washington, A. M. Voloshin, V. A. Daragan, K. H. Mayo, *Biopolymers* **1999**, *49*, 373 – 383.
[24] J. Koca, *Prog. Biophys. Mol. Biol.* **1998**, *70*, 137 – 173.
[25] D. Voet, J. G. Voet, C. W. Pratt, *Fundamentals of Biochemistry*, J. Wiley and Sons, New York, **1999**.
[26] P. Chakrabarti, D. Pal, *Prog. Biophys. Mol. Biol.* **2001**, *76*, 1 – 102.
[27] D. Pal, P. Chakrabarti, *Acta Crystallogr. D* **2000**, *56*, 589 – 594.
[28] M. Levitt, *Biochemistry* **1978**, *17*, 4277 – 4285.
[29] E. G. Hutchinson, J. M. Thornton, *Protein Sci.* **1994**, *3*, 2207 – 2216.
[30] V. Muñoz, L. Serrano, *Proteins* **1994**, *20*, 301 – 311.
[31] P. Koehl, M. Levitt, *Proc. Natl. Acad. Sci. USA* **1999**, *96*, 12 524 – 12 529.
[32] C. N. Pace, J. M. Scholtz, *Biophys. J.* **1998**, *75*, 422 – 427.
[33] M. Monné, M. Hermansson, G. von Heijne, *J. Mol. Biol.* **1999**, *288*, 141 – 145.
[34] P. Y. Chou, G. D. Fasman, *Biophys. J.* **1979**, *26*, 367 – 383.
[35] A. G. Street, S. L. Mayo, *Proc. Natl. Acad. Sci. USA* **1999**, *96*, 9074 – 9076.
[36] A. Perczel, I. Jákli, B. M. Foxman, G. D. Fasman, *Biopolymers* **1996**, *38*, 723 – 732.

 © 2003 Wiley-VCH Verlag GmbH & Co. KGaA, Weinheim

Molecular Electronics

Optical Logic Operation Based on Polymer Langmuir–Blodgett-Film Assembly**

*Jun Matsui, Masaya Mitsuishi, Atsushi Aoki, and Tokuji Miyashita**

For the development of nanotechnology, the design and fabrication of molecular electronics and photonics have become active areas of research. Recently several kinds of molecular devices, such as switches,[1–6] wires,[7–9] rectifiers,[10–13] and logic gates[14] have been reported. The molecular logic gate is an important device to enable information processing and computation at the molecular level. At present, several molecules that act as one of the three basic logic operations (AND, NOT, and OR) have been designed and synthesized. For the AND logic operation, most of the molecular logic gates have used chemical signals as inputs (or an input) and the performance has been limited to the solution phase.[14–19] To construct solid-state molecular logic devices, the immobilization of molecules onto solid substrates is essential. The Langmuir–Blodgett (LB) technique is one of powerful techniques to build up nanoassemblies onto solid supports. Heath et al. have succeeded in fabricating solid-state AND and OR logic gates by the deposition of a rotaxane onto a solid substrate using the LB technique.[20] In the device, an electrical signal (voltage and current) is used as an input and an output signal, so the device is similar in principle to conventional diode-based, wired logic gates.

Herein, a novel optical AND logic gate using polymer LB-film multi-assemblies is described. Fujihira and Gotoh have reported that molecular photodiodes can be constructed by LB-film multi-assemblies.[21] Our idea is based on the current rectification of the heterodeposited redox-polymer LB film that has been reported previously;[22] when visible light irradiates polymer LB films consisting of a ruthenium (sensitizer) containing monolayer and a ferrocene (electron donor) containing monolayer, the direction of photocurrent flow is completely controlled by the deposition order of the polymer monolayers containing the ruthenium and the ferrocene complex. This photocurrent rectification feature, which we call a "polymer nanosheets diode", has been applied to fabricate the AND logic gate with polymer LB films. Two

[*] Prof. T. Miyashita, Dr. J. Matsui, Dr. M. Mitsuishi, Dr. A. Aoki
Institute of Multidisciplinary Research for Advanced Materials (IMRAM)
Tohoku University
2-1-1 Katahira, Aoba-ku, Sendai 980-8577 (Japan)
Fax: (+81) 22-217-5642
E-mail: miya@tagen.tohoku.ac.jp

[**] This work was partially supported by a Grant-in-Aid for Scientific Research (No. 14205130) from The Ministry of Education Science, Sports, and Culture of Japan. J.M. thanks the Japan Society for the Promotion of Science for Young Scientists for a research fellowships.

Supporting information for this article is available on the WWW under http://www.angewandte.org or from the author.

 © 2003 Wiley-VCH Verlag GmbH & Co. KGaA, Weinheim DOI: 10.1002/anie.200250767

nanosheets diodes that operate at different wavelengths were configured to produce the AND logic gate. One nanosheets diode was constructed from a phenanthrene-based (Phen) polymer LB film and an electron-acceptor polymer LB film, and the other was constructed from anthracene-based (AMMA) polymer LB film and an electron-donor polymer LB film (Figure 1). In this optical AND logic gate, input

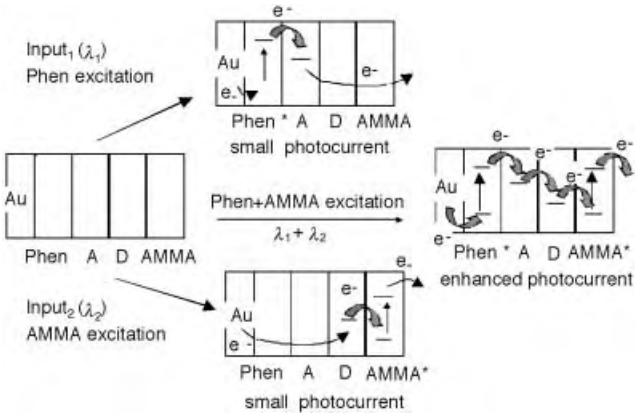


Figure 1. Schematic illustration for the concept of an AND logic-gate device using polymer LB films. A = electron-acceptor, D = electron-donor-polymer LB films.

signals are the excitation wavelengths of each chromophore and the output is the photocurrent, which is attributed to the interlayer charge-transfer between the chromophore layer and the donor or the acceptor layer. The phenanthrene and anthracene chromophores can be selectively excited because they have no overlap in their absorption spectra. In the selective excitation of phenanthrene or anthracene, photoinduced electron transfer from the photoexcited phenanthrene to the electron acceptor or from the electron donor to the photoexcited anthracene can occur independently. However, the magnitude of the photocurrent will be small because the unexcited layer acts as an insulating layer for the charge transport. On the other hand, in the case of the dual excitation, all the layers act not only as a charge-generating layer, but also as a charge-transporting layer. The direction of electron flow in the two photoinduced charge transfers is the same, so that the enhancement of photocurrent is expected (Figure 1).

The phenanthrene-based copolymer p(*t*PA/Phen) was prepared from free-radical copolymerization of 9-phenanthrylmethyl acrylate (Phen) with *tert*-pentylacrylamide (*t*PA), and the anthracene-based copolymer p(nPMA/AMMA) was prepared from 9-anthrylmethyl methacrylate (AMMA) with neopentyl methacrylamide (nPMA). The electron-acceptor copolymer, p(*t*PA/DNB), was prepared by the reaction of 3,5-dintrobenzoyl chloride (DNB) with p(*t*PA-*co*-2-hydroxymethyl acrylate) and the electron-donating copolymer, p(*t*PA/DMA) was synthesized by the reaction of 4-dimethylaminobenzylamine dihydrochloride (DMA) with p(*t*PA-*co*-*N*-acryloxysuccinimide; Figure 2). Mole contents of the functional groups were determined by UV/Vis spectroscopy. Stable monolayer formation of the copolymers on the water

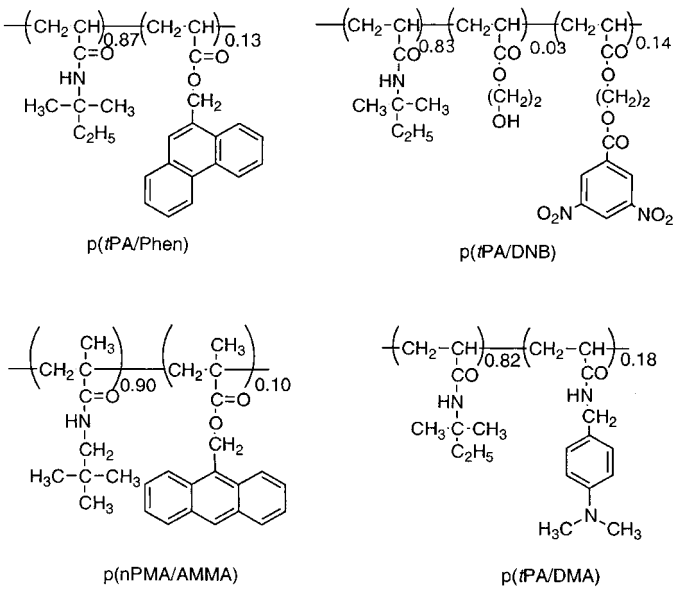


Figure 2. Chemical structure of the polymers.

surface was confirmed by surface pressure–area isotherm measurements and the monolayers can be transferred regularly onto a solid substrate in a tailor-made manner by using the LB technique (see Supporting Information for details of experiments).

The interlayer charge transfer between the p(*t*PA/Phen) layer and the p(*t*PA/DNB) layer or between the p(nPMA/AMMA) and p(*t*PA/DMA) layers in the heterodeposited LB film was investigated by fluorescence spectroscopy. The heterodeposited film structures are given in inset of Figure 3. A non-labeled polymer LB film (a *N*-dodecylacrylamide homopolymer (p(DDA)) LB film) was deposited on the quartz plate as a primary layer to prevent influence of the substrate on the fluorescence. The fluorescence of the phenanthrene chromophore was efficiently quenched when p(*t*PA/DNB) was deposited on the top of p(*t*PA/Phen) LB film (Figure 3a), and the anthracene fluorescence was also quenched by p(*t*PA/DMA) LB film (Figure 3b). As mentioned above, the quenching is caused by an interlayer electron transfer from the excited p(*t*PA/Phen) layer to the p(*t*PA/DNB) layer (oxidative quenching) and from the p(*t*PA/DMA) layer to the excited p(nPMA/AMMA) layer (reductive quenching). The energy-transfer quenching is ruled out because the overlap of the fluorescence of each chromophore with the electron donor or acceptor absorption was negligible (see Supporting Information).

For the AND logic operation, four polymer LB films were assembled as shown in the inset of Figure 4. From the previous reports, the thickness of each layer is estimated to be 1.0 nm.[23,24] In this film configuration a cathodic photocurrent is expected whichever chromophore was excited. The photocurrent was monitored as an output signal by using a three-electrode cell equipped with an Au electrode modified with the polymer LB films (working electrode), a platinum wire (counter electrode), a saturated calomel electrode (SCE; reference electrode), and 0.1 M $NaClO_4$ as supporting electro-

 © 2003 Wiley-VCH Verlag GmbH & Co. KGaA, Weinheim

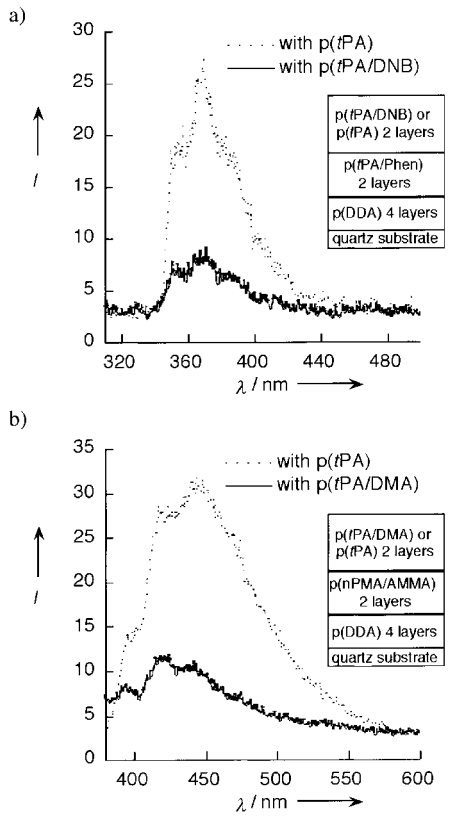
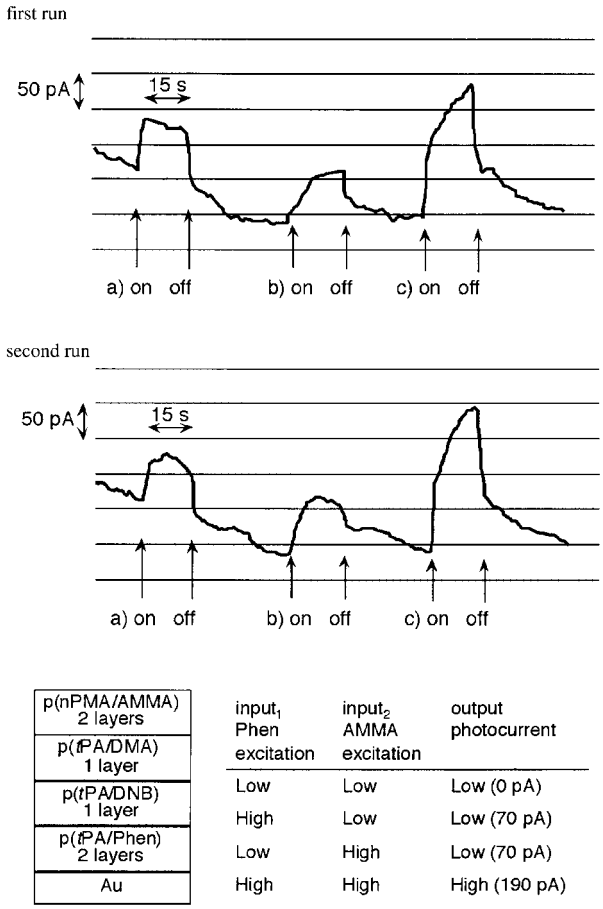


Figure 3. Fluorescence spectra of the heterodeposited film: a) phenanthrene fluorescence spectra with and without acceptor layers, b) anthracene fluorescence spectra with and without donor layers. Insets: Film structure for the fluorescence measurements.



input$_1$ Phen excitation	input$_2$ AMMA excitation	output photocurrent
Low	Low	Low (0 pA)
High	Low	Low (70 pA)
Low	High	Low (70 pA)
High	High	High (190 pA)

Figure 4. The photocurrent response of the AND logic gate for two monochromatic light beams. a) $\lambda_{ex} = 300$ nm (phenanthrene excitation) b) $\lambda_{ex} = 380$ nm (anthracene excitation) c) $\lambda_{ex} = 300$ nm and 380 nm (phenanthrene and anthracene excitation). Inset: film structure for the AND logic gate operation and truth table for the logic gate.

lyte. The solution was initially purged with N_2 for 30 min to remove oxygen. A 500-W xenon lamp and a 500-W deep UV lamp were used as the light source, and the interference filters (300 nm and 380 nm) were used to obtain monochromatic light. The irradiation light intensity at the substrate surface was measured with a power meter (0.5 mW cm^{-2} for 300 nm and 1.4 mW cm^{-2} for 380 nm). Figure 4 shows the photocurrent response of the polymer LB-film assembly. In the case of selective photoexcitation of the phenanthrene layer at 300 nm, almost 70 pA was generated by the interlayer charge transfer between phenanthrene and dinitrobenzene unit and also the selective photoexcitation of the anthracene layer at 380 nm produced approximately 70 pA by a similar manner. On the other hand, the excitation of both chromophore layers produced approximately 190 pA photocurrent. This is 1.4-times larger than the sum of the photocurrent obtained by selective photoexcitation (140 pA). This nonlinear response indicates that in the both-excitation condition, the layers are working not only as charge-generating layers but also as charge-transporting layers. Although these photocurrents were small, the reproducibility was confirmed by repeat measurements (Figure 4 second run). Furthermore, a difference between high and low states of a factor of 2.7 was achieved.

In conclusion, a novel concept for optical AND logic gates was proposed and its performance was clearly demonstrated for a polymer LB-film assembly. The AND logic gate was composed of two photoredox polymer nanosheet pairs, that is, p(*t*PA/Phen)/p(*t*PA/DNB) and p(nPMA/AMMA)/p(*t*PA/DMA) pairs. The input signals are the excitation of phenanthrene and anthracene, and the output signal is photocurrent. Although the high and low levels of the gates were separated only by a factor of 2.7, it will be increased with selecting a chromophore which has an absorbance at longer wavelength, a high charge mobility, and/or by modifying the layer structure. Moreover, the use of lasers as an excitation source will also increase the output photocurrent. The optimization of the layer structure and chromophore pairs is now in progress.

Received: December 13, 2002 [Z50767]

Keywords: charge transfer · chromophores · logic gates · molecular devices · thin films

[1] a) A. S. Lukas, S. E. Miller, M. R. Wasielewski, *J. Phys. Chem. B* **2000**, *104*, 931–940; b) A. S. Lukas, P. J. Bushard, M. R. Wasielewski, *J. Am. Chem. Soc.* **2001**, *123*, 2440–2441.

 © 2003 Wiley-VCH Verlag GmbH & Co. KGaA, Weinheim

[2] A. P. de Silva, H. Q. N. Gunaratne, T. Gunnlaugsson, A. J. M. Huxley, C. P. McCoy, J. T. Rademacher, E. T. Rice, *Chem. Rev.* **1997**, *97*, 1515 – 1566.
[3] C. P. Collier, J. O. Jeppesen, Y. Luo, J. Perkins, E. W. Wong, J. R. Heath, J. F. Stoddart, *J. Am. Chem. Soc.* **2001**, *123*, 12632 – 12641.
[4] J. Chen, M. A. Reed, A. M. Rawlett, J. M. Tour, *Science* **1999**, *286*, 1550 – 1551.
[5] L. Gobbi, P. Seiler, F. Diederich, V. Gramlich, C. Boudon, J. P. Gisselbrecht, M. Gross, *Helv. Chim. Acta* **2001**, *84*, 743 – 777.
[6] Special issue on Photochromism: Memories and Switches, *Chem. Rev.* **2000**, *100*, 1683 – 1890.
[7] R. Ziessel, A. Harriman, *Coord. Chem. Rev.* **1998**, *171*, 331 – 339.
[8] a) R. W. Wagner, J. S. Lindsey, *J. Am. Chem. Soc.* **1994**, *116*, 9759 – 9760; b) R. K. Lammi, R. W. Wagner, A. Ambroise, J. R. Diers, D. F. Bocian, D. Holten, J. S. Lindsey, *J. Phys. Chem. B* **2001**, *105*, 5341 – 5352.
[9] M. Mayor, M. Büschel, K. M. Fromm, J.-M. Lehn, J. Daub, *Chem. Eur. J.* **2001**, *7*, 1266 – 1273.
[10] G. J. Ashwell, D. S. Gandolfo, *J. Mater. Chem.* **2002**, *12*, 411 – 415.
[11] R. M. Metzger, T. Xu, I. R. Peterson, *J. Phys. Chem. B* **2001**, *105*, 7280 – 7290.
[12] A. Quintel, J. Hulliger, *Synth. Met.* **1999**, *107*, 183 – 190.
[13] S. Q. Zhou, Y. Q. Liu, W. F. Qui, Y. Xu, X. B. Huang, Y. S. Li, L. Jiang, D. B. Zhu, *Adv. Funct. Mater.* **2002**, *12*, 65 – 69.
[14] F. M. Raymo, *Adv. Mater.* **2002**, *14*, 401 – 414.
[15] a) A. P. de Silva, H. Q. N. Gunaratne, C. P. McCoy, *J. Am. Chem. Soc.* **1997**, *119*, 7891 – 7892; b) A. P. de Silva, I. M. Dexon, H. Q. N. Gunaratne, T. Gunnlaugsson, P. R. S. Maxwell, T. E. Rice, *J. Am. Chem. Soc.* **1999**, *121*, 1393 – 1394; c) A. P. de Silva, N. D. McClenaghan, *J. Am. Chem. Soc.* **2000**, *122*, 3965 – 3966.
[16] a) M. Asakawa, P. R. Ashton, V. Balzani, A. Credi, G. Mattersteig, O. A. Matthews, M. Montalti, N. Spencer, J. F. Stoddart, M. Venturi, *Chem. Eur. J.* **1997**, *3*, 1992 – 1996; b) A. Cred, V. Balzani, S. J. Langford, J. F. Stoddart, *J. Am. Chem. Soc.* **1997**, *119*, 2979 – 2981.
[17] a) F. Pina, A. Roque, M. M. Melo, I. Maestri, L. Belladelli, V. Balzani, *Chem. Eur. J.* **1998**, *4*, 1184 – 1192; b) F. Pina, M. Maestri, V. Balzani, *Chem. Commun.* **1999**, 107 – 114.
[18] a) D. Parker, J. A. G. Williams, *Chem. Commun.* **1998**, 245 – 246; b) T. Gunnlaugsson, D. A. MacDonail, D. Parker, *Chem. Commun.* **2000**, 93 – 94.
[19] H. F. Ji, R. Dabestani, G. M. Brown, *J. Am. Chem. Soc.* **2000**, *122*, 9306 – 9307.
[20] C. P. Collier, E. W. Wong, M. Belohradsky, F. M. Raymo, J. F. Stoddart, P. J. Kuekes, R. S. Williams, J. R. Heath, *Science* **1999**, *285*, 391 – 394.
[21] M. Fujihira, Y. Gotoh, in *Nanostructures based on molecular materials* (Eds.: W. Göpel, C. Ziegler), VCH, Weinheim, **1992**.
[22] A. Aoki, Y. Abe, T. Miyashita, *Langmuir* **1999**, *15*, 1463 – 1469.
[23] T. Taniguchi, Y. Yokoyama, T. Miyashita, *Macromolecules* **1997**, *30*, 3646 – 3649.
[24] Y. Guo, M. Mitsuishi, T. Miyashita, *Macromolecules* **2001**, *34*, 3548 – 3551.

 © 2003 Wiley-VCH Verlag GmbH & Co. KGaA, Weinheim

Probing Protein Folding

Incorporation of Selenomethionine into Proteins through Selenohomocysteine-Mediated Ligation**

*Gerard Roelfes and Donald Hilvert**

The chemical synthesis of moderate-sized proteins has benefited enormously from the development of chemoselective methods for the ligation of peptide fragments.[1] In this regard, the reaction of peptide thioesters with peptides containing an N-terminal cysteine has proved particularly powerful.[2] The thiol side chain of cysteine attacks the thioester and subsequent acyl transfer from sulfur to the amine yields a native peptide bond. Homocysteine,[3] sulfur-containing auxiliary groups,[4] and selenocysteine[5] have also been exploited to mediate ligations to thioesters, thus broadening the scope of the method. Herein we show that selenohomocysteine can also facilitate efficient peptide ligation (Scheme 1 a). Subsequent methylation of the resulting selenol affords selenomethionine at the ligation site, which is a useful probe for NMR spectroscopic[6] and X-ray crystallographic[7] investigations of biomolecules.

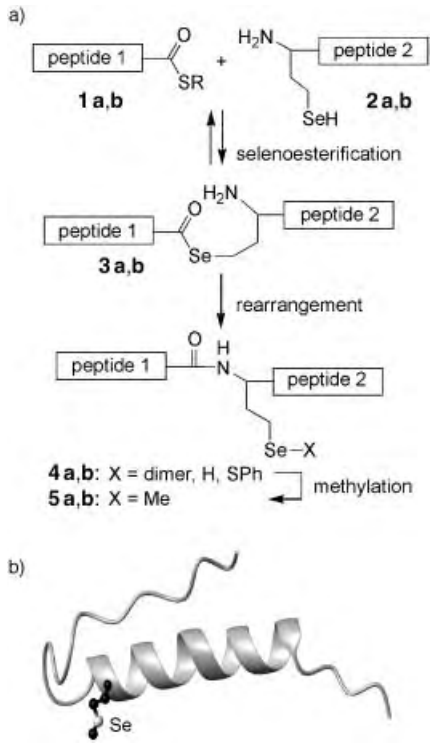
The strategy employed is illustrated by the model ligation of LYRAG-SEt with selenohomocystine. This reaction was carried out at a peptide concentration of 1 mM in Tris-HCl buffer (100 mM, pH 8.5; Tris = tris(hydroxymethyl)aminomethane) in the presence of guanidinium chloride (GdmCl; 6 M) and thiophenol (5 % v/v). Thiophenol helps to activate the thioester and also reduces the diselenide to the corresponding selenol. At pH 7–8, more than 90 % conversion was observed after 4 h, and the reaction was essentially complete within 20 h. Comparable results were obtained with homocysteine in control experiments.[5] The ligation product was isolated as a variable mixture of diselenide, a mixed selenosulfide (with thiophenol), and a species with the mass of the free selenol that was slowly converted into the diselenide upon exposure to air. The combined yield was 98 %. The reaction was somewhat slower in a phosphate buffer but also complete within 24 h. The addition of tris(2-carboxyethyl)phosphane hydrochloride (TCEP) to reduce the diselenide did not increase the rate of reaction, but did lead to the formation

[*] Prof. Dr. D. Hilvert, Dr. G. Roelfes
Laboratorium für Organische Chemie
Swiss Federal Institute of Technology (ETH)
ETH-Hönggerberg, 8093 Zürich (Switzerland)
Fax: (+41) 1-632-1486
E-mail: Hilvert@org.chem.ethz.ch

[**] We thank Brigitte Brandenberg and Bernhard Jaun for assistance with the NMR spectra, Richard Thomas for the analytical ultracentrifugation analysis, and the ETH Zürich and Novartis Pharma for financial support. G.R. wishes to thank the Netherlands Organisation for Scientific Research (NWO) for a Talent Fellowship.

Supporting Information for this article (including detailed experimental procedures, representative HPLC traces, a GdmCl titration curve, and analytical ultracentrifugation and CD data) is available on the WWW under http://www.angewandte.org or from the author.

 DOI: 10.1002/anie.200250830 © 2003 Wiley-VCH Verlag GmbH & Co. KGaA, Weinheim



Scheme 1. a) Schematic representation of a selenohomocysteine-ligation–methylation strategy. Model reaction: peptide 1 = LYRAG, peptide 2 = -CO_2H; seleno-bPP: peptide 1 = bPP(1-16), APLEPEYPGDNATPEQ-SEt, peptide 2 = bPP(18-36), -AQYAAELRRYINMLTRPRY-NH_2; b) MOLMOL[17] representation of the proposed structure of monomeric seleno-bPP based on the NMR structure of bPP from Ref. [12], which shows the position of the selenomethionine within the typical PP fold.

of more side products.[8] The diselenide was methylated under reducing conditions with methyl 4-nitrobenzenesulfonate, which has been successfully employed in the conversion of homocysteine into methionine.[3] Complete conversion was observed within 30 minutes in the presence of an excess of the methylating agent (2.5–10 equivalents based on the monomeric peptide) and TCEP in a 1:1 mixture of phosphate (200 mM, pH 6.0) and acetonitrile. The pure selenomethionine-containing hexapeptide was obtained from the reaction in 66% yield. Larger excesses of the methylating agent, higher pH values, or longer reaction times resulted in a lower yield and gave rise to numerous side products. That side reactions can be minimized by performing the reaction at a relatively low pH value, because of the low pK_a values of selenols, is an advantage over the methylation of homocysteine.

The utility of the selenohomocysteine ligation strategy was demonstrated by the synthesis of seleno-bPP, a variant of bovine pancreatic polypeptide (bPP) that contains selenomethionine at position 17 as a spectroscopic probe for folding studies. bPP is a member of the neuropeptide Y (NPY) family,[9] involved in the regulation of food uptake.[10] It is 36 amino acids long, has methionine groups at positions 17 and 30, and has a C-terminal carboxamide group. At high concentrations bPP is homodimeric[11] and each monomer adopts the so-called pancreatic-polypeptide (PP) fold (Scheme 1b), which consists of a polyproline helix docked onto the hydrophobic face of an α helix.[12]

Seleno-bPP was synthesized as shown in Scheme 1a. The bPP(1-16) fragment activated as a C-terminal thioester **1b** and bPP(17-36) containing an N-terminal selenohomocysteine **2b** were assembled on a safety-catch resin and Rink-amide resin, respectively, using standard Fmoc chemistry with HBTU/HOBt activation (Fmoc = 9-fluorenylmethoxycarbonyl, HBTU = *O*-(benzotriazol-1-yl)-*N*,*N*,*N*′,*N*′-tetramethyluronium hexafluorophosphate, HOBt = 1-hydroxy-1*H*-benzotriazole). Compound **2b** was stored as a diselenide and was regenerated in situ by reduction with excess thiophenol in the standard ligation buffer (Tris-HCl (100 mM), GdmCl (6 M), pH 8.5). As expected for ligations involving glutamine thioesters,[13] the reaction with **1b** was considerably slower than the model ligation with LYRAG-SEt. However, full conversion could be achieved when a fourfold excess of the thioester was employed and the reaction was allowed to proceed for at least five days. This procedure yielded the expected ligation product as the diselenide and a mixed selenosulfide (with thiophenol) in a combined yield of 59% after purification. Both compounds were methylated independently with a tenfold excess of methyl 4-nitrobenzenesulfonate under the conditions described above to give the selenomethionine-containing bPP derivative in 78% yield. The identity of the final product was confirmed by electrospray-ionization mass spectroscopy (ESI-MS; found: m/z 4272.2, calcd for average isotope distribution: m/z 4273.6).

Seleno-bPP is homodimeric as determined by conventional sedimentation-equilibrium analytical ultracentrifugation,[14] and its circular dichroism (CD) spectrum is identical to that reported for native bPP.[15] It undergoes reversible unfolding in the presence of guanidinium chloride.[14] The denaturation was monitored by CD, which showed a broad transition region. Fitting the data to a two-state model gave $\Delta G(H_2O) = 2.67 \pm 0.08$ kcal mol^{-1}, $m = 705$ cal mol^{-1}M^{-1}, and $[GdmCl]_{1/2} = 3.8$ M.

The unfolding of seleno-bPP was monitored as a function of GdmCl concentration by ^{77}Se NMR spectroscopy, which revealed equilibrium details that were not observable by CD spectroscopy (Figure 1). Relatively high protein concentrations (10.5–12.5 mM) were required as a result of the low natural abundance of ^{77}Se (7.58%). Nevertheless, in the absence of denaturant, the ^{77}Se NMR spectrum of the protein exhibits a single signal at $\delta = 46$ ppm with a linewidth of 101 Hz. In GdmCl (6 M) a cluster of peaks in the vicinity of the signal for free selenomethionine in solution ($\delta = 76.8$ ppm under the same conditions) is observed. Apparently, the denatured state in this case consists of several discrete conformations that are stable on the NMR time scale. At intermediate GdmCl concentrations covering the transition region of the CD unfolding curve, two very broad peaks are evident, which indicate the presence of multiple species that interconvert only slowly. As the GdmCl concentration is increased, the intensity of the signal at $\delta \approx 70$ ppm increases relative to that at higher field and can thus be confidently assigned to the denatured protein. This signal is also subject to a modest downfield shift, which can be ascribed to the presence of GdmCl, as it parallels the $\delta = 4.5$ ppm downfield

 © 2003 Wiley-VCH Verlag GmbH & Co. KGaA, Weinheim

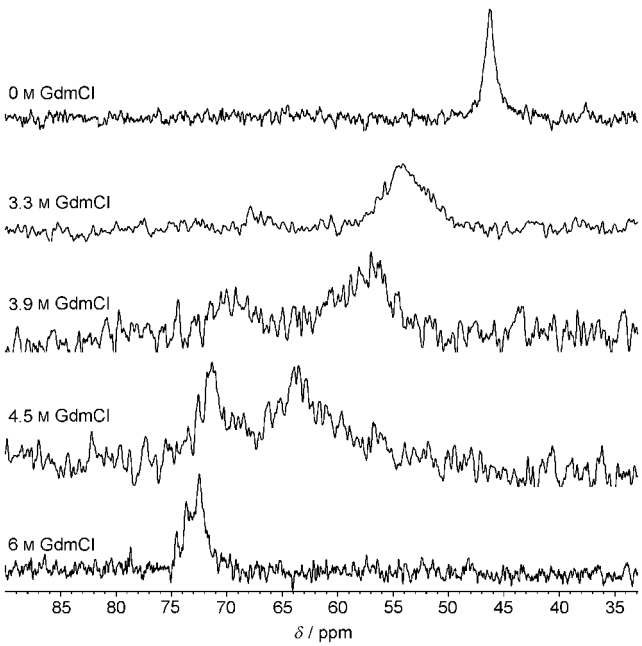


Figure 1. ^{77}Se NMR spectra of seleno-bPP at different GdmCl concentrations. Samples were measured in a solution of acetate in D_2O (150 mM, pH 4.2; uncorrected for the D effect) at 25 °C. Spectra were recorded at 95 MHz and the chemical shifts were referenced externally against Me_2Se (60% v/v) in $CHCl_3$. Chemical shifts were not corrected for the medium effect of GdmCl.

shift seen for free selenomethionine as the GdmCl concentration is increased from 0 to 6 M. The higher-field signal in the partially denatured samples is less readily assigned. However, based on the observed line broadening and chemical shifts it presumably represents an intermediate state that exhibits considerable dynamic behavior and is possibly in rapid equilibrium with the native protein.

A possible explanation for these observations is shown in Figure 2. The unfolding of the native dimeric protein (A) proceeds via an intermediate that further unfolds to give the denatured state (D). The intermediate could either be a monomeric species (B), or perhaps more likely, a dimer (C) in which the polyproline helices are no longer backfolded on the α helix, analogous to the structure of NPY.[16] A dynamic mixture of several intermediates is also possible.

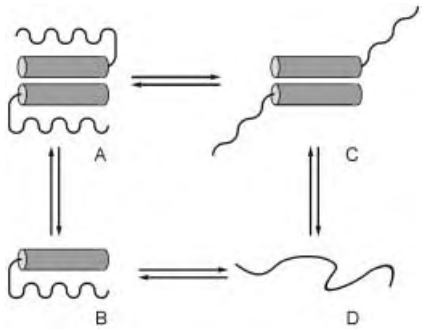


Figure 2. Schematic representation of the proposed unfolding mechanism of seleno-bPP.

In summary, selenohomocysteine-mediated ligation of peptides, followed by methylation of the resulting selenol, provides ready access to selenomethionine-containing peptides. The advantage of this strategy over the commonly used biosynthetic approach, with methionine auxotrophic strains supplemented with selenomethionine, is that it allows the site-selective introduction of a single selenomethionine into proteins in the presence of other methionines. As shown with seleno-bPP, this residue can provide unique information about the structure and dynamics of protein molecules.

Received: December 23, 2002 [Z50830]

Keywords: bioorganic chemistry · ligation · peptides · protein folding · selenium

[1] a) P. E. Dawson, S. B. H. Kent, *Annu. Rev. Biochem.* **2000**, *69*, 923–960; b) J. P. Tam, J. Xu, K. D. Eom, *Biopolymers* **2001**, *60*, 194–205; c) R. M. Hofman, T. W. Muir, *Curr. Opin. Biotechnol.* **2002**, *13*, 297–303.

[2] a) P. E. Dawson, T. W. Muir, I. Clark-Lewis, S. B. H. Kent, *Science* **1994**, *266*, 776–779; b) T. Wieland, E. Bokelmann, L. Bauer, H. U. Lang, H. Lau, *Justus Liebigs Ann. Chem.* **1953**, *583*, 129–149.

[3] J. P. Tam, Q. Yu, *Biopolymers* **1998**, *46*, 319–327.

[4] a) D. W. Low, M. G. Hill, M. R. Carrasco, S. B. H. Kent, P. Botti, *Proc. Natl. Acad. Sci. USA* **2001**, *98*, 6554–6559; b) J. Offer, C. N. C. Boddy, P. E. Dawson, *J. Am. Chem. Soc.* **2002**, *124*, 4642–4646.

[5] a) R. Quaderer, A. Sewing, D. Hilvert, *Helv. Chim. Acta* **2001**, *84*, 1197–1206; b) R. J. Hondal, B. L. Nilsson, R. T. Raines, *J. Am. Chem. Soc.* **2001**, *123*, 5140–5141; c) M. D. Gieselman, L. Xie, W. A. van der Donk, *Org. Lett.* **2001**, *3*, 1331–1334.

[6] a) N. P. Luthra, J. O. Odom in *The Chemistry of Organic Selenium and Tellurium Compounds, Vol. 1* (Eds.: S. Patai, Z. Rappaport), Wiley, Weinheim, **1986**, pp. 189–241; b) J. O. Boles, W. H. Tolleson, J. C. Schmidt, R. B. Dunlap, J. D. Odom, *J. Biol. Chem.* **1992**, *267*, 22217–22223.

[7] W. A. Hendrickson, J. R. Horton, D. M. LeMaster, *EMBO J.* **1990**, *9*, 1665–1672.

[8] The main side product (up to 18% yield) was the deselenated ligation product. Similar observations have been made in other selenium-mediated ligations.[5c]

[9] A. Bettio, A. G. Beck-Sickinger, *Biopolymers* **2001**, *60*, 420–437.

[10] G. Katsuura, A. Asakawa, A. Inui, *Peptides* **2002**, *23*, 323–329.

[11] M. Lerch, V. Gafner, R. Bader, B. Christen, G. Folkers, O. Zerbe, *J. Mol. Biol.* **2002**, *322*, 1117–1133.

[12] X. Li, M. J. Sutcliffe, T. W. Schwartz, C. M. Dobson, *Biochemistry* **1992**, *31*, 1245–1253.

[13] T. M. Hackeng, J. H. Griffin, P. E. Dawson, *Proc. Natl. Acad. Sci. USA* **1999**, *96*, 10068–10073.

[14] See Supporting Information.

[15] M. E. Noelken, P. J. Chang, J. R. Kimmel, *Biochemistry* **1980**, *19*, 1838–1843.

[16] a) R. Bader, A. Bettio, A. G. Beck-Sickinger, O. Zerbe, *J. Mol. Biol.* **2001**, *305*, 307–329; b) A. Bettio, M. C. Dinger, A. G. Beck-Sickinger, *Protein Sci.* **2002**, *11*, 1834–1844.

[17] R. Koradi, M. Billeter, K. Wüthrich, *J. Mol. Graphics* **1996**, *14*, 51–55.

 © 2003 Wiley-VCH Verlag GmbH & Co. KGaA, Weinheim

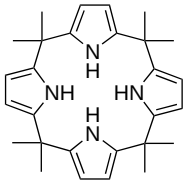
Anion Binding by Calix[n]bipyrroles

Calix[*n*]bipyrroles: Synthesis, Characterization, and Anion-Binding Studies**

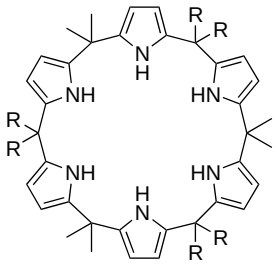
Jonathan L. Sessler, Deqiang An, Won-Seob Cho, and Vincent Lynch*

Anion-binding chemistry has emerged in recent years as one of the most intensely explored areas of supramolecular chemistry.[1,2] As a consequence, a number of elegant anion-binding systems are now known. Nonetheless, there remains a need for new receptors, particularly ones that are easy to make or which display unusual anion-binding characteristics. In 1996, the calix[4]pyrroles (for example, **1**), a venerable set of macrocycles dating from the late 1880s, were put forward as a new class of neutral anion-binding agents.[3] These simple-to-make, conformationally flexible macrocycles were found to bind small anions, such as fluoride, phosphate, and chloride, well in common aprotic solvents.[4–7] This observation has made the calix[4]pyrroles and their homologues of interest in a range applications that include anion sensing,[8] extraction,[9] and transport.[10] They have also been attached to solid supports and used to effect anion-specific separations.[11] In spite of their potential utility, the calix[4]pyrroles are plagued by binding "cavities" that are too small to make them efficient receptors for most larger anions, including specifically bromide and iodide in the halide series. Given this shortcoming, several research groups have worked to prepare so-called "higher order" calix[*n*]pyrroles ($n > 4$). In 1998, Eichen and co-workers reported the first syntheses of *meso*-substituted calix[6]pyrroles (for example, **2** and **3**).[12] Shortly thereafter, Kohnke and co-workers detailed a novel route based on the opening of the furan ring that permitted the synthesis of both calix[6]pyrrole **4** and calix[5]pyrrole **5**.[13] Contemporaneous with these latter efforts, our group reported one-pot syntheses of both β-decafluorocalix[5]pyrrole (**6**) and β-hexadecafluorocalix[8]pyrrole (**7**).[14] More recently, we have succeeded in isolating the corresponding β-dodecafluorocalix[6]pyrrole system (**8**).[15] Surprisingly, several of these larger systems did not show improved binding affinities for larger anions.[13d,16] This raises the question of whether other kinds of "expanded" calixpyrroles could be made that would indeed display enhanced selectivities for large anions. Here, we report the synthesis of calix[3]bipyrrole **10** and calix[4]bipyrrole **11**, representatives of a new class of calixpyrrole analogue containing bipyrrole (rather than pyrrole), and show that the first of these displays an affinity for bromide anions in dry acetonitrile that is greatly enhanced in both absolute and relative terms (that is, relative to the affinities of **1** and **10** for bromide and chloride anions, respectively).

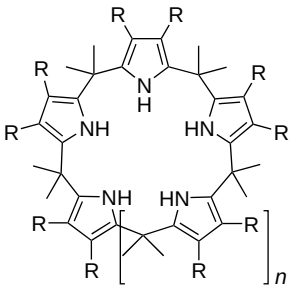
The synthesis of **10** and **11** is shown in Scheme 1. By analogy to the procedure used to prepare the parent calix[4]pyrrole **1**,[3–6] 2,2′-bipyrrole **9** was condensed with acetone in methanol in the presence of a catalytic amount of methanesulfonic acid. Bipyrrole **9** was synthesized in two steps from pyrrole and 2-pyrrolidinone as described previously in the literature.[17] Optimal conditions for the condensation involved stirring at room temperature for 2 h, followed by quenching with saturated aqueous sodium bicarbonate. The target macrocycles **10** and **11** were obtained in 24 and 29% yields, respectively, after purification by column chromatography (silica gel; dichloromethane eluent for **10**, followed by dichloromethane/ethyl acetate (98:2 v/v eluent) for **11**). Attempts to condense β-substituted bipyrroles, for example, 3,3′,4,4′-tetraethyl-2,2′-bipyrrole, proved unproductive. We attribute this latter lack of success to steric effects: interactions between the acetone-derived incipient *meso*-methyl groups and the β-alkyl substituents could be serving to inhibit both the various condensation steps and the ultimate ring-forming macrocyclization process.



1



2 R = phenyl
3 R = 4-pyridyl
4 R = CH_3



5 R = H, *n* = 1
6 R = F, *n* = 1
7 R = F, *n* = 4
8 R = F, *n* = 2

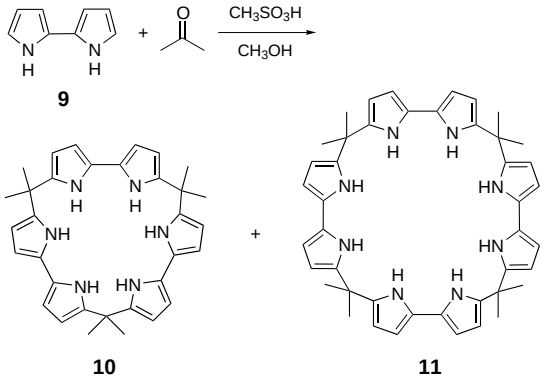
Compounds **10** and **11** were characterized by standard spectroscopic techniques (see Supporting Information). They

[*] Prof. J. L. Sessler, D. An, W.-S. Cho, V. Lynch
Department of Chemistry and Biochemistry
Institute for Cellular and Molecular Biology
The University of Texas at Austin
1 University Station—A5300, Austin, TX 78712-1167 (USA)
Fax: (+1) 512-471-7550
E-mail: sessler@mail.utexas.edu

[**] We thank the NIH for financial support (Grant No. GM 58907 to J.L.S.).

Supporting information for this article is available on the WWW under http://www.angewandte.org or from the author.

 © 2003 Wiley-VCH Verlag GmbH & Co. KGaA, Weinheim DOI: 10.1002/anie.200350941



Scheme 1. Synthesis of calix[3]bipyrrole **10** and calix[4]bipyrrole **11**.

were also characterized by X-ray diffraction analysis.[18] In the case of the calix[3]bipyrrole **10**, attempts to obtain diffraction grade crystals in the absence of an anion proved unsuccessful. However, crystals of the chloride anion complex of **10** were obtained by allowing a dichloromethane solution containing an excess of tetrabutylammonium chloride to undergo slow evaporation. X-ray structural analysis revealed that the calix[3]bipyrrole ligand adopts a conelike conformation, and that the six pyrrole NH protons are involved in hydrogen-bonding interactions to the chloride ion (Figure 1). The nitrogen-to-anion distances are in the range of 3.338(7)–3.382(8) Å, and the nitrogen-hydrogen-anion angles are in the range of 147.5–175.5°. As a result, the chloride anion resides 1.189(5) Å above the N_6 root-mean-square plane of the calix[3]bipyrrole core.

Diffraction-grade crystals of calix[4]bipyrrole **11** were grown from a tetrahydrofuran solution of the macrocycle layered between water and methanol. In this case, X-ray crystal analysis revealed that the calix[4]bipyrrole adopts a 1,3-alternate conformation in the solid state, with adjacent bipyrrole units oriented in opposite directions and each bipyrrole unit bonded to a tetrahydrofuran molecule through two NH(pyrrole)···O(THF) hydrogen bonds (Figure 2).[18] The two bipyrrole units at opposite positions are almost parallel to each other, while the plane of each bipyrrole unit is perpendicular to the plane of the tetrahydrofuran molecule hydrogen bonded to it.

The observation of a bound chloride anion in the solid-state structure of **10** led us to consider that it could act as an anion receptor in solution. Initial analyses were made by carrying out standard ^{1}H NMR titrations in [D_3]acetonitrile using the tetrabutylammonium chloride, bromide, and iodide salts (TBACl, TBABr, and TBAI) as the anion source. These analyses revealed evidence of very strong anion binding. For example, addition of approximately 0.1 equivalents of TBACl to an approximately 2 mM solution of calix[3]bipyrrole in [D_3]acetonitrile caused the pyrrole NH signal, originally

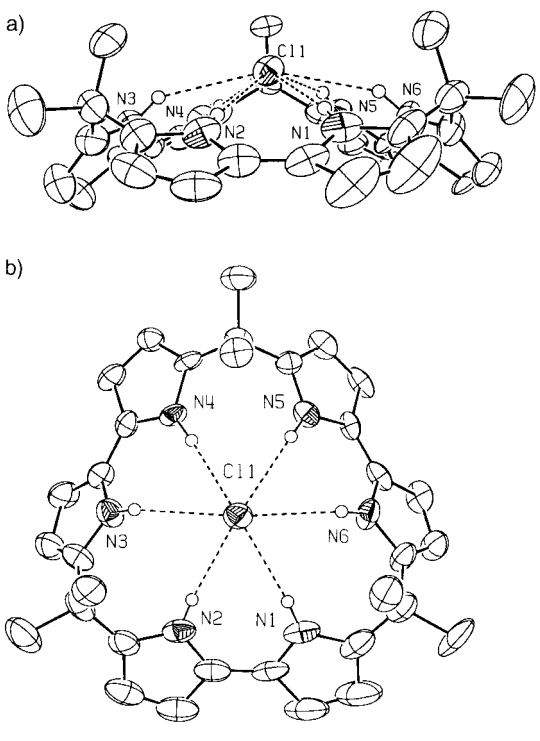


Figure 1. View of the molecular structure of the chloride complex of compound **10**·Cl. a) Side view; b) top view. Thermal ellipsoids are scaled to the 30% probability level. The molecule adopts a conelike conformation in the solid state. The chloride anion is bound to the calix[3]bipyrrole core through six NH···Cl bonding interactions (indicated by dashed lines).

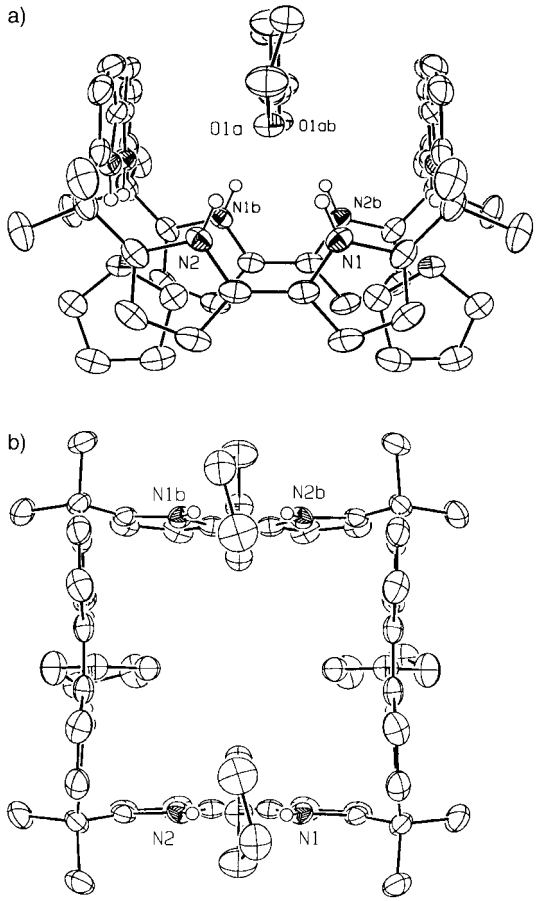


Figure 2. View of the molecular structure of **11**·4 THF. a) Side view; b) top view. Thermal ellipsoids are scaled to the 30% probability level. The molecule adopts a 1,3-alternate conformation in the solid state, with each bipyrrole unit being bound to a tetrahydrofuran molecule through two NH···O hydrogen bonds.

 © 2003 Wiley-VCH Verlag GmbH & Co. KGaA, Weinheim

present at $\delta = 8.52$ ppm, to split into two distinct signals, one at $\delta = 8.52$ ppm corresponding to the free calix[3]bipyrrole, and one at $\delta = 10.29$ ppm ascribed to the complex formed between calix[3]pyrrole and a chloride anion. Further additions of TBACl caused the siganl at $\delta = 8.52$ ppm to decrease in intensity, with a concomitent increase in the size of the signal at $\delta = 10.29$ ppm. The presence of the signal at $\delta =$ 8.52 ppm could no longer be discerned after the addition of about 0.7 equivalents, with further additions causing no apparent changes, either in the NH region, or in the spectrum as a whole. Such observations, which were seen also when TBABr was used as the anion source, preclude accurate assignments of either binding stoichiometry or association constants. However, they are consistent with strong binding and an equilibrium exchange process that is slow on the ^{1}H NMR time scale. In the case of TBAI in [D_3]acetonitrile, however, as well as in the cases of TBACl and TBABr in [D_6]DMSO, fast exchange was observed, with the NH signal moving to lower field in a monotonic manner upon the addition of increasing equivalents of anions. Good fits to 1:1 binding equilibria were obtained,[19] which allowed association constants K_a to be calculated in the usual way.[20] The resulting values (Table 1) provide support for the conclusion that receptor **10** displays affinities for bromide and iodide anions that are greatly enhanced relative to those of the parent system **1**.

Table 1: Association constants (M^{-1}) for the interaction of **10** and **1** with halide anions in acetonitrile and DMSO.[a]

Anion	Solvent	**10**	**1**	K_{rel}[e]
Cl^-	CH_3CN	110000[b]	140000[b]	0.79
	DMSO	9600[b]	1300[b]	
	[D_6]DMSO	15000[c]	1025[d]	14.6
Br^-	CH_3CN	100000[b]	3400[b]	29.4
	DMSO	440[b]	N.D.	
	[D_6]DMSO	450[c]	17[c]	26.5
I^-	CH_3CN	[f]	N.D.	
	[D_3]CH_3CN	9300[c]	17[c]	547
	[D_6]DMSO	N.D.	N.D.	

[a] Anions used in this assay were in the form of their tetrabutylammonium salts; values are the average of at least three separate measurements and are considered reproducible to ±15%; N.D.: not determined. [b] Value obtained from ITC titrations at 30°C. [c] Determined from ^{1}H NMR titrations carried out at 25°C. [d] From ref. [21]. [e] Represents the ratio of the association constants for **10** and **1**, respectively, recorded under identical conditions. [f] No reliable fit could be obtained.

Further studies of the anion-binding properties of receptor **10** were made using isothermal titration calorimetry (ITC). The advantages of this method in terms of permitting, for example, the analysis of calix[4]pyrrole···anion interactions characterized by high affinity have recently been highlighted by Schmidtchen.[7] In the present case, it allowed the association constants for the binding of both Cl^- and Br^- ions to **10** in dry acetonitrile to be determined, while also providing an independent confirmation of a representative subset of the K_a values originally determined by ^{1}H NMR titration as described above (see Table 1). In all cases, good fits to 1:1, but not 1:2 or 2:1, receptor:anion stoichiometries were obtained. Thus, the ITC measurements provide support for the notion that **10** binds a single halide anion (Cl^- or Br^-) under the solution-phase conditions of the ITC experiments, just as one would infer from the solid-state structure shown in Figure 1.[22] They also reinforce the conclusion drawn from the ^{1}H NMR analyses that calix[3]bipyrrole **10** is a good receptor for Br^- and I^- ions, both in absolute terms and when considered in comparison to calix[4]pyrrole **1**. Presumably, this observation reflects a better size- and geometry-based matching between the macrocyclic receptor and these larger anions, as well as the greater number of hydrogen-bond donor sites system **10** provides relative to **1**. Interestingly, detailed analysis of the ITC curves for **10** leads to the inference that in DMSO, but not CH_3CN, the binding process is dominated by entropic factors. Efforts to understand the origin of these observations, which are not seen for **1**, are ongoing.

In summary, we have described a new class of macrocyclic anion receptors, as well as a new member of the generalized calixpyrrole family. Current work is devoted to studying further the anion-binding properties of **10**, analyzing those of **11**, and preparing new macrocycles based on bipyrroles, terpyrroles, or combinations of these units and other heterocyclic building blocks, including simple, monomeric pyrroles.

Received: January 15, 2003 [Z50941]

Keywords: anions · calixpyrroles · halides · macrocycles · supramolecular chemistry

[1] D. B. Beer, P. A. Gale, *Angew. Chem.* **2001**, *113*, 502–532; *Angew. Chem. Int. Ed.* **2001**, *40*, 486–516.
[2] *Supramolecular Chemistry of Anions* (Eds.: A. Bianchi, K. Bowman-James, E. García-España), Wiley-VCH, New York, **1997**.
[3] P. A. Gale, J. L. Sessler, V. Král, V. Lynch, *J. Am. Chem. Soc.* **1996**, *118*, 5140–5141.
[4] P. A. Gale, J. L. Sessler, V. Král, *Chem. Commun.* **1998**, 1–8.
[5] J. L. Sessler, P. A. Gale in *The Porphyrin Handbook, Vol. 6* (Eds.: K. M. Kadish, K. M. Smith, R. Guilard), Academic Press, San Diego, **2000**, pp. 257–278.
[6] P. A. Gale, P. Anzenbacher, Jr., J. L. Sessler, *Coord. Chem. Rev.* **2001**, *222*, 57–102.
[7] F. P. Schmidtchen, *Org. Lett.* **2002**, *4*, 431–434.
[8] a) H. Miyaji, P. Anzenbacher, Jr., J. L. Sessler, E. L. Bleasdale, P. A. Gale, *Chem. Commun.* **1999**, 1723–1724; b) P. Anzenbacher, Jr., K. Jurisíkavá, J. L. Sessler, *J. Am. Chem. Soc.* **2000**, *122*, 9350–9351; c) H. Miyaji, W. Sato, J. L. Sessler, *Angew. Chem.* **2000**, *112*, 1847–1850; *Angew. Chem. Int. Ed.* **2000**, *39*, 1777–1780; d) J. L. Sessler, A. Gebauer, P. A. Gale, *Gazz. Chim. Ital.* **1997**, *127*, 723–726; e) P. A. Gale, M. B. Hursthouse, M. E. Light, J. L. Sessler, C. Warriner, R. Zimmerman, *Tetrahedron Lett.* **2001**, *42*, 6759–6762; f) P. A. Gale, L. J. Twyman, C. I. Handlin, J. L. Sessler, *Chem. Commun.* **1999**, 1851–1852.
[9] T. G. Levitskaia, M. Marquez, J. L. Sessler, J. A. Shriver, T. Vercoute, B. A. Moyer, *J. Am. Chem. Soc.*, submitted.
[10] a) J. L. Sessler, W. E. Allen, *CHEMTECH* **1999**, 16–24; b) J. L. Sessler, V. Král, T. V. Shishkanova, P. A. Gale, *Proc. Natl. Acad. Sci. USA* **2002**, *99*, 4848–4853.
[11] a) J. L. Sessler, P. A. Gale, J. W. Genge, *Chem. Eur. J.* **1998**, *4*, 1095–1099; b) J. L. Sessler, J. W. Genge, P. A. Gale, V. Král, *ACS Symp. Ser.* **2000**, *757*, 238–254.
[12] a) B. Turner, M. Botoshansky, Y. Eichen, *Angew. Chem.* **1998**, *110*, 2633–2637; *Angew. Chem. Int. Ed.* **1998**, *37*, 2475–2478;

 © 2003 Wiley-VCH Verlag GmbH & Co. KGaA, Weinheim

b) B. Turner, A. Shterenberg, M. Kapon, K. Suwinska, Y. Eichen, *Chem. Commun.* **2001**, 13 – 14; c) B. Turner, A. Shterenberg, M. Kapon, K. Suwinska, Y. Eichen, *Chem. Commun.* **2002**, 404 – 405; d) B. Turner, A. Shterenberg, M. Kapon, K. Suwinska, Y. Eichen, *Chem. Commun.* **2002**, 726 – 727.

[13] a) G. Cafeo, F. H. Kohnke, G. L. La Torre, A. J. P. White, D. J. Williams, *Angew. Chem.* **2000**, *112*, 1561 – 1563; *Angew. Chem. Int. Ed.* **2000**, *39*, 1496 – 1498; b) G. Cafeo, F. H. Kohnke, G. L. La Torre, A. J. P. White, D. J. Williams, *Chem. Commun.* **2000**, 1207 – 1208; c) G. Cafeo, F. H. Kohnke, G. L. La Torre, M. F. Parisi, R. P. Nascone, A. J. P. White, D. J. Williams, *Chem. Eur. J.* **2002**, *8*, 3148 – 3156; d) G. Cafeo, F. H. Kohnke, M. F. Parisi, R. P. Nascone, G. L. La Torre, D. J. Williams, *Org. Lett.* **2002**, *4*, 2695 – 2697.

[14] J. L. Sessler, P. Anzenbacher, Jr., J. A. Shriver, K. Jurisíková, H. Miyaji, V. Lynch, M. Marquez, *J. Am. Chem. Soc.* **2000**, *122*, 12061 – 12062.

[15] J. A. Shriver, PhD thesis, The University of Texas at Austin (USA), **2002**.

[16] Recently a detailed analysis of the chloride anion binding behavior of octafluorocalix[4]pyrrole and **6** was carried out in dry acetonitrile by isothermal calorimetry, and revealed association constants of 760000 and 47000 M^{-1} in the case of octafluorocalix[4]pyrrole and **6**, respectively: W.-S. Cho, J. L. Sessler, unpublished results. We consider these values more reliable than those determined by ^{1}H NMR titration methods as reported previously.[14]

[17] a) L. Groenendaal, H. W. I. Peerlings, J. L. J. van Dongen, E. E. Havinga, J. A. J. M. Vekemans, E. W. Meijer, *Macromolecules* **1995**, *28*, 116 – 123; b) U. Burger, F. Dreier, *Helv. Chim. Acta* **1980**, *63*, 1190 – 1197.

[18] a) Crystallographic summary for [**10**·Cl]·TBA·CH_2Cl_2. Very thin, light brown plates were grown by slow evaporation from dichloromethane, monoclinic, space group $P2_1/c$ (no. 14), $Z = 4$ in a cell of dimensions: $a = 12.6394(3)$, $b = 25.0959(6)$, $c = 16.5497(5)$ Å, $\beta = 108.614(1)°$, $V = 4974.9(2)$ Å^3, $\rho_{calcd} = 1.17$ g cm^{-3}, $\mu = 0.225$ mm^{-1}, $F(000) = 1896$. A total of 15672 reflections were measured ($2\theta_{max} = 50°$), 8657 unique ($R_{int} = 0.148$), on a Nonus Kappa CCD using graphite monochromatized $Mo_{K\alpha}$ radiation ($\lambda = 0.71073$ Å) at -120 °C. The structure was refined on F^2 to an $R_w = 0.169$, with a conventional $R = 0.142$ (3449 reflections with $F_o > 4[\sigma(F_o)]$), and GOF = 1.40 for 550 refined parameters. b) Crystallographic summary for **11**·4 THF. Light brown square plates were grown by layering a THF solution of the macrocyle over water and topping the THF with methanol, tetragonal, space group $I\bar{4}$ (no. 14), $Z = 4$ in a cell of dimensions $a = b = 16.4069(3)$, $c = 15.5522(2)$ Å, $V = 2840.51(9)$ Å^3, $\rho_{calcd} = 1.14$ g cm^{-3}, $\mu = 0.072$ mm^{-1}, $F(000) = 1056$. A total of 10600 reflections were measured ($2\theta_{max} = 55°$), 3277 unique ($R_{int} = 0.037$), on a Nonus Kappa CCD using graphite monochromatized $Mo_{K\alpha}$ radiation ($\lambda = 0.71073$ Å) at -120 °C. The structure was refined on F^2 to an $R_w = 0.0833$, with a conventional $R = 0.0391$ (2548 reflections with $F_o > 4[\sigma(F_o)]$), and a GOF = 1.03 for 249 refined parameters. CCDC-201040 ([**10**·Cl]·TBA·CH_2Cl_2) and CCDC-201041 (**11**·4 THF) contain the supplementary crystallographic data for this paper. These data can be obtained free of charge via www.ccdc.cam.ac.uk/conts/retrieving.html (or from the Cambridge Crystallographic Data Centre, 12 Union Road, Cambridge CB2 1EZ, UK; fax: (+44) 1223-336-033; or deposit@ccdc.cam.ac.uk).

[19] Binding stoichiometries were confirmed by independent Job plots; see the Supporting Information.

[20] C. S. Wilcox in *Frontiers in Supramolecular Organic Chemistry and Photochemistry* (Eds.: H.-J. Schneider, H. Dürr), VCH, Weinheim, **1991**, pp. 123 – 143.

[21] S. Camiolo, P. A. Gale, *Chem. Commun.* **2000**, 1129 – 1130.

[22] In the course of review, a referee noted with interest the fact that the affinity of calix[3]bipyrrole **10** for chloride anions is actually lower than that of calix[4]pyrrole **1** in acetonitrile, in spite of the greater number of potential NH donor sites in receptor **10** than in **1**. We rationalize this observation in terms of the poor size match between receptor **10** and a Cl^- ion. Specifically, we believe that the corresponding incommensurate binding geometry, as evidenced more by the unfavorable Cl-H-N angles seen in the solid state (ranging from 147.5–175.5°) than by the Cl···H-N hydrogen bond lengths, outweighs in an adverse sense the binding advantage that an increased number of hydrogen bonds would be expected to impart, at least in this relatively less polar solvent. This is not the case in DMSO. Here, the increased number of hydrogen-bond donor groups serves to overcome competition from the solvent, with the net result that stronger binding of a chloride anion is displayed by **10** relative to **1** in DMSO.

 © 2003 Wiley-VCH Verlag GmbH & Co. KGaA, Weinheim

Protonation of Cubylamine

Stereoelectronic, Strain, and Medium Effects on the Protonation of Cubylamine, a Janus-like Base**

José-Luis M. Abboud, Ilmar A. Koppel,* Ibon Alkorta, Ernest W. Della, Paul Müller, Juan Z. Dávalos, Peeter Burk,* Ivar Koppel, Viljar Pihl, and Esther Quintanilla*

In 1991 it was concluded on the basis of theoretical studies[1] that the amino group in cubylamine[2] (**1**NH_2, Scheme 1)

[*] Prof. Dr. J.-L. M. Abboud, Dr. J. Z. Dávalos, Eng. E. Quintanilla
Instituto de Química Física "Rocasolano", CSIC
C/Serrano, 119, 28006 Madrid (Spain)
Fax: (+34) 91-5855184
E-mail: jlabboud@iqfr.csic.es

Prof. Dr. I. A. Koppel, Prof. Dr. P. Burk, Dr. I. Koppel, Dr. V. Pihl
Institute of Chemical Physics, University of Tartu
2 Jakobi St. 51014 Tartu (Estonia)
Fax: (+372) 7-375-264
E-mail: ilmar@chem.ut.ee
peeter@chem.ut.ee

Dr. I. Alkorta
Instituto de Química Médica, CSIC
C/Juan de la Cierva, 3, 28006, Madrid (Spain)

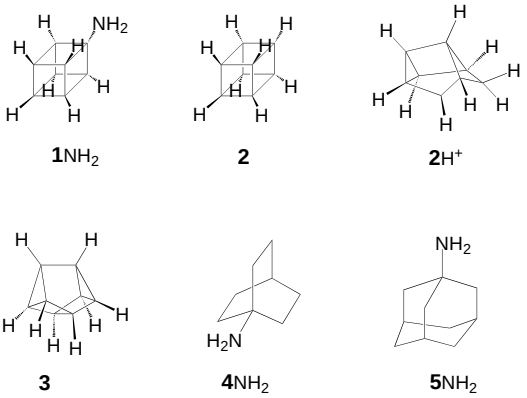
Prof. Dr. E. W. Della
Department of Chemistry, Flinders University
Bedford Park, South Australia 5042 (Australia)

Prof. Dr. P. Müller
Department of Organic Chemistry, University of Geneva
30, quai Ernest Ansermet, 1211 Geneva 4 (Switzerland)

[**] This work was supported by grants BQU2000-1497 (Spanish DGES) and 5226 (Estonian Science Foundation) and by a Joint Project CSIC-Estonian Academy of Sciences. "The Reactivity of the Strained Cage Molecules".

Supporting information for this article is available on the WWW under http://www.angewandte.org or from the author.

 DOI: 10.1002/anie.200350993 © 2003 Wiley-VCH Verlag GmbH & Co. KGaA, Weinheim



Scheme 1. Structures of cubylamine (**1**NH_2), cubane (**2**), tetracyclo[4.2.0.0^{2,4}.0^{3,8}]oct-7-ylium cation (**2**H^+), cuneane (**3**), bicyclo[2.2.2]oct-1-ylamine (**4**NH_2), and 1-adamantylamine (**5**NH_2).

interacts with the hydrocarbon moiety in a stereoelectronic fashion. To our knowledge, the potential consequences of this interesting feature were never explored. More recently we have shown[3] that the gas-phase protonation of the parent hydrocarbon, cubane (**2**), is irreversible and leads through ring opening to the formation of tetracyclo[4.2.0.0^{2,4}.0^{3,8}]oct-7-ylium cation (**2**H^+) which, on deprotonation, yields cuneane (**3**),[4] a less strained[5] isomer. These facts led us to study the protonation of **1**NH_2 in the gas phase (by using Fourier Transform Ion Cyclotron Resonance Spectroscopy, FT-ICR) and in solution (by means of potentiometric techniques as well as ^{1}H and ^{13}C NMR spectroscopy). The experimental findings were analyzed further by means of density functional theory (DFT) methods.[6]

We obtained the ^{1}H and ^{13}C NMR spectra of **1**NH_2 and its conjugate acid (see Supporting Information) and found that the ^{1}H and ^{13}C NMR shifts for **1**NH_2 are not only consistent with each other, but they are also in agreement with predicted shifts based on literature values for a number of monosubstituted cubanes.[7] Significantly, the data demonstrate that the cubic structure of the hydrocarbon framework of the parent hydrocarbon **2** is preserved in both **1**NH_2 and its conjugate acid. In addition, the ^{13}C chemical shifts of **2**,[8] **1**NH_2, and **1**NH_3^+ (assuming nitrogen protonation) from GIAO calculations[9] nicely correlate ($r^2 > 0.99$) with the experimental values.

The pK_a of **1**NH_3^+ in water at 25 °C (8.66 ± 0.02), which we measured,[10] can be compared to values given in Table 1 for other ammonium ions. There we see, for example, that **1**NH_3^+ is more acidic by two pK_a units than bicyclo[2.2.2]oct-1-ylammonium (**4**NH_3^+), a species having the same carbon content and a caged structure, and even more acidic than ammonium ion itself.

Table 1: Experimental pK_a and GB values for selected bases.

Base	pK_a[a]	GB [kcal mol^{-1}]
NH_3	9.24[b]	195.7[e]
CH_3NH_2	10.64[b]	206.6[e]
n-$C_3H_7NH_2$	10.53[b]	211.3[e]
bicyclo[2.2.2]oct-1-ylamine (**4**NH_2)	10.66[c]	217.8[e]
1-adamantylamine (**5**NH_2)	10.55 ± 0.02[d]	219.0[e]
1NH_2	8.66 ± 0.02[d]	(227.4 ± 2.3)[d,f]

[a] pK_a of the conjugate ion. [b] In kcal mol^{-1}. [b] From ref. [11]. [c] From ref. [12]. [d] This work. [e] From ref. [13]. [f] Apparent value.

To rationalize this result we carried out calculations at the B3LYP6-311 + G(d,p) level[14] (see Supporting Information). We found that the computed C–C bond lengths involving the carbon atom α to the amino group in **1**NH_2 (see Figure 1) fully

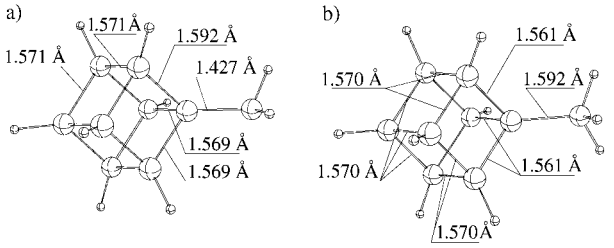


Figure 1. Selected geometry parameters for a) neutral and b) N-protonated cubylamine (B3LYP6-311 + G** data).

support the existence of a stabilizing stereoelectronic interaction, in which electron density is transferred from the amino group to the hydrocarbon moiety.[1] Furthermore, we have applied the NBO (natural bonding orbitals) methodology[15] to **1**NH_2 and found indeed a strong stabilizing interaction (14.2 kcal mol^{-1}) between the nitrogen lone pair and the antiperiplanar antibonding C–C orbital. This interaction, responsible for the elongation of the corresponding C–C bond, obviously disappears upon nitrogen protonation (see Figure 1). At the same level of theory the gas-phase basicity (GB) of **1**NH_2, assuming nitrogen protonation (i.e. the standard Gibbs energy change for Equation (1)), amounts

$$\mathbf{1}NH_3^+(g) \rightarrow \mathbf{1}NH_2(g) + H^+(g) \quad \Delta_r G^o(1) \qquad (1)$$

to 211.7 kcal mol^{-1}, a value close to the experimental value for the much less polarizable propylamine and significantly lower than GB(**4**NH_2) (see Table 1).

The intrinsic (gas-phase) basicity of **1**NH_2 (assuming protonation at nitrogen) is thus lower than expected on the basis of polarizability effects. The aqueous basicity of **1**NH_2 is also significantly lower than that of **4**NH_2 and other alicyclic and aliphatic primary amines. This is a very important fact, because these aqueous basicities are remarkably constant and very insensitive to polarizabilty effects,[16] a situation depicted in Figure 2. This implies the influence of a contribution other than polarizability.

All these results are consistent with **1**NH_2 behaving in solution as a nitrogen base weakened by electronic factors. In addition to the stereoelectronic interactions mentioned above, the most relevant electronic factors are likely hybridization effects originating in the large s character of the orbitals on the carbon bearing the amino group.[2b,17,18]

Our FT-ICR experiments show that under conditions of chemical ionization, **1**NH_2(g) is cleanly protonated to yield a

 © 2003 Wiley-VCH Verlag GmbH & Co. KGaA, Weinheim

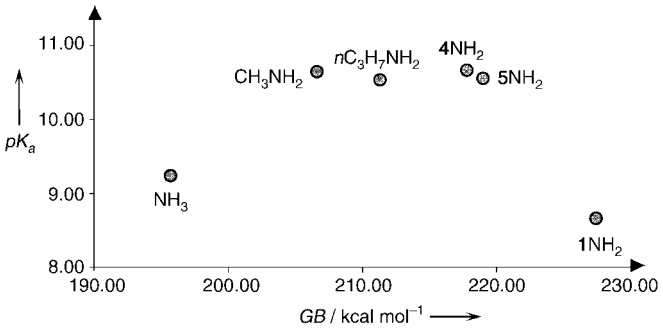


Figure 2. Correlation between gas-phase basicities and aqueous pK_a values for some amines.

cation $C_8H_{10}N^+$ (**6**H$^+$). Ion selection experiments were performed on mixtures of **1**NH_2(g) and a number of bases B of known GB to quantitatively examine the protonation of **1**NH_2(g) [Eq. (2)] and the deprotonation of **6**H$^+$ [Eq. (3)]

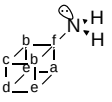
$$\mathbf{1}NH_2(g) + BH^+(g) \rightarrow \mathbf{6}H^+(g) + B(g) \quad \Delta_r G^o(2) \tag{2}$$

$$\mathbf{6}H^+(g) + B(g) \rightarrow \mathbf{6}(g) + BH^+(g) \quad \Delta_r G^o(3) \tag{3}$$

(details given in the Supporting Information). These experiments led to an "apparent gas-phase basicity" for **1**NH_2 of approximately 224.7 ± 2.3 kcal mol^{-1}. The structure of **6**H$^+$(g) has to be consistent with this finding.

The "apparent GB" of **1**NH_2(g) is appreciably higher than that of 1-adamantylamine (**5**NH_2, Scheme 1, GB = 219.0 kcal mol^{-1}), a primary amine endowed with a more polarizable framework and thus expected to be a stronger base in the gas phase. Cubylamine (**1**NH_2) is also 13 kcal mol^{-1} stronger than expected for nitrogen protonation (see above). These facts rule out the amino group as the basic center in the gas-phase molecule and, by analogy with the behavior of **2**(g), they suggest that **1**NH_2(g) is also undergoing ring opening on protonation.

There are six inequivalent carbon atoms in **1**NH_2 which can supposedly be the protonation centers (see Scheme 2). We summarize in Scheme 3 the structures and standard Gibbs energy changes computed at the B3LYP6-311 + G(d,p) level for the formation of all possible species **6**H$^+$(g) by protonation of **1**NH_2(g) in a one-step process as well as the most stable neutral products following deprotonation. Protonation at carbon f leads (without any barrier) to the N-protonated form **1**NH_3^+. Edge, face, and endohedral protonation of **1**NH_2 did not lead to independent minima, in analogy to **2**.[3]

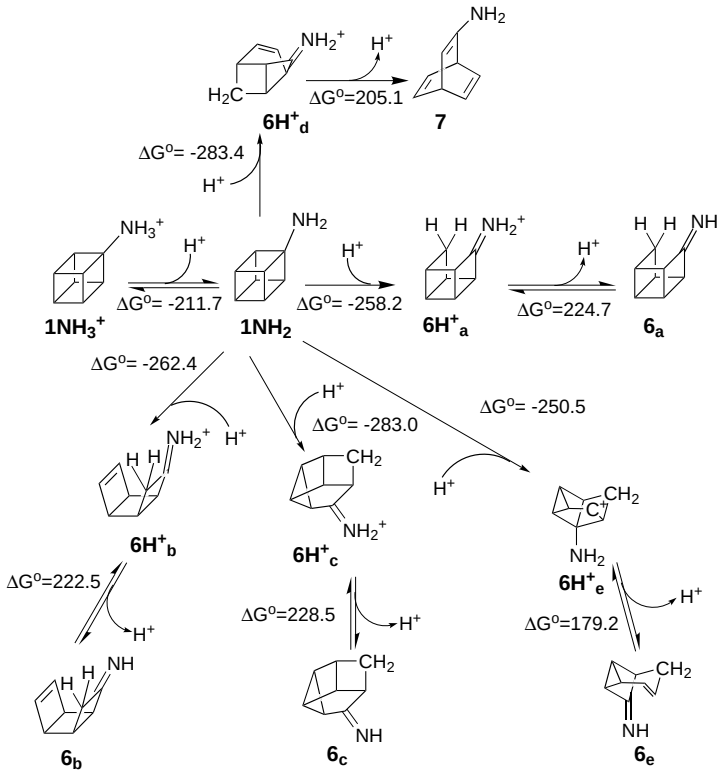


Scheme 2. Nonequivalent carbon atoms in **1**NH_2.

The computed Gibbs free energy changes of reaction (1) for carbon-protonated **1**NH_2(g) are at least 250.5 kcal mol^{-1}. Hence **1**NH_2(g) should be able to deprotonate the conjugate acids of bases with GB values of at least 250.5 kcal mol^{-1}. We maintain that the apparent GB for **1**NH_2(g) is appreciably smaller.

The fact that measurements in both the forward and reverse directions give the same basicity strongly suggests that kinetic factors are unimportant and that we are probing the properties of a single species, namely some (or all) of the ions **6**H^+_a–**6**H^+_e. Thus, when **1**NH_2 reacts in the gas phase with the ammonium ions mentioned above, it ring-opens to give a complex between one of these species and the deprotonated acid (i.e., reference base). The observable outcome is determined by the relative basicities of the ring-opened species and the reference amine, rather than by the difficulty of protonating the relevant carbon atom in **1**NH_2(g). There are important precedents of gas-phase isomerization through protonation[19]

Our computational results summarized in Scheme 3 are fully consistent with this concept, as iminium ions **6**H^+_a to **6**H^+_c can be deprotonated by bases with GB values in the



Scheme 3. Protonation of cubylamine at different sites and the preferred deprotonation of the resulting cations. All reaction free energies are given in kcal mol^{-1}.

range of 224.7 to 228.5 kcal mol^{-1} while the apparent GB of **1**NH_2 is 224.7 ± 2.3 kcal mol^{-1}. On these grounds, structures **6**H^+_d and **6**H^+_e can be excluded as the corresponding neutral bases (bicyclo[2.2.2]octa-2,5,7-trien-2-ylamine (**7**), GB = 204.4, and **6**$_e$, GB = 179.2 kcal mol^{-1}) are much weaker. On the other hand, in the light of the previous discussion, the formation of any of the structures **6**H^+_a to **6**H^+_c is possible and the formation of a mixture of these iminium ions can not be ruled out.

Last we draw attention to the importance of medium effects on the structure of protonated **1**NH_2. Although a number of cases have been reported wherein the structure of

 © 2003 Wiley-VCH Verlag GmbH & Co. KGaA, Weinheim

the protonated[20] or deprotonated[21] species is determined by the medium, this seems to be the first case involving a basic carbon center. Our computational results show that in the gas phase protonation followed by ring opening is favored over protonation at the amino group by 46.5–71.7 kcal mol^{-1}, and this large energetic advantage seems to be overrun in aqueous solution. On the other hand, we thought it unlikely that the stabilization of the ammonium ion **1**NH_3^+ through solvation could be so much larger than that of the iminium ions **6**H^+_a to **6**H^+_c. This led us to quantitatively estimate the corresponding changes in the Gibbs energies of solvation for these species, with water as the solvent, by using the the Polarized Continuum Model (PCM)[22] as implemented in the Gaussian 98 package. The corresponding Gibbs energy changes for solvation of the species **1**NH_3^+ and **6**H^+_a–**6**H^+_c are indeed quite close, −62.2, −59.6, −60.2 and −58.6 kcal mol^{-1}, respectively. It thus seems more likely that the release of energy attending the formation of the collision complex in the FT-ICR experiments is sufficient to overcome the activation barrier involved in the ring-opening process (as it is the case for **2**(g)) This energy release is absent in the reaction in solution.

Our results can be summarized as follows:

1) In the gas phase, **1**NH_2 is irreversibly protonated on the carbon atom, leading to the formation of iminium ions through ring opening.
2) In aqueous solution, **1**NH_2 is protonated on the amino nitrogen atom, and the cubic structure of the hydrocarbon moiety is preserved. The aqueous basicity of **1**NH_2 is appreciably lower than expected for a normal alicyclic amine. This effect is quite consistent with the stereoelectronic interaction between the amino group and the hydrocarbon framework as well as with the large *s* character of the orbitals on the carbon bearing the amino group.

Received: January 22, 2003 [Z50993]

Keywords: ab initio calculations · basicity · cubanes · density functional calculations · gas-phase reactions

[1] J. S. Murray, J. M. Seminario, P. Politzer, *Struct. Chem.* **1991**, *2*, 567 – 573.
[2] a) T. W. Cole, Jr., PhD thesis, The University of Chicago, **1966**; b) P. E. Eaton, C.-X. Yang, Y. Xiong, *J. Am. Chem. Soc.* **1990**, *112*, 3225 – 3226; c) For an important general reference on cubane and its derivatives, see, e.g., P. E. Eaton, *Angew. Chem.* **1992**, *104*, 1421 – 1422; *Angew. Chem. Int. Ed. Engl.* **1992**, *31*, 1399 – 1420.
[3] J.-L. M. Abboud, I. A. Koppel, J. Z. Dávalos, P. Burk, I. Koppel, E. Quintanilla, *Angew. Chem.* **2003**, *115*, 1074 – 1076, *Angew. Chem. Int. Ed.* **2003**, *42*, 1044 – 1046..
[4] L. Cassar, P. E. Eaton, J. Halpern, *J. Am. Chem. Soc.* **1970**, *92*, 6366 – 6368.
[5] Regarding strain in these and cognate species, see, e.g., a) D. W. Rogers, *J. Mol. Struct.* **2000**, *556*, 207 – 215; b) C. W. Earley, *J. Phys. Chem. A* **2000**, *104*, 6622 – 6627; c) K. Hassenbrück, H.-D. Martin, R. Walsh, *Chem. Rev.* **1989**, *89*, 1125 – 1146.
[6] The Gaussian 98 series of computer programs, Gaussian 98 (Revision A.7), M. J. Frisch, G. W. Trucks, H. B. Schlegel, G. E. Scuseria, M. A. Robb, J. R. Cheeseman, V. G. Zakrzewski, J. A. Montgomery, R. E. Stratmann, J. C. Burant, S. Dapprich, J. M. Millam, A. D. Daniels, K. N. Kudin, M. C. Strain, O. Farkas, J. Tomasi, V. Barone, M. Cossi, R. Cammi, B. Mennucci, C. Pomelli, C. Adamo, S. Clifford, J. Ochterski, G. A. Petersson, P. Y. Ayala, Q. Cui, K. Morokuma, D. K. Malick, A. D. Rabuck, K. Raghavachari, J. B. Foresman, J. Cioslowski, J. V. Ortiz, B. B. Stefanov, G. Liu, A. Liashenko, P. Piskorz, I. Komaromi, R. Gomperts, R. L. Martin, D. J. Fox, T. Keith, M. A. Al-Laham, C. Y. Peng, A. Nanayakkara, C. Gonzalez, M. Challacombe, P. M. W. Gill, B. G. Johnson, W. Chen, M. W. Wong, J. L. Andres, M. Head-Gordon, E. S. Replogle, J. A. Pople, Gaussian, Inc., Pittsburgh, PA, **1998**.
[7] See, e.g., a) J. T. Edward, P. G. Farrell, G. E. Langford, *J. Am. Chem. Soc.* **1976**, *98*, 3075 – 3085; b) T. Axenrod, B. Liang, A. Bashir-Hasemi, P. R. Dave, D. S. Reddy, *Magn. Reson. Chem.* **1991**, 88 – 91, and references therein.
[8] Experimental results from P. E. Eaton, *Tetrahedron* **1979**, *35*, 2189 – 2193.
[9] a) K. Wolinski, J. F. Hilton, P. Pulay, *J. Am. Chem. Soc.* **1990**, *112*, 8251 – 8260; b) R. Ditchfield, *Mol. Phys.* **1974**, *27*, 789 – 807; c) F. London, *J. Phys. Radium* **1938**, *8*, 397 – 409.
[10] The potentiometric method described in I. A. Koppel, J. Koppel, I. Koppel, I. Leito, V. Pihl, A. Wallin, L. Grehn, U. Ragnarsson, *J. Chem. Soc. Perkin Trans. 2* **1993**, 655 – 660. See also, A. Albert, E. P. Sergeant, *Ionization Constants of Acids and Bases*, Wiley, New York, **1962**.
[11] *Tables of Rate and Equilibrium Constants of Heterolytic Organic Reactions, Vol. 1(1)*, Supplementary Vol. 1(1–2) (Ed.: V. A. Palm), Viniti-Tartu State University, Moscow-Tartu, **1984**.
[12] W. Adcock, F. Anvia, G. Butt, A. , Cook, P. Duggan, C. A. Grob, S. Marriot, J. Rowe, M. Taagepera, R. W. Taft, R. W. Topsom, *J. Phys. Org. Chem.* **1991**, *4*, 353 – 360.
[13] E. P. L. Hunter, S. G. Lias, *J. Phys. Chem. Ref. Data* **1998**, *27*, 413 – 656.
[14] a) A. D. Becke, *J. Chem. Phys.* **1993**, *98*, 5648 – 5652; b) C. Lee, W. Yang, R. G. Parr, *Phys. Rev. B* **1988**, *37*, 785 – 789; c) S. H. Vosko, L. Wilk, M. Nusair, *Can. J. Phys.* **1980**, *58*, 1200 – 1211; d) P. J. Stephens, F. J. Devlin, C. F. Chabalowski, M. J. Frisch, *J. Phys. Chem.* **1994**, *98*, 11623 – 11627.
[15] a) A. E. Reed, L. A. Curtiss, F. Weinhold, *Chem. Rev.* **1988**, *88*, 899 – 926; b) Calculations performed using the NBO 3.1 Program, E. D. Glendening, A. E. Reed, J. E. Carpenter, F. Weinhold.
[16] a) R. W. Taft, R. D. Topsom, *Prog. Phys. Org. Chem.* **1987**, *16*, 1 – 80; b) D. C. Caskey, R. Damrauer, D. McGoff, *J. Org. Chem.* **2002**, *67*, 5098 – 5105.
[17] Estimated at ca. 31 %: a) E. W. Della, T. W. Hine, H. K. Patney, *J. Org. Chem.* **1977**, *42*, 2940 – 2945; b) T. W. Cole, Jr., C. J. Mayers, L. M. Stock, *J. Am. Chem. Soc.* **1974**, *96*, 4555 – 4557.
[18] Our own NBO calculations yield a 28.4 % s character.
[19] R. Wolfshütz, H. Schwarz, *Int. J. Mass Spectrom. Ion Phys.* **1980**,*33*, 291 – 297.
[20] See, e.g., a) J.-L. M. Abboud, J. L. G. de Paz, M. Yáñez, M. Esseffar, W. Bouab, M. El-Mouhtadi, R. Mokhlisse, E. Ballesteros, M. Herreros, R. Notario, *J. Am. Chem. Soc.* **1993**, *115*, 12468 – 12476; b) A. Bagno, G. Scorrano, *Acc. Chem. Res.* **2000**, *33*, 609 – 616; c) A. Bagno, B. Bujnicki, S. Bertrand, C. Comuzzi, F. Dorigo, P. Janvier, G. Scorrano, *Chem. Eur. J.* **1999**, *5*, 523 – 536.
[21] R. Notario, J. L. M. Abboud, C. Cativiela, J. I. García, M. Herreros, H. Homan, J. A. Mayoral, L. Salvatella, *J. Am. Chem. Soc.* **1998**, *120*, 13224 – 13229.
[22] a) V. Barone, M. Cossi, J. Tomasi, *J. Comput. Chem.* **1998**, *19*, 404 – 417; b) S. Miertus, J. Tomasi, *J. Chem. Phys.* **1982**, *65*, 239 – 245; c) M. Cossi, V. Barone, R. Cammi, J. Tomasi, *Chem. Phys. Lett.* **1996**, *255*, 327 – 331.

 © 2003 Wiley-VCH Verlag GmbH & Co. KGaA, Weinheim

Multiple-Scale Self-Organization

From Angstroms to Micrometers: Self-Organized Hierarchical Structure within a Polymer Film**

Teruaki Hayakawa and Shin Horiuchi*

Structural order over varying length scales is a commonly encountered phenomenon in nature, but achieving this in the synthetic world is a challenge.[1,2] Progress in synthesis and characterization of self-organizing synthetic materials has been astounding, and block copolymers have played a significant role in this process. They offer intriguing possibilities for preparation of materials with tunable structures and tailored properties.[3–10] However, the length scales attainable by self-assembly of block copolymers have been smaller than about 100 nm.[5b,6–10] In contrast, there have been recent reports on a self-assembly templating process for the creation of microsized structures.[11–13] In this templating process using water droplets, polymers with π-conjugated rod–coil-type architectures[12] or amphiphilic molecules[13] in the primary structure form hexagonally packed arrays of holes in the micrometer range in a thin polymer film. However, little attention has been paid to the formation of ordered structures on the nanometer-size scale by these approaches. For a wide range of advanced technological devices incorporating organic materials, it is desirable, advantageous, and often necessary that the hierarchical structures of these materials can be precisely controlled from the nano- to the micrometer regime.[5b] Here we report the creation of hierarchical structures from the molecular to the micrometer scale by using specifically designed block copolymers that self-organize at length scales from nanometers or angstroms to micrometers over areas in the square centimeter range.

Block copolymers with side chains can form regular nanoscale hierarchical structures through phase separation and intermolecular interactions,[5b,14] while the aromatic rigid-rod segments incorporated in rod–coil-type block copolymers form microsized structures, in contrast to the usual coil–coil-type block copolymers.[12] The incorporation of π-conjugated rigid-rod molecules in the side chain can thus play a role in forming both nano- and microsized structures and create the desired hierarchical structures over multiple length scales. For this purpose, we synthesized a semi-rod–coil block copolymer of styrene (ST) and an isoprene with oligothiophene-modified side chains (POTI), namely, PS_{400}-*b*-$POTI_{25}$ (**4**; the subscripts indicate the number of repeat monomer units; Figure 1), by esterifying a poly(styrene-*b*-substituted isoprene) block copolymer with an oligothiophene derivative.[15] The PS and POTI blocks in **4** represent coil and semi-rod segments, respectively. A poly(styrene-*b*-isoprene) block copolymer **1**

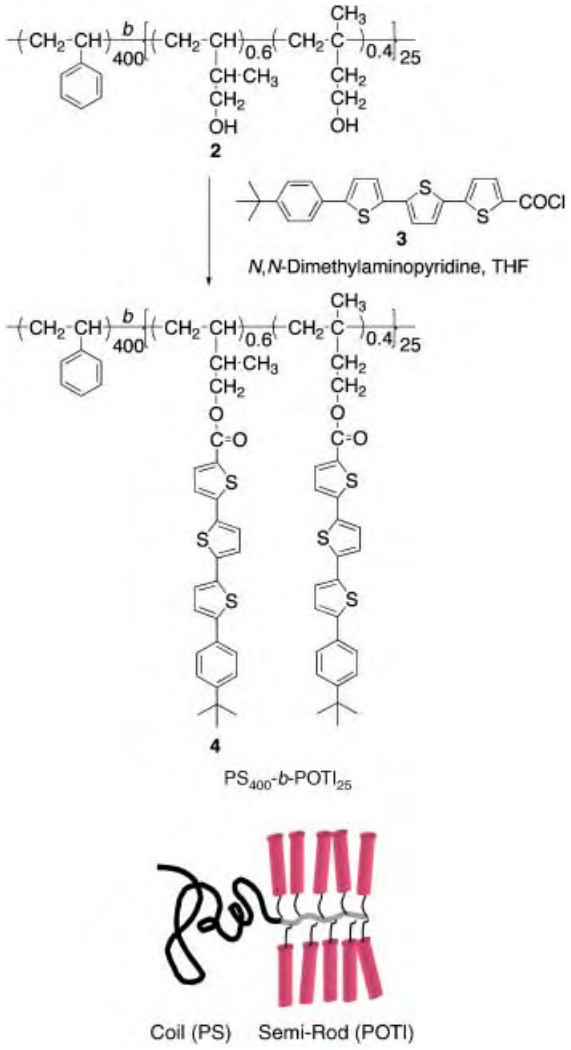


Figure 1. Synthesis and schematic representation of self-organizing semi-rod–coil block copolymer **4**.

was prepared by anionic polymerization of styrene monomers with 400 repeat units and isoprene monomers with 25 repeat units. Block copolymer **1** was modified by hydroboration of the polyisoprene block to yield poly(styrene-*b*-hydroxylated isoprene) block copolymer **2** with hydroxy groups in the polyisoprene block.[14] Oligothiophene with an acid terminus was synthesized by Stille coupling reactions.[16] Oligothiophene acid chloride **3** was esterified with **2** to obtain the target block copolymer **4**. Infrared and ^1H and ^{13}C NMR spectroscopy showed that the desired block copolymer **4** was obtained in quantitative yield without a side product. Gel permeation chromatography (GPC) indicated a narrow

[*] Dr. T. Hayakawa, Dr. S. Horiuchi
Research Center of Macromolecular Technology
National Institute of Advanced Industrial Science and Technology
1-1-1 Higashi, Tsukuba, Ibaraki 305-8565 (Japan)
Fax: (+81) 298-61-6327
E-mail: teru.hayakawa@aist.go.jp

[**] This work was supported by the New Energy and Industrial Technology Development Organization (NEDO) for the nanostructure polymer project. We thank Prof. T. Kajiyanma and Prof. A. Takahara for their useful suggestions, Dr N. Sundararajan for his valuable discussions, and the referees for their constructive comments.

Supporting information for this article is available on the WWW under http://www.angewandte.org or from the author.

 DOI: 10.1002/anie.200219877 © 2003 Wiley-VCH Verlag GmbH & Co. KGaA, Weinheim

polydispersity index of 1.08 and a number-average molecular weight M_n of 55000 (versus polystyrene standard in tetrahydrofuran).

Films were prepared from 0.2 mL of a 0.25 wt% polymer solution in CS_2 on a variety of substrates such as glass slides, silicon wafers, cured epoxy plates, polyimide films, and water surfaces by casting at room temperature (22 °C) under a moist air flow. The humidity and the flow rate were kept at 85% and 3.0 L min^{-1}, respectively. The solvent completely evaporated within 10–20 s, and a periodic microporous structure was instantly obtained over an area of 3 cm^2 (Figure 2). Observations under a polarized optical microscope (POM) and a scanning electron microscope (SEM) confirmed the formation of hexagonally packed micropores with a narrow size distribution (Figure 2a and b). The diameter of the open pores on the surface is approximately 1.3 μm (Figure 2d). A cross-sectional view (Figure 2c) shows a single layer with empty spheres, in which spheres with a diameter of 2.3 μm are separated from each other by thin walls of less than 100 nm.

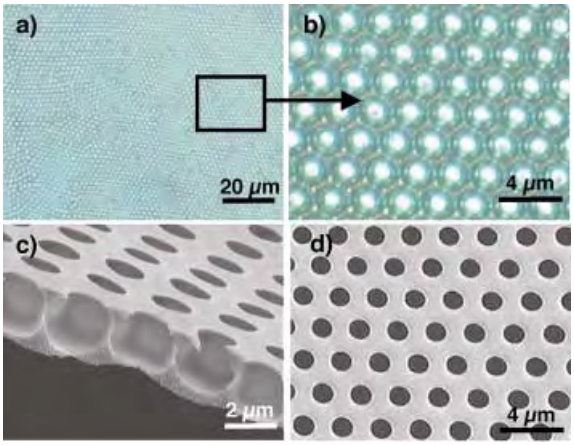


Figure 2. Self-organized microporous structure. The film of **4** was prepared from a 0.25 wt% solution under a moist air flow. a) Medium- and b) high-magnification optical micrographs of a hexagonally packed microporous structure on a glass slide. c) Side view and d) top view of SEM images of a).

This microporous film was sectioned perpendicular and horizontal to the substrate to give thin specimens which, after embedding in epoxy resin, were observed under a transmission electron microscope (TEM; Figure 3). Although the entire structure, especially that of the horizontally cross-sectioned film, is somewhat deformed during sectioning (Figure 3c and e), the film contains a nanoscale phase-separated structure characterized by layers perpendicular to the substrate with a periodicity of approximately 25 nm (Figure 3d, f, g, and h). A sulfur-distribution image created by electron spectroscopic imaging on an energy-filtering TEM (EFTEM) indicated that the phase-separated PS and POTI blocks aligned layer by layer due to the self-assembly characteristic of the diblock copolymer (Figure 3h). The phase-separated nanostructure of a nonmicroporous cast film prepared from the same solution was also investigated under the TEM. The TEM images (Figure 3a) revealed formation of a cylindrical nanostructure parallel to the substrate and a domain spacing of approximately 27 nm, in good agreement with that of the microporous film.

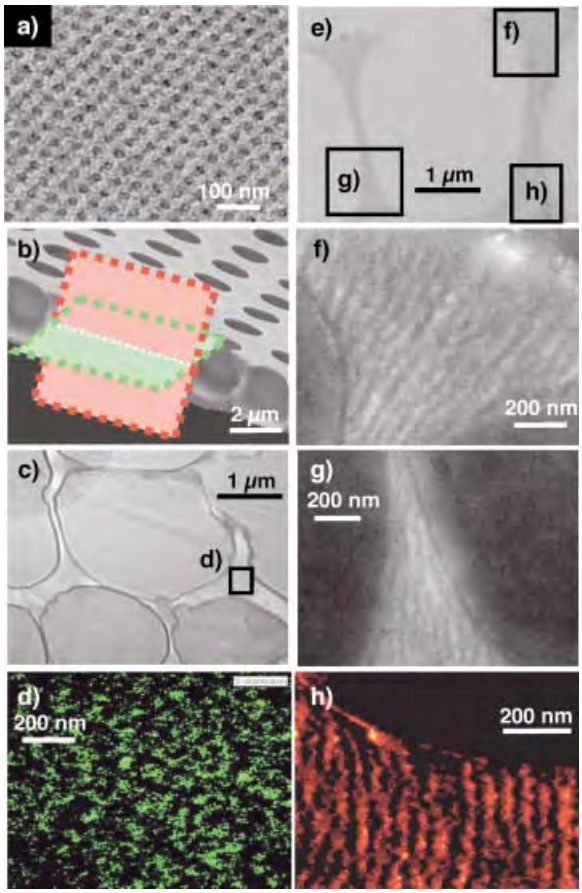


Figure 3. Self-organized phase-separated nanostructures, TEM images of cross sections of the microporous film (ca. 50 nm thick). Although the entire structure is somewhat deformed during sectioning, alignment layer-by-layer perpendicular to the substrate with a spacing of about 25 nm is apparent. a) Nonmicroporous film. b) Directions of cross-sectioned film. c) Horizontally cross-sectioned film. d) Sulfur-distribution image to detect POTI domains (green) in an unstained specimen by EFTEM. e) Perpendicularly cross-sectioned film. f, g) High-magnification micrographs of e) (red: POTI).

The mesophase structure of the block-copolymer thin film was investigated by differential scanning calorimetry (DSC), polarized optical microscopy, and X-ray diffraction (XRD). The DSC trace on the second heating showed three distinct thermal transitions (Figure 4a). The baseline shifts observed at 104 and 168 °C correspond to the glass transitions (T_g) of the PS and POTI blocks, respectively. Above the T_g temperature, an endothermic peak was observed at 238 °C, and a phase transition to an isotropic phase was found to occur around this temperature by means of POM observations. These transition temperatures showed very good agreement with those of the homopolymers. On the DSC traces of the homopolymers, the T_g of PS and POTI were 103 and 166 °C, respectively, and the phase transition of POTI from the smectic A mesophase to the isotropic phase was observed at

 © 2003 Wiley-VCH Verlag GmbH & Co. KGaA, Weinheim

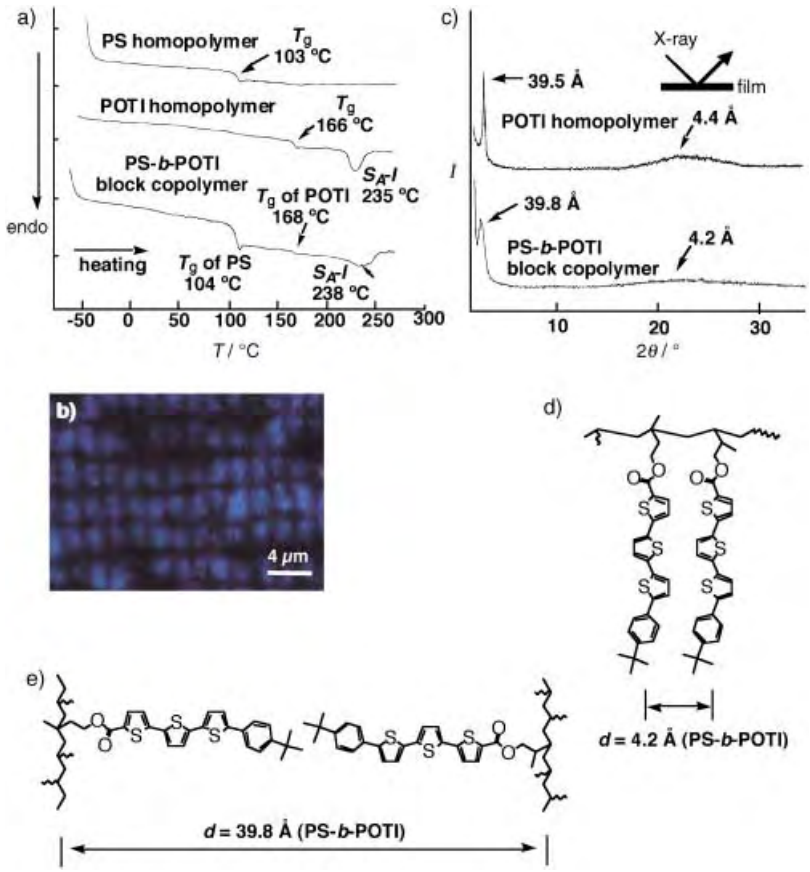


Figure 4. a) DSC traces of PS and POTI homopolymers and PS-*b*-POTI block copolymer. b) Polarized optical micrograph of microporous film in Figure 2 after thermal annealing at 170 °C for 1 min. c) X-ray diffraction pattern of film b). d, e) Schematic representation of proposed molecular arrangement of POTI polymer within the smectic A mesophase.

235 °C. Below T_g, the POTI homopolymer is in the glassy liquid-crystalline state with a smectic mesophase. Under the POM with crossed polarizers, a faint optical texture that maintains the hexagonal pore arrangement appears in a microporous film, prepared from 0.25 wt % solution, after heating from room temperature at 10 K min^{-1}, annealing for 1 min at 170 °C, that is, slightly above the T_g of POTI, and subsequent quenching to room temperature (Figure 4b). The XRD pattern after annealing at 170 °C showed a sharp inner reflection corresponding to the phase-separated layer structure, and a very broad outer reflection corresponding to the intermolecular spacing of oligothiophene molecules (Figure 4c). The layer spacing of 39.8 Å and the intermolecular spacing within the POTI layer of 4.2 Å are in good agreement with those of the POTI homopolymer film, and this suggests that the oligothiophene moieties in the POTI block are packed regularly to form a liquid crystalline smectic A mesophase within the phase-separated POTI nanodomains (Figure 4d and e). Thus, the semi-rod–coil block copolymer can form organized structures on three different length scales, ranging from angstroms to micrometers, by simple solvent casting and annealing (Figure 5). The combination of a liquid-crystal phase and phase-separated nanodomain structures formed by block copolymers has been reported before,[5b] and ordered microporous materials have been previously created by using rod–coil-type block copolymers.[12] This is the first report, however, that demonstrates three tiers of hierarchically organized structure created by molecular design and a simple process. Our synthetic approach for constructing such a highly organized structure is attachment of a rigid-rod molecule such as oligothiophene

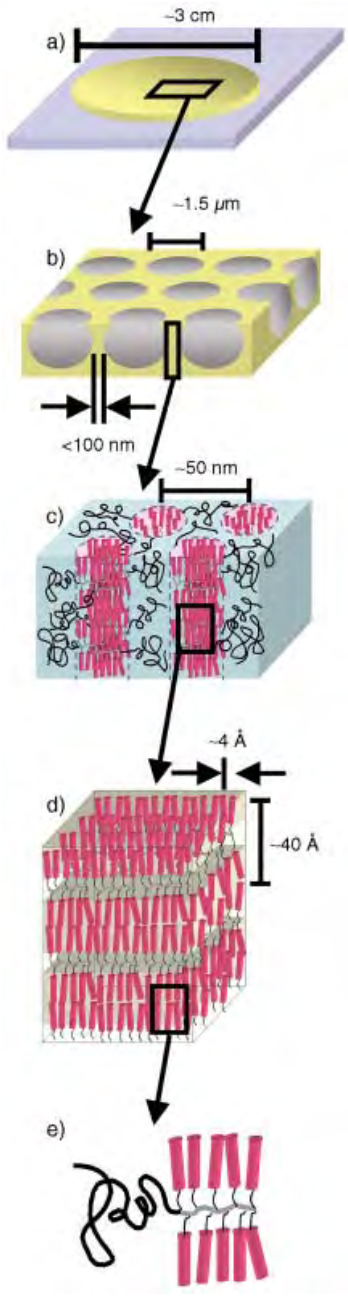


Figure 5. Schematic representation of self-organized hierarchical structure of **4**. a) Centimeter-sized film. b) Microsized porous structure. c) Nanosized phase-separated structure of PS and POTI blocks. d) Oligothiophene with molecularly orientated smectic A liquid-crystalline structure in POTI nanophase-separated domains. e) Molecular structure of **4**.

 © 2003 Wiley-VCH Verlag GmbH & Co. KGaA, Weinheim

onto the side chain of one block of the diblock copolymer. This has the advantage that functions such as electrical conductivity, optical storage, and photoluminescence can be added to the films.

The other advantage of the semi-rod–coil block copolymer over rod–coil block copolymers is that the ordered structure at the molecular level within the rod blocks can be fabricated by thermal treatment, because the side chain rod moieties can rearrange before complete isotropization of the block copolymer. Under the POM, film melting and micropores filling were gradually observed around 185 °C on heating at 10 K min^{-1} from room temperature. Annealing at 240 °C, that is, slightly above the phase-transition temperature from the smectic A to the isotropic phase, for 1 min and quenching to room temperature yields a "microembossed" pattern (Figure 6a) in which the pores are incompletely filled, and the height thus undulates in a regular fashion. The XRD pattern of the film indicated the same smectic A mesophase as shown in Figure 4c. This texture of the smectic A mesophase under the POM has a unique "ladder" pattern, for which the "ladder" corresponds to the top surface of the "embossed" pattern (Figure 6b). By focusing on the bottom surface of the "embossed" pattern, another texture with periodic microscale patterns was observed (Figure 6c). These optical textures indicate the creation of a micropatterned liquid crystalline film. Annealing at 260 °C for 1 min completely fills the pores to give a nonmicroporous film. A cross-sectional TEM image of this film shows the cylindrical phase-separated structure (Figure 6d and e), that is, annealing changes the direction of the cylinders from perpendicular to parallel to the bottom of the film, while the upper side just below the surface remains the same as it was just after casting. We also changed the depth of the pores by changing the annealing conditions. The possibility of such thermal fabrication is likely to extend the range of applications of these materials. For example, thermal treatment of the block-copolymer thin film leads to a surface that appears to have a microembossed pattern over areas of several square centimeters. These surfaces could be envisioned as being used as tunable diffraction gratings or holograms. Other examples include ordered microporous materials as templates for the patterning of functional materials in two or three dimensions. The experimental results presented above on the microporous structures also indicate the possibility of fixation or encapsulation of functional materials after patterning of the block copolymer film.

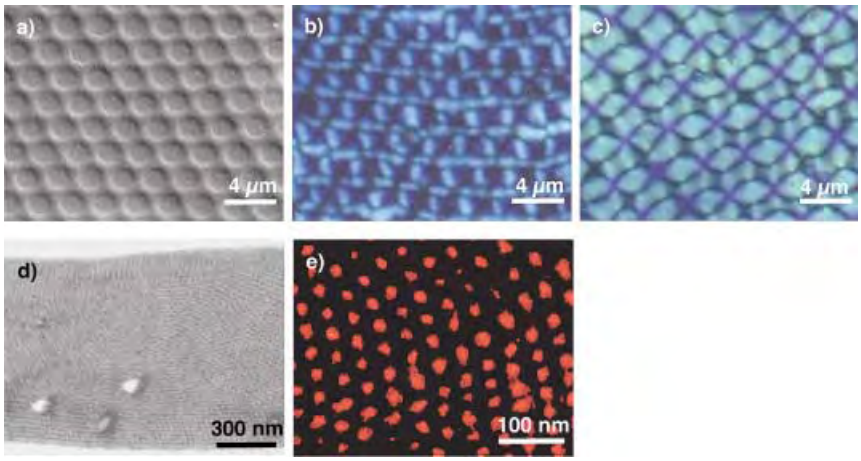


Figure 6. Micrographs of a thermally fabricated film. a) SEM micrograph of "embossed" pattern of the film in Figure 2, formed after annealing at 240 °C for 1 min. b) The "ladder"-pattern optical texture corresponds to the surface and c) to the bottom of the "embossed" pattern. d) TEM image of the cross section of completely filled film (ca. 50 nm thick) prepared by annealing at 260 °C for 1 min. The direction of the cylinder changes from perpendicular to parallel to the substrate. e) Sulfur-distribution image under the EFTEM.

The structure of the microporous films can be varied by means of the concentration of the polymer in the solution. For example, a 0.1 wt % solution leads to a single layer of pores open on both sides (Figure 7a), while a 1.0 wt % solution results in multiple layers of pores ordered in three dimensions (Figure 7b and c). The pore size can also be controlled from 1.2 to 4.5 μm by changing the solution concentration.

We have developed a new strategy for constructing highly ordered hierarchical structures by combining individual self-organizing components over multiple length scales. The materials prepared by this strategy and modified by further thermal fabrication are expected to have a wide range of applications in molecular optical or electronic devices, photonic band-gap materials, and sensors.

Received: August 2, 2002
Revised: February 10, 2003 [Z19877]

Keywords: block copolymers · hierarchical structures · microporous materials · nanostructures · self-assembly

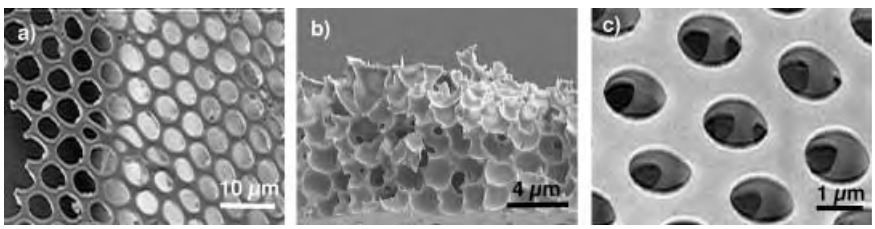


Figure 7. SEM images of a variety of microporous films. a) Film with a single layer of pores open on both sides and about 3.3 μm in diameter, prepared from 0.1 wt % casting solution. b) Side view of multilayer structure consisting of six layers, prepared from 1.0 wt % casting solution. c) Top view of micrograph b). Pores of the next layers can be seen through those of the top layer. The image shows the arrangement of pores of uniform size in multilayers.

 © 2003 Wiley-VCH Verlag GmbH & Co. KGaA, Weinheim

[1] G. M. Whitesides, J. P. Mathias, C. T. Seto, *Science* **1991**, *254*, 1312 – 1319; E. Kim, G. M. Whitesides, *Chem. Mater.* **1995**, *7*, 1257 – 1264; G. M. Whitesides, B. Grzybowski, *Science* **2002**, *295*, 2418 – 2421.
[2] G. A. Ozin, *Chem. Commun.* **2000**, 419 – 432.
[3] F. S. Bates, G. H. Fredrickson, *Annu. Rev. Phys. Chem.* **1990**, *41*, 525 – 557.
[4] Z. Li, W. Zhao, Y. Liu, M. H. Rafailovich, J. Sokolov, *J. Am. Chem. Soc.* **1996**, *118*, 10892 – 10893.
[5] a) C. K. Ober, G. Wegner, *Adv. Mater.* **1997**, *9*, 17 – 31; b) M. Muthukumar, C. K. Ober, E. L. Thomas, *Science* **1997**, *277*, 1225 – 1232.
[6] S. I. Stupp, V. LeBonheur, K. Walker, L. S. Li, K. E. Huggins, M. Keser, A. Amstutz, *Science* **1997**, *276*, 384 – 389.
[7] J. Ruokolainen, R. Mäkinen, M. Torkkeli, T. Mäkelä, R. Serimaa, G. ten Brinke, O. Ikkala, *Science* **1998**, *280*, 557 – 560.
[8] S. Walheim, E. Schäffer, J. Mlynek, U. Steiner, *Science* **1999**, *283*, 520 – 522.
[9] O. Illala, G. ten Brinke, *Science* **2002**, *295*, 2407 – 2409.
[10] S. Förster, T. Plantenberg, *Angew. Chem.* **2002**, *114*, 712 – 739; *Angew. Chem. Int. Ed.* **2002**, *41*, 688 – 714.
[11] M. Srinivasarao, D. Collings, A. Philips, S. Patel, *Science* **2001**, *292*, 79 – 83.
[12] G. Widawski, M. Rawiso, B. François, *Nature* **1994**, *369*, 387 – 389; S. A. Jenekhe, X. L. Chen, *Science* **1999**, *283*, 372 – 375.
[13] O. Karthaus, N. Maruyama, X. Cieren, M. Shimomura, H. Hasegawa, T. Hashimoto, *Langmuir* **2000**, *16*, 6071 – 6076.
[14] G. Mao, J. Wang, S. R. Clingman, C. K. Ober, *Macromolecules* **1997**, *30*, 2556 – 2567.
[15] Details of the molecular synthesis and polymerization studies are available as Supporting Information.
[16] J. K. Stille, *Angew. Chem.* **1986**, *98*, 504 – 519; *Angew. Chem. Int. Ed. Engl.* **1986**, *25*, 508 – 524.

 © 2003 Wiley-VCH Verlag GmbH & Co. KGaA, Weinheim

A 2D Molecule-Based Magnet

A Self-Assembled 2D Molecule-Based Magnet: The Honeycomb Layered Material $\{Co_3Cl_4(H_2O)_2[Co(Hbbiz)_3]_2\}$**

*José Ramón Galán-Mascarós and Kim R. Dunbar**

Research in the area of molecule-based magnets is rapidly expanding, owing, in part, to numerous breakthroughs in the past decade.[1] The preparation of solid-state architectures of varying dimensionalities from specifically tailored paramagnetic building blocks has proven to be very successful, and also clearly multidisciplinary. Materials science and supramolecular chemistry efforts have joined forces with classical organic and inorganic chemistry in the design of solid-state materials whose magnetic properties rival, and sometimes even exceed, those of classic inorganic solids.[2] The molecule-based strategy allows for the preparation of unusual materials that cannot otherwise be obtained, for example, materials that combine two or more physical properties in the same compound[3] or molecules with magnetic bistability.[4] The solid-state structures of the majority of molecule-based magnetic materials consist of extended networks of paramagnetic metal ions held in close proximity by bridging ligands that allow for magnetic exchange. The dimensionality of the system dictates the overall magnetic properties and can be controlled by the use of capping ligands[5] or templating counterions.[6]

Unfortunately, few ligands are capable of mediating sufficiently strong magnetic interactions between metal ions such that bulk magnetic ordering can occur. Apart from monoatomic ligands (such as oxide or halide bridges), the most effective bridging groups with respect to magnetic exchange interactions are cyanide,[7] dicyanamide,[8] and oxalate.[9] Common features of these ligands are that they contain only a small number of atoms, and that they offer a π as well as a σ pathway for magnetic superexchange interactions. Organic radicals have also been successfully applied

[*] Prof. K. R. Dunbar
Department of Chemistry
Texas A&M University
PO Box 30012, College Station, TX 77842-3012 (USA)
Fax: (+1) 979-845-7177
E-mail: dunbar@mail.chem.tamu.edu
Dr. J. R. Galán-Mascarós
Instituto de Ciencia Molecular
Universidad de Valencia
Dr. Moliner, 50, 46100 Burjasot (Spain)

[**] The authors thank the National Science Foundation for support through grants CHE-9906583 (PI) and NIRT DMR-0103455 and for equipment grants to purchase the CCD X-ray equipment (CHE-9807975) and the SQUID magnetometer (NSF-9974899). This work was also supported by the Ministerio de Ciencia y Tecnología (MCT project: BQU2002-01091). We thank Prof. E. Coronado for helpful discussions. Hbbiz = 2,2′-Hbibenzimidazole.

Supporting information for this article is available on the WWW under http://www.angewandte.org or from the author.

 DOI: 10.1002/anie.200250152 © 2003 Wiley-VCH Verlag GmbH & Co. KGaA, Weinheim

to the preparation of molecular magnets, with two of the best examples being families of metal–organic magnets based on TCNE and TCNQ.[10,11]

In our quest for new ligands to use as building blocks for new molecule-based magnets with new types of structural features, we discovered that 2,2′-bibenzimidazole (H_2bbiz, see structure) is capable of assembling homometallic structures that order ferromagnetically. This ligand and the related molecule 2,2′-biimidazole present multiple nitrogen-donor sites with the possibility of reversible protonation and deprotonation,[12] properties that have been capitalized upon in supramolecular chemistry for the preparation of multidimensional hydrogen-bonded networks.[13] The H_2bbiz molecule has also been used for the preparation of mononuclear,[14] dinuclear[15] and cyclic molecules[16] of second- and third-row metals with interesting photophysical properties, and in the preparation of models for bioinorganic systems.[17] Of more relevance to the present topic, we note that magnetic data for paramagnetic compounds of these ligands is limited to reports of a weakly antiferromagnetically coupled Ni dimer[18] and a poorly characterized magnet based on the bbiz ligand.[16a] Herein we present the synthesis, structural determination, and magnetic properties of a new molecule-based magnet based on Co^{II} ions and the $[Hbbiz]^-$ ligand.

The solvothermal reaction of $CoCl_2 \cdot x\,H_2O$ with H_2bbiz and KOH in a toluene/methanol mixture at 110 °C yields dark green single crystals of the title compound after several days. The structure of $\{Co_3Cl_4(H_2O)_2[Co(Hbbiz)_3]_2 \cdot 3\,C_7H_8 \cdot 9\,CH_3OH\}_\infty$, (**1**)[19] consists of neutral 2D layers (Figure 1) composed of octahedral units of $[Co^{II}(Hbbiz)_3]^-$ bridged by tetrahedral Co^{II} ions that are bound to the deprotonated N atoms of independent $Hbbiz^-$ ligands; Cl^- ions and water molecules complete the coordination sphere. The $[Co^{II}(Hbbiz)_3]^-$ moieties are in an octahedral environment with angles that deviate slightly from the ideal 90° (≈83° for the bite angle of the bibenzimidazole ligands) and regular Co–N bond lengths (1.92–1.95 Å). There are two crystallographically different tetrahedral sites, although the coordination environments for both sites are nearly identical, with two Cl^- ions and one water molecule being disordered over the three crystallographically unique positions. The tetrahedral sites clearly deviate from a regular tetrahedron as indicated by the different bond lengths observed for Co–N (2.01–2.03 Å) and the average Co–Cl/O separations (2.25–2.27 Å). The Cl^- ions and water molecules participate in hydrogen bonding to the remaining protons of the $Hbbiz^-$ molecules (Cl/O–N = 3.06 Å). The overall neutral framework consists of twelve-membered rings of alternating tetrahedral and octahedral Co^{II} ions, thereby creating an extended honeycomb hexagonal lattice. The three-atom bridge between metal centers leads to a short metal–metal separation of 5.79(2) Å.

Each layer is chiral, with all octahedral sites maintaining the same chirality, namely Δ or Λ. The overall structure is achiral, however, with alternating layers being of opposite chirality. The layers are offset from one other (Figure 2) in such a way that the phenyl rings point to the interstices of the cavities created by the interlocked rings in adjacent layers (≈ 18 Å diameter).

Magnetic susceptibility measurements carried out on 5 mg of crushed single crystals of $\{[Co_3Cl_4(H_2O)_2[Co(Hbbiz)_3]_2 \cdot 3\,C_7H_8 \cdot 9\,CH_3OH\}_\infty$ with an applied field of 1000 G revealed a room temperature $\chi_m T$ value of 14.2 emu K mol^{-1} (see Supporting Information). This value is higher than the

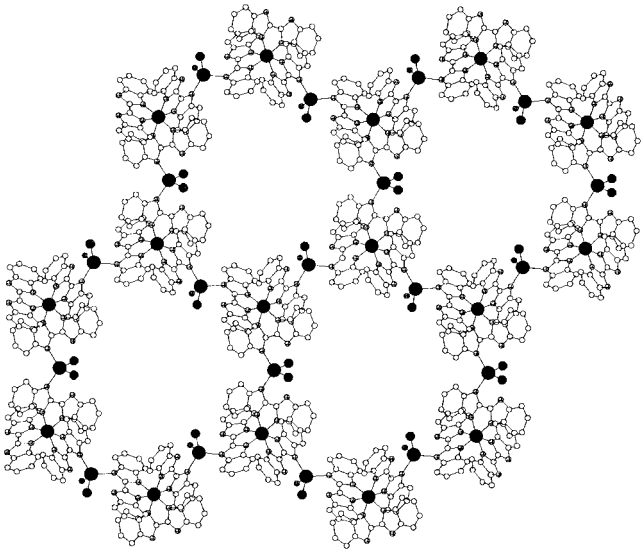


Figure 1. Top view of the 2D structure of the title compound $\{[Co_3Cl_4(H_2O)_2[Co(Hbbiz)_3]_2\}_\infty$.

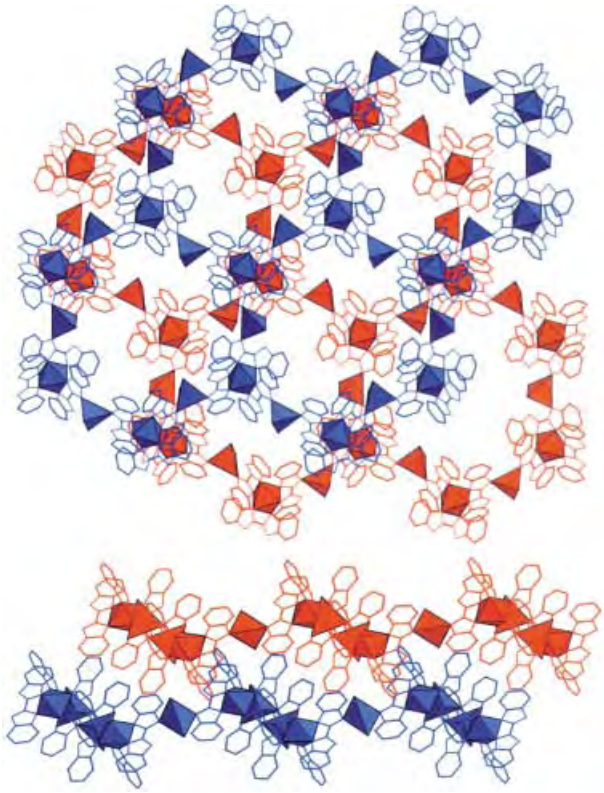


Figure 2. Top and side views of alternating layers in the title compound $\{[Co_3Cl_4(H_2O)_2[Co(Hbbiz)_3]_2\}_\infty$ showing the registry between layers.

 © 2003 Wiley-VCH Verlag GmbH & Co. KGaA, Weinheim

expected spin-only value, in accordance with the well-documented orbital contribution of octahedral Co^{II} ions. Upon lowering the temperature, $\chi_m T$ decreases, a feature that can be attributed to the spin–orbit coupling of the octahedral Co^{II} sites. The $\chi_m T$ value reaches a minimum at 42 K (11.8 emu K mol^{-1}) and then rapidly increases to a maximum of 19.2 emu K mol^{-1} at 7.5 K. These features correspond to an abrupt increase in χ_m around 15 K, which is an indication of the onset of magnetic ordering. Indeed, the AC magnetic susceptibility data (Figure 3) confirm the presence of net

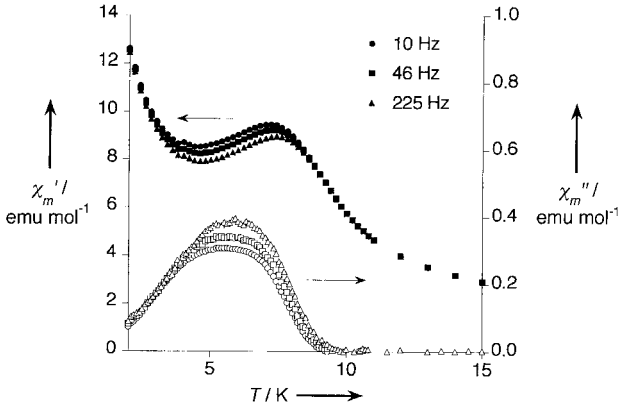


Figure 3. AC magnetic susceptibility (χ_m'; χ_m'' = out-of-phase) measurements for the title compound $\{[Co_3Cl_4(H_2O)_2[Co(Hbbiz)_3]_2\}_\infty$. T = temperature.

magnetization, as the data show a peak in both the χ_m' (in-phase) and χ_m'' (out-of-phase) signals below a $T_c = 9.0$ K (T_c = Curie temperature). The position of the maxima shows negligible frequency dependence over the range 1–1000 Hz. At very low temperatures χ_m' undergoes a slight increase which could be because of the presence of a paramagnetic contribution arising from defects in the crystal structure.

The magnetization of the sample at 2 K increases rapidly at low fields, with no saturation observed up to 5 T. The maximum value observed of 11.3 μ_B is lower that the expected value for a ferromagnetic ground state (~15 μ_B). The compound exhibits a hysteresis loop at 2 K (Figure 4) with a small coercive field of 155 G. These data do not allow for a precise understanding of the nature of the magnetic ordering. Based on the occupancy of the magnetic orbitals, it is reasonable to expect ferromagnetic superexchange to occur. The tetrahedral Co^{II} cations contain three unpaired electrons in the t_2 levels whereas the octahedral Co^{II} cations have one unpaired electron in a t_{2g} orbital set and two unpaired electrons in the e_g symmetry orbitals. The orthogonality of the t_2 and e_g orbitals is expected to favor ferromagnetic interactions, and, indeed, this pathway was found to dominate in compounds containing tetrahedral and octahedral Co^{II} ions,[20] although this factor depends on the relative orientation of the magnetic orbitals. If the ordering is ferromagnetic as proposed, the low saturation value for the magnetization is expected to be a consequence of the magnetic anisotropy of the octahedral Co^{II} ions in conjunction with strong spin canting within the layers which are noncentrosymetric. The structure of the magnet is quite

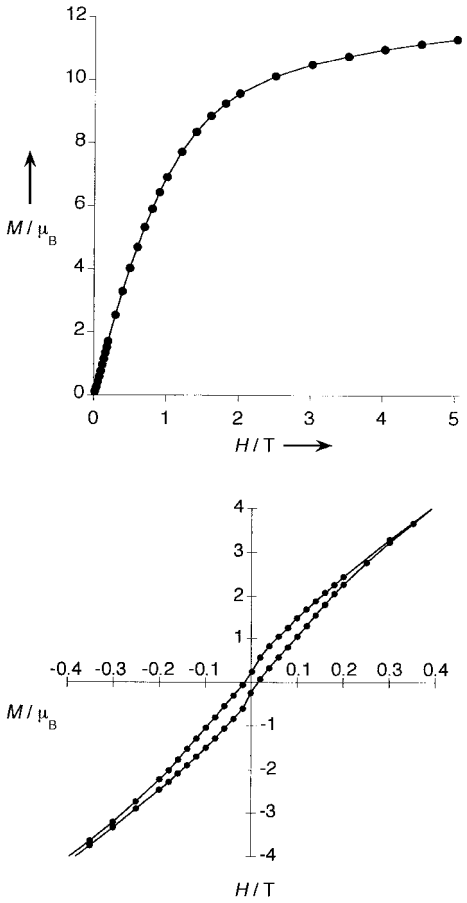


Figure 4. Field dependence of the magnetization (M; top) and hysteresis loop (bottom) at 2 K for the title compound $\{[Co_3Cl_4(H_2O)_2[Co(Hbbiz)_3]_2\}_\infty$. H = magnetic field strength.

complex, a fact that leads to questions about the exact dimensionality of the magnetic interactions in this system. Without pathways for magnetic exchange between the layers, the magnetic ordering could be quasi-2D.

The possibility of antiferromagnetic exchange, and ferrimagnetic ordering, seems less plausible than ferromagnetic interactions. In these cases, the three tetrahedral Co^{II} ions would align in an antiparallel fashion with the two octahedral Co^{II} cations. This situation would lead to very low magnetization values (~3 μ_B per one net Co^{II} atom which is far from the 11.3 μ_B observed at 5 T), and the slope would also be less steep owing to the field working against the antiferromagnetic interactions in the solid. In any case, to determine the sign of the magnetic exchange, either a model dimer compound or neutron diffraction studies will be needed.

In conclusion, $\{[Co_3Cl_4(H_2O)_2[Co(Hbbiz)_3]_2\}_\infty$ is the first molecule-based magnet of the 2,2′-bibenzimidazole ligand. The fact that the compound contains only one type of metal ion is important, as it represents a new strategy for preparing a family of magnetic materials with different paramagnetic transition metals. Preliminary data indicate that other homometallic compounds exhibit magnetic ordering as well, with critical temperatures as high as 40 K for the Mn^{II} derivative. The possibility of fully deprotonating the ligand is being

 © 2003 Wiley-VCH Verlag GmbH & Co. KGaA, Weinheim

contemplated as a means to produce additional novel architectures. Finally, it is noted that bimetallic networks should also be possible to prepare with this ligand, and these may prove to have even more interesting magnetic properties such as higher ordering temperatures, higher remnant magnetization and larger coercivities.

Experimental Section

The ligand 1,10-bibenzimidazole (H_2bbiz) was prepared according to a literature procedure.[21] $CoCl_2 \cdot 6H_2O$ (1 g, 4.2 mmol), H_2bbiz (0.09 g, 0.4 mmol) and KOH (0.2 g, 3.5 mmol) were suspended in a mixture of methanol (30 mL) and toluene (50 mL), and placed in a sealed teflon vessel. The suspension was heated to 110°C under autogeneous pressure. After seven days, chunky prismatic dark green crystals of $\{[Co_3Cl_4(H_2O)_2[Co(Hbbiz)_3]_2 \cdot 3C_7H_8 \cdot 9CH_3OH\}_\infty$ (**1**), were removed by filtration, washed with methanol and water, and dried in air. Elemental analysis for $C_{114}H_{118}Cl_4Co_5N_{24}O_{11}$: calcd: C 56.19, H 4.88, N 13.80; found: C 56.12, H 4.88, N 13.83.

CCDC-191616 contains the supplementary crystallographic data for this paper. These data can be obtained free of charge via www.ccdc.cam.ac.uk/conts/retrieving.html (or from the Cambridge Crystallographic Data Centre, 12 Union Road, Cambridge CB2 1EZ, UK; fax: (+44) 1223-336-033; or deposit@ccdc.cam.ac.uk).

Received: September 13, 2002
Revised: February 11, 2003 [Z50152]

Keywords: cobalt · coordination chemistry · imidazoles · magnetic properties

[1] "Magnetism: A Supramolecular Function": *NATO ASI Ser. C* **1996**, *484*.

[2] *MRS Bull.* **2000**, 21 – 71 special issue Eds.: J. S. Miller, A. J. Epstein).

[3] a) E. Coronado, J. R. Galán-Mascarós, C. J. Gómez-García,, V. Laukhin, *Nature* **2000**, *408*, 447 – 449; b) O. Sato, T. Iyoda, A. Fujishima, K. Hashimoto, *Science* **1996**, *272*, 704 – 705; c) K. Awaga, E. Coronado, M. Drillon, *MRS Bull.* **2000**, 52 – 57.

[4] R. Sessoli, D. Gatteschi, A. Caneschi, M. A. Novak, *Nature* **1993**, *365*, 141 – 143;b) H. J. Eppley, H.-L. Tsai, N. de Vries, K. Folting, G. Christou, D. N. Hendrickson, *J. Am. Chem. Soc.* **1995**, *117*, 301 – 317.

[5] a) M. Ohba, H. Okawa, *Coord. Chem. Rev.* **2000**, *198*, 313 – 328; b) J. A. Smith, J. R. Galán-Mascarós, R. Clérac, K. R. Dunbar, *Chem. Commun.* **2000**, 1077 – 1078; c) H. Z. Kou, S. Gao, B. Q. Ma, D. Z. Liao, *Chem. Commun.* **2000**, 1309 – 1310; d) F. Bellouard, M. Clemente-León, E. Coronado, J. R. Galán-Mascarós, C. J. Gómez-García, F. Romero, K. R. Dunbar, *Eur. J. Inorg. Chem.* **2002**, 1603 – 1606; e) E. Colacio, M. Ghazi, H. Stoeckli-Evans, F. Lloret, C. Perez, *Inorg. Chem.* **2001**, *40*, 4876 – 4883.

[6] a) M. Pilkington, M. Gross, P. Franz, M. Biner, S. Decurtins, H. Stockli-Evans, A. Neels, *J. Solid State Chem.* **2001**, *159*, 262 – 267; b) E. Coronado, M. Clemente-León, J. R. Galán-Mascarós, C. Giménez-Saiz, C. J. Gómez-García, E. Martínes-Ferrero, *J. Chem. Soc. Dalton Trans.* **2000**, 3955 – 3961.

[7] a) K. R. Dunbar, R. A. Heintz, *Prog. Inorg. Chem.* **1997**, *45*, 283 – 391; b) W. R. Entley, G. S. Girolami, *Inorg. Chem.* **1994**, *33*, 5156 – 5166; c) S. Ferlay, T. Mallah, R. Ouahés, P. Veillet, N. Verdaguer, *Nature* **1995**, *378*, 701 – 703.

[8] a) M. Kurmoo, C. J. Kepert, *New J. Chem.* **1998**, *22*, 1515 – 1524; b) J. L. Manson, C. R. Kmety, Q. Z. Huang, J. W. Lynn, G. M. Bendele, S. Pagola, P. W. Stephens, L. M. Liable-Sands, A. L. Rheingold, A. J. Epstein, J. S. Miller, *Chem. Mater.* **1998**, *10*, 2552 – 2560; c) S. R. Batten, P. Jensen, B. Moubaraki, K. S. Murray, R. Robson, *Chem. Commun.* **1998**, 439 – 440.

[9] a) E. Coronado, J. R. Galán-Mascarós, C. J. Gómez-García, J. M. Martínez-Agudo, *Inorg. Chem.* **2001**, *40*, 113 – 120; b) E. Coronado, J. R. Galán-Mascarós, C. J. Gómez-García, J. Ensling, P. Gütlich, *Chem. Eur. J.* **2000**, *6*, 552 – 563; c) H. Tamaki, Z. J. Zhong, N. Matsumoto, S. Kida, M. Koikawa, N. Achiwan, Y. Hashimoto, H. Okawa, *J. Am. Chem. Soc.* **1992**, *114*, 6974 – 6979.

[10] a) J. S. Miller, A. J. Epstein, *Angew. Chem.* **1994**, *106*, 399 – 432; *Angew. Chem. Int. Ed. Engl.* **1994**, *33*, 385 – 415; b) J. Zhang, J. Ensling, V. Ksenofontov, P. Gütlich, A. J. Epstein, J. S. Miller, *Angew. Chem.* **1998**, *110*, 676 – 679; *Angew. Chem. Int. Ed.* **1998**, *37*, 657 – 660; c) G. T. Yee, J. M. Manriquez, D. Dixon, R. S. McLean, D. M. Groski, R. B. Flippen, K. S. Narayan, A. J. Epstein, J. S. Miller, *Adv. Mater.* **1991**, *3*, 309 – 311.

[11] a) "Supramolecular Engineering of Synthetic Metallic Materials: Conductors and Magnets": K. R. Dunbar, J. Cowen, H. Zhao, R. A. Heintz, X. Ouyang, G. Grandinetti, *NATO ASI Ser. Ser. C* **1999**, *518*,353; b) J. Cowen, R. Clérac, R. A. Heintz, S. A. O'Kane, X. Ouyang, H. Zhao, K. R. Dunbar, *Mol. Cryst. Liq. Cryst. Sci. Technol. Sect. A* **1999**, *334*, 825 – 844; c) S. A. O'Kane, R. Clérac, H. Zhao, X. Ouyang, J. R. Galán-Mascarós, R. Heintz, K. R. Dunbar, *J. Solid State Chem.* **2000**, *152*, 159 – 173.

[12] T. Akutagawa, G. Saito, M. Kusunoki, K. Sakaguchi, *Bull. Chem. Soc. Jpn.* **1996**, *69*, 2487 – 2511.

[13] a) M. Tadokoro, K. Nakasuji, *Coord. Chem. Rev.* **2000**, *198*, 205 – 218; b) M. Tadokoro, K. Isobe, H. Uekusa, Y. Ohashi, J. Toyoda, K. Tashiro, K. Nakasuji, *Angew. Chem.* **1999**, *111*, 102 – 106; *Angew. Chem. Int. Ed.* **1999**, *38*, 95 – 98; c) M. Tadokoro, T. Shiomi, K. Isobe, K. Nakasuji, *Inorg. Chem.* **2001**, *40*, 5476 – 5478; d) C. A. Hester, R. G. Baughman, H. L. Collier, *Polyhedron* **1997**, *16*, 2893 – 2895.

[14] a) S. Rau, T. Büttner, C. Temme, M. Ruben, H. Görls, D. Walther, M. Duati, S. Fanni, J. G. Vos, *Inorg. Chem.* **2000**, *39*, 1621 – 1624; b) M. Leirer, G. Knör, A. Vogler, *Inorg. Chim. Acta* **1999**, *288*, 150 – 153; c) O. F. Danzeisen, M. Goanta, H. W. Rotter, G. Thiele, *Inorg. Chim. Acta* **1999**, *287*, 218 – 222.

[15] P. Majundar, S.-M. Peng, S. Goswami, *J. Chem. Soc. Dalton Trans.* **1998**, 1569 – 1574.

[16] K. D. Benkstein, J. T. Hupp, C. L. Stern, *Angew. Chem.* **2000**, *112*, 3013 – 3015; *Angew. Chem. Int. Ed.* **2000**, *39*, 2891 – 2893.

[17] a) M. A. Martinez-Lorente, F. Dahan, Y. Sanakis, V. Petrouleas, A. Bousseksou, J.-P. Tuchagues, *Inorg. Chem.* **1995**, *34*, 5346 – 5357; b) D. Boinnnard, P. Cassoux, V. Petrouleas, J.-M. Savariault, J.-P. Tuchagues, *Inorg. Chem.* **1990**, *29*, 4114 – 4122.

[18] M. Tadokoro, K. Sato, D. Shiomi, T. Takui, K. Itoh, *Mol. Cryst. Liq. Cryst. Sci. Technol. Sect. A* **1997**, *306*, 49 – 56.

[19] Crystal data for **1**: $C_{114}H_{118}Cl_4Co_5N_{24}O_{11}$, $M_r = 2436.77\ g\,mol^{-1}$, monoclinic, space group $C2/c$, $a = 32.4150(5)$, $b = 18.8240(7)$, $c = 20.4850$ Å, $\beta = 127.8221(13)°$, $V = 9873.6(6)$ Å^3; $Z = 4$; $\rho_{calc} = 1.639\ g\,cm^{-3}$; $2\theta_{max} = 42°$; $Mo_{K\alpha}$ radiation, $\lambda = 0.71069$ Å; $T = 293(2)$ K; 36176 reflections, of which 5266 are unique, and of which 3503 were included in the refinement ($I > 4\sigma$); solution by direct methods (SIR97, A. Altomare, M. C. Burla, M. Camalli, G. L. Cascarano, C. Giacovazzo, A. Guagliardi, A. G. G. Moliterni, G. Polidori, R. Spagna, *J. Appl. Crystallogr.* **1999**, *32*, 115 – 119) and refinement on F^2 by full-matrix least squares procedure (SHELXL-97, G. M. Sheldrick, University of Göttingen, Göttingen (Germany), **1997**); 356 parameters; all C, N, H and disordered solvent atoms were refined isotropically; H atoms from the monoprotronated Hbbiz ligands were found after successive Fourier transform cycles and refined with the restriction of maintaining a constant distance to the N atom they are bonded; all other H atoms were included in their calculated positions, except in disordered solvent molecules; disordered solvent molecules were assigned partial occupancy

 © 2003 Wiley-VCH Verlag GmbH & Co. KGaA, Weinheim

factors, and their positions restrained to maintain typical distances and shapes for toluene or methanol molecules; final values $R\ (F) = 0.0592$, $R_w\ (F^2) = 0.1423$.

[20] a) H. Kimagai, M. Ohba, K. Inoue, H. Okawa, *Chem. Lett.* **2002**, 1006 – 1007.

[21] M. C. Rezende, C. A. Marques, E. L. Dall'Oglio, C. Zucco, *Liebigs Ann.* **1997**, 925 – 929.

 © 2003 Wiley-VCH Verlag GmbH & Co. KGaA, Weinheim

Pseudorotaxanes on Gold

A Pseudorotaxane on Gold: Formation of Self-Assembled Monolayers, Reversible Dethreading and Rethreading of the Ring, and Ion-Gating Behavior**

*Kyungpil Kim, Woo Sung Jeon, Jin-Koo Kang, Jae Wook Lee, Sang Yong Jon, Taisun Kim, and Kimoon Kim**

Artificial molecular machines,[1] assemblies of a distinct number of molecular components designed to perform machinelike motions in response to appropriate external stimuli, have received much attention in recent years because of their potential applications in nanotechnology.[2] Pseudorotaxanes, a class of supramolecular species in which a molecular thread is encircled by a molecular bead, have been employed in the construction of prototype molecular machines because dethreading and rethreading movements of a thread through the center of a ring are reminiscent of the action of a linear motor. Although a number of molecular machines based on pseudorotaxanes were reported, their behavior in solution was mostly studied.[3–5] To realize the full potential of these molecules, however, they need to be organized on surfaces so that they behave coherently. Nevertheless, few studies on self-assembled monolayers (SAMs) of pseudorotaxanes on solid surfaces and their behavior have been reported.[6] Herein we report a self-assembled monolayer of a pseudorotaxane on gold and its machinelike behavior—reversible dethreading and rethreading of the ring. Furthermore, unprecedented ion-gating behavior associated with threading and dethreading is also reported.

Cucurbituril (CB[6]),[7,8] a macrocyclic cage compound comprising six glycoluril units, forms host–guest complexes with diaminoalkanes such as diaminobutane, the stability of which strongly depends on pH. Taking advantage of the pH-dependent complexation–decomplexation behavior of CB[6]-diaminoalkanes, we and others synthesized (pseudo)rotaxane-based molecular machines or switches working in solution.[9,10] To realize a molecular machine working on a gold surface, we have now designed and synthesized novel pseudorotaxane **1**[11] containing CB[6] threaded on a molecular string that consists of a diaminobutane unit as a station for the molecular bead, and a 1,2-dithiolane group[12] as an anchoring point toward a gold surface (Scheme 1).

A self-assembled monolayer (SAM) of the pseudorotaxane on gold is easily prepared by immersing a gold substrate in deionized water containing 1 mM of **1** for 24 h.[13] Figure 1a shows the reflectance FTIR spectrum of the SAM developed on the gold substrate. The peaks at 1755 cm^{-1} and 1474 cm^{-1} corresponding to CO and CN stretching motions of CB[6], respectively, confirm the attachment of the pseudorotaxane to the surface. The S(2p) peaks at 162.1 eV ($S(2p_{3/2})$) and 163.3 eV ($S(2p_{1/2})$) in X-ray photoelectron spectroscopy (XPS) are also consistent with the attachment of the 1,2-dithiolane group on the gold surface.[14]

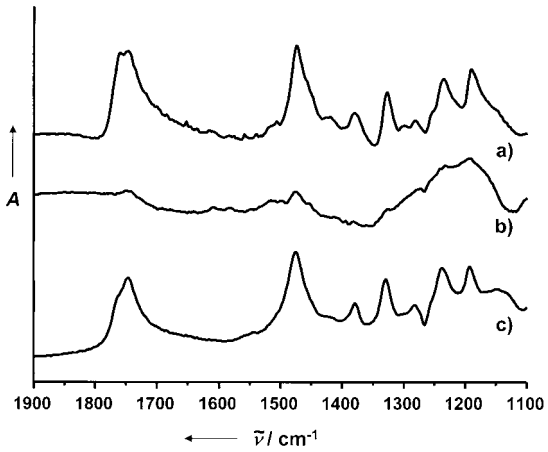


Figure 1. FTIR spectra of pseudorotaxane SAM: a) after preparation, b) after dethreading, and c) rethreading of CB[6].

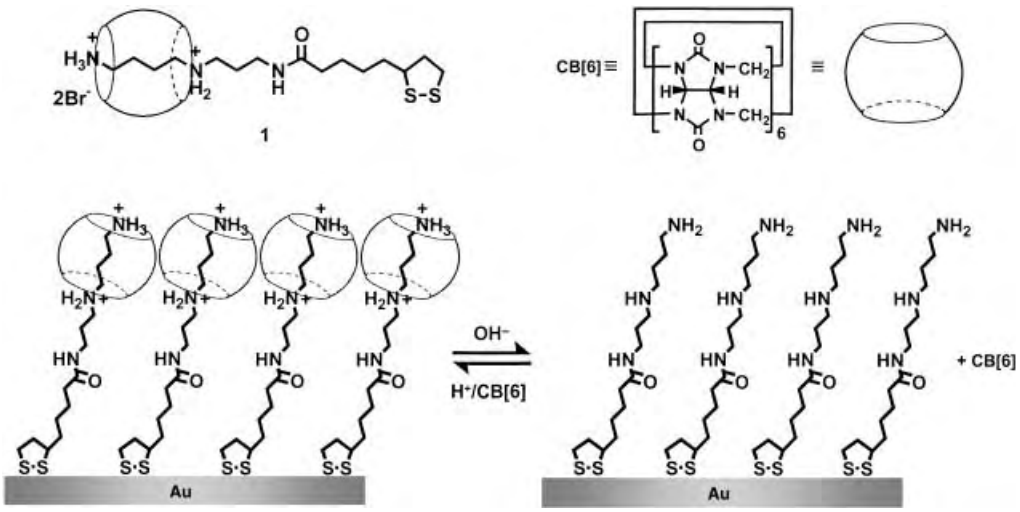
The reversible dethreading and rethreading of CB[6] in the pseudorotaxane SAM has been studied. Dethreading of CB[6] from the pseudorotaxane SAM is achieved by exposing it to 0.1M NaOH solution for 1 h, and rethreading of CB[6] is performed by soaking the substrate into 1 mM CB[6] in 0.1M ammonium chloride solution (pH ~5) with stirring for 10 h.

[*] Prof. Dr. K. Kim, K. Kim, W. S. Jeon, J.-K. Kang, Dr. J. W. Lee, Dr. S. Y. Jon
National Creative Research Initiative Center for Smart Supramolecules and
Department of Chemistry
Division of Molecular and Life Sciences
Pohang University of Science and Technology
San 31 Hyojadong, Pohang 790-784 (Republic of Korea)
Fax: (+82) 54-279-8129
E-mail: kkim@postech.ac.kr
Prof. Dr. T. Kim
Department of Chemistry, Hallym University
1 Ockchon-Dong, Chunchon
Kangwon-Do 200-702 (Republic of Korea)

[**] We gratefully acknowledge the Creative Research Initiative Program of the Korean Ministry of Science and Technology for support of this work and the Brain Korea 21 Program of the Korean Ministry of Education for graduate studentships to Kyungpil Kim, W. S. Jeon, and J.-K. Kang. We thank Tae Wan Kim for his contribution at the early stage of this work.

Supporting information for this article is available on the WWW under http://www.angewandte.org or from the author.

 DOI: 10.1002/anie.200250692 © 2003 Wiley-VCH Verlag GmbH & Co. KGaA, Weinheim



Scheme 1. Self-assembled monolayer of pseudorotaxane **1** on Au and dethreading and rethreading of molecular bead CB[6].

The dethreading and rethreading of CB[6] is confirmed by the disappearance and reappearance of the characteristic peaks of CB[6] in FTIR spectra (Figure 1 b and c). These processes are reversible and have been repeated up to three cycles with ~10–20% decrease in the intensities of FTIR signals in each cycle.

The pseudorotaxane monolayer formation, and dethreading and rethreading processes are monitored in situ by surface plasmon resonance (SPR) spectroscopy.[15,16] The following solutions are flowed over a gold substrate in sequence and the surface is washed with a HBS buffer solution (pH 7.4) after each solution is passed: 1) HBS buffer solution (pH 7.4) containing 0.5 mM of **1** and thioctic acid (1:1), 2) 0.1M NaOH solution, 3) 1 mM CB[6] in HBS solution, and 4) 0.1M NaOH solution. The resulting SPR sensorgram is shown Figure 2. A large change in resonance angle, which corresponds to increase in density to 0.49 ng mm^{-2}, after step 1 (and subsequent washing) is consistent with the formation of a mixed SAM of **1** and thioctic acid on the gold surface. The subsequent changes in resonance angle are consistent with dethreading and rethreading of CB[6]: after step 2, the density decreases to 0.23 ng mm^{-2}, which corresponds to ~80% dethreading of CB[6], and step 3 increases the density to 0.39 ng mm^{-2}, suggesting ~70% of CB[6] are rethreaded. The density decrease to 0.26 ng mm^{-2} after step 4 suggests that ~80% of CB[6] are dethreaded again.

The reversible threading and dethreading of the bulky CB[6] beads suggests that the pseudorotaxane SAM may behave as a gate. For example, it may block or allow the access of electroactive species to the electrode surface depending on the presence or absence of threaded CB[6]. To test this idea, the pseudorotaxane modified electrode was first treated with 1 mM thioctic acid in ethanol to fill up defect sites of the pseudorotaxane SAM.[17] The accessibility of the electrode surface to $[Fe(CN)_6]^{3-}$ was then examined by cyclic voltammetry. The defect-free pseudorotaxane SAM does not display any redox peaks in the cyclic voltammogram (Figure 3; ——). After dethreading CB[6], however, a quasireversible redox wave of $[Fe(CN)_6]^{3-}$ is observed (Figure 3, -----). This result suggests that dethreading of CB[6] opens up

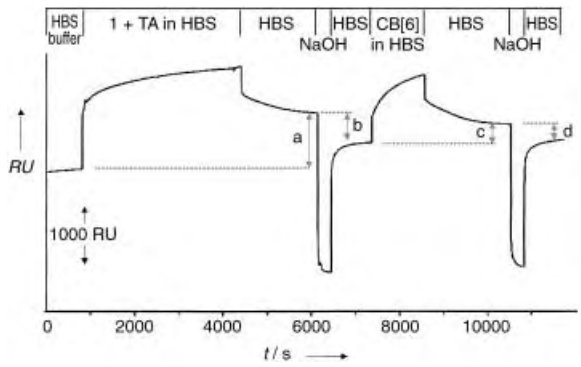


Figure 2. The SPR sensorgram showing reversible dethreading and rethreading of CB[6] in pseudorotaxane SAM: a) formation of mixed SAM of **1** and thioctic acid (TA), b) dethreading of CB[6], c) rethreading of CB[6] and d) dethreading of CB[6]. The top *x* axis represents the continuous flow of the indicated solutions.

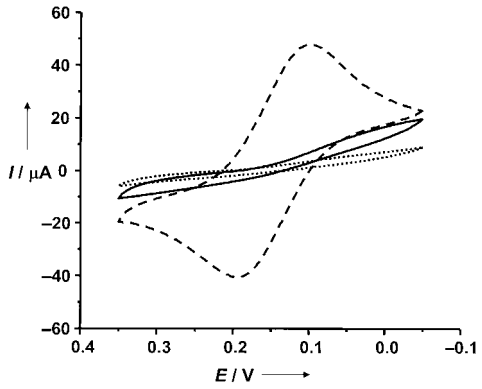


Figure 3. Cyclic voltammograms of $[Fe(CN)_6]^{3-}$ (0.5 mM) obtained with a) a gold electrode modified with SAM of **1** and thioctic acid (——), b) after dethreading of CB[6] (-----), and c) after treating with thioctic acid (•••••). Supporting electrolyte: 0.1 M KCl in universal buffer at pH 8.0; scan rate 0.1 V s^{-1}.

 © 2003 Wiley-VCH Verlag GmbH & Co. KGaA, Weinheim

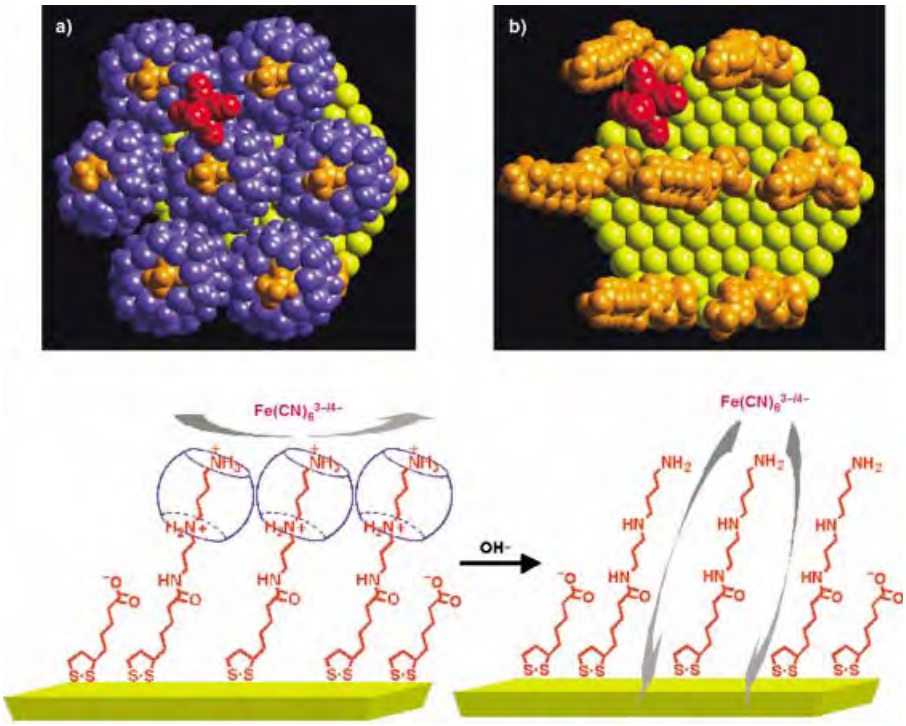


Figure 4. Space-filling (top) and chemical (bottom) representations of pseudorotaxane SAM of **1** on gold a) before and b) after dethreaded of CB[6] to illustrate that $[Fe(CN)_6]^{3-}$ can access the gold surface after dethreading. The string, CB[6] bead, $[Fe(CN)_6]^{3-}$ and gold surface are represented in orange, blue, red and yellow colors, respectively.

the "channels" through which the negatively charged $[Fe(CN)_6]^{3-}$ can now approach to the electrode surface and be reduced (Figure 4). Treatment of the CB[6]-dethreaded SAM with thioctic acid to fill up the exposed Au surface results in the disappearance of the redox wave of $[Fe(CN)_6]^{3-}$ (Figure 3, •••••).[18] Although further careful studies are needed, such an ion-gating phenomenon associated with threading and dethreading of pseudorotaxanes attached to electrode surfaces is unprecedented.

In summary, we have designed and constructed a pseudorotaxane SAM on a gold surface. The reversible dethreading and rethreading of CB[6] has been demonstrated by SPR and other experiments. Moreover, unprecedented ion-gating behavior associated with threading and dethreading of the molecular bead has been observed. This work may provide an insight in designing elaborate molecular machines on surface that may find useful applications in nanotechnology; we are currently working along this line.

Received: December 4, 2002 [Z50692]

Keywords: cyclic voltammetry · molecular devices · rotaxanes · self-assembly · supramolecular chemistry

[1] a) V. Balzani, A. Credi, F. M. Raymo, J. F. Stoddart, *Angew. Chem.* **2000**, *112*, 3484; *Angew. Chem. Int. Ed.* **2000**, *39*, 3348; b) Molecular machines special issues, *Acc. Chem. Res.* **2001**, *34*, 409–522.

[2] Electronic devices based on molecular machines have been reported. a) C. P. Collier, E. W. Wong, M. Belohradský, F. M. Raymo, J. F. Stoddart, P. J. Kuekes, R. S. Williams, J. R. Heath, *Science* **1999**, *285*, 391; b) C. P. Collier, G. Mattersteig, E. W. Wong, Y. Luo, K. Beverly, J. Sapaio, F. M. Raymo, J. F. Stoddart, J. R. Heath, *Science* **2000**, *289*, 1172.

[3] a) M. Asakawa, S. Iqbal, J. F. Stoddart, N. D. Tinker, *Angew. Chem.* **1996**, *108*, 1054; *Angew. Chem. Int. Ed. Engl.* **1996**, *35*, 976; b) A. Credi, V. Balzani, S. J. Langford, J. F. Stoddart, *J. Am. Chem. Soc.* **1997**, *119*, 2679; c) P. R. Ashton, R. Ballardini, V. Balzani, I. Baxter, A. Credi, M. C. T. Fyfe, M. T. Gandolfi, M. Gómez-López, M.-V. Martínez-Díaz, A. Piersanti, N. Spencer, J. F. Stoddart, M. A. J. P. White, D. J. Williams, *J. Am. Chem. Soc.* **1998**, *120*, 11932; d) E. Ishow, A. Credi, V. Balzani, F. Spadola, L. Mandolini, *Chem. Eur. J.* **1999**, *5*, 984; e) V. Balzani, A. Credi, G. Mattersteig, O. A. Matthews, F. M. Raymo, J. F. Stoddart, A. J. P. White, D. J. Williams, *J. Org. Chem.* **2000**, *65*, 1924.

[4] a) A. Mirzoian, A. E. Kaifer, *Chem. Eur. J.* **1997**, *3*, 1052; b) P. R. Ashton, V. Balzani, J. Becher, A. Credi, M. C. T. Fyfe, G. Mattersteig, S. Menzer, M. B. Nielsen, F. M. Raymo, J. F. Stoddart, M. Venturi, D. J. Williams, *J. Am. Chem. Soc.* **1999**, *121*, 3951; c) V. Balzani, J. Becher, A. Credi, M. B. Nielsen, F. M. Raymo, J. F. Stoddart, A. M. Talarico, M. Venturi, *J. Org. Chem.* **2000**, *65*, 1947; d) A. E. Kaifer, M. Gómez-Kaifer in *Supramolecular Electrochemistry*, Wiley-VCH, Weinheim, **1999**.

[5] a) R. Ballardini, V. Balzani, M. T. Gandolfi, L. Prodi, M. Venturi, D. Philp, H. G. Ricketts, J. F. Stoddart, *Angew. Chem.* **1993**, *105*, 1362; *Angew. Chem. Int. Ed. Engl.* **1993**, *32*, 1301; b) H. Murakami, A. Kawabuchi, K. Kotoo, M. Kinitake, N. Nakashima, *J. Am. Chem. Soc.* **1997**, *119*, 7605; c) A. M. Brouwer, C. Frochot, F. G. Gatti, D. A. Leigh, L. Mottier, F. Paolucci, S. Roffia, G. W. H. Wurpel, *Science* **2001**, *291*, 2124; d) P. R. Ashton, R. Ballardini, V. Balzani, E. C. Constable, A. Credi, O. Kocian, S. J. Langford, J. A. Preece, L. Prodi, E. R. Schofield, N. Spender, J. F. Stoddart, S. Wenger, *Chem. Eur. J.* **1998**, *4*, 2413.

[6] A pseudorotaxane tethered on the surface of a silica film was reported: S. Chia, J. Cao, J. F. Stoddart, J. I. Zink, *Angew. Chem.* **2001**, *113*, 2513; *Angew. Chem. Int. Ed.* **2001**, *40*, 2447. Tetrathiafulvalene (TTF) functionalized SAM on gold was reported. Cyclic voltammetric study with the SAM modified electrode in the presence of cyclobis(paraquat-*p*-phenylene) suggested reversible complexation between the TTF unit and the macrocycle. G. Cooke, F. M. A. Duclairoir, V. M. Rotello, J. F. Stoddart, *Tetrahedron Lett.* **2000**, *41*, 8163.

[7] For reviews on cucurbituril, see a) W. L. Mock, *Top. Curr. Chem.* **1995**, *175*, 1; b) P. Cintas, *J. Inclusion Phenom. Mol. Recognit. Chem.* **1994**, *17*, 205; c) W. L. Mock in *Comprehensive Supramolecular Chemistry, Vol. 2* (Ed.: F. Vögtle), Pergamon, Oxford, **1996**, p. 477. Cucurbituril homologues, cucurbit[*n*]uril ($n = 5$, 7 and 8) have been recently reported: J. Kim, I.-S. Jung, S.-Y. Kim,

 © 2003 Wiley-VCH Verlag GmbH & Co. KGaA, Weinheim

E. Lee, J.-K. Kang, S. Sakamoto, K. Yamaguchi, K. Kim, *J. Am. Chem. Soc.* **2000**, *122*, 540.
[8] Mechanically interlocked molecules incorporating CB[6]: a) D. Whang, Y.-M. Jeon, J. Heo, K. Kim, *J. Am. Chem. Soc.* **1996**, *118*, 11333; b) D. Whang, K. Kim, *J. Am. Chem. Soc.* **1997**, *119*, 451; c) D. Whang, K.-M. Park, J. Heo, K. Kim, *J. Am. Chem. Soc.* **1998**, *120*, 4899; d) S.-G. Roh, K.-M. Park, G.-J. Park, S. Sakamoto, K. Yamaguchi, K. Kim, *Angew. Chem.* **1999**, *111*, 672; *Angew. Chem. Int. Ed.* **1999**, *38*, 638; e) E. Lee, J. Heo, K. Kim, *Angew. Chem.* **2000**, *112*, 2811; *Angew. Chem. Int. Ed.* **2000**, *39*, 2699; f) E. Lee, J. Kim, J. Heo, D. Whang, K. Kim, *Angew. Chem.* **2001**, *113*, 413; *Angew. Chem. Int. Ed.* **2001**, *40*, 399; g) J. W. Lee, Y. H. Ko, S.-H. Park, K. Yamaguchi, K. Kim, *Angew. Chem.* **2001**, *113*, 768; *Angew. Chem. Int. Ed.* **2001**, *40*, 746; h) K.-M. Park, D. Whang, E. Lee, J. Heo, K. Kim, *Chem. Eur. J.* **2002**, *8*, 498; i) K.-M. Park, S.-Y. Kim, J. Heo, D. Whang, S. Sakamoto, K. Yamaguchi, K. Kim, *J. Am. Chem. Soc.* **2002**, *124*, 2140; j) K. Kim, *Chem. Soc. Rev.* **2002**, *31*, 96.
[9] W. L. Mock, J. Pierpont, *J. Chem. Soc. Chem. Commun.* **1990**, 1509.
[10] a) S. I. Jun, J. W. Lee, S. Sakamoto, K. Yamaguchi, K. Kim, *Tetrahedron Lett.* **2000**, *41*, 471; b) J. W. Lee, K. Kim, K. Kim, *Chem. Commun.* **2001**, 1042; c) J. W. Lee, S. W. Choi, Y. H. Ko, S.-Y. Kim, K. Kim, *Bull. Korean Chem. Soc.* **2002**, *23*, 1347.
[11] Synthetic details of **1** are given in the Supporting Information.
[12] a) A. Brajter-Toth, Q. Cheng, *Anal. Chem.* **1992**, *64*, 1998; b) J. Madoz, B. A. Kuznetov, F. J. Medrano, J. L. García, V. M. Fernández, *J. Am. Chem. Soc.* **1997**, *119*, 1043.
[13] Experimental details for SAM of **1** on gold are described in the Supporting Information.
[14] T. Ishida, N. Choi, *Langmuir* **1999**, *15*, 6799.
[15] a) J. Lahiri, L. Isaacs, J. Tien, G. M. Whitesides, *Anal. Chem.* **1999**, *71*, 777; b) C. D. Hodneland, M. Mrksich, *J. Am. Chem. Soc.* **2000**, *122*, 4235.
[16] BIACore 2000 and Pioneer Sensor Chip J1 Au surface were used for SPR studies. SPR measures the angle of light (θ) reflected from the backside of the gold substrate that has a minimum intensity. Changes in this angle ($\Delta\theta$) are linearly related to the index of refraction of the solution above the surface and therefore to the density of adsorbed molecules ($\Delta\theta$ of $0.10° = 1\ \mathrm{ng\,mm^{-2}} = 1000$ RU).
[17] a) Q. Cheng, A. Brajter-Toth, *Anal. Chem.* **1992**, *64*, 1998; b) Q. Cheng, A. Brajter-Toth, *Anal. Chem.* **1996**, *68*, 4180; c) V. P. Y. Gadzekpo, K. P. Xiao, H. Aoki, P. Bühlmann, Y. Umezawa, *Anal. Chem.* **1999**, *71*, 5109.
[18] In principle, complete rethreading of CB[6] would block the access of $[Fe(CN)_6]^{3-}$ to the electrode surface resulting in no redox wave of the electroactive species in cyclic voltammetry. However, as described in the text, the rethreading of the molecular bead is achieved only up to ~80% and therefore, a quasireversible redox wave of $[Fe(CN)_6]^{3-}$ is still observed with substantially decreased but significantly high peak currents even after rethreading. For this reason, fully reversible and perfect ion-gating behavior by dethreading and rethreading of the bead (induced by pH change of the solution) is not achieved with this system. We are currently working on other systems with better ion-gating behavior.

 © 2003 Wiley-VCH Verlag GmbH & Co. KGaA, Weinheim

Bistable Molecular Shuttles

Remarkable Positional Discrimination in Bistable Light- and Heat-Switchable Hydrogen-Bonded Molecular Shuttles**

Andrea Altieri, Giovanni Bottari, Francois Dehez, David A. Leigh, Jenny K. Y. Wong, and Francesco Zerbetto**

Stimuli-responsive molecular "shuttles"[1–11] (that is, mechanically interlocked molecules in which a macrocycle can be translocated between different sites in response to an external signal) all operate through the same basic principle. The external stimulus does not intrinsically induce directional motion of the macrocycle. Rather, it alters the equilibrium between different translational co-conformers by increasing the binding strength of the less populated station and/or destabilizing the initially preferred binding site. The motion of the components arises from the background thermal energy, the net result being a change in the position of the macrocycle through biased Brownian motion (Figure 1).

Given this mode of action, a major problem in designing photoactive shuttles that can function as practical components for molecular machinery is finding ways of generating sufficiently large, long lived, binding-energy differences between pairs of positional isomers.[2–10] A Boltzmann distribution at 298 K requires a value of $\Delta\Delta G$ between translational co-conformers of approximately 2 kcal mol^{-1} for 95% occupancy of one station. Achieving such discrimination in two states to form a positionally bistable shuttle (that is, both $\Delta\Delta G_{\text{orange-blue}}$ and $\Delta\Delta G_{\text{orange-green}} \geq 2$ kcal mol^{-1}) by modifying only intrinsically weak, noncovalent binding modes, without adding external reagents, presents a significant challenge. The problem has previously been overcome, in part, by using photochemistry to block the position of the macrocycle in single-binding-site rotaxanes.[5,10] In these systems the macrocycle is only able to sit on an azobenzene[5] or stilbene unit[10] in the *E* diastereomer of the rotaxane and must reside elsewhere in the *Z* form. Unfortunately, the integrity of macrocycle positioning in such systems is likely to be limited

[*] Prof. D. A. Leigh, A. Altieri, Dr. G. Bottari, Dr. J. K. Y. Wong
School of Chemistry, University of Edinburgh
The King's Buildings, West Mains Road, Edinburgh EH9 3JJ (UK)
Fax: (+44) 131-667-9085
E-mail: David.Leigh@ed.ac.uk

Prof. F. Zerbetto, Dr. F. Dehez
Dipartimento di Chimica "G. Ciamician"
Università degli Studi di Bologna
via F. Selmi 2, 40126 Bologna (Italy)
Fax: (+39) 051-2099456
E-mail: gatto@ciam.unibo.it

[**] This work was supported by the European Union Future and Emerging Technology Programme *MechMol*, the EPSRC and the MURST project "Dispositivi Supramolecolari". D.A.L. is an EPSRC Advanced Research Fellow (AF/982324)

Supporting information for this article is available on the WWW under http://www.angewandte.org or from the author.

 © 2003 Wiley-VCH Verlag GmbH & Co. KGaA, Weinheim DOI: 10.1002/anie.200250745

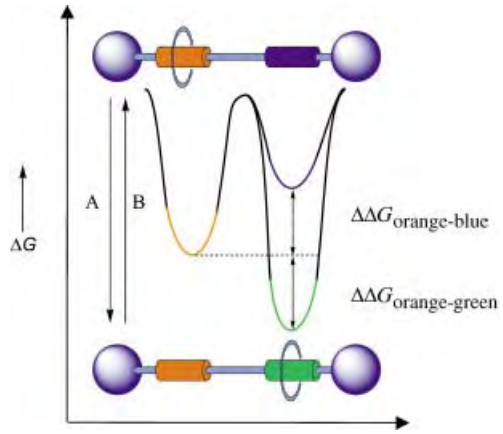


Figure 1. Macrocycle translation in a stimuli-responsive molecular shuttle. Stimulus A induces a blue-to-green transformation, and stimulus B induces a green-to-blue transformation. The equilibrium distribution of the macrocycle between two stations is determined by the difference in their binding energies ($\Delta\Delta G_{\text{orange-blue}}$, $\Delta\Delta G_{\text{orange-green}}$) and the temperature.

unless the thread is very short. Here we describe photo- and thermally responsive shuttles (**1**–**3**) in which the macrocycle moves over a relatively large distance (approximately 1.5 nm) between two discrete stations with remarkable positional integrity (even at room temperature), despite the fact that the discrimination between the binding sites is caused only by "matched" and "mismatched" hydrogen-bonding motifs. Each translational form is stable until a new stimulus is applied.

The basis for the new shuttles lies in the photochemical and thermal interconversion of fumaramide and maleamide groups.[12] The *trans*-olefin bisamide acts as an excellent template for the formation of benzylic amide macrocycle-based rotaxanes (for example, *E*-**4**; Figure 2) because the amide carbonyl groups of the thread are rigidly held in positions that fit the hydrogen-bond-donating sites of the forming macrocycle (an arrangement maintained even in crystals of *E*-**4** obtained from DMSO; Figure 2a).[13] Irradiation of fumaramide rotaxanes at 254 nm[14] produces the corresponding *cis*-maleamide rotaxane, in which the maximum number of intercomponent hydrogen bonds changes from four to two (Figure 2b), considerably reducing the binding strength[15] between the macrocycle and the thread. By incorporating a second binding site into the thread, we reasoned it might be possible to generate photoinduced, thermally reversible translation of the rotaxane components.

We prepared three different molecular shuttles (**1**–**3**; Scheme 1), each containing a fumaramide/maleamide site plus a non-photoactive second station with a predicted intermediate macrocycle-binding affinity. Since the transition state of the rotaxane-forming reaction is similar in structure to the final rotaxane,[16] it seemed likely that the macrocycle-binding affinity of a given station should be related to its ability to template the formation of the rotaxane. Several factors are known to affect both template efficacy and the nature of the intercomponent hydrogen-bonding interactions (NH···O=C bond lengths, angles etc.; Figure 2) including: the hydrogen-bond basicity of the functional groups (amides are superior to esters[13]), preorganization (fumaramide is superior to succinamide[17]), and distance between the binding sites (succinamide is superior to adipamide[18]).

Some features of the synthetic routes to **1**–**3** are noteworthy. Although *E*-**1** was prepared from the corresponding *trans*-olefin-containing *E*-**5** (an "*E* thread") in good yield, the other *E* threads could not be utilized owing to their insufficient solubility in solvents that do not disrupt hydrogen bonding. Rotaxanes *Z*-**2** and *Z*-**3** were therefore prepared from the corresponding *Z*-threads and converted to the *E* rotaxanes thermally (120 °C, 1–7 days, $C_2H_2Cl_4$, 80–95 %). In fact, the *E* isomers of each molecular shuttle could be converted to the *Z* forms with light (*E*→*Z*, direct irradiation at 254 nm, CH_2Cl_2, 30 min, 39–54 %; or with a catalytic benzophenone sensitizer at 350 nm, CH_2Cl_2, 5 min, 60–65 %) and back again through heating or reversible Michael addition (catalytic ethylenediamine, 60 °C, 4 h, 75–85 %).

Since the xylylene rings of the macrocycle shield encapsulated regions of the thread, the position of the macrocycle in

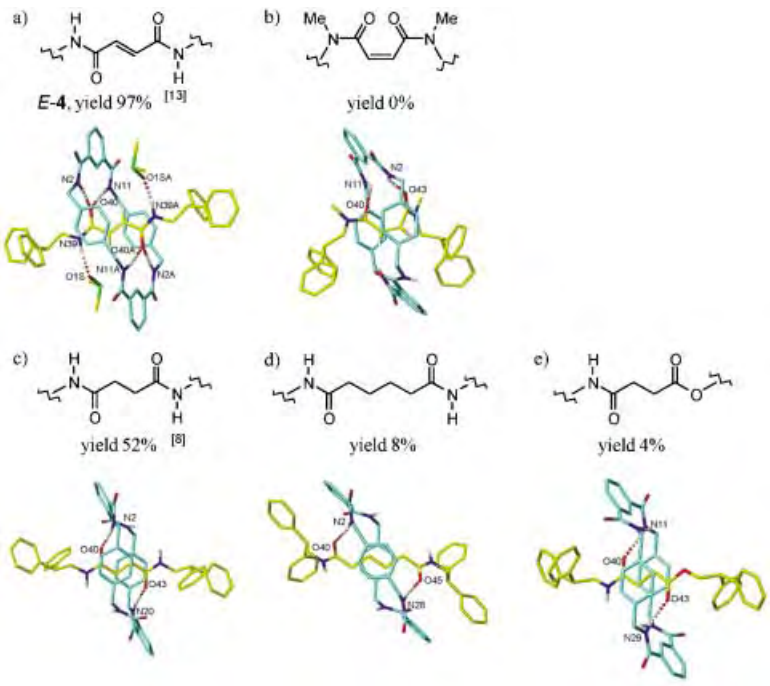
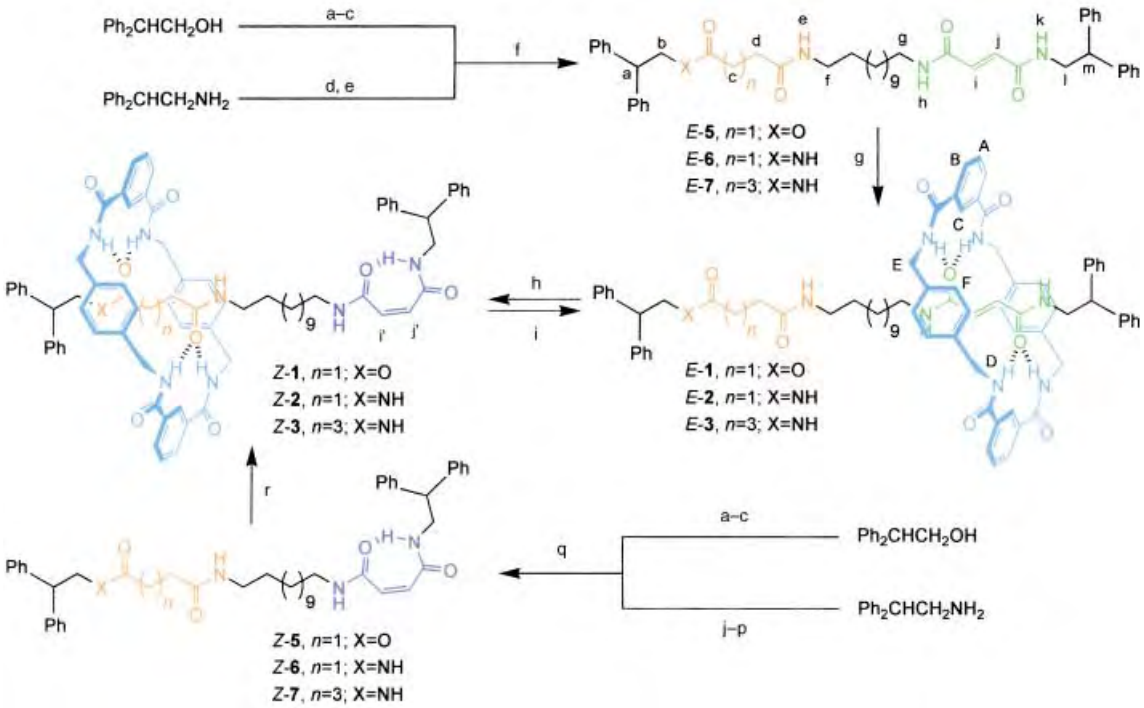


Figure 2. X-ray structures of model single-binding-site [2]rotaxanes showing hydrogen-bonding characteristics of predicted "strong" (a), "weak" (b), and "intermediate strength" (c–e) hydrogen-bonding stations; a) fumaramide rotaxane *E*-**4** crystallized from DMSO; b) *N*,*N*′-dimethyl derivative of the corresponding maleamide (*Z*) rotaxane; c) succinamide analogue of *E*-**4**; d) adipamide analogue of *E*-**4**; e) succinic amide ester analogue of *E*-**4**. Intramolecular hydrogen-bond lengths [Å] (and angles [°]): a) O40-HN2/O40A-HN2A 2.13 (173.7); O40-HN11/O40A-HN11A 1.89 (169.3); b) O40-HN11 2.08 (139.3); O43-HN2 2.00 (142.1); c) O40-HN2/O43-HN20 1.88 (165.3); d) O40-HN2/O45-HN28 2.00 (168.8); e) O40-HN11/O43-HN29 1.89 (156.1). Atoms: carbon (macrocycle), blue; carbon (thread), yellow; oxygen, red; nitrogen, dark blue; amide hydrogen, white. In all cases, the rotaxane "stoppers" are -CH_2CHPh_2 groups.

 © 2003 Wiley-VCH Verlag GmbH & Co. KGaA, Weinheim



Scheme 1. Synthesis of bistable molecular shuttles **1**–**3**. a) Succinic anhydride, Et_3N, CH_2Cl_2, 90%; b) $H_2N(CH_2)_{12}NHBoc$, 4-dimethylaminopyridine (DMAP), 1-(3-dimethylaminopropyl)-3-ethyl-carbodiimide hydrochloride (EDCI·HCl), CH_2Cl_2, 68%; c) trifluoroacetic acid, $CHCl_3$, quantitative; d) fumaric acid monoethylester, DMAP, EDCI·HCl, CH_2Cl_2, 85%; e) NaOH in H_2O, EtOH, 91%; f) DMAP, EDCI·HCl, DMF, *E*-**5**, 76%; g) isophthaloyl dichloride, *p*-xylylenediamine, Et_3N, $CHCl_3$, *E*-**1**, 57%; h) *hν* at 254 nm for 30 min, CH_2Cl_2, *Z*-**1**, 54%; *Z*-**2**, 48%; *Z*-**3**, 39%, or *hν* at 350 nm for 5 min, benzophenone, CH_2Cl_2, *Z*-**1**, 65%; *Z*-**2**, 65%; *Z*-**3**, 60%; i) $C_2H_2Cl_4$ at 120°C for 7 days, *E*-**1**, 80%; *E*-**2**, 80%; or 1 day, *E*-**3**, 95%; j) maleic anhydride, anhydrous THF, 75%; k) succinic anhydride, anhydrous THF, 95%; l) $SOCl_2$, 1,12-diaminododecane, CH_2Cl_2, 35%; m) adipic acid monoethylester, DMAP, EDCI·HCl, CH_2Cl_2, 86%; n) KOH in H_2O, EtOH, 95%; o) $H_2N(CH_2)_{12}NHBoc$, DMAP, EDCI·HCl, $CHCl_3$, 92%; p) trifluoroacetic acid, $CHCl_3$, quantitative; q) DMAP, EDCI.HCl, $CHCl_3$, *Z*-**5**, 70%; *Z*-**6**, 70%; *Z*-**7**, 70%; r) isophthaloyl dichloride, *p*-xylylenediamine, Et_3N, $CHCl_3$, *Z*-**1**, 2%; *Z*-**2**, 40%; *Z*-**3**, 20%. Boc = *tert*-butoxycarbonyl. Full experimental procedures can be found in the Supporting Information.[25]

$CDCl_3$ could be determined for each pair of rotaxane diastereomers by comparing the chemical shift of the protons in the rotaxane with those of the corresponding thread (or suitable model compounds in the case of *E*-**2** and *E*-**3**).[19] The spectra of *E*/*Z*-**1** and *E*/*Z*-**5** in $CDCl_3$ (400 MHz, 298 K) are shown in Figures 3 and 4. The H_i and H_j protons of the fumaramide group are shielded in the rotaxane *E*-**1**, compared to the thread *E*-**5**, by $\delta = 1.09$ and 1.02 ppm, whereas the chemical shifts of the H_c and H_d protons of the succinic amide ester group are similar in both compounds (Figure 3). In the maleamide isomer, the situation is completely reversed (Figure 4). The *Z* olefin protons ($H_{i'}$ and $H_{j'}$) resonate at almost identical chemical shifts in the rotaxane and thread, whereas the succinic amide ester methylene groups (H_c and H_d) are each shielded by > 1.3 ppm in the rotaxane. A similar series of shifts occurs in the ^{1}H NMR spectra of the other molecular shuttle pairs. Thus, even at 298 K, the occupancy of the fumaramide station in *E*-**1**, *E*-**2**, and *E*-**3** is greater than 95% (the limit we can determine with reasonable confidence using this method). The occupancy of the alternative, nonphotoactive station in the corresponding maleamide rotaxanes is similarly high for *Z*-**1** and *Z*-**2**. In *Z*-**3** the maleamide:adipamide occupancy ratio is reduced to approximately 15:85 (see Supporting Information), which corresponds to a $\Delta\Delta G$ of approximately 1.1 kcal mol^{-1}.

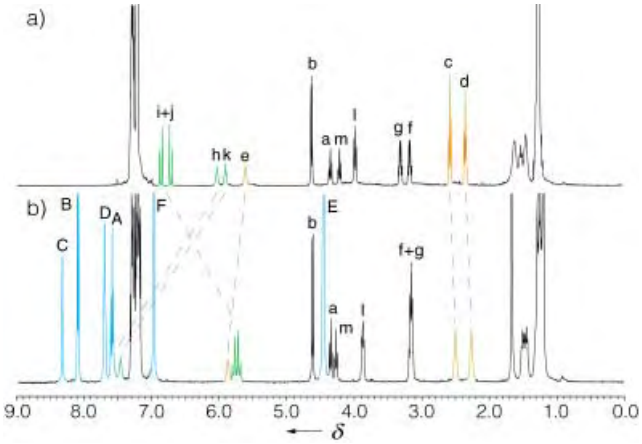


Figure 3. ^{1}H NMR spectra (400 MHz) of: a) Thread *E*-**5** and b) rotaxane *E*-**1** in $CDCl_3$ at 298 K. The assignments correspond to the lettering shown in Scheme 1.

It is interesting to note that our predictions of the relative station-binding affinities from rotaxane yield and hydrogen-bond lengths and angles are not completely accurate. Although the maleamide station is significantly populated in *Z*-**3**, the same station does not compete at all with the succinic amide ester site in *Z*-**1** (Figure 4), even though the yields[20]

 © 2003 Wiley-VCH Verlag GmbH & Co. KGaA, Weinheim

and X-ray structure suggest that the adipamide group should be a better binding site than the succinic amide ester.

Overall, the discrimination of the macrocycle for the different stations is excellent and, at temperatures which require substantial energy differences to significantly bias the population distribution, somewhat remarkable (most notably between the fumaramide and succinamide stations in *E*-**2**, which offer virtually identical hydrogen-bonding surfaces to the macrocycle). To probe this further, molecular modeling[16,17,21–24] was carried out by simulated annealing followed by geometrical optimization using the TINKER program with the MM3 force field. The difference in co-conformer stability for each pair of rotaxane diastereomers was calculated by comparing the energies (including zero point energies) of the occupied and unoccupied stations in each co-conformer to give the following $\Delta\Delta G$ values: a) 3.6 kcal mol^{-1} for *E*-**1** (fumaramide versus succinic amide ester occupancy), b) 2.9 kcal mol^{-1} for *Z*-**1** (succinic amide ester versus maleamide); c) 3.6 kcal mol^{-1} for *E*-**2** (fumaramide versus succinamide); d) 3.0 kcal mol^{-1} for *Z*-**2** (succinamide versus maleamide); e) 3.9 kcal mol^{-1} for *E*-**3** (fumaramide versus adipamide); f) 3.1 kcal mol^{-1} for *Z*-**3** (adipamide versus maleamide).

Whilst in each case there is probably overbinding as a result of solvation and folding not being included in the model, the calculations are broadly in agreement with the experimental results (that is, $\Delta\Delta G$ values are greater than 2 kcal mol^{-1}), although at this level they do not reproduce the anomalously poor binding of the adipamide station in *Z*-**3**.[20] However, the calculations do offer a simple explanation for why the positional discrimination is so good in these rotaxane systems: When they are not occupied, each station (except fumaramide) can intramolecularly hydrogen bond to itself, and so the positional isomer that has that station occupied must have at least one hydrogen bond less than the positional isomer with the fumaramide station occupied (Figure 5). The use of "self-binding" to compensate for the lack of station occupancy could prove a useful concept for driving submolecular motion in molecular machines that rely only on weak, noncovalent interactions.

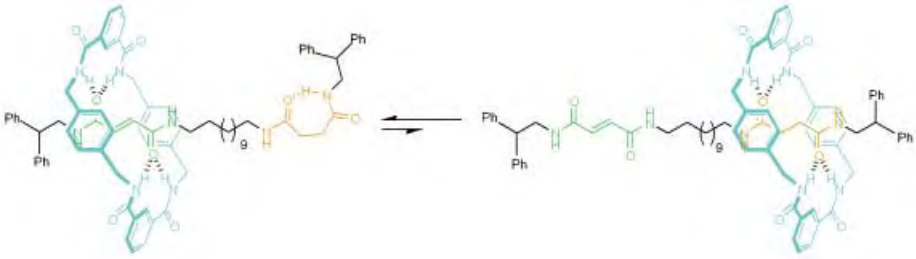


Figure 5. Translational isomerism in fumaramide-succinamide shuttle *E*-**2**.[25] Positional discrimination is excellent (greater than 95:5 at 298 K in $CDCl_3$) even though the fumaramide and succinamide stations present nearly identical surfaces to the macrocycle. The reason for this behavior is the self-binding of the succinamide station when it is unoccupied

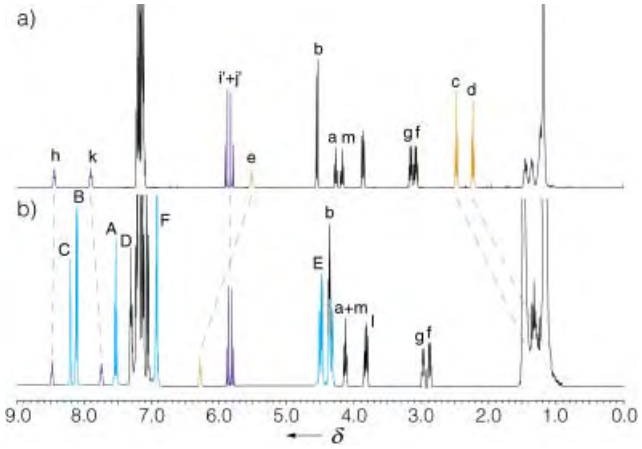


Figure 4. ^{1}H NMR spectra (400 MHz) of: a) Thread *Z*-**5** and b) rotaxane *Z*-**1** in $CDCl_3$ at 298 K.

Received: December 11, 2002 [Z50745]

Keywords: hydrogen bonds · macrocycles · molecular devices · photochemistry · rotaxanes

[1] For recent reviews see a) V. Balzani, A. Credi, F. M. Raymo, J. F. Stoddart, *Angew. Chem.* **2000**, *112*, 3484–3530; *Angew. Chem. Int. Ed.* **2000**, *39*, 3349–3391; b) Special issue on *Molecular Machines*: *Acc. Chem. Res.* **2001**, *34*, 409–522; c) Special issue on *Molecular Machines and Motors*: *Struct. Bonding (Berlin)* **2001**, *99*.

[2] A. C. Benniston, A. Harriman, *Angew. Chem.* **1993**, *105*, 1553–1555; *Angew. Chem. Int. Ed. Engl.* **1993**, *32*, 1459–1461.

[3] A. C. Benniston, A. Harriman, V. M. Lynch, *J. Am. Chem. Soc.* **1995**, *117*, 5275–5291.

[4] A. C. Benniston, *Chem. Soc. Rev.* **1996**, *25*, 427–436.

[5] H. Murakami, A. Kawabuchi, K. Kotoo, M. Kunitake, N. Nakashima, *J. Am. Chem. Soc.* **1997**, *119*, 7605–7606.

[6] P. R. Ashton, R. Ballardini, V. Balzani, A. Credi, K. R. Dress, E. Ishow, C. J. Kleverlaan, O. Kocian, J. A. Preece, N. Spencer, J. F. Stoddart, M. Venturi, S. Wenger, *Chem. Eur. J.* **2000**, *6*, 3558–3574.

[7] N. Armaroli, V. Balzani, J. P. Collin, P. Gaviña, J. P. Sauvage, B. Ventura, *J. Am. Chem. Soc.* **1999**, *121*, 4397–4408.

[8] A. M. Brouwer, C. Frochot, F. G. Gatti, D. A. Leigh, L. Mottier, F. Paolucci, S. Roffia, G. W. H. Wurpel, *Science* **2001**, *291*, 2124–2128.

[9] G. W. H. Wurpel, A. M. Brouwer, I. H. M. van Stokkum, A. Farran, D. A. Leigh, *J. Am. Chem. Soc.* **2001**, *123*, 11327–11328.

[10] C. A. Stanier, S. J. Alderman, T. D. W. Claridge, H. L. Anderson, *Angew. Chem.* **2002**, *114*, 1847–1850; *Angew. Chem. Int. Ed.* **2002**, *41*, 1769–1772.

[11] For examples featuring the use of stimuli other than light to induce shuttling in rotaxanes see a) R. A. Bissell, E. Córdova, A. E. Kaifer, J. F. Stoddart, *Nature* **1994**, *369*, 133–137; b) J. P. Collin, P. Gaviña, J. P. Sauvage, *New J. Chem.* **1997**, *21*, 525–528; c) C. Gong, H. W. Gibson, *Angew. Chem.* **1997**, *109*, 2426–2428; *Angew. Chem. Int. Ed. Engl.* **1997**, *36*, 2331–2333; d) A. S. Lane, D. A. Leigh, A. Murphy, *J. Am. Chem. Soc.* **1997**, *119*, 11092–11093; e) C. P. Collier, E. W. Wong, M. Belohradsky, F. M. Raymo, J. F. Stoddart, P. J. Kuekes, R. S. Williams, J. R. Heath, *Science* **1999**, *285*, 391–394; f) H. Shigekawa, K. Miyake, J.

 © 2003 Wiley-VCH Verlag GmbH & Co. KGaA, Weinheim

Sumaoka, A. Harada, M. Komiyama, *J. Am. Chem. Soc.* **2000**, *122*, 5411 – 5412; g) M. C. Jimenez-Molero, C. Dietrich-Buchecker, J. P. Sauvage, *Chem. Eur. J.* **2002**, *8*, 1456 – 1466; h) Y. Luo, C. P. Collier, J. O. Jeppesen, K. A. Nielsen, E. Delonno, G. Ho, J. Perkins, H. R. Tseng, T. Yamamoto, J. F. Stoddart, J. R. Heath, *ChemPhysChem* **2002**, *3*, 519 – 525.

[12] G. Campari, M. Fagnoni, M. Mella, A. Albini, *Tetrahedron: Asymmetry* **2000**, *11*, 1891 – 1906.

[13] F. G. Gatti, D. A. Leigh, S. A. Nepogodiev, A. M. Z. Slawin, S. J. Teat, J. K. Y. Wong, *J. Am. Chem. Soc.* **2001**, *123*, 5983 – 5989.

[14] The wavelength for the reaction has not yet been optimized (F. G. Gatti, S. León, J. K. Y. Wong, G. Bottari, A. Altieri, A. M. Farran Morales, S. J. Teat, C. Frochot, D. A. Leigh, A. M. Brouwer, F. Zerbetto, *Proc. Natl. Acad. Sci. USA* **2003**, *100*, 10 – 15).

[15] ^{1}H NMR experiments show that the macrocycle spins more than 10^6 times faster in the *Z* form of the rotaxane than the *E* form in CD_2Cl_2 at 233 K.

[16] G. Brancato, F. Coutrot, D. A. Leigh, A. Murphy, J. K. Y. Wong, F. Zerbetto, *Proc. Natl. Acad. Sci. USA* **2002**, *99*, 4967 – 4971.

[17] V. Bermudez, N. Capron, T. Gase, F. G. Gatti, F. Kajzar, D. A. Leigh, F. Zerbetto, S. W. Zhang, *Nature* **2000**, *406*, 608 – 611.

[18] D. A. Leigh and J. K. Y. Wong, unpublished results.

[19] Unlike rotaxanes with dipeptide stations separated by alkyl chains,[11d] *E*-**1**–**3** do not behave as solvent-switchable shuttles; even in [D_6]DMSO the fumaramide station is still occupied by the macrocycle for at least 85% of the time.

[20] The yield of the adipamide-maleamide rotaxane *Z*-**3** (20%) is reproducibly higher than that of the model single-site adipamide rotaxane shown in Figure 2 (8%). The significant differences in yield (and the anomalously poor binding of the adipamide unit to the macrocycle in *Z*-**3**) may indicate that the intramolecularly hydrogen-bonded nine-membered ring (S. H. Gellman, G. P. Dado, G.-B. Liang, B. R. Adams, *J. Am. Chem. Soc.* **1991**, *113*, 1164 – 1173) has differing stabilities in the one- and two-station adipamide threads and rotaxane *Z*-**3**.

[21] N. L. Allinger, Y. H. Yuh, J. H. Lii, *J. Am. Chem. Soc.* **1989**, *111*, 8551 – 8582.

[22] J. W. Ponder, F. Richards, *J. Comput. Chem.* **1987**, *8*, 1016 – 1024.

[23] F. Biscarini, M. Cavallini, D. A. Leigh, S. León, S. J. Teat, J. K. Y. Wong, F. Zerbetto, *J. Am. Chem. Soc.* **2002**, *124*, 225 – 233.

[24] In analogy to the MM3 H-bonding of (C)H atoms connected to sp^2 carbon atoms, we introduced a term to reproduce weak H-bonding of the acidic succinic methylene groups (well depth: 0.22 kcal mol^{-1}; equilibrium H-bonding separation: 2.78 Å).

[25] The rotaxane structures shown illustrate the position of the macrocycle on the thread and particularly favored intercomponent hydrogen-bonding motifs. Most of the low-energy co-conformations of the rotaxanes are probably folded with the unoccupied station folding back to hydrogen bond to the macrocycle.

 © 2003 Wiley-VCH Verlag GmbH & Co. KGaA, Weinheim

Saccharide Recognition

Self-Assembled Receptors that Stereoselectively Recognize a Saccharide

Tsutomu Ishi-i, Miguel A. Mateos-Timoneda, Peter Timmerman, Mercedes Crego-Calama, David N. Reinhoudt,* and Seiji Shinkai*

Saccharide recognition is very important for many processes occurring in nature, such as cell–cell interaction, carbohydrate transportation, and carbohydrate metabolism.[1,2] X-ray crystallographic analysis of saccharide–protein complexes has revealed that neutral and charged functionalities are preorganized in the three-dimensional binding pocket that recognizes saccharide molecules through hydrogen-bonding interactions.[3] This analysis has provided valuable information for the design of artificial saccharide receptors.[4–11] These receptors generally have a covalent scaffold decorated with neutral[4–10] and charged functionalites.[11] Recently, noncovalent synthesis[12] has led to new types of artificial receptors that self-assemble through multiple noncovalent interactions such as hydrogen-bonding[13] or metal–ligand interactions.[14] Hitherto, a self-assembled receptor for saccharide recognition has not yet been reported. Herein, we report the first example of carbohydrate recognition by a receptor that is self-assembled through hydrogen bonds. More importantly, this self-assembled receptor is able to recognize *O*-alkyl pyranosides stereoselectively.

Hydrogen-bonded tetrarosette assemblies $\mathbf{1}_3\cdot(BA)_{12}/(CYA)_{12}$ and $\mathbf{4}_3\cdot(BA)_{12}/(CYA)_{12}$ are formed from 15 components: 3 calix[4]arene tetramelamines **1** or **4** and 12 barbituric acid (BA) or cyanuric acid (CYA) derivatives (Scheme 1).[15,16] A total of 72 cooperative hydrogen bonds hold the building blocks together to form a fully assembled tetrarosette structure, with each floor of the assembly corresponding to one rosette motif (Figure 1, p. 2302). Tetramelamines **1** and **4** consist of two calix[4]arene units which are covalently connected through two urea moieties.

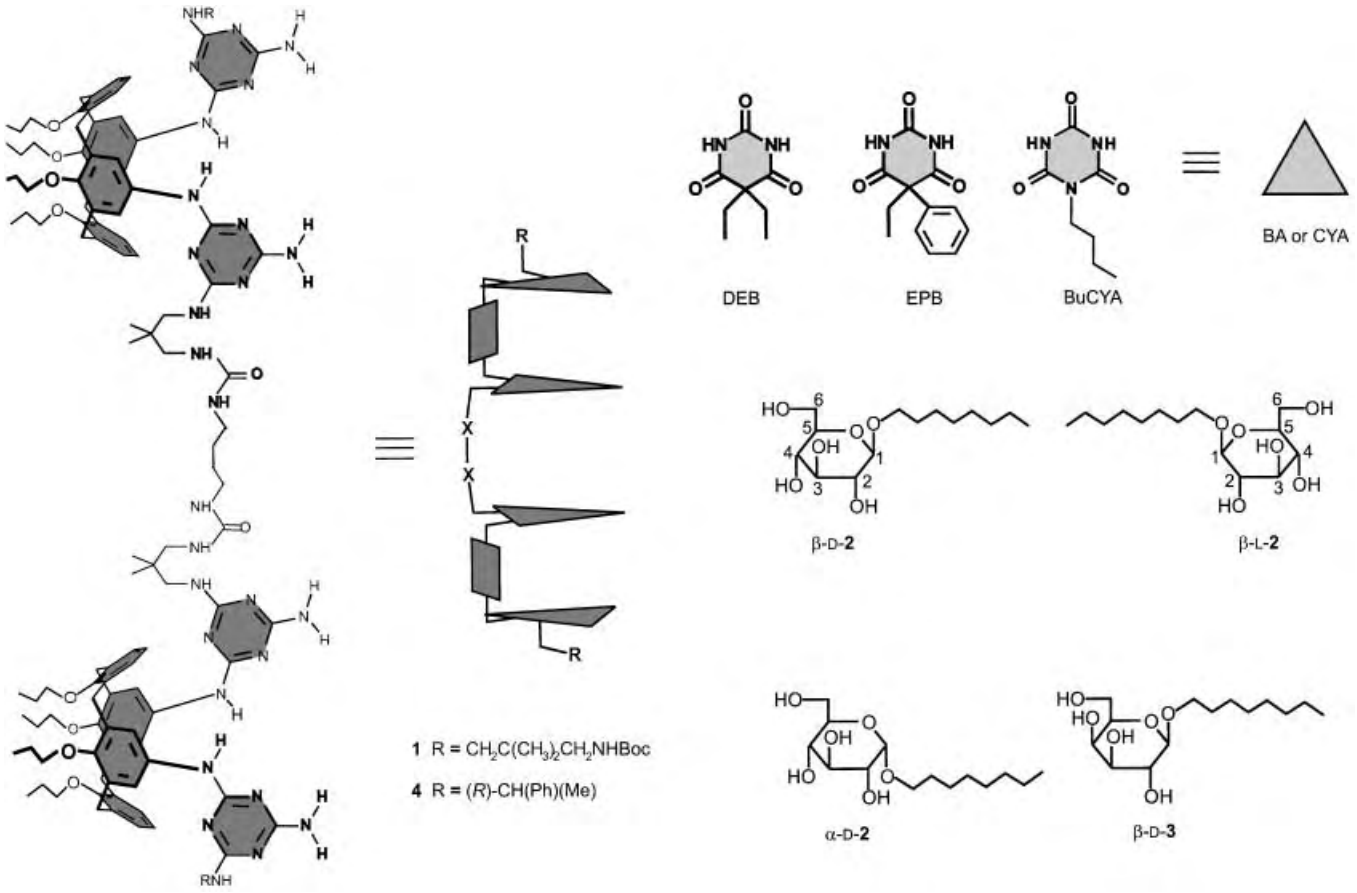
[*] Dr. M. Crego-Calama, Prof. D. N. Reinhoudt, Dr. T. Ishi-i,[+]
M. A. Mateos-Timoneda, P. Timmerman
Laboratory of Supramolecular Chemistry and Technology
MESA+ Research Institute
University of Twente
PO Box 217, 7500 AE Enschede (The Netherlands)
Fax: (+31) 53-489-4645
E-mail: m.crego-calama@ct.utwente.nl
d.n.reinhoudt@ct.utwente.nl

Prof. S. Shinkai
Chemotransfiguration Project
Japan Science and Technology Corporation (JST)
2432 Aikawa, Kurume, Fukuoka 839-0861 (Japan)

[+] Present address:
Institute of Advanced Material Study
Kyushu University
6-1 Kasuga-kohen, Kasuga, 816-8586 (Japan)

Supporting information for this article is available on the WWW under http://www.angewandte.org or from the author.

 © 2003 Wiley-VCH Verlag GmbH & Co. KGaA, Weinheim DOI: 10.1002/anie.200350956



Scheme 1. Structures of the building blocks. Boc = *tert*-butyloxycarbonyl.

This self-assembly process results in a total of six urea functionalities being positioned in the central cavity for saccharide recognition. In the absence of any source of chirality, the tetrarosette assembly is present as a racemic mixture of *P* and *M* enantiomers ((*P*)-$\mathbf{1}_3$·$(BA)_{12}$ and (*M*)-$\mathbf{1}_3$·$(BA)_{12}$) (Figure 1 a), while the introduction of chiral centers (*R* or *S*) in the assembly leads to the formation of exclusively one of the two possible diastereomers (Figure 1 b).[17]

Recognition of *n*-octyl β-D-glucopyranoside (β-D-**2**) by $\mathbf{1}_3$·$(DEB)_{12}$ (DEB = 5,5-diethylbarbituric acid) is reflected in the shifts and splitting of the signals in the ^{1}H NMR spectrum recorded in $CDCl_3$ (Figure 2, p. 2303). As expected, in addition to the original NH^A signal of the urea moiety, a new signal ($NH^{A'}$) corresponding to the complex formed between one of the isomers (*P* or *M*) of $\mathbf{1}_3$·$(DEB)_{12}$ and β-D-**2** is observed at lower magnetic field ($\Delta\delta = 0.05$ ppm, 10 equivalents of β-D-**2**). The downfield shift is possibly a result of the formation of one hydrogen bond between the urea carbonyl group of $\mathbf{1}_3$·$(DEB)_{12}$ and one hydroxy group of β-D-**2**. More important, similar shifts and splittings are observed for the H^{a2} and H^{c2} signals on the second and third rosette floors upon guest binding, whereas the corresponding signals on the first and fourth floors show no splitting. The intensities of the new signals ($H^{a2'}$ and $H^{c2'}$) slightly increase with the amount of β-D-**2** added, while the original signals decrease. This means that one of the two enantiomers from the racemic mixture of the *P* and *M* isomers of $\mathbf{1}_3$·$(DEB)_{12}$[15] recognizes the chiral guest stereoselectively and results in the formation of one diastereomeric complex.

This conclusion is supported by the induced signal in the circular dichroism (CD) spectrum. The racemic mixture of (*M*)-$\mathbf{1}_3$·$(DEB)_{12}$ and (*P*)-$\mathbf{1}_3$·$(DEB)_{12}$ is CD silent. The addition of β-D-**2** to this mixture induces a negative Cotton effect around 290–310 nm, clear evidence for the formation of a *P* rosette assembly (Figure 3; p. 2303).[17] As a result of the chiral recognition, the *P* enantiomer, which binds β-D-**2** more strongly, is amplified in the mixture as both enantiomers (*P* and *M*) are in dynamic equilibrium (Figure 4; p. 2304).[18] A ^{1}H NMR titration was also performed with *n*-octyl β-L-glucopyranoside (β-L-**2**). The chiral recognition of β-L-**2** by (*M*)-$\mathbf{1}_3$·$(DEB)_{12}$ is also reflected in the shifts and splitting of the signals in the ^{1}H NMR spectra recorded in $CDCl_3$. As expected, the appearance of a positive Cotton effect around 290–310 nm in the CD spectrum was observed, thus indicating the amplification of the *M*-rosette assembly.

The binding constants for the complexations of $\mathbf{1}_3$·$(DEB)_{12}$ with β-D-**2** and β-L-**2** can be estimated on the basis of the CD data to be approximately $20\,M^{-1}$ (ca. 9% diastereomeric excess).[19] The 1:1 stoichiometry of the complexes (*P*)-$\mathbf{1}_3$·$(DEB)_{12}$·(β-D-**2**) and (*M*)-$\mathbf{1}_3$·$(DEB)_{12}$·(β-L-**2**) was determined from a Job plot (see the Supporting Information).[20,21]

While similar chiral recognition of β-D-**2** by the different assembly $\mathbf{1}_3$·$(EPB)_{12}$ (EPB = 5-ethyl-5-phenyl barbituric acid) was found by ^{1}H NMR and CD spectroscopy, the cyanuric

 © 2003 Wiley-VCH Verlag GmbH & Co. KGaA, Weinheim

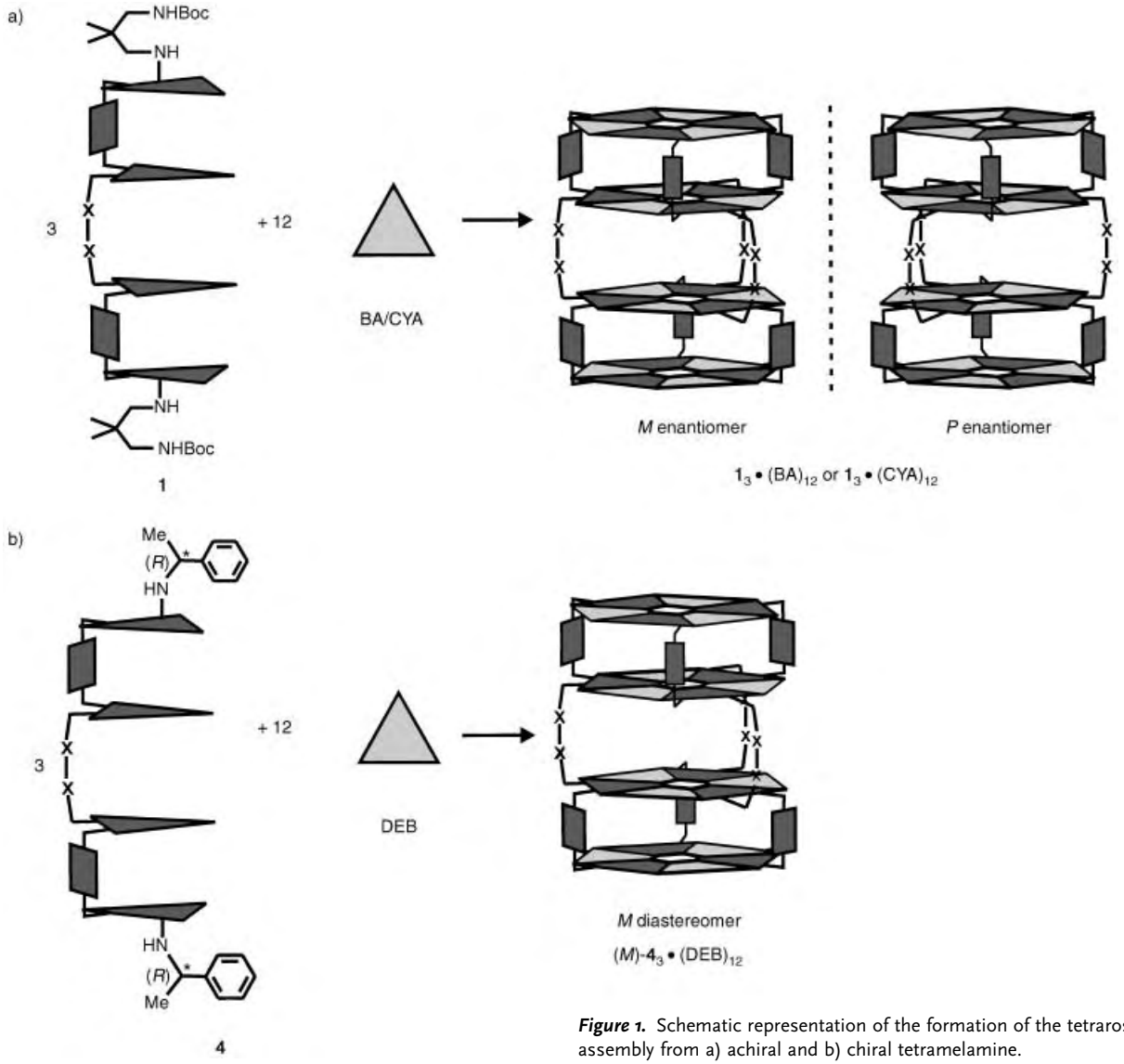


Figure 1. Schematic representation of the formation of the tetrarosette assembly from a) achiral and b) chiral tetramelamine.

acid based assembly $\mathbf{1}_3\cdot(\mathrm{BuCYA})_{12}$ did not show any shift or splitting in the ^{1}H NMR spectrum. Furthermore, the CD spectrum of this assembly upon addition of β-D-**2** remained unchanged.[22] Thus, this assembly does not complex the saccharide. This distinct behavior is most probably a consequence of the difference in the orbital electron distribution of BA and CYA.[23]

Computational studies (gas-phase MM calculation, Quanta 97/CHARMm 24.0) confirmed the observed enantioselectivity. In the complex with (P)-$\mathbf{1}_3\cdot(\mathrm{DEB})_{12}$, β-D-**2** is located in the cavity without any steric hindrance (Figure 5, p. 2304). A urea carbonyl group in the receptor forms a hydrogen bond with the hydroxy group at the 4-position of β-D-**2**. In contrast, the modeling study of the "mismatching" complex (P)-$\mathbf{1}_3\cdot(\mathrm{DEB})_{12}\cdot$(β-L-**2**) shows that the alkyl chain of β-L-**2** breaks the hydrogen-bonding network on the second rosette floor.

In contrast to β-D-**2**, its α isomer, *n*-octyl α-D-glucopyranoside (α-D-**2**), and epimer, *n*-octyl β-D-galactopyranoside (β-D-**3**), were not recognized by $\mathbf{1}_3\cdot(\mathrm{DEB})_{12}$, as indicated by the absence of shifts or splittings in the signals in the ^{1}H NMR spectra and the absence of CD signals. This trend in the complexation can be rationalized by the strength of the intramolecular hydrogen bonds in the pyranosides.[6–8]

Complexation experiments using chiral assemblies (M)-$\mathbf{4}_3\cdot(\mathrm{DEB})_{12}$ were performed to further probe the stereoselectivity of the recognition of saccharide by the tetrarosette assemblies. In this case, instead of the racemic mixture of receptors (P)-$\mathbf{1}_3\cdot(\mathrm{DEB})_{12}$ and (M)-$\mathbf{1}_3\cdot(\mathrm{DEB})_{12}$, the diastereomeric assembly (M)-$\mathbf{4}_3\cdot(\mathrm{DEB})_{12}$ was used as a complexing molecule.

The "mismatch" combination of receptor (M)-$\mathbf{4}_3\cdot(\mathrm{DEB})_{12}$ and β-D-**2** (Figure 6, p. 2305) does not show any changes in the ^{1}H NMR spectrum (see the Supporting Information). In contrast, recognition of *n*-octyl-β-L-glucopyranoside (β-L-**2**) by (M)-$\mathbf{4}_3\cdot(\mathrm{DEB})_{12}$ in the matching pair is reflected in the corresponding shifts in the ^{1}H NMR spectra recorded in $CDCl_3$ (see the Supporting Information). Similarly as observed for assembly $\mathbf{1}_3\cdot(\mathrm{DEB})_{12}$, the urea proton NH^A shifts to a lower magnetic field ($\Delta\delta = 0.10$ ppm, 10 equiva-

 © 2003 Wiley-VCH Verlag GmbH & Co. KGaA, Weinheim

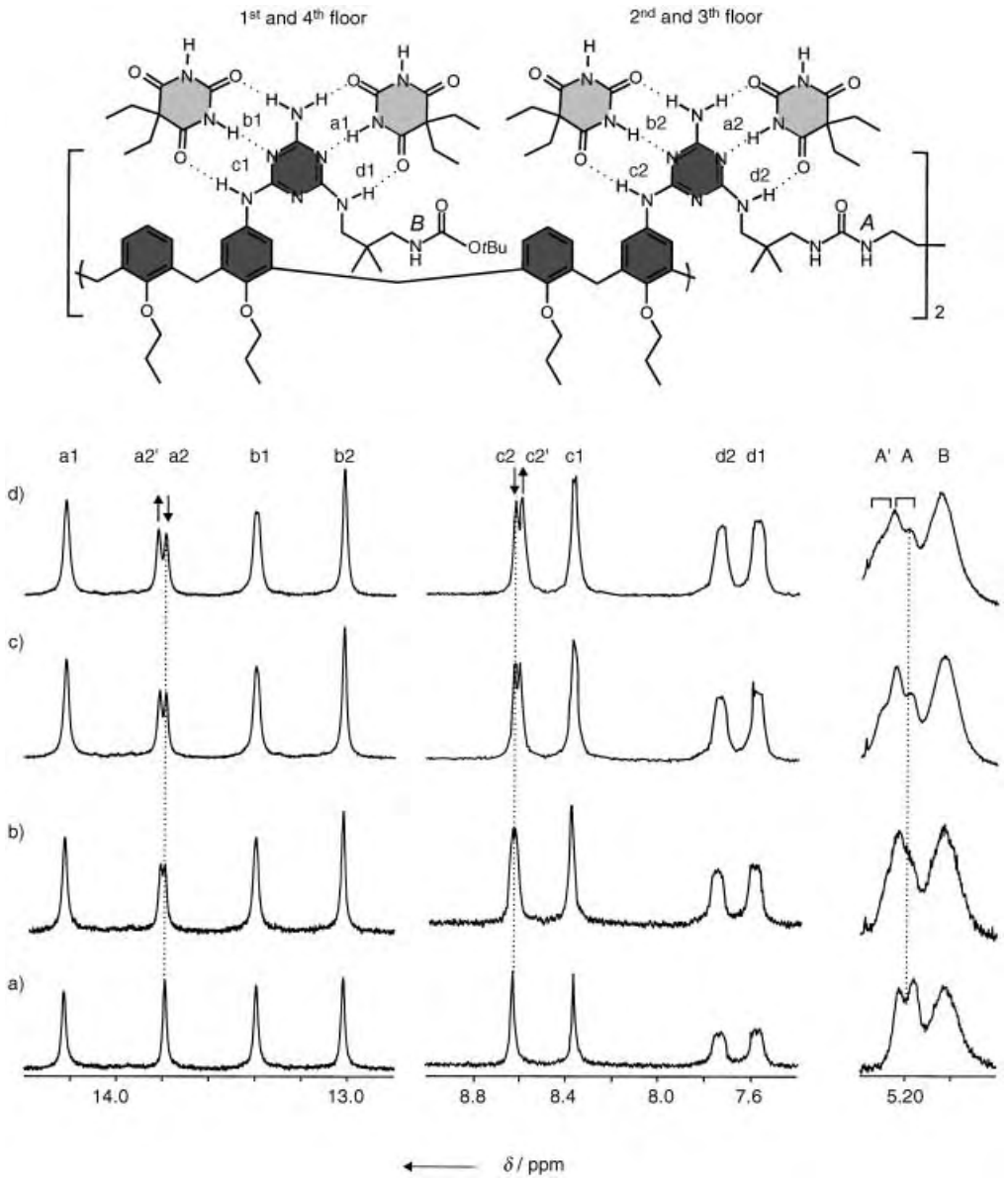
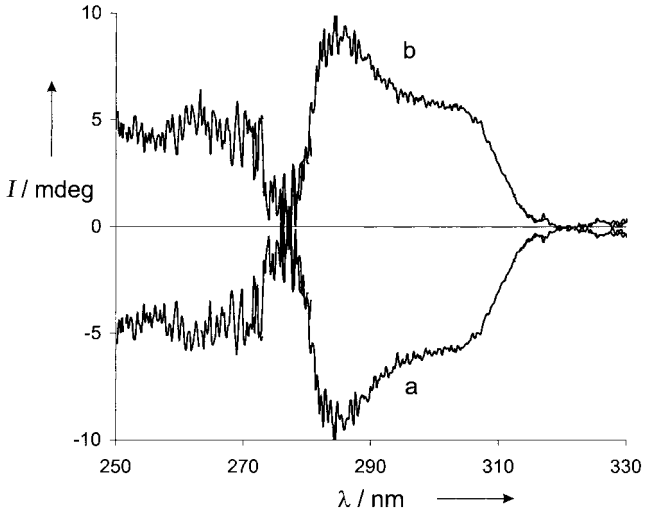


Figure 2. ^{1}H NMR spectra of $\mathbf{1}_3\cdot(DEB)_{12}$ (1 mM) in $CDCl_3$ at 20 °C in the presence of a) 0, b) 3, c) 5, and d) 10 equivalents of β-D-**2**.



lents of β-L-**2**) and shifts for H^{a2} and H^{c2} on the second and third rosette floors were observed, whereas the corresponding signals (H^{a1} and H^{c1}) on the first and fourth floors remained unchanged.

In contrast to what occurred in the complexation studies with the racemic mixture (M/P)-$\mathbf{1}_3\cdot(DEB)_{12}$, the addition of β-L-**2** to the chiral assembly (M)-$\mathbf{4}_3\cdot(DEB)_{12}$ does not result in measurable changes in the CD spectra (see Supporting Information). This observation means that the CD changes observed (see above) for the assembly $\mathbf{1}_3\cdot(DEB)_{12}$ definitely arise from the amplification of one of the enantiomers upon complexation.

Figure 3. CD spectra of $\mathbf{1}_3\cdot(DEB)_{12}$ (1 mM) in the presence of 10 equivalents of a) β-D-**2** and b) β-L-**2** in $CDCl_3$ (in a 0.01 cm width cell at 20 °C).

 © 2003 Wiley-VCH Verlag GmbH & Co. KGaA, Weinheim

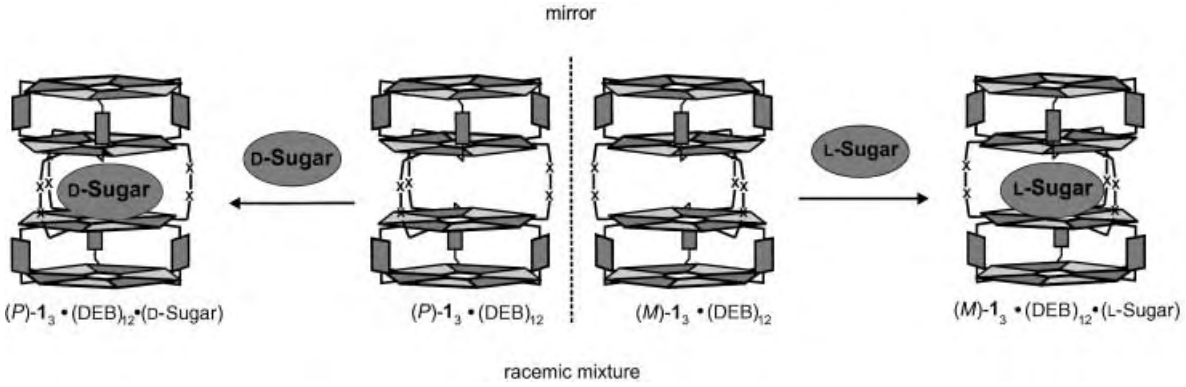


Figure 4. Schematic representation of the enantioselective recognition of saccharides by a racemic mixture of assemblies.

In conclusion, we have shown for the first time the complexation of a saccharide by a self-assembled receptor through hydrogen-bonding interactions. More importantly, the recognition of the monosaccharide occurs enantioselectively. This enantiomeric recognition of the saccharide allows the amplification of the best receptor from a racemic mixture of self-assembled receptors. Furthermore, the tetrarosettes are quite stable even in polar media (up to at least 60% methanol in $CDCl_3$). Further studies on saccharide recognition with similar assemblies in a polar environment are under investigation.

Received: January 16, 2003 [Z50956]

Keywords: carbohydrates · hydrogen bonds · molecular recognition · self-assembly · stereoselectivity

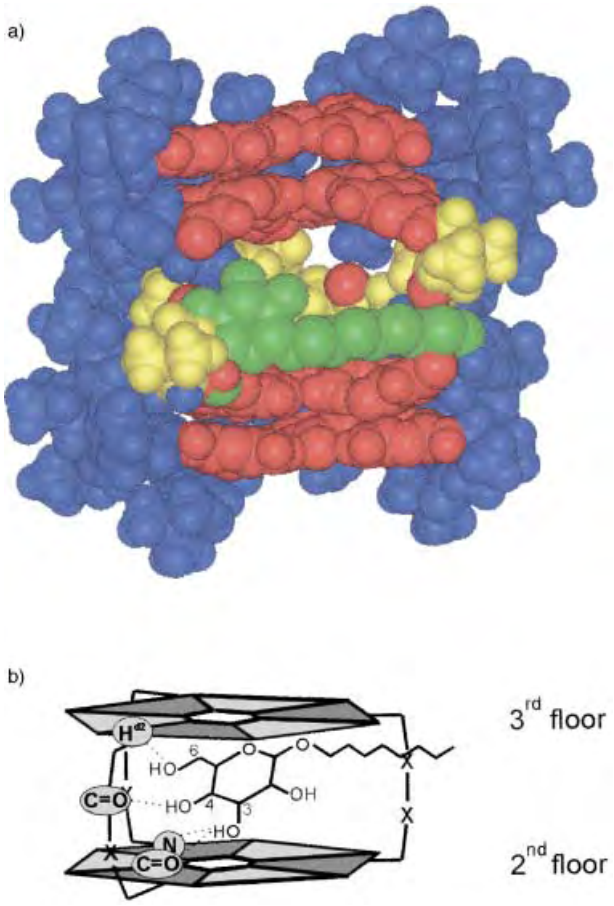


Figure 5. a) Computer simulated structures of (*P*)-**1**$_3$·(DEB)$_{12}$·(β-D-**2**) (a cross-sectional view of the assembly is depicted to show the environment inside the cavity occupied by the sugar; blue = calix[4]arene; red = rosette floors; green = saccharide; yellow = urea groups). b) Cartoon representation of (*P*)-**1**$_3$·(DEB)$_{12}$·(β-D-**2**) (for clarity reasons only the second and third floors of the tetrarosette assembly are shown).

[1] For review of saccharide recognition by hydrogen-bonding interactions, see A. P. Davis, R. S. Wareham, *Angew. Chem.* **1999**, *111*, 3160–3179; *Angew. Chem. Int. Ed.* **1999**, *38*, 2978–2996.

[2] For reviews of saccharide recognition by boronic acid receptors, see a) T. D. James, K. R. A. S. Sandanayake, S. Shinkai, *Angew. Chem.* **1996**, *108*, 2038–2050; *Angew. Chem. Int. Ed. Engl.* **1996**, *35*, 1910–1922; b) T. D. James, P. Linnane, S. Shinkai, *Chem. Commun.* **1996**, 281–288.

[3] a) R. U. Lemieux, *Chem. Soc. Rev.* **1989**, *18*, 347–374; b) F. A. Quiocho, *Pure Appl. Chem.* **1989**, *61*, 1293–1306; c) W. I. Weis, K. Drickhamer, *Annu. Rev. Biochem.* **1996**, *65*, 441–473; d) S. P. Spurlino, G.-Y. Lu, F. A. Quiocho, *J. Biol. Chem.* **1991**, *266*, 5202–5219.

[4] a) R. P. Bonar-Law, A. P. Davis, B. A. Murray, *Angew. Chem.* **1990**, *102*, 1497; *Angew. Chem. Int. Ed. Engl.* **1990**, *29*, 1407–1408; b) A. P. Davis, S. Menzer, J. J. Walsh, D. J. Williams, *Chem. Commun.* **1996**, 453–455; c) T. Mizutani, T. Kurahashi, T. Murakami, N. Matsumi, H. Ogoshi, *J. Am. Chem. Soc.* **1997**, *119*, 8991–9001; d) K. M. Bhattarai, A. P. Davis, J. J. Perry, C. J. Walter, *J. Org. Chem.* **1997**, *62*, 8463–8473; e) M. Inoue, J. Chiba, H. Nakazumi, *J. Org. Chem.* **1999**, *64*, 8170–8176; f) M. Mazik, H. Bandmann, W. Sicking, *Angew. Chem.* **2000**, *112*, 562–565; *Angew. Chem. Int. Ed.* **2000**, *39*, 551–554; g) M. Mazik, W. Sicking, *Chem. Eur. J.* **2001**, *7*, 664–670; h) J. M. Benito, M. Gómez-García, J. L. J. Blanco, C. O. Mellet, J. M. G. Fernández, *J. Org. Chem.* **2001**, *66*, 1366–1372.

[5] Y. Kikuchi, Y. Tanaka, S. Sutarto, K. Kobayashi, H. Toi, Y. Aoyama, *J. Am. Chem. Soc.* **1992**, *114*, 10302–10306.

[6] R. P. Bonar-Law, J. K. M. Sanders, *J. Am. Chem. Soc.* **1995**, *117*, 259–271.

[7] C.-Y. Huang, L. A. Cabell, E. V. Anslyn, *J. Am. Chem. Soc.* **1994**, *116*, 2778–2792.

[8] J. Cuntze, L. Owens, V. Alcázar, P. Seiler, F. Diederich, *Helv. Chim. Acta* **1995**, *78*, 367–390.

 © 2003 Wiley-VCH Verlag GmbH & Co. KGaA, Weinheim

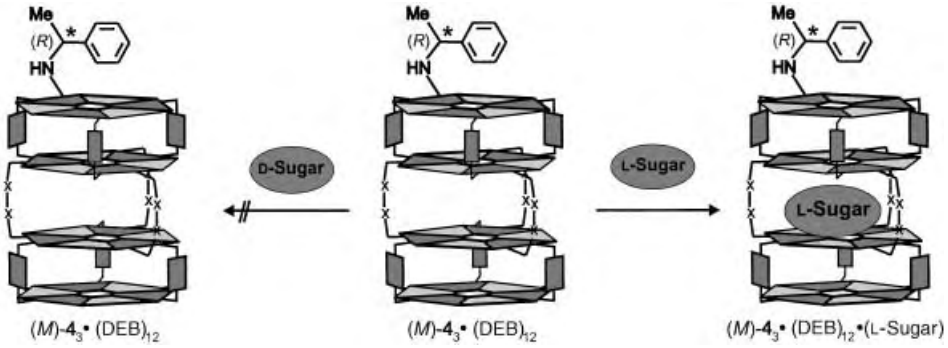


Figure 6. Schematic representation of the enantioselective recognition of saccharides by a chiral tetrarosette.

[9] a) K. M. Bhattarai, R. P. Bonar-Law, A. P. Davis, B. A. Murray, *J. Chem. Soc. Chem. Commun.* **1992**, 752 – 754; b) R. Liu, W. C. Still, *Tetrahedron Lett.* **1993**, *34*, 2573 – 2576; c) S. Anderson, U. Neidlein, V. Gramlich, F. Diederich, *Angew. Chem.* **1995**, *107*, 1722 – 1724; *Angew. Chem. Int. Ed. Engl.* **1995**, *34*, 1596 – 1600; d) D. K. Smith, F. Diederich, *Chem. Commun.* **1998**, 2501 – 2502; e) A. Bähr, A. S. Droz, M. Püntener, U. Neidlein, S. Anderson, P. Seiler, F. Diederich, *Helv. Chim. Acta* **1998**, *81*, 1931 – 1963; f) H.-J. Kim, Y.-H. Kim, J.-I. Hong, *Tetrahedron Lett.* **2001**, *42*, 5049 – 5052.

[10] a) A. P. Davis, R. S. Wareham, *Angew. Chem.* **1998**, *110*, 2397 – 2401; *Angew. Chem. Int. Ed.* **1998**, *37*, 2270 – 2273; b) O. Rusin, V. Král, *Chem. Commun.* **1999**, 2367 – 2368; c) O. Rusin, V. Král, *Tetrahedron Lett.* **2001**, *42*, 4235 – 4238; d) O. Rusin, K. Lang, V. Král, *Chem. Eur. J.* **2002**, *8*, 655 – 663.

[11] a) G. Das, A. D. Hamilton, *J. Am. Chem. Soc.* **1994**, *116*, 11 139 – 11 140; b) U. Neidlein, F. Diederich, *Chem. Commun.* **1996**, 1493 – 1494; c) G. Das, A. D. Hamilton, *Tetrahedron Lett.* **1997**, *38*, 3675 – 3678; d) A. S. Droz, F. Diederich, *J. Chem. Soc. Perkin Trans. 1* **2000**, 4224 – 4226; e) V. Král, O. Rusin, J. Charvátová, P. Anzenbacher, Jr., J. Fogl, *Tetrahedron Lett.* **2000**, *41*, 10 147 – 10 151; f) V. Král, O. Rusin, F. P. Schmidtchen, *Org. Lett.* **2001**, *3*, 873 – 876; g) J. Bitta, S. Kubik, *Org. Lett.* **2001**, *3*, 2637 – 2640; h) S. Tamaru, M. Yamamoto, S. Shinkai, A. B. Khasanov, T. W. Bell, *Chem. Eur. J.* **2001**, *7*, 5270 – 5276; i) S. Tamaru, S. Shinkai, A. B. Khasanov, T. W. Bell, *Proc. Natl. Acad. Sci. USA* **2002**, *99*, 4972 – 4976.

[12] D. N. Reinhoudt, M. Crego-Calama, *Science* **2002**, *295*, 2403 – 2407.

[13] a) M. M. Conn, J. Rebek, Jr., *Chem. Rev.* **1997**, *97*, 1647 – 1668; b) J. Rebek, Jr., *Acc. Chem. Res.* **1999**, *32*, 278 – 286; c) J. Rebek, Jr., *Chem. Commun.* **2000**, 637 – 643; d) L. J. Prins, P. Timmerman, D. N. Reinhoudt, *Angew. Chem.* **2001**, *113*, 2446 – 2492; *Angew. Chem. Int. Ed.* **2001**, *40*, 2382 – 2426.

[14] a) B. Linton, A. D. Hamilton, *Chem. Rev.* **1997**, *97*, 1669 – 1680; b) M. Fujita, *Chem. Soc. Rev.* **1998**, *27*, 417 – 425; c) D. L. Caulder, K. N. Raymond, *Acc. Chem. Res.* **1999**, *32*, 975 – 982; d) D. L. Caulder, K. N. Raymond, *J. Chem. Soc. Dalton Trans.* **1999**, 1185 – 1200; e) M. Fujita, K. Umemoto, M. Yoshizawa, N. Fujita, T. Kusukawa, K. Biradha, *Chem. Commun.* **2001**, 509 – 518.

[15] K. A. Jolliffe, P. Timmerman, D. N. Reinhoudt, *Angew. Chem.* **1999**, *111*, 983 – 986; *Angew. Chem. Int. Ed.* **1999**, *38*, 933 – 937.

[16] V. Paraschiv, M. Crego-Calama, T. Ishi-i, C. J. Padberg, P. Timmerman, D. N. Reinhoudt, *J. Am. Chem. Soc.* **2002**, *124*, 7638 – 7639.

[17] L. J. Prins, J. Huskens, F. de Jong, P. Timmerman, D. N. Reinhoudt, *Nature* **1999**, *398*, 498 – 502.

[18] a) T. Ishi-i, M. Crego-Calama, P. Timmerman, D. N. Reinhoudt, S. Shinkai, *Angew. Chem.* **2002**, *114*, 2004 – 2009; *Angew. Chem. Int. Ed.* **2002**, *41*, 1924 – 1929; b) T. Ishi-i, M. Crego-Calama, P. Timmerman, D. N. Reinhoudt, S. Shinkai, *J. Am. Chem. Soc.* **2002**, *124*, 14631 – 14641.

[19] In this chiral complexation, we assumed that the binding constant (K_P) of β-D-**2** with (*P*)-**1**$_3$·(DEB)$_{12}$ is much larger than that (K_M) with (*M*)-**1**$_3$·(DEB)$_{12}$. The K_P value can be obtained according to equations (1–5):$K_P = [(P)\text{-}\mathbf{1}_3\cdot(\mathrm{DEB})_{12}\cdot(\beta\text{-D-}\mathbf{2})]/[(M)\text{-}\mathbf{1}_3\cdot(\mathrm{DEB})_{12}]/[\beta\text{-D-}\mathbf{2}]$ (1)$[(P)\text{-}\mathbf{1}_3\cdot(\mathrm{DEB})_{12}] = [(M)\text{-}\mathbf{1}_3\cdot(\mathrm{DEB})_{12}] = \{(1-(de/100))/2\}\times[\mathbf{1}_3\cdot(\mathrm{DEB})_{12}]_0$ (2)$[\beta\text{-D-}\mathbf{2}] = [\beta\text{-D-}\mathbf{2}]_0-(de/100)\times[\mathbf{1}_3\cdot(\mathrm{DEB})_{12}]_0$ (3)$[(P)\text{-}\mathbf{1}_3\cdot(\mathrm{DEB})_{12}\cdot(\beta\text{-D-}\mathbf{2})] = (de/100)\times[\mathbf{1}_3\cdot(\mathrm{DEB})_{12}]_0$ (4)$de\,(\%) = (\mathrm{CD}_{obs}/\mathrm{CD}_{100\%\,de})\times 100$ (5)in which $[(P)\text{-}\mathbf{1}_3\cdot(\mathrm{DEB})_{12}\cdot(\beta\text{-D-}\mathbf{2})]$, $[(M)\text{-}\mathbf{1}_3\cdot(\mathrm{DEB})_{12}]$, $[(P)\text{-}\mathbf{1}_3\cdot(\mathrm{DEB})_{12}]$, and $[\beta\text{-D-}\mathbf{2}]$ are the concentrations of the corresponding species, $[\mathbf{1}_3\cdot(\mathrm{DEB})_{12}]_0$ and $[\beta\text{-D-}\mathbf{2}]_0$ are the initial concentrations of the host and guest, and *de*(%) is the diastereomeric excess of the *P* assemblies obtained from the ratio of observed and standard CD intensities (CD_{obs} and $\mathrm{CD}_{100\%\,de}$). The CD intensity (67 mdeg) at 300 nm in completely chiral (*M*)-**4**$_3$·(DEB)$_{12}$ is used as the reference ($\mathrm{CD}_{100\%\,de}$) because the CD spectral shape of (*M*)-**4**$_3$·(DEB)$_{12}$ almost coincides with that of **1**$_3$·(DEB)$_{12}$·(β-D-**2**) complex (see the Supporting Information). When $[\mathbf{1}_3\cdot(\mathrm{DEB})_{12}]_0 = 1$ mM, $[\beta\text{-D-}\mathbf{2}]_0 = 10$ mM, $\mathrm{CD}_{obs\,300\,nm} = 6$ mdeg, and $de = 9\%$, a K_p value can be estimated to be $20\,\mathrm{M}^{-1}$.

[20] A. Job, *Justus Liebigs Ann. Chem.* **1928**, *9*, 113 – 134.

[21] We also measured the MALDI-TOF mass spectra by using the Ag^+-labeling technique to detect the complex. However, only the parent ion peak of the assembly was observed at $m/z =$ 9978.0 (calcd for $C_{528}H_{684}N_{114}O_{78}Ag$, 9976.2). For a description of the MALDI-TOF mass spectrometry technique using Ag^+-labeling, see P. Timmerman, K. A. Jolliffe, M. Crego-Calama, J.-L. Weindmann, L. J. Prins, F. Cardullo, B. H. M. Snellink-Ruel, R. Fokkens, N. M. M. Nibbering, S. Shinkai, D. N. Reinhoudt, *Chem. Eur. J.* **2000**, *6*, 4104 – 4115.

[22] **1**$_3$·(BuCYA)$_{12}$ was obtained by two different methods:[15] 1) from **1**$_3$·(DEB)$_{12}$ upon exchange of DEB for BuCYA and 2) the direct mixing of **1** and BuCYA in toluene and subsequent heating (100 °C) and evaporation. Complexation with β-D-**2** was observed in neither case, even after two weeks or higher temperature (55 °C).

[23] The three-dimensional structure of DEB, which arises from the presence of a sp^3 carbon atom in the six-membered ring, is better suited for guest encapsulation, while the flatter structure of BuCYA is less favored because the complexed guest could be expelled more easily.

 © 2003 Wiley-VCH Verlag GmbH & Co. KGaA, Weinheim

DNA-Functionalized Au Nanoparticles

Living Templates for the Hierarchical Assembly of Gold Nanoparticles**

*Zhi Li, Sung-Wook Chung, Jwa-Min Nam, David S. Ginger, and Chad A. Mirkin**

Biological systems form sophisticated mesoscopic and macroscopic structures with tremendous control over the placement of nanoscopic building blocks within extended architectures. The promise of borrowing from nature's repertoire to organize inorganic materials on length scales relevant for applications in catalysis, photonics, and electronics has led to the pursuit of a variety of biotemplated and biomimetic strategies for the synthesis and assembly of nanoscale materials.[1–6] However, using such methods to independently control the organization of inorganic materials on multiple length scales has remained challenging.

Microorganisms including viruses, bacteria, and fungi, possess unique, structurally interesting motifs, and can reproduce quickly and inexpensively, which makes them attractive targets for use in directing materials synthesis. Their use in the fabrication of nanoscale materials has been dominated by studies of biomineralization processes, during which biological structures provide templates for, or even catalyze, naturally occurring as well as artificially induced reactions involving inorganic precursors.[7–15] Examples in nature of materials synthesis directed by microorganisms include the formation of iron oxides by bacteria, calcification in cyanobacteria, silica deposition in diatoms, and the formation of various other biogenic minerals by bacteria, lichen, algae, and fungi.[2,7,8] Other examples include the binding of metal ions to surface-layer proteins,[9] DNA,[10] virus protein cages,[11] or ordered protein assemblies[12] to initiate sites of nucleation for nanoparticle growth, and the synthesis of metallic nanocrystals through bioreduction of metal ions inside bacterial,[13] virus,[14] and fungal species.[15] Herein, we report a novel approach of using fungi to template the assembly of presynthesized and oligonucleotide-functionalized nanoparticles into ordered structures, thus allowing us to dynamically control the microscale structure of the resulting materials by relying on the fungi as living templates (Figure 1). Significantly, with this approach one can simultaneously control the organization and functionalization of the nanoscale building blocks by taking advantage of the preprogrammable interactions between the DNA-functionalized nanoparticles.

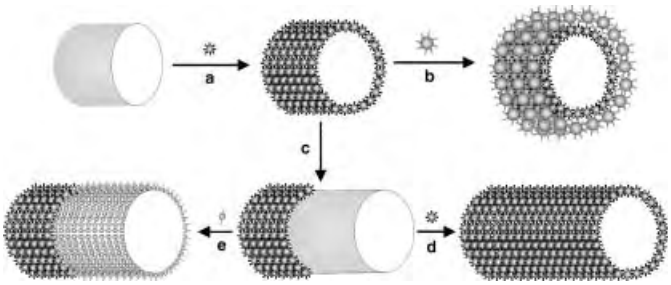


Figure 1. Schematic illustration of the use of a living hypha of a filamentous fungus as the template for the assembly of oligonucleotide-funtionalized Au nanoparticles into ordered microscopic structures. a) As the living fungal hypha grows, the Au nanoparticles (functionalized with single-stranded DNA) bind to its cell walls and a microscopic tube-shaped nanoparticle assembly is formed. b) Additional layers of nanoparticles functionalized with complementary oligonucleotide strands can be assembled onto the surface of the microscopic nanoparticle tube through DNA hybridization. c) The fungal hypha will continue to grow in a favorable environment and generate unmodified hyphae ends. d) and e) These fresh ends can be modified with new particles, thus providing control of the architecture along the growth axis.

In a typical experiment, 13-nm-diameter Au particles are prepared and modified with alkylthiol-capped oligonucleotide strands as previously reported.[16,17] On average, there are about 100 oligonucleotide strands chemically attached to each Au nanoparticle.[17] The modified Au nanoparticles are then dispersed in a culture solution (21 mM Na_2HPO_4, 11 mM KH_2PO_4, 9.3 mM NH_4Cl, 4.3 mM NaCl, 0.014 mM $CaCl_2$, 0.5 mM $MgSO_4$, 0.01 % glucose, ca. 7 nM Au particles). Subsequently, spores of a filamentous fungus, *Aspergillus niger*, are added to 20 mL of this media. Initially, this solution exhibits the characteristic intense red color of the Au nanoparticles (Figure 2a). After the fungal spores germinate, the hyphae grow and branch, while the Au nanoparticles in the media begin to assemble onto the surface of the hyphae. This results in the formation of a reddish purple macroscopic material that is phase-separated from the aqueous media and which consists of fungal mycelia heavily functionalized with nanoparticles (see below). The decrease in the red color of the media and concomitant formation of the reddish purple material can be visualized with the naked eye and have been characterized by UV/Vis spectroscopy (Figure 2b). These color changes are a direct consequence of particle assembly, which results in a red-shifting of the plasmon band associated with the gold nanoparticles—a well-documented phenomenon for other systems involving particle aggregation.[3a] Eventually, almost all of the Au nanoparticles are assembled by the fungi in the form of mycelia pellets, and the media loses its red color (Figure 2c). An optical microscope image of the mycelium fringe (Figure 2d) shows the hyphae (4–6 μm in diameter) of *Aspergillus niger*, which appear reddish purple in color.

[*] Prof. C. A. Mirkin, Z. Li, Dr. S.-W. Chung, J.-M. Nam, Dr. D. S. Ginger
Department of Chemistry and Institute for Nanotechnology
Northwestern University
2145 Sheridan Road, Evanston, IL 60208-3113 (USA)
Fax: (+1) 847-467-5123
E-mail: camirkin@chem.northwestern.edu

[**] C.A.M. acknowledges the AFOSR for financial support. In addition, this work was supported by the MRSEC program of the NSF (DMR-0076097) at the Materials Research Center of Northwestern University. Dr. W. A. Russin (BIF, Northwestern University) is acknowledged for his assistance with specimen processing and helpful discussions. In addition, we thank Dr. Y. Zhang and Prof. A. Lazarides for their valuable suggestions.

Supporting information for this article is available on the WWW under http://www.angewandte.org or from the author.

 © 2003 Wiley-VCH Verlag GmbH & Co. KGaA, Weinheim DOI: 10.1002/anie.200351231

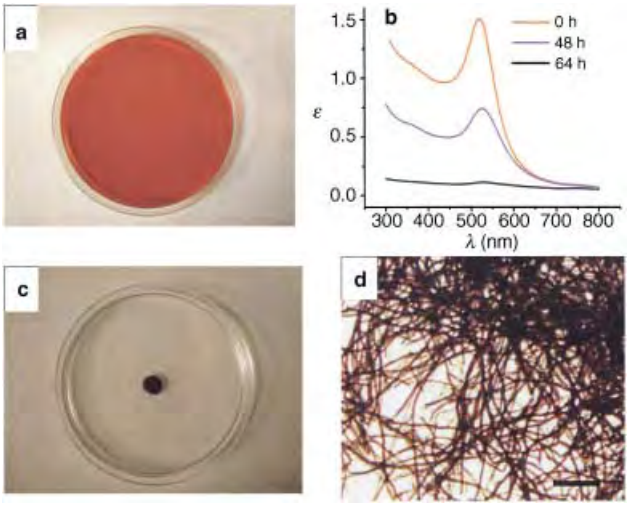


Figure 2. Au nanoparticles assembled by *Aspergillus niger*. a) Photograph of the culture media with an approximately 7 nM solution of 13-nm-diameter Au colloids immediately after introducing the fungal spores. The red color is characteristic of the Au colloid. b) UV/Vis spectra of the media during the mycelium growth process. Note that the time required for mycelia growth and nanoparticle assembly may vary from two days to more than one week. c) A reddish purple fungal mycelium is formed because of the fungal growth and Au nanoparticle assembly. Assembly of the particles onto the fungal surface depletes the solution of Au colloid. d) Optical microscope image of the fringe of the mycelium in (b). Regular branching hyphae (4–6 μm in diameter, tens of micrometers long) of *Aspergillus niger* with reddish purple color can be seen. The scale bar is 80 μm.

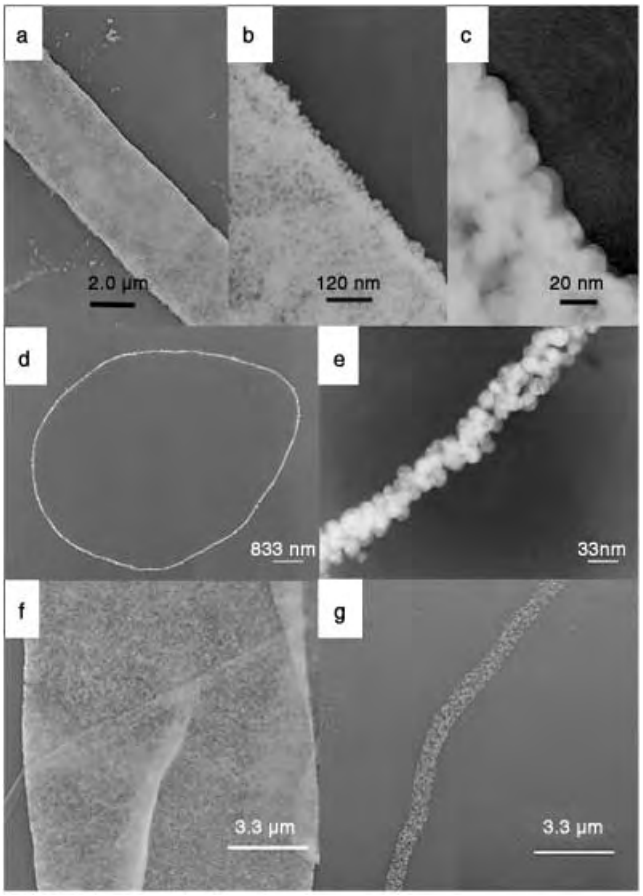


Figure 3. TEM images (unstained) of assemblies of Au nanoparticles templated by the fungal hyphae. a)–c) TEM images, at different magnifications, of the surface of an individual *Aspergillus niger* hypha heavily loaded with Au nanoparticles. d) Image of a thin section of an *Aspergillus niger* hypha loaded with Au nanoparticles embedded in epoxy resin. e) Higher magnification image of the "Au nanoparticle necklace" in (d). f) TEM image of the surface of an individual *Mucor hiemalis* hypha (ca. 12 μm in diameter) heavily loaded with Au nanoparticles. g) TEM image of the surface of an individual *Streptomyces venezuelae* hypha (ca. 0.8 μm in diameter) loaded with Au nanoparticles. Higher magnification TEM images of *Mucor hiemalis* and *Streptomyces venezuelae* hyphae in (f) and (g) are available in the Supporting Information.

Insight into the nanoparticle/fungal structure can be obtained by transmission electron microscopy (TEM). When air-dried directly on a TEM grid, the tube-shaped hyphae, loaded with nanoparticles, collapse to form thin nanoparticle-coated belt-shaped structures (Figure 3a–c). The tube shape of the nanoparticle assembly can be maintained if the mycelium is gradually dehydrated with acetone and then embedded in an epoxy resin by adding monomer to the solution and effecting thermal polymerization.[18] This was done to increase the rigidity of the material for subsequent sectioning and imaging experiments. An ultramicrotomed resin slice (approximately 80 nm thick) clearly shows that the nanoparticles assemble almost exclusively along the outer periphery of the hyphae, to form ring structures with diameters of 4–6 μm (Figure 3d). Higher magnification images show that these ring structures are made of the gold nanoparticles (Figure 3e).

When air-dried and compressed into thin films (ca. 0.2 mm), the fungal mats exhibit a golden hue and a faint metallic gloss resembling bulk gold (Figure 4a). Field emission scanning electron microscopy (FE-SEM) images show that the matted material consists of densely packed fibers with regular diameters (Figure 4b). Higher magnification TEM images show that each of these fibers derives from individual hyphae heavily functionalized with nanoparticles, which have not fused, presumably as a result of the protective oligonucleotide coating (Figure 4b; Figure 3a–c). The electrical conductivities of such films vary from 10^{-5} to 10^{-6} S cm^{-1} at room temperature, and exhibit an Arrhenius-like temperature dependence, characteristic of thermally activated charge transport between the individual Au nanoparticles (Figure 4c).[19] The semiconductive behavior and activation energy ($E_a = 1.62 \pm 0.05$ meV) of the Au-nanoparticle-assembled mycelium film are reminiscent of what has been observed for network assemblies of oligonucleotide-functionalized Au nanoparticles.[20]

Similar phenomena (nanoparticle assembly from solution and formation of fungal mats) can be observed with a variety of other common species of fungi and actinomycetes including *Penicillium notatum, Mucor hiemalis*, and *Streptomyces venezuelae*. These microorganisms grow into a range of characteristically species-dependent morphologies that allow the nanoparticles to be organized into tube-shaped structures with diameters ranging from about 12 (*Mucor hiemalis*) to 0.8 μm (*Streptomyces venezuelae*) and lengths of tens of micrometers (Figure 3f and g). At present we do not

 © 2003 Wiley-VCH Verlag GmbH & Co. KGaA, Weinheim

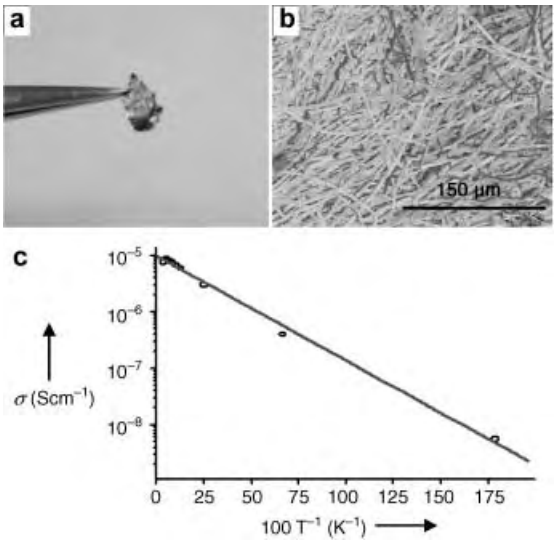


Figure 4. A thin film of gold formed from nanoparticle-fungal mycelia and its temperature-dependent electrical conductivity. a) A thin film (ca. 0.2 mm) formed by air-drying and compressing an *Aspergillus niger* mycelium loaded with oligonucleotide-functionalized 13-nm-diameter Au particles. b) FE-SEM image of the surface of the thin film in (a). Belt-shaped nanoparticle structures supported by fungal hyphae can be clearly seen. c) The electrical conductivity σ of the thin film in (a) as a function of temperature.

know the nature of the interaction between the particles and the surfaces of the fungi (for example, electrostatic versus chemical interaction). Nevertheless, the use of oligonucleotide-functionalized particles does not interfere with the assembly of the nanoparticles onto the fungal surfaces, and allows the use of sequence-specific DNA recognition properties to provide a second level of architectural control (Figure 1b).

Since the 13-nm-diameter gold particles are heavily loaded with single-stranded DNA, one can build secondary structures on the nanoscale into these micrometer-scale materials by using the sequence-specific recognition properties of their nanoparticle subcomponents. To demonstrate this capability, mycelia loaded with oligonucleotide-functionalized (5′-HS-C_6H_{12}-A_{10}AATATTGATAAGGAT-3′) 13 nm Au particles **1** were subsequently exposed to 30 nm Au particles functionalized with complementary 5′-hexylthiol-capped oligonucleotide strands (5′-HS-C_6H_{12}- A_{10}ATCCTTATCAATATT-3′). At 45 °C, the nanoparticles that make up the cottony mass hybridize with the complementary particles as evidenced by UV/Vis spectroscopy of the solution (see Supporting Information), which shows a gradual dissipation of the plasmon band (526 nm) associated with the dispersed particles, and TEM, which shows the formation of a concentric structure with two layers of different sized particles (Figure 5). Significantly, particles functionalized with DNA (30 nm, modified with 5′-hexylthiol-capped oligonucleotides, 5′-HS-C_6H_{12}- A_{10}TAACAATAATCCCTC-3′) that is noncomplementary to the 13-nm-diameter particles on the hyphae do not exhibit this behavior and remain dispersed in solution. Note that particle assembly can also be effected by using gold nanoparticles without oligonucleotide-functionalized surfaces

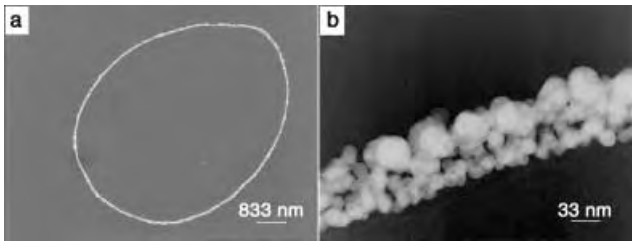


Figure 5. Double-layered nanoparticle ring structure. a) TEM image (unstained) of a thin section of an individual *Aspergillus niger* hypha, subsequently loaded with 13-nm-diameter Au particles, and then assembled with 30-nm-diameter Au particles through DNA hybridization. b) Higher magnification TEM image of the double-layered nanoparticle ring structure in (a) clearly shows the first layer of 13-nm-diameter Au particles and the second layer of 30-nm-diameter Au particles.

(for example, particles stabilized with bis(*p*-sulfonatophenyl)phenylphosphane dihydrate dipotassium salt (BSPP)). However, these particles do not allow one to control architecture through hybridization with other oligonucleotide-functionalized building blocks.

Finally, these fungal hyphae are truly living templates. Even after the dense assembly of Au particles, the mycelia will continue to grow as long as the culture media favors it (Figure 1c and d). Indeed, one can use fungal hyphae to assemble one type of particle in one solution, and then continue to assemble a second type of particle along the growing direction of the hyphae templates by changing the culture solution (Figure 1c and e). To illustrate this concept of axial arrangement of nanoparticles along the living templates as well as the living assembly process itself, an *Aspergillus niger* mycelia was first grown in the media culture containing 13-nm-diameter Au particles for about 50 h as described above, and then the surrounding solution was changed to a second culture media containing oligonucleotide-functionalized 5-nm-diameter Au nanoparticles (ca. 15 nM, only differing in particle size). After 5 h, the living assembly process was arrested when the hyphae were picked out from the growth media and air-dried onto a TEM grid (Figure 6a). As one scans along the hypha growth direction to the very end of the hypha, three different regions with different nanoparticle arrangements can be distinguished (Figure 6b–d). The region furthest from the end point of the hypha contains mainly 13-nm-diameter Au particles (Figure 6b), which assembled onto the hypha surface from the first culture media. On the other hand, only 5-nm-diameter Au particles from the second culture media can be seen in the region near the end point (Figure 6c). Between these two regions, there is a mixed region (ca. 2 μm along the hypha) containing a gradient of both 13- and 5-nm-diameter Au particles (Figure 6d; see also the Supporting Information).

In conclusion, this work provides an important example of how one can use macroscopic quantities of microorganisms as living templates to organize presynthesized nanoscale architectural components into structures with controllable micro- and nanoscale order. We anticipate that this strategy can be extended to a variety of other microorganisms, and that it could be used to construct hierarchical materials composed of

 © 2003 Wiley-VCH Verlag GmbH & Co. KGaA, Weinheim

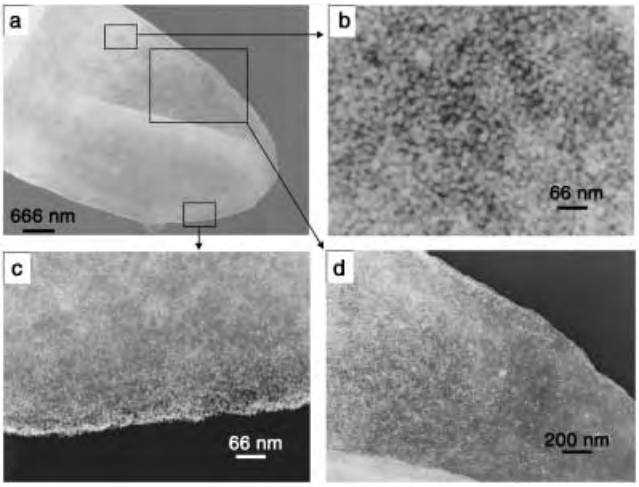


Figure 6. TEM images (unstained) of an apical growth zone of an *Aspergillus niger* hypha, grown consecutively in two culture media containing two different types of Au nanoparticles (diameters 13 nm and 5 nm, respectively), which shows the controlled distribution of these two different type of Au nanoparticles along the growth axis. a) TEM image of the whole end of the hypha, dried and captured on a carbon-coated copper grid. Three different regions with different arrangements of the nanoparticles can be distinguished as one examines sections along the hypha growth direction. b) Image of the region furthest from the apex of the hypha containing 13-nm-diameter Au paritcles. c) Image for the region closest to the apex of the hypha containing 5-nm-diameter Au paritcles. d) Transition region (ca. 2 μm along the hypha) containing a gradient of both 13- and 5-nm-diameter Au particles. Additional TEM images for (d) are available in the Supporting Information.

magnetic, semiconducting, and noble metal building blocks, thereby providing routes to high surface area macroscopic materials with novel and tailorable electronic, magnetic, optical, and catalytic properties that derive, in part, from the basic particles from which they are made.

Received: February 19, 2003 [Z51231]

Keywords: DNA · fungi · gold · nanostructures · template synthesis

[1] a) G. M. Whitesides, B. Grzybowski, *Science* **2002**, *295*, 2418 – 2421; b) M. Antonietii, C. Göltner, *Angew. Chem.* **1997**, *109*, 944 – 964; *Angew. Chem. Int. Ed. Engl.* **1997**, *36*, 910 – 928; c) C. M. Niemeyer, *Angew. Chem.* **2001**, *113*, 4254 – 4287; *Angew. Chem. Int. Ed.* **2001**, *40*, 4128 – 4158.

[2] a) S. Weiner, L. Addadi, *J. Mater. Chem.* **1997**, *7*, 689 – 702; b) S. Mann, *Biomineralization: Principles and Concepts in Bioinorganic Materials Chemistry*, Oxford University Press, Oxford, **2001**.

[3] a) C. A. Mirkin, R. L. Letsinger, R. C. Mucic, J. J. Storhoff, *Nature* **1996**, *382*, 607 – 609; b) A. P. Alivisatos, X. Peng, T. E. Wilson, K. P. Johnsson, C. J. Loweth, M. P. Bruchez, Jr., P. G. Schultz, *Nature* **1996**, *382*, 609 – 611.

[4] S. A. Davis, S. L. Burkett, N. H. Mendelson, S. Mann, *Nature* **1997**, *385*, 420 – 423.

[5] a) S.-W. Lee, C. Mao, C. Flynn, A. M. Belcher, *Science* **2002**, *296*, 892 – 895; b) Q. Wang, T. W. Lin, L. Tang, J. E. Johnson, M. G. Finn, *Angew. Chem.* **2002**, *114*, 477 – 480; *Angew. Chem. Int. Ed.* **2002**, *41*, 459 – 462.

[6] J. N. Cha, G. D. Stucky, D. E. Morse, T. J. Deming, *Nature* **2002**, *403*, 289 – 292.

[7] *Biomineralization in Lower Plants and Animals* (Eds.: B. S. C. Leadbeater, R. Riding), Clarendon Press, Oxford, **1986**.

[8] J. F. Banfield, S. A. Welch, H. Zhang, T. T. Ebert, R. L. Penn, *Science* **2000**, *289*, 751 – 754.

[9] W. Shenton, D. Pum,, U. B. Sleytr, S. Mann, *Nature* **1997**, *389*, 585 – 587.

[10] E. Braun, Y. Eichen, U. Sivan, G. Ben-Yoseph, *Nature* **1998**, *391*, 775 – 778.

[11] T. Douglas, M. Young, *Nature* **1998**, *393*, 152 – 155.

[12] S. Behrens, K. Rahn, W. Habicht, K.-J. Böhm, H. Rösner, E. Dinjus, E. Unger, *Adv. Mater.* **2002**, *14*, 1621 – 1625.

[13] T. Klaus, R. Joerger, E. Olsson, C.-G. Granqvist, *Proc. Natl. Acad. Sci. USA* **1999**, *96*, 13611 – 13614.

[14] E. Dujardin, C. Peet, G. Stubbs, J. N. Culver, S. Mann, *Nano Lett.* **2003**, *3*, 275 – 277

[15] a) P. Mukherjee, A. Ahmad, D. Mandal, S. Senapati, S. R. Sainkar, M. I. Khan, R. Ramani, R. Parischa, P. V. Ajayakumar, M. Alam, M. Sastry, R. Kumar, *Angew. Chem.* **2001**, *113*, 3697 – 3701; *Angew. Chem. Int. Ed.* **2001**, *40*, 3585 – 3588; b) P. Mukherjee, S. Senapati, D. Mandal, M. I. Khan, R. Kumar, M. Sastry, *ChemBioChem* **2002**, *3*, 461 – 463.

[16] J. J. Storhoff, R. Elghanian, R. C. Mucic, C. A. Mirkin, R. L. Letsinger, *J. Am. Chem. Soc.* **1998**, *120*, 1959 – 1964.

[17] Z. Li, R. Jin, C. A. Mirkin, R. L. Letsinger, *Nucleic Acids Res.* **2002**, *30*, 1558 – 1562.

[18] W. A. Russin, C. L. Trivett in *Microwave Techniques and Protocols* (Eds.: R. T. Giberson, R. S. Demaree, Jr.), Humana Press, Totowa, NJ, **2001**, pp. 25 – 35.

[19] M. Brust, D. Bethell, D. J. Schiffrin, C. J. Kiely, *Adv. Mater.* **1995**, *7*, 795 – 797.

[20] S.-J. Park, A. A. Lazarides, C. A. Mirkin, P W. Brazis, C. R. Kannewurf, R. L. Letsinger, *Angew. Chem.* **2000**, *112*, 4003 – 4006; *Angew. Chem. Int. Ed.* **2000**, *39*, 3845 – 3848.

 © 2003 Wiley-VCH Verlag GmbH & Co. KGaA, Weinheim

Protein Nanostructures

Direct-Write Dip-Pen Nanolithography of Proteins on Modified Silicon Oxide Surfaces**

*Jung-Hyurk Lim, David S. Ginger, Ki-Bum Lee, Jungseok Heo, Jwa-Min Nam, and Chad A. Mirkin**

The development of direct-write patterning methods for protein-based nanostructures is important for researchers working in the areas of proteomics, diagnostics, and materials science. Such methods could allow one to fabricate patterns of

[*] Prof. C. A. Mirkin, J.-H. Lim, D. S. Ginger, K.-B. Lee, J. Heo, J.-M. Nam
Department of Chemistry and Institute for Nanotechnology
Northwestern University
2145 Sheridan Road, Evanston, IL 60208-3113 (USA)
Fax: (+1) 847-467-5123
E-mail: camirkin@chem.northwestern.edu

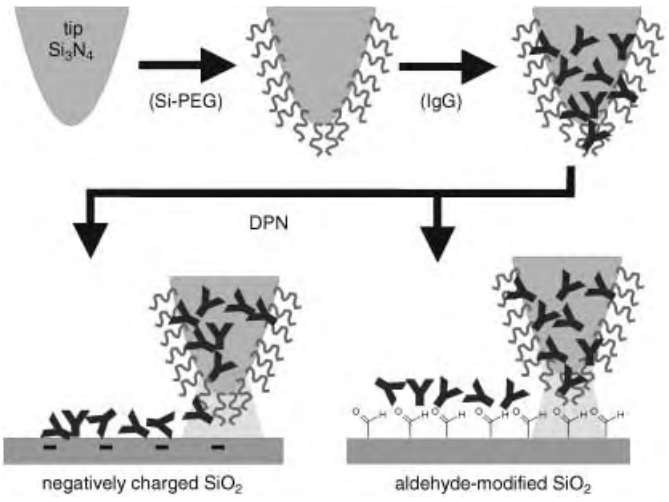
[**] C.A.M. acknowledges the AFOSR, DARPA, and NSF for support of this research. D.S.G. thanks the NIH for an NRSA Postdoctoral Fellowship (1 F32 HG02463).

 DOI: 10.1002/anie.200351256 © 2003 Wiley-VCH Verlag GmbH & Co. KGaA, Weinheim

nanostructures of extraordinary complexity, thus offering routes to important tools in the life sciences such as gene chips and proteomic arrays, as well as templates that could be used by chemists and materials scientists to build ordered two- and three-dimensional functional architectures.[1] Although direct-patterning approaches offer many potential advantages over indirect methods (such as facile processing and fabrication procedures, and elimination of the need for resists), they pose several challenges. Methods must be developed for facilitating the transport of the high-molecular-weight biomolecules from a coated tip to a substrate without sacrificing sub-100-nm resolution and patterning speed. Dip-pen nanolithography (DPN)[2] is a promising tool in this respect. However, in the area of protein arrays it has thus far been used primarily as a tool for making affinity arrays out of small organic molecules that can subsequently direct the assembly of proteins from solution. This indirect approach does not allow one to generate arrays made of more than one protein.

Three approaches have been taken in the direct patterning of proteins by DPN. The first involves the use of a chemically tailored form of collagen that has surface-binding groups built into it to help facilitate nanostructure adsorption.[3] This designer-protein approach, although powerful, can not be used generally by researchers interested in proteomic-array research. The second method involves the use of glass pretreated with 3-glycidoxypropyltrimethoxysilane;[4] with this technique, human chorionic gonadotropin could be patterned at the micrometer scale. However, the biological activity of the resulting patterns has not been demonstrated. The third approach involves the use of gold substrates and modified tips.[5] No general methods have been developed for using DPN to generate arrays of protein nanostructures through direct deposition on oxide substrates, the materials of choice in the microarray industry, while preserving the biological activity of the proteins. Herein, we present two strategies that offer patterning capabilities from the 50- to the 550-nm scale. This method complements other approaches to the indirect patterning of proteins on surfaces through techniques such as nanografting[6] and electron-beam lithography[7], as well as larger-scale patterning techniques such as microcontact printing.[8]

The approach described herein relies on the modification of an AFM tip with 2-[methoxypoly(ethyleneoxy)propyl]trimethoxysilane (Si-PEG), which forms a biocompatible and hydrophilic surface layer. This layer inhibits protein adsorption and reduces the activation energy required for protein transport from tip to surface. It also protects the proteins from denaturation on the tip surface.[9] In the absence of this tip coating, the protein inking solutions (500 $\mu g\,mL^{-1}$ in phosphate-buffered saline (PBS) at pH 7.3) do not wet the silicon nitride cantilevers. We have found that untreated cantilevers often produce inconsistent or low-density protein patterns. In addition to cantilever modification, we have developed two other strategies to facilitate ink transport and nanostructure formation, both of which involve silicon oxide surfaces. The first such strategy is the creation of a negatively charged surface through treatment with base[10] and the other is the use of an aldehyde-modified surface[11] (Scheme 1). After the formation of the desired surface the slides were rinsed with ethanol and cured under flowing nitrogen at 90–100 °C for 15 min. Proteins can be attached to such surfaces through electrostatic interactions between the positively charged parts of the protein and the negatively charged substrate surface in the first case,[12] or through covalent bonding between the aldehyde-modified surface and amine groups on the protein molecule in the second case.[11] The use of antirabbit immunoglobulin G (IgG, developed in goat, Sigma) is described herein as a representative example.



Scheme 1. Schematic representation of dip-pen nanolithography of proteins on two different modified surfaces.

In a typical DPN transport experiment, a Si-PEG-modified AFM tip was coated by immersing the tip in a solution containing the desired protein (500 $\mu g\,mL^{-1}$ in PBS buffer at pH 7.3) with glycerol (5 %) for 1 min. The tip was then mounted in the AFM and brought into contact (1.5 nN) with the substrate surface. Patterning of the proteins was performed at room temperature in a glove box with a controlled environment at a relative humidity of 60–90 %.[13] For probing of the biorecognition properties of the protein nanoarrays, the unpatterned region of the aldehyde-modified surface was passivated by immersing the sample in a 5 mM aqueous solution of amine-terminated oligo(ethylene glycol) ($n = 7$) for 20 min to impede nonspecific adsorption of proteins from the solution. The synthesis of amine-terminated oligo(ethylene glycol) was performed according to literature methods.[15]

By using these experimental conditions and the base-treated surfaces, we generated nanostructures composed of rabbit IgG and (fluorophore-labeled) antirabbit IgG in a direct-write fashion (Figures 1 and 2). The latter could be imaged by fluorescence microscopy as well as by AFM, thus allowing us to confirm the chemical identity of the transported material. The height profile of an antirabbit IgG pattern consisting of two parallel lines and three dots that was generated by direct-write DPN showed that each IgG feature was 8–10 nm high (Figure 1 a), which is consistent with the transfer of a monolayer of the protein to the negatively charged surface.[12,16] Protein arrays can be fabricated by repeating the procedure for forming a single dot feature

 © 2003 Wiley-VCH Verlag GmbH & Co. KGaA, Weinheim

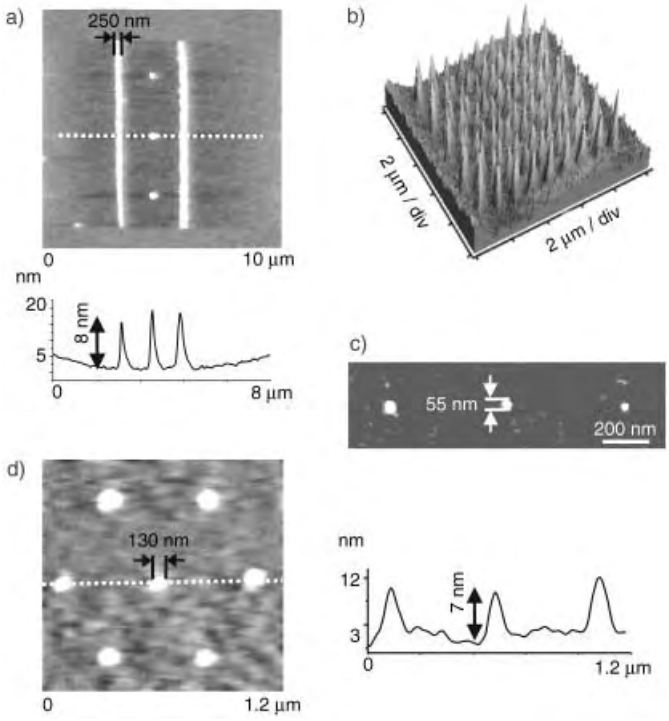


Figure 1. AFM topography images of protein nanostructures. a) Antirabbit IgG protein nanostructures on a negatively charged SiO_2 substrate written at 0.08 μm s^{-1} and corresponding line profile; b) 3D topography image of antirabbit IgG protein dot arrays (contact time = 3 s; div = division); c) tapping-mode image of antirabbit IgG protein dots (contact time = 0.5 s, set point = 0.5 nN); d) rabbit IgG nanostructures on an aldehyde-modified SiO_2 substrate (contact time = 2 s). AFM images were collected with an uncoated tip at a scan rate of 2 Hz.

(Figure 1b). For example, an array consisting of 85450-nm-diameter dots spaced 350 nm apart was fabricated from antirabbit IgG. The array was fabricated in less than 5 min with a holding time of 3 s for each dot.

The protein features studied thus far have been as large as 550 nm and as small as 55 nm (Figure 1c). Sub-100-nm protein features could be patterned successfully by using appropriate conditions (contact time = 0.5 s, contact force = 0.5 nN). We have demonstrated the generality of the electrostatic approach by patterning fluorophore-labeled antirabbit, -mouse, -goat, and -human IgG as well as unlabeled rabbit, mouse, goat, and human IgG. Certain proteins can also be patterned by DPN on aldehyde-derivatized surfaces (Figure 1d) by using the chemical approach adopted by MacBeath and Schreiber[11] for microarrays. In this approach, a reaction between aldehyde groups on the surface with primary amines (lysine and α-amines at their N termini) on the proteins results in the formation of Schiff bases and the immobilization of the proteins.[11]

Since the antirabbit IgG used in these experiments is labeled with a fluorophore, we can visualize patterns generated with it by fluorescence microscopy (Figure 2). Protein nanostructures with 550-nm line widths (Figure 2a) and dot arrays (450-nm dots, 6-μm spacing) can be visualized easily in this way (Figure 2b). A fluorescence image of the array represented by the 3D AFM image in Figure 1b is shown in Figure 2c. To demonstrate multiple protein-ink capabilities, two different fluorophore-labeled proteins, antirabbit IgG (Alexa Fluor 594) and antihuman IgG (Alexa Fluor 488) were deposited on aldehyde-derivatized surfaces by DPN in a serial fashion (Figure 2d). The line widths were determined by AFM rather than by fluorescence microscopy because of the resolution limitations of the optical technique. Finally, unlike many of the other inks studied thus far,[2] the transport of the protein structures described herein are not highly humidity dependent (over a 60–90% relative humidity). The most important factor controlling their transport seems to be set-point (large set-points lead to larger features and contact area). Many of the features generated in this study do not exhibit the uniform edges associated with the DPN transport of small ink molecules and DNA.[2,14] Indeed, transport in this case seems to be dominated by physical stamping rather than by diffusion from the tip to the surface.

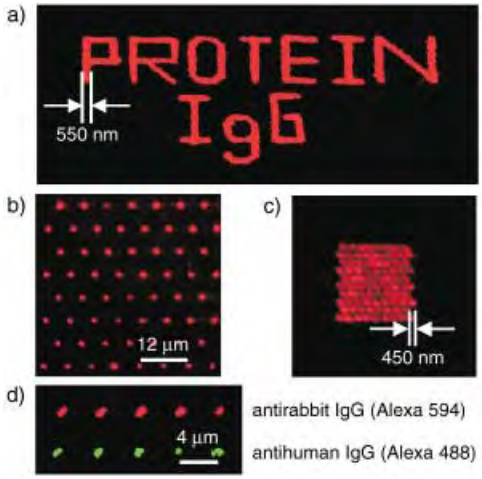


Figure 2. Fluorescence images of DPN-generated antirabbit IgG (labeled with Alexa 594) structures on a negatively charged SiO_2 surface (a–c): a) words (writing speed = 0.06 μm s^{-1}); b) dot arrays (contact time = 5 s); c) dot arrays (contact time = 3 s); d) two-component protein patterns formed by DPN on an aldehyde-derivatized SiO_2 surface (contact time = 5 s).

To test the biorecognition properties of the IgG nanostructures generated by DPN, a rabbit IgG and a human IgG pattern were immersed in a 5-μg mL^{-1} solution (PBS buffer, pH 7.3) of fluorophore-labeled antirabbit IgG (Alexa 594, red) and antihuman IgG (Alexa 488, green) for 30 min. After the substrate had been rinsed with PBS buffer (10 mM), Tween-20 solution (0.05%), and Milli-Q water, fluorescence microscopy showed that the antirabbit IgG had bound selectively to the rabbit IgG patterns (Figure 3a), and the antihuman IgG had bound to the human IgG patterns (Figure 3b). Cross-reactivity between the rabbit IgG and the human IgG was estimated to be approximately 20% based on the two-color-reading approach (compare red and green signals in Figure 3a and b).[17] It is very important that the proteins remain hydrated throughout all experimental steps to prevent their denaturation by drying.[11] The protein patterns that were either generated with the protein ink itself

 © 2003 Wiley-VCH Verlag GmbH & Co. KGaA, Weinheim

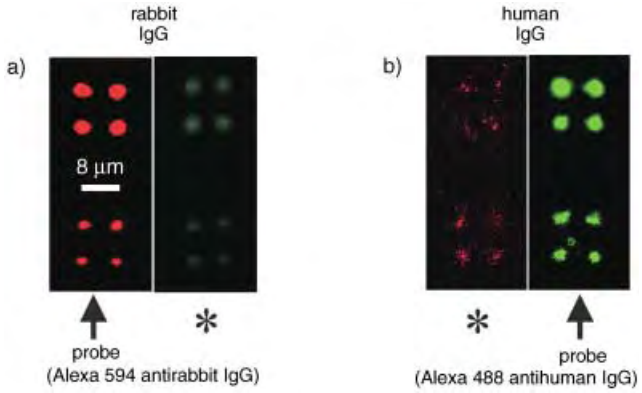


Figure 3. Probing biorecognition properties of the protein nanoarrays: a) a rabbit IgG slide; b) a human IgG slide. Both slides were incubated in a mixture of Alexa 594 labeled antirabbit IgG (red) and Alexa 488 labeled antihuman IgG (green). The images on the left probe the fluorescence of the red dye and those on the right probe the contributions from the green dye. A comparison of the two allows one to determine the extent of cross-reactivity. The images marked * are equivalent exposures and demonstrate the relatively low (< 20%) degree of nonspecific interaction between the patterned surfaces and the anti-IgGs.

(in the absence of glycerol) or exposed to air during experimental steps did not show selective protein–protein interactions. The glycerol apparently helps to hydrate the protein and inhibits denaturation.[11]

In conclusion, our studies show that DPN can be used to direct-write proteins on two different classes of SiO_2 substrates, which permits the use of both fluorescence and AFM detection methods. Importantly, the strategy we have developed provides a protocol for creating protein nanostructures on substrates while keeping their natural structures intact. When combined with multiple-pen AFM arrays,[2b,c,18] this approach could allow one to generate arrays of proteins rapidly with extraordinary complexity, almost at the resolution limit of physical-feature size (i.e. the size of the molecules).

Experimental Section

The negatively charged silicon wafers were prepared by literature methods.[19] Aldehyde-modified surfaces were prepared by cleaning oxidized silicon wafers with piranha solution (30% H_2O_2/H_2SO_4 (1:4); **Caution**: Piranha solutions are extremely dangerous and should be used with extreme caution) for 1 h, and then treating them with 3-aldehydepropyltrimethoxysilane (0.5% w/v solution in ethanol/water (95:5), adjusted to pH 5 with acetic acid, Bio-Connext, United Chemical Technologies) for 2 min.

DPN-patterning and AFM-imaging experiments were carried out with a ThermoMicroscopes CP atomic force microscope (AFM) driven by commercial lithography software (DPNWrite, DPN System-1, NanoInk Inc., Chicago, IL) and conventional silicon nitride cantilevers (force constant = 0.05 N m^{-1}). Tapping-mode images were taken with a Nanoscope IIIa and MultiMode microscope from Digital Instruments. Fluorescence images were obtained with a Zeiss Axiovert 100 microscope with a Hg lamp excitation source and standard filters.

Received: February 24, 2003 [Z51256]

Keywords: biorecognition · direct-write patterns · nanostructures · proteins · surface chemistry

[1] a) A. S. Blawas, W. M. Reichert, *Biomaterials* **1998**, *19*, 595; b) M. Schena, D. Shalon, R. Davis, P. O. Brown, *Science* **1995**, *270*, 467; c) J. M. Nam, S. J. Park, C. A. Mirkin, *J. Am. Chem. Soc.* **2002**, *124*, 3820.
[2] a) R. D. Piner, J. Zhu, F. Xu, S. Hong, C. A. Mirkin, *Science* **1999**, *283*, 661; b) S. Hong, J. Zhu, C. A. Mirkin, *Science* **1999**, *286*, 523; c) S. Hong, C. A. Mirkin, *Science* **2000**, *288*, 1808.
[3] D. L. Wilson, R. Martin, S. Hong, M. Cronin-Golomb, C. A. Mirkin, D. L. Kaplan, *Proc. Natl. Acad. Sci. USA* **2001**, *98*, 13660.
[4] A. Noy, A. E. Miller, J. E. Klare, B. L. Weeks, B. W. Woods, J. J. DeYoreo, *Nano Lett.* **2002**, *2*, 109.
[5] K. B. Lee, J. H. Lim, C. A. Mirkin, *J. Am. Chem. Soc.* **2003**, *125*, 5588.
[6] a) C.-H. Jang, B. D. Stevens, P. R. Carlier, M. A. Calter, W. A. Ducker, *J. Am. Chem. Soc.* **2002**, *124*, 12114; b) G.-Y. Liu, S. Xu, Y. L. Qian, *Acc. Chem. Res.* **2000**, *33*, 457; c) J. R. Kenseth, J. A. Harnisch, V. W. Jones, M. D. Porter, *Langmuir* **2001**, *17*, 4105.
[7] D. V. Nicolau, T. Taguchi, H. Taniguchi, S. Yoshikawa, *Langmuir* **1999**, *15*, 3845.
[8] J. P. Renault, A. Bernard, A. Bietsch, H. R. Bosshard, E. Delamarche, M. Kreiter, U. P. Wild, *J. Phys. Chem. B* **2003**, *107*, 703.
[9] A. Papra, N. Gadegaard, N. B. Larsen, *Langmuir* **2001**, *17*, 1457.
[10] M. Kosmulski, J. Hartikainen, E. Maczka, W. Janusz, J. B. Rosenholm, *Anal. Chem.* **2002**, *74*, 253.
[11] B. MacBeath, S. L. Schreiber, *Science* **2000**, *289*, 1760.
[12] K. B. Lee, S. J. Park, C. A. Mirkin, J. C. Smith, M. Mrksich, *Science* **2002**, *295*, 1702.
[13] We have found a high relative humidity to be an important factor in the transport of high-molecular-weight molecules from the tip to the surface.[14]
[14] L. M. Demers, D. S. Ginger, S. J. Park, Z. Li, S. W. Chung, C. A. Mirkin, *Science* **2002**, *296*, 1836.
[15] D. A. Neumayer, J. A. Belot, R. L. Feezel, C. Reedy, C. L. Stern, T. J. Marks, L. M. Liable-Sands, A. L. Rheingold, *Inorg. Chem.* **1998**, *37*, 5625.
[16] M. E. Browning-Kelley, K. Wadu-Mesthrige, V. Hari, G. Y. Liu, *Langmuir* **1997**, *13*, 343.
[17] Cross-reactivity was determined from the ratio of fluorescence-signal intensities in each pattern by using image-processing software (Adobe Photoshop 5.0, Adobe Systems, San Jose, CA). Before ratios were taken, the signals for each image were normalized by using the background intensity of the amine-terminated oligo(ethylene glycol) regions of the sample as the reference.
[18] M. Shang, D. Bullen, S. W. Chung, S. Hong, R. S. Kee, Z. Fan, C. A. Mirkin, C. Liu, *Nanotechnology* **2002**, *13*, 212.
[19] J. M. Berquier, H. Arribart, *Langmuir* **1998**, *14*, 3716.

 © 2003 Wiley-VCH Verlag GmbH & Co. KGaA, Weinheim

Cover Picture



David Barnes-Seeman, Seung Bum Park, Angela N. Koehler, and Stuart L. Schreiber*

Small-Molecule Microarrays have provided a robust and scalable means of searching for new small-molecule–protein interactions. The cover picture shows the protein calmodulin binding to a small molecule that was immobilized on a glass surface by using a novel slide/capture method. More about this method and its use is given by S. L. Schreiber et al. on page 2376 ff.

Contents

Obituary

Benno Hess (1922–2002) ——— 2330 | Biophysics and Self-Organization | *M. Engelhard and S. C. Müller*

Books

Modern Organocopper Chemistry – 2331 | Norbert Krause | *reviewed by S. R. Waldvogel*

Molecular Devices and Machines – 2331 | Vincenzo Balzani, Margherita Venturi, Alberto Credi | *reviewed by F. Vögtle, C. A. Schalley*

Chemically Speaking ——— 2332 | Carl C. Gaither, Alma E. Cavozos-Gaither | *reviewed by H.-J. Quadbeck-Seeger*

Practical Sonochemistry ——— 2333 | Timothy J. Mason, Dietmar Peters | *reviewed by N. E. Leadbeater*

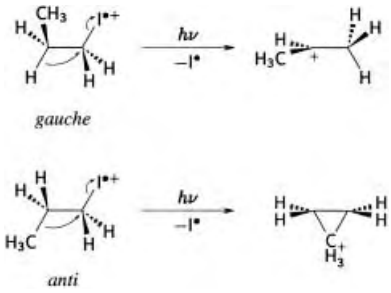
Microwaves in Organic Synthesis – 2334 | André Loupy | *reviewed by N. E. Leadbeater*

Highlights

Control of Chemical Reactivity

M. Goez* ——— 2336–2337

Conformation-Selective Laser Chemistry



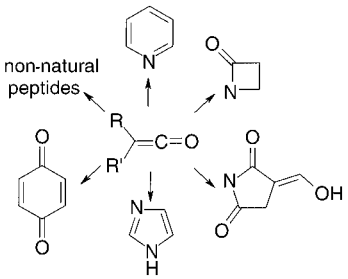
Selection of a conformer by a laser pulse and conformation-specific cleavage by a second laser pulse can be used to control the outcome of a chemical reaction. One of the most recent examples is the selective wavelength-dependent generation of either the 2-propyl cation or corner-protonated cyclopropane from 1-iodopropane (see scheme).

Minireviews

Ketene Synthesis and Reactions

A. Rafai Far* ——— 2340–2348

Ketenes in Polymer-Assisted Synthesis



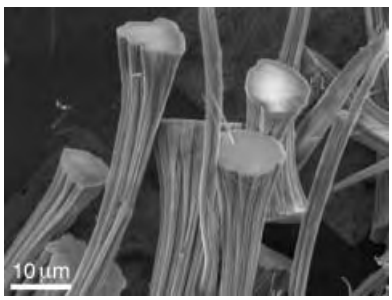
Ketenes, which are versatile intermediates in organic synthesis, have found a niche of their own in polymer-assisted organic transformations for the preparation of small-molecule libraries. Many of the methods of generating ketenes for such transformations are examined, and the scope of their reactions is discussed.

Reviews

Organization of Nanostructures

H. Cölfen, S. Mann* ——— 2350–2365

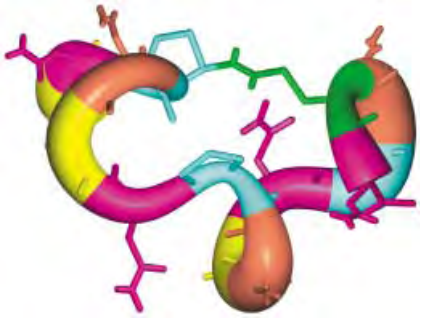
Higher-Order Organization by Mesoscale Self-Assembly and Transformation of Hybrid Nanostructures



The architecture of organization: By coupling synthesis, self-assembly, and transformation at the mesoscopic scale it should be possible to develop a chemistry of emergent structures based on the time- and scale-dependent coupling of interactive components. This review highlights how the interplay between the aggregation and crystallization of hybrid inorganic–organic building blocks can lead to complex single crystals, organized nanoparticle arrays, and embedded nanostructures with higher-order architecture (see picture).

© 2003 Wiley-VCH Verlag GmbH & Co. KGaA, Weinheim

Communications



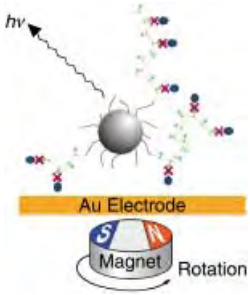
An optimized cyclic peptidomimetic (see picture) of the NPNA-repeat region in the circumsporozoite (CS) protein of *P. falciparum* was designed. When delivered to the immune system on human-compatible viruslike particles (virosomes), the mimetic effectively elicits sporozoite-binding antibodies. This virosome-mimotope (virotope) approach may be of general value for the design and testing of new synthetic-vaccine candidates.

Peptidomimetic Vaccine Design

B. Pfeiffer, E. Peduzzi, K. Moehle, R. Zurbriggen, R. Glück, G. Pluschke,* J. A. Robinson* _____ **2368 – 2371**

A Virosome-Mimotope Approach to Synthetic Vaccine Design and Optimization: Synthesis, Conformation, and Immune Recognition of a Potential Malaria-Vaccine Candidate

Taking DNA analysis for a spin: Amplified detection of viral DNA and single-base mutations in nucleic acids is accomplished by the thermally cycled incorporation of biotin labels into DNA replica associated with magnetic particles, by the electrocatalyzed biochemiluminescence transduction of the DNA recognition events, and by the rotation of the magnetic particles on electrode surfaces (see schematic representation).



Detecting Single-Base Mutations

F. Patolsky, Y. Weizmann, E. Katz, I. Willner* _____ **2372 – 2376**

Magnetically Amplified DNA Assays (MADA): Sensing of Viral DNA and Single-Base Mismatches by Using Nucleic Acid Modified Magnetic Particles

The importance of the pK_a value: Phenols, carboxylic acids, and compounds containing comparably acidic functional groups are covalently captured on a diazobenzylidene-functionalized glass surface. This new covalent slide-capture method has been used to print 6336 diversity-oriented synthesis-derived phenol-containing fused bicycles and tetracycles, from which new calmodulin ligands were identified (see schematic representation).



Diversity-Oriented Synthesis

D. Barnes-Seeman, S. B. Park, A. N. Koehler, S. L. Schreiber* _____ **2376 – 2379**

Expanding the Functional Group Compatibility of Small-Molecule Microarrays: Discovery of Novel Calmodulin Ligands

For the USA and Canada:
ANGEWANDTE CHEMIE International Edition (ISSN 1433-7851) is published weekly by Wiley-VCH PO Box 191161, D 69451 Weinheim, Germany. Air freight and mailing in the USA by Publications Expediting Inc. 200 Meacham Ave., Elmont, NY 11003. Periodicals postage paid at Jamaica NY 11431. US POSTMASTER: send address changes to *Angewandte Chemie*, Wiley-VCH, 111 River Street, Hoboken, NJ 07030. Annual institutional subscription price for institutions: Europe € 2998.00/3148.00. Outside Europe US$ 3718.00/3904.00 (valid for print or electronic/print and electronic delivery); for individuals who are personal members of a national chemical society, or whose institution already subscribes, or who are retired or self-employed consultants, print only (including postage and handling charges): Europe € 248.00/Outside Europe US$ 348.00.

 © 2003 Wiley-VCH Verlag GmbH & Co. KGaA, Weinheim

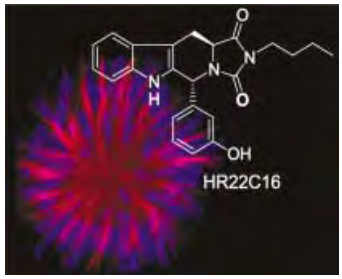
Contents

Probes for Cell Division

S. Hotha, J. C. Yarrow, J. G. Yang, S. Garrett, K. V. Renduchintala, T. U. Mayer, T. M. Kapoor* _ **2379 – 2382**

HR22C16: A Potent Small-Molecule Probe for the Dynamics of Cell Division

A high-throughput, microscopy-based chemical-genetic screen identified HR22C16, which causes a monoastral mitotic block, as a small-molecule probe for cell division (see picture). By using a diastereoselective, traceless solid-phase synthesis and biological assays, a more potent HR22C16 analogue was then identified. A photocaging strategy for HR22C16 was also developed to allow fast temporal control over the function of the target protein Eg5.

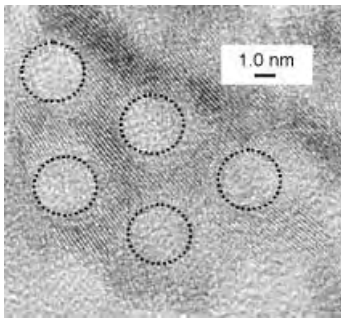


Crystallized Mesoporous Ta-Nb Oxide

T. Katou, B. Lee, D. Lu, J. N. Kondo, M. Hara, K. Domen* ____ **2382 – 2385**

Crystallization of an Ordered Mesoporous Nb–Ta Oxide

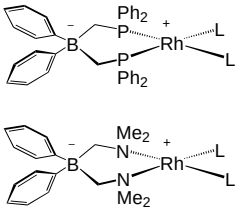
The ordered pore structure of 2D hexagonally ordered mesoporous niobium and tantalum mixed oxide has been successfully preserved during crystallization by filling the pores of the precursor with carbon prior to crystallization. Subsequent thermal treatment in an inert atmosphere produces the crystallized product without loss of the ordered mesoporous structure, and the carbon template is removed by calcination in air. Transmission electron microscopy and electron diffraction analyses clarify the preservation of the 2D hexagonally ordered mesoporous structure in single-crystal domains of about 100 nm.



Zwitterionic Catalysts

T. A. Betley, J. C. Peters* ___ **2385 – 2389**

Zwitterionic Relatives to the Classic $[(P–P)Rh(solv)_2]^+$ Ions: Neutral Catalysts Active for H–E Bond Additions to Olefins (E = C, Si, B)

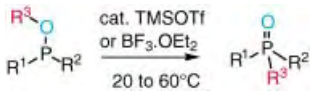


Formally zwitterionic bis(phosphanyl)- and bis(amino)borate rhodium(I) complexes (see picture) can catalytically mediate the hydrogenation, hydroacylation, hydroboration, and hydrosilation of double bonds. These neutral systems are shown to be highly active, even under conditions incompatible with their isostructural, but formally cationic, relatives.

Making Carbon – Phosphorus Bonds

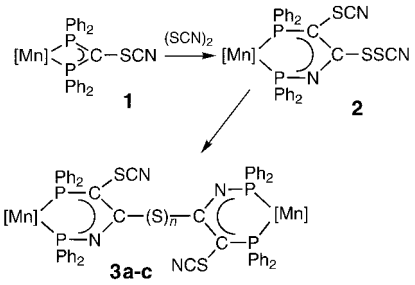
P.-Y. Renard,* P. Vayron, E. Leclerc, A. Valleix, C. Mioskowski* _ **2389 – 2392**

Lewis Acid Catalyzed Room-Temperature Michaelis–Arbuzov Rearrangement



The taming of the shrew! For the first time, a broadly applicable efficient room-temperature Arbuzov rearrangement is described. This reaction is accomplished through an atom-economical Lewis acid catalyzed process (see scheme, TMSOTf = trimethylsilyl trifluoromethanesulfonate). The method has been generalized to primary and activated secondary phosphites, phosphinites, and phosphonites.

 © 2003 Wiley-VCH Verlag GmbH & Co. KGaA, Weinheim

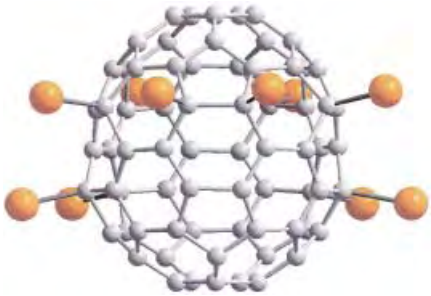


A remarkable lack of cleavage of the S–S bond characterizes the insertion of thiocyanogen into a P–C bond of **1** (see scheme) to afford **2**. Compound **2** is a valuable reagent for the synthesis of new dimetallic polysulfide derivatives (**3a–c**, $n = 2$–4). [Mn] = [Mn(CN*t*Bu)(CO)$_3$].

Thiocyanogen Insertion

J. Ruiz,* R. Quesada, V. Riera, M. Vivanco, S. García-Granda, M. R. Díaz ——— **2392 – 2395**

Insertion of Thiocyanogen into a P–C Bond and Subsequent Formation of Polysulfide Derivatives

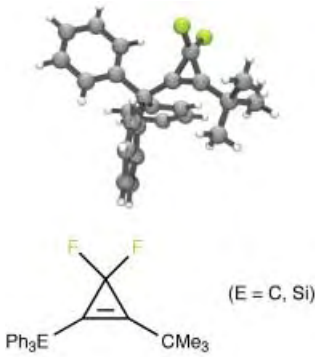


$C_{70}Br_{10}$ is the most stable and, apparently, the only product of the C_{70} bromination in pure bromine and in solution in *o*-dichlorobenzene. In accordance with the quantum chemical calculations, the ten bromine atoms (orange) form a belt in the equatorial region of the C_{70} molecule, with nine adjacent pairs of Br atoms located at the 1,4-positions and one pair at the 1,2-position.

Bromination of C_{70}: $C_{70}Br_{10}$

S. I. Troyanov,* A. A. Popov, N. I. Denisenko, O. V. Boltalina,* L. N. Sidorov, E. Kemnitz ——— **2395 – 2398**

The First X-ray Crystal Structures of Halogenated [70]Fullerene: $C_{70}Br_{10}$ and $C_{70}Br_{10}\cdot 3\,Br_2$

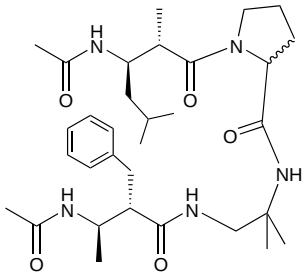


The end is in sight for the use of difluorocarbene (generated from toxic or inconvenient heavy-metal or gaseous reagents) in the preparation of geminal difluorocyclopropenyl compounds. A series of fluorinated alkynes now serve as precursors to these important small-ring systems (e.g. see picture) through a remarkably facile and convenient transformation initiated by *tert*-butyllithium.

Difluorocyclopropenes

A. K. Brisdon,* I. R. Crossley, K. R. Flower, R. G. Pritchard, J. E. Warren **2399 – 2401**

Ringing the Changes: A Remarkable Carbene-Free Synthesis of Difluorocyclopropenes



Diamine-linked *syn*-α,β-dialkyl β-amino acid residues (see picture) have been shown to exhibit parallel sheet secondary structure. Adoption of the parallel hairpin folding pattern is less strongly influenced by linker stereochemistry than for similar parallel hairpins in analogous α-peptide systems.

Foldamer Structure

J. M. Langenhan, I. A. Guzei, S. H. Gellman* ——— **2402 – 2405**

Parallel Sheet Secondary Structure in β-Peptides

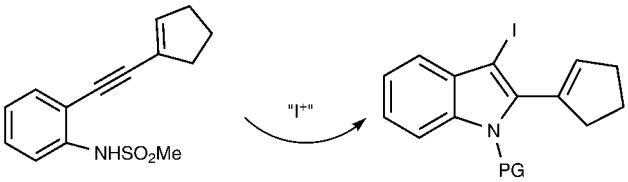
 © 2003 Wiley-VCH Verlag GmbH & Co. KGaA, Weinheim

Contents

Iodoindole Synthesis

J. Barluenga,* M. Trincado, E. Rubio, J. M. González ——— **2406 – 2409**

IPy_2BF_4-Promoted Intramolecular Addition of Masked and Unmasked Anilines to Alkynes: Direct Assembly of 3-Iodoindole Cores

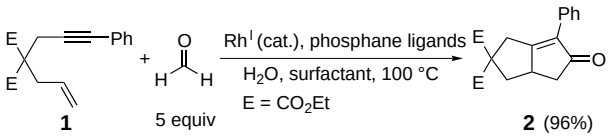


All at once! Indoles can be assembled and iodinated in a one-pot process (see scheme) from anilines and their derivatives. This metal-free addition of nitrogen compounds to alkynes is a clean reaction that is promoted by iodonium cations. Such a process provides a general pathway towards utilization of the biologically relevant indole core.

Dual Catalysis

K. Fuji, T. Morimoto,* K. Tsutsumi, K. Kakiuchi* ——— **2409 – 2411**

Aqueous Catalytic Pauson–Khand-Type Reactions of Enynes with Formaldehyde: Transfer Carbonylation Involving an Aqueous Decarbonylation and a Micellar Carbonylation

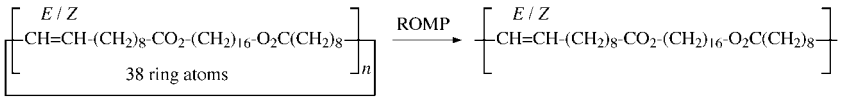


One rhodium(I) complex catalyzes two processes in an overall Pauson–Khand-type reaction of enynes such as **1** with formaldehyde in an aqueous medium to give bicyclic cyclopentenones such as **2** in excellent yields. The use of a water-soluble phosphane ligand in conjunction with a hydrophobic phosphane ligand in the presence of a surfactant promotes the decarbonylation of formaldehyde in the aqueous phase and the carbonylation of enynes in the micellar phase.

Macrocycle Polymerization

P. Hodge,* S. D. Kamau ——— **2412 – 2414**

Entropically Driven Ring-Opening-Metathesis Polymerization of Macrocyclic Olefins with 21–84 Ring Atoms



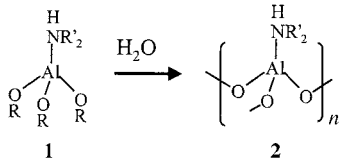
Giant rings make neat monomers: Macrocyclic olefins with up to 84, and possibly even more, ring atoms undergo ring-opening-metathesis polymerization (ROMP) to give high-molecular-weight polymers when the monomer is used neat or at very high concentration (see scheme). This type of ROMP is driven by entropy changes, unlike standard ROMP, which is carried out using strained cyclic monomers and is driven by the enthalpy change of the reaction.

Modified Aluminum Oxide

A. I. Kozlov, M. C. Kung,* W. M. Xue, H. H. Kung* ——— **2415 – 2418**

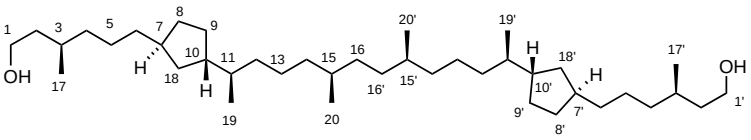
A "Soft-Chemical" Method To Synthesize Lewis Acid Surfaces of Aluminum Oxide

Stoichiometric hydrolysis of the monomeric adduct **1** formed from an amine and aluminum *tert*-butoxide provides aluminum oxide **2** with a high density of Lewis acidic Al surface ions and few hydroxy groups. The amine acts as a protection agent for the coordination site of Al. After the formation of the solid, the amine can be exchanged readily with other



Lewis bases, and the surface Al ions that the amine is coordinated to are catalytically active Lewis acid sites.

 © 2003 Wiley-VCH Verlag GmbH & Co. KGaA, Weinheim



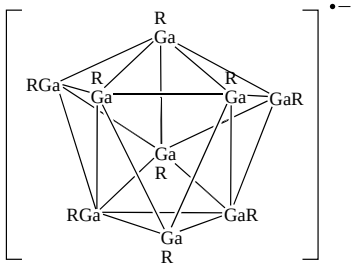
1

Archaea *Membrane Lipids*

E. Montenegro, B. Gabler, G. Paradies, M. Seemann, G. Helmchen* ——— **2419 – 2421**

Determination of the Configuration of an *Archaea* Membrane Lipid Containing Cyclopentane Rings by Total Synthesis

The fat controller: Thermoacidophilic *Archaea* possess membranes containing lipids consisting of mixtures of macrocyclic, 72-membered tetraethers composed of saturated isoprenoid chains linked to glycerol or higher sugars. Lipids of this type form highly stable liposomes and, therefore, are of commercial interest. The configurations of lipids containing cyclopentane units have now been determined by total synthesis of the diol **1**.

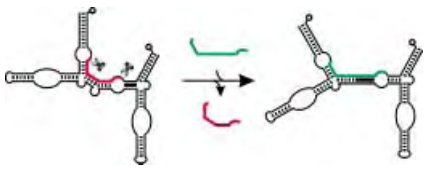


Reduction of a Gallium Cluster

W. Uhl,* L. Cuypers, W. Kaim, B. Schwederski, R. Koch ——— **2422 – 2423**

$[Ga_9(CMe_3)_9]^{\bullet-}$—A Persistent Cluster Radical Anion: Boron-Analogous Chemistry with the Heavier Homologue Gallium

Family resemblance: While the cluster chemistry of gallium generally proved to be quite different from that of the polyboranes or polyborates, the transfer of one electron to the nonagallium cluster $Ga_9(CMe_3)_9$ and the formation of its persistent radical anion emphasizes (see formula R = *t*Bu) the close relationship between gallium and boron. The reduction results in a considerable alteration of structural parameters, with the compression of the cluster parallel to its threefold rotation axis.



RNA Repair

R. Welz, K. Bossmann, C. Klug, C. Schmidt, H.-J. Fritz, S. Müller* ——— **2424 – 2427**

Site-Directed Alteration of RNA Sequence Mediated by an Engineered Twin Ribozyme

Repair of deletion mutations at the RNA level: A small synthetic twin ribozyme supports the insertion of four additional nucleotides into a predefined site of an arbitrarily chosen substrate RNA (see scheme). This method of RNA repair constitutes a novel approach to the therapy of medically relevant mutations.

Communications labeled with this symbol have been judged by two referees as being "very important papers".

The publication of Communications labeled with this symbol has been accelerated because of their topical or highly competitive nature.

The issues for May 2003 appeared online on the following dates
Issue 17: April 30. · Issue 18: May 8. · Issue 19: May 14. · Issue 20: May 21

 © 2003 Wiley-VCH Verlag GmbH & Co. KGaA, Weinheim

Sources

Product and Company Directory

You can start the entry for your company in "Sources" in any issue of *Angewandte Chemie*.

If you would like more information, please do not hesitate to contact us.

Wiley-VCH Verlag – Advertising Department
Tel.: 0 62 01 - 60 65 65
Fax: 0 62 01 - 60 65 50
E-Mail: MSchulz@wiley-vch.de

Service

Keywords ____ *2428*

Authors ____ *2429*

Vacancies ____ *2328, 2329*

Preview ____ *2431*



WILEY-VCH publishes for the scientific community, scientific societies and students worldwide. Our products are developed to anticipate and fulfill the needs of these users. Whether in print or online: we find the most effective medium, market expertise and cutting-edge content for specialized and interdisciplinary communities – world-wide.

Our successful chemistry publishing division, to which *Angewandte Chemie* and the family of European chemistry journals belong, is looking for

Chemists

as **Assistant Editors** to start as soon as possible.

Your responsibilities will include, in addition to supporting the associate and deputy editors:

- The formal assessment of manuscripts
- The processing of manuscripts from electronic coding to editing
- The control of page proofs

As our ideal candidate you have successfully completed a chemistry degree, have English as your first language and a good knowledge of German. You are experienced in using MS Office software and have a keen eye for detail. In addition you have good team and communication skills, as well as plenty of drive and enthusiasm.

Does this sound like you?
Then apply to:

WILEY-VCH Verlag GmbH & Co KGaA
Human Resources, Christiane Rabe
Boschstrasse 12
69451 Weinheim
Germany

Tel.: +49 6201 606-141
e-mail: *Crabe@wiley-vch.de*

WILEY-VCH

The place to be

http://www.wiley-vch.de

 © 2003 Wiley-VCH Verlag GmbH & Co. KGaA, Weinheim

Control of Chemical Reactivity

Conformation-Selective Laser Chemistry

*Martin Goez**

Keywords:
conformers · laser chemistry · molecular dynamics · photochemistry · rearrangement

Complete control over a chemical reaction is a fundamental challenge. To all probability, this will never be possible with thermal activation, for which the energy is distributed statistically among the different degrees of freedom of a molecule. Photochemical excitation, however, deposits energy much more selectively in a molecule, and can in principle be used to activate one particular bond only.

The ultimate strategy for completely specific photochemistry will most likely involve tailored multipulse laser methods operating on very short time scales:[1] After a particular point on an energy hypersurface has been reached by the action of a pulse, the wave function evolves under the influence of the Hamiltonian operator; if the details of this evolution are understood, delays and further excitations can be appropriately combined until a point on a hypersurface is reached, for which the desired reaction channel is open while all undesired ones are blocked.

At present, implementations of this strategy are still in their initial stages, although great progress has been made[2] and the approach certainly seems viable and highly promising. An extremely simplified variant is the use of (not necessarily very short) double pulses, the first of which prepares or selects a particular conformer from a pool of thermally available configurations, and the second initiates a chemical transformation; if different conformations lead to different products, selection of a conformer is equivalent to selection of a product. The potentially most serious limitation of this approach is that electronic excitation is often accompanied by rovibronic transitions, so one has to make sure that the reaction pulse does not undo the effect of the selection pulse by inducing unwanted conformational changes.

The first example is the selective generation of either the 2-propyl cation or corner-protonated cyclopropane from 1-iodopropane in a molecular beam.[3] Initially, the substrate is present as a mixture of two conformers, *anti* and *gauche*. Radical cations $C_3H_7I^{\bullet+}$ are obtained by resonant ionization in the vacuum ultraviolet (ca. 134 nm). Selective ionization is possible because the resonant transitions differ by 0.32 nm for the two conformers; hence, the application of a suitably tuned selection pulse produces $C_3H_7I^{\bullet+}$ either in the *anti* or in the *gauche* conformation. The resonant ionization is not accompanied by rotational transitions and generates the desired conformer of $C_3H_7I^{\bullet+}$ in a pure form. An interconversion of conformers is impossible during the short delay before the reaction pulse (100 ns) because of the low collision frequency (pressure $< 10^{-7}$ Torr) and rotational temperature (about 35 K) in the molecular beam. A reaction pulse of variable wavelength (480–700 nm) in the visible region then excites the radical cation to its first electronically excited state. As the latter is repulsive with respect to the C–I bond, dissociation to give a $C_3H_7^+$ carbocation and an iodine atom immediately occurs, thus precluding any conformational changes before cleavage of the bond.

The average kinetic-energy release $\langle T \rangle$ of the $C_3H_7^+$ fragment was determined by time-of-flight mass spectrometry (by evaluating the distribution of the times of flight when the laser polarization angle was set to 54.7° to avoid anisotropy effects). Plots of $\langle T \rangle$ as function of the photon energy gave straight lines in both cases so extrapolation to the point of intersection with the line $\langle T \rangle = 0$ yielded the threshold energy E_{th} for dissociation of the respective conformer. The E_{th} values were found to differ by 0.3 eV (*gauche* 1.3 eV, *anti* 1.6 eV). As this difference is 20 times higher than the energy difference of the two conformers of $C_3H_7I^{\bullet+}$, and as no evidence for a superposition of components was observed, the most natural conclusion is that each conformer possesses a unique pathway of dissociation, and that the products formed differ by 0.3 eV in their heats of formation.

Thermodynamic calculations gave a very simple explanation: assuming that the iodine atom is formed in its $^2P_{3/2}$ state, the computed reaction enthalpies for the dissociations [Eqs. (1) and (2)] closely reflect the experimentally observed values.

$$gauche\text{-}C_3H_7I^{\bullet+} + 1.40\,eV \xrightarrow{-I(^2P_{3/2})} 2\text{-}C_3H_7^+ \quad (1)$$

$$anti\text{-}C_3H_7I^{\bullet+} + 1.72\,eV \xrightarrow{-I(^2P_{3/2})} cyclo\text{-}C_3H_7^+ \quad (2)$$

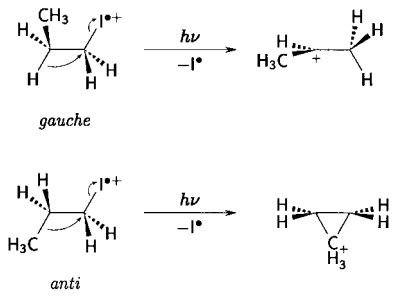
No such agreement can be reached for the $^2P_{1/2}$ state of the halogen, nor for formation of the 1-propyl cation, which is, in any case, known not to be a stable gas-phase species.

This picture was complemented by a high-level (CIS, single excitation configuration interaction) quantum-mechanical study of the reaction paths, which indicates that the group occupying the position *anti* with respect to the iodine

[*] Prof. Dr. M. Goez
Fachbereich Chemie
Martin-Luther-Universität Halle-Wittenberg
Kurt-Mothes-Strasse 2, 06120 Halle/Saale (Germany)
Fax: (+49) 345-55-27345
E-mail: goez@chemie.uni-halle.de

 © 2003 Wiley-VCH Verlag GmbH & Co. KGaA, Weinheim DOI: 10.1002/anie.200201626

atom assists in an S_N2-like manner during the cleavage of the C–I bond (Scheme 1). Further corroboration was obtained by a study of different iodobutanes, the results of which were consis-



Scheme 1. Cleavage of the C–I bond in the *gauche* and *anti* confomers of the radical cation of iodopropane is assisted by the group positioned *anti* to the iodine atom.

tent with the same type of neighboring group effects.[4] The corner-protonated cyclopropane in the reaction of the *anti* conformer is a known intermediate in 1,2-alkyl shifts of carbocations, that is, in Wagner–Meerwein rearrangements.[5]

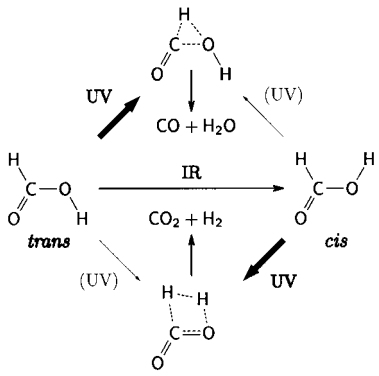
In remarkable contrast to excitation to the first excited state, no conformation specificity was observed when the wavelength of the reaction pulse was decreased to enable higher excited states to be reached: in these cases, dissociation was preceded by internal conversion to the ground state which was accompanied by interconversion of the conformations.[6]

While the information obtained about the product structures is inherently indirect with these gas-phase experiments, as a result of the detection principle, direct determinations were possible in the second, recently reported, example of conformation-selective laser chemistry,[7] where the substrate was formic acid in the solid state (argon matrix at 8 K), and detection was accomplished by FTIR spectroscopy.

The starting pool of molecules consists of practically the *trans* conformer only because the *cis* conformer has considerably higher energy (21.4 kJ mol^{-1}). The first O-H stretching overtone can be pumped by suitable IR selection pulses (alternately ca. 6930 and ca. 6934 cm^{-1}) which induces transitions between the conformers; when the irradiation intensity is high enough, a steady-state concentration ratio of 1:1 for the two conformers can be attained. Relaxation of *cis* formic acid to the *trans* conformer is not competitive because it occurs on a time scale of minutes under these conditions.

A reaction pulse of 193 nm excites the molecule to a repulsive electronic state, which again leads to instantaneous scission without prior equilibration of the conformations. There are three photodissociation channels: the excited formic acid can cleave to give $CO + H_2O$, $CO_2 + H_2$, or $HOC^{\bullet} + {}^{\bullet}OH$. The third possibility was not observed in these solid-state experiments, but the other two did occur, as observed by detection of the IR signals of CO and CO_2. Quantitative evaluation of the IR spectra showed that the CO_2/CO product ratio is about 0.2:1 for the *trans* conformer and about 2.6:1 for the *cis* conformer. Thus, quite clearly, cleavage of formic acid is conformation-selective. Scheme 2 sums up the findings, including the computed geometry of the transition states for the two dissociation channels.

The reason for the observed conformation selectivity or even specificity in the two examples seems to be that the preferred reaction channel is the one involving the least motion of the atoms (compare Schemes 1 and 2). This result is not surprising in view of the Hammond postulate. Although this postulate is usually taught and applied today in such a formulation as to allow a decision whether a transition state is reactant-like or product-like, Hammond's original wording, almost half a century ago, was much more general: "If two states … occur consecutively during a reaction



Scheme 2. Observed reaction channels for the photodissociation of formic acid.

process and have nearly the same energy content, their interconversion will involve only a small reorganization of molecular structure."[8] By reversing this argument, it is clear that, given alternative reaction pathways, the transition state needing the smallest structural change should be easiest to reach. For this reason, it is to be expected that many other photochemical reactions, either in the gas phase or in condensed media, could be controlled by conformation-selective laser chemistry in a similar manner as described.

[1] N. E. Henriksen, *Chem. Soc. Rev.* **2002**, *31*, 37–42, and references therein.
[2] T. Brixner, N. H. Damrauer, G. Gerber, *Adv. At. Mol. Opt. Phys.* **2001**, *46*, 1–54.
[3] S. T. Park, S. K. Kim, M. S. Kim, *Nature* **2002**, *415*, 306–308.
[4] S. T. Park, M. S. Kim, *J. Am. Chem. Soc.* **2002**, *124*, 7614–7621.
[5] M. Saunders, P. Vogel, E. L. Hagen, J. Rosenfeld, *Acc. Chem. Res.* **1973**, *6*, 53–59.
[6] S. T. Park, M. S. Kim, *J. Chem. Phys.* **2002**, *117*, 124–131.
[7] L. Khriachtchev, E. Maçôas, M. Pettersson, M. Räsänen, *J. Am. Chem. Soc.* **2002**, *124*, 10994–10995.
[8] G. S. Hammond, *J. Am. Chem. Soc.* **1955**, *77*, 334–338.

 © 2003 Wiley-VCH Verlag GmbH & Co. KGaA, Weinheim

Ketene Synthesis and Reactions

Ketenes in Polymer-Assisted Synthesis

*Adel Rafai Far**

Keywords:
combinatorial chemistry · heterocycles · reactive intermediates · solid-phase chemistry · synthesis design

Since its inception, ketene chemistry has developed into a unique and well-established source of useful transformations for conventional synthetic organic chemistry. It is, therefore, not surprising that soon after their movement from the realm of peptide and peptoid libraries to that of small molecules, combinatorial chemists have sought the benefits of ketene chemistry to satisfy their own synthetic needs. The ability of these versatile molecules to undergo reactions with nucleophiles, and to participate in cycloadditions and cyclocondensations, has been utilized for the preparation of diverse heterocyclic compounds, and has added to the advantages of polymer-assisted synthesis for rapid purification. Different types of ketenes and different methods for their generation have been involved, which illustrates the potential diversity of the chemistry. There is now a better grasp of the effect of the fragility of these sometimes transient molecules on the reactions involving solid supports, and this augurs well for the application of some of the more recent developments in ketene chemistry to the generation of small-molecule libraries.

1. Introduction

Since the report of the preparation of diphenylketene by Staudinger in 1905, ketene chemistry has consistently mirrored the progress in organic chemistry.[1] In fact, the unique ability of these sensitive and generally transient molecules to undergo [2+2] cycloadditions often gives ketenes a place of their own in organic synthesis.[2]

With the mainstreaming of combinatorial chemistry, matrix-assisted synthetic protocols have become precious commodities.[3] The necessity to deliver efficient methods in the preparation of structurally diverse molecules on supports has shed new light on the particularities of ketene chemistry, especially as the interests of combinatorial chemists has grown to include libraries of small molecules.

[*] Dr. A. Rafai Far
GlycoDesign Inc.
480 University Avenue
Toronto, ON M5G 1V2 (Canada)
Fax: (+1) 416-593-8988
E-mail: afar@glycodesign.com

1.1. On the Application of Ketene Chemistry to Supported Synthesis

Ketenes possess a typically transient nature: They react with electrophiles, nucleophiles, and free radicals and hence are sensitive to water and oxygen. In the absence of other possibilities, simple ketenes can dimerize and/or oligomerize. The consequence is that for any reagent to react with ketenes, the rate of the reaction must be faster than, or at least competitive with, the rates of ketene decomposition pathways.

In principle, the use of supports would permit any of these reactions to be driven to completion with a large excess of the desired ketene. In practice, however, what is often seen, especially with the insoluble supports, is a slowdown in the rates of the desired reactions, which results from the need for the reactions to occur across two phases.[4] This slowdown can drastically impede product formation, which consequently becomes negligible.

In this respect, reactive supported reagents are generally the best choice in polymer-assisted syntheses involving ketenes. Less reactive reagents might be compensated for by the use of soluble supports and/or more stable dialkyl or silyl ketenes. Fortunately, these limitations to the transposition of ketene chemistry from solution to solid supports have not prevented the use of these highly versatile molecules in polymer-assisted synthesis.

 © 2003 Wiley-VCH Verlag GmbH & Co. KGaA, Weinheim DOI: 10.1002/anie.200201594

2. Reactions of Ketenes with Polymer-Bound Reagents

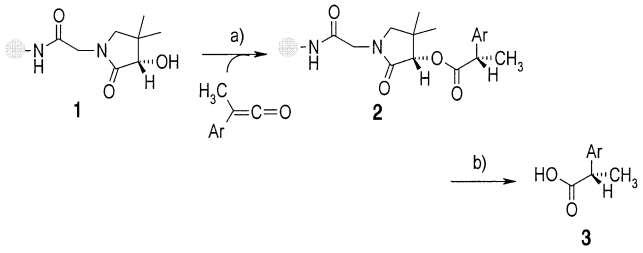
The addition of ketenes to the support is, in practice, the ideal case scenario, as a large excess of these sensitive reagents can be used to drive the reaction to completion. There are numerous examples of the involvement of ketenes in polymer-assisted synthesis, and these can be classified according to the method of generation of these transient compounds.

2.1. Dehydrohalogenation of Acid Halides

2.1.1. Esterification

The generation of ketenes from an acid halide by the base-mediated elimination of a hydrogen halide is perhaps the most simple and common approach. In fact, the sequence of the conversion of an acid to a ketene from the acid chloride and the subsequent reaction with a chiral alcohol is one of the oldest stereoselective reactions, and permits the origin of the stereochemistry to occur at the α position of the acid derivative.[5]

This approach was transposed to a solid-supported chiral alcohol **1** (Scheme 1).[6] This alcohol was treated with a aryl methyl ketene to generate an ester **2**, which can in turn be saponified to generate the chiral acid **3** in very high yield (>99%) and decent enantiomeric purity (*ee* > 80%). The saponification also releases the polymer-bound chiral alcohol, which can be recycled without loss of efficacy.



Scheme 1. a) Et_3N, THF; b) LiOH, H_2O, THF. Ar = aryl.

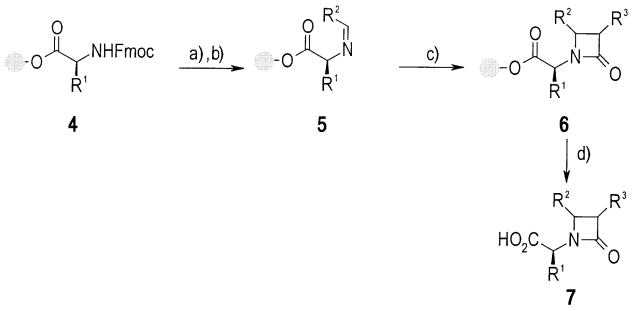


Adel Rafai Far, born in Iran in 1972, received a B.Sc. in biochemistry from McGill University. After gaining an M.Sc. with Prof. T. H. Chan at the same institution, he joined Prof. T. T. Tidwell (Univ. of Toronto) to prepare and study polymer-bound ketenes and allenes, receiving his Ph.D. in 2000. Postdoctoral research with Prof. J. Rebek, Jr. (Scripps, La Jolla) focussed on immobilization of large host molecules on polymer supports. In 2002, he joined GlycoDesign Inc., who develop proprietary drugs for cancer treatment and prevention of cardiovascular and chronic inflammatory diseases.

2.1.2. The Staudinger Reaction

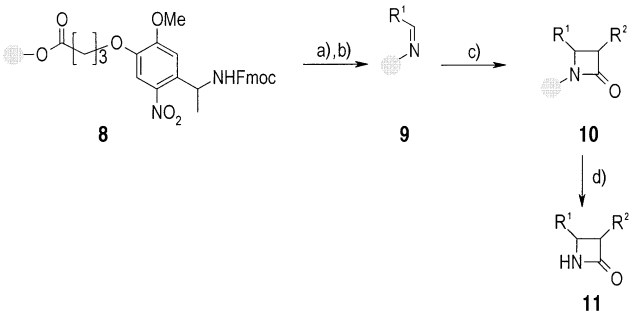
Given the importance of β-lactams to medicinal chemistry, it is not surprising that the Staudinger reaction has found a variety of uses in polymer-assisted synthesis. Perhaps one of the cornerstones of ketene chemistry, this reaction is the [2+2] cycloaddition of a ketene, generated in situ from an acid chloride and an amine base, with an imine to afford a β-lactam.[7]

In a seminal paper, Gallop and co-workers used sasrin, preloaded with an Fmoc-protected (Fmoc = 9-fluorenylmethoxycarbonyl) amino acid, as the starting material **4** (Scheme 2).[8] After deprotection, the resin yields a free



Scheme 2. a) 30% Piperidine in NMP; b) R^2CHO, $HC(OMe)_3$, CH_2Cl_2; c) R^3CH_2COCl, Et_3N, CH_2Cl_2; d) 3% CF_3COOH in CH_2Cl_2. NMP = *N*-methylpyrollidone. R^1 = alkyl, R^2 = alkyl, aryl, R^3 = alkyl, O-alkyl, O-aryl, *N*-phthalimidoyl.

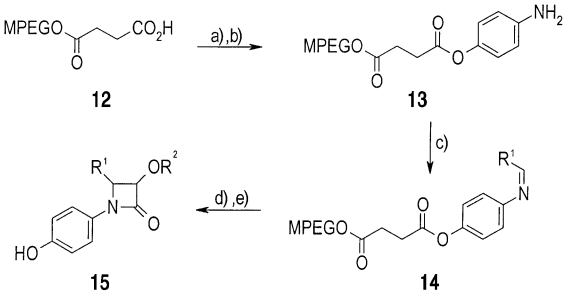
primary amine, which can be reacted with aldehydes, in the presence of trimethyl orthoformate as a desiccant, to afford the desired polymer-bound imines **5**. These, in turn, were treated with an acid chloride in the presence of triethylamine to produce the polymer-supported β-lactams **6**, which were liberated from the resin in good yields (58–97%) by treatment with CF_3COOH. The polymer-bound lactams can be further derivatized by Suzuki and Heck coupling reactions, upon selection of properly functionalized aldehydes, to form the imines.[9] The lesser substituted parent β-lactams **11** can be produced similarly through the use of the photolabile TentaGel B resin (**8**, Scheme 3).



Scheme 3. a) 30% Piperidine in NMP; b) R^1CHO, $HC(OMe)_3$, CH_2Cl_2; c) R^2CH_2COCl, Et_3N, CH_2Cl_2; d) *hν* (365 nm), DMSO. R^1 = alkyl, alkenyl, R^2 = *N*-phthalimidoyl.

 © 2003 Wiley-VCH Verlag GmbH & Co. KGaA, Weinheim

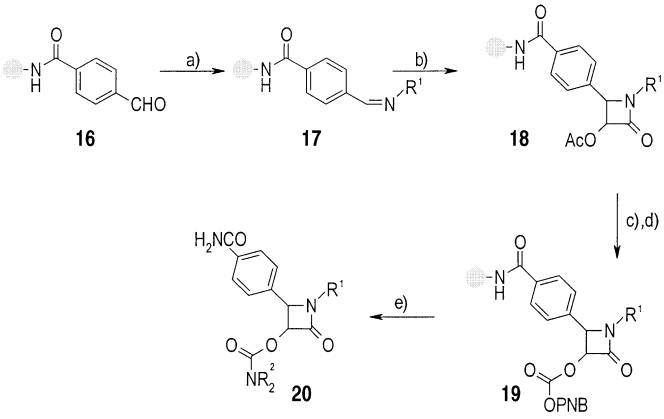
The stereochemical selectivity of this procedure, through the effect of chiral ketenes and chiral imines was also investigated.[10] In both cases only *cis* diasteromers were observed. The diastereoselectivities of the β-lactams produced were in a range of 8:1 to greater than 25:1 when using a ketene bearing a chiral oxazolidinone moiety, and a range of 2:1 to greater than 25:1 when using chiral aldehydes to form the imines. This method for preparing β-lactams has been extended to the use of poly(ethylene glycol) monomethyl ether (MPEGOH, $M_W = 5000\ g\,mol^{-1}$) as a soluble support (Scheme 4).[11]



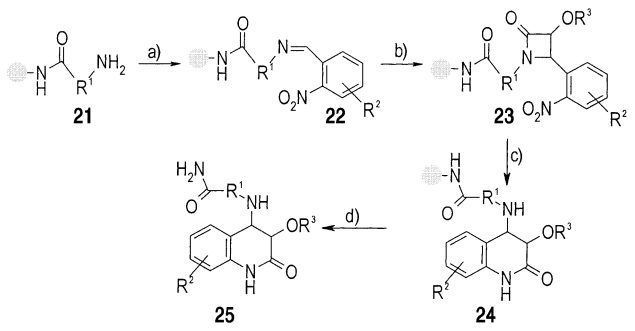
Scheme 4. a) 4-CbzNH(C_6H_4)OH, DCC, DMAP; b) H_2, Pd/C; c) R^1CHO, 90 °C; d) R^2OCH_2COCl, R_3N, CH_2Cl_2; e) H_2SO_4, MeOH, 60 °C. Cbz = carbobenzoxy, DCC = dicyclohexyl carbodiimide, DMAP = 4-dimethylaminopyridine. R^1 = alkyl, aryl, R^2 = benzyl, phenyl.

In all of the previous examples, the imine intermediate was generated from a polymer-bound amine, but it may also be generated from a polymer-bound aldehyde **16** (Scheme 5).[12] In this case acetoxyketene was used, and this allowed further modifications to give the carbamate products **20**. This approach also exclusively produces the *cis*-diastereomers of the lactams. This chemistry was extrapolated to the synthesis of enantiomerically enriched β-lactams starting from a polymer-bound version of Garner's aldehyde.[13]

β-Lactams are not only interesting as final targets but can also be used as interesting intermediates towards the preparation of other products. This was demonstrated by using substituted *o*-nitrobenzaldehydes in the preparation of imines **22** (Scheme 6), bound to a 4-methylbenzhydrylamine hydrochloride (MBHA) resin.[14] After formation of the β-lactams **23**, the nitro groups are reduced by tin(II) chloride and the resulting anilines open the four-membered ring to give, after cleavage from the resin, dihydroquinolinones **25** in excellent yields (68–100 %) and greater than 85 % purity.



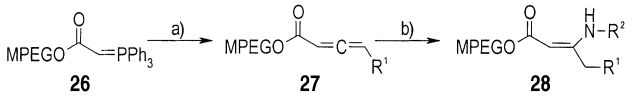
Scheme 5. a) R^1NH_2, 4 Å molecular sieves or $CH(OCH_3)_3$; b) $AcOCH_2COCl$, Et_3N, CH_2Cl_2; c) K_2CO_3, MeOH, CH_2Cl_2; d) *p*-nitrophenylchloroformate, DIPEA, CH_2Cl_2; e) R^2_2NH, CH_2Cl_2; f) 3 % CF_3COOH, CH_2Cl_2. DIPEA = *N*,*N*-diisopropylethylamine; PNB = *p*-nitrophenyl. R^1 = aryl, alkyl, R^2 = alkyl.



Scheme 6. a) Substituted *o*-nitrobenzaldehyde, Na_2SO_4, CH_2Cl_2; b) R^3OCH_2COCl, Et_3N, CH_2Cl_2; c) $SnCl_2$, DMF; d) HF/anisole (95:5). R^1 = arylene, alkanediyl, R^2 = O-alkyl, halogen, R^3 = aryl, acetyl.

2.1.3. *Reaction with Wittig Reagents*

The reaction of ketenes with stabilized Wittig reagents is a well-known and efficient method for the generation of allenes. The lack of reactivity of stabilized Wittig reagents on insoluble polymeric supports is, unfortunately, extremely detrimental to this reaction. However when MPEGOH is used as a soluble support, this becomes a very efficient way of generating polymer-bound allenecarboxylates **27** (Scheme 7).[15] These can, in turn, be used to generate polymer-bound enamines **28**, a class of reagents that are central to the preparation of heterocyclic compounds.

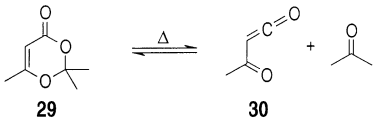


Scheme 7. a) R^1CH_2COCl, Et_3N, CH_2Cl_2; b) R^2NH_2, CH_2Cl_2. R^1 = aryl, acetyl, R^2 = alkyl.

2.2. *Thermal Decomposition of Ketene Precursors*

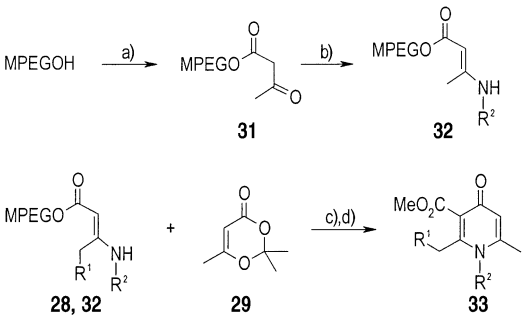
2.2.1. *4H-1,3-Dioxin-4-ones*

The retro-Diels–Alder-like thermal decomposition of 2,2,6-trimethyl-4*H*-1,3-dioxin-4-one (diketene acetone adduct **29**) efficiently generates acetyl ketene (**30**) [Eq. (1)].[16]



(1)

 © 2003 Wiley-VCH Verlag GmbH & Co. KGaA, Weinheim

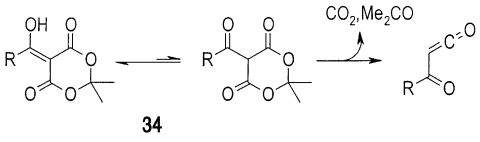


Scheme 8. a) **29**, PhMe, 130 °C (bath temperature); b) R^2NH_2, $HC(OCH_3)_3$, CH_2Cl_2; c) PhMe, 130 °C (bath temperature), repeat; d) KCN, MeOH, DMF, 60 °C. R^1 = alkyl, aryl, R^2 = alkyl.

Acetyl ketene (**30**) can then be trapped by MPEGOH to yield the parent acetoacetate **31**, which can, in turn, yield enamines **32** by treatment with primary amines in the presence of a dessicant (Scheme 8).[17] Acetyl ketene can also undergo cyclocondensation with enamines **28** or **32** to give 4-pyridones **33**.[15,17]

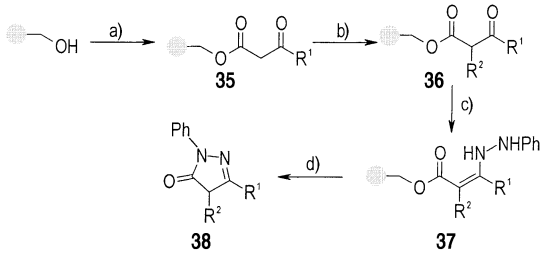
2.2.2. *Acylated Meldrum's Acid*

Meldrum's acid (2,2-dimethyl-1,3-dioxane-4,6-dione) reacts with aliphatic acyl chlorides in the presence of pyridine to give acyl derivative **34**,[18] in high yield, without the use of chromatography. These reagents are excellent sources of acyl ketenes through their thermal decomposition and have gained in popularity as a result of their facile preparation, as opposed to the time-consuming functionalization of 4*H*-1,3-dioxin-4-ones [Eq. (2)]. The ability of these ketenes to react with nucleophiles to give 1,3-dicarbonyl compounds, which are of interest in heterocyclic chemistry, has been widely exploited.

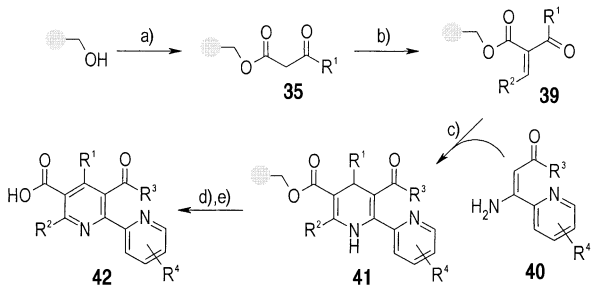


(2)

Acyl Meldrum's acid derivatives have been used in the esterification of hydroxy-functionalized resins.[19,20] The resulting β-ketoesters **35** can then be alkylated and condensed with phenyl hydrazine to give 1-phenylpyrazolones **38** in 52–95 % yield and 85–95 % purity (Scheme 9).[19] Such β-ketoesters **35** can also undergo Knoevenagel reactions with aldehydes, followed by Hantzsch condensations with enamines to give dihydropyridines that can be aromatized prior to cleavage from the resin (Scheme 10).[20] In this particular case, the method was used to generate 2,2′-bipyridines **42** in 47–79 % yield and 70–85 % purity.

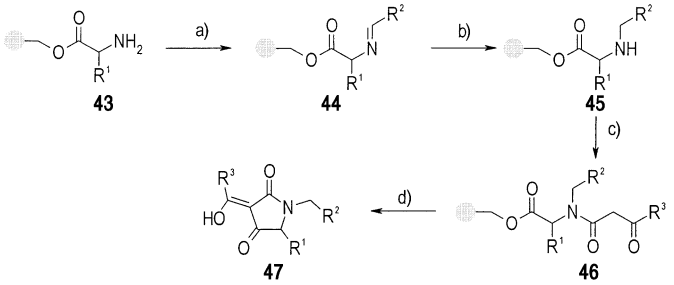


Scheme 9. a) Acyl Meldrum's acid derivative **34**, PhH (at reflux); b) R^2X, TBAF, THF; c) $PhNHNH_2$, THF, $HC(OCH_3)_3$; d) CF_3COOH, MeCN. TBAF = tetrabutylammonium fluoride. R^1, R^2 = alkyl.



Scheme 10. a) Acyl Meldrum's acid derivative **34**, PhMe, 70 °C; b) R^2CHO, piperidine, $HC(OCH_3)_3$, DMF, 65 °C; c) **40**, $HC(OCH_3)_3$, DMF, 80 °C; d) CAN, DMA; e) 3 % CF_3COOH in CH_2Cl_2. CAN = cerium(IV) ammonium nitrate, DMA = dimethylamine. R^1 = aryl, R^2, R^3 = alkyl, R^4 = alkyl, O-alkyl, halogen.

Polymer-bound amines **45** generated from polymer-bound amino acids **43** by reductive amination were also treated with acyl Meldrum's acid derivatives **34**, to give β-ketoamides **46** (Scheme 11)[21,22] that undergo an intramolecular cyclization, accompanied by cleavage from the resin, to give 3-acyltetramic acids **47** (tetramic acid = 2,4-pyrrolidinedione) in mediocre yields (11–61 %), but with excellent purity (80–100 %).

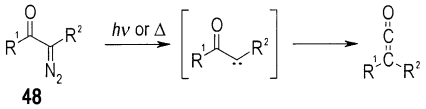


Scheme 11. a) R^2CHO, $HC(OCH_3)_3$, repeat; b) $NaCNBH_3$, DMF, AcOH, repeat; c) acyl Meldrum's acid derivative **34**, PhMe, 120 °C; d) 30 % DIPEA, dioxane, 80 °C. R^1, R^3 = alkyl, R^2 = aryl.

2.3. *Wolff Rearrangements*

Thermal or photochemical Wolff rearrangements are well-known methods for the generation of ketenes. These reactions stem from the decomposition of diazoketones **48** [Eq. (3)].[23]

This approach has been used in the Arndt–Eistert homologation, in which the carbon chain of a carboxylic acid

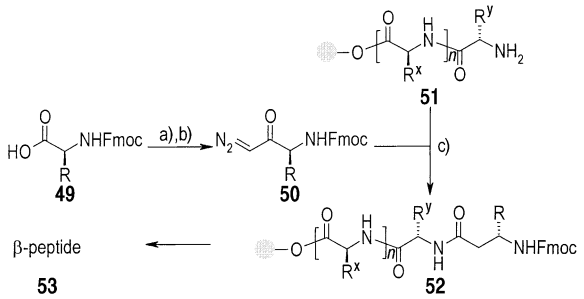


(3)

 © 2003 Wiley-VCH Verlag GmbH & Co. KGaA, Weinheim

is extended by one methylene unit with respect to its parent diazoketone.[24] This method has been applied to the preparation of enantiopure β-amino acid derivatives by extending the skeleton of the parent α-amino acids. Once incorporated into peptides (so-called β-peptides), these amino acids give rise to unusual properties, in particular, a number of very stable secondary structures.[25]

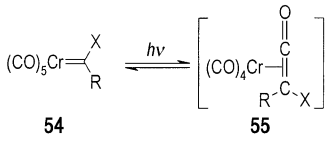
β-Peptides can be generated through conventional peptide coupling methods from the β-amino acids. Alternatively, the preparation can be made directly onto a solid support by the reaction of ketenes, generated through the Wolff rearrangement, and the amino terminal group of the peptide being synthesized using either the Wang resin or the 2-chlorotrityl resin, in the presence of silver benzoate as a mediator (Scheme 12).[26,27] More than one β-amino acid can be incorporated into the peptide by this method, which, in fact, can be made entirely of such amino acids.



Scheme 12. a) *i*BuOCOCl, NMM, THF; b) CH_2N_2, Et_2O; c) AgOBz, NMM, THF, 0 °C. NMM = *N*-methylmorpholine. R^x, R^y = amino acid side chain.

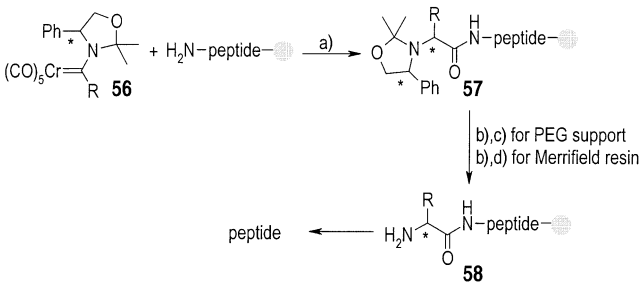
2.4. Photolysis of Chromium Carbene Complexes

The irradiation of chromium carbene complexes **54** is thought to give rise to short-lived chromium–ketene complexes **55**.[28] This complex reverts back to the carbene complex, if it is not otherwise trapped [Eq. (4)].



(4)

When chromium aminocarbene complexes **56** (Scheme 13) posessing a chiral auxiliary were photolyzed in the presence of an amino acid ester, dipeptides were formed in good yields (60–88 %), and with good diastereoselectivity (80–96 %).[29] This methodology allows the introduction of nonproteinogenic (nonnatural) α-amino acids into peptides (Scheme 13). It has been applied to both solid-phase peptide synthesis[30] and to the synthesis of peptides bound to a soluble poly(ethylene glycol) support.[31] Although the moderate yields obtained may be prohibitive in the synthesis of large peptides, it is certainly of interest in drug design, where small peptides are generally the standard.



Scheme 13. a) *hν*, CO (350 KPa), THF; b) 1 N HCl, MeOH or dioxane; c) H_2 (50 psi), $Pd(OH)_2/C$; d) $Pb(OAc)_4$, CH_2Cl_2, MeOH, then 1 N HCl. PEG = poly(ethylene glycol). R = alkyl.

3. Polymer-Bound Ketenes

As mentioned previously, the inherent instability of most ketenes makes them very sensitive substances. This has not prevented investigations on the use of polymer-bound ketenes in the synthesis of small-molecule libraries. Such ketenes belong to two broad categories: reactive ketenes used in intramolecular reactions and stable ketenes used in intermolecular reactions.

3.1. Intramolecular Reactions

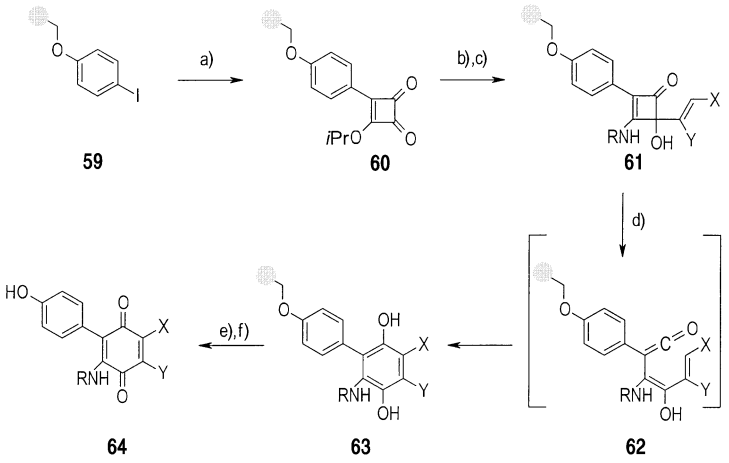
The Smith–Hoehn electrocyclization is a reaction sequence yielding phenols through the formation of a transient dienyl ketene from an appropriately derivatized cyclobutenone. This reaction has been widely exploited in recent years.[32] One such example is the polymer-bound cyclobutenedione **60**, prepared from squaric acid and the 4-iodophenyl ether of the Wang resin (Scheme 14).[33] Upon sequential treatment with an amine and an alkenyl lithium species, compound **60** is converted to the cyclobutenones **61**, which when heated in refluxing toluene undergo an electrocyclic ring-opening to give the polymer-bound ketenes **62**, which concomitantly cyclize to the hydroquinones **63**. Oxidation in air and treatment with CF_3COOH lead to the quinones **64** in rather low yields (0–53 %) after chromatography.

Acylamino ketenes cyclize to form interesting zwitterionic heterocyclic compounds known as münchnones, which possess a typically transient nature as a result of self-condensation. Bilodeau and Cunningham employed the cyclocondensation of münchnones with tosylimines to generate libraries of imidazoles (Scheme 15).[34] The polymer-bound münchnones **68** were generated from the acylated amino acids **66**, through dehydration to ketenes **67**. After the condensation reactions, the polymer-bound imidazoles **69** are freed from the resin in greater than 95 % purity after washing with CF_3COOH (90 % in H_2O) had removed most of the polymer-bound impurities.

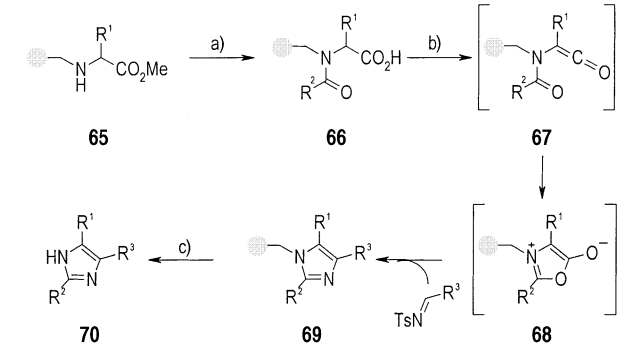
3.2. Stable Polymer-Bound Ketenes

As a result of the reactivity of ketenes, it would not be generally anticipated that polymer-bound ketenes would be

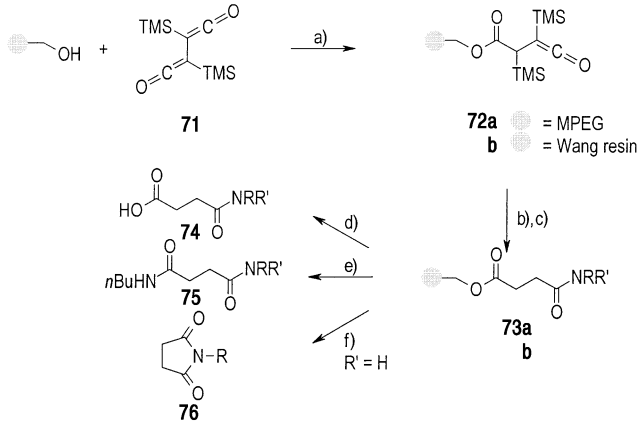
 © 2003 Wiley-VCH Verlag GmbH & Co. KGaA, Weinheim



Scheme 14. a) Isopropyl tributyltin squarate, $[PdCl_2(PPh_3)_2]$, CuI, DMF or *n*BuLi, then diisopropyl squarate, and then HCl in CH_2Cl_2; b) RNH_2, THF, 30 min; c) vinyllithium, −78 °C (X–CH=CH–Y = heterocycle); d) PhMe, reflux; e) air oxidation; f) 20% CF_3COOH in CH_2Cl_2. R = alkyl.



Scheme 15. a) R^2COCl, DIPEA, CH_2Cl_2, then KOH, dioxane/H_2O; b) EDC, CH_2Cl_2, 24–48 h, then R^3CHNTs; c) 90% CF_3COOH, H_2O, 1 h, then AcOH, 100 °C. EDC = 3-(3-dimethylaminopropyl)-1-ethylcarbodiimide. R^1 =, R^2 = aryl, R^3 = 3-, 4-pyridyl.

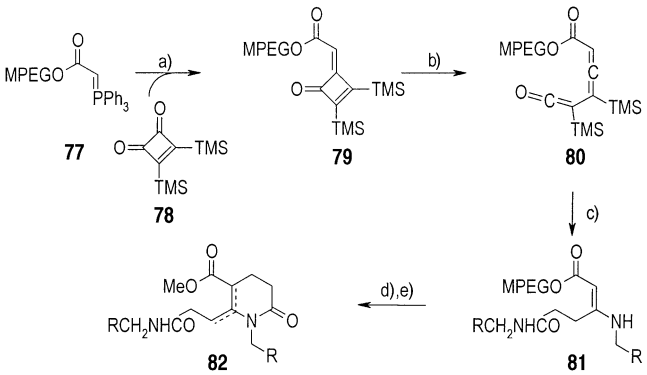


Scheme 16. a) Et_3N, CH_2Cl_2; b) $RR'NH_2$, CH_2Cl_2; c) TBAF, THF, AcOH; d) for **73b**: CF_3COOH, CH_2Cl_2, H_2O; e) for **73a**: *n*$BuNH_2$, PhMe; f) for **73a**: KCN, MeOH, DMF. R =, R′ = aryl, alkyl.

particularly useful, as side reactions are detrimental to the preparation of products of high purity. However, just as for the other less reactive cumulenes, stabilized ketenes may find applications, particularly when involved in reactions with nucleophiles.

In this respect, the particularly stable silylated ketenes were used. Reactions involving a ketenyl moiety of bisketene **71** proceed in a facile fashion; the reactivity of the remaining ketenyl moiety, however, is lower by orders of magnitude.[35] Therefore, the base-mediated reaction of **71** with either MPEGOH or the Wang resin cleanly gives the polymer-bound ketenes **72a** and **b** (Scheme 16).[17,36] These polymer-bound ketenes were used to immobilize amines as their succinamic esters **73**. Following desilylation the amines can be released as their succinamic acids **74**, succinamides **75**, or succinimides **76**. However, their reaction with alcohols is limited by competition with H_2O which, after cleavage, results in the increasing bulk of the alcohol being matched with increasing amounts of succinic anhydride.[36]

This set of experiments proves the viability of polymer-bound silylated ketenes. Such ketenes can also be generated on the polymer directly. For instance, the photochemical ring-opening of methylenecyclobutenones is an efficient method for the generation of allenyl ketenes.[37] Using MPEGOH as a support, the Wittig reagent **77** was treated with 3,4-bis(trimethylsilyl)cyclobut-3-ene-1,2-dione (**78**) to give the polymer-bound methylenecyclobutenone **79** (Scheme 17).[15,36] Photolytic ring-opening gave the stable polymer-bound silylated allenylketene **80**. Treatment of this ketene with an amine gave enamines **81**, which can be used to produce δ-lactams **82** by aza-annulation.



Scheme 17. a) CH_2Cl_2; b) *hν* (350 nm), CH_2Cl_2; c) RCH_2NH_2, CH_2Cl_2; d) acryloyl chloride, imidazole, THF, reflux; e) KCN, MeOH, DMF. R = alkyl.

4. Ketenes in Polymer-Assisted Synthesis

Although solid-phase organic synthesis is an unmatched method for the generation of huge libraries of compounds, it is rather time-consuming to develop. A viable alternative has been the adaptation of soluble substrates using polymer-bound reagents and scavengers.[38] This technique allows all of the conventional analytical tools, such as NMR spectroscopy and TLC, to be used for optimization of the synthetic

 © 2003 Wiley-VCH Verlag GmbH & Co. KGaA, Weinheim

protocol, and therefore reduces the time required for its development.

In an earlier case, the use of stable ketenes for the polymer-assisted preparation of the corresponding enantiomerically enriched acids through the asymmetric esterification of an immobilized chiral alcohol was examined (Scheme 1). A similar approach has been employed, which involved different chiral poly(tertiary amines) derived from cinchona alkaloids, prolinol, ephedrine, and (5*S*)-1-azabicyclo[3.1.0]hexane as catalysts in the esterification of methanol with methyl phenyl ketene to generate methyl 2-phenylpropionate in modest yields.[39]

However, the ketene is generated ideally from polymer-bound reagents and, as we have seen previously, the dehydrohalogenation of acyl halides is probably the most common method of generating reactive ketenes. Lectka and co-workers have devised a method in which a polymer-bound base, used as a packing material for a jacketed column cooled to −78 °C, effects the dehydrohalogenation.[40–43] When a solution of the acid chloride is added to the top of the column, a solution of the ketene percolates at the bottom and can be either trapped by another reagent or eluted through another column packed with a different polymer-bound reagent/scavenger for further transformations (Figure 1).

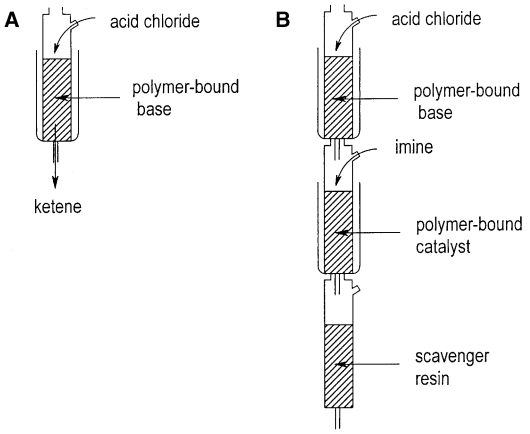
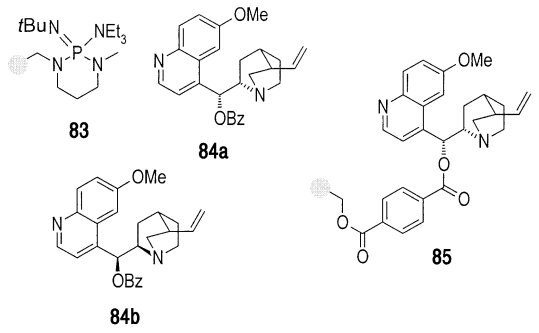
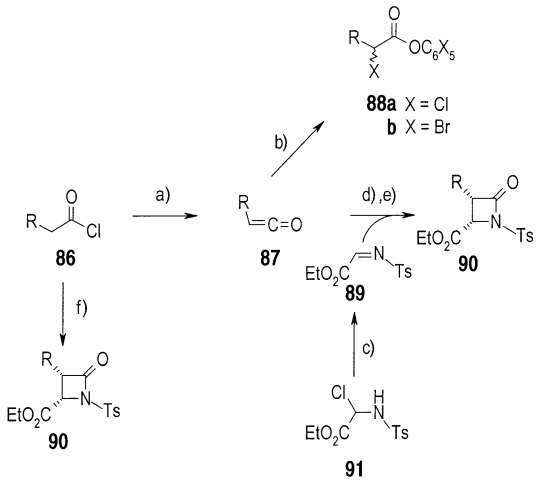


Figure 1. A) Setup for the polymer-mediated generation of ketenes; B) setup for the generation of β-lactams.

The polymer-bound form **83** of the phosphazene base 2-*tert*-butylimino-2-diethylamino-1,3-dimethylperhydro-1,3-diaza-2-phosphorine (BEMP, Scheme 18) is used to affect the dehydrohalogenation, and allows the generation of the ketene solution at −78 °C. This solution can be percolated onto a solution of a perhalocyclohexadienone in the presence of the cinchona alkaloids **84a** or **b** to generate the α-halo ester **88** of the corresponding perhalophenols (Scheme 19) in a stereoselective fashion ($ee \geq 90\,\%$).[40] In order to further extend the methodology to the Staudinger reaction, such ketene solutions can also be passed immediately through a second jacketed column packed with the polymer-bound cinchona alkaloid **85** (with an optimized linker to the resin) while a solution of an imine **89** is concomitantly introduced (Figure 1B).[41,42] The resulting crude β-lactam solution is passed through a final column packed with aminomethylated polystyrene, which serves to scavenge the final impurities. The imine solution can be preformed or can also be generated by passing a solution of the α-chlorosulfonamide **91** through another column packed with a mixture of celite and sodium hydride at −43 °C (Scheme 19).[42] In both cases, yields and stereoselectivities were similar.



Scheme 18. Reagents involved in polymer-assisted synthesis using acyl chlorides to generate ketenes.



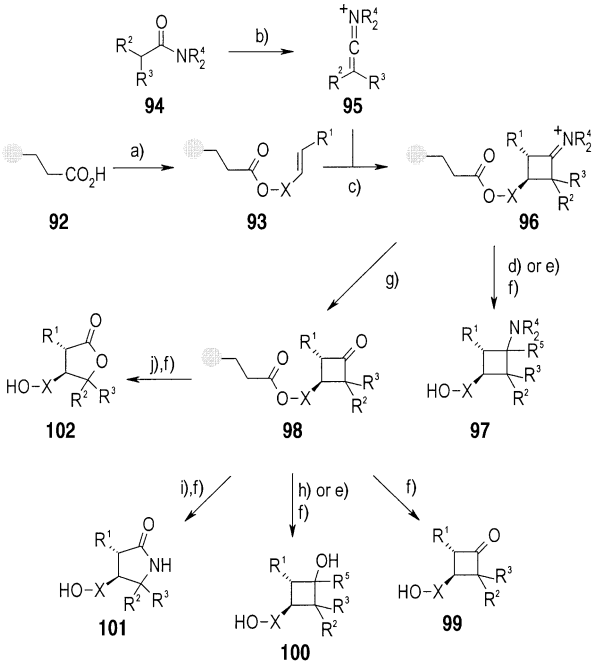
Scheme 19. a) **83**, THF, −78 °C; b) **84a** or **b**, perhalocyclohexadienone, THF, −78 °C; c) NaH, celite, THF, −43 °C; d) **89**, **85**, THF, −43 °C; e) aminomethylated polystyrene, THF; f) **85**, **89**, K_2CO_3 or NaH, THF, −43 °C. R = aryl, alkyl, alkenyl, O-phenyl, O-acetyl, halogen.

Finally, the use of the polymer-bound Cinchona alkaloid **85** as both the nucleophilic catalyst and the base effecting the dehydrohalogenation was investigated.[42,43] This rather precious polymeric reagent was regenerated in situ with K_2CO_3 or sodium hydride in a rather unusual solid-gel shuttle deprotonation between a solid and a gel. Although this β-lactam formation involves a single step, the presence of a regenerating base seems to induce some scrambling in its stereoselectivity. All of the polymers can be recycled by simply eluting washing solutions through the columns, which seems to have only a marginal effect on the reaction results.

 © 2003 Wiley-VCH Verlag GmbH & Co. KGaA, Weinheim

5. Reactions of Ketenimines with Solid Supports

Ketenimines are formally the imines of ketenes, and are generally generated by the dehydration of amides.[44] Ketenimines can be used as alternatives to ketenes in solid-phase synthesis, if the latter are not effective. Hence, whereas ketene–alkene [2+2] cycloadditions have not been reported using solid-phase supports, the corresponding reaction of ketenimines has been investigated (Scheme 20).[45] The reaction of keteniminium salts **95** with polymer-bound alkenes **93**



Scheme 20. a) Unsaturated alcohol, DIC, DMAP, CH_2Cl_2; b) triflic acid, CH_2Cl_2, 2,6-di-*tert*-butylpyridine, −10 °C; c) resin **93**, CH_2Cl_2, reflux; d) $Me_4NHB(OAc)_3$, CH_2Cl_2; e) MeMgCl, THF, −78 °C to −10 °C; f) KOTMS, MeOH, CH_2Cl_2; g) $NaHCO_{3(aq)}$, THF; h) $LiBH_4$, MeOH, THF; i) *o*-mesitylenesulfonylhydroxylamine, CH_2Cl_2; j) mCPBA, CH_2Cl_2. DIC = *N*,*N*′-diisopropylcarbodiimide, KOTMS = potassium trimethysilanolate, mCPBA = *m*-chloroperbenzoic acid. X = arylene, alkanediyl, R^1, R^3 = H, Me, R^2 = H, Me, Ph, R^4 = Me.

gives the desired cyclobutanone iminium salts **96**. Their reduction or treatment with methylmagnesium chloride leads, after release from the resin, to the corresponding cyclobutylamines **97**. On the other hand, hydrolysis leads to the cyclobutanones **98**, which are used as an intermediate in the generation of several scaffolds in a multiple-core combinatorial fashion. These reactions yielded cyclobutanones **99** (two examples), cyclobutanols **100** (six examples), γ-lactams **101** (two examples), and γ-lactones **102** (two examples). In this case, the production of a cyclobutanone, which would be the expected product of a [2+2] cycloaddition of ketenes and alkenes, and which derives from the keteniminium salt, is a demonstration of the correlation between the two species.

6. Summary and Outlook

As we have seen here, polymer-assisted synthesis has greatly benefited from the unique character of ketene chemistry. These versatile reagents have been applied to the preparation of a variety of heterocyclic compounds, and the advantages and limitations of the use of ketenes in the preparation of various small molecules have been fully assessed. The current work augurs well for the use of ketenes to generate diverse libraries. Until now, most attention has been focused on the Staudinger reaction, but the recent developments in ketene chemistry would certainly warrant further extrapolations of these reactions to polymeric supports. This is particularly true of intramolecular ketene reactions,[32] and especially of silylated ketenes, for which the scope and the set of possible reactions has been extended during the last decade.[46,47]

The author expresses his deepest gratitude to Professor Thomas T. Tidwell of the Department of Chemistry at the University of Toronto for useful comments and suggestions, as well as his thorough review of the manuscript.

Received: August 28, 2002
Revised: October 11, 2002 [M1594]

[1] See: T. T. Tidwell, *Ketenes*, Wiley, New York, **1995**, and references therein.
[2] See for example: a) J. A. Hyatt, P. W. Raynolds, *Org. React.* **1994**, *45*, 159–646; b) T. Machiguchi, T. Hasegawa, A. Ishiwata, S. Terashima, S. Yamabe, T. Minato, *J. Am. Chem. Soc.* **1999**, *121*, 4771–4786.
[3] See: a) *Combinatorial Peptide and Nonpeptide Libraries, a Handbook* (Ed.: G. Jung), VCH, Weinheim, **1996**; b) B. A. Bunin, *The Combinatorial Index*, Academic Press, San Diego, **1998**; c) F. Zaragoza Dörwald, *Organic Synthesis on Solid Phase*, Wiley-VCH, Weinheim, **2000**.
[4] For a review on the role of the support: P. Hodge, *Chem. Soc. Rev.* **1997**, *26*, 417–424.
[5] a) H. Pracejus, A. Tille, *Chem. Ber.* **1963**, *96*, 854–865; b) S. Winter, H. Pracejus, *Chem. Ber.* **1966**, *99*, 151–159.
[6] R. Akkari, M. Calmes, N. Mai, M. Rolland, J. Martinez, *J. Org. Chem.* **2001**, *66*, 5859–5865.
[7] C. Palomo, J. M. Aizpurua, I. Ganboa, M. Oiaride, *Eur. J. Org. Chem.* **1999**, 3223–3235.
[8] B. Ruhland, A. Bhandari, E. M. Gordon, M. A. Gallop, *J. Am. Chem. Soc.* **1996**, *118*, 253–254.
[9] B. Ruhland, A. Bombrun, M. A. Gallop, *J. Org. Chem.* **1997**, *62*, 7820–7826.
[10] C. M. L. Delpiccolo, E. G. Mata, *Tetrahedron: Asymmetry* **2002**, *13*, 905–910.
[11] a) V. Molteni, R. Annunziata, M. Cinquini, M. Benaglia, *Tetrahedron Lett.* **1998**, *39*, 1257–1260; b) M. Benaglia, M. Cinquini, F. Cozzi, *Tetrahedron Lett.* **1999**, *40*, 2019–2020; c) R. Annunziata, M. Benaglia, M. Cinquini, F. Cozzi, *Chem. Eur. J.* **2000**, *6*, 133–138.
[12] R. Singh, J. M. Nuss, *Tetrahedron Lett.* **1999**, *40*, 1249–1252.
[13] K. Gordon, M. Bolger, N. Khan, S. Balasubramanian, *Tetrahedron Lett.* **2000**, *41*, 8621–8625.
[14] Y. Pei, R. A. Houghten, J. S. Kiely, *Tetrahedron Lett.* **1997**, *38*, 3349–3352.
[15] A. Rafai Far, T. T. Tidwell, *J. Comb. Chem.* **1999**, *1*, 458–460.

 © 2003 Wiley-VCH Verlag GmbH & Co. KGaA, Weinheim

[16] C. Wentrup, W. Heilmeyer, G. Kollenz, *Synthesis* **1994**, 1219 – 1248.
[17] A. Rafai Far, T. T. Tidwell, *J. Org. Chem.* **1998**, *63*, 8636 – 8637.
[18] Y. Oikawa, K. Sugano, O. Yonemitsu, *J. Org. Chem.* **1978**, *43*, 2087 – 2088.
[19] L. F. Tietze, A. Steinmetz, F. Balkenhohl, *Bioorg. Med. Chem. Lett.* **1997**, *7*, 1303 – 1306.
[20] S. Tadesse, A. Bhandari, M. A. Gallop, *J. Comb. Chem.* **1999**, *1*, 184 – 187.
[21] L. Weber, P. Iaiza, G. Biringer, P. Barbier, *Synlett* **1998**, 1156 – 1158.
[22] S. P. Raillard, G. Ji, A. D. Mann, T. A. Baer, *Org. Process Res. Dev.* **1999**, *3*, 177 – 183.
[23] For a review see: H. Meier, K.-P. Zeller, *Angew. Chem.* **1975**, *87*, 43 – 54; *Angew. Chem. Int. Ed. Engl.* **1975**, *14*, 32 – 43.
[24] See: T. Ye, M. A. McKervey, *Chem. Rev.* **1994**, *94*, 1092 – 1160, and references therein.
[25] a) D. H. Appella, L. A. Christianson, I. L. Karle, D. R. Powell, S. H. Gellman, *J. Am. Chem. Soc.* **1996**, *118*, 13071 – 13072; b) D. Seebach, J. L. Matthews, A. Meden, T. Wessels, C. Baerlocher, L. B. McCusker, *Helv. Chim. Acta* **1997**, *80*, 173 – 182.
[26] R. E. Marti, K. H. Bleicher, K. W. Bair, *Tetrahedron Lett.* **1997**, *38*, 6145 – 6148.
[27] G. Guichard, S. Abele, D. Seebach, *Helv. Chim. Acta* **1998**, *81*, 187 – 206.
[28] For a review: L. S. Hegedus, *Tetrahedron* **1997**, *53*, 4105 – 4128.
[29] J. R. Miller, S. R. Pulley, L. S. Hegedus, S. DeLomabaert, *J. Am. Chem. Soc.* **1992**, *114*, 5602 – 5607.
[30] S. R. Pulley, L. S. Hegedus, *J. Am. Chem. Soc.* **1993**, *115*, 9037 – 9047.
[31] J. Zhu, L. S. Hegedus, *J. Org. Chem.* **1995**, *60*, 5831 – 5837.
[32] L. I. Smith, H. H. Hoehn, *J. Am. Chem. Soc.* **1939**, *61*, 2619-— 2624; L. A. Paquette, *Eur. J. Org. Chem.* **1998**, 1709 – 1728.
[33] P. A. Tempest, R. W. Armstrong, *J. Am. Chem. Soc.* **1997**, *119*, 7607 – 7608.
[34] M. T. Bilodeau, A. M. Cunningham, *J. Org. Chem.* **1998**, *63*, 2800 – 2801.
[35] a) A. D. Allen, T. T. Tidwell, *J. Org. Chem.* **1999**, *64*, 266 – 271; b) A. D. Allen, P. A. Moore, S. Missiha, T. T. Tidwell, *J. Org. Chem.* **1999**, *64*, 4690 – 4696.
[36] A. Rafai Far, PhD thesis, University of Toronto (Canada), **2000**.
[37] W. Huang, T. T. Tidwell, *Synthesis* **2000**, 457 – 470.
[38] a) D. L. Flynn, J. Z. Crich, R. V. Devraj, S. L. Hockerman, J. J. Parlow, M. S. South, S. Woodard, *J. Am. Chem. Soc.* **1997**, *119*, 4874 – 4881; b) R. J. Booth, J. C. Hodges, *J. Am. Chem. Soc.* **1997**, *119*, 4882 – 4886.
[39] a) T. Yamashita, H. Yasueda, N. Nakamura, *Chem. Lett.* **1974**, 585 – 588; b) T. Yamashita, H. Mitsui, H. Watanabe, N. Nakamura, *Polym. J.* **1981**, *13*, 179 – 181.
[40] H. Wack, A. E. Taggi, A. M. Hafez, W. J. Drury III, T. Lectka, *J. Am. Chem. Soc.* **2001**, *123*, 1531 – 1532.
[41] A. M. Hafez, A. E. Taggi, H. Wack, W. J. Drury III, T. Lectka, *Org. Lett.* **2000**, *2*, 3963 – 3965.
[42] A. M. Hafez, A. E. Taggi, W. J. Drury III, T. Lectka, *J. Am. Chem. Soc.* **2001**, *123*, 10853 – 10859.
[43] A. E. Taggi, A. M. Hafez, H. Wack, B. Young, D. Ferraris, T. Lectka, *J. Am. Chem. Soc.* **2002**, *124*, 6626 – 6635.
[44] J. B. Falmagne, C. Schmit, J. Escudero, H. Vanlierde, L. Ghosez, *Org. Synth. Coll.* **1993**, *8*, 306 – 309.
[45] R. C. D. Brown, J. Keily, R. Karim, *Tetrahedron Lett.* **2000**, *41*, 3247 – 3251.
[46] a) A. Pommier, J.-M. Pons, *Synthesis* **1993**, 441 – 459; b) A. Pommier, J.-M. Pons, *Synthesis* **1995**, 729 – 744.
[47] a) J. L. Loebach, D. M. Bennett, R. L. Danheiser, *J. Am. Chem. Soc.* **1990**, *120*, 9690 – 9691; b) J. L. Loebach, D. M. Bennett, R. L. Danheiser, *J. Org. Chem.* **1998**, *63*, 8380 – 8389; c) D. M. Bennett, I. Okamoto, R. L. Danheiser, *Org. Lett.* **1999**, *1*, 641 – 644.

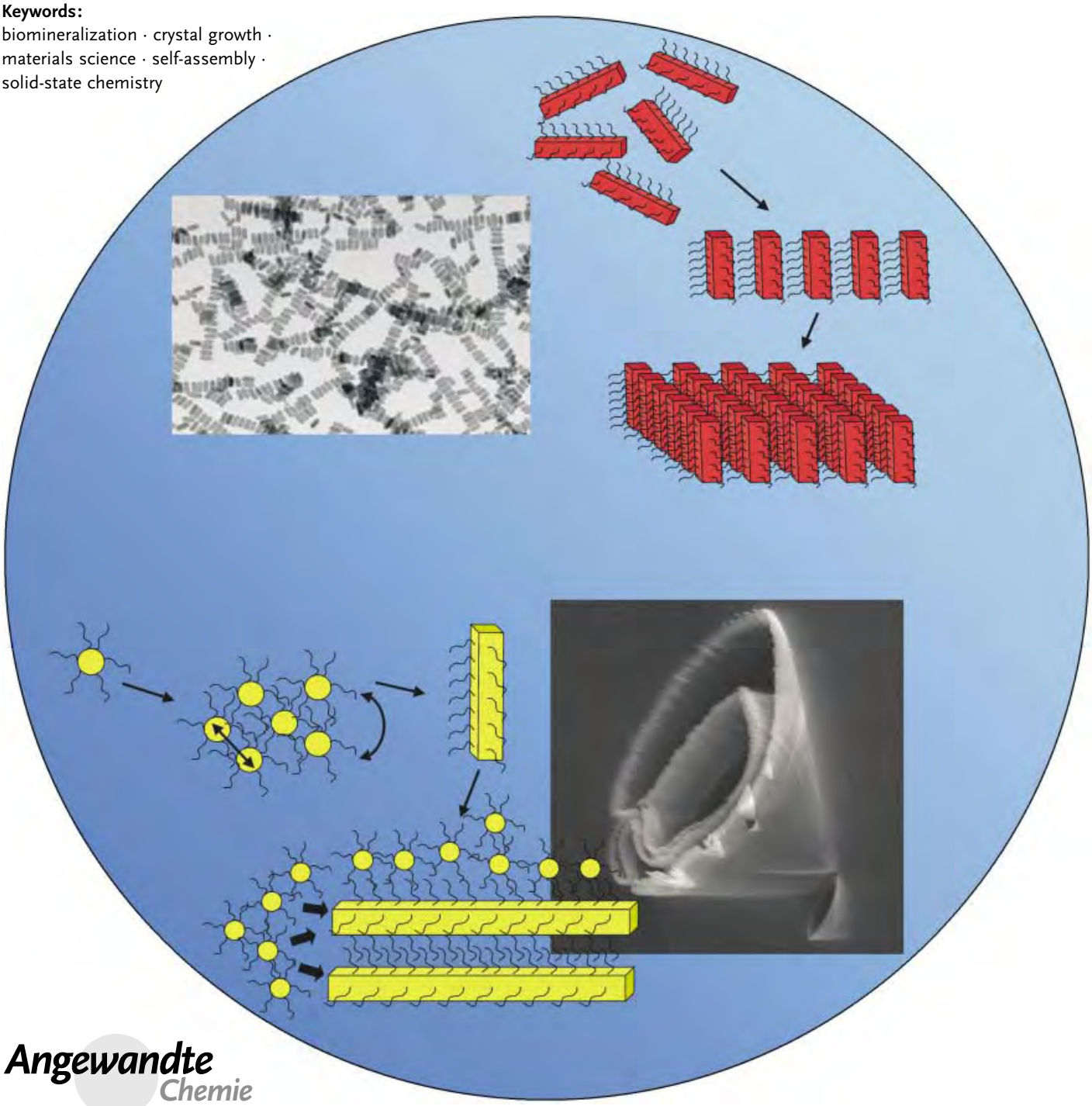
 © 2003 Wiley-VCH Verlag GmbH & Co. KGaA, Weinheim

Organization of Nanostructures

Higher-Order Organization by Mesoscale Self-Assembly and Transformation of Hybrid Nanostructures

*Helmut Cölfen and Stephen Mann**

Keywords:
biomineralization · crystal growth · materials science · self-assembly · solid-state chemistry



© 2003 Wiley-VCH Verlag GmbH & Co. KGaA, Weinheim
DOI: 10.1002/anie.200200562

The organization of nanostructures across extended length scales is a key challenge in the design of integrated materials with advanced functions. Current approaches tend to be based on physical methods, such as patterning, rather than the spontaneous chemical assembly and transformation of building blocks across multiple length scales. It should be possible to develop a chemistry of organized matter based on emergent processes in which time- and scale-dependent coupling of interactive components generate higher-order architectures with embedded structure. Herein we highlight how the interplay between aggregation and crystallization can give rise to mesoscale self-assembly and cooperative transformation and reorganization of hybrid inorganic–organic building blocks to produce single-crystal mosaics, nanoparticle arrays, and emergent nanostructures with complex form and hierarchy. We propose that similar mesoscale processes are also relevant to models of matrix-mediated nucleation in biomineralization.

From the Contents

1. Introduction 2351
2. Kinetic Control of Nucleation and Growth 2352
3. Aggregation-Mediated Pathways of Crystal Growth 2353
4. Mesoscale Self-Assembly of Nanoparticle Arrays 2356
5. Mesoscale Transformations and Emergent Nanostructures 2357
6. Mesoscale Transformations and Matrix-Mediated Nucleation in Biomineralization 2361
7. Summary and Outlook 2362

1. Introduction

It is self-evident that the organization and transformation of matter and energy are fundamental aspects of the universe. How these processes occur and the nature of the properties they encode are quintessential questions for all scientific disciplines past and present. In this regard, chemistry occupies the middle ground between physics and biology as it deals with the ordering and rearrangement of atoms at the molecular level, rather than the fundamental subatomic nature of matter or its animation in macroscopic time-dependent structures. Nanochemistry aims to extend the traditional length scales of synthetic chemistry and exploit the collective properties of organized assemblies produced by processes, such as, controlled crystallization and supramolecular complementarity. Although many approaches seek to mimic the information processing and sensing capabilities of biological nanostructures, they often lack the inherent materials-building properties typical of organisms, which are essential if nanostructures are to be organized across many length scales and used as functional materials within integrated systems. For this reason, strategies have been developed for the long-range organization and assembly of nanostructured phases. For example, chemical and microfabrication methods can be combined to produce externally patterned materials,[1,2] whereas spontaneous processes associated with solvent evaporation,[3,4] molecular cross-linking,[5,6] or programmed recognition[7–9] have been used to control the deposition of nanoparticle-based superlattices. Although promising, these approaches have disadvantages associated with the sequential processing and the physical fabrication, as well as limitations arising from the restricted number of superlattices available because of thermodynamic (packing) constraints on self-assembly. Indeed, structural organization in many of these systems depends on physics and crystal engineering rather than chemistry.

On the other hand, it should be possible to develop a chemistry of *organized matter* that couples together synthesis and self-assembly to produce, in situ, complex higher-order structures. In such cases, the embedding of structures over multiple length scales will arise as an emergent property that is not directly related to the smallest building blocks but is dependent on how these units evolve in time and space. Thus, different driving forces will operate at various stages along the synthesis–construction pathway such that these forces become superimposed mechanistically. For example, whereas localized molecular interactions can dominate ordering transitions on the nanoscale, surface forces are important in determining how nanostructures become assembled at the mesoscopic level. And beyond the colloidal regime, mechanical forces, such as internal strain, can drive transformations that result in macroscopic order.

It seems unlikely that significant levels of complexity can emerge for single-component systems as the scope for switching between these different length-scale-dependent regimes is severely limited by homogeneity. But increasing the number of interactive components should significantly enhance the diversity of emergent structures, particularly when inorganic and organic building blocks are present because of the

[*] Prof. S. Mann
School of Chemistry
University of Bristol
Bristol BS8 1TS (UK)
Fax: (+44) 117-929-0509
E-mail: s.mann@bristol.ac.uk
Dr. H. Cölfen
Max-Planck-Institut für Kolloid- und Grenzflächenforschung, Kolloidchemie
Forschungscampus Golm, 14424 Potsdam (Germany)

 DOI: 10.1002/anie.200200562 © 2003 Wiley-VCH Verlag GmbH & Co. KGaA, Weinheim

resulting disparate driving forces. In such circumstances, there needs to be a balance between the forces responsible for the self-organization of individual components and those required for mutual coassembly. If the former are predominant, then phase-separated structures will be synthesized, whereas domination of the latter can result in nonequilibrium conjugated architectures. This situation is exemplified by the hierarchical and hybrid nature of many biological minerals, which arise from an underlying synergy between the force fields of inorganic precipitation and biological organization.[10] Such materials illustrate the fundamental difference between notions of "organized" and "condensed" forms of matter, and have served as important archetypes in the biomimetic synthesis of higher-order structures.[11,12]

Underpinning the synthesis of emergent structures are two general engines of construction that propagate and integrate structures from the molecular to macroscopic scales: crystallization and aggregation. Herein, we focus on the relationships between these processes in the presence of inorganic–organic building blocks, particularly at the mesoscale level where aggregation and crystallization can become intimately linked to generate hybrid single-crystal mosaics (Section 3), coassembled nanoparticle arrays (Section 4), and embedded higher-order nanostructures (Section 5).

Because the driving force for crystallization can be very strong and readily sustained, it is not so easily embedded within the construction process unless subject to kinetic regulation. We therefore begin our discussion with the general case of kinetic control in nucleation and growth, which highlights the importance of phase transformations in sequential processes involving amorphous precursors and crystalline intermediates (Section 2). A model of crystal growth based on aggregation-mediated processes is then described and extended to consider the important influence of surface-adsorbed macromolecules and surfactants on crystal texture and composition (Section 3). This approach leads to the mesoscale self-assembly of inorganic–organic hybrid nanoparticles, which we consider first in regard to stable (nontransformable) inorganic building blocks with either crystalline or amorphous structures linked by organic connectors (Section 4). In contrast, in Section 5 we discuss the more complex situation in which aggregates consisting of metastable inorganic–organic building blocks undergo mesoscale transformations. We show that amorphous-to-crystalline transformations of the inorganic phase can be strongly coupled with organic mesophase transitions to produce emergent hybrid nanostructures with complex shapes and hierarchical organization. Finally, we propose that mesoscale transformations involving cooperative reorganization of coupled inorganic and organic components could be relevant in models of matrix-mediated nucleation in biomineralization (Section 6).

2. Kinetic Control of Nucleation and Growth

One of the many distinguishing features of biominerals is that they are produced in heterogeneous environments at ambient temperature and pressure and pH values close to neutral. In comparison, materials synthesis usually demands harsh conditions, and even so-called "soft-chemical" methods may involve hydrothermal or solvothermal procedures and extreme pH values, or conditions, such as, microwave radiation.[13,14]

Biological boundary conditions clearly limit the number and types of minerals that can be deposited from aqueous solutions but, on the other hand, increase the scope for controlled fabrication by shifting the reaction profile from themodynamic to kinetic driving forces. In general, kinetic control is based predominantly on the modification of the activation-energy barriers of nucleation, growth, and phase transformation (Figure 1). In such cases, crystallization often proceeds by a sequential process involving structural and compositional modifications of amorphous precursors and crystalline intermediates, rather than a single-step pathway.[15,16] How far these phase transformations proceed along a series of increasingly stable intermediates depends on the solubilities of the minerals and on the free energies of activation of their interconversions, all of which are strongly influenced by additives.[10] The corresponding changes in composition and structure usually occur by dissolution–renucleation processes closely associated with the surface and/or the interior of preformed particles. The nucleation of a particular crystalline phase is therefore highly heterogeneous and dependent on interfacial and hydrodynamic properties as well as reaction kinetics. Therefore, this process cannot be



Stephen Mann is Professor in the School of Chemistry and Director of the Centre for Organized Matter Chemistry at the University of Bristol. He received his B.Sc. in chemistry from the University of Science and Technology in Manchester in 1976, and was awarded a D.Phil. in 1982 from the University of Oxford He took up a lectureship at the University of Bath in 1984 followed by a full professorship in 1990. He subsequently moved to his current position in 1998. He was admitted as a Fellow of the Royal Society of Chemistry in 1996 and has obtained several awards including the Corday-Morgan Medal (1993) and Interdisciplinary Award (1999) from the Royal Society of Chemistry, and Vinci Science for Art Prize (1996).



Helmut Cölfen studied Chemistry at the University Duisburg and completed his Ph.D. in 1993 under the supervision of Prof. Dr. Werner Borchard. After a Postdoc at the University of Nottingham, with Prof. Stephen Harding, in 1995 he joined the Max-Planck-Institute of Colloids and Interfaces where he is a project leader in Prof. Markus Antonietti's group. After his habilitation in 2001, he was employed as senior scientist and head of the analytical service in the colloid chemistry department. Among his awards are the Hochschulabsolventenpreis of the Gerhard-Mercator University Duisburg and the Hermann Schnell award of the German Chemical Society (GDCh).

 © 2003 Wiley-VCH Verlag GmbH & Co. KGaA, Weinheim

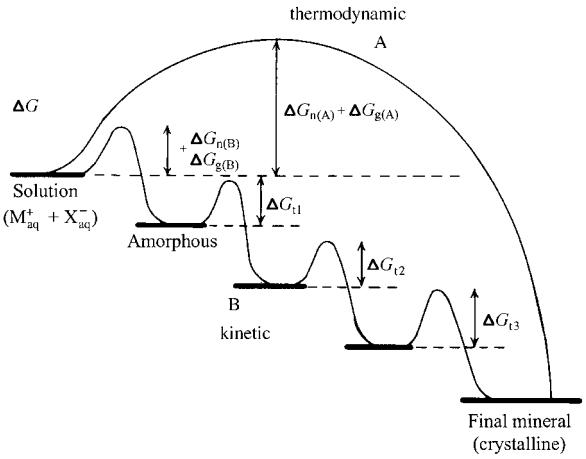


Figure 1. Crystallization pathways under thermodynamic and kinetic control. Whether a system follows a one-step route to the final mineral phase (pathway A) or proceeds by sequential precipitation (pathway B), depends on the free energy of activation (ΔG) associated with nucleation (n), growth (g), and phase transformation (t). Amorphous phases are common under kinetic conditions.

readily described by the classical model of nucleation, which is based on a thermodynamic treatment of the interplay between energy gain through bulk crystallization and energy loss through increase in surface area.[17]

Kinetically driven crystallization often involves an initial amorphous phase that may be nonstoichiometric, hydrated, and susceptible to rapid phase transformation. Amorphous calcium carbonate (ACC) for instance is highly soluble and rapidly transforms to calcite, vaterite, or aragonite unless kinetically stabilized. In biomineralization, this stabilization is achieved by ions such as Mg^{2+} and PO_4^{3-}, or by enclosing the amorphous phase in an impermeable sheath of organic macromolecules, such as polysaccharides[18] or mixtures of polysaccharides and proteins rich in glutamic acid, threonine, and serine.[19,20] Thus a significant number of stabilized ACC biominerals has now been documented in plant cystoliths,[21,22] snail shells,[23] ascidian spicules,[19,24] and crustacean exoskeletons.[25] In contrast, controlled phase transformation of ACC results in the deposition of calcite spicules in sea urchin larvae.[26,27] Interestingly, many biogenic calcites contain high levels (up to 30 mol%) of Mg^{2+} ions in the crystal lattice, and one possibility is that such high isomorphic substitution contents originate from associated Mg-rich ACC precursors. Although confirmation of these biogenic precursors has not yet been reported, laboratory experiments on calcite crystallization from supersaturated solutions containing a 4:1 Mg^{2+}:Ca^{2+} molar ratio in the absence or presence of polyasparate, polyacrylate, or macromolecules extracted from the high Mg-calcite skeleton of a coralline alga showed in each case that ACC phase transformation resulted in calcite crystals with Mg levels of approximately 20 mol%.[24] This level is significantly greater than the 10 mol% found in the thermodynamically stable Mg-calcite, and indeed such high substitution levels are unlikely to be attained under ambient conditions by a single-step crystallization process because the concomitant amounts of soluble Mg^{2+} ions required result in the kinetic precipitation of aragonite.

Kinetic control of crystallization can be achieved by modifying the interactions of nuclei and developing crystals with solid surfaces and soluble molecules.[28] Such processes influence the structure and composition of the nuclei, particle size, texture, habit and aggregation, and stability of intermediate phases. In biomineralization, for example, structured organic surfaces are considered to play a key role in organic-matrix-mediated deposition by lowering the activation energy of nucleation of specific crystal faces and polymorphs through interfacial recognition (see Section 6 for further details).[29] Soluble macromolecules and organic anions, as well as inorganic ions, such as Mg^{2+} and PO_4^{3-}, can also have a marked kinetic effect on crystallization, particularly with regard to polymorph selectivity and habit modification. These interactions can be highly specific; for example, proteins extracted either from calcite or aragonite-containing layers of the abalone shell induce the crystallization of calcite or aragonite, respectively, when added to supersaturated solutions of calcium hydrogen carbonate in the laboratory.[30] Atomic-force-microscope (AFM) studies[31] indicate that the macromolecules bind to growth sites on well-defined crystal surfaces and influence the kinetics of crystal growth from solution in accordance with the classical model of secondary nucleation.[32] Although there is much experimental evidence to support these molecular-based mechanisms, the studies usually concern macroscopic crystals with well-established faces and edges, so information about the early stages of growth at the colloidal level are not generally available. Significantly, as discussed in Section 3, recent studies indicate that aggregation of primary particles can be an important mechanism of crystallization at the mesoscopic length scale, particularly in kinetically controlled systems. The influence of macromolecules on this process has not been generally considered.

We now discuss aggregation-induced crystallization and extend this mechanism to inorganic–organic hybrid building blocks to highlight new insights into the design of synthesis routes to crystals with complex textures and morphologies, as well as organized assemblies of organically interconnected nanoparticles.

3. Aggregation-Mediated Pathways of Crystal Growth

The classical model of crystallization considers growth essentially as an amplification process in which stable nuclei are simply enlarged by unit-cell replication without incurring structural changes in the bulk or at the surface. In contrast, crystal growth by aggregation of preformed crystalline building blocks is a mesoscale assembly process that results in single crystals with iso-oriented mosaic textures (Figure 2). This process can occur through the coalescence of primary nanoparticles into colloidal aggregates, often of uniform size, and their subsequent internal restructuring to produce a crystallographically continuous particle.[33] Alternatively, nanoparticles can become attached stepwise to a growing

 © 2003 Wiley-VCH Verlag GmbH & Co. KGaA, Weinheim

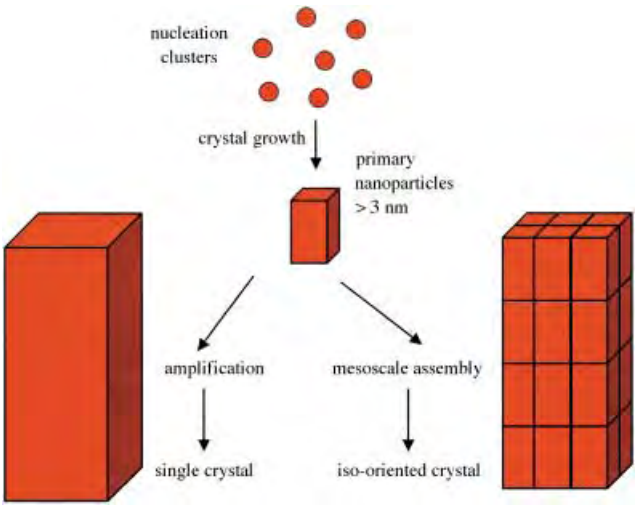


Figure 2. Alternative mechanisms of growth for single crystals.

assembly of aligned building blocks to produce, for example, chains of oriented nanocrystals.[34]

Aggregation-mediated crystallization appears to be prominent for solids, such as iron oxides,[35] cerium oxide,[36] copper oxalates,[33] and copper oxides,[37] which contain metal ions that readily undergo hydrolytic polymerization and cluster formation in aqueous solution. The resulting nanoparticles have surface charges that are highly sensitive to changes in pH value and ionic strength. Neutralization of surface species by the hydrolytic transformation of hydroxy (−OH) centers to oxo (−O−) bridges releases protons that can reduce the surface charge of dispersed nanoparticles to values equal to the isoelectric point, and thereby induce colloidal aggregation, which under appropriate conditions can occur concurrently with crystallization. For iron oxides, this generally requires hydrothermal aging of amorphous hydrated phases to produce well ordered nanocrystal superstructures,[38] whereas copper oxides crystallize directly upon neutralization-induced metal-ion hydrolysis.[37] In such cases, primary nanocrystals are nucleated, which subsequently aggregate as the surface charge is progressively reduced by hydrolysis. Because the onset of aggregation is coupled temporally with crystallization, the size and shape of the primary particles, as well as the colloidal aggregates, are often highly homogeneous. This is particularly the case when the primary nanoparticles are produced by a single nucleation event such that the building blocks are effectively consumed during the aggregation process.[39] For example, monodisperse CuO colloids, 300 nm in size, have been prepared from 20-nm-sized CuO nanocrystals by self-limiting aggregation.[37] In contrast, if the rate of nucleation and growth of the nanocrystals is constant throughout the aggregation process then the continuous supply of primary particles compensates for their consumption and polydispersity in aggregate size increases.

Transformation of nucleation clusters to stable crystalline building blocks will affect the structure, size, and shape of the primary particles, which in turn influence the mode of aggregation at the mesoscopic level. In particular, building blocks with high shape anisotropy, such as nanorods and nanodisks, will spontaneously align to produce crystals with analogous morphologies. Thus, changes in crystal habit can arise from modifications in the nanoscopic morphology of the building blocks, rather than by interactions between the crystal surfaces and environment as proposed in classical models of crystal growth. For example, variations in the morphology of colloidal hematite (α-Fe_2O_3) have been attributed to differences in the shape of nanoparticle building blocks.[40] Remarkably, even spherical primary particles can give rise to vectorial aggregation to produce ovoid or spindle-shaped aggregates.[37] This effect suggests that the interaction potential between the isometric building blocks is dependent on a multitude of factors, such as the actual combination of crystal faces expressed, electrostatic and dipolar fields associated with the aggregate, and hydrodynamic and van der Waals forces.

The controlled growth of a continuous single crystal from aggregated nanocrystals necessitates that the primary particles become aligned and interconnected along a common crystallographic axis. Studies have shown that crystallographically aligned chains of TiO_2 nanoparticles are produced under hydrothermal conditions at near flocculation conditions and close to the isoelectric point by oriented attachment of preformed nanocrystals.[34] A similar mechanism has been proposed for certain iron oxides[41] and ZnO nanorods.[42] In such cases, the nanocrystals are facetted and aligned by "docking" processes involving crystallographic fusion between certain high surface-energy faces. Moreover, stresses associated with defects caused by initial mismatching at the particle–particle interface might be sufficient to induce rotation of the crystallites into an aligned configuration.[43] It seems possible that such processes could also occur within aggregates, along with coherent restructuring at the particle–particle interfaces.[33,35,37,44] The latter could involve densification, and intra-aggregate reactivity and ripening. For example, in situ hydrolysis at the interfaces between adjacent metal-oxide nanoparticles could increase the density and expel occluded solvent from the interior of the hydrated aggregates. A high level uniformity in the size and shape of the primary particles is expected to facilitate long-range crystallographic coherence because of more efficient packing and epitaxial matching, provided that the interparticle forces resulting from the partial balancing of attractive van der Waals and repulsive electrostatic interactions are not so strong that the initial orientations are irreversibly fixed. Indeed, some degree of "error-correction" must operate if the colloidal aggregates are to restructure into well-ordered single crystals. In this regard, dynamic processes, such as jiggling of the nanoparticles within the aggregate by Brownian motion[41] or a modified Ostwald ripening process in which particles in crystallographic alignment are preferentially stabilized whilst non-aligned crystallites within the aggregates dissolve,[34] could be of key importance.

 © 2003 Wiley-VCH Verlag GmbH & Co. KGaA, Weinheim

3.1. Macromolecules and Crystal Textures

It is evident from many studies that soluble macromolecules can influence crystal habit by selective adsorption processes that lead to preferential growth inhibition for distinct crystal faces, in analogy to the adsorption of low-molar-mass additives or inorganic ions.[45] If such processes take place within a multistep growth mechanism, complex single-crystal morphologies, such as $BaSO_4$ flowerlike single-crystalline particles with forbidden 10-fold symmetry,[46] can be produced. In this case, the polymer additive interacts with primary $BaSO_4$ nanocrystals indicating that soluble macromolecules and surfactants can have marked effects on the very early stages of crystal growth. Moreover, macromolecules are expected to be associated with aggregation-based pathways of crystal growth for several reasons. It is well known that many polymers in solution can induce colloidal aggregation by enthalpic changes (surface binding and interparticle bridging), as well as nonadsorption entropic mechanisms (depletion flocculation).[47,48] This process is the molecular basis for polymeric scale inhibition. In addition, strong attractive interactions with the inorganic surface can arrest nucleation and change the shape and size of the primary clusters. In this way stabilized nanocrystals with anchored organic ligands (Figure 3) are produced. Such particles are hybrids consisting of inorganic cores and organic shells, and can undergo controlled aggregation in aqueous solutions to produce textured single crystals. Steric, van der Waals and hydrophilic–hydrophobic interactions involving the pendent chains of the adsorbed polymers or surfactants, as well as shape anisotropy, can influence the assembly of the primary particles. Moreover, modifications in crystal habit can arise from macromolecular-induced changes in the shape of the aggregating crystal nuclei rather than solution-based interactions at the particle surfaces.[33]

Strong binding interactions between the macromolecules and nanocrystals involved in aggregation-mediated crystal growth will tend to produce crystals containing significant levels of occluded organic molecules, which unless desorbed or cleaved during restructuring will be included in the internal composition and texture. For example, copper oxalate crystals grown in the presence of hydroxypropyl methycellulose have a polymer content of 0.4–1.5 wt %.[33] Likewise, levels of between 5–12 wt % and 4–30 wt % depending on the initial polymer concentration have been determined for $BaSO_4$[49] and ZnO[50] crystals, respectively. Functionalized latexes can also be incorporated into growing single crystals.[51] Intercalated macromolecules are common in many biominerals, such as the single-crystal Mg-calcite spines of the adult sea urchin that contain 0.02 wt % of protein, which is sufficient to modify their mechanical properties.[52] These biominerals, like their inorganic counterparts grown in the presence of polymers, are not only hybrid composites but exhibit modified domain structures. This situation is manifested in the corresponding X-ray diffraction patterns that show shortening of the coherence length and widening of the angular spread associated with the mosaic structure.[33,53,54]

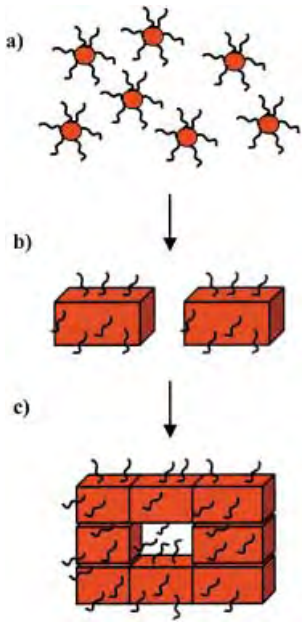


Figure 3. Influence of macromolecules and surfactants on crystallization by aggregation-mediated processes: a) spatially arrested nucleation of organic–inorganic hybrid clusters, b) size and shape modified hybrid nanocrystals, and c) controlled aggregation and formation of iso-oriented mosaic crystals with internal macromolecular-rich domains.

High concentrations of intercalated macromolecules will curtail restructuring within the nanocrystal aggregates with the consequence that crystallographic discontinuities will become prevalent as the hybrids increase in size. The corresponding changes in internal texture for $BaSO_4$ and $CaCO_3$ crystals have been revealed by thin sectioning and TEM analysis (Figure 4).[55,56] In both cases, the single crystals consist of a central region of oriented primary particles with sizes in the order of several tens of nanometers that are interspaced with polymer-rich domains. In contrast, the outer regions of the hybrid structure comprise considerably larger particles with a progressive increase in the angular spread. One possibility is that internal strain associated with defects

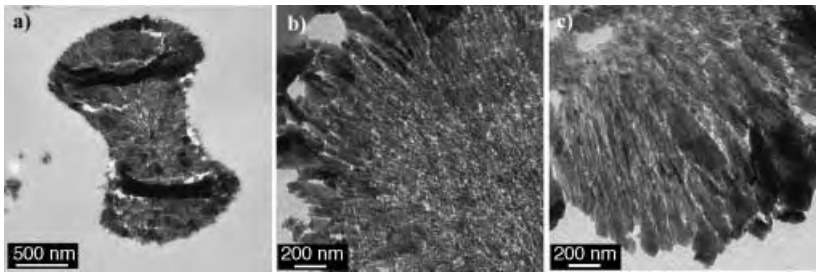


Figure 4. TEM micrographs of thin slices of dumbbell-shaped crystals grown in the presence of double hydrophilic block copolymers showing oriented internal domain structure. a) $BaSO_4$ crystal formed in the presence of 1 g L^{-1} poly(ethylene oxide)-*block*-poly(edta) at pH 5 (edta = ethylenediaminetetraacetic acid).[55] b) and c) central and edge regions, respectively, of $CaCO_3$ crystals precipitated in the presence of 1 g L^{-1} poly(ethylene oxide)-*block*-poly(methacrylic acid) at pH 10.[56]

 © 2003 Wiley-VCH Verlag GmbH & Co. KGaA, Weinheim

in the central region manifests itself in an increasing misalignment of the domains towards the outer edges of the aggregate where the energy can be more readily dissipated. This situation could lead to complex morphologies if the crystals continue to grow by solution processes because secondary nucleation would occur specifically at the misaligned surface sites to produce an angular spread of crystal outgrowths. The switching between aggregation and solution mechanisms could, for example, explain the time-dependent "rod-to-dumbbell-to-notched-sphere" evolution of forms that has been often observed when fluoroapatite,[57,58] calcium carbonate,[59,60] and barium sulfate[49,55] crystals grown in the presence of macromolecules, such as specially designed block-copolymer additives.[61] The transformation between rod, dumbbell, and spheroidal morphologies can be controlled to some extent by changes in the concentration ratio of polymer to mineral,[56] variations in the solvent composition in alcohol/water mixtures.[62] or by changing the strength of interaction between the polymer and crystal by variations in pH value.[55]

4. Mesoscale Self-Assembly of Nanoparticle Arrays

Implicit in the previous discussion is the assumption that occluded macromolecules do not completely prevent restructuring of the nanocrystal-containing aggregates. That is, crystallographically continuous junctions are formed between the nanocrystal building blocks even when significant numbers of defects are introduced. An interesting situation arises when the binding affinity of the organic molecules is sufficiently high that the nanocrystals are so highly stabilized that no further crystal growth can take place within the aggregates. In such cases, the nanoparticles can become ordered by organic interactions at the interfaces between the hybrid building blocks. If the nanocrystals have high shape anisotropy, then highly organized nanoparticle arrays and higher-order superstructures can spontaneously assemble (Figure 5).

The construction of organized nanoparticle-based structures by self-assembly or templating is a key goal of nanotectonics, as reviewed in detail elsewhere.[63,64] Herein we focus specifically on the mesoscale self-assembly of organic-coated crystalline nanoparticles. This process occurs readily, for example, in the presence of surface-anchored surfactant molecules.[4,65] In most cases, the nanoparticles (such as, Au Ag, CdSe(S)) are spherical so the corresponding superstructures have close-packed lattices in two or three dimensions. Hydrophobic interactions between surfactant molecules on adjacent nanoparticles drive the assembly, which is usually reversible unless interparticle cross-linkers are introduced to stabilize the superstructure. For example, organic dithiols have been used as bridging molecules in superlattices of hydrophobic Au nanoparticles.[66] Recent studies have focused on the mesoscale assembly of non-close-packed superstructures by using surfactant-coated nanoparticles with high shape anisotropy, such as nanorods of $BaCrO_4$,[67] Au,[68] and cobalt.[69] These nanocrystals have surfaces that are flat or exhibit low curvature, so the hydrophobic forces can be strengthened by collective intermolecular interactions, which, for example, result in stable surfactant bilayers between the inorganic particles. In such cases, disorder-to-order mesophase transitions associated with the pendent surfactant molecules are responsible for the strong interparticle driving force that can operate over long length scales to produce liquid-crystalline inorganic assemblies.[70]

The sensitivity of these ordering transitions to changes in the interaction potential between the crystal surface and associated surfactant molecules has been highlighted by using the interfacial activity of microemulsion-based reaction fields to interactively couple the synthesis of $BaCrO_4$ or $BaSO_4$ nanocrystals with their self-assembly into higher-order structures.[67] The reaction occurs at room temperature in unstirred isooctane that contains a mixture of $Ba(AOT)_2$ (AOT = bis(2-ethylhexyl)sulfosuccinate) reverse micelles and water-in-oil microemulsion droplets prepared from NaAOT and aqueous chromate or sulfate anions. When mixed together at a Ba^{2+}:CrO_4^{2-} (SO_4^{2-}) molar ratio of 1:1, slow exchange between the droplets gives rise to the spontaneous assembly in solution of linear chains of crystallographically aligned prismatic nanoparticles spaced at a distance of 2 nm from each other (Figure 6). Formation of the linear array depends

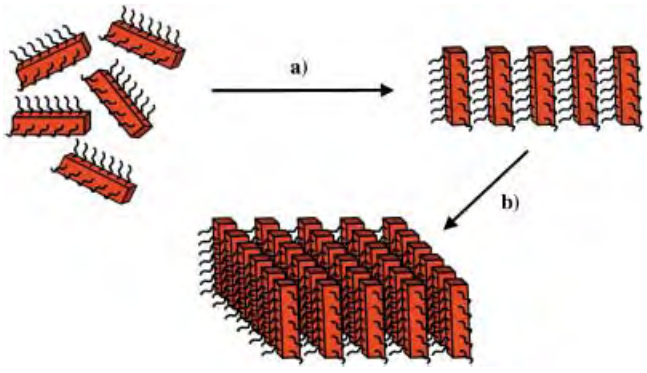


Figure 5. a) Mesoscale assembly of crystalline hybrid nanoparticles through face-specific surface conjugation or mesophase ordering between adsorbed organic molecules, b) higher-order assembly associated with 2D superstructure formation.

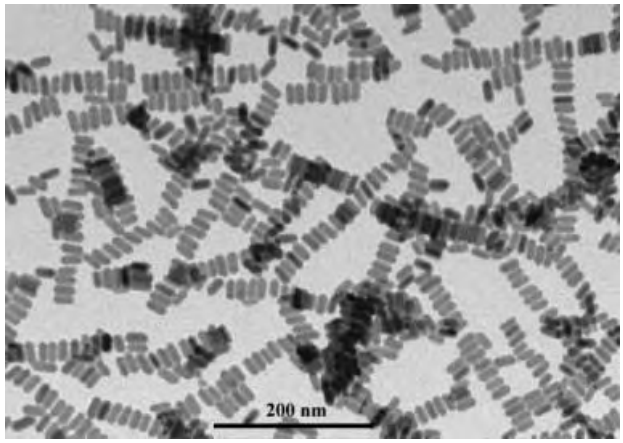


Figure 6. TEM image showing ordered chains of prismatic $BaCrO_4$ nanoparticles prepared in AOT microemulsions at $[Ba^{2+}]:[SO_4^{2-}] \approx 1$ and $w = 10$.

 © 2003 Wiley-VCH Verlag GmbH & Co. KGaA, Weinheim

on the uniformity in nanoparticle size and shape anisotropy, which facilitate crystal-face-specific interactions between the hydrophobic tails of surface-adsorbed surfactant molecules. The driving force for assembly appears to involve a mesophase transition in which the unordered pendent AOT molecules are organized into an interdigitated bilayer between adjacent nanoparticles. This process is sensitive to changes in the molar ratio of reactants, which can strengthen or weaken the binding of anionic AOT molecules to the surface of the growing nanoparticles. For example, no assembled chain structures are found if the anion concentration is two to five times less or greater than that of the Ba^{2+} ions. In the latter case, discrete crystalline nanoparticles are observed presumably because attractive interactions between the anionic headgroups of AOT and the crystal surface are significantly reduced by the negative surface charge associated with excess chromate or sulfate anions in the boundary layers. Thus, the surfactant molecules remain in a fluid state at the water–oil interface of the microemulsion droplets rather than being expelled from the interface and immobilized by surface anchoring, with the consequence that there is no significant driving force for interparticle bilayer formation. On the other hand, an excess of Ba^{2+} ions significantly increases the surfactant–inorganic-component interactions such that the assembly process becomes dependent on coupled mesoscale transformations, as described in detail in Section 5.

Mesoscale self-assembly of nanoparticle-based structures is also expected to occur in the presence of surface-adsorbed macromolecules such as polymers and biomolecules. Significantly, anchoring of biological macromolecules, such as DNA, antibodies, and biotinylated proteins, can significantly increase the informational content of the building blocks because the nondirectional electrostatic forces of the inorganic surface are replaced with organic sites for molecular recognition. For example, complementary single-stranded oligonucleotides can be attached to different populations of Au nanocrystals, and when mixed together give rise to spontaneous assembly because of base pairing and duplex formation between the particles.[71,72] Changing the number of bases in the synthetic oligonucleotides influences the interparticle separations, whereas variations in nanoparticle morphology can be used to produce anisotropic superstructures.[9]

It is well known that amphiphilic block copolymers exhibit mesophase transitions analogous to those observed for surfactant molecules, so the formation of assembled nanocrystal-based arrays should also be possible using surface-adsorbed synthetic macromolecules. To date, however, most examples of polymer-induced nanoparticle assembly involve phase separation of hydrophilic and hydrophobic segments, along with preferential demixing of the nanocrystals into one of these blocks.[73–76] On the other hand, polymer-induced nanoparticle assembly in aqueous solution has been generally concerned with amorphous building blocks. These include metastable phases, such as amorphous calcium carbonate and barium sulfate (see Section 6), as well as amorphous silica, which is stable at room temperature and pressure. In particular, poly(ethylene oxide) di- and triblock copolymers have been extensively used for the template-directed synthesis of ordered mesoporous silicas,[77–79] in which the aggregation of silica oligomers and primary particles is patterned by phase transitions that organize the macromolecules into hexagonal, lamellar, or cubic liquid-crystalline structures. Similar mechanisms involving the mesophase separation of cationic biomolecules, such as long-chain polyamines and proteins (silaffins), have been proposed to explain the nanoscale patterning of diatom biosilica.[80,81] These models propose that biosilica patterning occurs on various length scales because of consecutive phase separation of polyamine-containing droplets[80] or aggregates[81] associated with incipient polymerization and aggregate densification, respectively.

It is important to emphasize that in these polymer-based mechanisms the organization of the silica particles arises by exclusion of the building blocks from certain regions of space through phase separation (droplet/aggregate formation) or liquid-crystalline transitions. This situation is fundamentally different from the concerted assembly of hybrid building blocks, described in the first part of this section, in which nanocrystals are intimately interconnected with organic molecules. Moreover, unlike the nanocrystal systems described, the silica-based processes are transformable in the sense that the primary particles continue to grow to some extent during polymer-induced organization. This occurrence leads us to the interesting and important situation in which the assembly process proceeds by aggregation of hybrid building blocks consisting of amorphous interiors that are intrinsically unstable with respect to crystallization. In the next section, we discuss the influence of these transformations on the mesoscale assembly of hybrid nanomaterials.

5. Mesoscale Transformations and Emergent Nanostructures

Under certain circumstances, strong binding interactions between organic molecules and inorganic nuclei severely inhibit lattice construction such that colloidal aggregates containing hybrid primary particles with metastable amorphous cores are deposited. With time, however, the amorphous nanoparticles slowly crystallize within the aggregates, and this process can be strongly coupled with mesophase transitions involving surface-adsorbed polymers or surfactants (Figure 7). For example, growth of rod- and platelike nanocrystals would reduce the curvature imposed on the surface-anchored molecules, such that favorable changes in the inorganic lattice and organic bending energies can occur by cooperative mesoscale transformations. As these processes occur slowly within the confined field of the aggregates, nanocrystals with high shape anisotropy can be produced. Moreover, because the resulting nanocrystals are "coded" by the surface organization of the attached organic molecules, interparticle interactions involving, for example, hydrophobic interactions and bilayer interdigitation can lead to the in situ mesoscale assembly of interconnected hybrid nanostructures (Figure 7). The interactive nature of these processes determines the time-dependent coupling between crystallization and associated adaptations in the organization of the surface-

 © 2003 Wiley-VCH Verlag GmbH & Co. KGaA, Weinheim

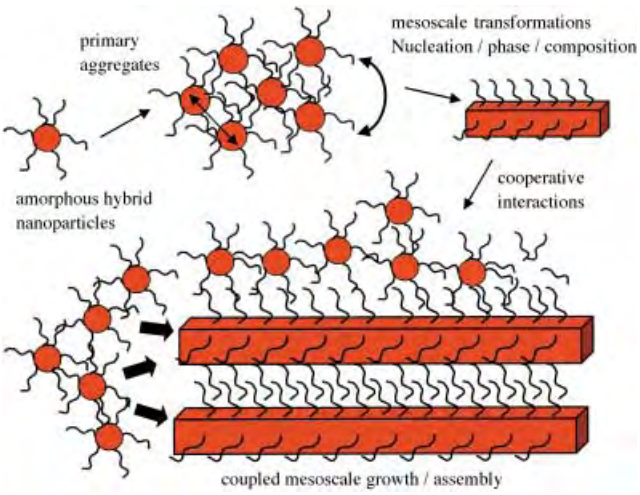


Figure 7. Proposed mechanism of coupled mesoscale transformations and emergent hybrid nanostructures. Transformation of the primary hybrid aggregates occurs by cooperative reorganization of the inorganic lattice energy (double-headed straight arrow) and mesostructure of the surface-adsorbed organic molecules (double-headed curved arrow). Higher-order cooperative interactions give rise to emergent behavior and the embedding of structures on different length scales.

attached molecules. As a consequence, a series of cooperative feedback loops can be established and the systems are then notable for their emergent properties that are expressed across a range of length scales.

The above concepts are based on several recent studies on the morphosynthesis of macroscopic structures consisting of higher-order assemblies of surfactant–inorganic-crystalline nanofilaments of $BaSO_4$, $BaCrO_4$, and Ba phosphotungstate,[82] $BaCO_3$,[83] $CaSO_4$,[84] or $CaCO_3$.[85] These structures were synthesized in water-in-oil microemulsions, but significantly, similar complex architectures can be prepared in aqueous supersaturation solutions. For example, barium sulfate and chromate nanofilament bundles and cones were obtained in aqueous solutions of anionic polyelectrolytes[86,87] or hydrophilic block copolymers with a polyanionic domain.[86,88] Nested neuronlike tangles of calcium phosphate nanofilaments have been prepared within aggregates of a partially alkylated poly(methacrylic acid)-*block*-poly(ethylene oxide) copolymer[89] or polyaspartate solutions,[90] in addition Ag nanowires[91] or calcite dumbbells[56] were produced from amorphous precursor particles in the presence of poly(ethylene oxide)-*block*-poly(methacrylic acid) copolymers.

The requirement for strong binding interactions between the adsorbed organic molecules and the inorganic surface during the nucleation and initial growth stages has been clearly demonstrated by changing the cation:anion molar ratio of reactions in microemulsions.[67,82] As discussed in Section 4, Ba^{2+}:CrO_4^{2-}(SO_4^{2-}) molar ratios of 1:1 or 1:5 give rise to surfactant-linked chains or discrete surfactant-coated nanoparticles as a result of intermediate and low levels of surfactant binding, respectively. In contrast, at molar ratios of 5:1, there is a large excess of Ba^{2+} ions such that the initially formed nanoparticles are positively charged and the anionic surfactant molecules are strongly adsorbed onto the inorganic surfaces. This produces amorphous rather than crystalline nanoparticles of $BaCrO_4$ and $BaSO_4$ that are constrained to 5 nm in size and which slowly aggregate because of hydrophobic interactions between the surface-anchored surfactant chains (Figure 8a). Amazingly, groups of nanoparticles line up in linear arrays that fuse together and crystallize into 5-nm-wide single filaments coated with AOT surfactant molecules (Figure 8b).[82] With time, other crystalline filaments are formed parallel to the original thread to produce a small bundle held together by surfactant bilayers (Figure 8c). The locking in of new filaments by surfactant interdigitation generates a bending force in the bundle to give a coiled spiral at one end, which can perpetuate throughout the whole length of the bundle to produce structures with helical and conelike forms.

The binding strength and corresponding degree of cooperativity associated with mesoscale disorder–order transformations and surfactant reorganization is not only influenced by the surface charge (molar ratio) but also the degree of hydration of the inorganic surface and surfactant headgroups. The amount of water in the above experiments is extremely small ([water]/[surfactant], molar ratio $w = 10$) but turns out to be optimal as lower water contents are not sufficient to drive the amorphous→crystal transformation, whereas higher levels increase the size of the droplets such that the crystallization process is no longer influenced by the surfactant membrane. Similar observations have been reported when different amounts of water-in-isooctane NaAOT microemulsions of constant droplet size ($w = 10$) are added to isooctane dispersions of alkylbenzenesulfonate-coated amorphous calcium carbonate (ACC) nanoparticles.[85] Hydration of the ACC nanoparticles results in aggregation followed by

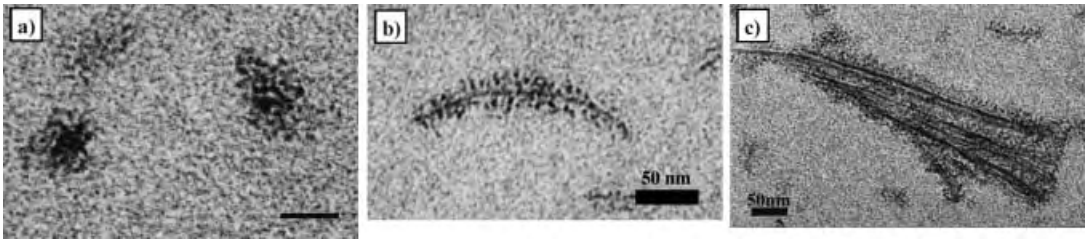


Figure 8. Early stages of $BaSO_4$ nanofilament formation in water-in-oil microemulsions:[82] a) aggregates of electron-dense 5-nm-sized surfactant-coated amorphous particles (1 h), b) nucleation and growth of crystalline nanofilament within a matrix of electron-dense nanoparticles (2–3 h), c) nucleation and growth of secondary filaments alongside the primary thread to produce aligned bundles (5 h). Scale bars = 50 nm.

 © 2003 Wiley-VCH Verlag GmbH & Co. KGaA, Weinheim

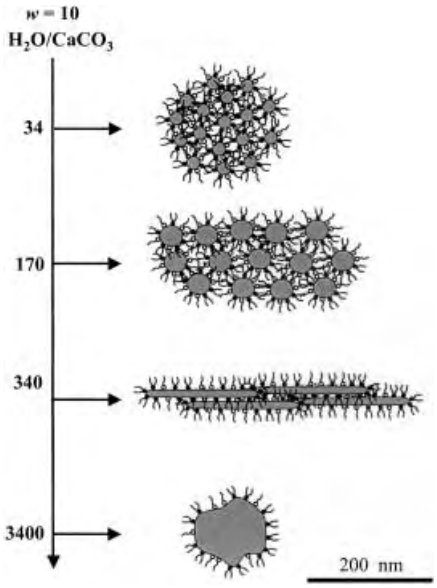


Figure 9. General scheme showing effect of [water droplet]/[amorphous $CaCO_3$ nanoparticle] ratio (n) at a constant [water]/[surfactant] molar ratio (w) of 10 on the types of hybrid-surfactant–vaterite nanostructures synthesized by microemulsion-mediated phase transformation of surfactant-stabilized ACC nanoparticles.[85] The aggregated structures are drawn approximately to scale.

water-induced crystallization and the formation of organized hybrid nanostructures by mesoscale transformations that are mediated by the extent of coupling at the surfactant–inorganic interface (Figure 9). Strong coupling in the presence of low amounts of water ($[H_2O]/[CaCO_3]$, $n = 34$) gives monodisperse spheroidal aggregates of densely packed 5-nm-diameter surfactant-coated vaterite nanoparticles, whereas weak interactions at $n = 3400$ produce discrete vaterite nanoparticles, 130 nm in size. Significantly, intermediate levels of coupling produce anisotropic nanostructures, such as spindle-shaped aggregates of 18-nm-sized vaterite nanoparticles ($n = 170$) and high aspect-ratio bundles of aligned 10-nm-wide twisted vaterite nanofilaments ($n = 340$), both of which are assembled by surfactant interdigitation between adjacent particles.

The above results indicate that the transformation pathways of amorphous barium sulfate or calcium carbonate are determined by the extent of water penetration into the primary cores and the effect of this on electrostatic interactions at the mineral–surfactant interface. The process can be coupled synergistically because the transformations take place in a hydrophobic solvent; thus it is very surprising that analogous nanostructures can be prepared in aqueous media containing certain water-soluble polymers. For example, the crystallization of $BaSO_4$ in the presence of a partially phosphonated poly(ethylene oxide)-*block*-poly(methacrylic acid) copolymer (PEO-*b*-PMAA-PO_3H_2) under quiescent conditions yields bundles of coiled single-crystalline nanofilaments[86] similar to those observed in the microemulsion-based system discussed above. Secondary nucleation of filaments preferentially along the length of the bundles gives rise to cone-shaped structures that splay outwards towards their growth edges (Figure 10a), possibly because of packing pressures associated with the increased thickness. The fiber bundles often show flat growth edges as a result of a self-healing mechanism in which surface defects are filled with nanoparticle building units under energy gain. Related studies on $BaCrO_4$ crystallization also in the presence of PEO-*b*-PMAA-PO_3H_2 showed that sheets of organized nanofilaments could be produced along with the cone-shaped bundles.[88]

Significantly, in common with the microemulsion systems, these polymer-mediated crystallization processes involve the presence of nanometer-sized amorphous precursor particles prior to the nucleation of crystalline nanofilaments. Whereas the water content was crucial for the surfactant-mediated stabilization of the amorphous precursor in the microemulsions, interactions between the amorphous phase and phosphonated block copolymer appear to be sufficiently strong that crystallization is inhibited even in the presence of a vast excess of water. The polymer-coated amorphous precursor particles slowly coalesce into colloidal aggregates (Figure 10b), followed by heterogeneous nucleation of the crystalline phase and anisometric growth (Figure 10c) in accordance with the model of coupled mesoscale transformation (see Figure 7).

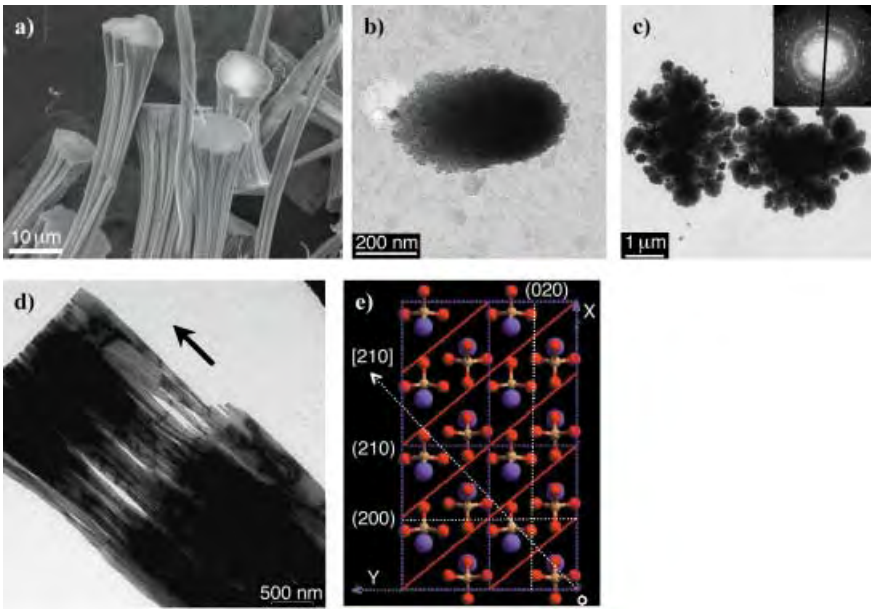


Figure 10. Crystallization of $BaSO_4$ in presence of 1 g L^{-1} PEO-*b*-PMAA-PO_3H_2 (21% phosphonation) at pH 5:[86] a) SEM image of mature $BaSO_4$ fiber bundles, b) TEM image showing aggregate of amorphous particles after 1 h, c) TEM image showing development of crystalline nanofilament bundles within cone-shaped aggregate of amorphous nanoparticles after 3 h. The cones nucleate on the TEM substrate and are viewed preferentially along their long axis, d) high-magnification TEM image showing growth edge and individual nanofilaments; arrow indicates the direction of the [210] axis, e) plot of barite crystal structure viewed perpendicular to the [210] axis (shown by arrow). The (210) face is identified by the red lines and contains coplanar Ba^{2+} and SO_4^{2-} ions.

 © 2003 Wiley-VCH Verlag GmbH & Co. KGaA, Weinheim

As for the surfactant-mediated microemulsion system, the high shape anisotropy indicates preferential adsorption and redistribution of polymer molecules onto certain crystal faces during growth. In the case of the phosphonated block copolymer, this leads to preferred growth along the [210] crystallographic axis, that is, perpendicular to the negatively charged (210) face (Figure 10d,e), which presumably does not interact as strongly with the anionic polymer as the faces parallel to the [210] axis. One possibility is that the vectorial growth is also facilitated by electric fields around the crystal nuclei that direct the attachment of amorphous primary particles present in the aggregate specifically to the tips of the nascent nanofilaments.[86] The high level of crystallographic coherence could also originate from the elimination of high-energy surfaces by oriented particle attachment at the ends of the growing nanofilaments, as observed in other systems (see Section 3).[34] It is remarkable that such vectorially controlled nanoparticle fusion leads to defect-free filaments that have a diameter of a few tens of nanometers but can grow as long as a hundred microns.

A remarkable feature of these systems is their emergent behavior in which self-similar structures become embedded in higher-order architectures as the length scale is extended from the meso to macro level. The cone structures appear to originate from single sheets of nanofilaments during the very early development stage by edge-to-edge attraction and fusion, followed by splaying as a result of lateral packing forces. The process is strongly temperature dependent as shown for $BaCrO_4$ where the self-similar structures develop by slow transformation over days at low temperature, whereas nanofilament sheets and spherical aggregates are produced at room temperature and 100 °C, respectively.[88] Amazingly, the cones are assembled within hierarchical architectures (Figure 11), particularly if the degree of phosphonation of the block copolymer is reduced such that the crystallization inhibition capacity is lowered to a level where higher-order interactions can take place. Multilevel architectures consisting of several generations of cones (Figure 11a) originate from the secondary nucleation of new cones on the rim of existing ones. Surprisingly, this stops the growth of the parent cone even though much of the original rim remains exposed, such that the growth edge becomes smooth and inert. A self-limiting growth mechanism has been proposed based on a critical length associated with the progressive increase in dipole moment along the nanofilaments as they extend in size.[88] Beyond this length, heterogeneous nucleation of a new generation of cones on the rim of the existing structures becomes energetically more favorable than further extension of the rim.

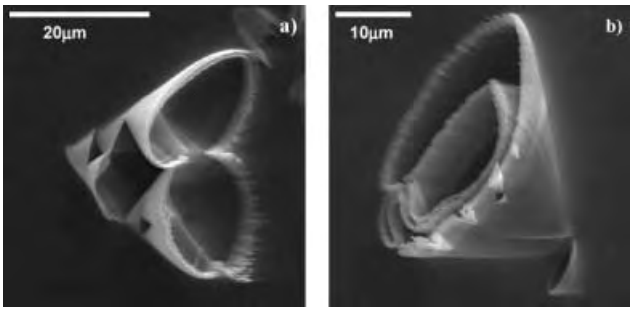


Figure 11. SEM images of higher-order $BaCrO_4$ nanofilament-based structures produced in the presence of 1 g L^{-1} PEO-*b*-PMAA-PO_3H_2 (1% phosphonation) at pH 5:[88] a) cone-on-cone and b) cone-in-core hierarchical forms.

It is noteworthy that similar hierarchical nanofilament-based cone structures have also been reported for the crystallization of $BaSO_4/BaCrO_4$ in the presence of low-molar-mass polyacrylate.[86,87] Although the hierarchical cone structures were only obtained within a limited window of experimental conditions, the much simpler molecular architecture of the polymer additive implies that at least three general requirements have to be fulfilled by the polymer. 1) the molecular length and/or structure must prevent bridging flocculation otherwise the transformation dynamics are severely curtailed. 2) rapid crystallization must be inhibited so that partially stabilized amorphous nanoparticles are produced. 3) the polymer must selectively adsorb on specific crystal faces once the nanocrystal is formed to induce vectorial growth and assembly. Although many polymers might meet these criteria, only a limited number have been identified to date.

The above examples indicate that the formation of macroscopic architectures with embedded structures involves a continuous supply of hybrid nanoparticle precursors to the growth sites of crystals formed initially in association with mesoscopic aggregates. This process can occur over relative long periods of time (days and weeks) as a result of the prolonged nucleation of the amorphous phase by slow release of sequestrated cations from soluble macromolecules, or by delayed aggregation associated with the solvation of surfactant molecules in hydrophobic solvents. In such cases, emergence of the multiscale structures from mesoscopic processes is also dependent on solution-based properties, so that changes in temperature and additive concentration can significantly influence the nature of the final products.[56,82,86,88] In contrast, other studies have highlighted alternative scenarios of morphosynthesis in which macroscopic deposits of the amorphous hybrid precursors are produced by phase separation from the reaction solution. The precursor can take the form of liquid droplets that are enriched in polymers, inorganic ions, and clusters—referred to as a polymer-induced liquid precursor (PILP) process[92]—which together act as a "solute melt" for catastrophic crystal nucleation. For example, liquid–liquid phase separation of $CaCO_3$/polyaspartate droplets gives rise to amorphous hybrid films by coalescence and sedimentation, followed by solidification into crystalline sectors often with nonequilibrium morphologies.[93] Similarly, catastrophic crystallization of calcium phosphate within phase-separated liquid droplets of polyaspartate or polyacrylate prior to sedimentation results in 300-μm diameter spheres with complex radially banded growth textures (Figure 12).[94] The large internal strain associated with rapid crystallization of the multilayered hybrid interior is sufficient to cause fragmentation into cone-shaped domains if the spheres are subjected to small mechanical forces.

 © 2003 Wiley-VCH Verlag GmbH & Co. KGaA, Weinheim



Figure 12. SEM micrograph of a fractured octacalcium phosphate–polyaspartate spheroid showing complex banded texture.[94] The sample was isolated after 45 min; scale bar, 50 μm.

Introduction of solid substrates into the above processes of inorganic–organic coupled mesoscale transformations can result in physical or chemical alignment of the nanostructures with an external surface. Indeed, in the case of the polymer-mediated $BaSO_4/BaCrO_4$ nanofilament superstructures heterogeneous nucleation on the glass walls or TEM grids (see Figure 10c) is fundamental to their formation; crystallization experiments in plastic bottles failed to reproduce the fibers. Thus, it should be possible in general to synthesize oriented assemblies of emergent nanostructures by interfacial control of hybrid mesoscale transformations using template surfaces with appropriate structure and chemistry. Moreover, similar strategies may be of direct relevance in organic-matrix-mediated processes of oriented nucleation in biomineralization, which we now discuss in detail.

6. Mesoscale Transformations and Matrix-Mediated Nucleation in Biomineralization

Although the study of biomineralization[95] has a long and venerable history, it is only during the last two decades that the field has become notable as a rich source of ideas and concepts in modern materials chemistry.[96,97] For centuries, knowledge of biomineralized systems has provided detailed and reliable descriptions of biologically produced inorganic deposits relevant to fields such as medicine, taxonomy, and paleontology. However, only with the input of physical-chemical principles during the 1960s and 70s did these diverse areas of biomineralization become integrated within a general conceptual framework. Above all, the introduction of key ideas borrowed from crystallization theory—such as supersaturation, nucleation and growth mechanisms, substrate-induced oriented nucleation (epitaxy), and habit modification—along with concurrent advances in instrumentation (notably, electron microscopy), played a central role in transforming the field. The coupling of these classical models with an increased knowledge of biological systems gave rise in particular to the notion of organic-matrix-mediated biomineralization, as elaborated in a seminal paper by Lowenstam in 1981.[98]

A key aspect of this theory concerns the role of molecular interactions in controlling oriented nucleation at the matrix–mineral interface.[99–101] The model proposes that a structural and geometric match exists between lattice spacings in certain crystal faces and distances that separate functional groups periodically arranged across an organic surface associated with a macromolecular matrix or lipid vesicle bilayer. The conventional view is that aqueous cations bind at these sites to form a 2D array, followed by binding of counteranions and cluster formation, which results in oriented nucleation as a result of the lowering of the activation energy for a specific crystallographic face (Figure 13, pathway A). A similar outcome can arise from the matrix binding of crystalline nuclei formed either directly from solution or by phase transformation of amorphous clusters in solution (Figure 13 pathway B). In this case, collective interactions involving crystal surfaces on the preformed nuclei and charged/polar groups on the organic matrix are responsible for the preferred crystallographic orientation.

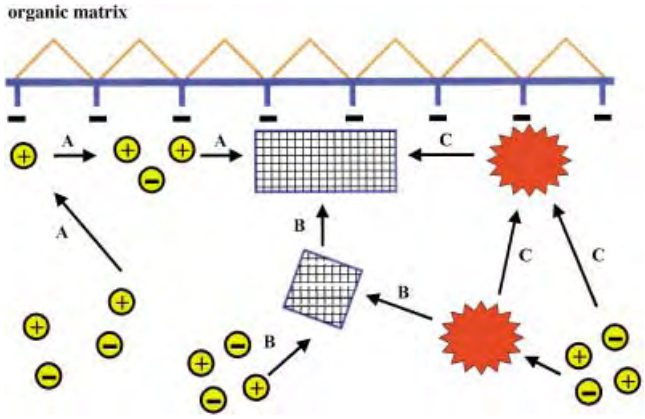


Figure 13. Classical and extended models of organic-matrix-mediated oriented nucleation in biomineralization. See text for details.

In light of the discussions in Section 5, we propose an alternative mechanism in which amorphous primary particles formed by ion or cluster binding at the organic surface undergo coupled matrix-mediated mesophase transformations that result in oriented crystallization (Figure 13, pathway C). As discussed above, depending on the nature and strength of interactions at the inorganic–organic interface, transformations of amorphous nanoparticles can become vectorially regulated within aggregates to produce crystallographically oriented hybrid nanostructures. Thus, it seems possible that the oriented nucleation and initial growth of biominerals could be determined by cooperative processes involving phase transformations at the mesoscopic level, as well as by molecular-based mechanisms such as described in classical theories of organic-matrix-mediated epitaxy.

Our extended model postulates that crystal nucleation and the initial stages of growth occur within an interfacial layer, such as a thin gel-like film of transformable macromolecules, some of which are anchored by connectors to the structural component of the organic matrix or vesicle bilayer

 © 2003 Wiley-VCH Verlag GmbH & Co. KGaA, Weinheim

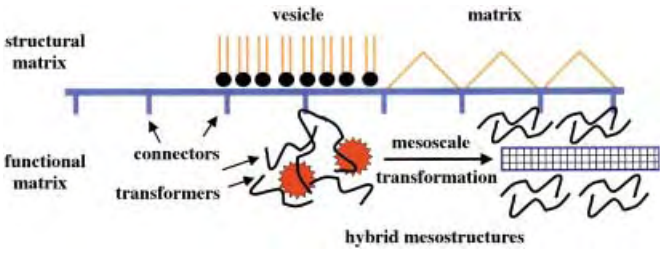


Figure 14. Matrix-mediated interfacial control of coupled mesoscale transformations in oriented nucleation and growth of biominerals.

(Figure 14). Possible candidate biomolecules include: sulfated polysaccharide PS2 in coccoliths,[102] multifunctional shell-matrix proteins, MSI60 and N16,[103] and lustrin A,[104] and collagen-binding proteins, such as osteonectin.[105] We propose that crystallization proceeds within this interfacial layer by mesoscale transformation of hybrid aggregates consisting of intimately associated amorphous inorganic nanoparticles and adsorbed macromolecules. In support of this mechanism, there are several examples of hybrid nanoparticles produced during the early stages of biomineralization, for example, in sea urchin embryo spiculogenic cells,[27] in association with coccolith polysaccharides,[106] rat dentin phosphoproteins,[107] phosphoproteins from several species of bivalve molluscs,[108] and as coatings on oyster shells.[109] The model considers crystallization to occur within these hybrid aggregates by coupled inorganic–organic interactions, as discussed in Section 5. The matrix is therefore no longer viewed as a static structural/functional template with binding potential for directed nucleation, but as comprising a dynamic interface that is inherently reactive and subject to mesoscale transformation. In addition, molecular recognition is not considered to be the principal driving force but is replaced by multilevel interactions that induce preferential orientation with respect to the structural matrix as an emergent property of the system.

It is important to note that similar processes could give rise to oriented crystallization even in the absence of a physical surface—for instance when the matrix is "internalized" within an isotropic gel monolith—provided that some stress field is imposed on the system. For example, the initial stages of enamel formation occur in a gel of amelogenin

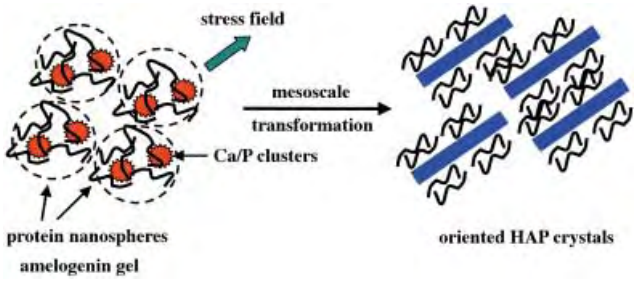


Figure 15. Stress-induced alignment of mesoscale transformations within gel-like organic matrices involved in biomineralization. The scheme shows a mechanism for oriented crystallization of hydroxyapatite (HAP) nanofilaments in dental enamel.

protein nanospheres,[110] and we propose that loading the organic aggregates with calcium phosphate clusters results in a coupled mesoscale transformation, which in the presence of an applied stress field produces an oriented array of ribbon-like carbonated hydroxyapatite nanocrystallites and associated macromolecules (Figure 15). The stress field could originate internally through progressive changes in densification, or externally through the action of adjacent cells. Similar mechanisms might apply to proteoglycans in cartilage,[111] and polysaccharides, such as chitin in mineralized molluscan teeth.[112]

7. Summary and Outlook

In this review we have attempted to establish some principles and concepts that elucidate the potential of synthesis-construction pathways involving mesoscale self-assembly and transformation processes. We have focused in particular on the interplay of aggregation and crystallization, and their influence on the cooperative reorganization of inorganic and organic building blocks and emergence of higher-order architectures with embedded structures. The following conclusions have been highlighted:

- Kinetic pathways of crystallization involve multistep pathways that if regulated, for example, by macromolecules and surfactants, could significantly increase the scope for controlled materials synthesis.
- Amorphous phases are prominent in kinetic pathways of crystallization and can be stabilized by organic macromolecules or transformed into crystalline phases, some of which (Mg-calcite, for example) may have high isomorphic substitutions.
- Crystal growth by the ordered aggregation of preformed crystalline building blocks is a mesoscale assembly process that results in single crystals with iso-oriented mosaic textures. The size and shape of the nanosized building blocks influence crystal morphology, and restructuring and/or oriented attachment at the particle–particle interfaces is required for long-range crystallographic continuity.
- Macromolecules and surfactants can bind to nanocrystal surfaces to produce inorganic–organic particles with shape and size specificity that can act as hybrid building blocks in aggregation-based pathways of crystal growth. Occlusion of surface-bound organic molecules influences the crystal texture and at high concentrations results in crystallographic discontinuities and the evolution of complex morphologies.
- Stabilized hybrid building blocks with shape anisotropy undergo mesoscale self-assembly to produce organized nanoparticle-based superstructures linked by organic connectors. The driving force for assembly can originate from disorder–order mesophase transitions, such as the formation of interparticle surfactant bilayers, or molecular recognition between biomolecules, such as single-stranded oligonucleotides. Another possibility not discussed in this review is the formation of hybrid nanocomposites through synthesis and self-assembly.[113,114]

 © 2003 Wiley-VCH Verlag GmbH & Co. KGaA, Weinheim

- Amphiphilic polymers can influence the assembly of amorphous silica nanoparticles by phase separation and liquid-crystalline phase transitions. These processes are influenced by incipient changes in aggregation and densification to produce patterned materials.
- Emergent processes involving coupled mesoscale transformations within aggregates of hybrid building blocks with metastable amorphous interiors can give rise to the spontaneous assembly of crystalline nanostructures with complex form and higher-order organization. Such structures are mediated by surface-adsorbed surfactants or polymers, and are propagated across a range of length scales to produce hierarchical self-similar architectures.
- Coupling of amorphous-to-crystal transformations with surfactant or macromolecular reorganization is strongly influenced by electrostatic interactions and the degree of hydration at the inorganic–organic interface, as well as the hydrophobic and van der Waals attractive forces between the surface-adsorbed organic molecules.

Finally, we used the above concepts to suggest some new ideas about oriented nucleation in biomineralization. The conventional model of molecular recognition at the organic–inorganic interface was extended to consider the role of matrix-mediated mesophase transformations involving aggregates of macromolecules and amorphous primary particles located at the organic surface or in the form of structured gels. In the past, biomineralization studies have inspired many novel approaches in materials research and nanochemistry,[115,116] which are now sufficiently developed that as illustrated in this review, new concepts are being generated that have potential biological relevance. Thus, the translation from biomineralization to biomimetics is no longer unidirectional but synergistic. We therefore expect that this increasing feedback loop will not only stimulate further research in the inorganic structures of life but also continue to drive our vision and imagination in laboratory studies on the chemistry of organized matter.

We thank Drs M. Li, L. M. Qi, and S. H. Yu for key experimental studies on the microemulsion-based and polymer-based syntheses of organized nanostructures and arrays, and Prof. A. Bigi and E. Boanini for collaborative studies on the growth of complex calcium phosphate spheroids.

Received: October 16, 2002 [A562]

[1] P. Yang, A. H. Rizvi, B. Messer, B. F. Chmelka, G. M. Whitesides, G. D. Stucky, *Adv. Mater.* **2001**, *13*, 427 – 431.
[2] W. Shenton, D. Pum, U. B. Sleytr, S. Mann, *Nature* **1997**, *389*, 585 – 587.
[3] C. B. Murray, C. R. Kagan, M. G. Bawendi, *Science* **1995**, *270*, 1335 – 1338.
[4] Z. L. Wang, *Adv. Mater.* **1998**, *10*, 13 – 30.
[5] R. P. Andres, J. D. Bielefeld, J. I. Henderson, D. B. Janes, V. R. Kolagunta, C. P. Kubiak, W. J. Mahoney, R. G. Osifchin, *Science* **1996**, *273*, 1690 – 1693.
[6] T. H. Galow, A. K. Boal, V. M. Rotello, *Adv. Mater.* **2000**, *12*, 576 – 579.
[7] C. A. Mirkin, R. L. Letsinger, R. C. Mucic, J. J. Storhoff, *Nature* **1996**, *382*, 607 – 609.
[8] S. Mann, W. Shenton, M. Li, S. Connolly, D. Fitzmaurice, *Adv. Mater.* **2000**, *12*, 147 – 150.
[9] E. Dujardin, L.-B. Hsin, C. R. C. Wang, S. Mann, *Chem. Commun.* **2001**, 1264 – 1265.
[10] S. Mann, *Angew. Chem.* **2000**, *112*, 3532 – 3548; *Angew. Chem. Int. Ed.* **2000**, *39*, 3392 – 3406.
[11] S. Mann, *Biomimetic Materials Chemistry*, VCH, New York, **1996**.
[12] *Biomimetics: Design and Processing of Materials* (Eds.: M. Sarikaya, I. A. Aksay), AIP Press, Woodbury, NY, **1995** (American Institute of Physics Series in Polymers and Complex Materials).
[13] M. Yoshimura, W. Suchanek, K. Byrappa, *MRS Bull.* **2000**, *9*, 17 – 25.
[14] S. H. Yu, *J. Ceram. Soc. Jpn.* **2001**, *109*, S65 – S75.
[15] J. Rieger, E. Hädicke, I. U. Rau, D. Boeckh, *Tenside Surfactants Deterg.* **1997**, *34*, 430 – 435.
[16] O. Söhnel, J. W. Mullin, *J. Cryst. Growth* **1982**, *60*, 239 – 250.
[17] The classical theory of nucleation considers the spontaneous formation of spherical molecular clusters with size-dependent free energies that continue to grow only when larger than the threshold value of the critical radius (D. H. Everett, *Basic Principles of Colloid Science*, The Royal Society of Chemistry, London, **1988**; O. Söhnel, J. Garside *Precipitation*, Butterworth-Heinemann, Oxford, **1992**). The model predicts the size of the critical nucleus and associated activation energy and nucleation rate, as well as their dependence on supersaturation, but is severely limited by a number of assumptions and simplifications. In particular, the structure and composition of the nucleus is considered to be the same as the bulk crystalline phase and the formation of subcritical supramolecular clusters or complexes (H. Cölfen, H. Schnablegger, A. Fischer, F. C. Jentoft, G. Weinberg, R. Schlögl, *Langmuir* **2002**, *18*, 3500 – 3509) and multistep assembly of large unit-cell structures are not addressed. Moreover, the experimental characterization of these transient solution species remains a major challenge, such that a quantitative/mechanistic analysis of nucleation is still to be developed.
[18] H. J. Arnott in, *Mechanisms of Biomineralization in Animals and Plants* (Eds.: M. Omori, N. Watabe), Tokai University Press, Tokyo, **1980**.
[19] J. Aizenberg, G. Lambert, L. Addadi, S. Weiner, *Adv. Mater.* **1996**, *8*, 222 – 226.
[20] J. Aizenberg, G. Lambert, S. Weiner, L. Addadi, *J. Am. Chem. Soc.* **2002**, *124*, 32 – 39.
[21] M. G. Taylor, K. Simkiss, G. N. Greaves, M. Okazaki, S. Mann, *Proc. R. Soc. London Ser. B* **1993**, *252*, 75 – 80.
[22] Y. Levi-Kalisman, S. Raz, S. Weiner, L. Addadi, *Adv. Funct. Mater.* **2002**, *12*, 43 – 48.
[23] B. Hasse, H. Ehrenberg, J. C. Marxen, W. Becker, M. Epple, *Chem. Eur. J.* **2000**, *6*, 3679 – 3685.
[24] S. Raz, S. Weiner, L. Addadi, *Adv. Mater.* **2000**, *12*, 38 – 42.
[25] A. Ziegler, *J. Struct. Biol.* **1994**, *112*, 110 – 116.
[26] E. Beniash, J. Aizenberg, L. Addadi, S. Weiner, *Proc. R. Soc. London Ser. B* **1997**, *264*, 461 – 465.
[27] E. Beniash, L. Addadi, S. Weiner, *J. Struct. Biol.* **1999**, *125*, 50 – 62.
[28] A. Tsortos, S. Ohki, A. Zieba, R. E. Baier, G. H. Nancollas, *J. Colloid Interface Sci.* **1996**, *177*, 257 – 262.
[29] S. Mann, D. D. Archibald, J. M. Didymus, T. Douglas, B. R. Heywood, F. C. Meldrum, N. J. Reeves, *Science* **1993**, *261*, 1286 – 1292.
[30] A. M. Belcher, X. H. Wu, R. J. Christensen, P. K. Hansma, G. D. Stucky, D. E. Morse, *Nature* **1996**, *381*, 56 – 58.
[31] C. A. Orme, A. Noy, A. Wierzbicki, M. T. McBride, M. Grantham, H. H. Teng, P. M. Dove, J. J. DeYoreo, *Nature* **2001**, *411*, 775 – 779.

 © 2003 Wiley-VCH Verlag GmbH & Co. KGaA, Weinheim

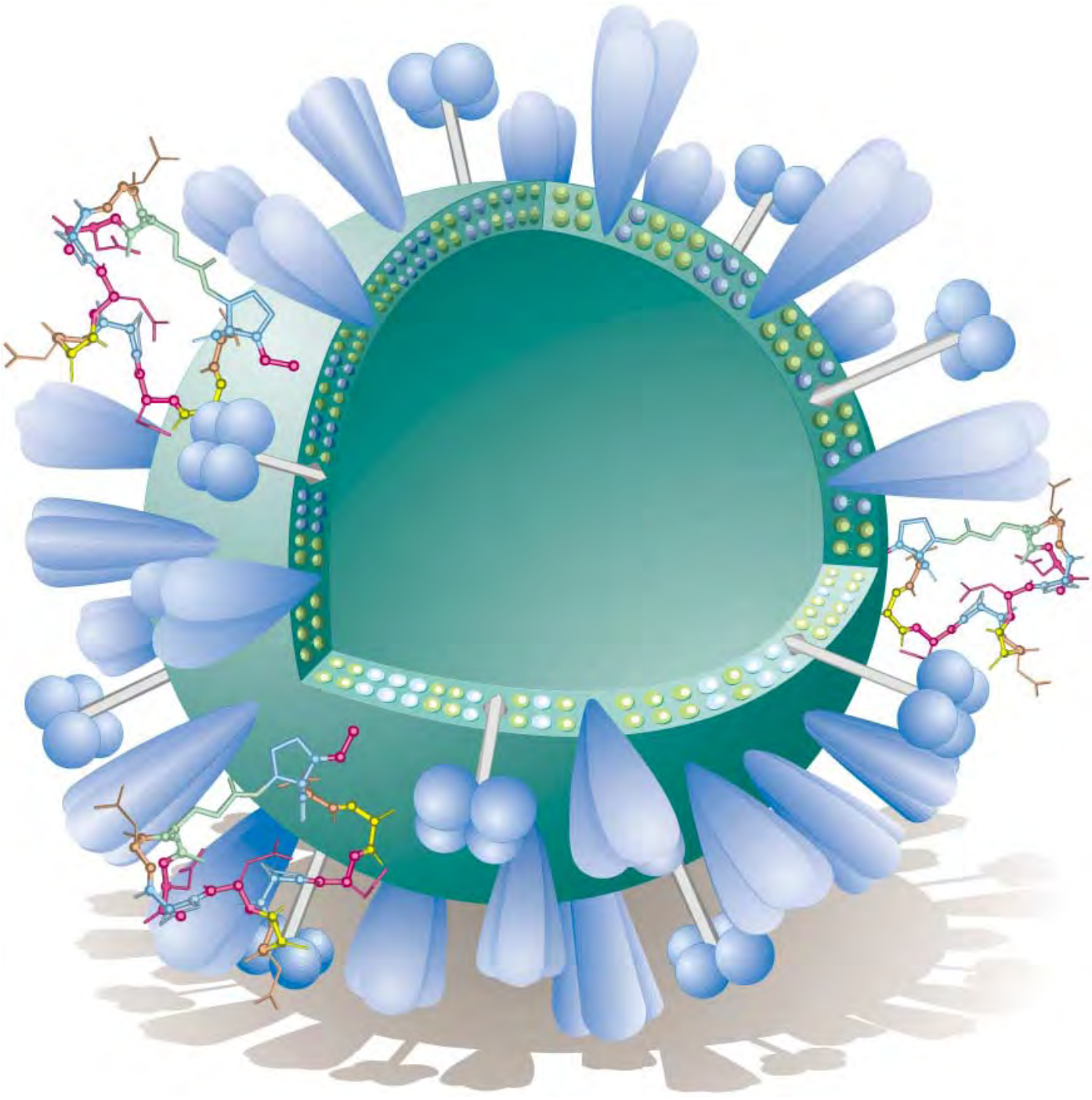
[32] The classical model of crystal growth is based on surface–solution interactions, which result in secondary nucleation, subjected to various conditions of rate limitation—which include mass transport, polynucleation, layer-by-layer growth, screw dislocations. Growth is through the addition of soluble ions, molecules, ion-pairs, and complexes to active sites on the existing crystal surface, such as kinks and steps. Various mechanistic equations have been derived: W. K. Burton, N. Cabrera, F. C. Frank, *Philos. Trans. R. Soc. London Ser. A* **1951**, *243*, 299 – 358.
[33] N. Jongen, P. Bowen, J. Lemaître, J. C. Valmalette, H. Hofmann, *J. Colloid Interface Sci.* **2000**, *226*, 189 – 198.
[34] R. L. Penn, J. F. Banfield, *Geochim. Cosmochim. Acta* **1999**, *63*, 1549 – 1557.
[35] E. Matijevic, P. Sheiner, *J. Colloid Interface Sci.* **1978**, *63*, 509 – 524.
[36] W. P. Hsu, L. Ronnquist, E. Matijevic, *Langmuir* **1988**, *4*, 31 – 37.
[37] S. H. Lee, Y. S. Her, E. Matijevic, *J. Colloid Interface Sci.* **1997**, *186*, 193 – 202.
[38] T. Sugimoto, Y. Wang, H. Itoh, A. Muramatsu, *Colloids Surf. A* **1998**, *134*, 265 – 279.
[39] V. Privman, D. V. Goia, J. Park, E. Matijevic, *J. Colloid Interface Sci.* **1999**, *213*, 36 – 45.
[40] M. Ocana, M. P. Morales, C. J. Serna, *J. Colloid Interface Sci.* **1995**, *171*, 85 – 91; M. Ocana, M. P. Morales, C. J. Serna, *J. Colloid Interface Sci.* **1999**, *212*, 317 – 323.
[41] J. F. Banfield, S. A. Welch, H. Zhang, T. T. Ebert, R. L. Penn, *Science* **2000**, *289*, 751 – 754.
[42] C. Pacholski, A. Kornowski, H. Weller, *Angew. Chem.* **2002**, *114*, 1234 – 1237; *Angew. Chem. Int. Ed.* **2002**, *41*, 1188 – 1191.
[43] M. Yeadon, M. Ghaly, J. C. Yang, R. S. Averback, J. M. Gibson, *Appl. Phys. Lett.* **1998**, *73*, 3208 – 3210.
[44] D. M. Murphy-Wilhelmy, E. Matijevic, *J. Chem. Soc. Faraday Trans. 1* **1984**, *80*, 536 – 570.
[45] J. H. Adair, E. Suvaci, *Curr. Opin. Colloid Interface Sci.* **2000**, *5*, 160 – 167.
[46] H. Cölfen, L. M. Qi, Y. Mastai, L. Börger, *Cryst. Growth Des.* **2002**, *2*, 191 – 196.
[47] "The Stability of Solid/Liquid Dispersions in the Presence of Polymers": B. Vincent in *Solid/Liquid Dispersions* (Ed.: T. F. Tadros), Academic Press, London, **1987**.
[48] G. J. Fleer, M. A. Cohen Stuart, J. M. H. Scheutjens, T. Cosgrove, B. Vincent, *Polymers at Interfaces*, Chapman Hall, London, **1993**.
[49] L. M. Qi, H. Cölfen, M. Antonietti, *Angew. Chem.* **2000**, *112*, 617 – 621; *Angew. Chem. Int. Ed.* **2000**, *39*, 604 – 607.
[50] A. Taubert, D. Palms, Ö. Weiss, M. T. Piccini, D. N. Batchelder, *Chem. Mater.* **2002**, *14*, 2594 – 2601.
[51] G. Wegner, P. Baum, M. Müller, J. Norwig, K. Landfester, *Macromol. Symp.* **2001**, *175*, 349 – 355.
[52] A. Berman, L. Addadi, S. Weiner, *Nature* **1988**, *331*, 546 – 548.
[53] A. Berman, J. Hanson, L. Leiserowitz, T. F. Koetzle, S. Weiner, L. Addadi, *Science* **1993**, *259*, 776 – 779.
[54] J. Aizenberg, J. Hanson, T. F. Koetzle, S. Weiner, L. Addadi, *J. Am. Chem. Soc.* **1997**, *119*, 881 – 886.
[55] L. M. Qi, H. Cölfen, M. Antonietti, *Chem. Mater.* **2000**, *12*, 2392 – 2403.
[56] H. Cölfen, L. M. Qi, *Chem. Eur. J.* **2001**, *7*, 106 – 116.
[57] R. Kniep, S. Busch, *Angew. Chem.* **1996**, *108*, 2788 – 2791; *Angew. Chem. Int. Ed. Engl.* **1996**, *35*, 2624 – 2626.
[58] S. Busch, H. Dolhaine, A. DuChesne, S. Heinz, O. Hochrein, F. Laeri, O. Podebrad, U. Vietze, T. Weiland, R. Kniep, *Eur. J. Inorg. Chem.* **1999**, 1643 – 1653.
[59] S. H. Yu, H. Cölfen, J. Hartmann, M. Antonietti, *Adv. Funct. Mater.* **2002**, *12*, 541 – 545.
[60] H. Cölfen, M. Antonietti, *Langmuir* **1998**, *14*, 582 – 589.
[61] H. Cölfen, *Macromol. Rapid Commun.* **2001**, *22*, 219 – 252.
[62] L. M. Qi, J. Li, J. M. Ma, *Chem. J. Chin. Univ.* **2002**, *23*, 1595 – 1597.
[63] S. A. Davis, M. Breulmann, K. H. Rhodes, B. Zhang, S. Mann, *Chem. Mater.* **2001**, *13*, 3218 – 3226.
[64] S. Mann, S. A. Davis, S. R. Hall, M. Li, K. H. Rhodes, W. Shenton, S. Vaucher, B. Zhang, *J. Chem. Soc. Dalton Trans.* **2000**, 3753 – 3763.
[65] X. Peng, L. Manna, W. Yang, J. Wickham, E. Scher, A. Kadavanich, A. P. Alivisatos, *Nature* **2000**, *404*, 59 – 61.
[66] M. Brust, D. Bethell, D. J. Schiffrin, C. J. Kiely, *Adv. Mater.* **1995**, *7*, 795 – 797.
[67] M. Li, H. Schnablegger, S. Mann, *Nature* **1999**, *402*, 393 – 395.
[68] B. Nikoobakht, Z. L. Wang, M. A. El-Sayed, *J. Phys. Chem. B* **2000**, *104*, 8635 – 8640.
[69] V. F. Puntes, K. M. Krishnan, A. P. Alivisatos, *Science* **2001**, *291*, 2115 – 2117.
[70] N. R. Jana, L. A. Gearheart, S. O. Obare, C. J. Johnson, K. E. Edler, S. Mann, C. J. Murphy, *J. Mater. Chem.*, **2002**, *12*, 2909 – 2912.
[71] C. A. Mirkin, R. L. Letsinger, R. C. Mucic, J. J. Storhoff, *Nature* **1996**, *382*, 607 – 609.
[72] A. P. Alivisatos, K. P. Johnsson, X. G. Peng, T. E. Wilson, C. J. Loweth, M. P. Bruchez, P. G. Schulz, *Nature* **1996**, *382*, 609 – 611.
[73] E. H. Tadd, J. Bradley, R. Tannenbaum, *Langmuir* **2002**, *18*, 2378 – 2384.
[74] J. P. Spatz, S. Mössmer, C. Hartmann, M. Möller, T. Herzog, M. Krieger, H. G. Boyen, P. Ziemann, B. Kabius, *Langmuir* **2000**, *16,* 407 – 415.
[75] Y. Boontongkong, R. E. Cohen, *Macromolecules* **2002**, *35*, 3647 – 3652.
[76] W. A. Lopes, H. M. Jaeger, *Nature* **2001**, *414*, 735 – 738.
[77] C. G. Göltner, S. Henke, M. C. Weissenberger, M. Antonietti, *Angew. Chem.* **1998**, *110*, 633 – 636; *Angew. Chem. Int. Ed.* **1998**, *37*, 613 – 616.
[78] D. Zhao, W. Huo, J. Feng, B. F. Chmelka, G. D. Stucky, *J. Am. Chem. Soc.* **1998**, *120*, 6024 – 6036.
[79] Many conventional surfactants have also been used to prepare mesoporous silicas, for example, C. T. Kresge, M. E. Leonowicz, W. J. Roth, J. C. Vartuli, J. S. Beck, *Nature* **1992**, *359*, 710 – 712.
[80] M. Sumper, *Science* **2002**, *295*, 2430 – 2433.
[81] E. G. Vrieling, T. P. M. Beelen, R. A. van Santen, W. C. Gieskes, *Angew. Chem.* **2002**, *114*, 1613 – 1616; *Angew. Chem. Int. Ed.* **2002**, *41*, 1543 – 1546.
[82] M. Li, S. Mann, *Langmuir* **2000**, *16*, 7088 – 7094.
[83] L. M. Qi, J. Ma, H. Cheng, Z. Zhao, *J. Phys. Chem. B* **1997**, *101*, 3460 – 3463.
[84] G. D. Rees, R. Evans-Gowing, S. J. Hammond, B. H. Robinson, *Langmuir* **1999**, *15*, 1993 – 2002.
[85] M. Li, S. Mann, *Adv. Functional Mater.,* **2002**, *12*, 773 – 779.
[86] L. M. Qi, H. Cölfen, M. Antonietti, M. Li, J. D. Hopwood, A. J. Ashley, S. Mann, *Chem. Eur. J.* **2001**, *7*, 3526 – 3532.
[87] S. H. Yu, M. Antonietti, H. Cölfen, *Nano Lett.*, **2003**, *3*, 379 – 382.
[88] S. H. Yu, H. Cölfen, M. Antonietti, *Chem. Eur. J.* **2002**, *8*, 2937 – 2945.
[89] M. Antonietti, M. Breulmann, C. G. Göltner, H. Cölfen, K. K. W. Wong, D. Walsh, S. Mann, *Chem. Eur. J.* **1998**, *4*, 2491 – 2500.
[90] A. Peytcheva, H. Cölfen, H. Schnablegger, M. Antonietti, *Colloid Polym. Sci.* **2002**, *280*, 218 – 227.
[91] D. B. Zhang, L. M. Qi, J. M. Ma, H. M. Cheng, *Chem. Mater.* **2001**, *13*, 2753 – 2755.
[92] L. B. Gower, D. A. Tirrell, *J. Cryst. Growth* **1998**, *191*, 153 – 160.
[93] L. B. Gower, D. J. Odom, *J. Cryst. Growth* **2000**, *210*, 719 – 734.

 © 2003 Wiley-VCH Verlag GmbH & Co. KGaA, Weinheim

[94] A. Bigi, E. Boanini, D. Walsh, S. Mann, *Angew. Chem.* **2002**, *114*, 2267 – 2270; *Angew. Chem. Int. Ed.* **2002**, *41*, 2163 – 2166.
[95] H. A. Lowenstam, S. Weiner, *On Biomineralization*, Oxford University Press, New York, **1989**, pp. 207 – 251.
[96] E. Bäuerlein, *Biomineralization: From Biology to Biotechnology and Medical Application*, Wiley-VCH, Weinheim, **2000**.
[97] S. Mann, *Biomineralization. Principles and Concepts in Bioinorganic Materials Chemistry*, Oxford University Press, Oxford, **2001**.
[98] H. A. Lowenstam, *Science* **1981**, *211*, 1126 – 1131.
[99] S. Mann, *Nature* **1988**, *332*, 119 – 124.
[100] S. Weiner, W. Traub, *Philos. Trans. R. Soc. London Ser. B* **1984**, *304*, 425 – 434.
[101] L. Addadi, S. Weiner, *Proc. Natl. Acad. Sci. USA* **1985**, *82*, 4110 – 4114.
[102] M. E. Marsh, D. P. Dickinson, *Protoplasma* **1997**, *199*, 9 – 17.
[103] T. Samata, N. Hayashi, M. Kono, K. Hasegawa, C. Horita, S. Akera, *FEBS Lett.* **1999**, *462*, 225 – 229.
[104] X. Shen, A. M. Belcher, P. K. Hansma, G. D. Stucky, D. E. Morse, *J. Biol. Chem.* **1997**, *272*, 32472 – 32481.
[105] J. D. Termine, *Rheumatology* **1986**, *10*, 499 – 509.
[106] M. E. Marsh, *Protoplasma* **1994**, *177*, 108 – 122.
[107] M. E. Marsh, *Biochemistry* **1989**, *28*, 339 – 345.
[108] M. E. Marsh, R. L. Sass, *J. Exp. Zool.* **1985**, *234*, 237 – 242.
[109] C. S. Sikes, A. P. Wheeler, A. Wierzbicki, R. M. Dillaman, L. De Luca, *Biol. Bull.* **1998**, *194,* 304 – 316.
[110] "Dental Enamel": A. G. Fincham, J. P. Simmer, *Ciba Found. Symp.* **1997**, *205*, 118 – 134.
[111] L. W. Fischer in *The Chemistry and Biology of Mineralized Tissues* (Ed.: W. T. Butler), EBSCO Media, Birmingham, AL, **1985**, pp. 188 – 195.
[112] J. Webb, D. J. Macey, S. Mann in *Biomineralization: Chemical and Biochemical Perspectives* (Ed.: S. Mann, J. Webb, R. J. P. Williams), VCH, Weinheim, **1989**, pp. 345 – 438.
[113] G. J. A. A. Soler-Illia, C. Sanchez, B. Lebeau, J. Paterin, *Chem. Rev.* **2002**, *102*, 4093.
[114] C. Sanchez, G. J. A. A. Soler-Illia, F. Ribot, C. Mayer, V. Cabuil, T. Lalot, *Chem. Mater.* **2001**, *13*, 3061.
[115] The loose translation of biomineralization concepts has inspired the synthesis-with-construction of organized nanostructures, oriented crystal arrays, microarchitectures with complex form, and hierarchical materials with structure and form extending across many length scales (A. H. Heuer, D. J. Fink, V. J. Laraia, J. L. Arias, P. D. Calvert, K. Kendall, G. L. Messing, J. Blackwell, P. C. Rieke, D. H. Thompson, A. P. Wheeler, A. Veis, A. I. Caplan, *Science* **1992**, *255*, 1098 – 1105; S. Mann, G. A. Ozin, *Nature* **1996**, *382*, 313 – 318; S. Mann, *Nature* **1993**, *365*, 499 – 505; S. Mann, S. L. Burkett, S. A. Davis, C. E. Fowler, N. H. Mendelson, S. D. Sims, D. Walsh, N. T. Whilton, *Chem. Mater.* **1997**, *9*, 2300 – 2310).
[116] Potential spin-offs from biomineral-inspired research include; a) oriented nucleation of inorganic crystals and thin films using functionalied organic surfaces ((B. R. Heywood, S. Mann, *Adv. Mater.* **1994**, *6*, 9 – 20; I. A. Aksay, M. Trau, S. Manne, I. Honma, N. Yao, L. Zhou, P. Fenter, P. M. Eisenberger, S. M. Gruner, *Science* **1996**, *273*, 892 – 898; J. Yang, F. C. Meldrum, J. H. Fendler, *J. Phys. Chem.* **1995**, *99*, 5500 – 5504; J. Aizenberg, A. J. Black, G. M. Whitesides, *Nature* **1999**, *398*, 495 – 498), b) use of bioorganic supramolecular structures, such as vesicles and lipid tubules, to direct the nucleation and growth of shaped inorganic materials (D. D. Archibald, S. Mann, *Nature* **1993**, *364*, 430 – 433; P. T. Tanev, T. J. Pinnavaia, *Science* **1996**, *271*, 1267 – 1269; J. D. Hartgerink, E. Beniash, S. I. Stupp, *Science* **2001**, *294*, 1684 – 1688; A. M. Seddon, H. M. Patel, S. L. Burkett, S. Mann, *Angew. Chem.* **2002**, *114*, 3114 – 3117; *Angew. Chem. Int. Ed.* **2002**, *41*, 2988 – 2991), c) new developments in the design of additives, such as block copolymers and dendrimers for control of crystal habit (ref. [57] and H. Cölfen, L. M. Qi, *Chem. Eur. J.* **2001**, *7*, 106 – 116; H. Cölfen, M. Antonietti, *Langmuir* **1998**, *14*, 582 – 589; J. J. J. M. Donners, B. R. Heywood, E. W. Meijer, R. J. M. Nolte, C. Roman, A. P. H. J. Schenning, N. A. J. M. Sommerdijk, *Chem. Commun.* **2000**, 1937 – 1938; K. Naka, Y. Tanaka, Y. Chujo, Y. Ito, *Chem. Commun.* **1999**, 1931 – 1932; J. M. Marentette, J. Norwig, E. Stockelmann, W. H. Meyer, G. Wegner, *Adv. Mater.* **1997**, *9*, 647 – 651; K. L. Robinson, J. W. V. M. Weaver, S. P. Armes, E. D. Marti, F. C. Meldrum, *J. Mater. Chem.* **2002**, *12*, 890 – 896), and d) developments in the laboratory synthesis of inorganic materials with complex form by using organized reaction systems (D. Walsh, S. Mann, *Nature* **1995**, *377*, 320 – 323; D. Walsh, J. D. Hopwood, S. Mann, *Science* **1994**, *264*, 1576 – 1578; D. Walsh, B. Lebeau, S. Mann, *Adv. Mater.* **1999**, *11*, 324 – 328; T. Hirai, S. Hariguchi, I. Komasawa, R. J. Davey, *Langmuir* **1997**, *13*, 6650 – 6653; L. B. Gower, D. A. Tirrell, *J. Cryst. Growth* **1998**, *191*, 153 – 160).

 © 2003 Wiley-VCH Verlag GmbH & Co. KGaA, Weinheim

Communications



Making the influenza virus look more like the malaria parasite could have important implications for synthetic-vaccine design. New synthetic mimotopes displayed on virosomes elicit a strong antibody response against the malaria parasite *P. falciparum*. For more information see the following Communication by Pluscke, Robinson, and co-workers.

DOI: 10.1002/anie.200250348
© 2003 Wiley-VCH Verlag GmbH & Co. KGaA, Weinheim

Peptidomimetic Vaccine Design

A Virosome-Mimotope Approach to Synthetic Vaccine Design and Optimization: Synthesis, Conformation, and Immune Recognition of a Potential Malaria-Vaccine Candidate

Bernhard Pfeiffer, Elisabetta Peduzzi, Kerstin Moehle, Rinaldo Zurbriggen, Reinhard Glück, Gerd Pluschke, and John A. Robinson**

Attempts to produce a vaccine against the malaria parasite *Plasmodium falciparum* have so far met with limited success. The molecules used to stimulate a protective antibody response have in general shown only poor efficacy in humans.[1] Synthetic peptides are attractive targets for vaccine design, as they are readily synthesized and are able to target specific antigens, but their use has suffered a number of drawbacks.[2] These include poor immunogenicity and poor mimicry of conformational epitopes, poor proteolytic stability, and the lack of a suitable delivery system in humans. To enhance immunogenicity, short peptides are usually coupled to a carrier protein and then injected together with an immunostimulatory adjuvant, which for humans is typically an alum-absorbed antigen.

We introduce herein an alternative approach to synthetic-vaccine design and optimization (see Figure 1), which involves the use of peptidomimetics delivered to the immune system on the surface of immunopotentiating reconstituted influenza virosomes (IRIVs).[3] The IRIVs are similar to liposomes, but contain influenza-derived, membrane-bound hemagglutinin and neuraminidase, which impart fusogenic activity and facilitate antigen delivery to immunocompetent cells. The potential advantages of IRIVs for vaccine delivery include their fusogenic activity, the surface display of molecularly defined antigens, and compatibility with both animals (e.g. mice) and humans.[4] Sequential rounds of mimetic optimization based on structure–activity relationships may ideally lead to vaccine candidates, which after appropriate preclinical profiling, can be tested in human clinical trials.[5] It is expected that the extensive clinical experience obtained with two IRIV-based vaccines already licensed[5] will facilitate the development of new IRIV-mimotope vaccine candidates. We illustrate this approach herein with a model system comprising the NPNA-repeat epitope from *Plasmodium falciparum*.

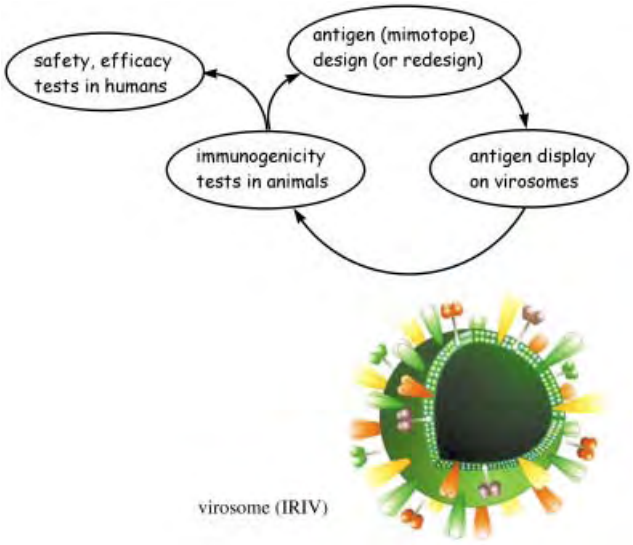


Figure 1. Using virosome technology, sequential cycles of design, testing and optimization of peptidomimetics in animal models can be followed by human clinical trials with the same molecularly defined adjuvant/delivery system.

One of the early synthetic malaria-vaccine candidates to be tested in humans was a linear $(NANP)_3$ peptide conjugated to tetanus toxin in alum.[6] This peptide mimics epitopes in the central repeat region $(NPNA)_{\approx 37}$ of the major surface protein on sporozoites, the circumsporozoite (CS) protein.[7,8] However, the efficacy of this construct in humans was poor. Building on these earlier studies, we describe below an improved NPNA mimetic incorporated into IRIVs and its potential as a new malaria-vaccine candidate.

A key step in the design of the new mimetic evolved from earlier studies[9] of **1** (Figure 2) as well as of linear $(NPNA)_n$

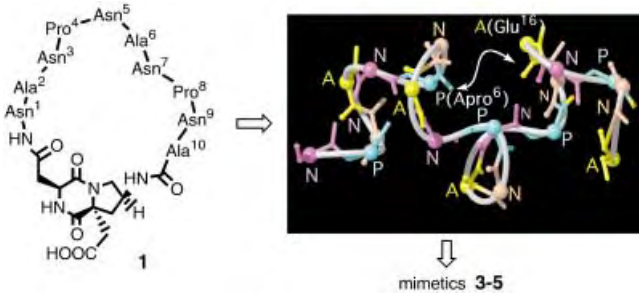


Figure 2. Mimetic **1** and a computer model of Ac-$(NPNA)_5$-NH_2 with a backbone conformation in which each NPNA motif adopts a helical β turn (see text). The arrows indicate the position of the proposed amide cross-link between (2*S*,3*R*)-3-aminoproline (Apro, residue 6) and glutamic acid (Glu, residue 16). Color coding: Asn = pink, Pro = cyan, Asn = coral, Ala = yellow. The C_α atoms are each marked along the ribbon with a ball.

[*] Prof. J. A. Robinson, Dr. B. Pfeiffer, Dr. K. Moehle
Institute of Organic Chemistry, University of Zurich
8057 Zurich, Winterthurerstrasse 190, 8057 Zürich (Switzerland)
Fax: (+41) 1-635-6833
E-mail: robinson@oci.unizh.ch

Prof. G. Pluschke, E. Peduzzi
Swiss Tropical Institute
Socinstrasse 57, 4002 Basel (Switzerland)
Fax: (41) 1-61-271-8654
E-mail: Gerd.Pluschke@unibas.ch

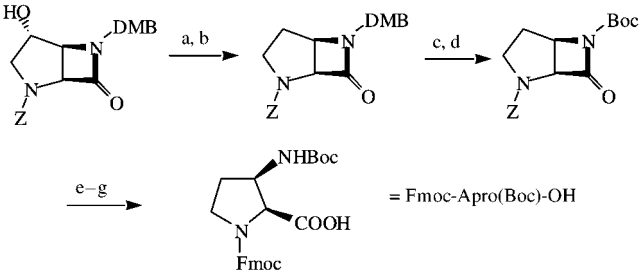
Dr. R. Zurbriggen
Pevion-Biotech
Rehhagstrasse 79, 3018 Bern (Switzerland)

Dr. R. Glück
Berna-Biotech
Rehhagstrasse 79, 3018 Bern (Switzerland)

Supporting information for this article is available on the WWW under http://www.angewandte.org or from the author.

 © 2003 Wiley-VCH Verlag GmbH & Co. KGaA, Weinheim DOI: 10.1002/anie.200250348

peptides.[10] Modeling and NMR spectroscopic studies suggested[9] that the central NPNA motif in **1** may adopt conformations in which the first Asn residue is in the β region of ϕ/ψ space (e.g. $-120/+120°$) and the next three residues Pro–Asn–Ala are each in the helical region (e.g. $-60/-40°$). Based on these ϕ/ψ angles, a computer model was built for the linear sequence Ac-$(NPNA)_5$-NH_2, such that this helical turn is tandemly repeated. The resulting model (which differs from previously reported theoretical models[11–13]) was stable in molecular-dynamics simulations (data not given), and displays a novel repetitious secondary structure (see Figure 2). Examination of the model suggested that this folded conformation could be stabilized by cross-linking an amino group at the β position of Pro 6 to a spatially adjacent side-chain carboxy group of Glu, to be used in turn as a replacement for Ala 16. This would require cyclic peptidomimetics **3**–**5** (Scheme 2), containing (2*S*,3*R*)-3-aminoproline (Apro)[16] at position 6 and glutamate at position 16 (Figure 2), linked by an amide bond. The required orthogonally protected (2*S*,3*R*)-3-aminoproline was prepared as shown in Scheme 1

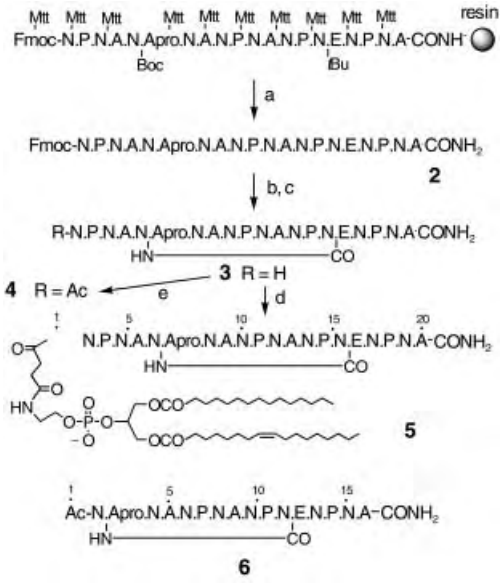


Scheme 1. Reagents and conditions: a) $(CF_3SO_2)_2O$, CH_2Cl_2, pyridine, 98%; b) $NaBH_4$, THF/DMF, 58%; c) $K_2S_2O_8$, Na_2HPO_4, MeCN/H_2O, 80%; d) $(Boc)_2O$, CH_2Cl_2, DMF, Et_3N, 76%; e) LiOH, THF, H_2O, 99%; f) Pd/C, MeOH, H_2, 93%; g) Fmoc-OSucc, iPr_2NEt, CH_2Cl_2, 68%. Apro = (2*S*,3*R*)-3-aminoproline; Boc = *tert*-butyloxycarbonyl; DMB = 3,4-dimethoxybenzyl; DMF = *N*,*N*-dimethylformamide; Fmoc = 9-fluorenylmethoxycarbonyl; Succ = succinimide.

The mimetic **4** and an analogue **5**, which was linked to a phospholipid for incorporation into IRIVs, were synthesized as shown in Scheme 2. The linear sequence was built through solid-phase Fmoc chemistry on Rink-amide MBHA resin (*Novabiochem*). After cleavage from the resin, the 3-amino group of Apro 6 and the carboxy group of Glu 16 could be coupled in high yield (> 90%) in DMF in the presence of HATU.

The conformation of **4** was studied by NMR spectroscopy in H_2O/D_2O (9:1) at pH 5. ^1H NMR spectra indicated the existence of a major conformer and two minor conformers (ratio 80:14:6), of which the latter two most likely arise from *cis–trans* isomerism at Asn–Pro peptide bonds, in analogy to earlier studies.[10,14,15]

Only the major form of **4** was considered further. 2D NOESY plots showed strong $d_{NN}(i,i+1)$ connectivities between the peptide NH groups of Asn 7 and Ala 8, and Ala 8 and Asn 9 in one NPNAN motif, Asn 11 and Ala 12, and Ala 12 and Asn 13 in the next, and between Asn 15 and Glu 16, and Glu 16 and Asn 17 in the last motif. These, together with



Scheme 2. Synthesis of mimetics. a) TFA, iPr_3SiH, H_2O (95:2.5:2.5); b) HATU, HOAt, DMF, iPr_2EtN; c) piperidine, DMF (20% v/v); d) succinyl-*rac*-1-palmitoyl-3-oleoyl-glycero-2-phosphoethanolamine, HATU, HOAt, iPr_2EtN; e) Ac_2O, pyridine/CH_2Cl_2. HATU = 2-(1H-7-azabenzotriazol-1-yl)-1,1,3,3-tetramethyluronium hexafluorophosphate; HOAt = 1-hydroxy-7-azabenzotriazole; Mtt = 4-methyltrityl; TFA = trifluoroacetic acid.

NOE interactions between Pro C_α-H and Ala N-H ($i+2$) in each motif, provide evidence for helical turns formed by the residues Asn 5–Asn 9, Asn 9–Asn 13, and Asn 13–Asn 17. The same pattern of NOE interactions was also found for **6** (Scheme 2). Signal overlap of side-chain resonances seen in the NMR spectrum of **4** was less severe for **6**. Mimetics **4** and **6** showed similar coupling patterns of ^3J (C_α-H, N-H) and amide-proton temperature coefficients (see Supporting Information) in their common substructures. However, the amide temperature coefficients were mostly more negative than −4 ppb/K and all the amide protons in **4** and **6** exchanged within a few minutes at pH 4 in D_2O, which suggests the absence of stable intramolecular hydrogen bonds involving the amide NHs.

Average solution structures were calculated for **4** and **6** by simulated annealing based on NOE-derived distance restraints, and gave similar results, except for the very flexible N- and C-termini in **4**. For example, the average structures for **6** could be clustered into four main families, as depicted in Figure 3 (see Supporting Information). The lack of convergence to a single structure reflects a low number of long range NOE restraints, which we presume is a result of significant backbone flexibility, compounded by problems of signal overlap. However, in some of the calculated structures the anticipated helical turns are populated (see Figure 4).

For immunological studies, the mimetic **5** was incorporated into IRIVs and then used to immunize BALB/c mice. After preimmunization with the IRIV-based influenza vaccine Inflexal Berna[17] (Berna Products), and three doses of **5**-IRIV, the sera of all immunized mice contained mimetic-specific antibodies, as demonstrated by ELISA (enzyme-

 © 2003 Wiley-VCH Verlag GmbH & Co. KGaA, Weinheim

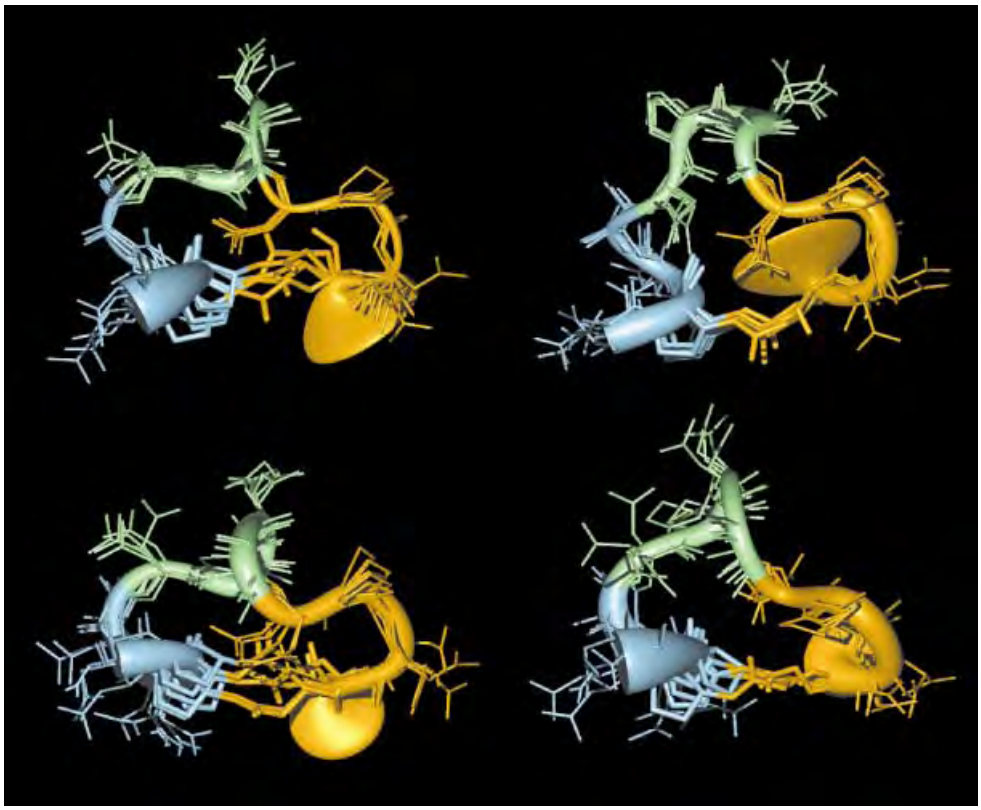


Figure 3. Average solution structures for **6** (Scheme 2). The calculated structures cluster into four main groups as shown. The sausage-shaped average backbone was calculated from the average displacement of the C_α atoms, which is represented by the spline radius. The first helical NPNA turn is in blue, the second in green, and the third in orange. The Apro 6–Glu 16 cross-link is at the bottom of the structure. The figure was prepared with MOLMOL.[20]



Figure 4. Superimposition of the computer model of Ac-$(NPNA)_5$-NH_2 shown in Figure 2 and average solution structures for **6** shown in Figure 3.

linked immunosorbent assay) (Figure 5a). The binding of anti-**5**-IRIV antisera to native circumsporozoite (CS) protein was analyzed by an indirect immunofluorescence assay using *P. falciparum* sporozoites. In all immunized animals a significant antisporozoite antibody response was detected. The specificity of the cross-reaction was demonstrated by a competition experiment (Figure 5b). Incubation of the antiserum with the sporozoites in the presence of **4** completely suppressed immunostaining. The IRIV formulations thus elicited a significant proportion of parasite-binding antibodies among the total antimimetic immune response. Priming of mice with influenza antigens has been found to enhance the humoral immune response against antigens delivered by virosomes.[5,18] Primed mice presumably reflect the situation in humans better than nonprimed mice, as most humans are already exposed to the influenza virus early in life. Currently it is not clear whether influenza antigen-specific helper T cells or antibodies are primarily responsible for the effects of influenza preimmunity.

The cross-reactivity of the antisera with peptidomimetic **1** was also analyzed by ELISA (data not shown). The sera from three of four mice immunized with **5**-IRIV cross-reacted with mimetic **1**. Interestingly, a helical NPNA turn (see above) is also possible in **1**.[9] That a significant part of the antibody response to **5**-IRIV cross-reacts with **1** also shows that these cross-reacting antibodies must not simply recognize the ends of the peptide backbone in **5**.

Monoclonal antibodies (mAbs) were prepared from spleen cells of mice immunized with **5**-IRIV, and two mAbs (EP3 and EP9) that bound both the mimetic **5**-IRIV and *P. falciparum* sporozoites were isolated. Both EP3 and EP9 have recently also been shown to inhibit the invasion of human-liver hepatocytes by live sporozoites in the midnanomolar range.[19] This inhibitory activity most likely arises as a result of binding by the mAbs of neutralizing epitopes on the parasite surface.

The cross-reactivity of EP3 and EP9 with peptidomimetic **1** and the linear peptide $(NANP)_{\approx 50}$ were also tested by ELISA. The results show that both EP3 and EP9 bind to **1**,

 © 2003 Wiley-VCH Verlag GmbH & Co. KGaA, Weinheim

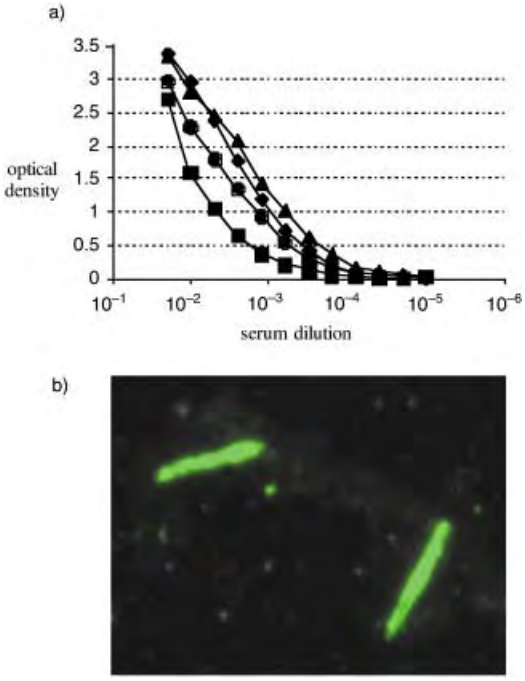


Figure 5. a) Serum IgG titers in BALB/c mice immunized three times with **5**-IRIV. ELISA was performed in microtiter plates coated with **5** and incubated with serial dilutions of the sera of individual mice. Bound IgG was detected using alkaline phosphatase-conjugated antibodies specific for mouse gamma heavy chains. No antibody binding was observed with uncoated plates and preimmune sera exhibited no significant antimimotope antibody titer in ELISA (data not shown). b) Immunofluorescence staining of *P. falciparum* sporozoites by mouse anti-**5**-IRIV antiserum, using a FITC-labeled secondary anti-mouse IgG antibody. No significant staining was observed with preimmune sera and incubation of the sporozoites in the presence of **4** suppressed immunostaining (data not shown). FITC = (fluorescein isothiocyanate).

whereas $(NANP)_{\approx 50}$ is only bound by EP9 and not by EP3 in ELISA. These data suggest that EP3 recognizes epitopes in both **5**-IRIV and on the parasite surface that are more poorly represented, if at all, in the linear peptide $(NANP)_{\approx 50}$.

The results show that the IRIV-bound peptidomimetic **5** effectively elicits sporozoite-binding antibodies, and also lead to a new proposal for the folded conformation of the NPNA-repeat region in the CS protein (Figure 2). A key issue now is whether the use of this peptidomimetic with the IRIV delivery system leads to a stronger antiparasite immune response in humans than in mice, as has been observed with other virosome-based vaccine candidates. In this case, influenza preimmunity may play a role, as suggested by the enhancing effects of influenza priming in mice. The suitability of virosomal mimetic formulations for use in humans will have to be evaluated in a phase I clinical safety and immunogenicity trial. At a later stage, efficacy trials will reveal whether the IRIV-based vaccine candidate offers improvements in protective efficacy over linear $(NANP)_3$ peptides delivered by the classical route.[6] The virotope approach, however, could also be applied to the design and testing of new combination vaccines targeted against multiple antigens and developmental stages of *P. falciparum*, or indeed against other infectious agents.

Received: October 11, 2002
Revised: January 31, 2003 [Z50348]

Keywords: antibodies · conformation analysis · immunochemistry · peptides · peptidomimetics

[1] M. Tsuji, E. G. Rodrigues, R. S. Nussenzweig, *Biol Chem.* **2001**, *382*, 553.
[2] *Ciba Foundation Symposium 119: Synthetic Peptides as Antigens* (Eds.: R. Porter, J. Whelan), Wiley, Chichester, UK, **1986**.
[3] R. Glück, *Vaccine* **1999**, *17*, 1782.
[4] I. P. Hunziker, R. Zurbriggen, R. Glueck, O. B. Engler, J. Reichen, W. J. Dai, W. J. Pichler, A. Cerny, *Mol. Immunol.* **2001**, *38*, 475.
[5] R. Zurbriggen, R. Glück, *Vaccine* **1999**, *17*, 1301.
[6] D. A. Herrington, D. F. Clyde, G. Losonsky, M. Cortesia, J. R. Murphy, J. Davis, S. Baqar, A. M. Felix, E. P. Heimer, D. Gillessen, E. Nardin, R. S. Nussenzweig, V. Nussenzweig, M. R. Hollingdale, M. M. Levine, *Nature* **1987**, *328*, 257; for other examples, see reference [1].
[7] F. Zavala, J. P. Tam, M. R. Hollingdale, A. H. Cochrane, I. Quakyi, R. S. Nussenzweig, V. Nussenzweig, *Science* **1985**, *228*, 1436.
[8] J. B. Dame, J. L. Williams, T. F. McCutchan, J. L. Weber, R. A. Wirtz, W. T. Hockmeyer, W. L. Maloy, J. D. Haynes, I. Schneider, D. Roberts, G. S. Sanders, E. P. Reddy, C. L. Diggs, L. H. Miller, *Science* **1984**, *225*, 593.
[9] R. Moreno, L. Jiang, K. Moehle, R. Zurbriggen, R. Glück, J. A. Robinson, G. Pluschke, *ChemBioChem* **2001**, *2*, 838.
[10] H. J. Dyson, A. C. Satterthwait, R. A. Lerner, P. E. Wright, *Biochemistry* **1990**, *29*, 7828.
[11] K. D. Gibson, H. A. Scheraga, *Proc. Natl. Acad. Sci. USA* **1986**, *83*, 5649.
[12] I. K. Roterman, K. D. Gibson, H. A. Scheraga, *J. Biomol. Struct. Dyn.* **1989**, *7*, 391.
[13] B. R. Brooks, R. W. Pastor, F. W. Carson, *Proc. Natl. Acad. Sci. USA* **1987**, *84*, 4470.
[14] C. Bisang, C. Weber, J. Inglis, C. A. Schiffer, W. F. van Gunsteren, I. Jelesarov, H. R. Bosshard, J. A. Robinson, *J. Am. Chem. Soc.* **1995**, *117*, 7904.
[15] C. Bisang, L. Jiang, E. Freund, F. Emery, C. Bauch, H. Matile, G. Pluschke, J. A. Robinson, *J. Am. Chem. Soc.* **1998**, *120*, 7439.
[16] For the starting bicyclic lactam, see: P. Angehrn, R. L. Charnas, K. Gubernator, E.-M. Gutknecht, C. Hubschwerlen, M. Kania, C. Oefner, M. G. P. Page, S. Sogabe, J.-L. Specklin, F. Winkler, *J. Med. Chem.* **1998**, *41*, 3961 – 3971.
[17] R. Glück, R. Mischler, B. Finkel, J. U. Que, B. Scarpa, S. J. Cryz, *Lancet* **1994**, *344*, 160.
[18] F. Poltl-Frank, R. Zurbriggen, A. Helg, F. Stuart, J. A. Robinson, R. Glück, G. Pluschke, *Clin. Exp. Immunol.* **1999**, *117*, 496 – 503.
[19] Full details of the immunological data will be published elsewhere.
[20] R. Koradi, M. Billeter, K. Wüthrich, *J. Mol. Graphics* **1996**, *14*, 51 – 55.

 © 2003 Wiley-VCH Verlag GmbH & Co. KGaA, Weinheim

Detecting Single-Base Mutations

Magnetically Amplified DNA Assays (MADA): Sensing of Viral DNA and Single-Base Mismatches by Using Nucleic Acid Modified Magnetic Particles**

*Fernando Patolsky, Yossi Weizmann, Eugenii Katz, and Itamar Willner**

Dedicated to Professor Dieter M. Kolb on the occasion of his 60th birthday

The detection of DNA has attracted significant recent research efforts directed to the analysis of genetic disorders, identification of pathogens, tissue matching, the detection of biological-warfare agents, and forensic applications.[1,2] The sensing of DNA involves two major challenges related to the sensitivity of the detection process and the specificity of DNA analysis, with the ultimate goal of detecting single-base mismatches. Amplified electronic DNA detection is accomplished by the coupling of biocatalytic (enzyme) conjugates to the nucleic acid/DNA recognition pair.[3–5] For example, the amplified analysis of the M13ϕ DNA was accomplished by the generation of biotin- or ferrocene-labeled replica followed by the biocatalyzed precipitation of an insoluble product on electrodes,[4] or the activation of a bioelectrocatalytic process,[5] respectively. Alternatively, the assembly of nanoarchitectures on surfaces with dendritic-type nucleic acid structures[6] or with layered functional particles[7] are extensively used to amplify DNA detection. Single-base-mismatch detection was reported by Heller and Caruana using thermally controlled hybridization.[8] The amplified single-base-mismatch detection was accomplished by the polymerase-induced incorporation of a biotin-labeled base into the primer sensing nucleic acid. Coupling of the avidin–enzyme[9a] or the avidin–Au nanoparticle[9b] conjugates enabled the secondary catalytic amplification of the sensing processes. Functional magnetic particles are often used in analytical assays for the separation of specific components from biological mixtures,[10] and for the elimination of non-specific adsorption.[11] Recently, functional magnetic particles were employed for the magnetoswitchable activation and deactivation of bioelectrocatalytic transformations[12] and of electrogenerated biochemiluminescence.[13] Also, magnetic particles were recently reported for the electrochemical analysis of DNA.[14] The use of rotating magnetic particles was recently reported as a means to enhance bioelectrocatalytic processes by convection-controlled (rather than diffusion-controlled) interactions of the substrate with the enzyme.[15] Wang and colleagues have recently employed nucleic acid functionalized magnetic particles for the amplified electrochemical detection of DNA by the catalytic deposition of silver on magnetic particles and Au-nanoparticle/DNA conjugates, followed by the electrochemical stripping of the resulting silver.[16] Herein we wish to report on the novel amplified detection of viral DNA and of single-base mismatches using nucleic acid functionalized magnetite particles and electrogenerated chemiluminescence as a transduction means. The magnetic particles have two complementary functions in the DNA detection schemes: a) They act as building units for the polymerase-induced incorporation of labels using thermally controlled replication cycles, b) the magnetic attraction of the labeled particles and their rotation on the electrode surface enables further amplified detection of DNA by electrogenerated chemiluminescence.

Magnetic particles (5-μm diameter) are modified with the thiolated primer **1** using the heterobifunctional cross-linker 3-maleimidopropionic acid *N*-hydroxysuccinimide ester, as outlined in Figure 1. The average coverage of the magnetic particles was determined by using the OliGreen reagent (Molecular Probes, Inc.) and corresponded to approximately 50000 oligonucleotide units per particle. The number of nucleic acids that were associated with the particles and accessible to an external enzyme was estimated by subjecting the **1**-functionalized magnetic particles to DNase and by the subsequent determination of the content of the DNA that is cleaved off. We find that around 20000 oligo units per particle are cleaved off, which implies that only about 40% of the particle-linked nucleic acids are accessible to the enzyme.

Figure 2 depicts the method for the amplified detection of the viral M13ϕ DNA (**2**) using the functional magnetic particles. The **1**-modified magnetic particles are hybridized with the M13ϕ ssDNA (7229 bases) and are subjected to polymerization in the presence of a mixture of dGTP, dATP, dCTP, and biotinylated dUTP (b-dUTP). The polymerization introduces into the replica a high number of biotin labels. The replication is followed by thermal cycles that result in the dissociation of the analyzed M13ϕ DNA, its re-hybridization with other oligonucleotide primers associated with the magnetic particles, and the subsequent polymerization and formation of new replica containing a high number of biotin

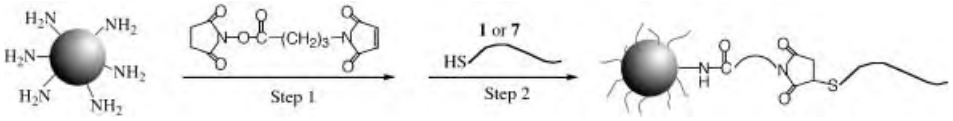


Figure 1. Alkylamine-coated magnetic particles are modified with cross-linker and then a thiolate primer.

[*] Prof. I. Willner, F. Patolsky, Y. Weizmann, Dr. E. Katz
Institute of Chemistry
The Farkas Center for Light-Induced Processes
The Hebrew University of Jerusalem
Jerusalem 91904 (Israel)
Fax: (+972) 2-6527-715
E-mail: willnea@vms.huji.ac.il

[**] This research is supported by the German–Israeli Program (DIP). The Max Planck Award for International Cooperation (I.W.) is gratefully acknowledged.

 © 2003 Wiley-VCH Verlag GmbH & Co. KGaA, Weinheim DOI: 10.1002/anie.200250379

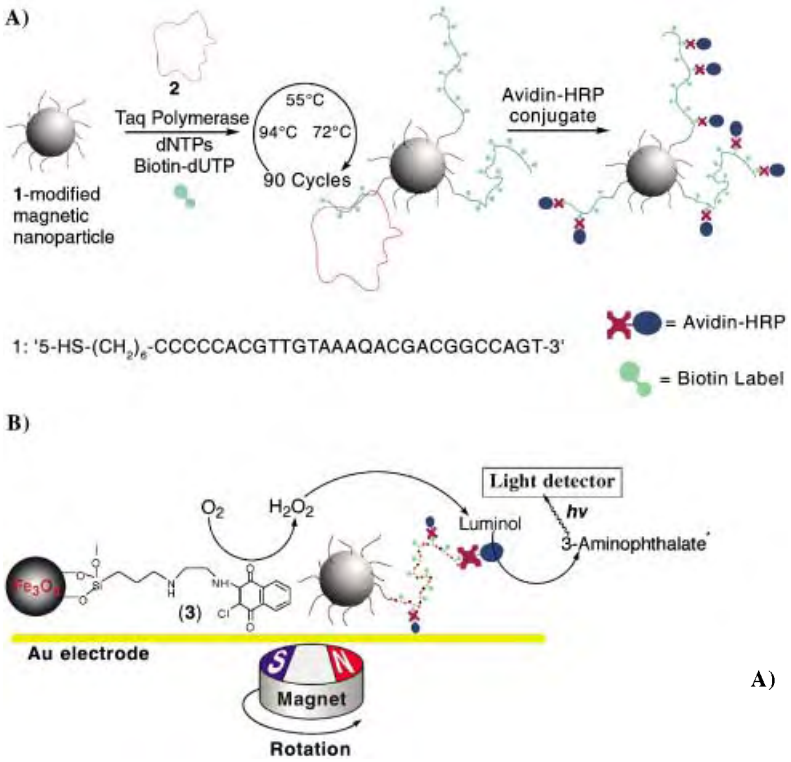


Figure 2. Amplified detection of viral DNA by multilabeled rotating magnetic particles: A) labeling of the nucleic acid replica on the particles with biotin units by using thermal cycles, B) generation of amplified chemiluminescence upon rotation of the functionalized magnetic particles on the electrode surfaces.

label units. By controlling the number of thermal cycles, the replication on the surface of the particles yields very high densities of biotin-labeled nucleic acids. The thermal cycles were conducted for 75 s each, which translate to a replication efficiency of about 250 bases per cycle. The resulting biotin-labeled magnetic particles are then separated by means of the external magnet, treated with avidin–horseradish peroxidase (HRP), separated again by the external magnet, and washed with a phosphate buffer solution. A mixture of the avidin-functionalized magnetic particles (1 mg) and naphthoquinone **3**-modified magnetic particles[12b] (Figure 2B) is then introduced into the electrochemical cell. The magnetic particles are then attracted to the electrode by means of the external magnet. Upon the application of a potential to the electrode that reduces the naphthoquinone to the respective hydroquinone, the electrocatalyzed reduction of O_2 to H_2O_2 occurs. The HRP-catalyzed oxidation of luminol by the electrogenerated H_2O_2 results in chemiluminescence and the emission of light. Figure 3A, curve a, shows the emitted light intensity upon analyzing M13ϕ DNA as in Figure 2, and by the application of a potential step on the electrode from 0 V to −0.5 V and back (the E^o value for the **3**-modified particles at pH 7 is −0.4 V versus SCE). In a control experiment in which all the analysis steps were applied on a sample that lacked M13ϕ DNA, no light emission was observed, which indicates that no non-specific adsorption of the avidin–HRP conjugate on the electrode, or on the magnetic particles, takes place, Figure 3A, curve e. The effect of the rotation of the magnetic particles, caused by rotating the external magnet, is depicted in Figure 3A, curves b–d. As the rotation speed of the magnetic particles is increased, the emitted light intensity increases, and a linear relationship between the intensity of emitted light and $\omega^{1/2}$ is observed (Figure 3B). The increase in the emitted light intensity is attributed to the fact that the rotating magnetic particles behave as catalytic rotating microelements, where the electrocatalyzed reduction of O_2 to H_2O_2 and the subsequent generation of chemiluminescence in the presence of luminol are controlled by convection rather than by the diffusion of O_2 and luminol to the particles associated with the conductive support.

At a constant rotation speed of the particles, the intensity of emitted light is controlled by the surface coverage of the labeled nucleic

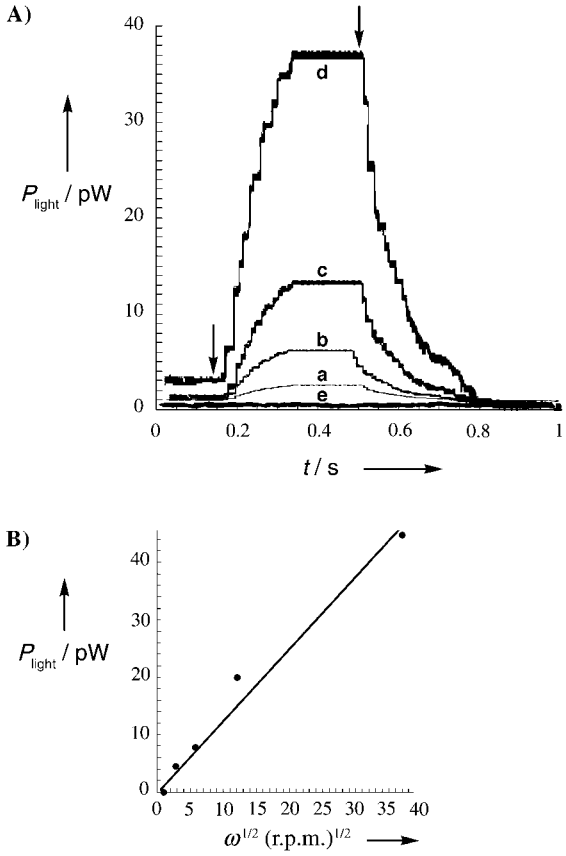


Figure 3. A) Chemiluminescence intensities upon the analysis of M13ϕ DNA (8×10^{-9} M) at different rotation speeds, a) 0 r.p.m., b) 60 r.p.m., c) 400 r.p.m., d) 2000 r.p.m., and curve e) chemiluminescence signal upon in the absence of M13ϕ DNA at 2000 r.p.m. B) Chemiluminescence intensities as a function of $\omega^{1/2}$ (ω = rotation speed). In all the experiments the chemiluminescence is generated by the application of a potential step from $E = 0.0$ V to $E = -0.5$ V and back versus SCE. Arrows indicate the times at which the potential was switched to −0.5 V and to 0.0 V, respectively. Data recorded in 0.01 M phosphate buffer pH 7.4 that includes luminol (1×10^{-6} M) under air.

 © 2003 Wiley-VCH Verlag GmbH & Co. KGaA, Weinheim

acid associated with the magnetic particles, and this relates to the concentration of M13ϕ DNA in the analyzed sample during the replication cycles. Figure 4 shows the emitted light intensity upon the analysis of different concentrations of M13ϕ DNA at a rotation speed of $\omega = 2000$ r.p.m. At $\omega =$ 2000 r.p.m. (Figure 4) we are able to sense the M13ϕ DNA with a detection limit that corresponds to 8.3×10^{-18} M, that translates to 50 copies per 10 μL.

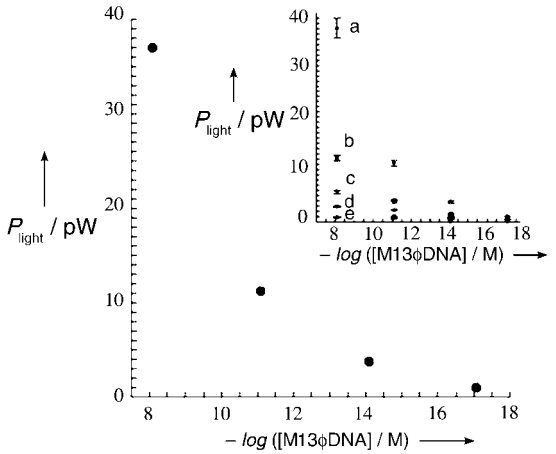


Figure 4. Calibration curve corresponding to the chemiluminescence intensities upon analyzing different concentrations of M13ϕ DNA at 2000 r.p.m. Inset: Calibration curve corresponding to the chemiluminescence intensities upon analyzing different concentrations of M13ϕ at a) 2000 r.p.m., b) 400 r.p.m., c) 60 r.p.m., d) 20 r.p.m., e) 0 r.p.m.

A related amplification path that uses functional magnetic particles was employed for the detection of single-base mismatches in DNA. This method is exemplified by the analysis of the mutant sequence **5**, where the G-base exchanges the A-base in the normal sequence gene **6** (Figure 5). The magnetic particles are functionalized with the nucleic acid **7** that is complementary to the mutant sequence **5** and the normal gene sequence **6**, up to one base prior to the mutation site. Interaction of the **7**-modified magnetic particles with the samples that include either **5** or **6** results in their hybridization with the particles. Treatment of the hybridized assemblies associated with the magnetic particles with polymerase and biotinylated-dCTP, followed by thermal dissociation/annealing/labeling cycles results in the multilabeling with biotin units of the magnetic particles incorporating **5**, whereas no biotin labels are introduced to the magnetic particles incorporating **6**. The subsequent interaction of the particles with the avidin–HRP conjugate, followed by the separation of the particles by means of the external magnet yield the biocatalytically labeled particles. Mixing of the resulting particles with the naphthoquinone **3**-modified particles in the electrochemical cell, followed by their attraction to the electrode by means of the external magnet, upon application of a potentential corresponding to −0.5 V, leads to the electrocatalyzed reduction of O_2 to H_2O_2. The electrogenerated H_2O_2 leads, in the presence of luminol, to the emission of light upon the analysis of **5**, while no light is detected upon the analysis of **6**. Rotation of the magnetic particles by means of the external magnet is then expected to amplify the emitted light since the electrogenerated chemiluminescence is controlled by convection of the respective substrates to the particles.

Figure 6A shows the emitted light intensity at rotation speeds of up to 2000 r.p.m. upon analyzing **5** and **6** as in Figure 5. A potential step from 0 V to −0.5 V and back is applied on the electrode to activate the electrocatalyzed reduction of O_2, and to drive the secondary chemiluminescent process. No light emission is observed upon the analysis of **6**, which indicates that no biotin labels were incorporated into the nucleic acid modified magnetic particles. Clearly, light emission is observed only upon the analysis of the mutant sequence. The intensity of the emitted light increases as the rotation speed of the particles is elevated, ($P_{light} \propto \omega^{1/2}$), again implying that the processes at the electrode support are controlled by convection. Figure 6B shows the light emitted upon analyzing different concentrations of **5**, at different rotation speeds. The mutant sequence **5** is analyzed with a detection limit of 1×10^{-17} M. Note that the concentration of **6** in the analyzed sample is 10^3-fold higher that of **5**, and still no light emission is observed upon analyzing **6**. This result implies that no non-specific association of the HRP conjugate to the magnetic particles occurs.

In conclusion, the present study has described the "magnetically amplified DNA analysis" (MADA) process. Several consecutive steps in the process lead to the overall amplification: 1) The thermal cyclic replication of the analyte on the magnetic particles leads to the incorporation of a high number of label units into the nucleic acids linked to the particles, 2) the electrocatalytic generation of O_2 at the electrode, and the coupled biocatalyzed light emission yield numerous product molecules or photons as a result of a single recognition event, 3) the rotation of the magnetic particles leads to the amplified light emission since the transport of the substrates for the electrocatalytic and biocatalytic processes at the particles are convection-controlled. Using these methods unprecedented sensitivities were achieved. The observed detection limit for the M13ϕ DNA is 8.3×10^{-18} M, (50 copies per 10 μL), and for the mutant sequence **5**, the detection limit corresponds to 1×10^{-17} M. These values were achieved with no attempt to optimize the analysis process (for example, optimization of

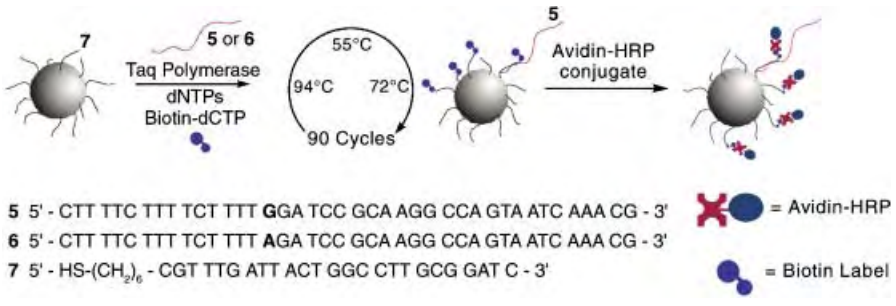


Figure 5. Amplified detection of a single-base mismatch in DNA by using rotating magnetic particles. See text for details.

 © 2003 Wiley-VCH Verlag GmbH & Co. KGaA, Weinheim

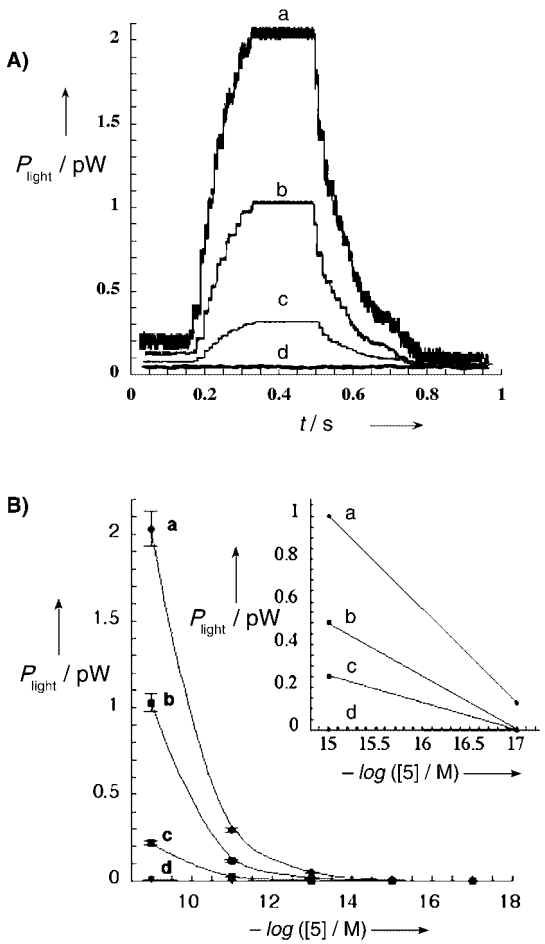


Figure 6. A) Chemiluminescence intensities upon the analysis of the mutant sequence **5** (1.4×10^{-9} M) at: a) 2000 r.p.m., b) 400 r.p.m., c) 60 r.p.m. The chemiluminescence intensity upon the analysis of the normal sequence **6** (1.4×10^{-6} M) at 2000 r.p.m. according to the method in Figure 5 is shown in curve (d). The conditions for the recording of the chemiluminescence are detailed in Figure 3. B) Calibration curves corresponding to the analysis of different concentrations of the mutant **5** at different rotation speeds: a) 2000 r.p.m., b) 400 r.p.m., c) 60 r.p.m., d) 0 r.p.m. Inset: Enlargement of calibration curves showing the chemiluminescence intensities at low concentrations of **5**.

the thermal incorporation of the biotin labels by the polymerization cycles). We believe, that by optimization of the process and further electronic amplification of the detected light signal, the method may be suitable for analyzing a few DNA molecules.

Experimental Section

Amine-functionalized borosilicate-based magnetic particles (5 μm, MPG Long Chain Alkylamine, CPG Inc.) and Biotin-21-dUTP (Clontech) were obtained from the firms indicated. The heterobifunctional cross-linker 3-maleimidopropionic acid N-hydroxysuccinimide ester, oligonucleotides **1**, **5**, **6**, and **7**, Avidin–HRP conjugate, dNTPs, Biotin-11-dCTP, Taq Polymerase, 10×PCR buffer, and all other compounds were purchased from Sigma and used as received.

Preparation of DNA-functionalized magnetic particles: the amino-functionalized magnetic particles (30 mg) were activated by reaction with the heterobifunctional cross-linker 3-maleimidopropionic acid *N*-hydroxysuccinimide ester (10 mg, Sigma) in DMSO (1 mL). After 4 h of incubation at room temperature, the particles were collected by using an external magnet and thoroughly washed with DMSO and water. The maleimido-activated particles were then reacted with 20–30 O.D. of the thiolated oligonucleotide in phosphate buffer 0.1M, pH 7.4 for a period of 8 h. (The thiolated nucleotide was freshly reduced with threo-4,4-dimercapto-2,3-butanediol (DTT) and separated on a Sephadex G-25 column prior to the reaction with the functionalized particles). Finally, the magnetic particles were washed with water and phosphate buffer 0.1M, pH 7.4. To keep the DNA-modified particles for periods longer than one week, 1% w/v sodium azide was added, and the particles were kept at 4°C. The oligonucleotide content on the magnetic particles, before and after enzymatic DNase treatment (10 units DNase, 30 min at 37°C) was measured by the use of the OliGreen reagent (ssDNA Quantitation Assay Kit Molecular Probes, Inc.).

Conditions for Thermal Cycles: a) For single-point-mutation detection: denaturation 30 s, 94°C; annealing 30 s, 55°C; polymerization 5 s, 72°C; b) For Viral-DNA detection: denaturation 30 s, 94°C; annealing 30 s, 55°C; polymerization 15 s, 72°C.

An Au-coated (50 nm gold layer) glass plate (Analytical-μSystem, Germany) was used as a working electrode (0.3 cm^2 area exposed to the solution). An auxiliary Pt electrode and a quasi-reference Ag electrode were made from wires of 0.5-mm diameter and added to the cell. The quasi-reference electrode was calibrated versus saturated calomel electrode (SCE) and the potentials are given versus SCE. An open electrochemical cell (230 μL) that includes the Au electrode in a horizontal position and a light detector linked to a fiber optic enabled easy light-emission measurements upon application of the appropriate potential to the modified working electrode. The electrochemical measurements were performed using a potentiostat (EG&G, model 283) connected to a computer (EG&G Software 270/250). All the measurements were performed in 0.01M phosphate buffer solution, pH 7.0, at room temperature. The electrochemically induced chemiluminescence was measured with a light detector (Laserstat, Ophir) linked to an oscilloscope (Tektronix TDS 220). The light detector was connected to the electrochemical cell by an optical fiber. The background electrolyte solution was equilibrated with air and included luminol, 1×10^{-6} M. A permanent magnet (NdFeB/zn-coated magnet 0.2 kOe) mounted on a rotating disx electrode system (EG&G, model 638) was used to rotate the particles.

Received: October 16, 2002
Revised: December 6, 2002 [Z50379]

Keywords: biosensors · chemiluminescence · DNA · magnetic particles

[1] a) E. K. Wilson, *Chem. Eng. News* **1998**, *76*(21), 47–49; b) S. R. Mikkelsen, *Electroanalysis* **1996**, *8*, 15–23.
[2] a) A. J. Bard, M. Rodriguez, *Anal. Chem.* **1990**, *62*, 2658–2662; b) K. M. Millan, S. R. Mikkelsen, *Anal. Chem.* **1993**, *65*, 2317–2323; c) M. Yang, M. E. McGovern, M. Thompson, *Anal. Chim. Acta* **1997**, *346*, 259–275.
[3] T. de Lumley-Woodyear, C. N. Campbell, E. Freeman, A. Freeman, G. Georgiuo, A. Heller, *Anal. Chem.* **1999**, *71*, 535–538.
[4] a) F. Patolsky, E. Katz, A. Bardea, I. Willner, *Langmuir* **1999**, *15*, 3703–3706; b) F. Patolsky, A. Lichtenstein, M. Kotler, I. Willner, *Angew. Chem.* **2001**, *113*, 2321–2325; *Angew. Chem. Int. Ed.* **2001**, *40*, 2261–2264; c) L. Alfonta, I. Willner, D. J. Throckmorton, A. K. Singh, *Anal. Chem.* **2001**, *73*, 5287–5295.
[5] F. Patolsky, Y. Weizmann, I. Willner, *J. Am. Chem. Soc.* **2002**, *124*, 770–772.
[6] J. Wang, M. Jiang, T. W. Nilsen, R. C. Getts, *J. Am. Chem. Soc.* **1998**, *120*, 8281–8282.

 © 2003 Wiley-VCH Verlag GmbH & Co. KGaA, Weinheim

[7] a) F. Patolsky, K. T. Ranjit, A. Lichtenstein, I. Willner, *Chem. Commun.* **2000**, 1025 – 1026; b) I. Willner, F. Patolsky, J. Wasserman, *Angew. Chem.* **2001**, *113*, 1913 – 1916; *Angew. Chem. Int. Ed.* **2001**, *40*, 1861 – 1864.
[8] D. J. Caruana, A. Heller, *J. Am. Chem. Soc.* **1999**, *121*, 769 – 774.
[9] a) F. Patolsky, A. Lichtenstein, I. Willner, *Nat. Biotechnol.* **2001**, *19*, 253 – 257; b) I. Willner, F. Patolsky, Y. Weizmann, B. Willner, *Talanta* **2002**, *56*, 847 – 856.
[10] a) P. Sharma, A. Lönneborg, P. Stougaard, *BioTechniques* **1993**, *15*, 610 – 611; b) P. Schraml, R. Shipman, P. Stulz, C. U. Ludwig, *Trends Genet.* **1993**, *9*, 70 – 71; c) H. C. Aasheim, T. Logtenberg, F. Larsen, *Methods Mol. Biol.* **1996**, *69*, 115 – 128.
[11] E. Palecek, S. Billova, L. Havran, R. Kizek, A. Miculkova, F. Jelen, *Talanta* **2002**, *56*, 919 – 930.
[12] a) R. Hirsch, E. Katz, I. Willner, *J. Am. Chem. Soc.* **2000**, *122*, 12053 – 12054; b) E. Katz, L. Sheeney-Haj-Ichia, I. Willner, *Chem. Eur. J.* **2002**, *8*, 4138 – 4148.
[13] L. Sheeney-Haj-Ichia, E. Katz, J. Wasserman, I. Willner, *Chem. Commun.* **2002**, 158 – 159.
[14] J. Wang, G. D. Liu, R. Polsky, A. Merkoci, *Electrochem. Commun.* **2002**, *4*, 722 – 726.
[15] E. Katz, I. Willner, *J. Am. Chem. Soc.* **2002**, *124*, 10290 – 10291.
[16] J. Wang, D. K. Xu, R. Polsky, *J. Am. Chem. Soc.* **2002**, *124*, 4208 – 4209.

 © 2003 Wiley-VCH Verlag GmbH & Co. KGaA, Weinheim

Diversity-Oriented Synthesis

Expanding the Functional Group Compatibility of Small-Molecule Microarrays: Discovery of Novel Calmodulin Ligands**

*David Barnes-Seeman, Seung Bum Park, Angela N. Koehler, and Stuart L. Schreiber**

Small molecules derived from diversity-oriented synthesis (DOS) that perturb the functions of proteins are facilitating explorations in biology. Small-molecule microarrays[1a,b,2] have proven robust and scalable[3] for the discovery of small-molecule–protein interactions that lead to small-molecule modulators of protein function.[1,4] Chlorinated slides have been used to print primary-alcohol-containing DOS-derived compounds.[2b] However, inspection of the literature suggests that synthetic routes yielding libraries of carboxylic acids or phenols outnumber those yielding primary alcohols.[5] In our own laboratory, DOS pathways leading to skeletally diverse products that use phenolic benzaldehydes as the first set of diversity elements have been developed,[6] and the phenolic products do not attach to chlorinated slides. We now report a new method for the covalent capture on a glass slide of phenols as well as compounds containing functional groups of at least comparable acidity.

A suitable surface must capture compounds of interest from 1-nL microcontact-printed spots in the absence of other reagents or additives and must be stable to handling in the atmosphere.

To address these requirements we focused on the development of diazobenzylidene-functionalized glass slides. Diazobenzylidenes are known to react selectively with heteroatoms that bear an acidic proton. Initial transfer of a proton from the heteroatom to the methine carbon atom of the diazobenzylidene is followed by nucleophilic displacement of N_2 by the heteroatom.

The glass slides derivatized with a diazobenzylidene moiety were prepared by coupling the toluenesulfonylhydrazone derived from 4-carboxybenzaldehyde (**1**) to γ-aminopropylsilane slides through formation of an amide bond (PyBOP, *i*Pr_2NEt, DMF) to yield a surface **B** as shown in Figure 1. Subsequent base-induced elimination yields the putative diazobenzylidene-derivatized glass slides (**C**).[7] Functionalization of these slides as small-molecule microarrays (**D**) was then facile with compounds containing acidic protons, such as phenols, carboxylic acids, and sulfonamides.

To test this approach, a robotic microarrayer was used to spot solutions of tetramethylrhodamine (**3**) in DMF, as well as synthetic FKBP12 ligands derivatized so as to present a phenol (**2a**), carboxylic acid (**2b**), primary alcohol (**2c**),

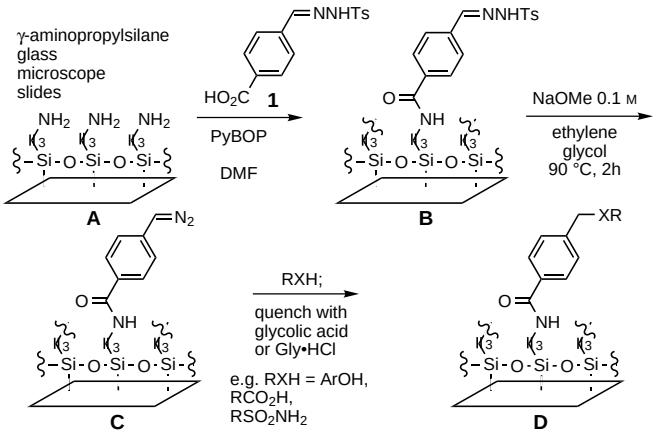


Figure 1. Preparation of diazobenzylidene-derivatized glass slides and covalent attachement of functional groups that bear an acidic proton. BOP = 1-benzotriazolyloxytris(dimethylamino)phosphonium hexafluorophosphate, Ts = toluene-4-sulfonyl.

[*] Prof. S. L. Schreiber, Dr. D. Barnes-Seeman, Dr. S. B. Park, Dr. A. N. Koehler
Howard Hughes Medical Institute
Department of Chemistry and Chemical Biology, and
Harvard Institute of Chemistry and Cell Biology (ICCB)
Harvard University, 12 Oxford St.
Cambridge, MA 02138 (USA)
Fax: (+1) 617-495-0751
E-mail: sls@slsiris.harvard.edu

[**] We are especially grateful to John Tallarico and Max Narovlyansky of the Harvard Institute of Chemistry and Cell Biology (ICCB) for donation of **2b** and synthesis resin, and to Jason Gatlin and Jennifer Raggio of the ICCB for their assistance with decoding. A.N.K. was supported by an Eli Lilly Predoctoral Fellowship. S.B.P. and D.B.-S. are Research Associates and S.L.S. is an Investigator at the Howard Hughes Medical Institute in the Department of Chemistry and Chemical Biology. We thank the National Institute for General Medical Sciences for support of this research, the National Cancer Institute (NCI), Merck KGaA, Merck & Co., and the Keck Foundation for support of the ICCB, and the NCI for support of the Initiative for Chemical Genetics (formerly known as the Molecular Target Laboratory).

Supporting information for this article is available on the WWW under http://www.angewandte.org or from the author.

 © 2003 Wiley-VCH Verlag GmbH & Co. KGaA, Weinheim DOI: 10.1002/anie.200351043

secondary alcohol (**2d**), and methyl ether (**2e**). The slides were then quenched with glycolic acid, washed extensively with DMF, THF, methanol, and phosphate-buffered saline, and probed with Cy5-FKBP12 (1 μg mL^{-1}),[8] a protein known to bind to derivatives **2a–e** (approximate dissociation constants for FKPB12 of 10 nM).[9] As shown in Figure 2, the visualization of the Cy5-FKBP12–small-molecule complexes are consistent with the immobilization of tetramethylrhodamine, phenol **2a**, and carboxylic acid **2b**, but not of **2c, 2d,** or **2e**.[10]

To test the reactivity of these diazobenzylidene slides further, 100 μM solutions[11] of biotin derivatives **4a–i** in DMF were printed in triplicate, with tetramethylrhodamine printed for reference. Probing this slide with 100 nM Cy5-streptavidin provided the differentially illuminated slide depicted in Figure 3. On the basis of these data, compounds **4c–i** were surmised to be attached to the glass slide, while **4a** and **4b** were not. Therefore, we conclude that functional groups that bear a proton with a p$K_a < 11$ (pK_a in DMSO < 19) are covalently attached to these slides, while those that bear a proton with a p$K_a > 16$ (pK_a in DMSO > 28) are not.

To demonstrate the ability of this covalent slide-capture method to identify new binding interactions between a protein and DOS-derived small molecules, 6336 phenol-containing fused bicycles and tetracycles,[5d] prepared in an encoded,[12] one-bead-one-stock solution[13] format, were printed and probed with Cy5-calmodulin (Figure 4).[14]

In order to prioritize the microarray positives prior to resynthesis, we have found it useful to retest qualitatively for the ability of the corresponding compound in solution to bind to the immobilized protein using surface plasmon resonance (SPR) spectroscopy (BIAcore). The initial secondary SPR screening was performed using compound (2 μL of a 1 mM DMF stock) directly from the original stock solutions used for microarray production. Of the 16 compounds on the microarray deemed positives, 13 showed qualitative binding to immobilized calmodulin based on the initial BIAcore analysis.[15] From this set, compounds **5, 6**, and **7** were resynthesized, purified, and their K_D values for calmodulin determined by SPR using steady-state affinity analysis. Compound **5** had a K_D value of 0.121 ± 0.03 μM, **6** a K_D value of 1.06 ± 0.09 μM, and **7** a K_D vlue of 20.7 ± 1 μM (Scheme 1).

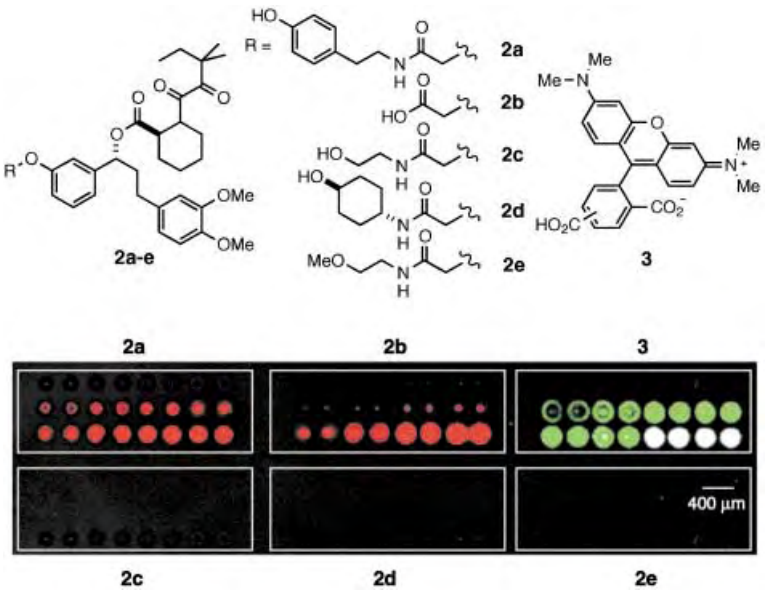


Figure 2. FKBP12 ligands (**2a–e**) and tetramethylrhodamine (**3**) printed on diazobenzylidene-derivatized slides. The DMF solutions were spotted in duplicate in serial twofold dilutions from 2 mM (lower right corner) to 1 μM (upper left corner).

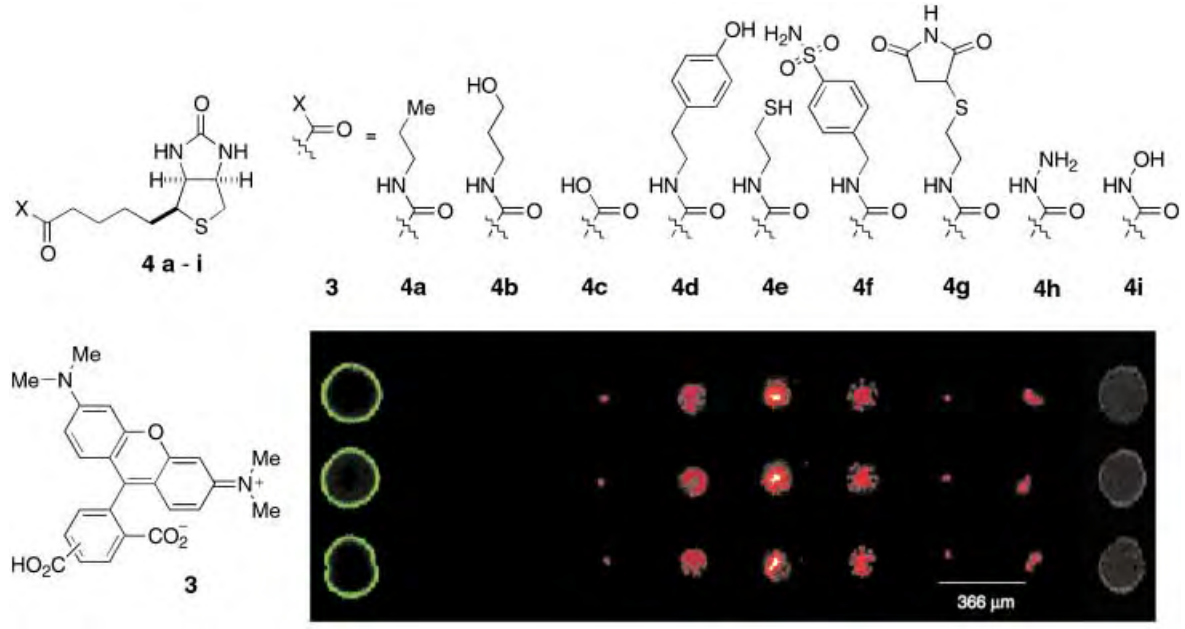


Figure 3. Tetramethylrhodamine (**3**) and biotin derivatives (**4a–i**) printed in triplicate at 100 μM and probed with 100 ng mL^{-1} Cy5-streptavidin. Estimated pK_a values (H_2O/DMSO): **4b** (16/28), **4c** (5/12), **4d** (10/18), **4e** (10/17), **4f** (10/16), **4g** (10/15), **4h** (11/19), **4i** (9/14).

 © 2003 Wiley-VCH Verlag GmbH & Co. KGaA, Weinheim

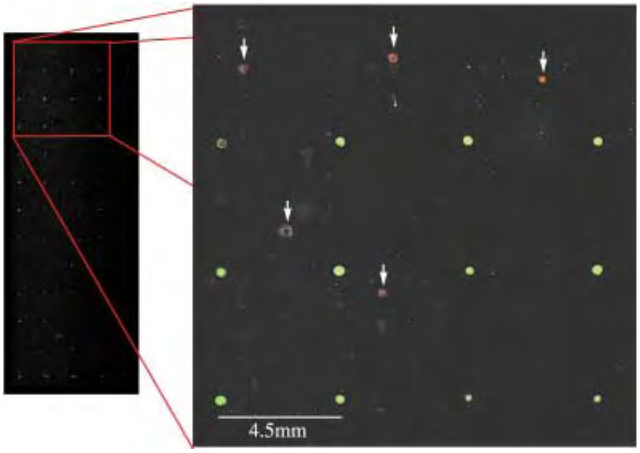
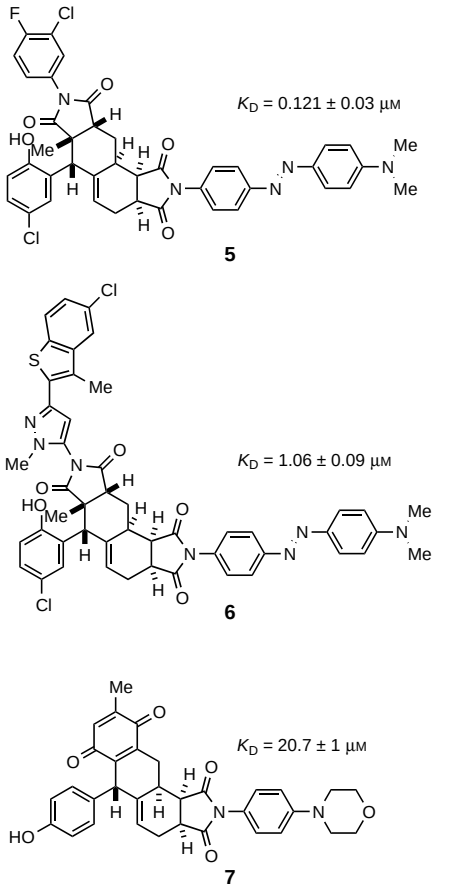


Figure 4. Diels–Alder polycycle array (6336 small molecules in total, approximately 1296 small molecules in the expanded view) probed with 3 $\mu g\,mL^{-1}$ Cy5-conjugated calmodulin. The positives for Cy5-calmodulin are false-colored red, and are indicated by white arrows. Tetramethylrhodamine makers, printed in the lower right-hand corner of each 12×12 subarray, are false-colored green.



Scheme 1. K_D values of calmodulin binders determined by surface plasmon resonance spectroscopy (BIAcore).

In conclusion, nonbiased[16] phenol-containing fused bicycles and tetracycles were immobilized as microarrays on diazobenzylidene slides. When they were probed with a protein, the observed positives corresponded well to binding interactions observed by SPR, where the protein is immobilized and the compound is free in solution.

Many sets of skeletally diverse small molecules derived from solid-phase, diversity-oriented syntheses should now be available in the manner described for high-density protein-binding assays that require minute quantities of synthetic compound. Also, the activated slides are simple and inexpensive to generate in large quantities and can be stored.[17] In contrast to the method previously reported for the covalent capture of primary alcohols,[2b] this new method includes an 11-atom spacer that may allow compounds to bind to deep pockets in proteins. Additionally, carboxylic acids and phenols are commonly found in collections of compounds currently prepared for screening.[5]

Diazobenzylidene slides serve a complementary function to chlorinated slides: the former captures phenols and carboxylic acids, but not primary alcohols, whereas the latter captures primary alcohols, but not phenols or carboxylic acids. The development of this new surface means that a significant number of compounds found in screening collections are now compatible with this high-throughput small-molecule–protein binding assay.

Received: January 23, 2003 [Z51043]

Keywords: carboxylic acids · combinatorial chemistry · phenols · small-molecule studies · surface chemistry

[1] a) F. G. Kuruvilla, A. F. Shamji, S. M. Sternson, P. J. Hergenrother, S. L. Schreiber, *Nature* **2002**, *416*, 653–657; b) A. N. Koehler, A. F. Shamji, S. L. Schreiber, *J. Am. Chem. Soc.*, submitted; c) D. S. Tan, M. A. Foley, B. R. Stockwell, M. D. Shair, S. L. Schreiber, *J. Am. Chem. Soc.* **1999**, *121*, 9073–9087; d) S. M. Sternson, J. B. Louca, J. C. Wong, S. L. Schreiber, *J. Am. Chem. Soc.* **2001**, *123*, 1740–1747; e) H. E. Pelish, N. J. Westwood, Y. Feng, T. Kirchhausen, M. D. Shair, *J. Am. Chem. Soc.* **2001**, *123*, 6740–6741; f) D. R. Spring, S. Krishnan, H. E. Blackwell, S. L. Schreiber, *J. Am. Chem. Soc.* **2002**, *124*, 1354.

[2] Small-molecule microarrays: a) G. MacBeath, A. N. Koehler, S. L. Schreiber, *J. Am. Chem. Soc.* **1999**, *121*, 7967–7968; b) P. J. Hergenrother, K. M. Depew, S. L. Schreiber, *J. Am. Chem. Soc.* **2000**, *122*, 7849–7850; c) J. R. Falsey, M. Renil, S. Park, S. Li, K. S. Lam, *Bioconjugate Chem.* **2001**, *12*, 346–353; d) N. Winssinger, J. L. Harris, B. J. Backes, P. G. Schultz, *Angew. Chem.* **2001**, *113*, 3254–3258; *Angew. Chem. Int. Ed.* **2001**, *40*, 3152–3155; e) N. Winssinger, S. Ficarro, P. G. Schultz, J. L. Harris, *Proc. Natl. Acad. Sci. USA* **2002**, *99*, 11139–11144; carbohydrate arrays: f) D. Wang, S. Liu, B. J. Trummer, C. Deng, A. Wang, *Nat. Biotechnol.* **2002**, *20*, 275–281; g) B. T. Houseman, M. Mrksich, *Chem. Biol.* **2002**, *9*, 443–454; h) S. Fukui, T. Feizi, C. Galustian, A. M. Lawson, W. G. Chai, *Nat. Biotechnol.* **2002**, *20*, 1011–1017; peptide protease substrate microarrays: i) C. M. Salisbury, D. J. Maly, J. A. Ellman *J. Am. Chem. Soc.* **2002**, *124*, 14868–14870.

[3] More than 1000000 discrete small-molecule–protein binding assays have been performed single-handedly to date with this method: A. N. Koehler, S. L. Schreiber, unpublished results.

[4] A. N. Koehler, P. Meneses, J. C. Wong, P. M. Howley, J. E. Bradner, P. T. Nghiem, Y.-S. Kim, X. Li, unpublished results.

[5] Inspection of the review series, "Comprehensive surveys of combinatorial library synthesis" reveals 160 routes yielding carboxylic acids, 30 routes yielding phenols, and 27 routes

 © 2003 Wiley-VCH Verlag GmbH & Co. KGaA, Weinheim

yielding primary alcohols: a) R. E. Dolle, *J. Comb. Chem.* **2002**, *4*, 369 – 418; b) R. E. Dolle, *J. Comb. Chem.* **2001**, *3*, 477 – 517; c) R. E. Dolle, *J. Comb. Chem.* **2000**, *2*, 383 – 433; d) R. E. Dolle, K. H. Nelson, Jr., *J. Comb. Chem.* **1999**, *1*, 235 – 282; e) R. E. Dolle, *Mol. Diversity* **1998**, *3*, 199 – 233.

[6] a) S. L. Schreiber, *Science* **2000**, *287*, 1964 – 1969; b) G. C. Micalizio, S. L. Schreiber, *Angew. Chem.* **2002**, *114*, 160 – 162; *Angew. Chem. Int. Ed.* **2002**, *41*, 152 – 154; c) G. C. Micalizio, S. L. Schreiber, *Angew. Chem.* **2002**, *114*, 3406 – 3410; *Angew. Chem. Int. Ed.* **2002**, *41*, 3272 – 3276; d) O. Kwon, S. B. Park, S. L. Schreiber, *J. Am. Chem. Soc.* **2002**, *124*, 13402 – 13405; e) S. Nagayama, M. M.-C. Lo, C. Neumann, L. Pérez, A. Vegas, K. Nakai, T. Arai, D. Lee, J. Sello, P. R. Andreana, A. K. Franz, S. J. Taylor, J. P. Rearick, D. E. A. Brittain, C. Chen, X. Li, unpublished results.

[7] Diazobenzylidene slides can be left at room temperature in the dark for at least three weeks with no noticeable deterioration in performance. They are typically stored at −20 °C.

[8] a) M. W. Harding, A. Galat, D. E. Uehling, S. L. Schreiber, *Nature* **1989**, *341*, 758 – 760; b) J. J. Siekierka, S. H. Y. Hung, M. Poe, C. S. Lin, N. H. Sigal, *Nature* **1989**, *341*, 755 – 757.

[9] D. A. Holt, J. I. Luengo, D. S. Yamashita, H.-J. Oh, A. L. Konialian, H.-Z. Yen, L. W. Rozamus, M. Brandt, M. J. Bossard, M. A. Levy, D. S. Eggleston, J. Liang, L. W. Schultz, T. J. Stout, J. Clardy, *J. Am. Chem. Soc.* **1993**, *115*, 9925 – 9938.

[10] **2a** and **3** were detectable when printed at as low as 15 μM, whereas **2b** was detectable when printed at as low as 31 μM.

[11] Compounds printed from aqueous solutions were also captured.

[12] H. E. Blackwell, L. Pérez, S. L. Schreiber, *Angew. Chem.* **2001**, *113*, 3529 – 3533; *Angew. Chem. Int. Ed.* **2001**, *40*, 3421 – 3425.

[13] a) H. E. Blackwell, L. Pérez, R. A. Stavenger, J. A. Tallarico, E. C. Eatough, M. A. Foley, S. L. Schreiber, *Chem. Biol.* **2001**, *8*, 1167 – 1182; b) P. A. Clemons, A. N. Koehler, B. K. Wagner, T. G. Sprigings, D. R. Spring, R. W. King, S. L. Schreiber, *Chem. Biol.* **2001**, *8*, 1183 – 1195.

[14] Cy5 detection was chosen to avoid conflict with compound autofluorescence in the Cy3 channel.

[15] Negative controls showed no effect. See the Supporting Information for details on BIAcore analysis.

[16] That is, not designed to interact with a given protein or class of proteins using structural motifs known to favor such binding.

[17] Printed slides are typically stored at −20 °C, with no noticeable deterioration over at least two months.

 © 2003 Wiley-VCH Verlag GmbH & Co. KGaA, Weinheim

Probes for Cell Division

HR22C16: A Potent Small-Molecule Probe for the Dynamics of Cell Division**

*Srinivas Hotha, Justin C. Yarrow, Janet G. Yang, Sarah Garrett, Kishore V. Renduchintala, Thomas U. Mayer, and Tarun M. Kapoor**

Proper cell division requires that each daughter cell receive a single and complete copy of DNA.[1] Errors in this process can lead to severe developmental defects and diseases in humans. To divide the genetic material, the cell assembles a multicomponent apparatus that converts chemical energy into mechanical energy for the transport of DNA. The entire process takes minutes, and several steps occur within seconds. Cell-permeable small molecules allow us to intervene in this process on this time scale, whereas genetic methods, including RNA interference, are too slow, effective on a time scale of hours to days.[2a] Although many small molecules, including taxol, disrupt cell division by binding to tubulin, only a few small molecules that target the numerous other proteins involved in cell division have been identified.[2b,c] A strategy referred to as "forward chemical genetics" is a particularly promising tool for the discovery of new small-molecule inhibitors.[3] In forward chemical genetics, small molecules are selected if they yield a desired cellular phenotype or perturbation. The identification of the target of this small molecule can then link a known or an unknown protein to the observed phenotype. The small molecule can then be used to study the function of the target protein in its cellular context.

Herein we report the discovery of HR22C16 (**1**, Figure 1), a new cell-permeable small-molecule inhibitor of cell division, identified by a high-throughput microscopy-based forward-chemical-genetic screen. We show that HR22C16 blocks cell division by targeting Eg5, a molecular-motor protein whose function is required for cell division ($IC_{50} = 800 \pm 10$ nM).[4a] Furthermore, we report an efficient, diastereoselective, traceless solid-phase synthesis of HR22C16 analogues.

[*] Dr. T. M. Kapoor, Dr. S. Hotha, J. G. Yang, S. Garrett, Dr. K. V. Renduchintala
Laboratory of Chemistry and Cell Biology
The Rockefeller University
1230 York Ave, New York, NY 10021 (USA)
Fax: (+1) 212-327-8177
E-mail: Kapoor@rockefeller.edu

J. C. Yarrow
Department of Cell Biology
Institute of Chemistry and Cell Biology
Harvard Medical School, Boston, MA 02115 (USA)

Dr. T. U. Mayer
Max Planck Institute for Biochemistry
Am Klopferspitz 18a, 82152 Martinsried/Munich (Germany)

[**] This work is supported by the NIH (GM65933) and the NCI (CA78048). SH is a Revson Fellow. JCY and SG are HHMI Predoctoral Fellows. TMK is a Pew Scholar.

Supporting information for this article is available on the WWW under http://www.angewandte.org or from the author.

 DOI: 10.1002/anie.200351173 © 2003 Wiley-VCH Verlag GmbH & Co. KGaA, Weinheim

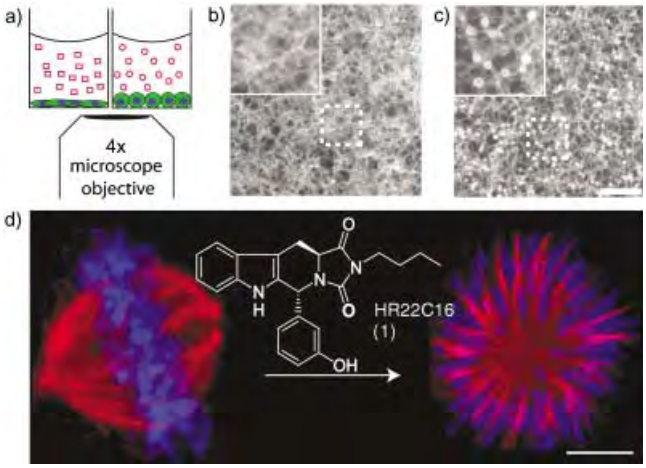


Figure 1. HR22C16 (**1**), a cell-division inhibitor discovered from a forward-chemical-genetic screen. a) Schematic representation of the assay. Vertebrate cells (BS-C-1) in a multiwell plate are stained for the actin cytoskeleton and imaged from below by using a 4× objective. Primary data from the screen show b) the effect of a compound that causes no morphological change (mostly flat cells with very few cells undergoing division) and c) the effect of HR22C16 with hundreds of cells blocked in mitosis as round cells (inset: 2.5×; scale bar: 250 μm). d) Configuration of microtubules (red: stained with antitubulin antibodies) and DNA (blue: stained with Hoechst 33342) in a control cell (left) and a HR22C16-treated cell (right; scale bar: 5 μm).

We have used these analogues in cellular and in vitro assays to clarify the structural basis of the activity of HR22C16 and to identify an Eg5 inhibitor that is approximately ninefold more potent than HR2216. Finally, guided by these studies, we have designed a photolabile protecting (photocaging) strategy for HR22C16 that allows fast temporal control over Eg5 function during cell division.

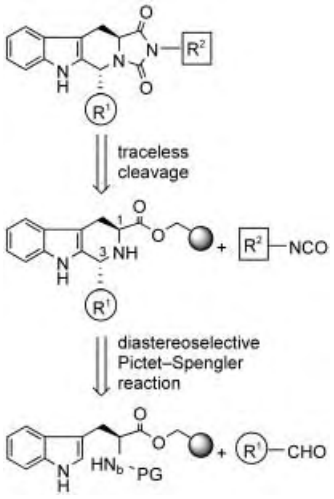
To identify small molecules that inhibit cell division we used the morphology of cells blocked in division as our readout, rather than limiting our search to one for an inhibitor of a particular protein. Cells are flat until they initiate cell division, when they adopt a round shape. Inhibition of cell division, then, increases the fraction of cells that exhibit a round morphology. Analysis by fluorescence microscopy (at only 4× magnification) provided a direct and simple readout for the inhibition of cell division. Based on this approach we examined the effects on mammalian cells of 16000 compounds from a collection of diverse small molecules.[5a,b] Figures 1b and 1c show primary data from this cell-based screen. Most compounds did not block cell division and therefore flat cells were mostly observed. In contrast, compounds that blocked cell division led to a higher proportion of round cells (i.e. dividing cells) and were easily detected by the eye or automated methods. HR22C16 (**1**) was discovered to be one of these compounds.

Subsequent examination of the microtubule cytoskeleton (red) and chromosomes (blue) in cells treated with HR22C16 revealed a monoaster phenotype (Figure 1d). Such a phenotype can arise in dividing cells by several mechanisms, including the loss of function of the ATPase Eg5, a motor protein that generates mechanical forces required for cell division.[4a] This phenotype is also obtained when cells are treated with the dihydropyrimidine monastrol, a known cell-permeable small-molecule Eg5 inhibitor ($IC_{50} = 14\ \mu M$).[4b] We used in vitro assays for Eg5 motor function and indeed found that HR22C16 inhibited Eg5 ($IC_{50} = 800 \pm 10$ nM).

HR22C16 is a new and potent inhibitor of a key enzyme involved in cell division. To understand and characterize the structural basis for the activity of HR22C16, we sought to develop an efficient solid-phase synthesis of HR22C16 analogues with defined stereochemistry. We envisaged that the HR22C16 scaffold could be generated by an initial Pictet–Spengler cyclization of tryptophan and an aldehyde, followed by treatment with an isocyanate to form the terminal hydantoin ring (Scheme 1). We recognized that the diastereoselectivity of the Pictet–Spengler cyclization would have to be examined carefully as a diastereoselective version of this reaction had not yet been reported on a solid support.[6] However, if successful, this transformation would not only provide access to HR22C16 analogues, but would also be useful for the synthesis of natural products in the sarpagine and ajmaline class.[7a]

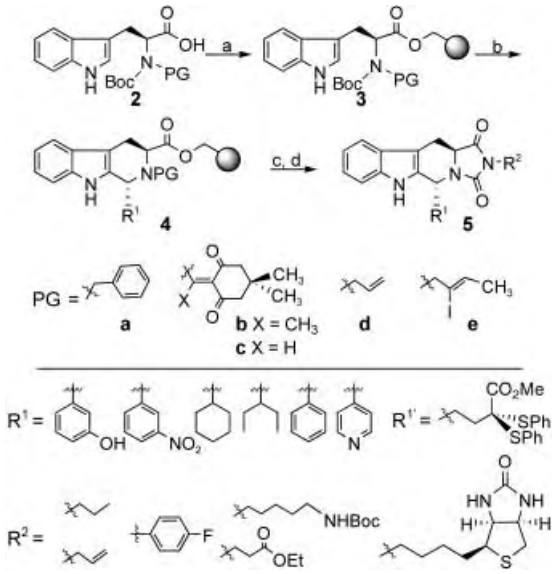
An additional key consideration was the cleavage of the products from the solid supports. We envisaged that the compounds could be attached to the solid support by the tryptophan carboxy group. After Pictet–Spengler cyclization, treatment with isocyanates would lead to formation of the hydantoin ring and concurrent cleavage of the ester bond, thus resulting in traceless release from the solid support.

Next, we required a protecting group for N_b that could be removed under homogeneous reaction conditions, as required for solid-phase synthesis, and that would allow diastereoselective Pictet–Spengler cyclization. In solution N_b-substituted tryptophan esters undergo the Pictet–Spengler cyclization to yield the 1,3-*trans* tetrahydro-β-carboline diastereoisomers preferentially.[7] We evaluated a number of protecting groups for N_b, including benzyl (**2a**), 4,4-dimethyl-2,6-dioxocyclohexylidene ethyl (**2b**), and 4,4-dimethyl-2,6-dioxocyclohexylidene methyl (**2c**; Scheme 2), but these protecting groups were either difficult to cleave under homogeneous conditions or did not afford any diastereoselectivity in the Pictet–



Scheme 1. Design of the traceless, diastereoselective solid-phase synthesis of diverse HR22C16 analogues. PG is a protecting group that induces transfer of asymmetry.

 © 2003 Wiley-VCH Verlag GmbH & Co. KGaA, Weinheim



Scheme 2. Diastereoselective traceless solid-phase synthesis of HR22C16 analogues. a) NovaSyn TG-S-OH (0.25 equiv; for aldehyde $R^{1\prime}$: Wang resin), 1,1′-carbonyldiimidazole (1 equiv), CH_2Cl_2, room temperature, 15 h; b) R^1CHO (20 equiv), trifluoroacetic acid (5% in CH_2Cl_2), 50°C, 24 h; c) $[Pd(PPh_3)_4]$ (0.4 equiv), *N*,*N*′-dimethylbarbituric acid (6 equiv), CH_2Cl_2, 50°C, 6 h; d) R^2NCO (10 equiv), THF, 55°C, 36 h.

Spengler cyclization. However, when the two readily cleavable groups N_b-allyl (**2d**) and N_b-(*Z*)-2-iodo-2-butenyl (**2e**) were used, the solid-phase Pictet–Spengler reaction with 3-hydroxybenzaldehyde afforded the products in good yields (>90%) and the *trans* isomer was favored over the *cis* isomer by 9:1.[5a] Notably, the solid-phase diastereoselective Pictet–Spengler cyclization of **3e** with 5-oxo-2,2-bis(phenylthio)pentanoic acid methyl ester ($R^{1\prime}CHO$)[8] yielded a key intermediate in the synthesis of the naturally occurring indole alkaloids corynantheidol and geissoschizine.[9] We are currently pursuing the diversity-oriented synthesis of analogues of these bioactive small molecules.

We carried out the diversity-oriented synthesis of HR22C16 analogues by first coupling N_b-Boc-N_b-allyl-L-tryptophan (**2d**) to hydroxy-TentaGel resin with 1,1′-carbonyldiimidazole (Scheme 2). The resin-bound amino acid **3d** was subjected to Pictet–Spengler cyclization conditions in the presence of various aldehydes, including heterocyclic, substituted aromatic, and aliphatic aldehydes.[5a,c] A key advantage of solid-phase chemistry is that large excesses of soluble reactants can normally be used to drive intermolecular reactions to completion. However, this feature does not apply to intramolecular cyclizations. We therefore devised a strategy to remove any uncyclized material that remained on the solid support. Toward this end, the resins were treated with propyl isocyanate after the Pictet–Spengler cyclization. Uncyclized starting material (typically <5%) was cleaved as the hydantoin to leave behind the desired N_b-allyl-1,2,3,4-tetrahydro-β-carboline. After Pd-mediated deprotection of the N_b-allyl functionality, the resin was treated with diverse isocyanates (R^2NCO). The hydantoin-forming reaction provided traceless cleavage of the HR22C16 analogues **5** from the solid support.[5a] Excess isocyanate was then removed by incubation with an amine scavenger resin. The average overall yield of HR22C16 analogues was 46%, and the products were obtained in >90% purity as determined by HPLC and ^1H NMR spectroscopic analysis.

Although our strategy can readily yield large libraries of HR22C16 analogues, we initiated our studies by synthesizing a small library of 50 compounds. Cell-based assays revealed that minor changes in the R^1 substitution on HR22C16 resulted in a marked decrease in potency.[5a] However, several analogues with variations in R^2 were active. These compounds were tested in in vitro assays with recombinant Eg5. Compound **6** (Figure 2) inhibited Eg5 motility with an IC_{50} value of 90 ± 40 nM, thus making it the most potent inhibitor currently available for this key cell-division protein.

The physical separation of genetic cargo during cell division (i.e. anaphase) typically takes 10–15 minutes in vertebrate cells. However, it has been reported that antimitotic agents, including the Eg5-inhibitor monastrol, take 10–15 minutes to achieve inhibitory concentrations inside cells.[10] Thus, greater temporal control in perturbing this process is critical. Light can be controlled with outstanding temporal and spatial precision to localize photochemistry noninvasively in a biological context. Photolabile protecting groups have been widely used to "cage" bioactive compounds for regulated physiological release.[11] When a caged compound is

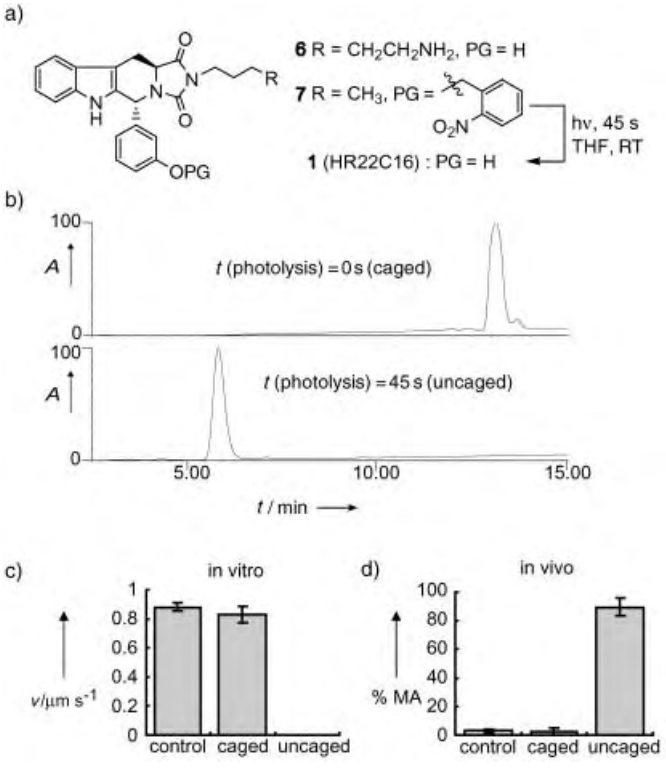


Figure 2. A strategy for the rapid photolytic release of "caged" HR22C16. a) Structures of HR22C16 analogues. b) HPLC analysis of photolysis. A 10 mM solution of **7** was completely uncaged upon exposure for 45 s to a He–Cd laser. Caged HR22C16 **7** does not c) inhibit Eg5 in in vitro motor assays (2.5 μM) or d) arrest cell division in human tumor cells (HeLa; 5.0 μM; control = dimethyl sulfoxide alone; %MA = percent monoastral spindles in mitotic cells). Uncaged HR22C16 blocks Eg5 function in both assays.

 © 2003 Wiley-VCH Verlag GmbH & Co. KGaA, Weinheim

used, cells are incubated to a point of equilibration with a caged inhibitor that does not block the function of its target. Then at the desired stage photolysis releases the active inhibitor to perturb the function of the target.

We envisaged that photocaging of HR22C16 would allow Eg5 to be inhibited with increased temporal precision. Based on our studies with HR22C16 analogues, we predicted that substitution at the phenolic moiety of HR22C16 would result in inactivation. Thus, we synthesized[5a] the *ortho*-nitrobenzyl ether **7** (Figure 2). Indeed, this "caged" HR22C16 analogue does not inhibit Eg5 in vitro or block cell division in a human tumor cell line. Compound **7** can be completely "uncaged" through the use of a He–Cd laser in under 45 seconds, with the release of active HR22C16. We anticipate that this strategy, combined with the use of more physiologically benign photolabile protecting groups such as brominated 7-hydroxycoumarin-4-ylmethyl, will provide the degree of temporal control needed to examine the complex dynamics of cell division. Furthermore, localized uncaging of HR22C16 analogues may allow spatial control over the inhibition of cell division, whereby a subset of dividing cells in an organelle (or tumor) in a living organism may be targeted.

In summary, we report the discovery of a novel antimitotic, HR22C16, identified by a forward-chemical-genetic screen. Our efficient solid-phase traceless synthesis of HR22C16 analogues has provided access to new tools for studying Eg5, including one molecule that is about 155-fold more potent than other available Eg5 inhibitors. Current efforts involve the use of "caged" HR22C16 to examine Eg5 function at high temporal resolution during cell division. The results of these studies will be reported in due course.

Received: February 13, 2003
Revised: April 14, 2003 [Z51173]

Keywords: antimitotics · inhibitors · molecular motors · photolysis · solid-phase synthesis

[1] For a review, see: T. J. Mitchison, E. D. Salmon, *Nat. Cell Biol.* **2001**, *3*, E17-E21.
[2] a) R. Micura, *Angew. Chem.* **2002**, *114*, 2369–2373; *Angew. Chem. Int. Ed.* **2002**, *41*, 2265–2269; b) C. M. Crews, R. Mohan, *Curr. Opin. Chem. Biol.* **2000**, *4*, 47–53; c) J. R. Peterson, T. J. Mitchison, *Chem. Biol.* **2002**, *9*, 1275–1285.
[3] S. L. Schreiber, *Bioorg. Med. Chem.* **1998**, *6*, 1127–1152.
[4] a) For a review, see: C. E. Walczak, T. J. Mitchison, *Cell* **1996**, *85*, 943–946; b) T. U. Mayer, T. M. Kapoor, S. J. Haggarty, R. W. King, S. L. Schreiber, T. J. Mitchison, *Science* **1999**, *286*, 971–974.
[5] a) See Supporting Information; b) The 16000-compound collection was obtained from ChemBridge Corporation; c) Analysis of HPLC and ^{1}H NMR spectroscopic data of solid-phase Pictet–Spengler-reaction products revealed the diastereoselectivity for each aldehyde to be (*trans*/*cis*): *m*-hydroxybenzaldehyde (9.0:1), benzaldehyde (7.6:1), *m*-nitrobenzaldehyde (8.5:1), cyclohexanecarboxaldehyde (10.5:1), 2-ethylbutyraldehyde (7.8:1), 4-pyridinecarboxaldehyde (9.6:1).
[6] Nondiastereoselective solid-phase Pictet–Spengler reactions: a) D. Bonnet, A. Ganesan, *J. Comb. Chem.* **2002**, *4*, 546–548; b) R. V. Connors, A. J. Zhang, S. J. Shuttleworth, *Tetrahedron Lett.* **2002**, *43*, 6661–6663; b) X. Li, L. Zhang, W. Zhang, S. E. Hall, J. P. Tam, *Org. Lett.* **2000**, *2*, 3075–3078; c) S. Vendeville, L. Bourel, E. Davioud-Charvet, P. Grellier, B. Deprez, C. Sergheraert, *Bioorg. Med. Chem. Lett.* **1999**, *9*, 437–442; d) H. Wang, A. Ganesan, *Org. Lett.* **1999**, *1*, 1647–1649; e) P. P. Fantauzzi, K. M. Yager, *Tetrahedron Lett.* **1998**, *39*, 1291–1294; f) J. P. Mayer, D. Bankaitis-Davis, J. Zhang, G. Beaton, K. Bjergarde, C. M. Andersen, B. A. Goodman, C. J. Herrera, *Tetrahedron Lett.* **1996**, *37*, 5633–5636; g) R. Mohan, Y.-L. Chou, M. M. Morrissey, *Tetrahedron Lett.* **1996**, *37*, 3963–3966; h) L. Yang, L. Guo, *Tetrahedron Lett.* **1996**, *37*, 5041–5044; i) K. Kalijuste, A. Undén, *Tetrahedron Lett.* **1995**, *36*, 9211–9214; k) B. Sauerbrei, V. Jungmann, H. Waldmann, *Angew. Chem.* **1998**, *110*, 1187–1190; *Angew. Chem. Int. Ed.* **1998**, *37*, 1143–1146.
[7] a) J. Li, T. Wang, P. Yu, A. Peterson, R. Weber, D. Soerens, D. Grubisha, D. Bennett, J. M. Cook, *J. Am. Chem. Soc.* **1999**, *121*, 6998–7010; b) E. D. Cox, J. M. Cook, *Chem. Rev.* **1995**, *95*, 1797–1842.
[8] For the synthesis of 5-oxo-2,2-bis(phenylthio)pentanoic acid methyl ester, see: G. Massiot, T. Mulamba, *J. Chem. Soc. Chem. Commun.* **1983**, 1147–1149; an α,β-unsaturated ester can be unmasked and cyclized.
[9] a) S. Yu, O. M. Berner, J. M. Cook, *J. Am. Chem. Soc.* **2000**, *122*, 7827–7828; b) L. E. Overman, A. J. Robichaud, *J. Am. Chem. Soc.* **1989**, *111*, 300–308; c) V. H. Rawal, C. Michoud, R. Monested, *J. Am. Chem. Soc.* **1993**, *115*, 3030–3031.
[10] S. Faruki, R. W. Cole, C. L. Rieder, *Cell Motil. Cytoskeleton* **2002**, *52*, 107–121.
[11] a) T. Furuta, S. S.-H. Wang, J. L. Dantzker, T. M. Dore, W. J. Bybee, E. M. Callaway, W. Denk, *Proc. Natl. Acad. Sci. USA* **1999**, *96*, 1193–1200; b) S. R. Adams, R. Y. Tsien, *Annu. Rev. Physiol.* **1993**, *55*, 755–784.

 © 2003 Wiley-VCH Verlag GmbH & Co. KGaA, Weinheim

Crystallized Mesoporous Ta-Nb Oxide

Crystallization of an Ordered Mesoporous Nb–Ta Oxide**

*Tokumitsu Katou, Byongjin Lee, Daling Lu, Junko N. Kondo, Michikazu Hara, and Kazunari Domen**

The preparation and application of mesoporous materials has been in recent years extended from silica-based materials to general inorganic materials such as oxides, sulfides and metals.[1] Applications now include catalysis, sorption, and

[*] Prof. K. Domen, T. Katou, Dr. J. N. Kondo, Prof. M. Hara
Chemical Resources Laboratory
Tokyo Institute of Technology, 4259
Nagatsuta-cho, Midori-ku, Yokohama, 226-8503 (Japan)
Fax: (+81) 45-924-5282
E-mail: kdomen@res.titech.ac.jp
Prof. K. Domen, Dr. B. Lee, Dr. D. Lu
Core Research for Evolutional Science and Technology (CREST)
Japan Science and Technology (Japan)

[**] This work was supported by the Core Research for Evolutional Science and Technology (CREST) program of the Japan Science and Technology (JST) Corporation.

Supporting information for this article is available on the WWW under http://www.angewandte.org or from the author.

 © 2003 Wiley-VCH Verlag GmbH & Co. KGaA, Weinheim DOI: 10.1002/anie.200250263

sensing, as well as nano devices. In particular, mesoporous transition-metal oxides are expected to be useful functional inorganic materials with a wide range of potential applications.[2] For example, mesoporous Ta_2O_5[3] and Mg–Ta mixed oxide[4] exhibit high photocatalytic activity for the decomposition of water into H_2 and O_2 under ultraviolet irradiation, and mesoporous SnO_2 with a uniform pore size has been investigated as a gas sensor.[5] The amorphous pore walls of most mesoporous materials, which offer only poor thermal and mechanical stability, restrict the range of applications of these materials; whereas a crystallized wall structure can be expected to provide better thermal and mechanical stability as well as superior electric and optical properties. The crystallization and crystallinity of mesoporous materials have therefore attracted much attention. Hybrid mesoporous materials (HMMs), prepared from alkoxysilane $(CH_3CH_2O)_3Si{-}C_6H_4{-}Si(OCH_2CH_3)_3$ and with a 2D hexagonal mesoporous structure, were recently reported to have periodically ordered phenyl groups.[6] The synthesis of mesoporous zeolite single-crystals has also been reported.[7] We reported the preparation of crystallized mesoporous Nb–Ta oxide (NbTa-TIT-1) consisting of single-crystal particles forming a wormholelike mesoporous structure.[8] This Nb–Ta oxide exhibits remarkable hydrothermal and mechanical stability, and the preparation of single-crystal particles in an ordered mesoporous structure would be of significant interest. We successfully synthesized a Nb–Ta mixed oxide with 2D hexagonally ordered mesoporous structure,[9] and attempted the preparation of a crystallized wall structure. However, the material obtained consisted of crystallized particles in a wormholelike mesoporous structure, which suggests that the wormhole structure is formed during crystallization regardless of the structure of the amorphous precursor. The pore diameter increases from 6 to 13 nm and the wall thickness remains widely distributed (4–8 nm) after crystallization, suggestive of considerable mass transfer during the process. These findings appear to indicate that it is difficult to preserve the original ordered mesoporous structure after crystallization by simple calcination in air.[10]

Nanoporous carbon materials were prepared from various mesoporous silica templates.[11] Recently, as one of the advanced applications, it was reported that highly ordered mesoporous silica can be regenerated from nanoporous carbon materials.[12] As such carbon materials exhibit excellent thermal stability in inert atmospheres.[11] Mesopores of ordered mesoporous Nb–Ta oxide filled with carbon may offer a means of preserving the ordered mesoporous structure during crystallization. We have examined this possibility by filling the mesopores of 2D hexagonally ordered Nb–Ta oxide with carbon prior to crystallization. The results of crystallization are presented herein.

Figure 1 shows a typical transmission electron microscopy (TEM) image and electron diffraction (ED) pattern (inset) of the 2D hexagonally ordered mesoporous Nb–Ta oxide, which was used as an amorphous precursor for crystallization. The preparation method was reported in detail previously.[9] The ordered mesoporous Nb–Ta oxide was then crystallized following the procedure shown in Figure 2. After crystallization, a peak attributed to an ordered mesoporous structure

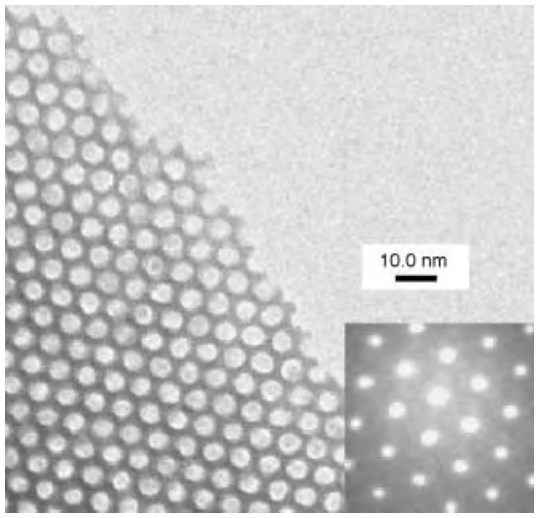


Figure 1. Representative TEM image and ED pattern (inset) of 2D hexagonally ordered mesoporous Nb–Ta oxide.

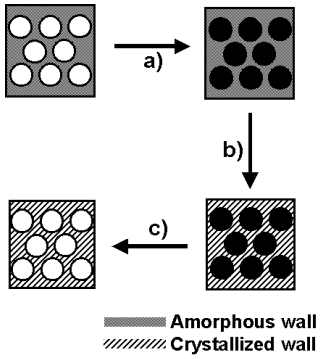


Figure 2. Conceptual scheme of the synthesis of mesoporous Nb–Ta oxide with 2D hexagonally ordered mesoporous structure and crystallized wall structure. a) Accumulation of polymerized furfuryl alcohol and subsequent carbonization at 823 K in vacuo. b) Crystallization of walls at 923 K under He. c) Removal of carbon by calcination at 773 K in air.

(d spacing = 6.8 nm) was observed in the powder X-ray diffraction (XRD) pattern (Figure 3). Wide-angle powder XRD revealed that a completely crystallized oxide phase, similar to that of NbTa-TIT-1[10], was prepared by calcination

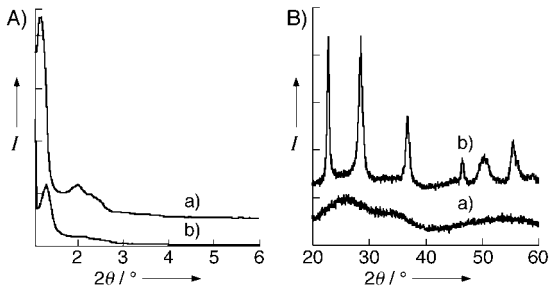


Figure 3. A) Low- and B) wide-angle powder XRD patterns a) before and b) after crystallization of 2D hexagonally ordered mesoporous Nb-Ta oxide. I = intensity, arbitrary units.

 © 2003 Wiley-VCH Verlag GmbH & Co. KGaA, Weinheim

of the Nb–Ta oxide in air. The detailed assignment of peaks in the wide-angle powder XRD pattern has also been given in a previous report.[8] These results imply the presence of both an ordered mesoporous structure and crystallized walls. Figure 4a shows the TEM image of a particle with 2D hexagonally ordered mesopore channels, having somewhat curved lines. The ED pattern for the whole particle consists of mixed spots on a ring pattern. As the size of the single-crystal domain is not clear from Figure 4, ED patterns were obtained for smaller areas. Figure 4b) is a TEM image in a 100 nm region with corresponding ED pattern (inset). The observed mesoporous region consists of a single crystalline domain. The presence of mesopores in a single-crystal domain can be directly observed in high-resolution (HR) TEM images. As indicated by the arrows in the inset of Figure 5a and b, the lattice fringes extend coherently across several mesopores, thus confirming the existence of mesopores in a single-crystal domain. Figure 5a and b, taken for the same particle, reveal different directions of lattice fringes. This is consistent with the fact that there are several single-crystal domains in a particle. In the HRTEM image taken along the pore channel axis (Figure 5c) lattice fringes can be seen in the walls around pores with almost the same size and arrangement of mesopores as prior to crystallization. From these results, the mixed spot ED pattern (Figure 4a inset) is attributable to the presence of several single-crystal domains in the particle within an ordered mesoporous structure. From energy-dispersive X-ray spectroscopy (EDX) analysis, an Nb/Ta ratio of about one was confirmed at approximately 10 points

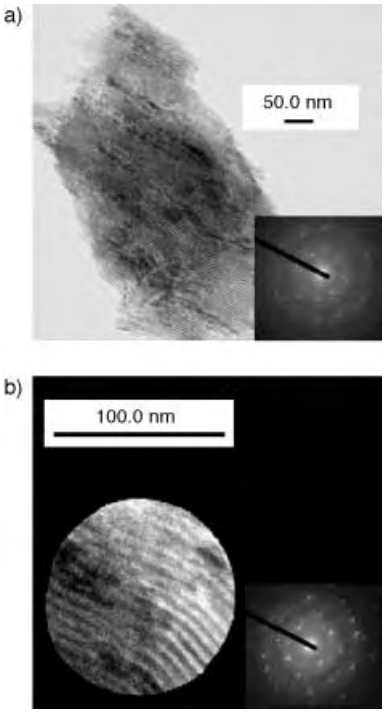


Figure 4. Typical TEM and ED analyses of NbTa-TIT-2. a) Image and ED pattern (inset) of a whole particle. b) Image and ED pattern (inset) of single-crystal domain of 100 nm.

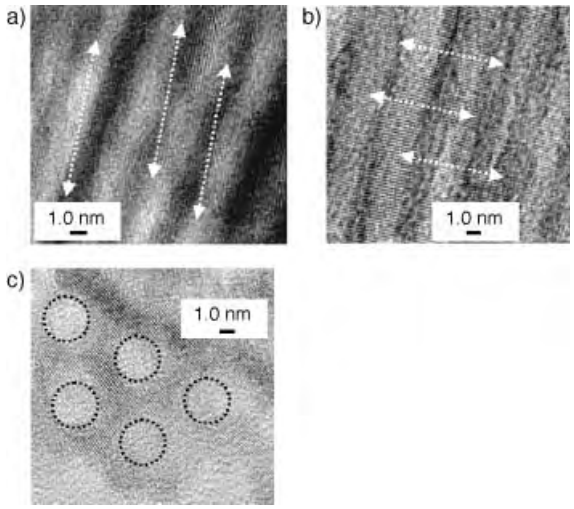


Figure 5. HRTEM images of NbTa-TIT-2. a) And b) lattice fringes in different orientations with respect to the pore channel direction. c) Lattice fringes on walls, viewed perpendicular to the pore channel axis.

(< ca. 5 nm size) on a particle in Figure 3a. This material is denoted NbTa-TIT-2, and represents a material obtained from a carbon-filled amorphous precursor with a 2D hexagonally ordered mesoporous structure.

The role of carbon in the preservation of the mesoporous structure was also examined. In the case of crystallization under helium at 923 K for 1 h in the absence of a carbon template, no peak was observed in the low 2θ region (1–6°) of the XRD results, and an N_2 uptake owing to the mesopores appeared at a relative pressure of around $P/P_0 = 0.8$ ($P_0 = 1 \times 10^5$ Pa). These results represent the physicochemical changes of NbTa-TIT-1 with the wormhole mesoporous structure, and differs markedly from the results for NbTa-TIT-2. Therefore, NbTa-TIT-2 cannot be constructed by calcination under helium without a carbon template. The mesoporous structure appears to be stabilized by the carbon template, thus preventing the structural change from a 2D hexagonal to a wormhole structure during crystallization.

According to the results shown in Figure 6, the N_2 uptake at $P/P_0 = 0.5$–0.7 for NbTa-TIT-2 is approximately a quarter of that of the amorphous precursor. The N_2 uptake at $P/P_0 = 0.8$ is derived from large pores, which increases markedly in size after crystallization of the amorphous precursor. In addition, the mesopore volume per gram decreases from 0.34 to 0.23 $mL\,g^{-1}$, probably owing to the collapse of mesopores. Therefore, approximately three quarters of the original mesopores (ca. 6.0 nm) of the amorphous precursor either are converted to larger pores or collapse after crystallization. Crystal domains with lower pore-wall periodicity are also observed by HRTEM. From the results obtained by XRD, N_2 isotherm and TEM image (see Supporting Information) before the removal of carbon (after crystallization of the pore walls), we regard the insufficient carbon content inside the pores of the sample as one of the reasons for the low yield of NbTa-TIT-2. Despite this low yield, the carbon templating method is still effective for controlling the mesoporous structure of crystallized mesoporous materials.

 © 2003 Wiley-VCH Verlag GmbH & Co. KGaA, Weinheim

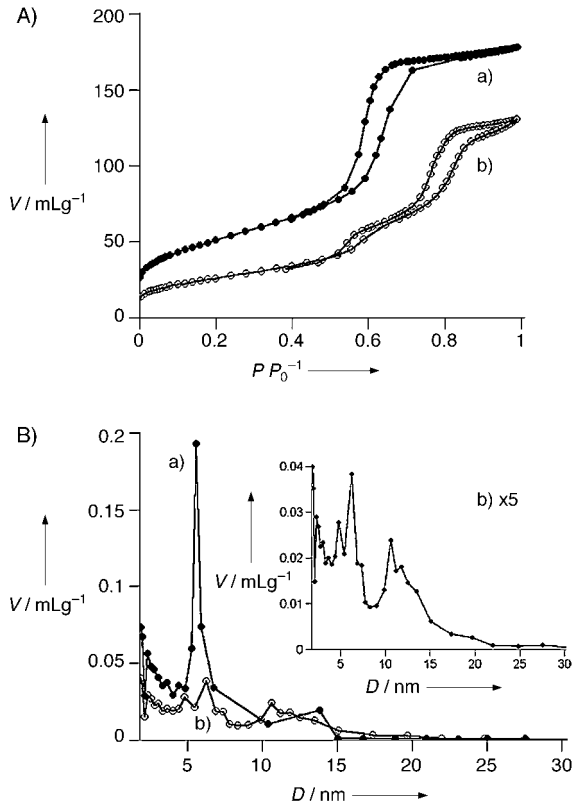


Figure 6. A) N_2 sorption isotherms and B) pore size distributions a) before and b) after crystallization of 2D hexagonally ordered mesoporous Nb–Ta oxide. V = volume of N_2 per gram of material.

Experimental Section

Two-dimensional hexagonal mesoporous Nb–Ta oxide, the amorphous precursor for crystallization, was synthesized based on a reported procedure.[9] The pore wall crystallization method is shown in Figure 2. Furfuryl alcohol vapor (0.023 mol h^{-1}) in nitrogen gas (30 mL min^{-1}) was passed through the amorphous precursor fixed in a reactor at 473 K for 2 h. The brown color of the resulting sample arises from the accumulation of polymerized furfuryl alcohol. The polymerized furfuryl alcohol in the brown sample was then changed to black carbon by carbonization at 823 K for 3 h in vacuo. The sample was subsequently crystallized by heating in a He atmosphere at 923 K for 2 h. The carbon template in the crystallized sample was then removed by calcination at 773 K for 15 h in air. Powder XRD patterns were obtained on a Rigaku RINT 2100 diffractometer with $Cu_{K\alpha}$ radiation. TEM images, ED patterns and EDX were obtained using a 200 kV JEOL JEM2010F microscope. N_2 sorption isotherms were measured using SA-3100 systems, and pore-size distributions were determined by Barett-Joyner-Halenda (BJH) analysis.

Received: September 30, 2002
Revised: March 13, 2002 [Z50263]

Keywords: crystal engineering · mesoporous materials · nanostructures · niobium · tantalum

[1] F. Schüth, *Chem. Mater.* **2001**, *13*, 3184 – 3195.
[2] P. Yang, D. Zhao, D. I. Margolese, B. F. Chemelka, G. D. Stucky, *Chem. Mater.* **1999**, *11*, 2813 – 2826; U. Ciesla, F. Schüth, *Microporous Mesoporous Mater.* **1999**, *27*, 131 – 149.
[3] Y. Takahara, J. N. Kondo, T. Takata, D. Lu, K. Domen, *Chem. Mater.* **2001**, *31*, 1194 – 1199.
[4] M. Uchida, J. N. Kondo, D. Lu, K. Domen, *Chem. Lett.* **2002**, 498 – 499.
[5] G.-J. Li, S. Kawi, *Talanta* **1998**, *45*, 759 – 766; T. Hyodo, N. Nishida, Y. Shimizu, M. Egashira, *Sens. Actuators B* **2002**, 209 – 215; F. Chen, M. Liu, *Chem. Commun.* **2000**, 2095 – 2096.
[6] S. Inagaki, S. Guan, T. Ohsuna, O. Terasaki, *Nature* **2002**, *416*, 304 – 307.
[7] I. Schmidt, A. Boisen, E. Gustavsson, K. Stahl, S. Pehrson, S. Dahl, A. Carlsson, C. J. H. Jacobsen, *Chem. Mater.* **2001**, *13*, 4416 – 4418; C. J. H. Jacobsen, C. Madsen, J. Houzvicka, I. Schmidt, A. Carlsson, *J. Am. Chem. Soc.* **2000**, *122*, 7116 – 7117.
[8] B. Lee, D. Lu, J. N. Kondo, K. Domen, *Chem. Commun.* **2001**, 2118 – 2119; B. Lee, T. Yamashita, D. Lu, J. N. Kondo, K. Domen, *Chem. Mater.* **2002**, *14*, 867 – 875.
[9] T. Katou, J. N. Kondo, D. Lu, K. Domen, *J. Mater. Chem.* **2002**, *12*, 1480 – 1483.
[10] T. Katou, B. Lee, D. Lu, J. N. Kondo, M. Hara, K. Domen, unpublished results.
[11] S. Jun, S. H. Joo, R. Ryoo, M. Kurk, M. Jaroniec, Z. Liu, T. Ohsuna, O. Terasaki, *J. Am. Chem. Soc.* **2000**, *122*, 10712 – 10713; M. Kurk, M. Jaroniec, R. Ryoo, S. H. Joo, *.J. Phys. Chem. B* **2000**, *104*, 7960 – 7968; S. H. Joo, S. J. Choi, I. Oh, J. Kwak, Z. Liu, O. Terasaki, R. Ryoo, *Nature* **2001**, *412*, 169 – 172.
[12] M. Kang, S. H. Yi, H. I. Lee, J. E. Yie, J. M. Kim, *Chem. Commun.* **2002**, 1944 – 1945; A. H. Lu, W. Schmidt, A. Taguchi, B. Spliethoff, B. Tesche, F. Schüth, *Angew. Chem.* **2002**, *114*, 3639 – 3642; *Angew. Chem. Int. Ed.* **2002**, *41*, 3489 – 3492.

 © 2003 Wiley-VCH Verlag GmbH & Co. KGaA, Weinheim

Zwitterionic Catalysts

Zwitterionic Relatives to the Classic [(P–P)-Rh(solv)$_2$]$^+$ Ions: Neutral Catalysts Active for H–E Bond Additions to Olefins (E = C, Si, B)**

*Theodore A. Betley and Jonas C. Peters**

Since their introduction by Osborne and Schrock three decades ago, cationic rhodium [(P–P)Rh(solv)$_2$]$^+$ complexes have been used as precatalysts for a wide range of E–H (E = C, Si, B) bond-forming processes.[1–4] Herein, we introduce a new and complementary class of neutral, formally zwitterionic rhodium complexes supported by bis(phosphanyl)- and bis(amino)borate ligands that provide an alternative

[*] Prof. J. C. Peters, T. A. Betley
Division of Chemistry and Chemical Engineering
Arnold and Mabel Beckman Laboratories of Chemical Synthesis
California Institute of Technology, Pasadena, CA 91125 (USA)
Fax: (+1) 626-577-4088
E-mail: jpeters@caltech.edu

[**] We thank the NSF (CHE-0132216), the ACS Petroleum Research Fund, and the Dreyfus Foundation for financial support. T.A.B. thanks the Department of Defense for a graduate research fellowship. Brian Stoltz and Jeremy May provided helpful discussions and a sample of 4-methyl-4-pentenal.

Supporting information for this article is available on the WWW under http://www.angewandte.org or from the author.

 DOI: 10.1002/anie.200250378 © 2003 Wiley-VCH Verlag GmbH & Co. KGaA, Weinheim

approach to the chemistry of the $[(P–P)Rh(solv)_2]^+$ complexes.[5] The rhodium(I) zwitterions introduced herein (Figure 1) feature a borate counteranion that is fastened within the ligand backbone and partially insulated from the coordinated metal center by tertiary phosphanes and amines.[6,7] These complexes are distinct from previously prepared bis(pyrazolyl)borate rhodium complexes,[8] where resonance delocalization of the borate charge is likely to be more prevalent.

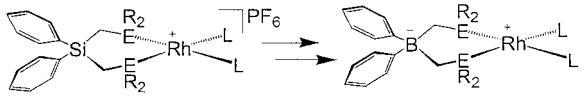


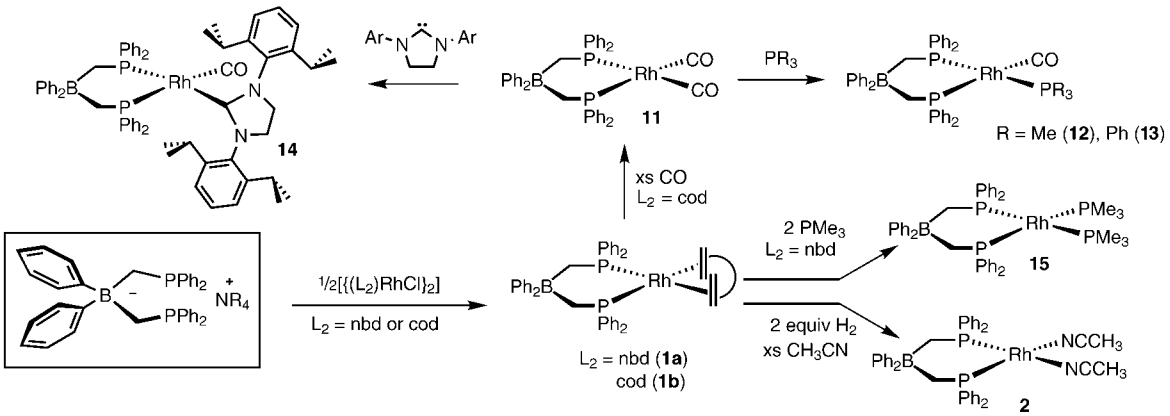
Figure 1. Catalyst systems featured herein. E = P, R = phenyl; E = N, R = methyl.

The key findings described in this report pertain to the catalytic activity and electrophilicity of the structurally similar zwitterionic and cationic complexes that are depicted in Figure 1. This comparative study shows that the phosphane-supported zwitterions are not only catalytically competent, but that they maintain their catalytic activity in both polar and nonpolar solvents, in contrast to their isostructural but cationic phosphane relatives. It is also shown that amine-chelated zwitterions are promising candidates for further catalytic development. The activity exhibited by these zwitterionic P- and N-chelated systems appears to be distinct from that of their corresponding N-donor bis(pyrazolyl)borate rhodium relatives, which seem to be relatively unsuitable for the reactions described herein.[8]

The synthetic and characterization data for each of the phosphane-chelated zwitterions is provided in the Supporting Information. The synthetic details for the amine-chelated complexes were recently communicated elsewhere.[7] Briefly, zwitterionic phosphane precatalysts were prepared in high yield by reaction of the diene–rhodium precursors $[\{(nbd)RhCl\}_2]$ and $[\{(cod)RhCl\}_2]$ with $[Ph_2B(CH_2PPh_2)_2]^-$ (nbd = norbornadiene; cod = cyclooctadiene; Figure 1). Hydrogenative removal of the norbornadiene ligand of $[\{Ph_2B(CH_2PPh_2)_2\}Rh(nbd)]$ (**1a**) occurred in the presence of acetonitrile to afford the complex $[\{Ph_2B(CH_2PPh_2)_2\}Rh(CH_3CN)_2]$ (**2**) (Scheme 1). The related amine-chelated complexes $[\{Ph_2B(CH_2NMe_2)_2\}Rh(nbd)]$ (**3**) and $[\{Ph_2B(CH_2NMe_2)_2\}Rh(CH_3CN)_2]$ (**4**) were similarly prepared.[7] The isostructural but cationic systems $[\{Ph_2Si(CH_2PPh_2)_2\}Rh(nbd)][PF_6]$ (**5**), $[\{Ph_2Si(CH_2PPh_2)_2\}Rh(CH_3CN)_2][PF_6]$ (**6**), $[\{Ph_2Si(CH_2NMe_2)_2\}Rh(nbd)][PF_6]$ (**7**), and $[\{Ph_2Si(CH_2NMe_2)_2\}Rh([D_6]acetone)_2][PF_6]$ (**8**) were independently prepared to allow comparisons of the reactivity.[9,10] The acetonitrile adducts for the cationic systems supported by $Ph_2PCH_2CH_2PPh_2$ (dppe) and $Ph_2PCH_2CH_2CH_2PPh_2$ (dppp), $[(dppe)Rh(CH_3CN)_2][PF_6]$ (**9**) and $[(dppp)Rh(CH_3CN)_2][PF_6]$ (**10**), were derived in a similar fashion from norbornadiene precursors that were previously reported.[11,4a]

Owing to their novelty, it was of interest to briefly canvass the structural characteristics and substitution chemistry of the phosphane-based zwitterions $[\{Ph_2B(CH_2PPh_2)_2\}RhL_2]$ (Scheme 1). Treatment of the cyclooctadiene analogue of **1a**, $[\{Ph_2B(CH_2PPh_2)_2\}Rh(cod)]$ (**1b**), with CO gas produced the dicarbonyl complex $[\{Ph_2B(CH_2PPh_2)_2\}Rh(CO)_2]$ (**11**) quantitatively. Dicarbonyl **11** underwent single substitution by PMe_3, PPh_3, and an N-heterocyclic carbene to produce the monocarbonyl adduct complexes $[\{Ph_2B(CH_2PPh_2)_2\}Rh(CO)(PMe_3)]$ (**12**), $[\{Ph_2B(CH_2PPh_2)_2\}Rh(CO)(PPh_3)]$ (**13**), and $[\{Ph_2B(CH_2PPh_2)_2\}Rh(CO)(carbene)]$ (**14**), respectively. The tetrakis(phosphane) complex $[\{Ph_2B(CH_2PPh_2)_2\}Rh(PMe_3)_2]$ (**15**) was available directly from **1a** by treatment with excess PMe_3.

The solid-state structures of complexes **1a**, **2**, **11**, and **14** were determined by X-ray diffraction studies.[12] The structures of **2** and **11** are displayed in Figure 2, and those of **1a** and **14** are available in the Supporting Information. In each case, the borate unit is locked rigidly in the backbone of the $[Ph_2B(CH_2PPh_2)_2]^-$ ligand at a distance of approximately 4 Å from the coordinated rhodium center. No inter- or intramolecular ion-pairing interactions are observed, consistent with the amine-chelated zwitterion that was characterized previously.[7] The $[Ph_2B(CH_2PPh_2)_2]^-$ ligand conformation for dicarbonyl **11** is distinct from its conformation in the other three structures and places the borate unit slightly closer (≈0.1 Å) to the bound rhodium center (Rh–B 3.908(3) Å in **11**). One possible explanation for this ligand distortion is that the borate unit is drawn closer to the metal center to



Scheme 1. Synthesis of zwitterionic $[\{Ph_2B(CH_2PPh_2)_2\}RhL_2]$ complexes.

 © 2003 Wiley-VCH Verlag GmbH & Co. KGaA, Weinheim

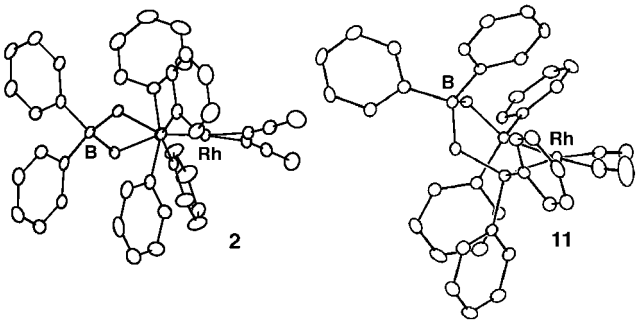


Figure 2. Molecular structures of **2** and **11** (ellipsoid representations, 50%; hydrogen atoms and residual solvent molecules are omitted for clarity).

compensate for the increased electrophilicity at the rhodium center because of the strongly π-acidic carbonyl ligands.

Complexes **1**–**4** are most simply described as zwitterions in which some of the borate unit's charge is dissipated through space and/or through the σ-bond framework of the ligand arms to the coordinated rhodium center. This situation might be anticipated to result in an appreciably more electron-rich metal center by comparison to an isostructural but cationic complex. This view is supported by the comparative IR data obtained for the carbonyl complexes **11** and $[\{Ph_2Si(CH_2PPh_2)_2\}Rh(CO)_2][PF_6]$ (**16**). The symmetric and antisymmetric vibrations for the zwitterion **11** in dichloromethane (2080 and 2029 cm^{-1}, respectively) are much lower in frequency than those for the cation **16** (2099 and 2056 cm^{-1}, respectively). Cationic **16** is electronically similar to the dppe- and dppp-supported dicarbonyl complexes, where both of the latter species exhibit vibrations at 2100 and 2056 cm^{-1}, respectively.[13] A similar trend has been observed for the amine-based systems.[7] The increased electron-richness of the zwitterions in comparison to their corresponding cations might be expected to attenuate or shut down their ability to mediate catalytic transformations, especially those reactions typical of electrophilic $[(P–P)Rh(solv)_2]^+$ complexes. Our data, however, suggests otherwise.

Comparative Catalytic Studies: Four model reactions were probed as exemplary of the $[(P–P)RhL_2]^+$ ions. These include the hydrogenation, hydroboration, and hydrosilation of styrene,[1–3] in addition to the hydroacylation of 4-methyl-4-pentenal, a transformation popularized by Bosnich and co-workers.[4] For each model study, we compared the catalytic activity of the isolated zwitterions to their cationic but structurally analogous cousins that incorporate a diphenylsilane unit in the phosphane backbone. To ensure that these Ph_2Si-based cationic systems give rise to activities similar to more conventional phosphane systems with all-carbon backbones, we also canvassed the reactivity of cationic congeners supported by dppe and dppp.

As a first catalytic screen, the norbornadiene adduct complexes **1a**, **3**, **5**, and **7** were assessed for their ability to mediate the hydrogenation of styrene to ethylbenzene in $[D_6]$acetone (monitored by ^1H NMR spectroscopy). For the neutral and cationic phosphane systems **1a** and **5**, hydrogenative removal of the norbornadiene ligands occurred rapidly, whereas the conversion of styrene to ethylbenzene proceeded more slowly (Table 1). The cationic systems $[(P–P)Rh(nbd)]^+$ ((P–P) = dppe, dppp) gave similar results. A possible mode of catalyst deactivation for the zwitterion **1a** is the formation of an arene-bridged Rh–Rh dimer. Unlike the cationic dimers that are broken up by coordinating solvents to provide catalytically active species,[4a–c] the zwitterionic dimer is very robust and requires forcing conditions to reform a monomeric species.[14]

Table 1: Styrene hydrogenation results.[a]

Entry	Catalyst		*T* [h][b]	TOF [h^{-1}][c]
1	$[\{Ph_2B(CH_2PPh_2)_2\}Rh(nbd)]$	**1a**	26	19
2	$[\{Ph_2Si(CH_2PPh_2)_2\}Rh(nbd)][PF_6]$	**5**	34	15
3	$[(dppe)Rh(nbd)][PF_6]$	–	44	11.4
4	$[(dppp)Rh(nbd)][PF_6]$	–	28	18
5	$[\{Ph_2B(CH_2NMe_2)_2\}Rh(nbd)]$	**3**	2.5	200
6	$[\{Ph_2Si(CH_2NMe_2)_2\}Rh(nbd)][PF_6]$	**7**	5	100

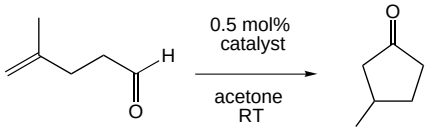
[a] Conditions: Rh catalyst (0.1 mol%) in $[D_6]$acetone (0.65 mL); H_2 (1 mL) at 1 atm added by syringe at 25 °C. [b] Time *T* to consume 50% of styrene as determined by ^1H NMR spectroscopy. [c] Turnover frequency (TOF) values expressed as mol of product per mol of catalyst per h.

Perhaps more intriguing was that the zwitterionic amine complex **3** exhibited activity far superior to both the neutral and cationic phosphane systems, and was twice as active as its cationic amine counterpart **7** (Table 1). Zwitterion **3** also proved tolerant to repeated addition of fresh styrene substrate. For further comparison, the related bis(pyrazolyl)borate complex $[\{Ph_2B(Pz)_2\}Rh(nbd)]$ was found to be completely inactive for the hydrogenation of styrene under similar conditions.[8] In fact, attempts to hydrogenatively remove the norbornadiene ligand from $[\{Ph_2B(Pz)_2\}Rh(nbd)]$ under the mild conditions used were unsuccessful.

The catalytic activity of the zwitterionic systems was more pronounced in the hydroacylation of the model substrate 4-methyl-4-pentenal ([Eq. (1)]; Table 2). The precatalysts used to canvass the hydroacylation of this substrate to racemic 3-methylcyclopentanone were the acetonitrile adduct complexes **2**, **4**, **6**, **9**, **10**, and the acetone adduct derivative **8**, which required in situ generation.[10] The turnover frequency (TOF) for hydroacylation of 4-methyl-4-pentenal by **2** was 40 times greater than its cationic phosphane counterparts **6**, **9,** and **10**. The data collected for the conventional phosphane systems **9** and **10** compares well with that for the diphenylsilane system **6**. This comparison suggests that the $[Ph_2Si(CH_2PPh_2)_2]$ ligand provides a good structural model for the anionic $[Ph_2B(CH_2PPh_2)_2]^-$ ligand, and also a good benchmark for comparing the activity of the zwitterionic systems to more familiar bis(phosphane)-supported catalysts. The activity of **2** also compares well with the BINAP catalyst systems of Bosnich and co-workers.[4] Their studies were typically performed in acetone, and more strongly coordinating solvents such as CH_3CN were strictly excluded as they act as catalyst poisons. The presence of CH_3CN likely attenuated the activity observed for the cationic species in entries 3–5 of Table 2. The disparity in hydroacylation activity between zwitterionic **2** and the cationic, phosphane catalysts could be

 © 2003 Wiley-VCH Verlag GmbH & Co. KGaA, Weinheim

Table 2: Hydroacylation results.[a]



(1)

Entry	Catalyst	Yield [%][b]	T[c]	TOF [h^{-1}]	
1	$[\{Ph_2B(CH_2PPh_2)_2\}Rh(CH_3CN)_2]$	**2**	99	5 min	2400
2	$[Ph_2B(CH_2NMe_2)_2]Rh(CH_3CN)_2$	**4**	95	30 min	380
3	$[\{Ph_2Si(CH_2PPh_2)_2\}Rh(CH_3CN)_2][PF_6]$	**6**	78	3 h	52
4	$[(dppe)Rh(CH_3CN)_2][PF_6]$	**9**	84	3 h	56
5	$[(dppp)Rh(CH_3CN)_2][PF_6]$	**10**	70	3 h	47
6	$[\{Ph_2Si(CH_2NMe_2)_2\}Rh(solv)_2][PF_6]$	**8**[d]	0	3 h	0

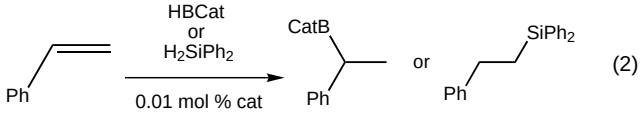
[a] Conditions: Rh catalyst (0.5 mol%) in $[D_6]$acetone (1.0 mL) at 25°C. [b] Determined by ^{1}H NMR spectroscopy. [c] Time *T* to consume starting material. [d] Hydrogenated in $[D_6]$acetone prior to substrate introduction; two equivalents of CD_3CN added to reaction mixture.

further amplified as a function of the solvent medium. For example, the activity of cationic **6** fell precipitously when solvents of varying polarities such as benzene, THF, and acetonitrile were employed (TOF for **6** = 15, 8, and 0 in these solvents, respectively). The decreasing activity is likely due to strong coordination of the donor solvent (CH_3CN), inability of THF or the substrate to break up intermediate Rh–Rh dimers, and poor solubility of the cation in benzene. In sharp contrast, zwitterionic **2** maintained TOF values near 2400 in all three solvent systems. Furthermore, the amine zwitterion **4** was also a relatively active catalyst for the hydroacylation reaction, superior to all cationic systems examined. Like zwitterionic **2**, **4** maintained its catalytic activity in benzene and in CH_3CN. While the in-situ-generated catalyst system $[\{Ph_2Si(CH_2NMe_2)_2\}Rh(acetone)_2]^+$ did afford racemic 3-methylcyclopentanone, the reaction was only 90% complete after 2 h and was completely inhibited when two equivalents of CH_3CN were added with substrate to the solution.

The precatalysts **2**, **4**, **6**, **9**, and **10** were next examined for the hydroboration and hydrosilation of styrene ([Eq. (2)]; Table 3). The cationic precatalyst **8** was also examined, though the data obtained for this system were highly irreproducible due to a propensity for the complex to precipitate Rh^0 upon reaction with the borane and silane reagents. For the hydroboration system, monitored in situ by ^{11}B NMR spectroscopy, only the branched product was obtained for all cases as determined by ^{1}H NMR spectroscopy.[15] The hydrosilation reactions, monitored by GC/MS and ^{1}H NMR spectroscopy, in all cases afforded a single anti-Markovnikov product, even when excess styrene was used. The cationic phosphane complexes **6, 9,** and **10** exhibited very similar activities that compared favorably with data that has been previously reported.[16] These cationic phosphane complexes were in general three to four times more active than the zwitterionic phosphane and amine complexes. However, the catalytic activity for all the cationic phosphane systems was completely shut down when an appreciable quantity of acetonitrile was present. Remarkably, the (phosphanyl)- and (amino)borate zwitterions were extremely tolerant to both acetonitrile and THF. For example, virtually no loss of activity was observed in 50/50 solvent mixtures of CH_3CN/THF and CH_3CN/acetone.

In summary, this study shows that zwitterionic phosphane and amine rhodium systems are promising catalysts for H–E addition reactions to olefins. The reactivity that the zwitterionic systems display parallels that of the cationic $[(P–P)RhL_2]^+$ systems with two important distinctions: The zwitterions are active in the presence of large quantities of a strongly coordinating donor solvent such as acetonitrile, which may reflect their attenuated electrophilicity in comparison to the cationic systems. Moreover, because the neutral systems are appreciably soluble in nonpolar hydrocarbons such as ben-

Table 3: Hydroboration and hydrosilation results.[a]



(2)

Catalyst	Reagent	Solvent	Yield [%][b]	*T* [h][c]	TOF [h^{-1}]
2	HBCat	THF	95	1.25	7600
2	HBCat	THF/CH_3CN	96	1.5	6400
4	HBCat	THF	93	1.5	6200
4	HBCat	THF/CH_3CN	94	1.65	5700
6	HBCat	THF	>99	0.5	20000
6	HBCat	THF/CH_3CN	0	24	0
9	HBCat	THF	92	1	9200
9	HBCat	THF/CH_3CN	0	24	0
10	HBCat	THF	98	0.75	13000
10	HBCat	THF/CH_3CN	0	24	0
2	H_2SiPh_2	acetone	98	1.5	6500
2	H_2SiPh_2	acetone/CH_3CN	96	1.5	6400
4	H_2SiPh_2	acetone	91	2	4600
4	H_2SiPh_2	acetone/CH_3CN	88	2	4400
6	H_2SiPh_2	acetone	>99	0.5	20000
6	H_2SiPh_2	acetone/CH_3CN	0	24	0
9	H_2SiPh_2	acetone	96	0.5	19200
9	H_2SiPh_2	acetone/CH_3CN	0	24	0
10	H_2SiPh_2	acetone	>99	0.5	20000
10	H_2SiPh_2	acetone/CH_3CN	0	24	0

[a] Conditions: Rh catalyst (0.01 mol%). [b] For hydroborations: determined by ^{11}B NMR spectroscopy based on borane conversion; for hydrosilations: determined by ^{1}H NMR spectroscopy based on styrene conversion. [c] Time elapsed to convert styrene.

 © 2003 Wiley-VCH Verlag GmbH & Co. KGaA, Weinheim

zene, they maintain their activity over a rather broad solvent polarity range. This solvent range is not spanned by more typical cationic catalysts, as illustrated by the cationic model complexes described in this study. We are encouraged to suggest that a zwitterionic approach to catalyst design will provide new systems with the potential for a high degree of functional group and solvent compatibility.

Received: October 16, 2002
Revised: February 10, 2003 [Z50378]

Keywords: borates · boron · hydrogenation · rhodium · zwitterions

[1] a) R. R. Schrock, J. A. Osborne, *J. Am. Chem. Soc.* **1971**, *93*, 3091; b) R. H. Crabtree, *Acc. Chem. Res.* **1979**, *12*, 331; c) "Homogeneous Catalysis": R. H. Crabtree, *The Organometallic Chemistry of the Transition Metals*, 3rd ed., Wiley, New York, **2001**, chap. 9, pp. 206–236.

[2] I. Ojima, *The Chemistry of Organic Silicon Compounds* (Eds.: S. Patai, Z. Rappoport), Wiley, New York, **1989**, chap. 25.

[3] a) K. Burgess, M. J. Ohlmeyer, *Chem. Rev.* **1991**, *91*, 1179, and references therein; b) D. A. Evans, G. C. Fu, A. H. Hoveyda, *J. Am. Chem. Soc.* **1988**, *110*, 6917.

[4] a) D. P. Fairlie, B. Bosnich, *Organometallics*, **1988**, *7*, 936; b) D. P. Fairlie, B. Bosnich, *Organometallics*, **1988**, *7*, 946; c) B Bosnich, *Acc. Chem. Res.* **1998**, *31*, 667.

[5] For another class of rhodium(I) zwitterions see: a) R. R. Schrock, J. A. Osborn, *Inorg. Chem.* **1970**, *9*, 2339; b) Z. Zhou, G. Facey, B. R. James, H. Alper, *Organometallics* **1996**, *15*, 2496; c) B. G. Van den Hoven, H. Alper, *J. Am. Chem. Soc.* **2001**, *123*, 10214.

[6] a) J. C. Thomas, J. C. Peters, *J. Am. Chem. Soc.* **2001**, *123*, 5100; b) C. C. Lu, J. C. Peters, *J. Am. Chem. Soc.* **2002**, *124*, 5272.

[7] T. A. Betley, J. C. Peters, *Inorg. Chem.* **2002**, *41*, 6541.

[8] For examples of bis(pyrazolyl)borate–rhodium(I) complexes see: a) M. Bortolin, U. E. Bucher, H. Ruegger, L. M. Venanzi, A. Albinati, F. Lianza, S. Trofimenko, *Organometallics* **1992**, *11*, 2514; b) M. J. Baena, M. L. Reyes, L. Rey, E. Carmona, M. C. Nicasio, P. J. Perez, E. Guitierrez, A. Monge, *Inorg. Chim. Acta* **1998**, *273*, 244. Hydrogenation-like catalysis by bis(pyrazolyl)-borate–rhodium(I) complexes has not, to our knowledge, been reported, in accord with our own observations using [{Ph_2B(pyrazolyl)$_2$}Rh(nbd)].

[9] The Supporting Information contains complete synthetic and characterization data for all new compounds.

[10] The complex [{$Ph_2Si(CH_2NMe_2)_2$}$Rh(CH_3CN)_2$][PF_6] could not be isolated due to problematic precipitation of Rh^0. [{$Ph_2Si(CH_2NMe_2)_2$}Rh(acetone)$_2$][PF_6] could be generated, but only in situ as it also proved unstable to a typical workup procedure.

[11] R. R. Schrock, J. A. Osborn, *J. Am. Chem. Soc.* **1976**, *98*, 4450.

[12] Summarized crystallographic data: [{$Ph_2B(CH_2PPh_2)_2$}Rh(CO)$_2$] (**11**): ($C_{40}H_{34}BO_2P_2Rh$), $M_r = 722.33$, yellow plate, collection temperature = 96 K, monoclinic, space group $P2_{1/n}$, $a = 9.8984(9)$, $b = 18.7925(16)$, $c = 18.1113(16)$ Å, $\beta = 98.108(2)$, $V = 3335.3(5)$ Å^3, $Z = 4$, $R_1 = 0.0433$ [$I > 2\sigma(I)$], GOF = 1.468. [{$Ph_2B(CH_2PPh_2)_2$}Rh$(CH_3CN)_2$]·THF (**2**): ($C_{42}H_{40}BN_2P_2Rh \cdot C_4H_8O$), $M_r = 820.52$, yellow cube, collection temperature = 98 K, monoclinic, space group $P2_{1/n}$, $a = 11.8228(9)$, $b = 16.4484(13)$, $c = 21.5822(17)$ Å, $\beta = 102.1030(10)$, $V = 4103.7(6)$ Å^3, $Z = 4$, $R_1 = 0.0425$ [$I > 2\sigma(I)$], GOF = 1.192. CCDC-195381 (**1a**), CCDC-195383 (**2**), CCDC-195382 (**11**), CCDC-195384 (**14**) contain the supplementary crystallographic data for this paper. These data can be obtained free of charge via www.ccdc.cam.ac.uk/conts/retrieving.html (or from the Cambridge Crystallographic Data Centre, 12 Union Road, Cambridge CB21EZ, UK; fax: (+44) 1223-336-033; or deposit@ccdc.cam.ac.uk).

[13] [(dppp)Rh$(CO)_2$][PF_6] was not previously reported and thus prepared in an analogous fashion to **14** and is reported in the Supporting Information. [(dppe)Rh$(CO)_2$][PF_6] was previously reported in ref [4b].

[14] The neutral "[{$Ph_2B(CH_2PPh_2)_2$}Rh^I]" unit can dimerize to a catalytically inactive [{[$Ph_2B(CH_2PPh_2)_2$]Rh}$_2$] complex presumably stabilized by phosphine aryl-rhodium(I) interactions, a process also common of cationic "[(P–P)Rh]$^+$" systems.[4] The dimer has limited solubility but has been characterized by ^{31}P and ^1H NMR spectroscopy, as well as ES·MS and combustion analysis (see Supporting Information). The presence of the [{[$Ph_2B(CH_2PPh_2)_2$]Rh}$_2$] dimer has been detected by ^{31}P NMR spectroscopy in situ during hydrogenation reactions with a 2% catalyst loading.

[15] C. Elschenbroich, A. Salzer, *Organometallics: A Concise Introduction*, 2nd ed., VCH, New York, **1992**.

[16] M. D. Fryzuk, L. Rosenberg, S. J. Rettig, *Organometallics* **1996**, *15*, 2871.

 © 2003 Wiley-VCH Verlag GmbH & Co. KGaA, Weinheim

Making Carbon-Phosphorus Bonds

Lewis Acid Catalyzed Room-Temperature Michaelis–Arbuzov Rearrangement**

Pierre-Yves Renard, Philippe Vayron, Eric Leclerc, Alain Valleix, and Charles Mioskowski**

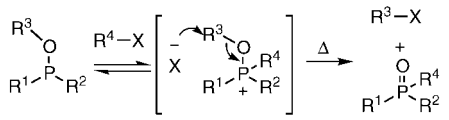
The Michaelis–Arbuzov rearrangement is one of the most extensively investigated reactions in organophosphorus chemistry, and is widely used in many fields of chemistry, from organic synthesis to catalyst design, to prepare phosphonates, phosphinates, and phosphane oxides.[1] This rearrangement involves the reaction of an ester of a trivalent phosphorus species $R^1R^2P{-}OR^3$ with alkyl halides R^4X. Although pentacoordinate phosphorane intermediates cannot be completely excluded,[1d] the generally accepted mechanism for this Michaelis–Arbuzov rearrangement (Scheme 1) involves formation of a phosphonium intermediate through nucleophilic addition of the phosphorus lone pair

[*] Dr. P.-Y. Renard, P. Vayron, E. Leclerc, A. Valleix
Service de Marquage Moléculaire et de Chimie Bioorganique
CEA Saclay, 91191 Gif sur Yvette Cedex (France)
Fax: (+33) 1-69-08-79-91
E-mail: pierre-yves.renard@cea.fr
Dr. C. Mioskowski
Laboratoire de synthèse bioorganique (UMR 7514)
faculté de pharmacie, université Louis Pasteur
74, route du Rhin 67401 Illkirch-Graffenstaden (France)
Fax: (+33) 3-90-24-43-06
E-mail: mioskow@aspirine.u-strasbg.fr

[**] This work was financially supported by the Délégation Générale pour L'Armement.

Supporting information for this article is available on the WWW under http://www.angewandte.org or from the author.

 DOI: 10.1002/anie.200250270 © 2003 Wiley-VCH Verlag GmbH & Co. KGaA, Weinheim



Scheme 1. Mechanism of the Michaelis–Arbuzov rearrangement.

to the alkyl halide. This first reversible step is followed by thermally induced intramolecular reaction of the conjugate nucleophile (halide X-) on the α carbon atom of the ester P–OR^3. The overall process gives the simultaneous formation of a new alkyl halide R^3X and a tetracoordinate phosphorus species.

Two main flaws have precluded wider use of this reaction. First, the drastic reactions conditions: apart from a with few particularly reactive halides, high reaction temperatures are required. Second, this reaction yields, together with the tetracoordinate P(=O) phosphorus target product, another alkyl halide R^3X. However, when this newly formed alkyl halide R^3X is more reactive, or less volatile than the initial alkyl halide R^4X, a troublesome competition takes place, and mixtures of phosphorylated products are obtained.[2] When desired, the higher reactivity of the second halide R^3X can be used to perform an "autocatalytic" Michaelis–Arbuzov rearrangement, by using catalytic amounts of the first alkyl halide R^4X (usually methyl iodide).[3] This latter "catalytic" reaction is still limited to a few reactive phosphites, and consumption of the catalyst yields, among other by-products, a corresponding amount of an undesired $R^1R^2R^4P(O)$ phosphorus (v) product.

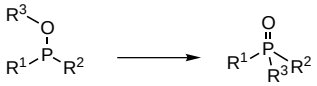
While the Arbuzov rearrangement has long been known, apart from the thermally induced alkyl-halide catalysis[3] already mentioned and the related iodine[4] or alkali-metal–iodide[5] catalysts, the only true thermal Arbuzov-rearrangement catalyst described to date is nickel(II) chloride.[1d,6] A few intramolecular rearrangements, limited to highly reactive phosphinites or requiring very high temperature or pressure, have been described,[7] and no efficient room-temperature catalysts have been described so far. Our idea was to test the use of oxophilic Lewis acids which could bind to the oxygen atom, and thus weaken the O–C bond, enhancing the reaction rate of the second, energy-requiring step of the Arbuzov rearrangement.

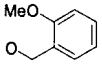
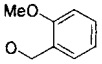
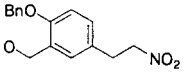
A first screening was conducted on methyl diphenylphosphinite (**1**; see Supporting Information), described as one of the most isomerization-sensitive phosphinites.[9] When the reaction was performed at room temperature, in $CDCl_3$ using 3 M phosphinite **1** and 5% Lewis acid catalyst, most of the Lewis acids described as epoxide ring-opening activators (and thus efficient oxygen-binding Lewis acids) did catalyze an efficient isomerization of **1** into methyldiphenylphosphane oxide (**2**). The best catalysts were found to be $BF_3{\cdot}OEt_2$ and trimethylsilyl trifluoromethane sulfonate (TMSOTf; 87 and 91% yield, respectively). Moderate heating (60 °C) resulted in complete transformation within an hour (see Supporting Information).

The reaction velocity proved to be moderately sensitive to substrate concentration and required a polar and aprotic solvent ($CHCl_3 > CH_2Cl_2 \approx CH_3CN \gg$ benzene, or toluene). Moreover, while an increase from 5 to 20 molar% of catalyst did somewhat speed up the reaction, use of over 50 molar% of catalyst diminished the reaction rate, and use of excess catalyst completely stopped the reaction. This observation, together with the substrate-concentration sensitivity, is a first indication of a bimolecular process involving both a catalyst-activated species and a phosphinite that is not coordinated to a Lewis acid (see below).

Optimized reaction conditions were then sought for a wide array of substrates. As illustrated in Table 1, addition of 5 molar% TMSOTf to phosphinite bearing primary *O*-alkyl

Table 1: Lewis acid promoted Arbuzov rearrangement of phosphinites.[a]



Entry	R^1	R^2	OR^3	Reaction conditions[b]	Reaction time [h]	Yield[c] [%]
1	Ph	Ph	OMe	A	72	87
2	Ph	Ph	OMe	B	72	91
3	Ph	Ph	OMe	C	1	98
4	Ph	Ph	OMe	D	1	95
5	Ph	Ph	OEt	C	18	85
6	Ph	Ph	OBn	A	72	87
7	Ph	Ph	OBn	C	3	90
8	Ph	Ph		C	18	86
9	Ph	Ph		C	2	91
10	Et	Et	OBn	A	72	92
11	Ph	Me	OMe	C	3	75
12	Ph	Me	OEt	C	18	63
13	Ph	Me		C	3	78[d]
14	Ph	Me		A	72	68
15	Ph	Me		C	18	44
16	Ph	*t*Bu	OBn	C	72	52
17	Ph	*t*Bu	OMe	C	72	47
18	Ph	*t*Bu		C	72	20[d]
19	*t*Bu	*t*Bu	OMe	E	72	degradation
20	cy[e]	cy	OMe	E	72	traces

[a] Unless stated, the reaction was performed at a phosphinite concentration of 1.0 M in chloroform with 5 mol% catalyst. [b] Reaction conditions: A: TMSOTf, 25 °C, B: $BF_3.OEt_2$, 20 °C, C: TMSOTf, 60 °C, D: BF_3OEt_2, 60 °C, E: no solvent, TMSOTf, 80 °C. [c] Yield of purified phosphane oxide. [d] 2 isomers 1:1. [e] Cyclohexyl.

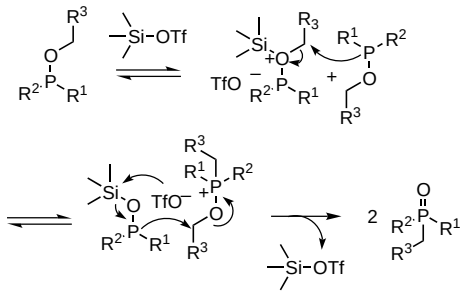
 © 2003 Wiley-VCH Verlag GmbH & Co. KGaA, Weinheim

groups initiated an Arbuzov rearrangement to phosphane oxide with fairly high yields in a few days at room temperature when the phosphorus(III) ester was reactive (methyl or benzyl, entries 1, 6, 10, and 14). Use of $BF_3.OEt_2$ also gave satisfactory results (entries 2, 4).

Interestingly, *O*-ethyl phosphinites, which are far less reactive in Arbuzov rearrangements, also isomerize when moderately (60 °C) heated (entries 5 and 12), as do activated phosphinites bearing secondary *O*-alkyl groups (*sec*-phenethyl esters, entries 8, 13, and 18).

Reaction is as yet limited to the migration of primary alkyl groups or activated secondary alkyl groups, as is the Arbuzov rearrangement involving alkyl halides. Sterically hindered alkyl substituents at the phosphorus center also dramatically hamper the rearrangement process (entries 18–20, and to a lesser extent, entries 16 and 17).

The reaction was then extended to less reactive phosphonites and phosphites. As illustrated in Table 2, Arbuzov rearrangement to the corresponding tetracoordinate phosphorus esters also readily occurred. As observed for the bimolecular Michaelis–Arbuzov rearrangement using alkyl halides, and as described for phosphinites (see Table 1), deactivation of the α carbon atom of the rearranging ester

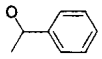
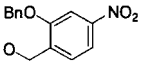


Scheme 2. Proposed mechanism for Lewis acid catalyzed Arbuzov rearrangement.

nylphosphite (**1**), corresponding to the oxonium intermediate).

- No alkyl trifluoromethane sulfonate has been observed in the crude reaction mixtures.
- No room-temperature TMSOTf-catalyzed rearrangement was observed with *S*-methyl diphenylphosphinithioite. This observation is in favor of an oxonium intermediate, since sulfur atoms are less susceptible towards silylation.
- An equimolar mixture of phosphinite **3** and **4** gave an approximately 1:1:1:1 mixture of all possible phosphane oxides **5**–**8** (Scheme 3), as indicated by both ^{31}P NMR spectroscopy and GC/MS experiments. Obtaining an approximately 1:1:1:1 mixture, although the kinetic rates for the migration of individual OMe and OEt groups are different (compare Table 1, entries 3 and 5), not only supports the bimolecular aspect of the mechanism, but also indicates that, if this mechanism is correct, the rate-limiting step is the second one (silyloxyphosphinite addition to the phosphonium intermediate).
- Addition of a catalytic (20%) amount of methyl trifluorome-

Table 2: TMSOTf-promoted Arbuzov rearrangement of phosphonites and phosphites.

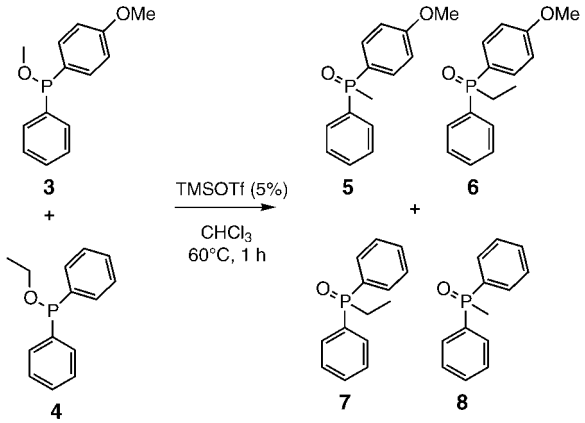
Entry	R^1	R^2	OR^3	Reaction conditions[a]	Yield[b] [%]
1	Ph	OMe	OMe	20 °C, 96 h	82
2	Ph	OEt	OEt	60 °C, 72 h	68
3	Ph			60 °C, 18 h	72
4	Ph	O*i*Pr	O*i*Pr	60 °C, 72 h	traces
5	OEt	OEt	OMe	20 °C, 96 h	80
6	OEt	OEt	OMe	60 °C, 18 h	96
7	OEt	OEt	OBn	60 °C, 18 h	87
8	OMe	OMe	OMe	60 °C, 18 h	98
9	OEt	OEt		60 °C, 3 h	93

[a] The reaction was performed at a concentration of 1.0 M in chloroform with 5 mol% catalyst. [b] Yield of phosphi(o)nates.

drastically lowers the rates of the reaction. A particularly high selectivity with respect to the migrating ester group was observed (benzyl > methyl ≫ ethyl, in the reactions given in entries 6 and 7, only traces of ethyl-migration products were detected).

As previously observed, with inhibition of the reaction by excess catalyst, and contrary to the intramolecular mechanism we originally proposed, much of the experimental evidence is strongly in favor of the bimolecular process outlined in Scheme 2.

- Whatever the oxophilic Lewis acid used (TMSOTf, TBSOTf (TBS = *tert*-butyldimethylsilyl, $Cl_2C{=}N(Me)_2^+$ TfO^-, $Sn(OTf)_2$, and BF_3OEt_2), the reaction occurred in the same way, and the detected reaction intermediates give similar ^{31}P NMR spectroscopy data (major peak at $\delta = 75.2$ to 75.4 ppm for the reaction with methyl diphe-



Scheme 3. Lewis acid catalyzed Arbuzov rearrangement of an equimolar amount of phosphinites **3** and **4**.

 © 2003 Wiley-VCH Verlag GmbH & Co. KGaA, Weinheim

thane sulfonate to **1** gave no rearrangement product **2** at room temperature. Only formation of the corresponding amounts of the quasi-phosphonium salt $[MeO(Ph)_2PMe]^+[OTf]^-$ was detected (^{31}P NMR: $\delta =$ 77.8 ppm in $CDCl_3$). Only heating the reaction mixture to 100 °C, without solvent, gave the formation of **2**, about 15 %, together with a mixture of starting phosphinite, and the oxidation product *O*-methyl diphenylphosphinate.

- Equimolar mixtures of phosphane oxide diastereoisomers (Table 1, entries 13 and 18) and racemic mixtures (Table 1, entry 8) were obtained, even when enantiomerically pure *sec*-phenethyl alcohols were used.
- For the Arbuzov rearrangement, a bimolecular process involving nucleophilic addition of phosphite to phosphonium has already been described,[8] and confirmed by kinetic experiments.[3b] This is actually the only possible mechanism when methyl triflate is used as a halide equivalent, since the nucleophilicity of the corresponding trifluoromethane sulfonate anion TfO^- is particularly low.[9]

In conclusion, we have demonstrated that use of an oxophilic Lewis acid, such as $BF_3.OEt_2$ or TMSOTf, could induce an Arbuzov-like rearrangement. The reaction conditions are particularly mild, since in most cases, room temperature or moderate heating are sufficient, which has not been described before for Arbuzov rearrangements. The scope of the reaction has been extended to phosphites, phosphinites, and phosphonites. As in the corresponding Arbuzov rearrangement using alkyl halides, the migrating groups are limited to both primary and activated secondary alkyl groups. The reaction mechanism has also been clarified, and a bimolecular process is proposed.

This room-temperature, catalyzed Arbuzov rearrangement, offers new reaction pathways for the synthesis of compounds containing carbon–phosphorus bonds, for example, key intermediates for the synthesis of both physiologically active drugs and basic chemical building blocks (via further Wittig or Horner–Wadsworth–Emmons reactions, for instance).

Received: October 1, 2002
Revised: December 18, 2002 [Z50270]

Keywords: Lewis acids · michaelis–arbuzov rearrangement · phosphorus · rearrangement

[1] a) A. Michaelis, R. Kaehne, *Ber. Dtsch. Chem. Ges.* **1898**, *31*, 1408; b) A. E. Arbuzov, *J. Russ. Phys. Chem. Soc.* **1906**, *38*, 687; c) The *Chemistry of Organophosphorus Compounds* (Ed.: F. H. Hartley), Wiley, New York, **1996**; d) A. K. Bhattacharya, G. Thyagarajan, *Chem. Rev.* **1981**, *81*, 415 – 430.

[2] M. Saady, L. Lebeau, C. Mioskowski, *Tetrahedron Lett.* **1995**, *36*, 5183 – 5186; M. Saady, L. Lebeau, C. Mioskowski, *Helv. Chim. Acta* **1995**, *78*, 670 – 678.

[3] a) J. E. Griffiths, A. B. Burg, *J. Am. Chem. Soc.* **1962**, *84*, 3442 – 3450; b) E. S. Lewis, D. Hamp, *J. Org. Chem.* **1983**, *48*, 2025 – 2029; c) H. J. Woerz, E. Quien, H. P. Latscha, *Z. Naturforsch. B* **1984**, *39*, 1706 – 1710.

[4] a) V. K. Yadav, *Synth. Commun.* **1990**, *20*, 239 – 246; b) H. Brunner, W. Zettlmeier, *Bull. Soc. Chim. Belg.* **1991**, *100*, 247 – 257.

[5] a) V. P. Kukhar', E. I. Sagina, *Zh. Obshch. Khim.* **1976**, *46*, 2686 – 2689; b) U. Rose, *J. Heterocycl. Chem.* **1991**, *28*, 2005 – 2012; c) K. Toshima, H. Yamagushi, T. Jyojima, Y. Nogushi, M. Nakata, S. Matsumura, *Tetrahedron Lett.* **1996**, *37*, 1073 – 1076.

[6] W. Flisch, P. Rußkamp, W. Langer, *Liebigs Ann. Chem.* **1985**, 1413 – 1421.

[7] a) T. Janecki, R. Bodalski, *Synthesis* **1990**, 799 – 801; b) R. S. Macomber, D. E. Rardon, D. M. Ho, *J. Org. Chem.* **1992**, *57*, 3874 – 3881; c) S. Demay, K. Harms, P. Knochel, *Tetrahedron Lett.* **1999**, *40*, 4981 – 4984; d) W. G. Bentrude, S. G. Lee, K. Akutagawa, W. Ye, Y. Charbonnel, *J. Am. Chem. Soc.* **1987**, *109*, 1577; e) D. Shukla, C. Lu, N. P. Schepp, W. G. Bentrude, L. J. Johnston, *J. Org. Chem.* **2000**, *65*, 6167 – 6172; f) T. Wada, Y. Sato, F. Honda, S.-I. Kawahara, M. Sekine, *J. Am. Chem. Soc.* **1997** *119*, 12710 – 12721; g) M. R. Banks, R. F. Hudson, *J. Chem. Soc. Perkin Trans. 2* **1989**, 463 – 467; h) A. E. Arbuzov, K. V. Nikonorov, *Zh. Obshch. Khim.* **1948**, *18*, 2008; h) V. Mark, *Mech. Mol. Migr.* **1969**, *2*, 319 – 437. Noteworthy is the spontaneous rearrangement of particularly activated triarylmethyl phosphorus-3-esters, for instance D. V. D. Hardy, H. H. Hatt, *J. Chem. Soc.* **1952**, 3778 – 3783, and references therein.

[8] a) P. Rumpf, *Bull. Soc. Chim. Fr.* **1951**, *18*, 128; b) T. B. Brill, S. J. Landon, *Chem. Rev.* **1984**, *84*, 577 – 585.

[9] a) K. S. Colle, E. S. Lewis, *J. Org. Chem.* **1978**, *43*, 571 – 574; b) E. S. Lewis, K. S. Colle, *J. Org. Chem.* **1981**, *46*, 4369 – 4372.

 © 2003 Wiley-VCH Verlag GmbH & Co. KGaA, Weinheim

Thiocyanogen Insertion

Insertion of Thiocyanogen into a P–C Bond and Subsequent Formation of Polysulfide Derivatives**

Javier Ruiz, Roberto Quesada, Víctor Riera, Marilín Vivanco, Santiago García-Granda, and M. Rosario Díaz*

Classical reactivity of thiocyanogen ($(SCN)_2$) involves the breaking of the sulfur–sulfur bond to give thiocyanate derivatives, and this pseudohalogen behavior has been widely applied in organic synthesis,[1] and in the field of coordination chemistry as well.[2] In contrast, to our knowledge the only example of a thiocyanogen reaction occurring

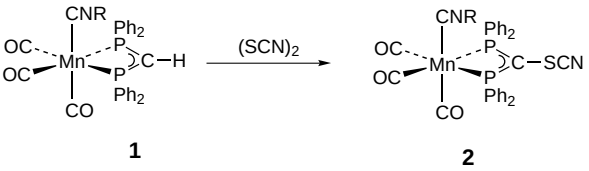
[*] Dr. J. Ruiz, R. Quesada, Prof. Dr. V. Riera, Dr. M. Vivanco
Departamento de Química Orgánica e Inorgánica
Facultad de Química
Universidad de Oviedo
33071 Oviedo (Spain)
Fax: (+34) 98-510-3446
E-mail: jruiz@sauron.quimica.uniovi.es
Dr. S. García-Granda, Dr. M. R. Díaz
Departamento de Química Física y Analítica
Facultad de Química
Universidad de Oviedo
33071 Oviedo (Spain)

[**] This work was supported by the Spanish DGES (Project 1FD97–0750) and by the Principado de Asturias (Project PR-01-GE-7).

 © 2003 Wiley-VCH Verlag GmbH & Co. KGaA, Weinheim DOI: 10.1002/anie.200250621

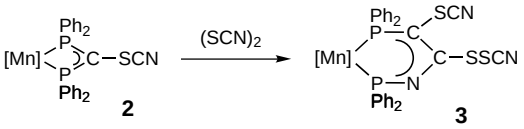
without cleavage of the S–S bond that has been described in the literature is the cycloaddition of $(SCN)_2$ with hexafluoroacetone, which leads to the formation of a 4H-dioxazine derivative.[3] Herein we describe a rare example of insertion of thiocyanogen into a P–C bond of a diphosphanylmethanide ligand, which initially proceeded without breaking the S–S bond leading later to the formation of a unique class of dimetallic polysulfides.

We have recently reported that the addition of $(SCN)_2$ to the diphosphanylmethanide complex *fac*-$[Mn(CNtBu)(CO)_3\{(PPh_2)_2CH\}]$ (**1**) allows the isolation of *fac*-$[Mn(CNtBu)(CO)_3\{(PPh_2)_2CSCN\}]$ (**2**) (Scheme 1). This reaction can be rationalized assuming a heterolytic cleavage of the S–S bond in the thiocyanogen molecule by the methanide carbon atom.[4] We have now found that a further treatment of **2** with $(SCN)_2$ leads to the insertion of this molecule into a P–C bond of the diphosphanylmethanide ligand yielding *fac*-$[Mn(CNtBu)(CO)_3\{(PPh_2)C(SCN)C(SSCN)N(PPh_2)\}]$ (**3**) (Scheme 2), which was isolated as a white solid. Noteworthy,



1 **2**

Scheme 1. Reaction of complex **1** with thiocyanogen to afford **2**. R = *t*Bu.

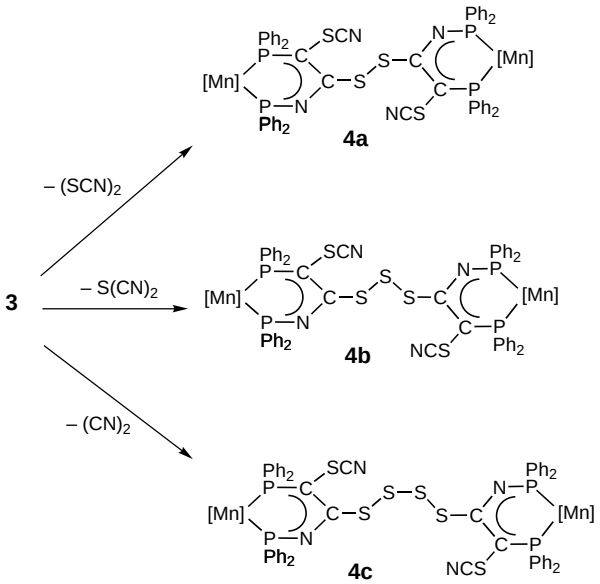


2 **3**

Scheme 2. Insertion reaction of thiocyanogen into a P–C bond of **2** to yield **3**. [Mn] = [Mn(CN*t*Bu)(CO)$_3$].

the reaction takes place instantaneously at room temperature, although the insertion implies the breaking of a rather strong P–C bond.[5] Insertion reactions of molecules into P–C bonds are very rarely encountered in the literature; examples are the insertion of nitriles either into the P–C bond of a phosphinidene complex,[6] or into a P–C bond of strained three-membered rings of 2H-azaphosphirene complexes,[7] and the insertion of electron-poor alkynes into a P–C bond of a coordinated phosphane ligand.[8]

Compound **3** was characterized spectroscopically, by elemental analysis, and by FAB mass spectrometry (see Experimental Section). Compound **3** slowly decomposes when left to stand in solution, thus precluding the preparation of single crystals for X-ray analysis. However, the elution of **3** through an alumina column in CH_2Cl_2/Hexane leads to the formation of the dimetallic complexes **4a, 4b**, and **4c**, in an approximate ratio of 6:4:1, respectively (Scheme 3). Compounds **4a–c** are unique polysulfide derivatives that contain a bridging chain of two to four sulfur atoms, and are formally



Scheme 3. Formation of the polysulfide dimetallic derivatives **4a, 4b** and **4c** from complex **3**. [Mn] = [Mn(CN*t*Bu)(CO)$_3$].

made from the coupling of two molecules of **3** with elimination of the pseudohalogen molecules $(SCN)_2$, $S(CN)_2$, and $(CN)_2$, respectively. This result can be compared with the S–S coupling process which allows the formation of the dimetallic disulfide $[(CO)_4Mn\{(PPh_2)_2C\text{-}S\text{-}S\text{-}C(PPh_2)_2\}Mn(CO)_4]$ on passing the complex $[Mn(CO)_4\{(PPh_2)_2C\text{-}S\text{-}I\}]$ through an alumina column, with elimination of I_2.[9] Since the formation of **4a, 4b**, and **4c** from **3** requires the scission of two S–S bonds, one S–S bond and one S–C bond, and two S–C bonds, respectively, the relative amount of each compound in the reaction mixture could be explained by considering the weakness of the S–S bond versus the S–C bond in the inserted thiocyanogen molecule. Complexes **4a–c** are all colorless and have very similar spectroscopic features and solubility, and therefore are difficult to characterize and separate. Thus, the IR spectra in the region where the CO and CN stretches are found are practically identical for the three species, and from the $^{31}P\{^1H\}$ NMR spectra the complexes can only be distinguished by slight differences in the chemical shift of one of the two non-equivalent phosphorus atoms (see Experimental Section). Nevertheless, the major species, **4a** and **4b**, could be separated by chromatography and were fully characterized, including the elucidation of their solid-state structures by X-ray crystallography.[10] The minor product **4c** could not be totally purified as it always contains some amount of **4b**, so its characterization is based mainly on the FAB mass spectrum.

The structure of **4a** (Figure 1) formally contains a thiocyanogen molecule inserted into two P–C (methanide) bonds of two diphosphanylmethanide complexes **2**, although, as stated above, its formation implies a process of S–S bonds breaking and forming. The structural features of the two related halves of the molecule are very similar. The octahedral coordination around each Mn atom involves three carbonyl groups, an isocyanide ligand and two chelating P atoms from the modified diphosphanylmethanide ligand.

 © 2003 Wiley-VCH Verlag GmbH & Co. KGaA, Weinheim

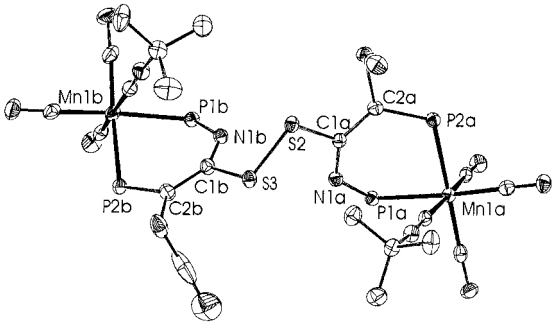


Figure 1. Molecular structure of **4a**. Hydrogen atoms and phenyl groups are omitted for clarity (ellipsoids set at the 30% probability level). Selected bond lengths [Å] and angles [°]: N1a-P1a 1.648(3), N1a-C1a 1.298(5), C1a-C2a 1.411(5), P2a-C2a 1.782(4), C1a-S2 1.824(4), P1b-N1b 1.645(3), N1b-C1b 1.301(5), C1b-C2b 1.398(5), P2b-C2b 1.785(4), C1b-S3 1.833(4), S2-S3 2.023(14), P1a-Mn1a-P2a 85.98(4), C1a-N1a-P1a 125.1(3), N1a-C1a-C2a 130.8(4), N1a-C1a-S2 116.7(3), C2a-C1a-S2 112.5(3), C1a-C2a-P2a 124.7(3), C1a-S2-S3 105.28(13), C1b-S3-S2 103.94(14), P1b-Mn1b-P2b 83.70(4), C1b-N1b-P1b, 126.4(3), N1b-C1b-C2b 131.8(4), N1b-C1b-S3 114.9(3), C2b-C1b-S3 113.3(2). Torsion angles [°]: N1a-C1a-S2-S3 5.9(3), C1a-S2-S3-C1b −93.70(18), S2-S3-C1b-N1b 19.9(3).

The bond lengths within the skeleton P1-N1-C1-C2-P2 of the expanded chelating ligand are shorter than single bonds, especially P1–N1 (1.646(3) Å on average) and N1–C1 (1.299(5) Å on average), as a result of the delocalization of the formal negative charge throughout the skeleton. The S2–S3 bond length (2.023(14) Å) is slightly shorter than that found in the cyclo-octasulfur molecule (2.06 Å), whereas the C1–S bond lengths (1.828(4) Å on average) are typical for a single bond. The structure of the trisulfide derivative **4b** (Figure 2) is closely related to **4a** with a more sulfur atom, the different bond distances and angles being very similar to those found for **4a**.

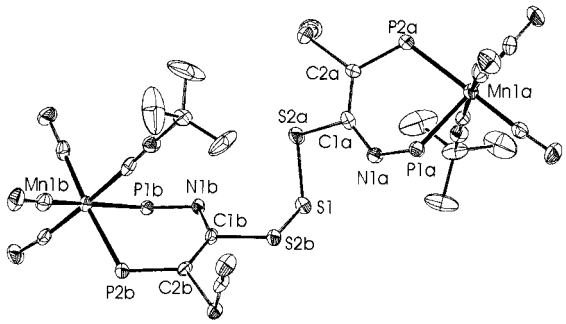


Figure 2. Molecular structure of **4b**. Hydrogen atoms and phenyl groups are omitted for clarity (ellipsoids set at the 20% probability level). Selected bond lengths [Å] and angles [°]: N1a-P1a 1.623(8), N1a-C1a 1.324(11), C1a-C2a 1.434(13), P2a-C2a 1.763(10), C1a-S2a 1.817(10), S2a-S1 2.020(4), S1-S2b 2.025(4), P1b-N1b 1.629(7), N1b-C1b 1.300(11), C1b-C2b 1.427(13), P2b-C2b 1.791(10), C1b-S2b 1.829(9), P1a-Mn1a-P2a 86.92(11), C1a-N1a-P1a 123.4(7), N1a-C1a-C2a 129.8(9), N1a-C1a-S2a 116.8(8), C2a-C1a-S2a 113.4(8), C1a-S2a-S1 103.2(4), C1a-C2a-P2a 125.1(7), S2a-S1-S2b 108.72(18), P1b-Mn1b-P2b 83.15(11), C1b-N1b-P1b, 123.6(7), N1b-C1b-C2b 130.4(8), N1b-C1b-S2b 117.0(7), C2b-C1b-S2b 112.6(7), C1b-C2b-P2b 123.5(3), C1b-S2b-S1 102.2(4). Torsion angles [°]: N1b-C1b-S2b-S1 −18.6(8), C1b-S2b-S1-S2a 80.6(4), S2b-S1-S2a-C1a 86.1(4), S1-S2a-C1a-N1a −3.7(9).

The length of the sulfur chains in compounds **4a–c** is essentially maintained when they are dissolved in organic solvents and left to stand for several days. When a mixture of **4b–c** is heated to reflux in toluene, some quantity of **4a** is formed, but mainly the starting materials decompose.

Preliminary results show that protonation of **3** with HBF_4 at the imino-nitrogen atom also produces the instantaneous scission of the inserted thiocyanogen molecule, thus giving a mixture of cationic dimetallic intermediates, which were converted to the same mixture of neutral compounds **4a–c** as above by deprotonation with KOH. It can be deduced that the interaction of **3** with alumina produces the same effect as that of a combined acid-base treatment with this complex.

In summary, we have found that thiocyanogen can be inserted into a P–C bond of a coordinated diphosphanylmethanide ligand under mild conditions, without breaking of the S–S bond, thus affording a new highly functionalized and very reactive diphosphanylmethanide ligand. The activation of S–S or S–C bonds in this ligand, with parallel S–S coupling processes, produces a number of unprecedented polysulfide derivatives that contain pendant carbonyl complexes of manganese(I). Experiments with the aim of inserting other unsaturated molecules into the P–C bonds of **3** are currently in progress.

Experimental Section

3: A solution containing $(SCN)_2$ (0.027 g, 0.230 mmol) was added dropwise to a solution of **2** (0.15 g, 0.226 mmol) with continuous stirring over five minutes at room temperature. The solution was then concentrated to 2 mL under vacuum. The addition of hexane (10 mL) produced the precipitation of a white solid; yield 85% (0.15 g). Elemental analysis (%) calcd for $C_{36}H_{29}MnN_4O_3P_2S_3$: C 55.53, H 3.75, N 7.19; found: C 54.58, H 3.97, N 6.92; IR (CH_2Cl_2): $\tilde{\nu}$ = 2172 (m) (CN*t*Bu), 2147 w (SCN), 2030 vs, 1967 cm^{-1} s (CO); ^1H NMR (300 MHz, CD_2Cl_2): δ = 7.96–7.04 (20H, Ph), 1.50 ppm (s, 9H, *t*Bu); $^{31}P\{^1H\}$ NMR (121.5 MHz, CH_2Cl_2/D_2O): δ = 70.8 (s, br), 47.1 ppm (s, br); FAB-MS (positive ion): *m*/*z*: 779 [M^+], 753 [M^+−CN], 721 [M^+−SCN], 689 [M^+−SSCN].

4a–c: Compound **3** (0.1 g, 0.128 mmol) was passed through an alumina column (activity degree III). Elution with CH_2Cl_2/hexane (1:1) afforded **4b** along with small amounts of **4c**, further elution with CH_2Cl_2/hexane (3:2) afforded **4a**. Both fractions were recrystallized in CH_2Cl_2/hexane to obtain **4a** and **4b** as colorless crystals. A second recrystallization of the first fraction provided **4c** as the major product in the mother liquor. **4a**: yield 30% (0.028 g). Elemental analysis (%) calcd for $C_{70}H_{58}Mn_2N_6O_6P_4S_4$: C 58.33, H 4.06, N 5.83; found: C 58.61, H 4.17, N 6.01; IR (CH_2Cl_2): $\tilde{\nu}$ = 2173 m (CN*t*Bu), 2142 w (SCN), 2025 vs, 1961 cm^{-1} s (CO); ^1H NMR (300 MHz, CD_2Cl_2): δ = 8.70–5.70 (40H, Ph), 1.60 ppm (s, 18H, *t*Bu); $^{31}P\{^1H\}$ NMR (121.5 MHz, CH_2Cl_2/D_2O): δ = 61.1 (s, br), 47.2 ppm (s, br); FAB-MS (positive ion): *m*/*z*: 1441 [M^+]. **4b**: yield 20% (0.019 g). Elemental analysis (%) calcd for $C_{70}H_{58}Mn_2N_6O_6P_4S_5$: C 57.06, H 3.97, N 5.70; found: C 56.85, H 4.05, N 5.98; IR (CH_2Cl_2): $\tilde{\nu}$ = 2174 (m) (CN*t*Bu), 2142 w (SCN), 2026 vs, 1963 cm^{-1} s (CO); ^1H NMR (300 MHz, CD_2Cl_2): δ = 8.19–6.97 (40H, Ph), 1.57 ppm (s, 18H, *t*Bu); $^{31}P\{^1H\}$ NMR (121.5 MHz, CH_2Cl_2/D_2O): δ = 64.6 (s, br), 47.4 ppm (s, br); FAB-MS (positive ion): *m*/*z*: 1473 [M^+].**4c**: IR (CH_2Cl_2): $\tilde{\nu}$ = 2174 m (CN*t*Bu), 2142 w (SCN), 2026 vs, 1963 cm^{-1} s (CO); $^{31}P\{^1H\}$ NMR (121.5 MHz, CH_2Cl_2/D_2O): δ = 67.6 (s, br), 47.5 ppm (s, br); FAB-MS (positive-ion): *m*/*z*: 1505 [M^+].

Received: November 25, 2002 [Z50621]

 © 2003 Wiley-VCH Verlag GmbH & Co. KGaA, Weinheim

Keywords: insertion · manganese · P ligands · polysulfides

[1] "The chemistry of cyanates and their thio derivatives": R. G. Guy in *The chemistry of functional groups, Part 2* (Ed.: S. Patai), Interscience, New York, **1977**, chap. 18, p. 833; E. Block, A. L. Schwan in *Comprehensive Organic Synthesis, Vol. 4* (Eds.: B. M. Trost, I. Fleming, M. F. Semmelhack), Pergamon, Oxford, **1991**, p. 348.

[2] See for instance: M. A. Bennett, M. I. Bruce, T. W. Matheson in *Comprehensive Organometallic Chemistry, Vol. 4* (Eds.: E. W. Abel, F. G. A. Stone, G. Wilkinson), Pergamon, Oxford, **1982**, p. 705; M. I. Bruce in *Comprehensive Organometallic Chemistry, Vol. 4* (Eds.: E. W. Abel, F. G. A. Stone, G. Wilkinson), Pergamon, Oxford, **1982**, p. 883; J. D. Odom in *Comprehensive Organometallic Chemistry, Vol. 1* (Eds.: E. W. Abel, F. G. A. Stone, G. Wilkinson), Pergamon, Oxford, **1982**, p. 289; R. J. Puddephatt in *Comprehensive Coordination Chemistry, Vol. 5* (Eds.: G. Wilkinson, R. D. Gillard, J. A. McCleverty), Pergamon, Oxford, **1987**, p. 887.

[3] H. W. Roesky, N. K. Homsy, M. Noltemeyer, G. M. Sheldrick, *Angew. Chem.* **1984**, *96*, 1002; *Angew. Chem. Int. Ed. Engl.* **1984**, *23*, 1000 – 1001.

[4] J. Ruiz, V. Riera, M. Vivanco, S. García-Granda, M. R. Díaz, *Organometallics* **1998**, *17*, 4562 – 4567.

[5] It is well established that the P–C bonds of diphosphanylmethanide ligands are significantly shorter than P–C single bonds, see for example: H. H. Karsch, A. Schier, *J. Chem. Soc. Chem. Commun.* **1994**, 2703 – 2704; H. H. Karsch, G. Grauvogl, M. Kawecki, P. Bissinger, O. Kumberger, A. Schier, G. Müller, *Organometallics* **1994**, *13*, 610 – 618; H. H. Karsch, U. Keller, S. Gamper, G. Müller, *Angew. Chem.* **1990**, *102*, 297; *Angew. Chem. Int. Ed. Engl.* **1990**, *29*, 295 – 296; J. Ruiz, V. Riera, M. Vivanco, M. Lanfranchi, A. Tiripicchio, *Organometallics* **1996**, *15*, 1082 – 1083.

[6] M. Schiffer, M. Scheer, *Angew. Chem.* **2001**, *113*, 3520 – 3523; *Angew. Chem. Int. Ed.* **2001**, *40*, 3413 – 3416.

[7] R. Streubel, H. Wilkens, P. G. Jones, *Chem. Eur. J.* **2000**, *6*, 3997 – 4000.

[8] Y. Yamamoto, K. Sugawara, *J. Chem. Soc. Dalton Trans.* **2000**, 2896 – 2897.

[9] J. Ruiz, M. Ceroni, O. V. Quinzani, V. Riera, O. E. Piro, *Angew. Chem.* **2001**, *113*, 226 – 228; *Angew. Chem. Int. Ed.* **2001**, *40*, 220 – 222.

[10] Diffraction data were collected on an Enraf–Nonius diffractometer at 293 K. The structures were solved by direct methods and refined by using full-matrix least squares on F^2 with all non-hydrogen atoms anisotropically defined. Crystal data for **4a** ($C_{70}H_{58}Mn_2N_6O_6P_4S_4$): $M_r = 1441.27$, triclinic, space group $P\bar{1}$, $a = 11.1915(7)$, $b = 17.3864(7)$, $c = 18.9243(9)$ Å, $\alpha = 104.540(3)$, $\beta = 94.546(5)$, $\gamma = 90.072(5)°$, $V = 3552.3(3)$ Å^3, $Z = 2$, $\rho_{calcd} = 1.347\ g\,cm^{-1-3}$, $F(000) = 1484$, $Cu_{K\alpha}$ radiation ($\lambda = 1.5418$ Å). For 13309 independent reflections and 947 parameters, final R indices [$I > 2\sigma I$]: $R1 = 0.0510$ and $wR_2 = 0.1315$. Crystal data for **4b** ($C_{70}H_{58}Mn_2N_6O_6P_4S_5$): $M_r = 1473.28$, triclinic, space group $P\bar{1}$, $a = 11.2755(4)$, $b = 16.4423(6)$, $c = 21.9661(11)$ Å, $\alpha = 72.807(2)$, $\beta = 77.227(2)$, $\gamma = 72.190(3)°$, $V = 3665.6(3$ Å^3, $Z = 2$, $\rho_{calcd} = 1.335\ g\,cm^{-1-3}$, $F(000) = 1516$, $Cu_{K\alpha}$ radiation ($\lambda = 1.5418$ Å). For 10418 independent reflections and 838 parameters, final R indices [$I > 2\sigma I$]: $R1 = 0.0663$ and $wR_2 = 0.1609$. CCDC-197197 and CCDC-197198 (**4a** and **4b**, respectively) contains the supplementary crystallographic data for this paper. These data can be obtained free of charge via www.ccdc.cam.ac.uk/conts/retrieving.html (or from the Cambridge Crystallographic Data Centre, 12 Union Road, Cambridge CB21EZ, UK; fax: (+44) 1223-336-033; or deposit@ccdc.cam.ac.uk).

 © 2003 Wiley-VCH Verlag GmbH & Co. KGaA, Weinheim

Bromination of C_{70}: $C_{70}Br_{10}$

The First X-ray Crystal Structures of Halogenated [70]Fullerene: $C_{70}Br_{10}$ and $C_{70}Br_{10}\cdot 3\,Br_2$**

Sergey I. Troyanov, Alexey A. Popov, Nadezhda I. Denisenko, Olga V. Boltalina,* Lev N. Sidorov, and Erhard Kemnitz*

In the past decade halogenated fullerenes have been intensely studied as versatile synthons in fullerene chemistry.[1] X-ray structural data were reported for various halo[60]fullerenes, including fluorides ($C_{60}F_{18}$, $C_{60}F_{36}$, and $C_{60}F_{48}$) and bromides: $C_{60}Br_6$,[2,3] $C_{60}Br_8$,[2,3] and $C_{60}Br_{24}$.[2,4] In addition, the structure of $C_{60}Cl_6$ has been suggested on the basis of NMR spectroscopy.[5]

In contrast, only modest progress has been made in the regioselective synthesis and structural characterization of halo[70]fullerenes. Fluorination of C_{70} has yielded complex mixtures of highly fluorinated products.[8] The most probable addition pattern in $C_{70}Cl_{10}$ was proposed based on its ^{13}C NMR spectrum.[9] The situation for bromo[70]fullerenes is even less clear; two theoretical studies have been published, each predicted a different addition pattern for bromo[70]fullerenes.[6,7] In one synthetic study, the direct bromination of C_{70} was claimed to yield $C_{70}Br_{24}$.[2] In another synthetic study, the product of C_{70} bromination with liquid Br_2 (as well as with Br_2 dissolved in CS_2 or $C_2H_2Cl_4$) was proposed to be $C_{70}Br_{14}$.[10] In our recent study, the available experimental evidence suggested that the product of C_{70} bromination was $C_{70}Br_{10}$.[11]

Herein, we confirm that the bromination of C_{70} produces $C_{70}Br_{10}$ and not $C_{70}Br_{14}$ or $C_{70}Br_{24}$. The evidence is the single-crystal X-ray structures of $C_{70}Br_{10}$ (**1**) and $C_{70}Br_{10}\cdot 3\,Br_2$ (**2**).

The bromination of C_{70} in neat bromine, in *o*-dichlorobenzene, or in carbon disulfide yielded crystalline $C_{70}Br_{10}$ or its crystalline dibromine solvates. The IR spectra of all crystalline products were similar and were in good agreement with the DFT-calculated spectrum shown in Figure 1. Thermogravimetric analysis reveals a two-step mass loss for the solvates formed by the direct bromination of C_{70}: the first step

[*] Dr. S. I. Troyanov, Dr. O. V. Boltalina, A. A. Popov, N. I. Denisenko, Prof. Dr. L. N. Sidorov
Chemistry Department
Moscow State University
119992 Moscow (Russia)
Fax: (+7) 095-9391-240
E-mail: troyanov@thermo.chem.msu.ru
ovbolt@lamar.colostate.edu

Prof. Dr. E. Kemnitz
Institut für Chemie
Humboldt-Universität Berlin
12489 Berlin (Germany)

[**] This work was partially supported by the Volkswagen Stiftung (grant 1/77 855), the Deutsche Forschungsgemeinschaft and the Russian Foundation for Basic Research (joint grant 436RUS113/1000/0-5, 03-03-04006, and 03-03-32756).

 DOI: 10.1002/anie.200351132 © 2003 Wiley-VCH Verlag GmbH & Co. KGaA, Weinheim

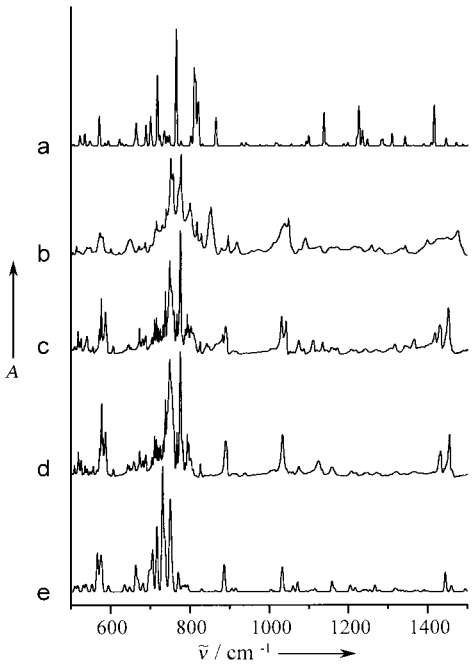


Figure 1. IR spectra of the bromo[70]fullerenes: a) simulated spectrum of $C_{70}Br_{14}$ with meridianal arrangement; b) experimental spectrum of "$C_{70}Br_{14}$" from reference [10] presented in absorbance units; experimental spectra of $C_{70}Br_{10}$ c) synthesized in neat bromine, d) in 1,2-dichlorobenzene, and e) simulated spectrum of $C_{70}Br_{14}$ with equatorial arrangement. *A* = relative absorbance (arbitary units).

(40–70 °C) was assigned to the release of the Br_2 solvate molecules leaving $C_{70}Br_{10}$; the second step (130–144 °C) was assigned to the decomposition of $C_{70}Br_{10}$ to C_{70} and Br_2. The formation of the bromine solvate was confirmed additionally by the X-ray single crystal structure of $C_{70}Br_{10}{\cdot}3\,Br_2$ (**2**) synthesized by brominating dilute *o*-dichlorobenzene solutions of C_{70}. Probably, the putative compound $C_{70}Br_{14}$ [10] corresponds to the bromine solvate of $C_{70}Br_{10}$. The IR spectrum of "$C_{70}Br_{14}$"[13] (Figure 1 b) is close to that of $C_{70}Br_{10}$ reported herein and differs drastically from the simulated spectrum for $C_{70}Br_{14}$ with meridianal bromine arrangement (Figure 1 a).

The molecular structure of $C_{70}Br_{10}$ in **1** has an idealized C_s symmetry (Figure 2). There are five pairs of symmetry-related Br atoms. The brominated sp^3 carbon atoms are located in a closed belt of ten hexagons around the C_{70} equator. Nine of the ten hexagons contain a pair of Br atoms in 1,4-positions; the remaining hexagon has a 1,2-addition pattern of Br atoms (Figure 3). This is the same addition pattern that was deduced from the NMR spectra for $C_{70}Cl_{10}$,[9] $C_{70}Ph_{10}$,[12] and $C_{70}H_{10}$.[13] The observed structure had been predicted in two theoretical studies[7,11] and was also considered as the most stable for the case of ten bulky groups attached to C_{70}.[14] The stabilizing factors of the observed addition pattern are the retention of conjugation in both hemispheres of the C_{70} cage and the absence of double bonds in pentagons. Note that the equatorial addition pattern in $C_{70}Br_{10}$ differs significantly from the meridianal pattern predicted earlier[6] for the still-unknown molecule $C_{70}Br_{14}$.

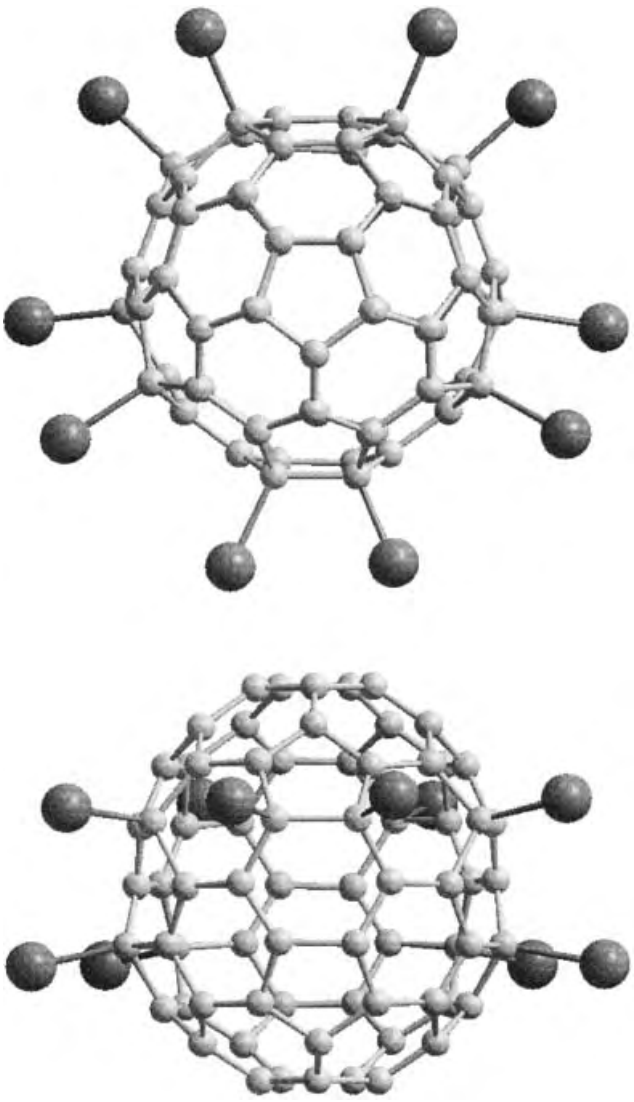


Figure 2. The top and side views of the $C_{70}Br_{10}$ molecule.

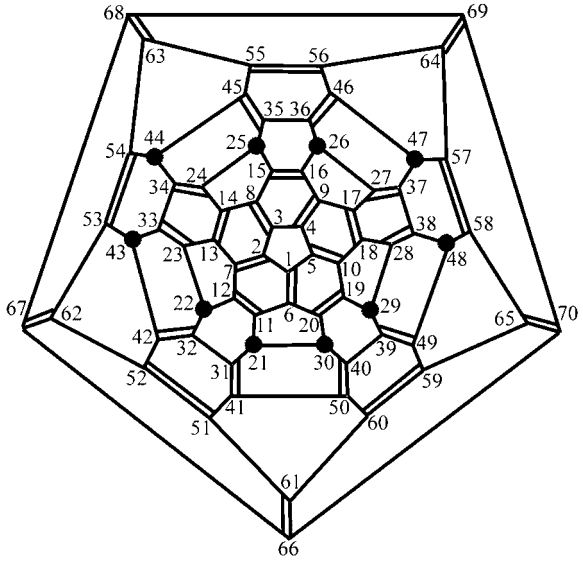


Figure 3. The Schlegel diagram and labeling Scheme for the $C_{70}Br_{10}$ molecule.

 © 2003 Wiley-VCH Verlag GmbH & Co. KGaA, Weinheim

The geometry parameters in the polar regions of $C_{70}Br_{10}$ remain substantially the same as those in the parent C_{70}. The averaged lengths for "single" and "double" C–C bonds are 1.44 Å and 1.40 Å, respectively, (Table 1) consistent with the values for C_{70}, 1.45 Å and 1.38 Å.[15] As expected, the most considerable perturbations of the carbon cage occur around the bromine-bearing carbon atoms. Significant bond lengthening was found for sp^2–sp^3 C–C (1.48(2)–1.54(2) Å; the analogous bonds in C_{70} 1.42–1.45 Å) and, in particular, for the unique sp^3–sp^3 C21–C30 bond (1.59(2) Å cf. 1.44 Å in C_{70}). The experimental $C_{70}Br_{10}$ molecular structure was found to be in a comparatively good agreement with the results of our DFT calculations (Table 1).

Additionally, a small (by 0.05 Å) shortening of the long axis of the ellipsoidal C_{70} molecule takes place upon bromination. The sp^3 C atoms are displaced from the geometric center of the molecule on average by 0.37 Å, whereas some adjacent sp^2 C atoms (C23, C24, C27, C28, C41, C42, C45, C46, C49, and C50) are further from the center by only 0.10 Å as compared with the analogous averaged distances in C_{70}.[15] C–Br bonds lie within a narrow range of 1.99–2.03(1) Å, in good agreement with data for three known C_{60} bromides, 1.99–2.01 Å.[3,4]

The X-ray single-crystal structure determination for the bromine solvate, $C_{70}Br_{10}\cdot 3Br_2$ (**2**), revealed the same molecular structure as that of the $C_{70}Br_{10}$ moiety, but with higher standard deviations for C–C (0.05 Å) and C–Br bonds (0.03 Å).

The packing in the crystal structures of **1** and **2** is shown in Figure 4. The shortest intermolecular separations in **1** are: C···C, 3.14–3.49 Å, C···Br, 3.26–3.31 Å, and Br···Br, 3.31–3.61 Å. In contrast to the dense packing in **1**, the structure of **2** has channels parallel to the *a* axis, in which Br_2 molecules are situated. The longer carbon cage axes of the $C_{70}Br_{10}$ molecules are oriented nearly parallel to the channels. Therefore, the shortest C···C separations, 3.36–3.54 Å, are between the top and bottom pentagons.

In summary, we have determined the first X-ray structures of halogenated [70]fullerene, containing $C_{70}Br_{10}$ molecule, which has a prominent beltlike arrangement of Br atoms in the equatorial region and is the most stable product of the C_{70} bromination.

Table 1: C–C and C–Br bonds (Å) in $C_{70}Br_{10}$ according to the averaged X-ray data for structure **1** and DFT calculations.

Bond	X-ray	Calc.	Bond	X-ray	Calc.
	North pole, C–C			South pole, C–C	
C(1)–C(2)	1.45(2)	1.438	C(31)–C(32)	1.44(2)	1.437
C(2)–C(3)	1.46(2)	1.455	C(35)–C(36)	1.49(2)	1.441
C(3)–C(4)	1.48(2)	1.439	C(41)–C(50)	1.48(2)	1.471
C(6)–C(11)	1.42(2)	1.430	C(41)–C(51)	1.42(2)	1.427
C(7)–C(12)	1.44(2)	1.431	C(42)–C(52)	1.40(2)	1.416
C(7)–C(13)	1.44(2)	1.445	C(45)–C(55)	1.42(2)	1.415
C(8)–C(14)	1.43(2)	1.447	C(51)–C(61)	1.44(2)	1.445
C(8)–C(15)	1.45(2)	1.433	C(52)–C(62)	1.43(2)	1.446
C(13)–C(23)	1.42(2)	1.414	C(53)–C(62)	1.44(2)	1.435
C(14)–C(24)	1.41(2)	1.415	C(54)–C(63)	1.44(2)	1.435
C(33)–C(34)	1.44(2)	1.441	C(55)–C(63)	1.45(2)	1.445
			C(66)–C(67)	1.48(2)	1.453
			C(67)–C(68)	1.43(2)	1.440
			C(68)–C(69)	1.42(2)	1.456
	North pole, C=C			South pole, C=C	
C(1)–C(6)	1.39(2)	1.411	C(31)–C(41)	1.42(2)	1.396
C(2)–C(7)	1.39(2)	1.398	C(32)–C(42)	1.42(2)	1.399
C(3)–C(8)	1.38(2)	1.401	C(35)–C(45)	1.37(2)	1.395
C(11)–C(12)	1.44(2)	1.379	C(51)–C(52)	1.42(2)	1.402
C(13)–C(14)	1.40(2)	1.401	C(53)–C(54)	1.38(2)	1.376
C(15)–C(16)	1.39(2)	1.377	C(55)–C(56)	1.43(2)	1.402
C(23)–C(33)	1.40(2)	1.395	C(61)–C(66)	1.38(2)	1.396
C(24)–C(34)	1.40(2)	1.396	C(62)–C(67)	1.40(2)	1.403
			C(63)–C(68)	1.38(2)	1.399
		Equatorial region, C(Br)–C(Br), C–C(Br), and C–Br			
C(11)–C(21)	1.43(2)	1.502	C(25)–C(35)	1.51(2)	1.504
C(21)–C(30)	1.59(2)	1.636	C(33)–C(43)	1.49(2)	1.504
C(21)–C(31)	1.52(2)	1.515	C(34)–C(44)	1.50(2)	1.504
C(12)–C(22)	1.48(2)	1.508	C(42)–C(43)	1.52(2)	1.526
C(15)–C(25)	1.52(2)	1.511	C(43)–C(53)	1.54(2)	1.510
C(22)–C(23)	1.52(2)	1.526	C(44)–C(45)	1.54(2)	1.527
C(22)–C(32)	1.52(2)	1.501	C(44)–C(54)	1.50(2)	1.510
C(24)–C(25)	1.53(2)	1.527	C(21)–Br(1)	2.03(1)	2.016
C(22)–Br(2)	2.01(1)	2.036	C(25)–Br(5)	1.99(1)	2.034
C(43)–Br(3)	2.00(1)	2.036	C(44)–Br(4)	2.00(1)	2.035

 © 2003 Wiley-VCH Verlag GmbH & Co. KGaA, Weinheim

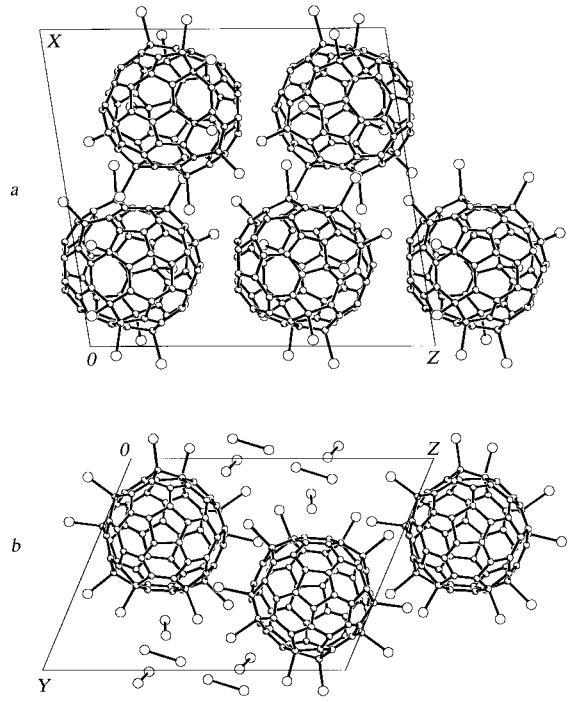


Figure 4. The packing in the crystal structure of a) $C_{70}Br_{10}$ and b) $C_{70}Br_{10}\cdot 3\,Br_2$.

Experimental Section

Two synthetic routes were used for the preparation of $C_{70}Br_{10}$. In the first procedure, a reaction of C_{70} (98.5%, TERMUSA) with an excess of liquid bromine was carried out at room temperature with a variation of the reaction time ranging from 5 min to several weeks. The orange solid separated by filtration had poor crystallinity. Alternatively, saturated solution of C_{70} in 1,2-dichlorobenzene (or in CS_2) reacted with excess bromine during 20–50 h. The fine crystalline orange product was stable in air for some weeks.

Small needles crystals of $C_{70}Br_{10}$ (**1**) were grown in glass ampoules by diffusion of Br_2 into concentrated solution of C_{70} in 1,2-dichlorobenzene during two months. Small crystals of $C_{70}Br_{10}\cdot 3Br_2$ (**2**) were precipitated in a similar ampoule after two weeks when a dilute solution of C_{70} was used.

Thermal properties were investigated with 3–5 mg samples by using differential scanning calorimetry (DSC) and thermogravimetric methods with METTLER TA300. IR spectra were recorded in KBr pellets on a Bruker IFS-113v FT spectrometer with an average of 128 scans and a resolution of 0.5 cm^{-1}.

Data collection for crystals of **1** ($0.16\times0.03\times0.03\ mm^3$) and **2** ($0.30\times0.08\times0.02\ mm^3$) was carried out on an IPDS diffractometer (Stoe) at 153 K and 170 K, respectively (graphite monochromatized $Mo_{K\alpha}$-radiation, $\lambda = 0.71073$ Å). $C_{70}Br_{10}$, **1**: monoclinic, $P2_1/c$, $a =$ 18.579(4), $b = 12.313(2)$, $c = 19.680(4)$ Å, $\beta = 98.64(3)°$, $V =$ 4451.0(15) $Å^3$, $Z = 4$. Reflections collected 35754, independent 9654. Structure solution with SHELXS-97. LS refinement (SHELXL-97) with anisotropic Br and isotropic C for 7563 reflections and 371 parameters converged to $wR_2 = 0.1115$ and $R_1 = 0.0553$. $C_{70}Br_{10}\cdot 3Br_2$, **2**: triclinic, $P\bar{1}$, $a = 11.400(3)$, $b = 13.973(4)$, $c =$ 18.165(5) Å, $\alpha = 111.78(4)$, $\beta = 93.19(4)$, $\gamma = 96.42(4)°$, $V =$ 2655.3(13) $Å^3$, $Z = 2$. Reflections collected 23593, independent 11828. LS refinement with anisotropic Br and isotropic C for 7946 reflections and 425 parameters gave the final values of $wR_2 = 0.3184$ and $R_1 = 0.1388$.[16]

The geometry optimization and vibrational spectra calculation were performed with the PRIRODA program[17] at the DFT level of theory employing PBE exchange-correlation functional[18] and a Gaussian-type basis set of TZ2P quality with effective core potential for bromine atoms.

Received: February 7, 2003 [Z51132]

Keywords: bromination · fullerenes · structure elucidation

[1] *Fullerenes; Chemistry, Physics and Technology* (Eds.: K. M. Kadish, R. S. Ruoff), Wiley-Interscience, New York, **2000**, p. 91.
[2] P. R. Birkett, P. B. Hitchcock, H. W. Kroto, R. Taylor, D. R. M. Walton, *Nature* **1992**, *357*, 479.
[3] S. I. Troyanov, P. A. Troshin, O. V. Boltalina, E. Kemnitz, *Fullerenes Nanotubes Carbon Nanostruct.* **2003**, *11*, 61.
[4] F. N. Tebbe, R. L. Harlow, D. B. Chase, D. L. Thorn, G. C. Campbell, J. C. Calabrese, N. Herron, R. J. Young, E. Wasserman, *Science* **1992**, *256*, 822.
[5] P. R. Birkett, A. G. Avent, A. D. Darwish, H. W. Kroto, R. Taylor, D. R. M. Walton, *J. Chem. Soc. Chem. Commun.* **1993**, 1230.
[6] R. Taylor, *J. Chem. Soc. Perkin Trans. 2* **1993**, 813.
[7] B. W. Clare, D. L. Kepert, *J. Mol. Struct. (Theochem)* **1999**, *491*, 249.
[8] R. Taylor, A. K. Abdul-Sada, O. V. Boltalina, J. K. Street, *J. Chem. Soc. Perkin Trans. 2* **2000**, 1013.
[9] P. R. Birkett, A. G. Avent, A. D. Darwish, H. W. Kroto, R. Taylor, D. R. M. Walton, *J. Chem. Soc. Chem. Commun.* **1995**, 683.
[10] G. Waidmann, M. Jansen, *Z. Anorg. Allg. Chem.* **1997**, *623*, 623.
[11] N. I. Denisenko, A. A. Popov, I. V. Kuvychko, O. V. Boltalina, N. V. Chelovskaya, *Proceedings - Electrochemical Society, Vol. 12* (Eds. K. Prakash, D. Guldi), Electrochemical Society Inc., Pennington, **2002**, p. 577.
[12] A. G. Avent, P. R. Birkett, A. D. Darwish, H. W. Kroto, R. Taylor, D. R. M. Walton, *Tetrahedron* **1996**, *52*, 5235.
[13] H. P. Spielmann, B. R. Weedon, M. S. Meier, *J. Org. Chem.* **2000**, *65*, 2755.
[14] A. D. Darwish, P. de Guio, R. Taylor, *Fullerenes Nanotubes Carbon Nanostruct.* **2002**, *10*, 261.
[15] H.-B. Bürgi, P. Venugopalan, D. Schwarzenbach, F. Diederich, C. Thilgen, *Helv. Chim. Acta* **1993**, *76*, 2155; S. I. Troyanov, *Russ. J. Inorg. Chem.* **2001**, *46*, 1612.
[16] CCDC-200994 (**1**) and -200995 (**2**) contain the supplementary crystallographic data for this paper. These data can be obtained free of charge via www.ccdc.cam.ac.uk/conts/retrieving.html (or from the Cambridge Crystallographic Data Centre, 12 Union Road, Cambridge CB2 1EZ, UK; fax: (+44) 1223-336-033; or deposit@ccdc.cam.ac.uk).
[17] D. N. Laikov, *Chem. Phys. Lett.* **1997**, *281*, 151.
[18] J. P. Perdew, K. Burke, M. Ernzerhof, *Phys. Rev. Lett.* **1996**, *77*, 3865.

 © 2003 Wiley-VCH Verlag GmbH & Co. KGaA, Weinheim

Difluorocyclopropenes

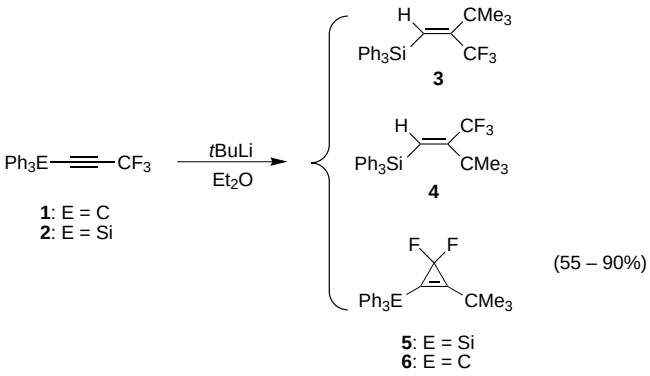
Ringing the Changes: A Remarkable Carbene-Free Synthesis of Difluorocyclopropenes**

Alan K. Brisdon, Ian R. Crossley, Kevin R. Flower, Robin G. Pritchard, and John E. Warren*

In recent years there has been resurgent interest in the chemistry of fluorinated compounds because of their potential pharmaceutical, agrochemical, and materials applications.[1] We have been investigating new methods for the selective introduction of small fluorocarbon fragments and have recently reported a new and facile route to trifluoropropynyl derivatives.[2] In seeking to extend to these systems our recent work on the reactivity of organometallic fluorovinyl compounds,[3] we have discovered a remarkable transformation, which results in the facile formation of *gem*-difluorocyclopropenyls in good yields.

The trifluoropropynyls $Ph_3EC{\equiv}CCF_3$ (**1**: E = C, **2**: E = Si) are readily prepared by the reaction of Ph_3EX (X = Cl, Br) with trifluoropropynyllithium ($LiC{\equiv}CCF_3$), derived from hydrofluorocarbon HFC-245fa ($CF_3CH_2CF_2H$) as we have previously described,[2] and isolated as air- and moisture-stable solids. These materials are characterized by singlet resonances at around $\delta_F = -50$ ppm in the ^{19}F NMR spectra, and three quartet signals in the ^{13}C NMR spectra, ($\delta_C = 90$–120 ppm), with infrared absorptions (C≡C stretch) at approximately 2200 cm^{-1}.

Given the versatility of silanes as organotransfer reagents[4] and in fluoro/hydro-desilylation chemistry,[5] compound **2** constitutes a potentially useful substrate for derivatization. The reaction of **2** with organolithium reagents was thus explored as a route to some novel β-CF_3-substituted vinylic systems. However, when an ethereal solution of **2** was treated with 1 equivalent of *t*BuLi at −78 °C and then allowed to warm to ambient temperature over 5 h, workup afforded an unexpected product mixture (Scheme 1). Multinuclear (^1H, ^{19}F) NMR studies revealed a significant proportion of (*Z*)-$Ph_3SiCH{=}C(tBu)CF_3$ (**3**), which was assigned on the basis of H-F coupling constants and a discernible NOE interaction between the alkenic and *tert*-butyl proton resonances, and trace levels of the *E* isomer **4** (*Z*/*E* 14:1). The major product (55% by integration) was characterized by a low-frequency singlet ^{19}F NMR resonance ($\delta_F = -103.1$ ppm) and additional



Scheme 1. Products from the *t*BuLi reaction with group 14 trifluoropropynyl derivatives.

tert-butyl resonances in the ^1H and ^{13}C NMR spectra; no further alkenic protons were observed. Efforts to separate these materials chromatographically proved unsuccessful, owing to their limited stability on the column, as did recrystallization. However, the slow evaporation of a dichloromethane/hexane solution, did afford isomerically enriched single crystals.

Surprisingly, X-ray analysis revealed the presence of both **4** (12%) and the *gem*-difluorocyclopropenyl **5** (88%, Figure 1), within the same crystal.[6] The presence of **5** is consistent with the observed NMR data, the low-frequency ^{19}F resonance being characteristic of other *gem*-difluorocyclopropenes.[7] Moreover, we observed three cyclopropenic

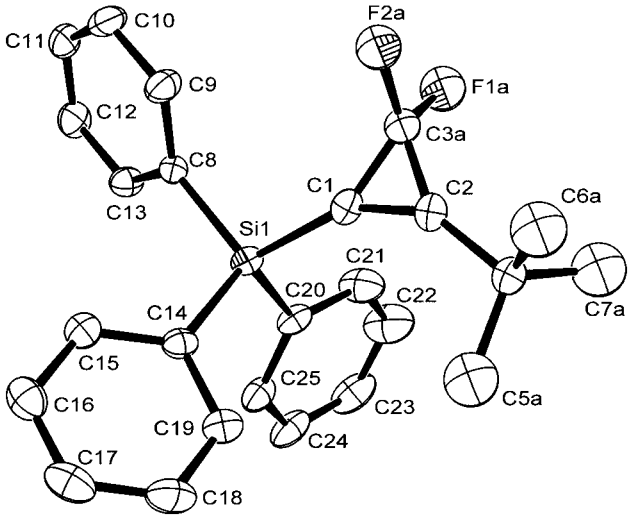


Figure 1. ORTEP representation of **5** with thermal ellipsoids set at the 30% probability level and hydrogen atoms omitted for clarity. The numbering scheme is directly transposable to compound **6**, with C1′ replacing Si1. Selected data (Å, °) for **5**. C1-C2 1.329(4), C2-C3 1.371(4), C1-C3 1.402(4), C3-F1a 1.384(4), C3-F2a 1.369(4); C2-C1-C3 60.2(2), C1-C2-C3 62.6(2), C2-C3-C1 57.27(19), Si1-C1-C2 151.2(2), C1-C2-C4 147.2(3). Selected data for **6**. C1-C2 1.324(3), C2-C3 1.427(3), C1-C3 1.429(3), C3-F1a 1.379(3), C3-F2a 1.375(3); C2-C1-C3 62.2(16), C1-C2-C3 62.47(15), C2-C3-C1 55.23(14), C1′-C1-C2 148.2(2), C1-C2-C4 152.0(3).

[*] Dr. A. K. Brisdon, I. R. Crossley, Dr. K. R. Flower, Dr. R. G. Pritchard, J. E. Warren
Department of Chemistry, UMIST
P.O. Box 88, Manchester, M60 1QD (UK)
Fax: (+44) 161-200-4559
E-mail: alan.brisdon@umist.ac.uk

[**] This work was supported by the Engineering and Physical Sciences Research Council (EPSRC) and UMIST. We gratefully acknowledge Honeywell Specialty Chemicals for a donation of HFC-245fa and the EPSRC for support of the UMIST NMR (GR/L52246), FT-IR/Raman (GR/M30135), and X-ray (Research Initiative Grant) facilities.

Supporting information for this article is available on the WWW under http://www.angewandte.org or from the author.

 DOI: 10.1002/anie.200250756 © 2003 Wiley-VCH Verlag GmbH & Co. KGaA, Weinheim

^{13}C NMR resonances in the region $\delta_C = 160$–100 ppm; each one a well-defined triplet.

The formation of **5** is optimized when **2** is treated with *t*BuLi at ambient temperature over 20 h, whereupon **5** accounts for 80% of the product mixture. Significantly, comparable conditions also result in cyclization of the trityl alkyne **1**, thus precluding the possibility that cyclization involves the participation of silicon d orbitals. Indeed, **1** has proven to be the most viable substrate, since difluorocyclopropene **6**[8] accounts for 90% of the reaction products.

This remarkably facile cyclization presumably occurs by elimination of LiF from the lithiated intermediate (*E*)-$Ph_3EC(Li)=C(tBu)CF_3$, driven by the steric strain associated with the introduction of a *t*Bu group *cis* to the Ph_3E fragment. This is supported by ab initio calculations of the related alkene (*E*)-$Me_3SiCH=C(tBu)CF_3$ at the B3LYP/6-311 + G* level,[9] which reveal an energy minimum with a significantly distorted geometry (Si-C=C = 140.1°, C=C-*t*Bu = 127.8°). Consequently, the eclipsing fluorine atom approaches the alkenic hydrogen center at 2.119 Å (C–F···H = 59.2°), significantly closer than the sum of the contact radii (2.67 Å).[10] This would be enhanced in the lithiated intermediate, thus predisposing it to elimination of LiF. Significantly, these distortions are also evident in the single-crystal structure of **4** (Figure 2),[11] obtained in a subsequent experiment. Once again, an extremely short H···F interaction (2.13(2) Å) is apparent, clearly enforced by an opening of the alkene geometry (Si-C=C = 139.37(18)°, C=C-*t*Bu = 127.4(2)°). The steric argument is supported by ongoing investigations of the interaction of **2** with other, smaller organolithium reagents, RLi (R = Ph, *n*Bu, Me) and $LiAlH_4$, whereupon cyclization occurs only at trace levels. Indeed, for the limiting case, (*E*)-$R_3SiCH=CHCF_3$ (**7**: R = Me), ab initio calculations reveal a more typical geometry (Si-C=C = 125.3°, C=C-H = 122.9°) with a significantly reduced H···F interaction (2.407 Å).[12] We note that similar Li···F interactions are also believed to play an important role in the mechanism of *ortho* metallation of fluoroaromatic compounds.[13]

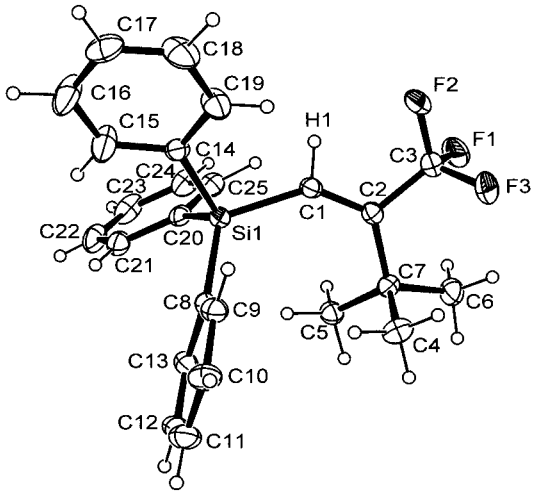


Figure 2. ORTEP representation of **4** with thermal ellipsoids set at the 30% probability level. Selected data (Å, °): C1-C2 1.341(3), C2-C3 1.510(3), C3-C1 1.345(3), C3-F2 1.344(3), C3-F3 1.345(3); C1-C2-C7 127.4(2), C1-C2-C3 115.9(2), Si1-C1-C2 139.37(18), C2-C1-C7 116.68(16), Si1-C1-H1 110.1(13).

The cyclization pathway is also inhibited when operating at reduced temperature. Thus, when **2** and *t*BuLi interact at −60 °C, **5** is obtained, along with **4**, only as a trace contaminant (2.5%) in admixture with **3** (95%). This preference for *syn* addition would suggest the intermediacy of a lithium π complex, favored by the decreased nucleophilicity of *t*BuLi under these conditions. Support for this has been obtained through the use of tmeda to enhance solvation, and thus nucleophilicity, of the *t*BuLi, which results in a lower specificity of addition. In these experiments, **3** was generated with varying amounts of the *E* isomer, consistent with inhibition of the π complex and also of LiF elimination to afford **5**.

In conclusion, the reaction of the group 14 trifluoropropynyl compounds $Ph_3EC{\equiv}CCF_3$ (E = C, Si) with sterically demanding organolithium reagents results in a facile and efficient cyclization to afford the respective triphenyl-2-*tert*-butyl-3,3-difluorocyclopropenyl compounds. This circumvents the use of difluorocarbene sources, as in more classical synthetic protocols, and is readily controlled under mild conditions. The potential for Si–C cleavage and selective transfer of organic components from organosilanes renders this discovery a significant advance in small-ring chemistry, which we continue to explore.

Experimental Section

Reagents were obtained from commercial vendors and used as supplied. NMR spectra were recorded as $CDCl_3$ solutions at 298 K, on Bruker DPX 200 (^{19}F NMR spectra at 188.310 MHz) or DPX 400 (^{13}C NMR and Dept-135 spectra at 100.155 MHz, ^1H NMR spectra at 400.4 MHz) spectrometers and referenced to external $CFCl_3$ and TMS, respectively.

2: A stirred solution of HFC-245fa (2.16 cm^3, 21.28 mmol) in diethyl ether (300 cm^3) was treated with *n*BuLi (2.5 M, 25.5 cm^3, 63.75 mmol) at −10 °C under N_2. After 15 min, Ph_3SiCl (4.15 g, 14.07 mmol) in diethyl ether (40 cm^3) was added, whilst maintaining the temperature at −10 °C. The mixture was then allowed to stir and attain ambient temperature overnight. Hexane (160 cm^3) was added to precipitate the inorganic salts, the settled mixture was then filtered through celite, and the filtrate was concentrated in vacuo. Purification on a silica column, eluting with 50:50 toluene/hexane, afforded **2** as a pale yellow solid (4.229 g, 85%). M.p. 110 °C; elemental analysis: calcd for $C_{21}H_{15}F_3Si$: C 71.6, H 4.3, F 16.2; found: C 71.9, H 4.5, F 16.0; $\delta_F = -50.4$ ppm; $\delta_C = 135.4$ (s; CH), 131.6 (s; C), 131.1 (s; CH), 128.8 (s; CH), 113.3 (q, $J_{CF} = 258.7$ Hz; CF_3), 93.8 (q, $J_{CF} = 51.6$ Hz; C_β), 90.3 ppm (q, $J_{CF} = 5.8$ Hz; C_α); $\delta_H = 7.7$–7.4 ppm (m; Ph); $\tilde{\nu}_{max}$ 2204 (C≡C str), 1245, 1151, 1114 cm^{-1} (C–F str).

1: M.p. 150 °C; elemental analysis: calcd for $C_{22}H_{15}F_3$: C 78.6, H 4.5, F 16.9; found: C 78.8, H 4.3, F 16.6; $\delta_F = -50.0$ ppm; $\delta_C = 143.2$ (s; C), 129.4 (s; CH), 128.8 (s; CH), 127.9 (s; CH), 114.8 (q, $J_{CF} = 256.9$ Hz; CF_3), 93.9 (q, $J_{CF} = 6.7$ Hz; C_α), 72.6 (q, $J_{CF} = 52.2$ Hz; C_β), 55.8 ppm (br s, Ph_3C); $\delta_H = 7.7$–7.4 (m; Ph); $\tilde{\nu}_{max}$ 2256 (C≡C str), 1276, 1145, 1091 cm^{-1} (C–F str).

Reaction with nucleophiles: Typically, a solution of **1** (0.500 g, 1.49 mmol) in diethyl ether (15 cm^3) was treated with *t*BuLi (1.5 M, 1.0 cm^3, 1.50 mmol) at ambient temperature under N_2 and stirred for 20 h. The reaction was quenched with methanol (3 cm^3) and hexane was added to precipitate the inorganic components, then filtered through celite, and the filtrate was concentrated in vacuo. Purification

 © 2003 Wiley-VCH Verlag GmbH & Co. KGaA, Weinheim

on silica, eluting with 50:50 CH_2Cl_2/hexane afforded the pure product **6** in 60% yield. M.p. 143°C; elemental analysis: calcd for $C_{26}H_{24}F_2$: C 83.4, H 6.5, F 10.2; found: C 83.2, H 6.8, F 10.5; $\delta_F = -105.9$ ppm; $\delta_C =$ 143.0 (s; C), 128.5 (s; CH), 127.2 (s; CH), 126.1 (s; CH), 136.1 (t, $J_{CF} =$ 10 Hz; C_β), 131.2 (t, $J_{CF} = 10.6$ Hz; C_α), 103.8 (t, $J_{CF} = 272$ Hz; CF_2), 58.1 (br s; Ph_3C), 30.3 (s; CMe_3), 27.1 ppm (s; $C(CH_3)_3$); $\delta_H = 7.7$–7.4 (m; Ph), 1.02 ppm (s; $(CH_3)_3$); $\tilde{\nu}_{max} = 1781$ (C=C str), 1292, 1147 cm^{-1} (C–F str).

5: $\delta_F = -103.1$ ppm; $\delta_C = 134.6$ (s; CH), 130.9 (s; C), 129.3 (s; CH), 127.1 (s; CH), 157.9 (t, $J_{CF} = 8.3$ Hz; C_β), 124.6 (t, $J_{CF} = 13.1$ Hz; C_α), 108.2 (t, $J_{CF} = 271$ Hz; CF_2), 29.7 (s; CMe_3), 27.4 ppm (s; $C(CH_3)_3$); $\delta_H = 7.7$–7.4 (m; Ph), 1.1 ppm (s; $(CH_3)_3$); $\tilde{\nu}_{max} = 1729$ (C=C str), 1261, 1149 cm^{-1} (C–F str).

3: M.p. 89°C; elemental analysis: calcd for $C_{25}H_{25}F_3Si$: C 73.2, H 6.1, F 13.9; found: C 73.4, H 6.1, F 13.5; $\delta_F = -60.7$ ppm (d, $J_{HF} =$ 1.5 Hz); $\delta_C = 134.7$ (s; CH), 134.1 (s; C); 128.6 (s; CH), 127.0 ($J_{SiC} =$ 29 Hz; CH), 155.7 (q, $J_{CF} = 23.7$ Hz; C_β), 126.2 (q, $J_{CF} = 4.8$ Hz; C_α), 123.2 (q, $J_{CF} = 279$ Hz; CF_3), 35.3 (s; CMe_3), 29.7 ppm (s; $C(CH_3)_3$); $\delta_H = 7.7$–7.4 (m; Ph), 6.9 (q, $J_{HF} = 1.5$ Hz; =CH), 1.06 ppm (s; $(CH_3)_3$); $\tilde{\nu}_{max} = 1429$ (C=C str), 1257, 1157, 1120 cm^{-1} (C–F str).

4: $\delta_F = -56.7$ ppm (d, $J_{HF} = 1.5$ Hz), $\delta_H = 7.7$–7.4 (m; Ph), 6.7 ppm (q, $J_{HF} = 1.5$ Hz; =CH), 1.1 (s; $(CH_3)_3$).

Crystallography: Single crystals were obtained by the slow evaporation of CH_2Cl_2/hexane solutions. Diffraction data were recorded on a Nonius κ-CCD 4-circle diffractometer using graphite-monochromated $Mo_{K\alpha}$ radiation ($\lambda = 0.71073$ Å) at 150(2) K. Structure data were solved by direct methods, with full-matrix least-squares refinement on F^2 using the SHELX-97[14] program; absorption corrections by the multiscan method were applied with the SORTAV program. Non-hydrogen atoms were refined with anisotropic thermal parameters: all hydrogen atoms were located in the data. Figures were generated using ORTEP-3 for Windows.[15] CCDC-199460 (**4**), -199461 (**5**), and -199462 (**6**) contain the supplementary crystallographic data for this paper. These data can be obtained free of charge via www.ccdc.cam.ac.uk/conts/retrieving.html (or from the Cambridge Crystallographic Data Centre, 12, Union Road, Cambridge CB21EZ, UK; fax: (+44) 1223-336-033; or deposit@ccdc.cam.ac.uk).

Ab inito calculations**:** Calculations were performed with the Gaussian 98 package, Revision A.7,[16] running on a Sun Enterprise HPC 4500 workstation. Geometries were optimized at the B3LYP/6-311+G* level and characterized as minima by frequency calculations.

Received: December 12, 2002 [Z50756]

Keywords: alkynes · cyclization · fluorine · small-ring systems · structure elucidation · synthetic methods

[1] a) R. Filler, Y. Kobayashi, *Biomedical Aspects of Fluorine Chemistry*, Kodasha/Elsevier, New York, **1982**; b) R. E. Banks, *Organofluorine Chemicals and Their Industrial Applications*, Ellis Horwood, Chichester, **1979**; c) R. E. Banks, *Organofluorine Chemistry: Principles and Commercial Applications*, Plenum Press, New York, **1994**; d) R. E. Banks, *Fluorine Chemistry at the Millennium: Fascinated by Fluorine*, Elsevier Science Ltd., Amsterdam, **2000**.

[2] A. K. Brisdon, I. R. Crossley, *Chem. Commun.* **2002**, 2420–2421

[3] A. K. Brisdon, I. R. Crossley, R. G. Pritchard, J. E. Warren, *Inorg. Chem.* **2002**, *41*, 4748- 4755.

[4] For example, see: a) G. L. Li, Y. H. Chen, J. R. Missert, A. Rungta, T. J. Dougherty, Z. D. Grossman, R. K. Pandey, *J. Chem. Soc. Perkin Trans. 1* **1999**, 1785–1788; b) L. Xue, L. Lu, S. D. Pedersen, Q. Liu, R. M. Narske, D. J. Burton, *J. Org. Chem.* **1997**, *62*, 1064–1071.

[5] For example, see: a) R. S. Dickson, H. P. Kirsch, *Aust. J. Chem.* **1972**, *25*, 1815–1818; b) B. Greedy, V. Gouverneur, *Chem. Commun.* **2001**, 233–234.

[6] Crystal data for $C_{25}H_{24}F_2Si$ (**5**): $0.25 \times 0.15 \times 0.05$ mm^3, monoclinic, $P121/n1$, $a = 15.7382(4)$ Å, $b = 8.8148(2)$ Å, $c =$ 16.2312(5) Å, $\alpha = 90.0000(10)$, $\beta = 103.0830(10)$, $\gamma =$ 90.0000(10)°, $V = 2193.29(10)$ $Å^3$, $\rho_{calcd} = 1.183$ $Mg\,m^{-3}$, $\theta_{max} =$ 27.45°, reflections/unique/parameters. 36277/4973/300, $F(000)$ 824, $\mu = 0.130$ mm^{-1}, $T_{max} = 1.039$, $T_{min} = 0.968$, $R = 0.0699$, $wR2 = 0.1515$, Largest diff. peak + hole 0.244, −0.218 e $Å^{-3}$.

[7] R. Eujen, B. Hoge, *J. Organomet. Chem.* **1995**, *503*, C51–C54.

[8] Crystal data for $C_{26}H_{24}F_2$ (**6**): $0.25 \times 0.25 \times 0.20$ mm^3, triclinic, $P\bar{1}$, $a = 9.6763(2)$ Å, $b = 9.9515(2)$ Å, $c = 11.8603(3)$ Å, $\alpha =$ 108.5100(10), $\beta = 99.078(2)$, $\gamma = 102.5900(10)$°, $V =$ 1024.67(10) $Å^3$, $\rho_{calcd} = 1.214$ $Mg\,m^{-3}$, $\theta_{max} = 27.55$°, reflections/unique/parameters 20467/4701/253, $F(000)$ 396, $\mu = 0.081$ mm^{-1}, $T_{max} = 0.9839$, $T_{min} = 0.9799$, $R = 0.0647$, $wR2 = 0.1736$, Largest diff. peak + hole 0.456, −0.470 e $Å^{-3}$.

[9] Selected geometric data (Å, °) for (*E*)-$Me_3SiCH{=}C(t\text{Bu})CF_3$: C1-C2 1.344, C2-C3 1.526, C3-F2 1.351, C3-F1 1.359, C3-F3 1.361; Si1-C1-C2 140.1, C1-C2-C7 127.8, C1-C2-C3 115.9, C3-C2-C7 116.2, Si1-C1-H1 106.8.

[10] A. Bondi, *J. Phys. Chem.* **1964**, *68*, 441–451.

[11] Crystal data for $C_{25}H_{25}F_3Si$ (**4**): $0.20 \times 0.25 \times 0.03$ mm^3, monoclinic, $P21/c$, $a = 14.5669(5)$ Å, $b = 9.8256(3)$ Å, $c =$ 15.4721(6) Å, $\alpha = 90$, $\beta = 90.4580(10)$, $\gamma = 90$°, $V =$ 2214.43(13) $Å^3$, $\rho_{calcd} = 1.231$ $Mg\,m^{-3}$, θ_{max} 24.98°, reflections/unique/parameters 13196/3837/362, $F(000)$ 864, $\mu =$ 0.139 mm^{-1}, $T_{max} = 0.9959$, $T_{min} = 0.9728$, $R = 0.0463$, $wR2 =$ 0.1128, Largest diff. peak + hole 0.215, −0.232 e $Å^{-3}$.

[12] Selected geometric data (Å, °) for **7**: C1-C2 1.333, C2-C3 1.498, C3-F2 1.349, C3-F1 1.358, C3-F3 1.358; Si1-C1-C2 125.3, C1-C2-H2 122.9, C1-C2-C3 124.3, C3-C2-H2 112.7, Si1-C1-H1 117.9.

[13] For example, see: W. Bauer, P. von R. Schleyer, *J. Am. Chem. Soc.* **1989**, *111*, 7191–7198; S. Takagishi, G. Katsoulos, M. Schlosser, *Synlett* **1992**, 360–362.

[14] G. M. Sheldrick, SHELX-97, University of Göttingen, Göttingen (Germany), **1998**

[15] ORTEP 3 for Windows: L. J. Farugia, *J. Appl. Crystallogr.* **1997**, *30*, 565.

[16] Gaussian 98 (Revision A.7), M. J. Frisch, G. W. Trucks, H. B. Schlegel, G. E. Scuseria, M. A. Robb, J. R. Cheeseman, V. G. Zakrzewski, J. A. Montgomery, R. E. Stratmann, J. C. Burant, S. Dapprich, J. M. Millam, A. D. Daniels, K. N. Kudin, M. C. Strain, O. Farkas, J. Tomasi, V. Barone, M. Cossi, R. Cammi, B. Mennucci, C. Pomelli, C. Adamo, S. Clifford, J. Ochterski, G. A. Petersson, P. Y. Ayala, Q. Cui, K. Morokuma, D. K. Malick, A. D. Rabuck, K. Raghavachari, J. B. Foresman, J. Cioslowski, J. V. Ortiz, B. B. Stefanov, G. Liu, A. Liashenko, P. Piskorz, I. Komaromi, R. Gomperts, R. L. Martin, D. J. Fox, T. Keith, M. A. Al-Laham, C. Y. Peng, A. Nanayakkara, C. Gonzalez, M. Challacombe, P. M. W. Gill, B. G. Johnson, W. Chen, M. W. Wong, J. L. Andres, M. Head-Gordon, E. S. Replogle, J. A. Pople, Gaussian, Inc., Pittsburgh, PA, **1998**.

 © 2003 Wiley-VCH Verlag GmbH & Co. KGaA, Weinheim

Foldamer Structure

Parallel Sheet Secondary Structure in β-Peptides**

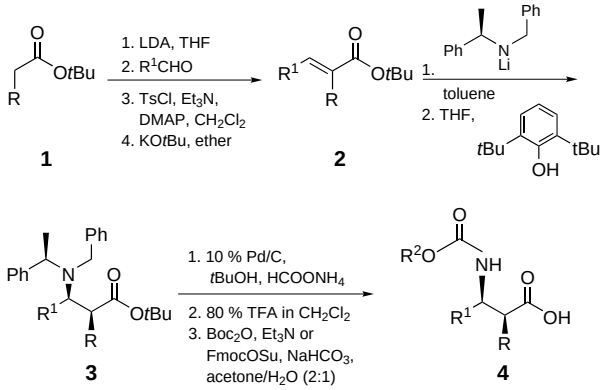
*Joseph M. Langenhan, Ilia A. Guzei, and Samuel H. Gellman**

Non-natural oligomers that adopt discrete conformations ("foldamers") are the focus of an extensive research effort.[1] β-Peptide foldamers[2] have been particularly interesting because several distinct secondary structures (for example, different types of helices, two kinds of reverse turns, and antiparallel sheet) can be induced by using appropriately substituted β-amino acid residues. Here we extend the secondary structure list by documenting parallel sheet secondary structure between α,β-*syn*-dialkyl β-amino acid residues, linked with a diamine connector, both in solution and in the solid state.[3]

A hairpin (that is, a strand–loop–strand motif) is the smallest possible increment of autonomous sheet secondary structure. The hairpin architecture has been widely employed to generate β-sheet model systems among conventional peptides[4] and to explore sheet secondary structure involving non-natural units, which include systems containing strand mimics,[5] nonpeptidic loops,[6] and α/β-amino acid combinations.[7] In proteins, two classes of secondary structure display long-range order, helices and sheets. Development of autonomously folding β sheets proved to be more difficult than creating autonomously folding α helices because noncovalent contacts within a helix occur between residues that are a fixed and short distance apart along the backbone, while noncovalent juxtapositions in sheet secondary structure do not involve fixed sequential relationships. Success in β-sheet design requires identification of appropriate strategies for linking the strand-forming segments.[4] Manipulation of the linker has allowed both antiparallel and parallel juxtapositions of β-strand segments among conventional peptides. The resulting model systems are invaluable tools for probing the forces that control β-sheet stability in natural peptides and proteins,[4] and for evaluating fundamental noncovalent interactions.[8] Small hairpin molecules should be useful for identifying the parameters that influence sheet secondary structure in unnatural foldamers, as has already been demonstrated for antiparallel β-peptide sheet.[3b,9]

Parallel hairpins[5c,f,6b,6c,10] require a reverse-turn unit that can link together two strand segments via their C or N termini; segments constructed from only α-, β-, or other amino acids cannot fulfill this need because they have only one N and one C terminus. The prolyl-(1,1-dimethyl)-1,2-diaminoethyl (Pro-DADME) unit has recently been identified as an effective reverse turn for both α- and γ-peptide strand segments.[11,12] Here we explore the Pro-DADME unit as a promoter of parallel sheet formation between β-peptide strands.

We have previously shown that antiparallel β-peptide sheet secondary structure is promoted by α,β-*syn*-dialkyl β-amino acid residues, which favor an *anti* torsion angle about the NC_β–$C_\alpha C(=O)$ bond.[9a,13] These residues form antiparallel hairpins in organic solvents when connected by either β-peptide[3b,9b–9d] or non-β-peptide linkers.[9a] Our initial studies utilized α,β-*syn*-dialkyl β-amino acids that had been synthesized from L-aspartic acid;[14] however, this methodology did not provide ready access to diverse side chains. Dialkyl β-amino acids have also been obtained by α-alkylation of β^3-substituted β-amino methyl esters, but this process results in mixtures of diastereomers, which are sometimes inseparable by chromatography.[15] We are now able to synthesize α,β-*syn*-dialkyl β-amino acids with high enantiomeric excesses by a route pioneered by Davies et al. (Scheme 1).[16] *E*-α,β-unsaturated *tert*-butyl esters **2** result from an aldol reaction between *tert*-butyl esters **1** and the appropriate aldehydes,



Scheme 1. Synthesis of α,β-*syn*-disubstituted β-amino acids. LDA = lithium diisopropylamide; DMAP = 4-dimethylamino pyridine; TFA = trifluroacetic acid; Boc = *t*-butyloxycarbonyl; FmocOSu = 9-fluorenylmethyloxycarbonyl-*N*-hydroxysuccinimide

followed by tosylation and subsequent potassium *tert*-butoxide-mediated elimination. These unsaturated esters undergo conjugate addition with lithium (*R*)-(+)-*N*-benzyl-*N*-α-methylbenzylamide under the reaction conditions developed by Davies and co-workers. The resultant amino esters **3** are then fully deprotected; the amino groups are reprotected with Boc or Fmoc groups, for solution or solid-phase synthesis, respectively. This general scheme can afford a variety of amino acids that contain β-alkyl groups and α-alkyl or α-aryl groups.

With appropriate reverse-turn and strand building blocks in hand, we synthesized hairpin **5**, in which two *N*-acetylated

[*] Prof. S. H. Gellman, J. M. Langenhan, Dr. I. A. Guzei[+]
Department of Chemistry
University of Wisconsin
1101 University Ave., Madison, WI 53706 (USA)
Fax: (+1) 608-265-4534
E-mail: gellman@chem.wisc.edu

[+] Correspondence regarding X-ray diffraction analysis should be addressed to I.A.G. (E-mail: iguzei@chem.wisc.edu).

[**] This research was supported by the U.S. National Institutes of Health (GM 56414). J.M.L. was supported in part by a National Science Foundation Predoctoral Fellowship. The NMR spectrometer was purchased in part with a U.S. National Institutes of Health grant (NIH 1 S10 RR13866-01).

 © 2003 Wiley-VCH Verlag GmbH & Co. KGaA, Weinheim DOI: 10.1002/anie.200350932

α,β-*syn*-dialkyl β-amino acid strand residues are connected by a D-Pro-DADME linker. Molecule **5** adopts a parallel hairpin conformation in the solid state (Figure 1; top).[17] Within the crystal, the hairpins are packed in a parallel fashion into columns (Figure 1; middle). There is a single intermolecular hydrogen bond between each hairpin molecule within these columns. The columns pack together in the manner shown in the lower section of Figure 1. Within each individual hairpin, the O(1)···H–N(5) and O(2)···H–N(4) separations (2.1 Å and 2.2 Å, respectively) strongly suggest the presence of two hydrogen bonds between the two β-peptide strands (Figure 1; top). This result demonstrates that the desired parallel sheet folding pattern is accessible to **5**, but, as with any crystal structure of an inherently flexible molecule, these solid-state data do not provide insight on the propensity for parallel-sheet formation.

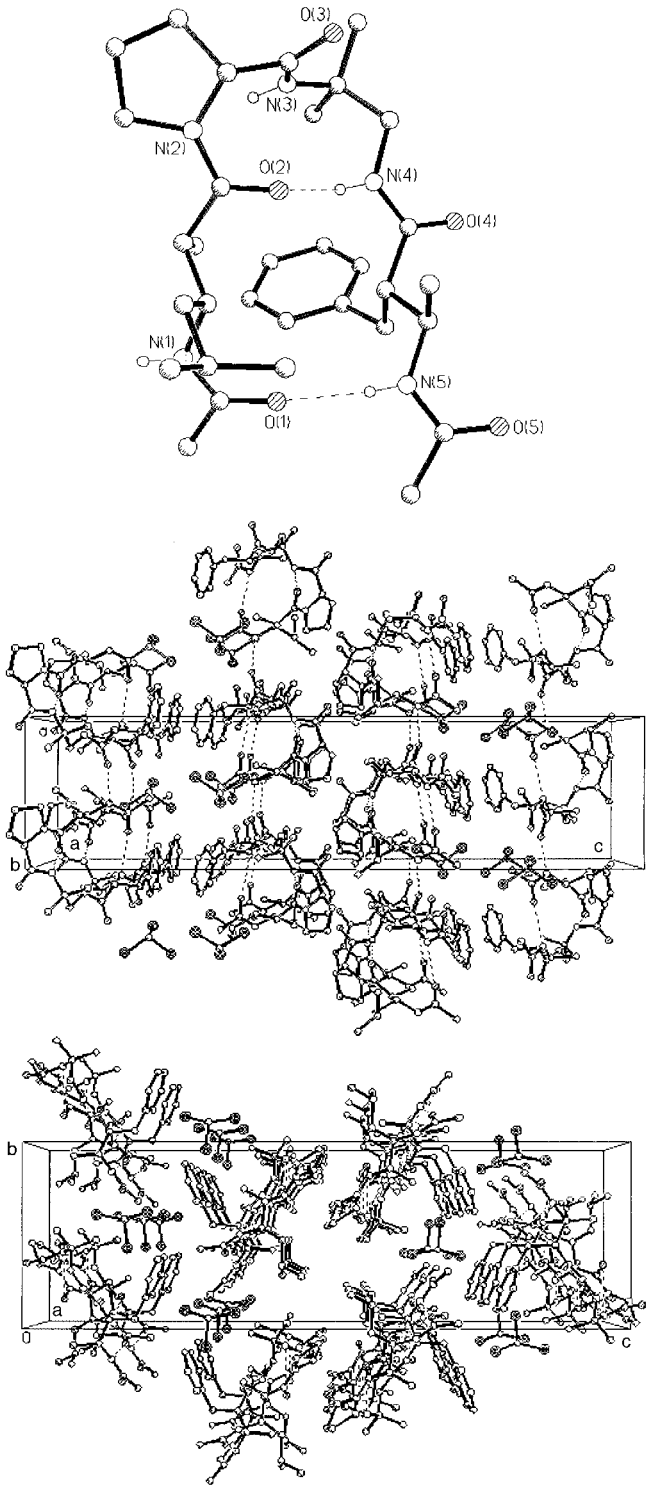
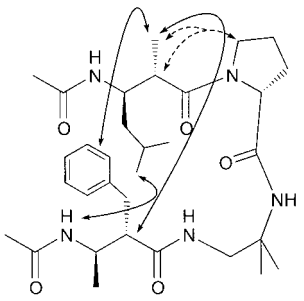


Figure 1. Top: The solid-state conformation of **5**. Hydrogen bonds are shown as dashed lines; middle: crystal packing diagram viewed along the *b* axis; bottom: crystal packing diagram viewed along the *a* axis.

To gain qualitative insight on the favorability of the hairpin conformation observed for **5** in the solid state, we examined this molecule by two-dimensional NMR spectroscopy in d_3-methanol at 4 °C. The chemical shifts for amide protons did not change between 0.05 mM and 5 mM, which is an indication that no aggregation of **5** occurs within this concentration range. All further experiments were performed at 5 mM. Because methanol is a protic solvent, a folding pattern stabilized exclusively by two internal hydrogen bonds should not be highly populated in this solvent. Detection of the hairpin conformation of **5** in methanol would suggest that other factors in addition to the hydrogen bonds preorganize **5** for parallel-sheet formation. Other secondary structures (helices[18] and antiparallel sheets[3b,9d]) have been detected among short β-peptides in methanol.

Two sets of proton resonances were observed for **5** in methanol, in a 93:7 ratio. We attribute this doubling of resonances to slow rotation about the tertiary amide C–N bond.[19] The proton resonances of the major conformer were fully assigned using COSY,[20] TOCSY,[21] and NOESY[22] measurements. Relatively strong NOEs were observed between the δ protons of the proline group and both the α proton and the α-methyl group of the adjacent residue (Scheme 2). Analogous NOEs involving the α proton of the proline group were not observed. These data establish the rotational state about the tertiary amide bond of the major rotamer as the *Z* configuration (as depicted in Scheme 2). This rotational state is consistent with the desired hairpin conformation. Most importantly, three interstrand NOEs were observed (Scheme 2). Each of these NOEs is consistent with the hairpin conformation observed in the solid state (Table 1); no NOEs inconsistent with the parallel hairpin structure were observed.

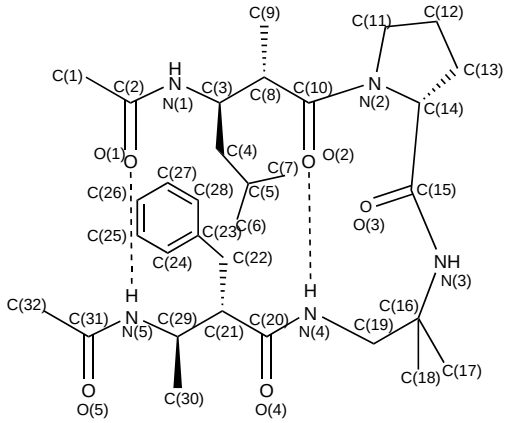


5

Scheme 2. NOEs observed for **5** in d_3-methanol that define the observed tertiary amide rotamer (dashed) and interstrand NOEs that establish a hairpin conformation in solution (solid).

 © 2003 Wiley-VCH Verlag GmbH & Co. KGaA, Weinheim

Table 1: Solid-state separations between protons of **5** for which NOEs are observed in solution (**5** or **6**)[a].



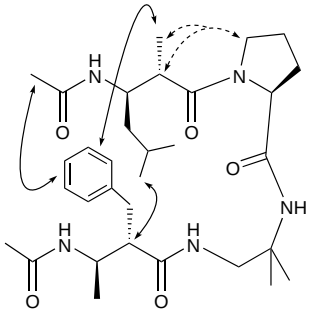
5

^{1}H atom	^{1}H atom	Separation [Å]
C(11)–H	C(8)–H	2.2
C(11)–H	C(9)–H	2.6
C(21)–H	C(9)–H	2.6
N(5)–H	C(6)–H	2.6
C(28)–H	C(9)–H	2.8
C(21)–H	C(6)–H	3.8
C(28)–H	C(1)–H	3.1

[a] For atoms that possess more than one proton, the smallest separation is reported. Protons on the phenyl ring (from C(24)–H to C(28)–H) could not be fully assigned. The separations reported involving the phenyl group are the shortest separations observed.

We and others have demonstrated that the α-peptide hairpin structure is dramatically influenced by the stereochemistry of the reverse-turn segment.[23] D-Pro-Gly and D-Pro-DADME reverse-turn segments induce antiparallel or parallel hairpin conformations, respectively; however, the enantiomeric L-Pro-Gly and L-Pro-DADME segments disallow folding. The stereochemistry of reverse-turn segments exerts a more subtle influence on antiparallel hairpin structure among β-peptides.[9c] For example, both an (*R*)-nipecotic acid-(*S*)-nipecotic acid segment and the enantiomeric (*S*)-nipecotic acid-(*R*)-nipecotic acid segment promote hairpin structure, but the *S*/*R* segment results in a larger population of a minor rotamer relative to the *R*/*S* segment (22% versus 6%), for α,β-syn-dialkyl β-amino acid strand residues with the absolute configuration of those used in the present study. Inspection of conventional Corey–Pauling–Koltun (CPK) models suggests that the possible minor rotamers do not allow hairpin folding. Therefore, this difference in the rotamer ratio indicates that the *R*/*S* reverse turn is slightly more effective than the *S*/*R* turn at promoting antiparallel sheet interactions between these strand residues.

We examined **6**, a diastereomer of **5** containing an L-Pro-DADME linker, to ascertain the influence exerted by the prolyl stereocenter on parallel hairpin formation in β-peptides. Molecule **6** displayed a 74:26 rotamer ratio in d_3-methanol at 5 mM, a concentration at which no aggregation occurs (4 °C). The proton resonances of the major rotamer were fully assigned using two-dimensional NMR spectroscopy. Strong NOEs between the δ protons of the proline group (but not the α protons) and both the α proton and the α-methyl group of the adjacent residue established a *Z* configuration about the tertiary amide in the major rotamer, as shown in Scheme 3. Several interstrand NOEs were observed (Scheme 3), which suggests the presence of a significant population of the hairpin conformation, with parallel-sheet interactions between the β-amino acid residues. No NOEs inconsistent with the desired hairpin conformation were observed (Table 1).



6

Scheme 3. NOEs observed for **6** in d_3-methanol that define the observed tertiary amide rotamer (dashed) and interstrand NOEs that establish a hairpin conformation in solution (solid).

The main difference between the D-Pro-DADME- and L-Pro-DADME-containing parallel hairpins (**5** and **6**, respectively) is the larger population of a minor rotamer in **6** (26%) relative to **5** (7%). This difference suggests that the L-Pro-DADME reverse turn of **6** is slightly less compatible with parallel-sheet interactions between α,β-*syn*-dialkyl β-amino acid residues (of the absolute configuration used in our studies) than is the D-Pro-DADME turn of **5**, because CPK modeling indicates that parallel sheet interactions are not possible if the tertiary amide configuration is *E*.

It is interesting that β-peptide hairpins, whether parallel or antiparallel, are less strongly influenced by reverse-turn stereochemistry than their α-peptide counterparts. For α-peptides, reverse-turn stereochemistry is important because the twist of the turn segment must be compatible with the twist preferred by the strand segments. β-Peptide strands may exhibit a significantly less pronounced twist than their α-peptide counterparts,[24] and therefore the local twist of the reverse-turn segment may be less influential in β-peptide sheet than for α-peptide sheet. Our demonstration of minimal systems for creating parallel sheet among β-peptides will enable a complete characterization of the factors that control this secondary structure.

Received: January 14, 2003 [Z50932]

Keywords: foldamers · NMR spectroscopy · peptides · secondary structure · structure elucidation

 © 2003 Wiley-VCH Verlag GmbH & Co. KGaA, Weinheim

[1] a) S. H. Gellman, *Acc. Chem. Res.* **1998**, *31*, 173; b) D. J. Hill, M. J. Mio, R. B. Prince, T. S. Hughes, J. S. Moore, *Chem. Rev.* **2001**, *101*, 3893.

[2] a) D. Seebach, J. L. Matthews, *Chem. Commun.* **1997**, *21*, 2015; b) R. P. Cheng, S. H. Gellman, W. F. DeGrado, *Chem. Rev.* **2001**, *101*, 3219.

[3] Intermolecular parallel-sheet structure has previously been observed in the solid state for two three-residue β-peptides. One of these peptides has a high intrinsic preference for helix formation in solution, which highlights the fact that solid-state data fail to provide insight on the intrinsic folding propensity of solvated molecules. See a) D. Seebach, M. Overhand, F. N. M. Kuhnle, B. Martinoni, L. Oberer, U. Hommel, H. Widmer, *Helv. Chim. Acta* **1996**, *79*, 913; b) D. Seebach, S. Abele, K. Gademann, B. Jaun, *Angew. Chem.* **1999**, *111*, 1700; *Angew. Chem. Int. Ed.* **1999**, *38*, 1595.

[4] a) S. H. Gellman, *Curr. Opin. Chem. Biol.* **1998**, *2*, 717; b) L. Serrano, *Adv. Protein Chem.* **2000**, *53*, 49; c) M. S. Searle, *J. Chem. Soc. Perkin Trans. 2* **2001**, 1011.

[5] a) J. M. Langenhan, J. D. Fisk, S. H. Gellman, *Org. Lett.* **2001**, *3*, 2559; b) D. S. Kemp, B. R. Bowen, *Tetrahedron Lett.* **1988**, *29*, 5081; c) J. S. Nowick, *Acc. Chem. Res.* **1999**, *32*, 287; d) J. S. Nowick, D. M. Chung, K. Maitra, S. Maitra, K. D. Stigers, Y. Sun, *J. Am. Chem. Soc.* **2000**, *122*, 7654; correction: J. S. Nowick, D. M. Chung, K. Maitra, S. Maitra, K. D. Stigers, Y. Sun, *J. Am. Chem. Soc.* **2001**, *123*, 1545; e) J. S. Nowick, J. M. Cary, J. H. Tsai, *J. Am. Chem. Soc.* **2001**, *123*, 5176; f) J. S. Nowick, E. M. Smith, J. W. Ziller, A. J. Shaka, *Tetrahedron* **2002**, *58*, 727; g) J. S. Nowick, K. S. Lam, T. V. Khasanova, W. E. Kemnitzer, S. Maitra, H. T. Mee, R. Lui, *J. Am. Chem. Soc.* **2002**, *124*, 4972.

[6] a) J. P. Schneider, J. W. Kelly, *Chem. Rev.* **1995**, *95*, 2169; b) D. Ranganathan, V. Haridas, S. Kurur, A. Thomas, K. P. Madhusudanan, R. Nagaraj, A. C. Kunwar, A. V. S. Sarma, I. L. Karle, *J. Am. Chem. Soc.* **1998**, *120*, 8448; c) I. G. Jones, W. Jones, M. North, *J. Org. Chem.* **1998**, *63*, 1505; d) R. R. Gardner, G.-B. Liang, S. H. Gellman, *J. Am. Chem. Soc.* **1999**, *121*, 1806; e) L. Belvisi, C. Gennari, A. Madder, A. Mielgo, D. Potenza, C. Scolastico, *Eur. J. Org. Chem.* **2000**, 695; f) B. Aguilera, G. Siegal, H. S. Overkleeft, N. J. Meeuwenoord, F. P. J. T. Rutjes, J. C. M. van Hest, H. E. Schoemaker, G. A. van der Marel, J. H. van Boom, M. Overhand, *Eur. J. Org. Chem.* **2001**, 1541.

[7] a) S. Hanessian, H. Yang, *Tetrahedron Lett.* **1997**, *38*, 3155; b) B. R. Huck, J. D. Fisk, S. H. Gellman, *Org. Lett.* **2000**, *2*, 2607; c) I. L. Karle, H. N. Gopi, P. Balaram, *Proc. Natl. Acad. Sci. USA* **2001**, *98*, 3716; d) H. N. Gopi, R. S. Roy, S. R. Raghothama, I. L. Karle, P. Balaram, *Helv. Chim. Acta* **2002**, *85*, 3313; e) I. L. Karle, H. N. Gopi, P. Balaram, *Proc. Natl. Acad. Sci. USA* **2002**, *99*, 5160.

[8] C. D. Tatko, M. L. Waters, *J. Am. Chem. Soc.* **2002**, *124*, 9372.

[9] a) S. Krauthauser, L. A. Christianson, D. R. Powell, S. H. Gellman, *J. Am. Chem. Soc.* **1997**, *119*, 11719; b) Y. J. Chung, L. A. Christianson, H. E. Stanger, D. R. Powell, S. H. Gellman, *J. Am. Chem. Soc.* **1998**, *120*, 10555; c) Y. J. Chung, B. R. Huck, L. A. Christianson, H. E. Stanger, S. Krauthauser, D. R. Powell, S. H. Gellman, *J. Am. Chem. Soc.* **2000**, *122*, 3995; d) X. Daura, K. Gademann, H. Schafer, B. Jaun, D. Seebach, W. F. van Gunsteren, *J. Am. Chem. Soc.* **2001**, *123*, 2393.

[10] a) D. S. Kemp, D. E. Blanchard, C. C. Muendel in *Peptides—Chemistry and Biology* (Eds.: J. Smith, J. River), ESCOM, Leiden, **1992**, p. 319; b) G. Wagner, M. Feigel, *Tetrahedron* **1993**, *49*, 10831; c) J. S. Nowick, S. Insaf, *J. Am. Chem. Soc.* **1997**, *119*, 10903; d) M. L. Skar, J. S. Svendsen, *Tetrahedron* **1997**, *53*, 17425; e) P. Chitnumsub, W. R. Fiori, H. A. Lashuel, H. Diaz, J. W. Kelly, *Bioorg. Med. Chem.* **1999**, *7*, 39; f) J. D. Fisk, S. H. Gellman, *J. Am. Chem. Soc.* **2001**, *123*, 343.

[11] J. D. Fisk, D. R. Powell, S. H. Gellman, *J. Am. Chem. Soc.* **2000**, *122*, 5443.

[12] M. G. Woll, J. R. Lai, I. A. Guzei, S. J. C. Taylor, M. E. B. Smith, S. H. Gellman, *J. Am. Chem. Soc.* **2001**, *123*, 11077.

[13] Y.-L. Zhao, Y.-D. Wu, *J. Am. Chem. Soc.* **2002**, *124*, 1570.

[14] a) C. W. Jefford, J. McNulty, *Helv. Chim. Acta* **1994**, *77*, 2142; b) C. W. Jefford, J. Wang, *Tetrahedron Lett.* **1993**, *34*, 1111.

[15] D. Seebach, S. Abele, K. Gademann, G. Guichard, T. Hintermann, B. Jaun, J. L. Matthews, J. V. Schreiber, *Helv. Chim. Acta* **1998**, *81*, 932.

[16] S. G. Davies, O. Ichihara, I. A. S. Walters, *J. Chem. Soc. Perkin Trans. 1* **1994**, 1141.

[17] Crystal data for $C_{32}H_{51}N_5O_5{\cdot}CHCl_3$: crystal size $0.43\times0.32\times0.26\,mm^3$, orthorhombic, $P2_12_12_1$, $a=9.1688(13)$, $b=11.3311(15)$, $c=36.444(5)$ Å, $V=3786.3(9)$ Å^3, $\rho_{calcd}=1.237\,Mg\,m^{-3}$, $2\theta_{max}=53.0°$, $Mo_{K\alpha}$ radiation ($\lambda=0.71073$ Å), ω scans, $T=100(1)$ K, 30860 independent and 7713 unique reflections. The data were corrected for Lorentz and polarization effects; the empirical absorption correction was performed with SADABS V2.03 (Bruker-AXS, 2001), $\mu=0.286\,mm^{-1}$, Tmax/min$^{-1}=0.93/0.89$. The structure was solved and refined usimg SHELXTL V6.10 (Bruker-AXS, 2000). All non-hydrogen atoms except C(15) and C(23) were refined with anisotropic displacement coefficients. All hydrogen atoms were included in the structure factor calculation at idealized positions and were allowed to ride on the neighboring atoms with relative isotropic displacement coefficients. The C(23) phenyl ring was refined with an idealized geometry. There is also one molecule of solvate chloroform in the asymmetric unit. The final least-squares refinement of 390 parameters against 7713 data (with 264 constraints) resulted in residuals R (based on F^2 for $I\geq2\sigma$) and wR (based on F^2 for all data) of 0.1111 and 0.2936, respectively. The slightly high R value results from the necessity of recording data from a weakly diffracting crystal. The final difference Fourier map was featureless. CCDC-200849 contains the supplementary crystallographic data for this paper. These data can be obtained free of charge via www.ccdc.cam.ac.uk/conts/retrieving.html (or from the Cambridge Crystallographic Data Centre, 12, Union Road, Cambridge CB2 1EZ, UK; fax: (+44) 1223-336-033; or deposit@ccdc.cam.ac.uk).

[18] a) D. Seebach, M. Overhand, F. N. M. Kuhnle, B. Martinoni, L. Oberer, U. Hommel, H. Widmer, *Helv. Chim. Acta* **1996**, *79*, 913; b) D. H. Appella, L. A. Christianson, I. L. Karle, D. R. Powell, S. H. Gellman, *J. Am. Chem. Soc.* **1996**, *118*, 13071; c) D. H. Appella, L. A. Christianson, D. A. Klein, D. R. Powell, X. L. Huang, J. J. Barchi, S. H. Gellman, *Nature* **1997**, *387*, 381.

[19] The difference in resonance ratios observed in *d*-chloroform versus d_3-methanol confirmed that resonance doubling is attributable to rotamers.

[20] W. P. Aue, E. Bartholdi, R. R. Ernst, *J. Chem. Phys.* **1976**, *64*, 2229.

[21] A. Bax, D. G. Davis, *J. Magn. Reson.* **1985**, *65*, 355.

[22] S. Macura, R. R. Ernst, *Mol. Phys.* **1980**, *41*, 95.

[23] a) T. S. Haque, J. C. Little, S. H. Gellman, *J. Am. Chem. Soc.* **1994**, *116*, 4105; b) S. K. Awasthi, S. Raghothama, P. Balaram, *Biochem. Biophys. Res. Commun.* **1995**, *216*, 375; c) I. L. Karle, S. K. Awasthi, P. Balaram, *Proc. Natl. Acad. Sci. USA* **1996**, *93*, 8189; d) T. S. Haque, J. C. Little, S. H. Gellman, *J. Am. Chem. Soc.* **1996**, *118*, 6975; e) T. S. Haque, S. H. Gellman, *J. Am. Chem. Soc.* **1997**, *119*, 2303; f) H. E. Stanger, S. H. Gellman, *J. Am. Chem. Soc.* **1998**, *120*, 4236; g) S. R. Raghothama, S. K. Awasthi, P. Balaram, *J. Chem. Soc. Perkin Trans. 2* **1998**, 137.

[24] J.-Q. Lin, S.-W. Luo, Y.-D. Wu, *J. Comput. Chem.* **2002**, *23*, 1551.

 © 2003 Wiley-VCH Verlag GmbH & Co. KGaA, Weinheim

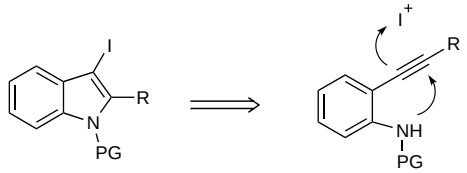
Iodoindole Synthesis

IPy_2BF_4-Promoted Intramolecular Addition of Masked and Unmasked Anilines to Alkynes: Direct Assembly of 3-Iodoindole Cores**

José Barluenga, Mónica Trincado, Eduardo Rubio, and José M. González*

Recently, organometallic transformations have been pursued with renewed interest to approach the elusive addition reaction of the N–H bond across alkynes.[1] As a cleaner alternative to the use of metal-containing reagents and catalysts we have developed useful reactions for C–C bond formation and cleavage, based on the iodinating reagent bis(pyridine)iodonium(I) tetrafluoroborate (IPy_2BF_4).[2] Herein, we present a powerful intramolecular addition of aniline and of several of its N-derivatives to alkynes, which relies on a simple iodination process. This new reaction entails a novel approach, and results in a general and valuable entry to the biological and synthetically relevant indole core.[3,4]

We have previously established a robust iodination of anilines that leads to the synthesis of substituted indoles via CuI-mediated cyclization of the corresponding *o*-((trimethylsilyl)ethynyl)aniline derivatives.[5] Certainly, new processes that selectively place additional functionality at the time of assembling the indole core are highly desirable.[6] Now, we illustrate a direct and clean entry to valuable 2-substituted-3-iodoindoles from readily available precursors. Thus, N-protected *o*-(alkynyl)anilines **1** furnish N-protected 3-iodoindoles **2** upon reaction with IPy_2BF_4,[2] the iodinating agent of choice to promote this process[7] (Scheme 1).

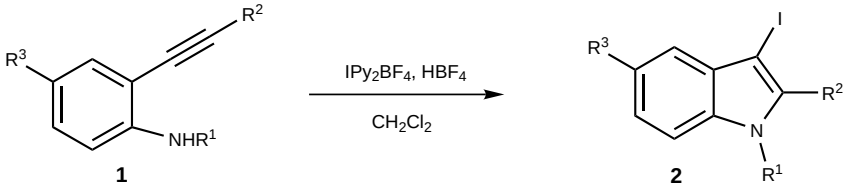


2 **1**

Scheme 1. 3-Iodoindole as a target from the iodocyclization of 2-alkynylaniline derivatives. PG = protecting group.

This C–N bond-formation reaction, which requires only a simple activation of the iodinating agent (namely, the addition of HBF_4 (1 equiv) to the reaction media), results in a versatile entry into 3-iodo-functionalised indoles (Table 1).[8] *N*-Boc derivatives gave satisfactory results when R^2 was an aryl or heteroaryl substituent (entries 1, 2, and 5).[9] However, when R^2 was an alkyl or 1-alkenyl group (entries 6, 7, and 10), the desired cyclization was very poor. Alternatively, for these functionalities, the related methanesulfonate derivative furnished indoles in moderate-to-good yield (entries 8, 9, and 11).

Table 1: Synthesis of indoles **2** from *o*-alkynyl aniline derivatives **1**, promoted by IPy_2BF_4.[a,b]



1 **2**

Entry	**1**	R^1	R^2	R^3	*t* [h][c]	*T* [°C]	**2**	Yield [%][d]
1	**1a**	CO_2tBu	Ph	H	15	−60	**2a**	68
2	**1b**	CO_2tBu	Ph	Me	8	−60	**2b**	76
3	**1c**	CO_2Me	Ph	H	24	−60	**2c**	53[e]
4	**1d**	*p*-$MeC_6H_4SO_2$	Ph	H	36	−60	**2d**	87
5	**1e**	CO_2tBu	3-thienyl	H	12	−20	**2e**	71
6	**1f**	CO_2tBu	1-cyclohexenyl	H	24	−60	**2f**	17[f]
7	**1g**	CO_2tBu	1-cyclopentenyl	H	15	−20	**2g**	10[f]
8	**1h**	$MeSO_2$	1-cyclopentenyl	H	15	−60	**2h**	61
9	**1i**	$MeSO_2$	Bn	H	15	−20	**2i**	54
10	**1j**	CO_2tBu	Bu	H	15	−20	**2g**	10[e]
11	**1k**	$MeSO_2$	Bu	H	24	−60	**2k**	84
12	**1l**	$MeSO_2$	Ph	H	48	−40	**2l**	74

[a] Indoles **2** were characterized by NMR spectroscopy, mass spectrometry, and gave analytical and/or HRMS data in agreement with the given structure. [b] IPy_2BF_4 (1.1 equiv), HBF_4 (1 equiv). [c] Determined as a function of the disappearance of **1**. [d] Based on the isolated indole **2**. [e] A cyclic urethane derivative was formed and isolated from the crude reaction mixture. [f] An allene structure was formed as major reaction product.

The feasibility of accomplishing a clean and efficient biscyclization process was satisfactorily tested with model compounds **3a** and **3b**. Upon iodination, **3a** provided a facile route to an interesting 1,4-phenyl-linked bisindole **4a**, as depicted in Scheme 2.

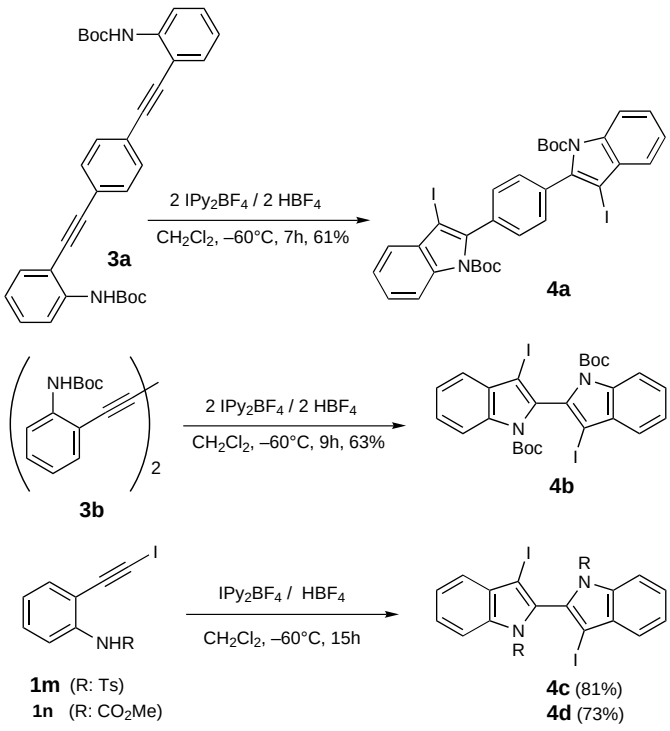
The butadiyne **3b**, readily accessible from the parent terminal alkyne, offers an attractive route to iodinated 2,2′-bisindolyl scaffolds **4b**, which have great potential in the preparation of naturally occurring bioactive compounds of

[*] Prof. Dr. J. Barluenga, M. Trincado, Dr. E. Rubio, Dr. J. M. González
Instituto Universitario de Química Organometálica "Enrique Moles"
Unidad Asociada al C.S.I.C.
Universidad de Oviedo, 33071 Oviedo (Spain)
Fax: (+34) 98-510-3450
E-mail: barluenga@sauron.quimica.uniovi.es

[**] This research was partially supported by the Principality of Asturias (PR-01-GE-9) and the Spanish DGI (MCT-01-BQU-3853). M.T. thanks Spanish M.E.C. for a FPU-fellowship.

Supporting information for this article is available on the WWW under http://www.angewandte.org or from the author.

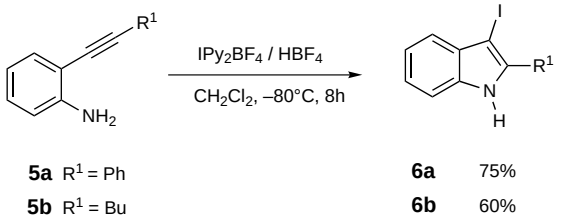
 © 2003 Wiley-VCH Verlag GmbH & Co. KGaA, Weinheim DOI: 10.1002/anie.200351303



Scheme 2. Biscyclization reactions. Boc = 1-butyloxycarbonyl; Ts = tosyl.

the indolocarbazole family, such as rebeccamycin.[10] With regard to these important building blocks, we have found that simple 2-iodoalkynylanilines **1m** and **1n** smoothly afford bisindole cores **4c** and **4d**. This remarkable result opens a short and valuable synthetic entry to complex indole frameworks.

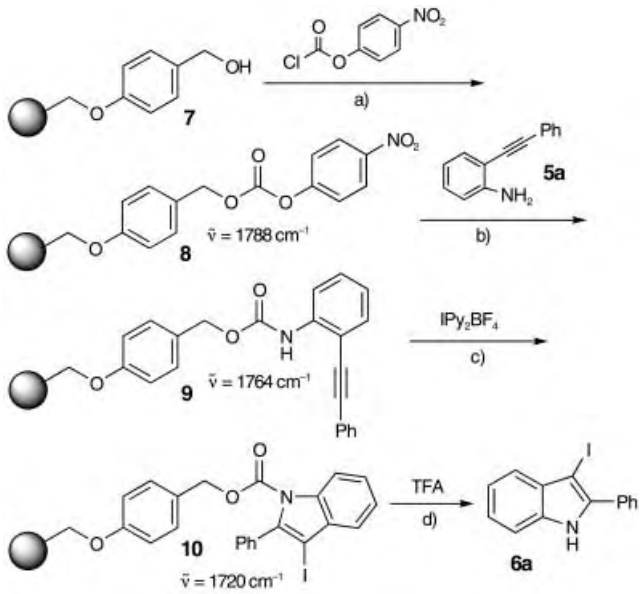
Protection of the N–H bond allows for efficient synthesis and handling of the target indoles. However, as depicted in Scheme 3, some unprotected anilines **5** were also efficient partners in this type of cyclization, which leads to the



Scheme 3. Cyclization of anilines; IPy_2BF_4 (1.1 equiv), HBF_4 (1 equiv).

corresponding free indoles.[11,12] To the best of our knowledge, these reactions represent the first examples of the addition of protected and unprotected anilines to internal alkynes, facilitated by a simple iodination reaction.

The solution chemistry reported above might be an interesting alternative pathway towards the first direct use of the key 3-iodoindole skeleton on a solid support. Thus, the binding of a carbamate group to the resin provides a convenient alternative for accomplishing the desired solid-



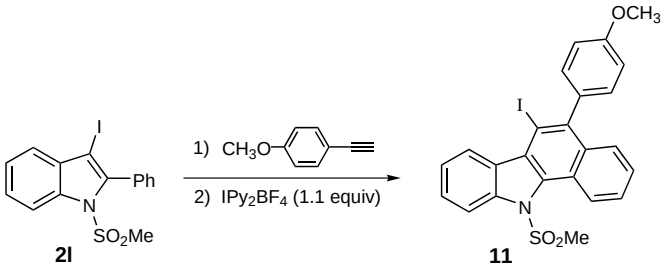
Scheme 4. a) Py, CH_2Cl_2, RT, 12 h; b) *N*,*N*-diisopropylethylamine (DIEA), HOBt·H_2O, DMF, CH_2Cl_2, 15 h; c) IPy_2BF_4 (2.2 equiv), HBF_4 (2.2 equiv), CH_2Cl_2, −20 °C, 24 h; d) trifluoroacetic acid (TFA)/CH_2Cl_2 (20 %), 1 h, RT. (31 % overall yield for four reaction steps).

phase indole synthesis (Scheme 4).[13] The approach of binding the resin to the moiety responsible for the N–C cyclization step has rarely been reported for the preparation of indoles.[14] A *p*-nitrophenyl-carbonate-modified Wang resin was used to prepare the desired carbamates from *o*-alkynylaniline.[15]

This system offers the first example of the solid-phase synthesis of an indole, promoted by a iodination process. As the versatile iodine functionality can be transformed on the resin using organometallic chemistry, this direct assembly of 3-iodoindole offers additional synthetic potential.[16]

Interestingly, this strategy of indole skeleton preparation yields iodinated compounds upon the cyclization step. Thus, it provides a unique entry to further build-related heterocyclic cores using the same reaction sequence. For instance, by following this approach, compound **2l** can be rapidly transformed into carbazole derivative **11** in two steps (Scheme 5).[17]

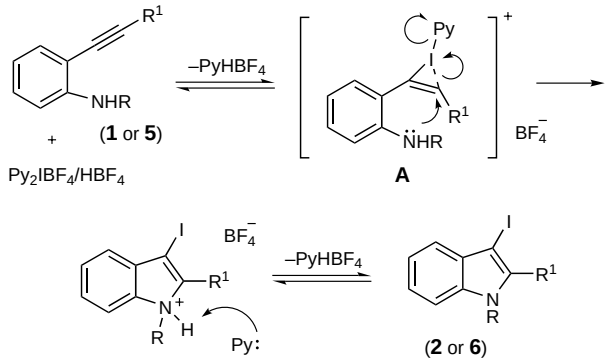
A tentative mechanistic interpretation to explain the formation of the observed indoles might reasonably assume a reaction path that implies an initial interaction of electro-



Scheme 5. Conversion of indole to carbazole skeleton. 1) $[PdCl_2(PPh_3)_2]$ (10 mol %), CuI (20 mol %), Et_2NH, RT, 15 h, 47 %; 2) HBF_4 (1 equiv), CH_2Cl_2, −80 °C, 15 h, 17 %.

 © 2003 Wiley-VCH Verlag GmbH & Co. KGaA, Weinheim

philic iodine with the alkynyl residue, to give the intermediate **A** (Scheme 6). Subsequent nucleophilic attack of nitrogen would lead to ring-closure. Only one equivalent of acid was used to activate the reagent in these reactions, therefore the second pyridine molecule might help to remove a proton from



Scheme 6. Proposed reaction mechanism.

the nitrogen atom, and result in the observed indole species.

In summary, both solution- and solid-phase strategies have been developed that result in an addition reaction of nitrogen to alkynes, which opens clean and synthetically competitive alternatives to the already established use of metal complexes. The reaction has been applied to the challenging field of the construction of the biologically relevant indole frame, where it proves to be the method of choice. Further studies on the scope of this method, and to gain insight into the unconventional formal cyclization–dimerization of 2-iodoalkynylanilines are in progress.

Experimental Section

All reactions were carried out under a positive pressure of nitrogen. Synthesis of **2a**: IPy_2BF_4 (0.41 g, 1.1 mmol, 1.1 equiv) was dissolved in dry CH_2Cl_2 (10 mL) and stirred for 5 min at room temperature. The solution was cooled to −60 °C, and HBF_4 (137 μL, 54% solution in Et_2O, 1.0 mmol, 1.0 equiv) was added. After 10 min, **1a** (293 mg, 1 mmol, 1 equiv) was added, and the solution was stirred (15 h) until the complete disappearance of **1a** was revealed by thin-layer chromatography (TLC). The reaction mixture was poured into 100 g of crushed ice and vigorously stirred, and then allowed to warm to room temperature. The organic layer was washed with a 5% aqueous solution of $Na_2S_2O_3$ (50 mL), dried over sodium sulfate, and then concentrated. The product was purified by column chromatography (silica gel, hexane/EtOAc 20:1) to give 285 mg of compound **2a**, as a white solid (mp 67–69 °C); $R_f = 0.71$ (hexane/EtOAc 3:1); ^{1}H NMR (300 MHz, $CDCl_3$): $\delta = 8.21$ (d, $J = 2$ Hz, 1H), 7.51–7.33 (m, 8H), 1.23 ppm (s, 9H); ^{13}C NMR (75 MHz, $CDCl_3$): $\delta = 149.2$ (s), 130.3 (s), 136.5 (s), 134.9 (s), 130.1 (s), 129.9 (d), 128.1 (d), 127.8 (d), 125.5 (d), 123.5 (d), 121.7 (d), 115.2 (d), 83.7 (s), 72.3 (s), 27.3 ppm (q); IR: ν_{max} (KBr): $\tilde{\nu}$1723 cm^{-1}; MS (70 eV, EI): m/z (%) = 419 (M^+, 59), 363 (100), 320 (49), 237 (47). Elemental analysis (%) calcd for $C_{19}H_{18}INO_2$: C 54.43, H 4.33, N 3.34; found: C 54.42, H 4.30, N 3.35.

Experimental procedures, spectral and analytical data for indoles **2**, **4**, **6**,and carbazole **11**, and solid-phase transformations are given in the Supporting Information.

Received: February 28, 2003 [Z51303]

Keywords: alkynes · cyclization · electrophilic addition · halogenation · nitrogen heterocycles

[1] For a recent account: a) M. Beller, C. Breindl, M. Eichberger, C. G. Hartung, J. Seayad, O. R. Thiel, A. Tillack, H. Trauthwein, *Synlett* **2002**, 1579–1594; For a selection of recent examples, see for instance: b) M. Tokunaga, M. Eckert, Y. Wakatsuki, *Angew. Chem.* **1999**, *111*, 3416–3419; *Angew. Chem. Int. Ed.* **1999**, *38*, 3222–3225; c) E. Haak, I. Bytschov, S. Doye, *Angew. Chem.* **1999**, *111*, 3584–3586; *Angew. Chem. Int. Ed.* **1999**, *38*, 3389–3391; d) J. S. Johnson, R. G. Bergman, *J. Am. Chem. Soc.* **2001**, *123*, 2923–2924; e) A. Tillack, I. García Castro, C. G. Hartung, M. Beller, *Angew. Chem.* **2002**, *114*, 2646–2648; *Angew. Chem. Int. Ed.* **2002**, *41*, 2541–2543; f) T. Shimada, Y. Yamamoto, *J. Am. Chem. Soc.* **2002**, *124*, 12670–12671.

[2] a) J. Barluenga, J. M. González, P. J. Campos, G. Asensio, *Angew. Chem.* **1988**, *100*, 1604–1605; *Angew. Chem. Int. Ed. Engl.* **1988**, *27*, 1546–1547; b) J. Barluenga, M. A. Rodríguez, J. M. González, P. J. Campos, *Tetrahedron Lett.* **1990**, *31*, 4207–4210; c) J. Barluenga, J. M. González, I. Llorente, P. J. Campos, *Angew. Chem.* **1993**, *105*, 928–929; *Angew. Chem. Int. Ed. Engl.* **1993**, *32*, 893–894; d) J. Barluenga, I. Llorente, L. J. Alvarez-García, J. M. González, P. J. Campos, M. R. Díaz, S. García-Granda, *J. Am. Chem. Soc.* **1997**, *119*, 6933–6934; e) J. Barluenga, G. P. Romanelli, L. J. Alvarez-García, I. Llorente, J. M. González, E. García-Rodríguez, S. García-Granda, *Angew. Chem.* **1998**, *110*, 3332–3334; *Angew. Chem. Int. Ed.* **1998**, *37*, 3136–3139; f) J. Barluenga, F. González-Bobes, S. R. Ananthoju, M. A. García-Martín, J. M. González, *Angew. Chem.* **2001**, *113*, 3491–3494; *Angew. Chem. Int. Ed.* **2001**, *40*, 3389–3392.

[3] Reviews on indole systems: a) R. J. Sundberg, *Indoles*, Academic Press, London, **1996**; b) G. W. Gribble, *J. Chem. Soc. Perkin Trans. 1* **2000**, 1045–1075; Palladium-mediated synthesis of indoles: c) J. J. Li, G. W. Gribble, *Palladium in Heterocyclic Chemistry*, Pergamon, Oxford, **2000**, pp. 73–181; d) R. C. Larock, *J. Organomet. Chem.* **1999**, *576*, 111–124; e) G. Battistuzzi, S. Cacchi, G. Fabrizi, *Eur. J. Org. Chem.* **2002**, 2671–2681.

[4] For recent indole preparations, see for instance: a) M. Beller, C. Breindl, T. H. Riermeier, A. Tillack, *J. Org. Chem.* **2001**, *66*,1403–1412; b) F. J. Fañanás, A. Granados, R. Sanz, J. M. Ignacio, J. Barluenga, *Chem. Eur. J.* **2001**, *7*, 2896–2907; c) A. Penoni, J. Volkmann, K. M. Nicholas, *Org. Lett.* **2002**, *4*, 699–701; d) D. M. Lindsay, W. Dohle, A. E. Jensen, F. Kopp, P. Knochel, *Org. Lett.* **2002**, *4*, 1819–1822; e) Y. Nakamura, T. Ukita, *Org. Lett.* **2002**, *4*, 2317–2320; f) C. Cao, Y. Shi, A. L. Odom, *Org. Lett.* **2002**, *4*, 2853–2856; g) H. Kusama, J. Takaya, N. Iwasawa, *J. Am. Chem. Soc.* **2002**, *124*, 11592–11593; i) S. Kamijo, Y. Yamamoto, *Angew. Chem.* **2002**, *114,* 3364–3367; *Angew. Chem. Int. Ed.* **2002**, *41*, 3230–3233; j) S. Kamijo, Y. Yamamoto, *J. Am. Chem. Soc.* **2002**, *124*, 11940–11945.

[5] a) J. Ezquerra, C. Pedregal, C. Lamas, J. Barluenga, M. Pérez, M. A. García-Martín, J. M. González, *J. Org. Chem.* **1996**, *61*, 5804–5812; see also; b) D. R. Adams, M. A. J. Duncton, J. R. A. Roffey, J. Spencer, *Tetrahedron Lett.* **2002**, *43*, 7581–7583.

[6] a) K. Iritani, S. Matsubara, K. Utimoto, *Tetrahedron Lett.* **1988**, *29*, 1799–1802; b) R. C. Larock, E. K. Yum, *J. Am. Chem. Soc.* **1991**, *113*, 6689–6690; c) R. C. Larock, E. K. Yum, M. D. Refvik, *J. Org. Chem.* **1998**, *63*, 7652–7662; d) A. Arcadi, S. Cacchi, G. Fabrizi, F. Marinelli, *Synlett* **2000**, 647–649; e) G. Battistuzzi, S. Cacchi, G. Fabrizi, F. Marinelli, L. M. Parisi, *Org. Lett.* **2002**, *4*, 1355–1358.

[7] Homopropargylic *s*ulfonamides related to methyl glycinate have been nicely cyclized by reaction with iodine, see: a) D. W. Knight, A. L. Redfern, J. Gilmore, *Chem. Commun.* **1998**, 2207–2208. However, under their reported conditions, our attempts to

 © 2003 Wiley-VCH Verlag GmbH & Co. KGaA, Weinheim

prepare **2k** from **1k** lead to a complex mixture of compounds, as revealed by both TLC monitoring of the reaction progress and NMR analysis of the crude products. We also checked the reaction at −60 °C; in this case, only the starting material was recovered. A sharp distinction was noticed when using either IPy_2BF_4 or I_2. A strong substrate dependence was previously observed in the iodine-promoted cyclization of homopropargyl alcohols; b) D. W. Knight, A. L. Redfern, J. Gilmore, *J. Chem. Soc. Perkin Trans. 1* **2002**, 622 – 628.

[8] a) G. W. Gribble, M. G. Saulnier, *J. Org. Chem.* **1983**, *48*, 607 – 609; b) Y. Kondo, A. Yoshida, S. Sato, T. Sakamoto, *Heterocycles* **1996**, *42*, 105 – 108; c) Y. Liu, G. W. Gribble, *Tetrahedron Lett.* **2000**, *41*, 8717 – 8721; d) Y. Liu, G. W. Gribble *Tetrahedron Lett.* **2001**, *42*, 2949 – 2951; e) H. Zhang, R. C. Larock, *J. Org. Chem.* **2002**, *67*, 7048 – 7056; f) H. Zhang, R. C. Larock, *J. Org. Chem.* **2002**, *67*, 9318 – 9330.

[9] For interesting bioactivity profiles of 2-arylindoles, see for instance: a) D. Shaw, G. C. Chicchi, J. M. Elliot, M. Kurtz, D. Morrison, M. P. Ridgil, N. Szeto, A. P. Watt, A. R. Williams, C. J. Swain, *Bioorg. Med. Chem. Lett.* **2001**, *11*, 3031 – 3034; b) C. A. Willoughby, S. M. Hutchins, K. G. Rosauer, M. J. Dhar, K. T. Chapman, G. G. Chicchi, S. Sadowski, D. H. Weinberg, S. Patel, L. Malkowitz, J. Di Salvo, S. G. Pachollok, K. Cheng, *Bioorg. Med. Chem. Lett.* **2002**, *12*, 93 – 96.

[10] For recent approaches to bioactive indolocarbazole alkaloids, see for instance: C. A. Merlic, Y. You, D. M. McInnes, A. L. Zechman, M. M. Miller, Q. Deng, *Tetrahedron*, **2001**, *57*, 5199 – 5212, and references therein.

[11] In this case, the reaction is more substrate dependent. Further studies are in progress to investigate alternative reaction paths.

[12] 2-Alkynylphenols undergo a similar reaction. Thus, *o*-(2-phenylethynyl)phenol gave 3-iodo-2-phenylbenzo[*b*]furan (78 % yield) after reaction with Ipy_2BF_4/HBF_4 for 6 h at room temperature. Similarly, *o*-(2-butylethynyl)phenol yielded 2-butyl-3-iodobenzo[*b*]furan upon reaction for 8 h (70 % yield).

[13] For a recent review, see: a) S. Bräse, C. Gil, K. Knepper, *Bioorg. Med. Chem.* **2002**, *10*, 2415 – 2437.

[14] For solid-phase studies using a related indole binding site, see: a) A. L. Smith, G. I. Stevenson, C. J. Swain, J. L. Castro, *Tetrahedron Lett.* **1998**, *39*, 8317 – 8320; b) H.-C. Zhang, H. Ye, A. F. Moretto, K. K. Brumfield, B. C. Maryanoff, *Org. Lett.* **2000**, *2*, 89 – 92; c) T. Y. H. Wu, S. Ding, N. S. Gray, P. G. Schultz, *Org. Lett.* **2001**, *3*, 3827 – 3830.

[15] a) A. Dressman, L. A. Spangle, S. W. Kaldor, *Tetrahedron Lett.* **1996**, *37*, 937 – 940; b) W. Huang, R. M. Scarborough, *Tetrahedron Lett.* **1999**, *40*, 2665 – 2668.

[16] Representative sp^2–sp coupling reactions are detailed in the Supporting Information.

[17] For a review on carbazole alkaloids, see: H.-J. Knölker, K. R. Reddy, *Chem. Rev.* **2002**, *102*, 4303 – 4427;b) for recent synthesis of substituted carbazoles, see: B. Witulski, C. Alayrac, *Angew. Chem.* **2002**,*114*, 3415 – 3418; *Angew. Chem. Int. Ed.* **2002**, *41*, 3281 – 3284; c) R. B. Bedford, C. S. J. Cazin, *Chem. Commun.* **2002**, 2310 – 2311; d) P. N. M. Botman, M. Postma, J. Fraanje, K. Goubitz, H. Schenk, J. H. Van Maarseveen, H. Hiemstra, *Eur. J. Org. Chem.* **2002**, 1952 – 1955.

 © 2003 Wiley-VCH Verlag GmbH & Co. KGaA, Weinheim

Dual Catalysis

Aqueous Catalytic Pauson–Khand-Type Reactions of Enynes with Formaldehyde: Transfer Carbonylation Involving an Aqueous Decarbonylation and a Micellar Carbonylation**

Koji Fuji, Tsumoru Morimoto, Ken Tsutsumi, and Kiyomi Kakiuchi**

Homogeneous catalysis by transition metal complexes has provided numerous excellent tools for synthetic organic chemists.[1] In most methods, the use of a single catalyst results in a unique type of transformation. Reports have recently also appeared on the use of a combination of different catalytic processes in one phase to catalyze one overall transformation.[2] In terms of synthetic organic chemistry, these methods permit convenient, one-pot catalytic transformations. We have already reported some catalytic transfer carbonylation reactions that involve two cooperative catalytic processes, the decarbonylation of aldehydes accompanied by the carbonylation of other organic substrates.[3] These carbonylation reactions do not involve the direct use of carbon monoxide.[4] Our goal was to develop a novel dual-catalysis system, in which each process proceeds simultaneously in a different reaction field. Such a system, to our knowledge, has not been successfully developed to date.

To investigate this strategy, we chose a microscopically biphasic system in an aqueous medium: a micellar phase surrounded by an aqueous phase. The solubility properties of formaldehyde with respect to organic substrates stimulated us to explore a system that consisted of the decarbonylation of formaldehyde in the aqueous phase and carbonylation of an organic substrate in the micelle. We herein describe this approach for an aqueous catalytic Pauson–Khand-type reaction of enynes in the presence of formaldehyde as the source of carbon monoxide (Scheme 1).[5,6]

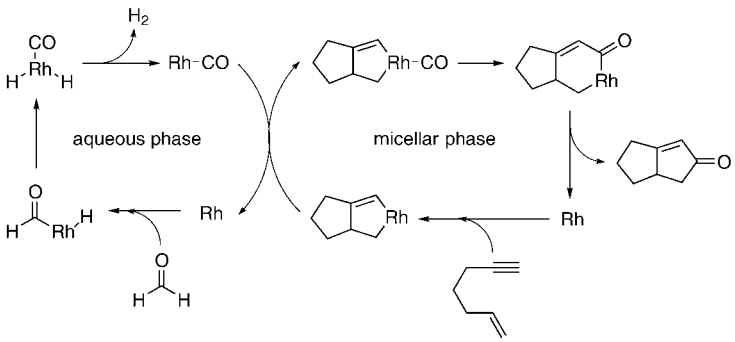
We first examined the reaction of enyne **1** with formaldehyde in water. The reaction of **1** with formaldehyde in the presence of SDS, a popular surfactant that is well-known for forming micelles, and a catalytic amount of $[RhCl(cod)]_2$/dppp in water at 100 °C afforded the desired carbonylated product **2** in 57% yield (Table 1, entry 1). Under conditions

[*] Dr. T. Morimoto, Prof. K. Kakiuchi, K. Fuji, Dr. K. Tsutsumi
Graduate School of Materials Science
Nara Institute of Science and Technology (NAIST)
Takayama, Ikoma, Nara 630-0192 (Japan)
Fax: (+81) 743-72-6089
E-mail: morimoto@ms.aist-nara.ac.jp
kakiuchi@ms.aist-nara.ac.jp

[**] This work was supported, in part, by a Sasagawa Scientific Research Grant from The Japan Science Society, and by a Pfizer Pharmaceuticals Inc. Award in Synthetic Organic Chemistry, Japan, through The Society of Synthetic Organic Chemistry, Japan, granted to T.M. We thank Ms. Yoshiko Nishikawa and Mr. Fumio Asanoma for assistance in obtaining HRMS and NMR spectra, respectively.

Supporting information for this article is available on the WWW under http://www.angewandte.org or from the author.

 DOI: 10.1002/anie.200351384 © 2003 Wiley-VCH Verlag GmbH & Co. KGaA, Weinheim

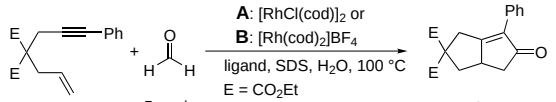


Scheme 1. Working hypothesis for aqueous transfer carbonylation.

reported previously,[3a] **2** was obtained in 53% yield along with unconverted **1** (14%) from a reaction for 24 h at 130°C with 10 equivalents of paraformaldehyde in xylene. The use of water as the solvent clearly resulted in an increase in reactivity, which is consistent with micelle formation in the reaction system. As is frequently observed for organic reactions in aqueous micellar systems, the encapsulation of reactants by a surfactant would lead to a higher effective concentration of reactants, thus resulting in acceleration of the reaction.[7] The use of excess formaldehyde (20 equiv) improved the yield of **2** to 82% (Table 1, entry 2), probably because of an increased amount of formaldehyde incorporated in the micelle.

When TPPTS, a water-soluble phosphane,[8] was used as a ligand instead of dppp, **1** was recovered in 82% yield with no detectable formation of **2** (Table 1, entry 3). The use of both dppp and TPPTS as ligands resulted in a dramatic increase in the yield of **2** (87%; Table 1, entry 4). Although reactions in which the more hydrophilic rhodium complex $[Rh(cod)_2]BF_4$ was used as the catalyst showed a similar trend as was found for $[RhCl(cod)]_2$, the yields of **2** were lower (Table 1, entries 5–7). The amount of SDS present also had an effect on the yield of **2** (Table 1, entries 8–12), which was obtained in nearly quantitative yield when 2 equivalents of SDS were used (Table 1, entry 12). Paraformaldehyde, a synthetic equivalent of formaldehyde, could also be utilized as a source of carbon monoxide in this aqueous system (Table 1, entry 13).

Table 1: Catalytic Pauson–Khand-type reaction of enyne **1** in the presence of formaldehyde in an aqueous medium.[a]



1 **2**

Entry	Cat.	Ligand (mol%)	SDS [equiv]	*t* [h]	Yield[b] [%]
1	**A**	dppp (10)	5.0	7	57
2[c]	**A**	dppp (10)	5.0	10	82 (17)
3	**A**	TPPTS (30)	5.0	6	0 (82)
4	**A**	dppp/TPPTS (10:10)	5.0	5	87
5	**B**	dppp (20)	5.0	10	44 (43)
6	**B**	TPPTS (30)	5.0	6	0 (65)
7	**B**	dppp/TPPTS (10:10)	5.0	7	65
8	**A**	dppp/TPPTS (10:10)	none	10	37 (47)
9	**A**	dppp/TPPTS (10:10)	0.1	10	59 (9)
10	**A**	dppp/TPPTS (10:10)	0.5	10	75 (4)
11	**A**	dppp/TPPTS (10:10)	1.0	10	88
12	**A**	dppp/TPPTS (10:10)	2.0	5	96
13[d]	**A**	dppp/TPPTS (10:10)	2.0	6	97

[a] Conditions: **1** (0.25 mmol), formaldehyde (37%; 0.1 mL, 1.25 mmol), H_2O (1.9 mL), catalyst **A** (5 mol%) or **B** (10 mol%), 100°C, N_2. [b] Yields of **2**. Values in parentheses are the yields of recovered **1**; in other cases, **1** was completely consumed. [c] Formaldehyde: 20 equiv. [d] Paraformaldehyde (5 equiv) was used instead of formaldehyde. cod = cyclooctadiene; dppp = 1,3-bis(diphenylphosphanyl)propane; SDS = sodium dodecylsulfate; TPPTS = triphenylphosphane-3,3′,3″-trisulfonic acid trisodium salt.

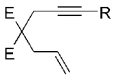
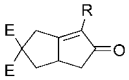
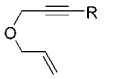
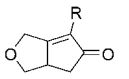
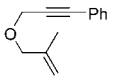
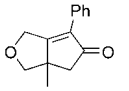
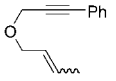
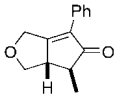
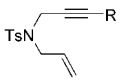
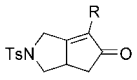
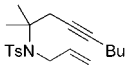
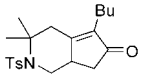
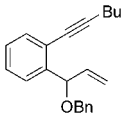
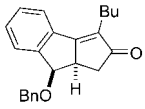
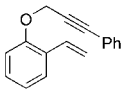
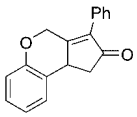
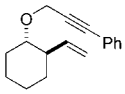
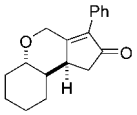
The high efficiency of this carbonylation system can not be rationalized simply by the high effective concentrations involved as a result of micelle formation. A plausible explanation for the dependence of the catalysis on the addition of TPPTS is that the decarbonylation occurs mainly in the aqueous phase when additional TPPTS is present,[9] and the actual carbonylation step takes place in the micelle. Evidently most of the formaldehyde exists in the aqueous phase because of its high solubility in water, whereas the enyne is incorporated into the micelle because of its hydrophobicity. The presence of both TPPTS and dppp would lead to the formation of two different types of rhodium(I) complexes: a water-soluble complex associated with TPPTS (hydrophilic), and a complex that is not associated with TPPTS (hydrophobic).[10] These factors would permit the dual catalytic cycles to each function more efficiently in the appropriate phase and thus lead to more efficient overall catalysis. Moreover, no reactants, including highly reactive species generated in each process, should be able to interfere with one another, thus permitting the catalysis to function more smoothly and with a higher degree of selectivity.

The present system is applicable to the carbonylation of a variety of enynes in excellent yields. Selected results are shown in Table 2. The use of analogues of **1**, in which a butyl or a methyl group replaces the phenyl group, also resulted in the formation of the carbonylated products in excellent yields (Table 2, entries 2 and 3). Reactions of substrates that contain a heteroatom such as oxygen or nitrogen in the tether between the alkene and the alkyne also afforded the corresponding bicyclic cyclopentenones (Table 2, entries 4–10, 12, and 13). Enynes with 1,1- and 1,2-disubstituted alkene portions were carbonylated smoothly (Table 2, entries 6 and 7), as were 1,7-enynes, which were converted into cyclopentenones fused to a six-membered ring (Table 2, entries 10, 12, and 13). When ring systems substituted at adjacent carbon centers with an alkene and an alkyne were used as substrates, the cyclocarbonylation proceeded efficiently and resulted in the formation of tricyclic cyclopentenones (Table 2, entries 11–13).

In summary, we have reported the development of an aqueous catalytic Pauson–Khand-type reaction of enynes in the presence of formaldehyde as a water-soluble source of carbon monoxide. The decarbonylation and the carbonylation processes are thought to take place independently in different phases of the reaction system, namely in the aqueous and micellar phases, respectively, which results in a more efficient catalytic carbonylation reaction. The use of the low-cost

 © 2003 Wiley-VCH Verlag GmbH & Co. KGaA, Weinheim

Table 2: Aqueous catalytic Pauson–Khand-type reactions of enynes with formaldehyde.[a]

Entry	Enyne	HCHO[b] [equiv]	*t* [h]	Product[c]	
1		5	5		96% (R = Ph)
2		5	8		84% (R = Bu)
3		10	5		89% (R = Me)
4[d]		100	2		87% (R = Ph)
5		20	5		81% (R = Bu)
6		10	4		94%
7[e]		10	5		94% (1.8:1)[f]
8		10	2		96% (R = Ph)
9		5	6		89% (R = Bu)
10		5	12		67%
11		20	6		91% (2.4:1)[f]
12		5	2		82%
13		5	4		93%[g]

[a] Conditions: enyne (0.25 mmol), $[RhCl(cod)]_2$ (0.0125 mmol), dppp (0.025 mmol), TPPTS (0.025 mmol), SDS (0.50 mmol), H_2O (1.9 mL), 100 °C, N_2. [b] Formaldehyde (37%) was used. [c] Yield of isolated product. [d] The reaction was carried out with formaldehyde (37%; 2.0 mL) as solvent and SDS (5.0 equiv) at 80 °C. [e] The enyne was used as an *E*/*Z* mixture (85:15). [f] Diastereomeric ratio was determined by GC. [g] Obtained as a single stereoisomer.

feedstock formaldehyde as the source of carbon monoxide gives rise to a more convenient Pauson–Khand-type reaction of enynes than the conventional reactions currently in use. This strategy has the potential to become a general protocol that could be used in a wide variety of carbonylation reactions. Further efforts are underway toward the elucidation of the mechanism of the dual catalysis, to improve our understanding of where the two processes occur and of the morphology of aggregation of the reagents. Applications to other carbonylation reactions are also under investigation.

Received: March 12, 2003 [Z51384]

Keywords: carbonylation · cyclization · enynes · homogeneous catalysis · Pauson–Khand reaction

[1] a) J. Tsuji, *Transition Metal Reagents and Catalysis: Innovations in Organic Synthesis*, Wiley, Chichester, **2000**; b) M. Beller, C. Bolm, *Transition Metals for Organic Synthesis: Building Blocks and Fine Chemicals*, Wiley-VCH, Weinheim, **1998**.

[2] For some recent examples, see: a) R. W. Barnhart, G. C. Bazan, T. Mourey, *J. Am. Chem. Soc.* **1998**, *120*, 1082; b) R. Grigg, V. Sridharan, M. York, *Tetrahedron Lett.* **1998**, *39*, 4139; c) C. Pellecchia, D. Pappalardp, G.-J. Gruter, *Macromolecules* **1999**, *32*, 4491; d) Z. J. A. Komon, X. Bu, G. C. Bazan, *J. Am. Chem. Soc.* **2000**, *122*, 1830; e) N. Jeong, S. D. Seo, *J. Am. Chem. Soc.* **2000**, *122*, 10220; f) P. A. Evans, J. E. Robinson, *J. Am. Chem. Soc.* **2001**, *123*, 4609; g) S. U. Son, K. H. Park, Y. K. Chung, *J. Am. Chem. Soc.* **2002**, *124*, 6838; h) K. H. Park, S. U. Son, Y. K. Chung, *Org. Lett.* **2002**, *4*, 4361; i) S. Ko, C. Lee, M.-G. Choi, Y. Na, S. Chang, *J. Org. Chem.* **2003**, *68*, 1607.

[3] a) T. Morimoto, K. Fuji, K. Tsutsumi, K. Kakiuchi, *J. Am. Chem. Soc.* **2002**, *124*, 3806; b) T. Morimoto, M. Fujioka, K. Fuji, K. Tsutsumi, K. Kakiuchi, *Chem. Lett.* **2003**, *32*, 154.

[4] For a rhodium-catalyzed Pauson–Khand-type reaction of enynes with cinnamaldehyde as the source of carbon monoxide in the absence of a solvent, see: a) T. Shibata, N. Toshida, K. Takagi, *Org. Lett.* **2002**, *4*, 1619; T. Shibata, N. Toshida, K. Takagi, *J. Org. Chem.* **2002**, *67*, 7446.

[5] For recent reviews of the Pauson–Khand-type reaction, see: a) Y. K. Chung, *Coord. Chem. Rev.* **1999**, *188*, 297; b) K. M. Brummond, J. L. Kent, *Tetrahedron* **2000**, *56*, 3263.

[6] For aqueous Pauson–Khand-type reactions of enynes with carbon monoxide, see: a) S. U. Son, S. I. Lee, Y. K. Chung, S.-W. Kim, T. Hyeon, *Org. Lett.* **2002**, *4*, 277; b) M. E. Krafft, J. A. Wright, L. V. R. Boñaga, *Tetrahedron Lett.* **2003**, *44*, 3417.

[7] a) S. Taşcioğlu, *Tetrahedron* **1996**, *52*, 11113; b) U. M. Lindstrom, *Chem. Rev.* **2002**, *102*, 2751, and references therein.

[8] For recent aqueous catalytic reactions using TPPTS as a ligand, see: a) M. C. K.-B. Djoman, A. N. Ajjou, *Tetrahedron Lett.* **2000**, *41*, 4845; b) C. Dupuis, K. Adiey, L. Charruault, V. Michelet, M. Savignac, J.-P. Genêt, *Tetrahedron Lett.* **2001**, *42*, 6523; c) V. Michelet, J.-C. Galland, L. Charruault, M. Savignac, J.-P. Genêt, *Org. Lett.* **2001**, *3*, 2065; d) L. W. Francisco, D. A. Moreno, J. D. Atwood, *Organometallics* **2001**, *20*, 4237; e) M. Lautens, A. Roy, K. Fukuoka, K. Fagnou, B. Martín-Mature, *J. Am. Chem. Soc.* **2001**, *123*, 5358; f) M. Lautens, M. Yoshida, *J. Org. Chem.* **2003**, *68*, 762.

[9] Even in the reaction in the presence of additional TPPTS, the decarbonylation probably does not proceed exclusively in the aqueous phase, because a hydrophobic combination of $[RhCl(cod)]_2$ and dppp catalyzed the carbonylation reaction in the absence of TPPTS (Table 1, entries 1 and 2).

[10] It has been reported that the use of both TPPTS and PPh_3 distributes the rhodium catalyst between the aqueous and the organic phases in the biphasic (toluene/water) hydroformylation of 1-octene: a) P. Kalck, M. Dessoudeix, S. Schwarz, *J. Mol. Catal. A* **1999**, *143*, 41; b) P. Kalck, M. Dessoudeix, *Coord. Chem. Rev.* **1999**, *190–192*, 1185.

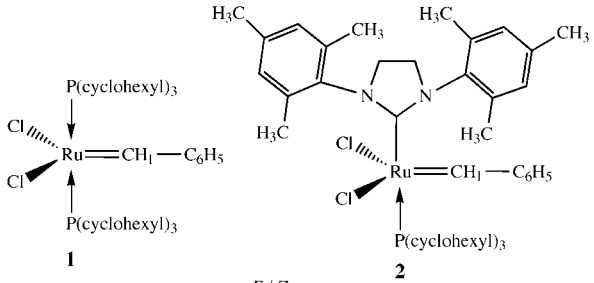
 © 2003 Wiley-VCH Verlag GmbH & Co. KGaA, Weinheim

Macrocycle Polymerization

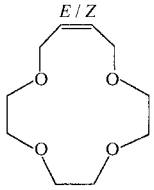
Entropically Driven Ring-Opening-Metathesis Polymerization of Macrocyclic Olefins with 21–84 Ring Atoms**

Philip Hodge and Stephen D. Kamau*

The ring-opening-metathesis polymerization (ROMP) of strained cyclic olefins has been studied extensively,[1,2] especially since Grubbs' catalyst **1**[3] and the more recently introduced "second-generation" Grubbs' catalyst **2**,[4] both of which are tolerant of many functional groups, became commercially available. The ROMP of strained cyclic olefins is mainly enthalpy-driven.

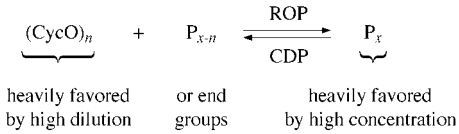


1 **2**



3

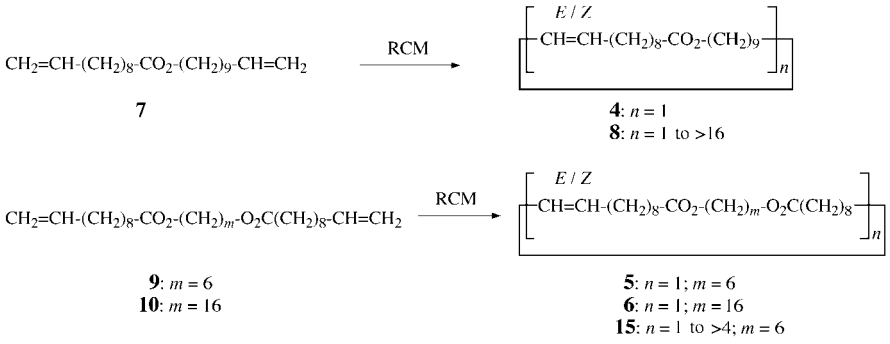
A relatively new type of ring-opening polymerization (ROP) exploits the well-known equilibria between cyclic oligomers and polymers[5–10] (Scheme 1). At high dilutions the equilibria lie heavily in favor of the cyclic oligomers, whereas at high concentrations they lie heavily in favor of the polymers. Thus, if one or more cyclic oligomers are taken neat as starting materials, and equilibrium is established, polymer synthesis results. The cyclic oligomers used as the feedstock are generally not strained, so the enthalpy change on polymerization is minimal. This type of polymerization is, therefore, mainly entropically driven, and so the process can be abbreviated ED-ROP. As a neat mixture the cyclic oligomers have relatively little translational entropy and the rings occupy limited conformations; conformational flexibility increases greatly upon conversion into polymers. Since ED-ROP is an equilibration process the polydispersity of the polymer is expected to have a value of 2.0. ED-ROP has been investigated for various types of macrocyclic oligomers,[11,12] but not for macrocyclic olefins.



Scheme 1. CycO = cyclic oligomer; P = polymer; CDP = cyclodepolymerization; "*x*" and "*n*" are degrees of polymerization.

Examples in which large, unstrained macrocycles (> 13 ring atoms) have been subjected to ROMP are rare,[2,13–15] and there only appear to be two examples in which the polymer has been formed in high yield, isolated, and characterized. The first was the ROMP of the 14-membered cyclic ether **3** in the presence of the catalyst **1**. This gave a polymer with $\bar{M}_n$ 65 900 ($\bar{M}_n$ = number-average molar mass).[2] The second example was the ROMP of ambrettolide, an unsaturated macrolide with 17 ring atoms.[13] A neat sample of this compound was polymerized in the presence of a catalyst prepared from tungsten hexachloride and tetramethyltin to give a polymer in 95% yield with $\bar{M}_n$ 95 000. Herein we show that when appropriate reaction conditions are used, unstrained macrocyclic olefins with up to 84, and possibly even more, ring atoms readily undergo entropically driven ROMP (ED-ROMP). Given that Grubbs and co-workers have recently reported an efficient method for the synthesis of very large macrocyclic olefins,[16] and that olefin-containing polymers are easily hydrogenated in the presence of decomposed metathesis catalysts,[17,18] ED-ROMP of large macrocyclic olefins is of more than theoretical interest.

In the present work the monomers **4**, **5**, and **6**, which have 21-, 28-, and 38-membered rings, respectively, were prepared



7

4: $n = 1$
8: $n = 1$ to >16

9: $m = 6$
10: $m = 16$

5: $n = 1$; $m = 6$
6: $n = 1$; $m = 16$
15: $n = 1$ to >4; $m = 6$

by ring-closing metathesis (RCM).[2,19–21] The monomer **4** had been synthesized previously by RCM in 70% yield.[20] In a similar procedure, the α,ω-diolefinic ester **7** and Grubbs' catalyst **1** (3 mol%) were slowly added over 24 h to dichloromethane at 25 °C to give a final concentration of 0.01 M. A mixture of cyclic oligomers **8** was thus produced in 76% yield. The cyclic structures were identified from the ^{1}H NMR spectrum of the product mixture, which indicated the absence

[*] Prof. P. Hodge, S. D. Kamau
Department of Chemistry, University of Manchester
Oxford Road, Manchester, M13 9PL (UK)
Fax: (+44) 161-275-4273
E-mail: philip.hodge@man.ac.uk

[**] We thank the Association of Commonwealth Universities for a PhD Studentship (to S.D.K.).

Supporting information for this article is available on the WWW under http://www.angewandte.org or from the author.

 © 2003 Wiley-VCH Verlag GmbH & Co. KGaA, Weinheim DOI: 10.1002/anie.200250842

of vinyl groups, and the MALDI-TOF mass spectrum, in which the only series of peaks were attributable to cyclic oligomers. Analytical gel-permeation chromatography (GPC) showed that the cyclic monomer **4** made up 52% of the mixture. Chromatography afforded **4** as an oil in 25% yield. ^{13}C NMR spectroscopic analysis showed that both geometric isomers were present (*E*/*Z* 55:45). Similar RCM of the α,ω-diolefinic diesters **9** and **10**, but at final olefin concentrations of just 0.006 M, gave the cyclic monomers **5** and **6**, respectively, each in 67% yield and with an *E*/*Z* ratio of 80:20.

The ED-ROMP of the monomer **4**, with 21 ring atoms, was carried out by treating a 40% w/v solution in dichloromethane under a stream of nitrogen at 40°C with Grubbs' second-generation catalyst **2** (1 mol%; Table 1, entry 1). The dichloromethane was allowed to evaporate into the nitrogen stream over 12 h and the polymer **11** was formed in 96% yield together with a mixture of cyclic oligomers (4%; see Scheme 1). The end groups of the polymer are derived from the catalyst. Once the system has reached equilibrium its composition should not change. However, the catalyst could be destroyed if necessary by reaction with methyl vinyl ether.[2] The presence of cyclic oligomers in the final mixture is to be expected, as even when neat monomers are used the final equilibrium position typically corresponds to approximately 2–3% of cyclic oligomers. Interestingly, 1) these recovered cyclic oligomers were a mixture and not just the cyclic monomer **4**, which indicates that they had also been involved in the equilibration, and 2) both the *E* and *Z* monomers reacted. The polymer formed had $\bar{M}_n$ 37000 and $\bar{M}_w$ 67500 ($\bar{M}_w$ = mass-average molar mass), based on GPC analysis (relative to a polystyrene standard). The FT-IR and ^1H NMR spectra were as expected for the polymer **11**. Note that the repeat units in the polymer **11** may be linked head-to-head, head-to-tail, or tail-to-tail.

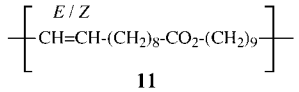
The cyclic monomers **5** and **6** (with 28 and 38 ring atoms, respectively) were polymerized under similar conditions, but with a reaction time in this case of just 10 min, to give the polymers **12** and **13**, respectively (Table 1, entries 3 and 4). The copolymer **14** was prepared by ED-ROMP of a mixture of the cyclic oligomers **5** and **6** (Table 1, entry 5). The monomer **6** was also polymerized by casting a film containing the metathesis catalyst **2** (1 mol%) from chloroform onto a microscope slide, followed by heating at 40°C (Table 1, entry 6). After 10 min the polymer **13** could be peeled off as a selfstanding film. GPC analysis showed it to have $\bar{M}_n$ 94000 and $\bar{M}_w$ 181700.

Table 1: ED-ROMP of various cyclic olefins with the metathesis catalyst **2** (1 mol%) at 40°C.[a]

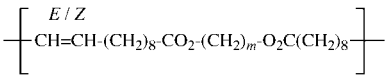
Entry	Monomer	*t*	Product ratio[b] c.o.[c]/polymer	Polymer	M_n ($\times 10^3$)[b]	M_w ($\times 10^3$)[b]
1	**4**	12 h	4:96	**11**	37.0	67.5
2	**8**	12 h	3:97	**11**	22.0	44.0
3	**5**	10 min	6:94	**12**	55.0	105.0
4	**6**	10 min	4:96	**13**	80.4	159.0
5	**5** + **6**[d]	10 min	10:90	**14**	74.4	135.0
6	**6**[e]	10 min	10:90	**13**	94.0	181.7
7	**15**	10 min	5:95	**12**	21.9	40.3

[a] See Experimental Section and main text for details of the procedure. [b] Based on GPC analysis. [c] Cyclic oligomers. [d] equimolar mixture. [e] Polymerized as a film on a microscope slide.

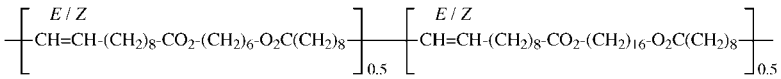
The feedstock for ED-ROMP need not be a pure monomer: a mixture of cyclic oligomers will suffice, but only cyclic compounds may be present. An alternative method to RCM for the synthesis of a mixture of cyclic oligomers is cyclodepolymerization (CDP).[2,22] This is simply the reverse of ED-ROP and it has been suggested that such reactions could form a basis for methods for recycling condensation polymers[12] (see Scheme 1). CDP involves the treatment of polymers in dilute solution, typically 2% w/v,[12] with a catalyst that will reversibly cleave the linkages between the polymer repeat units. As a result of the low concentration, the ring–chain equilibrium is shifted in favor of the cyclic oligomers. This method of cyclic-oligomer synthesis produces a cleaner product than RCM because very few end groups are present in the CDP system. Thus, the CDP product contains very few linear species. CDP is best carried out using the second-generation catalyst **2**. Treatment of the polymer **11** with **2** (1 mol%) in dichloromethane at 40°C for 2 h gave a mixture of cyclic oligomers **8** in 51% yield. GPC analysis showed the mixture **8** to consist of the cyclic monomer **4** (52%), cyclic dimer (30%), cyclic trimer (7%), cyclic tetramer (4%), and higher cyclic oligomers (7%). When these were polymerized under similar conditions to those used for the monomer **4**, the polymer **11** was produced in 97% yield with $\bar{M}_n$ 22000 and $\bar{M}_w$ 44000 (Table 1, entry 2). It was clear that the cyclic monomer, dimer, and trimer had undergone polymerization, which indicates that ED-ROMP occurs successfully with 21-, 42- and 63-membered macrocycles. The CDP of the polymer **12** under similar conditions to those used with the polymer **11** gave the cyclic oligomers **15** in 93% yield. GPC analysis showed the mixture to be composed of the cyclic monomer **5** (48%), cyclic dimer (17%), cyclic trimer (8%), and cyclic tetramer (5%). When the cyclic oligomers **15** were subjected to ED-ROMP under the standard conditions, the



11



12: *m* = 6
13: *m* = 16



14

 © 2003 Wiley-VCH Verlag GmbH & Co. KGaA, Weinheim

polymer **12** was reformed in 95% yield (Table 1 entry 7). GPC analysis of the product indicated that less than 2% of the cyclic dimer remained. Thus, ED-ROMP can be carried out successfully with a mixture of monomer, dimer, and trimer, thus showing that up to 84-membered rings can take part in ROMP.

To determine the effect of concentration on the yield of polymer, the monomer **4** was treated at various concentrations in dichloromethane with the second-generation catalyst **2** at 40 °C for 12 h, and the equilibrated mixture was analyzed by GPC. The results are summarized in Table 2. It is apparent from these experiments that the balance between cyclic oligomers and polymer is still heavily in favor of the latter at a concentration of 50% w/v. This observation suggests it may be possible to polymerize solid monomers in concentrated solutions at 40 °C.

Table 2: Distribution of cyclic oligomers and polymer obtained from equilibrations of **6** in dichloromethane at 40 °C with the catalyst **2** (1 mol%).

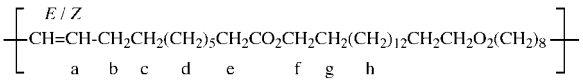
Entry	Initial conc.[a] [g/100 mL]	Product ratio[b] c.o.[c]/polymer	M_n ($\times 10^3$)[b]	M_w ($\times 10^3$)[b]
1	neat	4:96	36.8	67.4
2	50	3:97	33.4	60.1
3	2.0	57:43	16.2	25.5
4	0.5	100:0	–	–

[a] Initial concentration. [b] Based on GPC analysis. [c] Cyclic oligomers.

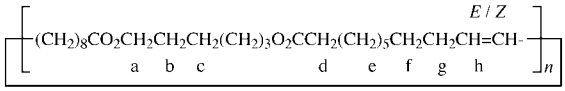
In conclusion, the range of cyclic olefins that can undergo ROMP can be increased substantially by using high monomer concentrations and ED-ROMP can be carried out successfully with macrocycles that have up to 84, and possibly even more, ring atoms. The $\bar{M}_n$ values obtained were as high as 94000 with polydispersities close to 2.0. Finally, when RCM is carried out in organic synthesis in the presence of very active metathesis catalysts, it should be borne in mind that equilibration of the cyclic monomer to give a series of cyclic oligomers may occur, that any polymer formed may be converted back into cyclic compounds by CDP, and that at high concentrations the cyclic oligomers may take part in ED-ROMP.

Experimental Section

Typical ED-ROMP: The cyclic oligomer **6** (100 mg, 0.179 mmol) was dissolved in dichloromethane (0.25 mL). The catalyst **2** (1.51 mg, 1 mol%) was then added and the mixture was stirred magnetically at 20 °C under a stream of nitrogen. The dichloromethane evaporated within 4 h to leave the polymeric product as a gum. A small portion of the product was analyzed by GPC (see Table 1 for results) and the rest was dissolved in dichloromethane and precipitated with methanol to give **13** (80 mg, 80%). ^{1}H NMR (300 MHz, $CDCl_3$): $\delta = 1.20$–1.40 (m, 44H, H-d and H-h), 1.58–1.70 (m, 8H, H-c and H-g), 1.94–2.04 (m, 4H, H-b), 2.30–2.38 (m, 4H, H-e), 4.04–4.14 (t, $J = 6.59$ Hz, 4H, H-f), 5.36–5.42 ppm (m, 2H, H-a).



CDP of **12:** The polymer **12** (200 mg, 0.474 mmol) was dissolved in dichloromethane (20 mL), and **2** (4.02 mg, 1 mol%) was added. The resulting mixture was stirred at 40 °C under nitrogen for 2 h. The solvent was then evaporated rapidly under vacuum and the product was purified by column chromatography (alumina, dichloromethane as eluent). This gave the mixture **14** as a gray, waxy solid (186 mg, 93%). ^{1}H NMR (300 MHz, $CDCl_3$): $\delta = 1.20$–1.50 (m, 24H, H-c and H-e), 1.58–1.74 (m, 8H, H-b and H-f), 1.94–2.10 (m, 4H, H-g), 2.26–2.36 (m, 4H, H-d), 4.00–4.20 (m, 4H, H-a), 5.35–5.45 ppm (m, 2H, H-h); MALDI-TOF mass spectrum of the product (doped with Na^+ in the form of NaBr, dithranol matrix) showed a series of mass peaks corresponding to a mixture of products, from the cyclic monomer (445, [monomer+Na]$^+$) to the cyclic hexamer (2558, [hexamer+Na]$^+$). The GPC analysis is given in the main text.



Received: December 23, 2002 [Z50842]

Keywords: alkenes · macrocycles · metathesis · ring-opening polymerization

[1] K. J. Ivin, J. C. Mol, *Olefin Metathesis and Metathesis Polymerization*, Academic Press, San Diego, **1997**, chap. 11–14.
[2] M. J. Marsella, H. D. Maynard, R. H. Grubbs, *Angew. Chem.* **1997**, *109*, 1147–1150; *Angew. Chem. Int. Ed. Engl.* **1997**, *36*, 1101–1103.
[3] P. Schwab, R. H. Grubbs, J. W. Ziller, *J. Am. Chem. Soc.* **1996**, *118*, 100–110.
[4] M. Scholl, S. Ding, C. W. Lee, R. H. Grubbs, *Org. Lett.* **1999**, *1*, 953–956.
[5] J. A. Semlyen, *Adv. Polym. Sci.* **1976**, *21*, 41–75.
[6] U. W. Suter in *Comprehensive Polymer Science, Vol. 5* (Eds.: G. Allen, J. C. Bevington), Pergamon, Oxford, **1989**, pp. 91–96.
[7] G. Ercolani, L. Mandolini, P. Mencareli, S. Roelens, *J. Am. Chem. Soc.* **1993**, *115*, 3901–3908.
[8] a) S. Kühling, H. Keul, H. Höcker, *Makromol. Chem.* **1992**, *193*, 1207–1217; b) H. Keul, R. Bacher, H. Höcker, *Makromol. Chem.* **1986**, *187*, 2579–2589.
[9] a) P. Hodge, Y. Zhuo, A. Ben-Haida, C. S. McGrail, *J. Mater. Chem.* **2000**, *10*, 1533–1537; b) C. L. Ruddick, P. Hodge, Z. Yang, R. L. Beddoes, M. Helliwell, *J. Mater. Chem.* **1999**, *9*, 2399–2406.
[10] H. M. Colquhoun, D. F. Lewis, P. Hodge, A. Ben-Haida, D. J. Williams, I. Baxter, *Macromolecules* **2002**, *35*, 6867–6882.
[11] D. J. Brunelle in *New Methods of Polymer Synthesis* (Eds.: J. R. Ebdon, G. C. Eastmond), Blackie, London, **1995**, chap. 6.
[12] P. Hodge, *React. Funct. Polym.* **2001**, *48*, 15–23.
[13] W. Ast, G. Rheinwald, R. Kerber, *Makromol. Chem.* **1976**, *177*, 1341–1348.
[14] H. Höcker, W. Reimann, L. Reif, K. Riebel, *J. Mol. Catal.* **1980**, *8*, 191–202.
[15] E. A. Ofstead, N. Calderon, *Makromol. Chem.* **1972**, *154*, 21–34.
[16] C. W. Bielawski, D. Benitez, R. H. Grubbs, *Science* **2002**, *297*, 2041–2044.
[17] M. D. Watson, K. B. Wagener, *Macromolecules* **2000**, *33*, 3196–3201.
[18] C. W. Bielawski, J. Louie, R. H. Grubbs, *J. Am. Chem. Soc.* **2000**, *122*, 12872–12873.
[19] R. H. Grubbs, S. J. Miller, G. C. Fu, *Acc. Chem. Res.* **1995**, *28*, 446–452.
[20] A. Fürstner, K. Langemann, *J. Org. Chem.* **1996**, *61*, 3942–3943.
[21] A. Fürstner, K. Langemann, *Synthesis* **1997**, 792–803.
[22] S. Dad, A. J. Hall, P. Hodge, *Polym. Prepr. Am. Chem. Soc. Div. Polym. Chem.* **2000**, *41*(1), 466–467.

 © 2003 Wiley-VCH Verlag GmbH & Co. KGaA, Weinheim

Modified Aluminum Oxide

A "Soft-Chemical" Method To Synthesize Lewis Acid Surfaces of Aluminum Oxide**

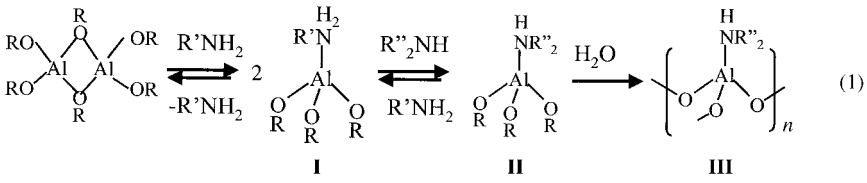
A. I. Kozlov, Mayfair C. Kung, W. M. Xue, and Harold H. Kung**

Many applications of metal oxides such as adsorption, separation, ion-exchange, and catalysis depend critically on surface properties, which include Brønsted acidity or basicity, Lewis acidity, and coordination unsaturation or redox properties of the surface metal ions. In order to generate the desired surface, it is common to perform postsynthesis treatments such as high-temperature calcination to dehydroxylate the surface or functionalization by reaction of the surface hydroxyl groups with various reagents. Here we report a method to generate a metal oxide with a specific surface property through synthesis instead of by postsynthesis treatment. We have synthesized an alumina that possesses a high density of surface Lewis acid sites, without resorting to postsynthesis high-temperature calcination, and has few hydroxyl groups relative to the material resulting from conventional preparation. The strategy is to protect the Lewis acid sites of Al with a base during hydrolysis to form the oxide. After the oxide is formed, the bound amine can be exchanged with other bases. The resulting alumina was an active catalyst for the aminolysis of epoxide. This concept of protecting the desired functionality during synthesis is applicable generally to other oxides having other surface properties.

This approach of protecting the Lewis acid site of an Al ion by forming an amine–aluminum adduct differs from the concept used in preparing oxides of uniform pore structures such as the M41S family of mesoporous siliceous oxides.[1,2] In those methods the self-assembly properties of the surfactants or surfactant–metal complexes are utilized to form structure-directing templates around which gelation of the inorganic precursor occurs. Various types of interactions between surfactants and inorganic species have been explored, including the direct charge–charge interaction between cationic surfactant and anionic inorganic species (and the counterpart anionic surfactant–cationic inorganic species), mediated charge–charge interaction in which the like-charged surfactant and inorganic species are separated by a mediator of opposite charged,[3] and hydrogen bonding between a neutral surfactant and neutral inorganic precursor.[4] By means of these techniques, transition[5–7] and post-transition metal oxides with structured mesopores have been prepared. Aluminum oxide has been prepared using these methods, and materials containing mesopores with narrow pore-size distributions can be obtained.[8–10]

In these methods the function of the surfactants is to provide structural templates around which the inorganic oxyhydroxy polymeric gel is formed. The chemistry of the gelation process remains largely the same as that in the hydrolysis of the inorganic metal ions in the absence of the surfactants, and the resulting surface properties of the final oxides are similar. In other cases, the surfactant ligand was employed to moderate the hydrolysis rate of the metal ion.[5] There has been no attempt to control the surface properties of the final oxide.

The common aluminum oxide precursors such as $AlCl_3$ and $Al(OR)_3$ are Lewis acids that exist as dimers (e.g., Al_2Cl_6) and oligomers (e.g., Al alkoxides). In the presence of a strong Lewis base such as an amine, these dimers and oligomers can be transformed into monomeric amine–Al acid–base adducts **I**. Thus, instead of serving as a structure-directing agent in the synthesis process, an amine can be used as a Lewis base to protect the Lewis acid site of Al by forming an adduct. After hydrolysis (→**III**), the resulting oxide surface would retain a high density of the amine-protected Al ions and be different from a hydroxyl-covered surface obtained by the conventional hydrolysis procedure. Equation (1) summarizes the steps involved.



(1)

Aluminum *tert*-butoxide exists as dimer in a toluene solution. Its ^{1}H NMR spectrum exhibits two singlets at $\delta =$ 1.39 and 1.51 ppm with a peak area ratio of 2:1 due to the terminal and bridging butoxy groups, respectively.[11] Addition of a primary amine such as propylamine, butylamine, or octylamine at room temperature resulted in the formation of a monomeric amine aluminum *tert*-butoxide adduct such as **I** (R = *t*Bu). The ^{1}H NMR spectrum of the monomer showed only one singlet at about $\delta = 1.47$ ppm (Figure 1). The transformation to the monomer was also supported by ^{13}C NMR spectroscopy. For the dimer $[Al(OtBu)_3]_2$ in toluene, the bridging *tert*-butyl groups gave rise to resonances at $\delta = 31.5$ and 76.2 ppm due to the methyl groups and the tertiary carbon, respectively, whereas the terminal *tert*-butyl groups gave rise to resonances at $\delta = 34.0$ and 69.1 ppm. For the monomer **I** only one type of *tert*-butyl groups was observed with resonances at $\delta = 34.3$ and 67.7 ppm. ^{27}Al NMR spectroscopy provided additional evidence. The peak at $\delta = 48.7$ ppm for the tetrahedral Al center in a dimeric species was replaced

[*] M. C. Kung, H. H. Kung, A. I. Kozlov, W. M. Xue
Department of Chemical Engineering
Northwestern University
Evanston, IL 60208-3120 (USA)
Fax: (+1) 847-467-1018
E-mail: m-kung@northwestern.edu
hkung@northwestern.edu

[**] This work was supported by the U.S. Department of Energy, Office of Science, Basic Energy Sciences.

 DOI: 10.1002/anie.200250581 © 2003 Wiley-VCH Verlag GmbH & Co. KGaA, Weinheim

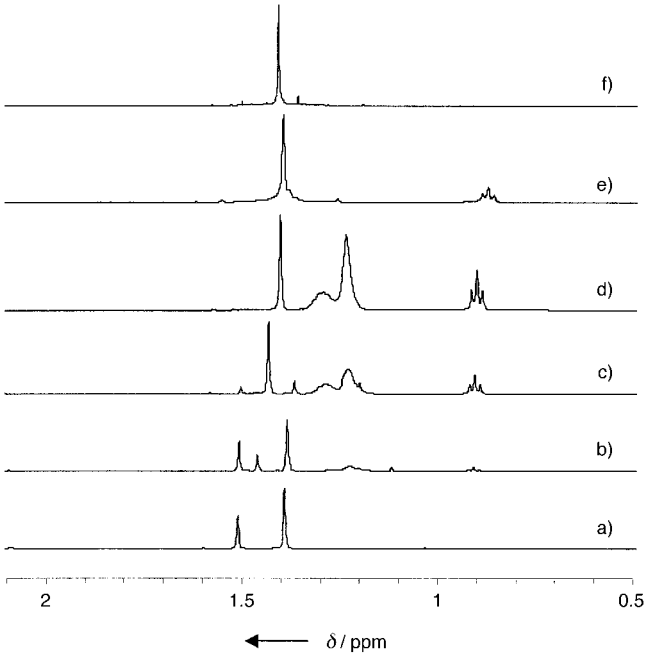


Figure 1. ^{1}H NMR spectra of solutions of $Al_2(OtBu)_6$ alone and as an adduct with various amines in [D_8]toluene. a) 6.4 wt% $Al_2(OtBu)_6$; b) adduct with *n*-octylamine (N/Al = 1.0); c) adduct with *n*-octylamine (N/Al = 4.7); d) adduct with *n*-octylamine (N/Al = 9.6); e) adduct with *n*-propylamine (N/Al = 3.0); f) adduct with piperidine (N/Al = 1.5).

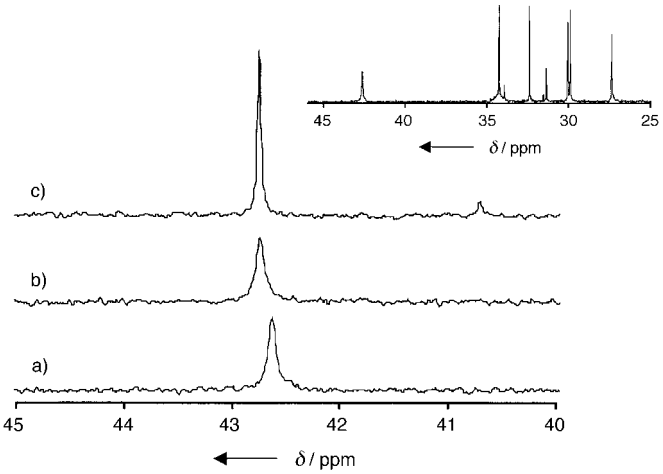


Figure 2. Variable-temperature ^{13}C NMR spectra of the $Al(OtBu)_3$–*n*-octylamine adduct at a) 20 °C, b) −30 °C, and c) −75 °C. Spectra recorded on dilute solutions of 0.4 M ($Al(OtBu)_3$) and 2 M octylamine in [D_8]toluene by using gated technique. The insert is the spectrum at 20 °C.

by a peak at $\delta = 62.9$ ppm with the formation of the monomeric species.

The transformation from dimer to monomer was slow at room temperature, and the equilibrium conversion increased when the ratio of amine to aluminum was increased. For octylamine, it took over 10 h to achieve equilibrium conversion, and a ratio of about 10 was required for complete conversion (Figure 1, spectrum d), whereas a lower ratio was sufficient for the reaction with propylamine (spectrum e). This method of preparing the amine–aluminum alkoxide monomer **I** is significantly simpler than the previously reported alcoholysis of $[Al(NMe_2)_3]_2$.[12,13]

At 25 °C primary amines bound to Al *tert*-butoxide exchange rapidly with the free amine in solution [Eq. (1)]. For example, the ^{13}C NMR resonance of the α carbon of octylamine at $\delta = 42.7$ ppm showed detectable broadening in the presence of Al *tert*-butoxide (Figure 2, spectrum a). The peak broadened further at −30 °C (spectrum b). When the sample was cooled further to −75 °C (spectrum c), the exchange was sufficiently slow that the resonances due to the bound amine and the free amine became distinguishable at $\delta = 40.7$ ppm and 42.8 ppm, respectively. A similar observation was obtained when propylamine was used instead of octylamine.

The rapid exchange between the free species and the bound species suggests that primary amines do not provide the desired protection of the Al coordination site. When the free amine was removed by purging with a flow of N_2 or by evacuation, $Al_2(OtBu)_6$ could be recovered. On the other hand, the more strongly basic piperidine can provide the protective function. However, piperidine does not react directly at a convenient rate with $Al_2(OtBu)_6$, probably due to steric hindrance. An adduct between piperidine and $Al(OtBu)_3$, **II,** can be obtained by reacting piperidine (piperidine/Al = 20) with $[Al(OtBu)_3(nPrNH_2)]$ in toluene (propylamine/Al = 10) at room temperature [Eq. (1)]. After 2 h the propylamine and most of the excess piperidine were removed by purging with N_2 for 12–20 h. The product was dried in vacuo at 25 °C for 2 h and then at 50 °C for 2 h. Throughout the process, the ^{1}H and ^{13}C NMR spectra of the mixture showed the presence of monomeric $Al(OtBu)_3$ and the absence of the dimer. The final solid could be redispersed in toluene. Its ^{1}H NMR spectrum shows new features not present in free piperidine. These peaks (and their assignments) are: a doublet at about $\delta = 3.1$ ppm (equatorial H of α-C), a quartet at about $\delta = 2.5$ ppm (axial H of α-C), a quartet at about $\delta = 0.95$ ppm (axial H of γ-C), a quartet at $\delta = 0.75$ ppm (axial H of β-C), and a broad doublet at $\delta = 1.25$ ppm. The α carbon atom of piperidine in this sample gives rise to two peaks at $\delta = 47.1$ and 45.96 ppm in the ^{13}C NMR spectrum. Their relative integrated areas are 1 and 0.46, respectively. From the ratio of the peak intensities of the piperidine and alkoxide, the N/Al ratio in this solution is close to 1.5, which suggests that some free piperidine remains.

Hydrolysis of the piperidine/Al alkoxide adduct **II** in toluene was conducted by introducing water to the gas phase with a stream of N_2 (100 mL min^{-1}) saturated with water at 30 °C until no Al *tert*-butoxide could be detected in solution by ^{1}H NMR spectroscopy. The resulting Al complex **III** was dried in vacuo at 60 °C to remove the toluene solvent, released *t*BuOH, and free piperidine. The ^{27}Al MAS NMR spectrum (MAS = magic angle spinning) of the dried solid showed a very pronounced peak at $\delta = 30$ ppm that could be due to pentacoordinated Al, in addition to the peaks at $\delta = 0$ ppm due to octadedral Al, and $\delta = 60$ ppm due to tetrahedral Al (Figure 3, spectrum a). The ratio of the peaks due to the tetrahedral and octahedral Al centers was much higher than that in a sample prepared without the formation of

 © 2003 Wiley-VCH Verlag GmbH & Co. KGaA, Weinheim

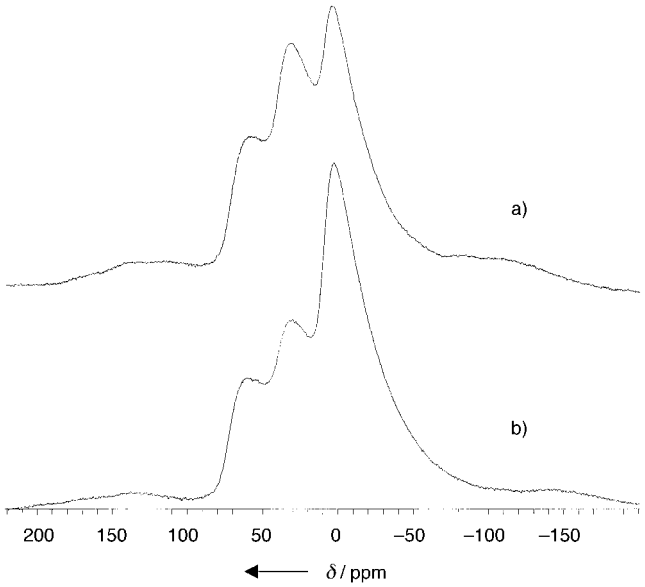


Figure 3. ^{27}Al MAS NMR spectra of the solids obtained from hydrolysis of a) piperidine-protected Al(O*t*Bu)$_3$; b) Al *tert*-butoxide in the presence of piperidine (unbound).

amine–Al alkoxide adduct (Figure 3, spectrum b). The dried solid had a BET surface area of 250 m^2g^{-1}. The DRIFT spectrum of the dried solid (Figure 4, spectrum a) showed strong peaks at $\nu = 1462$, 1388, and 1250 cm^{-1} due to piperidine bound to Lewis acid sites.[14,15] Peaks in the region $\nu = 2900$ cm^{-1} indicated that some *tert*-butanol or butoxide remained. After this dried solid had been refluxed in propylamine twice and then dried, a propylamine-exchanged sample (**IV**) was obtained, which gave the DRIFT spectrum in Figure 4b. The intensity of the C–H stretching band decreased substantially, although residual *t*Bu groups were still evident in the ^{13}C MAS NMR spectrum. The peaks at $\nu = 1595$, 1463, 1280, and 1253 cm^{-1} could be assigned to propylamine bound to Lewis acid sites.[14] If this

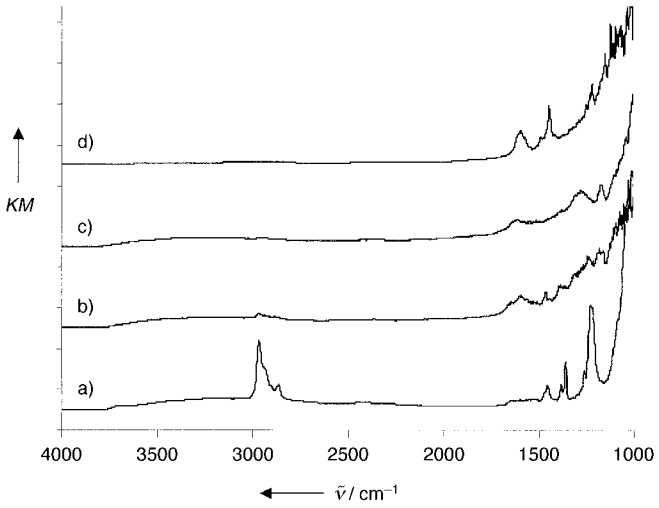
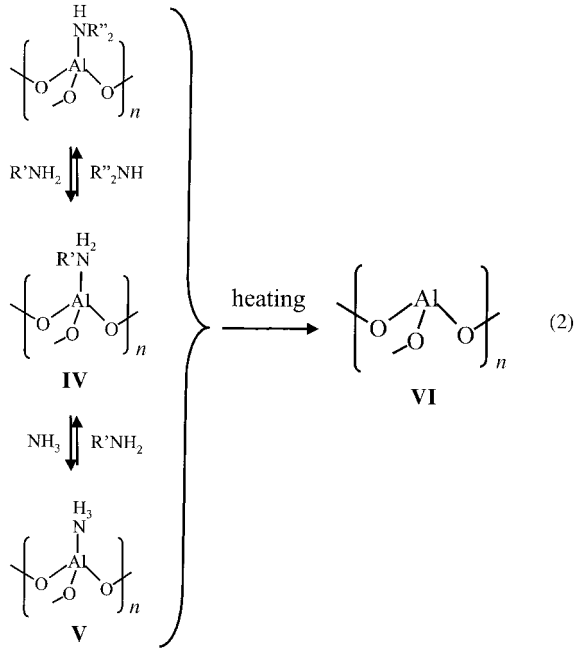


Figure 4. DRIFT spectra of: a) dried $C_5H_{10}NH$–Al_2O_3 formed from hydrolysis of $C_5H_{10}NH$–Al(O*t*Bu)$_3$; b) sample a exchanged with *n*$C_3H_7NH_2$; c) sample b exchanged with NH_3.

solid, in turn, was exposed to a stream of NH_3/He for 5 h at 25 °C, a solid (**V**) characterized by the spectrum in Figure 4c was obtained. Bands at 1615 and 1280 cm^{-1} indicated Lewis acid bound NH_3 group.[14,16] Thus, the amine coordinated to the Al Lewis acid center can be exchanged with other bases, as illustrated in Equation (2). In all these spectra, the absorption in the region near 3500 cm^{-1} was low, indicating that there were few hydroxyl groups in the samples. These solids were amorphous by X-ray diffraction.



(2)

Alumina **III** prepared using piperidine was tested as a catalyst for the aminolysis of epoxide by amine,[17,18] a class of reactions that may be useful in drug synthesis.[19] After cyclopentene oxide (5.0 mmol) and piperidine (5.0 mmol) had been heated in acetonitrile at reflux for 8 h in the absence of **III**, only 3% conversion of the epoxide was observed. However, in the presence of **III** (50 mg), 50% conversion quantitatively to the 1,2-amino alcohol was obtained after the same time period. On a per unit surface area basis, **3** was five times more active than conventional γ-Al_2O_3 activated in vacuo at 500 °C.

The bound amine in **IV** could be removed at elevated temperatures. A sample characterized by spectrum a in Figure 5 was obtained after **IV** had been heated in oxygen and then in vacuo at 400 °C for 30 min. Peaks due to coordinated piperidine disappeared. However, small peaks possibly due to surface nitro/nitrato groups remained, suggesting that some of the amine was oxidized. Pyridine was adsorbed on this sample readily to exhibit peaks at $\nu = 1445$ and 1615 cm^{-1} due to coordination to Lewis acid sites. A similar observation was made with the ammonia-exchanged sample **V**.

The alumina prepared using the amine–Al adduct contained a much higher ratio of Lewis acid sites to hydroxyl groups than conventionally prepared alumina. A sample (**VI**) prepared by thermally removing the bound propylamine was

 © 2003 Wiley-VCH Verlag GmbH & Co. KGaA, Weinheim

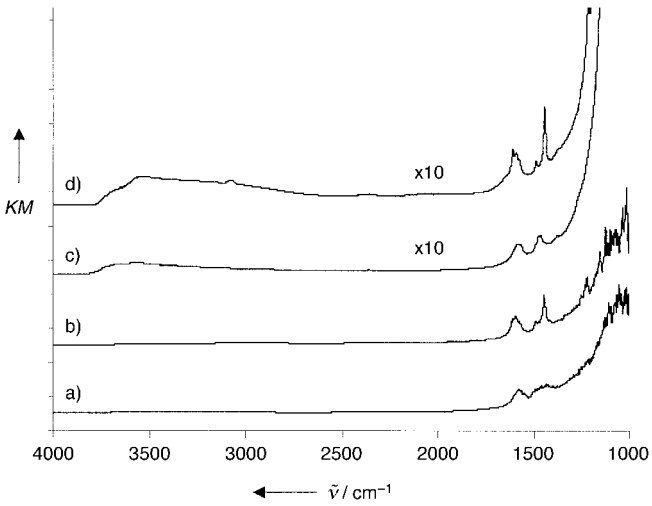


Figure 5. DRIFT spectra of pyridine adsorption on aluminas: a) $n$$C_3H_7NH_2$-exchanged sample **IV** after heating in O_2 and then in vacuo at 400 °C; b) sample a after pyridine adsorption; c) conventional γ-alumina after heating in vacuo at 400 °C; d) sample c after pyridine adsorption.

heated further in an O_2 stream containing 1.5% H_2O for 30 min. After the sample had been dried in He at 400 °C for 5 h, pyridine was adsorbed at 25 °C. The DRIFT spectra of the sample before and after pyridine adsorption (very similar to Figure 5, spectra a and b) showed rather low absorption in the OH stretching region (around 3500 cm^{-1}). The adsorbed pyridine showed bands at $\nu = 1612$, 1447, and 1223 cm^{-1}, indicative of adsorption on Lewis acid sites. On the other hand, a conventionally prepared γ-Al_2O_3 after the same water treatment and adsorption of pyridine exhibited spectra c and d, showing much more intense absorption in the OH region and much lower intensity of the peaks from adsorbed pyridine. Thus, the results reported here demonstrated that it is possible to exercise control of the surface properties of an oxide through the synthesis method.

Received: November 19, 2002 [Z50581]

Keywords: aluminum · amines · Lewis acids · oxides

[1] C. T. Kresge, M. E. Leonowicz, W. J. Roth, J. C. Vartuli, J. S. Beck, *Nature* **1992**, *359*, 710.
[2] J. S. Beck, J. C. Vartuli, W. J. Roth, M. E. Leonowicz, C. T. Kresge, K. D. Schmitt, C. T.-W. Chu, D. H. Olson, E. W. Sheppard, S. B. McCullen, J. B. Higgins, J. L. Schlenker, *J. Am. Chem. Soc.* **1992**, *114*, 10834.
[3] Q. Huo, D. I. Margolese, B. Ciesla, P. Feng, T. E. Gier, K. Sieger, R. Leon, P. M. Petroff, F. Schüth, G. D. Stucky, *Nature* **1994**, *368*, 317.
[4] P. T. Tanev, T. J. Pinnavaia, *Science* **1995**, *267*, 865.
[5] D. M. Antonelli, J. Y. Ying, *Angew. Chem.* **1996**, *108*, 461; *Angew. Chem. Int. Ed. Engl.* **1996**, *35*, 426.
[6] D. M. Antonelli, J. Y. Ying, *Angew. Chem.* **1995**, *107*, 2202; *Angew. Chem. Int. Ed. Engl.* **1995**, *34*, 2014.
[7] D. M. Antonelli, J. Y. Ying, *Chem. Mater.* **1996**, *8*, 874.
[8] P. Yang, D. Zhao, D. I. Margolese, B. F. Chmelka, G. D. Stucky, *Chem. Mater.* **1999**, *11*, 2813.
[9] S. A. Bagshaw, T. J. Pinnavaia, *Angew. Chem.* **1996**, *108*, 1180; *Angew. Chem. Int. Ed. Engl.* **1996**, *35*, 1102.
[10] F. Vaudry, S. Khodabandeh, M. E. Davis, *Chem. Mater.* **1996**, *8*, 1451.
[11] V. J. Shiner, Jr., D. Whitaker, V. P. Fernandez, *J. Am. Chem. Soc.* **1963**, *85*, 2318.
[12] M. H. Chisholm, V. F. Distasi, W. E. Streib, *Polyhedron* **1990**, *9*, 253.
[13] L. Mîinea, S. Suh, S. G. Bott, J.-H. Liu, W.-K. Chu, D. M. Hoffman, *J. Mater. Chem.* **1999**, *9*, 929.
[14] E. Jobson, A. Baiker, A. Wokaun, *J. Chem. Soc. Faraday Trans.* **1990**, *86*, 1131.
[15] D. Ouafi, F. Maugé, J. C. Duchet, J. C. Lavalley, *React. Kinet. Catal. Lett.* **1989**, *38*, 95.
[16] S. Rajagopal, T. L. Grimm, D. J. Collins, R. Miranda, *J. Catal.* **1992**, *137*, 453.
[17] G. H. Posner, D. Z. Rogers, *J. Am. Chem. Soc.* **1977**, *99*, 8207; G. H. Posner, D. Z. Rogers, *J. Am. Chem. Soc.* **1977**, *99*, 8214.
[18] Y. Harrak, M. D. Pujol, *Tetrahedron Lett.* **2002**, *43*, 819.
[19] M. Karpf, R. Trussardi, *J. Org. Chem.* **2001**, *66*, 2044.

 © 2003 Wiley-VCH Verlag GmbH & Co. KGaA, Weinheim

Archaea *Membrane Lipids*

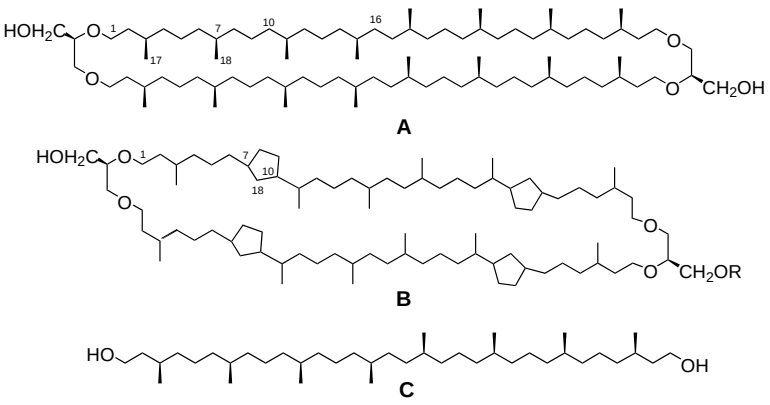
Determination of the Configuration of an *Archaea* Membrane Lipid Containing Cyclopentane Rings by Total Synthesis**

*Elvira Montenegro, Bert Gabler, Gesa Paradies, Matthias Seemann, and Günter Helmchen**

Dedicated to Professor Kurt Mislow on the occasion of his 80th birthday

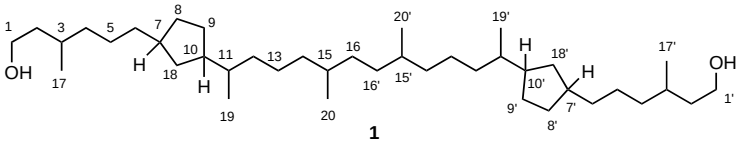
The *Archaea* are microorganisms that proliferate under extreme environmental conditions, such as high acidity, high temperature and/or high salt concentration.[1] *Archaea* are classified into three phenotypes on the basis of their living habitats: methanogens, halophiles, and thermoacidophiles. Among the distinctive features of the thermoacidophiles are their membranes. These contain lipids consisting of mixtures of macrocyclic, 72-membered tetraethers composed of saturated isoprenoid chains linked to glycerol or higher sugars.[2] Furthermore, compounds with up to eight five-membered rings were isolated. Typical tetraethers are compounds **A** and **B**.[3] Note that there is a relationship between **A** and **B** in that the five-membered rings of **B** can formally be generated by connecting CH_3 and CH_2 groups of **A**, for example C18 and C10.

During the last decade syntheses of ethers related to *archaea* membranes have been reported by several groups.[4]



In fact, the configuration of the macrocyclic tetraether **A** has been determined by total synthesis of the diol **C** and comparison with a sample of **C** obtained by degradation of natural **A**.[5] In the meantime, a synthesis of **A** has also been carried out.[6]

In contrast, the configurations of the compounds containing five-membered rings are largely unknown and, as a consequence, stereoselective synthesis of a lipid containing cyclopentane units has not been undertaken. De Rosa et al. obtained various pure diols with five-membered rings, among them **1**, by degradation of natural etherlipids and determined



1

their constitution by mass spectrometry and NMR spectroscopy.[7] Important features, revealed by ^{13}C NMR spectroscopy, are the C_2 symmetry of the structure of **1** and the *trans* configuration of the rings which was deduced by comparison of the ^{13}C NMR spectroscopy data with those of *cis*- and *trans*-1,3-dimethylcyclopentane.[8] Herein we report the determination of the complete relative and absolute configuration of the diol **1** by a stereoselective synthesis.

Before embarking on the considerable effort of the synthesis of **1**, it appeared wise to exclude possible configurations by comparing naturally derived C_{40} diol **1** with C_{20} model compounds. Exploiting the C_2 symmetry of **1**, the diastereomers **2a–d** (Scheme 1) were chosen as model compounds. The methylated center at C3 was assumed to be analogous to the all-methylated chain **C**, but all possible configurations in the 1,3-*trans*-disubstituted ring and the α-methyl group were considered.

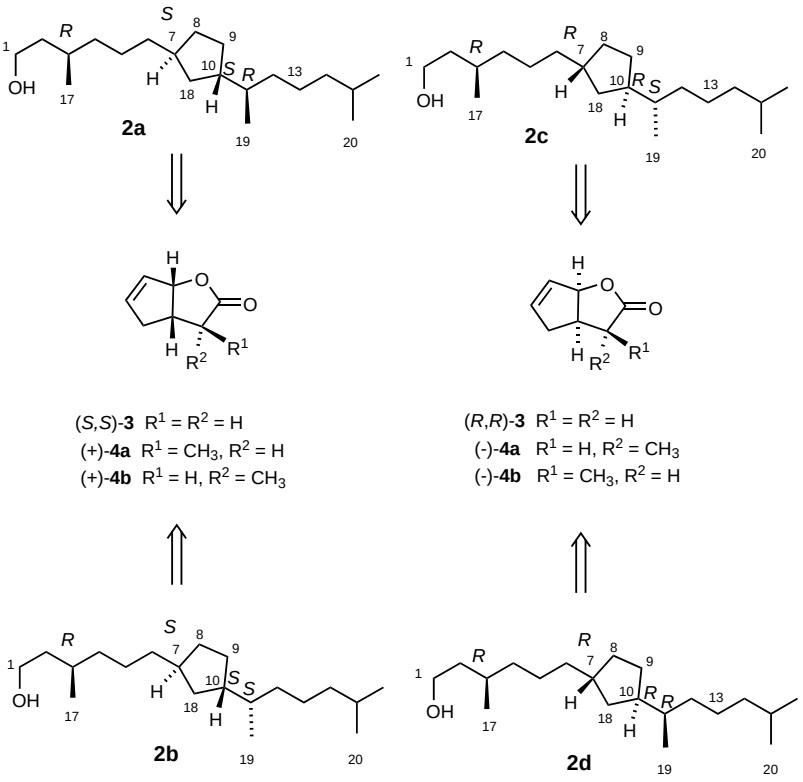
Our route to these compounds relies on lactones (*S*,*S*)-**3** and (*R*,*R*)-**3** as starting materials, available enantiomerically pure on a 100 g scale by asymmetric allylic substitution.[9] The CH_3 group corresponding to C19 was introduced by formation of the enolate (lithium diisopropylamide (LDA), THF, −78 °C) and alkylation with methyl iodide which proceeded with diastereoselectivity of **4a**:**4b** = 6:1; both lactones can be obtained in pure form by column chromatography.[10]

Compounds **2a–d** were synthesized by analogous routes. As a representative example, the synthesis of alcohol **2a** is described in Scheme 2. Bromide **5** was prepared from citronellol (98% *ee*), and transformed into an organocopper reagent which was coupled with lactone (+)-**4a** by an S_N2' reaction.[11] Reduction of the resulting acid **6** with $LiAlH_4$ gave the corresponding alcohol which was transformed into the tosylate **7**. Chain elongation by cross coupling tosylate **7** with 3-methylbutylmagnesium bromide, catalyzed by Li_2CuCl_4,[12] furnished the unsaturated precursor of **8** in high

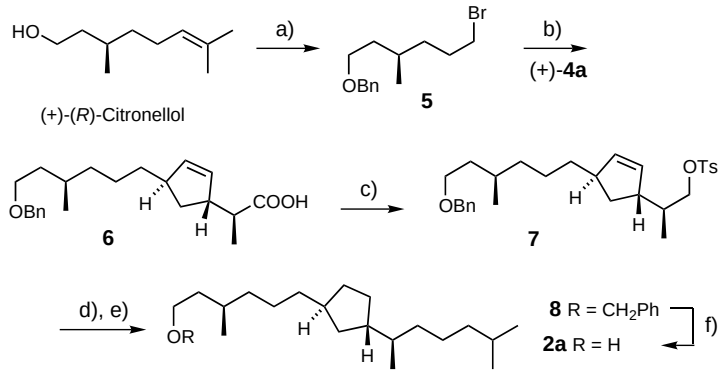
[*] Prof. Dr. G. Helmchen, Dr. E. Montenegro, Dr. B. Gabler, G. Paradies, Dr. M. Seemann
Organisch-chemisches Institut
Universität Heidelberg
Im Neuenheimer Feld 270, 69120 Heidelberg (Germany)
Fax: (+49) 6221-54-4205
E-mail: en4@ix.urz.uni-heidelberg.de

[**] We thank the Alexander von Humboldt Foundation for a postdoctoral fellowship to E. Montenegro, T. Weiss and W. Haseloff for recording the NMR spectra, K. Brödner and O. Tverskoy for experimental assistance, Dr. C. Kühl (Bernina Biosystems) for a sample of tetraether membrane lipids from *Archaea*, and Dr. T. Netscher (Hoffmann-La Roche) for (*R*)-citronellal.

 DOI: 10.1002/anie.200250629 © 2003 Wiley-VCH Verlag GmbH & Co. KGaA, Weinheim



Scheme 1. Model compounds **2a–d** and starting materials.



Scheme 2. Synthesis of model compound **2a**. a) 1. BnBr, NaH, DME, 0 °C→reflux, 4 h; 2. O_3, $NaBH_4$, $MeOH/CH_2Cl_2$ (1:1), −78 °C→RT, ≈12 h; 3. CBr_4, Ph_3P, Et_2O, RT, ≈12 h, 70% (3 steps); b) 1. Mg, THF, 65 °C; 2. CuBr·SMe_2, THF/SMe_2 (5:1), −78 °C; 3. (+)-**4a**, −78 °C→RT, ≈12 h, 80%; c) 1. $LiAlH_4$, THF, 65 °C; 2. TsCl, pyridine, 0 °C, 77% (2 steps); d) 3-methylbutyl magnesium bromide (3 equiv), 10 mol% Li_2CuCl_4, THF, −78 °C→0 °C, ≈12 h, 85%; e) $TsNHNH_2$, DME, NaOAc, H_2O, reflux, 2 h; f) $Pd(OH)_2/C$, H_2, AcOEt/MeOH (1:1), 1.1 atm, RT, ≈12 h, 88% (2 steps). Bn = benzyl, Ts = *p*-toluenesulfonyl, DME = dimethoxyethane.

yield. The double bond was reduced with diimine without the isomerization[13] which had occurred in a variety of transition-metal catalyzed hydrogenations. Finally, hydrogenation of benzyl ether **8** furnished the desired model compound **2a** in 32% overall yield from (+)-(*R*)-citronellol.

NMR spectra of isomers **2a–d** were recorded and the chemical shift assignments established by COSY, HMQC, HMBC, and DEPT experiments. Data were compared with those of diol **1** which was prepared by degradation of a mixture of tetraether lipids extracted from *Archaea Sulfolobus acidocaldarius*.[14] In Figure 1 the differences in ^{13}C chemical shift values are plotted for the cyclopentane ring and adjacent CH(Me) units. From these data, configurations **2b** and **2d** can be excluded.

The ^{13}C chemical shift values of the diastereomers **2a** and **2c** differ at most by 0.18 ppm. Thus, a decision between the two corresponding configurations for **1** on the basis of this NMR spectroscopy data is not possible. Nevertheless, these compounds were useful because it was found that the diastereomeric alcohols **2a–d** all display significantly different optical rotations (Figure 1). On the basis of this observation it was expected that comparison of the optical rotations of **1**, obtained by degradation and by total synthesis, would allow conclusive establishment of configuration. Accordingly, a synthesis of diol **1** was carried out.[15]

The synthesis of **1** starting from **7** involved chain elongation by a hydroisoprene unit followed by dimerization (Scheme 3). For chain elongation, a copper catalyzed cross-coupling of tosylate **7** (see Scheme 2) with a Grignard reagent prepared from bromide **9** was carried out. After removal of the protecting group, alcohol **10** was obtained and transformed into the corresponding bromide. Copper-catalyzed dimerization, reduction of the double bonds, and deprotection gave the diol **1** in 32% yield from **7**.

Samples of synthetic C_{40} diol **1** and **1** derived from *archaea* lipid displayed identical ^{13}C NMR spectra. All the resonance signals were assigned by 2D NMR spectroscopic techniques. Optical rotations of $[\alpha]_{436}^{20} = +14.7$ ($c = 1.00$, $CHCl_3$) for the synthetic diol **1** and $[\alpha]_{436}^{20} = +15.5$ ($c = 1.00$, $CHCl_3$) for the natural derived diol **1** were found. Thus, there is agreement within the range of precision of the measurement of optical rotation. Considering also the large differences in the optical rotations of the model compounds **2a–d** the proposed configuration of diol **1** is strongly supported.

In conclusion, the absolute and relative configuration of an *archaea* membrane lipid containing five-membered rings was determined for the first time. This was accomplished by

 © 2003 Wiley-VCH Verlag GmbH & Co. KGaA, Weinheim

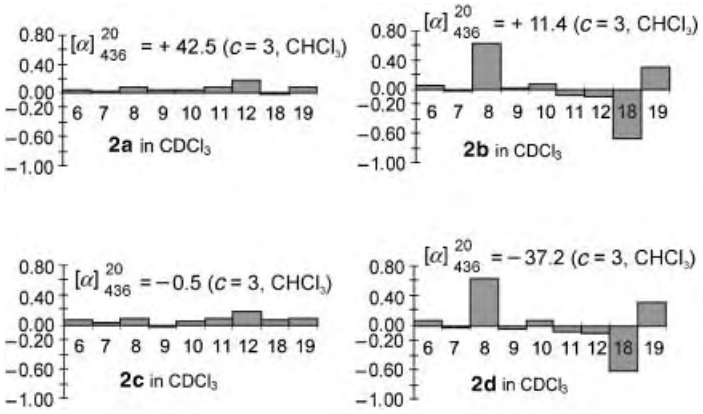
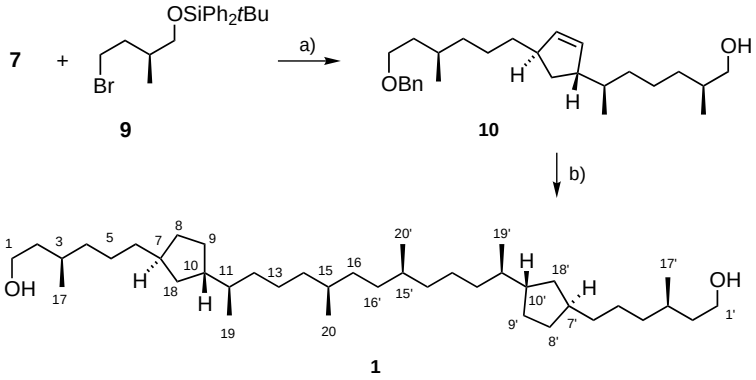


Figure 1. Differences in ^{13}C NMR chemical shifts of samples of diol **1** obtained by degradation of *Archaea* membrane lipids and of synthetic compound **2a–d** (125 MHz, $CDCl_3$). The *x* axis gives the number of the carbon atom and *y* axis the $\Delta\delta$ (δ(**2**)−δ(**1**)). In addition the optical rotations of **2a–d** are given.



Scheme 3. Synthesis of diol **1**. a) 1. **9**, Mg, THF, 65 °C; 2. 5 mol% Li_2CuCl_4, THF, −70 °C; 3. **7**, −70 °C→RT, ≈12 h; 4. Bu_4NF, THF, 85% (2 steps); b) 1. CBr_4, Ph_3P, Et_2O, RT, ≈12 h; 2. Mg (0.5 equiv), THF, 65 °C, 5 mol% Li_2CuCl_4, THF, 65 °C; 3. PtO_2, EtOAc, 2 h; 4. $Pd(OH)_2/C$, H_2, 4 bar, 38% (4 steps). Ts = *p*-toluenesulfonyl, DME = dimethoxyethane.

synthesis of the four model compounds **2a–d** and the diol **1** and comparison of their NMR spectroscopic and optical rotation data with those of diol **1** derived from natural *archaea* lipids.

Received: November 25, 2002 [Z50629]

Keywords: *archaea* membrane lipids · asymmetric synthesis · configuration determination · cross-coupling · natural products

[1] a) C. R. Woese, O. Kandler, M. L. Wheelis, *Proc. Natl. Acad. Sci. USA* **1990**, *87*, 4576–4759; b) G. Darland, T. D. Brock, W. Samsonoff, S. F. Conti, *Science* **1970**, *170*, 1416–1418; c) K. O. Stetter, *Naturwissenschaften* **1985**, *72*, 291–301; d) T. D. Brock, *Science* **1985**, *230*, 132–138.

[2] a) S. Thurl, PhD thesis, Technische Universität, Munich, **1986**; b) Y. Blériot, E. Untersteller, B. Fritz, P. Sinaÿ, *Chem. Eur. J.* **2002**, *8*, 240–246; c) A. J. Fairbanks, P. Sinaÿ, *Tetrahedron Lett.* **1995**, *36*, 893–896; d) M. De Rosa, A. Gambacorta, A. Gliozzi, *Microbiol. Rev.* **1986**, 70–80.

[3] "Archaeal Lipids": M. De Rosa, A. Gambacorta in *Chemical Methods in Bacterial Systematics* (Eds.: M. Goodfellow, A. G. O'Donell), Wiley, Chicester, **1994**, pp. 197–264.

[4] a) T. Eguchi, K. Arakawa, T. Terachi, K. Kakinuma, *J. Org. Chem.* **1997**, *62*, 1924–1933; b) T. Eguchi, T. Terachi, K. Kakinuma, *J. Chem. Soc. Chem. Commun.* **1994**, 7–8.

[5] a) C. H. Heathcock, B. L. Finkelstein, E. T. Jarvi, P. A. Radel, C. R. Hadley, *J. Org. Chem.* **1988**, *53*, 1922–1942.

[6] T. Eguchi, K. Ibaragi, K. Kakinuma, *J. Org. Chem.* **1998**, *63*, 2689–2698.

[7] a) M. De Rosa, S. De Rosa, A. Gambacorta, L. Minale, J. D. Bu'Lock, *Phytochemistry* **1977**, *16*, 1661–1965; b) M. De Rosa, S. De Rosa, *Phytochemistry* **1977**, *16*, 1909–1912.

[8] a) L. L. Yang, A. Haug, *Biochim. Biophys. Acta* **1979**, *573*, 308–320; b) H. Hanselaer, P. De Clercq, *Org. Magn. Reson.* **1980**, *13*, 376–379; c) M. Christl, H. J. Reich, J. D. Roberts, *J. Am. Chem. Soc.* **1971**, *93*, 3463–3468.

[9] a) G. Knühl, P. Sennhenn, G. Helmchen, *J. Chem. Soc. Chem. Commun.* **1995**, 1845–1846; b) S. Kudis, G. Helmchen, *Angew. Chem.* **1998**, *110*, 3210–3212; *Angew. Chem. Int. Ed.* **1998**, *37*, 3047–3050; c) S. Kudis, G. Helmchen, *Tetrahedron* **1998**, *54*, 10449–10456.

[10] a) V. K. Aggarwal, N. Monteiro, G. J. Tarver, R. McCague, *J. Org. Chem.* **1997**, *62*, 4665–4671.

[11] a) D. Curran, M.-H. Chen, D. Leszczweski, R. L. Elliott, D. M. Rakiewicz, *J. Org. Chem.* **1986**, *51*, 1612–1614; b) H. L. Goering, S. S. Kantner, *J. Org. Chem.* **1984**, *49*, 422–426.

[12] a) M. Tamura, J. Kochi, *Synthesis* **1971**, 303–305; b) G. Fouquet, M. Schlosser, *Angew. Chem.* **1974**, *86*, 50–51; *Angew. Chem. Int. Ed. Engl.* **1974**, *13*, 82–83.

[13] A. G. Schultz, T. J. Guzi, E. Larsson, R. Rahm, K. Thakkar, J. Bidlack, *J. Org. Chem.* **1998**, *63*, 7795–7805.

[14] The mixture of lipids was obtained from Bernina Biosystems, Munich. Degradation was carried out according to a method developed in the Arigoni goup (O. W. Gräther, PhD thesis, ETH Zürich, **1994**): reaction with HI followed by treatment of the resultant iodides with silver acetate to give acetates which were saponified.

[15] B. Gabler, PhD thesis, Universität Heidelberg, **1997**.

 © 2003 Wiley-VCH Verlag GmbH & Co. KGaA, Weinheim

Reduction of a Gallium Cluster

$[Ga_9(CMe_3)_9]^{\cdot-}$—a Persistent Cluster Radical Anion, Boron-Analogous Chemistry with the Heavier Homologue Gallium**

Werner Uhl, Lars Cuypers, Wolfgang Kaim, Brigitte Schwederski, and Rainer Koch*

Recently, we isolated the compound $Ga_9(CMe_3)_9$ (**1**)[1] which is a unique neutral cluster compound in the field of the heavier elements of the third main-group. Its molecular core consists of nine gallium atoms in an oxidation state +1, arranged as a tricapped trigonal prism elongated parallel to its threefold rotation axis. Similar boron clusters were reported with the subhalides B_9X_9 (X = Cl, Br), which gave the isolable and well-characterized anions $[B_9X_9]^-$ and $[B_9X_9]^{2-}$ on reduction.[2] According to the Wade rules the dianions may be described as closo clusters, while the monoanions represent nice examples of persistent cluster radical anions. Compared to the neutral boranes both anions are compressed along the threefold rotation axis.[2] Thus, compound **1** offers a the chance to systematically verify similarities or differences in the chemical behavior of boron and its heavier homologue gallium.

The redox potential for the reversible transfer of one electron to the cluster **1** was determined by cyclic voltammetry to be −1.74 V (relative to $[Fe(C_5H_5)_2]^{0/+}$).[1] A second reduction at a quite negative potential (−2.7 V) was found to be irreversible. To synthesize the corresponding radical we tried to reduce **1** by treatment with alkali metals in *n*-hexane, toluene, or THF, however, none of the reactions was successful. Decamethylcobaltocene seemed to be a suitable reducing agent,[3] strong enough for the reduction of **1** and soluble enough to allow the homogeneous reaction in organic solvents. We treated **1** with the metallocene in equimolar quantities in 1,2-difluorobenzene[4] and isolated deep green crystals of the product **2** [Eq. (1)], which, as a sign of a successful reaction, are insoluble in nonpolar solvents, such as pentane. Owing to its paramagnetism **2** did not give resolved NMR spectra.

$$Ga_9(CMe_3)_9\ (\mathbf{1}) + [Co(C_5Me_5)_2] \rightarrow [Co(C_5Me_5)_2]^+[Ga_9(CMe_3)_9]^-\ (\mathbf{2}) \quad (1)$$

[*] Prof. Dr. W. Uhl, Dr. L. Cuypers
Fachbereich Chemie der Philipps Universität Marburg
Hans-Meerwein-Strasse
35032 Marburg (Germany)
Fax: (+49) 6421-282-5653
E-mail: uhl@chemie.uni-marburg.de
Prof. Dr. W. Kaim, Dr. B. Schwederski
Institut für Anorganische Chemie
Universität Stuttgart (Germany)
Dr. R. Koch
Fachbereich Chemie der Carl von Ossietzky Universität Oldenburg (Germany)

[**] This work was supported by the Deutsche Forschungsgemeinschaft and the Fonds der Chemischen Industrie.

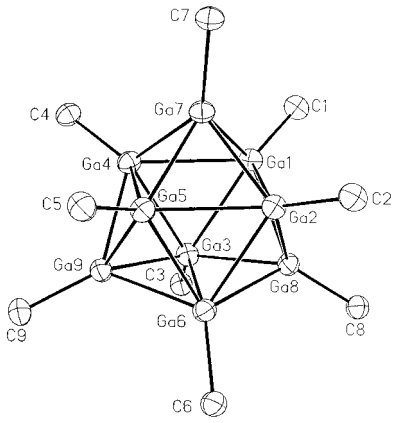


Figure 1. Molecular structure of the anion of **2**; only the α carbon atoms of the *tert*-butyl groups are shown. Selected bond lengths [pm]: Ga–Ga separations to the capping Ga atoms (Ga7, Ga8, Ga9): 254.67(5)–257.09(6) (av. 255.8), Ga–Ga separations along the edges of the triangles of the prism between the atoms Ga1, Ga3, Ga4 and Ga2, Ga5, Ga6: 273.57(6)–277.22(6) (av. 274.8), Ga1-Ga2 279.70(6), Ga3-Ga6 284.17(6), Ga4-Ga5 280.65(6) (av. 281.5), Ga-C 203.8 (av.).

The crystal-structure determination of **2**[5] revealed an ionic compound, $[Ga_9(CMe_3)_9]^-[Co(C_5Me_5)_2]^+$ (Figure 1), which possesses a deltahedral cluster radical anion and the 18 electron decamethylcobaltocenium cation. While the overall structure of **2** with a tricapped trigonal-prism core is quite similar to that of the starting compound **1**, there are significant differences with respect to the Ga–Ga separations. These differences are most pronounced along the edges of the trigonal prism parallel to the threefold rotation axis (Ga1–Ga2, Ga3–Ga6, Ga4–Ga5). Rather long distances of 298.8 pm were observed between these pairs of atoms in the neutral nonagallium compound **1**, which indicate only negligibly weak direct Ga–Ga bonding interactions. The addition of one electron causes a compression of the prism, and these distances are shortened significantly by 17 pm to 281.9 pm. Simultaneously, the edges of the triangles of the trigonal prism lengthen from 267.0 to 274.6 pm so that a more regular prism results. Smaller changes arose with respect to the distances to the capping gallium atoms (Ga7, Ga8, Ga9), which are shortened from 258.8 in **1** to 255.8 pm in **2**. For comparison, the Ga–Ga separations in tetrahedral clusters $Ga_4[C(SiMe_2R)_3]_4$ are on average 269 pm.[6] Standard structural parameters were observed for the cobaltocenium cation.[7] The compression of the cluster is comparable to that observed with boron subhalides. Thus, with respect to reactivity and bonding properties, there is a remarkably high similarity in the chemical behavior of boron and gallium clusters E_nR_n even though the reduction potentials for the halogenated boron clusters are much less negative than those of **1**.[2]

The changes in the cluster skeleton accompanying the formation of the radical anion are in complete accordance with the results of quantum-chemical calculations. The bonding in the neutral cluster is determined by interactions between the capping and the prism gallium atoms, which may be described by six Ga(prism)-Ga(cap)-Ga(prism) three-center bonds. In contrast, the direct interactions between the prism atoms are of negligible significance. The single electron

 © 2003 Wiley-VCH Verlag GmbH & Co. KGaA, Weinheim DOI: 10.1002/anie.200351123

of the radical anion is essentially localized in the p orbitals of Ga atoms (0.993 e^-), with the capping Ga atoms bearing most of the additional charge (80%). Mixing with the antibonding orbitals of the three-center bonds makes an important contribution to the stabilization of the cluster, which causes the shortening of the Ga–Ga separations along the edges of the prism parallel to the threefold rotation axis. Furthermore, this stabilization causes a slight shortening of the distances between the capping atoms and the atoms of the prism, as observed experimentally. The frontier orbitals of the neutral cluster and the radical anion are almost identical. The LUMO of **1** becomes semi-occupied through the addition of the unpaired electron in the transformation of neutral **1** into anionic **2**. That semi-occupied molecular orbital (SOMO) may pictorially be described as a belt across the rectangular faces of the prism mainly formed by p orbitals of the capping Ga atoms, which are arranged tangentially to the surface of the cluster and which are stabilized by contributions of the p orbitals of the prism atoms. The bond parameters predicted by theory as well as their alterations[8] are in excellent agreement with the values obtained by experiment.

An EPR signal of compound **2** was obtained only at low temperatures ($T < 110$ K). This fast-relaxation behavior is not unexpected for cluster radicals of the heavier main-group elements[9] and indicates closely arranged paramagnetic states and some contribution of spin-orbit coupling. Also, in a diluted, glassy frozen 1,2-difluorobenzene solution the signal is poorly resolved as a consequence of numerous overlapping lines of the complicated hyperfine structure (^{69}Ga: $I = {}^3/_2$, 60.1%; ^{71}Ga: $I = {}^3/_2$, 39.9%). A considerable, almost axial *g*-anisotropy ($g_{1,2} = 2.11$, $g_3 = 1.98$) was detected. The coupling constants to the metal atoms were estimated to be $a < 3$ mT, which in accordance with the *g*-factors verifies an at least partial spin delocalization in the cluster.[9]

With few exceptions, such as the tetrahedral tetragallium compounds, the cluster chemistry of gallium is dominated by metal-atom-rich metalloid skeletons,[10] which adopt structures quite different from those of the well-known deltahedral boron clusters.[11] In particular the facile synthesis of **2** by reduction of the neutral cluster **1** and the changes in the structural parameters connected with that electron transfer impressively show, however, the strong relationship between the heavier elements of the third main-group and their lightest homologue boron. The icosahedral compound $K_2[Al_{12}i Bu_{12}]$ shows a similar close relation between aluminum and boron.[12]

Experimental Section

1,2-Difluorobenzene was dried over molecular sieves (4 Å). $Ga_9(CMe_3)_9$[1] (0.151 g, 0.132 mmol) was dissolved in (7 mL) and added at room temperature to a solution of decamethylcobaltocene (0.047 g, 0.143 mmol)[3] also in 1,2-difluorobenzene (5 mL). The mixture was stirred for 1 h, color changed slightly from green to bright green. Two thirds of the solvent was removed in vacuum at room temperature. Dark green crystals of **2** were obtained by cooling the solution to −30 °C (yield: 0.161 g, 83% based on **1**). Decomposition (under argon, sealed capillary): 191 °C. IR (paraffin, CsBr plates): $\tilde{\nu} = 1505$ m (Cp*), 1462 vs, 1376 vs (paraffin), 1352s, 1268 m δCH_3, 1204 w, 1157 vs, 1099 w, 1075 w, 1021 m νCC; 967 w, 932 w CH_3 (rocking), 807 s $\nu_{as}C_3C$, 753 s, 722 s (Cp*), 512 m, 444 m νGa_9C_9, 362 cm^{-1} m δC_3C. UV/Vis (*n*-hexane): λ_{max} [nm] (log ε): 290 (5.2), 480 (4.0), 600 (3.5). ESR: X-Band measurement in glassy frozen 1,2-difluorobenzene solution at 4 K.

Received: February 6, 2003 [Z51123]

Keywords: cluster compounds · electron-deficient compounds · gallium · radical ions

[1] W. Uhl, L. Cuypers, W. Kaim, M. Wanner, R. Winter, R. Koch, W. Saak, *Angew. Chem.* **2001**, *113*, 589; *Angew. Chem. Int. Ed.* **2001**, *40*, 566.

[2] L. M. McKee, Z.-X. Wang, P. von R. Schleyer, *J. Am. Chem. Soc.* **2000**, *122*, 4781; H. Binder, R. Kellner, K. Vaas, M. Hein, F. Baumann, M. Wanner, R. Winter, W. Kaim, W. Hönle, Y. Grin, U. Wedig, M. Schultheiss, R. K. Kremer, H. G. von Schnering, O. Groeger, G. Engelhardt, *Z. Anorg. Allg. Chem.* **1999**, *625*, 1059.

[3] J. L. Robbins, N. Edelstein, B. Spencer, J. C. Smart, *J. Am. Chem. Soc.* **1982**, *104*, 1882; N. Connelly, W. E. Geiger, *Chem. Rev.* **1996**, *96*, 877.

[4] T. R. O'Toole, J. N. Younathan, B. P. Sullivan, T. J. Meyer, *Inorg. Chem.* **1989**, *28*, 3923.

[5] Crystal structure of **2**: Single crystals from 1,2-difluorobenzene at −30 °C, one solvent molecule per formula unit of **2** enclosed; $C_{56}H_{111}CoGa_9 \cdot C_6H_4F_2$, monoclinic, $P2_1/n$; $a = 1796.40(9)$, $b = 2091.47(9)$, $c = 1968.0(1)$ pm, $\beta = 96.078(4)$, $V = 7352.4(6)$ Å^3, $Z = 4$, $\rho_{calcd} = 1.432$ g cm^{-3}, crystal dimensions: $0.35 \times 0.20 \times 0.10$ mm, diffractometer Stoe IPDS, $Mo_{K\alpha}$ radiation, 193 K, measurement range: $2.8 < 2\Theta < 49.9°$, 12767 independent reflections, 9222 reflections $F > 4\sigma(F)$, $\mu = 3.50$ mm^{-1}, numerical absorption correction (min./max. transmission 0.424/0.706), programs SHELXTL PLUS REL 4.1 and SHELXL-93, 708 parameters, $R1 = 0.034$ and w$R2$ (all data) $= 0.082$, max./min. residual electron density: $0.669/-0.599 \times 10^{30}$ e m^{-3}. CCDC 202836 (**2**) contains the supplementary crystallographic data for this paper. These data can be obtained free of charge via www.ccdc.cam.ac.uk/conts/retrieving.html (or from the Cambridge Crystallographic Data Centre, 12 Union Road, Cambridge CB2 1EZ, UK; fax: (+44) 1223-336-033; or deposit@ccdc.cam.ac.uk).

[6] W. Uhl, W. Hiller, M. Layh, W. Schwarz, *Angew. Chem.* **1992**, *104*, 1378; *Angew. Chem. Int. Ed. Engl.* **1992**, *31*, 1364; W. Uhl, A. Jantschak, *J. Organomet. Chem.* **1998**, *555*, 263.

[7] D. Bellamy, N. G. Connelly, G. R. Lewis, A. G. Orpen, *CrystEngComm* **2002**, *4*, 68; X. Xie, T. Hughbanks, *Inorg. Chem.* **2002**, *41*, 1824.

[8] Results obtained by quantum-chemical calculations (UHF/6-31G(D)) for the radical anion $[Ga_9Me_9]^-$: 253.8–255.1 pm to the bridging Ga atoms, 274.7–275.7 pm for the edges of the triangles of the prism, 280.8–282.7 pm for the edges of the prism parallel to the threefold rotation axis.

[9] A. Haaland, K.-G. Martinsen, H. V. Volden, W. Kaim, E. Waldhör, W. Uhl, U. Schütz, *Organometallics* **1996**, *15*, 1146.

[10] G. Linti, H. Schnöckel, *Coord. Chem. Rev.* **2000**, *206*, 285; A. Schnepf, H. Schnöckel, *Angew. Chem.* **2002**, *114*, 3682; *Angew. Chem. Int. Ed.* **2002**, *41*, 3533; M. Kehrwald, W. Köstler, A. Rodig, G. Linti, T. Blank, N. Wiberg, *Organometallics* **2001**, *20*, 860.

[11] Polyborate analogous gallium cluster not possessing a deltahedral structure: A. Schnepf, G. Stößer, H. Schnöckel, *Z. Anorg. Allg. Chem.* **2000**, *626*, 1676.

[12] W. Hiller, K.-W. Klinkhammer, W. Uhl, J. Wagner, A *ngew. Chem.* **1991**, *103*, 182; *Angew. Chem. Int. Ed. Engl.* **1991**, *30*, 179; a radical anion formed by six equivalent aluminum atoms was detected by EPR spectroscopy: C. Dohmeier, M. Mocker, H. Schnöckel, A. Lötz, U. Schneider, R. Ahlrichs, *Angew. Chem.* **1993**, *105*, 1491; *Angew. Chem. Int. Ed. Engl.* **1993**, *32*, 1428.

 © 2003 Wiley-VCH Verlag GmbH & Co. KGaA, Weinheim

RNA Repair

Site-Directed Alteration of RNA Sequence Mediated by an Engineered Twin Ribozyme**

*Rüdiger Welz, Katrin Bossmann, Christian Klug, Christian Schmidt, Hans-Joachim Fritz, and Sabine Müller**

Recently, RNA has become a focus of investigations into novel therapeutic schemes; antisense RNA,[1] interfering RNA[2] and *trans*-cleaving ribozymes[3] are used to silence undesired gene expression. As an additional option with its own therapeutic potential, ribozymes may also be employed to specifically alter RNA sequences.[4] A general method of manipulating at will any chosen patch of any given mRNA sequence could open the door to phenotypic correction of genetic disorders without interfering with the corresponding DNA. This strategy requires an agent which promotes, in a strictly controlled fashion, two chain-cleavage events and two ligations. Herein we show that an engineered RNA of only 141 nucleotides (HP-TW5), derived from the hairpin ribozyme by tandem duplication (hence dubbed "twin ribozyme"), meets all the functional requirements of such an approach. Twin ribozyme HP-TW5 inserts four nucleotides into a predetermined site of an arbitrary model RNA. In the process, 16 nucleotides of the residing substrate sequence are exchanged for 20 nucleotides which are added to the reaction mixture as a separate, synthetic "repair" fragment. Up to 30% of the initial substrate is converted into insertion product.

The hairpin ribozyme is derived from the (−)-strand of *Tobacco ringspot* virus satellite RNA and catalyses the site-specific cleavage of suitable RNA substrates, to generate fragments with a 2′,3′-cyclic phosphate and a free 5′-OH terminus.[5] In the reverse reaction, the oxygen atom of the free 5′-OH group of one RNA fragment attacks the phosphorus atom of the cyclic 2′,3′-phosphate group of another, which results, through ring opening and the release of a 2′-OH unit, in ligating the two fragments. Because of the special conformational dynamics of the hairpin ribozyme, bond scission and ligation reach equilibrium long before products are released and thus, compared to other small, catalytic RNAs, such as the hammerhead ribozyme, ligation is especially efficient.[6] We decided to exploit the cleavage and ligation activity of the hairpin ribozyme in a scheme of site-directed and patchwise exchange of RNA sequence. This process should be brought about by an engineered twin ribozyme that is derived from the hairpin ribozyme by tandem duplication, and that catalyses two chain-cleavage and two ligation events in position *trans*.

To mimic the repair, at the RNA level, of a small deletion, twin ribozyme HP-TW5 was designed to promote the insertion of four specific nucleotides into a predetermined site of an arbitrarily defined substrate RNA (Figure 1). In the ribozyme/substrate complex, a stretch of four nucleotides in

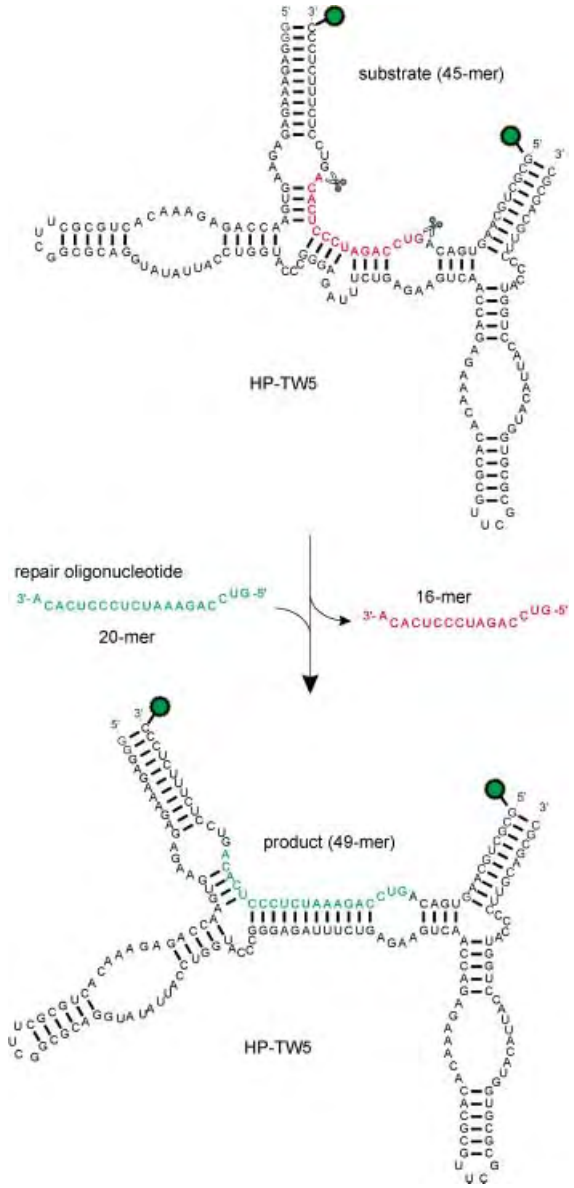


Figure 1. Reaction scheme for HP-TW5-mediated RNA repair. Substrate RNA is annealed to twin ribozyme HP-TW5 (top) and cleaved at two defined sites indicated by scissors symbols. The fragment extending between the two cleavage points (16-mer, red letters) is replaced on the ribozyme by the repair oligonucleotide (20-mer, green letters) which subsequently becomes ligated to the flanking substrate fragments to form the HP-TW5/product complex (bottom). Green circles indicate 5′- and 3′-terminal fluorescein moieties used for detection (see Figure 2).

[*] Dr. S. Müller, R. Welz, K. Bossmann, C. Schmidt
Institut für Chemie
Humboldt-Universität zu Berlin
Brook-Taylor-Strasse 2, 12489 Berlin (Germany)
Fax: (+49) 30-2093-7266
E-mail: s.mueller@chemie.hu-berlin.de
C. Klug, Prof. Dr. H.-J. Fritz
Abteilung Molekulare Genetik und Präparative Molekularbiologie
Institut für Mikrobiologie und Genetik der Georg-August-Universität Göttingen
Grisebachstrasse 8, 37077 Göttingen (Germany)

[**] This work was supported by Deutsche Forschungsgemeinschaft.

 © 2003 Wiley-VCH Verlag GmbH & Co. KGaA, Weinheim DOI: 10.1002/anie.200250611

the central part of the ribozyme strand (GAUU, see Figure 1), is looped out. Cleavage at both predetermined sites leads to a 16-mer that can easily dissociate from the ribozyme through the destabilizing influence of the single-strand loop. In contrast, the two RNA fragments flanking the cleavage sites form contiguous duplexes of 11 and 14 base pairs, respectively, and should thus preferentially remain bound to the ribozyme. The added "repair" oligonucleotide contains the four additional nucleotides complementary to the GAUU loop in the ribozyme strand. Hence, binding of this oligonucleotide to the gap left by dissociation of the 16-mer, extends the formerly interrupted double stranded stretch by four nucleotides and makes it, furthermore, contiguous. This feature, together with a moderate molar excess of repair oligonucleotide should favor product formation.

Validity of the experimental design was checked by analyzing the time course of the reaction. The assay is based on gel electrophoresis (in a DNA sequencer) of fluorescently labeled substrates and products in conjunction with numerical peak integration (for details see the Experimental Section).[7] Substrate RNA was incubated with an equimolar amount of ribozyme at 37 °C. The reaction was allowed to proceed for 4 h, after which the repair oligonucleotide (20-mer) was added in 2.7-fold excess (relative to the substrate) and the reaction left at 37 °C for another 2 h. Original data are presented in Figure 2. After 4 h, characteristic cleavage products are detected with 24 % of substrate RNA still present (Figure 2, lane 2). Addition of the repair fragment leads to formation of new products detected as two additional bands (lanes 3 and 4). These signals correspond to the 34/35-mers resulting from ligation of the 20-mer to either the 14- or 15-mer cleavage product and to the desired "repaired" RNA molecule (49-mer) resulting from ligation of the 20-mer to both fragments. Reaction for 2 h delivered 10 % of starting material as the 49-mer product with 5 % unprocessed substrate remaining (lane 3). After an additional 24 h at ambient temperature, further enrichment of products involving ligation to the repair 20-mer was observed and the ratio of product to initial substrate increased: 30 % of the substrate RNA was converted into 49-mer and 7 % left unchanged (lane 4).

The identity of the 49-mer product was established by sequence analysis (Figure 3). To this end, the reaction mixture of an analogous experiment (on a fivefold larger scale) was separated by gel electrophoresis and further enrichment of products involving ligation to the repair 20-mer was observed. The developing pattern was followed online and electrophoresis was stopped as soon as the peak of the 49-mer band had passed the laser beam (Figure 3 a). RNA was eluted from the gel, reverse transcribed, and the resulting cDNA amplified by polymerase chain reaction (PCR), then cloned and sequenced (see Experimental Section). As a reference, a sample of the initial substrate was treated identically (without prior gel electrophoresis). Figure 3 b shows the results of the electrophoresis of the two PCR products. Sequence analysis of the two samples delivered the data in Figure 3 c. Four independent clones of the 49-mer product were sequenced separately and with identical results (data not shown). Clearly, the tetranucleotide string AAUC has been inserted into the substrate sequence at the predetermined position.

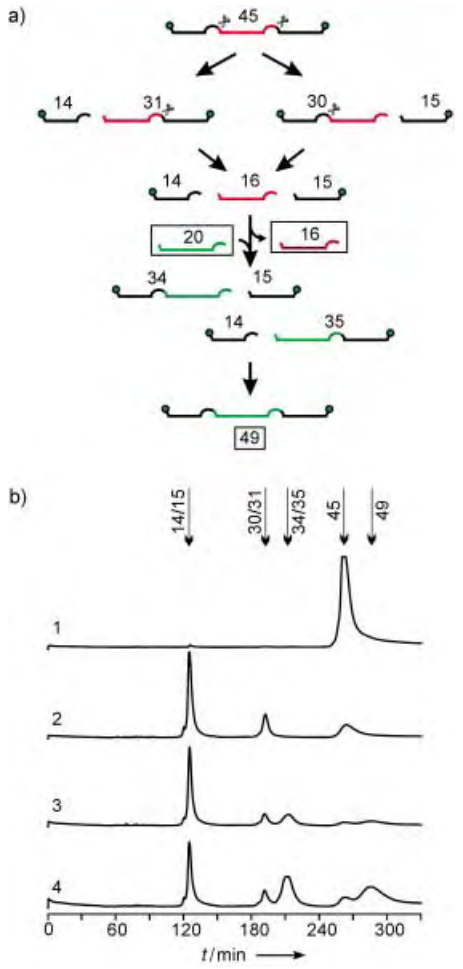


Figure 2. a) Fragmentation and ligation scheme (compare Figure 1). b) Monitoring the reaction. Lane 1: Start of cleavage reaction. Lane 2: Mixture after 4 h at 37 °C (immediately before addition of repair oligonucleotide). Lane 3: Mixture 2 h after addition of repair oligonucleotide (incubation at 37 °C continued). Lane 4: Mixture after an additional 24 h at room temperature (areas of peaks corresponding to chain lengths of 49 and 45 nucleotides indicate 30 % conversion to repair product and 7 % remaining substrate, respectively), for additional details see main text. Note that fragments differing in length by only one nucleotide are not resolved. This effect is a result of an accelerating influence of the 2′,3′-cyclic phosphate group on the 15-mer and differential effects of the fluorescein moiety at the 5′- or 3′-end. Peak heights are standardized by the data processing software so total peak integrals of different lanes are not constant.

The demonstration of feasibility of the new strategy described above makes it a model for the repair, at the RNA level, of a deletion mutation; the sequences bordering the deletion as well as the deletion itself had been defined arbitrarily. The basic hairpin ribozyme can be adapted to process different RNA sequences with remarkable flexibility and specificity[8] which should pave way for the design of twin ribozymes addressing genetic defects of medical relevance. Diseases that are caused by short deletions (e.g. Cystic Fibrosis[9]), are the most obvious first targets, but there is no reason to assume that the method should be confined to that class of mutations, even if one might expect that for replacements and insertions, the reaction could be less favored and

 © 2003 Wiley-VCH Verlag GmbH & Co. KGaA, Weinheim

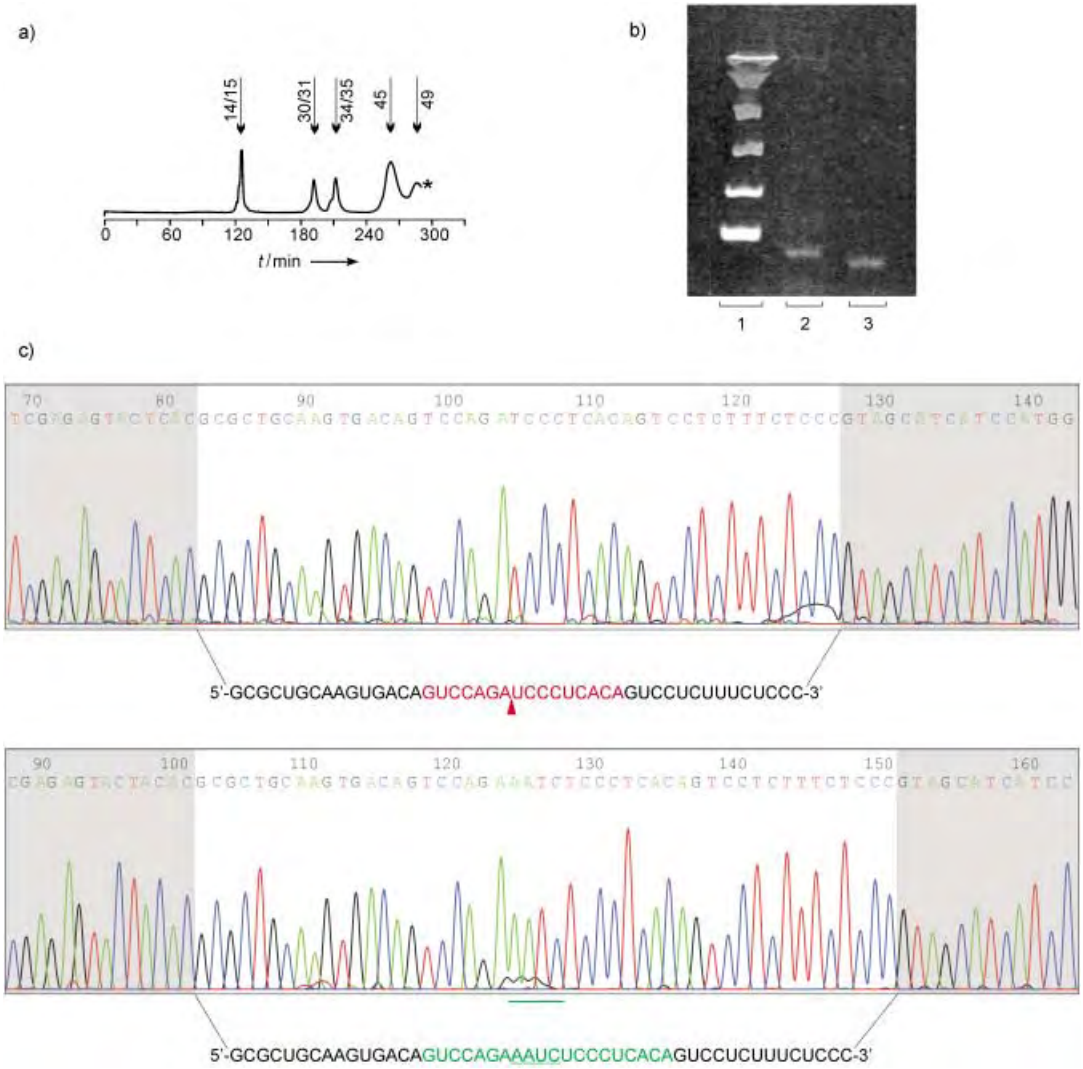


Figure 3. Product analysis. a) Tracing of preparative gel electrophoresis of reaction mixture (the asterisk denotes the time at which electrophoresis was stopped). b) Gel electrophoretic analysis (15% polyacrylamide) of PCR products. Lane 1: Marker DNAs; from bottom: 110, 147, 190, 242, 331, and 404 base pairs (bp). Lane 2: PCR product of cDNA obtained from the 49-mer eluted from preparative gel in (a) expected length: 96 bp. Lane 3: PCR of cDNA obtained from substrate RNA (expected length: 92 bp). c) DNA sequence analysis of PCR products derived from substrate (45-mer, top) and repair product (49-mer, bottom) after cloning in vector pCR4. The central windows correspond to substrate and product RNA sequence as indicated below the respective tracings, shaded flanking sequences are derived from PCR primers. The 16-mer replaced in the substrate sequence by the repair reaction is indicated in red; correspondingly, the sequence of the repair 20-mer is given in green. Within the substrate sequence, the red wedge indicates the target point of RNA repair; in the product sequence the inserted four nucleotides are underlined.

may require being driven by a larger excess of repair oligonucleotide.

Previously, an alternative scheme for correcting RNA sequences was introduced[4a] that exploits *trans* splicing by the group I intron ribozyme. In contrast to this latter system, which requires a large processing ribozyme fused to the reconstituting nucleotide segment plus the entire mRNA sequence downstream of the mutation, the twin ribozyme approach introduced here relies on a small ribozyme and a small repair oligonucleotide. The key advantage lies in that sequence alteration is achieved in a patchwise fashion and hence any accessible target sequence, irrespective of its location within the relevant mRNA, can be addressed with the same simple machinery. We expect this feature to enhance the prospects of RNA repair in future gene therapy.

Experimental Section

Synthesis of the twin ribozyme HP-TW5, the substrate, and the repair oligonucleotide. The twin ribozyme was transcribed in vitro from a double-stranded DNA template using T7 RNA polymerase.[7b] The template (total length: 158 base pairs) was generated from two synthetic DNAs (BioTeZ, Berlin), each 97 nucleotides long: 5′-TAA TAC GAC TCA CTA TAG GGA GAA AGA GAG *AAG TGA ACC AGA GAA* ACA CTG CGC TTC GGC G**CA GGT ATA TTA CCT GGT ACC CGG GAG ATT TCT GAG A**-3′ and 5′- GCG CTG CAA GGG *GTA CCA GGT AAT GTA* CCA CGC GCG AAC GCG TGT GTT TCT CTG GTT GAC T**TC TCA GAA ATC TCC CGG GTA CCA GGT AAT ATA CCT G**-3′. At their 3′-ends, the two strands overlap by 36 complementary bases (bold letters). To suppress spurious annealing, two short DNA fragments, 5′-TTC TCT GGT TCA CTT-3′ and 5′-TAC ATT ACC TGG TAC-3′ (BioTeZ), were added; these are complementary, on each strand, to

 © 2003 Wiley-VCH Verlag GmbH & Co. KGaA, Weinheim

a region outside the 36-base-pair-long primer/template duplex (italics). Enzymatic strand extension was carried out using DNA polymerase I (MBI Fermentas). Reaction conditions and product purification were as described in ref. [7b]

RNA substrates were chemically synthesized and end-labeled with fluorescein moieties by using an automated synthesizer (Gene Assembler Special, Amersham Pharmacia Biotech), then purified as described in ref. [10] The repair 20-mer containing a 2′,3′-cyclic phosphate group, was generated from a chemically synthesized 29-mer 5′-GUCCAGAAAUCUCCCUCACAGUCCUCUUU-3′ by cleavage with a wild type hairpin ribozyme (HP-WTTL, see ref. [11] for structure and reaction conditions). The product was purified in the same manner as the transcripts (see above).

Repair assay: a ribozyme stock solution (1 μM; 4 μL) was added to a stock solution of Tris-HCl (100 mM; 8 μL), pH 7.5, the mixture was heated at 90 °C for 1 min followed by incubation at 37 °C for 15 min. A $MgCl_2$ solution (4 μL; 50 mM) and a spermine solution (50 mM; 0.8 μL) were added, and after further 15 min at 37 °C, the reaction was started by addition of a substrate stock solution (2 μL; 2 μM). After 4 h, a stock solution of repair oligonucleotide (20-mer; 1.2 μL; 9 μM) was added to give final concentrations of 200 nM ribozyme and 200 nM substrate, 40 mM Tris-HCl, pH 7.5, 10 mM $MgCl_2$, 2 mM spermine, and 540 nM repair oligonucleotide. 2 μL aliquots were taken at time intervals as indicated in Figure 2b and added to a urea solution (4 μL; 7 M) containing 50 mM EDTA to stop the reaction. The samples were analyzed using an A.L.F. DNA sequencer (Amersham Pharmacia Biotech); data were processed with A.L.F. Fragment Manager software as described in ref. [7b]

Product analysis: The repair assay described above was repeated on a fivefold larger scale with all other parameters kept constant. The reaction mixture was equally distributed among the 40 slots of the polyacrylamide gel (this corresponds to approximately the same load per slot as in the analytical experiment). Development of the electrophoresis pattern was followed online and electrophoresis was stopped as soon as the slowest band had passed the laser beam. A ribbon of about 4-mm width was cut out across the entire gel at a height corresponding to the location of the photodiode array. A portion of about one tenth of that ribbon was cut and placed into a 2-mL Eppendorf cup with holes pierced into both bottom and lid and with a piece of BT1-membrane (Schleicher&Schuell, Dassel, Germany) jammed under the lid. RNA was electroeluted from the gel and onto the membrane by keeping the Eppendorf cup in a Biotrap-device (Schleicher&Schuell) with the lid side facing towards the cathode at 120 mA for 2 h and 20 min.

For reverse transcription, the BT1-membrane, together with H_2O (48 μL) and primer RREP1 RT (1.5 μL; 10 μM: 5′-Biotinyl-GGG AGA AAG AGG AC) was heated to 98 °C for 90 s, followed by incubation at 50 °C for 10 min. Finally, 10-fold concentrated RT-buffer (6 μL; 500 mM Tris-HCl, pH 8.3, 400 mM KCl, 10 mM DTT), AMV-Reverse Transcriptase "Enhanced" (1.5 μL; Sigma, Taufkirchen, Germany) and dNTPs (3 μL; 2.5 mM each) were added and the mixture was incubated at 42 °C for 1 h, after which the BT1-membrane piece was transferred into a PCR-reaction-mixture consisting of H_2O (55 μL), DTT (10 μL; 100 mM), dNTPs (8 μL; 2.5 mM each), primer RREP1 UP (5 μL; 10 μM: 5′-*CAC GGT GCT CGA GAG TAC TAC AC*G CGC TGC AAG TGA CA), primer RREP1 LO(5 μL 10 μM: 5′-*GAG ATA TAC CAT GGA TGA TGC TAC* GGG AGA AAG AGG AC), 10-fold concentrated PCR-buffer (10 μL) and Ampli-Taq solution (1 μL; Perkin-Elmer, Rodgau-Jügesheim, Germany). Regular letters correspond to substrate/product sequence flanking the core stretch exchanged during the repair reaction. Temperature cycles for PCR were as follows: 2 min 94 °C, 1 min 45 °C, 1 min 72 °C (two initial cycles); 1 min 94 °C, 1 min 70 °C, 30 s 72 °C (additional 35 cycles); after the last cycle, the temperature was kept at 72 °C for another 10 min. The reaction product was analyzed by electrophoresis through a 12% denaturing polyacrylamide gel. The PCR-product was ligated into the pCR4-vector from Invitrogen (Karlsruhe, Germany) using the TOPO-TA-Cloning-Kit (Invitrogen). Subsequent transformation of TOP10 cells (50 μL; Invitrogen) was performed by electroporation.[12] Four independent clones were picked and subjected to DNA sequence analysis (ABI Prism 377 DNA Sequencer). The same procedure, without preparative gel electrophoresis, was carried out with substrate RNA (45-mer).

Received: November 22, 2002 [Z50611]

Keywords: base deletions · gene therapy · ribozymes · RNA

[1] a) A. R. van der Krol, J. N. Mol, A. R. Stuitje, *Biotechniques* **1988**, *6*, 958–976; b) B. A. Sullenger, T. C. Lee, C. A. Smith, G. E. Ungers, E. Gilboa, *Mol. Cell. Biol.* **1990**, *10*, 6512–6523.

[2] a) S. M. Elbashir, J. Harborth, W. Lendeckel, A. Yalcin, K. Weber, T. Tuschl, *Nature* **2001**, *411*, 494–498; b) G. Sui, C. Soohoo, B. Affar el, F. Gay, Y. Shi, W. C. Forrester, *Proc. Natl. Acad. Sci. USA* **2002**, *99*, 5515–5520; c) M. Miyagishi, K. Taira, *Nat. Biotechnol.* **2002**, *20*, 497–500; d) N. S. Lee, T. Dohjima, G. Bauer, H. Li, M. J. Li, A. Ehsani, P. Salvaterra, J. Rossi, *Nat. Biotechnol.* **2002**, *20*, 500–505; e) C. P. Paul, P. D. Good, I. Winer, D. R. Engelke, *Nat. Biotechnol.* **2002**, *20*, 505–508.

[3] a) G. Bauer, P. Valdez, K. Kearns, I. Bahner, S. F. Wen, J. A. Zaia, D. B. Kohn, *Blood* **1997**, *89*, 2259–2267; b) F. Wong-Staal, E. M. Poeschla, D. J. Looney, *Hum. Gene Ther.* **1998**, *9*, 2407–2425; c) R. G. Amado, R. T. Mitsuyasu, G. Symonds, J. D. Rosenblatt, J. Zack, L. Q. Sun, M. Miller, J. Ely, W. Gerlach, *Hum. Gene Ther.* **1999**, *10*, 2255–2270; d) N. Usman, L. M. Blatt, *J. Clin. Invest.* **2000**, *106*, 1197–1202; e) P. A. Pavco, K. S. Bouhana, A. M. Gallegos, A. Agrawal, K. S. Blanchard, S. L. Grimm, K. L. Jensen, L. E. Andrews, F. E. Wincott, P. A. Pitot, R. J. Tressler, C. Cushman, M. A. Reynolds, T. J. Parry, *Clin. Cancer Res.* **2000**, *6*, 2094–2103; f) D. G. Macejak, K. L. Jensen, S. F. Jamison, K. Domenico, E. C. Roberts, N. Chaudhary, I. von Carlowitz, L. Bellon, M. J. Tong, A. Conrad, P. A. Pavco, L. M. Blatt, *Hepatology* **2000**, *31*, 769–776.

[4] a) B. A. Sullenger, T. R. Cech, *Nature* **1994**, *371*, 619–622; b) J. T. Jones, S. W. Lee, B. A. Sullenger, *Nat. Med.* **1996**, *2*, 643–648; c) L. A. Phylactou, C. Darrah, M. J. Wood, *Nat. Genet.* **1998**, *18*, 378–381; d) T. Watanabe, B. A. Sullenger, *Proc. Natl. Acad. Sci. USA* **2000**, *97*, 8490–8494; e) N. Lan, R. P. Howrey, S. W. Lee, C. A. Smith, B. A. Sullenger, *Science* **1998**, *280*, 1593–1596.

[5] a) P. A. Feldstein, J. M. Buzayan, G. Bruening, *Gene* **1989**, *82*, 53–61; b) A. Hampel, R. Tritz, *Biochemistry* **1989**, *28*, 4929–4933.

[6] X. Zhuang, H. Kim, M. J. Pereira, H. P. Babcock, N. G. Walter, S. Chu, *Science* **2002**, *296*, 1473–1476.

[7] a) W. Gläsner, R. Merkl, S. Schmidt, D. Cech, H.-J. Fritz, *Biol. Chem. Hoppe-Seyler* **1992**, *373*, 1223–1225; b) C. Schmidt, R. Welz, S. Müller, *Nucleic Acids Res.* **2000**, *28*, 886–894.

[8] A. Berzal-Herranz, S. Joseph, J. M. Burke, *Genes Dev.* **1992**, *6*, 129–134.

[9] J. R. Riordan, J. M. Rommens, B. Kerem, N. Alon, R. Rozmahel, Z. Grzelczak, J. Zielenski, S. Lok, N. Plavsic, J. L. Chou, M. L. Drumm, M. C. Iannuzzi, F. S. Collins, L. C. Tsui, *Science* **1989**, *245*, 1066–1073.

[10] R. Welz, S. Müller, *Tetrahedron Lett.* **2002**, *43*, 795–797.

[11] R. Welz, C. Schmidt, S. Müller, *Biochem. Biophys. Res. Commun.* **2001**, *283*, 648–654.

[12] W. J. Dower, J. F. Miller, C. W. Ragsdale, *Nucleic Acids Res.* **1988**, *16*, 6127–6145.

 © 2003 Wiley-VCH Verlag GmbH & Co. KGaA, Weinheim

Cover Picture



Teresa Carlomagno,* Marcel J. J. Blommers,* Jens Meiler, Wolfgang Jahnke, Thomas Schupp, Frank Petersen, Dieter Schinzer, Karl-Heinz Altmann, and Christian Griesinger*

The powerful antitumor agents, the epothilones, bind to tubulin and interfere with microtubule dynamics. Until now, no high-resolution structure for the tubulin–epothilone complex was available. NMR spectroscopy studies provide a high-resolution structure of epothilone bound to tubulin and show two major conformational changes of epothilone relative to the free conformation. These results correlate well with chemical-modification data. These findings and NMR techniques are discussed in the Communications by Carlomagno and co-workers on pp. 2511 – 2517.

Contents

News

Clusters: P. Braunstein recognized ——— 2444

Metal Catalysis: S. Gibson promotes women scientists

Organic Chemistry: Focus on small rings

Books

Enzyme Kinetics ——— 2445 — Alejandro G. Marangoni — *reviewed by M. Bertau*

Organic Ion Radicals ——— 2445 — Zory V. Todres — *reviewed by M. Schmittel*

Drug Design ——— 2446 — Darren R. Flower — *reviewed by H. Kubinyi*

Concise Chemistry of the Elements 2447 — Sławomir Siekierski, John Burgess — *reviewed by T. M. Klapötke*

Highlights

Helical Molecules and Aggregates

C. Schmuck* ——— 2448 – 2452

Molecules with Helical Structure: How To Build a Molecular Spiral Staircase



Helical structures can be formed in different ways: In rigid molecules through steric interactions and in flexible molecules through intramolecular noncovalent interactions or through supramolecular associations.

Minireviews

DNA-Mediated Charge Transfer

H.-A. Wagenknecht* ——— 2454 – 2460

Reductive Electron Transfer and Transport of Excess Electrons in DNA

Checking the traps: The transport of excess electrons in DNA has great potential for DNA chip technology. Radiolysis studies, for example, with mitoxanton as the electron acceptor and new photochemical assays (see scheme) have given new insights into the mechanisms of these processes.

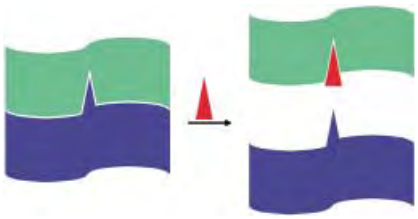


Reviews

Protein–Protein Interactions

T. Berg* ——— 2462 – 2481

Modulation of Protein–Protein Interactions with Small Organic Molecules



Does size matter? Can a drug-like molecule efficiently modulate the interaction between proteins in which the protein–protein interface (as indicated in the scheme) is many times larger than the small molecule itself? If so, how do you identify such organic molecules? Answers to these questions can be found in this review on the current research aimed at producing the next generation of drugs.

© 2003 Wiley-VCH Verlag GmbH & Co. KGaA, Weinheim

Communications

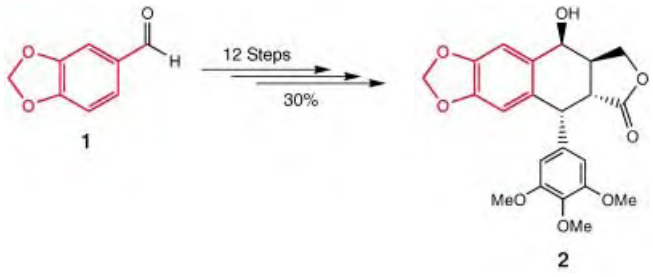
They do indeed exist, but not as expected: binary peroxide compounds of phosphorus. Whereas the peroxide P_2O_6 described by Schenk in 1937 still remains a presumption, the reaction of phosphorus(III) oxide with ozone at low temperature has led to the tetraozonide P_4O_{18} (see picture), the first defined binary peroxo compound of phosphorus. This is the oxygen-richest phosphorus compound known to date, and possibly could be used as a source for the generation of singlet oxygen under very mild conditions.



Tetraozonide of Phosphorus Oxide

A. Dimitrov, B. Ziemer, W.-D. Hunnius, M. Meisel* ——— **2484 – 2486**

The First Ozonide of a Phosphorus Oxide—Preparation, Characterization, and Structure of P_4O_{18}



1 2

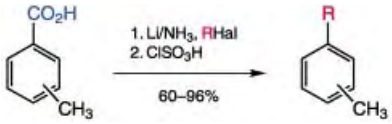
In only twelve steps the total synthesis of (−)-epipodophyllotoxin (**2**) has been completed starting from commercially available piperonal (**1**). The first stereocenter was formed under auxilary control, while the following epoxidation and radical cyclization proceeded with outstanding diastereoselectivity, which enabled the target molecule to be isolated in an overall yield of 30% and with 97% *ee*.

Epipodophyllotoxin Total Synthesis

U. Engelhardt, A. Sarkar, T. Linker* ——— **2487 – 2489**

Efficient Enantioselective Total Synthesis of (−)-Epipodophyllotoxin

Methyl-substituted arenes can be synthesized with high regioselectivity in only two steps through formal exchange of an aromatic carboxylic acid function with an alkyl substituent. The results obtained with toluic acid illustrate that good to very good yields can be obtained from inexpensive reagents (see scheme).



Regioselective Arene Alkylation

K. Vorndran, T. Linker* ——— **2489 – 2491**

Simple Two-Step *ipso* Substitution of Aromatic Carboxylic Acids by Alkyl Halides

For the USA and Canada:
ANGEWANDTE CHEMIE International Edition (ISSN 1433-7851) is published weekly by Wiley-VCH PO Box 191161, D 69451 Weinheim, Germany. Air freight and mailing in the USA by Publications Expediting Inc. 200 Meacham Ave., Elmont, NY 11003. Periodicals postage paid at Jamaica NY 11431. US POSTMASTER: send address changes to *Angewandte Chemie*, Wiley-VCH, 111 River Street, Hoboken, NJ 07030. Annual institutional subscription price for institutions: Europe € 2998.00/3148.00. Outside Europe US$ 3718.00/3904.00 (valid for print or electronic/print and electronic delivery); for individuals who are personal members of a national chemical society, or whose institution already subscribes, or who are retired or self-employed consultants, print only (including postage and handling charges): Europe € 248.00/Outside Europe US$ 348.00.

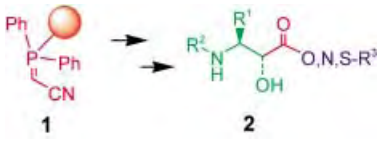
 © 2003 Wiley-VCH Verlag GmbH & Co. KGaA, Weinheim

Contents

Polymer-Supported Synthesis

S. Weik, J. Rademann* —— **2491 – 2494**

A Phosphorane as Supported Acylanion Equivalent: Linker Reagents for Smooth and Versatile C–C Coupling Reactions

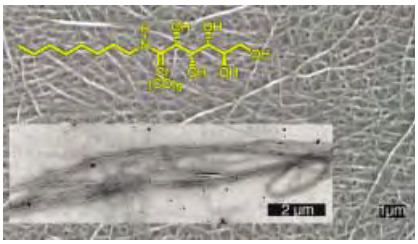


Smoothly linked: Polymer-supported phosphorane **1** is a C-nucleophile that can be acylated under mild reaction conditions. Diversely substituted α-ketocarbonyl and α-hydroxycarbonyl compounds **2** are furnished following to a reaction sequence including oxidative cleavage of the supported phosphoranes.

Organometallic Gelators

G. Bühler, M. C. Feiters, R. J. M. Nolte, K. H. Dötz* —— **2494 – 2497**

A Metal–Carbene Carbohydrate Amphiphile as a Low-Molecular-Mass Organometallic Gelator

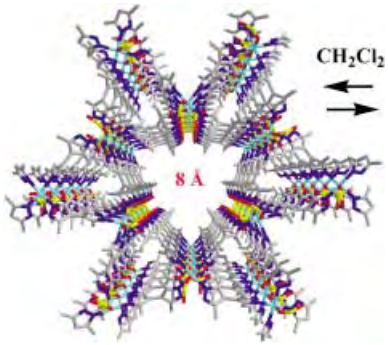


Stranded solvents: The aminocarbene chromium complex shown forms fiberlike aggregates of several μm length by self-assembly through noncovalent interactions. These strands allow an efficient immobilization of organic solvents in the form of a gel. The carbohydrate head group may induce supramolecular chirality in the aggregates.

Metal-Organic Zeolites

E. B. Rusanov, V. V. Ponomarova, V. V. Komarchuk, H. Stoeckli-Evans, E. Fernandez-Ibañez, F. Stoeckli, J. Sieler, K. V. Domasevitch* **2499 – 2501**

A Topology Paradigm for Metal-Organic Zeolites

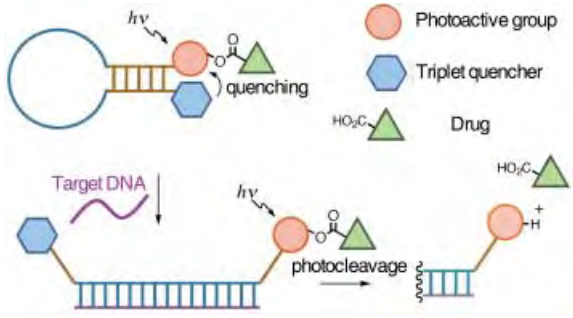


Unprecedented coordination polymers of hexagonal tungsten bronze topology represent a new type of metal–organic zeolites: the compounds have a microporous structure, they are thermally stable and are capable of the reversible adsorption of dichloromethane (see picture).

Phototriggered Molecular Release

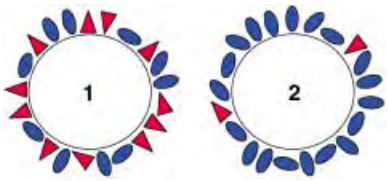
A. Okamoto, K. Tanabe, T. Inasaki, I. Saito* —— **2502 – 2504**

Phototriggered Drug Release from Functionalized Oligonucleotides by a Molecular Beacon Strategy



More than just a light switch: A phototriggered molecule-releasing system controlled through intramolecular triplet quenching by using a molecular beacon strategy with photoactive probe oligodeoxynucleotides (ODNs) has been developed (see picture).

 © 2003 Wiley-VCH Verlag GmbH & Co. KGaA, Weinheim

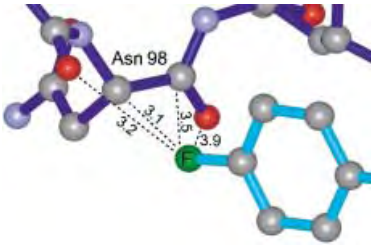


Positive discrimination: Confocal microscopy analysis has shown that TentaGel beads functionalized with unnatural carbohydrate-based ligands (**2**) can discriminate extremely well between carbohydrate-binding proteins labeled separately with fluorescein and tetramethylrhodamine (blue ellipsoids and red triangles, respectively) that recognize the same natural carbohydrate ligands (**1**, see schematic representation).

Carbohydrate Recognition

A. Basu, D. Kahne* ——— **2504 – 2506**

Overcoming Degeneracy in Carbohydrate Recognition

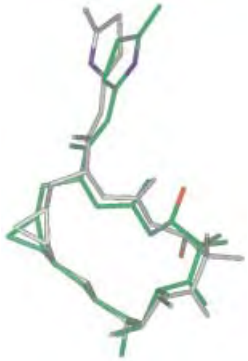


A highly fluorophilic environment comprising the H–C_α–C=O unit of Asn 98 in the active site of thrombin was identified by X-ray crystallography of a complex formed between the enzyme and a synthetic inhibitor (see partial X-ray structure, distances are in Angstroms). Short C–F···H–C_α and C–F···C=O contacts involving H–C_α–C=O fragments were also frequently observed in small-molecule X-ray crystal structures.

Mapping Enzyme Active Sites

J. A. Olsen, D. W. Banner,* P. Seiler, U. Obst Sander, A. D'Arcy, M. Stihle, K. Müller,* F. Diederich* ——— **2507 – 2511**

A Fluorine Scan of Thrombin Inhibitors to Map the Fluorophilicity/Fluorophobicity of an Enzyme Active Site: Evidence for C–F···C=O Interactions

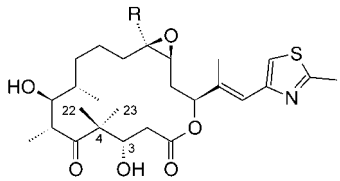


The tubulin-bound structure of epothilone A (shown in green) differs substantially from its free conformation (determined by X-ray crystallography, shown in gray). The new structural data correlate well with results from chemical modification experiments, giving a consistent picture of the functionally important regions of epothilone.

Structure of Bound Epothilone

T. Carlomagno,* M. J. J. Blommers* J. Meiler, W. Jahnke, T. Schupp F. Petersen, D. Schinzer, K.-H. Altmann C. Griesinger* ——— **2511 – 2515**

The High-Resolution Solution Structure of Epothilone A Bound to Tubulin: An Understanding of the Structure–Activity Relationships for a Powerful Class of Antitumor Agents



1a R = H (epothilone A)
1b R = CH_3 (epothilone B)

C–C torsion angles in HC-CCH_3 moieties can be measured by a new NMR experiment based on the measurement of CH–CH dipolar–dipolar cross-correlated relaxation rates and is demonstrated on a mixture of ^{13}C-labeled epothilone (**1**) and tubulin. The new pulse sequence is broadly applicable to any HC-CCH_3 moiety and therefore to a number of amino acid side chains in proteins.

Torsion Angles of Epothilones

T. Carlomagno,* V. M. Sánchez, M. J. J. Blommers, C. Griesinger* ——— **2515 – 2517**

Derivation of Dihedral Angles from CH–CH Dipolar–Dipolar Cross-Correlated Relaxation Rates: A C–C Torsion Involving a Quaternary Carbon Atom in Epothilone A Bound to Tubulin

 © 2003 Wiley-VCH Verlag GmbH & Co. KGaA, Weinheim

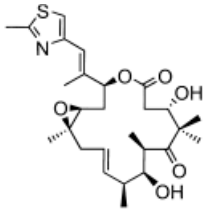
Contents

Antitumor Drugs

F. Yoshimura, A. Rivkin, A. E. Gabarda, T.-C. Chou, H. Dong, G. Sukenick, F. F. Morel, R. E. Taylor, S. J. Danishefsky* ——— **2518 – 2521**

Synthesis and Conformational Analysis of (*E*)-9,10-Dehydroepothilone B: A Suggestive Link between the Chemistry and Biology of Epothilones

The most potent epothilone analogue reported to date was obtained by incorporation of an *E* double bond at C9—C10 in the epothilone B series (see picture). Molecular modeling, NMR spectroscopic analysis, and chemical observations were used to rationalize the remarkable potency-enhancing effect of the double bond.



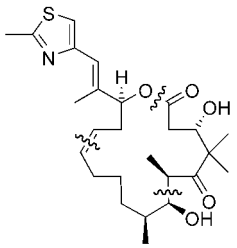
(*E*)-9,10-dehydroepothilone B

Solid-Phase Total Synthesis

R. I. Storer, T. Takemoto, P. S. Jackson, S. V. Ley* ——— **2521 – 2525**

A Total Synthesis of Epothilones Using Solid-Supported Reagents and Scavengers

A total synthesis of epothilone C (**1**) with concomitant formal synthesis of epothilone A is described, using immobilized reagents and scavengers to effect multistep synthetic transformations and purifications.

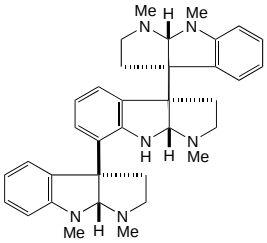


1

Alkaloid Total Synthesis

L. E. Overman,* E. A. Peterson ——— **2525 – 2528**

Enantioselective Total Synthesis of the Cyclotryptamine Alkaloid Idiospermuline



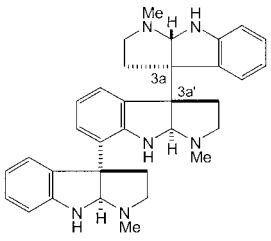
idiospermuline

Stereogenic quaternary carbons present the primary challenge in the syntheses of trispyrrolidinoindoline alkaloids such as idiospermuline. In its synthesis the two contiguous quaternary centers are expediently addressed by combining the lithium dienolate of a differentially protected dihydroisoindigo with a tartrate-derived electrophile. The third quaternary stereocenter is introduced by a catalytic asymmetric Heck reaction.

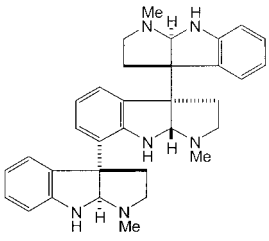
Alkaloid Total Synthesis

J. J. Kodanko, L. E. Overman* ——— **2528 – 2531**

Enantioselective Total Syntheses of the Cyclotryptamine Alkaloids Hodgkinsine and Hodgkinsine B



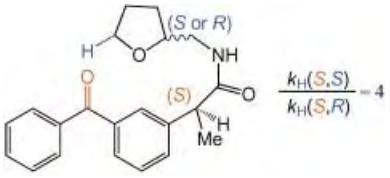
hodgkinsine



hodgkinsine B

A late-stage resolution of the *meso*-3a,3a′-bispyrrolidinoindoline unit of *rac*-**7** in a catalytic asymmetric transformation earmarks the remarkably short, ten-step, total syntheses of hodgkinsine and hodgkinsine B. The enantioselective total synthesis of hodgkinsine B establishes the relative and absolute configuration of this trispyrrolidinoindoline alkaloid.

 © 2003 Wiley-VCH Verlag GmbH & Co. KGaA, Weinheim



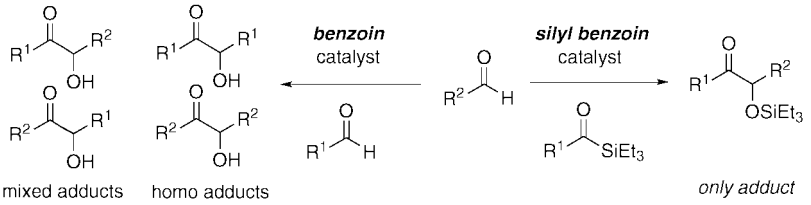
Chiral dyads of (*S*)-ketoprofen and (*S*)- or (*R*)-tetrahydrofurfurylamine show diastereomeric differentiation in photoinduced hydrogen abstractions, which could be directly followed by time-resolved observation of the ketone triplet state. A unimolecular rate constant of $k_H = 3.0 \times 10^5\ s^{-1}$ was found for the *S*,*S* diastereomer, while the *S*,*R* diastereomer reacts four times slower ($k_H = 7.5 \times 10^4\ s^{-1}$).

Photoinduced Hydrogen Abstraction

U. Pischel, S. Abad, L. R. Domingo, F. Boscá, M. A. Miranda* — **2531 – 2534**

Diastereomeric Differentiation in the Quenching of Excited States by Hydrogen Donors

---



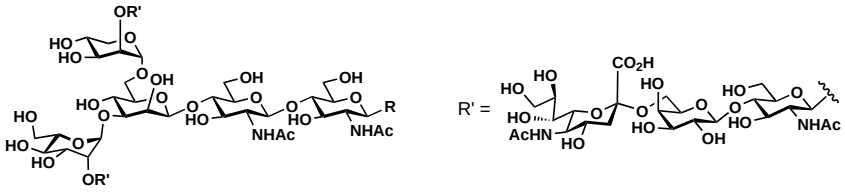
Side-stepping thermodynamics. In contrast to the traditional benzoin reaction, which can yield a mixture of homo and mixed adducts, only one regioisomer was obtained from the new cyanide-catalyzed silyl benzoin reaction between acylsilanes and aldehydes (see scheme).

Selective Benzoin Condensation

X. Linghu, J. S. Johnson* — **2534 – 2536**

Kinetic Control in Direct α-Silyloxy Ketone Synthesis: A New Regiospecific Catalyzed Cross Silyl Benzoin Reaction

---



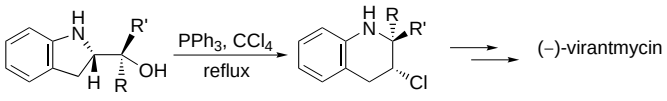
Egg yolk provided the starting disialyldecasaccharide for a highly efficient chemoenzymatic synthesis of a biantennary complex-type glycopeptide (see picture). Repetitive protection and deprotection steps required in oligosaccharide synthesis were thus avoided, and the desired glycopeptide was rapidly assembled on a solid phase (R = peptide).

Sialylglycopeptide Synthesis

N. Yamamoto, Y. Ohmori, T. Sakakibara, K. Sasaki, L. R. Juneja, Y. Kajihara* — **2537 – 2540**

Solid-Phase Synthesis of Sialylglycopeptides through Selective Esterification of the Sialic Acid Residues of an Asn-Linked Complex-Type Sialyloligosaccharide

---



Only nine steps away: PPh_3/CCl_4-mediated stereospecific rearrangement of α,α-disubstituted indoline-2-methanol to 2,2,3-trisubstituted optically active tetrahydroquinoline (see scheme) has been developed. The reaction was applied to the first total synthesis of natural virantmycin, in only nine steps from commercially available starting material.

Total Synthesis of Virantmycin

M. Ori, N. Toda, K. Takami, K. Tago, H. Kogen* — **2540 – 2543**

Stereospecific Construction of Contiguous Quaternary and Tertiary Stereocenters by Rearrangement from Indoline-2-methanol to 2,2,3-Trisubstituted Tetrahydroquinoline: Application to an Efficient Total Synthesis of Natural Virantmycin

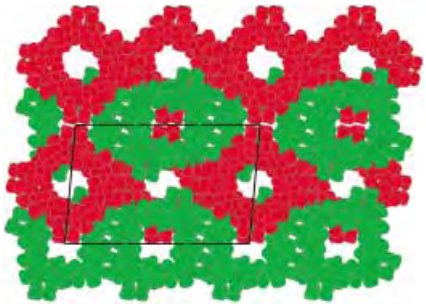
 © 2003 Wiley-VCH Verlag GmbH & Co. KGaA, Weinheim

Contents

Cyclic Dodecasaccharide Structure

M. Färnbäck, L. Eriksson, S. Senchenkova, K. Zych, Y. A. Knirel, Z. Sidorczyk, G. Widmalm* _____ **2543 – 2546**

Crystal Structure of a Cyclic Enterobacterial Common Antigen

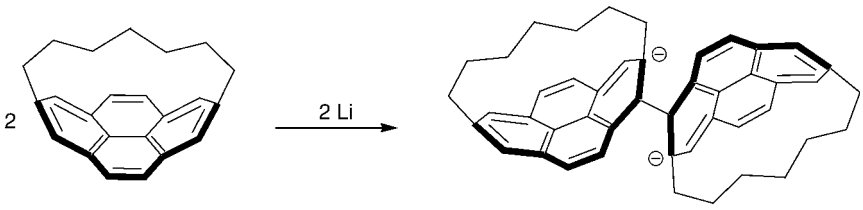


Two forms of a cyclic molecule, namely a rhomb and a square, are observed for an oligosaccharide, which has four repeating units that consist only of amino sugars (see picture). A relatively high water content (ca. 34%) can be discerned from the crystals, which were formed from a water/polyethylene glycol solution by utilizing a hanging-drop crystallization technique.

Pyrene Dimerization

I. Aprahamian, G. J. Bodwell, J. J. Fleming, G. P. Manning, M. R. Mannion, T. Sheradsky, R. J. Vermeij, M. Rabinovitz* _____ **2547 – 2550**

Reductive Dimerization of Tethered Pyrenes: Implications for the Reduction of Polcyclic Aromatic Hydrocarbons

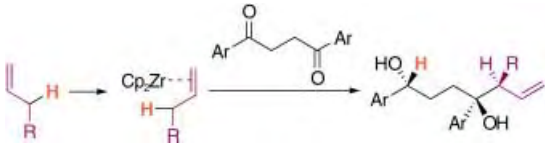


Pyrene reduction revisited: A reductive dimerization process is observed for strained pyrene derivatives, which occurs through single-electron reduction with lithium metal (see scheme). This process has implications for the reduction of pyrene itself. Various NMR methods can be utilized to characterize the products that result from such reactions.

Tandem Reduction–Allylation

K. Fujita, H. Shinokubo, K. Oshima* _____ **2550 – 2552**

Highly Diastereoselective Tandem Reduction–Allylation Reactions of 1,4-Diketones with Zirconocene–Olefin Complexes



Terminal alkenes act as dual nucleophiles in a zirconocene-mediated, highly 1,4-diastereoselective, tandem reduction–allylation reaction of 1,4-diketones. A zirconocene–alkene complex (in equilibrium with an allyl–zirconocene–hydride species) can deliver both hydride and an allyl group to a diketone, with control of the relative configuration of up to three new stereogenic centers (see scheme).

VIP Communications labeled with this symbol have been judged by two referees as being "very important papers".

The publication of Communications labeled with this symbol has been accelerated because of their topical or highly competitive nature.

Deadline for recruitment adverts

26/2003	June 12	Publication date: July 7
27/2003	June 20	Publication date: July 14

Angewandte Chemie International Edition
Advertising Sales Department:
Marion Schulz
Phone: 0 62 01 – 60 65 65
Fax: 0 62 01 – 60 65 50
E-Mail: MSchulz@wiley-vch.de

Place an advert in the printed version and have it made available online for 1 month, free of charge!

Service

Keywords _____ *2554*

Authors _____ *2555*

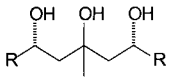
Vacancies _____ *A29*

Preview _____ *2557*

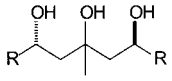
Corrigenda

In the Communication "Enantioselective C–C Bond Formation with Titanium(IV) Alkoxides—An Unusual Alkylation" by **R. Mahrwald** in *Angew. Chem. Int. Ed.* **2002**, *41*, 1361–1363 the structures of the triols **1a–c** and **2a–c** described therein must be revised. In fact **1a–c** and **2a–c** should be substituted, *meso*-configured tetrahydropyrans. Their identity was ascertained by comparison with X-ray crystal structure analyses of analogous compounds during subsequent studies. The originally accepted CH activation during this reaction with titanium(IV) alkoxides is apparently not involved in the real reaction mechanism. Further addition of aldehydes to alcohols, instead of to the corresponding titanium(IV) alkoxides, suggests that an elimination–addition mechanism analogous to a Prins reaction is involved. All the results and their interpretation will soon be published in a full paper. The author apologizes to the readers and referees for the mistakes in the publication.

Incorrect formulas:

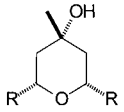


1a–c

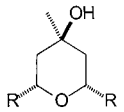


2a–c

Correct formulas:



1a–c



2a–c

In the Communication by **J. M. Thomas et al.** in *Angew. Chem. Int. Ed.* **2003**, *41*, 1520–1523 misleading statements were made in the first two sentences. The correct version is:

"The current, widely used and environmentally harmful industrial method of producing adipic acid (**2**) first entails the oxidation of cyclohexane in air, to a mixture of cyclohexanol and cyclohexanone using a homogeneous cobalt-containing catalyst. This mixture is then oxidized by nitric acid to adipic acid with extensive liberation of the greenhouse gas N_2O.[1,2]"

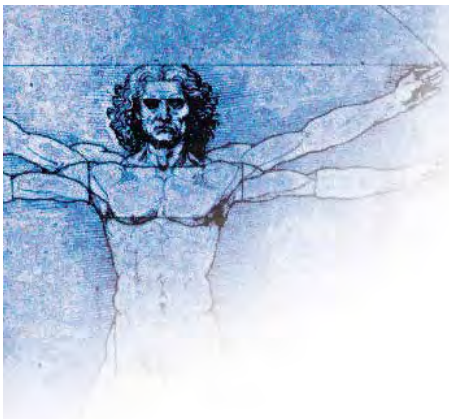
This replaces the passage:

"The current, widely used and environmentally harmful industrial method of producing adipic acid (**2**) first entails the oxidation of cyclohexane by nitric acid (with extensive liberation of the greenhouse gas N_2O) to a mixture of cyclohexanol and cyclohexanone.[1,2] This mixture is then rather inefficiently converted to adipic acid (and some other products) using a homogeneous cobalt-containing catalyst."

It has been drawn to the authors' attention (by Dr. J. H. Teles, BASF) that in current industrial practice in the production of adipic acid using nitric acid as an oxidant, the nitrous oxide liberated is decomposed to oxygen and nitrogen prior to release into the atmosphere, thereby avoiding environmental damage from this source.

In the legend to the cover picture on p. 2101 in Issue 19 of *Angew. Chem. Int. Ed.* the following acknowledgment was not included: "The authors thank B. Lafleuriel (CURRI-Visualization, ULP-Strasbourg) for generating the cover picture illustration." The editorial office apologizes for this omission.

 © 2003 Wiley-VCH Verlag GmbH & Co. KGaA, Weinheim



P. Braunstein Receives British and Italian Awards

Pierre Braunstein, CNRS research director at the University of Strasbourg (France), is to receive prestigious awards from both the British and the Italian Chemical Societies for his lifetime achievements. The research of his group is centered around coordination chemistry, in particular polytopic phosphorus ligands, enolate complexes, bimetallics with silicon ligands, and molecular clusters. He is the author of a Minireview on alkyl-, silyl-, and phosphane ligands in *Angewandte Chemie* and a co-editor of a reference work on metal clusters.[1] His Communication on "An Unusual Dynamic Fe-Hg-Pd Cluster with a Palladium(0) Fragment Stabilized by d^{10}–d^{10} Heterometallic Bonding" was featured on the cover of Issue 19/2003.[2] In 1993, Braunstein was elected Corresponding Member of the French Academy of Sciences and received the Grignard–Wittig Award from the French and German Chemical Societies in 1999.



P. Braunstein

This year, the Dalton (Inorganic) Division of the Royal Society of Chemistry (RSC) will award its Ronald Nyholm Lecture to him. It will be delivered on December 5, 2003, on the occasion of a symposium organized by the RSC and the Société Française de Chimie in Strasbourg. The title will be: "The chemistry of metals and ligands: new bonds, properties, and catalysts." The prize has been awarded annually by either the Dalton or the Education Division since 1973 in commemoration of the late Sir Ronald Nyholm, President of the RSC 1968–70. It is endowed with a silver medal and £ 500.

In addition, Braunstein is to receive the Paolo Chini Memorial Lecture from the Società Chimica Italiana (SCI) in memory of the late Professor Chini (University of Milan). It highlights progress in organometallic chemistry and has been awarded annually since 1981. The lecture on "Architectures and Functions Based on Metal–Metal Bonding" will be given on June 24, during the national meeting of the SCI in Torino (Italy).

S. Gibson: Giving Women Scientists More Visibility

This prize is not just for the winner: Part of the Rosalind Franklin Award presented by the Royal Society (Great Britain) is to be used for projects that raise the profile of women in science, engineering, and technology. As the first winner, Susan Gibson, Professor of Organic Chemistry at King's College in London (UK) will use part of the £ 30 000 to host prominent women scientists from around the world. "Giving women more visibility will help attract more women into science," she says.



S. Gibson

Her research group is interested in metal-mediated organic synthesis. Her Review announcing the catalytic age of the Pauson–Khand reaction was published in Issue 16/2003 of *Angewandte Chemie*. Therein, she points out how to meet the requirements of growing environmental awareness by designing synthetic metal-mediated transformations that involve only a catalytic use of toxic and expensive transition-metal species.[3]

Gibson is a member of the Editorial Board of *Chemistry—A European Journal*. She received her doctorate from the University of Oxford under the guidance of Stephen G. Davies and then worked with Albert Eschenmoser at ETH Zurich. She returned to the UK as a lecturer at the University of Warwick and, later, to Imperial College (London) before taking up a Chair at King's College in 1999. She is the mother of two children.

Small Rings with Large Impact

Under the guest editorship of Armin de Meijere, a thematic issue of *Chemical Reviews* devoted to cyclopropanes and related small rings was just published. The issue contains 18 contributions by chemists from all over the world. Recent progress regarding these seemingly fragile structures is presented: Topics range from spectroscopy to synthetic methodology and natural products. Heterocycles are discussed as well as asymmetry. "How far can we get a carbon atom and its homologues to bend their preferred bonding angles and accomodate unusual bonding situations?" de Meijere wonders in the introduction.

De Meijere has been a full professor of Organic Chemistry at the University of Göttingen (Germany) since 1989. Besides small-ring systems, he is interested in organometallic complexes and catalysis in organic synthesis. He is a member of the Editorial Board of *Chemistry—A European Journal*.

[1] a) P. Braunstein, N. M. Boag, *Angew. Chem.* **2001**, *113*, 2493; *Angew. Chem. Int. Ed.* **2001**, *40*, 2427; *Angew. Chem. Int. Ed.* **2001**, *40*, 2947, b) P. Braunstein, L. A. Oro, P. R. Raithby (Eds.), *Metal Clusters in Chemistry*, Wiley-VCH, Weinheim, **1999**.

[2] W. Schuh, P. Braunstein, M. Bénard, M.-M. Rohmer, R. Welter, *Angew. Chem.* **2003**, *115*, 2211; *Angew. Chem. Int. Ed.* **2003**, *42*, 2161.

[3] S. E. Gibson (née Thomas), A. Stevenazzi, *Angew. Chem.* **2002**, *115*, 1844; *Angew. Chem. Int. Ed.* **2003**, *42*, 1800.

 © 2003 Wiley-VCH Verlag GmbH & Co. KGaA, Weinheim

Helical Molecules and Aggregates

Molecules with Helical Structure: How To Build a Molecular Spiral Staircase

*Carsten Schmuck**

Keywords:
arenes · conformation analysis · foldamers · helical structures

Helical Compounds

Molecules with helical structure have fascinated chemists for may years now. Due to their nonplanar structure, such molecules are inherently chiral and exhibit interesting optical and electronic properties. In principle, molecules with such unusual topologies[1] can be synthesized through three different approaches: First, in rigid molecules steric effects can be used to enforce a helical structure. This is the case, for example, in the long-known and well-studied helicenes and their derivatives.[2] An increasing *ortho* annulation of aromatic ring systems first causes an increasing steric interaction between the H atoms on the terminal rings, leading to a nonplanar conformation. When the number of annulated arenes further increases, the terminal rings will overlap, giving rise to a helical conformation. Second, flexible molecules without any biased conformation can also give rise to defined structures through stabilizing intramolecular noncovalent interactions.[3] A classical example is the α helix found in proteins, which is stabilized by intramolecular hydrogen bonds between the amide groups of amino acid i and $i+4$ within a linear peptide strand.[4] As a result of the flexible nature of the underlying molecule (the linear peptide strand), helix formation in this case is a dynamic equilibrium process. Therefore, stable helices are only formed from α amino acids with chain lengths of more than 10 amino acids. In shorter chains the noncovalent interactions are not strong enough to compensate for the unfavorable entropy change associated with the folding of the flexible molecule.[5] Third, helical structures can also be formed through supramolecular interactions[6] of two or more molecules. This is, for example, the case in DNA, in which intermolecular hydrogen bonds between two complementary base strands give rise to the well-known double-helical conformation.[7]

Even though these examples show that molecular spiral staircases of various types have been well-known for a long time,[8] especially in the last few years a number of new compounds with helical structures have been described. We wish to present herein some examples that demonstrate the different ways in which such helical structures can be obtained: covalent synthesis of rigid molecules, the folding of flexible molecules as a result of intramolecular interactions, and structure formation by supramolecular complexation.

Rigid Molecules with Helical Structures

Vollhardt and co-workers recently reported the synthesis of the first helical phenylene.[9] [n]Phenylenes consist of n alternating benzene rings fused to $n-1$ cyclobutadiene rings. Phenylenes with $n > 5$ become helical and are thus chiral. Phenylenes have a larger ring size than the classical helicenes as a result of the intermediate cyclobutadiene σ spacer. The synthesis involved multiple cobalt-catalyzed cyclotrimerizations of a suitable alkyne-substituted arene (Scheme 1). This alkyne **3** can be synthesized in good yields by palladium-catalyzed coupling of iodoarenes **1** with Me_3Si-substituted alkyne **2**. The nonyne **3** thus obtained undergoes cobalt-catalyzed cyclization to the [7]phenylene **4** with the simultaneous formation of nine rings, six of which are formal cyclobutadiene units with an estimated strain energy of 300 kcal mol^{-1}. Even though the yield of this reaction is only 2%, this synthesis represents a general approach, which can also be used for the synthesis of higher homologues such as [8]- and [9]phenylene.[9b] These phenylenes are orange solids with a helical structure (Figure 1). According to ^{1}H NMR studies, this structure also predominates in solution. The conformational stability of the phenylenes is much lower than that of the helicenes. Temperature-dependent NMR studies provide a barrier of activation for the inversion of [7]phenylene of only 12.6 kcal mol^{-1}. This is only a third of the value of that of the [7]helicene (41.7 kcal mol^{-1}[2c]). Phenylenes are therefore much more flexible than their smaller relatives. Accordingly, an enantiomeric separation was thus far not possible.

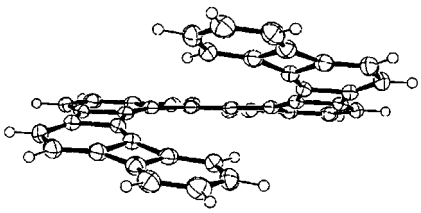
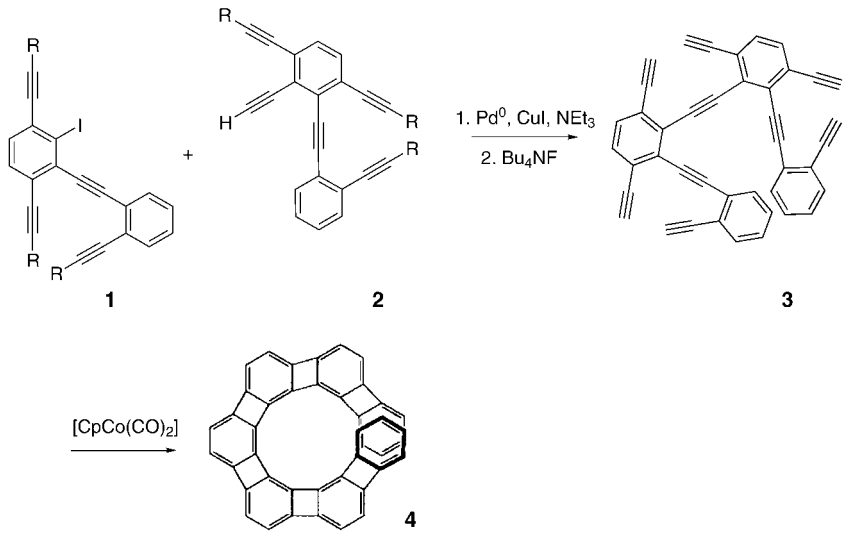


Figure 1. Structure of the helical [7]phenylene **4** in the solid state.

[*] Prof. Dr. C. Schmuck
Institut für Organische Chemie
Universität Würzburg
Am Hubland, 97074 Würzburg (Germany)
Fax: (+49) 931-888-4625
E-mail: schmuck@chemie.uni-wuerzburg.de

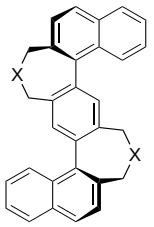
 © 2003 Wiley-VCH Verlag GmbH & Co. KGaA, Weinheim DOI: 10.1002/anie.200201625



1 2 3 4

Scheme 1. Synthesis of the cyclization precursor **3** by palladium-catalyzed Sonogashira coupling and its conversion into **4**. R = DMTS = dimethylthexylsilyl.

An alternative approach to rigid helical molecules represent the so-called "Geländer" helical molecules (molecules whose structure resemble the banisters of a spiral staircase) described

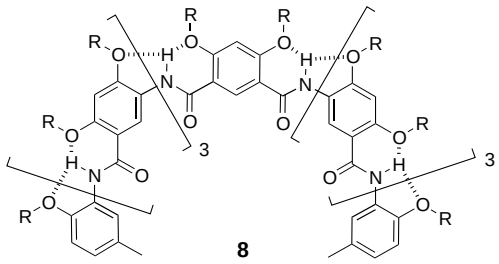


5

by Vögtle and co-workers.[10] These are *ortho*-bridged terphenylenes such as **5**, in which the helical structure results from steric interactions between the substituents *ortho* to the biaryl axis. Depending on the relative twist around each of the two biaryl axes, these molecules may exist in three different stable conformations: two enantiomeric chiral forms and one meso form. With suitable substituents at the terphenylene, the conformational stability is large enough that even an enantiomeric separation is possible.

Flexible Molecules with a Helical Secondary Structure

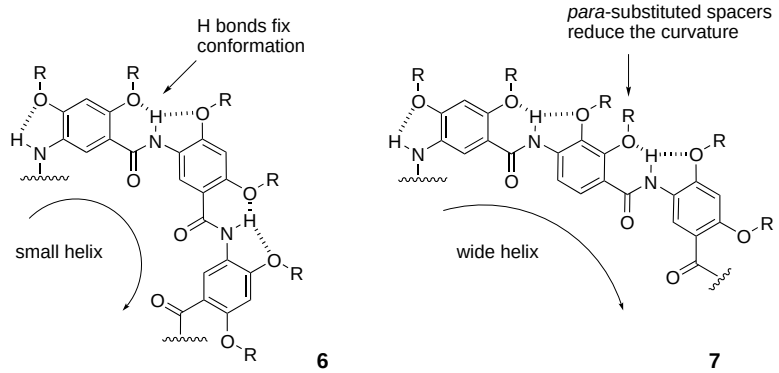
A new class of flexible molecules that adopt a helical conformation as a result of intramolecular interactions along their backbone are the oligoamides of general type **6**, which were recently introduced by Gong et al. (Scheme 2).[11] In these molecules, benzene rings are connected through amide bonds placed *meta* to each other on each benzene ring. Localized three-center hydrogen bonds between the amide hydrogen atom and alkoxy groups on the benzene ring lead to a curved conformation, which with increasing length of the oligoamide leads to helix formation. The nonamer **8** adopts, both in the solid state and in chloroform solution, a helical structure. As the amide linkages are slightly curved towards the NH side, the backbone is slightly opened up, leading to a helix with approximately seven benzene rings per turn and an inner diameter of 10 Å. The overlap of the last two aromatic rings in nonamer **8** within the helix can be proven spectroscopically by NOE interactions. According to these studies, the helical conformation seems to be predominant in solution. Even upon the addition of 50% DMSO to the solution in chloroform, the helical structure is still present, as the diagnostic NOE interactions of the two overlapping terminal rings can still be detected.



8

When *para*-aminobenzoic acid units are incorporated as linear spacers into the oligoamide, the diameter of the helix should increase (see **7**, Scheme 2). According to model calculations, the 21mer **9** (Figure 2), which consists of alternating *meta*- and *para*-connected building blocks, should form a helix with an inner diameter of 30 Å. An exact experimental structure elucidation was so far not possible. But again, in a spectroscopic study of solutions in chloroform, NOE interactions were detected, which suggest an interaction between the two ends of the oligoamide strand and hence indicate a helical conformation.

In contrast to the covalent helicenes or phenylenes, the structure of such



6 **7**

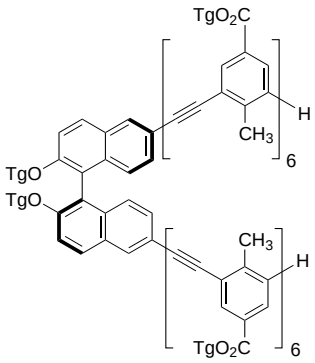
Scheme 2. Intramolecular hydrogen bonds stabilize a conformation within the oligoamides **6** and **7** and induces helix formation.

 © 2003 Wiley-VCH Verlag GmbH & Co. KGaA, Weinheim



Figure 2. The 21mer **9** adopts a helical conformation with a pore size of 30 Å according to preliminary NOESY studies.

foldamers strongly depends on external parameters. The conformation is based on intramolecular noncovalent interactions, whose strength is determined also by the surrounding factors such as the nature and polarity of the solvent.[12] Moore and Hill recently investigated the influence of 30 different solvents on the formation of helical structures in



Tg = $(CH_2CH_2O)_3CH_3$

10

conformationally flexible oligo(*m*-phenylene ethynylene) foldamers **10**.[13]

In this case, the intermolecular forces that give rise to helix formation are mainly hydrophobic or solvophobic interactions. Hence, with increasing polarity of the solvent, the extent of helical structures in the unfolded–folded conformational equilibrium increases, as could be shown by UV and CD spectroscopy (Figure 3). Whereas in chloroform mainly disordered random conformations predominate, a well-ordered helix is formed in methanol which is characterized by a strong Cotton effect. Depending on the solvent, nearly all helix ratios from 0 (completely unfolded) to 1 (completely folded) can be found.

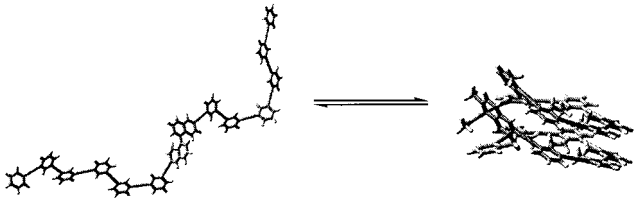


Figure 3. In the unfolded state (left), **10** contains both transoid and cisoid backbone conformations; in the helical conformation (right), only cisoid conformations occur.

An opposite effect of the solvent can be found in the oligopyridine amides **11** described by Lehn and co-workers (Scheme 3). The conformation of these oligomers, which are formed from alternating 2,6-diaminopyridine and 2,6-pyridinedicarboxylic acid units, is again based on hydrogen bonds.[14] An intramolecular interaction between the amide NH proton and the pyridine N atom is responsible for the curved conformation necessary for helix formation.

The X-ray single-crystal structure determination of **11** showed the presence of ellipsoid helices with an inner diameter of 5.5 ($n=2$) and 8 Å ($n=4$) (Figure 4). The longest strand examined so far, an undecamer ($n=4$), already extends to $2^1/_2$ helix turns. According to NMR spectroscopic studies, these helices are also present in chloroform solution. In DMSO however, at least the shorter oligomers do not adopt a helical conformation. The intramolecular hydrogen bonds are broken in DMSO as a result of competitive solvation of donor and acceptor sites by the solvent. Hence,

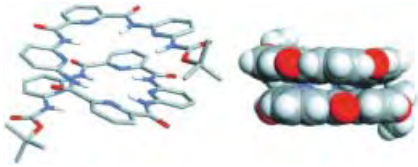
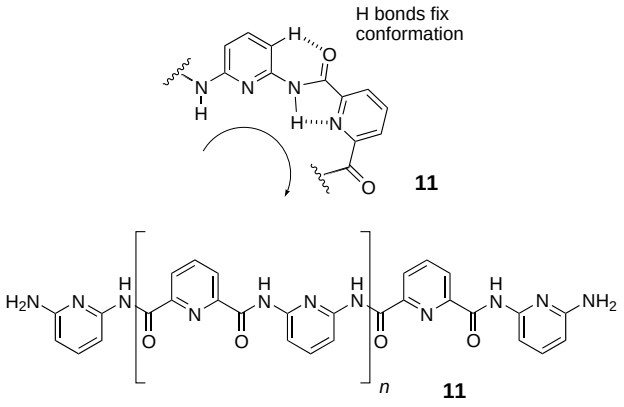


Figure 4. Solid-state structure of heptamer **11** ($n=2$).[14b]

the building blocks of the oligomer no longer adopt any preferred conformations and no stable secondary structure results.

Supramolecular helices

The oligoamide helices described by Lehn and co-workers can also further dimerize at higher concentrations, forming a stable double helix in solution.[14a,15] Within the double helix, the two oligomer strands are held together by arene–arene interactions between pyridine rings lying opposite each other. As before, intramolecular hydrogen bonds within each strand are responsible for the curvature of the helix. The formation of the double helix is accompanied by an unwinding of the individual helices, but the inner diameter of the



Scheme 3. Intramolecular hydrogen bonds within the oligopyridine **11** cause a curved conformation, which leads to helix formation in longer strands.

 © 2003 Wiley-VCH Verlag GmbH & Co. KGaA, Weinheim

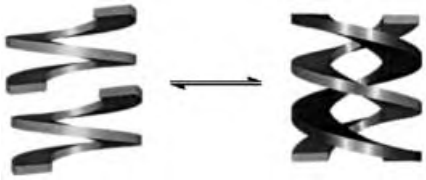


Figure 5. Two helical single strands **11** dimerize to form a supramolecular double helix.

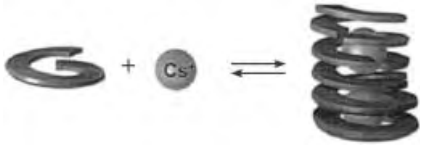
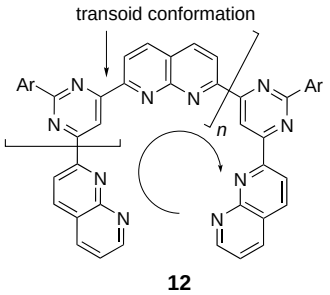


Figure 6. Only the interaction with the cation gives rise to the formation of a supramolecular helix from the oligomers **12**.[17]

central pore is not significantly affected (Figure 5).

The conformational behavior of fused heterocycles can also be exploited for helix formation, as shown by Lehn and co-workers.[16] 2,2′-Bipyridines and related heterocycles adopt a transoid conformation, which is biased towards helix formation in a similar way as the intramolecular hydrogen-bonded oligoamides by Lehn and co-workers[14] and Gong et al.[11] described above. In this context, it was recently shown that the use of naphthyridines instead of pyridines results in an opening of the structure, which allows now for the first time the inclusion of other molecules within the central pore of the helix[17]—a first step towards helical channels. For



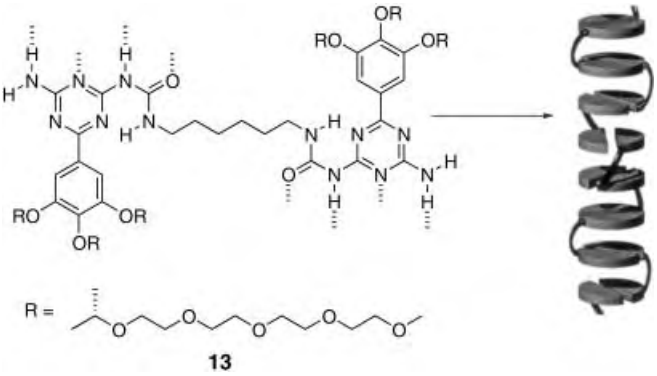
12

Scheme 4. In oligomer **12** interactions between the adjacent heterocycles result in a transoid conformation around the biaryl axis.

example, the naphthyridine pyrimidine oligomer **12** ($n = 2$, Scheme 4) adopts a conformation in solution ($CDCl_3$/CD_3CN) that represents a single helical turn. In the presence of alkali metal ions such as Cs^+, a supramolecular association of such individual helical springs occurs, leading to long hollow tubes in which, as the authors suggest, cations are incorporated (Figure 6). It is only this mutual interaction of two strands with one cation that stabilizes these supramolecular aggregates, as in the absence of cations only monomeric helices were observed. The formation of such cation channels is also supported by results from electrospray mass spectrometry and transmission electron microscopy.

As shown by Meijer and co-workers in recent years, supramolecular polymers[18] may also adopt a helical superstructure as a result of specific noncovalent interactions between the individual monomers.[19] In the case of the bifunctional ureido-*s*-triazine **13** (Figure 7), in addition to the hydrogen-bond driven dimerization of the head groups, π–π interactions between the aromatic rings cause the formation of columnar stacks. The chiral side chains further induce a helicity of these stacks, as could be shown by CD spectroscopy.

The examples presented herein demonstrate the various possibilities that exist today to obtain molecules with a helical conformation: from the synthesis of rigid molecules, in which helix formation minimizes steric strain, to flexible molecules with well-defined secondary structures, to supramolecular aggregates with a helical superstructure. Whether new material properties are associated with these molecules still has to be determined.



13

Figure 7. In supramolecular polymers of type **13**, additional π–π interactions are responsible for the formation of columnar stacks, which form a helix as a result of the chiral side chains.

[1] a) F. Vögtle, *Reizvolle Moleküle in der Organischen Chemie*, Teubner, Stuttgart, **1989**; b) H. Hopf, *Classics in Hydrocarbon Chemistry*, Wiley-VCH, Weinheim, **2000**.

[2] a) K. P. Meurer, F. Vögtle, *Top. Curr. Chem.* **1985**, *127*, 1; b) W. H. Laarhoven, W. J. C. Prinsen, *Top. Curr. Chem.* **1984**, *125*, 63; c) R. H. Martin, *Angew. Chem.* **1974**, *86*, 727; *Angew. Chem. Int. Ed. Engl.* **1974**, *13*, 649.

[3] D. J. Hill, M. J. Mio, R. B. Prince, T. S. Hughes, J. S. Moore, *Chem. Rev.* **2001**, *101*, 3893 – 4011.

[4] For a review article on protein folding, see: *Acc. Chem. Res.* **1998**, *31*, 697 – 773.

[5] A stabilization of such secondary structures is possible by using suitable templates or nonproteinogenic buildings blocks such as β amino acids; for review articles, see: a) J. S. Nowick, *Acc. Chem. Res.* **1999**, *32*, 287 – 296; b) S. H. Gellman, *Acc. Chem. Res.* **1998**, *31*, 173 – 180; c) J. S. Nowick, E. M. Smith, M. Pairish, *Chem. Soc. Rev.* **1996**, *25*, 401 – 415; d) J. P. Schneider, J. W. Kelly, *Chem. Rev.* **1995**, *95*, 2169 – 2187.

[6] a) H. J. Schneider, A. Yatsimirsky, *Principles and Methods in Supramolecular Chemistry*, Wiley, Chichester, **2000**; b) J. W. Steed, J. L. Atwood, *Supramolecular Chemistry*, Wiley, Chichester, **2000**; c) J.-M. Lehn, *Supramolecular Chemistry; Concepts and Perspectives*, VCH, Weinheim, **1995**; d) F. Vögtle, *Supramolecular Chemistry*, Wiley, Chichester, **1991**.

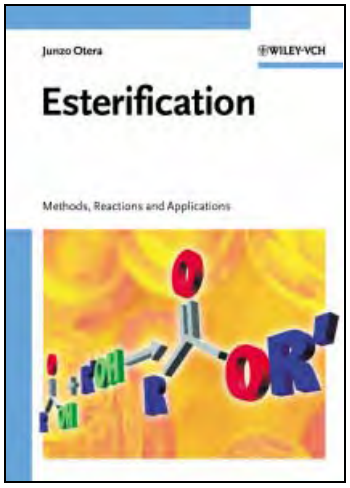
[7] W. Saenger, *Principles of Nucleic Acid Structure*, Springer, New York, **1984**.

[8] For reviews on older work, see: a) C. Piguet, G. Bernardinelli, G. Hopfgartner, *Chem. Rev.* **1997**, *97*, 2005 – 2062; b) A. E. Rowan, R. J. M. Nolte, *Angew. Chem.* **1998**, *110*, 65 – 71; *Angew. Chem. Int. Ed.* **1998**, *37*, 63 – 68; c) T. J. Katz, *Angew. Chem.* **2000**, *112*, 1997 – 1999; *Angew. Chem. Int. Ed.* **2000**, *39*, 1921 – 1923.

 © 2003 Wiley-VCH Verlag GmbH & Co. KGaA, Weinheim

[9] a) S. Han, A. D. Bond, R. L. Disch, D. Holmes, J. M. Schulmann, S. J. Teat, K. P. C. Vollhardt, G. D. Whitener, *Angew. Chem.* **2002**, *114*, 3357 – 3361; *Angew. Chem. Int. Ed.* **2002**, *41*, 3223 – 3227; b) S. Han, D. R. Anderson, A. D. Bond, H. V. Chu, R. L. Disch, D. Holmes, J. M. Schulmann, S. J. Teat, K. P. C. Vollhardt, G. D. Whitener, *Angew. Chem.* **2002**, *114*, 3361 – 3364; *Angew. Chem. Int. Ed.* **2002**, *41*, 3223 – 3230.
[10] B. Kiupel, C. Niederalt, M. Nieger, S. Grimme, F. Vögtle; *Angew. Chem.* **1998**, *110*, 3206 – 3209; *Angew. Chem. Int. Ed.* **1998**, *37*, 3031 – 3034.
[11] B. Gong, H. Zeng, J. Zhu, L. Yua, Y. Han, S. Cheng, M. Furukawa, R. D. Parra, A. Y. Kovalevsky, J. L. Mills, E. Skrzypczak-Jankun, S. Martinovic, R. D. Smith, C. Zheng, T. Szyperski, X. Zheng, *Proc. Natl. Acad. Sci. USA* **2002**, *99*, 11583 – 11588.
[12] a) G. A. Jeffrey, *An Introduction to Hydrogen Bonding*, Oxford University Press, New York, **1997**; b) J. Israelachvili, *Intermolecular and Surface Forces*, 2nd ed., Academic Press, London, **1992**.
[13] D. J. Hill, J. S. Moore, *Proc. Natl. Acad. Sci. USA* **2002**, *99*, 5053 – 5057.
[14] a) V. Berl, I. Huc, R. G. Khoury, M. J. Krische, J.-M. Lehn, *Nature* **2000**, *407*, 720 – 723; b) V. Berl, I. Huc, R. G. Khoury, J.-M. Lehn, *Chem. Eur. J.* **2001**, *7*, 2798 – 2809.
[15] V. Berl, I. Huc, R. G. Khoury, J.-M. Lehn, *Chem. Eur. J.* **2001**, *7*, 2810 – 2820.
[16] a) L. A. Cuccia, J.-M. Lehn, J.-C. Homo, M. Schmutz, *Angew. Chem.* **2000**, *112*, 239 – 243; *Angew. Chem. Int. Ed.* **2000**, *38*, 233 – 237; b) K. M. Gardinier, R. G. Khoury, J.-M. Lehn, *Chem. Eur. J.* **2000**, *6*, 4124 – 4131.
[17] A. Petitjean, L. A. Cuccia, J.-M. Lehn, H. Nierengarten, M. Schmutz, *Angew. Chem.* **2002**, *114*, 1243 – 1246; *Angew. Chem. Int. Ed.* **2002**, *41*, 1195 – 1198.
[18] For reviews, see: a) C. Schmuck, W. Wienand, *Angew. Chem.* **2001**, *113*, 4493 – 4499; *Angew. Chem. Int. Ed.* **2001**, *40*, 4363 – 4369; b) D. C. Sherrington, K. A. Taskinen, *Chem. Soc. Rev.* **2001**, *30*, 83 – 93.
[19] a) L. Brunsveld, J. A. J. M. Vekemans, J. H. K. K. Hirschberg, R. P. Sijbesma, E. W. Meijer, *Proc. Natl. Acad. Sci. USA* **2002**, *99*, 4977 – 4982; b) R. P. Sijbesma, E. W. Meijer, *Chem. Commun.* **2003**, 5 – 16.

Just a Must for Organic Chemists



ISBN 3-527-30490-8
*Approx *€ 139,- / sFr 205,-*

**The Euro price is* only valid for germany.

JUNZO OTERA, Okayama University of Science, Japan

Esterification
Methods, Reactions and Applications

2003. Approx XV, 435pp Hbk.

Here, Professor J. Otera brings together for the first time the combined knowledge about this elementary yet multifaceted reaction. Starting from the methodical basics right up to practical applications, this book represents a comprehensive overview of this type of reaction, saving readers time-consuming research among the literature – and not just in practical matters.

- First book bringing together widely spread knowledge about this important reaction
- Written by one of the leading chemists in the field of Esterification
- **All set to become a standard reference for every organic chemist**

Wiley-VCH Verlag
Fax: +49 (0)62 01 - 60 61 84
e-Mail: service@wiley-vch.de
www.wiley-vch.de

Register now for the free
WILEY-VCH Newsletter!
www.wiley-vch.de/home/pas

WILEY-VCH

50613032_kn

 © 2003 Wiley-VCH Verlag GmbH & Co. KGaA, Weinheim

DNA-Mediated Charge Transfer

Reductive Electron Transfer and Transport of Excess Electrons in DNA

*Hans-Achim Wagenknecht**

Keywords:
charge transfer · DNA · electron transfer · nucleosides

In principle, DNA-mediated charge transfer processes can be categorized as either oxidative hole transfer or reductive electron transfer. In research on DNA damage, major efforts have focused on the investigation of oxidative hole transfer or transport, resulting in insights on the mechanisms. On the other hand, the transport or transfer of excess electrons has a large potential for biomedical applications, mainly for DNA chip technology. Yet the mechanistic details of this type of charge transfer chemistry were unclear. In the last two years this mechanism has been addressed in γ-pulse radiolysis studies with randomly DNA-bound electron acceptors or traps. The major disadvantage of this experimental setup is that the electron injection and trapping is not site-selective. More recently, new photochemical assays for the chemical and spectroscopic investigation of reductive electron transfer and electron migration in DNA have been published which give new insights into these processes. Based on these results, an electron-hopping mechanism is proposed which involves pyrimidine radical anions as intermediate electron carriers.

1. Mechanisms of DNA-Mediated Hole Transfer and Hole Hopping

The possibility that the π-stacked array of base pairs in B-form DNA might serve as a pathway for charge migration was suggested over 40 years ago.[1] In the 1990s Barton et al. pioneered research in this area and published many articles about photoactivated charge transfer in DNA.[2,3] Since then, the fundamental question of whether DNA can serve as a medium for long-range charge transfer has been a subject of controversy.[4] The enormous interest in DNA-mediated charge transfer has been spurred by its relevance to oxidative DNA damage, which may cause apoptosis, mutations, and cancer.[5] Thus, most research groups have focused their work on the photochemically or photophysically induced oxidation of DNA,[6] in which one electron is removed from the DNA or the final acceptor (Ac) and transferred to the photoexcited charge donor (D). Such processes can be described as oxidative hole transfer or hole transport.

Most of the past experiments were performed according to the following strategy:[7]

1. Labeling of the DNA with redoxactive probes through intercalation and/or covalent linkages
2. Initiation of the charge transfer by photochemical or electrochemical techniques
3. Detection of the charge transfer processes.

DNA-mediated hole transfer or transport processes have been explored by numerous techniques, including spectroscopic measurements and the biochemical analysis of oxidative DNA lesions.[6,7] The two mechanisms most often discussed are the superexchange and the hopping mechanisms.[8] At this point it is generally accepted that charge transfer can occur through the DNA, and the discussion has moved on to its biological relevance.[9]

Initially the charge transfer processes were described in line with the Marcus theory as a superexchange mechanism (Figure 1a). The rate k_{CT} of this one-step tunneling process depends exponentially on the distance R between the donor (D) and acceptor (Ac), $k_{CT} \propto e^{-\beta R}$.[10] Four important observations were drawn from this interpretation:

1. Hole transfer by means of the superexchange mechanism is limited to short distances (< 10 Å).

[*] Dr. H.-A. Wagenknecht
Institute for Organic Chemistry and Biochemistry
Technical University of Munich
Lichtenbergstrasse 4, 85747 Garching (Germany)
Fax: (+49) 89-289-13210
E-mail: wagenknecht@ch.tum.de

 © 2003 Wiley-VCH Verlag GmbH & Co. KGaA, Weinheim DOI: 10.1002/anie.200301629

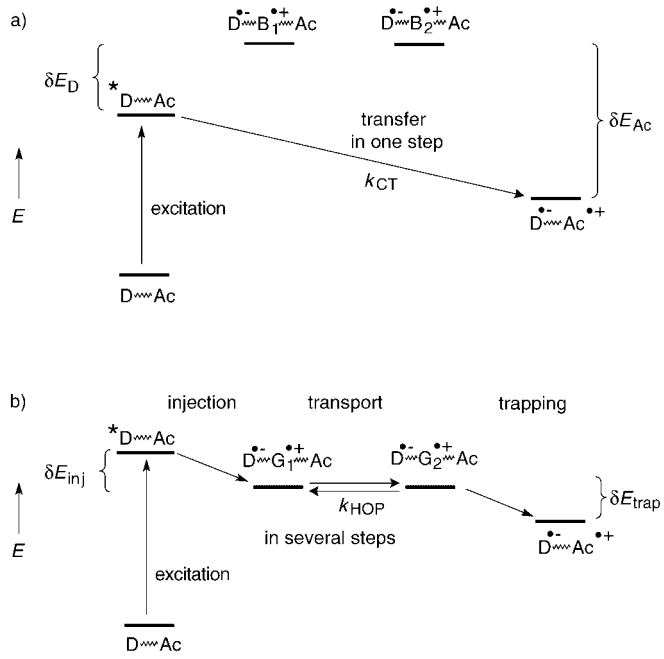


Figure 1. a) Superexchange mechanism for photoinduced DNA-mediated hole transfer and b) hopping mechanism of photoinduced hole transport in DNA. D = donor, Ac = acceptor, B = base, inj = injection, trap = trapping, CT = charge transfer.

2. Charge transfer reactions over short distances are very fast ($k_{CT} = 10^9$–10^{12} s^{-1}).
3. The typical β-value of DNA-mediated charge transfer is 0.6–0.8 $Å^{-1}$.
4. The intercalation of D and Ac is crucial for fast and efficient charge transfer.

In contrast to these observations other experiments and data[6,7] indicated that DNA-mediated hole transport can also result in reactions over long distances (up to 200 Å[11]), which indicates a very weak distance dependence. This observation led to the description of an alternative mechanism, the hopping model (Figure 1b). [8,12] Of the four DNA bases, guanine (G) is the most easily oxidized.[13,14] Hence, in the hopping mechanism the G radical cation ($G^{\bullet+}$) is proposed to serve as the intermediate hole carrier. Once the positive charge has been injected into the DNA base stack, it hops from G to G and can finally be trapped at a suitable Ac. Each hopping step is a tunneling process through the intervening adenine(A)–thymine(T) base pairs.[8,15] The overall rate of hole transport by hopping depends on the number of hopping steps (N), $k_{CT} \propto N^{-\eta}$ (η is a constant).[8] Lewis et al. were able to measure the rate for a single hopping step from G to GG, $k_{HOP} = 10^7$ s^{-1}.[16] Furthermore, Giese et al. proposed that adenines can play the role of the intermediate hole carriers if G is not present in the base sequence.[17]



H.-A. Wagenknecht, born in 1968, finished his studies in chemistry at the University of Freiburg with a thesis on glycosidase inhibitors (Prof. J. Lehmann). After completing his PhD thesis on synthetic models of chloroperoxidase in the group of Prof. W.-D. Woggon (Basel, Switzerland), he was awarded fellowships from the Swiss NSF, Novartis, and DFG to carry out postdoctoral research at the California Institute of Technology (Pasadena) in the group of Prof. J. K. Barton. Since 2000 he has led his own research group at the Technical University of Munich in work on DNA and carbohydrate modifications.

2. Reductive Electron Transfer and Transport of Excess Electrons

Reductive electron transfer or transport occurs if an electron from the photoexcited donor is injected into the DNA or transferred to the final electron acceptor. In contrast to the broad knowledge about the oxidative hole transfer and hole hopping in DNA, as described in the previous section, the mechanistic details of the transfer and migration of excess electrons remained unclear. This dearth of knowledge has been filled during the last two to three years, but a well-defined and suitable D–Ac system for time-resolved spectroscopic measurements has still not been found. The mechanisms of hole transfer and transport have been transferred to the problem of reductive electron transfer and excess electron migration.

Despite the uncertainty about the irreversibility of the experimentally determined potentials, the trend for the reducibility of DNA bases has been established to be T,U ≈ C > A > G (C = cytosine).[14,18] This trend has been corroborated recently by theoretical methods.[19] More detailed calculations of the electron affinities of DNA bases within the context of different base sequences in oligonucleotides were performed by Rösch et al., which predict that the strongest electron acceptors are 5′-XCY-3′ and 5′-XTY-3′ when X and Y are the pyrimidine bases C and T.[20] Both experiment and theory indicate that T and C are the bases that are most easily reduced and that their reduction potentials are very similar.

Accordingly, a hopping mechanism was proposed for the DNA-mediated transport of excess electrons over long distances,[12] in which all base pairs (T-A and C-G) are involved and the pyrimidine radical anions $C^{\bullet-}$ and $T^{\bullet-}$ serve as intermediate electron carriers. However, Steenken et al. found that $C^{\bullet-}$ and $T^{\bullet-}$ have substantially different basicities.[21] Thus, protonation of $C^{\bullet-}$ and $T^{\bullet-}$ by the complementary DNA bases or the surrounding water molecules could possibly interfere with the electron transfer and hopping.[21]

2.1. γ-Pulse Radiolysis Studies

Currently, most knowledge about the reductive electron transfer and the behavior of excess electrons in DNA comes from γ-pulse radiolysis studies.[22–26] Most of these studies were performed in frozen ice or glassy aqueous LiBr solutions of duplex DNA. The samples were γ-irradiated to generate solvated electrons, which reduce the DNA and initiate the DNA-mediated electron transfer or transport. The DNA was

 © 2003 Wiley-VCH Verlag GmbH & Co. KGaA, Weinheim

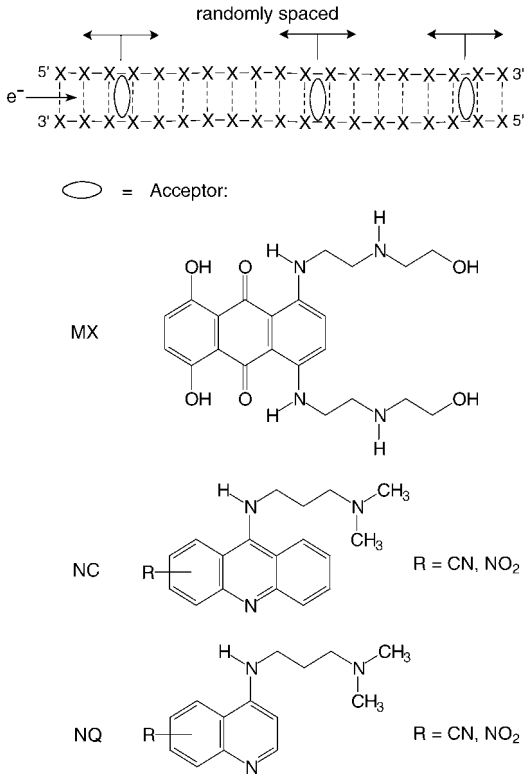


Figure 2. Mitoxantrone (MX), acridine (NC), and quinoline (NQ) derivatives as randomly bound electron acceptors in γ-pulse radiolysis experiments for the investigation of electron transfer and transport DNA.

doped with intercalated and randomly spaced electron traps, for example, mitoxantrone (MX, Figure 2). The intermediate radicals of the DNA bases and the acceptor were detected by ESR spectroscopy. The major disadvantage of this approach is that the electron injection and the electron trapping do not occur site-selectively. Nevertheless, a few remarkable and principle conclusions and implications can be drawn from these studies, which were performed mainly by Sevilla et al.[22]

Below 77 K electron transfer in DNA occurs by means of a superexchange mechanism. The average value of the distance dependence of the electron transfer rate, $\beta = 0.9\ \text{Å}^{-1}$, is not temperature dependent and clearly indicates that DNA at 77 K is not an especially effective conduit for the transfer of excess electrons. This result is in accord with oxidative hole transfer through the superexchange mechanism (see Section 1) and with single-step electron tunneling processes in proteins.[27]

The distance dependence of the electron transfer rate varies remarkably in different synthetic duplexes.[23] The β-values for electron tunneling were found to be $0.75\ \text{Å}^{-1}$ in poly(dA-dT)·poly(dA-dT) and $1.4\ \text{Å}^{-1}$ for poly(dI-dC)·poly(dI-dC), each measured in D_2O. The β-value for random-sequence DNA (from calf thymus) is intermediate at $0.92\ \text{Å}^{-1}$ in D_2O. Comparable measurements in H_2O gave a β-value of $0.83\ \text{Å}^{-1}$, indicating a moderate isotope effect. These results suggest that deuteron or proton transfer from inosine (I) or G to $C^{\bullet-}$ significantly slows but does not stop electron transfer.

At temperatures above 130 K irreversible deuteration of $T^{\bullet-}$ in D_2O competes with electron tunneling and acts as an irreversible sink for the electron. The electron transfer from one-electron-reduced cytosine ($C^{\bullet-}$) is apparently too slow to be observed at temperatures below 170 K. Above 170 K electron transfer proceeds as a thermally activated process, which involves also $C^{\bullet-}$ as the intermediate electron carrier. As mentioned previously, $C^{\bullet-}$ is presumably protonated by the complementary base G because it provides substantial stabilization energy.[21,24] This proton transfer is reversible and thermally activated, which suggests that the proton transfer in a C-G radical anion base pair does not limit the range of electron hopping in DNA.

Anderson et al. used nitroacridines and nitroquinolines as randomly bound electron acceptors in their γ-pulse radiolysis experiments (NC and NQ, Figure 2).[25] In agreement with the previously discussed results, these studies indicated that electron migration in DNA is strongly dictated by the activation energy. Bernhard et al. measured the yield of trapped radicals in crystalline DNA at 4 K to be 60% based on the number of radicals initially formed by irradiation.[26] Such an exceptionally high yield can only occur if the conductivity of the DNA crystals is very low. Interestingly, the qualitative features of the recorded spectra are consistent with a radical population dominated by one-electron-reduced C ($C^{\bullet-}$).

2.2. Photochemical Studies

The photochemical studies of electron injection and transport in DNA follow the experimental design already presented and discussed for the oxidative hole transfer chemistry (see Section 1).[7] Derivatives of flavines, stilbene diethers, and pyrenes have been used as photoexcitable electron donors and were covalently attached to the oligonucleotides. These donors differ significantly in their structure and redox properties.

Based on knowledge about the repair mechanism of DNA photolyases,[28] Carell et al. developed a DNA assay to investigate the migration of excess electrons, which consisted of two new DNA modifications (Figure 3)[29] 1) A flavine derivative was incorporated synthetically into oligonucleotides as an artificial nucleobase.[30] In its reduced, deprotonated, and photoexcited state, flavine has a redox potential of −2.8 V and is capable of reducing all four DNA bases.[31] 2) Additionally, a special T-T dimer was incorporated into the oligonucleotides, which lacks the connecting phosphodiester bridge between the 3′- and the 5′-hydroxy groups of the two ribofuranoside moieties.[32] Hence, cycloreversion of the T-T dimer, which is initiated by a one-electron reduction, yields a strand break of the oligonucleotide, which can be analyzed and quantified by HPLC analysis.

The splitting of the T-T dimer is the chemical result of electron transport through the DNA base stack. This interpretation is mainly based on the well-known redox properties of the flavin intercalator in its reduced and deprotonated state, and on the absence of the typical DNA base sequence dependence which would be observed in the case of a hole-

 © 2003 Wiley-VCH Verlag GmbH & Co. KGaA, Weinheim

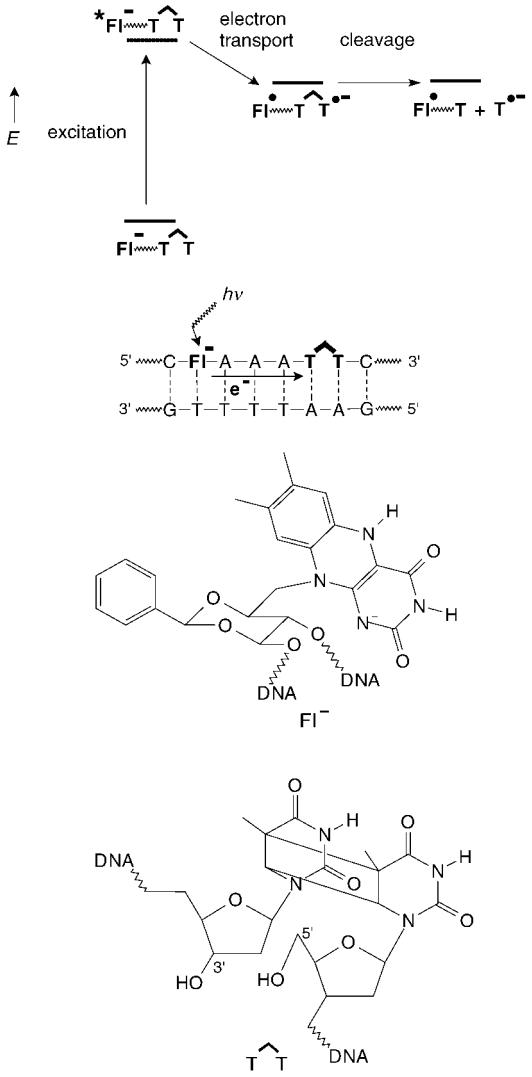


Figure 3. Chemical assay for the investigation of excess-electron migration in DNA. The splitting of the T-T dimer (T-T) is the chemical consequence of the photoinduced electron transfer from a distant flavine derivative as the charge donor (Fl^-).

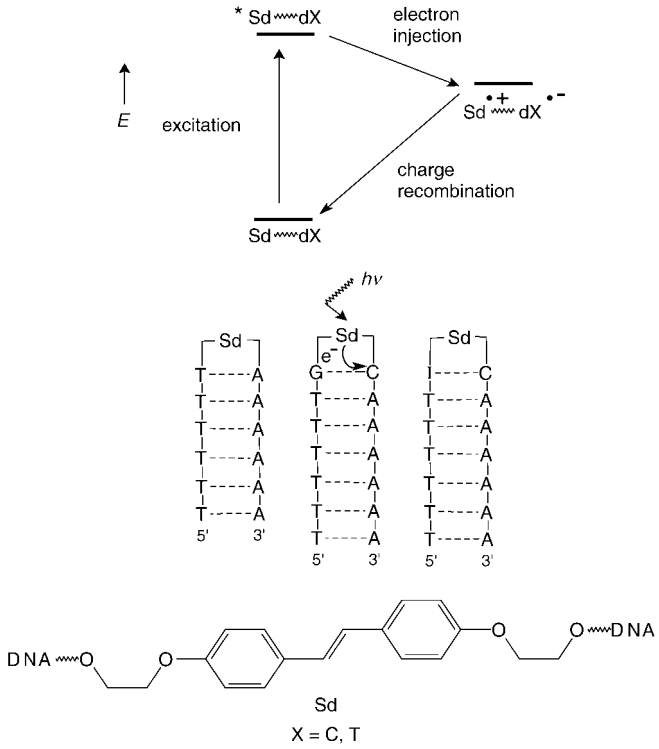


Figure 4. Electron injection into DNA hairpins capped with a stilbene diether derivative (Sd) as the electron donor.

hopping process. Based on the invariant irradiation conditions and the assumption that the electron injection efficiency is the same in all DNA duplexes, the observed yields of T-T dimer cleavage can be attributed to the different electron transport efficiencies. The amount of T-T dimer cleavage depends rather weakly on the distance to the flavine, which indicates a thermally activated electron-hopping process. This conclusion is clearly in agreement with the results of the γ-pulse radiolysis studies (see Section 2.1).

Lewis and Wasielewski et al. investigated the energetics and kinetics of the photoinduced electron injection into DNA hairpins that were synthetically capped by a stilbene diether derivative (Figure 4).[33] Based on the potentials for the nucleobases[14,18,20] and the corresponding oxidation potential (1.16 V vs. normal hydrogen electrode, NHE) and singlet energy ($E_{00} = 3.45$ eV) of the stilbene diether,[33] the reduction of C and T should be exergonic and the reduction of A and G should be endergonic. Thus, the driving force in this assay is completely different from that of the previously described flavine system.

In the present study the stilbene diether serves as the electron donor and the nucleobases T and C as electron acceptors.[33] The dynamics of the electron injection were determined by picosecond time-resolved laser spectroscopy. It is remarkable that the electron injection rates are faster when T is the electron acceptor ($> 2 \times 10^{12}\ s^{-1}$) than when C is the electron acceptor ($3.3 \times 10^{11}\ s^{-1}$). This indicates that in double-helical B-DNA the reduction potential of T is lower than that of C. This result is in accord with recent femtosecond time-resolved studies on the reduction of C and T with photoexcited 2-aminopurine[34] as well as with recent calculations of the electron affinities of single nucleobases,[19] but not with recent calculations by Rösch et al.[20]

Interestingly, Lewis et al. detected a small difference in the electron injection rate when C is used as the electron acceptor in different base pairs (C-G vs. C-I). The C-G base pair has a stronger hydrogen-bonding network than the C-I base pair. As a result, electron injection into the C-G base pair is slower ($3.3 \times 10^{11}\ s^{-1}$) than into the C-I base pair ($1.4 \times 10^{12}\ s^{-1}$). This indicates a small difference in the reduction potential of C as a result of different hydrogen bonding.

If the energetics are favorable, the locally excited state of pyrene (Py*) can act as a precursor state for an electron transfer to the DNA bases yielding the charge-separated state which consists of the pyrenyl radical cation $Py^{\bullet+}$ and the corresponding base radical anion. Based on the redox potential (1.5 V vs. NHE)[35] and the singlet energy of pyrene

 © 2003 Wiley-VCH Verlag GmbH & Co. KGaA, Weinheim

($E_{00} = 3.25$ eV),[35] the driving force of the electron transfer was estimated to be −0.5 to −0.6 eV when the reported reduction potentials of −1.1 and −1.2 V for U and C, respectively, are used.[18] Recently, Fiebig et al. reported a time-resolved study of the reduction of T and C by photoexcited 2-aminopurine, and derived redox potentials (vs. NHE) of −1.8 V and −1.9 V for the nonprotonated pairs $C^{\bullet-}$/C and $T^{\bullet-}$/T, respectively.[36] The significant pH dependence of the electrochemical redox potentials suggests that proton transfer is substantially involved in the reductive electron transport in DNA and must be interpreted as a proton coupling.

Pyrene-labeled oligonucleotides were used by Netzel et al. to investigate the quenching efficiency of the photoexcited pyrene emission (Py*) depending on the flanking nucleobases.[37] They established the following order for the quenching efficiencies: A < G < T < C. Emission spectra and lifetime measurements provided evidence for electron transfer from Py* to the pyrimidine bases C or T. This charge transfer assignment has been proven by nanosecond fluorescence lifetime measurements with 5-(pyren-1-yl)-2′-deoxyuridine (Py-dU).[38]

Most recently, our group prepared Py-dU and 5-(pyren-1-yl)-2′-deoxycytidine (Py-dC) by Suzuki–Miyaura cross-coupling reactions.[39] Subsequently, the properties and dynamics of the intramolecular electron transfer in Py-dU and Py-dC were characterized by steady-state fluorescence spectroscopy and femtosecond transient absorption spectroscopy in water at different pH values(Figure 5).[40] By comparing Py-dC and Py-dU as nucleoside models for electron transfer in DNA, we found that a small energy difference exists between $C^{\bullet-}$and $U^{\bullet-}$, which is in agreement with several calculations and experiments, as already discussed in the previous sections.

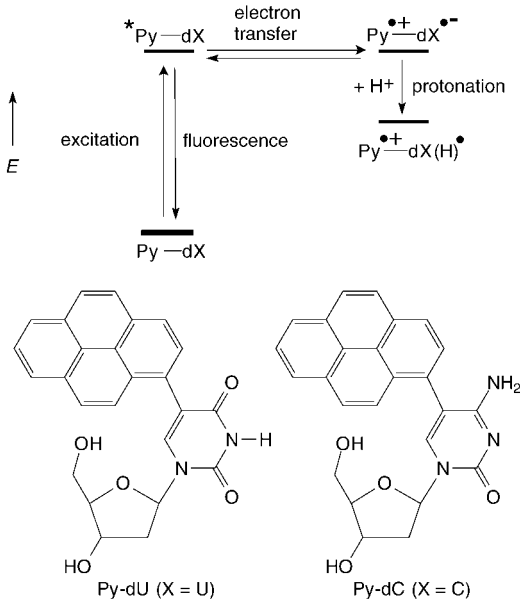


Figure 5. Pyrene-modified nucleosides as models for spectroscopic studies of the electron transport in DNA. When Py-dX (X = U or C) is excited at 340 nm, an intramolecular electron transfer occurs, yielding the charge-separated species Py^{+}-$dX^{\bullet-}$, which is protonated to form the diradical Py^{+}-$dX(H)^{\bullet}$.

Most importantly, we detected a difference in the basicity of the generated pyrimidine radical anions, which is significant for the understanding of electron migration in DNA, as mentioned originally by Steenken.[21] The nonprotonated radical anion of C ($C^{\bullet-}$) could not be observed in aqueous solution. Although the situation in water, where multiple hydrogen-bonding schemes are structurally and energetically feasible, cannot be directly compared with that in DNA, our results provide strong evidence that protonation of $C^{\bullet-}$ by the complementary DNA base G or the surrounding water molecules will occur rapidly. The time-resolved data at pH 5 show that the intramolecular electron transfer and protonation in Py-dU occurs within 4.7 ps and in Py-dC within 40 ps. During this time, the hydrogen-bonding network can readjust and stabilize the excess electron on the base by separating its spin from its charge. Although these processes must be microscopically reversible they may limit or ultimately terminate electron migration in DNA. Thus we suggest that $C^{\bullet-}$ cannot play a major role as an intermediate charge carrier. In contrast, $U^{\bullet-}$ or $T^{\bullet-}$ can act as stepping stones for electron hopping in DNA since protonation of these radical anions does not occur.

Using the nucleoside Py-dU, we prepared a range of pyrene-modified duplexes by means of phosphoramidite chemistry.[41] The covalently attached pyrene group is located outside the DNA base stack. Upon excitation, an intramolecular electron transfer in the Py-dU unit represents the injection of an excess electron into the DNA base stack. The significant differences between the prepared DNA duplexes are the bases located next to the Py-dU group. Based on the established trend for the reducibility of nucleobases,[14,18] we expect that $U^{\bullet-}$, which is formed upon photoexcitation, should be able to reduce only the adjacent pyrimidine bases C or T (see Figure 6). In keeping with this assumption, we detected a significant quenching of the Py* emission in the duplexes in which a T or a C flanked the Py-dU group. This observation can be attributed to a base-to-base electron transport process, which is supported by femtosecond time-resolved pump-probe laser spectroscopy measurements.

3. Conclusion and Outlook

From the γ-radiolysis studies as well as the different photochemical assays the following important conclusions can be drawn:

1. Below 77 K the transfer of excess electrons occurs by the superexchange mechanism; the rate is strongly distance dependent ($\beta = 0.9$ Å^{-1}), which is similar to that in oxidative hole transfer ($\beta = 0.7$ Å^{-1}).
2. Above 170 K electron migration in DNA occurs by means of a thermally activated hopping process.
3. Both pyrimidine radical anions $T^{\bullet-}$ and $C^{\bullet-}$ can play the role of the intermediate charge carrier. Electron hopping via $T^{\bullet-}$ seems to be more favorable since the reduction potential of T is slightly lower than that of C in double-helical B-DNA.
4. Proton transfer interferes with the electron transport in C-G base pairs but not in T-A base pairs. As a result, the

 © 2003 Wiley-VCH Verlag GmbH & Co. KGaA, Weinheim

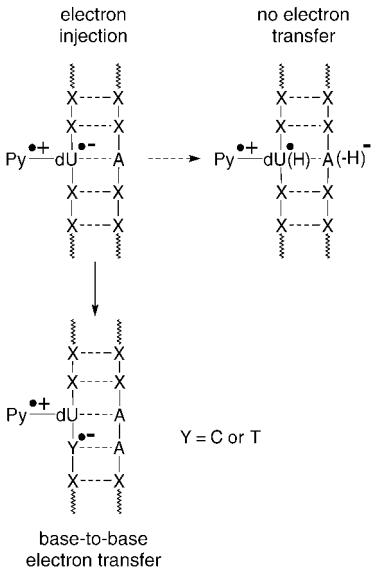


Figure 6. Electron injection into pyrene-modified DNA duplexes. Excitation of the Py-dU group results in charge separation, yielding the Py^{+}-$dU^{\bullet-}$ diradical, which corresponds to the injection of an excess electron into DNA. Efficient base-to-base electron transfer occurs only to adjacent pyrimidines (C or T).

protonation of $C^{\bullet-}$ in C-G base pairs decreases the electron transport efficiency and rate but does not stop electron migration in DNA.

Despite these efforts in understanding electron migration in DNA, a well-defined D-Ac DNA system for time-resolved spectroscopic investigations is still elusive. With such a system the rates of electron transport could be measured directly. Future experiments have to focus on 1) the dynamics of the electron injection process in more detail, 2) the distance dependence and base-sequence dependence of electron migration, 3) the rate of base-to-base electron transport in terms of the hopping model, and 4) the chemical reactivity of the radical anions in DNA that yield biologically or physiologically relevant DNA lesions.

Electron transfer chemistry in DNA has a large potential for biomedical applications, mainly for DNA chip technology. The high efficiency of DNA-mediated electron transport and its strong sensitivity towards structural pertubations caused by, for example, single base mismatches or DNA lesions offers a new approach for obtaining a highly sensitive electrochemical readout.[42,43]

Our work is supported by the Deutsche Forschungsgemeinschaft, the Volkswagen-Stiftung, and the Fonds der Chemischen Industrie. I am grateful to my co-workers Nicole Amann, Robert Huber, Peter Kaden, Elke Mayer, Stefan Mitschke, Manuela Rist, Linda Valis, and Clemens Wagner for their experimental contributions. I would also like to thank Dr. Torsten Fiebig, Technical University of Munich, and his coworkers for the fruitful collaboration and valuable discussions. I am also grateful to Professor Horst Kessler, Technical University of Munich, for his generous support.

Received: January 14, 2003 [M1629]

[1] D. D. Eley, D. I. Spivey, *Trans. Faraday Soc.* **1962**, *58*, 411–415.
[2] C. J. Murphy, M. R. Arkin, Y. Jenkins, N. D. Ghatlia, S. H. Bossmann, N. J. Turro, J. K. Barton, *Science* **1993**, *262*, 1025–1029.
[3] See the most recent review: E. M. Boon, J. K. Barton, *Curr. Opin. Struct. Biol.* **2002**, *12*, 320–329.
[4] a) S. Priyadarshy, S. M. Risser, D. N. Beratan, *J. Phys. Chem.* **1996**, *100*, 17678–17682; b) N. J. Turro, J. K. Barton, *J. Biol. Inorg. Chem.* **1998**, *3*, 201–209; c) Y. A. Berlin, A. L. Burin, M. A. Ratner, *Superlattices Microstruct.* **2000**, *28*, 241–252.
[5] a) P. O'Neill, E. M. Frieden, *Adv. Radiat. Biol.* **1993**, *17*, 53–120; b) B. Armitage, *Chem. Rev.* **1998**, *98*, 1171–1200; c) C. J. Burrows, J. G. Muller, *Chem. Rev.* **1998**, *98*, 1109–1151; d) D. Wang, D. A. Kreutzer, J. M. Essigmann, *Mutat. Res.* **1998**, *400*, 99–115; e) S. Kawanashi, Y. Hiraku, S. Oikawa, *Mutat. Res.* **2001**, *488*, 65–76.
[6] Recent reviews or recent publications of the different research groups: a) C. R. Treadway, M. G. Hill, J. K. Barton, *Chem. Phys.* **2002**, *281*, 409–428; b) B. Giese, *Curr. Opin. Chem. Biol.* **2002**, *6*, 612–618; c) F. D. Lewis, X. Liu, S. E. Miller, R. T. Hayes, M. R. Wasielewski, *J. Am. Chem. Soc.* **2002**, *124*, 3485–3487; d) M. Bixon, J. Jortner, *J. Am. Chem. Soc.* **2001**, *123*, 12556–12567; e) W. B. Davies, S. Hess, I. Naydnova, R. Haselsberger, A. Ogrodnik, M. D. Newton, M. E. Michel-Beyerle, *J. Am. Chem. Soc.* **2002**, *124*, 2422–2423; f) Y. A. Berlin, A. L. Burin, M. A. Ratner, *Chem. Phys.* **2002**, *275*, 61–74; g) U. Santhosh, G. B. Schuster, *J. Am. Chem. Soc.* **2002**, *124*, 10986–10987; h) V. Shafirovich, A. Dourandin, N. E. Geacintov, *J. Phys. Chem. B* **2001**, *105*, 8431–8435; i) C. Wan, T. Fiebig, O. Schiemann, J. K. Barton, A. H. Zewail, *Proc. Natl. Acad. Sci. USA* **2000**, *97*, 14052–14055.
[7] M. W. Grinstaff, *Angew. Chem.* **1999**, *111*, 3845–3851; *Angew. Chem. Int. Ed.* **1999**, *38*, 3629–3635.
[8] J. Jortner, M. Bixon, T. Langenbacher, M. E. Michel-Beyerle, *Proc. Natl. Acad. Sci. USA* **1998**, *95*, 12759–12765.
[9] a) A. Heller, *Faraday Discuss.* **2000**, *116*, 1–13; b) S. R. Rajski, B. A. Jackson, J. K. Barton, *Mutat. Res.* **2000**, *447*, 49–72; c) M. E. Núñez, G. Holmquist, J. K. Barton, *Biochemistry* **2001**, *40*, 12465–12471; d) M. E. Núñez, K. T. Noyes, J. K. Barton, *Chem. Biol.* **2002**, *9*, 403–415.
[10] R. A. Marcus, N. Sutin, *Biochim. Biophys. Acta* **1985**, *811*, 265–322.
[11] a) M. E. Núñez, D. B. Hall, J. K. Barton, *Chem. Biol.* **1999**, *6*, 85–97; b) P. T. Henderson, D. Jones, G. Hampikian, Y. Kan, G. B. Schuster, *Proc. Natl. Acad. Sci. USA* **1999**, *96*, 8353–8358.
[12] B. Giese, *Annu. Rev. Biochem.* **2002**, *71*, 51–70.
[13] S. Steenken, S. V. Jovanovic, *J. Am. Chem. Soc.* **1997**, *119*, 617–618.
[14] C. A. M. Seidel, A. Schulz, M. H. M. Sauer, *J. Phys. Chem.* **1996**, *100*, 5541–5553.
[15] J. Jortner, M. Bixon, A. V. Voityuk, N. Rösch, J. *Phys. Chem. A* **2002**, *106*, 7599–7606.
[16] F. D. Lewis, X. Liu, J. Liu, S. E. Miller, R. T. Hayes, M. R. Wasielewski, *Nature* **2000**, *406*, 51–53.
[17] a) B. Giese, M. Spichty, *ChemPhysChem* **2000**, *1*, 195–198; b) B. Giese, J. Amaudrut, A.-K. Köhler, M. Spormann, S. Wessely, *Nature* **2001**, *412*, 318–320.
[18] S. Steenken, J. P. Telo, H. M. Novais, L. P. Candeias, *J. Am. Chem. Soc.* **1992**, *114*, 4701–4709.
[19] a) S. S. Wesolowski, M. L. Leininger, P. N. Pentchev, H. F. Schaefer, III *J. Am. Chem. Soc.* **2001**, *123*, 4023–4028; b) X. Li, Z. Cai, M. D. Sevilla, *J. Phys. Chem. A* **2002**, *106*, 1596–1603.
[20] A. A. Voityuk, M.-E. Michel-Beyerle, N. Rösch, *Chem. Phys. Lett.* **2001**, *342*, 231–238.
[21] S. Steenken, *Free Radical Res. Commun.* **1992**, *16*, 349–379.

 © 2003 Wiley-VCH Verlag GmbH & Co. KGaA, Weinheim

[22] a) Y. Razskazovskii, S. G. Swarts, J. M. Falcone, C. Taylor, M. D. Sevilla, *J. Phys. Chem. B* **1997**, *101*, 1460 – 1467; b) A. Messer, K. Carpenter, K. Forzley, J. Buchanan, S. Yang, Y. Razskazovskii, Z. Cai, M. D. Sevilla, *J. Phys. Chem. B* **2000**, *104*, 1128 – 1136; c) Z. Cai, Z. Gu, M. D. Sevilla, *J. Phys. Chem. B* **2000**, *104*, 10406 – 10411; d) Z. Cai, M. D. Sevilla, *J. Phys. Chem. B* **2000**, *104*, 6942 – 6949.

[23] Z. Cai, X. Li, M. D. Sevilla, *J. Phys. Chem. B* **2002**, *106*, 2755 – 2762.

[24] X. Li, Z. Cai, M. D. Sevilla, *J. Phys. Chem. B* **2001**, *105*, 10115 – 10123.

[25] R. F. Anderson, G. A. Wright, *Phys. Chem. Chem. Phys.* **1999**, *1*, 4827 – 4831.

[26] M. G. Debije, M. T. Milano, W. A. Bernhard, *Angew. Chem.* **1999**, *111*, 2926 – 2930; *Angew. Chem. Int. Ed.* **1999**, *38*, 2752 – 2756.

[27] a) J. R. Winkler, H. B. Gray, *Chem. Rev.* **1992**, *92*, 369 – 379; b) S. S. Isied, M. Y. Ogawa, J. F. Wishart, *Chem. Rev.* **1992**, *92*, 381 – 394; c) M. R. Wasielewski, *Chem. Rev.* **1992**, *92*, 435 – 461.

[28] a) J.-S. Taylor, *Acc. Chem. Res.* **1994**, *27*, 76 – 82; b) A. Sancar, *Biochemistry* **1994**, *33*, 2 – 9; c) D. B. Sanders, O. Wiest, *J. Am. Chem. Soc.* **1999**, *121*, 5127 – 5134; d) T. Carell, L. T. Burgdorf, L. M. Kundu, M. Cichon, *Curr. Opin. Chem. Biol.* **2001**, *5*, 491 – 498; e) H. Komori, R. Masui, S. Kuramitsu, S. Yokoyama, T. Shibata, Y. Inoue, K. Miki, *Proc. Natl. Acad. Sci. USA* **2001**, *98*, 13560 – 13565.

[29] a) A. Schwögler, L. T. Burgdorf, T. Carell, *Angew. Chem.* **2000**, *112*, 4082 – 4085; *Angew. Chem. Int. Ed.* **2000**, *39*, 3918 – 3920; b) C. Behrens, L. T. Burgdorf, A. Schwögler, T. Carell, *Angew. Chem.* **2002**, *114*, 1841 – 1844; *Angew. Chem. Int. Ed.* **2002**, *41*, 1763 – 1766; c) C. Behrens, M. Ober, T. Carell, *Eur. J. Org. Chem.* **2002**, 3281 – 3289.

[30] A. Schwögler, T. Carell, *Org. Lett.* **2000**, *2*, 1415 – 1418.

[31] M. P. Scannell, D. J. Fenick, S.-R. Yeh, D. E. Falvey, *J. Am. Chem. Soc.* **1997**, *119*, 1971 – 1977.

[32] L. M. Kundu, L. T. Burgdorf, O. Kleiner, A. Batschauer, T. Carell, *ChemBioChem* **2002**, *3*, 1053 – 1060.

[33] a) F. D. Lewis, X. Liu, Y. Wu, S. E. Miller, M. R. Wasielewski, R. L. Letsinger, R. Sanishvili, A. Joachimiak, V. Tereshko, M. Egli, *J. Am. Chem. Soc.* **1999**, *121*, 9905 – 9906; b) F. D. Lewis, X. Liu, S. E. Miller, R. T. Hayes, M. R. Wasielewski, *J. Am. Chem. Soc.* **2002**, *124*, 11280 – 11281.

[34] C. Wan, T. Fiebig, O. Schiemann, J. K. Barton, A. H. Zewail, *Proc. Natl. Acad. Sci. USA* **2000**, *97*, 14052 – 14055.

[35] T. Kubota, K. Kano, T. Konse, *Bull. Chem. Soc. Jpn.* **1987**, *60*, 3865 – 3877.

[36] T. Fiebig, C. Wan, A. H. Zewail, *ChemPhysChem* **2002**, *3*, 781 – 788.

[37] M. Manoharan, K. L. Tivel, M. Zhao, K. Nafisi, T. Netzel, *J. Phys. Chem.* **1995**, *99*, 17461 – 17472.

[38] T. L. Netzel, M. Zhao, K. Nafisi, J. Headrick, M. S. Sigman, B. E. Eaton, *J. Am. Chem. Soc.* **1995**, *117*, 9119 – 9128.

[39] N. Amann, H.-A. Wagenknecht, *Synlett* **2002**, 687 – 691.

[40] a) N. Amann, E. Pandurski, T. Fiebig, H.-A. Wagenknecht, *Angew. Chem.* **2002**, *114*, 3084 – 3087; *Angew. Chem. Int. Ed.* **2002**, *41*, 2978 – 2980; b) M. Raytchev, E. Mayer, N. Amann, H.-A. Wagenknecht, T. Fiebig, unpublished results.

[41] N. Amann, E. Pandurski, T. Fiebig, H.-A. Wagenknecht, *Chem. Eur. J.* **2002**, *8*, 4877 – 4883.

[42] a) S. O. Kelley, E. M. Boon, J. K. Barton, N. M. Jackson, M. G. Hill, *Nucleic Acids Res.* **1999**, *27*, 4830 – 4837; b) E. M. Boon, D. M. Ceres, T. G. Drummond, M. G. Hill, J. K. Barton, *Nat. Biotechnol.* **2000**, *18*, 1096 – 1100; c) E. M. Boon, J. E. Salas, J. K. Barton, *Nat. Biotechnol.* **2002**, *20*, 282 – 286.

[43] G. Hartwich, D. J. Caruana, T. de Lumley-Woodyear, Y. Wu, C. N. Campbell, A. Heller, *J. Am. Chem. Soc.* **1999**, *121*, 10803 – 10812.

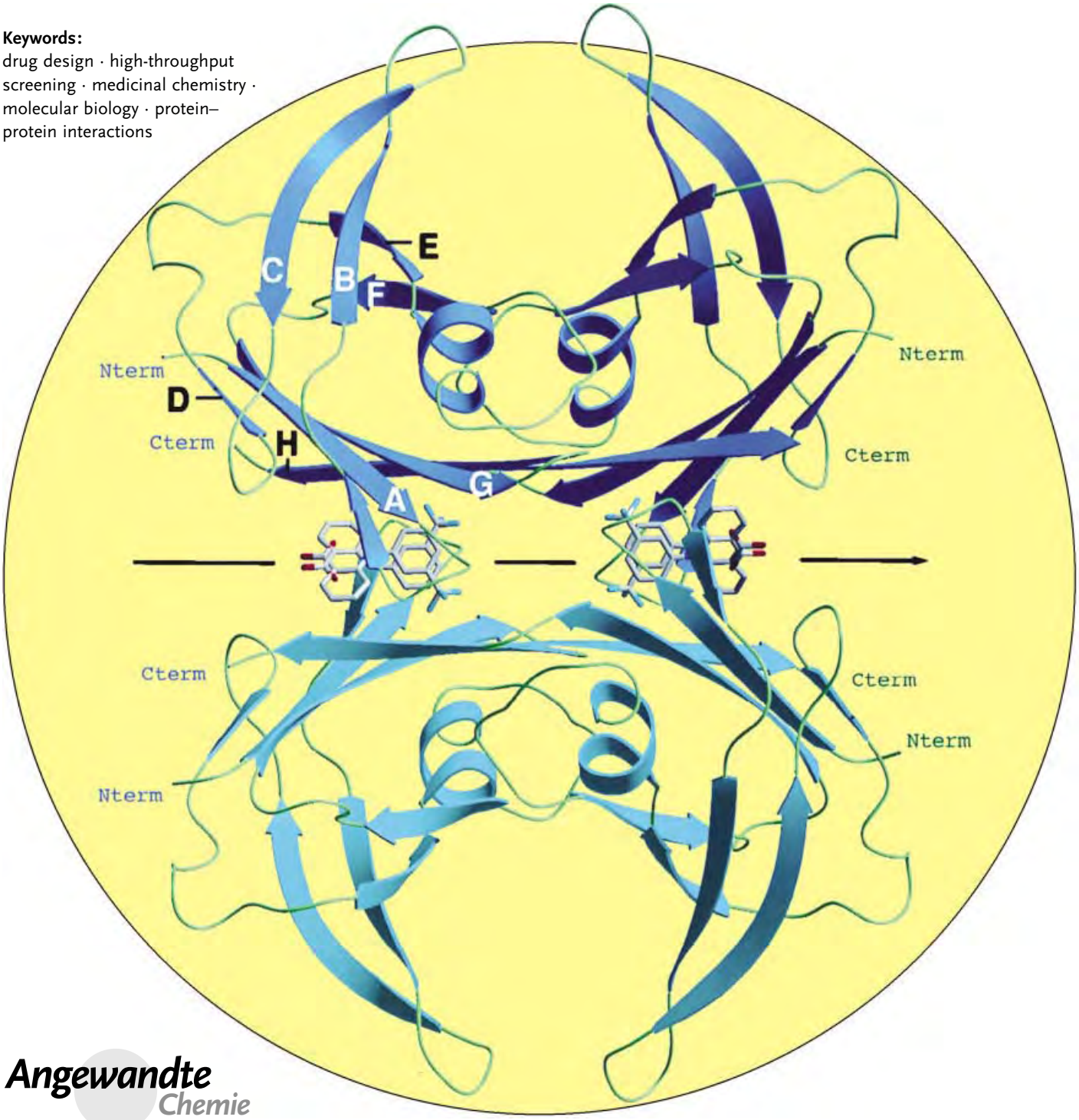
 © 2003 Wiley-VCH Verlag GmbH & Co. KGaA, Weinheim

Protein–Protein Interactions

Modulation of Protein–Protein Interactions with Small Organic Molecules

*Thorsten Berg**

Keywords:
drug design · high-throughput screening · medicinal chemistry · molecular biology · protein–protein interactions



 © 2003 Wiley-VCH Verlag GmbH & Co. KGaA, Weinheim DOI: 10.1002/anie.200200558

Many proteins exert their biological roles as components of complexes, and the functions of proteins are often determined by their specific interactions with other proteins. Because of the central importance of protein–protein interactions for cellular processes, the ability to interfere with specific protein–protein interactions provides a powerful means of influencing the function of selected proteins within the cell. Cell-permeable small organic modulators of protein–protein interactions are thus highly desirable tools both for the study of physiological cellular processes and for the treatment of numerous diseased states. Herein a number of protein–protein interactions that are considered to be pharmaceutical targets are presented, which will familiarize the reader with the strategies that have been employed for the successful identification of small molecule modulators of these protein–protein interactions. These encouraging examples suggest that combined research efforts in the areas of functional proteomics, assay development, and organic synthesis will open up novel possibilities for the treatment of human diseases in the future.

From the Contents

1. Introduction 2463

2. Peptides and Peptidomimetics Derived from Dimerization Interfaces 2464

3. Low-Molecular-Weight Modulators of Protein–Protein Interactions Identified through the Screening of Chemical Libraries 2467

4. Computational Approaches towards the Identification of Small-Molecule Modulators of Protein–Protein Interactions 2474

5. Summary and Outlook 2475

1. Introduction

One of the major challenges in biomedical research is that of gaining a thorough understanding of precisely how the expression of proteins within a cell translates into biological function. It has become evident that instead of acting in isolation, most proteins exert their functions as members of protein complexes.[1] The cellular function of a particular protein may be dependent on the exact composition of its protein complex. As a result of the central role of protein complexes in cellular processes, aberrant or inappropriate protein–protein interactions hold the potential to cause pathological conditions; conversely, the modulation of such protein–protein interactions by small organic molecules offers possibilities for the treatment of human diseased states.

The principal feasibility of using small organic molecules to target protein–protein interactions has been demonstrated impressively by a number of natural products. The taxane agents paclitaxel (Taxol),[2] a diterpenoid isolated from the bark of the Pacific yew tree (*Taxus brevifolia*), and its semisynthetic derivative docetaxel (Taxotère)[3] have been approved for the treatment of a number of human cancers. They bind to the β-subunit of the tubulin heterodimer and thereby stabilize the interactions between tubulin heterodimers, which leads to the accelerated polymerization of tubulin into microtubules. Since microtubules need to not only polymerize but also depolymerize during mitosis, microtubule stabilization by taxanes results in cell-cycle arrest, which ultimately leads to apoptosis (programmed cell death) of cancer cells. Further microtubule-stabilizing natural products[4] include laulimalide,[5] the epothilones A and B,[6] eleutherobin,[7] and discodermolide.[8] An analogue of epothilone B is currently in clinical trials.[9] Brefeldin A, a fungal metabolite[10] which is widely used in cell biology as an inhibitor of protein secretion, functions by stabilizing the protein–protein interaction between guanidine diphosphate (GDP) bound proteins of the Arf family and Sec7 domains.[11] The protein-binding ability of certain natural products was exploited by Schreiber and Crabtree in their pioneering design of CID (chemical inducer of dimerization) systems. Not only FK1012[12] (a dimeric form of the naturally occurring small molecule FK506), but also a fusion molecule comprised of FK506 and cyclosporin A,[13] as well as rapamycin and dimeric cyclosporin A,[14] were demonstrated to induce dimerization of genetically engineered receptors, which lacked their extracellular dimerization domains, and consequently to induce signal transduction and specific target-gene activation.[15] Similarly, FK506 and rapamycin were used to reconstitute the activity of transcription factors the functional domains of which had been separated and linked to the ligand-binding proteins of these organic molecules.[16] The continuation of this approach has recently yielded several novel CID systems.[17]

Even though these examples demonstrate the general feasibility of modulating protein–protein interactions with small organic molecules, the application of this principle to drug discovery research has posed a number of problems. The first difficulty arises over the identification of lead compounds to target protein–protein interactions for which no naturally occurring protein-binding small molecules are known. However, if the protein–protein interface consists of short continuous binding domains, peptidic binding-site mimics lend themselves as lead compounds for subsequent optimization. The existence of short continuous sequence motifs mediating the protein–protein interactions between integrins

[*] Dr. T. Berg
Max Planck Institute of Biochemistry
Department of Molecular Biology
Am Klopferspitz 18a, 82152 Martinsried (Germany)
Fax: (+49) 89-8578-2454
E-mail: berg@biochem.mpg.de

 DOI: 10.1002/anie.200200558 © 2003 Wiley-VCH Verlag GmbH & Co. KGaA, Weinheim

and their extracellular ligands has aided in the discovery of numerous small-molecule inhibitors to date, one of which is currently in clinical trials,[18] and two of which have even been approved for clinical use.[19] However, many protein–protein interfaces consist of noncontinuous binding epitopes in the primary protein sequence, which makes it difficult to rationally design binding-site mimics. Secondly, a recent study revealed that the area of the recognition sites in protein–protein complexes is usually greater than 1100 Å^2, with the exact area depending on the nature of the complex,[20] which vastly exceeds the potential binding area of a low-molecular-weight compound. Attempting to modulate such protein–protein interactions with low-molecular-weight compounds which satisfy the requirements for orally deliverable drugs appear to be unfeasible at first glance. However, it has been demonstrated that a minor fraction of the protein–protein interface residues can in fact account for the majority of the free energy of binding between proteins.[21] Such "hot spots" of binding free energy appear to be common in protein–protein interfaces.[22] Hot-spot amino acid residues tend to be clustered together at the center of a protein–protein interface and are surrounded by energetically less important amino acid residues that probably serve to occlude bulk solvent. The third difficulty is that protein–protein interfaces are often flat and may therefore lack binding sites for small molecules.[23] Despite these difficulties, a number of small organic modulators of large protein–protein interactions have been identified to date, some of which have been discussed in excellent earlier reviews.[24]

Herein, several pharmaceutically interesting protein–protein interactions which, for the most part, involve large, possibly discontinuous binding sites are discussed, and will familiarize the reader with the strategies employed for the identification of small molecule modulators (inhibitors as well as inducers and stabilizers) of these protein–protein interactions. The stategies covered in this review can be divided into three approaches: The first approach is the identification of peptides, derived from the interface between proteins, which are able to inhibit the interaction between the proteins by binding to one of the proteins in a competitive fashion. These peptides are subsequently optimized by the incorporation of non-natural amino acids or other chemical modifications. The latter criterion excludes many unmodified peptide inhibitors of protein–protein interactions, many of which were discovered by using phage-display technologies.[24d,25] The second approach is the in vitro or cell-based screening of chemical libraries for modulators of protein–protein interactions. The third approach is the virtual (in silico) screening of chemical databases for small molecules which are likely to bind to a hot spot of the corresponding protein–protein interaction. With the exception of molecules discussed in the first approach, this review will focus on nonpeptidic molecules. Protein–protein interactions mediated by short continuous binding domains which are involved in signal transduction (for example, interactions involving SH2[26] or SH3[27] domains) will not be discussed, nor will inhibitors of the interactions between integrins and proteins of the extracellular matrix be discussed as these have been extensively reviewed elsewhere.[18,19,28] The impressive progress made to date in the discovery of small-molecule modulators of protein–protein interactions highlights that the interplay between biological and synthetic organic chemical research can lead to major advances in future drug development.



Thorsten Berg, born 1967, studied chemistry at the University of Cologne on a studentship from the "Studienstiftung des deutschen Volkes" final-year project with Prof. E. Vogel). He received his Ph.D. in 1996 for his research on enantioselective synthesis under the supervision of Prof. D. Enders at the RWTH Aachen. He then performed postdoctoral studies at The Scripps Research Institute in La Jolla, USA, with Prof. K. D. Janda (1997–1998), and Prof. P. K. Vogt (1998–2001), where he established biochemical and cell-based assays to identify nonpeptidic antagonists of protein–protein interactions. He is currently a junior group leader at the Max Planck Institute of Biochemistry.

2. Peptides and Peptidomimetics Derived from Dimerization Interfaces

2.1. Inhibitors of HIV-1 Protease Dimerization

The protease encoded by the HIV-1 viral genome (HIV-1 protease) plays an essential role in the life cycle of the human immunodeficiency virus type 1 (HIV-1). It processes the gag and gag–pol HIV polypeptide precursors to functional viral proteins which are required for viral infection of further host cells.[29] Drugs currently used for the inhibition of HIV-1 protease in HIV-infected patients target the active site of the enzyme.[30] Our present inability to treat HIV-infections effectively is the result of constantly emerging viral mutations, which render the existing inhibitors ineffective.[31]

HIV-1 protease is a homodimeric enzyme; both catalytic site and substrate-binding pocket are only formed in the dimeric state.[32] Interestingly, the dimerization domains are highly conserved in HIV isolates, possibly because a mutation in that region in one protein molecule would require a matching mutation in another protein molecule to form a functional dimer.[33] Inhibition of HIV-1 protease subunit association was consequently suggested as an alternative molecular target for anti-HIV therapy since it is likely that inhibitors of HIV-1 protease subunit homodimerization would be less prone to drug resistance.

The dimerization interface of HIV-1 protease is largely composed of the N- and C-termini of the HIV-1 protease monomers which interdigitate to produce a four-stranded, antiparallel β sheet. While the area in the vicinity of the N- and C-termini comprises approximately half of the entire protein–protein interface, it accounts for more than 75% of the free energy of binding in the homodimer.[34] The feasibility of inhibiting HIV-1 protease by interface-derived peptides was initially demonstrated by Poorman et al. who reported that the tetrapeptide Ac-Thr-Leu-Asn-Phe-COOH derived from the C-terminus of HIV-1 protease inhibits the enzyme

 © 2003 Wiley-VCH Verlag GmbH & Co. KGaA, Weinheim

by a dissociative mechanism.[35] In an attempt to mimic the interdigitating termini of HIV-1 protease, Chmielewski et al. workers designed improved dimerization inhibitors bearing peptide sequences derived from the N-terminus of the enzyme cross-linked by a flexible linker to sequences derived from the C-terminus of the enzyme. Compound **1**, which inhibited HIV-1 protease with an IC_{50} of 350 nM (at 25 nM protease) by a dissociative mechanism, served as a starting point for structure–activity investigations aimed at the identification of HIV-1 protease subunit-association inhibitors with reduced molecular weight (Scheme 1).[36] Alanine scanning revealed the critical importance of the C-terminal residues of both peptide chains for the activity of the compounds.[37] Successive deletion of less-important N-terminal amino acids of compound **1** resulted in the peptide **2** ($IC_{50} = 9200$ nM), which acted through a competitive inhibition mode.[38] After the dissociative inhibition mode was recovered by replacing the Trp-OH residue of **2** with Phe-NH_2, the additional replacement of the isobutyl group of the leucine residue by a cyclohexyl group in compound **3** significantly improved the inhibitory activity ($IC_{50} = 680$ nM at 25 nM protease). Compound **3** might serve as a lead compound for medicinal chemistry efforts because of its reduced molecular weight (933 g mol^{-1}) compared with that of the starting compound **1** (1586 g mol^{-1}).

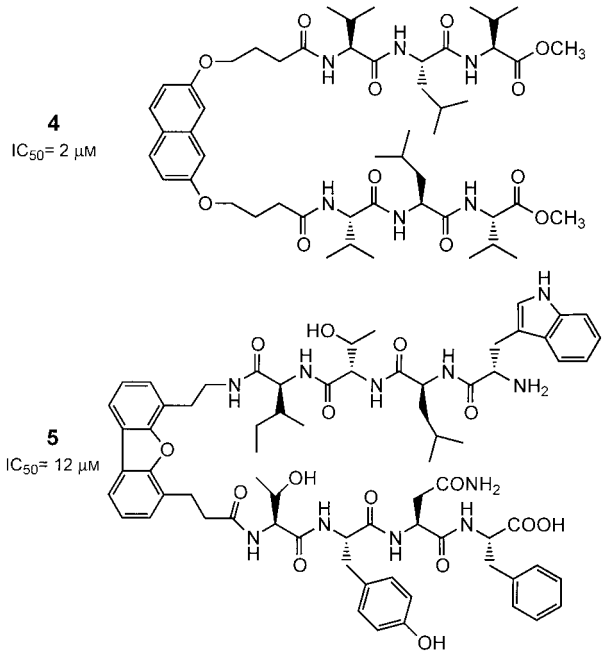
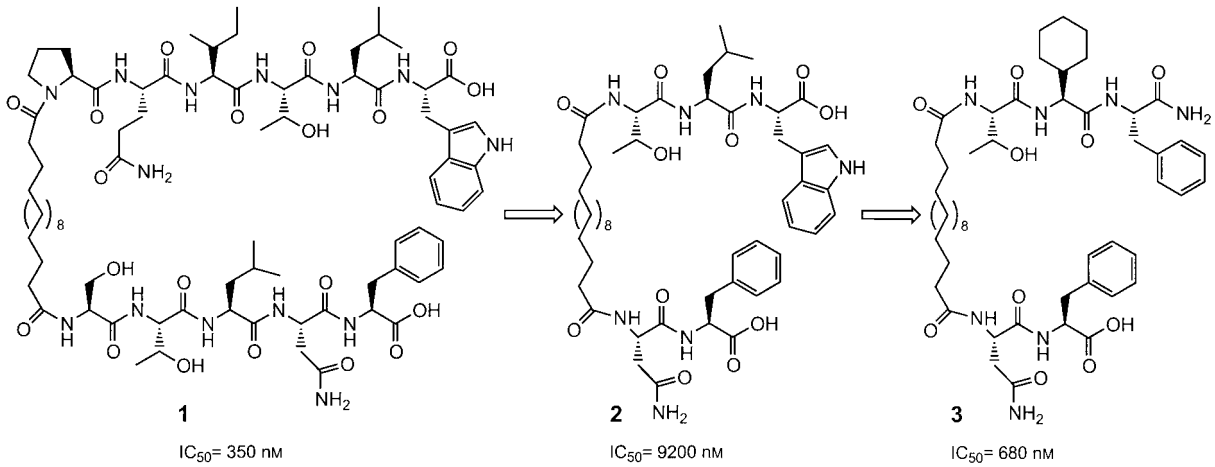


Figure 1. Interfacial HIV-1 protease inhibitors **4** and **5** bearing rigid cross-linkers.

It is conceivable that the flexibility of the alkyl tether used by Chmielewski et al. produces an unfavorable entropy term in the free interaction energy of the complex formed between the inhibitor and the monomeric protease. To investigate the hypothesis that the presence of more-rigid linker molecules between the peptide chains might produce more active dimerization inhibitors, Sicsic et al. cross-linked the peptide chains with aromatic groups.[39] The native N- and C-terminal tetrapeptide sequences were varied by amino acid substitutions and deletions. For convenience of synthesis, identical peptides were attached to each side of the constrained scaffold. The most active molecule, compound **4**, inhibited HIV-1 protease with an IC_{50} value of 2 μM (at 7.5 nM protease) by a dissociative mechanism (Figure 1). Of note is that this peptide sequence does not reproduce sequences involved in the antiparallel β sheet of HIV-1 protease. Kiso et al. fused the N- and C-terminal amino acids of HIV-1 protease to 4-(2-aminoethyl)-6-dibenzofuranpropionic acid and achieved inhibition of HIV-1 protease with an IC_{50} value of 12 μM (3.2–23.8 nM protease) by a dissociative mechanism (compound **5**).[40] While a direct comparison of the effect of the different linkers on the inhibitor potency is hampered by the nonidentical peptide chains and the assay conditions used, the compounds bearing the flexible alkyl tether display the best activities in this design series, which indicates that flexibility of the cross-linker may in fact be necessary for efficient binding of the peptide chains to the HIV-1 protease monomer. Consistent with this notion, the introduction of *cis*-



Scheme 1. Development of HIV-1 protease dimerization inhibitor **3** from **1**.

 © 2003 Wiley-VCH Verlag GmbH & Co. KGaA, Weinheim

and *trans* alkenyl groups or of an alkinyl group into the $(CH_2)_{14}$ linker of **1** reduces its inhibitory potency.[41]

Schramm et al. performed extensive mutational and deletion analysis as well as computer modeling of C-terminal HIV-1 protease sequences.[42] These efforts led to the identification of several *N*-palmitoyl-protected tripeptides which inhibit HIV-1 protease with IC_{50} values in the nanomolar concentration range. *N*-palmitoyl-Tyr-Glu-Leu-OH, which inhibits enzyme dimerization with an IC_{50} value of 150 nM (15–30 nM protease),[43] may be another lead structure for the development of HIV-1 protease dimerization inhibitors.

Natural-product inhibitors of HIV-1 dimerization present an interesting alternative to designed dimerization inhibitors, and will be discussed in this section to allow a direct comparison of the different approaches, even though they are not derived from the HIV-1 protease interface. Didemnaketal A (**6**), isolated from the ascidian *Didemnum sp.*, was shown to inhibit HIV-1 protease with an IC_{50} value of 2 μM (Figure 2).[44] Limited supply of **6** prevented the determination of the absolute configuration of the stereogenic centers in the pentaester side chain. The simplified synthetic analogue **7** which is more amenable to structural optimization was found to have an equal potency to that of didemnaketal A and to inhibit HIV-1 protease by a dissociative mechanism.[45] Because of their nonpeptidic character, didemnaketal **6** and its simplified analogue **7** are among the most promising lead structures for the development of HIV-1 protease subunit-association inhibitors.

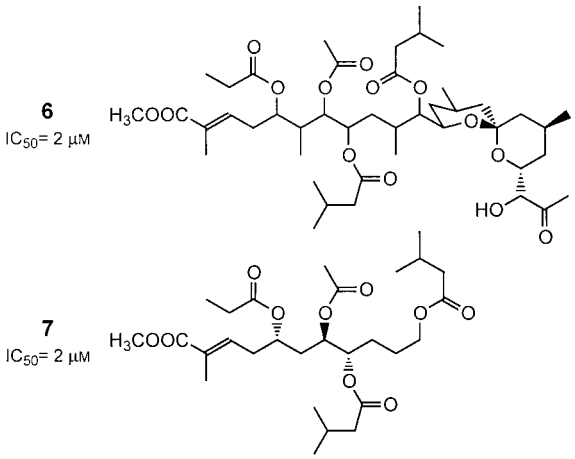


Figure 2. Didemnaketal A (**6**) and synthetic analogue **7**.

2.2. Inhibitors of Herpes Simplex Virus Ribonucleotide Reductase Dimerization

A large part of the world's population is infected with herpes simplex viruses (HSV) types 1 or 2 which cause a broad spectrum of diseases, which include labial and genital herpes.[46] Current drugs used for the treatment of HSV symptoms are nucleoside analogues (e.g. acyclovir), which are phosphorylated by the viral thymidine kinase and subsequently by cellular kinases to yield inhibitors of the viral DNA polymerase.[47] The viral enzyme ribonucleotide reductase, which converts ribonucleotide diphosphates into the corresponding deoxyribonucleotides, has been discussed as another potential target for the treatment of HSV-related symptoms.[48] HSV types 1 and 2 encode their own ribonucleotide reductases which were found to be important for viral virulence and reactivation from latency in mice.[49] The active form of ribonucleotide reductase results from association of the large subunit R1 with the small subunit R2.[50] The carboxy terminus of R2 was shown to be required for subunit dimerization,[51] and peptides derived from the C-terminus of R2 inhibited enzymatic activity by preventing subunit association.[52]

The hexapeptide Ala-Val-Val-Asn-Asp-Leu (**8**) derived from the C-terminus of HSV R2 served as the starting point for the development of enzyme-subunit-association inhibitors. Systematic side-chain variation[53] of this hexapeptide culminated in the discovery of BILD 1357 (**9**), which in an in vitro binding assay is at least 58000-fold more active than the native hexapeptide sequence ($IC_{50} < 1$ nM; Figure 3).[54] Despite its peptidic character, BILD 1357 efficiently inhibited HSV replication in tissue culture ($EC_{50} = 0.8$ μM against HSV-1, compared to 2 μM for acyclovir) and suppressed HSV-1 induced keratitis when applied as 0.3% cream in a mouse ocular model. The development of BILD 1357 impressively demonstrates the power of using short interface-derived peptides as lead structures for drug development.

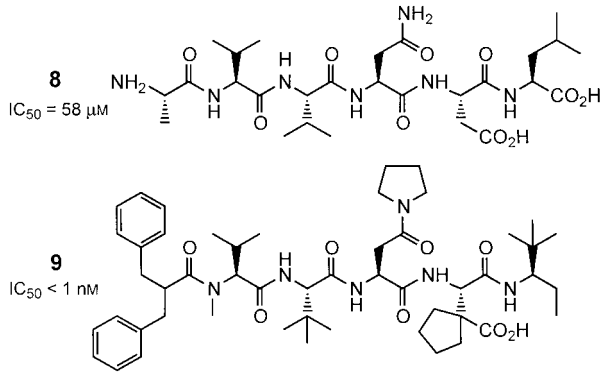


Figure 3. Peptide lead **8** and optimized HSV ribonucleotide reductase subunit-association inhibitor BILD 1357 (**9**).

2.3. Inhibitors of p53/Hdm2 Interactions

The tumor suppressor p53 is inactivated in the majority of human tumors, either by mis-sense mutations[55] or by binding to oncogenic proteins.[56] The function of p53 is to help maintain the genomic integrity of the cell by inducing cell-cycle arrest[57] and apoptosis (programmed cell death)[58] in response to DNA damage.[59] In more than 30% of human sarcomas, p53 inactivation can be linked to amplification of the gene coding for the oncoprotein Hdm2.[60] Interaction

 © 2003 Wiley-VCH Verlag GmbH & Co. KGaA, Weinheim

with Hdm2 inhibits p53 by two different mechanisms: first, Hdm2 binds to the transcriptional activation domain of p53 and thereby inhibits expression of p53 target genes. Second, a protein complex involving Hdm2 mediates nuclear export of p53 and subsequent degradation of p53 by cytoplasmic proteasomes.[61]

The X-ray structure of the complex formed by a p53-derived peptide and wild-type Hdm2 shows that amino acids 18–26 of p53 form an amphipathic α helix, which binds to an elongated hydrophobic Hdm2 cleft.[62] Residues Phe19, Trp23, and Leu26 of p53 form critical binding contacts along the cleft, and substitution of any of these amino acids for other natural amino acids dramatically reduces the binding affinity of p53 for Hdm2. Dodecapeptide **10**, which consists of amino acids 16–27 of p53, was shown to inhibit p53/Hdm2 interactions by binding to Hdm2 ($IC_{50} = 8.7$ μM in vitro, Table 1). Sequence optimization by phage display[63] and truncation identified the octapeptide **11** as an equally potent inhibitor. Substitution of residues not contacting the protein–protein interface by α,α′-substituted amino acids increased the helical propensity of the peptide and resulted in increased binding affinity of peptide **12** to Hdm2. Subsequent substitution of Tyr for phosphonomethylphenylalanine (Pmp) stabilized a salt bridge with the ε-amino group of a lysine residue in Hdm2 (compound **13**). Finally, binding activity was dramatically increased by substitution of Trp23 by 6-chlorotryptophan (ClTrp; compound **14**, $IC_{50} = 5$ nM). The chlorine atom of ClTrp fills the remaining space of the tryptophan-binding pocket of Hdm2 and thereby establishes additional van der Waals interactions with Hdm2.[64] In cellular assays, **14** led to activation and accumulation of p53, and caused p53-dependent cell-cycle arrest and apoptosis in an Hdm2-overexpressing tumor cell line.[65] Unfortunately, its low cellular permeability required the use of **14** at a concentration of 100 μM in these cellular assays.

Table 1: Peptide inhibitors of the p53/Hdm2 interaction.[a]

Compound		IC_{50} [μM]
10	Ac-Gln-Glu-Thr-Phe^{19}-Ser-Asp-Leu-Trp^{23}-Lys-Leu-Leu^{26}-Pro-NH_2	8.7
11	Ac-Phe^{19}-Met-Asp-Tyr-Trp^{23}-Glu-Gly-Leu^{26}-NH_2	8.9
12	Ac-Phe^{19}-Met-Aib-Tyr-Trp^{23}-Glu-Ac_3c-Leu^{26}-NH_2	2.2
13	Ac-Phe^{19}-Met-Aib-Pmp-Trp^{23}-Glu-Ac_3c-Leu^{26}-NH_2	0.3
14	Ac-Phe^{19}-Met-Aib-Pmp-ClTrp^{23}-Glu-Ac_3c-Leu^{26}-NH_2	0.005

[a] Abbreviations: Aib: α-aminoisobutyric acid; Pmp: phosphonomethylphenylalanine; ClTrp: 6-chlorotryptophan; Ac_3c:1-amino cyclopropanecarboxylic acid.

In two unrelated approaches, further inhibitors of the p53/Hdm2 interaction were identified. Screening of 53000 microbial extracts identified the fungal metabolite Chlorofusin as an inhibitor of the p53/Hdm2 interaction ($IC_{50} = 4.6$ μM in vitro).[66] This cyclic nonapeptide is composed of natural and unnatural amino acids and carries a chromophore. Meanwhile, Holak et al. found that certain chalcones (1,3-diphenyl-2-propen-1-ones) can bind to the tryptophan binding pocket of Hdm2 and can inhibit p53/Hdm2 interactions in the micromolar concentration range.[67]

3. Low-Molecular-Weight Modulators of Protein–Protein Interactions Identified through the Screening of Chemical Libraries

3.1. Inhibitors of the Interaction between Bcl-x_L or Bcl-2 and Bak-BH3 Domains

Drug resistance is a serious problem in cancer chemotherapy.[68] Most conventional chemotherapeutic agents damage cellular components, and this can result in a variety of post-damage responses. One of the desired effects is the induction of apoptosis, a highly regulated program of cellular suicide which plays an important role in the body's defense against cells that threaten to escape normal proliferation control mechanisms.[69] Overexpression of the anti-apoptotic *bcl-2* family genes *bcl-2* and *bcl-x_L* has frequently been observed in several solid human tumors, and has been linked to resistance of the tumors to chemotherapy.[70] Bcl-2 was furthermore validated as a tumor target by the effects of an antisense oligonucleotide (Genasense, Genta Inc., USA) which is currently being tested in clinical trials in combination with cytotoxic chemotherapy for the treatment of various cancers.[71] Bcl-2 and Bcl-x_L are assumed to prevent apoptosis by inhibiting the function of other, pro-apoptotic members of the Bcl-2 family, such as Bax and Bak, by binding to their BH3 (Bcl-2-homology 3) domain. Small-molecule inhibitors of the interactions between Bcl-2 or Bcl-x_L and the BH3 domain of pro-apoptotic Bcl-2 family proteins are therefore anticipated to restore the biological functions of pro-apoptotic Bcl-2 family members, and could possibly render drug susceptibility to cancers which are resistant to chemotherapy because of overexpression of anti-apoptotic Bcl-2 family genes.

To identify small-molecule inhibitors of the interaction between Bcl-x_L and the BH3 domain of Bak, Yuan et al.[72] set up an in vitro assay based on fluorescence polarization (FP).[73] This homogeneous assay is generally applicable for the analysis of protein–protein interactions if the molecular weight of the larger protein is considerably higher than the weight of the smaller protein or peptide, and can easily be adapted to a high-throughput format. The degree of interaction between the fluorescent-labeled BH3 domain of Bak and recombinant Bcl-x_L protein was assessed by analyzing the polarization of the emitted fluorescence upon excitation with polarized light (Figure 4). In the absence of an inhibitor compound, the small fluorescent-labeled BH3 peptide is bound to the larger Bcl-x_L protein. Since the spatial orientation of the large peptide/protein complex hardly changes between the time of fluorescence excitation and fluorescence emission, the polarization of the emitted fluorescence is relatively high. Inhibitors of Bcl-x_L/Bak-BH3 interactions liberate the small fluorescent-labeled BH3 peptide and are detected because of the increased rotational mobility of this peptide in the unbound state which leads to a reduction of the fluorescence polarization.

A commercially available library consisting of 16320 chemicals was screened, and three compounds termed BH3I-1 (**15**) BH3I-1′ (**16**), and BH3I-2 (**17**), were identified as inhibitors of the Bcl-x_L/Bak-BH3 interaction ($K_i = 2.4$–

 © 2003 Wiley-VCH Verlag GmbH & Co. KGaA, Weinheim

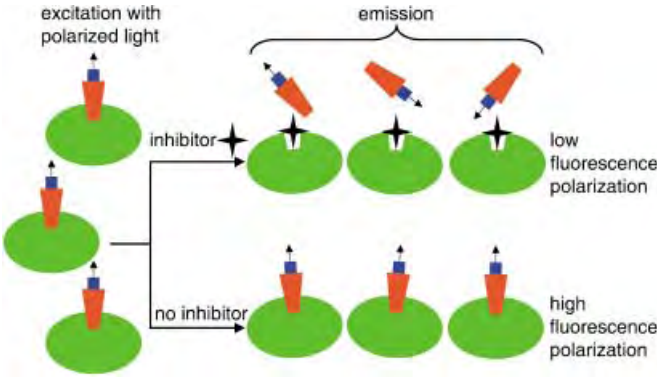
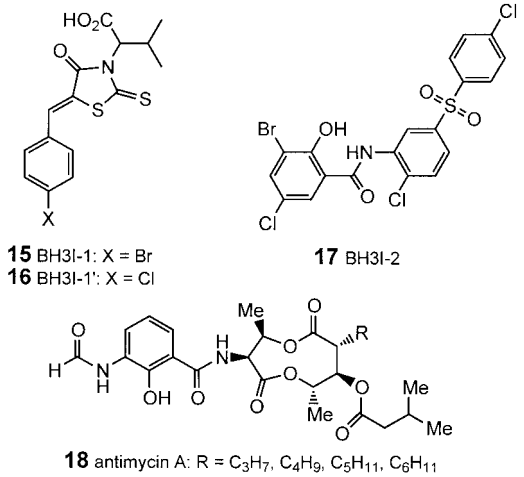


Figure 4. Principle of the fluorescence polarization assay used to screen for Bcl-x_L/Bak-BH3 inhibitors. Green oval: large Bcl-x_L protein; red cone: small BH3-peptide; blue square: fluorophore; arrow: transition vector of fluorescence emission.



15 BH3I-1: X = Br
16 BH3I-1': X = Cl
17 BH3I-2
18 antimycin A: R = C_3H_7, C_4H_9, C_5H_{11}, C_6H_{11}

Figure 5. Inhibitors of the interaction between Bcl-x_L and BH3 domains.

4.1 μM; Figure 5). Closely related analogues were also found to be Bcl-x_L/Bak-BH3 inhibitors. NMR spectroscopy experiments demonstrated that the inhibitor compounds target the BH3-binding pocket of Bcl-x_L. The Bcl-x_L/Bak-BH3 inhibitors restored the function of the pro-apoptotic Bcl-2 family members in cell culture, and allowed previously resistant cells to undergo apoptosis. Using an unrelated approach, Hockenbery et al. reported that a mixture of antimycin A isomers (**18**), previously used as an inhibitor of mitochondrial electron transfer, is also a competitive inhibitor of the binding of the BH3-domain of Bcl-2 or Bcl-x_L to a BH3 peptide.[74] The chemical optimization of these inhibitors could lead to novel approaches in the treatment of cancers resistant to chemotherapy.

3.2. Inhibitors of Myc/Max Dimerization

The transcription factor c-Myc is estimated to be involved in one out of seven human cancer deaths.[75] In Burkitt's lymphoma and other lymphoid malignancies, the c-*myc* gene is translocated into the vicinity of an immunoglobulin enhancer, which results in constitutive overexpression.[76] The c-*myc* gene is also amplified in lung[77] and breast carcinomas,[78] and elevated expression of the c-Myc protein is found in the majority of colon carcinomas.[79] Targeted overexpression of c-*myc* causes hematopoetic tumors in transgenic mice,[80] and sustained activation of c-Myc is sufficient to induce premalignant changes in the skin epidermis.[81] Since the oncogenic activity of c-Myc entirely depends on binding to its activation partner Max,[82] inhibitors of c-Myc/Max interactions have the potential to regulate c-Myc activity and be of pharmacological interest for the treatment of cancers that depend on sustained activation of c-Myc.

c-Myc and Max belong to the basic helix-loop-helix leucine zipper (bHLH-LZ) protein family. From the crystal structure of the related Max/Max homodimer,[83] it is to be assumed that the Myc/Max dimer forms a parallel, left-handed, four-helix bundle, with each monomer containing two α-helical segments separated by a loop. While the basic region and the N-terminal helices mediate binding to specific DNA sequences in the promoters of c-Myc target genes, the dimerization interface consists of the C-terminal helix motif and the leucine zipper, which forms a parallel, two stranded α-helical coiled coil. The protein–protein interface is formed by mostly hydrophobic, buried, amino acid residues.[84]

As a result of the parallel alignment and the identical length of the dimerization motifs of c-Myc and Max, a binding assay based on fluorescence resonance energy transfer (FRET)[85] is ideally suited to screen for inhibitors of the Myc/Max interaction. FRET can occur between two fluorophores if the emission spectrum of the donor fluorophore overlaps with the absorption spectrum of the acceptor fluorophore. As the efficiency of FRET is dependent on the inverse sixth power of the distance between the fluorophores, this method allows the analysis of binding equilibria between molecules fused to two suitable fluorophores. Vogt et al.[86] expressed the dimerization domains of c-Myc and Max as fusion proteins with cyan fluorescent protein (CFP) and yellow fluorescent protein (YFP), respectively. Upon excitation of CFP, the close proximity between the fluorophores in the c-Myc/Max dimer allowed for energy transfer from CFP to YFP (Figure 6). Inhibitors of c-Myc/Max dimerization-domain interactions increased the average distance between the c-Myc and Max polypeptides and thereby decreased the amount of energy transferred between the fluorophores,

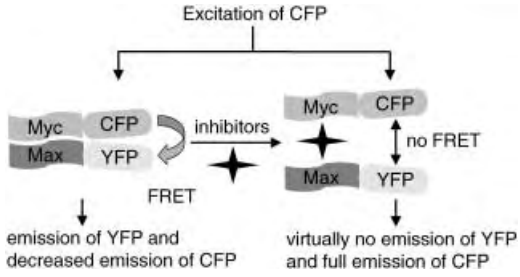


Figure 6. Simplified principle of the FRET assay used to screen for Myc/Max inhibitors.

 © 2003 Wiley-VCH Verlag GmbH & Co. KGaA, Weinheim

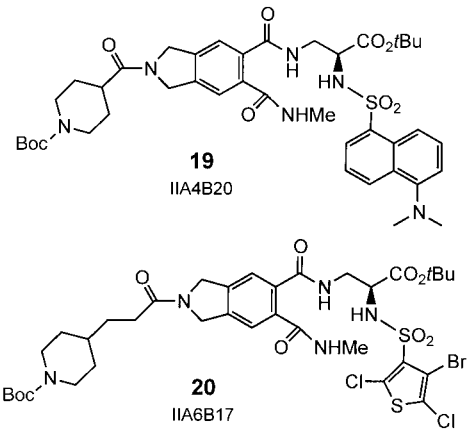


Figure 7. Structures of Myc/Max inhibitors IIA4B20 (**19**) and IIA6B17 (**20**).

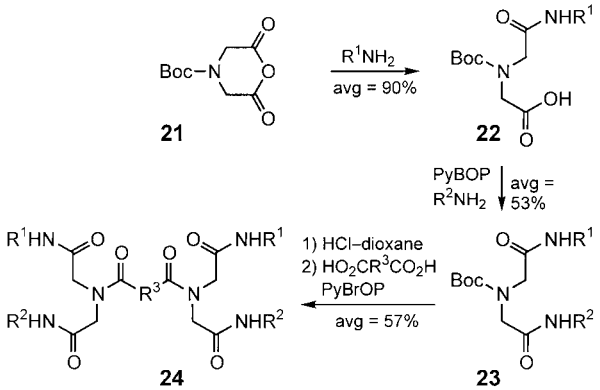
which led to characteristic changes in the fluorescence spectrum.

Screening of chemical libraries encompassing approximately 7000 compounds[87,96] resulted in the discovery of four small-molecule antagonists of c-Myc/Max dimerization-domain interactions which were subsequently validated in independent in vitro assays. The two most active inhibitors in vitro, IIA4B20 (**19**) and IIA6B17 (**20**; Figure 7), also inhibited c-Myc-induced oncogenic transformation of chicken embryo fibroblasts with IC_{50} values of approximately 20 μM. Improved inhibitors of c-Myc/Max interactions which may emerge from secondary libraries could not only serve as lead structures for drug development, but might also be useful as molecular tools to aid in the identification of downstream target genes of c-Myc.[88]

3.3. Inhibitors of MMP2/Integrin $\alpha_v\beta_3$ Interactions

Tumor growth is dependent on the formation of new blood vessels, a process termed angiogenesis.[89] The early steps of angiogenesis involve the branching of endothelial cells from the existing vasculature, which requires remodeling of the vascular basal lamina and the extracellular matrix (ECM).[90] Matrix metalloproteinases (MMPs) in the extracellular environment are responsible for breaking down the basal lamina and the ECM.[91] Unfortunately, since MMPs have a broad range of functions in the adult organism, active-site inhibitors of MMPs possess damaging side effects,[92] which limit their the clinical use as anti-angiogenic agents. Another therapeutic avenue toward the prevention of angiogenesis in tumors emerged when one family member, MMP-2, was found to associate with the integrin $\alpha_v\beta_3$ on the surface of invasive angiogenic vascular cells and melanoma cells in vivo,[93] and inhibition of the MMP-2/$\alpha_v\beta_3$ interaction by a polypeptide comprising the $\alpha_v\beta_3$-binding domain of MMP-2 was shown to disrupt angiogenesis.[94] Hence, inhibition of the MMP-2/$\alpha_v\beta_3$ interaction by small organic molecules may provide an alternative entry point for the treatment of cancer.

In an attempt to identify small-molecule inhibitors of MMP-2/$\alpha_v\beta_3$ interactions as antiangiogenic agents, an interdisciplinary research group led by Boger and Cheresh monitored the interactions between MMP-2 and $\alpha_v\beta_3$ in the presence of members of a chemical library.[95] This library was synthesized by combining six different amines R^1 with 10 different amines R^2 through a iminodiacetic acid linker.[96] Dimerization of each of the 60 single compounds **23** with a mixture of 10 rigid dicarboxylic acids R^3 provided 60 compound mixtures **24** consisting of 10 different compounds each (Scheme 2).



Scheme 2. Synthesis of the chemical library containing inhibitors of the MMP-2/$\alpha_v\beta_3$ interaction; Boc = *tert*-butoxycarbonyl, PyBOP = benzotriazol-1-yl tripyrrolidinophosphonium hexafluorophosphate, PyBrOP = bromotripyrrolidinophosphonium hexafluorophosphate, avg = average yield.

In the absence of precise structural information about the MMP2-$\alpha_v\beta_3$ interface, binding between $\alpha_v\beta_3$ and MMP-2 was analyzed in an enzyme-linked immunosorbent assay (ELISA). Purified $\alpha_v\beta_3$ was first coated on the surface of a microtiter plate, followed by incubation of the immobilized $\alpha_v\beta_3$ with biotinylated MMP-2 in the presence of the screening compounds (Figure 8). Finally, an anti-biotin antibody coupled to the enzyme horseradish peroxidase (HRP) was added, and the extent of MMP-2/$\alpha_v\beta_3$ binding in the presence of the screening compounds was quantified colorimetrically by using an HRP substrate.

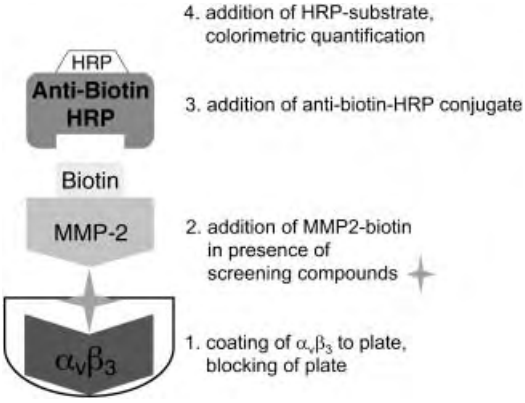
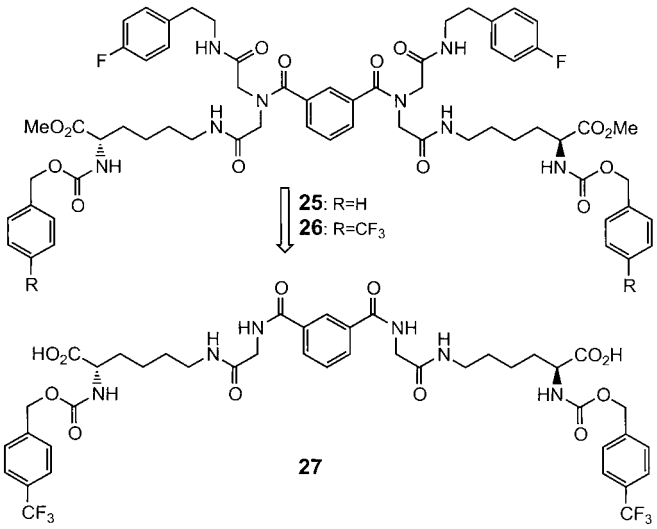


Figure 8. Set-up of the ELISA used to screen for inhibitors of the MMP-2/$\alpha_v\beta_3$interaction.

 © 2003 Wiley-VCH Verlag GmbH & Co. KGaA, Weinheim



Scheme 3. Development of MMP-2/$\alpha_v\beta_3$ inhibitors.

Deconvolution of active mixtures identified compound A6B10C4 (**25**) as an inhibitor of the MMP-2/$\alpha_v\beta_3$ interaction (79% inhibition at 3 μM compound; Scheme 3). It is noteworthy that the enantiomer of **25** has no inhibitory activity, which demonstrates the importance of stereochemistry for the design of small-molecule modulators of protein–protein interactions. Structural optimization resulted in the identification of compound **26** and its simplified analogue **27,** which was more suited for in vivo testing because of its improved solubility and lower molecular weight ($IC_{50} = 1$ μM for both compounds in the in vitro binding assay). Both **26** and **27** specifically bound to $\alpha_v\beta_3$, not to MMP-2, in a dose-dependent manner. The ability of $\alpha_v\beta_3$-infected melanoma cells to degrade the main constituent of the basal lamina (collagen IV) was inhibited by **27** in the low micromolar concentration range. Compound **27** also inhibited angiogenesis and tumor growth in vivo without suppressing MMP-2 activation. The identification of compound **27** demonstrates the principal feasibility of targeting the MMP2/$\alpha_v\beta_3$ interaction with small organic molecules, and raises hope that in the future aberrant angiogenesis in cancers may be treatable with drugs that cause less detrimental side effects.

3.4. Inhibitors of Binding of TNF-α to Its Receptor TNFRc1

The cytokine tumor-necrosis factor alpha (TNF-α) plays an important role in the inflammatory response to tissue injury and various viral and bacterial infections.[97] TNF-α forms homotrimers which bind to the TNF-α receptors 1 and 2 and induce receptor trimerization.[98] Depending on the cellular context, trimerization of the TNF-α receptor 1 (TNFRc1) can lead to activation of the immune system by the NF-κB signaling pathway. Since aberrantly increased TNF-α activity may also lead to tissue damage, inhibitors of TNF-α are of clinical interest for the treatment of autoimmune diseases, such as rheumatoid arthritis or Crohn's disease.[99] These pathological conditions are currently being treated with anti-TNF-α antibodies and soluble receptor molecules, which act by sequestering TNF-α.[100] Inhibition of the interaction between TNF-α and its receptor TNFRc1 may be an alternative approach for inhibition of TNF-α activity.

Carter and co-workers set up a solid-phase binding assay to screen chemical libraries for antagonists of the TNF-α/TNFRc1 interaction. To this end, the TNF-α receptor TNFRc1 was immobilized on microtiter plates, and binding of fluorescent-labeled TNF-α to its receptor was quantified in the presence of the screening compounds. The screen identified *N*-alkyl 5-arylalkylidene-2-thioxo-1,3-thiazolidin-4-ones as antagonists for the TNF-α/TNFRc1 interaction.[101] The most active compound IW927 (**28**; Figure 9) inhibited the

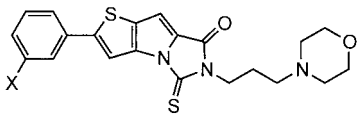


Figure 9. Inhibitors of binding of TNF-α to its receptor TNFRc1.

TNF-α/TNFRc1 interaction with an apparent IC_{50} value of 50 nM and also blocked TNF-α-stimulated phosphorylation of IκB, an intermediate event in the activation of NF-κB signaling. Surprisingly, the activity of the compounds decreased by up to 1000-fold when the binding assays were performed in the dark. Detailed X-ray crystallographic and other investigations of the binding mode of the analogue compound IV703 (**29**) revealed that this inhibitor reversibly bound to TNFRc1 with only micromolar affinity in the absence of light. Under normal lighting conditions, the nitrophenyl ring of **29** subsequently became covalently attached to the backbone nitrogen of an alanine residue of TNFRc1, thereby preventing the binding of TNF-α to its receptor. Since in a living organism activation of the compounds by light is not generally feasible, the activity of the compounds in the dark must be used to judge their utility. The data suggest that caution should be exercised when analyzing the biological activity of compounds containing an *N*-alkyl 5-arylalkylidene-2-thioxo-1,3-thiazolidin-4-one core.

3.5. Inhibitors of LFA-1/ICAM-1 Interactions

The binding of activated leukocyte function-associated antigen-1 (LFA-1) to its endothelial-cell-ligand intercellular adhesion molecule-1 (ICAM-1, CD54) is an important step in the migration of leukocytes from the bloodstream to the surrounding tissues during the early stages of inflammation.[102] The integrin LFA-1, expressed on all leukocytes,[103] consists of a large α_L subunit (CD11a) and a small β_2 subunit (CD18) and is activated by exposure to cytokines and pro-inflammatory mediators.[104] In addition to this role in the early stages of inflammation, the interaction between LFA-1 on the surface of T cells and ICAM-1 provides a strong costimulatory signal during T-cell activation.[105] T-cell activation and proliferation is a crucial component of the immune

response. Inhibitors of the LFA-1/ICAM-1 interaction consequently have the potential to inhibit both the inflammatory and the immune response. Inhibitors of the LFA-1/ICAM-1 interaction developed for the treatment of inflammatory diseases[106] and graft rejection after transplantation[107] have mostly been based on monoclonal antibodies[108] directed against CD11a, the α-chain of LFA-1. CD11a contains a multidomain β-propeller motif. Between two of the domains of the β-propeller, a domain referred to as the "I-domain" is inserted.[109] Part of the I-domain is a magnesium-cation-binding domain, called the "metal-ion-dependent adhesion site" (MIDAS),[110] which is directly involved in the interaction of CD11a with ICAMs.

Lovastatin, a drug clinically used for lowering cholesterol levels,[111] was identified as an inhibitor of LFA-1/ICAM-1 interactions in an LFA-1-dependent adhesion assay.[112] A lovastatin analogue, LFA703, with improved activity (IC_{50} = 200 nM in a solid-phase binding assay) was subsequently identified and found to suppress the inflammatory response in a mouse model of acute inflammation.[113] LFA451 (**30**; IC_{50} = 40 nM; Figure 10) is the most active statin inhibitor of the LFA-1/ICAM-1 interaction identified to date.[114] Another

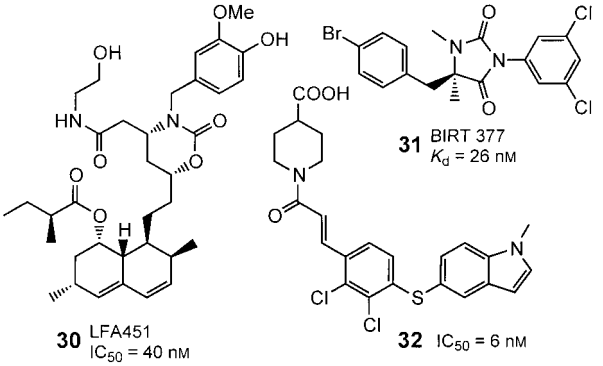
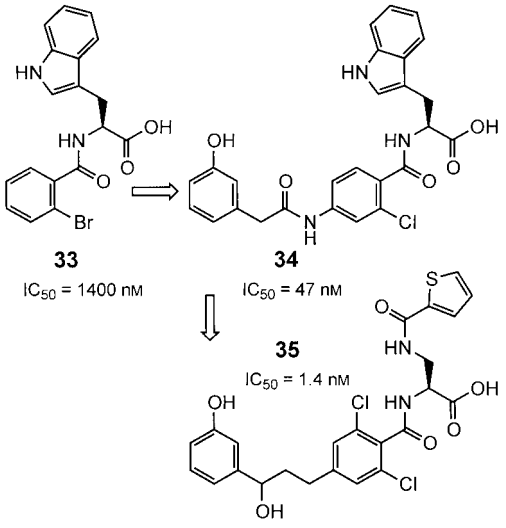


Figure 10. Inhibitors of the LFA-1/ICAM-1 interaction.

research group discovered the hydantoin BIRT377 (**31**) as a nanomolar antagonist for the LFA-1/ICAM-1 interaction by screening of proprietary chemical libraries and subsequent lead optimization.[115] Interestingly, the authors report that the enantiomer of BIRT377 is 35-times less potent, once again emphasizing the importance of stereoselective synthesis for the discovery of small-molecule modulators of protein–protein interactions. Scientists at the company Abbott (and ICOS) identified *p*-arylthio cinnamides[116] as antagonists for the LFA-1/ICAM-1 interaction, and performed extensive structure–activity relationship (SAR) studies using an NMR-spectroscopy-based model of the complex formed between the compounds and their LFA-1 binding site. This investigation ultimately resulted in the identification of compound **32** as a nanomolar inhibitor (IC_{50} = 6 nM in a solid-phase binding assay).[117] Compound **32** was shown to inhibit cell migration by blocking LFA-1/ICAM1 interactions in vivo, which suggests that it may reduce the severity of an in vivo inflammatory reaction.

Structural investigations indicated that none of the inhibitors mentioned above directly inhibit ICAM-1 binding by interacting with the MIDAS site of LFA-1. Instead, they bind to a site within the I-domain of LFA-1 with suggested regulatory function, thereby preventing an allosteric change required for LFA-1 to achieve a conformation that binds ICAM-1 with high affinity.[118] This allosteric regulation of protein–protein interactions is an interesting approach as it circumvents potential difficulties encountered when targeting large, possibly discontinuous protein–protein interfaces with small molecules.

The most potent inhibitor of LFA-1/ICAM-1 interactions to date was identified by an approach involving rational design.[119] The LFA-1 binding epitope of ICAM-1 consists of residues Glu34, Lys39, Met64, Tyr66, Asn68, and Gln73.[120] Molecular modeling and alanine scanning identified the sequence motif Arg-Gly-Asp-Met-Pro as a mimic of the ICAM-1 residues Glu34 and Lys39. Analysis of disulfide-constrained, cyclized, heptapeptide libraries based on the Arg-Gly-Asp-Met-Pro epitope led to the identification of the inhibitor peptide H_2N-Cys-Gly-Tyr(m)-Asp-Met-Pro-Cys-COOH (Tyr(m) = *meta*-tyrosine). During the course of these studies, *ortho*-bromobenzoyl tryptophan (**33**) was identified as an inhibitor of the LFA-1/ICAM-1 interaction in independent investigations. Alignment of *ortho*-bromobenzoyl tryptophan with the C-terminus of H_2N-Cys-Gly-Tyr(m)-Asp-Met-Pro-Cys-COOH suggested that a three-atom extension at the 4-position of the benzoyl ring of *ortho*-bromobenzoyl tryptophan could mimic the *meta*-phenol group of *meta*-tyrosine. In fact, compound **34** is 30-times more active than *ortho*-bromobenzoyl tryptophan **33** (Scheme 4). Further optimization led to the discovery of **35**, which inhibited LFA-1/ICAM-1 interactions with an IC_{50} value of 1.4 nM in an in vitro binding assay. Compound **35** was demonstrated to inhibit LFA-1-mediated lymphocyte proliferation and adhesion in vitro, and is equivalent to an anti-CD11a antibody in its potency of inhibition of the immune response in vivo. It is conceivable that **35** truly mimics the LFA-1 binding epitope of ICAM-1, since some of the functional groups of the LFA-1 binding epitope of ICAM-1 are also in compound **35**.



Scheme 4. Development of LFA/ICAM-1 inhibitor **35**.

 © 2003 Wiley-VCH Verlag GmbH & Co. KGaA, Weinheim

3.6. Inhibitors of iNOS Dimerization

Nitric oxide has been implicated in a wide range of physiological functions related to the central nervous system, the cardiovascular system, and the immune system.[121] Nitric oxide is able to function as a rapidly reversible, specific, and local signal-transduction molecule, but also as a nonspecific mediator of tissue damage.[122] Nitric oxide is synthesized from L-arginine by a family of enzymes, the nitric oxide synthases (NOS), through the arginine–nitric oxide pathway.[123] NOS isoforms are enzymatically active only as homodimers.[124] Since inducible nitric oxide synthase (iNOS) has been implicated in the pathogenesis of a number of inflammatory and autoimmune diseases,[125] small-molecule inhibitors of iNOS are potentially of therapeutic use.

Based on previous observations that phenylimidazoles inhibit iNOS activity,[126] Devlin et al. designed a structurally related chemical library containing a pyrimidineimidazole core.[127] Screening of this library in a cell-based assay measuring NO production resulted in the identification of the iNOS inhibitor **36** ($IC_{50} = 1.1$ nM; Figure 11). Surprisingly,

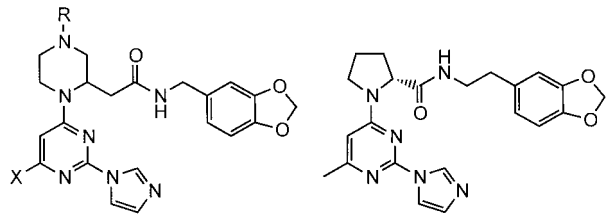


Figure 11. iNOS inhibitors.

this compound was unable to inhibit partially purified recombinant human iNOS in its natural dimeric form. Therefore, the authors speculated that **36** inhibited the dimerization of iNOS monomers to enzymatically active homodimers. Indeed, size-exclusion chromatography of cellular extracts revealed that the inhibitor analogue **37** inhibited the intracellular association of iNOS monomers. More importantly, an X-ray structure of the inhibitor **37** bound to the monomeric oxygenase domain of iNOS showed that **37** occupied the iNOS active site and thereby induced allosteric changes in the monomer which prevented the formation of stable homodimers. The most active compound **38** ($IC_{50} = 0.5$ nM) was demonstrated to be a highly selective and cell-permeable research tool for the study of cellular iNOS functions.[128] This example demonstrates once more that dimeric enzymes may be inhibited not only by active-site inhibitors, but also by inhibitors of enzyme subunit association (see Sections 2.1 and 2.2).

3.7. Agonists of the EPO Receptor

The production of red blood cells is regulated by the hormone erythropoietin (EPO).[129] Like other cytokines, EPO activates its receptor by binding to two receptor molecules which leads to receptor dimerization.[130] Binding of EPO, a 34 kDa glycoprotein, to the erythropoietin receptor (EPOr) leads to proliferation and differentiation of erythroid progenitors into red blood cells.[131] In humans, EPO is primarily produced in the kidney,[132] and anemias caused by kidney failure[133] are currently treated with recombinant EPO.[134] As EPO needs to be administered by repeated injection, orally administered small-molecule EPO mimics would be highly desirable.[135]

While the inhibition of protein–protein interactions with a small molecule requires the molecule to bind to only one of the proteins in a fashion that inhibits the interactions between the two proteins, inducing the interactions between two proteins requires simultaneous binding of the small molecule to both proteins in a productive fashion. Inducing the dimerization of two EPO receptor molecules could hence be achieved by either a receptor-binding molecule which is displayed in two or multiple copies on a dendrimer, or by a symmetrical compound which uses only one set of its functional groups for binding one receptor molecule. Following the first approach, Qureshi et al. identified compound **39** from a chemical library as a compound that binds to the EPO receptor (Figure 12).[136] Subsequently, eight copies of **39** were arranged on a central core to allow for simultaneous binding of at least two EPO-binding molecules to the EPO receptor. Compound **40** binds to the EPO receptor with slightly higher affinity than compound **39** (when calculated on a monomer basis), and in contrast to **39**, is able to induce receptor dimerization in vitro ($EC_{50} = 15.9$ μM). Compound **40** activates the EPO receptor in a manner similar to that of EPO itself; for example, it supports the proliferation of several tumor-cell lines expressing the EPO receptor and induces differentiation of human progenitor cells into colonies of erythrocytic lineage in tissue culture.

Following the second approach, Boger and co-workers screened a C_2-symmetrical chemical library for molecules that bind to the EPO receptor.[137] The same chemical library that was used in the search for inhibitors of MMP2/$\alpha_v\beta_3$ interactions was used in the primary screen for EPO-binding molecules, and the same compound A6B10C4 (**25**) was identified, albeit with much lower affinity for its target. Structural optimization of **25** resulted in the discovery of compound A7B10C1 (**41**; Figure 13) which inhibited binding of EPO to its receptor by 45% (at 50 μM) and increased proliferation of an EPO-dependent cell line by up to 175%. A similar compound, A1B10C1 (**42**), was equally as active as compound **40** at nanomolar concentrations, but has a significantly lower molecular weight. The data suggest that compounds A7B10C1 (**41**) and A1B10C1 (**42**) may act as weak partial agonists of the EPO receptor, although the possibility that the compounds affect alternative downstream targets cannot be ruled out.

 © 2003 Wiley-VCH Verlag GmbH & Co. KGaA, Weinheim

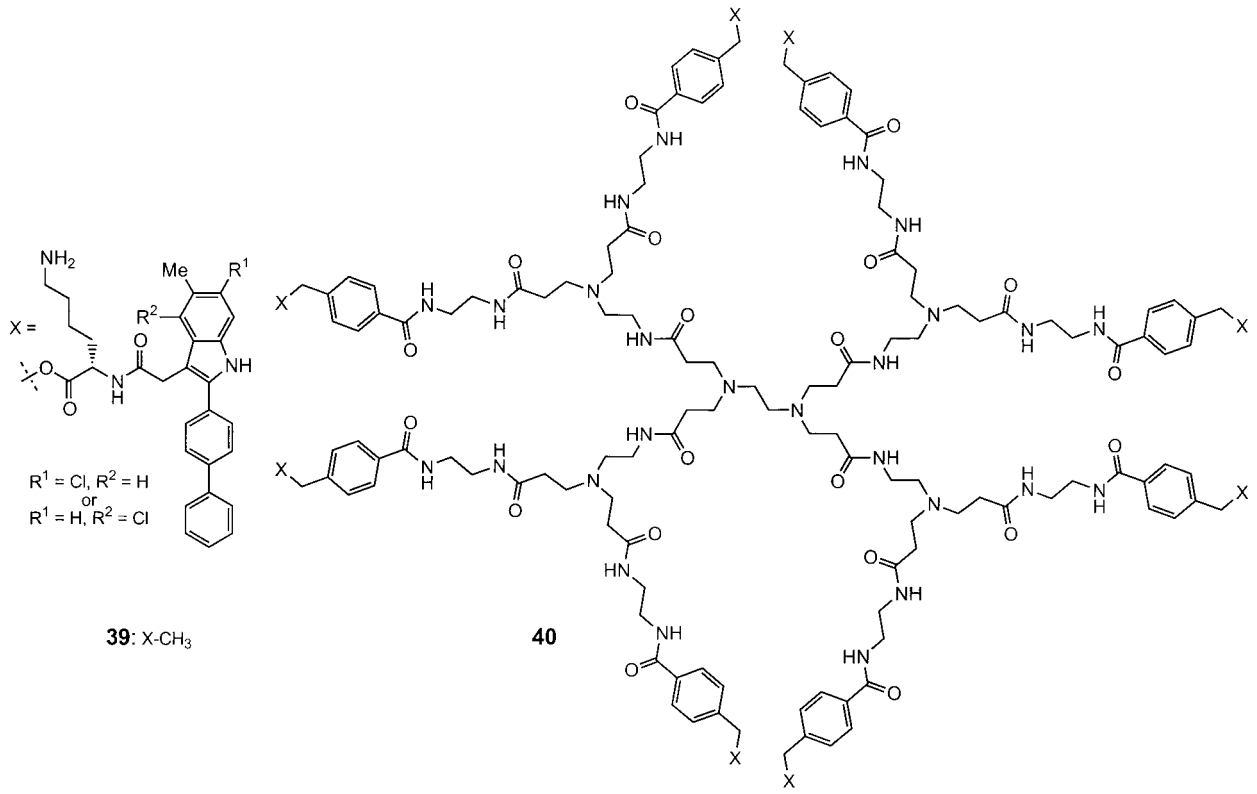


Figure 12. EPO mimetics by Qureshi et al.[136]

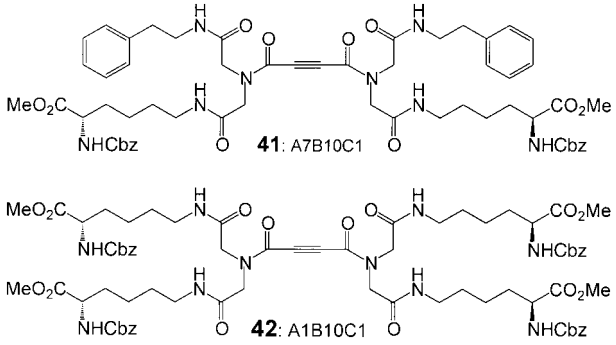


Figure 13. Small-molecule EPO mimics by Boger et al.[137] Cbz = benzyloxycarbonyl.

3.8. Agonists for the Interaction Between Mutated Human Growth Hormone and Its Mutated Receptor

Human growth hormone (hGH) participates in the regulation of normal human growth and development.[138] In a similar manner to the EPO–EPO receptor system (Section 3.7), binding of hGH to its receptor leads to receptor dimerization and activation. The interaction between hGH and the extracellular domain of its receptor (hGHbp) has been extensively analyzed by approaches including X-ray-structural[139] and mutational analysis.[21,140] The discovery that a central region in the receptor, dominated by the two tryptophan residues Trp 104 and Trp 169, accounts for more than three quarters of the binding free energy was one of the landmarks of protein–protein interaction research, and led to the initial postulation of the hot spot theory (see Introduction).[21] Schultz et al. have used this interaction as a model system to design a small-molecule switch for protein–protein interactions.[141] In the hGH/hGHbp complex, Trp 104 of hGHbp tightly packs against Thr 175 of hGH. Mutation of both residues to glycine reduced the binding affinity between hormone and receptor by a factor of 10^6. A library of roughly 200 indole analogues was then screened for molecules that could restore the protein–protein interaction. 5-Chloro-2-trichloromethyl benzimidazole (**43**; Figure 14) increased the binding affinity of the mutant hormone to the mutant receptor by more than 1000-fold at a concentration of 100 μM ($K_d = 260$ nM). The mutated hormone–receptor pair mediated growth-hormone signaling in the presence of **43**. This example demonstrates that glycine mutations of amino acid side chains which significantly contribute to the overall binding free energy of a given protein–protein interaction can be partially compensated by small organic molecules possessing similar chemical features as the wild-type amino acid side chains.

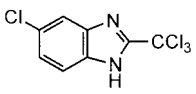


Figure 14. Agonist of the mutated hGH/hGHbp hormone/receptor system.

3.9. Stabilization of Transthyretin Tetramers

Insoluble protein fibrils resulting from the self-assembly of a conformational intermediate are implicated as causative agents in several human amyloid diseases, including Alzheimer's disease, familial amyloid polyneuropathy, and senile

 © 2003 Wiley-VCH Verlag GmbH & Co. KGaA, Weinheim

systemic amyloidosis. The latter two diseases are caused by deposition of insoluble transthyretin (TTR) fibrils in the peripheral nerves and heart tissue.[142] TTR, a tetrameric protein found in plasma and cerebral spinal fluid, binds to and transports thyroxine[143] and the retinol binding protein.[144] The formation of insoluble TTR amyloid fibrils requires as an intermediate step the dissociation of the TTR tetramer to monomers with altered tertiary structure.[145] Studies by Kelly et al. showed that the TTR-ligand thyroxine inhibited TTR amyloid formation by stabilizing the TTR tetramer against dissociation, and thereby demonstrated that small organic molecules could be used to interfere with TTR-associated amyloid fibril formation.[146] Since the hormonal activity of thyroxine-like molecules makes them undesirable as drugs, other small molecules which were thought to complement the binding site of TTR were screened for their ability to inhibit TTR amyloid fibril formation. The nonsteroidal anti-inflammatory drug (NSAID) flufenamic acid (FLU; **44**) was found to potently inhibit amyloid fibril formation in vitro (Figure 15).[147] The X-ray structure of the FLU–TTR com-

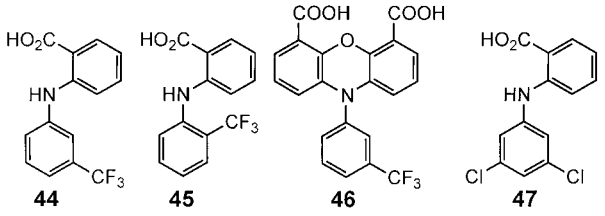


Figure 15. Inhibitors of transthyretin amyloid fibril formation.

plex showed that two FLU molecules are bound to the TTR tetramer, and that FLU stabilizes the TTR tetramer by mediating intersubunit hydrophobic interactions and intersubunit hydrogen bonds. Further screening of chemicals, some of which were structurally related to FLU, indicated that good stabilization of TTR tetramers requires a molecule with at least two aromatic rings, one of which needs to carry an acidic functional group.[148] Unfortunately, undesirable side effects known to accompany the prolonged use of FLU (**44**) prevent its clinical use as an amyloidosis inhibitor. Screening of other NSAIDs showed that diclofenac (Voltaren), flurbiprofen, and resveratrol also strongly inhibited the formation of TTR amyloid fibrils in vitro.[149] Detailed crystallographic investigations of the drug–TTR interactions and molecular modeling led to the development of the potent inhibitors of TTR fibril formation, *ortho*-trifluoromethylphenyl anthranilic acid (*o*-FLU; **45**) and *N*-(*meta*-trifluoromethylphenyl)-phenoxazine-4,6-dicarboxylic acid (PHENOX; **46**).[150] The superior ability of PHENOX and other *N*-phenyl phenoxazine ligands to stabilize the TTR tetramer was confirmed by mass spectrometry studies.[151] Furthermore, the diclofenac analogue **47** was found to be potentially more suitable than diclofenac for the treatment of TTR-associated amyloidosis, as it was not only a potent inhibitor in vitro, but also partitioned more effectively than diclofenac into TTR in human plasma.[152] These studies are an impressive demonstration of the ability of small organic ligands to interfere with amyloid fibril formation.[153]

4. Computational Approaches towards the Identification of Small-Molecule Modulators of Protein–Protein Interactions

4.1. Structure-Based Discovery of Inhibitors of Bcl-2/Bak Interactions

The significance of the interaction between the anti-apoptotic proteins Bcl-2 or Bcl-x_L and pro-apoptotic Bcl-2 family members through the BH3 domain has been discussed in Section 3.1. As an alternative method to the random in vitro screening of chemical libraries, two research groups screened databases of small molecules for compounds likely to bind to the BH3-peptide binding pocket of Bcl-2. Since the solution structure of Bcl-2[154] had not been published at the time these studies were initiated, the Bcl-2 structure was modeled from the data available for the homologue Bcl-x_L on its own[155] or in complex with the BH3 domain of Bak.[156] Huang et al.[157] screened a virtual database consisting of 193 833 chemicals. They selected 53 compounds, 28 of which were obtained for in vitro screening in a fluorescence polarization assay (see Section 3.1). The mixture of diastereoisom-

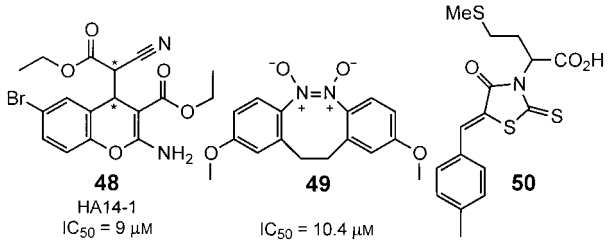
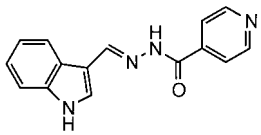


Figure 16. Inhibitors of the interaction between Bcl-x_L and BH3 domains identified by virtual screening or similarity searching.

ers of compound HA14–1 (**48**; Figure 16) inhibited the interaction between Bcl-2 and the Bak-BH3 peptide in vitro ($IC_{50} = 9\ \mu M$) and induced apoptosis in a tumor cell line overexpressing Bcl-2.

In a similar approach, the research groups of Wang and Yang screened the National Cancer Institute (USA) three-dimensional (3D) database consisting of 206 876 compounds for molecules complementary to the BH3-peptide binding pocket of the modeled Bcl-2 protein.[158] Out of 35 molecules selected for in vitro screening, seven compounds inhibited the Bcl-2/Bak-BH3 interaction with IC_{50} values of less than 15 μM in a fluorescence polarization assay. By NMR spectroscopy compound **49** (Figure 16) was shown to bind to the BH3 binding site in Bcl-x_L. It inhibited cell growth and induced apoptosis in Bcl-2-expressing cancer cell lines in the low micromolar range. The potency of compound **49** correlated with the Bcl-2 expression levels in cancer cells, which indicates that the compound may exert a specific effect on Bcl-2. In another approach, Wagner et al. searched chemical databases for molecules similar to the previously identified Bcl-x_L/Bak-BH3 inhibitors **15**–**17**.[159] 93 selected molecules were further investigated by performing molecular-docking calculations, and compound **50** was identified as another Bcl-

x_L/Bak-BH3 inhibitor. It is noteworthy that the different classes of inhibitors of the interaction between the anti-apoptotic Bcl-2 family members (Bcl-2 and Bcl-x_L) and the BH3 domain of Bak discussed in this review (**15**–**17**, **50**, **18**, **48**, **49**) do not show obvious structural similarity to each other. All these compounds have IC_{50} values in the low micromolar range and low molecular weights which should make them promising starting points for drug discovery.



51 TJU103

Figure 17. Inhibitor of CD4/MHC class II interactions, TJU103.

4.2. Inhibitors of CD4/MHC Class II Interactions

$CD4^+$ T cells, whilst essential for the immune response, participate in the pathogenesis of a number of diseases including various autoimmune diseases,[160] allogenic organ transplant rejection,[161] and graft-versus-host disease following bone-marrow transplantation.[162] The interaction between CD4 and the major histocompatibility complex class II (MHC class II) on the surface of antigen presenting cells is a critical step in the activation of $CD4^+$ T cells.[163] Small-molecule inhibitors of the CD4/MHC class II interaction therefore have the potential to be immunosuppressive agents in the treatment or prevention of these diseases.

CD4 is a glycoprotein expressed on the surface of helper T cells which consists of four immunoglobulin(Ig)-like extracellular domains termed D1–D4.[164] The MHC class II complex expressed on the surface of antigen-presenting cells is a heterodimeric glycoprotein. Antigenic peptides taken up from the local environment become associated with the MHC class II dimer prior to their display on the cell surface, and the MHC class II–peptide complex is recognized by the T-cell receptor (TCR). This interaction is stabilized by a second association between the MHC class II dimer itself and CD4.[165] The structure of the CD4/MHC class II complex is unclear, but it is believed that the interface may involve many contact sites over a large surface area.[166] In an attempt to search for potential small-molecule binding pockets within the CD4 protein, surface ligand-binding site-searching algorithms,[167,168] solvent-accessible-surface-area calculations,[169] as well as analyses of the electrostatic properties of CD4 surface structures were performed on the D1 domain of CD4.[170] A binding pocket in the D1 domain of CD4 consistent with available mutational data was identified.[171,166c] Interestingly, a cyclic heptapeptide mimicking a surface loop which is part of the proposed binding pocket had previously been shown to inhibit stable CD4/MHC class II interactions and CD4-mediated immune responses in vitro and in vivo.[172] An X-ray structural analysis of the human CD4 D1 domain was used as a receptor for molecular docking.[173] Members of a virtual library consisting of approximately 150000 commercially available compounds were judged by the criteria of both shape complementarity and force-field energy using a molecular-docking program.[168] The 1000 best-scoring compounds by each of the two criteria were visually inspected for compounds with distinctive chemical structures, receptor binding modes, and electrostatic and shape complementarity. Of the 41 compounds finally chosen for testing in a CD4/MHC class II cell-adhesion assay, eight displayed inhibitory activity (31–74% inhibition at 100 μM). Compound TJU103 (**51**; Figure 17; $IC_{50} \approx 90$ μM) was nontoxic to lymphocytes in vivo and appeared to specifically inhibit $CD4^+$ T-cell mediated responses. TJU103 exhibited significant inhibition of immune responses in animal models of autoimmune disease and transplant rejection.[174]

5. Summary and Outlook

Herein three general approaches were described by which small-molecule modulators of protein–protein interactions can be identified, and a number of studies in which these approaches have been employed to identify modulators of protein–protein interactions with potential therapeutic use in the treatment of human diseases was illustrated. All three of these approaches have resulted in the discovery of highly potent modulators of protein–protein interactions, which are active in the micromolar or even low nanomolar concentration range. Each approach has its own advantages and limitations, and the approach best applied to a specific protein–protein target depends on the nature of the respective protein–protein interaction and on the availability of structural data.

The identification of inhibitory peptides and peptidomimetics derived from dimerization interfaces (Section 2) requires that the respective interfaces, whilst not necessarily continuous as a whole, possess short continuous amino acid sequences which contribute significantly to the overall affinity between the monomeric protein subunits. If this requirement is met, the approach allows for the straightforward identification of inhibitor peptides from the primary amino acid sequence of the protein that can serve as lead compounds for subsequent medicinal chemistry efforts. However, not all protein–protein interfaces contain such continuous peptide interaction sequences, and in the absence of these sequences or sufficient knowledge of the interface this approach is not applicable. In addition, problems related to the generally poor metabolic stability and low bioavailability of peptides need to be overcome.[175]

The second approach discussed, that of screening combinatorial chemical libraries for modulators of protein–protein interactions (Section 3), may be more relevant to drug-discovery research, since it can result in the identification of nonpeptidic compounds. It does not require prior knowledge about the structure of the dimerization interfaces, even though such information can be helpful for setting-up assays amenable to high-throughput screening of chemical libraries. The drawback of this approach is the large number of compounds which need to be analyzed, which makes screening expensive. It is noteworthy that even though structural information about the protein–protein interactions was

 © 2003 Wiley-VCH Verlag GmbH & Co. KGaA, Weinheim

available, in most of the examples discussed in Section 3, the majority of research groups used nontargeted libraries for the primary screening. This occurrence is presumably because the translation of such structural knowledge into predictions about the nature of chemical entities which could be suitable for the modulation of a given protein–protein interaction tends to be difficult. The selection of the targeted chemical library used to screen for iNOS inhibitors (Section 3.6.) was not based on structural information about the protein–protein interface, but on the structure of previously known inhibitors. The finding that the inhibitors identified in the studies acted by inhibiting enzyme-subunit association was unexpected. Only in two of the examples discussed in Section 3 was the selection of primary screening compounds directly based on structural information about the respective protein–protein interface. In the screen for agonists of the interaction between the mutated human-growth hormone and its mutated receptor (Section 3.8.), the screening compounds were selected to compensate for the loss of a functional group resulting from the mutation in the receptor. In the studies aimed at identifying stabilizers of transthyretin tetramers (Section 3.9.), only compounds with structures known to complement the binding site of the tetramers were screened. In both of the latter two studies, screening hits could be obtained from smaller libraries, thereby demonstrating the utility of structural information for the identification of organic molecules which modulate the protein–protein interaction.

Virtual screening of chemical databases (Section 4) can be used to preselect molecules which are more likely to bind to a hot spot of a protein–protein interaction, and thereby modulate it. In the two examples covered in Section 4, approximately 20% of the compounds selected in silico had reasonable biological activity in vitro. This rate of success is much higher than that obtained in the screens of untargeted libraries covered in Section 3, which shows that when possible, virtual screening of chemical databases is a valuable tool. Narrowing down the search in this way saves a great deal of time and expense, since only those compounds that are likely to affect the respective protein–protein interactions need to be synthesized or purchased, and analyzed in laboratory assays. Unfortunately, this approach requires detailed structural information about the protein dimer interfaces from NMR spectroscopy or X-ray studies, which in many cases is not available. Furthermore, the plasticity of protein–protein interfaces makes protein-structure-based predictions of chemical entities which are suitable for the modulation of the respective interaction an even more challenging task.[176]

The fact that several of the low-molecular-weight modulators of protein–protein interactions described in this review display specific effects in tissue culture and in animal models of disease provides further evidence that previous reservations about the feasibility of the modulation of protein–protein interactions using small organic molecules may have been unjustified. Small-molecule inhibitors of protein–protein interactions need not necessarily bind to the protein–protein interface, but can also bind to allosteric protein sites and thereby induce a conformational change that disfavors the protein–protein interaction, as demonstrated for the inhibition of the LFA-1/ICAM-1 interaction (Section 3.5.) and of iNOS dimerization (Section 3.6.). This mode of activity circumvents problems related to the targeting of large protein–protein interfaces lacking binding sites for small molecules.

The systematic identification of small-molecule entities that bind to specific protein domains would be a major breakthrough in the field. This step would allow small-molecule libraries composed of preselected domain-specific compounds to be used in screening for modulators of selected protein–protein interactions, provided that the respective protein domains contribute significantly to the overall binding free energy between the proteins. Possible approaches towards this goal include the tethering of small-molecule ligands to targeted protein sites, to identify even weak protein binders.[177] The affinity of molecules which bind weakly to adjacent protein sites may be increased by covalently linking them,[178] as applied in the technique SAR by NMR spectroscopy.[179] As many natural products evolved to bind specific proteins, the identification of their protein binding sites as well as the synthesis and screening of libraries of such protein-binding natural products would present additional promising approaches furthering our understanding of the interactions between small molecules and proteins. This process could translate into a more systematic approach for the identification of modulators of protein–protein interactions in the future.[180]

In addition to the approaches mentioned above, scientific progress in this research area will be driven by advances in a number of disciplines. New technologies for the analysis of protein–protein interactions and an improved understanding of the relevance of these interactions for human disease will contribute to the identification of novel therapeutic targets. High-resolution NMR spectroscopy or X-ray structures of proteins and protein complexes will allow the virtual screening of chemical databases for small-molecule modulators of numerous protein–protein interactions and will facilitate lead-compound optimization. Further advances in assay development and screening technologies will allow even more rapid high-throughput screening of chemical libraries. Finally, the importance of synthetic organic chemistry cannot be over-emphasized, since it is the organic chemist who synthesizes the chemical libraries used for screening and who optimizes potential lead compounds. The particular importance of stereoselective synthesis for the modulation of protein–protein interactions with low-molecular-weight compounds is clear in view of those small molecules the biological activity of which was demonstrated to depend on the correct stereochemistry (for example, compounds **25** and **31**). Combined research efforts in the aforementioned disciplines are very likely to open new avenues for the identification of drug candidates against hitherto unconsidered or unknown disease targets.

I extend my thanks to Professor Dr. Axel Ullrich for his enthusiastic support of my research. I would like to thank Drs. Ulrich Kruse, Oliver Brümmer, Joel Goldberg, Torsten Keßler, and especially Angela Hollis, M.Sc., for critical reading of the manuscript. The picture of the transthyretin tetramer stabilized

by two flufenamino acid molecules shown in the frontispiece was reproduced with permission from ref. [147] (Copyright 2002, The National Academy of Sciences, USA).

Received: September 23, 2002 [A558]

[1] a) A.-C. Gavin, M. Bösche, R. Krause, P. Grandi, M. Marzioch, A. Bauer, J. Schultz, J. M. Rick, A.-M. Michon, C.-M. Cruciat, M. Remor, C. Höfert, M. Schelder, M. Brajenovic, H. Ruffner, A. Merino, K. Klein, M. Hudak, D. Dickson, T. Rudi, V. Gnau, A. Bauch, S. Bastuck, B. Huhse, C. Leutwein, M.-A. Heurtier, R. R. Copley, A. Edelmann, E. Querfurth, V. Rybin, G. Drewes, M. Raida, T. Bouwmeester, P. Bork, B. Seraphin, B. Kuster, G. Neubauer, G. Superti-Furga, *Nature* **2002**, *415*, 141 – 147; b) Y. Ho, A. Gruhler, A. Heilbut, G. D. Bader, L. Moore, S.-L. Adams, A. Millar, P. Taylor, K. Bennett, K. Boutilier, L. Yang, C. Wolting, I. Donaldson, S. Schandorff, J. Shewnarane, M. Vo, J. Taggart, M. Goudreault, B. Muskat, C. Alfarano, D. Dewar, Z. Lin, K. Michalickova, A. R. Willems, H. Sassi, P. A. Nielsen, K. J. Rasmussen, J. R. Andersen, L. E. Johansen, L. H. Hansen, H. Jespersen, A. Podtelejnikov, E. Nielsen, J. Crawford, V. Poulsen, B. D. Sørensen, J. Matthiesen, R. C. Hendrickson, F. Gleeson, T. Pawson, M. F. Moran, D. Durocher, M. Mann, C. W. V. Hogue, D. Figeys, M. Tyers, *Nature* **2002**, *415*, 180 – 183.

[2] E. K. Rowinsky, *Semin. Oncol.* **1997**, *24*, S19-1–S19-12.

[3] D. Guénard, F. Guéritte-Vogelein, P. Potier, *Acc. Chem. Res.* **1993**, *26*, 160 – 167.

[4] a) S. J. Stachel, K. Biswas, S. J. Danishefsky, *Curr. Pharm. Des.* **2001**, *7*, 1277 – 1290; b) M. Kavallaris, N. M. Verrills, B. T. Hill, *Drug Resist. Updates* **2001**, *4*, 392 – 401.

[5] a) S. L. Mooberry, G. Tien, A. H. Hernandez, A. Plubrukarn, B. S. Davidson, *Cancer Res.* **1999**, *59*, 653 – 660; b) A. K. Ghosh, Y. Wang, *J. Am. Chem. Soc.* **2000**, *122*, 11027 – 11028; c) I. Paterson, C. De Savi, M. Tudge, *Org. Lett.* **2001**, *3*, 3149 – 3152; d) J. Mulzer, E. Öhler, *Angew. Chem.* **2001**, *113*, 3961 – 3964; *Angew. Chem. Int. Ed.* **2001**, *40*, 3842 – 3846.

[6] a) D. M. Bollag, P. A. McQueney, J. Zhu, O. Hensens, L. Koupal, J. Liesch, M. Goetz, E. Lazarides, C. M. Woods, *Cancer Res.* **1995**, *55*, 2325 – 2333; b) K. C. Nicolaou, N. Winssinger, J. Pastor, S. Ninkovic, F. Sarabia, Y. He, D. Vourloumis, Z. Yang, T. Li, P. Giannakakou, E. Hamel, *Nature* **1997**, *387*, 268 – 272.

[7] T. Lindel, P. R. Jensen, W. Fenical, B. H. Long, A. M. Casazza, J. Carboni, C. R. Fairchild, *J. Am. Chem. Soc.* **1997**, *119*, 8744 – 8745.

[8] a) E. ter Haar, R. J. Kowalski, E. Hamel, C. M. Lin, R. E. Longley, S. P. Gunasekera, H. S. Rosenkranz, B. W. Day, *Biochemistry* **1996**, *35*, 243 – 250; b) D. T. Hung, J. Chen, S. L. Schreiber, *Chem. Biol.* **1996**, *3*, 287 – 293.

[9] H. M. McDaid, S. Mani, H. J. Shen, F. Muggia, D. Sonnichsen, S. B. Horwitz, *Clin. Cancer Res.* **2002**, *8*, 2035 – 2043.

[10] E. Härri, W. Loeffler, H. P. Sigg, H. Stähelin, C. Tamm, *Helv. Chim. Acta* **1963**, *46*, 1235 – 1243.

[11] A. Peyroche, B. Antonny, S. Robineau, J. Acker, J. Cherfils, C. L. Jackson, *Mol. Cell* **1999**, *3*, 275 – 285.

[12] D. M. Spencer, T. J. Wandless, S. L. Schreiber, G. R. Crabtree, *Science* **1993**, *262*, 1019 – 1024.

[13] P. J. Belshaw, S. N. Ho, G. R. Crabtree, S. L. Schreiber, *Proc. Natl. Acad. Sci. USA* **1996**, *93*, 4604 – 4607.

[14] P. J. Belshaw, D. M. Spencer, G. R. Crabtree, S. L. Schreiber, *Chem. Biol.* **1996**, *3*, 731 – 738.

[15] a) D. M. Spencer, P. J. Belshaw, L. Chen, S. N. Ho, F. Randazzo, G. R. Crabtree, S. L. Schreiber, *Curr. Biol.* **1996**, *6*, 839 – 847; b) B. R. Stockwell, S. L. Schreiber, *Curr. Biol.* **1998**, *8*, 761 – 770.

[16] a) V. M. Rivera, T. Clackson, S. Natesan, R. Pollock, J. F. Amara, T. Keenan, S. R. Magari, T. Phillips, N. L. Courage, F. Cerasoli, Jr., D. A. Holt, M. Gilman, *Nat. Med.* **1996**, *2*, 1028 – 1032; b) S. N. Ho, S. R. Biggar, D. M. Spencer, S. L. Schreiber, G. R. Crabtree, *Nature* **1996**, *382*, 822 – 826.

[17] a) P. J. Belshaw, S. N. Ho, G. R. Crabtree, S. L. Schreiber, *Proc. Natl. Acad. Sci. USA* **1996**, *93*, 4604 – 4607; b) S. J. Kopytek, R. F. Standaert, J. C. Dyer, J. C. Hu, *Chem. Biol.* **2000**, *7*, 313 – 321; c) M. A. Farrar, J. Alberola-Ila, R. M. Perlmutter, *Nature* **1996**, *383*, 178 – 181; d) C. T. Rollins, V. M. Rivera, D. N. Woolfson, T. Keenan, M. Hatada, S. E. Adams, L. J. Andrade, D. Yaeger, M. R. van Schravendijk, D. A. Holt, M. Gilman, T. Clackson, *Proc. Natl. Acad. Sci. USA* **2000**, *97*, 7096 – 7101; e) J. F. Amara, T. Clackson, V. M. Rivera, T. Guo, T. Keenan, S. Natesan, R. Pollock, W. Yang, N. L. Courage, D. A. Holt, M. Gilman, *Proc. Natl. Acad. Sci. USA* **1997**, *94*, 10618 – 10623.

[18] a) M. A. Dechantsreiter, E. Planker, B. Mathä, E. Lohof, G. Hölzemann, A. Jonczyk, S. L. Goodman, H. Kessler, *J. Med. Chem.* **1999**, *42*, 3033 – 3040; b) T. Taga, A. Suzuki, I. Gonzalez-Gomez, F. H. Gilles, M. Stins, H. Shimada, L. Barsky, K. I. Weinberg, W. E. Laug, *Int. J. Cancer* **2002**, *98*, 690 – 697.

[19] a) G. Proimos, *J. Thromb. Thrombolysis* **2001**, *11*, 99 – 110; b) J. C. O'Shea, J. E. Tcheng, *Expert Opin. Pharmacother.* **2002**, *3*, 1199 – 1210.

[20] L. Lo Conte, C. Chothia, J. Janin, *J. Mol. Biol.* **1999**, *285*, 2177 – 2198.

[21] T. Clackson, J. A. Wells, *Science* **1995**, *267*, 383 – 386.

[22] A. A. Bogan, K. S. Thorn, *J. Mol. Biol.* **1998**, *280*, 1 – 9.

[23] a) S. Jones, J. M. Thornton, *Proc. Natl. Acad. Sci. USA* **1996**, *93*, 13 – 20; b) R. Preißner, A. Goede, C. Frömmel, *J. Mol. Biol.* **1998**, *280*, 535 – 550.

[24] a) P. L. Toogood, *J. Med. Chem.* **2002**, *45*, 1543 – 1558; b) D. A. Ockey, T. R. Gadek, *Expert Opin. Ther. Pat.* **2002**, *12*, 393 – 400; c) A. G. Cochran, *Curr. Opin. Chem. Biol.* **2001**, *5*, 654 – 659; d) A. G. Cochran, *Chem. Biol.* **2000**, *7*, R85 – R94; e) R. Zutshi, M. Brickner, J. Chmielewski, *Curr. Opin. Chem. Biol.* **1998**, *2*, 62 – 66.

[25] J. F. Smothers, S. Henikoff, P. Carter, *Science* **2002**, *298*, 621 – 622.

[26] a) S. M. Violette, W. C. Shakespeare, C. Bartlett, W. Guan, J. A. Smith, R. J. Rickles, R. S. Bohacek, D. A. Holt, R. Baron, T. K. Sawyer, *Chem. Biol.* **2000**, *7*, 225 – 235; b) B. Gay, S. Suarez, G. Caravatti, P. Furet, T. Meyer, J. Schoepfer, *Int. J. Cancer* **1999**, *83*, 235 – 241; c) C. García-Echeverría, *Curr. Med. Chem.* **2001**, *8*, 1589 – 1604.

[27] a) S. V. Sharma, C. Oneyama, Y. Yamashita, H. Nakano, K. Sugawara, M. Hamada, N. Kosaka, T. Tamaoki, *Oncogene* **2001**, *20*, 2068 – 2079; b) C. Oneyama, H. Nakano, S. V. Sharma, *Oncogene* **2002**, *21*, 2037 – 2050.

[28] S. L. Goodman, G. Hölzemann, G. A. G. Sulyok, H. Kessler, *J. Med. Chem.* **2002**, *45*, 1045 – 1051, zit. Lit.

[29] a) N. E. Kohl, E. A. Emini, W. A. Schleif, L. J. Davis, J. C. Heimbach, R. A. Dixon, E. M. Scolnick, I. S. Sigal, *Proc. Natl. Acad. Sci. USA* **1988**, *85*, 4686 – 4690; b) S. Seelmeier, H. Schmidt, V. Turk, K. von der Helm, *Proc. Natl. Acad. Sci. USA* **1988**, *85*, 6612 – 6616.

[30] D. R. Kaul, S. K. Cinti, P. L. Carver, P. H. Kazanjian, *Pharmacotherapy* **1999**, *19*, 281 – 298.

[31] S. G. Deeks, M. Smith, M. Holodniy, J. O. Kahn, *JAMA J. Am. Med. Assoc.* **1997**, *277*, 145 – 153.

[32] a) M. A. Navia, P. M. D. Fitzgerald, B. M. McKeever, C.-T. Leu, J. C. Heimbach, W. K. Herber, I. S. Sigal, P. L. Darke, J. P. Springer, *Nature* **1989**, *337*, 615 – 620; b) M. Miller, J. Schneider, B. K. Sathyanarayana, M. V. Toth, G. R. Marshall, L. Clawson, L. Selk, S. B. H. Kent, A. Wlodawer, *Science* **1989**, *246*, 1149 – 1152.

[33] A. Gustchina, I. T. Weber, *Proteins Struct. Funct. Genet.* **1991**, *10*, 325 – 339.

[34] M. J. Todd, N. Semo, E. Freire, *J. Mol. Biol.* **1998**, *283*, 475 – 488.

 © 2003 Wiley-VCH Verlag GmbH & Co. KGaA, Weinheim

[35] Z.-Y. Zhang, R. A. Poorman, L. L. Maggiora, R. L. Heinrikson, F. J. Kézdy, *J. Biol. Chem.* **1991**, *266*, 15591 – 15594.
[36] R. Zutshi, J. Franciskovich, M. Shultz, B. Schweitzer, P. Bishop, M. Wilson, J. Chmielewski, *J. Am. Chem. Soc.* **1997**, *119*, 4841 – 4845.
[37] M. D. Shultz, J. Chmielewski, *Bioorg. Med. Chem. Lett.* **1999**, *9*, 2431 – 2436.
[38] M. D. Shultz, M. J. Bowman, Y.-W. Ham, X. Zhao, G. Tora, J. Chmielewski, *Angew. Chem.* **2000**, *112*, 2822 – 2825; *Angew. Chem. Int. Ed.* **2000**, *39*, 2710 – 2713.
[39] A. Bouras, N. Boggetto, Z. Benatalah, E. de Rosny, S. Sicsic, M. Reboud-Ravaux, *J. Med. Chem.* **1999**, *42*, 957 – 962.
[40] M. Song, S. Rajesh, Y. Hayashi, Y. Kiso, *Bioorg. Med. Chem. Lett.* **2001**, *11*, 2465 – 2468.
[41] L. G. Ulysse, J. Chmielewski, *Bioorg. Med. Chem. Lett.* **1998**, *8*, 3281 – 3286.
[42] a) H. J. Schramm, A. Billich, E. Jaeger, K.-P. Rücknagel, G. Arnold, W. Schramm, *Biochem. Biophys. Res. Commun.* **1993**, *194*, 595 – 600; b) H. J. Schramm, J. Boetzel, J. Büttner, E. Fritsche, W. Göhring, E. Jaeger, S. König, O. Thumfart, T. Wenger, N. E. Nagel, W. Schramm, *Antiviral Res.* **1996**, *30*, 155 – 170.
[43] H. J. Schramm, E. de Rosny, M. Reboud-Ravaux, J. Büttner, A. Dick, W. Schramm, *Biol. Chem.* **1999**, *380*, 593 – 596.
[44] B. C. M. Potts, D. J. Faulkner, J. A. Chan, G. C. Simolike, P. Offen, M. E. Hemling, T. A. Francis, *J. Am. Chem. Soc.* **1991**, *113*, 6321 – 6322.
[45] X. Fan, G. R. Flentke, D. H. Rich, *J. Am. Chem. Soc.* **1998**, *120*, 8893 – 8894.
[46] R. J. Whitley in *Fields Virology* (Eds.: B. N. Fields, D. M. Knipe, P. M. Howley), Lippincott-Raven, Philadelphia, **1996**, pp. 2297 – 2342.
[47] J. E. Reardon, T. Spector, *Adv. Pharmacol.* **1991**, *22*, 1 – 27.
[48] P. Reichard, *Annu. Rev. Biochem.* **1988**, *57*, 349 – 374.
[49] a) J. G. Jacobson, D. A. Leib, D. J. Goldstein, C. L. Bogard, P. A. Schaffer, S. K. Weller, D. M. Coen, *Virology* **1989**, *173*, 276 – 283; b) J. M. Cameron, I. McDougall, H. S. Marsden, V. G. Preston, D. M. Ryan, J. H. Subak-Sharpe, *J. Gen. Virol.* **1988**, *69*, 2607 – 2612; c) C. R. Brandt, R. L. Kintner, A. M. Pumfery, R. J. Visalli, D. R. Grau, *J. Gen. Virol.* **1991**, *72*, 2043 – 2049; d) Y. Yamada, H. Kimura, T. Morishima, T. Daikoku, K. Maeno, Y. Nishiyama, *J. Infect. Dis.* **1991**, *164*, 1091 – 1097; e) A. D. Idowu, E. B. Fraser-Smith, K. L. Poffenberger, R. C. Herman, *Antiviral Res.* **1992**, *17*, 145 – 156.
[50] A. J. Darling, E. M. McKay, R. Ingemarson, V. G. Preston, *Virus Genes* **1989**, *2*, 187 – 194.
[51] D. Filatov, R. Ingemarson, A. Gräslund, L. Thelander, *J. Biol. Chem.* **1992**, *267*, 15816 – 15822.
[52] a) R. L. Krogsrud, E. Welchner, E. Scouten, M. Liuzzi, *Anal. Biochem.* **1993**, *213*, 386 – 394; b) N. Moss, R. Déziel, J. Adams, N. Aubry, M. Bailey, M. Baillet, P. Beaulieu, J. DiMaio, J.-S. Duceppe, J.-M. Ferland, J. Gauthier, E. Ghiro, S. Goulet, L. Grenier, P. Lavallée, C. Lépine-Frenette, R. Plante, S. Rakhit, F. Soucy, D. Wernic, Y. Guindon, *J. Med. Chem.* **1993**, *36*, 3005 – 3009.
[53] a) M. Liuzzi, R. Déziel, N. Moss, P. Beaulieu, A.-M. Bonneau, C. Bousquet, J. G. Chafouleas, M. Garneau, J. Jaramillo, R. L. Krogsrud, L. Lagacé, R. S. McCollum, S. Nawoot, Y. Guindon, *Nature* **1994**, *372*, 695 – 698; b) N. Moss, P. Beaulieu, J.-S. Duceppe, J.-M. Ferland, J. Gauthier, E. Ghiro, S. Goulet, L. Grenier, M. Llinas-Brunet, R. Plante, D. Wernic, R. Déziel, *J. Med. Chem.* **1995**, *38*, 3617 – 3623.
[54] N. Moss, P. Beaulieu, J.-S. Duceppe, J.-M. Ferland, M. Garneau, J. Gauthier, E. Ghiro, S. Goulet, I. Guse, J. Jaramillo, M. Llinas-Brunet, E. Malenfant, R. Plante, M. Poirier, F. Soucy, D. Wernic, C. Yoakim, R. Déziel, *J. Med. Chem.* **1996**, *39*, 4173 – 4180.
[55] M. S. Greenblatt, W. P. Bennett, M. Hollstein, C. C. Harris, *Cancer Res.* **1994**, *54*, 4855 – 4878.
[56] M. Scheffner, B. A. Werness, J. M. Huibregtse, A. J. Levine, P. M. Howley, *Cell* **1990**, *63*, 1129 – 1136.
[57] D. Schwartz, V. Rotter, *Semin. Cancer Biol.* **1998**, *8*, 325 – 336.
[58] Y. Shen, E. White, *Adv. Cancer Res.* **2001**, *82*, 55 – 84.
[59] N. D. Lakin, S. P. Jackson, *Oncogene* **1999**, *18*, 7644 – 7655.
[60] J. D. Oliner, K. W. Kinzler, P. S. Meltzer, D. L. George, B. Vogelstein, *Nature* **1992**, *358*, 80 – 83.
[61] D. A. Freedman, A. J. Levine, *Cancer Res.* **1999**, *59*, 1 – 7.
[62] P. H. Kussie, S. Gorina, V. Marechal, B. Elenbaas, J. Moreau, A. J. Levine, N. P. Pavletich, *Science* **1996**, *274*, 948 – 953.
[63] a) V. Böttger, A. Böttger, S. F. Howard, S. M. Picksley, P. Chène, C. Garcia-Echeverria, H.-K. Hochkeppel, D. P. Lane, *Oncogene* **1996**, *13*, 2141 – 2147; b) A. Böttger, V. Böttger, C. García-Echeverría, P. Chène, H.-K. Hochkeppel, W. Sampson, K. Ang, S. F. Howard, S. M. Picksley, D. P. Lane, *J. Mol. Biol.* **1997**, *269*, 744 – 756.
[64] a) P. Chène, J. Fuchs, J. Bohn, C. García-Echeverría, P. Furet, D. Fabbro, *J. Mol. Biol.* **2000**, *299*, 245 – 253; b) C. García-Echeverría, P. Chène, M. J. J. Blommers, P. Furet, *J. Med. Chem.* **2000**, *43*, 3205 – 3208.
[65] C. García-Echeverría, P. Furet, P. Chène, *Bioorg. Med. Chem. Lett.* **2001**, *11*, 2161 – 2164.
[66] S. J. Duncan, S. Grüschow, D. H. Williams, C. McNicholas, R. Purewal, M. Hajek, M. Gerlitz, S. Martin, S. K. Wrigley, M. Moore, *J. Am. Chem. Soc.* **2001**, *123*, 554 – 560.
[67] R. Stoll, C. Renner, S. Hansen, S. Palme, C. Klein, A. Belling, W. Zeslawski, M. Kamionka, T. Rehm, P. Mühlhahn, R. Schumacher, F. Hesse, B. Kaluza, W. Voelter, R. A. Engh, T. A. Holak, *Biochemistry* **2001**, *40*, 336 – 344.
[68] M. M. Gottesman, *Annu. Rev. Med.* **2002**, *53*, 615 – 627.
[69] a) S. W. Lowe, A. W. Lin, *Carcinogenesis* **2000**, *21*, 485 – 495; b) R. W. Johnstone, A. A. Ruefli, S. W. Lowe, *Cell* **2002**, *108*, 153 – 164.
[70] Y. Gutierrez-Puente, P. Zapata-Benavides, A. M. Tari, G. Lopez-Berestein, *Semin. Oncol.* **2002**, *29, Suppl. 11*, 71 – 76.
[71] R. J. Klasa, A. M. Gillum, R. E. Klem, S. R. Frankel, *Antisense Nucleic Acid Drug Dev.* **2002**, *12*, 193 – 213.
[72] A. Degterev, A. Lugovskoy, M. Cardone, B. Mulley, G. Wagner, T. Mitchison, J. Yuan, *Nat. Cell Biol.* **2001**, *3*, 173 – 182.
[73] J. C. Owicki, *J. Biomol. Screening* **2000**, *5*, 297 – 306.
[74] S.-P. Tzung, K. M. Kim, G. Basañez, C. D. Giedt, J. Simon, J. Zimmerberg, K. Y. J. Zhang, D. M. Hockenbery, *Nat. Cell Biol.* **2001**, *3*, 183 – 191.
[75] a) M. Henriksson, B. Lüscher, *Adv. Cancer Res.* **1996**, *68*, 109 – 182; b) C. V. Dang, *Mol. Cell. Biol.* **1999**, *19*, 1 – 11.
[76] a) A. Gerbitz, J. Mautner, C. Geltinger, K. Hörtnagel, B. Christoph, H. Asenbauer, G. Klobeck, A. Polack, G. W. Bornkamm, *Oncogene* **1999**, *18*, 1745 – 1753; b) R. Dalla-Favera, M. Bregni, J. Erikson, D. Patterson, R. C. Gallo, C. M. Croce, *Proc. Natl. Acad. Sci. USA* **1982**, *79*, 7824 – 7827.
[77] C. D. Little, M. M. Nau, D. N. Carney, A. F. Gazdar, J. D. Minna, *Nature* **1983**, *306*, 194 – 196.
[78] D. J. Liao, R. B. Dickson, *Endocr.-Relat. Cancer* **2000**, *7*, 143 – 164.
[79] M. D. Erisman, P. G. Rothberg, R. E. Diehl, C. C. Morse, J. M. Spandorfer, S. M. Astrin, *Mol. Cell. Biol.* **1985**, *5*, 1969 – 1976.
[80] D. W. Felsher, J. M. Bishop, *Mol. Cell* **1999**, *4*, 199 – 207.
[81] S. Pelengaris, T. Littlewood, M. Khan, G. Elia, G. Evan, *Mol. Cell* **1999**, *3*, 565 – 577.
[82] B. Amati, M. W. Brooks, N. Levy, T. D. Littlewood, G. I. Evan, H. Land, *Cell* **1993**, *72*, 233 – 245.
[83] A. R. Ferré-D'Amaré, G. C. Prendergast, E. B. Ziff, S. K. Burley, *Nature* **1993**, *363*, 38 – 45.
[84] P. Lavigne, M. P. Crump, S. M. Gagné, R. S. Hodges, C. M. Kay, B. D. Sykes, *J. Mol. Biol.* **1998**, *281*, 165 – 181.

 © 2003 Wiley-VCH Verlag GmbH & Co. KGaA, Weinheim

[85] T. Förster, *Ann. Phys.* **1948**, *2*, 55 – 75.
[86] T. Berg, S. B. Cohen, J. Desharnais, C. Sonderegger, D. J. Maslyar, J. Goldberg, D. L. Boger, P. K. Vogt, *Proc. Natl. Acad. Sci. USA* **2002**, *99*, 3830 – 3835.
[87] D. L. Boger, J. K. Lee, J. Goldberg, Q. Jin, *J. Org. Chem.* **2000**, *65*, 1467 – 1474.
[88] a) A. Menssen, H. Hermeking, *Proc. Natl. Acad. Sci. USA* **2002**, *99*, 6274 – 6279; b) H. A. Coller, C. Grandori, P. Tamayo, T. Colbert, E. S. Lander, R. N. Eisenman, T. R. Golub, *Proc. Natl. Acad. Sci. USA* **2000**, *97*, 3260 – 3265; c) C. Grandori, R. N. Eisenman, *Trends Biochem. Sci.* **1997**, *22*, 177 – 181.
[89] W. Risau, *Nature* **1997**, *386*, 671 – 674.
[90] Extracellular matrix: complex network of polysaccharides and proteins secreted by cells, serves as structural element in tissues; basal lamina: thin mat of extracellular matrix that separates epithelial sheets and other cell types from connective tissue.
[91] I. E. Collier, S. M. Wilhelm, A. Z. Eisen, B. L. Marmer, G. A. Grant, J. L. Seltzer, A. Kronberger, C. He, E. A. Bauer, G. I. Goldberg, *J. Biol. Chem.* **1988**, *263*, 6579 – 6587.
[92] a) S. Wojtowicz-Praga, J. Torri, M. Johnson, V. Steen, J. Marshall, E. Ness, R. Dickson, M. Sale, H. S. Rasmussen, T. A. Chiodo, M. J. Hawkins, *J. Clin. Oncol.* **1998**, *16*, 2150 – 2156; b) A. H. Drummond, P. Beckett, P. D. Brown, E. A. Bone, A. H. Davidson, W. A. Galloway, A. J. H. Gearing, P. Huxley, D. Laber, M. McCourt, M. Whittaker, L. M. Wood, A. Wright, *Ann. N. Y. Acad. Sci.* **1999**, *878*, 228 – 235.
[93] P. C. Brooks, S. Strömblad, L. C. Sanders, T. L. von Schalscha, R. T. Aimes, W. G. Stetler-Stevenson, J. P. Quigley, D. A. Cheresh, *Cell* **1996**, *85*, 683 – 693.
[94] a) P. C. Brooks, S. Silletti, T. L. von Schalscha, M. Friedlander, D. A. Cheresh, *Cell* **1998**, *92*, 391 – 400; b) A. Pfeifer, T. Kessler, S. Siletti, D. A. Cheresh, I. M. Verma, *Proc. Natl. Acad. Sci. USA* **2000**, *97*, 12227 – 12232.
[95] a) D. L. Boger, J. Goldberg, S. Silletti, T. Kessler, D. A. Cheresh, *J. Am. Chem. Soc.* **2001**, *123*, 1280 – 1288; b) S. Silletti, T. Kessler, J. Goldberg, D. L. Boger, D. A. Cheresh, *Proc. Natl. Acad. Sci. USA* **2001**, *98*, 119 – 124.
[96] a) D. L. Boger, P. Ducray, W. Chai, W. Jiang, J. Goldberg, *Bioorg. Med. Chem. Lett.* **1998**, *8*, 2339 – 2344; b) D. L. Boger, J. Goldberg, W. Jiang, W. Chai, P. Ducray, J. K. Lee, R. S. Ozer, C.-M. Andersson, *Bioorg. Med. Chem.* **1998**, *6*, 1347 – 1378.
[97] G. Kollias, E. Douni, G. Kassiotis, D. Kontoyiannis, *Immunol. Rev.* **1999**, *169*, 175 – 194.
[98] V. Baud, M. Karin, *Trends Cell Biol.* **2001**, *11*, 372 – 377.
[99] B. A. Beutler, *J. Rheumatol.* **1999**, *26, Suppl. 57*, 16 – 21.
[100] L. W. Moreland, *J. Rheumatol.* **1999**, *26, Suppl. 57*, 7 – 15.
[101] P. H. Carter, P. A. Scherle, J. K. Muckelbauer, M. E. Voss, R.-Q. Liu, R. L. A. Thompson, A. J. Tebben, K. A. Solomon, Y. C. Lo, Z. Li, P. Strzemienski, G. Yang, N. Falahatpisheh, M. Xu, Z. Wu, N. A. Farrow, K. Ramnarayan, J. Wang, D. Rideout, V. Yalamoori, P. Domaille, D. J. Underwood, J. M. Trzaskos, S. M. Friedman, R. C. Newton, C. P. Decicco, *Proc. Natl. Acad. Sci. USA* **2001**, *98*, 11879 – 11884.
[102] A. van de Stolpe, P. T. van der Saag, *J. Mol. Med.* **1996**, *74*, 13 – 33.
[103] R. O. Hynes, *Cell* **1992**, *69*, 11 – 25.
[104] C. G. Gahmberg, *Curr. Opin. Cell Biol.* **1997**, *9*, 643 – 659.
[105] G. A. van Seventer, Y. Shimizu, K. J. Horgan, S. Shaw, *J. Immunol.* **1990**, *144*, 4579 – 4586.
[106] R. S. Cotran, T. Mayadas-Norton, *Pathol. Biol.* **1998**, *46*, 164 – 170.
[107] E. K. Nakakura, R. A. Shorthouse, B. Zheng, S. M. McCabe, P. M. Jardieu, R. E. Morris, *Transplantation* **1996**, *62*, 547 – 552.
[108] a) C. J. Cornejo, R. K. Winn, J. M. Harlan, *Adv. Pharmacol.* **1997**, *39*, 99 – 142; b) A. Fischer, W. Friedrich, A. Fasth, S. Blanche, F. Le Deist, D. Girault, F. Veber, J. Vossen, M. Lopez, C. Griscelli, M. Hirn, *Blood* **1991**, *77*, 249 – 256; c) M. Hourmant, B. Le Mauff, Y. Le Meur, J. Dantal, D. Cantarovich, M. Giral, P. Caudrelier, G. Albericci, J.-P. Soulillou, *Transplantation* **1994**, *58*, 377 – 380.
[109] Y. Takada, T. Kamata, A. Irie, W. Puzon-McLaughlin, X. P. Zhang, *Matrix Biol.* **1997**, *16*, 143 – 151.
[110] J. O. Lee, P. Rieu, M. A. Arnaout, R. Liddington, *Cell* **1995**, *80*, 631 – 638.
[111] A. W. Alberts, J. Chen, G. Kuron, V. Hunt, J. Huff, C. Hoffman, J. Rothrock, M. Lopez, H. Joshua, E. Harris, A. Patchett, R. Monaghan, S. Currie, E. Stapley, G. Albers-Schonberg, O. Hensens, J. Hirshfield, K. Hoogsteen, J. Liesch, J. Springer, *Proc. Natl. Acad. Sci. USA* **1980**, *77*, 3957 – 3961.
[112] J. Kallen, K. Welzenbach, P. Ramage, D. Geyl, R. Kriwacki, G. Legge, S. Cottens, G. Weitz-Schmidt, U. Hommel, *J. Mol. Biol.* **1999**, *292*, 1 – 9.
[113] G. Weitz-Schmidt, K. Welzenbach, V. Brinkmann, T. Kamata, J. Kallen, C. Bruns, S. Cottens, Y. Takada, U. Hommel, *Nat. Med.* **2001**, *7*, 687 – 692.
[114] K. Welzenbach, U. Hommel, G. Weitz-Schmidt, *J. Biol. Chem.* **2002**, *277*, 10590 – 10598.
[115] a) T. A. Kelly, D. D. Jeanfavre, D. W. McNeil, J. R. Woska, Jr., P. L. Reilly, E. A. Mainolfi, K. M. Kishimoto, G. H. Nabozny, R. Zinter, B.-J. Bormann, R. Rothlein, *J. Immunol.* **1999**, *163*, 5173 – 5177; b) K. Last-Barney, W. Davidson, M. Cardozo, L. L. Frye, C. A. Grygon, J. L. Hopkins, D. D. Jeanfavre, S. Pav, C. Qian, J. M. Stevenson, L. Tong, R. Zindell, T. A. Kelly, *J. Am. Chem. Soc.* **2001**, *123*, 5643 – 5650.
[116] G. Liu, J. T. Link, Z. Pei, E. B. Reilly, S. Leitza, B. Nguyen, K. C. Marsh, G. F. Okasinski, T. W. von Geldern, M. Ormes, K. Fowler, M. Gallatin, *J. Med. Chem.* **2000**, *43*, 4025 – 4040.
[117] a) M. Winn, E. B. Reilly, G. Liu, J. R. Huth, H.-S. Jae, J. Freeman, Z. Pei, Z. Xin, J. Lynch, J. Kester, T. W. von Geldern, S. Leitza, P. DeVries, R. Dickinson, D. Mussatto, G. F. Okasinski, *J. Med. Chem.* **2001**, *44*, 4393 – 4403; b) Z. Pei, Z. Xin, G. Liu, Y. Li, E. B. Reilly, N. L. Lubbers, J. R. Huth, J. T. Link, T. W. von Geldern, B. F. Cox, S. Leitza, Y. Gao, K. C. Marsh, P. DeVries, G. F. Okasinski, *J. Med. Chem.* **2001**, *44*, 2913 – 2920; c) G. Liu, J. R. Huth, E. T. Olejniczak, R. Mendoza, P. DeVries, S. Leitza, E. B. Reilly, G. F. Okasinski, S. W. Fesik, T. W. von Geldern, *J. Med. Chem.* **2001**, *44*, 1202 – 1210.
[118] a) J. R. Woska, Jr., D. Shih, V. R. Taqueti, N. Hogg, T. A. Kelly, T. K. Kishimoto, *J. Leukocyte Biol.* **2001**, *70*, 329 – 334; b) J. R. Huth, E. T. Olejniczak, R. Mendoza, H. Liang, E. A. S. Harris, M. L. Lupher, Jr., A. E. Wilson, S. W. Fesik, D. E. Staunton, *Proc. Natl. Acad. Sci. USA* **2000**, *97*, 5231 – 5236.
[119] T. R. Gadek, D. J. Burdick, R. S. McDowell, M. S. Stanley, J. C. Marsters, Jr., K. J. Paris, D. A. Oare, M. E. Reynolds, C. Ladner, K. A. Zioncheck, W. P. Lee, P. Gribling, M. S. Dennis, N. J. Skelton, D. B. Tumas, K. R. Clark, S. M. Keating, M. H. Beresini, J. W. Tilley, L. G. Presta, S. C. Bodary, *Science* **2002**, *295*, 1086 – 1089.
[120] K. L. Fisher, J. Lu, L. Riddle, K. J. Kim, L. G. Presta, S. C. Bodary, *Mol. Biol. Cell* **1997**, *8*, 501 – 515.
[121] a) S. Moncada, R. M. J. Palmer, E. A. Higgs, *Pharmacol. Rev.* **1991**, *43*, 109 – 142; b) F. Murad, *Angew. Chem.* **1999**, *111*, 1976 – 1989; *Angew. Chem. Int. Ed.* **1999**, *38*, 1856 – 1868; c) R. F. Furchgott, *Angew. Chem.* **1999**, *111*, 1990 – 2000; *Angew. Chem. Int. Ed.* **1999**, *38*, 1870 – 1880; d) L. J. Ignarro, *Angew. Chem.* **1999**, *111*, 2002 – 2013; *Angew. Chem. Int. Ed.* **1999**, *38*, 1882 – 1892; e) S. Pfeiffer, B. Mayer, B. Hemmens, *Angew. Chem.* **1999**, *111*, 1824 – 1844; *Angew. Chem. Int. Ed.* **1999**, *38*, 1714 – 1731.
[122] V. L. Dawson, T. M. Dawson, *Adv. Pharmacol.* **1995**, *34*, 323 – 342.
[123] S. Moncada, A. Higgs, *N. Engl. J. Med.* **1993**, *329*, 2002 – 2012.

 © 2003 Wiley-VCH Verlag GmbH & Co. KGaA, Weinheim

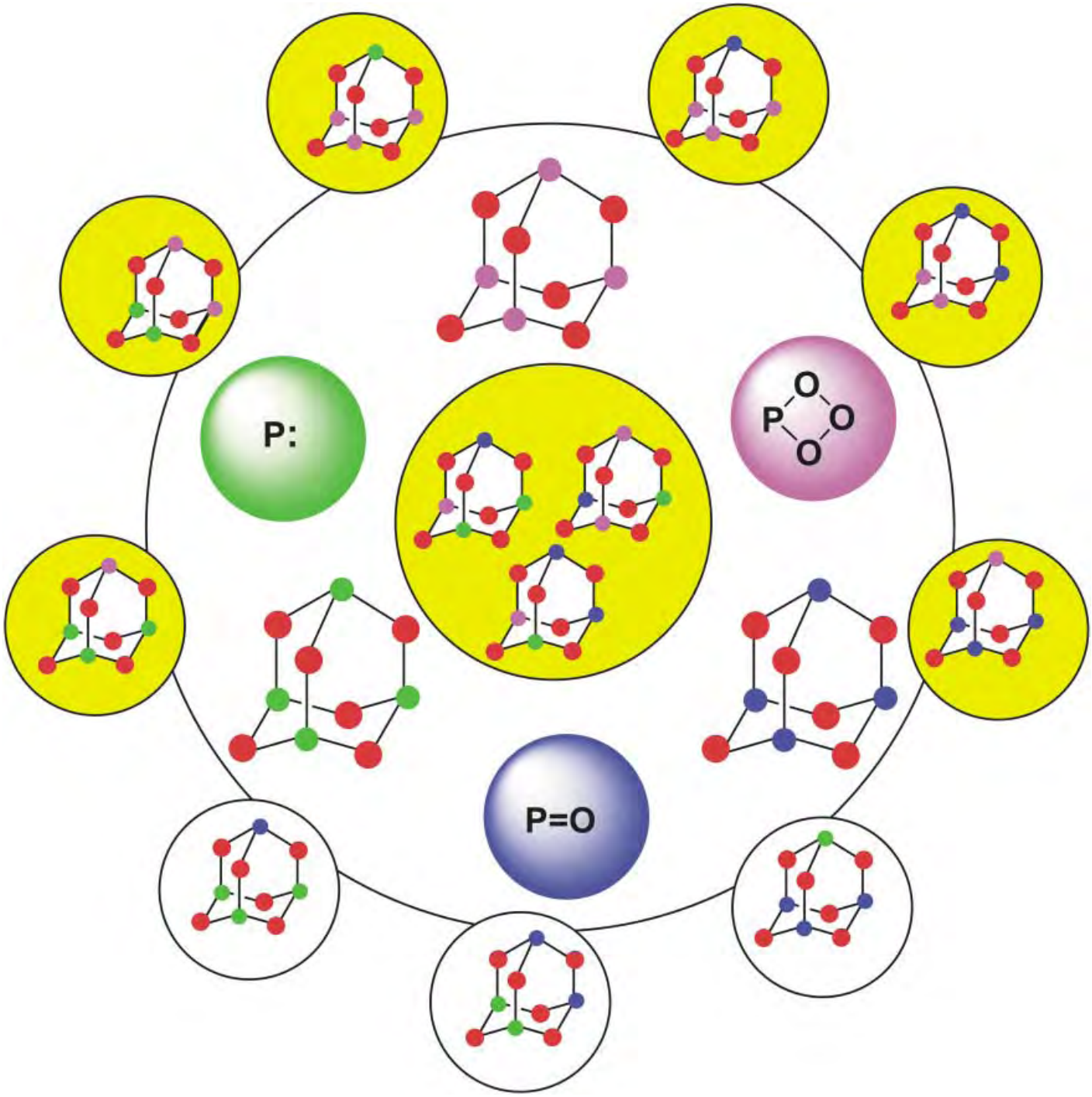
[124] W. K. Alderton, C. E. Cooper, R. G. Knowles, *Biochem. J.* **2001**, *357*, 593 – 615.
[125] a) C. Nathan, *J. Clin. Invest.* **1997**, *100*, 2417 – 2423; b) D. O. Stichtenoth, J. C. Frolich, *Br. J. Rheumatol.* **1998**, *37*, 246 – 257.
[126] a) D. J. Wolff, A. Lubeskie, S. Umansky, *Arch. Biochem. Biophys.* **1994**, *314*, 360 – 366; b) R. M. Chabin, E. McCauley, J. R. Calaycay, T. M. Kelly, K. L. MacNaul, G. C. Wolfe, N. I. Hutchinson, S. Madhusudanaraju, J. A. Schmidt, J. W. Kozarich, K. K. Wong, *Biochemistry* **1996**, *35*, 9567 – 9575.
[127] K. McMillan, M. Adler, D. S. Auld, J. J. Baldwin, E. Blasko, L. J. Browne, D. Chelsky, D. Davey, R. E. Dolle, K. A. Eagen, S. Erickson, R. I. Feldman, C. B. Glaser, C. Mallari, M. M. Morrissey, M. H. Ohlmeyer, G. Pan, J. F. Parkinson, G. B. Phillips, M. A. Polokoff, N. H. Sigal, R. Vergona, M. Whitlow, T. A. Young, J. J. Devlin, *Proc. Natl. Acad. Sci. USA* **2000**, *97*, 1506 – 1511.
[128] E. Blasko, C. B. Glaser, J. J. Devlin, W. Xia, R. I. Feldman, M. A. Polokoff, G. B. Phillips, M. Whitlow, D. S. Auld, K. McMillan, S. Ghosh, D. J. Stuehr, J. F. Parkinson, *J. Biol. Chem.* **2002**, *277*, 295 – 302.
[129] S. B. Krantz, *Blood* **1991**, *77*, 419 – 434.
[130] a) C.-H. Heldin, *Cell* **1995**, *80*, 213 – 223; b) J. A. Wells, *Curr. Opin. Cell Biol.* **1994**, *6*, 163 – 173.
[131] W. Jelkmann, *Physiol. Rev.* **1992**, *72*, 449 – 489.
[132] S. T. Koury, M. C. Bondurant, M. J. Koury, *Blood* **1988**, *71*, 524 – 527.
[133] F. Valderrábano, *Kidney Int.* **1996**, *50*, 1373 – 1391.
[134] J. L. Spivak, *Annu. Rev. Med.* **1993**, *44*, 243 – 253.
[135] D. L. Boger, J. Goldberg, *Bioorg. Med. Chem.* **2001**, *9*, 557 – 562.
[136] S. A. Qureshi, R. M. Kim, Z. Konteatis, D. E. Biazzo, H. Motamedi, R. Rodrigues, J. A. Boice, J. R. Calaycay, M. A. Bednarek, P. Griffin, Y.-D. Gao, K. Chapman, D. F. Mark, *Proc. Natl. Acad. Sci. USA* **1999**, *96*, 12156 – 12161.
[137] J. Goldberg, Q. Jin, Y. Ambroise, S. Satoh, J. Desharnais, K. Capps, D. L. Boger, *J. Am. Chem. Soc.* **2002**, *124*, 544 – 555.
[138] R. K. Chawla, J. S. Parks, D. Rudman, *Annu. Rev. Med.* **1983**, *34*, 519 – 547.
[139] A. M. de Vos, M. Ultsch, A. A. Kossiakoff, *Science* **1992**, *255*, 306 – 312.
[140] a) B. C. Cunningham, J. A. Wells, *J. Mol. Biol.* **1993**, *234*, 554 – 563; b) J. A. Wells, B. C. Cunningham, G. Fuh, H. B. Lowman, S. H. Bass, M. G. Mulkerrin, M. Ultsch, A. M. deVos, *Recent Prog. Horm. Res.* **1993**, *48*, 253 – 275.
[141] Z. Guo, D. Zhou, P. G. Schultz, *Science* **2000**, *288*, 2042 – 2045.
[142] M. D. Benson, M. R. Wallace in *The Metabolic Basis of Inherited Disease* (Eds.: C. R. Scriver, A. L. Beaudet, W. S. Sly, D. Valle), McGraw-Hill, New York, **1989**, pp. 2439 – 2460.
[143] L. Bartalena, J. Robbins, *Clin. Lab. Med.* **1993**, *13*, 583 – 598.
[144] H. L. Monaco, M. Rizzi, A. Coda, *Science* **1995**, *268*, 1039 – 1041.
[145] Z. Lai, W. Colón, J. W. Kelly, *Biochemistry* **1996**, *35*, 6470 – 6482.
[146] G. J. Miroy, Z. Lai, H. A. Lashuel, S. A. Peterson, C. Strang, J. W. Kelly, *Proc. Natl. Acad. Sci. USA* **1996**, *93*, 15051 – 15056.
[147] S. A. Peterson, T. Klabunde, H. A. Lashuel, H. Purkey, J. C. Sacchettini, J. W. Kelly, *Proc. Natl. Acad. Sci. USA* **1998**, *95*, 12956 – 12960.
[148] a) P. W. Baures, S. A. Peterson, J. W. Kelly, *Bioorg. Med. Chem.* **1998**, *6*, 1389 – 1401; b) P. W. Baures, V. B. Oza, S. A. Peterson, J. W. Kelly, *Bioorg. Med. Chem.* **1999**, *7*, 1339 – 1347.
[149] T. Klabunde, H. M. Petrassi, V. B. Oza, P. Raman, J. W. Kelly, J. C. Pacchettini, *Nat. Struct. Biol.* **2000**, *7*, 312 – 321.
[150] a) V. B. Oza, H. M. Petrassi, H. E. Purkey, J. W. Kelly, *Bioorg. Med. Chem. Lett.* **1999**, *9*, 1 – 6; b) H. M. Petrassi, T. Klabunde, J. Sacchettini, J. W. Kelly, *J. Am. Chem. Soc.* **2000**, *122*, 2178 – 2192.
[151] M. G. McCammon, D. J. Scott, C. A. Keetch, L. H. Greene, H. E. Purkey, H. M. Petrassi, J. W. Kelly, C. V. Robinson, *Structure* **2002**, *10*, 851 – 863.
[152] a) H. E. Purkey, M. I. Dorrell, J. W. Kelly, *Proc. Natl. Acad. Sci. USA* **2001**, *98*, 5566 – 5571; b) V. B. Oza, C. Smith, P. Raman, E. K. Koepf, H. A. Lashuel, H. M. Petrassi, K. P. Chiang, E. T. Powers, J. Sachettinni, J. W. Kelly, *J. Med. Chem.* **2002**, *45*, 321 – 332.
[153] a) J. C. Sacchettini, J. W. Kelly, *Nat. Rev. Drug Discovery* **2002**, *1*, 267 – 275; b) P. Kuner, B. Bohrmann, L. O. Tjernberg, J. Näslund, G. Huber, S. Celenk, F. Grüninger-Leitch, J. G. Richards, R. Jakob-Rœtne, J. A. Kemp, C. Nordstedt, *J. Biol. Chem.* **2000**, *275*, 1673 – 1678; c) B. Bohrmann, M. Adrian, J. Dubochet, P. Kuner, F. Müller, W. Huber, C. Nordstedt, H. Döbeli, *J. Struct. Biol.* **2000**, *130*, 232 – 246; d) J. McLaurin, D.-S. Yang, C. M. Yip, P. E. Fraser, *J. Struct. Biol.* **2000**, *130*, 259 – 270.
[154] A. M. Petros, A. Medek, D. G. Nettesheim, D. H. Kim, H. S. Yoon, K. Swift, E. D. Matayoshi, T. Oltersdorf, S. W. Fesik, *Proc. Natl. Acad. Sci. USA* **2001**, *98*, 3012 – 3017.
[155] a) S. W. Muchmore, M. Sattler, H. Liang, R. P. Meadows, J. E. Harlan, H. S. Yoon, D. Nettesheim, B. S. Chang, C. B. Thompson, S.-L. Wong, S.-L. Ng, S. W. Fesik, *Nature* **1996**, *381*, 335 – 341; b) M. Aritomi, N. Kunishima, N. Inohara, Y. Ishibashi, S. Ohta, K. Morikawa, *J. Biol. Chem.* **1997**, *272*, 27886 – 27892.
[156] M. Sattler, H. Liang, D. Nettesheim, R. P. Meadows, J. E. Harlan, M. Eberstadt, H. S. Yoon, S. B. Shuker, B. S. Chang, A. J. Minn, C. B. Thompson, S. W. Fesik, *Science* **1997**, *275*, 983 – 986.
[157] J.-L. Wang, D. Liu, Z.-J. Zhang, S. Shan, X. Han, S. M. Srinivasula, C. M. Croce, E. S. Alnemri, Z. Huang, *Proc. Natl. Acad. Sci. USA* **2000**, *97*, 7124 – 7129.
[158] I. J. Enyedy, Y. Ling, K. Nacro, Y. Tomita, X. Wu, Y. Cao, R. Guo, B. Li, X. Zhu, Y. Huang, Y.-Q. Long, P. P. Roller, D. Yang, S. Wang, *J. Med. Chem.* **2001**, *44*, 4313 – 4324.
[159] A. A. Lugovskoy, A. I. Degterev, A. F. Fahmy, P. Zhou, J. D. Gross, J. Yuan, G. Wagner, *J. Am. Chem. Soc.* **2002**, *124*, 1234 – 1240.
[160] a) T. D. Brumeanu, C. A. Bona, S. Casares, *Int. Rev. Immunol.* **2001**, *20*, 301 – 331; b) J. J. Goronzy, C. M. Weyand, *Curr. Dir. Autoimmun.* **2001**, *3*, 112 – 132; c) H. Schulze-Koops, P. E. Lipsky, *Curr. Dir. Autoimmun.* **2000**, *2*, 24 – 49.
[161] B. Watschinger, *Nephrol. Dial. Transplant.* **1995**, *10*, 1556 – 1558.
[162] A. C. Fischer, P. P. Ruvolo, R. Burt, L. R. Horwitz, E. C. Bright, J. M. Hess, W. E. Beschorner, A. D. Hess, *J. Immunol.* **1995**, *154*, 3713 – 3725.
[163] a) D. A. A. Vignali, *Behring Inst. Mitt.* **1994**, *94*, 133 – 147; b) D. A. A. Vignali, C. Doyle, M. S. Kinch, J. Shin, J. L. Strominger, *Philos. Trans. R. Soc. London Ser. B* **1993**, *342*, 13 – 24.
[164] a) P. J. Maddon, S. M. Molineaux, D. E. Maddon, K. A. Zimmerman, M. Godfrey, F. W. Alt, L. Chess, R. Axel, *Proc. Natl. Acad. Sci. USA* **1987**, *84*, 9155 – 9159; b) K. Bowers, C. Pitcher, M. Marsh, *Int. J. Biochem. Cell Biol.* **1997**, *29*, 871 – 875.
[165] a) C. Doyle, J. L. Strominger, *Nature* **1987**, *330*, 256 – 259; b) K. Eichmann, *Angew. Chem.* **1993**, *105*, 56 – 66; *Angew. Chem. Int. Ed. Engl.* **1993**, *32*, 54.
[166] a) J. Wang, Y. Yan, T. P. J. Garrett, J. Liu, D. W. Rodgers, R. L. Garlick, G. E. Tarr, Y. Husain, E. L. Reinherz, S. C. Harrison, *Nature* **1990**, *348*, 411 – 4418; b) D. Lamarre, A. Ashkenazi, S. Fleury, D. H. Smith, R.-P. Sekaly, D. J. Capon, *Science* **1989**, *245*, 743 – 7746; c) S. Fleury, D. Lamarre, S. Meloche, S.-E. Ryu, C. Cantin, W. A. Hendrickson, R.-P. Sekaly, *Cell* **1991**, *66*, 1037 – 1049.
[167] K. P. Peters, J. Fauck, C. Frömmel, *J. Mol. Biol.* **1996**, *256*, 201 – 2213.

 © 2003 Wiley-VCH Verlag GmbH & Co. KGaA, Weinheim

[168] E. C. Meng, B. K. Shoichet, I. D. Kuntz, *J. Comput. Chem.* **1992**, *13*, 505 – 524.
[169] B. Lee, F. M. Richards, *J. Mol. Biol.* **1971**, *55*, 379 – 400.
[170] S. Li, J. Gao, T. Satoh, T. M. Friedman, A. E. Edling, U. Koch, S. Choksi, X. Han, R. Korngold, Z. Huang, *Proc. Natl. Acad. Sci. USA* **1997**, *94*, 73 – 78.
[171] a) L. K. Clayton, M. Sieh, D. A. Pious, E. L. Reinherz, *Nature* **1989**, *339*, 548 – 551; b) D. Lamarre, A. Ashkenazi, S. Fleury, D. H. Smith, R.-P. Sekaly, D. J. Capon, *Science* **1989**, *245*, 743 – 746.
[172] a) T. Satoh, J. M. Aramini, S. Li, T. M. Friedman, J. Gao, A. E. Edling, R. Townsend, U. Koch, S. Choksi, M. W. Germann, R. Korngold, Z. Huang, *J. Biol. Chem.* **1997**, *272*, 12175 – 12180; b) A. E. Edling, S. Choksi, Z. Huang, R. Korngold, *J. Neuroimmunol.* **2001**, *112*, 115 – 128.
[173] S.-E. Ryu, P. D. Kwong, A. Truneh, T. G. Porter, J. Arthos, M. Rosenberg, X. Dai, N.-h. Xuong, R. Axel, R. W. Sweet, W. A. Hendrickson, *Nature* **1990**, *348*, 419 – 426.
[174] a) Z. Huang, S. Li, R. Korngold, *Biopolymers* **1997**, *43*, 367 – 382; b) A. E. Edling, S. Choksi, Z. Huang, R. Korngold, *J. Autoimmun.* **2002**, *18*, 169 – 179.
[175] C. Adessi, C. Soto, *Curr. Med. Chem.* **2002**, *9*, 963 – 978.
[176] a) H. Gohlke, G. Klebe, *Angew. Chem.* **2002**, *114*, 2764 – 2798; *Angew. Chem. Int. Ed.* **2002**, *41*, 2644 – 2676; b) W. L. DeLano, M. H. Ultsch, A. M. de Vos, J. A. Wells, *Science* **2000**, *287*, 1279 – 1283.
[177] D. A. Erlanson, A. C. Braisted, D. R. Raphael, M. Randal, R. M. Stroud, E. M. Gordon, J. A. Wells, *Proc. Natl. Acad. Sci. USA* **2000**, *97*, 9367 – 9372.
[178] a) P. J. Hajduk, G. Sheppard, D. G. Nettesheim, E. T. Olejniczak, S. B. Shuker, R. P. Meadows, D. H. Steinman, G. M. Carrera, Jr., P. A. Marcotte, J. Severin, K. Walter, H. Smith, E. Gubbins, R. Simmer, T. F. Holzman, D. W. Morgan, S. K. Davidsen, J. B. Summers, S. W. Fesik, *J. Am. Chem. Soc.* **1997**, *119*, 5818 – 5827; b) D. J. Maly, I. C. Choong, J. A. Ellman, *Proc. Natl. Acad. Sci. USA* **2000**, *97*, 2419 – 2424.
[179] S. B. Shuker, P. J. Hajduk, R. P. Meadows, S. W. Fesik, *Science* **1996**, *274*, 1531 – 1534.
[180] a) R. Breinbauer, I. R. Vetter, H. Waldmann, *Angew. Chem.* **2002**, *114*, 3002 – 3015; *Angew. Chem. Int. Ed.* **2002**, *41*, 2878 – 2890; b) D. Brohm, S. Metzger, A. Bhargava, O. Müller, F. Lieb, H. Waldmann, *Angew. Chem.* **2002**, *114*, 319 – 323; *Angew. Chem. Int. Ed.* **2002**, *41*, 307 – 311.

 © 2003 Wiley-VCH Verlag GmbH & Co. KGaA, Weinheim

Communications



P_4O_{18}, the first defined binary peroxo compound in the P/O binary system, was obtained by the reaction of ozone with P_4O_6. This reaction paves the way to related, hitherto-unknown phosphorus ozonides (yellow circles). Details on the synthesis and properties of P_4O_{18}, the most-oxygen-rich phosphorus compound known to date, are given by M. Meisel et al. on the following pages.

DOI: 10.1002/anie.200351135
© 2003 Wiley-VCH Verlag GmbH & Co. KGaA, Weinheim

Tetraozonide of Phosphorus Oxide

The First Ozonide of a Phosphorus Oxide—Preparation, Characterization, and Structure of P_4O_{18}**

*Anton Dimitrov, Burkhard Ziemer, Wolf-Dietrich Hunnius, and Manfred Meisel**

Since 1961 it has been known that ozone reacts at low temperatures with a large number of esters of the orthophosphonic acid, $(RO)_3P$, and depending on the structures of the starting phosphites, labile adducts of different stability are formed.[1] Analogous to the primary ozonides, well-known from organic chemistry, these compounds could be classified as inorganic covalent ozonides. Extensive studies by several groups have opened up the application of these compounds as oxidizing agents as well as a source for the generation of singlet oxygen.[2] The ^{31}P-chemical shifts of numerous phosphorus ozonides appear in the range typical for five-coordinate phosphorus compounds, which led to the assumption that a trioxaphosphetane ring should be present in these compounds. That the reaction between phosphites and ozone does indeed represent a electrophilic [1+3] cycloaddition of the ozone on the nucleophilic phosphorus atom of the $\sigma^3\lambda^3$-phosphite was recently exemplified by Dimitrov and Seppelt with the determination of the crystal structure of a trioxaphosphetane phosphorane, the ozonide of the bicyclic phosphite 4-ethyl-1-phospha-2,6,7-trioxabicyclo[2.2.2]octane.[3]

In our investigations on the ozonization behavior of phosphorus compounds we have been interested in the reaction of ozone with low-valent phosphorus oxides, especially with phosphorus(III) oxide P_4O_6, to establish whether it is possible to synthesize binary phosphorus oxides with a higher oxygen to phosphorus ratio than 2.5 (corresponding to P_4O_{10}).

All the molecular binary phosphorus oxides of the formula P_4O_{6+n} ($n = 0$–4) have been isolated as pure compounds and characterized structurally.[4] In some textbooks on Inorganic Chemistry[5] a phosphorus peroxide of the composition "P_2O_6" has been mentioned,[6] which is said to be formed by the reaction of P_4O_{10} with O_2 in a hot discharge tube (5 kV) and is stable up to 130 °C. Unfortunately its existence could not be confirmed up to now. We initially tried to reproduce the results of Schenk and Rehaag[6] under slightly modified conditions. However, in the ^{31}P MAS NMR spectrum of the product obtained we neither observed additional signals to those attributed to P_4O_{10} nor was there any indication from the Raman spectra for the presence of a phosphorus peroxide in this product.

The reaction of phosphorus(III) oxide with ozone at room temperature results in a mixture of P_4O_{10} and phosphorus(III/V) oxides.[7] But till now no data are available on the reaction of P_4O_6 with ozone at low temperature in organic solvents. Therefore, we were interested to investigate to what extent phosphorus(III) oxide would behave similarly to the cyclic phosphites on reaction with ozone under very mild conditions.

Indeed, P_4O_6 reacts, analogously to the cyclic phosphites, with O_3 at −78 °C in CH_2Cl_2 resulting in the [1+3] cycloaddition products. After the addition of 4 mol of O_3 per mol of P_4O_6 no further reaction was observed. After pumping off the excess ozone and some of the solvent at −78 °C, we obtained a white solid as crude product. In solution or as a suspension in CH_2Cl_2, this solid starts to decompose on gentle warming above −35 °C with the gradual evolution of O_2. In contrast, the thermal decomposition of the dry powder without solvent is explosive.

The decomposition product was identified by ^{31}P MAS NMR and Raman spectroscopy as phosphorus(V) oxide together with small amounts of the phosphorus(III/V) oxide P_4O_9. The ^{31}P NMR spectrum of the recrystallized product (dissolved in CD_2Cl_2) shows only one signal at $\delta = -66.3$ ppm at −70 °C, which we assign to the tetraozonide of P_4O_6.

The composition and structure of the new tetraozonide P_4O_{18} (**1**) was confirmed by an X-ray crystal-structure analysis[8] (Figure 1). The structure of **1** can be derived like

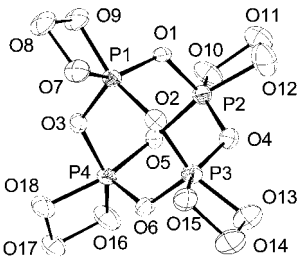


Figure 1. Structure of **1** (ORTEP representation with 60% probability ellipsoids).

the structures of P_4O_6 and P_4O_{10} starting from a P_4 tetrahedron, because the four phosphorus atoms adopt positions in the crystal which correspond to a slightly distorted tetrahedron. Within the accuracy of the determination, D_2 symmetry is present; the opposite P–P distances of 283, 289, and 296 pm respectively, are equal. The angles between the edges on the surface faces of the tetrahedron are distorted and found to be 57.3, 59.9, and 62.3°, respectively. By taking the oxygen atoms into consideration the D_2 symmetry no longer holds, which corresponds to the general position of **1** in the unit cell. Details of the structure are collected in Table 1.

Each P atom is surrounded by a distorted square pyramid comprising five O atoms. O3 and O1 represent the tips of the

[*] Prof. Dr. M. Meisel, Dr. A. Dimitrov, Dr. B. Ziemer
Institut für Chemie
Humboldt Universität zu Berlin
Brook-Taylor-Strasse 2, 12489 Berlin (Germany)
Fax: (+49) 30-2093-7468
E-mail: manfred.meisel@chemie.hu-berlin.de
Dr. W.-D. Hunnius
Institut für Anorganische und Analytische Chemie
Freie Universität Berlin
Fabeckstrasse 34–36, 14195 Berlin (Germany)

[**] This work was supported by the Fonds der Chemischen Industrie. A.D. is much obliged to the public authorities for the State Program of financial support, continuously offered since 1992 to the evaluated scientists of the former Academy of Science of the GDR. We thank Dr. A.-R. Grimmer for solid-state NMR spectroscopic assistance.

 © 2003 Wiley-VCH Verlag GmbH & Co. KGaA, Weinheim DOI: 10.1002/anie.200351135

Table 1: Bond lengths [pm] and bond angles [°] at the P atoms 1–4 of **1**.

[a]	P1	P2	P3	P4
P–O(c)	159.0(4)	159.5(4)	159.9(4)	160.4(4)
	164.4(4)	161.0(4)	162.4(4)	161.3(4)
	164.7(4)	163.9(4)	163.8(4)	164.3(4)
P–O(l)	162.7(4)	161.8(4)	163.3(4)	163.7(5)
	164.4(5)	166.2(5)	164.6(5)	164.1(4)
O(l)–O(l)	145.6(6)	144.6(6)	145.2(6)	144.8(6)
	145.4(6)	146.6(6)	146.4(6)	146.6(6)
O(a)-P-O(b)	107.9(2)	104.4(2)	101.6(2)	101.1(2)
	103.3(2)	112.3(2)	105.9(2)	107.2(2)
	104.1(2)	100.5(2)	103.2(2)	104.0(2)
	99.9(2)	100.0(3)	104.7(2)	102.2(2)
O(c)-P-O(c)	104.1(2)	104.4(2)	103.2(2)	102.2(2)
	99.9(2)	100.5(2)	101.6(2)	101.1(2)
	94.2(2)	95.3(2)	94.7(2)	94.7(2)
O(l1)-P-O(c)	107.9(2)	112.3(2)	104.7(2)	107.2(2)
	147.4(2)	142.6(2)	152.8(2)	149.6(2)
	86.2(2)	85.3(2)	86.2(2)	87.4(2)
O(l2)-P-O(c)	103.3(2)	100.0(3)	105.9(2)	104.0(2)
	155.6(2)	157.9(2)	150.0(2)	154.2(2)
	87.1(2)	87.7(2)	86.7(2)	86.0(2)
O(l)-O(l)-P	93.6(3)	94.5(3)	93.6(3)	94.2(3)
	93.0(3)	93.4(3)	93.6(3)	93.4(3)
O(l)-P-O(l)	79.9(2)	79.3(2)	79.5(2)	79.5(2)
O(l)-O(l)-O(l)	92.4(3)	91.9(4)	92.0(4)	92.0(3)
Σ internal angles $PO(l)_3$	358.9	359.1	358.7	359.1
O(l)-P-O(l)-O(l)	±7.2(3)	±7.0(3)	±8.3(3)	±6.9(3)
O(b)-O(b)-O(b)-O(b)	±5.8(3)	±11.3(3)	±2.0(3)	±3.3(3)

[a] c: cage; l: ligand; a: apical; b: basal.

pyramids around P1 and P2, respectively, and O6 forms the common tip of the pyramids surrounding P3 and P4. Analogous to the structure of a phosphorus ozonide described by Dimitrov and Seppelt,[3] all P–O bonds pointing to the tips of the pyramids in **1** are significantly shorter than those pointing to O atoms of the pyramid bases. The bond angles between the O atom at the apex and the other four O atoms (average values) are 103.8° at P1, 104.3° at P2, 103.8° at P3, and 103.6 at P4, and are thus close to the value of about 105° expected for a square pyramid. Every phosphorus atom is situated by 38 to 40 pm above its base surface. Evidently, the spiro character of the P atoms in this ozonide determines the preference for the tetragonal-pyramidal coordination. Another possible coordination, for example trigonal-bipyramidal, is not observed.

Within the P_4O_{18} molecule the four pyramids are connected through common corners formed by the atoms O1 to O6 (Figure 2). These O atoms build an octahedron, whose unoccupied center is the midpoint of the adamantane cage. The connectivity of the pyramids with each other differs remarkably: one tip-to-tip (P3/P4 over O6), two base-to-tip (P1/P2 over O1, P1/P4 over O3), and three base-to-base

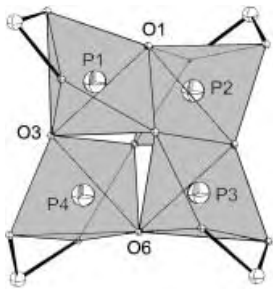


Figure 2. Connection of the four tetragonal pyramids within the adamantane cage.

connections (P1/P3 over O2, P2/P3 over O4, and P2/P4 over O5).

The Raman spectrum of **1** recorded at −80 °C shows besides the expected bands for the adamantane cage[9] the three prominent bands at 901, 887, and 870 cm^{-1} that were assigned by Dimitrov and Seppelt as the characteristic Raman bands of the PO_3 ring.[3] The Raman spectrum measured at −30 °C shows that the decrease in the intensity of these bands occurs simultaneously with the vigorous liberation of O_2 and the formation of phosphorus(v) oxide P_4O_{10}.

In summary, the results of our investigations show that the series P_4O_{6+n} can be extended up to $n = 12$. We have succeeded in the synthesis and structure analysis of the oxygen-richest binary phosphorus compound (with 4.5 oxygen atoms per phosphorus atom) of the formula P_4O_{18} known to date. Besides P_4O_6 with four $\sigma^3\lambda^3$- and P_4O_{10} with four $\sigma^4\lambda^5$-, P_4O_{18} with four $\sigma^5\lambda^5$-phosphorus atoms represents a further final member of the series of binary phosphorus–oxygen compounds having the adamantane-like structure. Taking into consideration the coordination number of 3 for the trivalent, and of 4 or 5 for the pentavalent phosphorus atoms of the adamantane cage, there are 15 binary phosphorus–oxygen compounds possible, of which only the five known oxides P_4O_{6+n} ($n = 0$–4) and the new tetraozonide P_4O_{18} have been synthesized and structurally characterized up to now (Figure 3). These 15 binary compounds with adamantane-like

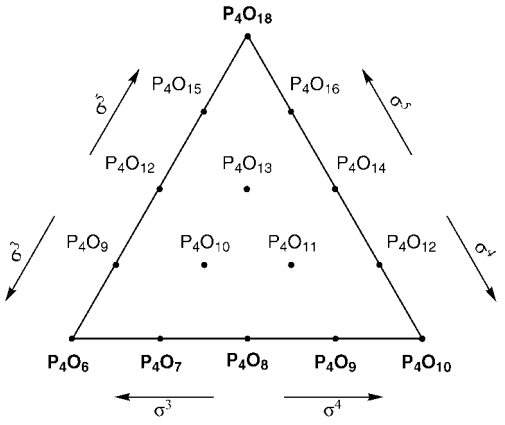


Figure 3. Triangle diagram of all possible binary phosphorus–oxygen compounds with an adamantane cage structure formed by combination of the structural elements ≡P, ≡PO, and $\equiv PO_3$.

 © 2003 Wiley-VCH Verlag GmbH & Co. KGaA, Weinheim

structure can be derived by combination of the three structural elements ≡P, ≡PO, ≡PO_3. They are depicted in Figure 3 in the triangle diagram based on the coordination numbers σ^3, σ^4, and σ^5 as selected coordinates (the known compounds are printed in bold). The adamantane-cage structures of the compounds at the corner of the triangle contain only one kind of phosphorus atom, those on the sides two kinds, and those within the triangle three kinds.

By applying the presented reaction it should be possible to synthesize further new binary phosphorus–oxygen compounds from the diagram in Figure 3, for example, by reacting the phosphorus(III/V) oxides P_4O_{6+n} ($n = 0$–3) with various stoichiometric amounts of ozone or by a partial decomposition of "oligoozonide" precursors.

Experimental Section

All experiments were performed under a purified dry inert gas atmosphere (argon) in a glove box and/or on glass high-vacuum line. P_4O_6 was purified by multiple distillation under reduced pressure, CH_2Cl_2 was refluxed over CaH_2 and freshly distilled prior to use.

The ^{31}P solid-state and ^{31}P liquid NMR spectra were recorded on 400 and 300 MHz Bruker spectrometers, respectively, at the appropriate ^{31}P frequencies using 85 % $H_3{}^{31}PO_4$ as an external standard, the Raman spectra were recorded on a Bruker-RPS 100 S instrument (Nd:YAG laser excitation at 1064 nm).

Synthesis of **1**: P_4O_6 (967 mg, 4.4 mmol) was dissolved in CH_2Cl_2 (19.5 mL) in a 50-mL Schlenk tube. An O_2/O_3 stream at a flow rate of about 3 L h^{-1} (5 vol. % ozone generated by a self-built ozonizer at 11 kV) was bubbled through the 0.23 M solution at −78 °C until it turned from colorless to blue, due to the dissolved ozone at the end of the reaction. After the excess ozone and some of the solvent had been removed under vacuum at −78 °C, **1** decomposed on warming slowly to room temperature; about 345 mL O_2 (equivalent to 3.5 mmol per mmol P_4O_6; normal conditions, determined pneumatically) evolved. After separation and drying, 1.223 g of the decomposition product was obtained, which was identified by its ^{31}P MAS NMR and Raman spectra as P_4O_{10} contaminated with small amounts of P_4O_9.

After its synthesis, **1** was isolated by removing the CH_2Cl_2 from the reaction mixture under vacuum at −78 °C. After the separation of the solid precipitate, the supernatant solvent was removed under argon by using a precooled syringe. The resulting crude product of **1** was dried by performing several cycles of evacuation and refilling with dry argon at −78 °C. *The dry powder is extremely explosive and has to be handled very carefully and in small amounts only!* In contrast, the handling of **1** under CH_2Cl_2 is relatively harmless; in this way we could prepare and handle all samples for our investigations.

The Raman spectra of **1** were recorded on powder samples kept in sealed 4-mm glass tubes (containing small amounts of CH_2Cl_2). The bands of the glass tube and the dichloromethane were subtracted digitally.

The low-temperature Raman spectra (−80 °C) showed three characteristic groups of bands, which are assigned to the bending mode vibrations ($\tilde{\nu} = 392$ (90), 407 cm^{-1} (60)), the stretching mode vibrations of the adamantane cage ($\tilde{\nu} = 598$ (50), 619 (shoulder), 606 (5), 798 cm^{-1} (35)), and the stretching mode vibrations of the trioxaphosphetane (PO_3) ring ($\tilde{\nu} = 870$ (20), 887 (25), 901 cm^{-1} (100)). The approximate values of the intensities are given in parentheses.

The crude product from the ozonization, partially dissolved and partially suspended in CH_2Cl_2 was sealed in a glass tube, and kept at −78 °C. The emulsion-like consistency of the solution was maintained by daily shaking of the tube. After 2–3 weeks colorless rodlike crystals of **1** were obtained, from which after repeated attempts under argon at −80 °C a single crystal suitable for X-ray analysis was isolated. The temperature-sensitive single crystal was prepared in a cold stream of nitrogen. Data collection was carried out on an IPDS diffractometer (Stoe & Cie) at 180 K using graphite-monochromated $Mo_{K\alpha}$ radiation and a cryostream cooler (Oxford Cryosystems). The data set was collected in steps of $\varphi = 1.1°$ up to 198° (180 images). The measured intensities were corrected for background, Lorentz, polarization, and crystal decay effects. The structure was solved[10] and refined[11] with the SHELX 97 program (see reference [8]). Further details on the crystal structure investigations may be obtained from the Fachinformationszentrum Karlsruhe, 76344 Eggenstein-Leopoldshafen, Germany (fax: (+49) 7247-808-666; e-mail: crysdata@fiz-karlsruhe.de), on quoting the depository number CSD-412901.

Received: February 7, 2003 [Z51135]

Keywords: cycloaddition · ozone · ozonization · phosphorus

[1] Q. E. Thomson, *J. Am. Chem. Soc.* **1961**, *83*, 846–851.
[2] G. D. Mendenhall in *Advances in Oxygenated Processes, Vol. 2* (Ed.: A. L. Baumstark), JAI, Greenwich, CT, **1990**, pp. 203–231.
[3] A. Dimitrov, K. Seppelt, *Eur. J. Inorg. Chem.* **2001**, 1929–1932.
[4] a) J. Clade, F. Frick, M. Jansen, *Adv. Inorg. Chem.* **1994**, *41*, 327–388; b) S. Strojek, M. Jansen, *Z. Naturforsch. B* **1997**, *52*, 906–910.
[5] N. N. Greenwood, A. Earnshaw, *Chemie der Elemente*, VCH, Weinheim, **1990**, p. 647.
[6] P. W. Schenk, H. Rehaag, *Z. Anorg. Allg. Chem.* **1937**, *233*, 403–410.
[7] C. C. Miller, *Philos. Trans. R. Soc. London* **1929**, 1823–1847.
[8] Crystal data for **1**; P_4O_{18}, orthorhombic, space group $P2_12_12_1$ (no.19); crystal size $0.50 \times 0.15 \times 0.12$ mm, $a = 909.47(17)$, $b = 1423.55(18)$, $c = 836.66(12)$ pm, $V = 1083.2(3) \times 10^6$ pm^3, $\rho_{calcd} = 2.526$ g cm^{-3}, $Z = 4$, $F(000) = 816$, $\mu(Mo_{K\alpha}) = 0.822$ mm^{-1}; data collection: diffractometer STOE Ipds, $Mo_{K\alpha}$ irradiation (71.073 pm), $T = 180(2)$ K, scan mode: φ-oscillation, $(h,k,l) = (\pm 11, \pm 15, \pm 10)$, 2Θ range = 5.32–51.00°, 6739 measured, 1916 unique reflections, $R_{int} = 0.129$, 1693 reflections with $I > 2\sigma(I)$, no absorption correction, $T_{min}/T_{max} = 0.784/0.908$; refinement: least-squares (full matrix) on F^2, 200 parameters, 1916 reflections used, $R1 = \Sigma\,||F_o| - |F_c||/\Sigma\,|F_o| = 0.0623$ $[F_o > 4\sigma(F_o)]$, $wR2 = [\Sigma w(F_o^2 - F_c^2)^2/\Sigma w(F_o^2)^2]^{1/2} = 0.1195$ (all), GoF = 1.025 (all), weighting parameters $w = 1/[\sigma^2(F_o^2) + (aP)^2 + bP]$ $(P = (F_o^2 + 2F_c^2)/3)$: $a = 0.060$, $b = 0.0$, $\rho_{final}(max/min) = 0.596/-0.558 \times 10^{-6}$ e pm^{-3}.
[9] A. R. S. Valentin, B. Engels, S. D. Peyerimhoff, J. Clade, M. Jansen, *J. Phys. Chem. A* **1998**, *102*, 3690–3696.
[10] G. M. Sheldrick, *Acta Crystallogr. Sect. A* **1990**, *46*, 467–473 cited for SHELXS.
[11] G. M. Sheldrick, SHELXL-97, Program for Crystal Structure Refinement, University of Göttingen, Göttingen (Germany), **1997**.

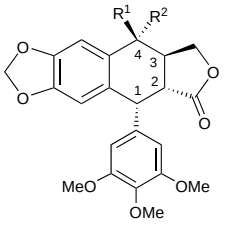
 © 2003 Wiley-VCH Verlag GmbH & Co. KGaA, Weinheim

Epipodophyllotoxin Total Synthesis

Efficient Enantioselective Total Synthesis of (−)-Epipodophyllotoxin**

*Ulrike Engelhardt, Arunkanti Sarkar, and Torsten Linker**

(−)-Epipodophyllotoxin (**1a**) is the C-4 epimer of (−)-podophyllotoxin (**1b**), a naturally occurring aryltetralin lignan with antimitotic activity.[1] Furthermore, (−)-epipodophyllotoxin (**1a**) represents the aglycon of the very potent clinical antitumor drugs etoposide and teniposide, which are used for the treatment of small cell lung cancer and Kaposi's sarcoma.[2] Therefore, various synthetic strategies were developed for podophyllotoxin and its analogues.[3] Initiated by the pioneering work of Meyers and co-workers, asymmetric total syntheses became more and more attractive during the last few years and ranged from auxiliary control to enzymatic approaches.[4] However, many steps were required and only moderate yields and stereoselectivities were achieved. Herein we describe a new efficient total synthesis of (−)-epipodophyllotoxin (**1a**) which involves only twelve reaction steps and occurs in high stereoselectivities and in 30% overall yield.

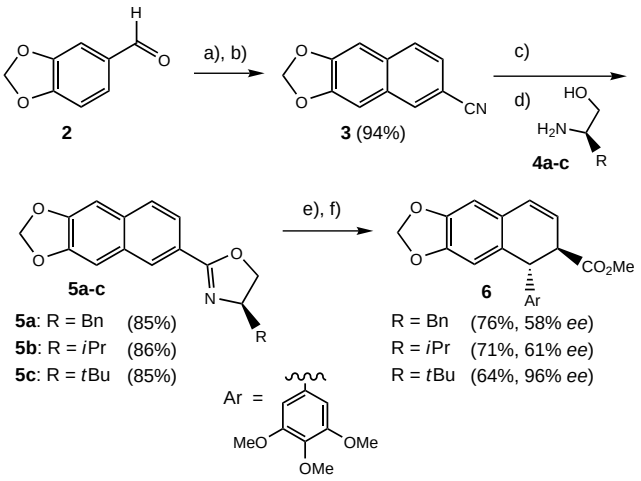


R^1 = OH, R^2 = H: (–)-Epipodophyllotoxin (**1a**)

R^1 = H, R^2 = OH: (–)-Podophyllotoxin (**1b**)

Our strategy was based on the stereoselective introduction of the OH group at C-4 and the carbon substituent at C-3 in the last reaction steps, thus enabling simple 1,2-dihydronaphthalenes to be employed as precursors. The naphthalenic nitrile **3** was synthesized in excellent yield by an anellation of commercially available piperonal (**2**; Scheme 1).

The elegant oxazoline strategy developed by Meyers and co-workers[5] was the method of choice to introduce the aryl substituent at C-1. Furthermore, the nitrile **3** was the ideal precursor for such auxiliaries, since the corresponding imidate was obtained quantitatively with hydrochloric acid in ethanol, and reaction with the chiral amino alcohols **4**[6] afforded the



Scheme 1. Synthesis of the 1,2-dihydronaphthalene **6** via the oxazolines **5** by auxiliary control. a) LDA, 4,4-diethoxybutyronitrile, −78 °C, 1 h; b) H_2SO_4 (20%), MeOH, 65 °C, 1.5 h; c) HCl, EtOH, 0 °C, 12 h; d) amino alcohol **4**, $CHCl_3$, 61 °C, 24–48 h; e) ArBr, *t*BuLi, −35 °C, 5 d; f) $MeSO_3H$, MeOH, 65 °C, 48 h. LDA = lithium diisopropylamide.

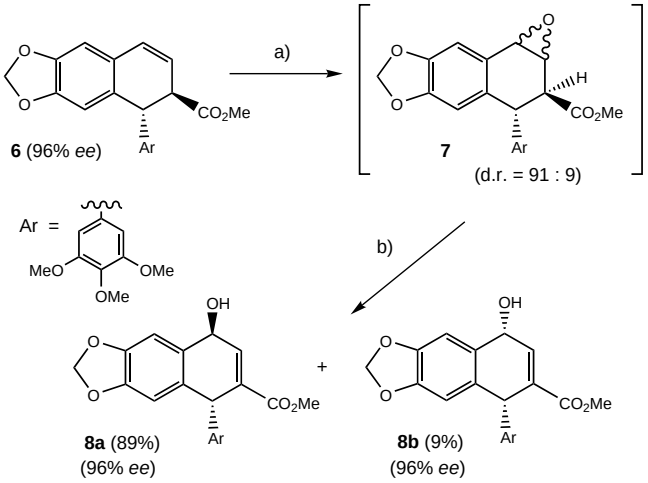
oxazolines **5** in good overall yield (Scheme 1). The subsequent addition of trimethoxyphenyllithium required thorough optimization of the reaction conditions. Thus, quenching of the aza enolate intermediate with 2-propanol, by using the same protocol as employed by Meyers and co-workers in the total synthesis of (−)-podophyllotoxin,[4a] afforded only the thermodynamically more stable 1,4-dihydronaphthalene. Another problem was the sensitivity of the desired product to oxidation, which led to naphthalenic systems. For the same reason, the attempted kinetic resolution of *rac*-**6** by Jacobsen epoxidation failed, although model studies in our research group showed promising prospects.[7] The best results were obtained by quenching the reaction mixture with methanesulfonic acid and the direct transformation of the chiral auxiliary into the methyl ester. This sequence led to the isolation of 1,2-dihydronaphthalenes **6** in moderate yields and in analytically pure form.[8] The exclusive formation of the *trans* diastereomer can be rationalized by thermodynamic control, and is in accordance with the literature.[9] The enantiomeric excess (*ee*) was unequivocally determined by HPLC on a chiral stationary phase. As expected, the *tert*-butyl auxiliary afforded the highest *ee* value, and was used for the further total synthesis.

The singlet oxygen ene reaction seemed to be the method of choice to introduce the OH group at C-4, since the desired allylic alcohol **8a** would be formed directly after reduction. However, the 1,2-dihydronaphthalene **6** was too labile and led again to oxidation side products, which arise as a result of the high reactivity of singlet oxygen and attack at the electron-rich aromatic rings. This result is in accordance with our previous studies with model compounds.[10] Thus, the epoxidation of the sensitive double bond was achieved with dimethyl dioxirane and enabled the reaction to be performed under very mild conditions.[11] Indeed, the desired epoxides **7** were obtained quantitatively with high stereoselectivity (Scheme 2). The stereochemical outcome of the epoxidation can be rationalized through steric interactions with the

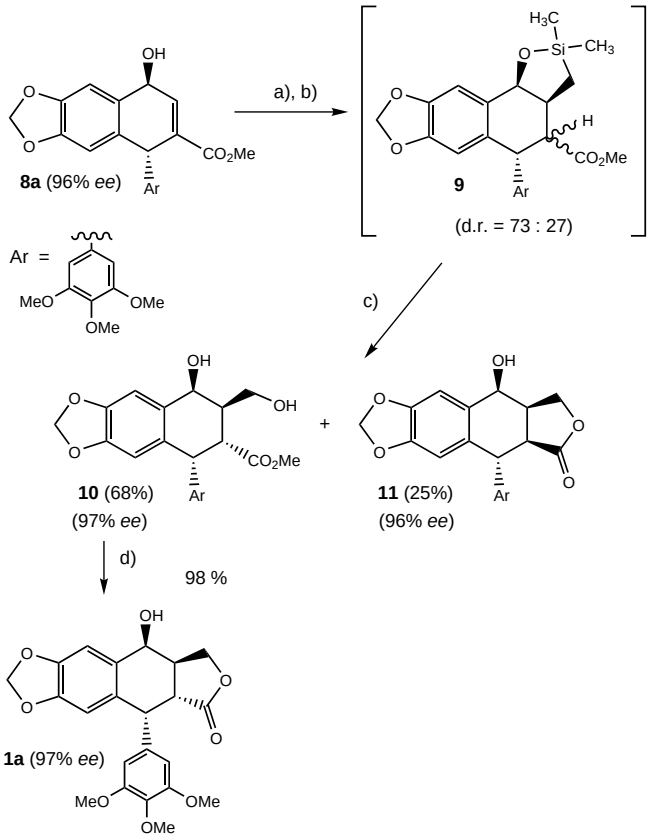
[*] Prof. Dr. T. Linker, Dr. U. Engelhardt, Dr. A. Sarkar
Department of Chemistry
University of Potsdam
Karl-Liebknecht-Strasse 24–25, 14476 Golm (Germany)
Fax: (+49) 331-977-5056
E-mail: linker@chem.uni-potsdam.de

[**] This work was supported by the Fonds der Chemischen Industrie, the Deutsche Forschungsgemeinschaft, and the Alexander von Humboldt Foundation.

 DOI: 10.1002/anie.200351086 © 2003 Wiley-VCH Verlag GmbH & Co. KGaA, Weinheim



Scheme 2. Diastereoselective oxidation of the 1,2-dihydronaphthalene **6**. a) Dimethyl dioxirane (0.06 M), CH_2Cl_2, 0 °C, 4 h; b) $LiN(SiMe_3)_2$, THF, −78 °C, 10 min, NH_4Cl, 20 °C, 2 h.



Scheme 3. Diastereoselective C–C bond formation by radical cyclization and final steps to (−)-epipodophyllotoxin (**1a**). a) NEt_3, $ClSiMe_2CH_2Br$; CH_2Cl_2, 0 °C, 6 h; b) $HSnBu_3$, AIBN, benzene, 80 °C, 10 h; c) KF, $KHCO_3$, H_2O_2 (30 %), THF, 20 °C, 12 h; d) molecular sieves (4 Å), $ZnCl_2$, THF, 66 °C, 12 h. AIBN = azobisisobutyronitrile.

trimethoxyaryl group, which is in accordance to our previous studies.[12] The intermediates **7** were highly labile and were therefore not isolated, but were directly deprotonated in the position α to the ester group. This epoxide opening afforded the desired *trans*-configured allylic alcohol **8a** in 89 % overall yield and in an analytically pure form (Scheme 2).[8]

The crucial step of our total synthesis was the regio- and stereoselective introduction of a hydroxymethylene group at C-3. For this purpose we employed a silicon-tethered radical reaction, which was developed for simple cyclohexenols.[13] The radical precursor was generated in situ by the reaction of the allylic alcohol **8a** with commercially available chlorosilane. Homolysis of the carbon–bromine bond in the presence of tri-*n*-butyltin hydride afforded radicals, which attacked the double bond intramolecularly. This cyclization is directed by the hydroxy group at C-4 and proceeds with exclusive regio- and stereoselectivity. On the other hand, the final H-atom transfer step was less selective, but the desired epimer was the main product. The carbon–silicon bond of the intermediate **9** was directly oxidized with hydrogen peroxide to afford the corresponding alcohols.[14] Furthermore, the *cis*-configured epimer directly undergoes a lactonization under the reaction conditions, which allowed the convenient separation of both products. Thus, the diol **10** and lactone **11**, which are both naturally occurring analogues of (−)-podophyllotoxin **1b**, were isolated in high overall yield (Scheme 3). The total synthesis was completed by the Lewis acid catalyzed lactonization of the methyl ester **10**. Thus, (−)-epipodophyllotoxin (**1a**) was isolated in 98 % yield and 97 % *ee*. The spectroscopic and analytical data was identical to that of the natural product.[8]

In conclusion, the total synthesis of (−)-epipodophyllotoxin (**1a**) has been accomplished in only twelve steps starting from commercially available piperonal (**2**), with the final product isolated in 30 % overall yield and 97 % *ee*. The advantage of our strategy consists of the introduction of the C-4 oxygen and C-3 carbon substituents in the late steps of the synthesis. Of particular note is that the radical C–C bond formation occurred with especially high regio- and stereoselectivity.

Received: February 3, 2003 [Z51086]

Keywords: antitumor agents · chiral auxiliaries · enantioselectivity · natural products · total synthesis

[1] a) D. C. Ayres, J. D. Loike, *Lignans. Chemical, biological and clinical properties*, Cambridge University Press, Cambridge, **1990**; b) R. S. Ward, *Nat. Prod. Rep.* **1993**, *10*, 1–28; c) R. S. Ward, *Nat. Prod. Rep.* **1997**, *14*, 43–74.

[2] a) B. F. Issell, F. M. Muggia, S. K. Carter, *Etoposide(VP-16). Current Status and New Developments*, Academic Press, New York, **1984**; b) H. F. Stähelin, A. von Wartburg, *Cancer Res.* **1991**, *51*, 5–15; c) T. F. Imbert, *Biochimie* **1998**, *80*, 207–222; d) Y. Damayanthi, J. W. Lown, *Curr. Med. Chem.* **1998**, *5*, 205–252.

[3] Reviews: a) R. S. Ward, *Tetrahedron* **1990**, *46*, 5029–5041; b) R. S. Ward, *Synthesis* **1992**, 719–730; c) R. S. Ward, *Nat. Prod. Rep.* **1999**, *16*, 75–96.

[4] a) R. C. Andrews, S. J. Teague, A. I. Meyers, *J. Am. Chem. Soc.* **1988**, *110*, 7854–7858; b) R. Van Speybroeck, H. Guo, J. Van der Eycken, M. Vandewalle, *Tetrahedron* **1991**, *47*, 4675–4682; c) E. J. Bush, D. W. Jones, *J. Chem. Soc. Chem. Commun.* **1993**, 1200–1201; d) S. B. Hadimani, R. P. Tanpure, S. V. Bhat,

 © 2003 Wiley-VCH Verlag GmbH & Co. KGaA, Weinheim

Tetrahedron Lett. **1996**, *37*, 4791 – 4794; e) D. B. Berkowitz, S. Choi, J.-H. Maeng, *J. Org. Chem.* **2000**, *65*, 847 – 860.

[5] Reviews: a) M. Reuman, A. I. Meyers, *Tetrahedron* **1985**, *41*, 837 – 860; b) T. G. Gant, A. I. Meyers, *Tetrahedron* **1994**, *50*, 2297 – 2360; c) A. I. Meyers, *J. Heterocycl. Chem.* **1998**, *35*, 991 – 1002.

[6] These amino alcohols are commercially available or can be synthesized (K. Drauz, W. Jahn, M. Schwarm, *Chem. Eur. J.* **1995**, *1*, 538 – 540). However, we thank Degussa AG, Germany, for the generous gift of the auxiliaries **4**.

[7] T. Linker, F. Rebien, G. Tóth, A. Simon, J. Kraus, G. Bringmann, *Chem. Eur. J.* **1998**, *4*, 1944 – 1951.

[8] Selected analytical data of key intermediates: 1,2-dihydronaphthalene **6**: m.p. 118–120 °C; $[\alpha]_D^{31} = -189.5$ ($c = 1.01$, $CHCl_3$); ^{1}H NMR (300 MHz, $CDCl_3$): $\delta = 3.58$ (ddd, $J = 8.5$, 4.5, 2.0 Hz, 1H, H-2), 3.64 (s, 3H, CO_2Me), 3.79 (s, 6H, OMe-3′), 3.83 (s, 3H, OMe-4′), 4.43 (d, $J = 8.5$ Hz, 1H, H-1), 5.81 (dd, $J = 9.5$, 4.5 Hz, 1H, H-3), 5.90–5.96 (m, 2H, OCH_2O), 6.41 (s, 2H, H-2′), 6.42 (s, 1H, H-8), 6.50 (dd, $J = 9.5$, 2.0 Hz, 1H, H-4), 6.64 ppm (s, 1H, H-5); ^{13}C NMR (75 MHz, $CDCl_3$): $\delta = 46.1$ (d, C-1), 48.4 (d, C-2), 52.1 (q, CO_2*Me*), 56.0 (q, OMe-3′), 60.7 (q, OMe-4′), 100.9 (t, OCH_2O), 105.4 (d, C-2′), 106.9 (d, C-5), 109.2 (d, C-8), 121.7 (d, C-3), 126.4 (s, C-4a), 128.6 (d, C-4), 130.2 (s, C-8a), 136.8 (s, C-4′), 138.5 (s, C-1′), 146.4 (s, C-7), 147.2 (s, C-6), 153.1 (s, C-3′), 173.6 ppm (s, CO); elemental analysis calcd for $C_{22}H_{22}O_7$: C 66.32, H 5.57; found: C 66.31, H 5.56. Allylic alcohol **8a**: m.p. 163 °C; $[\alpha]_D^{20} = +104.8$ ($c = 1.0$, $CHCl_3$, 96 % *ee*); ^{1}H NMR (300 MHz, $CDCl_3$): $\delta = 2.17$ (d, $J = 10.2$ Hz, 1H, OH), 3.74 (s, 3H, CO_2Me), 3.78 (s, 9H, 3 OMe), 4.93 (d, $J = 3.7$ Hz, 1H, H-1), 5.34 (ddd, $J = 10.2$, 3.7, 2.8 Hz, 1H, H-4), 5.91–5.95 (m, 2H, OCH_2O), 6.30 (s, 2H, H-2′), 6.65 (s, 1H, H-8), 7.13 (s, 1H, H-5), 7.20 ppm (d, $J = 2.8$ Hz, 1H, H-3); ^{13}C NMR (75 MHz, $CDCl_3$): $\delta = 45.6$ (d, C-1), 51.9 (q, CO_2*Me*), 55.9 (q, OMe-3′), 60.6 (q, OMe-4′), 65.6 (d, C-4), 101.0 (t, OCH_2O), 104.8 (d, C-2′), 106.3 (d, C-5), 107.6 (d, C-8), 128.7, 130.0, 132.3, 136.3 (4 × s, C-2, C-4a, C-8a, C-4′), 138.9 (s, C-1′), 139.4 (d, C-3), 146.8, 147.4 (2 × s, C-6, C-7), 153.0 (s, C-3′), 166.3 ppm (s, CO); elemental analysis calcd for $C_{22}H_{22}O_8$: C 63.76, H 5.35; found: C 63.53, H 5.56. (−)-Epipodophyllotoxin (**1a**): m.p. 180 °C (Ref.:[4b] 182 °C); $[\alpha]_D^{31} = -88.4$ ($c = 0.52$, $CHCl_3$, 97 % *ee*) (Ref.:[4b] $[\alpha]_D^{31} = -72.0$ ($c = 0.70$, $CHCl_3$, 98 % *ee*)); ^{1}H NMR (500 MHz, $CDCl_3$): $\delta = 1.81$ (d, $J =$ 4.3 Hz, 1H, OH), 2.84 (dddd, $J = 14.1$, 10.6, 7.9, 3.4 Hz, 1H, H-3), 3.29 (dd, $J = 14.1$, 5.1 Hz, 1H, H-2), 3.74 (s, 6H, OMe-3′), 3.80 (s, 3H, OMe-4′), 4.36 (dd, $J = 10.6$, 8.5 Hz, 1H, OCH_aH_bC), 4.39 (dd, $J = 8.5$, 7.9 Hz, 1H, OCH_aH_bC), 4.62 (d, $J = 5.1$ Hz, 1H, H-1), 4.88 (dd, $J = 4.3$, 3.4 Hz, 1H, H-4), 5.98 (d, $J = 1.3$ Hz, 1H, OCH_aH_bO), 6.00 (d, $J = 1.3$ Hz, 1H, OCH_aH_bO), 6.28 (s, 2H, H-2′), 6.56 (s, 1H, H-8), 6.88 ppm (s, 1H, H-5); ^{13}C NMR (125 MHz, $CDCl_3$): $\delta = 36.3$ (d, C-3), 40.5 (d, C-2), 43.8 (d, C-1), 56.3 (q, OMe-3′), 60.8 (q, OMe-4′), 66.9 (d, C-4), 67.6 (t, CH_2OH), 101.6 (t, OCH_2O), 108.2 (d, C-2′), 108.9 (d, C-5), 110.5 (d, C-8), 131.8, 132.0 (2s, C-4a, C-8a), 135.0 (s, C-4′), 137.2 (s, C-1′), 147.5, 148.6 (2s, C-6, C-7), 152.6 (s, C-3′), 175.0 ppm (s, CO).

[9] A. I. Meyers, B. A. Barner, *J. Org. Chem.* **1986**, *51*, 120 – 122.

[10] T. Linker, F. Rebien, G. Tóth, *Chem. Commun.* **1996**, 2585 – 2586.

[11] a) W. Adam, R. Curci, J. O. Edwards, *Acc. Chem. Res.* **1989**, *22*, 205 – 211; b) W. Adam, J. Bialas, L. Hadjiarapoglou, *Chem. Ber.* **1991**, *124*, 2377.

[12] T. Linker, K. Peters, E.-M. Peters, F. Rebien, *Angew. Chem.* **1996**, *108*, 2662 – 2664; *Angew. Chem. Int. Ed. Engl.* **1996**, *35*, 2486 – 2489.

[13] Reviews: a) M. Bols, T. Skrydstrup, *Chem. Rev.* **1995**, *95*, 1253 – 1277; b) L. Fensterbank, M. Malacria, S. M. Sieburth, *Synthesis* **1997**, 813 – 854.

[14] Review: G. R. Jones, Y. Landais, *Tetrahedron* **1996**, *52*, 7599 – 7662.

 © 2003 Wiley-VCH Verlag GmbH & Co. KGaA, Weinheim

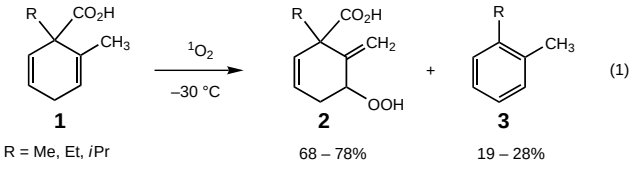
Regioselective Arene Alkylation

Simple Two-Step *ipso* Substitution of Aromatic Carboxylic Acids by Alkyl Halides**

*Katja Vorndran and Torsten Linker**

The transformation of arenes is still an important topic in organic chemistry and serves as a key step in many industrial syntheses. The controlled formation of carbon–carbon bonds to arenes is of special interest, but the classical Friedel–Crafts alkylation exhibits only moderate regioselectivity.[1] This disadvantage can be avoided by using modern methodologies such as the Heck reaction or the Stille and Suzuki coupling,[2] since an *ipso* substitution of bromides or other functional groups on the aromatic ring affords exclusively one regioisomer. However, the synthesis of the precursors is often tedious. Aromatic carboxylic acids offer an attractive alternative for C–C coupling reactions as they are inexpensive and easily available. Herein we describe a practical and efficient protocol for a formal two-step *ipso* substitution of such arenes by alkyl halides which is characterized by simple reagents, high yields, and the exclusive formation of one regioisomer.

During the course of our investigations on the photooxygenation of 1,4-cyclohexadienes **1**[3] we observed the surprising formation of arenes **3** as well as the expected hydroperoxides **2** [Eq. (1)]. Our first mechanistic rationaliza-



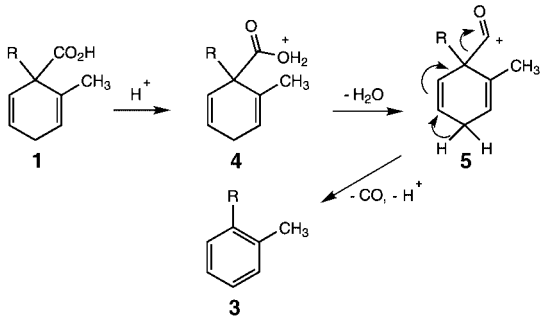
tion was based on an acid-catalyzed Grob fragmentation of the hydroperoxides **2**.[4] To prove this hypothesis, the photooxygenations were conducted in the presence of one equivalent of sulfuric acid. Indeed, the yield of the arenes **3** was increased to over 70%. Alternatively, an oxidative or free-radical decarboxylation of the cyclohexadienecarboxylic acids **1** might be possible, which were reported to occur in moderate yields using lead tetraacetate.[5] However, a control experiment performed in an argon atmosphere clearly indicated that the arenes **3** are formed without oxygen in the sole presence of sulfuric acid.

[*] Prof. Dr. T. Linker, Dr. K. Vorndran
Department of Chemistry
University of Potsdam
Karl-Liebknecht-Strasse 24-25, 14476 Golm (Germany)
Fax: (+49) 331-977-5056
E-mail: linker@chem.uni-potsdam.de

[**] This work was supported by the Fonds der Chemischen Industrie and the Deutsche Forschungsgemeinschaft.

 DOI: 10.1002/anie.200351087 © 2003 Wiley-VCH Verlag GmbH & Co. KGaA, Weinheim

The first step of the aromatization is the protonation of the carboxylic acid with the stronger mineral acid (Scheme 1). The intermediate cation **4** can dehydrate to the acylium ion **5**, which after *decarbonylation* and deprotonation affords the arenes **3**. This mechanism was confirmed by the detection of carbon monoxide in the gas phase by IR spectroscopy and by reduction of Pd^{II} to Pd^{0}. Therefore, an oxidative *decarboxylation* can be excluded and the herein described transformation is a formal retro-Koch reaction.[6]



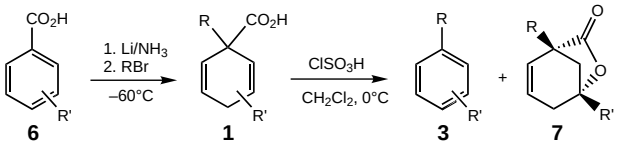
Scheme 1. Proposed mechanism for the acid-catalyzed aromatization of the cyclohexadienes **1**.

We investigated the influence of various acids on the decarbonylations in order to further improve the yields of the arenes **3** for synthetic applications. The best results were obtained with chlorosulfonic acid, since it is not only a strong mineral acid but exhibits dehydrating properties as well. Indeed, the desired products **3** could now be isolated in over 90% yield; thus the Birch reduction/protonation reaction sequence offers a valuable procedure for the highly regioselective synthesis of alkyl-substituted arenes. Such decarbonylations were hitherto unknown for 1,4-cyclohexadienecarboxylic acids, but are in accordance with the conversion of citric acid into acetonedicarboxylic acid.[7]

The applicability of our new methodology was examined in the reaction of a variety of 1,4-cyclohexadienes **1** with chlorosulfonic acid (Table 1). In addition to the regioisomeric benzoic acids **6b–d**, unsubstituted benzoic acid (**6a**) can be used as the starting material. The advantage of this strategy is that the Birch reduction/alkylation proceeds very smoothly.[8] Indeed, the desired arenes **3a–f** and **3j–l** can be isolated in high to excellent yields in only two steps from the reaction of **1** with chlorosulfonic acid (Table 1). The slightly lower yields with the unsubstituted cyclohexadienes **1a–c** are attributable to the higher volatility of the products **3a–c** and the resulting problems during the work-up. Interestingly, *meta*-toluic acid (**6c**) affords lactones **7** as well as the expected arenes **3g–i**. This result can be rationalized in terms of a competing protonation of the electron-rich double bond on forming the carbocation **8**, which is intramolecularly trapped by the acid group (Scheme 2).

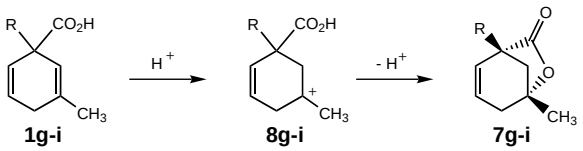
In summary, the Birch reduction/protonation reaction sequence offers a simple and highly regioselective alkylation of arenes. Excellent yields of *ortho*- and *para*-substituted products are obtained, whereas lactones were isolated as by-products with 3-methylbenzoic acid. The formation of the arenes proceeds mechanistically through a protonation, dehydration, and subsequent decarbonylation reaction. Furthermore, no toxic lead tetraacetate is required. The herein described formal *ipso* substitution should be of special interest for further synthetic applications as it uses simple and cheap reagents, and offers the possibility of performing the Birch reduction with various aromatic carboxylic acids and electrophiles.

Table 1: Two-step *ipso* substitution of the aromatic carboxylic acids **6** to afford the arenes **3**.



	R′	R	Yield [%][a] 1	3	7
6a	H	Me	**1a** [96]	**3a** [74]	**7a** [0]
6a	H	Et	**1b** [99]	**3b** [76]	**7b** [0]
6a	H	*i*Pr	**1c** [98]	**3c** [89]	**7c** [0]
6b	*ortho*-Me	Me	**1d** [98]	**3d** [95]	**7d** [0]
6b	*ortho*-Me	Et	**1e** [74]	**3e** [86]	**7e** [0]
6b	*ortho*-Me	*i*Pr	**1f** [98]	**3f** [98]	**7f** [0]
6c	*meta*-Me	Me	**1g** [99]	**3g** [32]	**7g** [53]
6c	*meta*-Me	Et	**1h** [89]	**3h** [38]	**7h** [52]
6c	*meta*-Me	*i*Pr	**1i** [89]	**3i** [35]	**7i** [49]
6d	*para*-Me	Me	**1j** [92]	**3j** [81]	**7j** [0]
6d	*para*-Me	Et	**1k** [87]	**3k** [87]	**7k** [0]
6d	*para*-Me	*i*Pr	**1l** [86]	**3l** [93]	**7l** [0]

[a] Yield of isolated product after column chromatography on silica gel, crystallization, or distillation.



Scheme 2. Proposed mechanism for the acid-catalyzed formation of the lactones **7**.

Experimental Section

Lithium (1.60 g, 230 mmol) was added in small portions at −60 °C to a solution of the carboxylic acid **6** (100 mmol) in liquid ammonia (400 mL) until a blue color persisted. After 30 min at this temperature, the alkyl halide (400 mmol) was added slowly over a period of 5 min. The ammonia was evaporated overnight and the residue was dissolved in water (400 mL). Concentrated hydrochloric acid was then added to give pH 1–2 and the solution extracted with *tert*-butyl methyl ether (3 × 200 mL). The combined organic phases were washed with water (100 mL) and then dried over sodium sulfate. After removal of the solvent, the 1,4-cyclohexadienecarboxylic acids **1** could be used directly for the next step or were purified by recrystallization.

The 1,4-cyclohexadienecarboxylic acid **1** (10 mmol) was dissolved in dichloromethane (20 mL) and chlorosulfonic acid (1.16 g, 10 mmol) was added at 0 °C, which resulted in the evolution of carbon monoxide. After 10 min the solution was neutralized with a saturated solution of sodium hydrogen carbonate. The aqueous phase was then

 © 2003 Wiley-VCH Verlag GmbH & Co. KGaA, Weinheim

extracted with dichloromethane (4 × 20 mL) and the combined organic phases were dried over sodium sulfate. After removal of the solvent, the arenes **3** were purified by distillation or by column chromatography on silica gel.

Received: February 3, 2003 [Z51087]

Keywords: arenes · protonation · reaction mechanisms · reduction · synthetic methods

[1] a) G. A. Olah, *Friedel-Crafts and Related Reactions*, Intersience, New York, **1963**–**1964**; b) R. M. Roberts, A. A. Khalaf, *Friedel–Crafts alkylation Chemistry: A Century of Discovery*, Marcel Dekker, New York, **1984**. However, Friedel–Crafts acylations proceed with higher regioselectivity (see, for example, M. Eissen, J. O. Metzger, *Chem. Eur. J.* **2002**, *8*, 3580 – 3585).

[2] Heck reaction: R. F. Heck, *Org. React.* **1982**, *27*, 345 – 390; A. de Meijere, F. E. Meyer, *Angew. Chem.* **1994**, *106*, 2473 – 2506; *Angew. Chem. Int. Ed. Engl.* **1994**, *33*, 2379 – 2411; S. Bräse, A. de Meijere in *Metal-Catalyzed Cross-Coupling Reactions* (Eds.: F. Diederich, P. J. Stang), Wiley-VCH, Weinheim, **1998**, pp. 99 – 166; Stille coupling: V. Farina, V. Krishnamurthy, W. J. Scott, *Org. React.* **1997**, *50*, 1 – 652; Suzuki coupling: A. Suzuki in *Metal-Catalyzed Cross-Coupling Reactions* (Eds.: F. Diederich, P. J. Stang), Wiley-VCH, Weinheim, **1998**, pp. 49 – 97; S. Kotha, K. Lahiri, D. Kashinath, *Tetrahedron* **2002**, *58*, 9633 – 9695.

[3] a) T. Linker, L. Fröhlich, *Angew. Chem.* **1994**, *106*, 2064 – 2066; *Angew. Chem. Int. Ed. Engl.* **1994**, *33*, 1971 – 1972; b) T. Linker, L. Fröhlich, *J. Am. Chem. Soc.* **1995**, *117*, 2694 – 2697.

[4] a) C. A. Grob, P. W. Schiess, *Angew. Chem.* **1967**, *79*, 1 – 14; *Angew. Chem. Int. Ed. Engl.* **1967**, *6*, 1 – 15; b) C. A. Grob, *Angew. Chem.* **1969**, *81*, 543 – 554; *Angew. Chem. Int. Ed. Engl.* **1969**, *8*, 535 – 546.

[5] a) A. J. Baker, A. C. Goudie, *J. Chem. Soc. Chem. Commun.* **1972**, 951; b) A. J. Birch, J. Slobbe, *Tetrahedron Lett.* **1976**, 2079 – 2082; c) G. Binmore, J. C. Walton, L. Cardellini, *J. Chem. Soc. Chem. Commun.* **1995**, 27 – 28.

[6] a) C. W. Bird, *Chem. Rev.* **1962**, *62*, 283 – 302; b) Y. T. Eidus, A. L. Lapidus, K. V. Puzitskii, B. K. Nefedov, *Russ. Chem. Rev.* **1973**, *42*, 199 – 213.

[7] a) J. v. Pechmann, *Justus Liebigs Ann. Chem.* **1891**, *261*, 151 – 172; b) F. Germer (Boehringer), Ger. 1,160,841, **1964** [*Chem. Abstr.* **1964**, *60*, 6753c].

[8] a) H. van Bekkum, C. B. van den Bosch, G. van Minnen-Pathuis, J. C. de Mos, A. M. van Wijk, *Recl. Trav. Chim. Pays-Bas* **1971**, *90*, 137 – 149; b) P. W. Rabideau, Z. Marcinow, *Org. React.* **1992**, *42*, 1 – 334.

 © 2003 Wiley-VCH Verlag GmbH & Co. KGaA, Weinheim

Polymer-Supported Synthesis

A Phosphorane as Supported Acylanion Equivalent: Linker Reagents for Smooth and Versatile C–C Coupling Reactions**

*Steffen Weik and Jörg Rademann**

Polymer supports are employed widely in diversity-oriented organic chemistry, either in solid-phase synthesis in which products are assembled on a cleavable linker moiety,[1] or in polymer-assisted solution-phase (PASP) synthesis using polymer reagents and scavengers.[2–4] Recently, we introduced novel polymer reagents for important organic transformations including alkylating[5] and oxidating polymers.[6,7] To establish more complex reaction sequences including C–C coupling steps, polymer-supported carbanion equivalents would be an ideal addition to the synthetic repertoire in polymer-assisted synthesis. Lithiated dithioacetals[8–10] have been described as polymer-supported carbanion equivalents, however, these reagents are strongly basic and are thus of no use for the efficient parallel synthesis of sensitive products. Ideally, the successful method should allow reactions with easily available building blocks, under smooth, neutral conditions, and further derivatization after the C–C coupling step.

To establish polymer-supported acyl anion equivalents **1**, several different concepts were investigated (Scheme 1). The results for the reactions of polymer-supported thiazolinium salts (Y = 2-thiazolidenyl) and polymer-supported dialkyl hydrazones ($Y = NNR_2$) with amino acid electrophiles **2** will be reported in due course. As a third approach, phosphoranes were investigated as polymer-supported acyl anion equivalents (Y = P). The norstatine isostere **3** (Scheme 1) was selected as a synthetic target for our study of carbanion equivalents as it represents a class of potent protease inhibitors of metallo and aspartate proteases.[11,12]

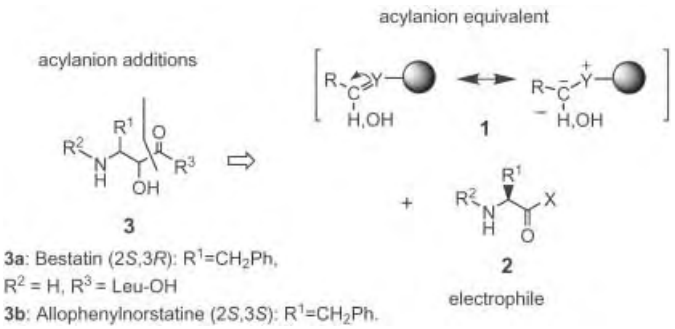
Polystyrene-bound triphenylphosphane (**4**; Scheme 2; 1.2 $mmol\,g^{-1}$) is a classical polymer reagent,[13,14] which is routinely employed in supported halogenation, Mitsunobu,

[*] Dr. J. Rademann, Dipl.-Chem. S. Weik
Institute for Organic Chemistry
Eberhard-Karls University Tübingen
Auf der Morgenstelle 18, 72076 Tübingen (Germany)
Fax: (+49) 7071-29-5560
E-mail: joerg.rademann@uni-tuebingen.de

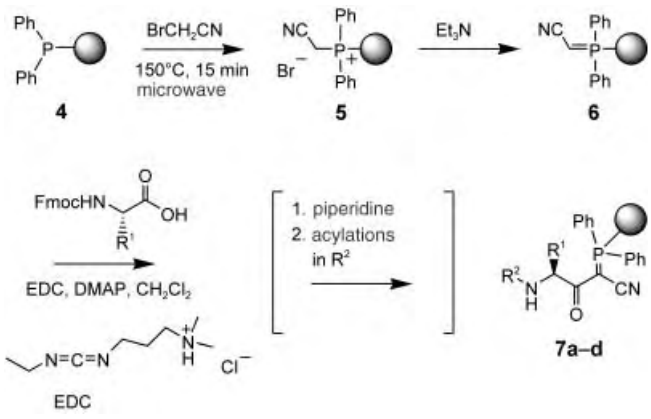
[**] Part of this work was presented at the ORCHEM 2002 in Bad Nauheim (Germany). We gratefully acknowledge generous support from Prof. G. Jung and from Prof. M. E. Maier, Tübingen, the Strukturfonds of the University of Tübingen, DFG project "Reactive Intermediates in Polymeric Gels" (Ra 895/2), from the Fonds der Chemischen Industrie, Novabiochem AG (Läufelfingen, Switzerland), and Personal Chemistry GmbH (Konstanz (Germany)). We thank Andreas Petri, Bojan Bister and Daniel Bischoff for analytical support.

Supporting information (representative spectra of compounds **9**–**23**) for this article is available on the WWW under http://www.angewandte.org or from the author.

 DOI: 10.1002/anie.200351190 © 2003 Wiley-VCH Verlag GmbH & Co. KGaA, Weinheim



Scheme 1. Three pathways to construct the novel acyl anion equivalents **1** were investigated to identify a general concept allowing for variations in positions R^1, R^2, and R^3. Bestatin (**3a**) as well as allophenylnorstatine (**3b**) represent the norstatine family **3** of potent protease inhibitors.



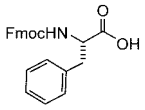
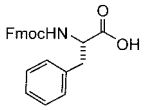
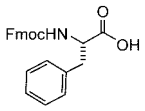
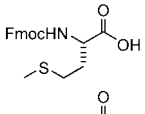
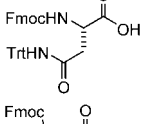
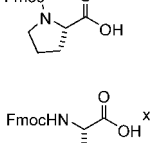
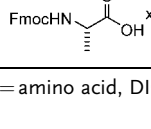
Scheme 2. Supported phosphorane **6** was constructed by alkylation of triphenylphosphane resin **4** under microwave irradiation, followed by proton abstraction. Acylation of **6** to give the acylphosphoranes **7a–d** was best effected by activation with the condensing agent EDC. EDC = *N*-(3-dimethylaminopropyl)-*N*′-ethylcarbodiimide hydrochloride, DMAP = 4-*N*,*N*-dimethylaminopyridine, Fmoc = 9-fluorenylmethoxycarbonyl.

and Wittig reactions.[14,15] To our knowledge this is the first report using it as a starting point for polymer-supported acyl anion equivalents. Compound **4** was alkylated with bromoacetonitrile in toluene under microwave irradiation (150 °C, 15 min) yielding phosphonium salt **5** quantitatively (elemental analysis; Scheme 2). Compound **5** was converted by treatment with triethylamine into the stable and storable phosphorane **6** which has a characteristic yellow color.

The coupling of protected amino acids to **6** was investigated employing various condensation agents. Reactions were monitored by ATR-IR (ATR = attenuated total reflection), yields could be quantified by spectrophotometric Fmoc-determination. The success of the acylations depended critically on the rigorous exclusion of water (see Table 1, entries 1 and 7), which indicates the comparably low nucleophilicity of cyanophosphorane **6**. The method of choice was preactivation with EDC as condensing agent with DMAP in CH_2Cl_2 yielding up to 90 % of the acylation product in single couplings. The base-labile Fmoc-protecting group was not affected by the phosphorane. Thus, the R^1 position could be varied conveniently starting from a selection of representative amino acids (Table 2, entries 1–6). Fmoc-protected acyl cyanophosphoranes **7a–d** were deprotected (25 % piperidine, DMF) allowing for variations in the liberated amino position R^2 (Table 2, entries 7–14).

Finally, the acyl cyanophosphoranes were efficiently cleaved by oxidation, either employing ozonolysis at −78 °C or by using freshly distilled 3,3-dimethyl dioxirane[16] at room temperature (Scheme 3). Cleavage was accompanied by decoloration of the resin and released the α,β-diketo nitriles **8**. Compounds **8** are highly activated electrophiles that were converted in situ with O-, N-, and S-nucleophiles, to give the α-keto esters **9**–**17**, the α-keto amide **18**, and the α-keto thioester **19** (Table 2). Excess of non-volatile N-nucleophiles employed in this reaction was

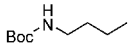
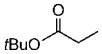
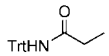
Table 1: Coupling yields to polymer-supported acylanion equivalents determined by spectroscopic quantification of Fmoc groups.

Entry	Amino acid	Conditions[a]	Product	Yield [%]
1		5 equiv AA, 5 equiv DIC, 5 equiv HOBt·H_2O, 0.75 equiv DMAP, CH_2Cl_2, RT	**7a**	0
2		5 equiv AA, 5 equiv DIC, 0.75 equiv DMAP, CH_2Cl_2, RT	**7a**	60
3		5 equiv AA, 5 equiv EDC, 0.75 equiv DMAP, CH_2Cl_2, RT	**7a**	90
4		5 equiv AA, 5 equiv EDC, 0.75 equiv DMAP, CH_2Cl_2, RT	**7b**	83
5		5 equiv AA, 5 equiv EDC, 0.75 equiv DMAP, CH_2Cl_2, RT	**7c**	81
6		5 equiv AA, 5 equiv EDC, 0.75 equiv DMAP, CH_2Cl_2, RT	**7d**	54
7		5 equiv AA, 5 equiv EDC, 0.75 equiv DMAP, CH_2Cl_2, RT	**7e**	0

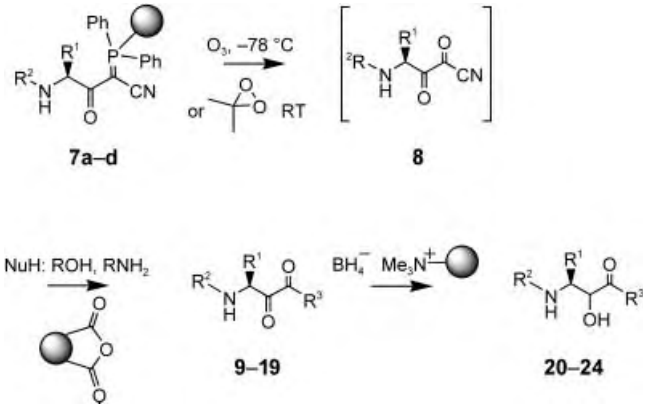
[a] AA = amino acid, DIC = diisopropylcarbodiimide, HOBt = Hydroxybenzotriazol.

 © 2003 Wiley-VCH Verlag GmbH & Co. KGaA, Weinheim

Table 2: Variations of the α-ketocarbonyl products in the isosteric building block (R^1 position), in the N-terminal (R^2) and C-terminal (R^3) positions.[a]

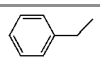
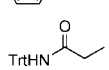
Entry	Product	R^1	R^2	R^3	Yield [%]	Purity [%]
1	**9**		Fmoc	OMe	65 (32 mg)	88
2	**10**		Fmoc	OMe	54 (24 mg)	86
3	**11**		Fmoc	OMe	50 (29 mg)	72
4	**12**		Fmoc	OMe	55 (28 mg)	88
5	**13**		Fmoc	OMe	59 (43 mg)	99
6	**14**		Fmoc	OMe	63 (31 mg)	87
7	**15**		Ac-Ser(*t*Bu)-Ile	OMe	30 (17 mg)	71
8	**16**		Ac-Asp(*t*Bu)-Val	OMe	43 (25 mg)	80
9	**17**		Ac		55 (28 mg)	80
10	**18**		Ac		53 (18 mg)	68[b]
11	**19**		Ac		38 (20 mg)	62

[a] Yields were determined by weight, purities were determined by HPLC (detection at 214 nm) combining the signals assigned to the product equilibrium. [b] Purities of amide products were determined after the reduction step.



Scheme 3. Oxidative cleavage of acylcyanophosphoranes **7**. The intermediary diketo nitriles **8** react with O-, N-, and S-nucleophiles yielding the respective α-keto esters **9**–**17**, the α-keto amide **18**, and the α-keto thioester **19**. Reduction of the α-keto products gives the α-hydroxy esters **20**–**23** and the α-hydroxy amide **24**.

Table 3: Reduction of ketoesters, and -amides.

Entry	Product	R^1	R^2	R^3	Yield [%]	Purity [%]
1	**20**		Ac	OMe	76 (42 mg)	72
2	**21**		Ac-Ser(*t*Bu)-Ile	OMe	87 (25 mg)	84
3	**22**		Ac-Asp(*t*Bu)-Val	OMe	90 (6.3 mg)	79
4	**23**		Fmoc	OMe	>95 (37 mg)	62
5	**24**		Ac		>95 (18.8 mg)	68

removed by using polymer-supported anhydride as a scavenger resin (7.5 equiv, 60 °C).

Products **9**–**18** were obtained in yields between 43 and 65 % in five (**9**–**14**) to 11 (**15**, **16**) synthetic steps. In all the examples this corresponds to an average of >90 % per step. Reversed-phase HPLC-MS revealed that the ketocarbonyl products were in equilibrium with the respective hydrate and cyanohydrine adducts. The keto products could be characterized by mass spectrometry and by fully assigned NMR spectra (^{1}H, ^{13}C, HSQC, and COSY) in $CDCl_3$. The purities of α-keto esters were generally above 70 %; purities of amide products were determined after the reduction step.[17]

In the final step, direct conversion of the α-keto compounds into the α-hydroxy esters **20**–**23** and α-hydroxy amide **24** was accomplished with the reducing polystyrylmethyl-bound trimethylammonium borohydride resin (10 equiv, 12 h) (Scheme 3, Table 3).[18,19] Under the selected conditions both diastereomers were obtained in roughly equal amounts and could be fully assigned by NMR spectroscopy after purification by reversed-phase HPLC. The asymmetric reduction of α-ketocarbonyl compounds has been reported in the literature.[20]

In summary, we have established a powerful novel concept of polymer-supported acyl anion equivalents that has been demonstrated to allow the addition of a large variety of easily accessible activated carboxylic acids. Diversity in all relevant positions of the core structure **3** could be smoothly obtained. The supported acyl anion reagents form a novel class of reagent linkers, which combine the intermediary immobilization of a substrate with a C–C coupling as transformation step. Variations with respect to electrophiles, on-bead transformations, and the cleavage reaction are currently under investigation.

Experimental Section

6: Triphenylphosphane polystyrene (0.5 g, 1.2 mmol g^{-1}, 0.6 mmol, 1 % divinylbenzene, 100–200 mesh, Novabiochem) was suspended in dry toluene (3 mL). After addition of bromoacetonitrile (199 μL, 3 mmol) the vial was sealed and heated by microwave irradiation (15 min, 150 °C, Personal Chemistry Creator). Following cooling to room temperature the vial was opened. The resin was collected by

 © 2003 Wiley-VCH Verlag GmbH & Co. KGaA, Weinheim

filtration, washed with dry toluene, CH_2Cl_2 and Et_2O (3 × each) and dried. Elemental analysis (%) calcd: N 1.05; found: 1.02. The obtained triphenylphosphonium bromide resin was suspended in dry CH_2Cl_2 (5 mL) and triethylamine (418 μL, 3 mmol) was added. The mixture was agitated (2 h, RT), the solid collected by filtration, washed (MeOH, THF, CH_2Cl_2), and dried in vacuo. IR (ATR): $\tilde{\nu}$ = 3057, 3024, 2923, 2851, 2150, 1945, 1751, 1600, 1492, 1452, 1437, 1261, 1183, 1115, 1028, 749, 697, 539 cm^{-1}. **7**: EDC (101 mg, 0.525 mmol), DMAP (10 mg, 0.079 mmol), and Fmoc-protected amino acid (0.525 mmol) were dissolved in dry CH_2Cl_2 (3 mL) and stirred for 5 min. Cyanophosphorane polystyrene **6** (100 mg, 1.05 mmol g^{-1}, 0.105 mmol) was added and the reaction mixture was agitated (12 h, RT). The resin was collected by filtration, washed (MeOH, DMF, THF, CH_2Cl_2, and Et_2O), and dried in vacuo. Coupling yields were measured by spectroscopic Fmoc-determination (see Table 1).
Oxidative cleavage of resins yielding α-ketomethyl esters or α-keto amides **9**–**17**: **7a**–**d** were suspended in a mixture of dry CH_2Cl_2 and the respective alcohol (2:1) under N_2-atmosphere. At −78 °C the suspension was purged with ozone until a blue-green color remains (5–10 min). Excess ozone was removed by a stream of N_2. After warming to RT the mixture was stirred (4 h) and filtered. The resin was washed (CH_2Cl_2) and the solvents were removed in vacuo. **18**: Ozonolytic resin cleavage was conducted as described with dry CH_2Cl_2 as the only solvent. After ozone removal at −78 °C, the precooled solution of an amine (1.5 equiv in respect to the resin loading determined by Fmoc-cleavage, CH_2Cl_2, −78 °C) was added by syringe. The reaction mixture was kept at −78 °C (30 min), was then warmed to RT and stirred for 2 h. Excess amine was scavenged in a sealed vessel by the addition of macroporous anhydride resin (Novabiochem, 7.5 equiv, 60 °C, 12 h). The resin was collected by filtration, washed with CH_2Cl_2, and the solvent was removed in vacuo. Products **9**–**19** were characterized by NMR spectroscopy and LC-MS; purities and yields are given in Table 2.

Received: February 17, 2003 [Z51190]

Keywords: C–C coupling · carbanions · combinatorial chemistry · protease inhibitors · solid-phase synthesis

[1] F. Zaragoza Dörwald, *Solid-Phase Synthesis*, Wiley-VCH, Weinheim, **2000**.
[2] A. Kirschning, H. Monenschein, R. Wittenberg, *Angew. Chem.* **2001**, *113*, 670–701; *Angew. Chem. Int. Ed.* **2001**, *40*, 650–679.
[3] S. V. Ley, I. R. Baxendale, R. M. Bream, P. S. Jackson, A. G. Leach, D. A. Longbottom, M. Nesi, J. S. Scott, R. I. Storer, S. J. Taylor, *J. Chem. Soc. Perkin Trans. 1* **2000**, *23*, 3815–4195.
[4] a) J. Rademann in *Methods in Enzymol.*, **2003**, in press; b) J. Rademann, W. Kraas, B. Dörner, *Nachr. Chem.* **2000**, *48*, 280–283.
[5] J. Rademann, J. Smerdka, G. Jung, P. Grosche, D. Schmid, *Angew. Chem.* **2001**, *113*, 390–393; *Angew. Chem. Int. Ed.* **2001**, *40*, 381–385.
[6] G. Sorg, A. Mengel, G. Jung, J. Rademann, *Angew. Chem.* **2001**, *113*, 4532–4535; *Angew. Chem. Int. Ed.* **2001**, *40*, 4395–4397.
[7] S. Weik, G. Nicholson, G. Jung, J. Rademann, *Angew. Chem.* **2001**, *113*, 1489–1492; *Angew. Chem. Int. Ed.* **2001**, *40*, 1436–1439.
[8] V. Bertini, F. Lucchesini, M. Pocci, A. De Munno, *Tetrahedron Lett.* **1998**, *39*, 9263–9266.
[9] V. Bertini, F. Lucchesini, M. Pocci, A. De Munno, *J. Org. Chem.* **2000**, *65*, 4839–4842.
[10] F. Lucchesini, V. Bertini, M. Pocci, E. Micali, A. De Munno, *Eur. J. Org. Chem.* **2002**, 1546–1550.
[11] R. Nishizawa, T. Saino, T. Takita, H. Suda, T. Aoyagi, H. Umezawa, *J. Med. Chem.* **1977**, *20*, 510–515.
[12] T. Mimoto, N. Hattori, H. Takaku, S. Kisanuki, T. Fukazawa, K. Terashima, R. Kato, S. Nojima, S. Misawa, T. Ueno, J. Imai, H. Enomoto, S. Tanaka, H. Sakikawa, M. Shintani, H. Hayashi, Y. Kiso, *Chem. Pharm. Bull.* **2000**, *48*, 1310–1326.
[13] W. Heitz, R. Michels, *Angew. Chem.* **1972**, *84*, 296–297; *Angew. Chem. Int. Ed. Engl.* **1972**, *12*, 298–299.
[14] W. Heitz, R. Michels, *Justus Liebigs Ann. Chem.* **1973**, 227–230.
[15] M. H. Bolli, S. V. Ley, *J. Chem. Soc. Perkin Trans. 1* **1998**, 2243–2246.
[16] W. Adam, Y.-Y. Chan, D. Cremer, J. Gauss, D. Scheutzow, M. Schindler, *J. Org. Chem.* **1987**, *52*, 2800–2803.
[17] The decarbonylated amide was identified as a by-product of **18**. It could be removed by chromatography after the reduction step. To our knowledge, the decarbonylation of activated α-keto acids has not been described, a possible mechanism is currently under investigation.
[18] B. Sansoni, O. Sigmund, *Naturwissenschaften* **1961**, *48*, 598–599.
[19] H. W. Gibson, F. C. Bailey, *J. Chem. Soc. Chem. Commun.* **1977**, 815.
[20] H. H. Wasserman, M. Xia, A. K. Petersen, M. R. Jorgensen, E. A. Curtis, *Tetrahedron Lett.* **1999**, *40*, 6163–6166.

 © 2003 Wiley-VCH Verlag GmbH & Co. KGaA, Weinheim

Organometallic Gelators

A Metal–Carbene Carbohydrate Amphiphile as a Low-Molecular-Mass Organometallic Gelator**

*Gunnar Bühler, Martinus C. Feiters, Roeland J. M. Nolte, and Karl Heinz Dötz**

Dedicated to Professor Ernst Otto Fischer

In recent years the interest in molecules that form supramolecular structures by self-assembly through noncovalent interactions has increased considerably.[1] The formation of such supramolecular aggregates may give three-dimensional (3D) networks that are suited for gelation of a solvent. In contrast to macromolecular networks, these supramolecular aggregates can easily be disintegrated by adding a cosolvent, application of mechanical stress, or heating, because no chemical bonds need to be broken. Amphiphiles bearing a polar carbohydrate head group which is connected to an alkyl

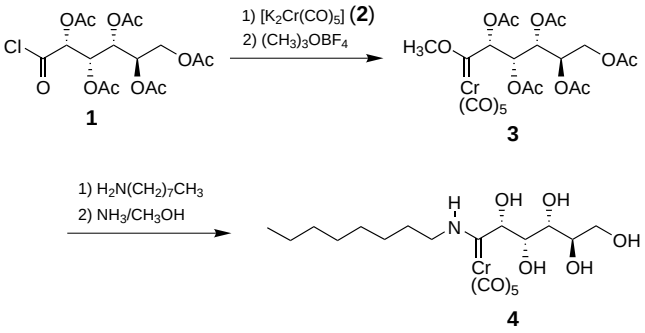
[*] Prof. Dr. K. H. Dötz, G. Bühler
Kekulé-Institut of Organic Chemistry and Biochemistry
University of Bonn
Gerhard Domagk-Strasse 1, 53121 Bonn (Germany)
Fax: (+49) 228-735-813
E-mail: doetz@uni-bonn.de
Dr. M. C. Feiters, Prof. Dr. R. J. M. Nolte
Department of Organic Chemistry, NSRIM
University of Nijmegen
Toernooiveld, 6525 ED Nijmegen (Netherlands)

[**] We thank Femke de Loos, Dennis Vriezema, Huub Geurts (Nijmegen), and Prof. Dr. H. Fischer (Konstanz) for practical and technical support.

 © 2003 Wiley-VCH Verlag GmbH & Co. KGaA, Weinheim DOI: 10.1002/anie.200351134

chain by an amide functionality can form various supramolecular aggregates in aqueous media.[2] Some derivatives of this type of alkyl aldonamides are excellent gelators for a variety of organic solvents.[3]

Our interest in carbohydrate-functionalized transition-metal carbene complexes[4] prompted us to synthesize pentacarbonyl[D-*gluco*-hex(*N*-*n*-octylamino)-1-ylidene]chromium (**4**; Scheme 1) an organometallic isolobal analogue of *N*-*n*-octyl-D-gluconamide.[2]



Scheme 1. Synthesis of carbene complex **4**.

The pentacarbonyl chromate **2** adds to the pentaacetylated gluconic acid chloride **1** to form an anionic acyl complex which undergoes subsequent O-methylation to give carbene complex **3**.[4a] The aminocarbene complex **4** is formed by aminolysis followed by deprotection under basic conditions. With regard to the restricted rotation about the carbene carbon–nitrogen bond only the *Z* isomer is obtained, as confirmed by comparison of NMR spectroscopic data of **4** with those reported for other aminocarbene–chromium complexes.[5]

The exchange of the carbonyl-oxygen atom, which is supposed to play an important role in the aggregation of *N*-*n*-octyl-D-gluconamide,[2,3] for the apolar pentacarbonylchromium fragment leads to an increased solubility of the resulting carbene complex **4** in organic solvents; on the other hand, **4** is almost insoluble in water. In this context, it is quite remarkable that the incorporation of the bulky organometallic fragment into the carbohydrate head group does not suppress the gelating ability.

Upon heating to 70–75 °C followed by cooling to room temperature the metal carbene **4** forms thermoreversible gels within a few minutes in chloroform, dichloromethane, benzene, toluene, and mixtures of these solvents. The yellow gels in chloroform are more or less turbid, depending on the concentration of **4** (0.35–1.3 wt %). Unexpectedly, the nature of the gels also depends on the cooling rate: If the solutions are cooled rapidly, turbid gels are formed within a few seconds; if cooled slowly, the gels appear to be clear. The gels formed in chloroform are quite stable towards mechanical agitation, and no visible change could be observed after storage for several weeks at room temperature. The gel-to-solution phase-transition temperatures (T_{gel}) of gels formed upon slow cooling were determined by using the "falling ball method"[6] for various concentrations (Table 1). The T_{gel} values observed for rapidly cooled, turbid gels are about 5–10 °C lower than for the slowly cooled gels. The gels of **4** in benzene and toluene, even at concentrations of about 1 wt %, are readily disintegrated by light mechanical agitation; sometimes precipitation of **4** was observed within a few hours. Addition of chloroform to benzene or toluene (wt/wt up to 1:4 chloroform:benzene/toluene) affords more rigid gels at concentrations of **4** of above 0.5 wt %. Again, the turbidity of these yellow gels depends on the chloroform content. The T_{gel} values are listed in Table 1; again slowly cooled gels are more stable.

Table 1: T_{gel} values for various solvents (mixtures) at various concentrations.

Solvent (mixture)[a]	T_{gel} (1 wt %)	T_{gel} (0.7 wt %)	T_{gel} (0.5 wt %)
$CHCl_3$	48–54[b]	45–51	30–32
$CHCl_3/C_7H_8$ 1:1	72	57–59	50–55
$CHCl_3/C_7H_8$ 3:1	62	57	54–55
$CHCl_3/C_7H_8$ 1:3	65–68	61–63	57–59
$CHCl_3/C_6H_6$ 1:1	68	53–54	—[c]
$CHCl_3/C_6H_6$ 3:1	60	51	—[c]
$CHCl_3/C_6H_6$ 1:3	63–67	57–59	—[c]

[a] wt/wt. [b] 1.3 wt %. [c] No gelation observed.

Electron micrographs (SEM and TEM, with or without metal shadowing or sputtering) of the gels show dense networks (Figure 1 A, B) of long fibers which account for the rigidity gels. TEM-micrographs of Pt shadowed (45°) samples (Figure 1 A) prepared from gels in chloroform and dichloromethane revealed flat tapelike aggregates with a maximum height of about 13 nm, but most of the tapelike fibers do not show a shadow at all, which indicates that the height of the aggregates is below the TEM resolution (< 3–

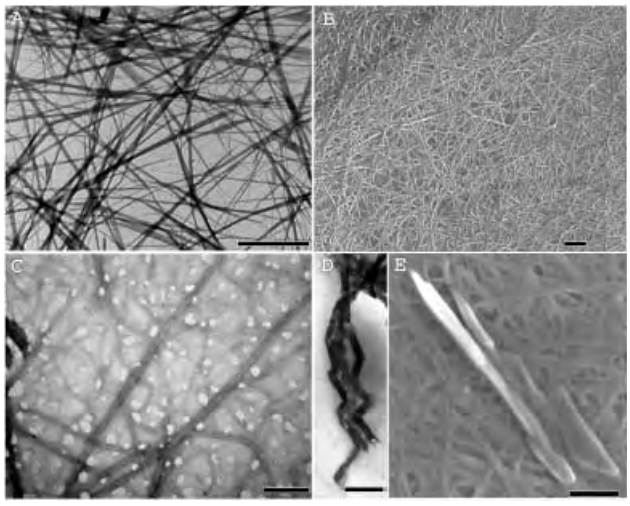


Figure 1. A) TEM, gel in $CHCl_3$, 0.78 wt %, Pt shadowing at 45°, the scale bar corresponds to 2 μm; B) SEM, gel in benzene/chloroform 1:1, 0.71 wt %, the scale bar corresponds to 2 μm; C) TEM, gel in toluene/chloroform 1:1, 0.74 wt %, the scale bar corresponds to 500 nm; D) TEM, gel in benzene/chloroform 1:3, 0.89 wt %, the scale bar corresponds to 500 nm; E) SEM, gel in toluene/chloroform 1:1, 0.74 wt %, Pd/Au sputtering, the scale bar corresponds to 500 nm.

 © 2003 Wiley-VCH Verlag GmbH & Co. KGaA, Weinheim

4 nm). The width ranges from 16 nm to >200 nm and appears to be independent of the length of the aggregates. Micrographs of aged gels (two weeks at 4 °C) show identical structures.

Micrographs of gels of **4** in mixtures of benzene or toluene and chloroform (various concentrations and amounts of chloroform) reveal the presence of extended aggregates with diameters varying from 80 to 120 nm (Figure 1 C). A higher electron-scattering density is observed at the edges of these structures, which indicates an accumulation of material; thus, these structures are more likely to resemble tubes than tapes. These tubes appear to be flat, probably a because of a loss of solvent from their inner space under the vacuum conditions required for electron microscopy. Furthermore tubelike aggregates can be seen in combination with rolled-up flat layers as precursors of tubules (Figure 1 D, E).

Temperature-dependent circular-dichroism (CD) experiments using a 4×10^{-3} M gel of **4** in chloroform revealed a thermoreversible CD effect (Figure 2 a). At temperatures below T_{gel} the effect was strong whereas it decreased gradually on heating and disappeared completely at approximately 50 °C. After the third heating cycle the sign for the low-wavelength transition at 260 nm changed from positive to negative on cooling the sample. A similar change of sign in CD spectra has been reported for azobenzene-appended cholesterol derivatives and was found to depend on the cooling rate of heated solutions of the gelator molecules.[7]

The corresponding UV/Vis spectra (Figure 2 b) showed no significant temperature dependence. The observed bands can be assigned to the aminocarbene pentacarbonylchromium moiety as follows: 350 nm (metal-to-ligand charge transfer), 320 nm (ligand-field transition) and 270–260 nm (ligand-to-metal charge transfer).[8] Although a linear dichroistic effect cannot be precluded, we expect that its possible contribution to the observed dichroism is only small. The dichroism may reflect the formation of chiral supramolecular structures from the fibers observed by electron microscopy; these ordered structures collapse at higher temperatures.

Temperature-dependent ^{1}H NMR spectroscopy experiments of gels in $CDCl_3$ (0.7 wt %), CD_2Cl_2 (0.8 wt %), and a mixture of $CDCl_3/C_6D_6$ (1/1, 0.8 wt %) revealed a strong broadening of all the resonance signals at room temperature, including the signal arising from traces of undeuterated solvent. Increasing the temperature resulted in a decrease of the half-width of all the resonance signals. At temperatures slightly below the boiling point of the solvent some signals of the alkyl chain and the undeuterated solvent were well resolved whereas all the other signals remained broad. Even though all the samples appear to be clear solutions at these temperatures and spinning conditions, this behavior suggests that even at high temperatures molecules are still aggregated—however, to less extent, as indicated by free rotation within the alkyl chain.

IR spectra of solutions of **4** in methanol show three carbonyl bands with peaks at $\tilde{\nu}=2053$ (A_1), 1968 (B_1), and 1930–1920 cm^{-1} (A_1^2+E) that are characteristic for aminocarbene pentacarbonylchromium complexes of local C_{4v} symmetry. IR spectra of chloroform gels of **4** revealed two additional strong absorptions at $\tilde{\nu}=1889$ and 1878 cm^{-1}; the other bands were shifted to $\tilde{\nu}=2055$ (A_1), 1976 cm^{-1} (B_1), and the broad band sharpened at $\tilde{\nu}=1926$ cm^{-1}. With decreasing concentrations of **4** the gels turn to highly viscous fluids and finally to solutions. Corresponding IR spectra (Figure 3 b) showed the gradual decrease of the bands $\tilde{\nu}=1889$ and 1878 cm^{-1} while the other bands increasingly resemble those observed in solution. Similar results were obtained by heating

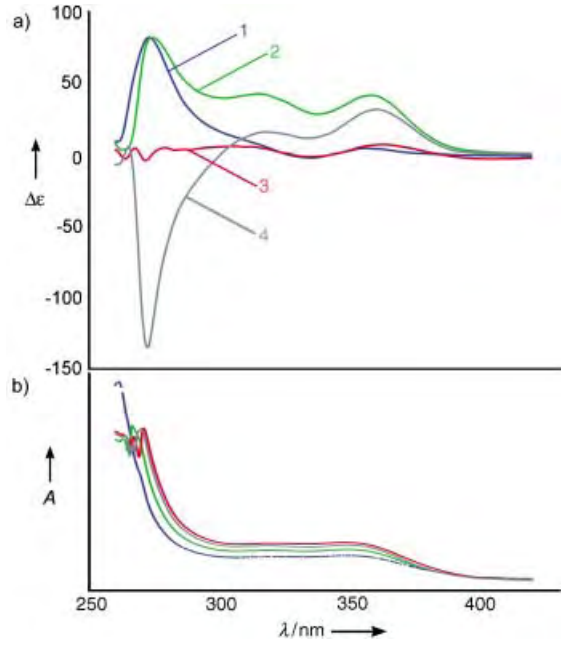


Figure 2. CD (a) and UV/Vis spectra (b): 1) originally prepared gel at 25 °C; 2) after cooling to 25 °C; 3) after heating to 50 °C; 4) after third heating to 55 °C and cooling to 25 °C.

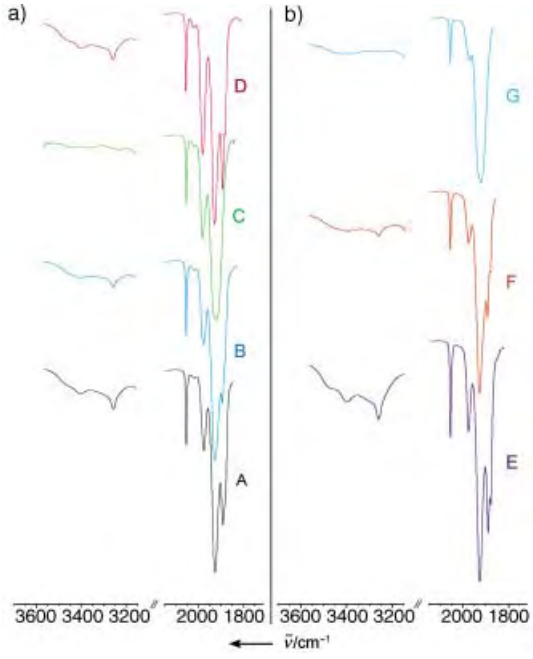


Figure 3. IR spectra of a gel in $CHCl_3$, a) 1.0 wt % at A) 25 °C, B) 40 °C, C) 55 °C, D) 25 °C (cooled from 55 °C); b) at 25 °C and E) 1 wt %, F) 0.4 wt % (viscous fluid), G) 0.2 wt % (solution).

 © 2003 Wiley-VCH Verlag GmbH & Co. KGaA, Weinheim

a gel to 55 °C; upon cooling the sample the bands centered at $\tilde{\nu} = 1889$ and 1878 cm^{-1} reappeared (Figure 3 a). Furthermore the bands arising from hydrogen bonded OH and/or NH groups ($\tilde{\nu} = 3200$–$3500\ cm^{-1}$) disappeared upon continuous dilution or heating.

The observed effects may reflect the molecular packing effects on fiber formation which result from hindered rotation around the metal–carbene bond, reducing the local C_{4v} symmetry of the pentacarbonyl chromium fragment. Clearly, the self-assembly of **4** arises from hydrogen bonding involving the hydroxy groups and the amino function, as indicated by the disappearance of the corresponding IR bands upon disintegration of the gel. Furthermore, the appearance of the "low-energy" bands at $\tilde{\nu} = 1889$ and $1878\ cm^{-1}$ which decrease in intensity upon dilution may be rationalized in terms of intermolecular hydrogen bonding involving one or more carbonyl ligands in the gel state.[9]

In conclusion, aminocarbene chromium complex **4** is an efficient gelator for typical chlorinated and aromatic solvents and mixtures thereof. Its aggregation behavior depends on both the solvent (mixture) and on the cooling rate. It is the first organometallic low-molecular-mass gelator bearing a direct transition-metal-to-carbon bond, a promising feature relevant for supramolecular catalysis based on a variety of catalytically active, and in particular late, transition-metal centers. Further studies aim at a better understanding of the self-assembly process and at the formation of chiral macrostructures arising from chiral induction by the carbohydrate head group.

Experimental Section

All reactions involving organometallic compounds were carried out under argon atmosphere in dry reaction vessels. All the solvents were distilled, dried, and stored under argon over molecular sieve (4 Å). Silica gel (0.063–0.200 mm) was degassed in vacuum and stored under argon before being used as the stationary phase for column chromatography.

For the preparation of the gel samples the solvents (quality p.a.) were saturated with argon by freeze, pump, and thaw cycles and stored over molecular sieve (4 Å). Compound **4** (approximately 8 mg) was filled into a screw-cap tube and the solvent (mixture) was added by syringe in an argon-filled glove box. The exact concentration was determined by differential weighting. Compound **4** was dissolved by heating in an oil bath (75 °C) or by a heat-gun under continuous shaking. Afterwards the samples were cooled down rapidly in a water bath at 5 °C or slowly in a water bath in which the temperature was reduced from 60 °C by 1 °C per minute. The samples for SEM/TEM were left to cool down at room temperature.

For the determination of T_{gel}[6] a glass ball (radius 1.5 mm, weight 36 mg) was placed on the gel surface and the samples were heated in a water bath by 0.3 °C per minute. As soon as the ball started subsiding into the gel, the corresponding temperature was denoted as T_{gel}. TEM/SEM-experiments were carried out on JEOL-JEM 1010/JEOL-JSM 6330F microscopes; all pictures were taken digitally. For sample preparation carbon-coated copper grids (mesh 200 or 150) were placed on the surface of the gels for a short time. The gel samples were partly destroyed by knocking the test tube forcefully on the table to provide a "print" of the inner volume of the gel. This procedure was carried out in an argon-filled glove box.

NMR spectra were recorded on a BRUKER DRX 500. The gels were prepared in the NMR tubes under argon atmosphere. The CD experiments were carried out on a JASCO J-720 spectropolarimeter. The gel was put into a thermoadjustable 0.2-mm quartz sample cell by syringe.

4: In a Schlenk tube, **3** (2.56 g, 4.29 mmol) was dissolved in a mixture of methanol (20 mL) and dichloromethane (20 mL) and cooled to −78 °C. *n*-Octylamine (0.71 mL, 4.3 mmol) was dissolved in dichloromethane and added by syringe. The reaction mixture was stirred for 0.5 h and allowed to warm slowly to −40 °C. At this temperature most of the dichloromethane was removed in vacuum. Afterwards a saturated solution of ammonia in methanol was added (50 mL), the cooling vessel was removed, and the reaction mixture was left to reach room temperature. After 6 h of stirring the solvent and excess ammonia were removed in vacuum, and the resulting brown oil was purified by column chromatography (silica gel, dichloromethane, change to dichloromethane:methanol 8:1, −5 °C) to provide **4** as a yellow solid (1.04 g, 2.16 mmol, 50 %) after removal of solvents. Elemental analysis (%) calcd for $C_{19}H_{29}CrNO_{10}$: C 47.21, H 6.05, N 2.90; found: C 47.32, H 6.23, N 2.89; ^{1}H NMR (CD_3OD, 500 MHz): $\delta = 5.07$ (s, 1 H), 4.56 (s, 1 H), 3.81 (m, 1 H), 3.92 (t, $^3J(H,H) = 7.4$ Hz, 2 H), 3.79 (dd, $^3J(H,H) = 10.9$ Hz, $^3J(H,H) = 3.0$ Hz, 1 H), 3.71 (m, 1 H), 3.65 (dd, $^3J(H,H) = 10.9$ Hz, $^3J(H,H) = 5.8$ Hz, 1 H), 1.79 (p, $^3J(H,H) = 7.4$ Hz, 2 H), 1.47 (m, 2 H), 1.42–1.28 (m, 8 H), 0.92 ppm (t, 3 H); ^{13}C NMR (CD_3OD, 125 MHz): $\delta = 264.59$, 223.98, 219.52, 87.82, 76.61, 73.05, 68.89, 64.71, 53.71, 32.92, 30.38, 30.35, 30.23, 27.74, 23.68, 14.41 ppm; FAB-MS: m/z: 371 [$M^{+\cdot}$·4 CO].

Received: February 7, 2003 [Z51134]

Keywords: amphiphiles · carbene ligands · carbohydrates · chromium · gels

[1] a) D. Philp, J. F. Stoddart, *Angew. Chem.* **1996**, *108*, 1242–1286; *Angew. Chem. Int. Ed. Engl.* **1996**, *35*, 1154–1196; b) D. J. Abdallah, R. G. Weiss, *Adv. Mater.* **2000**, *12*, 1237–1247.

[2] a) B. Pfannemüller, W. Welte, *Chem. Phys. Lipids* **1985**, *37*, 227–240; b) J. H. Fuhrhop, P. Schnieder, E. Boekema, W. Helfrich, *J. Am. Chem. Soc.* **1988**, *110*, 2861–2867; c) J.-H. Fuhrhop, W. Helfrich, *Chem. Rev.* **1993**, *93*, 1565–1582; d) D. A. Frankel, D. F. O'Brien, *J. Am. Chem. Soc.* **1994**, *116*, 10057–10069.

[3] R. J. H. Hafkamp, M. C. Feiters, R. J. M. Nolte, *J. Org. Chem.* **1999**, *64*, 412–426.

[4] a) K. H. Dötz, W. Straub, R. Ehlenz, K. Peseke, R. Meisel, *Angew. Chem.* **1995**, *107*, 2023–2025; *Angew. Chem. Int. Ed. Engl.* **1995**, *34*, 1856–1858; b) K. H. Dötz, C. Jäkel, W.-C. Haase, *J. Organomet. Chem.* **2001**, *617–618*, 119–132.

[5] E. Moser, E. O. Fischer, *J. Organomet. Chem.* **1969**, *16*, 275–282.

[6] A. Takahashi, M. Sakai, T. Kato, *Polym. J.* **1980**, *12*, 335–341.

[7] K. Murata, M. Aoki, T. Suzuki, T. Harada, H. Kawabata, T. Komori, F. Ohseto, K. Ueda, S. Shinkai, *J. Am. Chem. Soc.* **1994**, *116*, 6664–6676.

[8] A. Hafner, L. S. Hegedus, G. deWeck, B. Hawkins, K. H. Dötz, *J. Am. Chem. Soc.* **1988**, *110*, 8413–8421.

[9] Hydrogen bonding to carbonyl ligands in the crystalline state of metal complexes has been established by single-crystal X-ray analysis in some rare examples: D. Braga, F. Grepioni, P. Sabatino, G. R. Desiraju, *Organometallics* **1994**, *13*, 3532–3543; the coordination of Lewis acids to the oxygen terminus of carbonyl ligands is well known and the resulting shifts in the IR spectra can be correlated with our observations with respect to a weaker interaction: D. F. Shriver, *J. Organomet. Chem.* **1975**, *94*, 259–271.

 © 2003 Wiley-VCH Verlag GmbH & Co. KGaA, Weinheim

Metal-Organic Zeolites

A Topology Paradigm for Metal-Organic Zeolites**

*Eduard B. Rusanov, Vira V. Ponomarova, Vasiliy V. Komarchuk, Helen Stoeckli-Evans, Elena Fernandez-Ibañez, Fritz Stoeckli, Joachim Sieler, and Konstantin V. Domasevitch**

Coordination polymers that afford controllable cavities and incorporate different guest molecules may provide structural prototypes for the design of porous host lattices for applications such as adsorption,[1,2] ion exchange[3] and heterogeneous catalysis.[4] The elaboration of such materials is a considerable challenge, as only a few of the previously synthesized solids are stable to the loss of the initially accumulated guests and capable of taking up small organic molecules in the resulting molecular holes.[1] New insights into the development of approaches for the engineering of metal–organic zeolites are possible on the basis of topological considerations.[5] Attractive metal–organic-zeolite models of metal–organic frameworks may be predicted for novel "2D building blocks" of semiregular topology[6] (Figure 1 b and c) that are expanded in a third direction by pillaring.[7] In this case, initial plane tiling by a set of different polygons, instead of uniform square grids as in $[Cu(bipy)_2SiF_6]$,[2] generates closely packed molecular triangles (cf. molecular hexagons)

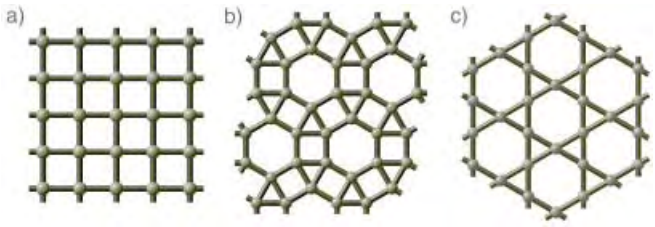


Figure 1. Four-connected plane nets of significance for chemical topology: a) regular 4^4 tiling, b),c) semiregular nets.

[*] Dr. K. V. Domasevitch, Dr. V. V. Ponomarova, V. V. Komarchuk
Inorganic Chemistry Department, Kiev University
Volodimirska Street 64, Kiev 01033 (Ukraine)
Fax: (+380) 44-296-2467
E-mail: dk@anorgchemie.univ.kiev.ua
Dr. E. B. Rusanov
Institute of Organic Chemistry
Murmanskaya Str. 5, Kiev-94, 02094 (Ukraine)
Prof. Dr. J. Sieler
Institut für Anorganische Chemie, Universität Leipzig
Linnéstrasse 3, 04103 Leipzig (Germany)
Prof. Dr. H. Stoeckli-Evans, E. Fernandez-Ibañez, Prof. Dr. F. Stoeckli
Chemistry Department, University of Neuchâtel
Av. de Bellevaux 51, Neuchâtel, 2007 (Switzerland)

[**] The authors gratefully acknowledge support from Deutsche Forschungsgemeinschaft and an INTAS Fellowship grant (KVD) YSF 2002-310.

Supporting information for this article is available on the WWW under http://www.angewandte.org or from the author.

with very open regions within the network. Thus, the free space appears to be concentrated, and the resulting framework of relatively low overall porosity, which is stable and robust, could maintain large cages for guest molecules. Realistic prototypes of such arrays are provided by the structures of purely inorganic materials—tungsten bronzes.[6b]

Herein, we report how the combination of the inherent functional features of organic and inorganic counterparts allows an especially effective implementation of this assembly scenario, and the generation of a target coordination network with unprecedented hexagonal tungsten bronze topology. Despite the fact that the angles at the net vertex (2×60, $2\times120°$) do not match the demands of a typical coordination environment around octahedrally coordinated transition-metal ions, the desired connectivity may be tuned by the conformational flexibility of the organic linker. First, the 3,3′,5,5′-tetramethylsubstituted 4,4′-bipyrazolyl ligand (4,4′-bpz) acts as an angular linker.[8] Its frame includes two planar pyrazolyl fragments, which have an angle of rotation around 60–80° and the resulting noncollinear orientation of two N–M vectors makes possible the assembly of the desired flat coordination net. Second, these coordination layers $[M(4,4'\text{-bpz})_2]_n$, formed by the octahedrally coordinated metal ions and two equivalents of the bridging 4,4′-bpz ligands, have a rich and versatile functionality for cross-linking into a 3D superstructure. Each four-coordinate point $M(pyrazole)_4$ of the layer provides, in the two axial directions, six binding sites that include coordination positions at the metal atom, and four hydrogen bond donating NH groups of the coordinated pyrazole ligands. Thus, dense interconnection of the layers and generation of a rigid 3D network is feasible by the rational choice of an anionic counterpart to fit perfectly this set of binding sites.

The 3D structure of a new family of framework solids $[M(4,4'\text{-bpz})_2\{S_2O_6\}]_n$ **1** (M = Co **1a**, Zn **1b**, Cd **1c**) is supported by cooperation of bridging functions of organic and inorganic linkers. The 2D $[M(4,4'\text{-bpz})_2]_n$ linkage exists as a triangular so-called Kagomé network[9] (Figure 2) and dithionate anions are used as pillars. The present 2D metal-organic subunit is a isomer of "square grids" and represents a mode of plane tiling by a combination of molecular triangles and hexagons in 2:1 ratio, instead of a 4^4 regular tiling topology. The fragments $[M(4,4'\text{-bpz})_2]_6$ are distorted and adopt a roughly triangular shape that eliminates possible centers of inversion and the entire 3D structure is chiral. Dithionates are perfectly suited as pillars for the 1:4 metal–pyrazole coordination, as two oxygen atoms complete the octahedral environment of the metal atoms and the remaining four oxygen atoms form relatively strong NH···O hydrogen bonds with all available adjacent pyrazolyl groups (Scheme 1, Figure 3). This complementary set of donor/acceptor interactions, and effective shielding of the S_2O_6 linkers by eight methyl groups, presumably has an impact on the high thermal stability of the compounds, which remains unchanged in air up to 590 K.[10] Noteworthy, simple inorganic dithionates themselves are much less stable and readily loose SO_2 upon heating.

Successive planes of $[M(4,4'\text{-bpz})_2]_n$ are stacked with an interlayer separation of approximately 7.97 Å, and the entire

 DOI: 10.1002/ange.200250534 © 2003 Wiley-VCH Verlag GmbH & Co. KGaA, Weinheim

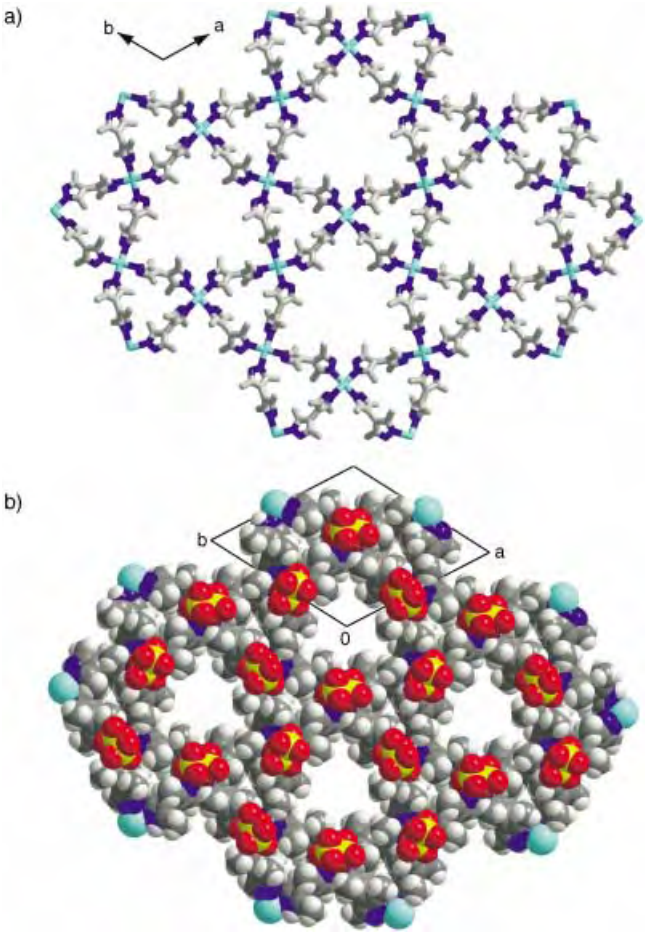
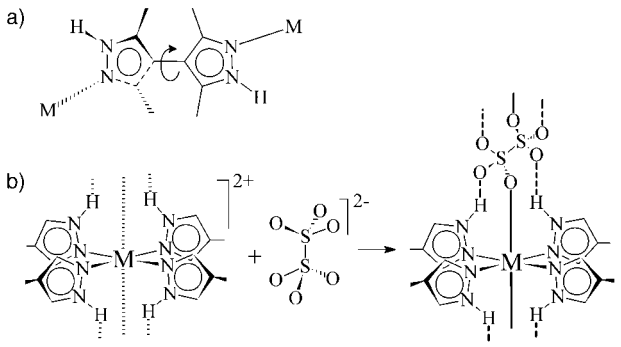


Figure 2. Structure of the 2D $[M(4,4'\text{-bpz})_2]_n$ (M = Co, Zn, Cd) network (a), and space-filling representation of the entire structure viewed down the *c* axis, which shows the cylindrical channels of about 8 Å size and how the bulky organic ligands shield the dithionate pillars (b).



Scheme 1. a) 3,3′,5,5′-tetramethyl-4,4′-bipyrazolyl as an angular connector between two metal atoms; b) Illustration of how the functionality of the dithionate ion is complementary for 1:4 metal-pyrazole units.

structure has channels down the *c* axis. The total unpopulated area for **1a** is 737 Å^3 per unit cell or about 29% of the crystal volume.[11] The channels have inner dimensions of about 8 Å and are accessible for small guest molecules (Figure 2b). Indeed, the compounds are capable of the reversible adsorption of dichloromethane, as was found from vapor adsorption

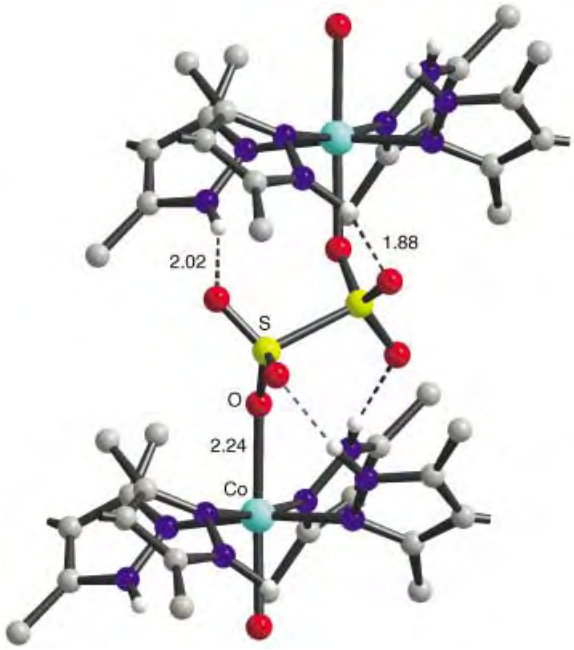


Figure 3. Function of dithionate group as a linker between metal–organic layers.

and by immersion calorimetry studies[12] for **1a** (M = Co) and **1c** (M = Cd). The CH_2Cl_2 vapour adsorption isotherms showed reversible type I behavior and were analyzed in the framework of Dubinin's theory,[13] which was developed for the filling of micropores in carbons and zeolites. A logarithmic plot of the Dubinin-Astakhov Equation (1):

$$N_a\ (\text{mmol g}^{-1}) = N_{ao}^{-(A/E)^n};\ A\ (\text{kJ mol}^{-1}) = RT\ln(ps/p) \qquad (1)$$

leads to a single line for exponent $n = 4$. In the case of activated carbons and zeolites with relatively wide micropores, n is usually close to 2. A higher value, as in this case, corresponds to pores with higher adsorption energies.[13] The overall fit leads to a characteristic energy $E = 10.3$ kJ mol^{-1}, the limiting amount filling the micropores $N_{ao} = 2.53$ mmol (215 mg) g^{-1}, and assuming a liquidlike state of the condensate, the apparent micropore volume W_o is 0.16 cm^3 g^{-1} or 0.19 cm^3 cm^{-3}. That is, comparable with the values obtained for zeolites; ranging from 0.18 for analcine to 0.47 cm^3 cm^{-3} for zeolite A. Immersion calorimetry experiments at 293 K suggest enthalpies $-\Delta_i H$ of -54 (**1a**) and -45 J g^{-1} (**1c**) versus the expected value of -33 J g^{-1}, calculated by using the adsorption data. This may be regarded as a satisfactory correlation and confirms a similar behavior of **1a** and **1c** towards CH_2Cl_2.

In conclusion, our study introduces a novel 3D coordination architecture as an attractive prototype for the development of metal-organic zeolites. We believe that further expansion of the pillaring strategy into a family of semiregular plane nets could provide new structural types with alternating closely packed and very open regions. This approach would simplify the generation of robust solids with pores that are large enough for useful adsorption applications.

 © 2003 Wiley-VCH Verlag GmbH & Co. KGaA, Weinheim

Experimental Section

Slow interdiffusion of the solutions of 0.086 g (0.26 mmol) $CoS_2O_6 \cdot 6H_2O$ in 5 mL methanol and 0.100 g (0.52 mmol) 4,4′-bpz[15] in 5 mL methanol and 5 mL chloroform afforded pink dithionate $[Co(4,4'\text{-bpz})_2\{S_2O_6\}] \cdot n H_2O$ ($n = 2$) **1a**·$n H_2O$. Compound **1a** readily loses guest water in air within minutes, without collapse of the 3D structure to give $[Co(4,4'\text{-bpz})_2\{S_2O_6\}]$ **1a** (yield: 0.118 g, 75 %). By using the same conditions zinc **1b** and cadmium **1c** complexes were crystallized as colorless blocks.

Crystallographic measurements were made at 153 K using a STOE Image Plate Diffraction System with $Mo_{K\alpha}$ radiation ($\lambda = 0.71073$ Å). The structures were solved by direct methods and refined by full-matrix least-squares in the anisotropic approximation for all non hydrogen atoms by using SHELXS-86 and SHELXL-93.[16] For **1a** the site of the guest water molecule was refined with partial occupancy, 0.5. All crystals were trigonal, space group *P*321 (No. 150), $Z = 3$. Crystal data: **1a**, $C_{20}H_{28}CoN_8O_6S_2$, $M = 599.55$, $a = b = 19.329(1)$, $c = 7.7651(4)$ Å, $V = 2512.5(3)$ Å^3, $\rho_{calcd} = 1.189$ g cm^{-3}, $2\theta_{max} = 52.0°$, 2878 unique data, $R_1 = 0.036$, absolute structure parameter $x = -0.05(2)$; **1a**·H_2O, $C_{20}H_{30}CoN_8O_7S_2$, $M = 617.57$, $a = b = 19.311(3)$, $c = 7.772(2)$ Å, $V = 2510.0(8)$ Å^3, $\rho_{calcd} = 1.226$ g cm^{-3}, $2\theta_{max} = 51.8°$, 2624 unique data, $R_1 = 0.036$, $x = 0.02(2)$. **1b**, $C_{20}H_{28}N_8O_6S_2Zn$, $M = 603.98$, $a = b = 19.298(4)$, $c = 7.967(2)$ Å, $V = 2569.5(10)$ Å^3, $\rho_{calcd} = 1.171$ g cm^{-3}, $2\theta_{max} = 51.8°$, 2025 unique data, $R_1 = 0.055$, $x = 0.18(3)$. Cadmium complex **1c** is isomorphous: $a = b = 19.877(1)$, $c = 8.0067(6)$ Å. CCDC 195428–195430 (**1a**, **1a**·H_2O, **1b**) contains the supplementary crystallographic data for this paper. These data can be obtained free of charge via www.ccdc.cam.ac.uk/conts/retrieving.html (or from the Cambridge Crystallographic Data Centre, 12 Union Road, Cambridge CB21EZ, UK; fax: (+44) 1223-336-033; or deposit@ccdc.cam.ac.uk).

The adsorption isotherms of CH_2Cl_2 were determined gravimetrically[12] at 293, 308 and 318 K for **1a** and at 308 K for **1c**, in the range of relative pressures $10^{-4} < p/ps^{-1} < 0.2$, following out-gassing at 383 K for 12–15 h (10^{-4} Torr). Immersion calorimetry experiments were carried out at 293 K on samples of 0.050–0.100 g by using a *Tian–Calvet* type calorimeter. The accuracy varies between 3 and 5 %, depending on the absolute energy liberated in the process (usually 1 to 20 J) and on the amount of solid used. The enthalpy of immersion was calculated within the framework of Dubinin's theory.[12,13]

Received: November 12, 2002 [Z50534]

Keywords: crystal engineering · inclusion compounds · microporous materials · self-assembly · zeolites

[1] K. Seki, *Chem. Commun.* **2001**, 1496–1497; M. Kondo, T. Yoshitomi, K. Seki, H. Matsuzaka, S. Kitagawa, *Angew. Chem. Int. Ed. Engl.* **1997**, *36*, 1725–1727; H. Li, M. Eddaoudi, M. O'Keeffe, O. M. Yaghi, *Nature* **1999**, *402*, 276–279; M. Eddaoudi, H. Li, O. M. Yaghi, *J. Am. Chem. Soc.* **2000**, *122*, 1391–1397; L. C. Tabares, J. A. R. Navarro, J. M. Salas, *J. Am. Chem. Soc.* **2001**, *123*, 383–387; Y.-H. Liu, Y.-L. Lu, H.-C. Wu, J.-C. Wang, K.-L. Lu, *Inorg. Chem.* **2002**, *41*, 2592–2597, and references therein.

[2] S. Noro, S. Kitagawa, M. Kondo, K. Seki, *Angew. Chem.* **2000**, *112*, 2161–2164; *Angew. Chem. Int. Ed.* **2000**, *39*, 2082–2084.

[3] B. F. Hoskins, R. Robson, *J. Am. Chem. Soc.* **1990**, *112*, 1546–1554.

[4] M. Fujita, Y. J. Kwon, S. Washizu, K. Ogura, *J. Am. Chem. Soc.* **1994**, *116*, 1151–1152; S. Noro, S. Kitagawa, M. Yamashita, T. Wada, *Chem. Commun.* **2002**, 222–223.

[5] R. Robson, *J. Chem. Soc. Dalton Trans.* **2000**, 3735–3744; B. Moulton, M. J. Zaworotko, *Chem. Rev.* **2001**, *101*, 1629–1658.

[6] a) A. F. Wells, *Three-Dimensional Nets and Polyhedra*, Wiley-Interscience, New York, **1977**; b) A. F. Wells, *Structural Inorganic Chemistry*, 5th ed., Clarendon, Oxford, **1986**.

[7] M. J. Zaworotko, *Chem. Commun.* **2001**, 1–9; S. Subramanian, M. J. Zaworotko, *Angew. Chem.* **1995**, *107*, 2295–2297; *Angew. Chem. Int. Ed. Engl.* **1995**, *34*, 2127–2129.

[8] I. Boldog, E. B. Rusanov, A. N. Chernega, J. Sieler, K. V. Domasevitch, *Angew. Chem.* **2001**, *113*, 3543–3546; *Angew. Chem. Int. Ed.* **2001**, *40*, 3435–3438; I. Boldog, E. B. Rusanov, A. N. Chernega, J. Sieler, K. V. Domasevitch, *J. Chem. Soc. Dalton Trans.* **2001**, 893–897; V. V. Ponomarova, V. V. Komarchuk, I. Boldog, A. N. Chernega, J. Sieler, K. V. Domasevitch, *Chem. Commun.* **2002**, 436–437; I. Boldog, E. B. Rusanov, J. Sieler, S. Blaurock, K. V. Domasevitch, *Chem. Commun.* **2003**, 740–741.

[9] 2D Kagomé networks themselves were recently discovered by:B. Moulton, J. Lu, R. Hajndl, S. Hariharan, M. J. Zaworotko, *Angew. Chem.* **2002**, *114*, 2945–2948; *Angew. Chem. Int. Ed.* **2002**, *41*, 2821–2824; M. Eddaoudi, J. Kim, D. Vodak, A. Sudik, J. Wachter, M. O'Keeffe, O. M. Yaghi, *Proc. Natl. Acad. Sci. USA* **2002**, *99*, 4900–4904.

[10] The TGA curve for hydrated **1a** shows 4.4 % weight loss (ca. $-1.4 H_2O$) to 425 K, then release of SO_2 at 590 K, which is followed by further decomposition at 650 K. For comparison, the most stable inorganic dithionate, $K_2S_2O_6$, looses SO_2 at 530 K.

[11] PLATON/PLUTON version Jan. 1999 A. L. Spek, *Acta Crystallogr. Sect. A* **1990**, *46*, C34.

[12] R. C. Bansal, J. B. Donnet, F. Stoeckli, *Active Carbon*, Marcel Dekker, New York, **1988**, pp. 119–162; F. Stoeckli in *Porosity in Carbons* (Ed.: J. Patrick), Arnold, London, **1995**, pp. 67–92.

[13] F. Stoeckli, *Russ. Chem. Bull. Int. Ed.* **2001**, *50*, 2265–2272; M. M. Dubinin in *Progress in Surface and Membrane Science, Vol. 19* (Ed.: D. A. Cadenhead), Academic Press, London, **1975**, pp. 1–69.

[14] B. Garrot, G. Couderc, M. H. Simonot-Grange, F. Stoeckli, *Microporous Mesoporous Mater.* **2002**, 52, 199–206.

[15] W. L. Mosby, *J. Chem. Soc.* **1957**, 3997–4003.

[16] G. M. Sheldrick, *Acta Crystallogr. Sect. A* **1990**, *46*, 467–473; G. M. Sheldrick, SHELXL-93, Program for Crystal Structure Refinement from Diffraction Data, University of Göttingen, Göttingen (Germany), **1993**.

 © 2003 Wiley-VCH Verlag GmbH & Co. KGaA, Weinheim

Phototriggered Molecular Release

Phototriggered Drug Release from Functionalized Oligonucleotides by a Molecular Beacon Strategy

*Akimitsu Okamoto, Kazuhito Tanabe, Takeshi Inasaki, and Isao Saito**

DNA hybridization biosensors offer considerable promise for obtaining sequence information of genes in a fast and simple manner. Various DNA probes that give signals in a sequence-specific fashion, as represented by molecular beacons, have been widely used.[1–3] However, there are very few DNA probes that release functional molecules on recognition of the target sequence.[4,5] The sequence-specific molecule-releasing system that is triggered by external stimulation, such as irradiation would be a very powerful tool for gene analysis.

Herein we report for the first time a molecule-releasing system controllable by an intramolecular quenching based on a molecular-beacon strategy by using photoactive probe oligodeoxynucleotides (ODNs). The photoreaction of the probe ODN containing a photoactive group and a triplet quencher at both ends of the strand was very inefficient when it was in the closed-form ODN (a stem-and-loop structure), whereas irradiation of the open-form ODN hybridized with the complementary DNA resulted in a rapid release of the functional molecule from the ODN (see Figure 1).

ODN sequences for the molecule-releasing system were designed according to the molecular-beacon strategy.[1] Phenacyl ester[6–8] as a photocleavable group via a triplet excited state, and substituted naphthalene[9,10] as a triplet quencher

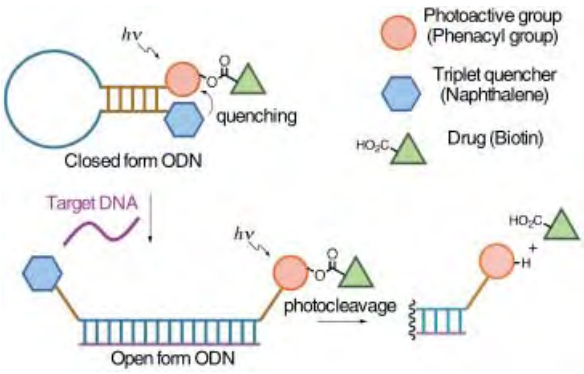


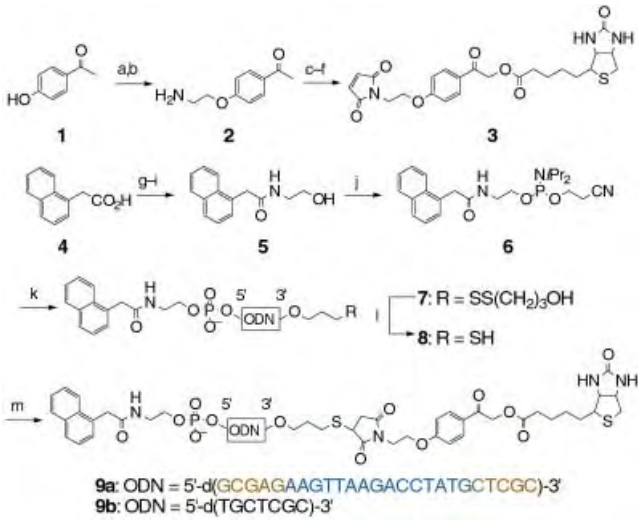
Figure 1. Outline for the phototriggered drug release from functionalized oligonucleotides by a molecular beacon strategy.

[*] Prof. I. Saito, Dr. A. Okamoto, K. Tanabe, T. Inasaki
Department of Synthetic Chemistry and Biological Chemistry
Faculty of Engineering
Kyoto University and
SORST, Japan Science and Technology Corporation
Kyoto 606–8501 (Japan)
Fax: (+81) 75-753-5676
E-mail: saito@sbchem.kyoto-u.ac.jp

Supporting information for this article is available on the WWW under http://www.angewandte.org or from the author.

were incorporated into the 3′- and 5′-ends of the ODN, respectively. The stem of the closed-form ODN keeps a phenacyl ester and a naphthalene ring in close proximity to each other, causing the efficient triplet quenching, as in the case of a molecular beacon. In contrast, when the probe ODN is transformed to the open form by hybridization with target DNA,[1] photocleavage of the phenacyl ester proceeds very smoothly under irradiation, because the photoactive phenacyl ester is far away from the naphthalene quencher.

The synthetic route for the functionalized ODN is shown in Scheme 1. The photocleavable phenacyl ester **3**, which has both a maleimide functional group to be connected to thiol-



Scheme 1. Reagents and conditions: a) K_2CO_3, *N*-(2-bromoethyl)phthalimide, acetone, reflux, 10 h, 23%; b) 40% methylamine, 2:1 chloroform-methanol, RT, 5 h, 64%; c) maleic anhydride, toluene, reflux, 5 h; d) sodium acetate, acetic acid, reflux, 1.5 h, 49% in two steps; e) $PhMe_3NBr_3$, THF, RT, 3 h, 35%; f) (+)-biotin, triethylamine, DMF, RT, 2 h, 76%; g) thionyl chloride, reflux, 2 h; h) $TBDMSO(CH_2)_2NH_2$, THF, RT, 12 h, 43% in two steps; i) TBAF, THF, RT, 3 h, 82%; j) $(iPr_2N)_2PO(CH_2)_2CN$, 1*H*-tetrazole, acetonitrile, RT, 1.5 h, quant.; k) DNA autosynthesizer, then 28% ammonia, 55 °C, 12 h; l) 5 mM dithiothreitol, 25 mM sodium phosphate (pH 8.4), 23 °C, 12 h, quant.; m) 0.5 mM **3**, 250 mM sodium phosphate (pH 7.0), 23 °C, overnight, quant.

modified DNA and a biotin unit as a leaving functional molecule, was prepared from 4-hydroxyacetophenone (**1**). Naphthalene phosphoramidite, **6**, was prepared from 1-naphthylacetic acid (**4**) in four steps. ODNs containing both a naphthalene unit at the 5′ end and a disulfide unit at the 3′ end were synthesized by using a DNA synthesizer by a conventional phosphoramidite method. The disulfide group of the given ODNs **7** was reduced to thiol by dithiothreitol, and then coupled with **3** to give ODNs **9a** and **9b** that were equipped with a photoactive group and a quencher at each end.

We initially investigated the efficiency of the photoreaction of ODN **9a** by irradiation at 312 nm before and after hybridization with the complementary target DNA 5′-d(CATAGGTCTTAACTT)-3′. The irradiation of a solution of **9a** in 15 mM sodium cacodylate (pH 7.0) and 2-propanol (2:1) was

 © 2003 Wiley-VCH Verlag GmbH & Co. KGaA, Weinheim DOI: 10.1002/anie.200250832

conducted at 0 °C for 10 seconds, and the disappearance of **9a** was monitored by HPLC. The conversion of closed-form **9a**[11] was relatively inefficient (5% conversion, $k_{obs} = 0.03\ \mu M\ s^{-1}$), whereas irradiation of open form **9a** hybridized with the complementary strand resulted in an efficient degradation (25% conversion, $k_{obs} = 0.17\ \mu M\ s^{-1}$). These results clearly indicate that a structural change caused by hybridization of **9a** with the complementary DNA strongly affects the consumption of **9a**.[12]

To obtain photoproducts, we examined the irradiation of a shorter single-stranded ODN **9b**, and analyzed the reaction products by mass spectrometry. With five minutes of irradiation, **9b** was completely consumed and afforded the product mixture. The molecular weight [$(M-H)^-$] of the reaction products given by MALDI-TOF mass spectrometry was 2775.49, thus indicating the formation of acetophenone **10b** (calcd 2775.99) (Scheme 2). Such reductive cleavage of phenacyl ester was also confirmed in the photolysis of a model system, 4-methoxyphenacyl ester of biotin.[6,13,14]

We next quantified the biotin that was released from **9a** by the photolysis of the phenacyl ester. After irradiation at 312 nm of a solution of **9a** (200 pmol), the photoproduct mixture was isolated filtration through a centrifugal filter and mixed with a solution of the complex of avidin and 2-((4′-hydroxyphenyl)azo)benzoic acid (HABA).[15,16] Then, the decrease of the absorbance at 500 nm (A_{500}) originating from the avidin-HABA complex was monitored. The decrease of A_{500} is known to be caused by the displacement of HABA from the avidin-HABA complex by the released biotin.[16] The amount of biotin that was released from **9a** was determined by using a calibration curve of A_{500} given from control experiments (Figure 2). Irradiation of closed-form **9a** resulted in a slight decrease of A_{500}, corresponding to 12% biotin release. In contrast, a drastic decrease of A_{500} corresponding to 84% biotin release was observed in the presence of complementary ODN 5′-d(CATAGGTCTTAACTT)-3′. The efficiency of biotin release was significantly altered by the conformational change of **9a** by hybridization with the target DNA sequence. These results strongly suggest that naphthalene attached to the 5′ end of **9a** acts as an effective intramolecular quencher in closed form **9a** and suppresses photodegradation of the phenacyl ester, which readily occurred in open-form **9a**.

In summary, we have demonstrated for the first time a phototriggered molecule-releasing system by using a molecular beacon strategy. Hybridization of the photoactive probe ODN with the complementary target DNA resulted in a rapid photolytic cleavage of phenacyl ester with the release of biotin, although closed form ODN before hybridization suppresses biotin release due to the intramolecular triplet quenching. The drug release occurs effectively by UV irradiation when a specific sequence has been recognized. This new drug-releasing system will facilitate the rational design of a well-controllable prodrug for gene analysis.

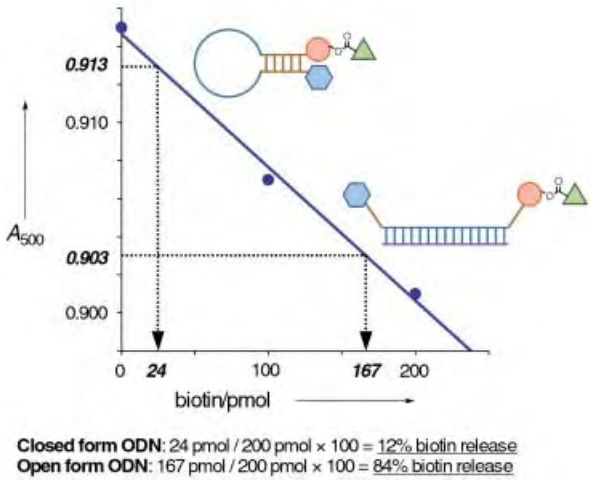
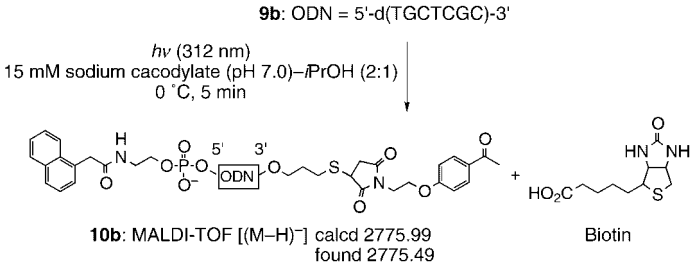


Figure 2. Quantification of biotin released from **9a**. Irradiation (312 nm) of 200 pmol of **9a** in the presence or absence of the complementary ODN 5′-d(CATAGGTCTTAACTT)-3′ was carried out in 15 mM sodium cacodylate (pH 7.0)-*i*PrOH (2:1) at RT with a monochromator (JASCO CRM-FD, 300 W Xe lamp, 40 counts; one count of irradiation approximately corresponds to a surface energy of 0.02 $J\,cm^{-2}$). After the reaction mixture was filtered through a Microcon centrifugal filter (YM-3, 3000 NMWL), the filtrate was mixed with a solution of avidin-HABA complex (0.43 mg of ImmunoPure Avidin, PIERCE and 62.5 μg of ImmunoPure HABA, PIERCE) in 86 mM sodium phosphate (pH 7.2) and 130 mM sodium chloride, and then the absorbance at 500 nm (A_{500}) of the mixture was measured. The amount of released biotin was quantified by using a linear fit (the blue solid line, $y = -7.0 \times 10^{-5}x + 0.9147$; $R = 0.9966$) based on A_{500} of an avidin-HABA solution in the presence of 0, 100, and 200 pmol of biotin.



Scheme 2.

Received: December 23, 2002 [Z50832]

Keywords: · drug delivery · molecular devices · oligonucleotides · photolysis

[1] S. Tyagi, F. R. Kramer, *Nat. Biotechnol.* **1996**, *14*, 303–308.
[2] S. Tyagi, D. P. Btaru, F. R. Kramer, *Nat. Biotechnol.* **1998**, *16*, 49–53.
[3] A. S. Piatek, S. Tyagi, A. C. Pol, A. Telenti, L. P. Miller, F. R. Kramer, D. Alland, *Nat. Biotechnol.* **1998**, *16*, 359–363.
[4] Z. Ma, J.-S. Taylor, *Proc. Natl. Acad. Sci. USA* **2000**, *97*, 11159–11163.
[5] Z. Ma, J.-S. Taylor, *Bioorg. Med. Chem.* **2001**, *9*, 2501–2510.
[6] J. C. Sheehan, K. Umezawa, *J. Org. Chem.* **1973**, *38*, 3771–3774.
[7] K. Zhang, J. E. T. Corrie, V. R. N. Munasinghe, P. Wan, *J. Am. Chem. Soc.* **1999**, *121*, 5625–5632.

 © 2003 Wiley-VCH Verlag GmbH & Co. KGaA, Weinheim

[8] P. G. Conrad II, R. S. Givens, J. F. W. Weber, K. Kandler, *Org. Lett.* **2000**, *2*, 1545 – 1547.
[9] R. S. Givens, A. Jung, C.-H. Park, J. Weber, W. Bartlett, *J. Am. Chem. Soc.* **1997**, *119*, 8369 – 8370.
[10] R. S. Givens, J. F. W. Weber, P. G. Conrad II, G. Orosz, S. L. Donahue, S. A. Thayer, *J. Am. Chem. Soc.* **2000**, *122*, 2687 – 2697.
[11] Closed-form **9a** was stable at room temperature. The T_m was 40.4 °C in 10 mM sodium cacodylate (pH 7.0) and 1 mM NaCl.
[12] A control ODN that does not have a 5′ triplet quencher **9a**–naph was also tested. Very rapid degradation was observed for both closed form **9a**–naph and open form **9a**–naph hybridized with the complementary strand (59% and 55% conversion, respectively).
[13] A solution of 4-methoxyphenacyl ester of biotin (0.14 mmol) in acetonitrile/2-propanol/water (1:4:2, v/v/v) was irradiated at 312 nm with a transilluminator for 3.5 h at room temperature. The reaction mixture was purified by silica gel chromatography to give 4-methoxyacetophenone and biotin in 59% yield.
[14] Several peaks were detected by HPLC in the reaction mixture of **9b**, suggesting that the mixture contains several photoproducts in addition to product **10b** as given by MALDI-TOF mass. For a solution containing duplex ODN 5′-d(GCGAGAAGTTAA-GACCTATGCTCGC)-3′/5′-d(CATAGGTCTTAACTT)-3′ and 4-methoxyphenacyl ester of biotin, 8% consumptions of ODN were observed for 60 s irradiation. Further conversion of **10b** by irradiation was not observed.
[15] N. M. Green, *Biochem. J.* **1965**, *94*, 23c-24c.
[16] H. Hofstetter, M. Morpurgo, O. Hofstetter, E. A. Bayer, M. Wilchek, *Anal. Biochem.* **2000**, *284*, 354 – 366.

 © 2003 Wiley-VCH Verlag GmbH & Co. KGaA, Weinheim

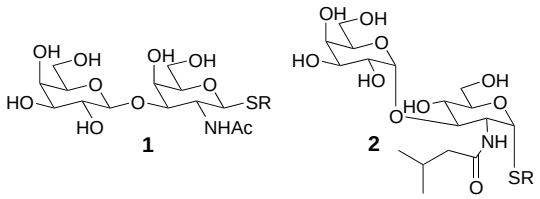
Carbohydrate Recognition

Overcoming Degeneracy in Carbohydrate Recognition**

*Amit Basu and Daniel Kahne**

Protein binding to cell-surface carbohydrates is a key event in many important biological processes, including fertilization, development, inflammation, and cancer.[1] These events and the responses they trigger are difficult to study and to inhibit selectively because protein receptors for carbohydrates frequently have overlapping or degenerate binding specificities.[2] For example, the tetrasaccharide sialyl Lewis X present on endothelial cells and neutrophils binds to at least three different proteins, E-, P-, and L-selectin during the initiation of the inflammatory response.[3] For the study of recognition processes or events involving carbohydrate-binding proteins (lectins), it would be useful to have ligands that bind to one protein in the presence of other proteins that have similar binding specificities. Herein we show that it is indeed possible to find carbohydrate ligands that are specific for one among a group of carbohydrate-binding proteins that have the same nominal binding selectivity.

We previously reported the synthesis of a 1300-member combinatorial library of di- and trisaccharides on TentaGel beads.[4] This library was screened against *Bauhinia purpurea* (BP) lectin, which recognizes ligands terminating with the disaccharide Galβ1-3GalNAc (**1**, Scheme 1). We found that an unnatural carbohydrate (**2**) binds better to BP than all the other carbohydrates present in the library, which included the thioglycoside derivative of the natural ligand **1**.[4,5] This result showed that carbohydrate-binding proteins can discriminate one particular carbohydrate ligand among a large collection of related carbohydrates.[6] Furthermore, we have shown that the nature of the polyvalency of the ligand affects the selectivity of BP for **2** versus **1**.[5b] However, if unnatural carbohydrate ligands are to be used to probe carbohydrate–protein recognition processes, the binding specificity must be reciprocal; that is, not only must the lectin bind one particular carbohydrate ligand in the presence of related ligands, but the ligand in question must bind that protein selectively in the presence of other proteins that have the same nominal binding specificity.[7] It is not a forgone conclusion that a ligand selected in a screen will be specific for the protein used in the selection, particularly if the protein is known to be promiscuous with respect to natural ligands (see above). Therefore, the central question we sought to answer in this study is whether **2** would be specific for BP only, or whether it would exhibit some level of degeneracy in its interactions with lectins that bind **1**.



Scheme 1. Structures of the natural (**1**) and hit (**2**) ligands attached to TentaGel resin. R = $SC_6H_4OCH_2CONH$TentaGel or photocleavable linker (see reference [13]).

To evaluate whether the binding selectivity of ligand **2** was reciprocal, we studied whether **2** could discriminate between the BP lectin and that from *Arachis hypogaea* (AH), which also recognizes ligands terminating with disaccharide **1**.[5b,8] We prepared TentaGel beads functionalized with **1** or **2** and incubated them with mixtures of BP and AH.[9,10] To facilitate detection of the proteins, BP was labeled with fluorescein (BP-F) and AH was modified with tetramethylrhodamine (AH-T). Fluorescein and tetramethylrhodamine have distinct fluorescence emission wavelengths, which allows the separate detection of both proteins on individual beads. The beads were incubated with the mixture of proteins and then examined with a confocal microscope.[11,12] Beads which were functionalized with ligand **1** had strong emissions at

[*] Prof. D. Kahne, Dr. A. Basu
Department of Chemistry
Princeton University
Princeton, NJ 08544 (USA)
Fax: (+1) 609-258-2617
E-mail: dkahne@princeton.edu

[**] This work was supported by the ONR. We thank Joe Goodhouse for assistance with the confocal microscopy measurements.

 © 2003 Wiley-VCH Verlag GmbH & Co. KGaA, Weinheim DOI: 10.1002/anie.200250859

the wavelengths for both fluorescein and tetramethylrhodamine, thus showing that both lectins were bound simultaneously to the beads (Figure 1). In contrast, the fluorescence from AH-T on beads containing **2** was barely above background levels, while the fluorescence from BP-F was very strong. Hence, ligand **2**, which was originally identified by screening a combinatorial library of carbohydrates for binding to BP lectin, binds that lectin almost exclusively, even in the presence of another lectin that has the same nominal binding selectivity.

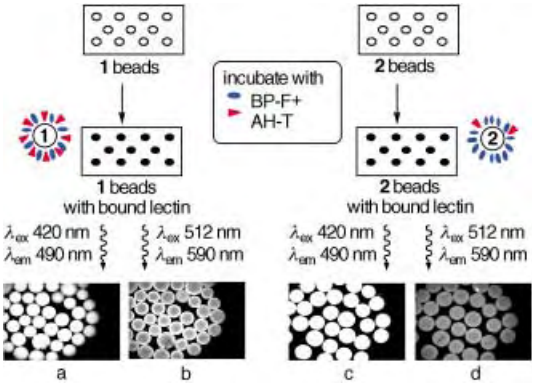


Figure 1. Confocal microscope images of the binding of a solution of BP-F and AH-T to TentaGel Beads functionalized with **1** or **2**. a) Fluorescein emission from BP-F bound to **1**; b) tetramethylrhodamine emission from AH-T bound to **1**; c) fluorescein emission from BP-F bound to **2**; d) tetramethylrhodamine emission from AH-T bound to **2**.

These initial experiments showed that beads derivatized with ligand **2** were quite selective for the BP lectin over AH. We next sought to determine if we could use carbohydrate-derivatized beads to isolate BP lectin from a mixture of lectins which all recognize ligands terminating in disaccharide **1**. The ligands **1** and **2** were attached to beads using a photocleavable linker that can be cleaved under mild conditions to release carbohydrate-bound lectins into solution.[13] Lectins that are bound nonspecifically to the resin itself or that have denatured on the surface should not be released upon cleaving the carbohydrates.

In the event, carbohydrate-derivatized beads **1** and **2** were incubated with a solution containing a mixture of three lectins which all bind to ligand **1**: BP, *Agaricus bisporus* (AB), and *Vicia villosa* (VV).[14,15] After washing the beads, they were photolyzed to release the bound lectins into solution. The solution was filtered to remove excess albumin from the buffer and then the filtrate concentrated and analyzed by using denaturing gel electrophoresis followed by silver staining. The final results of this experiment are shown in Figure 2. The beads derivatized with the natural ligand bound all three lectins in similar amounts as shown by the presence of bands representing all three proteins in lane 1.[16] In contrast, beads derivatized with ligand **2** bound BP lectin almost exclusively (lane 2). Most importantly, this experiment demonstrates that unnatural carbohydrates can be used to extract proteins from a mixture with a selectivity suitable for subsequent analysis, such as sequencing. The preceding

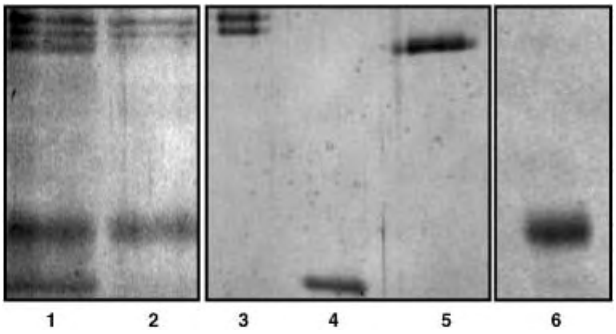


Figure 2. Denaturing gels showing lectin release from TentalGel beads functionalized with **1** or **2** after photocleavage. Lane 1: lectins bound to beads containing **1**. Lane 2: lectins bound to beads containing **2**. Lane 3: BP lectin. Lane 4: AB lectin. Lane 5: VV lectin. Lane 6: avidin.

results illustrate that degeneracy in carbohydrate recognition can be overcome by the use of unnatural carbohydrates in place of the natural ligands.[17]

A specific carbohydrate ligand for that receptor was identified by screening a library of polyvalent carbohydrates against a particular protein receptor. This unnatural carbohydrate ligand bound avidly to the protein it was screened against, but not to other proteins, including proteins that recognize the same natural carbohydrate ligand. Carbohydrate-derivatized beads or surfaces have clear applications in protein isolation and extraction as well as in sensors for detecting carbohydrate-binding proteins.[5a,18] Recent developments in carbohydrate microarray technology, coupled with advances in oligosaccharide synthesis, will result in the identification of a large number of protein targets which bind and interact with oligosaccharides.[19] Perhaps more interesting, unnatural carbohydrate ligands that are specific for particular carbohydrate-binding proteins could be useful tools for probing biological processes or pathways involving monovalent or multivalent carbohydrate–protein recognition events.[20]

Received: December 27, 2002 [Z50859]

Keywords: carbohydrates · fluorescent probes · glycoconjugates · lectins · oligosaccharides

[1] a) M. Fukuda, O. Hindsgaul, *Molecular Glycobiology*, Oxford University Press, New York, **1994**; b) S. Hakomori, Y. Zhang, *Chem. Biol.* **1997**, *4*, 97–104; c) A. Varki, *Glycobiology* **1993**, *3*, 97–130; d) R. Dwek, *Chem. Rev.* **1996**, *96*, 683–720; e) H. Lis, N. Sharon, *Chem. Rev.* **1998**, *98*, 637–674; f) P. M. Rudd, T. Elliott, P. Cresswell, I. A. Wilson, R. A. Dwek, *Science* **2001**, *291*, 2370–2376.

[2] R. C. Hughes, *Biochem. Soc. Trans.* **1997**, *25*, 1194–1198.

[3] a) C. R. Bertozzi, *Chem. Biol.* **1995**, *2*, 703–708; b) E. E. Simanek, G. J. McGarvey, J. A. Jablonowski, C.-H. Wong, *Chem. Rev.* **1998**, *98*, 833–862; c) A. Varki, *Proc. Natl. Acad. Sci. USA* **1994**, *91*, 7390–7397.

[4] R. Liang, L. Yan, J. Loebach, M. Ge, Y. Uozumi, K. Sekanina, N. Horan, J. Gildersleeve, C. Thompson, A. Smith, K. Biswas, W. C. Still, D. Kahne, *Science* **1996**, *274*, 1520–1522.

 © 2003 Wiley-VCH Verlag GmbH & Co. KGaA, Weinheim

[5] a) N. Horan, L. Yan, H. Isobe, G. M. Whitesides, D. Kahne, *Proc. Natl. Acad. Sci. USA* **1999**, *96*, 11782 – 11786; b) R. Liang, J. Loebach, N. Horan, M. Ge, C. Thompson, L. Yan, D. Kahne, *Proc. Natl. Acad. Sci. USA* **1997**, *94*, 10554 – 10559.

[6] Polyvalent carbohydrate ligands have been shown to amplify the intrinsic selectivity of lectin–saccharide recognition: K. H. Mortell, R. V. Weatherman, L. L. Kiessling, *J. Am. Chem. Soc.* **1996**, *118*, 2297 – 2298.

[7] Two lectins which recognize a monovalent ligand with similar affinities have been shown to have very different binding constants for the dimeric forms of the ligands: R. V. Weatherman, K. H. Mortell, M. Chervenak, L. L. Kiessling, E. J. Toone, *Biochemistry* **1996**, *35*, 3619 – 3624. A series of lectins with overlapping specificities has also been shown to exhibit differences in the mode of binding with a series of related oligosaccharides, thus indicating that the mechanism of binding degeneracy is not uniform: M. Chervenak, E. J. Toone, *Biochemistry* **1995**, *34*, 5685 – 5695.

[8] W. J. Peumans, E. J. M. Van Damme, *Crit. Rev. Biochem. Mol. Biol.* **1998**, *33*, 209 – 258.

[9] The disaccharides **1** and **2** were prepared by using previously reported procedures: N. R. Horan, PhD thesis, Princeton University, **1999**.

[10] Two eppendorf tubes were charged with small portions (1 mg) of either **1** or **2**. The beads were washed with phosphate-buffered saline containing tween (PBST; 3 × 500 μL, 10 min), followed by incubation with PBST containing 3% bovine serum albumin (BSA; 500 μL, 30 min) and washing with PBST with 1% BSA (3 × 500 μL, 5 min). The beads were incubated with a mixture of BP-F and AH-T (100 μL, each protein at 250 μg mL^{-1}, 3 h). After washing the beads with PBST (2 × 500 μL, 5 min), they were transferred to a Terasaki multiwell plate and visualized under a confocal microscope.

[11] R. Quarrell, T. D. W. Claridge, G. W. Weaver, G. Lowe, *Mol. Diversity* **1995**, *1*, 223 – 232.

[12] The confocal images indicate that BP-F freely partitions through the resin, while AH-T is only surface-bound. This variability in protein partitioning has been reported previously.[11] Other research groups have noted that the catalytic efficiency of enzymes in on-bead assays is dependent on the nature of the solid support, and have suggested that not all portions of a resin bead are equally accessible to the enzyme; see a) J. P. Morken, T. M. Kapoor, S. Feng, F. Shirai, S. L. Schreiber, *J. Am. Chem. Soc.* **1998**, *120*, 30 – 36; J. Vagner, G. Barany, S. Lam, K. V. Krchnak, N. Sepetov, J. A. Ostrem, P. Strop, M. Lebl, *Proc. Natl. Acad. Sci. USA* **1996**, *93*, 8194 – 8199; b) Y. W. Cheung, C. Abell, S. Balasubramanian, *J. Am. Chem. Soc.* **1997**, *119*, 9568 – 9569; c) M. T. Burger, P. A. Bartlett, *J. Am. Chem. Soc.* **1997**, *119*, 12697 – 12698; for the use of various methods of spectroscopic analysis to examine the efficiency of chemical reactions at the exterior and interior of polymer beads, see d) S. R. McAlpine, S. L. Schreiber, *Chem. Eur. J.* **1999**, *5*, 3528 – 3532; e) J. Kress, A. Rose, J. G. Frey, W. S. Brocklesby, M. Ladlow, G. W. Mellor, M. Bradley, *Chem. Eur. J.* **2001**, *7*, 3880 – 3883; f) J. Rademann, M. Barth, R. Brock, H.-J. Egelhaaf, G. Jung, *Chem. Eur. J.* **2001**, *7*, 3884 – 3889; g) R. A. Farrer, G. T. Copeland, M. J. R. Previte, M. M. Okamoto, S. J. Miller, J. T. Fourkas, *J. Am. Chem. Soc.* **2002**, *124*, 1994 – 2003; h) S. R. McAlpine, C. W. Lindsley, J. C. Hodges, D. M. Leonard, G. F. Filzen, *J. Comb. Chem.* **2001**, *3*, 1 – 5; i) R. Liu, J. Marik, K. S. Lam, *J. Am. Chem. Soc.* **2002**, *124*, 7678 – 7680.

[13] a) A. Borchardt, S. D. Liberles, S. R. Biggar, G. R. Crabtree, S. L. Schreiber, *Chem. Biol.* **1997**, *4*, 961 – 968; b) C. P. Holmes, D. G. Jones, *J. Org. Chem.* **1995**, *60*, 2318 – 2319.

[14] The affinities of the lactol of **1** for BP, AH, and VV lectins, respectively, are 0.2, 0.79, and 0.89 mM; a) S. Sueyoshi, T. Tsuji, T. Osawa, *Carbohydr. Res.* **1988**, *178*, 213 – 224; b) A. M. Wu, S. Sugii, *Carbohydr. Res.* **1991**, *213*, 127 – 143.

[15] Two eppendorf tubes were charged with small portions (1 mg) of either **1** or **2**. The beads were washed with PBST (3 × 500 μL, 10 min), followed by incubation with PBST containing 0.5% biotinylated BSA (1 mL, 30 min) and washing with PBST (3 × 1 mL, 5 min). The beads were incubated with a solution containing a mixture of the BP, AB, and VV lectins (500 μL, 50 μg mL^{-1} of each lectin, 2 h). The beads were washed with PBS (2 × 500 μL, 5 min) and water (1 × 500 μL, 5 min), transferred to siliconized Pyrex test tubes, and suspended in water (500 μL). The test tubes were placed in a Rayonet photoreactor and irradiated at a wavelength of 300–400 nm for 1 h. The water was removed, and the beads were washed with water (500 μL). The combined aqueous solutions were added to TetraLink avidin resin (75 μL, Promega) and vortexed briefly. The supernatant was removed, and the avidin resin was washed with additional water (500 μL). Lyophilization of the combined washes (1.5 mL) was followed by denaturing gel electrophoresis on a 15% polyacrylamide gel and silver staining.

[16] The avidin in lanes 1 and 2 is derived from the avidin-linked resin that was used to remove the biotinylated BSA present on the beads which prevented nonspecific lectin adhesion to the solid support. Densitometry of the gel confirmed that the amount of AB in lane 2 was negligible.

[17] For other examples of breaking degeneracy in biological recognition processes by a bump-hole approach, see P. J. Alaimo, M. A. Shogren-Knaak, K. M. Shokat, *Curr. Opin. Chem. Biol.* **2001**, *5*, 360 – 367, and references therein.

[18] a) S. R. Haseley, J. P. Kamerling, J. F. G. Vliegenthart, *Top. Curr. Chem.* **2002**, *218*, 93 – 114; b) B. T. Houseman, M. Mrksich, *Top. Curr. Chem.* **2002**, *218*, 1 – 44.

[19] a) D. Wang, S. Liu, B. J. Trummer, C. Deng, A. Wang, *Nat. Biotechnol.* **2002**, *20*, 275 – 281; b) B. T. Houseman, M. Mrksich, *Chem. Biol.* **2002**, *9*, 443 – 454; c) O. J. Plante, E. R. Palmacci, P. H. Seeberger, *Science* **2001**, *291*, 1523 – 1527; d) F. Fazio, M. C. Bryan, O. Blixt, J. C. Paulson, C.-H. Wong, *J. Am. Chem. Soc.* **2002**, *124*, 14397 – 14402.

[20] a) M. Mammen, S.-K. Choi, G. M. Whitesides, *Angew. Chem.* **1998**, *110*, 2908 – 2953; *Angew. Chem. Int. Ed.* **1998**, *37*, 2754 – 2794; b) J. E. Gestwicki, L. L. Kiessling, *Nature* **2002**, *415*, 81 – 84; c) U. S. Eggert, N. Ruiz, B. V. Falcone, A. A. Branstrom, R. C. Goldman, T. J. Silhavy, D. Kahne, *Science* **2001**, *294*, 361 – 364.

 © 2003 Wiley-VCH Verlag GmbH & Co. KGaA, Weinheim

Mapping Enzyme Active Sites

A Fluorine Scan of Thrombin Inhibitors to Map the Fluorophilicity/Fluorophobicity of an Enzyme Active Site: Evidence for C–F···C=O Interactions**

Jacob A. Olsen, David W. Banner, Paul Seiler, Ulrike Obst Sander, Allan D'Arcy, Martine Stihle, Klaus Müller,* and François Diederich**

The modulation of pharmacokinetic properties by fluorine substitution has become a well-established strategy for lead optimization[1] and has resulted in a large number (ca. 150) of fluorinated drugs in clinical use. The substitution of hydrogen by fluorine often causes minimal steric effects despite their different van der Waals radii (1.20 and 1.47 Å, respectively),[1,2] while a number of properties, such as lipophilicity, pK_a values, and metabolic stability, can be affected in a favorable way. Multiple fluorination of aromatic rings changes the quadrupole moment,[3] which profoundly affects aromatic–aromatic interactions.[4] The bioisosteric replacement of hydrogen by fluorine also affects enzyme–ligand binding affinity and selectivity, as shown for inhibitors of carboxypeptidase A,[5] stromelysin A,[6] carbonic anhydrase,[7] and chymotrypsin.[8]

In the same way as an active-site environment can be described as being hydrophilic or lipophilic, it could also be classified as being either fluorophilic or fluorophobic because of the unique properties of fluoro-organic compounds. Teflon and other fluorinated compounds clearly are neither hydrophilic nor hydrophobic.[9] Understanding the nature and intrinsic properties of fluorophilic/fluorophobic environments is therefore of great interest for structure-based lead design and optimization.

We recently reported a family of inhibitors of thrombin with a rigid tricyclic core that show nearly identical binding geometries in the structurally well-defined active site of this trypsin-like serine protease from the blood coagulation cascade.[10,11] We have recently started to systematically exchange one or more H atoms for F atoms in various positions of these inhibitors to explore the fluorophilicity/fluorophobicity of the thrombin active site. Here we report the results of a fluorine scan involving the benzylic residue that undergoes edge-to-face interactions with the indole ring of Trp 215 in the spacious hydrophobic D pocket of the enzyme (Figure 1).[12]

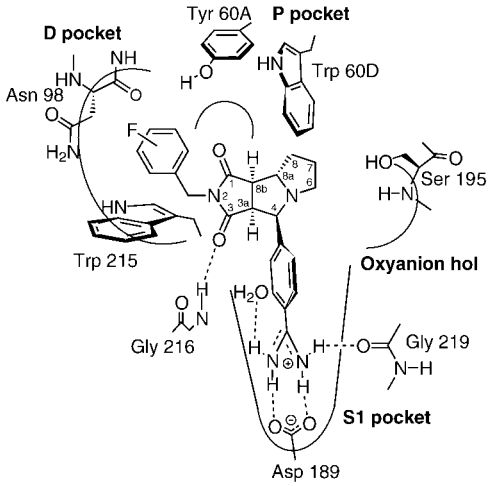
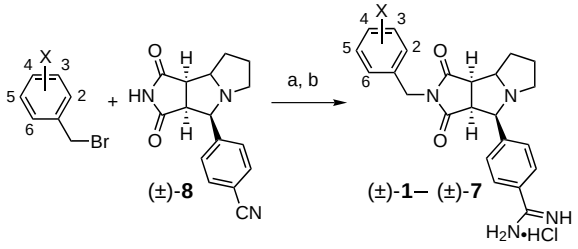


Figure 1. Schematic representation of the binding mode of the tricyclic inhibitors in the active site of thrombin. Only the (3a*S*,4*R* 8a*S*,8b*R*)-configured enantiomer is bound, as determined from the X-ray crystallographic analysis.[10] In addition to the catalytic triad flanked by the oxyanion hole, the active site can be described in terms of selectivity pocket (S1), a small proximal pocket (P), and a large hydrophobic distal (D) pocket.

Benzyl derivative (±)-**1**[10c] and a series of six mono-, di- and pentafluorinated inhibitors (±)-**2**–(±)-**7** (Scheme 1) were prepared by alkylation of (±)-**8** (which was obtained by 1,3-dipolar cycloaddition from maleimide, 4-formylbenzonitrile, and L-proline) followed by a Pinner reaction.[10c,13] Their activity against thrombin and trypsin was determined as previously described.[14] The results were surprising (Table 1): whereas five fluorinated inhibitors ($K_i = 0.27$ to 0.61 μM) showed a potency similar to that of non-fluorinated (±)-**1** ($K_i = 0.31$ μM), the *para*-monofluorinated derivative (±)-**4** was much more active, with $K_i = 0.057$ μM



Scheme 1. Synthesis of inhibitors (±)-**1** to (±)-**7**. a) K_2CO_3, [18]crown-6 (10%), toluene, reflux, 58–86%; b) 1. AcCl, MeOH, CH_2Cl_2, 5 °C; 2. NH_3 in MeOH, 65 °C, 40–79%.

[*] Dr. D. W. Banner, Prof. Dr. K. Müller, Dr. U. Obst Sander, A. D'Arcy, M. Stihle
Pharma Research Basel, Discovery Chemistry
F. Hoffmann–La Roche Ltd
4070 Basel (Switzerland)
Fax: (+41) 61-688-7408
E-mail: david.banner@roche.com
klaus.mueller@roche.com
Prof. Dr. F. Diederich, Dr. J. A. Olsen, P. Seiler
Laboratorium für Organische Chemie
ETH-Hönggerberg, HCI
8093 Zürich (Switzerland)
Fax: (+41) 1-632-1109
E-mail: diederich@org.chem.ethz.ch

[**] We thank Dr. T. Tschopp for the measurement of enzyme inhibition constants. J.A.O. thanks the Carlsberg Foundation for a fellowship. The research was supported by the ETH Research Council and F. Hoffmann–La Roche Ltd.

Supporting information for this article is available on the WWW under http://www.angewandte.org or from the author.

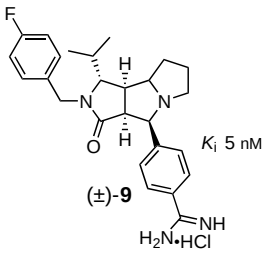
 DOI: 10.1002/anie.200351268 © 2003 Wiley-VCH Verlag GmbH & Co. KGaA, Weinheim

Table 1: Activities of the fluorinated thrombin inhibitors and selectivities with respect to trypsin.

Inhibitor	X (R^1)	K_i [μM][a]	Selectivity[b]
(±)-**1**	—	0.31	15
(±)-**2**	2-F	0.50	9.8
(±)-**3**	3-F	0.36	26
(±)-**4**	4-F	0.057	67
(±)-**5**	2,6-F_2	0.61	9.0
(±)-**6**	3,5-F_2	0.59	25
(±)-**7**	1,2,3,4,5-F_5	0.27	44

[a] The uncertainty of the measured K_i values is ±20%. [b] K_i(trypsin)/K_i(thrombin).

($\Delta\Delta G_{(\pm)\text{-}\mathbf{1}\rightarrow(\pm)\text{-}\mathbf{4}} = -1.05 \pm 0.17$ kcal mol^{-1}). Furthermore, this compound showed by far the best selectivity against trypsin in the series tested. We subsequently synthesized inhibitor (±)-**9**, with an isopropyl group to fill the P pocket, by a previously reported route.[10a–b] Compound (±)-**9** with a K_i value of 5 nM is to date our most potent thrombin inhibitor with a 413-fold selectivity over trypsin.



The binding mode of (±)-**4** at the thrombin active site was investigated by X-ray crystallography at 1.67-Å resolution (Figure 2).[15] Not surprisingly, only the 3a*S*,4*R*,8a*S*,8b*R* enantiomer is bound, as we had already shown for related thrombin inhibitors.[10a,b] Superimposition with a previously reported X-ray crystal structure of thrombin complexed with an inhibitor having a piperonyl group pointing into the D pocket[10a] revealed an identical binding mode for both inhibitors (see the Supporting Information). This result supports our modeling-based assumption that all fluorinated inhibitors have identical binding geometries.

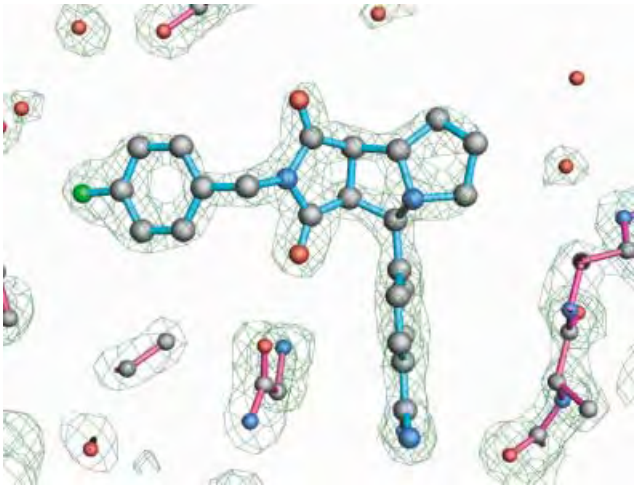


Figure 2. $2F_oF_c$ electron density contoured at 0.6 e Å^{-3}. All the inhibitor atoms are well-ordered. The slightly weaker electron density for the pyrrolidine ring hints at pseudorotation, although the temperature factors after constrained refinement have acceptably low values of approximately 20 Å^2.[15]

The F atom of (±)-**4** is in remarkably close contact with the H–C_α–C=O moiety of Asn 98 (Figure 3), as indicated by the short distances d(F···Cα) of 3.1 Å (d(F···H_α): 2.1 Å,

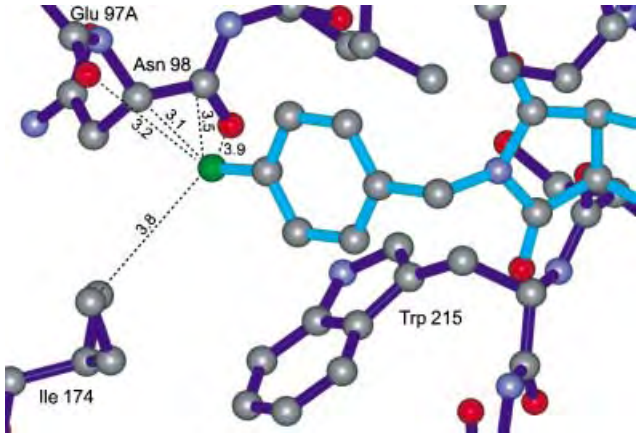
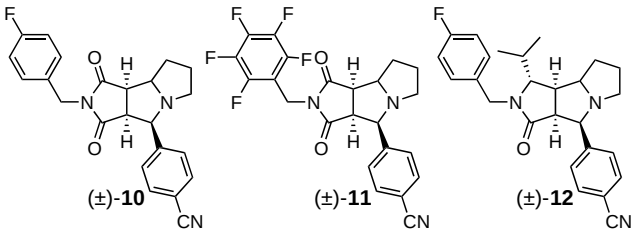


Figure 3. Binding mode of the 4-fluorobenzyl moiety in the D pocket of thrombin.[15] All F contacts with the protein within a distance of less than 4.0 Å are shown with dotted lines.

α(F···H–C_α): 157°) and d(F···C=O): 3.5 Å (α(F···C=O): 96°, α(F···C(0)–pseudotrigonal axis of the carbonyl system): 28°).[16] The ability of the H–C_α bond to act as an H-bond donor is increasingly being recognized, and calculations show that weak C=O···H–C_α H bonds contribute significantly in stabilizing the folded structure of proteins.[17] Desiraju and coworkers obtained evidence for weak C–F···H–C interactions from crystal structures of fluorobenzenes.[18] In addition, it was recently reported that C–F···H–C interactions stabilize duplex formation with RNA having unnatural fluorinated bases.[19] Whether the observed C–F···H–C_α interaction should be classified as a weak H bond is a matter of discussion.[20] The enhanced positive polarization of the H atom *ortho* to the F substituent presumably enhances the edge-to-face interaction of the inhibitor with Trp 215 (Figure 3).[21] We believe, however, that a particularly comfortable positioning of the F atom, with its direct polar interactions with the H–C_α–C=O moiety of Asn 98, is the major determinant for the large increase in activity seen for (±)-**4** relative to the other inhibitors in the series.

Organofluorine interactions with carbonyl groups, as seen in the thrombin complex with (±)-**4**, have to the best of our knowledge not been reported in the literature. We therefore analyzed the small-molecule X-ray crystal structures of the nitrile precursors (±)-**10**, (±)-**11**, and (±)-**12** to inhibitors (±)-**4**, (±)-**7**, and (±)-**9**, respectively, to obtain further insight into fluorophilic environments.[22]

 © 2003 Wiley-VCH Verlag GmbH & Co. KGaA, Weinheim



A C–F···H–C_α–C(O) contact similar to the one in the thrombin complex was found in the crystal-packing environment of (±)-**12**, as indicted by d(F···H_α): 2.41 Å,[23] d(F···C_α): 3.37 Å, and α(F···H-C_α): 148° (Figure 4). The F atom is rather

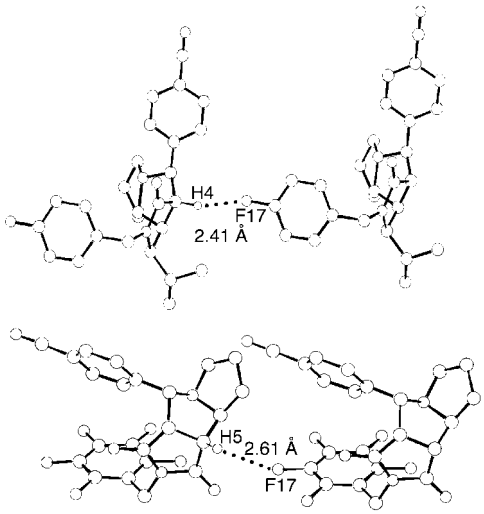


Figure 4. Short intermolecular C–F···H–C_α–C=O contacts[23] observed in the X-ray crystal packing of (±)-**11** (bottom) and (±)-**12** (top).[22]

distant from the C=O unit (d(F···C=O): 4.53 Å and α(F···C=O): 110°). Two similar C–F···H–C_α interactions were identified, though at longer F···H distances (2.65 and 2.74 Å), in the crystal of (±)-**10** (see the Supporting Information).[23] In the first case, the F atom is also in contact with a C=O group (d(F···C=O): 3.40 Å, d(F···O=C): 3.06 Å, α(F···C=O): 63°).

Analysis of the crystal packing of compound (±)-**11** revealed an additional C–F···H–C_α–C=O contact (d(F···H_α): 2.61 Å,[23] d(F···C_α): 3.27 Å, α(F···H-C_α): 119°, Figure 4). In this case the F atom is also in contact with the carbonyl group (d(F···C=O): 3.63 Å, d(F···O=C): 3.30 Å, α(F···C=O): 65°).

These findings prompted us to search the Cambridge Structural Database (CSD)[24] for intermolecular interactions between C–F and C=O moieties in crystals of fluorine-containing organic carbonyl derivatives in which the C=O group is flanked by one or two C, N, or O atoms. The search was limited to well-resolved (R factor < 7.5%, no disorder) neutral organic molecules, excluding metallorganic or polymeric compounds, with an intermolecular (nonbonded) distance between a C-bound F atom and a carbonyl C atom in the range of 2.5 Å < d_1(F···C=O) < 4.0 Å. The search resulted in 573 hits, with a total of 1091 occurrencies of close F···C=O contacts. There are quite a number of cases (43 occurrencies, Figure 5) with contact distances significantly below the sum of the van der Waals radii of C and F atoms (ca. 3.3 Å), which indicates there is an attractive interaction between the two polar groups.

An analysis of the relative orientation of the two interacting units in terms of the nonbonded distance d_1(F···C=O), the two angles α_1 and α_2 (Figure 5), as well as the pseudotorsional angle θ (C–F···C=O, Figure 5 and see the Supporting Information) reveals that the F atoms prefer a position close to the pseudotrigonal axis of the carbonyl unit

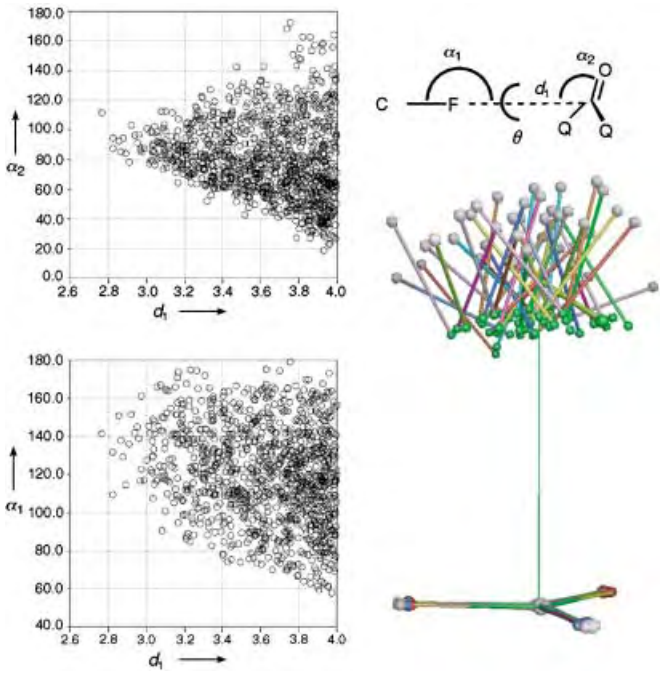


Figure 5. Scatterplots of α_1 versus d_1 (upper left) and α_2 versus d_1 (lower left) of 1091 occurrencies of close C–F···C=O contacts with 2.5 Å < d_1 < 4.0 Å obtained from 573 hits of the CSD search of fluorine-containing organic carbonyl derivatives (Q = C, N, O). Right: Superposition of 43 intermolecular C–F···Q(CO)Q subunits with 2.77 Å < d_1 < 3.09 Å extracted from the crystal structures and superimposed on the carbonyl unit (pointing backwards to the right). The thin vertical line marks the pseudotrigonal axis of the carbonyl system (norm of the Q(CO)Q plane).

at short contact distances. The C–F bond is generally inclined to the F–C axis with angles (α_1) adopting values typically between 100°–160°, but rarely 180°, at short to middle-range contact distances. There appears to be no preference in terms of *anti*, *syn*, or other orientations of the C–F unit relative to the C=O bond, even for the closest contacts. No systematic change of either the C–F or C=O bond lengths in response to the nonbonded distance d_1(F···C=O) could be found (see the Supporting Information). Thus, there are no indications of a covalent component in these C–F···C=O interactions, which are probably best described in terms of multipolar interactions between the intrinsically polar C–F and C=O units.

The crystal structures with short intermolecular contact distances of 2.9 Å < d_1(F···C=O) < 3.1 Å were examined in more detail using the modeling system Moloc:[16] the close

 © 2003 Wiley-VCH Verlag GmbH & Co. KGaA, Weinheim

intermolecular contacts were identified, the relevant substructural units extracted from the crystal structures, and superimposed with respect to the carbonyl system. The plot (Figure 5, right) shows the narrow cone around the pseudo-trigonal axis of the carbonyl group (cone angle ca. 12°) within which the fluorine atom of a closely interacting C–F bond unit prefers to be located.[25]

In view of our observation that the fluorine atom in the thrombin inhibitor complex also appears to be in close contact to a C_α–H bond α next to the C=O group, we analyzed a subset of structures containing at least one such bond in terms of close contacts of the C–F unit to both the C=O and the C_α–H unit.

Interestingly, while there is an expected correlation between the nonbonded distances d_3(F···C_α) and d_1(F···C=O) (Figure 6, left), the scatter plot of d_2(F···H–C_α) versus d_1(F···C=O) (Figure 6, right) clearly shows that a close contact of the fluorine atom with the carbonyl group does not

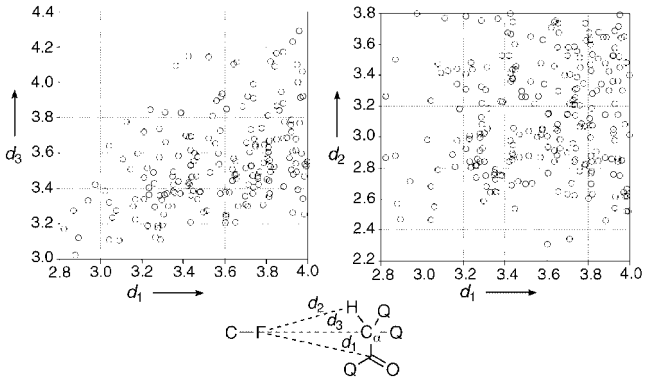


Figure 6. Scatterplots of nonbonded contact distances d_3(F···H–Cα) versus d_1 (left) and d_2(F···C_α) versus d_1 (right) for a total of 246 occurrencies in the subset of 132 crystal structures in which the C=O group is attached to at least one C atom carrying at least one H atom.

necessarily imply a close C–F···H–C_α contact. Conversely, there are clear cases where the F atom interacts predominantly with the C_α–H unit, but is somewhat more remote from the carbonyl group. Thus, there appears to be a range of possibilities for a C–F unit to engage in potentially attractive contacts. It is gratifying to see that the pair of values of 3.1 Å and 3.5 Å observed for the F···C_α and F···C=O nonbonded contact distances, respectively, in the thrombin inhibitor complex lies essentially in the domain of the scatter plot obtained for corresponding contacts in small-molecule crystal structures (Figure 6, left).

In conclusion, the combination of X-ray crystal-structure analysis of a protein–ligand complex, small-molecule X-ray crystallography, and database mining has for the first time shown that H–C_α–C=O fragments provide a pronounced fluorophilic environment. The high propensity of H–C_α–C=O units in the active sites of proteins suggests that such F interactions could be effectively exploited for enhancing ligand affinity or selectivity in structure-based design.

Received: February 24, 2003 [Z51268]

Keywords: fluorine · inhibitors · medicinal chemistry · molecular recognition · structure elucidation · thrombin

[1] a) K. Park, N. R. Kitteringham, P. M. O'Neill, *Annu. Rev. Pharmacol. Toxicol.* **2001**, *41*, 443–470; b) D. O'Hagan, H. S. Rzepa, *Chem. Commun.* **1997**, 645–652; c) B. E. Smart, *J. Fluorine Chem.* **2001**, *109*, 3–11.
[2] M. Schlosser, D. Michel, *Tetrahedron* **1996**, *52*, 99–108.
[3] J. Hernández-Trujillo, A. Vela, *J. Phys. Chem.* **1996**, *100*, 6524–6530.
[4] For a review, see E. A. Meyer, R. K. Castellano, F. Diederich, *Angew. Chem.* **2003**, *115*, 1244–1287, *Angew. Chem. Int. Ed.* **2003**, *42*, 1210–1250.
[5] J. A. Ippolito, D. W. Christianson, *Int. J. Biol. Macromol.* **1992**, *14*, 193–197.
[6] B. C. Finzel, E. T. Baldwin, G. L. Bryant, Jr., G. F. Hess, J. W. Wilks, C. M. Trepod, J. E. Mott, V. P. Marshall, G. L. Petzold, R. A. Poorman, T. J. O'Sullivan, H. J. Schostarez, M. A. Mitchell, *Protein Sci.* **1998**, *7*, 2118–2126.
[7] a) C.-Y Kim, J. S. Chang, J. B. Doyon, T. A. Baird, Jr., C. A. Fierke, A. Jain, D. W. Christianson, *J. Am. Chem. Soc.* **2000**, *122*, 12125–12134; b) R. D. Madder, C.-Y. Kim, P. P. Chandra, J. B. Doyon, T. A. Baird, Jr., C. A. Fierke, D. W. Christianson, J. G. Voet, A. Jain, *J. Org. Chem.* **2002**, *67*, 582–584.
[8] A. Kashima, Y. Inoue, S. Sugio, I. Maeda, T. Nose, Y. Shimohigashi, *Eur. J. Biochem.* **1998**, *255*, 12–23.
[9] F. T. T. Huque, K. Jones, R. A. Saunders, J. A. Platts, *J. Fluorine Chem.* **2002**, *115*, 119–128.
[10] a) U. Obst, V. Gramlich, F. Diederich, L. Weber, D. W. Banner, *Angew. Chem.* **1995**, *107*, 1874–1877; *Angew. Chem. Int. Ed. Engl.* **1995**, *34*, 1739–1742; b) U. Obst, D. W. Banner, L. Weber, F. Diederich, *Chem. Biol.* **1997**, *4*, 287–295; c) U. Obst, P. Betschmann, C. Lerner, P. Seiler, F. Diederich, V. Gramlich, L. Weber, D. W. Banner, P. Schönholzer, *Helv. Chim. Acta* **2000**, *83*, 855–909; d) P. Betschmann, S. Sahli, F. Diederich, U. Obst, V. Gramlich, *Helv. Chim. Acta* **2002**, *85*, 1210–1245.
[11] For recent examples of other thrombin inhibitors, see a) J. Z. Ho, T. S. Gibson, J. E. Semple, *Bioorg. Med. Chem. Lett.* **2002**, *12*, 743–748; b) S. Hanessian, E. Therrien, K. Granberg, I. Nilsson, *Bioorg. Med. Chem. Lett.* **2002**, *12*, 2907–2911; c) for a review, see J. B. M. Rewinkel, A. E. P. Adang, *Curr. Pharm. Des.* **1999**, *5*, 1043–1075.
[12] The term fluorine scan has been coined in a recent report on a computational fluorine scan of biotin, see B. Kuhn, P. A. Kollman, *J. Am. Chem. Soc.* **2000**, *122*, 3909–3916.
[13] All new compounds were fully characterized by m.p., IR, ^{1}H and ^{13}C NMR spectroscopy, MS, and HR-MS or elemental analysis.
[14] K. Hilpert, J. Ackermann, D. W. Banner, A. Gast, K. Gubernator, P. Hadváry, L. Labler, K. Müller, G. Schmid, T. B. Tschopp, H. van de Waterbeemd, *J. Med. Chem.* **1994**, *37*, 3889–3901.
[15] Crystals of human α-thrombin of C_2 symmetry were grown in the presence of a carboxy-terminal hirudin peptide (des-amino Asp55 hirudin55–65) as the inhibitor in the anion-binding exosite, but with no active-site inhibitor. Compound (±)-**4** was diffused into the crystals for 6 h from a 2.5 mM solution containing 30% PEG3350, 100 mM NaCl, and 100 mM Na^+/K^+ pH 7.4 phosphate buffer. One crystal was flash-frozen in liquid N_2, and diffraction data were measured on a Delft Instruments FR591 X-ray generator, run at 50 kV/100 mA, equipped with an Osmic focussing monochromator and an Oxford Cryostream cooler run at 100 K. The Marresearch345 image plate detector was placed 120 mm from the crystal and scanned with 0.15 mm pixel size. Exposure times were 180 s for 1.0° frames, and a profuse amount of data was obtained by collecting 720 frames. Data were processed to 1.67-Å resolution using XDS (W. Kabsch, *J. Appl. Crystallogr.* **1993**, *26*, 795–800). Unit-cell

 © 2003 Wiley-VCH Verlag GmbH & Co. KGaA, Weinheim

dimensions were $a = 70.69$, $b = 71.48$, $c = 72.80$ Å, and $\beta = 100.53°$. For 284109 observations of 38758 reflections, the merging R factor on intensities was 3.3% and in the outermost data shell (1.67 Å–1.74 Å) 14.9%, with $I/\sigma I = 33.5$ overall and 9.7 in the outermost shell. Model building with Moloc[16] and refinement with CNX (A. T. Brünger, P. D. Adams, G. M. Clore, W. L. DeLano, P. Gros, R. W. Grosse-Kunstleve, J.-S. Jiang, J. Kuszewski, M. Nilges, N. S. Pannu, R. J. Read, L. M. Rice, T. Simonson, G. L. Warren, *Acta Crystallogr. D* **1998**, *54*, 905–921) gave final overall crystallographic R factors of 17.9% (working) and 20.5% (free), with values in the outer shell of 22.8 and 24.9%, respectively, for 2296 protein atoms, 30 inhibitor atoms, one Na^+ ion, one Ca^{2+} ion, and 404 water molecules. The inhibitor density is very clear (Figure 2): the refined temperature factors for the inhibitor range from 14 (amidinium moiety) to 26 Å^2. PDB code: 10YT.

[16] a) P. R. Gerber, K. Müller, *J. Comput.-Aided Mater. Des.* **1995**, *9*, 251–268; b) Gerber Molecular Design (http://www.moloc.ch). The distances and angles were obtained with the Moloc modeling/visualization program. The position of the H_α atom of Asn98 is based on stereochemical consideration with a C···H distance of 1.08 Å.

[17] R. Vargas, J. Garza, D. A. Dixon, B. P. Hay, *J. Am. Chem. Soc.* **2000**, *122*, 4750–4755.

[18] V. R. Thalladi, H.-C. Weiss, D. Bläser, R. Boese, A. Nangia, G. R. Desiraju, *J. Am. Chem. Soc.* **1998**, *120*, 8702–8710.

[19] J. Parsch, J. W. Engels, *J. Am. Chem. Soc.* **2002**, *124*, 5664–5672.

[20] J. D. Dunitz, R. Taylor, *Chem. Eur. J.* **1997**, *3*, 89–98.

[21] A. Matsushima, T. Fujita, T. Nose, Y. Shimohigashi, *J. Biochem.* **2000**, *128*, 225–232.

[22] CCDC 203566–203568 ((±)-**10**–(±)-**12**) contain the supplementary crystallographic data for this paper. These data can be obtained free of charge via www.ccdc.cam.ac.uk/conts/retrieving.html (or from the Cambridge Crystallographic Data Centre, 12 Union Road, Cambridge CB2 1EZ, UK; fax: (+44) 1223-336-033; or deposit@ccdc.cam.ac.uk). Further details are found as Supporting Information.

[23] The H positions are based on stereochemical consideration with a C···H distance of 1.08 Å.

[24] CSD Version 5.24, November **2002**, which holds over 270000 small-molecule crystal structures.

[25] The F···C=O interaction bears some structural resemblance to the interaction of nucleophiles with the carbonyl groups investigated: B. Bürgi, J. D. Dunitz, *Acc. Chem. Res.* **1983**, *16*, 153–161.

 © 2003 Wiley-VCH Verlag GmbH & Co. KGaA, Weinheim

Structure of Bound Epothilone

The High-Resolution Solution Structure of Epothilone A Bound to Tubulin: An Understanding of the Structure–Activity Relationships for a Powerful Class of Antitumor Agents**

Teresa Carlomagno, Marcel J. J. Blommers,* Jens Meiler, Wolfgang Jahnke, Thomas Schupp, Frank Petersen, Dieter Schinzer, Karl-Heinz Altmann, and Christian Griesinger**

Most of the drugs available today for the treatment of cancer are based on the inhibition of cell proliferation and induction of cell death by apoptosis. At the molecular level, the majority of cytotoxic agents interfere with DNA function. However, a prominent subclass of compounds, including paclitaxel (taxol), exert their cytotoxic activity by perturbing microtubule dynamics. In 1993, Höfle, Reichenbach, and coworkers reported the isolation and characterization of a novel class of cytotoxic polyketide macrolides from the myxobacterium *Sorangium cellulosum*, which were named epothilones (**1**).[1,2] The interest in these natural products immediately soared when it was found that epothilones are microtubule stabilizers and that they inhibit cell proliferation through a mechanism of action analogous to that of the renowned clinical anticancer drug taxol.[3] Epothilones exhibit extraordinary antiproliferative activity in vitro and they efficiently induce cell death in paclitaxel-resistant tumor cell lines at up to 5000-fold

[*] Dr. T. Carlomagno,[++] Prof. Dr. C. Griesinger, Dr. J. Meiler[+]
Max-Planck-Institut für Biophysikalische Chemie
Am Fassberg 11, 37077 Göttingen (Germany)
Fax: (+49) 551-201-2202
E-mail: taco@nmr.mpibpc.mpg.de
cigr@nmr.mpibpc.mpg.de

Dr. M. J. J. Blommers,[++] Dr. W. Jahnke
Core Technologies, Novartis Pharma AG
P.O. Box, 4002 Basel (Switzerland)
Fax: (+41) 61-324-2686
E-mail: marcel_jj.blommers@pharma.novartis.com

Dr. T. Schupp, Dr. F. Petersen
Lead Discovery Center, Novartis Pharma AG
P.O. Box, 4002 Basel (Switzerland)

Dr. K.-H. Altmann
Corporate Research, Novartis Pharma AG
P.O. WKL-136.5.22, 4002 Basel (Switzerland)

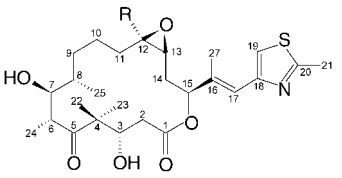
Prof. Dr. D. Schinzer
Chemisches Institut, Universität Magdeburg
Universitätsplatz 2, 39106 Magdeburg (Germany)

[+] Present address: University of Washington
BOX 357350, Seattle, WA 98195 (USA)

[++] Both authors have contributed equally.

[**] This work was supported by the MPG, the DFG (Gr1112/11-1, Schi 230/14-1) and the Fonds der Chemischen Industrie. J.M. was supported by a stipend by the Fonds der Chemischen Industrie. Dr. G. Rihs and H. R. Walter of Novartis Pharma AG are thanked for the structure of epothilone A by X-ray crystallography. Dr. M. O. Steinmetz is acknowledged for his work to determine the polymerization state of tubulin in the NMR sample.

 DOI: 10.1002/anie.200351276 © 2003 Wiley-VCH Verlag GmbH & Co. KGaA, Weinheim



1a: R = H (epothilone A)
1b: R = CH_3 (epothilone B)

lower concentrations than taxol.[3–5] In addition, they are more soluble than taxol in water,[2,4] which allows delivery in vivo with non-chremaphor-containing formulation vehicles, thus eliminating formulation-based side effects (major hypersensitivity reactions (HSR)).[6] The potential clinical utility of epothilones is supported by in vivo experiments with epothilone B in a variety of nude mouse human-tumor models.[4,7]

Shortly after the elucidation of the absolute stereochemistry of epothilone B by a combination of X-ray crystallography and chemical degradation studies,[2] routes for the total synthesis of the epothilones were devised.[8–10] To date, more than 20 total syntheses of epothilones A and B have been published.[8–14] At the same time several hundred analogues have been prepared and their biological activity investigated, which has led to a remarkably comprehensive understanding of the structure–activity relationships (SAR) for epothilone-derived structures.[11,12,15,16] Recently, the structure of a 2D tubulin polymer sheet in complex with docetaxel (taxotere) was solved at 3.7-Å resolution by electron crystallography.[17] However, in the absence of information on the bioactive conformation of epothilones any 3D model of the tubulin–epothilone complex remains uncertain.[18–23]

Herein we describe the conformation of epothilone A bound to tubulin, as determined by NMR spectroscopy in aqueous solution. This structure provides the first piece of experimental information on the active conformation of this class of microtubule stabilizers. The conformational differences observed between the X-ray crystal structure and the tubulin-bound conformation of epothilone A allow the rationalization of the biological data available on the tubulin-polymerization activity of several epothilone derivatives.

Both epothilones A and B, the two major naturally occurring epothilone variants, displace ^{3}H-taxol from tubulin ($K_i = 1.4$ and 0.71 μM for epothilone A and epothilone B, respectively),[5] indicating that the tubulin-binding sites of the epothilones and taxol overlap.

The high molecular weight of the tubulin–epothilone complex (~100 kDa) renders a tight complex a difficult target for NMR-based structural studies. However, if the binding of the ligand to the receptor is weak ($K_d > 10$ μM, $K_{off} > 100$ Hz), transferred nuclear Overhauser enhancement (trNOE)[24] and transferred cross-correlated relaxation (trCCR)[25,26] methods can be employed to unravel the conformation of epothilones in complex with tubulin. When a ligand is in fast exchange with the receptor, its spectroscopic properties result from the weighted average of those of the free and the bound conformation. NOE interactions and CCR rates are directly proportional to the correlation time of the molecule, and their average is governed by the contribution of the bound conformation, as a result of the considerably larger correlation time of the complex relative to the free ligand. Fortunately, the kinetic and thermodynamic properties of the complex between epothilone A and tubulin are in the desirable range for trNOE and trCCR experiments, as indicated by the negative sign of the NOE cross-peaks in a 100:1 mixture of epothilone A with tubulin. The trNOE and trCCR data are in agreement with a K_d in the range of 10–100 μM. Evidence for *specific* binding of epothilone A to tubulin is provided by the restoration of the NOE spectrum of free epothilone A upon addition of epothilone B to the mixture, which proves the quantitative displacement of epothilone A from tubulin by the tighter binder epothilone B. The existence of specific and transient binding of epothilone A to tubulin enables the structural analysis of the active conformation of the epothilones by NMR.

A crucial provision for the structural investigation of the epothilone–tubulin complex in solution is the prevention of tubulin polymerization. Electron microscopy and gel electrophoresis show that substitution of Mg^{2+} with Ca^{2+}[27] and D_2O as solvent[28] are sufficient to prevent tubulin polymerization. Samples were stable for approximately one week.

The tubulin-bound conformation of epothilone A was calculated from 46 interproton-distance restraints and seven torsion-angle restraints measured for a 0.5 mM solution of epothilone A in water in the presence of 5 μM tubulin. The distance restraints were derived from transferred NOE experiments. To filter out spin-diffusion-mediated peaks, only those signals with opposite sign to the diagonal peaks in a transferred ROESY experiment were taken into account. The dihedral-angle restraints were obtained by measuring CH–CH dipolar–dipolar and CH–CO dipolar–CSA transferred CCR rates for 60–70% ^{13}C-labeled epothilone A. The transferred cross-correlated relaxation (trCCR) experiments[25,26] were indispensable to obtain a unique description of the bound conformation, as more than one structure of the macrolide ring is compatible with the same H–H distance set (NOE intensities). The seven trCCR rates defined the torsion angles O1-C1-C2-C3, C1-C2-C3-C4, C2-C3-C4-C5, C5-C6-C7-C8, C12-C13-C14-C15, C13-C14-C15-O1, and C14-C15-C16-C17. One particular problem in the determination of the bound conformation of epothilone was the stereospecific assignment of the two methyl groups at C4, which turned out to be opposite to the published assignment (see Experimental Section for details).[2]

The tubulin-bound conformation of epothilone A is shown in green in Figure 1 and is compared with the free (unbound) conformation of epothilone A determined by X-ray crystallography,[29] which is shown in gray. We chose to compare the tubulin-bound conformation of epothilone with the X-ray structure and not with the solution structure available in CD_2Cl_2, because of the extensive flexibility of epothilone in solution in the absence of tubulin.[30] However, the most populated conformer in solution is indeed very similar to the X-ray conformer. The position of the thiazole nitrogen atom (blue in Figure 1) and of the 3-OH group (red), which are important for the delineation of a pharmocophore model, change significantly upon binding.

A comparison of the torsion angles of epothilone A in the tubulin-bound (green) and in the free (gray) conformation

 © 2003 Wiley-VCH Verlag GmbH & Co. KGaA, Weinheim

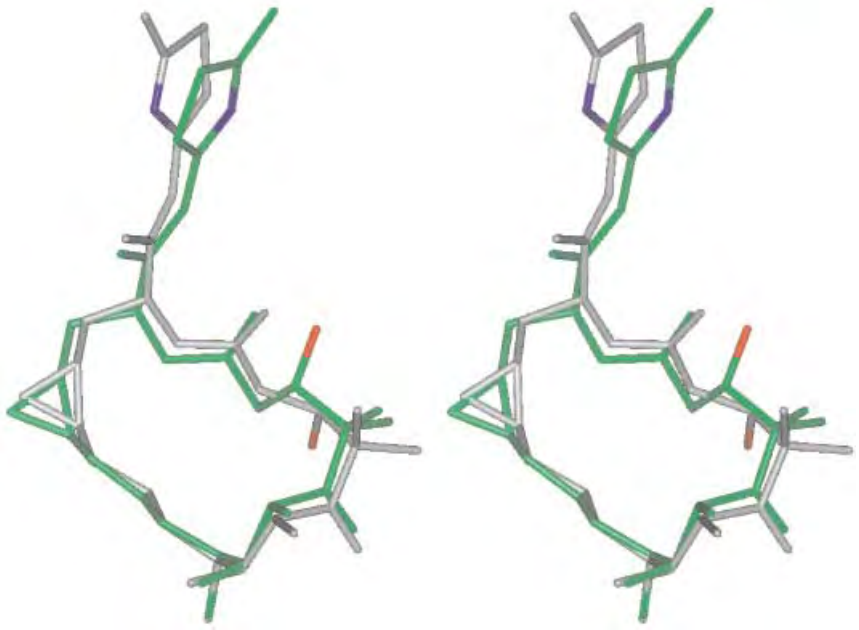


Figure 1. Stereoview of a comparison of the tubulin-bound conformation of epothilone A in aqueous solution (green) with the free conformation determined by X-ray crystallography[29] (gray). Hydrogen atoms have been removed for clarity. The conformational change that occurs in the O1–C6 region is clearly visible and is associated with a significant shift in the position of the 3-OH group (in red). A second key feature of the bound structure is the 180° change in the orientation of the side chain, which liberates the nitrogen atom (in blue) of the thiazole ring from the bulky Me27 group and makes it accessible to hydrogen-bonding donors.

(Table 1) reveals two major changes: the first occurs in the O1–C6 region and the second affects the orientation of the thiazole ring with respect to the C16–C17 double bond. In the lower region of the macrocycle, both cross-correlated relaxation rates (see preceding paper) and NOE data define the conformational change of the dihedral angle C2-C3-C4-C5, which switches from a *gauche*+ to a *gauche*− conformation, while the variations of the dihedral angles O1-C1-C2-C3 (+*anti*-periplanar to −*anti*-clinal) and C3-C4-C5-C6 result from the adjustment of the macrocycle to the modified torsion around the C3–C4 bond. The observed conformational change in the O1–C6 region of the ring primarily affects the position of the protons at C2, and of the 3-OH group. The two protons at C2 move towards the inner part of the ring. At the same time the oxygen atom attached to C3, which points to the inside of the macrocycle in the free conformation, moves towards the exterior by 3.8 Å (i.e. it now points away from the macrocycle). Neither the C5-C6-C7-C8 dihedral angle, determined by trCCR, nor the C10–C15 region exhibit any significant conformational change upon binding to tubulin. The latter finding corroborates a recent study in which the conformation of the macrocycle in the epoxide region is investigated with analogues of epothilone B and D.[31]

The second significant difference between the free and tubulin-bound conformations of epothilone occurs in the side chain that bears the thiazole ring. The C16-C17-C18-C19 dihedral angle changes from an *anti*-periplanar to a *syn*-periplanar conformation. This finding is substantiated by a strong NOE interaction between the protons of Me27 and H19 together with a significant weakening of the NOE interaction between H17 and H19 compared with that observed for epothilone A in aqueous solution and in the absence of tubulin. The eclipsed rotamer is energetically disfavored as a result of the steric hindrance between Me27 and H19. However, in this conformation, the nitrogen atom of the thiazole ring becomes more accessible for potential hydrogen-bonding formation with functional groups of proteins, which may more than offset an intrinsically disfavored epothilone side-chain conformation.

The tubulin-bound conformation of epothilone described herein is consistent with the wealth of chemical modification data available for this class of compounds. Epothilones are quite sensitive to chemical modifications in the C4–C8 region. The inversion of the stereochemistry at C3 also results in a considerable loss of potency in the induction of tubulin polymerization.[32] On the other hand, α,β-unsaturated (*trans* C2–C3 double bond) analogues of epothilones A and B are almost as active as the natural products. A very recent report by Vite and co-workers also showed that the replacement of the hydroxy group at C3

Table 1: Comparison of the dihedral angles of the tubulin-bound and the free conformations of epothilone A.

Dihedral angle	Tubulin-bound conformation [°]	Free conformation [°]
C1-C2-C3-C4	−152.5 ± 0.2	165.4
C2-C3-C4-C5	−51.7 ± 0.1	73.0
C3-C4-C5-C6	−43.0 ± 1.8	−75.9
C4-C5-C6-C7	156.4 ± 0.5	145.6
C5-C6-C7-C8	−70.0 ± 0.8	−64.0
C6-C7-C8-C9	−74.8 ± 0.3	−79.2
C7-C8-C9-C10	164.1 ± 0.8	159.0
C8-C9-C10-C11	−171.9 ± 0.4	176.8
C9-C10-C11-C12	−178.0 ± 0.4	174.8
C10-C11-C12-C13	−129.2 ± 0.5	−112.8
C11-C12-C13-C14	4.1 ± 0.1	−1.9
C12-C13-C14-C15	76.3 ± 0.1	93.9
C13-C14-C15-O1	−62.6 ± 1.0	−82.6
C14-C15-O1-C1	179.5 ± 0.5	159.6
C15-O1-C1-C2	176.3 ± 1.3	174.2
O1-C1-C2-C3	−124.3 ± 1.2	156.7
C14-C15-C16-C17	−129.7 ± 1.3	−118.5
C15-C16-C17-C18	180.0 ± 0.2	176.0
C16-C17-C18-N	180.0 ± 0.3	−7.6

The values given for the tubulin-bound conformation result from averaging over the ten lowest-energy conformations. The values given for the free conformation result from crystal structure analysis of epothilone A in methyl *tert*-butyl ether ($CH_3OC(CH_3)_3$) solvate.[29] This conformation, as well as crystal packing, is nearly identical to that of epothilone B,[2] although the two compounds crystallize from different solvents.

 © 2003 Wiley-VCH Verlag GmbH & Co. KGaA, Weinheim

with a cyano moiety leads to a compound that retains high biological activity.[33]

The hydroxy group attached to C3 is one of the biologically most relevant sites. In the free conformation, this OH group points towards the inner part of the ring and its oxygen atom is not easily accessible for the formation of external hydrogen bonds; conversely, in the tubulin-bound conformation, the 3-OH group points outwards, which makes the oxygen atom a potentially better acceptor of hydrogen bonding from tubulin side chains. This observation is consistent with chemical modification data, which underline the importance of the stereochemistry at C3 and therefore of the position of the 3-OH group. On the other hand, the fact that α,β-unsaturated epothilone analogues are almost as active as the natural compound indicates that the OH group is not crucial for tight binding to tubulin. This finding does not necessarily contradict the hypothesis of the existence of hydrogen bonding between the 3-OH of epothilone and tubulin side chains, as a double bond can also function as an electron donor.

The second profound conformational change observed upon binding of epothilone to tubulin concerns the orientation of the thiazole side chain, which undergoes a 180° rotation around the C17–C18 bond to liberate the nitrogen atom of the thiazole ring from the hindrance of the methyl group C27. It might be speculated that the nitrogen atom is now better available for hydrogen-bonding formation with a tubulin side chain. The potential role of the nitrogen atom as an hydrogen-bonding acceptor is corroborated by chemical modification data: the tubulin polymerization activity is retained upon substitution of the thiazole ring with a 2-pyridyl moiety, whereas the incorporation of a 3-pyridyl residue causes a notable decrease in the biological activity.[21] The recognition that the nitrogen atom of the thiazole ring may be involved in a hydrogen bond is highly relevant, as it might change the way of projecting new pharmacophore models for the orientation of epothilone in the tubulin-binding pocket. To date, all pharmacophore models are based on the attempted overlapping of the thiazole ring of epothilone with either the 2-OCOPh or the C3′-Ph of taxol. Nevertheless, the indubitable relevance of the nitrogen atom of the thiazole ring as an hydrogen-bonding acceptor opens the way to new pharmacophore models in which the nitrogen atom overlaps with a hydrogen-bonding acceptor in taxol. This new working hypothesis is currently under investigation in our laboratory.

So far, the design and synthesis of new potent analogues of epothilones was based on the available crystal structure of free epothilone. This has led to the discovery of candidates with promising properties, which, however, are still closely related to the parent compound. Potent analogues with structures deviating more strongly from the natural products might have a higher potential for alterations in the overall pharmacological profile. In addition, such compounds might be synthetically more readily accessible than closely related analogues of the natural products. The design of such analogues will be greatly aided by the knowledge described herein about the conformation of epothilone in its tubulin-bound state.

Experimental Section

All NMR experiments were performed on Bruker DRX 600 MHz or Avance 700 MHz spectrometers. The NOE constraints used to calculate the structure of the tubulin-bound conformation of epothilone were obtained from "transferred-NOE" experiments for a solution of epothilone A (0.5 mM) and tubulin (5 μM) in D_2O at mixing times of 100, 200, and 300 ms. The tr-ROESY experiment had a mixing time of 60 ms with CW irradiation at a field strength of 3500 Hz. CH–CH cross-correlated relaxation rates (trCCR-rates) for the determination of the C1-C2-C3-C4, C5-C6-C7-C8, C12-C13-C14-C15, and C13-C14-C15-C16 torsion angles were measured in HCCH correlation experiments, which were adapted from the original pulse program[34] to achieve the desired selectivity on the various epothilone moieties. The O-C1-C2-C3 torsion angle was measured in a dipole-CSA (CSA = chemical-shift anisotropy) trCCR experiment that was adapted from that used to measure CCR rates in the protein backbone.[35] The C2-C3-C4-C5 and C14-C15-C16-C17 torsion angles were measured with the help of a newly developed trCCR experiment.[36]

Tubulin was obtained from cytoskeleton (bovine brain, T238). The protein was dialyzed against calcium phosphate (3 mM), pH 7.0, lyophilized, and dissolved in D_2O prior to each measurement. All the trCCR experiments were acquired for a solution of ^{13}C-labeled epothilone A (0.5 mM) and tubulin (5 μM) in D_2O. ^{13}C-labeled epothilone was obtained by shake flask fermentation with the myxobacterium *Sorangium cellulosum* So ce90 by using a high-epothilone-producing mutant, BCE99/41 (Novartis strain collection). The fermentation was performed by growing the strain in medium (1000 mL) containing ^{13}C-labeled starch ($^{13}C_6$, 98%; 20 g) as carbohydrate source. Yields: epothilone A (20 mg) and epothilone B (15 mg), incorporation rate: 60–70% ^{13}C.

The assignment of the two diastereotopic methyl groups had to be established as it was essential to determine the dihedral angle around the C3–C4 bond by cross-correlated relaxation and consequently detect the large conformational change that takes place in this region upon binding to tubulin. Owing to the paucity of protons around the C3–C4 bond and to the conformational averaging present in this region for epothilone in solution in the absence of tubulin, the stereospecific assignment of the methyl groups could not be carried out by a combination of NOE interactions and $^3J_{CH}$ coupling constants. Therefore, we relied on the combination of NOE experiments, $^3J_{C,H}$ and $^3J_{C,C}$ couplings constants ($^3J_{C2,C5}$, $^3J_{C2,C22}$, and $^3J_{C2,C23}$) measured for epothilone B in the absence of tubulin at −20 °C in dimethylformamide. Under these conditions, the macrocycle can assume two conformations around the C3–C4 bond. Two pictures are compatible with the measured set of $^3J_{C,H}$ ($^3J_{C22,H3} \approx {}^3J_{C5,H3} > {}^3J_{C23,H3}$): 1) C22 = pro-*R*, C23 = pro-*S*, and a mixture of *gauche*+ and *trans* conformations around the C3–C4 bond; 2) pro*S*-C22, pro*R*-C23, and a mixture of *gauche*+ and *gauche* − conformations around the C3–C4 bond. The measured set of $^3J_{C,C}$ couplings ($^3J_{C2,C5} < {}^3J_{C2,C23} < {}^3J_{C2,C22}$) unequivocally confirms alternative 2. The resulting stereospecific assignment is opposite to that previously published.[2]

The structure of the tubulin-bound conformation of epothilone was determined by using the simulated annealing protocol, including NMR restraints, of the X-PLOR program.[37] The force field was adapted to include atom types occurring in epothilone A. Bond lengths and angles were taken from the X-ray structure of the free conformation. In addition, the force field included 46 NOE restraints and seven dihedral angles derived from trCCR rates. From a random starting point, an initial energy minimization of 50 steps, a high-temperature phase (32.5 ps, 6500 steps, 2000 K) and two cooling phases (25.0 ps, 5000 steps, 2000 K → 1000 K/10.0 ps, 2000 steps, 1000 K → 100 K) were performed. The closest local minimum was reached by applying a final energy minimization of 200 steps. This protocol was repeated 100 times. Within the ten lowest energy structures, all dihedral angles have a standard deviation of less than 2° and the RMSD of the positions of the heavy atoms is 0.044 Å.

Received: February 25, 2003 [Z51276]

 © 2003 Wiley-VCH Verlag GmbH & Co. KGaA, Weinheim

Keywords: natural products · NMR spectroscopy · structure elucidation · structure–activity relationships · tubulin

[1] G. Höfle, K. Bedorf, K. Gerth, *Chem. Abstr.* **1993**, *120*, 52841.
[2] G. Höfle, N. Bedorf, H. Steinmetz, D. Schomburg, K. Gerth, H. Reichenbach, *Angew. Chem.* **1996**, *108,* 1671 – 1672; *Angew. Chem. Int. Ed. Engl.* **1996**, *35*, 1567 – 1569.
[3] D. M. Bollag, P. A. McQueney, J. Zhu, O. Hensens, L. Koupal, J. Liesch, M. Goetz, E. Lazarides, C. M. Woods, *Cancer Res.* **1995**, *55*, 2325 – 2333.
[4] K.-H. Altmann, M. Wartmann, T. O'Reilly, *Biochim. Biophys. Acta* **2000**, *1470*, M79-M91.
[5] J. Kowalski, P. Giannakakou, E. Hamel, *J. Biol. Chem.* **1997**, *272*, 2534 – 2541.
[6] E. K. Rowinsky, *Annu. Rev. Med.* **1997**, *48*, 353 – 374.
[7] K.-H. Altmann, G. Bold, G. Caravatti, N. End, A. Florsheimer, V. Guagnano, T. O'Reilly, M. Wartmann, *Chimia* **2000**, *54*, 612 – 621.
[8] A. Balog, D. Meng, T. Kamenecka, P. Bertinato, D.-S. Su, E. J. Sorensen, S. J. Danishefsky, *Angew. Chem.* **1996**, *108*, 2976 – 2978; *Angew. Chem. Int. Ed. Engl.* **1996**, *35*, 2801 – 2803.
[9] Z. Yang, Y. He, D. Vourloumis, H. Vallberg, K. C. Nicolaou, *Angew. Chem.* **1997**, *109*, 170 – 173; *Angew. Chem. Int. Ed. Engl.* **1997**, *36*, 166 – 168.
[10] D. Schinzer, A. Limberg, A. Bauer, O. M. Böhm, M. Cordes, *Angew. Chem.* **1997**, *109*, 543 – 544; *Angew. Chem. Int. Ed. Engl.* **1997**, *36*, 523 – 524.
[11] K. C. Nicolaou, F. Roschangar, D. Vourloumis, *Angew. Chem.* **1998**, *110*, 2120-2153; *Angew. Chem. Int. Ed.* **1998**, *37*, 2014 – 2045.
[12] C. R. Harris, S. J Danishefsky, *J. Org. Chem.* **1999**, *64*, 8434 – 8456.
[13] J. Mulzer, H. J. Martin, M. Berger, *J. Heterocycl. Chem.* **1999**, *36*, 1421 – 1436.
[14] K. C. Nicolaou, A. Ritzen, K. Namoto, *J. Chem. Soc. Chem. Commun.* **2001**, 1523 – 1535.
[15] K.-H. Altmann, M. Wartmann, T. O'Reilly, *Biochim. Biophys. Acta* **2000**, *1470*, M79-M91.
[16] M. Wartmann, K.-H. Altmann, *Curr. Med. Chem. - Anti-cancer Agents* **2002**, *2*, 123 – 148.
[17] E. Nogales, S. G. Wolf, K. H. Downing, *Nature* **1998**, *391*, 199 – 203.
[18] J. D. Winkler, P. H. Axelsen, *Bioorg. Med. Chem. Lett.* **1996**, *6*, 2963 – 2966.
[19] M. Wang, X. Xia, Y. Kim, D. Hwang, J. M. Jansen, M. Botta, D. C. Liotta, J. P. Snyder, *Org. Lett.* **1999**, *1*, 43 – 46.
[20] I. Ojima, S. Chakravarty, T. Inoue, S. Lin, L. He, S. B. Horwitz, S. D. Kuduk, S. J. Danishefsky, *Proc. Natl. Acad. Sci. USA* **1999**, *96*, 4256 – 4261.
[21] K. C. Nicolaou, R. Scarpelli, B. Bollbuck, B. Werschkun, M. M. A. Pereira, M. Wartmann, K. H. Altmann, D. Zaharevitz, R. Gussio, P. Giannakakou, *Chem. Biol.* **2000**, *7*, 593 – 599.
[22] P. Giannakakou, R. Gussio, E. Nogales, K. H. Downing, D. Zaharevitz, B. Bollbuck, G. Poy, D. Sackett, K. C. Nicolaou, T. Fojo, *Proc. Natl. Acad. Sci. USA* **2000**, *97*, 2904 – 2909.
[23] L. He, P. G. Jagtap, D. G. I. Kingston, H.-J. Shen, G. A. Orr, S. B. Horwitz, *Biochemistry* **2000**, *39*, 3972 – 3978.
[24] F. Ni, *Prog. Nucl. Magn. Reson. Spectrosc.* **1994**, *26*, 517 – 606.
[25] T. Carlomagno, I. C. Felli, M. Czech, R. Fischer, M. Sprinzl, C. Griesinger, *J. Am. Chem. Soc.* **1999**, *121*, 1945 – 1948.
[26] M. J. J. Blommers, W. Stark, C. E. Jones, D. Head, C. E. Owen, W. Jahnke, *J. Am. Chem. Soc.* **1999**, *121*, 1949 – 1953.
[27] F. Solomon, *Biochemistry* **1977**, *16*, 358 – 363.
[28] G. Chakrabarti, S. Kim, M. L. Gupta, Jr., J. S. Barton, R. H. Himes, *Biochemistry* **1999**, *38*, 3067 – 3072.
[29] G. Rihs, H. R. Walter, unpublished results.
[30] R. E. Taylor, J. Zajicek, *J. Org. Chem.* **1999**, *64*, 7224 – 7228.
[31] R. E. Taylor, Y. Chen, A. Beatty, D. C. Myles, Y. Zhou, *J. Am. Chem. Soc.* **2003**, *125*, 26 – 27.
[32] K. C. Nicolaou, D. Vourloumis, T. Li, J. Pastor, N. Winssinger, Y. He, S. Ninkovic, F. Sarabia, H. Vallberg, F. Roschangar, N. P. King, M. Ray, V. Finlay, P. Giannakakou, P. Verdier-Pinard, E. Hamel, *Angew. Chem.* **1997**, *109*, 2181 – 2187; *Angew. Chem. Int. Ed. Engl.* **1997**, *36*, 2097 – 2103.
[33] A. Regueiro-Ren, K. Leavitt, S.-H. Kim, G. Höfle, M. Kiffe, J. Z. Gougoutas, J. D. DiMarco, F. Y. F. Lee, C. R. Fairchild, B. H. Long, G. D. Vite, *Org. Lett.* **2002**, *4*, 3815 – 3818.
[34] I. C. Felli, C. Richter, C. Griesinger, H. Schwalbe, *J. Am. Chem. Soc.* **1999**, *121*, 1956.
[35] D. W. Yang, R. Konrat, L. E. Kay, *J. Am. Chem. Soc.* **1999**, *121*, 11938 – 11940.
[36] See following manuscript in this issue: T. Carlomagno, V. M. Sanchez, M. J. J. Blommers, C. Griesinger, *Angew. Chem.* **2003**, *115*, 2619 – 2621; *Angew. Chem. Int. Ed.* **2003**, *42*, 2515 – 2517.
[37] A. T. Bruenger, *X-PLOR A System for X-ray Crystallography and NMR* (Yale University Press, New Haven), **1992**.

 © 2003 Wiley-VCH Verlag GmbH & Co. KGaA, Weinheim

Torsion Angles of Epothilones

Derivation of Dihedral Angles from CH–CH Dipolar–Dipolar Cross-Correlated Relaxation Rates: A C–C Torsion Involving a Quaternary Carbon Atom in Epothilone A Bound to Tubulin**

Teresa Carlomagno, Víctor M. Sánchez, Marcel J. J. Blommers, and Christian Griesinger**

Cross-correlated relaxation (CCR) rates constitute a valid alternative to coupling constants for the determination of dihedral angles.[1] For high-molecular-weight systems the measurement of scalar coupling constants poses serious problems caused by large linewidths and by differential relaxation effects.[2] Conversely, CCR measurements are feasible also for molecules of large size and have been successfully employed in the past years to determine dihedral angles in biomolecules.[3–6] We have recently reported the usage of cross-correlated relaxation rates to derive angular

[*] Dr. T. Carlomagno, Prof. Dr. C. Griesinger, Dr. V. M. Sánchez
Max-Planck-Institut für Biophysikalische Chemie
Am Fassberg 11, 37077 Göttingen (Germany)
Fax: (+49) 551-201-2201
E-mail: taco@nmr.mpibpc.mpg.de
cigr@nmr.mpibpc.mpg.de

Dr. M. J. J. Blommers
Novartis Pharma AG
P.O. Box, 4002 Basel (Switzerland)

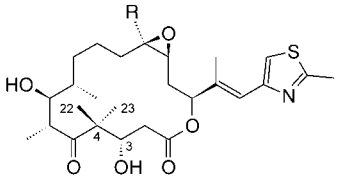
[**] This work was supported by the MPG, the DFG and the Fonds der Chemischen Industrie. V.M.S. is supported by the EU through a Marie Curie fellowship. All measurements were performed at the Large Scale Facility for Biomolecular NMR in Frankfurt (HPRI-1999-CT-00014). The authors thank T. Schupp and F. Petersen of Novartis Pharma AG for the preparation of ^{13}C-labeled epothilone.

 DOI: 10.1002/anie.200350950 © 2003 Wiley-VCH Verlag GmbH & Co. KGaA, Weinheim

structural information for a small ligand weakly bound to a macromolecule.[7,8] Similarly to "transferred-NOEs",[9,10] "transferred-CCR rates" are informative of the bound conformation of the ligand when the complex is in the fast-exchange regime on the NMR timescale. Information on the bound conformation of the ligand cannot be obtained from coupling constants, because their value is independent of the molecular correlation time.[7]

Herein we introduce a pulse sequence that measures CH–CH cross-correlated relaxation in a H^aC^a–$C^b(CH_3)^c$ moiety, in which the second C atom is quaternary. This rate allows the calculation of the dihedral angle about the C^a—C^b bond.

We have applied the pulse sequence to a 100:1 mixture of ^{13}C-labeled epothilone A (**1**) and tubulin to determine the dihedral angle about the C3—C4 bond of epothilone in its bound conformation. Epothilones are very potent antitumor drugs that exert cytotoxic activity by binding to the 100-kDa tubulin α/β heterodimers.[11a] Their conformation in the bound state is not known, whereas the unbound conformation was previously determined by X-ray crystallography.[11b] The equilibrium and kinetic constants of the epothilone A–tubulin complex ($K_D = 10$–100 μM) render it suitable for "transferred" CCR experiments. Furthermore, it could be shown by competition experiments with the strong specific binder epothilone B that there is only one specific binding site for epothilone A. A sample of ^{13}C-labeled epothilone A was obtained by growing the myxobacterium *Sorangium cellulosum* on ^{13}C-rich medium.



1a R = H (epothilone A)
1b R = CH_3 (epothilone B)

The dihedral angle about the C3—C4 bond of epothilone is accessible by measuring the dipolar–dipolar CCR rates between the C3–H vector and the C22–H or C23–H vectors. The direction of the three C—H bonds in each methyl group is averaged, as a consequence of the fast rotation around the C4—C22 and C4—C23 bonds. Therefore, the C22–H and C23–H vectors assume an average orientation that is collinear with the C4—C22 and C4—C23 bonds, respectively.

The pulse sequence used for the measurement of the $\Gamma_{CH,CH}$ rate between the C3–H vector and the $(C22/23–H)_{av.}$ vectors is shown in Figure 1. Two experiments are recorded, yielding a cross and a reference spectrum (quantitative Γ approach).[12,13] The CCR rate is extracted from the ratio of peak intensities in the cross and reference experiments. The pulse sequence is optimized for maximum sensitivity of the cross experiment: the $8H_z^{22/23}C_y^{22/23}C_z^{4}C_y^{3}$ coherence present at point c is transformed by $\Gamma_{C23–H,C3–H}$ into $8C_x^{22/23}C_z^{4}C_x^{3}H_z^{3}$ with an efficiency equal to $3\sinh(\Gamma_{C22/23–H,C3–H}T_{rel})\cosh^2(\Gamma_{C22/23–H,C3–H}T_{rel})$. The $8C_x^{22/23}C_z^{4}C_x^{3}H_z^{3}$ term is then transformed into H_x^3 for detection. The delays are optimized for optimal refocusing and defocusing of the couplings. Selective π pulses on the carbon atoms prevent loss of magnetization to other passively coupled carbons. The details of the coherence transfers are provided in Figure 1 and its legend.

The cross and reference spectra are shown in Figure 2. Two peaks are observed in the reference spectrum at the chemical shifts of C22 and C23 in ω_1 and the chemical shift of H3 in ω_2. In the cross-spectrum, the C23(ω1)–H3(ω2) peak is missing, indicating that the dipolar–dipolar CCR between the $(C23–H)_{av.}$ vector and the C3–H vector is close to zero. The quantitative value for the two CCR rates can be extracted according to [Eq. (1)] (I_{cross} and I_{ref} are the intensities of the peaks in the cross and reference experiment, respectively and Γ indicates the cross-correlated relaxation rate).

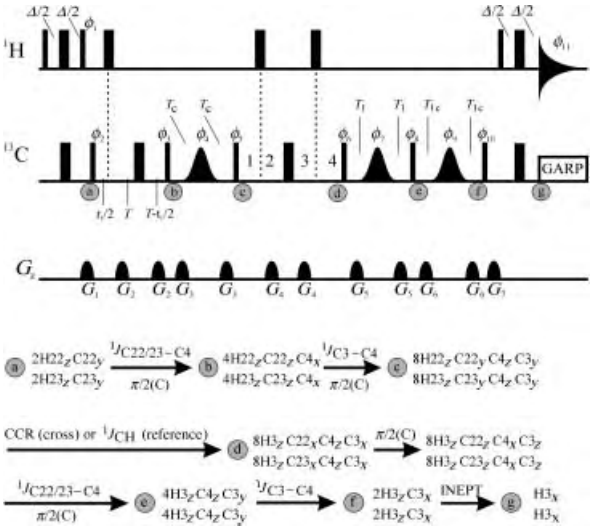


Figure 1. Pulse sequence for the measurement of dipolar–dipolar cross-correlated relaxation between the $(C22/23–H)_{av.}$ vector and the C3–H vector in epothilone. $\Delta = 1/(2^1J_{C,H}) = 7$ ms; $T = 1/(4^1J_{C,C}) = 7$ ms; $T_c = 1/(4^1J_{C,C}) = 7$ ms; $T_1 = 1/(8^1J_{C,C}) = 3.5$ ms; $T_{1c} = T_c$. Delays 1–4 are equal to $T_{rel}/4$ ($T_{rel} = 1/^1J_{C,C} = 28$ ms) in the cross-experiment; in the reference experiment, delay 1 = $T_{rel}/4+\Delta/8$ = delay 3 and delay 2 = $T_{rel}/4-\Delta/8$ = delay 4. $\phi_1 = y$; $\phi_2 = x, -x$; $\phi_3 = 2(y), 2(-y)$; $\phi_5 = 4(x), 4(-x)$; $\phi_6 = 8(y), 8(-y)$; $\phi_8 = x$; $\phi_{10} = y$; $\phi_{11} = 2(x,-x), 4(-x,x), 2(x,-x)$; $\phi_4 = \phi_7 = \phi_9 = x$. The pulses with phase ϕ_4 and ϕ_9 are Q3 pulses of 768 ms duration, centered at $\delta = 63$ ppm, to invert C3 and C4 selectively (C3 resonates at 70.9 ppm and C4 at 53.0 ppm); the pulse with phase ϕ_7 is a Q3 pulse with a duration of 512 ms centered at $\delta = 37$ ppm, to invert the C22/23 and C4 selectively (C22 resonates at $\delta = 19.1$ ppm and C23 at $\delta = 21.7$ ppm). The proton carrier was at $\delta = 4.78$ ppm and the carbon carrier at $\delta = 37$ ppm; spectral widths were 4807.69 Hz for ^{1}H and 8333.33 Hz for ^{13}C. Carbon decoupling in acquisition consisted of a GARP modulated pulse train at 2.38 kHz field strength.

$$I_{cross}/I_{ref} = \tanh(\Gamma T_{rel})/[\sin^2(\pi J_{C,H}\Delta/2)\cos^2(\pi J_{C,H}\Delta/2)] \quad (1)$$

The measured CCR rates between the C3–H vector and the $(C23–H)_{av.}$ and $(C22–H)_{av.}$ vectors are 0.1 ± 0.1 and -1.4 ± 0.4, respectively. The error was calculated applying error propagation theory, assuming that the noise represents the experimental uncertainty of the peak intensities.

The dependence of the two CCR rates on the C2-C3-C4-C5 dihedral angle θ is given in [Eq. (2)] and [Eq. (3)].

$$\Gamma_{C23–H,C3–H} = -0.3296\, k\, S^2 \tau_c P_2[\cos^2 109.7^o \sin^2 109.7^o \cos(\theta)] \quad (2)$$

$$\Gamma_{C22–H,C3–H} = -0.3296\, k\, S^2 \tau_c P_2[\cos^2 109.7^o \sin^2 109.7^o \cos(\theta - 120^o)] \quad (3)$$

 © 2003 Wiley-VCH Verlag GmbH & Co. KGaA, Weinheim

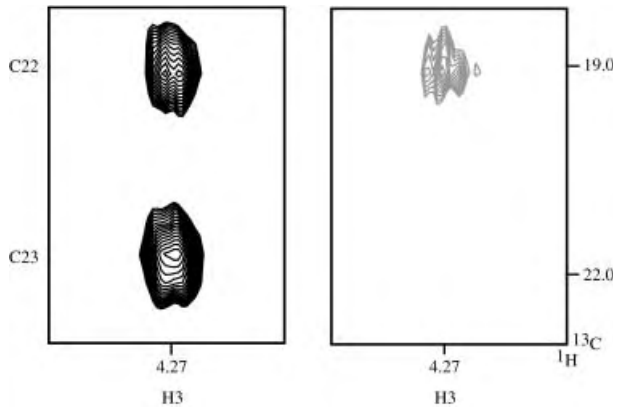


Figure 2. Reference (left) and cross-spectra (right) acquired with the sequence of Figure 1 on a Bruker DRX 600 MHz spectrometer. The peaks visible in the reference spectrum are at the chemical shift of C22 ($\delta = 19.1$ ppm) and C23 ($\delta = 21.7$ ppm) in the ^{13}C dimension and at the chemical shift of H3 ($\delta = 4.27$ ppm) in the ^{1}H dimension. The cross-experiment was four times longer than the reference experiment. During the experiment, 1024 and 64 complex points were acquired in t_2 and t_1, respectively. The final matrices were 2048×128 points. The gray lines represent negative contours. The sample contained 0.5 mM epothilone A and 5 μM tubulin dissolved in D_2O.

The $(C22–H)_{av.}$ and $(C23–H)_{av.}$ vectors lie along the direction defined by the C4–C22 and C4–C23 bonds, respectively. The CCR rates $\Gamma_{C22–H,C3–H}$ and $\Gamma_{C23–H,C3–H}$ are scaled by $P_2[\cos 109.7°] = {}^1/_2[3\cos^2(109.7°)-1] = -0.3296$ as a result of the averaging of the C–H directions in each methyl group, ($k = (\gamma_C\gamma_H h\mu_0/8\pi^2)^2$, τ_c is the effective correlation time of the molecule, θ is the torsion angle C^2-C^3-C^4-C^5 and S^2 is the order parameter accounting for internal motions.)

A graphical representation of the dependence of the two CCR rates on the torsion angle θ is shown in Figure 3 for a τ_c of 0.74 ns, which is the effective τ_c of epothilone in the presence of 5 μM tubulin, as estimated from other CCR measurements, and an order parameter $S^2 = 0.8$ to account for

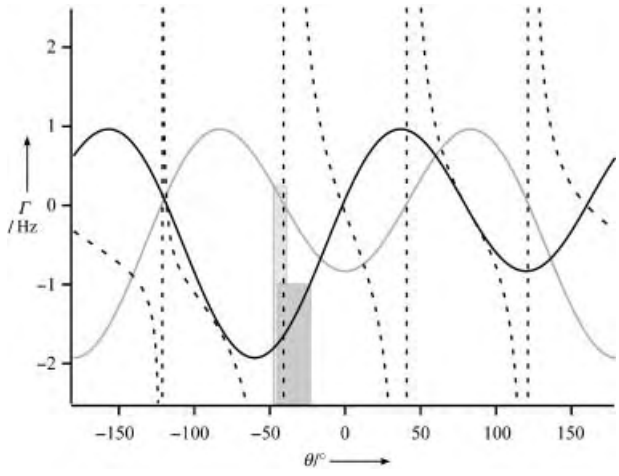


Figure 3. Dependence of the two cross-correlated relaxation rates $\Gamma_{C22–H,C3–H}$ (in black) and $\Gamma_{C23–H,C3–H}$ (in gray) on the dihedral angle θ(C^2-C^3-C^4-C^5). The two gray shadowed regions represent the value of θ that satisfy the measured CCR rates. The dashed curve represents the ratio $\Gamma_{C23–H,C3–H}/\Gamma_{C23–H,C3–H}$.

internal motions. The stereospecific assignment of the methyl groups (C22 in *pro-S* and C23 in *pro-R*) was obtained by the combination of NOE interactions and $^3J_{H,C}$ and $^3J_{C,C}$ coupling-constant data for epothilone B in the absence of tubulin and is opposite to that reported in the literature.[11b,14]

The dihedral angle θ that complies with the ratio between the two CCR rates is $-45 \pm 5°$. We used the ratio of the two CCR rates, instead of the rates themselves, to determine the dihedral angle because this approach is independent of both the correlation time and the internal motion order parameter S^2, if equal internal reorientation of all the C–H vectors is assumed.

The change in the θ dihedral angle from the gauche+ conformation in the free form to the gauche− conformation in the bound form is supported by transferred-NOE data. The structure of the bound form of epothilone determined by transferred-NOE and transferred-CCR was reported in the previous communication.[14]

The new experiment allows the determination of X-C^a-C^b-Y dihedral angles by CCR rates when X is a proton and Y is a methyl group. The method is broadly applicable to any HC-CCH_3 moiety, and therefore to a number of amino acid side chains in proteins.

Received: January 16, 2003 [Z50950]

Keywords: conformation analysis · dihedral angle · natural products · NMR spectroscopy · tubulin

[1] B. Reif, M. Hennig, C. Griesinger, *Science* **1997**, *276*, 1230–1233.
[2] a) G. S. Harbison, *J. Am. Chem. Soc.* **1993**, *115*, 3026–3027; b) T. J. Norwood, *J. Magn. Reson. Ser. A* **1993**, *104*, 106.
[3] D. Yang, K. H. Gardner, L. E. Kay, *J. Biomol. NMR* **1998**, *11*, 213–220.
[4] D. Yang, R. Konrat, L. E. Kay, *J. Am. Chem. Soc.* **1997**, *119*, 11938–11940.
[5] E. Chiarparin, P. Pelupessy, R. Ghose, G. Bodenhausen, *J. Am. Chem. Soc.* **2000**, *122*, 1758–1761.
[6] P. Pelupessy, E. Chiarparin, R. Ghose, G. Bodenhausen, *J. Biomol. NMR* **1999**, *14*, 277–280.
[7] T. Carlomagno, I. C. Felli, M. Czech, R. Fischer, M. Sprinzl, C. Griesinger, *J. Am. Chem. Soc.* **1999**, *121*, 1945–1948.
[8] M. J. J. Blommers, W. Stark, C. E. Jones, D. Head, C. E. Owen, W. Jahnke, *J. Am. Chem. Soc.* **1999**, *121*, 1949–1953.
[9] a) F. Ni, *Prog. Nucl. Magn. Reson. Spectrosc.* **1994**, *26*, 517; b) L. Y. Lian, I. L. Barsukov, M. J. Sutcliffe, K. H. Sze, G. C. K. Roberts, *Methods Enzymol.* **1994**, *239*, 657–707.
[10] a) G. M. Clore, A. M. Gronenborn, *J. Magn. Reson.* **1982**, *48*, 402–417; b) G. M. Clore, A. M. Gronenborn, *J. Magn. Reson.* **1982**, *53*, 423–442.
[11] a) G. Höfle, N. Bedorf, K. Gerth, *Chem. Abstr.* **1993**, *120*, 52841; b) G. Höfle, N. Bedorf, H. Steinmetz, D. Schomburg, K. Gerth, H. Reichenbach, *Angew. Chem. Int. Ed. Engl.* **1996**, *35*, 1567–1569; *Angew. Chem.* **1996**, *108*, 1671–1673.
[12] I. C. Felli, C. Richter, C. Griesinger, H. Schwalbe, *J. Am. Chem. Soc.* **1999**, *121*, 1956–1957.
[13] T. Carlomagno, M. J. J. Blommers, J. Meiler, B. Cuenoud, C. Griesinger, *J. Am. Chem. Soc.* **2001**, *123*, 7364–7370.
[14] See previous manuscript in this issue: T. Carlomagno, M. J. J. Blommers, J. Meiler, W. Jahnke, T. Schupp, F. Petersen, D. Schinzer, K.-H. Altmann, C. Griesinger, *Angew. Chem.* **2003**, *115*, 2511–2515; *Angew. Chem. Int. Ed.* **2003**, *42*, 2615–2619.

 © 2003 Wiley-VCH Verlag GmbH & Co. KGaA, Weinheim

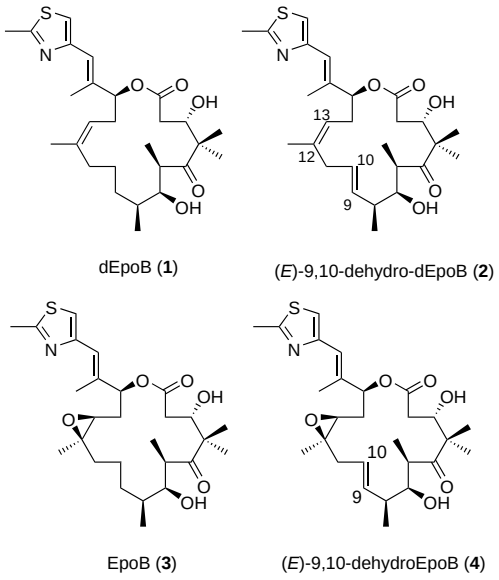
Antitumor Drugs

Synthesis and Conformational Analysis of (*E*)-9,10-Dehydroepothilone B: A Suggestive Link between the Chemistry and Biology of Epothilones**

*Fumihiko Yoshimura, Alexey Rivkin, Ana E. Gabarda, Ting-Chao Chou, Huajin Dong, George Sukenick, Florence F. Morel, Richard E. Taylor, and Samuel J. Danishefsky**

The substantial multidisciplinary interest in epothilones, fueled by their emergence as promising anticancer drug candidates, has led to a worldwide effort to synthesize new analogues[1] and to establish their structure–activity relationships with a view to identifying and developing later-generation agents for clinical evaluation.[2] Human clinical trials of several epothilones as drugs, seeking to assess issues of toxicity, optimal dosage, and efficacy, are well underway. For example, 12,13-desoxyepothilone (**1**, dEpoB),[3] which was initially developed in our laboratory by total synthesis, is now undergoing human clinical trials after showing promising activity in in vivo tests.[4]

In our early studies we had found that epothilone B (**3**, EpoB),[5] which contains an epoxide at C12–C13, is significantly more cytotoxic than is its 12,13-desoxy analogue (**1**, dEpoB).[6] However, from the perspective of therapeutic index, the desoxy compound seemed to us to be much more promising.[7] More recently, we reported the total synthesis of (*E*)-9,10-dehydro-12,13-desoxyepothilone B (**2**), using a stereoselective ring-closing metathesis reaction as a key step.[8] The incorporation of unsaturation at C9–C10 over and above the usual *Z*-12,13 double bond (see compound **2**) resulted in a marked increase in in vitro potency of the drug. The beneficial effects of the incremental C9–C10 unsaturation have been extended to in vivo experiments in xenograft mice. Moreover, compound **2** enjoys major pharmacokinetic advantages over dEpoB (**1**). These twin benefits allowed a decrease in the dosing levels for **2** relative to **1** in xenograft experiments by an order of magnitude.[8a] Accordingly, we wondered if the incorporation of a double bond at C9–C10 in epothilone B, with the epoxide intact (i.e. (*E*)-9,10-dehydroEpoB (**4**)) would alter the biological profile of the drug in the same manner.



In practice, epoxidation of **2** with 2,2′-dimethyldioxirane (DMDO) proceeded with high chemoselectivity at the more substituted C12–C13 double bond to give **4** (corresponding to the natural series in the configuration of the epoxide linkage) and its non-natural diastereomer (**5**) in 87% yield with a 1:2.6 ratio (Scheme 1). The stereochemical assignment of the epoxides was secured by selective reduction of the C9–C10 double bonds of **4** and **5** with diimide.[9] Examination of the spectral properties of these reduction products revealed that EpoB (**3**) had arisen from the minor epoxidation product of **2**, that is, **4**. Correspondingly, reduction of the major epoxidation product **5** afforded 12,13-bis-*epi*-EpoB (**6**). The preference for α epoxidation[10] in the case of **2** stands in striking contrast to the highly stereoselective epoxidation of dEpoB,[11,2b] which occurs from the β face,[10] leading to EpoB (**3**) (see below).[3b]

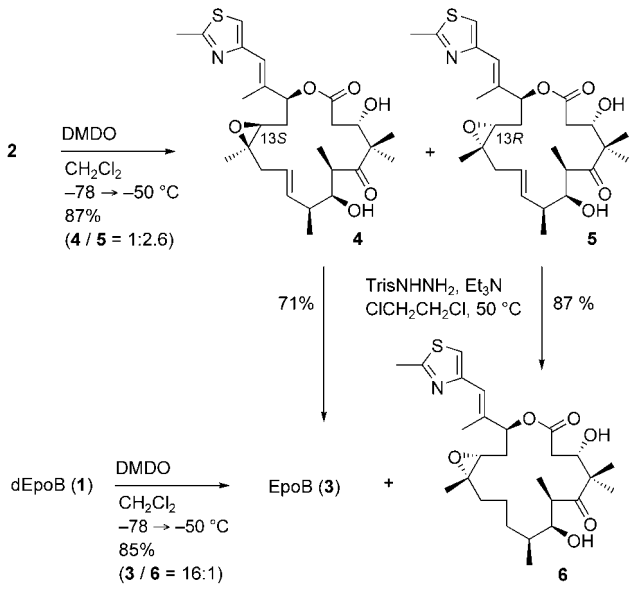
(*E*)-9,10-Dehydroepothilone B (**4**) was evaluated against a variety of cell types for an early assessment of its antitumor potential. As shown in Table 1, the compound exhibits high cytotoxic activity against a variety of sensitive and resistant tumor cell lines. A direct comparison of **4** with EpoB (**3**) indicates that this new analogue, **4**, is nearly three times as potent as **3** itself. Interestingly, **5** and **6** in the non-natural (13*R*)-α-epoxide series display much lower in vitro activity than **3** and **4**, respectively.

[*] Prof. S. J. Danishefsky, Dr. F. Yoshimura, Dr. A. Rivkin, Dr. A. E. Gabarda
Laboratory for Bioorganic Chemistry
Sloan-Kettering Institute for Cancer Research
1275 York Avenue, New York, NY 10021 (USA)
Fax: (+1) 212-772-8691
E-mail: s-danishefsky@ski.mskcc.org
and
Department of Chemistry, Columbia University
Havemeyer Hall, 3000 Broadway, New York, NY 10027 (USA)
Dr. T.-C. Chou, Dr. H. Dong
Preclinical Pharmacology Core Facility
Sloan-Kettering Institute for Cancer Research
Dr. G. Sukenick
NMR Analytical Core Facility
Sloan-Kettering Institute for Cancer Research
F. F. Morel, Prof. R. E. Taylor
Department of Chemistry and Biochemistry
Walther Cancer Research Center, University of Notre Dame
Notre Dame, IN 46556-5670 (USA)

[**] This work was supported by the National Institutes of Health (CA-28824). F.Y. is a Uehara Memorial Foundation Fellow. A.R. is a NIH Cancer Pharmacology Fellow (T32-CA62948). A.E.G. is a MSKCC Experimental Therapeutics Center Fellow. We thank Ms. Sylvi Rusli (NMR Core Facility, CA-02848) and Mrs. Anna Dudkina for mass spectral analyses.

Supporting information for this article is available on the WWW under http://www.angewandte.org or from the author.

 © 2003 Wiley-VCH Verlag GmbH & Co. KGaA, Weinheim DOI: 10.1002/anie.200351407



Scheme 1. Synthesis of **4** and EpoB (**3**).

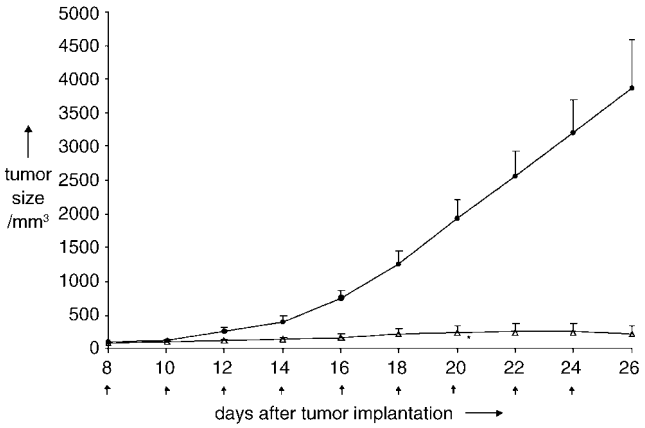


Figure 1. Therapeutic effect of (*E*)-9,10-dehydroEpoB (**4**) in nude mice bearing MX-1 xenograft (6 h intravenous infusion, $n = 4$). ● Control (sacrificed on day 26). △Dosage: 0.4 mg kg^{-1}, administered every other day, nine doses in total (25% of the mice had died by day 25, after 9 doses, 25% of the tumors had disappeared by day 34).

Table 1: In vitro cytotoxicities (IC_{50}) with tumor cell lines.[a]

Compounds	IC_{50} [μM][a]		
	CCRF-CEM	CCRF-CEM/VBL_{100}	CCRF-CEM/taxol
1 (dEpoB)	0.0036	0.016	0.0046
2	0.0009	0.0042	0.0012
3 (EpoB)	0.00062	0.0037	0.0011
4	0.00023	0.00032	0.00042
5	0.0134	0.0959	0.0802
6	0.083	0.4519	0.1507

[a] XTT assay following 72 h inhibition. CCRF-CEM is a human T cell acute lymphoblastic leukemia cell line. The CCRF-CEM/VBL and CCRF-CEM/taxol cell lines all overexpress P-glycoprotein and display a multidrug-resistance phenotype to MDR-associated oncolytics.[13]

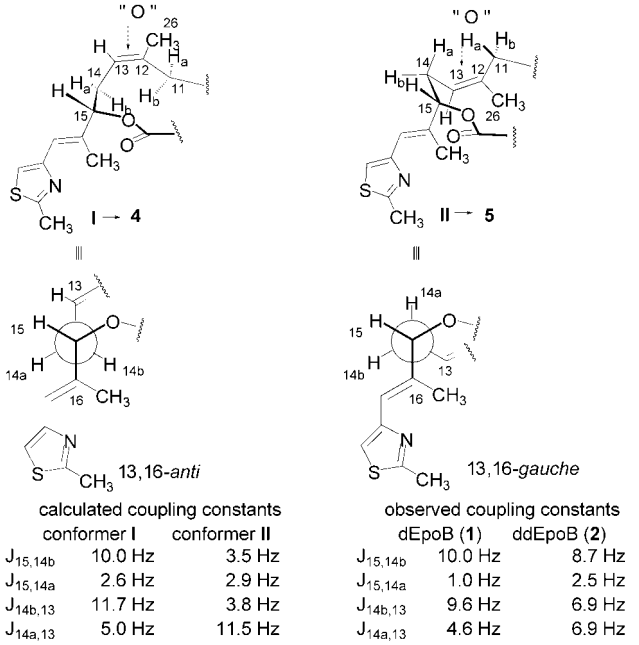


Figure 2. Conformation of the C11–C14 region of desoxy-epothilone.

The high cytotoxic activity of **4** encouraged us to determine its in vivo efficacy in nude mice bearing human tumor xenografts. As shown in Figure 1, compound **4** demonstrated remarkable potency in inhibiting the growth of implanted tumors at much lower dosages (0.4 mg kg^{-1}) relative to **3**. Compound **4** is, to our knowledge, the *most potent epothilone* of established in vivo efficacy.[12]

The dramatic difference in the stereochemistry of epoxidation of **2** relative to that observed in the case of **1** suggested that the conformational properties of these compounds in solution might be quite different. It was particularly intriguing to attempt to use the knowledge thus gained through a chemical perspective to gain insight into the conformational characteristics of the epothilones in solution.

To rationalize the stereochemistry of the epoxidation, we explored the conformation of **2** by both computational and NMR spectroscopy techniques.[14] Molecular-mechanics-based conformational analysis suggested that the C11–C14 region of **2** has a greater flexibility than dEpoB (**1**). The two extreme conformations for this region are depicted in Figure 2. In the 13,16-*anti* conformer (**I**), the C12–C13 double bond adopts an *anti* conformation with respect to the C16–C17 double bond. In contrast, in the 13,16-*gauche* conformer **II**, C12=C13 is in a *gauche* relationship with respect to C16=C17.

Our computational models projected the following characteristic coupling constants for these two boundary conformations: conformer **I**: $J_{15,14b} = 10.0$ Hz, $J_{15,14a} = 2.6$ Hz, $J_{14b,13} = 11.7$ Hz, $J_{14a,13} = 5.0$ Hz and conformer **II**: $J_{15,14b} = 3.5$ Hz, $J_{15,14a} = 2.9$ Hz, $J_{14b,13} = 3.8$ Hz, $J_{14a,13} = 11.5$ Hz. The observed ^{1}H NMR coupling constants for dEpoB (**1**) ($J_{15,14b} = 10.0$ Hz, $J_{15,14a} = 1.0$ Hz, $J_{14b,13} = 9.6$ Hz, $J_{14a,13} = 4.6$ Hz) and for (*E*)-9,10-dehydro-EpoB (**2**) ($J_{15,14b} = 8.7$ Hz, $J_{15,14a} = 2.5$ Hz, $J_{14b,13} = 6.9$ Hz, $J_{14a,13} = 6.9$ Hz), suggest that the population density of conformations converging toward **II** is higher in the case of **2** than in the case of **1**.

 © 2003 Wiley-VCH Verlag GmbH & Co. KGaA, Weinheim

Epoxidation of both boundary conformers **I** and **II** would be expected to occur *exo* to the macrolide ring, thus leading to epoxides **4** and **5**, respectively. Given Curtin–Hammett considerations,[15] it seems unlikely that a small increase in the population of conformer type **II** in (*E*)-9,10-dehydro-dEpoB (**2**) could, in itself, account for the shift to α selectivity[10] in the epoxidation reaction. It is more likely that the introduction of 9,10-unsaturation lowers the barrier of interconversion of **I** and **II**, with the latter being the more reactive conformer.

Computational studies in conjunction with NMR spectroscopic analysis prompt the notion that the incorporation unsaturation at C9–C10 leads to an increase in the flexibility of the C11–C14 region and has a substantial impact on the mean conformation of the polypropionate region of **2**. Analysis of the relevant ^{1}H NMR coupling constants also points to a significant difference in the H6–H7 dihedral angle of dEpoB (**1**) ($J_{6,7} = < 1.0$ Hz) and 9,10-dehydro-dEpoB (**2**) ($J_{6,7} = 6.5$ Hz). Significantly, the coupling constants in this region of the spectrum of **2** suggest an increase in conformational population in the direction observed in both the X-ray crystal structure of EpoB[5b] and in its solution NMR spectrum (Figure 3). Although we cannot be certain of the overall conformation of the macrolide while bound to tubulin, it

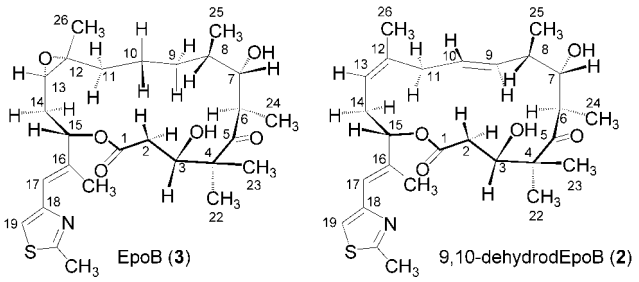


Figure 3. Preferred conformation of EpoB and 9,10-dehydro-dEpoB.

should be noted that the *trans* geometry of C9–C10 rigidifies the C8-C9-C10-C11 torsion angle to 180° and stabilizes the position of the C25 methyl group through a minimization of $A_{1,3}$ strain (Figure 3). These findings lead to the suggestion that the notable increase in biological activity of **2** relative to **1** reflects the impact of the double bond at C9–C10 on the conformation of the polypropionate region.

Furthermore, comparison of the H6–H7 coupling constants (**4** (3.8 Hz), **5** (1.8 Hz), **3** (4.2 Hz), **6** (< 1.0 Hz)) suggests that the long-range conformational guidance provided by the epoxides is in the same direction as that favored by the (*E*)-9,10 double bond of **2**. Moreover, the NMR spectroscopic data show that the long-range conformational guidance depends on the stereochemistry of the epoxides. Only the naturally configured β-epoxides (**3** and **4**) modulate the polypropionate region to populate the highly bioactive conformation. In contrast, long-range modulation by the non-natural α-epoxide series (**5** and **6**) is sharply attentuated. This finding nicely accounts for the higher cytotoxic activity in the natural EpoB series (**3** and **4**) relative to the non-natural α-epoxide series (**5** and **6**).

In summary, we have used molecular modeling and NMR spectroscopic analysis to account for the preferred (α) stereochemistry of epoxidation of the C12–C13 double bond of **2**. Through this epoxidation, we have synthesized the most active epothilone known, **4**, which demonstrated remarkable in vivo efficacy in xenografts. The arguments used to account for the stereochemistry of epoxidation of **2**, closely coordinated modeling, and NMR spectroscopic analysis serve to rationalize the remarkable potency-enhancing effect of the (*E*)-9,10 double bond in this series. We also account for the potency enhancement of the naturally configured β-epoxides (**3** and **4**) and lack of enhancement from the corresponding non-natural α-epoxides (**5** and **6**). While these studies are focused on the epothilones, they point to modalities in drug discovery of wider generality.

Received: March 14, 2003 [Z51407]

Keywords: antitumor agents · conformational analysis · natural products · structure–activity relationships

[1] For reviews of epothilone chemistry and biology, see: a) K. C. Nicolaou, A. Ritzén, K. Namoto, *Chem. Commun.* **2001**, 1523; b) K. H. Altmann, M. Wartmann, T. O'Reilly, *Biochim. BioPhys. Acta* **2000**, *1470*, M79; c) C. R. Harris, S. J. Danishefsky, *J. Org. Chem.* **1999**, *64*, 8434; d) K. C. Nicolaou, F. Roschangar, D. Vourloumis, *Angew. Chem.* **1998**, *110*, 2014; *Angew. Chem. Int. Ed.* **1998**, *37*, 2120.

[2] For recent examples of syntheses of novel epothilone analogues, see: a) A. Regueiro-Ren, K. Leavitt, S.-H. Kim, G. Höfle, M. Kiffe, J. Z. Gougoutas, J. D. DiMarco, F. Y. F. Lee, C. R. Fairchild, B. H. Long, G. D. Vite, *Org. Lett.* **2002**, *4*, 3815; b) R. E. Taylor, Y. Chen, A. Beatty, D. C. Myles, Y. Zhou, *J. Am. Chem. Soc.* **2003**, *125*, 27; c) S. C. Sinha, J. Sun, *Angew. Chem.* **2002**, *114*, 1439; *Angew. Chem. Int. Ed.* **2002**, *41*, 1381; d) K. C. Nicolaou, A. Ritzén, K. Namoto, R. M. Buey, J. F. Diaz, J. M. Andreu, M. Wartmann, K. H. Altmann, A. O'Brate, P. Giannakakou, *Tetrahedron* **2002**, *58*, 6413; e) J. W. Bode, E. M. Carreira, *J. Org. Chem.* **2001**, *66*, 6410.

[3] a) C. R. Harris, S. D. Kuduk, A. Balog, K. Savin, P. W. Glunz, S. J. Danishefsky, *J. Am. Chem. Soc.* **1999**, *121*, 7050; b) D. Meng, P. Bertinato, A. Balog, D.-S. Su, T. Kamenecka, E. J. Sorensen, S. J. Danishefsky, *J. Am. Chem. Soc.* **1997**, *119*, 10073.

[4] For more information about clinical trials of dEpoB, visit: www.kosan.com.

[5] a) G. Höfle, N. Bedorf, K. Gerth, H. Reichenbach, (GBF), DE-B 4138042, **1993**; b) G. Höfle, N. Bedorf, H. Steinmetz, D. Schomburg, K. Gerth, H. Reichenbach, *Angew. Chem.* **1996**, *108*, 1671; *Angew. Chem. Int. Ed. Engl.* **1996**, *35*, 1567; c) K. Gerth, N. Bedorf, G. Höfle, H. Irschik, H. Reichenbach, *J. Antibiot.* **1996**, *49*, 560.

[6] D.-S. Su, A. Balog, D. Meng, P. Bertinato, S. J. Danishefsky, Y.-H. Zheng, T.-C. Chou, L. He, S. B. Horwitz, *Angew. Chem.* **1997**, *109*, 2178; *Angew. Chem. Int. Ed. Engl.* **1997**, *36*, 2093.

[7] T.-C. Chou, X. G. Zhang, X. G.; C. R. Harris, S. D. Kuduk, A. Balog, K. A. Savin, J. R. Bertino, S. J. Danishefsky, *Proc. Natl. Acad. Sci. USA* **1998**, *95*, 9642.

[8] a) A. Rivkin, F. Yoshimura, A. E. Gabarda, T.-C. Chou, H. Dong, W. P. Tong, S. J. Danishefsky, *J. Am. Chem. Soc.* **2003**, *125*, 2899; b) for the interfacing of these findings with earlier claims, see: J. D. White, R. G. Carter, K. F. Sundermann, M. Wartmann, *J. Am. Chem. Soc.* **2001**, *123*, 5407, and references in [8a].

 © 2003 Wiley-VCH Verlag GmbH & Co. KGaA, Weinheim

[9] a) K. Biswas, H. Lin, J. T. Njardarson, M. D. Chappel, T.-C. Chou, Y. Guan, W. P. Tong, L. He, S. B. Horwitz, S. J. Danishefsky, *J. Am. Chem. Soc.* **2002**, *124*, 9825; b) N. J. Cusack, C. B. Reese, A. C. Risius, B. Roozpeikar, *Tetrahedron* **1976**, *32*, 2157; c) M. S. Ermolenko, P. Potier, *Tetrahedron Lett.* **2002**, *43*, 2895.
[10] The terms α and β epoxidation anticipate the stereostructure of the products presented in structures **4** and **5**.
[11] S. J. Stachel, S. J. Danishefsky, *Tetrahedron Lett.* **2001**, *42*, 6785.
[12] It remains to be established whether this remarkable level of potency can be translated to achieve clinically useful therapeutic margins; for recent examples of alternative highly potent epothilone analogues, see: a) K. H. Altmann, G. Bold, G. Caravatti, A. Flörsheimer, V. Guagnano, M. Wartmann, *Bioorg. Med. Chem. Lett.* **2000**, *10*, 2765; b) K. C. Nicolaou, R. Scarpelli, B. Bollbuck, B. Werschkun, M. M. A. Pereira, M. Wartmann, K.-H. Altmann, D. Zaharevitz, R. Gussio, P. Giannakakou, *Chem. Biol.* **2000**, *7*, 593.
[13] T.-C. Chou, O. A. O'Connor, W. P. Tong, Y. Guan, Z.-G. Zhang, S. J. Stachel, C. Lee, S. J. Danishefsky, *Proc. Natl. Acad. Sci. USA* **2001**, *98*, 8113.
[14] For leading articles, see reference [2b] and: a) R. E. Taylor, J. Zajicek, *J. Org. Chem.* **1999**, *64*, 7224; for additional references, see: b) J. D. White, K. F. Sudermann, M. Wartmann, *Org. Lett.* **2002**, *4*, 995; c) K. W. Lee, J. M. Briggs, *J. Comput.-Aided Mol. Des.* **2001**, *15*, 41.
[15] a) D. Y. Curtin, *Rec. Chem. Prog.* **1954**, *15*, 111; b) E. L. Eliel, *Stereochemistry of Carbon Compounds*, McGraw-Hill, New York, **1962**, pp. 151 – 152, 237 – 238.

 © 2003 Wiley-VCH Verlag GmbH & Co. KGaA, Weinheim

Solid-Supported Total Synthesis

A Total Synthesis of Epothilones Using Solid-Supported Reagents and Scavengers**

*R. Ian Storer, Toshiyasu Takemoto, Philip S. Jackson, and Steven V. Ley**

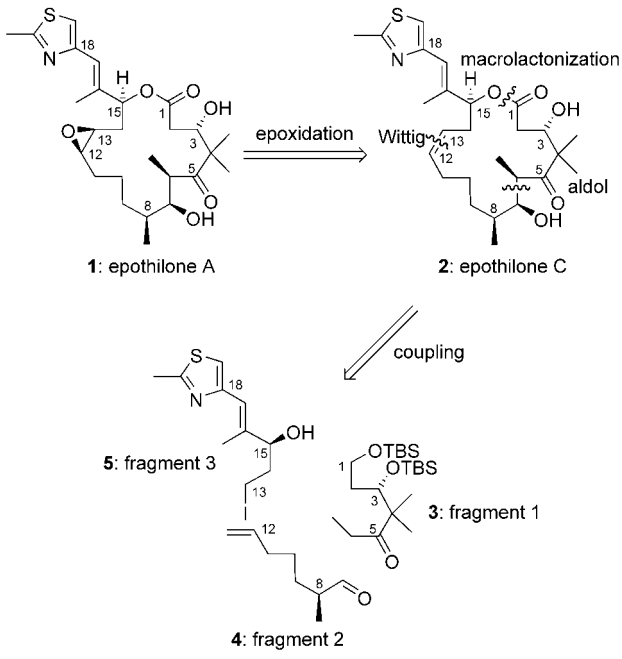
The epothilone natural products[1] exhibit extraordinary cytotoxic biological activity by promoting GTP-independent tubulin polymerization. This mode of action inhibits the growth of tumors by inducing mitotic arrest, followed by cell apoptosis. Mechanistic investigations have revealed that the epothilones bind competitively to the same, or overlapping, sites in β-tubulin as taxol.[2] However, certain epothilones exhibit a higher activity than taxol, even against multiple-drug-resistant cells, and are more soluble in water, making them interesting drug candidates.

Several total syntheses of both natural and analogous epothilones have been reported reported since the disclosure of their biological importance.[3–12] However, as a result of the complexity of these molecules, all previous synthetic programs have required extensive silica-gel chromatography to provide material free from contaminating by-products. Although acceptable in the research laboratory, such processes cannot be efficiently accommodated within larger-scale production, nor are they appropriate for the high-throughput preparation of libraries of analogues, in which speed and simplicity of operation are important criteria.

In recent years we have begun to explore the utility of commercially available immobilized reagents and scavengers[13] in the synthesis of drugs and natural products.[14] The combined application of these tools has been shown to provide versatile methods for molecular conversion and elimination of impurities, thereby offering the opportunity to avoid conventional approaches to reaction quenching, extraction, and purification.

Herein we describe how immobilized reagents and scavengers have been employed in a multistep sequence leading to epothilones A (**1**) and C (**2**), avoiding frequent use of conventional workup and purification procedures, including flash-column chromatography, recrystallization, and distillation (Scheme 1).

Our approach to the 16-membered macrocycle is similar to several previously published syntheses in that it utilizes a stereoselective union of three fragments by lithium aldol (C6–C7) and Wittig (C12–C13) reactions, followed by macrolactonization (C1–C15) to provide epothilone C (**2**; Scheme 1).[7,8,15] Epoxidation can then be applied to the



Scheme 1. Synthetic plan.

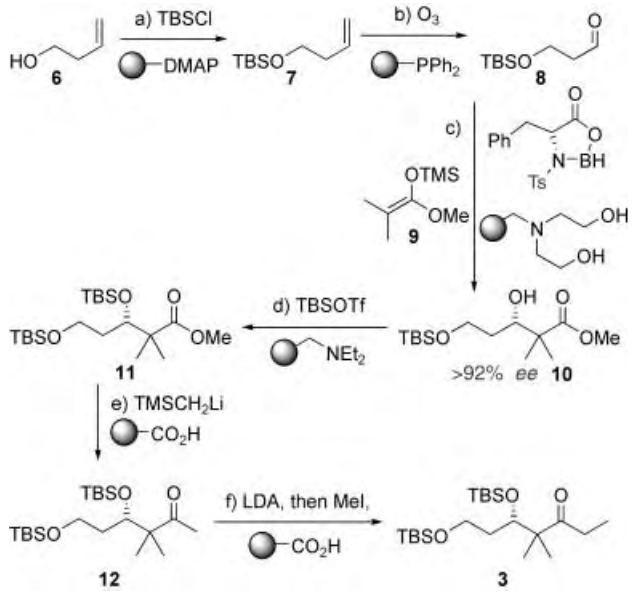
[*] Prof. S. V. Ley, R. I. Storer, Dr. T. Takemoto, Dr. P. S. Jackson
University Chemical Laboratories, University of Cambridge
Lensfield Road, Cambridge, CB2 1EW (UK)
Fax: (+44) 1223-336-442
E-mail: svl1000@cam.ac.uk

[**] We gratefully acknowledge financial support for this work from AstraZeneca (to I.R.S.), the EPSRC (to P.S.J.), Merck Sharp & Dohme (to P.S.J.), Sankyo Co. Ltd., Japan (to T.T.), a B.P. endowment (to S.V.L.), and a Novartis Research Fellowship (to S.V.L.). The authors would like to thank Dr. Dearg Brown of AstraZeneca for support and useful discussions and Dr. Karl-Heinz Altmann of Novartis, Switzerland for a generous donation of authentic materials.

 DOI: 10.1002/anie.200351413 © 2003 Wiley-VCH Verlag GmbH & Co. KGaA, Weinheim

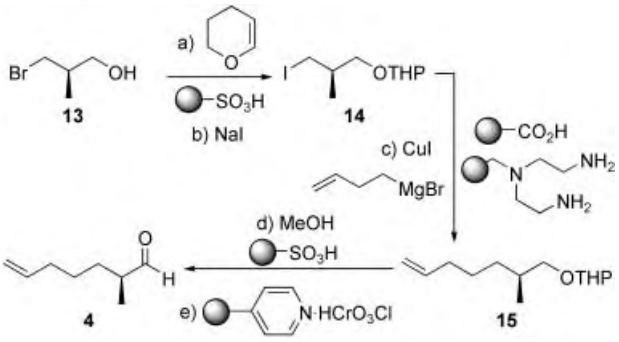
C12–C13 double bond to complete the synthesis of epothilone A (**1**).[5]

The stereogenic center in fragment 1 (**3**) was efficiently installed by using Kiyooka's asymmetric Lewis acid catalyzed Mukaiyama aldol methodology between readily accessible aldehyde **8** and silyl enol ether **9**[16] in a similar manner to the groups of Mulzer and Taylor.[10,11] Sulfonamide-protected D-phenylalanine in combination with borane gave optimal results, providing the desired alcohol adduct **10** in >92% *ee* (Scheme 2).[17] The reaction was quenched by the addition of a small amount of water and Amberlite IRA-743, a boron-specific scavenging resin, allowing efficient separation of the desired product and quantitative recovery of the amino acid. A silyl protecting group was introduced by using *tert*-butyldimethylsilyl triflate in the presence of basic diethylaminomethyl polystyrene. Ester **11** was converted into ethyl ketone fragment 1 (**3**) by the single addition of (trimethylsilylmethyl)lithium followed by monoalkylation. Both steps were quenched by a supported carboxylic acid to neutralize the reactions and scavenge the lithium ions.[10]



Scheme 2. Synthesis of fragment 1.[18] a) TBSCl (1.4 equiv), PS DMAP (2.0 equiv, 1.49 mmol g^{-1}), CH_2Cl_2, room temperature, 2.5 h, 96%; b) O_3, CH_2Cl_2, −78 °C, 20 min, then PS PPh_3 (1.5 equiv, 3.3 mmol g^{-1}), −78 °C→RT, 12 h, 93%; c) *N*-Ts-D-phenylalanine (1.2 equiv), BH_3·THF (1.05 equiv, 1.5 M), CH_2Cl_2, 0 °C→RT, 1 h, then **8** (1.0 equiv), −94 °C, 15 min, then **9** (1.0 equiv), −94 °C→−78 °C, 105 min, then H_2O (5 equiv), Amberlite IRA-743 (1.3 equiv), −78 °C→RT, 6 h, 93% (92% of *N*-Ts-D-phenylalanine recovered); d) TBSOTf (2.0 equiv), diethylaminopolystyrene (5.0 equiv, 3.2 mmol g^{-1}), CH_2Cl_2, 0 °C→RT, 165 min, then MeOH (25 equiv), room temperature, 1 h, 100%; e) (trimethylsilylmethyl)lithium (2.2 equiv, 1.0 M pentane), pentane, 0 °C, 195 min, then MeOH (50 equiv), 0 °C→RT, 5 h, then Amberlite IRC-50 (2.5 equiv, ~5.0 mmol g^{-1}), room temperature, 75 min, 100%; f) LDA (2.3 equiv), THF, −78 °C→−15 °C, 30 min, then MeI (3.1 equiv), −78 °C→−40 °C, 2 h, then Amberlite IRC-50 (12 equiv, ~5.0 mmol g^{-1}), room temperature, 2 h, 94%. TBS = *tert*-butyldimethylsilyl, PS = polymer-supported, DMAP = 4-dimethylaminopyridine, Tf = trifluoromethanesulfonyl, LDA = lithium diisopropylamide, Ts = *para*-toluenesulfonyl, TMS = trimethylsilyl.

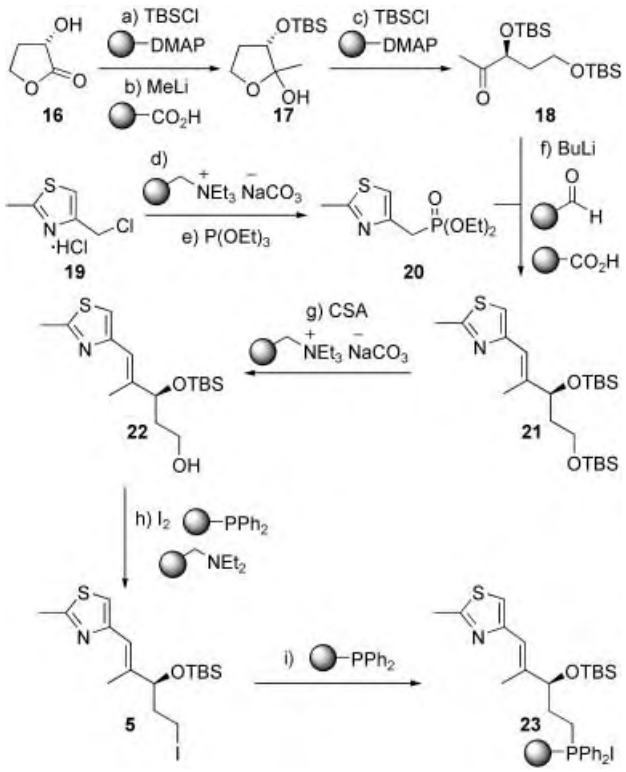
Synthesis of aldehyde fragment 2 (**4**) utilized a popular strategy that allowed access from a commercially available "(*R*)-Roche ester" derivative. Protection of (*R*)-(−)-3-bromo-2-methyl-1-propanol (**13**) as the tetrahydropyranyl acetal was achieved with polymeric sulfonic acid catalysis and was followed by a Finkelstein halide exchange to provide the more reactive primary iodide **14** (Scheme 3). Workup required addition of diethyl ether and silica gel to bind any remaining dissolved inorganic salts prior to filtration. CuI-mediated substitution with 3-butenylmagnesium bromide, followed by Amberlite IRC-50 acidic quench and a trisamine copper scavenge, yielded desired alkene **15**. Acid-catalyzed deprotection in methanol and oxidation of the corresponding alcohol with pyridinium chlorochromate on alumina, provided fragment 2 (**4**).



Scheme 3. Synthesis of fragment 2. a) 3,4-Dihydropyran (1.02 equiv), PS TsOH (0.05 equiv, 4.2 mmol g^{-1}), neat, 30 min, 100%; b) NaI (3 equiv), 2-butanone, 75 °C, 1 h, then Et_2O, silica-gel filtration, 96%; c) CuI (1.0 equiv), 3-butenylmagnesium bromide (4.0 equiv), THF, −10 °C→0 °C, 2 h, then Amberlite IRC-50 (3.0 equiv, ~5.0 mmol g^{-1}) and PS trisamine (3.0 equiv, 4.36 mmol g^{-1}), room temperature, 24 h, 97%; d) MP-TsOH (0.04 equiv, 4.2 mmol g^{-1}), MeOH, RT, 7 h 30 min, 97%; e) pyridinium chlorochromate on Al_2O_3 (3.0 equiv, 1.0 mmol g^{-1}), CH_2Cl_2, room temperature, 3.5 h, 80%. MP = macroporous polymer.

A precedented, convergent route was applied to the formation of thiazole fragment 3 (**5**). A commercially available lactone derivative of malic acid was used to provide the necessary stereochemistry at C15. Silyl protection of *S*-(−)-α-hydroxy-γ-butyrolactone (**16**) was followed by the addition of 1 equivalent of methyllithium to give lactol **17**, which was subsequently trapped as the open-chain ketone **18** upon the formation of a second TBS ether (Scheme 4).[6] In parallel, the hydrochloride salt of 4-chloromethyl-2-methylthiazole (**19**) was deprotonated with polymer-supported carbonate, before heating with excess triethylphosphite to yield phosphonate **20**. The residual triethylphosphite was subsequently removed under reduced pressure.[6] Deprotonation of phosphonate **20** with butyllithium, followed by a Horner–Wadsworth–Emmons olefination with ketone **18** provided thiazole adduct **21**. An excess of the phosphonate anion was used, which was later scavenged by a polymeric benzaldehyde equivalent, followed by the addition of silica gel to bind the polar phosphorus by-products. This provided the desired *E*-trisubstituted olefin **21** after simple filtration. Selective deprotection of the primary hydroxy group was effected in

 © 2003 Wiley-VCH Verlag GmbH & Co. KGaA, Weinheim



Scheme 4. Synthesis of fragment 3. a) TBSCl (1.4 equiv), PS DMAP (2.0 equiv, 1.49 mmol g^{-1}), CH_2Cl_2, RT, 1 h 30 min, 97%; b) MeLi (1.05 equiv), THF, −78 °C, 1 h, then Amberlite IRC-50 (20 equiv, ~10 mmol g^{-1}), 98%; c) TBSCl (1.48 equiv), PS DMAP (2.0 equiv, 1.49 mmol g^{-1}), CH_2Cl_2, room temperature, 2.5 h, 98%; d) PS carbonate (2 equiv, 3.5 mmol g^{-1}), MeOH, room temperature, 45 min, 98%; e) triethylphosphite (1.2 equiv), neat, 160 °C, 3.5 h, 84%; f) **20** (3.5 equiv), *n*BuLi (3.5 equiv), THF/hexanes, −78 °C, then **18** (1.0 equiv), −78 °C→RT, 1.5 h, then PS benzaldehyde (5.0 equiv, 1.2 mmolg-1) and Amberlite IRC-50 (10 equiv, ~5 mmol g^{-1}), 105% by mass w.r.t. ketone **18**; g) CSA (1.5 equiv), MeOH/CH_2Cl_2 (1:1), 0 °C, 2.5 h, then PS carbonate (2.2 equiv, 3.5 mmol g^{-1}), 2 h, 104%; h) iodine (4.0 equiv), PS PPh_3 (5.0 equiv, 3.3 mmol g^{-1}), imidazole (6.0 equiv), MeCN/Et_2O (3:1), then diethylaminomethylpolystyrene (8.0 equiv, 3.2 mmol g^{-1}), Amberlite IRC-50 (13.0 equiv, ~5 mmol g^{-1}), toluene, room temperature, 105 min, 73%; i) PS PPh_3 (1.0 equiv, 3.3 mmol g^{-1}), toluene, 90 °C, 18 h. CSA = 10-camphorsulfonic acid.

acidic solution and quenched by a polymer-supported carbonate, before conversion of the resulting alcohol **22** into iodide **5** by treatment with polymer-supported triphenylphosphane and iodine. The corresponding resin-bound phosphonium iodide salt **23** of fragment 3 was then formed, in preparation for Wittig coupling, by heating iodide **5** with polymer-supported triphenylphosphane in toluene. This final "catch" step also permitted separation from minor phosphorus contaminants that had remained following the olefination coupling.

Aldol coupling between fragments 1 (**3**) and 2 (**4**) generates two new stereocenters, so a highly diastereoselective process was required. Coupling at C6–C7 has been extensively investigated on a wide variety of substrates, and shown to be highly sensitive to proximal and remote functionality in both fragments.[9,19] Our approach, although bearing close analogy to those already published, incorporates a novel fragment combination of ketone **3** and aldehyde **4**.[20] The use of freshly prepared lithium diisopropylamide in THF reliably gave excellent selectivity (>13:1) for the desired anti-Felkin–Anh adduct **24**,[21] with an excess of the aldehyde required to force the reaction to completion. After quenching with acetic acid, diamine polymer was added to scavenge excess acid and aldehyde fragment from the crude reaction mixture. Protection of aldol adduct **24** followed by ozonolysis, using polymer-supported triphenylphosphane to reduce the ozonide, efficiently gave aldehyde **25** in preparation for Wittig coupling with fragment 3 (**5**).

Treatment of immobilized phosphonium salt **23** with excess sodium bis(trimethylsilyl)amide followed by washing with dry THF allowed the isolation of the corresponding salt-free ylide.[22] Coupling of aldehyde **25** with this ylide installed the necessary *cis* olefin exclusively (Scheme 5). Selective primary alcohol deprotection yielded **26**, which after a two-step oxidation with catalytic TPAP in the presence of NMO[23] followed by polymer-supported chlorite, gave the corresponding carboxylic acid.[24] Selective removal of the allylic TBS ether by using excess TBAF[25] provided hydroxy acid **27** in readiness for macrolactonization.[8]

Macrolactonization of linear hydroxy acid **27** proceeded under Yamaguchi conditions, using a polymer-supported DMAP equivalent, to furnish the required 16-membered lactone.[8,12] Polymeric sulfonic acid resin was used not only to remove both TBS protecting groups, but also to protonate the thiazole nitrogen atom and to capture the natural product as an ion-exchanged salt. Unbound impurities were removed by washing the resin with dichloromethane, before subsequent release of epothilone C by using a basic solution of ammonia in methanol. Having obtained the natural product as a mixture containing over 90% of the desired diastereoisomer, the material was then finally purified by flash column chromatography to provide pure epothilone C (**2**). Epoxidation of epothilone C has been shown to proceed with facial selectivity to provide a formal synthesis of epothilone A (**1**).[3]

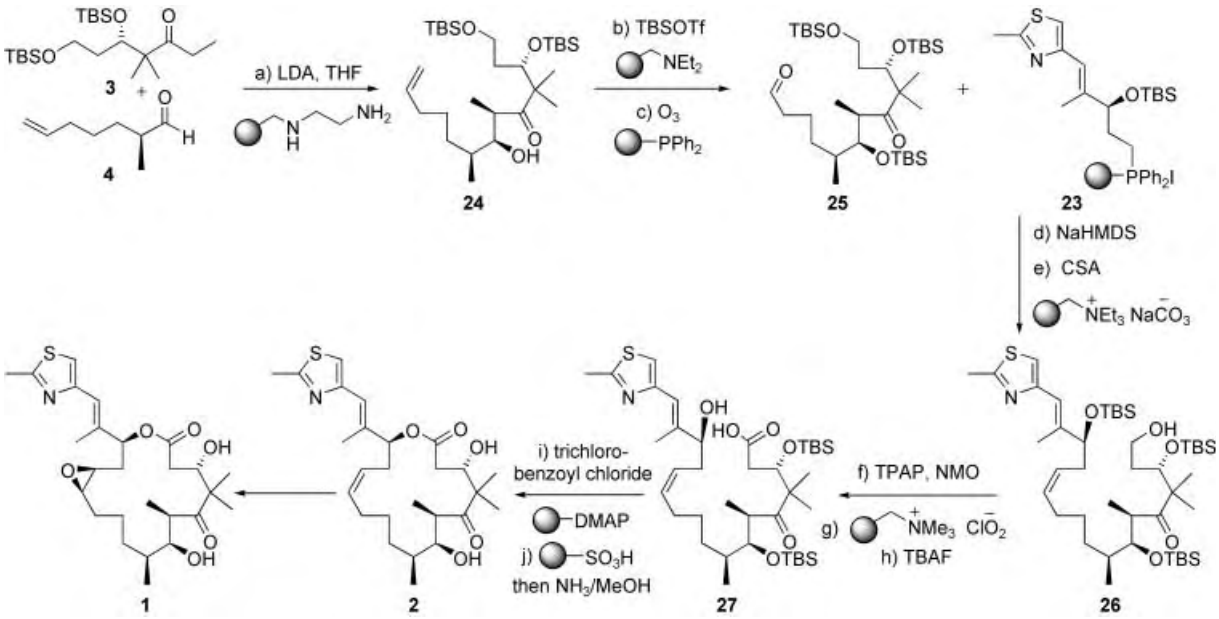
In summary, we have demonstrated the scope and utility of supported reagents and scavenging techniques within a multistep synthesis by stereoselectively providing epothilone C in 29 steps overall and with a longest linear sequence of only 17 steps from commercially available materials.[26] The high selectivity and overall efficiency is comparable with the best of the previous conventional syntheses. As epothilone C is the most challenging target that has been synthesized by using solid-phase reagent and scavenging techniques, we hope that this will encourage their future integration alongside conventional methods for application within general synthesis programs.

Received: March 17, 2003 [Z51413]

Keywords: aldol reaction · antitumor agents · natural products · polyketides · polymers

[1] a) G. H. Höfle, N. Bedorf, H. Steinmetz, D. Schomburg, K. Gerth, H. Reichenbach, *Angew. Chem.* **1996**, *108*, 1671; *Angew.*

 © 2003 Wiley-VCH Verlag GmbH & Co. KGaA, Weinheim



Scheme 5. Fragment coupling and cyclization. a) LDA (1.6 equiv), THF, −78 °C→−40 °C, 1.5 h, then aldehyde **4** (1.5 equiv), −78 °C, 20 min, then AcOH (5 equiv), −78 °C→RT, 30 min, then PS diamine (4.8 equiv, 3.0 mmol g^{-1}), room temperature, 2 h, 100% (13.5:1); b) TBSOTf (1.5 equiv), diethylaminopolystyrene (3.0 equiv, 3.2 mmol g^{-1}), CH_2Cl_2, 0 °C→RT, 205 min, then MeOH (3.0 equiv), room temperature, 2 h, 99%; c) O_3, CH_2Cl_2, −78 °C, 20 min, then PS PPh_3 (5.0 equiv, 3.3 mmol g^{-1}), −78 °C→RT, 15 h, 100%; d) phosphonium salt **23** (2.5 equiv), NaHMDS (10.0 equiv), THF, room temperature, 15 min, then THF wash, then aldehyde **25** (1.0 equiv), −78 °C→−40 °C, 15 min, 93%; e) CSA (1.0 equiv), $MeOH/CH_2Cl_2$ (1:1), 0 °C, 4 h, 99%; f) TPAP (0.05 equiv), NMO (1.5 equiv), CH_2Cl_2, 0 °C→RT, 3 h 10 min, then Et_2O through silica pad, 93%; g) PS chlorite (2 equiv, ~0.5 mmol g^{-1}), PS dihydrogenphosphate (3 equiv, ~0.5 mmol g^{-1}), 2-methyl-2-butene (5 equiv, 2 M in THF), *t*BuOH/H_2O (1:2), room temperature, 6 h, 99%; h) TBAF (6 equiv, 1 M in THF), THF, room temperature, 12 h, 95%; i) 2,4,6-trichlorobenzoylchloride (10.0 equiv), triethylamine (12 equiv), room temperature, 50 min, then added to PS DMAP (20 equiv), THF/toluene (1:25), 80 °C, 2.5 h; j) PS TsOH (12 equiv, 1.5 mmol g^{-1}), CH_2Cl_2, 1 h, then CH_2Cl_2 and Et_2O wash, then release with NH_3 (2 M in MeOH), 81% (over two steps), k) reference [4]. HMDS = bis(trimethylsilyl)amide, NMO = 4-methylmorpholine *N*-oxide, TBAF = tetrabutylammonium fluoride, TPAP = tetra-*N*-propylammonium perruthenate.

Chem. Int. Ed. Engl. **1996**, *35*, 1567; b) K. Gerth, N. Bedorf, G. Höfle, H. Irschik, H. Reichenbach, *J. Antibiot.* **1996**, *49*, 560.

[2] a) R. J. Kowalski, E. Terhaar, R. E. Longley, S. P. Gunasekera, C. M. Lin, B. V. Day, E. Hamel, *Mol. Biol. Cell* **1995**, *6*, 2137; b) D. M. Bollag, P. A. McQueney, J. Zhu, O. Hensens, L. Koupal, J. Liesch, M. Goetz, E. Lazarides, C. M. Woods, *Cancer Res.* **1995**, *55*, 2325; c) J. D. Winkler, P. H. Axelsen, *Bioorg. Med. Chem. Lett.* **1996**, *6*, 2963; d) P. F. Muhlradt, F. Sasse, *Cancer Res.* **1997**, *57*, 3344; e) R. J. Kowalski, P. Giannakakou, E. Hamel, *J. Biol. Chem.* **1997**, *272*, 2534.

[3] A. Balog, D. F. Meng, T. Kamenecka, P. Bertinato, D. S. Su, E. J. Sorensen, S. Danishefsky, *Angew. Chem.* **1996**, *108*, 2976; *Angew. Chem. Int. Ed. Engl.* **1996**, *35*, 2801.

[4] a) D. S. Su, D. F. Meng, P. Bertinato, A. Balog, E. J. Sorensen, S. J. Danishefsky, Y. H. Zheng, T. C. Chou, L. F. He, S. B. Horwitz, *Angew. Chem.* **1997**, *109*, 775; *Angew. Chem. Int. Ed. Engl.* **1997**, *36*, 757; b) A. Balog, C. Harris, K. Savin, X. G. Zhang, T. C. Chou, S. J. Danishefsky, *Angew. Chem.* **1998**, *110*, 2821; *Angew. Chem. Int. Ed.* **1998**, *37*, 2675; c) M. D. Chappell, S. J. Stachel, C. B. Lee, S. J. Danishefsky, *Org. Lett.* **2000**, *2*, 1633; d) K. C. Nicolaou, Y. He, D. Vourloumis, H. Vallberg, F. Roschangar, F. Sarabia, S. Ninkovic, Z. Yang, J. I. Trujillo, *J. Am. Chem. Soc.* **1997**, *119*, 7960; e) Z. Yang, Y. He, D. Vourloumis, H. Vallberg, K. C. Nicolaou, *Angew. Chem.* **1997**, *109*, 170; *Angew. Chem. Int. Ed. Engl.* **1997**, *36*, 166; f) K. C. Nicolaou, S. Ninkovic, F. Sarabia, D. Vourloumis, Y. He, H. Vallberg, M. R. V. Finlay, Z. Yang, *J. Am. Chem. Soc.* **1997**, *119*, 7974; g) K. C. Nicolaou, Y. He, F. Roschangar, N. P. King, D. Vourloumis, T. H. Li, *Angew. Chem.* **1998**, *110*, 89; *Angew. Chem. Int. Ed.* **1998**, *37*, 84; h) J. Mulzer, G. Karig, P. Pojarliev, *Tetrahedron Lett.* **2000**, *41*, 7635; i) H. J. Martin, M. Drescher, J. Mulzer, *Angew. Chem.* **2000**, *112*, 591; *Angew. Chem. Int. Ed.* **2000**, *39*, 581; j) J. W. Bode, E. M. Carreira, *J. Am. Chem. Soc.* **2001**, *123*, 3611; k) J. W. Bode, E. M. Carreira, *J. Org. Chem.* **2001**, *66*, 6410; l) R. E. Taylor, G. M. Galvin, K. A. Hilfiker, Y. Chen, *J. Org. Chem.* **1998**, *63*, 9580; m) A. Fürstner, C. Mathes, C. W. Lehmann, *Chem. Eur. J.* **2001**, *7*, 5299; n) A. Fürstner, C. Mathes, K. Grela, *Chem. Commun.* **2001**, 1057; o) J. D. White, K. F. Sundermann, R. G. Carter, *Org. Lett.* **1999**, *1*, 1431; p) J. D. White, R. G. Carter, K. F. Sundermann, *J. Org. Chem.* **1999**, *64*, 684; q) J. D. White, R. G. Carter, K. F. Sundermann, M. Wartmann, *J. Am. Chem. Soc.* **2001**, *123*, 5407; r) N. Martin, E. J. Thomas, *Tetrahedron Lett.* **2001**, *42*, 8373; s) D. Sawada, M. Kanai, M. Shibasaki, *J. Am. Chem. Soc.* **2000**, *122*, 10521; t) D. Sawada, M. Shibasaki, *Angew. Chem.* **2000**, *112*, 215; *Angew. Chem. Int. Ed.* **2000**, *39*, 209; u) M. Valluri, R. M. Hindupur, P. Bijoy, G. Labadie, J. C. Jung, M. A. Avery, *Org. Lett.* **2001**, *3*, 3607; v) R. M. Hindupur, B. Panicker, M. Valluri, M. A. Avery, *Tetrahedron Lett.* **2001**, *42*, 7341; w) S. C. Sinha, J. Sun, G. P. Miller, M. Wartmann, R. A. Lerner, *Chem. Eur. J.* **2001**, *7*, 1691; x) S. A. May, P. A. Grieco, *Chem. Commun.* **1998**, 1597; y) M. Kalesse, M. Quitschalle, E. Claus, K. Gerlach, A. Pahl, H. H. Meyer, *Eur. J. Org. Chem.* **1999**, 2817; z) J. Sun, S. C. Sinha, *Angew. Chem.* **2002**, *114*, 1439; *Angew. Chem. Int. Ed.* **2002**, *41*, 1381; aa) B. Zhu, J. S. Panek, *Org. Lett.* **2000**, *2*, 2575; ab) B. Zhu, J. S. Panek, *Eur. J. Org. Chem.* **2001**, 1701; ac) M. S. Ermolenko, P. Potier, *Tetrahedron Lett.* **2002**, *43*, 2895; ad) C. R. Harris, S. D. Kuduk, A. Balog, K. Savin, P. W. Glunz, S. J. Danishefsky, *J. Am. Chem. Soc.* **1999**, *121*, 7050.

 © 2003 Wiley-VCH Verlag GmbH & Co. KGaA, Weinheim

[5] D. F. Meng, P. Bertinato, A. Balog, D. S. Su, T. Kamenecka, E. J. Sorensen, S. J. Danishefsky, *J. Am. Chem. Soc.* **1997**, *119*, 10073.
[6] a) D. Schinzer, A. Limberg, A. Bauer, O. M. Bohm, M. Cordes, *Angew. Chem.* **1997**, *109*, 543; *Angew. Chem. Int. Ed. Engl.* **1997**, *36*, 523; b) D. Schinzer, A. Bauer, O. M. Bohm, A. Limberg, M. Cordes, *Chem. Eur. J.* **1999**, *5*, 2483; c) D. Schinzer, A. Bauer, J. Schieber, *Chem. Eur. J.* **1999**, *5*, 2492.
[7] K. C. Nicolaou, N. Winssinger, J. Pastor, S. Ninkovic, F. Sarabia, Y. He, D. Vourloumis, Z. Yang, T. Li, P. Giannakakou, E. Hamel, *Nature* **1997**, *387*, 268.
[8] K. C. Nicolaou, F. Sarabia, S. Ninkovic, Z. Yang, *Angew. Chem.* **1997**, *109*, 525; *Angew. Chem. Int. Ed. Engl.* **1997**, *36*, 539.
[9] a) K. C. Nicolaou, D. Hepworth, M. R. V. Finlay, N. P. King, B. Werschkun, A. Bigot, *Chem. Commun.* **1999**, 519; b) G. Koch, O. Loiseleur, D. Fuentes, A. Jantsch, K. H. Altmann, *Org. Lett.* **2002**, *4*, 3811; c) Z. C. Wu, F. Zhang, S. J. Danishefsky, *Angew. Chem.* **2000**, *112*, 4679; *Angew. Chem. Int. Ed.* **2000**, *39*, 4505.
[10] J. Mulzer, A. Mantoulidis, E. Ohler, *J. Org. Chem.* **2000**, *65*, 7456.
[11] R. E. Taylor, Y. Chen, *Org. Lett.* **2001**, *3*, 2221.
[12] Z. Y. Liu, Z. C. Chen, C. Z. Yu, R. F. Wang, R. Z. Zhang, C. S. Huang, Z. Yan, D. R. Cao, J. B. Sun, G. Li, *Chem. Eur. J.* **2002**, *8*, 3747.
[13] a) S. V. Ley, I. R. Baxendale, R. N. Bream, P. S. Jackson, A. G. Leach, D. A. Longbottom, M. Nesi, J. S. Scott, R. I. Storer, S. J. Taylor, *J. Chem. Soc. Perkin Trans. 1* **2000**, 3815, and references therein; b) A. Kirschning, H. Monenschein, R. Wittenberg, *Angew. Chem.* **2001**, *113*, 670; *Angew. Chem. Int. Ed.* **2001**, *40*, 650, and references therein.
[14] I. R. Baxendale, S. V. Ley, M. Nesi, C. Piutti, *Tetrahedron* **2002**, *58*, 6285, and references therein.
[15] K. C. Nicolaou, Y. He, D. Vourloumis, H. Vallberg, Z. Yang, *Angew. Chem.* **1996**, *108*, 2554; *Angew. Chem. Int. Ed. Engl.* **1996**, *35*, 2399.
[16] a) S. Kiyooka, *Rev. Heteroat. Chem.* **1997**, *17*, 245; b) S. Kiyooka, *J. Synth. Org. Chem. Jpn.* **1997**, *55*, 313; c) S. Kiyooka, H. Maeda, M. Abu Hena, M. Uchida, C. S. Kim, M. Horiike, *Tetrahedron Lett.* **1998**, *39*, 8287.
[17] Enantiomeric excess determined by ^{1}H NMR spectroscopy (Mosher esters).
[18] All yields quoted are based on mass recovery, assuming quantitative conversion into products.
[19] C. R. Harris, S. D. Kuduk, A. Balog, K. A. Savin, S. J. Danishefsky, *Tetrahedron Lett.* **1999**, *40*, 2267.
[20] It was necessary to perform a filtration through silica gel to remove baseline impurities from ketone fragment 1 (**3**) prior to the aldol coupling.
[21] The same reaction also proceeded well in diethyl ether, although the selectivity appeared to be more capricious, varying from 10:1 to as high as >30:1.
[22] M. H. Bolli, S. V. Ley, *J. Chem. Soc. Perkin Trans. 1* **1998**, 2243.
[23] W. P. Griffith, S. V. Ley, G. P. Whitcombe, A. D. White, *J. Chem. Soc. Chem. Commun.* **1987**, 1625.
[24] T. Takemoto, K. Yasuda, S. V. Ley, *Synlett* **2001**, 1555.
[25] It proved to be necessary to perform an aqueous workup to remove the excess TBAF from the reaction.
[26] Although no attempt was made to recycle or regenerate the immobilized reagents, owing to the scale of this particular synthesis, recycling remains an option for larger-scale processes.

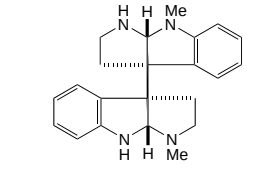
 © 2003 Wiley-VCH Verlag GmbH & Co. KGaA, Weinheim

Alkaloid Total Synthesis

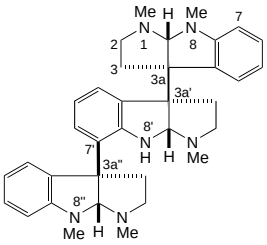
Enantioselective Total Synthesis of the Cyclotryptamine Alkaloid Idiospermuline**

Larry E. Overman and Emily A. Peterson*

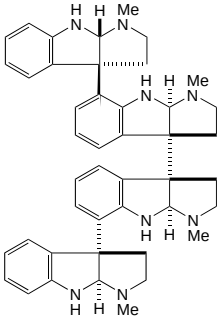
A remarkable group of alkaloids that link together up to eight pyrrolidinoindoline units has been isolated from higher plants.[1] (−)-Chimonanthine (**1**) is representative of the simplest of these. In higher order members of this group,



(–)-chimonanthine (**1**)



idiospermuline (**2**)



quadrigemine C (**3**)

exemplified by idiospermuline (**2**) and quadrigemine C (**3**), additional pyrrolidinoindoline units are attached at their benzylic quaternary stereocenters to *peri* positions of the aromatic ring of other pyrrolidinoindoline fragments. Stimulated by the unusual structures and varied biological activities of these cyclotryptamine alkaloids,[1] we have developed chemistry to access these complex, configurationally diverse alkaloids by stereocontrolled total synthesis.[2] We report herein the first total synthesis of the trispyrrolidinoindoline alkaloid idiospermuline (**2**), a naturally occurring cholinergic antagonist isolated recently from the seeds of *Idiospermum australiense*, a rare tree found in lowland rain forests of North Queensland, Australia.[3]

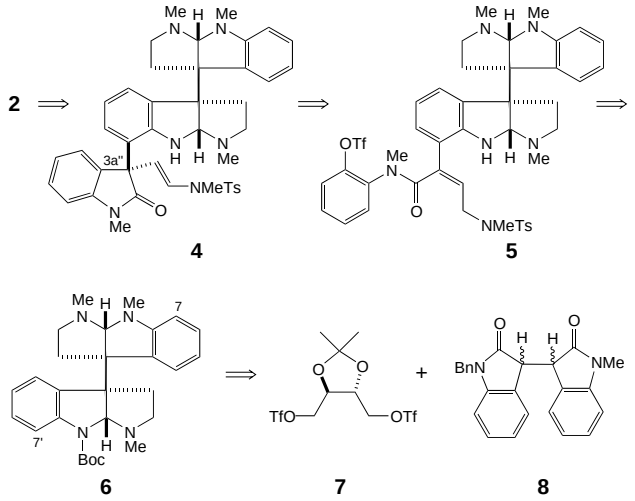
[*] Prof. Dr. L. E. Overman, E. A. Peterson
Department of Chemistry
University of California, Irvine
516 Rowland Hall, Irvine, CA 92697-2025 (USA)
Fax: (+1) 949-824-3866
E-mail: leoverma@uci.edu

[**] This research was supported by the General Medical Sciences Institute of the NIH (grant GM-30859). NMR and mass spectra were determined at UC Irvine with instruments purchased with the assistance of the NSF and NIH shared instrumentation programs.

Supporting information for this article is available on the WWW under http://www.angewandte.org or from the author.

 DOI: 10.1002/anie.200351260 © 2003 Wiley-VCH Verlag GmbH & Co. KGaA, Weinheim

Idiospermuline (**2**) contains three all-carbon-substituted quaternary centers, two of which are vicinal (3a and 3a′) and the third (3a″), a diaryl-substituted quaternary carbon of the flanking pyrrolidinoindoline subunit. Two of the three indoline nitrogens (8 and 8″) carry methyl substituents, a structural feature that is rarely seen in polypyrrolidinoindoline alkaloids.[1] The synthesis plan we followed is outlined in antithetic format in Scheme 1. We envisaged forming the diaryl-substituted quaternary stereocenter by catalytic asym-

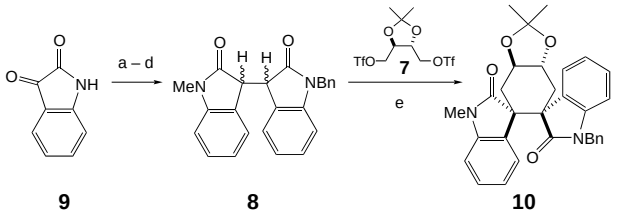


Scheme 1. Retrosynthesis of idiospermuline (**2**). Bn = benzyl, Boc = *tert*-butoxycarbonyl, Tf = trifluoromethanesulfonyl, Ts = toluenesulfonyl.

metric Heck cyclization of the heptacyclic triflate **5**.[4] This latter intermediate would be assembled from the (−)-chimonanthine congener **6**, whose contiguous quaternary carbons we saw as arising from the combination of tartrate-derived dielectrophile **7** and the lithium dienolate generated from dihydroisoindigo **8**.[2c] The asymmetric Heck cyclization step in this sequence would explore the utility of this transformation for appending a precursor of a pyrrolidinoindoline onto a chiral 3a,3a′-bispyrrolidinoindoline moiety.[5] The unsymmetrical methylation pattern of **2**, as well as the requirement to differentiate the two *peri* positions of **6** (7 and 7′), would be addressed expediently by simply beginning the synthesis with a dihydroisoindigo derivative having different substituents on the oxindole nitrogens.

This total synthesis endeavor commenced with the preparation of differentially functionalized dihydroisoindigo **8** (Scheme 2). Following a straightforward sequence, isatin (**9**) was *N*-benzylated[6] and then condensed with oxindole to provide the corresponding isoindigo. Methylation of this latter intermediate, followed by catalytic hydrogenation of the product over PtO_2 furnished **8** in 65% overall yield, and only one chromatographic purification was required in this four-step sequence.

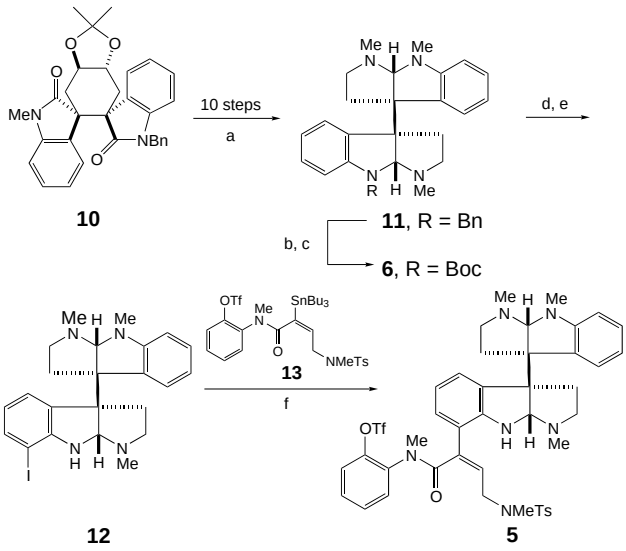
The first critical step in the synthesis was the combination of the lithium dienolate of dihydroisoindigo **8** with enantiopure ditriflate **7** (Scheme 2),[2c] a union that could produce four distinct C_1-symmetric dialkylation products. Detailed examination of this reaction revealed that solvent, temper-



Scheme 2. Reaction conditions: a) NaH, BnBr, DMF, RT; b) oxindole, AcOH, HCl, 110 °C (75%, 2 steps); c) Cs_2CO_3, MeI, DMF, RT; d) PtO_2, H_2, EtOAc, RT (87%,2 steps; e) 2 equiv LHMDS, 9:1 THF:HMPA, **7**, −40 °C (75%). DMF = dimethylformamide, HMPA = hexamethylphosphoramide, LHMDS = lithium bis(trimethylsilyl)amide, RT = room temperature.

ature, and concentration were all important factors in determining stereoselection.[7] The highest selectivity in generating the desired hexacyclic product **10** was realized by forming the lithium dienolate of **8** with LHMDS at −40 °C in a 9:1 mixture of THF/HMPA (0.05 M substrate concentration) and allowing this intermediate to react with **7** at this temperature.[8,9] These optimized conditions provided cyclohexanediol derivative **10** in 75% yield. Selective formation of **10** requires approach of the chiral dielectrophile from the *re* face of the prostereogenic dienolate, followed by cyclization of the resulting monoalkylated product without chelate organization.[2c,8]

Elaboration of **10** by a ten-step sequence analogous to that developed in our earlier total syntheses of (−)- and (+)-chimonanthine[2b,c] provided enantiopure 3a,3a′-bispyrrolidinoindoline **11** in 49% overall yield (Scheme 3).[10] Removal of the benzyl group of **11** with Na/NH_3, followed by Boc

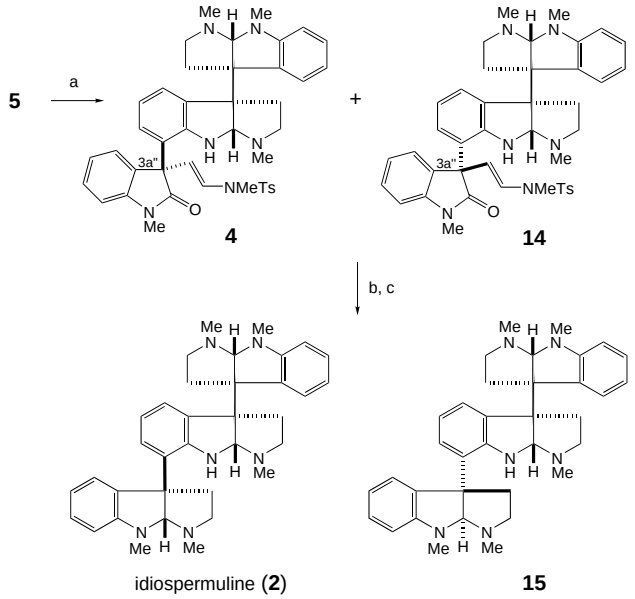


Scheme 3. Reaction conditions: a) for details of this sequence, see the Supporting Information (49% overall yield); b) Na, NH_3, THF, −78 °C (99%); c) Boc_2O, NaHMDS, THF, −78 °C (74%); d) 1) sBuLi, TMEDA, Et_2O, −78 °C; 2) diiodoethane, −78 to 0 °C (90%); e) TMSOTf, CH_2Cl_2, RT (94%); f) **13**, $Pd_2dba_3{\cdot}CHCl_3$, P(2-furyl)$_3$, CuI, NMP, RT (94%). dba = *trans*,*trans*-dibenzylideneacetone, NMP = 1-methyl-2-pyrrolidinone, TMEDA = *N*,*N*,*N*′,*N*′-tetramethylethylenediamine, TMSOTf = trimethylsilyl trifluoromethanesulfonate.

 © 2003 Wiley-VCH Verlag GmbH & Co. KGaA, Weinheim

protection of the resulting indoline, delivered **6** in 74% yield over the two steps. *ortho*-Lithiation of **6** with *s*BuLi at −78°C in pentane/TMEDA, quenching of the derived aryllithium intermediate with excess diiodoethane, and removal of the Boc group from the resulting product gave iodide derivative **12** in 85% yield.[11] The remaining carbon framework of idiospermuline was introduced by chemoselective Stille cross-coupling of **12** with the readily available stannyl butenanilide **13**[12] to furnish (*Z*)-butenanilide derivative **5** in 94% yield.[5,13]

With the Heck cyclization precursor in hand, we directed efforts toward construction of the 3a″ diaryl-substituted quaternary stereocenter. Substrate-controlled Heck cyclization of **5** using simple chelating diphosphane ligands such as bis(1,4-diphenylphosphanyl)butane (dppb) favored formation of the desired 3a″ *R* diastereomer **4**, albeit with poor selectivity (Scheme 4). Optimum stereoselection in forming **4** was realized with $Pd(OAc)_2$ as the precatalyst and (*S*)-Tol-BINAP ((*S*)-2,2′-bis(di-*p*-tolylphosphanyl)-1,1′-binaphthyl) as the ligand (Table 1).[4b,14] With this catalyst, cyclization of **5** in acetonitrile at 80°C in the presence of excess 1,2,2,6,6-pentamethylpiperidine (PMP) provided epimers **4** and **14** in 97% yield and a 6:1 ratio. Identical cyclization using (*R*)-Tol-BINAP provided **4** and **14** in a 1:18 ratio, reflecting in this case a match of substrate and catalyst control.[15]



Scheme 4. Reaction conditions: a) 10 mol% $Pd(OAc)_2$, 20 mol% diphosphane ligand, PMP, MeCN, 80°C (see Table 1); b) $Pd(OH)_2$, 1500 psi H_2, 80°C, EtOH, (90%); c) 1) Red-Al, toluene, RT; 2) Na, NH_3, THF, −78°C, (a 6:1 mixture of **4** and **14** yields **2** (47%) and **15** (16%), 2 steps).

Table 1: Heck cyclizations of (*Z*)-butenanilide **5**.

Entry	Ligand	Yield [%]	**4**:**14**
1	dppb	90	2.5:1
2	*rac*-Tol-BINAP	97	1:1.8
3	(*S*)-Tol-BINAP	97	6:1
4	(*R*)-Tol-BINAP	99	1:18

The total syntheses of idiospermuline (**2**) and its 3a″,8a″ isomer **15** were completed as follows: As epimers **4** and **14** were not readily separated, the 6:1 mixture of these products produced by cyclization of **5** with the Pd/(*S*)-Tol-BINAP catalyst was advanced to the end of the synthesis where **2** and **15** could be separated readily by preparative HPLC. This conversion began with catalytic hydrogenation using palladium hydroxide on carbon at high hydrogen pressure to provide the corresponding saturated sulfonamides. The oxindole carbonyl group of these intermediates then was reduced with sodium bis(2-methoxyethoxy)aluminum hydride (Red-Al) in toluene at room temperature,[16] and the resulting product was immediately exposed to excess sodium in ammonia at −78°C. After purification by preparative HPLC, idiospermuline (**2**), $[\alpha]_D = -267$ ($c = 0.85$ $CHCl_3$),[17] was isolated in 47% overall yield from the mixture of Heck products. Synthetic idiospermuline (**2**) was identical to a natural sample by comparison of ^1H NMR, ^{13}C NMR, CD, and HRMS data, as well as by HPLC coinjection.[18] An analogous sequence carried out with the 1:18 mixture of **4** and **14** generated from **5** with the Pd/(*R*)-Tol-BINAP catalyst gave 3a″,8a″-bisepiidiospermuline (**15**) in 57% yield.

The total synthesis of idiospermuline (**2**) described herein and that of hodgkinsine reported in the following communication[19] are the first total syntheses of trispyrrolidinoindoline alkaloids. Starting with isatin, idiospermuline was formed in 6% overall yield by way of 14 isolated and purified intermediates. This stereocontrolled total synthesis demonstrates for the first time the use of our dienolate dialkylation chemistry[2,8] for enantioselective preparation of unsymmetrical 3a,3a′-bispyrrolidinoindolines. It also provides another illustration of the ability of asymmetric intramolecular Heck reactions to generate compounds having congested quaternary carbon centers in high yield and the first demonstration of using such a transformation to elaborate a pyrrolidinoindoline unit at C7 of a chiral 3a,3a′-bispyrrolidinoindoline fragment.

Received: February 24, 2003 [Z51260]

Keywords: alkaloids · alkylation · asymmetric catalysis · C–C coupling · Heck reaction

[1] For a recent review, see: U. Anthoni, C. Christophersen, P. H. Nielsen, *Alkaloids: Chemical and Biological Perspectives, Vol. 13* (Ed.: S. W. Pelletier), Pergamon, New York, **1999**, pp. 163–236.

[2] a) J. T. Link, L. E. Overman, *J. Am. Chem. Soc.* **1996**, *118*, 8166–8167; b) L. E. Overman, D. V. Paone, B. A. Stearns, *J. Am. Chem. Soc.* **1999**, *121*, 7702–7703; c) L. E. Overman, J. F. Larrow, B. A. Stearns, J. M. Vance, *Angew. Chem.* **2000**, *112*, 219–221; *Angew. Chem. Int. Ed.* **2000**, *39*, 213–215.

[3] R. K. Duke, R. D. Allan, G. A. R. Johnston, K. N. Mewett, A. D. Mitrovic, C. C. Duke, T. W. Hambley, *J. Nat. Prod.* **1995**, *58*, 1200–1208.

[4] a) M. Oestreich, P. R. Dennison, J. J. Kodanko, L. E. Overman, *Angew. Chem.* **2001**, *113*, 1485–1489; *Angew. Chem. Int. Ed.* **2001**, *40*, 1439–1442; b) A. B. Dounay, K. Hatanaka, J. J. Kodanko, M. Oestreich, L. E. Overman, L. A. Pfeifer, M. M.

 © 2003 Wiley-VCH Verlag GmbH & Co. KGaA, Weinheim

Weiss, *J. Am. Chem. Soc.* **2003**, *125*, in press (ASAP Web release April 23, 2003).
[5] The utility of this transformation for attaching precursors of pyrrolidinoindoline fragments to a *meso* bis-3a,3a′-bispyrrolidinoindoline moiety was demonstrated in our recent total synthesis of quadrigemine C, see: A. D. Lebsack, J. T. Link, L. E. Overman, B. A. Stearns, *J. Am. Chem. Soc.* **2002**, *124*, 9008–9009.
[6] R. L. Autrey, F. C. Tahk, *Tetrahedron* **1967**, *23*, 901–917.
[7] These studies were guided by our earlier systematic studies of the related condensation of **7** with the dibenzyl analogue of **8** en route to (−)-chimonanthine.[2c,8]
[8] For a detailed study and analysis of a related dialkylation reaction, see S. B. Hoyt, L. E. Overman, *Org. Lett.* **2000**, *2*, 3241–3244.
[9] The HMPA additive was necessary not only to reduce chelation during the intramolecular alkylation step,[8] but also to solvate the substrate at low temperature.
[10] See the Supporting Information for reagents and yields for each step in the elaboration of **10** to **11**.
[11] For examples of *ortho*-lithiation of *N*-(*tert*-butoxy)indolines see: a) M. Iwao, T. Kuraishi, *Org. Synth.* **1996**, *73*, 85–93; b) S. P. Govek, L. E. Overman, *J. Am. Chem. Soc.* **2001**, *123*, 9468–9469, and reference [5].
[12] Stannyl butenanilide **13** is available in two steps from *N*-methylpropargylamine and 3-methylbenzoxazolinone, see the Supporting Information.
[13] a) V. Farina, B. Krishnan, *J. Am. Chem. Soc.* **1991**, *113*, 9585–9595; b) V. Farina, S. Kapadia, B. Krishnan, C. Wang, L. S. Liebeskind, *J. Org. Chem.* **1994**, *59*, 5905–5911; c) L. S. Liebeskind, R. W. Fengl, *J. Org. Chem.* **1990**, *55*, 5359–5364.
[14] (*S*)-Tol-BINAP = (*S*)-2,2′-bis(di-*p*-tolylphosphanyl)-1,1′-binaphthyl: H. Takaya, K. Mashima, K. Koyano, M. Yagi, H. Kumobayashi, T. Taketomi, S. Akutagawa, R. Noyori, *J. Org. Chem.* **1986**, *51*, 629–635.
[15] HPLC analysis was used to determine the diastereometric ratios in all cyclizations except that with (*R*)-Tol-BINAP. In this case a small impurity coeluted with the minor product **4**; thus, high-temperature ^{1}H NMR (360 K, for coalescence of rotamer signals) was used to determine the diastereomer ratio.
[16] X.-F. Pei, S. Bi, *Heterocycles* **1994**, *39*, 357–360.
[17] The rotation of **2** was reported erroneously as $[\alpha]_D = -2.5$ (c = 1.0, $CHCl_3$).[3] The rotation of natural **2**[18] measured in our hands (c = g/100 mL) is $[\alpha]_D = -241$ (c = 0.2, $CHCl_3$).
[18] We thank Professor Rujee K. Duke for providing this sample.
[19] J. J. Kodanko, L. E. Overman, *Angew. Chem.* **2003**, *115*, 2632–2635; *Angew. Chem. Int. Ed.* **2003**, *42*, 2528–2531 (following communication in this issue).

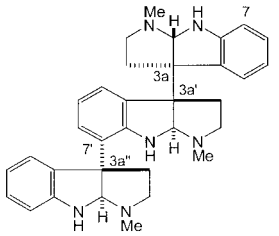
 © 2003 Wiley-VCH Verlag GmbH & Co. KGaA, Weinheim

Alkaloid Total Synthesis

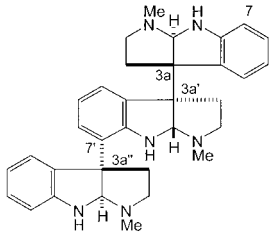
Enantioselective Total Syntheses of the Cyclotryptamine Alkaloids Hodgkinsine and Hodgkinsine B**

*Jeremy J. Kodanko and Larry E. Overman**

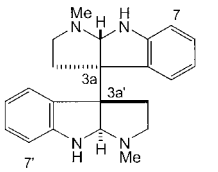
Hodgkinsine (**1**), first isolated in 1961 from the leaves of a shrub (*Hodgkinsonia frutescens*) growing in the coastal and tableland region of tropical Queensland, Australia,[1] was later identified in the alkaloid extracts of numerous members of



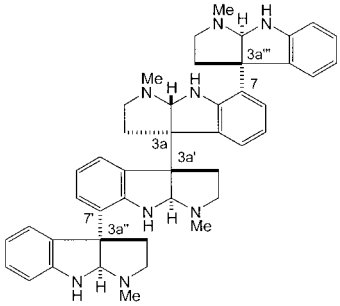
hodgkinsine (**1**)



hodgkinsine B (**2**)



meso-chimonanthine (**3**)



quadrigemine C (**4**)

the *Psychotria* genus,[2] including *P. colorata*, a plant traditionally used in the Brazilian Amazon as a remedy for pain.[3] Early chemical[1,4] and mass spectrometric evidence,[5] the latter complicated by the facile fragmentation of the C3a–C3a′ bond connecting the contiguous benzylic quaternary carbons, suggested that hodgkinsine was a N_b-methyltryptamine-derived dimer akin to chimonanthine and calycanthine. Single-crystal X-ray analysis of the trimethiodide

[*] Prof. Dr. L. E. Overman, J. J. Kodanko
Department of Chemistry
University of California, Irvine
516 Rowland Hall, Irvine, CA 92697-2025 (USA)
Fax: (+1) 949-824-3866
E-mail: leoverma@uci.edu

[**] This research was supported by the General Medical Sciences Institute of the NIH (grant GM-30859). NMR and mass spectra were determined at UC Irvine with instruments purchased with the assistance of the NSF and NIH shared instrumentation programs. We thank Professor Luisella Verotta, Università degli Studi, Milano, Italy, for a sample of hodgkinsine B and its characterization data.

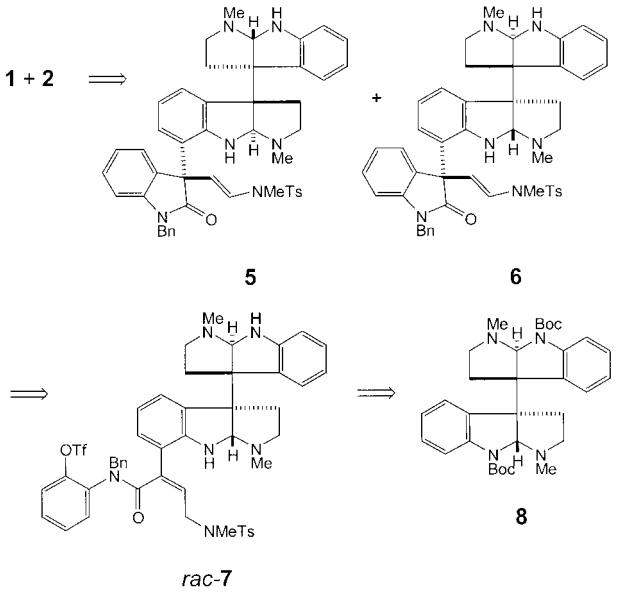
Supporting information for this article is available on the WWW under http://www.angewandte.org or from the author.

 © 2003 Wiley-VCH Verlag GmbH & Co. KGaA, Weinheim DOI: 10.1002/anie.200351261

derivative subsequently established that hodgkinsine (**1**) is composed of three pyrrolidinoindoline units,[6] and it is thus the first member of the higher order polypyrrolidinoindoline alkaloids to be fully characterized.[7]

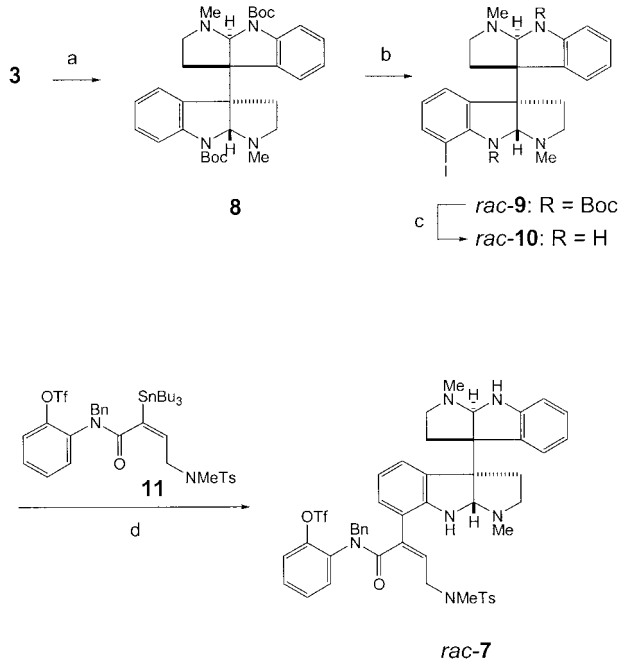
Recent pharmacological studies have shown hodgkinsine (**1**) to be a micromolar agonist of the μ-opiod receptor and to show potent dose-dependent analgesic activity against capsaicin-induced pain, the latter of which also implies the involvement of NMDA receptors.[8] In this communication we report the first total synthesis of hodgkinsine (**1**) as well as its stereoisomer **2**, a previously undisclosed alkaloid isolated from Amazon *Psychotria* species for which the name hodgkinsine B has been suggested.[9]

The approach we pursued (Scheme 1) to synthesize hodgkinsine (**1**) and hodgkinsine B (**2**) was based on a number of considerations. The vicinal quaternary stereocenters of **1** and **2** (3a and 3a′) have opposite relative configurations, making the hexacyclic 3a,3a′-bispyrrolidinoindoline moieties of these alkaloids similar to those of *meso*-chimonanthine (**3**) and quadrigemine C (**4**).[2b,7] In both alkaloids the third all-carbon-substituted quaternary stereocenter C3a″ has the *R* absolute configuration. What differentiates hodgkinsine and hodgkinsine B is the opposite absolute configurations of their contiguous quaternary stereocenters. Thus, the synthetic problem in preparing **1** and **2** reduces to selectively joining a pyrrolidinoindoline having the *R* absolute configuration at C3a″ to either the enantiotopic C7 or C7′ *peri* position of *meso*-chimonanthine (**3**). We envisioned accomplishing this stereochemical differentiation by catalyst-controlled asymmetric Heck cyclization of the racemic triflate *rac*-**7** to generate the octacyclic oxindoles **5** and **6**.[10,11] This late-stage catalytic asymmetric transformation would resolve the *meso*-3a,3a′-bispyrrolidinoindoline unit of *rac*-**7** while appending the diaryl-substituted quaternary stereocenter C3a″. The heptacyclic triflate *rac*-**7** in turn would be accessed from the known di-*tert*-butoxycarbonyl derivative **8** of *meso*-chimonanthine in a fashion similar to that employed in our recent total synthesis of quadrigemine C (**4**).[12]



Scheme 1. Retrosynthesis for hodgkinsine (**1**) and hodgkinsine B (**2**).

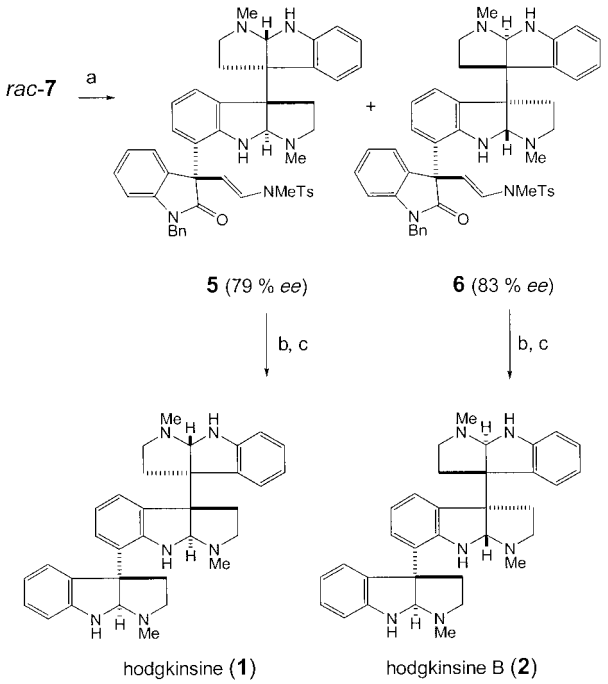
meso-Chimonanthine (**3**), the starting point for preparing hodgkinsine (**1**) and hodgkinsine B (**2**), is available by stereocontrolled total synthesis,[13] or more conveniently in 30% overall yield from tryptamine by a recently reported three-step, stereorandom sequence.[14] After conversion of **3** to dicarbamate **8** (Scheme 2),[12] this latter intermediate was *ortho*-lithiated by reaction with 2 equiv *sec*-butyllithium at −78 °C in THF containing 2 equiv TMEDA.[15] Quenching of the resulting lithium species with an excess of 1,2-diiodoethane delivered the monoiodide *rac*-**9** in 64% yield. Cleavage of the Boc groups followed by Stille cross-coupling of *rac*-**10** with stannane **11**[10b,12] furnished the racemic intramolecular Heck precursor *rac*-**7** in 39% overall yield from *meso*-chimonanthine (**3**).



Scheme 2. Reaction conditions: a) Boc_2O, THF, RT; NaHMDS (77%, ref. [13]); b) 1) sBuLi, TMEDA, THF, −78 °C; 2) diiodoethane, −78 °C to 0 °C (64%); c) TMSOTf, CH_2Cl_2 (97%); d) **10**, $Pd_2(dba_3)\cdot CHCl_3$, P(2-furyl)$_3$, CuI, DMA, RT (81%). Boc = *tert*-butoxycarbonyl, dba = dibenzylideneacetone, DMA = *N*,*N*-dimethylacetamide, NaHMDS = sodium bis(trimethylsilyl)amide, RT = room temperature, TMEDA = *N*,*N*,*N*′,*N*′-tetramethylethylenediamine, TMSOTf = trimethylsilyl trifluoromethanesulfonate.

The critical catalyst-controlled Heck cyclization of *rac*-**7** was investigated in some detail (Scheme 3 and Table 1). First we established that there was little substrate-controlled diastereoselection in the cyclization of *rac*-**7** with palladium catalysts containing achiral diphosphane ligands such as dppb (**5**:**6** = 2:1). Of the chiral, enantiopure diphosphanes screened, Tol-BINAP[16] provided the highest degree of catalyst control.[17] With this ligand, stereoselectivity was

 © 2003 Wiley-VCH Verlag GmbH & Co. KGaA, Weinheim



Scheme 3. Reaction conditions: a) 10% $Pd(OAc)_2$, 20% (*R*)-Tol-BINAP, PMP, MeCN, 80°C, (93%,1:1 ratio of **5**:**6**); b) $Pd(OH)_2$, 80 psi H_2, EtOH, 80°C; c) Na/NH_3 −78°C, NH_4Cl quench (29%, 2 steps).

Table 1: Intramolecular Heck reactions of *rac*-**7**.[a]

Ligand	Solvent	Base	Yield of % **5** [%] (% *ee*)[b]	Yield of **6** [%] (% *ee*)[b]
dppb[c]	MeCN	PS[d]	50 (–)	24 (–)
(*R*)-BINAP	MeCN	PS[d]	40 (68)	38 (69)
(*R*)-Tol-BINAP[e]	MeCN	PS[d]	37 (78)	37 (82)
(*S*)-Cy-BINAP[f]	MeCN	PS[d]	7[g] (11)[h]	6[g] (6)
(*R*)-Tol-BINAP	DMA	PS[d]	31 (71)	28 (82)
(*R*)-Tol-BINAP	toluene	PS[d]	24 (55)	24 (48)
(*R*)-Tol-BINAP	MeCN	PMP[i]	48 (79)	45 (83)

[a] Conditions: 10 mol% $Pd(OAc)_2$, 20 mol% ligand, 4.0 equiv base, substrate concentration (0.05 M), 12 h. [b] Determined by HPLC analysis with a Chiracel OD-R column. [c] dppb = 1,4-bis(diphenylphosphanyl)butane. [d] PS = 1,8-bis(dimethylamino)naphthalene (Proton-Sponge). [e] (*R*)-Tol-BINAP = (*R*)-2,2′-bis(di-*p*-tolylphosphanyl)-1,1′-binaphthyl. [f] (*S*)-Cy-BINAP = (*S*)-2,2′-bis(dicyclohexylphosphanyl)-1,1′-binaphthyl. [g] Yields measured by HPLC with an internal standard (2-aminophenol). [h] The major enantiomer formed is *ent*-**5**. [i] PMP = 1,2,2,6,6-pentamethylpiperidine.

slightly enhanced in more polar solvents, whereas the yields of **5** and **6** were improved upon substitution of PMP (1,2,2,6,6-pentamethylpiperidene) for 1,8-bis(dimethylamino)naphthalene (Proton-Sponge). Temperature changes over the range 65–80°C had no discernable effect on enantioselectivity. Under optimized conditions Heck cyclization of *rac*-**7** in acetonitrile at 80°C using the catalyst generated from 10 mol% $Pd(OAc)_2$ and 20 mol% (*R*)-Tol-BINAP provided a separable 1:1 mixture of diastereomers **5** (48% yield) and **6** (45% yield). The enantiopurity of these products (**5** 79% *ee*, **6** 83% *ee*) shows that under these conditions (*R*)-Tol-BINAP regulated stereoselection at the newly formed quaternary center to the extent of 9:1.

Saturation of the alkene double bonds of **5** and **6**, followed by reductive deprotection–cyclization of the dihydro products with Na/NH_3 and NH_4Cl[12] furnished hodgkinsine (**1**) and hodgkinsine B (**2**), each in 29% overall yield (Scheme 3). NMR spectra (^1H and ^{13}C) for synthetic **1** at room temperature and at 243 K were identical to those reported for natural hodgkinsine.[2e] Synthetic **2** was identical to an authentic sample of hodgkinsine B (**2**) by comparison of ^1H and ^{13}C NMR spectroscopic and mass spectrometric data and by HPLC coinjection.[18a] Synthetic **1** (79% *ee*) showed an optical rotation $[\alpha]_D^{27} = -25$ ($c = 0.8$, $CHCl_3$); rotations at the D line in $CHCl_3$ ranging from −26 to −42 (typically at $c = 1$) have been reported for natural samples of hodgkinsine.[2a,e,19] Synthetic **2** (83% *ee*) showed an optical rotation $[\alpha]_D^{27} = -55$ ($c = 0.8$, $CHCl_3$), whereas $[\alpha]_D^{27} = -77$ ($c = 1$, $CHCl_3$) was reported for a natural sample.[18b]

In summary, the first total syntheses of hodgkinsine (**1**) and hodgkinsine B (**2**) were accomplished from tryptamine by highly concise sequences of ten total steps. The alkaloid products were produced in enantioenriched form (~80% *ee*) and in 1.5% overall yield. The stereorational total synthesis of **2** establishes the relative and absolute configuration of this *Psychotria* natural product. To the best of our knowledge, the conversion of *rac*-**7** to enantioenriched **5** and **6** represents the first successful use of an asymmetric intramolecular Heck reaction for resolution.[20] This work, together with our recent enantioselective total syntheses of idiospermuline[21] and quadrigemine C,[12] firmly establishes the utility of catalytic asymmetric Heck cyclizations for appending pyrrolidinoindoline units in stereocontrolled fashion to hindered *peri* positions of either chiral or *meso* 3a,3a′-bispyrrolidinoindoline (chimonanthine) fragments. This chemistry, and the diastereoselective dialkylation chemistry we developed contemporaneously for preparing either enantiomer of chiral 3a,3a′-bispyrrolidinoindolines,[13b,c,22] should allow a wide variety of polypyrrolidinoindoline alkaloids and their analogues to be prepared by stereocontrolled chemical synthesis. Use of these tools to prepare all eight hodgkinsine stereoisomers and preliminary pharmacological assessment of this series will be reported elsewhere.

Received: February 24, 2003 [Z51261]

Keywords: alkaloids · asymmetric catalysis · C–C coupling · chiral resolution · Heck reactions

[1] E. F. L. J. Anet, G. K. Hughes, E. Ritchie, *Aust. J. Chem.* **1961**, *14*, 173–174.

[2] a) N. K. Hart, S. R. Johns, J. A. Lamberton, R. E. Summons, *Aust. J. Chem.* **1974**, *27*, 639–646; b) F. Libot, C. Miet, N. Kunesch, J. E. Poisson, J. Pusset, T. Sévenet, *J. Nat. Prod.* **1987**, *50*, 468–473; c) F. Guéritte-Voegelein, T. Sévenet, J. Pusset, M.-T. Adeline, B. Gillet, J. C. Beloeil, D. Guénard, P. Potier, *J. Nat. Prod.* **1992**, *55*, 923–930; d) N. H. Lajis, Z. Mahmud, R. F. Toia,

 © 2003 Wiley-VCH Verlag GmbH & Co. KGaA, Weinheim

Planta Med. **1993**, *59*, 383 – 384; e) L. Verotta, T. Pilati, M. Tatò, E. Elisabetsky, T. A. Amador, D. S. Nunes, *J. Nat. Prod.* **1998**, *61*, 392 – 396; f) V. Jannic, F. Guéritte, O. Laprévote, L. Serani, M.-T. Martin, T. Sévenet, P. Potier, *J. Nat. Prod.* **1999**, *62*, 838 – 843.

[3] L. Verotta, F. Orsini, M. Sbacchi, M. A. Scheildler, T. A. Amador, E. Elisabetsky, *Bioorg. Med. Chem.* **2002**, *10*, 2133 – 2142.

[4] B. Robinson, *Chem. Ind.* **1963**, 218 – 227.

[5] J. B. Hendrickson, R. Göschke, R. Rees, *Tetrahedron* **1964**, *20*, 565 – 579.

[6] a) J. Fridrichsons, M. F. Mackay, A. McL. Mathieson, *Tetrahedron Lett.* **1967**, 3521 – 3524; b) J. Fridrichsons, M. F. Mackay, A. McL. Mathieson, *Tetrahedron* **1973**, 85 – 92.

[7] For a recent review, see: U. Anthoni, C. Christophersen, P. H. Nielsen in *Alkaloids: Chemical and Biological Perspectives, Vol. 13* (Ed.: S. W. Pelletier), Permagnon, New York, **1999**, pp. 163 – 236.

[8] T. A. Amador, L. Verotta, D. S. Nunes, E. Elisabetsky, *Planta Med.* **2000**, *66*, 770 – 772.

[9] a) L. Verotta, F. Peterlongo, E. Elisabetsky, T. A. Amador, D. S. Nunes, *J. Chromatogr. A* **1999**, *841*, 165 – 176; b) L. Verotta, personal communication to L. E. O., November 12, **2002**.

[10] a) M. Oestreich, P. R. Dennison, J. J. Kodanko, L. E. Overman, *Angew. Chem.* **2001**, *113*, 1485 – 1489; *Angew. Chem. Int. Ed.* **2001**, *40*, 1439 – 1442; b) A. B. Dounay, K. Hatanaka, J. J. Kodanko, M. Oestreich, L. E. Overman, L. A. Pfeifer, M. M. Weiss, *J. Am. Chem. Soc.* **2003**, *125*, in press (ASAP Web release April 23, 2003).

[11] For a recent review of the use of catalytic asymmetric intramolecular Heck reactions in the synthesis of natural products, see; L. E. Overman, A. B. Dounay, *Chem. Rev.* **2003**, *103*, in press.

[12] A. D. Lebsack, J. T. Link, L. E. Overman, B. A. Stearns, *J. Am. Chem. Soc.* **2002**, *124*, 9008 – 9009.

[13] a) J. T. Link, L. E. Overman, *J. Am. Chem. Soc.* **1996**, *118*, 8166 – 8167; b) L. E. Overman, D. V. Paone, B. A. Stearns, *J. Am. Chem. Soc.* **1999**, *121*, 7702 – 7703; c) L. E. Overman, J. F. Larrow, B. A. Stearns, J. M. Vance, *Angew. Chem.* **2000**, *112*, 219 – 221; *Angew. Chem. Int. Ed.* **2000**, *39*, 213 – 215.

[14] H. Ishikawa, H. Takayama, N. Aimi, *Tetrahedron Lett.* **2002**, *43*, 5637 – 5639.

[15] a) M. Iwao, T. Kuraishi, *Org. Synth.* **1996**, *73*, 85 – 93; b) Approximately 1 equiv *s*BuLi apparently is tied up by complexation to one or more of the heteroatoms of **8**. When **8** was treated with 1 equiv *s*BuLi, *rac*-**9** was obtained in only 9 % yield and 74 % of **8** was recovered.

[16] H. Takaya, K. Mashima, K. Koyano, M. Yagi, H. Kumobayashi, T. Taketomi, S. Akutagawa, R. Noyori, *J. Org. Chem.* **1986**, *51*, 629 – 635.

[17] The cyclization of *rac*-**7** failed when the following commercially available chiral ligands were used: (*R*)-(+)-2-[2-(diphenylphosphanyl)phenyl-4-(1-methylethyl)-4,5-dihydrooxazole (Pfaltz ligand); (1*S*,2*S*)-(−)-1,2-diaminocyclohexane-*N*,*N*′-bis(2′diphenylphosphanylbenzoyl) (Trost ligand).

[18] a) Kindly provided by Professor Louisa Verotta. b) L. Verotta unpublished results conveyed to L. E. O., January 14, **2003**.

[19] F. Libot, N. Kunesch, J. Poisson, M. Kaiser, H. Duddeck, *Heterocycles* **1988**, *27*, 2381 – 2386.

[20] An earlier attempt by Shibasaki and co-workers to use an intramolecular Heck reaction to resolve a chiral intermediate produced only one of two possible diasteromers in measurable yield, see: S. Honzawa, T. Mizutani, M. Shibasaki, *Tetrahedron Lett.* **1999**, *40*, 311 – 314.

[21] L. E. Overman, E. A. Peterson, *Angew. Chem.* **2003**, *115*, 2629 – 2632; *Angew. Chem. Int. Ed.* **2003**, *42*, 2525 – 2528 (preceding communication in this issue).

[22] S. B. Hoyt, L. E. Overman, *Org. Lett.* **2000**, *2*, 3241 – 3244.

 © 2003 Wiley-VCH Verlag GmbH & Co. KGaA, Weinheim

Photoinduced Hydrogen Abstraction

Diastereomeric Differentiation in the Quenching of Excited States by Hydrogen Donors**

*Uwe Pischel, Sergio Abad, Luis R. Domingo, Francisco Boscá, and Miguel A. Miranda**

Photoinduced hydrogen transfer and electron transfer to excited states of carbonyl compounds are two of the most intensively investigated fundamental processes in photochemistry.[1–3] Numerous studies have been performed to elucidate the mechanisms as well as to determine ways to control these processes, and have involved variation of the electronic nature of the excited state (n,π* versus π,π*)[4,5] and its multiplicity, that is, singlet- versus triplet-state photochemistry.[6,7] Electronic donor properties, such as bond dissociation energies and ionization potentials,[1,4,7,8] structural features, namely, stereoelectronic and steric hindrance effects,[9,10] and the influence of the chemical surrounding (solvent polarity, hydrogen bonding) have also been investigated.[11–14]

However, relatively little is known about diastereomeric differentiation in the intramolecular quenching of excited states, which is basically related to the search for asymmetric photoreactions, and is another phenomenon which could control the kinetics of hydrogen- or electron-transfer processes.[15–17] Recently, studies were performed on the intramolecular exciplex-mediated quenching of triplet states in diastereomeric dyads consisting of 2-arylpropionic acid derivatives and electron donors of biological importance, namely, tyrosine and tryptophan.[18,19] Other studies focused on the chiral control of intramolecular charge-transfer quenching of ketone triplets in solution and in the solid state.[20,21] Reports on related intermolecular quenching are rather scarce and are also focused mainly on exciplex-mediated processes.[22,23]

Although the possibility of conformational control of photoinduced hydrogen abstractions in Norrish type II reac-

[*] Prof. Dr. M. A. Miranda, Dr. U. Pischel, Dipl.-Chem. S. Abad, Dr. F. Boscá
Instituto de Tecnología Química
Universidad Politécnica de Valencia, UPV-CSIC
Av. de los Naranjos s/n, 46022 Valencia (Spain)
Fax: (+34) 96-3877-809
E-mail: mmiranda@qim.upv.es
Prof. Dr. L. R. Domingo
Departamento de Química Orgánica
Facultad de Ciencias Químicas
Universidad de Valencia
Doctor Molliner 50, 46199 Burjassot, Valencia (Spain)

[**] Financial support by MCYT (Grant no. BQU2001-2725) is gratefully acknowledged. U.P. thanks the Deutsche Forschungsgemeinschaft for a research fellowship.

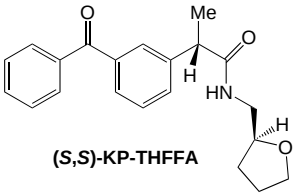
Supporting information for this article is available on the WWW under http://www.angewandte.org or from the author.

 DOI: 10.1002/anie.200250442 © 2003 Wiley-VCH Verlag GmbH & Co. KGaA, Weinheim

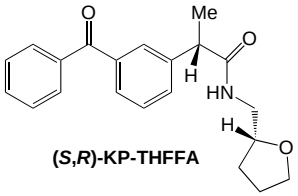
tions[24,25] or photoenol formation[26] has been reported, diastereomeric differentiation of a hydrogen donor by an excited chromophore remains unprecedented. Just recently such an effect was observed in hydrogen abstractions in dyads comprised of a chiral benzophenone derivative, namely, (*S*)-ketoprofen (KP), and a chiral 1,4-cyclohexadiene.[27] Unfortunately, the lifetime of the triplet state of ketoprofen in the investigated dyads was too short for direct kinetic characterization. Thus, a hydrogen donor with lower interaction efficiency, that is, a chiral tetrahydrofuran derivative, seemed to be a promising choice to circumvent this problem. The intermolecular rate constant for the triplet quenching of benzophenone by this ether is known to be 30 times lower than for 1,4-cyclohexadiene ($9.6\times10^{6}\,\text{M}^{-1}\,\text{s}^{-1}$ versus $2.9\times10^{8}\,\text{M}^{-1}\,\text{s}^{-1}$) in benzene.[28] Furthermore, a higher selectivity in the quenching reaction can be anticipated as a result of the lower reactivity of tetrahydrofuran which might result in a significant discrimination between both diastereomers (similar to the reactivity-selectivity principle).

Ketoprofen is a known photosensitizer similar to benzophenone which is photophysically well-characterized,[29] with special emphasis devoted to its photobiological importance.[30] Since benzophenone can be considered as the classical carbonyl chromophore, our investigations regarding diastereomeric differentiation during hydrogen-abstraction reactions are expected to provide deeper insights into a photochemical mechanism of general interest.

The dyads (*S*,*S*)-KP-THFFA and (*S*,*R*)-KP-THFFA were synthesized from (*S*)-ketoprofen (KP) and (*S*)- or (*R*)-tetrahydrofurfurylamine ((*S*)- or (*R*)-THFFA) by condensation in the presence of 1-ethyl-3-(3-dimethylamino)propylcarbodiimide (EDC) in dichloromethane. Analysis of the products by ^{1}H and ^{13}C NMR spectroscopy confirmed their identity. The UV/Vis absorption spectra of both isomers in acetonitrile are characterized by a weak absorption at 338 nm, which corresponds to the n,π* transition, and a much stronger band at 254 nm, which is typical for the π,π* absorption. These bands are similar to those obtained for the benzophenone chromophore.



(*S*,*S*)-KP-THFFA



(*S*,*R*)-KP-THFFA

Laser flash photolysis studies on the nanosecond timescale using the 355-nm output of a Nd:YAG laser (full width of half maximum height: ca. 10 ns, 10 mJ pulse^{-1}) were performed to clarify the role of diastereomeric differentiation in the primary step of the photoreduction of the carbonyl function, namely, transfer of a hydrogen atom to the triplet-excited chromophore. A transient with absorption maxima at 325 and 530 nm was formed immediately in both cases (Figure 1, inset) upon excitation of nitrogen-bubbled solutions of the diastereomers (9.5×10^{-4} M) in acetonitrile. The

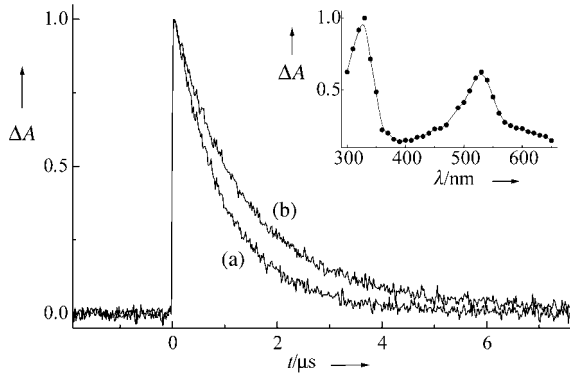


Figure 1. Transient decay for solutions of a) (*S*,*S*)-KP-THFFA and b) (*S*,*R*)-KP-THFFA in acetonitrile (9.5×10^{-4} M) under nitrogen at 525 nm upon excitation at 355 nm. The inset shows the corresponding transient spectrum of (*S*,*S*)-KP-THFFA 20–120 ns after the laser flash.

position of these bands and the ratio between their intensities (A_{325}/A_{530} ca. 1.6:1) lead to an unambiguous assignment of this transient to the triplet–triplet absorption (the triplet state) of the ketoprofen chromophore.[29–31] The ketyl radical of ketoprofen has similar absorption maxima (330 and 540 nm), but with a much larger ratio of the intensities of the two bands. The kinetics of the transient was measured at $\lambda_{obs}=525$ nm and shown to consist of a major fast component and a minor slow component (lifetime ca. 3.4–3.8 μs). The latter might be caused by the decay of biradicals formed as a result of hydrogen abstraction. Based on the transient spectrum, the major fast component can be ascribed to the triplet decay, which is significantly different for the two diastereomers: $\tau_T=0.95$ μs for (*S*,*S*)-KP-THFFA and 1.20 μs for (*S*,*R*)-KP-THFFA. The corresponding decay traces are shown in Figure 1. This result provides kinetic evidence for diastereomeric differentiation in the photoinduced hydrogen-transfer process. The triplet lifetime of ketoprofen itself under the same experimental conditions is $\tau_0=1.32$ μs. The intramolecular rate constant for hydrogen abstraction (k_H) was determined from the following relationship [Eq. (1)].

$$k_H = 1/\tau_T - 1/\tau_0 \qquad (1)$$

A unimolecular rate constant of $k_H=3.0\times10^{5}\,\text{s}^{-1}$ is found for the *S*,*S* diastereomer, while the *S*,*R* diastereomer reacts four times slower ($k_H=7.5\times10^{4}\,\text{s}^{-1}$).

To rule out the possibility that the diastereomeric differentiation found for the dyads simply reflects the result of different conformational pre-organization of the diastereomers, the intermolecular triplet quenching of (*S*)-KP by the acetamides of (*S*)- and (*R*)-THFFA was examined. Remarkably, true chiral recognition was actually observed in this experiment. The respective bimolecular quenching rate constants were 3.8×10^{7} and $2.0\times10^{7}\,\text{M}^{-1}\,\text{s}^{-1}$, thus, the enantioselectivity factor was 1.9. Although this value is smaller than that found in the intramolecular case, as would be expected from the higher degrees of freedom, it is still quite substantial and deserves further investigation. This chiral recognition could be associated with restricted approach geometries, probably as a result of hydrogen-bonding interactions

 © 2003 Wiley-VCH Verlag GmbH & Co. KGaA, Weinheim

between the carboxy group of (*S*)-KP and the NH group of the acetamides of (*S*)- and (*R*)-THFFA.

The ketyl radicals formed (biradicals in the case of an intramolecular hydrogen transfer) remain difficult to assign in the transient spectrum for the following reasons: 1) the ketyl radical is generated only in a relatively small amount (maximum 30% quenching effect for (*S*,*S*)-KP-THFFA) and 2) a significant amount of long-lived light-absorbing transients (LAT) is formed during irradiation of the dyads, as evidenced by an increase in the absorbance at approximately 330 nm (Figure 2).[32] However, although LAT complicate the

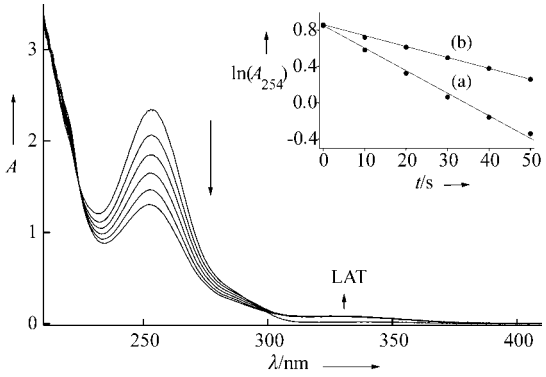
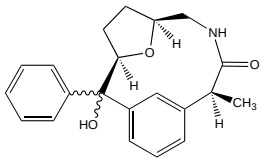


Figure 2. Steady-state irradiation of a solution of (*S*,*R*)-KP-THFFA in nitrogen-bubbled acetonitrile at $\lambda_{exc} = 254$ nm. The UV/Vis spectra were taken in time intervals of 10 s. The inset shows the respective plots for the decrease of the absorbance at 254 nm for a) (*S*,*S*)-KP-THFFA and b) (*S*,*R*)-KP-THFFA.

analysis of the transient spectra, they provide clear-cut evidence for the hydrogen-transfer process.

The influence of stereochemistry on the decomposition of the dyads under steady-state irradiation was tested in an additional experiment. The decay of the band at 254 nm in nitrogen-saturated solutions was followed during the irradiation time (Figure 2). Significant differences were noted between the two diastereomers, similar to the situation for the analogous ketoprofen–cyclohexadiene dyad,[27] with (*S*,*R*)-KP-THFFA being more photostable than the *S*,*S* diastereomer. Logarithmic plots of absorbance versus irradiation time yielded straight lines (Figure 2, inset), whose slopes point to a difference factor of 2. Again, similar to the kinetic observation of the triplet, the *S*,*S* compound reacts more efficiently, although with a somewhat lower differentiation.

Finally, isolation of the major photoproducts was accomplished by means of preparative HPLC. The NMR data (see Supporting Information) confirm the unambiguous formation of biradical recombination products, as reported for other benzophenone–hydrogen-donor dyads.[27,33] Hydrogen is surprisingly not abstracted from the more highly substituted OCHR group, but from the OCH_2 group. Molecular modeling studies (ab initio B3LYP6-31G* DFT and semiempirical AM1 calculations; see Supporting Information) on the transition states for both pathways revealed a higher activation energy (by 1.8 kcal mol^{-1}) for hydrogen abstraction from the methine group, presumably as a result of a higher ring strain in the resulting cyclophane-like photoproduct (Scheme 1).



Scheme 1. Diastereomeric photoproducts of (S,S)-KP-THFAF.

In conclusion, kinetic evidence for diastereomeric differentiation is presented for a classical textbook example of a hydrogen-abstraction process. The concept is supported by photoproduct studies and quantum-chemical calculations.

Received: October 25, 2002
Revised: March 13, 2003 [Z50442]

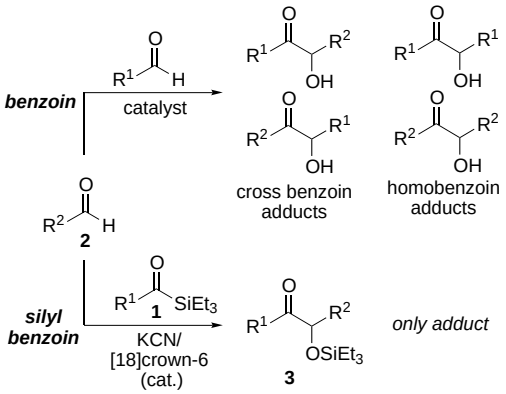
Keywords: diastereoselectivity · hydrogen transfer · ketones · laser chemistry · photochemistry

[1] J. C. Scaiano, *J. Photochem.* **1973**, *2*, 81–118.
[2] S. G. Cohen, A. Parola, G. H. Parsons, *Chem. Rev.* **1973**, *73*, 141–161.
[3] W. M. Nau, *Ber. Bunsen-Ges.* **1998**, *102*, 476–485.
[4] P. J. Wagner, R. J. Truman, A. E. Puchalski, R. Wake, *J. Am. Chem. Soc.* **1986**, *108*, 7727–7738.
[5] W. J. Leigh, E. C. Lathioor, M. J. S. Pierre, *J. Am. Chem. Soc.* **1996**, *118*, 12339–12348.
[6] W. M. Nau, F. L. Cozens, J. C. Scaiano, *J. Am. Chem. Soc.* **1996**, *118*, 2275–2282.
[7] U. Pischel, W. M. Nau, *J. Am. Chem. Soc.* **2001**, *123*, 9727–9737.
[8] J. B. Guttenplan, S. G. Cohen, *J. Am. Chem. Soc.* **1972**, *94*, 4040–4042.
[9] D. Griller, J. A. Howard, P. R. Marriott, J. C. Scaiano, *J. Am. Chem. Soc.* **1981**, *103*, 619–623.
[10] M. von Raumer, P. Suppan, E. Haselbach, *Helv. Chim. Acta* **1997**, *80*, 719–724.
[11] P. J. Wagner, A. E. Kemppainen, *J. Am. Chem. Soc.* **1969**, *91*, 3085–3087.
[12] A. A. Gorman, C. T. Parekh, M. A. J. Rodgers, P. G. Smith, *J. Photochem.* **1978**, *9*, 11–17.
[13] J. D. Simon, K. S. Peters, *J. Am. Chem. Soc.* **1982**, *104*, 6542–6547.
[14] W. M. Nau, U. Pischel, *Angew. Chem.* **1999**, *111*, 3126–3129; *Angew. Chem. Int. Ed.* **1999**, *38*, 2885–2888.
[15] H. Rau, *Chem. Rev.* **1983**, *83*, 535–547.
[16] Y. Inoue, *Chem. Rev.* **1992**, *92*, 741–770.
[17] A. G. Griesbeck, U. J. Meierhenrich, *Angew. Chem.* **2002**, *114*, 3279–3286; *Angew. Chem. Int. Ed.* **2002**, *41*, 3147–3154.
[18] M. A. Miranda, A. Lahoz, R. Martínez-Mánez, F. Boscá, J. V. Castell, J. Pérez-Prieto, *J. Am. Chem. Soc.* **1999**, *121*, 11569–11570.
[19] M. A. Miranda, A. Lahoz, F. Boscá, M. R. Metni, F. B. Abdelouahab, J. V. Castell, J. Pérez-Prieto, *Chem. Commun.* **2000**, 2257–2258.
[20] R. Boch, C. Bohne, J. C. Scaiano, *J. Org. Chem.* **1996**, *61*, 1423–1428.
[21] J. N. Moorthy, S. L. Monahan, R. B. Sunoj, J. Chandrasekhar, C. Bohne, *J. Am. Chem. Soc.* **1999**, *121*, 3093–3103.
[22] T. Yorozu, K. Hayashi, M. Irie, *J. Am. Chem. Soc.* **1981**, *103*, 5480–5484.
[23] T. Nishiyama, K. Mizuno, Y. Otsuji, H. Inoue, *Chem. Lett.* **1994**, 2227–2228.

 © 2003 Wiley-VCH Verlag GmbH & Co. KGaA, Weinheim

[24] J. C. Dalton, K. Dawes, N. J. Turro, D. S. Weiss, J. A. Barltrop, J. D. Coyle, *J. Am. Chem. Soc.* **1971**, *93*, 7213 – 7221.
[25] F. D. Lewis, R. W. Johnson, *J. Am. Chem. Soc.* **1972**, *94*, 8914 – 8916.
[26] J. C. Netto-Ferreira, J. C. Scaiano, *J. Am. Chem. Soc.* **1991**, *113*, 5800 – 5803.
[27] M. A. Miranda, L. A. Martínez, A. Samadi, F. Boscá, I. M. Morera, *Chem. Commun.* **2002**, 280 – 281.
[28] W. Adam, J. N. Moorthy, W. M. Nau, J. C. Scaiano, *J. Org. Chem.* **1997**, *62*, 8082 – 8090.
[29] L. J. Martínez, J. C. Scaiano, *J. Am. Chem. Soc.* **1997**, *119*, 11066 – 11070.
[30] F. Boscá, M. L. Marin, M. A. Miranda, *Photochem. Photobiol.* **2001**, *74*, 637 – 655.
[31] R. V. Bensasson, J.-C. Gramain, *J. Chem. Soc. Faraday Trans. 1* **1980**, *76*, 1801 – 1810.
[32] N. Filipescu, F. L. Minn, *J. Am. Chem. Soc.* **1968**, *90*, 1544 – 1547.
[33] R. Breslow, P. Kalicky, *J. Am. Chem. Soc.* **1971**, *93*, 3540 – 3541.

 © 2003 Wiley-VCH Verlag GmbH & Co. KGaA, Weinheim



Scheme 1. Benzoin and silyl benzoin addition reactions.

Selective Benzoin Condensation

Kinetic Control in Direct α-Silyloxy Ketone Synthesis: A New Regiospecific Catalyzed Cross Silyl Benzoin Reaction**

*Xin Linghu and Jeffrey S. Johnson**

Dedicated to Professor Maurice Brookhart on the occasion of his 60th birthday

The benzoin condensation remains arguably the most direct method for synthesis of α-hydroxy ketones and is the quintessential reaction of an acyl anion equivalent. The utility of the traditional benzoin condensation is well documented, but its principal limitation arises in the coupling of two different aldehydes: the product distribution of the cross benzoin condensation is generally determined by the relative stability of the four possible products (Scheme 1).[1] The usual consequences of this energetic constraint are product mixtures or lack of access to the higher energy regioisomer. Since generation of an acyl anion equivalent in situ by the reaction of an aldehyde with cyanide ion or a thiazolium ylide is the key step in the benzoin and related condensations,[2–6] we speculated that alternative methods of acyl anion formation that place the reaction under kinetic control might circumvent the aforementioned limitations.[7] In this context, the generation of silyloxy nitrile anions from acylsilanes by cyanide-promoted [1,2] Brook rearrangement of acylsilanes was particularly intriguing.[8–10] Phase-transfer-catalyzed alkylation[11,12] and acylation[13] reactions of these species are known, but the analogous carbonyl addition reactions[14,15] under catalytic conditions have not been reported to the best of our knowledge. The purpose of this paper is to document new catalyzed silyl benzoin addition reactions of acylsilanes **1** and aldehydes **2** that facilitate complete regiochemical control in direct α-silyloxy ketone synthesis (Scheme 1).

Preliminary experiments indicated that KCN/[18]crown-6 is an effective catalyst[16] for the silyl benzoin addition between benzoyl triethylsilane and benzaldehyde. An operationally convenient reaction time (2 h) was realized with 10 mol% [18]crown-6 and 0.3 equiv KCN. The reaction was possible with less catalyst (e.g., 0.1 equiv KCN); however, the reaction time increased to 12 h. To evaluate the generality of the silyl benzoin reaction, the substrate scope was studied by using a variety of acylsilanes and aldehydes (Table 1).

Collectively, the catalyzed reactions between aryl acylsilanes and aryl or heterocyclic aldehydes gave good to excellent yields of the product α-silyloxy ketones at ambient temperature (Table 1, entries 1–11). Most reaction times were less than 3 h. Electronically diverse substrates were tolerated and displayed little difference in reactivity. A sterically demanding substrate reacted without a decrease in yield or increase in reaction time (entry 10). The more challenging aryl–alkyl′ and alkyl–aryl′ benzoin adducts were obtained in moderate to good yields (entries 12–16). Efforts to synthesize alkyl–alkyl′ acyloins possessing enolizable protons on both reaction partners have to date been low yielding.

There are several noteworthy features of the silyl benzoin addition. First, the nascent secondary hydroxy group is protected as its derived silyl ether in situ. Second, no competing homobenzoin adducts are observed. Finally, either regioisomeric benzoin adduct may be prepared simply through judicious selection of the acylsilane and aldehyde (cf. **3b**/**3c** in entries 2 and 3, **3d**/**3e** in entries 4 and 5, **3f**/**3g** in entries 6 and 7, **3h**/**3i** in entries 8 and 9, and **3o**/**3p** in entries 15 and 16). By way of comparison, thiazolium-ylide-catalyzed benzoin reaction between benzaldehyde and isobutyraldehyde provides a 2:1 mixture of regioisomeric cross acyloins,[17] while the analogous cross silyl benzoin reaction gives only one isomer, **3l** (entry 12). Benzoin reaction of *p*-

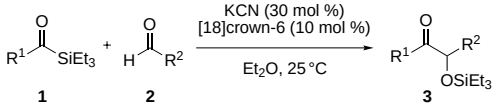
[*] Prof. J. S. Johnson, X. Linghu
Department of Chemistry
University of North Carolina, Chapel Hill
Chapel Hill, NC 27599-3290 (USA)
Fax: (+1) 919-962-2388
E-mail: jsj@unc.edu

[**] The authors acknowledge partial funding of this work by the Donors of the Petroleum Research Fund, administered by the American Chemical Society (PRF #37868-G1) and Research Corporation (Research Innovation Award to J.S.J.).

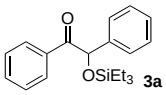
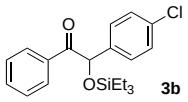
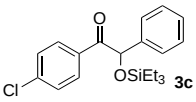
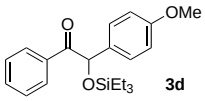
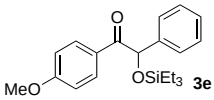
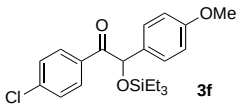
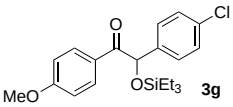
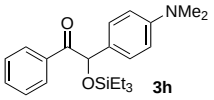
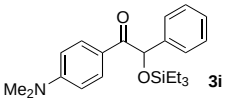
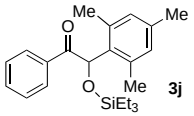
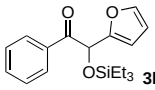
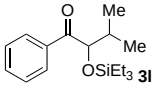
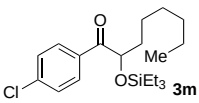
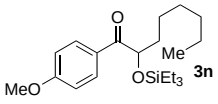
Supporting information for this article is available on the WWW under http://www.angewandte.org or from the author.

 © 2003 Wiley-VCH Verlag GmbH & Co. KGaA, Weinheim DOI: 10.1002/anie.200250554

Table 1: Catalyzed silyl benzoin addition reactions of acylsilanes and aldehydes.[a]



1 **2** **3**

Entry	R^1	R^2	Product	Yield [%][b]
1	Ph	Ph	 **3a**	90
2	Ph	4-ClPh	 **3b**	82
3	4-ClPh	Ph	 **3c**	86
4	Ph	4-MeOPh	 **3d**	79
5	4-MeOPh	Ph	 **3e**	85
6	4-ClPh	4-MeOPh	 **3f**	80
7	4-MeOPh	4-ClPh	 **3g**	80
8	Ph	4-Me_2NPh	 **3h**	66[c]
9	4-Me_2NPh	Ph	 **3i**	95[c]
10	Ph	mesityl	 **3j**	85
11	Ph	2-furyl	 **3k**	75
12	Ph	isopropyl	 **3l**	66
13	4-ClPh	*n*-hexyl	 **3m**	75
14	4-MeOPh	*n*-hexyl	 **3n**	51

anisaldehyde with benzaldehyde under cyanide catalysis allows access to only the thermodynamic isomer (hydroxy derivative of **3e**).[1] In contrast, entries 4 and 5 demonstrate that the kinetic control inherent in the acylsilane reaction circumvents this issue and provides access to both regioisomers.

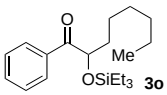
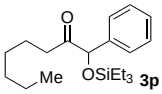
To account for the observed results, a silyl version of the Lapworth–Schowen benzoin condensation mechanism is proposed in Scheme 2.[2,18] Nucleophilic addition of a metal cyanide to acylsilane **1** generates the tetrahedral intermediate **1a,** which undergoes a [1,2] Brook rearrangement to afford the siloxy nitrile anion intermediate **1b**.[19] Addition to aldehyde **2** followed by 1,4-silyl migration gives alkoxide intermediate **1d**. Retrocyanation leads to the product α-silyloxy ketone **3** and the metal cyanide needed to engage another equivalent of acylsilane, thus completing the catalytic cycle.

Having established a new direct method to form unsymmetrical α-silyloxy ketones, we wished to explore the possibility of effecting a second catalyzed construction of a carbon–carbon bond in the same pot (Scheme 3). Thus, benzoyl *tert*-butyldimethylsilane (**4**) and *p*-chlorobenzaldehyde (**5**) participated in a silyl benzoin addition catalyzed by KCN/[18]crown-6. Upon consumption of the acylsilane (TLC analysis), ethyl cyanoformate was added. The α-silyloxy ketone intermediate **6** underwent a sequential catalyzed cyanation, 1,4-silyl migration, and *O*-acylation with ethyl cyanoformate to afford silyl cyanohydrin carbonate **7** in 91% yield as a single regioisomer (d.r. = 77:23, relative stereochemistry unassigned).[20] Conveniently, orthogonal protection of the product's two hydroxy groups is an inherent characteristic of the reaction. This result also demonstrates the utility of other silyl groups in the cross silyl benzoin addition.

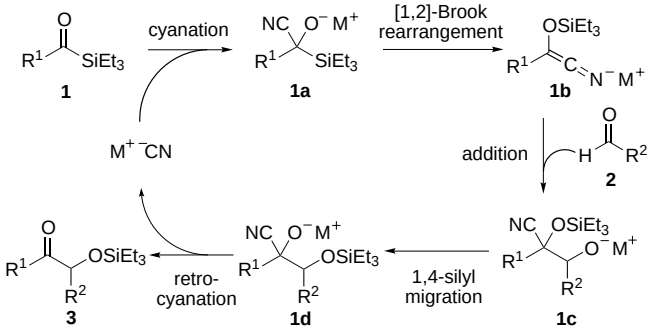
In summary, cyanide-catalyzed silyl benzoin reactions have been developed to afford unsymmetrical silyl ether protected benzoin adducts with complete regiocontrol. A sequential silyl benzoin addition/cyanation–*O*-acylation reaction that resulted in two new C–C bonds was achieved in excellent yield. The operationally simple reaction proceeds at ambient temperature and provides a convenient method for direct introduction of the protected α-hydroxy ketone moiety. Asymmetric modification of both reactions is a current focus of research.

© 2003 Wiley-VCH Verlag GmbH & Co. KGaA, Weinheim

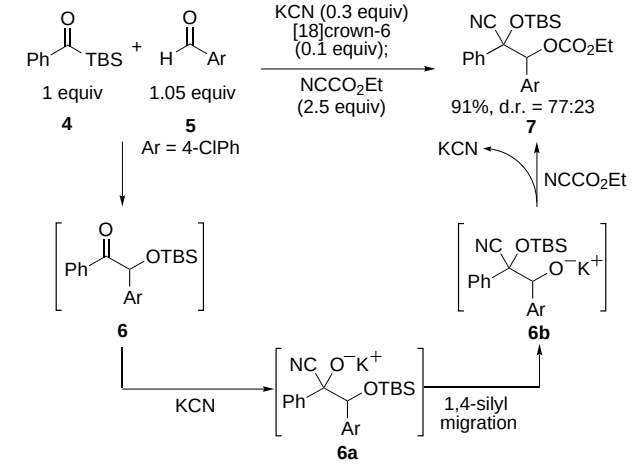
Table 1: (Continued)

Entry	R^1	R^2	Product	Yield [%][b]
15	Ph	*n*-hexyl	 **3o**	70
16	*n*-hexyl	Ph	 **3p**	51[d]

[a] $R^1C(O)SiEt_3$ (1.0 equiv), R^2CHO (1.1 equiv), [18]crown-6 (0.1 equiv), and KCN (0.3 equiv) in Et_2O at 25 °C for 1–5 h unless otherwise noted. See Supporting Information for details. [b] Yield of isolated analytically pure material. [c] Reaction time = 10 h. [d] $R^1C(O)SiEt_3$ (1.0 equiv), R^2CHO (4.0 equiv), [18]crown-6 (0.3 equiv), and KCN (0.5 equiv) in Et_2O at 25 °C.



Scheme 2. Proposed mechanism for the cross silyl benzoin addition reaction.



Scheme 3. Sequential one-pot silyl benzoin addition/cyanation–acylation reaction. TBS = *tert*-butyldimethylsilyl.

Experimental Section

Representative procedure: Synthesis of **3a**: A dry round-bottom flask with a magnetic stir bar was charged with acylsilane (104 mg, 0.47 mmol), KCN (8.0 mg, 0.12 mmol), [18]crown-6 (13 mg, 0.047 mmol), and Et_2O (8 mL). To the resulting mixture was added neat benzaldehyde (53 μL, 0.52 mmol) by syringe. The reaction mixture was stirred at 25 °C under N_2 until the starting material was consumed (2.5 h, TLC analysis). To the reaction mixture was added H_2O (15 mL). The mixture was stirred for 5 min before the organic layer was separated and the aqueous layer was extracted with Et_2O (3 × 15 mL). The organic extracts were combined and dried ($MgSO_4$), and the solvent was removed with a rotary evaporator. The product was purified by flash chromatography, eluting with 33:1 hexanes/EtOAc to afford **3a** as a clear oil (140 mg, 90% yield). Analytical data for **3a**: ^1H NMR (400 MHz, $CDCl_3$): $\delta = 8.02$–8.00 (m, 2H), 7.53–7.51 (m, 2H), 7.46–7.42 (m, 1H), 7.35–7.30 (m, 4H), 7.25–7.21 (m, 1H), 5.77 (s, 1H), 0.88 (t, $J = 8.0$ Hz, 9H), 0.64–0.57 ppm (m, 6H); $^{13}C\{^1H\}$ NMR (100 MHz, $CDCl_3$): $\delta = 198.8$, 139.0, 134.5, 132.8, 129.8, 128.5, 128.1, 127.7, 125.8, 80.0, 6.6, 4.7 ppm; IR (thin film): $\tilde{\nu} = 3087$, 3062, 3029, 2957, 2913, 2877, 1700, 1680, 1598, 1579, 1493, 1448, 1413, 1277, 1238, 1190, 1119, 1071, 1004, 980, 850, 764, 745, 606 cm^{-1}; TLC (33:1 hexanes/EtOAc) $R_f = 0.17$; elemental analysis (%) calculated for $C_{20}H_{26}O_2Si$: C 73.57, H 8.03; found: C 73.22, H 8.05.

Received: November 14, 2002 [Z50554]

Keywords: benzoin condensation · ketones · phase-transfer catalysis · rearrangements · umpolung

[1] W. S. Ide, J. S. Buck, *Org. React.* **1948**, *4*, 269–304.
[2] A. Lapworth, *J. Chem. Soc.* **1903**, *83*, 995.
[3] R. Breslow, R. Kim, *Tetrahedron Lett.* **1994**, *35*, 699–702.
[4] H. Stetter, H. Kuhlmann, *Org. React.* **1991**, *40*, 407–496.
[5] For an example of a highly enantioselective enzyme-catalyzed aryl–aryl cross benzoin reaction, see: P. Dünkelmann, D. Kolter-Jung, A. Nitsche, A. S. Demir, P. Siegert, B. Lingen, M. Baumann, M. Pohl, M. Müller, *J. Am. Chem. Soc.* **2002**, *124*, 12084–12085.
[6] Highly enantioselective homobenzoin reactions are known. See, for example: D. Enders, U. Kallfass, *Angew. Chem.* **2002**, *114*, 1822–1824; *Angew. Chem. Int. Ed.* **2002**, *41*, 1743–1745.
[7] M. D. Rozwadowska, *Tetrahedron* **1985**, *41*, 3135–3140.
[8] A. G. Brook, *Acc. Chem. Res.* **1974**, *7*, 77–84.
[9] H. J. Reich, R. C. Holtan, C. Bolm, *J. Am. Chem. Soc.* **1990**, *112*, 5609–5617.
[10] W. H. Moser, *Tetrahedron* **2001**, *57*, 2065–2084.
[11] A. Degl'Innocenti, A. Ricci, A. Mordini, G. Reginato, V. Colotta, *Gazz. Chim. Ital.* **1987**, *117*, 645–648.
[12] K. Takeda, Y. Ohnishi, *Tetrahedron Lett.* **2000**, *41*, 4169–4172.
[13] X. Linghu, D. A. Nicewicz, J. S. Johnson, *Org. Lett.* **2002**, *4*, 2957–2960.
[14] S. Hünig, G. Wehner, *Chem. Ber.* **1979**, *112*, 2062–2067.
[15] D. Saleur, J. P. Bouillon, C. Portella, *Tetrahedron Lett.* **2001**, *42*, 6535–6537.
[16] D. A. Evans, L. K. Truesdale, *Tetrahedron Lett.* **1973**, 4929–4932.
[17] H. Stetter, G. Daembkes, *Synthesis* **1977**, 403–404.
[18] J. P. Kuebrich, R. L. Schowen, M.-S. Wang, M. E. Lupes, *J. Am. Chem. Soc.* **1971**, *93*, 1214–1220.
[19] This may be contrasted with fluoride-promoted acylation reactions of acylsilanes: a) A. Degl'Innocenti, S. Pike, D. R. M. Walton, *J. Chem. Soc. Chem. Commun.* **1980**, 1201–1202; b) D. Schinzer, C. H. Heathcock, *Tetrahedron Lett.* **1981**, *22*, 1881–1884.
[20] Details of the proof of the regiochemistry may be found in the Supporting Information.

 © 2003 Wiley-VCH Verlag GmbH & Co. KGaA, Weinheim

Sialylglycopeptide Synthesis

Solid-Phase Synthesis of Sialylglycopeptides through Selective Esterification of the Sialic Acid Residues of an Asn-Linked Complex-Type Sialyloligosaccharide**

*Naoki Yamamoto, Yoshiko Ohmori, Tohru Sakakibara, Ken Sasaki, Lekh Raj Juneja, and Yasuhiro Kajihara**

Glycoproteins and glycopeptides contain O- or N-linked oligosaccharides on their peptide backbones and play a central role in several biological events.[1] Thus, it is essential to be able to synthesize glycoproteins and glycopeptides for use as probes to study their biological roles.[2–4]

A chemoenzymatic method based on the solid-phase chemical synthesis of peptides and the enzymatic attachment of a sialyloligosaccharide to the peptide by the endoglycosidase enzyme Endo M has been reported for the synthesis of N-linked sialylglycopeptides.[3a,4] However, as the enzyme used is not commercially available and as the enzymatic method often requires substrate specificity,[5] chemical synthesis is essential for the preparation of pure sialyloligosaccharides. To date there has been no solid-phase chemical synthesis of glycopeptides with the N-linked complex-type biantennary sialyloligosaccharide structure that is commonly found on glycoproteins reported, as there are two major problems concerning the solid-phase synthesis of these compounds.

The first of these problems is the tendency of the sialyl linkage of glycopeptides to undergo acid-catalyzed hydrolysis in the presence of 95% trifluoroacetic acid (TFA) during the final cleavage step in solid-phase glycopeptide synthesis.[6] Both α-2,6 and α-2,3 sialyl linkages are very labile, but particularly the former. If α-2,6 sialyloligosaccharides are to resist acid hydrolysis, an electron-withdrawing group such as an acetyl group should be used as a protecting group.[3g] Another way to avoid hydrolysis of the sialyl linkage is to use a sophisticated linker such as HYCRON, which can be cleaved under mild conditions.[7]

The second problem is the quantity of complex-type sialyloligosaccharide required. If 10 mg of a decapeptide (M_W ca. 1000) is to be attached to a complex-type biantennary sialyloligosaccharide (M_W ca. 2000) by solid-phase peptide synthesis, at least 20 mg of the oligosaccharide must be used. Unverzagt and Prahl have developed a highly efficient chemoenzymatic method for the synthesis of such large oligosaccharides.[3j,8] However, 20 mg of a complex-type biantennary sialyloligosaccharide would be a very valuable sample, which would take several months to prepare by a chemical or chemoenzymatic method. The sialylglycopeptide **1** is available in multigram quantities from eggs.[9] If the sialyloligosaccharide part of **1** could be used for the solid-phase chemical synthesis of sialylglycopeptides, research on the biological role of sialylglycopeptides could be advanced.

The sialylglycopeptide **1** can be converted into the asparaginyl sialyloligosaccharide **2** upon treatment with the enzyme Actinase E (Scheme 1).[4a] However, as this Asn-linked oligosaccharide **2** contains three carboxylic acid groups, selective protection of the carboxylic acid groups on the sialic acid residues would be essential for solid-phase glycopeptide synthesis, in which undesired amide condensations must be avoided. Herein we describe solutions to these problems, and the resulting efficient solid-phase synthesis of an N-linked sialylglycopeptide via the sialyloligosaccharide **4**.

We investigated various conditions in our search for a selective esterification of the sialic acid carboxylic acid groups and found that the use of Cs_2CO_3 and BnBr[10] afforded the desired disialyloligosaccharide dibenzyl ester **4** in 85% yield from **3** (Scheme 1).[11,12] Compound **3** was in turn prepared by adding an Fmoc group to the asparagine residue of **2**. The ^{1}H NMR spectrum of **3** showed enhanced broadening of the AcN-H and C_1-H signals of the Asn-linked 2-acetamido-2-deoxy-β-D-glucopyranosyl residue and of the β-methylene proton signals of the asparagine residue, relative that of **2**. This observation may indicate that clustering of the Fmoc groups occurs, as a result of the hydrophobic nature of the aqueous solution. Selective neutralization by Cs_2CO_3 in water and subsequent selective benzyl esterification of the sialic acid residues might then take place because of the steric bulk of the clustered Fmoc groups. Even though three equivalents of Cs_2CO_3 (3 equiv of Cs to each sialic acid residue) were used, the triply esterified product was not obtained. We also found that compound **4** was stable in 95% aqueous TFA for three hours;[13] that is, under typical conditions for the cleavage of products from peptides in solid-phase synthesis. This resistance to acid may be a result of the steric bulk of the benzyl esters around the sialyl linkages.

We took advantage of this new finding and attempted the stepwise, solid-phase assembly of an N-linked sialylglycopeptide. As a target compound we chose the sequence ALLVNSS (79–85), which is part of the pharmaceutically important glycoprotein hormone erythropoietin (EPO).[14]

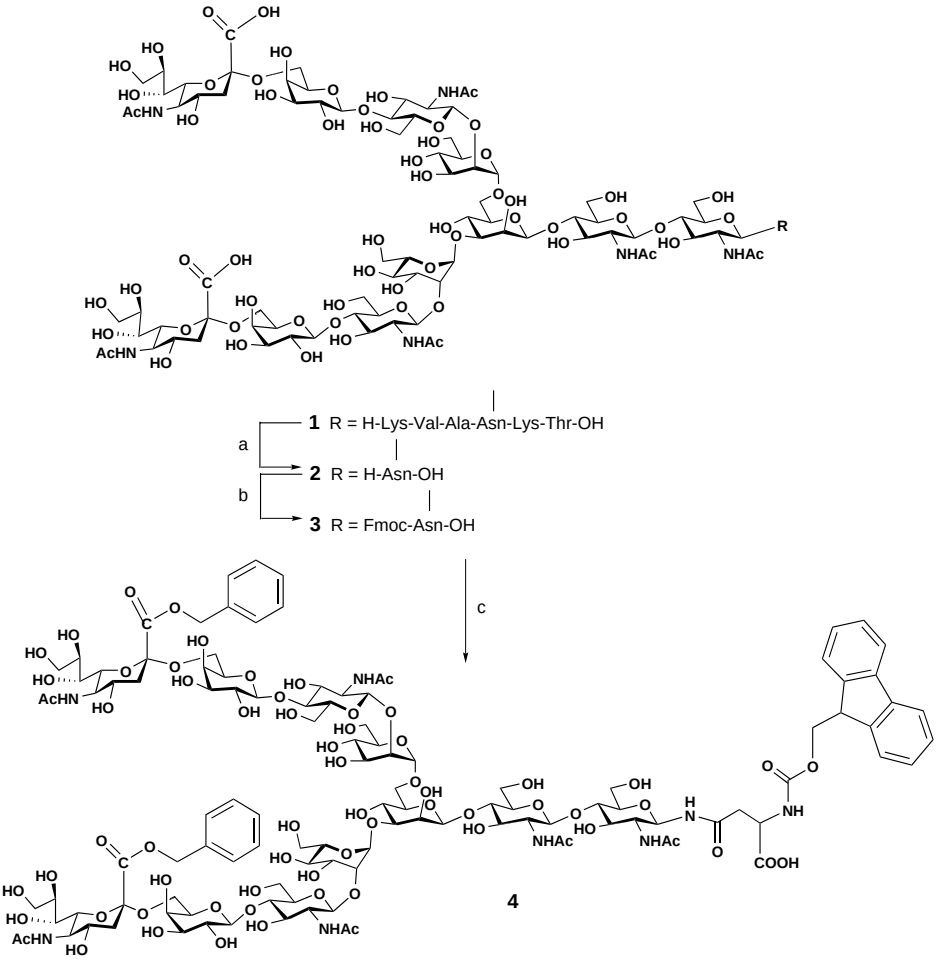
The N-linked sialylglycopeptide synthesis was performed on the poly(ethylene glycol)–poly(dimethylacrylamide) copolymer (PEGA) resin, which contains the acid-labile linker hydroxymethylphenoxyacetic acid (HMPA)[15] (Scheme 2). The first amino acid, serine, was coupled as Fmoc-Ser(*t*Bu)-OH by activation with 1-(mesitylenesulfonyl)-3-nitro-1,2,4-triazole (MSNT) and *N*-methylimidazole. The second serine residue was coupled in the presence of 1-hydroxybenzotriazole (HOBt) and diisopropylcarbodiimide (DIPCDI). At this point, the oligosaccharide was introduced through reaction with glycosylated Fmoc-Asn-OH **4** in the

[*] Prof. Dr. Y. Kajihara, N. Yamamoto, Y. Ohmori, T. Sakakibara
Graduate School of Integrated Science
Yokohama City University
22-2, Seto, Kanazawa-ku, Yokohama, 236-0027 (Japan)
Fax: (+81) 45-787-2370
E-mail: kajihara@yokohama-cu.ac.jp
K. Sasaki, L. R. Juneja
Central Research Laboratories, Taiyo Kagaku Co., Ltd.
1–3, Takaramachi, Yokkaichi, Mie, 510-0844 (Japan)

[**] We thank Dr. Michio Sasaoka (Otsuka Chemical Co., LTD) for supporting this work.

Supporting information for this article is available on the WWW under http://www.angewandte.org or from the author.

 DOI: 10.1002/anie.200250572 © 2003 Wiley-VCH Verlag GmbH & Co. KGaA, Weinheim



Scheme 1. Reagents: a) Actinase E, Tris-HCl buffer, NaN_3, pH 7.5, 86%; b) Fmoc-OSucc, $NaHCO_3$, acetone, H_2O, 68%; c) Cs_2CO_3, H_2O, then BnBr, DMF, 85%. Tris = tris(hydroxymethyl)aminomethane, Fmoc-OSucc = 9-fluorenylmethyl *N*-succinimidyl carbonate.

presence of the coupling reagent 2-(1*H*-9-azobenzotriazole-1-yl)-1,1,3,3-tetramethyluronium hexafluorophosphonate (HATU) and diisopropylethylamine (DIPEA) in DMF/DMSO (1:1) for 24 hours. The yield for this coupling step was 38%, based on the Fmoc-fullvene estimation method.[15] The other amino acids of the peptide in **5** were coupled as activated pentafluorophenol (OPfp) esters, in the presence of the catalyst 3,4-dihydro-3-hydroxy-4-oxo-1,2,3-benzotriazine (Dhbt-OH).[15] However, the coupling of Fmoc-Val-OPfp was monitored based on the disappearance of the yellow Dhbt-OH color and stopped at 85% conversion. If coupling with Val was continued, esterification of the hydroxyl groups on the oligosaccharide occurred.[16]. The coupling of the other amides (Leu, Leu, Ala) by the OPfp method took place quantitatively and the reactions were monitored in the same way, based on the disappearance of the Dhbt-OH color. In these cases no esterification of the hydroxy groups of the oligosaccharide was observed. After construction of the glycopeptide, the sialylglycopeptide was deprotected and cleaved from the resin by treatment with TFA/water (95:5) for three hours. As expected, the sialyl linkage was resistant to this acid treatment. Hydrolysis of the benzyl esters was carried out with aqueous sodium hydroxide at pH 11. This reaction was carefully monitored by ^{1}H NMR spectroscopy, and we could confirm that no epimerization of any of the amino acid α-carbon centers occurred. The crude product was then subjected to reversed-phase HPLC purification (Figure 1), and the pure sialylglycopeptide **5** thus obtained was characterized by ^{1}H NMR spectroscopy (2D-TOCSY, 2D-NOESY).[17]

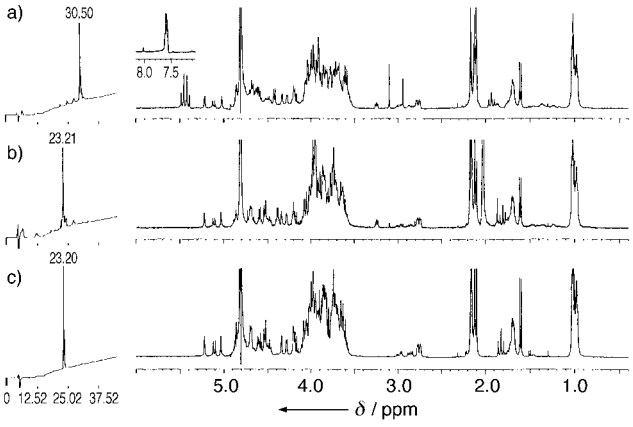
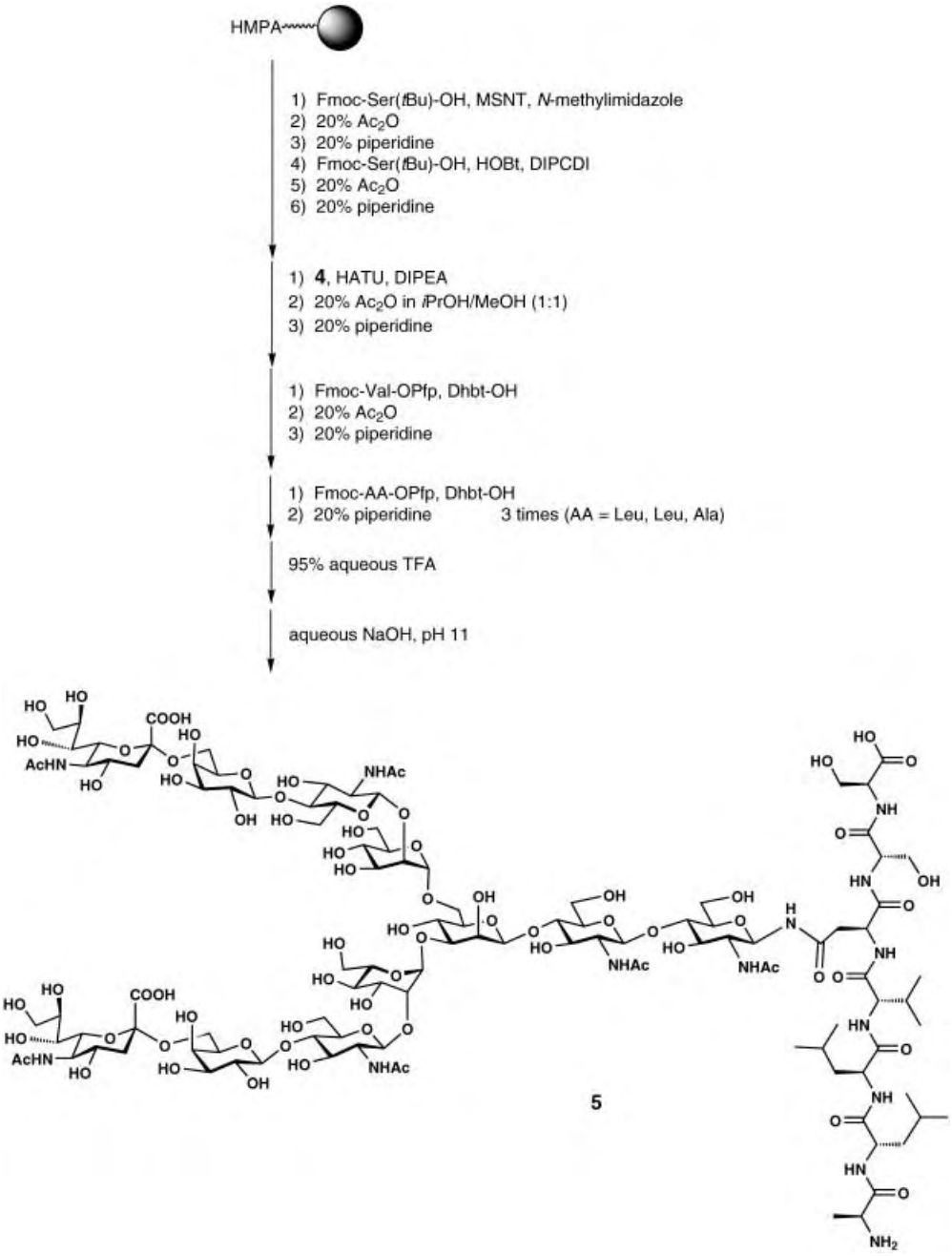


Figure 1. HPLC traces with corresponding ^{1}H NMR spectra: a) crude sample after cleavage from the resin with 95% TFA; b) crude sample after NaOH treatment of (a); c) sialylglycopeptide **5** after purification by HPLC.

 © 2003 Wiley-VCH Verlag GmbH & Co. KGaA, Weinheim



Scheme 2. Solid-phase synthesis of the sialylglycopeptide **5**.

In conclusion, we have developed a selective esterification method for the sialic acid residues of asparagine-linked sialyloligosaccharides, which has enabled us to perform the first solid-phase chemical synthesis of an Asn-linked sialylglycopeptide. This method should be applicable to the synthesis of large sialylglycopeptides and sialylglycoproteins by native chemical ligation and intein methods,[18] and ultimately allow the investigation of the roles of sialyloligosaccharides in biological systems.

Received: November 18, 2002 [Z50572]

Keywords: glycopeptides · oligosaccharides · sialic acids · solid-phase synthesis

[1] a) R. A. Dwek, *Chem. Rev.* **1996**, *96*, 683–720; b) A. Varki, *Glycobiology* **1993**, 3, 97–130.
[2] a) H. Herzner, T. Reipen, M. Schultz, H. Kunz, *Chem. Rev.* **2002**, *102*, 4495–4537; b) B. G. Davis, *Chem. Rev.* **2002**, *102*, 579–601; c) P. Sears, C. H. Wong, *Science* **2001**, *291*, 2344–2350; d) O. Seitz, *ChemBioChem* **2000**, *1*, 214–246; e) L. S. Marcaurelle, C. R. Bertozzi, *Chem. Eur. J.* **1999**, *5*, 1384–1390.
[3] a) S. E. O'Connor, J. Pohlmann, B. Imperiali, I. Saskiawan, K. Yamamoto, *J. Am. Chem. Soc.* **2001**, *123*, 6187–6188; b) S. K.

 © 2003 Wiley-VCH Verlag GmbH & Co. KGaA, Weinheim

George, T. Schwientek, B. Holm, C. A. Reis, H. Clausen, J. Kihlberg, *J. Am. Chem. Soc.* **2001**, *123*, 11117 – 11125; c) K. M. Koeller, M. E. B. Smith, C. H. Wong, *J. Am. Chem. Soc.* **2000**, *122*, 742 – 743; d) S. E. O'Connor, B. Imperiali, *Chem. Biol.* **1998**, *5*, 427 – 437; e) Y. Nakahara, Y. Nakahara, Y. Ito, T. Ogawa, *Carbohydr. Res.* **1998**, *309*, 287 – 296; f) K. Witte, O. Seitz, C. H. Wong, *J. Am. Chem. Soc.* **1998**, *120*, 1979 – 1989; g) M. Elofsson, L. A. Salvador, J. Kihlberg, *Tetrahedron* **1997**, *53*, 369 – 390; h) K. Witte, P. Sears, R. Martin, C. H. Wong, *J. Am. Chem. Soc.* **1997**, *119*, 2114 – 2118; i) L. X. Wang, M. Tang, T. Suzuki, K. Kitajima, Y. Inoue, S. Inoue, J. Q. Fan, Y. C. Lee, *J. Am. Chem. Soc.* **1997**, *119*, 11136 – 11146; j) C. Unverzagt, *Tetrahedron Lett.* **1997**, *38*, 5627 – 5630; k) O. Seitz, C. H. Wong, *J. Am. Chem. Soc.* **1997**, *119*, 8766 – 8776.

[4] a) M. Mizuno, K. Haneda, R. Iguchi, I. Muramoto, T. Kawakami, S. Aimoto, K. Yamamoto, T. Inazu, *J. Am. Chem. Soc.* **1999**, *121*, 284 – 290; b) K. Yamamoto, K. Fujimori, K. Haneda, M. Mizuno, T. Inazu, H. Kumagai, *Carbohydr. Res.* **1998**, *305*, 415 – 422.

[5] Another method (not on a solid phase) involves the use of sialyltransferases: Following the synthesis of an asialoglycopeptide, sialic acid can be attached by using sialyltransferase.[3j] However, this enzymatic reaction is not quantitative and the incomplete sialylation results in a time-consuming purification. See: a) T. Miyazaki, H. Sato, T. Sakakibara, Y. Kajihara, *J. Am. Chem. Soc.* **2000**, *122*, 5678 – 5694; b) T. Miyazaki, T. Sakakibara, H. Sato, Y. Kajihara, *J. Am. Chem. Soc.* **1999**, *121*, 1411 – 1412; c) S. Sabesan, J. O. Duus, P. Domaille, S. Kelm, J. C. Paulson, *J. Am. Chem. Soc.* **1991**, *113*, 5865 – 5866; d) D. H. Joziasse, W. E. C. M. Schiphorst, D. H. Van den Eijnden, J. A. Van Kuik, H. Van Halbeek, J. F. G. Vliegenthart, *J. Biol. Chem.* **1987**, *262*, 2025 – 2033.

[6] For the α-2,3 sialyl linkage in the glycopeptide, Kunz and coworkers (N. Bézay, G. Dudziak, A. Liese, H. Kunz, *Angew. Chem.* **2001**, *113*, 2350 – 2353; *Angew. Chem. Int. Ed.* **2001**, *40*, 2292 – 2295) and Nakahara et. al[3e] showed that esterified and lactonized O-linked sialyltrisaccharides, respectively, are resistant toward acid treatment in the final step of solid-phase peptide synthesis.

[7] a) O. Seitz, H. Kunz, *J. Org. Chem.* **1997**, *62*, 813 – 826; b) M. Rösch, H. Herzner, W. Dippold, M. Wild, D. Vestweber, H. Kunz, *Angew. Chem.* **2001**, *113*, 3954 – 3957; *Angew. Chem. Int. Ed.* **2001**, *40*, 3836 – 3839.

[8] a) I. Prahl, C. Unverzagt, *Angew. Chem.* **2002**, *114*, 4434 – 4437; *Angew. Chem. Int. Ed.* **2002**, *41*, 4259 – 4262; b) C. Unverzagt, *Carbohydr. Res.* **1998**, *305*, 423 – 431; c) C. Unverzagt, *Angew. Chem.* **1996**, *108*, 2507 – 2510; *Angew. Chem. Int. Ed. Engl.* **1996**, *35*, 2350 – 2353.

[9] A. Seko, M. Kotetsu, M. Nishizono, Y. Enoki, H. R. Ibrahim, L. R. Juneja, M. Kim, T. Yamamoto, *Biochim. Biophys. Acta* **1997**, *1335*, 23 – 32.

[10] T. W. Greene, P. G. Wuts, *Protective Groups in Organic Synthesis*, 2nd ed., Wiley, New York, **1991**, p. 228.

[11] This structure was confirmed by ^{1}H NMR spectroscopic analysis and HRMS analysis. The signals for the anomeric protons of the two galactose residues were shifted upfield by 0.12 ppm and the two axial proton signals of the deoxygenated carbon atom (C-3) of the two sialic acid residues were shifted downfield by 0.13 ppm relative to those of **3**. No other proton signals were shifted relative to **3**.

[12] For the benzyl esterification of sialic acid in the synthesis of a sialyldisaccharylpeptide, see: S. Keil, C. Claus, W. Dippold, H. Kunz, *Angew. Chem.* **2001**, *113*, 379 – 382; *Angew. Chem. Int. Ed.* **2001**, *40*, 366 – 369.

[13] ^{1}H NMR spectroscopic data showed that the sialyl linkage of the benzyl diester **4** did not undergo acid-catalyzed hydrolysis in 95 % TFA solution (see the Supporting Information).

[14] F. K. Lin, S. Suggs, C. H. Lin, J. K. Browne, R. Smalling, J. C. Egrie, K. K. Chen, G. M. Fox, F. Martin, Z. Stabinsky, S. M. Badrawi, P. H. Lai, E. Goldwasser, *Proc. Natl. Acad. Sci. USA* **1985**, *82*, 7580 – 7584.

[15] E. Meinjohanns, M. Meldal, H. Paulsen, R. A. Dwek, K. J. Bock, *J. Chem. Soc. Perkin Trans. 1* **1998**, 549 – 560.

[16] This undesired esterification was observed by HPLC after the release of the glycopeptide from the solid phase. When this sample was treated with aqueous NaOH (pH 11), many peaks were simplified in the HPLC trace.

[17] As seen in the Supporting Information, the NOESY data show an NOE interaction between Asn-N-H and Val-C_α-H. This interaction indicates that Asn is linked to Val in the sialylglycopeptide **5**. Furthermore, acid treatment (40 mM HCl, 80 °C, 1 h) of the sialylglycopeptide **5** afforded the corresponding asialoglycopeptide quantitatively, which indicates that the carboxylic acid moieties of the sialic acid residues are not linked to the amino acid during the solid-phase synthesis, because of the benzyl ester protecting groups.

[18] a) T. J. Tolbert, C. H. Wong, *J. Am. Chem. Soc.* **2000**, *122*, 5421 – 5428; b) D. Macmillan, C. R. Bertozzi, *Tetrahedron* **2000**, *56*, 9515 – 9525.

 © 2003 Wiley-VCH Verlag GmbH & Co. KGaA, Weinheim

Total Synthesis of Virantmycin

Stereospecific Construction of Contiguous Quaternary and Tertiary Stereocenters by Rearrangement from Indoline-2-methanol to 2,2,3-Trisubstituted Tetrahydroquinoline: Application to an Efficient Total Synthesis of Natural Virantmycin**

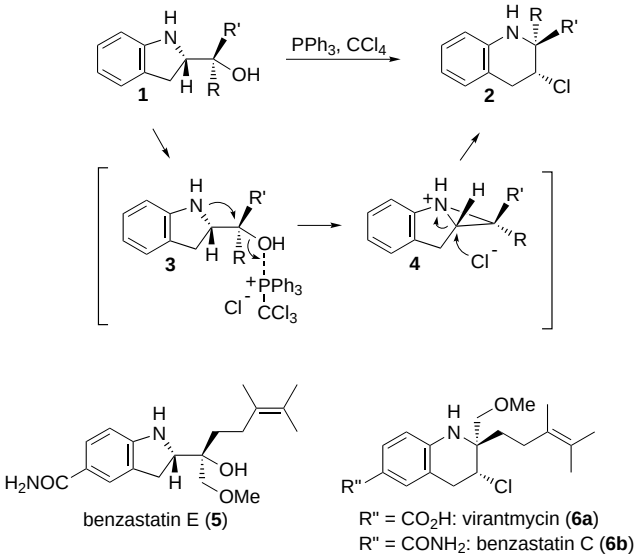
*Mayuko Ori, Narihiro Toda, Kazuko Takami, Keiko Tago, and Hiroshi Kogen**

The stereoselective construction of chiral quaternary stereocenters is one of the most challenging problems in synthetic organic chemistry.[1] Substituted tetrahydroquinolines and tetrahydroisoquinolines have attracted considerable attention from organic and medicinal chemists, primarily because they display a wide range of physiological activities.[1c,2] These ring systems are present in various important natural products.[2] Moreover, chiral quaternary centers are often essential for these compounds. For example, chiral contiguous quaternary and tertiary stereocenters are found in virantmycin (**6a**),[3] a potent antiviral agent (Scheme 1). Recently, Shibasaki et al. reported an elegant synthesis of 1,1-disubstituted tetrahy-

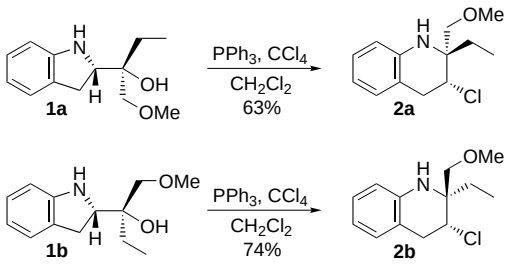
[*] Dr. H. Kogen, M. Ori, N. Toda, K. Takami, Dr. K. Tago
Exploratory Chemistry Research Laboratories
Sankyo Co., Ltd.
1-2-58 Hiromachi, Shinagawa-ku, Tokyo 140-8710 (Japan)
Fax: (+81) 3-5436-8570
E-mail: hkogen@shina.sankyo.co.jp

[**] We thank Prof. Satoshi Ōmura (Kitasato Institute) for providing copies of NMR spectra of natural virantmycin and Mr. Youji Furukawa (Sankyo) for X-ray analysis.

 © 2003 Wiley-VCH Verlag GmbH & Co. KGaA, Weinheim DOI: 10.1002/anie.200351069



Scheme 1.



Scheme 2.

droisoquinolines by a catalytic, enantioselective Reissert-type reaction.[1c] However, efficient stereoselective synthesis of 2,2-disubstituted tetrahydroquinolines still remains to be solved. Herein we describe an indoline-2-methanol to tetrahydroquinoline rearrangement in which contiguous quaternary and tertiary stereogenic centers are constructed in one step. This reaction was successfully applied to an efficient total synthesis of natural virantmycin (**6a**).

Kim et al. reported the isolation from *Streptomyces nitrosporeus* 30643 of a novel class of indoline alkaloids, that is benzastatins such as benzastatin E (**5**), and tetrahydroquinoline alkaloids, namely, benzastatin C (**6b**) and its congeners, which are structurally related to virantmycin (**6a**).[4] The structures of these alkaloids suggested that an aziridine intermediate, such as **4**, is involved in their biosyntheses.[5] Based on this hypothesis, we designed the triphenylphosphane/CCl_4-mediated rearrangement from α,α-disubstituted indoline-2-methanol **1** to 2,2,3-trisubstituted tetrahydroquinoline **2** via the aziridine **4**, followed by ring opening by attack of chloride anion (Scheme 1).[6] This type of rearrangement is a useful method of accessing various chiral 2,2,3-trisubstituted tetrahydroquinoline derivatives in conjunction with our previously developed, highly diastereoselective synthesis of optically active α,α-disubstituted indoline-2-methanol compounds **1** by Grignard addition to 2-acylindoline.[7]

We investigated the reaction by using optically active alcohol **1a**[7] as starting material (Scheme 2). Treatment of **1a** with PPh_3 (3 equiv) and CCl_4 (10 equiv) in CH_2Cl_2 under reflux for 30 min afforded tetrahydroquinoline **2a** as a single isomer in 63% yield. The same treatment of diastereomer **1b**[7] gave **2b** as a sole isomer in 74% yield.[8,9] Relative configurations of **2a** and **2b** were determined by comparison with the corresponding authentic racemic samples, reported by Shirahama et al.[10] The absolute configuration of **2a** was determined to be 2*R*,3*R* by X-ray analysis of (1*S*,2*R*,4*R*)-(−)-camphorsultam[11] derivative **7** (Figure 1),[12] which was derived from **2a** in a two-step sequence. Treatment of **2b** with nBu_3SnH and azobisisobutyronitrile afforded the dechlorinated derivative, which was identical with the dechlorinated compound derived from **2a** except for the optical rotation. On the basis of these results, the rearrangement is considered to be stereospecific.[13] Table 1 presents the results of the rearrangement of various chiral indoline-2-methanol derivatives. All the reactions provide single isomers in moderate to good yield.[14] The reaction of **1c** (enantiomer of **1a**) provided the antipode of **2a** (entry 1). Use of polymer-supported triphenylphosphane gave the same result (entry 6). Thus, this rearrangement provides a new method for the synthesis of various optically active 2,2,3-trisubstituted tetrahydroquinolines.

The utility of this reaction was clearly demonstrated by an efficient total synthesis of the potent antiviral agent virantmycin (**6a**)[3] in its natural form. Several total syntheses of (±)- or *ent*-virantmycin are known.[15,16] However, the naturally occurring form of virantmycin has not been synthesized to date. The synthesis of (−)-virantmycin is outlined in Scheme 3. Acylindoline **9**,[7] which was prepared from commercially available (*S*)-(−)-indoline-2-carboxylic acid (**8**) in four steps (37%), was treated with iodine monochloride to afford iodide **10** in 91% yield. Iodide **10** was subjected to diastereoselective Grignard addition[7] with 2,3-dimethyl-3-pentenylmagnesium bromide[17] to give *tert*-alcohols as a 95/5 mixture of separable isomers, as determined by HPLC analysis of the product mixture. The Boc protecting group of the major isomer was removed by treatment with HCO_2H to afford **11**.[18] The resulting amino alcohol **11** was treated with tri-*n*-butylphosphane (20 equiv)[19] and CCl_4 (30 equiv) to provide tetrahydroquinoline **12** as a single isomer in 45% yield. The tetrahydroquinoline **12** was carbonylated by reaction with 1 atm of CO in H_2O/DMF in the presence of catalytic $Pd(OAc)_2$ and K_2CO_3 to give

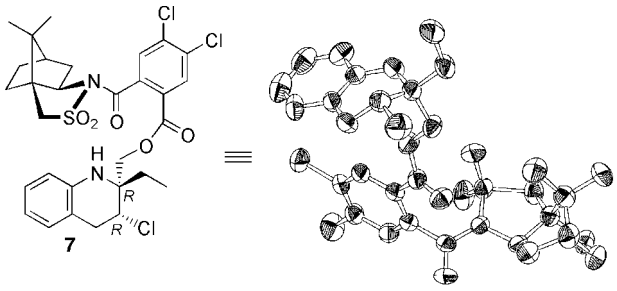
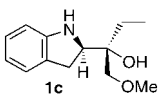
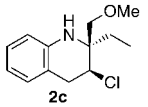
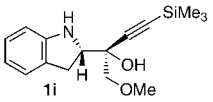
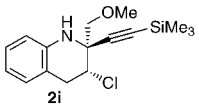
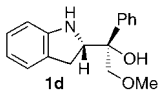
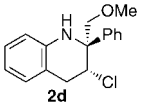
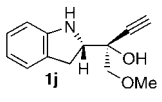
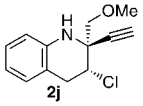
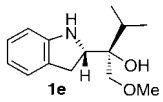
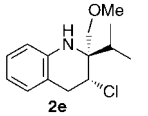
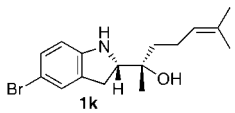
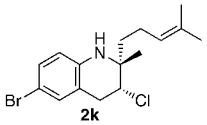
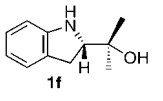
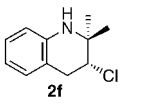
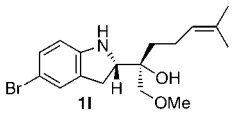
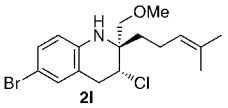
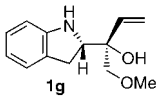
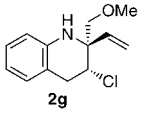
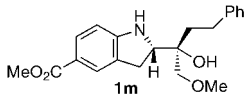
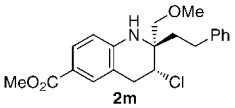
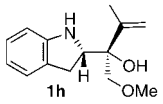
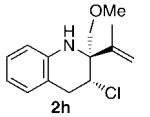
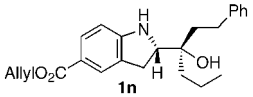
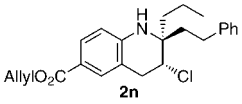


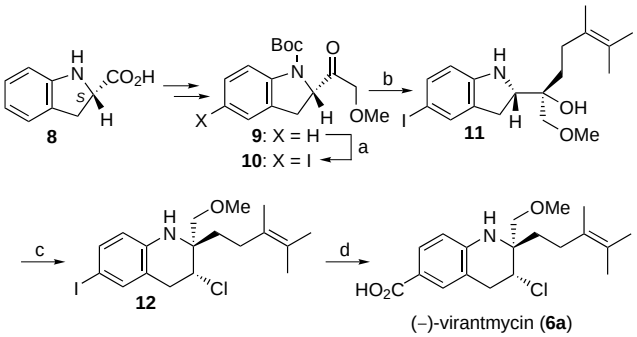
Figure 1. X-ray structure of the (1*S*,2*R*,4*R*)-(−)-camphorsultam derivative of **2a**.

 © 2003 Wiley-VCH Verlag GmbH & Co. KGaA, Weinheim

Table 1: Rearrangement of indoline **1** to tetrahydroquinoline **2**.

Entry[a]	Indoline **1**[b]	Tetrahydroquinoline **2**[c]	Yield [%][d]	Entry[a]	Indoline **1**[b]	Tetrahydroquinoline **2**[c]	Yield [%][d]
1	 **1c**	 **2c**	63	7	 **1i**	 **2i**	63
2	 **1d**	 **2d**	63	8	 **1j**	 **2j**	55
3	 **1e**	 **2e**	53	9	 **1k**	 **2k**	62
4	 **1f**	 **2f**	65	10	 **1l**	 **2l**	41
5	 **1g**	 **2g**	31	11	 **1m**	 **2m**	50
6	 **1h**	 **2h**	37 (44)[e]	12	 **1n**	 **2n**	52

[a] All the reactions conducted were with Ph_3P (3 equiv) and CCl_4 (10 equiv), except for entry 6. [b] For synthesis of indoline **1**, see ref. [7]. [c] The absolute stereochemistry was tentatively assigned by analogy with the reaction mechanism, except for **2c** (enantiomer of **2a**). [d] Yield of isolated product after column chromatography. [e] Polymer-supported triphenylphosphane (5 equiv) was used.



Scheme 3. Reagents and conditions: a) ICl, 2,6-di-*tert*-butyl-4-methylpyridine, CH_2Cl_2, 0 °C→RT, 91 %; b) 1) $Me_2C{=}C(Me)(CH_2)_2MgBr$, THF, −78 °C, 73 %; 2) HCO_2H, CH_2Cl_2, 50 °C, 59 %; c) $(nBu)_3P$, CCl_4, CH_2Cl_2, reflux, 45 %; d) CO 1 atm, K_2CO_3, $Pd(OAc)_2$, H_2O/DMF, RT, 53 % (80 % based on recovered starting material); Boc = 1,1-dimethylethoxycarbonyl.

(−)-virantmycin (**6a**) in 53 % yield (80 % based on recovered starting material). Synthetic **6a** was identical in all respects to natural virantmycin[3,16] [^{1}H NMR, ^{13}C NMR spectra, and $[\alpha]_D^{24} = -15.0$ ($c = 0.84$ in $CHCl_3$) (ref.[16,20] $[\alpha]_D^{18} = -11.1$ ($c = 0.175$ in $CHCl_3$))]. This synthesis required only nine steps from indoline **8**.

In summary, we have developed a novel synthesis of chiral trisubstituted tetrahydroquinolines in which contiguous quaternary and tertiary stereogenic centers are constructed in analogy to the hypothetical biosynthetic pathway. The reaction was applied to the first total synthesis of natural virantmycin in only nine steps from commercially available starting material. We believe that our rearrangement reaction provides some support for the proposed biosynthetic pathway of virantmycin and related tetrahydroquinoline alkaloids via an aziridine intermediate. Further applications of this methodology to complex polycyclic tetrahydroquinoline alkaloids are underway.

Experimental Section

2a: Triphenylphosphane (135 mg, 0.420 mmol) was added to a solution of **1a** (31 mg, 0.14 mmol) and CCl_4 (135 μL, 1.40 mmol) in CH_2Cl_2 (3 mL) at 40 °C (bath temp.). The mixture was stirred under reflux for 1 h, and then concentrated. Purification by column chromatography on silica gel (*n*-hexane/AcOEt 10/1 to 2/1) gave tetrahydroquinoline **2a** as a colorless oil (21 mg, 63 %): $[\alpha]_D^{24} = +7.2$ ($c = 0.45$ in $CHCl_3$); ^{1}H NMR (400 MHz, $CDCl_3$): $\delta = 7.01$ (t, $J =$ 8.1 Hz, 1H), 6.96 (d, $J = 8.1$ Hz, 1H), 6.63 (t, $J = 8.1$ Hz, 1H), 6.53 (d, $J = 8.1$ Hz, 1H), 4.33 (dd, $J = 6.6$, 5.2 Hz, 1H), 3.99 (br s, 1H), 3.53 (d, $J = 9.2$ Hz, 1H), 3.48 (d, $J = 9.2$ Hz, 1H), 3.35 (s, 3H), 3.30 (dd, $J =$ 16.8, 5.2 Hz, 1H), 3.05 (dd, $J = 16.8$, 6.6 Hz, 1H), 1.76 (dq, $J = 14.9$, 7.3 Hz, 1H), 1.66 (dq, $J = 14.9$, 7.3 Hz, 1H), 0.92 ppm (t, $J = 7.3$ Hz, 3H); ^{13}C NMR (100 MHz, $CDCl_3$): $\delta = 142.3$, 129.4, 127.4, 117.6, 117.2, 114.7, 73.5, 59.4, 57.6, 57.0, 33.9, 27.2, 7.1 ppm; IR ($CHCl_3$ solution): $\tilde{\nu} = 3422$, 2972, 2935, 2896, 1607, 1588, 1482, 1312, 1260, 1112, 980, 960, 834 cm^{-1}; HRMS calcd for $C_{13}H_{18}NOCl$ [M^+]: 239.1077; found 239.1075.

2b: $[\alpha]_D^{24} = -30.2$ ($c = 0.67$ in $CHCl_3$); ^{1}H NMR (500 MHz, $CDCl_3$): $\delta = 7.01$ (t, $J = 8.0$ Hz, 1H), 6.97 (d, $J = 8.0$ Hz, 1H), 6.67 (t, $J = 8.0$ Hz, 1H), 6.57 (d, $J = 8.0$ Hz, 1H), 4.44 (dd, $J = 7.0$, 5.0 Hz, 1H), 3.99 (br s, 1H), 3.42 (1H, d, $J = 9.5$ Hz), 3.40 (d, $J = 9.5$ Hz, 1H),

 © 2003 Wiley-VCH Verlag GmbH & Co. KGaA, Weinheim

3.35 (s, 3H), 3.24 (dd, $J = 16.5$, 5.0 Hz, 1H), 3.09 (dd, $J = 16.5$, 6.5 Hz, 1H), 1.82 (dq, $J = 14.5$, 7.5 Hz, 1H), 1.72 (dq, $J = 14.5$, 7.5 Hz, 1H), 0.94 ppm (t, $J = 7.3$ Hz, 3H); ^{13}C NMR (125 MHz, $CDCl_3$): $\delta = 142.1$, 129.3, 127.3, 117.8, 117.7, 115.0, 75.1, 59.3, 57.9, 57.5, 34.0, 25.4, 7.5 ppm; IR ($CHCl_3$ solution): $\tilde{\nu} = 3424$, 2972, 2935, 2883, 1607, 1588, 1498, 1481, 1307, 1156, 1111, 962 cm^{-1}; HRMS: calcd for $C_{13}H_{18}NOCl$ [M^+]: 239.1077, found: 239.1081.

Received: January 30, 2003 [Z51069]

Keywords: alkaloids · natural products · rearrangement · total synthesis

[1] a) K. Fuji, *Chem. Rev.* **1993**, *93*, 2037; b) E. J. Corey, A. Guzman-Perez, *Angew. Chem.* **1998**, *110*, 402; *Angew. Chem. Int. Ed.* **1998**, *37*, 388; c) K. Funabashi, H. Ratni, M. Kanai, M. Shibasaki, *J. Am. Chem. Soc.* **2001**, *123*, 10784.

[2] I. Gallou-Dagommer, P. Gastaud, T. V. Rajan Babu, *Org. Lett.* **2001**, *3*, 2053, and references therein.

[3] S. Ōmura, A. Nakagawa, *Tetrahedron Lett.* **1981**, *22*, 2199.

[4] a) W. G. Kim, J. P. Kim, C. J. Lim, K. H. Lee, I. D. Yoo, *J. Antibiot.* **1996**, *49*, 20; b) W. G. Kim, J. P. Kim, I. D. Yoo, *J. Antibiot.* **1996**, *49*, 26; c) W. G. Kim, J. P. Kim, H. Koshino, K. Shin-Ya, H. Seto, I. D. Yoo, *Tetrahedron* **1997**, *53*, 4309. For the total synthesis of benzastatin E, see ref. [7].

[5] S. E. Yoo, J. H. Kim, K. Y. Yi, *Bull. Korean Chem. Soc.* **1999**, *20*, 139. Yoo et al. speculated on an alternative biosynthetic pathway for these alkaloids. See ref. [4c].

[6] Cossy et al. reported a ring-expansion reaction of *N*-benzylpyrrolidine-2-methanol derivatives to *N*-3-chloropiperidine derivatives using MsCl (Ms = methanesulfonyl). They reported that the rearrangement does not proceed with α,α-disubstituted *N*-benzylpyrrolidine-2-methanol derivatives. J. Cossy, C. Dumas, D. Gomez Pardo, *Eur. J. Org. Chem.* **1999**, 1693. Under the same conditions, α,α-disubstituted indoline-2-methanols do not undergo the rearrangement reaction, probably because of steric hindrance.

[7] N. Toda, M. Ori, K. Takami, K. Tago, H. Kogen, *Org. Lett.* **2003**, *5*, 269.

[8] The same reactions of corresponding α-monosubstituted or unsubstituted indoline-2-methanols gave complex mixtures.

[9] No racemization occurs during the rearrangement, this is confirmed by the resulting tetrahydroquinoline **2a** which is optically pure by chiral HPLC analysis. Daicel Chiralcel OJ ($\varnothing = 0.46$ cm × 25 cm), *n*-hexane/*i*PrOH (95/5), 1 mL min^{-1}.

[10] Y. Morimoto, F. Matsuda, H. Shirahama, *Tetrahedron* **1996**, *52*, 10609.

[11] N. Harada, N. Koumura, M. Robillard, *Enantiomer* **1997**, *2*, 303.

[12] CCDC 202237 (**7**) contains the supplementary crystallographic data for this paper. These data can be obtained free of charge via www.ccdc.cam.ac.uk/conts/retrieving.html (or from the Cambridge Crystallographic Data Centre, 12 Union Road, Cambridge CB2 1EZ, UK; fax: (+44) 1223-336-033; or deposit@ccdc.cam.ac.uk).

[13] There is no direct evidence for the formation of an aziridine intermediate such as **4**. A stepwise sequence may be possible (1. formation of tertiary chloride; 2. intermolecular cyclization to an aziridine; 3. ring opening by the attack of chloride anion). However, we could not obtain the tertiary chloride by treatment of **1a** with various chlorinating agents. Also, treatment of **1a** under Mitsunobu conditions gave no aziridine compound (starting material was recovered). For the ring-opening reaction of an aziridine, such as **4**, with chloride anions to provide tetrahydroquinoline **2**, see ref. [10].

[14] All the other products were highly polar materials which were not isolated.

[15] Syntheses of (±)-virantmycin: a) M. L. Hill, R. A. Raphael, *Tetrahedron Lett.* **1986**, *27*, 1293; b) M. L. Hill, R. A. Raphael, *Tetrahedron* **1990**, *46*, 4587; c) Y. Morimoto, F. Matsuda, H. Shirahama, *Synlett* **1991**, 202 and ref. [10]; d) H. Steinhagen, E. J. Corey, *Org. Lett.* **1999**, *1*, 823.

[16] Synthesis of *ent*-virantmycin: Y. Morimoto, F. Matsuda, H. Shirahama, *Tetrahedron* **1996**, *52*, 10631.

[17] A. N. De Silva, C. L. Francis, D. Ward, *Aust. J. Chem.* **1993**, *46*, 1657.

[18] The configurations of the newly created asymmetric centers in the Grignard adduct were determined after NOE experiments on the acetonide derivative of **11**. See ref. [7].

[19] When we used triphenylphosphane in the reaction, an undesired deiodinated product and an indole derivative (dehydration followed by isomerization) were obtained. However, using tri-*n*-butylphosphane instead of triphenylphosphane prevented these side reactions.

[20] Initially, the optical rotation of (−)-virantmycin was reported as −0.05 in ref. [3]. Later, the optical rotation of (−)-virantmycin was reexamined and reported as −11.1 by Shirahama and co-workers.[16]

 © 2003 Wiley-VCH Verlag GmbH & Co. KGaA, Weinheim

Cyclic Dodecasaccharide Structure

Crystal Structure of a Cyclic Enterobacterial Common Antigen**

*Magnus Färnbäck, Lars Eriksson, Sof'ya Senchenkova, Krystyna Zych, Yuriy A. Knirel, Zygmunt Sidorczyk, and Göran Widmalm**

Carbohydrates have several functions in nature and, among other things, they are involved in biochemical regulation and trafficking processes.[1] Likewise, bacteria have different types

[*] Prof. Dr. G. Widmalm, M. Färnbäck
Department of Organic Chemistry
Arrhenius Laboratory, Stockholm University
106 91 Stockholm (Sweden)
Fax: (+46) 8-154-908
E-mail: gw@organ.su.se

M. Färnbäck, Dr. L. Eriksson
Division of Structural Chemistry
Arrhenius Laboratory, Stockholm University
106 91 Stockholm (Sweden)

S. Senchenkova, Dr. Y. A. Knirel
N. D. Zelinsky Institute of Organic Chemistry
Russian Academy of Sciences
119991 Moscow (Russia)

K. Zych, Prof. Dr. Z. Sidorczyk
Department of General Microbiology
Institute of Microbiology and Immunology
University of Lodz, Banacha 12/16
90-237 Lodz (Poland)

[**] This work was supported by a grant from the Swedish Research Council.

 DOI: 10.1002/anie.200351250 © 2003 Wiley-VCH Verlag GmbH & Co. KGaA, Weinheim

of polysaccharides on their surfaces and in their outer membranes. A certain species of bacteria usually carries both a specific and a common type of polysaccharide. All members of the enterobacteriaceae family share an antigen known as the enterobacterial common antigen (ECA), which normally is found as a phosphoglycolipid conjugate in the outer membrane of the bacteria.[2] However, the biological importance of ECA is so far not known. In some cases cyclic ECA structures are also produced,[3] but the most common type of cyclic carbohydrate oligomers are the cyclodextrins that are composed of α-(1→4)-linked glucosyl residues ranging from hexamers to hexaicosamers.[4] Crystal structures of other cyclic glycans have also been reported.[5,6] In the present communication, we describe the crystal structure of a cyclic dodecasaccharide of ECA, in which the repeating unit is composed of three amino sugars, namely, →3)-α-D-Fuc*p*4NAc-(1→4)-β-D-Man*p*NAcA-(1→4)-α-D-Glc*p*NAc-(1→ (Figure 1).

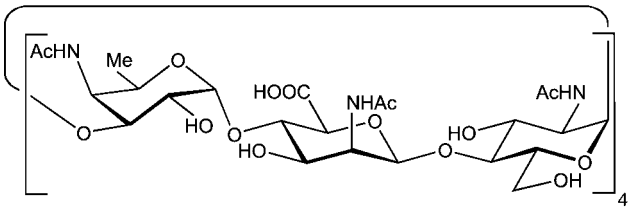


Figure 1. Structure of the cyclic enterobacterial common antigen dodecasaccharide ($cECA_{12}$) having a repeating unit of →3)-α-D-Fuc*p*4-NAc-(1→4)-β-D-Man*p*NAcA-(1→4)-α-D-Glc*p*NAc-(1→.

An ECA preparation from *Proteus penneri* strain 17 was shown to exist as a cyclic dodecasaccharide ($cECA_{12}$), since the FAB mass spectrum revealed the pseudomolecular ion at *m*/*z* 2429.89, which corresponds to $[M+H]^+$[7] and showed good agreement with previously published ^1H and ^{13}C NMR data of a cyclic ECA dodecasaccharide from a *Plesiomonas shigelloides* strain.[8] It was noted by serendipity that crystals of $cECA_{12}$ had formed in the NMR tube. Subsequently, a preliminary investigation of the brittle crystals revealed that the unit cell consisted of four molecules (data not shown).

A systematic investigation was now performed where $cECA_{12}$ was crystallized employing the hanging-drop technique, by which prism-like crystals (monoclinic space group *C*2) were formed. Data were collected with a rotating anode and synchrotron radiation, and the structure was solved by direct methods, which reveal that the asymmetric unit is composed of two symmetry-independent parts, each containing half of the cyclic dodecasaccharide.[9] The two different $cECA_{12}$ molecules are denoted **A** and **B**. The former adapts the form of a slightly tilted rhomb, while the latter adapts an almost perfect square. One half of each molecule is related to the other half by crystallographic symmetry, thus forming a complete $cECA_{12}$ unit (Figure 2). Each side is composed of a repeating unit that is followed by a sharp turn at the (1→3)-linkage. A similar structure was also found in a prior molecular dynamics simulation.[8] The sugar rings all adopt the $^4C_1$ chair conformation and the glycosidic torsion angles

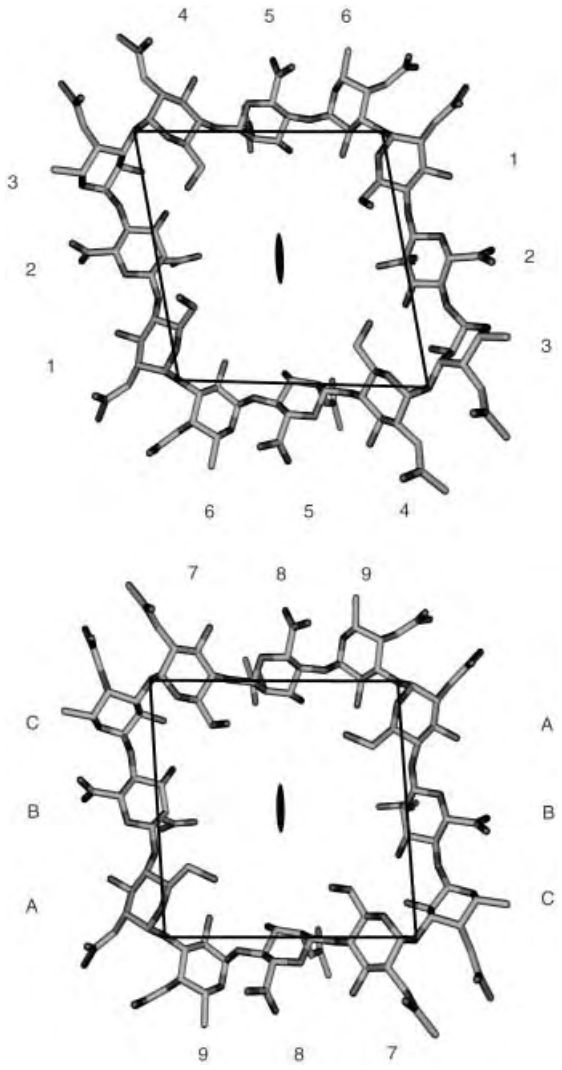


Figure 2. Stick representation of the two crystal forms of $cECA_{12}$ including the one-character sugar residue labeling 1–6 in **A** and 7–C in **B**. Hydrogen atoms are removed for clarity.

lead to a *syn* relationship[10] between adjacent residues. The ϕ versus ψ scatter plot (Figure 3) reveals a grouping of torsional angles[11] according to each glycosidic linkage, with the largest range observed for the fucosyl residue. A summary of the glycosidic torsion angles is compiled in Table 1.

The crystal packing is shown in Figure 4. The molecules are arranged in layers in the *ac* plane and stack in the *b* direction. There are different orientations observed in the *ac* plane, with two symmetry independent $cECA_{12}$ environments exhibited. Molecule **A** is surrounded by four **B** molecules and two **A** molecules in the *ac* plane, while molecule **B** is surrounded solely by four **A** molecules. Two distinct layers are present throughout the structure. They are identical and related to each other through *c* centering. The columns consist solely of either **A** or **B** molecules.

A noticeable feature of $cECA_{12}$ is the positioning of the *N*-acetyl groups. On the mannuronosyl residues the *N*-acetyl groups protrude out from the plane of $cECA_{12}$, that is, all in the same direction (see Figure 2). The next molecule along

 © 2003 Wiley-VCH Verlag GmbH & Co. KGaA, Weinheim

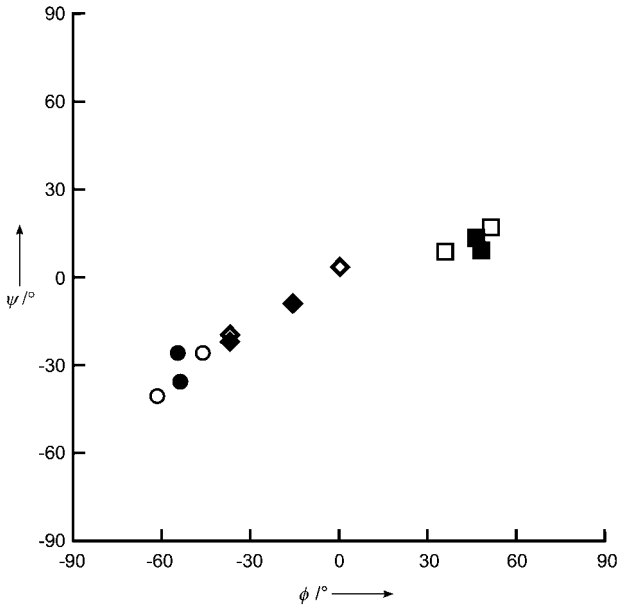


Figure 3. Scatter plot of the glycosidic torsion angles of the crystal structure of $cECA_{12}$. Glucosyl residues are denoted by circles, fucosyl residues by diamonds, and mannuronosyl residues by squares. Open and closed symbols refer to molecules **A** and **B**, respectively.

Table 1: Glycosidic torsion angles in the two crystal forms of $cECA_{12}$.

Residue	A			B		
	Label	ϕ [°]	ψ [°]	Label	ϕ [°]	ψ [°]
→4)-α-D-Glc*p*NAc-(1→	1	−46	−26	7	−55	−26
→4)-β-D-Man*p*NAcA-(1→	2	36	9	8	48	9
→3)-α-D-Fuc*p*4NAc-(1→	3	0	4	9	−37	−22
→4)-α-D-Glc*p*NAc-(1→	4	−62	−41	A	−54	−36
→4)-β-D-Man*p*NAcA-(1→	5	52	17	B	46	14
→3)-α-D-Fuc*p*4NAc-(1→	6	−37	−20	C	−16	−9

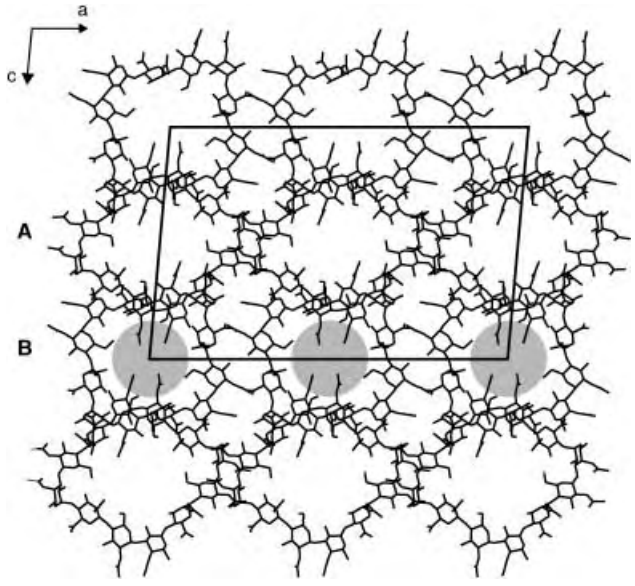


Figure 4. Crystal packing including the unit cell of $cECA_{12}$ viewed along the *b* axis. The shaded regions highlight the channels closed by *N*-acetyl groups on glucosyl and fucosyl residues. Water molecules are not displayed.

the *b* axis is turned upside down and translated by half a molecule, and its *N*-acetyl groups are in close vicinity of two of the *N*-acetyl groups in the former molecule. The *N*-acetyl groups on adjacent glucosyl and fucosyl residues extend in a parallel manner (see shaded regions in Figure 4) at the corners of $cECA_{12}$.

Channels are formed along the *b* axis, mainly through molecule **A**. The channels through the **B** molecules are closed by *N*-acetyl groups on glucosyl and fucosyl residues protruding from adjacent molecules (solely of type **A**) above and below molecule **B**. This feature is not observed for molecule **A**. Instead, the channel is filled to a greater extent with partially disordered water molecules. Of those that could be located, all are geometrically arranged to form hydrogen bonds to either the sugars or to other water molecules.

A few intramolecular hydrogen bonds are indicated between residues. Both molecules **A** and **B** show a similar hydrogen-bond network with hydrogen bonds between O2 in the fucosyl residue and O3 in the mannuronosyl residue, as well as between O3 in the glucosyl residue and O5 in the mannuronosyl residue, based on the distance between donor and acceptor atoms in the range 2.7–3.3 Å. Molecule **B** also displays an additional hydrogen bond between O6 in the glucosyl residue and O2 in the fucosyl residue when the hydroxymethyl group of the donor has the *gauche*/*trans* (*gt*) conformation, but not when it has the *gauche*/*gauche* (*gg*) conformation. Although both the *gg* and *gt* conformations are present for the glucosyl residues in **A**, the latter hydrogen bond is not formed.

In larger cyclic crystal structures, solvent molecules make up a significant part of the volume of the unit cell.[12] Likewise, the $cECA_{12}$ crystal contains a large amount of water (~34% by weight or ~6 water molecules per sugar residue in the unit cell, if a volume of 29.7 $Å^3$ is assumed).[13] In the analysis of hydrogen-bonding patterns, 30 water molecules were localized per $cECA_{12}$ unit, all of which participate in interactions to either the sugar residues or to other water molecules. The identified water molecules amount to approximately half of those present per $cECA_{12}$ unit.

In conclusion, the crystal structure of a cyclic oligosaccharide has been determined. Its characterization is of special interest since only amino sugars are found in the repeating unit and in another form they are the constituents of a polysaccharide anchored in outer bacterial membranes. Future studies should include analysis of NMR relaxation-time data to investigate whether the ϕ versus ψ variation observed in the crystal structure can be reconciled with our previous NMR and simulation studies of $cECA_{12}$.

Experimental Section

Proteus penneri strain 17 (1410-75) was cultivated using a procedure previously described.[14] A lipopolysaccharide (LPS) preparation was obtained by extraction of dry bacterial mass with a hot phenol/water mixture and purified by treatment with a cold aqueous solution of CCl_3CO_2H (50%) followed by dialysis of the supernatant. Degradation of LPS was performed with an aqueous acetic acid solution (1%) at 100 °C for 2 h and the product was fractionated by gel permeation chromatography and lyophilized. The resulting polysaccharide preparation (700 mg) was suspended in water (10.5 mL) and centrifuged

 © 2003 Wiley-VCH Verlag GmbH & Co. KGaA, Weinheim

(13000 *g*, 20 min). The precipitate was washed with water (7 mL), centrifuged as above, and the combined supernatant was concentrated in vacuum and fractionated on a column (70 × 2.5 cm) of Sephadex G-50 (Pharmacia) in 0.05 M pyridinium acetate buffer (pH 4.5). Fractions containing ECA were collected (90 mg). An NMR sample of ECA in D_2O was prepared (~100 mg mL^{-1}), from which prism-like crystals with dimensions up to 0.3 × 0.3 × 0.1 mm formed. These crystals were investigated with X-ray diffraction methods using an IPDS system.

For further investigations, larger crystals of a higher quality were desired. ECA was crystallized employing the hanging-drop technique from an aqueous solution (~100 mg mL^{-1}) containing PEG-400 (40%). Crystals formed as slightly irregular prisms, up to 0.5 mm in length. The structure was solved from data obtained from the STOE IPDS data set with direct methods using the density modification technique available in SHELXD.[15] Attempts to use the direct methods available in SHELXS97[16] failed. Both halves of the $cECA_{12}$ structure in the asymmetric unit, with the exception of some side chains, were visible in the initial electron-density maps. Nonexchangeable hydrogen atoms were added at calculated geometrical positions. Several bond length restraints were applied using standard bond lengths[17] and some conformational features, such as *N*-acetyl group planarity, with the DFIX and FLAT command available in SHELXH.

Water molecules were located from the electron-density difference map and kept if they were located at a reasonable distance (2.6–3.2 Å) from suitable hydrogen acceptors or donors, together with the observation that they did not diverge in the least-squares refinement. Not all water molecules in the cavities could be located, probably as a result of high disorder. The remaining solvent-accessible volume was calculated with PLATON.[18]

Received: February 24, 2003 [Z51250]

Keywords: carbohydrates · polysaccharides · structure elucidation · X-ray diffraction

[1] *Essentials of Glycobiology* (Eds.: A. Varki, R. Cummings, J. Esko, H. Freeze, G. Hart, J. Marth), Cold Spring Harbor Laboratory Press, Cold Spring Harbor, **1999**.
[2] H.-M. Kuhn, U. Meier-Dieter, H. Mayer, *FEMS Microbiol. Rev.* **1988**, *54*, 195–222.
[3] A. Dell, J. Oates, C. Lugowski, E. Romanowska, L. Kenne, B. Lindberg, *Carbohydr. Res.* **1984**, *133*, 95–114.
[4] K. Gessler, I. Usón, T. Takaha, N. Krauss, S. M. Smith, S. Okada, G. M. Sheldrick, W. Saenger, *Proc. Natl. Acad. Sci. USA* **1999**, *96*, 4246–4251.
[5] M. Sawada, T. Tanaka, Y. Takai, T. Hanafusa, T. Taniguchi, M. Kawamura, T. Uchiyama, *Carbohydr. Res.* **1991**, *217*, 7–17.
[6] G. M. Bradbrook, K. Gessler, G. L. Côté, F. Momany, P. Biely, P. Bordet, S. Pérez, A. Imberty, *Carbohydr. Res.* **2000**, *329*, 655–665.
[7] E. V. Vinogradov, Y. A. Knirel, J. E. Thomas-Oates, A. S. Shashkov, V. L. L'vov, *Carbohydr. Res.* **1994**, *258*, 223–232.
[8] M. Staaf, C. Höög, B. Stevensson, A. Maliniak, G. Widmalm, *Biochemistry* **2001**, *40*, 3623–3628.
[9] $T = 293$ K, crystal dimensions: 0.08 × 0.10 × 0.15 mm, monoclinic, space group C_2, $Z = 4$, $a = 46.42(2)$, $b = 13.542(2)$, $c = 30.15(1)$ Å, $\beta = 95.15(5)°$, $V = 18875(12)$ Å^3, $\rho_{calcd} = 1.023$ g cm^{-3}. Data measured with a STOE IPDS (Stoe & Cie, Darmstadt, Germany) on a rotating anode equipped with a graphite monochromator set to diffract $Mo_{K\alpha}$ ($\lambda = 0.71073$ Å) and a BRUKER SMART 1k (Bruker AXS GmbH, Karlsruhe, Germany) diffraction system using synchrotron radiation, ($\lambda \approx 0.856$ Å) at beam line I711, MAXLAB, Lund, Sweden. The crystal was mounted in a glass capillary with some residual mother liquor. Scan mode: area detector φ-scans (STOE IPDS) and ω-scans (BRUKER SMART). Three data sets, one from the in-house STOE IPDS and two from the BRUKER SMART system were scaled and merged to a common data set. A total of 52476 reflections were measured of which 17543 were independent with $R_{int} = 0.143$. The structure was solved by direct methods (SHELXD). The non-hydrogen carbohydrate skeleton was refined with anisotropic displacement parameters and water oxygen atoms were refined with isotropic displacement parameters. Hydrogen atoms were not placed on water oxygen atoms. All 17543 independent reflections were used in the full-matrix least-squares calculation (SHELXH97) against F^2. Number of refined parameters = 1633, $2\theta_{max} = 64.0°$ ($\lambda \approx 0.856$ Å), $R1 = 0.129$, $wR2 = 0.316$ for 5409 reflections with $F^2 \geq 2\sigma(F^2)$, max shift/esd = 0.12 in the final model. Lorentz and polarization corrections were applied during data reduction with STOE diffractometer control software for the STOE IPDS data set and SAINT 5.5 for the BRUKER data. Absorption correction with XRED 1.09 (STOE), $\mu = 0.92$ cm^{-1}, transmission factors were min: 0.98, max: 0.99. Residual electron density: min: 0.37 e Å^{-3}; max: 0.50 e Å^{-3}. CCDC-202591 contains the supplementary crystallographic data for this paper. These data can be obtained free of charge via www.ccdc.cam.ac.uk/conts/retrieving.html (or from the Cambridge Crystallographic Data Centre, 12, Union Road, Cambridge CB2 1EZ, UK; fax: (+44) 1223-336-033; or deposit@ccdc.cam.ac.uk).
[10] C. Höög, C. Landersjö, G. Widmalm, *Chem. Eur. J.* **2001**, *7*, 3069–3077.
[11] Definition of ϕ and ψ torsion angles: H1(m)–C1(m)–On($m+1$)–Cn($m+1$) and C1(m)–On($m+1$)-Cn($m+1$)–Hn($m+1$), respectively, where m denotes a sugar residue and n denotes a linkage position.
[12] J. R. Dias, R. A. Pascal, Jr., J. Morrill, A. J. Holder, H. Gao, C. Barnes, *J. Am. Chem. Soc.* **2002**, *124*, 4647–4652.
[13] M. Gerstein, C. Chothia, *Proc. Natl. Acad. Sci. USA* **1996**, *93*, 10167–10172.
[14] K. Kotelko, W. Gromska, M. Papierz, Z. Sidorczyk, D. Krajewska, K. Szer, *J. Hyg. Epidemiol. Microbiol. Immunol.* **1977**, *21*, 271–284.
[15] G. M. Sheldrick, T. R. Schneider in *Methods in Macromolecular Crystallography* (Eds.: D. Turk, L. Johnson), IOS Press, Amsterdam, **2001**, pp. 72–81.
[16] G. M. Sheldrick, SHELX-98, Program for the Solution of Crystal Structures, University of Göttingen, Göttingen (Germany), **1998**
[17] *International Tables for Crystallography, Vol. C* (Ed.: A. J. C. Wilson), Kluwer, Dordrecht, **1995**.
[18] A. L. Spek, PLATON, University of Utrecht, The Netherlands.

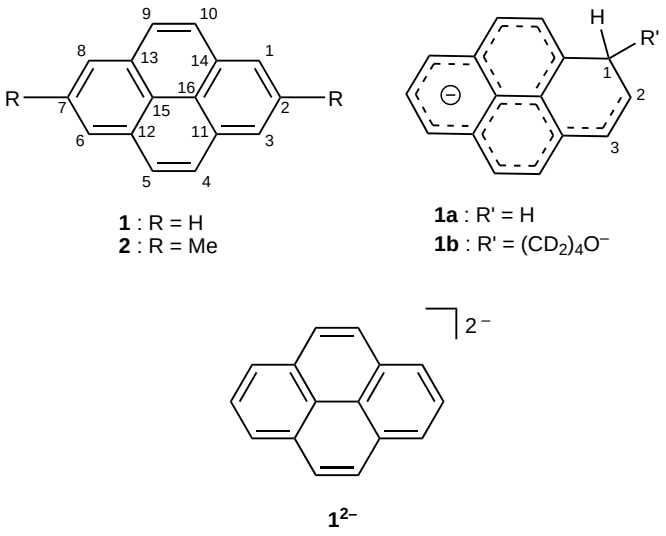
 © 2003 Wiley-VCH Verlag GmbH & Co. KGaA, Weinheim

Pyrene Dimerization

Reductive Dimerization of Tethered Pyrenes: Implications for the Reduction of Polcyclic Aromatic Hydrocarbons**

*Ivan Aprahamian, Graham J. Bodwell, James J. Fleming, Gregory P. Manning, Michael R. Mannion, Tuvia Sheradsky, Rudolf J. Vermeij, and Mordecai Rabinovitz**

The reduction of polycyclic aromatic hydrocarbons (PAHs) with alkali metals can, in some cases, afford a reductive dimerization process. This process takes place in systems that have the capability of forming a stable anionic subunit and concentrating a high electron density on a specific carbon atom, which will eventually form a new σ bond.[1] Such behavior has been recently reported in the reduction of indenocorannulene, which undergoes a four-step reductive dimerization/bond-cleavage process.[1d] The reduction of pyrene (**1**) and 2,7-dimethylpyrene (**2**) with alkali metals has been thoroughly studied.[2] The reduction affords different products depending on solvent, counterion, and temperature. Three primary diamagnetic species can be detected when **1** (Scheme 1) is reduced with lithium metal in [D_8]THF: a protonated pyrene monoanion (**1a**), a dianion ($\mathbf{1}^{2-}$), and a solvent-molecule-incorporated monoanion (solvent cleavage; **1b**).[2c] The same results are obtained when **2** is reduced with lithium metal. Protonation of the monoanion radicals of **1** and **2**, and the solvent cleavage by their respective dianions at room temperature, illustrate that these species are very reactive. Another aspect of interest in the chemistry of pyrene is its aromatic character. Recent reports suggest that imparting nonplanarity in pyrene, by tethering two remote positions, does not significantly decrease the magnetic anisotropy effect of its nucleus in the neutral state.[3] To evaluate the effect of strain on the reduction of pyrene, two curved systems, [7](2,7)pyrenophane (**3**; Scheme 2)[3a] and [2]metacyclo[2](2,7)pyrenophane (**4**)[4] were reduced with lithium metal in [D_8]THF, and the reduction process was followed by NMR spectroscopy. The two-electron reduction of strained pyrene moieties affords totally unexpected results. A new σ bond is formed, to avoid strained antiaromaticity.[5] A careful and detailed follow up of the reduction process of **3** and **4** led to the observation of unexpected and hitherto unknown intermediary one-electron reduction products.[6] A reductive dimerization process is observed for the radical anions of **3** and **4** instead of protonation, as is the case in **1** and **2**. Thus, the strain-relieving process in the dianions of **3** and **4** is preceded by an intermolecular σ-bond formation, which results from electron coupling. Each pyrene moiety in the dimerization, protonation, and solvent-cleavage products has the same local symmetry because the reactions all occur at the same carbon atom. This makes it very difficult to distinguish between these products using standard ^{1}H and ^{13}C NMR

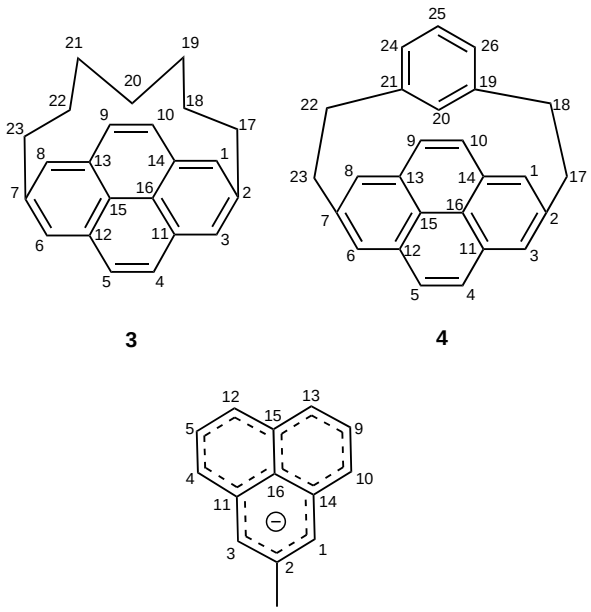


1 : R = H
2 : R = Me

1a : R' = H
1b : R' = $(CD_2)_4O^-$

$\mathbf{1}^{2-}$

Scheme 1. Structures of pyrene molecules (**1** and **2**), the protonated and solvent-incorporated pyrene monoanions (**1a** and **b**), and the dianion ($\mathbf{1}^{2-}$).



3 **4**

5

Scheme 2. Structures of [7](2,7)pyrenophane (**3**), [2]metacyclo[2](2,7)-pyrenophane (**4**), and the 2-methylphenalenyl anion (**5**).

[*] Prof. M. Rabinovitz, I. Aprahamian, Prof. T. Sheradsky
Department of Organic Chemistry
The Hebrew University of Jerusalem
Jerusalem 91904 (Israel)
Fax: (+972) 2-652-7547
E-mail: mordecai@vms.huji.ac.il
Prof. G. J. Bodwell, J. J. Fleming, Dr. G. P. Manning, M. R. Mannion, Dr. R. J. Vermeij
Department of Chemistry
Memorial University of Newfoundland
St. John's, NL, A1B 3X7 (Canada)

[**] We are grateful to the United States–Israel Binational Science Foundation (BSF) (M.R.) and the Natural Sciences and Engineering Research Council (NSERC) of Canada (G.J.B.) for financial support.

 DOI: 10.1002/anie.200351376 © 2003 Wiley-VCH Verlag GmbH & Co. KGaA, Weinheim

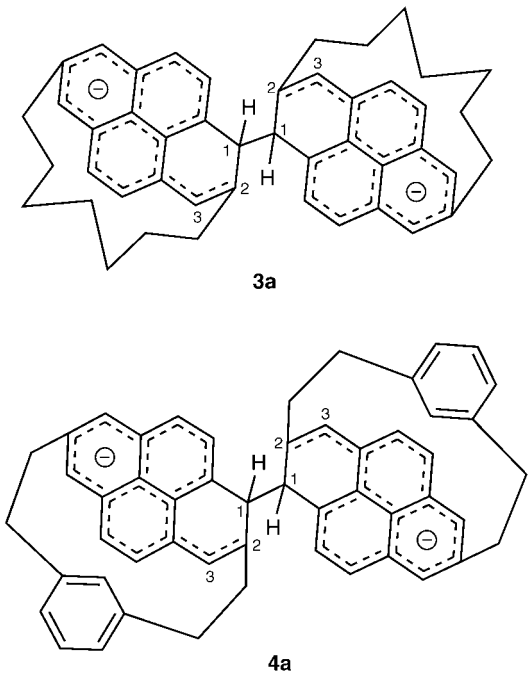
Table 1: The NMR data of hydrogen and carbon atoms H6 and C6 of the different reduction products of **1**, **2**, **3**, and **4**.

	δH6 [ppm]	δC6 [ppm]	$^1J_{C,H}$ [Hz]	$^3J_{H,*H}$ [Hz]	Integration
Dimerization	3.2–3.4	48.3–48.7	128–130	~10	1 H atom
Protonation	4.0–4.2[a]	34.0–35.0[a]	124–125[b]	not observed	2 H atoms
Solvent Cleavage	3.7–3.8[a]	43.0–48.0[a]	124–125[b]	not observed	1 H atom

[a] Taken from ref. [2]. [b] See ref. [8]

experiments. However, based on our recent findings,[1d,5] it is now possible to suggest some basic rules of thumb that can help distinguish the products by way of standard 2D NMR experiments and simple integration (Table 1).

The reduction of **3** (colorless) and **4** (pale yellow) with lithium metal, which is accompanied by color change, gives the diamagnetic species **3a** (claret; Scheme 3) and **4a** (brown), which both give complex ^{1}H and ^{13}C NMR spectra (Table 2). The ^{1}H NMR spectrum of **3a** exhibited no dynamic processes over a wide range of temperatures (165–273 K). In addition, it is noteworthy that the signal of hydrogen atom H6 is shifted to high field. The ^{13}C NMR spectrum exhibits a signal at an extremely high field ($\delta = 48.3$ ppm; assigned to C6, see Table 2) with a one-bond coupling constant ($^1J_{C6,H6}$) of 128.3 Hz. The rest of the carbon atoms are divided into two groups, of which one ($\delta = 99$–119 ppm) is at a higher field than the other ($\delta = 129$–143 ppm). The ^{7}Li NMR spectrum showed an absorption at $\delta = 0$ ppm, which implies the presence of solvent-separated ion pairs. Long-range CH-correlation experiments (heteronuclear multiple-bond correlation (HMBC)) conducted on species **3a** afforded three-bond interactions that helped to fully assign the carbon spectra. In addition, a long-range correlation between carbon atom C6 and hydrogen atom H6, which resides on C6, was observed.[7] In the short-range CH-correlation (proton-coupled heteronuclear single quantum coherence signal-improved (HSQCSI)) experiment, a coupling between hydrogen atom H6 and its symmetrical equivalent was observed from the ^{13}C satellites ($^3J_{H6,*H6'} = 10.3$ Hz).[8] Similar results were obtained for ion **4a** (Table 2).[9]



Scheme 3. Structures of the dimeric species **3a** and **4a**.

The high-field absorption of carbon atom C6 in species **3a** and **4a**, and the magnitude of its $^1J_{C,H}$ coupling constant are compatible with an sp^3-hybridized carbon atom. This means that the high-field shift of both carbon atom C6 and hydrogen atom H6 is a result of rehybridization. The HMBC experiments and the $^3J_{H6,*H6'}$ coupling constant indicate that a reaction has taken place between two identical C6 carbon atoms of separate molecules, thus forming the sp^3-hybridized carbons, which in turn lowers the symmetry of the system. These arguments can also be applied to differentiate between the products of protonation, dimerization, and solvent cleavage (Table 1).

The dimerization of two units of **2** and **3** can be explained by means of a radical coupling at carbon atom C6. It has been previously shown for pyrene that position C6 (and its symmetrical counterparts) has the highest spin density for the odd electron in the monoanion radical,[10] which rationalizes the high reactivity of this site and the likelihood of it undergoing radical coupling. Such radical coupling will leave a negative charge on carbon atom C7 that can be delocalized

Table 2: ^{13}C NMR and ^{1}H NMR (in parenthesis) chemical shifts, in ppm, of the pyrene moiety of **3**, **3a**, **4**, and **4a** in [D$_8$]THF.[a]

	C1 (H1)	C2	C3 (H3)	C4 (H4)	C5 (H5)	C6 (H6)	C7	C8 (H8)	C9 (H9)	C10 (H10)	C11	C12	C13	C14	C15	C16
3	130.8 (7.50)	131.0	130.8 (7.50)	127.2 (7.80)	127.2 (7.80)	130.8 (7.50)	131.0	130.8 (7.50)	127.2 (7.80)	127.2 (7.80)	132.9	132.9	132.9	132.9	131.5	131.5
3a	119.3 (5.62)	135.5	114.8 (5.71)	110.0 (5.95)	129.7 (5.98)	48.3[b] (3.22)	99.4	129.6 (5.78)	131.9 (6.63)	102.7 (5.71)	142.7	105.2	110.6	142.2	140.6	135.8
4	130.5 (7.10)	134.7	128.6 (7.50)	126.6 (7.60)	126.6 (7.60)	128.6 (7.50)	134.7	130.5 (7.10)	126.9 (6.50)	126.9 (6.50)	133.8	133.8	132.2	132.2	131.2	131.2
4a	118.3 (5.24)	131.4	114.1 (5.82)	109.3 (6.02)	129.1 (5.91)	48.7[c] (3.41)	95.7	129.0 (5.87)	129.8 (6.26)	102.6 (5.26)	143.0	103.5	113.1	142.5	140.5	135.8
5[d]	104.3	135.2	104.3	103.1	128.1	–	–	–	128.1	103.1	144.7	103.1	103.1	144.5	144.7	137.6

[a] The ^{13}C NMR of **5** is also added for comparison. [b] $^1J_{C6,H6} = 128.2$ Hz, $^3J_{H,*H} = 10.3$ Hz. [c] $^1J_{C6,H6} = 130.0$ Hz, $^3J_{H,*H} = 10.6$ Hz. [d] Taken from ref. [11].

 © 2003 Wiley-VCH Verlag GmbH & Co. KGaA, Weinheim

over the remainder of the pyrene moiety. The ^{13}C NMR spectra show that this is indeed the case, as carbon atom C7 is shifted to high field. In addition it can be seen that the negative charge is distributed over alternating carbon atoms on the periphery of a phenalene unit, which explains why two sets of carbon atoms are observed in the ^{13}C NMR spectra. The good agreement between the carbon chemical shifts of the phenalene moiety of **3a** and **4a** and those of the 2-methylphenalenyl anion (**5**; Scheme 2)[11] supports this conclusion.

The nonplanarity of the pyrene unit in **3** and **4**, which is induced by the tether, imparts an element of asymmetry to each half of the respective dimers. This leads to the possibility of different diastereomeric reduced species, depending on the position of the connection. Even if one assumes that the new σ bond forms on the less hindered *exo* faces of the pyrene moieties, two possible products still remain: a *meso* or a D/L pair. From the data available, it appears as though only one diastereoisomer dominates. Unfortunately, it is not possible to fully assign the relative stereochemistry of the dimers, although it is apparent from the above-mentioned $^3J_{H,*H}$ coupling constants ($^3J_{H6,*H6} = 10.3$ Hz for **3a** and $^3J_{H6,*H6} = 10.6$ Hz for **4a**) that they adopt an *anti* conformation about the new σ bond.

The fact that the same behavior is observed in both **3** and **4** implies that the isolated benzene ring in **4** has little or no effect on the overall reduction process. This also indicates that electron transfer through the "cyclophane hub" is minimal.[12] Moreover, under very similar reduction conditions, the nonplanar systems **3** and **4** afford a reductive dimerization process (major product) whereas the planar systems, **1** and **2**, undergo protonation (minor product). It is noteworthy that both processes are accompanied by the production of an aromatic phenalenyl anion entity,[13] which stabilizes the negative charge in the system.

The difference between the two sets of systems is the alkane tether. This has the dual function of enforcing nonplanarity on the polycyclic aromatic portion of the systems and increasing their solubility; this is evident from the comparatively high solubility of **3** and **4**. It seems that nonplanarity does not significantly alter the spin distribution in the radical anion of all the systems as protonation and dimerization take place at the same carbon atom. However the full effect of nonplanarity in such systems is not yet understood.[14]

With respect to solubility, the effect of the tether on the systems is better understood. In our experiments, some precipitate was seen along with the protonation products of **1** and **2**. The solubility of the precipitate increased with temperature, but no diamagnetic species, other than the protonation product was observed in the NMR spectra. Müllen et al. previously reported that at low temperatures, the radical anion of **1** might be in equilibrium with a diamagnetic dimer, which undergoes cleavage at higher temperatures.[2c] Taking the above-mentioned facts into consideration, it is possible to postulate that a dimeric product is also afforded from **1** and **2** but cannot be observed by NMR spectroscopy because of its low solubility.[15] Edlund et al. have encountered such a case with the reduction of azulene, where a dimeric precipitate was formed, which upon further reduction was cleaved to afford the azulene dianion.[1b]

Compounds **3** and **4** afford a reductive dimerization process upon a single-electron reduction, prior to the formation of an intramolecular σ bond. This process was not observed in the planar systems **1** and **2**. It is possible to see that differentiating between dimerization, protonation, and solvent cleavage can be achieved by the use of simple NMR experiments (Table 1). The $^2J_{C,H}$ and $^3J_{H,*H}$ couplings obtained from the HMBC and proton-coupled HSQCSI experiments, respectively, can be used as a means of detecting the formation of novel and unexpected dimeric compounds.

Received: March 12, 2003 [Z51376]

Keywords: aromaticity · cyclophanes · dimerization · NMR spectroscopy · polycyclic anions

[1] a) E. D. Bergmann, *Chem. Rev.* **1968**, *68*, 41–84; b) U. Edlund, B. Eliasson, *J. Chem. Soc. Chem. Commun.* **1982**, 950–952; c) M. Baumgarten, K. Müllen, *Top. Curr. Chem.* **1994**, *169*, 1–103; d) I. Aprahamian, R. E. Hoffman, T. Sheradsky, D. V. Preda, M. Bancu, L. T. Scott, M. Rabinovitz, *Angew. Chem.* **2002**, *114*, 1788–1791; *Angew. Chem. Int. Ed.* **2002**, *41*, 1712–1715.

[2] a) K. Müllen, *Helv. Chim. Acta* **1978**, *61*, 2307–2317; b) A. Minsky, A. Y. Meyer, M. Rabinovitz, *J. Am. Chem. Soc.* **1982**, *104*, 2475–2482; c) C. Schnieders, K. Müllen, W. Huber, *Tetrahedron* **1984**, *40*, 1701–1711; d) B. Eliasson, T. Lejon, U. Edlund, *J. Chem. Soc. Chem. Commun.* **1984**, 591–592.

[3] a) G. J. Bodwell, J. J. Fleming, M. R. Mannion, D. O. Miller, *J. Org. Chem.* **2000**, *65*, 5360–5370; b) G. J. Bodwell, J. N. Bridson, M. K. Cyrański, J. W. J. Kennedy, T. M. Krygowski, M. R. Mannion, D. O. Miller, *J. Org. Chem.* **2003**, *68*, 2089–2098; c) G. J. Bodwell, J. N. Bridson, T. J. Houghton, J. W. J. Kennedy, M. R. Mannion, *Angew. Chem.* **1996**, *108*, 1418–1420; *Angew. Chem. Int. Ed. Engl.* **1996**, *35*, 1320–1321; d) G. J. Bodwell, J. N. Bridson, T. J. Houghton, J. W. J. Kennedy, M. R. Mannion, *Chem. Eur. J.* **1999**, *5*, 1823–1827.

[4] I. Aprahamian, G. J. Bodwell, D. O. Miller, M. Rabinovitz, T. Sheradsky, R. J. Vermeij, in preparation.

[5] I. Aprahamian, G. J. Bodwell, J. J. Fleming, G. P. Manning, M. R. Mannion, T. Sheradsky, R. J. Vermeij, M. Rabinovitz, *J. Am. Chem. Soc.* **2003**, *125*, 1720–1721.

[6] The difficulty in observing the product of the first reduction step (one-electron reduction), stems from the readiness with which it undergoes further reduction (within a few minutes) to afford the two-electron reduction product, reported in ref. [5].

[7] This is, in fact, a $^2J_{C,H}$ (not a $^3J_{C,H}$) correlation.

[8] Compounds **1** and **2** were reduced for comparison: Although the specified interaction in the HMBC is possible in both **1a, 1b,** and their equivalents in **2,** neither it nor the specific HSQCSI coupling were observed for them in our experiments.

[9] A higher concentration of **4** is needed to see this process clearly. In addition, **4a** is less stable than **3a**, as its stability is highly dependent on temperature, and it tends to cleave rapidly above 240 K.

[10] G. J. Hoijtink, J. Townsend, S. I. Weissman, *J. Chem. Phys.* **1961**, *34*, 507–508.

[11] M. A. Hempenius, W. Heinen, P. P. J. Mulder, C. Erkelens, H. Zuilhof, J. Lugtenburg, J. Cornelisse, *J. Phys. Org. Chem.* **1994**, *7*, 296–302.

[12] a) F. Gerson, W. B. Martin, Jr., C. Wydler, *Helv. Chim. Acta* **1976**, *59*, 1365–1370; b) E. Shabtai, M. Rabinovitz, B. König, B.

 © 2003 Wiley-VCH Verlag GmbH & Co. KGaA, Weinheim

Knieriem, A. de Meijere, *J. Chem. Soc. Perkin Trans. 2* **1996**, 2589 – 2595.
[13] I. Sethson, D. Johnels, U. Edlund, A. Sygula, *J. Chem. Soc. Perkin Trans. 2* **1990**, 1339 – 1341.
[14] I. Aprahamian, G. J. Bodwell, J. J. Fleming, G. P. Manning, M. R. Mannion, B. L. Merner, T. Sheradsky, R. J. Vermeij, M. Rabinovitz, unpublished results.
[15] It seems that the two methyl groups in **2** are not sufficient to increase the solubility of the dimer.

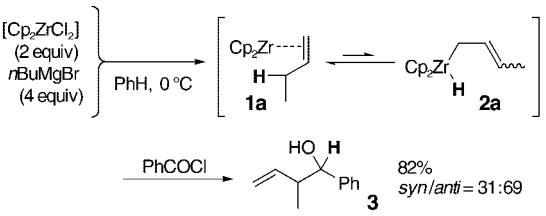
 © 2003 Wiley-VCH Verlag GmbH & Co. KGaA, Weinheim

Tandem Reduction–Allylation

Highly Diastereoselective Tandem Reduction–Allylation Reactions of 1,4-Diketones with Zirconocene–Olefin Complexes**

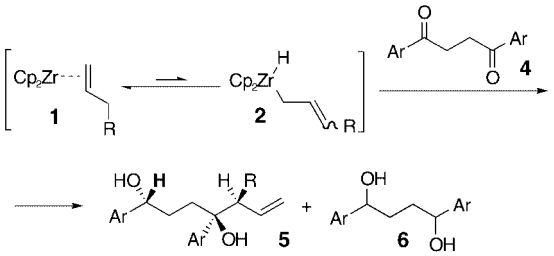
*Kazuya Fujita, Hiroshi Shinokubo, and Koichiro Oshima**

Since the development by Negishi et al. of a convenient method for the generation of low-valent zirconocene species,[1] the reaction of zirconocene–alkene complexes with a variety of unsaturated compounds has been regarded as a powerful tool for carbon–carbon bond-forming processes.[2] Recently, we found that [Cp_2Zr(1-alkene)] **1**, prepared at 0 °C in benzene, reacted with acid chlorides to provide homoallylic alcohols **3** (Scheme 1).[3] In this reaction, the [Cp_2Zr(alkene)] serves as a donor both of hydride and of an allyl group. We assume that an equilibrium exists between zirconocene–allyl–hydride complex **2a** and zirconocene–alkene complex **1a** through reversible allylic C–H bond cleavage of the coordinating alkene.[4] On the basis of this finding, we envisaged the application of [Cp_2Zr(alkene)] complexes as dual nucleophiles in reactions with diketones. We discovered that a tandem reduction–allylation reaction of 1,4-diketones takes place in the presence of a [Cp_2Zr(1-alkene)] complex with a high level of 1,4-diastereoselectivity. To our knowledge this is the first example of the 1,4-diastereoselective allylation of ketones.[5]



Scheme 1. Reaction of [Cp_2Zr(1-butene)] with benzoyl chloride.

The treatment of [Cp_2ZrCl_2] (2.0 equiv) with *n*PrMgBr (4.0 equiv) in benzene at 0 °C provided [Cp_2Zr(propene)] (**1b**, R = H). 1,4-Diketone **4a** (Ar = 3,5-$F_2(C_6H_3)$) was added to this mixture and the reduction of one carbonyl group and allylation at the other occurred to provide 1,4-diol **5a** in 64 % yield with excellent diastereoselectivity (Scheme 2, Table 1, entry 1). By-product **6a** was also obtained in 6 % yield.[6] The reaction of **1b** with other aromatic 1,4-diketones is summarized in Table 1 (entries 2–9).[7] Most of the reactions proceeded in satisfactory yields, although the use of electron-rich aromatic 1,4-diketones such as **4h** resulted in lower yields (Table 1, entry 8).[8] Ether and ester functionalities are also tolerated under the reaction conditions (e.g. Table 1, entry 9).



Scheme 2. Reaction of [Cp_2Zr(1-alkene)] complexes with 1,4-diketones.

Table 1: Conversion of 1,4-diketones into *anti* 1,4-diols.[a]

Entry	4	Ar	R	5 (%Yield)	*anti*/*syn*	6 (%Yield)
1[b]	**a**	3,5-$F_2(C_6H_3)$	H	**a** (64)	96:4	**a** (6)
2[b]	**b**	Ph	H	**b** (57)	94:6	**b** (18)
3[b]	**c**	3-$CF_3(C_6H_4)$	H	**c** (60)	92:8	**c** (11)
4[b]	**d**	4-$CF_3(C_6H_4)$	H	**d** (62)	92:8	**d** (16)
5[b]	**e**	4-Br(C_6H_4)	H	**e** (52)	>99:1	**e** (13)
6[b]	**f**	4-Cl(C_6H_4)	H	**f** (60)	96:4	**f** (9)
7[b]	**g**	4-F(C_6H_4)	H	**g** (62)	96:4	**g** (7)
8[b]	**h**	4-MeO(C_6H_4)	H	**h** (29)	91:9	**h** (36)
9[b]	**i**	4-*t*BuO_2C(C_6H_4)	H	**i** (62)	97:3	**i** (13)
10[c]	**a**	3,5-$F_2(C_6H_3)$	Me	**j** (76)	97:3	**a** (5)
11[c]	**b**	Ph	Me	**k** (54)	95:5	**b** (17)
12[c]	**c**	3-$CF_3(C_6H_4)$	Me	**l** (78)	96:4	**c** (11)
13[c]	**d**	4-$CF_3(C_6H_4)$	Me	**m** (62)	92:8	**d** (16)
14[c]	**e**	4-Br(C_6H_4)	Me	**n** (70)	97:3	**e** (14)
15[c]	**f**	4-Cl(C_6H_4)	Me	**o** (81)	97:3	**f** (11)
16[c]	**g**	4-F(C_6H_4)	Me	**p** (62)	96:4	**g** (7)
17[d]	**a**	3,5-$F_2(C_6H_3)$	Et	**q** (66)	95:5	**a** (16)
18[e]	**a**	3,5-$F_2(C_6H_3)$	*n*Pr	**r** (59)	96:4	**a** (21)
19[f]	**a**	3,5-$F_2(C_6H_3)$	Ph	**s** (71)	>99:1	**a** (6)

[a] Reaction conditions: [Cp_2ZrCl_2] (2.0 mmol), benzene (30 mL), Grignard reagent (1.0 M in THF, 4.0 mmol), 1,4-diketone (1.0 mmol), 0 °C. Grignard reagents used: [b] *n*PrMgBr. [c] *n*BuMgBr. [d] *n*PentMgBr. [e] *n*HexMgBr. [f] Ph(CH_2)$_3$MgBr.

[*] Prof. Dr. K. Oshima, K. Fujita, Dr. H. Shinokubo
Department of Material Chemistry
Graduate School of Engineering, Kyoto University
Yoshida, Sakyo-ku, Kyoto 606-8501 (Japan)
Fax: (+81) 75-753-4863
E-mail: oshima@fm1.kuic.kyoto-u.ac.jp

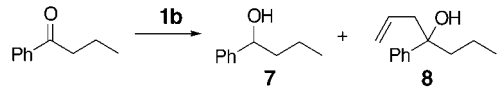
[**] This work was supported by Grants-in-Aid for Scientific Research from the Ministry of Education, Culture, Sports, Science, and Technology of Japan. We thank Prof. Tamejiro Hiyama and Dr. Masaki Shimizu (Kyoto University) for X-ray crystallographic analysis. K.F. acknowledges the JSPS for financial support.

Supporting information for this article is available on the WWW under http://www.angewandte.org or from the author.

 © 2003 Wiley-VCH Verlag GmbH & Co. KGaA, Weinheim DOI: 10.1002/anie.200351480

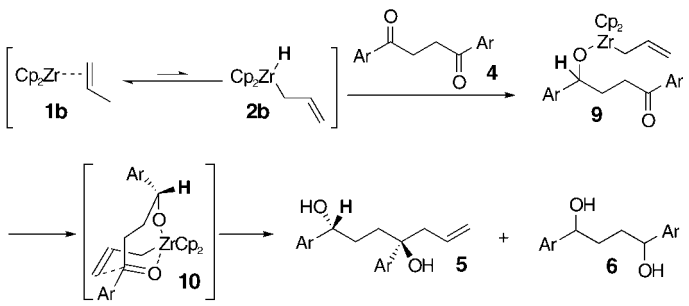
Especially rewarding was the high level of *anti*/*syn* stereoselectivity displayed by the reaction (>95:5 in most cases), with respect to the two OH-bearing carbon centers.[9] The relative 1,4-stereochemistry of the major isomer was assigned as *anti* based on the X-ray crystallographic analysis of **5e**.

To elucidate the order in which the nucleophilic attacks by hydride and the allyl group take place, we examined the reactivity of zirconocene complex **1b** toward phenyl propyl ketone (Scheme 3). Analysis of the crude mixture indicated



Scheme 3. Reaction of [Cp_2Zr(propene)] with phenyl propyl ketone.

predominant formation of **7** along with a trace amount of the allylated adduct **8**. This result clearly suggests that hydride transfer occurs prior to that of the allyl moiety.[10] Consequently, we propose the reaction mechanism depicted in Scheme 4 for the formation of the *anti* 1,4-diols. Thus,

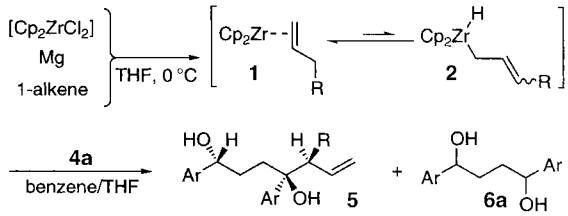


Scheme 4. Proposed reaction pathway.

[Cp_2Zr(propene)] (**1b**), through its equilibrium with **2b**, delivers hydride to one of the carbonyl carbon centers of a 1,4-diketone **4** to yield an allylzirconium alkoxide **9**. Subsequent intramolecular addition of the allyl group on zirconium to the other carbonyl carbon atom then takes place with the formation of an *anti* 1,4-diol **5**.

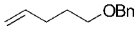
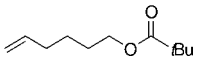
We next turned our attention to tandem reduction–3-alkenylation reactions with other 1-alkenes. The results are listed in Table 1 (entries 10–19). For example, the treatment of 1,4-diketone **4a** with [Cp_2ZrCl_2] (2.0 equiv), after prior treatment of the latter with *n*BuMgBr (4.0 equiv), resulted in the formation of **5j** in 76% yield with excellent 1,4,5-diastereoselectivity (Table 1, entry 10). The alkenylation reactions proceeded with perfect 4,5-*syn* selectivity as well as with excellent 1,4-*anti* stereoselectivity.[11] The use of pentyl, hexyl, and 3-phenylpropyl Grignard reagents also allowed the formation of the corresponding homoallylic alcohols with excellent stereoselectivity (Table 1, entries 17, 18, and 19).

The preparation of the requisite Grignard reagents is laborious. It is known that a zirconocene–olefin complex can be prepared from [Cp_2ZrCl_2] and Mg metal in the presence of the 1-alkene.[12] [Cp_2Zr(1-alkene)] complexes prepared in this way were also found to serve as dual nucleophiles, and the desired 1,4-diols were obtained in reasonable yields with excellent stereoselectivity (Scheme 5). Table 2 summarizes the reduction–3-alkenylation reactions of 1,4-diketone **4a** with several olefins. Ether and ester groups were tolerated under the reaction conditions (Table 2, entries 3 and 4). Thus, the reaction allows the facile preparation of various functionalized 1,4-diols.



Scheme 5. Preparation of zirconocene complexes with magnesium metal.

Table 2: Synthesis of *anti* 1,4-diols from 1-alkenes.[a]

Entry	Alkene	**5**	Yield [%]	1,4-*anti*/*syn*	Yield of **6a** [%]
1		**q**	68	96:4	9
2		**s**	53	>99:1	0
3		**t**	68	>99:1	0
4		**u**	44	>99:1	0

[a] Reaction conditions: [Cp_2ZrCl_2] (3.0 mmol), Mg (4.5 mmol), alkene (6.0 mmol), 1,4-diketone (1.0 mmol), benzene/THF (25/5 mL), 0°C.

In conclusion, we have disclosed a highly 1,4-stereoselective tandem reduction–3-alkenylation of 1,4-diketones with zirconocene–alkene complexes. Reduction of one of the carbonyl groups, followed by intramolecular transfer of the allyl group, enables excellent levels of diastereocontrol of three stereocenters. Investigations into the further utility of zirconocene–alkene complexes as dual nucleophiles is currently underway in our laboratory.

Experimental Section

*n*PrMgBr (1.0 M in THF, 4.0 mL, 4.0 mmol) was added dropwise to a mixture of [Cp_2ZrCl_2] (585 mg, 2.0 mmol) in benzene (30 mL) at 0°C. The resulting viscous black suspension was stirred for 30 min at 0°C, then a solution of **4a** (310 mg, 1.0 mmol) in benzene (2 mL) was added. The reaction mixture was stirred for a further 5 h at 0°C, then was poured into aqueous HCl. This mixture was extracted with hexane/ethyl acetate, and the organic extracts were dried and concentrated. Purification on silica gel provided **5a** (228 mg, 0.64 mmol) in 64% yield.

Received: March 25, 2003 [Z51480]

Keywords: allylation · C-H activation · domino reactions · reduction · zirconium

 © 2003 Wiley-VCH Verlag GmbH & Co. KGaA, Weinheim

[1] E.-I. Negishi, F. E. Cederbaum, T. Takahashi, *Tetrahedron Lett.* **1986**, *27*, 2829.

[2] For leading reviews, see: a) E.-I. Negishi, T. Takahashi, *Acc. Chem. Res.* **1994**, *27*, 124; b) E.-I. Negishi, D. Y. Kondakov, *Chem. Soc. Rev.* **1996**, *25*, 417; c) E.-I. Negishi, T. Takahashi, *Bull. Chem. Soc. Jpn.* **1998**, *71*, 755; d) T. Takahashi, M. Kotora, R. Hara, Z. Xi, *Bull. Chem. Soc. Jpn.* **1999**, *72*, 2591.

[3] K. Fujita, H. Yorimitsu, H. Shinokubo, K. Oshima, *J. Am. Chem. Soc.* **2001**, *123*, 12115.

[4] It has been shown that zirconocene–olefin complex **1** and allyl–zirconocene–hydride complex **2** are in an equilibrium that is significantly shifted toward **1**: V. K. Dioumaev, J. F. Harrod, *Organometallics* **1997**, *16*, 1452; see also: E.-I. Negishi, J. P. Maya, D. Choueiry, *Tetrahedron* **1995**, *51*, 4447.

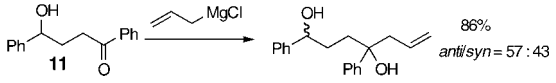
[5] The 1,4-diastereoselective methylation of γ-alkoxy aldehydes has been reported: a) M. T. Reetz, K. Kesseler, S. Schmidtberger, B. Wenderoth, R. Steinbach, *Angew. Chem.* **1983**, *95*, 1007; *Angew. Chem. Int. Ed. Engl.* **1983**, *22*, 989; b) M. T. Reetz, *Angew. Chem.* **1984**, *96*, 542; *Angew. Chem. Int. Ed. Engl.* **1984**, *23*, 556.

[6] ^{13}C NMR spectroscopic analysis indicated that 1,4-diol **6a** had formed as a mixture of isomers. We assume that **6** resulted from the intermolecular reduction of intermediate **9** by zirconocene hydride **2b**. The formation of double reduction product **6** is suppressed by conducting the reaction under high dilution conditions.

[7] When 1,5-diketones or 1,6-diketones were used in place of 1,4-diketones, trace amounts of the expected products were isolated along with products of double reduction. Nucleophilic addition reactions did not occur with 1,3-diketones because of enolization of these substrates.

[8] In contrast to aromatic 1,4-diketones, the reaction of 5,8-dodecadione with **1b** afforded the desired adduct in only 15% yield.

[9] The reaction of γ-hydroxyketone **11** with allylmagnesium chloride exhibited no diastereoselectivity.



[10] This order of sequential nucleophilic attack was also found in the reaction of zirconocene–alkene complex **1** with acid chlorides; see reference [3].

[11] The relative 4,5-configuration of the diols was assigned by comparison of their spectral data with those reported for analogues; see: Y. Kataoka, I. Makihara, T. Yamagata, K. Tani, *Organometallics* **1997**, *16*, 4788.

[12] a) E.-I. Negishi, S. J. Holmes, J. M. Tour, J. A. Miller, *J. Am. Chem. Soc.* **1985**, *107*, 2568; b) K. Miura, M. Funatsu, H. Saito, H. Ito, A. Hosomi, *Tetrahedron Lett.* **1996**, *37*, 9059; c) S. Thanedar, M. F. Farona, *J. Organomet. Chem.* **1982**, *235*, 65.

 © 2003 Wiley-VCH Verlag GmbH & Co. KGaA, Weinheim

Cover Picture



Yoshiaki Nishibayashi, Masato Yoshikawa, Youichi Inada, Marilyn Daisy Milton, Masanobu Hidai,* and Sakae Uemura*

A One-Pot Sequential Reaction for the ruthenium- and platinum-catalyzed preparation of a trisubstituted furan from a propargylic alcohol and acetone in good yield with high regioselectivity is shown. Two different catalysts, the thiolate-bridged diruthenium complex [Cp*RuCl(μ_2-SMe)RuCp*Cl] (Cp* = C_5Me_5) and $PtCl_2$, sequentially promote each catalytic cycle in the same medium. For more information, see the Communication by M. Hidai, S. Uemura, and co-workers on pp. 2681 ff.

Contents

Meeting Reviews

Molecule-Based Magnetic Materials — 2570 – 2572 — Eugenio Coronado, Fernando Palacio and Jaume Veciana

Books

Chirality in Natural and Applied Science — 2573 — W. J. Lough, I. W. Wainer — *reviewed by D. Heller*

Biomimetic Materials and Design — 2574 — Angela K. Dillow, Anthony M. Lowman — *reviewed by J. Frahn*

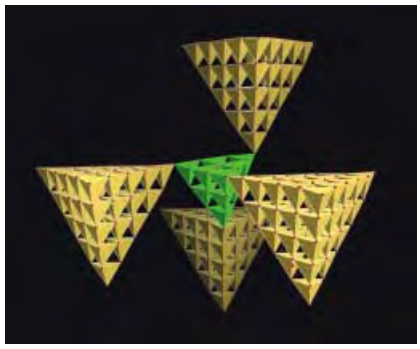
Highlights

Supertetrahedral Sulfides

G. Férey* — 2576 – 2579

Supertetrahedra in Sulfides: Matter against Mathematical Series?

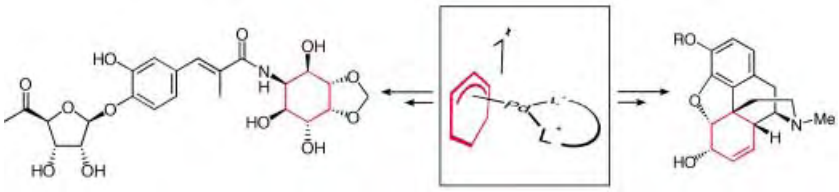
The game continues... Self-assembled sulfide supertetrahedra can be used to generate porous solids with unusual electoluminescence and semiconducting properties. Recent advances, including the discovery of corner-linked superclusters (see picture) and super-supertetrahedral clusters, may lead to materials, the properties of which could be superior to the best quantum dots known to date.



Pd in Natural Product Synthesis

T. Graening, H.-G. Schmalz* — 2580 – 2584

Pd-Catalyzed Enantioselective Allylic Substitution: New Strategic Options for the Total Synthesis of Natural Products



As versatile as Nature: Pd-catalyzed enantioselective allylic substitution is a powerful reaction in modern synthetic chemistry. The reactions of cyclic allylic substrates (see figure) have recently been proven to be of particular value as they lead to novel and highly efficient strategies in the total synthesis of various natural products.

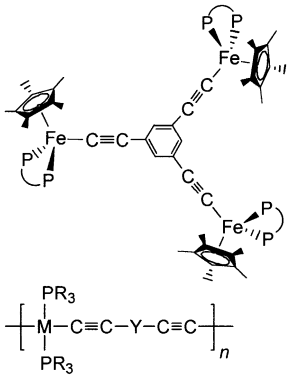
Reviews

Transition-Metal Alkyne Complexes

N. J. Long,* C. K. Williams — 2586 – 2617

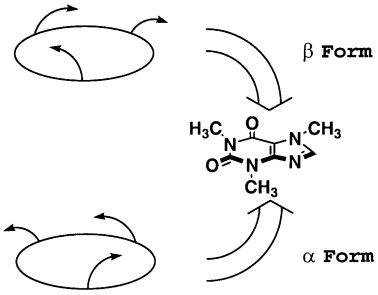
Metal Alkynyl σ Complexes: Synthesis and Materials

The M–C≡C structural unit, which can be used to establish a wide variety of molecular topologies (see, for example, the tris(ferrocenylalkynyl) complex and the molecular rigid-rod polymer shown), together with the increasing importance of material properties such as electron transfer, nonlinear optical behavior, and luminescence, combine to make transition-metal alkynyl complexes, especially as oligomers and polymers, of particular current interest.



© 2003 Wiley-VCH Verlag GmbH & Co. KGaA, Weinheim

Communications



Telling top and bottom apart: Supramolecular receptors can discriminate between the "top" and "bottom" sides of a single guest molecule, such as caffeine (see picture). This reversible enantiofacial differentiation results in the preferential formation of the α or β complexes.

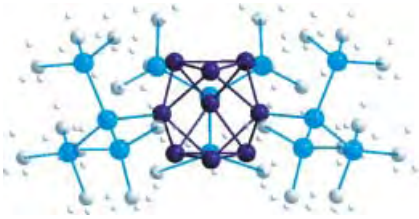
Stereoselective Complex Formation

M. C. Schopohl, C. Siering, O. Kataeva, S. R. Waldvogel* ——— **2620 – 2623**

Reversible Enantiofacial Differentiation of a Single Heterocyclic Substrate by Supramolecular Receptors

---

"Naked" but refined! The reaction of germanium(I) bromide with Li{Si(SiMe$_3$)$_3$} gives the polyhedral Ge$_9$ cluster ion [Ge$_9${Si(SiMe$_3$)$_3$}$_3$]$^-$ (see structure), in which only three of the nine germanium atoms are bound to a ligand, the remaining germanium atoms are naked. The unusually high solubility of this cluster opens the possibility of using it as a starting material for further reactions.



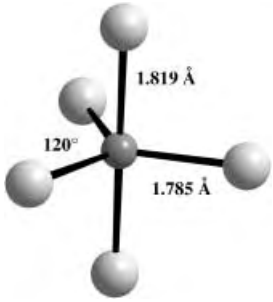
A Soluble Germanium Cluster

A. Schnepf* ——— **2624 – 2625**

[Ge$_9${Si(SiMe$_3$)$_3$}$_3$]$^-$: A Soluble Polyhedral Ge$_9$ Cluster Stabilized by Only Three Silyl Ligands

---

Welcome to the family: The previously unknown discrete pentafluoroaluminate [(CH$_3$)$_4$N]$^+_2$[AlF$_5$]$^{2-}$ salt, a missing link of the homoleptic fluoroaluminate family, is synthesized from [(CH$_3$)$_4$N]$^+$[AlF$_4$]$^-$ and [(CH$_3$)$_4$N]$^+$F$^-$. IR and Raman spectroscopic data along with ^{27}Al MAS NMR spectroscopy investigations reveal a perfect and unperturbed trigonal-bipyramidal structure (see picture).



Discrete Fluoroaluminates

U. Groß,* D. Müller, E. Kemnitz* ——— **2626 – 2629**

Coordination Geometry of the Discrete Pentafluoroaluminate Dianion [AlF$_5$]$^{2-}$

A breath of fresh air: Air oxidation of [*n*Bu$_4$N]$_2$[Ni^{II}(1-nor)$_3$Br], prepared from [*n*Bu$_4$N]$_2$[Ni^{II}Br$_4$] and 1-norbornyllithium generates the title pseudotetrahedral organometallic complex in which a nickel center with the formal oxidation state of +4 is present (see structure; Ni purple, Br brown, C black, H green).



High-Oxidation-State Ni Complex

V. Dimitrov,* A. Linden —— **2631 – 2633**

A Pseudotetrahedral, High-Oxidation-State Organonickel Compound: Synthesis and Structure of Bromotris(1-norbornyl)nickel(IV)

For the USA and Canada:
ANGEWANDTE CHEMIE International Edition (ISSN 1433-7851) is published weekly by Wiley-VCH PO Box 191161, D 69451 Weinheim, Germany. Air freight and mailing in the USA by Publications Expediting Inc. 200 Meacham Ave., Elmont, NY 11003. Periodicals postage paid at Jamaica NY 11431. US POSTMASTER: send address changes to *Angewandte Chemie*, Wiley-VCH, 111 River Street, Hoboken, NJ 07030. Annual institutional subscription price for institutions: Europe € 2998.00/3148.00. Outside Europe US$ 3718.00/3904.00 (valid for print or electronic/print and electronic delivery); for individuals who are personal members of a national chemical society, or whose institution already subscribes, or who are retired or self-employed consultants, print only (including postage and handling charges): Europe € 248.00/Outside Europe US$ 348.00.

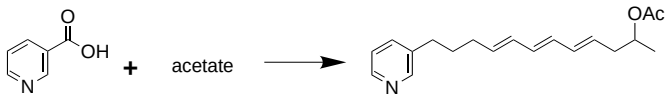
 © 2003 Wiley-VCH Verlag GmbH & Co. KGaA, Weinheim

Contents

Biosynthesis of Alkylpyridines

A. Cutignano, A. Tramice, S. De Caro, G. Villani, G. Cimino, A. Fontana* ——— **2633 – 2636**

Biogenesis of 3-Alkylpyridine Alkaloids in the Marine Mollusc *Haminoea Orbignyana*



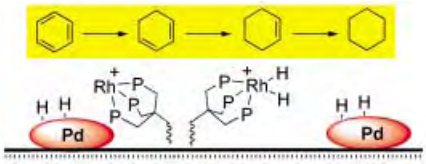
Fruits of the sea: Alkylpyridine alkaloids are a family of marine natural products, the structures of which are all related to each other by the presence of a biogenetically common motif, an alkyl chain linked to C-3 of a six-membered nitrogen heterocycle. We report the first experimental evidence for the biosynthesis of alkylpyridines (see scheme).

Single-Site/Dispersed-Metal Catalyst

C. Bianchini,* V. Dal Santo, A. Meli, S. Moneti, M. Moreno, W. Oberhauser, R. Psaro, L. Sordelli, F. Vizza ——— **2636 – 2639**

Hydrogenation of Arenes over Catalysts that Combine a Metal Phase and a Grafted Metal Complex: Role of the Single-Site Catalyst

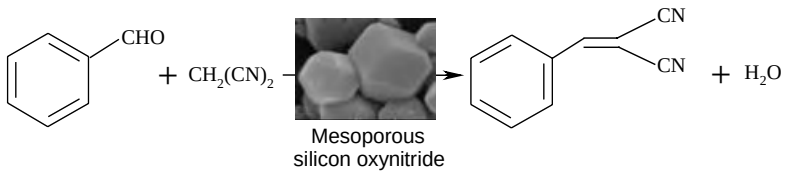
Cooperating catalysts: The combined single-site/dispersed-metal catalyst [Rh(cod)(sulphos)]–Pd^0/SiO_2 (cod = cyclooctadiene; sulphos = $^-O_3S(C_6H_4)CH_2C(CH_2PPh_2)_3$) is more efficient than the dispersed-metal catalyst Pd^0/SiO_2 for the hydrogenation of arenes to cycloalkanes. The grafted rhodium moieties and the palladium particles in [Rh(cod)(sulphos)]–Pd^0/SiO_2 cooperate to speed up the hydrogenation of arenes (see scheme).



Mesoporous Basic Catalysts

Y. Xia, R. Mokaya* ——— **2639 – 2644**

Highly Ordered Mesoporous Silicon Oxynitride Materials as Base Catalysts

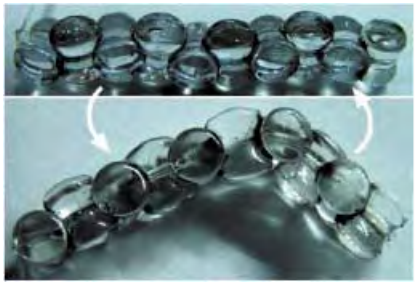


Basically, a good catalyst: The introduction of NH_x species into the framework of mesoporous silicas results in silicon oxynitride materials and generates basic sites, which exhibit considerable catalytic activity for the Knoevenagel condensation reaction (see scheme). The well-ordered mesoporous oxynitrides have a high surface area and pore volume and are attractive as alternative basic catalysts, especially for large-molecule transformations.

Self-Healing Systems

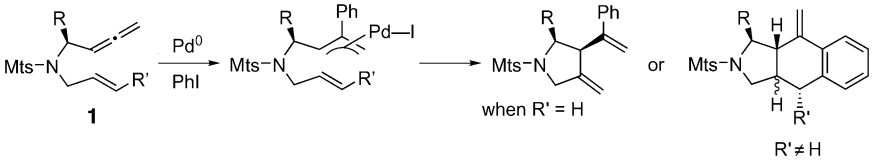
M. Boncheva, G. M. Whitesides* ——— **2644 – 2647**

Self-Healing Systems Having a Design Stimulated by the Vertebrate Spine



The organization of the vertebrate spine was the source of the concepts used to design self-healing structures. These structures comprise mm-sized beads self-assembled on elastomeric threads and connected by solder joints. The structures spontaneously realign and heal (top) after breaking and dislocation (bottom).

 © 2003 Wiley-VCH Verlag GmbH & Co. KGaA, Weinheim

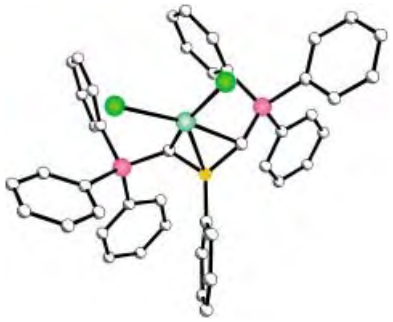


Cyclizations of Allenenes

H. Ohno, K. Miyamura, Y. Takeoka, T. Tanaka* ——— 2647 – 2650

Palladium(0)-Catalyzed Tandem Cyclization of Allenenes

Tri- and tetracyclic heterocycles were formed through the tandem cyclization of allenenes **1** upon treatment with an aryl iodide, potassium carbonate, and catalytic $[Pd(PPh_3)_4]$ (see scheme). The reactivity of the palladium(II) intermediates could be controlled by substitution (R′) at the olefin terminus (Mts = 2,4,6-trimethylphenylsulfonyl).

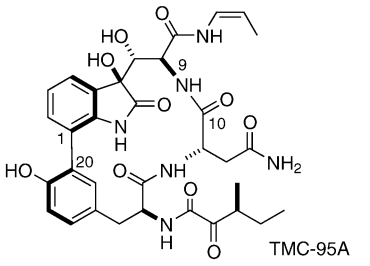


A Zwitterionic Chelating Ligand

F. Jiang, P. J. Shapiro,* F. Fahs, B. Twamley ——— 2651 – 2653

Phenyl{bis(triphenylphosphanemethylenido)}borane: A Zwitterionic Chelating Ligand Exhibiting Allyl-Type Coordination

When complexed to transition-metal atoms, the zwitterionic ligand phenyl{bis(triphenylphosphanemethylenido)}borane behaves like a neutral analogue of the η^3-allyl ligand. Syntheses and X-ray crystal structures of the ligand and its complexes with $ZrCl_4$ and $PdCl_2$ (depicted) are described (Pd = cyan, B = yellow, P = pink, Cl = green, C = white).

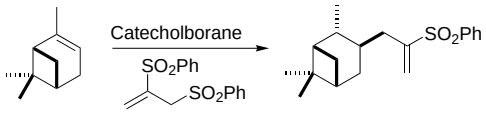


Natural Product Synthesis

M. Inoue,* H. Sakazaki, H. Furuyama, M. Hirama* ——— 2654 – 2657

Total Synthesis of TMC-95A

A Suzuki–Miyaura coupling reaction to form C1—C20, macrolactamization at N9—C10, and a mild decarboxylative *anti* elimination to selectively introduce the (*Z*)-1-propenylamide are key steps in a highly convergent and completely stereoselective synthesis of the potent proteasome inhibitor TMC-95A (see structure).



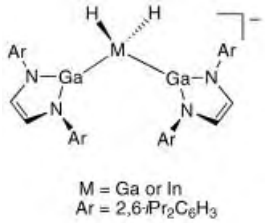
Hydroallylation of Alkenes

A.-P. Schaffner, P. Renaud* 2658 – 2660

Tin-Free Radical Allylation of *B*-Alkylcatecholboranes

Organoboranes, prepared in situ by hydroboration of olefins with catecholborane, are efficiently allylated with allyl sulfones by a radical fragmentation process (see scheme). This hydroallylation of alkenes proved to be general for a wide range of alkenes and allyl sulfones.

The first covalently bonded metal complexes derived from an anionic gallium carbene analogue (see picture) show remarkable thermal stability in the solid state. This fact suggests that gallium(I) heterocycles should prove to be versatile ligands towards both main-group and transition-metal fragments.



Anionic Gallium Carbene Analogue

R. J. Baker, C. Jones,* M. Kloth, J. A. Platts ——— 2660 – 2663

Synthesis and Structural Characterization of Thermally Stable Group 13 Hydride Complexes Derived from a Gallium(I) Carbene Analogue

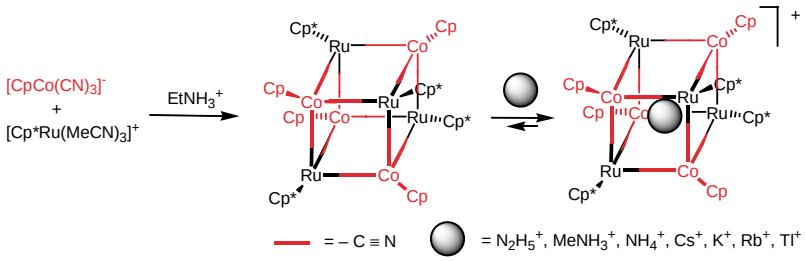
 © 2003 Wiley-VCH Verlag GmbH & Co. KGaA, Weinheim

Contents

Containers for Cations

S. C. N. Hsu, M. Ramesh, J. H. Espenson, T. B. Rauchfuss* ——— **2663 – 2666**

Membership Rules for a Molecular Box: The Admission Process and Protection Provided to Guest Molecules

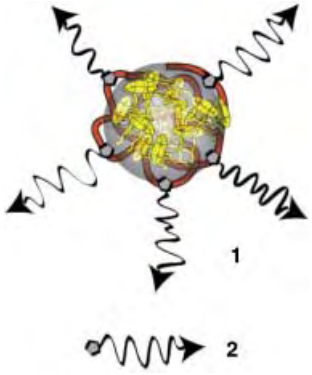


Crate chemistry: The inclusion dynamics of molecular boxes has been studied by virtue of the synthesis of the voided ionophilic packing crate $[\{CpCo(CN)_3\}_4(Cp^*Ru)_4]$ ($Cp = C_5H_5$ $Cp^* = C_5Me_5$). Numerous ions can then be inserted into the box (see scheme). The box exhibits the highest formation constant known for Cs^+ ions. Once inside, ions are insulated from chemical attack, such as amine-deprotonation or H–D exchange.

Viruslike DNA Particles

G. Zuber,* L. Zammut-Italiano, E. Dauty, J.-P. Behr ——— **2666 – 2669**

Targeted Gene Delivery to Cancer Cells: Directed Assembly of Nanometric DNA Particles Coated with Folic Acid

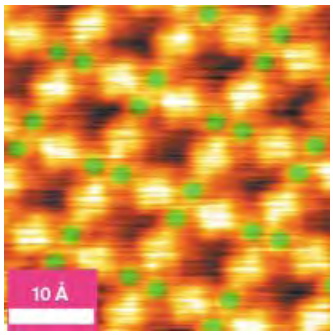


A synthetic viruslike particle: Monomolecular condensation of a gene into a 30-nm particle was performed by the DNA-templated air oxidation of a cationic thiol detergent to a gemini lipid (depicted in yellow). A folic acid coating was added (in the form of the DNA-binding folate-containing compounds represented schematically by **2**) and the resulting DNA particles **1** were shown to be nanometric and stable, and to enter cells through the folic acid receptor.

Metal–Organic Network Assembly

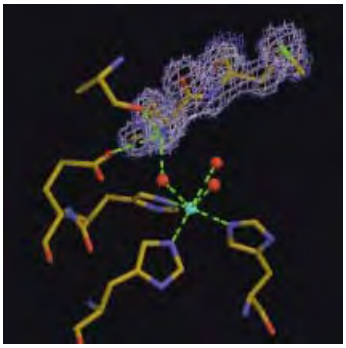
A. Dmitriev, H. Spillmann, N. Lin,* J. V. Barth,* K. Kern* ——— **2670 – 2673**

Modular Assembly of Two-Dimensional Metal–Organic Coordination Networks at a Metal Surface



Impressive iron networks: Two-dimensional metal–organic coordination networks have been prepared by the vacuum deposition of organic polytopic linkers and metal atoms on a copper surface. This unprecedented technique enabled the modular assembly of open Fe–carboxylate grids (see image, Fe atoms in green) that possess regularly spaced, identically shaped cavities. The structure and composition of the networks can be tuned by controlling the deposition parameters.

© 2003 Wiley-VCH Verlag GmbH & Co. KGaA, Weinheim

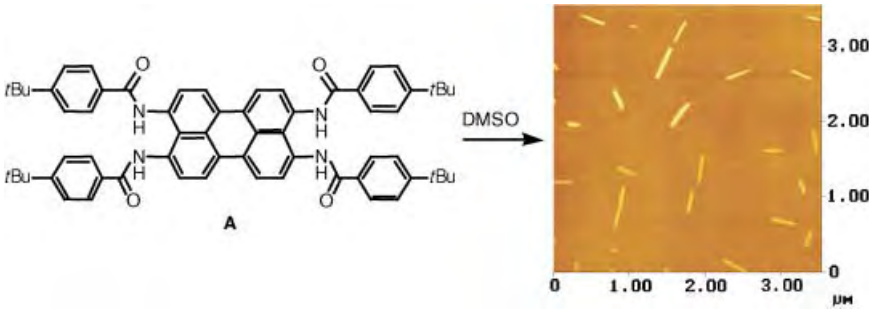


A helicoidal filament results from the approach of the N-terminus of the mutated variant of the catalytic domain of MMP-12 with the catalytic zinc center of another molecule (see X-ray structure); adjacent filaments are arranged in double helices. The N-terminal fragment is proposed to be analogous to an N-terminal polypeptide product after cleavage. Crystals yield two contrasting structures, in which the NH_3^+ ion is either triply hydrogen bonded, or only exhibits van der Waals interactions.

Matrix Metalloproteinases

I. Bertini,* V. Calderone, M. Fragai, C. Luchinat, S. Mangani, B. Terni ——— **2673 – 2676**

X-ray Structures of Binary and Ternary Enzyme-Product-Inhibitor Complexes of Matrix Metalloproteinases

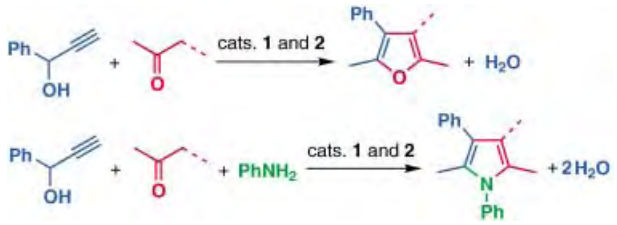


A new class of perylene-derived dyes, tetra(carboxamido)perylenes, has been obtained by a generally applicable synthetic method. Derivative **A** is shown to form nanocrystalline aggregates in DMSO which display significantly modified photophysical behavior with respect to the monomer and were studied by using atomic force microscopy techniques.

Perylene-Derived Dyes

L. H. Gade,* C. H. Galka, R. M. Williams,* L. De Cola, M. McPartlin, B. Dong, L. Chi ——— **2677 – 2681**

Synthesis, Photophysical Properties, and Nanocrystal Formation of a New Class of Tetra-N-Substituted Perylenes



Two cats. in the same pot: The two catalysts [Cp*RuCl(μ_2-SMe)$_2$RuCp*Cl] (**1**) and $PtCl_2$ (**2**) promote a sequence of catalytic cycles in the same medium. Tri- or tetrasubstituted furans or pyrroles are afforded in moderate to good yields with high regioselectivities from the catalyzed reactions of propargylic alcohols with ketones or with ketones and anilines, respectively (see scheme; cats. = catalysts).

One-Pot Sequential Reactions

Y. Nishibayashi, M. Yoshikawa, Y. Inada, M. D. Milton, M. Hidai,* S. Uemura* ——— **2681 – 2684**

Novel Ruthenium- and Platinum-Catalyzed Sequential Reactions: Synthesis of Tri- and Tetrasubstituted Furans and Pyrroles from Propargylic Alcohols and Ketones

 © 2003 Wiley-VCH Verlag GmbH & Co. KGaA, Weinheim

Contents

Ferrous Complexes

O. L. Sydora, P. T. Wolczanski,*
E. B. Lobkovsky ——— **2685 – 2687**

Ferrous Wheels, Ellipse $[(t\mathrm{Bu_3SiS})\mathrm{FeX}]_n$, and Cube $[(t\mathrm{Bu_3SiS})\mathrm{Fe}(\mathrm{CCSi}t\mathrm{Bu_3})]_4$

The shapes of things to come: The use of the extremely bulky $t\mathrm{Bu_3SiS}$ ligand has enabled the synthesis of rare ferrous wheels (depicted), a unique ellipse, and an uncommon ferrous cube based on tetrahedral coordination. Fe = red, Cl = green, S = orange, Si = blue, C = gray.



Communications labeled with this symbol have been judged by two referees as being "very important papers".

The publication of Communications labeled with this symbol has been accelerated because of their topical or highly competitive nature.

Looking for outstanding employees?

Do you need another expert for your excellent team?
... Chemists, PhD Students, Managers, Professors, Sales Representatives...

Place an advert in the printed version and have it made available online for 1 month, free of charge!

Angewandte Chemie International Edition
Advertising Sales Department: Marion Schulz
Phone: 0 62 01 - 60 65 65
Fax: 0 62 01 - 60 65 50
E-Mail: MSchulz@wiley-vch.de

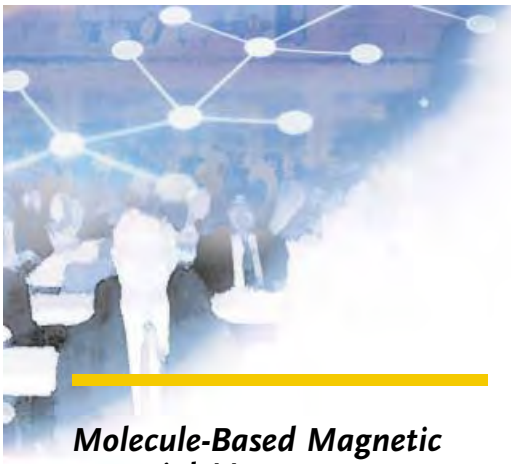
Service

Keywords ——— *2688*

Authors ——— *2689*

Vacancies ——— *2569*

Preview ——— *2691*



Molecule-Based Magnetic Materials**

Eugenio Coronado,* Fernando Palacio, and Jaume Veciana

From bulk magnets to multifunctional materials and nanomagnets

The perennial pursuit to develop new molecule-based magnets, particularly with higher critical temperatures T_c, is still on the agenda. Two examples of room temperature magnets exist but they contain metals. The search for **purely organic high-T_c magnets** is still a challenge.

K. Awaga (Nagoya Univ., Japan) reported that benzo[1,2-*d*:4,5-*d*']bis[1,3,2]dithiazole cation radical $[BBDTA]^{\bullet+}$ in the form of its $[GaCl_4]^-$ salt is diamagnetic when solvated with CH_3CN, but orders ferromagnetically at 6.7 K when desolvated.[1] This temperature is an order of magnitude greater than that typically observed for organic ferromagnets. K. Takeda (Kyushu Univ., Japan) reported that application of 17 kbar pressure to the canted antiferromagnet $4\text{-}NCC_6F_4CN_2S_2$ discovered by J. M. Rawson (Univ. Cambridge, UK; $T_c = 35.5$ K) led to the doubling of the T_c to 70 K—the highest ever reported ordering temperature for an organic magnet under pressure.

Dealing with metals, an unexplored possibility is that of designing new magnets based on the interaction of 3d/4d and 4d/5d transition metal ions, as well as on p–f interactions. An interesting family of new **3d/4d ferrimagnets** formulated as $[Mn_2(tea)Mo(CN)_7]\cdot x H_2O$ (tea: triethanolamine) with critical temperatures as high as 106 K was described by J. P. Sutter (ICMCB, France). These results demonstrate the potential offered by second- and third-row transition metal ions for the future development of molecule-based magnets. **p/f Ferrimagnets** comprised of $S = 7/2$ Gd^{3+} with either 7,7,8,8-tetracyano-*p*-quinodimethanide, $[TCNQ]^{\bullet-}$, or tetracyanoethanide, $[TCNE]^{\bullet-}$, were reported by K. R. Dunbar (Texas A&M Univ., USA) and J. S. Miller (Univ. Utah, USA) to order below 3 K. Hence, weak exchange couplings which involve highly screened orbitals can lead to magnetic ordering albeit at low temperatures.

In addition to new materials with greater critical temperatures and different magnetic coupling mechanisms, multifunctional magnetic materials, which display coexistence or synergism with another physical (or chemical) property, as well as the so-called single-molecule magnets (SMMs) are sought. Appealing examples of **multifunctional materials**, include chiral, photomagnetic, magneto-optical materials, and magnetic conductors. **Chiral magnets** became an important class of dual-function materials because they can show a coupling between optical activity and ferromagnetism. Coordination compounds of this kind which show 1- to 3D structural motifs were investigated by several groups from Europe and Japan.[2] Still, it remains to be demonstrated that these materials exhibit magneto-chiral dichroism and that their spins adopt a chiral arrangement when the materials are ordered. **Molecule-based photomagnets** are of considerable interest for data storage and signal processing applications. Over the last six years, photo-induced magnetism (PIM) was observed, generated, and studied in many different materials, primarily as Prussian-blue-structured materials, in Japan, Europe, and the United States. The correlation of PIM with structural changes induced by photo-irradiation was elusive and has thwarted major progress in the area. K. Hashimoto (Univ. Tokyo, Japan) reported a large geometrical distortion of single-crystalline $CsCo^{II}[W^{V}(CN)_8](3\text{-}NC_5H_4CN)_2$ associated with a photoinduced transition from a paramagnetic to a ferrimagnetic phase. His group also observed the novel "time-dependent photomagnetism" phenomenon in $RbMn^{II}[Fe^{III}(CN)_6]$. In a magnetically ordered phase, this compound is demagnetized upon irradiation with a laser pulse at 3 K. Switching off the laser results in the recovery of the initial magnetization. In addition to the "light-tunable magnets", **spin crossover materials** are another important class of bistable, switchable materials whose magnetic properties and color can be reversibly changed by light, temperature, or pressure, which may lead to promising applications such as thermal displays, optical devices, and pressure sensors. Relatedly, J. A. Real (ICMol Univ. Valencia, Spain) reported cyanide-bridged Fe^{II}–M bimetallic 3D networks (M: Ni^{II}, Pd^{II}, Pt^{II}, Cu^{I}, Ag^{I}, Au^{I}) to have cooperative spin transitions with large hysteresis and dramatic color changes. Similar effects were observed by O. Sato (Kanagawa Academy of Science and Technology, Japan) in mononuclear iron(III) complexes which exhibit strong π–π intermolecular interactions. This strategy afforded the first observation of Light-Induced Excited Spin State Trapping (LIESST)[3] for iron(III). Additionally, remarkable advances in the physics of these materials were reported, for example, the triggering of the spin crossover phenomenon through application of pulsed high magnetic fields in $Co^{II}(H_2(fsa)_2en)py_2$

[*] Prof. Dr. E. Coronado
Instituto de Ciencia Molecular
Universidad de Valencia
Doctor Moliner 50, 46100 Burjasot (Spain)
Fax: (+34) 96-354-4415
E-mail: eugenio.coronado@uv.es
Prof. Dr. F. Palacio
Instituto de Ciencia de Materiales de Aragón
CSIC – Universidad de Zaragoza (Spain)
Prof. Dr. J. Veciana
Instituto de Ciencia de Materiales de Barcelona
CSIC (Spain)

[**] VIIIth International Conference on Molecule-based Magnets, ICMM 2002, October 5–10, Valencia, Spain. ICMM 2002 was supported in part by the European Science Foundation (Programme on Molecular Magnets), the Generalitat Valenciana and the Spanish Ministry of Science and Technology. We thank J. S. Miller for his critical comments to improve the manuscript.

 © 2003 Wiley-VCH Verlag GmbH & Co. KGaA, Weinheim

(H_2(fsa)$_2$en: *N*,*N*′-ethylenebis(3-carboxysalicylaldiminate) by A. Bousseksou, LCC Toulouse, France.

Significant progress was made in the development of multifunctional materials which combine magnetic and conducting properties. The interleaving of bis(ethylenedithio)tetrathiafulvalene, BEDT–TTF, known to support conductivity and even superconductivity, with a magnetically ordered inorganic system led to the development of the first molecular material which is both a ferromagnet and a metallic conductor.[4] This strategy opened the way to the design of novel **ferromagnetic molecular conductors** from Mn^{II}–Cr^{III} and Co^{II}–Cr^{III} bimetallic tris(oxalato) anionic layers which alternate with BEDT-TTF-type cationic layers, as reported by J. R. Galán-Mascarós and E. Coronado (ICMol Univ. Valencia, Spain). Another important class of materials are the **magnetic superconductors**. In those formed by bis(ethylenedithio)tetraselenafulvalene (BETS) and the magnetic $S = 5/2$ $[FeX_4]^-$ (X: Cl, Br) anions, novel physical phenomena like the observation of field-induced superconductivity have been found by H. Kobayashi's group (IMS-Okazaki, Japan). A third class of materials of interest are the **TTF-based magnets** reported by S. S. Turner and P. Day (Royal Institution, London, UK). The compounds are formed by mixed stacks of $TTF^{\bullet+}$ and sulfur-containing magnetic anions that promote interion S···S contacts and π-stacking. This results in significant exchange interactions between the two components and in magnetic ordering.

The term multifunctional magnetic materials is not limited to materials in which magnetism is combined with another physical property. A chemical property such as solvent adsorption capability can also be added. Two interesting examples with nanoporous structures that may have applications as magnetic solvent sensors were reported by D. Ruiz-Molina and J. Veciana (ICMAB Barcelona, Spain) and by T. Ishida (Univ. of Electro-Communications, Tokyo, Japan) and co-workers. The former reported a spongelike magnet obtained with the metal radical strategy by using a tricarboxilic substituted radical and Cu ions, while the latter detailed a solvato-magnetic molecular material which was obtained by using a Cu complex with a nitronyl nitroxide radical.

Single-molecule nanomagnets exhibit a slow relaxation of the magnetization with a magnetic hysteresis analogous to bulk magnets, but with quantum effects.[5] These features were first observed for the $Mn_{12}O_{12}(O_2CCH_3)_{16}(OH_2)_4$ cluster. Subsequently, significant efforts have been devoted to identify new SMMs and to investigate their new physical properties. Although the blocking temperature has yet to be increased above liquid-helium temperatures, key advances have been made. These include 1) G. Christou (Univ. Florida, Gainsville, USA) and D. Hendrickson (Univ. California, San Diego, USA) reported exchange-biased quantum tunneling in a supramolecular dimer comprised of two antiferromagnetically coupled tetramanganese SMMs. 2) The observation of resonant quantum tunneling between spin multiplet states reported by R. Sessoli (Univ. Florence, Italy) for an octanuclear iron(III) cluster which lacks an inversion center. Here, the individual spins have different magnetic anisotropy and efficient admixing occurs between the ground ($S = 10$) and the first excited ($S = 9$) state. Resonant tunneling occurs at those fields for which levels which belong to different multiplets can be brought in coincidence. 3) The observation by M. Evangelisti (Leiden Univ., The Netherlands) of long-range magnetic order in a tetramanganese $S = 9/2$ SMM prepared by G. Christou. At 0.21 K and in the absence of a magnetic field, magnetic ordering is observed and can be suppressed by applying a magnetic field as small as 500 Oe. An incoherent quantum tunneling with a sufficiently fast spin–lattice relaxation mechanism at very low temperatures was proposed to explain this surprising result. Like SMM clusters, some chain molecules also exhibit bistability and slow relaxation of the magnetization, for example the compound Co(hfac)$_2$(NITR) (hfac: hexafluoroacetylacetonate; NITR: nitronyl nitroxide radical) reported by Sessoli, Gatteschi, and coworkers (Univ. Florence, Italy). These compounds are called **single-chain magnets**. Bimetallic Mn^{III}-Ni^{II} and Fe^{III}-Co^{II} chain complexes which show similar behavior were presented by H. Miyasaka, M. Yamashita (Tokyo Metropolitan Univ., Japan), and R. Clérac (CRPP, Pessac, France), as well as F. Lloret and M. Julve (ICMol Univ. Valencia, Spain), and others, respectively. The slow magnetic relaxation of these systems suggests that information may be stored magnetically in smaller devices because the hysteresis seems to be related to a cooperative behavior within the chain without requiring interchain interactions. Tunneling of the magnetization in these systems is a very active research thrust.

From materials to applications

Applications of molecule-based magnets are the target of increasing study, as there is growing interest in the exploration of their benefits in molecule-based electronics, information storage, and other nanotechnologies. Over the last few years, we have witnessed many families of materials with improved magnetic properties, and many more are expected. While most materials were crystalline, some significant progress was made in preparing these materials as **thin films and nanoparticles**, or deposited/inserted on/into solid supports, or embedded in polymeric matrices. The controlled supramolecular organization of molecule-based magnets and SMMs is making steady progress. D. R. Talham (Univ. Florida, Gainesville, USA) organized 2-D nanostructures by using Langmuir–Blodgett (LB) techniques to build films of isolated monolayers, bilayers, or organized multilayers of molecule-based magnets. Dealing with SMMs and other nanomaterials, C. Rovira (ICMAB, Barcelona, Spain) reported that Mn_{12} could be placed onto the surface of a polymeric thin film. H. Nishide (Waseda Univ., Japan) showed that nanometer-sized high-spin polyradicals could be deposited and even patterned on a silicon surface. Atomic force (AFM) and magnetic force microscopies (MFM) were successfully used in these studies to produce images of the obtained single-molecule-based magnetic quantum dots, which may be important for information storage and

 © 2003 Wiley-VCH Verlag GmbH & Co. KGaA, Weinheim

quantum computing applications. T. Sugawara (Univ. Tokyo, Japan) described the decoration of the surface of gold nanoparticles with thiol-functionalized nitronyl nitroxide radicals. Spectroscopic measurements reveal that the nitroxide spins are magnetically coupled with the gold conduction electrons to provide a magnetic quantum dot.

Spintronics is an important emerging area involving magnetoresistive materials. It may lead to faster computer operations and communications with less power consumption. Conventional semiconductors, such as Si, and conventional metals, such as Cu, have equal electron densities of opposite spin. In electronic devices, electric fields are used to manipulate these electrons regardless of their spin orientation. Spintronics takes advantage of the spin as well as the charge on the electrons, and makes use of charges with one principal spin direction. This has been achieved in semiconductors, such as Mn-doped GaAs, at low temperatures, but the memory of the spin orientation can be lost quickly for such high atomic number materials. Studies on thin films of the semiconducting $V(TCNE)_2$ magnet, which remains magnetic above room temperature, were reported by A. J. Epstein (Ohio State Univ., USA) and J. S. Miller (Univ. Utah, USA), and demonstrated this to be a feasible spintronic material.

Challenges and Opportunities

Scientific interest and curiosity, which were initially mainly focused on synthesizing new molecule-based materials, have evolved towards the development of more complex materials with one or more specific properties, as well as to materials processing aimed at applications. The molecule or nanoscale options for information storage, quantum computing etc., are increasingly being explored and new phenomena, such as spintronics, are being incorporated into the field to further stimulate the design of new materials with a clear trend towards molecule-based electronics.

One future research avenue will be associated with one of the intrinsic characteristics of molecules: their small dimensions. The synthesis of molecular nanomagnets already demonstrated that the design of new functional molecular nanoscale materials will bring new and unexpected surprises and applications. Organization and controlled positioning of magnetic molecules or materials in one, two, or three dimensions is an important objective for the future. Finally, multifunctionality is a general trend in the materials community, and molecule-based materials are attracting much attention in this regard as they are already known to exhibit technologically important properties traditionally considered to be solely available for atom-based inorganic solids (magnetic ordering, electrical conductivity, superconductivity, ferroelectricity,...).[6]

But the use of organic synthetic methods to modulate and combine properties justifies the optimism offered by the molecular approach for the development of new materials unparalleled in the world of atom-based solid-state chemistry. We can imagine in this context new dual-function materials such as ferromagnetic (super)conductors and chiral (super)conductors, or materials which combine ferromagnetism, (super)conductivity or liquid-crystallinity with the bistability provided by SMMs or spin crossover molecules. We look forward to the advances in the development of new materials as well as new phenomena to be reported in ICMM 2004 in Japan.

[1] W. Fujita, K. Awaga, *Chem. Phys. Lett.* **2003**, *367*, 385.

[2] For an example of this new type of material see: M. Minguet, D. Luneau, E. Lhotel, V. Villar, C. Paulsen, D. B. Amabilino, J. Veciana, *Angew. Chem.* **2002**, *114*, 606; *Angew. Chem. Int. Ed.* **2002**, *41*, 586.

[3] P. Gütlich, A. Hauser, H. Spiering, *Angew. Chem.* **1994**, *106*, 2109; *Angew. Chem. Int. Ed. Engl.* **1994**, *33*, 2024.

[4] E. Coronado, J. R. Galán-Mascarós, C. J. Gómez-García, V. Laukhin, *Nature* **2000**, *408*, 447.

[5] D. Gatteschi, R. Sessoli, *Angew. Chem.* **2003**, *115*, 278; *Angew. Chem. Int. Ed.* **2003**, *42*, 268.

[6] J. S. Miller, *Adv. Mater.* **1990**, *2*, 98.

 © 2003 Wiley-VCH Verlag GmbH & Co. KGaA, Weinheim

Supertetrahedral Sulfides

Supertetrahedra in Sulfides: Matter against Mathematical Series?

*Gérard Férey**

Keywords:
electroluminescence · microporous materials · nanomaterials · sulfides · supertetrahedra

In the Beginning was the Game! To Perforate Dense Matter

Even now, Cronstedt[1] could not imagine the consequences of his discovery of the natural zeolite stilbite, the first porous solid to have been found by a chemist. At least as a first step, most of the consequences relate to the curiosity of chemists and their need to do better and better, just for the challenge. But how many surprises would the players uncover?

The mimicking of nature began in the middle of the 19th Century with the first synthetic homologue of natural zeolite[2] (levynite), formed from a mixture of dense phases (Al_2O_3 and SiO_2) in an alkaline medium. In the resulting phase, alkaline ions and water played the role of a cutter (template) for the original dense structures, and the elimination of water (through heating) gave rise to the porosity of the structure. This concept was further developed[3] when organic molecules (mainly quaternary ammonium ions and amine groups) replaced the alkaline ions. The modular character of the length of the carbon chain led to an explosion of new porous solids with increasing pore dimensions, the inorganic skeleton remaining mainly composed of AlO_4, SiO_4 and, additionally, PO_4 tetrahedra when the porous aluminophosphates were discovered.[4]

[*] Prof. G. Férey
Institut Universitaire de France &
Institut Lavoisier
UMR CNRS 8637, UVSQ
45, Avenue des Etats-Unis
78035 Versailles Cedex (France)
Fax: (+33) 1-3925-4358
E-mail: ferey@chimie.uvsq.fr

Along with many variations developed around that theme, some other breakthroughs occurred later, which mainly concerned oxides[5] and, to a lesser extent, oxyfluorides:[6] The introduction of six-coordinate cations into the frameworks (rather than four),[7] the discovery of magnetic porous solids[8] where transition-metal atoms fully replaced aluminum in the skeleton, the first studies on the mechanisms of the formation of these solids,[6c,9] and so on. The aim of such developments was to increase the size of the pores,[10] mainly by adjusting the characteristics of the template, for improved applications of this family of solids (such as, catalysis, gas separation, nanoreactors). One of the last breakthroughs concerned the discovery of porous sulfides, which possess supertetrahedral frameworks, and about which this highlight is dedicated.

The Porous Sulfides and Mathematical Extrapolation

The known classes of open-framework materials are overwhelmingly dominated by oxide or mixed oxide/fluoride matrices. In 1989, however, Bedard et al.[11] proposed to extend this class of materials to metal sulfide compounds by using the same principle of perforating dense matter with the use of organic templates. Two recent reviews[5,12] report the progress with these topics up to 1999.

From the point of view of crystal chemistry, the choice of sulfides presents many advantages: a) The larger ionic radius of the S^{2-} ion, compared to those of oxide and fluoride ions, favors tetrahedral coordination for the cations and therefore allows the discovery of sulfide homologues of zeolites, b) in the eventuality of such structures, the higher polarisability of the S^{2-} ion implies more flexibility for the T-S-T angles that exist between tetrahedra (109–161°), when compared to those with oxides (140–145°) and, consequently, more flexible frameworks that better accommodate the shape of the template and, more surprisingly, c) the arrangement of the tetrahedra in the starting dense matter remains unchanged.

In principle (Figure 1 a–d), the perforation of a dense phase (here ZnS or sphalerite) by templates can create holes that are surrounded by groups of, for example, four- (T2), ten- (T3), or twenty- (T4) corner-sharing tetrahedra, according to the size and the charge of the template. Whatever the arrangement of these superclusters, the supertetrahedra obey some mathematical rules. According to O'Keeffe et al.,[13] the number of tetrahedra (T atoms) in a Tp supertetrahedron is the p^{th} tetrahedral number $t_p = p(p+1)(p+2)/6$. The number of distinct vertexes (S atoms) in one supertetrahedron is t_{p+1}. In a continuous framework, each of the four outmost vertexes of a supertetrahedron is shared with another supertetrahedron, so that the overall composition is T_xS_y with $x = t_p$ and $y = t_{p+1} - 2$. Therefore, the compositions of T2, T3, and T4 supertetrahedra are T_4S_8, $T_{10}S_{18}$, and $T_{20}S_{33}$, respectively.

The first T2 structure appeared in 1987,[14a] but the interest in supertetrahedra began after the work of Yaghi et al.[14b] who showed that the adamantanoid cluster $(NMe_4)_4Ge_4S_{10}$ reacts with manganese acetate in water at room temperature to give a three-dimensional

 © 2003 Wiley-VCH Verlag GmbH & Co. KGaA, Weinheim DOI: 10.1002/anie.200201621

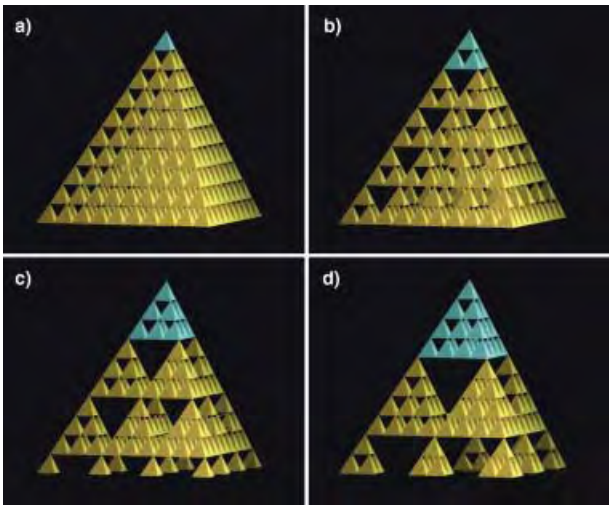


Figure 1. The principle of building supertetrahedra from the dense sphalerite structure: a) A part of the sphalerite structure limited to a large tetrahedron corresponding to an edge of ten primitive tetrahedra (in blue); b) assembly of T2 supertetrahedra with the same sphalerite topology (the supertetrahedron, in blue, contains four metal centers); c) assembly of T3 supertetrahedra built on the same principle; d) assembly of T4.

(3D) network ($(NMe_4)_2MnGe_4S_{10}$); several similar compounds appeared later.[14c–e] The game was then to increase the size of the supertetrahedra, with the risk that enlarging the size of the hole was advantageous for the undesired interpenetration of two identical subnetworks, which was indeed frequently observed. However, using an incrementation strategy, the Yaghi and O'Keeffe research group isolated[15a,b] three non-interpenetrating indium sulfides, ASU-31, 32, and 34, with T3 supertetrahedra (ASU = Arizona State University), while interpenetrating examples were also discovered.[15c] The same group[13] and another[16] recently succeeded in the third incremental step (T4); the T4 cluster $[M_4In_{16}S_{33}]^{10-}$ containing in this case a divalent metal M (M = Mn, Co, Zn, Cd) as well as indium. With such discoveries, there was hope that this series might be continued, based on the same mathematical rules, for example, $T_{35}S_{54}$, $T_{56}S_{82}$, and so on. The edge of the supertetrahedra corresponds to *n* times the S–S distance in the primitive tetrahedron and the size of the cavity increasing accordingly.

Moreover, these extended frameworks, the series of which has been augmented recently with networks containing M^{4+}/M^{3+} ions,[17] can present new structure types (T4)[16] but are very often the upper homologues of well-known basic topologies (aristotypes), such as diamond (T3),[15c] sodalite (T2, T3),[15a] cristobalite (T2, T3, T4),[13,14a,15b] or CrB_4 (T2, T3),[15a] and provide nice examples of the concept of scale chemistry[18] ("the larger the bricks, the larger the pores"). It is worth noting that the flexibility of the T-S-T angles compared to the rigidity of the corresponding T-O-T angles leads, in these superframeworks, to contracted versions of the aristotypes.[13,15a]

Breaking Off

T5, the next term in the series, was much sought after. Two recent papers[19,20] described its nature, but the results mark a break from the previous evolution. The striking feature common to the two structures concerns the T5 cluster itself. Whereas the lower cluster homologues are complete, one core atom is missing in both T5 structures (Figure 2a), and the formula corresponds to $\square_1T_{34}S_{54}$ ($\square$ = missing atom). Moreover, when T5 is the only type of cluster in the structure,[20] the solid is two-dimensional (2D). Surprisingly, in the second solid,[19] 3D character is preserved because of the presence, for the first time, of two types of superclusters, T3 and T5, linked at their corners (Figure 2b). This clearly indicates that T5 represents a limit for the

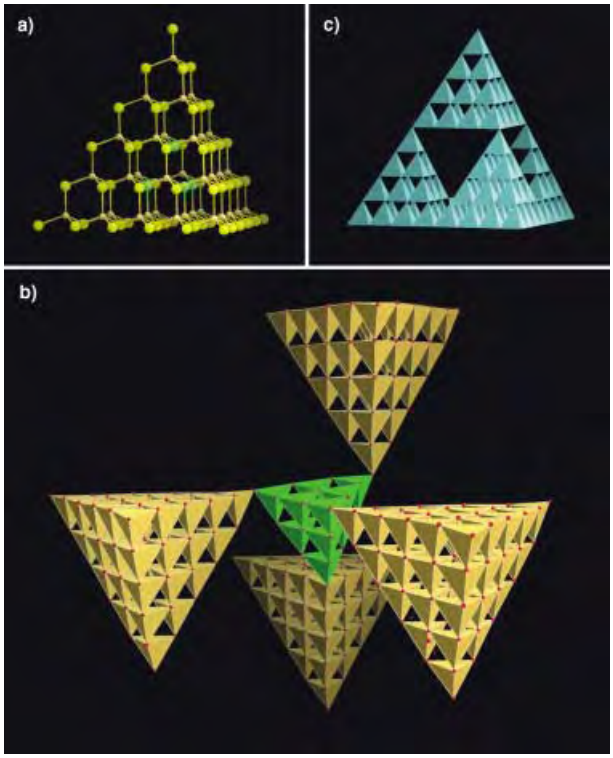


Figure 2. a) Ball-and-stick representation of the defect-containing T5 cluster; the four sulfur atoms surrounding the vacancy are indicated in green; b) ordered arrangement of T3 and T5 supertetrahedra in the structure of ref. [19]; c) the T4,2 cluster.

 © 2003 Wiley-VCH Verlag GmbH & Co. KGaA, Weinheim

initial evolution, an interesting problem which needs to be addressed to answer the fundamental questions regarding the primitive evolution and the reasons for the break in the series.

And After the Game, Questions...

Of course, the first question concerns the defective nature of the T5 topology, since both examples given above have the same characteristics. It is evident that there is no obvious reason to explain the behavior, but some suggestions can be offered.

The first reflection takes into account some chemical observations. Looking at the evolution of the nature of the cations involved in the T*n* series, T2 involved a mixture of tetra- and divalent ions (Ge^{4+} and Mn^{2+}, $(NMe_4)_2MnGe_4S_{10}$),[14b] T3 contained exclusively trivalent metal ions (In^{3+}, ASU-32: $In_{10}S_{18}(C_{11}H_{24}N_2)_3(H_2O)_7$),[15] T4 introduced divalent metal ions (mainly Cd^{2+}) as well as In^{3+} (CdInS-44: $Cd_4In_{16}S_{33}(C_{10}H_{28}N_4)_{2.5}(H_2O)_{20}$),[13] while the pure T5 structure $[Cd_6In_{28}S_{54}\{(CH_3)_4N\}_{12}(HSCH_2COOH)_2)_{3.5}]$[20] leads to a trend in the formal charges for the clusters, as folllows: $[T2]^{2-}$, $[T3]^{6-}$, $[T4]^{10-}$, and $[T5]^{12-}$. The progressive introduction of lower valences, which limits the expansion of the negative charge of the cluster (a charge too negative would render the solid unstable), is in agreement with the upper infinite limit corresponding to the neutral solid CdS with the sphalerite structure. For T5, if a vacancy was not present, the negative charge would be too small ($[T5]^{10-}$ or $[T5]^{9-}$ if the vacancy is occupied by Cd or In, respectively). It seems that, once more, the building unit accommodates its condensation (here by the creation of a defect in the structural building unit) according to the charge density of the template, the precipitation being explained either by equalization of the electronegativities of the groups[6c,d] or by the host–guest charge-density-matching principle.[21] However, the latter does not help to explain (when assimilating the charge density to the C/N ratio of the template) the evolution in the whole series.

A more interesting evolution, already noted by Feng et al.,[19] relates to the negative charge per metal site within the overall framework of the cluster, which decreases in steps from T2 (−1) to T5 (−0.35) via T3 (−0.6) and T4 (−0.5). This could be an interesting indicator for further synthesis.

However, it is not only electronic reasons that explain the evolution and the breaking of the trend; the chemical conditions also play a major role. The novel material[19] that contains both T3 and T5 morphologies (noting that $[(NMe_4)_2MnGe_4S_{10}]$ is a combination of T1 and T2) provides a good illustration of this point. Indeed, the comparison between the synthesis conditions of the latter and ASU-32, which only contains T3 clusters, are exactly the same (identical concentrations, ratios, and template). Only temperature and time differ (135 °C and 5 days for ASU-32; 190 °C and 16 days for $[(NMe_4)_2MnGe_4S_{10}]$) which seems to show that increasing time and temperature favor larger clusters. This interesting feature poses questions about the mechanism of formation of these supertetrahedra. Any tentative explanation of the formation requires a thorough in situ study of the succession of the appearance of these phases, as was carried out by Parise[22] on Ge_4S_{10}-based solids.

The last question concerns templates and their exact role. If it is obvious that their shape, combined with the flexibility of the T-S-T angles, directly influences the shape and the dimensions of the cavities, the situation is more complicated than for alumino- and gallophosphates.[6c,d] Is there a direct relation between their charge and the size of the cluster? Do they play the role of structure-directing or space-filling agents, or both? The fact that all the solids lose their templates proportionally with temperature, with no observed plateau corresponding to the empty solid, left the question open. It is noteworthy that, before the recent paper of Feng[24] and the description of the porous solid UCR20, previous papers did not mention the porosity of these solids, despite the large dimensions of all the cages; the framework representing between 20 and 45 % of the total space.

Open Windows

These concern both fundamental research and applications. Defective T5 clusters with one metal vacancy may tempt chemists to consider them as the first term in a new series, after the break, by increasing the number of vacancies with the number of metallic sites in the cluster. As noted by Feng et al.,[19] one might have imagined until recently that the game may be continued by creating "a whole family of coreless nanoclusters with sizes larger than T5". The series would be continued by a T6 cluster with a missing T2 core ($\square_4M_{52}X_{84}$), a T7 cluster with a missing T3 core ($\square_{10}M_{74}X_{120}$), a T8 cluster with a missing T4 core ($\square_{20}M_{100}\square_1X_{164}$), and so on, with the aim of creating clusters with inter- and intracluster pores. However, although the idea is brilliant, the intracluster concept is not so obvious since, even if there are 4, 10, and 20 metallic defects, they do not create real internal space (only the volume of a cation) and the series must reach T8 before an anionic vacancy with an internal pore the same diameter as a sulfur atom is achieved. But conceptually, the approach was very interesting, even if it will not reach the fascinating dimensions of the Mo oxide-based hollow spheres recently described by Müller et al.[23]

This was true until very recently, but a discovery by Yaghi and O'Keeffe once more breaks the series.[24] Very recently, they described a super-supertetrahedral cluster with 214 atoms and 80 tetrahedra. The topology is the same as a T2 cluster (which contains four single tetrahedra), but this time, each single tetrahedra is replaced by T4 supertetrahedra. The latter leave an octahedral vacancy at the center of the cluster with a volume of 1855 Å^3! This striking feature requires a change in the notation of the supertetrahedra by using two numbers *p* and *q*. Specifically, T*p*,*q* will be used to describe a T*q* supertetrahedron of T*p* supertetrahedra. The first term of this new series (Figure 2c) is therefore T4,2.

In addition to the numerous ideas stated by Ozin[12] for biological applications, the potential applications of these solids are also evident. First of all, they are ion exchangers (except for two examples[13,24]) and can accept mono-

 © 2003 Wiley-VCH Verlag GmbH & Co. KGaA, Weinheim

and divalent cations in good yield. This means that, even if no porosity measurements were performed, the cavities containing the templates are accessible. However, the most attractive application, which renders these solids close to nanomaterials, concerns their semiconducting character (a band gap of 3 eV) and it is meritorious of Li et al.[20] to have discussed this point. Indeed, these materials are, in many ways, far superior to colloidal nanoparticles (classical quantum dots). The periodical arrangement of the clusters (dots) and cavities (antidots) in the crystal presents many advantages compared to the randomly distributed colloids, particularly in providing opportunities for studying the collective physical phenomena attributed to interactions between individual dots (energy transfer, excitonic splitting, etc.), the regular distance between the dots giving rise to strong interdot coupling. The first measurements by Li show that the density of states near the top of the valence band, larger than that of normal III–V semiconductors, is dominated by sulfur lone-pair orbitals. This situation gives rise, according to Li, to a small band dispersion, and the band-edge transitions are sharp, which will be useful for efficient laser and solar devices. This unusual family of solids is therefore promised a brilliant future, despite the unresolved questions concerning their formation.

[1] A. F. Cronstedt, *Akad. Handl. Stockholm* **1756**, *17*, 120.

[2] H. de Sainte Claire Deville, *C. R. Hebd. Seances Acad. Sci.* **1862**, *54*, 324.

[3] R. M. Barrer, J. W. Baynham, F. W. Bultitude, W. M. Meier, *J. Chem. Soc.* **1959**, 195.

[4] S. T. Wilson, B. M. Lok, C. A. Messina, T. R. Cannan, E. M. Flanigen, *J. Am. Chem. Soc.* **1982**, *104*, 1146.

[5] A. K. Cheetham, G. Férey, T. Loiseau, *Angew. Chem.* **1999**, *111*, 3466; *Angew. Chem. Int. Ed.* **1999**, *38*, 3268.

[6] E. M. Flanigen, R. L. Patton, US Patent 4073865, **1978**; J. L. Guth, H. Kessler, R. Wey, *Stud. Surf. Sci. Catal.* **1986**, *28*, 121; G. Férey, *J. Fluorine Chem.* **1995**, *72*, 187; G. Férey, *C. R. Acad. Sci. Ser. IIc* **1998**, *1*, 1.

[7] J. B. Parise, *Inorg. Chem.* **1985**, *24*, 4312.

[8] M. Cavellec, D. Riou, J. M. Grenèche, G. Férey, *Zeolites* **1996**, *17*, 250; M. Cavellec, D. Riou, J. M. Grenèche, G. Férey, *J. Magn. Magn. Mater.* **1996**, *163*, 173.

[9] S. Oliver, A. Kuperman, G. A. Ozin, *Angew. Chem.* **1998**, *110*, 48; *Angew. Chem. Int. Ed.* **1998**, *37*, 46; S. Neeraj, S. Natarajan, C. N. R. Rao, *Angew. Chem.* **1999**, *111*, 3688; *Angew. Chem. Int. Ed.* **1999**, *38*, 3480.

[10] G. Férey, A. K. Cheetham, *Science* **1999**, *283*, 1125.

[11] R. L. Bedard, S. T. Wilson, D. Vail, J. M. Bennett, E. M. Flanigen, *Stud. Surf. Sci. Catal.* **1989**, *49*, 375.

[12] R. W. J. Scott, M. J. MacLachlan, G. A. Ozin, *Curr. Opin. Solid State Mater. Sci.* **1999**, *4*, 113.

[13] H. Li, J. Kim, T. L. Groy, M. O'Keeffe, O. M. Yaghi, *J. Am. Chem. Soc.* **2001**, *123*, 4867.

[14] a) I. G. Dance, R. G. Garbutt, D. C. Craig, M. L. Scudder, *Inorg. Chem.* **1987**, *26*, 4057; b) O. M. Yaghi, Z. Sun, D. A. Richardson, T. L. Groy, *J. Am. Chem. Soc.* 1994, 116, 807; c) K. Tan, A. Darovsky, J. B. Parise, *J. Am. Chem. Soc.* **1995**, *117*, 7039; d) K. Tan, K. Younghee, J. B. Parise, A. Darovsky, *Chem. Mater.* **1996**, *8*, 448; e) C. L. Cahill, J. B. Parise, *Chem. Mater.* **1997**, *9*, 4807.

[15] a) H. Li, A. Laine, M. O'Keeffe, O. M. Yaghi, *Science* **1999**, *283*, 1145; b) H. Li, M. Eddaoudi, A. Laine, M. O'Keeffe, O. M. Yaghi, *J. Am. Chem. Soc.* **1999**, *121*, 6096; c) C. L. Cahill, Y. Ko, J. B. Parise, *Chem. Mater.* **1998**, *10*, 19.

[16] C. Wang, Y. Li, X. Bu, N. Zheng, O. Zivkovic, C.-S. Yang, P. Feng, *J. Am. Chem. Soc.* **2001**, *123*, 11506.

[17] N. Zheng, X. Bu, B. Wang, P. Feng, *Science* **2002**, *298*, 2366.

[18] G. Férey, *J. Solid State Chem.* **2000**, *152*, 37.

[19] C. Wang, Y. Li, X. Bu, N. Zheng, P. Feng, *J. Am. Chem. Soc.* **2002**, *124*, 10268.

[20] W. Su, X. Juang, J. Li, H. Fu, *J. Am. Chem. Soc.* **2002**, *124*, 12944.

[21] a) X. Bu, P. Feng, G. D. Stucky, *Science* **1997**, *278*, 2080; b) P. Feng, X. Bu, G. D. Stucky, *Nature* **1997**, *388*, 735.

[22] C. L. Cahill, Y. Ko, J. C. Hanson, K. Tan, J. B. Parise, *Chem. Mater.* **1998**, *10*, 1453.

[23] A. Müller, E. Krickemeyer, H. Bögge, M. Schmidtmann, S. Roy, A. Berkle, *Angew. Chem.* **2002**, *114*, 3756; *Angew. Chem. Int. Ed.* **2002**, *41*, 3604.

[24] H. Li, J. Kim, M. O'Keeffe, O. M. Yaghi, *Angew. Chem.* **2003**, *115*, 1863; *Angew. Chem. Int. Ed.* **2003**, *42*, 1819.

 © 2003 Wiley-VCH Verlag GmbH & Co. KGaA, Weinheim

Pd in Natural Product Synthesis

Pd-Catalyzed Enantioselective Allylic Substitution: New Strategic Options for the Total Synthesis of Natural Products

*Timm Graening and Hans-Günther Schmalz**

Keywords:
asymmetric synthesis · desymmetrization · homogeneous catalysis · natural products · palladium

The enantioselective version of palladium-catalyzed allylic substitution, sometimes referred to as AAA (asymmetric allylic alkylation), has emerged as a powerful synthetic tool.[1] Since the first report of a stoichiometric AAA reaction in the 1970s,[2] it took almost 20 years of research until effective catalytic systems based on chiral ligands were developed. The major challenge in conducting such reactions enantioselectively arises from the fact that both the departure of the allylic leaving group, resulting in the formation of a cationic π-allyl–Pd complex and, in most cases, the attack of the nucleophile occur on the π face of the substrate opposite to the metal. Asymmetric induction therefore proceeds remote to the employed chiral ligands. However, some particularly successful concepts to address this issue have been devised, and over 100 catalysts have been developed.[3]

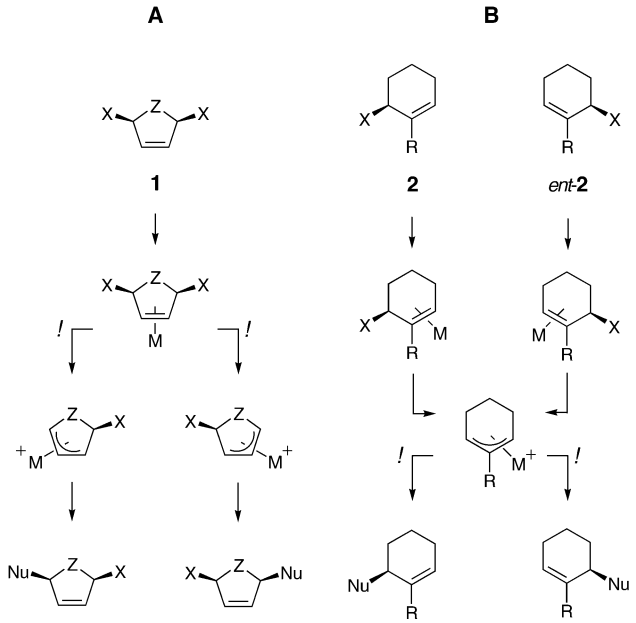
Besides high levels of asymmetric induction, advantages of the AAA methodology are a broad tolerance towards functional groups and, in contrast to many other catalytic asymmetric methods, a great flexibility in the bond type to be formed. For instance, H, O, N, S, P, and C nucleophiles can be employed. Among the many new opportunities thus arising for the synthetic chemist,[4] AAA reactions of cyclic substrates of type **1** and **2** have recently proven to be of particular value as they



1 Z = CH_2CH_2, CH_2, O *rac*-**2**

lead to novel and highly efficient strategies in the total synthesis of natural products. The abundance of the corresponding cyclic subunits in natural products together with the inherent potential in controlling the stereochemistry of cyclic scaffolds in the course of a synthesis makes these building blocks very attractive.

The reactions of *meso* compounds **1** and those of chiral cyclohexenes **2** with allylic leaving groups X differ in the nature of the enantiodiscriminating step (pathways **A** and **B**, respectively, in Scheme 1). In the substitution of *meso* compounds of type **1** (path **A**), the formation of the intermediate η^3-π-allyl–metal complex (ionization) constitutes the enantiodiscriminating step. The nucleophile is then introduced at the least-hindered allyl terminus with overall retention of configuration. Following path **B**, substrates of type **2** can be employed as racemic mixtures. With



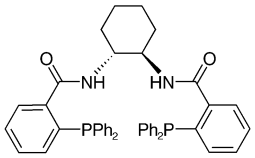
Scheme 1. Different reaction pathways of the Pd-catalyzed substitution of *meso*-**1** (path A) and *rac*-**2** (path B).

[*] Prof. Dr. H.-G. Schmalz,
Dipl.-Chem. T. Graening
Institut für Organische Chemie
Universität zu Köln
Greinstrasse 4, 50939 Köln (Germany)
Fax: (+49) 221-470-3064
E-mail: schmalz@uni-koeln.de

 © 2003 Wiley-VCH Verlag GmbH & Co. KGaA, Weinheim DOI: 10.1002/anie.200301644

the formation of the π-allyl complex, the stereochemical information of the substrate is lost and in this case the attack of the nucleophile from the face opposite to the metal represents the enantiodiscriminating step. According to Trost, this deracemization process can be regarded as a DYKAT (dynamic kinetic asymmetric transformation).[4] Both pathways allow the selective induction of chirality and make up the starting point of some very efficient natural product syntheses published recently.

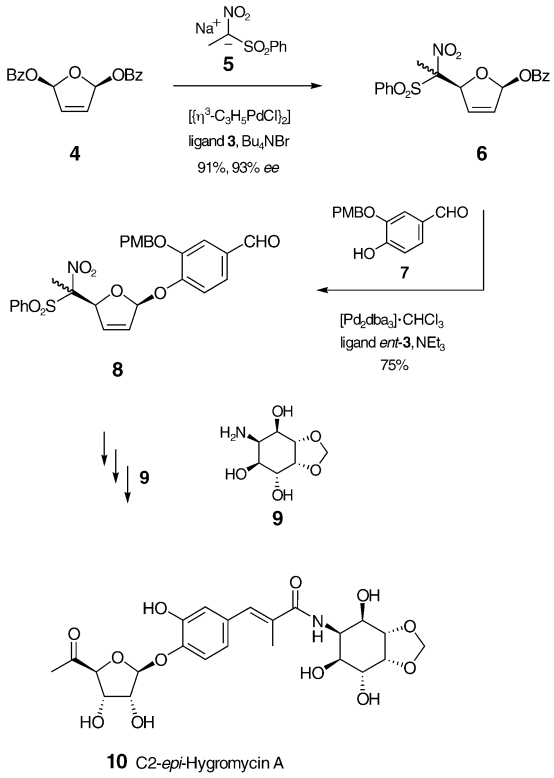
In a synthesis of *epi*-hygromycin A (Scheme 2) Trost et al. made use of four Pd-catalyzed allylic-substitution reactions employing versatile diphosphane bisamide ligands of type **3** in all cases.[5]



3

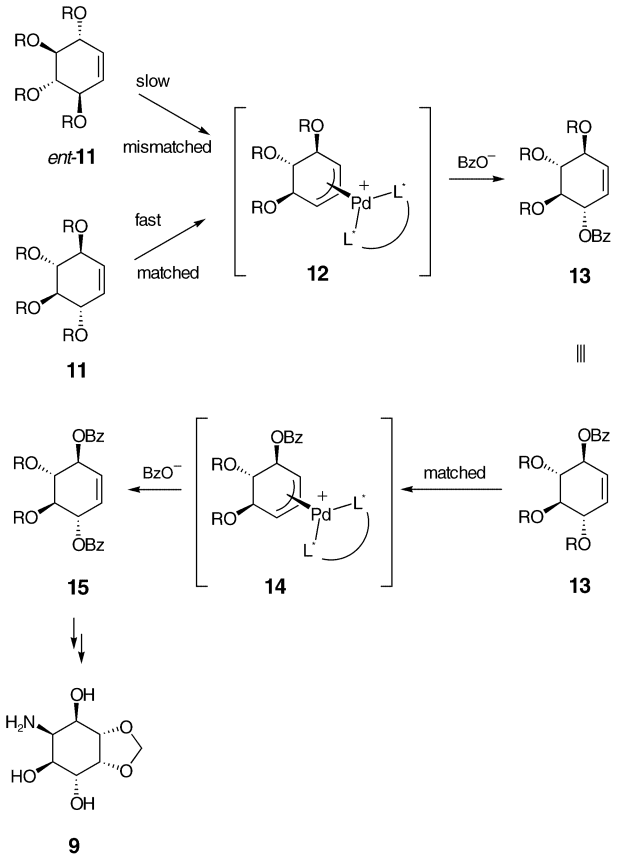
As a result of a larger bite angle of the phosphane groups, these ligands are believed to envelop the allylic system. The reaction of the *meso*-dihydrofuran **4** with the nucleophile **5** as an acyl anion equivalent afforded the monosubstitution product **6** in excellent yield and enantioselectivity (93% *ee*). The second allylic substitution was carried out with the ligand *ent*-**3**. Although a chiral ligand is not necessary in this case, a higher reactivity was observed. Moreover, the phenolic glycoside **10** was formed with perfect *cis* diastereoselectivity, in contrast to a previous synthesis in which the glycosylation step led to an anomeric mixture. The subsequent steps in the synthesis of **10** involved dihydroxylation of the double bond, Horner–Wadsworth–Emmons olefination, and attachment of the aminocyclitol moiety **9**.

The synthesis of the aminocyclitol building block **9** (Scheme 3) started from the readily available racemic conduritol tetraester *rac*-**11**. In a remarkable twofold asymmetric allylic substitution process, both enantiomers were converted into the same bisbenzoate **15** by employing the chiral ligand **3**.[5b] The ionization of the tetraesters **11** and *ent*-**11** proceeded with different reaction



10 C2-*epi*-Hygromycin A

Scheme 2. Synthesis of *epi*-hygromycin A by Trost and co-workers. PMB = *para*-methoxybenzyl, dba = *trans*,*trans*-dibenzylideneacetone.



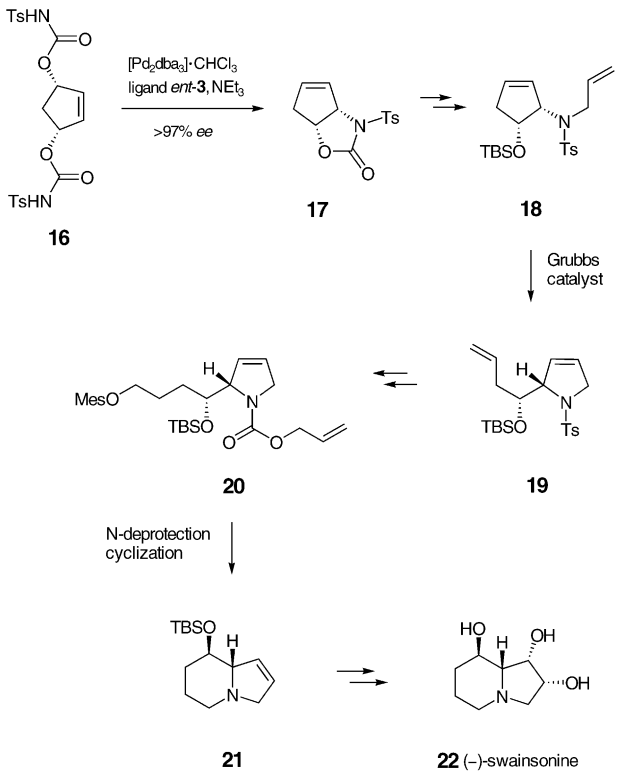
Scheme 3. Synthesis of aminocyclitol **9** by a twofold allylic substitution/deracemization strategy. Bz = benzoyl.

 © 2003 Wiley-VCH Verlag GmbH & Co. KGaA, Weinheim

rates, representing matched and mismatched cases, respectively. With the tetraacetate *rac*-**11** (R = Ac) a nearly perfect kinetic resolution was observed and only 50 % (i.e. the enantiomer **11**) of the starting material was converted. When the leaving group was changed from an acetate to a more reactive alkyl carbonate, both enantiomers were rapidly converted into complex **12**. Attack of the benzoate nucleophile led initially to the enantiomerically pure monosubstitution product **13** ($R = CO_2CH_2CCl_3$), which still bears an allylic leaving group (with the same configuration as in the matched substrate **11**). A second substitution then gave rise to conduritol tetraester **15** (> 99 % *ee*). Reductive cleavage of the carbonate groups R and desymmetrization by derivatization of one of the homotopic hydroxy groups was followed by five further steps to yield the required aminocyclitol derivative **9**.

Notably, the straightforward strategy used for the synthesis of the glycoside part of *epi*-hygromycin A was not based on a sugar-derived starting material from the chiral pool. Instead, the *meso* compound **4** was used, which is not suited for common enzymatic desymmetrization methods.

AAA reactions also provide easy access to chiral nitrogen-substituted cyclopentene derivatives, which may serve as building blocks for the synthesis of alkaloids, as demonstrated by Blechert and co-workers. In a recent synthesis of (−)-swainsonine (**22**, Scheme 4) the key intermediate **17** was prepared by an intramolecular substitution of one of the enantiotopic carbamate groups of **16**.[6a] As demonstrated earlier, ligand **3** gives excellent *ee* in this transformation if NEt_3 is used as a base.[6b] The cyclization product **17** already contains the two vicinal stereocenters found in (−)-swainsonine (**22**). Upon treatment of the allyltosylamide **18** with the Grubbs catalyst under an atmosphere of ethylene, a remarkable ring-opening/ring-closing-metathesis cascade took place. In the reaction, the oxygen-bearing stereocenter was transferred to the side chain of the newly formed dihydropyrrole **19**. Only a few more steps were required to set up the indolizidine framework, and the synthesis was completed by dihydroxylation and deprotection.

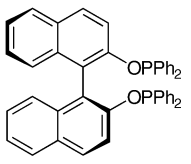


16 17 18 19 20 21 **22** (–)-swainsonine

Scheme 4. Synthesis of (−)-swainsonine by Blechert and co-workers. TBS = *tert*-butyldimethylsilyl, Ts = *para*-toluenesulfonyl.

In the synthesis of (+)-juvabione (**31**) by Bergner and Helmchen (Scheme 5), two Pd-catalyzed allylic substitutions were used to attach the side chains onto the cyclohexene ring.[7] At first, asymmetric alkylation of cyclohexenylacetate (*rac*-**24**) with lithium dimethyl malonate in the presence of ligand **23** afforded **25** in 91 % yield with 95 % *ee*. After a sequence of Krapcho decarbomethoxylation, saponification, iodolactonization, and dehydrohalogenation, the enantiomerically pure key intermediate **26** was obtained, which was also used in the synthesis of (−)-wine lactone.[7b] Fully diastereoselective α-methylation afforded the lactone **27** in which the C=C bond is favorably positioned for a second allylic substitution. The 2-acyloxymalonate **28** was used as a formyl anion equivalent in the second Pd-catalyzed allylation, which proceeded with complete regio- and diastereoselectivity to give **29**. The final part of the synthesis was initiated by reduction and glycol cleavage to liberate the masked carboxy group. This was followed by methylation and isomerization of the double bond to yield **30**, which was finally converted into (+)-juvabione (**31**) in three steps.

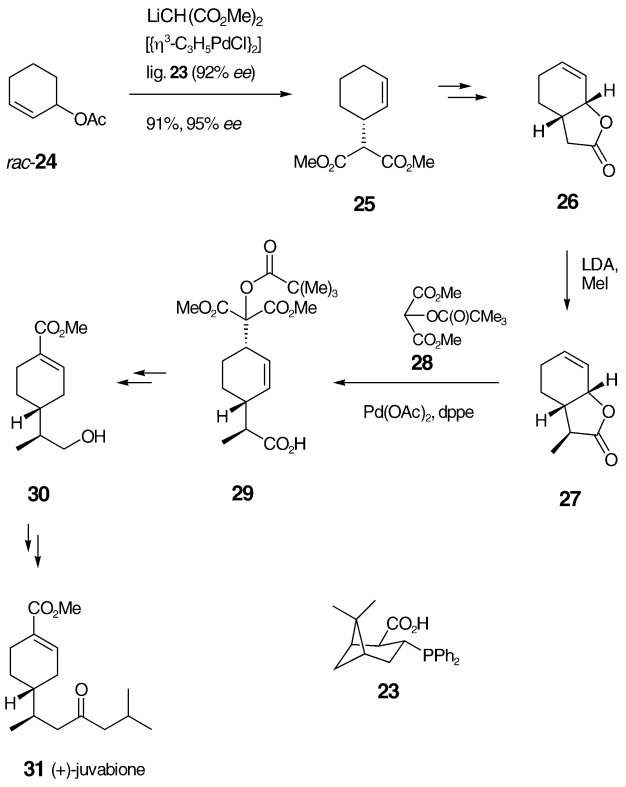
Recently it was demonstrated by Mori et al. that the use of *N*-sulfonated *ortho*-bromoaniline as a nucleophile in an AAA process of type **B** paves the way for a simple assembly of optically active indolines by means of a Heck cyclization. On this basis, a new strategy for the synthesis of *Strychnos* alkaloids was devised and demonstrated in the synthesis of (−)-dehydrotubifoline (**42**) and (−)-tubifoline (Scheme 6).[8] In the first step, the Pd-catalyzed reaction of the cyclohexene *rac*-**34** with the anilide **33** in the presence of (*S*)-binapo (**32**) as a



32

chiral ligand yielded the building block **35** in 84 % *ee*. After recrystallization enantiomerically pure **35** was obtained. A nitrile group was introduced and Heck cyclization of **36** gave rise to the

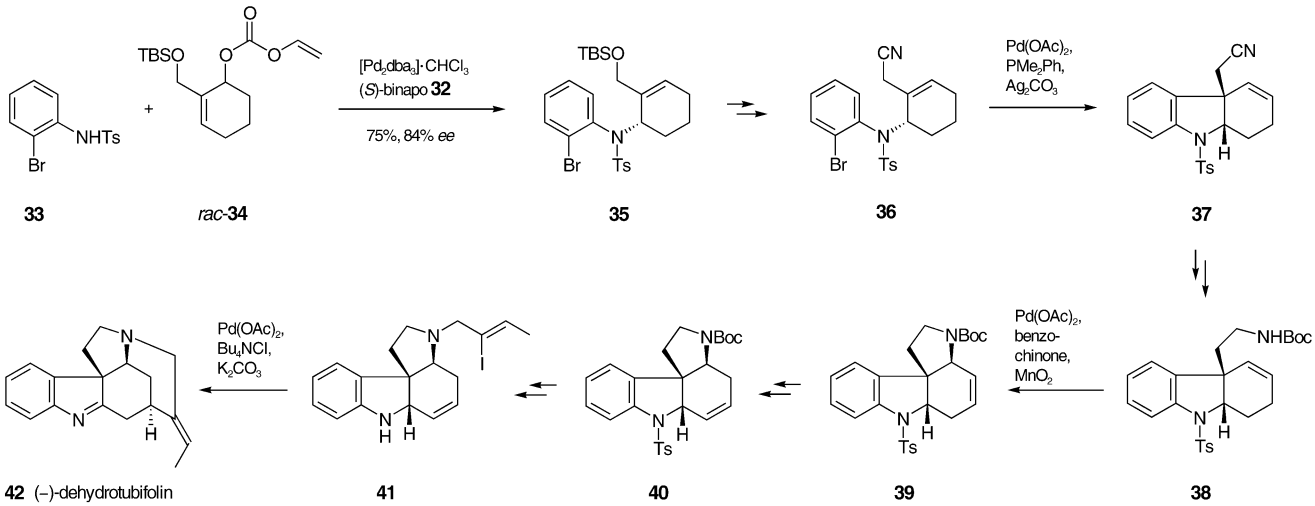
 © 2003 Wiley-VCH Verlag GmbH & Co. KGaA, Weinheim



Scheme 5. Synthesis of (+)-juvabione by Helmchen and Bergner. dppe = 1,2-Bis(diphenylphosphanyl)ethane.

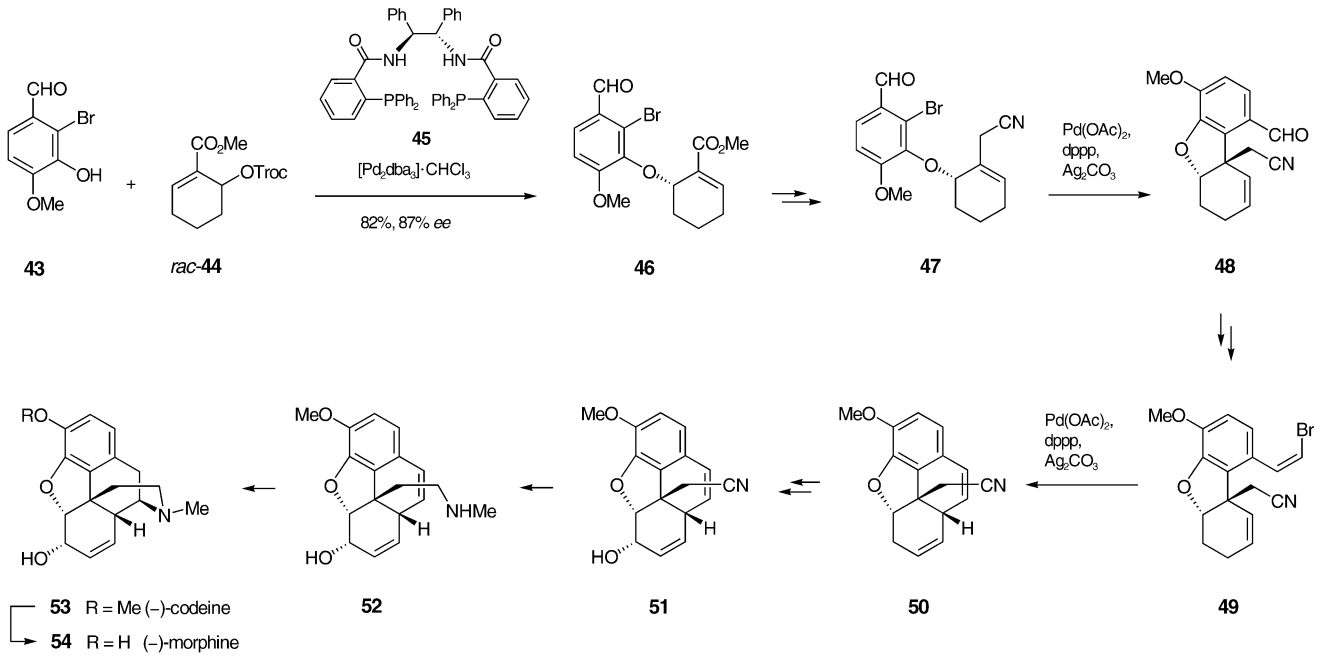
annulated indoline **37**, in which the crucial quaternary stereocenter had been installed. This delivered the cyclohexene double bond in the correct position for the cyclization of **38** to **39** through Pd-mediated allylic oxidation. The double bond was shifted further by one position in a four-step sequence to set the stage for the final Heck cyclization. After removal of the *N*-protecting groups and alkylation of the more reactive pyrrolidine nitrogen atom with a iododalkene C_4-unit (→**41**), a Heck reaction directly afforded the target compound **42**. The synthesis is characterized by the fact that all cyclizations are performed in a fully diastereoselective manner using Pd-catalyzed reactions and that the absolute stereochemical information was established in the initial AAA reaction.

In a spectacular synthesis of (−)-codeine (**53**) and (−)-morphine (**54**, Scheme 7) Trost and Tang followed a related general strategy for the stereocontrolled construction of a complex cyclic framework around a cyclohexane ring.[9] Asymmetric allylic substitution of *rac*-**44** with the functionalized phenol **43** afforded the key intermediate **46** (87% *ee*). The enantiomeric purity was enhanced to 96% *ee* by recrystallization at the stage of the homologous nitrile **47**. In an intramolecular Heck reaction, the second (quaternary) stereocenter was established with complete diastereoselectivity. The product **48** also served as an intermediate in the total synthesis of (−)-galanthamine.[9b] For the synthesis of morphine, the common intermediate **48** was first converted into the bromoalkene (*Z*)-**49** before a second Heck cyclization was used to build up the phenanthrene scaffold with a correctly placed double bond. Allylic oxidation of **50** (SeO_2, then Dess–Martin periodinane reagent) followed by diastereoselective reduction with DIBAH (diisobutylaluminum hydride) gave the alcohol **51**, which was then converted into the secondary amine **52**. The final cyclization by means of a photochemically induced intramolecular hydroamination yielded (−)-codeine (**53**, R = Me), from which (−)-morphine (**54**, R = H) was prepared by a known protocol. A noteworthy feature of this latest synthesis of



Scheme 6. Synthesis of (−)-dehydrotubifoline by Mori et al. following an AAA/Heck cyclization strategy. Boc = *tert*-butyloxycarbonyl.

 © 2003 Wiley-VCH Verlag GmbH & Co. KGaA, Weinheim



Scheme 7. Synthesis of (−)-morphine by Trost and Tang. Troc = 2,2,2,-trichloroethoxycarbonyl, dppp = bis(diphenylphosphanyl)propane.

the prominent target molecule morphine is the masterly use of the double bond in the pivotal cyclohexene ring to serve as a platform for three successive Pd-catalyzed transformations.[10]

The few selected examples discussed herein show only a facet of the synthetic scope of asymmetric allylic substitution. Besides the manifold options for further transformation of the double bond of the AAA reaction products, the true synthetic power arises from the variety of functionalized building blocks that can be enantioselectively joined in a convergent manner.

[1] For recent reviews, see: a) B. M. Trost, C. Lee in *Catalytic Asymmetric Synthesis*, 2nd ed. (Ed.: I. Ojima), Wiley-VCH, New York, **2000**, pp. 593–649; b) A. Pfaltz, M. Lautens in *Comprehensive Asymmetric Catalysis* (Ed.: E. N. Jacobsen, A. Pfaltz, H. Yamamoto), Springer, Heidelberg, **1999**, pp. 833–886; c) B. M. Trost, D. L. Van Vranken, *Chem. Rev.* **1996**, *96*, 395; d) G. Helmchen, *J. Organomet. Chem.* **1999**, *576*, 203.

[2] B. M. Trost, T. J. Dietsche, *J. Am. Chem. Soc.* **1973**, *95*, 8200.

[3] a) T. Hayashi, *Pure Appl. Chem.* **1988**, *60*, 7; b) C. G. Frost, J. M. J. Williams, *Tetrahedron Lett.* **1993**, *34*, 2015; c) P. von Matt, A. Pfaltz, *Angew. Chem.* **1993**, *105*, 614; *Angew. Chem. Int. Ed. Engl.* **1993**, *32*, 566; d) J. Sprinz, G. Helmchen, *Tetrahedron Lett.* **1993**, *34*, 1769; e) B. M. Trost, *Acc. Chem. Res.* **1996**, *29*, 355.

[4] For synthetic applications of AAA reactions, see: B. M. Trost, *Chem. Pharm. Bull.* **2002**, *50*, 1.

[5] a) B. M. Trost, O. Dirat, J. Dudash, Jr., E. J. Hembre, *Angew. Chem.* **2001**, *113*, 3770; *Angew. Chem. Int. Ed.* **2001**, *40*, 3658; b) B. M. Trost, J. Dudash, Jr., E. J. Hembre, *Chem. Eur. J.* **2001**, *7*, 1619.

[6] a) N. Buschmann, A. Rückert, S. Blechert, *J. Org. Chem.* **2002**, *67*, 4325; b) B. M. Trost, D. E. Patterson, *J. Org. Chem.* **1998**, *63*, 1339.

[7] a) E. J. Bergner, G. Helmchen, *J. Org. Chem.* **2000**, *65*, 5072; b) E. J. Bergner, G. Helmchen, *Eur. J. Org. Chem.* **2000**, 419.

[8] a) M. Mori, M. Nakanishi, D. Kajishima, Y. Sato, *Org. Lett.* **2001**, *3*, 1913; b) for a related strategy, see: H. Yoshizaki, H. Satoh, Y. Sato, S. Nukui, M. Shibasaki, M. Mori, *J. Org. Chem.* **1995**, *60*, 2016.

[9] a) B. M. Trost, W. Tang, *J. Am. Chem. Soc.* **2002**, *124*, 14542; b) B. M. Trost, W. Tang, *Angew. Chem.* **2002**, *114*, 2919; *Angew. Chem. Int. Ed.* **2002**, *41*, 2795.

[10] For recent reviews on morphine syntheses, see: a) B. H. Novak, T. Hudlicky, J. W. Reed, J. Mulzer, D. Trauner, *Curr. Org. Chem.* **2000**, *4*, 343; b) P. R. Blakemore, J. D. White, *Chem. Commun.* **2002**, 1159.

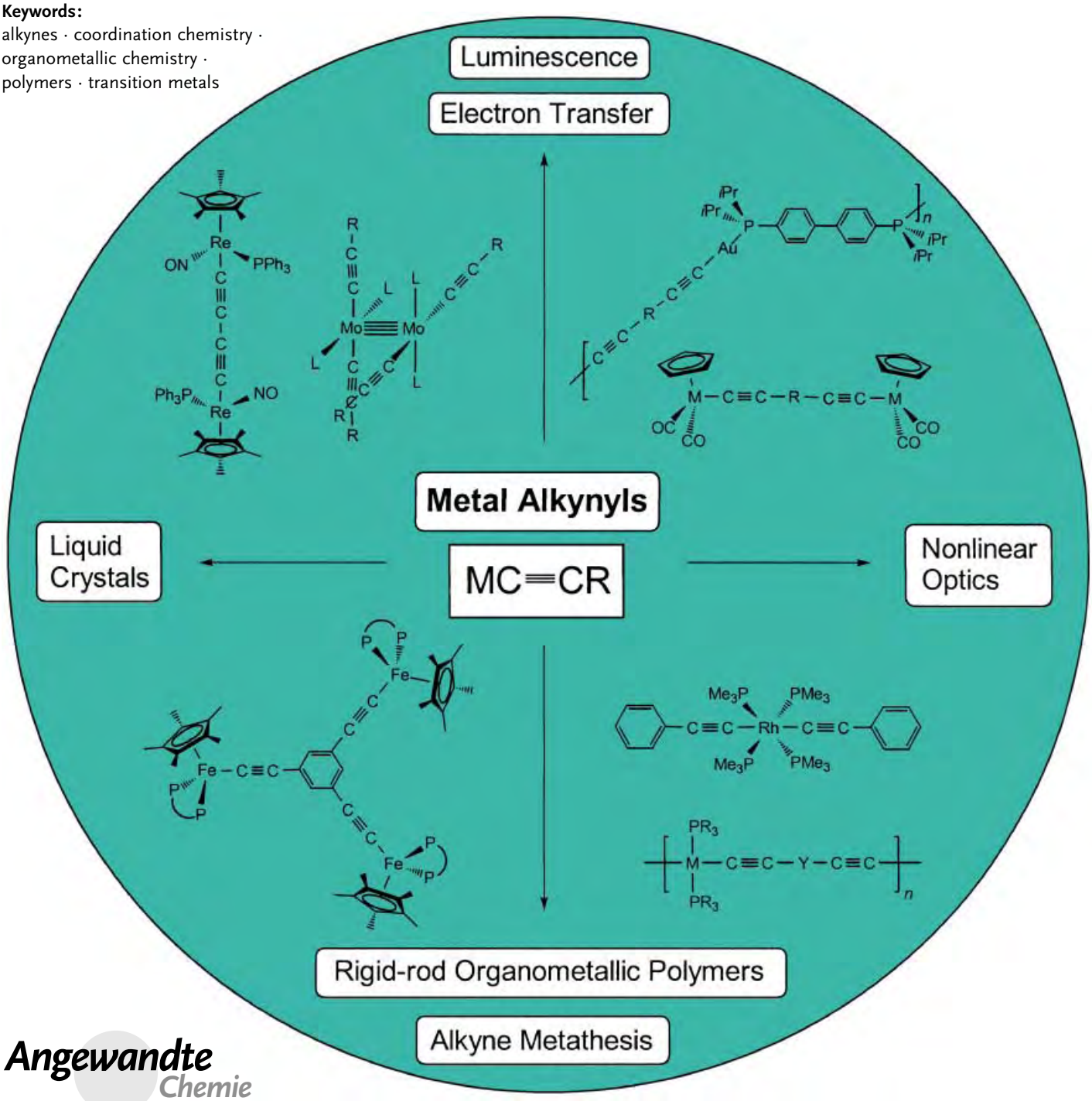
 © 2003 Wiley-VCH Verlag GmbH & Co. KGaA, Weinheim

Transition-Metal Alkyne Complexes

Metal Alkynyl σ Complexes: Synthesis and Materials

Nicholas J. Long and Charlotte K. Williams*

Keywords:
alkynes · coordination chemistry · organometallic chemistry · polymers · transition metals



 © 2003 Wiley-VCH Verlag GmbH & Co. KGaA, Weinheim DOI: 10.1002/anie.200200537

Metal alkynyl complexes hold a fascination for synthetic chemists, structural chemists, and materials scientists alike. Harnessing the unique overlap of metal and carbon orbitals is a challenge that can be overcome in many ways and hence, there are many synthetic routes toward M−C≡C− bond-forming reactions that utilize a wide variety of transition-metal and alkynyl reagents. Some methods can be widely applied, while others are specific to a particular metal or compound. The linear geometry of the alkynyl unit and its π-unsaturated character have led to metal alkynyls becoming attractive building blocks for molecular wires and polymeric organometallic materials, which can possess interesting properties, such as optical nonlinearity, luminescence, liquid crystallinity, and electrical conductivity. A unique, multifaceted approach, often combining talents from all three of the above chemical disciplines, has served as a driving force behind the intense research into the development of metal alkynyl σ complexes, the progress of which, particularly in the last ten years, is summarized in this review.

From the Contents

1. Introduction	2587
2. Bonding in Metal Alkynyl Complexes	2588
3. Classical Routes to Metal Alkynyl Complexes	2588
4. Metal Alkynyl Complexes: Ni, Pd, Pt	2589
5. Metal Alkynyl Complexes: Co, Rh, Ir	2594
6. Metal Alkynyl Complexes: Fe, Ru, Os	2596
7. Metal Alkynyl Complexes: Mn, Re	2602
8. Metal Alkynyl Complexes: Cr, Mo, W	2603
9. Metal Alkynyl Complexes: Cu, Ag, Au	2604
10. Other Metal Alkynyl Complexes	2607
11. Summary and Outlook	2612

1. Introduction

The study of transition-metal alkynyl σ complexes has, since the mid-1980's, been an intense area of research, which encompasses complexes with just one alkynyl group bound to the metal, through to polymers that contain as many as 10000 M−C≡C− linkages in the polymeric chain. In 1982, Nast[1] published a review on the coordination chemistry of metal alkynyl complexes based on approximately 200 papers. There are now in excess of 20000 papers that deal, in some way, with metal alkynyl species. The scope of the research is broad, and covers not only those areas that are of "traditional" interest to organometallic chemists, but also reflects the interest in utilizing these species in materials science. All carbon-rich systems are well-known,[2,3] and the interest in metal-containing conjugated polymers has grown rapidly due to their technological potential.[4–12] The introduction of a metal center or a metallocene unit into the conjugated polymeric chain may introduce a range of properties (that is, redox, magnetic, optical, and electronic properties) that differ from those of conventional organic polymers. The normally polymeric or, at least, oligomeric "rigid-rod" alkynyl species have particularly promising electronic and structural properties, which include nonlinear optical effects,[13–16] luminescence and photoconductivity,[17–22] electronic communication ("molecular wires"),[23] and liquid crystallinity.[24] Such promise is mainly a result of their linear structure, high stability, and π-electron conjugation. The C≡C bonds also constitute a focus for reactivity studies; in particular, there has been intense studies regarding: 1) The formation of cluster compounds,[25–30] in which the alkynyl ligand bridges multiple metal centers,[30,31] 2) reactions where the ligand is transformed into a vinylidene, allenylidene, or cummulenylidene[32–35] and 3) the coupling and cleavage reactions with early transition-metal centers.[36–38]

The synthesis and chemistry of metal alkynyls is a very topical and diverse area of interest and we have necessarily had to be selective in our coverage by concentrating on literature from the past ten years. A periodic-group approach toward the various metal complexes and syntheses has been adopted, which highlights the generalities of many of the synthetic methods. Through the combination of σ (η^1) and/or π (η^2) bonding there are many coordination modes available to alkynes, but we have chosen to focus on the various modern M−C≡C− σ-bond forming reactions, which are relevant not only for simple monomeric metal alkynyls but also for their increasingly important polymeric analogues.

Along with synthetic methods, the properties of metal alkynyls and their application in materials science is also reviewed herein; the majority of the applied examples currently known feature σ-bonded species, usually with linear geometry. There will not be an in-depth discussion on

[*] Dr. N. J. Long, Dr. C. K. Williams
Department of Chemistry
Imperial College of Science, Technology and Medicine
South Kensington, London, SW7 2AY (UK)
Fax: (+44) 207–594–5804
E-mail: n.long@ic.ac.uk

 DOI: 10.1002/anie.200200537 © 2003 Wiley-VCH Verlag GmbH & Co. KGaA, Weinheim

π-donating (η^2) interactions, which is a rapidly expanding area in its own right, but where materials applications of such species remain unexplored to date.

Many other excellent review articles listed here feature metal alkynyl complexes in some way, but as far as we are aware, this is the first article to review solely the synthesis of transition-metal alkynyl complexes, their structural diversity, and their application in materials science.

2. Bonding in Metal Alkynyl Complexes

Transition-metal alkynyl complexes can be regarded as complexes of the $HC{\equiv}C^-$ ligand, which is isoelectronic with CN^-, CO, and N_2. The stoichiometry, color, and magnetic properties of these complexes are closely related to the corresponding cyanide complexes, and the alkynyl ligand can also be thought of as a pseudohalide because of its behavior in complex formation and precipitation reactions. Thus, the chemistry of transition-metal alkynyl complexes often falls into the category of classical coordination chemistry, rather than organometallic chemistry.[1]

There is a simple frontier-orbital relationship between alkynyl and cyanide ligands, and from wide-ranging spectroscopic and magnetic studies, the two ligands are shown to occupy similar "strong-field" positions in the spectrochemical series. Thus, alkynyl ligands can be interpreted as being good σ and π donors and poor π acceptors, compared to other ligands within the series. In 1995, Manna, John, and Hopkins[39] produced an excellent review of the bonding in metal alkynyl complexes, based on molecular-orbital calculations, photoelectron and electronic spectroscopy, X-ray crystallographic studies, and vibrational spectroscopic results. Photoelectron spectroscopy and calculations indicate significant overlap between the filled metal d orbitals and the filled π system of the alkynyl moiety. The energy difference between the HOMO metal d orbitals and the LUMO π* alkynyl orbitals appears to be too large (ca. 15 eV) for π-accepting behavior,[39] unless there are strong π-acceptor substituents in conjugation with the alkynyl unit.

Extended Hückel band calculations and photoelectron spectroscopic measurements[40–42] on metal polyyne systems $[L_nM{-}C{\equiv}C{-}R{-}C{\equiv}C{-}]_n$ show that the highest occupied crystal orbital (HOCO) has predominantly metal d orbital character and is delocalized along the entire chain through the ML_n groups ($n = 2$, square planar; $n = 4$, octahedral). Extension of the conjugation length of the alkyne spacer group is suggested to lower the optical band gap by lowering the energy of the lowest unoccupied crystal orbital (LUCO; predominantly alkynyl π* character). The metal can also have a significant influence, with four-coordinate d^8 square-planar metal centers favored over six-coordinate d^6 octahedral units, because of the greater conduction bandwidth of the former (ca. 0.4 eV).[40]

3. Classical Routes to Metal Alkynyl Complexes

The conventional synthesis of transition-metal alkynyl σ complexes is achieved either by the reaction of metal halides with anionic alkynylating agents, such alkali-metal,[43] magnesium,[44,45] or copper(I)[44,45] alkynyl compounds, or alternatively by direct dehydrohalogenation[46] in the reaction between metal halides and active alkynes that possess electron-withdrawing substituents.

Until recently, the majority of σ-alkynyl complexes were prepared by the interaction of either an alkali-metal or an alkaline-earth-metal alkynyl complex $RC{\equiv}CM$ (M = Li, Na, Mg, etc.) with a transition-metal halide L_nMX (X = Cl, Br, I), or the neutral alkyne itself with a transition-metal complex. The former is a displacement reaction, in which the alkynyl anion acts as a nucleophile and the metal center as an electrophilic substrate. Both routes feature sensitive reagents and generally give low yields of desired products and a range of by-products.

Organometallic compounds of the alkaline-earth metals are difficult to access because of their enhanced reactivity and decreased kinetic stability, and those that are known are generally linked to species exhibiting metal–π interactions. However, there has been an increase in the studies of σ-alkynyl derivatives, and a family of calcium, strontium, and barium triphenylsilylethynyl derivatives have recently been characterized.[47]



Nick Long, born in Bristol in 1965, obtained a B.Sc. from the University of Durham and a Ph.D. from the University of Exeter in 1989 under the supervision of Prof. Edward Abel and Dr. Tony Osborne. Subsequently he moved to the University of Cambridge to become the "Adrian Research Fellow" and then "Temporary Lecturer in Inorganic Chemistry". In 1995, he moved to Imperial College, London where he was promoted to "Senior Lecturer" in 1999 and "Reader in Inorganic Chemistry" in 2002. Among his areas of interest are multidentate, hemilabile N, S, P-donor ferrocene ligands, substituted phthalocyanines, and aza-macrocycles, and transition metal alkynyl complexes. He has also written a textbook entitled Metallocenes.



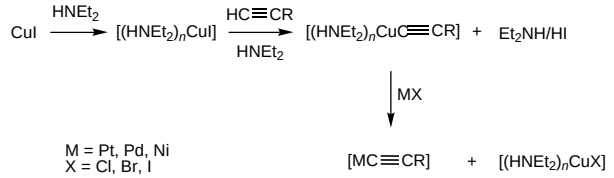
Charlotte Williams, born in Gloucester in 1975, received her B.Sc. in 1998 from Imperial College, London, and went on to complete her Ph.D there in 2001 under the supervision of Dr. Nicholas J. Long and Prof. Vernon C. Gibson with research on novel ferrocenediyl ligands and their potential for catalysis. She is currently a postdoctoral researcher at the University of Minnesota, working in the research groups of Prof. William B. Tolman and Prof. Marc Hillmyer.

 © 2003 Wiley-VCH Verlag GmbH & Co. KGaA, Weinheim

4. Metal Alkynyl Complexes: Ni, Pd, Pt

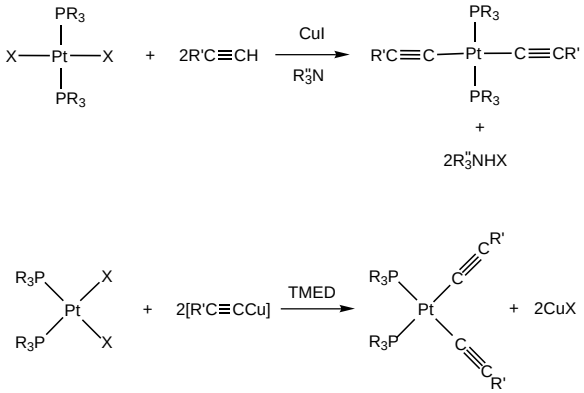
4.1. Copper-Catalyzed Dehydrohalogenation

In 1970, Hagihara and co-workers developed a route to σ-alkynyl derivatives of transition metals by direct dehydrohalogenation through the reaction between Group 10 metal halides and active alkynes with electron-withdrawing substituents.[46] Seven years later, the same group published a novel, more general method that involved copper(I)-catalyzed dehydrohalogenation of metal halides in an amine solvent (Scheme 1). This route, which generally used diethylamine,



Scheme 1. Synthesis of metal alkynes by copper(I)-catalyzed dehydrohalogenation.

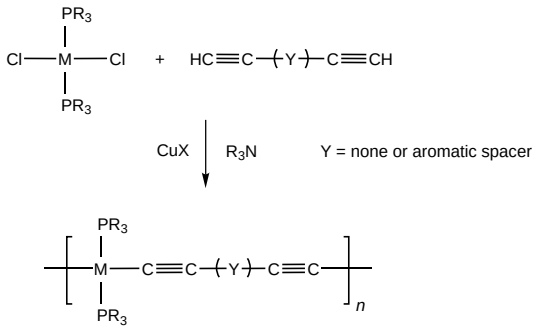
diisopropylamine, or piperidine under reflux, enabled the synthesis of mono- or dialkynyl compounds, with a *trans*-orientation of the ligands around the square-planar metal centers.[48,49] A route to the *cis* derivatives was also developed by using *N*,*N*,*N*′,*N*′-tetramethylethylenediamine (TMED; Scheme 2).[50a]



Scheme 2. Formation of *cis*-dialkynylplatinum complexes.

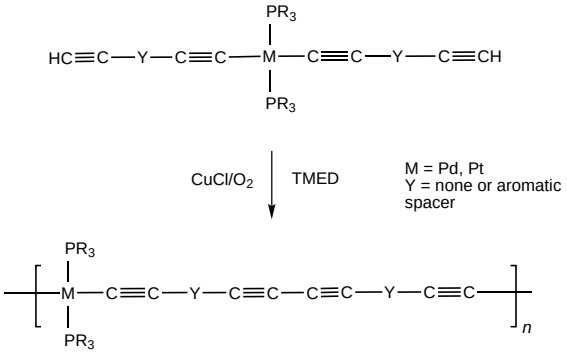
The preparation of compounds with terminal alkynyl protons requires a large amount of alkyne to prevent further reactions that give oligomers or polymers. Slow isomerization between the *cis* and *trans* forms was observed for solutions in amines under reflux, with cuprous halides accelerating the isomerization process. The less stable *cis* isomers can be obtained at lower temperatures and should be stored below −20 °C to avoid decomposition. The first polymers to be prepared by this route were reported in 1975,[50b] and despite being of only low molecular weight, they were soluble as a result of using solubilizing P*n*Bu$_3$ groups bound to Pt and Pd. These groups enhance interactions between the solvent and polymer-chain segments and decrease intramolecular interactions between the polymer chains. Accordingly, the solubility decreases in the order R = *n*Bu > Et > Me. The pioneering work of the Hagihara research group[4,50] has led to the preparation of many rigid-rod σ-bonded alkynyl polymers with molecular weights (M_w) greater than 10^6. Three general copper-catalyzed methods can be utilized:

- Dehydrohalogenation: In this process a cuprous halide acts as a catalyst in the dehydrohalogenation reaction between diterminal alkynes and transition-metal halides. An amine acts as both an acid acceptor and as the solvent, and polymerization proceeds smoothly at room temperature or under reflux (Scheme 3).[51,52]



Scheme 3. Formation of rigid-rod σ-alkynyl polymers by copper-catalyzed dehydrohalogenation.

- Oxidative coupling: In this method, a catalytic amount of a cuprous halide and O_2 (which is employed in organic synthesis in Hay's coupling reaction[53]) is used to couple species with two terminal alkynyl groups (Scheme 4).[54] This is a useful preparative route as there is no stoichiometric restriction on a reactant bearing identified functional groups, and the degree of polymerization is normally high. In dehydrohalogenation reactions, the degree of polymerization depends on the exact ratio of the reacting monomers. In general, both methods work extremely well for Pt (M_w of ca. 100000), less well for Pd (M_w of ca. 20000), but not at all for Ni, as a result of the

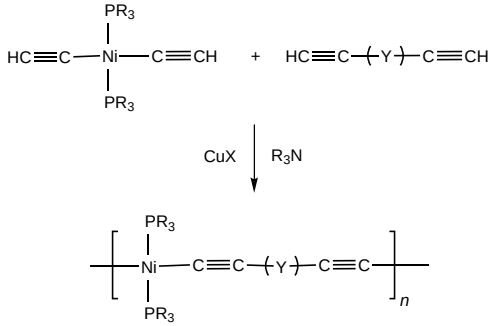


Scheme 4. Homocoupling of di(terminal) alkynes by Hay's coupling reaction.

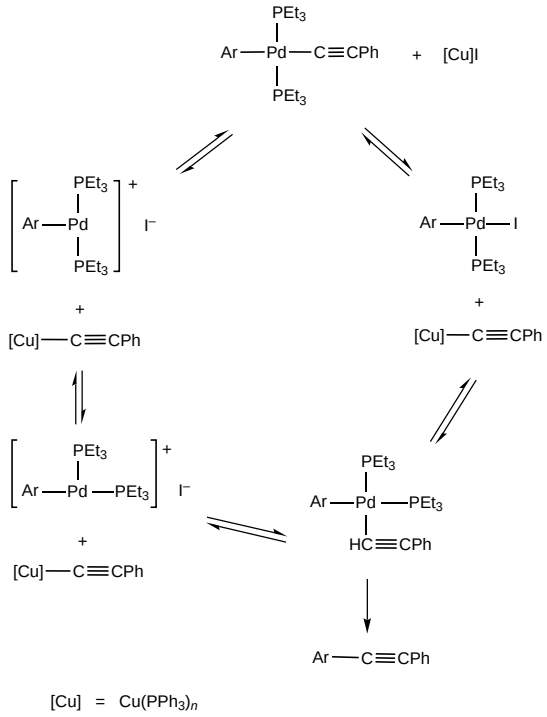
 © 2003 Wiley-VCH Verlag GmbH & Co. KGaA, Weinheim

decomposition of dihalonickel complexes in amine solvents and/or reaction of the nickel centers with the oxidative-coupling reagent.

- Alkynyl-ligand exchange: The third copper-catalyzed route involves an alkynyl-ligand exchange process in amine solvents and is utilized largely to produce Ni-containing polymers.[55] A small amount of PR_3 is added to prevent decomposition of the polymer, and is essential for suppressing phosphane dissociation from the metal center (Scheme 5).



Scheme 5. Copper-catalyzed alkynyl ligand exchange.



Scheme 6. Mechanism of copper-catalyzed formation of metal alkynes.

These general methods have been widely utilized for several reasons: 1) The degree of polymerization is easily controlled;2) the electronic properties of the polymer can be tailored by the attachment of various end groups (through substitution reactions) and the incorporation of an almost limitless number of terminal alkynes; 3) mixed-metal polymers can be synthesized;4) the distance between metal centers in the polymer chain can be varied according to the preparative method used. Oxidative polymerization yields polymers in which the metal atoms are separated by approximately twice the distance of those formed by dehydrohalogenation reactions.

4.1.1. ***Mechanism***

Yamamoto et al. have studied the mechanism of the reactions of Group-10-metal alkynyl complexes in detail. They reported that migration of the alkynyl ligand from a Cu alkynyl complex to a Pd center appears to be reversible, and that the equilibrium can result in a mixture of products.[56] Two possible mechanisms are proposed to explain the formation of a coupling product; the first involves the CuI-induced removal of a PEt_3 ligand from a Pd complex, which induces dissociative reductive elimination of the aryl and alkynyl ligands from $[Pd(Ar)(C{\equiv}CPh)(PEt_3)]$. The other mechanism is shown in Scheme 6, and suggests that alkynyl-ligand transfer between Pd and Cu gives a mixture of *trans*- and *cis*-$[PdAr(C{\equiv}CPh)(PEt_3)_2]$; the *cis* complex seems to undergo rapid reductive elimination. There is no such equilibrium for Pt alkynyl complexes and no coupling products are observed because of the high stability of the complexes. The highly stable Pt–C bond is attributed to significant back-donation from the alkynyl group to the Pt center.

Intermolecular alkynyl-ligand transfer in Pd^{II} and Pt^{II} complexes has been thoroughly investigated.[57] Alkynyl-ligand transfer between dialkynyl complexes and diiodo species of Pd and Pt is observed, which leads to comproportionation of the Pd complexes or ligand transfer from Pd to Pt depending on the nature of the alkynyl group and the reaction conditions. It is evident that the metal center, the substituent on the alkynyl ligand, and the catalyst used are all crucial in these ligand-transfer reactions.

4.1.2. ***Limitations***

The main limitation of these routes is the use of amines as solvents. Many complexes of transition metals that are not in Group 10 are either insoluble in amines or, if soluble, decompose readily in such a harsh solvent.

4.1.3. ***Polymer Properties***

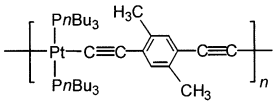
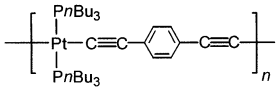
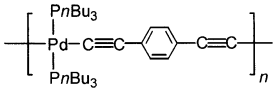
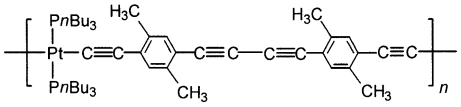
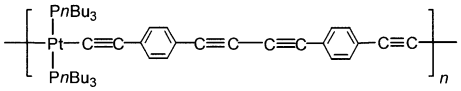
As stated previously, alkynyl polymers are one of the most studied types of organometallic polymers,[5,6,10,11] largely as a result of the synthetic versatility of the reaction, but also because of the unique properties of the polymer products. Such polymers, which contain highly polarizable transition-metal units and have a degree of π-conjugation along the rigid-rod polymer backbone, have been shown to possess varying degrees of third-order nonlinear optical (NLO) susceptibility, liquid-crystalline properties, and electrooptic behavior.

 © 2003 Wiley-VCH Verlag GmbH & Co. KGaA, Weinheim

4.1.3.1. Nonlinear Optical Properties

Polymeric materials with extended π conjugation are known to have an important role in third-order nonlinear optics, and an enhancement of the effective conjugation through increasing the π-delocalization length has been recognized as a way of achieving large third-order optical nonlinearities.[58,59] Organometallic systems have shown promise in this area[13–15] and indeed, the platinum polyynes discussed here, exhibit large hyperpolarizabilities γ that are comparable to inorganic semiconductors such as InSb (1700×10^{-36} esu) and Ge (1300×10^{-36} esu),[60–62] and higher than those of their purely organic counterparts. Table 1 lists the γ values for some metal polyynes, which exemplifies that type of metal, arene spacer, and length of conjugation are all important.

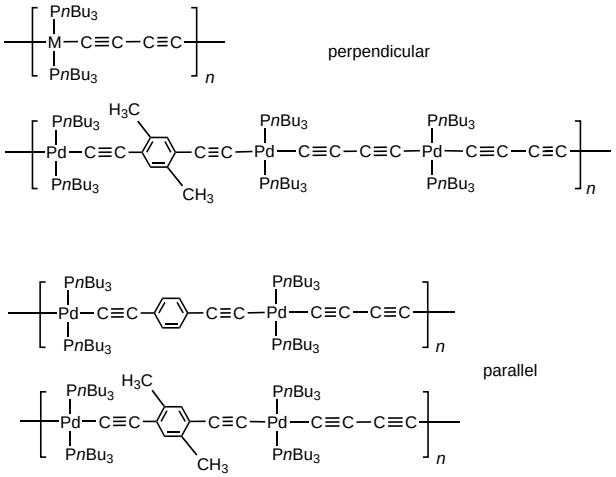
Table 1: The third-order nonlinear optical hyperpolarizabilities of some metal polyynes.

Compound	γ [$\times 10^{-35}$ esu]
	56
	102
	390
	181
	856

Some recent second- and third-order NLO measurements have been carried out on a series of "push-pull" symmetrical and unsymmetrical Pt^{II} bisalkynyl complexes.[63] The inclusion of ferrocenyl (push) and nitro (pull) groups has led to promising second-harmonic generation (SHG) effects, whilst pull-pull (acceptor groups at either side) or push-push substituents modify the delocalization of π electrons associated with the central Pt atom, and can therefore tune the third-order NLO properties.

4.1.3.2 Liquid-Crystalline Properties

Metal polyynes represent the first examples of lyotropic liquid-crystalline materials that involve transition metals. Following studies on other rigid-rod polymers such as polyamides and polyisocyanates,[64] it may be expected that concentrated solutions of the Pt and Pd polymers would form nematic liquid crystals in trichloroethene.[65–67] NMR studies using a rotating probe suggested that the main chain of the polymer could be orientated in a direction perpendicular or parallel to the applied magnetic field.[68,69] Polymers with diethynyl aromatic bridges were aligned parallel to the field whilst those composed of only dialkynyl units were arranged perpendicular to it, probably as a result of to the negative magnetic anisotropy of the C≡C bonds (Scheme 7).[69]



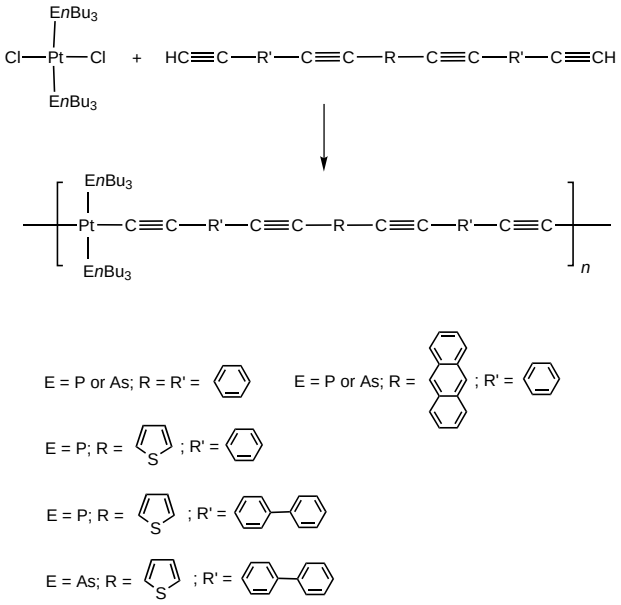
Scheme 7. Liquid-crystalline palladium polyynes.

4.1.3.3. Optical Spectroscopy and Band-Gap Studies

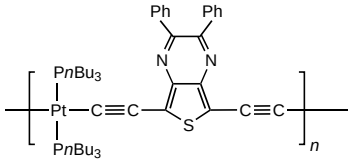
Optical absorption, photoluminescence spectroscopic studies, and Extended Hückel calculations have shown that metal polyynes possess a delocalized polymer backbone, where the electronic structure can be modified by the nature of the transition metal, the coligands, and the aromatic spacer.[18,19,70–73] By utilizing an adaptation of the dehydrohalogenation route developed by Hagihara et al., a series of platinum polyynes were prepared with a variety of aromatic spacer groups (Scheme 8). The polymers exhibit strong metal-to-ligand charge-transfer (MLCT) absorptions and the platinum polyynes have a much smaller band gap (the lowest-energy HOMO–LUMO transition in the polymer) than the analogous dialkynyl monomers. This behavior is indicative of increasing π-conjugation along the polymer, as exemplified by the trialkynyl-bridged polymer, which exhibits a lower optical band gap than the dialkynyl analogue (3.12 versus 3.23 eV).

With band gaps of approximately 3 eV, the polymers can be classified as wide-band-gap semiconductors or insulators in their undoped state, and compare unfavorably with some conjugated organic polymers (< 1 eV).[74] Recently however, a platinum polyyne has been formed with a band gap of 1.77 eV: The concept of alternating electron-donor (*n*-butylphosphane-substituted platinum(II) alkynyl) and acceptor (electron-deficient thieno [3,4-*b*]pyrazine) units was used to obtain a soluble deep-blue polymer, which was formed in 43% yield through Cu-catalyzed dehydrohalogenation routes in diisopropylamine (Scheme 9).[17] Other spacer groups recently utilized in platinum(II) alkynyl species include electron-rich ferrocenylfluorene (2.1 ev),[75] the donor–accep-

 © 2003 Wiley-VCH Verlag GmbH & Co. KGaA, Weinheim

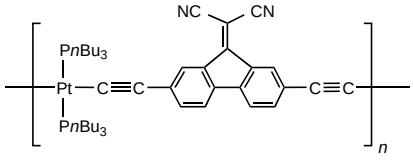


Scheme 8. Synthesis of some platinum polyynes with different aromatic spacer groups.



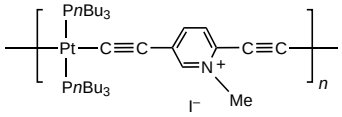
Scheme 9. A low band-gap platinum polyyne with donor and acceptor units.

tor bithiazolediyl unit (2.35 eV),[76] pyridyl units,[77] 9-acridone and dansyl (5-(dimethylamino)naphthalene-1-sulfonyl) for blue luminescence,[78] porphyrins,[79] and most interestingly, the donor–acceptor 9-dicyanomethylenefluorene-2,7-diyl unit (Scheme 10),[80] with a band gap of 1.58 eV that is currently the lowest reported for a metal polyyne species. The authors suggest that electron-withdrawing groups at the periphery exert a more pronounced influence on narrowing the band gaps of these polymers than electron-donating substituents.



Scheme 10. An example of a compound with a low band-gap with 9-dicyanomethylenefluorene-2,7-diyl as a donor–acceptor spacer.

Similar polymers with diethynylpyridine units have been synthesized,[81,82] and as with all the rigid-rod organometallic polymers, these systems exhibit π–π* transitions at lower energy than the corresponding monomers, which signifies delocalization along the polymer backbone (Scheme 11).



Scheme 11. A platinum polyyne with quaternized pyridine units.

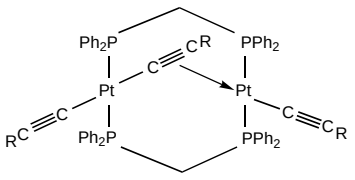
Quaternization of the N atom on the pyridine ring leads to improved electron delocalization and yields a stable polymer with positive charges on the polymer backbone.

4.1.3.4. ***Luminescence***

Detailed surveys of the luminescence of polynuclear metal alkynyl complexes have recently reported[20,21] that the first luminescent platinum(II) complex containing an alkynyl ligand, the dinuclear platinum(II) phenylethynylidene complex $[Pt_2(\mu\text{-}C{=}CHPh)(C{\equiv}CPh)(PEt_3)_3Cl]$, which dates back to 1989, was found to exhibit red-orange luminescence at 77 K.[83]

Site-selective luminescence of mononuclear Pt^{II}-alkynyl complexes[84] has been found in *trans*-$[Pt(C{\equiv}CH)_2(PEt_3)_2]$ and *trans*-$[Pt(C{\equiv}CPh)_2(PEt_3)_2]$, which exhibit an intense vibronically structured emission in rigid glasses at 77 K. The emissive state has $Pt\rightarrow\pi^*(C{\equiv}C)$ MLCT character through excitation into the low-energy MLCT absorption bands. Masai and co-workers[85] have made similar assignments on the mononuclear series *trans*-$[M(C{\equiv}CR)_2L_2]$ (M = Ni, Pt, Pd). The lowest-lying band was assigned as a transition between the $\pi(C{\equiv}CR)$ and $\pi^*(C{\equiv}CR)$ orbitals, with strong charge-transfer character resulting from the mixing of the $\pi^*(C{\equiv}CR)$ and the $(n+1)$ *p* orbitals of the metal center. The polymers $[Pt(C{\equiv}C)_m\text{-}(PnBu_3)_2]_n$ also exhibit vibronically structured emission bands, which originate from π–π* excited states that are localized on alkynyl moieties.[18,19]

The dinuclear platinum(II)alkynyl complexes $[Pt_2(\mu\text{-}dppm)_2(\mu\text{-}C{\equiv}C{-}R)(C{\equiv}C{-}R)_2]^+$ (Scheme 12; R = various aromatic groups, dppm = bis(diphenylphosphanyl)methane), which have "A-frame" structures, show interesting luminescence properties and have been extensively studied by Yam and co-workers.[86,87] The first isolation of a binuclear Pt^{II} A-frame alkynyl complex was reported in 1987,[88] achieved by the reaction of $[Pt(dppm\text{-}P,P')Cl_2]$ with $LiC{\equiv}Ct$Bu in boiling THF. The electron-richness and steric bulk of the *tert*-butyl group was thought to be crucial in the formation of the structure, and for not giving face-to-face dimers of the type $[Pt_2(\mu\text{-}dppm)(C{\equiv}CR)_4]$, which are formed when R = phenyl or tolyl. However, an analogous homobimetallic Pt^{II} A-frame complex with the less bulky and less electron-rich phenyl-



Scheme 12. A dinuclear platinum alkyne unit with an "A-frame" structure. R = *p*-$MeOC_6H_4$, *p*-EtC_6H_4, *p*-$EtOC_6H_4$, Ph, *t*Bu.

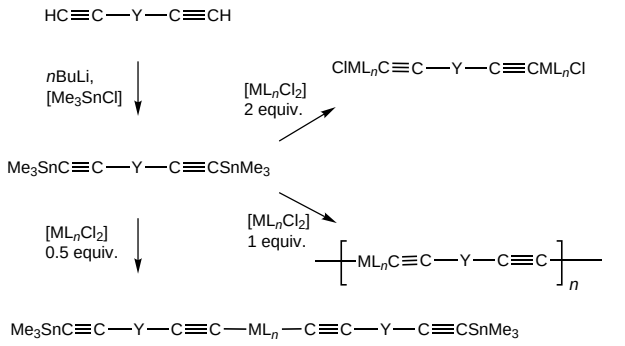
 © 2003 Wiley-VCH Verlag GmbH & Co. KGaA, Weinheim

alkynyl ligand has been synthesized by the deprotonation of phenylalkyne by mercury(II) acetate. The phenylalkynyl mercury complex that is formed is then reacted with $[Pt(dppm)_2Cl_2]$ in refluxing ethanol to yield the A-frame product in reasonable yield.

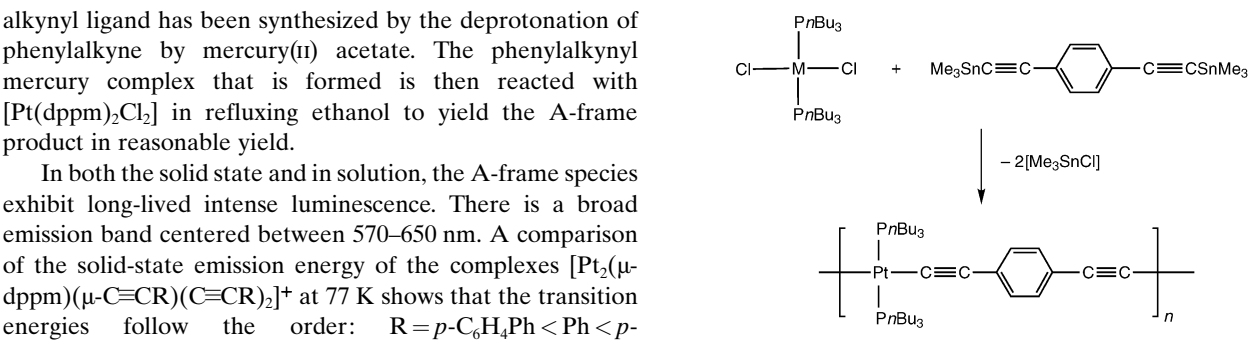
In both the solid state and in solution, the A-frame species exhibit long-lived intense luminescence. There is a broad emission band centered between 570–650 nm. A comparison of the solid-state emission energy of the complexes $[Pt_2(\mu\text{-}dppm)(\mu\text{-}C{\equiv}CR)(C{\equiv}CR)_2]^+$ at 77 K shows that the transition energies follow the order: $R = p\text{-}C_6H_4Ph < Ph < p\text{-}C_6H_4OCH_3 < p\text{-}C_6H_4CH_2CH_3 < p\text{-}C_6H_4OCH_2CH_3 < t$Bu. This trend supports the theory regarding the effect of increasing the π–π* transition energy of the alkynyl ligand and, thus, the involvement of the π*(C≡CR) orbital in the transition.

4.2. Metathesis Reactions Using Trimethylstannyl Reagents

One method that avoids using harsh amine solvents has been developed by Lewis and co-workers. They utilized a metathesis reaction that was first reported by Lappert et al.,[89] which involves trimethyltin reagents and metal halides (primarily chlorides; Scheme 13). Lewis and co-workers have synthesized a variety of monomers, dimers, and polymers by using a number of trimethylstannyl alkynyl ligands in different ratios with metal chlorides, and performing CuI-catalyzed reactions in toluene or chlorinated solvents (Scheme 14).[18,90–92] Although an extra step is required to synthesize the trimethylstannyl ligands (that is, treatment of the alkyne with *n*BuLi followed by $[Me_3SnCl]$[93]) and careful handling of toxic $[Me_3SnCl]$ is required, the route avoids amine solvents and opens up the generality of the method. Stoichiometric treatment of bis(trimethylstannyl)ethyne with *trans*-$[MCl_2(nBu_3P)_2]$ affords polymers in excellent yield (Scheme 15), which in the case for M = Pt were found to have average molecular weights up to $M_w = 210\,000$, which is, on average, 30 000 Da higher than for those prepared by the dehydrohalogenation route of Hagihara et al.



Scheme 14. Illustration of the versatility of trimethylstannyl alkynyl ligands.



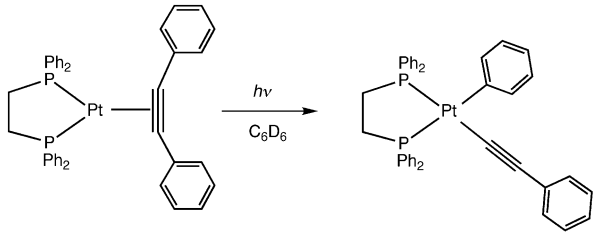
Scheme 15. Formation of a high molecular weight platinum polyyne by trimethylstannyl metathesis.

However, as with the dehydrohalogenation route, the analogous Ni and Pd polymers were obtained with much lower molecular weights ($M_w = 20\,000$–$30\,000$). The complexes reported were all symmetrical, although Wrackmeyer et al.[94] formed the unsymmetrical dialkynyl complexes *trans*-$[Pt(Et_3P)_2(C{\equiv}CR)(C{\equiv}CR')]$ (R = Me, Ph; R′ = H) by the reaction of *trans*-$[Pt(Et_3P)_2(Cl)(C{\equiv}CR)]$ with $Me_3SnC{\equiv}CR$. Slow conversion of unsymmetrical to symmetrical alkynyls in solution was observed and was believed to be accelerated through the presence of $[Me_3SnCl]$.

4.3. Synthesis through C–C Bond Activation

The cleavage of C–C bonds under mild conditions is currently an active area of research in organometallic chemistry, and activation of an unstrained C–C bond can be achieved in the presence of highly reactive species by forcing the target molecule into close proximity to the metal center.[38,95,96]

Jones and co-workers have reported the synthesis of various Pt^0 diphenylacetylene complexes with chelating P,N or P,P ligands (Scheme 16), and the cleavage of the C(sp)–C(sp^2) bond in diphenylacetylene. The η^2-alkyne complexes are quantitatively converted into their oxidation products under photolytic conditions.[97] It is interesting to note that the oxidative addition of diphenylacetylene to the metal center can be reversible; on thermal activation, Pt η^2-alkynyl complexes are reformed. Similar reversible cleavage has been



Scheme 16. Transition from η^2 to η^1 alkynyl coordination to a platinum center.

© 2003 Wiley-VCH Verlag GmbH & Co. KGaA, Weinheim

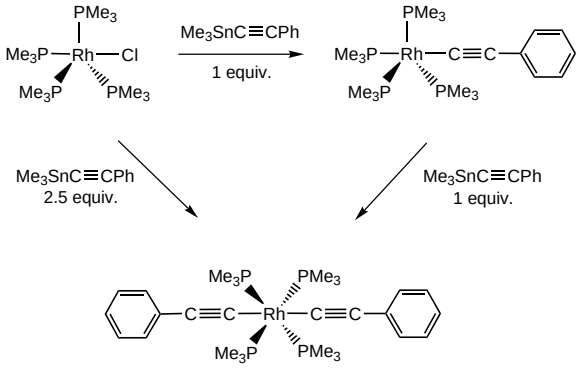
observed in Ni^0 complexes[96] and thermal and photochemical Si–C bond activation has been noted in donor-stabilized Pt^0 η^2-alkyne complexes.[98]

5. Metal Alkynyl Complexes: Co, Rh, Ir

Group 9 transition-metal alkynyl complexes have not been well studied, which is mainly as a result of the instability of the metal centers and the difficulty in characterizing some of the complexes produced. However, some novel and unusual synthetic routes have been developed that utilize the coordinatively (un)saturated properties of the metal centers.

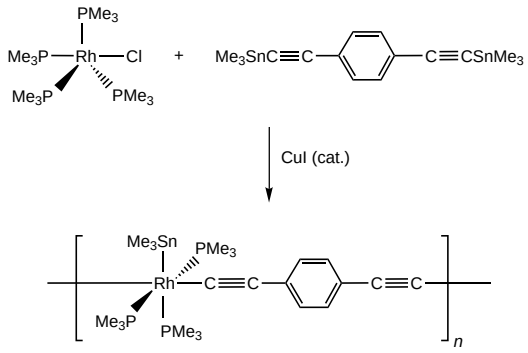
5.1. Synthesis Using Trimethylstannyl Reagents

Synthesis of the first monoalkynyl complexes of rhodium was achieved by Lappert et al.,[89] when they prepared $[Rh(PMe_3)_3(C{\equiv}CPh)]$. Lewis et al. utilized the trimethylstannyl route to synthesize the novel *mer*,*trans*-$[Rh^{III}(PMe_3)_3SnMe_3(C{\equiv}CPh)_2]$ by treating this complex with trimethylstannylethynylbenzene (Scheme 17).[91,92,99] The proposed mechanism involves oxidative addition of a second trimethylstannylalkyne molecule to the known monoalkynyl species. As the dialkynyl complex was shown to have a *trans* arrangement of the alkynyl ligands, it was a suitable building block for the production of rigid-rod oligomers and polymers (Scheme 18). The poor solubility of these white solids in organic solvents could be overcome by replacement of the trimethylphosphane groups with tri-*n*-butylphosphane units, whereas substitution with triphenylphosphane groups resulted in complexes with lower solubility. In addition, dialkynyl complexes synthesized by this route were found to have a *cis* configuration, in contrast to the *trans* configuration usually observed.

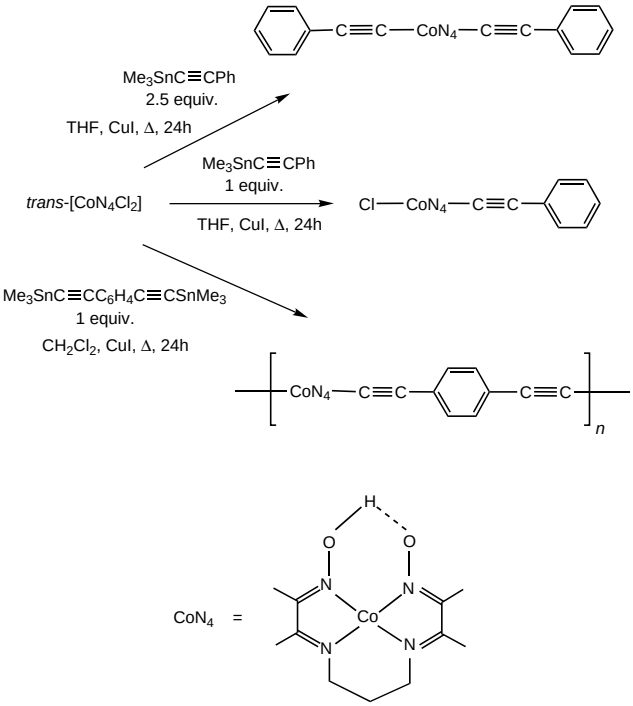


Scheme 17. Formation of rhodium alkynyls by using trimethylstannyl reagents.

The trimethylstannyl route has been used for the synthesis of Co^{III} analogues, although an N_4 pseudomacrocyclic species is required to stabilize the Co center.[100] Mono-, di-, and polymeric alkynyl σ complexes have been formed



Scheme 18. Formation of rigid-rod rhodium alkynyl polymers.



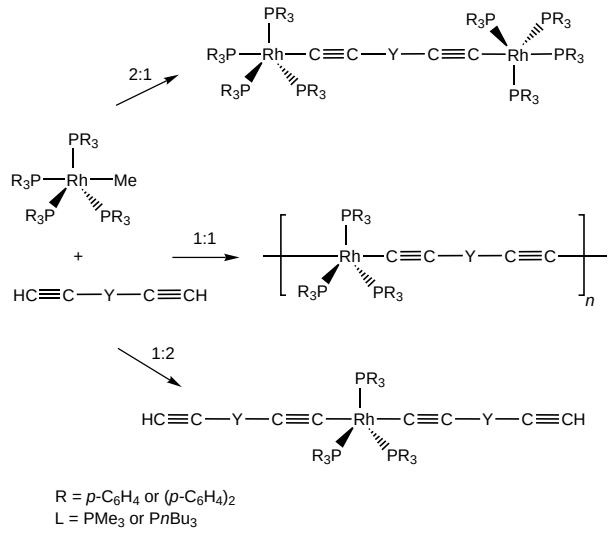
Scheme 19. Formation of cobalt alkynyl species by utilizing an N_4 pseudomacrocyclic ligand.

(Scheme 19); IR spectroscopy indicates that the ν(C≡C) absorption decreases on going from the monoalkynyl complex to the polymeric species, which is an indication of increased π-electron conjugation. As with the Group 10 transition metals, the IR bands decrease in energy owing to an increase in the metal-mediated interactions between the alkynylic units. However, the reduction in the absorbance is less pronounced in this case than for the Group 10 analogues, which may be a reflection of the degree of overlap between the metal center and the π(C≡C) orbitals.

5.2. Synthesis through the Elimination of Methane

A novel route to monomeric, oligomeric, and polymeric rhodium complexes was pioneered by Marder and co-work-

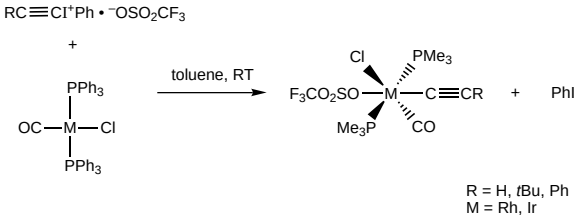
ers[101,102] through the direct oxidative addition of terminal alkynes to [L_4RhMe] species, with loss of methane (in analogy to the synthesis of [Co(PMe)$_4$(C≡CPh)] reported by Klein et al.[103] Terminal alkynes were found to react cleanly with [Rh(PMe)$_4$]Cl by oxidative addition to give *cis*-[Rh(PMe$_3$)$_4$(C≡CR)(H)]Cl.[104] The structure of this octahedral complex, as determined by X-ray crystallography, exhibited bond lengths that indicated a lack of π back-donation from the Rh d orbitals to alkynyl π* orbitals. Reaction of the same complex with two equivalents of a dialkynyl ligand yields dinuclear cations of the form [Rh(PMe$_3$)$_4$(H)(C≡C–X–C≡C)Rh(PMe)$_4$]$^{2+}$, which upon treatment with an aqueous base (e.g., KOH) gives the neutral dinuclear Rh^I species [Rh(PMe$_3$)$_4$(C≡C–X–C≡C)-Rh(PMe$_3$)$_4$]. The same synthetic strategy was utilized to produce Rh^I oligomers and polymers, with the elimination of methane and loss of a phosphane ligand (Scheme 20). When L = PMe$_3$, insoluble polymers are produced, while the use of P*n*Bu$_3$ leads to soluble products; however, characterization of these species is still difficult. The polymers can also be prepared from [Rh(PBu$_3$)$_4$]BPh$_4$, MeLi, and one equivalent of HC≡C–C$_6$H$_4$–C≡CH.



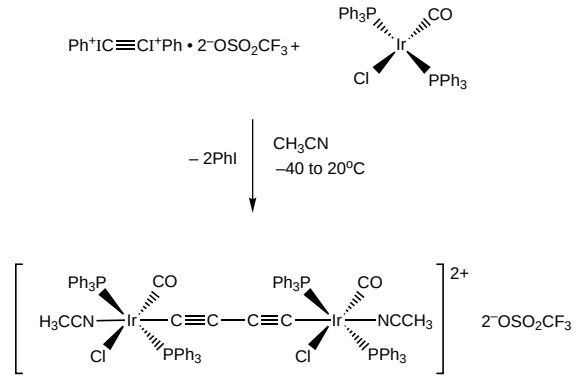
Scheme 20. Synthesis of rhodium alkynyl oligomers and polymers by elimination of methane and loss of a phosphane ligand.

5.3. Synthesis with Alkynyliodonium Triflates

Stang et al. proposed a very different route of Rh and Ir alkynyl complexes[105] by substitution reactions of the square-planar metal(I) centers with alkynyliodonium triflate species, in which the transition-metal complex effectively acts as a nucleophile and the iodonium species as an electrophile, that is, by using an RC≡C$^+$ synthon and an "umpolung" of the normal alkyne reactivity (Scheme 21). The yields of Rh^{III} and Ir^{III} hexacoordinated complexes formed by this route were excellent (80–90%), which was later developed to prepare a number of cationic bimetallic diynes[106] (Scheme 22). However, this method has not yet been expanded to other transition metals.



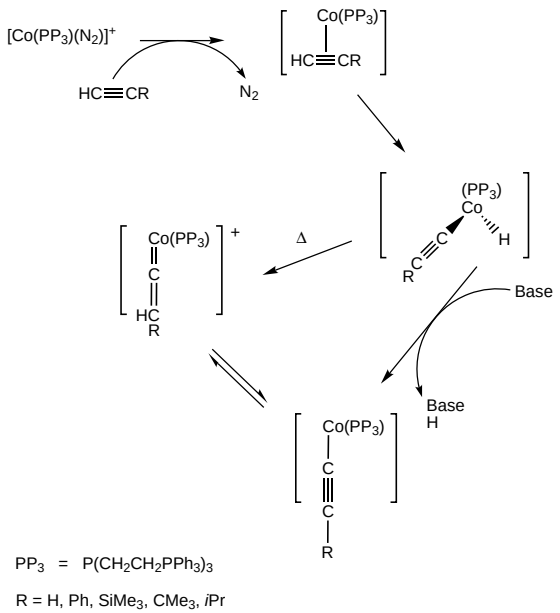
Scheme 21. Synthesis of rhodium and iridium alkynyls by using alkynyliodonium triflates.



Scheme 22. Formation of cationic iridium diynes.

5.4. Synthesis with N_2 or H_2 Elimination

Bianchini et al. reported a synthetic route to Co^{III} alkynyl complexes through the elimination of N_2.[107] A thorough investigation of the reaction mechanism focussed on the factors controlling alkynyl/vinylidene interconversion (Scheme 23), which suggested that N_2 is easily removed to give a 16-electron species that reacts with terminal alkynes to

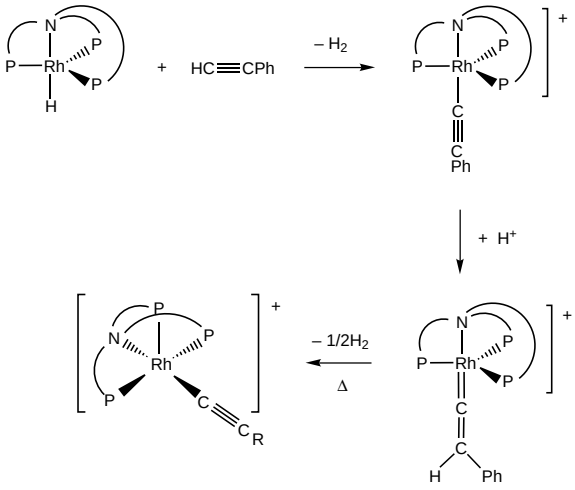


Scheme 23. Synthesis of cobalt alkynyls by elimination of N_2.

 © 2003 Wiley-VCH Verlag GmbH & Co. KGaA, Weinheim

form π-bonded alkyne products and vinylidene complexes as the kinetic and thermodynamic products, respectively. Between the π-bound alkyne and vinylidene forms, the system evolves through a third species, a Co^{III} hydride alkynyl complex, which is more thermodynamically stable than the π-bound alkyne but less stable than the vinylidene complex. It was shown that the electronic nature of the R group determined the temperature at which the hydride-alkyne-to-vinylidene rearrangement occurs. The stability of the hydride alkyne decreases in the order: $R = SiMe_3 \gg Ph > H \gg CMe_3 >$ Pr = pentane. To date, questions about the nature of the migrating hydrogen species, in particular whether it migrates as a proton or as a hydride ion, are yet to be answered. Parallel studies of the 16-electron Rh fragment showed no conversion from the hydride alkyne complex to the vinylidene complex, which may result from the greater strength of the Rh–H bond, when compared to the Co–H bond.[107]

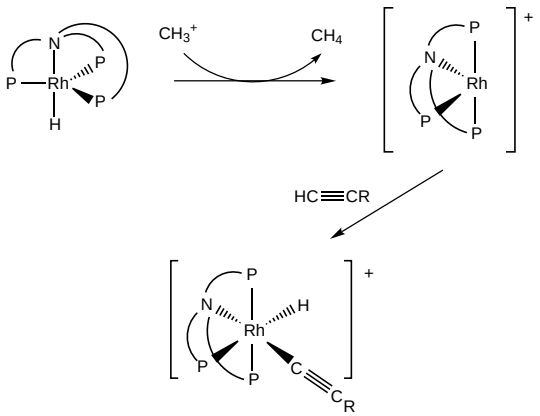
Whilst focussing on the transformation of vinylidene ligands, Bianchini and co-workers have formed some novel Rh alkynyl σ complexes through the elimination of H_2 and the incorporation of stabilizing tetradentate ligands of the form $N(CH_2CH_2PPh_2)_3$ (denoted "NP_3") or $P(CH_2CH_2PPh_2)_3$ ("PP_3") around the Rh center[108] (Scheme 24). The reaction



Scheme 24. Formation of rhodium alkynyls by elimination of H_2.

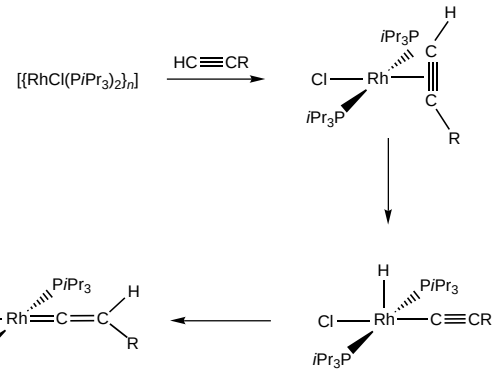
can also be carried out through the elimination of methane in the electrophilic attack of the trigonal-bipyramidal hydrides [(NP_3)RhH] and [(PP_3)RhH] by CH_3^+ species (from MeO-SO_2CF_3). The resultant 16-electron fragment [(NP_3)Rh]$^+$ reacts with terminal alkynes to give *cis*-hydride alkynyl complexes of Rh^{III} with a wide variety of substituents[109] (Scheme 25). The overall aim of the study was to form a new family of terminal vinylidene and vinylphosphonium complexes of Rh^I, synthesized by electrophilic attack at the β-carbon atom of the σ-bonded alkynyl ligand.

Some novel Rh^{III} alkynyl complexes have been synthesized by Werner and co-workers[110] during their investigations into vinylidene transition-metal complexes. The highly reactive rhodium complex $[RhCl(PiPr_3)_2]_n$ is an excellent starting material for such reactions. Coordination of a terminal alkyne



Scheme 25. Use of a stabilizing tetradentate ligand in the formation of rhodium alkynyls.

to the metal center is followed by an intramolecular oxidative addition (Scheme 26). Alkynyl(hydrido)rhodium(III) complexes are thus formed, which can then undergo hydrogen transfer from the metal center to the β-carbon atom of the ligand to form the vinylidene complex. The kinetic stability of the product depends on the R group on the alkynyl ligand; if R = *t*Bu, the reaction can be stopped and the alkyne complex can be isolated. Some interesting dimetallic species have been prepared using buta-1,3-diyne and hexa-1,5-diyne ligands.[111]



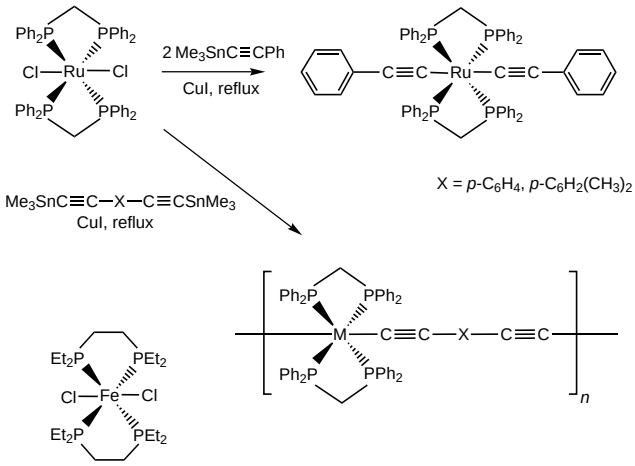
Scheme 26. Formation of rhodium alkynyls by intramolecular oxidative addition with subsequent vinylidene formation.

6. Metal Alkynyl Complexes: Fe, Ru, Os

6.1. Copper-Catalyzed Trimethylstannyl Routes

In an extension of the methodology of utilizing trimethylstannylalkynes, Lewis and co-workers have investigated the incorporation of Fe^{II},[112,113] Ru^{II}[114,115] and Os^{II}[116–118] centers into mono-, di-, and polymeric alkynyl systems. Such methods were found to be particularly reliable for the synthesis of *trans*-oriented di- and polyalkynyl Ru^{II} complexes (with the stabilizing ligands bis(diphenylphosphanyl)ethane (dppe) and bis(diphenylphosphanyl)methane (dppm); also for Os^{II} (with dppm) and Fe^{II} (with diethylphospanylethane (depe); Scheme 27 and Figure 1). The Fe complexes could only be

 © 2003 Wiley-VCH Verlag GmbH & Co. KGaA, Weinheim



Scheme 27. Synthesis of Group 8 metal alkynyls by using trimethylstannyl reagents.

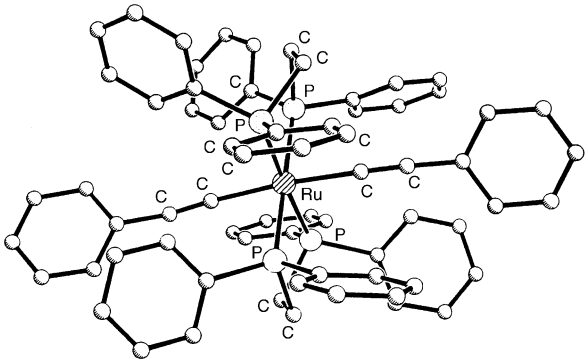


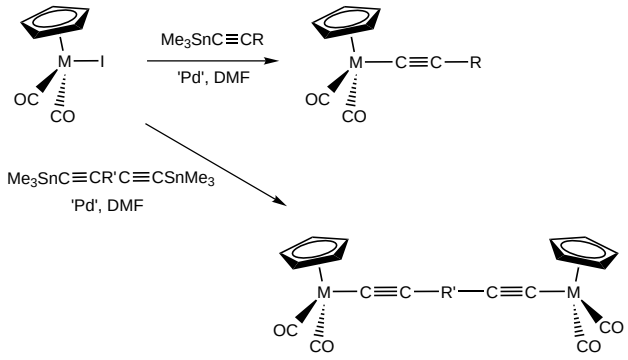
Figure 1. Molecular structure of $[Ru(dppe)_2(C{\equiv}CC_6H_5)_2]$.[114]

stabilized and isolated with depe, while dppm was used as the necessary bidentate phosphane ligand for the Os complexes. The complexes are generally soluble in organic solvents, although the incorporation of a xylene spacer group increases the solubility, along with the polymeric chain length ($M_w =$ 173000). Purity of the starting materials and an exact 1:1 stoichiometry is crucial in obtaining a high degree of polymerization. In general, for Ru dppm species, soluble polymers of high molecular weight ($M_w > 55000$) were formed using this CuI-catalyzed method, and were of a higher degree of polymerization than the corresponding dppe systems. UV/Vis spectra of the iron dialkynyl species show an increased $d_{\pi-\pi^*}$ overlap when compared to the analogous Group 10 transition-metal species. However, the method was not successful in preparing monoalkynyl species when starting with mixtures of the dihalide reagents; mono- and disubstituted products were usually obtained and required lengthy purification.

It should be noted that similar mono- and dialkynyl complexes of Ru^{II} with CO and PEt_3 ligands can be formed through treatment of *trans*-$[Ru(CO)_2(PEt_3)_2Cl_2]$ with $LiC{\equiv}CSiMe_3$.[119]

6.2. Palladium-Catalyzed Trimethylstannyl Routes

Lo Sterzo et al. utilized the trimethylstannyl route to form Fe and Ru alkynyl complexes in a stepwise fashion using half-sandwich cyclopentadienyl metal centers. Rather than using bulky phosphanes, carbonyl moieties were incorporated along with an iodo ligand that was then coupled with the trimethylstannylalkynyl reagents (Scheme 28).[120–123] The use of a



M = Fe, Ru; R = H, alkyl, Ph; R' = nothing, thiophene

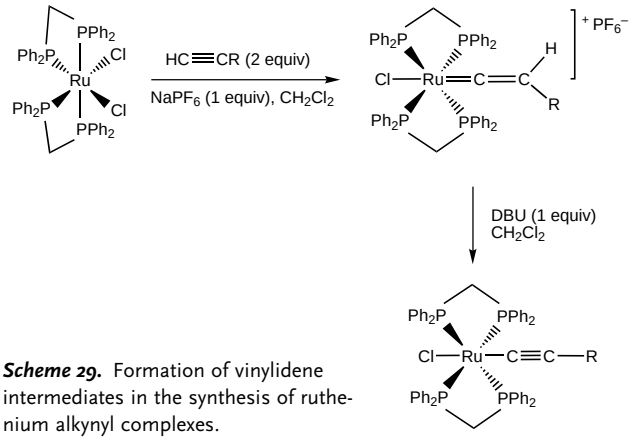
Scheme 28. Formation of metal alkyne half-sandwich complexes by palladium-catalyzed trimethylstannylation.

catalytic amount of palladium, usually 5 mol% of $[PdCl_2(CH_3CN)_2]$ in DMF at room temperature, was of particular note. In fact, it was found that the coupling reaction (known in organic synthesis as the Stille reaction[124,125]) did not form products, even under forcing conditions. Addition of $PdCl_2$ to the reaction mixture also did not affect the reaction, which led to the conclusion that Pd^0 centers are responsible for the promotion of metal–carbon bond formation. In support of this hypothesis, $[Pd(PPh_3)_4]$ was found to be as effective, in terms of consumption of starting material and reaction rate, as $[PdCl_2(CH_3CN)_2]$. In fact, $[PdCl_2(CH_3CN)_2]$ must be reduced to a Pd^0 center in situ by a slight excess of the stannane before it enters the catalytic cycle, and use of $[Pd(PPh_3)_4]$ can lead to side reactions, such as the substitution of CO ligands by PPh_3. Fischer and co-workers[126,127] have also utilized similar Stille-coupling techniques to form heterobimetallic complexes with propynylidene and pentadiynylidene bridges (see Section 8). The role of palladium catalysis in C–C and M–C bond formation, with particular focus on alkynes, was well summarized by Lo Sterzo in 1999.[128]

6.3. Synthesis through Vinylidene Formation

An efficient, stepwise approach to mono- and unsymmetrical dialkynyl ruthenium compounds, pioneered by Dixneuf and co-workers, is provided by vinylidene formation.[129–133] Their initial findings illustrated that *cis*-$[RuCl_2(Ph_2PCH_2CH_2PPh_2)_2]$ readily activates terminal alkynes to produce stable and isolable vinylidene complexes

in excellent yields. $NaPF_6$ is crucial for the production of a 16-electron Ru intermediate by displacement of a chloride ligand. The vinylidene species are then deprotonated by either passing a solution through a short alumina column or, preferably, by the addition of DBU (1,8-diazabicyclo[5.4.0]undec-7-ene; 1 equiv) in CH_2Cl_2. Both reactions are carried out at room temperature, and give the *trans*-chloro alkynyl metal derivatives (Scheme 29). Surprisingly, it was not

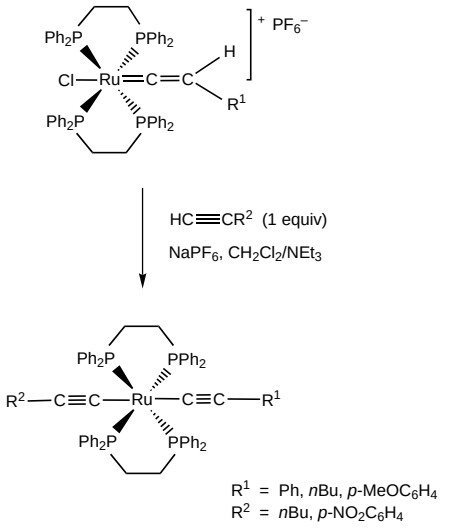


Scheme 29. Formation of vinylidene intermediates in the synthesis of ruthenium alkynyl complexes.

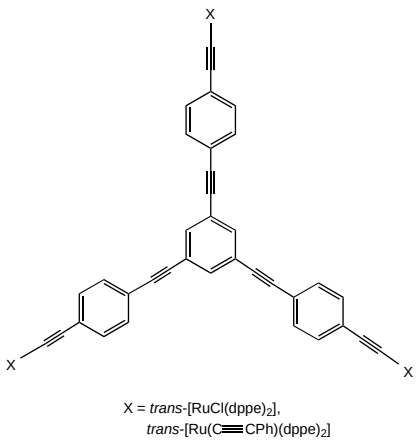
possible to directly introduce two alkynyl groups at the metal center under these conditions (compare the Sn routes of Lewis et al.), but the addition of triethylamine, $NaPF_6$, and more alkynyl ligand (3 equiv) could achieve this aim. These conditions allowed the formation of unsymmetrical bisalkynyl ruthenium(II) complexes, when starting from a monovinylidene complex (Scheme 30).

This method, or a combination of it with the trimethylstannyl route, led to the formation of a wide range of symmetric and unsymmetric Ru^{II} and Os^{II} bisalkynyl complexes. The main aspects of these investigations included: 1) The bonding, spectroscopy, and electrochemistry of the complexes through electron-donating and withdrawing ligands, 2) NLO properties, and 3) the synthesis of electron-transfer/mixed-valence complexes.

1) It was shown[117] that the alkynyl ligand and the auxiliary ligand share a role in determining the ease of oxidation at the metal center, whilst changes in the UV/Vis spectrum illustrate the influence of electron-withdrawing and electron-donating ligands.
2) Second-order NLO studies focussed on the unsymmetrical derivatives; the basic requirements for large second-order hyperpolarizability values (β)[13] being: a) an asymmetric charge distribution, brought about by having substituents with high donor and acceptor abilities at positions *para* to each other, b) a pathway for π-conjugated electrons, and c) an optimized π-electron conjugation length; metal alkynyl σ complexes were thought to be good candidates. Utilizing the synthetic methods of Dixneuf et al., Humphrey and co-workers prepared a range of rigid-rod Ru^{II} alkynyl σ complexes with a variety of substituents on the alkynyl ligands, and performed systematic NLO studies.[134–138] They used methods, such as the Kurtz powder technique, electric-field-induced second-harmonic generation (EFISH), hyper-Rayleigh scattering, and semi-empirical calculations, such as ZINDO to suggest that for these complexes, centrosymmetry withstanding, there is: a) a non-additive effect of *trans*-disposed ligands, b) a significant increase in the value of β upon incorporation of a strong acceptor substituent, c) a substantial increase in the value of β on chain lengthening, and d) a more efficient NLO response using 1,3,5-substituted aryl bridges (leading to dendrimers), than for linear polymers. Other work[139,140] on the third-order NLO properties of a Ru^{II} alkynyl dendrimeric species (Scheme 31), using the same synthetic methodology, indicated that: a) there was no loss of optical transparency, b) there was a nonlinear increase in the second hyperpolarizability γ, and c) there was a dramatic enhancement of two-photon absorption.
3) The M^{II} alkynyl dimetallic complexes (M = Fe, Ru, Os) were viewed as model systems to evaluate the capability

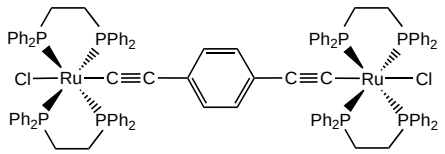


Scheme 30. Formation of unsymmetrical ruthenium bis(alkynyl) complexes.



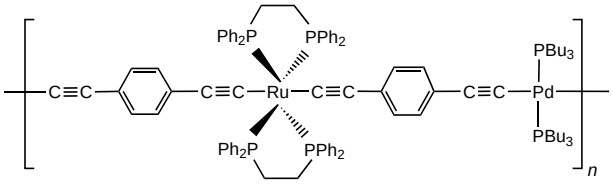
Scheme 31. Octopolar ruthenium alkynyl complexes.

 © 2003 Wiley-VCH Verlag GmbH & Co. KGaA, Weinheim



Scheme 32. A dimetallic alkynyl complex as model for studying electron transfer properties.

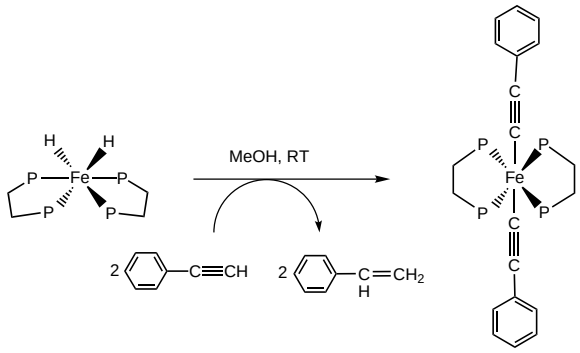
of communication between metal centers. The cyclic voltammogram for the diruthenium complex shown in Scheme 32 shows two reversible one-electron redox waves for the formation of the mono- and dicationic species, that is, the Ru^{III}/Ru^{II} and Ru^{III}/Ru^{III} systems. The separation of 360 mV is indicative of communication between the ruthenium centers through the 1,4-diethynylbenzene bridge.[131] A more detailed study[118] involving dinuclear metal alkynyl σ complexes was carried out on Fe, Ru, and Os metal centers, which studied the influence of various diethynyl spacers, that is, 1,4-benzene, 1,3-benzene, 2,5-xylene, 2,5-pyridine, and 2,5-thiophene. Electrochemistry, coulometry, and optical absorbance studies were used to show that communication between the metal centers through a bridging unit is affected by the nature of the bridge (the thiophene spacer allowed greatest communication) or the terminal metal fragments, and mixed-valence oxidized species possess a delocalized allenylidene structure and can be classified as a "Class II" mixed-valence species, after Robin and Day. [141] Similar studies to probe the interactions between the metal moiety and the organic fragment by Wolf and co-workers[142] have synthesized some Ru^{II} mono- and bis(oligothienylalkynyl) complexes, using a combination of the vinylidene method and the CuI-catalyzed $Bu_3SnC{\equiv}CR$ approach. Cyclic voltammetry and electronic spectroscopy indicate that the π system of the conjugated oligothienyl ligands interacts strongly with the metal center. The donating Ru^{II} group decreases the energy of the π–π* transition in the oligothienyl ligands, which is decreased further when Ru^{II} is oxidized to Ru^{III}. The reversibility of the $Ru^{II/III}$ oxidation wave improves as the length of the ligand is increased, which indicates that stabilization of the Ru^{II} species occurs via delocalization of positive charge from the metal to the oligothioenyl ligand. Dixneuf et al. have combined their original approach to Ru alkynyl complexes and the Cu-catalyzed dehydrohalogenation process (used for the Group 10 transition metals) to form heterobimetallic polyyne complexes (M_w = ca. 15000) with alternating {Ru(dppe)$_2$} and {Pd(P*n*Bu$_3$)$_2$} moieties along the polymer backbone (Scheme 33).[131] This is the first example of a polymer with a mixed coordination environment (d^6/d^8). Electrochemical measurements show that there is only one redox wave for the Ru^{II}/Ru^{III} couple, indicative of a lack of communication between the Ru centers through the Pd bridges, which can be thought of an insulating units.



Scheme 33. A heterobimetallic polyyne complex formed by copper-catalyzed dehydrohalogenation.

6.4. Synthesis of Complexes with Molecular Hydrogen

Dihydride complexes of Fe^{II}, such as *cis*-[$FeH_2(P{-}P)_2$] (P–P = $R_2PCH_2CH_2PR_2$; R = Me, Et, *n*Pr)[143,144] are basic and can be reversibly protonated by alcohols to yield complexes with molecular hydrogen. These species are readily substituted by many ligands (e.g., Cl^-, PR_3), with loss of H_2.[145,146] Terminal alkynes are acidic enough to protonate the dihydride complexes and then react to initially give an alkynyl metal hydride, and then a metal dialkynyl complex[147] (Scheme 34). The formation of styrene as a by-product

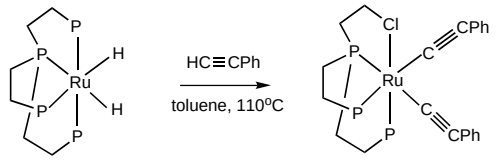


Scheme 34. Formation of an iron dialkynyl complex by elimination of H_2.

suggests that the terminal alkyne not only acts as a proton source but also serves to remove H_2. The dialkynyl complexes formed were seen as precursors to oligomers or polymers. High pressures were found to aid the reaction to give monoalkynyl complexes; at 800 mPa, the yield increased from 8% to 95% and the reaction time decreased from 24 h to 30 min. It was concluded that the volume of activation for the formation of monoalkynyl hydride species was large and negative and that increasing the pressure aided the formation of the molecular H_2 complex, which, in turn, accelerated the rate of alkyne substitution.

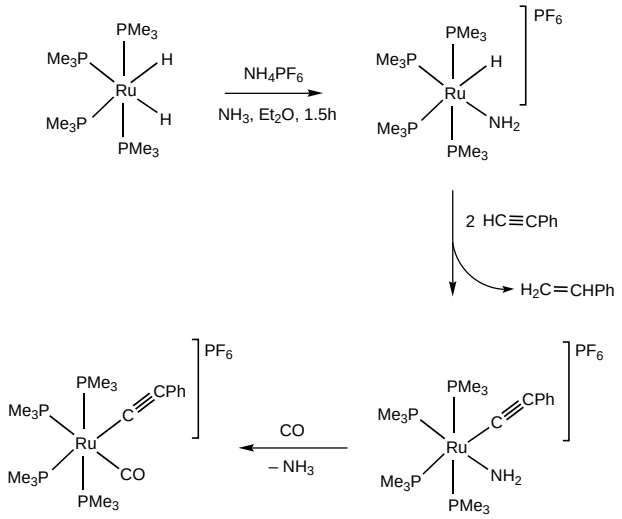
Bianchini et al. have also used this method with *cis*-[$(PP_3)RuH_2$] ($PP_3 = P(CH_2CH_2PPh_2)_3$) used as a catalyst precursor for the regio- and stereoselective dimerization of HC≡CPh[148] (Scheme 35). Mechanistic studies suggested that the following steps were involved: 1) Insertion of a 1-alkyne into a Ru–H bond, 2) reductive σ-coupling of a hydride with a vinyl group, 3) displacement of the resulting alkene by a 1-alkyne group, 4) hydroruthenation of the 1-alkyne, and 5) σ-bond metathesis between C_{sp}–H and Ru–C_{sp^2} moieties.

 © 2003 Wiley-VCH Verlag GmbH & Co. KGaA, Weinheim



Scheme 35. Formation of a ruthenium dialkynyl complex by utilizing a stabilizing tetradentate phosphane ligand.

The reactivities of dihydridoruthenium complexes with alkynes, via cationic intermediates, have been investigated (Scheme 36).[149] The yields of the moderately air-stable complexes are virtually quantitative, and the *cis*-bisalkynyl species can be formed in the same way. It is noteworthy that the cationic complex does not need to be heated for reaction, and substitution occurs at room temperature, whereas heating is necessary to substitute the neutral complex [Ru(P-$Me_3)_4$(H)(H)]. The cationic intermediate catalyzes alkynyl dimerization, to exclusively give the *Z* isomer. Oro and co-workers have studied parallel Os systems, in which the same phenomenon, that is, the formation of mono- and bisalkynyls via osmium hydride intermediates, has been observed.[150]



Scheme 36. Formation of a ruthenium alkynyl from a dihydrido complex.

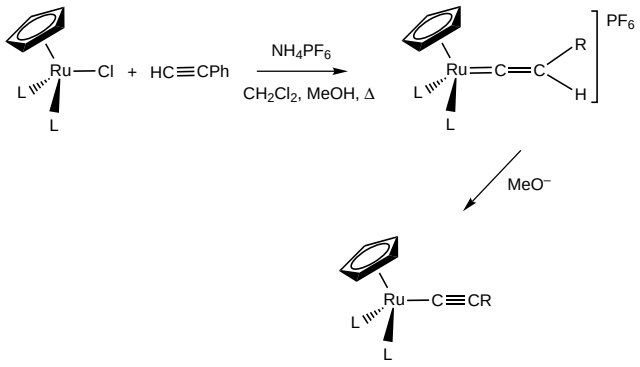
6.5. The Sodium Methoxide Method

An efficient synthetic route toward iron species using methoxide reagents was developed by Field et al.[151] Addition of the terminal mono- or dialkynyl ligand to a solution of freshly cut sodium in methanol, followed by dropwise addition of the iron halide complex leads to the formation of the metal alkynyl complex in reasonable yield. This route has been used to form a number of dinuclear Fe^{II} dialkynyl species,[118] in which it was found that exact stoichiometries were essential, only particular dialkynyl bridging ligands were successfully incorporated, and efforts to synthesize Ru and Os analogues resulted in decomposition of the *trans*-dialkynyl metal complexes.

By utilizing this synthetic method, a range of Ru^{II} and Ru^{III} bisalkynyl σ complexes supported by a tetradentate macrocyclic tertiary amine ligand (16-TMC = 1,5,9,13-tetramethyl-1,5,9,13-tetraazacyclohexadodecane) have been formed.[152] The N_4 ligand is optically transparent in the UV/Vis spectral region, thus permitting MLCT or ligand-to-metal charge-transfer (LMCT) transitions to be observed using optical spectroscopy. Low-energy ν(C≡C) stretching vibrations were observed by IR spectroscopy, and the strong σ-donating strength of the tertiary amine ligand is manifest in substantial metal-to-alkynyl π back-bonding. The N_4 ligand can also kinetically stabilize highly oxidized species, such as $[Ru^{IV}(C{\equiv}CAr)^2]^{2+}$. Oxidation of the Ru^{II} alkynyl complexes yields low-energy vibronic UV/Vis absorption bands, which are tentatively assigned as $p_\pi(ArC{\equiv}C){\rightarrow}d_{\pi^*}(Ru^{III})$ LMCT transitions.

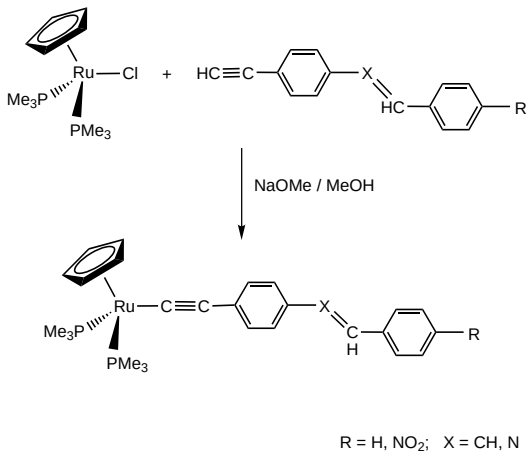
6.6. Cyclopentadienyl and Arene Ruthenium(II) Alkynyls

Alkynyl cyclopentadienyl ruthenium (and osmium) σ complexes have been comprehensively studied, largely because of their ease of preparation.[153] They are often formed by the reaction of a Ru halide (normally the chloride) and a terminal alkynyl ligand to give a vinylidene cation. This can be isolated, but is often deprotonated in situ in methoxide solution to afford the σ-bonded alkynyl products in good yields (Scheme 37).[154–156] The complexes have come to the



Scheme 37. Synthesis of cyclopentadienylruthenium σ-alkynyls.

fore largely because of interest in their NLO attributes, as the electron-donating capability of the ruthenium moiety has been found to be beneficial in enhancing second-order molecular hyperpolarizability effects.[157] Lin et al. have built up extended chains and varied conjugation bridges from a Ru center using, for example, conjugated pyridine,[158,159] thienyl, or pyridyl metal units.[160] They showed that pyridinium derivatives exhibit efficient charge transfer from the ruthenium donor to the organic acceptor. In addition, Jia and co-workers[161] have produced a range of fully conjugated bimetallic pentamethylcyclopentadienyl Ru complexes bridged with C_5H and related ligands, while Bruce et al.



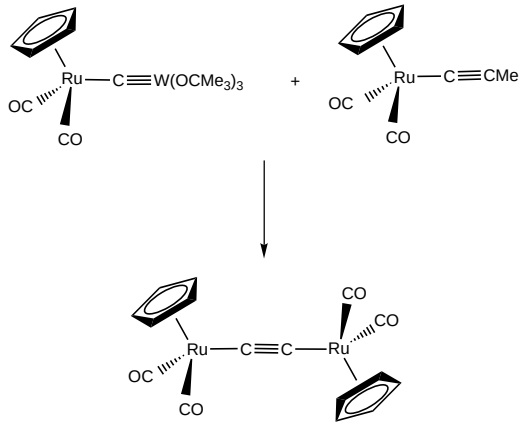
Scheme 38. Formation of half-sandwich ruthenium alkynyls for nonlinear optical measurements.

have formed a series of $\{(C_5H_5)Ru(PPh_3)_2\}$-capped C_4 chains, and obtained five different oxidation states for ruthenium.[162]

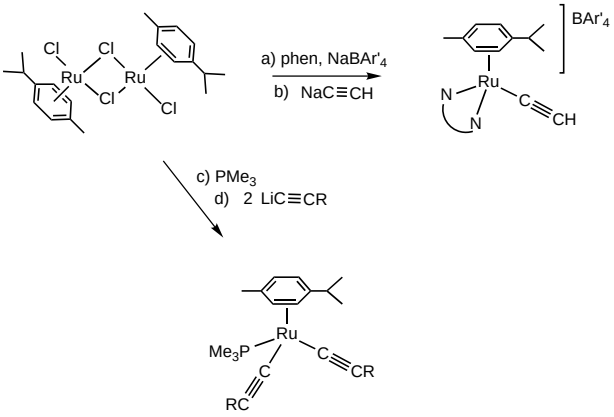
Humphrey et al. have carried out a systematic NLO study on (η^5-C_5H_5)Ru-centered complexes with various phosphane and σ-bonded alkynyl ligands (Scheme 38).[163–165] The complexes were designed to be of the donor–acceptor type and thus, their second-order NLO responses were analyzed. An increase in hyperpolarizability could be achieved by: 1) increasing electron density at the metal center (replacing PPh_3 by PMe_3), 2) increasing the acceptor strength of the alkynylarene (replacing H by NO_2), 3) decreasing the metal–alkynyl M−C bond lengths, and 4) optimizing the orientation of the alkynylarene group.

A novel alkyne metathesis reaction between −W≡C− and −C≡CMe units resulted in the formation of dimetallic ethynediyl complexes (Scheme 39); a number of metals can be incorporated by this method.[166] (further discussion on alkyne metathesis can be found in Section 10.6.).

In contrast to the cyclopentadienyl derivatives, much less is known about (arene)Ru^{II} alkynyl complexes,[167] mainly owing to their general instability. Some interesting recent studies report that cationic monoalkynyl complexes and a



Scheme 39. Formation of dimetallic ethynediyl complexes by alkyne metathesis.



Scheme 40. Synthesis of (arene)ruthenium alkynyls.

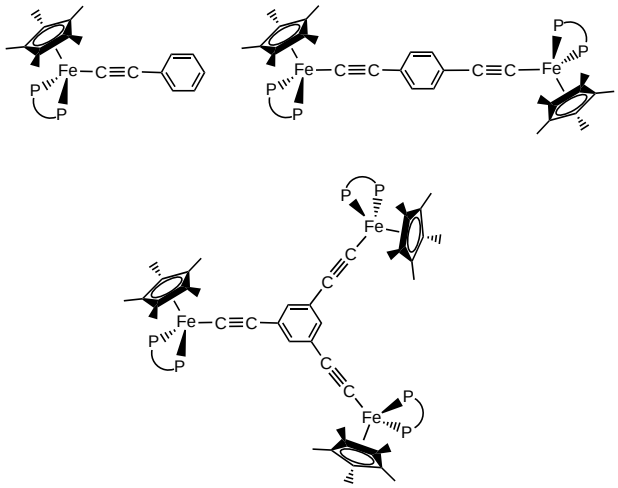
neutral bisalkynyl complex have been synthesized (Scheme 40),[168,169] in which the non-isolated intermediate $[RuCl(cym)(phen)]BAr'_4$ (cym = cymene, phen = 1,10-phenanthroline) is involved. Stirring with an excess of the sodium acetylide for 12 h yield the alkynyl complex. For substituted alkynes, lithium reagents were used and to increase the reactivity, the chloride ligand was substituted by the more labile triflate ligand. The bisalkynyl complex can eventually be formed by using an excess of the lithium phenylalkyne. This pseudotetrahedral piano-stool complex has a similar angle between the alkynyl groups as that which is found in the "tweezer-like" bimetallic complexes with Group 4 transition-metallocene fragments (see below) and perhaps could also be used as a metalloligand.

6.7. Cyclopentadienyl Iron(II) Alkynyl Complexes

There is much interest in molecular electronics and the formation of "molecular wires". The consequences of intramolecular long-distance electron transfer are crucial in such domains as biology, solid-state chemistry, and materials science. The study of compounds in which a conjugated pathway spans two transition-metal centers has featured complexes with alkynyl-bridged {Cp*Fe(dppe)} units.[23,170–175] In a series of papers, Lapinte and co-workers described the synthesis and characterization of organometallic molecules containing one, two, and three electron-rich {Cp*Fe(dppe)} units linked to a connecting arene group through an ethynyl spacer group (Scheme 41). The species are formed, as with the Ru analogues, through the reaction of terminal alkynes and [M]−X complexes in the presence of a halide-ion abstractor to form the vinylidene species, which can then be deprotonated by base.

A Pd/Cu-catalyzed cross-coupling reaction ($[(Ph_3P)_2PdCl_2]$ (10 mol%), CuI (20 mol%), HN*i*Pr_2, 50–85 °C) has also been utilized for use with half-sandwich compounds.[175–177] The species can be oxidized and stabilized, and a wide range of mixed-valence delocalized complexes with differing carbon-atom bridge lengths have been isolated. Each metal center can be oxidized individually, and so compounds can be prepared and isolated with multiple

 © 2003 Wiley-VCH Verlag GmbH & Co. KGaA, Weinheim



Scheme 41. A range of cyclopentadienyliron(II) alkynyls.

oxidation states. Detailed investigations have indicated that: 1) Direct linking of the spacer group to the metal center by a metal–carbon σ bond promotes electronic coupling, 2) electron delocalization occurs over a distance of approximately 12–15 Å, 3) there are nanosized magnetic interactions, and 4) the intramolecular electron-transfer rate could be controlled by molecular properties such as conformational changes and electronic density. After oxidation, electron density is still located mainly at the iron center, which is efficiently protected by the bulk of the ligands in the {Cp*Fe(dppe)} unit. Recently, these materials have been the subject of NLO studies. Although there are the familiar problems with optical transparency, the materials do show reasonable second-order hyperpolarizability and the NLO activity is controlled by one-electron redox processes (that is, an electroswitch), which may give rise to potentially useful switchable NLO materials of the future.[178]

The length of the conjugating bridge has also been the focus of investigations regarding the complex [Fp*-$(C\equiv C)_n$-Fp*] ($n = 1$–4, 6; Fp* = $(\eta^5$-$C_5Me_5)Fe(CO)_2$).[179,180] The oligomeric complexes were prepared by conventional Cu-catalyzed oxidative coupling, with the longest example, the dodecahexynediyl derivative ($n = 6$), formed by oxidative dimerization of the hexatriynyl complex in the presence of a catalytic amount of CuCl·TMED. X-ray structural analysis shows it to be a linear but slightly twisted structure, but electronic communication studies have not been reported to date.

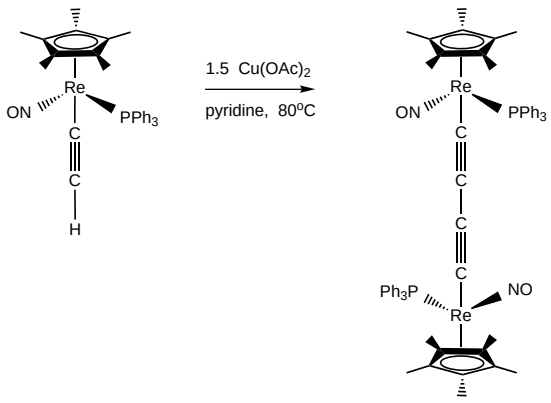
7. Metal Alkynyl Complexes: Mn, Re

Research into alkynyl complexes of the Group 7 transition metals has been dominated in recent years by investigations into the synthesis of long chains of sp-hybridized carbon atoms that span two metal centers, often featuring Re. However, σ-bonded alkynyl complexes of Re^I were obtained, albeit in very low yield, in 1968 by the treatment of rhenium carbonyl bromide complexes with organolithium reagents.[181]

Attempts to prepare analogous Mn complexes by similar procedures were unsuccessful. The first alkynyl carbonyl σ complex of Mn^I was prepared in 1982 by the reaction of a pentacarbonyl manganate anion with a salt of the triphenyl-(phenylethynyl)phosphonium ion.[182] Since then, several methods have been successful in synthesizing new Mn^I alkynyl σ complexes[183]:

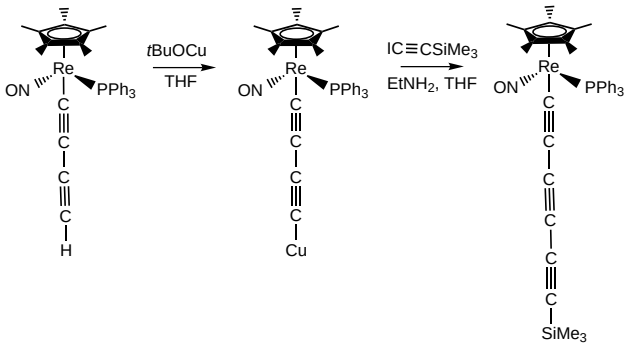
1) The reaction of bromomanganese carbonyl complexes with Ag^I and Cu^I alkynyls: This reaction worked reasonably well, but it was found that a decrease in the number of CO ligands led to a decrease in the lability of the Mn–Br bonds and hence, the reaction time increased.
2) The reaction of perchloromanganese carbonyl complexes with 1-alkynes and a base: The yield of the products formed using this route were low but could sometimes be improved by using NEt_3 as the base.
3) CO replacement in alkynyl σ complexes: By using this process, some novel Mn phosphane alkynyl complexes could be synthesized and isolated.

Compounds in which "wirelike" unsaturated chains of carbon atoms span two metal centers are attracting attention from fundamental and applied viewpoints.[9,184–186] Gladysz and co-workers[187–190] have, amongst others, investigated the methodology of the construction of longer sp-hybridized carbon-atom chains, such as for species that constitute models for the polymeric carbon allotrope "carbyne". A number of synthetic strategies have been employed in the synthesis of chains with an even or odd (much less common) number of carbon atoms. Starting from the sterically congested and strongly π-donating chiral rhenium end-group [$(\eta^5$-$C_5Me_5)$-Re(NO)(PPh_3)], alkynes can be attached and homocoupled using known reactions of organic terminal alkynes (i.e., the Eglinton reaction; $Cu(OAc)_2$ in pyridine; Scheme 42).[191] Analogous C_8, C_{12}, C_{16}, and C_{20} species can be formed in this way, and the cross-coupling of ethynyl and butadiynyl complexes can give C_6 species, but it was found that coupling with the Glaser reaction catalyst (O_2 and CuCl) was not so effective. For the syntheses of 1,3,5-hexatriynyl and 1,3,5,7-octatetraynyl complexes, the Cadiot–Chodkiewicz reaction was important,[192,193] that is, by formation of a preformed Cu alkynyl complex, and avoiding the use of lithiating agents.



Scheme 42. Formation of a dirhenium alkynyl by the Eglington coupling reaction.

 © 2003 Wiley-VCH Verlag GmbH & Co. KGaA, Weinheim

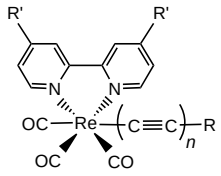


Scheme 43. Synthesis of a rhenium oligoyne species.

It is noted that the best methods for C≡C bond-forming reactions are difficult to predict (Scheme 43).[194] The solid-state structures of the hexatri- and octatetraynes have unusual, markedly curved chains of sp-hybridized carbon atoms, [194] much more so than in previously reported analogues.

A feature of the general coupling routes is that chains with an odd number of carbon atoms, which possess unique electronic characteristics, are much less common as more sophisticated synthetic strategies are required.[195] Heterobimetallic systems have also been studied,[195–198] which have been subjected to cylic voltammetry, magnetic, and optical analysis to attempt to understand the electronic communication processes involved, in a similar way to the work of Lapinte, discussed previously in Section 6.7. Theoretical calculations and the physical properties of the dirhenium compounds suggest that the HOMOs of the longer polymers were likely to have appreciable metal d and alkynyl π character. Cyclic voltammograms for the smaller oligomers show two chemically reversible one-electron oxidation processes under suitable conditions, however for the longer chain compounds, the E^o values approach each other, and at C_{20} they merge to give a single (two-electron) oxidation. This perhaps, signifies the chain length at which the two centers start to behave independently.

A series of simple mono- and dinuclear pentacarbonylrhenium(I) alkynyl complexes of the form $[Re(CO)_5(C{\equiv}CR)]$ and $[(OC)_5Re{-}C{\equiv}C{-}Re(CO)_5]$ have been synthesized[199] and the first luminescent Re^I alkynyl complex, prepared by the reaction of a metal halide and lithium alkynyl species, was reported by Yam and co-workers in 1995.[200] Upon excitation at $\lambda > 350$ nm, the complexes show intense and long-lived orange-red luminescence in the solid state and in solution at room temperature. As the alkynyl ligand becomes more electron-donating in character, the more electron-rich the Re center becomes and, consequently, the MLCT transition decreases in energy. The extensive luminescence of Re^I alkynyl complexes has recently been reviewed[201] and highlights include: 1) The formation of diynyl and triynyl compounds[202,203] (Scheme 44) where it was noted that there is a blue shift in the emission spectrum upon extending the carbon chain. This differs from the common concept of tuning the emission energy towards the red end of the spectrum by extending the number of alkynyl units in organic polyynes.



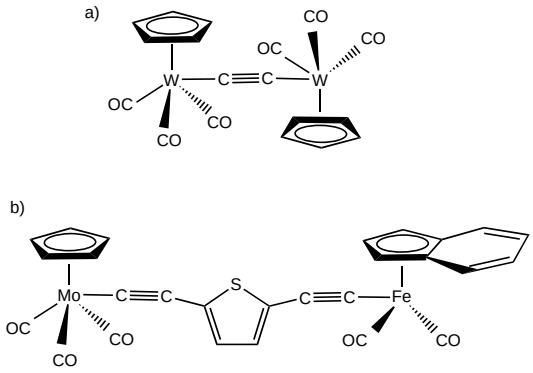
n = 2, 3; R = *t*Bu, Me; R' = H, Ph, $SiMe_3$

Scheme 44. Mononuclear tricarbonylrhenium(I) alkynyls.

2) The formation of mixed-metal alkynyl complexes through the use of Re^I alkynyl complexes with terminal $-C{\equiv}CH$ groups as metalloligands. An interesting series of Cu^I–Re^I alkynyl complexes[204] have been prepared by σ-coordination of the metal alkynyl to a trinuclear Cu^I diphosphane unit, which facilitates the possible tuning of emission energies.

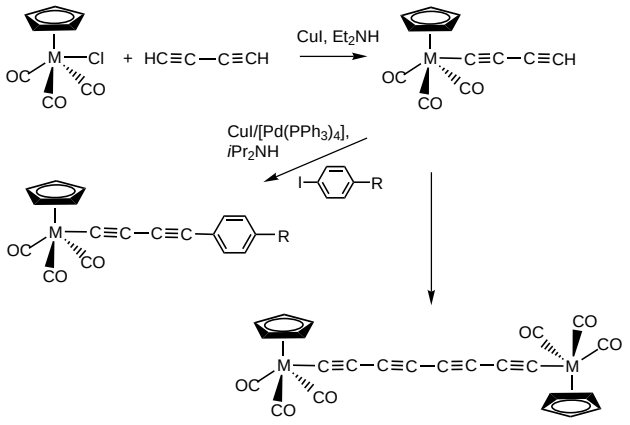
8. Metal Alkynyl Complexes: Cr, Mo, W

Early work in the field of Group 6 transition-metal alkynyl σ complexes by Ruff[205–207] using alkynyl anions and/or thermal activation was superceded in 1992 by more reliable syntheses using dinitrogen binding centers to form *trans*-$[M(C{\equiv}CR)_2(dppe)_2]$ from *trans*-$[M(N_2)(dppe)_2]$.[208] The stability of the Group 6 metal alkynyls is not high, and the use of a cyclopentadienyl ligand has proved to be beneficial. Lin et al.[209] transformed a bridging ketene to form a dinuclear alkynyl σ complex (Scheme 45a). The Pd-catalyzed trimethylstannyl route utilized by Lo Sterzo for Ru alkynyl complexes can also be applied here.[122] A catalytic amount (5 mol%) of $[PdCl_2(CH_3CN)_2]$ in DMF enables the preparation of a range of alkynyl species, and some interesting heterobimetallic complexes can be synthesized (Scheme 45b). In a study analogous to that which yielded the Re polyyndiyl complexes, Bruce et al.[210] prepared a series of unsaturated C_n chain units capped by the same or different ML_n groups at each end. The buta-1,3-diyne ligand, which is amenable to substitution, has proved to be a suitable reagent, and a series of W and Mo complexes of the form [M(C≡CC≡



Scheme 45. Homo- and heterobimetallic alkynyls featuring Group 6 metals.

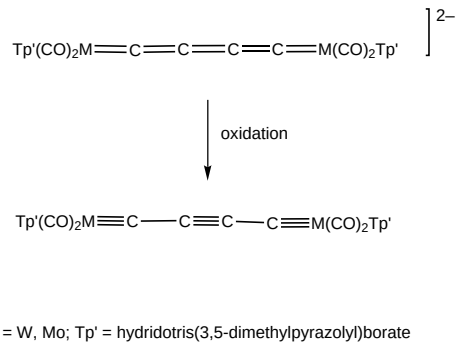
 © 2003 Wiley-VCH Verlag GmbH & Co. KGaA, Weinheim



Scheme 46. Half-sandwich tungsten and molybdenum buta-1,3-diyl complexes. M = W, Mo.

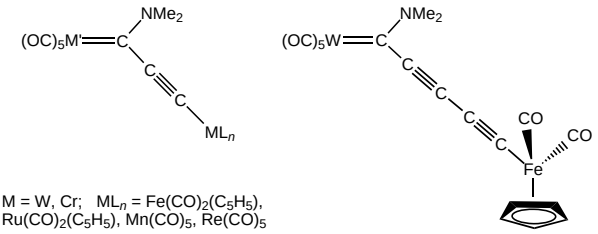
CH)$(CO)_3$Cp] have been efficiently prepared (Scheme 46). The terminal alkynyl complexes undergo facile cross-coupling reactions with aryl and vinyl halides in the presence of basic amines and a mixed Cu^I/Pd^0 catalyst. There is also the possibility of oxidative homocoupling under the mild Hay conditions (CuCl/TMED/O_2); the tetraynediyl complexes produced are reasonably light-sensitive. Following this, the reactivity of the diynes with $[Co_2(CO)_8]$ shows that one of the C≡C bonds is readily coordinating if the R group on the alkynyl is small enough, and further interaction between the metal carbonyl groups results in the expulsion of CO and the formation of clusters.[211] An interesting series of heterobimetallic systems, largely with C_4 chains, have been formed by using similar Cu^I-catalyzed coupling reactions.[212] A range of end groups can be incorporated, for example, $\{(C_5H_5)W(CO)_3\}$, $\{(C_5H_5)Fe(C_5H_4)\}$,[213] $\{(C_5H_5)Fe(CO)_2\}$, $\{Rh(CO)(PPh_3)_2\}$, and $\{Au(PPh_3)\}$, and the electronic interactions between the metal centers can be investigated.

Templeton and co-workers reported the unusual M≡C–C≡C–C≡M structure, in which two robust carbyne moieties are bridged by an alkynyl unit,[214] through the oxidation of a dianionic C_4 cumulene (Scheme 47). The $(OC)_5W{=}C$ unit has been used by Fischer and co-workers[126,127] to form heterobimetallic complexes with an odd number of carbon atoms in the π-conjugated bridge, that is, C_3R and C_5R species (Scheme 48). Two slightly different routes were developed:



M = W, Mo; Tp' = hydridotris(3,5-dimethylpyrazolyl)borate

Scheme 47. Formation of metal carbyne species with linking alkyne units.

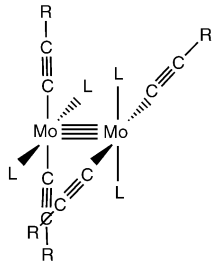


Scheme 48. Heterobimetallic complexes featuring varying lengths of π-conjugated bridge.

1) A Pd-catalyzed coupling of a C-stannylated ethynyl (or butadiynyl) carbene complex with a metal halide, and 2) the nucleophilic substitution of a lithiated ethynyl (or butadiynyl) complex with a metal halide. These methods are only of use for certain complexes, but are useful in not being restricted to carbonyl-containing transition-metal complexes with a strongly electrophilic carbonyl carbon atom, and larger extendable systems should be possible.

Very recently, molybdenum alkynyl complexes have been utilized as alkynyl-transfer reagents.[215] The complexes $[Mo(C{\equiv}CR)(\eta^3\text{-allyl})(CO)_2(phen)]$ feature long $Mo{-}C_{alkynyl}$ bond lengths that can be easily cleaved. Reaction of the Mo alkynyl species (a crystalline nonhygroscopic solid for R = Ph) with trimethyltin chloride efficiently gives $Me_3SnC{\equiv}$CPh, which illustrates its efficiency as an alkynylation reagent. Arene ruthenium alkynyl complexes can also be formed by this synthetic route.

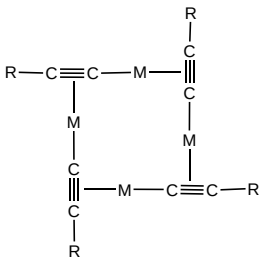
Finally, an unusual series of alkynyl-substituted complexes with quadruple bonds of the type $[M_2(C{\equiv}CR)_4(PMe_3)_4]$ (M = Mo, W; R = alkyl, C_6H_5, $SiMe_3$) have been synthesized (Scheme 49), and the parent C≡CH species was structurally characterized.[216,217]



Scheme 49. Alkynyl-substituted molybdenum complexes featuring Mo–Mo quadruple bonds.

9. Metal Alkynyl Complexes: Cu, Ag, Au

Alkynyl σ complexes of the Group 11 transition metals have been known for some time and are largely synthesized from metal salts and terminal alkynes or alkali-metal reagents.[44,218,219] Their structures are often complicated, such as polymeric systems with alkyne units that are σ-bonded to one metal center and π-bound to another (Scheme 50). Cu^I alkynyls have aroused a lot of interest due to their highly flexible bonding modes,[220,221] with common

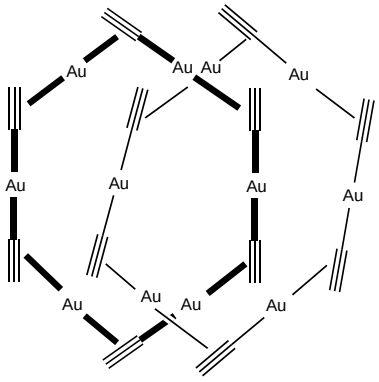


Scheme 50. A schematic structure showing σ- and π-alkynyl metal interactions.

motifs including the μ_3–η^1 type, of which the triangular Cu^I alkynyls $[Cu_3(\mu\text{-dppm})_3(\mu_3\text{–}\eta^1\text{–C}\equiv\text{C–Ph})]^{2+}$[222] and $[Cu_3(\mu\text{-dppm})_3(\mu_3\text{–}\eta^1\text{-C}\equiv\text{C-Ph})_2]^{+}$[223] are known, and those complexes where the alkyne group bridges two copper ions, that is, the $Cu_2(\mu$-alkyne) unit.[224,225]

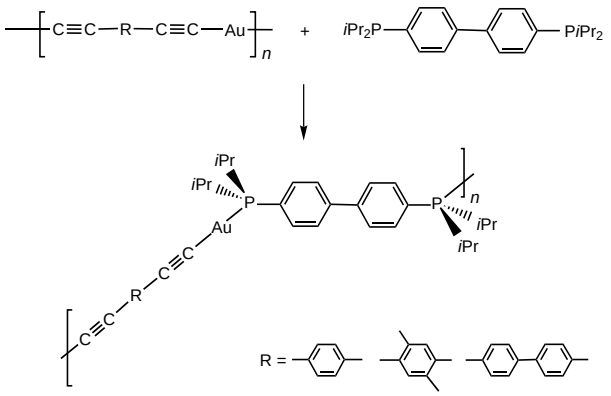
Silver alkynyl complexes are also well known[44,226] and, as for Cu, a series of trinuclear Ag^I alkynyl complexes $[Ag_3(\mu\text{-dppm})_3(\mu_3\text{-}\eta^1\text{-C}\equiv\text{C-R})]^{2+}$ have been reported.[227,228] The molecular structures of Au^I alkynyl complexes tend to be very different from those of their Cu^I and Ag^I analogues. This is because the common coordination geometry of Au^I is either two- (linear) or three-coordinate (trigonal planar). Au^I alkynyl complexes exhibit short Au···Au contacts (owing to relativistic effects) and a wide range of molecular structures.[229,230] In recent years, oligomeric and polymeric conjugated rigid-rod species containing linear Au^I centers have become topical.[231] Mingos et al. have characterized a novel catenane structure of the compound $[\{[Au(C\equiv C\mathit{t}Bu)]_6\}_2]$, where the ethynyl ligands adopt both η^1 and η^2 coordination modes (Scheme 51).[232]

Dinuclear Au^I diarylalkynyl complexes $[Au\text{–}C\equiv C\text{–}Ar\text{–}C\equiv C\text{–}Au]_n$ (Ar = arene spacer group) can be formed from $[AuCl(SMe_2)]$ and the appropriate aryl dialkyne.[233,234] These can then be treated with aryl diidocyanides to form polymers of the type $[Ar\text{–}C\equiv C\text{–}Ar\text{–}C\equiv C\text{–}Au\text{–}C{=}N\text{–}R\text{–}N{=}C]_n$.[233–235] Unfortunately, these polymers suffer from a lack of solubility, which hampers attempts at characterization and most likely results in low-molecular-weight oligomeric materials. However, the dinuclear species $[RN{=}C\text{–}Au\text{–}C\equiv C\text{–}Ar\text{–}C\equiv C\text{–}Au\text{–}C{=}NR]$ and $[RC\equiv C\text{–}Au\text{–}C{=}N\text{–}Ar\text{–}N{=}C\text{–}Au\text{–}C\equiv CR]$ can be characterized, and whilst molecular in solution, the compounds associate in the solid state through π-stacking [235] or intermolecular Au···Au interactions.[233] The weak Au···Au interactions, which arise from relativistic London forces, are thought to have similar strengths to hydrogen bonds (ca. 5–10 kcal mol^{-1}).[236] Such interactions may explain the insolubility of the polymers with the possibility of cross-linking of the linear rigid-rods and formation of a three-dimensional network.



Scheme 51. Schematic structure of the [2]catenane $[\{Au(C\equiv C\mathit{t}Bu)_6\}_2]$.

Analogous diphosphane-bridged structures have been formed either by reacting $[AuC\equiv CArC\equiv CAu]_x$ with the corresponding diphosphanes or from the reactions of gold phosphane halide dimers with the appropriate diethynylarene in the presence of a base[237] (Scheme 52). Atlhough they are



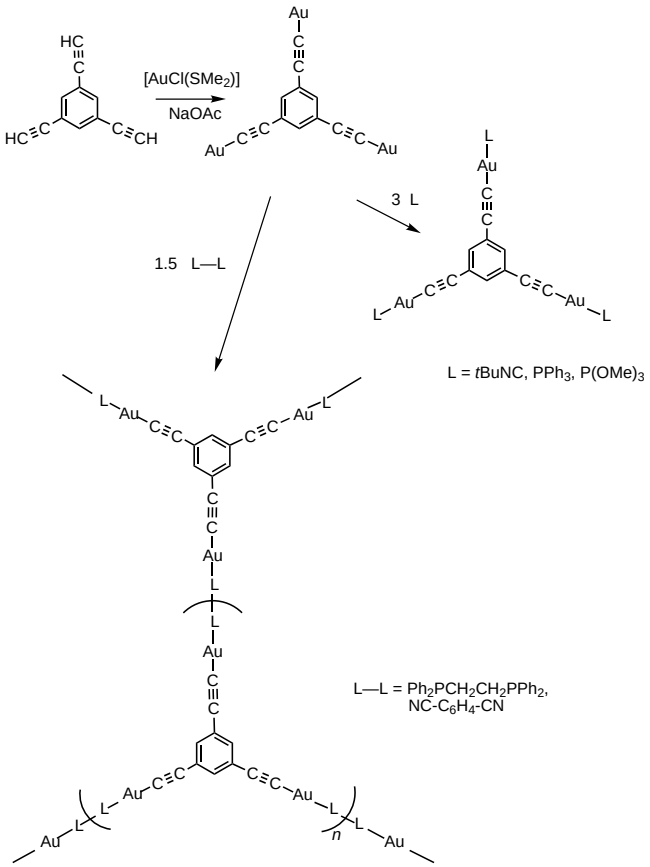
Scheme 52. Synthesis of diphosphane-bridged gold alkynyls.

not strictly linear rigid-rod species, owing to the incorporation of P atoms, models suggest that the polymers have a linear structure about the gold centers, with the diphosphane spacer groups arranged in an *anti* configuration. The species are partially soluble in chlorinated solvents, and have average molecular weights of 15000–18000. Gold-containing rings and catenanes have been formed through fine-tuning of the steric and electronic properties of both the alkynyl species and the other ligands present in the complexes. The self-assembly of gold-containing rings and catenanes has been reported,[238] and further molecular topologies can be expected.

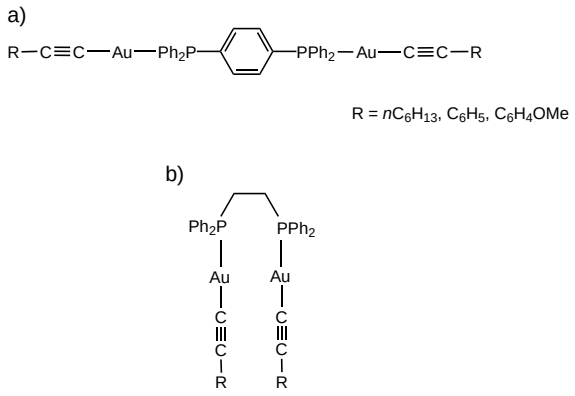
An interesting addition to the topical field of dendrimer chemistry from Puddephatt et al. took trifunctional core molecules, such as 1,3,5-triethynylaurylbenzene, and extended them to polymeric species (Scheme 53).[239] Intramolecular Au···Au separations (3.15 Å), along with strong luminescence and a long-lived excited state[240] were noted for a series of dinuclear and tetranuclear Au^I alkynyl complexes of the form $[Au_2(\mu\text{-dppb})(C\equiv CR)_2]$ and $[Au_4(\mu_4\text{-tppb})(C\equiv CR)_4]$ (dppb = 1,4-bis(diphenylphosphanyl)benzene, tppb = 1,2,4,5-tetrakis(diphenylphosphanyl)benzene; Scheme 54a).

Copper(I) alkynyls have been shown to be suitable for the chemical vapor deposition (CVD) of pure copper films.[241–243] In the search for new materials, a series of mixed-metal Au–Cu alkynyl complexes have been prepared using $[(Ph_3P)AuC\equiv CR]$ (R = organic or organometallic group). Structural characterization shows that the alkynyl ligands

 © 2003 Wiley-VCH Verlag GmbH & Co. KGaA, Weinheim

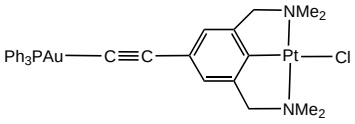


Scheme 53. Formation of gold alkynyl dendrimeric species.



Scheme 54. Gold(I) alkynyls with bridging phosphane groups.

are σ-bonded to the Au^I center and π-bonded to the Cu^I center.[244] In addition, van Koten et al. prepared an interesting series of mixed-metal alkynyl complexes utilizing the anionic, potentially tridentate "NCN" pincer ligand (NCN = 2,6-$(NMe_2)_2$–$C_6H_3CH_2^-$).[245] A Pt center can coordinate to the conjugated π system, and is further stabilized by the N donor units of the ligand framework; such complexes are precursors to a range of heterobimetallic compounds (Scheme 55). Electronic communication between the metal centers is observed and longer chains of repeating metal alkynyl units can be envisaged.



Scheme 55. A heterobimetallic complex with a "NCN" pincer-type ligand.

9.1. Luminescence

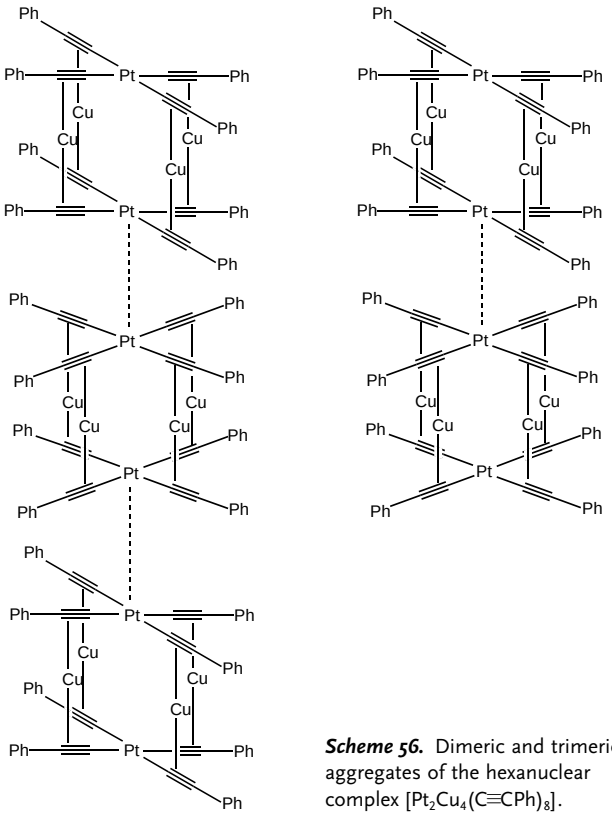
Metal alkynyls of the Group 11 transition metals exhibit interesting photophysical and photochemical properties, in particular luminescence, which have been the subject of a recent review by Yam et al.[21] The trinuclear Cu^I alkynyl complexes $[Cu_3(\mu\text{-dppm})_3(\mu_3\text{-}\eta^1\text{-}C{\equiv}C\text{-}R)_2]$ have long-lived and intense luminescence in both the solid state and in solution, and the alkynyl groups seem to be involved in the formation of excited states in the complexes.[246] The emission is proposed to originate from a LMCT [alkynyl→Cu_3] effect (a rare phenomenon when compared with MLCT, but ubiquitous to the Group 11 alkynyl complexes). This work has been extended to luminescent rigid-rod oligomers based on triangular M_3 building blocks, from which a hexanuclear species $[Cu_3(\mu\text{-dppm})_3(\mu_3\text{-}\eta^1\text{-}C{\equiv}C\text{-}C_6H_4\text{-}C{\equiv}C\text{-}p)Cu_3(\mu\text{-dppm})_3]^{4+}$ was isolated.[247] A very long-lived, intense orange-yellow emission is observed from this complex, and the excited state of the species is proposed to possess substantial ^{3}LMCT (alkynyl→Cu) character, probably in tandem with a metal-centered d–s triplet state.

Compared to their Cu and Au homologues, the photochemistry of Ag^I alkynyl complexes is not well known, largely because of the photosensitivity of many silver compounds. However, tri- and hexanuclear Ag^I alkynyl complexes, analogous to the above copper species, are known. The complexes show strong and long-lived green luminescence upon photoexcitation, which again is largely a result of substantial ^{3}LMCT (alkynyl→Cu/Ag) character in the excited state.

Fornies and co-workers have studied a series of di- and polynuclear alkynyl platinum complexes, in which electrophilic Cu^I, Ag^I, and Au^I centers are π-coordinated to platinum alkynyl complexes (Scheme 56).[248,249] These species can be precursors for polynuclear assemblies, because of the versatility of the alkynyl ligands, which can form strong σ bonds to metal centers and can also coordinate in a η^2 fashion to a second metal fragment. The $[PtCu_4(C{\equiv}CPh)_8]$ cluster exhibits solid-state aggregation via M···M interactions and the dimeric[250] and trimeric[251] structures possess rich luminescent properties.

The photophysics and photochemistry of the luminescent Au^I complexes have been studied in detail. The first report on the luminescence of Au^I alkynyl complexes in 1993 featured the emissive behavior of $[Au_2(\mu\text{-dppe})_2(C{\equiv}C{-}Ph)_2]$ (Scheme 54b).[252] A series of Au^I alkynyl complexes with bridging phosphanes or alkynyl groups has been studied, which were prepared either by the reaction of RC≡CH with the appropriate Au^I chlorophosphane precursor in the presence of a base, or by depolymerization of $[\{Au(C{\equiv}CR)\}_n]$ with the phosphane.[253] The strong luminescence observed ion these

 © 2003 Wiley-VCH Verlag GmbH & Co. KGaA, Weinheim



Scheme 56. Dimeric and trimeric aggregates of the hexanuclear complex $[Pt_2Cu_4(C{\equiv}CPh)_8]$.

complexes is thought to arise from intraligand π–π* (alkynyl ligand) or $^1[\sigma(Au{-}P){\rightarrow}\pi^*$ (alkynyl)] transitions. A metal–metal-bond-to-ligand charge-transfer (MMLCT) $1[d_{\sigma^*}(Au{-}Au){\rightarrow}\pi^*(C{\equiv}C{-}R)]$ assignment is also possible as there is a red shift in the absorption going from the mononuclear to the trinuclear complex.

Puddephatt et al.[235] noted that the rigid-rod conjugated Au^I oligomeric complexes are emissive at room temperature in both the solid state or solution. There is a distinct red shift in the solid state compared to the solution state, which probably results from stacking interactions between the phenyl rings of the alkynyl and isocyanide groups of two neighboring molecules. In the bridging phosphane complexes reported by Yam,[240] it was found that increasing the number of PPh_2 substituents to the central phenyl ring rendered the ring more electron-deficient and caused a red shift in transition energy. The extinction coefficients were roughly parallel to the number of gold alkynyl units in the complexes, which suggests a possible application for these complexes as light-harvesting devices.

9.2. Nonlinear Optics

Humphrey et al. have synthesized a range of Au^I alkynyl σ complexes as part of their continuing investigations into organometallic complexes for nonlinear optics. They have used standard reactions of metal dihalides and terminal alkynes in a sodium methoxide solution to form compounds with a systematic variation in the length and nature of the alkynyl ligand.[165,254,255] NLO measurements on the various metal species found that the trend for the donating power and first-order hyperpolarizability values was in the order: $\{Ru(PPh_3)_2(C_5H_5)\} > \{Ni(PPh_3)(C_5H_5)\} > \{Au(PPh_3)\}$; the Au complexes suffer from weak donor-bridge-acceptor compositions and use of the chiral phosphane (+)-neomenthyldiphenylphosphane did not serve to improve the response.

Third-order NLO properties of silver phenylalkynyl and related complexes were recently reported,[256] in which the response was enhanced by the incorporation of Ag d electrons into the conjugated π system. The magnitude of the response is highly dependent upon the extent of π delocalization, and follows the order: silver phenylacetylide polymer > silver phenylacetylide double salt > polyphenylacetylene polymer > tetrameric triphenylphosphane silver phenylacetylide cluster; this trend can be attributed to the decreasing length of π conjugation.

10. Other Metal Alkynyl Complexes

10.1. Mercury Alkynyl Complexes

Studies of mercury(II) alkynyl complexes are sparse compared to their isoelectronic (Au^I, Ag^I) counterparts.[257] Such complexes were first synthesized in 1926 by the addition of a dilute alcoholic solution of the appropriate alkyne to excess potassium tetraiodo mercurate.[258] Monoalkynyl complexes [Hg(C≡CR)X] can be obtained by a ligand-exchange reaction between HgX_2 and the mercury dialkynyl species $[Hg(C{\equiv}CR)_2]$.[259,260] The characterization of mercury alkynyl complexes is problematic because of their instability ; some NMR studies have been reported,[261] along with limited X-ray crystallographic characterization. The structure of a dimercury dialkynyl complex has been reported recently (Figure 2),

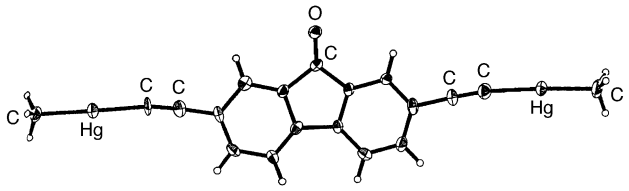


Figure 2. X-ray crystal structure of a dimercury dialkynyl complex.[262]

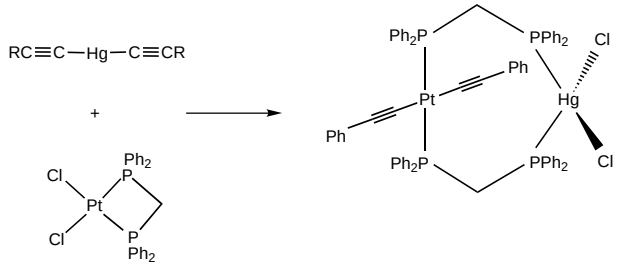
which was prepared by the classical dehydrohalogenation reaction between the alkyne and an alkyl mercury(II) chloride in the presence of a base.[262] Hg^{II} alkynyl complexes possess a strong driving force for aggregation in the solid state, largely through mercurophilic attractions, combined with Hg···C≡C interactions. These species have been utilized for their luminescence,[263] but more importantly as ligand-transfer reagents. The reaction of dialkynyl mercury species and *cis*-$[PtCl_2(CO)L]$ has been thoroughly investigated, and has been shown to occur in a stereospecific fashion (Scheme 57).[264] An unusual alkynyl-transfer reaction is observed between $[Pt(dppm)_2Cl_2]$ and a series of $[Hg(C{\equiv}CR)_2]$ species.[265] The

 © 2003 Wiley-VCH Verlag GmbH & Co. KGaA, Weinheim



Scheme 57. Alkynyl transfer between $[Hg(C{\equiv}CR)_2]$ and *cis*-$[PtCl_2(CO)L]$.

reaction occurs readily and nearly quantitatively, and involves the formation of an eight-membered ring containing both platinum and mercury (Scheme 58).

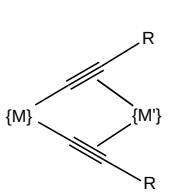


Scheme 58. Alkynyl transfer between $[Hg(C{\equiv}CR)_2]$ and $[Pt(dppm)_2Cl_2]$.

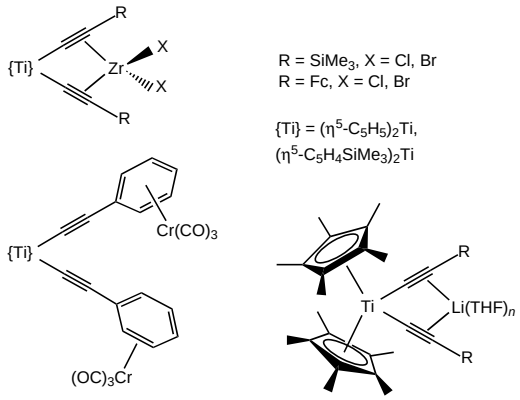
10.2. Titanocene and Zirconocene Alkynyl σ Complexes

Mono- and dialkynyl titanocene complexes of the type $[\{Ti\}(R)(C{\equiv}CR')]$ ($\{Ti\} = (\eta^5\text{-}C_5H_5)_2Ti$, $(\eta^5\text{-}C_5H_4SiMe_3)_2Ti$; $R = Cl$, CH_2SiMe_3; $R' =$ organic group} and $[\{Ti\}\{(C{\equiv}C)_nR''\}_2]$ ($R'' =$ organic group) have been of interest due to their potential use as organometallic "π-tweezers",[266] and as model compounds for the study of intra- and/or intermolecular electron-transfer reactions. These complexes can be used form homo- and, more importantly, heterodinuclear complexes, in which the alkynyl ligand spans the two transition-metal atoms through σ and π bonding.

The alkynyl titanocene σ complexes are prepared by facile substitution of the chloride ligand in titanocene dichloride with the appropriate alkynyl species, usually using classical dehydrohalogenation routes. The coordination properties of the σ-bound alkynyl ligands are of great interest, in that they can also act as π-bonded "tweezer" systems for a range of transition metals (Scheme 59). Interest in the π-bound



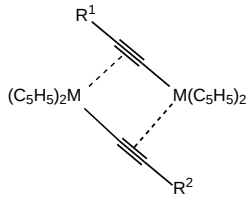
Scheme 59. σ- and π-electrron interactions in alkynyl "tweezer" complexes.



Scheme 60. Examples of σ- and π-bound titanocene-based alkynyl complexes.

coordination chemistry has led to many studies which have been comprehensively reviewed elsewhere,[266,267] and of which some examples are shown in Scheme 60.[268–270]

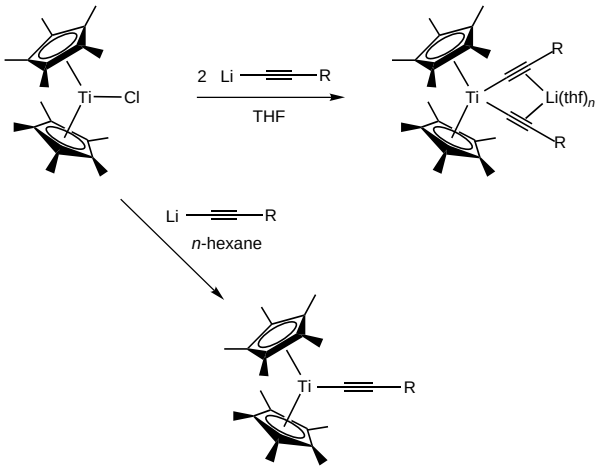
As with the Pt^0 complexes, some interesting single-bond cleavage reactions with early-transition-metal units have been observed, which have been reviewed along with the general chemistry of titanocenes and zirconocene complexes with diynes and polyynes.[37,38] For example, Rosenthal et al.[271] have reported the reaction of the titanocene complex $[Cp_2Ti(Me_3SiC_2SiMe_3)]$ with the disubstituted butadiyne $Me_3SiC{\equiv}CC{\equiv}CSiMe_3$, in which the starting butadiyne is split by the generated "titanocene" to yield the dinuclear complex $[Cp_2Ti(\mu\text{-}\eta^1{:}\eta^2\text{-}C{\equiv}CSiMe_3)]_2$ (Scheme 61). Similar results are



Scheme 61. Dinuclear "metallocene" complexes featuring η^1- and η^2-alkynyl bonding modes.

obtained with the zirconocene analogue. The same research group have also studied the reactivity of the mono(η^1-alkynyl)titanocene(III) complexes $[Cp^*_2Ti(C{\equiv}CR)]$ ($R = Me$, tBu),[272] which were obtained by the salt-elimination reaction of $[Cp^*_2TiCl]$ with $LiC{\equiv}CR$ in hexane; in THF however, the titanium(III) "ate" complexes $[Cp^*_2Ti(C{\equiv}CR)_2Li(thf)_n]$ were formed ($R =$ Ph, tBu, $SiMe_3$; Scheme 62). Reactivity studies are reported with, for example, carbon dioxide, with the ate species ($R = t$Bu) yielding a permethyl titanocene carboxylate complex $[Cp^*_2(OCC{\equiv}Ct\text{Bu})]$ through insertion of CO_2 into the acetylenic σ bond, whereas for $R =$ Ph, reaction with CO_2 gives the stable bisalkynyl permethyl titanocene $[Cp^*_2Ti(C{\equiv}CPh)_2]$ without coupling of the alkynyl groups or insertion of CO_2 into the alkynyl σ bond.[273]

 © 2003 Wiley-VCH Verlag GmbH & Co. KGaA, Weinheim



Scheme 62. Reactions of titanocene(III) chloride with lithium alkynyls.

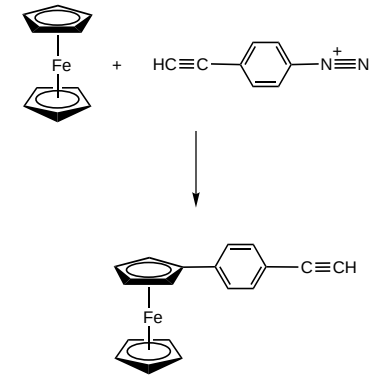
10.3. Alkyne Complexes with Metal Clusters

The reaction of alkynes with metal clusters[274] will not be discussed in this review as η^2 interactions and π bonding predominate, but it should be noted that interesting chemistry, structures, and redox properties are exhibited by, for example, cobalt carbonyl,[275–279] osmium carbonyl[280–284] and ruthenium carbonyl[285–287] complexes, as well as some mixed-metal (Fe, Mo, W) species.[288,289]

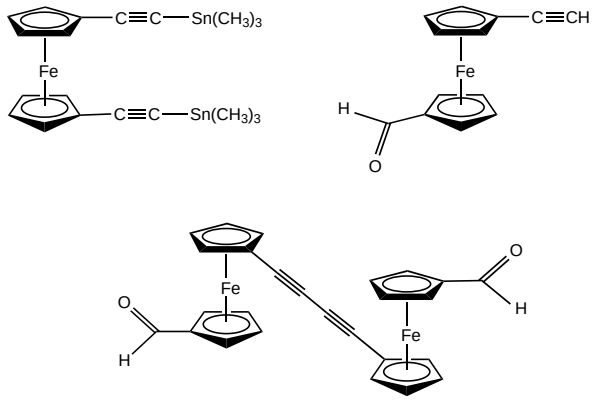
10.4. Ferrocenyl Alkyne Complexes

Ferrocenyl alkyne complexes and their derivatives are not strictly metal alkynyl species, but they have been increasingly investigated in the last decade. Interesting carbon-rich materials or metallo σ-bonded complexes are now well known and have been largely studied for their electronic communication behavior, usually by incorporation of a redox center into one-dimensional delocalized polymers.

The numerous routes to ethynylferrocene and doubly ethynylated species (1,2 or 1,1′-diethynylferrocene) have been summarized.[290] A number of methodologies have been used, which include using acetophenone as a starting material, the conversion of aldehydes into terminal alkynes by Vilsmeier and Wittig reactions, and the dehydration of acetylferrocenes.[291] One direct reaction involves the coupling of ferrocene with a terminal alkyne through a one-pot diazotisation/arylation reaction (Scheme 63). 1,2-Alkynylated ferrocenes[292] are reasonably stable, which contrasts greatly with 1,1′-diethynylferrocene, the instability of which is exemplified in the formation of ansa-ferrocenes with four carbon-atom bridges,[293] and disubstituted alkynylferrocene species, which have only been isolated through the incorporation of alkyl, aryl, thioaryl, or trimethylsilyl groups. The stepwise conversion of functional substituents has recently been investigated using *ortho*-lithiation (with lithium diisopropylamide (LDA)) of bromoferrocene,[294] the stannylation of diethynylferrocenes,[295] and semi-masked acetyl- or formyl-ferrocenyl-substituted alkynes,[290,296] which have



Scheme 63. Formation of ferrocenyl alkynes by "one-pot" diazotization.

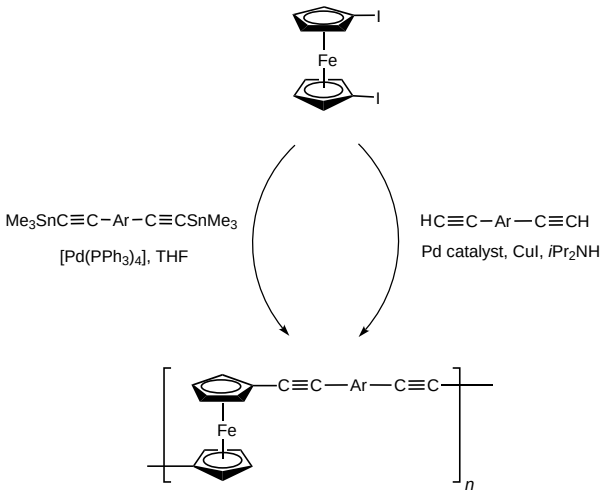


Scheme 64. Semi-masked substituted ferrocenyl alkynes.

shown synthetic value (Scheme 64). Ferrocenyl alkynes have been incorporated into polymers by the Pd-catalyzed polycondensation of 1,1′-dihaloferrocenes with terminal alkynes[297,298] or trimethylstannyl-stabilized species (Scheme 65).[299] Electrochemical oxidation of the polymers highlights that an exchange of electrons exists between the ferrocene units and hence, delocalization along the π-conjugated main chain. The polymers themselves are insulators, but can be converted into semiconducting materials with a conductivity of 10^{-7} to 10^{-4} S cm^{-1} by the formation of adducts with iodine.[298] However, the incorporation of square-planar Pt^{II} units within the polymer structure causes any ferrocene–ferrocene interactions to disappear.[295] Detailed charge-transfer and delocalization studies have been carried out with ferrocenylethynyl end groups that are bridged by, for example, oligothiophene,[300] or substituted fluorene units,[301] the synthesis of which utilizes the usual Pd/Cu-catalyzed coupling routes. To enhance delocalization, the oxidation potentials of the bridge and the metal center should be matched as closely as possible. Analogous ferrocenyl species are known with up to five vinylene–phenylene subunits, which give an effective conjugation pathway of approximately 50 Å, and thus serve as model systems for "molecular wires".[302]

In recent years, the ethynylferrocene ligand and its derivatives have been used to prepare complexes with Pt^{II},[295,303,304] Mn^{I},[305] Ru and Os,[131,306–310]

 © 2003 Wiley-VCH Verlag GmbH & Co. KGaA, Weinheim

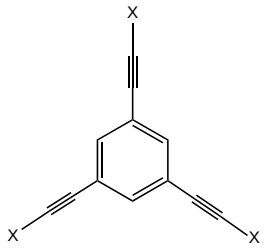


Scheme 65. Pd-catalyzed formation of ferrocenyl polyynes.

$[Co_2(CO)_6]$[276,311,312] and titanocene.[313] Chemical and electrochemical oxidation leads to heterobinuclear mixed-valence complexes,[314] which can generally be described as Robin and Day "Class II" mixed-valence species.[307]

A series of first-generation dendrimers that feature ferrocenyl, ruthenium, and osmium units around the periphery of a 1,3,5-triethynylbenzene core have been synthesized from vinylidenes by Pd/Cu-catalyzed dehydrohalogenation methods (Scheme 66 and Figure 3).[315–317] Electrochemical investigations suggest electronic communication amongst the peripheral metal centers through the organic linkages of the Ru^{II} or Os^{II} derivatives; the analogous ferrocenyl derivatives do not exhibite such behavior as these units appear to act independently of each other.

Experiments to synthesize homo- and heterometallic complexes, in which metal centers are bridged by linear π-conjugated organic groups have led to the development of conjugated pyridyl ligands with end-capping ferrocene groups (Scheme 67).[318–321]



Scheme 66. Ferrocenyl and metal alkynyl complexes featuring a 1,3,5-triethynylbenzene core.

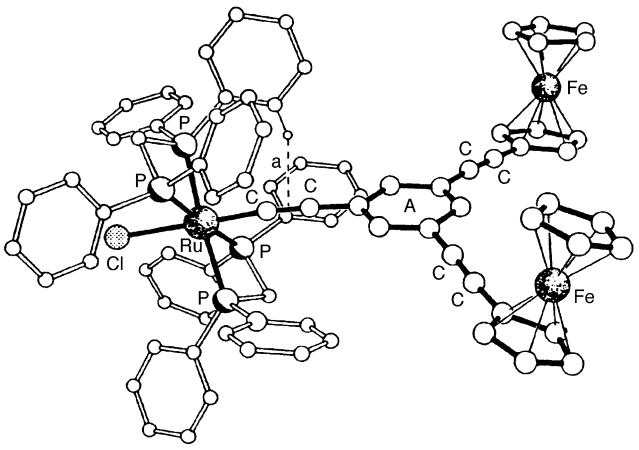
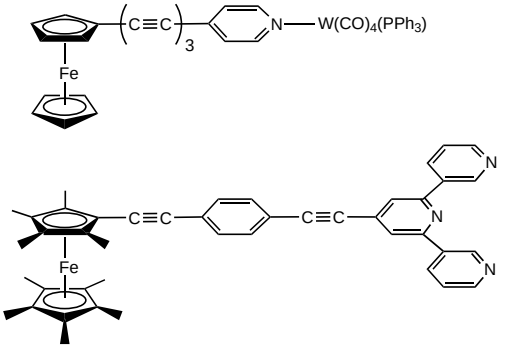


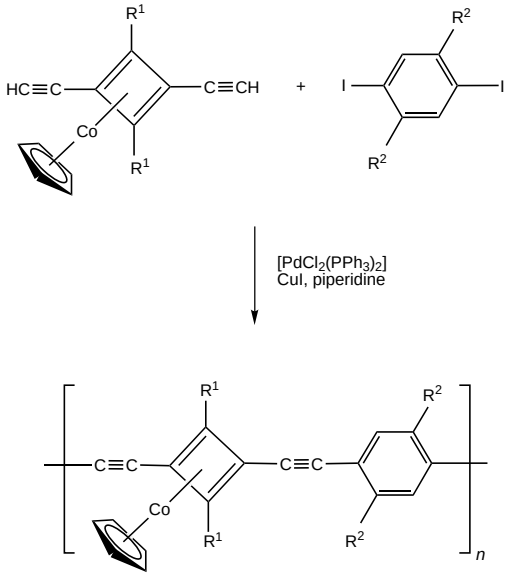
Figure 3. Molecular structure of a trisubstituted species featuring one ruthenium and two ferrocenyl units.[317]



Scheme 67. Ferrocenyl alkynes with pyridyl substituents.

10.5. Half-Sandwich Alkynyl Complexes

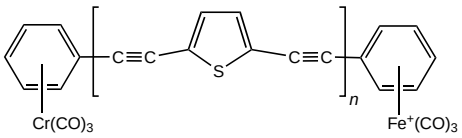
Novel thermotropic liquid crystalline behavior has been exhibited by a series of rigid-rod organocobalt polyynes with complexed cyclobutadiene units in the main chain.[322] Although not direct metal alkynyls, these novel organometallic polymers offer conjugation, unusual aggregation and structural properties, and novel liquid crystalline behavior. The species can be synthesized by CuI-catalyzed dehydrohalogenation, in piperidene with $[PdCl_2(PPh_3)_2]$ (5%) as catalyst (Scheme 68). When thiophene is included in the main



Scheme 68. Synthesis of rigid-rod organocobalt polyynes.

 © 2003 Wiley-VCH Verlag GmbH & Co. KGaA, Weinheim

chain, smectic lyotropic liquid crystalline phases are adopted.[323] By similar palladium-catalyzed coupling reactions bimetallic π-conjugated complexes based on (η^5-cyclohexadienyl)iron cations and (η^6-arene)chromium moieties and joined by alkynyl ligands and aromatic spacers have been formed (Scheme 69).[324] These mixed-metal dipole complexes have been evaluated for nonlinear optical effects by hyper-Rayleigh scattering.

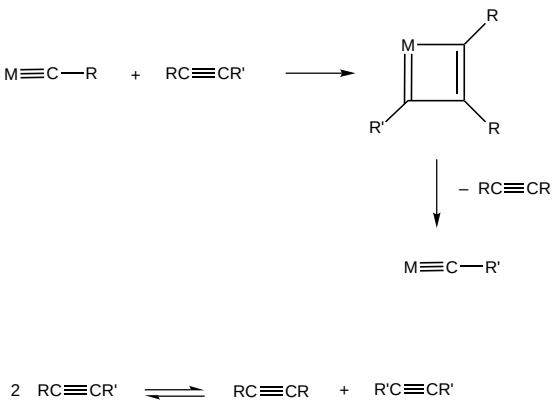


Scheme 69. A mixed-metal dipolar aromatic alkyne.

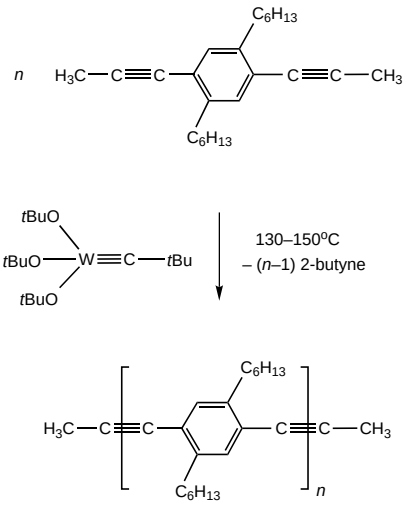
Bunz gives an excellent critique on the palladium-catalyzed coupling of terminal alkynes and aromatic bromides or iodides in amine solvents.[3] Substrate structure and the choice of halide, catalyst, copper co-catalyst, amine, and solvent are all crucial to the effectiveness of the reaction; that is, aryl iodides couple best in the presence of piperidene as base, whilst aryl bromides seem to work better with diisopropylamine. In the review article,[3] Bunz also discusses Mo/W-catalyzed alkyne metathesis, which they have utilized for the formation of high molecular weight poly(aryleneethynylene)s.

10.6. Alkyne Metathesis

Alkyne metathesis is a reaction in which alkylidene components of disubstituted alkynes are scrambled statistically to give all possible alkynes (Scheme 70).[325] These metathesis reactions in homogeneous solution have been known since 1974,[326] but the field only advanced significantly when Schrock et al. showed that well-defined molybdenum– or tungsten–carbyne complexes are active in this metathesis reaction.[327] In 1997, Weiss et al.[328] reported the first use of Schrock's high oxidation state tungsten–carbyne species for the formation of a range of poly(aryleneethynylene)s (Scheme 71) and showed that the method was competitive

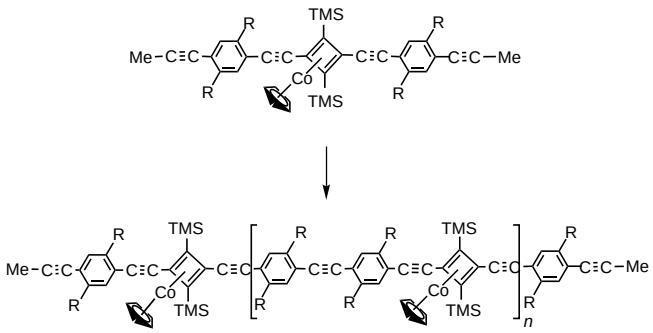


Scheme 70. The alkyne metathesis reaction.



Scheme 71. Formation of poly(arylenethynylene)s by using a tungsten–carbyne alkyne metathesis catalyst.

with Pd-catalyzed couplings. Although the Schrock catalyst is very active at 80 °C, it is also extremely sensitive to air and moisture and so the monomers have to be rigorously dried and purified before use. Thus, simple "instant" catalysts derived from "off-the-shelf" reagents such as [$Mo(CO)_6$] and 4-chlorophenol or 4-trifluoromethylphenol have been developed.[3,329–331] This methodology is very effective for hydrocarbon monomers, though the high temperatures required (130–150 °C) and aggressive phenols/solvents may ultimately lead to degradation of organometallic monomers. However, by diyne metathesis, where the organometallic units are separated by two phenylene–ethynylene groups (Scheme 72), stability and a more robust reagent nature is conferred.

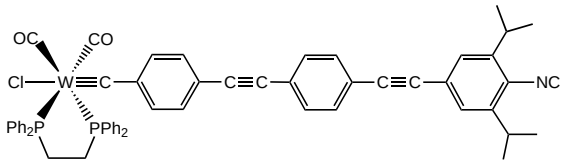


Scheme 72. Formation of organometallic polyynes by using "instant" alkyne metathesis catalysts. TMS = trimethylsilyl.

Another important type of alkyne metathesis reaction, ring-closing alkyne metathesis, has been used especially for the formation of large rings that contain a *cis* double bond. A range of [$Mo\{N(aryl)(tBu)\}_3Cl$] species have been developed as catalysts and shown to be active catalysts at room temperature and tolerant to an array of polar functional groups.[332–335] This method is undoubtedly important for carbon-based systems and although not as ubiquitous as

 © 2003 Wiley-VCH Verlag GmbH & Co. KGaA, Weinheim

alkene metathesis, alkyne metathesis is an attractive option that requires further investigation. Future work will surely include developments aimed at more metal alkynyl systems, following the W-catalyzed alkyne metathesis reaction reported by Selegue and Koutsantonis (Section 6.6)[166] and utilizing the type of metal alkylidyne species, as synthesized by Mayr and Yin Yu in 1999 (Scheme 73).[336]



Scheme 73. A tungsten–carbyne species with an aryleneethynyl ligand.

11. Summary and Outlook

In conclusion, it is clear that research into metal alkynyl σ complexes has a great deal to offer in many ways—particularly with regard to synthesizing novel organometallic compounds with unusual molecular topologies and/or unique physical properties. It could be argued that there are now enough M−C≡C− bond-forming reactions to choose from. Virtually all the transition metals can be reacted to form metal alkynyl complexes with the palladium- and/or copper-catalyzed dehydrohalogenation routes being a clear favorite as there is application to many metal centers. Other routes, such as using trimethylstannyl reagents or via vinylidene intermediates are generally more limited in their application to the middle/late transition metals and to ruthenium and osmium, respectively. Methods that utilize alkynyliodoinium triflates or the elimination of small molecules (CH_4, H_2, or N_2) that have to date been specific for certain transition metals may yet be applied more widely, but the growing interest in alkyne metathesis is most likely to provide novel synthetic development in M−C≡C− bond formation.

Greater advances are expected in designing the shape and reactivity of the transition metal centers. Linear rigid-rod polymers are the "backbone" of this field but chiral compounds, well-characterized and -defined polymers and block co-polymers, and three-dimensional multimetallic structures all featuring metal alkynyls are significantly underdeveloped, if known at all.

In our opinion, it is the application of metal alkynyls to materials science that will show the greatest advances in the next decade or so. The formation of larger, extended, conjugated networks will improve intramolecular electron transfer and hopefully demonstrate that these "molecular wires" can have true technological importance in optic and electronic building blocks. The design of new topological structures and arrays could lead to nanoscale materials with unique catalytic and mechanical properties. With the development of "supramolecular chemistry" and sophisticated X-ray diffraction techniques, strategic metal/ligand design can only improve and excite. The materials properties that are already known such as optical nonlinearity, luminescence, and liquid crystallinity will continue to be focussed upon and enhanced through greater processability and a better understanding of structure–property relationships. There will surely also be further, as yet undiscovered, physical and material properties of these complexes and this combined with greater control and design of molecular topologies and innovative chemical synthesis ensures a bright and exciting future for metal alkynyls.

The majority of this review was written in September 2001 during a study visit/lecture tour based at the University of Hong Kong. N.J.L. is grateful to the Royal Society of Chemistry for a Journals Grant to Authors that financed the visit and to Professors Vivian Yam and Wing-Tak Wong for their kind hospitality in the Department of Chemistry, University of Hong Kong.

Received: May 29, 2002 [A537]

[1] R. Nast, *Coord. Chem. Rev.* **1982**, *47*, 89.
[2] *Modern Acetylene Chemistry* (Eds.: P. J. Stang, F. Diederich), VCH, Weinheim, **1995**.
[3] U. H. F. Bunz, *Chem. Rev.* **2000**, *100*, 1605, and references therein.
[4] N. Hagihara, K. Sonogashira, S. Takahashi, *Adv. Polym. Sci.* **1981**, *41*, 151.
[5] R. P. Kingsborough, T. W. Swager, *Prog. Inorg. Chem.* **1999**, *48*, 123.
[6] P. Nguyen, P. Gomez-Elipe, I. Manners, *Chem. Rev.* **1999**, *99*, 1515.
[7] U. H. F. Bunz, Y. Rubin, Y. Tobe, *Chem. Soc. Rev.* **1999**, *28*, 107.
[8] C. Bruneau, P. H. Dixneuf, *Acc. Chem. Res.* **1999**, *32*, 311.
[9] *J. Organomet. Chem.* **1999**, *578* (special issue: "Carbon-rich Organometallics").
[10] I. Manners, *Angew. Chem.* **1996**, *108*, 1712; *Angew. Chem. Int. Ed. Engl.* **1996**, *35*, 1602.
[11] P. F. H. Schwab, M. D. Levin, J. Michl, *Chem. Rev.* **1999**, *99*, 1869.
[12] T. Yamamoto, *Bull. Chem. Soc. Jpn.* **1999**, *72*, 621.
[13] N. J. Long, *Angew. Chem.* **1995**, *107*, 37; *Angew. Chem. Int. Ed. Engl.* **1995**, *34*, 21.
[14] S. R. Marder in *Inorganic Materials* (Eds.: D. W. Bruce, D. O'Hare), Wiley, Chichester, **1996**, p. 121.
[15] S. Barlow, D. O'Hare, *Chem. Rev.* **1997**, *97*, 637.
[16] I. R. Whittal, A. M. McDonagh, M. G. Humphrey, *Adv. Organomet. Chem.* **1998**, *42*, 291.
[17] M. Younus, A. Kohler, S. Cron, N. Chawdhury, M. R. A. Al-Madani, M. S. Khan, N. J. Long, R. H. Friend, P. R. Raithby, *Angew. Chem.* **1998**, *110*, 3180; *Angew. Chem. Int. Ed.* **1998**, *37*, 3036.
[18] J. Lewis, M. S. Khan, A. K. Kakkar, B. F. G. Johnson, T. B. Marder, H. B. Fyfe, F. Wittmann, R. H. Friend, A. E. Day, *J. Organomet. Chem.* **1992**, *425*, 165.
[19] N. Chawdhury, A. Kohler, R. H. Friend, M. Younus, N. J. Long, P. R. Raithby, J. Lewis, *Macromolecules* **1998**, *31*, 722.
[20] V. W. W. Yam, K. K. W. Lo, K. M. C. Wong, *J. Organomet. Chem.* **1999**, *578*, 3.
[21] V. W. W. Yam, *Acc. Chem. Res.* **2002**, *35*, 555.
[22] M. J. Irwin, J. J. Vittal, R. J. Puddephatt, *Organometallics* **1997**, *16*, 3541.
[23] F. Paul, C. Lapinte, *Coord. Chem. Rev.* **1998**, *178–180*, 431.
[24] D. W. Bruce in *Inorganic Materials* (Eds.: D. W. Bruce, D. O'Hare), Wiley, Chichester, **1996**, 429.

 © 2003 Wiley-VCH Verlag GmbH & Co. KGaA, Weinheim

[25] G. Jaouen, A. Marinetti, B. Mentzen, R. Muin, S.-Y. Saillard, B. G. Sayer, M. J. McGlinchey, *Organometallics* **1982**, *1*, 753.
[26] S. J. Chiang, Y. Chi, P. C. Su, S. M. Peng, G. H. Lee, *J. Am. Chem. Soc.* **1994**, *116*, 11181.
[27] T. Wiedmann, V. Weinrich, B. Wagner, C. Robl, W. Beck, *Chem. Ber.* **1991**, *124*, 1363.
[28] M. I. Bruce, G. A. Koutsantonis, E. R. T. Tiekink, *J. Organomet. Chem.* **1991**, *407*, 391.
[29] P. J. Low, K. A. Udachin, G. D. Enright, A. J. Carty, *J. Organomet. Chem.* **1999**, *578*, 103.
[30] P. J. Low, M. I. Bruce, *Adv. Organomet. Chem.* **2002**, *48*, 71.
[31] S. Lotz, P. H. van Rooyen, R. Meyer, *Adv. Organomet. Chem.* **1995**, *37*, 219.
[32] M. I. Bruce, *Chem. Rev.* **1991**, *91*, 197.
[33] H. Werner, *Angew. Chem.* **1990**, *102*, 1109; *Angew. Chem. Int. Ed. Engl.* **1990**, *29*, 1077.
[34] D. Touchard, P. H. Dixneuf, *Coord. Chem. Rev.* **1998**, 178–180, 409.
[35] M. I. Bruce, *Chem. Rev.* **1998**, *99*, 2797.
[36] H. Lang, M. Weinmann, *Synlett* **1996**, 1.
[37] R. Choukroun, P. Cassoux, *Acc. Chem. Res.* **1999**, *32*, 494.
[38] U. Rosenthal, P.-M. Pellny, F. G. Kircbauer, V. V. Burlakov, *Acc. Chem. Res.* **2000**, *33*, 119.
[39] J. Manna, K. J. John, M. D. Hopkins, *Adv. Organomet. Chem.* **1995**, *38*, 79.
[40] G. Frapper, M. Kertesz, *Inorg. Chem.* **1993**, *32*, 732.
[41] D. L. Lichtenberger, S. K. Renshaw, A. Wong, C. D. Tagge, *Organometallics* **1993**, *12*, 3522.
[42] D. L. Lichtenberger, S. K. Renshaw, R. M. Bulluck, *J. Am. Chem. Soc.* **1993**, *115*, 3276.
[43] M. L. H. Green, *Organometallic Compounds* (Eds.: G. E. Coates, M. L. H. Green, K. Wade), Methuen, London, 3rd. ed., **1968**.
[44] M. I. Bruce, R. Clark, J. Howard, P. Woodward, *J. Organomet. Chem.* **1972**, *42*, C107.
[45] O. M. Abu Salah, M. I. Bruce, *J. Chem. Soc. Dalton Trans.* **1974**, 2302.
[46] P. J. Kim, H. Masai, K. Sonogashira, N. Hagihara, *Inorg. Nucl. Chem. Lett.* **1970**, *6*, 181.
[47] D. C. Green, U. Englisch, K. Ruhlandt-Senge, *Angew. Chem.* **1999**, *111*, 345; *Angew. Chem. Int. Ed.* **1999**, *38*, 354.
[48] K. Sonogashira, T. Yatake, Y. Tohda, S. Takahashi, N. Hagihara, *J. Chem. Soc. Chem. Commun.* **1977**, 291.
[49] K. Sonogashira, N. Hagihara, S. Takahashi, *Macromolecules* **1977**, *10*, 879.
[50] a) K. Sonogashira, Y. Fujikura, T. Yatake, N. Toyoshima, S. Takahashi, N. Hagihara, *J. Organomet. Chem.* **1978**, *145*, 101; b) Y. Fujikura, K. Sonogashira, N. Hagihara, *Chem. Lett.* **1975**, 1067.
[51] K. Sonogashira, S. Kataoka, S. Takahashi, N. Hagihara, *J. Organomet. Chem.* **1978**, *160*, 319.
[52] S. Takahashi, H. Morimoto, E. Murata, S. Kataoka, K. Sonogashira, N. Hagihara, *J. Polym. Sci. Polym. Chem. Ed.* **1982**, *20*, 565.
[53] A. S. Hay, *J. Org. Chem.* **1962**, *27*, 3320.
[54] S. Takahashi, E. Murata, K. Sonogashira, N. Hagihara, *J. Polym. Sci. Polym. Chem. Ed.* **1980**, *18*, 661.
[55] K. Sonogashira, K. Ohga, S. Takahashi, N. Hagihara, *J. Organomet. Chem.* **1980**, *188*, 237.
[56] K. Osakada, R. Sakata, T. Yamamoto, *Organometallics* **1997**, *16*, 5354.
[57] K. Osakada, M. Hamada, T. Yamamoto, *Organometallics* **2000**, *19*, 458.
[58] "Nonlinear Optical Properties of Polmers": A. J. Heeger, J. Orenstein, D. R. Ulrich, *Mater. Res. Soc. Symp. Proc.* **1987**, 109.
[59] *Nonlinear Optical and Electroactive Polymers* (Eds.: P. N. Prasad, D. R. Ulrich), Plenum, New York, **1988**.
[60] S. Guha, C. C. Frazier, P. L. Porter, K. Kang, S. Finberg, *Opt. Lett.* **1989**, *14*, 952.
[61] C. C. Frazier, S. Guha, W. P. Chen, M. P. Cockerham, P. L. Porter, E. A. Chauchard, C. H. Lee, *Polymer* **1987**, *28*, 553.
[62] W. J. Blau, H. J. Byrne, D. J. Cardin, A. P. Davey, *J. Mater. Chem.* **1991**, *1*, 245.
[63] R. D'Amato, A. Furlani, M. Colapietro, G. Portalone, M. Casalboni, M. Falconieri, M. V. Russo, *J. Organomet. Chem.* **2001**, *627*, 13.
[64] S. M. Anaroni, *Macromolecules* **1979**, *12*, 94.
[65] S. Takahashi, E. Murata, M. Kariya, K. Sonogashira, N. Hagihara, *Macromolecules* **1979**, *12*, 1016.
[66] S. Takahashi, H. Morimoto, Y. Takai, K. Sonogashira, N. Hagihara, *Mol. Cryst. Liq. Cryst.* **1981**, *72*, 101.
[67] A. Abe, N. Kimura, S. Tabata, *Macromolecules* **1991**, *24*, 6238.
[68] S. Takahashi, Y. Takai, H. Morimoto, K. Sonogashira, N. Hagihara, *Mol. Cryst. Liq. Cryst.* **1982**, *82*, 139.
[69] S. Takahashi, Y. Takai, H. Morimoto, K. Sonogashira, *J. Chem. Soc. Chem. Commun.* **1984**, 3.
[70] M. S. Khan, A. K. Kakkar, N. J. Long, J. Lewis, P. Raithby, P. Nguyen, T. B. Marder, F. Wittmann, R. H. Friend, *J. Mater. Chem.* **1994**, *4*, 1227.
[71] N. J. Long, A. J. P. White, D. J. Williams, M. Younus, *J. Organomet. Chem.* **2002**, *649*, 94.
[72] C. J. Adams, S. L. James, P. R. Raithby, *Chem. Commun.* **1997**, 2155.
[73] C. J. Adams, S. L. James, X. Liu, P. R. Raithby, L. J. Yellowlees, *J. Chem. Soc. Dalton Trans.* **2000**, 63.
[74] M. Karikoni, C. Kitamura, S. Tanaka, Y. Yamashita, *J. Am. Chem. Soc.* **1995**, *117*, 6791.
[75] W.-Y. Wong, W.-K. Wong, P. R. Raithby, *J. Chem. Soc. Dalton Trans.* **1998**, 2761.
[76] W.-Y. Wong, S.-M. Chan, K.-H. Choi, K.-W. Cheah, W.-K. Chan, *Macromol. Rapid Commun.* **2000**, *21*, 453.
[77] W.-Y. Wong, W. T. Wong, K. K. Cheung, *J. Chem. Soc. Dalton Trans.* **1995**, 1379.
[78] W.-Y. Wong, K.-H. Choi, K.-W. Cheah, *J. Chem. Soc. Dalton Trans.* **2000**, 113.
[79] A. Ferri, G. Polzoneeti, S. Licoccia, R. Paolesse, D. Favretto, P. Traldi, M. V. Russo, *J. Chem. Soc. Dalton Trans.* **1998**, 4063.
[80] W.-Y. Wong, K. -H. Choi, G.-L. Lu, J. -X. Shi, *Macromol. Rapid Commun.* **2001**, *22*, 461.
[81] K. A. Bunten, A. K. Kakkar, *J. Mater. Chem.* **1995**, *5*, 2041.
[82] K. A. Bunten, A. K. Kakkar, *Macromolecules* **1996**, *29*, 2885.
[83] E. Baratt, E. A. Boudreaux, J. N. Demas, P .G. Lenhert, C. M. Lukehart, A. T. McPhail, D. R. McPhail, J. B. Myers, L. Sacksteder, W. R. True, *Organometallics* **1989**, *8*, 2417.
[84] L. Sacksteder, E. Baratt, B. A. DeGraff, C. M. Lukehart, J. N. Demas, *Inorg. Chem.* **1991**, *30*, 2468.
[85] H. Masai, K. Sonogashira, N. Hagihara, *Bull. Chem. Soc. Jpn.* **1971**, *44*, 2226.
[86] V. W. W. Yam, L. P. Chau, T. F. Lai, *Organometallics* **1993**, *12*, 2197.
[87] V. W. W. Yam, P. K. Y. Yeung, L. P. Chan, W. M. Kwok, D. L. Phillips, K. L. Yu, R. W. K. Wong, H. Yan, Q. J. Meng, *Organometallics* **1998**, *17*, 2590.
[88] N. W. Alcock, T. J. Kemp, P. G. Pringle, P. Bergamini, O. Traverso, *J. Chem. Soc. Dalton Trans.* **1987**, 1659.
[89] B. Cetinkaya, M. F. Lappert, J. McMeeking, D. E. Palmer, *J. Chem. Soc. Dalton Trans.* **1973**, 1202.
[90] B. F. G. Johnson, A. K. Kakkar, M. S. Khan, J. Lewis, A. E. Dray, R. H. Friend, F. Wittmann, *J. Mater. Chem.* **1991**, *1*, 485.
[91] S. J. Davies, B. F. G. Johnson, M. S. Khan, J. Lewis, *J. Chem. Soc. Chem. Commun.* **1991**, 187.
[92] M. S. Khan, S. J. Davies, A. K. Kakkar, D. Schwartz, B. Lin, B. F. G. Johnson, J. Lewis, *J. Organomet. Chem.* **1992**, *424*, 87.
[93] M. E. Wright, *Macromolecules* **1989**, *22*, 3256.

 © 2003 Wiley-VCH Verlag GmbH & Co. KGaA, Weinheim

[94] A. Sebald, C. Stader, B. Wrackmeyer, *J. Organomet. Chem.* **1986**, *311*, 233.
[95] B. Rybtchinski, D. Milstein, *Angew. Chem.* **1999**, *111*, 98; *Angew. Chem. Int. Ed.* **1999**, *38*, 870.
[96] J. J. Garcia, W. D. Jones, *Organometallics* **2000**, *19*, 5544, and references therein.
[97] C. Muller, C. N. Iverson, R. J. Lachicotte, W. D. Jones, *J. Am. Chem. Soc.* **2001**, *123*, 9718.
[98] C. Muller, R. J. Lachicotte, W. D. Jones, *Organometallics* **2002**, *21*, 1190.
[99] M. S. Khan, S. J. Davies, A. K. Kakkar, D. Schwartz, B. Lin, B. F. G. Johnson, J. Lewis, *J. Organomet. Chem.* **1992**, *425*, 165.
[100] M. S. Khan, N. A. Pasha, A. K. Kakkar, P. R. Raithby, J. Lewis, K. Fuhrmann, R. H. Friend, *J. Mater. Chem.* **1992**, *2*, 759.
[101] D. Zargarian, P. Chow, N. J. Taylor, T. B. Marder, *J. Chem. Soc. Chem. Commun.* **1989**, 540.
[102] H. B. Fyfe, M. Mlekuz, D. Zargarian, N. J. Taylor, T. B. Marder, *J. Chem. Soc. Chem. Commun.* **1991**, 188.
[103] H. F. Klein, H. H. Karsch, *Chem. Ber.* **1975**, *108*, 944.
[104] T. B. Marder, D. Zargarian, J. C. Calabrese, T. H. Herskovitz, D. Milstein, *J. Chem. Soc. Chem. Commun.* **1987**, 1484.
[105] P. J. Stang, C. M. Crittell, *Organometallics* **1990**, *9*, 3191.
[106] P. J. Stang, R. Tykwinski, *J. Am. Chem. Soc.* **1992**, *114*, 4411.
[107] C. Bianchini, A. Meli, M. Peruzzini, F. Zanobini, P. Zanello, *Organometallics* **1990**, *9*, 241.
[108] C. Bianchini, F. Laschi, F. Ottaviani, M. Peruzzini, P. Zanello, *Organometallics* **1988**, *7*, 1660.
[109] C. Bianchini, D. Masi, A. Meli, M. Peruzzini, J. A. Ramirez, A. Vacca, F. Zanobini, *Organometallics* **1989**, *8*, 2179.
[110] T. Rappert, O. Nurnberg, H. Werner, *Organometallics* **1993**, *12*, 1359.
[111] O. Gevert, J. Wolf, H. Werner, *Organometallics* **1996**, *15*, 2806.
[112] S. J. Davies, B. F. G. Johnson, J. Lewis, P. R. Raithby, *J. Organomet. Chem.* **1991**, *414*, C51.
[113] B. F. G. Johnson, A. K. Kakkar, M. S. Khan, J. Lewis, *J. Organomet. Chem.* **1991**, *409*, C12.
[114] Z. Atherton, C. W. Faulkner, S. L. Ingham, A. K. Kakkar, M. S. Khan, J. Lewis, N. J. Long, P. R. Raithby, *J. Organomet. Chem.* **1993**, *462*, 265.
[115] A. J. Hodge, S. L. Ingham, A. K. Kakkar, M. S. Khan, J. Lewis, N. J. Long, D. G. Parker, P. R. Raithby, *J. Organomet. Chem.* **1995**, *488*, 205.
[116] M. Younus, N. J. Long, P. R. Raithby, J. Lewis, *J. Organomet. Chem.* **1998**, *570*, 55.
[117] M. Younus, N. J. Long, P. R. Raithby, J. Lewis, N. A. Page, A. J. P. White, D. J. Williams, M. C. B. Colbert, A. J. Hodge, M. S. Kahn, D. G. Parker, *J. Organomet. Chem.* **1999**, *578*, 198.
[118] M. C. B. Colbert, J. Lewis, N. J. Long, P. R. Raithby, M. Younus, A. J. P. White, D. J. Williams, N. N. Payne, L. Yellowlees, D. Beljonne, N. Chawdhury, R. H. Friend, *Organometallics* **1998**, *17*, 3034.
[119] Y. Sun, N. J. Taylor, A. J. Carty, *Organometallics* **1992**, *11*, 4301.
[120] R. Crescenzi, C. Lo Sterzo, *Organometallics* **1992**, *11*, 4301.
[121] E. Viola, C. Lo Sterzo, R. Crescenzi, G. Frackey, *J. Organomet. Chem.* **1995**, *493*, 55.
[122] E. Viola, C. Lo Sterzo, F. Trezzi, *Organometallics* **1996**, *15*, 4352.
[123] C. Lo Sterzo, *J. Chem. Soc. Dalton Trans.* **1992**, 1989.
[124] J. K. Stille, *Angew. Chem.* **1986**, *98*, 504; *Angew. Chem. Int. Ed. Engl.* **1986**, *25*, 505.
[125] J. K. Stille, J. H. Simpson, *J. Am. Chem. Soc.* **1987**, *109*, 2138.
[126] C. Hartbaum, G. Roth, H. Fischer, *Chem. Ber.* **1997**, *130*, 479.
[127] C. Hartbaum, H. Fischer, *Chem. Ber.* **1997**, *130*, 1063.
[128] C. Lo Sterzo, *Synlett* **1999**, *11*, 1704.
[129] P. Haquette, N. Pirio, D. Touchard, L. Toupet, P. H. Dixneuf, *J. Chem. Soc. Chem. Commun.* **1993**, 163.
[130] D. Touchard, C. Morice, V. Cadierno, P. Haquette, L. Toupet, P. H. Dixneuf, *J. Chem. Soc. Chem. Commun.* **1994**, 859.
[131] O. Lavastre, M. Even, P. H. Dixneuf, A. Pacreau, J. Vairon, *Organometallics* **1996**, *15*, 1530.
[132] O. Lavastre, J. Plass, P. Bachmann, S. Guesmi, C. Moinet, P. H. Dixneuf, *Organometallics* **1997**, *16*, 184.
[133] D. Touchard, P. Haquette, S. Guesmi, L. Le Pichon, A. Daridor, L. Touplet, P. H. Dixneuf, *Organometallics* **1997**, *16*, 3640.
[134] A. M. McDonagh, I. R. Whittall, M. G. Humphrey, B. W. Skelton, A. H. White, *J. Organomet. Chem.* **1996**, *519*, 229.
[135] A. M. McDonagh, I. R. Whittall, M. G. Humphrey, D. C. R. Hockless, B. W. Skelton, A. H. White, *J. Organomet. Chem.* **1996**, *523*, 33.
[136] A. M. McDonagh, M. P. Cifuentes, I. R. Whittall, M. G. Humphrey, M. Samoc, B. Luther-Davies, D. C. R. Hockless, *J. Organomet. Chem.* **1996**, *526*, 99.
[137] I. R. Whittall, M. G. Humphrey, S. Houbrechts, J. Maes, A. Persoons, S. Schmid, D. C. R. Hockless, *J. Organomet. Chem.* **1997**, *544*, 277.
[138] S. K. Hurst, M. P. Cifuentes, J. P. L. Morrell, N. T. Lucas, I. R. Whittall, M. G. Humphrey, I. Asselberghs, A. Persoons, M. Samoc, B. Luther-Davies, A. C. Willis, *Organometallics* **2001**, *20*, 4664, and references therein.
[139] A. M. McDonagh, M. G. Humphrey, M. Samoc, B. Luther-Davies, *Organometallics* **1999**, *18*, 5195.
[140] A. M. McDonagh, M. G. Humphrey, M. Samoc, B. Luther-Davies, S. Houbrechts, T. Wada, H. Sasabe, A. Persoons, *J. Am. Chem. Soc.* **1999**, *121*, 1405.
[141] M. B. Robin, P. Day, *Adv. Inorg. Chem. Radiochem.* **1967**, *10*, 247.
[142] Y. Zhu, D. B. Millet, M. O. Wolf, S. J. Rettig, *Organometallics* **1999**, *18*, 1930.
[143] M. V. Baker, L. D. Field, D. J. Young, *J. Chem. Soc. Chem. Commun.* **1988**, 546.
[144] M. V. Baker, L. D. Field, *J. Organomet. Chem.* **1988**, *354*, 31.
[145] L. D. Field, A. V. George, T. W. Hambley, E. Y. Malouf, D. J. Young, *J. Chem. Soc. Chem. Commun.* **1990**, 931.
[146] L. D. Field, A. V. George, E. Y. Malouf, I. H. Slip, T. W. Hambley, *Organometallics* **1991**, *10*, 3842.
[147] L. D. Field, A. V. George, *J. Organomet. Chem.* **1993**, *454*, 217.
[148] C. Bianchini, D. Mesi, M. Peruzzini, F. Zanobini, P. Frediani, *Organometallics* **1994**, *13*, 4616.
[149] T. Rappert, A. Yamamoto, *Organometallics* **1994**, *13*, 4984.
[150] J. Espuelas, M. A. Esteruelas, F. J. Lahoz, L. A. Oro, C. Valero, *Organometallics* **1993**, *12*, 663.
[151] L. D. Field, A. V. George, F. Laschi, E. Y. Malouf, P. Zanello, *J. Organomet. Chem.* **1992**, *435*, 347.
[152] M. Y. Choi, M. C. W. Chan, S. Zhang, K. K. Cheung, C. M. Che, K. Y. Wong, *Organometallics* **1999**, *18*, 2074.
[153] S. G. Davies, J. P. McNally, A. J. Smallridge, *Adv. Organomet. Chem.* **1990**, *30*, 1.
[154] M. I. Bruce, R. C. Wallis, *Aust. J. Chem.* **1979**, *32*, 1471.
[155] M. I. Bruce, A. G. Swincer, *Adv. Organomet. Chem.* **1983**, *22*, 59.
[156] M. I. Bruce, G. A. Koutsantonis, *Aust. J. Chem.* **1991**, *44*, 207.
[157] W. M. Laidlaw, R. G. Denning, T. Verbiest, E. Chauchard, A. Persoons, *Nature* **1993**, *363*, 58.
[158] J. T. Lin, S. S. Sun, J. J. Wu, L. S. Lee, K. J. Lin, Y. F. Huang, *Inorg. Chem.* **1995**, *34*, 2323.
[159] J. T. Lin, S. S. Sn, J. J. Wu, Y. C. Liaw, K. J. Lin, *J. Organomet. Chem.* **1996**, *517*, 217.
[160] I. Y. Wu, J. T. Lin, J. Luo, S. S. Sun, C. S. Li, K. J. Lin, C. Tsai, C. C. Hsu, J. L. Lin, *Organometallics* **1997**, *16*, 2038.
[161] H. P. Xia, W. F. Wu, W. S. Ng, I. D. Williams, G. Jia, *Organometallics* **1997**, *16*, 2940.
[162] M. I. Bruce, P. J. Low, K. Costuas, J.-F. Halet, S. P. Best. G. A. Heath, *J. Am. Chem. Soc.* **2000**, *122*, 1949.

[163] I. R. Whittall, M. P. Cifuentes, M. J. Costigan, M. G. Humphrey, S. C. Goh, B. W. Skelton, A. H. White, *J. Organomet. Chem.* **1994**, *471*, 193.
[164] I. R. Whittall, M. G. Humphrey, D. C. R. Hockless, B. W. Skelton, A. H. White, *Organometallics* **1995**, *14*, 3970.
[165] M. G. Humphrey, I. R. Whittall, *Organometallics* **1996**, *15*, 1935.
[166] G. A. Koutsantonis, J. P. Selegue, *J. Am. Chem. Soc.* **1991**, *113*, 2316.
[167] H. Le Bozec, K. Ouzzine, P. H. Dixneuf, *Organometallics* **1991**, *10*, 2768.
[168] D. Carmona, C. Vega, F. J. Lahoz, R. Atencio, L. A. Oro, M. P. Lamata, F. Viguri, E. San Jose, *Organometallics* **2000**, *19*, 2273.
[169] C. Menendez, D. Morales, J. Perez, V. Riera, D. Miguel, *Organometallics* **2001**, *20*, 2775.
[170] N. Le Narvor, C. Lapinte, *J. Chem. Soc. Chem. Commun.* **1993**, 357.
[171] N. Le Narvor, C. Lapinte, *Organometallics* **1995**, *14*, 634.
[172] T. Weyland, C. Lapinte, G. Frapper, M. J. Calhorda, J. F. Halet, L. Toupet, *Organometallics* **1997**, *16*, 2024.
[173] T. Weyland, K. Costuas, A. Mari, J. F. Halet, C. Lapinte, *Organometallics* **1998**, *17*, 5569.
[174] T. Weyland, K. Costuas, L. Toupet, J. F. Halet, C. Lapinte, *Organometallics* **2000**, *19*, 4228.
[175] R. Denis, L. Toupet, F. Paul, C. Lapinte, *Organometallics* **2000**, *19*, 4240.
[176] R. Denis, T. Weyland, F. Paul, C. Lapinte, *J. Organomet. Chem.* **1997**, *545–546*, 615.
[177] S. Le Stang, D. Lenz, F. Paul, C. Lapinte, *J. Organomet. Chem.* **1999**, *572*, 189.
[178] T. Weyland, I. Ledoux, S. Brasselet, J. Zyss, C. Lapinte, *Organometallics* **2000**, *19*, 5235.
[179] M. Akita, M. C. Chung, A. Sakaurai, S. Sugimoto, M. Terada, M. Tanaka, Y. Moro-oka, *Organometallics* **1997**, *16*, 4882.
[180] M. Sakurai, M. Akita, Y. Moro-oka, *Organometallics* **1999**, *18*, 3241.
[181] M. I. Bruce, D. A. Harbourne, F. Waugh and F. G. A. Stone, *J. Chem. Soc. A* **1968**, 353.
[182] N. A. Ustnyuk, V. N. Vinogradova, P. V. Petrovski, *Izv. Akad. Nauk SSSR Ser. Khim.* **1982**, *3*, 680.
[183] D. Miguel, V. Riera, *J. Organomet. Chem.* **1985**, *293*, 379.
[184] H. Lang, *Angew. Chem.* **1994**, *106*, 569; *Angew. Chem. Int. Ed. Engl.* **1994**, *33*, 547.
[185] W. Beck, B. Niemer, M. Wieser, *Angew. Chem.* **1993**, *105*, 969; *Angew. Chem. Int. Ed. Engl.* **1993**, *32*, 923.
[186] U. Bunz, *Angew. Chem.* **1996**, *108*, 1047; *Angew. Chem. Int. Ed. Engl.* **1996**, *35*, 969.
[187] For example: W. Weng, T. Bartik, M. T. Johnson, A. M. Arif, J. A. Gladysz, *Organometallics* **1995**, *14*, 889.
[188] T. Bartik, B. Bartik, M. Brady, R. Dembinski, J. A. Gladysz, *Angew. Chem.* **1996**, *108*, 487; *Angew. Chem. Int. Ed. Engl.* **1996**, *35*, 414.
[189] M. Brady, W. Weng, Y. Zhou, J. W. Seyler, A. J. Amoroso, A. M. Arif, M. Bohme, G. Frenking, J. A. Gladysz, *J. Am. Chem. Soc.* **1997**, *119*, 775.
[190] W. E. Meyer, A. J. Amoroso, C. R. Horn, M. Jaeger, J. A. Gladysz, *Organometallics* **2001**, *20*, 1115.
[191] G. Eglinton, W. McCrae, *Adv. Org. Chem.* **1963**, *4*, 225.
[192] P. Cadiot, W. Chodkiewicz in *Chemistry of Acetylenes* (Ed.: H. G. Viehe), Marcel Dekker, New York, **1969**.
[193] For overview: K. Sonogashira in *Metal Catalyzed Cross-Coupling Reactions* (Eds.: F. Diederich, P. J. Stang), Wiley-VCH, Weinheim, **1998**.
[194] R. Dembinski, T. Lis, S. Szafert, C. L. Mayne, T. Bartik, J. A. Gladysz, *Organometallics* **1999**, *578*, 229.
[195] R. Dembinski, S. Szafert, P. Haquette, T. Lis, J. A. Gladysz, *Organometallics* **1999**, *18*, 5438.
[196] T. Bartik, W. Weng, J. A. Ramsden, S. Szafert, S. B. Falloon, A. M. Arif, J. A. Gladysz, *J. Am. Chem. Soc.* **1998**, *120*, 11071.
[197] S. B. Falloon, S. Szafert, A. M. Arif, J. A. Gladysz, *Chem. Eur. J.* **1998**, *4*, 1033.
[198] R. Dembinski, T. Bartik, B. Bartik, M. Jaeger, J. A. Gladysz, *J. Am. Chem. Soc.* **2000**, *122*, 810.
[199] J. Heidrich, M. Steimann, A. Appel, W. Beck, J. R. Phillips, W. C. Trogler, *Organometallics* **1990**, *9*, 1296.
[200] V. W. W. Yam, V. C. Y. Lau, K. K. Cheung, *Organometallics* **1995**, *14*, 2749.
[201] V. W. W. Yam, *Chem. Commun.* **2001**, 789.
[202] V. W. W. Yam, S. H. F. Chong, K. K. Cheung, *Chem. Commun.* **1998**, 2121.
[203] V. W. W. Yam, S. H. F. Chong, *Organometallics* **2000**, *19*, 5092.
[204] V. W. W. Yam, W. K. M. Fung, K. M. C. Wong, V. C. Y. Lau, K. K. Cheung, *Chem. Commun.* **1998**, 727.
[205] J. K. Ruff, *Inorg. Chem.* **1968**, *7*, 1821.
[206] J. K. Ruff, *Inorg. Chem.* **1969**, *8*, 86.
[207] J. K. Ruff, *Inorg. Chem.* **1971**, *10*, 387.
[208] A. Hills, D. L. Hughes, N. Kashef, M. A. N. D. A. Lemos, A. J. L. Pombeiro, R. L. Richards, *J. Chem. Soc. Dalton Trans.* **1992**, 1775.
[209] M. C. Chen, Y. J. Sai, C. T. Chen, Y. C. Lin, T. W. Tseng, G. H. Lee, Y. Wang, *Organometallics* **1991**, *10*, 378.
[210] M. I. Bruce, M. Ke, P. J. Low, B. W. Skelton, A. H. White, *Organometallics* **1998**, *17*, 3539.
[211] M. I. Bruce, J.-F. Halet, S. Kahlal, P. J. Low, B. W. Skelton, A. H. White, *J. Organomet. Chem.* **1999**, *578*, 155.
[212] M. I. Bruce, B. C. Hall, P. J. Low, M. E. Smith, B. W. Skelton, A. H. White, *Inorg. Chim. Acta* **2000**, *300–302*, 633.
[213] M. I. Bruce, M. E. Smith, B. W. Skelton, A. H. White, *J. Organomet. Chem.* **2001**, *637–639,* 484.
[214] B. E. Woodworth, P. S. White, J. L. Templeton, *J. Am. Chem. Soc.* **1997**, *119*, 828.
[215] J. Perez, L. Riera, V. Riera, S. Garcia-Granda, E. Garcia-Rodriguez, D. Miguel, *Chem. Commun.* **2002**, 384.
[216] T. C. Stoner, R. F. Dallinger, M. D. Hopkins, *J. Am. Chem. Soc.* **1990**, *112*, 5651.
[217] T. C. Stoner, S. J. Geib, M. D. Hopkins, *Angew. Chem.* **1993**, *105*, 457; *Angew. Chem. Int. Ed. Engl.* **1993**, *32*, 409.
[218] *Organometallics* (Eds.: C. Elschenbroich, A. Slatzer), VCH, New York, **1989**, **1993**.
[219] For a recent reference on π-coordination of Ag and Cu, see: D. Rais, D. M. P. Mingos, R. Vilar, A. J. P. White, D. J. Williams, *Organometallics* **2000**, *19*, 5209, and references therein.
[220] B. J. Hathaway in *Comprehensive Coordination Chemistry, Vol. 5* (Eds.: G. Wilkinson, R. D. Gillard, J. A. McCleverty), Pergamon, Oxford, **1987**, p. 533.
[221] G. van Koten, S. L. James, J. T. B. H. Jastrzebski in *Comprehensive Organometallic Chemistry II, Vol. 3* (Eds.: E. W. Abel, F. G. A. Stone, G. Wilkinson), Pergamon, Oxford, **1995**, p. 57.
[222] M. P. Gamasa, J. Gimeno, E. Lastra, A. Aguirre, S. Garcia-Granda, *J. Organomet. Chem.* **1989**, *378*, C11.
[223] J. Diez, M. P. Gamasa, J. Gimeno, A. Aguirre, S. Garcia-Granda, *Organometallics* **1991**, *10*, 380.
[224] D. L. Reger, M. F. Huff, *Organometallics* **1990**, *9*, 2807.
[225] D. L. Reger, M. F. Huff, *Organometallics* **1992**, *11*, 69.
[226] R. J. Lancashire in *Comprehensive Coordination Chemistry, Vol. 5* (Eds.: G. Wilkinson, R. D. Gillard, J. A. McCleverty), Pergamon, Oxford, **1987**, p. 775.
[227] V. W. W. Yam, W. K. M. Fung, K. K. Cheung, *Organometallics* **1997**, *16*, 2032.
[228] C. F. Wang, S. M. Peng, C. K. Chan, C. M. Che, *Polyhedron* **1996**, *15*, 1853.
[229] R. J. Puddephatt in *Comprehensive Coordination Chemistry, Vol. 5* (Eds.: G. Wilkinson, R. D. Gillard, J. A. McCleverty), Pergamon, Oxford, **1987**, p. 861.

 © 2003 Wiley-VCH Verlag GmbH & Co. KGaA, Weinheim

[230] A. Grohmann, H. Schmidbaur in *Comprehensive Organometallic Chemistry II, Vol. 3* (Eds.: E. W. Abel, F. G. A. Stone, G. Wilkinson), Pergamon, Oxford, **1995**, p. 1.
[231] R. J. Puddephatt, *Chem. Commun.* **1998**, 1055.
[232] D. M. P. Mingos, J. Yau, S. Menzer, D. J. Williams, *Angew. Chem.* **1995**, *107*, 2045; *Angew. Chem. Int. Ed. Engl.* **1995**, *34*, 1894.
[233] M. J. Irwin, G. Jia, N. C. Payne, R. J. Puddephatt, *Organometallics* **1996**, *15*, 51.
[234] G. Jia, N. C. Payne, J. J. Vittal, R. J. Puddephatt, *Organometallics* **1993**, *12*, 4771.
[235] M. J. Irwin, J. J. Vittal, R. J. Puddephatt, *Organometallics* **1997**, *16*, 3541.
[236] J. Li, P. Pyykko, *Chem. Phys. Lett.* **1992**, *197*, 586.
[237] G. Jia, R. J. Puddephatt, J. D. Scott, J. J. Vittal, *Organometallics* **1993**, *12*, 3565.
[238] C. P. McArdle, M. C. Jennings, J. J. Vittal, R. J. Puddephatt, *Chem. Eur. J.* **2001**, *7*, 3572.
[239] M. J. Irwin, L. Manojlovic-Muir, K. W. Muir, R. J. Puddephatt, D. S. Yufit, *Chem. Commun.* **1997**, 219.
[240] V. W. W. Yam, S. W. K. Choi, K .K. Cheung, *Organometallics* **1996**, *15*, 1734.
[241] A. Jain, K.-M. Chi, T. T. Kodas, M. J. Hampden-Smith, J. D. Farr, M. F. Paffett, *Chem. Mater.* **1991**, *3*, 995.
[242] H. K. Shin, K.-M. Chi, J. Farkas, M. J. Hampden-Smith, T. T. Kodas, E. N. Duesler, *Inorg. Chem.* **1992**, *31*, 424.
[243] H. Lang, K. Kohler, L. Zsolnai, *Chem. Ber.* **1995**, *128*, 519.
[244] H. Lang, S. Kochler, S. Back, G. Rheinwald, G. van Koten, *Organometallics* **2001**, *20*, 1968.
[245] S. Back, R. A. Gossage, H. Lang, G. van Koten, *Eur. J. Inorg. Chem.* **2000**, 1457.
[246] V. W. W. Yam, W. K. M. Tung, K. K. Cheung, *Organometallics* **1998**, *17*, 3293.
[247] V. W. W. Yam, W. K. M. Fung, K. K. Cheung, *Chem. Commun.* **1997**, 963.
[248] J. Fornies, E. Lalinde, *J. Chem. Soc. Dalton Trans.* **1996**, 2587.
[249] I. Ara, J. Fornies, J. Gomez, E. Lalinde, M. T. Moreno, *Organometallics* **2000**, *19*, 3137.
[250] V. W. W. Yam, K.-L. Yu, K.-K. Cheung, *J. Chem. Soc. Dalton Trans.* **1999**, 2913.
[251] J. P. H. Charmant, J. Fornies, J. Gomez, E. Lalinde, R. I. Merino, M. T. Moreno, A. G. Orpen, *Organometallics* **1999**, *18*, 3353.
[252] D. Li, X. Hong, C. M. Che, W. C. Lo, S. M. Peng, *J. Chem. Soc. Dalton Trans.* **1993**, 2929.
[253] V. W. W. Yam, S. W. K. Choi, *J. Chem. Soc. Dalton Trans.* **1996**, 4227.
[254] I. R. Whittall, M. G. Humphrey, M. Samoc, B. Luther-Davies, D. C. R. Hockless, *J. Organomet. Chem.* **1997**, *544*, 189.
[255] R. H. Naulty, M. P. Cifuentes, M. G. Humphrey, S. Houbrechts, C. Boulton, A. Persoons, G. A. Heath, D. C. R. Hockless, B. Luther-Davies, M. Samoc, *J. Chem. Soc. Dalton Trans.* **1997**, 4146.
[256] B. K. Teo, Y. H. Xu, B. Y. Zhong, Y. K. He, H. Y. Chen, W. Qian, Y. J. Deng, Y. H. Zhou, *Inorg. Chem.* **2001**, *40*, 6794.
[257] D. Rais, Ph.D. Thesis, Imperial College, London, **2002**.
[258] J. R. Johnson, W. L. McEwen, *J. Am. Chem. Soc.* **1926**, *48*, 469.
[259] Y. Imai, K. Aida, *Bull. Chem. Soc. Jpn.* **1979**, *52*, 2875.
[260] M. Cano, E. Squivel, A. Santos Marcias, L. Ballester Reventos, *J. Inorg. Nucl. Chem.* **1977**, *39*, 1153.
[261] A. Sebald, B. Wrackmeyer, *Spectrochim. Acta Part A* **1982**, *38*, 163.
[262] W.-Y. Wong, K.-H. Choi, G.-L. Lu, J.-X. Shi, A.-Y. Lai, S.-M. Chan, *Organometallics* **2001**, *20*, 5446.
[263] F. Bolletta, D. Fabbri, M. Lombardo, L. Prodi, C. Trombini, N. Zaccheroni, *Organometallics* **1996**, *15*, 2415.
[264] R. J. Cross, M. F. Davidson, *J. Chem. Soc. Dalton Trans.* **1986**, 1987.
[265] C. R. Langrick, D. M. McEwan, P. G. Pringle, B. L. Shaw, *J. Chem. Soc. Dalton Trans.* **1983**, 2487.
[266] H. Lang, D. S. A. George, G. Rheinwald, *Coord. Chem. Rev.* **2000**, *206–207*, 101.
[267] H. Lang, T. Stein, *J. Organomet. Chem.* **2002**, *641*, 41.
[268] H. Lang, N. Mansilla, G. Rheinwald, *Organometallics* **2001**, *20*, 1592.
[269] S. Kocher, H. Lang, *J. Organomet. Chem.* **2002**, *641*, 62.
[270] F. G. Kirchbauer, P.-M. Pellny, H. Sun, V. V. Burlakov, P. Arndt, W. Baumann, A. Spannenberg, U. Rosenthal, *Organometallics* **2001**, *20*, 5289.
[271] U. Rosenthal, A. Ohff, W. Baumann, R. Kempe, A. Tillack, V. V. Burlakov, *Organometallics* **1994**, *13*, 2903.
[272] F. G. Kirchbauer, S. Pulst, B. Heller, W. Baumann, U. Rosenthal, *Angew. Chem.* **1998**, *110*, 2029; *Angew. Chem. Int. Ed.* **1998**, *37*, 1925.
[273] F. G. Kirchbauer, P.-M. Pellny, H. Sun, V. V. Burlakov, P. Arndt, W. Baumann, A. Spannenberg, U. Rosenthal, *Organometallics* **2001**, *20*, 5289.
[274] *Metal Clusters in Chemistry, Vols. 1–3* (Eds.: P. Braunstein, L. A. Oro, P. R. Raithby), Wiley-VCH, **1999**.
[275] J. Lewis, B. Lin, M. S. Khan, M. R. A. Al-Mandhary, P. R. Raithby, *J. Organomet. Chem.* **1994**, *484*, 161.
[276] C. J. McAdam, N. W. Duffy, B. H. Robinson, J. Simpson, *Organometallics* **1996**, *15*, 3935.
[277] D. Osella, L. Milone, C. Nervi, M. Ravera, *J. Organomet. Chem.* **1995**, *488*, 1.
[278] D. Osella, G. Cavigiolio, M. Vincenti, A. Vessieres, I. Laios, G. Leclerq, E. Napolitano, R. Fiaschi, G. Jaouen, *J. Organomet. Chem.* **2000**, *595*, 242.
[279] N. Esho, B. Davies, J. Lee, R. Dembinski, *Chem. Commun.* **2002**, 332.
[280] R. D. Adams, B. Qu, *Organometallics* **2000**, *19*, 2411.
[281] R. D. Adams, B. Qu, M. D. Smith, *J. Organomet. Chem.* **2001**, *637–639*, 514.
[282] O. A. Kizas, V. V. Krivyth, E. V. Vorontsov, O. L. Tok, F. M. Dolgushin, A. A. Koridze, *Organometallics* **2001**, *20*, 4170.
[283] D. Braga, F. Grepioni, B. F. G. Johnson, J. Lewis, J. A. Lunnis, *J. Chem. Soc. Dalton Trans.* **1992**, 1101.
[284] T. Bin Wen, Y. K. Cheung, J. Z. Yao, W. T. Wong, Z. Y. Zhou, G. C. Jia, *Organometallics* **2000**, *19*, 3803.
[285] Y. Chi, A. J. Carty, P. Blenkiron, E. Delgado, G. D. Enright, W. Wang, S.-M. Peng, G.-H. Lee, *Organometallics* **1996**, *15*, 5269.
[286] E. Delgado, Y. Chi, W. Wang, G. Hogarth, P. J. Low, G. D. Enright, S.-M. Peng, G. H. Lee, A. J. Carty, *Organometallics* **1998**, *17*, 2936.
[287] E. N. M. Ho, Z. Y. Lin, W. T. Wong, *Chem. Eur. J.* **2001**, *7*, 258.
[288] P. Mathur, M. O. Ahmed, A. K. Dash, M. G. Walawalkar, V. G. Puranik, *J. Chem. Soc. Dalton Trans.* **2000**, 2916.
[289] P. Mathur, *Adv. Organomet. Chem.* **1997**, *41*, 243.
[290] H. Schottenberger, J. Lukasser, E. Reichel, A. Gallis Muller, G. Steiner, H. Koapcka, K. Wurst, K. H. Ongania, K. Kirchner, *J. Organomet. Chem.* **2001**, *637–639*, 558.
[291] G. Doisneau, G. Balavoine, T. Fillebeen-Khan, *J. Organomet. Chem.* **1992**, *425*, 113.
[292] U. H. F. Bunz, *J. Organomet. Chem.* **1995**, *494*, C8.
[293] J. K. Pudelski, M. R. Callstrom, *Organometallics* **1992**, *11*, 2757.
[294] I. R. Butler, A. L. Boyes, G. Kelly, S. C. Quayle, T. Herzig, J. Scewezyk, *Inorg. Chem. Commun.* **1999**, *2*, 403.
[295] N. J. Long, A. J. Martin, R. Vilar, A. J. P. White, D. J. Williams, M. Younus, *Organometallics* **1999**, *18*, 4261.
[296] W. Steffen, M. Laskoski, G. Collins, U. H. F. Bunz, *J. Organomet. Chem.* **2001**, *630*, 132.
[297] T. Yamamoto, T. Morikita, T. Maruyama, K. Kubota, M. Katada. *Macromolecules* **1997**, *30*, 5390.

[298] T. Morikita, T. Yamamoto, *J. Organomet. Chem.* **2001**, *637–639*, 809.
[299] S. L. Ingham, M. S. Khan, J. Lewis, N. J. Long, P. R. Raithby, *J. Organomet. Chem.* **1994**, *470*, 153.
[300] Y. Zhu, M. O. Wolf, *J. Am. Chem. Soc.* **2000**, *122*, 10121.
[301] W.-Y. Wong, G.-L. Lu, K.-F. Ng, C.-K. Wong, K.-H. Choi, *J. Organomet. Chem.* **2001**, *637–639*, 159.
[302] A. Hradsky, B. Bildstein, N. Schuler, H. Schottenberger, P. Jaitner, K.-H. Ongania, K. Wurst, J.-P. Launay, *Organometallics* **1997**, *16*, 392.
[303] W.-Y. Wong, G.-L. Lu, K. F. Ng, K. H. Choi, Z. Lin, *J. Chem. Soc. Dalton Trans.* **2001**, 3250.
[304] C. J. McAdam, E. J. Blackie, J. L. Morgan, S. A. Mole, B. H. Robinson, J. Simpson, *J. Chem. Soc. Dalton Trans.* **2001**, 2362.
[305] M. C. B. Colbert, A. J. Edwards, J. Lewis, N. J. Long, N. A. Page, D. G. Parker, P. R. Raithby, *J. Chem. Soc. Dalton Trans.* **1994**, 2589.
[306] M. C. B. Colbert, S. L. Ingham, J. Lewis, N. J. Long, P. R. Raithby, *J. Chem. Soc. Dalton Trans.* **1994**, 2215.
[307] M. C. B. Colbert, J. Lewis, N. J. Long, P. R. Raithby, A. J. P. White, D. J. Williams, *J. Chem. Soc. Dalton Trans.* **1997**, 99.
[308] E. Ruba, K. Mereiter, R. Schmid, K. Kirchner, H. Schottenberger, *J. Organomet. Chem.* **2001**, *637–639*, 70.
[309] Y. Zhu, O. Clot, M. O. Wolf, G. P. A. Yap, *J. Am. Chem. Soc.* **1998**, *120*, 1812.
[310] D. Osella, R. Robetto, C. Nervi, M. Ravera, R. D'Amato, M. V. Russo, *Inorg. Chem. Commun.* **1998**, *1*, 239.
[311] E. Champeil, S. M. Draper, *J. Chem. Soc. Dalton Trans.* **2001**, 1440.
[312] C. J. McAdam, N. W. Duffy, B. H. Robinson, J. Simpson, *J. Organomet. Chem.* **1997**, *527*, 179.
[313] S. Back, H. Pritzkow, H. Lang, *Organometallics* **1998**, *17*, 41.
[314] M. Sato, Y. Kawata, H. Shintate, Y. Habata, S. Akabori, K. Unoura, *Organometallics* **1997**, *16*, 1693.
[315] H. Fink, N. J. Long, A. J. Martin, G. Opromolla, A. J. P. White, D. J. Williams, P. Zanello, *Organometallics* **1997**, *16*, 2646.
[316] N. J. Long, A. J. Martin, F. Fabrizi de Biani, P. Zanello, *J. Chem. Soc. Dalton Trans.* **1998**, 2017.
[317] N. J. Long, A. J. Martin, A. J. P. White, D. J. Williams, M. Fontani, F. Laschi, P. Zanello, *J. Chem. Soc. Dalton Trans.* **2000**, 3387.
[318] J. T. Lin, J. J. Wu, C.-S. Li, Y. S. Wen, K.-J. Lin, *Organometallics* **1996**, *15*, 5028.
[319] U. Siemeling, U. Vorfeld, B. Neumann, H. G. Stammler, M. Fontani, P. Zanello, *J. Organomet. Chem.* **2001**, *637–639*, 733.
[320] S. Kocher, H. Lang, *J. Organomet. Chem.* **2001**, *637–639*, 198.
[321] S.-S. Sun, D. T. Tran, O. S. Odongo, A. J. Lees, *Inorg. Chem.* **2002**, *41*, 132.
[322] M. Altmann, U. H. F. Bunz, *Angew. Chem.* **1995**, *107*, 603; *Angew. Chem. Int. Ed. Engl.* **1995**, *34*, 569.
[323] M. Altmann, V. Enkelmann, G. Lieser, U. H. F. Bunz, *Adv. Mater.* **1995**, *7*, 726.
[324] J.-P. Tranchier, R. Chavignon, D. Prim, A. Auffrant, J. G. Planas, F. Rose-Munch, E. Rose, G. R. Stephenson, *Tetrahedron Lett.* **2001**, *42*, 3311.
[325] R. R. Schrock, *J. Chem. Soc. Dalton Trans.* **2001**, 2541, and references therein.
[326] U. H. F. Bunz, L. Kloppenburg, *Angew. Chem.* **1999**, *111*, 503; *Angew. Chem. Int. Ed.* **1999**, *38*, 478, and references therein.
[327] S. A. Krouse, R. R. Schrock, *Macromolecules* **1989**, *22*, 2569, and references therein.
[328] K. Weiss, A. Michel, E. M. Auth, U. H. F. Bunz, T. Mangel, K. Mullen, *Angew. Chem.* **1997**, *109*, 520; *Angew. Chem. Int. Ed. Engl.* **1997**, *36*, 506.
[329] W. Steffen, B. Kohler, M. Altmann, U. Scherf, K. Stitzer, H.-C. zur Loye, U. H. F. Bunz, *Chem. Eur. J.* **2001**, *7*, 117.
[330] W. Steffen, U. H. F. Bunz, *Macromolecules* **2000**, *33*, 9518.
[331] G. Brizius, N. G. Pschirer, W. Steffen, K. Stitzer, H.-C. zur Loye, U. H. F. Bunz, *J. Am. Chem. Soc.* **2000**, *122*, 12435.
[332] Y.-C. Tsai, P. L. Diaconescu, C. C. Cummins, *Organometallics* **2000**, *19*, 5260.
[333] C. C. Cummins, *Prog. Inorg. Chem.* **1998**, *47*, 685.
[334] A. Furstner, C. Mathes, C. W. Lehmann, *Chem. Eur. J.* **2001**, *7*, 5299.
[335] A. Fürstner, C. Mathes, C. W. Lehmann, *J. Am. Chem. Soc.* **1999**, *121*, 9453.
[336] A. Mayr, M. P. Yin Yu, *J. Organomet. Chem.* **1999**, *577*, 223.

 © 2003 Wiley-VCH Verlag GmbH & Co. KGaA, Weinheim

Stereoselective Complex Formation

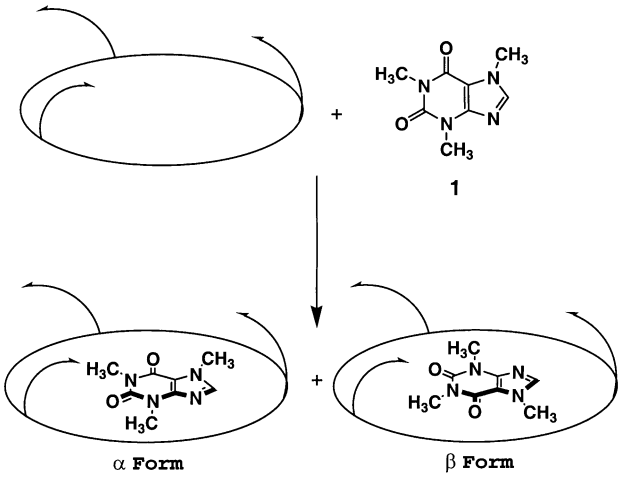
Reversible Enantiofacial Differentiation of a Single Heterocyclic Substrate by Supramolecular Receptors**

*Matthias C. Schopohl, Carsten Siering, Olga Kataeva, and Siegfried R. Waldvogel**

Dedicated to Professor Manfred T. Reetz on the occasion of his 60th birthday

For successful chiral induction in enantioselective transformations, a preceding equilibrium of substrate coordination and recognition is essential. In the case of prochiral substrates the two enantiotopic faces have to be differentiated. A reversible interaction serving this requirement is pivotal for the catalytic use of chiral information. This principle is well established for the coordination of carbonyl groups by Lewis acids.[1] Furthermore, it was successfully applied in transition-metal catalysis to allyl and other multiple bond systems.[2] An extension of that principle towards bigger, aromatic systems turned out to be difficult. Employment of tricarbonylchromium or cyclopentadienyliron fragments results in complex formation at both enantiotopic faces of the π system. Subsequent separation of the enantiomeric complexes provides the pure antipodes. However, these reactions require stoichiometric amounts of the achiral transition-metal reagents, and subsequent resolution of the racemate.[3] Therefore, an alternative is highly desirable; reversible enantiofacial differentiation based on supramolecular interaction could be the key. Self-assembly of supramolecular systems can also involve an enantiofacial discrimination, when some components are chirally modified.[4] Unfortunately, these methods are not applicable to the differentiation of a single molecule.

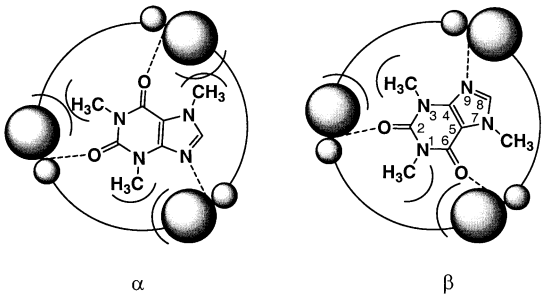
Herein, we present a novel concept for the enantiofacial differentiation of single substrate molecules by supramolecular interactions. Receptors based on triphenylene ketals were employed, these have already been successfully used in the first artificial caffeine receptor (Scheme 1).[5] The huge electron-rich aromatic triphenylene platform, combined with three arms capable of hydrogen bonding, offers molecular recognition of C_3 and pseudo C_3-symmetric electron-deficient guest molecules, such as caffeine (**1**). When a prochiral guest is absorbed by the receptor one of its enantiotopic faces will be pointing towards the triphenylene moiety. This situation gives rise to planar chirality, which influences both the π systems. The two chiral complexes are described as α- and β-form.[6] Interconversion of these isomers requires the dissociation of the complexes. To preferentially form one of these planar chiral aggregates an asymmetric modification of the receptor is required.[7] The resulting diastereomeric complexes with prochiral guests will be detectable by spectroscopic means.



Scheme 1. Illustration of the enantiofacial differentiation of heterocyclic substrates, such as caffeine.

For our investigations caffeine was selected as the guest. The steric demands of the alkyl groups on the hypoxanthine moiety will cause repulsive interactions with the substituents, of various sizes, on the arms of the receptor, and lead to a preferential orientation of the guest in the receptor. (Scheme 2).

For an enantiofacial differentiation it is necessary to place the same stereogenic information close to each of the hydrogen-bond donors because, in terms of binding to the oxygen atom of the C-6 carbonyl group and to the N-9 nitrogen atom, similar steric requirements are necessary. The



Scheme 2. Representation of the interaction between chirally modified receptors and caffeine.

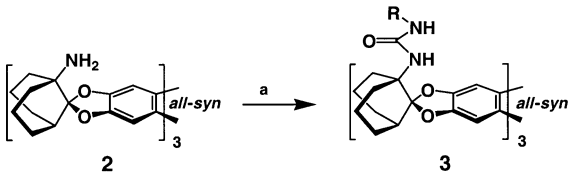
[*] Dr. S. R. Waldvogel, M. C. Schopohl, C. Siering
Westfälische Wilhelms-Universität Münster
Organisch-Chemisches Institut
Corrensstrasse 40, 48149 Münster (Germany)
Fax: (+49) 251-83-39772
E-mail: waldvog@uni-muenster.de.
Dr. O. Kataeva
A. E. Arbuzov Institute of Organic and Physical Chemistry
Russian Academy of Sciences
Arbuzov-Str. 8, Kazan 420088 (Russia)

[**] The work was supported by the Deutsche Forschungsgemeinschaft, the State Nordrhein-Westfalen and the Sonderforschungsbereich 424. Chiral amines were kindly donated by the BASF AG. We cordially thank Birgit Wibbeling for the measurements of the numerous samples for X-ray analysis. We particularly thank Prof. Dr. Dieter Hoppe for the fruitful discussions and the support in this project.

Supporting information for this article is available on the WWW under http://www.angewandte.org or from the author.

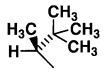
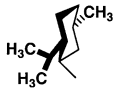
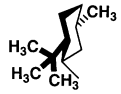
 © 2003 Wiley-VCH Verlag GmbH & Co. KGaA, Weinheim DOI: 10.1002/anie.200351102

synthesis of the optically pure receptors was accomplished by treating α chiral isocyanates[8] with the trisamine **2** (Scheme 3).[5] Column chromatography then provided the analytically pure receptors **3** (Table 1).[9]



Scheme 3. a) RNCO, NEt_3, CH_2Cl_2, 0 °C.

Table 1: Synthesis of the receptors.

Compound	R–	Yield [%]
3a		49
3b		66
3c		63
3d		47

The α chiral substituents on the urea moieties have a preferential conformation in which the differently sized groups are positioned on opposite sides of the urea moiety. The selection of appropriate chiral systems was based on molecular modeling studies.[10] The readily available (*S*)-phenethyl system turned out not to be very efficient as after complex formation the phenyl substituents turn away. The anisotropy effect of the phenyl groups induces remarkably different chemical shifts for the resonance signals of the caffeine methyl groups of the diastereomeric complexes, which were observed in variable-temperature NMR spectroscopy experiments; the resonance signals for the methyl substituents on N-7 differ by 0.25 ppm. A preference for one of the two forms was not detected (Table 2). In receptor **3b** the phenyl groups of **3a** are replaced by *tert*-butyl moieties. At low temperature a distinct enantiofacial differentiation of **1** in **3b** was detected in the NMR spectra, and molecular-modeling studies suggest a significant preference for the β form. This selectivity is caused by the repulsive interaction between the N-7 methyl group of caffeine and the *tert*-butyl fragments of the receptor. The β complex allows a more favorable orientation of these methyl groups of the guest with respect to the smaller substituents of the α chiral subunit.

Table 2: Enantiofacial differentiation in solution.[a]

Host–guest complex	Diastereomeric ratio	Preference[b]
3a+**1**	1:1[c]	–
3b+**1**	3 ± 0.5:1[c]	β
3c+**1**	3.4 ± 0.6:1[d]	α
3d+**1**	≥ 9:1[d]	α

[a] variable temperature ^{1}H NMR spectroscopy: concentration of **3** and **1** each 10 mM in CD_2Cl_2, 360 MHz, 193 K. [b] Molecular-modeling studies. [c] Integrals for the resonance signals of $NH_{(distal)}$ of the receptor and of H-8 of **1** yield consistent results. [d] Difference NMR spectra with [8-D]caffeine.

To improve the enantiofacial differentiation other α chiral subunits, which reach far into the cavity of the receptor were introduced. The (−)-menthol-derived substructure in **3c** has two methyl groups meeting these requirements. Additionally, the six-membered ring has a higher conformational stability. Based on the inverted stereogenic information of the α chiral moiety, the supramolecular complex will prefer the α form. A significant increase of the enantiofacial differentiation is not observed since the isopropyl groups of the menthyl system occupy a specific conformation in which the C–H substituent points into the coordination space which results in a facial discrimination of the same extent as in **3b**. The low-temperature NMR spectra showed an inconvenient overlap of the resonance signals for the caffeine guest and the multiplets of **3c**. Employing [8-D]caffeine circumvented this problem.[11] Comparison of the NMR spectra of both complexes provided the assignment of the imidazole proton of the caffeine. A difference spectrum enables this effect to be quantified (Figure 1).

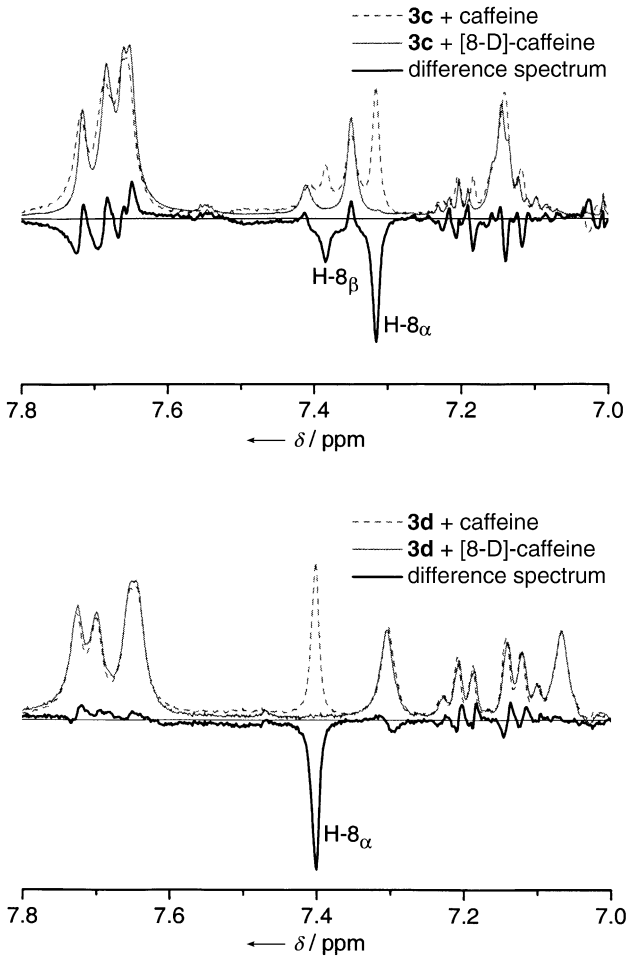


Figure 1. Difference NMR spectra of caffeine and [8-D]caffeine complexes of **3c** (top) and **3d** (bottom).

 © 2003 Wiley-VCH Verlag GmbH & Co. KGaA, Weinheim

By installing the 8-methylmenthyl moiety the remaining C-H unit of **3c** was substituted by a methyl group to give **3d**. The strongly restricted chiral coordination space for the heterocyclic guest leads to an excellent enantiofacial differentiation. However, as a result of the limited resolution of the signals in the NMR spectrum, only a minimum diastereomeric ratio is given (Table 2).

The caffeine complexes of the receptors **3b**–**3d** gave suitable crystals for X-ray analysis.[12] In all the systems these investigations gave a consistent picture of enantiofacial differentiation both in solution as well as in the solid state. Thus for the combination of **3b** with **1**, the crystal structure shows that exclusively the β form is present (Figure 2). When caffeine is placed into the menthyl substituted receptor **3c** it behaves as though it were in a cage. Thus, both diastereomeric forms were found in the crystalline phase. For occupation of the disfavored β form, one arm of the receptor has to turn through about 40°. The caffeine molecule and the arm of the receptor are disordered in this particular complex which is a result of the partial formation of the α complex at this specific position. When a structural relationship between both disorders is anticipated, a cautious estimation reveals a α:β ratio of at least 60:40,[13] which is a direct consequence of the enantiofacial discrimination.

As a result of the installation of a further methyl group into the menthyl system, the host–guest aggregate between **3d** and **1** shows a definite enantiofacial preference, even in the solid state. In the crystal structure the α form was found exclusively as a single independent complex. Through steric interaction with cocrystallized methanol, caffeine is pushed slightly away from the central position in the receptor, and the π systems of both guest and host are tilted by 5.3° from the coplanar arrangement. One arm of the receptor also experiences this change in orientation which contributes to the long-range order in the solid state.

In conclusion, chirally modified receptors based on triphenylene ketals are capable of enantiofacial differentiation of single guest molecules, such as caffeine. An excellent discrimination which arises exclusively from repulsive interactions can be achieved by steric modifications of the cavity. Both spectroscopic studies in solution and investigations of the caffeine complexes in the solid state resulted in a consistent picture of enantiofacial differentiation. The chiral modification of the bicyclic backbone will be the next target to give access to enantiofacially protected substrates and allow the effect to be exploited in catalysis.

Received: February 4, 2003 [Z51102]

Keywords: caffeine · chirality · pi interactions · receptors · supramolecular chemistry

[1] S. Saito, H. Yamamoto in *Modern Carbonyl Chemistry* (Ed.: J. Otera), Wiley-VCH, Weinheim, **2000**, pp. 33–67.
[2] B. M. Trost, M. J. Krische, R. Radinov, G. Zanoni, *J. Am. Chem. Soc.* **1996**, *118*, 6297–6298; W.-H. Fung, W.-Y. Yu, C.-M. Che, *J. Org. Chem.* **1998**, *63*, 7715–7726, and references therein.

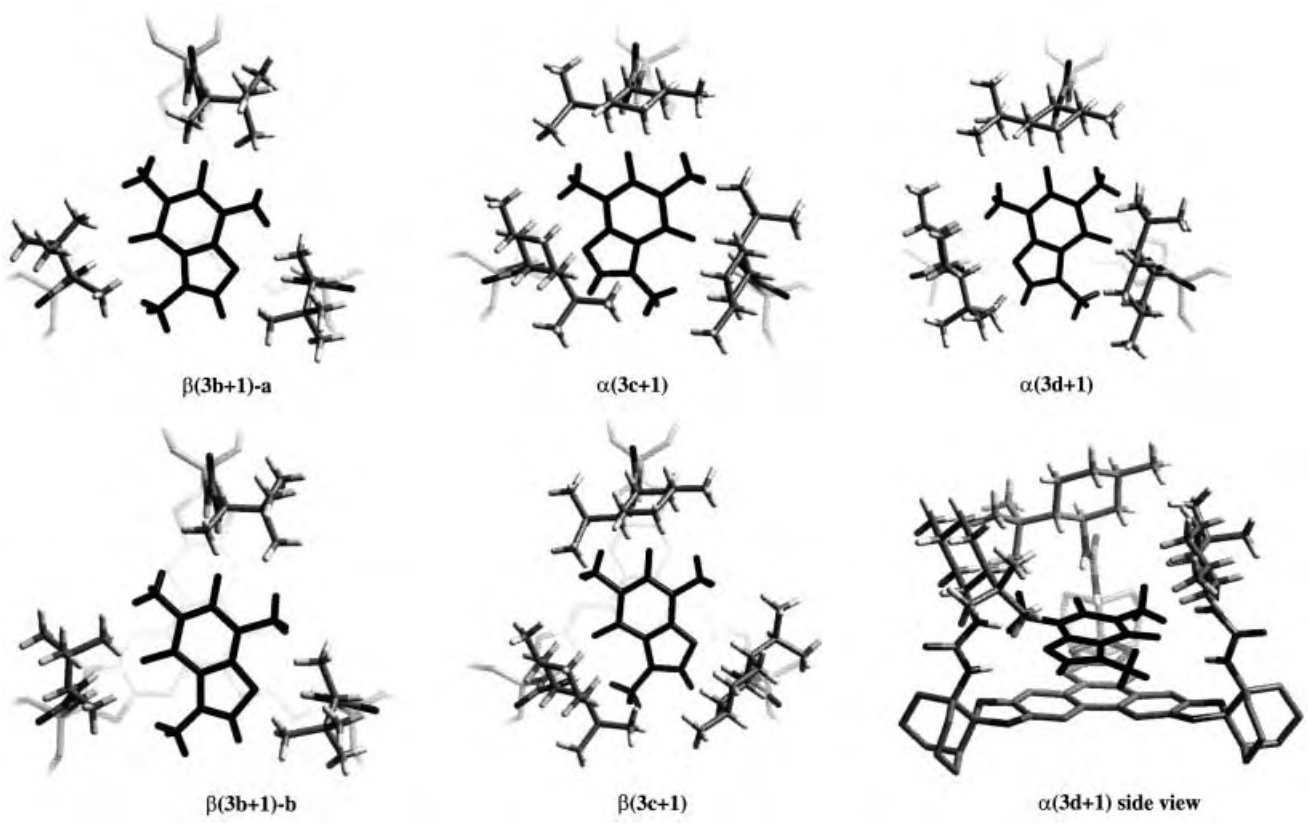


Figure 2. Molecular structures of the caffeine complexes.

 © 2003 Wiley-VCH Verlag GmbH & Co. KGaA, Weinheim

[3] F. Rose-Munch, E. Rose in *Modern Arene Chemistry* (Ed.: D. Astruc), Wiley-VCH, Weinheim, **2002**, pp. 368 – 399; D. Astruc in *Modern Arene Chemistry* (Ed.: D. Astruc), Wiley-VCH, Weinheim, **2002**, pp. 400 – 434.

[4] L. J. Prins, R. Hulst, P. Timmerman, D. N. Reinhoudt, *Chem. Eur. J.* **2002**, *8*, 2288 – 2301; L. J. Prins, J. Huskens, F. De Jong, P. Timmerman, D. N. Reinhoudt, *Nature* **1999**, *398*, 498 – 502; A. L. Marlow, E. Mezzina, G. P. Spada, S. Masiero, J. T. Davis, G. Gottarelli, *J. Org. Chem.* **1999**, *64*, 5116 – 5123.

[5] S. R. Waldvogel, R. Fröhlich, C. A. Schalley, *Angew. Chem.* **2000**, *112*, 2580 – 2583; *Angew. Chem. Int. Ed.* **2000**, *39*, 2472 – 2475.

[6] I. A. Rose, K. R. Hanson, K. D. Wilkinson, M. J. Wimmer, *Proc. Natl. Acad. Sci. USA* **1980**, *77*, 2439 – 2441.

[7] The solid-state structure of the achiral receptor with caffeine is a conglomerate of both racemic complex species (see ref. [5]).

[8] Enantiopure isocyanates were synthesized analogous to: R. Reck, J. C. Jochims, *Chem. Ber.* **1982**, *115*, 860 – 870. (*S*)-phenethylamine und (2*S*)-2-amino-3,3-dimethylbutane were donated by the BASF AG, Ludwigshafen. (1*R*,2*S*,5*R*)-5-Methyl-2-(methylethyl)-cyclohexylamine and (1*R*,2*S*,5*R*)-2-(1,1-dimethylethyl)-5-methyl-cyclohexylamine were obtained by reduction of the oximes: H. Feltkamp, F. Koch, T. N. Thanh, *Justus Liebigs Ann. Chem.* **1967**, *707*, 78 – 86.

[9] **3**: Transformation according to ref. [5]. The subsequent purification of **3a**–**d** was performed by column chromatography on silica using ethyl acetate/cyclohexane or ethyl acetate/toluene elutant mixtures. The solvent molecules of **3a, 3b**, and **3d** were verified by NMR spectroscopy. **3a**: m.p. 245 °C (dec); ^{1}H NMR (400 MHz, $CDCl_3$, 25 °C, TMS): $\delta = 1.09$ (d, 9H, $^3J = 6.8$ Hz, CH_3), 1.65–1.68 (m, 12H, bicycle), 2.02–2.24 (m, 21H, bicycle), 2.83–2.93 (m, 6H, bicycle), 4.37 (s br, 3H, NCH), 4.64–4.68 (m, 6H, N-H), 6.93–7.09 (m, 15H, phenyl), 7.64 (s, 3H, triphenylene), 7.75 ppm (s, 3H, triphenylene); ^{13}C NMR (100 MHz, $CDCl_3$, 25 °C, TMS): $\delta = 20.96$, 21.01, 23.50, 28.26, 34.10, 34.37, 38.03, 50.59, 57.68, 101.47, 102.08, 121.83, 124.55, 124.66, 125.57, 127.00, 128.54, 143.79, 147.26, 147.53, 157.00 ppm; elemental analysis (%) calcd for $C_{72}H_{78}N_6O_9 \cdot 1.5\,H_2O$ (1198.42): C 72.16, H 6.81, N 7.01; found: C 72.04, H 6.60, N 7.14; MS(ES$^+$) *m*/z 1193.7 $[M+Na]^+$; $[\alpha]_D^{20} = +20.2°$ ($c = 0.48$, CH_2Cl_2). **3b**: m.p. 230 °C (dec); ^{1}H NMR (400 MHz, $CDCl_3$, 25 °C, TMS): $\delta = 0.73$ (s, 27H, *t*Bu), 0.84 (d, 9H, $^3J = 6.4$ Hz, CH_3), 1.69–1.71 (m, 12H, bicycle), 2.04–2.31 (m, 21H, bicycle), 2.76–2.86 (m, 6H, bicycle), 3.32 (s br, 3H, NCH), 4.13 (d, 3H, $^3J = 9.2$ Hz, NH_{distal}), 4.38 (s, 3H, $NH_{proximal}$), 7.79 (s, 3H, triphenylene), 7.80 ppm (s, 3H, triphenylene); ^{13}C NMR (100 MHz, $CDCl_3$, 25 °C, TMS): $\delta = 16.54$, 21.01, 21.06, 26.17, 28.30, 28.33, 34.28, 34.35, 34.77, 34.80, 38.26, 53.99, 57.71, 101.68, 122.17, 124.56, 124.71, 147.38, 147.58, 157.14 ppm; elemental analysis (%)calcd for $C_{66}H_{90}N_6O_9 \cdot 0.5\,CH_2Cl_2$(1196.46): C 69.22, H 7.95, N 7.28; found: C 69.00, H 7.81, N 7.10; MS(ES$^+$) *m*/*z* 1112.0 $[M+H]^+$; 1133.9 $[M+Na]^+$; 1149.9 $[M+K]^+$; $[\alpha]_D^{20} = +26.1°$ ($c = 0.55$, CH_2Cl_2). **3c**: m.p. 185 °C (dec); ^{1}H NMR (400 MHz, $CDCl_3$, 25 °C, TMS): $\delta = 0.49$–0.92 (m, 39H, menthyl; selected signals: 0.53 (q, menthyl, $^3J = 12$ Hz), 0.69, 0.70 (d, $^3J = 5.6$ Hz, 6.0 Hz, 9a′-H, 9b′-H), 0.75 (d, $^3J = 7.2$ Hz, 7′-H)), 1.19–1.22 (m, 3H, menthyl), 1.49 (d br, 6H, $^3J = 10$ Hz, menthyl), 1.63–1.87 (m, 6H, menthyl; 12H, bicycle), 2.01–2.34 (m, 21H, bicycle); 2.80–2.90 (m, 6H, bicycle), 3.21 (s br, 3H, 1′-H), 3.84 (d, 3H, $^3J = 8.8$ Hz, NH_{distal}), 4.34 (s br, 3H, $NH_{proximal}$), 7.80 ppm (s, 3H, triphenylene), 7.81 (s, 3H, triphenylene); ^{13}C NMR (100 MHz, $CDCl_3$, 25 °C, TMS): $\delta = 16.04$, 21.02, 21.07, 21.19, 22.09, 23.75, 26.40, 28.35, 28.36, 31.83, 34.28, 34.50, 38.46, 43.90, 48.55, 50.85, 56.16, 58.06, 101.53, 122.16, 124.56, 124.70, 147.47, 147.63, 156.91 ppm; elemental analysis (%) calcd for $C_{78}H_{108}N_6O_9$ (1273.73): C 73.55, H 8.55, N 6.60; found: C 73.27, H 8.54, N 6.28; MS(ES$^+$) *m*/*z* 1274.1 $[M+H]^+$; 1296.1 $[M+Na]^+$; $[\alpha]_D^{20} = -26.9°$ ($c = 0.51$, CH_2Cl_2). **3d**: m.p. 205 °C (dec); ^{1}H NMR (400 MHz, $CDCl_3$, 25 °C, TMS): $\delta = 0.54$–0.98 (m, 48H, menthyl; selected signals: 0.69 (d, $^3J = 5.6$ Hz, 7′-H), 0.79 (s, 9′-H)), 1.19–1.23 (m, 3H, menthyl), 1.43–1.48 (m, 3H, menthyl), 1.64–1.75 (m, 18H, menthyl + bicycle), 2.01–2.33 (m, 21H, bicycle), 2.79–3.05 (m, 6H, bicycle), 3.34 (s br, 3H, 1′-H), 3.68–3.95 (m, 3H, NH_{distal}), 4.34 (s br, 3H, $NH_{proximal}$), 7.76 (s, 3H, triphenylene), 7.82 ppm (s, 3H, triphenylene); ^{13}C NMR (100 MHz, $CDCl_3$, 25 °C, TMS): $\delta = 21.04$, 21.14, 21.87, 27.32, 28.33, 28.38, 29.30, 31.75, 33.04, 34.89, 38.29, 45.36, 51.17, 51.21, 58.00, 101.53, 101.61, 122.07, 124.57, 124.68, 147.58, 147.62, 155.98 ppm; elemental analysis (%) calcd for $C_{81}H_{114}N_6O_9$·toluene·ethylacetate (1496.05): C 73.86, H 8.76, N 5.62; found: C 73.53, H 8.53, N 5.87; MS(ES$^+$) *m*/*z* 1338.9 $[M+Na]^+$; $[\alpha]_D^{20} = -29.8°$ ($c = 0.49$, CH_2Cl_2).

[10] Molecular-modelling studies were performed with MacroModel 7.3. Minimization occurred by employing the AMBER* force field. Molecular-dynamics simulations were applied until convergent energy behavior was reached (300 K, > 5 ns, solvent $CHCl_3$).

[11] [8-D]caffeine: By treatment of 8-bromocaffeine with $LiBD_4$ similar to: G. Chauviere, C. Viode, J. Perie, *J. Heterocycl. Chem.* **2000**, *37*, 119 – 126.

[12] Crystals were obtained by slow evaporation of a solution of equimolar amounts of **3b**–**d** with **1** in cyclohexane/dichloromethane/methanol mixtures. For further details see the Supporting Information. CCDC-202934 for **3b** + **1**, CCDC-202932 for **3c** + **1**, CCDC-202933 for **3d** + **1** contain the supplementary crystallographic data for this paper. These data can be obtained free of charge via www.ccdc.cam.ac.uk/conts/retrieving.html (or from the Cambridge Crystallographic Data Centre, 12 Union Road, Cambridge CB2 1EZ, UK; fax: (+44) 1223-336-033; or deposit@ccdc.cam.ac.uk).

[13] One arm of the receptor molecule is disordered over two positions, all the carbon atoms of the disordered part were revealed from the difference Fourier electron density maps, and were refined isotropically with all C–C bonds in the cyclohexyl moiety being set equal. The caffeine molecule was found to be disordered over two major positions as well, with multiple small residual peaks of electron density in the plane of the caffeine molecule giving evidence for the presence of other minor orientations or of caffeine motion in the plane. Thus, the geometry of caffeine was fixed to be the same as in **3d** + **1**. Based on this inaccuracy, only an approximate ratio is given; probably the amount of α complex is higher.

 © 2003 Wiley-VCH Verlag GmbH & Co. KGaA, Weinheim

A Soluble Germanium Cluster

$[Ge_9\{Si(SiMe_3)_3\}_3]^-$: A Soluble Polyhedral Ge_9 Cluster Stabilized by Only Three Silyl Ligands**

*Andreas Schnepf**

Germanium cluster compounds containing nine atoms are well known in the form of Zintl anions.[1] They can be prepared from the corresponding Zintl phase (e.g. K_4Ge_9) by using ethylenediamine and subsequently crystallized as isolated units, with [2.2.2]cryptand, for example.[2] The structure of the Ge_9 Zintl anions can be described as distorted, capped square antiprisms or as distorted tricapped trigonal prisms.[3] Herein the first synthesis of a ligand-stabilized Ge_9 cluster compound to be prepared from metastable Ge^I bromide is described.

Treating dissolved Ge^I bromide, prepared by a cocondensation technique,[4] with $Li\{Si(SiMe_3)_3\}$ at −78 °C followed by slow warming of the reaction mixture to room temperature, gives a dark red solution, which after workup yields orange crystals that contain the Ge cluster anion $[Ge_9\{Si(SiMe_3)_3\}_3]^-$ (**1**). Single-crystal X-ray diffraction confirms that **1** is a Ge_9 cluster in which only three of the nine Ge atoms are bound to a ligand (Figure 1 a). The crystal structure shows one $Li(thf)_4^+$ ion per cluster, which indicates that the cluster has a charge of −1.

The structure of **1** can be described as a tricapped trigonal prism, in which the core of the trigonal prism has an *a*:*h* ratio of 1:1.27. In the Ge_3 three-ring of naked Ge atoms the Ge–Ge bonds are 267 pm, whereas the bonds between the naked Ge atoms and the ligand-bound Ge atoms are 253 pm, thus the Ge atoms with the higher coordination number form the shorter Ge–Ge bonds. In this respect this cluster differs from the Zintl anions, in which the Ge atoms with the higher coordination numbers form the longer Ge–Ge bonds.[3] This topological difference shows that the formation of a two-electron two-center (2e2c) bond to a ligand[5] also changes the bonding situation within the cluster, causing a shortening of the Ge–Ge bonds between the naked and ligand-bound Ge atoms. The special role of the ligands in **1** is emphasized by a comparison with the EPh_2-functionalized Ge_9 cluster $[Ge_9(EPh_2)_2]^{2-}$ (E = Bi, Sb),[6] in which Sevov and Ugrinov found no significant change in the Ge_9 skeleton.

In terms of electronic structure **1** also differs from the Zintl anions, which can normally be described by Wades rules[7] in which the Ge atom is assumed to have a free electron pair.[3] Thus, the Ge_9^{4-} ion has 22 skeletal electrons ($2n+4$), which is the electron count for a nido cluster, and in agreement with this, the ion is found as a capped quadratic antiprism.[8] Assuming that the ligand-bound Ge atoms in **1** contribute three electrons to the cluster core then **1** also has 22 skeletal electrons. Thus a capped quadratic antiprism structure could also be expected. This structure however, seems to be energetically unfavorable for **1** as instead of this structure a tricapped trigonal prism is preferred.

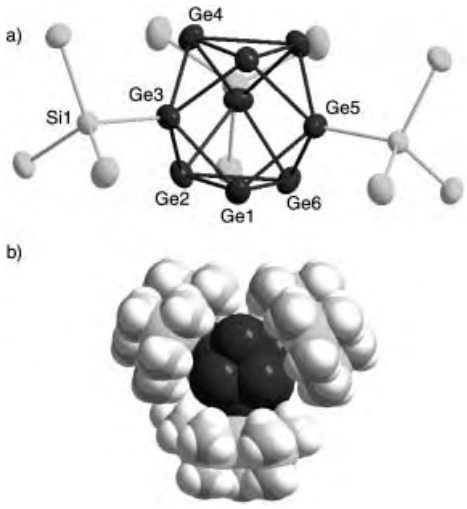


Figure 1. a) Molecular structure of $[Ge_9\{Si(SiMe_3)_3\}_3]^-$ (**1**); the methyl groups are omitted for clarity (thermal ellipsoids set at 50% probability). b) Space-filling model of **1** (view along the C_3 axis); selected interatomic distances [pm] and angles [°]: Ge1-Ge2 268.12(10), Ge2-Ge6 265.44(12), Ge2-Ge3 252.58(9), Ge1-Ge3 252.51(8), Ge3-Ge4 252.70(8), Ge2···Ge4 344.3(1), Ge3···Ge5 364.6(1), Ge3-Si1 236.95(14); Ge2-Ge3-Ge4 85.94(4), Ge2-Ge1-Ge6 59.34(3), Ge1-Ge3-Ge2 64.10(3), Ge3-Ge1-Ge5 92.34(4).

DFT calculations[9] were carried out for the model compound $[Ge_9H_3]^-$ (**1′**) to analyze the electronic properties within the cluster. The computed Ge–Ge distances (Ge–Ge 274, Ge–GeH 257 pm) were found to be close to those observed experimentally in **1** . An analysis of the energies of the individual molecular orbitals shows a significant leap of 2.2 eV in the orbital energy between the HOMO-10 and the HOMO-11, a result that supports the presence of 22 skeletal electrons mentioned above. The energy difference between the other individual high-lying molecular orbitals is between 0.2 and 1.1 eV. Further, these results from the quantum-chemical calculations show that the bonding electrons in the cluster core of **1′** are, like those in Zintl anions, highly delocalized.[10]

Cluster **1** is thus the second example, after $[Ge_8\{N(SiMe_3)_2\}_6]$,[11] of a ligand-stabilized Ge cluster containing naked Ge atoms, in which the bonding electrons are delocalized, a result which indicates that the introduction of naked Ge atoms into a ligand-stabilized cluster causes a delocalization of the bonding electrons in the cluster core.

In addition to the structural and electronic differences between **1** and the known Ge_9 clusters, the high solubility of **1** is also unusual. Cluster **1** dissolves in THF or in toluene to

[*] Dr. A. Schnepf
Institut für Anorganische Chemie
Universität Karlsruhe (TH)
Engesserstrasse, Geb. 30.45, 76128 Karlsruhe (Germany)
Fax: (+49) 721-608-4854
E-mail: schnepf@aoc2.uni-karlsruhe.de

[**] The financial support of the DFG through the program "Semiconductors and Metal Clusters as Building Blocks for Organized Structures" is gratefully acknowledged. Thanks also go to K. Weiss for mass spectrometry measurements and Prof. H. Schnöckel for helpful discussions.

 © 2003 Wiley-VCH Verlag GmbH & Co. KGaA, Weinheim DOI: 10.1002/anie.200250683

which a small amount of THF has been added, and naturally this solubility is an important factor which may allow follow-up reactions to be performed with the cluster. A possible point of attack would be the naked Ge atoms which, as shown in Figure 1b are only partially shielded by the ligands.[12] A further feature of the $[Ge_9R_3]^-$ cluster presented here is that by electrospray ionization (ESI)[13] the cluster can be transferred, intact into the gas phase[14] opening the possibility of gas-phase reactions with **1**.

Experimental Section

Liquid germanium at 1550 °C was treated with HBr and the resulting gas particles were subsequently condensed with a solvent mixture of toluene:N*n*Pr$_3$ (5:1) at −196 °C. The Cocondensate (20 mmol GeBr) was then warmed to −78 °C, which gave an emulsion of a dark red oil in a pale yellow solution. At −78 °C the emulsion was treated with Li{Si(SiMe$_3$)$_3$}·3 THF (11.79 g, 25 mmol) dissolved in toluene, and slowly warmed to room temperature to give a dark red solution. Removal of solvent in vacuum left a dark red oil. Extraction of this oil with pentane gave a dark red pentane extract from which orange crystals formed on reducing the volume of pentane. Recrystallization from THF gave orange crystals of $[Ge_9\{Si(SiMe_3)_3\}_3]Li(thf)_4$·3 THF (400 mg, 0.2 mmol).

^{1}H NMR (250 MHz, [D$_8$]THF): $\delta = 0.241$ (s, SiMe$_3$), 1.720 (br s, CH$_2$), 3.581 ppm (br s, CH$_2$); ^{13}C NMR (63 MHz, [D$_8$]THF): $\delta = 3.09$ ppm (CH$_3$); ^{29}Si{^{1}H} NMR (50 MHz, [D$_8$]THF): $\delta = -9.82$ (SiMe$_3$), −108.19 ppm (Si). IR(KBr): $\tilde{\nu} = 2952, 2890, 1259, 1242, 1093, 1041, 835, 687, 623\ cm^{-1}$. Crystal structure data of $[Ge_9\{Si(SiMe_3)_3\}_3]$-$Li(thf)_4$·3 THF: $M_r = 1907.98\ g\,mol^{-1}$, dimensions $0.5 \times 0.4 \times 0.2$ mm, monoclinic, space group $P2(1)/m$, $a = 13.536(3)$, $b = 22.872(5)$, $c = 16.156(3)$ Å, $\beta = 109.76(3)$, $V = 4707(1)$ Å^3, $Z = 2$, $\rho_{calcd} = 1.346\ g\,cm^{-3}$, $\mu_{Mo} = 3.020\ mm^{-1}$, $2\theta_{max} = 46.44°$, 24320 measured reflections, 6881 independent reflections ($R_{int.} = 0.0644$), numerical absorption correction (min/max transmission 0.1893/0.4898), $R_1 = 0.0375$, $wR_2 = 0.0877$. Stoe IPDS diffractometer ($Mo_{K\alpha}$ radiation), $\lambda = 0.71073$ Å, 200 K). The structure was solved by direct methods, solved against F^2, and refined for all observed reflections; programs: SHELXS and SHELXL (G. M. Sheldrick, Universität Göttingen). CCDC-198411 contains the supplementary crystallographic data for this paper. These data can be obtained free of charge via www.ccdc.cam.ac.uk/conts/retrieving.html (or from the Cambridge Crystallographic Data Centre, 12 Union Road, Cambridge CB2 1EZ, UK; fax: (+44) 1223-336-033; or deposit@ccdc.cam.ac.uk).

Received: December 2, 2002 [Z50683]

Keywords: cluster compounds · DFT calculations · germanium · silicon

[1] L. Diehl, K. Khodadadeh, D. Kummer, L. Strähle, *Chem. Ber.* **1976**, *109*, 3404.
[2] J. D. Corbett, D. G. Adolphson, D. J. Merryman, P. A. Edwards, F. J. Armatis, *J. Am. Chem. Soc.* **1975**, *97*, 6267; J. D. Corbett, *Angew. Chem.* **2000**, *112*, 683; *Angew. Chem. Int. Ed.* **2000**, *39*, 671.
[3] J. D. Corbett, *Struct. Bonding (Berlin)* **1997**, *87*, 157.
[4] A. Schnepf, R. Köppe, *Z. Anorg. Allg. Chem.* **2002**, *628*, 2914.
[5] The length of the Ge–Si bond (236.5 pm) resembles that in $[Ge_4(SitBu_3)_4]$ (238 pm): N. Wiberg, W. Hochmuth, H. Nöth, A. Appel, M. Schmidt-Amelunxen, *Angew. Chem.* **1996**, *108*, 1437; *Angew. Chem. Int. Ed. Engl.* **1996**, *35*, 1333.
[6] A. Ugrinov, S. C. Sevov, *J. Am. Chem. Soc.* **2002**, *124*, 2442.
[7] K. Wade, *Adv. Inorg. Chem. Radiochem.* **1976**, *18*, 1.
[8] C. H. E. Belin, J. D. Corbett, A. Cisar, *J. Am. Chem. Soc.* **1977**, *99*, 7163; V. Queneau, S. C. Sevov, *Angew. Chem.* **1997**, *109*, 1842; *Angew. Chem. Int. Ed. Engl.* **1997**, *36*, 1754.
[9] Quantum-chemical calculations were carried out with the RI-DFT version of the Turbomole program packet by employing the Becke–Perdew 86 functionals. The basis sets were of SVP quality. The electronic structure was analyzed by using Ahlrichs–Heinzmann population analysis based on occupation numbers. Turbomole: O. Treutler, R. Ahlrichs, *J. Chem. Phys.* **1995**, *102*, 346; BP 86 functional: J. P. Perdew, *Phys. Rev. B* **1986**, *33*, 8822; A. D. Becke, *Phys. Rev. A* **1988**, *38*, 3098; RI-DFT: K. Eichkorn, O. Treutler, H. Öhm, M. Häser, R. Ahlrichs, *Chem. Phys. Lett.* **1995**, *240*, 283; SVP: A. Schäfer, H. Horn, R. Ahlrichs, *J. Chem. Phys.* **1992**, *97*, 2571; Ahlrichs–Heinzmann population analysis: E. R. Davidson, *J. Chem. Phys.* **1967**, *46*, 3320; K. R. Roby, *Mol. Phys.* **1974**, *27*, 81; R. Heinzmann, R. Ahlrichs, *Theor. Chim. Acta* **1976**, *42*, 33; C. Erhardt, R. Ahlrichs, *Theor. Chim. Acta* **1985**, *68*, 231.
[10] In accordance with an Ahlrichs–Heinzmann population analysis[9] both three-center and four-center bonding contributions are present: for example, the three-center SEN (SEN = shared electron number) between the three naked Ge atoms has a value of 0.319. Also the different Ge–Ge bond lengths in **1** are reflected in the two-center SENs: thus the SEN between two naked Ge atoms is 0.89, whereas the SEN between a naked and a ligand-bound Ge atom is 1.01.
[11] A. Schnepf, R. Köppe, *Angew. Chem.* **2003**, *115*, 940; *Angew. Chem. Int. Ed.* **2003**, *42*, 911.
[12] Thus here a possible method for linking together individual Ge_9 units is presented, an area in which interesting results have recently been reported: T. F. Fässler, *Angew. Chem.* **2001**, *113*, 4289; *Angew. Chem. Int. Ed.* **2001**, *40*, 4161.
[13] D. A. Laude, E. Stevenson, J. M. Robinson in *Electrospray Ionization Mass Spectrometry* (Ed.: R. B. Cole), Wiley, New York, **1997**, p. 291.
[14] In a first experiment with an FT mass spectrometer (Ionspec) the molecular peak of the $[Ge_9\{Si(SiMe_3)_3\}_3]^-$ ion with the expected isotope ratios could be detected.

 © 2003 Wiley-VCH Verlag GmbH & Co. KGaA, Weinheim

Discrete Fluoroaluminates

Coordination Geometry of the Discrete Pentafluoroaluminate Dianion $[AlF_5]^{2-}$**

Udo Groß, Dirk Müller, and Erhard Kemnitz**

Aluminumfluorides and the complex fluoroaluminate salts occur as inorganic polymers consisting of Al–F octahedrons bridged at shared corners. Exceptions are mineral cryolite, $Na_3[AlF_6]$, made up of discrete octahedrons and the tetrahedral $[AlF_4]^-$ species formed as salts with large organic cations,[1] and for which some single-crystal structural analyses have been published.[2] The work of Sengupta and Sen published in a communication in 1979[3] on preparation of tetra- and pentacoordinate fluoroaluminates in aqueous media is not reproducible, and the reported IR data are not in agreement with the published structures. Our investigations, in particular the ^{27}Al magic-angle spinning (MAS) NMR and IR spectroscopic results have shown that according to this preparative route predominantly tetrafluoroaluminates and their hydrates are formed. The existence of hydrazinium (1+) pentafluoroaluminates[4] as linear arrangement of octahedrons in chains has been suggested from a new spectroscopic study by Milicev and Rathen[5]. In fluoroaluminate melts, which are of importance for the industrial aluminum production by electrolysis, ionic equilibria of the known hexafluoro- and tetrafluoroaluminates are assumed but also the presence of $[AlF_5]^{2-}$ ions is proposed.[6] To our knowledge fluoroaluminates with a coordination number of five are unknown.[7]

The isolated homoleptic pentafluoroaluminate anion, $[AlF_5]^{2-}$, with D_{3h} symmetry is apparently the global minimum on the potential hypersurface and clearly a stable species according to our quantum-chemical ab initio molecular orbital (MO) calculations.[8] This complex ion is isoelectronic with the $[SiF_5]^-$ ion and the PF_5 molecule. Geometry optimization was carried out on a Hartree–Fock level using different basis sets. The MP2 approximation for the electron correlation was applied to the optimized HF/6-31G* geometry. The bond lengths thus calculated, $Al–F_{ax} = 181.9$ pm and $Al–F_{eq} = 178.5$ pm, are in accord with earlier LDF calculations.[9] The vibrational bands determined by these calculations are, after scaling, in good agreement with our experimental IR and Raman spectroscopy results for the trigonal bipyramidal $[AlF_5]^{2-}$ ion.

All the fluoroaluminates in this study with coordination numbers at aluminum sites smaller than six are moisture sensitive and their handling has to be carried out under dry conditions. Although the hydrolysis of Al–F bonds is nearly negligible because of the small amount of covalent bonding, but the coordinatively unsaturated central atom allows the addition of water as a donor to form octahedral structures.

In course of our investigations of isolated tetrahedral tetrafluoroaluminates reactions with tetramethylammonium fluoride (TMAF)[10] were carried out in non-aqueous solvents according to Equation (1) to yield the title compound.

$$[(CH_3)_4N]^+[AlF_4]^- + [(CH_3)_4N]^+F^- \rightarrow [(CH_3)_4N]^+_2[AlF_5]^{2-} \quad (1)$$

$[(CH_3)_4N]_2^+[AlF_5]^{2-}$ was formed as white, thermally stable but moisture sensitive salt, insoluble in acetonitrile. The formation of the pentafluoroaluminate in a mixture of differently coordinated discrete fluoroaluminates is also observed in the reactions given in Equation (2), where in

$$AlCl_3 + 3\,[(CH_3)_4N]^+F^- \rightarrow [AlF_3] + 3\,[(CH_3)_4N]^+Cl^- \quad (2a)$$

$$[AlF_3] + 2\,[(CH_3)_4N]^+F^- \rightarrow [(CH_3)_4N]^+[AlF_4]^- \quad (2b)$$

dry acetonitrile aluminum trichloride is treated with five equivalents of TMAF to give a Cl–F substitution reaction as well as F^- ion addition.

AlF_3 is formed by halogen exchange and subsequently gives the higher coordinate homoleptic fluoroaluminates $[(CH_3)_4N]^+[AlF_4]^-$, $[(CH_3)_4N]^+_2[AlF_5]^{2-}$, and $[(CH_3)_4N]^+_3[AlF_6]^{3-}$ by further reaction with TMAF. The tetrafluoroaluminate is the major constituent of the product mixture, which is in accord with the substantially greater fluoride-ion affinity of the intermediate AlF_3 in comparison with the higher coordinate fluoroaluminates. Product concentrations of Equation (2) were obtained from ^{27}Al MAS NMR spectra. Clearly, higher coordinate fluoroaluminates can be prepared with a great excess of TMAF.

DTG/DTA-MS (differential thermal gravity/differential thermal analysis) investigations of $[(CH_3)_4N]^+_3[AlF_6]^{3-}$ show that the less-fluorine-containing aluminates are formed by thermal decomposition [Eq (3)].

$$[(CH_3)_4N]^+_3[AlF_6]^{3-} \xrightarrow{\Delta} [(CH_3)_4N]^+_2[AlF_5]^{2-} + CH_3F + N(CH_3)_3 \xrightarrow{\Delta} [(CH_3)_4N]^+[AlF_4]^- \cdots \quad (3)$$

Finally, the thermodynamically stable α AlF_3 is formed via, the at 450 °C occurring, metastable θ AlF_3 phase [see Eq. (4)].[11] This can be an alternative route to defined fluoroaluminates.

Because of the extremely poor solubility in nearly all conceivable polar solvents, the growth of single crystals of $[(CH_3)_4N]^+_2[AlF_5]^{2-}$ has not been successful to date, and structural analysis has had to be by spectroscopic methods. Besides the complete elemental analysis of $[(CH_3)_4N]^+_2[AlF_5]^{2-}$, the ^{27}Al MAS NMR spectra (Figure 1) are clear indication of the presence of the $[AlF_5]^{2-}$ ion. From

[*] Dr. U. Groß, Prof. Dr. E. Kemnitz
Institut für Chemie
Humboldt-Universität zu Berlin
Brook-Taylor-Strasse 2, 12489 Berlin (Germany)
Fax: (+49) 30-2093-7277
E-mail: udo.gross@chemie.hu-berlin.de
erhard.kemnitz@chemie.hu-berlin.de
Dr. D. Müller
Institut für Angewandte Chemie
Richard-Willstätter-Strasse 12, 12489 Berlin (Germany)

[**] Thanks are due to Dr. M. Schneider, ACA Berlin, for the diffraction measurements and indexing of peaks.

Supporting information for this article is available on the WWW under http://www.angewandte.org or from the author.

 © 2003 Wiley-VCH Verlag GmbH & Co. KGaA, Weinheim DOI: 10.1002/anie.200350885

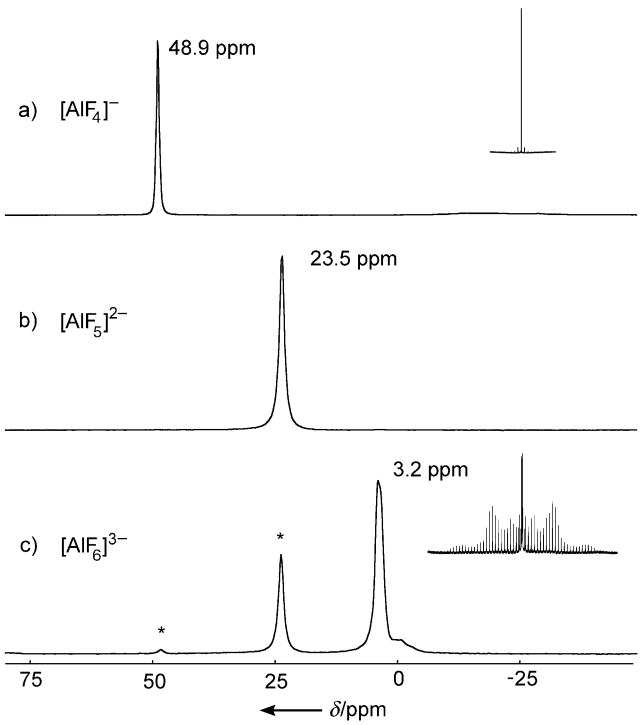


Figure 1. ^{27}Al MAS NMR spectra of a) $[(CH_3)_4N]^+[AlF_4]^-$, b) $[(CH_3)_4N]^+_2[AlF_5]^{2-}$, and c) $[(CH_3)_4N]^+_3[AlF_6]^{3-}$. Spectrum (c) shows traces (*) of (b) and (a). The inset shows the satellite transitions.

the ^{27}Al MAS NMR spectrum, the chemical shift is $\delta =$ 23.5 ppm (aqueous $[Al(H_2O)]^{3+}$ ion as external standard). The line width of the NMR signal amounts to 139 Hz at a rotational frequency of the sample of 10 kHz and is comparable to solution spectra. The static signal shows a half-width of 3050 Hz, which is essentially a result of dipole–dipole interactions with the surrounding fluorine nuclei. The very small line width for a quadrupolar ^{27}Al nucleus with a nuclear spin $^5/_2$ shows that the anion structure is highly symmetric and the quadrupolar coupling and the dipolar interaction of fluorine are negligibly small. In contrast, corner-shared pentafluoroaluminates with a polymer chain structure of $[AlF_{4/1}F_{2/2}]^{2-}_{\infty}$ units exhibit quadrupolar coupling constants (QCC) in the ^{27}Al MAS NMR spectra of about 12–13 MHz and chemical-shift values in a broad range of lower frequencies.[12]

Figure 1 shows the ^{27}Al MAS NMR spectrum of the $[AlF_5]^{2-}$ ion and for comparison spectra of the discrete $[AlF_4]^-$ and $[AlF_6]^{3-}$ ions. In the complete MAS NMR spectrum of the $[AlF_6]^{3-}$ ion the rotational side bands of satellite transitions, caused by first-order perturbation theory quadrupolar interaction, can be seen as well as the central resonance signal. Calculating this spectrum based on an axial symmetric model of the electric tensor, the field gradient QCC is estimated to be 1.6 MHz.

From the solid-state NMR spectra it seems clear that the single, but intense, resonance signal of the product at $\delta =$ 23.5 ppm confirms a quantitative conversion in the stoichiometric reaction of Equation (1) . Other ^{27}Al MAS NMR measurements of educt $[(CH_3)_4N]^+[AlF_4]^-$ gave the up to now unknown ^{27}Al chemical shift of the tetrahedral $[AlF_4]^-$ ion in a solid as $\delta = 48.9$ ppm. The perfect tetrahedral structure of this ion is unperturbed, as is to be seen from the half-width of 127 Hz and the QCC < 0.1 MHz. These data along with the recently published chemical-shift values of octahedral fluoroaluminates[12] allow the extrapolation of a new chemical shift scale of ^{27}Al δ values for fluoroaluminates depending on their coordination number (Figure 2). With increasing coordination numbers at the central aluminum the Al–F bond length increases, as expected, and the shielding of the ^{27}Al nucleus also increases with the chemical shift values moving linearly to higher magnetic fields (Table 1).

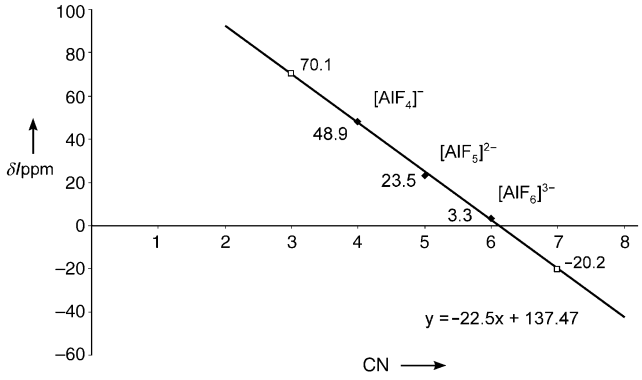


Figure 2. ^{27}Al chemical shifts of fluoroaluminates as a function of coordination numbers (CN) at aluminum. ◆ = experimental value, □ = extrapolated value, —— = regression line.

Table 1: ^{27}Al MAS NMR spectroscopy data for discrete fluoroaluminates.

Compound[a]	δ [ppm]	$\Delta\tilde{\nu}_r$ [Hz][b]	$\Delta\tilde{\nu}_{stat}$ [Hz]	QCC [MHz][c]
$[M]^+[AlF_4]^-$	48.9	127	1920	< 0.1
$[M]^+_2[AlF_5]^{2-}$	23.5	139	3050	< 0.2
$[M]^+_3[AlF_6]^{3-}$	3.2	223	–	1.6

[a] M = NMe_4, NEt_4, NBu_4. [b] Rotational frequency 10 kHz. [c] Estimated from first-order satellites.

The linearity of δ and coordination number makes extrapolation to coordination numbers three and seven at central aluminum atoms possible. Thus, NMR spectroscopic evidence could demonstrate the existence of these species. Although the coordination number seven is unlikely, it should not be excluded, especially in high temperature melts. Coordination number three seems possible to realize, for example, by matrix isolation from the existing complex AlF_3·HF, the MO-calculated[13] dissociation energy of which is only 53.5 kJ mol^{-1}.

Evidence for the structure of the homoleptic pentafluoroaluminate ion comes from IR and Raman spectroscopic studies. According to the VSEPR model molecules of type XY_5 are expected to have D_{3h} or C_{4v} symmetry. Quantum-chemical ab initio calculations suggest the probable structure of the $[AlF_5]^{2-}$ ion to be D_{3h} (Figure 3).[8,9]

The trigonal-bipyramidal (D_{3h}) structure XY_5 has eight fundamental vibrations; six of them are Raman active, five are IR active. Nine of these eleven bands are clearly seen in

 © 2003 Wiley-VCH Verlag GmbH & Co. KGaA, Weinheim

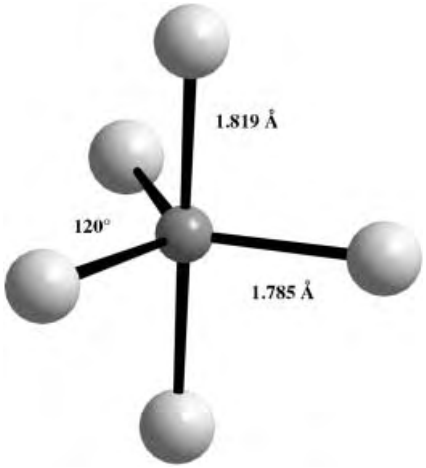


Figure 3. Calculated[8] trigonal-bipyramidal structure of the $[AlF_5]^{2-}$ ion.

the spectrum; the remaining two bands are weak, as expected, and are partly obscured. The Raman spectrum is dominated by bands of the tetramethylammonium ion.[10] The fundamental vibrations of point group D_{3h} are $2\,A_1'$, $2\,A_2''$, $3\,E'$, and $1\,E''$. The most characteristic and intense band of the Raman spectra is the vibration ν_1, that is, the symmetric stretch of the equatorial AlF_3 group (Figure 4); in the IR spectrum ν_5 and ν_3, the antisymmetric stretching vibrations of the equatorial AlF_3 group and the axial AlF_2 group dominate (Table 2). Comparing the wave numbers of the axial and equatorial vibrations of Al–F bonds of one symmetry type shows higher wave numbers are observed for equatorial Al–F bonds because of the shorter Al–F bond lengths and larger force constants. According to our ab initio calculations[8] the equatorial Al–F bonds are 178.5 pm and the axial ones are 181.9 pm.

When comparing the equatorial valence vibration ν_1 along the row of discrete fluoroaluminates (Table 2), the wave numbers decrease from $\tilde{\nu} = 634$ ($[AlF_4]^-$), 563 ($[AlF_5]^{2-}$), and 540 cm^{-1} ($[AlF_6]^{3-}$), which shows a weakening of the Al–F bonds with increasing coordination at aluminum. This pattern is also in accord with the increasing Al–F bond length found experimentally and by calculations. With regard to the intensities of the vibrations the experimental rule for molecules of symmetry D_{3h} is again confirmed $\nu_5 > \nu_3 > \nu_1 > \nu_2$.

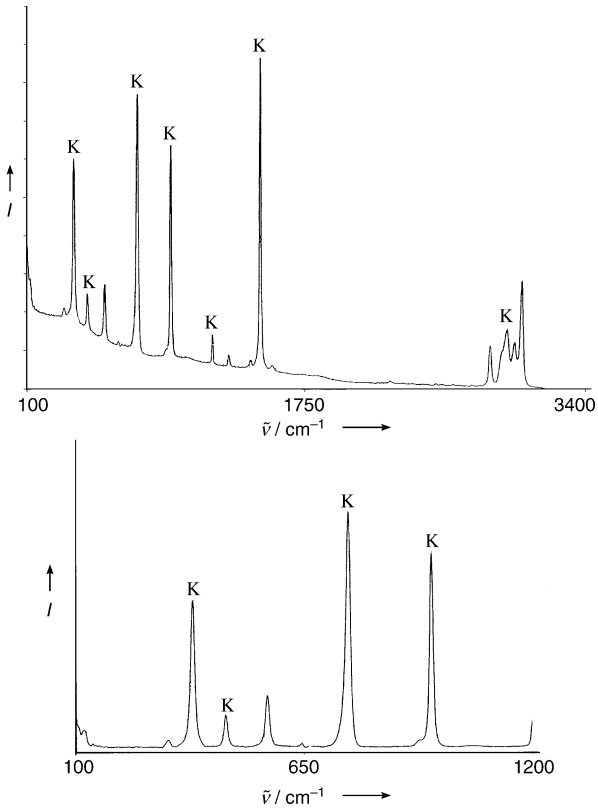


Figure 4. Laser Raman spectra of $[(CH_3)_4N]^+_2\,[AlF_5]^{2-}$ a) $\tilde{\nu} = 100$–3400 cm^{-1}, b) $\tilde{\nu} = 100$–1200 cm^{-1}, C = cation.

The reactivity of the $[AlF_5]^{2-}$ ion is characterized by reactions with electron-pair donating molecules, for example, water or similar basic species, to give coordinatively saturated Al centers. Evidence for such reactions comes from IR and NMR spectroscopy. The transformation to octahedral geometry causes drastic changes in the IR spectra, while ^{27}Al MAS NMR resonance signals are shifted by about 40 ppm upfield.[12] With the "naked" fluoride, TMAF, hexafluoroaluminate is generated. The lower reactivity is caused by the very poor solubility of the $[AlF_5]^{2-}$ ion and, its weak Lewis acidity.

The reverse reaction, that is, splitting of the fluoride ions from the complex fluoroaluminate ion, takes place under thermal conditions at elevated temperatures. Stepwise

Table 2: Anionic bands in the IR and Raman spectra of $[(CH_3)_4N]^+_2[AlF_5]^{2-}$ and their assignment to the point group D_{3h}.

Assignment	Symmetry type/ selection rule	Vibration	Raman		IR	
			$\tilde{\nu}$ [cm^{-1}]	rel. Intensity	$\tilde{\nu}$ [cm^{-1}]	rel. Intensity
ν_1	A_1' Ra, p	ν_s AlF_3 eq	563	10		
ν_2	A_1' Ra, p	ν_s AlF_2 ax	464 sh	0.1		
ν_3	A_2'' IR	ν_{as} AlF_2 ax			601	vs
ν_4	A_2'' IR	γ AlF_3 eq			354	
ν_5	E′ IR, Ra, dp	ν_{as} AlF_3 eq	644	0.9	675	vs
ν_6	E′ IR, Ra, dp	δ AlF_3 eq			374	
ν_7	E′ IR, Ra, dp	δ AlF_2 ax	117 sh	0.1	117	w
ν_8	E″ Ra, dp	ρ AlF_2 ax	322	2.0		

 © 2003 Wiley-VCH Verlag GmbH & Co. KGaA, Weinheim

decomposition starts at 296 °C under formation of the $[AlF_4]^-$ ion and of AlF_3 at 424 °C [Eq. (4)].

$$[(CH_3)_4N]^+{}_2[AlF_5]^{2-} \xrightarrow{\Delta} [(CH_3)_4N]^+[AlF_4]^- + CH_3F + N(CH_3)_3 \xrightarrow{\Delta} AlF_3 + CH_3F + N(CH_3)_3 \quad (4)$$

Thermoanalysis (DTA/DTG MS) reveals that the thermal decomposition occurs in two endothermic steps (see Supporting Information). The weight loss is as calculated, 34.4 % for the first and 68.8 % for both the degradation steps. AlF_3 is obtained above 700 °C via metastable intermediates in the thermodynamically most stable α modification, CH_3F and trimethylamine are expelled from the system as gases.

From the powder diffraction pattern of the microcrystalline solid (see Supporting Information) the lattice constants $a = 18.34$, $b = 13.98$, $c = 4.03$ Å were calculated. The crystallographic axes confirm an orthorhombic unit cell.

Experimental Section

1: Tetramethylammonium tetrafluoroaluminate (354 mg, 2 mmol) and tetramethylammonium fluoride (205 mg, 2.2 mmol) were stirred for 5 h at 25–35 °C in dry CH_3CN (30 mL). The resulting white solid was collected by filtration, washed with acetonitrile, and dried. Elemental analysis (%) calcd for $C_8H_{24}AlF_5N_2$ (270.2): C 35.1, H 8.9, N 10.1, Al 9.7, F 34.4; found: C 35.5, H 8.9, N 10.3, Al 10.0, F 35.2.
2: $AlCl_3$ (134 mg, 1 mmol) and TMAF (465 mg, 5 mmol) were heated at 35 °C in dry CH_3CN (30 mL) for 5 h. The solvent was removed under vacuum to give a white moisture sensitive solid. The mixture of compounds and their concentrations were estimated by ^{27}Al-MAS-NMR ($[AlF_4]^-$ 88 %, $[AlF_5]^{2-}$ 7 %, $[AlF_6]^{3-}$ 5 %).
NMR spectra were recorded with a Varian Unity plus 500 at 130.2 MHz with rotational speed of 10 kHz. Vibrational spectra were measured with a Laser FT-Raman spectrometer (Bruker RFS 100) and a FT-IR (Perkin-Elmer 2000) as KBr and CsI tablets between 100–4000 cm^{-1}. Elemental analysis were carried out by the Mikro-analytisches Labor Beller/Matthies Göttingen, Germany.

Received: January 3, 2003 [Z50885]

Keywords: fluoroaluminate · IR spectroscopy · Raman spectroscopy · solid-state NMR spectroscopy · structure elucidation

[1] P. Bukovec, J. Siftar, *Monatsh. Chem.* **1975**, *106*, 483 – 490.
[2] a) N. Herron, R. L. Harlow, D. L. Thorn, *Inorg. Chem.* **1993**, *32*, 2985 – 2986; b) M. Ferbinteanu, H. W. Roesky, F. Cimpoesu, M. Atanasov, S. Körke, R. Herbst-Irmer, *Inorg. Chem.* **2001**, *40*, 4947 – 4955.
[3] A. K. Sengupta, K. Sen, *Indian J. Chem. Sect. A* **1979**, *17*, 107 – 108.
[4] W. Pugh, M. C. B. Hotz, *J. Chem. Soc.* **1953**, 2493 – 2495.
[5] S. Milicev, A. Rathen, *Eur. J. Solid State Inorg. Chem.* **1991**, *28*, 557 – 566.
[6] B. Gilbert, E. Robert, E. Tixhon, J. E. Olsen, T. Ostvold, *Inorg. Chem.* **1996**, *35*, 4198 – 4210.
[7] CAS-Database research with SciFinder Scholar 2000.
[8] G. Scholz, U. Groß, E. Kemnitz, unpulished results.
[9] F. Bouyer, G. Picard, J.-J. Legendre, *Int. J. Quantum Chem.* **1994**, *52*, 927 – 934.
[10] K. O. Christe, W. W. Wilson, R. D. Wilson, R. Bau, J. A. Feng, *J. Am. Chem. Soc.* **1990**, *112*, 7619 – 7625.
[11] N. Herron, D. L. Thorn, R. L. Harlow, G. A. Jones, J. B. Parise, J. A. Fernandez-Baca, T. Vogt, *Chem. Mater.* **1995**, *7*, 75 – 83.
[12] D. Müller, U. Bentrup, *Z. Anorg. Allg. Chem.* **1989**, *575*, 17 – 25.
[13] L. A. Curtis, G. Scholz, *Chem. Phys. Lett.* **1993**, *205*, 550 – 554.

 © 2003 Wiley-VCH Verlag GmbH & Co. KGaA, Weinheim

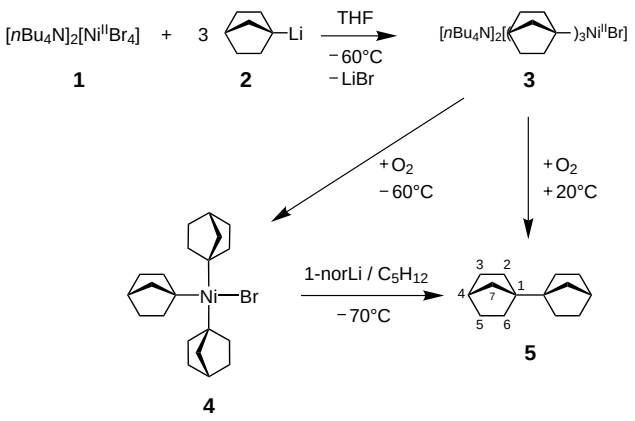
High-Oxidation-State Ni Complex

A Pseudotetrahedral, High-Oxidation-State Organonickel Compound: Synthesis and Structure of Bromotris(1-norbornyl)nickel(IV)**

Vladimir Dimitrov and Anthony Linden*

The organometallic chemistry of late transition metals in high oxidation states has been of considerable interest because of its relevance to certain catalytic reactions.[1–4] Organonickel compounds in the formal oxidation state +4 have been obtained by the oxidation of decamethylnickelocene[5] and in a trinickelacarborane complex.[6] The first examples of octahedral diorganonickel(IV) compounds containing σ-bonded methyl and acylphenolato ligands were reported only recently.[7] The occurrence of tetracoordinate organonickel(IV) intermediates has been proposed in some cases,[8] but there are no previous reports of the isolation of a tetrahedral nickel(IV) compound containing σ-bonded organic ligands. Herein we report the preparation of a tris(1-norbornyl)nickelate(II) complex and its oxidation, which results in the formation of a diamagnetic pseudotetrahedral triorganonickel(IV) compound. The tetrakis(1-norbornyl) compounds of the first-row metals, with the exception of nickel, are rare examples of high oxidation state homoleptic transition-metal alkyl complexes with extraordinarily high stability.[9]

Previously, we prepared several 1-norbonyl complexes of Ni^{II}, which include the nickelate(II) salt $Li[CpNi(1\text{-nor})_2]$ ($Cp = C_5H_5$), starting from nickelocene.[10] For the preparation of the tris(1-norbornyl)nickel(II) complex anion we now started from the pale blue compound $[n\mathrm{Bu_4N}]_2[Ni^{II}Br_4]$ (**1**). The reaction of **1** with three equivalents of 1-norbornyllithium (**2**) in THF at −60 °C gave a blue-green solution of the anionic complex **3** (Scheme 1). The reaction with four equivalents of **2** also produced **3** and not the tetrakis(1-norbonyl)nickel(II) complex, as was demonstrated by a subsequent transformation. Note that all previously reported nickel complexes of the type $Li_2[Ni^{II}R_4]$ are yellow.[11] Complex **3** could not be isolated because it decomposed during removal of the solvent, but it could be characterized by NMR spectroscopy after preparation in [D_8]THF (Table 1). A solution of **3** in THF can be handled at room temperature for 1 h without decomposition. By following analogous procedures reported in the literature,[12] complex **3** was oxidized at −60 °C by bubbling air through this THF solution. The resulting nickel(IV) complex **4** was isolated by pentane extraction and crystallization as a red-brown crystalline solid. Compound **4** is stable in air for several days. On heating, it decomposes at 131–133 °C without melting. Conversely, decomposition of **4** occurs rapidly in solution, as shown by the NMR spectra of one-hour-old solutions which indicated the presence of small quantities of dinorbornane. In the mass spectrum (EI-MS), only dinorbornane was detected, formed as a result of an elimination reaction. The high stability of the complex can be attributed to the strong σ-bond-donor capability of the 1-norbornyl group, which provides the necessary electron density for stabilizing the formal +4 oxidation state. The strong electron-donating ability of the 1-norbonyl ligand was demonstrated in a previous investigation.[13] In addition, the electron-donating ability of the bromo ligand can also contribute to the stabilization of the coordinatively and electronically unsaturated complex **4**.[14]



Scheme 1. Preparation of **4** by air oxidation of **3**.

Interestingly, when the oxidation of **3** was carried out at room temperature, only dinorbornane (**5**) could be isolated.[15] A similar elimination reaction was observed in the reaction of iodine with $Li_2[NiMe_4]\cdot 2\,THF$ and $Li_2[NiPh_4]\cdot 4\,THF$.[8a,11a] The formation of dinorbornane also occurred during attempts to exchange the bromine atom in **4** with a 1-norbornyl group by treating **4** with **2** in pentane at −70 °C (Scheme 1). Consequently, it seems unlikely that tetrakis(1-norbornyl)nickel(IV) can be prepared by this method.

Complexes **3** and **4** were characterized by NMR spectroscopy (Table 1). For the nickel(II) complex **3** the ^{13}C resonance signal of the coordinating carbon atom is shifted up field, and

Table 1: ^{13}C NMR spectroscopy chemical shift values of **3** and **4**.[a]

Compound	C-1	C-2,6	C-3,5	C-4	C-7
$[n\mathrm{Bu_4N}]_2[Ni^{II}(1\text{-nor})_3Br]$ (**3**)	20.19	35.65	30.39	34.49	44.79
$[Ni^{IV}(1\text{-nor})_3Br]$ (**4**)	68.79	35.99	31.58	32.83	45.69

[a] Chemical shifts δ (in ppm relative to TMS) measured in [D_8]THF, at 75.5 MHz, for numbering of C atoms, see **5** in Scheme 1.

[*] Dr. V. Dimitrov
Institute of Organic Chemistry
Bulgarian Academy of Sciences
Acad. G. Bonchev str. bl.9, 1113 Sofia (Bulgaria)
Fax: (+359) 2-8700-225
E-mail: vdim@orgchm.bas.bg
Dr. A. Linden
Institute of Organic Chemistry
University of Zürich
Winterthurerstrasse 190, 8057 Zürich (Switzerland)

[**] We thank the Swiss National Science Foundation and the "Dr. Helmut Legerlotz Stiftung" of the Institute of Organic Chemistry, University of Zürich for generous financial support. We thank Prof. M. Hesse, Prof. H. Lehmkuhl, Prof. R. Taube, and Prof. K.-H. Thiele for helpful discussions.

 DOI: 10.1002/anie.200219383 © 2003 Wiley-VCH Verlag GmbH & Co. KGaA, Weinheim

its chemical shift is comparable with those of related nickel(II) complexes.[10,11c] The ^{13}C resonance signal of the coordinating bridgehead C atom in **4** is shifted down field, which is in agreement with the trend observed for the corresponding Ti^{IV},[16a] Fe^{IV},[16b] and Co^{V}[17] compounds.[18] The remaining sharp resonance signals, which are not shifted from their normal positions, indicate the diamagnetic nature of **4**. In addition, EPR measurements showed that **4** is diamagnetic in the temperature range 77–298 K.

To support the spectroscopic and chemical evidence for the nickel(IV) complex **4**, an X-ray crystallographic analysis was carried out. The Ni atom is four-coordinate with almost tetrahedral geometry, but the tetrahedron is stretched in the direction of the Br atom, so that the C-Ni-C angles are all significantly smaller than the normal tetrahedral angle, while the Br-Ni-C angles are correspondingly larger (Figure 1).

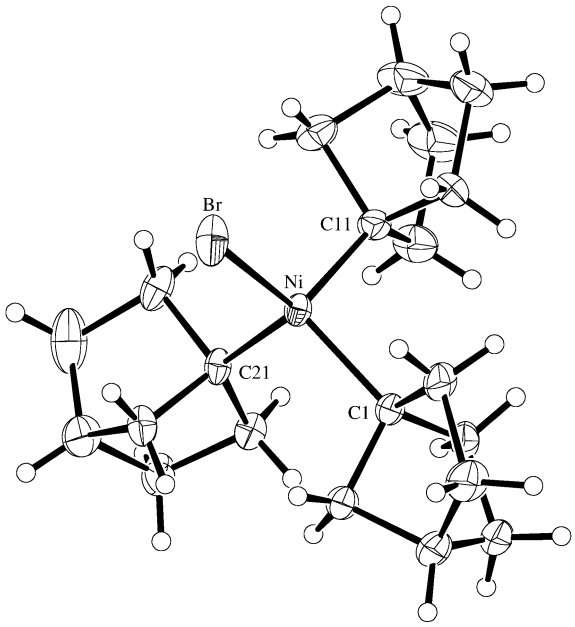


Figure 1. ORTEP plot of the structure of compound **4** (thermal ellipsoids set at 50% probability). Selected bond lengths [Å] and angles [°]: Ni–Br 2.3858(5), Ni–C1 1.931(3), Ni–C11 1.931(3), Ni–C21 1.937(3); Br-Ni-C1 123.84(10), Br-Ni-C11 116.08(10), Br-Ni-C21 113.36(9), C1-Ni-C11 98.18(14), C1-Ni-C21 100.14(13), C11-Ni-C21 101.83(14).

Furthermore, there are 15 C···H and H···H intramolecular contacts that are 0.10–0.31 Å shorter than the sum of the van der Waals radii of the relevant atoms. In contrast, there are no unusually short intramolecular contacts involving the Br atom. The ligand-field requirements of a true tetrahedrally coordinated nickel(IV) atom are inconsistent with the measured diamagnetism of the compound. However, the distortions of the tetrahedron correspond to lowering of symmetry from T_d to C_{3v}, which splits the energies of the t_2 orbitals and produces one orbital of lower energy. In the pseudotetrahedral arrangement of **4**, the observed lowering of symmetry evidently splits the orbital energies sufficiently to allow pairing of all six d electrons, which leads to the observed diamagnetism.

In conclusion, we have prepared and structurally characterized a pseudotetrahedral organonickel compound in the formal oxidation state +4. Being diamagnetic it seems to be the first low-spin tetracoordinate organonickel compound with d^6 configuration. This and the remarkable stability of the new compound are consistent with the ability of the 1-norbornyl ligand to stabilize metals in high oxidation states.

Experimental Section

All operations were carried out by using standard Schlenk techniques under an Ar atmosphere. The solvents were prepared free of oxygen and moisture by standard methods. The starting compounds **1**[19] and **2**[16c] were prepared according to literature procedures.

3 in [D_8]THF: Three equivalents of **2** (0.0404 g, 0.40 mmol) were added to a suspension of **1** (0.1103 g, 0.13 mmol) in [D_8]THF (1 mL) at −60 °C, and the mixture was stirred for 1 h at this temperature and then insoluble material was removed by filtration. For NMR spectroscopy investigations, 0.6 mL of the solution of **3** in [D_8]THF was transferred into a NMR tube.

4: Three equivalents of **2** (0.16 g, 1.56 mmol) were added to a suspension of **1** (0.43 g, 0.50 mmol) in THF (15 mL) at −60 °C, and the mixture was stirred for 1 h at this temperature and then insoluble material was removed by filtration. Dry air was bubbled through the blue-green solution for 1 min, the mixture was allowed to warm to room temperature, and all volatile materials were removed. The residue was extracted with pentane, and insoluble material was removed by filtration. After concentration, the solution was cooled to −20 °C and the crystalline solid collected by filtration to give a brown solid, which was recrystallized three times from pentane/Et_2O to give 0.115 g (55%) of **4** as red-brown crystals. Crystals for crystallographic analysis were obtained from pentane/Et_2O by slow evaporation of the solvents.

Data for **4**: decomposition at 131–133 °C; elemental analysis (%) calcd: C 59.48, H 7.84, Br 18.84, Ni 13.84; found: C 59.25, H 7.97, Br 18.53, Ni 13.50.

Crystal data for **4**: crystals from pentane/Et_2O; $C_{21}H_{33}BrNi$, $M_r = 424.10$; orthorhombic, space group *Pbca*, $a = 17.1432(2)$, $b = 12.0680(1)$, $c = 18.5311(3)$ Å, $V = 3833.79(8)$ Å^3, $Z = 8$, $\rho = 1.469$ g cm^{-3}, crystal dimensions: $0.03 \times 0.20 \times 0.30$ mm, $T = -113$ °C, Nonius Kappa CCD diffractometer, graphite-monochromated $Mo_{K\alpha}$ radiation, $\lambda = 0.71073$ Å, $\mu = 3.102$ mm^{-1}, $2\theta_{max} = 55°$, 102373 measured reflections of which 4391 were unique and 3531 had $I > 2\sigma(I)$. The intensities were corrected for Lorentzian and polarization effects, as well as for absorption.[20] The structure was solved by direct methods using SHELXS97[21a] and refined on F^2 by full-matrix least-squares methods using SHELXL97.[21b] The H atoms were placed in geometrically calculated positions and were allowed to ride on their parent atom with $U_{iso}(H) = 1.2\,U_{eq}(C)$. The refinement of 208 parameters using 4390 reflections gave $R(F) = 0.0430$ ($I > 2\sigma(I)$ data), $Rw(F^2) = 0.1025$ (all data), GOF on F^2 1.061, $\Delta\rho_{max} = 0.85$ e Å^{-3}. CCDC-185226 (**4**) contains the supplementary crystallographic data for this paper. These data can be obtained free of charge via www.ccdc.cam.ac.uk/conts/retrieving.html (or from the Cambridge Crystallographic Data Centre, 12 Union Road, Cambridge CB21EZ, UK; fax: (+44) 1223-336-033; or deposit@ccdc.cam.ac.uk).

Received: May 24, 2002
Revised: March 3, 2003 [Z19383]

Keywords: coordination modes · nickel · norbornyl ligands · oxidation

 © 2003 Wiley-VCH Verlag GmbH & Co. KGaA, Weinheim

[1] M. Ohff, A. Ohff, M. E. van der Boom, D. Milstein, *J. Am. Chem. Soc.* **1997**, *119*, 11687.

[2] a) S. Stahl, J. A. Labinger, J. E. Bercaw, *Angew. Chem.* **1998**, *110*, 2298; *Angew. Chem. Int. Ed.* **1998**, *37*, 2180; b) R. J. Puddephatt, *Angew. Chem.* **2002**, *114*, 271; *Angew. Chem. Int. Ed.* **2002**, *41*, 261.

[3] a) S. B. Duckett, R. N. Perutz, *Organometallics* **1992**, *11*, 90; b) K. Ezbiansky, P. I. Djurovich, M. LaForest, D. J. Sinning, R. Zayes, D. H. Berry, *Organometallics* **1998**, *17*, 1455.

[4] a) M. Brookhart, B. E. Grant, *J. Am. Chem. Soc.* **1993**, *115*, 2151; b) M. Brookhart, B. E. Grant, C. P. Lenges, M. H. Prosenc, P. S. White, *Angew. Chem.* **2000**, *112*, 1742; *Angew. Chem. Int. Ed.* **2000**, *39*, 1676.

[5] U. Kölle, F. Khouzami, H. Leuken, *Chem. Ber.* **1982**, *115*, 1178.

[6] C. G. Salentine, C. E. Strouse, M. F. Hawthorne, *J. Am. Chem. Soc.* **1976**, *98*, 841.

[7] a) H.-F. Klein, A. Bickelhaupt, T. Jung, G. Cordier, *Organometallics* **1994**, *13*, 2557; b) H.-F. Klein, A. Bickelhaupt, M. Lemke, H. Sun, A. Brand, T. Jung, C. Röhr, U. Flörke, H.-J. Haupt, *Organometallics* **1997**, *16*, 668; c) H.-F. Klein, X. Li, H. Sun, R. Beck, U. Flörke, H.-J. Haupt, *Inorg. Chim. Acta* **2000**, *298*, 63.

[8] a) M. F. Semmelhack, P. M. Helquist, L. D. Jones, *J. Am. Chem. Soc.* **1971**, *93*, 5908; b) R. Taube, D. Steinborn, H. Drevs, P. N. Chuong, N. Stransky, J. Langlotz, *Z. Chem.* **1988**, *28*, 381.

[9] B. K. Bower, H. G. Tennent, *J. Am. Chem. Soc.* **1972**, *94*, 2512.

[10] a) H. Lehmkuhl, V. Dimitrov, *J. Organomet. Chem.* **1996**, *519*, 69; b) H. Lehmkuhl, V. Dimitrov, *J. Organomet. Chem.* **1996**, *519*, 83; c) H. Lehmkuhl, V. Dimitrov, unpublished results.

[11] a) R. Taube, G. Honymus, *Angew. Chem.* **1975**, *87*, 291; *Angew. Chem. Int. Ed. Engl.* **1975**, *14*, 261; b) H.-O. Frölich, B. Hipler, B. Hofmann, *J. Organomet. Chem.* **1992**, *430*, 133; c) H.-O. Frölich, R. Wyrwa, H. Görls, *J. Organomet. Chem.* **1992**, *441*, 169; d) D. Steinborn, F. Becke, R. Boese, *Inorg. Chem.* **1995**, *34*, 2625.

[12] a) The complex $Li[Cr^{III}Mes_4]\cdot 4THF$ was oxidized in air to $[Cr^{IV}Mes_4]$ (Mes = 2,4,6-trimethylphenyl): W. Seidel, I. Bürger, *Z. Anorg. Allg. Chem.* **1976**, *426*, 155; b) $[Mo^{IV}Mes_4]$ was prepared by air oxidation of $Li[Mo^{III}Mes_4]\cdot 4THF$: W. Seidel, I. Bürger, *J. Organomet. Chem.* **1979**, *171*, C45.

[13] The donor influence of the 1-norbornyl ligand was determined by ^{13}C NMR spectroscopy investigations on (1-nor)Hg compounds and comparison with the data of other alkyl ligands: V. Dimitrov, K.-H. Thiele, R. Radeglia, *Z. Anorg. Allg. Chem.* **1983**, *503*, 177; see also ref. [8b].

[14] K. Fagnou, M. Lautens, *Angew. Chem.* **2002**, *114*, 26; *Angew. Chem. Int. Ed.* **2002**, *41*, 26.

[15] Data of **5**: a) ^{13}C NMR (300 MHz, $[D_8]$THF, 20 °C, TMS): $\delta =$ 51.05 (C-1), 40.79 (C-7), 37.94 (C-4), 32.73 (C-2,6), 31.49 ppm (C-3,5); MS (70 eV): *m*/*z* (%): 190 (40) [M^+], 161 (100); elemental analysis (%) calcd: C 88.35, H 11.65; found: C 88.11, H 11.78; b) The crystal structure of **5** was also determined and will be published elsewhere.

[16] a) V. Dimitrov, K.-H. Thiele, D. Schenke, *Z. Anorg. Allg. Chem.* **1985**, *527*, 85; b) K.-H. Thiele, V. Dimitrov, D. Schenke, A. Krüger, A. Rusina, *Wiss. Z. Tech. Hochsch. "Carl Schorlemmer" Leuna-Merseburg* **1986**, *28*, 197; c) V. Dimitrov, K.-H. Thiele, A. Zschunke, *Z. Anorg. Allg. Chem.* **1982**, *494*, 144.

[17] E. K. Byrne, K. H. Theopold, *J. Am. Chem. Soc.* **1989**, *111*, 3887.

[18] The preparation of tetrakis(1-camphenyl) compounds of Ti^{IV}, Zr^{IV},and Hf^{IV} has been described; the ^{13}C NMR data are comparable with those of the corresponding tetrakis(1-norbornyl) derivatives: D. Schenke, K.-H. Thiele, *J. Organomet. Chem.* **1990**, *382*, 109.

[19] H. Lehmkuhl, K. Mehler, G. Hauschild, *Chem. Ber.* **1983**, *116*, 438.

[20] R. H. Blessing, *Acta Crystallogr. Sect. A* **1995**, *51*, 33.

[21] a) G. M. Sheldrick, SHELXS97, Program for the Solution of Crystal Structures, University of Göttingen, Göttingen (Germany), **1997**; b) G. M. Sheldrick, SHELXL97, Program for the Refinement of Crystal Structures, University of Göttingen, Göttingen (Germany), **1997**.

 © 2003 Wiley-VCH Verlag GmbH & Co. KGaA, Weinheim

Biosynthesis of Alkylpyridines

Biogenesis of 3-Alkylpyridine Alkaloids in the Marine Mollusc *Haminoea Orbignyana***

*Adele Cutignano, Annabella Tramice, Salvatore De Caro, Guido Villani, Guido Cimino, and Angelo Fontana**

In comparison with our knowledge of terrestrial plant and microbial systems, little is known about the biogenesis of secondary metabolites in marine organisms, such as sponges, tunicates, algae and molluscs.[1] Although most of these compounds show more than one analogy with terrestrial metabolites, there are a few categories of products that seem to be structurally specific to marine species. One such group of compounds is formed by 3-alkylpyridine alkaloids (also named 3-alkylpiperidine alkaloids), a family of natural products that encompasses a very heterogeneous collection of molecules sharing an hypothetical common origin from a putative 3-alkylpyridine precursor (or a biochemical analogue).[2] Although several new members of this class of products were characterized over the last decade from Haplosclerida sponges[3] and Cephalaspidea molluscs,[4] no biosynthetic study has been reported in the literature to date. Herein, we describe the biosynthesis of haminol-2 (**1**) in the Mediterranean mollusc *Haminoea orbignyana*, the first in vivo evidence on the biogenesis of 3-alkylpyridines in marine organisms.

Mediterranean molluscs of the genus *Haminoea* (Opisthobranchia: Cephalaspidea) are chemically characterized by the presence of oxygenated 3-alkylpyridines, commonly named haminols, which when secreted in the mucus act as alarm pheromones inducing escape reaction in conspecifics.[5] The structure of **1**, which was first isolated along with its deacetyl derivative, **2**, from *H. orbignyana*,[5b] exemplifies well

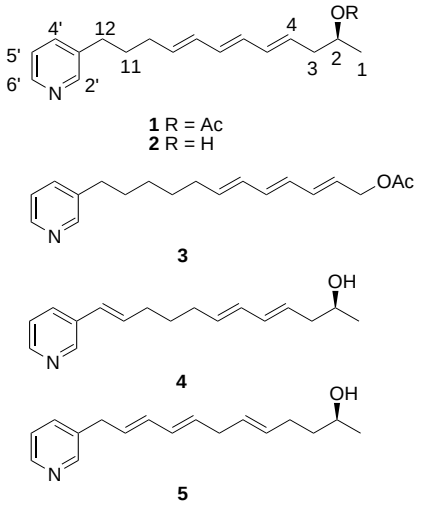
[*] Dr. A. Fontana, Dr. A. Cutignano, Dr. A. Tramice, Dr. S. De Caro, Dr. G. Villani, Dr. G. Cimino
Istituto di Chimica Biomolecolare (ICB) del CNR
Via Campi Flegrei 34
80078, Pozzuoli (Napoli) (Italy)
Fax: (+39) 081-804-1770
E-mail: afontana@icmib.na.cnr.it

[**] The authors are grateful to the "Servizio NMR dell'ICB" for the technical support. The work has been partially supported by a grant of PharmaMar s.a. (Madrid, Spain).

Supporting information for this article is available on the WWW under http://www.angewandte.org or from the author.

 DOI: 10.1002/anie.200250642 © 2003 Wiley-VCH Verlag GmbH & Co. KGaA, Weinheim

the peculiar characteristics of cephalaspidean alkylpyridines that, with the exception of **3**, has a polyunsaturated 12-membered chain with a hydroxy group at the *S*-configured C-2 center (e.g., **4** and **5**).[5]



To test the ability of *H. orbygniana* to produce de novo haminol-1 (**2**) and **1**, two preliminary experiments were performed by feeding either [2-^{14}C]-acetic acid (30 specimens, 0.3 μCi/specimen) or nicotinic acid-carboxy-^{14}C (18 specimens, 0.5 μCi/specimen). After the injection, the animals were starved three days in an aquarium before carrying out the extraction and purification of the secondary metabolites. Significant levels of radioactivity were recovered in the haminols (**1** and **2**) from both experiments, thus proving the de novo origin of the alarm pheromones in the cephalaspideans. Notably, incorporation of radioactive nicotinic acid into **2** and **1** provided the first evidence for the involvement of this molecule in the biogenesis of 3-alkylpyridines. To confirm these unexpected results and address the biosynthesis of **1** in *H. orbignyana*, other two groups of molluscs were injected twice over four days with either d_4-nicotinic acid ethyl ester or [1-^{13}C]-acetic acid. A third population of opisthobranchs was frozen and kept as control sample. Organic extracts of treated and control animals were prepared by soaking the frozen specimens in acetone, and **1** was purified from the resulting Et_2O-soluble fractions by radial TLC (8:2 *n*-hexane/ethyl acetate) on Chromatotron (Harrison Research). The analysis of the biosynthetic experiments was preceded by a complete assignment of the NMR data of **1** (^{1}H NMR: 400 MHz, $CDCl_3$, 19 °C; ^{13}C NMR: 100 MHz, $CDCl_3$, 19 °C; Table 1).

A feeding experiment with [D_4]nicotinic acid ethyl ester led to the labeling of the pheromones. In fact, after the injection of the deuterated precursor to 50 specimens of *H. orbignyana*, LC-MS (APCI; atmospheric pressure chemical ionization) analysis of the resulting product, **1**, showed a MS pseudomolecular ion at $m/z = 304$, which substantiated the retention of the four deuterium atoms (natural, $m/z = 300$ [$C_{19}H_{25}NO_2 + H^+$]; labeled, $m/z = 304$ [$C_{19}H_{21}D_4NO_2 + H^+$]). In SIM mode, integration of the HPLC peaks associated with natural and labeled **1** suggested that 5% of the whole content

Table 1: NMR data of haminol-2 (**1**) from natural and labeled samples.

	δ(^{1}H)	δ(^{13}C)	% Apparent Enrichment[a]
1	1.20, s	19.5	−4.7
2	4.93, m	70.3	23.8
3	2.35, m; 2.31, m	39.2	−5.5
4	5.59, m	128.5	33.5
5	6.09, m	131.6	−3.3
6	6.09, m	130.7	33.6
7	6.09, m	133.3	0.0
8	6.09, m	131.1	25.3
9	5.67, m	133.8	−6.6
10	2.14, bq	32.1	23.1
11	1.73, m	30.6	−3.7
12	2.62, t	32.4	−2.1
2′	8.44, bs	149.9	6.0
3′	–	137.5	5.6
4′	7.49, bd	135.9	6.0
5′	7.20, dd	123.3	36.0
6′	8.44, bs	147.1	6.7
CO_{Ac}	–	170.6	116.5
Me_{Ac}	2.01, s	21.3	–

[a] From feeding experiments with [1-^{13}C]-acetic acid. The apparent enrichment was expressed as variation of the peak intensity in labeled and natural samples. Spectra were normalized to the signal at $\delta =$ 21.3 ppm (methyl group of the acetyl residue) and the values were calculated on the basis of the following formula: (labeled signal−natural signal)/natural signal.

of the pheromone derived from the exogenous precursor. The final evidence that nicotinic acid (**6**) was incorporated into the molecule of **1** came with ^{2}H NMR analysis (Figure 1). In fact, the ^{2}H NMR (62 MHz, CH_2Cl_2, 19 °C) spectrum (Figure 1, top) of labeled **1** showed three peaks at $\delta = 8.40$ (H-2′ and H-6′), 7.20 (H-5′), and 7.49 ppm (H-4′), which were in good agreement with the signals of the pyridine ring in the isotopically natural sample (Figure 1, bottom). The integration of these three resonances indicated a ratio of 2:1:1, thus confirming that there was complete retention of deuterium

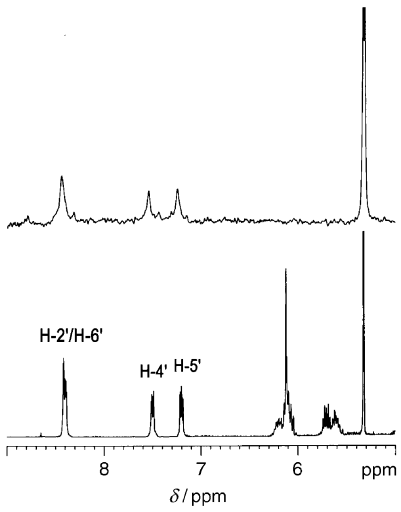


Figure 1. Incorporation of [D_4]nicotinic acid in haminol-2 (**1**): ^{2}H NMR (62 MHz, CH_2Cl_2, 19 °C) spectrum (top) and ^{1}H NMR (400 MHz, CD_2Cl_2, 19 °C) spectrum (bottom).

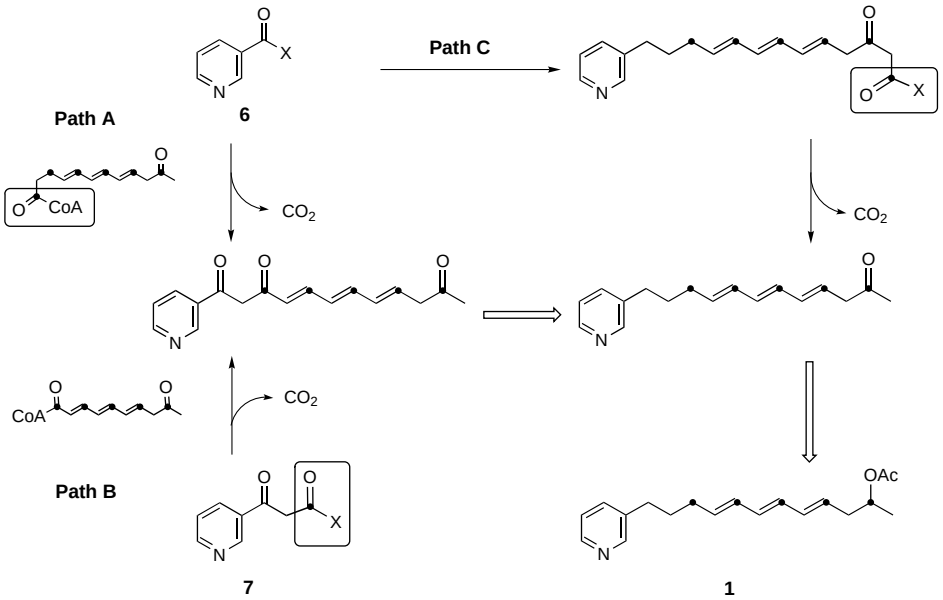
 © 2003 Wiley-VCH Verlag GmbH & Co. KGaA, Weinheim

during the biosynthesis and ruling out any change of the oxidation state of the pyridine. This was of particular interest since dihydropyridine intermediates are required for the decarboxylation of the nicotinic acid.[6] The presence of all deuterium atoms implied, therefore, the preservation of the carboxylic carbon of **6**, thus proving the incorporation of an intact molecule of the precursor. This result was also in full agreement with the results of the labeling of **1** recorded by feeding experiments with [1-^{14}C]-nicotinic acid.

Once the origin of both the C-12 center and the pyridine ring of **1** had been established, the question of the biosynthesis of the alkyl chain remained. A comparison of the ^{13}C NMR spectra of **1** from natural and treated molluscs demonstrated that C-2, C-4, C-6, C-8, and C-10 had been enriched after the injection of [1-^{13}C]-acetic acid(Table 1). The labeling pattern confirmed the acetogeninic origin of the alkyl chain and suggested that the hydroxy group at C-2 could be directly derived from the carbonyl moiety of an acetate unit. As expected, no incorporation was evident at C-12, whereas we recorded a significant increase of the signals for the acetyl group (C-1, $\delta = 170.6$ ppm) and C-5′ ($\delta =$ 123.3 ppm) of the pyridine moiety (Table 1). This latter finding is consistent with the involvement of acetate-derived glyceraldehyde 3-phosphate in the formation of nicotinic acid.[6] Although the experiments with ^{13}C-labeled acetates proved the incorporation of five acetate units into the aliphatic part of **1**, they did not clarify the mechanism leading to the assembly of the pheromone molecule. In fact, three different pathways could be proposed on the basis of the experimental data (Scheme 1). Paths A and B involve the condensation of a hexa- or pentaketide moieties with the nicotinic derivatives **6** and **7**, respectively. On the other hand, path C relies on incorporation of acetate via a polyketide biogenesis by using nicotinic acid as starter unit. In this view, the double bond position of **1** is not in agreement with the classical reduction of the growing polyketide intermediates, which suggests that shift of the double bonds might occur during the biosynthetic process. Every path described in Scheme 1, however, implies the loss of one carbon atom by decarboxylation of the acetate-derived chain.

In conclusion, this work proves the de novo biosynthesis of **1** in *H. orbignyana* and confirms the pioneering data reported by Fenical and co-workers with *Navanax inermis*.[7] The experiments prove the origin of the pyridine ring and C-12 from nicotinic acid, as well as the contribution of acetate to the formation of the alkyl chain. On the other hand, the way of assembling the molecule needs to be studied in more detail. Unfortunately, injection of ^{13}C-doubly labeled acetic acid, which should shed definitive light on these aspects, did not give clear evidence because of the limited number of molluscs (six specimens) that were available for the experiment. However, the polyketide route of Path C (Scheme 1) seems to us more likely, although nicotinic acid, or a metabolic equivalent, has been never reported as the starting unit in the biosynthesis of polyketides. This hypothesis is, however, not groundless if one considers the many examples of similar molecules that can be loaded by polyketide synthases of bacteria and fungi.[8] The short life-cycle of *H. orbignyana* (only 5–6 weeks) strongly limited our possibility of performing other feeding experiments (for example, with doubly labeled acetate) to shed light on these unresolved aspects.

Finally, as stated above, 3-alkylpyridines are generally envisaged as precursors of polycyclic sponge compounds including some of the most intriguing structures ever isolated from marine organisms, such as saraines[9] and manzamines.[10] Based on previous proposals, Andersen and co-workers have suggested a unified pathway for the biosynthesis of monomeric and oligomeric members of this family of natural products.[3] As already put forth by Baldwin and Whitehead,[11] one of the key points of this hypothesis is the origin of



Scheme 1. Possible pathways for the biosynthesis of **1**, based upon [1-^{13}C]-acetic acid (·) labeling studies. **X** is for -OH or a metabolically equivalent residue. Squares indicate the carbon atoms eventually lost by decarboxylation.

 © 2003 Wiley-VCH Verlag GmbH & Co. KGaA, Weinheim

the 3-alkylpyridine motif from the condensation of ammonia, a C_{10} unit (a symmetrical dialdehyde) and a C_3 unit (an acrolein equivalent). Our data are not in agreement with this part of the proposal of Andersen and co-workers, although paths A and B closely resemble the biomimetic synthesis of keramaphidin B published by Baldwin.[11b] Yet, we cannot exclude that the biosynthesis of alkylpyridines in marine sponges may involve steps different from those occurring in *H. orbignyana.*

Received: November 27, 2002
Revised: March 24, 2003 [Z50642]

Keywords: alkaloids · biosynthesis · ecology · natural products

[1] a) D. J. Faulkner, *Nat. Prod. Rep.* **2002**, *19*, 1 – 48, and references therein; b) A. Fontana, G. Cimino, *Recent Res. Dev. Org. Chem.* **2001**, *5*, 89 – 105; c) B. S. Moore, *Nat. Prod. Rep.* **1999**, *16*, 653 – 674; d) W. H. Gerwick, M. A. Roberts, A. Vulpanovici, D. L. Ballantine, *Adv. Exp. Med. Biol.* **1999**, *447*, 211 – 218; e) W. H. Gerwick, *Biochim. Biophys. Acta* **1994**, *1211*, 243 – 255; f) M. J. Garson, *Nat. Prod. Rep.* **1989**, *6*, 143 – 170.

[2] a) M. Tsuda, J. Kobayashi, *Heterocycles* **1997**, *46*, 765 – 794; b) I. Kitigawa, M. Kobayashi, *Gazz. Chim. Ital.* **1993**, *123*, 321 – 325; c) J. E. Baldwin, C. R. Whitehead, *Tetrahedron Lett.* **1992**, *33*, 2059 – 2062; d) G. Cimino, G. Scognamiglio, A Spinella, E. Trivellone, *J. Nat. Prod.* **1990**, *53*, 1519 – 1525.

[3] R. J. Andersen, R. W. M. van Soest, F. Kong in *Alkaloids: Chemical and Biological Perspectives, Vol. 10* (Ed.: S. W. Pelletier), Pergamon, London, **1996**, pp. 301 – 355, and references therein.

[4] G. Cimino, M. L. Ciavatta, A. Fontana, M. Gavagnin in *Bioactive Compounds from Natural Sources*, (Ed.: C. Tringali), Taylor and Francis, **2001**, pp. 577 – 637.

[5] a) G. Cimino, A. Passeggio, G. Sodano, A. Spinella, G. Villani, *Experientia* **1991**, *47*, 61 – 63; b) A. Spinella, L. A. Alvarez, A. Passeggio, G. Cimino, *Tetrahedron* **1993**, *49*, 1307 – 1314.

[6] J. Mann in *Natural products: their chemistry and biological significance. Alkaloids*, (Eds.: J. Mann, R. S. Davidson, J. B. Hobbs, D. V. Banthorpe, J. B. Harborne), Longman, London, **1994**, pp. 389 – 446.

[7] W. Fenical, H. L. Sleeper, V. J. Paul, M. O. Stallard, H. H. Sun, *Pure Appl. Chem.* **1979**, *51*, 1865 – 1874.

[8] J. Staunton, B. Wilkinson, *Top. Curr. Chem.* **1998**, *195*, 49 – 92.

[9] a) G. Cimino, S. De Stefano, G. Scognamiglio, G. Sodano, E. Trivellone, *Bull. Soc. Chim. Belg.* **1986**, *95*, 783 – 800; b) G. Cimino, A Spinella, E. Trivellone, *Tetrahedron Lett.* **1989**, *30*, 133 – 136; c) G. Cimino, C. A. Mattia, L. Mazzarella, R. Puliti, G. Scognamiglio, A Spinella, *Tetrahedron* **1989**, *45*, 3863 – 3872.

[10] a) R. Sakai, T. Higa, C. W. Jefford, G. Berardinelli, *J. Am. Chem. Soc.* **1986**, *108*, 6404 – 6405; b) R. Sakai, S. Kohmoto, T. Higa, C. W. Jefford, G. Berardinelli, *Tetrahedron Lett.* **1987**, *28*, 5493 – 5946.

[11] a) J. E. Baldwin, R. C. Whitehead, *Tetrahedron Lett.* **1992**, *33*, 2059 – 2062; b) J. E. Baldwin, T. D. W. Claridge, A. J. Culshaw, F. A. Heupel, V. Lee, D. R. Spring, R. C. Whitehead, R. J. Boughtflower, I. M. Mutton, R. J. Upton, *Angew. Chem.* **1998**, *110*, 2806 – 2808; *Angew. Chem. Int. Ed.* **1998**, *37*, 2661 – 2663.

 © 2003 Wiley-VCH Verlag GmbH & Co. KGaA, Weinheim

Single-Site/Dispersed-Metal Catalyst

Hydrogenation of Arenes over Catalysts that Combine a Metal Phase and a Grafted Metal Complex: Role of the Single-Site Catalyst**

Claudio Bianchini, Vladimiro Dal Santo, Andrea Meli, Simonetta Moneti, Marta Moreno, Werner Oberhauser, Rinaldo Psaro, Laura Sordelli, and Francesco Vizza*

In comparison with the separate components, the combination on the same support material of dispersed palladium nanoparticles and grafted molecular rhodium complexes has provided evidence of improved activity in the hydrogenation of arenes.[1] It was proposed that the catalytic efficiency is a consequence of a hydrogen-spillover process that would enhance specifically the hydrogenation activity of the molecular catalyst.[1] A recent study of the hydrogenation of arenes with a catalyst obtained by silica sol–gel coentrapment of metallic palladium and $[Rh(cod)(\mu\text{-}Cl)]_2$ disagrees with the hydrogen-spillover hypothesis and suggests that the action of both metals is caused by a synergistic effect;[2] however, no explanation of the nature of this effect has been forthcoming. Herein, we provide a rationale for this synergistic effect, and show that the grafted rhodium complex speeds up the hydrogenation of arenes to cyclic dienes.

Three different heterogeneous catalysts were tested in the hydrogenation of some arenes in *n*-pentane at relatively low temperature (40–60 °C) and 30 bar H_2. A highly dispersed palladium metallic phase and the Rh^I complex [Rh(cod)(sulphos)] (cod = cyclooctadiene; sulphos = $^-O_3S(C_6H_4)CH_2\text{-}C(CH_2PPh_2)_3$) were separately supported on high-surface-area porous silica . A calcination/reduction procedure of silica-supported $PdCl_2$ was employed to prepare Pd^0/SiO_2, **1**, with a metal content of about 10 wt %, while the Rh^I complex was grafted by using a known procedure involving hydrogen bonds between silanols of the support and sulfonate groups from the sulphos ligand.[3] The single-site catalyst, [Rh(cod)-(sulphos)]/SiO_2, **2** (Figure 1 A) with a metal content of about 0.5 wt %, was previously employed to catalyze the hydrogenation and hydroformylation of olefins in either gas–solid or liquid–solid phase.[3a] Upon hydrogenation, the cod ligand

[*] Dr. C. Bianchini, Dr. A. Meli, Dr. S. Moneti, Dr. M. Moreno, Dr. W. Oberhauser, Dr. F. Vizza
Istituto di Chimica dei Composti Organometallici (ICCOM) – CNR
Via J. Nardi 39, 50132 Firenze (Italy)
Fax: (+39)055–2478366
E-mail: bianchin@fi.cnr.it
Dr. V. Dal Santo, Dr. R. Psaro, Dr. L. Sordelli
Istituto di Scienze e Tecnologie Molecolari (ISTM) – CNR
Via C. Golgi 19, 20133 Milano (Italy)

[**] This work was partially supported by the RTN contract HPRN-CT-2002-00196, and a bilateral project CNR/FONACIT. M.M. acknowledges a contribution from the European Commission for a postdoctoral grant (Marie Curie Contract no. HPMF-CT-2000–00568).

Supporting information for this article is available on the WWW under http://www.angewandte.org or from the author.

 © 2003 Wiley-VCH Verlag GmbH & Co. KGaA, Weinheim DOI: 10.1002/anie.200250667

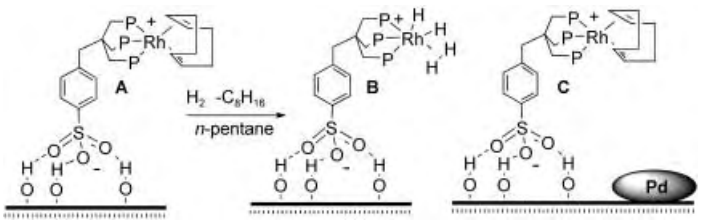


Figure 1. Sketches of the precursors employed in this study.

in **2** is removed as cyclooctane and replaced in the metal coordination sphere by hydride ligands.[3a] Studies of model compounds showed that the most likely stucture of Rh^{III} tetrahydride is nonclassical (Figure 1B).[4] The third catalyst, [Rh(cod)(sulphos)]–Pd^0/SiO_2 ,**3** , was obtained by straightforwardly tethering the Rh^I precursor [Rh(cod)(sulphos)] onto **1** by using the same procedure adopted for **2** (Figure 1C).[3]

The high resolution transmission electron-microscopy (HRTEM) analysis of **1** showed a uniform particle dispersion with a narrow distribution centered at 1.65 nm, which is in good agreement with the value estimated from the EXAFS data. The surface area was found to decrease from 344 to 304 $m^2 g^{-1}$ with a corresponding decrease in the pore volume from 1.19 to 1.02 $cm^3 g^{-1}$. Diffuse reflectance infrared fourier transform spectroscopy (DRIFTS) and extended X-ray absorption fine-structure (EXAFS) measurements showed [Rh(cod)(sulphos)] to be tethered through hydrogen bonds on preformed **1** with no change in the chemical environment of the rhodium center. The surface area and pore volume for **3** were 284 $m^2 g^{-1}$ and 0.95 $cm^3 g^{-1}$, respectively. HRTEM data were consistent with a uniform palladium-particle dispersion with a mean size of 1.79 nm. Table 1 reports data obtained for the hydrogenation of benzene, toluene, styrene, and ethylbenzene. A unique sample of **3** containing a Pd/Rh molar ratio of 17.6:1 was used in all reactions. Irrespective of the arene, the combined single-site/dispersed-metal catalyst **3** was from four to six times more active than **1**, while **2** proved to be totally inactive. In contrast, the grafted Rh^I complex was as active as **1** for the hydrogenation of the styrene double bond (entries 7, 8).

Catalyst **3** was also the best for the hydrogenation of cyclohexa-1,3-diene (Table 2). The presence of the grafted Rh^I complex apparently minimizes the amount of benzene produced by the dehydrogenation of cyclohexa-1,3-diene over the Pd particles (see entries 1 and 3).[5] The ability of supported Pd^0 particles to disproportionate cyclohexa-1,3-diene to benzene and cyclohexene is well-known, and the hydrogenation of benzene to cyclohexa-1,3-diene was proved to be the rate limiting step along the reduction to cyclohexane.[5]

Table 2: Hydrogenation of cyclohexa-1,3-diene with **1**, **2** or **3**.[a]

Entry	Catalyst	Substrate/ M ratio	% Conversion[b] (TOF, M)[c] benzene	cyclohexene	cyclohexane
1	**1**	525	27 (284)	5 (52)	68 (714)
2	**2**	9200	0	11 (2024)	2 (368)
3	**3**	525/9200	6 (63, Pd)	6 (63, Pd)	88 (924 Pd)

[a] Experimental conditions: **1** (9.86 wt% Pd), 0.044 mmol Pd; **2** (0.56 wt% Rh), 0.0025 mmol Rh; **3** (0.56 wt% Rh, 9.86 wt% Pd), 0.044 mmol Pd, 0.0025 mmol Rh; 30 bar H_2, 30 mL *n*-pentane, 25 °C, 30 min, 1500 rpm. [b] Average values over at least three runs. [c] Mol product (mol M h)$^{-1}$ (M = Pd, Rh; TOF = turnover frequency).

Control experiments of the dehydrogenation of cyclohexa-1,3-diene under N_2 proved that **1** is an effective disproportionation catalyst (cyclohexane 2%, cyclohexene 46%, benzene 48% under the conditions of Table 2), while **2** is unable to perform such a reaction.

Finally, **1** proved much better than **2** for the hydrogenation of cyclohexene to cyclohexane (Table 3 entries 1, 3), and did not promote the dehydrogenation of cyclohexene as shown by a reaction under N_2 (Table 3, entry 2).

A number of independent experiments were performed to gain further insight into the role played by the tethered Rh^I catalyst in the hydrogenation of benzene. The hydrogenation was carried out in the presence of a mechanical mixture of **1** and **2** under the experimental conditions of Table 1, entry 3. No appreciable synergistic effect was observed, the conversion to cyclohexane being almost identical to that obtained with **1** alone.

Table 1: Hydrogenation of arenes with **1**, **2** or **3**.[a]

Entry	Catalyst	*T* [°C]	Substrate	Substrate/M ratio	% Conversion[b] (TOF, M)[c] product
1	**1**	40	benzene	525	4 (11) cyclohexane
2	**2**	40	benzene	9200	0
3	**3**	40	benzene	525/9200	15 (39, Pd) cyclohexane
4	**1**[d]	40	toluene	426	4 (8) methylcyclohexane
5	**2**[e]	40	toluene	7520	0
6	**3**[f]	40	toluene	426/7520	16 (32, Pd) methylcyclohexane
7	**1**	60	styrene	400	97 (194) ethylbenzene; 3 (6) ethylcyclohexane
8	**2**	60	styrene	8750	98 (4287) ethylbenzene
9	**3**	60	styrene	400/8750	81 (162, Pd) ethylbenzene; 19 (38 Pd) ethylcyclohexane
10	**1**	60	ethylbenzene	400	3 (6) ethylcyclohexane
11	**2**	60	ethylbenzene	8750	0
12	**3**	60	ethylbenzene	400/8750	20 (40, Pd) ethylcyclohexane

[a] Experimental conditions: **1** (9.86 wt% Pd), 0.044 mmol Pd; **2** (0.56 wt% Rh), 0.0025 mmol Rh; **3** (0.56 wt% Rh, 9.86 wt% Pd), 0.044 mmol Pd, 0.0025 mmol Rh; 30 bar H_2; 30 mL *n*-pentane, 2 h, 1500 rpm. [b] Average values over at least three runs. [c] Mol product (mol M h)$^{-1}$ (M = Pd, Rh). [d] 0.088 mmol Pd. [e] 0.005 mmol Rh. [f] 0.088 mmol Pd, 0.005 mmol Rh.

 © 2003 Wiley-VCH Verlag GmbH & Co. KGaA, Weinheim

Table 3: Hydrogenation of cyclohexene to cyclohexane with **1**, **2** or **3**.[a]

Entry	Catalyst	Substrate/M ratio	% Conversion[b] (TOF, M)[c]
1	**1**	525	99.8 (1048)
2[d]	**1**	525	0
3	**2**	9200	0.5 (92)
4	**3**	525/9200	100 (1050 Pd)

[a] Experimental conditions: **1** (9.86 wt% Pd), 0.044 mmol Pd; **2** (0.56 wt% Rh), 0.0025 mmol Rh; **3** (0.56 wt% Rh, 9.86 wt% Pd), 0.044 mmol Pd, 0.0025 mmol Rh; 30 bar H_2; 30 mL *n*-pentane, 25 °C, 30 min, 1500 rpm. [b] Average values over at least three runs. [c] Mol product (mol M h)$^{-1}$ (M = Pd, Rh). [d] Under 1 bar N_2.

The known Rh^I complex $[Rh(CO)_2(sulphos)]$, unable to hydrogenate double bonds,[3a] was anchored over **1**, and the resulting combined molecular–nanoparticle catalyst was used to hydrogenate benzene under the conditions of Table 1. The conversion to cyclohexane (4%) was similar to that observed in the presence of **1** alone (Table 1, entry 1).

Both **2** and the molecular precursor [Rh(cod)(sulphos)] did not hydrogenate arenes, irrespective of the phase variation, even at very high H_2 pressure, which rules out the promoting effect of an eventual hydrogen spillover promoted by palladium particles, and the action of leached Rh^I catalyst, respectively.

The hydrogenation of cyclohexa-1,3-diene in the presence of **2** under the conditions of Table 2, entry 2 was quenched after 30 min by depressurising the reactor, which was then replenished with N_2 (Figure 2). The solid compound was collected by filtration, dried in vacuo and treated with MeOD/[D_7]DMF (1:1, v/v) under N_2 to break the hydrogen bonds between the support and the molecular complex.[3] $^{31}P\{^1H\}$ and ^1H NMR spectra of the resulting solution showed the formation of $[Rh(\eta^4\text{-}C_6H_8)(sulphos)]$.[6] Crystals of $[Rh(\eta^4\text{-}C_6H_8)(sulphos)]\cdot 2\,MeOH$ were obtained by reacting [Rh(cod)(sulphos)] with cyclohexa-1,3-diene in MeOH and authenticated by a single-crystal X-ray analysis.[7] The structure consists of discrete molecules of $[Rh(\eta^4\text{-}C_6H_8)(sulphos)]$ with MeOH filling holes in the lattice (ORTEP drawing, Figure 2). Three *fac* phosphorus atoms and two double bonds from cyclohexa-1,3-diene coordinate the rhodium center in a distorted square-pyramidal geometry. The bond distances and angles are typical of metal complexes with either sulphos or $MeC(CH_2PPh_2)_3$ (triphos) and η^4-dienes.[3a,8]

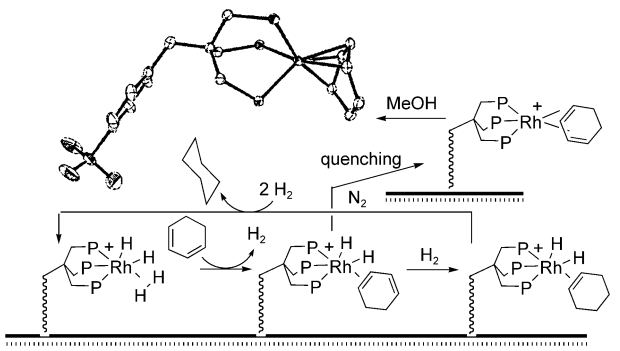


Figure 2. Proposed mechanism for the formation of $[Rh(\eta^4\text{-}C_6H_8)(sulphos)]$.

The possibility that rhodium metal, eventually formed upon partial decomposition of the grafted complex, might contribute to enhance the hydrogenation activity of the palladium catalyst was ruled out on the basis of five recycling experiments that gave comparable conversions. Washing the recycled catalyst with MeOH to remove the grafted rhodium complex gave a much less active catalyst with a conversion to cyclohexane similar to that observed with **1** alone. Mechanistic details for cyclohexa-1,3-diene hydrogenation to cyclohexene were provided for $[Ir(\eta^4\text{-}C_6H_8)(triphos)]^+$.[9]

The incorporation of the experimental evidence reported above leads us to conclude that 1) an intimate contact between the Pd nanoparticles and the Rh single sites in the mixed catalyst **3** is mandatory to observe improved activity in the hydrogenation of arenes to cycloalkanes; 2) the inhibition of diene disproportionation by the grafted rhodium complex, though important, cannot account alone for the increased conversions to cycloalkanes. These conversions are at least four times higher than those obtained with **1**, and even under the precondition that all cyclic dienes undergo disproportionation over palladium the total production of cycloalkane would not have been more than two times higher than that obtained with palladium alone. It is therefore reasonable to conclude that the grafted rhodium moieties cooperate with the palladium nanoparticles in promoting the hydrogenation of arenes to cyclic 1,3-dienes.

A simplified mechanism for the overall hydrogenation of benzene to cyclohexane is proposed in Figure 3, in which the rate-limiting hydrogenation of benzene to cyclohexa-1,3-diene is assisted by both palladium and rhodium centers. In view of the catalytic results reported in Table 2 and Table 3,

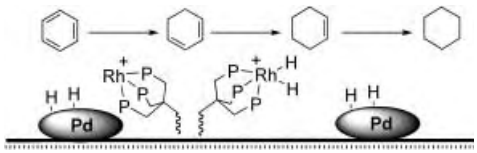


Figure 3. Proposed mechanism for the hydrogenation of benzene by **3**.

cyclohexa-1,3-diene should be more rapidly reduced to cyclohexene at rhodium, while cyclohexene should be predominantly reduced at palladium. The intimate mechanism of the Pd–Rh interaction in the first hydrogenation step is still rather obscure, yet its discovery is of paramount importance as it may open the door to the rational design of a new generation of tailored heterogeneous catalysts for diverse applications through appropriate combinations of supported metals and grafted molecular complexes.

Experimental Section

Details of the synthesis and characterization of the heterogeneous catalysts **1**, **2**, and **3** and of the complex $[Rh(\eta^4\text{-}C_6H_8)(sulphos)]$ are described in the Supporting Information.

Hydrogenation procedure: A stainless steel Parr reactor (100 mL), equipped with a temperature and pressure controller, and a paddle stirrer was charged with the appropriate amount of catalyst, the

 © 2003 Wiley-VCH Verlag GmbH & Co. KGaA, Weinheim

unsaturated substrate, *n*-pentane (30 mL), and H_2 (30 bar). The ensemble was heated to the appropriate temperature and then stirred (1500 rpm) for the desired time, after which the vessel was cooled to ambient temperature and depressurised. The liquid contents were analysed by GC and GC–MS. Above 1500 rpm, the rates were independent of the agitation speed at all the temperatures studied, thus indicating the absence of mass transfer resistance.

Received: December 2, 2002
Revised: March 13, 2003 [Z50667]

Keywords: arenes · heterogeneous catalysis · hydrogenation · palladium · rhodium

[1] a) H. Gao, R. J. Angelici, *J. Am. Chem. Soc.* **1997**, *119*, 6937; b) H. Yang, H. Gao, R. J. Angelici, *Organometallics* **2000**, *19*, 622, and references therein.

[2] R. Abu-Reziq, D. Avnir, I. Miloslavski, H. Schumann, J. Blum, *J. Mol. Catal. A* **2002**, *185*, 179.

[3] a) C. Bianchini, D. G. Burnaby, J. Evans, P. Frediani, A. Meli, W. Oberhauser, R. Psaro, L. Sordelli, F. Vizza, *J. Am. Chem. Soc.* **1999**, *121*, 5961; b) C. Bianchini, P. Barbaro, V. Dal Santo, R. Gobetto, A. Meli, W. Oberhauser, R. Psaro, F. Vizza, *Adv. Synth. Catal.* **2001**, *343*, 41; c) C. Bianchini, V. Dal Santo, A. Meli, W. Oberhauser, R. Psaro, F. Vizza, *Organometallics* **2000**, *19*, 2433.

[4] V. I. Bakhmutov, C. Bianchini, M. Peruzzini, F. Vizza, E. Vorontsov, *Inorg. Chem.* **2000**, *39*, 1655.

[5] a) A. Bunjes, I. Eilks, M. Pahlke, B. Ralle, *J. Chem. Educ.* **1997**, *74*, 1323; b) L. Cerveny, S. Rehurkova, *Collect. Czech. Chem. Commun.* **1987**, *52*, 2909; c) L. Cerveny, P. Kluson, I. Paseka, *React. Kinet. Catal. Lett.* **1991**, *43*, 533.

[6] NMR Data ([D_7]DMF, 20 °C, *J* in Hz): $^{31}P\{^1H\}$ NMR (81.01 MHz): $\delta = 11.0$ ppm (d, $^1J(P,Rh) = 122.6$); ^1H NMR (200.13 MHz): $\delta = 7.88$ (d, $^3J(H,H) = 8.1$, 2H; *m*-H-$SO_3C_6H_4$), 7.71 (d, $^3J(H,H) = 8.1$, 2H; *o*-H-$SO_3C_6H_4$), 7.30 (m, 6H; *p*-H-PPh_2), 7.2–7.1 (m, 24H; *o*- and *m*-H-PPh_2), 6.61 (m, 2H; CH-C_6H_8), 3.52 (s, 2H; CH_2C), 3.45 (m, 2H; CH-C_6H_8), 2.91 (br s, 6H; CH_2P), 1.35 (m, 2H; Hβ(CH_2)-C_6H_8), 1.23 ppm (m, 2H; Hα(CH_2)-C_6H_8).

[7] *Crystal data*: yellow crystals ($0.3 \times 0.25 \times 0.25$ mm), monoclinic, space group $P2_1/n$, $a = 13.513(5)$, $b = 18.308(5)$, $c = 19.539(5)$ Å, $\beta = 94.350(5)°$, $V = 4820(3)$ Å^3, $Z = 4$, $\rho_{calcd} = 1.415$ g cm^{-3}, $\mu = 0.546$ mm^{-1}, $Mo_{K\alpha}$ ($\lambda = 0.71609$ Å), $T = 293(2)$ K, 6674 independent reflections. Refinement on all data converged at $R_1 = 0.0678$, $wR_2 = 0.1113$, GOF = 0.9912. CCDC-198527 contains the supplementary crystallographic data for this paper. These data can be obtained free of charge via www.ccdc.cam.ac.uk/conts/retrieving.html (or from the Cambridge Crystallographic Data Centre, 12 Union Road, Cambridge CB2 1EZ, UK; fax: (+44) 1223-336-033; or deposit@ccdc.cam.ac.uk).

[8] a) C. Bianchini, P. Frediani, V. Herrera, M. V. Jiménez, A. Meli, L. Rincón, R. Sánchez-Delgado, F. Vizza, *J. Am. Chem. Soc.* **1995**, *117*, 4333; b) C. Bianchini, K. G. Caulton, C. Chardon, M.-L. Double, O. Eisenstein, S. A. Jackson, T. J. Johnson, A. Meli, M. Peruzzini, W. E. Streib, F. Vizza, *Organometallics* **1994**, *13*, 2010.

[9] C. Bianchini, K. G. Caulton, K. Folting, A. Meli, M. Peruzzini, A. Polo, F. Vizza, *J. Am. Chem. Soc.* **1992**, *114*, 7290.

 © 2003 Wiley-VCH Verlag GmbH & Co. KGaA, Weinheim

Mesoporous Basic Catalysts

Highly Ordered Mesoporous Silicon Oxynitride Materials as Base Catalysts**

*Yongde Xia and Robert Mokaya**

The discovery of mesoporous silicates by researchers at the Mobil company a decade ago, was a significant step in expanding the range of ordered zeolite-type materials beyond the microporous range and into the mesoporous regime.[1] However, purely siliceous mesoporous materials have neutral silica frameworks, which limits their applications in the fields of catalysis, ion exchange or adsorption. To obtain mesoporous solids with potential for use as catalysts, it is necessary to introduce heteroatoms and/or organic functional moieties that have specific active sites, into or onto the silica framework.[2] For example when Si in a mesoporous silica framework is substituted by other metal ions, M^{n+}, (where M^{n+} may be tetravalent, Ti^{4+}, V^{4+}, Sn^{4+} or trivalent, Al^{3+}, Fe^{3+}, Ga^{3+})[3,4] the framework either maintains electroneutrality (for M^{4+}) or acquires an overall negative charge (for M^{3+}) that may be compensated for by cations (e.g. protons). The M^{4+} ion substituted silica materials may be used as redox catalysts while M^{3+} ion substituted materials can function as solid acid or basic catalysts when protons or alkali/alkaline earth cations are the charge balancing ions respectively. In both cases the number and strength of the active sites generated generally depends on the amount and nature of the heteroatom. An extensively studied example is that of aluminum-containing mesoporous silica materials, which have attracted attention because of their potential application as solid acid catalysts.[4]

Although most metal-ion (i.e., cation) substituted mesoporous silica frameworks can be prepared by direct synthesis or by post-synthesis grafting methods, it is now thought that grafted materials are more catalytic active than their directly prepared analogues because of the higher accessibility of active sites.[5] However, in contrast to the abundance of research on cation-modified mesoporous silica materials, there are very few reports on framework "anion-modified" materials. Anion modified frameworks have been extensively studied for other classes of materials. For example when amorphous silica,[6] microporous aluminosilicate/aluminophosphate,[7] or aluminum vanadate[8] are treated with ammonia at high temperatures, the oxygen in their framework is partially displaced by nitrogen or NH_x species (to generate oxynitride frameworks), which have active sites capable of catalysing base-catalyzed reactions. As a consequence of the

[*] Dr. R. Mokaya, Dr. Y. Xia
School of Chemistry
University of Nottingham
University Park, Nottingham NG7 2RD (UK)
Fax: (+44) 115-951-3562
E-mail: r.mokaya@nottingham.ac.uk

[**] The authors are grateful to the EPSRC for financial support and the Royal Society for an equipment grant. The assistance of Dr P. Licence with the catalysis work is gratefully acknowledged.

 DOI: 10.1002/anie.200350978 © 2003 Wiley-VCH Verlag GmbH & Co. KGaA, Weinheim

amorphous nature of the pore walls of mesoporous silica materials, NH_x species can be immobilized/incorporated onto the surface of mesoporous silica frameworks via high-temperature treatment in the presence of ammonia or nitrogen.[6,9] This affords new types of mesostructured solid base materials with high surface area and pore volume.

Basic mesoporous materials may be prepared by one of three other routes;[10] 1) cation exchange with alkali (e.g., Na^+, K^+, Cs^+) metal ions, 2) impregnation with basic salts and 3) functionalisation with organic moieties (e.g., amines), which are basic. These methods, however, suffer from various disadvantages, such as competition from acidic sites and a low cation exchange capacity (which limits number of possible basic sites) for route 1), while route 2) and 3) suffer from problems with leaching along with structural degradation and a drastic decrease in textural properties (surface area, pore volume and pore size).[2,10] Herein, we report a synthesis route to mesoporous base catalysts, which exhibit excellent mesostructural ordering and considerable catalytic activity. We present the synthesis of structurally well-ordered anion (NH_x species) modified mesoporous-silica materials and also report on their catalytic activity for the base catalysed Knoevenagel condensation reaction. The materials were obtained by reacting cubic phase mesoporous silica with ammonia (a process hereinafter referred to as nitridation) at high temperature to obtain nitrogen-containing mesoporous-silica materials. The high structural ordering of the nitrogen-containing mesoporous materials reported here benefits from the use of high-quality sodium-free Si-MCM-48 as the starting material.[11] The use of Na-free Si-MCM-48 allowed us to use an optimised (i.e., relatively high) nitridation temperature—the presence of sodium ions in mesoporous silicas is known to have a detrimental effect on thermal/hydrothermal stability.[11,12] An optimised nitridation temperature preserved the mesoporous structure from collapse and allowed the ammonia molecules to react efficiently with silanol groups and/or bridging oxygen on the host Si-MCM-48 material. We show that NH_x species are incorporated onto the N-containing MCM-48 materials and generate basic sites, which exhibit considerable catalytic activity for the Knoevenagel condensation reaction. The resulting well-ordered mesoporous oxynitride materials, which have high surface area and pore volume, are likely to be attractive as alternative basic catalysts especially for large molecule transformations.

The structural ordering of the parent Si-MCM-48 and ammonia treated MCM-48 materials was assessed by powder X-ray diffraction (XRD). As shown in Figure 1, all the XRD patterns are typical for highly ordered MCM-48 materials with an intense *d* spacing (211) diffraction peak and several well-resolved higher order peaks in the 2θ range of 3–6°, which can be indexed to *Ia3d* cubic structure.[1] The synthesized and calcined Si-MCM-48 materials have different d_{211} spacing (37.6 Å and 35.4 Å respectively), which indicates a 6% contraction of the MCM-48 lattice after calcination. However, after being subjected to thermal treatment at 900 °C in a flow of ammonia gas, the resulting N-containing materials (designated as N-MCM-48A and N-MCM-48B for materials derived from nitridation of calcined or as-synthesized Si-MCM-48 respectively) exhibit similar d_{211} spacing of about

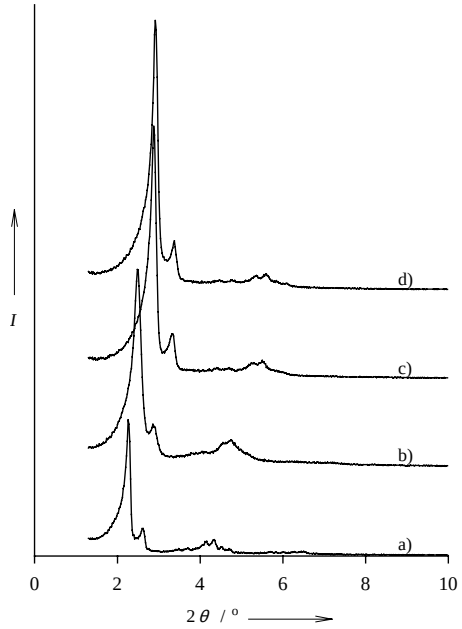


Figure 1. Powder XRD patterns of a) as-synthesized Si-MCM-48, b) calcined Si-MCM-48 and nitrided c) N-MCM-48A and d) N-MCM-48B materials.

30.3 Å. Noteworthy, when the parent Si-MCM-48 was subjected to heat treatment at 900 °C in air for the same duration as for the nitridation reaction (i.e., 20 h) it was virtually destroyed (surface area and pore volume reduced to 62 $m^2 g^{-1}$ and 0.07 $cm^3 g^{-1}$ respectively). This implies that an ammonia atmosphere is an important factor in maintaining structural ordering during nitridation. Interestingly, the intensity of the d_{211} diffraction peak for both nitrided materials is higher than that of the respective parent materials as shown in Figure 1.

The nitridation reaction occurs according to the following schemes

$$\equiv Si{-}OH + NH_3 \rightarrow \equiv Si{-}NH_2 + H_2O$$

and/or

$$\equiv Si{-}O{-}Si\equiv + NH_3 \rightarrow \equiv Si{-}NH{-}Si\equiv + H_2O \text{ or } \equiv Si{-}NH_2 + \equiv Si{-}OH$$

Given that synthesized mesoporous silica materials have a higher concentration of silanol groups than their calcined analogues,[13] it is reasonable to expect sample N-MCM-48B, which was obtained by nitridation of the synthesized Si-MCM-48, to have a higher NH_x density on its surface. Elemental analysis (see Table 1) confirmed that sample N-MCM-48B contained 14.7 wt % of N, which corresponded to a Si:N:O molar ratio of 1:0.65:1.025 while N-MCM-48A obtained by nitridation of calcined Si-MCM-48 had a N content of 11.4 wt % which is close to a Si:N:O molar ratio of 1:0.5:1.25.

The quality and structural ordering of the parent Si-MCM-48 and N-MCM-48 materials were also evaluated by N_2 sorption studies. The N_2 sorption isotherms of the materials

 © 2003 Wiley-VCH Verlag GmbH & Co. KGaA, Weinheim

Table 1: Elemental composition, *d* spacing and textural properties of studied MCM-48 materials.

Sample	N content [wt%]	d_{211} spacing [Å]	Surface area per gram [$m^2 g^{-1}$]	Pore volume per gram [$cm^3 g^{-1}$]	Pore size [Å]
Si-MCM-48		35.4	1247	1.10	34.1
N-MCM-48A	11.4	30.4	1340	0.65	20.0
N-MCM-48B	14.7	30.3	1487	0.66	17.8

are presented in Figure 2 and the corresponding textural properties are summarized in Table 1. Both Si-MCM-48 and N-MCM-48 exhibit type IV isotherms with a typical capillary condensation step into uniform pores without hysteresis. This indicates that both Si-MCM-48 and the N-MCM-48 samples

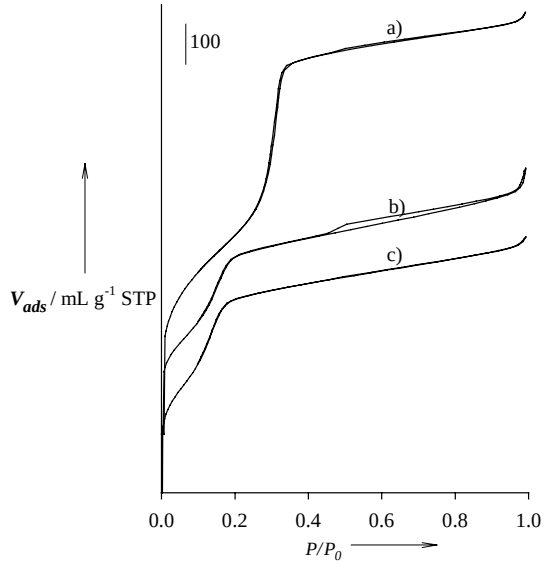


Figure 2. Nitrogen sorption isotherms of a) calcined Si-MCM-48 and nitride, b) N-MCM-48A, and c) N-MCM-48B materials. P/P_0 is partial pressure.

have good structural ordering. The capillary condensation step for Si-MCM-48 is in the relative pressure range 0.25–0.35 while the N-MCM-48 samples exhibit pore filling steps in the relative pressure range 0.15–0.22, thus indicating that the high-temperature treatment in ammonia results in a significant reduction in pore size. As shown in Table 1 the pore size of the N-MCM-48 materials is in the super-microporous to lower mesopore range. The reduction in pore size after nitridation arises from contraction of the lattice occasioned by the relatively severe thermal treatment at 900 °C. Indeed as noted above, extended (20 h) calcination at 900 °C virtually destroys the parent Si-MCM-48 material. Pore-wall thickening after nitridation also contributes to pore size reduction. The wall thickness of Si-MCM-48 was 11 Å compared to 14.1 Å and 15.1 Å for N-MCM-48A and N-MCM-48B respectively. However, the structural changes resulting from the thermal treatment in ammonia are not necessarily at the expense of pore uniformity or structural ordering as evidenced in Figure 1 and Figure 2.

Both Si-MCM-48 and the N-MCM-48 materials have a surface area per gram in the range 1200–1500 $m^2 g^{-1}$, which is typical for highly ordered MCM-48 materials.[1,11] However, the N-MCM-48 materials retain only 60% of the pore volume of the parent Si-MCM-48 material. This is consistent with the pore size contraction observed. The pore size contraction is expected to have a much greater effect on the pore volume than on the surface area, which is observed to increase slightly after nitridation. We note that a slight increase in surface area after nitridation has previously been observed for other types of porous materials.[6–8] The overall picture that emerges from the textural parameters is that upon nitridation of well-ordered Si-MCM-48, the resulting N-MCM-48 materials retain good structural ordering despite a significant decrease in pore volume and pore size.

The excellent structural ordering of the N-MCM-48 materials was also evidenced by transmission electron microscopy (TEM) as shown by the representative TEM image in Figure 3. Well-ordered pore channels are observed, thus indicating the excellent ordering of the nitrided materials. From the TEM micrograph it is possible to estimate a pore



Figure 3. Representative TEM image of nitrided N-MCM-48A.

channel diameter of 2 nm, which is similar to the pore size obtained from nitrogen sorption studies (Table 1). The particle morphology of the Si-MCM-48 and N-MCM-48 materials was investigated by scanning electron microscopy (SEM) and representative SEM images are shown in Figure 4. The Si-MCM-48 material exhibits well-formed cubic (rhombic dodecahedral) crystal-like particles (Figure 4a) of diameter in the range of 0.5–2 μm. The N-MCM-48A material (Figure 4b) also displays cubic crystal-like particles of diameter in the range 0.5–1 μm while the N-MCM-48B sample is made up of cubic particles, which, in some cases, appear to be bunched together but with a discernable particle size of 0.5–2 μm as shown in Figure 4c. It is worthwhile to note that the

 © 2003 Wiley-VCH Verlag GmbH & Co. KGaA, Weinheim

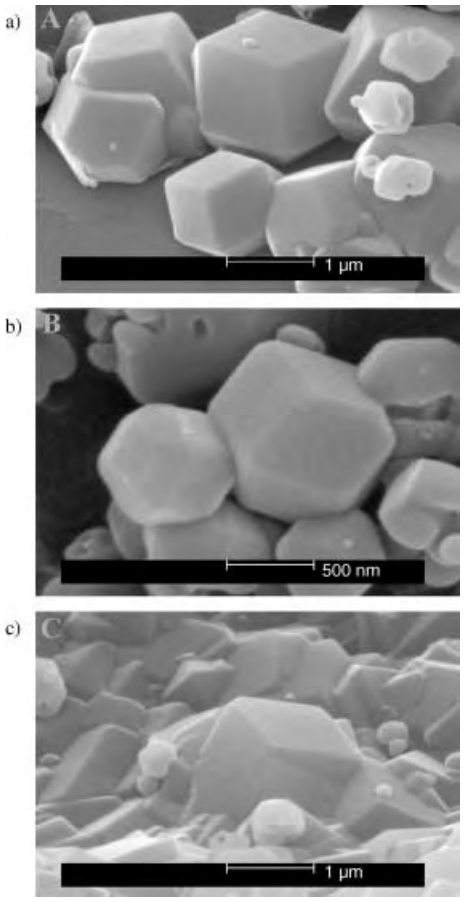


Figure 4. Representative SEM images of a) calcined Si-MCM-48 and nitrided b) N-MCM-48A and c) N-MCM-48B materials.

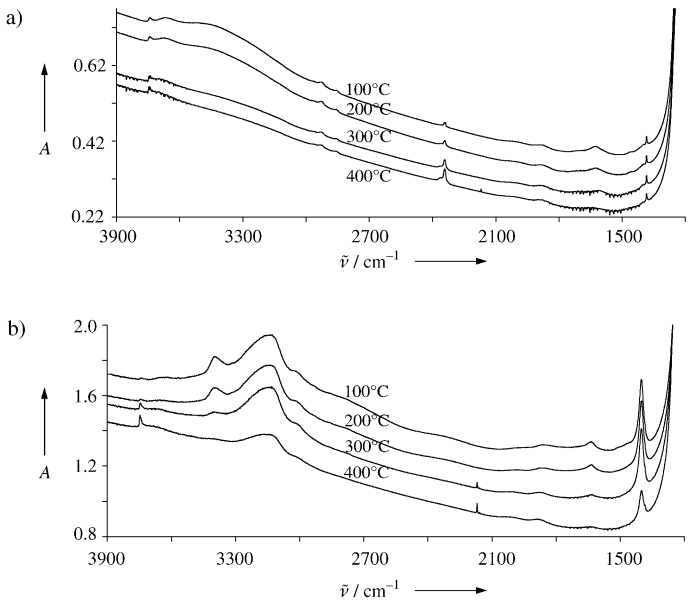
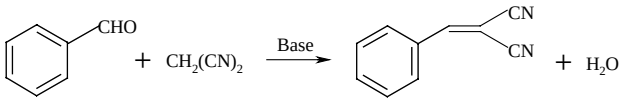


Figure 5. IR spectrum of a) calcined Si-MCM-48 and b) nitrided N-MCM-48A samples evacuated in vacuo at the temperatures shown. A = Absorbance.

"bunching" appearance shown in Figure 4c for sample N-MCM-48B is also observed for the N-MCM-48A and Si-MCM-48[11] and is therefore not a unique feature of sample N-MCM-48B. The particle morphology is therefore largely maintained after nitridation. The retention of particle morphology after nitridation has previously been reported for other types of porous oxides.[14]

Infrared spectroscopy was used to ascertain the presence of NH or NH_2 groups on the surface of the nitrided MCM-48 materials. Pure silica MCM-48 (Figure 5a) exhibits very low absorbance bands from Si–OH ν(OH) at 3743 cm^{-1} and adsorbed water at 3673 cm^{-1} and 1620 cm^{-1} along with several small peaks attributed to ν(CH) and δ(CH) which were also observed at about 2900 cm^{-1} and 1384 cm^{-1} arising from the presence of trace amount of surfactant on the sample. The peaks at 2340 cm^{-1} and 1860 cm^{-1} come from the overtones and combination bands of lattice vibrations. The main effect of increasing the evacuation temperature from 100 °C to 400 °C was the gradual decrease of the intensity of peaks attributed to adsorbed water. The N-containing MCM-48 sample (N-MCM-48A, Figure 5b) on the other hand displays several very strong absorbance bands at 3396 cm^{-1} and 3147 cm^{-1}, which are attributed to the stretching NH bands ν(N–H).[6,7,15] The strong absorbance bands at 1401 cm^{-1} and 1639 cm^{-1} can be assigned to $\delta_{as}(NH_4^+)$ of NH_3 bonded to a Si–OH hydroxyl group and the presence of adsorbed NH_3 or/and water.[8,15] On increasing the evacuation temperature from 100 °C to 400 °C, the intensities of absorbance bands from all the NH_x species (including ν(NH) from Si–NH–Si and Si–NH_2 at 3396 cm^{-1} and 3147 cm^{-1} and $\delta_{as}(NH_4^+)$ from NH_4^+ at 1401 cm^{-1}) decrease gradually. The bands at 3147 cm^{-1} and 1401 cm^{-1} are, however, still observed after thermal treatment at 400 °C in a vacuum, thus indicating that at least part of the NH_x species incorporated into the mesoporous silica are thermal stable up to 400 °C.

The Knoevenagel condensation reaction has been shown to be a useful probe of the basicity of solids when carried out with a series of methylene groups of varying pK_a, and it has been used to evaluate the basicity of solid bases such as amorphous silicon oxynitride, silicon imidonitride or aluminophosphates oxynitride.[6–8,16,17] To explore the catalytic properties of the MCM-48 silicon oxynitride materials, Knoevenagel condensation between benzaldehyde and malononitrile (Scheme 1) was preformed at 60 °C under an inert



Scheme 1. Knoevenagel condensation reaction between benzaldehyde and malononitrile.

atmosphere. The catalytic data is presented in Figure 6. It was found that whilst pure silica MCM-48 exhibited negligible catalytic activity, N-MCM-48 materials were active catalysts for the test reaction. After a 3 h reaction time, both N-MCM-48A and N-MCM-48B achieved conversions of 78% and 96% respectively to give 1,1-dicyanophenylethylene with a selectivity of 100%. The higher conversion over N-MCM-48B is consistent with its higher nitrogen content. No Michael

 © 2003 Wiley-VCH Verlag GmbH & Co. KGaA, Weinheim

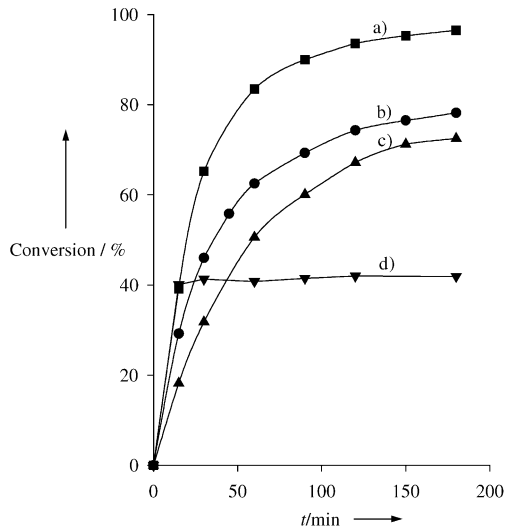


Figure 6. Conversion as a function of time in the Knoevenagel condensation reaction of malononitrile with benzaldehyde at 60 °C in toluene solution catalyzed by; a) N-MCM-48B, b) N-MCM-48A, c) MgO and conversion as a function of time d) after removal of the catalyst (N-MCM-48B) by filtration of the reaction mixture. The reaction had previously been allowed to proceed for 15 min in the presence of the N-MCM-48B catalysts during which a conversion of 40% was attained. t = Reaction time.

addition products, which involve the reaction of malononitrile with the double bond of the 1,1-dicyanophenylethylene, were detected under our reaction conditions. The Michael addition reaction is known to require stronger basic sites or higher reaction temperatures than Knoevenagel condensation,[17] thus suggesting that either there are no strong basic sites on the surface of N-MCM-48 materials, or that higher temperatures are required for Michael addition to occur.[17] The latter is more likely since we did not observe Michael addition even for a commercially available MgO catalyst which is known to have strong basic sites. The absence of Michael addition at a reaction temperature of 60 °C is consistent with previous results.[17] Noteworthy, the catalytic activities achieved by the N-MCM-48 materials were higher than that of the commercially available MgO catalyst (see Figure 6). We infer that the higher overall conversion on the N-MCM-48 catalysts arises from a higher content of basic site (compared to MgO). This inference is consistent with the higher surface area and pore volume per gram of the mesostructured N-MCM-48 oxynitride materials (1200–1500 $m^2 g^{-1}$ and ca. 0.65 $cm^3 g^{-1}$) compared to 44 $m^2 g^{-1}$ and 0.26 $cm^3 g^{-1}$ for the commercial MgO catalyst.

It is important to note that water is one of the products of the Knoevenagel condensation reaction and that the N-MCM-48 oxynitrides would, to some extent, be hydrolytically sensitive to water. Any hydrolysis of the oxynitrides would yield ammonia. Furthermore, since the N-MCM-48 materials were nitrided under a flow of ammonia and given that ammonia is known to catalyze the Knoevenagel condensation reaction homogeneously, it was important to verify that the observed catalytic activity was from the solid N-MCM-48 oxynitride materials and not ammonia. Therefore a control experiment was performed as follows; a catalytic reaction was carried out with N-MCM-48B as catalyst and stopped after 15 min at 40% conversion. The reaction mixture was then cooled and filtered to remove the solid N-MCM-48B catalyst after which the catalyst free filtrate was heated to 60 °C and conversion monitored as a function of time. As shown in Figure 5d, no increase in conversion was observed (i.e., the composition of the filtrate remained unchanged). This observation from the control experiment rules out any contribution to the observed catalytic activity from a homogeneously catalyzed reaction of ammonia. We therefore believe[8,16] that the presence of NH_x species on the N-MCM-48 materials is responsible for the observed catalytic activity.

In summary, we have presented here an attractive route for the preparation of mesoporous base catalysts that are well ordered and have a high surface area, pore volume and catalytic activity. The resulting materials are both truly mesoporous and, as far as we can tell, entirely basic in character. They exhibit considerable thermal stability and do not appear to suffer from leaching (of the basic sites) during catalysis. The method described herein is not limited to MCM-48 and may be used to prepare mesoporous oxynitride materials from other types of mesostructured silicas or metal substituted silicas. There is also scope, by the nitridation route, to prepare acid/base mesoporous materials where the ratio of acidity to basicity is readily controlled. Such highly ordered novel mesoporous oxynitride or acid/base materials with high surface area and pore volume are attractive and may find use as alternative solid catalytic materials.

Experimental Section

High-quality sodium-free Si-MCM-48 was synthesized by using a method in which cetyltrimethylammonium hydroxide (CTAOH) was used simultaneously as a structure director and also to control the pH of the synthesis gel.[11] Typically, 2.14 g of fumed silica was added to 30 g of a 10% CTAOH stirring solution. The mole ratio of the gel mixture of SiO_2:CTAOH:H_2O was 1:0.28:42. After the reaction mixture was stirred for 2 h at room temperature, it was transferred to a teflon-lined autoclave and heated at 135 °C for 24 h. The autoclave was cooled to room temperature and the solid product isolated by filtration and repeatedly washed with a large amount of distilled water. After the product was air-dried at room temperature, part of the dry material was calcined in air at 550 °C for 6 h to yield calcined Si-MCM-48. For nitridation, 0.2 g of calcined or synthesized Si-MCM-48 was placed in an alumina boat and inserted into a flow-through tube furnace. Prior to thermal treatment, the tube furnace was purged by Ar for 30 min, then further purged with NH_3 for another 30 min. The NH_3 flow rate was 100 mL min^{-1}, the temperature of the furnace was increased at a ramp rate of 5 K min^{-1} to 900 °C and maintained for 20 h under the NH_3 atmosphere. The furnace was then cooled down to RT and purged again with Ar for 30 min. The nitrided sample obtained from calcined Si-MCM-48 was designated N-MCM-48A and that obtained from synthesized Si-MCM-48 was designated N-MCM-48B.

Powder XRD analysis was performed by using a Philips 1710 powder diffractometer with Cu K_α radiation (40 kV, 40 mA). Nitrogen sorption isotherms and textural properties of the materials were determined at 77 K by using nitrogen in a conventional volumetric technique by a Coulter SA3100 sorptometer. Before analysis the samples were oven dried at 150 °C and evacuated for 12 h at 200 °C

 © 2003 Wiley-VCH Verlag GmbH & Co. KGaA, Weinheim

under vacuum. The surface area was calculated using the BET method based on adsorption data in the partial pressure (P/P_0) range 0.05–0.2 and total pore volume was determined from the amount of the nitrogen adsorbed at $P/P_0 \approx 0.99$. Elemental analysis was carried out on the nitrided samples by using a CHNS analyzer (Fishons EA 1108). Infrared spectra were recorded using a Perkin Elmer 2000 FTIR spectrometer on self-supporting sample wafers in a pyrex vacuum IR cell. Prior to the collection of spectra the samples were heated in the cell for 2 h at increasing temperature, after which the spectra were recorded at room temperature. Scanning electron microscopy (SEM) images were recorded using a JEOL JSM-820 scanning electron microscope. Samples were mounted using a conductive carbon double-sided sticky tape. A thin (ca. 10 nm) coating of gold sputter was deposited onto the samples to reduce the effects of charging. Transmission electron microscopy (TEM) images were recorded on a JEOL 2000-FX electron microscope operating at 200 kV. Samples for analysis were prepared by spreading them on a holey carbon film supported on a grid.

The Knoevenagel condensation test reactions were performed under an inert atmosphere (N_2), in a flask that was fitted with a reflux condenser. The flask containing a mixture of redistilled benzaldehyde (10 mmol), malononitrile (10 mmol) and 40 mL toluene was immersed in an oil bath and the reaction mixture was stirred with a bar magnet. Once the mixture reached the reaction temperature (60 °C), 0.05 g catalyst was added into the flask. Samples of the reaction mixture were then periodically withdrawn by a filtering syringe and analyzed by a GC-17A gas chromatography to obtain the extent of conversion (%) as a function of reaction time.

Received: January 21, 2003 [Z50978]

Keywords: basicity · heterogeneous catalysis · knoevenagel condensation · mesoporous materials · silicon

[1] a) C. T. Kresge, M. E. Leonowicz, W. J. Roth, J. C. Vartuli, J. S. Beck, *Nature* **1992**, *359*, 710; b) J. S. Beck, J. C. Vartulli, W. J. Roth, M. E. Leonowicz, C. T. Kresge, K. D. Schmitt, C. T. W. Chu, D. H. Olson, E. W. Sheppard, S. B. McCullen, J. B. Higgings, J. L. Schlenker, *J. Am. Chem. Soc.* **1992**, *114*, 10834.

[2] a) A. P. Wight, M. E. Davis, *Chem. Rev.* **2002**, *102*, 3589; b) J. Y. Ying, C. P. Mehnert, M. S. Wong, *Angew. Chem.* **1999**, *111*, 58; *Angew. Chem. Int. Ed.* **1999**, *38*, 56; c) A. Corma, *Chem. Rev.* **1997**, *97*, 2373; d) D. T. On, D. Desplantier-Giscard, C. Danumah, S. Kaliaguine, *Appl. Catal. A* **2001**, *222*, 299.

[3] a) P. T. Tanev, M. Chibwe, T. J. Pinnavaia, *Nature* **1994**, *368*, 321; b) P. T. Tanev, T. J. Pinnavaia, *Science* **1995**, *267*, 865; c) J. V. Walker, M. Morey, H. Carlsson, A, Davidson, G. D. Stucky, *J. Am. Chem. Soc.* **1997**, *119*, 6921; d) L. X. Dai, K. Tabata, E. Suzuki, T. Tatsumi, *Chem. Mater.* **2001**, *13*, 208; e) R. Mokaya, W. Jones, *J. Catal.* **1997**, *172*, 211; f) T. M. Abdel Fattah, T. J. Pinnavaia, *J. Chem. Soc. Chem. Commun.* **1996**, 665; g) B. Echchahed, A. Moen, D. Nicholson, L. Bonneviot, *Chem. Mater.* **1997**, *9*, 1716; h) P. van der Voort, E. F. Vansant, *J. Phys. Chem. B* **1999**, *103*, 10102; i) M. Froba, R. Kohn, G. Bouffaud, *Chem. Mater.* **1999**, *11*, 2858.

[4] a) R. Mokaya, *Angew. Chem.* **1999**, *111*, 3079; *Angew. Chem. Int. Ed.* **1999**, *38*, 2930; b) R. Mokaya, *Adv. Mater.* **2000**, *12*, 1681; c) R. Mokaya, *ChemPhysChem* **2002**, *3*, 360; d) A. S. O'Neil, R. Mokaya, M. Poliakoff, *J. Am. Chem. Soc.* **2002**, *124*, 10636; e) S. C. Shen, S. Kawi, *Langmuir* **2002**, *18*, 4720.

[5] R. D. Oldroyd, J. M. Thomas, T. Maschmeyer, P. A. MacFaul, D. W. Snelgrove, K. U. Ingold, D. M. Wayner, *Angew. Chem.* **1996**, *108*, 2966; *Angew. Chem. Int. Ed. Engl.* **1996**, *35*, 2787.

[6] a) P. W. Lednor, R. Derutter, *J. Chem. Soc. Chem. Commun.* **1991**, 1625; b) P. W. Lednor, *Catal. Today* **1992**, *15*, 243; c) G. Busca, V. Losenzelli, G. Porcile, *Mater. Chem. Phys.* **1986**, *14*, 123.

[7] a) M. J. Climent, A. Corma, V. Fornes, A. Frau, R. Guil-Lopez, S. Iborra, J. Primo, *J. Catal.* **1996**. *163*, 392; b) P. Grange, P. Bastians, R. Conanec, R. Marchand, Y. Laurent, *Appl. Catal. A* **1994**, *114*, L191; c) S. Ernst, M. Hartmann, S. Sauerbeck, T. Bongers, *Appl. Catal. A* **2000**, *200*, 117; d) J. Xiong, Y. Ding, H. Zhu, L. Yan, X. Liu, L. Lin, *J. Phys. Chem. B* **2003**, *107*, 1366.

[8] a) H. M. Wiame, C. M. Cellier, P. Grange, *J. Phys. Chem. B* **2000**, *104*, 591; b) H. Wiame, C. Cellier, P. Grange, *J. Catal.* **2000**, *190*, 406.

[9] a) M. P. Kapoor, S. Inagaki, *Chem. Lett.* **2003**, *32*, 94; b) H. Yoshida, Y. Inaki, Y. Kajita, K. Ito, T. Hattori, *Stud. Surf. Sci. Catal.* **2002**, *143*, 837; c) J. E. Haskouri, S. Cabrera, F. Sapina, J. Latorre, C. Guillen, A. Beltran-Porter, D. Beltran-Porter, M. D. Marcos, P. Amoros, *Adv. Mater.* **2001**, *13*, 192.

[10] J. Weitkamp, M. Hunger, U, Rymsa, *Microporous Mesoporous Mater.* **2001**, *48*, 255.

[11] Y. D. Xia, R. Mokaya, *J. Mater. Chem.* **2003**, *13*, 657.

[12] T. R. Pauly, V. Petkov, Y. Liu, S. J. L. Billinge, T. J. Pinnavaia, *J. Am. Chem. Soc.* **2002**, *124*, 97.

[13] J. Chen, Q. Li, R. Xu, F. Xiao, *Angew. Chem.* **1995**, *107*, 2898; *Angew. Chem. Int. Ed. Engl.* **1995**, *34*, 2694.

[14] a) T. Suehiro, J. Tatami, T. Meguro, S. Matsuo, K. Komeya, *J. Eur. Ceram. Soc.* **2002**, *22*, 521; b) T. Suehiro, J. Tatami, T. Meguro, K. Komeya, S. Matsuo, *J. Am. Ceram. Soc.* **2002**, *85*, 715.

[15] a) S. Delsarte, M. A. Centeno, P. Grange, *J. Non-Cryst. Solids* **2002**, *297*, 189; b) R. L. Puurunen, A. Root, P. Sarv, M. M. Viitanen, H. H. Brongersma, M. Lindblad, A. O. I. Krause, *Chem. Mater.* **2002**, *14*, 720; c) T. Blasco, A. Corma, L. Fernandez, V. Fornes, R. Guil-Lopez, *Phys. Chem. Chem. Phys.* **1999**, *1*, 4493.

[16] J. S. Bradley, O. Vollmer, R. Rovai, U. Specht, F. Lefebvre, *Adv. Mater.* **1998**, *10*, 938.

[17] M. J. Climent, A. Corma, R. Guil-Lopez, S. Iborra, *Catal. Lett.* **2001**, *74*, 161.

 © 2003 Wiley-VCH Verlag GmbH & Co. KGaA, Weinheim

Self-Healing Systems

Self-Healing Systems Having a Design Stimulated by the Vertebrate Spine**

*Mila Boncheva and George M. Whitesides**

This work describes the design of two self-healing systems comprising mm-sized beads connected by elastomeric threads. Axial compressive stress exerted by the thread, and capillary interactions between drops of molten solder patterned on the beads, lead to their self-assembly into linear rods; cooling the solder makes the rods rigid. We demonstrate

[*] Prof. G. M. Whitesides, Dr. M. Boncheva
Department of Chemistry and Chemical Biology
Harvard University
Cambridge, MA 02138 (USA)
Fax: (+1) 617-495-9857
E-mail: gwhitesides@gmwgroup.harvard.edu

[**] This work was supported by DARPA.

 © 2003 Wiley-VCH Verlag GmbH & Co. KGaA, Weinheim DOI: 10.1002/anie.200351010

the spontaneous realignment of the structures after breaking and dislocation.

We and others have used biomimetic approaches to design molecular and macroscale systems imitating the internal structure[1,2] and the principles of organization[3–7] of biological systems, or biological processes.[8–12] One distinguishing characteristic of living systems is their ability to heal themselves. Self-healing in living systems, however, involves complex cascades of out-of-equilibrium processes, and is therefore still difficult to reproduce in man-made systems.[13,14]

The design of self-healing structures is of considerable interest in engineering and microtechnology. One approach consists in developing so-called "smart" or self-healing materials, such as polymers,[15,16] ceramics,[17] and glasses.[18,19] Another approach can be based on self-assembly: after disruption, self-assembled systems return to their ordered state, provided that that state is a thermodynamic minimum.[20] Herein, we propose a strategy for designing self-healing, self-aligning structures, based on self-assembly of mm-sized components. The design of one system is inspired by (and loosely modeled on) the vertebrate spine; the design of the second one is modeled on the traction splints used for therapy of spinal fractures.

The spine consists of rigid, structural elements—vertebrae—separated by elastomeric discs and connected to one another by ligaments and muscles (Figure 1, top). The spine, like many other biological structures, serves several functions simultaneously: it provides both strength and flexibility to the body, dampens shock, and protects the spinal cord.[21]

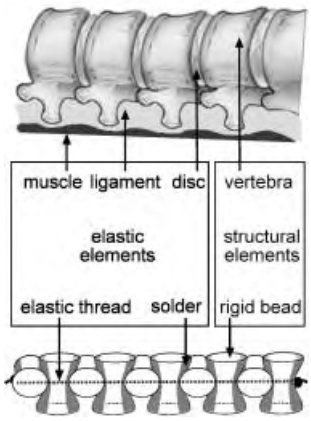


Figure 1. Common features of the design of a vertebrate spine (top) and the self-assembling systems of mm-sized components (bottom). Both systems consist of rigid structural elements connected by elastomeric elements.

The structures we used share with the spine the design of a set of rigid structural units connected by elastomeric element(s) (Figure 1, bottom). In both systems, the structural components, which mimic the function (if not the structure) of vertebrae, were hourglass-shaped polyurethane beads that have a hole through the waist. The beads were patterned with rectangular patches of copper covered with solder (Figure 2a). We strung the beads together onto an elastic thread

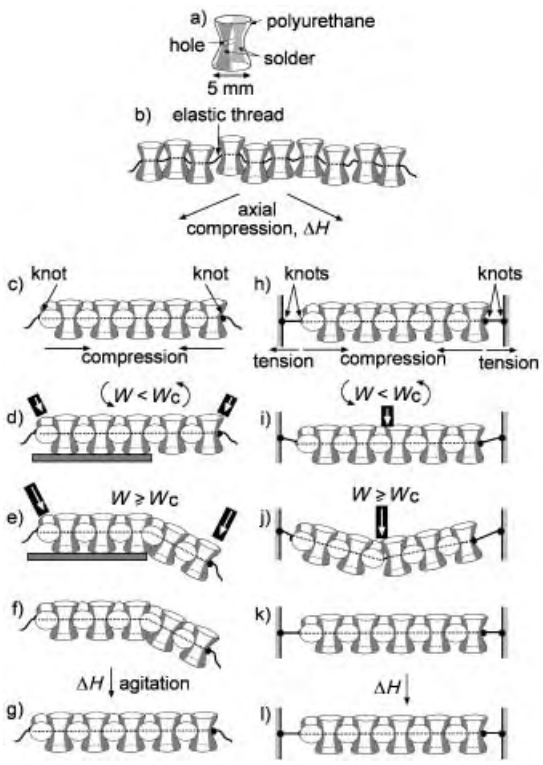


Figure 2. Design of self-aligning systems mimicking the spine of vertebrates. a) One structural element (bead). b) A string of ten beads on an elastic thread. Two types of structures were generated from this string: c)–g) a rigid rod in which only compressive forces acted on the beads; h)–l) a rigid rod in which compressive and tensile forces acted on the beads. The direction of the forces acting in each of these systems is shown schematically as arrows. These structures could support weight W (schematically shown as white arrows) applied to both ends (d) or to a point in the middle (i), but broke into two parts (e), j) when the applied weight exceeded the critical weight of $W_c \approx 250$ g. f), k) After removing the weight, the structure shown in e) remained dislocated, while the structure shown in j) spontaneously realigned. g), l) Both structures recovered their structure and mechanical strength after removing the weight, heating under water to a temperature above the melting point of the solder, and cooling to room temperature.

(Figure 2b, Figure 3a), and secured the ends of the thread by tying large knots; the thread mimicked the function of muscles and ligaments of the spine. In both designs, the elastic thread put the systems in compression, and the beads self-aligned with the long axes of adjacent beads perpendicular. In the first system (Figure 2c–2g), we cut the length of thread close to the knots; in this system, as in the human spine, compressive forces were the only type of force acting on the beads in the string (Figure 2c). In a second system (Figure 2h–2l), we cut the length of thread to extend approximately 1 cm beyond the knots, and tied the ends around a holder; we selected the width of this holder such that the length of the string between the beads and the holder was kept under tension. In this system, two types of forces were acting on the beads: compressive and counteracting tensile forces (Figure 2h). The regions of the thread that exerted tensile forces on the beads mimic the action of traction splints used to stabilize fractures and dislocations by counteracting the compression.

 © 2003 Wiley-VCH Verlag GmbH & Co. KGaA, Weinheim

When heated to a temperature above the melting point of the solder, the droplets of solder on neighboring beads fused, and connected the beads into a compact linear rod (Figure 3b, 3e); the drops of metal thus mimic one function of the discs connecting the bone vertebrae in the spine. After cooling, the solidified solder rendered the structures sufficiently strong mechanically to support weight of up to approximately 250 g.[22] The weight was applied manually to the end of the rod, or to an arbitrary point in the middle, by using the piston of a syringe (Figure 2d, 2i).

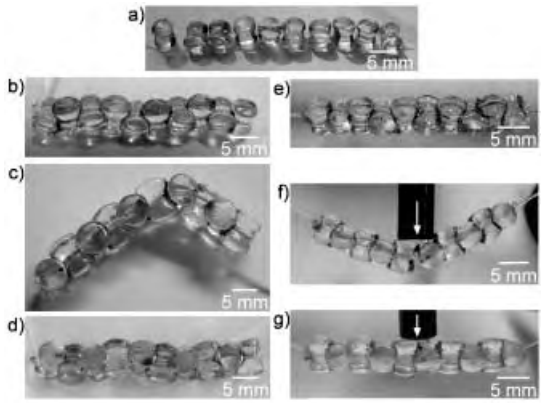


Figure 3. Properties of the self-aligning systems that mimic a vertebrate spine. a) A loose string of ten beads on an elastic thread. b), e) Rigid linear structures generated from the string shown in a). c), f) The same structures when a weight of 250 g was applied to both ends (c), or at a point in the middle of the string of beads (f). d), g) The structures after removing the weight and heating under water to 55 °C. A weight of 100 g was applied to the middle portion of the structure shown in g). The arrows in f), and g) indicate the direction of the applied weight.

Upon exceeding this load, the structures broke into two parts, still connected by the thread (Figure 2e, 2j; Figure 3c, 3f). The fracture occurred either in the middle of a solder drop, or at the interface between solder and copper. When the applied weight was removed, the structure of the string of beads differed in the two systems. In the system in which only compressive forces were acting, the two parts remained dislocated (Figure 2f); in the system in which both compressive and tensile forces were acting, the structure spontaneously realigned to its initial, linear configuration because of the tension applied by the taut thread (Figure 2k). The strings of beads were transferred to water heated to 55 °C. The droplets of molten metal at the point of fracture melted and fused, or molten solder rewetted the copper. Manual agitation of the vessel containing the dislocated structure for about 2 min led to spontaneous realignment of the two parts (Figure 2g). The resulting structures, when cooled to room temperature, were indistinguishable from the structures before the fracture (Figure 2g, 2l, Figure 3d, 3g). They could again support weight applied to the point that had been fractured and healed. We repeated the breaking–heating–cooling cycles three times, and observed indistinguishable behavior in each case.

We have designed two self-healing structures that are loosely analogous to a vertebrate spine and a spine under splint traction, using a system of millimeter-sized, solid beads that self-align under axial compressive or tensile stress. The combination of the shapes of the units and the forces exerted by the elastomeric connectors tends to return the system to a linear configuration; analogous forces act on the spine. The compressive element in the system—the elastic thread—plays a role both in maintaining the relative positions of the beads after breaking, and in keeping the system under compression.

Our self-healing systems differ from their biological counterpart in most details: the structures are not flexible; the entire array of complex biological processes involved in tissue repair is replaced by the coalescence and solidification of drops of solder; the self-healing of the systems is initiated externally, by increasing the temperature of the surrounding aqueous solution.

The effectiveness of the two systems differed considerably. The system in which only compressive forces acted on the beads required external agitation to realign, while realignment of the dislocated parts occurred spontaneously in the system in which both compressive and tensile forces acted on the beads. While the first system is structurally a more accurate mimic of the vertebrate spine, the second one is functionally more efficient.

Synthetic self-healing composites open one promising route to the fabrication of structures that can heal without external mediation.[15] Our results suggest an alternative approach to the design of self-healing structures: instead of fabricating a monolithic structure made entirely of a *self-healing material*, it is possible to design a *composite, self-healing structure* comprising rigid and elastic elements, and self-healing joints. This design offers several advantages: 1) the rigid elements can be made of any material, that is, the choice is not limited only to self-healing composites; 2) the structure aligns spontaneously to its initial configuration; 3) the structure can be fractured and healed multiple times at the same joint; in contrast, self-healing in composite materials depends on the availability of healing agent at the point of fracture, and can therefore occur only once at a given point.

This work demonstrates that by using biomimetic (and medical-mimetic) design in a self-assembling system, one can build structures that are mechanically strong, self-aligning, and self-repairing. Such structures can find application as weight-bearing elements in devices where external repair is not possible because of inaccessibility, or is difficult because of the small size of the structures.

Experimental Section

The beads were prepared by replica molding in UV-curable mercapto-ester (NOA-81, Norland Optical Products) by using poly(dimethylsiloxane) (PDMS) molds (Sylgard 184, Dow Corning) and porcelain masters (Beadworks, Cambridge, MA). We placed the beads in PDMS molds that covered their entire surface, except for two rectangular patches around the holes. A 10 nm thick adhesive layer of titanium and a 400 nm thick layer of copper were evaporated thermally onto the exposed rectangular surfaces of the beads. After removing the molds, we dipped the beads into molten solder (T_m = 47 °C, Small Parts, Inc., http://www.smallparts.com); the solder was

 © 2003 Wiley-VCH Verlag GmbH & Co. KGaA, Weinheim

kept under water brought to pH 1 with HCl to dissolve oxides formed on its surface. The solder wetted only the patterns of copper. We strung the beads together manually onto stretched elastic threads (Stretch Magic, Pepperell Braiding Company), and secured the threads by tying large knots next to the beads at the end of the sequence. In one string, we cut the thread close to the knots. We mounted the other string of beads on a holder by tying the ends of the string on the holder; we selected the width of this holder such that the portions of the string extending between the sequence of beads and the holder were kept under tension. The strings of beads were then immersed in hot water ($T = 55\,^{\circ}C$) for 2 min. The drops of solder melted; to minimize the high interfacial energy of the molten metal/water interface[23] ($\approx 400\ ergs\,cm^{-2}$), droplets of molten metal patterned on neighboring beads fused. On cooling the strings of beads, a compact, rigid structure was generated.

Received: January 23, 2003 [Z51010]

Keywords: materials science · mechanical properties · self-assembly · self-healing

[1] B. L. Smith, T. E. Schaeffer, M. Viani, J. B. Thompson, N. A. Frederick, J. Kindt, A. Belcher, G. D. Stucky, D. E. Morse, P. K. Hansma, *Nature* **1999**, *399*, 761.
[2] W. J. Clegg, K. Kendall, N. M. Alford, T. W. Button, J. D. Birchhall, *Nature* **1990**, *347*, 455.
[3] Y. Yin, Y. Lu, B. Gates, Y. Xia, *J. Am. Chem. Soc.* **2001**, *123*, 8718.
[4] W. T. S. Huck, J. Tien, G. M. Whitesides, *J. Am. Chem. Soc.* **1998**, *120*, 8267.
[5] I. S. Choi, N. Bowden, G. M. Whitesides, *Angew. Chem.* **1999**, *111*, 3265; *Angew. Chem. Int. Ed.* **1999**, *38*, 3078.
[6] M. Weck, I. S. Choi, N. L. Jeon, G. M. Whitesides, *J. Am. Chem. Soc.* **2000**, *122*, 3546.
[7] A. Terfort, G. M. Whitesides, *Adv. Mater.* **1998**, *10*, 470.
[8] T. D. Clark, M. Boncheva, J. M. German, M. Weck, G. M. Whitesides, *J. Am. Chem. Soc.* **2002**, *124*, 18.
[9] M. Boncheva, D. H. Gracias, H. O. Jacobs, G. M. Whitesides, *Proc. Natl. Acad. Sci. USA* **2002**, *99*, 4937.
[10] J. H. Tortai, N. Bonifaci, A. Denat, *IEEE Trans. Dielectr. Electr. Insul.* **2002**, *9*, 3.
[11] H. Heywang, *Colloid Polym. Sci.* **1976**, *254*, 139.
[12] M. H. Dickinson, C. T. Farley, R. J. Full, M. A. R. Koehl, R. Kram, S. Lehman, *Science* **2000**, *288*, 100.
[13] G. J. Tortora, S. R. Grabowski, *Principles of Anatomy and Physiology*, 9th ed., J. Wiley & Sons, New York, **1999**.
[14] I. V. Yannas, *Tissue and Organ Regeneration in Adults*, Springer, New York, **2001**.
[15] S. R. White, N. R. Sottos, P. H. Geubelle, J. S. Moore, M. R. Kessler, S. R. Sriram, E. N. Brown, S. Viswanathan, *Nature* **2001**, *409*, 794.
[16] R. Sharad, *Polym. Mater. Sci. Eng.* **2002**, *87*, 129.
[17] M. S. Morrow, D. E. Schechter, H. E. Huey, Q. S. Wang, P. A. Eggleston, *Ceram. Trans.* **2001**, *111*, 329.
[18] S. M. Wiederhorn, P. R. Townsend, *J. Am. Ceram. Soc.* **1970**, *53*, 486.
[19] J. R. Varner, *Glass Res.* **2001**, *10–11*, 33.
[20] G. M. Whitesides, M. Boncheva, *Proc. Natl. Acad. Sci. USA* **2002**, *99*, 4769.
[21] T. J. Lovely in *Operative Spine Surgery* (Eds.: W. C. Welch, G. B. Jacobs, R. P. Jackson), Appleton & Lange, Stamford, CT, **1999**, p. 238.
[22] R. R. A. Syms, E. M. Yeatman, V. M. Bright, G. M. Whitesides, *J. MEMS* **2003**, in press.
[23] T. L. Breen, J. Tien, S. R. J. Oliver, T. Hadzic, G. M. Whitesides, *Science* **1999**, *284*, 948.

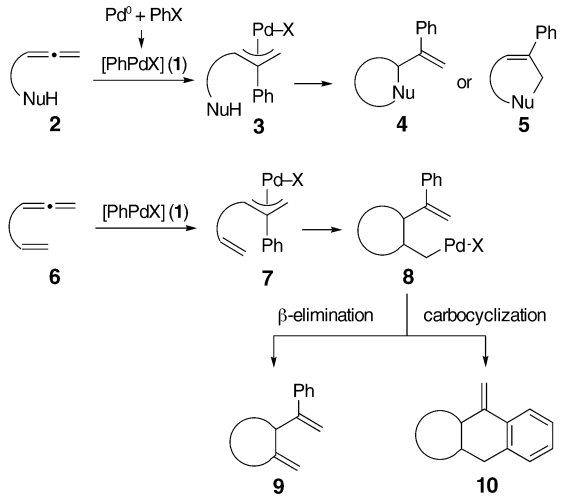
 © 2003 Wiley-VCH Verlag GmbH & Co. KGaA, Weinheim

Cyclizations of Allenenes

Palladium(0)-Catalyzed Tandem Cyclization of Allenenes**

*Hiroaki Ohno, Kumiko Miyamura, Yusuke Takeoka, and Tetsuaki Tanaka**

Allenes have become more versatile intermediates in organic synthesis as a result of recent developments in transition-metal-catalyzed reactions.[1,2] In particular, allenes of general type **2**, which bear a nucleophilic moiety such as a nitrogen- or oxygen-containing functional group, are a well-known class of compounds that undergo a variety of palladium(0)-catalyzed cyclizations to form cyclic products **4** or **5** (Scheme 1).[3]



Scheme 1. Palladium-catalyzed cyclization of allenes.

Recent studies in this area revealed that three-[4] or four-membered heterocycles[5] could also be synthesized efficiently by the palladium-catalyzed cyclization of allenes **2**. In sharp contrast, however, palladium-catalyzed reactions of allenes that contain an additional multiple bond have scarcely been studied.

In analogy to the reactions of allenes **2**, which terminate with the intramolecular reaction of the π-allyl palladium intermediate with a nucleophile, the allenene **6** could undergo a tandem cyclization of the type shown in Scheme 1 under

[*] Prof. Dr. T. Tanaka, Dr. H. Ohno, K. Miyamura, Y. Takeoka
Graduate School of Pharmaceutical Sciences
Osaka University
1-6 Yamadaoka, Suita, Osaka 565-0871 (Japan)
Fax: (+81) 6-6879-8214
E-mail: t-tanaka@phs.osaka-u.ac.jp

[**] We thank Dr. S. Aoki, Graduate School of Pharmaceutical Sciences, Osaka University, for NMR analyses. This work was supported by a Sasakawa Scientific Research Grant from the Japan Science Society.

Supporting information for this article is available on the WWW under http://www.angewandte.org or from the author.

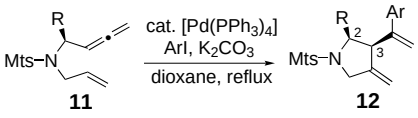
 DOI: 10.1002/anie.200351011 © 2003 Wiley-VCH Verlag GmbH & Co. KGaA, Weinheim

similar conditions. Thus, the π-allyl palladium(II) intermediate **7**, formed by the reaction of the allenene **6** with the phenyl palladium(II) halide **1**, would be converted into the intermediate **8** by carbocyclization.[6] If β-hydride elimination then predominated, a monocyclic product **9** would be produced. However, further carbocyclization onto the aromatic ring[7] would lead to a tricyclic product such as **10** in a single step. Suppression of both β-hydride elimination in **8** and the potential Heck-type reaction between the aryl halide and the vinyl group in **6** would be required for a tandem cyclization to take place.

Recently, some palladium-catalyzed carbocyclization reactions of bisallenes,[8] allenynes,[9] and allenenes[10] were reported.[11] However, as far as we are aware there has been no report of a palladium(0)-catalyzed tandem cyclization of an allene that contains an additional multiple bond.[12] Herein we report the first palladium(0)-catalyzed tandem carbocyclization of allenenes for the synthesis of tri- and tetracyclic nitrogen heterocycles.

With a view to synthesizing a variety of nitrogen heterocycles, we prepared the substrates **11a–c** through the diethylzinc-mediated reductive synthesis of amino allenes catalyzed by palladium(0),[13] followed by *N*-allylation. In an initial experiment, we found that the carbocyclization of allenenes and subsequent β-hydride elimination proceeded efficiently upon treatment with iodobenzene and potassium carbonate in the presence of a catalytic amount of $[Pd(PPh_3)_4]$ (Table 1). The reaction of **11a** in refluxing dioxane provided the 2,3-*cis*-pyrrolidine **12a** in 60% yield as the only isolable product (Table 1, entry 1).[14] The use of other solvents, such as MeCN, DMF, or DMSO, resulted in lower yields. Whereas the use of 4-iodoanisole and 4-iodotoluene as the aryl halide gave comparable results (Table 1, entries 2 and 3), only 36% of the pyrrolidine **12d** was obtained when the reaction was carried out with the electron-poor 1-iodo-4-nitrobenzene (Table 1, entry 4). Furthermore, the substituent α to the allene was found to be extremely important for the efficiency of the cyclization. Thus, the allenenes **11b** and **11c**, which have an effectively smaller α substituent than **11a** (R = Bn and *i*Bu, respectively) required prolonged reaction times for the complete consumption of the starting materials (Table 1, entries 5 and 6). Moreover, no cyclized product was isolated when the corresponding unsubstituted allenene (R = H) was used.[15] We speculate that the bulky α substituent stabilizes the conformation required for the carbocyclization.

Table 1: Stereoselective synthesis of 2,3-*cis*-pyrrolidines **12** by the palladium(0)-catalyzed carbocyclization of allenenes **11**.[a]

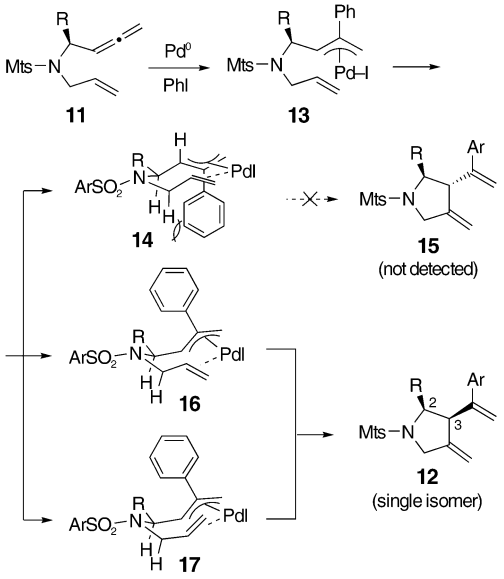


11 **12**

Entry	Allenene	R	ArI	*t* [h]	Product	Yield [%][b]
1	**11a**	*i*Pr	PhI	4.5	**12a**	60
2	**11a**	*i*Pr	4-MeOPhI	3	**12b**	60
3	**11a**	*i*Pr	4-MePhI	8	**12c**	56
4	**11a**	*i*Pr	4-NO_2PhI	11	**12d**	36
5	**11b**	Bn	PhI	24	**12e**	58
6[c]	**11c**	*i*Bu	PhI	24	**12f**	46

[a] Reactions were carried out in the presence of $[Pd(PPh_3)_4]$ (10 mol%), ArI (2 equiv), and K_2CO_3 (2 equiv) in dioxane under reflux. [b] Yields of isolated products. The 2,3-*trans* products were not observed (2,3-*cis*/*trans* > 98:2). [c] Increased amounts of ArI (4 equiv) and K_2CO_3 (4 equiv) were used. Mts = 2,4,6-trimethylphenylsulfonyl.

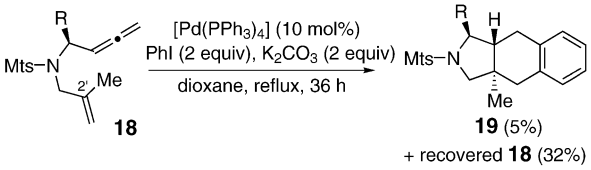
The observed 2,3-*cis* selectivity in the pyrrolidine formation can be rationalized as shown in Scheme 2. If a π-allyl palladium(II) intermediate **13** underwent carbocyclization via the conformation **14**, the 2,3-*trans*-pyrrolidine **15** would be obtained. However, an unfavorable steric interaction between the pseudoaxial hydrogen atoms and the phenyl group in **14** destabilizes this conformer. Thus, ring formation proceeds preferentially via the more abundant conformers **16** and/or **17** to yield the *cis*-pyrrolidine **12** as a single isomer.



Scheme 2. Stereoselective formation of 2,3-*cis*-pyrrolidines **12**.

Next, we investigated inhibition of the β-hydride elimination to promote the desired tandem cyclization. We expected that the replacement of the β-hydrogen atom with an alkyl group would suppress the β-hydride elimination and allow another carbopalladation step. However, the introduction of a methyl group at the 2′-position dramatically decreased the reactivity of the allenene, and the desired tricyclic product **19** was obtained from the 2′-methylated allenene **18** in just 5% yield after 36 h (Scheme 3).

We then anticipated that the introduction of a substituent at the olefin terminus (3′-position) would impede the required arrangement of the palladium center relative to the hydrogen

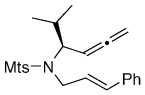
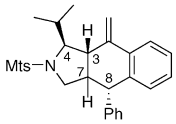
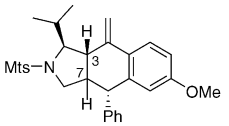
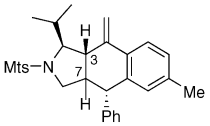
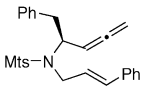
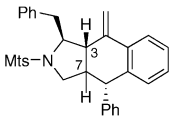
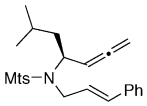
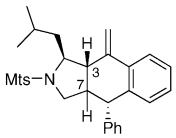
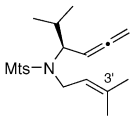
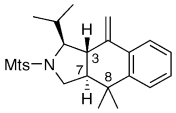


Scheme 3. Reaction of the 2′-methylated allenene **18**.

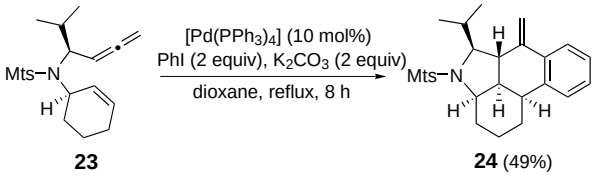
 © 2003 Wiley-VCH Verlag GmbH & Co. KGaA, Weinheim

atom for β-hydride elimination to occur.[16,17] Fortunately, we found that the *N*-(*E*)-cinnamyl derivative **20a** reacted to give a separable mixture of the benzoisoindole derivatives **21a** and **22a** in moderate yields (41 and 10%, respectively) upon treatment with a catalytic amount of palladium(0), iodobenzene, and potassium carbonate in dioxane (Table 2, entry 1). These cyclized products were characterized by ^{1}H NMR, ^{13}C NMR, NOE, and COSY spectroscopic analysis, and the structure of **21a** was also confirmed by HMQC and HMBC analysis. This is the first example of a palladium(0)-catalyzed tandem cyclization of allenenes. 4-Iodoanisole and 4-iodotoluene could also be used for this transformation (Table 2, entries 2 and 3). The *N*-cinnamylamino allenes **20b** and **20c**, in which the α substituent is effectively smaller, also reacted to afford the expected tricyclic products, although prolonged reaction times were required (23–29 h). An improvement of the yields of the desired cyclized products was hampered by the formation of unidentified by-products. Substituents other than a phenyl group at the olefin terminus can also promote the tandem cyclization. Thus, the reaction of the *N*-(3,3-dimethylallyl)amino derivative **20d** yielded the expected cyclized product **21f** with geminal dimethyl substitution at C8 in a stereoselective manner. In all the cases listed in Table 2 the stereoselectivity of the first cyclization (which dictates the relative configuration at C3 and C4 in the product) was opposite to that observed in the formation of the pyrrolidines (Table 1).[14] Furthermore, although the stereoselectivities at C7 were not very high, the configurations of the other two stereocenters (C3 and C8) created in the reaction were controlled completely. We assume that the steric bulk of the cinnamyl group interferes in the first cyclization to hinder the formation of the 3,7-*cis* product.

Table 2: Palladium(0)-catalyzed tandem cyclization of allenenes **20**.[a]

Entry	Substrate	ArI	*t* [h]	Product	Yield [%][b]
1		PhI	7.5		
	20a			**21a** (3,7-*trans*)	41
				22a (3,7-*cis*)	10
2	**20a**	4-MeOPhI	3.5		
				21b (3,7-*trans*)	43
				22b (3,7-*cis*)	20
3	**20a**	4-MePhI	7		
				21c (3,7-*trans*)	37
				22c (3,7-*cis*)	18
4		PhI	23		
	20b			**21d** (3,7-*trans*)	30
				22d (3,7-*cis*)	24
5		PhI	29		
	20c			**21e** (3,7-*trans*)	25
				22e (3,7-*cis*)	17
6		PhI	28		
	20d			**21f**	42

[a] Reactions were carried out in the presence of $[Pd(PPh_3)_4]$ (10 mol%), ArI (2 equiv), and K_2CO_3 (2 equiv) in dioxane under reflux. [b] Yields of isolated products.



23 **24** (49%)

Scheme 4. Synthesis of the tetracyclic compound **24**.

Finally, we investigated the reaction of the *N*-cyclohexenyl derivative **23** (Scheme 4). Exposure of **23** to the standard cyclization conditions led to the formation of the desired tetracyclic compound **24** as a single isomer. The structure of **24** was confirmed by NMR analysis, including NOE and COSY experiments. This result clearly indicates the utility of our tandem cyclization as a novel method for the synthesis of complex heterocycles.

In conclusion, we have developed a novel tandem cyclization of allenenes for the synthesis of tri- and tetracyclic nitrogen heterocycles. This study demonstrated that allenes

 © 2003 Wiley-VCH Verlag GmbH & Co. KGaA, Weinheim

with an additional multiple bond can undergo a tandem cyclization in the presence of a palladium(0) catalyst and an aryl iodide and that complex heterocyclic skeletons can be constructed from readily prepared allenenes. Further investigations to improve the yields of the reactions and our understanding of the observed stereoselectivity are in progress in our laboratory, as well as the synthesis of other hetero- and carbocycles by this method.

Received: January 23, 2003 [Z51011]

Keywords: allenes · cyclization · domino reactions · heterocycles · palladium

[1] For recent reviews, see: a) R. Zimmer, C. U. Dinesh, E. Nandanan, F. A. Khan, *Chem. Rev.* **2000**, *100*, 3067 – 3125; b) A. S. K. Hashmi, *Angew. Chem.* **2000**, *112*, 3737 – 3740; *Angew. Chem. Int. Ed.* **2000**, *39*, 3590 – 3593; c) R. W. Bates, V. Satcharoen, *Chem. Soc. Rev.* **2002**, *31*, 12 – 21; d) J. A. Marshall, *Chem. Rev.* **2000**, *100*, 3163 – 3186; e) Y. Yamamoto, U. Radhakrishnan, *Chem. Soc. Rev.* **1999**, *28*, 199 – 207; see also: f) A. Hoffman-Röder, N. Krause, *Angew. Chem.* **2002**, *114*, 3057 – 3059; *Angew. Chem. Int. Ed.* **2002**, *41*, 2933 – 2935.

[2] For recent examples, see: a) M. Meguro, Y. Yamamoto, *J. Org. Chem.* **1999**, *64*, 694 – 695; b) Y. Horino, M. Kimura, Y. Wakamiya, T. Okajima, Y. Tamaru, *Angew. Chem.* **1999**, *111*, 123 – 126; *Angew. Chem. Int. Ed.* **1999**, *38*, 121 – 124; c) A. S. K. Hashmi, L. Schwarz, J.-H. Choi, T. M. Frost, *Angew. Chem.* **2000**, *112*, 2382 – 2385; *Angew. Chem. Int. Ed.* **2000**, *39*, 2285 – 2288; d) M. Shanmugasundaram, M.-S. Wu, C.-H. Cheng, *Org. Lett.* **2001**, *3*, 4233 – 4236; e) S.-K. Kang, Y.-H. Ha, B.-S. Ko, Y. Lim, J. Jung, *Angew. Chem.* **2002**, *114*, 353 – 355; *Angew. Chem. Int. Ed.* **2002**, *41*, 343 – 345; f) S.-K. Kang, K.-J. Kim, Y.-T. Hong, *Angew. Chem.* **2002**, *114*, 1654 – 1656; *Angew. Chem. Int. Ed.* **2002**, *41*, 1584 – 1586; g) H. Ohno, H. Hamaguchi, M. Ohata, T. Tanaka, *Angew. Chem.* **2003**, *115*, 1791 – 1795; *Angew. Chem. Int. Ed.* **2003**, *42*, 1749 – 1753.

[3] For some more recent examples, see: a) B. M. Trost, P.-Y. Michellys, V. J. Gerusz, *Angew. Chem.* **1997**, *109*, 1837 – 1839; *Angew. Chem. Int. Ed. Engl.* **1997**, *36*, 1750 – 1753; b) S. K. Kang, K.-J. Kim, *Org. Lett.* **2001**, *3*, 511 – 514; c) K. Hiroi, Y. Hiratsuka, K. Watanabe, I. Abe, F. Kato, M. Hiroi, *Tetrahedron: Asymmetry* **2002**, *13*, 1351 – 1353; d) S. Ma, W. Gao, *J. Org. Chem.* **2002**, *67*, 6104 – 6112; e) G. Liu, X. Lu, *Org. Lett.* **2001**, *3*, 3879 – 3882; f) S. Ma, Z. Shi, *Chem. Commun.* **2002**, 540 – 541.

[4] a) H. Ohno, A. Toda, Y. Miwa, T. Taga, E. Osawa, Y. Yamaoka, N. Fujii, T. Ibuka, *J. Org. Chem.* **1999**, *64*, 2992 – 2993; b) S. Ma, S. Zhao, *J. Am. Chem. Soc.* **1999**, *121*, 7943 – 7944; c) H. Ohno, M. Anzai, A. Toda, S. Ohishi, N. Fujii, T. Tanaka, Y. Takemoto, T. Ibuka, *J. Org. Chem.* **2001**, *66*, 4904 – 4914; d) H. Ohno, *Yakugaku Zasshi* **2001**, *121*, 733 – 741; e) S. Ma, N. Jiao, S. Zhao, J. Hou, *J. Org. Chem.* **2002**, *67*, 2837 – 2847; for other related reactions, see: f) H. Ohno, H. Hamaguchi, T. Tanaka, *Org. Lett.* **2001**, *3*, 2269 – 2271; g) H. Ohno, K. Ando, H. Hamaguchi, Y. Takeoka, T. Tanaka, *J. Am. Chem. Soc.* **2002**, *124*, 15255 – 15266.

[5] a) M. Anzai, A. Toda, H. Ohno, Y. Takemoto, N. Fujii, T. Ibuka, *Tetrahedron Lett.* **1999**, *40*, 7393 – 7397; b) F. P. J. T. Rutjes, K. C. M. F. Tjen, L. B. Wolf, W. F. J. Karstens, H. E. Schoemaker, H. Hiemstra, *Org. Lett.* **1999**, *1*, 717 – 720; c) S.-K. Kang, T.-G. Baik, A. N. Kulak, *Synlett* **1999**, 324 – 326; see also: Ref. [4c].

[6] For excellent reviews on related palladium-catalyzed carbocyclizations, see: a) W. Oppolzer, *Angew. Chem.* **1989**, *101*, 39 – 53; *Angew. Chem. Int. Ed. Engl.* **1989**, *28*, 38 – 52; b) E. Negishi, C. Copéret, S. Ma, S.-Y. Liou, F. Liu, *Chem. Rev.* **1996**, *96*, 365 – 393.

[7] For recent examples of carbocyclization onto an arene ring, see: a) T. Nishimura, K. Ohe, S. Uemura, *J. Am. Chem. Soc.* **1999**, *121*, 2645 – 2646; b) T. Harayama, H. Akamatsu, K. Okamura, T. Miyagoe, T. Akiyama, H. Abe, Y. Takeuchi, *J. Chem. Soc. Perkin Trans. 1* **2001**, 523 – 528; c) M. A. Campo, R. C. Larock, *J. Am. Chem. Soc.* **2002**, *124*, 14326 – 14327; d) M. Toyota, A. Ilangovan, R. Okamoto, T. Masaki, M. Arakawa, M. Ihara, *Org. Lett.* **2002**, *4*, 4293 – 4296; e) C. C. Hughes, D. Trauner, *Angew. Chem.* **2002**, *114*, 1639 – 1642; *Angew. Chem. Int. Ed.* **2002**, *41*, 1569 – 1572.

[8] S.-K. Kang, T.-G. Baik, A. N. Kulak, Y.-H. Ha, Y. Lim, J. Park, *J. Am. Chem. Soc.* **2000**, *122*, 11529 – 11530.

[9] S. Shin, T. V. RajanBabu, *J. Am. Chem. Soc.* **2001**, *123*, 8416 – 8417.

[10] a) J. Franzén, J. Löfstedt, I. Dorange, J.-E. Bäckvall, *J. Am. Chem. Soc.* **2002**, *124*, 11246 – 11247; b) J. Löfstedt, J. Franzén, J.-E. Bäckvall, *J. Org. Chem.* **2001**, *66*, 8015 – 8025.

[11] For other cyclizations of allenenes, allenynes, or bisallenes, see: a) H. Urabe, T. Takeda, D. Hideura, F. Sato, *J. Am. Chem. Soc.* **1997**, *119*, 11295 – 11305; b) K. M. Brummond, J. Lu, *J. Am. Chem. Soc.* **1999**, *121*, 5087 – 5088; c) P. A. Wender, F. Glorius, C. O. Husfeld, E. Langkopf, J. A. Love, *J. Am. Chem. Soc.* **1999**, *121*, 5348 – 5349; d) C. H. Oh, S. H. Jung, C. Y. Rhim, *Tetrahedron Lett.* **2001**, *42*, 8669 – 8671; e) S.-K. Kang, Y.-H. Ha, D.-H. Kim, Y. Lim, J. Jung, *Chem. Commun.* **2001**, 1306 – 1307; f) Q. Shen, G. B. Hammond, *J. Am. Chem. Soc.* **2002**, *124*, 6534 – 6535; g) C. Mukai, I. Nomura, K. Yamanishi, M. Hanaoka, *Org. Lett.* **2002**, *4*, 1755 – 1758; h) S.-K. Kang, B.-S. Ko, D.-M. Lee, *Tetrahedron Lett.* **2002**, *43*, 6693 – 6696; i) K. M. Brummond, H. Chen, P. Sill, L. You, *J. Am. Chem. Soc.* **2002**, *124*, 15186 – 15187.

[12] A palladium(II)-catalyzed domino cyclization of allenynes in the presence of LiBr under oxygen at atmospheric pressure was recently reported: B. Alcaide, P. Almendros, C. Aragoncillo, *Chem. Eur. J.* **2002**, *8*, 1719 – 1729.

[13] a) H. Ohno, A. Toda, S. Oishi, T. Tanaka, Y. Takemoto, N. Fujii, T. Ibuka, *Tetrahedron Lett.* **2000**, *41*, 5131 – 5134; b) H. Ohno, K. Miyamura, T. Tanaka, S. Oishi, A. Toda, Y. Takemoto, N. Fujii, T. Ibuka, *J. Org. Chem.* **2002**, *67*, 1359 – 1367.

[14] Confirmation of the stereochemistry of the cyclized products was based on NOE analysis (see the Supporting Information).

[15] The reaction of the unsubstituted allenene (R = H) led to a complex mixture of unidentified products.

[16] R. F. Heck, *Acc. Chem. Res.* **1979**, *12*, 146 – 151.

[17] Although the *syn* β-elimination generally predominates, a base-induced *anti* elimination by an E_2 mechanism can occur in limited cases. See, for example: a) J. M. Takacs, E. C. Lawson, F. Clement, *J. Am. Chem. Soc.* **1997**, *119*, 5956 – 5957; b) I. Schwarz, M. Braun, *Chem. Eur. J.* **1999**, *5*, 2300 – 2305, and references therein.

 © 2003 Wiley-VCH Verlag GmbH & Co. KGaA, Weinheim

A Zwitterionic Chelating Ligand

Phenyl{bis(triphenylphosphanemethylenido)}-borane: A Zwitterionic Chelating Ligand Exhibiting Allyl-Type Coordination**

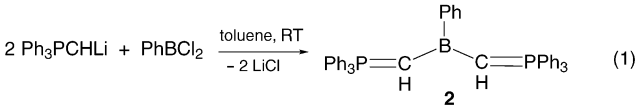
Feilong Jiang, Pamela J. Shapiro, Faysal Fahs, and Brendan Twamley*

The ability of phosphorus ylides to form stable organometallic complexes with both main-group metal atoms and transition-metal atoms has been known for some time.[1] The dipolar resonance form available to these molecules, by placing a formal negative charge on the carbon, makes them very effective Lewis bases that in some cases have been substituted for phosphane ligands to form even more active transition-metal organometallic catalysts.[2]

Recent work in our group employing Ph_3PCH_2 as a Lewis base adduct for the boron in borylidene bridged ansa-zirconocene complexes[3] led to the serendipitous discovery of an unusual bonding motif between a boron-bridged bis(ylide) ligand and zirconium tetrachloride. Complex **1** (Figure 1)[4] was isolated reproducibly with a yield of 14% as a product from the reaction intended to bond Ph_3PCH_2 to a borylidene bridged bis(indenyl)zirconium species similar to the ones reported by Reetz et al.[5] The unusual allyl-type coordination between the boron-bridged diylide ligand and zirconium prompted us to pursue the synthesis of the ligand by a more direct route to determine if additional coordination chemistry with this novel, zwitterionic, chelating ligand might be accessed.

Boron-bridged diylide compounds similar to the ligand in **1** were reported in 1986 by Bestmann and Arenz,[6] who prepared the compounds by treating alkyldichloroboranes with four equivalents of phosphonium ylide. Related triphenyl- and tri-*tert*-butyl-phosphiniminatoborane derivatives were reported by Dehnicke and co-workers[7] and by Stephan and co-workers.[8] Until now, however, the coordination of these molecules to metal atoms has not been reported.

Initial efforts to prepare the ligand in complex **1** by treating $PhBCl_2$ with either four equivalents of Ph_3PCH_2 or with two equivalents of the ylide in the presence of triethylamine were unsuccessful and afforded only the ylide adduct $PhCl_2B(CH_2PPh_3)$. Therefore, we used the lithium salt of the ylide[9] to prepare the desired ligand **2** as a benzene-soluble yellow powder in 68% yield [Eq. (1)].



(1)

Two independent but structurally similar molecules were found in the asymmetric unit of the crystal (Figure 2).[4] In both molecules of **2** one triphenylphosphane group adopts a *syn* orientation and the other an *anti* orientation relative to the boron-diylide backbone instead of the double *syn* arrangement that they exhibit in the zirconium complex. The B–C(ylide) bond lengths (av. 1.521(7) Å) are at the low end of the 1.50–1.64 Å range for B–C single bonds in the Cambridge Crystallographic Database[10] and noticeably shorter than the B–C(phenyl) bond in each molecule (av. 1.598(2) Å). The P–C(ylide) bond lengths (av. 1.689(2) Å) are

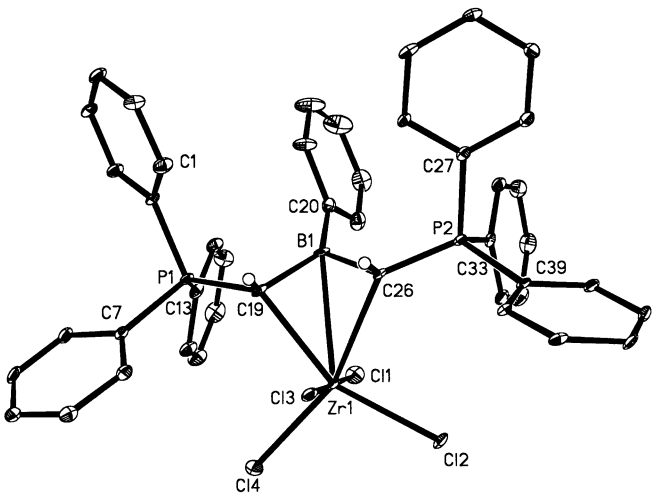


Figure 1. ORTEP drawing of complex **1** with thermal ellipsoids at the 30% probability level. Selected bond lengths [Å] and angles [°]: Zr1–B1 2.754(4), Zr1–C19 2.434(3), Zr1–C26 2.469(3), Zr–Cl1 2.4068(11), Zr1–Cl2 2.4360(11), Zr1–Cl3 2.4980(11), Zr1–Cl4 2.4076(12), B1–C19 1.544(6), B1–C26 1.532(5), B1–C20 1.587(5), P1–C19 1.748(3), P2–C26 1.734(4), C26-B1-C19 110.0(3), C26-Zr-C19 61.83(12), Cl1-Zr-Cl3 179.23(4), Cl2-Zr-Cl4 106.64(4).

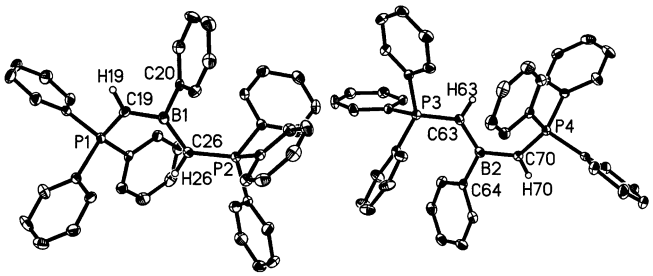


Figure 2. ORTEP drawings of two independent molecules of **2**. Thermal ellipsoids are at the 30% probability level. Selected bond lengths [Å] and angles [°]: B1–C19 1.513(5), B1–C26 1.530(5), B1–C20 1.595(5), B2–C63 1.522(5), B2–C70 1.518(5), B2–C64 1.600(5), P1–C19 1.691(3), P2–C26 1.689(3), P3–C63 1.693(3), P4–C70 1.682(3), C19-B1-C26 124.1(3), C63-B2-C70 122.9(3).

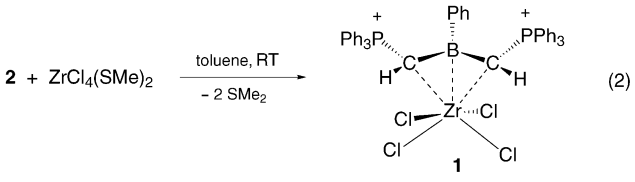
[*] Prof. P. J. Shapiro, Dr. F. Jiang, F. Fahs, Dr. B. Twamley
Department of Chemistry
University of Idaho
Moscow, ID 83844–2343 (USA)
Fax: (+1) 208-885-5785
E-mail: shapiro@uidaho.edu

[**] This work was supported by The Dow Chemical Company and partially by the donors of the Petroleum Research Fund, administered by the American Chemical Society. We are grateful to Dr. Alex Blumenfeld for his assistance with NMR data acquisition.

 DOI: 10.1002/anie.200351056 © 2003 Wiley-VCH Verlag GmbH & Co. KGaA, Weinheim

longer than the P–C bond of free Ph_3PCH_2 (1.661(8) Å), consistent with a reduction in P–C(ylide) π-bonding. These bonds are still substantially shorter than the P–C(ylide) bond length of 1.7919(14) Å in the donor–acceptor complex $Ph_3PCH_2B(C_6F_5)_3$.[11] A PM3 calculation on the molecule gave an energy optimized conformation with both phosphonium moieties in *syn* positions. The HOMO of the molecule consists almost entirely of nonbonding p-orbital density on the ylide carbons, which should be conducive to their coordination to metals. The HOMO-1 is π-bonding between the boron and these two carbons, with no contribution from either phosphorus atom. Significantly, the HOMO and HOMO-1 orbitals for the ligand are essentially identical in appearance to the corresponding molecular orbitals of an allyl ligand.[12]

Complex **1** was prepared directly by reacting **2** with $ZrCl_4(SMe_2)_2$ in toluene [Eq. (2)]. The complex is exceptionally sensitive to protonolysis, forming $[Ph_3PCH_3]Cl$, and must be stored at low temperature (−30 °C) under N_2. Another X-ray crystallographic analysis of the complex was undertaken to confirm that the structure of this complex was identical to that of the species obtained earlier by an indirect route.



(2)

The structure of **1** (Figure 1) can be regarded as pseudo-octahedral, with the ylide carbons occupying two sites of an equatorial plane, Cl2 and Cl4 at the other two equatorial positions, and Cl1 and Cl3 at *trans* axial positions. Although the Zr–B distance of 2.754(4) Å is significantly longer than distances between the zirconium and the ylide carbon atoms (av. 2.45(2) Å), it is well within the sum of the van der Waals radii of the two atoms.[13] Ab initio calculations at the 3-21G* level on the model complex $[(H_3PCH)_2BH]ZrCl_4$ affords an energy optimized geometry that is remarkably close to that of **2**. When an initial geometry that places the Zr, B, and ylide carbon atoms in the same plane is used, the final optimized geometry bends the boron toward zirconium with a Zr–B distance of 2.754 Å and Zr–C(ylide) distances of 2.453 Å.

To determine if ligand **2** and its allyl-type binding mode could be extended to other metal atoms, **2** was reacted with *trans*-$[PdCl_2(SMe_2)_2]$ to give **3** (Figure 3). An allyl-type bonding motif between the ligand and the palladium is again observed. In this case, however, one phosphonium group is *anti* and the other is *syn*, making the complex asymmetric. The presence of two different, weakly coupled phosphorus signals in the ^{31}P NMR spectrum, and the presence of two different methine proton signals with different couplings to phosphorus in the ^{1}H NMR spectrum indicate that the asymmetric geometry of the complex is retained in solution. The boron atom approaches the metal center more closely relative to the ylide carbons in **3** than it does in the zirconium complex (0.08 Å av. difference in **3** versus 0.3 Å av. difference in **1**). The Pd^{II} complex is also considerably more stable than the Zr^{IV} complex both in solution and upon storage as a solid under N_2 at ambient temperature.

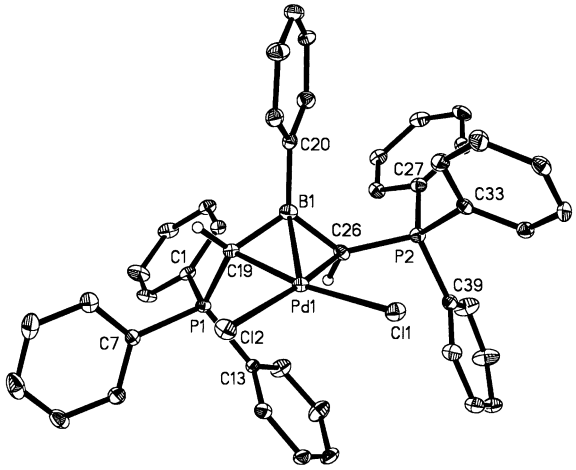


Figure 3. ORTEP drawing of complex **3** with thermal ellipsoids at the 30% probability level. Selected bond lengths [Å] and angles [°]: Pd1–C26 2.140(4), Pd1–C19 2.094(4), Pd1–B1 2.200(5), Pd1–Cl1 2.3705(11), Pd1–Cl2 2.3604, Cl1-Pd1-Cl2 93.45(4), P1-C19-Pd 112.8(2), P2-C26-Pd 128.8(2).

In summary, ligand **2** behaves like a boron-containing analogue of a η^3-allyl ligand when attached to both early and late transition-metal systems. As a neutral, zwitterionic ligand, **2** offers an interesting alternative to other neutral bidentate ligands containing phosphanes,[14] imines,[15] and nucleophilic carbenes[16] that are currently popular in transition-metal-mediated catalysis. Furthermore, it should be possible to fine-tune the electronic and steric properties of the ligand by varying the substituent on boron and the phosphonium ylide components.

Experimental Section

All manipulations were carried out under an argon or nitrogen atmosphere. NMR spectra were recorded on Bruker AMX 300 and Bruker AVANCE 500 spectrometers. H_3PO_4(aq, 80%) and $BF_3{\cdot}Et_2O$ were used as external references for ^{31}P and ^{11}B NMR assignments, respectively. ^{1}H chemical shifts were referenced to residual proton signals from the deuterated solvent. ^{13}C NMR chemical shifts were also referenced to the solvent peaks. Ph_3PCH_2[17] and $Zr(SMe_2)_2Cl_4$[18] were prepared as described in the literature. Elemental analyses were determined by Desert Analytics (Tuscon, AZ). Theoretical calculations were performed with the MacSpartan Plus program (**1996**, Wavefunction, Inc., Irvine CA).

1: A solution of $Zr(SMe_2)_2Cl_4$ (373 mg, 1.04 mmol) in 30 mL toluene was added to a stirring solution of **2** (667 mg, 1.04 mmol) in toluene (150 mL) at −78 °C. The reaction was allowed to warm to room temperature and a light yellow precipitate began to form. After 18 h, the precipitate was isolated by filtration and dried in vacuo (yield: 736 mg, 74%). ^{1}H NMR (300 MHz, $CDCl_3$, 25 °C): $\delta = 7.60$–7.54 (m, 12H; PC_6H_5), 7.51–7.45 (m, 6H; PC_6H_5), 7.38–7.33 (m, 12H; PC_6H_5), 6.63 (tt, $^{3}J(H,H) = 7.3$ Hz, $^{4}J(H,H) = 1.5$ Hz, 1H; BC_6H_5) 6.42 (dd,, $^{3}J(H,H) = 6.8$ Hz, $^{4}J(H,H) = 1.5$ Hz, 2H; BC_6H_5), 6.30 (t, $^{3}J(H,H) = 7.4$ Hz, 2H; BC_6H_5) 4.23 ppm (d, $^{2}J(P,H) = 7.9$ Hz, 2H; BCHP);

 © 2003 Wiley-VCH Verlag GmbH & Co. KGaA, Weinheim

$^{13}C\{^1H\}$ NMR (125.7 MHz, $CDCl_3$, 25 °C): $\delta = 134.5$ (pseudo t, $J(C,P) = 4.9$ Hz; $P(C_6H_5)_3$), 134.1 (d, $J(C,P) = 10.4$ Hz; $P(C_6H_5)_3$), 133.0 (s, $B(C_6H_5)$), 131.2 (d, $J(P,C) = 12.5$ Hz; $P(C_6H_5)_3$), 129.3 (pseudo t, $J(C,P) = 6.0$ Hz; $P(C_6H_5)_3$), 126.5 (s; $B(C_6H_5)$), 125.8 ppm (s; $B(C_6H_5)$). No ^{13}C resonance was observed for the ylide methine carbons although a cross peak at $\delta = 51$ ppm with the ylide methine hydrogens was observed in a heteronuclear multiple-quantum coherence (HMQC) experiment. $^{31}P\{^1H\}$ (121.4 MHz, CD_2Cl_2, 25 °C): $\delta = 27.0$ ppm; ^{11}B NMR (160.4 MHz, CD_2Cl_2, 25 °C): $\delta =$ 33 ppm. X-ray quality crystals of **1** were grown from a concentrated CH_2Cl_2 solution cooled at −30 °C for several days. Elemental analysis calcd (%) for $C_{44}H_{37}BCl_4P_2Zr{\cdot}CH_2Cl_2$: C 55.97 , H 4.07; found C 56.03, H 4.12.

2: $PhBCl_2$ (635 mg, 4.00 mmol) was injected by syringe into a stirring solution of Ph_3PCHLi (2.26 g, 8.02 mmol) in toluene (120 mL) at −78 °C. The reaction mixture was stirred for 8 h at room temperature affording an orange suspension that was isolated by filtration, washed with pentane (2 × 30 mL) and dried in vacuo (yield: 1.74 g, 68 %). ^1H NMR (300 MHz, C_6D_6, 25 °C): $\delta = 7.7$–7.6 (br m,14 H; C_6H_5), 7.0–6.9 (m, 21 H; C_6H_5), 1.50 ppm (d, 2 H, $^2J(P,H) = 13.8$ Hz; PCH); $^{13}C\{^1H\}$ NMR (125.7 MHz, C_6D_6, 25 °C): 134.9 (d, $J(C,P) = 9.5$ Hz), 133.3 (s), 131.3 (d, $J(C,P) = 2.8$ Hz), 130.7 (d, $J(C,P) = 2.5$ Hz) 129.0 (d, $J(C,P) = 12$ Hz), 127.0 (s), 124.9 ppm (s). A very broad ^{13}C signal at $\delta = 34$ ppm is attributed to the ylide methine carbons. $^{31}P\{^1H\}$ NMR (121.4 MHz, C_6D_6, 25 °C): $\delta = 18.2$ ppm; ^{11}B NMR (160.4 MHz, C_6D_6, 25 °C): $\delta = 50$ ppm. X-ray quality crystals of **2** were obtained by layering pentane over a concentrated benzene solution of the ligand and storing the mixture at 4 °C for several days. Elemental analysis calcd (%) for $C_{44}H_{37}BP_2$: C 82.76, H 5.84; found: C 2.70, H 5.88.

3: Toluene (120 mL) was added to a mixture of $Pd(SMe_2)_2Cl_2$ (483 mg, 1.60 mmol) and **2** (1.02 g, 1.60 mmol) and the reaction mixture was stirred for 36 h at room temperature. A dark-orange slurry formed, and the precipitate was isolated by filtration, washed with toluene (30 mL), and dried under vacuum to afford a light brown solid (yield: 758 mg, 58 %): ^1H NMR (300 MHz, CD_2Cl_2, 25 °C): $\delta =$ 8.0–7.8 (m, 5 H; C_6H_5), 7.7–7.3 (m, 28 H; C_6H_5), 6.99–6.91 (m, 2 H; C_6H_5), 3.10 (d, $^2J(P,H) = 13.3$ Hz, 1 H; PCH), 3.05 ppm (d, $^2J(P,H) =$ 4.2 Hz, 1 H; PC*H*). $^{13}C\{^1H\}$ (125.7 MHz, CD_2Cl_2, 25 °C): $\delta = 135.94$ (d, $J(C,P) = 3.0$ Hz), 135.15 (d, $J(C,P) = 9.8$ Hz), 134.63 (d, $J(C,P) =$ 11 Hz), 133.98 (d, $J(C,P) = 2.9$ Hz), 133.21 (d, $J(C,P) = 2.6$ Hz), 133.0, 131.2 (d, $J(C,P) = 13$ Hz), 129.85 (d, $J(C,P) = 12$ Hz), 129.2 (br d, $J(C,P) = 11$ Hz) 128.0 (s), 126.9 (s), 126.5 (s), 125.8 ppm (s). No ^{13}C resonance was observed for the ylide methine carbons although a cross peak at $\delta = 31$ ppm with the ylide methine hydrogens was observed in an HMQC experiment. $^{31}P\{^1H\}$ NMR: (121.4 MHz, CD_2Cl_2, 25 °C): $\delta = 29.0$ (d, $^4J(P,P) = 3.1$ Hz), 26.0 ppm (d, $^4J(P,P) =$ 3.3 Hz). ^{11}B NMR (160.4 MHz, CD_2Cl_2, 25 °C): $\delta = 35$ ppm. X-ray quality crystals of **3** were grown from a CH_2Cl_2 solution cooled at −30 °C for several days. Elemental analysis calcd (%) for $C_{44}H_{37}BCl_2P_2Pd{\cdot}CH_2Cl_2$: C 60.00, H 4.33; found: C 58.01, H 4.46.

Received: January 30, 2003 [Z51056]

Keywords: allyl ligands · boranes · palladium · ylides · zirconium

[1] H. Schmidbaur, *Angew. Chem.* **1983**, *95*, 980; *Angew. Chem. Int. Ed. Engl.* **1983**, *22*, 907, and references therein.

[2] a) K. Alexander, O. Starzewski, J. Witte, *Angew. Chem.* **1988**, *100*, 861; *Angew. Chem. Int. Ed. Engl.* **1988**, *27*, 839; b) K. Alexander, O. Starzewski, L. Born, *Organometallics* **1992**, *11*, 2701.

[3] P. J. Shapiro, *Eur. J. Inorg. Chem.* **2001**, 321, and references therein.

[4] Crystal data for $\mathbf{1}{\cdot}CH_2Cl_2$ and **2** and $\mathbf{3}{\cdot}CH_2Cl_2$ was collected by using a Bruker SMART APEX diffractometer with monochromated $Mo_{K\alpha}$ radiation ($\lambda = 0.71073$ Å): $\mathbf{1}{\cdot}CH_2Cl_2$: 81 K, triclinic, $P\bar{1}$, $a = 11.199(2)$, $b = 12.298(3)$, $c = 17.622(4)$ Å, $\alpha = 85.84(3)$, $\beta = 84.40(3)$, $\gamma = 68.07(3)°$, $V = 2238.8(10)$, $Z = 2$, $\rho_{calc} = 1.419\ mg\,m^{-3}$, $2\theta_{max} = 56.8°$, $\mu = 0.706\ mm^{-1}$, 496 parameters, 11 106 independent reflections ($R_{int} = 0.0669$), 7779 with $I > 2(\sigma)I$, $R1 = 0.0597$, $wR2 = 0.1276$. **2**: 203 K, triclinic, $P\bar{1}$, $a = 9.925(2)$, $b = 19.215(4)$, $c = 19.233(4)$ Å, $\alpha = 102.03(3)$, $\beta = 92.66(3)$, $\gamma = 103.61(3)°$, $V = 3469.0(14)$, $Z = 4$, $\rho_{calc} = 1.223\ mg\,m^{-3}$, $2\theta_{max} = 50°$, $\mu = 0.156\ mm^{-1}$, 847 parameters, 12 207 independent reflections ($R_{int} = 0.0819$), 6826 with $I > 2(\sigma)I$, $R1 = 0.0629$, $wR2 = 0.1174$. $\mathbf{3}{\cdot}CH_2Cl_2$: 82 K, monoclinic, $P2_1/n$, $a = 11.479(2)$, $b = 17.301(4)$, $c = 20.108(4)$ Å, $\beta = 91.64(3)°$, $V = 3992.1(14)$, $Z = 4$, $\rho_{calc} = 1.499\ mg\,m^{-3}$, $2\theta_{max} = 55.2°$, $\mu = 0.846\ mm^{-1}$, 478 parameters, 9215 independent reflections ($R_{int} = 0.0939$), 6758 with $I > 2(\sigma)I$, $R1 = 0.0560$, $wR2 = 0.1110$. Hydrogen atoms on C19, C26 (**1, 2**) and C63 and C70 (**2**) were located on the difference map and then added geometrically using a riding model. There are residuals of 1.68 and 1.03 e Å^{-3} ca. 1 Å from the Zr center in $\mathbf{1}{\cdot}CH_2Cl_2$. CCDC 202606–202608 (**1**–**3**, respectively) contain the supplementary crystallographic data for this paper. These data can be obtained free of charge via www.ccdc.cam.ac.uk/conts/retrieving.html (or from the Cambridge Crystallographic Data Centre, 12, Union Road, Cambridge CB2 1EZ, UK; fax: (+44) 1223-336-033; or deposit@ccdc.cam.ac.uk).

[5] M. T. Reetz, M. Willuhn, C. Psiorz, R. Goddard, *J. Chem. Soc. Chem. Commun.* **1999**, 1105.

[6] H.-J. Bestmann, T. Arenz, *Angew. Chem.* **1986**, *98*, 571; *Angew. Chem. Int. Ed. Engl.* **1986**, *25*, 559.

[7] M. Möhlen, B. Neumüller, K. Dehnicke, *Z. Anorg. Allg. Chem.* **1998**, *624*, 177.

[8] S. Courtenay, J. Y. Mutus, R. W. Schurko, D. W. Stephan, *Angew. Chem.* **2002**, *114*, 516; *Angew. Chem. Int. Ed.* **2002**, *41*, 498.

[9] E. J. Corey, J. Kang, *J. Am. Chem. Soc.* **1982**, *104*, 4724.

[10] F. H. Allen, O. Kennard, *Chem. Des. Autom. News* **1993**, *8*(1), 1; F. H. Allen, O. Kennard, *Chem. Des. Autom. News* **1993**, *8*(1), 31.

[11] S. Döring, G. Erker, R. Fröhlich, O. Meyer, K. Bergander, *Organometallics* **1998**, *17*, 2183.

[12] R. H. Crabtree, *The Organometallic Chemistry of the Transition Metals*, 3rd. ed., John Wiley & Sons, New York, **2001**, p. 122.

[13] A. Bondi, *J. Phys. Chem.* **1964**, *68*, 441.

[14] J. Ledford, C. S. Schultz, D. P. Gates, P. S. White, J. M. DeSimone, M. Brookhart, *Organometallics* **2001**, *20*, 5266.

[15] S. D. Ittel, L. K. Johnson, M. Brookhart, *Chem. Rev.* **2000**, *100*, 1169.

[16] a) W. A. Herrmann, C.-P. Reisinger, M. Spiegler, *J. Organomet. Chem.* **1998**, *557*, 93; b) A. J. Arduengo, T. Bannenberg, *Strem Chem.* **2002**, *XVIV*, 1, and references therein.

[17] H. Schmidbaur, H. Stuhler, W. Vornberger, *Chem. Ber.* **1972**, *105*, 1084.

[18] E. C. Lund, T. Livinghouse, *Organometallics* **1990**, *9*, 2426.

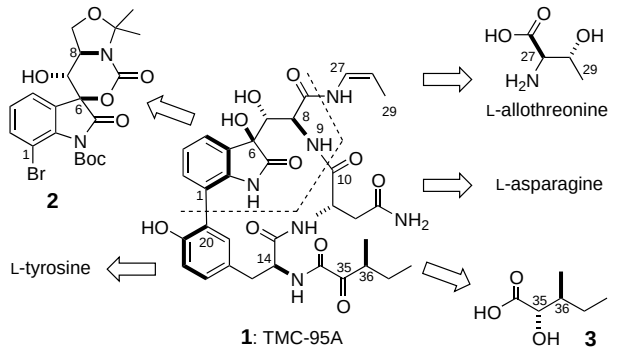
 © 2003 Wiley-VCH Verlag GmbH & Co. KGaA, Weinheim

Natural Product Synthesis

Total Synthesis of TMC-95A**

Masayuki Inoue, Hayato Sakazaki, Hidetomo Furuyama, and Masahiro Hirama**

A proteasome is a multicatalytic protease that is involved in a variety of biologically important processes, including immune responses, cell-cycle control, metabolic adaptation, stress response, and cell differentiation.[1] The selective inhibition of proteasomes may therefore be a means of controlling these essential pathways.[2] TMC-95A (**1**, Scheme 1) and its C36 epimer TMC-95B are potent proteasome inhibitors that bind

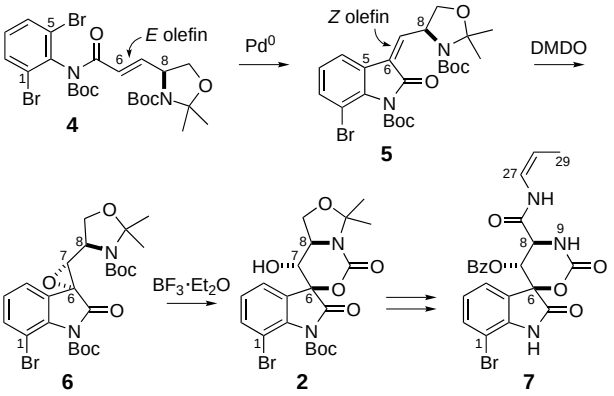


Scheme 1. Synthetic approach to TMC-95A. Boc = *tert*-butoxycarbonyl

to enzymes noncovalently with IC_{50} values at low nanomolar levels.[3] Thus, TMC-95 may provide unique insight into the detailed biological functions of proteasomes. Recently, the X-ray crystallographic structure of a complex of **1** with a proteasome was reported,[4] which has allowed the design of novel TMC-95 analogues with tailored biological activities.[5]

The intriguing biological profile and the structural complexity of TMC-95 immediately generated considerable interest within the synthetic community, and chemical syntheses have been pursued by several research groups.[6,7] These efforts have culminated in a total synthesis of TMC-95A/B by Lin and Danishefsky,[8] and a formal synthesis by Albrecht and Williams.[9] This report details a new solution to the stereoselective construction of TMC-95A.

The most notable features of TMC-95A from the perspective of the synthetic chemist are the highly oxidized tryptophan moiety, the (*Z*)-1-propenylamide, the 3-methyl-2-oxopentanoic acid side chain with the configurationally unstable methyl-substituted C36 center, and the aryl–oxindole ring junction (C1–C20) (Scheme 1). It was envisaged that the macrolactam structure could be assembled by a Suzuki–Miyaura coupling reaction (C1–C20) and peptide bond formation (N9–C10).[8–11] To avoid epimerization at the C36 stereocenter, we planned to introduce 3-methyl-2-oxopentanoic acid as the reduced form **3**, and to generate the C35 ketone in the final stage of the synthesis. We previously reported a stereoselective synthesis of the northern part of the molecule[6] (**7**, Scheme 2) with the following



Scheme 2. Synthesis of the northern part of TMC-95A. DMDO = 3,3-dimethyldioxirane.[6]

key features: 1) a *Z*-selective Mizoroki–Heck reaction to construct the oxindole structure (**4**→**5**), 2) diastereoselective epoxidation (**5**→**6**), 3) a 6-endo epoxide ring opening reaction to establish the stereochemistry of the C6 and C7 stereocenters (**6**→**2**), and 4) decarboxylative *anti* elimination under Mitsunobu conditions[12] to create the (*Z*)-1-propenylamide **7**. However, removal of the carbamate in **7** to liberate the N9 amine was unsuccessful despite extensive experimentation, which revealed the chemical instability of the propenylamide both in strongly acidic and in strongly basic media. Accordingly, we decided to construct the propenylamide after macrolactam formation, although the applicability of our method in a more complex structure remained uncertain.[13]

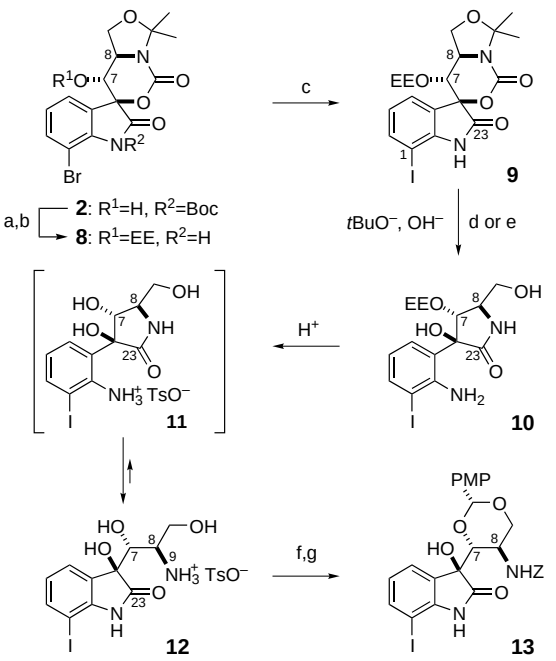
Our modified route started with the previously reported compound **2** (Scheme 3). The Boc group of **2** was selectively removed with $Mg(ClO_4)_2$ in acetonitrile,[14] and the C7 secondary alcohol was protected as its ethoxyethyl (EE) ether to afford **8** in 94% yield for the two steps. For effective biaryl coupling, the bromide **8** was converted into the corresponding iodide **9** in 86% yield through metalation with *n*BuLi and subsequent addition of diiodoethane without affecting the potentially reactive carbamate. The carbamate group of **9** was in fact extremely resistant to removal under a variety of conditions in the next step. Finally, it was found that the "anhydrous hydroxide" method of Gassman et al.[15] with *t*BuOK (15 equiv) and H_2O (10 equiv) transformed **9** into the aniline **10** (74% yield), in which both the carbamate and the acetonide had been hydrolyzed.

[*] Dr. M. Inoue, Prof. Dr. M. Hirama, H. Sakazaki, H. Furuyama
Department of Chemistry
Graduate School of Science, Tohoku University
Sendai 980-8578 (Japan)
Fax: (+81) 22-217-6566
E-mail: inoue@ykbsc.chem.tohoku.ac.jp
hirama@ykbsc.chem.tohoku.ac.jp

[**] Dr. Jun Kohno, Tanabe Seiyaku Co. (Japan), is gratefully acknowledged for providing natural TMC-95A for comparative analysis.

Supporting information for this article is available on the WWW under http://www.angewandte.org or from the author.

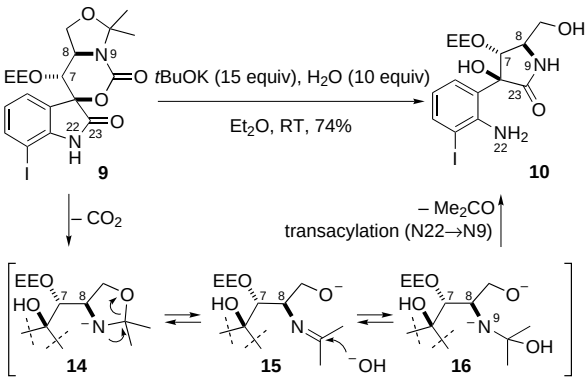
 © 2003 Wiley-VCH Verlag GmbH & Co. KGaA, Weinheim DOI: 10.1002/anie.200351130



Scheme 3. Reagents and conditions: a) $Mg(ClO_4)_2$, MeCN, 50 °C; b) ethyl vinyl ether, PPTS, THF, 35 °C, 94% from **2**; c) *n*BuLi, ICH_2CH_2I, THF, −60 °C→room temperature, 86%; d) *t*BuOK (15 equiv), H_2O (10 equiv), Et_2O, room temperature, 74%; e) *t*BuOK (15 equiv), H_2O (10 equiv), Et_2O, room temperature; then H_2O, TsOH, MeOH, room temperature; f) ZCl, Et_3N, DMF, 0 °C→room temperature, 55% from **9**; g) *p*-$MeOC_6H_4CH(OMe)_2$, TsOH, THF, 84%. DMF = dimethylformamide, PMP = *p*-methoxyphenyl, PPTS = pyridinium *p*-toluenesulfonate, TsOH = *p*-toluenesulfonic acid, Z = benzyloxycarbonyl.

The most plausible mechanism for this interesting outcome is depicted in Scheme 4: Compound **14**, generated upon loss of the carbamate group in **9** by decarboxylation, is in equilibrium with the imine **15**, which can undergo attack by a hydroxy anion to give **16**. Expulsion of acetone from **16** and transacylation from N22 to the more nucleophilic N9 then results in the formation of **10**.

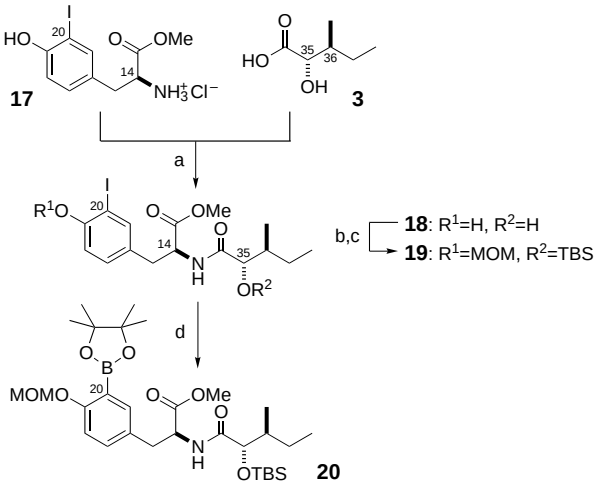
As shown in Scheme 3, regeneration of the oxindole structure from the aniline **10**, accompanied by loss of the ethoxyethyl group, was realized by lowering the pH value



Scheme 4. Possible reaction mechanism for **9**→**10**.

with *p*-toluenesulfonic acid to give **12** as a salt. The formation of **12** over **11** in acidic media is attributable to the preferential protonation of the more basic N9 amine of **12**.[16] The transformation from **9** to **12** was performed more practically in one pot by treating **9** under the Gassman conditions before sequentially introducing water, methanol, and TsOH. The liberated amine of **12** was then protected as its benzyl carbamate (55% yield from **9**), and the 1,3-diol was masked as its *p*-methoxybenzylidene acetal to produce the tryptophan fragment **13** (84% yield), suitably protected for the next reaction sequence.

We then turned our attention to the synthesis of the coupling partner of **13** (**20**, Scheme 5). The iodotyrosine derivative **17**[17] and the α-hydroxycarboxylic acid **3**[18] were prepared from L-tyrosine and L-isoleucine, respectively. After

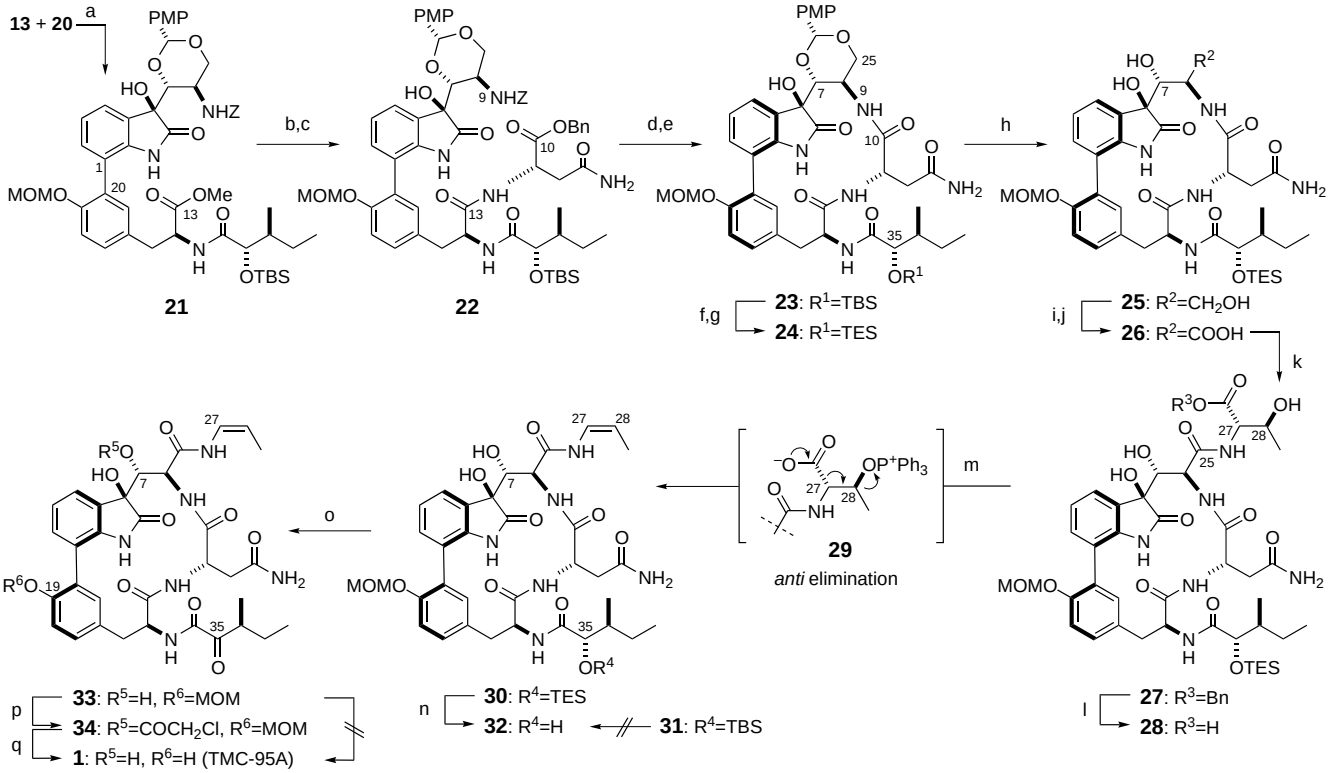


Scheme 5. Reagents and conditions: a) **3** (2 equiv), EDC·HCl, HOBt, 4-methylmorpholine, DMF, 0 °C, 56%; b) MOMCl, K_2CO_3, acetone, 85%; c) TBSOTf, 2,6-lutidine, CH_2Cl_2, 0 °C, 88%; d) bis(pinacolato)diboron, $[Pd(dppf)Cl_2]$, KOAc, DMSO, 80 °C, 71%. DMSO = dimethylsulfoxide, dppf = 1,1′-bis(diphenylphosphany)ferrocene, EDC = ethylcarbodiimide chloride, HOBt = 1-hydroxy-1*H*-benzotriazole, MOM = methoxymethyl, TBSOTf = *tert*-butyldimethylsilyl trifluoromethanesulfonate.

condensation of these two structural units in the presence of EDC and HOBt (56% yield), selective protection of the phenolic hydroxy group of **18** as its methoxymethyl ether, followed by protection of the remaining C35 alcohol with TBS, produced **19** in 75% yield over the two steps. The protected iodide **19** was converted into the aryl boronate **20** in 71% yield by palladium-mediated borylation.[19]

The C1−C20 biaryl bond was formed by treating the two advanced intermediates **13** and **20** with a catalytic amount of $[Pd(PPh_3)_4]$ and Na_2CO_3 in aqueous DME at 95 °C to give the adduct **21** in 84% yield (Scheme 6).[11,20] Basic hydrolysis of the methyl ester **21**, followed by amidation with L-asparagine benzyl ester, afforded **22** in 75% yield. Hydrogenolysis of both the benzyloxycarbonyl (Z) and benzyl groups gave a seco acid, which was subjected to cyclization in the presence of EDC and HOAt to afford the macrolactam **23** in 78% yield. In this way, the macrocyclic structure was constructed effectively through the assembly of three key fragments.

 © 2003 Wiley-VCH Verlag GmbH & Co. KGaA, Weinheim



Scheme 6. Reagents and conditions: a) **20** (1.5 equiv), $[Pd(PPh_3)_4]$, Na_2CO_3, DME/H_2O (4:1), 95 °C, 84 %; b) LiOH, THF/H_2O (1:1), 0 °C; c) H-Asn-OBn·TFA, EDC·HCl, HOBt, DMF, 0 °C, 75 % from **21**; d) H_2, $Pd(OH)_2$/C, THF/H_2O (1:1); e) EDC·HCl, HOAt, DMF, 0 °C, 78 % from **22**; f) TBAF, 4-Å MS, THF, 86 %; g) TESCl, imidazole, DMF, 85 %; h) $Zn(OTf)_2$, EtSH, $NaHCO_3$, CH_2Cl_2, 100 %; i) SO_3·pyr, Et_3N, CH_2Cl_2/DMSO (3:1), room temperature; j) $NaClO_2$, NaH_2PO_4, 2-methyl-2-butene, *t*BuOH/H_2O (5:1), room temperature; k) L-allo-Thr-OBn·TFA, EDC·HCl, HOBt, DMF, 0 °C, 67 % from **25**; l) H_2, $Pd(OH)_2$/C, THF/H_2O (1:2); m) DEAD, PPh_3, 4-Å MS, 0 °C→room temperature, 59 % from **27**; n) HF·pyridine, THF, 79 %; o) Dess–Martin periodinane, CH_2Cl_2, 80 %; p) $(ClCH_2CO)O$, pyridine, CH_2Cl_2, 0 °C; q) aqueous HCl (1 N)/THF (3:1), room temperature; then saturated aqueous $NaHCO_3$, 64 % from **33**. Bn = benzyl; DEAD = diethyl azodicarboxylate, DME = 1,2-dimethoxyethane, HOAt = 1-hydroxy-7-azabenzotriazole, MS = molecular sieves, pyr = pyridine, TBAF = tetrabutylammonium fluoride, TES = triethylsilyl, TFA = trifluoroacetic acid.

We had thus reached a critical stage of the total synthesis: introduction of the (*Z*)-propenylamide, construction of the dicarbonyl moiety, and the final deprotection. First, the TBS group of the C35 alcohol was exchanged for TES (**23**→**24**) for facile deprotection at a later stage. The PMP acetal was then removed with zinc triflate and ethanethiol in the presence of $NaHCO_3$ as a buffer[21] to afford the triol **25** in 73 % yield over three steps. Selective oxidation of the C25 primary alcohol of **25** allowed differentiation of the oxidation levels of C7 and C25 and led to the carboxylic acid **26** in two steps. Attachment of L-allothreonine benzyl ester to **26** produced **27** (67 % yield from **25**), which was then subjected to hydrogenolysis to provide the β-hydroxycarboxylic acid **28**. Subsequent treatment of **28** with PPh_3 and DEAD[12] in the presence of molecular sieves induced dehydrative decarboxylation at room temperature and led to the isomerically pure (*Z*)-propenylamide **30** in 59 % yield over the two steps.[6,22] The geometry of the resultant olefin is thought to be defined through the Grob-type *anti* elimination of **29**.[23] Thus, the applicability of this method in a complex setting was clearly demonstrated. The neutral nature and high chemoselectivity of the reaction should make it suitable for use in the synthesis of a wide variety of TMC-95 analogues and other compounds containing enamides.[8,24]

To adjust the oxidation level to that of the natural product, the C35 alcohol in **30** had to be deprotected. A TBS-protected compound **31** had been prepared by a similar route to **30**, but extensive investigations had failed to identify conditions that would allow the selective removal of the TBS group while leaving the rest of the molecule intact. However, the TES group in **30** was readily removed and the alcohol **32** was obtained in 79 % yield upon treatment of **30** with HF·pyridine. Selective oxidation of the C35 alcohol of **32** in the presence of the C7 alcohol with Dess–Martin periodinane[25] then afforded MOM-protected TMC-95A **33** in 80 % yield.

The final deprotection step proved to be nontrivial because of the intrinsic instability of the enamide. Various attempts to remove the MOM group of **33** under acidic conditions led to a complex mixture of products, and TMC-95A (**1**) was obtained in only minute amounts. The free C7 alcohol may be responsible for these difficulties as it may react in an intramolecular fashion with the propenylamide to form a six-membered ring.[26] Therefore, the alcohol at C7 was temporarily protected as its chloroacetyl ester (**33**→**34**), which indeed suppressed the side reactions. Exposure of **34** to HCl (1N)/THF and then saturated aqueous $NaHCO_3$ in one pot effectively afforded fully synthetic TMC-95A (**1**) in 64 % yield from **33** without destruction of the enamide or the

 © 2003 Wiley-VCH Verlag GmbH & Co. KGaA, Weinheim

stereochemistry of epimerizable C36 center. The physical data (^{1}H NMR, IR, MS) for the synthetic material were identical to those for the natural product.[3,8]

In summary, an efficient, highly convergent total synthesis of TMC-95A has been achieved. The key transformations in this synthesis are 1) a new deprotection protocol for the removal of the hindered carbamate and the acetonide of **9**, 2) conversion of the aniline **10** into the oxindole **12** by lowering the pH value, 3) a Suzuki–Miyaura coupling reaction and macrolactamization to efficiently create the macrocyclic framework **23**, and 4) a mild decarboxylative *anti* elimination to selectively produce the (*Z*)-1-propenylamide as part of a complex structure. The chemistry and biology of TMC-95A are being investigated further in our laboratory.

Received: February 7, 2003 [Z51130]

Keywords: biaryls · macrocycles · natural products · olefination · total synthesis

[1] For reviews on the biology of proteasomes, see: a) M. Bochtler, L. Ditzel, M. Groll, C. Hartmann, R. Huber, *Annu. Rev. Biophys. Biomol. Struct.* **1999**, *28*, 295; b) K. Tanaka, *J. Biochem.* **1998**, *123*, 195; c) A. Hershko, A. Ciechanover, *Annu. Rev. Biochem.* **1998**, *67*, 425.

[2] For reviews on proteasome inhibitors, see: a) A. F. Kisselev, A. L. Goldberg, *Chem. Biol.* **2001**, *8*, 739; b) J. Myung, K. B. Kim, C. M. Crews, *Med. Res. Rev.* **2001**, *21*, 245; c) D. H. Lee, A. L. Goldberg, *Trends Cell Biol.* **1998**, *8*, 397.

[3] a) J. Kohno, Y. Koguchi, M. Nishio, K. Nakao, M. Kuroda, R. Shimizu, T. Ohnuki, S. Komatsubara, *J. Org. Chem.* **2000**, *65*, 990; b) Y. Koguchi, J. Kohno, M. Nishio, K. Takahashi, T. Okuda, T. Ohnuki, S. Komatsubara, *J. Antibiot.* **2000**, *53*, 105.

[4] M. Groll, Y. Koguchi, R. Huber, J. Kohno, *J. Mol. Biol.* **2001**, *311*, 543.

[5] M. Kaiser, M. Groll, C. Renner, R. Huber, L. Moroder, *Angew. Chem.* **2002**, *114*, 817; *Angew. Chem. Int. Ed.* **2002**, *41*, 780.

[6] M. Inoue, H. Furuyama, H. Sakazaki, M. Hirama, *Org. Lett.* **2001**, *3*, 2863.

[7] a) D. Ma, Q. Wu, *Tetrahedron Lett.* **2001**, *42*, 5279; b) S. Lin, S. J. Danishefsky, *Angew. Chem.* **2001**, *113*, 2020; *Angew. Chem. Int. Ed.* **2001**, *40*, 1967; c) B. K. Albrecht, R. M. Williams, *Tetrahedron Lett.* **2001**, *42*, 2755; d) D. Ma, Q. Wu, *Tetrahedron Lett.* **2000**, *41*, 9089.

[8] S. Lin, S. J. Danishefsky, *Angew. Chem.* **2002**, *114*, 530; *Angew. Chem. Int. Ed.* **2002**, *41*, 512.

[9] B. K. Albrecht, R. M. Williams, *Org. Lett.* **2003**, *5*, 197.

[10] For recent reviews on biaryl synthesis, see: a) J. Hassan, M. Sévignon, C. Gozzi, E. Schulz, M. Lemaire, *Chem. Rev.* **2002**, *102*, 1359; b) P. Lloyd-Williams, E. Giralt, *Chem. Soc. Rev.* **2001**, *30*, 145; c) S. P. Stanforth, *Tetrahedron* **1998**, *54*, 263.

[11] For reviews on the Suzuki–Miyaura reaction, see: a) A. Suzuki, *J. Organomet. Chem.* **1999**, *576*, 147; b) A. Suzuki in *Metal-catalyzed Cross-coupling Reactions* (Eds.: F. Diederich, P. J. Stang), Wiley-VCH, Weinheim, **1998**, p. 49; c) N. Miyaura, A. Suzuki, *Chem. Rev.* **1995**, *95*, 2457.

[12] For reviews on the Mitusnobu reaction, see: a) O. Mitsunobu, *Synthesis* **1981**, 1; b) D. L. Hughes, *Org. React.* **1992**, *42*, 335.

[13] Lin and Danishefsky constructed the (*Z*)-1-propenylamide through ingenious use of the thermal rearrangement of an α-silylallylamide in the final stage of their total synthesis.[8]

[14] J. A. Stafford, M. F. Brackeen, D. S. Karanewsky, N. L. Valvano, *Tetrahedron Lett.* **1993**, *34*, 7873.

[15] a) P. G. Gassman, W. N. Schenk, *J. Org. Chem.* **1977**, *42*, 918; b) P. G. Gassman, P. K. G. Hodgson, R. J. Balchunis, *J. Am. Chem. Soc.* **1976**, *98*, 1275.

[16] a) P. A. Thio, M. J. Kornet, *J. Heterocycl. Chem.* **1971**, *8*, 479; b) M. Nakagawa, S. Kato, H. Fukazawa, Y. Hasegawa, J. Miyazawa, T. Hino, *Tetrahedron Lett.* **1985**, *26*, 5871.

[17] J. Chiarello, M. M. Joullie, *Synth. Commun.* **1988**, *18*, 2211.

[18] M. Winitz, L. Bloch-Frankenthal, N. Izumiya, S. M. Birnbaum, C. G. Baker, J. P. Greenstein, *J. Am. Chem. Soc.* **1956**, *78*, 2423.

[19] T. Ishiyama, M. Murata, N. Miyaura, *J. Org. Chem.* **1995**, *60*, 7508.

[20] S. Boisnard, A.-C. Carbonnelle, J. Zhu, *Org. Lett.* **2001**, *3*, 2061.

[21] K. C. Nicolaou, C. A. Veale, C.-K. Hwang, J. Hutchinson, C. V. C. Prasad, W. W. Ogilvie, *Angew. Chem.* **1991**, *103*, 304; *Angew. Chem. Int. Ed. Engl.* **1991**, *30*, 299.

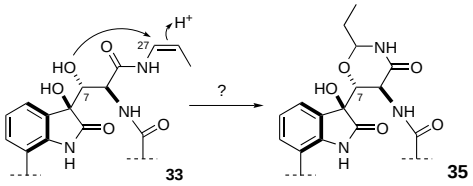
[22] S. V. Pansare, J. C. Vederas, *J. Org. Chem.* **1989**, *54*, 2311.

[23] a) J. Mulzer, A. Pointner, A. Chucholowski, G. Brüntrup, *J. Chem. Soc. Chem. Commun.* **1979**, 52; b) J. Mulzer, O. Lammer, *Angew. Chem. Suppl.* **1983**, 887.

[24] For selected examples of the preparation of enamides, see: a) S. Sergeyev, M. Hesse, *Synlett* **2002**, 1313; b) P. Ribéreau, M. Delamare, S. Célanire, G. Quéguiner, *Tetrahedron Lett.* **2001**, *42*, 3571; c) R. Shen, J. A. Porco, Jr., *Org. Lett.* **2000**, *2*, 1333; d) B. B. Snider, F. Song, *Org. Lett.* **2000**, *2*, 407; e) K. Kuramochi, H. Watanabe, T. Kitahara, *Synlett* **2000**, 397; f) T. Mecozzi, M. Petrini, *Synlett* **2000**, 73; g) N. M. Laso, B. Quiclet-Sire, S. Z. Zard, *Tetrahedron Lett.* **1996**, *37*, 1605; h) U. Schmidt, A. Lieberknecht, *Angew. Chem.* **1983**, *95*, 575; *Angew. Chem. Int. Ed. Engl.* **1983**, *22*, 550; i) U. Redeker, N. Engel, W. Steglich, *Tetrahedron Lett.* **1981**, *22*, 4263; j) J. K. Stille, Y. Becker, *J. Org. Chem.* **1980**, *45*, 2139.

[25] D. B. Dess, J. C. Martin, *J. Am. Chem. Soc.* **1991**, *113*, 7277.

[26] The attempted isolation of **35** was unsuccessful, presumably because of its instability under the reaction conditions.



 © 2003 Wiley-VCH Verlag GmbH & Co. KGaA, Weinheim

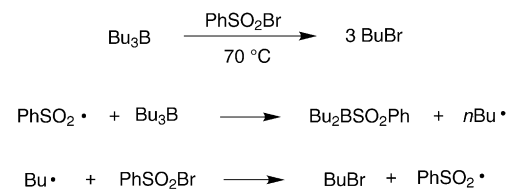
Hydroallylation of Alkenes

Tin-Free Radical Allylation of *B*-Alkylcatecholboranes**

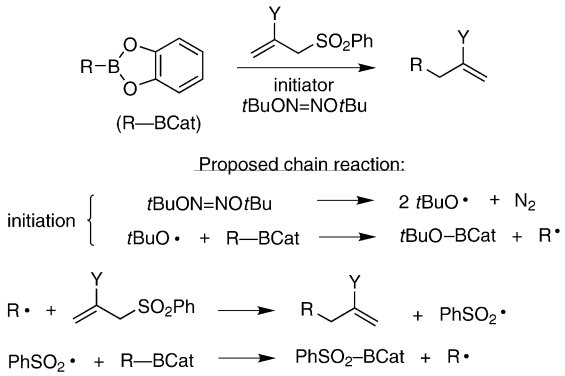
*Arnaud-Pierre Schaffner and Philippe Renaud**

For many years organoboron chemistry has been a privileged field of research for synthetic organic chemists. Following the spectacular development of radical chemistry in organic synthesis,[1] the use of organoboranes has recently led to many novel and useful synthetic applications such as hydroxylation reactions and conjugate additions.[2] These recent reports have shown that *B*-alkylcatecholboranes readily undergo radical substitution at boron and are therefore particularly good precursors for radical chain reactions.[3] However, at the moment, the method is limited mainly to conjugate addition to enones[3a] and to other activated olefins in the presence of a chain-transfer reagent.[3b,e] This last reaction is very general; however, the direct reaction of the radical with the chain-transfer reagent may be an important side reaction with weakly activated alkenes. This problem is well known in radical conjugate addition mediated by tin hydride (Giese reaction),[4] and the reduced radical precursor is a significant side product. In tin chemistry the problem has been solved by the development of the fragmentation method based on the use of allylstannanes.[5] Allylstannanes are employed as a radical trap and as chain-transfer reagents. In this communication we report an efficient fragmentation process for the allylation of organoboranes. *B*-Alkylcatecholboranes, prepared in situ by hydroboration of olefins with catecholborane, can be allylated efficiently with allyl sulfones. This tin-free radical method parallels the allylstannane-mediated radical allylation. Interestingly, this radical approach complements nicely Knochel's procedure for the allylation of organoboranes, which requires transmetalation to organozinc derivatives.[6]

In 1972 Davies and Roberts established that benzenesulfonyl bromide is a suitable reagent for the bromination of tri-*n*-butylborane (Scheme 1).[7] They assumed that this reaction was a radical chain process in which a benzenesulfonyl radical displaces an alkyl radical from tri-*n*-butylborane. Their observation incited us to try a similar radical chain process for the allylation of *B*-alkylcatecholboranes using easily available allyl sulfones (Scheme 2).[8] Since phenyl sulfones are employed, the fragmentation produces a stable phenyl-



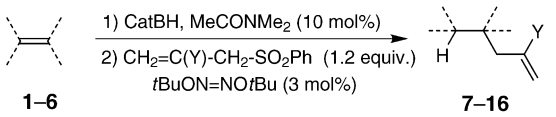
Scheme 1. Bromination of tri-*n*-butylborane according to Davies and Roberts.



Scheme 2. Proposed approach for the radical allylation of *B*-alkylcatecholboranes.

sulfonyl radical that should react with *B*-alkylcatecholborane to sustain the chain reaction. Oxygen-centered radicals react efficiently with *B*-alkylcatecholboranes. Therefore, di-*tert*-butylhyponitrite was chosen as an initiator due to its easy availability and practicability to furnish *tert*-butoxyl radical in refluxing dichloromethane.[9] The thermal properties of this initiator should allow us to run a one-pot hydroboration/radical reaction sequence by taking advantage of the very mild, efficient, and cost-effective hydroboration conditions developed by Fu and Garett.[10]

The whole transformation represents formally a reductive allylation or hydroallylation of alkenes [Eq. (1)]. The reaction was first tested with 2-(methoxycarbonyl)prop-2-en-1-yl



(1)

phenyl sulfone as the radical trap (Y = COOEt). The results are summarized in Table 1. The desired products **7**–**11** were obtained in satisfactory to excellent yields by using only 1.2 equivalents of the allyl sulfones with primary (entries 1, 2), secondary (entries 3, 4), and tertiary alkyl radicals (entry 5). The nonsubstituted allyl sulfones react also under these conditions and provide the volatile allylated products **12** and **13** in moderate yields (entries 6, 7). Finally, other allylic sulfones bearing a sulfonyl group (Y = $PhSO_2$) and a bromine atom (Y = Br) were found to react equally well (entries 8–10). The stereochemical outcome of all these reactions is rationalized in a straightforward manner: the hydroboration

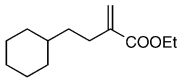
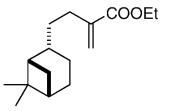
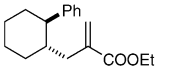
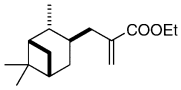
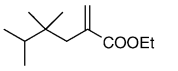
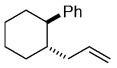
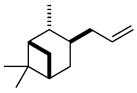
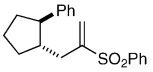
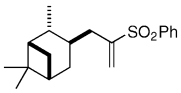
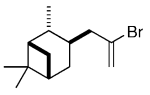
[*] Prof. Dr. P. Renaud, A.-P. Schaffner
University of Berne
Department of Chemisty and Biochemistry
Freiestrasse 3, 3000 Berne 9 (Switzerland)
Fax: (+41) 31-631-3426
E-mail: philippe.renaud@ioc.unibe.ch

[**] This work was supported by the Swiss National Science Foundation (grants 21-67106.01 and 7SUPJ062348). We thank Callery Chemical Company (Pittsburgh) and Z&S Handel AG (Kloten) for the gift of catecholborane.

Supporting information for this article is available on the WWW under http://www.angewandte.org or from the author.

 © 2003 Wiley-VCH Verlag GmbH & Co. KGaA, Weinheim DOI: 10.1002/anie.200351171

Table 1: Reductive allylation of alkenes according to Equation (1).

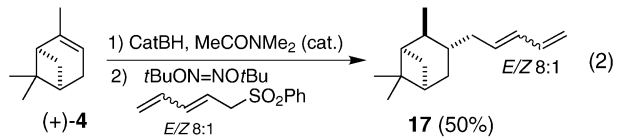
Entry	Alkene		Product		Yield [%]	d.r.
1		**1**		**7**	55	–
2		**2**		**8**	62	90/10
3		**3**		**9**	76	90/10
4		(−)-**4**		**10**	89	96/4
5		**5**		**11**	65	–
6		**3**		**12**	56	90/10
7		(−)-**4**		**13**	52	95/5
8		**6**		**14**	74	97/3
9		(−)-**4**		**15**	89	96/4
10		(−)-**4**		**16**	58	96/4

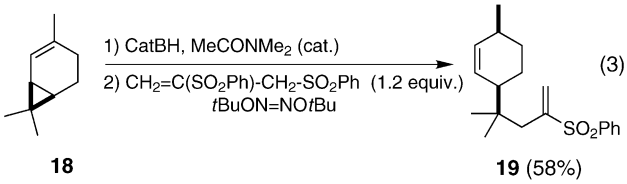
(entries 2, 4, 7, 9, 10) and the radical reaction (entries 3, 4, 6–10) both occur from the less hindered face.

Interestingly, this allylation process seems to be very general. For instance, introduction of a dienyl moiety using penta-2,4-dienyl phenyl sulfone has been achieved [Eq. (2)].[11] The modest yield for the conversion of **4** to **17** (50%) is due to the instability of the dienyl sulfone, which readily polymerizes.[12]

Finally, the radical nature of the process was demonstrated by running an allylation reaction with (+)-2-carene (**18**) [Eq. (3)]. In this radical probe experiment the intermediate cyclopropylmethyl radical undergoes ring opening to give the homoallylic radical, which is trapped by the allylic sulfone to produce **19**. We previously established that in this system no ring opening occurs during the hydroboration step.[13]

In conclusion we have developed a one-pot procedure for the hydroallylation of alkenes. We have demonstrated that *B*-alkylcatecholboranes, easily generated by hydroboration of alkenes with catecholborane, can be allylated with a variety of allyl sulfones by using a fragmentation process. Interestingly, due to the exceptional reactivity of *B*-alkylcatecholboranes towards sulfonyl radicals, excellent yields are obtained with only 1.2 equivalents of the radical trap. The radical nature of the key step is of high interest for further applications of this chemistry in radical cascade reactions for the formation of one or more cycles. Radical chain reactions involving sulfonyl radicals and *B*-alkylcatecholborane are expected to become an important method for tin-free radical reactions.





Experimental Section

General procedure: Catecholborane (0.8 mL, 7.5 mmol) was added dropwise at 0 °C to a solution of olefin (3.0 mmol) and *N*,*N*-dimethylacetamide (28.0 μL, 0.3 mmol) in CH_2Cl_2 (2.0 mL) under nitrogen. The reaction mixture was heated at reflux for 5 h. MeOH (0.20 mL, 4.8 mmol) was added at 0 °C and the solution was stirred for 15 min at room temperature. The sulfone (3.6 mmol) was then added, the solution was warmed at reflux, and di-*tert*-butylhyponitrite (15 mg, 0.09 mmol) was added every hour. The reaction was monitored by GCMS. At the end of the reaction the solution turned to black. The crude product was purified by flash chromatography over silica gel.

Phenyl 1-{[(1*S*,2*R*,3*R*,5*S*)-2,6,6-trimethylbicyclo[3.1.1]hept-3-yl]-methyl}vinyl sulfone (**15**): The reaction was conducted following the general procedure starting from (−)-α-pinene (**4**) (0.409 g, 3 mmol). Flash chromatography (hexane/EtOAc 4:1) afforded **15** (0.848 g, 89%) as a colorless oil. ^{1}H NMR (300 MHz, $CDCl_3$): $\delta = 7.93$–7.83 (m, 2H), 7.64–7.45 (m, 3H), 6.41 (s, 1H), 5.80 (s, 1H), 2.52 (dd, $J =$ 15.1, 3.7 Hz, 1H), 2.24 (m, 1H), 2.06 (m, 1H), 1.95–1.69 (m, 3H), 1.54 (m, 1H), 1.23 (m, 2H), 1.13 (s, 3H), 0.93 (m, 3H), 0.86 (s, 3H), 0.61 ppm (d, $J = 9.6$ Hz, 1H). ^{13}C NMR (75 MHz, $CDCl_3$): $\delta = 149.3$, 139.2, 133.4, 129.1, 128.2, 124.6, 47.9, 43.7, 41.6, 38.6, 34.1, 34.2, 33.9, 27.9, 22.8, 21.2 ppm. MS (EI): *m*/*z* 319 [M^++1], 246, 218, 177, 137, 81, 55, 41. HRMS (ESI-MS) calculated for $C_{19}H_{27}O_2S$ ([M+1]$^+$): 319.1731; found: 319.1729.

 © 2003 Wiley-VCH Verlag GmbH & Co. KGaA, Weinheim

Supporting information for this article (experimental procedures and characterizations of compounds **7**–**17** and **19**) is available on the WWW under http://www.angewandte.org or from the author.

Received: February 13, 2003 [Z51171]

Keywords: allylation · allylic compounds · boron · hydroboration · radical reactions · sulfones

[1] a) B. Giese, *Radicals in Organic Synthesis: Formation of Carbon–Carbon Bonds*, Pergamon, Oxford, **1986**; b) W. B. Motherwell, D. Crich, *Free Radical Chain Reactions in Organic Synthesis*, Academic Press, London, **1992**; c) J. Fossey, D. Lefort, J. Sorba, *Free Radicals in Organic Synthesis*, Wiley, Chichester, **1995**; d) *Radicals in Organic Synthesis, Vol. 1 and 2* (Eds.: P. Renaud, M. P. Sibi), Wiley-VCH, Weinheim, **2001**.

[2] a) C. Ollivier, P. Renaud, *Chem. Rev.* **2001**, *101*, 3415; b) H. Yorimitsu, K. Oshima in *Radicals in Organic Synthesis, Vol. 1* (Eds.: P. Renaud, M. P. Sibi), Wiley-VCH, Weinheim, **2001**, p. 11.

[3] a) C. Ollivier, P. Renaud, *Chem. Eur. J.* **1999**, *5*, 1468; b) C. Ollivier, P. Renaud, *Angew. Chem.* **2000**, *112*, 946; *Angew. Chem. Int. Ed.* **2000**, *39*, 925; c) C. Ollivier, R. Chuard, P. Renaud, *Synlett* **1999**, 807; d) C. Cadot, P. I. Dalko, J. Cossy, C. Ollivier, R. Chuard, P. Renaud, *J. Org. Chem.* **2002**, *67*, 7193; see also: e) C. Cadot, J. Cossy, P. I. Dalko, *Chem. Commun.* **2000**, 1017.

[4] See ref. [1a] for an extensive discussion of the Giese reaction.

[5] For a recent review, see: I. J. Rosenstein in *Radicals in Organic Synthesis, Vol. 1* (Eds.: P. Renaud, M. P. Sibi), Wiley-VCH, Weinheim, **2001**, p. 50.

[6] a) F. Langer, L. Schwink, A. Devasagayaraj, P.-Y. Chavant, P. Knochel, *J. Org. Chem.* **1996**, *61*, 8229; b) A. Boudier, C. Darcel, F. Flachsmann, L. Micouin, M. Oestreich, P. Knochel, *Chem. Eur. J.* **2000**, *6*, 2748.

[7] A. G. Davies, B. P. Roberts, *Acc. Chem. Res.* **1972**, *5*, 387.

[8] The use of sulfones for radical allylation has been reported. For a review, see: a) F. Bertrand, F. Le Guyader, L. Liguori, G. Ouvry, B. Quiclet-Sire, S. Seguin, S. Z. Zard, *C. R. Acad. Sci. Ser. IIc* **2001**, *4*, 547; b) S. Z. Zard, *Angew. Chem* **1997**, *109*, 724; *Angew. Chem. Int. Ed. Engl.* **1997**, *36*, 672; c) C. Chatgilialoglu, C. Ferreri, M. Ballestri, D. P. Curran, *Tetrahedron Lett.* **1996**, *37*, 6387; d) C. Chatgilialoglu, A. Alberti, M. Ballestri, D. Macciantelli, D. P. Curran, *Tetrahedron Lett.* **1996**, *37*, 6391; e) B. Quiclet-Sire, S. Z. Zard, *J. Am. Chem. Soc.* **1996**, *118*, 1209; f) I. Y. Ryu, S. Kreimerman, T. Niguma, S. Minaka, M. Komatsu, Z. Y. Luo, D. P. Curran, *Tetrahedron Lett.* **2001**, *42*, 947; g) J. Xiang, J. Evarts, A. Rivkin, D. P. Curran, P. L. Fuchs, *Tetrahedron Lett.* **1998**, *39*, 4163; h) S. Kim, C. J. Lim, *Angew. Chem.* **2002**, *114*, 3399; *Angew. Chem. Int. Ed.* **2002**, *41*, 3265; for free radical mediated 1,3-rearrangements of allylic sulfones, see: i) E. D. Phillips, G. H. Whitham, *Tetrahedron Lett.* **1993**, *34*, 2537; E. D. Phillips, G. H. Whitham, *Tetrahedron Lett.* **1993**, *34*, 2541; j) T. A. K. Smith, G. H. Whitham, *J. Chem. Soc. Perkin Trans. 1* **1989**, 313; T. A. K. Smith, G. H. Whitham, *J. Chem. Soc. Perkin Trans. 1* **1989**, 319; k) D. J. Knight, P. Lin, G. H. Whitham, *J. Chem. Soc. Perkin Trans. 1* **1987**, 2707; l) A. Padwa, D. N. Kline, S. S. Murphree, P. E. Yeske, *J. Org. Chem.* **1992**, *57*, 298; m) A. Padwa, W. H. Bullock, A. D. Dyszlewski, *Tetrahedron Lett.* **1987**, *28*, 3193; n) A. Padwa, W. H. Bullock, A. D. Dyszlewski, *J. Org. Chem.* **1990**, *55*, 955; o) V. Barre, D. Uguen, *Tetrahedron Lett.* **1987**, *28*, 6045; p) R. D. Baechler, P. Bentley, L. Deuring, S. Fisk, *Tetrahedron Lett.* **1982**, *23*, 2269.

[9] For the preparation of di-*tert*-butyl hyponitrite, see: a) G. D. Mendenhall, *Tetrahedron Lett.* **1983**, *24*, 451; b) J. T. Banks, J. C. Scaiano, W. Adam, R. S. Oestrich, *J. Am. Chem. Soc.* **1993**, *115*, 2473.

[10] C. E. Garett, G. C. Fu, *J. Org. Chem.* **1996**, *61*, 3224.

[11] Pentadienylation of radicals with penta-2,4-dienyltributylstannane has been reported: a) T. Toru, T. Yoneda, T. Okumura, Y. Watanabe, Y. Ueno, *Trends in Org. Chem.* **1990**, 43; b) Y. Watanabe, T. Yoneda, T. Okumura, Y. Ueno, T. Toru, *Bull. Chem. Soc. Jpn.* **1993**, *66*, 3030; c) G. A. Kraus, B. Andersh, Q. Su, J. Shi, *Tetrahedron Lett.* **1993**, *34*, 1741; d) Y. Landais, D. Planchenault, *Tetrahedron* **1995**, *51*, 12097.

[12] The unstable penta-2,4-dienyl phenyl sulfone was used immediately after its preparation. Preparation: T. B. Chen, J. J. Burger, E. R. De Waard, *Tetrahedron Lett.* **1977**, 4527. Use in radical polymerization: M.-O. Zink, D. Colombani, P. Chaumont, *Eur. Polym. J.* **1997**, *33*, 1433.

[13] See ref. [3a, c, d].

 © 2003 Wiley-VCH Verlag GmbH & Co. KGaA, Weinheim

Anionic Gallium Carbene Analogue

Synthesis and Structural Characterization of Thermally Stable Group 13 Hydride Complexes Derived from a Gallium(I) Carbene Analogue**

Robert J. Baker, Cameron Jones, Marc Kloth, and Jamie A. Platts*

The chemistry of aluminum(I) and gallium(I) compounds is a rapidly expanding area.[1] Within this field neutral metal(I) alkyl and aryl compounds have been widely used as ligands in complexes with both main group and transition metals.[2] In related work, the neutral, monomeric six-membered aluminum and gallium carbene analogues, [:M{N(Ar)C(Me)}$_2$CH], M = Al[3] or Ga,[4] Ar = C$_6$H$_3$*i*Pr$_2$-2,6, were developed and shown to contain singlet lone pairs at the metal centers, which reside in orbitals that are approximately sp-hybridized. Despite this work, the coordination chemistry of these carbene analogues has not been widely examined and only one metal complex, [Fe(CO)$_4${Ga[N(Ar)C(Me)]$_2$CH}], was reported,[5] though a borane complex, [B(C$_6$F$_5$)$_3${Ga-[N(Ar)C(Me)]$_2$CH}], was also described.[6] Two related anionic gallium(I) heterocycles, [:Ga{NC(R)C(H)}$_2$]$^-$, were developed by Schmidbaur et al. (R = *t*Bu)[7] and ourselves (R = Ar, **1**)[8] and these can be thought of as valence isoelectronic analogues of the ubiquitous *N*-heterocyclic-carbene (NHC) class of ligand. In light of the ever increasing importance of NHCs as ligands in main-group and transition-metal chemistry,[9] the initiation of a study of the coordination

[*] Prof. C. Jones, Dr. R. J. Baker, Dipl.-Eng. M. Kloth, Dr. J. A. Platts
Department of Chemistry
University of Wales, Cardiff
P.O. Box 912, Park Place, Cardiff CF10 3TB (UK)
Fax: (+44) 2920-874-030
E-mail: jonesca6@cardiff.ac.uk

[**] This work was supported in part by the Engineering and Physical Sciences Research Council (UK).

Supporting information for this article is available on the WWW under http://www.angewandte.org or from the author.

 © 2003 Wiley-VCH Verlag GmbH & Co. KGaA, Weinheim DOI: 10.1002/anie.200351281

chemistry of heterocycles, such as **1** was thought to be of considerable interest. In view of our recent success in stabilizing group 13 trihydrides through their complexation by NHCs,[10] we have begun such a study aimed at examining the reactivity of **1** towards $[MH_3(L)]$, M = Al, Ga or In, L = Lewis base. The preliminary results of this investigation are reported herein.

The reaction of an ethereal solution of **1** with $[AlH_3(NMe_3)]$ in a 2:1 soichiometry led to a considerable aluminum and gallium metal deposition upon warming the reaction mixture to room temperature. This was accompanied by the formation of the ionic tetraamido gallium complex $[Ga\{[NC(Ar)C(H)]_2\}_2][K(DME)_4]$, which was isolated in moderate yield after recrystallization from DME. The same product was obtained when the reaction was carried out in 1:1 or 3:1 stoichiometries, though with lower yields. Compound **2** was characterized crystallographically and spectroscopically[11,12] and presumably forms via an unknown intermediate which is unstable at room temperature. It was originally thought this decomposition process involved the generation of the free diazabutadiene, $(ArN=C)_2$, which was doubly reduced an excess of **1** to give the observed product. However, this was discounted as intentionally treating $(ArN=C)_2$ with **1** led to no reaction.

An indication of the nature of the intermediate in the decomposition process that affords **2** might come from the analogous reactions of **1** with tertiary amine adducts of GaH_3 and InH_3 in a 2:1 stoichiometry (Scheme 1). These reactions gave high yields of the novel trimetallic group 13 hydride complexes, **3** and **4**. When these reactions were carried out in 1:1 or 3:1 stoichiometries, the same products were formed but with reduced yields. It is noteworthy that the lithium counterion in **4** originates from LiBr, which is generated as an inseparable by-product in the in situ preparation of $[InH_3(NMe_3)]$.[10] The mechanisms of formation of **3** and **4** are unknown but presumably involve an initial elimination of KH to form neutral intermediates, $[MH_2(Ga\{NC(R)C(H)\}_2)]$, M = Ga or In, which are then coordinated by a second equivalent of **1** to give the observed anionic complexes, $[MH_2(Ga\{NC(Ar)C(H)\}_2)_2]^-$. Both compounds are remarkably thermally stable in the solid state and, indeed, the decomposition temperature of **4** (116 °C) is comparable with that of the most stable InH_3–carbene complex yet reported, $[InH_3(IMes)]$, IMes = :CN(Mes)C_2H_2N(Mes), Mes = mesityl (dec. 115 °C).[10]

The spectroscopic data for **3** and **4** fully support their proposed structures. In particular, the ^{1}H NMR spectra of **3** and **4** exhibit broad resonances corresponding to their hydride ligands. These resonances occur at higher fields than those normally seen for neutral MH_3 complexes, which reflects the expected greater shielding of the hydride ligands in the anionic systems. In addition, the infrared spectra of **3** and **4**, recorded in Nujol, display strong, broad absorptions at $\tilde{\nu}$ = 1769 and 1632 cm^{-1}, which lie in the normal frequency ranges for Ga–H and In–H stretches respectively.[10,13]

Both compounds were crystallographically characterized[12] and the molecular structure of **3** and the structure of the anionic component of **4** are depicted in Figures 1 and 2 respectively. These structures reveal that the anion of each

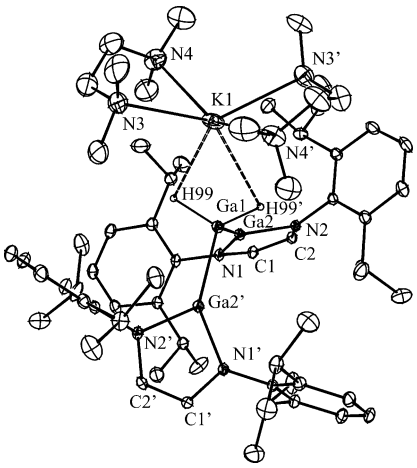
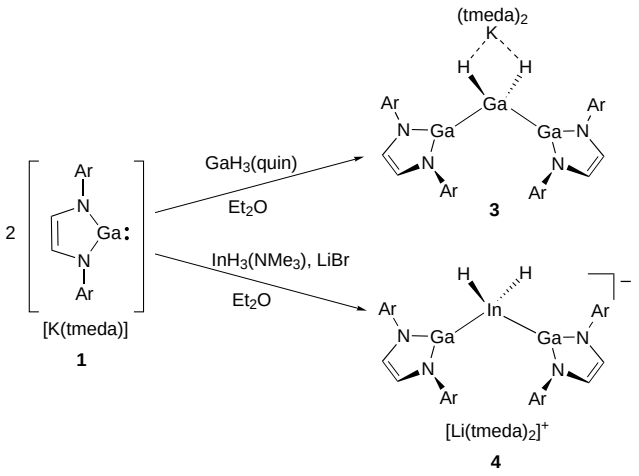


Figure 1. Molecular structure of **3**. Selected bond lengths [Å] and angles [°]: Ga1-Ga2 2.4071(9), Ga1-H99 1.49(6), Ga2-N1 1.877(4), Ga2-N2 1.886(4), C1-C2 1.357(7), N1-C1 1.399(6), N2-C2 1.381(6), K1-H99 2.87(6), K1-N3 2.760(7), K1-N4 2.920(9), Ga2-Ga1-Ga2′ 107.24(4), Ga2-Ga1-H99 111(2), Ga2′-Ga1-H99 106(2), H99-Ga1-H99′ 116(2), N1-Ga2-N2 86.98(16), N1-Ga2-Ga1 142.88(12), N2-Ga2-Ga1 129.68(11), C1-N1-Ga2 110.4(3), C2-N2-Ga2 110.0(3). Symmetry transformation: $-x+1, y, -z+1/2$.



Scheme 1. Syntheses of compounds **3** and **4**, quin = quinuclidine.

compound contains a chain of three metal atoms connected by two M–Ga bonds. In the case of **3**, comparisons can be made with $[Ga\{Ga(GePh_3)_3\}_2][Li(THF)_4]$,[14] though in that case the central Ga atom is two-coordinate and the terminal Ga centers are four-coordinate. With respect to **4**, there are no previously reported compounds containing Ga_2In chains but In_3 chains are relatively common, as in, for example, $[In\{C(SiMe_3)_3\}\{\mu\text{-Br-Li}(THF)_4\}\{In[C(SiMe_3)_3](\mu\text{-Br})\}_2]$.[15] The hydride ligands of **3** and **4** were located from difference maps and refined isotropically. Those in **3** bridge the Ga and K centers to effectively form a contact ion pair. The central group 13 metal atom in each complex has a distorted tetrahedral environment whilst the gallium heterocycles are essentially planar and contain trigonal planar metal centers.

 © 2003 Wiley-VCH Verlag GmbH & Co. KGaA, Weinheim

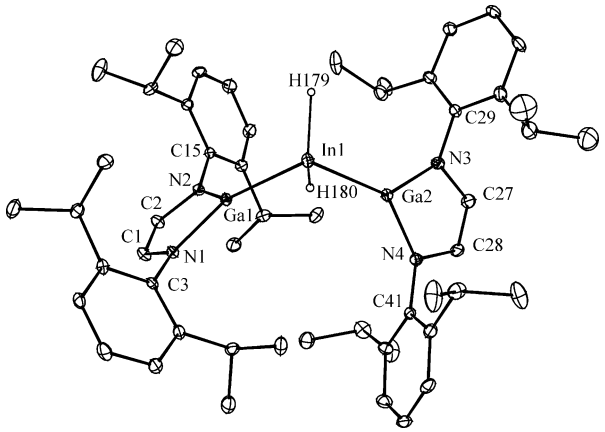


Figure 2. Structure of the anionic component of **4**. Selected bond lengths [Å] and angles [°]: In1-Ga2 2.5921(8), In1-Ga1 2.5983(8), In1-H179 1.72(2), In1-H180 1.73(2), Ga1-N1 1.896(4), Ga1-N2 1.883(4), Ga2-N3 1.885(5), Ga2-N4 1.880(5), N1-C1 1.400(7), N2-C2 1.383(7), N3-C27 1.405(7), N4-C28 1.394(7), C1-C2 1.331(7), C27-C28 1.336(8), Ga1-In1-Ga2 103.19(3), Ga2-In1-H179 101(2), Ga1-In1-H179 108(2), Ga2-In1-H180 110(2), Ga1-In1-H180 110(2), H179-In1-H180 123(3), N2-Ga1-N1 86.09(18), N3-Ga2-N4 86.8(2), N2-Ga1-In1 136.44(13), N1-Ga1-In1 137.39(13), N3-Ga2-In1 135.11(14), N4-Ga2-In1 138.08(14).

The Ga–Ga bonds in **3** (2.4071(9) Å) are normal for single, covalent Ga–Ga interactions (cf. 2.4232(7) Å in [(GaI{N-(*t*Bu)C(H)}$_2$)$_2$])[8] but significantly shorter than the only structurally characterized Ga→Ga dative interaction, that is, 2.506(3) Å in [(Tp$^{t\mathrm{Bu}_2}$)Ga→GaI$_3$], Tp$^{t\mathrm{Bu}_2}$ = tris(3,5-di-*tert*-butylpyrazolyl)hydroborate.[16] There are no crystallographically characterized examples of Ga–In interactions for comparison with **4** but the average Ga–In bond length in this compound, 2.595 Å, is well within the sum of the covalent radii, 2.75 Å, for these two elements.[17] Although of low accuracy, the M–H bond lenghts in **3** and **4** are similar to those in previously reported adducts of MH$_3$, M = Ga or In.[10,13] Finally, an examination of the geometry of the heterocycles in **3** and **4** reveals that they have significantly shorter Ga–N bond lengths (**3** av. = 1.882 Å, **4** av. = 1.886 Å) and more obtuse N-Ga-N angles (**3** 86.98(16)°, **4** av. = 86.44°) than those in the free gallium(I) heterocycle (Ga–N av. = 1.970 Å, N-Ga-N 83.02(11)°).[8] In fact, these values are close to those observed in related gallium(II)-diazabutadiene complexes, for example, [(GaI{N(*t*Bu)C(H)}$_2$)$_2$],[8] and arise from a loss of charge from the heterocyclic Ga centres to the central MH$_2$ fragment upon formation of **3** and **4**. It is noteworthy that a similar shortening of the Ga–N bond lengths in gallium donor ligand of [(Tp$^{t\mathrm{Bu}_2}$)Ga→GaI$_3$] occurs upon complex formation.

This effect in **3** and **4** has been examined by preliminary Density Functional calculations[18] which have been carried out on the model anions, [MH$_2$(Ga{NC(Me)C(H)}$_2$)$_2$]$^-$, M = Ga (**5**) or In (**6**). The fully optimized geometries of these compounds are similar to those of the anions in **3** and **4** taking into account the steric differences between the theoretical and experimental situations. Significantly, the Ga–N distances (**5** av. = 1.900 Å, **6** av. = 1.900 Å) and the N-Ga-N angles (**5** av = 85.66°, **6** av. = 85.74°) are comparable with those in **3**, **4** and Ga^{II} diazabutadiene complexes. In addition, there is a significant development of negative charge on the central metal atoms and MH$_2$ fragments (**5** M–0.35, MH$_2$–0.77; **6** M–0.09, MH$_2$–0.63) relative to the gallium atoms of the heterocycles (**5** av. = +1.04, **6** av. = +0.96).

In summary, we have prepared the first covalently bonded metal complexes derived from an anionic gallium carbene analogue, one of which contains the first example of a structurally authenticated In–Ga bond. The remarkable thermal stability of these complexes suggests that gallium(I) heterocycles such as **1** should prove to be versatile ligands towards both main-group and transition-metal fragments, especially considering the importance of their isoelectronic NHC counterparts in coordination chemistry. We are currently exploring this potential in addition to examining the controlled decomposition of **3** and **4** in solution and will report on these studies in forthcoming publications.

Experimental Section

3: A solution of [:Ga{NC(Ar)C(H)}$_2$][K(tmeda)] (0.50 g, 0.84 mmol) in Et$_2$O (15 cm^3) was added to a solution of [GaH$_3$(quinuclidine)] (0.08 g, 0.43 mmol) in Et$_2$O (10 cm^3) at −78 °C over 5 mins. The resulting suspension was allowed to warm to 25 °C, filtered and the filtrate concentrated to about 10 cm^3. Slow cooling of the filtrate to −35 °C yielded yellow crystals of **3**, (0.39 g, 71 %). m.p. 128–131 °C (decomp.); ^{1}H NMR (400 MHz, C$_6$D$_6$, 298 K): δ = 1.00 (d, 24 H, ^3J(H,H) = 6.8 Hz, CH$_3$), 1.20 (d, 24 H, ^3J(H,H) = 6.9 Hz, CH$_3$), 1.75 (s, 24 H, NCH$_3$), 1.89 (s, 8 H, NCH$_2$), 2.17 (br. s, 2 H, GaH$_2$), 3.56 (sept., 8 H, ^3J(H,H) = 6.8 Hz, CH), 6.19 (s, 4 H, NCH), 6.96 (t, 4 H, ^3J(H,H) = 7.3 Hz, *p*-ArH), 7.07 ppm (d, 8 H, ^3J(H,H) = 7.6 Hz, *m*-ArH); ^{13}C NMR (100.6 MHz, C$_6$D$_6$, 298 K): δ = 23.3 (CH$_3$), 24.2 (CH$_3$), 26.7 (CH), 44.2 (NCH$_3$), 56.2 (NCH$_2$), 120.9 (CN), 121.6 (*m*-ArC), 123.5 (*p*-ArC), 145.2 (*o*-ArC), 146.1 ppm (*ipso*-ArC); IR (Nujol): $\tilde{\nu}$ = 1769 cm^{-1} (br. s, Ga-H); MS/APCI *m*/*z* (%): 377 [(ArNC)$_2$H$^+$, 100]. **4**: A solution of [:Ga{NC(Ar)C(H)}$_2$][K(tmeda)] (0.50 g, 0.84 mmol) in Et$_2$O (15 cm^3) was added over 5 mins to a solution of [InH$_3$(NMe$_3$)], generated in situ (0.42 mmol) in Et$_2$O (10 cm^3), at −78 °C. The resulting suspension was allowed to warm to −30 °C and kept at this temperature for 24 h, after which it was filtered, and the filtrate was warmed to −15 °C and concentrated to about 10 cm^3. Slow cooling of the filtrate to −35 °C yielded yellow crystals of **4**, (0.33 g, 63 %). m.p. 116–118 °C (decomp.); ^{1}H NMR (100.6 MHz, CD$_2$Cl$_2$, 243 K): δ = 0.85 (d, 24 H, ^3J(H,H) = 6.6 Hz, CH$_3$), 1.08 (d, 24 H, ^3J(H,H) = 6.6 Hz, CH$_3$), 2.18 (s, 24 H, NCH$_3$), 2.34 (s, 8 H, NCH$_2$), 2.93 (br. s, 2 H, InH$_2$), 3.27 (sept., 8 H, ^3J(H,H) = 6.6 Hz, CH), 5.86 (s, 4 H, NCH), 7.03 ppm (m, 12 H, *p*-ArH and *m*-ArH); ^{13}C NMR (100.6 MHz, CD$_2$Cl$_2$, 243 K): δ = 24.0 (CH$_3$), 25.4 (CH$_3$), 27.5 (CH), 46.6 (NCH$_3$), 57.1 (NCH$_2$), 121.3 (CN), 122.5 (*m*-ArC), 123.9 (*p*-ArC), 145.8 (*o*-ArC), 146.8 ppm (*ipso*-ArC); IR (Nujol): $\tilde{\nu}$ = 1632 cm^{-1} (br. s, In-H); MS/APCI *m*/*z* (%): 377 [(ArNC)$_2$H$^+$, 100]. Reproducible elemental analyses of **3** and **4** could not be obtained because of the highly air and moisture sensitive nature of these compounds.

Received: February 26, 2003 [Z51281]

Keywords: density functional calculations · group 13 elements · hydrides · metal–metal interactions · structure elucidation

[1] A. Schnepf, H. Schnöckel, *Angew. Chem.* **2002**, *114*, 3682–3704; *Angew. Chem. Int. Ed.* **2002**, *41*, 3532–3552, and references therein.

[2] G. Linti, H. Schnöckel, *Coord. Chem. Rev.* **2000**, *206–207*, 285–319, and references therein.

[3] C. Cui, H. W. Roesky, H.-G. Schmidt, M. Noltemeyer, H. Hao, F. Cimpoesu, *Angew. Chem.* **2000**, *112*, 4444 – 4446; *Angew. Chem. Int. Ed.* **2000**, *39*, 4274 – 4276.
[4] N. J. Hardman, B. E. Eichler, P. P. Power, *Chem. Commun.* **2000**, 1991 – 1992.
[5] N. J. Hardman, R. J. Wright, A. D. Phillips, P. P. Power, *J. Am. Chem. Soc.* **2003**, *125*, 2667 – 2679.
[6] N. J. Hardman, P. P. Power, J. D. Gorden, C. L. B. Macdonald, A. H. Cowley, *Chem. Commun.* **2001**, 1866 – 1867.
[7] a) E. S. Schmidt, A. Jockisch, H. Schmidbaur, *J. Am. Chem. Soc.* **1999**, *121*, 9758 – 9759; b) E. S. Schmidt, A. Schier, H. Schmidbaur, *J. Chem. Soc. Dalton Trans.* **2001**, 505 – 507.
[8] R. J. Baker, R. D. Farley, C. Jones, M. Kloth, D. M. Murphy, *J. Chem. Soc. Dalton Trans.* **2002**, 3844 – 3850.
[9] W. A. Herrmann, *Angew. Chem.* **2002**, *114*, 1342 – 1363; *Angew. Chem. Int. Ed.* **2002**, *41*, 1290 – 1309, and references therein.
[10] C. Jones, *Chem. Commun.* **2001**, 2293 – 2298, and references therein.
[11] full synthetic and spectroscopic data for compound **2** have been submitted as supplementary material.
[12] Crystal data for **2**.DME: $C_{72}H_{122}GaKN_4O_{10}$ $M = 1312.56$, triclinic, space group $P\bar{1}$, $a = 13.143(3)$, $b = 14.958(3)$, $c = 19.431(4)$ Å, $\alpha = 82.72(3)$, $\beta = 85.37(3)$, $\gamma = 86.19(3)°$, $V = 3770.7(13)$ Å^3, $Z = 2$, $\rho_{calcd.} = 1.156$ g cm^{-3}, $F(000) = 1424$, $\mu Mo_{K\alpha} = 0.475$ mm^{-1}, $T = 150(2)$ K, 16894 unique reflections [$R_{int} = 0.0801$], R (on F) 0.0596, wR (on F^2) 0.1172 ($I > 2\sigma(I)$); **3**.C_6H_{14}: $C_{70}H_{120}Ga_3KN_8$ $M = 1322.00$, monoclinic, space group $C2/c$, $a = 21.747(4)$, $b = 14.984(3)$, $c = 26.082(5)$ Å, $\beta = 112.91(3)°$, $V = 2191.5(8)$ Å^3, $Z = 4$, $\rho_{calcd.} = 1.122$ g cm^{-3}, $F(000) = 2832$, $\mu Mo_{K\alpha} = 1.118$ mm^{-1}, $T = 150(2)$ K, 6949 unique reflections [$R_{int} = 0.0513$], R (on F) 0.0647, wR (on F^2) 0.1729 ($I > 2\sigma(I)$); **4**: $C_{64}H_{106}Ga_2InLiN_8$ $M = 1248.77$, monoclinic, space group $P2_1$, $a = 13.113(3)$, $b = 20.708(4)$, $c = 26.528(5)$ Å, $\beta = 103.19(3)°$, $V = 7013(2)$ Å^3, $Z = 4$, $\rho_{calcd.} = 1.183$ g cm^{-3}, $F(000) = 2640$, $\mu Mo_{K\alpha} = 1.129$ mm^{-1}, $T = 150(2)$ K, 22113 unique reflections [$R_{int} = 0.0673$], R (on F) 0.0442, wR (on F^2) 0.0860 ($I > 2\sigma(I)$). CCDC-204734 **2**, CCDC-204735 **3**, CCDC-204736 **4** contain the supplementary crystallographic data for this paper. These data can be obtained free of charge via www.ccdc.cam.ac.uk/conts/retrieving.html (or from the Cambridge Crystallographic Data Centre, 12 Union Road, Cambridge CB2 1EZ, UK; fax: (+44) 1223-336-033; or deposit@ccdc.cam.ac.uk).
[13] C. Jones, G. A. Koutsantonis, C. L. Raston, *Polyhedron* **1993**, *12*, 1829 – 1848.
[14] G. Linti, A. Rodig, W. Kostler, *Z. Anorg. Allg. Chem.* **2001**, *627*, 1465 – 1476.
[15] W. Uhl, F. Schmock, G. Geisler, *Z. Anorg. Allg. Chem.* **2002**, *628*, 1963 – 1966.
[16] M. C. Kutchta, J. B. Bonanno, G. Parkin, *J. Am. Chem. Soc.* **1996**, *118*, 10914 – 10915.
[17] J. Emsley, *The Elements*, 2nd ed., Clarendon, Oxford, **1991**, p. 77, 91.
[18] Geometries of **5** and **6** were optimized in Gaussian 98 by using the mPW91 functional with the 6-311 + G(d) basis set on Ga, C, N, and H atoms and LANL2DZ basis set and core potential for In. Atomic charge, orbital population, and bonding analyses were carried out by using the NBO scheme. See supplementary material for full details.

 © 2003 Wiley-VCH Verlag GmbH & Co. KGaA, Weinheim

Containers for Cations

Membership Rules for a Molecular Box: The Admission Process and Protection Provided to Guest Molecules**

*Sodio C. N. Hsu, Maya Ramesh, James H. Espenson, and Thomas B. Rauchfuss**

Molecular containers are the smallest possible agents for sensing, sorting, and sequestering ions and molecules.[1] Molecular cages based on transition-metal vertices often easily self-assemble, and those with inorganic frameworks are of special interest because their rigidity, uncommon in organic ligands,[2–5] could give rise to high selectivity with respect to guest size.

Prussian Blue (PB) and its variants[6–8] are insoluble cyanometallate polymers consisting of boxlike subunits that exhibit ion-exchange behavior. We and others have previously described molecular PB analogues with encapsulated cations.[9–12] Lacking so far, however, are examples of empty (or voided) ionophilic boxes, which could provide insights into the ion-inclusion process, which is fundamentally relevant to the behavior of PB analogues and the design of a new class of ion-sequestering agents.[13]

We have previously reported that the cage $[Cs\subset\{CpCo(CN)_3\}_4(Cp^*Ru)_4]^+$ ($\mathbf{Cs\subset Co_4Ru_4^+}$; $Cp^* = C_5Me_5$, $Cp = C_5H_5$) forms by the cesium-ion templated condensation of $[CpCo(CN)_3]^-$ and $[Cp^*Ru(NCMe)_3]^+$.[14] When the cesium ion is omitted from this recipe, an intractable mixture is obtained. Herein we report that when mediated by the templating ion $EtNH_3^+$ self-assembly indeed proceeds to give the empty molecular box $[\{CpCo(CN)_3\}_4(Cp^*Ru)_4]$ ($\mathbf{Co_4Ru_4}$) in high purity and good yield (Figure 1).

In contrast to $EtNH_3^+$, $MeNH_3^+$ templates self-assembly with inclusion to form $\mathbf{MeNH_3\subset Co_4Ru_4^+}$. The high selectivity of these molecular containers is highlighted by comparison of the van der Waals volumes of the $MeNH_3^+$ (43.3 Å^3) and $EtNH_3^+$ (60.2 Å^3) ions.

In addition to ESI-MS and ^{1}H NMR spectroscopy, $\mathbf{Co_4Ru_4}$ was also characterized crystallographically, the results of which indicate that the cage interior is indeed empty, despite its large volume ($\approx$135 Å^3 based on internuclear distances). The availability for the first time of an empty ionophilic box enables the study of ion binding with respect to kinetic and

[*] Prof. Dr. T. B. Rauchfuss, Dr. S. C. N. Hsu, Dr. M. Ramesh
Department of Chemistry
University of Illinois at Urbana-Champaign
Urbana, IL 61801 (USA)
Fax: (+1) 217-333-2685
E-mail: rauchfuz@uiuc.edu
Prof. Dr. J. H. Espenson
Ames Laboratory, Department of Chemistry
Iowa State University, Ames, IA 50011 (USA)

[**] This research was funded by the US Department of Energy.

Supporting information (kinetic data) for this article is available on the WWW under http://www.angewandte.org or from the author.

 DOI: 10.1002/anie.200219562 © 2003 Wiley-VCH Verlag GmbH & Co. KGaA, Weinheim

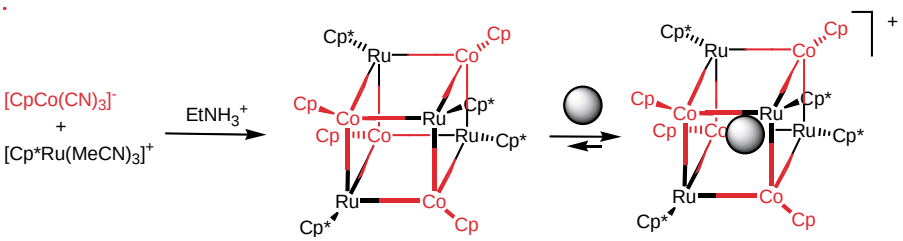


Figure 1. Formation of empty and filled molecular boxes; ● = $N_2H_5^+$, $MeNH_3^+$, NH_4^+, Cs^+, K^+, Rb^+, Tl^+; — = −CN.

thermodynamic selectivities. We found that $\mathbf{Co_4Ru_4}$ readily binds K^+, Rb^+, Cs^+, Tl^+, NH_4^+, $MeNH_3^+$, and $N_2H_5^+$ ions (see Figure 1) but not the smaller Na^+ ion ($r_{ionic} = 1.16$ Å) or divalent cations.

The kinetic selectivity of $\mathbf{Co_4Ru_4}$ was probed by treatment of THF solutions of $\mathbf{Co_4Ru_4}$ with an MeCN solution equimolar in KPF_6 and CsOTf (OTf = CF_3SO_3) and then monitoring the process by NMR spectroscopy or ESI-MS spectrometry. These reactions rapidly formed $\mathbf{K{\subset}Co_4Ru_4^+}$ together with ≈3% $\mathbf{Cs{\subset}Co_4Ru_4^+}$. Whereas the K^+ ion inserts more rapidly, $\mathbf{Cs{\subset}Co_4Ru_4^+}$ is the only complex detected after seven days (Figure 2a,b). We propose that the smaller size of the K^+ ion ($r_{ionic} = 1.52$ Å) facilitates its insertion, but as a result of a better fit (ionic radius versus box volume) and affinity for π CN ligands,[15,16] the Cs^+ ion ($r_{ionic} = 1.81$ Å) is thermodynamically preferred. In another ion-competition experiment, the cation of NH_4PF_6 ($r_{ionic} \approx 1.75$ Å)[17] was shown to insert at approximately the same rate as that of CsOTf, but subsequent equilibration is immeasurably slow. For $MeNH_3BF_4$ versus CsOTf, the $MeNH_3^+$ ion inserts faster than the Cs^+ ion, although there is a subsequent slower conversion into $\mathbf{Cs{\subset}Co_4Ru_4^+}$ (Figure 2c,d).

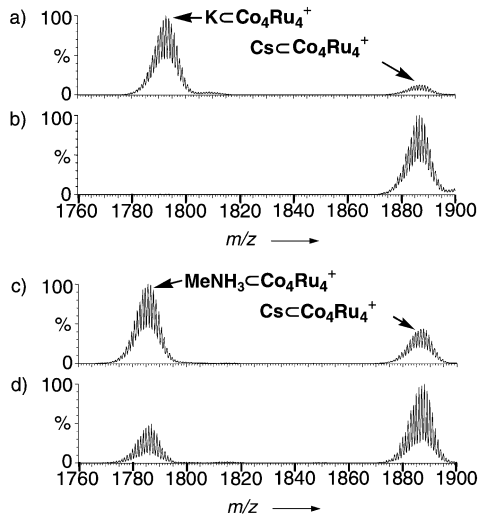


Figure 2. Electrospray mass spectra for a 0.0057 M MeCN solution of $\mathbf{Co_4Ru_4}$ upon treatment with 2 equivalents each of KPF_6 and CsOTf after 10 min (a) and after seven days (b), and after treatment with two equivalents each of $MeNH_3BF_4$ and CsOTf after 10 min (c) and after seven days (d).

In terms of mechanism, the collective evidence points to ion insertion into $\mathbf{Co_4Ru_4}$ through a $\{Co_2Ru_2(CN)_4\}$ "window". The differing kinetic and thermodynamic selectivities of $\mathbf{Co_4Ru_4}$ (see above) can best be explained if the cage remains intact during ion insertion. Labeling experiments are consistent with this view. We found that THF solutions of $\mathbf{Co_4Ru_4}$ and its close analogue $[\{CpCo(CN)_3\}_4\{(C_5Me_4Et)Ru\}_4]$ ($\mathbf{Co_4Ru_4'}$) reacted with CsOTf to give $\mathbf{Cs{\subset}Co_4Ru_4^+}$ (*m*/*z*: 1886) and $\mathbf{Cs{\subset}Co_4Ru_4'^+}$ (*m*/*z*: 1942), respectively. Products of scrambling, such as $[Cs{\subset}\{CpCo(CN)_3\}_4(Cp^*Ru)_3\{(C_5Me_4Et)Ru\}]^+$ were not observed. The results of these labeling experiments could also be explained if insertion of the Cs^+ ion occurred by rupture of a single Ru–N bond followed by admission of the Cs^+ ion through this opening in an otherwise intact box. Arguing against labile Ru–N linkages is the inertness of $\mathbf{Co_4Ru_4}$ towards Et_4NCN; it is very unlikely that any exposed ruthenium site could resist attack by the CN^- ion, an extremely potent nucleophile.

Kinetic measurements revealed that the rate of conversion of $\mathbf{K{\subset}Co_4Ru_4^+}$ into $\mathbf{Cs{\subset}Co_4Ru_4^+}$ slowed during the course of the reaction, which reflects the build-up of free K^+ ions that increasingly compete with the entering Cs^+ ions [Eq. (1) and (2)].

$$\mathbf{K{\subset}Co_4Ru_4^+} \underset{k_{-1}}{\overset{k_1}{\rightleftharpoons}} K^+ + \mathbf{Co_4Ru_4} \qquad (1)$$

$$Cs^+ + \mathbf{Co_4Ru_4} \xrightarrow{k_2} \mathbf{Cs{\subset}Co_4Ru_4^+} \qquad (2)$$

A dissociative ion-exchange process is indicated, whereby the rate-limiting step is loss of the K^+ ion from $\mathbf{K{\subset}Co_4Ru_4^+}$ followed by uptake of the Cs^+ ion. A rate equation for the kinetic model describing this two-step process can be formulated, provided k_{-1}/k_2 is known (details in Supporting Information). The ratio of the rates of insertion of K^+ and Cs^+ ions into $\mathbf{Co_4Ru_4}$, k_{-1}/k_2, was determined from competition experiments (see above), the rates of ion insertion into $\mathbf{Co_4Ru_4}$ being fast relative to the rate of ion exchange. Plots of $\{(k_{-1}/k_2)[\mathbf{K{\subset}Co_4Ru_4^+}] - a\ln[\mathbf{K{\subset}Co_4Ru_4^+}]\}$ versus time were linear under conditions where $[Cs^+]_0 > 10[\mathbf{K{\subset}Co_4Ru_4^+}]_0$. Four sets of kinetic measurements allowed us to determine $k_1 = 1.2 \times 10^{-4}\ s^{-1}$ (60 °C). The rate of formation of $\mathbf{K{\subset}Co_4Ru_4^+}$ (k_{-1}) was shown to be 135 $s^{-1}M^{-1}$, even at room temperature. From k_1 and this lower bound for k_{-1}, K_K, the binding constant for K^+ ions by $\mathbf{Co_4Ru_4}$ (defined in this case as k_{-1}/k_1), is approximately 10^6. Previous competition experiments on $[M{\subset}\{Cp^*Rh(CN)_3\}_4\{Mo(CO)_3\}_4]^{3-}$ (which cannot be obtained as a voided box) showed that the Cs^+ ion binds $> 10^4$ more strongly than the K^+ ion;[12] extrapolating to the present case, we estimate that K_{Cs} is $> 10^{10}$.

The slow ion-exchange rates and cagelike structure suggest that $\mathbf{Co_4Ru_4}$ should chemically protect its guests. To assess this protection, we examined the H–D exchange of the guest in $\mathbf{NH_4{\subset}Co_4Ru_4^+}$. The ^1H NMR signal for

 © 2003 Wiley-VCH Verlag GmbH & Co. KGaA, Weinheim

$\mathbf{NH_4{\subset}Co_4Ru_4^+}$ appears as a 1:1:1 triplet, indicative of the absence of proton exchange. The signal is unaffected by exposure of the compound to D_2O for several hours, whereas ammonium ions characteristically undergo H–D exchange at diffusion-limited rates at neutral pH value.[18] H–D exchange is accelerated somewhat in the presence of free ND_4BF_4, and is complete in around 25 h at room temperature in MeCN solution. Deuteration occurs by proton transfer, not by exchange of the ammonium ions since we can detect the initial formation of $\mathbf{NDH_3{\subset}Co_4Ru_4^+}$, as indicated by its distinctive coupling pattern in the ^{1}H NMR spectrum. The guest cation in $\mathbf{NH_4{\subset}Co_4Ru_4^+}$ is completely unaffected by quinuclidine, which is a stronger base than ammonia (pK_a = 19.56 vs. 16.46).[19] ^{14}N and ^{1}H NMR measurements (Figure 3) show that H–D exchange between ND_4^+ and $\mathbf{MeNH_3{\subset}Co_4Ru_4^+}$ is also slow.

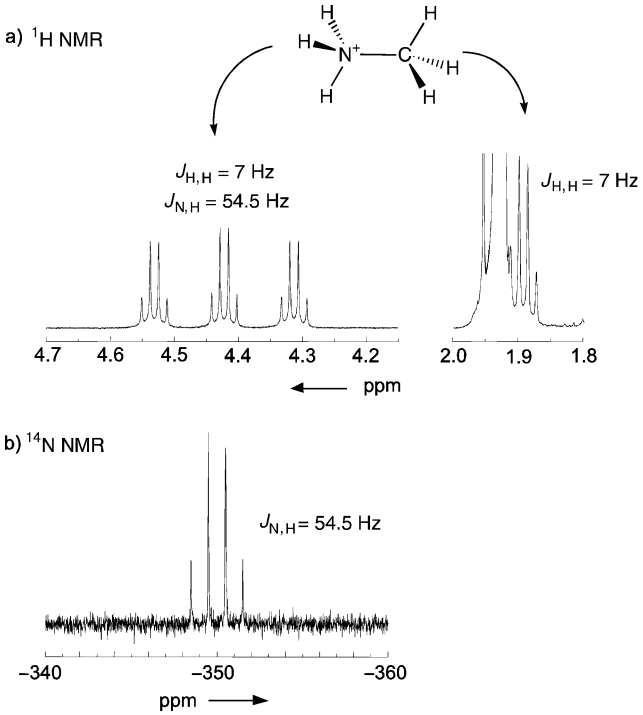


Figure 3. a) 500 MHz ^{1}H NMR spectrum of $\mathbf{MeNH_3{\subset}Co_4Ru_4^+}BF_4^-$, b) ^{14}N NMR spectrum of $\mathbf{MeNH_3{\subset}Co_4Ru_4^+}BF_4^-$ (in CD_3CN).

To summarize, an ionophilic molecular box has been synthesized with the aid of a templating ion. The kinetic and thermodynamic selectivities are distinctive, in large measure because of the pronounced effects of atomic size on the binding and ion-exchange rates. The cage indeed shields guest ions from reagents in the surrounding solution.

Experimental Section

Co_4Ru_4: A solution of PPN[$CpCo(CN)_3$] (290 mg, 0.39 mmol; PPN = triphenyl[(triphenylphosphanylidene)amino]phosphonium) and $EtNH_3BF_4$ (13 mg, 0.10 mmol) in MeCN (50 mL) was added to a solution of [$Cp^*Ru(NCMe)_3$]PF_6 (197 mg, 0.39 mmol) in MeCN (20 mL). After 5 h, the red microcrystals were collected and then extracted into Et_2O (50 mL). Evaporation gave dark red microcrystals, yield: 140 mg (80%). ^{1}H NMR ([D_8]THF; 500 MHz): δ = 1.67 (s, 60H), 5.35 ppm (s, 20H). ESI-MS (*m*/*z*): 1754 ([H{$CpCo(CN)_3$}$_4$($Cp^*Ru)_4$]$^+$). FAB (*m*/*z*): 1753 ([{$CpCo(CN)_3$}$_4$-($Cp^*Ru)_4$]$^+$). Elemental analysis (%) calcd for $C_{72}H_{80}Co_4N_{12}Ru_4$: C 49.32, H 4.60, N 9.59; found: C 49.01, H 4.93, N 9.78

$MeNH_3{\subset}Co_4Ru_4$: A solution of PPN[$CpCo(CN)_3$] (290 mg, 0.39 mmol) and $MeNH_3BF_4$ (12 mg, 0.10 mmol) in MeCN (50 mL) was added to a solution of [$Cp^*Ru(NCMe)_3$]PF_6 (197 mg, 0.39 mmol) in MeCN (20 mL). After 2 h, the solvent volume was reduced (to approximately 10 mL) to produce dark-red microcrystals of [$MeNH_3{\subset}${$CpCo(CN)_3$}$_4$($Cp^*Ru)_4$]PF_6, which were washed with cold MeCN (2 mL); yield: 135 mg (71%). IR (KBr): $\tilde{\nu}_{CN}$ = 2158, 2127 cm^{-1}; ^{1}H NMR (CD_3CN): δ = 1.66 (s, 60H), 1.89 (q, $J_{H,H}$ = 7 Hz, 3H; $CH_3NH_3^+$), 4.09 (q of t, $J_{H,H}$ = 7 Hz, $J_{N,H}$ = 55 Hz, 3H; $CH_3NH_3^+$), 5.57 ppm (s, 20H); ^{14}N NMR ([D_6]acetone, vs. MeCN;): δ = −71.65 (Co-CN-Ru), −349.9 ppm (q, $CH_3NH_3^+$, $J_{N,H}$ = 55 Hz); ESI-MS *m*/*z* 1786 ([$MeNH_3{\subset}${$CpCo(CN)_3$}$_4$($Cp^*Ru)_4$]$^+$); elemental analysis (%) calcd for $C_{73}H_{86}Co_4F_6N_{13}PRu_4$: C 45.42, H 4.49, N 9.43; found: C 45.36, H 4.66, N 9.57. The same species can be synthesized by treatment of a solution of **Co_4Ru_4** with $MeNH_3BF_4$.

Ion Competition Experiments: **Co_4Ru_4** with CsO_3SCF_3 versus KPF_6. (similar for Cs^+ versus $MeNH_3^+$ and Cs^+ versus NH_4^+). A solution of **Co_4Ru_4** (10 mg, 0.0057 mmol) in THF (10 mL) was added in one portion to a well-stirred homogeneous solution of both CsO_3SCF_3 (3.2 mg, 0.0114 mmol) and KPF_6 (2.1 mg, 0.0114 mmol) in MeCN (1 mL). The reaction was monitored by ESI-MS (sample concentration = 10^{-11} mol μL^{-1}). Experiments were run in duplicate.

Kinetics of ion exchange: The differential and integrated rate laws for the kinetic model in Equations (1) and (2) are:

$$d[\mathbf{Cs{\subset}Co_4Ru_4^+}]/dt = (k_1[\mathbf{K{\subset}Co_4Ru_4^+}][Cs^+])/\{(k_{-1}/k_2)[K^+] + [Cs^+]\}$$

integrating:

$$(k_{-1}/k_2)[\mathbf{K{\subset}Co_4Ru_4^+}] - a(\ln[\mathbf{K{\subset}Co_4Ru_4^+}]) = -k_1[Cs^+]t + X$$

where

$$a = [Cs^+]_0 + (k_{-1}/k_2)[\mathbf{K{\subset}Co_4Ru_4^+}]_0$$

$$k_{-1}/k_2 = 32.8 \text{ (in THF:6 MeCN)}$$

$$X = (k_{-1}/k_2)[\mathbf{K{\subset}Co_4Ru_4^+}]_0 - a(\ln[\mathbf{K{\subset}Co_4Ru_4^+}]_0)$$

The value of k_{-1}/k_2 = 32.8 was obtained by addition of a solution of **Co_4Ru_4** to a solution equimolar in KPF_6 and CsOTf (where $[K^+]_0 = [Cs^+]_0 \gg [\mathbf{Co_4Ru_4}]_0$) in 1:6 THF:$CD_3CN$ solution followed by integration of the C_5H_5 NMR signals at δ = 5.605 and 5.609 ppm. The measurements were taken for $[Co_4Ru_4]$:([KPF_6] or [CsOTf]) = 1:2, 1:3, and 1:4. Kinetic rate measurements were monitored for 12 h at 60 °C in 1:6 THF:CD_3CN solvent mixture. All four experiments employed 2.21×10^{-3} M [$\mathbf{K{\subset}Co_4Ru_4^+}]_0$; measurements where $[Cs^+]_0$ was 0.0221, 0.0663 M, 0.0884 M, and 0.1105 M gave $k_1 = 1.2 \times 10^{-4}$ s^{-1}. Crystal data: $C_{90}H_{107}Co_4N_{21}Ru_4$, M_r2122.97, cubic, *I*23; $a = b = c$ = 18.014(3) Å; $\alpha = \beta = \gamma = 90°$; V = 5872(3) Å^3; Z = 2; ρ_{calcd} = 1.206 Mg m^{-3}, $F(000)$ = 2156, 175 parameters: $R1$ = 0.0408, $wR2$ = 0.963, GOF = 1.007 for all 1798 data ($I > 2\sigma(I)$). Single crystals of **Co_4Ru_4** were mounted on glass fibers using Paratone-N (Exxon) and were analyzed on a Siemens Platform/CCD automated diffractometer at 193 K. Data were processed using SAINT.[20] The structures were solved using direct methods and refined using full-matrix least-squares analysis on F^2 using the program SHELXTL.[21] Hydrogen atoms were fixed in idealized positions with thermal parameters 1.2 times those of the attached carbon atoms. Data were corrected for absorption on the basis of integration. CCDC-187755 contains the supplementary crystallographic data for this paper. These data can be obtained free of charge via www.ccdc.cam.ac.uk/conts/retrieving.html (or from the Cambridge Crystallographic Data Centre, 12 Union Road, Cambridge CB2 1EZ, UK; fax: (+44) 1223-336-033; or deposit@ccdc.cam.ac.uk).

Received: June 19, 2002
Revised: January 15, 2003 [Z19562]

 © 2003 Wiley-VCH Verlag GmbH & Co. KGaA, Weinheim

Keywords: cage compounds · cations · cobalt · cyanide · host–guest systems · ruthenium

[1] D. J. Cram, *Nature* **1992**, *356*, 29.
[2] J.-M. Lehn, *Supramolecular Chemistry*, VCH, Weinheim, **1995**.
[3] F. Vögtle, *Supramolecular Chemistry*, Wiley, New York, **1991**.
[4] F. Hof, S. L. Craig, C. Nuckolls, J. Rebek, Jr., *Angew. Chem.* **2002**, *114*, 1556; *Angew. Chem. Int. Ed.* **2002**, *41*, 1488.
[5] P. V. Bonnesen, T. J. Haverlock, N. L. Engle, R. A. Sachleben, B. A. Moyer, *ACS Symp. Ser.* **2000**, *757*, 26.
[6] A. G. Sharpe, *The Chemistry of Cyano Complexes of the Transition Metals*, Academic Press, London, **1976**.
[7] F. Herren, P. Fischer, A. Ludi, W. Hälg, *Inorg. Chem.* **1980**, *19*, 956.
[8] K. R. Dunbar, R. A. Heintz, *Prog. Inorg. Chem.* **1997**, *45*, 283.
[9] K. K. Klausmeyer, T. B. Rauchfuss, S. R. Wilson, *Angew. Chem.* **1998**, *110*, 1808; *Angew. Chem. Int. Ed.* **1998**, *37*, 1694.
[10] S. M. Contakes, K. K. Klausmeyer, R. M. Milberg, S. R. Wilson, T. B. Rauchfuss, *Organometallics* **1998**, *17*, 3633.
[11] J. L. Heinrich, P. A. Berseth, J. R. Long, *Chem. Commun.* **1998**, 1231.
[12] K. K. Klausmeyer, S. R. Wilson, T. B. Rauchfuss, *J. Am. Chem. Soc.* **1999**, *121*, 2705.
[13] K. L. Nash, R. E. Barrans, R. Chiarizia, M. L. Dietz, M. P. Jensen, P. G. Rickert, B. A. Moyer, P. V. Bonnesen, J. C. Bryan, R. A. Sachleben, *Solvent Extr. Ion Exch.* **2000**, *18*, 605.
[14] S. M. Contakes, M. L. Kuhlman, M. Ramesh, S. R. Wilson, T. B. Rauchfuss, *Proc. Natl. Acad. Sci. USA* **2002**, *99*, 4889.
[15] J. C. Bryan, K. Kavallieratos, R. A. Sachleben, *Inorg. Chem.* **2000**, *39*, 1568.
[16] G. W. Gokel, L. J. Barbour, R. Ferdani, J. Hu, *Acc. Chem. Res.* **2002**, *35*, 878.
[17] R. D. Shannon, *Acta Crystallogr. Sect. A* **1976**, *32*, 751.
[18] C. L. Perrin, T. J. Dwyer, P. Baine, *J. Am. Chem. Soc.* **1994**, *116*, 4044.
[19] K. Izutsu, *Acid–Base Dissociation Constants in Dipolar Aprotic Solvents, Vol. 35*, Blackwell, Oxford, **1990**.
[20] Bruker AXS, Inc., Madison, WI (USA), **2001**.
[21] G. M. Sheldrick, University of Göttingen, Göttingen (Germany), **1997**.

 © 2003 Wiley-VCH Verlag GmbH & Co. KGaA, Weinheim

Viruslike DNA Particles

Targeted Gene Delivery to Cancer Cells: Directed Assembly of Nanometric DNA Particles Coated with Folic Acid**

Guy Zuber, Liliane Zammut-Italiano, Emmanuel Dauty, and Jean-Paul Behr*

This work is dedicated to Marc Zuber and Marie-Hélène Fauré

Gene therapy is gaining credit as a means to fight cancer from an angle other than radio- and chemotherapies.[1] However, it has yet to enjoy any real success because viral vectors are immunogenic, thus excluding repetitive treatment, and because gene delivery is too complex to be achieved with a single carrier molecule.[2] Therefore, effective multicomponent delivery vectors need to be developed.[3–5] The core of synthetic vectors is invariably a polycation capable of inducing condensation of anionic DNA. Conversion of the filiform DNA macromolecule into a compact particle improves both its chemical stability and physical properties. However, DNA compaction by cationic liposomes or polymers is a quasi-irreversible process that leads to the formation of 0.2–1-μm-sized microprecipitates containing hundreds of DNA molecules per particle.[6] For the transfection of cells in culture dishes, large complexes are advantageous because they sediment onto the cells. However, as one would expect, in animal models their gene-delivery properties are weak as a result of size-restricted diffusion.[7] In light of these factors, we have designed a novel synthetic DNA supramolecular assembly with key viral properties, such as diffusion and cell recognition.

We have developed a general method for the monomolecular condensation of genes that leads to a monodisperse and stable population of particles 30 nm in diameter.[8] The technique takes advantage of the condensation of DNA by a cationic cysteine-based detergent. This is a reversible interaction that can be used to drive the system entropically toward the largest number of particles. Particle stability is obtained subsequently by template-assisted oxidative dimerization of the detergent into a gemini lipid (see Figure 1, first two steps). As our goal is for particles to reach distant tumor metastases after injection into the blood stream, particles had to be protected from capture by liver macrophages and had to

[*] Dr. G. Zuber, L. Zammut-Italiano, E. Dauty, J.-P. Behr
Laboratoire de Chimie Génétique associé CNRS/ULP Strasbourg
Faculté de Pharmacie
Route du Rhin, 67401 Illkirch (France)
Fax: (+33) 3-9024-4306
E-mail: zuber@bioorga.u-strasbg.fr

[**] Many thanks to A. Fraley for proofreading of the manuscript and to A.-M. Aubertin and J.-L. Gendrault for access to the electron microscope.

Supporting information for this article is available on the WWW under http://www.angewandte.org or from the author.

 © 2003 Wiley-VCH Verlag GmbH & Co. KGaA, Weinheim DOI: 10.1002/anie.200250446

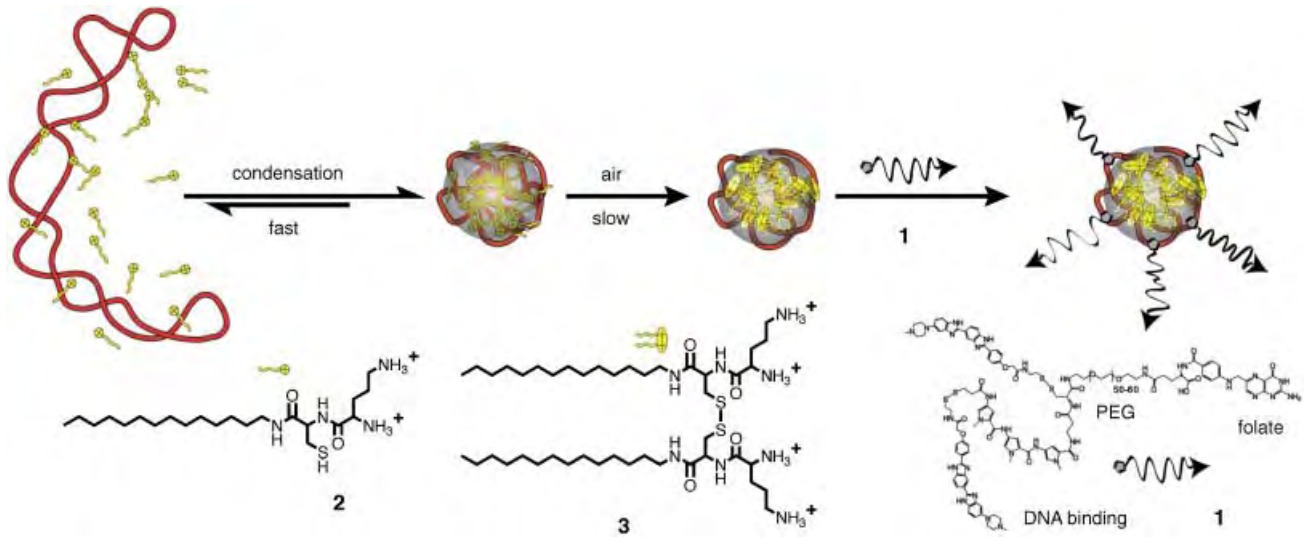
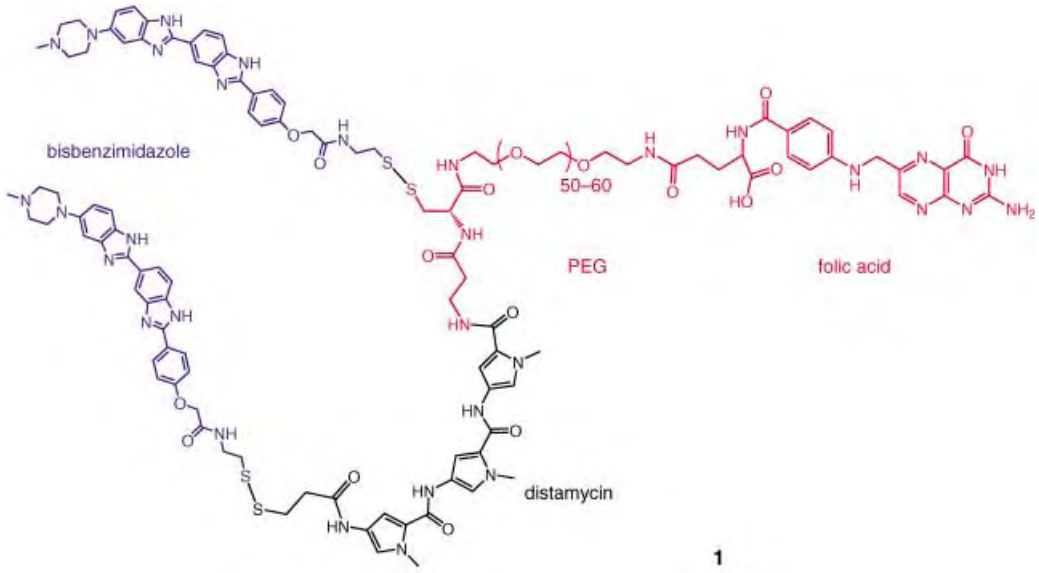


Figure 1. Stepwise assembly of stealth nanometric DNA particles. Plasmid DNA is condensed with a cationic cysteine detergent under aerobic conditions. The resulting gemini lipid–DNA particles are coated with a polyethyleneglycol–folate envelope that is anchored to the DNA by a minor-groove-binding moiety.

be equipped with a ligand that allows binding to and entry into cancer cells.

The biodistribution of different particle types, including liposomes, has been shown to benefit greatly from coating with a layer of polyethyleneglycol (PEG).[9] This effect is a result of the inertness of the polyether backbone, combined with brushtype polymer crowding, which prevents opsonization and capture by macrophages. Fast-dividing cancer cells overexpress the folic acid (vitamin B6) receptor,[10] which is capable of engulfing, besides folic acid, particles as large as the SV40[11] and Ebola viruses.[12] We therefore planned to cover the monomolecular DNA particles with a folate–PEG envelope. The envelope was anchored to the particle surface with a strong DNA-minor-groove-binding agent prepared from distamycin[13] and Hoechst 33258. Finally, as the PEG coat may also interfere with the release of DNA into the cell nucleus, linkages that can be broken by the cytoplasm were introduced into the molecule in the form of reducible disulfide bonds, to give compound **1**.



The synthesis of compound **1** was performed according to standard methods[14] by linking a distamycin central domain to folic acid by means of a commercially available heterobifunctional PEG. For the distamycin portion, the pyrrole amino acids were synthesized and then oligomerized stepwise. Bisbenzimidazole (Hoechst dye 33258) was *O*-alkylated and activated as a 2-pyridyl disulfide derivative. The final compound **1** was obtained by treating the distamycin–PEG–folate conjugate with 2 equivalents of the bisbenzimidazole fragment and purified by HPLC. It was characterized by UV and MALDI-TOF mass spectrometry ($M_w = 4479$ Da).

Preliminary binding studies of **1** to 5.5 Kbp pCMVLuc plasmid DNA were performed by agarose gel electrophoresis (Figure 2, lanes 1–4). Compound **1** induced concentration-dependent DNA retardation and reduced ethidium bromide staining of DNA, both of which are indicative of strong binding. The bulk reducing power inside cells is known to arise from millimolar concentrations of glutathione.[15] As an intracellular reversibility test, **1**–DNA complexes were incubated with 1 mM glutathione. A 15-min incubation period was sufficient to restore ethidium bromide staining and plasmid mobility (Figure 2, lane 4; a slight amount of plasmid retardation and blue fluorescence were observed as a result of some residual bisbenzimidazole binding to the plasmid).

 © 2003 Wiley-VCH Verlag GmbH & Co. KGaA, Weinheim

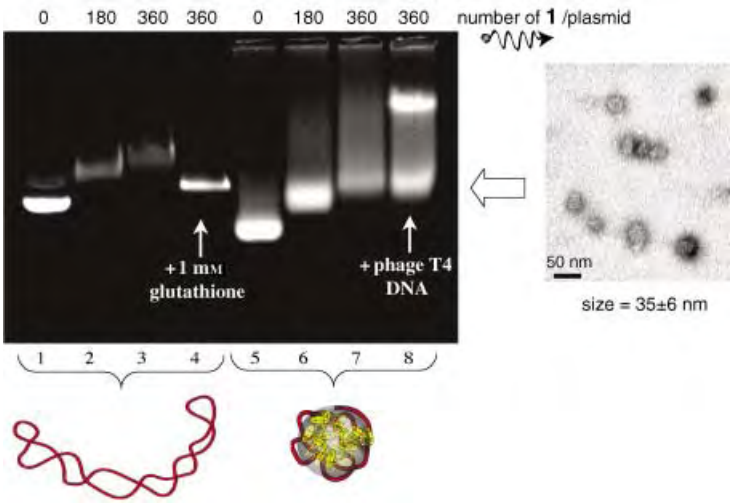


Figure 2. Agarose gel electrophoresis shows complex formation between DNA, the cationic detergent, and compound **1**. Plasmid DNA (30 μM-base pairs (bp), lane 1) was mixed with increasing amounts of **1** (1 μM, lane 2 and 2 μM, lanes 3 and 4). Lane 4: DNA–**1** complexes were incubated for 15 min with glutathione (1 mM). Lanes 5–8: nanometric **3**–DNA particles were prepared as in Figure 1. After overnight incubation, compound **1** (1 μM, lane 6 and 2 μM, lanes 7 and 8) was added to the particles. Lane 8: 1 h incubation of the complexes with phage T4 DNA. Image: Transmission-electron-microscopy picture of the final **3**–DNA–**1** complexes shows monomolecular DNA condensation into compact particles.

The preparation of the monomolecular DNA particles was carried out as described previously.[8] Thus, anionic DNA was condensed with an equimolar charge amount of the cationic detergent ornithyl-cysteine tetradecylamide (**2**), which was allowed to dimerize overnight under aerobic conditions (Figure 1). The electrophoretic mobility of the condensed DNA species through the agarose gel (Figure 2, lane 5) was found to be faster than reptation of the elongated DNA molecule (Figure 2, lane 1). Addition of the bulky conjugate **1** to the particles somewhat decreased their mobility (Figure 2, lanes 6 and 7). **3**–pDNA–**1** particles were stable in the presence of excess DNA (Figure 2, lane 8), thus indicating a quasi-irreversible binding of **1** to the particle surface.

The morphology of the PEG–folate-enveloped particles was observed by transmission electron microscopy[16] (Figure 2). Complexes appeared as a rather homogeneous population ($n = 53$) of compact particles with an average size of 35 ± 6 nm, indicative of monomolecular plasmid-DNA condensation.[17] If it is assumed that every molecule of **1** present binds to the DNA, the enveloped particles prepared as in Figure 2, lane 7 were each coated with 360 molecules of PEG–folate, which corresponds to approximately one PEG polymer per 10 nm^2. Such polymer density is within the range of the so-called "weakly overlapping mushroom regime",[9] and therefore should both provide stealth properties and allow folate-receptor-binding to the particles.

The cellular fate of the particles was tracked by using fluorescence-activated cell sorting (FACS) and confocal microscopy. KB cells derived from a human nasopharyngeal cancer line were chosen as a target because they conditionally express a large number of folic acid receptors upon folic acid starvation. Particles were made fluorescent with the DNA-intercalating dye YOYO (36 molecules/plasmid) and were incubated for 3 h with folate-receptor-expressing KB cells.[18] FACS analysis showed about a tenfold increase over background of the average cellular fluorescence (Figure 3). KB cells that did not overexpress the folate receptor did not show enhanced fluorescence, thus confirming specific and homogeneous folate-receptor-mediated cell binding. The combination of faster diffusion as a result of monomolecular DNA compaction,[19] stability, and cell specificity highlight the potential of these complexes for in vivo gene delivery.

To examine whether binding was followed by endocytosis, 1-μm optical sections were taken through the median plane of the cells by confocal fluorescence microscopy.[20] As shown in Figure 4, complexes ended up in large perinuclear endosomal compartments. A similar picture was observed previously for classical transfection agents such as cationic lipids.[21] However, in contrast to the latter compounds, folate complexes were poor transfection agents (ca. 0.5 pg luciferase/mg cell protein with the pCMVluc plasmid).

In an effort to understand this discrepancy, we studied the cell-binding thermodynamics by FACS. Half saturation of the receptor was obtained for a

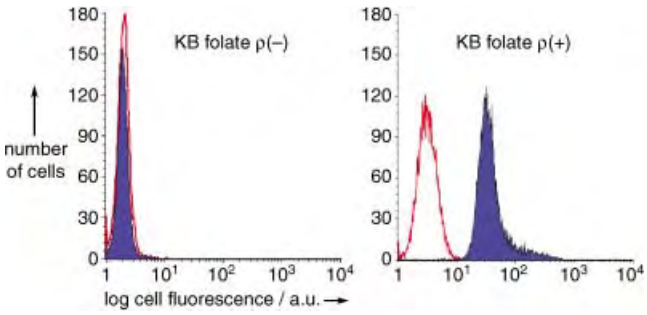


Figure 3. **3**–DNA–**1** complexes specifically bind to folate-receptor-expressing KB cells (KB folate ρ(+)). Cells were incubated for 3 h with fluorescent DNA complexes and sorted by cytometry according to their fluorescence. Only cells overexpressing the folic acid receptor (right graph) show an increased fluorescence (filled trace) over untreated cells (hollow trace).

particle concentration of about 5 nM (Figure 4). This value is close to the affinity measured for folic acid itself,[22] thus ruling out the cooperative binding of each particle to multiple folic acid receptors. The total number of plasmid molecules internalized at saturation (10^5) is within the range that was estimated for cationic lipid-mediated transfection.[21,23] It is therefore unlikely that the observed low transfection level is a result of insufficient cell entry through the folate receptor. However, if the PEG envelope is not removed in endosomes, it may prevent DNA release.

In summary, we have demonstrated that a synthetic DNA supramolecular assembly with diffusion and cell-recognition properties can be built. However, these do not yet exhibit

 © 2003 Wiley-VCH Verlag GmbH & Co. KGaA, Weinheim

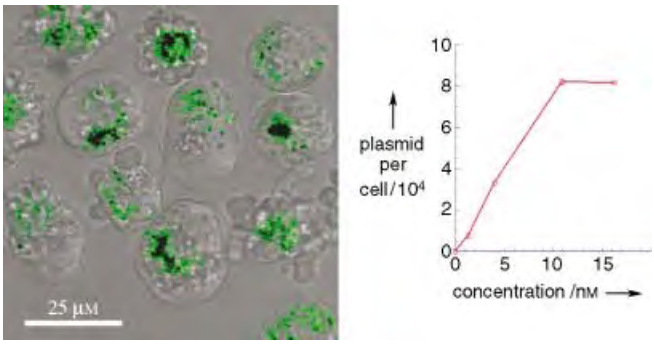


Figure 4. Intracellular fate of the fluorescent **3**–DNA–**1** particles in KB folate ρ(+) cells as shown by confocal microscopy after 3 h incubation. The particle binding isotherm shows an affinity of 5 nM for the receptor and up to 8×10^4 particles internalized per cell.

molecular functions such as endosome release and intracellular trafficking to the nucleus. Classical transfection has been shown to benefit greatly from "proton sponges" able to buffer the acidity of endo- or lysosomes[24] as well as from nuclear-localization-signal peptides conjugated to the DNA.[25,26] Work is currently in progress toward the incorporation of such additional features into ligand-bearing nanometric DNA particles.

Received: October 28, 2002
Revised: March 3, 2003 [Z50446]

Keywords: cell recognition · DNA binding · nanostructures · supramolecular chemistry · transfection

[1] K. K. Hunt, S. A. Vorburger, *Science* **2002**, *297*, 415.
[2] N. Somia, I. M. Verma, *Nat. Rev. Genet.* **2000**, *1*, 91.
[3] M. Ogris, E. Wagner, *Drug Discovery Today* **2002**, *7*, 479.
[4] C. M. Ward, *Curr. Opin. Mol. Ther.* **2000**, *2*, 182.
[5] J. D. Hood, M. Bednarski, R. Frausto, S. Guccione, R. A. Reisfeld, R. Xiang, D. A. Cheresh, *Science* **2002**, *296*, 2404.
[6] M. X. Tang, F. C. Szoka, *Gene Ther.* **1997**, *4*, 823.
[7] S. M. Zou, P. Erbacher, J. S. Remy, J. P. Behr, *J. Gene Med.* **2000**, *2*, 128.
[8] E. Dauty, J. S. Remy, T. Blessing, J. P. Behr, *J. Am. Chem. Soc.* **2001**, *123*, 9227.
[9] J. Y. Wong, T. L. Kuhl, J. N. Israelachvili, N. Mullah, S. Zalipsky, *Science* **1997**, *275*, 820.
[10] J. Sudimack, R. J. Lee, *Adv. Drug Delivery Rev.* **2000**, *41*, 147.
[11] L. Pelkmans, J. Kartenbeck, A. Helenius, *Nat. Cell Biol.* **2001**, *3*, 473.
[12] S. Y. Chan, C. J. Empig, F. J. Welte, R. F. Speck, A. Schmaljohn, J. F. Kreisberg, M. A. Goldsmith, *Cell* **2001**, *106*, 117.
[13] J. W. Trauger, E. E. Baird, P. B. Dervan, *Nature* **1996**, *382*, 559.
[14] See Supporting Information.
[15] G. Bellomo, M. Vairetti, L. Stivala, F. Mirabelli, P. Richelmi, S. Orrenius, *Proc. Natl. Acad. Sci. USA* **1992**, *89*, 4412.
[16] Electron microscopy was performed on a Philips EM410 apparatus operated at 80 kV. Samples were transferred onto ultrathin-carbon-film grids (Ted Pella, CA, USA, 1822-F, formvar removed) by placing the grid on top of a 10 μL drop of the sample for 1 min. From one side of the grid the excess fluid was wicked away, then the grid was placed on a 100-μL water drop for 30 s to wash, excess fluid was again removed, the grid was placed for 1 min on a 60-μL drop of freshly filtered uranyl acetate (1.33 %), the excess fluid was again wicked away, and the grid was air dried.
[17] The volume of the 5500-bp DNA is 11800 nm^3 if hexagonal packing is assumed, in analogy with: J. A. Schellman, N. Parthasarathy, *J. Mol. Biol.* **1984**, *175*, 313. The DNA was neutralized with 2700 lipid molecules. If hydrated-lipid molecular dimensions of 0.8 $nm^2\times4$ nm are assumed, this gives a total volume of 20440 nm^3 for the complex, that is, a sphere of 34-nm diameter.
[18] KB cells were cultured in Dubelcco's modified Eagles medium (DMEM; Sigma, St Quentin, France) containing heat-inactivated fetal calf serum (10 %), glutamine (2 mM), penicillin (100 units mL^{-1}), and streptomycin (100 μg mL^{-1}) at 37 °C in a 5 %-humidified CO_2 atmosphere. Overexpression of the folic acid receptor was induced by growing the cells for three passages in folic acid depleted DMEM (FDMEM). For flow cytometry, particles were labeled with YOYO-1 (Molecular Probes, OR, USA; 1 YOYO/150 bp) by mixing the plasmid with YOYO before addition of the detergent. Cells were harvested by trypsination, washed with FDMEM, collected by centrifugation, and suspended in serum-free FDMEM. The cells (final concentration of 10^5 cells mL^{-1}) were then mixed with labeled particles in a total volume of 1 mL of serum-free DMEM and were incubated for 3 h at 37 °C in a 5 %-humidified atmosphere. DMEM (3 mL) containing calf-thymus DNA (200 μg mL^{-1}) was then added to account for nonspecific binding and the cells were collected by centrifugation and suspended in phosphate-buffered saline (PBS) with bovine serum albumin (BSA; 1 %). Flow cytometric analysis was performed on a FAC-StarPlus apparatus (Becton Dickinson, San Jose, USA) with an argon laser (excitation at 488 nm). Granulation, size, and fluorescence intensity (emission 515 nm) were recorded at a rate of 300 cells s^{-1}. Data were analyzed using cellQuest software. Calibration of the fluorescence intensity was performed by using 6-μm calibrated beads ($\lambda_{ex}=488$ nm, $\lambda_{em}=515$ nm). Quantum yields of FITC-labeled BSA, DNA-bound YOYO, and calibration beads were measured on a spectrofluorophotometer (Shimadzu RF-5301PC); FITC = fluorescein isothiocyanate.
[19] A. S. Verkman, *Trends Biochem. Sci.* **2002**, *27*, 27.
[20] KB folate ρ(+) cells were incubated for 3 h with fluorescent complexes and recovered as described[18] for cytometric analysis. Cells resuspended in FDMEM were deposited on chambered cover slides (Nalge Nunc, USA, Lab-Tek 155383). Images of living cells were collected on an AMRC-1024ES confocal laser scanning system equipped with an Eclipse TE300 microscope (Nikon) by using a 60× water-immersion objective. Series of 512 × 512 pixel images were acquired at different focal planes (*z* series) with a displacement of 1 mm between images. Green fluorescence, obtained from the 488-nm excitation line of an argon/krypton laser, and phase-contrast micrographs were loaded in the green and blue channels of the digital color image, respectively. Image contrast was corrected by using Adobe Photoshop software.
[21] J. Zabner, A. J. Fasbender, T. Moninger, K. A. Poellinger, M. J. Welsh, *J. Biol. Chem.* **1995**, *270*, 18997.
[22] S. Wang, P. S. Low, *J. Controlled Release* **1998**, *53*, 39.
[23] F. Labat-Moleur, A. M. Steffan, C. Brisson, H. Perron, O. Feugeas, P. Furstenberger, F. Oberling, E. Brambilla, J. P. Behr, *Gene Ther.* **1996**, *3*, 1010.
[24] O. Boussif, F. Lezoualch, M. A. Zanta, M. D. Mergny, D. Scherman, B. Demeneix, J. P. Behr, *Proc. Natl. Acad. Sci. USA* **1995**, *92*, 7297.
[25] M. A. Zanta, P. Belguise-Valladier, J. P. Behr, *Proc. Natl. Acad. Sci. USA* **1999**, *96*, 91.
[26] L. J. Branden, A. J. Mohamed, C. I. Smith, *Nat. Biotechnol.* **1999**, *17*, 784.

 © 2003 Wiley-VCH Verlag GmbH & Co. KGaA, Weinheim

Metal–Organic Network Assembly

Modular Assembly of Two-Dimensional Metal–Organic Coordination Networks at a Metal Surface

Alexandre Dmitriev, Hannes Spillmann, Nian Lin, Johannes V. Barth,* and Klaus Kern**

The construction of complex assemblies using molecular building blocks is paramount for the development of novel functional materials. A rich variety of molecular nanostructures and architectures with well-defined shapes and geometries have been obtained using transition-metal centers and concepts from coordination chemistry.[1–3] Metal–organic coordination networks (MOCNs) have been realized with specific topologies and a high structural stability.[4–12] MOCNs may exhibit intriguing properties, for example, molecular recognition, functionalities for heterogeneous asymmetric catalysis, and inclusion phenomena.[13–19] Moreover, for many applications the controlled nanoscale fabrication of functional molecular architectures at well-defined substrates is desirable.[20–22] However, most of the surface-supported assemblies reported to date are stabilized by relatively weak interactions, such as hydrogen bonding, van der Waals, or electrostatic forces, which implies a limited thermal stability.[23–25] Very recently, more robust one-dimensional (1D) nanostructures stabilized by metal–ligand interactions and the formation of metal–organic complexes at surfaces have been reported.[26–28]

Here we present a new strategy to fabricate surface-supported MOCNs at a well-defined metal surface under ultrahigh vacuum (UHV) conditions. The sequential deposition of 1,2,4-benzenetricarboxylic acid (trimellitic acid, tmla) molecules and Fe atoms on a clean Cu(100) substrate gives rise to the formation of 2D surface-supported open networks, stabilized by relatively strong lateral metal–organic coordination bonds. The MOCNs were investigated at the molecular level by scanning tunneling microscopy (STM). The precise control of the concentration ratio of the components allows for the assembly of distinct architectures. This approach opens up new possibilities for the bottom-up fabrication of low-dimensional functional materials.

The necessary precursors for surface-supported MOCNs are organic layers of a well-defined tmla phase, obtained by deposition of submonolayer tmla on the Cu(100) substrate. Figure 1 shows the corresponding well-ordered 2D domains,

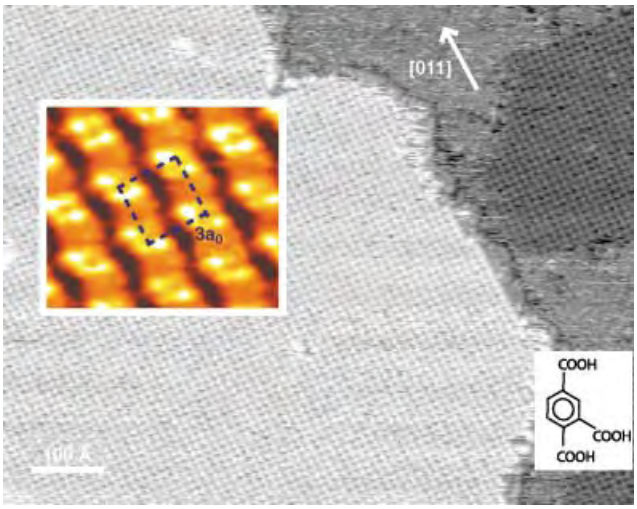


Figure 1. STM topography showing the 1,2,4-benzenetricarboxylic acid (tmla, shown bottom right) precursor layer deposited on a Cu(100) surface at 400 K. Domains comprising a commensurate regular structure of flat-lying molecules are resolved. The inset shows a high-resolution image with the [3 × 3] unit cell of the molecular layer. Individual tmla molecules are resolved as a four-lobe oval protrusion with a length of 8 Å.

with a superstructure oriented along the Cu(100) high-symmetry directions. They extend over entire terraces and are commensurate with the underlying Cu substrate. The arrangement of the molecules is characterized by a [3 × 3] unit cell. A detailed experimental (using near-edge X-ray absorption fine structure spectroscopy (NEXAFS)) and theoretical (using density functional theory) analysis of this phase suggests that it consists of molecules with their aromatic ring slightly tilted out of the surface plane.[29] In view of the chemical reactivity of the substrate and the elevated temperature employed in the preparation,[29] it is expected that deprotonation of the carboxylic acid groups occurs, which is analogous to findings for other carboxylic acids on Cu surfaces under comparable conditions.[27–30] However, based on current experimental evidence, the intriguing possibility of an intramolecular hydrogen bond at the carboxylic groups in the *ortho* position of the adsorbed species cannot be ruled out. A further interesting feature of this phase is that it comprises homochiral domains, since the prochiral tmla molecules become chiral upon confinement to two dimensions, as discussed in more detail elsewhere.[29]

Upon deposition of Fe atoms onto the tmla layer, the carboxylate groups readily react with the transition-metal adatoms. STM analysis (Figure 2a) reveals the formation of an extended regular network oriented along the principal directions of the substrate, at a coverage of one Fe atom to one tmla molecule. The network single domains are oriented along a substrate high-symmetry direction and are up to 100 × 100 nm in size, frequently covering entire substrate terraces (areas with compact islands, presumably from Fe aggregation, and other defects account for approximately 20% of the total surface). The MOCN contains anisotropic cavities and can be found in two 90°-rotational domains, reflecting the symmetry of the substrate.

[*] Dr. N. Lin, Prof. Dr. K. Kern, A. Dmitriev, Dr. H. Spillmann
Max-Planck-Institut für Festkörperforschung
70569 Stuttgart (Germany)
Fax: (+49) 711-689-1079
E-mail: n.lin@fkf.mpg.de
k.kern@fkf.mpg.de
Dr. J. V. Barth, Prof. Dr. K. Kern
Institut de Physique des Nanostructures
Ecole Polytechnique Fédérale de Lausanne
1015 Lausanne (Switzerland)
E-mail: johannes.barth@epfl.ch

 © 2003 Wiley-VCH Verlag GmbH & Co. KGaA, Weinheim DOI: 10.1002/anie.200250610

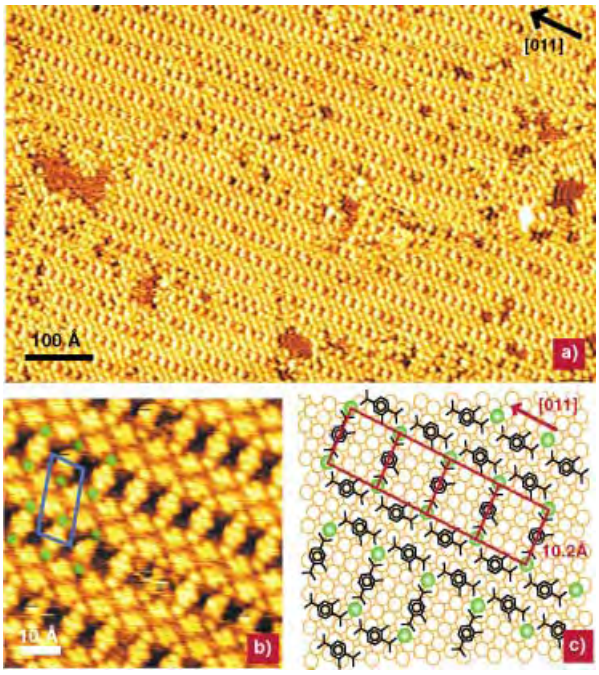


Figure 2. A "double-row MOCN" assembled by tuning the coverage ratio to one Fe atom per tmla molecule. a) Large-scale STM topography showing the regularly ordered network structure that comprises anisotropic cavities; b) high-resolution STM image revealing the four-lobe molecular structure. Single protrusions at the points of intersection throughout the network are associated with Fe atoms, laterally coordinated by tmla carboxylato moieties. The unit cell of the network is marked in blue and Fe atoms around are colored green; c) tentative model for the double-row Fe–carboxylate MOCN. The side carboxylate groups are assumed to be oriented perpendicular to the surface. Fe atoms (green) are arranged in a ladder-type structure with a 10.2×10.2 Å repeat unit.

High-resolution STM analysis (Figure 2b) allows individual tmla molecules to be distinguished; their characteristic four-lobe features are similar to the molecular resolution in the pure organic layer, which indicates that the flat adsorption geometry is preserved. Paired molecular rows running along the [011] direction have formed under the influence of the incorporated Fe atoms. The paired rows are interconnected by individual molecules oriented in the direction perpendicular to the rows. Thus this structure is designated "double-row MOCN". At the points of intersection bright protrusions are resolved, which are associated with the deposited Fe atoms, similar to the STM imaging of metal atoms in related compounds formed at the Cu(100) surface.[27,28] The relative orientation of the molecules with respect to the metal atoms indicates that the *para* carboxylate groups of tmla point towards the Fe atoms, which can be attributed to the formation of a lateral coordination bond. Consequently, the entire structure can be understood as an open-network-type Fe–carboxylate arrangement, stabilized by metal–ligand interactions.

A tentative geometrical model for the double-row MOCN based on an analysis of STM data is presented in Figure 2c. We assume that both Fe atoms and phenyl rings reside at the energetically preferential hollow sites of the substrate.[28,31] The Fe atoms in the double-row MOCN form ladders with a square $4a \times 4a$ repeat unit (the surface lattice parameter of Cu(100), $a = 2.55$ Å). Each Fe atom interacts with three tmla molecules: The data suggest that a unidentate linkage exists to the two neighboring molecules from the double row, along with a bidentate coupling to the isolated species in the perpendicular orientation. This arrangement implies a distorted fourfold coordination for each Fe atom, a configuration frequently encountered in 3D square-planar metal carboxylates.[32] However, it is important to note that with the present system the charge on both adsorbed tmla molecules and Fe atoms is strongly affected by the electrons of the metal surface, which effectively screen the adsorbate species and, in particular, prevent determination of the Fe oxidation state (for a more detailed discussion of this issue see Ref. [27]). In the model we assume that a too close distance of the laterally noncoordinated carboxylato groups at the *ortho* positions is avoided by their 90° rotation out of the surface plane. This behavior is suggested from a theoretical analysis of tmla bonding in the organic layer,[29] and is also a well-known conformational adaptation for carboxylic acids in solution chemistry. Furthermore the *ortho* side groups are placed randomly, since we found that they do not influence the primary frame structures of the MOCNs.[33] The effective cavity envelope is $\approx 3 \times 10$ Å, as estimated from high-resolution STM analysis. The stoichiometric Fe/tmla ratio in the model structure is determined to be 0.66, which falls below the necessary 1:1 ratio required for network formation.[34]

A second network type, designated "single-row MOCN", is obtained by increasing the adsorbate coverage ratio to two Fe atoms per tmla molecule. STM analysis (Figure 3a) shows that MOCNs with different topologies are formed. These MOCNs again follow the high-symmetry directions of the substrate and grow in extended islands. Two types of structures comprising different cavities can be discerned, which are designated the α and β phases, respectively. These structures always develop simultaneously, which signals that they are close in composition and energy. In the corresponding high-resolution STM data (Figure 3b,c) the positioning of the constituents is revealed. The networks consist of a sequential arrangement of individual tmla molecules and Fe atoms, which are identified by their respective imaging characteristics, similar to those in the double-row MOCN. In the α phase (Figure 3b) a rectangular unit cell and a cavity of similar shape and size as that in the double-row MOCN is identified. However, the cavity density is increased because the cavities in the α phase are separated by single tmla molecules, in contrast to the double-row structures where the cavities are separated by pairs of tmla molecules in one direction (Figure 2). Two 90° rotational domains are found in the α phase (inset, Figure 3a), which originate from its anisotropic shape. In the β phase (Figure 3c) a square unit cell comprising cavities of concave edges is found in a continuous 2D Fe–carboxylate network. The essential difference between the α and β phases is in the symmetry of the Fe–carboxylate linkage in the intersection points of the MOCNs. While it is always identical in the α phase, an alternating orientation of the Fe pairs at each intersection is found for the

 © 2003 Wiley-VCH Verlag GmbH & Co. KGaA, Weinheim

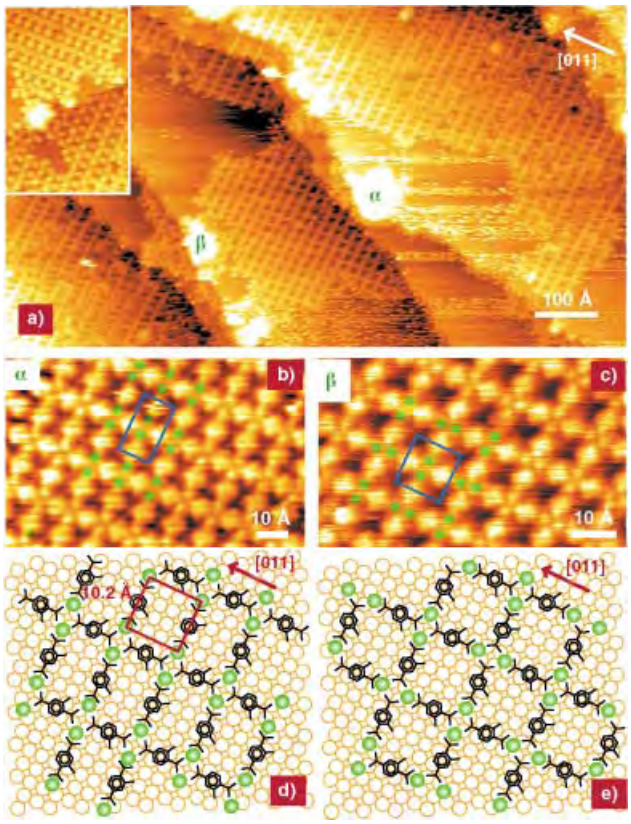


Figure 3. A "single-row MOCN" assembled by tuning the coverage ratio to two Fe atoms per tmla molecule. a) STM topography showing two species of regularly ordered networks, designated the α and β phases. In the inset, both 90°-rotational domains of the α phase are depicted; b,c) high-resolution STM images show that the detailed arrangement of Fe and tmla in both the α and β phases is resolved. A rectangular and square unit cell is characteristic for the networks of the α and β phases, respectively; d,e) tentative models that identify the α and β phases as MOCN isomers (coding as in Figure 2). Although both phases have the same stochiometry and contain Fe atoms with identical coordination environments, their geometrical arrangement is different.

β phase. This is illustrated by the corresponding models (Figure 3 d,e), which also show that the integral coordination of each Fe atom is equivalent for both phases. However, in the α phase a given tmla molecule has either two bidentate or four unidentate linkages to two Fe atoms, whereas in the β phase for every given molecule both bidentate and unidentate bonding are encountered at its extremities. Apparently the energy change associated with this subtle difference is small, which is understood as the reason for the simultaneous evolution of both phases under the employed conditions. Thus the two phases of the single-row MOCNs are closely related and can be regarded as structural isomers, which is a common finding for metal–organic frameworks.[10] In analogy with the double-row MOCN, the ideal 1:1 Fe/tmla stoichiometric coverage ratio for single-row MOCNs falls below the actual 2:1 value required for network formation.[34]

With the present system only the carboxylato groups in the *para* position seem to be integral for the formation and final topology of the encountered MOCNs, whereas the remaining side group is not directly involved in metal–organic complexation. Unfortunately the detailed positioning of side groups in the various network structures cannot be unambiguously determined by the STM data obtained, which is associated with the distortion of the molecules upon adsorption and the weak contribution of this moiety to the tunneling current. Note that the presence of the side group will nevertheless be important for the functionality of the cavity. For example, it may result in the formation of two mirror-symmetric MOCN cavities, since tmla is a 2D chiral species.

It is interesting to address the potential functionality of the obtained MOCNs. Firstly, the single- and double-row structures contain magnetic atoms which are periodically arranged. It is expected that the organic linkers mediate magnetic coupling between the Fe atoms, similar to effects in related metal–organic magnetic structures.[35,36] The ladder formations and 2D metal–organic linkages in the double-row and single-row MOCNs thus represent nanoscale magnetic arrangements with distinct symmetry. On the other hand, the obtained networks provide a regular arrangement of cavities with well-defined shape and chemistry. Finally, the MOCNs are of potential use as templates for 3D molecular architectures, such as nanoporous lattices.

In conclusion, we have succeeded in the rational design of 2D metal–organic networks, formed in situ under UHV conditions by sequential deposition of the organic linker molecule trimellitic acid and Fe atoms on a Cu(100) surface. The subtle variation of the relative quantities of the constituents that are deposited allows can steer the modular assembly of distinct metal–carboxylate network architectures. Our results indicate that, in general, 2D metal–organic coordination networks can be synthesized at well-defined surfaces. It is suggested that this approach opens novel avenues for the fabrication of nanoscale functional materials.

Experimental Section

Iron atoms and tmla molecules were co-deposited on the metal surface in a standard UHV chamber with a base pressure of $\sim 3 \times 10^{-10}$ mbar. A Cu(100) surface was prepared by repeated cycles of Ar^+ sputtering and subsequent annealing to 800 K, by which flat terraces of up to 50 nm width separated by monatomic steps were obtained. Tmla (99 + %, Sigma-Aldrich Chemie GmbH) was deposited by organic molecular beam epitaxy (OMBE) from a Knudsen-cell-type evaporator, held at 415 K during deposition. Fe atoms were evaporated using an electron-beam heating evaporator. To hinder Fe–Cu surface intermixing, which can be encountered in the pure Fe/Cu(100) system,[37] Fe was always deposited on an organic layer. Both tmla and Fe deposition were performed at a substrate temperature of 400 K to increase mobility and reactivity of the adsorbates and, thus, to allow for the formation of ordered structures. Coverages below full monolayer saturation were employed for the tmla precursor layers, in order to leave space for the formation of the more open network structures. STM experiments employing the constant-current mode were performed in situ following cooling to room temperature.

Received: November 22, 2002
Revised: March 12, 2003 [Z50610]

Keywords: coordination compounds · iron · nanomaterials · scanning tunneling microscopy · vacuum deposition

 © 2003 Wiley-VCH Verlag GmbH & Co. KGaA, Weinheim

[1] S. Leininger, B. Olenyuk, P. J. Stang, *Chem. Rev.* **2000**, *100*, 853.
[2] G. F. Swiegers, T. J. Malefetse, *Chem. Rev.* **2000**, *100*, 3483.
[3] B. J. Holliday, C. A. Mirkin, *Angew. Chem.* **2001**, *113*, 2076; *Angew. Chem. Int. Ed.* **2001**, *40*, 2022.
[4] J. Y. Lu, M. A. Lawandy, J. Li, T. Yuen, C. L. Lin, *Inorg. Chem.* **1999**, *38*, 2695.
[5] P. J. Stang, N. E. Persky, J. Manna, *J. Am. Chem. Soc.* **1997**, *119*, 4777.
[6] D. Venkataraman, G. B. Gardner, S. Lee, J. S. Moore, *J. Am. Chem. Soc.* **1995**, *117*, 11600.
[7] M. Fujita, Y. J. Kwon, S. Washizu, K. Ogura, *J. Am. Chem. Soc.* **1994**, *116*, 1151.
[8] L. R. MacGillivray, R. H. Groeneman, J. L. Atwood, *J. Am. Chem. Soc.* **1998**, *120*, 2676.
[9] S. R. Batten, R. Robson, *Angew. Chem.* **1998**, *110*, 1558; *Angew. Chem. Int. Ed.* **1998**, *37*, 1460.
[10] B. Moulton, M. J. Zaworotko, *Chem. Rev.* **2001**, *101*, 1629.
[11] M. Eddaoudi, D. B. Moler, H. Li, B. Chen, T. M. Reineke, M. O'Keeffe, O. M. Yaghi, *Acc. Chem. Res.* **2001**, *34*, 319.
[12] Y. Cui, O. R. Evans, H. L. Ngo, P. S. White, W. Lin, *Angew. Chem. Int. Ed.* **2002**, *114*, 1207; *Angew. Chem. Int. Ed.* **2002**, *41*, 1159.
[13] H. Li, M. Eddaoudi, M. O'Keeffe, O. M. Yaghi, *Nature* **1999**, *402*, 276.
[14] J. S. Seo, D. Whang, H. Lee, S. I. Jun, J. Oh, Y. J. Jeon, K. Kim, *Nature* **2000**, *404*, 982.
[15] G. B. Gardner, D. Venkataraman, J. S. Moore, S. Lee, *Nature* **1995**, *374*, 792.
[16] O. M. Yaghi, G. Li, H. Li, *Nature* **1995**, *378*, 703.
[17] S. S.-Y. Chui, S. M.-F. Lo, J. P. H. Charmant, A. G. Orpen, I. D. Williams, *Science* **1999**, *283*, 1148.
[18] B. Chen, M. Eddaoudi, S. T. Hyde, M. O'Keeffe, O. M. Yaghi, *Science* **2001**, *291*, 102.
[19] C. J. Kepert, T. J. Prior, M. J. Rosseinsky, *J. Am. Chem. Soc.* **2000**, *122*, 5158.
[20] C. P. Collier, E. W. Wong, M. Belohradský, F. M. Raymo, J. F. Stoddart, P. J. Kuekes, R. S. Williams, J. R. Heath, *Science* **1999**, *285*, 391.
[21] G. P. Lopinski, D. D. M. Wayner, R. A. Wolkow, *Nature* **2000**, *406*, 48.
[22] C. Joachim, J. K. Gimzewski, A. Aviram, *Nature* **2000**, *408*, 541.
[23] T. Yokoyama, S. Yokoyama, T. Kamikado, Y. Okuno, S. Mashiko, *Nature* **2001**, *413*, 619.
[24] J. V. Barth, J. Weckesser, C. Cai, P. Günter, L. Bürgi, O. Jeandupeux, K. Kern, *Angew. Chem.* **2000**, *112*, 1285; *Angew. Chem. Int. Ed.* **2000**, *39*, 1230; J. V. Barth, J. Weckesser, G. Trimarchi, M. Vladimirova, A. De Vita, C. Cai, H. Brune, P. Günter, K. Kern, *J. Am. Chem. Soc.* **2002**, *124*, 7991.
[25] M. Böhringer, K. Morgenstern, W.-D. Schneider, R. Berndt, F. Mauri, A. De Vita, R. Car, *Phys. Rev. Lett.* **1999**, *83*, 324.
[26] D. G. Kurth, N. Severin, J. P. Rabe, *Angew. Chem.* **2002**, *114*, 3833; *Angew. Chem. Int. Ed.* **2002**, *41*, 3681.
[27] N. Lin, A. Dmitriev, J. Weckesser, J. V. Barth, K. Kern, *Angew. Chem.* **2002**, *114*, 4973; *Angew. Chem. Int. Ed.* **2002**, *41*, 4779.
[28] P. Messina, A. Dmitriev, N. Lin, H. Spillmann, M. Abel, J. V. Barth, K. Kern, *J. Am. Chem. Soc.* **2002**, *124*, 14000.
[29] A. Dmitriev, H. Spillmann, N. Lin, P. Messina, M. Abel, A. Seitsonen, M. Parrinello, J. V. Barth, K. Kern, unpublished results **2002**.
[30] C. C. Perry, S. Haq, B. G. Frederick, N. V. Richardson, *Surf. Sci.* **1998**, *409*, 512.
[31] A. Dmitriev, N. Lin, J. Weckesser, J. V. Barth, K. Kern, *J. Phys. Chem. B* **2002**, *106*, 6907.
[32] R. C. Mehrotra, R. Bohra, *Metal Carboxylates*, Academic Press, London, **1983**.
[33] In fact, by using 1,4-benzenedicarboxylic acid (terephtalic acid, TPA), a molecule with two carboxylic groups at *para* positions, exactly the same MOCN structures can be fabricated, which proves that the side group does not play a significant role in the MOCN formation.
[34] This difference is attributed to the effective loss of Fe atoms in other surface chemical processes, that is, the entire amount of deposited Fe is not employed in coordination network formation. Decoration of substrate step edges, and in particular Fe island formation are frequently suggested from inspection of STM topographs. In addition, a small percentage of the Fe atoms might be lost in substrate atom-exchange processes.
[35] E. Breuning, M. Ruben, J.-M. Lehn, F. Renz, Y. Garcia, V. Ksenofontov, P. Gütlich, E. Wegelius, K. Rissanen, *Angew. Chem.* **2000**, *112*, 2563; *Angew. Chem. Int. Ed.* **2000**, *39*, 2504.
[36] B. Moulton, J. Lu, R. Hajndl, S. Hariharan, M. J. Zaworotko, *Angew. Chem.* **2002**, *114*, 2945; *Angew. Chem. Int. Ed.* **2002**, *41*, 2821.
[37] D. D. Chambliss, K. E. Johnson, *Phys. Rev. B* **1994**, *50*, 5012.

 © 2003 Wiley-VCH Verlag GmbH & Co. KGaA, Weinheim

Matrix Metalloproteinases

X-ray Structures of Binary and Ternary Enzyme-Product-Inhibitor Complexes of Matrix Metalloproteinases**

Ivano Bertini, Vito Calderone, Marco Fragai, Claudio Luchinat, Stefano Mangani, and Beatrice Terni*

Matrix metalloproteinases (MMP) are a class of extracellular zinc-containing peptidases that are involved in a variety of tissue-remodeling activities, and whose misfunction/misregulation is implicated in several pathologies ranging from arthritis rheumatoides to metastatic processes.[1–5] Such proteins, which may be bound to the outer cell membrane or

[*] Prof. I. Bertini, Dr. M. Fragai, Prof. S. Mangani, Dr. B. Terni
Magnetic Resonance Center and Department of Chemistry
University of Florence
via Luigi Sacconi, 6, 50019 Sesto Fiorentino (Italy)
Fax: (+39) 055-457-4271
E-mail: bertini@cerm.unifi.it

Dr. V. Calderone, Prof. S. Mangani
Department of Chemistry
University of Siena (Italy)

Prof. C. Luchinat
Magnetic Resonance Center and
Department of Agricultural Biotechnology
University of Florence (Italy)

[**] This work was supported by Ente Cassa di Risparmio di Firenze; Fondo per gli investimenti della ricerca di base (MIUR), contract RBNE01TTJW; Fondo integravito speciale per la ricerca (MIUR), "Modeling di strutture di metalloproteine e delle internazioni proteinafarmaco e proteina-proteina. We are grateful to the staff of the ID-14-1- beam line of the European Synchrotron Facility for technical assistance during the X-ray data collection.

Supporting information for this article is available on the WWW under http://www.angewandte.org or from the author.

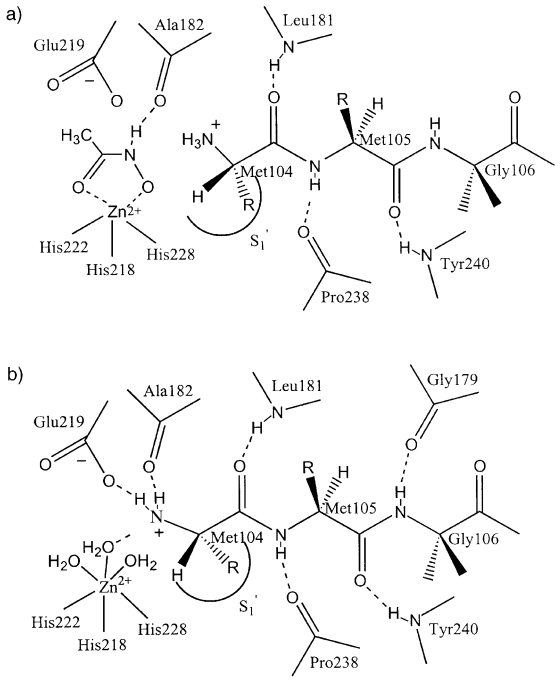
 DOI: 10.1002/anie.200350957 © 2003 Wiley-VCH Verlag GmbH & Co. KGaA, Weinheim

released into the matrix as soluble molecules, are composed of a prodomain, a catalytic domain, and a hemopexin-like (or substrate-recognition) domain.[3,6–8] The prodomain is folded back into the active-site crevice and acts as an inhibitor until it is cleaved by a protease (or another MMP) to produce the active enzyme form.[7,9,10] The catalytic mechanism of MMP has been proposed[11,12] to parallel that of thermolysin.[13,14] The peptide substrate is believed to enter the active-site crevice and interact with the catalytic zinc ion through the carbonyl group of the scissile peptide bond, while the peptide NH group is hydrogen bonded to the carbonyl carbon atom of Ala 182 (MMP-12 numbering). The zinc-bound water molecule is activated by hydrogen bonding to the catalytically essential Glu 219 residue. The coordinated water molecule then transfers the proton to Glu 219 while attacking the peptide carbonyl carbon atom, and the proton is finally transferred to the terminal nitrogen atom of the amino leaving group when the peptide bond is broken.[11,12] While structures mimicking transition-state analogues are available to support this mechanism,[15] none of the approximately 80 MMP structures available to date can be taken as representative of enzyme-product complexes after the hydrolytic event.

In the case of MMP-1 (fibroblast collagenase), a catalytic domain that was three residues longer in the N-terminal end showed a filamentous structure with the N-terminal residues 102–104 entering the active-site cavity of an adjacent molecule.[11] However, the NH_2 and CO groups of Leu 102 were found to chelate the catalytic zinc ion in an unproductive self-inhibitory adduct.[11] Metal chelation by the N-terminal residue is also typical of tissue inhibitors of metalloproteinases (TIMPs), proteins that act as physiological inhibitors of MMPs.[16–18]

We have expressed the F171D mutant of the catalytic domain of MMP-12 bearing two additional N-terminal methionine residues, Met 104–Met 105, before the catalytic Glu 106–Asn 258 domain. The F171D mutation has been designed to enhance solubility without altering the catalytic activity and the reaction mechanism.[19] We report here the structures of the above MMP-12 constructions obtained from crystals grown in the presence of acetohydroxamic acid (AHA), a weak zinc-directed inhibitor. In these structures, the N-terminal Met 104–Met 105 residues of one domain are hosted into the active cleft of the following domain, with an arrangement similar to that described above for MMP-1.[11] One of these structures is the first example of a non-inhibited zinc site, while in the other the small AHA ligand blocks the catalytic zinc site. In both cases, there is room for the amino terminal group to assume product-like arrangements.

Crystals of MMP-12 catalytic domains can be obtained under a relatively wide range of solute conditions, and the structures are solved to resolutions ranging from 2.15 to 1.5 Å. In all cases, the catalytic domains are chained to one another forming double helices whose arrangement will be described in detail elsewhere. The asymmetric unit of the $P3_1$ cell always comprises six different molecules, three from one chain and three from an adjacent chain. In all cases, the structure of the MMP-12 domain is almost identical to the recently published structures of strongly inhibited forms.[20,21] The six independent molecules are labeled A–F. Molecule B hosts the N-terminal methionine residues of A, C hosts those of B, and A those of C, crystallographically related to C through two successive 3_1 symmetry operations. Likewise, in the adjacent chain, E hosts the N terminals of D, F hosts those of E, and D hosts those of F′. As the six molecules in the unit cell are inequivalent, the relative orientations of the relevant species and fragments in the active-site crevice are not necessarily identical. However, it appears that the A-B-C chain is virtually identical to the D-E-F chain, while differences are seen within each chain, that is, $A \approx D \neq B \approx E \neq C \approx F$. In all cases, the N-terminal Met residue of an adjacent MMP molecule is positioned in such a way that the hydrophobic *S*-CH_3 terminus points towards the inner part of the main hydrophobic S_1' site (see Scheme 1 a,b) and is close to the



Scheme 1.

Tyr 240 ring. The Met 104 carbonyl group is hydrogen-bonded to the NH group of Leu 181, the NH group of Met 105 is hydrogen-bonded to the carbonyl group of Pro 238, and the carbonyl group of Met 105 is hydrogen-bonded to the NH group of Tyr 240. However, there are differences in the zinc ligand(s) and in the position of the N-terminal NH_3^+ group, which is the part of the molecule which is closest to the catalytic zinc ion. These different arrangements are best illustrated by molecules B and E of a crystal diffracting at 1.85 Å (**1**) and by molecules A and D of another crystal diffracting at 2.15 Å (**2**). The detailed crystallization conditions of **1** and **2** are reported in the Supporting Information.

In molecules A and D of **2**, an AHA molecule is bound to the zinc ion (Figure 1 a). AHA binds in a bidentate fashion, as is typical for MMPs, with the oxygen atom of the O-N-H moiety pointing towards the metal center, and with the hydrogen atom involved in a hydrogen bond with the

 © 2003 Wiley-VCH Verlag GmbH & Co. KGaA, Weinheim

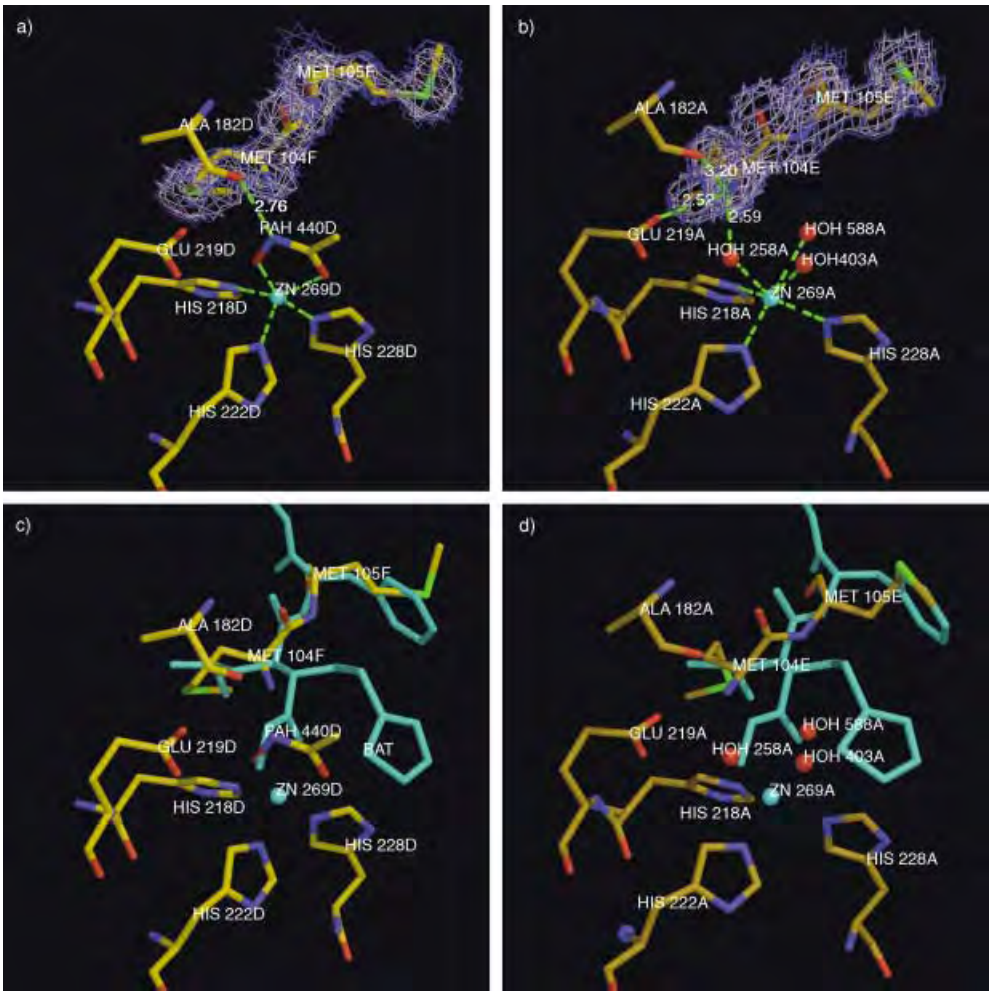


Figure 1. $2F_o–F_c$ density map (blue) contoured at 1σ and $F_o–F_c$ omit map (pink) contoured at 3σ around the Met 104, Met 105, and Gly 106 residues of molecules C′ in A (a) and molecules D in E (b), which shows two different arrangements of the N-terminal residues within the cavity. Panels c) and d) show the superposition of batimastat to the N-terminal residues in the arrangements described in a) and b), respectively.

backbone carbonyl group of Ala 182 (Figure 2a, Supporting Information). The CO moiety of AHA is also bound to the metal center, and oriented towards the His 222 ring. The structural features of the active site occupied by the N-terminal and AHA molecule are summarized in Scheme 1a.

Conversely, in molecules B and E of **1** there is no electron density from the solute ligand. The zinc ion appears to be coordinated by three water molecules (Figure 2b, Supporting Information) in a reasonably regular octahedral fashion (Figure 1b). The lack of the AHA ligand in this case allows the N-terminal NH_3^+ group to move by about 1 Å towards the metal center and to drastically change its hydrogen-bonding pattern. All three N-terminal hydrogen atoms are now engaged in hydrogen bonds; the first is formed with one of the metal-coordinated water molecules, another with the carbonyl group of Ala 182, and the third with the carboxylate group of the catalytically essential Glu 219 residue. Finally, a further hydrogen bond (besides those with the NH group of Leu 181, the carbonyl group of Pro 238 and the NH group of Tyr 240, also observed in molecules A and D of **2**) is formed between the NH group of Gly 106 and the carbonyl group of Gly 179. Overall, this arrangement of the N-terminal Met–Met residue (Scheme 1b) would correspond beautifully to the amine product after hydrolysis and before its release, in accordance with the widely accepted proposals for the mechanism of MMP and of other endopeptidases.[11–14] Recent calculations[22,23] confirm that the arrangement of the amine product observed here is the most energetically plausible one along the catalytic pathway.

These results are, therefore, the first examples of MMP structures demonstrating possible arrangements of enzyme–amine product complexes; the present findings are even more valuable when compared with the X-ray structure of the catalytic domain of MMP-1,[11] as well as with a variety of MMP complexes with strong inhibitors. Besides the unique and catalytically competent arrangement of the N-terminal NH_3^+ group of Met 104, all the other hydrogen-bonding interactions of the N-terminal residues 104–106 are also observed in the self-inhibited MMP-1 structure.[11] In short, and neglecting the zinc-bound Leu 102 residue in MMP-1, there is a perfect match between Thr 103, Glu 104, and Gly 105 in the MMP-1 cavity, and Met 104, Met 105, and Gly 106 in the MMP-12 cavity of molecules B and E of **1**. Four hydrogen-bonding interactions are maintained, and are

 © 2003 Wiley-VCH Verlag GmbH & Co. KGaA, Weinheim

indeed observed in several complexes that the catalytic domain forms with TIMPs[24] and the prodomain.[25] These interactions are among the crucial interactions for the proper positioning of the substrate, and are apparently maintained in the amine product. In this light, the position of the N-terminal Met residue in molecules A and D of **2**, pushed away from its hydrogen-bonding interactions in the immediate neighborhood of the metal center by the bulkier metal-coordinated AHA molecule (Scheme 1a), could be representative of a further detachment step of the amine product. Interestingly, strong chemical inhibitors, such as batimastat,[21] match the arrangement of the N-terminal Met residue in molecules A and D of **2** better than that in molecules B and E of **1** (compare Figure 1c and 1d). Therefore, the binding modes observed here for N-terminal peptides suggest that improved S_1'-directed drugs could mimic the present Gly-Met-Met tripeptide by actually exploiting as many as seven of its eight hydrogen bonds, and be optimally positioned to carry a metal ligand. The latter could actually be attached to the terminal amino group, which could still maintain two of its three hydrogen bonds (with the CO group of Ala 182 and the carboxylate group of Glu 219) and replace the third hydrogen bond by a covalent link with the metal-binding moiety.

Experimental Section

The cDNA of the F171D mutant of the MMP12 catalytic domain was obtained using a "quick-change" site-directed mutagenesis kit. The protein was expressed as an inclusion body, purified by FPLC, and refolded, as has been widely reported for MMPs.[19,26–30]

Crystals of the catalytic domain of MMP-12 belonging to the trigonal space group $P3_1$ ($a = b = 125.44$, $c = 72.34$ Å for **1**; $a = b = 123.84$, $c = 69.73$ Å for **2**) were obtained from a solution containing PEG 6000 and 200 mM AHA in Tris-HCl buffer at pH 8.0. Structural details are available in the Supporting Information.

Received: January 16, 2003 [Z50957]

Keywords: enzymes · inhibitors · metalloproteins · peptides · structure elucidation

[1] W. G. Stetler-Stevenson, R. Hewitt, *Semin. Cancer Biol.* **1996**, *7*, 147–154.
[2] L. Steinman, *Cell* **1996**, *85*, 299–302.
[3] N. Borkakoti, *Progr. Biophys. Mol. Biol.* **1998**, *70*, 73–94.
[4] M. Whittaker, C. D. Floyd, P. Brown, A. J. Gearing, *Chem. Rev.* **1999**, *99*, 2735–2776.
[5] N. Borkakoti, *J. Mol. Med.* **2000**, *78*, 261–268.
[6] J. Li, P. Brick, M. C. O'Hare, T. Skarzynski, L. F. Lloyd, V. A. Curry, I. M. Clark, H. F. Bigg, B. L. Hazleman, T. E. Cawston, *Structure* **1995**, *3*, 541–549.
[7] E. Morgunova, A. Tuuttila, U. Bergmann, M. Isupov, Y. Lindqvist, G. Schneider, K. Tryggvason, *Science* **1999**, *284*, 1667–1670.
[8] I. Massova, L. P. Kotra, R. Fridman, S. Mobashery, *FASEB J.* **1998**, *12*, 1075–1095.
[9] E. B. Springman, E. L. Angleton, H. Birkedal-Hansen, H. E. van Wart, *Proc. Natl. Acad. Sci. USA* **1990**, *87*, 364–368.
[10] H. E. van Wart, H. Birkedal-Hansen, *Proc. Natl. Acad. Sci. USA* **1990**, *87*, 5578–5582.
[11] B. Lovejoy, A. M. Hassell, M. A. Luther, D. Weigl, S. R. Jordan, *Biochemistry* **1994**, *33*, 8207–8217.
[12] R. E. Babine, S. L. Bender, *Chem. Rev.* **1997**, *97*, 1359–1472.
[13] B. W. Matthews, *Acc. Chem. Res.* **1988**, *21*, 333–340.
[14] H. M. Holden, B. W. Matthews, *J. Biol. Chem.* **1988**, *263*, 3256–3260.
[15] A. L. Gall, M. Ruff, R. Kannan, P. Cuniasse, A. Yiotakis, V. Dive, M. C. Rio, P. Basset, D. Moras, *J. Mol. Biol.* **2001**, *307*, 577–586.
[16] G. Murphy, F. Willenbrock, *Methods Enzymol.* **1995**, *248*, 496–510.
[17] F. X. Gomis-Ruth, K. Maskos, M. Betz, A. Bergner, R. Huber, K. Suzuki, N. Yoshida, H. Nagase, K. Brew, G. P. Bourenkov, H. Bartunik, W. Bode, *Nature* **1997**, *389*, 77–81.
[18] K. Brew, D. Dinakarpandian, H. Nagase, *Biochim. Biophys. Acta* **2000**, *1477*, 267–283.
[19] L. Banci, I. Bertini, A. Ciulli, M. Fragai, C. Luchinat, B. Terni, unpublished results.
[20] H. Nar, K. Werle, M. M. T. Bauer, H. Dollinger, B. Jung, *J. Mol. Biol.* **2001**, *312*, 743.
[21] R. Lang, A. Kocourek, M. Braun, H. Tschesche, R. Huber, W. Bode, K. Maskos, *J. Mol. Biol.* **2001**, *312*, 731–742.
[22] V. Pelmenschikov, E. M. Siegbahn, *Inorg. Chem.* **2002**, *41*, 5659–5666.
[23] V. Pelmenschikov, M. R. Blomberg, P. E. Siegbahn, *J. Biol. Inorg. Chem.* **2002**, *7*, 284–298.
[24] C. Fernandez-Catalan, W. Bode, R. Huber, D. Turk, J. J. Calvete, A. Lichte, H. Tschesche, K. Maskos, *EMBO J.* **1998**, *17*, 5238–5248.
[25] P. A. Elkins, Y. S. Ho, W. W. Smith, C. A. Janson, K. J. D'Alessio, M. S. McQueney, M. D. Cummings, A. M. Romanic, *Acta Crystallogr. D Biol. Crystallogr.* **2002**, *58*, 1182–1192.
[26] A. A. Parkar, M. D. Stow, K. Smith, A. K. Panicker, J. P. Guilloteau, R. Jupp, S. J. Crowe, *Protein Expression Purif.* **2000**, *20*, 152–161.
[27] Q. Z. Ye, L. L. Johnson, D. J. Hupe, V. Baragi, *Biochemistry* **1992**, *31*, 11231–11235.
[28] H. Oneda, K. Inouye, *J. Biochem.* **1999**, *126*, 905–911.
[29] B. Lovejoy, A. R. Welch, S. Carr, C. Luong, C. Broka, R. T. Hendricks, J. A. Campbell, K. A. Walker, R. Martin, H. van Wart, M. F. Browner, *Nat. Struct. Biol.* **1999**, *6*, 217–221.
[30] S. Rowsell, P. Hawtin, C. A. Minshull, H. Jepson, S. M. Brockbank, D. G. Barratt, A. M. Slater, W. L. McPheat, D. Waterson, A. M. Henney, R. A. Pauptit, *J. Mol. Biol.* **2002**, *319*, 173–181.

 © 2003 Wiley-VCH Verlag GmbH & Co. KGaA, Weinheim

Perylene-Derived Dyes

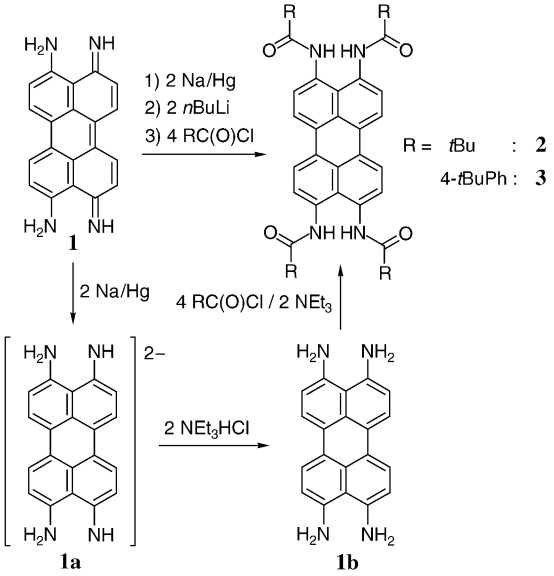
Synthesis, Photophysical Properties, and Nanocrystal Formation of a New Class of Tetra-N-Substituted Perylenes**

Lutz H. Gade, Christian H. Galka, René M. Williams,* Luisa De Cola, Mary McPartlin, Bin Dong, and Lifeng Chi*

Perylenes as pigments and fluorescent dyes have found wide ranging applications in very diverse fields of current research.[1–3] There are very few examples of tetra-N-substituted perylenes to be found in the literature to date which is because of the cumbersome nature of the established preparative methods.[4] We recently discovered a novel and efficient route to 4,9-diaminoperylenequinone-3,10-diimines[5] and showed that it is possible to convert these quinoidal systems to the reduced 3,4,9,10-tetraaminoperylenes,[6] a class of compounds which has very recently been cited in the patent literature of photovoltaic devices.[7]

However, these tetraaminoperylenes have extremely negative redox potentials, which leads to their instantaneous reoxidation when exposed to air and makes them impossible to manipulate under the conditions normally encountered in dye chemistry. Herein we report the first successful stabilization of such derivatives in the form of their carboxamides. In a sense, these compounds are perylene derivatives that are inversely functionalized with respect to the ubiquitous perylenebisimides.[8,9] Furthermore we show that these compounds can form very interesting rod-shaped structures that are promising candidates as building blocks in self-assembled functional nanostructures.

The treatment of 4,9-diaminoperylenequinone-3,10-diimine (**1**)[5a,6] with two molar equivalents of sodium amalgam or potassium metal in THF and subsequent deprotonation of the dianion **1a** with two equivalents of *n*-butyllithium gave a nonisolable tetraanionic intermediate. The addition of four molar equivalents of pivalyl chloride and 4-*tert*-butylbenzoyl chloride to this intermediate gave the corresponding carboxamides 3,4,9,10-[*t*BuC(O)NH]$_4$C$_{20}$H$_8$ (**2**) and 3,4,9,10-[(4′-*t*BuPh)C(O)NH]$_4$C$_{20}$H$_8$ (**3**) with a high yield. (Scheme 1). An equally efficient preparative route involves the neutral tetraaminoperylene **1b** obtained by controlled protonation of **1a** and subsequent coupling with the carboxyl chlorides.



Scheme 1. Synthesis of the tetra(carboxamido)perylenes **2** and **3**.

Whereas compound **2** is readily soluble in polar solvents, such as CH_2Cl_2, THF, or dimethyl sulfoxide, the 4-*tert*-butylphenyl substituted derivative **3** is much less so and only dissolves readily in DMSO. Both compounds were characterized by elemental analysis, ^{1}H and ^{13}C NMR spectroscopy, and infrared spectroscopy.

Crystals of compound **2** suitable for an X-ray diffraction study were grown from dimethyl sulfoxide at room temperature. The molecule of **2** has exact crystallographic C_i symmetry (Figure 1a) with two dimethyl sulfoxide solvent molecules hydrogen bonded to two centrosymmetrically related carboxamido hydrogen atoms of **2** through their oxygen atoms (O1s···H1N 2.30 Å).[10] There is evidence of hydrogen bonding between the two adjacent independent carboxamido groups (N(1)···H(2N) 2.06 Å).

The most remarkable feature of the molecular structure of **2** is the lack of coplanarity of the perylene core and its carboxamido substituents (Figure 1b). The aromatic hydrocarbon core shows a slight twisting (maximum deviation from planarity 0.15 Å for C(1)) but the two independent carboxamido groups are markedly rotated relative to this plane

[*] Prof. L. H. Gade, Dr. C. H. Galka
Laboratoire de Chimie Organométallique et de Catalyse (UMR 7513)
Institut Le Bel
Université Louis Pasteur
4, rue Blaise Pascal, 67070 Strasbourg (France)
Fax: (+33) 390-241-531
E-mail: gade@chimie.u-strasbg.fr
Dr. R. M. Williams, Prof. L. De Cola
Molecular Photonic Materials
Institute of Molecular Chemistry
Universiteit van Amsterdam
Nieuwe Achtergracht 166, 1018 WV Amsterdam (The Netherlands)
Fax: (+31) 20-525-6456
E-mail: williams@science.uva.nl
Prof. M. McPartlin
Dept. Of Health and Human Sciences
London Metropolitan University
Holloway Road, London N7 8DB (UK)
B. Dong, Priv.-Doz. Dr. L. Chi
Physikalisches Institut
Westfälische-Wilhelms-Universität Münster
Wilhelm-Klemm-Str. 10, 48149 Münster (Germany)

[**] We are grateful to the CNRS (France), the Institut Universitaire de France, the Deutsche Forschungsgemeinschaft and the EPSRC (UK), for funding. L.F.C., L.D.C., and R.M.W. thank Prof. Dr. H. Fuchs for his stimulating contributions.

 DOI: 10.1002/anie.200351348 © 2003 Wiley-VCH Verlag GmbH & Co. KGaA, Weinheim

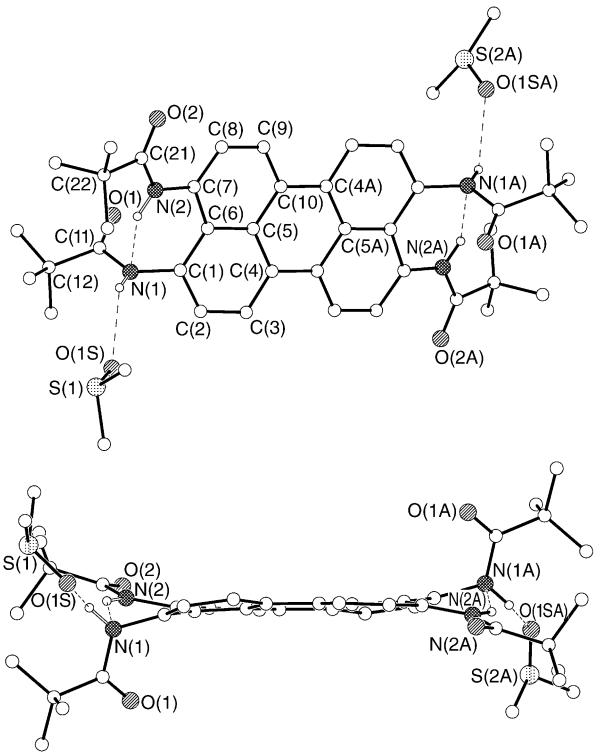


Figure 1. Molecular structure of compound **2**. Views orthogonally to the polyaromatic plane (a) and along a bisecting vector in the perylene unit (b) showing the distortion of the four carboxamido groups out of the molecular plane.

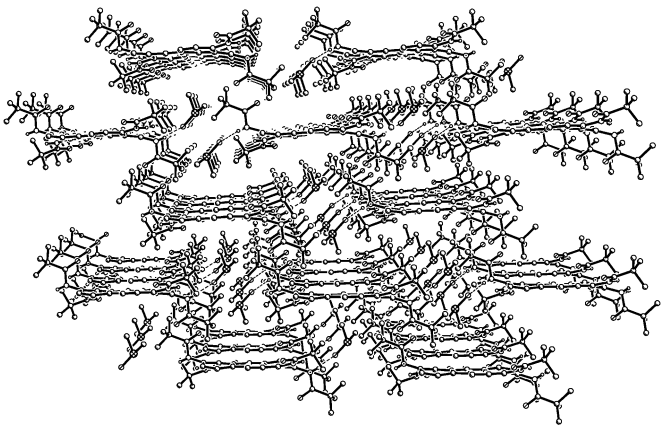


Figure 2. The packing of the perylene layers in the crystal.

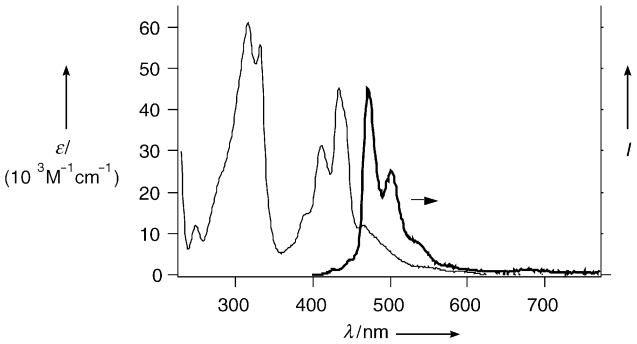


Figure 3. UV/Vis absorption and emission spectra of compound **3** in dichloromethane. The emission was recorded upon 392 nm excitation of 7×10^{-6} M solution by using a 400 nm cutoff filter. I = intensity, λ = wavelength.

(dihedral angles N(1)-O(1)-C(11)-C(12) 86.2°; N(2)-O(2)-C(21)-C(22) 22.8°). This marked overall twisting of the molecule may be attributed to mutual repulsion between the bulky pivalyl substituents. We note that deviations from planarity of perylene units were reported and studied previously.[11]

The carbon–carbon bond lengths C(2)–C(3), C(8)–C(9), and C(4)–C(10A) of 1.386(4), 1.394(5), and 1.469(4) Å, respectively, are similar to the corresponding interatomic distances in the unsubstituted parent perylene (1.394(3) and 1.476(3) Å)[12] as well as those established for a large number of perylene tetracarboximides.[13]

The molecules in the crystal are all parallel and arranged in approximately planar layers, each consisting of rows of molecules running along the *b* axes of the unit cells (Figure 2a); adjacent rows are separated by the hydrogen-bonded solvent DMSO molecules. The parallel layers aggregate in an "AB pattern" (Figure 2) with alternate layers lying above each other, and adjacent layers staggered. This arrangement appears to be unique in perylene chemistry.

Both **2** and **3** are dark orange-red in the solid state, and yellow to red, depending on the concentration, in dichloromethane solution. Although the composition and structures of the two compounds appear to be very similar, their absorption and emission characteristics differ significantly.[14,15] The UV/Vis apsorption and emission spectra of compound **3**, recorded in CH_2Cl_2, are shown in Figure 3. The symmetry observed in the relation between the absorption and emission spectra of this derivative is a clear indication of its monomeric nature at the concentration chosen in this study (7×10^{-6} M). The fluorescence quantum yield is $\Phi_{fl}=0.092$ with a lifetime of $\tau_{fl}=1.77$ ns for compound **3**. From the overlap of the spectra of the two compounds, the singlet state energies are determined to be 460 and 507 nm ($^1E_{00}=2.7$ and 2.45 eV) for **3** and **2**, respectively.

The UV/Vis absorption spectra of compound **2** in dichloromethane turned out to be virtually concentration independent. However, whereas compound **3** is only sparingly soluble in dichloromethane, its behavior in DMSO is very different and at high concentrations (10^{-2} M) gives rise to magenta solutions. Upon dilution, compound **3** display significantly altered photophysics (Figure 4) indicating aggregation. The absorption is strongly red-shifted and broadened relative to the monomer, with a maximum at 574 nm ($\varepsilon=3\times10^4$ mol^{-1}cm^{-1}), while the emission of the aggregated form is located at 690 nm, and has much lower quantum yield (10^{-2}).

A fresh magenta solution of the compound at high concentration (10^{-3} M) was studied with scanning probe microscopy (AFM-tapping mode; AFM = atomic force microscopy) (Figure 5).[16] The sample consists of long rod-type structures with a length between 100 and 400 nm, a width of approximately 40 nm and a height of only 2 nm. The observed structures can best be described as nanocrystals.[17] Related structures have been studied,[17a–b] which were made

 © 2003 Wiley-VCH Verlag GmbH & Co. KGaA, Weinheim

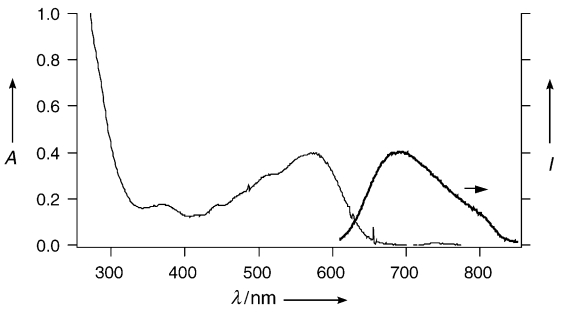


Figure 4. UV/Vis absorption ($l = 1$ mm) and emission spectra of the magenta aggregated form of compound **3** in DMSO. Concentration is 1.3×10^{-4} M; the emission was recorded upon 500 nm excitation by using a 550 nm cutoff filter. A = Absorbance.

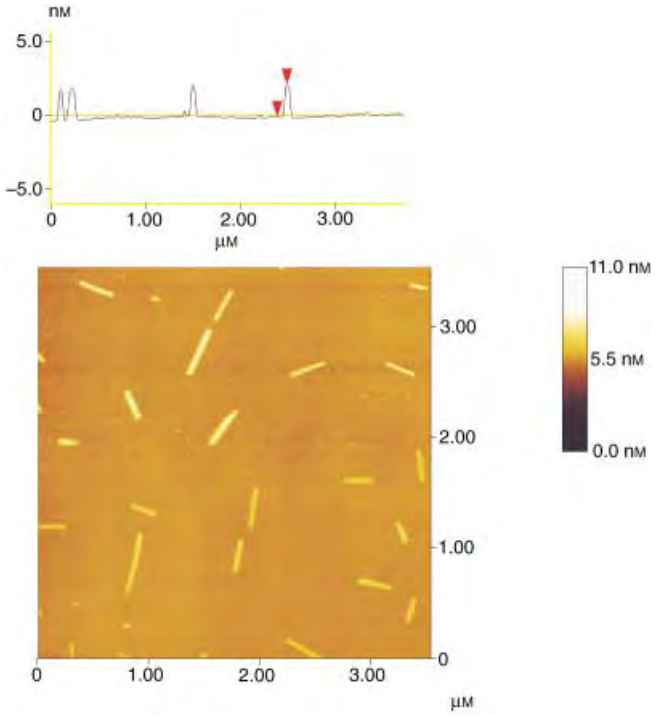


Figure 5. AFM image obtained with a purple solution of compound **3** in DMSO (10^{-3} M) on mica by using the tapping mode. The top section shows a height profile, which indicates a very narrow height distribution.

by the reprecipitation method (involving injection of perylene solutions into hot water).[17c] They can be considered a special form of "Scheibe" or *J* aggregates[17d–g] because of their linear rod-type shape even though we do not have a direct spectroscopic evidence of their nature. Noteably, the solvent, DMSO, plays a major role in the formation of the rods, and it is the only solvent in which it was possible to grow such nanocrystals.

From the assumption that the molecular network in the crystallites of **3** is similar to that established for compound **2** by single-crystal X-ray diffraction, an interesting picture of these Scheibe polymers emerges. Since the unit cell, which in the case of **2** contains one perylene molecule, has dimensions in the order of 1 nm, the nanocrystal rods generated by the stacking of molecular units would contain two molecules in one dimension. We observed that the length of the rods is sensitive to the concentration of the solution from which they are obtained (maximum lengths of several microns). A coalescence effect was observed with AFM, by adjusting the concentration of the solution, although the thickness of the aggregates remained essentially unchanged.

Given the proposed molecular stacking, the transition dipole moment (along the long axis of the molecule) is most likely to be perpendicular to the long axis of the nanocrystal, a notion which we plan to establish in a future systematic structural study of related derivatives. The possibility of assembling nanosize rods is essential for the construction of nanoelectronic devices, and the molecular assembly of conducting self-assembled wires remains a challenge in this field.

In this first investigation into a new class of perylene-derived dyes we have shown that the chosen synthetic approach to the tetra-N-substituted derivatives opens up the possibility of a wide range of further modifications of the chromophores, in particular their use in extended functional supramolecular arrays based on well-defined building principles, such as nanoscopic rods. We are currently aiming to construct a more rigid auxochromic periphery, which is thought to increase the emission quantum yields of these fluorescent dyes, thus bringing them closer to potential applications.

Experimental Section

Preparation of 3,4,9,10-$[RC(O)NH]_4C_{20}H_8$: A solution of compound **1** (310 mg = 1.00 mmol) in THF (30 mL) was slowly added at ambient temperature to freshly prepared sodium amalgam (Na: 2.00 mmol). After stirring the deep blue solution for 3 days, a 2.5 M solution of *n*-butyllithium in *n*-hexane (1.00 mL = 2.50 mmol) was added. After the reaction mixture was stirred for another 18 h at ambient temperature the blue-violet solution was decanted from the metallic mercury by using canula–septa techniques. The solution of the tetraanion, thus obtained, was slowly added to a solution of 4.10 mmol of the acid chloride dissolved in cooled THF (−30 °C, 40 mL). After the product mixture was stirred for 48 h at ambient temperature the solvent was removed in vacuo and the residue washed with water (100 mL), acetone (20 mL) and, finally, *n*-pentane (30 mL). After recrystallization from DMSO, compounds **2** and **3** were obtained as air stable, orange microcrystalline solids, which were washed with diethyl ether and then dried in vacuo.

3,4,9,10-$[t\text{BuC(O)NH}]_4C_{20}H_8$ (**2**): Yield: 78 %. M.p.: 268 °C. ^{1}H NMR (400.13 MHz, $(CD_3)_2SO$, 295 K): $\delta = 1.29$ (s, 36 H, $C(CH_3)_3$), 7.73 (d, 4 H, $^3J_{HaHb} = 8.4$ Hz, H^a, $C_{20}H_8$), 8.31 (d, 4 H, H^b, $C_{20}H_8$), 9.64 ppm (s, 4 H, NH). $\{^1H\}^{13}$C NMR (100.61 MHz, $(CD_3)_2SO$, 295 K): $\delta = 27.3$ ($C(CH_3)_3$), 39.6 ($C(CH_3)_3$), 121.1 (CH, $C_{20}H_8$), 124.1 (CH, $C_{20}H_8$), 124.5 (C, $C_{20}H_8$), 128.2 (C, $C_{20}H_8$), 129.2 (C, $C_{20}H_8$), 134.3 (CN, $C_{20}H_8$), 178.3 ppm (CO). IR (KBr): $\tilde{\nu} = 3340$ (vbr m), 3119 (vw), 2965 (s), 2932 (m), 2906 (m), 2870 (m), 1680 (s), 1623 (s), 1591 (s), 1519 (br vs), 1479 (s), 1430 (m), 1398 (m), 1366 (m), 1285 (vs), 1202 (s), 1172 (s), 1138 (vs), 1104 (s), 1050 (m), 1015 (m), 931 (m), 819 (m), 629 (w), 571 cm^{-1}(w); elemental analysis calcd. for $C_{40}H_{48}N_4O_4$ ($M_r = 648.85$): C 74.05, H 7.46, N 8.63; found: C 73.99, H 7.32, N 8.45.

3,4,9,10-$[(4'\text{-}t\text{BuPh})C(O)NH]_4C_{20}H_8$ (**3**): Yield: 66 %, M.p.: 286 °C (dec.); ^{1}H NMR (200.13 MHz, $(CD_3)_2SO$, 295 K): $\delta = 1.26$ (s, 36 H, $C(CH_3)_3$), 7.27 (d, 8 H, $^3J_{H2H3} = 8.4$ Hz, H^3, C_6H_4), 7.71 (d, 4 H, $^3J_{HaHb} = 8.3$ Hz, H^a, $C_{20}H_8$), 7.83 (d, 8 H, H^2, C_6H_4), 8.42 (d, 4 H, H^b, $C_{20}H_8$), 10.74 ppm (s, 4 H, NH); $\{^1H\}^{13}$C NMR (100.61 MHz, $(CD_3)_2SO$, 295 K): $\delta = 31.3$ ($C(CH_3)_3$), 34.9 ($C(CH_3)_3$), 118.8 (C, $C_{20}H_8$), 121.3

 © 2003 Wiley-VCH Verlag GmbH & Co. KGaA, Weinheim

(CH, $C_{20}H_8$), 125.0 (CH, C_6H_4), 125.1 (CH, $C_{20}H_8$), 127.1 (C, $C_{20}H_8$), 128.1 (CH, C_6H_4), 129.1 (C, $C_{20}H_8$), 131.6 (C, C_6H_4), 133.7 (CN, $C_{20}H_8$), 154.6 (C, C_6H_4), 165.9 ppm (CO); IR (KBr): $\tilde{\nu}$ = 3385 (vbr m), 3274 (vbr m), 3058 (w), 2963 (vs), 2906 (m), 2869 (m), 1655 (s), 1611 (m), 1593 (m), 1524 (vs), 1497 (vs), 1461 (s), 1409 (s), 1363 (m), 1301 (s), 1265 (vs), 1106 (br s), 1020 (s), 848 (m), 816 (s), 703 cm^{-1} (m); elemental analysis calcd. for $C_{64}H_{64}N_4O_4$ (M_r = 953.24): C 80.64, H 6.77, N 5.88; found: C 80.37, H 6.61, N 5.86. UV/Vis data. **2**: $\lambda_{max}(\varepsilon)$ = 271 (33690), 382 (14960), 442 (36020), 465 nm (45980 $M^{-1}cm^{-1}$); **3**: $\lambda_{max}(\varepsilon)$ = 248 (11860), 316 (61154), 332 (55497), 390 (sh) (14560), 412 (31155), 434 (45010), 466 nm (sh) (11859 $M^{-1}cm^{-1}$).

X-ray Crystallographic Study of **2**: X-ray intensity data were collected on an Enraf-Nonius CAD4 diffractometer. Formula $C_{40}H_{48}N_4O_4 \cdot 2(C_2H_6OS)$, Crystal size 0.4 × 0.2 × 0.1 mm, M = 808.08, triclinic, space group $P\bar{1}$ (No. 2), a = 10.0280(16), b = 10.213(2), c = 11.504(2) Å, α = 84.843(13), β = 72.388(15), γ = 74.140(15)°, V = 1080.2(3) $Å^3$, Z = 1, ρ_{calc} = 1.238 $g\,cm^{-3}$, $\lambda(Mo_{K\alpha})$ = 0.71073 Å, μ = 0.174 mm^{-1}, $F(000)$ = 432. Reflections collected: 5832, Data/restraints/parameters = 2188/0/287, GOF = 1.100, R_1 = 0.0634, wR_2 = 0.1752, max and min $\Delta\rho$ = +0.644/−0.467 e $Å^{-3}$. The structure was solved using direct methods (SHELXL 97).[18] The asymmetric unit only contains one half of a perylene molecule and a DMSO molecule, the other half being generated by the symmetry operation −x + 2, −y, −z + 2). The amino hydrogen atoms were directly located and their positions refined. All other hydrogen atoms were placed in calculated positions with displacement parameters set equal 1.2 U_{eq} (or 1.5 U_{eq} for methyl groups) of the parent carbon atoms. The DMSO molecule in the asymmetric unit was disordered in a 50:50 ratio between two sites. In the final cycles of full-matrix least-squares refinement the non-hydrogen atoms (except for the disordered carbon atom C3S of the DMSO molecule) were assigned anisotropic displacement parameters. CCDC 205348 contains the supplementary crystallographic data for this paper. These data can be obtained free of charge via www.ccdc.cam.ac.uk/conts/retrieving.html (or from the Cambridge Crystallographic Data Centre, 12 Union Road, Cambridge CB2 1EZ, UK; fax: (+44) 1223-336-033; or deposit@ccdc.cam.ac.uk).

Received: March 7, 2003 [Z51348]

Keywords: dyes · fluorescence · perylenes · scanning probe microscopy · self-assembly

[1] a) H. Zollinger, *Color Chemistry*, 2nd ed., VCH, Weinheim, **1991**; b) W. Herbst, K. Hunger, *Industrial Organic pigments, Production, Properties, Applications*, Wiley-VCH, Weinheim, **1997**; c) H. Kaiser, J. Lindner, H. Langhals, *Chem. Ber.* **1991**, *124*, 529; d) P. M. Kazmaier, R. Hoffmann, *J. Am. Chem. Soc.* **1994**, *116*, 9684; e) R. Reisfeld, G. Seybold, *Chimia* **1990**, *44*, 295; f) F. Würthner, *Nachr. Chem.* **2001**, *49*, 1284.

[2] Selected references: a) J. Lukác, H. Langhals, *Chem. Ber.* **1983**, *116*, 3524; b) H. Langhals, *Chem. Ber.* **1985**, *118*, 4641; c) H. Langhals, *Chimia* **1994**, *48*, 503; d) L. Feiler, H. Langhals, K. Polborn, *Liebigs Ann.* **1995**, 1229; e) H. Langhals, J. Gold, *J. Prakt. Chem.* **1996**, 338, 654; f) H. Langhals, P. von Unold, M. Speckbacher, *Liebigs Ann.* **1997**, 467; g) H. Langhals, W. Jona, *Eur. J. Org. Chem.* **1998**, 847; h) H. Langhals, H. Jaschke, U. Ring, P. von Unold, *Angew. Chem.* **1999**, *111*, 143; *Angew. Chem. Int. Ed.* **1999**, *38*, 201; i) M. Adachi, Y. Nagao, *Chem. Mater.* **1999**, *11*, 2107; j) H. Langhals, F. Süßmeier, *J. Prakt. Chem.* **1999**, *341*, 309; k) H. Langhals, S. Kirner, *Eur. J. Org. Chem.* **2000**, 365; l) K. D. Belfield, K. J. Schafer, M. D. Alexander, Jr., *Chem. Mater.* **2000**, *12*, 1184; m) T. Sakamoto, C. Pac, *J. Org. Chem.* **2001**, *66*, 94; n) S. Demmig, H. Langhals, *Chem. Ber.* **1988**, *121*, 225; o) D. Dotcheva, M. Klapper, K. Müllen, *Macromol. Chem. Phys.* **1994**, *195*, 1905; p) H. Quante, P. Schlichting, U. Rohr, Y. Geerts, K. Müllen, *Macromol. Chem. Phys.* **1996**, *197*, 4029; q) U. Rohr, P. Schlichting, A. Böhm, M. Groß, K. Meerholz, C. Bräuchle, K. Müllen, *Angew. Chem.* **1998**, *110,* 1463; *Angew. Chem. Int. Ed.* **1998**, *37*, 1434.

[3] a) C. Göltner, D. Pressner, K. Müllen, H. W. Spieß, *Angew. Chem.* **1993**, *105*, 1722; *Angew. Chem. Int. Ed. Engl.* **1993**, *32*, 1660; b) C. W. Struijk, A. B. Sieval, J. E. J. Dakhorst, M. van Dijk, P. Kimkes, R. B. M. Koehorst, H. Donker, T. J. Schaafsma, S. J. Picken, A. M. van de Craats, J. M. Warman, H. Zuilhof, E. J. R. Sudhölter, *J. Am. Chem. Soc.* **2000**, *122*, 11057; c) R. A. Cormier, B. A. Gregg, *J. Phys. Chem. B* **1997**, *101*, 11004; d) P. Schlichting, U. Rohr, K. Müllen, *J. Mater. Chem.* **1998**, *8*, 2561; e) B. A. Gregg, R. A. Cormier, *J. Phys. Chem. B* **1998**, *102*, 9952; f) R. A. Cormier, B. A. Gregg, *Chem. Mater.* **1998**, *10*, 1309; g) G. P. Wiederrecht, B. A. Yoon, M. R. Wasielewski, *Adv. Mater.* **2000**, *12*, 1533; h) V. Gama, R. T. Henriques, G. Bonfait, M. Almeida, A. Meetsma, S. van Smaalen, J. L. de Boer, *J. Am. Chem. Soc.* **1992**, *114*, 1986; i) A. Smirnov, D. B. Fulton, A. Andreotti, J. W. Petrich, *J. Am. Chem. Soc.* **1999**, *121*, 7979; j) T. G. Dax, H. Falk, *Monatsh. Chem.* **2000**, *131*, 1217; k) B. Immitzer, H. Falk, *Monatsh. Chem.* **2000**, *131*, 1167; l) T. G. Dax, C. Etzlstorfer, H. Falk, *Monatsh. Chem.* **2000**, *131*, 1115; m) F. Würthner, A. Sautter, C. Thalacker, *Angew. Chem.* **2000**, *112*, 1298; *Angew. Chem. Int. Ed.* **2000**, *39*, 1243.

[4] a) A. Zinke, E. Unterkreuter, *Monatsh. Chem.* **1919**, *40*, 405; b) A. Zinke, W. Hirsch, E. Brozek, *Monatsh. Chem.* **1929**, *51*, 205.

[5] a) K. W. Hellmann, C. H. Galka, I. Rüdenauer, L. H. Gade, I. J. Scowen, M. McPartlin, *Angew. Chem.* **1998**, *110*, 2053; *Angew. Chem. Int. Ed.* **1998**, *37*, 1948; b) K. W. Hellmann, C. H. Galka, L. H. Gade, A. Steiner, D. S. Wright, T. Kottke, D. Stalke, *J. Chem. Soc. Chem. Commun.* **1998**, 549.

[6] L. H. Gade, C. H. Galka, K. W. Hellmann, R. M. Williams, L. De Cola, I. J. Scowen, M. McPartlin, *Chem. Eur. J.* **2002**, *8*, 3732.

[7] a) M. Tamano, S. Maki (Toyo Ink MFG Co., Ltd), EP 0965629A, **1999**; b) S. Onikubo, M. Tamano (Toyo Ink MFG Co., Ltd), JP 2000150152A, **2000**; c) S. Onikubo, M. Tamano (Toyo Ink MFG Co., Ltd), JP 2000150161A, **2000**; d) M. Tamano, S. Onikubo (Toyo Ink MFG Co., Ltd), JP 2000068058A, **2000**.

[8] H. Langhals, *Heterocycles* **1995**, *40*, 477.

[9] a) F. Würthner, A. Sautter, *J. Chem. Soc. Chem. Commun.* **2000**, 445; b) F. Würthner, A. Sautter, D. Schmid, P. J. A. Weber, *Chem. Eur. J.* **2001**, *7*, 894.

[10] The DMSO solvent molecules adopt two different orientations with the result that the asymmetric unit of the triclinic crystal consists of a half molecule of **2** with two disordered DMSO molecules of half occupancy.

[11] a) D. M. Donaldson, J. M. Roberts, J. G. White, *Proc. R. Soc.* **1953**, *A220*, 311; b) C. Zannoni, A. Arcioni, P. Cavatorta, *Chem. Phys. Lipids* **1983**, *32*, 179; c) L. B.-A. Johansson, J. Karolin, H. Langhals, S. Reichherzer, N. von Füner, K. Polborn, *J. Chem. Soc. Faraday Trans.* **1993**, *89*, 49.

[12] a) H. Bock, C. Näther, Z. Havlas, *J. Am. Chem. Soc.* **1995**, *117*, 3869; b) C. Näther, H. Bock, Z. Havlas, T. Hauck, *Organometallics* **1998**, *17*, 4707.

[13] a) F. Graser, E. Hädicke, *Liebigs Ann. Chem.* **1980**, 1994; b) F. Graser, E. Hädicke, *Liebigs Ann. Chem.* **1984**, 483; c) G. Klebe, F. Graser, E. Hädicke, J. Berndt, *Acta Crystallogr. Sect. B* **1989**, *45*, 69; d) E. Hädicke, F. Graser, *Acta Crystallogr. Sect. C* **1986**, *42*, 189.

[14] Emission spectra were recorded on a SPEX Fluorolog I (1681) instrument equipped with an R928 photomultiplier (Products for Research) and were measured on dilute solutions by using a 395 nm (emission-path) cut-off filter. Corrections for the photomultiplier sensitivity were applied to the emission spectra. For determination of the emission quantum yields, using the "optical dilute relative method",[13a] bis(di-*tert*-butylphenyl)perylenebisi-

mide in air-saturated dichloromethane ($\Phi_{em} = 0.99$)[13b] was used as a standard. Quantum yields and lifetimes are reported or air saturated dichloromethane solutions. The excitation wavelength was 392 nm, and the optical density of both the reference and the sample was adjusted to 0.1 (1 cm) at this wavelength. Absorption spectra were recorded on a Hewlett Packard 8453 diode array spectrophotometer, using 1 nm bandwidth. Time resolved emission was recorded with a Hamamatsu C-5680 streak camera equipped with an M 5677 sweep unit. Excitation was performed with a LTB, MGS 450 TD nitrogen laser (337 nm, 600 ps) operating at 10 Hz. a) J. N. Demas, G. A. Crosby, *J. Phys. Chem.* **1971**, *75*, 991; b) W. E. Ford, P. V. Kamat, *J. Phys. Chem.* **1987**, *91*, 6373.

[15] Compound **2** displays rather sharp absorption features, with maxima observed at 271, 382, 442, 466 nm (see also Experimental Section) and a tailing band, with the last maximum at 572 nm, which is significantly beyond the emission maximum at 530 nm (the typical wavelength for the first emission maximum for perylenebisimides). The position of the absorption band maximum at 466 nm and symmetrically featured emission band at 530 nm indicates a rather large stokes shift of 2591 cm^{-1}. The emission at 530 nm, which we attribute to single, nonaggregated dye molecules, displays a moderate quantum yield of emission ($\Phi_{fl} = 0.091$) with a normal fluorescence lifetime ($\tau_{fl} = 4.4$ ns). Remarkably both the absorption and emission maxima of 3,4,9,10-[(4′-*t*BuPh)C(O)NH]$_4$C$_{20}$H$_8$ (**3**) are blue-shifted with respect to the pivalyl-substituted compound **2**. It appears that the larger amide substituents introduce steric crowding at the N-amido functions, making them turn out of the plane of the aromatic ring system, thus canceling the enhanced conjugation and red shift (auxochromic effect) as observed with **2**, and making the absorption and emission characteristics much more like perylene itself. Absorption maxima are observed at 248, 316, 323, 390 (sh), 411, 434, and 465 nm, and vibrationally resolved emission is displayed at 471, 501, and 537 nm (sh). The Stokes shift based on the 434 and 471 nm maxima is 1810 cm^{-1}.

[16] For scanning force microscopy (SFM) investigations, the substance was dissolved in DMSO and dropped onto freshly cleaved mica surfaces and dried in vacuo. SFM inspections were performed with a commercial instrument (Digital Instruments, Nanoscope IIIa, Dimension 3000, Santa Barbara, CA) running in the tapping mode. Silicon cantilevers (Nanosensors) with a resonant frequency of 250–350 kHz were used for the experiments. AFM images obtained under identical conditions with compound **3** from a saturated dichloromethane only displayed a featureless aggregation, which indicates that this phenomenon is directly associated with the incorporation of the solvent.

[17] a) T. Onodera, T. Oshikiri, H. Katagi, H. Kasai, S. Okada, H. Oikawa, M. Terauchi, M. Tanaka, H. Nakanishi, *J. Cryst. Growth* **2001**, *229*, 586; b) J. I. Niitsuma, T. Fujimura, T. Itoh, H. Kasai, S. Okada, H. Oikawa, H. Nakanishi, *Int. J. Mod. Phys. B* **2001**, *15*, 3901; c) H. Kasai, H. S. Nalwa, H. Oikawa, S. Okada, H. Matsuda, N. Minami, A. Kakuta, K. Ono, A. Mukoh, H. Nakanishi, *Jpn. J. Appl. Phys. Part 2* **1992**, *31*, L1132-L1134; d) D. A. Higgins, P. F. Barbara, *J. Phys. Chem.* **1995**, *99*, 3; e) D. A. Higgins, J. Kerimo, D. A. Van den Bout, P. F. Barbara, *J. Am. Chem. Soc.* **1996**, *118*, 4049; f) H. Yao, S. Sugiyama, R. Kawabata, H. Ikeda, O. Matsuoka, S. Yamamoto, N. Kitamura, *J. Phys. Chem. B* **1999**, *103*, 4452; g) J. A. Tuszynski, M. F. Jorgensen, D. Mobius, *Phys. Rev. E* **1999**, *59*, 4374.

[18] G. M. Sheldrick, SHELXS-97, Program for the Solution of Crystal Structures, University of Göttingen, Göttingen (Germany), **1997**

 © 2003 Wiley-VCH Verlag GmbH & Co. KGaA, Weinheim

One-Pot Sequential Reactions

Novel Ruthenium- and Platinum-Catalyzed Sequential Reactions: Synthesis of Tri- and Tetrasubstituted Furans and Pyrroles from Propargylic Alcohols and Ketones**

Yoshiaki Nishibayashi, Masato Yoshikawa, Youichi Inada, Marilyn Daisy Milton, Masanobu Hidai, and Sakae Uemura**

Studies on multiple catalysts within the same medium to obtain desired products from simple starting materials are one of the current and important topics in synthetic chemistry.[1] The action of multiple catalysts lessens the reaction time and the yield loss by avoiding the isolation and purification of intermediates in multiple step sequences. Some interesting results in which multiple and different transition metal catalysts work in the same medium were reported,[2] but in most cases the reaction conditions, such as reaction temperature and reaction atmosphere, need to be changed on the way, or the successive addition of catalysts is necessary according to the reaction steps.[3]

Quite recently, we reported the ruthenium-catalyzed efficient propargylic substitution reactions of propargylic alcohols with various heteroatom- and carbon-centered nucleophiles to give the corresponding functionalized propargylic products in high yields with complete regioselectivities.[4] Noteworthy, the reactions are catalyzed only by thiolate-bridged diruthenium complexes[5] such as $[Cp^*RuCl(\mu_2\text{-}SR)_2RuCp^*Cl]$ ($Cp^* = \eta^5\text{-}C_5Me_5$; R = Me (**1a**), *i*Pr (**1b**), *n*Pr (**1c**)). The result prompted us to investigate the transition metal-catalyzed sequential reaction of functionalized propargylic products, which have a terminal alkyne, because organic compounds with a terminal alkyne are known to be converted into more valuable compounds by various transition metal catalysts.[6,7] We have now found a novel sequential reaction system by using heterobimetallic

[*] Prof. Dr. S. Uemura, Dr. Y. Nishibayashi, M. Yoshikawa, Y. Inada, Dr. M. D. Milton
Department of Energy and Hydrocarbon Chemistry
Graduate School of Engineering
Kyoto University
Yoshida, Sakyo-ku, Kyoto 606–8501 (Japan)
Fax: (+81) 75-753-3573
E-mail: uemura@scl.kyoto-u.ac.jp
Prof. Dr. M. Hidai
Department of Materials Science and Technology
Faculty of Industrial Science and Technology
Tokyo University of Science
Noda, Chiba 278–8510 (Japan)
Fax: (+81) 471-23-9362
E-mail: hidai@rs.noda.sut.ac.jp

[**] This work was supported by a Grant-in-Aid for Scientific Research (No. 13305062) from the Ministry of Education, Science, Sports, and Culture of Japan.

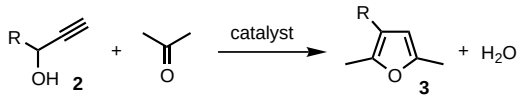
Supporting information for this article is available on the WWW under http://www.angewandte.org or from the author.

 DOI: 10.1002/anie.200351170 © 2003 Wiley-VCH Verlag GmbH & Co. KGaA, Weinheim

catalysts to give the corresponding tri- and tetra-substituted furans and pyrroles in moderate to high yields with complete regioselectivity from the reaction of propargylic alcohols with ketones in the presence of a catalytic amount of both **1a** and $PtCl_2$. In this reaction system, two different catalysts simultaneously promote their catalytic cycles in the same medium. Preliminary results are described herein.

Treatment of 1-phenyl-2-propyn-1-ol (**2a**) in acetone in the presence of **1a** (10 mol%), NH_4BF_4 (20 mol%), and $PtCl_2$ (20 mol%) at reflux temperature for 36 h afforded 2,5-dimethyl-3-phenylfuran (**3a**) in 75% yield as measured by GLC (64% yield of the isolated product; Table 1, entry 1). A prolonged reaction time improved the yield of **3a** (Table 1, entries 2 and 3). The reaction proceeded even in the presence of smaller quantities of **1a** (5 mol%) and $PtCl_2$ (10 mol%; Table 1, entry 4). Noteworthy, the bimetallic system of **1a** and $PtCl_2$ is essential to promote the catalytic formation of **3a** effectively. Other transition-metal complexes, such as $Pd(OAc)_2$, $[PdCl_2(MeCN)_2]$ and $PdCl_2$ were ineffectual, while $AuCl_3$[8] worked effectively but an intermediate diketone was also formed (see below; Table 1, entry 5). The use of various propargylic alcohols resulted in the formation of the corresponding 3-aryl and 3-alkenyl substituted 2,5-dimethylfurans (**3b**–**3h**) in moderate to high yields with a complete regioselectivity (Table 1, entries 6–12). Unfortunately, the reaction of 1-cyclohexyl-2-propyn-1-ol did not proceed at all (Table 1, entry 13).

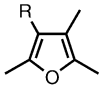
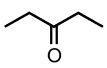
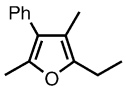
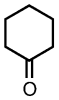
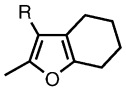
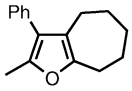
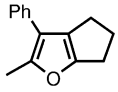
Table 1: Reaction of propargylic alcohol (**2**) with acetone in the presence of $[Cp^*RuCl(\mu\text{-}SMe)_2RuCp^*Cl]$ (**1a**) and $PtCl_2$.[a]



Entry	R	Cat (mol%)	t [h]	Yield of **3** [%][b]
1	Ph (**2a**)	**1a** (10) and $PtCl_2$ (20)	36	**3a**, 64 (75)[c]
2	Ph (**2a**)	**1a** (10) and $PtCl_2$ (20)	72	**3a**, 69
3	Ph (**2a**)	**1a** (10) and $PtCl_2$ (10)	100	**3a**, (83)[c]
4	Ph (**2a**)	**1a** (5) and $PtCl_2$ (10)	110	**3a**, (74)[c]
5	Ph (**2a**)	**1a** (10) and $AuCl_3$ (20)	36	**3a**, (36)[c,d]
6	*p*-MeC_6H_4 (**2b**)	**1a** (10) and $PtCl_2$ (20)	72	**3b**, 65
7	*p*-$MeOC_6H_4$ (**2c**)	**1a** (10) and $PtCl_2$ (20)	36	**3c**, 52
8	*p*-FC_6H_4 (**2d**)	**1a** (10) and $PtCl_2$ (20)	72	**3d**, 57
9	*p*-ClC_6H_4 (**2e**)	**1a** (10) and $PtCl_2$ (20)	72	**3e**, 74
10	*p*-$CF_3C_6H_4$ (**2f**)	**1a** (10) and $PtCl_2$ (20)	36	**3f**, 54
11	2-naphthyl (**2g**)	**1a** (10) and $PtCl_2$ (20)	72	**3g**, 64
12	$Ph_2C{=}CH$- (**2h**)	**1a** (10) and $PtCl_2$ (20)	36	**3h**, 29
13	cyclohexyl (**2i**)	**1a** (10) and $PtCl_2$ (20)	36	**3i**, 0

[a] All the reactions of **2** (0.60 mmol) with acetone (30 mL) were carried out in the presence of catalysts and NH_4BF_4 (20 mol%) at reflux temperature. [b] Yield of isolated compound. [c] Yield obtained by GLC. [d] 3-Phenyl-2,5-hexanedione was also formed with 27% yield obtained by GLC.

Table 2: Reaction of propargylic alcohol (**2**) with ketone in the presence of $[Cp^*RuCl(\mu\text{-}SMe)_2RuCp^*Cl]$ (**1a**) and $PtCl_2$.[a]

Entry	**2**	Ketone	Furan (**3**)	Yield of **3**, %[b]
1	R = Ph (**2a**)			R = Ph, 72 (**3j**)
2	R = *p*-MeC_6H_4 (**2b**)			R = *p*-MeC_6H_4, 78 (**3k**)
3	R = *p*-FC_6H_4 (**2d**)			R = *p*-FC_6H_4, 65 (**3l**)
4[c]	R = Ph (**2a**)			85 (**3m**)
5	R = Ph (**2a**)			R = Ph, 75 (**3n**)
6	R = *p*-FC_6H_4 (**2d**)			R = *p*-FC_6H_4, 75 (**3o**)
7	R = *p*-ClC_6H_4 (**2e**)			R = *p*-ClC_6H_4, 69 (**3p**)
8	R = Ph (**2a**)			66 (**3q**)
9	R = Ph (**2a**)			0 (**3r**)

[a] All the reactions of **2** (0.60 mmol) with ketone (30 mL) were carried out in the presence of **1a** (0.06 mmol), $PtCl_2$ (0.12 mmol) and NH_4BF_4 (0.12 mmol) at reflux temperature for 36 h. [b] Isolated yield. [c] For 72 h.

Reactions of propargylic alcohols with other ketones were similarly carried out. Typical results are shown in Table 2. Formation of the corresponding 3-aryl-2,4,5-trimethylfurans (**3j**–**3l**) was observed in the reactions of propargylic alcohols (**2a**, **2b**, **2d**) with 2-butanone (Table 2; entries 1–3). The reaction of **2a** with 3-pentanone under the same reaction conditions gave 2-ethyl-3,5-dimethyl-4-phenylfuran (**3m**) in 85% yield (Table 2, entry 4). Noteworthy, the formation of other regioisomers of furans was not observed in all cases. The reactions of various propargylic alcohols with cyclohexanone gave the expected 3-aryl-2-methyl-4,5,6,7-tetrahydrobenzofurans (**3n**–**3p**) in high yields (Table 2, entries 5–7). From **2a** and cycloheptanone, 2-methyl-3-phenyl-5,6,7,8-tetrahydro-4*H*-cyclohepta[*b*]furan (**3q**) was obtained in 66% yield, but no reaction occurred with cyclopentanone (Table 2, entries 8 and 9, respectively).

To obtain some information of the reaction mechanism, the relationship between the product yields and the reaction time was investigated in the reaction between **2a** and acetone in the presence of **1a** and $PtCl_2$ (Figure 1). This time profile indicates the following: At first, **2a** is transformed rapidly into γ-ketoalkyne (**4a**) by the catalysis of **1a** (Scheme 1, step a).[4b] Then, hydration of the alkyne moiety in **4a** by the produced H_2O slowly gives the 1,4-diketone, **5a**, by the catalysis of $PtCl_2$ (Scheme 1, step b).[9] Intramolecular cyclization of the produced diketone then follows, which results in the formation of the furan, **3a**, also by the catalysis of $PtCl_2$ (Scheme 1, step c).[9b] This result clearly indicates that two different

 © 2003 Wiley-VCH Verlag GmbH & Co. KGaA, Weinheim

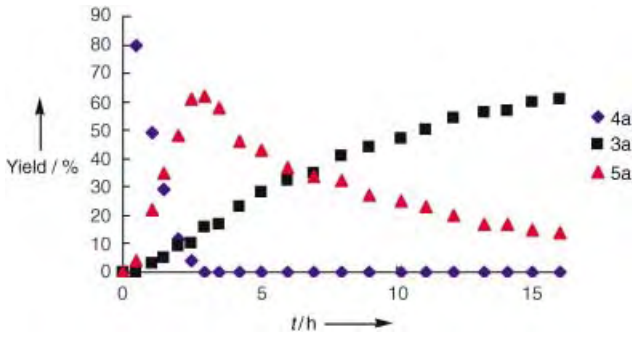
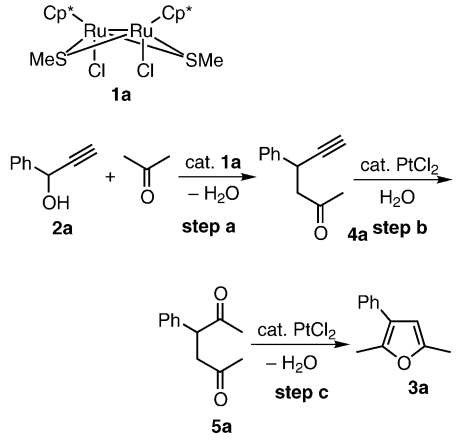
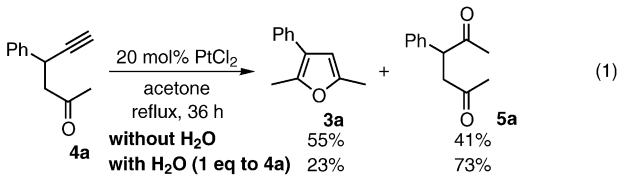


Figure 1. Time profile of the reaction of propargylic alcohol (**2a**) with acetone in the presence of [Cp*RuCl(μ-SMe)$_2$RuCp*Cl] (**1a**; 10 mol%) and $PtCl_2$ (20 mol%).



Scheme 1. Reaction of 1-phenyl-2-propyn-1-ol with acetone in the presence of [Cp*RuCl(μ-SMe)$_2$RuCp*Cl] and $PtCl_2$.

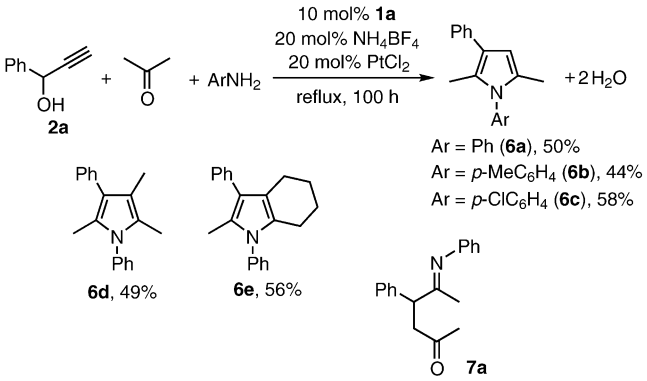
catalysts, such as **1a** and $PtCl_2$, can promote their catalytic cycles in the same medium. Separately, the transformation of **4a** into **3a** and **5a** was confirmed in the presence of $PtCl_2$ [Eq. (1)]. However, even upon adding stoichiometric



(1)

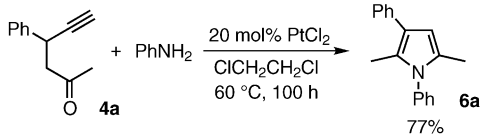
amounts of water to **4a**, its conversion into **3a** via **5a** was slower than that in the present reaction system, thus showing that the coexistence of **1a** and $PtCl_2$ promotes this conversion more smoothly.

When the above new catalytic reactions were carried out in the presence of aniline derivatives (5 equiv relative to **2a**), the corresponding tri- and tetra-substituted pyrroles (**6**) were produced in moderate isolated yields with complete regioselectivity (Scheme 2).[10] No formation of the corresponding furans and other regioisomers of **6** was observed in all cases. Nucleophilic attack of anilines on the carbon-carbon triple bond in **4a** catalyzed by $PtCl_2$ may give the corresponding



Scheme 2. Reactions of 1-phenyl-2-propyn-1-ol with ketones and anilines in the presence of [Cp*RuCl(μ-SMe)$_2$RuCp*Cl] and $PtCl_2$.

imines (**7a**).[11] Cyclization of **7a** catalyzed by $PtCl_2$ may produce the substituted pyrrole (**6a**). It was confirmed that the reaction of **4a** with aniline in the presence of $PtCl_2$ afforded **6a** in 77% isolated yield [Eq. (2)]. This result

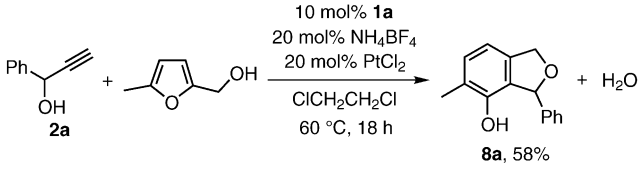


(2)

indicates that sequential three-component coupling reaction by the catalysis of **1a** and $PtCl_2$ occurs in the same medium.

The bimetallic system of **1a** and $PtCl_2$ can be applied to other sequential catalytic reactions. A typical example is shown in Scheme 3. The reaction of propargylic alcohol (**2a**) with 5-methyl-2-furylmethanol in the presence of a catalytic amount of both **1a** and $PtCl_2$ in 1,2-dichloroethane at 60 °C for 18 h afforded the corresponding phenol derivative **8a** in 58% yield.[12] Propargylation of the furylmethanol with **2a** was promoted by **1a** to give the corresponding furylmethyl propargylic ether,[4a] which was subsequently transformed into the corresponding phenol derivative by the so far known catalysis of $PtCl_2$.[13]

In summary, we have found novel ruthenium- and platinum-catalyzed sequential reactions to afford the corresponding tri- and tetra-substituted furans or pyrroles[14] from propargylic alcohols with ketones, or with ketones and anilines, respectively, in moderate to good yields with high regioselectivities. Two different kinds of catalysts **1a** and $PtCl_2$ sequentially promote each catalytic cycle in the same medium. Some phenol derivatives can also be prepared from propargylic alcohols and furylmethanol by this bimetallic



Scheme 3. Reaction of 1-phenyl-2-propyn-1-ol with 5-methyl-2-furylmethanol in the presence of [Cp*RuCl(μ-SMe)$_2$RuCp*Cl] and $PtCl_2$.

 © 2003 Wiley-VCH Verlag GmbH & Co. KGaA, Weinheim

system. Further investigations involving the elucidation of the detailed reaction mechanism and broadening the scope of this sequential catalytic systems are currently in progress.

Experimental Section

A typical experimental procedure for the reaction of 1-phenyl-2-propyn-1-ol (**2a**) with acetone catalyzed by [Cp*RuCl(μ_2-SMe)$_2$-RuCp*Cl] (**1a**) and $PtCl_2$ is described below. Complex **1a** (38 mg, 0.06 mmol), NH_4BF_4 (12 mg, 0.12 mmol), and $PtCl_2$ (31 mg, 0.12 mmol) were placed in a 50 mL flask under N_2. Anhydrous acetone (30 mL) was added, and then the mixture was magnetically stirred at room temperature. After the addition of **2a** (79 mg, 0.60 mmol), the reaction flask was kept at reflux temperature for 36 h. The solvent was concentrated under reduced pressure by an aspirator, and then the residue was purified by TLC (SiO_2) with EtOAc-hexane (1/9) to give 2,5-dimethyl-3-phenylfuran[15] (**3a**) as a colorless oil (66.5 mg, 0.38 mmol, 64% yield); ^{1}H NMR (270 MHz, $CDCl_3$): $\delta =$ 2.28 (s, 3H), 2.40 (s, 3H), 6.10 (s, 1H), 7.21–7.37 ppm (m, 5H); ^{13}C NMR (67.5 Hz, $CDCl_3$): $\delta = 12.9$, 13.4, 106.9, 121.4, 126.0, 127.3, 128.5, 134.5, 145.8, 149.7 ppm.

Received: February 13, 2003 [Z51170]

Keywords: domino reactions · heterocycles · homogeneous catalysis · platinum · ruthenium

[1] For recent reviews, see a) L. F. Tietze, *Chem. Rev.* **1996**, *96*, 115; b) E. K. Beuken, B. L. Feringa, *Tetrahedron* **1998**, *54*, 12985; c) G. Poli, G. Giambastiani, A. Heumann, *Tetrahedron* **2000**, *56*, 5959.

[2] For recent examples: examples where two catalysts activated different functional groups in the same medium, a) M. Sawamura, M. Sudoh, Y. Ito, *J. Am. Chem. Soc.* **1996**, *118*, 3309; b) S. Kamijo, Y. Yamamoto, *Angew. Chem.* **2002**, *114*, 3364; *Angew. Chem. Int. Ed.* **2002**, *41*, 3230, and references therein. Examples where two different catalytic cycles proceeded in the same medium, c) R. W. Barnhart, G. C. Bazan, T. Mourey, *J. Am. Chem. Soc.* **1998**, *120*, 1082; d) N. Jeong, S. D. Seo, J. Y. Shin, *J. Am. Chem. Soc.* **2000**, *122*, 10220; e) Z. J. A. Komon, G. M. Diamond, M. K. Leclerc, V. Murphy, M. Okazaki, G. C. Bazan, *J. Am. Chem. Soc.* **2002**, *124*, 15280.

[3] For recent examples, see a) P. A. Evans, J. E. Robinson, *J. Am. Chem. Soc.* **2001**, *123*, 4609; b) B. M. Choudary, N. S. Chowdari, S. Madhi, M. L. Kantam, *Angew. Chem.* **2001**, *113*, 4755; *Angew. Chem. Int. Ed.* **2001**, *40*, 4620; c) J. L. Christopher, W. Bielawski, R. H. Grubbs, *J. Am. Chem. Soc.* **2001**, *123*, 11312; d) T. Shimada, K. Mukaide, A. Shinohara, J. W. Han, T. Hayashi, *J. Am. Chem. Soc.* **2002**, *124*, 1584; e) J. Tian, N. Yamagiwa, S. Matsunaga, M. Shibasaki, *Angew. Chem.* **2002**, *114*, 3788; *Angew. Chem. Int. Ed.* **2002**, *41*, 3636; f) S. U. Son, K. H. Park, Y. K. Chung, *J. Am. Chem. Soc.* **2002**, *124*, 6838; g) B. M. Trost, M. R. Machacek, *Angew. Chem.* **2002**, *114*, 4887; *Angew. Chem. Int. Ed.* **2002**, *41*, 4693; h) A. E. Sutton, B. A. Seigal, D. F. Finnegan, M. L. Snapper, *J. Am. Chem. Soc.* **2002**, *124*, 13390.

[4] a) Y. Nishibayashi, I. Wakiji, M. Hidai, *J. Am. Chem. Soc.* **2000**, *122*, 11019; b) Y. Nishibayashi, I. Wakiji, Y. Ishii, S. Uemura, M. Hidai, *J. Am. Chem. Soc.* **2001**, *123*, 3393; c) Y. Inada, Y. Nishibayashi, M. Hidai, S. Uemura, *J. Am. Chem. Soc.* **2002**, *124*, 15172; d) Y. Nishibayashi, G. Onodera, Y. Inada, M. Hidai, S. Uemura, *Organometallics* **2003**, *22*, 873.

[5] The thiolate-bridged diruthenium complexes (**1**) were found to provide unique bimetallic reaction sites for activation and transformation of various terminal alkynes, see: Y. Nishibayashi, M. Yamanashi, I. Wakiji, M. Hidai, *Angew. Chem.* **2000**, *112*, 3031; *Angew. Chem. Int. Ed.* **2000**, *39*, 2909, and references therein.

[6] a) K. Ohe, T. Yokoi, K. Miki, F. Nishino, S. Uemura, *J. Am. Chem. Soc.* **2002**, *124*, 526; b) K. Miki, F. Nishino, K. Ohe, S. Uemura, *J. Am. Chem. Soc.* **2002**, *124*, 5260; c) Y. Nishibayashi, Y. Inada, M. Hidai, S. Uemura, *J. Am. Chem. Soc.* **2002**, *124*, 7900; d) Y. Nishibayashi, M. Yoshikawa, Y. Inada, M. Hidai, S. Uemura, *J. Am. Chem. Soc.* **2002**, *124*, 11846; e) Y. Nishibayashi, Y. Inada, M. Yoshikawa, M. Hidai, S. Uemura, *Angew. Chem.* **2003**, *115*, 1533; *Angew. Chem. Int. Ed.* **2003**, *42*, 1495.

[7] For recent examples, see a) J. L. Pail, S. Dérien, C. Bruneau, B. Demerseman, L. Toupet, P. H. Dixneuf, *Angew. Chem.* **2001**, *113*, 2996; *Angew. Chem. Int. Ed.* **2001**, *40*, 2912; b) M. Méndez, M. P. Muñoz, C. Nevado, D. J. Cárdenas, A. M. Echavarren, *J. Am. Chem. Soc.* **2001**, *123*, 10511; c) A. Fürstner, F. Stelzer, H. Szillat, *J. Am. Chem. Soc.* **2001**, *123*, 11863; d) Y. Sheng, D. G. Musaev, K. S. Reddy, F. E. McDonald, K. Morokuma, *J. Am. Chem. Soc.* **2002**, *124*, 4149; e) B. M. Trost, M. T. Rudd, *J. Am. Chem. Soc.* **2002**, *124*, 4178; f) K.-L. Yeh, B. Liu, C.-Y. Lo, H.-L. Huang, R.-S. Liu, *J. Am. Chem. Soc.* **2002**, *124*, 6510; g) H. Kusama, J. Takaya, N. Iwasawa, *J. Am. Chem. Soc.* **2002**, *124*, 11592.

[8] A. Stephen, K. Hashmi, L. Schwarz, J.-H. Choi, T. M. Frost, *Angew. Chem.* **2000**, *112*, 2382; *Angew. Chem. Int. Ed.* **2000**, *39*, 2285.

[9] a) W. Hiscox, P. W. Jennings, *Organometallics* **1990**, *9*, 1997; b) W. Baidossi, M. Lahav, J. Blum, *J. Org. Chem.* **1997**, *62*, 669; c) E. Mizushima, K. Sato, T. Hayashi, M. Tanaka, *Angew. Chem.* **2002**, *114*, 4745; *Angew. Chem. Int. Ed.* **2002**, *41*, 4563.

[10] A novel one-pot pyrrole synthesis has been reported, see R. U. Braun, K. Zeitler, T. J. J. Muller, *Org. Lett.* **2001**, *3*, 3297.

[11] Nucleophilic addition of amines on a C≡C triple bond mediated by a platinum complex has been reported, see a) T. E. Müller, A.-K. Pleier, *J. Chem. Soc. Dalton Trans.* **1999**, 583; b) T. E. Müller, M. Beller, *Chem. Rev.* **1998**, *98*, 675, and references therein.

[12] The molecular structure of **8a** was unambiguously determined by X-ray analysis. CCDC 203160 contains the supplementary crystallographic data for this paper. These data can be obtained free of charge via www.ccdc.cam.ac.uk/conts/retrieving.html (or from the Cambridge Crystallographic Data Centre, 12 Union Road, Cambridge CB2 1EZ, UK; fax: (+44) 1223-336-033; or deposit@ccdc.cam.ac.uk).

[13] a) A. S. K. Hashmi, T. M. Frost, J. W. Bats, *J. Am. Chem. Soc.* **2000**, *122*, 11553; b) B. Martín-Matute, D. J. Cárdenas, A. M. Echavarren, *Angew. Chem.* **2001**, *113*, 4890; *Angew. Chem. Int. Ed.* **2001**, *40*, 4754.

[14] For recent examples of the preparation of substituted furans and pyrroles, see a) C.-F. Lee, L.-M. Yang, T.-Y. Hwu, A.-S. Feng, J.-C. Tseng, T.-Y. Luh, *J. Am. Chem. Soc.* **2000**, *122*, 4992; b) A. V. Kel′in, A. W. Sromek, V. Gevorgyan, *J. Am. Chem. Soc.* **2001**, *123*, 2074; c) J. A. Marshall, E. A. V. Devender, *J. Org. Chem.* **2001**, *66*, 8037; d) A. V. Kel′in, V. Gevorgyan, *J. Org. Chem.* **2002**, *67*, 95; e) J. T. Kim, A. V. Kel′in, V. Gevorgyan, *Angew. Chem.* **2003**, *115*, 102; *Angew. Chem. Int. Ed.* **2003**, *42*, 98.

[15] T. S. Balaban, M. Hiegemann, *Tetrahedron* **1992**, *48*, 9827.

 © 2003 Wiley-VCH Verlag GmbH & Co. KGaA, Weinheim

Ferrous Complexes

Ferrous Wheels, Ellipse $[(t\mathrm{Bu_3SiS})\mathrm{FeX}]_n$, and Cube $[(t\mathrm{Bu_3SiS})\mathrm{Fe(CCSi}t\mathrm{Bu_3})]_4$**

Orson L. Sydora, Peter T. Wolczanski, and Emil B. Lobkovsky*

Dedicated to Roald Hoffmann

The controlled aggregation of low-coordinate, transition-metal complexes can lead to the generation of unusual oligomers, polymers or clusters. Inspired by Hoffmann's treatise on tetrahedral units as building blocks,[1,2] we sought "XMY" species as potential monomers for $[\mathrm{M}(\mu\text{-X})(\mu\text{-Y})]_n$, an oligomer or polymer based on the *edge*-connectivity of tetrahedra. Literature precedent[3] suggested the use of bulky thiolate and halide ligands as the μ-X and μ-Y linkages.

Treatment of $[\{(\mathrm{Me_3Si})_2\mathrm{N}\}_2\mathrm{Fe}]_2$ with four equivalents $t\mathrm{Bu_3SiSH}$[4] afforded orange $[\{(t\mathrm{Bu_3SiS})\mathrm{Fe}\}_2(\mu\text{-SSi}t\mathrm{Bu_3})_2]$ (**1**, 86%) akin to trigonal-based dimers prepared by Holm et al.,[5,6] hence desymmetrization was viewed as one means toward oligomerization. $\mathrm{FeX_2(thf)_2}$ and one equivalent of $t\mathrm{Bu_3SiSNa(thf)}_x$ ($x = 1.4$–1.7) were stirred for 18–24 h to provide yellow $[(\mathrm{X_2Fe})(\mu\text{-SSi}t\mathrm{Bu_3})_2\{\mathrm{FeX(thf)}\}]\mathrm{Na(thf)_4}$ (**2a**, X = Cl, 74%; **2b**, X = Br, 86%) and *cis*-$[\{\mathrm{I(thf)Fe}\}_2(\mu\text{-SSi}t\mathrm{Bu_3})_2]$ (**3**, 75%) upon isolation. The structures of **1**, **2b** and **3** were determined by single-crystal X-ray crystallography, and quenching studies ($\mathrm{D_2O/DCl}$ in $\mathrm{D_3COD}$) suggested that **2a** has the same thiolate:THF ratio (1:3.9) as **2b**. Elemental analyses were indeterminate, probably because of variable desolvation. Each complex has a μ_{eff} consistent with an $S = 2$ ground state (Evans' method [7] in $[\mathrm{D_8}]$THF) and little orbital contribution: **2a**, 4.8 μ_B; **2b**, 4.5 μ_B; **3**, 4.8 μ_B.

If the solvent (THF) was removed after the above procedures, and the remaining solids were heated under vacuum (**2a**, 80 °C, 1.5 h; **2b**, 79 °C, 2 h); **3**, 117 °C, 5 h) and extracted into benzene, then desolvation and aggregation occurred, but not to the expected polymers. Instead, ferrous wheels $[\mathrm{Fe}(\mu\text{-X})(\mu\text{-SSi}t\mathrm{Bu_3})]_n(\mathrm{C_6H_6})_m$ (X = Cl, $n = 12$, **4a**, 45%;[8] X = Br, $n = 12$, **4b**, 72%)[9] and the ferrous ellipse $[\mathrm{Fe}(\mu\text{-I})(\mu\text{-SSi}t\mathrm{Bu_3})]_{14}(\mathrm{C_6H_6})_m$ (**5**, 16%)[10] were isolated by crystallization. The structures of these complexes were determined by single-crystal X-ray crystallography,[11] but the benzene molecules of solvation, determined from quenching studies to be ~0.5–1.0 equivalent per Fe atom, exhibited significant disorder, and were removed from the refinement by using PLATON methods.

[*] Prof. P. T. Wolczanski, O. L. Sydora, E. B. Lobkovsky
Department of Chemistry & Chemical Biology
Baker Laboratory
Cornell University
Ithaca, New York 14853 (USA)
Fax: (+1) 607-255-4137
E-mail: ptw2@cornell.edu

[**] We thank the US National Science Foundation for support of this research, and Zoltan Gal for experimental assistance. Wheel X = Cl, Br, $n = 12$; ellipse X = I, $n = 14$.

The chloride ferrous wheel, **4a** (Figure 1), packs in a tetragonal array of columns; the bromide derivative, **4b**, is isomorphous. The wheels consist of edge-shared tetrahedra, with the inner diameter comprises μ-X ligands, and the periphery composed of $\mu\text{-SSi}t\mathrm{Bu_3}$ linkages. The orientation of each shared tetrahedral edge alternates relative to the ring plane such that the three different transannular X···X separations are basically the same (**4a**, 9.484 (29) Å av; **4b**, 9.483 (22) Å av) Because of the greater size of Br ion, the iron atoms in **4b** are slightly displaced towards the outside of the wheel relative to **4a.**

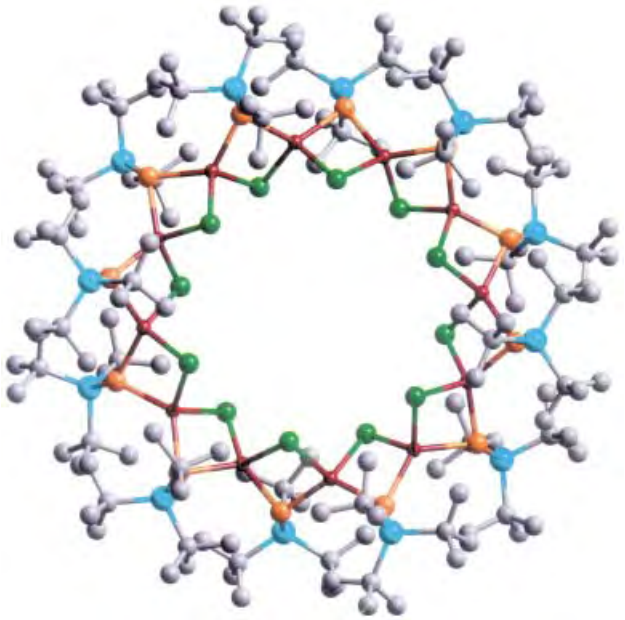


Figure 1. Molecular view of $[\mathrm{Fe}(\mu\text{-Cl})(\mu\text{-SSi}t\mathrm{Bu_3})]_{12}$ (**4a**) Fe = red, Cl = green, S = orange, Si = blue, C = gray; pertinent interatomic distances (Å) and angles (°): $d(\mathrm{FeS})_{av} = 2.340$ (9); transannular $d(\mathrm{Cl\cdots Cl})_{av} = 9.484$ (29); $d(\mathrm{FeCl})_{av} = 2.339$ (9); $d(\mathrm{Fe\cdots Fe})_{av} = 3.127$ (44); $(\mathrm{Cl\text{-}Fe\text{-}Cl})_{av} = 103.5$ (13); $(\mathrm{S\text{-}Fe\text{-}S})_{av} = 124.8$ (6); $(\mathrm{Fe\text{-}S\text{-}Fe})_{av} = 83.9$ (14); $(\mathrm{Fe\text{-}Cl\text{-}Fe})_{av} = 83.9$ (15); $(\mathrm{Cl\text{-}Fe\text{-}S})_{av} = 93.3$ (5), 121.0 (14). $[\mathrm{Fe}(\mu\text{-Br})(\mu\text{-SSi}t\mathrm{Bu_3})]_{12}$ (**4b**) is isomorphous: $d(\mathrm{FeS})_{av} = 2.339$ (6); transannular $d(\mathrm{Br\cdots Br})_{av} = 9.483$ (22); $d(\mathrm{FeBr})_{av} = 2.474$ (9); $d(\mathrm{Fe\cdots Fe})_{av}$ of 3.171 (51); $(\mathrm{Br\text{-}Fe\text{-}Br})_{av} = 103.6$ (15); $(\mathrm{S\text{-}Fe\text{-}S})_{av} = 127.4$ (8); $(\mathrm{Fe\text{-}S\text{-}Fe})_{av} = 85.4$ (18); $(\mathrm{Fe\text{-}Br\text{-}Fe})_{av} = 79.7$ (17); $(\mathrm{Br\text{-}Fe\text{-}S})_{av} = 94.7$ (7), 117.7 (13).

The iodide ellipse, **5** (Figure 2) is constructed of tetrahedra linked on the perimeter by $\mu\text{-SSi}t\mathrm{Bu_3}$ ligands, and internally by bridging iodides. Ellipse **5** also packs in columnar fashion, and has transannular $d(\mathrm{I\cdots I})$ of 11.101 (2), 11.499 (2), 12.402 (2) and 13.469 (2) Å. The tetrahedra form a ring with the iodides inside, despite the $d(\mathrm{FeI})_{av} = 2.672$ (11) Å that is substantially longer than $d(\mathrm{FeS})_{av} = 2.342$ (7) Å. Now the iron atoms are even further apart than in **4a** and **4b**, and those tetrahedra nearest the foci exhibit metric parameters consistent with slightly greater strain. The wheels and ellipse are unusual examples of ferrous-based rings with a tetrahedral motif, of which $[\mathrm{Fe_{12}(SePh)_{24}}]$ of Fenske and Fischer is the first documented example.[12] The sulfide cluster $[\mathrm{Na_2Fe^{III}_{14}Fe^{II}_4S_{30}}]^{8-}$ contains tetrahedral $\mathrm{FeS_4}$ units, but it is a mixed valence compound,[13] as is $[\mathrm{Fe_6S_6I_6}]^{2-}$.[14] An eight-

 DOI: 10.1002/anie.200351143 © 2003 Wiley-VCH Verlag GmbH & Co. KGaA, Weinheim

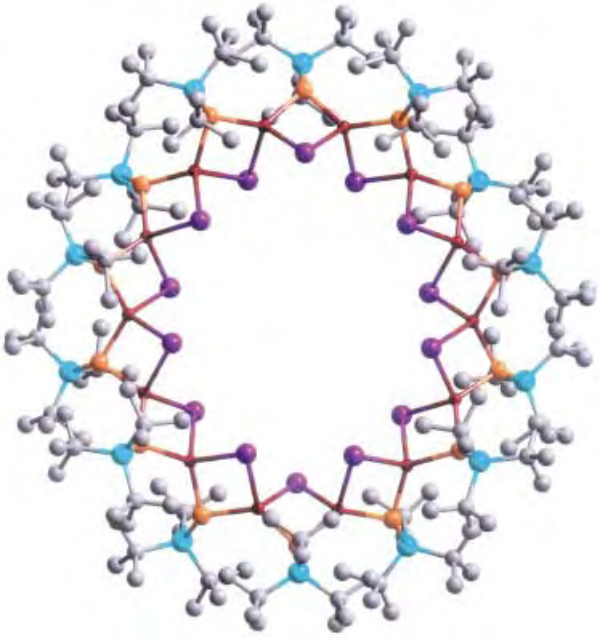


Figure 2. Molecular view of $[Fe(\mu\text{-}I)(\mu\text{-}SSi\ t\text{Bu}_3)]_{14}$ (**5**) Fe = red, I = purple, S = orange, Si = blue, C = gray; pertinent interatomic distances (Å) and angles (°): $d(FeS)_{av}$ = 2.342 (7); transannular $d(I\cdots I)$ = 11.101 (2), 11.499 (2), 12.402 (2), 13.469 (2); $d(FeI)_{av}$ = 2.672 (11); $d(Fe\cdots Fe)_{av}$ = 3.238 (46); $(I\text{-}Fe\text{-}I)_{av}$ = 101.6 (7); near foci (Fe-I-Fe) = 72.98 (10), other $(Fe\text{-}I\text{-}Fe)_{av}$ of 75.1 (9); near foci (S-Fe-S) = 132.13 (17), other $(S\text{-}Fe\text{-}S)_{av}$ of 125.0 (9); near foci (I-Fe-S) = 112.85 (12) and 115.35 (16), other $(I\text{-}Fe\text{-}S)_{av}$ of 117.0 (6).

membered Fe^{II} wheel of sulfide cubes, $[\{(Cy_3P)FeS\}_2Fe_2S_2]_4$ has been prepared,[15] but all remaining iron wheels are based on octahedral Fe^{III}.[16–21]

What is the aggregation state if only one ligand can bridge? The treatment of **4b** with one equivalent of LiCC-Si*t*Bu$_3$ per mole of Fe (chosen in part for size compatibility) afforded the ferrous cube $[\{(t\text{Bu}_3\text{SiCC})Fe(\mu\text{-}SSi\text{-}t\text{Bu}_3)\}_4(C_6H_6)_3]$ (**6** (67%)).[11,22] The cube is nearly perfect (Figure 3), with $S\text{-}Fe\text{-}S_{av}$ = 90.6 (8)° and $Fe\text{-}S\text{-}Fe_{av}$ = 89.4 (8)°. Thiolate-containing cubes with a ferrous-only core are rarely observed,[15–21,23] although a ferrous acetylide phosphaneimide derivative is known.[24]

The magnetic properties of **4a**, **4b**, **5** and **6** were briefly examined. When a Heisenberg $S = 2$ quantum infinite chain model[25] is applied (10 K to 290 K), chloride wheel **4a** is essentially a simple paramagnet, with $J = 0.0$ at both 0.5 and 2.0 T. When a similar approach was used with the bromide wheel, the fits at 1.0 ($R^2 = 97.6$) and 4.0 T ($R^2 = 98.0$) were not as satisfactory, especially below 100 K, but J remained weakly antiferromagnetic (−0.7 and −1.0 cm^{-1} respectively). The temperature dependence of χ_{mol}/Fe for **5** was not properly fit by any model, and μ_{eff} = 3.6 (1.0, 4.0 T) at 23 °C. Thiolate acetylide cube **6** was fit to a tetrahedral array of iron(II) centers according to the Kambe method,[26] and it exhibited no significant interactions (0.5, 2.0 T; $J = 0.1$, 0.3 cm^{-1}; μ_{eff}(295 K) = 5.7, 5.4 μ_B). Most wheels based on octahedral Fe^{III} motifs have modest antiferromagnetic behavior,[16–21] although certain Mn^{III} (O_h),[27] Cr^{III} (O_h),[28] and Ni^{II}[29] wheels have manifested ferromagnetic properties.

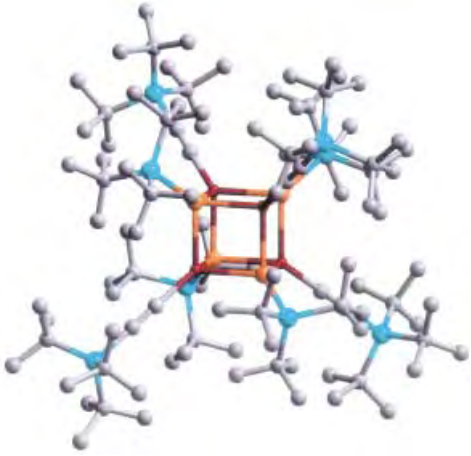


Figure 3. Molecular view of $[(t\text{Bu}_3\text{SiCC})Fe(\mu\text{-}SSi t\text{Bu}_3)]_4$ (**6**), Fe = red, Si = blue, C = gray; pertinent interatomic distances (Å) and angles (°): $d(FeC)_{av}$ = 1.996 (12); $d(FeS)_{av}$ = 2.460 (3); $(S\text{-}Fe\text{-}S)_{av}$ = 90.6 (8); $(Fe\text{-}S\text{-}Fe)_{av}$ = 89.4 (8); $(S\text{-}Fe\text{-}C)_{av}$ = 124.9 (8).

Use of the extremely bulky *t*Bu$_3$SiS ligand has enabled the synthesis of rare ferrous wheels, a unique ellipse, and an uncommon ferrous cube based on tetrahedral coordination. Extensions to other first-row elements and further scrutiny of the magnetic properties of these compounds is underway.[30]

Experimental Section

All manipulations were performed by using either a glovebox (N_2) or high vacuum techniques (Ar), and dried deoxygenated solvents. **1**: A 50 mL flask was charged with $[\{(Me_3Si)_2N\}_2Fe]_2$ (1.099 g, 2.918 mmol), *t*Bu$_3$SiSH (1.357 g, 5.836 mmol and benzene (25 mL) at 23 °C. The reaction mixture was stirred for 30 min, after which the volatiles removed, and the resulting brown solid was subjected to dynamic vacuum for 3 h. This material was dissolved in pentane, filtered and cooled to −78 °C to provide orange **1** (1.308 g, 86%). ^{1}H NMR (400 MHz, C_6D_6, 23 °C, TMS): $\delta = 1.91$ ($\tilde{\nu}_{1/2} = 200$ Hz), 3.63 ($\tilde{\nu}_{1/2} = 200$ Hz). Elemental analysis calcd (%) for $C_{24}H_{54}Si_2S_2Fe$: C 55.56, H 10.49; found: C 55.3, H 10.6.

2a: A 50 mL flask was charged with $NaSSi t\text{Bu}_3(thf)_{1.48}$ (0.250 g, 0.692 mmol), $FeCl_2(thf)_2$ (0.188 g, 0.694 mmol) and THF (20 mL). The pale yellow solution was stirred for 18 h, filtered and allowed to evaporate to give **2a** (0.271 g, 74%). ^{1}H NMR (400 MHz, [D$_8$]THF, 23 °C, TMS): $\delta = 9.11$ ($\tilde{\nu}_{1/2} = 940$ Hz). Elemental analysis calcd (%) for $[\{Cl_2Fe\}(\mu\text{-}SSi t\text{Bu}_3)_2\{FeCl(thf)\}]Na$ (desolvated), $C_{28}H_{62}Cl_3Si_2S_2Fe_2Na$: C 43.32, H 8.07, Cl 13.70; found: C 42.5, H 8.2, Cl 13.4.

2b: A 50 mL flask was charged with $NaSSi t\text{Bu}_3(thf)_{1.68}$ (0.325 g, 0.865 mmol), $FeBr_2(thf)_2$ (0.311 g, 0.864 mmol) and THF (20 mL). The pale yellow solution was stirred for 18 h, filtered and the solvent allowed to evaporate to give 0.446 g **2b** (86%). ^{1}H NMR (400 MHz, [D$_8$]THF, 23 °C, TMS): $\delta = 12.46$ ($\tilde{\nu}_{1/2} = 280$ Hz). Elemental analysis calcd (%) for $[(Cl_2Fe)(\mu\text{-}SSi t\text{Bu}_3)_2\{FeCl(thf)\}]Na(thf)$ (desolvated), $C_{32}H_{70}Br_3Si_2S_2Fe_2Na$: C 42.67, H 7.87, Br 21.29; found: C 42.3, H 7.9, Br 21.8.

3: A 50 mL flask was charged with (0.504 g, 1.34 mmol) $NaSSi t\text{Bu}_3(thf)_{1.68}$, (0.608 g, 1.34 mmol) $FeI_2(thf)_2$ and THF (25 mL). The yellow solution was stirred for 24 h, filtered and the solvent was removed. The yellow solid was heated under vacuum at 98 °C for 2 h, extracted into benzene (40 mL) and filtered. Slow evaporation of the solvent afforded **3** (0.485 g, 75%) after 5 days. ^{1}H NMR (400 MHz, [D$_8$]THF, 23 °C, TMS): $\delta = 6.82$ ($\tilde{\nu}_{1/2} = 140$ Hz). Elemental analysis calcd (%) for $[(IFe)_2(\mu\text{-}SSi t\text{Bu}_3)]_2$ (desolvated), $C_{12}H_{27}SiSIFe$: C,

 © 2003 Wiley-VCH Verlag GmbH & Co. KGaA, Weinheim

34.79; H, 6.58; I, 30.63. Found: C, 33.4; H, 6.4; I, 27.7. **4a**: A 50 mL flask was charged with **2a** (0.271 g, 0.255 mmol) and heated under vacuum at 80 °C for 1.5 h. The product was extracted with benzene and filtered, and yellow crystalline **4a** (0.082 g, 45 %) deposited after slow evaporation of the solvent (6 days). Elemental analysis calcd (%) for $[Fe(\mu\text{-}Cl)(\mu\text{-}SSi\textit{t}Bu_3)]_{12}$(desolvated), $C_{12}H_{27}ClSiSFe$: C 44.64, H 8.45, Cl 10.98; found: C 43.9, H 8.4, Cl, 9.9. **4b**: A 100 mL flask was charged with $NaSSi\textit{t}Bu_3(thf)_{1.40}$ (0.801 g, 2.25 mmol), $FeBr_2(thf)_2$ (0.736 g, 2.28 mmol), and THF (50 mL). The mixture was stirred at 23 °C for 24 h, and the solvent was removed to yield a yellow solid. The solid was heated at 79 °C under vacuum for 2 h, then extracted into benzene and filtered. After slow evaporation of the solvent (5 days), yellow crystals of the product formed (0.739 g, 72 %). Elemental analysis calcd (%) for $[Fe(\mu\text{-}Br)(\mu\text{-}SSi\textit{t}Bu_3)]_{12}$-(desolvated), $C_{12}H_{27}BrSiSFe$: C 39.24, H 7.42, Br 21.75; found: C 39.7, H 7.3, Br 21.8.
5: A 50 mL flask was charged with $NaSSi\textit{t}Bu_3(thf)_{1.56}$ (0.301 g, 0.820 mmol), $FeI_2(thf)_2$ (0.371 g, 0.817 mmol), and THF (20 mL). The mixture was stirred at 23 °C for 24 h, and the solvent was removed to yield a yellow solid. The solid was heated at 117 °C under vacuum for 5 h, then extracted into benzene and filtered. After slow evaporation of the solvent (7 days), dark yellow crystals formed (0.064 g, 16 %). Suitable elemental analyses could not be obtained. **6**: A 12 mL darkened vial was charged with **4a** (0.099 g, 0.222 mmol), $LiCCSSi\textit{t}Bu_3(OEt_2)_{0.28}$ (0.059 g, 0.235 mmol), and benzene (8 mL). The solution was stirred for 10 h, filtered, and the solvent slowly evaporated over 4 days to provide dark yellow crystalline **6** (0.079 g 67 %).

Received: February 10, 2003 [Z51143]

Keywords: cluster compounds · iron · magnetic properties · S ligands

[1] C. Zheng, R. Hoffmann, D. R. Nelson, *J. Am. Chem. Soc.* **1990**, *112*, 3784 – 3791.
[2] H. Hartl, F. Mahdjour-Hassan-Abadi, *Angew. Chem.* **1994**, *106*, 1929 – 1931; *Angew. Chem. Int. Ed. Engl.* **1994**, *33*, 1841 – 1842.
[3] I. G. Dance, *Polyhedron* **1986**, *5*, 1037 – 1104.
[4] N. Wiberg, *Coord. Chem. Rev.* **1997**, *163*, 217 – 252.
[5] P. P. Power, S. C. Shoner, *Angew. Chem.* **1991**, *103*, 308 – 309; *Angew. Chem. Int. Ed. Engl.* **1991**, *30*, 330 – 332; F. M. MacDonnell, K. Ruhlandt-Senge, J. J. Ellison, R. H. Holm, P. P. Power, *Inorg. Chem.* **1995**, *34*, 1815 – 1822.
[6] T. Komuro, H. Kawaguchi, K. Tatsumi, *Inorg. Chem.* **2002**, *41*, 5083 – 5090.
[7] D. F. Evans, *J. Chem. Soc.* **1959**, 2003 – 2005; E. M. Schubert, *J. Chem. Educ.* **1992**, *69*, 62.
[8] **4a**: tetragonal; $P\bar{4}2_1c$; $a = 23.3716$ (7), $c = 24.0912$ (11) Å; $V = 13159.4$ (8) Å^3; $Z = 8$; $C_{36}H_{81}Cl_3S_3Si_3Fe_3$ (benzenes removed); $T = 173$ (2) K; $\lambda = 0.71073$; 46598 reflections, 9453 independent ($R_{int} = 0.0726$); $R1 = 0.0506$ ($I > 2\sigma(I)$), $wR2 = 0.1445$; $\mu = 0.951$ mm^{-1} (SADABS); full-matrix, least squares on F^2.
[9] **4b**: tetragonal; $P\bar{4}2_1c$; $a = 23.542$ (5), $c = 24.086$ (8) Å; $V = 13349$ (6)) Å^3; $Z = 8$; $C_{36}H_{81}Br_3S_3Si_3Fe_3$ (benzenes removed); $T = 173$ (2) K; $\lambda = 0.71073$; 17324 reflections, 5190 independent ($R_{int} = 0.0976$); $R1 = 0.0615$ ($I > 2\sigma(I)$), $wR2 = 0.1414$; $\mu = 2.605$ mm^{-1}; full-matrix, least squares on F^2.
[10] **5**: orthorhombic; $Cmca$; $a = 38.173$ (6), $b = 24.296$ (4), $c = 35.977$ (5) Å; $V = 33367$ (9)) Å^3; $Z = 16$; $C_{44}H_{93.5}I_{3.5}S_{3.5}Si_{3.5}Fe_{3.5}$ (benzenes removed); $T = 173$ (2) K; $\lambda = 0.71073$; 104844 reflections, 10375 independent ($R_{int} = 0.0961$); $R1 = 0.0762$ ($I > 2\sigma(I)$), $wR2 = 0.1952$; $\mu = 2.055$ mm^{-1}; full-matrix, least squares on F^2.
[11] CCDC-203239 (**4a**), CCDC-203238 (**4b**), CCDC-203240 (**5**) and CCDC-203237 (**6**) contain the supplementary crystallographic data for this paper. These data can be obtained free of charge via www.ccdc.cam.ac.uk/conts/retrieving.html (or from the Cambridge Crystallographic Data Centre, 12 Union Road, Cambridge CB2 1EZ, UK; fax: (+44) 1223-336-033; or deposit@ccdc.cam.ac.uk).
[12] D. Fenske, A. Fischer, *Angew. Chem.* **1995**, *107*, 340 – 342; *Angew. Chem. Int. Ed. Engl.* **1995**, *34*, 307 – 309.
[13] J.-F. You, B. S. Snyder, G. C. Papaefthymiou, R. H. Holm, *J. Am. Chem. Soc.* **1990**, *112*, 1067 – 1076.
[14] W. Saak, G. Henkel, S. Pohl, *Angew. Chem.* **1984**, *96*, 153 – 154; *Angew. Chem. Int. Ed. Engl.* **1984**, *23*, 150 – 151.
[15] H.-C. Zhou, R. H. Holm, *Inorg. Chem.* **2003**, *42*, 11 – 21; C. Goh, B. M. Segal, J. Huang, J. R. Long, R. H. Holm, *J. Am. Chem. Soc.* **1996**, *118*, 11844 – 11853.
[16] K. L. Taft, S. J. Lippard, *J. Am. Chem. Soc.* **1990**, *112*, 9629 – 9630; K. L. Taft, C. D. Delfs, G. C. Papaefthymiou, S. Foner, D. Gatteschi, S. J. Lippard, *J. Am. Chem. Soc.* **1994**, *116*, 823 – 832; S. P. Watton, P. Fuhrmann, L. E. Pence, A. Caneschi, A. Cornia, A. Cornia, G. L. Abbati, S. J. Lippard, *Angew. Chem.* **1997**, *109*, 2917 – 2919; *Angew. Chem. Int. Ed. Engl.* **1997**, *36*, 2774 – 2776.
[17] A. Caneschi, A. Cornia, S. J. Lippard, *Angew. Chem.* **1995**, *107*, 511 – 513; *Angew. Chem. Int. Ed. Engl.* **1995**, *34*, 467 – 469; G. L. Abbati, A. Cornia, A. C. Fabretti, W. Malavasi, L. Schenetti, A. Caneschi, D. Gatteschi, *Inorg. Chem.* **1997**, *36*, 6443 – 6446; A. Caneschi, A. Cornia, A. C. Fabretti, D. Gatteschi, *Angew. Chem.* **1999**, *111*, 1372 – 1374; *Angew. Chem. Int. Ed.* **1999**, *38*, 1295 – 1297.
[18] C. Benelli, S. Parsons, G. A. Solan, R. E. P. Winpenny, *Angew. Chem.* **1996**, *108*, 1967 – 1970; *Angew. Chem. Int. Ed. Engl.* **1996**, *35*, 1825 – 1828.
[19] R. W. Saalfrank, I. Bernt, E. Uller, F. Hampel, *Angew. Chem.* **1997**, *109*, 2596 – 2599; *Angew. Chem. Int. Ed. Engl.* **1997**, *36*, 2482 – 2485; O. Waldmann, R. Koch, S. Schromm, J. Schülein, P. Müller, I. Bernt, R. W. Saalfrank, F. Hampel, E. Balthes, *Inorg. Chem.* **2001**, *40*, 2986 – 2995.
[20] C. P. Raptopoulou, V. Tangoulis, E. Devlin, *Angew. Chem.* **2002**, *114*, 2492 – 2495; *Angew. Chem. Int. Ed.* **2002**, *41*, 2386 – 2389.
[21] S.-X. Liu, S. Lin, B.-Z. Lin, C.-C. Lin, J.-Q. Huang, *Angew. Chem.* **2001**, *113*, 1118 – 1121; *Angew. Chem. Int. Ed.* **2001**, *40*, 1084 – 1087.
[22] **6**: cubic; $P2_13$; $a = 23.8617$ (17) Å; $V = 13586.4$ (17)) Å^3; $Z = 12$; $C_{40.67}H_{72}S_{1.33}Si_{2.66}Fe_{1.33}$; $T = 173$ (2) K; $\lambda = 0.71073$; 49628 reflections, 6526 independent ($R_{int} = 0.1949$); $R1 = 0.0685$ ($I > 2\sigma(I)$), $wR2 = 0.1379$; $\mu = 0.664$ mm^{-1}; full-matrix, least squares on F^2.
[23] H. Link, A. Decker, D. Fenske, *Z. Anorg. Allg. Chem.* **2000**, *626*, 1567 – 1574.
[24] U. Riese, K. Harms, J. Pebler, K. Dehnicke, *Z. Anorg. Allg. Chem.* **1999**, *625*, 746 – 754.
[25] T. Smith, S. A. Friedberg, *Phys. Rev.* **1968**, *176*, 660 – 665; R. Dingle, M. E. Lines, S. L. Holt, *Phys. Rev.* **1969**, *187*, 643 – 648.
[26] K. Kambe, *J. Phys. Soc. Jpn.* **1950**, *5*, 48 – 51.
[27] G. L. Abbati, A. Cornia, A. C. Fabretti, A. Caneschi, D. Gatteschi, *Inorg. Chem.* **1998**, *37*, 1430 – 1431.
[28] E. J. L. McInnes, C. Anson, A. K. Powell, A. J. Thomson, S. Poussereau, R. Sessoli, *Chem. Commun.* **2001**, 89 – 90.
[29] A. J. Blake, C. M. Grant, S. Parsons, J. M. Rawson, R. E. P. Winpenny, *J. Chem. Soc. Chem. Commun.* **1994**, 2363 – 2364.
[30] D. Gatteschi, A. Caneschi, L. Pardi, R. Sessoli, *Science* **1994**, *265*, 1054 – 1058.

 © 2003 Wiley-VCH Verlag GmbH & Co. KGaA, Weinheim

Cover Picture

Chandrakala Pidathala, Linh Hoang, Nicola Vignola, and Benjamin List*



A feather in the cap of the aldol reaction. The cover picture shows the amino acid (*S*)-proline surrounded by some new catalytic asymmetric intramolecular aldolizations, which are described by B. List et al. on page 2785 ff. Another example of the ever-increasing number of proline-catalyzed reactions are *enolexo* aldolizations. Despite these exciting discoveries, it is often forgotten that almost half of the 250 tonnes of proline produced each year is isolated from chicken feathers!

Contents

News

S. Mann Elected Fellow of the Royal Society ____ 2703

W. Lubitz Receives Bruker Prize

D. Seebach Receives Prize during Liebig Memorial Colloquium

Books

Aqueous Organometallic Catalysis ____ 2704 — Ferenc Joó — *reviewed by Boy Cornils*

Enzyme Kinetics ____ 2705 — Alejandro G. Marangoni — *reviewed by Thorsten Friedrich*

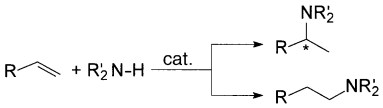
Highlights

Hydroamination

P. W. Roesky,* T. E. Müller* **2708 – 2710**

Enantioselective Catalytic Hydroamination of Alkenes

Catalytically to chirality: Enantioselective catalytic hydroamination (see scheme) is one of the major challenges in synthetic organic and organometallic chemistry and offers a very attractive synthetic pathway to chiral amines. Recent progress made with this reaction is presented.

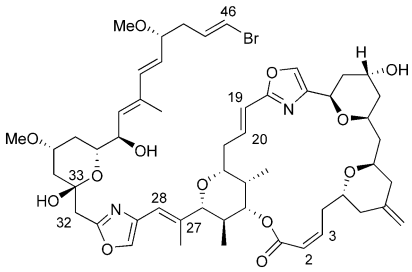


Macrolide Syntheses

L. O. Haustedt, I. V. Hartung, H. M. R. Hoffmann* ____ **2711 – 2716**

The Total Syntheses of Phorboxazoles—New Classics in Natural Product Synthesis

The marine sponge metabolites phorboxazoles A (see structural formula) and B were the targets of several clever total syntheses, whose special features are described in this Highlight. Now that the synthetic entry to these compounds has been cleared, their cytostatic activity can be studied thoroughly in vitro and in vivo.



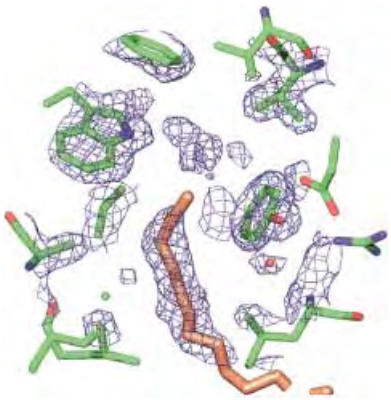
Reviews

Structure-Based Drug Design

A. M. Davis,* S. J. Teague, G. J. Kleywegt ____ **2718 – 2736**

Application and Limitations of X-ray Crystallographic Data in Structure-Based Ligand and Drug Design

A main source of information on protein–ligand complexes is X-ray crystallography. In the structure shown oleic acid (orange) is complexed to an IFABP mutant (green); the experimentally determined electron density is represented by a blue mesh. Uncertainties in the atomic model can have far-reaching consequences when this model is subsequently used in manual design, docking, scoring, and virtual screening.



Communications



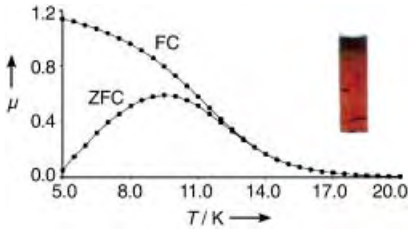
Extensions and compressions on the molecular scale: A synthetic oligomer unfolds from a helical to a linear conformation upon partial and selective protonation and refolds into another helical conformation upon further protonation (see scheme).

pH-Induced Changes in Conformation

C. Dolain, V. Maurizot, I. Huc* ——— **2738 – 2740**

Protonation-Induced Transition between Two Distinct Helical Conformations of a Synthetic Oligomer via a Linear intermediate

Moldable magnetism: Tunable photomagnetism is exhibited by homogeneous, optically transparent, moldable silica xerogel nanocomposites containing the ferromagnetic Prussian blue analogue $K_xCo_y^{II}[Fe^{III}(CN)_6]_z$. These materials also show a blue-shifted intervalence charge-transfer band and superparamagnetic behavior. The picture shows the temperature dependence of the field-cooled (FC) and zero-field-cooled (ZFC) dc magnetization μ of a xerogel sample (inset).

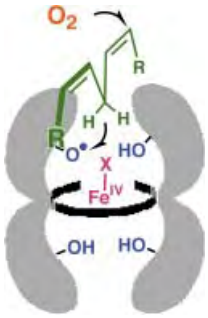


Photomagnetic Nanocomposites

J. G. Moore, E. J. Lochner, C. Ramsey, N. S. Dalal, A. E. Stiegman* **2741 – 2743**

Transparent, Superparamagnetic $K_x^ICo_y^{II}[Fe^{III}(CN)_6]$–Silica Nanocomposites with Tunable Photomagnetism

Impressions of enzymes: A stable naphthoxyl radical was formed in the cavity of an iron porphyrin by peroxy acid oxidation. The intermediate was characterized by spectroscopic methods. This reaction was applied to the catalytic oxygenation of *Z,Z*-1,4-diene regio- and stereoselectively to give the corresponding alcohol under an O_2 atmosphere (see picture). This is the first example of a mimic of the active site of the prostaglandin H synthases.



Stereoselective Oxygenation

E. Matsui, Y. Naruta,* F. Tani, Y. Shimazaki ——— **2744 – 2747**

An Active-Site Model of Prostaglandin H Synthase: An Iron "Twin-Coronet" Porphyrin with an Aryloxyl Radical Overhang and Its Catalytic Oxygenation of 1,4-Diene

For the USA and Canada:
ANGEWANDTE CHEMIE International Edition (ISSN 1433-7851) is published weekly by Wiley-VCH PO Box 191161, D 69451 Weinheim, Germany. Air freight and mailing in the USA by Publications Expediting Inc. 200 Meacham Ave., Elmont, NY 11003. Periodicals postage paid at Jamaica NY 11431. US POSTMASTER: send address changes to *Angewandte Chemie*, Wiley-VCH, 111 River Street, Hoboken, NJ 07030. Annual institutional subscription price for institutions: Europe € 2998.00/3148.00. Outside Europe US$ 3718.00/3904.00 (valid for print or electronic/print and electronic delivery); for individuals who are personal members of a national chemical society, or whose institution already subscribes, or who are retired or self-employed consultants, print only (including postage and handling charges): Europe € 248.00/Outside Europe US$ 348.00.

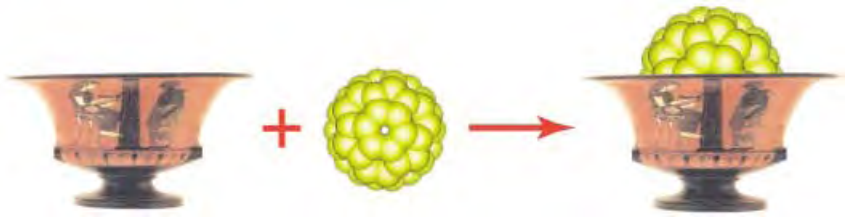
 © 2003 Wiley-VCH Verlag GmbH & Co. KGaA, Weinheim

Contents

Fullerenes in Calixarenes

G.-B. Pan, J.-M. Liu, H.-M. Zhang, L.-J. Wan,* Q.-Y. Zheng, C.-L. Bai* ——— **2747 – 2751**

Configurations of a Calix[8]arene and a C_{60}/Calix[8]arene Complex on a Au(111) Surface

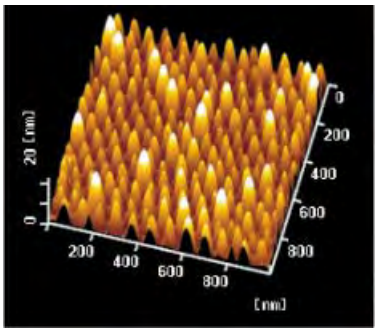


Having a ball: Molecules of a calix[8]arene derivative, and the inclusion complex it forms with C_{60} (see schematic), can be adsorbed onto a Au(111) surface in solution to yield self-organized highly ordered arrays. The structures of the two arrays have been investigated by scanning tunnelling microscopy, which gives clear evidence of the inclusion of the fullerene molecules. The stable configuration and well-defined arrays should be useful for the construction of nanostructures.

Polymer-Coated Gold Nanoparticles

K. Ohno, K. Koh, Y. Tsujii, T. Fukuda* ——— **2751 – 2754**

Fabrication of Ordered Arrays of Gold Nanoparticles Coated with High-Density Polymer Brushes



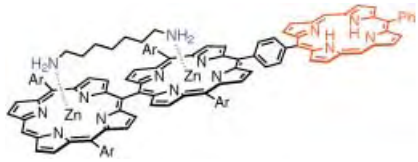
A brush with gold: Gold nanoparticles with a narrow size distribution have been coated with well-defined, high-density polymer brushes (see AFM image) by means of surface-initiated living radical polymerization. The gold nanoparticles have formed a 2D array with a high degree of structural order and exceptional controllability of the interparticle distance.

meso–meso-*Linked* Zn^{II} *Diporphyrin*

H. Shinmori, T. K. Ahn, H. S. Cho, D. Kim,* N. Yoshida, A. Osuka* ——— **2754 – 2758**

Dihedral-Angle Modulation of *meso–meso*-Linked Zn^{II} Diporphyrin through Diamine Coordination and Its Application to Reversible Switching of Excitation Energy Transfer

The dihedral angle between the two porphyrins in *meso–meso*-linked Zn^{II} diporphyrin can be modulated effectively by adding 1,7-diaminoheptane, which coordinates at the both Zn^{II} centers (see picture). This mechanical torsion gives rise to a decrease in the energy of the S_1 state in the *meso–meso*-linked Zn^{II}-diporphyrin subunit, and results in the change



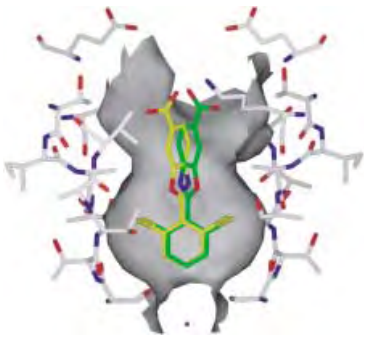
in direction of the energy transfer in the excited state. This process can be reversed by adding acetic acid.

Small-Molecule Inhibitors

H. Razavi, S. K. Palaninathan, E. T. Powers, R. L. Wiseman, H. E. Purkey, N. N. Mohamedmohaideen, S. Deechongkit, K. P. Chiang, M. T. A. Dendle, J. C. Sacchettini, J. W. Kelly* ——— **2758 – 2761**

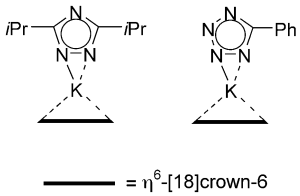
Benzoxazoles as Transthyretin Amyloid Fibril Inhibitors: Synthesis, Evaluation, and Mechanism of Action

Benzoxazoles pevent misfolding: Benzoxazole-based inhibitors of transthyretin (TTR) amyloid fibril formation are among the most effective found to date. They stabilize TTR against both acid-mediated misfolding and urea denaturation by raising the activation barrier to tetramer dissociation, the rate-limiting step for amyloid formation. The figure depicts the cocrystal structure of one of the better benzoxazole inhibitors bound to TTR.



 © 2003 Wiley-VCH Verlag GmbH & Co. KGaA, Weinheim

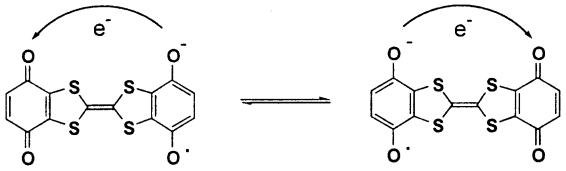
Potassium slips a disk: A novel slipped η^2-coordination mode with differing K–N separations is found in the complexes (3,5-diisopropyltriazolato)([18]crown-6)-potassium and (phenyltetrazolato)([18]crown-6)potassium (see diagram), which are thus extremely rare examples of terminal η^2 coordination of nitrogen-rich azolato ligands.



Azolato Coordination Modes

W. Zheng, M. J. Heeg, C. H. Winter* ——— 2761 – 2764

Coordination of 3,5-Diisopropyl-1,2,4-triazolato and 5-Phenyltetrazolato Ligands to the $[K([18]crown-6)]^+$ Fragment: Structural Insight into the Coordination of Nitrogen-Rich Azolato Ligands to Single Metal Centers

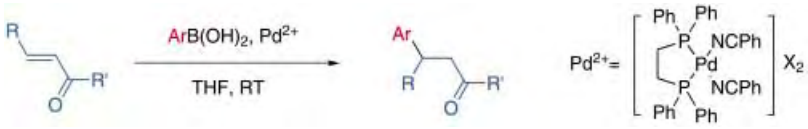


Radical bridge design: The diquinone-tetrathiafulvalene (TTF) species shown exhibits effective electron coupling between the quinone centers which is mediated by the TTF bridge. Stepwise one-electron reduction of the molecule occurs, and the observed potential difference between reduction events is an indication that reduction of the second quinone unit is affected by the radical species already formed on the other side of the bridge.

Organosulfur Conducting Bridges

N. Gautier, F. Dumur, V. Lloveras, J. Vidal-Gancedo, J. Veciana, C. Rovira,* P. Hudhomme* ——— 2765 – 2768

Intramolecular Electron Transfer Mediated by a Tetrathiafulvalene Bridge in a Purely Organic Mixed-Valence System



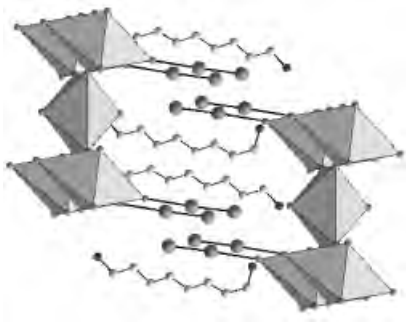
A cationic palladium complex was found to be an efficient catalyst for the 1,4-addition of aryl boronic acids to enones at room temperature (see scheme; X = ClO_4, OTf, BF_4, PF_6, or SbF_6); T_f = trifluoromethanesulfonyl).

Pd and B in 1,4-Additions

T. Nishikata, Y. Yamamoto, N. Miyaura* ——— 2768 – 2770

Conjugate Addition of Aryl Boronic Acids to Enones Catalyzed by Cationic Palladium(II)–Phosphane Complexes

Chemistry with a golden touch: The first examples of organic-based mixed-valent Au^I/Au^{III} layered perovskites are reported (see picture). The crystal structures of the new hybrid compounds feature $[AuI_2]^-/[AuI_4]^-$ layers pillared by I_3^- ions and appropriate organic dications. The measured optical band gaps of the new organic–inorganic semiconductors are smaller than the value for $Cs_2Au_2I_6$.



Gold(I)/Gold(III) Perovskites

VIP

L. M. Castro-Castro, A. M. Guloy* ——— 2771 – 2774

Organic-Based Layered Perovskites of Mixed-Valent Gold(I)/Gold(III) Iodides

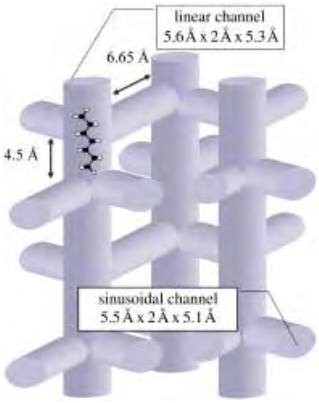
 © 2003 Wiley-VCH Verlag GmbH & Co. KGaA, Weinheim

Contents

Alkane Adsorption on Zeolites

J. F. M. Denayer,* K. De Meyer, J. A. Martens, G. V. Baron — **2774 – 2777**

Molecular Competition Effects in Liquid-Phase Adsorption of Long-Chain *n*-Alkane Mixtures in ZSM-5 Zeolite Pores

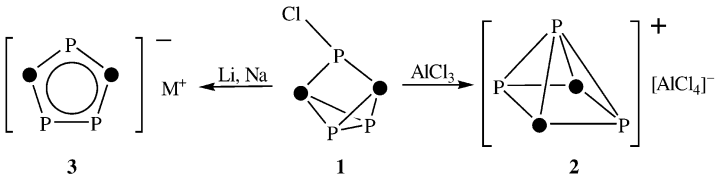


Picking on the short one: Molecular arrangement of long-chain hydrocarbon mixtures in the 2D pore system of ZSM-5 (depicted) causes strong and unexpected selectivity effects to occur. The formation of azeotropes and selective uptake of the shortest molecule from mixtures is observed for a range of hydrocarbon mixtures, and has significant implications for separative applications.

Phosphorus–Carbon Compounds

J. M. Lynam, M. C. Copsey, M. Green,* J. C. Jeffery, J. E. McGrady, C. A. Russell,* J. M. Slattery, A. C. Swain — **2778 – 2782**

Selective Preparation of the $[3,5\text{-}t\mathrm{Bu}_2\text{-}1,2,4\text{-}C_2P_3]^-$ Ion and Synthesis and Structure of the Cationic Species *nido*-$[3,5\text{-}t\mathrm{Bu}_2\text{-}1,2,4\text{-}C_2P_3]^+$, Isoelectronic with $[C_5R_5]^+$



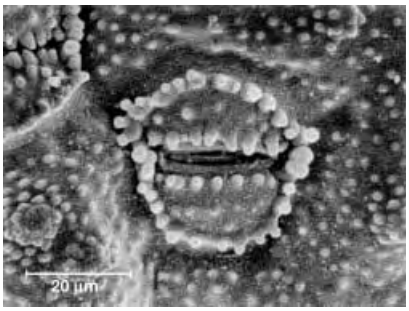
Building pyramids: The first P–C cluster, namely, the novel nido species **2**, is readily prepared from **1** (● = C*t*Bu), which is also an excellent precursor for the selective synthesis of the anion **3**. DFT calculations show that there is a switch in the global minimum, on the introduction of three P atoms (⟷CH) into the $[C_5H_5]^+$ ion, from cyclic-unsaturated to saturated cage species, such as **2**.

Zeolites from Plant Leaves

V. Valtchev,* M. Smaihi, A.-C. Faust, L. Vidal — **2782 – 2785**

Biomineral-Silica-Induced Zeolitization of *Equisetum Arvense*

Turning over a new leaf: Leaves of *Equisetum Arvense* can be successfully treated to yield zeolite-type structures which, after calcination, are transformed into a micro-/mesoporous material which keeps all of the morphological features of the vegetal template (see SEM image). Faithful zeolitization of the plant structure is induced by the highly reactive biomorphic silica deposited in the epidermal surface of the plant.



Enolexo *Aldol Reactions*

C. Pidathala, L. Hoang, N. Vignola, B. List* — **2785 – 2788**

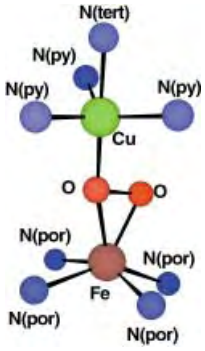
Direct Catalytic Asymmetric *Enolexo* Aldolizations



32 years after the first, and still the only, catalytic asymmetric intramolecular aldol reaction was published in this journal, the proline-catalyzed Hajos–Parrish–Eder–Sauer–Wiechert reaction is extended for the first time to catalytic asymmetric *enolexo* aldolizations. The process provides substituted cyclohexanes in excellent diastereo- and enantioselectivities. For example, heptanedial is converted into the corresponding cyclic *anti*-configured aldol in 99% *ee* (see scheme).

 © 2003 Wiley-VCH Verlag GmbH & Co. KGaA, Weinheim

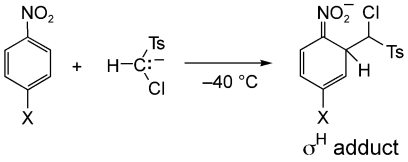
A stable bridge: A peroxo-bridged Fe–O_2–Cu complex (see picture) was synthesized and isolated as crystals. The X-ray structure analysis revealed that the Fe–O_2–Cu moiety has a μ-η^2:η^1 coordination mode; a peroxo ligand is bound to Fe in a side-on fashion with only one oxygen atom of the peroxide bound to Cu. The two metal ions (high-spin Fe^{III} and Cu^{II}) were strongly coupled in an antiferromagnetic fashion, thus resulting in a total spin of $S = 2$.



Peroxo-Bridged Heme–Copper Complex

T. Chishiro, Y. Shimazaki, F. Tani, Y. Tachi, Y. Naruta,* S. Karasawa, S. Hayami, Y. Maeda ——— 2788 – 2791

Isolation and Crystal Structure of a Peroxo-Bridged Heme – Copper Complex

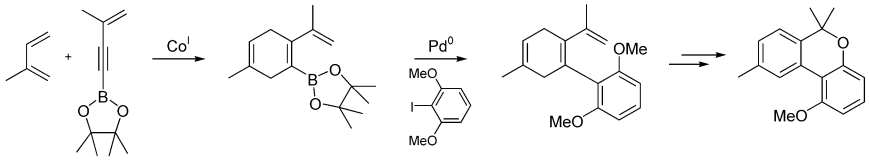


Mononitrobenzene derivatives and 1-chloro-1-arylsulfonyl-methyl anions react with formation of stable σ^H adducts (see scheme; Ts = tosyl) which are observed by UV/Vis and NMR spectroscopy. The generally accepted energy profiles for vicarious nucleophilic substitutions with σ^H adducts as high-energy intermediates have to be revised.

Vicarious Substitutions

T. Lemek,* M. Mąkosza, D. S. Stephenson, H. Mayr* ——— 2793 – 2795

Direct Observation of the Intermediate in Vicarious Nucleophilic Substitutions of Hydrogen



Versatile building blocks with a dihydroaromatic vinylic boron substructure can be generated efficiently by cobalt-catalyzed Diels–Alder reactions and used in Suzuki coupling reactions for the synthesis of functionalized polycyclic compounds (see scheme).

Catalytic Diels–Alder Reactions

G. Hilt,* K. I. Smolko ——— 2795 – 2797

Alkynylboronic Esters as Efficient Dienophiles in Cobalt-Catalyzed Diels–Alder Reactions

Communications labeled with this symbol have been judged by two referees as being "very important papers".

The publication of Communications labeled with this symbol has been accelerated because of their topical or highly competitive nature.

Looking for outstanding employees?

Do you need another expert for your excellent team?
... Chemists, PhD Students, Managers, Professors, Sales Representatives...

Place an advert in the printed version and have it made available online for 1 month, free of charge!

Angewandte Chemie International Edition
Advertising Sales Department: Marion Schulz
Phone: 0 62 01 - 60 65 65
Fax: 0 62 01 - 60 65 50
E-Mail: MSchulz@wiley-vch.de

Service

Keywords ——— *2798*

Authors ——— *2799*

Vacancies ——— *2707, 2802*

Preview ——— *2803*

 © 2003 Wiley-VCH Verlag GmbH & Co. KGaA, Weinheim

Corrigenda

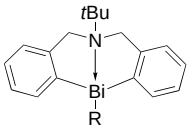
In the Communication "A Zeolite Structure (ITQ-13) with Three Sets of Medium-Pore Crossing Channels Formed by 9- and 10-Rings" by **A. Corma et al.** in *Angew. Chem.* **2003**, *115*, 1188–1191; *Angew. Chem. Int. Ed.* **2003**, *42*, 1156–1159, it should have been made clear early on in the manuscript that the synthesis of the ITQ-13 material was first reported in a patent published in 2002 (T. Boix, M. Puche, M. A. Camblor, A. Corma, US Patent 6 471 941 B1, **2002**; reference [12] in the manuscript). Furthermore, owing to an editorial error the reference to this patent was wrongly introduced into the *Experimental Section*, where reference [13] should read reference [12] and vice versa.

We apologize to our readers and to the authors of the above mentioned patent if this mistake has resulted in any misunderstanding.

Avelino Corma
Corresponding Author

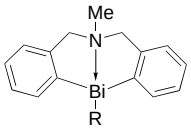
Peter Gölitz
Editor

In the Communication by **S. Shimada, M. Tanaka et al.** published in *Angew. Chem. Int. Ed.* **2003**, *42*, 1845–1848, the incorrect formula was printed on p. 1845. The correct formula is that shown below. Furthermore, the e-mail address for Professor Tanaka should be m.tanaka@res.titech.ac.jp.



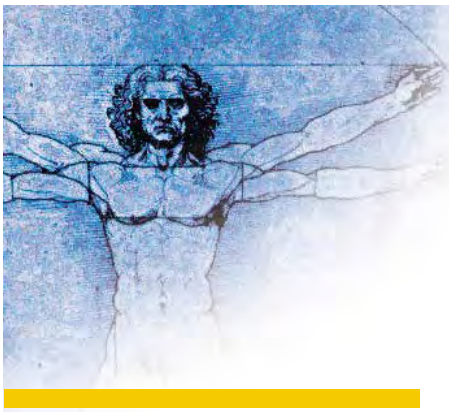
3a – 3g

3a: R = Ph
3b: R = 3,5-$(CF_3)_2C_6H_3$-
3c: R = 3,4-$(CH_2O_2)C_6H_3$-
3d: R = 2,4,6-$(MeO)_3C_6H_2$-
3e: R = CH_2=C(Me)-
3f: R = Br
3g: R = Cl



4

 © 2003 Wiley-VCH Verlag GmbH & Co. KGaA, Weinheim



S. Mann Elected Fellow of the Royal Society

Each year, the Royal Society elects 42 new Fellows and 6 new Foreign Members on the basis of their scientific achievements. The Royal Society, Britain's academy of science, has some 1300 members and can look back on a tradition of almost 350 years. This year, Nobel Laureates Alan MacDiarmid[1] and Klaus von Klitzing are among the newly elected, as well as Stephen Mann, Professor of Inorganic and Materials Chemistry at the University of Bristol (UK).



S. Mann

Mann received his BSc in chemistry from the University of Science and Technology in Manchester (UK) in 1976, and was awarded a DPhil from the University of Oxford (UK) in 1982. He took up a lectureship at the University of Bath (UK) in 1984, and was made a full Professor in 1990. Mann moved to his current position in 1998. He is a member of the International Advisory Board of *Angewandte Chemie*.

Mann's research is centered around "The Chemistry of Form", as he put it in his Review in *Angewandte Chemie* in 2000,[2a] and ranges from biomineralization to template-directed synthesis, self-assembled inorganic materials, and mesostructured inorganic–organic hybrid materials.[2b]

W. Lubitz Receives Bruker Prize

The Bruker Prize in Electron Paramagnetic Resonance (EPR) Spectroscopy was presented to Wolfgang Lubitz, Director of the Max Planck Institute of Radiation Chemistry in Mülheim an der Ruhr (Germany), from the Electron Spin Resonance Group of the Royal Society of Chemistry in April. Lubitz was recognized for his achievements in the development and application of EPR techniques. The Prize Lecture was entitled "Signals from the Reaction Center: Applications of EPR in Photosynthesis".



W. Lubitz

Lubitz completed his doctorate (1977) and habilitation (1982) at the Freie Universität Berlin under the guidance of Harry Kurreck (organic chemistry) and Klaus Möbius (physics) in EPR and ENDOR (electron–nuclear double resonance) spectroscopic studies of organic radicals.[3a] Subsequently, he worked with George Feher (University of California, San Diego) on photosynthetic reaction centers and became a Professor of Physics at the University of Stuttgart (Germany) in 1989. Lubitz succeeded Horst T. Witt as a full Professor of Physical Chemistry at the Max Volmer Institute of Biophysical Chemistry (Technische Universität Berlin) in 1991 and joined the Max Planck Society in 2000.

The work of Lubitz's research group has contributed significantly to the understanding of photosynthesis by means of these techniques[3b] in combination with methods in theoretical chemistry and molecular biology. More generally, Lubitz is interested in hydrogenases, radical enzymes, metal centers in proteins and their role in photosystem II, and the design and synthesis of artificial proteins with metal cofactors.

D. Seebach Receives Prize during Liebig Memorial Colloquium

On the occasion of the 200th anniversary of the birth of Justus von Liebig, the Gesellschaft Deutscher Chemiker (GDCh, German Chemical Society) unveiled a memorial plaque outside the Liebig Museum in Giessen (Germany). During the accompanying Colloquium, the August Wilhelm von Hofmann Memorial Medal was presented to Professor Dieter Seebach (ETH Zurich, Switzerland) for his achievements in organic synthesis. Currently, his research interests are focused on chiral dendrimers and β-peptides.[4]



Hofmann (1818–1892) was the founding President of the German Chemical Society (1867). Prior to that he had worked in England for 20 years and had served there as President of the Chemical Society from 1861.[5] The Medal is awarded at irregular intervals to non-German chemists and to German scientists who are not chemists, for services to chemistry.

[1] A. G. MacDiarmid, *Angew. Chem.* **2001**, *113*, 2649; *Angew. Chem. Int. Ed.* **2001**, *40*, 2581.
[2] a) S. Mann, *Angew. Chem.* **2000**, *112*, 3632; *Angew. Chem. Int. Ed.* **2000**, *39*, 3392; b) H. Cölfen, S. Mann, *Angew. Chem.* **2003**, *115*, 2452; *Angew. Chem. Int. Ed.* **2003**, *42*, 2350.
[3] a) H. Kurreck, B. Kirste, W. Lubitz, *Angew. Chem.* **1984**, *96*, 171; *Angew. Chem. Int. Ed. Engl.* **1984**, *23*, 173; b) W. Lubitz, F. Lendzian, R. Bittl, *Acc. Chem. Res.* **2002**, *35*, 313.
[4] K. Gademann, A. Häne, M. Rueping, B. Jaun, D. Seebach, *Angew. Chem.* **2003**, *115*, 1573; *Angew. Chem. Int. Ed.* **2003**, *42*, 1534.
[5] C. Meinel, *Angew. Chem.* **1992**, *104*, 1293; *Angew. Chem. Int. Ed. Engl.* **1992**, *31*, 1265.

 © 2003 Wiley-VCH Verlag GmbH & Co. KGaA, Weinheim

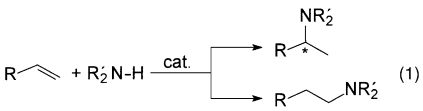
Asymmetric Synthesis of Amines

Enantioselective Catalytic Hydroamination of Alkenes

Peter W. Roesky and Thomas E. Müller**

Keywords:
asymmetric synthesis · chiral ligands · homogeneous catalysis · hydroamination · iridium · lanthanides

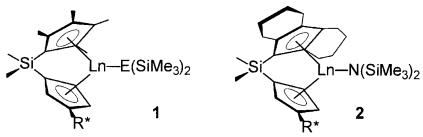
The catalytic addition of an organic amine R_2N-H bond to alkenes or alkynes (hydroamination) to give nitrogen containing molecules is of great interest for academic and industrial research. Since today most amines are made in multistep syntheses, hydroamination would offer the most attractive alternative synthetic route. It was shown, that hydroamination can be catalyzed by transition metals (d- and f-block) and alkali metals.[1] Depending on the catalytic system either an activation of the C–C multiple bond or the N–H bond takes place. Alkene or alkyne activation is usually accomplished with late-transition metals through coordination of the C–C multiple bond to the metal center. In contrast, the amino function can be activated by alkali or early transition metals, which generate an amido species, or by N–H oxidative addition to electron-rich transition metals. Depending on the nature of the catalysts and the substrates either Markovnikov or anti-Markovnikov products are obtained [Eq. (1)]. The scope of



(1)

catalytic hydroamination has been reviewed recently.[1–6]

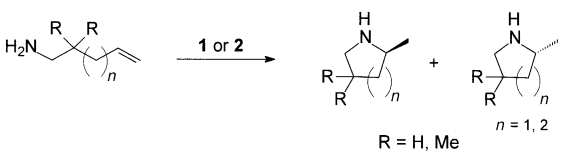
Today, the vast number of enantioselective syntheses of molecules bearing an amine functionality use classical stoichiometric reactions with chiral auxiliaries or utilize enantiomerically pure starting materials.[7] As a result of the increasing interest in the hydroamination reaction some research groups have started to investigate the enantioselective R_2N-H addition to C–C double bonds. In early transition-metal chemistry Marks et al. implemented C_1-symmetric organolanthanide *ansa*-metallocene catalysts of the type $[Me_2Si(\eta^5\text{-}C_5Me_4)(\eta^5\text{-}C_5H_3R^*)LnE(SiMe_3)_2]$ (**1**)[8–10] (R* = (−)-menthyl, (+)-neomenthyl, (−)-phenylmenthyl; Ln = La, Nd, Sm, Y, Lu; E = CH, N) and $[Me_2Si(\eta^5\text{-}OHF)(\eta^5\text{-}C_5H_3R^*)LnN(SiMe_3)_2]$ (**2**)[11] (OHF = octahydrofluorenyl; R* = (−)-menthyl; Ln = Sm, Y, Lu) in the enantioselective and diastereoselective hydroamination/cyclization of aminoalkenes. Compounds **1** and **2** catalyze the cyclization of, for example, 1-amino-4-pentenes to 2-methylpyrrolidines and of 1-amino-5-hexenes to 2-methylpiperidines, generating a new asymmetric center adjacent to the heterocyclic nitrogen atom [Eq. (2)].



Using **1** as the catalyst 2,2-dimethyl-1-aminopent-4-ene is cyclized with 53% *ee* at 25 °C (74% *ee* at −30 °C) and turnover frequencies as high as 93 h^{-1}. In general, the turnover frequencies decrease with decreasing ion radius of the metal center. The configuration of the product and the enantiomeric excess depends on the chiral group R* and the ion radius of the lanthanide metal. The product stereochemistry can be understood in terms of olefin insertion via a chairlike, seven-membered transition state.

Compound **2** was used to convert 1-amino-5-hexenes into 2-methylpiperidines with enantioselectivities up to 67%. Compared to **1**, compound **2** only provides greater enantioselectivities with sterically encumbered substrates. In both cases the reaction kinetics were zero order in substrate and first order in catalyst concentration over at least three half-lives. The kinetics are thus in agreement with activation of the amine and rate-determining insertion of the alkene group.[12] Compound **2** (Ln = Sm) was also used for the enantioselective hydroamination/cyclization of aminodienes. Preliminary studies reveal that the cyclization of 1-amino-5,7-octadiene to the corresponding piperidine proceeds with up to 69% *ee*.[13]

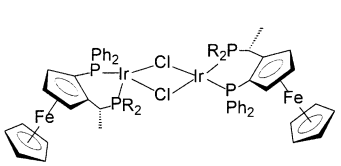
Togni et al.[14,15] developed an enantioselective version of the known iridium-catalyzed hydroamination reaction.[16,17] The binuclear, chloride bridged complexes **3**–**7** which have chiral chelating diphosphanes in their coordi-



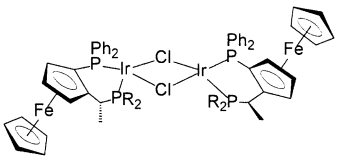
(2)

[*] Prof. Dr. P. W. Roesky
Institut für Chemie
Freien Universität Berlin
Fabeckstrasse 34–36
14195 Berlin (Germany)
Fax: (+49) 30-838-52440
E-mail: roesky@chemie.fu-berlin.de
Dr. T. E. Müller
Institut für Technische Chemie II
Technische Universität München
Lichtenbergstrasse 4
85747 Garching (Germany)
Fax: (+49) 89-28913544
E-mail: thomas.mueller@ch.tum.de

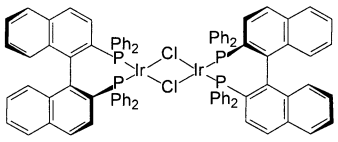
 © 2003 Wiley-VCH Verlag GmbH & Co. KGaA, Weinheim DOI: 10.1002/anie.200301637



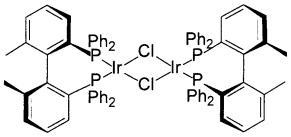
trans-**3** (R = Cy, [{IrCl((*R*,*S*)-Josiphos)}$_2$])
trans-**4** (R = Ph)
trans-**5** (R = 3,5-Me$_2$C$_6$H$_3$)



cis-**3** (R = Cy)
cis-**4** (R = Ph)
cis-**5** (R = 3,5-Me$_2$C$_6$H$_3$)

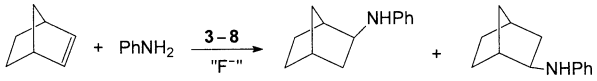


6 ([{IrCl((*S*)-binap)}$_2$])



7 ([{IrCl((*R*)-biphemp)}$_2$])

nation spheres were prepared. The unseparated *cis*/*trans* mixtures of these compounds were used as catalyst precursors in the intermolecular hydroamination of norbornene with aniline [Eq. (3)].



(3)

Addition of fluoride ions (as 1,1,1,3,3,3-hexakis(dimethylamino)diphosphazenium fluoride) as cocatalyst increased the activity and enantioselectivities. Using **6** as the catalyst, up to 95% enantiomeric excess were observed. The highest turnover frequencies of 3.4 h^{-1} were observed when **3** was employed as catalyst. These reactions were performed without solvent and at a catalyst concentration of 1 or 2 mol% Ir.

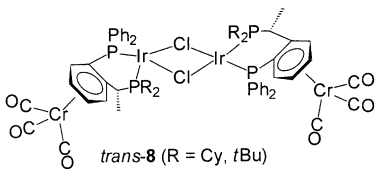
In a similar approach planar chiral arene chromium tricarbonyl complexes, [{η^6-(*pR*,*R*)[(PR$_2$)CHMe]C$_6$H$_4$PPh$_2$}Cr(CO)$_3$] (R = Cy (cyclohexyl), Ph), were used as ligands to generate binuclear, chloride-bridged iridium complexes **8**.[18,19] The compounds **8** were used as catalyst precursors in the intermolecular hydroamination of norbornene with aniline. The study compared the complexes **8** (employed as inseparable *cis*/*trans* mixture) with the corresponding ferrocene-based Josiphos-ligated complexes **3** and its *t*Bu derivative. Reactions were performed in aniline at 60°C for 96 h using 0.1 mol% of catalyst. An even higher enantiomeric excess (up to 70%) was obtained in comparison to the ferrocene ligated complexes (13% and 64% *ee*), however, only traces of product were isolated.

In contrast to the results found for the iridium-based catalysts, the bidentate ferrocenyl Josiphos system did not afford active catalysts for nickel systems. On the other hand Ni^{II} complexes containing the chiral tridentate ferrocenyl Pigiphos ligand, [Ni(Pigiphos)(thf)](ClO$_4$)$_2$ have been found to efficiently catalyze the enantioselective hydroamination of activated olefins with both anilines and aliphatic amines [Eq. (4); EWG = electron-withdrawing group] at room temperature.[20] The most remarkable result in this series concerns the hydroamination of methacrylonitrile with morpholine that gave the product in quantitative yield and 69% *ee*.

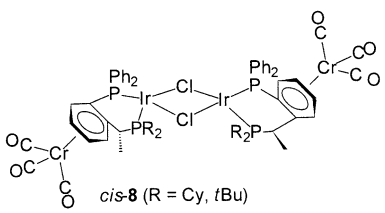
The palladium catalyzed hydroamination of anilines to 1,3-dienes was investigated by Hartwig et al.[21] This group evaluated a large number of potential catalysts for the hydroamination reaction by a colorimetric method which allowed the rapid determination of the concentration of unreacted anilines at the end of the reaction. Anilines (educt) but not allylic amines (product) react with furfural to give a red product. The experiments showed that complexes formed in situ from [{Pd(π-allyl)Cl}$_2$] and PPh$_3$ in the presence of 10% trifluoracetic acid (TFA) are very active for the hydroamination of aromatic amines. Experiments with optically active phosphanes instead of PPh$_3$ showed good conversions but little or no stereoselectivity. Although slower, the same reaction with the chiral phosphane ligand **9**, but without acid as cocatalyst, showed a promising stereoselectivity and conversion of various arylamines and cyclohexadienes [Eq. (5)].

Under optimized reaction conditions enantioselectivities up to 95% were observed. In a more detailed study, it was shown that—in the presence of acid, the catalyst [{Pd(π-allyl)Cl}$_2$], and **9**—at the metal center, the product exchanges with free amine as fast as it is formed, and therefore, loses its optical activity. Thus, the kinetic selectivity of the catalytic system may be the same in the presence and absence of acid; the exchange process leads to the apparent reduction in selectivity.[22]

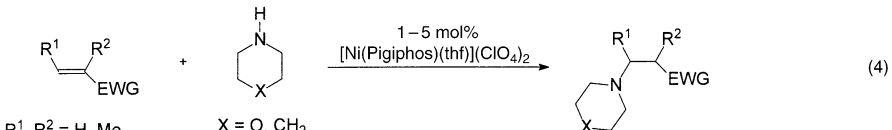
Also, the enantioselective addition of aniline to vinylarenes can be per-



trans-**8** (R = Cy, *t*Bu)



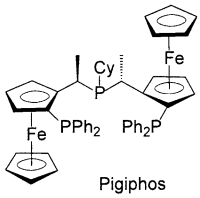
cis-**8** (R = Cy, *t*Bu)



R^1, R^2 = H, Me
EWG = CN, COOR

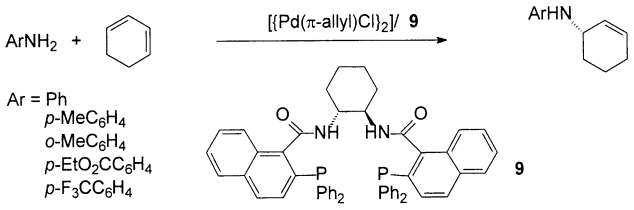
X = O, CH$_2$

(4)



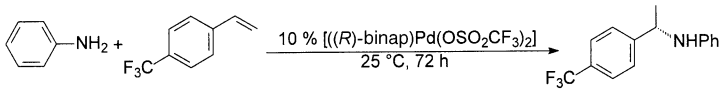
Pigiphos

 © 2003 Wiley-VCH Verlag GmbH & Co. KGaA, Weinheim



(5)

formed with palladium catalysts.[23] As outlined above this requires irreversible addition of the amine to the olefin. Reaction of aniline with *p*-trifluoromethylstyrene catalyzed by [((*R*)-binap)-$Pd(OSO_2CF_3)_2$] at 25 °C gave the addition product in 81 % yield and 81 % enantioselectivity [Eq. (6)]. Analysis of the enantioselectivity throughout the reaction showed a constant value at both low and high conversion. Reaction of vinylnaphthalene with aniline at 45 °C with the same catalyst gave quantitative yields and 64 % enantioselectivity.



(6)

The enantioselective catalytic hydroamination is one of the major challenges in synthetic organic and organometallic chemistry. An enantioselective hydroamination offers a very attractive synthetic pathway to chiral amines. As shown herein only a few catalysts for the enantioselective hydroamination are known to date. So far, these systems have only limited applications. As a result of the increasing research efforts in the enantioselective catalytic hydroamination new and spectacular examples of this reaction will most likely follow in the near future.

[1] T. E. Müller, M. Beller, *Chem. Rev.* **1998**, *98,* 675 – 703.
[2] M. Johannsen, K. A. Jørgensen, *Chem. Rev.* **1998**, *98,* 1689 – 1708.
[3] D. M. Roundhill, *Chem. Rev.* **1992**, *92,* 1 – 27.
[4] T. E. Müller in *Encyclopedia of Catalysis* (Ed.: J. T. Horváth), Wiley, New York, **2002**.
[5] J. Seayad, A. Tillack, C. G. Hartung, M. Beller, *Adv. Synth. Catal.* **2002**, *344*, 795 – 813.
[6] M. Nobis, B. Drießen-Hölscher, *Angew. Chem.* **2001**, *113*, 4105 – 4108; *Angew. Chem. Int. Ed.* **2001**, *40,* 3983 – 3985.
[7] F. J. Sardina, H. Rapoport, *Chem. Rev.* **1996**, *96*, 1825 – 1872.
[8] M. A. Giardello, V. P. Conticello, L. Brard, M. Sabat, A. L. Rheingold, C. L. Stern, T. J. Marks, *J. Am. Chem. Soc.* **1994**, *116*, 10212 – 10240.
[9] M. A. Giardello, V. P. Conticello, L. Brard, M. R. Gagné, T. J. Marks, *J. Am. Chem. Soc.* **1994**, *116*, 10241 – 10254.
[10] M. R. Gagné, L. Brard, V. P. Conticello, M. A. Giradello, C. L. Stern, T. J. Marks, *Organometallics* **1992**, *11*, 2003 – 2005.
[11] M. R. Douglass, M. Ogasawara, S. Hong, M. V. Metz, T. J. Marks, *Organometallics* **2002**, *21*, 283 – 292.
[12] M. R. Gagné, C. L. Stern, T. J. Marks, *J. Am. Chem. Soc.* **1992**, *114*, 275 – 294.
[13] S. Hong, T. J. Marks, *J. Am. Chem. Soc.* **2002**, *124*, 7886 – 7887.
[14] R. Dorta, P. Egli, F. Zürcher, A. Togni, *J. Am. Chem. Soc.* **1997**, *119*, 10857 – 10858.
[15] N. Bieler, P. Egli, R. Dorta, A. Togni, M. Eyer (Lonza A.G.), EP 0 909 762A2, **1999**, [*Chem. Abstr.* **1999**, *130*, 305622].
[16] A. L. Casalnuovo, J. C. Calabrese, D. Milstein, *J. Am. Chem. Soc.* **1988**, *110*, 6738 – 6744.
[17] M. Aizenberg, D. Milstein, T. H. Tulip, *Organometallics* **1996**, *15*, 4093 – 4095.
[18] D. Vasen, A. Salzer, F. Gerhards, H.-J. Geis, R. Stürmer, N. H. Bieler, A. Togni, *Organometallics* **2000**, *19*, 539 – 546.
[19] S. E. Gibson, H. Ibrahim, *Chem. Commun.* **2002**, *21*, 2465 – 2473.
[20] L. Fadini, A. Togni, *Chem. Commun.* **2003**, 30 – 31.
[21] O. Löber, M. Kawatsura, J. F. Hartwig, *J. Am. Chem. Soc.* **2001**, *123*, 4366 – 4367.
[22] J. Pawlas, Y. Nakao, M. Kawasura, J. F. Hartwig, *J. Am. Chem. Soc.* **2002**, *124*, 3669 – 3679.
[23] M. Kawatsura, J. F. Hartwig, *J. Am. Chem. Soc.* **2000**, *122*, 9546 – 9547.

 © 2003 Wiley-VCH Verlag GmbH & Co. KGaA, Weinheim

Macrolide Syntheses

The Total Syntheses of Phorboxazoles—New Classics in Natural Product Synthesis

*Lars Ole Haustedt, Ingo V. Hartung, and H. M. R. Hoffmann**

Keywords:
antitumor agents · macrolides · phorboxazoles · synthesis design · total synthesis

In September 1995 at the Eighth Symposium on Marine Natural Products in Santa Cruz de Tenerife, Spain, the phorboxazoles first caught the interest of natural products chemists. The phorboxazoles had been isolated by Molinski and co-workers from the marine sponge *Phorbas* sp. found in the Indian Ocean.[1] The structures as well as the relative and absolute configurations were elucidated from 2D NMR and NOESY experiments, Mosher ester analysis, correlation with synthetic compounds, and CD spectroscopy.[2] The phorboxazole skeleton consists of six rings—including two 2,4-disubstituted oxazoles—and 15 stereogenic centers organized into a macrolide (C1–C26) and a side-chain substructure (C27–C46). Phorboxazoles A and B differ only in the absolute configuration at C13. Both compounds show exceptional cytostatic activity and antifungal activity against *Candida albicans* but no antibacterial activity against *E. coli*, *Pseudomonas aeruginosa*, and *Staphylococcus aureus*. Phorboxazoles A and B were tested against the 60 tumor cell lines of the U.S. National Cancer Institute (NCI), and they effected in vitro inhibition of cell growth with mean GI_{50} values of $< 1.6 \times 10^{-9}$ M. Phorboxazole A induced cell cycle arrest in the S phase in Burkitt lymphoma cells and showed neither inhibition of tubulin polymerization nor interference with the microtubules. Since selective modulation of cell cycles by natural and synthetic compounds is of both scientific and pharmaceutical importance,[3] the phorboxazoles and (semi)synthetic analogues are attractive compounds for detailed in vitro and in vivo investigations to determine their biological target and mode of action. These investigations largely depend on a synthetic entry to the phorboxazole skeleton.

[*] Prof. H. M. R. Hoffmann, Dr. L. O. Haustedt, Dr. I. V. Hartung
Institut für Organische Chemie
Universität Hannover
Schneiderberg 1B
30167 Hannover (Germany)
Fax: (+49) 511-762-3011
E-mail:
hoffmann@mbox.oci.uni-hannover.de

The Forsyth Synthesis (1998)

The first total synthesis of phorboxazole A was completed by Forsyth and co-workers in early 1998.[4] They relied on a highly convergent strategy for the assembly of the phorboxazole skeleton, employing three fragments of comparable complexity (C3–C17, C18–C30, and C31–C46) (Figure 1).

A most elegant and unprecedented feature of the Forsyth synthesis is the biomimetic assembly of the oxazole units. This assembly commenced with the formation of the C16–C18 oxazole from a C3–C17 amino alcohol and a C18–C30 carboxylic acid by application of the Wipf protocol (yellow box in Figure 1).[5] Amide formation was followed by oxidation to yield the amide aldehyde. Aromatization to give the 2,4-disubstituted oxazole involved bromooxazoline formation and subsequent dehydrobromination. The C1–C23 macrocycle was closed by an intramolecular Still–Gennari olefination of a C3 aldehyde with C1–C2 bis-(2,2,2-trifluoroethyl)phosphonoacetate, thus forming

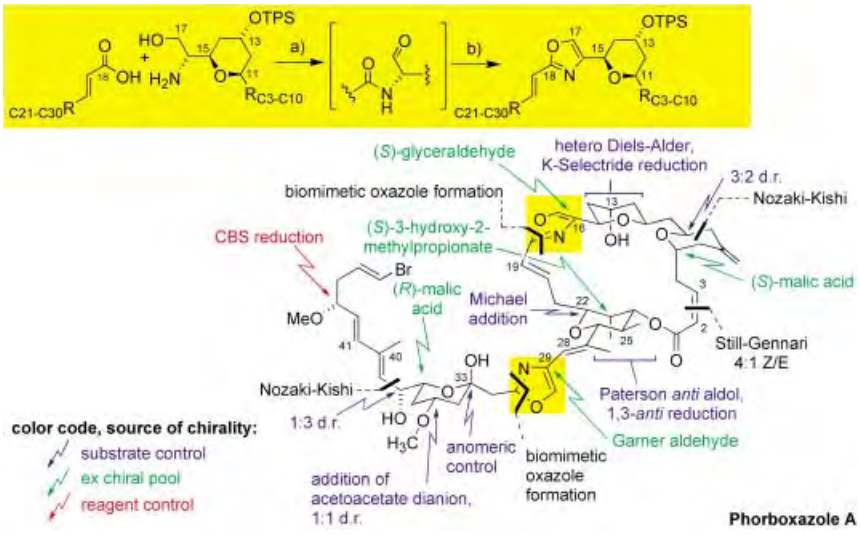


Figure 1. The Forsyth synthesis of phorboxazole A.[4] a) 1) EDCI·MeI, HOBt, 2) DMP; b) 1) $(BrCCl_2)_2$, PPh_3, 2,6-tBu_2-4-Me-C_5NH_2, 2) DBU (67% overall). EDCI = *N*′-3′-dimethylaminopropyl-*N*-ethylcarbodiimide, DBU = 1,8-diazabicyclo[5.4.0.]undec-7-ene, DMP = Dess–Martin periodinane, HOBt = 1-hydroxybenzotriazole, K-Selectride = potassium tris(*sec*-butyl)borohydride, TPS = *tert*-butyldiphenylsilyl.

DOI: 10.1002/anie.200301643
© 2003 Wiley-VCH Verlag GmbH & Co. KGaA, Weinheim

the intermediate with a C2–C3 double bond in 77% yield as a 4:1 mixture of *Z* and *E* isomers. Finally, the second biomimetic formation of an oxazole unit (C29–C31) completed the skeleton assembly although in significantly lower yield (22%) than that for the C16–C18 oxazole synthesis (67%).

For the construction of the remote stereogenic center at C43 Forsyth et al. relied on Corey's oxazaborolidine-catalyzed reduction protocol. In contrast to this reagent-controlled method (highlighted in red), all other stereocenters, which are clustered around C5–C15, C22–C26, and C33–C38, were either taken from abundant chiral starting materials (highlighted in green) or generated in a substrate-directed manner (highlighted in blue).

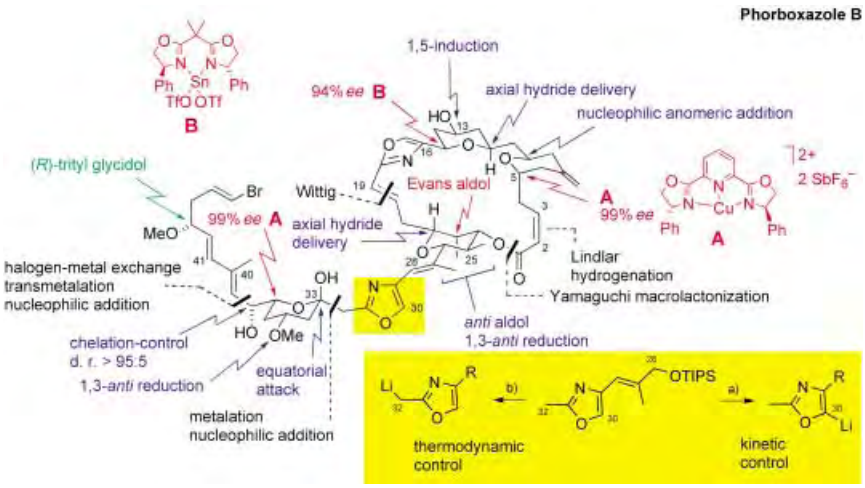


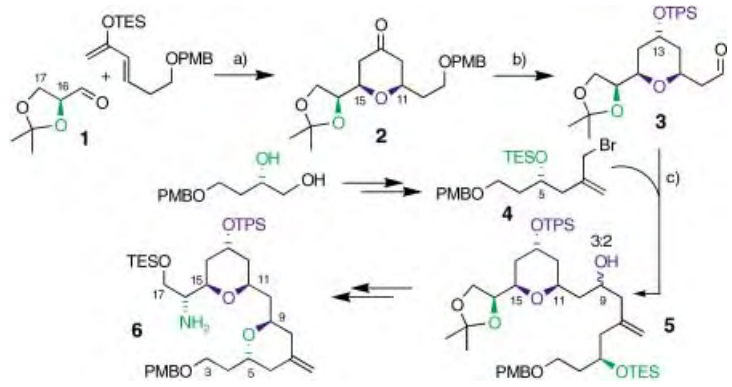
Figure 2. The Evans synthesis of phorboxazole B.[6] a) LDA, THF, −78 °C; b) $LiNEt_2$, THF, −78 °C. LDA = lithium diisopropylamide, TIPS = triisopropylsilyl.

This strategy is exemplified by Forsyth's synthesis of the C3–C17 fragment (Scheme 1). Starting from (*S*)-glyceraldehyde acetonide **1** an *endo*-selective BF_3-mediated hetero-Diels–Alder reaction formed the *syn*-C11/C15 tetrahydropyran (THP) fragment **2** as the major product in a 16:4:1 mixture with *exo* cycloadducts. The C13 axial hydroxy group was generated diastereoselectively by substrate-controlled reduction with bulky K-Selectride as the hydride source. The formation of the C11, C13, and C15 stereocenters was therefore guided by the intermediate stereocenter at C16, which is removed en route to the natural product. Finally, Nozaki–Kishi coupling of **3** with allylic bromide **4**, which was derived from (*S*)-malic acid, generated homoallylic alcohol **5** as a 3:2 mixture of C9 epimers. The unwanted diastereomer was removed and recycled by Mitsunobu inversion. This sequence developed during the race for the first total synthesis illustrates a drawback of Forsyth's substrate-controlled strategy: In several instances absence of a substrate-intrinsic stereochemical bias led to a mixture of diastereomers, which necessitated additional recycling steps.

The Evans Synthesis (2000)

The first total synthesis of phorboxazole B was completed by the Evans group in 2000.[6] Their retrosynthetic analysis differs significantly from Forsyth's strategy in that only two fragments of equal complexity (C1–C19 and C20–C38) are employed and the C39–C46 side chain is added late in the synthesis (Figure 2). Fragment assembly started with an *E*-selective Wittig olefination ($E/Z > 95:5$) to generate the C19–C20 double bond followed by a Yamaguchi macrolactonization. In order to avoid isomers at the C2–C3 double bond, the (*Z*)-alkene was masked as a triple bond and regenerated after macrolactonization by Lindlar hydrogenation ($Z/E > 95:5$). Addition of the C39–C46 side chain had been achieved initially by a chemoselective halogen–metal exchange of a vinyl iodide (in the presence of the terminal vinyl bromide) with *tert*-butyllithium and subsequent addition to a C1–C38 aldehyde to yield a 1:2 mixture of C38 epimers. When the initially formed vinyllithium species was transmetalated with magnesium bromide, the desired C38 diastereomer was formed almost exclusively (>20:1) by chelation-controlled nucleophilic addition. The synthesis of the C20–C38 fragment included the regioselective α-metalation of the C29–C32 methyloxazole with lithium diethylamide (yellow box in Figure 2) and subsequent diastereoselective addition to the C33–C37 lactone to generate the C33 hemiacetal.

This phorboxazole synthesis features an array of asymmetric catalytic processes developed in the Evans laboratory over the years. Only the forlorn stereocenter at C43 is derived from a chiral starting material, while the other stereocenters are either formed by li-



Scheme 1. a) 1) $BF_3{\cdot}OEt_2$, Et_2O, −78 °C, 2) TBAF, TsOH, THF, 60% (2 steps), 16:4:1 d.r.; b) 1) K-Selectride, THF, 2) TPSCl, Et_3N, 3) DDQ, CH_2Cl_2, 4) DMP, 70% (4 steps); c) $CrCl_2/NiCl_2$, THF, 80%, 3:2 d.r. TBAF = tetrabutylammonium fluoride, DDQ = 2,3-dichloro-5,6-dicyano-*p*-benzoquinone, PMB = *p*-methoxybenzyl, TES = triethylsilyl.

 © 2003 Wiley-VCH Verlag GmbH & Co. KGaA, Weinheim

gand- and auxiliary-controlled asymmetric reactions or are generated with high substrate control.

The elegance of the Evans synthesis and their brilliant retrosynthetic analysis is exemplified by the synthesis of the C4–C19 fragment (Scheme 2). The C5 stereocenter was formed with perfect stereoselection by addition of bis(trimethylsilyl)dienol ether **7**, which functions as an efficient polyacetate aldol equivalent, to (benzyloxy)acetaldehyde in the presence of the copper(II)-Phpybox catalyst **A** (Figure 2).[7] Axial nucleophilic attack at a cyclic oxonium ion[8] formed in situ from the anomeric acetate **9** resulted in the diastereoselective formation of the C9 stereocenter (89:11 d.r.). Addition of a silylketene acetal to α-oxazole aldehyde **11** catalyzed by [Sn((*S*,*S*)-Ph-box)](OTf)$_2$ (Figure 2) allowed the stereocontrolled generation of the C15 hydroxy group.[9] Addition of dibutylboryl enolate derived from ketone **10** to β-silyloxyaldehyde **13** afforded the aldol product **14** under 1,5-*anti* induction.[10] Finally, the C11 stereocenter was set by axial nucleophilic hydride delivery to a cyclic oxonium ion.

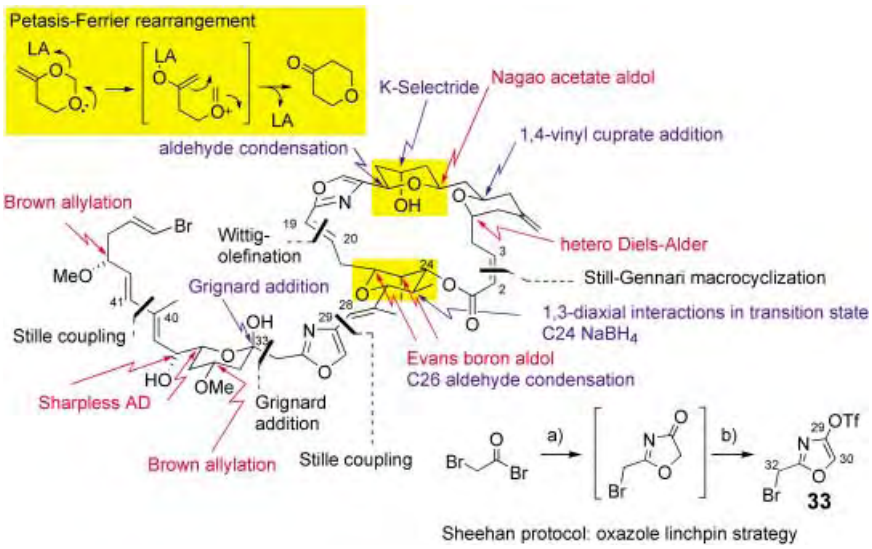
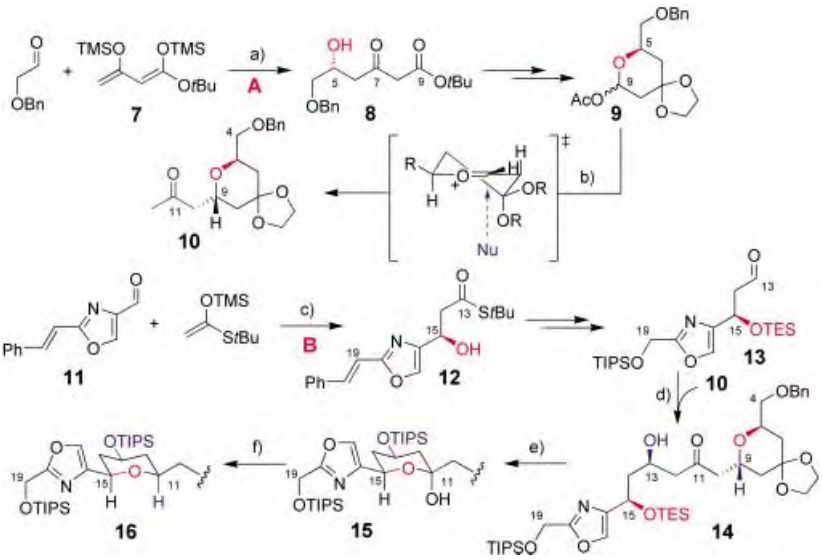


Figure 3. The Smith synthesis of phorboxazole A. [11] a) AgOCN, CH_2N_2; b) Et_3N, Tf_2O.

The Smith Synthesis (2001)

The Smith total synthesis of phorboxazole A, which was completed in 2001,[11] features the application of the Petasis–Ferrier rearrangement for the construction of two of the four tetrahydropyran units (yellow box in Figure 3). In 1996 Petasis described the rearrangement of enol acetals to give tetrahydropyranones. This process is related to earlier investigations by Ferrier et al. on enol ether rearrangements induced by mercuric ions. However, never before was the enol acetal rearrangement used on such challenging targets. It has proved to be very valuable for the assembly of highly functionalized *cis*-substituted tetrahydropyran ring systems.

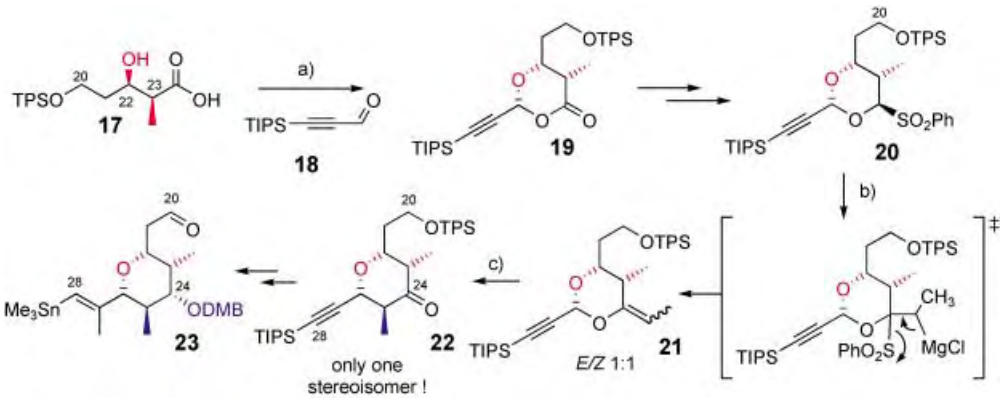


Scheme 2. a) 2 mol% **A**, CH_2Cl_2, 85%, >99% *ee*; b) TMSOTf, 2-(trimethylsiloxy)propene, cat. pyr, CH_2Cl_2, 89%, 89:11 d.r.; c) 10 mol% **B**, CH_2Cl_2, 91%, 94% *ee*; d) nBu_2BOTf, iPr_2NEt, CH_2Cl_2, 82%, >95:5 d.r.; e) 1) TIPSOTf, CH_2Cl_2, 99%, 2) HF·pyr, pyr, THF, H_2O, 99%; f) $BF_3{\cdot}OEt_2$, Et_3SiH, CH_2Cl_2, 96%, >95:5 d.r. TMS = trimethylsilyl, OTf = trifluoromethanesulfonate, pyr = pyridine.

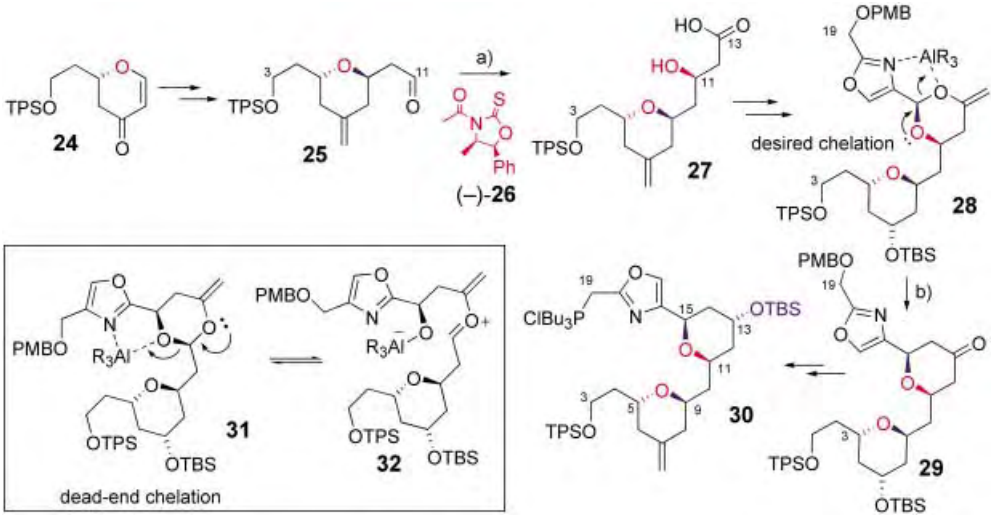
The synthesis of the central and most complex *cis*-substituted C22–C26 THP system started with the condensation of β-hydroxy acid **17**, which was prepared under Evans aldol conditions, with propargyl aldehyde **18** (Scheme 3). A 3:1 mixture of *cis* and *trans* acetals was obtained, from which the *trans* acetal could be recycled. After conversion of dioxanone **19** into sulfone **20**, a Julia-type reaction with an α-halo Grignard reagent generated the enol ether **21** without stereocontrol of the *exo* double-bond geometry. However, in the presence of Me_2AlCl the Petasis–Ferrier rearrangement took place, and pyranone **22** was formed exclusively in high yield. This observation was explained by the boatlike transition state of the *E* isomer, caused by 1,3-diaxial interactions in the chair transition state, in contrast to the chairlike transition state of the *Z* isomer. Diastereoselective reduction of the C24 ketone in **22** was achieved with sodium borohydride.

The C5–C9 *trans*-substituted THP system was built up from Danishefsky's diene and a protected β-hydroxyaldehyde in a hetero-Diels–Alder reaction (Scheme 4). 1,4-Vinyl cuprate addition, hydroboration, generation of the *exo*-

 © 2003 Wiley-VCH Verlag GmbH & Co. KGaA, Weinheim



Scheme 3. a) 1) HMDS, 2) TMSOTf, 66% *cis* + 19% *trans* (2 steps); b) *n*BuLi, 1-chloro-1-iodoethane, *i*PrMgCl, −78 °C, 95%, *E*/*Z* 1:1; c) Me_2AlCl, CH_2Cl_2, 91%. DMB = 3,4-dimethoxybenzyl, HMDS = hexamethyldisilazane.



Scheme 4. a) 1) $Sn(OTf)_2$, (−)-**26**, *N*-ethylpiperidine, 92%, 10:1 d.r., 2) LiOH, H_2O_2, 98%; b) Me_2AlCl, CH_2Cl_2, −78 °C, 89%.

methylene functionality by a Wittig reaction and oxidation of the C11 primary alcohol delivered aldehyde **25**, which was ready for a Nagao aldol reaction using a tin enolate (92%, 10:1 d.r.). The resulting C3–C13 β-hydroxycarboxylic acid **27** was condensed with an oxazole aldehyde to generate a dioxanone. By use of the Petasis modification of the Tebbe reagent, the enol acetal required for the Petasis–Ferrier rearrangement was established. In the presence of Me_2AlCl even this highly functionalized C3–C19 segment underwent the rearrangement cleanly. Reduction of the C13 ketone using K-selectride selectively formed the axial hydroxy group. In prior investigations Smith had shown that the vinyl acetal **31** was resistent to the rearrangement conditions due to a dead-end chelation with the neighboring oxazole nitrogen. 1,3-Transposition of the enol ether oxygen allowed the successful rearrangement of **28** to the desired tetrahydropyranone system.

After conversion of the C19 hydroxy group into the phosphonium chloride, the C19–C20 double bond was established in high yield (94%) and *E* selectivity (*E*/*Z* 12:1) by condensation with aldehyde **23**. One further key feature of the Smith synthesis is the application of the 2,4-disubstituted difunctional oxazole **33** (Figure 3) as a linchpin for the combination of the acyclic precursor of the macrolide core and the functionalized side chain. Revisiting a protocol developed in 1949 by Sheehan, Smith et al. used bromoacetyl bromide, silver isocyanate, and diazomethane to generate a 2-bromomethyl-4-trifluoromethanesulfonyloxyoxazole. Oxazole **33** is perfectly suited at one terminus for a Stille cross-coupling reaction and at the other for a Grignard addition to a C33–C46 lactone side chain. Finally, a Still–Gennari olefination was applied to form the macrolide (95%, *Z*/*E* 4:1).

The Pattenden Synthesis (2003)

In their total synthesis of phorboxazole A Pattenden et al. utilized a fragment-coupling strategy combining features of the Evans and Forsyth syntheses.[12] In contrast to the Evans synthesis, this fragment assembly started with the diastereoselective addition of a metalated C20–C32 oxazole to a C33–C46 lactone. Next, the C19–C20 double bond was set by Wittig olefination, and finally macrolide ring closure was achieved by an intramolecular Still–Gennari olefination. Thus, this highly efficient fragment

 © 2003 Wiley-VCH Verlag GmbH & Co. KGaA, Weinheim

assembly employing three segments of roughly equal complexity (C3–C19, C20–C32, C33–C46) might well be suitable for providing compounds for studies of the structure–activity relationship (SAR). For the generation of the stereocenters Pattenden relied both on reagent control (e.g. Brown allylation for C13, C15, and C35) and substrate control (e.g. an intramolecular oxyanion Michael addition for C11) as well as on chiral building blocks (e.g. malic acid for C43 and D-xylose for C37–C38).

The Williams Synthesis (2003)

The fourth synthesis of phorboxazole A was completed by the group of D. R. Williams and is characterized by a far-reaching asymmetric allylation strategy (Figure 4).[13] Originally established in Williams's hennoxazole synthesis, the in situ transmetalation protocol, which employs an allylstannane, boron tribromide, and (*R*,*R*)- or (*S*,*S*)-1,2-diamino-1,2-diphenylethane as the chiral controller, was adapted in this phorboxazole synthesis (yellow box in Figure 4). The chiral ligand had been introduced by Corey in enantioselective Diels–Alder reactions and asymmetric allylations. The boron bromide ligand system built up from the C_2-symmetric ligand and BBr_3 is used as a chiral electrophilic boron atom ready for the S_E2' transmetalation step with the allylic stannane, which is derived from malic acid.

The diastereofacial selectivity of the addition is determined solely by the chiral auxiliary. An iterative asymmetric allylation process allowed construction of all stereocenters (except C13) in the C5–C15 bistetrahydropyran region. Ring closure towards the THP systems was achieved by mesylation and subsequent S_N2 displacement. The C13 hydroxy functionality was generated under substrate control by using LS-Selectride. The allylation strategy was utilized a third time for the generation of the C37 stereocenter. As a result, three of the four tetrahydropyran systems were established by using the asymmetric in situ transmetalation–allylation strategy.

As seen before in the Smith synthesis, a 2,4-disubstituted oxazole was used as a bifunctional linchpin for the convergent assembly of fragments. In

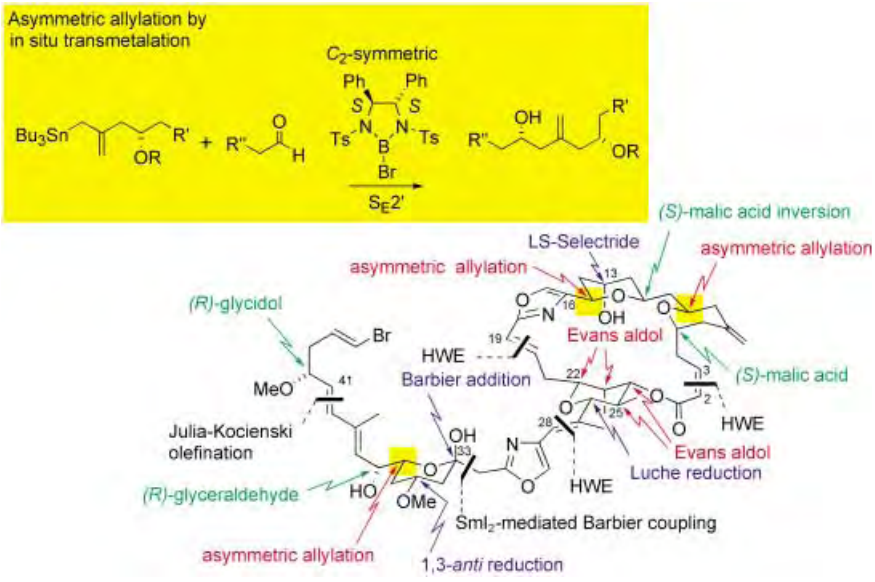


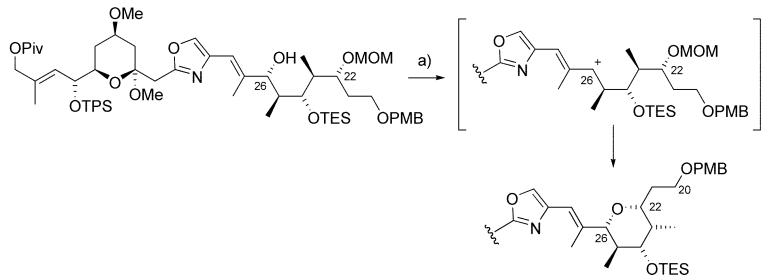
Figure 4. The Williams synthesis of phorboxazole A. [13] LS-Selectride = lithium tris(1,3-dimethylbutyl)borohydride, HWE = Horner–Wittig–Emmons olefination.

contrast to the Smith group, Williams et al. used a masked iodomethyloxazole aldehyde for this purpose. First, a SmI_2-mediated Barbier coupling of the C28–C32 iodomethyloxazole with the C33–C46 aldehyde yielded a 1:1 diastereomeric mixture of C33 alcohols. Subsequently, the oxazole aldehyde was set free by a deprotection–oxidation sequence and combined with a C20–C27 β-ketophosphonate in a Horner–Wadsworth–Emmons reaction, which delivered the trisubstituted C27–C28 olefin with excellent *E* selectivity.

The C22–C26 stereopentade had been created by two successive Evans aldol processes, in which four contiguous stereocenters had been generated (Scheme 5). Under Luche conditions the C26 ketone could be reduced regio- and diastereoselectively. In a very elegant manner, the C22–C26 tetrahydropyran was established by internal capture of a transoid allylic cation at C26 by the C22 oxygen atom with concomitant cleavage of the MOM ether (Scheme 5). The configuration at C26 in the neutral precursor is irrelevant in this cyclization step. Finally, the macrolide was formed by Wittig olefination (C19–C20, >95:5 *E*/*Z*) and intramolecular Horner–Wadsworth–Emmons olefination (C2–C3, 4:1 *Z*/*E*).

SAR Studies

Preliminary results from SAR studies were reported by Uckun and Forsyth.[14] Seven synthetic analogues were tested against three different human cancer cell lines. These studies revealed that the macrolide, the central C29–C31 oxazole, and the C39–C46 side chain are necessary for anticancer activity, whereas the C45–C46 vinyl bromide and the free C33 hemiketal can be replaced by an alkyne and a mixed ketal, respective-



Scheme 5. a) Tf_2O, pyr, CH_2Cl_2, −20 °C, 12 h, 55 %. MOM = methoxymethyl.

 © 2003 Wiley-VCH Verlag GmbH & Co. KGaA, Weinheim

ly. It was speculated from these results that the biological activity might depend on multiple point contacts on a cell receptor. In addition, the rigid C27–C31 vinyloxazole substructure might place the macrolide and side-chain substructures in the necessary relative orientation for receptor binding. In this context, further SAR studies are necessary to identify a minimal pharmacophore. As the configuration of C38 is thought to play a crucial role in the overall molecular shape of phorboxazole, a variation of this stereocenter is of special interest as well as deletions within the macrolide core structure.

The work on the phorboxazoles demonstrates how the judicious application and development of reagent and substrate control as well as the chiral pool have successfully enabled chemists to tackle a most challenging stereochemical problem. Besides improving known protocols and inventing new ones in the race for the phorboxazoles, researchers have shown how important creativity and nonlinear thinking can be. Total synthesis remains a yardstick for measuring the progress of organic chemistry and natural product chemistry.

[1] P. A. Searle, T. F. Molinski, *J. Am. Chem. Soc.* **1995**, *117*, 8126.

[2] a) P. A. Searle, T. F. Molinski, L. J. Brzezinski, J. W. Leahy, *J. Am. Chem. Soc.* **1996**, *118*, 9422; b) T. F. Molinski, *Tetrahedron Lett.* **1996**, *37*, 7879; c) T. F. Molinski, L. J. Brzezinski, J. W. Leahy, *Tetrahedron: Asymmetry* **2002**, *13*, 1013.

[3] D. T. Hung, T. F. Jamison, S. L. Schreiber, *Chem. Biol.* **1996**, *3*, 623.

[4] a) C. J. Forsyth, F. Ahmed, R. D. Cink, C. S. Lee, *J. Am. Chem. Soc.* **1998**, *120*, 5597; b) C. S. Lee, C. J. Forsyth, *Tetrahedron Lett.* **1996**, *37*, 6449; c) R. D. Cink, C. J. Forsyth, *J. Org. Chem.* **1997**, *62*, 5672; d) F. Ahmed, C. J. Forsyth, *Tetrahedron Lett.* **1998**, *39*, 183.

[5] P. Wipf, S. Lim, *J. Am. Chem. Soc.* **1995**, *117*, 558.

[6] a) D. A. Evans, D. M. Fitch, T. E. Smith, V. J. Cee, *J. Am. Chem. Soc.* **2000**, *122*, 10033; b) D. A. Evans, V. J. Cee, T. E. Smith, D. M. Fitch, P. S. Cho, *Angew. Chem.* **2000**, *112*, 2633; *Angew. Chem. Int. Ed.* **2000**, *39*, 2533; c) D. A. Evans, D. M. Fitch, *Angew. Chem.* **2000**, *112*, 2636; *Angew. Chem. Int. Ed.* **2000**, *39*, 2536.

[7] D. A. Evans, M. S. Kozlowski, J. A. Murry, C. S. Burgey, K. R. Campos, B. T. Connell, R. J. Staples, *J. Am. Chem. Soc.* **1999**, *121*, 669.

[8] M. D. Lewis, J. K. Cha, Y. Kishi, *J. Am. Chem. Soc.* **1982**, *104*, 4976.

[9] D. A. Evans, D. W. C. MacMillan, K. R. Campos, *J. Am. Chem. Soc.* **1997**, *119*, 10859.

[10] D. A. Evans, P. J. Coleman, B. Côté, *J. Org. Chem.* **1997**, *62*, 788.

[11] a) A. B. Smith III, K. P. Minbiole, P. R. Verhoest, M. Schelhaas, *J. Am. Chem. Soc.* **2001**, *123*, 10942; b) A. B. Smith III, P. R. Verhoest, K. P. Minbiole, M. Schelhaas, *J. Am. Chem. Soc.* **2001**, *123*, 4834; c) A. B. Smith III, K. P. Minbiole, P. R. Verhoest, T. J. Beauchamp, *Org. Lett.* **1999**, *1*, 913; d) A. B. Smith III, P. R. Verhoest, K. P. Minbiole, J. J. Lim, *Org. Lett.* **1999**, *1*, 909.

[12] a) M. A. González, G. Pattenden, *Angew. Chem.* **2003**, *115*, 1293; *Angew. Chem. Int. Ed.* **2003**, *42*, 1255; b) T. Ye, G. Pattenden, *Tetrahedron Lett.* **1998**, *39*, 319; c) G. Pattenden, A. T. Plowright, J. A. Tornos, T. Ye, *Tetrahedron Lett.* **1998**, *39*, 6099; d) A. T. Plowright, G. Pattenden, *Tetrahedron Lett.* **2000**, *41*, 983.

[13] a) D. R. Williams, A. A. Kiryanov, U. Emde, M. P. Clark, M. A. Berliner, J. T. Reeves, *Angew. Chem.* **2003**, *115*, 1296; *Angew. Chem. Int. Ed.* **2003**, *42*, 1258; b) D. R. Williams, M. P. Clark, U. Emde, M. A. Berliner, *Org. Lett.* **2000**, *2*, 3023; c) D. R. Williams, M. P. Clark, M. A. Berliner, *Tetrahedron Lett.* **1999**, *40*, 2287.

[14] F. M. Uckun, C. J. Forsyth, *Bioorg. Med. Chem. Lett.* **2001**, *11*, 1181.

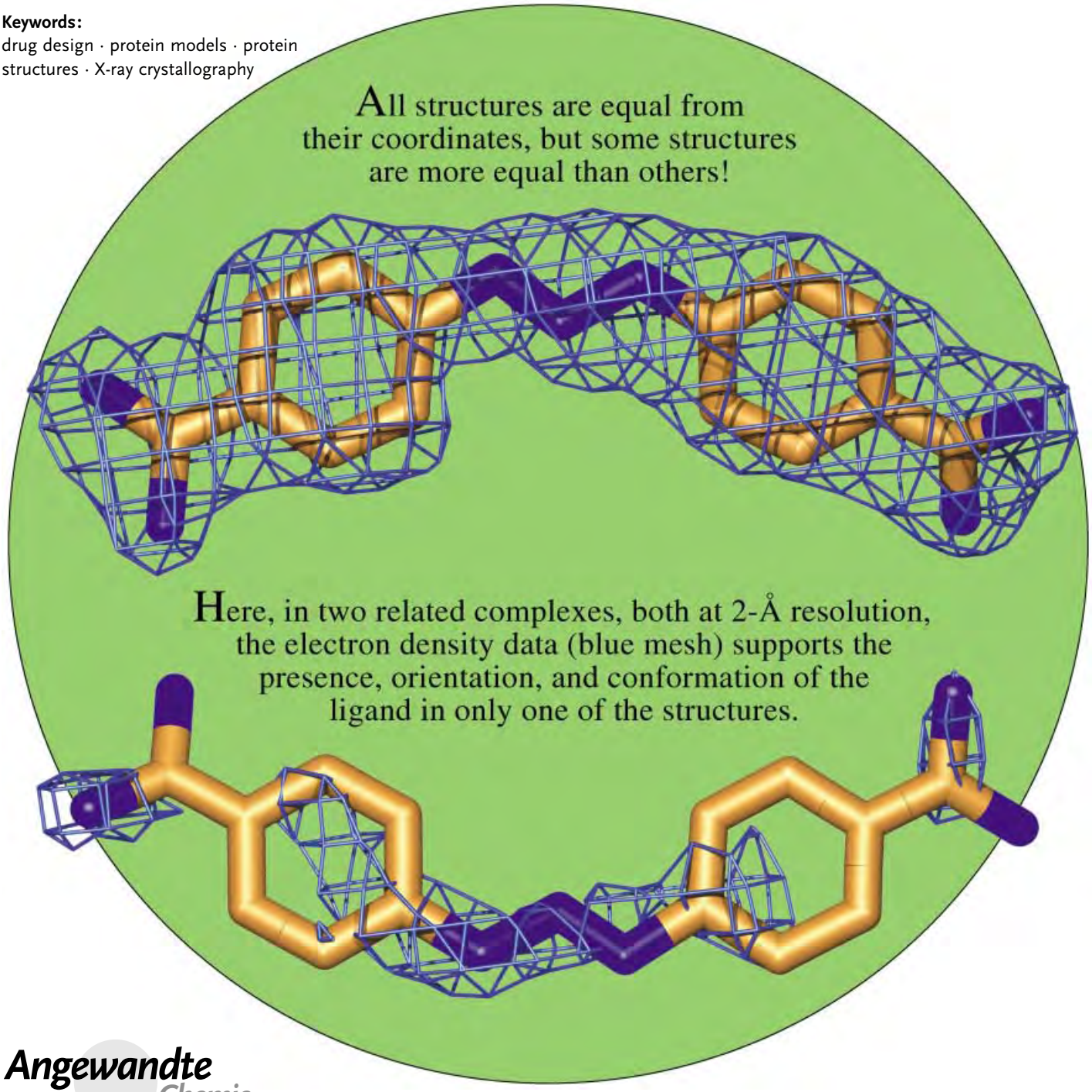
 © 2003 Wiley-VCH Verlag GmbH & Co. KGaA, Weinheim

Structure-Based Drug Design

Application and Limitations of X-ray Crystallographic Data in Structure-Based Ligand and Drug Design

Andrew M. Davis, Simon J. Teague, and Gerard J. Kleywegt*

Keywords:
drug design · protein models · protein structures · X-ray crystallography



© 2003 Wiley-VCH Verlag GmbH & Co. KGaA, Weinheim
DOI: 10.1002/anie.200200539

Structure-based design usually focuses upon the optimization of ligand affinity. However, successful drug design also requires the optimization of many other properties. The primary source of structural information for protein–ligand complexes is X-ray crystallography. The uncertainties introduced during the derivation of an atomic model from the experimentally observed electron density data are not always appreciated. Uncertainties in the atomic model can have significant consequences when this model is subsequently used as the basis of manual design, docking, scoring, and virtual screening efforts. Docking and scoring algorithms are currently imperfect. A good correlation between observed and calculated binding affinities is usually only observed only when very large ranges of affinity are considered. Errors in the correlation often exceed the range of affinities commonly encountered during lead optimization. Some structure-based design approaches now involve screening libraries by using technologies based on NMR spectroscopy and X-ray crystallography to discover small polar templates, which are used for further optimization. Such compounds are defined as leadlike and are also sought by more traditional high-throughput screening technologies. Structure-based design and HTS technologies show important complementarity and a degree of convergence.

From the Contents

1. Introduction 2719
2. Structure-Based Design of Ligands and Drugs 2720
3. Limitations in the Use of X-ray Data 2723
4. PDB Files Used in Docking and Scoring Studies 2728
5. Assessing the Validity of Structure Models 2729
6. Automated Docking and Scoring 2730
7. Convergence of Screening and Structure-Based Design 2732
8. Summary and Outlook 2733

1. Introduction

The use of protein structure information in drug discovery is often termed structure-based design, and it encompasses a number of technologies (Table 1). Although many pharmaceutical companies invested heavily in structure-based design in the 1980s, by the 1990s it appeared passé, as the industry focused upon the new great hope for drug discovery—modern high-throughput screening (HTS) of compounds produced by combinatorial chemistry.

Presently, however, structure-based design is undergoing a renaissance. This renewed interest has a number of drivers. Advances in molecular biology have made possible the reliable production of homogeneous, natural or modified proteins suitable for rapid, iterative crystallographic and NMR studies of ligand–protein complexes. Mutagenesis of these cloned and expressed proteins allows direct probing of ligand–receptor interactions.[28] A better understanding of the energetics of ligand–receptor interactions has been derived from a combination of mutagenesis with classical physical-organic chemistry investigations,[29] X-ray crystallography,[13] and thermodynamic measurements.[30] The hardware and software available to computational chemists has improved dramatically and so has the quality and speed of ligand docking algorithms. This has taken the subjectivity out of the placement of virtual structures into a protein's active site. It has also opened up the possibility of using structural information in lead generation. Virtual screening of large collections of compounds, or even larger virtual libraries, can be undertaken almost routinely with tools like DOCK,[6] GOLD,[8] FLEX-X,[7] and SLIDE.[23] Likewise, the prediction of physical properties from structures has improved greatly. Currently much emphasis is being placed upon computationally filtering by physical properties to remove nondruglike compounds[31,32] in order to frontload HTS or to guide library design.

The revolution in computer technology is showing no signs of slowing down, with current Linux farms allowing many hundreds of parallel calculations to be made in acceptable timescales. By means of Seti technology[33] over PC networks, researchers at the University of Oxford are using 1.2 million household PCs to screen 3.2 billion virtual structures in 13 protein active sites in a search for novel anticancer agents.[34] Another important driver is the increasingly high cost and competitiveness of drug discovery and development. This requires the process to be not only faster, but also smarter.[35] Although HTS is useful in the hunt for novel leads, screening of small subsets chosen by virtual screening can be very useful when the structure of the protein is available. This is especially true when other factors preclude HTS of the entire company file. The possibilities for successful structure-based design have never been greater.

[*] Dr. A. M. Davis, Dr. S. J. Teague
AstraZeneca R&D Charnwood
Bakewell Road, Loughborough
Leicestershire LE11 5RH (United Kingdom)
Fax: (+44) 150-964-5576
E-mail: andy.davis@astrazeneca.com
Dr. G. J. Kleywegt
Department of Cell and Molecular Biology
Uppsala University, Biomedical Centre
Box 596, SE-75124 Uppsala (Sweden)

 DOI: 10.1002/anie.200200539 © 2003 Wiley-VCH Verlag GmbH & Co. KGaA, Weinheim

Table 1: A selection of current structure-based design technologies.

Technology	Objective	Programs/Tools
X-ray crystallography Protein NMR spectroscopy Homology modeling	Protein structure generation	O,[1] CNS,[2] X-PLOR,[3] CCP4, [4] MODELLER[5]
Ligand docking	Prediction of bound ligand conformation	Manuel docking, DOCK,[6] Flex-X[7] GOLD[8]
Receptor interaction mapping	Ligand optimization	GRID,[9] MCSS, [10] RELIBASE,[11] SUPERSTAR[12]
Scoring	Affinity prediction	GLIDE, GOLD, LUDI,[13] DOCKSCORE,[14] SmoG2001[15]
3D QSAR	Affinity prediction	CATALYST,[16] COMFA,[17] GOLPE[18]
De novo design	Automated ligand design	LEAPFROG,[19] LUDI CombiSMoG,[20] SPROUT[21]
Pharmacophore searching	Potential lead retrieval from real or virtual databases	CATALYST, UNITY[22]
Virtual screening	Lead selection from a virtual library guided by a docking into a protein structure	DOCK, Flex-X, GLIDE GOLD, SLIDE[23]
Structure-based screening	Lead selection guided by direct observation of the ligand–protein interaction	SAR-by-NMR,[24] SHAPES,[25] CRYSTALLEAD,[26] high-throughput crystallography[27]

Structure-based design and the technologies listed in Table 1 are an extremely active area of research and have been extensively and frequently reviewed.[36–40] However, these new technologies may not suffice, since their successful application still has some severe limitations. The aim of structure-based design is the optimization of ligand potency, which is usually measured in a simple in vitro competitive inhibition or binding assay. However, the aim of all pharmaceutical research projects is the discovery of a candidate drug. Here, we highlight the distinction between ligand design and drug design, and illustrate the difference with case histories from studies on HIV-protease, neuraminidase, carbonic anhydrase, and renin inhibitors. In most cases the protein structure used in the structure-based design process has been determined by X-ray crystallography rather than NMR spectroscopy. The latter technique is limited by constraints on the molecular size of the protein and the requirement for multiple isotopic labeling. Since all the technologies listed in Table 1 depend upon protein structural information, we highlight some of the pitfalls and limitations in protein structure determination by X-ray crystallographic methods that might otherwise mislead the unwary user. Addressing these ambiguities may lead to further opportunities, which we highlight in this review.

2. Structure-Based Design of Ligands and Drugs

Structure-based design is often loosely termed structure-based drug design or rational drug design. Usually the processes described could be termed more accurately structure-based ligand design, since the objective is to optimize the potency of a ligand in a simple in vitro assay. Drug design requires optimization of many other properties including dissolution, absorption, metabolic stability, plasma protein binding, distribution, elimination, toxicological profile, cost of synthesis, and pharmaceutical



Simon Teague, born in 1959 in Worcester (UK), gained his PhD at the University of Nottingham in the group of Professor G. Pattenden. He carried out postdoctoral work with Professor A. I. Meyers at Colorado State University (USA). He is now a Principle Scientist at AstraZeneca R&D Charnwood (UK). His research interests are lead generation methodologies and the study of drug–receptor interactions.



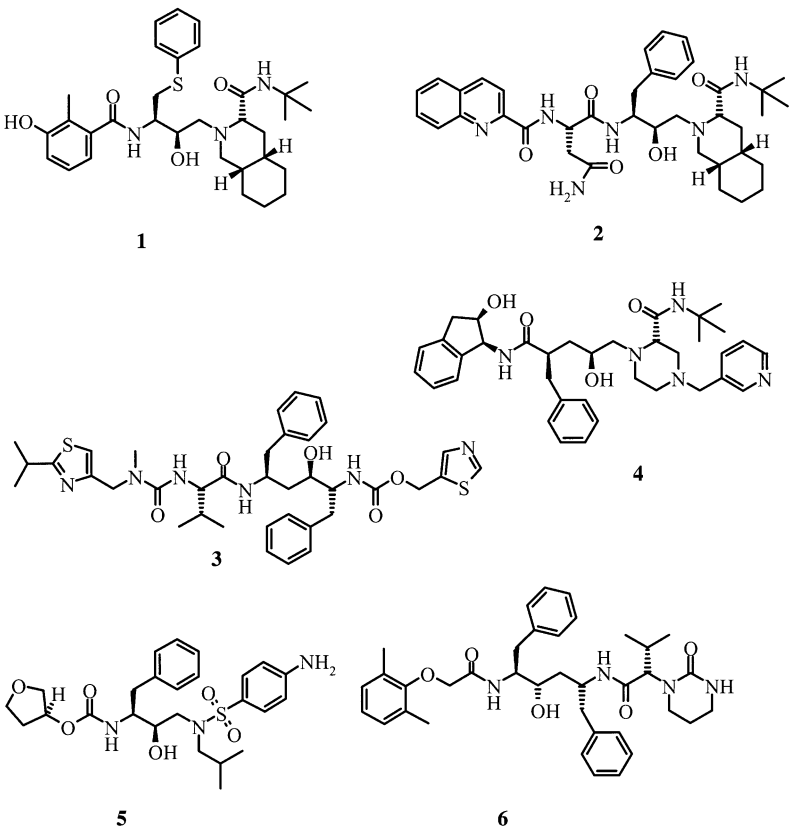
Andy Davis, born in 1961 in Wells, Somerset (UK), gained his BSc degree from Imperial College, London, and his PhD at the University of Huddersfield with Professor M. I. Page for studies on the kinetics and mechanism of rearrangements of penicillins. He is now Associate Director of Physical Chemistry at AstraZeneca R&D Charnwood. His interests are the energetics of ligand–receptor interactions, QSAR methods, and the cooperative application of physical-organic and computational chemistry to drug discovery.

 © 2003 Wiley-VCH Verlag GmbH & Co. KGaA, Weinheim

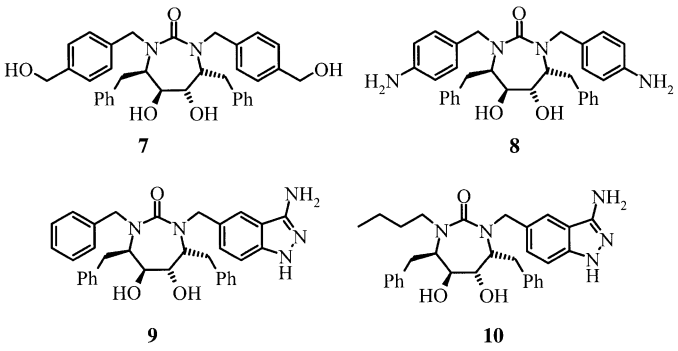
properties. Structure-based design has already contributed to the discovery of a number of very important drugs such as the peptidomimetic HIV-protease inhibitors nelfinavir (**1**), saquinavir (**2**), ritonavir (**3**), indinavir (**4**), amprenavir (**5**), and lopinavir (**6**, Scheme 1).

Peptidomimetic HIV-protease inhibitors are already in clinical use. Although these drugs are successful commercially and clinically, they have distinct therapeutic limitations, and the search for more effective inhibitors continues. Poor bioavailability has been reported for saquinavir, and variable bioavailability for a number of members of this class of agents. They also suffer from moderate to high clearance, nonlinear phamacokinetics, and very significant interactions with other drugs. In addition they are substrates for p-glycoprotein efflux proteins. These effects are very significant clinically since the drugs may be excluded from certain organs, which provides the virus with a safe haven[41,42] from which it may reemerge. The market for HIV proteases may well accept improved inhibitors with more favorable absorption, distribution, metabolism, and elimination (ADME) properties. Agents with improved properties sometimes displace first generation drugs, as was the case for the antihypertensive calcium channel antagonist amlodipine, which largely replaced nifedipine.

The HIV-protease inhibitor DMP323 (**7,** IC_{50} = 0.031 nM) was discovered by structure-based design (Scheme 2) and progressed into clinical development. Its development illustrates a number of important and recurring themes[43,44] in the progress from a ligand to an effective drug. The clinical trials of **7** were terminated due to poor bioavailability caused by low solubility and metabolic instability associated with the benzyl alcohol groups. An excellent ligand proved to be a suboptimal drug. A second clinical candidate entered development, DMP450 (**8**), which displayed improved affinity along with better solubility and good bioavailability in humans. In phase II DMP450 was found to have only modest potency in patients. Dupont–Merck reentered the discovery phase of the project, again utilizing a structure-based approach, but this time including a potency assay in whole plasma. This aimed to address the deficiency of DMP450, which was perceived to be its high plasma protein binding. Plasma protein binding affects all drugs in vivo and largely depends upon lipophilicity and charge. It modulates the concentration of the drug in free plasma, which drives efficacy. Dupont–Merck's latest clinical candidates are DMP 850 (**9**) and DMP851 (**10,** Scheme 2), both of which have improved potency in whole blood , as well as increased solubility and bioavailability. The second and third phases of the program were focused upon incorporating druglike properties whilst maintaining ligand potency.



Scheme 1. The peptidomimetic HIV-protease inhibitors nelfinavir (**1**), saquinavir (**2**), ritonavir (**3**), indinavir (**4**), amprenavir (**5**), and lopinavir (**6**).



Scheme 2. The HIV-protease inhibitors DMP323 (**7**), DMP450 (**8**), DMP850 (**9**), and DMP851 (**10**).

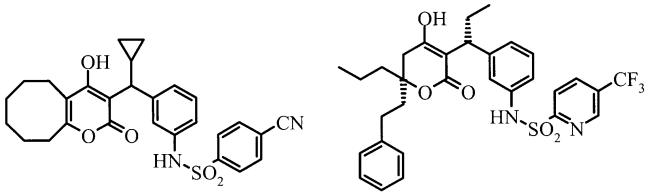
Similar problems were also encountered with Pharmacia–Upjohn's pyrone sulfonamide inhibitors of HIV protease.[45] Broad screening of a "diverse" subset identified warfarin as an interesting but weak inhibitor. Similarity searching identified a related compound, phenprocoumon, as a potential



Gerard J. Kleywegt obtained a degree in chemistry from the University of Leiden (The Netherlands) in 1986 and his doctorate from the University of Utrecht in 1991. After a short time with a commercial software company, he moved to Sweden to join Alwyn Jones's protein crystallography laboratory in Uppsala. He is currently working as an independent investigator at Uppsala University, and has been the coordinator of the Swedish Structural Biology Network (SBNet) since its inception in 1994. In 2001 he was awarded a research fellowship by the Royal Swedish Academy of Sciences.

 © 2003 Wiley-VCH Verlag GmbH & Co. KGaA, Weinheim

lead. The use of X-ray structural information led to PNU-103017 (**11**, Scheme 3), which although a potent HIV-protease inhibitor with excellent phamacokinetics, failed to demonstrate sufficient cellular activity due to its high plasma protein binding. Again, optimization aimed at reducing plasma protein binding and increasing potency resulted in an improved clinical candidate, tipranavir (**12**, Scheme 3).

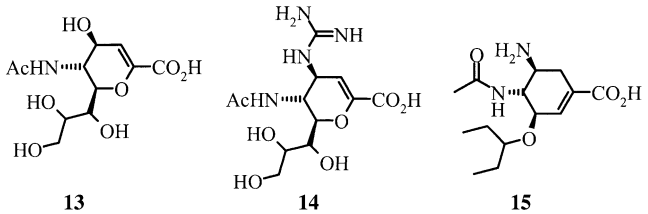


11 **12**

Scheme 3. The HIV-protease inhibitors PNU-103017 (**11**) and tipranavir (**12**).

A second case study is provided by the search for neuraminidase inhibitors. Neuraminidase has been an important target for antiinfluenza therapy for many years. Mark von Itzstein and his group at Monash University used the program GRID in an attempt to identify binding hotspots in the active site of neuraminidase to guide compound design.[46] GRID suggested replacement of the 4-hydroxy group in **13** by a basic moiety (Scheme 4). Replacement of the hydroxy by the basic guanidinyl group resulted in a 5000-fold increase in affinity. This compound, zanamivir (**14**), was subsequently developed by GlaxoSmithKline and marketed as the first neuraminidase-based antiinfluenza drug, Relenza.

Zanamivir is a very polar molecule and is dosed topically to the lung by means of dry-powder inhalation.[47] However, Gilead Pharmaceuticals were able to obtain sufficient potency without incorporation of either the strongly basic guanidine group or the polar glycerol side chain by replacement of the glycerol chain with a 1-ethylpropoxy group.[48] This group participates in favorable hydrophobic contacts and induces movements in protein side chains, which result in the formation of an additional salt bridge between Glu 276 and Arg 244. This design process resulted in oseltamivir carboxylate (**15**), a compound with more moderate polarity and charge. The zwitterionic parent is unsuitable as an oral drug, but the ethyl ester prodrug allows the compound to be absorbed orally. Oseltamivir is marketed by Hoffman–La Roche as Tamiflu. This was the first oral antiinfluenza drug, and in the first six weeks of sales in the USA Tamiflu took 40 % of the neuraminidase inhibitor market from Relenza.[49]

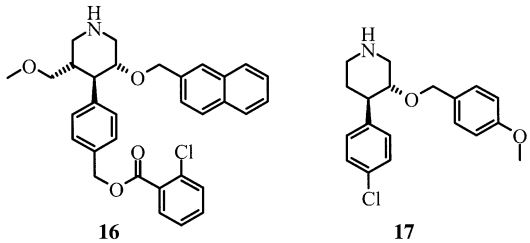


13 **14** **15**

Scheme 4. Neuraminidase inhibitors.

More balanced polarity, charge, and lipophilicity in Tamiflu resulted in a more acceptable physical property profile and considerable commercial success.

The search for renin inhibitors affords a third case study of the importance of considering ADME properties and the difference between ligands and drugs. Many of the world's pharmaceutical companies have attempted to discover renin inhibitors. The structure of murine renin became available in 1984[50] and that of the human renin in 1989.[51] Before 1989, structure-based design programs utilized homology models of renin based on the aspartyl peptidases endothiapepsin, penicillopepsin, and rhizopuspepsin. With the availability of high-resolution X-ray structures to guide compound design, it might have been expected that by now this target would have yielded a drug. But all these renin programs failed to discover low-molecular-weight agents. Potent ligands were developed but not drugs.[52] Further development of the compounds found was discontinued owing to variable bioavailability and/or excessive production costs. Availability of detailed structural information had not aided the rational design of potent inhibitors with an acceptable pharmacokinetic profile. However, the pharmaceutical industry has not given up on this target. Recently, researchers at Roche have described compound **16**,[53] a renin inhibitor in the nM-range, which was developed from the HTS hit **17** (26 μM, Scheme 5). With a molecular weight of 550 Da compound **16** is one of the smallest, most druglike ligands to have been discovered and is furthest from the peptidic ligands of the 1990s. Both the lead



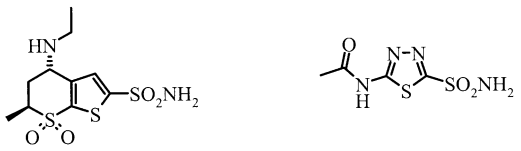
16 **17**

Scheme 5. Renin inhibitors.

and the potent ligand designed from it induce major conformational changes in the renin active site. Interestingly, these changes had not been observed previously, during a decade of X-ray crystallographic study, with peptidic ligands. These observations represent a new starting point for drug design programs. This is clearly not the end of the renin story, and it will be fascinating to see how modern discovery paradigms deal with this old target.

Structure-based design also contributed to the discovery of the carbonic anhydrase II (CA-II) inhibitor dorzolamide (**18**, Scheme 6), the first topical treatment for glaucoma.[54,55] Based on structural information, the methyl group was introduced into the thienothiopyran ring system, which stabilizes the alkylamino substituent in what would otherwise be the less favorable pseudo-axial conformation. The 4-alkylamino substituent induces a conformational change in the catalytically important residue His 64 causing it to occupy a position that is not observed for ligands bearing an N

 © 2003 Wiley-VCH Verlag GmbH & Co. KGaA, Weinheim

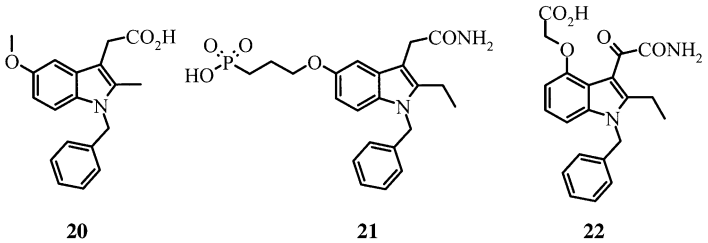


18 19

Scheme 6. Compounds for the treatment of glaucoma.

substituent smaller than ethyl. Introduction and optimization of the alkylamino substituent also enabled the manipulation of lipophilicity and solubility, which are critical factors for ocular penetration and formulation of a topical agent. Oral sulfonamide diuretics such as acetazolamide (**19**, Scheme 6) were used to treat glaucoma some forty years before the introduction of the topical agent dorzolamide.[56] Inhibition of carbonic anhydrase systemically has a myriad of consequences, and this limits the utility of oral, nonselective inhibitors. A nonselective agent must be present at very high concentrations in the blood in order to saturate carbonic anhydrase I, which is expressed at high levels in red blood cells. Only then can an efficacious level of the free drug be achieved, which results in inhibition of CA-II in the eye. With dorzolamide, because of the high local concentrations that can be achieved by topical treatment, and its selectivity for CA-II, an efficacious local concentration can be achieved at a 200-fold lower plasma concentration than would be required from an oral dose of acetazolamide. Carbonic anhydrase binding to red blood cells and its selectivity for CA-II totally dominates the pharmacokinetics of dorzolamide; its $t_{1/2}$ for elimination is approximately 120 days.

As might be anticipated, for topical agents the differences between a ligand and a drug are somewhat less. The pharmacodymanic and pharmacokinetic properties of dorzolamide are totally dominated by its affinity and selectivity for CA-II. In this sense, its properties as a ligand for its receptor have largely determined its success as a drug. This is not typical of drug discovery programs, however, since they are more frequently aimed at therapy through oral administration. More recently, structure-based design has been employed in the discovery of several agents that are now nearing market. For instance inhibitors of human nonpancreatic secretory phospholipase A2 (hnps-PLA2) have been obtained starting from the screening hit **20** (Scheme 7). Large movements of side chains were necessary to accommodate these inhibitors, and the movements would have been difficult to predict from the native structure.[57] The structures of a sequence of increasingly potent inhibitors such as **21** complexed with hnps-PLA2 were determined by X-ray analysis, and overall a 1000-fold improvement in potency in vitro was obtained. The study has resulted in LY315920 (**22**, Scheme 7), which is undergoing phase II clinical evaluation in inflammatory disease.[58] It will be interesting to see if this ligand proves to be an effective drug.



20 21 22

Scheme 7. Potential inhibitors of hnps-PLA2.

These examples illustrate the distinction between ligands and drugs. As these areas are relatively mature, the successes and difficulties can be viewed in the context of the whole journey from the initial concept to a drug in the clinic. The HIV protease, neuraminidase, and renin case studies are instructive when viewed in the light of the current understanding of druglike properties. The use of protein structural information in ligand optimization often leads to the maintenance and incorporation of polar interactions while the lipophilic contacts are increased in order to increase potency. However, the combination of these two strategies may not result in compounds with good druglike properties. The use of protein structural information in conjunction with in vitro potency determination may tempt medicinal chemists into designing ligands that are not drugs. High potency is not necessarily the most important requirement for a drug. The importance of ADME properties as well as potency is now recognized in most drug discovery programs. In order to be effective, the concentration of free drug must be maintained at a level at which the binding site on the target protein is significantly occupied throughout the dosing interval. This is a function of dose, clearance, plasma protein binding, intrinsic potency, volume of distribution, and dosing interval. Furthermore, an acceptable margin is required between the maximum concentration achieved at a therapeutic dose and the concentration that produces toxic side effects. The drug's pharmacodynamics and pharmacokinetics must be such that it meets these requirements at the desired dosing frequency.

Limiting the size, charge, and lipophilicity of a ligand in order to fulfill ADME requirements can limit the number of interactions made between the ligand and the residues composing the binding pocket. This limits the affinity that can be derived from interactions at the ligand–protein interface. This problem can be particularly acute where the ligand occupies a large binding site and mimics a large natural substrate, as is the case with many peptidases. The problem can sometimes be solved by using small ligands, which induce structural changes in the protein to fit the ligand. Greater affinity is obtained from a small ligand when it intercepts or induces a conformation of the protein, which produces a complex of lower total free energy. This is often the result of the ligand making favorable hydrophobic interactions with residues made available as a consequence of inherent conformational mobility of the protein.

3. Limitations in the Use of X-ray Data

A number of common and implicit assumptions are made by chemists who use protein structural data during structure-based design. These need to be highlighted, since they are often overlooked or even forgotten. First, we briefly define basic crystallography

 © 2003 Wiley-VCH Verlag GmbH & Co. KGaA, Weinheim

terms, which aid in the interpretation of X-ray crystal structures. Then we discuss possible pitfalls and caveats in the structure determination, which are important for users of such structures.

3.1. Basic Crystallography Terms

In a crystallographic (X-ray diffraction) experiment, the raw data consists of the positions and intensities of the reflections as measured in the diffraction pattern of the crystal. From these intensities, the structure-factor amplitudes can be calculated (roughly as the square root of the intensities). Once the phases of the structure factors are also known (i.e., once the "phase problem" has been solved), Fourier transformation of the structure factors provides a map, which is a three-dimensional matrix of numbers that represent the local electron density.[59] Where there are many electrons (and, hence, heavier atoms) the density is higher than in places where (on average) there are few electrons. It is now the task of the crystallographer to interpret the electron density in terms of a discrete atomic model.[60] This is typically an iterative process, in which the crystallographer (or in favorable cases even a computer program) builds a part of the model and then refines this. The refinement program will make small changes to the model by adjusting parameters such as the atomic coordinates, which improve the ability of the model to explain the experimental data. Simultaneously, geometric and other restraints and constraints are enforced onto the model to ensure that it is chemically reasonable. With an improved model, new maps can be calculated that may reveal further details, for example, previously missing or uninterpretable density for loops, ligand, solvent molecules, etc. The crystallographer can then add these. Simultaneously, the crystallographer should be on the lookout for possible errors in the current model and correct them if possible.[61]

Besides coordinates, atoms in the model typically have a "temperature factor" (also known as B factors or atomic displacement parameters) to model the effects of static and dynamic disorder in the crystal. Except at high resolution (typically, better than ~1.5 Å), where there are sufficient reflections to warrant refinement of anisotropic temperature factors (requiring six parameters per atom), temperature factors are usually constrained to be isotropic (requiring only one parameter per atom). The isotropic temperature factor of an atom is related to the atom's mean-square displacement. In most cases temperature factors provide a useful relative indication of the reliability of different parts of the model. If they are high, for example, for a lysine side chain, this usually means that little or no electron density was observed for the atoms in that side chain, and that the coordinates are therefore less reliable.

Figure 1 shows the atomic coordinate records of a crystallographically determined structure stored in the Protein Data Bank (PDB).[62] Figure 1a gives an example of crucial information in the REMARK records of PDB entries. Inspection of these notes and of a validation report (e.g., the WHAT IF report on the PDBREPORT web site or the PROCHECK report on the PDBsum web site) is highly recommended. In this case, the structure of crambin has been determined (PDB entry 1EJG). Crambin exists in two isoforms that differ in two residues (either Pro22/Leu25 or Ser22/Ile25), and both forms were present in the crystal. The two sequence heterogeneities have been modeled as alternative conformations for residues 22 and 25, but due to format restrictions, only one sequence is recorded in the sequence records.

Figure 1b shows a fragment of a PDB file from the same entry. The basic information about the atoms in the model is listed on "cards" (records, lines). These begin with ATOM for protein or nucleic acid components or HETATM for entities that are ligands, ions, metals, and solvent molecules. The second item on each line is simply a sequential index number of that atom. In the first line atom 136 is the amide nitrogen atom (N) of the valine (VAL) residue A8. "A" is the chain name, "8" the residue number. The "A" before the residue symbol "VAL" signifies that this atom is statically disordered. This means that this atom is observed in more than one location in the electron density, and the various instances are labeled "A", "B", "C", etc. Indeed, the third line in the figure contains the alternative location "B" of this atom. The three real numbers that follow the residue number—"6.382, 2.222, 13.070"—are the Cartesian coordinates (x, y, and z) of the atom in orthogonal Å. The fourth number is the occupancy of the position. This is a number between zero and one, which indicates the fraction of the amide nitrogen atom of valine A8 that occurs in this location. Here, the first conformation has been given an occupancy is 0.55, and line 3 shows that the alternative conformation B accounts for the remaining 0.45. Note that quite a few programs that read and process PDB files ignore alternative conformations completely. When the occupancy of ligands and solvent molecules is refined or set to a number less than one, this implies that they occupy the position in only a fraction of the molecules in the crystal, or for only a fraction of the time, or a combination of both. The fifth number, 1.92 in line 1, is the value of the isotropic temperature factor (B factor). Line 2 reveals that this atom has been modeled anisotropically, (this involves six parameters per atom which are listed on the ANISOU card), but the isotropic equivalent value is always listed as the fifth real number of the ATOM (or HETATM) card. At the end of each card the atomic symbol of the chemical element of the atom is listed, since this cannot always be deduced unambiguously from the atom's name.

An important parameter in crystallographic studies is the resolution of the data, which is expressed in Å, where lower numbers signify higher resolution. The higher the resolution, the more experimental data, and the more reliable (in terms of accuracy and precision) one may expect the resulting model to be. At high resolution (<1.5 Å) the model is probably more than 95% a consequence of the observed data.[63] However, at lower resolution (>2.5 Å), the modeling of details in protein structures is much more subjective than is widely appreciated.[64] This can be understood by calculating typical data-to-parameter ratios, that is, the ratio of the number of experimental observations and the number of adjustable parameters (atomic coordinates, parameters asso-

 © 2003 Wiley-VCH Verlag GmbH & Co. KGaA, Weinheim

a)

```
HEADER    PLANT PROTEIN                                 02-MAR-00   1EJG
TITLE     CRAMBIN AT ULTRA-HIGH RESOLUTION: VALENCE ELECTRON DENSITY.
...
REMARK 999 PRO/SER22:LEU/ILE25 ISOFORMS ARE MODELLED
REMARK 999 AS ALTERNATE CONFORMERS IN COORDINATE RECORDS.
REMARK 999 BECAUSE OF FORMAT RESTRICTIONS, ONLY PRO22/LEU25
REMARK 999 ISOFORM IS REPRESENTED IN THE SEQUENCE RECORDS.
```

b)

```
ATOM    136  N  AVAL A   8       6.382   2.222  13.070  0.55  1.92           N
ANISOU  136  N  AVAL A   8      421    149    160     33    -23    -35       N
ATOM    137  N  BVAL A   8       6.695   2.072  13.037  0.45  1.88           N
ATOM    138  CA AVAL A   8       5.099   2.259  12.380  0.55  2.32           C
ANISOU  138  CA AVAL A   8      397    258    224     16    -22   -120       C
ATOM    139  CA BVAL A   8       5.471   2.048  12.164  0.45  1.94           C
ATOM    140  C   VAL A   8       5.208   3.386  11.373  1.00  2.63           C
ANISOU  140  C   VAL A   8      380    402    213     71    -42   -209       C
ATOM    141  O   VAL A   8       4.712   3.302  10.238  1.00  2.67           O
ANISOU  141  O   VAL A   8      378    434    200     39    -31   -178       O
ATOM    142  CB AVAL A   8       3.944   2.394  13.375  0.55  3.36           C
ANISOU  142  CB AVAL A   8      376    635    262    186      4   -244       C
ATOM    143  CB BVAL A   8       4.263   1.630  13.035  0.45  3.05           C
ATOM    144  CG1AVAL A   8       2.629   2.981  12.701  0.55  4.22           C
ANISOU  144  CG1AVAL A   8      326    856    420    159     34   -159       C
ATOM    145  CG1BVAL A   8       3.580   2.930  13.664  0.45  3.89           C
ATOM    146  CG2AVAL A   8       3.635   1.036  13.955  0.55  4.82           C
ANISOU  146  CG2AVAL A   8      771    684    376    230    -61   -385       C
ATOM    147  CG2BVAL A   8       3.136   1.077  12.028  0.45  4.17           C
ATOM    148  H  AVAL A   8       6.374   2.231  14.084  0.55  2.27           H
ATOM    149  H  BVAL A   8       6.648   2.059  14.045  0.45  5.91           H
...
END
```

Figure 1. a) An example of crucial information presented on REMARK records in PDB entries. b) Fragment of a PDB file from the same entry. The basic information about the atoms in the model is listed on "cards" (records, lines). For a complete description please refer to the text.

ciated with the temperature factors, and occupancies amongst others) in the model. For an average protein structure at a resolution of 2 Å, this ratio is slightly greater than two, but at ~2.7 Å it becomes less than unity. Whereas gross errors in the structure are unlikely to persist to the publication stage if the resolution is high, once the resolution becomes >2 Å, the balance shifts. Some published protein models appear to have been more determined by the crystallographer's imagination than by any experimental data.[63] In fact, in the 1980s the first reports of some of the "hottest" protein crystal structures, some of which were also prime drug targets, contained extremely serious errors.[65] Examples included HIV-1 protease, photoactive yellow protein, the small subunit of RuBisCO, D-Ala-D-Ala peptidase, ferredoxin, metallothionein, gene V binding protein, and the GTP-binding domain of Ha-ras p21.

Recently, the structure of a complex between botulinum neurotoxin type B protease and the inhibitor BABIM was published,[66] and the structure and experimental data were deposited in the PDB (entry 1FQH). However, subsequent critical analysis of the electron-density maps revealed that these did not support the placement of the inhibitor as stated in the earlier paper, and the structural conclusions based on it were withdrawn by the authors.[67]

Another trap to be aware of (and one that many crystallographers have fallen into) is the derivation of "high-resolution information" from low-resolution models. For instance, in a typical 3-Å structure the uncertainty in the position of the individual atoms can easily be 0.5 Å or more. Nevertheless, many such models have been described where hydrogen-bonding distances are listed with a precision (note: not accuracy!) of 0.01 Å (probably because the program that generated these distances used that particular precision) and solvent-accessible surface areas with a precision of 1 Å^2.

The ability of the model to explain the experimental data is usually assessed by means of the (conventional) *R*-value, which is defined in Equation (1).

$$R = \left(\sum \| F_{\mathrm{obs}} | - \mathrm{scale}\, | F_{\mathrm{calcd}} \| \right) / \left(\sum | F_{\mathrm{obs}} | \right) \qquad (1)$$

Here, F_{obsd} are the experimental structure-factor amplitudes, F_{calcd} are the structure-factor amplitudes calculated from the model, and the sums extend over all observed reflections. However, when more and more parameters are introduced into the model, the *R*-value can be made almost arbitrarily small (this is called "over-fitting the data"). In 1992 Brünger[68] introduced the concept of cross-validation in

 © 2003 Wiley-VCH Verlag GmbH & Co. KGaA, Weinheim

crystallographic refinement, and with it the free *R*-value (*R*free), whose definition is identical to that of the conventional *R*-value, except that the free *R*-value is calculated for a small subset of reflections that is never used in the refinement of the model. The free *R*-value therefore measures how well the model predicts experimental observations that are not used to fit the model. Until a few years ago a conventional *R*-value below 0.25 was generally considered a sign that a model was essentially correct. While this is probably true at high resolution, it was subsequently shown for several intentionally mistraced models that these could be refined to deceptively low conventional *R*-values.[65,69] Brünger suggests a threshold value of 0.40 for the free *R*-value, that is, models with free *R*-values greater than 0.40 should be treated with caution.[70,71] Since the difference between the conventional and free *R*-value is partly a measure of the extent to which the model overfits the data (i.e., some aspects of the model improve the conventional but not the free *R*-value and are therefore likely to fit noise rather than signal in the data), this difference (*R*free $-$ *R*) should be small for the final model, ideally < 0.05.

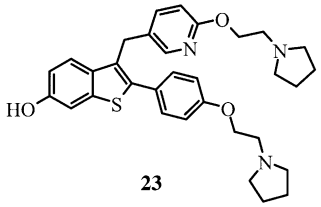
3.2. Uncertainty in the Identity or Location of Protein or Ligand Atoms

It is often forgotten that an X-ray crystal structure is one crystallographer's subjective interpretation of an observed electron-density map expressed in terms of an atomic model. This structure is treated by chemists undertaking structure-based design as if it were at perfect resolution, independent of the resolution at which the structure was actually determined and ignoring the interpolations, assumptions, biases, and sometimes mistakes incorporated by the crystallographer.

Uncertainties can involve the identity of important atoms like those in the binding pocket. For instance at a resolution typical for macromolecules (~2 Å) the relative positions of the δN and δO atoms of asparagine and γN and γO atoms of glutamine side chains cannot usually be determined directly from the electron density since they are isoelectronic. The decision as to which density feature should be assigned to N and O should be based on inspection of the local hydrogen-bonding networks. However, these decisions may have to be made before solvent molecules have been added to the model and hence be based on incomplete hydrogen-bonding networks. Moreover, in low-resolution structures many of the solvent entities are not resolved in the electron density and can therefore not be modeled, thereby further complicating the analysis. A careful crystallographer will verify the assignment in the final model, but in general the users of the model should treat the final assignment with caution. This is also borne out by large-scale analysis of the hydrogen-bonding patterns involving histidine, glutamine, and asparagine residues with the program WHAT IF,[72] as listed on the PDBREPORT web site.[73] This analysis suggests that as many as one in six of all histidine, asparagine, and glutamine residues in the PDB may have been modeled in a "flipped" orientation.

Uncertainties can also occur at the level of whole residues. This is the case for flexible residues, which often diffract so weakly that no clear electron density is observed for them. This is quite common for the side chains of surface residues, but may also be found in some active sites, particularly with the flexible side chains of lysine and glutamate. Analysis of real-space density fits[74] shows that most poorly defined residues are, in order of improving average fit to the density, Lys < Glu < Arg, Gln < Asp, Asn. The crystallographer knows they are present from the amino-acid sequence, and so they are incorporated into the structure in a conformation commonly observed for that residue in databases of high-resolution structures. The final conformation of the side chain, as viewed by the chemist, can be the product of intelligent guesswork and the van der Waals term in the refinement program's force field, rather than experimentally observed electron density. It is also quite common for whole sections of the protein to give little or no observable electron density. Sometimes these parts are mobile loops and these can have great functional significance also, by virtue of this greater mobility.[75] In other cases, entire domains may be invisible in the electron-density maps.

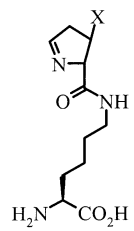
Similar ambiguities apply when the bound ligand is considered. For instance, the position of pyridine nitrogen atom cannot usually be determined from the electron density alone. This fact will introduce uncertainty into many crystal structures containing a molecule with an asymmetrically substituted pyridine. For instance, during the study of benzo[*b*]thiophene inhibitors of thrombin, compound **23** was complexed and a structure built based on the measured



23

electron density. The C3 pyridyl ring was oriented arbitrarily so that the nitrogen atom resides in the more hydrophilic of the two possible environments. This is a reasonable assumption, but not the result of direct experimental observation and so is still uncertain.

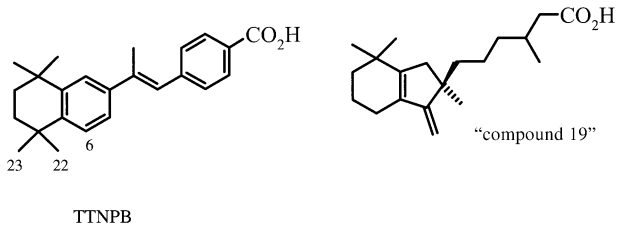
An example of how ambiguous X-ray crystallographic data can be when the exact chemical composition of a ligand or residue is not known was encountered recently. The exact identity of the twenty-second genetically encoded amino acid pyrrolysine **24**,[76] present in *Methanosarcina barkeri* monomethylamine methyltransferase (MtmB), is still unknown even though a 1.55-Å resolution structure of the protein is available. The X substituent is a methyl, ammonium, or hydroxy group.



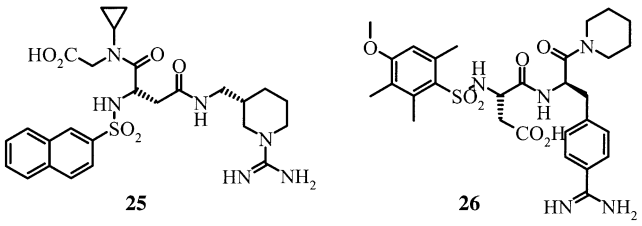
24

On the other hand, sometimes (careful) crystallography can reveal cases of mistaken identity. For example, when the structure of cellular retinoic-acid-binding protein type 2 (CRABP2) in complex with a synthetic retinoid was solved, it was assumed that the ligand

 © 2003 Wiley-VCH Verlag GmbH & Co. KGaA, Weinheim



Scheme 8. Postulated and actual CRABP2 ligand.



Scheme 9. Thrombin inhibitors napsagatran (**25**) and CRC220 (**26**).

was TTNPB (Scheme 8).[77] The ligand was built and fitted to the density, but the maps stubbornly suggested that there was something wrong. The density failed to cover the whole ligand, and features in the map suggested that there ought to be a carbon-like atom at a distance of ~1.5 Å from C6, and that atoms C22 and C23 should be removed from the model. After double-checking the identity of the ligand with the chemists, the crystallographers found that the ligand that was actually complexed to the protein was "compound 19" (Scheme 8). The structure of this ligand made perfect sense in terms of the density (Figure 2), and the refinement of the structure could be completed successfully. However, had the resolution been 3 Å instead of 2.2 Å, the error might well have gone undetected.

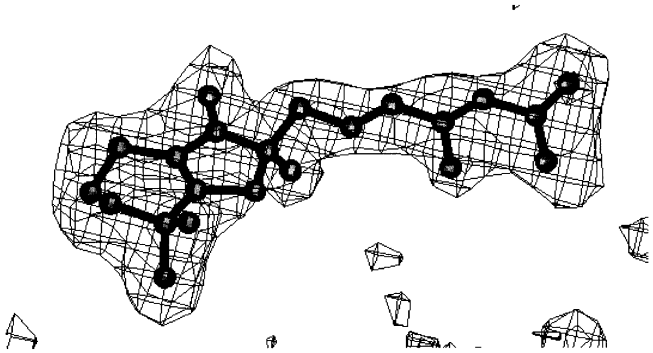
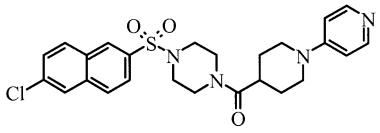


Figure 2. Electron density for and structure of "compound 19" in complex with CRABP2.

Since the presence of hydrogen atoms is inferred rather than observed, the tautomeric state of histidine or of bound ligands containing tautomeric groups cannot be determined directly. The latter problem is rather common in studies involving acid isosteres. Similarly, the state of ionization of the ligand or protein cannot be observed. It is usually assumed that the charged state of the protein is known. However, the pK_a values of common acidic or basic side chains can differ drastically from their normal values as measured in water, when they are located in the microenvironment of a protein active site.[78] Even when the protonation states of key active-site residues and the ligand are known, these may change upon complexation. Enthalpies of complexation measured by isothermal titration calorimetry, in aqueous buffers with different enthalpies of ionization, established that the Roche thrombin inhibitor napsagatran (**25**, Scheme 9) binds to thrombin incorporating an additional proton.[79] An inhibitor with a similar structure, CRC220 (**26**), from Behring binds to thrombin without an additional proton. This difference in ionization, upon binding to the protein, was supported by different orientations of the ligands when the structures of the complexes with thrombin were determined by X-ray crystallography.

3.3. Effect of Crystallization Conditions

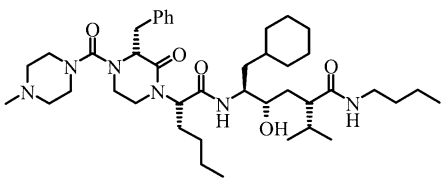
The conditions required to crystallize a protein or to optimize diffraction may not be the same as those employed in the biological assay. This may affect the reliability of rationalization and prediction of structure–activity relations (SAR) from sequential protein–ligand complexes. The influence of crystallization conditions is often unknown or not considered, but numerous examples highlight its importance. An unusual cubic form of trypsin was observed when it was complexed with compound **27** at pH 7.[80] The same ligand–protein complex crystallized at pH 8 shows a different ligand



27

conformation, active-site conformation, and crystal morphology. Normally the pH during protein crystallization has no effect upon the formation of various crystal forms, but in the case of **27** the pH affects the protonation state of the ligand and thereby alters its binding mode, which in turn precludes the normally observed packing of the protein.

The terminal methylpiperazine ring of Abbott inhibitor A-70450 (**28**) was found to exist in a chair conformation in the crystal structure of secreted aspartic protease 2X crystallized at pH 4.5.[81] But in a subsequent study the methylpiperazine group was observed to assume a boat conformation when the complex was crystallized at pH 6.5.[82]



28

 © 2003 Wiley-VCH Verlag GmbH & Co. KGaA, Weinheim

The recently identified genetically encoded amino acid pyrrolysine adopts two conformations in MtmB. The occupancies of the two conformations depend upon whether the precipitating salt was sodium chloride or ammonium sulfate.[76] When ammonium sulfate is used as the precipitating agent, additional density adjacent to C2 of the ring suggests the addition of ammonia from the buffer to the imine of pyrrolysine. The change in occupancy of the two conformations appears to be controlled by new hydrogen bonds formed between this nitrogen atom and Glu259 and Gln333.

Two crystal forms of human pancreatic α-amylase were also observed at different pH values. The flexible loop, which is typical of mammalian α-amylases, was shown to exist in two conformations, which suggests that loop closure is pH sensitive.[83] Likewise, pH-sensitive changes in conformation have been observed for glycinamide ribonucleotide transformylase,[84] *Aspergillus* pectin lyase A,[85] glutathione synthetase,[86] influenza matrix protein M1[87] and ribonuclease A.[88]

3.4. Identification and Location of Water Molecules

Identification of water molecules in the electron-density maps can be a problem. Water, sodium ion, and ammonium ion—common constituents in crystallization media—cannot always be distinguished based on their density alone, because they are isoelectronic. The local environment must be taken into account in order to decide how a solvent feature in the electron-density map is best interpreted. Such issues are easily missed, especially by less experienced crystallographers.

The location of water molecules can also be problematic. Unless the resolution is high, the presence or absence of water molecules cannot be determined with certainty, and it becomes a subjective matter whether a feature in the density should be ignored as noise or modeled as a water molecule. However, uncritical addition of solvent molecules (each of which introduces four adjustable parameters, x, y, and z coordinates and an isotropic temperature factor, into the model) provides the crystallographer with an excellent means of absorbing problems in both the experimental data and the atomic model.[63,69] Addition of water molecules is then simply used to artificially reduce the differences between observed and calculated structure-factor amplitudes.

When crystallographers determine the same structure at similar resolution, their water structures are bound to reveal many discrepancies. For example, the structure of transforming growth factor-β2 was determined by two independent laboratories at similar resolutions, 1.8 Å (1TGI) and 1.95 Å (1TFG).[89] There are 58 water molecules in 1TGI with an average temperature factor of 31.8 Å^2 and 84 water molecules in 1TFG with an average temperature factor of 43.3 Å^2. In 1TFG the 54 water molecules common also to 1TGI have much lower temperature factors (average 34 Å^2) than the 30 extra water molecules (average 60 Å^2), which suggests that the latter have a much lower level of reliability. The structure of human interleukin 1β was determined independently in four different laboratories at similar resolution.[90] The four models contained between 83 and 168 water molecules, but a mere 29 of these were in common to all four models. Interestingly, although all 29 belong to the first layer of solvation, not all of them are buried. In a final example the structure of poplar leaf plastocyanin was subjected to two separate refinements by independent laboratories who used the same set of synchrotron X-ray data at 1.6 Å.[91] The two groups used two different refinement protocols and agreed not to communicate until each was convinced that their refinement calculations were complete. The structures contained 171 and 189 water molecules, respectively, but only 159 water molecules were common to both structures within 1 Å. While it can be a matter of subjectivity to decide whether the electron density supports the presence of a water molecule at a particular location, a water molecule that does not form a single hydrogen bond to any other atom is almost certainly an artefact. Statistics from the protein verification tool WHAT IF,[72] found at the PDBREPORT web site[73] identify 99 793 water molecules in 10 857 structures deposited in the PDB that have no hydrogen bonds to any other atom in the structure (September 2002).

It may simply be worth remembering that at the resolution usually encountered in structures in pharmaceutical discovery projects, the electron density for water molecules that are not well ordered is often difficult to distinguish from noise. The importance of water in binding energetics and kinetics should not be overlooked (although it sometimes is). Water is the "third party" in the ligand–receptor interaction.[92] Depending on the hydrogen-bonding environment of influential water molecules, it may be energetically favorable for a ligand to displace the water molecule, form a hydrogen bond to it, or not to interact with it. With uncertainties over which water molecules are displaced, and which are not displaced from the active site upon ligand binding, water molecules are often completely removed in virtual screening campaigns. This oversimplification may affect the accuracy of docking and scoring.

4. PDB Files Used in Docking and Scoring Studies

An important criterion in the choice of protein–ligand complexes used to validate docking and scoring programs is the resolution of the structure. But even at high resolution the ligand may still not be well defined, as recently highlighted by Boström.[93] The structure in PDB entry 1PME was determined to a resolution of 2.0 Å, however the planar methanesulfonyl group present in the ligand is chemically unlikely. Similarly, the 3-phenylpropylamine ligand in structure 1TNK, which was determined to a resolution of 1.8 Å, contains a tetrahedral aromatic carbon atom bound to the propylamine chain. Visual inspection would reject these structures, so it is surprising that 1TNK also features in the validation set for Flex-X. One lesson is that whereas high-quality dictionaries of acceptable bond lengths, angles, and torsions are available for amino and nucleic acids in model refinement, the same is not true for complexed ligands. This is because of the huge diversity of small molecules compared to amino and nucleic acids. The Hetero-Compound Information Centre, Uppsala, (HIC-Up[94]) has made available ready-made dictionaries for

 © 2003 Wiley-VCH Verlag GmbH & Co. KGaA, Weinheim

commonly used crystallographic protein modeling software (CNS, X-PLOR, TNT, and O) as an aid to crystallographers.[95] A similar service is provided by the PRODRG server.[96] Also accessible through the HIC-Up site is a basic validation tool, HETZE, which checks the PDB file of a ligand for acceptable ranges of bond lengths, angles, and torsions.

Sometimes complexes are selected as docking targets, even though the experimental evidence is not sufficiently strong for an unequivocal decision on the ligand orientation. For instance, the position of the carboxylate group of oleic acid in a mutant rat intestinal fatty acid binding protein (IFABP) was ambiguous when the electron density was examined.[97] Indeed, the crystallographers report three positions for the carboxylate group in the deposited PDB file (1ICN), with occupancies of approximately 0.3 for each. Surprisingly, this complex, despite its uncertain structure, was selected as a validation structure when Flex-X was tested with the DOCKSCORE scoring function[14] and GOLD. In hindsight then, it may not be surprising that Flex-X and GOLD failed to reproduce any of the observed conformations of oleic acid. Flex-X calculated that the highest scoring conformation for oleic acid is rotated 180° in the active site relative to the orientation reported in the PDB file. It was suggested that the original crystallographic assignment for the position of oleic acid was incorrect and that the orientation predicted by Flex-X was in better agreement with the electron density. However, limited rerefinement of the model from which the carboxylate groups were removed, against the original experimental data, but with current methodology reveals no clear density for the carboxylate group at either end of the ligand (Figure 3a–c). Normally, in this family of proteins, two arginine residues are involved in binding the carboxylate group of the ligand. Wild-type IFABP is already the odd one out in the family, since one of the arginine residues is involved in a salt bridge with an aspartate residue. In the present structure the remaining arginine was mutated to glutamine, and therefore it seems unlikely that there is any driving force to cajole the carboxylate group of the fatty acid into entering the interior cavity of the protein. Instead, it seems more likely that the carboxylate group sticks out into the solvent. Such a binding mode has been observed in the crystal structure of another fatty-acid-binding protein.[98] Moreover, subsequent NMR experiments by Jackoby et al. on the mutant complex[99] showed that the carboxylate group of the ligand is exposed to solvent.

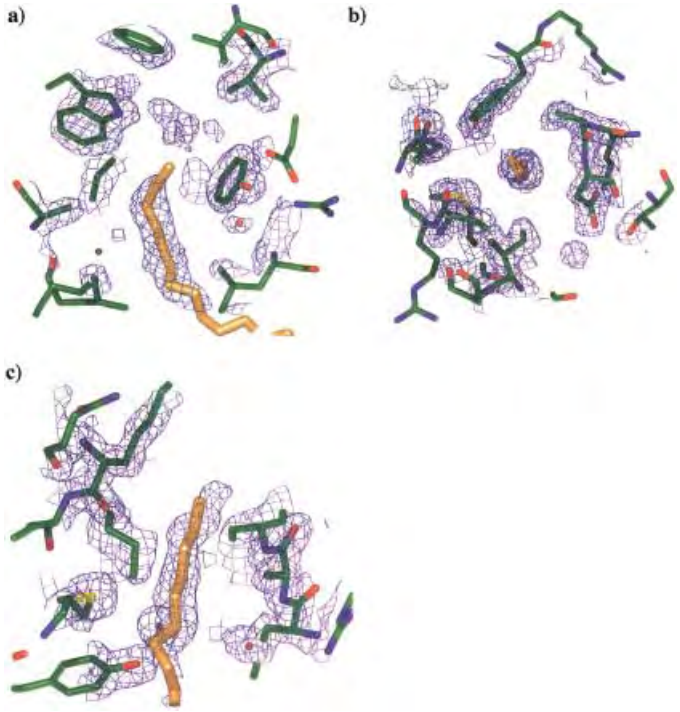


Figure 3. a) Oleic acid complexed to an IFABP mutant after limited refinement (data not shown). Although some extraneous electron density (blue mesh) is visible, it is neither possible nor sensible to assign it to the ligand's carboxylate moiety. b) Electron density near the opposite end of the ligand. It is clear that there is no density to support either the presence of the carboxylate group or any contacts with main-chain amides. This view is from outside the protein into the ligand-binding cavity. c) Electron density at the other end of the ligand model shows that the ligand points into the solvent. Most likely the carboxylate group is located here, but due to disorder there is no density for it.

Recently, the Cambridge Crystallographic Data Centre and Astex Technology Ltd have produced a "clean" list of protein–ligand complexes for validating docking and scoring algorithmns.[100] All entries in the "clean" list have been checked manually to exclude protein–ligand complexes that contain factual or structural errors in the PDB file, unlikely ligand conformations, and severe protein–ligand clashes, as well as those complexes in which the crystallographically related protein chains influence the binding geometry.

5. Assessing the Validity of Structure Models

In view of the uncertainties concerning the validity of X-ray structures deposited in the PDB, about which even experts disagree, the average user does well to proceed with caution. The degree of confidence in the position of a particular atom or residue can be assessed by using the temperature factors, occupancies, and occasionally remarks, all of which are deposited with the atomic coordinates. If the structure factors are also deposited, electron-density maps can be calculated and superimposed on the structure. Examination of the structure together with the electron-density map is highly recommended.[101] This enables users of the refined model to assess the quality of the fit of the model to the density (data). Issues that can be addressed include the overall reliability of the model, together with the position, orientation, conformation, and geometry of specific residues and ligands. This level of detailed visualization is generally only available in specialist crystallographic modeling tools such as O, but the program DEEP VIEW, which is freely available on the internet allows full visualization of PDB files together with electron-density maps.[102] It is not always possible to inspect the density, since this requires that the structure factor data have been deposited with the PDB by the crystallographer. Although most journals now have strict deposition policies, a recent

 © 2003 Wiley-VCH Verlag GmbH & Co. KGaA, Weinheim

survey found that for only ~30% of all crystal structures in the PDB could electron-density maps be calculated.[103] Interestingly, it appears that more structure factors are deposited for structures with low than for those with high free *R*-values. This curious observation suggests that the worse the model is, the less likely it is that the crystallographer will deposit the experimental data that the structure is supposed to explain. Jones and co-workers have developed the Uppsala Electron Density Server[104] to facilitate objective assessment of the quality of the fit of the model to the electron density of any PDB entry for which structure factors are available.[74]

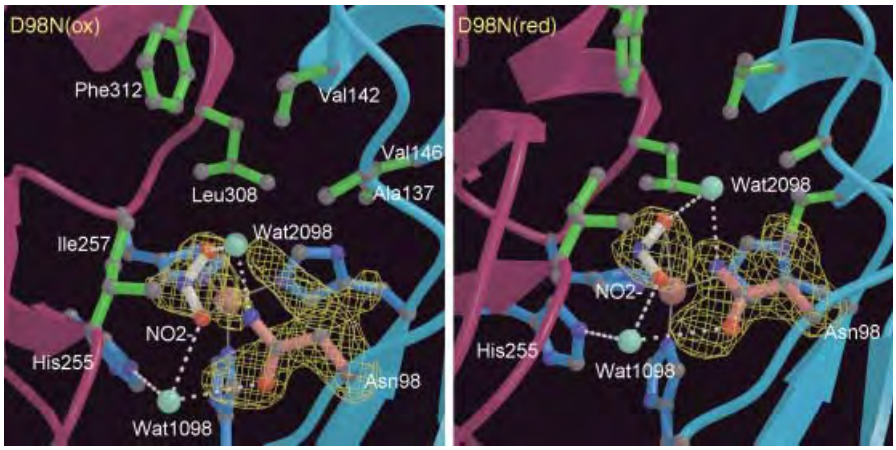


Figure 4. Active sites of the oxidized and reduced forms of a nitrite reductase. The electron density associated with Asn98 (brown mesh) is only partly filled, consistent with multiple conformations for this residue. Similarly the poor fit around the bound nitrite group indicates disorder (reproduced from ref. [107] with permission).

Before expending considerable resources on the exploitation of a protein–ligand structure, medicinal chemists and protein modelers would do well to assess the overall reliability of the model. An introductory tutorial for nonexperts is available on the internet.[63,105] Subsequently, researchers should assess the reliability of any crucial residues, water molecules, and bound ligands, either by interacting directly with the crystallographer who determined the structure or by reading the literature. Scrutiny of the REMARK records in the PDB entry and inspection of the temperature factors and occupancies is recommended. Treating a PDB entry as a simple array of atom coordinates at perfect resolution is a gross oversimplification and can easily lead to false assumptions concerning the model.

Two examples, from many which might be chosen, illustrate the point. Two molecules of 1-deoxynojirimycin were observed bound in the active site of glucoamylase from *Aspergillus awamori* varX100 in a structure determined at 2.4-Å resolution.[106] One of the ligands shows strong electron density, whereas the second molecule appears to occupy the second binding site only partially. The authors comment that the "secondary binding site for 1-deoxynorjirimycin should be regarded with caution and may not reflect the true binding of the substrate to the second subsite". With such uncertainty a medicinal chemist might expect that the second site would be left empty in the deposited coordinate file. In fact, the PDB entry contains both 1-deoxynojirimycin molecules, albeit that the second one is flagged in a way that makes perfect sense to crystallographers, but which inexpert users of the structure files are almost bound to overlook. The choice of whether to include partially occupied binding sites or multiple side chain conformations is largely arbitrary. For instance, disorder was observed for both the nitrite ligand and an active site asparagine residue in the mutant Asp98Asn form of *Alcaligenes faecalis* S-6 nitrite reductase,[107] in a structure determined at 2.0-Å resolution (Figure 4). Although the electron density clearly shows two binding conformations for Asn98, this time only one conformation is reported in the PDB entry.

Confidence in a model can be gained when multiple, independently determined protein–ligand complexes are available, at very good resolution, and when the electron-density maps are inspected closely. Important factors can then be assessed such as the position of influential water molecules,[108] the degree of flexibility in residues neighboring the active site, and assumptions that may influence the success of structure-based design and docking studies.

Assumptions crystallographers make in modeling the electron density may appear minor when one considers the correctness of an entire ligand–protein structure. However, these assumptions can have a profound effect when the structure is used subsequently as the basis for a structure-based design project. While some of these problems are minimized at high resolution (< 1.5 Å), many structure-based design projects routinely rely on protein structures determined at significantly lower resolutions than this. The structure generated from the electron density may be good. In any one target or ligand series, protein flexibility may be unimportant. It is possible that sensible decisions about influential water molecules can be made. The binding site may be wholly contained within a single copy of the protein and therefore little influenced by other copies of the protein in the unit cell. Therefore there may be many situations in which current manual design and docking and scoring programs have utility. However, great care should be exercised and assumptions in the structure should be assessed continuously.

6. Automated Docking and Scoring

Successful structure-based design requires accurate and reliable docking algorithms and the ability to predict the affinity of the docked ligand for the target structure. Many of the standard packages have been reviewed recently (Table 1).[39] The most widely used programs at present are probably DOCK, Flex-X, and GOLD. GOLD is arguably the most rigorously validated docking algorithm presently avail-

 © 2003 Wiley-VCH Verlag GmbH & Co. KGaA, Weinheim

able. It utilizes an algorithm that allows full ligand flexibility during docking, while protein flexibility is limited to very small movements in the protein active site, for instance rotation of OH groups to allow for optimal H-bonding. The GOLD web site includes some examples of successful docking, including that of a peptide ligand into actinidin and of GMP into ribonuclease T1. Its web site also provides access to overlays of all the docked ligands from the validation set with the deposited conformation taken from the PDB file.[109] Indeed one of its most attractive features is the rigorous and self-critical validation of the program.

The GOLD validation methodology is typical of docking and scoring evaluations. It is based on redocking calculations where the ligand is docked back into its own receptor pocket. This is not representative of the actual design process, however, where a single or at best a small number of protein structures are utilized to dock many ligands. The test is also somewhat artificial in that the protein conformation is predetermined, the approximate binding site indicated, and various assumptions made concerning the ionization state of individual residues. A recent survey of the success of redocking using the PROLEADS program has succinctly highlighted the deficiency of redocking as an objective way of assessing a new docking algorithm.[110] Six or more protein–ligand complexes were taken for a single target. Although PROLEADS was successful 76% of the time at redocking individual ligands into their own active sites, it was successful only 45% of the time in docking another ligand from the set to that same active site. Small, apparently insignificant, changes in the protein structure around the ligands are enough to adversely affect the chances of successful docking. The study was carried out for ligands of the proteins thrombin, thermolysin, and neuraminidase.

Successful ligand design also requires accurate scoring of a molecule's potency. Scoring allows the ranking of multiple docked conformations and/or the prediction of binding energy. Scoring of docked conformations is recognized as a major weakness in current algorithms. While it would be anticipated that scoring functions do rather well at predicting the potency of complexes that were used in the derivation/training set for that scoring function, the most objective assessment of performance is how well they predict new complexes. Three commonly used scoring methods are master equations, knowledge-based functions, and trainable functions.

Approaches based on master equations are implemented in a number of leading algorithms, of which the LUDI scoring function was the first and most widely imitated. The total binding energy is partitioned into contributions from hydrophobic, hydrogen-bonding, and charge interactions, corrections for suboptimal hydrogen-bond geometry, and the energetic cost of the degrees of freedom for bond rotation lost upon binding. The coefficients of the LUDI master equation SCORE1 were determined initially by regression analysis of the interactions observed by X-ray structure determination of 45 ligand–protein complexes together with the affinities of each ligand for its cognate receptor. These are in good agreement with independent assessments of the contributions to binding obtained from thermodynamic measurements. For instance, the contribution of hydrophobic interactions is scored at $0.17\ kJ\,A^{-2}\,mol^{-1}$, which is in good agreement with estimates of $0.12\ kJ\,A^{-2}\,mol^{-1}$ from solvent-partitioning measurements and detailed SAR studies.[111,112] The contributions of hydrogen bonds are scored at $4.7\ kJ\,mol^{-1}$ per hydrogen bond. This value is also in reasonable agreement with estimates of up to $6.3\ kJ\,mol^{-1}$ derived from detailed study of tyrosyl t-RNA synthase, a value of $2–6\ kJ\,mol^{-1}$ from physical-organic studies on vancomycin,[113] and SAR studies on sugars binding to glycogen phosphorylase.[114]

Knowledge-based approaches (SmoG,[15] DRUG-SCORE,[14] and PMF[115]) are currently receiving considerable interest. Knowledge-based potentials are derived from evaluations of close contacts between atoms in a large selection of protein–ligand complexes by means of statistical mechanics. Binding energy is represented as the sum of free energies of interatomic ligand–protein contacts, which are calculated from their frequencies of occurrence in the complexes. The knowledge-based approach implemented in SmoG2001 gave a root-mean-square error (RMSE) of 1.69 log units in predicting the potency of a test set of 77 complexes. The authors compared SmoG2001 with SCORE1 (LUDI) by using the same test set and found that SCORE1 (LUDI) gave an RMSE of 3.47 log units, which suggests that SmoG2001 is a considerable improvement upon SCORE1 in prediction.

One drawback of master-equation or knowledge-based approaches is that the relative contribution of different types of interactions to ligand affinity may change between families of active sites, because of differences in hydration or polarity within the active site.[116] However, the scoring function for VALIDATE can be trained on the series of interest in contrast to a generic scoring function.[117] A large number of ligand–protein complexes, covering a sufficient range of potencies, are required, since the approach is based on QSAR methods. Physicochemical descriptors are calculated for the ligand and the ligand–protein complex and are correlated against affinity in order to generate empirical predictive models. Thus, VALIDATE was trained by using 39 HIV-protease inhibitor complexes having a potency range of $pK_i = 6.4–11.4$.[118] This HIV-protease VALIDATE model was then used to predict the binding constants of 363 HIV-protease inhibitors reported in the literature. Actual versus predicted affinities for the validation set are given in Figure 5.

The current performance of scoring functions such as LUDI, SmoG2001, and VALIDATE in predicting potency is usually insufficient to be useful in optimizing leads. Here the aim is usually to convert a lead having 1–10 μM activity into a potential development candidate having 1–10 nM activity. This 100- to 1000-fold increase in potency appears to be within the random error of these scoring functions. However, this is not universally the case. One successful example where scoring was applied in lead optimization was in the design of peptidic HIV-protease inhibitors at Merck.[119] The scoring was calculated based on consideration of the electrostatic and steric interaction energies after energy minimization of the docked ligand (**22**) in the protein active site. Although the absolute prediction of potency depended upon which protein structure was used for the dockings, the correlation between

 © 2003 Wiley-VCH Verlag GmbH & Co. KGaA, Weinheim

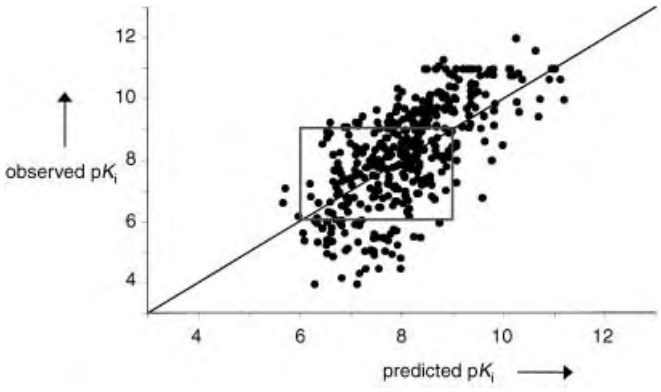


Figure 5. A plot of observed pK_i values versus values predicted by VALIDATE II for a test set of HIV-protease inhibitors not used to train VALIDATE II. The line of unity is displayed. The box indicates the 1000-fold potency range in which lead-optimization projects typically operate (reproduced from ref. [118] with permission).

predicted potency and actual potency was remarkably good, as were predictions on novel compounds, which were subsequently synthesized.

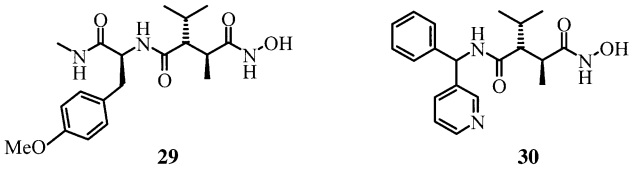
A further major assumption underlying the use of docking and scoring programs is that the receptor is not flexible, or at least that receptor flexibility is an infrequent occurrence. This assumption has been questioned recently, and a number of examples of induced fit and protein flexibility have been reviewed.[120] Indeed, induced fit appears common for drug-like compounds rather than being an infrequent occurrence.[121] The incorporation of protein flexibility into automated docking and scoring algorithms is presently an important focus. Several approaches are being taken to try to address this problem, with various degrees of rigor. These include the use of a "soft" scoring function, which allows some overlap between the ligand and the protein, protein-ensemble approaches in which the protein is represented as a composite of a number of different conformations, and constrained molecular dynamics simulations in explicit water.[122–124]

It is sometimes possible to overcome the uncertainties in the scoring functions by using them to design combinatorial arrays of putative ligands rather than individual compounds. For instance, Multiple Copy Simultaneous Search (MCSS) was used to identify subsites within the picornaviral capsid ligand-binding site.[125] This information was applied to the design of targeted libraries and hits obtained. Interestingly, because of induced fit, the position of one of the ligands was reproduced only when protein side chains were allowed to move. The authors comment that the advantage of libraries over individual compounds is that the scoring function for selecting ligands need not be highly accurate. The scoring function is required only to have enough information to guide and focus libraries. Even though small changes in protein structure do occur upon ligand binding, a combinatorial approach ensured that the appropriate ligands were synthesized anyway. Combinatorial chemistry and structure-based design were combined to provide a useful tool.

7. Convergence of Screening and Structure-Based Design

Many drug discovery programs demonstrate an important complementarity between HTS and structure-based design. HTS often yields many weak leads, and chemists make intuitive decisions about which leads to follow. Structural studies can dramatically influence the priority placed upon a particular hit.

Obtaining structural information on chemically diverse leads can reveal hitherto unsuspected mobility in active-site residues. These observations can provide new insights and opportunities for optimization. Combinatorial chemistry can be used to probe areas of the binding pocket in the search for new interactions. For instance, MMP3 inhibitors have been developed[126] by replacement of the N-methylacetamido group in **29** by phenyl (Scheme 10). This unexpected replacement was discovered by applying combinatorial chemistry and subsequently explained by X-ray crystallography. Structural information on the induced binding site prompted further rounds of design and evaluation, leading to replacement of the *p*-methoxyphenyl group by pyridyl (**30**).

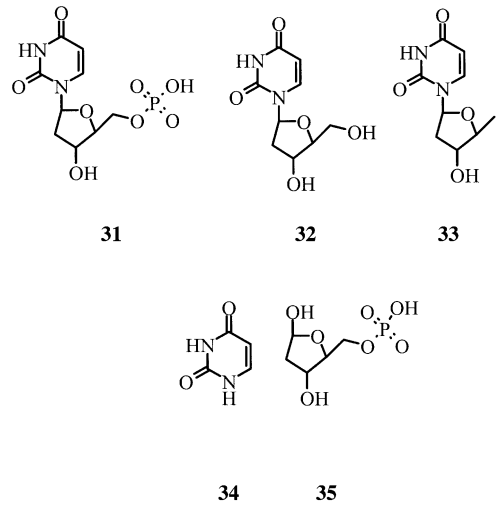


Scheme 10. MMP3 inhibitors.

The design criteria for an ideal HTS compound library have been shifting from mere diversity towards "druglike" properties and even further towards "leadlike" libraries[127,128] and compound collections. The lead optimization process tends to result in compounds with increased molecular weight and complexity,[129] and this has resulted in an intense search for methods to identify small leadlike templates. NMR spectroscopy and X-ray crystallography may be superior to HTS for identifying small ligands since low-molecular-weight ligands may not contain enough functionality to demonstrate significant inhibition at the concentrations typically used in HTS. The VERTEX SHAPES,[25] Fesik's SAR-by-NMR,[24] and high-throughput crystallography approaches,[26,27] are being utilized increasingly to find small binding motifs with activities in the mM-to μM-range that can be effective starting points. This strategy also allows for the rapid design of new hybrid structures. Surprising observations are often made concerning binding orientations of ligands and the mobility of binding site residues.

The additivity of substrate fragments in an enzyme–ligand binding site was demonstrated with thymidylate synthase complexed with fragments of deoxyuridine monophosphate, **31**–**35** (Scheme 11).[130] The complexes show considerable fidelity of binding orientation, which suggests a modular approach to ligand design by utilizing small molecular fragments. The advantage of NMR spectroscopic and crystallographic techniques is that fragments which bind in the

 © 2003 Wiley-VCH Verlag GmbH & Co. KGaA, Weinheim



31 32 33 34 35

Scheme 11. Deoxyuridine monophosphate fragments.

millimolar range can be used and spatial information obtained. The disadvantages include expense, high dependence on solubility of the fragments, modest numbers of templates screened, and labor-intensive analysis. Typically protein crystals may not be tolerant of the high concentrations of compounds and DMSO used. 1D NMR techniques are typically used as a preselection tool. The elegance of these approaches has led to the setup of a number of small start-up companies offering the techniques as part of a collaborative effort. The assumption that a number of low-affinity templates can be combined to yield a molecule with an affinity greater than the sum of these components is implicit in these techniques. However the common practice of obtaining affinity with one subsection of a molecule and then addressing ADME requirements by adding further groups is fraught with difficulty. For drug design the requirement is often to achieve the required properties by using a limited number of atoms such that parts of the molecule address several property objectives simultaneously.

Some screening technologies like SAR-by-NMR or high-throughput crystallography have greater information content but more limited throughput than traditional HTS screens. Virtual and property-based screening methods can be used to address this when they are used to pick a subset of the total compound collection. Sometimes virtual screening and HTS campaigns are run in parallel. Pharmacia screened their 400000-compound corporate library against protein tyrosine phosphatase-1B in parallel with a virtual screen of 235000 commercially available compounds with DOCK3.5.[131] Whereas the HTS screen identified 85 compounds with $IC_{50} < 100\ \mu M$, a 0.021% hit rate, the virtual screen identified 365 high-scoring molecules, of which 127 (34.8%) inhibited with $IC_{50} < 100\ \mu M$. The authors acknowledge, however, that the presence of plasma protein in the HTS screen artificially depressed its hit rate, whereas the compounds identified by DOCK were screened in the absence of plasma protein. Even with this bias in favor of the virtual screen, this is still an encouraging result. Ultimately the test for any screening output is the usefulness of the compounds as starting points for a project program, where consideration of ADME properties may well provide part of the selection criteria.

In another example, ligands for factor Xa were selected from a virtual library by using PRO-SELECT. The library of putative ligands had been obtained by enumeration of compounds derived by attachment of a set of substituents around core templates.[132] As a control, a similar sized library was also synthesized, based on reasonable medicinal chemistry principles, but without the application of PRO-SELECT. A tenfold enhancement in activity was claimed for the PRO-SELECT set. Likewise when inhibitors of cathepsin D were derived from a library of compounds, synthesized by parallel methods, and guided by structure-based design, enrichments of two- to sevenfold were found compared to the activities of a similar number of compounds selected from a diverse chemical library.[133]

8. Summary and Outlook

Structure-based drug design has contributed to the discovery of a number of drugs and late-stage clinical candidates. It is now common for a series of ligand–protein structures to be available in discovery projects. Where several ligands have been identified, more information is usually obtained by determining complexes with dissimilar ligands than by determining several in which the ligands are structurally closely related. Perversely, the persuasiveness of structural information allied to seductively high in vitro potency can constitute a barrier in the journey from ligand design to drug discovery. The use of ADME data alongside primary screening is now becoming routine in the pharmaceutical industry. The traditional approach of maintaining or including polar interactions while increasing in vitro potency using hydrophobicity is unacceptable if that is achieved at the expense of other druglike properties.

The availability of X-ray derived structural information on protein–ligand complexes is increasing, and this is a useful tool in lead optimization. However, the ambiguities associated with structural models derived from X-ray data may not be fully appreciated. The process of deriving an atomic model from electron density data disguises uncertainties in the identity and position of ligand, water, and protein atoms. The observed ligand and protein conformation can be affected by crystallization conditions. It can be difficult for even the most conscientious medicinal chemist to avoid drawing misleading conclusions.

These ambiguities have important consequences for the application of structure-based design methodologies. Calculation of binding affinities is currently too imprecise to guide design in the narrow range of affinities observed during the optimization of a lead compound to a drug. The use of docking and scoring tools to design combinatorial chemistry libraries makes some allowance for the inaccuracies of scoring functions, and cases already exist that demonstrate an important complementarity between these technologies. Virtual and property-based screening also has utility for the choice of compound subsets for low-throughput screens, which are not amenable to HTS. The prevalence of induced fit

 © 2003 Wiley-VCH Verlag GmbH & Co. KGaA, Weinheim

in ligand–protein interactions also adds complexity to predicting affinities, but at the same time offers new opportunities in ligand design. At present the ability to predict the protein movement and its consequences upon ligand binding is limited. However, it does appear that hydrophobic residues, particularly Phe, Tyr, and Trp and those residues associated with function, are often implicated. In summary, the opportunities for structure-based design have never been greater.

Received: June 5, 2002
Revised: October 2, 2002 [A539]

[1] T. A. Jones, J. Y. Zou, S. W. Cowan, M. Kjeldgaard, *Acta Crystallogr. Sect. A* **1991**, *47*, 110–119.
[2] A. T. Brunger, P. D. Adams, G. M. Clore, W. L. DeLano, P. Gros, R. W. Grosse-Kunstleve, J. S. Jiang, J. Kuszewski, M. Nilges, N. S. Pannu, R. J. Read, L. M. Rice, T. Simonson, G. L. Warren, *Acta. Crystallogr. Sect. D* **1998**, *54*, 905–921.
[3] A. T. Brünger, *" X-PLOR. A System for Crystallography and NMR"*, Yale University, New Haven, CT, USA, **1990**.
[4] Collaborative Computational Project Number 4, *Acta Crystallogr. Sect. D* **1994**, *50*, 760–763.
[5] M. A. Marti-Renom, A. Stuart, A. Fiser, R. Sanchez, F. Melo, A. Sali, *Annu. Rev. Biophys. Biomol. Struct.* **2000**, *29*, 291–325.
[6] C. M. Oshiro, I. D. Kuntz, J. S. Dixon, *J. Comput.-Aided Mol. Des.* **1995**, *9*, 113–130.
[7] M. Rarey, B. Kramer, T. Lengauer, G. Klebe, *J. Mol. Biol.* **1996**, *261*, 470–489.
[8] G. Jones, P. Willett, R. C. Glen, A. R. Leach, R. Taylor, *J. Mol. Biol.* **1997**, *267*, 727–748.
[9] P. J. Goodford, *J. Med. Chem.* **1985**, *28*, 849–857.
[10] A. Miranker, M. Karplus, *Proteins Struct. Funct. Genet.* **1991**, *11*, 29–34.
[11] M. Hendlich, *Acta Crystallogr. Sect. D* **1998**, *54*, 1178–1182.
[12] M. L. Verdonk, J. C. Cole, R. Taylor, *J. Mol. Biol.* **1999**, *289*, 1093–1108.
[13] H. J. Bohm, *J. Comput. -Aided. Mol. Des.* **1994**, *8*, 243–256.
[14] H. Gohlke, M. Hendlich, G. Klebe, *J. Mol. Biol.* **2000**, *295*, 337–356.
[15] A. V. Ishchencko, E. I. Shakhnovich, *J. Med. Chem.* **2002**, *45*, 2770–2780.
[16] P. W. Sprauge, *Perspect. Drug Discovery Des.* **1995**, *3*, 1–20.
[17] R. D. Cramer, D. E. Patterson, J. D. Bunce, *J. Am. Chem. Soc.* **1988**, *110*, 5959–5967.
[18] M. Baroni, G. Constantino, G. Cruciani, D. Riganelli, R. Valigi, S. Clementi, *Quant. Struct.-Act. Relat.* **1993**, *12*, 9–20.
[19] LEAPFROG Tripos Inc., 1699 South Hanley Rd., St Louis, MO, 63144, USA.
[20] B. A. Grzybowski, A. V. Ishenko, J. Shamada, E. I. Shakhnovich, *Acc. Chem. Res.* **2002**, *35*, 261–269.
[21] V. J. Gillet, W. Newell, P. Mata, G. Myatt, S. Sike, Z Zsoldos, A. P. Johnson, *J. Chem. Inf. Comput. Sci.* **1994**, *34*, 207–217.
[22] UNITY 4.2.1 Tripos Inc., 1699 South Hanley Rd., St Louis, MO, 63144, USA.
[23] V. Schnecke, C. A. Swanson, E. D. Getzoff, J. A. Tainer, L. A. Kuhn, *Proteins Struct. Funct. Genet.* **1998**, *33(1)*, 74–87.
[24] S. B. Shuker, P. J. Hajduk, R. P. Meadows, S. W. Fesik, *Science* **1996**, *274*, 1531–1534.
[25] J. Fejzo, C. A. Lepre, J. W. Peng, G. W. Bemis, Ajay, M. A. Murko, J. M. Moore, *Chem. Biol.* **1999**, *6*, 755–769.
[26] V. L. Neinaber, P. L. Richardson, V. Klighofer, J. J. Bouska, V. L. Giranda, J. Greer, *Nat. Biotechnol.* **2000**, *18*, 1105–1108.
[27] T. L. Blundell, H. Joti, C. Abell, *Nat. Rev. Drug Discovery* **2002**, *1*, 145–154.
[28] A. R. Fersht, J. P. Shi, J. Knill-Jones, D. M. Lowe, A. J. Wilkinson, D. M. Blow, P. Brick, Carter, M. M. Y. Waye, G. Winter, *Nature* **1985**, *314*, 235–238.
[29] D. H. Williams, M. S. Searle, J. P. Mackay, U. Gerhard, R. A. Maplestone, *Proc. Natl. Acad. Sci. USA* **1993**, *90*, 1172–1178.
[30] T. G. Davies, J. R. H. Tame, R. E. Hubbard, *Perspect. Drug Discovery Des.* **2000**, *20*, 29–42.
[31] C. A. Lipinski, F. Lombardo, B. W. Dominy, P. J. Feeney, *Adv. Drug Delivery Rev.* **1997**, *23*, 2–25.
[32] Ajay, W. P. Walters, M. A. Murcko, *J. Med. Chem.* **1998**, *41*, 3314–3324.
[33] http://setiathome.ssl.berkeley.edu/.
[34] http://www.chem.ox.ac.uk/curecancer.html.
[35] A. M. Davis, J. Dixon, C. J. Logan, D. W. Payling, in *Pharmacokinetic Challenges in Drug Discovery*, (Eds.: O. Pelkonen, A. Baumann, A. Reichel) Springer, Berlin, **2002**, 1–32.
[36] M. A. Murko, P. R. Caron, P. S. Charifson, *Annu. Rep. Med. Chem.* **1999**, *34*, 297–306.
[37] G. Schneider, H.-J. Bohm, *Drug Discovery Today* **2002**, *7*, 64–70.
[38] R. E. Babine, S. L. Bender, *Chem. Rev.* **1997**, *97*, 1359–1472.
[39] M. Stahl, M. Rarey, G. Klebe, *Methods and Principles in Medicinal Chemistry Volume 14 Bioinformatics—From Genome to Drug*, (Ed.: Thomas Lengauer), Wiley-VCH, **2002**, pp. 137–170.
[40] M. G. Bursavich, D. H. Rich, *J. Med. Chem.* **2002**, *45*, 541–558.
[41] M. T. Huisman, J. W. Smit, H. R. Wiltshire, R. M. W. Hoetelmans, J. H. Beijnen, A. H. Schinkel, *Mol. Pharmacol.* **2001**, *59*, 806–813.
[42] G. C. Williams, P. J. Sinko, *Adv. Drug Delivery Rev.* **1999**, *39*, 211–238.
[43] V. de Lucca, P. Y. S. Lam, *Drugs Future* **1998**, *23*, 987–994.
[44] J. D. Rodgers, P. Y. S. Lam, B. L. Johnson, H. Wang, S. S. Ko, S. P. Seitz, G. L. Trainor, P. S. Anderson, R. M. Klabe, L. T. Bacheler, B. Cordova, S. Garber, C. Reid, M. R. Wright, C.-H. Chang, S. Erickson-Viitanen, *Chem. Biol.* **1998**, *5*, 597–608.
[45] P. A. Aristoff, *Drugs Future* **1998**, *23*, 995–999.
[46] M. von Itzstein, W.-Y. Wu, G. B. Kok, M. S. Pegg, J. C. Dyason, B. Jin, T. V. Phan, M. L. Smythe, H. F. White, S. W. Oliver, P. M. Colman, J. N. Varghese, D. M. Ryan, J. M. Woods, R. C. Bethell, V. J. Hotham, J. M. Cameron, C. R. Penn, *Nature* **1993**, *363*, 418–423.
[47] Physicians' Desk Reference, 55. edition, Thomson Medical Economics, Montvale, **2001**, p. 1454.
[48] C. U. Kim, W. Lew, M. A. Williams, H. Liu, L. Zhang, S. , Swaminathan, N. Bischofberger, M. S. Chen, D. B. Mendel, C. Y. Tai, W. G. Laver, R. C. Stevens, *J. Am. Chem. Soc.* **1997**, *119*, 681–690.
[49] R&D Insight, **2000**, ADIS International Ltd., Chester, United Kingdom.
[50] M. A. Navia, J. P. Springer, M. Poe, J. Boger, K. Hoogsteen, *J. Biol. Chem.* **1984**, *259*, 12714–12717.
[51] A. R. Sielecki, K. Hayakawa, M. Fujinaga, M. E. P. Murphy, M. Frazer, A. K. Muir, C. T. Carilli, J. A. Lewicki, J. D. Baxter, M. N. G. James, *Science* **1989**, *243*, 1341–1351.
[52] M. A. Navia, P. R. Chaturvedi, *Drug Discovery Today* **1996**, *1*, 179–189.
[53] C. Oefner, A. Binggeli, V. Breu, D. Bur, J.-P. Clozel, A. D′Arcy, A. Dorn, W. Fischli, F. Gruninger, R. Guller, G. Hirth, H. P. Marki, S. Mathews, M. Miuller, R. G. Ridley, H. Stadler, E. Viera, M. Wilhelm, F. K. Winkler, W. Wostl, *Chem. Biol.* **1999**, *6*, 127–131.
[54] H. Kubinyi, *J. Recept. Signal Transduction Res.* **1999**, *19*, 15–39.
[55] J. Greer, J. W. Erickson, J. J. Baldwin, M. D. Varney, *J. Med. Chem.* **1994**, *37*, 1035–1054.
[56] G. S. Ponticello, M. F. Sugre, B. Plazonnet, G. Durand-Cavagna, *Pharm. Biotechnol.* **1998**, *11*, 555–574.

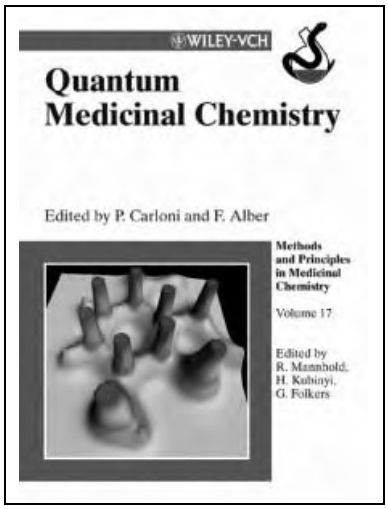
 © 2003 Wiley-VCH Verlag GmbH & Co. KGaA, Weinheim

[57] R. W. Schevitz, N. J. Bach, D. G. Carlson, N. Y. Chirgadze, D. K. Clawson, R. D. Dillard, S. E. Draheim, L. W. Hartley, N. D. Jones, E. D. Mihelich, J. L. Olkowski, D. W. Snyder, C. Sommers, J.-P. Wery, *Nat. Struct. Biol.* **1995**, *2*, 458 – 465.
[58] E. D. Mihelich, R. W. Schevitz, *Biochim. Biophys. Acta* **1999**, *1441*, 223 – 228.
[59] J. Drenth, *Principles of Protein X-ray Crystallography*, Springer-Verlag, New York, **1994**.
[60] T. A. Jones, M. Kjeldgaard, *Methods Enzymol.* **1997**, *277*, 173 – 208.
[61] G. J. Kleywegt, T. A. Jones, *Methods Enzymol.* **1997**, *277*, 208 – 230.
[62] a) F. C. Bernstein, T. F. Koetzle, G. J. B. Williams, E. F. Meyer, Jr., M. D. Brice, J. R. Rodgers, O. Kennard, T. Shimanouchi, M. Tasumi, *J. Mol. Biol.* **1977**, *112*, 535 – 542; b) http://www.rcsb.org/pdb.
[63] G. J. Kleywegt, *Acta Crystallogr. Sect. D* **2000**, *56*, 249 – 265.
[64] G. J. Kleywegt, T. A. Jones in *Making the Most of Your Model* (Eds.: W. N. Hunter, J. M. Thornton, S. Bailey), SERC Daresbury Laboratory, Warrington, **1995**, pp. 11 – 24.
[65] C. I. Brändén, T. A. Jones, *Nature* **1990**, *343*, 687 – 689.
[66] M. A. Hanson, T. K. Oost, C. Sukonpan, D. H. Rich, R. C. Stevens, *J. Am. Chem. Soc.* **2000**, *122*, 11268 – 11269.
[67] M. A. Hanson, T. K. Oost, C. Sukonpan, D. H. Rich, R. C. Stevens, *J. Am. Chem. Soc.* **2002**, *124*, 10248.
[68] A. T. Brünger, *Nature* **1992**, *355*, 472 – 475.
[69] G. J. Kleywegt, T. A. Jones, *Structure* **1995**, *3*, 535 – 540.
[70] A. T. Brünger, *Methods Enzymol.* **1997**, *277*, 366 – 396.
[71] G. J. Kleywegt, A. T. Brünger, *Structure* **1996**, *4*, 897 – 904.
[72] R. W. W. Hooft, G. Vriend, C. Sander, E. E. Abola, *Nature* **1996**, *381*, 272.
[73] http://www.cmbi.kun.nl/gv/pdbreport.
[74] J. Y. Zou, M. R. Harris, T. Taylor, A. Wählby, G. J. Kleywegt, T. A. Jones, unpublished results.
[75] J. F. Leszczynski, G. D. Rose, S. Milton, *Science* **1986**, *234*, 849 – 855.
[76] B. Hao, W. Gong, T. K. Ferguson, M. Carey, J. A. Krzycki, M. K. Chan, *Science* **2002**, *296*, 1462 – 1466.
[77] G. J. Kleywegt, T. Bergfors, H. Senn, P. Le Motte, B. Gsell, K. Shudo, T. A. Jones, *Structure* **1994**, *2*, 1241 – 1258.
[78] A. Fersht, *Enzyme Structure and Mechanism*, Freeman, New York, **1985**, pp. 155 – 175.
[79] G. Klebe, M. Bohm, F. Dullweber, U. Gradler, H. Gohlke, M. Hendlich, in *Molecular Modelling and Prediction of Bioactivity* (Eds.: K. Gundertofte, F. S. Jorgensen), Kluwer/Plenum, New York, **2000**, pp. 103 – 110.
[80] M. T. Stubbs, S. Reyda, F. Dullweber, M. Moller, G. Klebe, D. Dorsch, W. W. K. R. Mederski, H. Wurziger, *Chembiochem* **2002**, *3*, 246 – 249.
[81] S. M. Cutfield, E. J. Dodson, B. F. Anderson, P. C. E. Moody, C. J. Marshall, P. A. Sullivan, J. F. Cutfield, *Structure* **1995**, *3*, 1261 – 1271.
[82] C. Abad-Zapatero, R. Goldman, S. W. Muchmore, C. Hutchins, K. Stewart, J. Navaza, C. D. Payne, T. L. Ray, *Protein Sci.* **1996**, *5*, 640 – 652.
[83] V. Nahoum, G. Roux, V. Anton, P. Rouge, A. Puigserver, H. Bischoff, B. Henrissat, F. Payan, *Biochem. J.* **2000**, *346*, 201 – 208.
[84] Y. So, M. M. Yamashita, S. E. Greasley, C. A. Mullen, J. H. Shim, P. A. Jennings, S. J. Benkovic, L. A. Wilson, *J. Mol. Biol.* **1998**, *281*, 485 – 499.
[85] O. Mayans, M. Scott, I. Connerton, T. Gravesen, J. Benen, J. Visser, R. Rickersgill, J. Jenkins, *Structure* **1997**, *5*, 677 – 689.
[86] K. Matsuda, K. Mizuguchi, T. Nishioka, H. Kato, N. Go, J. Oda, *Protein Eng.* **1996**, *9*, 1083 – 1092.
[87] "Options for the Control of Influenza IV": A. Harris, F. Forouhar, S. Qiu, S. Shihong, L. M. Bingdong, Int. Congress Series, **2001**, *1219*, 405 – 410.
[88] R. Berisio, F. Sica, V. S. Lamzin, K. S. Wilson, A. Zagari, L Mazzarella, *Acta Crystallogr. Sect. D* **2002**, *58*, 441 – 450.
[89] S. Daopin, D. R. Davies, *Acta Crystallogr. Sect. D* **1994**, *50*, 85 – 92.
[90] D. H. Ohlendorf, *Acta Crystallogr. Sect. D* **1994**, *50*, 808 – 812.
[91] B. A. Fields, H. H. Bartsch, H. D. Bartunik, F. Cordes, J. M. Guss, H. C. Freeman, *Acta Crystallogr. Sect. D* **1994**, *50*, 709 – 730.
[92] J. E. Ladbury, *Chem. Biol.* **1996**, *3*, 973 – 980.
[93] J. Boström, *J. Comp-Aided Mol. Des.* **2001**, *15*, 1137 – 1152.
[94] G. J. Kleywegt, T. A. Jones, *Acta Crystallogr. D* **1998**, *54*, 1119 – 1131.
[95] http://xray.bmc.uu.se/hicup.
[96] D. M. F. van Aalten, R. Bywater, J. B. C. Findlay, M. Hendlich, R. W. W. Hooft, G. Vriend, *J. Comput. Aided Mol. Des.* **1996**, *10*, 255 – 262.
[97] J. Eads, J. C. Sacchettini, A. Kromminga, J. I. Gordon, *J. Biol. Chem.* **1993**, *268*, 26375 – 26385.
[98] J. Thompson, N. Winter, D. Terwey, J. Bratt, L. Banaszak, *J. Biol. Chem.* **1997**, *272*, 7140 – 7150.
[99] M. G. Jakoby, K. R. Miller, J. J. Toner, A. Bauman, L. Cheng, E. Li, D. P. Cistola, *Biochemistry* **1993**, *32*, 872 – 878.
[100] J. W. M. Nissink, C. Murray, M. Hartshorn, M. L Verdonk, J. C. Cole, R. Taylor, *Proteins Struct. Funct. Genet.* **2002**, *49*, 457 – 471.
[101] E. E. Abola, A. Bairoch, W. C. Barker, S. Beck, D. A. Benson, H. Berman, G. Cameron, C. Cantor, S. Doubet, T. J. P. Hubbard, T. A. Jones, G. J. Kleywegt, A. S. Kolastar, A. Van Kuik, A. M. Lest, H.-W. Mewes, D. Neuhaus, F. Pfeiffer, L. F. TenEyck, R. J. Simpson, G. Stoesser, J. L. Sussman, Y. Tateno, A. Tsugita, E. L. Ulrick, J. F. G. Vliegenthart, *Bio-Essays* **2000**, *22*, 1024 – 1034.
[102] http://www.expasy.ch/spdbv.
[103] G. J. Kleywegt, T. A. Jones, *Structure*, **2002**, *10*, 465 – 472.
[104] http://fsrv1.bmc.uu.se/eds.
[105] http://xray.bmc.uu.se/embo2001/modval.
[106] E. M. S. Harris, A. E. Aleshin, L. M. Firsov, R. B. Honzatko, *Biochemistry* **1993**, *32*, 1618 – 1626.
[107] M. J. Boulanger, M. E. P. Murphy, *Biochemistry* **2001**, *40*, 9132 – 9141.
[108] P. C. Sanschagrin, L. A. Kuhn, *Protein Sci.* **1998**, *7*, 2054 – 2064.
[109] http://www.ccdc.cam.ac.uk/prods/gold/value.html.
[110] C. W. Murray, C. A. Baxter, A. D. Frenkel, *J. Comput.-Aided Mol. Des.* **1999**, *13*, 547 – 562.
[111] C. Hansch, *Acc. Chem. Res.* **1993**, *26*,147 – 153.
[112] C. Hansch, D. Hoekman, H. Gao, *Chem. Rev.* **1996**, *96*, 1045 – 1075.
[113] D. H. Williams, M. S. Westwell, *Chem. Soc. Rev.* **1998**, *27*, 57 – 64.
[114] I. P. Street, C. R. Armstrong, S. G. Withers, *Biochemistry* **1986**, *25*, 6021 – 6027.
[115] I. Muegge, Y. C. Martin, *J. Med. Chem.* **1999**, *42*, 791 – 804.
[116] H.-J. Bohm, M. Stahl, *Med. Chem. Res.* **1999**, *9*, 445 – 462.
[117] R. D. Head, M. L. Smythe, T. I. Oprea, C. L. Waller, S. M. Green, G. R. Marshall, *J. Am. Chem. Soc.* **1996**, *118*, 3959 – 3969.
[118] T. I. Oprea, G. R. Marshall, *Perspect. Drug Discovery Des.* **1998**, *9–11*, 35 – 61.
[119] M. K. Holloway, J. M. Wai, T. A. Halgren, P. M. D. Fitzgerald, J. P. Vacca, B. D. Dorsey, R. B. Levin, W. J. Thompson, L. J. Chen, S. J. deSolms, N. Gaffin, A. K. Ghosh, E. A. Giuliani, S. L. Graham, J. P. Guare, R. W. Hungate, T. A. Lyle, W. M. Sanders, T. J. Tucker, M. Wiggins, C. M. Wiscount, O. W.

 © 2003 Wiley-VCH Verlag GmbH & Co. KGaA, Weinheim

Woltersdorf, S. D. Young, P. L. Darke, J. A. Zugay, *J. Med. Chem.* **1995**, *38*, 305 – 317.
[120] A. M. Davis, S. J. Teague, *Angew. Chem.* **1999**, *111*, 778 – 792; *Angew. Chem. Int. Ed.* **1999**, *38*, 736 – 749.
[121] R. Najmanovich, J. Kuttner, V. Sobolev, M. Edelman, *Proteins Struct. Funct. Genet.* **2000**, *39*, 261 – 268.
[122] P. Goodford, *Alfred Benzon Symp.* **1998**, *42*, 215 – 230.
[123] V. Schnecke, L. Kuhn, *Perspect. Drug Discovery Des.* **2000**, *20*, 171 – 190.
[124] A. C. Anderson, R. H. O'Neil, T. S. Surti, R. M. Stroud, *Chem. Biol.* **2001**, *8*, 445 – 457.
[125] D. Joseph-McCarthy, S. K. Tsang, D. J. Filman, J. M. Hogle, M. Karplus, *J. Am. Chem. Soc.* **2001**, *123*, 12758 – 12769.
[126] A. Rockwell, M. Melden, R. A. Copeland, K. Hardman, C. P. Decicco, W. F. DeGrado, *J. Am. Chem. Soc.* **1996**, *118*, 10337 – 10338.
[127] A. M. Davis, T. I. Oprea, S. J. Teague, P. D. Leeson, *Angew. Chem.* **1999**, *111*, 3962 – 3967; *Angew. Chem. Int. Ed.* **1999**, *38*, 3743 – 3748.
[128] T. I. Oprea, A. M. Davis, S. J. Teague, P. D. Leeson, *J. Chem. Inf. Comput. Sci.* **2001**, *41*, 1308 – 1315.
[129] M. Hann, A. R. Leach, . G. Harper, *J. Chem. Inf. Comput. Sci.* **2001**, *41*, 856 – 864.
[130] T. J. Stout, C. R. Sage, R. M. Stroud, *Structure* **1998**, *6*, 839 – 848.
[131] T. N. Doman, S. L. McGovern, B. J. Witherbee, T. P. Kasten, R. Kurumbail, W. C. Stallings, D. T. Connolly, B. K. Shoichet, *J. Med. Chem.* **2002**, *45*, 2213 – 2221.
[132] J. W. Leibeshuetz, S. D. Jones, P. J. Morgan, C. W. Murray, A. D. Rimmer, J. M. E. Roscoe, B. Waszkowycz, P. M. Welsh, W. A. Wylie, S. C. Young, H. Martin, J. Mahler, L. Brady, K. Wilkinson, *J. Med. Chem.* **2002**, *45*, 1221 – 1232.
[133] E. K. Kick, D. C. Roe, A. G. Skillman, G. Lui, T. J. A. Ewing, Y. Sun, I. D. Kuntz, J. A. Ellman, *Chem. Biol.* **1997**, *4*, 297 – 307.

NEW +++ NEW +++ NEW +++ NEW



ISBN 3-527-30456-8
€ 139,-* / sFr 205,-

*Der Euro-Preis ist ausschließlich gültig für Deutschland.

PAOLO CARLONI, SISSA / ISAS, Trieste, Italy, and FRANK ALBER, The Rockefeller University, New York, USA (eds.)

Quantum Medicinal Chemistry

2003. XIII, 281pp Hbk

Tailored to the Needs of Pharmaceutical Chemists

Everyone relies on the power of computers, including chemical and pharmaceutical laboratories. Increasingly faster and more exact simulation algorithms have made quantum chemistry a valuable tool in the search for active substances. This book cleverly combines the theoretical basics with example applications from chemistry and pharmaceutical research and so will appeal to both beginners as well as experienced users of quantum chemical methods. For anyone striving to stay ahead in this rapidly evolving field.

This title is also available online at www.interscience.wiley.com/onlinebooks

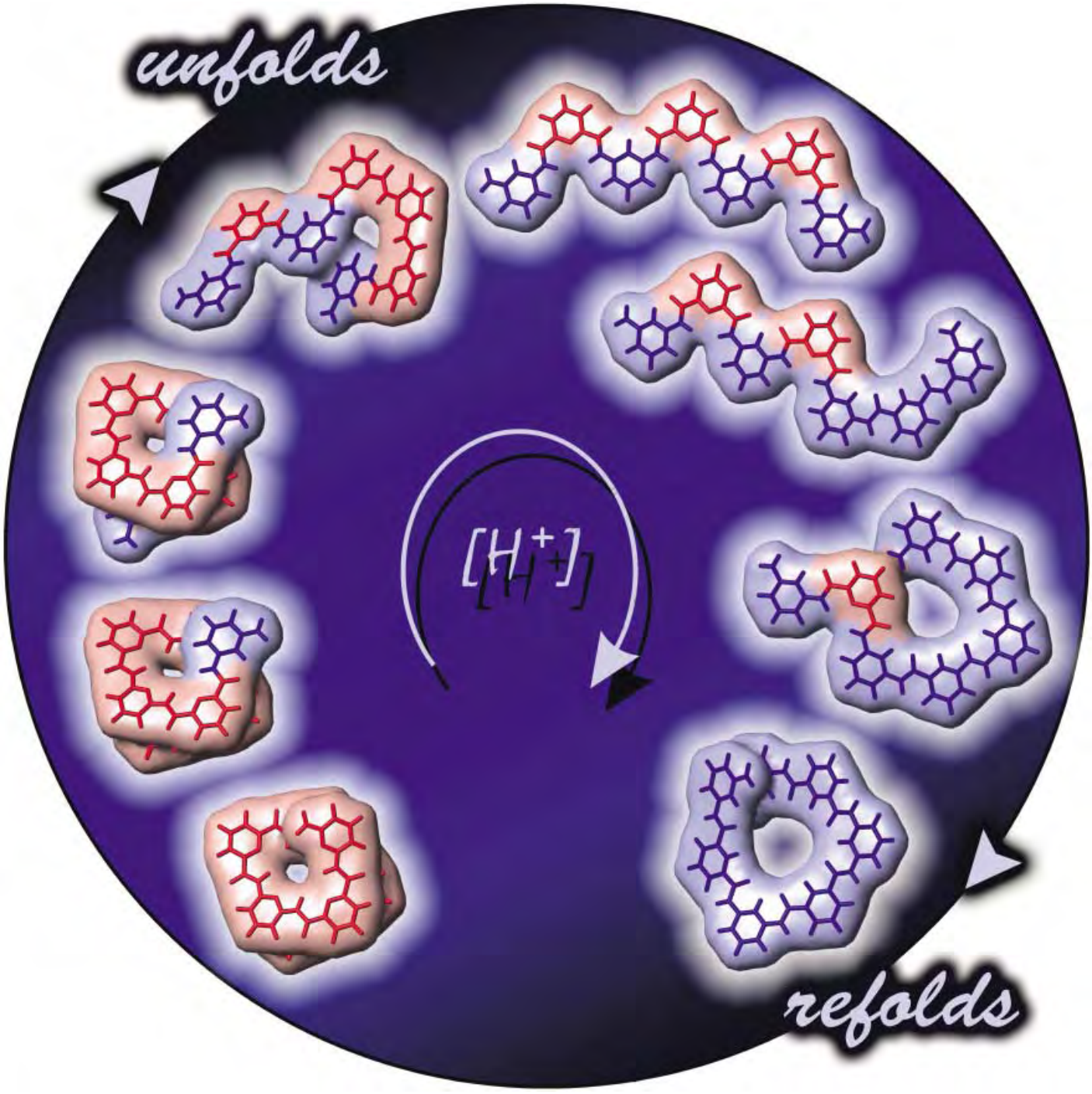
Wiley-VCH Verlag
Fax: +49 (0)6201 606 184
e-Mail: service@wiley-vch.de
www.wiley-vch.de

Register now for the free
WILEY-VCH Newsletter!
www.wiley-vch.de/home/pas

WILEY-VCH

50403032_kn

Communications



Molecular machines can convert energy into controlled molecular motions of large amplitude. Selective protonation of an oligoamide strand leads to an extension of the initial helical conformation to a linear structure, which then refolds into another helix. For more information see the following communication by Huc and co-workers.

DOI: 10.1002/anie.200351080
© 2003 Wiley-VCH Verlag GmbH & Co. KGaA, Weinheim

pH-Induced Changes in Conformation

Protonation-Induced Transition between Two Distinct Helical Conformations of a Synthetic Oligomer via a Linear Intermediate**

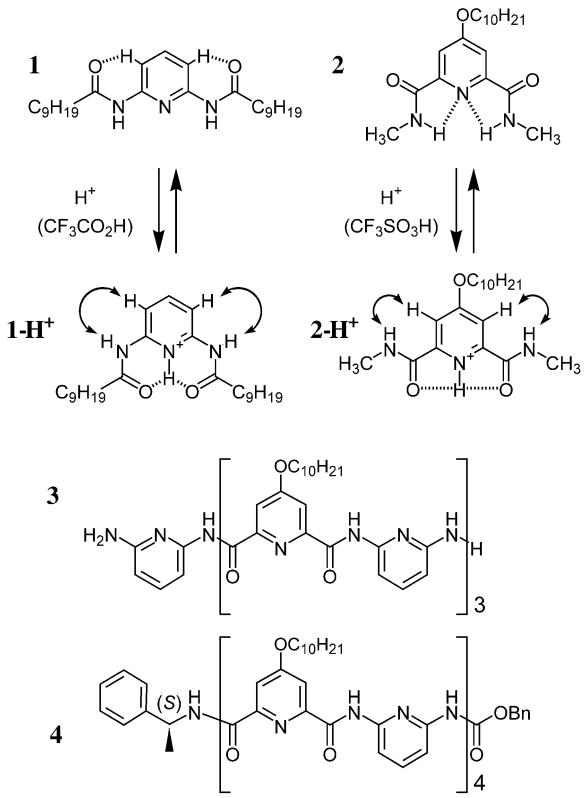
*Christel Dolain, Victor Maurizot, and Ivan Huc**

Dedicated to Dr. Christian Rolando

Designed molecular and supramolecular structures held together by noncovalent interactions have been increasing in size and complexity.[1] They provide frames within which or between which controlled dynamic structural changes of large amplitude (molecular motions) can be envisaged such as rotations and translations or combinations thereof.[2] Interest in these so-called molecular machines is fueled by their relation to important natural phenomena and by the prospect of elaborating useful chemical devices. Molecular motions can be triggered by various means (e.g., ion binding, electron transfer, and light excitation) and can often be reverted by simply removing or reversing the triggering stimuli.[2] Here, we present an original system in which a large conformational change caused by protonation is formally reverted not only upon deprotonation but also upon further protonation: helical oligopyridine–dicarboxamide strands unfold to an extended linear conformation upon partial protonation,[3] which upon full protonation refolds to a helix related to (though distinct from) the initial state.

Oligoamides prepared from 2,6-pyridinedicarboxylic acids and 2,6-diaminopyridines adopt stable helical conformations in the solid state as well as in solution in organic solvents and in water.[4–6] The bending of the strands into helices arises from the strongly preferred conformations of 2,6-bis(carbonylamino)pyridine units and 2,6-pyridinedicarboxamide units, which are both stabilized by intramolecular hydrogen bonds as in **1** and **2** (Scheme 1).

We speculated that protonation at the pyridine nitrogen of these units should affect their conformational preferences and investigated their behavior in the presence of acids of various strengths: CF_3CO_2H (TFA, $pK_a = 0$), CH_3SO_3H (MsOH, $pK_a = -2$), and CF_3SO_3H (TfOH, $pK_a = -16$). When 1 equiv MsOH is added to a solution of **1** in $CDCl_3$, protonation is shown to occur quantitatively, leading to the conformation shown in Scheme 1, in which the carbonyl groups form hydrogen bonds with the pyridinium N^+H and not with H^3 aryl protons. The following observations support for this conformation: 1) A sharp signal for the pyridinium N^+H is observed at very low field ($\delta = 17$ ppm); 2) Protonation causes downfield shifts of the NMR signals of H^4 and NH protons and an upfield shift of the signal of H^3 as the neighboring carbonyl oxygen moves farther away; 3) NOE experiments with **1**-H^+ reveal a strong correlation between the amide proton and the adjacent aromatic proton, and no correlation with the pyridinium N^+H;[7] 4) The proposed conformation is also adopted in the solid by all four 2,6-bis(carbonylamino)pyridinium derivatives listed in the CCDB.[8]



Scheme 1. Changes in the conformations of **1** and **2** upon protonation to give **1**-H^+ and **2**-H^+, respectively, and structures of **3** and **4**. The double-headed arrows indicate relevant NOE correlations seen in the ^{1}H NMR spectra of **1**-H^+ and **2**-H^+.

When TFA is used instead of MsOH, **1** is also protonated but roughly four equivalents of acid are needed.[7] On the other hand, pyridinedicarboxamide **2** is not protonated by TFA[7] and only partially by MsOH.[9] The electron-withdrawing effect of the carbonyl groups and the intramolecular hydrogen bonds apparently decrease the basicity of the pyridine nitrogen. Quantitative protonation of **2** is achieved upon adding TfOH, which results in an upfield shift of the signals of aromatic and amide protons, and the development of a pyridinium signal. NOE experiments with **2**-H^+ show a correlation between the amide proton and the neighbor aryl proton.[7] Again, this indicates a 180° rotation about the aryl-amide linkages, presumably caused by the larger strength of a $N^+H\cdots OC$ hydrogen bond with respect to a $CH^3\cdots OC$ hydrogen bond (Figure 1).

[*] Dr. I. Huc, C. Dolain, V. Maurizot
Institut Européen de Chimie et Biologie
16 Av. Pey Berland, 33607 Pessac Cedex (France)
Fax: (+33) 5-5796-2226
E-mail: i.huc@iecb-polytechnique.u-bordeaux.fr

[**] This work was supported by the Région Aquitaine and the CNRS (predoctoral fellowships to V.M. and C.D.). We thank Dr. V. Berl and Prof. M. J. Krische for stimulating discussions at an early stage of this project, and Dr. E. J. Dufourc and C. Simon for assistance with NMR measurements.

Supporting information for this article is available on the WWW under http://www.angewandte.org or from the author.

 © 2003 Wiley-VCH Verlag GmbH & Co. KGaA, Weinheim DOI: 10.1002/anie.200351080

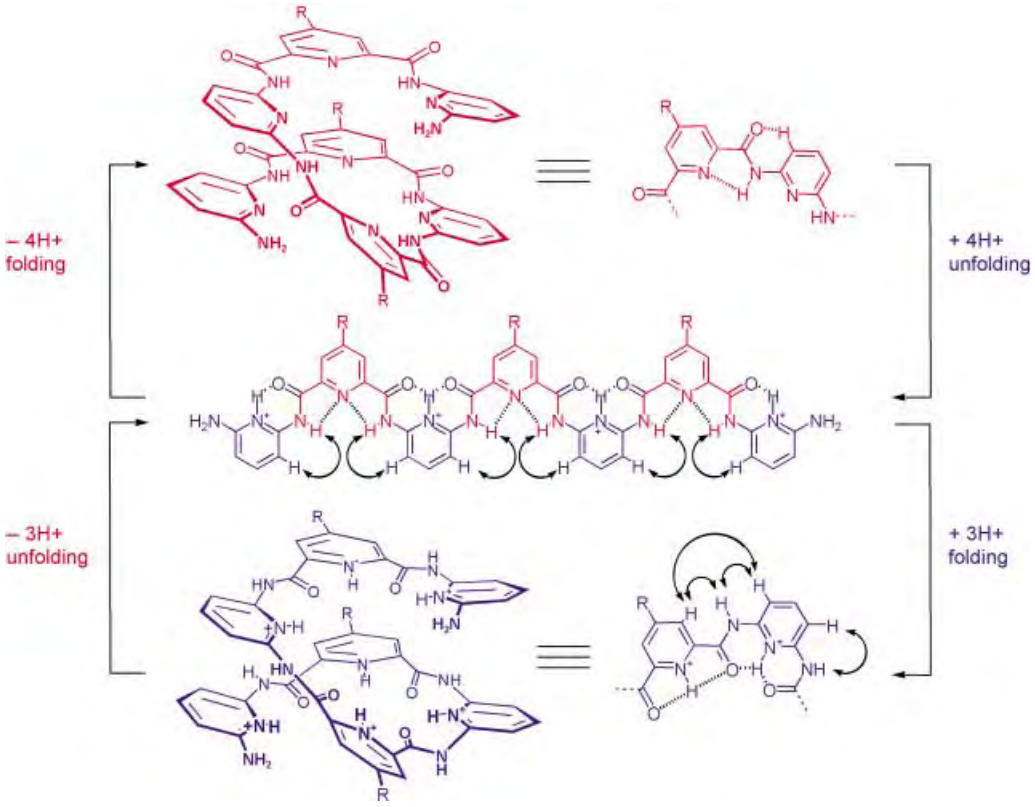
In oligomeric strands **3** and **4**, protonation at each pyridine site is expected to cause local conformational changes that may cooperatively affect the structure of the whole molecule. According to the behavior of **1** and **2**, TFA should protonate all four diaminopyridine units of **3** and only them, giving rise to an extended linear conformation (Scheme 2). When a 1 mM solution of **3** in $CDCl_3$ is titrated with TFA, the initial sharp ^1H NMR spectrum of the single helix broadens extensively as partially protonated species equilibrate and sharpens again when saturation is reached (20 equiv TFA).[7,10] The linear conformation of **3**-$(H^+)_4$ is demonstrated by NOESY spectra which show that each amide proton correlates with only one proton: the H^3 proton of the neighbor aminopyridine ring (Scheme 2 and Figure 1a).

The conformational preferences of **1**-H^+ and **2**-H^+ led us to speculate that the protonation of **3**-$(H^+)_4$ to give **3**-$(H^+)_7$ may result in the folding of the linear extended strand into a helix (Scheme 2). Heptaprotonation was achieved by treating **3** with an excess of TfOH. The ^1H NMR spectrum shows the signals of the expected four different pyridinium protons at $\delta = 15.5$, 14.9, 11.6, and 11.5 ppm, which can be assigned unambiguously.[11] The signals of the amide protons are found at $\delta = 10.1$, 9.6 and 9.7 ppm and partly overlap with the signal of TfOH. In NOESY experiments each amide signal shows two correlations: one with the H^3 proton of the neighbor diaminopyridine ring, and one with the H^3 proton of the neighbor pyridinedicarbonyl ring (Scheme 2 and Figure 1b). Moreover, these two aromatic protons also directly correlate. No correlation is observed between the amides and the pyridiniums, which is consistent with the helical structure proposed for **3**-$(H^+)_7$.

Circular dichroism (CD) measurements of **4** were performed to corroborate the NMR data obtained with **3**. The terminal chiral (*S*)-(1-phenyl)ethylamino group of **4** shifts the equilibrium between the right- and left-handed helical conformations, which gives rise to a CD signal in the absorption region of the oligoamide associated with its helical conformation. Upon addition of TFA, this signal progressively disappears (Figure 2a) and is restored upon neutralization with excess Et_3N. This is consistent with the proposed transition from the helical conformation to the linear strand for **4**-$(H^+)_4$. No chiral induction is possible in the latter, and only the CD bands belonging to the chiral terminal group are observed ($\lambda < 280$ nm).

Titration of **4** with TfOH initially results in a similar decrease of CD intensity as the diaminopyridine units are protonated, but it is then followed by the appearance of a new signal in the absorption region of the pyridinium chromophores as the pyridinedicarbonyl units are protonated as well (Figure 2b).[12] The oligomeric sequence of **4**-$(H^+)_8$ therefore adopts a chiral conformation, in agreement with the helix proposed on the basis of NMR data.

In summary, the conformational preferences of **1**, **2**, **1**-H^+, and **2**-H^+, on the one hand, and the large difference in pK_{BH^+} between **1**-H^+ and **2**-H^+, on the other hand, translate into selective protonations and conformational changes in oligoamides such as **3** and **4** that give rise to an unprecedented pH-controlled equilibrium between a nonprotonated helix, a



Scheme 2. The equilibria between the helical conformation of **3** (top), the linear conformation of **3**-$(H^+)_4$ (middle), and the helical conformation of **3**-$(H^+)_7$ (bottom) Protonated units are represented in blue and nonprotonated units are in red. The double-headed arrows indicate relevant observed NOE correlations.

 © 2003 Wiley-VCH Verlag GmbH & Co. KGaA, Weinheim

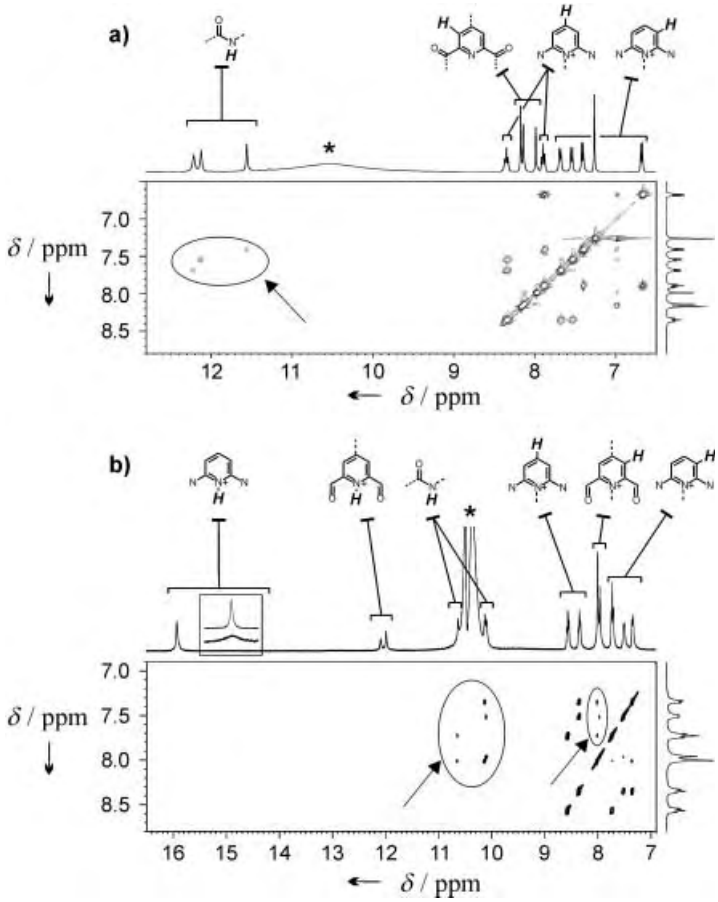


Figure 1. 400 MHz ^{1}H NMR NOESY spectra at 298 K of a) **3**-$(H^+)_4(CF_3CO_2^-)_4$ (20 mM in $CDCl_3$ in the presence of 20 equiv TFA); the asterisk marks the signal of CF_3CO_2H, the arrow marks relevant correlations; b) **3**-$(H^+)_7(CF_3SO_3^-)_4$ (20 mM in TfOH); the asterisk marks the residual signal of CF_3SO_3H after presaturation, arrows mark relevant correlations. Because of exchange phenomena, the presaturation causes the disappearance of the terminal pyridinium signal at $\delta = 14.9$ ppm. If the signal is not presaturated, it is broad at 298 K and sharp at 273 K (inset).

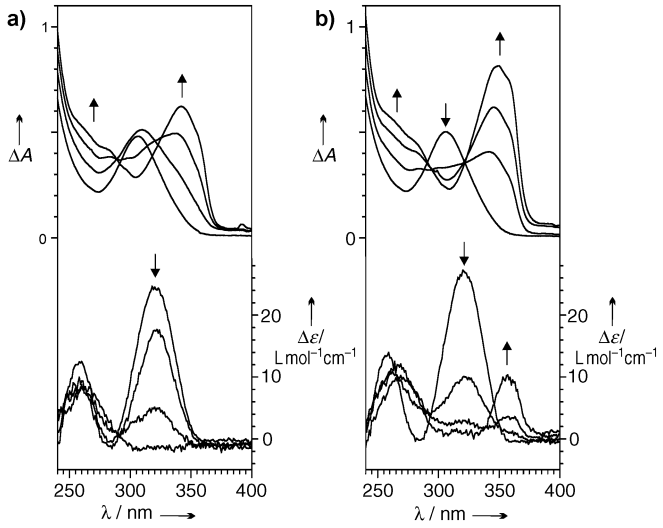


Figure 2. UV/Vis absorption (top) and CD (bottom) spectra of (*S*)-**4** (1 mM in $CHCl_3$ at −10 °C in a 0.1-mm cell) in the presence of acids. The arrows indicate the evolution of the spectra in the presence of a) 0, 30, 50, and 80 equiv TFA and b) 0, 2, 4, and 15 equiv TfOH.

partially protonated linear strand, and a fully protonated helix distinct from the nonprotonated helix. This system may be considered as an "or" logic gate, which gives a CD signal in neutral or very acidic media but not in slightly acid medium. Upon tuning the pK_a of the pyridine nitrogens, using for example electron-donating or -withdrawing groups in position 4, one can hope to combine protonated and nonprotonated pyridine units in even more complex structural patterns and molecular motions.

Received: February 3, 2003 [Z51080]

Keywords: chirality · conformation analysis · helical structures · hydrogen bonds · supramolecular chemistry

[1] J.-M. Lehn, *Supramolecular Chemistry–Concepts and Perspectives*, VCH, Weinheim, **1995**.
[2] For reviews: *Special Issue on Molecular Machines* (Ed.: J. F. Stoddart), *Acc. Chem. Res.* **2001**, *34*, 409; V. Balzani, F. Credi, M. Raymo, J. F. Stoddart, *Angew. Chem.* **2000**, *112*, 3484; *Angew. Chem. Int. Ed.* **2000**, *39*, 3348.
[3] For related examples of unfolding of bent or helical conformers: P. S. Corbin, S. C. Zimmermann, *J. Am. Chem. Soc.* **2000**, *122*, 3779; M. Barboiu, J.-M. Lehn, *Proc. Natl. Acad. Sci. USA* **2002**, *99*, 5201; H. Nakako, R. Nomura, T. Masuda, *Macromolecules* **2001**, *34*, 1496; M. Fujiki, *J. Am. Chem. Soc.* **2000**, *122*, 3336; J. Lie, G. B. Schuster, K.-P. Cheon, M. M. Green, J. V. Selinger, *J. Am. Chem. Soc.* **2000**, *122*, 2603.
[4] For a recent and extensive review on the folding properties of synthetic molecular strands see: D. J. Hill, M. J. Mio, R. B. Prince, T. S. Hughes, J. S. Moore, *Chem. Rev.* **2001**, *101*, 3893.
[5] N. C. Singha, D. N. Sathyanarayana, *J. Mol. Struct.* **1997**, *403*, 123; V. Berl, I. Huc, R. G. Khoury, J.-M. Lehn, *Chem. Eur. J.* **2001**, *7*, 2798; I. Huc, V. Maurizot, H. Gornitzka, J.-M. Léger, *J. Chem. Soc. Chem. Commun.* **2002**, 578.
[6] For related systems see: B. Gong, *Chem. Eur. J.* **2001**, *7*, 4337, and references therein; Y. Hamuro, S. J. Geib, A. D. Hamilton, *J. Am. Chem. Soc.* **1997**, *119*, 10587.
[7] See supporting information.
[8] S. J. Geib, S. C. Hirst, C. Vicent, A. D. Hamilton, *J. Chem. Soc. Chem. Commun.* **1991**, 197; R. P. Dixon, S. J. Geib. , A. D. Hamilton, *J. Am. Chem. Soc.* **1992**, *114*, 365; R. Ostaszewski, Z. Urbanczyk-Lipkowska, *J. Mol. Struct.* **1999**, *474*, 197.
[9] The data cannot be interpreted unambiguously. The addition of MsOH causes some variations in chemical shifts, which suggests that protonation occurs, but no pyridinium signal is observed. The titrations are complicated by the poor miscibility of $CDCl_3$ and MsOH, and cosolvents interfere with the protonation.
[10] Protonation also causes the dissociation of the double helices formed by these oligomers, see: V. Berl, I. Huc, R. G. Khoury, M. J. Krische, J.-M. Lehn, *Nature* **2000**, *407*, 720; V. Berl, I. Huc, R. G. Khoury, J.-M. Lehn, *Chem. Eur. J.* **2001**, *7*, 2810.
[11] The assignment is based on the comparison of this spectrum to the spectra of shorter oligomers, and on the integration and the values of the chemical shifts of these signals: the signals at higher field belong to the pyridinedicarbonyl units, and the signals at lower field belong to the diaminopyridine units; the less deshielded and broader signal at $\delta = 14.9$ ppm is assigned to the terminal pyridinium unit, which can form a hydrogen bond with only one carbonyl group.
[12] The band induced in the pyridinium chromophores becomes faint at very high TfOH concentration (above 30 equiv) or in the presence of MeOH, presumably because of a weaker induction in protic medium.

 © 2003 Wiley-VCH Verlag GmbH & Co. KGaA, Weinheim

Photomagnetic Nanocomposites

Transparent, Superparamagnetic $K_x^I Co_y^{II}[Fe^{III}(CN)_6]$–Silica Nanocomposites with Tunable Photomagnetism

*Joshua G. Moore, Eric J. Lochner, Chris Ramsey, Naresh S. Dalal, and A. E. Stiegman**

There has been considerable interest in molecular magnets based on the Prussian blue class of transition-metal cyanide complexes.[1] Pioneering work on these materials has realized a broad range of ferro- and ferrimagnetic solids with Curie points ranging from cryogenic to above room temperature.[2,3] A parallel interest also exists in the development of nanocomposite structures containing nanoscale magnetic particles exhibiting single-domain magnetic behavior.[4–6] Investigations of magnetic nanocomposites is driven by their novel properties and their potential as new magnetic, optical, and electronic materials. With one exception,[7] however, the Prussian blue class of magnetic materials has not been produced as nanoparticles, and, to the best of our knowledge, there have been no reports of their incorporation into composite structures. Herein we report the fabrication of a new nanocomposite material containing $K_xCo_y^{II}[Fe^{III}(CN)_6]_z$, a ferromagnetic analogue of Prussian blue, in a porous silica matrix. This material is made by a controlled multicomponent sol–gel synthesis in which the precipitation of the Prussian blue analogue is arrested at nanoscale dimensions by gelation of the silica network. The resulting materials are homogeneous, optically transparent, and exhibit superparamagnetic and tunable photomagnetic behavior. We believe that this study suggests a new approach for utilizing the Prussian blue class of magnetic materials in advanced optical and magnetic applications.

Homogeneous silica xerogels containing cyanide-bridged Co^{II}/Fe^{III} centers were made by incorporation of both transition-metal components during the solution phase of the synthesis. To obtain homogeneous materials reproducibly, conditions were optimized for the amount of water and the concentration and molar ratio of Co^{II} and ferricyanide by following previously developed procedures.[8,9] In the optimized preparation, Co^{II} nitrate was dissolved in methanol and added to tetramethylorthosilicate. Aqueous potassium ferricyanide was added to this solution to give a 1:1 Co:Fe molar ratio. Upon mixing, the solution turns dark purple, which suggests the formation of the mixed-valence complex. At concentrations up to 0.03 mol % total-metal to silicon (Fe + Co/Si), the solution remained transparent through gelation, aging, and drying, and ultimately yielded a homogeneous, optically transparent xerogel (Figure 1, inset). The spectrum of this glass (Figure 1) is qualitatively similar to that of the bulk materials, with a broad intervalence charge-transfer band in the visible region between 450 and 650 nm and a sharp, higher energy peak around 400 nm. However, the maximum of the intervalence band lies at 452 nm

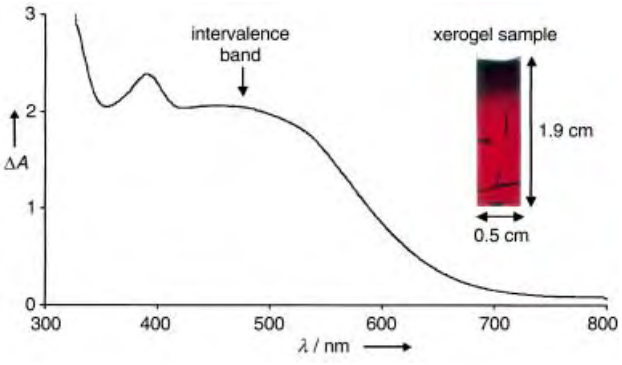


Figure 1. The optical absorption spectrum of a 0.03 mol % Co^{II}/Fe^{III} xerogel (inset) shows an intervalence charge-transfer band in the range 450–650 nm with a maximum at 452 nm.

(22 124 cm^{-1}) which is blue-shifted by approximately 2900 cm^{-1} from that of the bulk materials. To determine whether the magnetic behavior was singular, the magnetic susceptibility of these materials was measured as a function of temperature and field strength.[10] Bulk $M_x^I Co_y^{II}[Fe^{III}(CN)_6]_z$ (M^I = alkali-metal cation) shows ferromagnetic behavior in its field-cooled (FC) magnetization, with a Curie temperature of 14.0 K.[11,12] However, this complex, along with other first-row Prussian blue analogues, also shows blocking behavior in the zero-field-cooled (ZFC) magnetization, which has been attributed to spin-glass properties arising from defects in the lattice.[13,14] While it might be expected that a dilute dispersion of $K_xCo_y^{II}[Fe^{III}(CN)_6]_z$ in a xerogel would exhibit only simple paramagnetic behavior, the FC and ZFC magnetization as a function of temperature for a 0.03 mol % Co^{II}/Fe^{III} xerogel (Figure 2a) indicates more complex behavior. The FC magnetization parallels that of the bulk complex above 5 K but has a lower Curie temperature ($T_c \approx 13$ K). The ZFC magnetization curve shows a well-defined peak at 10 K. Above this temperature, the FC and ZFC magnetization curves converge and become coincident. This magnetization behavior is characteristic of blocking in a superparamagnetic system of small, single-domain particles or, as it is in the bulk, the glass transition in a spin glass.[15] Measurement of the magnetization as a function of field strength at 5 K, below the blocking temperature (Figure 2b), reveals hysteretic behavior that reaches a magnitude of 7.08×10^3 emu mol^{-1} at 5 kOe with a coercive field of approximately 0.41 kOe. From room temperature down to the blocking temperature (10 K) no hysteresis is observed (Figure 2c). These observations are also consistent with both spin-glass and superparamagnetism. However, the hysteresis loops measured under FC and ZFC conditions at 5 K are identical and symmetric about the center; this is one of the defining characteristics of super-

[*] Prof. A. E. Stiegman, J. G. Moore, C. Ramsey, Prof. N. S. Dalal
The Department of Chemistry and Biochemistry
Florida State University
Tallahassee, FL 32306 (USA)
Fax: (+1) 850-644-6605
E-mail: stiegman@chem.fsu.edu
E. J. Lochner
Materials Research and Technology Center (MARTECH)
Florida State University
Tallahassee, FL 32306 (USA)

 DOI: 10.1002/anie.200250409 © 2003 Wiley-VCH Verlag GmbH & Co. KGaA, Weinheim

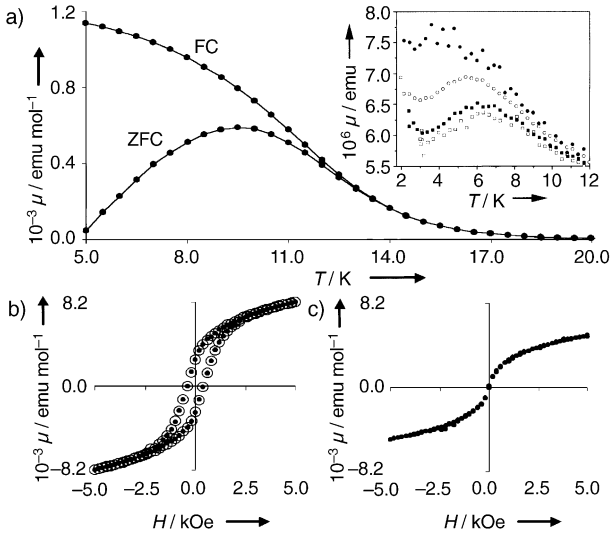


Figure 2. a) Field-cooled (FC) and zero-field-cooled (ZFC) dc magnetization versus temperature curves at $H = 100$ Oe [inset: frequency dependence of ac susceptibility: 100 (●), 1000 (○), 5000 (■), and 10000 Hz (□)]. b) FC (●) and ZFC (○) hysteresis loops at $T = 5$ K. c) Hysteresis loop at $T = 13$ K.

paramagnetism and suggests that this property, possibly superimposed by the inherent spin-glass properties of the bulk, is present in these materials.[15,16] This conclusion is also consistent with ac susceptibility data (Figure 2, inset), which show a significant frequency-dependent, thermally activated magnetization reversal dynamics with an activation energy of 29 ± 1 K ($160\,\mathrm{J\,mol^{-1}}$) and $\tau_0 = 3 \times 10^{-6}$ s. This frequency dependence is a unique property of these materials and is significantly different from that of the bulk, as frequency dependence has not been observed in this composition.

Support for a superparamagnetic origin of the magnetic properties and an explanation of the blue shift in the absorption spectrum is provided by the observation of $K^{I}_{x}Co^{II}_{y}[Fe^{III}(CN)_6]_z$ nanoparticles in the silica matrix. These particles can be observed directly by transmission electron microscopy, which reveals small domains, approximately 8–10 nm in size, distributed in the amorphous matrix (Figure 3). The strong diffraction of these domains verifies that they are crystalline, and quantitative analysis of the electron diffraction pattern (Figure 3, inset) yields d spacings identical to those of bulk $Co^{II}_{3}[Fe^{III}(CN)_6]_2$, and hence they can be unambiguously assigned to the mixed-valence compound. Since the synthesis of these materials is carried out by mixing solutions of the various components to form a homogeneous sol–gel solution, the formation of nanoparticles must occur spontaneously during some phase of the process. Given the large formation constants for Prussian blue analogues, the existence of nanoparticles in the matrix (as opposed to bulk phase-separated regions) strongly suggest that gelation of the silica effectively arrests the precipitation of $K^{I}_{x}Co^{II}_{y}[Fe^{III}(CN)_6]_z$ and sequesters the particles. We believe this to be the first time that nanoparticles of this type of materials have been generated in this way.

Among the most interesting properties of bulk $C^{I}_{x}Co^{II}_{y}[Fe^{III}(CN)_6]_z$ is its photomagnetism, which was first

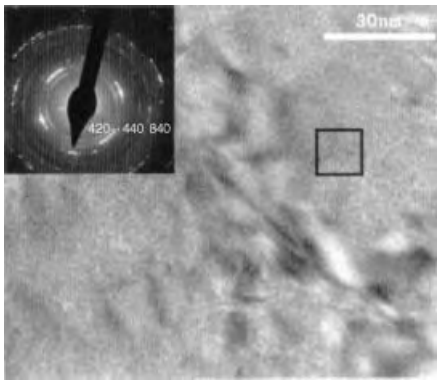


Figure 3. TEM image of a powdered Co^{II}/Fe^{III} xerogel showing nanoparticle crystalline structures with a size of 8–10 nm (inset: indexed diffraction pattern of the nanoparticles shown).

reported by Hashimoto.[12] Specifically, incidence of red light ($\lambda \approx 600$ nm) at temperatures below 150 K results in a net increase in the magnetization of the bulk material. This increase in magnetization can be erased by heating or irradiation with higher energy light ($\lambda \approx 450$ nm). As shown in Figure 4a, an analogous photomagnetic effect is observed in the nanocomposite system: irradiation of the glass ($\lambda \geq 550$ nm) results in an increase in magnetization, which, on returning to thermal equilibrium after the radiation source is extinguished, amounts to 7.6%. As with the bulk material, this magnetization could be decreased by irradiation with blue light ($\lambda = 448$ nm). Photomagnetic behavior in these materials arises from the presence of diamagnetic Co^{III}/Fe^{II} impurity sites in the $C^{I}_{x}Co^{II}_{y}[Fe^{III}(CN)_6]_z$ lattice. Absorption of light by these impurities at low temperature results in electron transfer to create a paramagnetic Co^{II}/Fe^{III} metastable state that increases the magnetization of the bulk.[12] Detailed studies of the system indicated that, on increasing the ligand-field strength around the Co^{II} centers, electron transfer from cobalt to iron occurs and generates more Co^{III}/Fe^{II} defect sites. These additional defect sites increase the magnitude of the photomagnetic effect.[17–19] In the bulk materials modification of the ligand field around cobalt is accomplished by the addition of alkali-metal cations, which change the stoichiometry of the complex and increase the degree of nitrogen coordination around the metal centers.[17,20] We found that, because of the porous nature of the silica matrix, direct substitution of the cobalt centers by ammine and other higher field ligands can be accomplished cleanly and in a highly controlled fashion. As shown in Figure 4b, passing ammonia over the composite results in continuous spectral changes that are highly isosbestic. The broad intervalence charge-transfer band is replaced by a single peak (470 nm) characteristic of hexammine Co^{III} centers, which suggests that diamagnetic defect sites have been created. Measurement of the magnetization of the composite as a function of ammine doping shows a steady decrease in magnetization, and the materials become diamagnetic at the highest levels of doping. Changes in the magnitude of the photomagnetic effect as a function of exposure to ammonia are shown in Figure 4c. With small exposure increments the magnetization increases until a maximum is reached at about 9.4% above that of the doped

 © 2003 Wiley-VCH Verlag GmbH & Co. KGaA, Weinheim

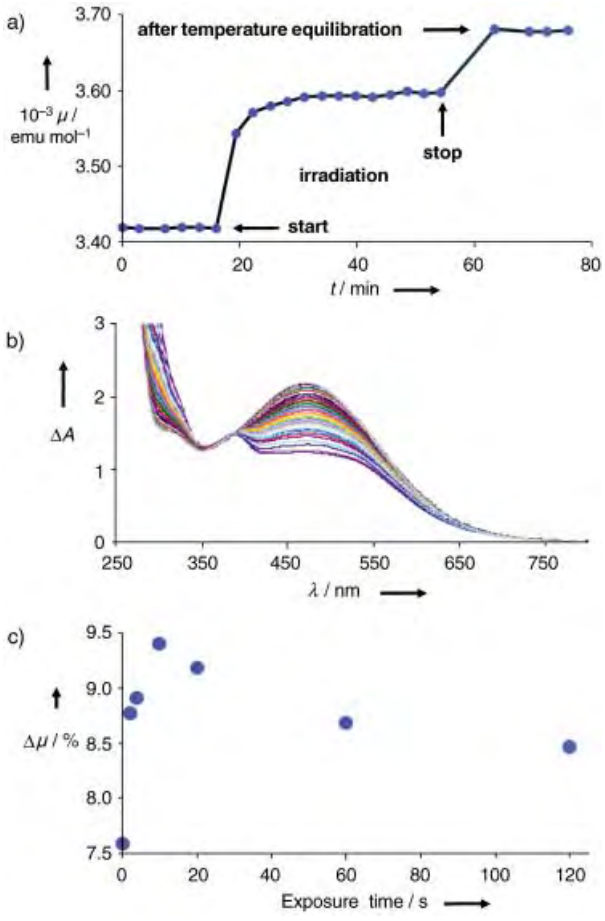


Figure 4. a) Photomagnetic effect at $\lambda \geq 550$ nm, $H = 500$ Oe, and $T = 5$ K. b) A series of optical absorption spectra taken every 30 min while anhydrous ammonia flowed over a 0.03 mol% Co^{II}/Fe^{III} xerogel. c) Percentage increase in magnetization of NH_3-substituted xerogels as a function of NH_3 exposure time (10 μL dose).

but nonirradiated composite. Above this threshold the photomagnetic effect decreases, and at high degrees of substitution the effect vanishes. This change is consistent with observations on the bulk material, which show that large numbers of the diamagnetic Co^{III}/Fe^{II} defect sites result in significantly diminished photomagnetism. In the bulk material this has been explained as arising from an increased rigidity in the lattice as the number of Co^{III}/Fe^{II} sites increases. This rigidity can no longer accommodate the bond-length increases that accompany the electron transfer of the Co^{II}/Fe^{III} sites to the metastable state.[17], Although such a rigidity effect may also be acting in the nanocrystals, high degrees of ammine substitution may ultimately result in disruption of the CN bridge with concomitant deactivation of the electron-transfer pathway, which would also degrade the effect.

Experimental Section

The 0.03% Co^{II}/Fe^{III} xerogel was made in the following manner: a solution of H_2O (4.6 mL), methanol (20.8 mL), and an aqueous solution of $K_3[Fe(CN)_6]$ (2.2 mM; 13.9 mL) was added dropwise to a solution containing tetramethylorthosilicate (30.3 mL), methanol (16.4 mL), and $Co(NO_3)_2$ (2.2 mM; 13.9 mL) in methanol, which gives an overall concentration of 0.31 mM for each metal. Then 4 mL of solution was placed into polystyrene cuvettes for gelation, aging, and drying phases. After gelation the xerogel has 12% of the original volume with a final concentration of each metal of approximately 3 mM.

Received: October 22, 2002 [Z50409]

Keywords: cobalt · iron · magnetic properties · nanostructures · sol–gel processes

[1] K. R. Dunbar, R. A. Heintz in *Progress in Inorganic Chemistry, Vol 45*, John Wiley & Sons, New York, **1997**, p. 283.
[2] S. Ferlay, T. Mallah, R. Ouahes, P. Veillet, M. Verdaguer, *Nature* **1995**, *378*, 701.
[3] W. R. Entley, G. S. Girolami, *Science* **1995**, *268*, 397.
[4] E. Cattaruzza, F. Gonella, G. Mattei, P. Mazzoldi, D. Gatteschi, C. Sangregorio, M. Falconieri, G. Salvetti, G. Battaglin, *Appl. Phys. Lett.* **1998**, *73*, 1176.
[5] I. S. Edelman, R. Ivantsov, A. Vasiliev, S. Stepanov, E. Kornilova, T. Zarubina, *Physica B* **2001**, *301*, 203.
[6] B. H. Sohn, R. E. Cohen, *Chem. Mat.* **1997**, *9*, 264.
[7] S. Vaucher, J. Fielden, M. Li, E. Dujardin, S. Mann, *Nano Lett.* **2002**, *2*, 225.
[8] M. D. Curran, T. E. Gedris, A. E. Stiegman, G. A. Plett, *Chem. Mat.* **1999**, *11*, 1120.
[9] M. D. Curran, D. D. Poore, A. E. Stiegman, *Chem. Mat.* **1998**, *10*, 3156.
[10] dc magnetic measurements were made with a superconducting quantum interference device (SQUID; Quantum Design MPMS XL-7). ac measurements were made on a Quantum Design PPMS.
[11] S. Juszczyk, C. Johansson, M. Hanson, A. Ratuszna, G. Malecki, *J. Phys. Condens. Matter* **1994**, *6*, 5697.
[12] O. Sato, T. Iyoda, A. Fujishima, K. Hashimoto, *Science* **1996**, *272*, 704.
[13] W. E. Buschmann, J. S. Miller, *Inorg. Chem.* **2000**, *39*, 2411.
[14] D. A. Pejakovic, J. L. Manson, J. S. Miller, A. J. Epstein, *Synth. Met.* **2001**, *122*, 529.
[15] J. K. Vassiliou, V. Mehrotra, M. W. Russell, E. P. Giannelis, R. D. McMichael, R. D. Shull, R. F. Ziolo, *J. Appl. Phys.* **1993**, *73*, 5109.
[16] J. L. Garcia, A. Lopez, F. J. Lazaro, C. Martinez, A. Corma, *J. Magn. Magn. Mater.* **1996**, *158*, 272.
[17] A. Bleuzen, C. Lomenech, V. Escax, F. Villain, F. Varret, C. C. D. Moulin, M. Verdaguer, *J. Am. Chem. Soc.* **2000**, *122*, 6648.
[18] C. C. D. Moulin, F. Villain, A. Bleuzen, M. A. Arrio, P. Sainctavit, C. Lomenech, V. Escax, F. Baudelet, E. Dartyge, J. J. Gallet, M. Verdaguer, *J. Am. Chem. Soc.* **2000**, *122*, 6653.
[19] V. Escax, A. Bleuzen, C. C. D. Moulin, F. Villain, A. Goujon, F. Varret, M. Verdaguer, *J. Am. Chem. Soc.* **2001**, *123*, 12536.
[20] The magnetic properties of this and other Prussian blue analogues are dependent on the exact composition of the complex, including the amount of alkali-metal present in the lattice. In the case of the nanocomposite materials reported here, the total amount of metals is so low that an accurate determination of the amount of K^+ ions present in the lattice of the nanoparticles (as opposed to the gross quantity present in the material as a whole) proved impossible by conventional techniques. Bulk $K^I_xCo^{II}_y[Fe^{III}(CN)_6]_z$ made under the same conditions of stoichiometry and concentrations was found, from X-ray fluorescence and FTIR measurements, to have the formula $K_{0.27}Co^{II}_{1.33}[Fe^{III}(CN)_6]$, which is close to that of the materials studied by Sato et al.[12], but we cannot assert that this composition is retained in the nanoparticles.

 © 2003 Wiley-VCH Verlag GmbH & Co. KGaA, Weinheim

Stereoselective Oxygenation

An Active-Site Model of Prostaglandin H Synthase: An Iron "Twin-Coronet" Porphyrin with an Aryloxyl Radical Overhang and Its Catalytic Oxygenation of 1,4-Diene**

Eiki Matsui, Yoshinori Naruta, Fumito Tani, and Yuichi Shimazaki*

The tyrosyl radical acts as a mediator for electron-/proton-transfer reactions coupled to metal redox centers in various metalloenzymes in spite of its instability under aerobic conditions.[1] Among several metalloenzymes utilizing the tyrosyl radical, prostaglandin H synthases (PGHSs), which catalyze the addition of two equivalents of dioxygen to arachidonic acid (AA) in the formation of prostaglandin H_2 (PGH_2), contain a tyrosyl residue (Tyr385 for PGHS-1) located 10 Å from the heme unit in the peroxidase active site.[2] The essential steps of the reaction are 1) generation of the tyrosyl radical (Tyr-O•) by a rapid intramolecular electron transfer from tyrosine to an oxoiron(IV) porphyrin π cation radical and 2) regio- and stereoselective H• radical abstraction of the 13-*pro-S* hydrogen from AA and trapping of the resultant radical with O_2.[3] The intrinsic instability of aryloxyl radicals becomes an obstacle in aryloxyl-radical-mediated organic synthesis[4] in spite of its potential utility. Herein we report the formation of an aryloxyl radical close to the metal center of a binaphthol-bridged iron "twin-coronet" porphyrin (TCP), which is investigated as a PGHS model, and its catalytic and stereoselective hydroxylation of 1,4-diene under aerobic conditions. Ferric TCP **1**,[5] which has D_2 symmetry, has four naphthol groups, tightly bound between *meso*-phenyl groups, which form rigid, hydrophobic, chiral cavities on both faces of the porphyrin ring (Figure 1). In this complex, hydroxy groups are situated in the cavity and do not directly coordinate to the Fe ion.

The oxidation of the model complex **1** with *m*-chloroperbenzoic acid (*m*CPBA) results in the formation of a new species **1′** distinguishable in the UV/Vis spectrum (Figure 2) with a concomitant color change from brown to red-brown, which is distinct from the typical *m*CPBA-oxidized species, $[Fe^{IV}(=O)\mathbf{P}]^{+\bullet}$, of an iron porphyrin (**P** = porphyrin).[6] The

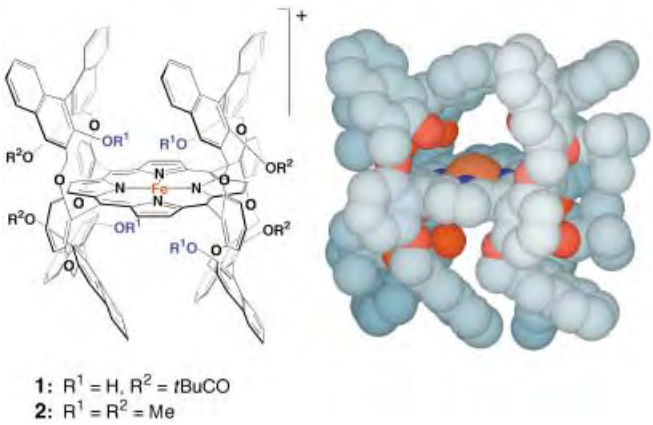


Figure 1. Left: Iron "twin-coronet" porphyrin **1,** as a PGHS model, and a methyl derivative (**2**). Right: Computer-generated model of **1**. Hydrogen atoms are omitted for clarity.

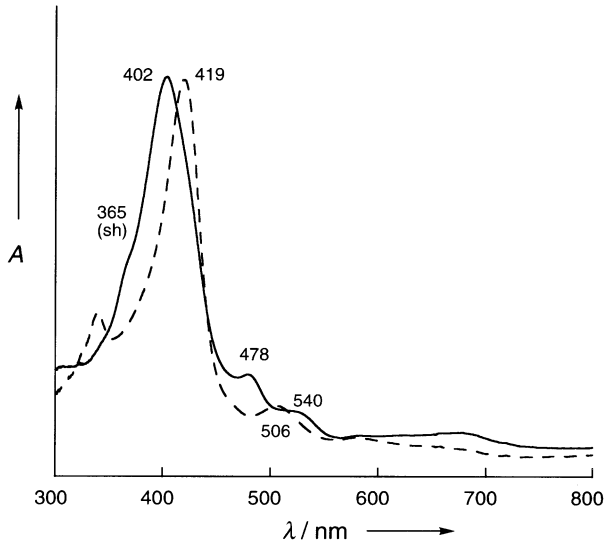


Figure 2. UV/Vis spectra of **1** (– – –, 1.66×10^{-5} M) and the oxidized species **1′**(——) with *m*CPBA (2.5 equiv) in CH_2Cl_2 at −40 °C.

oxidized species **1′** exhibits absorption bands at 365 and 478 nm as well as at 402 (Soret) and 540 nm (Q), which are characteristic of an iron(IV) porphyrin.[7] The bands at 365 and 478 nm are assigned to the corresponding naphthoxyl radical (Np-O•) based on comparison of the spectroscopic evidence with the reported spectra of 2-nahthoxyl radical:[8] the ESR spectrum of **1′** (Figure 3) is dominated by a signal at $g = 2.0046$ no signals arising from Fe^{III} centers are detected after complete conversion. In a frozen solution, **1′** gives a single ESR signal without any splitting, though its solution spectra show hyperfine couplings assigned to the naphthoxyl radical.[9] No signals arising from to Fe^{IV} centers could be detected, because this species is ESR silent. Quantifying the radical by double integration with 2,2,6,6-tetramethyl-1-piperidinyloxy (TMPO) as an external standard showed that **1** was converted into the corresponding Np-O• in 74% yield, which indicates efficient formation of **1′** within experimental error.

[*] Prof. Dr. Y. Naruta, Dr. E. Matsui, Dr. F. Tani, Dr. Y. Shimazaki
Institute for Fundamental Research of Organic Chemistry
Kyushu University
Higashi-ku, Fukuoka 812-8581 (Japan)
Fax: (+81) 92-642-2715
E-mail: naruta@ms.ifoc.kyushu-u.ac.jp

[**] This work was supported by Grants-in-Aids for COE Research (No. 08CE2005), for Scientific Research on Priority Areas (No. 11228207) from MEXT, and for Scientific Research (A) (No. 14204073) and Exploratory Research (No. 14654115) from JSPS. The P & P project "Green Chemistry", Kyushu University, partly supported this research.

Supporting information for this article (spectral data on compounds **1** and **1′**) is available on the WWW under http://www.angewandte.org or from the author.

 © 2003 Wiley-VCH Verlag GmbH & Co. KGaA, Weinheim DOI: 10.1002/anie.200250431

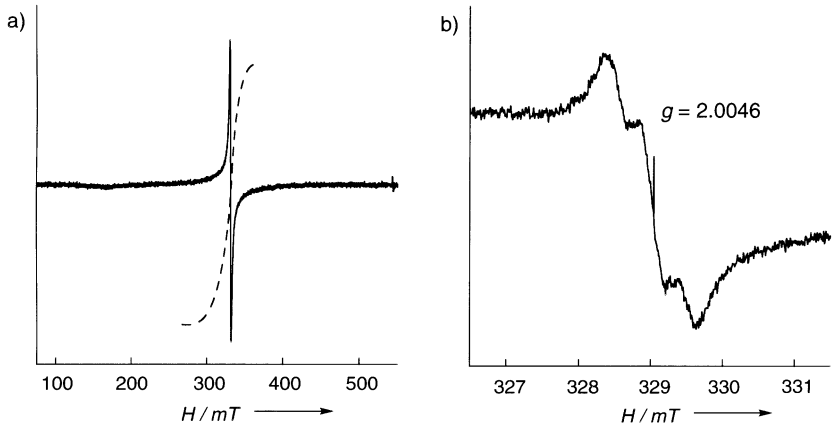


Figure 3. a) ESR spectrum of the oxidized species **1′** (——, 1.66×10^{-3} M) in CH_2Cl_2 at 77 K, and double integration of its signal (– – –). b) Its solution state ESR spectrum CH_2Cl_2 at 183 K. Magnification of $g=2$ region.

In resonance Raman spectroscopy of **1′**, selective excitation ($\lambda_{ex}=476.5$ nm) of the absorption band corresponding to the Np-O$^{\bullet}$ moiety indicates two scattered bands, 1579 and 1525 cm^{-1}, in the same region as the corresponding phenoxyl radicals (Figure 4).[10] Upon Soret-band excitation ($\lambda_{ex}=$ 406.7 nm), two porphyrin marker bands are observed at 1368 ($\tilde{\nu}_4$) and 1569 cm^{-1} ($\tilde{\nu}_2$). The latter is at higher wavenumber by 13 cm^{-1} than the corresponding band of the ferric species **1** (1556 cm^{-1}). These frequencies are very similar to those of the nonradical Fe^{IV} porphyrin species (1369 and 1565 cm^{-1}).[11] All the spectroscopic data support **1′** being an Fe^{IV} species, possibly Fe^{IV}=O, with a single naphthoxyl radical moiety. No scattered bands that could be assigned to $\tilde{\nu}$(Fe=O) are observed presumably because of this units instability and photolability, even at low laser power in a spinning cell (and in the presence of various axial bases).

Consequently, it is concluded that **1′** [Fe^{IV}(X)/Np-O$^{\bullet}$] (X = =O or axial ligands) is formed upon heterolysis of the perbenzoate adduct of the ferric porphyrin **1**, either through the compound I ([Fe^{IV}(=O)**P**]$^{+\bullet}$) and subsequent intramolecular electron transfer or through a concerted and direct pathway. The cyclic voltammogram of **1** in CH_2Cl_2 (0.1 M Bu_4NClO_4 as a supporting electrolyte) has an irreversible wave at $E_{pa}=+0.61$ V (vs. Ag/AgCl) and a quasi-reversible wave at $E_{1/2}=+0.77$ V. The former wave is assigned to the redox couple Np-OH/Np-O$^{\bullet}$[12] and the latter to Fe^{III}/Fe^{IV}.[13] Thus, the Fe^{IV}**P** has sufficient potential to oxidize the naphthol moiety.

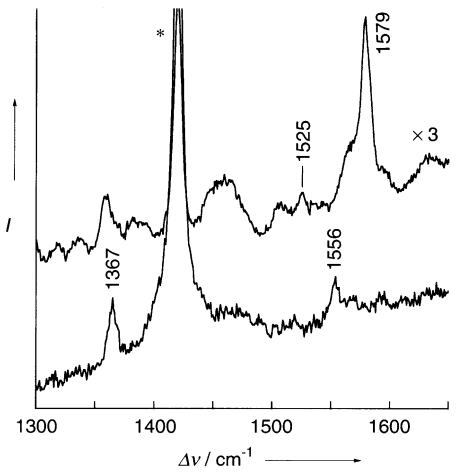


Figure 4. High-frequency region of resonance Raman spectra of **1** (lower line, 1.66×10^{-4} M) and the oxidized species **1′** (upper line). $\lambda_{ex}=476.5$ nm; *= solvent peak.

The titration of **1′** with *N*,*N*-dimethylaniline (DMA) as an efficient reducing agent[14] at −30 °C under N_2 indicates complete recovery of **1** upon addition of one molar equivalent of the substrate. There are clear isosbestic points in the UV/Vis spectra and a simultaneous decrease of the absorption bands corresponding to the Np-O$^{\bullet}$ and Fe^{IV} units (see Supporting Information). Evidence for this reduction process is also confirmed in the ESR spectra by the appearance of the signals assigned to Fe^{III} centers and the simultaneous decrease in the signals of the Np-O$^{\bullet}$ species upon addition of DMA. When 4-*cis*-7-*cis*-undeca-4,7-diene (**3**) is added instead of DMA under anaerobic conditions and the reaction is monitored by UV/Vis spectroscopy, the solution of **1′** also undergoes regeneration of **1**. Since, of the two redox active residues in **1′**, only the Np-O$^{\bullet}$ unit is considered to be reactive to the diene, these results suggest that both the Np-O$^{\bullet}$ and the Fe^{IV} units are involved in this reaction and intramolecular electron transfer from Np-OH to Fe^{IV}[15] occurs as the second step as a result of the higher oxidation potential of the $Fe^{III/IV}$ couple compared to the Np-OH/Np-O$^{\bullet}$ couple. Consequently, one **1′** molecule contains two oxidation equivalents which could react with two mole of the diene.

The radical intermediate **1′** was applied to the oxygenation of the 1,4-diene. This process is the fundamental reaction of PGH synthases. In the single-turnover reaction, addition of an excess amount of the diene **3** to the solution of **1′** generated by the *m*CPBA oxidation of **1** at −35 °C under O_2 atmosphere (1 atm) results in the formation of the corresponding dienyl hydroperoxide, which is stable at this temperature. After purging with N_2 and elevation to ambient temperature[16] (or treatment with Ph_3P), 5-*trans*-7-*cis*-undeca-5,7-diene-4-ol (**4**) was obtained in 156% yield, based on the amount of the iron TCP **1**, in good regio- and stereoselectivities (5*E*,7*Z*:5*E*,7*E* ≈ 5:1) as confirmed by GC-MS/^{1}H NMR spectroscopic analyses and by comparison with authentic samples. Further, this oxygenation is a catalytic reaction: **1**, diene (**3**, 30 molar equivalents relative to **1**), and *m*CPBA (12.5 molar equivalents relative to **1**) at −35 °C under O_2 give the dienyl alcohol **4** in 132% yield, based on the amount of *m*CPBA (catalyst turnover number (TON) = 16.5).

To rule out the possibility of oxidation side reaction(s) involving species other than **1′**, the reaction of the diene with several oxoiron species was investigated. When the [Fe^{IV}(=O)**P**]$^{+\bullet}$, formed by reaction of octamethyl TCP **2** with *m*CPBA, reacted with the diene **3**, only a trace amount

 © 2003 Wiley-VCH Verlag GmbH & Co. KGaA, Weinheim

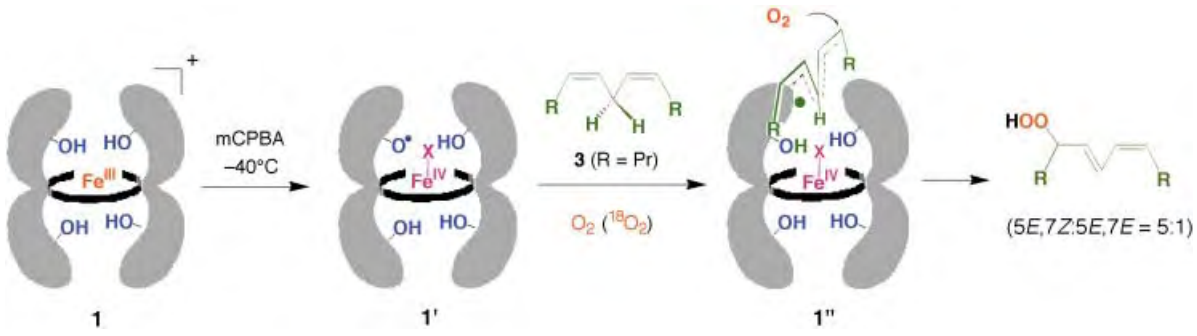


Figure 5. Formation of oxidized species **1**′ and regio- and stereoselective oxygenation of (4*Z*,7*Z*)-undeca-4,7-diene (**3**).

(< 5 %) of the corresponding monoepoxide was observed at −35 °C.[17] A separately prepared ferryl complex [Fe^{IV}(=O)**P**] (containing a different porphyrin ligand) does not show any reactivity toward the diene.[18] Thus, the observed dienyl alcohol **4** is formed only in the reaction with **1**′. Other potential oxidants can be excluded from the present oxygenation reaction. This oxygenation reaction with **1**′ could proceed through regioselective H· abstraction at 6-CH_2 of the diene by the naphthoxyl radical followed by stereoselective O_2 addition to produce the corresponding 5-*trans*-7-*cis*-4-hydroperoxyundeca-5,7-diene (Figure 5).[19] Since the hydroperoxide reacts very slowly with **1** below −30 °C, a stoichiometric amount of *m*CPBA is required for this catalytic oxygenation. It is worth noting that the observation of high stereoselectivity suggests that the resultant dienyl radical, generated after the hydrogen-atom abstraction step, is quickly trapped with O_2 in the cavity before it can escape to the solvent medium. The free stereoisomerization of the resultant pentadienyl radical could be restricted in the cavity formed by rigid naphthalene groups.

This oxygenation reaction is tightly coupled with the formation of dienyl radicals, because by-products, such as epoxides, ketones, are not detected in the reaction mixture. The alcohol product is not obtained in the absence of either of the components. A labeling experiment with $^{18}O_2$ (^{18}O, 95 %), indicates quantitative incorporation of labeled oxygen in the alcohol. Both [$^{18}O_2$]*m*CPBA and $H_2{}^{18}O$, which can act as alternative oxygen sources, do not give the labeled alcohol. Moreover, after the reaction, the catalyst **1** is recovered without decomposition.

In conclusion, FeTCP is considered to be a good active-site model for PGHSs. Selective hydroperoxidation of a 1,4-diene by this catalyst is also considered to be an artificial lipoxygenase reaction,[20] which usually results in a complex mixture of products.[21] This is the first example of a model system utilizing the unstable Ar-O· radical as a mediator in catalytic oxygenation reactions and provides important insights into the catalytic oxygenation mechanism of PGHSs.

Experimental Section

Complexes **1**,[5] **2**,[22] and (4*Z*,7*Z*)-undeca-4,7-diene,[23] were prepared as previously reported.

*m*CPBA oxidation of **1**: To a CH_2Cl_2 solution of **1** (1.66×10^{-5} M), *m*CPBA (2.5 molar equiv) was added at −40 °C in a 1 cm^3 cuvette (light-path length 2 mm) under N_2 atmosphere. The time-course of the UV/Vis spectral change was observed at 30 s intervals. ESR spectra were obtained at 77 and 183 K on a JES TE-300 spectrometer (JEOL) operating at 9.36 GHz equipped with a RMC CRYO SYSTEMS CT-470-ESR; microwave frequency: 100 kHz, modulation amplitude: 10 G, and microwave power: 1 mW. Resonance Raman spectra were obtained on a SpectraPro-300i spectrometer (Acton Research Co.) with a 2400-groove grating, a Beamlok 2060 Kr^+ laser and a Stabilite 2017 Ar^+ laser (Spectra Physics), a holographic supernoch filter (Kaiser Optical), and LN-1100PB CCD detector (Princeton Instruments) cooled with liquid N_2. Spectra were collected in spinning cells (2-cm diameter, 1500 rpm) at −80 °C at excitation wavelengths $\lambda_{ex} = 406.7$ or 476.5 nm (10 mW).

Catalytic oxygenation of (4*Z*,7*Z*)-undeca-4,7-diene (**3**): *m*CPBA (0.25 mL, 8.27×10^{-2} M in CH_2Cl_2) was slowly added to a stirred CH_2Cl_2 solution (10 mL) containing **1** (8.29×10^{-7} mole) and **3** (2.5×10^{-5} mole) at −35 °C under O_2 (or $^{18}O_2$) atmosphere (1 atm). After the reaction mixture was stirred for 30 min, portions of the *m*CPBA solution were added at 30-min intervals (0.25 mL × 4), after which the solution was stirred for a further 30 min, followed by substitution of the dissolved O_2 with N_2. The reaction mixture was allowed to stand to ambient temperature and was directly analyzed by a GC-MS (model JMS SUN200; JEOL), with tridecane as an internal standard. The resultant alcohols were isolated by flash column chromatography and their spectra were compared with authentic samples.

Received: October 25, 2002
Revised: February 14, 2003 [Z50431]

Keywords: enzyme models · iron · porphyrinoids · radical ions · redox chemistry

[1] Recent reviews: R. P. Pesavento, W. A. van der Donk, *Adv. Protein Chem.* **2001**, *58*, 317–385; J. Stubbe, W. A. van der Donk, *Chem. Rev.* **1998**, *98*, 705–762.
[2] Recent reviews: L. J. Marnett, S. W. Rowlinson, D. C. Goodwin, A. S. Kalgutkar, C. A. Lanzo, *J. Biol. Chem.* **1999**, *274*, 22903–22906; W. L. Smith, D. L. DeWitt, R. M. Garavito, *Annu. Rev. Biochem.* **2000**, *69*, 145–182.
[3] R. Dietz, W. Nastainczyk, H. H. Ruf, *Eur. J. Biochem.* **1988**, *171*, 321–328; S. Peng, N. M. Okeley, A.-L. Tsai, G. Wu, R. J. Kiulmacz, W. A. van der Donk, *J. Am. Chem. Soc.* **2002**, *124*, 10785–10796.
[4] A catechol/semiquinone couple was utilized in galactose oxidase models: P. Chaudhuri, M. Hess, J. Müller, K. Hildenbrand, E. Bill, T. Weyhermüller, K. Wieghardt, *J. Am. Chem. Soc.* **1999**, *121*, 9599–9610, and references therein.
[5] M. Matsu-ura, F. Tani, S. Nakayama, N. Nakamura, Y. Naruta, *Angew. Chem.* **2000**, *112*, 2083–2086; *Angew. Chem. Int. Ed.*

 © 2003 Wiley-VCH Verlag GmbH & Co. KGaA, Weinheim

2000, *39*, 1989 – 1991; F. Tani, M. Matsu-ura, S. Nakayama, M. Ichimura, N. Nakamura, Y. Naruta, *J. Am. Chem. Soc.* **2001**, *123*, 1133 – 1142; M. Matsu-ura, F. Tani, Y. Naruta, *J. Am. Chem. Soc.* **2002**, *124*, 1941 – 1950.

[6] As a control experiment, *m*CPBA oxidation of the octamethyl derivative **2** under the same conditions gave the corresponding green-colored oxoiron(IV) π cation radical (**2′**) UV/Vis:, $\lambda_{max} =$ 419 (Soret) and 550–750 nm (porphyrin π cation radical). Its ESR traces at 4 K indicate rhombic signals at $g_{eff} = 3.69$ and 2.00. These values are similar to those previously reported: H. Fujii, T. Yoshimura, H. Kamada, *Inorg. Chem.* **1996**, *35*, 2373 – 2377.

[7] J. T. Groves, Z. Gross, M. K. Stern, *Inorg. Chem.* **1994**, *33*, 5065 – 5072.

[8] 2-Nahthoxyl radical ($\lambda_{max} = 355$ and 480 nm); T. Nath, P. Neta, *J. Phys. Chem. A* **1998**, *102*, 7081 – 7085.

[9] The simulation of the signal assumes three major hyperfine couplings for $H^{6'}$, $H^{8'}$, and one of CH_2 protons at the C-2′ position. The detailed analysis will be reported elsewhere.

[10] R. Schnepf, A. Sokolowski, J. Müller, V. Bachler, K. Wieghardt, P. Hildebrandt, *J. Am. Chem. Soc.* **1998**, *120*, 2353 – 2364.

[11] K. Jayaraj, J. Terner, A. Gold, D. A. Roberts, R. N. Austin, D. Mandon, R. Weiss, E. Bill, M. Müther, A. X. Trautwein, *Inorg. Chem.* **1996**, *35*, 1632 – 1640.

[12] In consideration of the pH dependence of the redox potential of Ar-O(H)/Ar-O•, the redox potential ($E = +0.4$–0.5 V vs. Ag/AgCl in CH_2Cl_2) of 2-naphthol (at pH 7) is estimated from the corresponding value ($E = +0.69$ V vs. the normal hydrogen electrode (NHE) in H_2O) of 2-naphtholate (at pH 13). See, ref. [8] and C. Li, M. Z. Hoffman, *J. Phys. Chem. B* **1999**, *103*, 6653 – 6656.

[13] C. Swistak, X. H. Mu, K. M. Kadish, *Inorg. Chem.* **1987**, *26*, 4360 – 4366.

[14] S. B. Karki, J. P. Dinnocenzo, J. P. Jones, K. R. Korzekwa, *J. Am. Chem. Soc.* **1995**, *117*, 3657 – 3664.

[15] N. Colclough, J. R. L. Smith, *J. Chem. Soc. Perkin Trans. 2* **1994**, 1139 – 1149.

[16] Upon being left to stand at room temperature, the hydroperoxide converts into the corresponding alcohol with a constant stereoisomeric ratio and without formation of any by-products by the ferric porphyrin catalyst **1**. This highly selective transformation of hydroperoxide/alcohol was confirmed by the separate reaction of the isolated hydroperoxide with **1**. The detailed mechanism will be discussed elsewhere.

[17] The reaction of the diene **3** with oxoiron(IV) porphyrin π cation radical **2′** at −35 °C also gave a trace amount (< 5 %) of the corresponding monoepoxide without any of the accompanying dienyl alcohols.

[18] *meso*-Tetramesitylporphinatoiron(II) was converted into the corresponding [Fe^{IV}(=O)**P**] species by the treatment with O_2 in toluene according to the reported method; A. L. Balch, *J. Am. Chem. Soc.* **1984**, *106*, 7779 – 7785. Addition of the diene **3** to this ferryl porphyrin solution at −35 °C resulted in the complete recovery of the diene. It is generally accepted that a ferryl complex does not catalyze H-abstraction or oxygen-atom transfer.

[19] Ordinary autoxidation of the diene in air gives the same hydroperoxide without any stereoselectivity (5-*trans*-7-*cis*:5-*trans*-7-*trans* = 1:1).

[20] H. Kuhn, B. J. Thiele, *FEBS Lett.* **1999**, *449*, 7 – 11; S. Yamamoto, *Biochim. Biophys. Acta* **1992**, *1128*, 117 – 131.

[21] R. Nagata, S. Morimoto, I. Saito, *Tetrahedron Lett.* **1990**, *31*, 4485 – 4488.

[22] Y. Naruta, F. Tani, N. Ishihara, K. Maruyama, *J. Am. Chem. Soc.* **1991**, *113*, 6865 – 6872.

[23] H. A. J. Carless, R. J. Batten, *J. Chem. Soc. Perkin. Trans. 1* **1987**, 1999 – 2007.

 © 2003 Wiley-VCH Verlag GmbH & Co. KGaA, Weinheim

Fullerenes in Calixarenes

Configurations of a Calix[8]arene and a C_{60}/Calix[8]arene Complex on a Au(111) Surface**

Ge-Bo Pan, Jun-Min Liu, Hui-Min Zhang, Li-Jun Wan, Qi-Yu Zheng, and Chun-Li Bai**

Calixarenes and fullerenes have novel properties that make them ideal materials for nanoscale electronic devices.[1–4] If fullerenes can be placed within a calixarene to form an ordered array, it could be possible to operate them and fabricate nanoscale circuits. As an essential prerequisite, the configurations of calixarenes and fullerenes included within calixarene units at a solid surface must be understood to construct the nanoscalar architecture. Calixarenes have a highly flexible molecular conformation, which is important in various chemical reactions and host–guest chemistry.[5,6] To understand the variety of molecular conformations that exist, resolution at the atomic or submolecular level is important, and is a challenging research activity in calixarene studies.

Herein, we report the results of the construction and investigation of a calix[8]arene derivative, OBOCMC8 ($C_{104}H_{128}O_{24}$),[7] and the inclusion of C_{60} in OBOCMC8 (C_{60}/OBOCMC8). Scheme 1a illustrates the chemical insertion of the buckyball into the calix structure,[8,9] and the structures of the calixarene and the inclusion complex are shown in Scheme 1b and c, respectively. Well-ordered arrays of OBOCMC8 and C_{60}/OBOCMC8 can be constructed on a Au(111) surface, and are clearly observed by scanning tunneling microscopy (STM). The results directly demonstrate a stable conformation of OBOCMC8 and the possibility of C_{60} inclusion.

The electrochemical behavior of the Au(111) surface in a solution containing OBOCMC8 and C_{60}/OBOCMC8 was investigated by cyclic voltammetry. Cyclic voltammograms (CVs) were recorded in 0.1M $HClO_4$ using the so-called hanging meniscus method. After recording the standard CV of a bare Au(111) surface, a small amount of OBOCMC8 solution was added into the electrochemical cell. As a result, the oxidation peak, which is found at +1.3 V for Au(111)

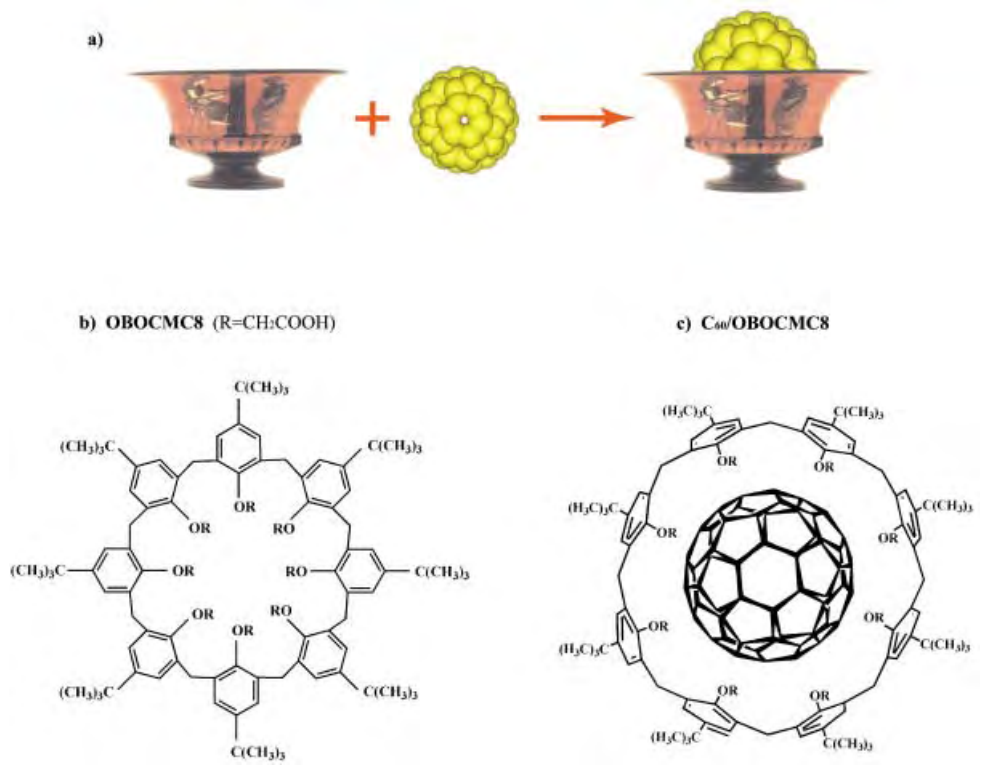
[*] Prof. Dr. L.-J. Wan, Prof. Dr. C.-L. Bai, G.-B. Pan,[+] J.-M. Liu,[+] Dr. H.-M. Zhang, Dr. Q.-Y. Zheng
Institute of Chemistry
Chinese Academy of Sciences
Beijing 100080 (China)
Fax: (+86) 10-6255-8934
E-mail: wanlijun@iccas.ac.cn
clbai@iccas.ac.cn

[+] Also at the Graduate School of Chinese Academy of Sciences Beijing (China)

[**] This work was supported by the National Natural Science Foundation of China (Nos. 20025308, 20177025, and 20121301), the National Key Project on Basic Research (Grants G2000077501 and 2000078100) and the Chinese Academy of Sciences.

Supporting information for this article is available on the WWW under http://www.angewandte.org or from the author.

 DOI: 10.1002/anie.200350432 © 2003 Wiley-VCH Verlag GmbH & Co. KGaA, Weinheim



Scheme 1. a) Schematic representation of the formation of the C_{60}/OBOCMC8 complex; b,c) molecular structures of OBOCMC8 and C_{60}/OBOCMC8, respectively.

(against a reversible hydrogen electrode (RHE)), is shifted to a more positive value. It is suggested that OBOCMC8 is adsorbed onto the Au(111) surface, which suppresses surface oxidation. No additional peaks are observed in the double-layer region, which suggests that no phase transition occurs. A similar result is obtained in the solution containing C_{60}/OBOCMC8. The CVs of Au(111) in different solutions are shown in the Supporting Information.

After achieving the atomic resolution of the Au(111) substrate, a small amount of saturated OBOCMC8 solution (in 0.1M $HClO_4$) was added in an STM cell; the electrode potential of Au(111) was held at 0.6 V. Figure 1a shows a typical large-scale STM image (20 nm × 20 nm) acquired for an OBOCMC8 adlayer with a bias voltage of −100–−250 mV and a set-point current of 500–1000 pA. A highly ordered OBOCMC8 array extends over the flat terrace of the Au(111) surface. The important features in the image are the well-ordered dark depressions. The structural details are revealed by a higher resolution STM image (Figure 1b), which shows that the array consists of regular "calices". Each "calix", with an associated dark depression, can be clearly observed in the image. The chemical structure of OBOCMC8 suggests that it may be adsorbed on Au(111) through either the *tert*-butyl, carboxyl, or the phenyl groups. The carboxyl–gold interaction might be stronger than those of the phenyl and *tert*-butyl groups, as has been described elsewhere.[10,11] The distance between the centers of the dark depressions is 1.2 ± 0.1 nm along the **A** direction (equivalent to the ⟨121⟩ direction; Figure 1b), and 1.7 ± 0.1 nm along the **B** direction. The molecular rows in the **A** and **B** directions cross each other at an angle of 95 ± 2°. These distances compare favorably to the size of the OBOCMC8 molecule and, therefore, each calix appearing in the STM image can be assigned as an individual OBOCMC8 molecule. The surrounding protrusion and dark depression can be attributed to the phenyl units and the molecular cavity, respectively. This feature can be more clearly seen in the height-shaded surface plot shown in Figure 1c. Based on the above analysis, a schematic model can be constructed for the ordered array of OBOCMC8 (Figure 1d). A rhombic unit cell is outlined in the model. The molecules are arranged in an upright orientation and form a depression in the center, which has a calix-like shape. The schematic model is consistent with the observed molecular array.

After recording the STM image at 0.6 V, the electrode potential was scanned in increments of 10 mV in both negative and positive directions. Almost identical images of the OBOCMC8 array as those shown in Figure 1 are observed in the potential region of 0 to 1.0 V, which indicates that no structural transformation occurs in this range; the molecular array with ordered calices is always seen. The molecules retain the same configuration and structural symmetry, which suggests that the molecule–substrate and intermolecular interactions play important roles in immobilizing molecular conformations.

The experimental procedure described above was also applied to investigate the array of C_{60}/OBOCMC8 on Au(111) in 0.1M $HClO_4$. After the atomic image of the Au(111) surface was obtained, a small amount of saturated C_{60}/OBOCMC8 solution was injected directly into the STM

 © 2003 Wiley-VCH Verlag GmbH & Co. KGaA, Weinheim

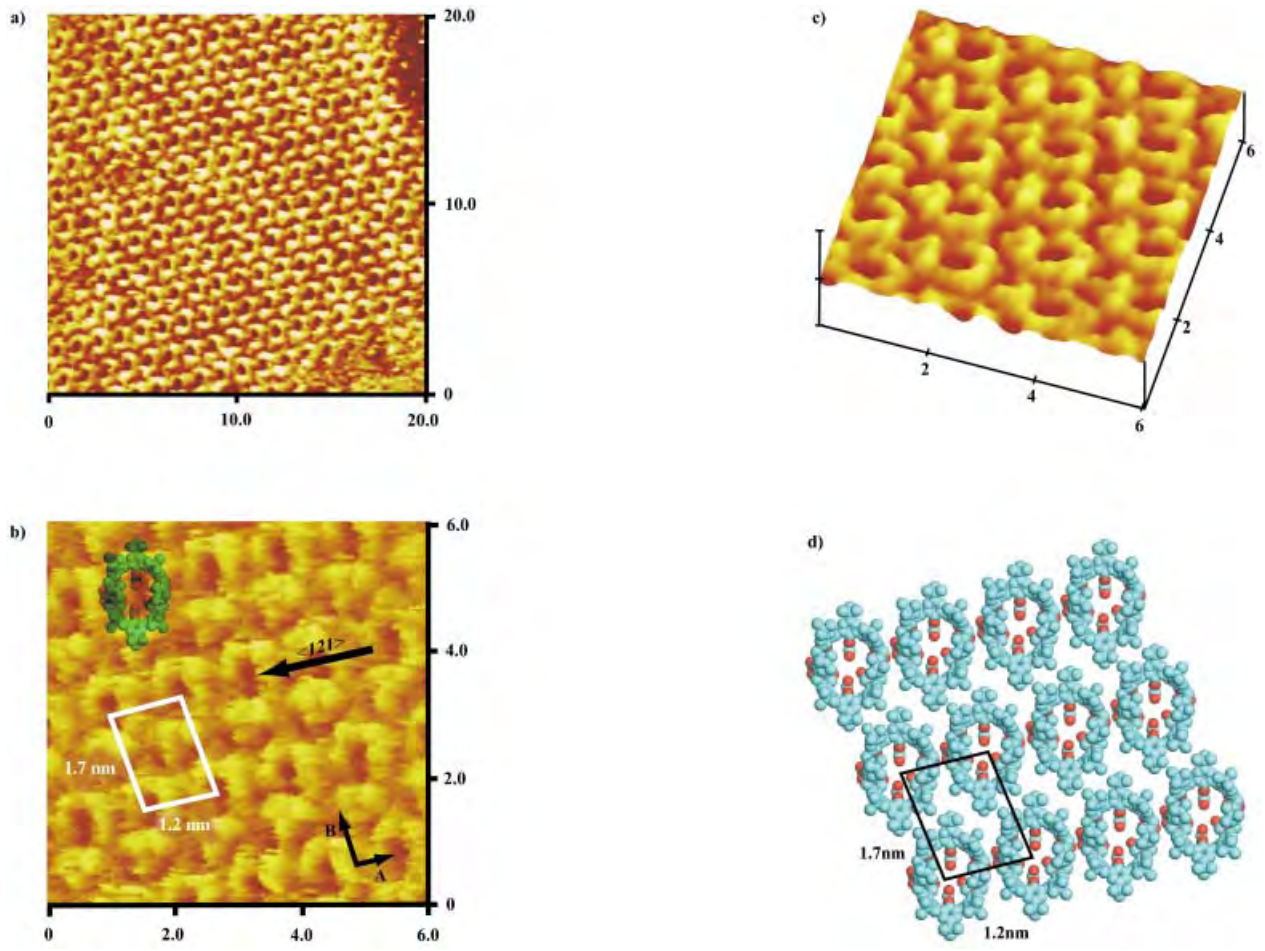


Figure 1. A typical large-scale STM image (a) of an OBOCMC8 array on a Au(111) surface, and a top view (b) and height-shaded surface plot (c) of the same OBOCMC8 array, recorded using high-resolution STM; d) a proposed structural model for the ordered array of OBOCMC8. The bias voltage and tunneling current were −213 mV and 670 pA, respectively. The scales are given in nm.

cell; again, the electrode potential of the Au(111) substrate was held at 0.6 V. After approximately 30 min, a completely different pattern is observed. Figure 2a shows an STM image, taken with a bias voltage of −100–−200 mV and a set-point current of 500–1300 pA. It is evident that the flat Au(111) surface is now covered by a highly-ordered C_{60}/OBOCMC8 array, which is free of molecular defects over the whole 25 nm × 25 nm area observed. This array extends over wide, flat terraces of more than 50 nm × 50 nm in area. An interesting feature of the C_{60}/OBOCMC8 array is the well-ordered bright spots, which can be clearly seen in the image. The feature is different from the dark depressions appearing in pure OBOCMC8 array (Figure 1), which suggests the existence of C_{60} associated with the OBOCMC8 molecule.

A higher resolution STM image (Figure 2b) shows that the molecular rows of the array are parallel to the ⟨121⟩ direction of the underlying Au(111) substrate, and cross each other at an angle of either 60° or 120°, within an experimental error of ±2°, to form a two-dimensional hexagonal lattice with associated bright spots. The structural symmetry of the C_{60}/OBOCMC8 array is significantly different from that of OBOCMC8. From careful observation, it can be seen that each individual bright spot (as indicated by the arrow; Figure 2b) is surrounded by a circular protrusion. The nearest distance between the centers of the bright spots is approximately 1.4 ± 0.1 nm, which is comparable to the size of the C_{60}/OBOCMC8 complex, as estimated from a molecular model. The C_{60}/OBOCMC8 complex tends toward having an upright orientation on the Au(111) surface; the molecular structure suggests that the carboxyl groups are responsible for this arrangement. Therefore, the bright spot and circular protrusion can be assigned as C_{60}, *tert*-butyl, and phenyl units, respectively. In other words, the cavity of the OBOCMC8 molecule is now filled with a C_{60} unit, observed as the additional bright spot in the STM image.[8,9] The STM images prove that the calix in C_{60}/OBOCMC8 complex retains an upright configuration despite containing a buckyball, which has been synthetically included within the calix structure.[8,9] This structural feature can be more clearly seen in the height-shaded surface plot shown in Figure 2c. C_{60} molecules appear within protrusions throughout the array. On the basis of the STM results, a tentative model for the C_{60}/OBOCMC8 array can be proposed (Figure 2d), in which a unit cell with a parameter of 1.4 nm is outlined.

After recording the STM images at 0.6 V, the electrode potential was scanned incrementally in 10 mV stages between

 © 2003 Wiley-VCH Verlag GmbH & Co. KGaA, Weinheim

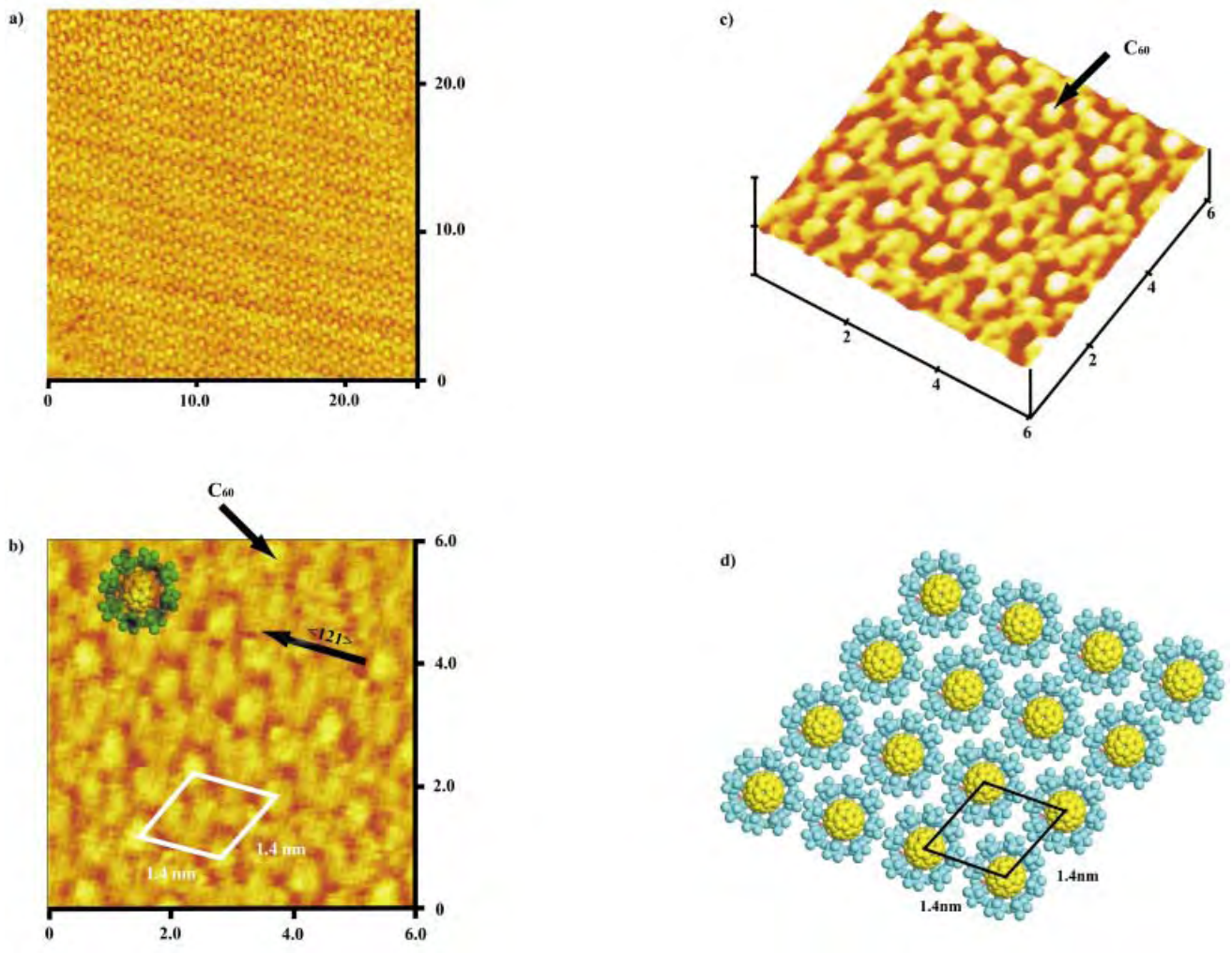


Figure 2. A typical large-scale STM image (a) of an C_{60}/OBOCMC8 array on a Au(111) surface, and a top view (b) and height-shaded surface plot (c) of the same C_{60}/OBOCMC8 array, recorded using high-resolution STM; d) a proposed structural model for the ordered array of C_{60}/OBOCMC8. The bias voltage and tunneling current were −140 mV and 1.0 nA, respectively. The scales are given in nm.

0 and 1.0 V; an identical structure for the C_{60}/OBOCMC8 array is always observed. There was no evidence for structural transformations or the release of C_{60} from the OBOCMC8 calix, even in the negative potential region, where molecular desorption from the Au(111) surface takes place. It is important to point out that different STM contrasts have been observed for both OBOCMC8 and C_{60}/OBOCMC8 arrays in the present experiment when the bias voltage between tip and substrate is varied; this phenomenon has been described in a previous study under vacuum and ambient conditions.[12] The images shown in the communication give clear structural details under the indicated imaging conditions. However, the different image contrasts could not produce different structures, even under conditions that resulted in unclear images. It is obvious that more straightforward experimental techniques, such as IR spectroscopy, and theoretical calculations must be applied to obtain further structural information to support the models suggested in this preliminary study. A more detailed investigation is now in progress.

In summary, the molecules of OBOCMC8 and C_{60}/OBOCMC8 can adsorb onto a Au(111) surface and self-organize into ordered adlayers. The configurations of the two molecules are clearly revealed by high-resolution STM images. OBOCMC8 molecules adsorb onto the substrate with an upright orientation. The intrinsic cavity of the molecule appears as a dark depression. The structure of the C_{60}/OBOCMC8 array is completely different, in that bright spots corresponding to C_{60} molecules can be clearly resolved in individual C_{60}/OBOCMC8 units. The contents of the calix could be changed to other fullerenes, clusters, and organic molecules by utilizing various methods. The stable configuration and well-defined array should be useful for nanostructure construction and for nanodevices.

Experimental Section

OBOCMC8 was synthesized by the method described in the literature.[13] C_{60} was inserted into the intrinsic cavity of OBOCMC8 by the method reported by Atwood and Shinkai.[8,9] OBOCMC8 and C_{60} (1:1 stoichiometry) were dissolved in dry toluene and heated under reflux for 4 h. After this procedure, a green-yellow solid, the C_{60}/OBOCMC8 complex, was formed.

 © 2003 Wiley-VCH Verlag GmbH & Co. KGaA, Weinheim

Single-crystal beads of Au were prepared by the crystallization of a molten ball formed at the end of a pure Au wire in a hydrogen–oxygen flame.[14] Au(111) facets on the beads were used for STM observation. For voltammetric measurements, the bead was cut and mechanically polished with successively finer grades of Al_2O_3. Before each measurement, the electrode was further annealed and quenched in deionized (Millipore) water, saturated with hydrogen.

A solution of 0.1 M $HClO_4$ was prepared from ultrapure $HClO_4$ solution (Kanto Chemical Co., Japan) and deionized water. Saturated aqueous solutions of OBOCMC8 and C_{60}/OBOCMC8 were prepared for STM and electrochemical analysis. The solutions were deaerated with high-purity nitrogen before experiments were carried out. Cyclic voltammetry experiments were performed by the hanging meniscus method with an EG&G PAR (Princeton Applied Research) Basic Electrochemical System. A reversible hydrogen electrode and a platinum wire were used as the reference and counter electrodes, respectively. All potentials are reported versus a reversible hydrogen electrode (RHE) in 0.1 M $HClO_4$.

In situ STM measurements were carried out with a Nanoscope E microscope (Digital Instrument Inc., Santa Barbara, CA). The tunneling tips were prepared from an electrochemically etched tungsten wire (0.25 mm in diameter) in 0.6 M KOH. The sidewalls of the tips were sealed with transparent nail polish to minimize the faradaic current.

The molecular models of OBOCMC8 and C_{60}/OBOCMC8 were built and optimized by the AM1 method included in the HyperChem 6.0 package (Hypercube, Inc.). The interatomic separations and molecular sizes quoted in this study were estimated from these molecular models.

Received: October 24, 2002
Revised: April 2, 2003 [Z50432]

Keywords: calixarenes · electrochemistry · fullerenes · gold · inclusion complexes · scanning tunneling microscopy

[1] L. Mandolini, R. Ungaro, *Calixarenes in Action*, Imperial College Press, London, **2000**.
[2] P. Janda, T. Krieg, L. Dunsch, *Adv. Mater.* **1998**, *10*, 1434 – 1438.
[3] P. R. Birkett, *Annu. Rep. Prog. Chem. Sect. A* **2000**, *96*, 467 – 490.
[4] J. G. Hou, J. L. Yang, H. Q. , Wang, Q. X. Li, C. G. Zeng, L. F. Yuan, B. Wang, D. M. Chen, Q. S. Zhu, *Nature* **2001**, *409*, 304 – 305.
[5] C. D. Gutsche, *Calixarenes*, Royal Society of Chemistry, Cambridge, **1989**.
[6] C. D. Gutsche, *Calixarenes Revisited*, Royal Society of Chemistry, Cambridge, **1998**.
[7] OBOCMC8: 5,11,17,23,29,35,41,47-octa-*tert*-butyl-49,50,51,52,53,54,55,56-octakis(carboxymethoxy)calix[8]arene.
[8] T. Suzuki, K. Nakashima, S. Shinkai, *Chem. Lett.* **1994**, 469 – 472.
[9] J. L. Atwood, G. A. Koutsantonis, C. L. Raston, *Nature* **1994**, *368*, 229.
[10] G.-B. Pan, L.-J. Wan, Q.-Y. Zheng, C.-L. Bai, *Chem. Phys. Lett.* **2003**, *367*, 711 – 716.
[11] T. Sakai, A. Ohira, M. Sakata, C. Hirayama, M. Kunitake, *Chem. Lett.* **2001**, 782 – 783.
[12] H. S. Lee, S. Iyengar, I. H. Musselman, *Langmuir* **1998**, *14*, 7475 – 7483.
[13] I. Alam, C. D. Gutsche, *J. Org. Chem.* **1990**, *55*, 4487 – 4489.
[14] G.-B. Pan, L.-J. Wan, Q.-Y. Zheng, C.-L. Bai, K. Itaya, *Chem. Phys. Lett.* **2002**, *359*, 83 – 88.

 © 2003 Wiley-VCH Verlag GmbH & Co. KGaA, Weinheim

Polymer-Coated Gold Nanoparticles

Fabrication of Ordered Arrays of Gold Nanoparticles Coated with High-Density Polymer Brushes**

*Kohji Ohno, Kyoungmoo Koh, Yoshinobu Tsujii, and Takeshi Fukuda**

The synthesis and characterization techniques of monodisperse nanoparticles have rapidly developed, thus stressing the importance of organizing those particles into an ordered assembly to obtain new properties, which may arise from their collective interactions in the ordered state.[1,2] Sun et al. reported that controlled evaporation of solvent with nanoparticles dispersed in it, followed by thermal treatment led to a self-organized, close-packed assembly of the particles.[3,4] Several groups created ordered arrays of nanoparticles by using the Langmuir-Blodgett (LB) technique[5,6] or the self-organization of block copolymers.[7] These studies, however, only provided ordered arrays of nanoparticles with a limited area and controllability of interparticle distance.

We recently applied the surface-initiated living radical-polymerization (LRP) technique[8–14] to form polymer brushes on Au-nanoparticle surfaces with a controlled chain length and chain-length distribution, and a graft density as high as 0.3 chains nm^{-2}.[15] In a solvent-cast film of the Au-nanoparticle–polymer hybrid as observed by transmission electron microscope (TEM), the metal cores of the hybrid particles were uniformly dispersed in the matrix of the brush polymer without forming any aggregates. However, this Au-nanoparticle assembly was poorly ordered, mainly because of the broad size distribution of the Au nanoparticles (relative standard deviation $\sigma = 49.7\,\%$). In this work, we have attempted to broaden the science and technology of the Au nanoparticle coated with a high-density polymer brush, with the aim of fabricating ordered and controllable assemblies of metal particles.

A narrowly size-distributed Au nanoparticle with LRP-initiating groups was synthesized by a simple one-pot reaction as follows: An aqueous solution of citric acid trisodium salt (140 mM, 20 mL) was quickly added to vigorously stirring boiling water (1.5 L) containing tetrachloroaurate (230 mg). After 5 min, the reaction was cooled in an ice bath for 10 min. To this mixture the initiator 11,11′-dithiobis[1-(2-bromo-2-methylpropionyloxy)undecane][10] (70 mg) dissolved in THF (500 mL) was added, and this mixture was stirred for another 12 h. The resulting crude Au nanoparticles were purified by using a reported method.[15] TEM revealed that the average

[*] Prof. Dr. T. Fukuda, Dr. K. Ohno, K. Koh, Dr. Y. Tsujii
Institute for Chemical Research, Kyoto University
Uji, Kyoto 611-0011 (Japan)
Fax: (+81) 774-38-3170
E-mail: fukuda@scl.kyoto-u.ac.jp

[**] This work was supported in part by a Grant-in-Aid for Scientific Research (Grant-in-Aid 14205131, 14750695) from the Ministry of Education, Culture, Sports, Science and Technology, Japan.

 DOI: 10.1002/anie.200250850 © 2003 Wiley-VCH Verlag GmbH & Co. KGaA, Weinheim

diameter of the purified particles was about 12 nm, with a fairly narrow size distribution ($\sigma = 11.4\,\%$).

The copper-mediated LRP[16] of methyl methacrylate (MMA) was carried out with the initiator-coated Au nanoparticles by using a reported method.[15] The resultant Au-nanoparticle–poly(methyl methacrylate) (PMMA) hybrids were purified repeatedly by a fractional reprecipitation technique, and it was confirmed by gel permeation chromatography (GPC) that the thus purified Au-nanoparticle–PMMA hybrids contained no free polymers.[15] The $\bar{M}_n$ values of the PMMAs cleaved from the Au-nanoparticle surface were 12000, 28000, and 62000, and their polydispersity indexes $\bar{M}_w/\bar{M}_n$ were 1.23, 1.33, and 1.49, respectively, according to GPC. The graft density was estimated to be about 0.4 chains nm^{-2} for each of the three samples. This figure means that an Au nanoparticle has on average 180 PMMA grafts on its surface.

Each of the Au-nanoparticle–PMMA hybrids thus prepared was dissolved in benzene at a concentration about 1 mg mL^{-1}. The solution was deposited onto the surface of purified water in a circular Langmuir trough equipped with a circular compression barrier.[17] The surface film was compressed at a constant speed of 60 mm^2 min^{-1} by the circular barrier. The surface pressure π was measured by a filter paper Wilhelmy plate. A typical isotherm of the surface pressure, π, versus occupied area, A, is given in Figure 1. In this example, π deviates from zero at a critical surface pressure, A_{crit}, of 13600 nm^2 per particle. With a further compression, π increases gradually at first, and passing through a shoulder at around $A = 8000$, it increases steeply for A smaller than about 5000 nm^2 per particle. The other Au-nanoparticle–PMMA hybrids showed qualitatively a similar behavior.

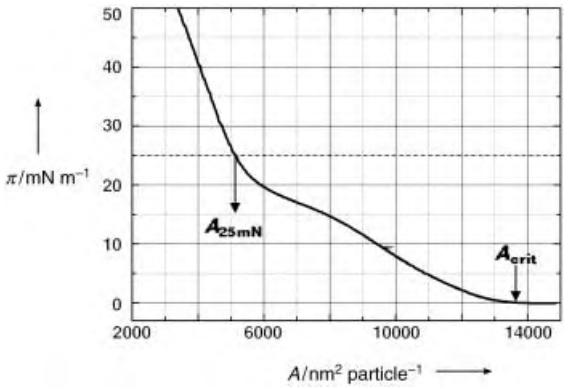


Figure 1. Isotherm of the surface pressure, π, versus occupied area A for the surface film of Au-nanoparticle–PMMA hybrid. $\bar{M}_n$ of the graft polymer is 28000.

All the surface films of Au-nanoparticle–PMMA hybrids were successfully transferred onto a carbon-coated copper TEM grid mounted on a glass plate (sputtered with reduced-pressure air just before use) by the LB deposition (vertical lifting-up) technique at a constant π of 25 mN m^{-1} and a constant speed of 1 mm min^{-1}. Figures 2a–d shows the TEM images of the transferred films. For comparison, the TEM image of the initiator-coated Au-nanoparticle monolayer is

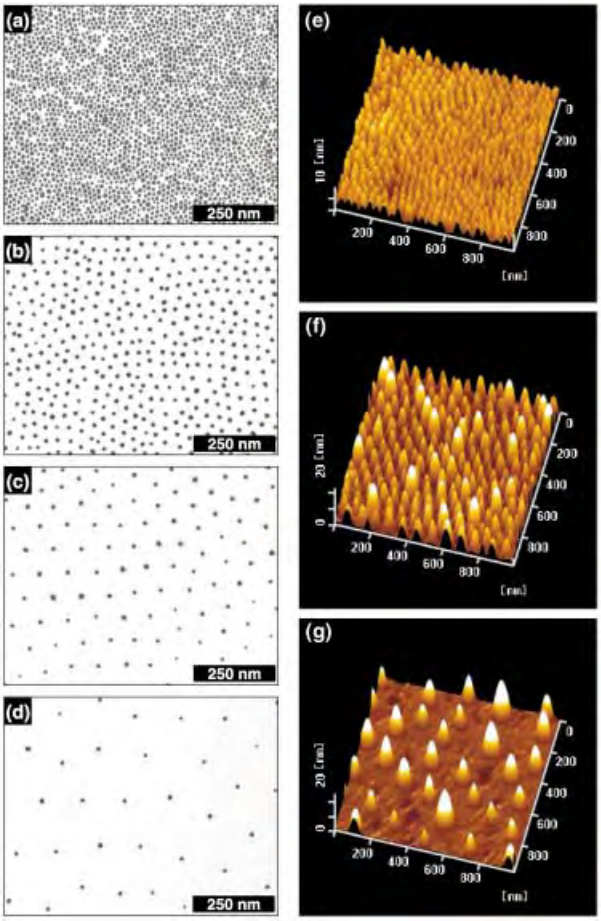


Figure 2. TEM micrographs of the transferred films of (a) initiator-coated Au nanoparticles and (b–d) Au-nanoparticle–PMMA hybrids: $\bar{M}_n$ of the PMMA graft = (b) 12000, (c) 28000, and (d) 62000. (e–g) AFM images of the transferred films of Au-nanoparticle–PMMA hybrids: $\bar{M}_n$ of the PMMA graft = (e) 12000, (f) 28000, and (g) 62000.

also shown (Figure 2a), which was prepared under exactly the same conditions as for the Au-nanoparticle–PMMA films, except that a mixture of THF/chloroform (1:1 by volume) was used as the solvent. The TEM images show that the Au-nanoparticle cores visible as dark circles are uniformly dispersed throughout the film, while the PMMA chains, which should be forming fringes surrounding the Au-nanoparticle cores, are invisible because of their much lower electron density. Noteworthy are the high degree of positional order of the Au-nanoparticle cores present in the hybrid films and the strong dependence of the interparticle distance on the chain length of PMMA grafts. Questions now arise as to the detailed structure of the monolayer film, of the individual hybrid particles, and the conformation of the individual PMMA grafts on the substrate and hence at the air–water surface.

To shed light on these questions, we have observed the same monolayer films transferred onto a freshly cleaved mica substrate (at $\pi = 25$ mN m^{-1}) on an atomic force microscope (AFM, Seiko Instruments Inc., SPA-400). The AFM images given in Figure 2e–g exhibit protrusions whose height and thickness both increase with increasing chain length of

 © 2003 Wiley-VCH Verlag GmbH & Co. KGaA, Weinheim

PMMA grafts. In the AFM image in Figure 2g, for example, the protrusions are standing on the rather flat but rough surface, which is not the substrate (mica) surface but a PMMA matrix, as a mica surface should look perfectly smooth at this magnification. The mean height of the protrusions measured from the lowest surface of the matrix is about 20 nm, which roughly compares to the size of the "compact core–shell model" consisting of the Au-nanoparticle core and the PMMA shell of the bulk density (Figure 3a). These observations suggest the structural model of the hybrid film as is schematically illustrated in Figure 3c.

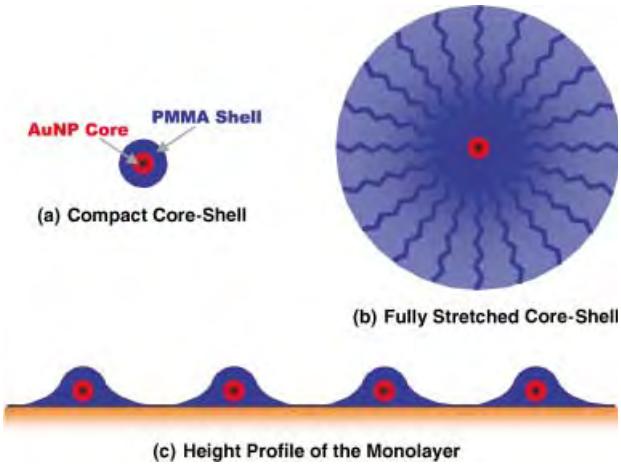


Figure 3. Schematic representations of (a) the compact core-shell model, (b) the fully stretched core-shell model, and (c) the height profile of the Au-nanoparticle–PMMA ($\bar{M}_n = 28000$) hybrid monolayer on the substrate surface transferred at 25 mN m^{-1}.

Figure 4 shows the mean nearest-neighbor center-to-center distance D of the Au-nanoparticle–PMMA hybrid at $\pi = 25$ mN m^{-1} (D_{25mN}) as a function of the PMMA graft molecular weight. Figure 4 also shows the D value at $A = A_{crit}$ calculated with $D_{crit} = D_{25mN}(A_{crit}/A_{25mN})^{1/2}$, where A_{crit} and A_{25mN} are the values of A read from the π–A isotherm (cf. Figure 1). The diameters of the compact core–shell model and the "fully stretched core–shell model" are also shown. (The diameter is equal to D for the 2D hexagonal close packing of spherical models.) The latter model consists of the Au-nanoparticle core and the PMMA shell whose size is equal to that of the PMMA chains radially stretched in all *trans* conformation (Figure 3b). Figure 4 shows that D_{25mN} is much larger than the diameter of the compact core–shell model. It is as large as about half that of the fully stretched core–shell model. This means that the PMMA shell is not compact but has an extremely large extension in the film-surface direction, thus producing the strong hindrance against compression. This picture is consistent with the AFM observation presented above. According to Rondelez et al.,[18] PMMA at the air–water interface has a slightly negative second virial coefficient and the radius of gyration R_G proportional to $M^{0.57}$. This factor means that even though water does not dissolve PMMA, it swells PMMA and allows it to have a random coil conformation at the air–water interface. If, then,

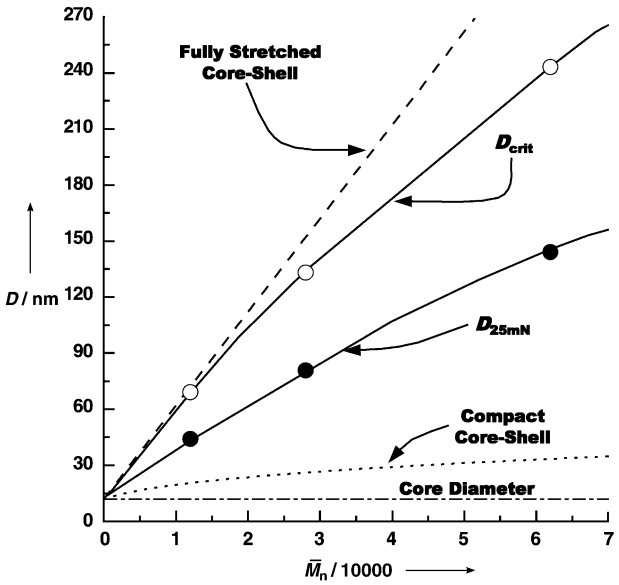


Figure 4. Plot of the mean nearest-neighbor center-to-center distance D as a function of $\bar{M}_n$ of the PMMA graft. The broken and dotted lines represent the diameters of the fully stretched and compact core–shell models, respectively.

we assume that the PMMA chains on the Au-nanoparticle surface have the random coil conformation suggested above, we estimate the size of the PMMA shell to be about the same as that of the compact core–shell model (the thickness of the "compact" shell is already quite large because of the high graft density). Even more surprising is the magnitude of D_{crit}. This parameter will characterize the critical surface concentration[18] at which the PMMA fringes from different particles begin to overlap with each other. Figure 4 shows that D_{crit} is nearly as large as the diameter of the fully stretched core–shell model. This strongly suggests that the fringe PMMA chains are nearly fully stretched at the air–water interface.

We reported that the PMMA brush formed on a silicon wafer with a similarly high surface density[8] and swollen by toluene had an equilibrium film thickness as much as 80 to 90% of the end-to-end distance of the fully stretched PMMA chain.[19,20] Namely the PMMA chains in this high-density brush were almost fully extended. This phenomenon was interpreted as being a consequence of the strong anisotropic interactions among polymer chains arising from the high surface density. The observations described above show that a similar phenomenon does occur in a 2D system like the air–water interface. Aside from the difference in dimensionality, the surface on which the brush is formed is spherical in the work reported herein, not flat like the silicon wafer used in previous work.[19,20] Accordingly, the polymer density decreases with increasing distance from the core center. For a fixed core diameter, the anisotropic interaction that causes the chain extension will, therefore, become weaker as the chain length of the brush increases. This effect manifests itself in the downward curvature observed for both the D_{crit} and D_{25mN} versus $\bar{M}_n$ plot in Figure 4.

In conclusion, we have synthesized a narrowly size-distributed Au nanoparticle coated with a well-defined,

 © 2003 Wiley-VCH Verlag GmbH & Co. KGaA, Weinheim

high-density PMMA. Because of the high surface density and the controlled chain length, the PMMA grafts at the air–water interface exert interparticle interactions of an extremely long range, a range comparable to the full length of the PMMA chain. Consequently, the Au nanoparticles form a 2D array with a high degree of structural order and exceptionally wide controllability of the interparticle distance. Owing to the simplicity and versatility of surface-initiated LRP, this work may be extended to other metal and semiconductor nanoparticles for their 2D or 3D ordered assemblies with wide controllability of lattice parameters. The degree of structural order attainable by this strategy depends primarily on the size uniformity of the nanoparticles.

Received: December 27, 2002
Revised: February 20, 2003 [Z50850]

Keywords: gold · nanostructures · nanotechnology · ordered arrays · polymers

[1] D. L. Feldheim, C. D. Keating, *Chem. Soc. Rev.* **1998**, *27*, 1.
[2] C. P. Collier, T. Vossmeyer, J. R. Heath, *Annu. Rev. Phys. Chem.* **1998**, *49*, 371.
[3] S. Sun, C. B. Murray, D. Weller, L. Folks, A. Moser, *Science* **2000**, *287*, 1989.
[4] S. Sun, H. Zeng, *J. Am. Chem. Soc.* **2002**, *124*, 8204.
[5] J. R. Heath, C. M. Knobler, D. V. Leff, *J. Phys. Chem. B* **1997**, *101*, 189.
[6] J. J. Brown, J. A. Porter, C. P. Daghlian, U. J. Gibson, *Langmuir* **2001**, *17*, 7966.
[7] J. P. Spatz, S. Mössmer, C. Hartmann, M. Möller, T. Herzog, M. Krieger, H.-G. Boyen, P. Ziemann, B. Kabius, *Langmuir* **2000**, *16*, 407.
[8] M. Ejaz, S. Yamamoto, K. Ohno, Y. Tsujii, T. Fukuda, *Macromolecules* **1998**, *31*, 5934.
[9] T. von Werne, T. E. Patten, *J. Am. Chem. Soc.* **2001**, *123*, 7494.
[10] R. R. Shah, D. Merreceyes, M. Husemann, I. Rees, N. L. Abbott, C. J. Hawker, J. L. Hedrick, *Macromolecules* **2000**, *33*, 597.
[11] J. Pyun, K. Matyjaszewski, T. Kowalewski, D. Savin, G. Patterson, G. Kickelbick, N. Huesing, *J. Am. Chem. Soc.* **2001**, *123*, 9445.
[12] J.-B. Kim, M. L. Bruening, G. L. Baker, *J. Am. Chem. Soc.* **2000**, *122*, 7616.
[13] H. Mori, A. Boker, G. Krausch, A. H. E. Müller, *Macromolecules* **2001**, *34*, 6871.
[14] R. A. Sedjo, B. K. Mirous, W. J. Brittain, *Macromolecules* **2000**, *33*, 1492.
[15] K. Ohno, K. Koh, Y. Tsujii, T. Fukuda, *Macromolecules* **2002**, *35*, 8989.
[16] T. E. Patten, J. Xia, T. Abernathy, K. Matyjaszewski, *Science* **1996**, *272*, 866.
[17] M. Matsumoto, Y. Tsujii, K. Nakamura, T. Toshimoto, *Thin Solid Films* **1996**, *280*, 238.
[18] D. Poupinet, R. Vilanove, F. Rondelez, *Macromolecules* **1989**, *22*, 2491.
[19] S. Yamamoto, M. Ejaz, Y. Tsujii, M. Matsumoto, T. Fukuda, *Macromolecules* **2000**, *33*, 5602.
[20] S. Yamamoto, M. Ejaz, Y. Tsujii, T. Fukuda, *Macromolecules* **2000**, *33*, 5608.

 © 2003 Wiley-VCH Verlag GmbH & Co. KGaA, Weinheim

meso–meso-*Linked Zn^{II} Diporphyrin*

Dihedral-Angle Modulation of *meso–meso*-Linked Zn^{II} Diporphyrin through Diamine Coordination and Its Application to Reversible Switching of Excitation Energy Transfer**

Hideyuki Shinmori, Tae Kyu Ahn, Hyun Sun Cho, Dongho Kim, Naoya Yoshida, and Atsuhiro Osuka**

Control of intramolecular excitation-energy transfer (EET) and electron transfer (ET) has been a subject of considerable attention in light of its importance in molecular electronics including artificial photosynthesis,[1] molecular sensing systems,[2] molecular devices,[3] and so forth. When the direction of an intramolecular EET reaction can be switched at will by external physical and/or chemical input, it provides a switching EET module as a component of molecular devices.[4]

Recently, we reported the synthesis of *meso–meso*-linked diporphyrins, whose Soret band is split into two bands by an exciton coupling but the conjugative electronic interaction between the porphyrin chromophores in the diporphyrin is weak because of the nearly perpendicular conformation, despite the direct *meso–meso* linkage.[5] Thus, a decrease in the dihedral angle of diporphyrin, from an average of 90° to an oblique geometry, is expected to lead to an enhancement in the electronic coupling within the diporphyrin, which has been confirmed by permanently distorted *meso–meso*-linked diporphyrins bridged by a strap of variable length.[6] Namely, the decrease in the dihedral angle between the porphyrin rings in the diporphyrin causes progressive lowering of the S_1-state energy and an increase in energy of the HOMO orbital in addition to the spectral changes from two Soret bands to four Soret bands, which is a consequence of symmetry change from D_{2d} to D_2.

Herein we report reversible switching of intramolecular EET direction on the basis of the dihedral angle control of *meso–meso*-linked Zn^{II} diporphyrin through 1,7-diaminohep-

[*] Prof. D. Kim, Dr. T. K. Ahn, Dr. H. S. Cho
Center for Ultrafast Optical Characteristics Control and
Department of Chemistry, Yonsei University
Seoul 120–749 (Korea)
Fax: (+82) 2-2123-2434
E-mail: dongho@yonsei.ac.kr
Prof. A. Osuka, Dr. H. Shinmori, Dr. N. Yoshida
Department of Chemistry, Graduate School of Science
Kyoto University, and
Core Research for Evolutional Science and Technology (CREST)
Japan Science and Technology Corporation
Sakyo-ku, Kyoto 606–8502 (Japan)
Fax: (+81) 75-753-3970
E-mail: osuka@kuchem.kyoto-u.ac.jp

[**] The work at Yonsei University was financially supported by the Creative Research Initiatives Program of the Ministry of Science and Technology of Korea. N.Y. thanks the JSPS Research Fellowship for Young Scientists.

Supporting information for this article is available on the WWW under http://www.angewandte.org or from the author.

 © 2003 Wiley-VCH Verlag GmbH & Co. KGaA, Weinheim DOI: 10.1002/anie.200351177

tane coordination. First, coordination behaviors of α,ω-diaminoalkanes ($H_2N(CH_2)_nNH_2$, ***n*DA**) to *meso–meso*-linked Zn^{II} diporphyrin **1** have been examined in terms of association ability and association mode, by changing the molecular length of ***n*DA**.[7] In the absence of an amine, the absorption spectrum of **1** exhibits split Soret bands at 416 and 451 nm in toluene.[5] Following the changes in the absorption spectra upon the addition of ***n*DA** to the corresponding solutions, we determined the association constants (K_a) on the basis of 1:1 complex formation (Table 1). A jump in K_a was observed between 1,6-diaminohexane (**6DA**) and 1,7-diaminoheptane (**7DA**), and between 1,9-diaminononane (**9DA**) and 1,10-diaminodecane (**10DA**). Figure 1 shows typical contrasting coordination behaviors of 1,5-diaminopentane (**5DA**) and **7DA** towards **1**. The addition of **5DA** to a toluene solution of **1** caused the red shift of Soret bands to 424 and 459 nm with several isosbestic points (Figure 1a). These spectral changes, which are common for ***n*DA** shorter than **5DA** and for monoaminoalkanes, can be interpreted in terms of the coordination of two diamine molecules to **1** without affecting an averaged perpendicular conformation. Conversely, a similar addition of **7DA** to a toluene solution of **1** gave rise to markedly different spectral changes, from two Soret bands to four Soret bands (λ_{max} = 412 (shoulder), 427, 462, and 472 (shoulder) nm) as well as red shifts of Q bands from 540 (shoulder) and 553 nm to 554, 575, respectively, and the appearance of a band at 629 nm (Figure 1b). The resultant absorption spectral features of complex **7DA–1** are, both in the Soret band and Q band regions, quite similar to those of permanently distorted *meso–meso*-linked diporphyrin **2** bridged by a 1,4-dioxyteteramethylene strap (Scheme 1). It

Table 1: Association constants of **1** with ***n*DA** in toluene at 25 °C. Association constants have been calculated assuming a 1:1 complex.

n	K_a [$\times 10^4$ M^{-1}]	*n*	K_a [$\times 10^4$ M^{-1}]
2	9.0	8	710
4	11	9	690
5	16	10	2600
6	10	12	910
7	160		

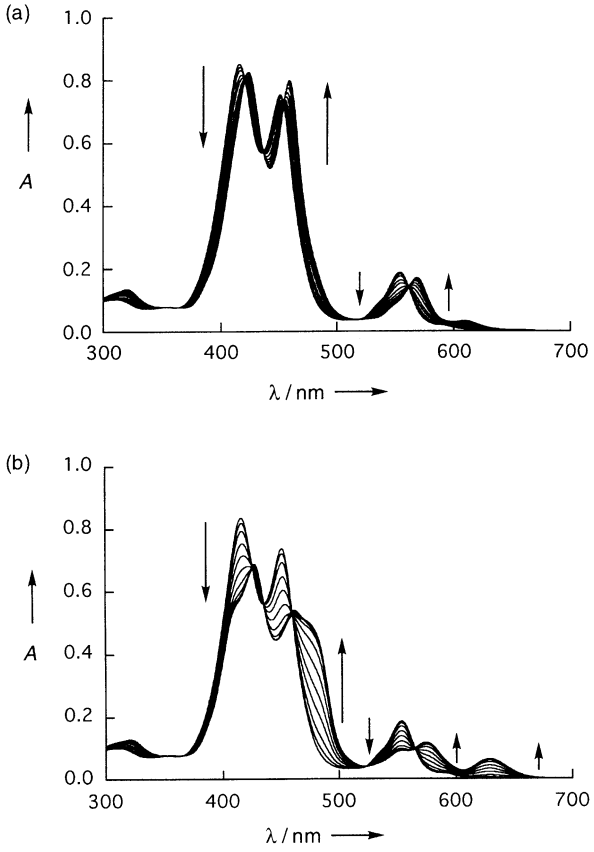
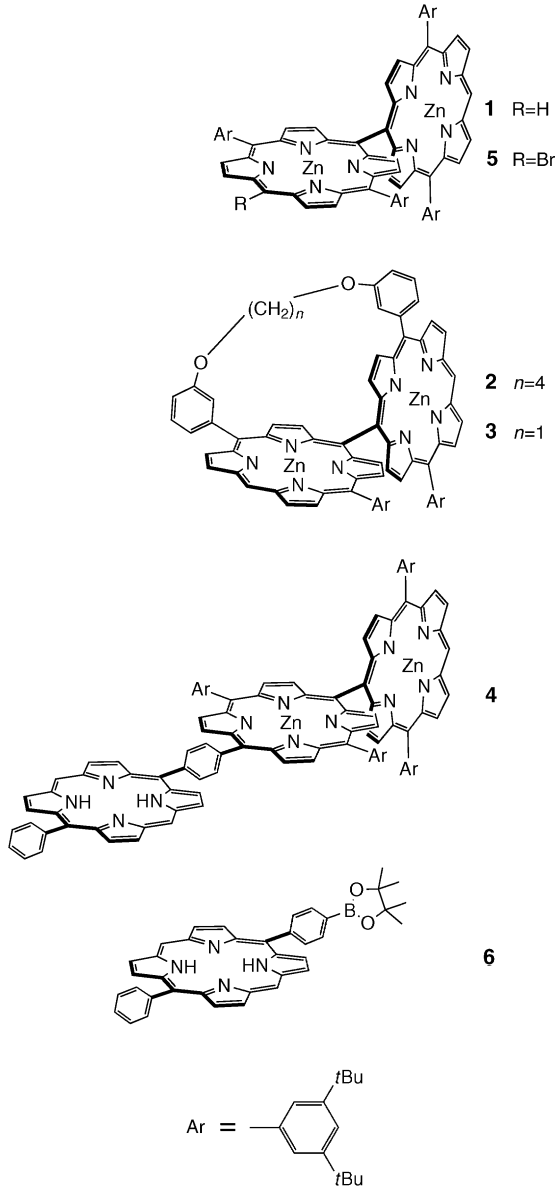


Figure 1. Absorption spectra of **1** (3.5×10^{-6} M) with **5DA** (a) and **7DA** (b) in toluene at 25 °C: [**5DA**] = 0–1.6×10^{-4} M; [**7DA**] = 0–3.5×10^{-5} M. *A* = absorption.



Scheme 1. Structure of the porphyrins referred to.

 © 2003 Wiley-VCH Verlag GmbH & Co. KGaA, Weinheim

is thus conceivable that the association of **7DA** with **1** takes place through two amino groups coordinated to the two zinc centers, hence forcing a tilt of the two porphyrins from a dihedral angle of about 90° to a decreased dihedral angle. Association constants of **1** with longer diamines such as **10DA** and **12DA** are apparently larger than that with **7DA**, but the resulting complexes exhibit an absorption spectra similar to that of the **5DA–1** complex, thus suggesting that these long diamines have sufficient molecular length to form a 1:1 complex without affecting the average perpendicular conformation of the *meso–meso*-linked Zn^{II} diporphyrin. Job plots indicate a 1:1 molecular ratio for the formation of complexes **7DA–1** and **10DA–1** (Supporting Information). Different association modes between complexes **5DA–1** and **7DA–1** are also evident in the fluorescent spectra (Figure 2), which feature modest spectral changes in the former, and a distinct red shift and intensity enhancement in the latter. The fluorescence spectrum of complex **7DA–1** (Figure 2b) is reminiscent of that of the distorted diporphyrin **2** coordinated with amine, which again indicates a change in the dihedral angle of **1** upon the association of **7DA**. Among the α,ω-diaminoalkanes examined, **7DA** is the most effective in inducing the distorted conformation as judged from the optical properties of the complexes formed. Judging from the X-ray crystal structure of the Cu^{II} analogue of **2**, the coordination of **7DA** reduces the dihedral angle from nearly 90° to 60–70°.[6b] The absorption and fluorescence spectra of **7DA–2** complex are quite similar to those of more distorted diporphyrin **3** bridged by a dioxymethylene strap, in which the dihedral angle is estimated to be less than 50°.[6b] Therefore, it is likely that **7DA** is ideally suited for changing the dihedral angle of the *meso–meso*-linked Zn^{II} diporphyrin and the additional torsional strain imposed by the coordination of **7DA** is effective for the modulation of the interporphyrin electronic interaction. Furthermore it is noteworthy that the addition of acetic acid to a solution of complexes **7DA–1** or **7DA–2** restores the original absorption and fluorescence spectra of **1** or **2**, plausibly through a simple acid–base reaction without affecting the Zn^{II} metallation. Thus these torsional changes can be effected in a reversible manner.

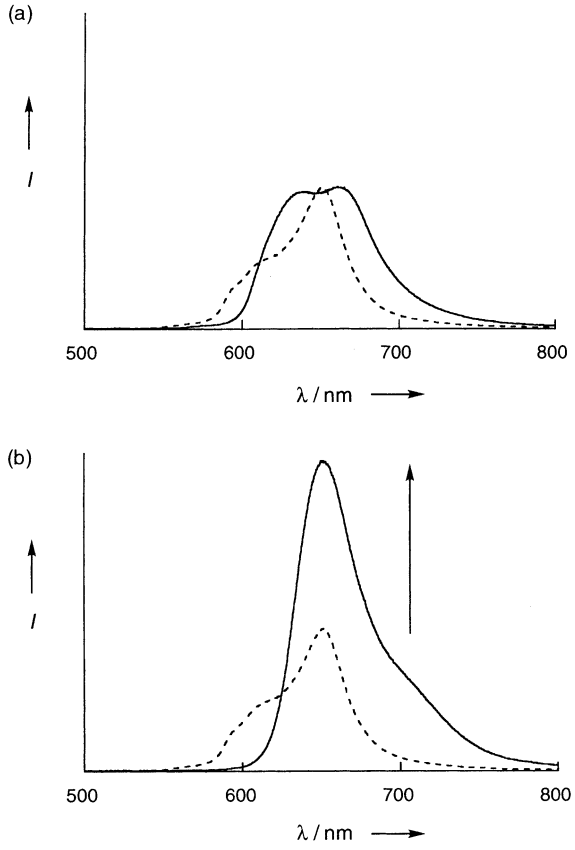


Figure 2. Fluorescence spectra of **1** (3.5×10^{-6} M) with **5DA** (a) and **7DA** (b) in toluene at 25 °C: $\lambda_{ex}=435$ nm, [**5DA**] = 0 (-----) or 2.9×10^{-4} M (——); [**7DA**] = 0 or 8.0×10^{-6} M. *I* = intensity (arbitrary units).

With these reversible modulations of the optical properties of **1** at our disposal, we have explored a molecular system that enables reversible switch in direction of the EET. We designed triporphyrin **4**, in which a *meso–meso*-linked Zn^{II}-diporphyrin unit is covalently linked to a 5,15-diaryl free-base porphyrin through a 1,4-phenylene bridge. Model **4** was prepared by the Suzuki coupling reaction of bromide **5** with boronate **6** ($[Pd(PPh_3)_4]$, K_2CO_3, toluene) in 81 % yield.[8] The absorption spectrum of **4** is almost identical to the sum of those of **1** and the monomer of 5,15-diaryl free-base porphyrin, thus indicating negligible electronic interaction in the ground state. The steady-state fluorescence spectrum of **4** arises only from the 5,15-diaryl free-base porphyrin, thus indicating the nearly quantitative EET from the *meso–meso*-linked Zn^{II}-diporphyrin subunit to the free-base porphyrin subunit. The addition of **7DA** to a toluene solution of **4** caused distinct spectral changes in the absorption spectra, which are essentially the same as those observed for **1**, thus suggesting a similar decrease in the dihedral angle of the *meso–meso*-linked diporphyrin. Interestingly, the fluorescence spectrum of **4** exhibits a clear change of the emitting chromophore, from the 5,15-diaryl free-base porphyrin in free **4** to the *meso*–meso-linked Zn^{II}-diporphyrin in **7DA–4** complex (Figure 3a). These results indicate that the intramolecular EET direction can be switched upon the addition of **7DA**. Furthermore, the addition of acetic acid to complex **7DA–4** recovers the original absorption and fluorescence spectra of the free **4** (Figure 3b), hence restoring the intramolecular EET from the Zn^{II} diporphyrin to the free base porphyrin, probably through liberation of **7DA** from the Zn^{II}-diporphyrin moiety.[9]

The intramolecular EET processes have been examined by picosecond time-resolved transient absorption spectroscopy. Figure 4a shows the transient absorption spectra of free **4** taken by excitation at 580 nm, mainly pumping the *meso–meso*-linked Zn^{II}-diporphyrin part of the molecule. The spectrum at 1 ps delay time indicates strong bleaching bands at 450 and 555 nm because of the formation of the singlet excited state of the Zn^{II} diporphyrin. These bleaching bands disappear rapidly with $\tau = 5.5$ ps (Supporting Information) followed by an increase of a new bleaching band at 500 nm arising from the formation of the singlet excited state of the free base porphyrin with $\tau = 5.0$ ps as can be seen in the spectrum at 50 ps delay time and the temporal profile at

 © 2003 Wiley-VCH Verlag GmbH & Co. KGaA, Weinheim

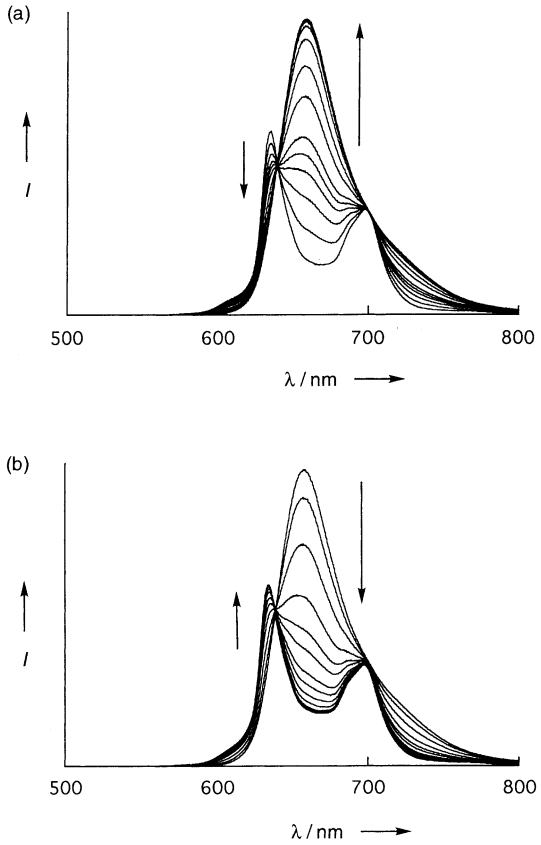


Figure 3. Fluorescence spectra of **4** (1.8×10^{-6} M) with **7DA** in toluene at 25 °C: $\lambda_{ex}=468$ nm, [**7DA**] = 0–1.7×10^{-5} M, (a). Fluorescence spectra of **4** (1.8×10^{-6} M) and **7DA** (6.7×10^{-6} M) plus acetic acid, [acetic acid] = 0–2.6×10^{-2} M, (b).

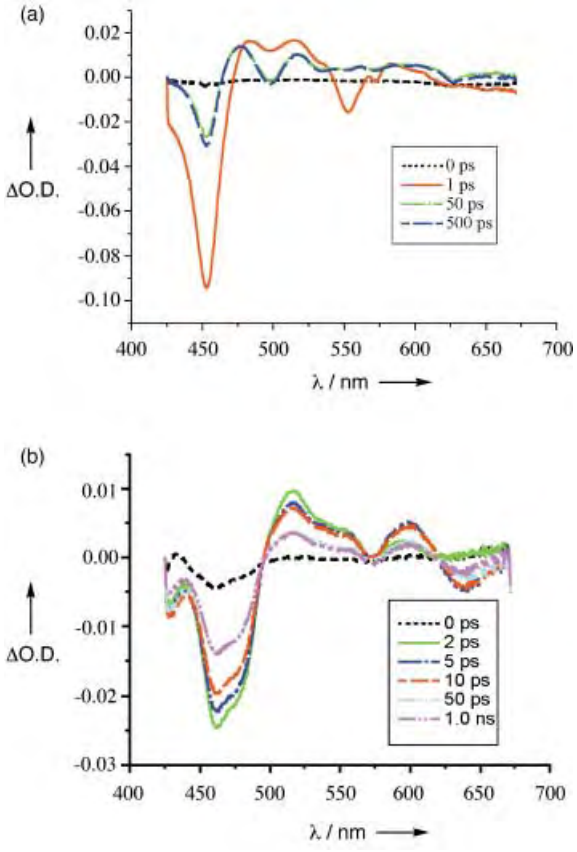


Figure 4. Transient absorption spectra of **4** in toluene by excitation at 580 nm (a) and of **7DA–4** complex by excitation at 400 nm (b). O.D. = optical density.

500 nm (Supporting Information). These results unambiguously indicate the efficient intramolecular EET from the Zn^{II}-diporphyrin to the free base porphyrin part with $k_{EET}=2\times10^{11}\ s^{-1}$. The resultant singlet excited state of the free-base porphyrin has a lifetime of about 9 ns, as determined by the fluorescence lifetime measurement, and thus is not quenched by the Zn^{II}-diporphyrin moiety. This result provides firm evidence for the occurrence of EET, not electron transfer. The reverse EET in **7DA–4** complex was more difficult to detect owing to larger absorbance of the Zn^{II}-diporphyrin in comparison with that of the free-base porphyrin unit, which did not allow a selective excitation of the latter. Figure 4b shows the transient absorption spectra of complex **7DA–4** taken by excitation at 400 nm that corresponds to the pumping of the Zn^{II} diporphyrin and the free base porphyrin roughly in a 1:1.5 ratio. At 462 nm, at which the bleaching arises from the superposition of the singlet excited states of the Zn^{II} diporphyrin complexed with **7DA** as well as from the free base porphyrin, the temporal profile has revealed a rapid recovery with $\tau\approx10$ ps, which is assignable to the EET from the free base porphyrin to the Zn^{II} diporphyrin.

As demonstrated above, the dihedral angle between the two porphyrins in the *meso–meso*-linked Zn^{II} diporphyrin can be modulated effectively upon the addition of **7DA** through the 1:1 coordination at both Zn^{II} centers. This mechanical torsion gives rise to a decrease in the S_1-state energy in the *meso–meso*-linked Zn^{II}-diporphyrin subunit, which, in turn, can be erased upon the addition of acetic acid in a reversible manner. This sequence, when applied to the triporphyrin model **4**, nearly completes the switch in the direction of the intramolecular EET. Further extension of this methodology is currently being investigated in our laboratories.

Experimental Section

Triporphyrin **4**: *meso*-Brominated *meso–meso* Zn^{II} diporphyrin **5** (10 mg, 0.006 mmol), porphyrin boronate **6** (30 mg, 0.051 mmol), K_2CO_3 (44 mg, 0.32 mmol), and $Pd(PPh_3)_4$ (1.2 mg, 0.001 mmol) were dissolved in dry toluene (7 mL). The solution was degassed by three freeze–pump–thaw cyles and then heated to 80 °C for 17 h under argon. The reaction mixture was cooled to room temperature, and the solvent was removed by evaporation. The desired porphyrin was separated by silica-gel column chromatography (eluent; CH_2Cl_2:hexane = 1:1) and was further purified by recrystallization from CH_2Cl_2 and MeOH to give **4** as a violet solid. Yield; 10 mg, 81 %. ^{1}H NMR (500 MHz, $CDCl_3$, 25 °C, TMS): $\delta=10.45$ (s, 2H, *meso*), 10.41 (s, 1H, *meso*), 9.62 (d, $J=5$ Hz, 2H, Por-β), 9.60 (d, $J=5$ Hz, 2H, Por-β), 9.53 (d, $J=5$ Hz, 2H, Por-β), 9.51 (d, $J=5$ Hz, 2H, Por-β), 9.48 (d, $J=5$ Hz, 2H, Por-β), 9.26 (d, $J=5$ Hz, 2H, Por-β), 9.21 (d, $J=5$ Hz, 2H, Por-β), 9.15 (d, $J=5$ Hz, 2H, Por-β), 8.80 (d, $J=5$ Hz, 2H, Por-β), 8.77 (d, $J=5$ Hz, 2H, Por-β), 8.78 and 8.73 (d-d, $J=8$ Hz, 4H, Phenylene), 8.35–8.32 (m, 2H, Ph), 8.22 (d, $J=5$ Hz, 2H, Por-β), 8.19 (d, $J=2$ Hz, 4H, Ar), 8.16 (d, $J=5$ Hz, 2H, Por-β), 8.14 (d, $J=2$ Hz, 4H, Ar), 7.86–7.84 (m, 3H, Ph), 7.76 (t, $J=2$ Hz, 2H, Ar), 7.73 (t, $J=2$ Hz, 2H,

 © 2003 Wiley-VCH Verlag GmbH & Co. KGaA, Weinheim

Ar), 1.50 ppm (s, 36H, *t*Bu), 1.48 (s, 36H, *t*Bu); MALDI-TOF MS *m*/*z* 1955, calcd for $C_{128}H_{122}N_{12}Zn_2$ 1955; UV/Vis (toluene): $\lambda_{max}(\log\varepsilon) =$ 410(5.64), 458(5.49), 500(4.59), 541(4.65), 558(4.82), 601(4.05), and 633(3.52) nm; fluorescence (toluene): $\lambda_{max} = 634$ and 698 nm.

Received: February 13, 2003
Revised: April 14, 2003 [Z51177]

Keywords: coordination modes · energy transfer · molecular devices · porphyrinoids · zinc

[1] a) M. R. Wasielewski, *Chem. Rev.* **1992**, *92*, 435; b) D. Gust, T. A. Moore, A. L. Moore, *Acc. Chem. Res.* **1993**, *26*, 198; c) K. Maruyama, A. Osuka, *Pure Appl. Chem.* **1990**, *62*, 1511.

[2] a) T. D. James, K. Sandanayake, S. Shinkai, *Angew. Chem.* **1994**, *106*, 2287; *Angew. Chem. Int. Ed. Engl.* **1994**, *33*, 2207; b) R. Krämaer, *Angew. Chem.* **1998**, *110*, 804; *Angew. Chem. Int. Ed.* **1998**, *37*, 772; c) L. Fabbrizzi, M. Licchelli, P. Pallavicini, L. Parodi, *Angew. Chem.* **1998**, *110*, 838; *Angew. Chem. Int. Ed.* **1998**, *37*, 800.

[3] a) D. Holten, D. F. Bocian, J. S. Lindsey, *Acc. Chem. Res.* **2002**, *35*, 57; b) A. P. de Silva, N. D. McClenaghan, *J. Am. Chem. Soc.* **2000**, *122*, 3965; c) A. P. de Silva, H. Q. N. Gunnaratne, C. P. McCoy, *Nature* **1993**, *364*, 42; d) A. Credi, V. Balzani, S. Langford, J. F. Stoddart, *J. Am. Chem. Soc.* **1997**, *119*, 2679.

[4] a) J. Walz, K. Ulrich, H. Port, H. C. Wolf, J. Wonner, F. Effenberger, *Chem. Phys. Lett.* **1993**, *213*, 321; b) H. Shiratori, T. Ohno, K. Nozaki, A. Osuka, *Chem. Phys. Lett.* **2000**, *320*, 631; c) T. B. Norsten, N. R. Brabda, *J. Am. Chem. Soc.* **2001**, *123*, 1784; d) A. Osuka, D. Fujikane, H. Shinmori, S. Kobatake, M. Irie, *J. Org. Chem.* **2001**, *66*, 3913; e) J. L. Bahr, G. Kodis, L. de la Garza, S. Lin, A. L. Moore, T. A. Moore, D. Gust, *J. Am. Chem. Soc.* **2001**, *123*, 7124; d) P. A. Liddell, G. Kodis, A. L. Moore, T. A. Moore, D. Gust, *J. Am. Chem. Soc.* **2002**, *124*, 7668.

[5] a) A. Osuka, H. Shimidzu, *Angew. Chem.* **1997**, *109*, 93; *Angew. Chem. Int. Ed. Engl.* **1997**, *36*, 135; b) A. Nakano, A. Osuka, I. Yamazaki, T. Yamazaki, Y. Nishimura, *Angew. Chem.* **1998**, *110*, 3172; *Angew. Chem. Int. Ed.* **1998**, *37*, 3023; c) N. Aratani, A. Osuka, Y. H. Kim, D. H. Jeong, D. Kim, *Angew. Chem.* **2000**, *112*, 1517; *Angew. Chem. Int. Ed.* **2000**, *39*, 1458; d) Y. H. Kim, D. H. Jeong, D. Kim, S. C. Jeoung, H. S. Cho, S. Kim, N. Aratani, A. Osuka, *J. Am. Chem. Soc.* **2001**, *123*, 76.

[6] a) N. Yoshida, A. Osuka, *Org. Lett.* **2000**, *2*, 2963; b) N. Yoshida, T. Ishizuka, A. Osuka, D. H. Jeong, H. S. Cho, D. Kim, Y. Matsuzaki, A. Nogami, K. Tanaka, *Chem. Eur. J.* **2003**, *9*, 58.

[7] J. K. M. Sanders in *The Porphyrin Handbook, Vol. 3* (Eds.: K. M. Kadish, K. M. Smith, R. Guillard), Academic Press, San Diego, **2000**, pp. 347–368.a) Examples of conformational changes induced by the coordination of diamines to Zn^{II} diporphyrins; C. A. Hunter, M. N. Meah, J. K. M. Sanders, *J. Chem. Soc. Chem. Commun.* **1988**, 692; b) H. L. Anderson, C. A. Hunter, J. K. M. Sanders, *J. Chem. Soc. Chem. Commun.* **1989**, 226; c) I. P. Danks, T. G. Lane, I. O. Sutherland, M. Yap, *Tetrahedron* **1992**, *48*, 7679; d) M. J. Crossley, L. G. Mackay, A. C. Try, *J. Chem. Soc. Chem. Commun.* **1995**, 1925; e) X. Huang, B. H. Rickman, B. Borhan, N. Berova, K. Nakanishi, *J. Am. Chem. Soc.* **1998**, *120*, 6185.

[8] a) X. Zhou, K. S. Chan, *J. Org. Chem.* **1998**, *63*, 99; b) A. G. Hyslop, M. A. Kellett, P. M. Ivovine, M. J. Therien, *J. Am. Chem. Soc.* **1998**, *120*, 12676; c) L. Yu, J. S. Lindsey, *Tetrahedron* **2001**, *57*, 9285; d) N. Aratani, A. Osuka, *Org. Lett.* **2001**, *3*, 4213.

[9] The observed fluorescence upon addition of acetic acid was the same as that of nonprotonated free-base porphyrin, thus excluding the formation of dicationic species in toluene solution. As about 1000-fold excess of acetic acid was needed to recover the fluorescence of the free base porphyrin in **7DA–4**, therefore the switching cycle only occurs once at the present stage.

 © 2003 Wiley-VCH Verlag GmbH & Co. KGaA, Weinheim

Small-Molecule Inhibitors

Benzoxazoles as Transthyretin Amyloid Fibril Inhibitors: Synthesis, Evaluation, and Mechanism of Action**

*Hossein Razavi, Satheesh K. Palaninathan, Evan T. Powers, R. Luke Wiseman, Hans E. Purkey, Nilofar N. Mohamedmohaideen, Songpon Deechongkit, Kyle P. Chiang, Maria T. A. Dendle, James C. Sacchettini, and Jeffery W. Kelly**

Transthyretin (TTR) is one of twenty nonhomologous proteins, the misfolding, aggregation, and deposition (amyloidogenesis) of which is linked to amyloid disease.[1,2] TTR is a homotetramer composed of 127 amino acid subunits[3] that carries thyroxine[4] and holo-retinol binding protein[5] in the blood. The TTR tetramer is non-amyloidogenic, but undergoes dissociation, monomer misfolding, and misassembly into numerous aggregated structures including amyloid under partially denaturing conditions (for example, at low pH values).[6] Amyloidogenesis by wild type (wt) TTR appears to cause senile systemic amyloidosis,[7] whereas amyloidogenesis by one of over 80 TTR mutants results in either familial amyloid polyneuropathy[8] or cardiomyopathy.[9] Incorporation of T119M *trans*-suppressor subunits into tetramers otherwise composed of disease-associated subunits (such as V30M or L55P) inhibits amyloidogenesis in vitro and ameloriates disease in V30M carriers by increasing the dissociative activation barrier and thereby kinetically stabilizing the tetramer.[10,11] TTR has two largely unoccupied thyroxine

[*] Prof. J. W. Kelly, Dr. H. Razavi, Prof. E. T. Powers, R. L. Wiseman, Dr. H. E. Purkey, S. Deechongkit, K. P. Chiang, M. T. A. Dendle
Department of Chemistry and
The Skaggs Institute for Chemical Biology
The Scripps Research Institute
La Jolla, CA 92037 (USA)
Fax: (+1) 858-784-9610
E-mail: jkelly@scripps.edu
Dr. S. K. Palaninathan, Dr. N. N. Mohamedmohaideen, Prof. J. C. Sacchettini
Department of Biochemistry and Biophysics
Texas A & M University (USA)

[**] This work was supported by the NIH (DK 46335), the Skaggs Institute for Chemical Biology, and the Lita Annenberg Hazen Foundation. H.R. thanks the Skaggs Institute for Chemical Biology for a postdoctoral fellowship. Additional support was provided by the Robert A. Welch Foundation (J.C.S). Use of the Argonne National Laboratory Structural Biology Center beam lines at the Advanced Photon Source was supported by the United States Department of Energy, Office of Energy Research, under contract W-31-109-ENG-38. Use of the BioCARS Sector 14 was supported by the National Institutes of Health National Center for Research Resources. We thank the General Clinical Research Center of The Scripps Research Institute (supported by NIH grant RR00833) for providing blood plasma through the normal donor blood drawing program.

Supporting information for this article (experimental and crystallographic details) is available on the WWW under http://www.angewandte.org or from the author.

 © 2003 Wiley-VCH Verlag GmbH & Co. KGaA, Weinheim DOI: 10.1002/anie.200351179

binding sites that are created by its quaternary structural interface.[12] The tetramer can be stabilized by small-molecule-binding to these sites, potentially providing a means to treat TTR amyloid disease with small-molecule drugs.[13] Many families of compounds have been discovered, the binding of which stabilizes the tetrameric ground state to a degree proportional to the small-molecule dissociation constants K_{d1} and K_{d2}.[11] This binding also effectively increases the dissociative activation barrier and inhibits amyloidosis by kinetic stabilization.[11] Such inhibitors are typically composed of two aromatic rings, with one ring bearing halogen substituents and the other bearing hydrophilic substituents.[13–20] Benzoxazoles substituted with a carboxylic acid at C4–C7 and a halogenated phenyl ring at C2 also appeared to complement the TTR thyroxine binding site. A small library of these compounds was therefore prepared by dehydrocyclization of *N*-acyl amino hydroxybenzoic acids (Scheme 1).[21,22]

The benzoxazoles were evaluated by using a series of analyses of increasing stringency. A previously developed fibril-formation assay was used as the first screen.[13,15] wt TTR (3.6 μM) was incubated for 30 min (pH 7, 37 °C) with a test compound (7.2 μM). Since at least one molecule

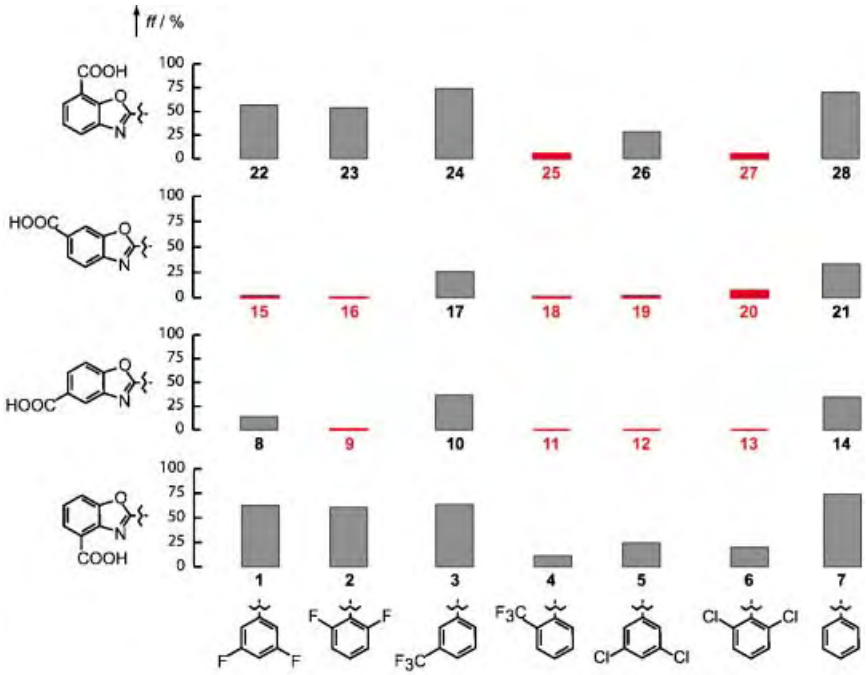
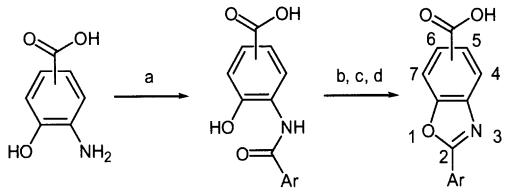


Figure 1. Suppression of TTR fibril formation by compounds **1**–**28**. The position of the carboxy group on the benzoxazole is shown on the left-hand side, while the C2 phenyl ring is shown at the bottom. The bars indicate the percent fibril formation (*ff*), that is, the amount of fibrils formed from TTR in the presence of **1**–**28** relative to the amount formed by TTR in the absence of inhibitor (which is defined as 100%). The most effective compounds (lowest *ff*) are indicated in red.



Scheme 1. General synthesis of benzoxazoles: a) ArCOCl, THF, pyridine (Ar = phenyl, 3,5-difluorophenyl, 2,6-difluorophenyl, 3,5-dichlorophenyl, 2,6-dichlorophenyl, 2-(trifluoromethyl)phenyl, and 3-(trifluoromethyl)phenyl); b) $TsOH \cdot H_2O$ (Ts = tosyl), refluxing xylenes; c) $TMSCHN_2$, benzene, MeOH; d) LiOH, THF, MeOH, H_2O (8–27% yield over four steps).

of the test compound must bind to each molecule of TTR tetramer to be able to stabilize it, a test compound concentration of 7.2 μM is only twice the minimum effective concentration. The pH value was then adjusted to 4.4, the optimal pH for fibrilization. The amount of amyloid formed after 72 h (37 °C) in the presence of the test compound was determined by turbidity at 400 nm and is expressed as % fibril formation (*ff*), 100% being the amount formed by TTR alone. Of the 28 compounds tested, 11 reduced fibril formation to negligible levels ($ff < 10\%$; Figure 1, red bars).

The 11 most-active compounds were then evaluated for their ability to bind selectively to TTR over all other proteins in the blood.[23] Human blood plasma (TTR conc. 3.6–5.4 μM) was incubated for 24 h with the test compound (10.8 μM) at 37 °C. The TTR and any bound inhibitor were immunoprecipitated using a sepharose-bound polyclonal TTR antibody. The TTR with or without bound inhibitor was liberated from the resin at high pH value, and the inhibitor:TTR stoichiometry was ascertained by HPLC analysis (Figure 2).[23] Benzoxazoles with carboxylic acids in the 5- or 6-position, and 2,6-dichlorophenyl (**13**, **20**) or 2-trifluoromethylphenyl (**11**, **18**) substituents at the 2-position displayed the highest binding stoichiometries. In particular, **20** exhibited excellent inhibitory activity and binding selectivity. Hence, its mechanism of action was characterized further.

To confirm that **20** inhibits TTR fibril formation by binding strongly to the tetramer, isothermal titration calo-

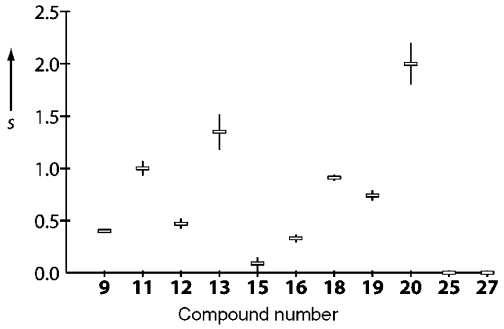


Figure 2. Stoichiometry (*s*) of benzoxazoles bound to TTR after incubation in human blood plasma; the maximum possible value of *s* is 2. The thin vertical lines indicate the measurement error. The stoichiometries shown are not corrected for wash-associated loss of small molecules and therefore are lower limits for the true stoichiometries.

 © 2003 Wiley-VCH Verlag GmbH & Co. KGaA, Weinheim

rimetry (ITC) and sedimentation velocity experiments were conducted with wt TTR. ITC showed that two equivalents of **20** bind with average dissociation constants of $K_{d1} = K_{d2} = 55$ (± 10) nM under physiological conditions. These values are comparable to the dissociation constants of many other highly efficacious TTR amyloidogenesis inhibitors. For the sedimentation velocity experiments, TTR (3.6 μM) was incubated with **20** (3.6 μM, 7.2 μM, 36 μM) under optimal fibrilization conditions (72 h, pH 4.4, 37 °C). The tetramer (55 kDa) was the only detectable species in solution with **20** at 7.2 or 36 μM. Some large aggregates formed with **20** at 3.6 μM, but the TTR remaining in solution was tetrameric.

T119M subunit inclusion and small-molecule binding both prevent TTR amyloid formation by raising the activation barrier for tetramer dissociation.[11] The ability of an inhibitor to do this is most rigorously tested by measuring its efficacy at slowing tetramer dissociation in 6 M urea, a severe denaturation stress.[11] Thus, the rates of TTR tetramer dissociation in 6 M urea in the presence and absence of **20**, **21**, or **27** were compared (Figure 3). TTR (1.8 μM) was completely dena-

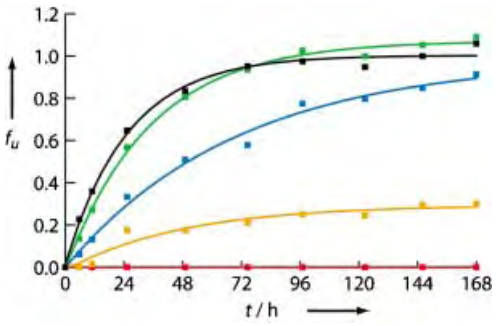


Figure 3. Dissociation as a function of time (t) for wt TTR (1.8 μM) in 6 M urea without inhibitor (——), or in the presence of 3.6 μM of **20** (——), **21** (——), or **27** (——), or 1.8 μM **20** (——). The dimensionless extent of tetramer dissociation (f_u, or fraction unfolded) was determined from the intensity of the circular dichroism spectrum at 215–218 nm. Although this is a measure of secondary structure, it corresponds indirectly to tetramer dissociation because dissociation must precede denaturation, and monomer denaturation is virtually irreversible and instantaneous in 6 M urea (the half time for denaturation is approximately 70 ms).

tured after 168 h in 6 M urea. In contrast, **20** at 3.6 μM prevented tetramer dissociation for at least 168 h (> 3 × the half-life of TTR in human plasma). With an equimolar amount of **20**, only 27% of TTR denatured in 168 h. Compound **27** (3.6 μM) was much less able to prevent tetramer dissociation (90% unfolding after 168 h), even though it was active in the fibril formation assay. Compound **21** did not hinder the dissociation of TTR at all. These results show that inhibitor binding to TTR is necessary but not sufficient to kinetically stabilize the TTR tetramer under strongly denaturing conditions; it is also important that the dissociation constants are very low (or that the off rates are very slow). Also, the arrangement of functional groups on **20** is apparently optimal for stabilizing the TTR tetramer; moving the carboxylic acid from C6 to C7, as in **27**, or removing the chlorines, as in **21**, severely diminishes its activity.

The role of the substituents in **20** is evident from its cocrystal structure with TTR (Figure 4). Compound **20** orients its two chlorine atoms near halogen binding pockets 2 and 2′ (so-called because they are occupied by iodine atoms when thyroxine binds to TTR). The 2,6 substitution pattern

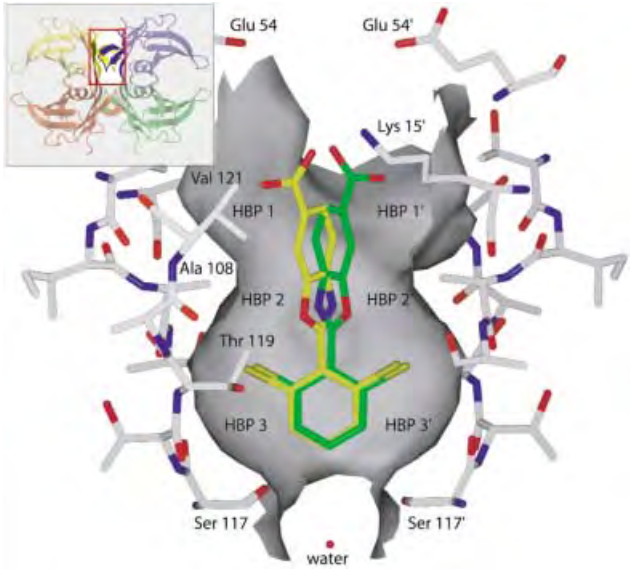


Figure 4. X-ray cocrystal structure of **20** bound to TTR. The green and yellow structures represent its two symmetry equivalent binding modes. The surface of the binding site is shown in gray. Equivalent residues in different subunits are distinguished with primed and unprimed residue numbers, as are the pairs of halogen binding pockets (HBPs). The inset shows an entire TTR tetramer (each subunit colored differently) with the binding site highlighted. Details of the crystal structure are given in the Supporting Information.

on the phenyl ring forces the benzoxazole and phenyl rings out of planarity, optimally positioning the carboxylic acid on the benzoxazole unit to hydrogen bond with the ε-NH_3^+ groups of Lys 15/15′. Hydrophobic and van der Waals interactions between the aromatic rings of **20** and the side chains of Leu 17, Leu 110, Ser 117, and Val 121 contribute additional binding energy (the side chains of Leu 17 and leu 110 obscure the view of **20** in Figure 4 and were therefore omitted for clarity).

In summary, 28 benzoxazole compounds were each prepared in four steps. Many of these compounds effectively inhibited TTR amyloid formation in vitro and bound selectively to TTR in blood plasma. Urea denaturation experiments demonstrated that **20** was particularly effective at kinetic stabilization of the TTR tetramer. The X-ray crystal structure of the TTR–**20** complex provides a structural basis for understanding its ability to stabilize the native state. The benzoxazole compounds presented here represent a new class of TTR inhibitors that may have better pharmacological properties than those described previously.[13–20] Their efficacy in vivo will be determined in animal models for TTR amyloidosis.[24]

 © 2003 Wiley-VCH Verlag GmbH & Co. KGaA, Weinheim

Experimental Section

The general procedure for benzoxazole synthesis and complete characterization of the products (^{1}H and ^{13}C NMR spectroscopy and high-resolution mass spectra) are given in the Supporting Information. The analytical ultracentrifugation and X-ray crystallography experiments are also detailed in the Supporting Information. The procedures for the fibril formation assay,[13,15] the immunoprecipitation assay,[23] ITC[14,20] and urea-induced dissociation kinetics[11] have been described elsewhere.

Received: February 13, 2003 [Z51179]

Keywords: aggregation · bioorganic chemistry · drug design · inhibitors · structure–activity relationships

[1] J. D. Sipe, *Crit. Rev. Clin. Lab. Sci.* **1994**, *31*, 325.
[2] J. W. Kelly, *Curr. Opin. Struct. Biol.* **1996**, *6*, 11.
[3] C. C. Blake, M. J. Geisow, S. J. Oatley, B. Rerat, C. Rerat, *J. Mol. Biol.* **1978**, *121*, 339.
[4] L. Bartalena, J. Robbins, *Clin. Lab. Med.* **1993**, *13*, 583.
[5] H. L. Monaco, *Biochim. Biophys. Acta* **2000**, *1482*, 65.
[6] J. W. Kelly, W. Colon, Z. Lai, H. A. Lashuel, J. McCulloch, S. L. McCutchen, G. J. Miroy, S. A. Peterson, *Adv. Protein Chem.* **1997**, *50*, 161.
[7] R. E. McCarthy III, E. K. Kasper, *Clin. Cardiol.* **1998**, *21*, 547.
[8] V. Plante-Bordeneuve, G. Said, *Curr. Opin. Neurobiol.* **2000**, *13*, 569.
[9] D. R. Jacobson, R. D. Pastore, R. Yaghoubian, I. Kane, G. Gallo, F. S. Buck, J. N. Buxbaum, *N. Engl. J. Med.* **1997**, *336*, 466.
[10] P. Hammarstrom, F. Schneider, J. W. Kelly, *Science* **2001**, *293*, 2459.
[11] P. Hammarstrom, R. L. Wiseman, E. T. Powers, J. W. Kelly, *Science* **2003**, *299*, 713.
[12] J. C. Sacchettini, J. W. Kelly, *Nat. Rev. Drug Discov.* **2002**, *1*, 267..
[13] G. J. Miroy, Z. Lai, H. A. Lashuel, S. A. Peterson, C. Strang, J. W. Kelly, *Proc. Natl. Acad. Sci. USA* **1996**, *93*, 15051.
[14] S. A. Peterson, T. Klabunde, H. A. Lashuel, H. Purkey, J. C. Sacchettini, J. W. Kelly, *Proc. Natl. Acad. Sci. USA* **1998**, *95*, 12956.
[15] P. W. Baures, S. A. Peterson, J. W. Kelly, *Bioorg. Med. Chem.* **1998**, *6*, 1389.
[16] P. W. Baures, V. B. Oza, S. A. Peterson, J. W. Kelly, *Bioorg. Med. Chem.* **1999**, *7*, 1339.
[17] V. B. Oza, H. M. Petrassi, H. E. Purkey, J. W. Kelly, *Bioorg. Med. Chem. Lett.* **1999**, *9*, 1.
[18] T. Klabunde, H. M. Petrassi, V. B. Oza, P. Raman, J. W. Kelly, J. C. Sacchettini, *Nat. Struct. Biol.* **2000**, *7*, 312.
[19] H. M. Petrassi, T. Klabunde, J. Sacchettini, J. W. Kelly, *J. Am. Chem. Soc.* **2000**, *122*, 2178.
[20] V. B. Oza, C. Smith, P. Raman, E. K. Koepf, H. A. Lashuel, H. M. Petrassi, K. P. Chiang, E. T. Powers, J. Sacchettinni, J. W. Kelly, *J. Med. Chem.* **2002**, *45*, 321.
[21] M. Terashima, M. Ishii, *Synthesis* **1982**, 484.
[22] M. R. DeLuca, S. M. Kerwin, *Tetrahedron* **1997**, *53*, 457.
[23] H. E. Purkey, M. I. Dorrell, J. W. Kelly, *Proc. Natl. Acad. Sci. USA* **2001**, *98*, 5566.
[24] M. H. Teng, J. Y. Yin, R. Vidal, J. Ghiso, A. Kumar, R. Rabenou, A. Shah, D. R. Jacobson, C. Tagoe, G. Gallo, J. Buxbaum, *Lab. Invest.* **2001**, *81*, 385.

 © 2003 Wiley-VCH Verlag GmbH & Co. KGaA, Weinheim

Azolato Coordination Modes

Coordination of 3,5-Diisopropyl-1,2,4-triazolato and 5-Phenyltetrazolato Ligands to the $[K([18]crown-6)]^+$ Fragment: Structural Insight into the Coordination of Nitrogen-Rich Azolato Ligands to Single Metal Centers**

*Wenjun Zheng, Mary Jane Heeg, and Charles H. Winter**

There is considerable interest in the coordination chemistry of anionic, five-membered, heterocyclic N ligands.[1–6] Much of this activity has centered on pyrazolato ligands,[1] and many new and unexpected coordination modes have been documented recently.[2] Theoretical predictions regarding the high stability of the pentazolate (N_5^-) ion suggest that metal complexes of this ligand might be stable enough to allow isolation.[5] Recent tantalizing results in this area include the first experimental detection of the N_5^- ion (in the gas phase),[6] as well as isolation and characterization of metal complexes containing the isoelectronic P_5^- ligand.[7] As experimental work moves inexorably toward ligands with higher nitrogen content,[3,4,6,8–10] a considerable barrier to development remains the formation of insoluble oligomeric or polymeric complexes in which the nitrogen atoms of the heterocyclic ligands bridge metal ions.[3,9,10] Coordination modes of 1,2,4-triazolato and tetrazolato ligands to single metal centers remain poorly developed so far. Several examples of η^1 coordination of 1,2,4-triazolato and tetrazolato ligands are known.[3,4,11] However, η^2 coordination of 1,2,4-triazolato ligands to single metal centers has only recently been reported for $[(t\mathrm{Bu_2pz})_3\mathrm{Ti}(\eta^2\text{-}\mathrm{Me_2tz})]$ ($t\mathrm{Bu_2pz}$ = 3,5-di-*tert*-butylpyrazolato, $\mathrm{Me_2tz}$ = 3,5-dimethyltriazolato)[4] and $[\mathrm{Ti}(\eta^2\text{-}i\mathrm{Pr_2tz})_4]$ ($i\mathrm{Pr_2tz}$ = 3,5-diisopropyl-1,2,4-triazolato).[8] A related compound, benzotriazolatopotassium, contains η^2 bonding interactions within a more complex bridging structure.[9] η^2 Bonding interactions within more complex bridging coordination modes of tetrazolato ligands are restricted to $[\{(\mathrm{C_5H_4(CH_3)})_2\mathrm{Ln}(\mu{:}\eta^2(N,N'),\eta^1(N')\text{-Phttz})\}_2]$ (Ln = Yb, Gd, Dy, Er; Phttz = 5-phenyltetrazolato)[12a] and 5-cyanotetrazolatocesium.[12b] Other structurally authenticated coordination modes of 1,2,4-triazolato and tetrazolato ligands have not been reported to date.

Herein, we report the synthesis, structure, and properties of 3,5-diisopropyl-1,2,4-triazolato and 5-phenyltetrazolato complexes of the ([18]crown-6)potassium fragment. These complexes exhibit slipped terminal η^2 coordination of the

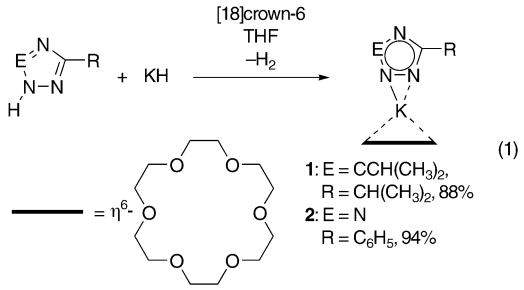
[*] Professor Dr. C. H. Winter, Dr. W. Zheng, Dr. M. J. Heeg
Department of Chemistry
Wayne State University
Detroit, MI 48202 (USA)
Fax: (+1) 313-577-8289
E-mail: chw@chem.wayne.edu

[**] We thank the Office of Naval Research (contract number N00014-21-0-866) and the National Science Foundation (grant number CHE-9807269) for support of this research.

 DOI: 10.1002/anie.200250485 © 2003 Wiley-VCH Verlag GmbH & Co. KGaA, Weinheim

heterocyclic ligands to the metal centers. The potassium ion normally bonds to anionic five-membered nitrogen heterocyclic ligands with a variety of bridging coordination modes,[9,13,14] so the terminal coordination described herein is particularly novel. In addition, the results suggest that (pentazolato)([18]crown-6)potassium is a potential target for stabilization of the pentazolate ion on a metal center.

Treatment of 3,5-diisopropyltriazole[15a] or 5-phenyltetrazole[15b] with potassium hydride and [18]crown-6 in THF at ambient temperature led to slow hydrogen evolution and formation of (3,5-diisopropyl-1,2,4-triazolato)([18]crown-6)potassium (**1**, 88%) and (5-phenyltetrazolato)([18]crown-6)potassium (**2**, 94%) as white crystalline solids [Eq. (1)]. Complexes **1** and **2** can be alternatively prepared by a two-



(1)

step sequence in which the potassium salts are formed first, and are then treated with [18]crown-6. Both **1** and **2** are very soluble in alcohols and hot THF, and are easily crystallized from the latter. The microanalytical data are consistent with the proposed formulations, and the ^{1}H and ^{13}C{^{1}H} NMR spectroscopy data in [D$_4$]methanol show the expected signals for the nitrogen heterocycles and [18]crown-6 ligands. The single set of signals for the isopropyl groups in **1** and the sharp single resonances of the [18]crown-6 ligands in **1** and **2** suggest that the ligands are involved in dynamic exchange processes in solution at room temperature.

Complexes **1** and **2** exist in the solid state as monomers that contain η^6-[18]crown-6 ligands[2c,16] and slipped η^2-3,5-diisopropyl-1,2,4-triazolato (in **1**) or slipped η^2-phenyltetrazolato (in **2**) ligands (Figures 1 and 2).[17] There are no intermolecular bonding interactions. The K–N bond lengths in **1** (2.709(3), 3.304(3) Å) and **2** (2.744(2), 3.102(3) Å) indicate slipped η^2 bonding,[19] as opposed to the more common idealized η^2 bonding. Roesky, Mösch-Zanetti and co-workers previously documented a difference in bond length of 0.475 Å as an example of extreme slippage in an aluminum complex containing an η^2-pyrazolato ligand.[19c] The bond-length difference of 0.595 Å in **1** is similar to, or slightly shorter than, that in the aforementioned aluminum pyrazolato complex, given the difference in ionic radii between potassium (1.38 Å) and aluminum (0.535 Å).[20] By the same argument, the bond-length difference in **2** of 0.358 Å clearly places it within the regime of slipped η^2 bonding. The shorter K–N bond lengths in **1** and **2** are comparable to those in [K(Ph$_2$pz)(thf)]$_6$ (2.76–2.87 Å),[13] while the longer K–N bond lengths are comparable to or longer than the related values in structurally characterized [K([18]crown-6)(en)]$^+$ fragments (2.88–3.08 Å; en = ethylenediamine).[16d,e] The K–O bond lengths (**1**, 2.789–2.934 Å; **2**, 2.777–2.926 Å) are similar to those in other potassium complexes containing η^6-[18]crown-6 ligands.[2c,16] In **1**, the KN$_2$ plane and triazolato ligand core are nearly coplanar (angle between least-squares planes: 2.1°). By contrast, the corresponding planes in **2** deviate from coplanarity by 19.5°. Interestingly, **2** exists as the η^2-1,2 isomer, as opposed to the η^2-2,3 isomer. We have previously reported molecular orbital calculations that predict the η^2-1,2 and η^2-2,3 isomers to differ in energy by less than 0.8 kcal mol^{-1} in model titanium complexes.[4a] In the case of **2**, formation of the 1,2 isomer may be a result of the higher basicity of the N atoms.

Complexes **1** and **2** contain slipped η^2-azolato ligands, in which one K–N bond is 0.36–0.60 Å longer than the other. Slipped η^2-pyrazolato ligands have been documented in several different metal complexes,[19] but the asymmetry in

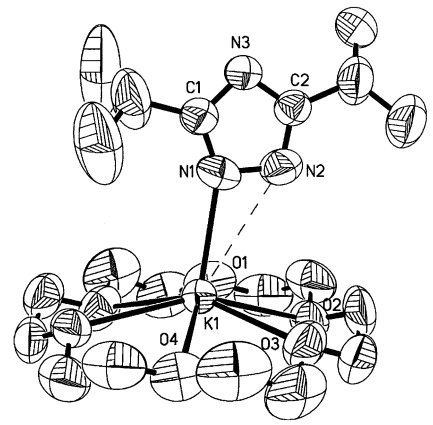


Figure 1. Perspective view of **1**. Selected interatomic distances [Å] and angles [°]: K1–N1 2.709(3), K1–N2 3.304(3), K1···N3 4.902(3), K1–O1 2.789(2), N1–N2 1.380(4), C1–N1 1.293(4), C1–N3 1.329(4); C1-N1-K1 151.0(3), C2-N2-K1 157.3(2), N1-K1-O1 91.19(10), N2-K1-O2 73.31(8), N2-K1-O1 84.29(9), N1-K1-N2 24.02(9).

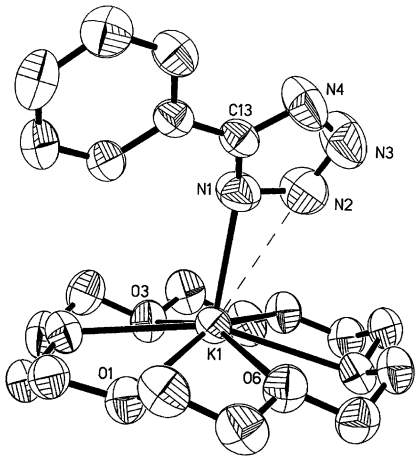


Figure 2. Perspective view of **2**. Selected bond lengths [Å] and angles [°]: K1–N1 2.744(2), K1–N2 3.102(3), K1–O1 2.926(3), N1–N2 1.341(3), N2–N3 1.299(3), N3–N4 1.342(3); K1-N2-N3 160.22(17), K1-N1-C13 153.62(13), N1-K1-N2 25.60(5).

 © 2003 Wiley-VCH Verlag GmbH & Co. KGaA, Weinheim

the metal–nitrogen bond lengths was clearly attributable to steric crowding. In **1** and **2**, the steric demands of the C-bound substituents of the azolato ligands are not particularly high, and so the slipped η^2 bonding cannot be a result of to steric crowding. The structural distortions observed in **1** and **2**, that is, the slipped η^2 coordination modes and the bending in **2**, must reflect optimization of the bonding interactions between the azolato ligands and the potassium center. The bending in **2** suggests that the basicity of the in-plane nitrogen lone pairs is reduced in tetrazolato ligands to the point where the out-of-plane π orbitals may be similar in energy. The results of this study are of fundamental importance, and have implications for efforts to prepare metal complexes containing pentazolato ligands. In particular, **2** is thermally stable and shows no tendency to undergo cycloreversion to benzonitrile and (azido)([18]crown-6)potassium.[21] Accordingly, it is possible that (pentazolato)([18]crown-6)potassium may exhibit a similar stability toward loss of dinitrogen, and might therefore possess sufficient thermal stability to allow its isolation. The slipped η^2-azolato ligands in **1** and **2** suggest that a similar coordination mode could be present in (pentazolato)([18]-crown-6)potassium. However, extrapolation of the bending observed in **2** to the pentazolato ligand raises the intriguing possibility that (pentazolato)([18]crown-6)potassium may exist with a facial η^2-pentazolato ligand or even an η^5-pentazolato ligand. In this vein, similar bending features have been found in related 1,2,4-di-*tert*-butyltriphospholylato and 1,4,2-di-*tert*-butylstibadiphospholylato complexes of lanthanide ions.[22] Additionally, recent theoretical studies predicted that bis(η^5-pentazolato)iron(II) is stable thermodynamically and may have sufficiently thermal stability to allow isolation.[5a,b]

Experimental Section

Complexes **1** and **2** were not noticeably affected by short exposure to air, but were hygroscopic upon extended exposure. Accordingly, all manipulations were performed under a purified argon atmosphere using standard Schlenk techniques.

1: A mixture of 3,5-diisopropyl-1,2,4-triazole (1.53 g, 10.0 mmol), potassium hydride (0.42 g, 10.5 mmol), and [18]crown-6 (2.77 g, 10.5 mmol) in THF (100 mL) was stirred at ambient temperature for 5 h until hydrogen evolution was complete. The volatile components were then removed under reduced pressure, and the resulting residue was washed with hexane to afford **1** as an analytically pure white solid (4.01 g, 88%); m.p. 167°C; ^{1}H NMR (400 MHz, CD_3OD, 23°C, TMS): $\delta = 3.61$ (s, 24H; OCH_2), 3.01 (septet, $^2J = 7.2$ Hz, 2H; CH), 1.27 ppm (d, $^2J = 7.2$ Hz, 12H; CH_3); ^{13}C{^{1}H} NMR (100 MHz, CD_3OD, 23°C, TMS): $\delta = 168.23$ (s; NCCH), 71.33 (s; OCH_2), 29.15 (s; *C*HCH_3), 22.59 ppm (s; CH_3); MS (EI): *m*/*z* (%): 303 (100) [K([18]crown-6)]$^+$; Elemental analysis (%) calcd for $C_{20}H_{38}KN_3O_6$: C 52.72, H 8.41, N 9.22; found: C 52.59, H 8.34, N 9.24. Single crystals suitable for X-ray diffraction analysis were obtained from THF/hexane (1/1) at −20°C.

2: In a fashion similar to the preparation of **1**, reaction of 5-phenyltetrazole (1.46 g, 10.0 mmol), potassium hydride (0.42 g, 10.5 mmol), and [18]crown-6 (2.77 g, 10.5 mmol) afforded **2** as a white solid (4.22 g, 94%); m.p. 157°C; ^{1}H NMR (400 MHz, CD_3OD, 23°C, TMS): $\delta = 7.27$, 7.28 (m, 5H; aromatic CH), 3.41 ppm (s, 24H; OCH_2); ^{13}C{^{1}H} NMR (100 MHz, CD_3OD, 23°C, TMS): $\delta = 162.93$ (s; tetrazolato ring CN), 131.42 (s; Ph ring CH), 129.71 (s; overlapping Ph ring CH and *ipso*-C), 127.73 (s; Ph ring CH), 71.31 ppm (s; CH_2); MS (EI): *m*/*z* (%): 303 (100) [K([18]crown-6)]$^+$; Elemental analysis (%) calcd for $C_{19}H_{29}KN_4O_6$: C 50.88, H 6.52, N 12.49; found: C 50.32, H 6.46, N 12.55. Single crystals suitable for X-ray diffraction analysis were obtained from THF at ambient temperature.

Received: November 6, 2002
Revised: December 16, 2002 [Z50485]

Keywords: coordination modes · N ligands · potassium · pyrazolates

[1] For reviews on pyrazolato complexes, see a) F. Nief, *Eur. J. Inorg. Chem.* **2001**, 891–904; b) J. E. Cosgriff, G. B. Deacon, *Angew. Chem.* **1998**, *110*, 298–299; *Angew. Chem. Int. Ed.* **1998**, *37*, 286–287; c) G. La Monica, G. A. Ardizzoia, *Prog. Inorg. Chem.* **1997**, *46*, 151–238; d) A. P. Sadimenko, S. S. Basson, *Coord. Chem. Rev.* **1996**, *147*, 247–297; e) S. Trofimenko, *Prog. Inorg. Chem.* **1986**, *34*, 115–210; f) S. Trofimenko, *Chem. Rev.* **1972**, *72*, 497–508.

[2] For selected recent examples of pyrazolato coordination modes to single metal centers, see a) η^1: L. R. Falvello, J. Fornies, A. Martin, R. Navarro, V. Sicilia, P. Villarroya, *Chem. Commun.* **1998**, 2429–2430 (C-bonded); W. Zheng, H. W. Roesky, M. Noltemeyer, *Organometallics* **2001**, *20*, 1033–1035 (N-bonded); b) η^2: G. B. Deacon, C. M. Forsyth, A. Gitlits, R. Harika, P. C. Junk, B. W. Skelton, A. H. White, *Angew. Chem.* **2002**, *114*, 3383–3385; *Angew. Chem. Int. Ed.* **2002**, *41*, 3249–3251; G. B. Deacon, E. E. Delbridge, B. W. Skelton, A. H. White, *Angew. Chem.* **1998**, *110*, 2373–2373; *Angew. Chem. Int. Ed.* **1998**, *37*, 2251–2252; I. A. Guzei, A. G. Baboul, G. P. A. Yap, A. L. Rheingold, H. B. Schlegel, C. H. Winter, *J. Am. Chem. Soc.* **1997**, *119*, 3387–3388; c) η^3: G. B. Deacon, E. E. Delbridge, C. M. Forsyth, *Angew. Chem.* **1998**, *110*, 1880–1882; *Angew. Chem. Int. Ed.* **1999**, *38*, 1766–1767; d) η^5: J. R. Perera, M. J. Heeg, H. B. Schlegel, C. H. Winter, *J. Am. Chem. Soc.* **1999**, *121*, 4536–4537; A. Steiner, G. T. Lawson, B. Walfort, D. Leusser, D. Stalke, *J. Chem. Soc. Dalton Trans.* **2001**, 219–221; G. B. Deacon, A. Gitlits, P. W. Roesky, M. R. Bürgstein, K. C. Lim, B. W. Skelton, A. H. White, *Chem. Eur. J.* **2001**, *7*, 127–138.

[3] Recent review on the coordination chemistry of 1,2,4-triazole-derived ligands: J. G. Haasnoot, *Coord. Chem. Rev.* **2000**, *200–202*, 131–185.

[4] For leading references to the coordination chemistry of 1,2,4-triazolato and tetrazolato ligands, see a) C. Yélamos, K. R. Gust, A. G. Baboul, M. J. Heeg, H. B. Schlegel, C. H. Winter, *Inorg. Chem.* **2001**, *40*, 6451–6462; b) N. C. Mösch-Zanetti, M. Ferbinteanu, J. Magull, *Eur. J. Inorg. Chem.* **2002**, 950–956.

[5] Selected recent papers describing theoretical studies on N_5^- ions and metal complexes thereof: a) J. Frunzke, M. Lein, G. Frenking, *Organometallics* **2002**, *21*, 3351–3359; b) M. Lein, J. Frunzke, A. Timoshkin, G. Frenking, *Chem. Eur. J.* **2001**, *7*, 4155–4163; c) L. A. Burke, R. N. Butler, J. C. Stephens, *J. Chem. Soc. Perkin Trans. 2* **2001**, 1679–1684; d) S. Fau, K. J. Wilson, R. J. Bartlett, *J. Phys. Chem. A* **2002**, *106*, 4639–4644; e) L. Gagliardi, G. Orlandi, S. Evangelisti, B. O. Roos, *J. Chem. Phys.* **2001**, *114*, 10733–10737; f) X. Wang, H.-R. Hu, A. Tian, N. B. Wong, S.-H. Chien, W.-K. Li, *Chem. Phys. Lett.* **2000**, *329*, 483–489; g) S. A. Perera, R. J. Bartlett, *Chem. Phys. Lett.* **1999**, *314*, 381–387; h) M. N. Glukhovtsev, P. von R. Schleyer, C. Maerker, *J. Phys. Chem.* **1993**, *97*, 8200–8206.

[6] A. Vij, J. G. Pavlovich, W. W. Wilson, V. Vij, K. O. Christie, *Angew. Chem.* **2002**, *114*, 3177–3180; *Angew. Chem. Int. Ed.* **2002**, *41*, 3051–3054.

[7] For selected leading references to P_5^- complexes, see E. Urzenius, W. W. Brennessel, C. J. Cramer, J. E. Ellis, P. von R. Schleyer, *Science* **2002**, *295*, 832–834; P. Sekar, M. Scheer, A.

 © 2003 Wiley-VCH Verlag GmbH & Co. KGaA, Weinheim

Voigt, R. Kirmse, *Organometallics* **1999**, *18*, 2833 – 2837; O. J. Scherer, T. Hilt, G. Wolmershäuser, *Organometallics* **1998**, *17*, 4110 – 4112; M. Detzel, G. Friedrich, O. J. Scherer, G. Wolmershäuser, *Angew. Chem.* **1995**, *107*, 1454 – 1456; *Angew. Chem. Int. Ed. Engl.* **1995**, *34*, 1321 – 1325; A. K. Hughes, V. J. Murphy, D. O'Hare, *J. Chem. Soc. Chem. Commun.* **1994**, 163 – 164; B. Rink, O. J. Scherer, G. Wolmershäuser, *Chem. Ber.* **1995**, *128*, 71 – 73; B. Rink, O. J. Scherer, G. Heckmann, G. Wolmershäuser, *Chem. Ber.* **1992**, *125*, 1011 – 1016.

[8] N. C. Mösch-Zanetti, M. Hewitt, T. R. Schneider, J. Magull, *Eur. J. Inorg. Chem.* **2002**, 1181 – 1185.

[9] P. C. Andrews, W. Clegg, R. E. Mulvey, P. A. O'Neil, H. M. M. Wilson, *J. Chem. Soc. Chem. Commun.* **1993**, 1142 – 1143.

[10] For leading references to complexes with bridging tetrazolato ligands, see L. Carlucci, G. Ciani, D. M. Proserpio, *Angew. Chem.* **1999**, *111*, 3700 – 3704; *Angew. Chem. Int. Ed.* **1999**, *38*, 3488 – 3492; E. O. John, R. D. Willett, B. Scott, R. L. Kirchmeier, J. M. Shreeve, *Inorg. Chem.* **1989**, *28*, 893 – 897.

[11] Crystallographically characterized η^1-1,2,4-tetrazolato and η^1-tetrazolato ligands coordinated to single metal centers from a Cambridge Crystallographic Database search (version 5.23, April 2002): R. Hage, J. G. Haasnoot, J. Reedijk, R. Wang, E. M. Ryan, J. G. Vos, A. L. Spek, A. J. M. Duisenberg, *Inorg. Chim. Acta* **1990**, *174*, 77 – 85; B. E. Buchanan, J. G. Vos, M. Kaneko, W. J. M. van der Putten, J. M. Kelly, R. Hage, R. A. G. de Graaff, R. Prins, J. G. Haasnoot, J. Reedijk, *J. Chem. Soc. Dalton Trans.* **1990**, 2425 – 2431; R. Hage, J. P. Turkenburg, R. A. G. De Graaff, J. G. Haasnoot, J. Reedijk, *Acta Crystallogr. Sect. C* **1989**, *45*, 381 – 383; S. Bhandari, C. G. Frost, C. E. Hague, M. F. Mahon, K. C. Molloy, *J. Chem. Soc. Dalton Trans.* **2000**, 663 – 669; S. Bhandhari, M. F. Mahon, K. C. Molloy, J. S. Palmer, S. F. Sayers, *J. Chem. Soc. Dalton Trans.* **2000**, 1053 – 1060; T. M. Becker, J. A. Krause-Bauer, C. L. Homrighausen, M. Orchin, *Polyhedron* **1999**, *18*, 2653 – 2571; K. D. Demadis, E.-S. El Samanody, T. J. Meyer, P. S. White, *Inorg. Chem.* **1998**, *37*, 838 – 839; B. Morosin, R. G. Dunn, R. Assink, T. M. Massis, J. Fronaberger, E. N. Duesler, *Acta Crystallogr. Sect. C* **1997**, *53*, 1609 – 1611; R. Guilard, I. Perrot, A. Tabard, P. Richard, C. Lecomte, Y. H. Liu, K. M. Kadish, *Inorg. Chem.* **1991**, *30*, 27 – 37; R. Das, P. Paul, K. Nag, K. Venkatsubramanian, *Inorg. Chim. Acta* **1991**, *185*, 221 – 227.

[12] a) X.-G. Zhou, Z.-E. Huang, R.-F. Cai, L.-X. Zhang, X.-F. Hou, X.-J. Feng, X.-Y. Huang, *J. Organomet. Chem.* **1998**, *563*, 101 – 112; b) H. P. H. Arp, A. Decken, J. Passmore, D. J. Wood, *Inorg. Chem.* **2000**, *39*, 1840 – 1848.

[13] C. Yélamos, M. J. Heeg, C. H. Winter, *Inorg. Chem.* **1998**, *37*, 3892 – 3894.

[14] For potassium complexes of tris(pyrazolyl)borate and related ligands, see Z. Hu, S. M. Gorun, *Inorg. Chem.* **2001**, *40*, 667 – 671; C. Janiak, S. Temizdemir, S. Dechert, *Inorg. Chem. Commun.* **2000**, *3*, 271 – 275; H. V. R. Dias, J. D. Gorden, *Inorg. Chem.* **1996**, *35*, 318 – 324; H. V. R. Dias, W. Jin, H.-J. Kim, H.-L. Lu, *Inorg. Chem.* **1996**, *35*, 2317 – 2328; C. Janiak, *Chem. Ber.* **1994**, *127*, 1379 – 1385.

[15] a) R. Grüner, Z. Benes, E. Schuber, M. Arman, *Monatsh. Chem.* **1927**, *48*, 37 – 46; b) Purchased commercially.

[16] For selected recent reports on structurally characterized complexes containing the $[K([18]crown-6)]^+$ fragment, see a) S. Neander, F. E. Tio, R. Buschumann, U. Behrens, F. Olbrich, *J. Organomet. Chem.* **1999**, *582*, 58 – 65; b) S. Neander, U. Behrens, F. Olbrich, *J. Organomet. Chem.* **2000**, *604*, 59 – 67; c) M. C. Cassani, Y. K. Gun'ko, P. B. Hitchcock, A. G. Hulkes, A. V. Khvostov, M. F. Lappert, A. V. Protechenko, *J. Organomet. Chem.* **2002**, *647*, 71 – 83; d) C. Downie, Z.-J. Tang, A. M. Guloy, *Angew. Chem.* **2000**, *112*, 346 – 348; *Angew. Chem. Int. Ed.* **2000**, *39*, 338 – 340; e) T. F. Fässler, R. Hoffmann, *Angew. Chem.* **1999**, *111*, 526 – 529; *Angew. Chem. Int. Ed.* **1999**, *38*, 543 – 545.

[17] X-ray structure determinations: The data were collected on a Siemens/Bruker P4-CCD instrument at 295(2) K with graphite-monochromated $Mo_{K\alpha}$ radiation ($\lambda = 0.71073$ Å). The structures were solved and refined on all F^2 with the programs of SHELXS-97.[18] **1**: $C_{20}H_{38}KN_3O_6$, $M_r = 455.63$, monoclinic, space group $P2(1)/c$, $a = 14.2681(15)$, $b = 9.8984(12)$, $c = 18.767(2)$ Å, $\beta = 103.605(3)°$, $V = 2576.1(5)$ Å^3, $Z = 4$, $\rho_{calcd} = 1.175$ g cm^{-3}, crystal size: $0.50 \times 0.40 \times 0.20$ mm, $F(000) = 984$, $\mu(Mo_{K\alpha}) = 0.242$ mm^{-1}. The total number of reflections measured was 18035 in the range $4 \le 2\theta \le 57°$, of which 5968 were unique. Final R indices: $R_1 = 0.0624$ ($I > 2\sigma(I)$) and $wR_2 = 0.2221$ (all data). Max./min. residual electron density: 0.61/−0.30 e Å^{-3}. **2**: $C_{19}H_{29}KN_4O_6$, $M_r = 448.56$, monoclinic, space group Cc, $a = 14.309(14)$, $b = 10.584(10)$, $c = 16.512(16)$ Å, $\beta = 114.93(2)°$, $V = 2268(4)$ Å^3, $Z = 4$, $\rho_{calcd} = 1.314$ g cm^{-3}, crystal size: $0.40 \times 0.40 \times 0.20$ mm, $F(000) = 952$, $\mu(Mo_{K\alpha}) = 0.275$ mm^{-1}. The total number of reflections measured was 8049 in the range $5 \le 2\theta \le 56.60°$, of which 4406 were unique. Final R indices: $R_1 = 0.0247$ ($I > 2\sigma(I)$) and $wR_2 = 0.0611$ (all data). Max./min. residual electron density: 0.12/−0.10 e Å^{-3}. CCDC-196712 (**1**) and CCDC-196713 (**2**) contain the supplementary crystallographic data for this paper. These data can be obtained free of charge via www.ccdc.cam.ac.uk/conts/retrieving.html (or from the Cambridge Crystallographic Data Centre, 12 Union Road, Cambridge CB2 1EZ, UK; fax: (+44) 1223-336-033; or deposit@ccdc.cam.ac.uk).

[18] G. M. Sheldrick, SHELXL-97, Program for Crystal Structure Refinement, University of Göttingen, Göttingen, Germany, **1997**.

[19] a) I. A. Guzei, G. P. A. Yap, C. H. Winter, *Inorg. Chem.* **1997**, *36*, 1738 – 1739; b) D. Pfeiffer, M. J. Heeg, C. H. Winter, *Angew. Chem.* **1998**, *110*, 2674 – 2676; *Angew. Chem. Int. Ed.* **1998**, *37*, 2517 – 2519; c) W. Zheng, N. C. Mösch-Zanetti, T. Blunck, H. W. Roesky, M. Noltemeyer, H.-G. Schmidt, *Organometallics* **2001**, *20*, 3299 – 3303.

[20] N. N. Greenwood, A. Earnshaw, *Chemistry of the Elements*, 2nd ed., Butterworth-Heinemann, Oxford, **1997**, pp. 75, 222.

[21] T. Koritsanszky, J. Buschmann, P. Luger, A. Knöchel, M. Patz, *J. Am. Chem. Soc.* **1994**, *116*, 6748 – 6756.

[22] G. B. Deacon, E. E. Delbridge, G. D. Fallon, C. Jones, D. E. Hibbs, M. B. Hursthouse, B. W. Skelton, A. H. White, *Organometallics* **2000**, *19*, 1713 – 1721; unpublished results described in G. K. Clentsmith, F. G. N. Cloke, P. B. Hitchcock, M. D. Francis, J. F. Nixon, A. G. Avent, *Eur. J. Inorg. Chem.* **2001**, 898.

 © 2003 Wiley-VCH Verlag GmbH & Co. KGaA, Weinheim

Organosulfur Conducting Bridges

Intramolecular Electron Transfer Mediated by a Tetrathiafulvalene Bridge in a Purely Organic Mixed-Valence System**

Nicolas Gautier, Frédéric Dumur, Vega Lloveras, José Vidal-Gancedo, Jaume Veciana, Concepció Rovira, and Piétrick Hudhomme**

Tetrathiafulvalene (TTF) and its derivatives have been successfully used as building blocks of low-dimensional organic conductors and superconductors where intermolecular electron-transfer phenomena play a key role in the electronic transport properties.[1] Important results have been also achieved using TTFs as versatile strong π-donor systems in materials chemistry,[2] particularly in intramolecular charge-transfer materials for donor–acceptor molecules[3] or in photoinduced electron transfer when linked to [60]fullerene.[4] However, TTF has never been used as a bridge to promote electron conduction between two groups. Nowadays, unimolecular electronic devices are at the forefront of research in nanotechnology because of the anticipated limits to the further miniaturization of microelectronics.[5] Moreover, direct electronic conduction through single molecules has recently been demonstrated[6] showing the potential use of integrated molecular-sized devices. As a consequence, there is great interest in studying the role of various parameters that govern the intramolecular electron-transfer (IET) rates. Mixed-valence compounds are the prototypes of molecules able to undergo fast electron transfer through a bridge. Such systems have been widely used to study IET between redox centers of both inorganic[7] and organic nature,[8] with the aim of understanding electron-transfer processes to aid the design of molecular wires.[9]

One way to test the electron conduction through TTF is to use it as a bridge between two redox moieties in a mixed-valence system. Consequently, our target molecule was the TTF-diquinone **1**, Q-TTF-Q, since the *p*-benzoquinone groups are particularly useful organic redox centers to generate mixed-valence systems[10] that form persistent radical anions upon reduction.[11] The behavior of **1** has been studied by electrochemistry and ESR spectroscopy, and we have also performed the synthesis of the TTF-monoquinone **2**, TTF-Q, as a model compound.

Syntheses of **1** and **2** were achieved using the same key intermediate 2-oxo-1,3-dithiole derivative **7** (Scheme 1). The iminium salt **4** was prepared according to a previously described procedure.[12] After quantitative conversion to the 2-thioxo-1,3-dithiole **5**, the hydroquinone functionalities were protected using acetyl or silyl groups by well-established reactions. Further transchalcogenation of **6a** and **6b** furnished the 2-oxo-1,3-dithiole derivatives **7** in excellent yields. The triethylphosphite coupling methodology was applied to **7a** and the resulting TTF derivative **8** was transformed into the bis(1,4-hydroquinone)-TTF derivative by subsequent methanolysis in a methoxide solution and subsequent treatment with *p*-toluenesulfonic acid (PTSA). Without isolating the later intermediate, the fused Q-TTF-Q system **1** was obtained as green-blue crystals by selective oxidation using 2,3-dichloro-5,6-dicyano-1,2-benzoquinone (DDQ).To obtain the TTF-Q assembly **2**, the Horner–Wadsworth–Emmons olefination approach was applied to create the TTF core,[13] which involved the 2-oxo-1,3-dithiole functionality and the anion of phosphonate **9**.[14] After deprotection of the silyl groups of compound **10**, subsequent oxidation with *p*-benzoquinone afforded compound **2** as green crystals.

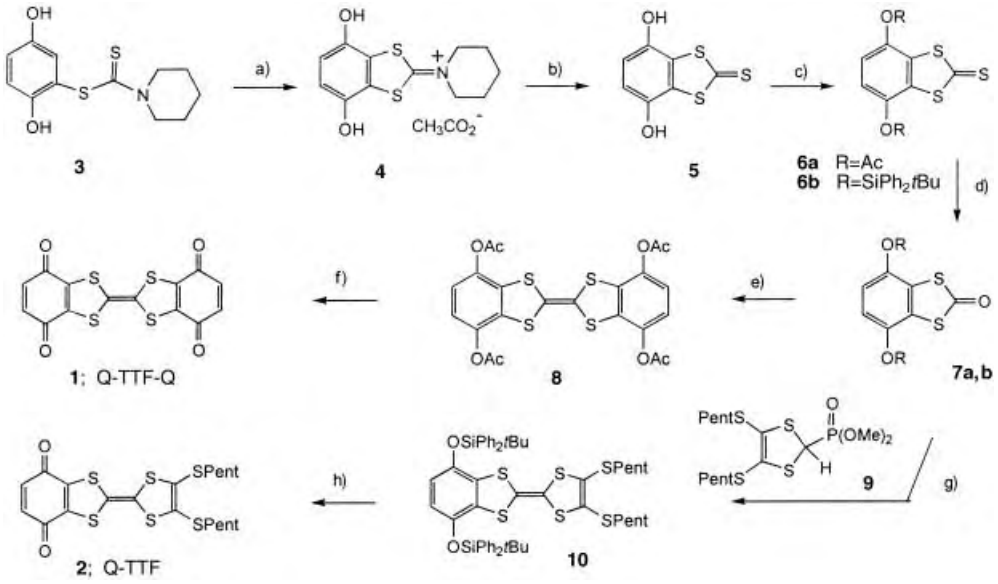
The cyclic voltammogram of **1** showed two one-electron reversible oxidation waves at $E^0_{ox1} = +0.99$ and $E^0_{ox2} = +1.36$ V (versus a Ag/AgCl electrode), which are characteristic for the TTF moiety, and two distinguishable reversible waves at $E^1_{red} = -0.20$ and -0.28 V, which correspond to the stepwise one-electron reduction of each *p*-quinone moiety. The potential difference of $\Delta E = 0.08$ V between the two waves indicates that the reduction of the second *p*-quinone group is somewhat affected by the presence of the first $Q^{-\bullet}$ center, and suggests that an effective electronic coupling exists between both Q centers, which is mediated by the TTF bridge.

We have studied the intramolecular electron-transfer process in the Q-TTF-$Q^{-\bullet}$ mixed-valence system by temperature-dependent ESR spectroscopy. Electrochemical or chemical reduction[15] of model compound **2** gives the TTF-$Q^{-\bullet}$, which gives an ESR spectrum that is characterized by three lines with 1:2:1 intensities that result from coupling with two equivalent aromatic protons ($a_H = 2.50$ G). This ESR spectrum was singularly invariant over a wide temperature range (270–360 K) and also with concentration, which shows that there is no intermolecular electron transfer in this system. In contrast, the ESR spectrum of the TTF-bridged mixed-valence anion radical Q-TTF-$Q^{-\bullet}$ changes upon cooling from 340 to 260 K (Figure 1). While the spectrum at 260 K was essentially identical to that of model compound TTF-$Q^{-\bullet}$ (three lines in 1:2:1 intensity, $a_H = 2.47$ G), the spectrum at temperatures higher than 340 K is characterized by the coupling of four equivalent aromatic protons (five lines in 1:4:6:4:1 intensity, $a_H = 1.23$ G; Figure 1a).[16] As the temperature is gradually lowered from 340 to 260 K, the alternate lines broaden and disappear because of extensive dynamic electron exchange between both of the Q electrophores through the TTF bridge (Scheme 2).[17] The lowest temper-

[*] Dr. C. Rovira, V. Lloveras, Dr. J. Vidal-Gancedo, Prof. J. Veciana
Institut de Ciència de Materials de Barcelona (CSIC)
Campus Universitari de Bellaterra, 08193 Cerdanyola (Spain)
Fax: (+34) 93-5805-729
E-mail: cun@icmab.es
Prof. P. Hudhomme, Dr. N. Gautier, Dr. F. Dumur
Ingénierie Moléculaire et Matériaux Organiques
UMR 6501, 2 Bd Lavoisier, Université d'Angers
49045 Angers (France)
Fax: (+33) 2-4173-5405
E-mail: pietrick.hudhomme@univ-angers.fr

[**] This work was partially supported by grants from the MENRT (for N.G.), the "Ville d'Angers" (for F.D.), DGI-Spain BQU2000-1157, and DURSI-Catalunya 2001SGR-00362. This research was undertaken as part of the European collaborative COST Program (Action D14/0004/99).

 DOI: 10.1002/anie.200250587 © 2003 Wiley-VCH Verlag GmbH & Co. KGaA, Weinheim



Scheme 1. Syntheses of **1** and **2**. Reagents: a) *p*-benzoquinone then glacial AcOH, 80 °C, 96%; b) $Na_2S{\cdot}9H_2O$, MeOH, 98%; c) Ac_2O, Et_3N, 80% for **6a**; $Ph_2tBuSiCl$, DMF, imidazole, 86% for **6b**; d) $Hg(OAc)_2$, CH_2Cl_2/glacial AcOH, 88% for **7a**, 85% for **7b**; e) Δ, $P(OEt)_3$, 45%; f) MeONa/MeOH, then PTSA and H_2O, then DDQ, 57%; g) phosphonate **9**, *n*BuLi, THF, −78 °C to 20 °C, 90%; h) nBu_4NF/THF then *p*-benzoquinone, 75%.

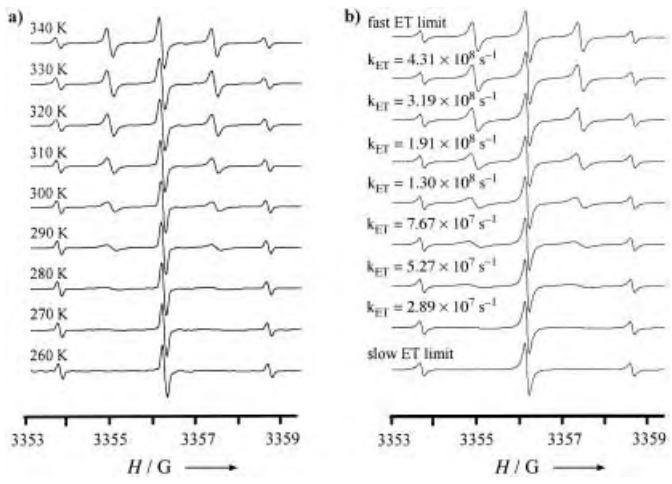
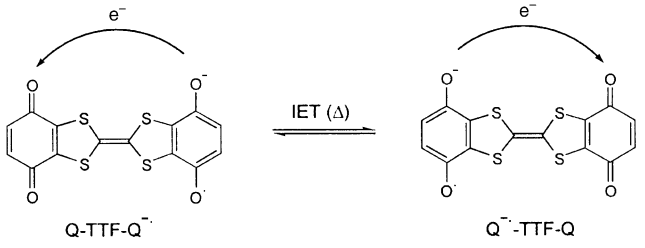


Figure 1. Experimental (a) and simulated (b) ESR spectra of $\mathbf{1}^{-\cdot}$ at different temperatures in ethyl acetate/*tert*-butanol (10:1) with PPh_4Br.



Scheme 2. Electron exchange through the TTF bridge.

ature spectrum unequivocally demonstrates that the odd electron of Q-TTF-$Q^{-\cdot}$ is localized on one particular Q unit on the ESR time scale, and as the temperature is raised the activation energy barrier is overcome, which promotes a faster IET process between the two Q moieties.

The dynamics of the intramolecular exchange process was theoretically simulated[18] (Figure 1b) and first-order rate constants for the thermally activated IET process were extracted by fitting the experimental ESR spectra. The simulation leads to a linear Arrhenius plot over the 330–270 K temperature range, which gives the activation parameters: $E_{act} = 7.96\ \text{kcal mol}^{-1}$; $\log A = 13.9$ ($\Delta G^{\ddagger}_{298K} = 6.4\ \text{kcal mol}^{-1}$; $\Delta H^{\ddagger} = 7.4\ \text{kcal mol}^{-1}$; $\Delta S^{\ddagger} = 3.1$ e.u.). The activation parameters for compound **1** are close to those previously reported for the anthracene-diquinone anion radical.[10e] This is one of the very few cases of an intervalence system for which the IET process can be followed by ESR spectroscopy,[8a,b,d,l,10e] which allows an accurately determination of the rate constant for thermally activated electron transfer. Figure 1 shows the results obtained in a 10:1 mixture of ethyl acetate/*tert*-butanol. However, the rate constants of the electron-transfer (ET) process have been determined in different solvents, which gives rise to different rate constants because of energy variations resulting from solvent reorganization. For example, the rate constants at 300 K are very similar in dichloromethane and ethyl acetate ($k_{ET} = 2.58 \times 10^8\ \text{s}^{-1}$ and $2.10 \times 10^8\ \text{s}^{-1}$, respectively) and of the same order in the 10:1 mixture of ethyl acetate/*tert*-butanol ($k_{ET} = 1.30 \times 10^8\ \text{s}^{-1}$), whereas in *tert*-butanol the ET process is slower ($k_{ET} = 2.89 \times 10^7\ \text{s}^{-1}$). It is important to indicate that the thermally activated IET process can only be fully studied using the 10:1 ethyl acetate/*tert*-butanol mixture, since other solvent systems exhibit interfering precipitation processes. As a result of the high insolubility of the monoanion radical species in any solvent, we have not been able to generate the corresponding dianion by chemical reduction or electrochemical reduction at −0.5 V.

The high insolubility of the Q-TTF-$Q^{-\cdot}$ mixed-valence species also prevents the quantitative study of the IET process by Vis/NIR spectroelectrochemical methods, since the com-

 © 2003 Wiley-VCH Verlag GmbH & Co. KGaA, Weinheim

pound starts to precipitate after passing a very small quantity of charge. Nevertheless, by deconvoluting the Vis/NIR spectra at different reduction steps, a broad charge-transfer band centered around 1300 nm is clearly observed for the generated Q-TTF-$Q^{-\bullet}$ mixed-valence species. Moreover, this band is completely absent for both the neutral species and in the TTF-$Q^{-\bullet}$ model compound.

The Q-TTF-$Q^{-\bullet}$ species is, therefore, a prototypical class II mixed-valence system involving moderately coupled redox centers.[19]

In summary, we have obtained a new, purely organic mixed-valence compound in which the existence of a temperature-dependent intramolecular electron transfer has not only been undoubtedly established but for which the rate constant for the thermally activated IET process has been accurately determined. In addition, this is the first time that a bridge exhibiting a strong electron-donating character, such as TTF, has been used in a mixed-valence system. The results here demonstrate that TTF is a suitable molecular bridge for the promotion of intramolecular electron transfer between two redox centers and constitutes a natural route towards the measurement of an electrical current through metal-TTF-metal nanojunctions. In that sense, TTF can be considered as the prototype of a huge family of electron donors in which the ionization potential (I_D) is small and can be tuned by changing the substituents and the conjugated extension. These characteristics are very important since one of the criteria for a good donor molecular wire is that the I_D value must be small, and must closely match the work function of the metal layer that acts as an electrode.[6c] We are currently working on the introduction of conjugated spacers between the 1,3-dithiole moieties of compound **1** to elongate the TTF bridge, and also on the utilization of other redox centers to replace *p*-benzoquinone groups.

Received: November 20, 2002
Revised: March 3, 2003 [Z50587]

Keywords: electron transfer · mixed-valent compounds · molecular electronics · quinones · tetrathiafulvalene

[1] a) J. M. Williams, J. R. Ferraro, R. J. Thorn, K. D. Carlson, U. Geiser, H. H. Wang, A. M. Kini, M. H. Whangbo, *Organic Superconductors (including fullerenes)*, Prentice Hall, Englewood Cliffs, NJ, **1992**; b) *Organic conductors. Fundamentals and applications* (Ed.: J. P. Farges), Marcel Dekker, New York, **1994**.

[2] a) M. R. Bryce, *J. Mater. Chem.* **2000**, *10*, 589 – 598; b) J. L. Segura, N. Martín, *Angew. Chem.* **2001**, *113*, 1416 – 1455; *Angew. Chem. Int. Ed.* **2001**, *40*, 1372 – 1409.

[3] M. R. Bryce, *Adv. Mater.* **1999**, *11*, 11 – 23.

[4] N. Martín, L. Sánchez, B. Illescas, I. Pérez, *Chem. Rev.* **1998**, *98*, 2527 – 2547.

[5] Molecular electronics is a field of study that proposes the miniaturization and the use of a single molecule to function as the key component in future devices. See J. M. Tour, A. M. Rawlett, M. Kozaki, Y. Yao, R. C. Jagessar, S. M. Dirk, D. W. Price, M. A. Reed, C.-W. Zhou, J. Chen, W. Wang, I. Campbell, *Chem. Eur. J.* **2001**, *7*, 5118 – 5134, and references therein.

[6] a) L. A. Bumm, J. Arnold, M. T. Cygan, T. D. Dunbar, T. P. Burgin, L. Jones II, D. L. Allara, J. M. Tour, P. S. Weiss, *Science*, **1996** *271*, 1705 – 1707; b) M. A. Reed, C. Zhou, C. J. Muller, T. P. Burgin, J. M. Tour, *Science* **1997**, *278*, 252 – 254; c) R. M. Metzger, *Acc. Chem. Res.* **1999**, *32*, 950 – 957; d) C. P. Collier, E. W. Wong, M. Belohradsky, F. M. Raymo, J. F. Stoddart, P. J. Kuekes, R. S. Williams, J. R. Heath, *Science* **1999**, *285*, 391 – 394; e) C. Joachim, J. K. Gimzewski, A. Aviram, *Nature* **2000**, *408,* 541 – 548; f) J. M. Tour, *Acc. Chem. Res.* **2000**, *33*, 791 – 804; g) *Electron Transfer in Chemistry, Vol. 3* (Eds.: F. Scandola, C. Chiorboli, M. T. Indelli, M. A. Rampi), Wiley-VCH, New York, **2001**.

[7] a) R. J. Crutchley, *Adv. Inorg. Chem.*, **1994**, *41*, 273 – 325; b) "Molecular-level Electronics": A. P. de Silva in *Electron Transfer in Chemistry, Vol. 5* (Ed.: V. Balzani), Wiley, New York, **2001**.

[8] a) F. S. Nelsen, J. A. Thomson-Colon, M. J. Katfory, *J. Am. Chem. Soc.* **1994**, *116*, 1589; b) J. Bonvoisin, J.-P. Launay, C. Rovira, J. Veciana, *Angew. Chem.* **1994**, *106*, 2190 – 2193; *Angew. Chem. Int. Ed. Engl.* **1994**, *33*, 2106 – 2109; c) K. Lahlil, A. Moradpour, C. Bowlas, F. Menou, P. Cassoux, J. Bonvoisin, J.-P. Launay, G. Dive, D. Dehareng, *J. Am. Chem. Soc.* **1995**, *117*, 9995 – 10002; d) F. S. Nelsen, R. F. Ismagilov, D. A. Trieber, *Science* **1997**, *278,* 846 – 849; e) C. Lambert, G. Nöll, *Angew. Chem.* **1998**, *110*, 2239 – 2242; *Angew. Chem. Int. Ed.* **1998**, *37*, 2107 – 2110; f) C. Lambert, G. Nöll, *J. Am. Chem. Soc.* **1999**, *121*, 8434 – 8442; g) D. Ruiz-Molina, J. Sedó, C. Rovira, J. Veciana in *Handbook of Advanced Electronic and Photonic Materials and Devices, Vol. 3* (Ed.: H. S. Nalwa), Academic Press, San Diego, **2001**, pp. 303 – 327; h) J.-P. Launay, *Chem. Soc. Rev.* **2001**, *30*, 386 – 397; i) C. Rovira, D. Ruiz-Molina, O. Elsner, J. Vidal-Gancedo, J. Bonvoisin, J.-P. Launay, J. Veciana, *Chem. Eur. J.* **2001**, *7*, 240 – 250; j) M. Mayor, M. Büschel, K. M. Fromm, J.-M. Lehn, J. Daub, *Chem. Eur. J.* **2001**, *7*, 1266 – 1272; k) C. Lambert, G. Nöll, J. Schelter, *Nat. Mater.* **2002**, *1*, 69 – 73; l) S. V. Lindeman, S. V. Rosokha, D. Sun, J. K. Kochi, *J. Am. Chem. Soc.* **2002**, *124*, 842 – 855.

[9] S. Creager, C. J. Yu, C. Bamdad, S. O'Connor, T. MacLean, E. Lam, Y. Chong, G. T. Olsen, J. Luo, M. Gozin, J. F. Kayyem, *J. Am. Chem. Soc.* **1999**, *121*, 1059 – 1064.

[10] Polycondensed aryl rings were previously used as a bridge for the intramolecular electron transfer between two *p*-benzoquinones in mixed-valence compounds; a) T. H. Jozefiak, L. L. Miller, *J. Am. Chem. Soc.* **1987**, *109*, 6560 – 6561; b) T. H. Jozefiak, J. E. Almlöf, M. W. Feyereisen, L. L. Miller, *J. Am. Chem. Soc.* **1989**, *111*, 4105 – 4106; c) J. E. Almlöf, M. W. Feyereisen, T. H. Jozefiak, L. L. Miller, *J. Am. Chem. Soc.* **1990**, *112*, 1206 – 1214; d) L. L. Miller, C. A. Liberko, *Chem. Mater.* **1990**, *2*, 339 – 340; e) S. F. Rak, L. L. Miller, *J. Am. Chem. Soc.* **1992**, *114*, 1388 – 1394.

[11] Landolt-Börnstein, New series, *Vol. 11/17e* **1986**, p. 206, and references therein.

[12] Yields were improved by the use of piperidine instead of pyrrolidine. D. Sun, M. Krawiec, W. H. Watson, *J. Chem. Crystallogr.* **1997**, *27*, 515 – 526.

[13] C. Boulle, O. Desmars, N. Gautier, P. Hudhomme, M. Cariou, A. Gorgues, *Chem. Commun.* **1998**, 2197 – 2198.

[14] Phosphonate **9** was synthesized according to an established procedure; A. J. Moore, M. R. Bryce, *Synthesis* **1991**, 26 – 28.

[15] Chemical reduction of Q-TTF and Q-TTF-Q was performed with Cu metal in CH_2Cl_2 or ethyl acetate/*tert*-butanol (10:1) solutions containing tetraphenylphosphonium bromide. Electrochemical reduction was carried out using a solution of nBu$_4$NPF$_6$ (0.2 M in CH_2Cl_2).

[16] As the coupling constant a_H is dependent on the spin density, the delocalization of the electron over both quinone groups means that this constant is half as large for compound **1** as for **2**.

[17] A. Hudson, G. R. Luckhurst, *Chem. Rev.* **1969**, *69,* 1961.

 © 2003 Wiley-VCH Verlag GmbH & Co. KGaA, Weinheim

[18] J. Heinzer, *Mol. Phys.* **1971**, *22*, 167; *Quantum Chemistry Program Exchange* **1972**, No. 209. We thank Prof. A. Lund for a copy of this program.
[19] M. B. Robin, P. Day, *Adv. Inorg. Chem. Radiochem.* **1967**, *10*, 247. Mixed-valence compounds are classified in three categories. Class I: the redox centers are completely localized and behave as separated entities; Class II: intermediate coupling between the mixed-valence centers exists; Class III: the system is completely delocalized and the redox centers show intermediate valence states.

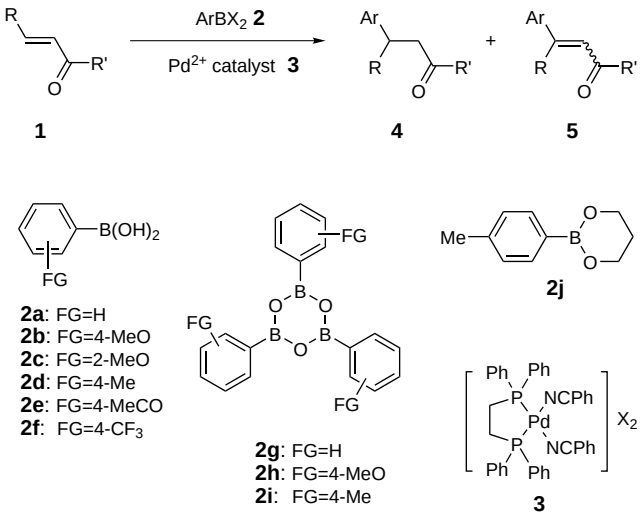
 © 2003 Wiley-VCH Verlag GmbH & Co. KGaA, Weinheim

Pd and B in 1,4-Additions

Conjugate Addition of Aryl Boronic Acids to Enones Catalyzed by Cationic Palladium(II)–Phosphane Complexes

*Takashi Nishikata, Yasunori Yamamoto, and Norio Miyaura**

Rhodium(I) complexes are excellent catalysts for the 1,4-addition of aryl or 1-alkenyl boron,[1] silicon,[2] and tin[3] compounds to α,β-unsaturated carbonyl compounds. Various addition reactions analogous to copper-catalyzed reactions of lithium and magnesium reagents have been carried out that involve a catalytic cycle starting from transmetalation to yield an aryl or 1-alkenyl rhodium(I) intermediate. In contrast to the formation of O-bound enolates in the insertion of enones into a C–Rh bond,[4] a palladium catalyst yields C-bound enolates, resulting in β-hydride elimination.[5] Thus, the reaction of enones with RPdX, generated in situ by transmetalation of PdX_2 with an organometallic reagent or by the oxidative addition of RX to a palladium(0) complex, affords Heck coupling products with precipitation of palladium black. However, there are some reports that palladium(II) complexes catalyze 1,4-addition to enones. Products of a simple Michael-type reaction often predominate over the insertion–elimination products of the Heck reaction.[6] Cacchi et al. demonstrated the palladium(II)-catalyzed 1,4-addition of ArHgCl or $SnAr_4$ to enones in acidic water in the presence of Bu_4NCl.[7] In connection with our interest in metal-catalyzed reactions of organoboron compounds,[8] we report herein the 1,4-addition of aryl boronic acids and boroxines **2** to α,β-unsaturated carbonyl compounds **1**, catalyzed by cationic palladium(II) complexes (Scheme 1). $[Pd(dppe)(PhCN)_2]X_2$ **3**[9] (dppe = 1,2-bis(diphenylphophanyl)ethane) was found to be an excellent catalyst for the reaction at room temperature. The catalysts were designed on the basis of the findings of Espinet and co-workers that cationic palladium enolates are much more susceptible to hydrolytic C–Pd-bond cleavage than are neutral species.[10] Their high Lewis acidity and the very smooth insertion of a C–C or C–N double bond into a C–Pd bond are also great advantages of cationic palladium(II) catalysts[11], which have been demonstrated in the palladium-catalyzed Diels–Alder reaction,[12] Mannich reaction,[13] Wacker process,[14] and polymerization of alkenes.[15]



Scheme 1. Palladium(II)-catalyzed 1,4-addition of aryl boron compounds to α,β-unsaturated carbonyl compounds.

Table 1 shows the effects of the catalyst, the type of boron compound, and the presence of a base in the addition of phenylboronic acid (**2a**), *p*-tolylboronic acid (**2d**), the boroxine **2i**, and the boronic ester **2j** to 2-cyclohexenone. Neutral palladium complexes such as $[PdCl_2(dppe)]$ were not effective

Table 1: Pd^{2+}-catalyzed reaction of 2-cyclohexenone with aryl boron compounds **2**.[a]

Entry	Catalyst	2	Additive (equiv)[b]	Yield [%][c]	4/5
1	$[PdCl_2(dppe)]$	**a**[d]	K_2CO_3 (1)	0	
2	**3** ($X=ClO_4$)$_2$	**a**[d]	K_2CO_3 (1)	52	90:10
3	**3** ($X=OTf$)$_2$	**a**[d]	K_2CO_3 (1)	43	96:4
4	**3** ($X=BF_4$)$_2$	**a**[d]	K_2CO_3 (1)	48	89:11
5	**3** ($X=PF_6$)$_2$	**a**[d]	K_2CO_3 (1)	59	96:4
6	**3** ($X=SbF_6$)$_2$	**a**[d]	K_2CO_3 (1)	63	95:5
7	**3** ($X=SbF_6$)$_2$	**a**[d]	none	63	>99:1
8	**3** ($X=SbF_6$)$_2$	**d**[e]	none	77	>99:1
9	**3** ($X=SbF_6$)$_2$	**d**[e]	H_2O (33)	95	>99:1
10	**3** ($X=SbF_6$)$_2$	**i**	none	43	>99:1
11	**3** ($X=SbF_6$)$_2$	**i**	H_2O (1.5)	91	>99:1
12	**3** ($X=SbF_6$)$_2$	**i**	H_2O (3)	95	>99:1
13	**3** ($X=SbF_6$)$_2$	**i**	H_2O (10)	89	>99:1
14	**3** ($X=SbF_6$)$_2$	**j**	none	54	>99:1
15	**3** ($X=SbF_6$)$_2$	**j**	H_2O (1)	40	>99:1

[a] All reactions were carried out in THF (6 mL) at 20°C for 23 h in the presence of 2-cyclohexenone (1 mmol), a phenyl- or *p*-tolylboron compound (1.5 mmol), a palladium(II) catalyst (5 mol%), and base or H_2O (if used). [b] Equivalents with respect to the boron compound. [c] Yields of isolated products based on 2-cyclohexenone starting material. [d] **2a**/**2g** = 68:32. [e] **2d**/**2i** = 87:13.

[*] Prof. Dr. N. Miyaura, T. Nishikata, Y. Yamamoto
Division of Molecular Chemistry
Graduate School of Engineering, Hokkaido University
Sapporo 060-8628 (Japan)
Fax: (+81) 11-706-6561
E-mail: miyaura@org-mc.eng.hokudai.ac.jp

 © 2003 Wiley-VCH Verlag GmbH & Co. KGaA, Weinheim DOI: 10.1002/anie.200350888

(Table 1, entry 1), but cationic palladium–dppe complexes of ClO_4^-, OTf^-, BF_4^-, PF_6^-, and SbF_6^- catalyzed the reaction at room temperature (Table 1, entries 1–6). Although variation of the counteranion had no significant effect, the catalyst efficiency was greatly dependent on the phosphane ligand. Of the catalysts tested, the dppe complex was found to be the best choice, as the use of dppp (1,3-bis(diphenylphosphanyl)-propane), (*S*)-binap ((*S*)-2,2′-bis(diphenylphosphanyl)-1,1′-binaphthyl) and PPh_3 complexes resulted in no reaction. The cationic benzonitrile complexes are bench-stable catalysts that required no activation. The presence of benzonitrile was critical: The use of a nitrile-free catalyst generated in situ from $[PdCl_2(dppe)]$ and $AgSbF_6$ resulted in 45% yield, and the use of electron-poor benzonitrile complexes such as $[Pd(dppe)(4\text{-}CF_3C_6H_4CN)_2](SbF_6)_2$ led to less than 1% yield. Although K_2CO_3 was used to accelerate the reaction[8] and the yields were indeed highly dependent on the bases employed ($K_2CO_3 > KHCO_3 > Et_3N$), the use of a base always resulted in the formation of a Heck product (4–11%), whereas Heck products were negligible in the absence of a base (Table 1, entry 7). The reaction proceeded smoothly in less polar solvents, such as THF, dioxane, and cyclohexane, but was very slow in donating solvents such as *N,N*-dimethylformamide (DMF) and MeCN.

The reaction requires the presence of water, as does the analogous rhodium-catalyzed reaction.[1] The reactions with *p*-tolylboronic acid (**2d**, boronic acid/boroxine = 87:13) and tris(*p*-tolyl)boroxine (**2i**) resulted in 77% and 43% yields, respectively, in the absence of water (Table 1, entries 8 and 10). Both yields improved to 95% upon the addition of water to the boronic acid or boroxine, which are in equilibrium in an aqueous solution (Table 1, entries 9 and 12).[16] On the other hand, all attempts at using boronic esters were unsuccessful. The reactions of all five- and six-membered boronic esters tested occurred in low yields in either the presence or the absence of water (for example, Table 1, entries 14 and 15).

Results of the 1,4-addition of aryl boronic acids and boroxines to representative α,β-unsaturated carbonyl compounds at room temperature are summarized in Table 2. The reaction of 2-cyclopentenone with phenylboronic acid (**2a**, boronic acid/boroxine = 68:32) occurred in 63% yield in the absence of water, in 78% yield when water was added to the boronic acid, and in 91% yield when a mixture of the corresponding boroxine **2g** and water was used (Table 2, entries 1–3). These reactions selectively provided 1,4-addition products, whereas a Heck product was selectively formed in the presence of K_2CO_3 (Table 2, entry 4). Although various boronic acids gave the best yields in the presence of water in reactions with 2-cyclohexenone or 2-cycloheptenone (Table 2, entries 5–8 and 11), the presence of water was not critical for reactions with *p*-acetyl and *p*-trifluoromethylphenylboronic acid (Table 2, entries 9 and 10). An NMR spectroscopic study indicated that these two compounds were pure boronic acid with no accompanying boroxine. The protocol was easily extended to acyclic α,β-unsaturated ketones and aldehydes with a primary alkyl, secondary alkyl, or phenyl substituent on the β carbon atom (Table 2, entries 12–21). In most reactions 5 mol% of the catalyst was used. However, the loading could be decreased to less than 1 mol%: An almost quantitative yield was found in a reaction in which only 0.5 mol% of the catalyst was used (Table 2, entry 13). In contrast to the rhodium-catalyzed reaction, which gave a mixture of 1,4- and 1,2-addition products from enals,[17] the palladium catalysts selectively yielded 1,4-addition products (Table 2, entries 20 and 21). On the other hand, the addition of boronic acids to α,β-unsaturated esters was very slow, and Heck-coupling products predominated (Table 2, entry 22). No reaction was observed for the addition to *N*-benzylcrotonamide.

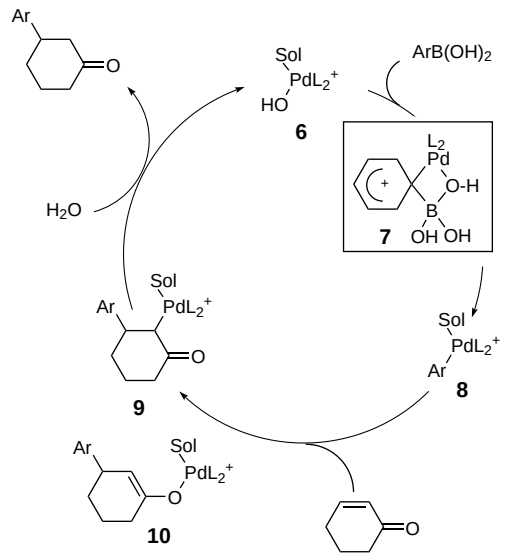
Table 2: 1,4-Addition of aryl boronic acids and boroxines.[a]

Entry	1	2	Product	Yield [%][b]
1	2-cyclopentenone	**a**	**4a**	63
2	2-cyclopentenone	**a**/H_2O[c]	**4a**	78
3	2-cyclopentenone	**g**/H_2O[d]	**4a**	91
4[e]	2-cyclopentenone	**a**	**5a**[f]	48
5	2-cyclohexenone	**a**/H_2O[c]	**4b**	87
6	2-cyclohexenone	**b**/H_2O[c]	**4c**	80
7	2-cyclohexenone	**c**/H_2O[c]	**4d**	95
8	2-cyclohexenone	**d**/H_2O[c]	**4e**	95
9	2-cyclohexenone	**e**	**4g**	96
10	2-cyclohexenone	**f**	**4h**	94
11	2-cycloheptenone	**a**/H_2O[c]	**4i**	87
12	(*E*)-$C_5H_{11}CH{=}CHCOCH_3$	**a**	**4j**	92
13[g]	(*E*)-$C_5H_{11}CH{=}CHCOCH_3$	**a**	**4j**	97
14	(*E*)-*i*-$C_3H_7CH{=}CHCOCH_3$	**a**/H_2O[c]	**4k**	82
15	(*E*)-$PhCH{=}CHCOCH_3$	**a**/H_2O[c]	**4l**	83
18	(*E*)-$PhCH{=}CHCOPh$	**a**	**4m**	92
20	(*E*)-$CH_3CH{=}CHCHO$	**g**/H_2O[d]	**4n**	83
21	(*E*)-$C_3H_7CH{=}CHCHO$	**a**/H_2O[c]	**4o**[h]	76
22	$CH_2{=}CHCO_2Et$	**a**	**4p**	5[i]

[a] All reactions were carried out at 20°C for 23 h in the presence of 2-cyclohexenone (1 mmol), an aryl boron compound (1.5 mmol), and $[Pd(dppe)(PhCN)_2](SbF_6)_2$ (5 mol%) in THF (6 mL), unless otherwise noted. The ratios of boronic acid/boroxine were: **2a**: 68:32, **2b**: 68:32, **2c**: 100:0, **2d**: 87:13, **2e**: 100:0, and **2f**: 100:0. [b] Yields of isolated products, after purification by chromatography. [c] The reaction was conducted in THF/H_2O (10:1, 6 mL). [d] An aryl boroxine (0.5 mmol) and water (3 mmol) were used in place of the boronic acid. [e] K_2CO_3 (1.2 mmol) was used. [f] 3-Phenyl-2-cyclopentene was formed selectively. [g] Catalyst used: 0.5 mol%. [h] 1,3-Diphenyl-1-hexanone (1.6%) was also obtained. [i] Ethyl cinnamate (31%) was also isolated.

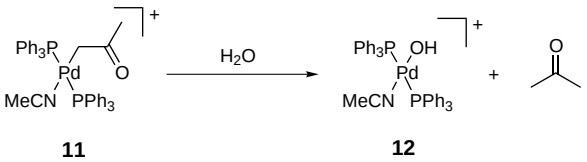
A proposed catalytic cycle involving transmetalation, insertion, and hydrolytic C–Pd-bond cleavage is shown in Scheme 2. Organoboronic acids are inert to neutral palladium(II) halides, but they easily undergo transmetalation with cationic platinum(II) and palladium(II) complexes.[8,18] Although the mechanism has not yet been fully elucidated, the high reactivity of the cationic species suggests that a transmetalation occurs through a Wheland intermediate **7** to produce a cationic aryl palladium(II) species **8**.[19] Because of the difficulty in preventing double transmetalation to **6**, which results in the formation of a homocoupling product (Ar–Ar) and palladium black, palladium(II) complexes have rarely been used in reactions that occur through such a catalytic cycle, which starts with a transmetalation. However, the high turnover number of the catalyst observed in entry 13 of Table 2 indicates that the next insertion step is sufficiently fast to prevent a second transmetalation to **8**. Insertion of a C–C double bond into a C–Pd bond proceeds for electron-deficient alkenes, and this process can be further accelerated

 © 2003 Wiley-VCH Verlag GmbH & Co. KGaA, Weinheim



Scheme 2. Proposed catalytic cycle. Sol = solvent molecule.

when cationic palladium complexes are used, as has been demonstrated in the Heck reaction.[5] Nucleophilic addition may occur with delivery of an aryl nucleophile to the β carbon atom of an enone to yield a C- or O-bound palladium enolate (**9** or **10**). As was demonstrated by Espinet and co-workers (Scheme 3),[10] the C-bound enolate **9** is the sole species that undergoes hydrolytic bond cleavage upon treatment with water. It is not yet known whether this process involves direct C–Pd-bond cleavage or the transformation of **9** into **10** before protonolysis (Scheme 2).



11 **12**

Scheme 3. Protonolysis of C-bound palladium enolates (Espinet).

In conclusion, the efficiency of cationic palladium(II) catalysts was demonstrated in the 1,4-addition of aryl boronic acids to α,β-unsaturated carbonyl compounds. Because of the simple experimental procedure and the neutral conditions of this reaction, extension to an asymmetric version is under investigation in our laboratories.

Experimental Section

All cationic palladium(II) complexes were synthesized by reported procedures.[9]

General procedure: A flask charged with a palladium catalyst (0.05 mmol) and an aryl boronic acid (1.5 mmol) or boroxine (0.5 mmol) was flushed with argon. A solvent (6 mL), an enone (1.0 mmol), and water (if used, 0.054 mL for a boroxine and 0.6 mL for a boronic acid) were then added successively. The reaction mixture was stirred for 23 h at room temperature (20–25 °C), then the product was extracted with diethyl ether, washed with K_2CO_3 (0.5 M), and dried over $MgSO_4$. Chromatography on silica gel gave the analytically pure product.

Received: January 3, 2003 [Z50888]

Keywords: boron · enones · Michael addition · palladium · synthetic methods

[1] a) T. Hayashi, M. Takahashi, Y. Takaya, M. Ogasawara, *J. Am. Chem. Soc.* **2002**, *124*, 5052; b) S. Sakuma, M. Sakai, R. Itooka, N. Miyaura, *J. Org. Chem.* **2000**, *65*, 5951; c) T. Hayashi, T. Senda, Y. Takaya, M. Ogasawara, *J. Am. Chem. Soc.* **1999**, *121*, 11591; d) Y. Takaya, M. Ogasawara, T. Hayashi, M. Sakai, N. Miyaura, *J. Am. Chem. Soc.* **1998**, *120*, 5579; e) M. Sakai, H. Hayashi, N. Miyaura, *Organometallics* **1997**, *16*, 4229; for a review, see: f) K. Fagnou, M. Lautens, *Chem. Rev.* **2003**, *103*, 169.
[2] a) M. Murata, R. Shimazaki, M. Ishikura, S. Watanabe, Y. Masuda, *Synthesis* **2002**, 717; b) T. Koike, X. Du, A. Mori, K. Osakada, *Synlett* **2002**, 301; c) S. Oi, Y. Honma, Y. Inoue, *Org. Lett.* **2002**, *4*, 667.
[3] a) S. Oi, M. Moro, H. Ito, Y. Honma, S. Miyano, Y. Inoue, *Tetrahedron* **2002**, *58*, 91; b) T. Huang, Y. Meng, S. Venkatraman, D. Wang, C.-J. Li, *J. Am. Chem. Soc.* **2001**, *123*, 7451.
[4] G. A. Sough, R. G. Bergmann, C. H. Heathcock, *J. Am. Chem. Soc.* **1989**, *111*, 938.
[5] T. Jeffery in *Advances in Metal-Organic Chemistry, Vol. 5* (Ed.: L. S. Liebeskind), JAI, Greenwich, **1996**, p. 153.
[6] a) J. P. Konopelski, K. S. Chu, G. R. Negrete, *J. Org. Chem.* **1991**, *56*, 1355; b) A. Wada, H. Yasuda, S. Kanamoto, *Synthesis* **1988**, 771.
[7] S. Cacchi, D. Misiti, G. Palmieri, *Tetrahedron* **1981**, *37*, 2941.
[8] N. Miyaura, *Top. Curr. Chem.* **2002**, *219*, 11.
[9] J. A. Davis, E. R. Hartley, S. G. Muray, *J. Chem. Soc. Dalton Trans.* **1980**, 2246.
[10] A. C. Albéniz, N. M. Catalina, P. Espinet, R. Redón, *Organometallics* **1999**, *18*, 5571.
[11] A. Yamamoto, *J. Organomet. Chem.* **1995**, *500*, 337.
[12] K. Mikami, K. Aikawa, Y. Yusa, *Org. Lett.* **2002**, *4*, 95.
[13] A. Fujii, E. Hagiwara, M. Sodeoka, *J. Am. Chem. Soc.* **1999**, *121*, 5450.
[14] M. J. Gaunt, J. B. Spencer, *Org. Lett.* **2001**, *3*, 25.
[15] M. Brookhart, M. I. Wagner, *J. Am. Chem. Soc.* **1994**, *116*, 3641.
[16] Y. Tokunaga, H. Ueno, Y. Shimomura, T. Seno, *Heterocycles* **2002**, *57*, 787.
[17] M. Ueda, N. Miyaura, *J. Org. Chem.* **2000**, *65*, 4450.
[18] a) K. Siegmann, P. S. Pregosin, L. M. Venanzi, *Organometallics* **1989**, *8*, 2659; b) S. Darses, T. Jeffery, J.-P. Genet, *Tetrahedron Lett.* **1996**, *37*, 3857; c) S.-K. Kang, H.-W. Lee, S.-B. Jang, P.-S. Ho, *J. Org. Chem.* **1996**, *61*, 4720.
[19] B. Crociani, F. D. Bianca, P. Uguagliati, L. Canovese, A. Berton, *J. Chem. Soc. Dalton Trans.* **1991**, 71.

 © 2003 Wiley-VCH Verlag GmbH & Co. KGaA, Weinheim

Gold(I)/Gold(III) Perovskites

Organic-Based Layered Perovskites of Mixed-Valent Gold(I)/Gold(III) Iodides**

*Laura M. Castro-Castro and Arnold M. Guloy**

One of the most appealing handles in the design and synthesis of multifunctional hybrid materials is the wide choice of available molecular building blocks, in which one can combine properties that are often difficult to achieve in extended solids. The choices are often guided by the desire to combine distinct properties attributable to each organic and inorganic component.[1–2] Critical to the design of organic–inorganic hybrid materials is the control and exploitation of relevant supramolecular and noncovalent interactions. The establishment of a clear understanding of tunable noncovalent interactions useful for the design of complex supramolecular architectures is currently a growing field of research.[3]

Organic cations combined with polarizable inorganic moieties, such as heavy-metal halides (Br and I) and polyhalides, provide interesting chemical systems where moderately strong noncovalent interactions can be investigated. Recent investigations on heavy metal iodide and polyiodide systems have revealed surprising results, including complex supramolecular structures, unprecedented physical properties, and novel chemical bonding descriptions.[4–5]

Mixed-valent gold(I/III) halides, such as $Cs_2Au_2X_6$, have received significant attention because of their similarities with $BaBiO_3$ and its superconducting derivatives.[6] The crystal structure of $Cs_2Au^IAu^{III}X_6$ (X = Cl, Br, I) can be derived from a tetragonal distortion of the cubic perovskite ABX_3 structure, in which the network of corner-shared ABX_6 octahedra disproportionates into distinct BX_2 (linear $Au^II_2^-$) and BX_4 (square planar $Au^{III}I_4^-$) units.[7–11] The class II mixed-valent perovskites of $BaBiO_3$ and $Cs_2Au_2X_6$ have been shown to exhibit interesting optical and electronic behavior, as well as, novel transport properties by substitution (doping) or application of high pressures, respectively.[6–8]

The introduction of mixed valency in the inorganic components of hybrid materials, thus providing another handle in modulating their electronic properties, has remained relatively unexplored. Attempts to prepare organic-based analogues of Au^{III} and mixed-valent $Au^{I/III}$ halides were reported as early as 1914.[12] However, the poorly crystalline dark solids obtained from these studies were not structurally characterized and were incompletely analyzed. Surprisingly, no investigations were subsequently reported to confirm or rectify the results of the initial studies.[12] Our exploratory studies, aimed at preparing new hybrid compounds of mixed-valent gold (I/III), led to the synthesis and characterization of two new organic-based mixed-valent $Au^{I/III}$ iodides: $[NH_3(CH_2)_8NH_3]_2[(Au^II_2)(Au^{III}I_4)(I_3)_2]$ (**1**) and $[NH_3(CH_2)_7NH_3]_2[(Au^II_2)(Au^{III}I_4)(I_3)_2]$ (**2**).

The monoclinic crystal structure of **1** (Figure 1) features layers of corner-shared nominal AuI_6 octahedra stacked along the *a* axis, with interlayer distances of 15.5 Å.[13] Adjacent perovskite gold iodide layers are displaced by 5.8 Å along the *c* axis. Each inorganic sheet features two nonequivalent Au atoms corresponding to mixed-valent $Au^{I/III}$ iodide ions of linear $[Au^II_2]^-$ and square-planar $[Au^{III}I_4]^-$ units. Tetragonally compressed nominal octahedron around each $[Au^II_2]^-$ unit is completed by four coplanar iodide ions ($d_{Au^I\cdots I} = 3.278(1)$ Å) from neighboring $[Au^{III}I_4]^-$ units. Similarly, an elongated octahedra around each $[Au^{III}I_4]^-$ unit is completed by two apical iodine atoms ($d_{Au^{III}\cdots I} = 3.752(7)$ Å) from I_3^- ions sandwiched between the gold iodide layers. The observed structural behavior, typical for mixed-valent gold (I/III) halides, has been described as a breathing-mode distortion.[10] It is noteworthy that the I_3^- ions directed at the nearest $[Au^{III}I_4]^-$ units are strongly polarized ($d_{I\text{-}I} = 2.798(3)$, 3.093(4 Å). To our knowledge, this is the first report of polyiodides taking part in a network of mixed-valent $Au^{I/III}$. The organic dications, oriented nearly perpendicular to the inorganic layers, are confined between anionic sheets and tethered by parallel triiodide molecules.

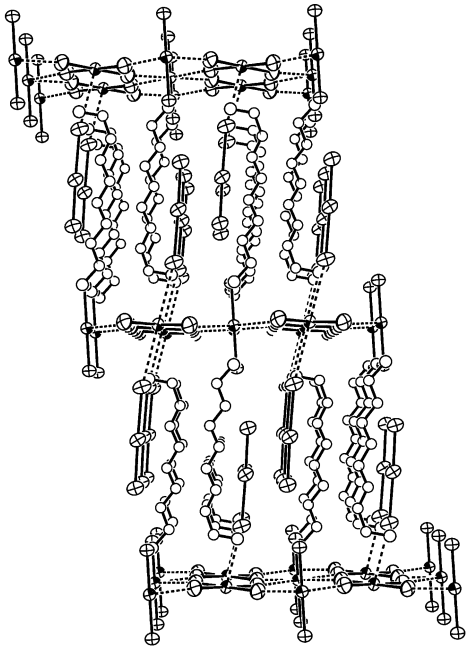


Figure 1. A [010] view of the crystal structure of (**1**). Gold and iodine atoms are represented as octant-shaded and crossed-hatched ellipsoids (75%), respectively. Light atoms are represented as small open spheres (C) and open ellipsoids (N).

[*] Prof. A. M. Guloy, L. M. Castro-Castro
Department of Chemistry
University of Houston, Houston, Texas, 77204–5641 (USA)
Fax: (+1) 713-743–2787
E-mail: aguloy@uh.edu

[**] This work was supported by the R.A. Welch Foundation, the Texas Center for Superconductivity at UH, and the National Science Foundation (CAREER Award, DMR-9733587). The authors are also grateful to Prof. P. S. Halasyamani for the TGA measurements.

 DOI: 10.1002/anie.200350929 © 2003 Wiley-VCH Verlag GmbH & Co. KGaA, Weinheim

The crystal structure of **2** (Figure 2) is similar to that of **1**.[14] The significant structural differences between **1** and **2** are effected by the different conformations of the organic cations. The organic dications in **2**, $(NH_3(CH_2)_7NH_3)^{2+}$, have completely staggered *anti* conformations, but the $(NH_3(CH_2)_8NH_3)^{2+}$ dications in **1** exhibit a *gauche* conformation at the terminal amine closest to the inorganic layers. The

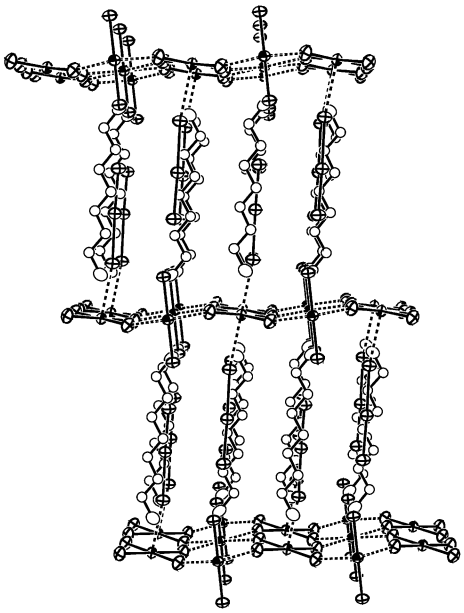


Figure 2. A [010] view of the crystal structure of (**2**). Gold and iodine atoms are represented as octant-shaded and crossed-hatched ellipsoids (75%), respectively. Carbon and nitrogen atoms are represented as small open spheres and open ellipsoids, respectively.

molecular conformations result in nearly identical cation lengths of 10.13 and 10.04 Å for **1** and **2**, respectively. Compound **2** exhibits shorter noncovalent Au···I distances: $d_{Au^{III}\cdots I} = 3.500(3$ Å, $d_{Au^{I}\cdots I} = 3.235(3)$ and 3.248(3 Å. The polarization of I_3^- ions in **2** is also enhanced with $d_{I-I} = 2.794(2)$, 3.103(2) Å. Attempts to prepare layered derivatives with other diamine homologues have been unsuccessful. The observed structural behavior of **1** and **2** affirms the crucial role of organic cation templates in the structural stability and flexibility of hybrid layered perovskites.[15] Different dication conformations also result in different cation–triiodide layered arrangements in **1** and **2**. Denser cation–triiodide arrangements in **2** result in greater buckling of the inorganic layer, as reflected by greater tilt between the nominal $Au^{III}I_6$ and $Au^{I}I_6$ octahedra. The pillaring of the mixed-valent gold-iodide perovskite layer by I_3^- units also results in nonbonding (I···I) contacts between the terminal iodide ions of the AuI_2^- and I_3^- units of 3.75 Å in **1,** and 3.56 Å in **2**.

Compounds **1** and **2** differ from $Cs_2Au_2I_6$ in that the nominal octahedral coordination of the Au^{III} center in **1** and **2** is completed by two asymmetric I_3^- units, as illustrated in Figure 3. The perovskite structure of $Cs_2Au_2I_6$ is more 3D than that exhibited by **1** and **2**. Noncovalent Au···I distances in $Cs_2Au_2I_6$ are: $d_{Au^{III}\cdots I} = 3.460(3)$ Å; $d_{Au^{I}\cdots I} = 3.212(2)$ Å are slightly shorter. However, the Au–I bond lengths for the



Figure 3. Representation of the inorganic substructures of **1** (left), **2** (center) and $Cs_2Au_2I_6$ (right). Gold and iodine atoms are shown as light and dark spheres, respectively. The structural parameters for $Cs_2Au_2I_6$ were obtained from reference [10].

AuI_2^- and AuI_4^- units in **1**, **2** and $Cs_2Au_2I_6$ are very similar. It has been shown that I_3^- structurally and electronically substitutes for the $[AuI_2]^-$ unit in some $[AuI_4]^-/[AuI_2]^-$ derivatives to form $[AuI_4]^-/I_3^-$ analogues.[3,16] The electronic behavior of the I_3^- ion differs from $[AuI_2]^-$ ion with respect to charge-transfer interactions.

Charge transfer in $Cs_2Au_2I_6$ and analogous $Au^{I/III}$ halides was reported to predominantly occur within $[AuI_2–AuI_4]$ perovskite layers, similar to the sheets observed in **1** and **2**.[17] Thus it is reasonable to expect that **1** and **2** would still preserve the most important electronic interactions present in the inorganic parent perovskites. Diffuse reflectance measurements indicate optical band gaps of 1.14 and 0.95 eV for **1** and **2**, respectively.[18] These values compare with the reported optical band gap of 1.31 eV for $Cs_2Au_2I_6$.[20] The unexpectedly narrower band gaps of **1** and **2** can be attributed to induced electronic interactions between I_3^- and the AuI_2^-–AuI_4^- perovskite layers absent in $Cs_2Au_2I_6$. The polarization and subsequent distortion of the I_3^- ions in **1** and **2** manifests the relative strength of the interactions. DFT calculations on **2** reveal a net dipole moment of 2.18 D for I_3^-, with the more negative end of I_3^- ion directed towards the Au^{III} center. The calculated molecular electrostatic potential surface indicates an asymmetric distribution of the electron densities suggesting the possibility of I_2 removal. The DFT calculations on **2** also indicate that the AuI_2^-–I_3^- interactions are significantly weaker than the AuI_4^-–I_3^- interactions. Although structural similarities between the $[AuI_2]^-$ and $[I_3]^-$ units are substantial, subtle differences in their electronic behavior provides an additional handle in fine tuning the electronic properties of mixed-valent gold iodides.

Thermogravimetric analysis (TGA) was performed on **2** to assess compound stability and the possibility of I_2 removal. The first step in the TGA curve occurs above 85 °C and is consistent with the loss of an equivalent of I_2, according to the following reaction [Eq(1)]:

$$[NH_3(CH_2)_7NH_3]_2[(Au^{I}I_2)(Au^{III}I_4)(I_3)_2] \rightarrow [NH_3(CH_2)_7NH_3]_2[(Au^{I}I_2)(Au^{III}I_4)(I_3)(I)] + I_2 \quad (1)$$

Decomposition occurs above 155 °C, forming metallic gold and Au^{I} iodides.

 © 2003 Wiley-VCH Verlag GmbH & Co. KGaA, Weinheim

Our findings reveal the exciting potential of organic-based mixed-valent gold(I/III) iodide polyiodides as tunable electronic materials. An intriguing possibility is the pillaring of the perovskite layers with other polyiodides and appropriate organic cations. Moreover, hybrid gold iodide polyiodides provide interesting chemical systems wherein significant noncovalent interactions and hyperpolarizabilities may be systematically investigated and exploited. The complete characterization of their electronic structures and measurement of the more relevant physical properties of these and other related compounds are currently in progress.

Experimental Section

A solution of $HAuCl_4$ (1 mL, 0.05 mol L^{-1}) was treated with stoichiometric amounts of 1,8-diaminooctane and 1,7-diaminoheptane. Six drops of iodine solution (5% w/w) in concentrated HI were added and a black precipitate was readily obtained. Shiny black crystals were recovered after the reaction mixture was left undisturbed for 4–6 weeks. The same compounds were also synthesized, in high yield, through solid-state reactions by using stoichiometric amounts of AuI, the corresponding amine, and excess I_2 (~10×) in sealed glass tubes under vacuum. The reaction tubes were heated to 160°C for 10 days and slowly cooled to room temperature. The solution method yielded well-crystallized samples suitable for single-crystal X-ray diffraction. Chemical composition was confirmed by elemental analysis and results agree with theoretical values within the experimental error.[21] Magnetic susceptibility of **1**, measured from 5 to 300 K, corresponds to normal diamagnetic behavior.[22] All theoretical calculations on the triiodide molecule were performed by using the Gaussian 98 software package. All calculations made use of the B3LYP hybrid functional and the Stuttgart-group basis set as implemented on Gaussian 98.[23] TGA was carried out on a SIEKO TG/DTA 320 instrument. The sample was heated at a rate of 2°C min^{-1} under a flowing nitrogen atmosphere.

Received: January 13, 2003
Revised: April 8, 2003 [Z50929]

Keywords: gold · hybrid materials · iodine · mixed-valent compounds · noncovalent interactions

[1] a) P. Day, *Philos. Trans. R. Soc. London Ser. A* **1985**, *314*, 145; b) J. Takada, H. Awaji, M. Koshioka, A. Nakajima, W. A. Nevin, *Appl. Phys. Lett.* **1992**, *61*, 2184; c) P. G. Lacroix, R. Clement, K. Nakatani, J. Zyss, I. Ledoux, *Science* **1994**, *263*, 658; d) L. Ouahab, *Chem. Mater.* **1997**, *9*, 1909.

[2] a) D. B. Mitzi, S. Wang, C. A. Feild, C. A. Chess, A. M. Guloy, *Science* **1995**, *267*, 1473; b) D. B. Mitzi, *Prog. Inorg. Chem.* **1999**, *48*, 1; c) C. R. Kagan, D. B. Mitzi, C. D. Dimitrakopoulos, *Science* **1999**, *286*, 945.

[3] a) J.-M. Lehn, *Supramolecular Chemistry*, VCH, Weinheim, **1995**; b) P. Metrangolo, G. Resnati, *Chem. Eur. J.* **2001**, *7*, 2511; c) D. Quiñonero, C. Garau, C. Rotger, A. Frontera, P. Ballester, A. Costa, P. M. Deyà, *Angew. Chem.* **2002**, *114*, 3539–3542; *Angew. Chem. Int. Ed.* **2002**, *41*, 3389–3393.

[4] a) A. J. Blake, R. O. Gould, S. Parsons, C. Radek, M. Schröder, *Angew. Chem.* **1995**, *107*, 2563; *Angew. Chem. Int. Ed. Engl.* **1995**, *34*, 2374; b) Z. Tang, A. M. Guloy, *J. Am. Chem. Soc.* **1999**, *121*, 452; c) A. M. Guloy, Z. Tang, P. B. Miranda, V. I. Srdanov, *Adv. Mater.* **2001**, *13*, 833; d) T. Hertzsch, F. Budde, E. Weber, J. Hulliger, *Angew. Chem.* **2002**, *114*, 2385–2388; *Angew. Chem. Int. Ed.* **2002**, *41*, 2281–2284.

[5] a) G. A. Landrum, R. Hoffmann, *Angew. Chem.* **1998**, *110*, 1989–1992; *Angew. Chem. Int. Ed.* **1998**, *37*, 1887–1890; b) G. A. Landrum, N. Goldberg, R. Hoffmann, *New J. Chem.* **1998**, *22*, 883; c) L. Kloo, J. Rosdahl, P. H. Svensson, *Eur. J. Inorg. Chem.* **2002**, 1203.

[6] a) R. J. Cava, B. Batlogg, J. J. Krajewski, R. Farrow, L. W. Rupp, A. E. White, K. Short, W. F. Peck, T. Kometani, *Nature* **1988**, *332*, 814; b) A. W. Sleight, J. L. Gillson, P. E. Bierstedt, *Solid State Commun.* **1975**, *17*, 27.

[7] M. B. Robin, P. Day, *Adv. Inorg. Chem. Radiochem.* **1967**, *10*, 247.

[8] a) N. Kojima, M. Hasegawa, H. Kitagawa, T. Kikegawa, O. Shimomura, *J. Am. Chem. Soc.* **1994**, *116*, 11368; b) N. Kojima, N. Matsushita, *Coord. Chem. Rev.* **2000**, *198*, 251.

[9] a) H. L. Wells, *Am. J. Sci.* **1922**, *3*, 315; b) H. L. Wells, *Am. J. Sci.* **1922**, *3*, 417; c) N. Elliot, L. Pauling, *J. Am. Chem. Soc.* **1938**, *60*, 1846.

[10] N. Matsushita, H. Kitagawa, N. Kojima, *Acta Crystallogr. Sect. C* **1997**, *53*, 663.

[11] D. Weber, *Z. Naturforsch. B* **1978**, *33*, 862.

[12] S. D. Gupta, *J. Am. Chem. Soc.* **1914**, *36*, 747.

[13] Crystallographic data for $[NH_3(CH_2)_8NH_3]_2[(AuI_2)(AuI_4)(I_3)_2]$: monoclinic, space group $C2/m$ (no.12), $a = 32.1710(6)$, $b = 7.7846(2)$, $c = 8.8640(2)$ Å, $\beta = 103.17(0)°$, $V = 2161.46(2)$ Å^3, $\rho_{calc} = 3.395$ g cm^{-3}, $Z = 2$, $F(>4\sigma) = 1908$, $\lambda = 0.71073$ Å, $T = 223$ K, 6797 measured reflections, 2662 independent reflections. Single-crystal X-ray analysis was performed by using a Siemens SMART diffractometer equipped with a 1 K CCD area detector. Empirical absorption correction was applied by using ψ-scans. The structures were solved by direct methods and refined by full-matrix least-squares calculations. Thermal parameters of all non-H atoms were treated anisotropically. Hydrogen atoms were located at ideal positions using a riding model. All calculations were made by using the Siemens SHELXTL crystallographic package resulting in $R(\text{int}) = 0.0555$, $R_1 = 0.0388$, $wR_2 = 0.1006$.[24]

[14] Crystallographic data for $[NH_3(CH_2)_7NH_3]_2[(AuI_2)(AuI_4)(I_3)_2]$: triclinic, space group $P\bar{1}$ (no. 2), $a = 7.8197(1)$, $b = 8.6794(1)$, $c = 15.9093(2)$ Å, $\alpha = 80.87(0)°$, $\beta = 77.22(0)°$, $\gamma = 89.50(0)°$, $V = 1039.29(64)$ Å^3, $\rho_{calc} = 3.485$ g cm^{-3}, $Z = 1$, $F(>4\sigma) = 2844$, $\lambda = 0.71073$ Å, $T = 223$ K, 6478 measured reflections, 4490 symmetry-independent reflections. Empirical absorption correction was applied using SADABS. $R(\text{int}) = 0.0385$, $R_1 = 0.0534$, $wR_2 = 0.1423$. CCDC-197203 and CCDC 197204 (**1** and **2**) contain the supplementary crystallographic data for this paper. These data can be obtained free of charge via www.ccdc.cam.ac.uk/conts/retrieving.html (or from the Cambridge Crystallographic Data Centre, 12 Union Road, Cambridge CB2 1EZ, UK; fax: (+44) 1223-336-033; or deposit@ccdc.cam.ac.uk).

[15] J. Guan, Z. Tang, A. M. Guloy, *Chem. Commun.* **1999**, 1833.

[16] a) P. H. Svensson, J. Rosdahl, L. Kloo, *Chem. Eur. J.* **1999**, *5*, 305; b) P. H. Svensson, G. Raud, L. Kloo, *Eur. J. Inorg. Chem.* **2000**, 1275.

[17] a) N. Kojima, H. Kitagawa, *J. Chem. Soc. Dalton Trans.* **1994**, 327; b) H. Kitagawa, N. Kojima, T. Nakajima, *J. Chem. Soc. Dalton Trans.* **1991**, 3121.

[18] Optical diffuse reflectance measurements were made at room temperature for pure samples of compounds **1** and **2** by using a Cary 500 double beam, double monochromator spectrometer. Several single crystals were placed on a sample holder within a Praying-Mantis apparatus. Polytetrafluoroethylene was used as a standard background reference (100% reflectance). Absorption data were calculated from the reflectance data using the Kubelka-Munk function:[19] $[\alpha/S = (1-R)^2/2R]$, where R is the reflectance at a given wavelength, α is the absorption coefficient and S is the scattering coefficient. The electronic excitation energy, E_g, is extracted from the $(\alpha/S)^2$ versus energy plot.

 © 2003 Wiley-VCH Verlag GmbH & Co. KGaA, Weinheim

[19] a) W. W. Wendlandt, H. G. Hecht, *Reflectance Spectroscopy*, Interscience Publishers, New York, **1966**; b) G. Kotiim, *Reflectance Spectroscopy*, Springer, New York, **1969**.
[20] X. L. Liu, K. Matsuda, Y. Moritomo, A. Nakamura, N. Kojima, *Phys. Rev. B* **1999**, *59*, 7925.
[21] Chemical analysis was performed by SEM. Crystalline samples were placed on an adhesive carbon tape attached to a brass disk. No carbon coating was necessary for these narrow band gap semiconductors. The samples were then bombarded with a 15 eV electron beam over at least 15 1-micron diameter areas, to determine the elements present and to then average the ratio of gold and iodine. Compositional precision was found to be within 5% error. Data was collected by using a JEOL JSM 6400 scanning electron microscope equipped with a wave-dispersive spectrometer (WDS).
[22] The diamagnetic behavior of compound **1** (25 mg pellet sample) was examined by using an Oxford VSM instrument at a magnetic field of 0.01 T.
[23] a) Gaussian 98 (Revision A.7), M. J. Frisch, G. W. Trucks, H. B. Schlegel, G. E. Scuseria, M. A. Robb, J. R. Cheeseman, V. G. Zakrzewski, J. A. Montgomery, R. E. Stratmann, J. C. Burant, S. Dapprich, J. M. Millam, A. D. Daniels, K. N. Kudin, M. C. Strain, O. Farkas, J. Tomasi, V. Barone, M. Cossi, R. Cammi, B. Mennucci, C. Pomelli, C. Adamo, S. Clifford, J. Ochterski, G. A. Petersson, P. Y. Ayala, Q. Cui, K. Morokuma, D. K. Malick, A. D. Rabuck, K. Raghavachari, J. B. Foresman, J. Cioslowski, J. V. Ortiz, B. B. Stefanov, G. Liu, A. Liashenko, P. Piskorz, I. Komaromi, R. Gomperts, R. L. Martin, D. J. Fox, T. Keith, M. A. Al-Laham, C. Y. Peng, A. Nanayakkara, C. Gonzalez, M. Challacombe, P. M. W. Gill, B. G. Johnson, W. Chen, M. W. Wong, J. L. Andres, M. Head-Gordon, E. S. Replogle, J. A. Pople, Gaussian, Inc., Pittsburgh, PA, **1998**; b) C. Lee, W. Yang, R. G. Parr, *Phys. Rev. B* **1988**, *37*, 785; c) B. Miehlich, A. Savin, H. Stoll, H. Preuss, *Chem. Phys. Lett.* **1989**, *157*, 200; d) A. D. Becke, *J. Chem. Phys.* **1993**, *98*, 5648; e) T. Leininger, A. Nicklass, H. Stoll, M. Dolg, P. Schwerdtfeger, *J. Chem. Phys.* **1996**, *105*, 1052.
[24] G. M. Sheldrick, O. R. Gould, *Acta Crystallogr. Sect. B* **1995**, *51*, 423.

 © 2003 Wiley-VCH Verlag GmbH & Co. KGaA, Weinheim

Alkane Adsorption on Zeolites

Molecular Competition Effects in Liquid-Phase Adsorption of Long-Chain *n*-Alkane Mixtures in ZSM-5 Zeolite Pores**

Joeri F. M. Denayer, Kurt De Meyer, Johan A. Martens, and Gino V. Baron*

Zeolite adsorbents play a vital role in molecular separation technology, industrial catalysis and pollution control. In spite of its relevance to these areas, few fundamental studies have thus far been devoted to the adsorption of mixtures. The complexity of the molecular filling patterns of zeolite micropores directed earlier investigations, rather, into the adsorption of a single compound. Herein, we report the investigation of the adsorption of binary mixtures of *n*-alkanes with chain lengths up to C_{22} from the liquid phase on ZSM-5 zeolite, and the discovery of unexpected selectivities depending on subtle differences in the number of carbon atoms. In some *n*-alkane mixtures, the uptake of the lighter molecule was favored, whereas in other mixtures the heavier molecule was preferred. With other alkane combinations, azeotropic behavior of the adsorbate phase was also encountered. Systematic exploration of binary mixtures in the carbon range C_5–C_{22} led to the identification of the underlying mechanisms.

Intriguing effects in the adsorption of single components in microporous environments, such as zeolites were found recently. For example, ferrierite behaves as a 1D pore system for long-chain *n*-alkane molecules ($> C_5$), whereas only shorter molecules can exploit its full 2D pore system.[1–4] With ferrierite and ZSM-22, the siting of dibranched alkane seems to depend subtly on their size. At low coverage the dibranched alkanes adsorb in parallel to the outer surface of the zeolite and as coverage increases, additional molecules adsorb in such a manner that propyl and butyl groups point into the pores.[5] Other studies focused on the relationship between pore size and energy of interaction of pure substances.[6,7] Efforts have been made in the study of adsorption of hydrocarbons on ZSM-5 and Silicalite-1. These zeolites have the MFI framework topology are among the most studied zeolites in the field of adsorption, diffusion and catalysis.[8] The pore system of these zeolites comprises linear channels, with a free pore diameter of 5.6×5.3 Å, that are

[*] Dr. Ir. J. F. M. Denayer, Ir. K. De Meyer, Prof. Dr. Ir. G. V. Baron
Department of Chemical Engineering, Vrije Universiteit Brussel
Pleinlaan 2, 1050 Brussel (Belgium)
Fax: (+32) 2-629-32-48
E-mail: Joeri.denayer@vub.ac.be
Prof. Dr. Ir. J. A. Martens
Center for Surface Chemistry and Catalysis
Katholieke Universiteit Leuven
Kasteelpark Arenberg 23, 3001 Leuven (Belgium)

[**] This research was financially supported by FWO Vlaanderen. J.F.M.D. is grateful to the F.W.O.-Vlaanderen, for a fellowship as postdoctoral researcher. J.A.M. acknowledges the Flemish government for financial support through a concerted research action (G.O.A.).

 © 2003 Wiley-VCH Verlag GmbH & Co. KGaA, Weinheim DOI: 10.1002/anie.200351012

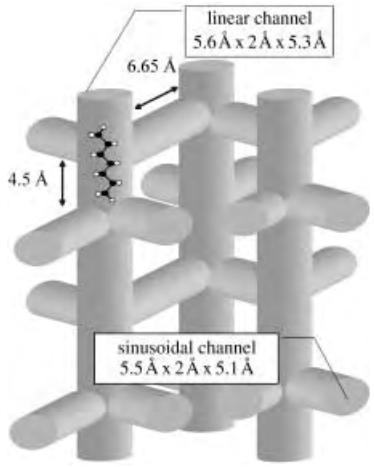


Figure 1. Schematic presentation of the structure of ZSM-5.

intersecting with sinusoidal channels, with free diameters of 5.5×5.1 Å (Figure 1). The length of a linear channel segment between two intersections is 4.5 Å. The sinusoidal channel segments measure 6.65 Å. Each unit cell contains four intersections, four sinusoidal segments and four linear segments.

Adsorption isotherms of *n*- and isoalkanes on MFI type zeolites deviate from the usual Langmuir isotherm and contain a "kink" at a compound specific partial pressure. These kinks coincide with abrupt changes in adsorption enthalpy and entropy, ascribed to a transition from adsorption in one type of channel to both types and the intersections.[9–15] For example, isobutane is adsorbed in the channel intersections at low pressure, while at high pressure, the isobutane molecules invade the channel segments too.[16] For *n*-alkanes, sometimes contradicting adsorption models were proposed to explain experimental adsorption isotherms. Short alkanes were postulated to adsorb in the entire pore system, or in the intersections.[13,14,17] C_9 and C_{10} *n*-alkanes preferentially fill the sinusoidal channel and C_6-C_8 alkanes the straight channels.[17] According to another study, alkanes longer than C_4 occupied the sinusoidal channels.[13] A similar, confusing picture emerged from theoretical calculations, such as Configurational-bias Monte-Carlo and Molecular Dynamic approaches. In some studies short alkanes were found to adsorb in all regions.[18–20] Other studies showed selective adsorption in sinusoidal channels or in the intersections.[21,22] At low temperatures, longer alkanes are positioned in the straight channels but are distributed over the entire pore system at higher temperatures.[18] Configurational-bias Monte-Carlo simulations revealed a "commensurate freezing" phenomenon of hexane and heptane in the sinusoidal channels.[23] At low partial pressure, the alkanes move freely in the sinusoidal channels, and prevent other molecules from adsorbing in the linear channels. At higher pressures, molecules are frozen in the sinusoidal channels allowing the filling of linear channel segments as well.[23]

In mixtures, theoretically the selectivity for the shortest molecule increases with increasing loading.[24,25] This happens because the vacant sites in the pores can best be filled by the smallest molecules.[26] Until now, theoretical approaches have been applied to predict the behavior of mixtures of much shorter alkane than the ones studied in the present work.[27]

For some representative binary alkane mixtures, compositions in the adsorbed phase (X_i) are plotted versus the compositions of the external liquid phase (Y_i) in Figure 2. Preferential adsorption of the longest alkane chain was

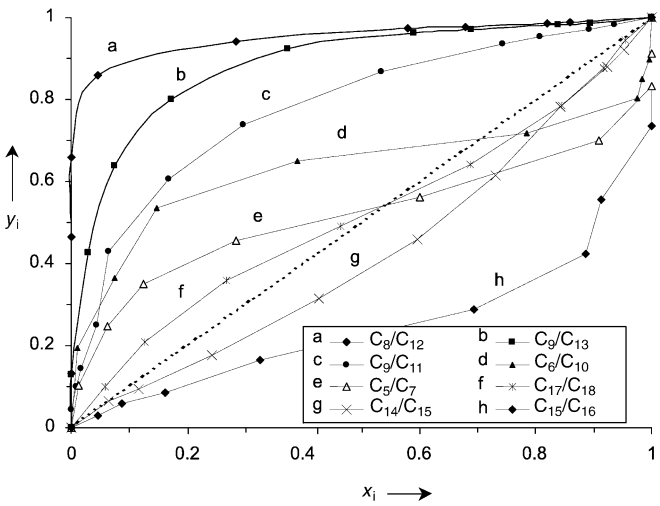


Figure 2. Selectivity diagrams for the adsorption of some binary alkane mixtures on ZSM-5. See also Table 1.

observed with C_8/C_{12}, C_9/C_{13}, and C_9/C_{11} (Figure 2; a–c). In the C_{14}/C_{15}, and C_{15}/C_{16} mixtures, the lightest alkane was selectively adsorbed (Figure 2; g, h). With C_6/C_{10}, and C_5/C_7 mixtures, the adsorbate phase behaved as an azeotrope (Figure 2; d, e). Azeotropic behavior was identified by a reversal of selectivity, at a specific composition where adsorbate and liquid have identical composition.[28] Thus the behavior of ZSM-5 zeolite is entirely different from mesoporous adsorbents, which do not discriminate among short and long alkanes when adsorbed from a liquid phase.[29]

The behavior of investigated *n*-alkane mixtures, in terms of the formation of azeotropes, or selective adsorption of the longest or shortest molecule, is summarized in Table 1.[30] Selective adsorption of the short alkane compound was observed with C_{14}/C_{15} and C_{15}/C_{16}, azeotropic behavior with C_5/C_7, C_6/C_7, C_6/C_8, C_7/C_8, C_6/C_{10}, C_{13}/C_{14}, C_{17}/C_{18}, and C_{20}/C_{22}. Selective adsorption of the heaviest molecule occurred with C_5/C_6, C_6/C_{14}, C_8/C_9, C_8/C_{12}, C_9/C_{11}, C_9/C_{12}, and C_9/C_{13}. In Table 1, the adsorption selectivity is further quantified by two parameters, namely 1) the external mole fraction (X_{ext}) of short chains needed to obtain an equimolar concentration in the pores, and 2) the mole fraction of long chains in the pores (X_{int}) at an equimolar composition in the external liquid phase. The adsorption selectivity was most pronounced with C_8/C_{12}. For example, the C_8 mole fraction in the external liquid phase must exceed 0.99 to reach a 50:50 mixture inside the pores (Table 1, entry 8). The very pronounced selectivity for C_{15} versus C_{16}, that is alkanes with a difference in chain length of one C atom, is striking (Table 1, entry 14: $X_{ext} = 0.10$).

 © 2003 Wiley-VCH Verlag GmbH & Co. KGaA, Weinheim

Table 1: Summary of the behavior encountered in the adsorption of alkane mixtures on ZSM-5

Entry	Mixture	Adsorption behavior[a]	X_{ext}[b]	X_{int}[b]	Pore filling [%][c]
1	C_5/C_7	A	0.59	0.53	75–85
2	C_5/C_6	L	0.66	0.65	72–87
3	C_6/C_7	A	0.42	0.66	89–87
4	C_6/C_8	A	0.55	0.52	85–64
5	C_6/C_{10}	A	0.87	0.67	81–85
6	C_6/C_{14}	L	0.86	0.73	85–100
7	C_8/C_9	L	0.82	0.80	64–74
8	C_8/C_{12}	L	>0.99	0.97	66–92
9	C_9/C_{11}	L	0.89	0.85	74–89
10	C_9/C_{12}	L	0.91	0.91	74–92
11	C_9/C_{13}	L	0.96	0.95	74–100
12	C_{13}/C_{14}	A	0.44	0.65	~100
13	C_{14}/C_{15}	S	0.37	0.38	~100
14	C_{15}/C_{16}	S	0.10	0.23	~100
15	C_{17}/C18	A	0.52	0.52	~100
16	C_{20}/C_{22}	A	0.45	0.46	~100

[a] A = azeotrope formation; L = longest chain adsorbed preferentially at all mixture compositions; S = shortest chain adsorbed preferentially at all mixture compositions. [b] X_{ext} = external mole fraction of shortest chain at equimolar concentration in the pores; X_{int} = mole fraction of longest chain in the pores at equimolar composition in the external liquid phase. [c] Pore filling, first figure: pure short alkane; second figure: pure long alkane.[30]

The remarkable adsorption selectivity of ZSM-5 should reflect a special organization of the *n*-alkane molecules in this specific pore system. The straight and sinusoidal pore segments are narrow and impose stretching of the alkyl chains along the pore axis, and minimize intermolecular interactions. The strong interaction with the pore walls implies a high adsorption enthalpy but also a significant loss of freedom, and strongly negative adsorption entropy. At high loading, the dense packing of the molecules contributes a second, negative contribution to the adsorption entropy. This compaction limits the reorganization capabilities and mobility of individual molecules in the adsorbate phase.

Mixtures of alkanes heavier than C_{12} completely fill up the pores (Table 1, entries 12–16, last column). The complete filling of the 2D pore system of ZSM-5 by long alkanes requires a very high flexibility and degree of organization. Pronounced adsorption selectivity for the short chain is observed with C_{14}/C_{15} and C_{15}/C_{16}. The chain length of C_{14} corresponds to the length of two sinusoidal channel segments and an intersection, but also fits into two linear-channel segments and two intersections. The length of a C_{15} molecule exceeds the dimensions of two sinusoidal-channel segments and an intersection but still fits into two linear-channel segments and two intersections. A stretched C_{16} molecule does not fit into either of these combinations, and thus always blocks an additional intersection compared to C_{15} or C_{14}. We ascribe the favorable adsorption of C_{14} and C_{15} to this matching with characteristic dimensions of the pore system. With other long-chain alkanes matching less with the characteristic pore lengths, such as C_{13}/C_{14}, C_{17}/C_{18}, and C_{20}/C_{22}, selectivities are less pronounced (Figure 2, f and Table 1, entries 12, 15 and 16).

A similar reasoning in terms of the matching of alkyl-chain lengths and pore-segment lengths explains the behavior of mixtures containing C_5 or C_6. These molecules fit neatly into a sinusoidal channel segment, whereas longer alkanes block intersections. Admixing C_5 or C_6 with a longer alkane fitting less well with a characteristic pore length gives rise to azeotrope behavior (C_5/C_7, C_6/C_7, C_6/C_8, C_6/C_{10}). These mixtures fill the pores only partially (Table 1, entries 1–5). At low concentration of the long chain, it is preferentially adsorbed because of its higher adsorption enthalpy. From a critical concentration of these long chains on, C_5 or C_6 adsorption is preferred because of their better fitting with the sinusoidal channels. This reversal of selectivity, depending on concentration, explains the azeotropic behavior.

In two further experiments, alkanes with excellent matching with specific structural elements of the pore architecture were mixed, namely (C_5/C_6 and C_6/C_{14}). As expected, adsorption of the long chain was preferred.

A last series of experiments was performed with alkanes with chain lengths in between the optima of C_5–C_6 and C_{14}–C_{15} (C_8/C_9, C_8/C_{12}, C_9/C_{11}, C_9/C_{12}, C_9/C_{13}, Table 1, entries 7–11). As expected for situations with partial pore filling (Table 1), the selective adsorption of the longest chain was observed.

The practical applicability of the observed adsorption effects was verified by performing preparative separation chromatography experiments with selected mixtures. Figure 3 shows the breakthrough profiles of a C_8/C_{12} mixture obtained with a 12 cm HPLC column filled with ZSM-5. Pure octane elutes first, and dodecane is selectively accumulated in the ZSM-5 adsorbent.

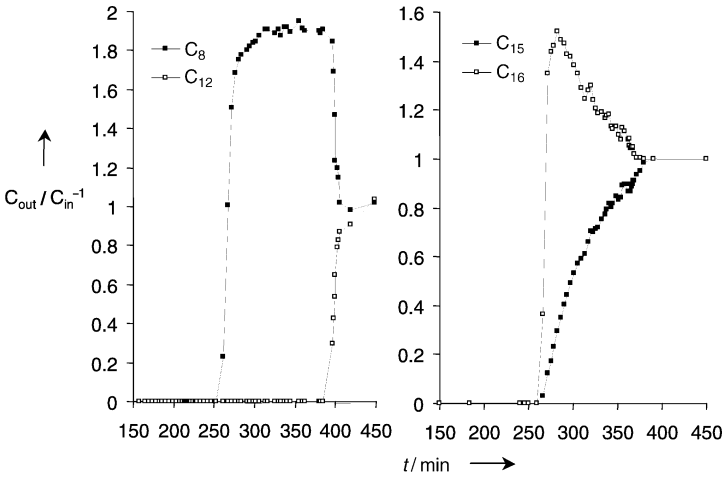


Figure 3. Breakthrough profiles of equimolar mixtures of octane and dodecane (left) and pentadecane and hexadecane (right) on a 12 cm column packed with ZSM-5.

 © 2003 Wiley-VCH Verlag GmbH & Co. KGaA, Weinheim

Only when the pores are saturated with dodecane do we observe its sharp breakthrough. A similar experiment was performed with a C_{15}/C_{16} mixture (Figure 3). The eluent is clearly enriched in C_{16}, and C_{15} is retained on the column, thus reflecting the adsorption equilibrium (Table 1, entry 14).

In conclusion, the adsorption of binary alkane mixtures can be rationalized in terms of the agreement between lengths of alkyl chains and channel segments. With alkanes not capable of filling the entire pore system, preferential adsorption of the longest chain is encountered with mixtures of alkanes in which both fit with the channel system, or with mixtures of alkanes of which neither fit. Azeotrope formation or preferential adsorption of the shortest chain is encountered in all other cases. The present findings can be exploited in molecular separation and catalytic-conversion processes. Many zeolites show 2D and 3D intersecting tubular pore systems. Probably, similar systems exist in related zeolite materials.

Experimental Section

Batch adsorption experiments were performed with an H-ZSM-5 zeolite (CBV 8014, Zeolyst, Si/Al = 40). Zeolite samples (~1 g) were put in 10 mL glass vials. After regeneration overnight at 673 K, the vials were immediately sealed with a cap containing a septum to avoid water uptake. Mixtures of two linear alkanes in a nonadsorbing solvent (*iso*-octane, 99.5 % purity, Acros) were prepared so to obtain 14 liquid mixtures of different composition. The total concentration of the adsorbing components was between 0.12 and 0.15 $g\,g^{-1}$. Immediately after the samples were sealed and weighed, about 10 mL of the mixture was injected through the septum into vials containing zeolite, and another 10 mL was added to a vial without zeolite, which was to be used as blank sample. Samples were kept at 277 K, so that no compounds could evaporate, and were stirred continuously. Liquid samples were taken after 24 h and 48 h, to check if equilibrium between the adsorbed and bulk phase had occurred, and analyzed in a GC with a flame ionization detector (FID). For every binary mixture, a calibration line was obtained by analysis of the blank samples. This approach guaranteed a very high precision in the calculation of the amounts adsorbed, obtained by calculation of the mass balance:

$$q_{\mathrm{sorbate}} = \left(\frac{(\mathrm{wt}\,\%_{\mathrm{blanco}} - \mathrm{wt}\,\%_{\mathrm{zeolite}})\,(m^0_{\mathrm{sorbate}} + m^0_{\mathrm{solvent}})}{100\,\rho_{\mathrm{sorbate}}\,m_{\mathrm{zeolite}}} \right)$$

Breakthrough experiments were performed by HPLC. A column (120 mm length, 4.9 mm internal diameter) was packed with zeolite and regenerated overnight under N_2 flow at 400 °C. Dried *iso*-octane was used as a nonadsorbing carrier. Firstly, the HPLC setup and column were flushed with *iso*-octane. Subsequently, a mixture of *iso*-octane and equimolar trace amounts of adsorbates were pumped (0.1 $mL\,min^{-1}$) over the column. Liquid samples were taken every four minutes and analyzed by GC.

Received: January 24, 2003 [Z51012]

Keywords: · adsorption · alkanes · zeolites

[1] W. J. M. Van Well, X. Cottin, J. W. de Haan, R. A. Van Santen, B. Smit, *Angew. Chem.* **1998**, *110*, 1142 – 1144; *Angew. Chem. Int. Ed.* **1998**, *37*, 1081 – 1083.

[2] W. J. M. Van Well, X. Cottin, J. W. de Haan, B. Smit, G. Nivarthy, J. A. Lercher, J. H. C. Van Hooff, R. A. Van Santen, *J. Phys. Chem. B* **1998**, *102*, 3945 – 3951.

[3] W. J. M. Van Well, X. Cottin, B. Smit, J. H. C. Van Hooff, R. A. Van Santen, *J. Phys. Chem. B* **1998**, *102*, 3952 – 3958.

[4] F. Eder, J. A. Lercher, *J. Phys. Chem. B* **1997**, *101*, 1273 – 1278.

[5] J. A. Z. Pieterse, S. Veefkind-Reyes, K. Seshan, J. A. Lercher, *J. Phys. Chem. B* **2000**, *104*, 5715 – 5723.

[6] S. Savitz, F. Siperstein, R. J. Gorte, A. L. Myers, *J. Phys. Chem. B* **1998**, *102*, 6865 – 6872.

[7] K. F. Czaplewski, T. L. Reitz, Y. J. Kim, R. Q. Snurr, *Microporous Mesoporous Mater.* **2002**, 56, 55 – 64.

[8] G. T. Kokotailo, S. L. Lawton, D. H. Olson, W. M. Meier in *Atlas of zeolite structure types* (Eds.: W. M. Meier, D. H. Olson, C. Baerlocher), Elsevier, New York, **1996**, pp. 146 – 147.

[9] Y. Yang, L. V. C. Rees, *Microporous Mater.* **1997**, *12*, 117 – 122.

[10] B. Millot, A. Methivier, H. Jobic, *J. Phys. Chem. B* **1998**, *102*, 3210 – 3215.

[11] O. Talu, C.-J. Guo, D. T. Hayhurst, *J. Phys. Chem.* **1989**, *93*, 7294 – 7298.

[12] M. S. Sun, O. Talu, D. B. Shah, *J. Phys. Chem.* **1996**, *100*, 17276 – 17280.

[13] R. E. Richards, L. V. C. Rees, *Langmuir* **1987**, *3*, 335 – 340.

[14] W. Zhu, J. M. van der Graaf, L. J. P. van den Broeke, F. Kapteijn, J. A. Moulijn, *Ind. Eng. Chem. Res.* **1998**, *37*, 1934 – 1942.

[15] W. J. M. van Well, J. P. Wolthuizen, B. Smit, J. H. C. Van Hooff, R. A. Van Santen, *Angew. Chem.* **1995**, *107*, 2765 – 2767; *Angew. Chem. Int. Ed. Engl.* **1995**, *34*, 2543 – 2544.

[16] W. Zhu, F. Kapteijn, J. A. Moulijn, *Phys. Chem. Chem. Phys.* **2000**, *2*, 1989 – 1995.

[17] P. A. Jacobs, H. K. Beyer, J. Valyon, *Zeolites* **1981**, *1*, 161 – 168.

[18] E. J. Maginn, A. T. Bell, D. N. Theodorou, *J. Phys. Chem.* **1995**, *99*, 2057 – 2079.

[19] B. Smit, J. I. Siepmann, *J. Phys. Chem.* **1994**, *98*, 8442 – 8452.

[20] R. L. June, A. T. Bell, D. N. Theodorou, *J. Phys. Chem.* **1992**, *96*, 1051 – 1060.

[21] J. B. Nicholas, F. R. Trouw, J. E. Mertz, L. E. Iton, A. J. Hopfinger, *J. Phys. Chem.* **1993**, *97*, 4149 – 4163.

[22] J. O. Titiloye, S. C. Parker, F. S. Stone, C. R. A. Catlow, *J. Phys. Chem.* **1991**, *95*, 4038 – 4044.

[23] B. Smit, T. L. M. Maesen, *Nature* **1995**, *374*, 42 – 44.

[24] J. Talbot, *AIChE J.* **1997**, *43*, 2471 – 2478.

[25] D. M. Ruthven, K. F. Loughlin, K. A. Holborow, *Chem. Eng. Sci.* **1973**, *28*, 701.

[26] R. Krishna, S. Calero, B. Smit, *Chem. Eng. J.* **2002**, *88*, 81 – 94.

[27] R. Krishna, B. Smit, S. Calero, *Chem. Soc. Rev.* **2002**, *31*, 185 – 194.

[28] D. M. Ruthven, *Principles of adsorption and adsorption processes*, Wiley-Interscience, New York, **1984**, p. 111.

[29] J. F. M. Denayer, A. Bouyermaouen, G. V. Baron, *Ind. Eng. Chem. Res.* **1998**, *37*, 3691 – 3698.

[30] The pore filling is defined as the number of adsorbed alkane carbon atoms in the experimental conditions divided by the maximum number of alkane carbon atoms that can be adsorbed in the pore system of ZSM-5 multiplied by 100.

 © 2003 Wiley-VCH Verlag GmbH & Co. KGaA, Weinheim

Phosphorus–Carbon Compounds

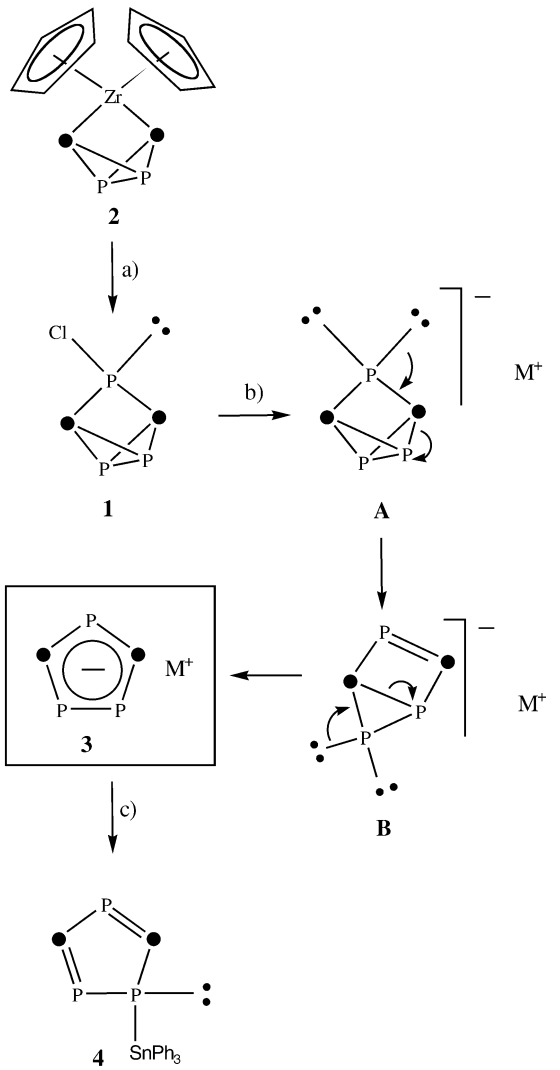
Selective Preparation of the $[3,5\text{-}t\mathrm{Bu}_2\text{-}1,2,4\text{-}C_2P_3]^-$ Ion and Synthesis and Structure of the Cationic Species *nido*-$[3,5\text{-}t\mathrm{Bu}_2\text{-}1,2,4\text{-}C_2P_3]^+$, Isoelectronic with $[C_5R_5]^+$**

Jason M. Lynam, May C. Copsey, Michael Green, John C. Jeffery, John E. McGrady, Christopher A. Russell,* John M. Slattery, and Anthony C. Swain*

Dedicated to Professor Manfred Regitz

There has been significant progress in the chemistry of transition-metal complexes carrying the η^5-3,5-$t\mathrm{Bu}_2$-1,2,4-C_2P_3 ligand.[1] Although the isolobal relationship P⟷CH and diagonal relationship P/C suggest that complexes carrying this ligand should behave like the corresponding η^5-cyclopentadienyl-substituted analogues, recent work has shown that the phosphorus-containing systems exhibit subtle differences in both bonding and reactivity.[2–4] This situation suggests that further investigations could be rewarding. In a new approach to this chemistry we focused on the reactivity of the interesting tricyclic C_2P_3 compound **1** (Scheme 1), first reported by Regitz et al.[5] First, we used this species as a convenient starting point for a new selective synthetic approach to the aromatic ion $[3,5\text{-}t\mathrm{Bu}_2\text{-}1,2,4\text{-}C_2P_3]^-$ (**3**). Second, and again reflecting on the consequences of replacing CH groups by isolobal P atoms, we explored the possibility of utilizing **1** as a precursor to cations $[C_2t\mathrm{Bu}_2P_3]^+$, isoelectronic with $[C_5R_5]^+$.

The published synthetic pathways to the anion **3**,[6–8] which derive from earlier work by Becker et al.,[9,10] involve reaction of P≡C*t*Bu with alkali metals (M). However, this procedure is unselective, and to obtain pure **3** it is necessary to repeatedly recrystallize the moisture-sensitive alkali-metal salts to remove the second product of these reactions, the $[2,4,5\text{-}t\mathrm{Bu}_3\text{-}1,3\text{-}C_3P_2]^-$ ion. Therefore, we recognized that if the full potential of this area was to be realized, it was important to devise a more efficient and selective pathway to **3**. We reasoned that if the tricyclic compound **1**, which is readily formed in good to excellent yield by treating the readily accessible zirconium complex **2** with PCl_3,[5] was treated with an alkali metal in THF, the anionic species **A** should be generated (Scheme 1). We then hypothesized that such a species should undergo consecutive ring-opening reactions (**A**→**B**→**3**) and thus selectively provide the desired anion.



Scheme 1. a) PCl_3; b) M, THF, −MCl; c) Ph_3SnCl, −MCl (● = C*t*Bu; ·· = lone pair; M = Li, Na.

Reaction (RT, 2 h, THF) of **1** with Li or Na metal leads to quantitative formation of the lithium or sodium salt of **3**, which confirms our ring-opening hypotheses. Both Li·**3** and Na·**3** react quantitatively with Ph_3SnCl to give the known compound $3,5\text{-}t\mathrm{Bu}_2\text{-}1\text{-}SnPh_3\text{-}1,2,4\text{-}C_2P_3$ (**4**), which has been shown to be a valuable reagent for the syntheses of complexes of the η^5-C_2P_3 ligand.[7]

We believed that **1** might react with Lewis acids to provide an entry point to the cationic $[C_2t\mathrm{Bu}_2P_3]^+$ manifold, related to the isoelectronic pentamethylcyclopentadienyl cation, a species that has recently attracted considerable attention.[11–15] In particular, in view of the isolobal relationship P⟷CH, and

[*] Prof. M. Green, Dr. C. A. Russell, Dr. J. M. Lynam, M. C. Copsey, Dr. J. C. Jeffery, J. M. Slattery, Dr. A. C. Swain
School of Chemistry
University of Bristol
Cantock's Close, Bristol BS8 1TS (UK)
Fax: (+44) 117-929-0509
E-mail: michael.green@bristol.ac.uk
chris.russell@bristol.ac.uk
Dr. J. E. McGrady
Department of Chemistry
University of York
Heslington, York, YO10 5DD (UK)

[**] We thank the Leverhulme Trust (Emeritus Research Fellowship for M.G.), the Royal Society (University Research Fellowship for C.A.R.), the Ramsay Memorial Fellowship Trust (Research Fellowship for J.M.L.), the University of Bristol (M.G., C.A.R., J.M.L.), and the EPSRC (A.C.S., M.C.C., J.M.S.) for financial support. We would also like to thank Dr. Simon Duckett (York) for helpful discussions concerning the interpretation of NMR spectra.

 © 2003 Wiley-VCH Verlag GmbH & Co. KGaA, Weinheim DOI: 10.1002/anie.200351096

Stohrer and Hoffmann's conclusion[16] that a dynamic Jahn–Teller system of C_{2v} $[CH]_5^+$ ion geometries can be accessed by interaction of an empty p orbital centered on C(3) with the σ* levels of a tricyclo[2.1.0.0^{2,5}]pentane unit, abstraction of a chloride anion from the P–Cl bond of **1** might lead via a phosphenium cation to the formation of the unknown $[C_2tBu_2P_3]^+$ ions and potentially interesting structures.

Our attempt to achieve this by treating **1** with $SbCl_5$ was unsuccessful in that chlorination of the P–P bond occurred to give $SbCl_3$ and the known compound **5** (Scheme 2).[5] However, reaction (20 °C, CH_2Cl_2, 10 min) of **2** with a stoichiometric amount of $AlCl_3$ produced a colorless solution from which a small amount of white precipitate separated. This solid redissolved on gentle warming, and storage of the resulting solution at 20 °C for 24 h furnished colorless crystalline blocks. A single-crystal X-ray diffraction study of this compound showed it to have the Wadeian structure *nido*-$[3,5\text{-}tBu_2\text{-}1,2,4\text{-}C_2P_3]^+[AlCl_4]^-$ (**6**) (Figure 1). The molecule is essentially ion-separated, with $[AlCl_4]^-$ ions loosely linked by long-range Cl···P interactions (ranging from 3.37 to 3.58 Å) to a cluster cation that is isoelectronic with the hypothetical $[C_5Me_5]^+$ cation.

The cation consists of three phosphorus and two *t*BuC units arranged in a pseudo square-based-pyramidal geometry, consisting of a diamond-shaped P_2C_2 base (with alternating P and C units) capped by an apical four-coordinate P atom. This is a 14-electron *nido* cluster, based on an octahedron with one missing vertex, in which the carbon atoms occupy the sites of lowest connectivity. The basal P–C bonds are all approximately equal (ca. 1.80 Å), whereas the P–C bonds to the apical P atom are significantly longer (2.00 Å). The P-C-P angles in the basal unit are approximately 100°, whereas the C-P-C angles are considerably more compressed (79°). All the bond angles subtended at the apical phosphorus atom by adjacent basal atoms are extremely acute (ca. 50°).

The structure of **6** is an analogue of that predicted by Hoffmann[16] for the $[C_5H_5]^+$ ion and also to the species *nido*-2-*t*Bu-1,2-PCB_3H_5 prepared by the reaction of P≡C*t*Bu with

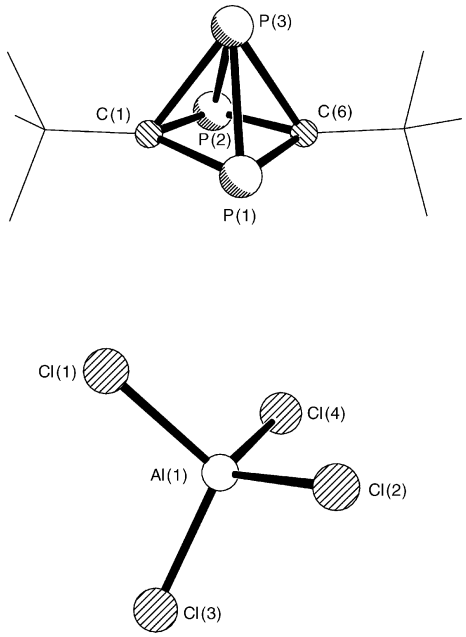
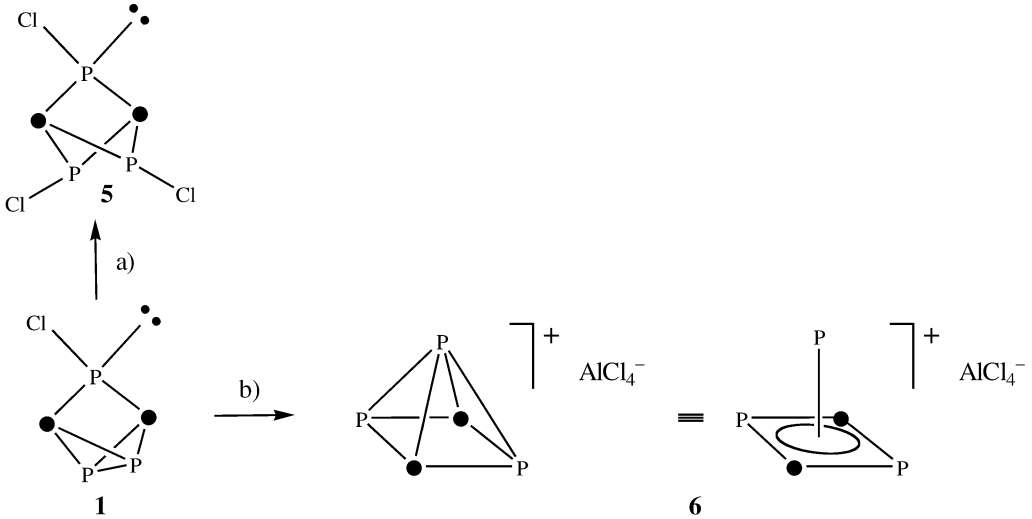


Figure 1. Crystal structure of **6**. H atoms have been omitted for clarity. Only one of the two independent molecules in the unit cell is shown. Selected bond lengths [Å] and angles [°]: P(1)–C(1) 1.8009(15), P(1)–C(6) 1.8037(15), P(1)–P(3) 2.2367(7), P(2)–C(1) 1.8011(15), P(2)–C(6) 1.8020(16), P(2)–P(3) 2.2517(8), P(3)–C(1) 1.9955(16), P(3)–C(6) 2.0022(15); C(1)-P(1)-C(6) 79.30(7), C(1)-P(1)-P(3) 58.04(5), C(6)-P(1)-P(3) 58.24(5), C(1)-P(2)-C(6) 79.34(7), C(1)-P(2)-P(3) 57.72(5), C(6)-P(2)-P(3) 57.93(5), C(1)-P(3)-C(6) 70.25(6), C(1)-P(3)-P(1) 49.97(4), C(6)-P(3)-P(1) 49.99(5), C(1)-P(3)-P(2) 49.73(5), C(6)-P(3)-P(2) 49.70(5), P(1)-P(3)-P(2) 75.93(2), P(1)-C(1)-P(2) 100.10(7), P(1)-C(1)-P(3) 71.99(6), P(2)-C(1)-P(3) 72.55(6). Selected bond lengths [Å] and angles [°] for the second independent molecule in the unit cell (P(6) is the apical phosphorus atom): P(4)–C(16) 1.7981(16), P(4)–C(11) 1.8013(16), P(4)–P(6) 2.2540(8), P(5)–C(16) 1.8018(16), P(5)–C(11) 1.8083(15), P(5)–P(6) 2.2287(7), P(6)–C(16) 1.9934(16), P(6)–C(11) 1.9955(16); C(16)-P(4)-C(11) 79.29(7), C(16)-P(4)-P(6) 57.63(5), C(11)-P(4)-P(6) 57.67(5), C(16)-P(5)-C(11) 79.01(7), C(16)-P(5)-P(6) 58.14(5), C(11)-P(5)-P(6) 58.13(5), C(16)-P(6)-C(11) 70.30(6), C(16)-P(6)-P(5) 50.14(5), C(11)-P(6)-P(5) 50.32(5), C(16)-P(6)-P(4) 49.63(5), C(11)-P(6)-P(4) 49.70(5), P(5)-P(6)-P(4) 76.19(2), P(4)-C(11)-P(5) 100.03(7), P(4)-C(11)-P(6) 72.63(6), P(5)-C(11)-P(6) 71.54(6).



Scheme 2. a) $SbCl_5$, CH_2Cl_2, $-SbCl_3$; b) $AlCl_3$, CH_2Cl_2 (● = C*t*Bu, ·· = lone pair).

 © 2003 Wiley-VCH Verlag GmbH & Co. KGaA, Weinheim

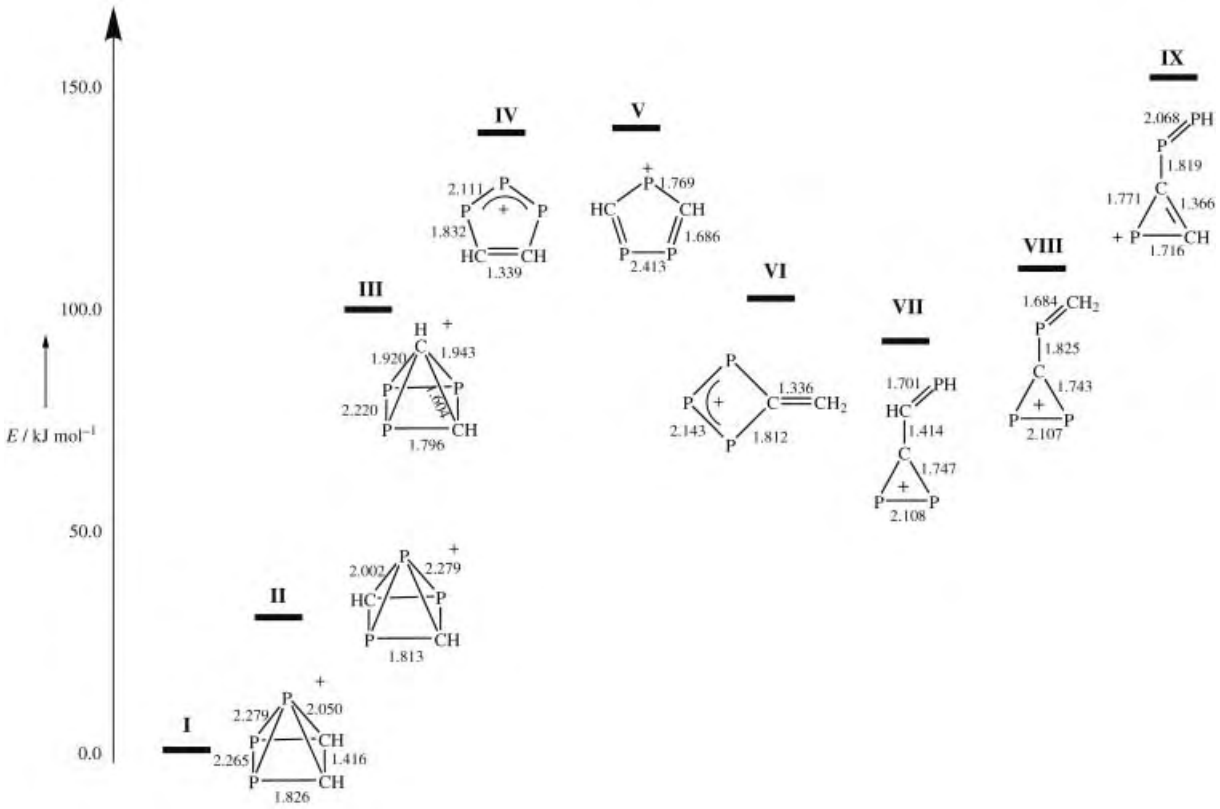


Figure 2. Optimized structural parameters and relative energies E of $[C_2H_2P_3]^+$ isomers.

B_4H_{10}.[17] Recent calculations have shown, however, that the vinylcyclopropenyl and cyclopentadienyl cations are more stable isomers of the $[C_5H_5]^+$ ion than a square-based-pyramidal structure.[18,19] These observations encouraged us to survey systematically the potential-energy surface (PES) of the model cation $[C_2H_2P_3]^+$ at the B3LYP/6-311G** level. Optimized structural parameters and relative energies of the most stable isomers are summarized in Figure 2. In contrast to the isomers of the $[C_5H_5]^+$ ion the most stable structures on the PES for $[P_3C_2H_2]^+$ ions are square-based pyramids, the lowest lying of which, **I**, has two basal phosphorus atoms in a 2,3-arrangement. Structure **II**, which has the same connectivity as **6**, is 24.4 kJ mol^{-1} higher in energy, and its optimized structural parameters are remarkably similar to those in the crystal structure of **6**. The third possible square-based pyramid, structure **III**, with a CH group in the apical position, is 99.8 kJ mol^{-1} higher in energy than **I**. A survey of species located on the PES of $[C_5H_5]^+$ led us to investigate additional isomers based on the cyclopentadienyl (**IV** and **V**) methylenecyclobutenyl (**VI**) and vinylcyclopropenyl (**VII**, **VIII**, and **IX**) structures.[*] However, even the most stable of these alternative structures (**VII**) lies 83.5 kJ mol^{-1} above the global minimum **I**. The calculations therefore imply that **6** is not the most stable isomer of the $[C_2tBu_2P_3]^+$ ion, despite the fact that it is formed in the experiment. We cannot rule out the possibility that **6** crystallized preferentially, and that analogues of **I** and **II**, undergoing rapid exchange, are present in our experiments. However, if one considers that **6** is formed by abstraction of a chloride anion from **1**, then it would be the kinetic product of the reaction. It might be possible to access structure **I** from **II** if **III** is invoked as an intermediate. However, the barrier for the conversion of **II** into **III** is calculated to be rather high (115 kJ mol^{-1}), and this implies that **6** is the only species of the $[P_3C_2R_2]^+$ manifold that is present.

Phosphorus compounds have a striking structural resemblance to carbon compounds. However, as is shown here and in valence isomers of tetraphosphabenzene and phosphorus analogues of amidinium salts, any isomers that are high in energy as a result of the constraint of bond angles (i.e., strain energy) will be much more stable on the hypersurface for the phosphorus analogues.[20] Most significantly, the stability of the planar cyclopentadienyl, methylenecyclobutenyl, and vinylcyclopropenyl analogues is much reduced in the phosphorus-containing systems because of the inefficient π–π overlap in double bonds involving atoms of the second period. As a result, there is a distinct switch in global minimum from cyclic unsaturated species to saturated cages with high connectivity.

The ^{1}H, ^{13}C, and ^{27}Al NMR spectra of **6** in CD_2Cl_2 solution are consistent with the solid-state structure. Curiously, however, no signals attributable to **6** could be observed in the ^{31}P NMR spectrum of **6** over the temperature range −100 to +30 °C. Further calculations shed some light on this rather

[*] We considered many alternative linkage isomers of the methylenecyclobutenyl and vinylcyclopropenyl structures; only the most stable are shown in Figure 2.

 © 2003 Wiley-VCH Verlag GmbH & Co. KGaA, Weinheim

puzzling observation. The NMR spectroscopic chemical-shift values of the ^{31}P nuclei in structure **II** were calculated to be $\delta = -532$ (apical) and $\delta = 246$ (basal) ppm. The value for the apical phosphorus atom is in good agreement with that found for *nido*-2-*t*Bu-1,2-PCB_3H_5.[17] The lack of signals at these chemical shifts in our spectra led us to conclude that a fluxional process was occurring, the result of which was to exchange the apical and basal phosphorus atoms. A similar process was predicted by Stohrer and Hoffmann[16] in their analysis of bond-stretch isomerism and polytopal rearrangements within the $[C_5H_5]^+$ manifold. Here, exchange of basal and apical carbon atoms is predicted to occur via a C_{2v} transition state. In the case of the $[P_3C_2H_2]^+$ manifold, a similar C_{2v}-symmetric transition state was located (one imaginary frequency), only 37.0 kJ mol^{-1} higher in energy than **II** and thus allowing facile exchange of apical and basal phosphorus atoms (Figure 3).

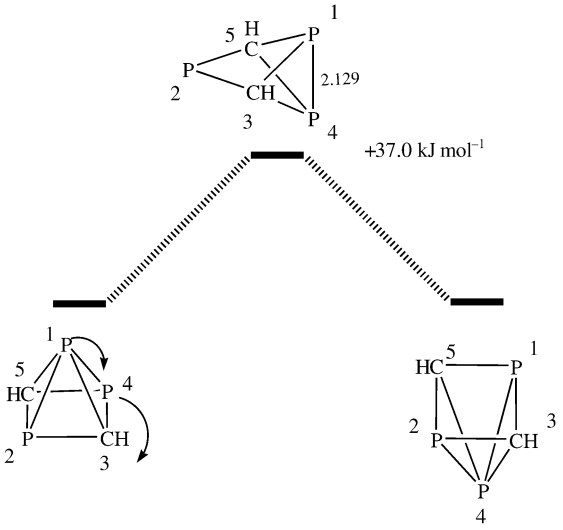


Figure 3. Facile exchange of apical and basal phosphorus atoms.

This result allowed us to calculate the rate constant for this exchange process for a range of temperatures, and ^{31}P NMR spectra were simulated using these data. At 298 K the simulated spectrum exhibited a single resonance at $\delta = -12$ ppm with a line width at half height ($\omega_{1/2}$) of about 3000 Hz, and at 183 K two peaks at $\delta = -532$ and 246 ppm were predicted, with a line width of about 100 Hz. The poor solubility of **6** and the calculated broadening of the signals provides an explanation for our inability to observe, even at low temperature, any signal in the ^{31}P NMR spectrum of this species. Consistent with this rapid exchange of apical and basal phosphorus atoms, signals arising from **6** in the ^{13}C NMR spectrum all show significant broadening.

From a synthetic standpoint, the synthesis of **6** by a Lewis acid promoted ring-opening reaction of **1** represents a new approach to phosphorus–carbon clusters. These compounds were previously prepared from P≡C*t*Bu, either by thermolysis or by reaction with various transition-metal species or Lewis acids,[21,22] synthetic approaches which have to date not provided access to molecules such as **6**. Interestingly, the cation of **6** obeys Wade's rules and is in fact the first example of a cationic phosphorus–carbon cluster.

In conclusion we have shown that the tricyclic C_2P_3 compound **1** can selectively ring open to give in high yield the anion **3** and the novel nido cation **6**.

Experimental Section

3·M: In a typical experiment, compound **1** (172 mg, 0.65 mmol) was dissolved in THF (5 mL) and added to a suspension of Na pieces (100 mg, 4.34 mmol) in THF (5 mL). The resulting mixture was stirred for 2 h, after which time it had turned deep red, which indicated formation of **2**: an NMR spectrum recorded at this time indicated that conversion into **2** was essentially quantitative. The solution was then filtered, cooled to −30 °C, and a solution of Ph_3SnCl (272 mg, 0.71 mmol) in THF (10 mL) added in portions, which caused an instant color change to yellow. Conversion into compound **4** was again quantitative, as shown by ^{31}P NMR spectroscopy.

The reaction with Li could be accomplished in the same manner by using an excess of Li metal that had been activated by sonication.

6: $AlCl_3$ (87 g, 0.65 mmol) was added to a stirred solution of **1** (172 mg, 0.65 mmol) in CH_2Cl_2 (5 mL). After stirring the mixture for 10 min, a white solid was observed to form in the colorless solution. The solid redissolved on gentle heating. Storage for 16 h at 20 °C yielded a good crop of colorless blocks of **6**. ^1H NMR (25 °C, 299.9 MHz, CD_2Cl_2): $\delta = 1.01$ ppm (s, $C(CH_3)_3$); ^{27}Al NMR (25 °C, 78.2 MHz, CD_2Cl_2): $\delta = 102.2$ ppm (s, $AlCl_4^-$); ^{13}C NMR (25 °C, 75.4 MHz, CD_2Cl_2): $\delta = 29.5$ (apparent q, 3.0 Hz, $C(CH_3)_3$), 31.2 (br, $C(CH_3)_3$); 32.8 ppm (br, P_3C_2*t*Bu).

All density functional calculations were performed with the Gaussian 98 program.[23] The natures of the minima and transition states were confirmed by vibrational analysis (zero or one imaginary frequency, respectively). Shielding parameters σ were calculated by using the GIAO formalism,[24] and converted into chemical shifts δ by using $\delta = 328.5 - \sigma$ ppm, where 328.5 ppm is the absolute shielding parameter for the ^{31}P reference standard, 85 % H_3PO_4.[25]

Crystal structure for **6**: $C_{20}H_{36}Al_2Cl_8P_6$, $M_r = 799.87$, $T = 173(2)$ K, monoclinic, space group $P2(1)/n$, $a = 10.529(2)$, $b = 21.520(4)$, $c = 16.354(3)$ Å, $\beta = 95.95(3)°$, $V = 3685.6(13)$ Å^3, $Z = 4$, $\rho_{calcd} = 1.442$ Mg m^{-3}, $\mu = 0.933$ mm^{-1}, $3.14 \le 2\theta \le 54.96°$. X-ray measurements were made using a Bruker APEX area-detector diffractometer with $Mo_{K\alpha}$ radiation ($\lambda = 0.71073$ Å)[26] on a single crystal of **6** of size $0.2 \times 0.2 \times 0.1$ mm that was coated in perfluoropolyether oil and mounted on a glass fiber. Of the 25669 reflections collected, 8453 were independent. Intensities were integrated[27] from several series of exposures, each exposure covering 0.3° in ω, and the total data set was a hemisphere. Absorption corrections were applied, based on multiple and symmetry-equivalent measurements.[28] The structure was solved by direct methods[29] and refined by least-squares methods on F^2 values for all reflections[30] with weighting $w^{-1} = \sigma^2(F_o^2) + (0.0267\,P)^2$, where $P = [\max(F_o^2, 0) + 2F_c^2]/3$, to final values of $R1 = 0.0256$ [$I > 2\sigma(I)$] and $wR2 = 0.0575$ (all data). Largest peak and hole in the final difference map were 0.462 and −0.179 e Å^{-3}. All non-hydrogen atoms were assigned anisotropic displacement parameters and refined without positional constraints. All hydrogen atoms were constrained to ideal geometries and refined with fixed isotropic displacement parameters. CCDC-202457 contains the supplementary crystallographic data for this paper. These data can be obtained free of charge via www.ccdc.cam.ac.uk/conts/retrieving.html (or from the Cambridge Crystallographic Data Centre, 12 Union Road, Cambridge CB2 1EZ, UK; fax: (+44) 1223-336-033; or deposit@ccdc.cam.ac.uk).

Received: February 4, 2003 [Z51096]

 © 2003 Wiley-VCH Verlag GmbH & Co. KGaA, Weinheim

Keywords: anions · cations · density functional calculations · phosphorus · phosphorus heterocycles

[1] K. B. Dillon, F. Mathey, J. F. Nixon, in *Phosphorus, The Carbon Copy*, Wiley, Chichester, **1998**.

[2] T. Clark, A. Elvers, F. W. Heinemann, M. Hennemann, M. Zeller, U. Zenneck, *Angew. Chem.* **2000**, *112*, 2174; *Angew. Chem. Int. Ed.* **2000**, *39*, 2087.

[3] K. Al-Ktaifeni, J. C. Green, P. B. Hitchcock, J. F. Nixon, *J. Chem. Soc. Dalton Trans.* **2001**, 1726.

[4] F. G. N. Cloke, J. C. Green, P. B. Hitchcock, J. F. Nixon, *J. Chem. Soc. Dalton Trans.* **2000**, 3534.

[5] P. Binger, T. Wettling, R. Schneider, F. Zurmühlen, U. Bergsträsser, J. Hoffmann, G. Maas, M. Regitz, *Angew. Chem.* **1991**, *103*, 208; *Angew. Chem. Int. Ed. Engl.* **1991**, *30*, 207.

[6] R. Bartsch, J. F. Nixon, *Polyhedron* **1989**, *8*, 2407.

[7] A. Elvers, F. W. Heinemann, B. Wrackmeyer, U. Zenneck, *Chem. Eur. J.* **1999**, *5*, 3143.

[8] C. Callaghan, G. K. B. Clentsmith, F. G. N. Cloke, P. B. Hitchcock, J. F. Nixon, D. M. Vickers, *Organometallics* **1999**, *18*, 793.

[9] G. Becker, G. Gresser, W. Uhl, *Z. Naturforsch. B* **1981**, *36*, 16.

[10] G. Becker, W. Becker, R. Kuebl, H. Schmidt, U. Webber, M. Westhausen, *Nova Acta Leopold.* **1985**, *59*, 55.

[11] J. M. Lambert, L. Lin, V. Rassolov, *Angew. Chem.* **2002**, *114*, 1487; *Angew. Chem. Int. Ed.* **2002**, *41*, 1429; Corrigendum: J. M. Lambert, L. Lin, V. Rassolov, *Angew. Chem.* **2002**, *114*, 1716; *Angew. Chem. Int. Ed.* **2002**, *41*, 1642.

[12] M. Otto, D. Scheschkewitz, M. M. Midland, J. M. Lambert, G. Bertrand, *Angew. Chem.* **2002**, *114*, 2379; *Angew. Chem. Int. Ed.* **2002**, *41*, 2275.

[13] T. Müller, *Angew. Chem.* **2002**, *114*, 2380; *Angew. Chem. Int. Ed.* **2002**, *41*, 2276.

[14] J. B. Lambert, *Angew. Chem.* **2002**, *114*, 2382; *Angew. Chem. Int. Ed.* **2002**, *41*, 2278.

[15] J. N. Jones, A. H. Cowley, C. L. B. Macdonald, *Chem. Commun.* **2002**, 1520.

[16] W.-D. Stohrer, R. Hoffmann, *J. Am. Chem. Soc.* **1972**, *94*, 1661.

[17] P. Condick, M. A. Fox, R. Greatrex, C. Jones, D. L. Ormsby, *Chem. Commun.* **2002**, 1448.

[18] J. Feng, J. Leszczynski, B. Weiner, M. C. Zerner, *J. Am. Chem. Soc.* **1989**, *111*, 4648.

[19] M. N. Glukhovtsev, R. D. Bach, S. Laiter, *J. Phys. Chem.* **1996**, *100*, 10952.

[20] a) Y. Canal, D. Bourisson, A. Baceiredo, H. Gornitzka, W. W. Schoeller, G. Bertrand, *Science* **1998**, *279*, 2080; b) T. Kato, H. Gornitzka, A. Baceiredo, W. W. Schoeller, G. Bertrand, *Science* **2000**, *289*, 754.

[21] A. Mack, M. Regitz, *Chem. Ber.* **1997**, *130*, 823.

[22] M. M. Al-Ktaifani, W. Bauer, U. Bergsträßer, B. Breit, M. D. Francis, F. W. Heinemann, P. B. Hitchcock, A. Mack, J. F. Nixon, H. Pritzkow, M. Regitz, M. Zeller, U. Zenneck, *Chem. Eur. J.* **2002**, *8*, 2622.

[23] Gaussian 98 (Revision A.7), M. J. Frisch, G. W. Trucks, H. B. Schlegel, G. E. Scuseria, M. A. Robb, J. R. Cheeseman, V. G. Zakrzewski, J. A. Montgomery, R. E. Stratmann, J. C. Burant, S. Dapprich, J. M. Millam, A. D. Daniels, K. N. Kudin, M. C. Strain, O. Farkas, J. Tomasi, V. Barone, M. Cossi, R. Cammi, B. Mennucci, C. Pomelli, C. Adamo, S. Clifford, J. Ochterski, G. A. Petersson, P. Y. Ayala, Q. Cui, K. Morokuma, D. K. Malick, A. D. Rabuck, K. Raghavachari, J. B. Foresman, J. Cioslowski, J. V. Ortiz, B. B. Stefanov, G. Liu, A. Liashenko, P. Piskorz, I. Komaromi, R. Gomperts, R. L. Martin, D. J. Fox, T. Keith, M. A. Al-Laham, C. Y. Peng, A. Nanayakkara, C. Gonzalez, M. Challacombe, P. M. W. Gill, B. G. Johnson, W. Chen, M. W. Wong, J. L. Andres, M. Head-Gordon, E. S. Replogle, J. A. Pople, Gaussian, Inc., Pittsburgh, PA, **1998**.

[24] a) R. Ditchfield, *Mol. Phys.* **1974**, *27*, 789; b) K. Wolinski, J. F. Hinton, P. Pulay, *J. Am. Chem. Soc.* **1990**, *112*, 8251.

[25] C. J. Jameson, A. De Dios , A. K. Jameson, *Chem. Phys. Lett.* **1990**, *167*, 575.

[26] SMART diffractometer control software, Siemens Analytical X-ray Instruments Inc., Madison, WI, **1998**.

[27] SAINT Integration Software, Siemens Analytical X-ray Instruments Inc., Madison, WI, **1994**.

[28] SADABS: A program for absorption correction with the Siemens SMART system, Siemens Analytical X-ray Instruments Inc., Madison, WI, **1996**.

[29] G. M. Sheldrick, SHELX-S, Bruker Analytical X-ray Instruments Inc., Madison, WI, **1997**.

[30] G. M. Sheldrick, SHELXTL, Bruker Analytical X-ray Instruments Inc., Madison, WI, **1998**.

Zeolites from Plant Leaves

Biomineral-Silica-Induced Zeolitization of *Equisetum Arvense***

Valentin Valtchev, Monique Smaihi, Anne-Catherine Faust, and Loic Vidal*

The performance of bulk materials often depends on the size and habit of the primary particles, and their ordering into hierarchical structures. In the area of catalysis and separation processes, ordered materials with well-defined periodic structures and controlled sizes are highly desired. Hierarchical porous structures combine the benefits of each pore-size regime and are expected to lead to higher efficiency and new applications in catalytic and separation processes, biomolecular separations, and chromatographic supports.[1] The most commonly used approach for the fabrication of such materials is the application of sacrificial templates, which after the synthesis of the inorganic framework are dissolved or volatilized by heating. The template approach, first employed for the preparation of zeolite-type materials, where small organic molecules are used for directing the microporosity,[2] was extended to the formation of mesoporous[3] and macroporous[4] structures. By employing dual templates, hierarchical porous materials with combinations of micro-/meso-

[*] Dr. V. Valtchev, A.-C. Faust
Laboratoire de Materiaux Mineraux
UMR–7016 CNRS, ENSCMu, UHA
3 rue Alfred Werner, 68093 Mulhouse, Cedex (France)
E-mail: V.Valtchev@uha.fr
Dr. M. Smaihi
IEM, UMR 5635 CNRS-ENSCM-UM2, CNRS
1919 route de Mende, 34293 Montpellier Cedex 5 (France)
Dr. L. Vidal
Institut de Chimie de Surface et Interface
UPR–9069 CNRS
15, rue Jean Starcky, 68057 Mulhouse, Cedex (France)

[**] V.V. is grateful to the Bavarian–French Foundation and the CNRS/DFG bilateral program for financial support. *Equisetum arvense* is also known as the Field Horsetail.

 © 2003 Wiley-VCH Verlag GmbH & Co. KGaA, Weinheim DOI: 10.1002/anie.200351175

pores,[5] meso-/macropores,[6] micro-/macropores[7] and micro-/meso-/macropores[8] were synthesized. Thus, a high level of control was achieved and materials with up to three different pore sizes were synthesized, however, the morphology of these hierarchical structures is far from being controlled.

Nature provides many examples of biological specimens with complicated morphologies and hierarchically built anatomies that are completely petrified, and in which the organic structures are substituted by minerals. Laboratory simulation of this process may provide materials where complex anatomy is combined with specific macromorphology. Recently, laboratory zeolitization of silica cells from diatoms (single-celled algae) providing a micro-/macroporous material was reported.[9,10] Crystallization of the zeolite was induced from seeds, since the reactivity of the fossilized biogenic silica seems to be very low, which does not allow direct crystallization of the zeolite. In addition, by the adsorption of zeolite nanocrystals followed by a hydrothermal treatment, wood cellular structures were transformed into micro-/macroporous zeolite structures.[11] Aggregation of silicalite-1 nanocrystals on biological macrotemplates was used for the preparation of micro-/macroporous fibers[12] and spongelike monoliths.[13] Previous studies have shown that the utilization of biological templates requires the application of zeolite seeds. On the other hand, the most perfect replication of biogenic materials in nature is by silica that is transported in solution and deposited in an amorphous form.[14] Although zeolites are silicates and water transport is an important stage in their formation, successful laboratory zeolitization of biological templates without the use of seeds has not been reported. Thus, the application of zeolite seeds appeared to be indispensable for the synthesis of zeolites on biological macrotemplates.

Herein, we report the in situ zeolitization of a vegetal macrotemplate, induced by the biogenic silica of a fresh plant. The content of silica in dry *Equisetum arvense* used for the present study was about 13 wt%, and is deposited in discrete knobs and rosettes at the epidermal surface.[15] The ^{29}Si NMR spectrum of the freeze-dried plant is typical of amorphous silica.[16] Thus, *Equisetum arvense* offers a perfect surface for zeolitization where easily accessible, highly reactive amorphous silica is exposed.

Leaves of the plant were subjected to hydrothermal treatment with a precursor solution that yielded silicalite-1 (MFI-type structure) crystals.[17] The crystallization of silicalite-1 was accomplished after 24 h treatment. A series of experiments that varied the duration of the hydrothermal treatment from 4–24 h was performed. Analysis of the biological macrotemplate and the mother liquor showed that zeolite formation at the surface of *Equisetum arvense* overtook that observed in solution. The first trace of silicalite-1 on the surface of the plant was detected after 6 h hydrothermal treatment, followed by a rapid increase of the zeolite content. In contrast, silicalite-1 crystallization in the mother liquor took place over the 12–24 h period, which is in good agreement with literature data.[18] The enhanced nucleation on *Equisetum arvense*, in comparison with that in the solution, clearly showed that the epidermal surface of the plant was not a simple support for nucleation and subsequent zeolite formation. The high rate of zeolite formation on the epidermal surface of the plant results from the interaction of the highly reactive initial mixture with biogenic silica, which induces a fast and uniform nucleation. Figure 1 shows the effect of one- and two-step hydrothermal treatments on the amount of crystallized zeolite. The halo emanating from the organic part of the composite decreased after the second

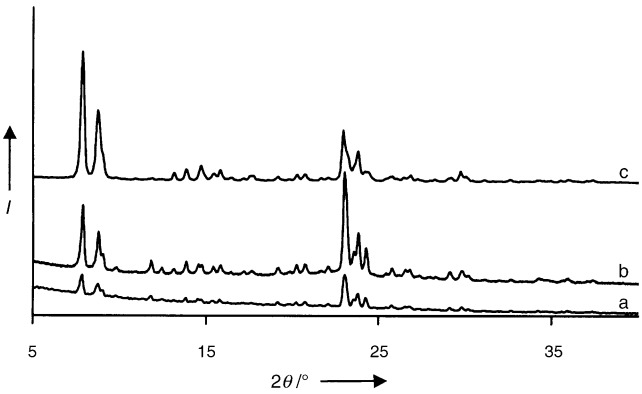


Figure 1. X-ray diffraction patterns of silicalite-1/*Equisetum arvense* composites obtained by one- (a) and two-step (b) synthetic procedures, and the pure silicalite-1 replica (c) of the plant obtained after calcination of the two-step material.

crystallization procedure. Only pure, highly crystalline silicalite-1 was observed in the calcined material (600 °C for 5 h).

The amounts of silicalite-1 deposited after one and two synthesis steps were determined by thermogravimetric analysis (TGA). After one step, a weight loss of 50.1 wt% was recorded, of which 6.02 wt% was attributed to the loss of water, and the remaining 44 wt% results from thermal degradation of the plant tissues and the tetrapropylammonium (TPA) template. After two hydrothermal steps the total weight loss was about 36.9 wt%, where the weight loss through water was only 0.7 wt%, while that resulting from the decomposition of TPA and the biological macrotemplate was about 36 wt%. It is difficult, however, to evaluate the content of each of the templates because of the overlapping of the corresponding peaks.

Figure 2 shows the zeolitized *Equisetum arvense* leaves, viewed at various magnifications by scanning electron microscopy (SEM), after the hydrothermal treatment and calcination procedure. The morphology of the leaves is maintained after combustion of the organic tissue (Figure 2a,b). It can be seen that the silicalite-1 replica (Figure 2c) retains much of the detail observed in the original plant structure (Figure 2d). Also of note are the extremely small silicalite-1 crystallites that grow on the surface, the size of which is approximately at the resolution limit of the SEM instrument; according to dynamic light scattering (DLS) measurements, the size of the silicalite-1 crystals formed in the solution is approximately 90 nm. An investigation by transmission electron microscopy (TEM) showed that crystallites grown at the epidermal surface of *Equisetum arvense* are much smaller, and range from 20 to 40 nm (Figure 2e,f). The TEM images reveal that

 © 2003 Wiley-VCH Verlag GmbH & Co. KGaA, Weinheim

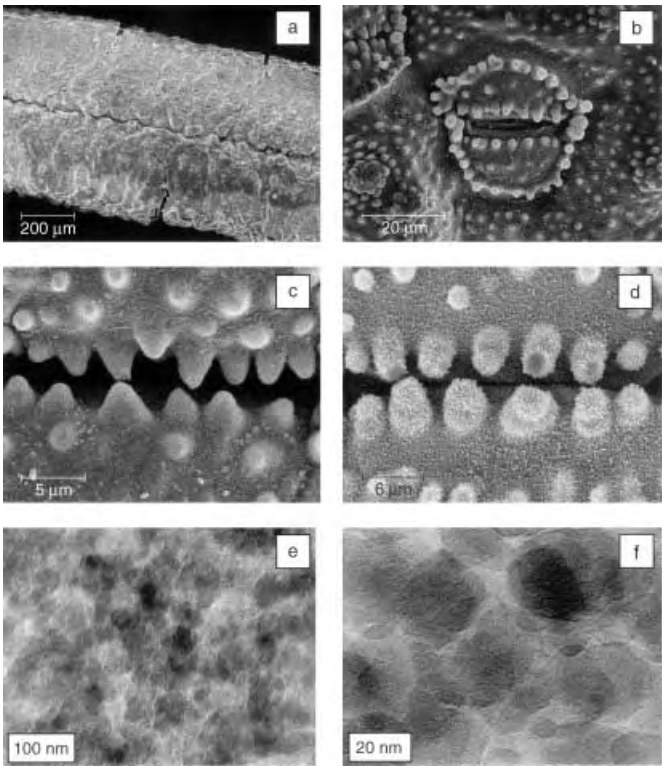


Figure 2. Low-(a) and higher (b) magnification views of the silicalite-1 replica of a leaf of *Equisetum arvense*. The silicalite-1 replica of a stomata structure (c) is compared with the original plant structure (d), where fine filaments covering the leaf can be seen; e,f) TEM images at two magnifications show the lattice fringes of the silicalite-1 nanocrystals within the homogeneous zeolite layer.

the crystals are fairly uniform in size (Figure 2e). These results prove that the reactive biomineral silica promotes zeolite nucleation at the epidermal surface. Thus, a very homogeneous fine silicalite-1 film is formed, and even the nanometer-scale morphological details of the plant are replicated.

Initially, the leaves showed a relatively high Brunnauer–Emmet–Teller (BET) surface area ($3.9\ m^2 g^{-1}$) for a dense centimeter-sized material, which is probably a result of the nanosized silica particles exposed throughout the epidermal membrane. After a single-step hydrothermal synthesis, the BET surface area of the as-synthesized product increased to $58\ m^2 g^{-1}$. This value is indicative of the very small nanocrystallites formed on the biological template. After calcination, the sample showed a BET surface area of $217\ m^2 g^{-1}$, which is two orders of magnitude higher than natural *Equisetum arvense* leaves. This value, however, is lower than that of a highly crystalline MFI-type material, which reveals that after the one-step synthesis, a dense material with low specific surface area is still present. The second synthesis step substantially reduces the amount of non-zeolite material, and the calcined sample showed a BET surface area of $383\ m^2 g^{-1}$, which is in accordance with a highly crystalline MFI-type material. However, a total single-point pore volume of $0.92\ cm^3 g^{-1}$ was measured for the two-step material (of which the micro- and mesopores contribute 0.13 and $0.79\ cm^3 g^{-1}$, respectively), which does not correspond to that of a microporous MFI-type material. The value corresponding to the micropore volume is somewhat below that of a highly crystalline sample of silicalite-1 (about $0.18\ cm^3 g^{-1}$), which reveals the presence of some non-zeolitic material after the second hydrothermal synthesis. The type I adsorption/desorption isotherms of the calcined samples synthesized by one- and two-step hydrothermal treatments show the microporous character of the materials (Figure 3a and b). A steep rise in the gas uptake at low relative pressures corresponds to

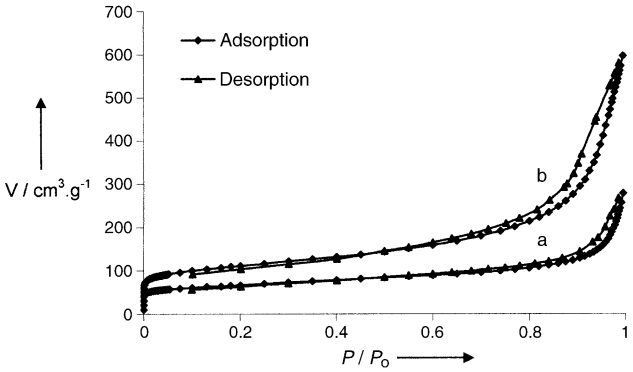


Figure 3. Adsorption/desorption isotherms of the calcined samples prepared by one- (a) and two-step (b) synthetic procedures.

the filling of micropores with N_2. In contrast to pure microporous materials, the steep uptake at low relative pressures is not followed by a flat curve. Instead, an inclination of the curve with an increase of the pressure can be observed. At high relative pressure the upward turn with a hysteresis loop is indicative of the generation of intercrystalline mesoporosity. Thus, the zeolitization of *Equisetum arvense* yields a material with combined micro- and mesoporosity.

Results of small-angle X-ray scattering (SAXS) analysis are in good agreement with the TEM observations and the N_2 adsorption measurements, that is, uniform nanoparticles and a secondary porosity were detected. SAXS data obtained for dried *Equisetum arvense* leaves do not show fractal behavior nor microporosity features (Figure 4a). In contrast, SAXS data obtained after hydrothermal treatment of the fibers exhibits three $\boldsymbol{Q}$-vector domains in the ranges $\boldsymbol{Q} < 5 \times 10^{-3}\ Å^{-1}$, $5 \times 10^{-3} < \boldsymbol{Q} < 2 \times 10^{-2}\ Å^{-1}$, and $2 \times 10^{-2}\ Å^{-1} < \boldsymbol{Q}$ (Figure 4b). These $\boldsymbol{Q}$-vector domains correspond to scattering from mesopores (or small macropores), micropores, and the surface of the crystallites, respectively. The slope deviation observed in the log–log plot of the SAXS curves at $5 \times 10^{-3}\ Å^{-1}$ indicates a mean nanocrystallite size of about 30 nm. The power law behavior of the scattering intensities (that is, a linear increase with decreasing $\boldsymbol{Q}$ with a slope equal to -4) for $\boldsymbol{Q} > 2 \times 10^{-2}\ Å^{-1}$ suggests that these particles possess a smooth surface.

Although no special tests were performed, the difference in the strength of the silicalite-1 replicas prepared by one- and two-step synthesis procedures is easily distinguishable. The one-step synthesized material retained the macromorphological features of the plant leaves. However, the fibrous structure easily disintegrates when a simple laboratory

 © 2003 Wiley-VCH Verlag GmbH & Co. KGaA, Weinheim

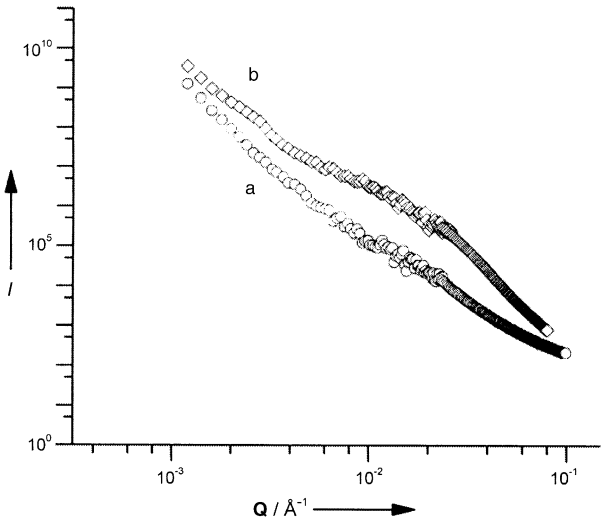


Figure 4. SAXS profiles of *Equisetum arvense* leaves before (a) and after (b) hydrothermal treatment.

operation is performed. In contrast, the replicas obtained by the two-step synthesis are stable, rigid, and can be destroyed only under applied pressure; no destruction was observed during the laboratory manipulations performed with this material. Further increase of the strength of *Equisetum arvense* silicalite-1 replicas might be achieved either by an additional synthetic step, or by a hydrothermal treatment with a precursor gel that does not contain an organic structure-directing agent. In the latter case, subsequent calcination to open the zeolite microporosity is not necessary, and thus flexible fibrous zeolite/*Equisetum arvense* composites might be prepared.

In conclusion, highly reactive silica in plants can promote zeolite crystallization. The large amount of silica found in the epidermal surface of *Equisetum arvense* facilitates zeolite nucleation providing homogeneously and densely distributed zeolite nuclei. Thus a micro-/mesoporous material which retains all of the morphological features of the plant was obtained.

This study opens up routes for the zeolitization of silica-containing plants and the preparation of materials with controlled porosity and specific macromorphological features. The large variety of microporous aluminosilicates and numerous silica-containing plants present tremendous possibilities for tailoring such materials. The reactivity of biomorphous silica can most probably be used to promote the nucleation of other silicate materials that crystallize under soft hydrothermal conditions.

Received: February 13, 2003 [Z51175]

Keywords: biomimetic synthesis · mesoporous materials · silicates · zeolites

[1] D. Zhao, P. Yang, B. F. Schmelka, G. D. Stucky, *Chem. Mater.* **1999**, *11*, 1174.
[2] R. Szostak, *Molecular Sieves*, 2nd ed., Blackie Academic&Professional, London, **1998**, p. 359.
[3] J. C. Vartuli, W. J. Roth, J. S. Beck, S. B. McCullen, C. T. Kresge in *Molecular Sieves: Science and Technology, Vol. I* (Eds.: H. G. Karge, J. Weitcamp), Springer, Berlin, **1998**, p. 97.
[4] O. D. Velev, E. W. Kaler, *Adv. Mater.* **2000**, *12*, 531.
[5] L. Tosheva, V. Valtchev, J. Sterte, *Microporous Mesoporous Mater.* **2000**, *35–36*, 621.
[6] O. D. Velev, P. M. Tessier, A. M. Lenhoff, E. W. Kaler, *Nature* **1999**, *401*, 548.
[7] Y.-J. Lee, J. S. Lee, Y. S. Park, K. B. Yoon, *Adv. Mater.* **2001**, *13*, 1259.
[8] K. H. Rhodes, S. A. Davis, F. Caruso, B. Zhang, S. Mann, *Chem. Mater.* **2000**, *12*, 2832.
[9] M. W. Anderson, S. M. Holmes, N. Hanif, C. S. Cundy, *Angew. Chem.* **2000**, *112*, 2819; *Angew. Chem. Int. Ed.* **2000**, *39*, 2707.
[10] Y. Wang, Y. Tang, A. Dong, X. Wang, N. Ren, Z. Gao, *J. Mater. Chem.* **2002**, *12*, 1812.
[11] A. Dong, Y. Wang, Y. Tang, N. Ren, Y. Zhang, Y. Yue, Z. Gao, *Adv. Mater.* **2002**, *14*, 926.
[12] B. Zhang, S. A. Davis, N. H. Mendelson, S. Mann, *Chem. Commun.* **2000**, 781.
[13] B. Zhang, S. A. Davis, S. Mann, *Chem. Mater.* **2002**, *14*, 1369.
[14] R. K. Iler in *The Chemistry of Silica*, Wiley, New York, **1979**, p. 88.
[15] P. B. Kaufman, W. C. Wilber, R. Schmid, N. S. Najati, *Am. J. Bot.* **1971**, *58*, 309.
[16] R. Berterma, R. Tacke, *Z. Naturforsch. B* **2000**, *55*, 459.
[17] *Equisetum arvense* was collected from the campus of the University of Haute Alsace (Mulhouse, France). After being dried at room temperature, the leaves were subjected to one or two hydrothermal treatments with a precursor mixture containing 9 TPA:25 SiO_2:420 H_2O:100 EtOH. The syntheses were performed at 100 °C for 24 h.
[18] A. E. Persson, B. J. Schoeman, J. Sterte, J.-E. Otterstedt, *Zeolites* **1994**, *14*, 557.

 © 2003 Wiley-VCH Verlag GmbH & Co. KGaA, Weinheim

Enolexo *Aldol Reactions*

Direct Catalytic Asymmetric *Enolexo* Aldolizations**

*Chandrakala Pidathala, Linh Hoang, Nicola Vignola, and Benjamin List**

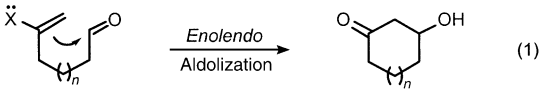
The aldol reaction is an exceptionally useful strategic C–C bond-forming reaction for the stereoselective construction of cyclic and acyclic molecules. As a result, several catalytic

[*] Dr. B. List, C. Pidathala, L. Hoang, N. Vignola
The Scripps Research Institute
Department of Molecular Biology
10550 North Torrey Pines Road, La Jolla, CA 92037 (USA)
Fax: (+1) 858-784-7028
E-mail: blist@scripps.edu

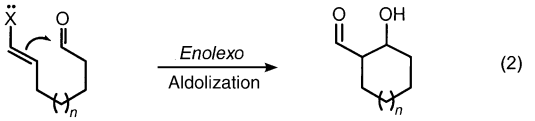
[**] Generous support by the NIH (RO1 GM-63914) is most gratefully acknowledged. The cover picture was designed by Mike Pique (Scripps Institute) using a proline image attributed to K. N. Houk and S. Bahmanyar (UCLA). Chicken artwork courtesy of Sheri Hoeger, www.madstencilist.com © 2000.

 DOI: 10.1002/anie.200351266 © 2003 Wiley-VCH Verlag GmbH & Co. KGaA, Weinheim

asymmetric intermolecular variants, both indirectly, with preformed enolate equivalents, and directly involving unmodified carbonyl compounds have been described.[1] Remarkably, however, there is still only one catalytic asymmetric intramolecular aldol reaction, the proline-catalyzed Hajos–Parrish–Eder–Sauer–Wiechert reaction.[2] While the usefulness of this process has been illustrated in a broad context,[3] only 6-*enolendo* aldolizations [Eq. (1), $n=1$] have been described so far. Direct catalytic asymmetric *enolexo* aldolizations [Eq. (2)] are unknown. Herein we describe the first and highly enantioselective examples of this process.



(1)



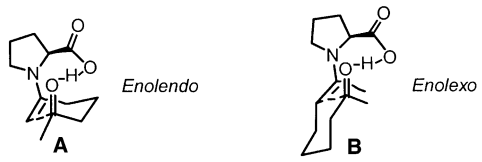
(2)

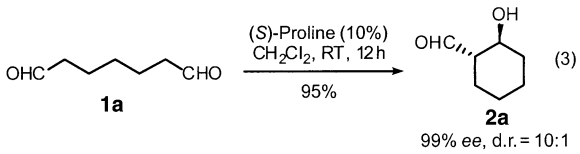
6-*Enolendo* aldolizations are very common and favored according to the Baldwin rules.[4,5] The only catalytic asymmetric variant of this process, the Hajos–Parrish–Eder–Sauer–Wiechert reaction has not been extended to different ring sizes, nor have any proline-catalyzed *enolexo* aldolizations [Eq. (2)] been described.[6] Although Baldwin-favored in the formation of 3–7 membered rings, *enolexo* aldolizations are less studied[7] and direct catalytic asymmetric variants are unknown.[8]

Recently, we discovered the first proline-catalyzed asymmetric intermolecular aldol reactions[9–11] and proposed a unified one-proline enamine catalysis mechanism of both inter- and intramolecular aldol reactions.[12–14] By inspecting possible transition-state models, we realized that in addition to the established 6-*enolendo* aldolizations via transition state **A**, proline should also catalyze corresponding 6-*enolexo* aldolizations via the chairlike assembly **B**. Such reactions should provide a highly stereoselective pathway to useful *trans*-1,2-disubstituted cyclohexanes.

Indeed, the reaction of heptanedial[15] (**1a**) with a catalytic amount of (*S*)-proline in dichloromethane gave aldol **2a** in high yield and diastereoselectivity, and with excellent enantioselectivity [Eq. (3)].[16,17]

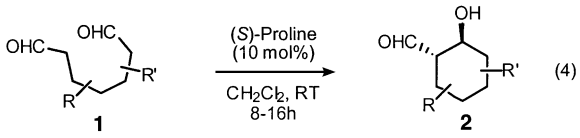
With this encouragement, we decided to study the scope of this





(3)

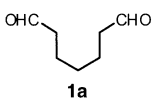
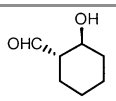
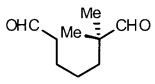
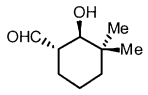
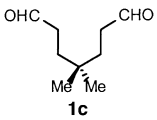
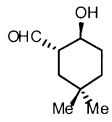
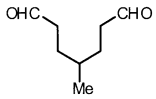
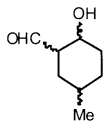
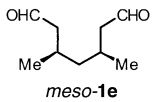
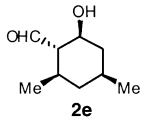
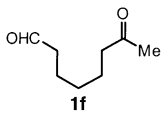
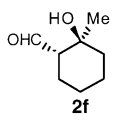
proline-catalyzed 6-*enolexo* aldolization. Various pentane-1,5-dialdehydes (pimelaldehydes; **1**) were prepared[18] and then treated with a catalytic amount of (*S*)- or (*R*)-proline in dichloromethane [Eq. (4), Table 1]. Both **1b** and **1c** provided



(4)

the corresponding cyclic aldols **2b** and **2c** in high yields and excellent diastereo- and enantioselectivities. Surprisingly, we found that a single substituent in the 4-position has an unfavorable effect on the stereoselectivity of the cycloaldo-

Table 1: Proline-catalyzed *enolexo* aldolizations of dicarbonyl compounds. Yields refer to diols obtained after in situ $NaBH_4$ reduction.

Dicarbonyl	Yield [%]	Products	*ee* [%]	d.r. [%]
 **1a**	95	 **2a**	99	10:1
 **1b**	74	 **2b**	98	>20:1
 **1c**	75	 **2c**	97	>20:1
 **1d**	76	 **2d**	75,89,95,8	22:5:5:1
 *meso*-**1e**	88	 **2e**	99	1:1
 **1f**	92	 **2f**	99	2:1

 © 2003 Wiley-VCH Verlag GmbH & Co. KGaA, Weinheim

lization. This effect was demonstrated with 4-methyl-substituted **1d**, which provided all four possible diastereomeric aldols of **2d** upon treatment with proline; the resulting aldols were obtained in a 22:5:5:1 ratio and in 75, 89, >95, and 8% *ee*, respectively. Explaining the lowered stereoselectivity in this case is difficult without calculating the relative energies of all reasonable transition states.[12] Even if the enamine is fixed to having *E* geometry, and boat conformations are excluded (as in **B**), the transition states may still vary in an axial versus equatorial 4-substituent and/or enamine double bond, and in the *anti* versus *syn* relationship of the carboxylic acid to the olefin. We also investigated the behavior of the *meso*-configured dialdehyde **1e** under our reaction conditions. Four stereogenic centers may be created simultaneously in a catalytic asymmetric desymmetrization of this substrate. We found the two expected *anti*-configured aldols (**2e** and **2e′**) to be formed in equal amounts and in 99 and 75% *ee*, respectively. That the proline-catalyzed *enolexo* aldolization is not limited to dialdehydes was illustrated in the reaction of ketoaldehyde **1f**, which gave tertiary aldol **2f** (d.r. = 2:1), in 99% *ee* (minor isomer 95% *ee*).

In summary, we have described the first and highly enantioselective proline-catalyzed *enolexo* aldolization of dicarbonyl compounds. This reaction provides β-hydroxy cyclohexane carbonyl derivatives that are of potential widespread usage in target-oriented synthesis. This *anti*-diastereoselective proline-catalyzed *enolexo* aldolization nicely complements alternative methodologies such as the highly enantio- and *syn*-diastereoselective baker's yeast reduction of β-keto esters.[19] An advantage of the aldolization methodology is that both enantiomeric products can be accessed simply by using either (*S*)- or (*R*)-proline, whereas the biocatalysis route is limited to products of a single absolute configuration.[20] Applications in natural product synthesis and further extensions of proline-catalyzed inter- and intramolecular aldolizations are forthcoming.

Experimental Section

Typical aldolization procedure: Dicarbonyl **1** (1 mmol) was dissolved in dry dichloromethane (10 mL) and treated with (*S*)- or (*R*)-proline (12 mg, 0.1 mmol, 10%). The mixture was stirred at room temperature until the starting material had disappeared (8–16 h). Aldols **2** can be isolated after standard aqueous work-up, but are unstable over extended time periods at room temperature. Stable diols are obtained by in situ reduction with $NaBH_4$ followed by an aqueous work-up, as described elesewhere.[11d,21]

Received: February 24, 2003 [Z51266]

Keywords: aldol reaction · amino acids · asymmetric catalysis · organocatalysis

[1] For some recent reviews and accounts, see: a) J. S. Johnson, D. A. Evans, *Acc. Chem. Res.* **2000**, *33*, 325–335; b) T. D. Machajewski, C.-H. Wong, *Angew. Chem.* **2000**, *112*, 1406–1430; *Angew. Chem. Int. Ed.* **2000**, *39*, 1352–1374; c) B. Alcaide, P. Almendros, *Eur. J. Org. Chem.* **2002**, 1595–1601; d) S. E. Denmark, R. A. Stavenger, *Acc. Chem. Res.* **2000**, *33*, 432–440; e) S. G. Nelson, *Tetrahedron: Asymmetry* **1998**, *9*, 357–389; f) M. Shibasaki, H. Sasai, T. Arai, T. Iida, *Pure Appl. Chem.* **1998**, *70*, 1027–1034; g) E. M. Carreira, R. A. Singer, *Drug Discovery Today* **1996**, *1*, 145–150.

[2] a) Z. G. Hajos, D. R. Parrish, German Patent DE 2102623, **1971**; b) U. Eder, G. R. Sauer, R. Wiechert, German Patent DE 2014757, **1971**; c) U. Eder, G. Sauer, R. Wiechert, *Angew. Chem.* **1971**, *83,* 492–493; *Angew. Chem. Int. Ed. Engl.* **1971**, *10,* 496–497; d) Z. G. Hajos, D. R. Parrish, *J. Org. Chem.* **1974**, *39*, 1615–1621; Related enantiogroup-differentiating aldol cyclodehydrations have been described, see: C. Agami, N. Platzer, H. Sevestre, *Bull. Soc. Chim. Fr.* **1987**, *2*, 358–360.

[3] Reviews: a) N. Cohen, *Acc. Chem. Res.* **1976**, *9*, 512–517; b) K. Drauz, A. Kleemann, J. Martens, *Angew. Chem.* **1982**, *94*, 590–613; *Angew. Chem. Int. Ed. Engl.* **1982**, *21*, 584–608; c) E. R. Jarvo, S. J. Miller *Tetrahedron* **2002**, *58*, 2481–2495; d) B. List, *Tetrahedron* **2002**, *58*, 5572–5590; e) P. I. Dalko, L. Moisan, *Angew. Chem.* **2001**, *113*, 3840–3864; *Angew. Chem. Int. Ed.* **2001**, *40*, 3726–3748.

[4] a) J. E. Baldwin, M. J. Lusch, *Tetrahedron* **1982**, *38*, 2939–2947; b) J. E. Baldwin, *J. Chem. Soc. Chem. Commun.* **1976**, 734–736.

[5] Cycloaldolizations are formally *enolexo*- or *enolendo-exo-trig* processes. However, since all intramolecular aldolizations are by definition *exo-trig* processes, we refer to these processes simply as *enolexo* or *enolendo* aldolizations.

[6] For a proline-catalyzed *enolexo* aldolization in a dynamic kinetic resolution, see: R. B. Woodward et al. , *J. Am. Chem. Soc.* **1981**, *103*, 3210–3213; Also see: C. Agami, N. Platzer, C. Puchot, H. Sevestre, *Tetrahedron* **1987**, *43*, 1091–1098.

[7] For selected non-enantioselective variants, see: a) R. B. Woodward, F. Sondheimer, D. Taub, K. Heusler, W. M. MacLamore, *J. Am. Chem. Soc.* **1952**, *74*, 4223–4251; b) E. J. Corey, R. L. Danheiser, S. Chandrasekaran, P. Siret, G. E. Keck, J. L. Gras, *J. Am. Chem. Soc.* **1978**, *100*, 8031–8034; c) H. Hagiwara, H. Ono, N. Komatsubara, T. Hoshi, T. Suzuki, M. Ando, *Tetrahedron Lett.* **1999**, *40*, 6627–6630.

[8] For two indirect catalytic enantioselective *enolexo* aldolizations, see: a) Romo's organocatalytic asymmetric *syn*-diastereospecific intramolecular, nucleophile-catalyzed aldol-lactonization (NCAL): G. S. Cortez, R. L. Tennyson, D. Romo, *J. Am. Chem. Soc.* **2001**, *123*, 7945–7946; b) Krische's catalytic asymmetric carbometallative aldol cycloreduction, which is a tandem catalytic asymmetric conjugate addition followed by a *syn*-diastereoselective *enolexo* aldolization: D. F. Cauble, J. D. Gipson, M. J. Krische, *J. Am. Chem. Soc.* **2003**, *125*, 1110–1111.

[9] a) B. List, R. A. Lerner, C. F. Barbas III, *J. Am. Chem. Soc.* **2000**, *122*, 2395–2396; b) W. Notz, B. List, *J. Am. Chem. Soc.* **2000**, *122*, 7386–7387; c) B. List, P. Pojarliev, C. Castello, *Org. Lett.* **2001**, *3*, 573–575.

[10] a) A. B. Northrup, D. W. C. MacMillan, *J. Am. Chem. Soc.* **2002**, *124*, 6798–6799 (This important paper describes an intermolecular variant of the reaction discussed here); b) A. Córdova, W. Notz, C. F. Barbas III, *J. Org. Chem.* **2002**, *67*, 301–303; c) A. Bøgevig, N. Kumaragurubaran, K. A. Jørgensen, *Chem. Commun.* **2002**, 620–621, Also see: A. Bøgevig, K. Juhl, N. Kumaragurubaran, W. Zhuang, K. A. Jørgensen, *Angew. Chem.* **2002**, *114*, 1868–1871; *Angew. Chem. Int. Ed.* **2002**, *41*, 1790–1793; N. Halland, P. S. Aburel, K. A. Jørgensen, *Angew. Chem.* **2003**, *115*, 685–689; *Angew. Chem. Int. Ed.* **2003**, *42*, 661–665.

[11] For the first proline-catalyzed asymmetric intermolecular Mannich, Michael, and α-amination reactions, see a) B. List, *J. Am. Chem. Soc.* **2000**, *122*, 9336–9337; b) B. List, P. Pojarliev, W. T. Biller, H. J. Martin, *J. Am. Chem. Soc.* **2002**, *124*, 827–833; c) B. List, P. Pojarliev, H. J. Martin, *Org. Lett.* **2001**, *3*, 2423–2425; d) B. List, *J. Am. Chem. Soc.* **2002**, *124*, 5656–5657. For recent highlights, see: a) M. Movassaghi, E. N. Jacobsen, *Science* **2003**, 298, 1904–1905; b) S. Borman, *Chem. Eng. News* **2002**, *80*, 35–

 © 2003 Wiley-VCH Verlag GmbH & Co. KGaA, Weinheim

37; c) H. Gröger, J. Wilken, *Angew. Chem.* **2001**, *113*, 545 – 548; *Angew. Chem. Int. Ed.* **2001**, *40*, 529 – 532.
[12] a) S. Bahmanyar, K. N. Houk, *J. Am. Chem. Soc.* **2001**, *123*, 9922 – 9923; b) S. Bahmanyar, K. N. Houk, *J. Am. Chem. Soc.* **2001**, *123*, 11273 – 11283; c) S. Bahmanyar, K. N. Houk, H. J. Martin, B. List, *J. Am. Chem. Soc.* **2003**, *125,* 2475 – 2479; d) L. Hoang, S. Bahmanyar, K. N. Houk, B. List, *J. Am. Chem. Soc.* **2003**, *125*, 16 – 17.
[13] For additional supporting density functional theory calculations, see: a) K. N. Rankin, J. W. Gauld, R. J. Boyd, *J. Phys. Chem. A* **2002**, *106*, 5155 – 5159; b) M. Arnó, L. R. Domingo, *Theor. Chem. Acc.* **2002**, *108*, 232 – 239.
[14] B. List, *Synlett* **2001**, 1675 – 1686.
[15] M. Daumas, Y. Vo-Quang, L. Vo-Quang, F. Le Goffic, *Synthesis* **1989**, 64 – 65.
[16] Comparison of the literature NMR data and optical rotation of the known diol of aldol **2a** (T. Kakuchi, A. Namuri, H. Kaga, T. Ishibashi, M. Obata, K. Yokota, *Macromolecules* **2000**, *33*, 3964 – 3969) confirmed the expected absolute and relative configuration. The *ee* value of the aldol products was typically determined from chiral-phase HPLC after in situ conversion to a chromogenic enone by a Horner–Wadsworth–Emmons reaction ($MeCOCH_2PO(OMe)_2$, LiOH, THF).
[17] The analogous proline-catalyzed 5-*enolexo* aldolization of hexanedial is less selective (d.r. = 2:1; *ee*(*anti*) = 79 %, *ee*(*syn*) = 37 %).
[18] Substituted pimelaldehydes **1** were routinely prepared from commercially available substituted cyclohexanones through α-carbomethoxylation (NaH, $MeOCO_2Me$) and retro-Dieckman condensation using either NaOMe or Cs_2CO_3 (R. G. Salomon, M. F. Salomon, *J. Org. Chem.* **1975**, *40*, 1488 – 1492; P. Tundo, S. Memoli, M. Selva, , WO 02/14257, **2000**.) Diisobutylaluminium hydride reduction (or LAH reduction followed by PCC oxidation) of the resulting diesters then provided the desired pimelaldehydes **1** in acceptable overall yields.
[19] See for example: a) M. Bertau, M. Bürli, E. Hungerbühler, P. Wagner, *Tetrahedron: Asymmetry* **2001**, *12*, 2103 – 2107; b) V. Spiliotis, D. Papahatjis, N. Ragoussis, *Tetrahedron Lett.* **1990**, *31*, 1615 – 1616.
[20] Alternative highly efficient and enantioselective ruthenium-catalyzed β-keto ester reductions can be diastereounselective: a) R. Noyori, T. Ohkuma, M. Kitamura, H. Takaya, N. Sayo, H. Kumobayashi, S. Akutagawa, *J. Am. Chem. Soc.* **1987**, *109*, 5856 – 5858; b) M. Kitamura, T. Ohkuma, M. Tokunaga, R. Noyori, *Tetrahedron: Asymmetry* **1990**, *1*, 1 – 4; c) J. P. Genêt, X. Pfister, V. Ratovelomanana-Vidal, C. Pinel, J. A. Laffitte, *Tetrahedron Lett.* **1994**, *35*, 4559 – 4562.
[21] All new compounds gave satisfactory ^1H and ^{13}C NMR spectra, as well as high-resolution mass spectroscopic analysis.

 © 2003 Wiley-VCH Verlag GmbH & Co. KGaA, Weinheim

Peroxo-Bridged Heme–Copper Complex

Isolation and Crystal Structure of a Peroxo-Bridged Heme–Copper Complex**

Takefumi Chishiro, Yuichi Shimazaki, Fumito Tani, Yoshimitsu Tachi, Yoshinori Naruta, Satoru Karasawa, Shinya Hayami, and Yonezo Maeda*

The reaction of dioxygen with transition metal complexes is important from the standpoint of O_2 binding and activation in biological systems.[1] Cytochrome c oxidase (CcO), which a catalyzes four electron reduction of O_2 to water, has a unique heme/nonheme copper dinuclear core in its active site.[2] A number of heme-based iron–copper dinuclear complexes have been synthesized to elucidate the mechanism of O_2 reduction in CcO.[3–6] We reported the reaction of O_2 with tetraphenylporphyrin (TPP)-Fe^{II}-linked tris(2-pyridylmethyl)amine (TPA)–Cu^{I} dinuclear complexes and the formation of peroxo-bridged dinuclear species Fe–O_2–Cu with a moderate stability in CH_3CN at room temperature.[4] Karlin et al. also reported a similar dioxygen reaction with both the analogous dinuclear complexes[5d] and the 1:1 mixture of the heme and the Cu complex.[5e,6] Although these peroxo-bridged dinuclear species were characterized by various spectroscopic methods, the detailed structure of Fe^{III}–O_2–Cu^{II} moiety has not been clarified. Moreover, to the best of our knowlege, the isolation and structure of such a heterodimetallic peroxo-bridged complex has never been reported. Herein, we describe the first report of the isolation and crystal structure of a peroxo-bridged heme–copper dinuclear complex.

We prepared a dinuclear complex, [(TMP)Fe^{II}-(5MeTPA)Cu^{I}]BPh_4 (**1**, TMP-5MeTPA = 10,15,20-tris(2,4,6-trimethylphenyl)-5-(2′-bis((5″-methyl-2″-pyridylmethyl)aminomethyl)pyridine-5′-carboxyamidophenyl)-porphyrin). The UV/Vis spectrum of **1** in CH_3CN showed absorption maxima at 428 and 534 nm. When **1** was exposed to O_2 in CH_3CN at −30 °C (Scheme 1), the 428 and 534 nm bands disappeared

[*] Prof. Dr. Y. Naruta, T. Chishiro, Dr. Y. Shimazaki, Dr. F. Tani, Dr. Y. Tachi
Institute for Fundamental Research of Organic Chemistry
Kyushu University, Higashi-ku, Fukuoka 812-8581 (Japan)
Fax: (+81) 92-642-2715
E-mail: naruta@ms.ifoc.kyushu-u.ac.jp

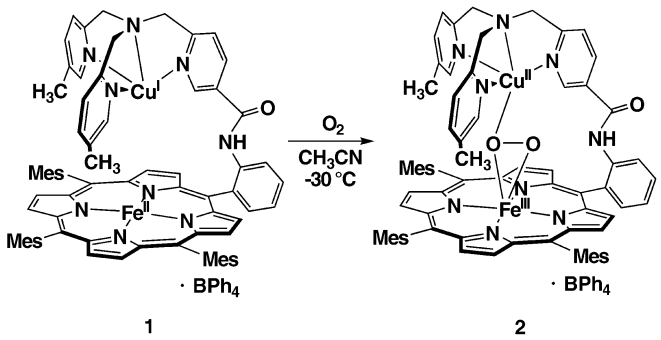
Dr. S. Karasawa
Graduate School of Pharmaceutical Sciences
Kyushu University, Higashi-ku, Fukuoka 812-8582 (Japan)

Dr. S. Hayami, Prof. Dr. Y. Maeda
Graduate School of Sciences, Kyushu University
Higashi-ku, Fukuoka 812-8581 (Japan)

[**] This work was supported by the Grants-in-Aid for COE Research (No. 08CE2005) and for Science Research on Priority Areas (Nos. 09235225 and 11228207) from MEXT and for Scientific Research (A) (No. 14204073) from JSPS. The P&P project, Green Chemistry, of Kyushu University partly supported this research.

Supporting information for this article is available on the WWW under http://www.angewandte.org or from the author.

 © 2003 Wiley-VCH Verlag GmbH & Co. KGaA, Weinheim DOI: 10.1002/anie.200351415



Scheme 1. Formation of [(TMP)Fe^{III}-(O_2)-(5MeTPA)Cu^{II})]BPh_4 (**2**) from [(TMP)Fe^{II}-(5MeTPA)Cu^{I}]BPh_4 (**1**) and dioxygen.

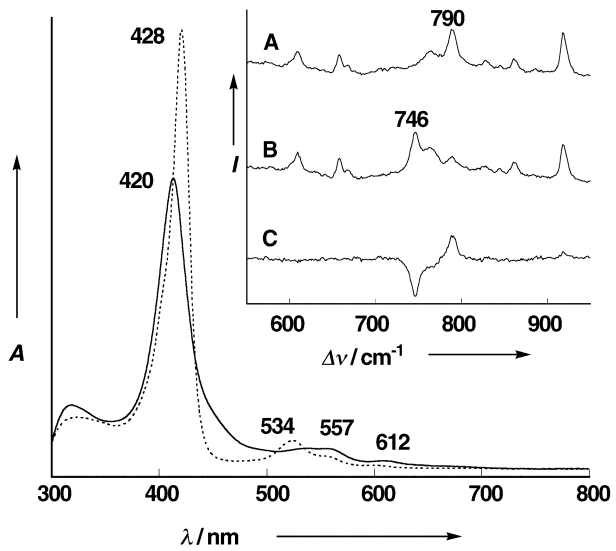


Figure 1. UV/Vis absorption spectra of **1** (-----) and **2** (——) in CH_3CN at −30 °C; inset. resonance Raman spectra of **2** (in CH_3CN, room temperature, λ_{ex} = 413.1 nm), A: $^{16}O_2$, B: $^{18}O_2$, C: A-B.

and bands at 420, 557 and 612 nm appeared (Figure 1), thus indicating the formation of a peroxo-bridged Fe–O_2–Cu species, as we described previously.[4] This peroxo species exhibited much higher stability in the CH_3CN solution than the previously reported analogues,[7] on account of the steric hindrance by the multiple methyl groups. The solution of the peroxo complex could be kept at −30 °C for several days without decomposition finally yielding dark-purple crystals. The formula of the crystals was determined as [(TMP)Fe^{III}-(O_2)-(5MeTPA)Cu^{II}]BPh_4 (**2**) from the elemental analysis and ESI-mass spectrum. The UV/Vis spectrum of the redissolved solution of **2** in CH_3CN (λ_{max} (ε, $M^{-1}cm^{-1}$) = 420 (126000), 557 (8500), 612 (3500) nm) was in good agreement with that of the peroxo complex before the isolation. The resonance Raman spectrum of **2** in CH_3CN exhibited an isotope sensitive band at 790 ($^{16}O_2$)/746 ($^{18}O_2$) cm^{-1} (Figure 1, inset), which was assigned to peroxy ν(O–O) as were the analogues reported previously.[4] These results clearly indicate the successful isolation of the peroxo complex **2**. The decomposition of **2** was not observed for a sample that was left for several months in the solid state, even at room temperature.

The crystal structure of **2** was determined by single-crystal X-ray analysis (Figure 2).[8] The Fe–O_2–Cu moiety has a μ-η^2:η^1 coordination mode; both oxygen atoms (O(2) and O(3)) of the peroxo ligand bind to Fe(1) while only O(2) binds to Cu(1). The observed O–O bond length (1.460(6) Å) is reasonable for a peroxo ligand,[9] although this value is larger than those of other side-on peroxo-metalloporphyrins.[10–12] The Fe(1)–O(2)–Cu(1) unit is almost linear with the angle 166.0(3)°, being similar to that of the heme–copper μ-oxo species (Fe-O-Cu = 171.1(3)°).[5c] The μ-η^2:η^1 coordination mode in metal-peroxo species has been reported for the rhodium(III), vanadium(V) and palladium(II) homodinuclear complexes.[13] However, in those cases, the M-O-M units are bent with an angle 103 ≤ M-O-M ≤ 133°.

The iron ion is coordinated by the four pyrrole nitrogen atoms and the two oxygen atoms of the peroxo ligand. The peroxo ligand is bound to Fe(1) in a side-on mode eclipsing the two Fe–N bonds (Fe(1)–N(5) and Fe(1)–N(7)). The two Fe–O bond lengths are 2.031(4) (Fe(1)-O(2)) and 1.890(6) (Fe(1)-O(3)) Å. In mononuclear side-on peroxo–M–porphyrin complexes (M = Ti^{III},[10] Mo^{VI},[11] or Mn^{III}[12]) the M–O bond lengths are almost identical. On the other hand, the Fe(1)–O(2) bond length in complex **2** is considerably longer than that of Fe(1)–O(3), probably as a result of the coordination of Cu(1) to O(2). The iron ion lies 0.595(10) Å above the least-square plane based on the pyrrole nitrogen atoms towards the peroxo ligand. This displacement is also found in peroxo–M–por-

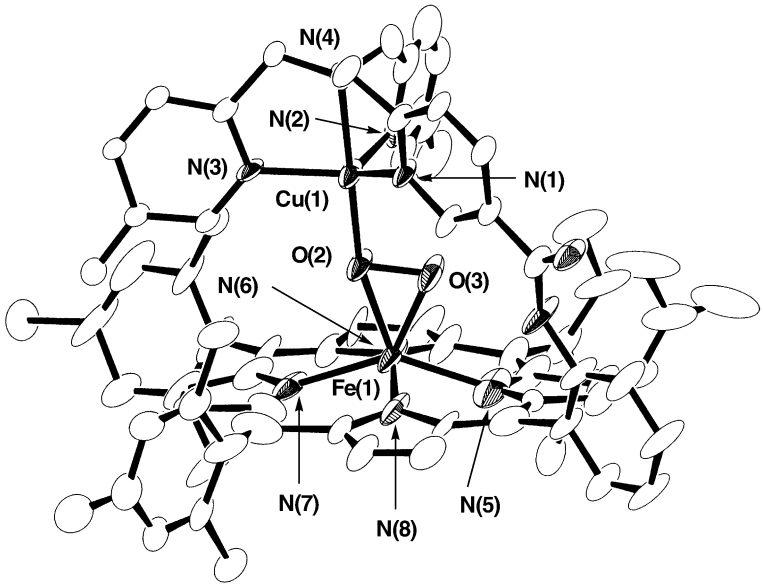


Figure 2. ORTEP view of [(TMP)Fe^{III}-(O_2)-(5MeTPA)Cu^{II})]$^+$ in crystals of **2** drawn with the thermal elliposids at the 30% probability level. All hydrogen atoms are omitted for clarity. Selected bond length [Å] and angles [°]: Cu(1)-O(2) 1.915(5), Cu(1)···O(3) 2.657(7), Fe(1)-O(2) 2.031(4), Fe(1)-O(3) 1.890(6), O(2)-O(3) 1.460(6), Cu(1)-N(1) 2.054(8), Cu(1)-N(2) 2.15(1), Cu(1)-N(3) 2.035(6), Cu(1)-N(4) 2.061(6), Fe(1)-N(5) 2.15(1), Fe(1)-N(6) 2.08(1), Fe(1)-N(7) 2.18(1), Fe(1)-N(8) 2.03(2), Cu(1)-O(2)-Fe(1) 166.0(3), Cu(1)-O(2)-O(3) 103.0(4).

 © 2003 Wiley-VCH Verlag GmbH & Co. KGaA, Weinheim

phyrin complexes (M = Ti^{III},[10] or Mn^{III}[12]) and is consistent with the EXAFS structure of peroxo–iron(III) porphyrin.[14b]

The structure of the TPA-Cu-O-O unit is similar with that of the *trans*-(μ-1,2-peroxo)dicopper(II) complex derived from $[(TMPA)Cu^{I}(CH_3CN)]^+$ (TMPA = tris(2-pyridylmethyl)-amine) and dioxygen.[15] The copper ion is pentacoordinated with a distorted trigonal-bipyramidal geometry by the three pyridine nitrogen atoms, the one tertiary nitrogen atom and the one oxygen atom of the peroxo ligand. Cu(1) is displaced 0.319(2) Å out of the N(1), N(2), N(3) trigonal plane away from the tertiary nitrogen N(4) toward O(2) of the peroxo ligand. The Cu(1)-O(2) bond length (1.915(5) Å) and the Cu(1)-O(2)-O(3) angle (103.0(4)°) are close to those of the *trans*-(μ-1,2-peroxo)dicopper(II) complex.[15]

Evidence that the peroxo ligand bridges the iron and the copper ions is also obvious from magnetic studies. The peroxo complex **2** is ESR inactive at 4 K. The magnetic susceptibility of **2** was measured from 10 to 300 K. The determined effective magnetic moment is 4.65 μ_B and temperature independent within this temperature range. This magnetic moment is consistent with a spin-only value of $S = 2$ ($\mu_{eff} = 4.90\ \mu_B$), therefore, **2** is assigned as a paramagnetic species with an overall $S = 2$ spin state. The Mössbauer spectrum of **2** (77 K, zero field) showed a sharp quadrupole doublet with parameters ($\Delta E_q = 1.17\ mm\,s^{-1}$, $\delta = 0.56\ mm\,s^{-1}$) typical for high-spin Fe^{III} compound (see Supporting Information), and is in good agreement with those of peroxo-bound iron(III)-porphyrin complexes.[5e,14c] Based on these results, the iron ion has a high-spin d^5 configuration ($S = 5/2$), and is strongly coupled with the copper(II) ion ($S = 1/2$) in an antiferromagnetic fashion. This strong interaction between the metal ions is mediated by the bridging peroxo ligand.

In conclusion, we synthesized and characterized a peroxo-bridged iron-copper complex **2**. The successful isolation of **2** was confirmed by the elemental analysis and various spectroscopic methods. The X-ray structure analysis of **2** revealed that the Fe–O_2–Cu moiety has a μ-η^2:η^1 coordination mode. To the best our knowlege, this is the first example of the structure determination of a peroxo-bridged heterodinuclear complex. Further, this is the first X-ray structure of an "iron"-porphyrin complex with a side-on peroxo ligand.[14] Complex **2** is a paramagnetic species with a spin state of $S = 2$, as the bridging peroxo ligand mediates the strong antiferromagnetic coupling between the high-spin iron(III) and the copper(II) ions. Further studies of **2** are in progress in our laboratory.

Experimental Section

$[(TMP)Fe^{II}(5MeTPA)]$ was prepared by the similar procedure reported in reference [4].

Synthesis of complex **2**: $[(TMP)Fe^{II}(5MeTPA)]$ (48 mg, 42 mmol), $[Cu(CH_3CN)_4]OTf$ (18 mg, 42 mmol) and $NaBPh_4$ (16 mg, 42 mmol) were dissolved in CH_3CN (20 mL) and cooled to −30 °C. The resulting solution was exposed to dry O_2 gas for 30 min, and then stored at −30 °C for 5 days, to give **2** (32 mg, 25 mmol, 60 %) as dark purple crystals. Elemental analysis (%) calcd for $C_{98}H_{87}N_9O_3Cu_1Fe_1B_1$: C 75.02, H 5.59, N 8.03; found: C 74.64, H 5.59, N 7.87, ESI-MS: *m*/*z*: $[(TMP)Fe^{III}(^{16}O_2)(5MeTPA)Cu^{II}]^+$, 1248.

The ^{18}O-labeled peroxo complex for Raman experiment was synthesized and isolated by the same procedure. ESI-MS: *m*/*z*: $[(TMP)Fe^{III}(^{18}O_2)(5MeTPA)Cu^{II}]^+$, 1252.

Received: March 17, 2003 [Z51415]

Keywords: copper · iron · peroxo ligands · porphyrinoids

[1] a) M. Sono, M. P. Roach, E. D. Coulter, J. H. Dawson, *Chem. Rev.* **1996**, *96*, 2841; b) R. E. White, M. J. Coon, *Annu. Rev. Biochem.* **1980**, *49*, 315; c) I. C. Gausalus, J. R. Meeks, J. D. Lipsoomb, P. Debrunner, E. Munck, *Molecular Mechanism of Oxygen Activation* (Ed.: O. Hayashi), Academic Press, New York, **1974**, chap. 14, p. 559; d) M. Costas, K. Chen, L. Que, Jr., *Coord. Chem. Rev.* **2000**, *200*, 517; e) W. J. Ingleden, M. Bacon, *Biochem. Soc. Trans.* **1991**, *19*, 613.

[2] a) S. Iwata, C. Ostermeier, B. Ludwig, H. Michel, *Nature* **1995**, *376*, 660; b) C. Ostermeier, A. Harrenga, U. Ermler, H. Michel, *Proc. Natl. Acad. Sci. USA* **1997**, *94*, 10547; c) T. Tsukihara, H. Aoyama, E. Yamashita, T. Tomizaki, H. Yamaguchi, K. Shinzawa-Itoh, R. Nakashima, R. Yano, S. Yoshikawa, *Science* **1995**, *269*, 1069; d) T. Tsukihara, H. Aoyama, E. Yamashita, T. Tomizaki, H. Yamaguchi, K. Shinzawa-Itoh, R. Nakashima, R. Yano, S. Yoshikawa, *Science* **1996**, *272*, 1136; e) S. Yoshikawa, K. Shinzawa-Itoh, R. Nakashima, R. Yano, E. Yamashita, N. Inoue, M. Yao, M. J. Fei, C. P. Libei, T. Mizushima, H. Yamaguchi, T. Tomizaki, T. Tsukihara, *Science* **1998**, *280*, 1723; f) J. Abramson, S. Riistama, G. Larsson, A. Jasaitis, M. Svensson-Ek, L. Laakkonen, A. Puustinen S. Iwata, M. Wirkström, *Nat. Struct. Biol.* **2002**, *7*, 910.

[3] a) J. P. Collman, L. Fu, P. C. Hermann, X. Zhang, *Science* **1997**, *275*, 949; b) J.-O. Baeg, R. H. Holm, *Chem. Commun.* **1998**, 571; c) F. Tani, Y. Matsumoto, Y. Tachi, T. Sasaki, Y. Naruta, *Chem. Commun.* **1998**, 1731; d) R. Boulatov, J. P. Collman, I. M. Shiryaeva, C. P. Sunderland, *J. Am. Chem. Soc.* **2002**, *124*, 11923, and references therein.

[4] a) T. Sasaki, N. Nakamura, Y. Naruta, *Chem. Lett.* **1998**, 351; b) Y. Naruta, T. Sasaki, F. Tani, Y. Tachi, N. Kawato, N. Nakamura, *J. Inorg. Biochem.* **2001**, *83*, 239.

[5] a) A. Nanthakumar, S. Fox, N. N. Murthy, K. D. Karlin, *J. Am. Chem. Soc.* **1997**, *119*, 3898; b) H. V. Obias, G. P. F. van Strijdonck, D.-H. Lee, M. Ralle, N. J. Blackburn, K. D. Karlin, *J. Am. Chem. Soc.* **1998**, *120*, 9696; c) T. D. Ju, R. A. Ghiladi, D.-H. Lee, G. P. F. van Strijdouck, A. S. Woods, R. J. Cotter, J. V. G. Young, K. D. Karlin, *Inorg. Chem.* **1999**, *38*, 2244; d) R. A. Ghiladi, T. D. Ju, D.-H. Lee, P. Moënne-Loccoz, S. Kaderli, Y. M. Neuhold, A. D. Zuberbühler, A. S. Woods, R. J. Cotter, K. D. Karlin, *J. Am. Chem. Soc.* **1999**, *121*, 9885; e) R. A. Ghiladi, K. R. Hatwell, K. D. Karlin, H.-W. Huang, P. Moënne-Loccoz, C. Krebs, B. H. Huynh, L. A. Marzilli, R. J. Cotter, S. Kaderli, A. D. Zuberbühler, *J. Am. Chem. Soc.* **2001**, *123*, 6183.

[6] Collman et al. have also reported the dioxygen reaction with different types of iron(II)- or cobalt(II)-porphyrin-linked copper(I) dinuclear complexes and the formation of the corresponding peroxo species: J. P. Collman, *Inorg. Chem.* **1997**, *36*, 5145, and references therein.

[7] The peroxo complex **2** in CH_3CN solution is stable for several days at room temperature. It gradually decomposes, to give the mixture of corresponding μ-oxo and μ-hydroxo complexes, as reported in ref. [4] and [5]. Detailed studies of the decomposition mechanism are in progress.

[8] The X-ray experiments for complexes **2** were carried out on a Rigaku RAXIS imaging plate area detector with graphite monochromated $Cu_{K\alpha}$ radiation ($\lambda = 1.54178$ Å). The crystal was mounted on a glass fiber. The data were collected ($3.5 \le 2\theta \le 136.5°$) at −150 °C. To determine the cell constant and

orientation matrix, three oscillation photographs were taken with an oscillation angle of 5.0° and exposure time of 60 s per degree for each frame. Intensity data were collected by taking 180 oscillation photographs with an oscillation angle of 5.0° and exposure time of 90 s per degree for each frame. Refraction data were corrected for both Lorentz and polarization effects. **2**: $C_{98}H_{87}N_9O_3Cu_1Fe_1B_1$, dark purple crystals, monoclinic, $P2_1/n$, $a = 14.2898(4)$, $b = 13.0041(3)$, $c = 50.368(1)$ Å, $\beta = 91.4898(7)°$, $V = 9356.6(4)$ Å^3, $Z = 4$, $\rho_{calcd} = 1.114$ g cm^{-3}, 91575 reflections collected, 15999 reflections used and 1126 parameters. $R = 0.095$ ($I > 3.0\sigma(I)$), $R_W = 0.223$. CCDC-205246 (**2**) contains the supplementary crystallographic data for this paper. These data can be obtained free of charge via www.ccdc.cam.ac.uk/conts/retrieving.html (or from the Cambridge Crystallographic Data Centre, 12 Union Road, Cambridge CB2 1EZ, UK; fax: (+44) 1223-336-033; or deposit@ccdc.cam.ac.uk).

[9] a) F. A. Cotton, G. Wilkinson, C. A. Murillo, M. Bochmann, *Advanced Inorganic Chemistry*, 6th ed., Wiley, New York, **1999**, p. 450; b) J. S. Valentine, *Chem. Rev.* **1973**, *73*, 235; c) L. Vaska, *Acc. Chem. Res.* **1976**, *9*, 175.

[10] a) R. Guilard, M. Fontesse, P. Fournari, C. Lecomte, J. Protas, *J. Chem. Soc. Chem. Commun.* **1976**, 161; b) R. Guilard, J.-H. Latour, C. Lecomte, J.-C. Marchon, J. Protas, D. Ripoll, *Inorg. Chem.* **1978**, *17*, 1228.

[11] B. Chevrier, T. Diebold, R. Weiss, *Inorg. Chim. Acta* **1976**, *19*, L57.

[12] a) B. M. Hoffman, C. J. Weschler, F. Basolo, *J. Am. Chem. Soc.* **1976**, *98*, 5473; b) R. B. VanAtta, C. E. Strouse, L. K. Hanson, J. S. Valentine, *J. Am. Chem. Soc.* **1987**, *109*, 1425.

[13] a) M. J. Bennett, P. B. Donaldson, *J. Am. Chem. Soc.* **1971**, *93*, 3307; b) M. J. Bennett, P. B. Donaldson, *Inorg. Chem.* **1977**, *16*, 1585; c) V. Suchá, M. Sivák, J. Tyrsenová, J. Marek, *Polyhedron* **1997**, *16*, 2837; d) T. Miyaji, M. Kujime, S. Hikichi, Y. Moro-oka, M. Akita, *Inorg. Chem.* **2002**, *41*, 5286.

[14] a) E. McCandlish, A. R. Miksztal, M. Nappa, A. Q. Sprenger, J. S. Valentine, J. D. Stong, T. G. Spiro, *J. Am. Chem. Soc.* **1980**, *102*, 4268; b) P. Friant, J. Goulon, J. Fischer, L. Ricard, M. Schappacher, R. Weiss, M. Momenteau, *Nouv. J. Chim.* **1985**, *9*, 33; c) J. N. Burstyn, J. A. Roe, A. R. Miksztal, B. A. Shaevitz, G. Lang, J. S. Valentine, *J. Am. Chem. Soc.* **1988**, *110*, 1382.

[15] Z. Tyeklár, R. R. Jacobson, N. Wei, N. N. Murthy, J. Zubieta, K. D. Karlin, *J. Am. Chem. Soc.* **1993**, *115*, 2677.

 © 2003 Wiley-VCH Verlag GmbH & Co. KGaA, Weinheim

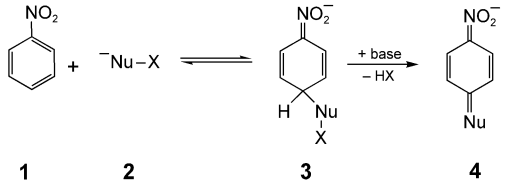
Vicarious Substitutions

Direct Observation of the Intermediate in Vicarious Nucleophilic Substitutions of Hydrogen**

Tadeusz Lemek, Mieczysław Mąkosza, David S. Stephenson, and Herbert Mayr**

In memory of Janusz Baran

Vicarious nucleophilic substitution has proven to be a general method for the direct replacement of hydrogen atoms in electron-deficient aromatic rings.[1] As shown in Scheme 1, the reaction has been postulated to proceed through the energetically high-lying intermediate σ^H adduct **3**.[2] Depending on the reagents and reaction conditions, nucleophilic addition (formation of **3**) or 1,2-elimination (formation of **4**) may be the rate-determining step.[2b]

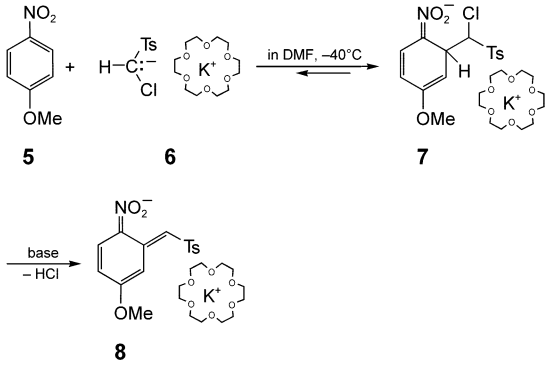


Scheme 1. Vicarious nucleophilic substitution of hydrogen.[1]

This mechanism is in accord with all experimental evidence so far acquired, including substituent effects,[2a] kinetic isotope effects,[2b,c] and leaving-group dependence.[2d,e] However, σ^H adducts have generally been considered as short-lived intermediates[2a] which have never been directly observed.[3]

Herein we report the first UV/Vis and NMR spectroscopic observation of σ^H adducts from an α halogen-substituted carbanion and mononitro-substituted benzene derivatives, which allows us to observe directly the individual steps of vicarious nucleophilic substitutions and to determine the rates of the addition steps.

Nucleophilic addition: Addition of 4-nitroanisole (**5**) to colorless solutions of 7–50 equivalents of the carbanion **6**,[4] the most intensively studied carbanion in vicarious nucleophilic substitutions (Scheme 2), results in the formation of a yellow product with $\lambda_{max} = 408$ nm (Figure 1). Since the intensity of the final absorbance does not depend on the concentration of **6**, the conversion of **5** into the σ^H adduct **7** must be complete.



Scheme 2. Stepwise formation of **8** by vicarious nucleophilic substitution from the chloro-4-tolylsulfonyl methyl anion **6** and nitroanisole (**5**).

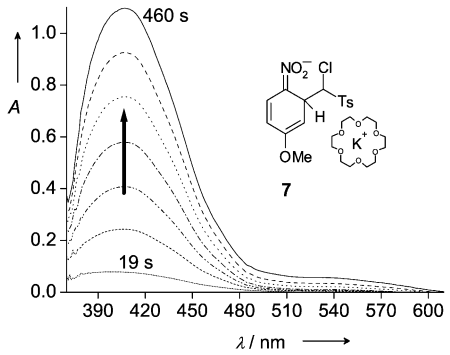


Figure 1. Formation of the σ^H adduct **7** from **6** (0.01 M) and **5** (2×10^{-4} M) in DMF at −40 °C.

When the reactions were run with $[\mathbf{6}]_0 \geqslant [\mathbf{5}]_0$ (pseudo-first-order conditions), linear plots of $\ln(A_\infty - A_t)$ versus t were observed, which indicate first-order kinetics with respect to arene. From the slopes of these plots, the pseudo-first-order rate constants $k_{1\psi}$ were derived, which were plotted against [**6**] to yield the second-order rate constant k_2 (Figure 2).

To confirm the identity of the σ^H intermediate, the reaction of **5** with **6** was also investigated by NMR spectroscopy. A 0.02 M solution of **7** was obtained by adding equimolar amounts of *t*BuOK and of **5** dissolved in [D_8]THF successively to a solution of $TsCH_2Cl$ (Ts = tosyl) and [18]crown-6 in [D_8]THF at −78 °C. The ^{1}H NMR (400 MHz) spectrum taken at −40 °C indicated the presence of two diastereoisomers in a 1:3 ratio, which are tentatively assigned the molecular structures shown in Scheme 3. The structure of the major diastereoisomer could further be corroborated by its ^{13}C NMR spectrum.[5]

Elimination: When the solution of **7** is produced from **5** (2×10^{-4} M) with excess of **6** (5×10^{-3} M) in DMF at −40 °C, the

[*] Dr.-Ing. T. Lemek, Prof. Dr. H. Mayr, Dr. D. S. Stephenson
Department Chemie
Ludwig-Maximilians-Universität München
Butenandtstrasse 5–13 (Haus F), 81377 München (Germany)
Fax: (+49) 89-2180-77717
E-mail: tadeusz.lemek@cup.uni-muenchen.de
herbert.mayr@cup.uni-muenchen.de
Prof. Dr. M. Mąkosza
Institute of Organic Chemistry
Polish Academy of Sciences
Kasprzaka 44, 01-224 Warszawa (Poland)

[**] We thank the Alexander von Humboldt Foundation for a fellowship to T.L., as well as the Deutsche Forschungsgemeinschaft and the Fonds der Chemischen Industrie for financial support.

 DOI: 10.1002/anie.200351352 © 2003 Wiley-VCH Verlag GmbH & Co. KGaA, Weinheim

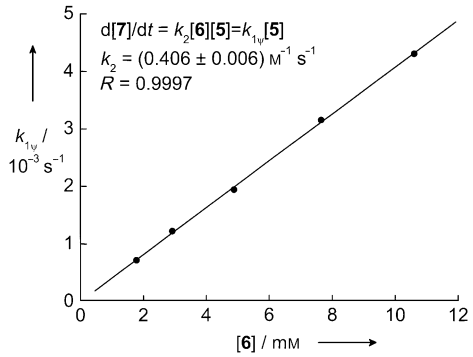
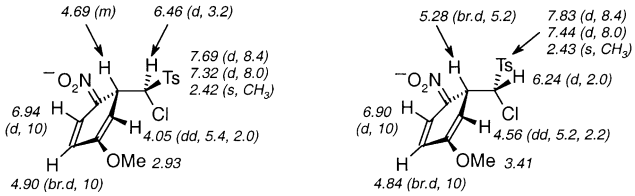


Figure 2. Pseudo-first-order rate constants of the addition reactions of **5** with **6** in DMF at −40 °C ($[\mathbf{6}]_0 \gg [\mathbf{5}]_0$).



7, minor diastereoisomer **7**, major diastereoisomer

Scheme 3. Chemical shift values from ^{1}H NMR spectroscopy of a 1:3 mixture of the two diastereoisomers of **7** assigned by a COSY experiment (−40 °C, [D$_8$]THF, δ [ppm], in parentheses: J [Hz]).

UV/Vis spectra show a slow decrease of the absorbance of **7** at $\lambda_{max} = 408$ nm (< 10 % within 30 min), which is accompanied by the appearance of a new absorption band with $\lambda_{max} = 534$ nm arising from the elimination process **7**→**8** formulated in Scheme 2. The small value of the absorbance at $\lambda = 534$ nm in Figure 1 indicates that this subsequent reaction is almost negligible during the formation of **7** from **5** and **6**.

In accord with previous investigations,[2b] the conversion of **7** into **8** can be accelerated by the addition of extra base, for example *t*BuOK, the standard base for vicarious nucleophilic substitution on a preparative scale. Figure 3 illustrates that **7** and **8** have comparable absorption coefficients at λ_{max} of both ions, and the observation of the isosbestic point demonstrates the absence of further long-lived intermediates. Since the rate of the conversion of **7** into **8** does not increase linearly with the concentration of *t*BuOK, rate constants for this process have not been determined.

NMR spectroscopic investigation of the conversion of **7** into **8** showed different behavior of the two diastereoisomers. When a 0.02 M solution of the potassium [18]crown-6 salt of **7** in [D$_8$]THF was warmed to −20 °C, slow disappearance of the signals of the minor diastereoisomer of **7** and the growth of signals arising from **8** was observed, while the signals of the major diastereoisomer of **7** remained unaffected. Conversion of both diastereoisomers of **7** into **8** occurred when **7** was treated with an excess of *t*BuOK at approximately −40 °C and warmed to room temperature.

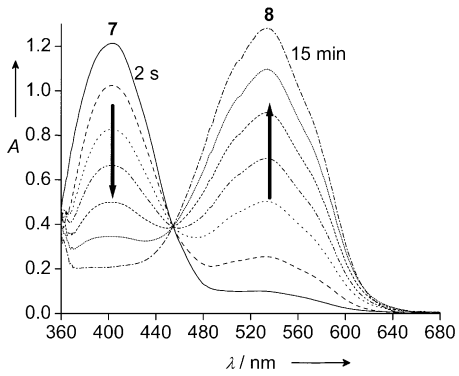
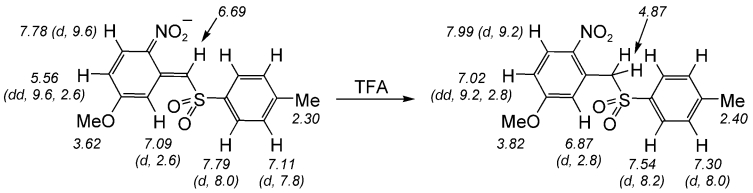


Figure 3. Formation of the anion **8** by treatment of the σ^H adduct **7** (2×10^{-4} M) with *t*BuOK (2×10^{-2} M; DMF, −40 °C). The color of the reaction mixture changes from yellow to purple.

While *anti*-elimination of HCl converts the minor diastereoisomer of **7** directly into the *E* isomer of **8**, the corresponding *Z* isomer of **8** is expected to be formed by *anti*-elimination from the major diastereoisomer. It is not clear whether the exclusive formation of the *E* isomer of **8** is a result of stereoisomerization at the stage of **7** (by deprotonation–reprotonation of **7** at the CHCl position) or a result of base-induced isomerization of the *Z* isomer of **8** into the thermodynamically more favorable *E* isomer of **8**. Stereomutation of the two stereoisomers of **7** by retroaddition (→**5** + **6**) is excluded because the formation of **8** from the major stereoisomer requires the presence of a higher concentration of base.

Treatment of the purple solution of **8** with trifluoroacetic acid (TFA) led to decolorization because of the formation of **9**, which gave spectra consistent with those in the literature (Scheme 4).[6]



8 **9**

Scheme 4. Chemical shift values from ^{1}H NMR spectroscopy of the nitrotosyl-substituted benzyl anion **8** and its protonation product, **9** (in [D$_8$]THF).

Since the same reaction cascade, quantitative formation of a σ^H adduct followed by slow elimination of HCl was also observed by the reaction of **6** with 4-bromonitrobenzene, it is concluded that in contrast to current opinion[2a] the initially formed σ^H adducts are often not high-energy intermediates, but are usually formed in exergonic reactions of α halocarbanions with nitroarenes.

Received: March 7, 2003 [Z51352]

Keywords: aromatic substitution · carbanions · elimination · kinetics · nucleophilic substitution

 © 2003 Wiley-VCH Verlag GmbH & Co. KGaA, Weinheim

[1] a) M. Mąkosza, J. Winiarski, *Acc. Chem. Res.* **1987**, *20*, 282 – 289; b) M. Mąkosza, *Synthesis* **1991**, 103 – 111; c) M. Mąkosza, *Pol. J. Chem.* **1992**, *66*, 3 – 23; d) M. Mąkosza, *Chem. Unserer Zeit* **1996**, *30*, 134 – 140; e) M. Mąkosza, *Russ. Chem. Bull.* **1996**, *45*, 491 – 503; f) M. Mąkosza, K. Wojciechowski, *Liebigs Ann.* **1997**, 1805 – 1816; g) F. Terrier, *Nucleophilic Aromatic Displacement: The Influence of the Nitro Group*, VCH, New York, **1991**; h) O. N. Chupakin, V. N. Charushin, H. C. van der Plas, *Nucleophilic Aromatic Substitution of Hydrogen*, Academic Press, San Diego, **1994**; i) S. Ostrowski, *Pol. J. Chem.* **2001**, *75*, 1661 – 1687; j) O. V. Donskaya, G. V. Dolgushin, V. A. Lopyrev, *Chem. Heterocycl. Compd.* **2002**, *38*, 371 – 383; O. V. Donskaya, G. V. Dolgushin, V. A. Lopyrev, *Khim. Geterotsikl. Soedin.* **2002**, 435 – 449.

[2] a) M. Mąkosza, A. Kwast, *J. Phys. Org. Chem.* **1998**, *11*, 341 – 349; b) M. Mąkosza, T. Lemek, A. Kwast, F. Terrier, *J. Org. Chem.* **2002**, *67*, 394 – 400; c) T. Glinka, M. Mąkosza, *J. Org. Chem.* **1983**, *48*, 3860 – 3861; d) S. Ostrowski, M. Mąkosza, *Tetrahedron* **1988**, *44*, 1721 – 1726; e) M. Mąkosza, T. Ziobrowski, M. Serebriakov, A. Kwast, *Tetrahedron* **1997**, *53*, 4739 – 4750.

[3] For reactions of carbanions, which contain leaving groups, with highly electrophilic arenes yielding stable σ^H adducts which do not undergo β elimination, see: a) G. P. Stahly, B. C. Stahly, J. R. Maloney, *J. Org. Chem.* **1988**, *53*, 690 – 692; b) G. P. Stahly, *J. Fluorine Chem.* **1989**, *45*, 431 – 433; c) S. Ostrowski, M. Mąkosza, *J. Organomet. Chem.* **1989**, *367*, 95 – 100; d) P. Müller, G. Bernardinelli, S. Motallebi, *Helv. Chim. Acta* **1990**, *73*, 1242 – 1249; see also: e) F. Terrier, R. Goumont, M. J. Pouet, J. C. Halle, *J. Chem. Soc. Perkin Trans. 2* **1995**, 1629 – 1637.

[4] The carbanion **6** ($\lambda_{max} = 317$ nm) formed instantaneously (< 0.1 s) when a solution of *t*BuOK (0.2 mmol) in THF (0.8 mL) was added to a solution of 1 equivalent of chloro 4-tolylsulfonyl methane and 1 equivalent of [18]crown-6 in DMF (20 mL) at −40 °C.

[5] ^{13}C NMR ([D_8]THF, 100.7 MHz): $\delta = 21.77$ (q, CH_3), 41.98 (d), 54.56 (q, OCH_3), 74.09 (d), 87.99 (d), 109.59 (d), 113.27 (s), 127.13 (d), 129.68 (d), 130.67 (d), 136.73 (s), 145.92 (s), 157.97 ppm (s).

[6] a) W. Verboom, E. O. H. Orlemans, H. J. Berga, H. W. Scheltinga, D. N. Reinhoudt, *Tetrahedron* **1986**, *42*, 5053 – 5064; b) M. Mąkosza, Z. Wróbel, *J. Prakt. Chem.* **1992**, *334*, 131 – 134.

 © 2003 Wiley-VCH Verlag GmbH & Co. KGaA, Weinheim

Catalytic Diels–Alder Reactions

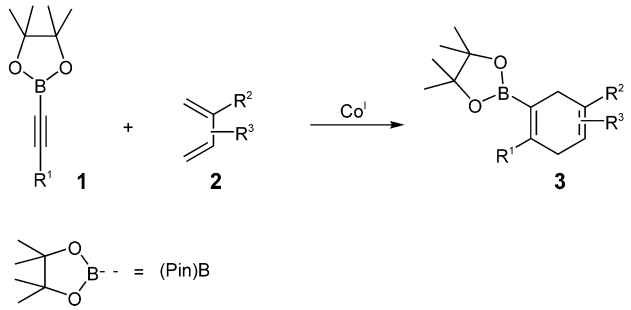
Alkynylboronic Esters as Efficient Dienophiles in Cobalt-Catalyzed Diels–Alder Reactions

Gerhard Hilt and Konstantin I. Smolko*

In memory of Konstantin Smolko

The palladium-catalyzed Suzuki coupling of boron-functionalized aromatic and vinylic building blocks has been established as a useful tool for carbon–carbon bond formation in organic synthesis.[1] The synthesis of vinylic boron compounds by thermal Diels–Alder reactions is rare, since the low reactivity of alkynylboronic esters[2] and the instability of 2-boron-functionalized 1,3-dienes[3] prohibit the efficient use of these materials in these reactions.

In contrast to the thermal Diels–Alder reactions with alkynylboronic esters, the cobalt(I)-catalyzed cycloaddition[4] of alkynylboron compounds **1** with the acyclic 1,3-dienes **2** proceeds under very mild conditions to generate the corresponding dihydroaromatic vinylboron compounds **3** in good yield (Scheme 1).[5] A catalyst system consisting of $[CoBr_2(dppe)]$ (dppe = bis(diphenylphosphanyl)ethane), ZnI_2, and Zn powder has proven to be very effective for the reaction of the alkynylboron compounds.



Scheme 1. Regioselective cobalt(I)-catalyzed Diels–Alder reaction of alkynylboronic esters with 1,3-dienes.

Alkynyl pinacol boronic esters, alkynyl diisopropylboronic esters, and alkynyl-9-BBN boranes can all be used as the dienophilic alkyne component. The latter cycloadducts are much more difficult to isolate than the pinacol derivatives, which can be purified by regular column chromatography on silica gel.

The reaction of the alkynylboron compounds with isoprene generates predominantly the regioisomer in which the methyl group of the diene and the boronic ester functionality have a *meta* relationship. Both the regioselectivity and the stability of the adducts increased on going from the 9-BBN derivatives to the isopropyl boronic esters to the pinacol boronic esters (Table 1). For the latter adducts the regioselectivity is generally very good ($> 95 : < 5$).[6] In most cases the other regioisomer could only be detected in traces.[7]

Based on the effective control of the regiochemistry, the mild reaction conditions, and the good yields of the sensitive dihydroaromatic products, we investigated the subsequent reactions of the cycloadducts as a platform for the efficient synthesis of more complex products. The complexity of the products could be increased significantly by palladium-catalyzed Suzuki coupling reactions (Scheme 2). The reaction sequence consisting of the cobalt-catalyzed Diels–Alder reaction, Suzuki coupling giving **4,** and mild oxidation with DDQ to yield **5** can be performed as a one-pot operation without isolation of the intermediates. The dihydroaromatic vinylic boron compounds **3** can be used in sp^2/sp^2 and sp^2/sp coupling reactions with the corresponding halides to generate intermediates **4**. Thus building blocks can be connected to give more complex polyfunctionalized structures (Table 2).

[*] Prof. Dr. G. Hilt, K. I. Smolko
Fachbereich Chemie
Philipps-Universität Marburg
Hans-Meerwein-Strasse, 35043 Marburg (Germany)
Fax: (+49) 6421-282-5677
E-mail: hilt@chemie.uni-marburg.de

 DOI: 10.1002/anie.200351404 © 2003 Wiley-VCH Verlag GmbH & Co. KGaA, Weinheim

Table 1: Results of the cobalt(I)-catalyzed Diels–Alder reaction with alkynylboronic esters.

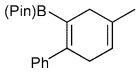
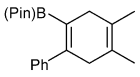
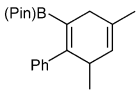
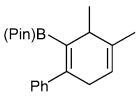
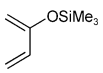
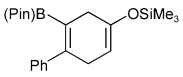
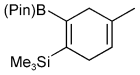
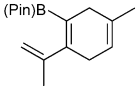
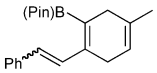
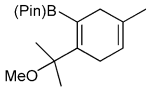
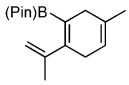
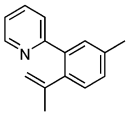
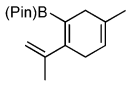
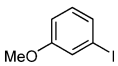
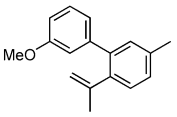
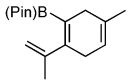
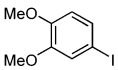
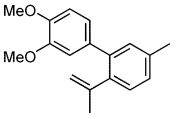
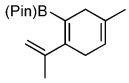
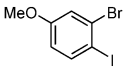
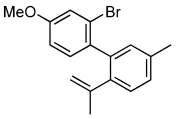
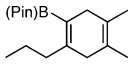
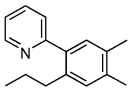
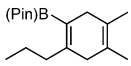
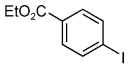
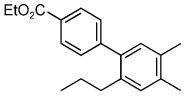
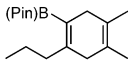
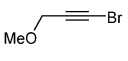
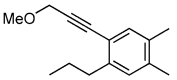
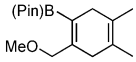
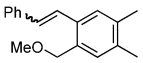
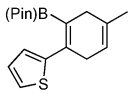
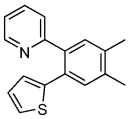
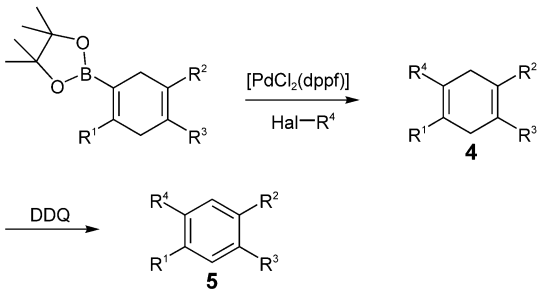
Entry	R^1	Diene	Product	Yield [%]
1	Ph			85
2	Ph			76
3	Ph			71
4	Ph			68
5	Ph			61
6	$SiMe_3$			85
7				91
8				63
9				76

Table 2: Results of the reaction sequence consisting of Diels–Alder reaction, Suzuki coupling, and DDQ oxidation.

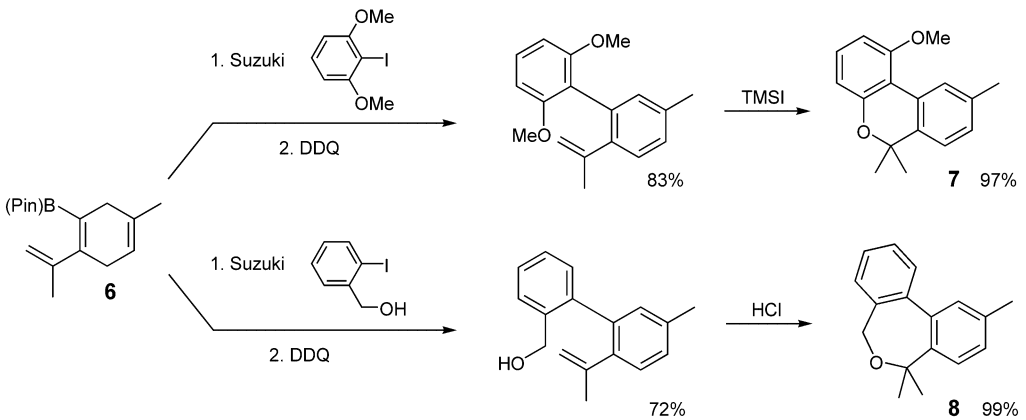
Entry	**3**	R-Hal	**5**	Yield [%][a]
1				83
2				89
3				85
4				85
5				73
6				83
7				68
8				75
9				63

[a] Yield over three steps.



Scheme 2. Suzuki coupling of the dihydroaromatic boron derivatives and subsequent oxidation. dppf = bis(diphenylphosphanyl)ferrocene, DDQ = dichlorodicyanobenzoquinone.

Tricyclic compounds can be prepared efficiently when the Suzuki coupling of the isopropenyl substituents building block **6** with alkoxy-functionalized aromatic halides is followed by oxidation with DDQ and cleavage of the ether with trimethylsilyl iodide (Scheme 3). Spontaneous cyclization[8] gives the framework of the family of cannabinoid natural products **7**. Structural variations are easily accessible by this



Scheme 3. Synthesis of heterocyclic compounds from polyfunctionalized dihydroaromatic boron compounds. TMSI = trimethylsilyl iodide.

 © 2003 Wiley-VCH Verlag GmbH & Co. KGaA, Weinheim

modular approach. For example, the Suzuki coupling of 2-iodobenzylic alcohol and the following acid-catalyzed cyclization generates the structurally related product **8** in good yield. These and other reactions of dihydroaromatic boron compounds give an indication of the synthetic potential of this new class of compounds, which we are currently investigating.

Experimental Section

Synthesis of 2-(5-methyl-2-thiophen-2-yl-phenyl)pyridine (Table 2, entry 9): A 10-mL Schlenk flask was charged with [$CoBr_2$(dppe)] (31 mg, 0.05 mmol, 5 mol%), ZnI_2 (100 mg, 0.31 mmol, 31 mol%), and zinc dust (22 mg, 0.3 mmol, 30 mol%) in dry dichloromethane under a nitrogen atmosphere. After addition of 4,4,5,5-tetramethyl-(2-thiophen-2-yl-ethynyl)-1,3,2-dioxaborolane (234 mg, 1.0 mmol) and isoprene (82 mg, 1.2 mmol) the mixture was stirred for 16 h at ambient temperature (GC, GCMS monitoring). The solvents were removed, and the residue was dissolved in THF (5 mL) and aqueous NaOH solution (10%, 2 mL). Then 2-bromopyridine (170 mg, 1.1 mmol) and [$PdCl_2$(dppf)] (70 mg, 0.1 mmol, 10 mol%) were added. The solution was stirred over night at ambient temperature then diluted with water (20 mL) and diethyl ether (30 mL). The aqueous phase was extracted with diethyl ether (2 × 20 mL), washed with brine, and dried over Na_2SO_4. After the solvent was removed, the residue was dissolved in benzene (10 mL) and DDQ (300 mg, 1.32 mmol) was added in one portion. After 10 min basic $Na_2S_2O_3$ solution (10% $Na_2S_2O_3$ and 10% NaOH, 20 mL) was added and the mixture was stirred for another 5 min. The aqueous phase was extracted with diethyl ether (2 × 20 mL), washed with brine, and dried over Na_2SO_4. The crude product was purified by column chromatography on silica gel, eluting with pentane/diethyl ether (10:1), and the product was obtained as an oily mass (158 mg, 0.63 mmol, 63%). ^{1}H NMR (C_6D_6, 300 MHz): $\delta = 2.33$ (s, 3H), 6.57 (dd, 1H, $J = 3.5$ Hz, 1.2 Hz), 6.77 (dd, 1H, $J = 3.6$ Hz, 5.2 Hz), 6.97–7.20 (m, 4H), 7.33–7.47 (m, 2H), 7.41 ppm (dd, $J = 1.9$ Hz, 7.7 Hz); ^{13}C NMR (C_6D_6, 75 MHz): $\delta = 21.0$, 121.6, 124.9, 125.3, 126.7, 127.0, 129.2, 130.2, 130.6, 131.1, 135.4, 137.9, 139.6, 142.9, 149.3, 159.3 ppm; IR (KBr): $\tilde{\nu} = 3066$ (m), 2919 (m), 1587 (s), 1562 (s), 1464 (s), 1429 (s), 818 (s), 789(s), 747 (s), 698 cm^{-1} (s); MS (EI): m/z (%): 250 (M^+−1, 100), 235 (7), 218 (13), 194 (22), 180 (4), 118 (5), 108 (5), 95 (3); HRMS: calcd for $C_{16}H_{12}NS$ (M^+−H): 250.0690, found: 250.0669.

Received: March 14, 2003 [Z51404]

Keywords: alkynes · boron compounds · Diels–Alder reactions · dihydroaromatic compounds · Suzuki reaction

[1] A. Suzuki, *Pure Appl. Chem.* **1994**, *66*, 213; A. Suzuki in *Metal-Catalyzed Cross-Coupling Reactions* (Eds.: F. Diederich, P. J. Stang), Wiley-VCH, Weinheim, **1998**, chapt. 2, p. 49.

[2] D. S. Matteson, J. O. Wasserbillig, *J. Org. Chem.* **1963**, *28*, 366; M. A. Silva, S. C. Pellegrinet, J. M. Goodman, *J. Org. Chem.* **2002**, *67*, 8203; D. A. Singleton, S.-W. Leung, *J. Org. Chem.* **1992**, *57*, 4796; S.-W. Leung, D. A. Singleton, *J. Org. Chem.* **1997**, *62*, 1955; D. A. Singleton, S.-H. Leing, *J. Organomet. Chem.* **1997**, *544*, 157; for an application in the Dötz reaction see: M. W. Davies, C. N. Johnson, J. P. A. Harrity, *J. Org. Chem.* **2001**, *66*, 3525; for an application in [3+2]-cycloadditions see: W. M. Davies, R. A. J. Wybrow, C. N. Johnson, J. P. A. Harrity, *Chem. Commun.* **2001**, 1558; for the synthesis of the alkynylboron derivatives see: H. C. Brown, N. G. Bhat, M. Srebnik, *Tetrahedron Lett.* **1988**, *29*, 2631.

[3] N. Guennouni, C. Rasset-Deloge, B. Carboni, M. Vaultier, *Synlett* **1992**, 581; A. Kamabuchi, N. Miyaura, A. Suzuki, *Tetrahedron Lett.* **1993**, *34*, 4827; M. Shimizu, T. Kurahashi, T. Hiyama, *Synlett* **2001**, 1006; J. Renoud, C.-D. Graf, L. Oberer, *Angew. Chem.* **2000**, *112*, 3231; *Angew. Chem. Int. Ed.* **2000**, *39*, 3101; F. Carreaux, F. Posseme, B. Carboni, A. Arrieta, B. Lecea, F. P. Cossio, *J. Org. Chem.* **2002**, *67*, 9153.

[4] For previous reports on cobalt-catalyzed reactions see: G. Hilt, F.-X. du Mesnil, S. Lüers, *Angew. Chem.* **2001**, *113*, 408; *Angew. Chem. Int. Ed.* **2001**, *40*, 387; G. Hilt, K. I. Smolko, *Synlett* **2002**, 1081.

[5] When Bu_4NBH_4 was used as reducing agent for the generation of the active cobalt(I) catalyst, side reactions such as the reduction of the triple bond were observed.

[6] The regioselectivity can be explained by steric effects as well as by an insertion of the alkynylboron derivative into the intermediate cobaltacycle in terms of a Michael addition.

[7] Traces of a side product could be detected by GC and GCMS, which could be either a regioisomer or a double-bond isomer (1,3-cyclohexadiene derivative).

[8] Traces of water should be present so the reaction can reach completion within 5 minutes.

 © 2003 Wiley-VCH Verlag GmbH & Co. KGaA, Weinheim